Appeneix 4.2-10 to Appendix 4.2-12, Appendix A-F, Appendix 4.2-13 to Appendix 4.2-14. Volume XII

Foth and Van Dyke and Associates, Inc.
Green Bay, Wisconsin: Foth and Van Dyke, [s.d.]

https://digital.library.wisc.edu/1711.dl/PDOL7B65H2B6Z83

Appendix 4.2-10

Numerical Simulation of Potential Solute Transport at the Proposed Zinc and Copper Mine Near Crandon, Wisconsin

Note: In November 1996 NMC submitted the above titled report to the WDNR and USCOE for review. The WDNR issued a letter dated November 17, 1997, to NMC containing comments on the report. To respond to those comments, HSI GeoTrans, Inc. prepared an April 28, 1998 report titled *Update to: Numerical Simulation of Potential Solute Transport at the Proposed Zinc and Copper Mine Near Crandon, Wisconsin.* In January 1999 HSI GeoTrans, Inc. issued a report titled *Update No. 2 to: Numerical Simulation of Potential Solute Transport at the Proposed Zinc and Copper Mine Near Crandon, Wisconsin.* The 1999 update was prepared to make the project's transport modeling work consistent with the flow model update issued by HSI GeoTrans, Inc. in August 1998, and the revised TMA footprint based on the depyritization concept. On June 21, 1999, HSI GeoTrans issued *Addendum No. 1 to: Update No. 2 to: Numerical Simulation of Potential Solute Transport at the Proposed Zinc and Copper Mine Near Crandon, Wisconsin.* The addendum presents an updated solute transport modeling analysis based on the correction of a discrepancy in the project's HELP model results. On March 27, 2000, HSI GeoTrans, Inc. issued *Update No. 3 to: Numerical Simulation of Potential Solute Transport at the Proposed Zinc and Copper Mine Near Crandon, Wisconsin.* Update No. 3 presents an updated solute transport model based on WDNR's review of the TMA *Groundwater Quality Performance Evaluation* contained in Appendix 4.2-12. These updates and Addendum No. 1 have been incorporated into Appendix 4.2-10 and immediately follow the original report.

The update addresses comments received from the Wisconsin Department of Natural Resources on November 17, 1997. This update addresses the following key items with respect to the TMA submodel:

- Revised model structure based on the 1998 revisions to the regional groundwater flow model.
- Inclusion of revised percolation rates based on the extension of a drainage layer along the upper sideslopes of the TMA.
- Inclusion of the TMA reclaim pond.
- Revised grid boundaries.
- Sensitivity analysis on vertical dispersivity.
- Particle tracking simulations to assess flow paths from the TMA.
- Detailed cross sections showing model layers.
- Calibration to CFC data.
- Sensitivity analysis on a global increase in hydraulic conductivity of the glacial deposits.
- Sensitivity analysis on TMA percolation rates.

This update also addresses the following items pertaining to the mine reflood model:

- Modeled cross sections showing particle starting positions, model layering, and the crown pillar.
- Sensitivity analysis on the starting positions of particles.
- Sensitivity analysis on hydraulic conductivity of the mine backfill.

You will note that sensitivity analyses covered in the November 1996 report are not repeated in the update to the report. Also, final compliance boundary concentrations are addressed in the forthcoming revised groundwater quality performance evaluation.

Should you have any questions concerning this document, please call me at (715) 478-3393.

Sincerely,

Gordon Reid
Manager of Engineering
Nicolet Minerals Company

MLD2\93C049\GBAPP\61690.61\4000

NUMERICAL SIMULATION OF POTENTIAL SOLUTE TRANSPORT AT THE PROPOSED ZINC AND COPPER MINE NEAR CRANDON, WISCONSIN

NOVEMBER 20, 1996

GeoTrans, inc.

TABLE OF CONTENTS

LIST OF TABLES

LIST OF FIGURES

1 INTRODUCTION

1.1 PROJECT DESCRIPTION

On February 15, 1994 Crandon Mining Company (CMC) issued to the Wisconsin Department of Natural Resources (WDNR) a Notice of Intent with a Detailed Scope of Study (NOI/SOS) informing the agency of its plan to seek permits and mine a zinc and copper deposit located in Forest County, Wisconsin, approximately five miles south of the City of Crandon (Foth & Van Dyke, 1994). The location of the Crandon ore body is shown in Figure 1.1. The ore body is long and tabular with an approximate width of 100 feet, north-south, and a strike length of 4900 feet, east-west. Based on the results of drilling, the mineable ore body extends to an approximate depth of 2200 feet.

The operating plan calls for mining the deposit via underground mining methods. This will involve both intercepting groundwater and removing it prior to entry into areas being mined and collecting and treating groundwater that bypasses the intercept system. Ore from the deposit will be physically concentrated on-site prior to shipment for further processing. Tailings from the processed ore will be used to backfill the mine workings, or will be pumped to an engineered tailings management area constructed with a composite liner and collection system and composite cap. The NOI/SOS described in detail the environmental studies that were conducted as part of the permitting process. An extensive description of the project is included in the Mine Permit Application (Foth & Van Dyke, 1995a).

As part of the project studies outlined in the NOI/SOS, a broad spectrum of environmental issues were studied, including archaeology, biology, blasting, geology and soils, groundwater, noise, topography, surface water, tailings management, waste characterization, water management, wetlands, etc. This report describes in detail the solute transport modeling that was performed as part of the environmental studies for the permit process. The solute transport model is a tool that was used to assess potential groundwater quality impacts of tailings management and mine closure activities. A separate groundwater flow modeling report provides estimates of mine water inflow and quantifies potential impacts of the mine water inflow on the overlying glacial aquifer and the subsequent impact on the lakes and streams.

1.2 OBJECTIVES OF STUDY

Solute transport modeling was performed to meet two primary objectives:

- to evaluate Tailings Management Area (TMA) compliance with groundwater standards,
- to evaluate groundwater quality in the glacial aquifer following mine reflooding.

Results from the solute transport modeling study are incorporated into related environmental studies. Results are also used in the impact section of the project's Environmental Impact Report (EIR) to evaluate compliance with groundwater standards and regulations.

1.3 METHOD OF INVESTIGATION

The objectives described in Section 1.2 are accomplished through the development of a numerical model that is capable of simulating the transport of dissolved constituents in the groundwater and from evaluation of flow directions during and following mine operations. This type of an analysis integrates available data and allows a hydrogeologic evaluation with extensive physical complexities (e.g. heterogeneity and other non-uniform parameter distributions). Predictions of future hydrologic changes on the system can be made, as well as an assessment of the sensitivity of various parameters on model results. The TMA transport model differs from the previously documented flow model in that it computes concentrations at points within the model, instead of the hydraulic heads that were computed by the flow model.

The generalized modeling process begins with development of a conceptual hydrogeological model. The conceptual model includes definition of hydrostratigraphic units, boundary conditions, sources, and sinks. The conceptual model is transformed into a mathematical model, consisting of governing groundwater flow and solute transport equations, which is solved by a computer program. The numerical groundwater flow model is calibrated to observed conditions. Model calibration is an iterative process of adjusting and revising model features and/or parameters, within hydrogeological reason, in order to test the conceptual understanding of the system and to match modeled results to field measured values. After the model is calibrated, predictive simulations are performed.

The solute transport modeling for this study uses the results of a regional groundwater flow model as its basis for representing the hydrogeological system. Detailed descriptions of the conceptual model, model construction, calibration, sensitivity analysis, and predictions are contained in GeoTrans (1996). The three-dimensional solute transport modeling documented in this report expands upon a two-

dimensional cross-sectional analysis that was documented in an earlier version of the groundwater modeling report. The earlier modeling report was completed in September 1995 and submitted to the WDNR, U.S. Army Corps of Engineers (COE), and other interested parties for review. That study and report were the subject of several meetings with the regulators. The discussions from those meetings has resulted in the modeling effort being updated. The primary change for the solute transport analysis was to extend the model to three dimensions. This report, along with the flow modeling report that was submitted in August 1996, serves to update and replace the September 1995 report on groundwater modeling.

Construction of the TMA solute transport model consisted of focusing the model domain used in the regional flow model on the vicinity of the TMA and it's proposed compliance boundary and increasing the resolution of computational points within that area. The stratigraphic layering and hydraulic parameters used in the solute transport model are therefore nearly identical to those used for the TMA area of the regional flow model. The construction of the solute transport model is discussed in detail in Section 2.1

The solute transport model uses parameters and boundary conditions derived from the calibrated regional groundwater flow model. In this sense, the groundwater flow aspects of the solute transport model are calibrated. Comparison of the solute transport model flow field to the groundwater model flow field as well as to observed field data were made to verify calibration. The results of this comparison is provided in Section 2.2. Calibration of solute transport properties is not possible.

Groundwater quality in the glacial aquifer following mine reflooding was assessed by analyzing flow paths and velocities of particles originating in the mined ore body. This advective solute transport model used the calibrated regional groundwater flow model directly. Therefore, additional model construction and calibration were not necessary to evaluate groundwater quality in the glacial aquifer following mine reflooding.

Predictive simulations of the potential groundwater quality impacts of tailings management and mine closure activities were also made. The predictive simulations with parameters that were based on model calibration and best available data are referred to as the Best Engineering Judgement (BEJ) simulations. Confidence in the ability of the model to represent the natural system was obtained from the multiple calibrations and sensitivity analysis performed with the groundwater flow model. In addition, a series of sensitivity simulations were performed on the solute transport model predictions. Sensitivity analysis involved running the models with a range of parameter values in order to determine which parameters are most influential in the model and system. These sensitivity simulations formed the basis for the Practical Worst Case (PWC) simulations. The PWC simulations represents a combination of

possible, but unlikely factors that could cause impacts to be in excess of those predicted by the BEJ simulation.

1.4 CONCEPTUAL MODEL

Separate conceptual models exist for each of the two objectives of the solute transport modeling study. The first deals with leakage of dissolved constituents from the engineered TMA facility. The second deals with water flowing upwards out of the ore body into the glacial aquifer system following mine closure.

The simulated mechanisms for solute transport from the TMA into the glacial system include movement of water through the lined facility during operation of each TMA basin, movement of water through the covered and lined facility following closure of each TMA basin, and postulated degradation of the Flexible Membrane Liner (FML) at some time in the future. These hypothetical events are assumed to be sequential. The first two events during which leakage is considered, operation and closure, are of known duration. Degradation of the FML, if it occurs, would happen at an unknown time in the future. A reasonable FML life was therefore assumed.

The conceptual model involves precipitation entering the TMA basins either by direct input during operation or through the composite liner (including FML and clay liner) and clay cap following closure. Tailings water is assumed to bypass the leachate collection system and percolate through the FML. Leakage through the FML was based on HELP model calculations completed by Foth andVan Dyke as part of the development of the TMA Feasibility Report/Plan of Operation. These calculations consider the amount of leakage that would result from a scenario involving an assumed number of holes in the FML and are standard for landfill design and assessment. The leakage through the FML is assumed to enter the unsaturated zone and travel vertically to the glacial aquifer system. The transit time in the unsaturated zone is likely on the order of many years or decades (EMC, 1985). For purposes of this analysis, two events were considered, entry of solute to the groundwater system on the first day of operation as the BEJ case and entry of solute to the groundwater system following cessation of mining activities as a sensitivity simulation. Once solute enters the groundwater system, it is assumed to be advected along groundwater flow paths toward groundwater discharge points. Along the route to discharge points, the solute mixes with resident groundwater and is dispersed through travel along tortuous paths in the saturated groundwater system. No geochemical reactions, such as adsorption or decay, are assumed to occur. Disregarding geochemical reactions is conservative with respect to travel time (adsorption) and with respect to concentrations at the compliance boundary (decay). As will be discussed in CMC's final Waste Characterization Report, concentrations within the source area are assumed to vary through time.

The conceptual model of flow through the mine workings is only possible after the mine has been reflooded following cessation of mining activities. Flow through the upper part of the mined workings into the glacial system is postulated to occur because there is a slight upward head gradient on the western end of the ore body under current conditions. The possibility therefore exists for flow passing through the upper mine workings, coming in contact with backfilled tailings and exiting the western part of the ore body. The analysis that was conducted assessed groundwater flowpaths resulting from post mining conditions. This scenario involved assessment of flow through the mine, once the mined area had been backfilled with tailings.

1.5 NUMERICAL MODELING APPROACH

Waste characterization studies documented in Foth & Van Dyke (1995b) indicate that source term concentration of some constituents will be in excess of applicable groundwater standards if these concentrations were considered at a compliance boundary. However, scoping calculations documented in the TMA Feasibility Report (Foth & Van Dyke, 1995c) indicate that concentrations will be reduced at least ten-fold between the source term and the proposed compliance boundary. Although the ten-fold reduction in concentration is sufficient for most constituents to comply with groundwater standards, a more sophisticated approach of computing concentrations at the compliance boundary and at points in between was desired. Numerical modeling was selected as the tool to address such complexities as changing flow directions due to cessation of mining operations, a changing source term, and the need to efficiently assess parameter sensitivity and Practical Worst Case situations.

Two separate numerical analyses, one for the TMA leak scenario and one for the mine reflooding scenario were made. For the TMA leak scenario, the entire history of solute transport was simulated, from entry of solute to the groundwater flow system until occurrence of a significant decline in concentration at the proposed compliance boundary. The model simulates flow in the saturated zone only, from point of entry to the glacial system to the proposed compliance boundary or nearby hydrologic boundary. Relative concentrations are used, such that reductions in concentrations at the proposed compliance boundary are expressed as a fraction of the input term. A superposition approach is used to account for time-variant changes in source concentrations. The advantage that this method has over using constituent specific concentrations is that a single simulation can be used for a variety of constituents. Actual concentrations can be calculated by multiplying the source concentration by the relative concentration computed by the model. A demonstration of the superposition and relative concentration method is provided in Section 2.3.

A three-dimensional model was used to evaluate groundwater flow in the vicinity of the TMA. The model uses a greater resolution of nodes, both vertically and

horizontally, than the regional groundwater flow model. The model uses parameters and boundary conditions derived from the regional groundwater flow model. Solute transport properties were obtained from the technical literature. Determination of site specific solute transport properties such as dispersivity and retardation by field methods was not considered necessary or practical. Instead of conducting field tests, reasonable ranges of solute transport parameters were tested with the model in the sensitivity analysis. Reasonable ranges for dispersivity were based on Gelhar, et al (1992). Retardation was conservatively assumed to not occur. The possible ranges in concentrations and travel time were evaluated with the model and discussed as a Practical Worst Case.

The regional groundwater flow model was used to simulate the potential for upward flow, out of the ore body and into the glacial system, following mine closure and reflooding. This flowpath currently occurs and is the result of hydraulic conductivity differences between the ore body, bedrock, and glacial system. The model evaluated future flowpaths resulting from decreased hydraulic conductivities in the ore body caused by backfilling with coarse tailings. The model was based on site-specific conditions and how they would be altered as a part of mine backfilling operations. The results of these simulations indicated that particle travel times to the compliance boundary would be very long. This finding eliminated the need to perform a detailed evaluation of solute transport from the ore body.

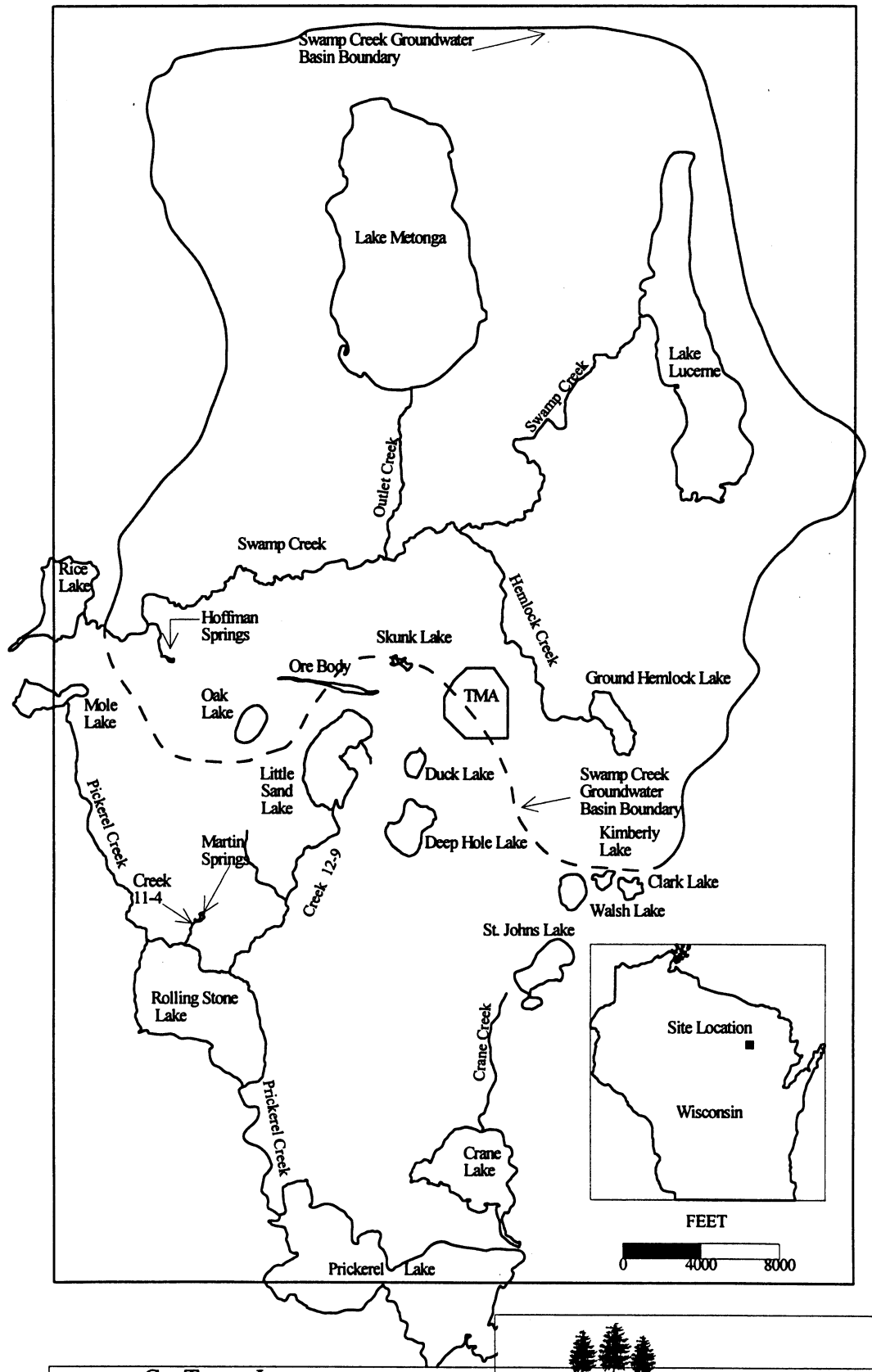

GeoTrans, Inc.		
REVISED	DATE	DESCRIPTION

CHECKED BY: RTH	DATE: NOV 96
APPROVED BY: PFA	DATE: NOV 96
APPROVED BY:	DATE:

Crandon Mining Company

FIGURE 1.1
Location Map

Scale: AS SHOWN	Date: NOV 1996
Prepared By: GeoTrans, Inc.	By: PV

2 TAILINGS MANAGEMENT AREA MODEL

Groundwater transport of solutes originating at the Tailings Management Area (TMA) was simulated with a numerical model covering an area much smaller than that of the regional groundwater flow model (GeoTrans, 1996) (Figure 2.1). The TMA sub-model was built from the same data set used to construct the regional model, as explained in Section 2.1. Section 2.2 demonstrates that the sub-model produces results that are consistent with those of the regional model.

Full details of the TMA design appear in a separate report (Foth & Van Dyke, 1995c). As shown in Figure 2.2, the TMA will consist of cells 1 through 4, each with three regions: base, sideslope with drainage, and sideslope without drainage. The TMA cells will be operated on a phased schedule, with TMA 1 receiving the first mine tailings, TMA 2 beginning operations about seven years later, and so on. The exfiltration rate from the TMA to the groundwater will be much smaller than the natural precipitation recharge rate because of the engineered liner and drainage system (Foth & Van Dyke, 1995c). Within each cell, the exfiltration rate will vary depending on the region (base, sideslope with drainage, or sideslope without drainage). Modeled variations in the TMA exfiltration rate are explained in detail in Section 2.3.

The mine tailings in the TMA may contain many constituents to be monitored (e.g. sulfate, iron, manganese, calcium, etc.). The concentration of these constituents in the pore water of the tailings will depend on many factors, including the availability of air in the pores. A characterization of the pore water chemistry is currently being conducted as a separate study. To account for tailings concentrations that vary from constituent to constituent and that vary over the life of the TMA, this report presents a generalized approach to transport modeling that involves unit-response curves and superposition (Section 2.3.2). With this method, the results presented here will be applicable to a variety of constituents, even accounting for source concentration changes over time as the tailings chemistry changes. Thus, results from the ongoing tailings characterization study can be combined with the results here to evaluate regulatory compliance for a variety of constituents.

Uncertainty in model predictions is addressed with an approach analogous to the one used in the regional groundwater modeling report (GeoTrans, 1996). First, reasonable flow and transport parameters were used to make Best Engineering Judgement (BEJ) predictions. Then, various sensitivity simulations were conducted to determine the sensitivity of the predictions to variations in the chosen parameters. Finally, a combination of conservative and unlikely parameters were used to make Practical Worst Case (PWC) predictions. In the regional groundwater flow model, the

quantities of concern were mine inflow rate, lake level changes, streamflow changes, and the magnitude and extent of groundwater drawdown. For the TMA sub-model, the primary quantity of concern is the concentration of constituents at the proposed compliance boundary located 1200 feet from the edge of the TMA. Model predictions are presented in Section 2.4.

2.1 NUMERICAL MODEL DESIGN

This section describes the design and construction of the solute transport model. The computer code selected for use is described, along with the associated input data. Input data include grid location and spacing, boundary conditions, and aquifer parameters.

2.1.1 CODE SELECTION

MT3D^{96} (Zheng, 1996) was selected in consultation with WDNR for three-dimensional modeling of solute transport at the Crandon site. MT3D^{96} was originally developed as MT3D for the USEPA. MT3D^{96} is the first major upgrade of the code since 1992. It is commercially available through organizations such as the International Ground Water Modeling Center (IGWMC) and Scientific Software, Inc.

MT3D^{96} is a three-dimensional model for simulating solute transport processes in fully saturated porous media. The transport model is structured such that it can be used in conjunction with any block-centered finite-difference flow model such as the MODFLOW (McDonald and Harbaugh, 1988) model. MODFLOW was the groundwater flow model used for the regional model (GeoTrans, 1996). MT3D^{96} can be used to simulate changes in concentration of single species soluble constituents in groundwater considering advection, dispersion, and some simple chemical reactions. The chemical reactions include equilibrium controlled linear or non-linear adsorption and first-order irreversible decay or biodegradation.

Following solution of the flow field by MODFLOW, or another finite-difference code, MT3D^{96} uses one of four solution techniques to solve for concentrations. Three of the solution techniques, Method of Characteristics, Modified Method of Characteristics, and Hybrid Method of Characteristics, are particle based. An explicit finite-difference solution option is also offered. The finite difference solution was selected for application at the Crandon site because it is significantly more efficient than the particle based methods.

MT3D^{96} was developed for the USEPA for solute transport applications. It is generally accepted by state and federal regulators as a tool for solving solute transport problems. MT3D^{96} was used for verification of the cross-sectional solute transport modeling performed using FTWORK (Faust, et al, 1989) in the original groundwater

modeling report (GeoTrans, 1995). MT3D[96] was selected in favor of FTWORK for this application because the conversion of data sets to MT3D[96] was more expeditious than to FTWORK.

2.1.2 GRID DESIGN AND DISCRETIZATION

The TMA sub-model covers a 7000-foot by 7000-foot square rotated 35 degrees west of north (Figure 2.1). The model extends approximately 200 feet past the proposed 1200-foot compliance boundary on the northwest, southwest, and southeast sides, and to Hemlock Creek on the northeast side (Figure 2.3). The model grid consists of 70 rows and 70 columns, with uniform 100-foot grid spacing in either direction. The orientation was chosen such that model rows approximately line up with the flow direction from the TMA to Hemlock Creek, increasing numerical accuracy. Since Hemlock Creek is a natural flow boundary, all cells on the far side of the stream (to the east and north of the stream) are inactive in the model.

Vertically, the glacial overburden in the subsurface is divided into seven layers based on stratigraphic changes interpreted from the hydrogeologic cross sections documented in GeoTrans (1996). These cross sections were based on observed data from geological drilling programs. The method for vertical discretization is the same as that used for the regional groundwater flow model, and is explained in that report (GeoTrans, 1996). However, regional model layers 2 and 3, which primarily represent the outwash strata, are sub-divided into 5 layers for the TMA sub-model to increase the resolution of flow and transport in these higher-conductivity layers. The conversion from regional model layering to TMA sub-model layering is depicted in Figure 2.4. Regional model layer 1 (primarily Late Wisconsinan Till) is the same as TMA sub-model layer 1. Regional model layer 2 is evenly divided into three parts, becoming TMA sub-model layers 2, 3 and 4. Similarly, regional model layer 3 is evenly divided into two parts, becoming TMA sub-model layers 5 and 6. Regional model layer 4 (primarily Pre- to Early- Wisconsinan Till and massive saprolite) is the same as TMA sub-model layer 7. Bedrock layers 5, 6, and 7 of the regional flow model are not represented in the TMA sub-model because flow across the bedrock/glacial interface is very limited away from the mine. Note that it is conservative for concentrations computed at the proposed compliance boundary to assume that the solute plume does not spread vertically beyond the limits of the glacial overburden. The sensitivity of predictions to flow across the bedrock/glacial interface is addressed in Section 2.4.3. A contour map of topography is shown in Figure 2.5. The bottom elevations for all seven layers of the TMA sub-model are shown in Figures 2.6 through 2.12.

In order to calculate hydraulic conductivity in the model, the makeup of each model cell was calculated in terms of fractional content of each of the geological units present. For this purpose, only the saturated portion of the layers are considered (see GeoTrans, 1996 for a more detailed description of the method). The water table

elevation used to determine saturated thickness was derived from measurements made in 1984, and is shown in Figure 2.13. The saturated thicknesses of all seven model layers are shown in Figures 2.14 through 2.20. Note that zero-thickness cells, which represent areas above the water table, are inactive in the model.

2.1.3 MODEL PARAMETERS AND BOUNDARY CONDITIONS

The hydraulic conductivities for the geologic units (Table 2.1) were taken from the calibrated, BEJ regional groundwater model. As in the regional model, there are two zones of hydraulic conductivity for the coarse outwash (Figure 2.21). This zonation is based on a number of factors including grain size analyses, slug test results, potentiometry, and model calibration. The hydraulic conductivity used in the zone is supported by a chlorofluorocarbon (CFC) travel time analysis conducted by the USGS (Saad, 1996). The conductivity zonation is discussed in further detail in the regional groundwater flow report (GeoTrans, 1996). The hydraulic conductivity at each cell is calculated from the conductivity values for each geologic material (Table 2.1) and each cell's fractional content. The cell-wide hydraulic conductivities are computed with the ACALC program, also described in the regional groundwater flow report (GeoTrans, 1996).

Six types of flow boundaries are used to model the area: 1) no-flow at the base of the model and on the far side of Hemlock Creek, 2) specified head along the northwestern, southwestern, and southeastern edges of the model grid, 3) a head-dependent flux or river-type boundary for Hemlock Creek, 4) a head-dependent flux or drain-type boundary for the discharge wetlands around Hemlock Creek, 5) head dependent or river-type boundaries for the seepage wetlands in the eastern part of the model, and 6) specified flux to represent areal recharge derived from precipitation. The cell locations for specified head, river-type and drain-type boundaries are shown in Figure 2.22.

The no-flow boundary at the base of the model is valid because flow across the bedrock/glacial interface is very limited in this area. It was observed during model calibration (discussed in Section 2.2) that without mining, the modeled groundwater head in the lowest glacial layer changes little when the bedrock is removed. When the mine is in operation, flow becomes less downward when the bedrock is removed, which would tend to limit spreading of the plume and raise the maximum concentration at the proposed compliance boundary. Therefore, not including the bedrock in the solute transport model is conservative with regard to computed concentrations of the proposed compliance boundary because the computed concentrations are higher than they would be had the bedrock been included. To verify the appropriateness of the boundary, a sensitivity simulation was conducted where flow and solute transport across the glacial bedrock interface was represented by a head-dependent flux boundary.

Since Hemlock Creek is a receiving stream with groundwater from both sides contributing to flow, it is a natural groundwater divide for the glacial aquifer. This is also evident from plots of modeled head in layers 1 through 4 of the regional flow model (GeoTrans, 1996, Figures 5.2 through 5.5 and 7.7). Thus all cells to the northeast of Hemlock Creek were set inactive, effectively creating a no-flow boundary on the far side of the creek. This conceptualization means that all water flowing to the northeast from the TMA must exit through Hemlock Creek or its adjoining wetlands.

There are no natural groundwater boundaries along the northwest, southwest and southeast edges of the model. Therefore, heads along these boundaries were specified in the TMA sub-model. They were computed directly from the regional flow model using three-dimensional linear interpolation (from regional model cell-center-points to sub-model cell-center-points). The MODFLOW General-Head-Boundary (GHB) package was used to specify heads at these locations. To ensure that the head values in the cells along these edges is equal to the specified boundary head, the conductance used for each GHB cell is set to a sufficiently high value (1.0E6 ft^2/day). Using the GHB package for specified heads instead of setting the cells to constant-head in the MODFLOW Basic package makes it easy to change the value of the boundary heads from stress period to stress period during the simulation. The boundary heads change in response to cessation of mining and when TMA construction reduces areal recharge. Specified head boundaries were applied at all seven layers along the model edges (except layer 1 cells where the saturated thickness is zero).

Hemlock Creek was modeled with the MODFLOW River package using parameters identical to those used in the regional flow model (Table 2.1). The stage in the stream was taken from topographic maps similar to the one shown in Figure 2.5, and varies from 1578.63 feet-msl in row 70 to 1578.20 feet-msl in row 1. The conductance at each river cell was calculated as the length of the creek (which varies from cell to cell) times the width of the creek (14.0 feet) times the hydraulic conductivity of the creekbed (1.0 ft/day, which is 3.5E-4 cm/sec) divided by the thickness of the creekbed (1.0 foot). The river bottom elevation was set 2.0 feet below the river stage (representing a 1.0-foot water depth and a 1.0-foot thick creekbed). The river boundary that was used to represent Hemlock Creek was applied to the uppermost active layer (either layer 1 or layer 2). Application to only the uppermost layer is consistent with a conceptual model of a shallow, partially penetrating stream.

The discharge wetlands around Hemlock Creek were modeled with the MODFLOW Drain package using parameters identical to those used in the regional flow model (Table 2.1). The elevations for these boundaries were taken from topographic maps similar to the one shown in Figure 2.5. The conductance of each drain cell was calculated as the area of the wetland in the cell times the hydraulic conductivity of the wetland-bottom sediments (0.318 ft/day, which is 1.12E-4 cm/sec), divided by the thickness of the wetland-bottom sediments (1.0 foot). Discharge

wetland boundaries were applied to the uppermost active layer (either layer 1 or layer 2).

The small seepage wetlands adjacent to the discharge wetlands were modeled with the MODFLOW River package using parameters identical to those used in the regional flow model (Table 2.1). The elevations and conductances were derived in the same manner as for the discharge wetlands, with a sediment hydraulic conductivity of 0.00318 ft/day (1.12E-6 cm/sec) and a sediment thickness of 5.0 feet. The bottoms of the wetland sediments were set 7.0 feet below the wetland elevation (representing a 2.0-foot water depth and a 5.0-foot sediment thickness). Seepage wetland boundaries were applied to the uppermost active layer (either layer 1 or layer 2).

Areal recharge is applied to the uppermost active layer using the MODFLOW Recharge package. The default recharge rate applied over most of the model is 10 in/yr (2.283E-3 ft/day). The recharge rate was set to zero at Hemlock Creek, the discharge wetlands, and the seepage wetlands. Recharge zones were identified for modeling the TMA exfiltration over time in the transport simulations. These zones, shown in Figure 2.23, are model representations of the four TMA cells, each with three regions. Additional zones represent the five runoff basins adjacent to the TMA. The TMA and runoff-basin zones were used in predictive simulations to model exfiltration rates that change over time. Further details on exfiltration rates are provided in Section 2.3.1.

Two additional parameters, effective porosity and dispersivity, are required when simulating solute transport. Effective porosity represents the portion of the soil/water medium that is available for transport, or the ratio of interconnected pore space to total volume of geologic material. As described in the regional flow model report (GeoTrans, 1996, Section 3.2.6.2), the effective porosity of the glacial sediments is between 15 and 35 percent. As with the regional model, the BEJ porosity was set at 25 percent for all sediments, and varied in the sensitivity analysis. Dispersivity is a length scale for spreading of solute. The solute disperses primarily because of the random, tortuous pathways of varying lengths and varying directions that are available for solute transport. Dispersivity is not a measurable quantity, but in many applications, the longitudinal dispersivity (that is, dispersivity in the direction of flow) is roughly one-tenth to one-hundredth of the model length scale (Gelhar, et al, 1992). It is often assumed that the transverse dispersivities (perpendicular to flow) in the horizontal and vertical directions are one-tenth of the longitudinal dispersivity. For the purpose of the BEJ simulation, the longitudinal dispersivity was set at 50 feet (roughly one-sixtieth of the distance from the center of the TMA to the proposed compliance boundary), and the transverse dispersivities were set at 5 feet. The length scale for molecular diffusion (on the order of microns) is insignificant compared to these dispersivity values, therefore molecular diffusion is not simulated. Dispersivity values were varied as a part of the sensitivity analysis.

To be conservative and applicable to many constituents, retardation (sorption and desorption of solute to and from soil solids) and chemical decay were not considered in the model. This is equivalent to setting the retardation factor of the solute transport model to 1.0 and the first order decay constant to zero.

2.2 MODEL CALIBRATION

The TMA sub-model was constructed as a "zoomed-in" version of the regional groundwater flow model. As such, it should produce results that are consistent with those of the regional model. To verify this, the TMA sub-model was run with stresses that represent steady-state (October 1984) pre-mining conditions. The groundwater head field computed by the TMA sub-model was then compared to the head field computed by the regional model in the vicinity of the TMA. Head values at well locations were also compared to observed water levels to verify that the TMA sub-model is reasonably calibrated to field conditions.

2.2.1 COMPARISON TO THE REGIONAL GROUNDWATER FLOW MODEL

In the steady-state, pre-mining simulation, the TMA sub-model produces a head field very similar to that produced by the regional flow model. Note that the specified heads along the northwestern, southwestern, and southeastern boundaries were interpolated from computed heads in the steady-state, pre-mining simulation of the regional flow model. Figure 2.24 demonstrates the similarity of the computed water table elevations in the TMA submodel and the regional model. Noting that the center of TMA sub-model layer 3 is the same as the center of regional model layer 2, Figure 2.25 shows the similarity of computed head in the outwash for the two models. Similarly, noting that the center of TMA sub-model layer 7 is the same as the center of regional model layer 4, Figure 2.26 reveals the consistency of the models at the base of the glacial aquifer.

2.2.2 COMPARISON TO FIELD DATA

Figure 2.27 shows the locations of water level measurements in the area, with symbols that indicate the magnitude of differences between modeled and observed values or residuals. As expected, the residuals at these wells are very similar to those of the regional model, as demonstrated in Table 2.2. Of particular importance, note that the water level at EX-10, which is near the groundwater high for the model, is matched well. This means that the overall gradient from the TMA to Hemlock Creek is reasonably approximated, 0.00381 modeled versus 0.00388 observed. This gradient governs the movement of solute in transport simulations.

2.3 TRANSPORT SIMULATION METHODOLOGY

In order to simulate solute transport, sources must be specified in terms of flux rates and source concentrations. For the TMA sub-model, the source flux rate is a complicated function in space and time, and the source concentrations vary from constituent to constituent and are currently being estimated in another study. In this subsection, the modeled representation of the source flux is discussed. Subsequently, a general approach for simulating an unknown and constituent-specific source concentration that varies over time is presented.

2.3.1 TMA EXFILTRATION RATES

When a TMA cell is active (that is, it is receiving or has already received tailings), the water exfiltrating through the engineered liner and drain system becomes the source infiltration flux for groundwater transport. Note that it is conservatively assumed that the entire amount of exfiltrated water travels immediately through the unsaturated zone beneath the TMA to reach the water table.

The complete design and operation of the TMA is presented in a separate report (Foth & Van Dyke, 1995c and subsequent addenda). Each TMA cell is designed to receive mine tailings for 7 to 12 years, after which a protective cap is placed over each cell. For the purposes of this study it was assumed that each TMA cell's FML remains intact for 140 years after the cell is capped, a 150 year life. At that time, it is assumed that the water within the tailings is released to the groundwater. Following this postulated FML degradation it was further assumed that a constant infiltration rate (equal to the amount of water entering the TMA through the cap) prevails. The exfiltration rate in each year of activity was derived in the TMA design report using the HELP model.

In order to create a manageable number of stress periods for the transport model, the active period of a TMA cell was divided into 8 phases, labeled A through H in Table 2.3. These phases were designed to represent periods where the exfiltration rate is approximately constant for a unique TMA cell. Phases A through H are staggered for the four TMA cells, as each cell becomes active at a different elapsed time. Phases A and B represent operational phases of the TMA (unique to each cell), when tailings are being received. Phases C through F represent the period when the cap is on and the FML has not degraded. The exfiltration rate decreases during these phases due to cap placement. Phase G represents the first year after degradation of the FML, and phase H represents the final, constant exfiltration rate resulting from a capped TMA with the FML degraded. It is important to note that phases G and H assume that the FML is no longer intact, and that this is a very conservative assumption. In Table 2.3, the exfiltration rates are listed for each TMA region (base, sideslope with drainage, and sideslope without drainage) for each phase.

The operation of the four TMA cells is staggered in time such that TMA cell 2 begins receiving tailings two years before the cap is in place over TMA cell 1, TMA cell 3 begins operation 2 years before TMA 2 is capped, and TMA 4 starts two years before TMA 3 is capped. A detailed time line of the phase sequence for each TMA cell is shown in Figure 2.28. Note that the duration of operational phases A and B is different for the different cells, because of different capacities. In order to properly simulate every phase change at every cell, the model is made up of 28 stress periods of varying lengths, as shown in Figure 2.28 and listed in Table 2.4. Tables 2.5 through 2.8 provide detailed lists of modeled exfiltration rates for each TMA cell by stress period. Using these rates, the total modeled flux is plotted versus time in Figure 2.29. Figure 2.30 shows the cumulative volume of water exfiltrated from the TMA over time, and demonstrates that the spatial and temporal discretization used for the TMA sub-model conservatively approximates the design specifications. Note that prior to operation, TMA cells 2, 3, and 4 receive the default recharge rate of 10 in/yr (2.283E-3 ft/day) containing no solute (phase X in Tables 2.3 and 2.5-2.8), and do not contribute to the total TMA flux reflected in Figures 2.29 and 2.30.

Each stress period was simulated as steady-state for flow, meaning that flow field changes take effect immediately. This simplifies the modeling approach considerably and should not lead to any significant errors in the prediction of concentration.

2.3.2 SUPERPOSITION OF SOURCES

Simulation of multiple constituents could present several problems from a practical standpoint. First, source term concentrations for each constituent are in the process of being developed in a separate study, and their absolute concentrations are not currently available. Second, the time varying nature of source term concentration is unique for each constituent. In order to overcome these potential problems, a general approach using unit concentration sources is used in this report. Using the principal of superposition and scaleable unit concentration sources, it is possible to account for source concentrations that vary over the life of the TMA and constituent specific source concentrations. The process is explained here.

Consider a simulation (call it Simulation A) that has a source concentration equal to 1.0 ppm over the entire life of each TMA cell (that is, starting at time zero for TMA 1, time 7 years for TMA 2, etc. and continuing indefinitely). The result of the simulation is a prediction of concentration at every cell in the model at all times resulting from the unit-concentration source. To then determine the concentration in groundwater at a specific time and place of a specific constituent that (hypothetically) has a constant concentration in the tailings, the modeled concentration at that time and place is multiplied (or scaled) by the actual source concentration of the constituent. Another constituent, having a source concentration twice as large as the first would be

scaled in the same way resulting in a modeled concentration also twice as large as that for the first constituent. Thus, using unit-concentration sources makes it easy to apply results from a single simulation to multiple constituents, after the simulation is complete.

Now consider a constituent that does *not* have a constant concentration over the life of the TMA. Instead, phases A-C (higher exfiltration) are characterized by one source concentration, C_A, and phases D-H (lower exfiltration) are characterized by another concentration C_B, because the capping of the tailings has changed the chemistry in the pore water. Additionally, suppose that sometime after phase H begins and the FML has degraded, the chemistry in the tailings changes yet again due to (hypothesized) oxidation, and the constituent under consideration is then characterized by concentration C_C. To account for these hypothesized changes, two additional simulations (Simulation B and Simulation C) are performed. In simulation B, the source concentration is again 1.0 ppm, but it is only applied during phases D-H at each TMA cell (the source concentration is zero prior to the beginning of phase D). Simulation C begins in the final, steady-state stress period of the model (that is, stress period 28), when the exfiltration rate from each TMA is equal to the rate through the cap (phase H). The unit concentration source is applied at TMA 1, then after 10 years at TMA 2, then after 6 more years at TMA 3, then after 6 more years at TMA 4, corresponding to the lag times between the hypothesized FML degradations as shown on the time line in Figure 2.28.

Simulations A, B, and C can then be used to compute the concentration at any point, and at any time, regardless of the magnitude of the source concentrations C_A, C_B, and C_C. Once the source concentrations are known for a constituent and the time to (hypothesized) oxidation is estimated, the principle of superposition is used to compute the constituent-specific concentration in the groundwater. The process is illustrated in Figure 2.31. First the simulations are run to generate unit response functions. At a given model cell, the functions are curves of concentration versus time, or unit response curves as shown in Figure 2.31. The unit response curve for Simulation A is scaled by the constituent specific concentration C_A. The unit response curve for Simulation B is scaled by the amount of increase from C_A to C_B (negative if the concentration decreases), and the unit response curve for Simulation C is scaled by the amount of increase from C_B to C_C. The scaled response curve for Simulation C is also offset by the estimated time between assumed FML degradation and the source being oxidized. The three scaled response curves are then added (or superimposed) to yield the function of concentration versus time that is sought for the constituent. This process can be repeated for any number of constituents without need of re-executing the simulations.

The method of superposition applied in this manner is valid because of the linear nature of the underlying differential equations that govern solute transport. A validation of the method with actual simulation results is presented in Section 2.4.2.

2.3.3 OTHER CHANGING BOUNDARY CONDITIONS

In this configuration, model time zero is the beginning of TMA operation, which is approximately coincidental with the beginning of mining. Mine operation is modeled with the specified-head boundary conditions along the model edges. Allowing for 30 years of mine operation and 2 years for recovery, the mine is assumed to be in post-operation mode after 32 years in the model. The specified heads used at the beginning of the simulation, for stress periods 1 and 2, were interpolated from a steady-state simulation with the regional model that had zero recharge in TMA 1 only (default recharge in the other three) and the mine in operation. In stress periods 3 through 7, specified heads were interpolated from a regional model simulation with the mine operating and TMA cells 1 and 2 receiving zero recharge. Specified heads for stress periods 8 through 10 were taken from a simulation with mine operation and zero recharge in TMA 1, 2 and 3. In stress periods 11 through 14, the specified heads were computed from a regional model simulation with zero recharge over the entire TMA and the mine in operation. Finally, in stress periods 15 through 28, the mine is no longer in operation, and the specified head values are interpolated from a regional model simulation made with a backfilled mine and zero recharge over the entire TMA. Assuming zero recharge for active TMA cells in the regional model, instead of using actual values derived in Section 2.3.1, is a good approximation for regional flow modeling, because the TMA exfiltration rates are orders of magnitude less than the default recharge of 10 in/yr (2.283E-3 ft/day). Because the discrepancy between recharge rates derived from the regional model and actual computed recharge rates is small, use of specified heads interpolated directly from the regional model is appropriate.

The runoff basins around the TMA do not receive tailings and thus have a source concentration of zero. They do, however contribute additional recharge to the groundwater due to the collection of water from the TMA cap. In the model, each runoff basin recharge zone (Figure 2.23) contributes 13 in/yr (2.968E-3 ft/day), beginning when the nearest TMA cell becomes active. The additional 3 in/yr over default recharge assumes an average 30-day period each year with 2 feet of standing water in the runoff basin which is underlain by 1 foot of fine grained (conductivity of 1.0E-6 cm/sec, or 2.8E-3 ft/day) sediment. Because the runoff basins are a small portion of the total model area, the transport results are not sensitive to the runoff basin recharge rate.

2.4 MODEL PREDICTIONS

Using MODFLOW with MT3D[96] in finite-difference mode, BEJ, sensitivity, and PWC simulations were conducted. The results are BEJ and PWC predictions of unit

concentration response curves at the proposed compliance boundary. These curves will be used (in the EIR) to compute proposed compliance boundary concentrations for specific constituents of concern. In order to demonstrate the use of the unit response curves, a hypothetical example is used. This example also provides the base simulation for verification and sensitivity simulations.

2.4.1 BEST ENGINEERING JUDGEMENT

Using the BEJ parameters listed in Table 2.1, and the methodology explained in Section 2.3, BEJ unit response functions were computed with the MT3D[96] transport modeling code. Focusing on the proposed compliance boundary, 1200 feet from the outer edge of the TMA, unit-response curves (normalized concentration versus time) were computed for each cell shown in Figure 2.32. These curves can be scaled with constituent-specific source concentrations and summed to produce a profile of concentration versus time at each proposed compliance cell for the constituent of concern.

Figure 2.33 shows the maximum concentration unit-response curves for all three BEJ superposition simulations. Note that different cells may contain the maximum concentration at different times during the simulations. Thus, the curves in Figure 2.33 represent the concentration at a point that moves with time, always at the point on the proposed compliance boundary with the maximum concentration.

To demonstrate the use of the unit-response curves produced by the three BEJ simulations, a hypothetical example was considered. Suppose a constituent of concern is sulfate, and that the initial source concentration is 2,000 ppm. During post-cap phases C-G, the concentration of sulfate hypothetically increases to 4,000 ppm in the tailings pore water. And starting (as a worst case) at the very beginning of phase H (time 150 years for TMA 1), the concentration escalates to 40,000 ppm (see Table 2.9). In this example, to determine the sulfate concentration at the proposed compliance boundary, all of the unit-response curves (one for each proposed compliance boundary cell) for Simulation A are multiplied by 2,000. The unit-response curves for Simulation B are also multiplied by 2,000 (i.e. 4,000 - 2,000). And the unit-response curves for Simulation C are multiplied by 36,000 (i.e. 40,000 - 4,000). At each proposed compliance cell, the scaled-response curves are summed to yield the modeled sulfate concentration versus time. Figure 2.34 shows how this superposition method works. Note that the curves in Figure 2.34 represent a moving point that is always at the point on the proposed compliance boundary with the maximum total sulfate concentration. Because of this, Figure 2.34 exhibits a "kink" of approximately 40 years as the point of maximum concentration shifts from a point on the western proposed compliance boundary to a point on the eastern proposed compliance boundary. In this example, it is evident that the initial source concentration, though the lowest of the three source concentrations, produces the greatest concentration at the proposed compliance

boundary. This occurs because the TMA exfiltration rate is much larger during phases A through C than it is during phases D through H

To better understand the movement of solute through the aquifer from the TMA cells to the proposed compliance boundary, several snapshots of the modeled concentration plumes (plan view) are shown for this example in Figures 2.35 through 2.42. These figures show the maximum modeled concentration in any cell, following scaling and superposition, regardless of layer. The figures show the TMA cells beginning operation in succession, the initial movement of the solute plume to the west and toward the mine, and the eventual movement of the plume to the northeast, toward Hemlock Creek. Using the cross-section line A-A' shown in Figure 2.43, the modeled plume is viewed in cross-section in Figures 2.48 through 2.51. Note that the discontinuity in the curves in Figures 2.33 and 2.34 at time 50 years occurs when the point of maximum concentration moves from a point on the proposed compliance boundary west of the TMA to a point on the proposed compliance boundary northeast of the TMA.

2.4.2 VERIFICATION OF METHODOLOGY

Two verification simulations were performed to demonstrate: 1) that the method of superposition, as used in the preceding sulfate example, is accurate, and 2) that the numerical solution method for the transport equations is appropriate.

To demonstrate the accuracy of the superposition method, a single simulation was conducted with the source concentrations explicitly specified in the model. That is, the concentration for phases A through C was set to 2,000 ppm in the model input, the concentration for phases D through G was set to 4,000 ppm, and the concentration for phase H was set to 40,000 ppm. It is important to remember that these concentrations are hypothetical and are not the actual source concentrations for sulfate, and that the time of concentration increase to 40,000 ppm was arbitrarily set to the very beginning of phase H (the method is valid for an increase any time after phase H starts). The model was run once and concentration at the proposed compliance boundary cells was recorded. Figure 2.52 shows that the results of this model are practically identical to the results obtained with superposition, as expected.

To check the validity of the finite-difference method for solving the transport problem, the same hypothetical sulfate example was run with MT3D[96] using another solution technique called the Method Of Characteristics (MOC). The MOC technique solves the solute transport equation by moving and dispersing particles that represent solute. This is much more computationally intensive than the finite difference method, therefore causing excessively long simulation times. A single 650-year simulation takes about 11.5 days on a 166MHz pentium-processor computer. As with the previous

verification simulation, all source concentrations were specified explicitly in the model input, eliminating the need to perform multiple simulations for superposition.

The results of this simulation indicate that the MOC solution predicts concentrations that are similar, but slightly higher than the finite difference solution. Figure 2.53 compares concentration versus time at the proposed compliance boundary for the two solution methods. On average, the concentrations computed by MOC are 9.4 percent higher for the 650 year simulation than those computed by the finite difference method. The peak concentration is approximately 12.5 percent higher for the MOC method. The reason that the finite difference solution gives lower concentrations may be due to numerical dispersion, resulting in a "smearing" of the concentration front. This hypothesis may be supported by detailed inspection of areal concentration contour plots, which show a slightly sharper plume shape for the MOC solution. However, there are other factors that could cause the small difference that is observed. These factors are inherent to the basic differences between MOC and finite difference, including the need to interpolate concentration and velocity in MOC, the need to perform particle tracking in MOC, and differences in time stepping. Therefore it cannot be said with certainty that a particular solution technique is better or more accurate than the other. The two solutions presented here are as similar as other verifications presented for less complex problems. For example, the two dimensional benchmark problem presented in the MT3D[96] documentation shows differences that are on the same order as the differences observed between MOC and finite difference. From a practical standpoint, the two solutions presented here are similar and this exercise provides verification that the finite difference solution technique is working properly.

2.4.3 SENSITIVITY ANALYSIS

Seven sensitivity simulations were conducted to assess the effect of parameter uncertainty on model predictions. These simulations involved independent variations of key parameters in the model. Each simulation was based on the hypothetical sulfate example with concentrations explicitly specified (Figure 2.52, solid line). The sensitivity simulations were run to 300 years to capture the concentration peak. As in the flow model report, the sensitivity simulations that caused results that were less favorable than the BEJ simulation were considered for the Practical Worst Case. For the transport model, these simulation cause an increase in the peak concentration or decrease in the time to peak concentration. The simulations are summarized in Table 2.10 and described below.

Lowering the effective porosity to 0.1 causes concentrations to peak more quickly, a higher peak concentration, and a lower long-term concentration (< 150 years), than in the BEJ simulation (Figure 2.54). This observation is intuitive since lowering porosity causes higher interstitial velocities.

Lowering the longitudinal dispersivity from 50 feet to 25 feet causes concentrations to increase slightly over the BEJ simulation (Figure 2.55). Lowering the transverse dispersivity from 5 feet to 2.5 feet causes an increase in concentrations (Figure 2.55) which is most prevalent following the initial peak, after 150 years. The decrease in dispersivity apparently causes a sharper, more defined concentration front than in the BEJ case.

Figure 2.56 shows the effect of lowering the horizontal hydraulic conductivity of the outwash and areal recharge rate by a factor of two. This change in parameters causes the peak concentration to be lower than in the BEJ case, but for higher concentrations to persist longer than in the BEJ case. This result is apparently dominated by the slower velocity that occurs because of the lower hydraulic conductivities.

Lowering the vertical hydraulic conductivity of the glacial deposits by a factor of ten causes a slightly higher peak concentration, a slower time to peak, but a more persistent long-term concentration than in the BEJ simulation (see Figure 2.56). The result is apparently caused because the plume does not migrate as deep into the system, and therefore does not spread as much as in the BEJ simulation.

Figure 2.57 shows the results of sensitivity simulations where boundary conditions in the solute transport model were varied. One of these simulations evaluated the effect of assuming in the BEJ simulation that solute reached the water table instantaneously. In this sensitivity simulation, the solute was assumed to enter the groundwater system some time after mining operations had ended and the groundwater system had rebounded to pre-mine development conditions. In contrast to the BEJ simulation, which models two flow fields, one westerly during mining operations and a second north-easterly after mining operations have ended, this simulation only has a single flow field which is north-easterly. The results of this simulation, shown in Figure 2.57, indicate that the BEJ simulation gives a higher peak and overall higher concentrations than the simulation where solute is assumed to enter the system some time after mining operations have ended. Presumably, concentrations in the two flow field case are higher because the westerly flow, which already has solute in it, has to pass below the TMA source term again once the flow reverses. This causes additional solute to be added to this parcel of water.

The second sensitivity simulation that assessed boundary conditions involved including the effect of flow into the bedrock. General head boundary conditions were attached to the base of the solute transport model to allow a small amount of flow to enter and exit the bedrock. Hydraulic heads and conductances were interpolated from the regional model. The results of this simulation, shown in Figure 2.57, indicate that allowing some flow into and out of the bedrock actually reduces concentrations at the

proposed compliance boundary. The concentration reduction is most likely caused by the further vertical spreading of the plume and additional mixing.

2.4.4 PRACTICAL WORST CASE

The sensitivity simulations indicate that lower porosity, lower dispersivity, and lower vertical conductivity can all lead to higher concentrations at the proposed compliance boundary. Combining the low-range of probable values for these parameters results in the following PWC parameters (also listed in Table 2.11): 1) the effective porosity is decreased to 10 percent, 2) the longitudinal and transverse dispersivities are reduced to 25 feet and 2.5 feet, respectively, and 3) the vertical conductivity of all geological units is reduced by a factor of 10. All other parameters are the same as those listed in Table 2.1.

Three unit-concentration simulations were conducted with the PWC parameters. The results from these simulations (Figure 2.58) can be combined using superposition. For the hypothetical sulfate example, the superposition method is illustrated in Figure 2.59. Comparison of Figures 2.59 and 2.34 shows that the peak concentration for this example is about three times greater with PWC parameters than with BEJ parameters. PWC concentration plumes are shown in plan view in Figures 2.60 through 2.67, and in cross-sectional view in Figures 2.68 through 2.75.

2.5 SUMMARY OF TAILINGS MANAGEMENT AREA MODEL RESULTS

Transport in groundwater of solute originating from the Tailings Management Area was simulated using the MT3D[96] model. The model was designed specifically to focus on the area near the TMA as defined by the regulatory proposed compliance boundaries. The TMA model was constructed based on input parameters and boundary conditions from the regional groundwater flow model. However, grid resolution was improved both vertically and horizontally over the regional model in order to accurately model the potential movement of solute.

A generalized analysis method was created that enabled simulation of multiple constituents and a changing source term concentration without having to make numerous simulations. This method was verified and described in detail in the report text. Data regarding TMA exfiltration rates versus time were based on HELP model calculations by Foth and Van Dyke, while relative source term concentration versus time data were based on the waste characterization studies. The analysis described in this report developed BEJ response functions for three phases of TMA operation, corresponding to changes in source term concentration. Once source term concentrations are known for specific constituents, groundwater concentrations at the proposed compliance boundary can be computed by scaling and combining the response functions documented herein. A hypothetical set of source term concentrations for

sulfate was used to demonstrate the applicability of the generalized simulation methodology. The sulfate example was also used in the sensitivity simulations.

Sensitivity analysis was performed by varying aquifer parameters and solute transport properties. Combinations of the most influential parameters in the sensitivity analysis constituted the Practical Worst Case simulation. The response functions presented in this report will be used to determine both the BEJ groundwater concentrations and Practical Worst Case groundwater concentrations at the proposed compliance boundary. These groundwater concentrations will be documented for specific constituents in an update to the impact section of the EIR.

Table 2.1 Best Engineering Judgement model parameters

Geologic Unit or Boundary	Parameter	Value
All Geologic Units	Effective Porosity	0.25
	Longitudinal Dispersivity	50.0 ft
	Horizontal Transverse Dispersivity	5.0 ft
	Vertical Dispersivity	5.0 ft
Late Wisconsinan Till	Horizontal Hydraulic Conductivity	0.80 ft/day
	Vertical Hydraulic Conductivity	0.40 ft/day
Coarse Outwash	Default Zone Horizontal Hydraulic Conductivity	60.2 ft/dy
	Default Zone Vertical Hydraulic Conductivity	6.02 ft/day
	Low Zone Horizontal Hydraulic Conductivity	7.3 ft/day
	Low Zone Vertical Hydraulic Conductivity	0.73 ft/day
Fine Outwash	Horizontal Hydraulic Conductivity	15.0 ft/day
	Vertical Hydraulic Conductivity	1.50 ft/day
Pre- to Early-Wisconsinan Till and Massive Saprolite	Horizontal Hydraulic Conductivity	0.80 ft/day
	Vertical Hydraulic Conductivity	0.10 ft/day
Ancient Lacustrine	Horizontal Hydraulic Conductivity	0.80 ft/day
	Vertical Hydraulic Conductivity	0.16 ft/day
Ice Margin Contact Deposit	Horizontal Hydraulic Conductivity	0.80 ft/day
	Vertical Hydraulic Conductivity	0.16 ft/day
Hemlock Creek	Width	14.0 ft
	Creekbed Vertical Hydraulic Conductivity	1.0 ft/day
	Creekbed Sediment Thickness	1.0 ft
	Water Depth	1.0 ft
Discharge Wetlands	Bottom Sediment Vertical Hydraulic Conductivity	0.318 ft/day
	Bottom Sediment Thickness	1.0 ft
Seepage Wetlands	Bottom Sediment Vertical Hydraulic Conductivity	0.00318 ft/day
	Bottom Sediment Thickness	5.0 ft
	Water Depth	2.0 ft

Table 2.2 Modeled and observed steady-state water levels (feet)

WELL ID	October 1984 Observed Water Level	TMA Submodel		Regional Flow Model	
		Water Level	Residual	Water Level	Residual
DMB-1A	1594.78	1593.91	-0.87	1594.00	-0.78
DMB-4	1593.73	1589.29	-4.44	1591.28	-2.45
DMB-5	1593.50	1593.72	0.22	1593.61	0.11
DMB-5A	1592.58	1593.72	1.14	1593.61	1.03
DMB-6	1593.80	1592.92	-0.88	1592.85	-0.95
DMB-8	1588.58	1585.69	-2.89	1586.34	-2.24
EX-10AL	1594.62	1594.34	-0.28	1594.21	-0.41
EX-10AU	1594.72	1594.34	-0.38	1594.30	-0.42
EX-10BL	1595.14	1594.50	-0.64	1594.62	-0.52
EX-10BU	1596.06	1594.84	-1.22	1594.62	-1.44
EX-11AL	1593.93	1593.69	-0.24	1593.58	-0.35
EX-11AU	1593.47	1593.69	0.22	1593.58	0.11
EX-11BL	1594.19	1593.70	-0.49	1593.82	-0.37
EX-11BU	1593.37	1593.89	0.52	1594.05	0.68
EX-11CL	1593.80	1593.91	0.11	1593.95	0.15
EX-12AL	1593.83	1593.79	-0.04	1593.51	-0.32
EX-12AU	1593.73	1593.79	0.06	1593.51	-0.22
EX-12BL	1593.73	1593.81	0.08	1593.78	0.05
EX-12BU	1594.03	1594.01	-0.02	1594.02	-0.01
EX-7AL	1582.32	1580.83	-1.49	1580.46	-1.86
EX-7BL	1581.27	1580.83	-0.44	1580.46	-0.81
EX-7BU	1579.66	1580.82	1.16	1580.21	0.55
EX-7CL	1578.61	1580.61	2.00	1579.96	1.35
EX-8AL	1584.68	1581.12	-3.56	1580.71	-3.97
EX-8AU	1582.97	1581.12	-1.85	1580.71	-2.26
EX-8BL	1579.85	1581.11	1.26	1580.34	0.49
EX-8BU	1579.89	1580.63	0.74	1579.91	0.02
EX-9AU	1594.32	1592.81	-1.51	1592.58	-1.74
EX-9BL	1594.52	1592.93	-1.59	1592.77	-1.75
EX-9BU	1594.62	1593.18	-1.44	1592.94	-1.68
G41-B12	1593.90	1593.18	-0.72	1593.13	-0.77
G41-E13	1594.52	1593.75	-0.77	1593.66	-0.86
G41-E17	1592.78	1592.70	-0.08	1592.65	-0.13
G41-G13	1594.49	1594.09	-0.40	1593.84	-0.65
G41-G14A	1593.83	1594.33	0.50	1594.01	0.18
G41-G14B	1593.90	1594.09	0.19	1593.92	0.02
G41-G14C	1594.39	1594.31	-0.08	1594.33	-0.06
G41-G14D	1594.23	1594.08	-0.15	1593.97	-0.26
G41-G14E	1594.06	1594.28	0.22	1594.27	0.21
G41-G14F	1593.73	1594.04	0.31	1593.88	0.15
G41-G15	1593.90	1593.93	0.03	1593.73	-0.17
G41-G15A	1593.70	1594.13	0.43	1594.11	0.41
G41-G15B	1593.73	1594.13	0.40	1594.11	0.38
G41-H18B	1592.52	1593.00	0.48	1592.90	0.38
G41-H9	1594.00	1590.33	-3.67	1589.67	-4.33
G41-K13	1593.37	1592.25	-1.12	1592.26	-1.11
G41-K13A	1594.09	1592.57	-1.52	1592.52	-1.57
G41-M11	1579.89	1581.14	1.25	1581.02	1.13
G41-P16	1579.33	1585.22	5.89	1585.32	5.99
SG-WP-6	1577.20	1579.87	2.67	1580.46	3.26
SG-WP-7	1578.15	1579.46	1.31	1579.18	1.03
Mean Residual			**-0.23**		**-0.33**
Mean Absolute Residual			**1.06**		**1.02**
Root Mean Square Residual			**1.60**		**1.58**

Table 2.3 Basis for TMA phases and flux rates

Phase	Description	Duration (years)	Basis for Exfiltration Rate
X	Pre-construction	0-23[1]	Regional model calibrated value
A	First Phase of Operation	2-4[1]	Table 6.7-17 maximum[2]
B	Second Phase of Operation	5-8[1]	Table 6.7-18 maximum
C	Cap in Place Part 1	1	Table 6.7-19 Year 1
D	Cap in Place Part 2	6	Table 6.7-19 Average for Years 2-7
E	Cap in Place Part 3	20	Table 6.7-19 Average for Years 8-25
F	Cap in Place Part 4	113	Table 6.7-19 Years 41-140
G	Degraded FML Part 1	1	Table 6.7-19 Year 141
H	Degraded FML Steady-State	N/A	Table 6.7-19 Years 231-240

Phase	Base		Sideslope with drainage		Sideslope without drainage	
	Rate(in/yr)	Rate(ft/d)	Rate(in/yr)	Rate(ft/d)	Rate(in/yr)	Rate(ft/d)
X	10	2.283E-03	10	2.283E-03	10	2.283E-03
A	0.000328	7.489E-08	0	0.000E+00	10	2.283E-03
B	0.000387	8.836E-08	0	0.000E+00	0.595868	1.360E-04
C	0.000171	3.904E-08	0	0.000E+00	0.217444	4.964E-05
D	0.000037	8.447E-09	0	0.000E+00	0.000348	7.945E-08
E	0.000011	2.511E-09	0	0.000E+00	0.000033	7.534E-09
F	0.000004	9.132E-10	0	0.000E+00	0.000003	6.849E-10
G	0.013495	3.081E-06	0.000005	1.142E-09	0.012844	2.932E-06
H	0.000100	2.283E-08	0	0.000E+00	0.000104	2.374E-08

Notes

[1] Varies by TMA Cell

[2] During the first phase of operation, the TMA sideslope without drainage receives full recharge (from regional model) with a concentration of zero.

Table 2.4 TMA sub-model stress periods

Stress Period	Time (years)			Time (days)		
	Start	Duration	End	Start	Duration	End
1	0	4	4	0	1460	1460
2	4	3	7	1460	1095	2555
3	7	2	9	2555	730	3285
4	9	1	10	3285	365	3650
5	10	1	11	3650	365	4015
6	11	5	16	4015	1825	5840
7	16	1	17	5840	365	6205
8	17	2	19	6205	730	6935
9	19	1	20	6935	365	7300
10	20	3	23	7300	1095	8395
11	23	2	25	8395	730	9125
12	25	1	26	9125	365	9490
13	26	5	31	9490	1825	11315
14	31	1	32	11315	365	11680
15	32	4	36	11680	1460	13140
16	36	2	38	13140	730	13870
17	38	8	46	13870	2920	16790
18	46	6	52	16790	2190	18980
19	52	6	58	18980	2190	21170
20	58	91	149	21170	33215	54385
21	149	1	150	54385	365	54750
22	150	9	159	54750	3285	58035
23	159	1	160	58035	365	58400
24	160	5	165	58400	1825	60225
25	165	1	166	60225	365	60590
26	166	5	171	60590	1825	62415
27	171	1	172	62415	365	62780
28	172	478	650	62780	174470	237250

Table 2.5 TMA 1 flux rates by stress period

Stress Period	Phase	Exfiltration Rate (ft/day)		
			Sideslope	
		Base	With Drainage	Without Drainage
1	A	7.489E-08	0.000E+00	2.283E-03
2	B	8.836E-08	0.000E+00	1.360E-04
3	B	8.836E-08	0.000E+00	1.360E-04
4	C	3.904E-08	0.000E+00	4.964E-05
5	D	8.447E-09	0.000E+00	7.945E-08
6	D	8.447E-09	0.000E+00	7.945E-08
7	E	2.511E-09	0.000E+00	7.534E-09
8	E	2.511E-09	0.000E+00	7.534E-09
9	E	2.511E-09	0.000E+00	7.534E-09
10	E	2.511E-09	0.000E+00	7.534E-09
11	E	2.511E-09	0.000E+00	7.534E-09
12	E	2.511E-09	0.000E+00	7.534E-09
13	E	2.511E-09	0.000E+00	7.534E-09
14	E	2.511E-09	0.000E+00	7.534E-09
15	E	2.511E-09	0.000E+00	7.534E-09
16	F	9.132E-10	0.000E+00	6.849E-10
17	F	9.132E-10	0.000E+00	6.849E-10
18	F	9.132E-10	0.000E+00	6.849E-10
19	F	9.132E-10	0.000E+00	6.849E-10
20	F	9.132E-10	0.000E+00	6.849E-10
21	G	3.081E-06	1.142E-09	2.932E-06
22	H	2.283E-08	0.000E+00	2.374E-08
23	H	2.283E-08	0.000E+00	2.374E-08
24	H	2.283E-08	0.000E+00	2.374E-08
25	H	2.283E-08	0.000E+00	2.374E-08
26	H	2.283E-08	0.000E+00	2.374E-08
27	H	2.283E-08	0.000E+00	2.374E-08
28	H	2.283E-08	0.000E+00	2.374E-08

Table 2.6 TMA 2 flux rates by stress period

Stress Period	Phase	Exfiltration Rate (ft/day)		
		Base	Sideslope	
			With Drainage	Without Drainage
1	X	2.283E-03	2.283E-03	2.283E-03
2	X	2.283E-03	2.283E-03	2.283E-03
3	A	7.489E-08	0.000E+00	2.283E-03
4	A	7.489E-08	0.000E+00	2.283E-03
5	A	7.489E-08	0.000E+00	2.283E-03
6	B	8.836E-08	0.000E+00	1.360E-04
7	B	8.836E-08	0.000E+00	1.360E-04
8	B	8.836E-08	0.000E+00	1.360E-04
9	C	3.904E-08	0.000E+00	4.964E-05
10	D	8.447E-09	0.000E+00	7.945E-08
11	D	8.447E-09	0.000E+00	7.945E-08
12	D	8.447E-09	0.000E+00	7.945E-08
13	E	2.511E-09	0.000E+00	7.534E-09
14	E	2.511E-09	0.000E+00	7.534E-09
15	E	2.511E-09	0.000E+00	7.534E-09
16	E	2.511E-09	0.000E+00	7.534E-09
17	E	2.511E-09	0.000E+00	7.534E-09
18	F	9.132E-10	0.000E+00	6.849E-10
19	F	9.132E-10	0.000E+00	6.849E-10
20	F	9.132E-10	0.000E+00	6.849E-10
21	F	9.132E-10	0.000E+00	6.849E-10
22	F	9.132E-10	0.000E+00	6.849E-10
23	G	3.081E-06	1.142E-09	2.932E-06
24	H	2.283E-08	0.000E+00	2.374E-08
25	H	2.283E-08	0.000E+00	2.374E-08
26	H	2.283E-08	0.000E+00	2.374E-08
27	H	2.283E-08	0.000E+00	2.374E-08
28	H	2.283E-08	0.000E+00	2.374E-08

Table 2.7 TMA 3 flux rates by stress period

Stress Period	Phase	Exfiltration Rate (ft/day)		
		Base	Sideslope	
			With Drainage	Without Drainage
1	X	2.283E-03	2.283E-03	2.283E-03
2	X	2.283E-03	2.283E-03	2.283E-03
3	X	2.283E-03	2.283E-03	2.283E-03
4	X	2.283E-03	2.283E-03	2.283E-03
5	X	2.283E-03	2.283E-03	2.283E-03
6	X	2.283E-03	2.283E-03	2.283E-03
7	X	2.283E-03	2.283E-03	2.283E-03
8	A	7.489E-08	0.000E+00	2.283E-03
9	B	8.836E-08	0.000E+00	1.360E-04
10	B	8.836E-08	0.000E+00	1.360E-04
11	B	8.836E-08	0.000E+00	1.360E-04
12	C	3.904E-08	0.000E+00	4.964E-05
13	D	8.447E-09	0.000E+00	7.945E-08
14	D	8.447E-09	0.000E+00	7.945E-08
15	E	2.511E-09	0.000E+00	7.534E-09
16	E	2.511E-09	0.000E+00	7.534E-09
17	E	2.511E-09	0.000E+00	7.534E-09
18	E	2.511E-09	0.000E+00	7.534E-09
19	F	9.132E-10	0.000E+00	6.849E-10
20	F	9.132E-10	0.000E+00	6.849E-10
21	F	9.132E-10	0.000E+00	6.849E-10
22	F	9.132E-10	0.000E+00	6.849E-10
23	F	9.132E-10	0.000E+00	6.849E-10
24	F	9.132E-10	0.000E+00	6.849E-10
25	G	3.081E-06	1.142E-09	2.932E-06
26	H	2.283E-08	0.000E+00	2.374E-08
27	H	2.283E-08	0.000E+00	2.374E-08
28	H	2.283E-08	0.000E+00	2.374E-08

Table 2.8 TMA 4 flux rates by stress period

Stress Period	Phase	Exfiltration Rate (ft/day)		
		Base	Sideslope	
			With Drainage	Without Drainage
1	X	2.283E-03	2.283E-03	2.283E-03
2	X	2.283E-03	2.283E-03	2.283E-03
3	X	2.283E-03	2.283E-03	2.283E-03
4	X	2.283E-03	2.283E-03	2.283E-03
5	X	2.283E-03	2.283E-03	2.283E-03
6	X	2.283E-03	2.283E-03	2.283E-03
7	X	2.283E-03	2.283E-03	2.283E-03
8	X	2.283E-03	2.283E-03	2.283E-03
9	X	2.283E-03	2.283E-03	2.283E-03
10	X	2.283E-03	2.283E-03	2.283E-03
11	A	7.489E-08	0.000E+00	2.283E-03
12	A	7.489E-08	0.000E+00	2.283E-03
13	B	8.836E-08	0.000E+00	1.360E-04
14	C	3.904E-08	0.000E+00	4.964E-05
15	D	8.447E-09	0.000E+00	7.945E-08
16	D	8.447E-09	0.000E+00	7.945E-08
17	E	2.511E-09	0.000E+00	7.534E-09
18	E	2.511E-09	0.000E+00	7.534E-09
19	E	2.511E-09	0.000E+00	7.534E-09
20	F	9.132E-10	0.000E+00	6.849E-10
21	F	9.132E-10	0.000E+00	6.849E-10
22	F	9.132E-10	0.000E+00	6.849E-10
23	F	9.132E-10	0.000E+00	6.849E-10
24	F	9.132E-10	0.000E+00	6.849E-10
25	F	9.132E-10	0.000E+00	6.849E-10
26	F	9.132E-10	0.000E+00	6.849E-10
27	G	3.081E-06	1.142E-09	2.932E-06
28	H	2.283E-08	0.000E+00	2.374E-08

Table 2.9 Hypothetical concentration phases for sulfate

Description	Flow Phases	Source Concentration (ppm)	Beginning Time[1]
Operational	A-C	2,000	Start of flow phase A
Post-Cap	D-H	4,000	Start of flow phase D
Oxidized	H	40,000	Start of flow phase H[2]

Notes

[1]Varies by TMA Cell

[2]As a conservative assumption, the oxidized concentration begins one year after assumed degradation of the flexible membrane liner.

Table 2.10 Summary of sensitivity simulations

Description of Simulation	Parameter Variation(s)	Peak Concentration (ppm)	Time to Peak (years)
Best Engineering Judgement (BEJ)	None	2.88	125
Lower Effective Porosity	Effective Porosity = 0.10	7.28	60
Lower Longitudinal Disprsivity	Longitudinal Dispersivity = 25.0 ft	2.97	130
Lower Transverse Disprsivity	Transverse Dispersivity (horizontal and vertical) = 2.5 ft	2.97	150
Lower Transmissivity and Recharge	Horizontal Hydraulic Conductivity (all units) x 0.5 Default Recharge Rate = 5 in/yr	1.67	200
Lower Vertical Conductivity	Vertical Hydraulic Conductivity (all units) x 0.1	2.96	155
Post-Mine Flow Field	Fixed Head Boundaries from Post-Mine Regional Model Simulations	2.63	125
Bedrock Flow	General Head Boundaries at Model Base from Regional Model Simulations	2.41	75

Table 2.11 Practical Worst Case model parameters

Geologic Unit or Boundary	Parameter	Value [1]
All Geologic Units	Effective Porosity	**0.10**
	Longitudinal Dispersivity	**25.0 ft**
	Horizontal Transverse Dispersivity	**2.5 ft**
	Vertical Dispersivity	**2.5 ft**
Late Wisconsinan Till	Horizontal Hydraulic Conductivity	0.80 ft/day
	Vertical Hydraulic Conductivity	**0.040 ft/day**
Coarse Outwash	Default Zone Horizontal Hydraulic Conductivity	60.2 ft/dy
	Default Zone Vertical Hydraulic Conductivity	**0.602 ft/day**
	Low Zone Horizontal Hydraulic Conductivity	7.3 ft/day
	Low Zone Vertical Hydraulic Conductivity	**0.073 ft/day**
Fine Outwash	Horizontal Hydraulic Conductivity	15.0 ft/day
	Vertical Hydraulic Conductivity	**0.150 ft/day**
Pre- to Early-Wisconsinan Till and Massive Saprolite	Horizontal Hydraulic Conductivity	0.80 ft/day
	Vertical Hydraulic Conductivity	**0.010 ft/day**
Ancient Lacustrine	Horizontal Hydraulic Conductivity	0.80 ft/day
	Vertical Hydraulic Conductivity	**0.016 ft/day**
Ice Margin Contact Deposit	Horizontal Hydraulic Conductivity	0.80 ft/day
	Vertical Hydraulic Conductivity	**0.016 ft/day**
Hemlock Creek	Width	14.0 ft
	Creekbed Vertical Hydraulic Conductivity	1.0 ft/day
	Creekbed Sediment Thickness	1.0 ft
	Water Depth	1.0 ft
Discharge Wetlands	Bottom Sediment Vertical Hydraulic Conductivity	0.318 ft/day
	Bottom Sediment Thickness	1.0 ft
Seepage Wetlands	Bottom Sediment Vertical Hydraulic Conductivity	0.00318 ft/day
	Bottom Sediment Thickness	5.0 ft
	Water Depth	2.0 ft

[1] Bold values indicate changes from Best Engineering Judgement model parameters.

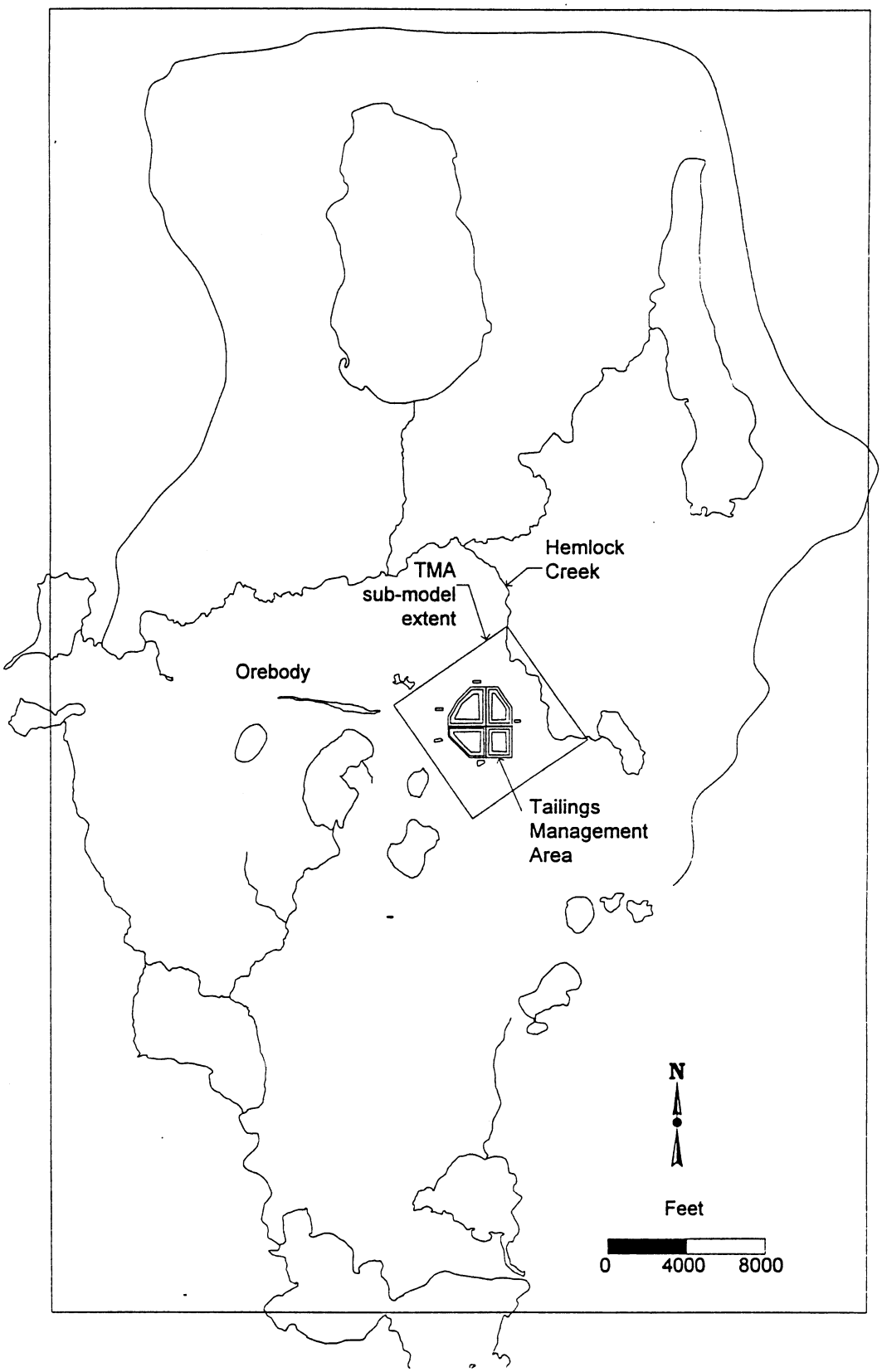

GeoTrans, inc.

REVISED	DATE	BY	DESCRIPTION

CHECKED BY:	PV	DATE: NOV 96
APPROVED BY:	RTH	DATE: NOV 96
APPROVED BY:	PFA	DATE: NOV 96

Crandon Mining Company

Figure 2.1
Tailings Management Area and TMA sub-model location map

Scale: 1" = 8000'	Date: Nov 1996
Prepared By: GeoTrans, Inc.	By: GWC

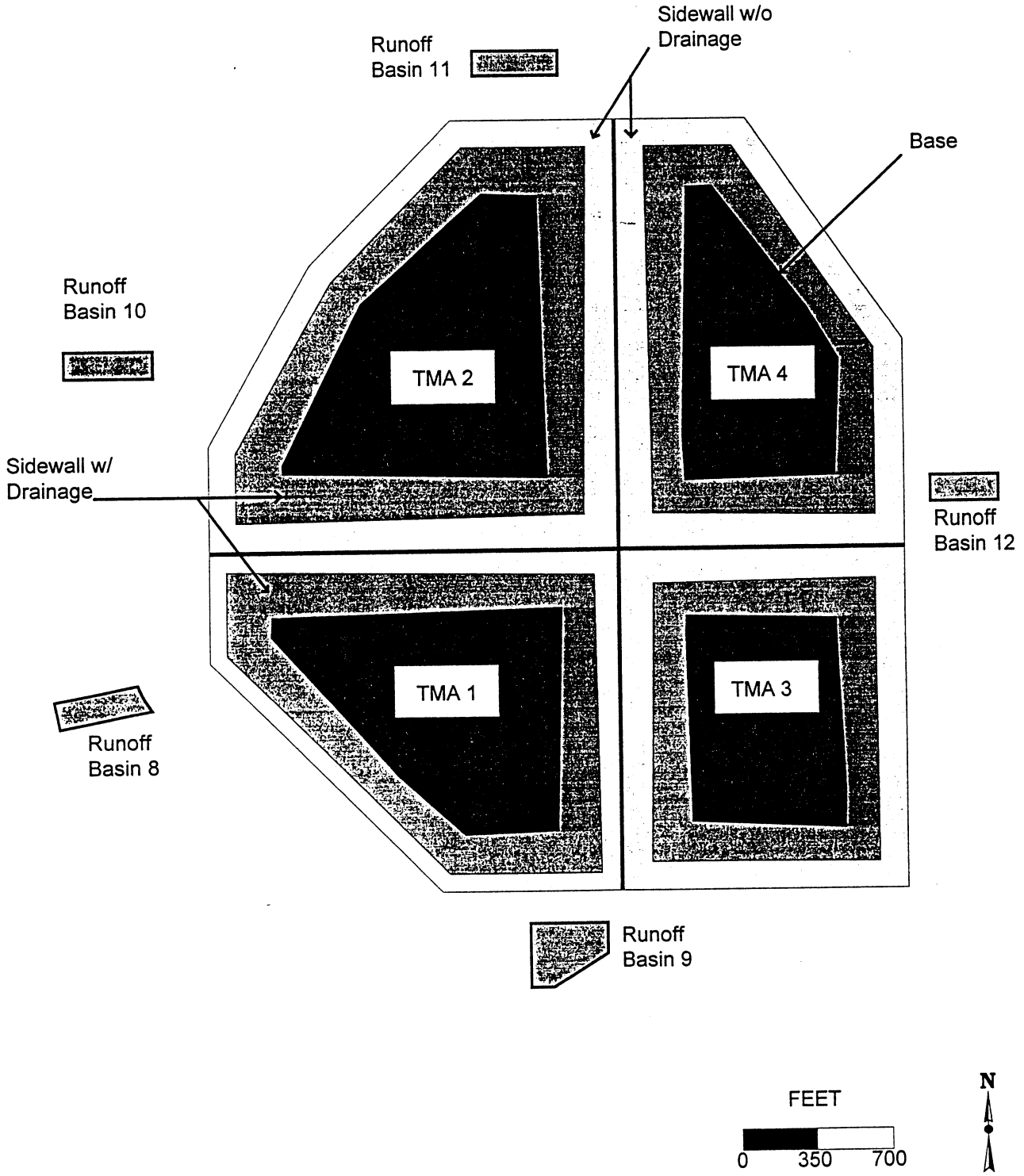

GeoTrans, inc.			
REVISED	DATE	BY	DESCRIPTION

CHECKED BY: PV	DATE: NOV 96
APPROVED BY: RTH	DATE: NOV 96
APPROVED BY: PFA	DATE: NOV 96

Crandon Mining Company

Figure 2.2
Tailings Management Area detail

Scale: 1" = 700'	Date: Nov 1996
Prepared By: GeoTrans, Inc.	By: GWC

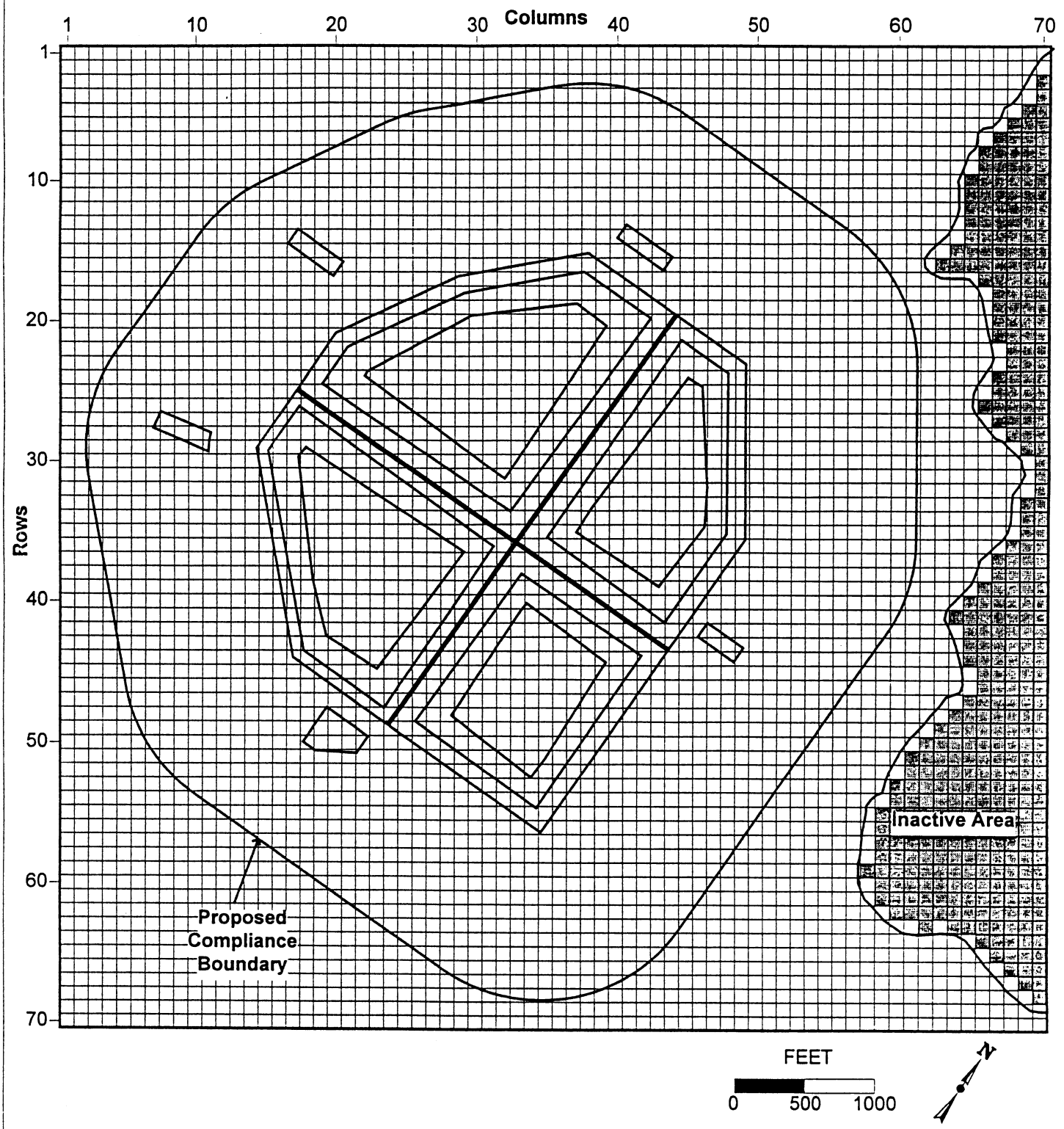

GeoTrans, inc.			
REVISED	DATE	BY	DESCRIPTION

CHECKED BY: PV	DATE: NOV 96
APPROVED BY: RTH	DATE: NOV 96
APPROVED BY: PFA	DATE: NOV 96

Crandon Mining Company

Figure 2.3
Model grid

Scale: 1" = 1000'	Date: Nov 1996
Prepared By: GeoTrans, Inc.	By: GWC

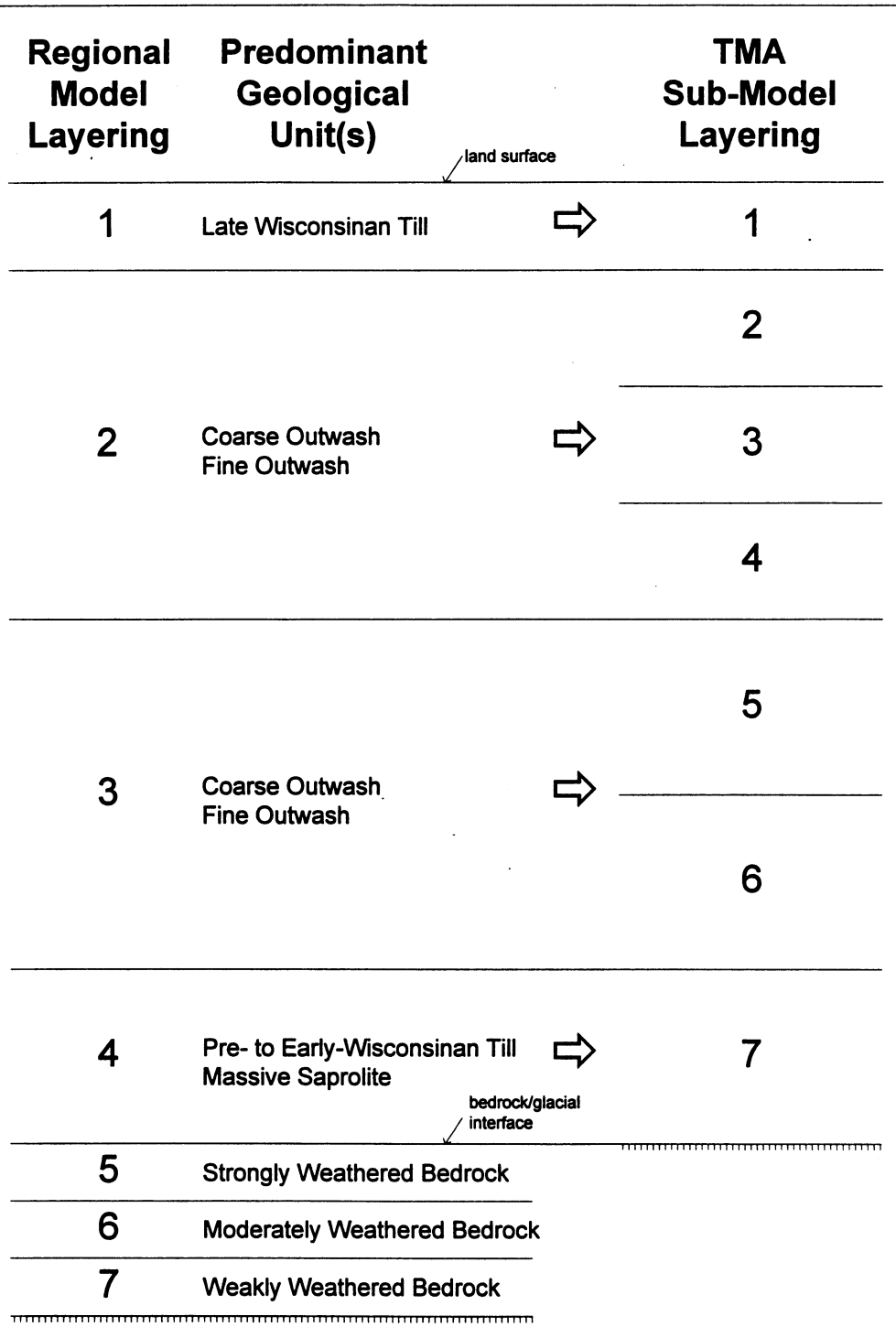

GeoTrans, inc.			
REVISED	DATE	BY	DESCRIPTION

CHECKED BY: PV	DATE: NOV 96
APPROVED BY: RTH	DATE: NOV 96
APPROVED BY: PFA	DATE: NOV 96

Crandon Mining Company

Figure 2.4
Model layering

Scale: Not to scale	Date: Nov 1996
Prepared By: GeoTrans, Inc.	By: GWC

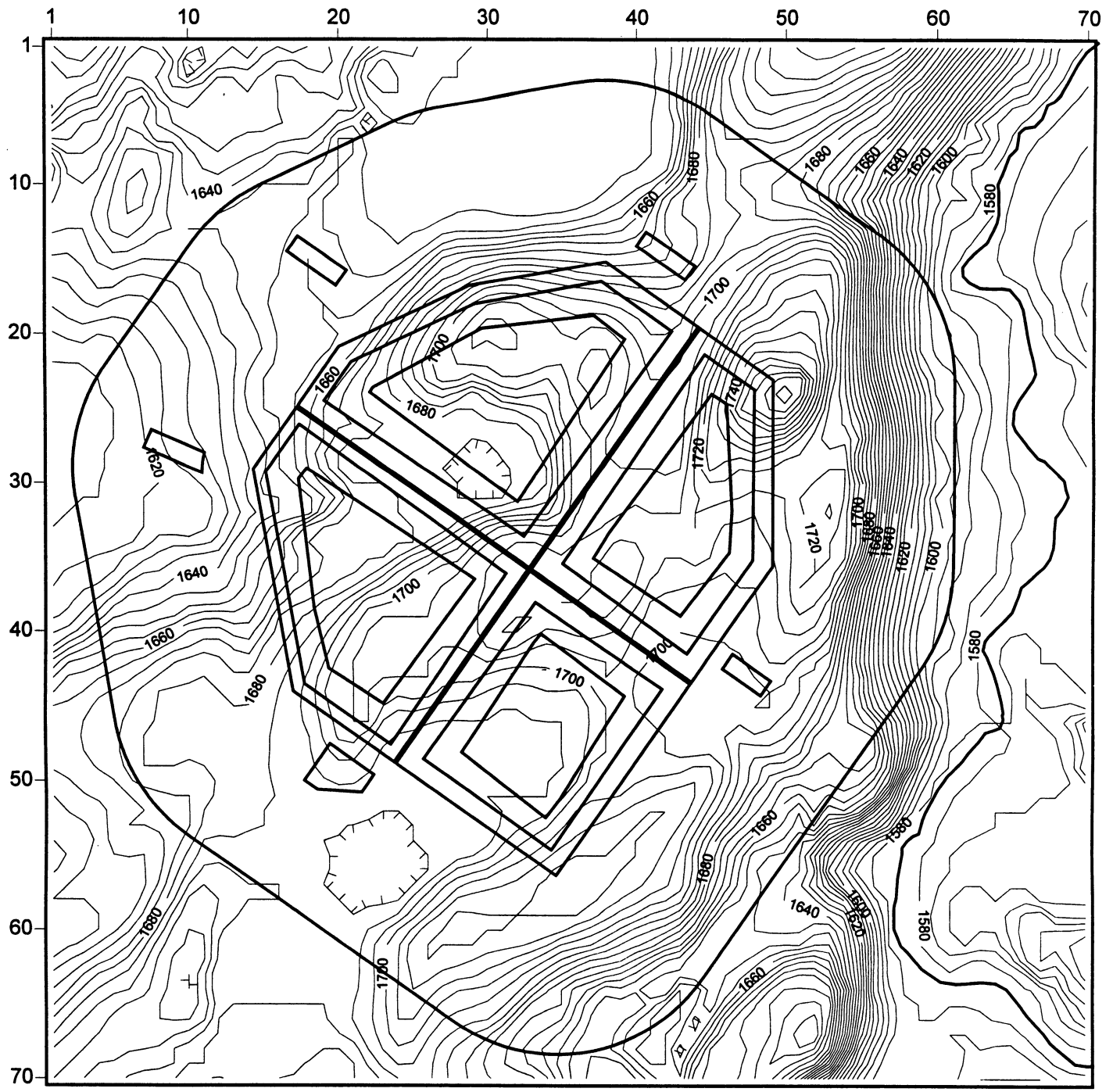

Notes:
Contour interval is 5 feet.
Elevation datum is mean sea level.

GeoTrans, inc.

REVISED	DATE	BY	DESCRIPTION

CHECKED BY: PV	DATE: NOV 96
APPROVED BY: RTH	DATE: NOV 96
APPROVED BY: PFA	DATE: NOV 96

Crandon Mining Company

Figure 2.5
Topographic elevation

Scale: 1" = 1000'	Date: Nov 1996
Prepared By: GeoTrans, Inc.	By: GWC

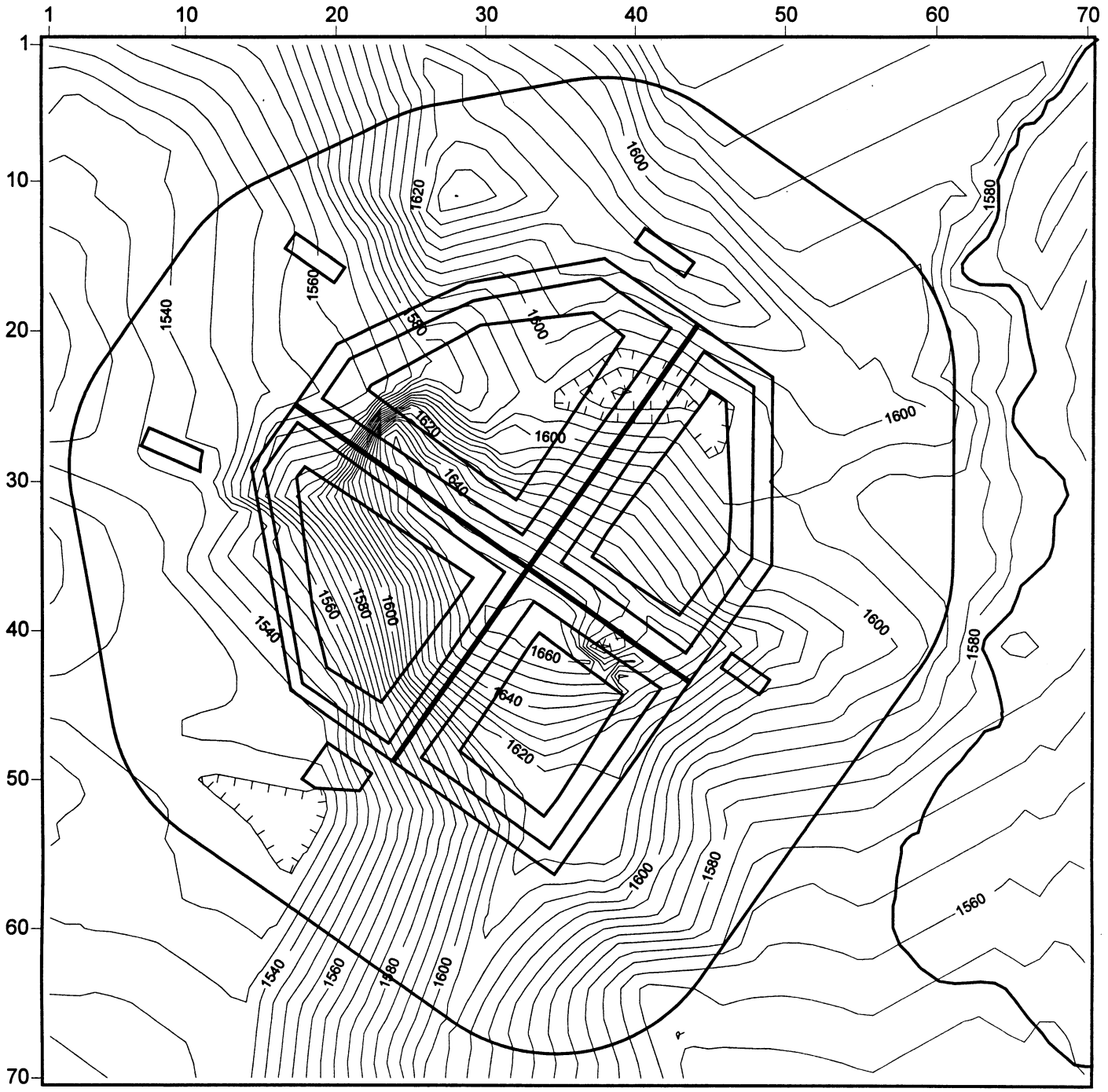

Notes:
Contour interval is 5 feet.
Elevation datum is mean sea level.

GeoTrans, inc.			
REVISED	DATE	BY	DESCRIPTION

CHECKED BY: PV	DATE: NOV 96
APPROVED BY: RTH	DATE: NOV 96
APPROVED BY: PFA	DATE: NOV 96

Crandon Mining Company

Figure 2.6
Elevation of the bottom of model layer 1

Scale: 1" = 1000'	Date: Nov 1996
Prepared By: GeoTrans, Inc.	By: GWC

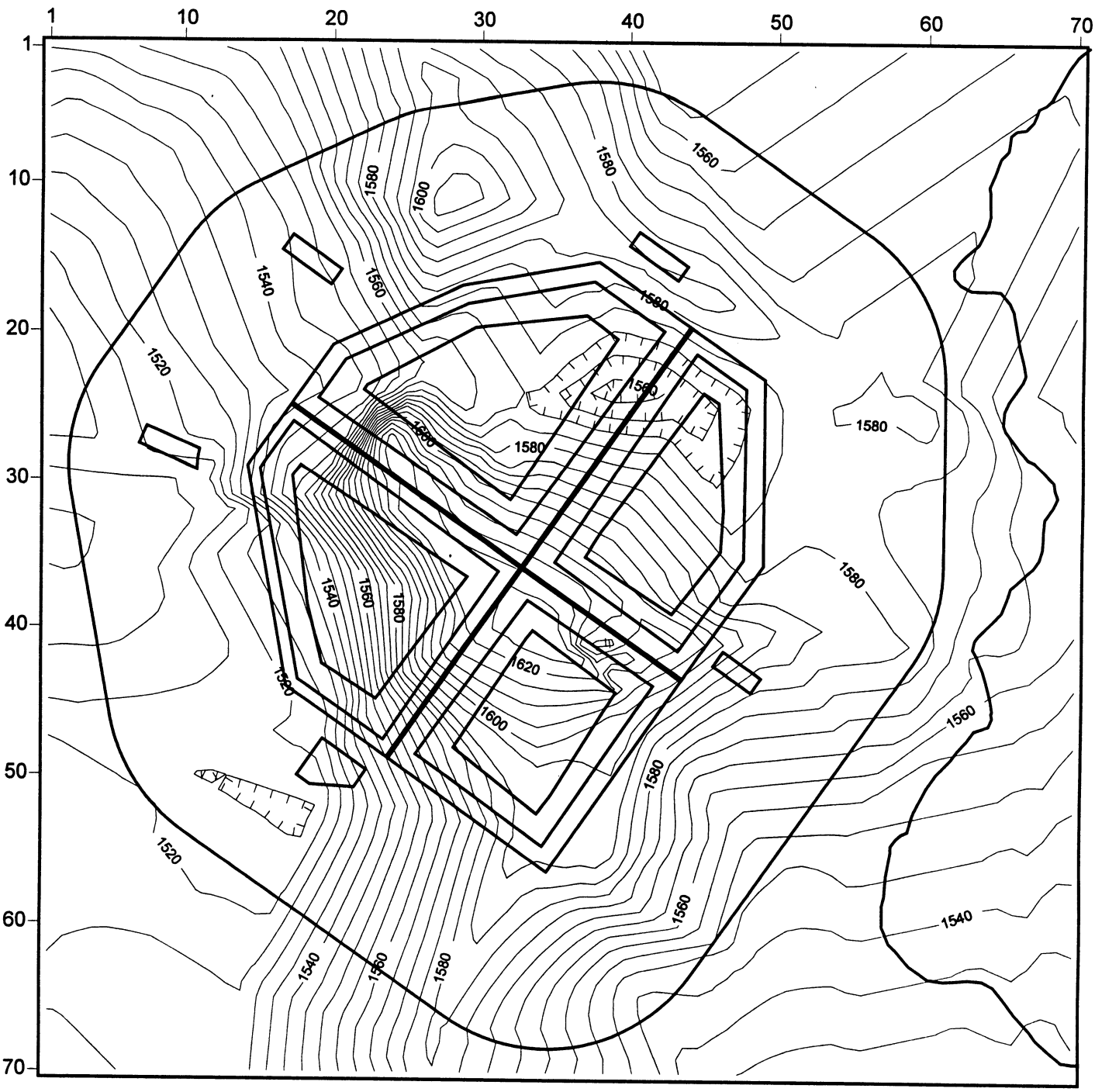

Notes:
Contour interval is 5 feet.
Elevation datum is mean sea level.

GeoTrans, inc.

REVISED	DATE	BY	DESCRIPTION

CHECKED BY: PV	DATE: NOV 96
APPROVED BY: RTH	DATE: NOV 96
APPROVED BY: PFA	DATE: NOV 96

Crandon Mining Company

Figure 2.7
Elevation of the bottom of model layer 2

Scale: 1" = 1000'	Date: Nov 1996
Prepared By: GeoTrans, Inc.	By: GWC

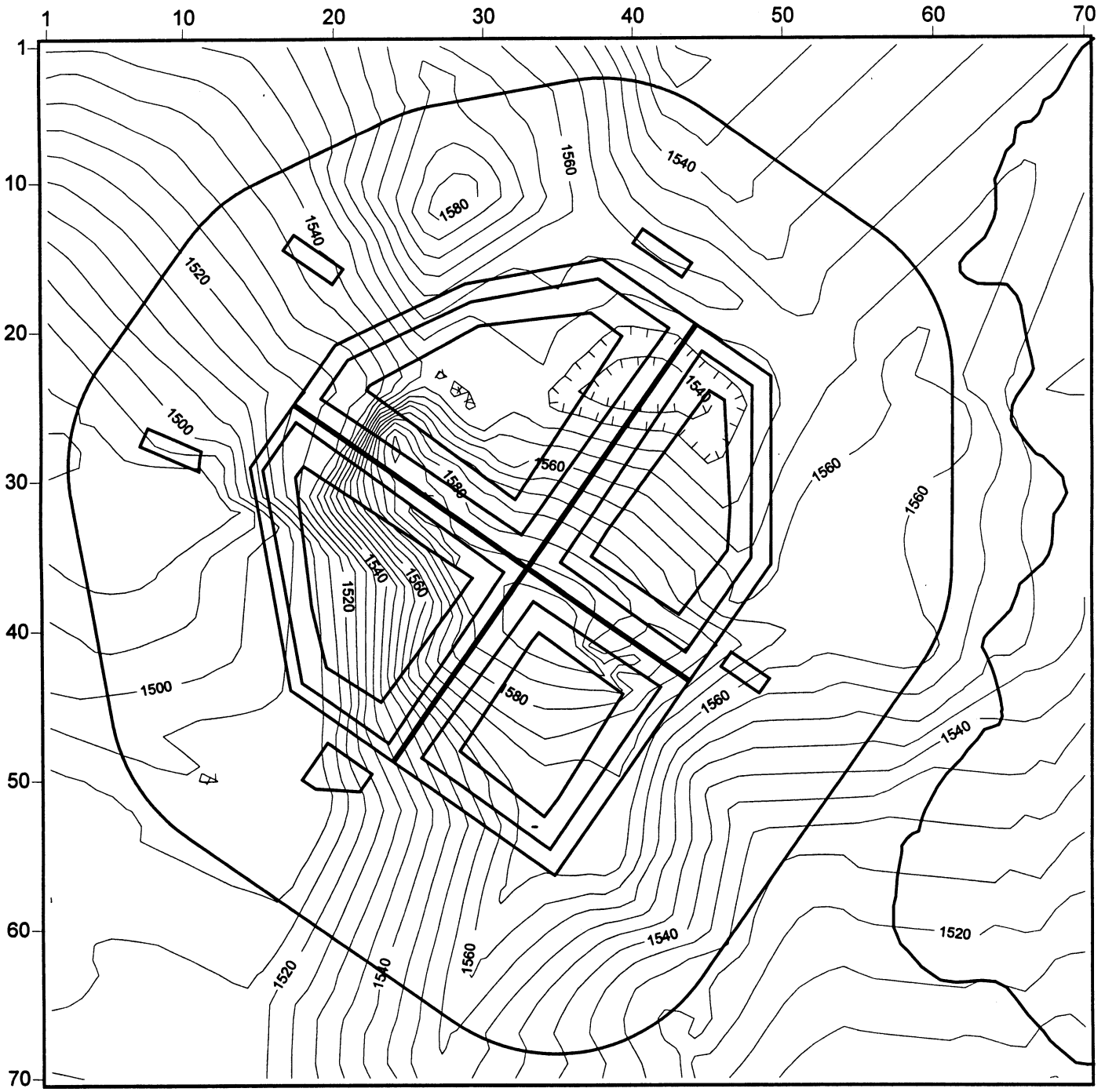

Notes:
Contour interval is 5 feet.
Elevation datum is mean sea level.

GeoTrans, inc.			
REVISED	DATE	BY	DESCRIPTION

CHECKED BY: PV	DATE: NOV 96
APPROVED BY: RTH	DATE: NOV 96
APPROVED BY: PFA	DATE: NOV 96

Crandon Mining Company

Figure 2.8
Elevation of the bottom of model layer 3

Scale: 1" = 1000'	Date: Nov 1996
Prepared By: GeoTrans, Inc.	By: GWC

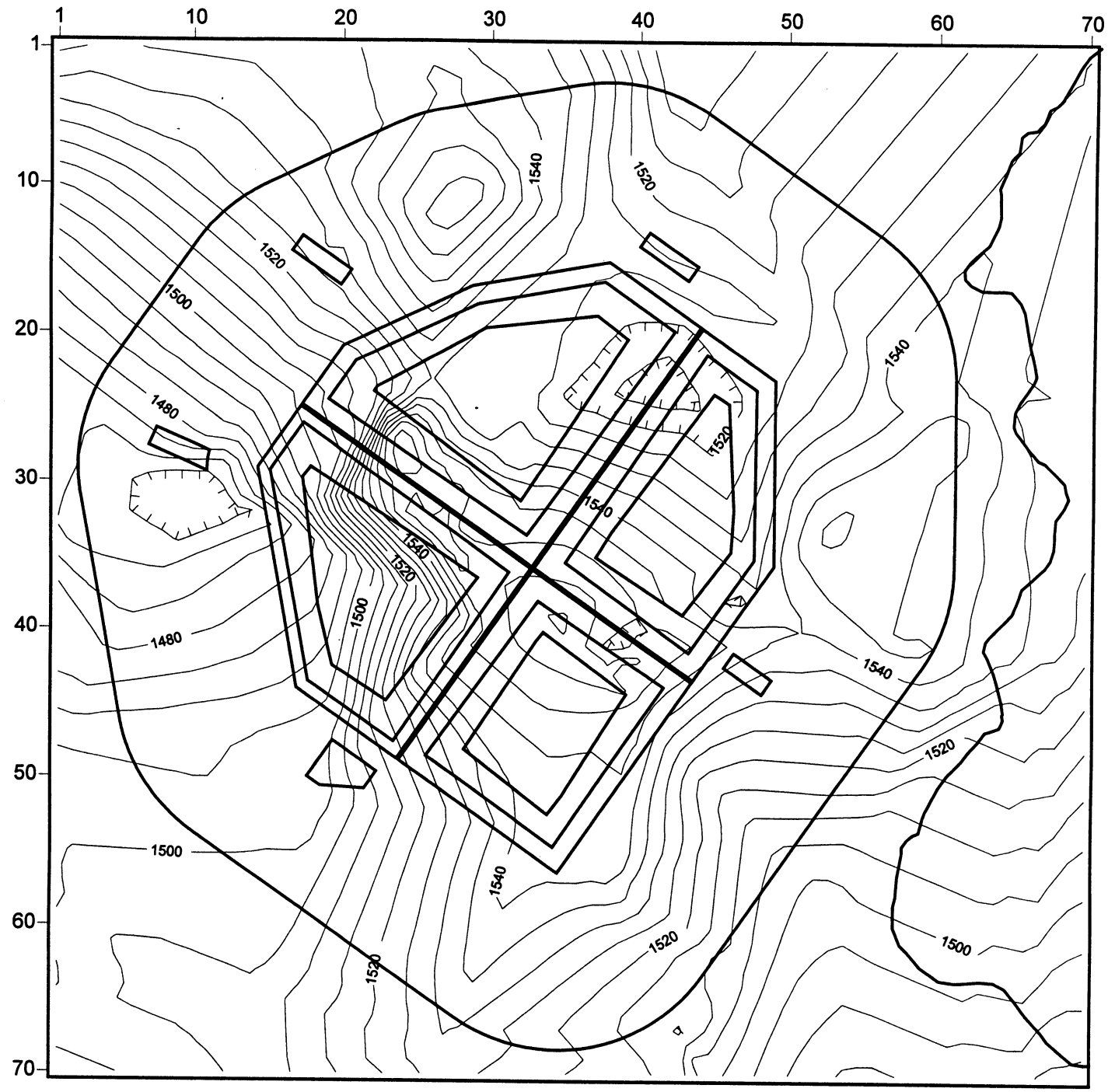

Notes:
Contour interval is 5 feet.
Elevation datum is mean sea level.

GeoTrans, inc.			
REVISED	DATE	BY	DESCRIPTION

CHECKED BY: PV	DATE: NOV 96
APPROVED BY: RTH	DATE: NOV 96
APPROVED BY: PFA	DATE: NOV 96

Crandon Mining Company

Figure 2.9
Elevation of the bottom of model layer 4

Scale: 1" = 1000'	Date: Nov 1996
Prepared By: GeoTrans, Inc.	By: GWC

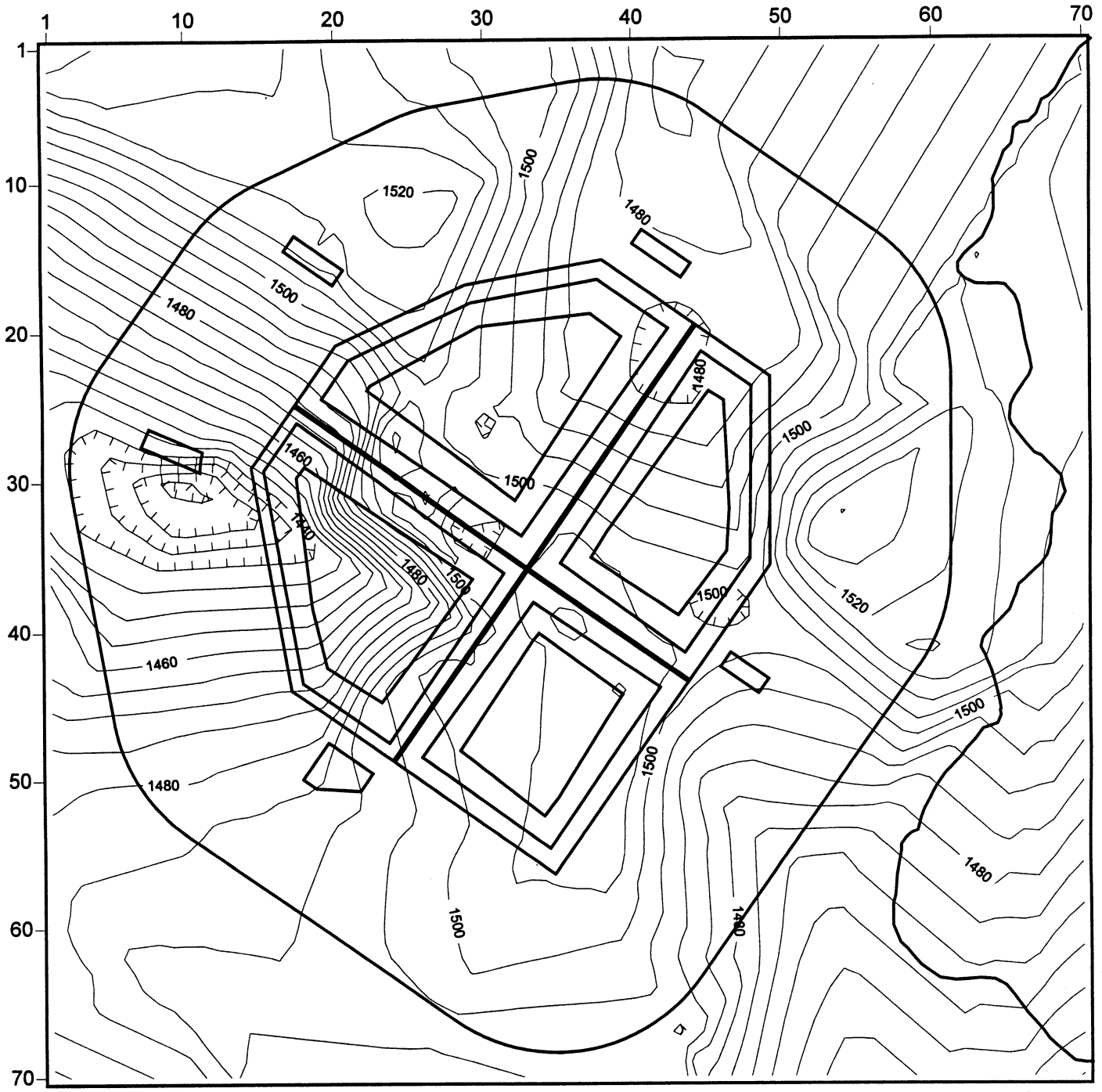

Notes:
Contour interval is 5 feet.
Elevation datum is mean sea level.

GeoTrans, inc.			
REVISED	DATE	BY	DESCRIPTION

CHECKED BY: PV	DATE: NOV 96
APPROVED BY: RTH	DATE: NOV 96
APPROVED BY: PFA	DATE: NOV 96

Crandon Mining Company

Figure 2.10
Elevation of the bottom of model layer 5

Scale: 1" = 1000'	Date: Nov 1996
Prepared By: GeoTrans, Inc.	By: GWC

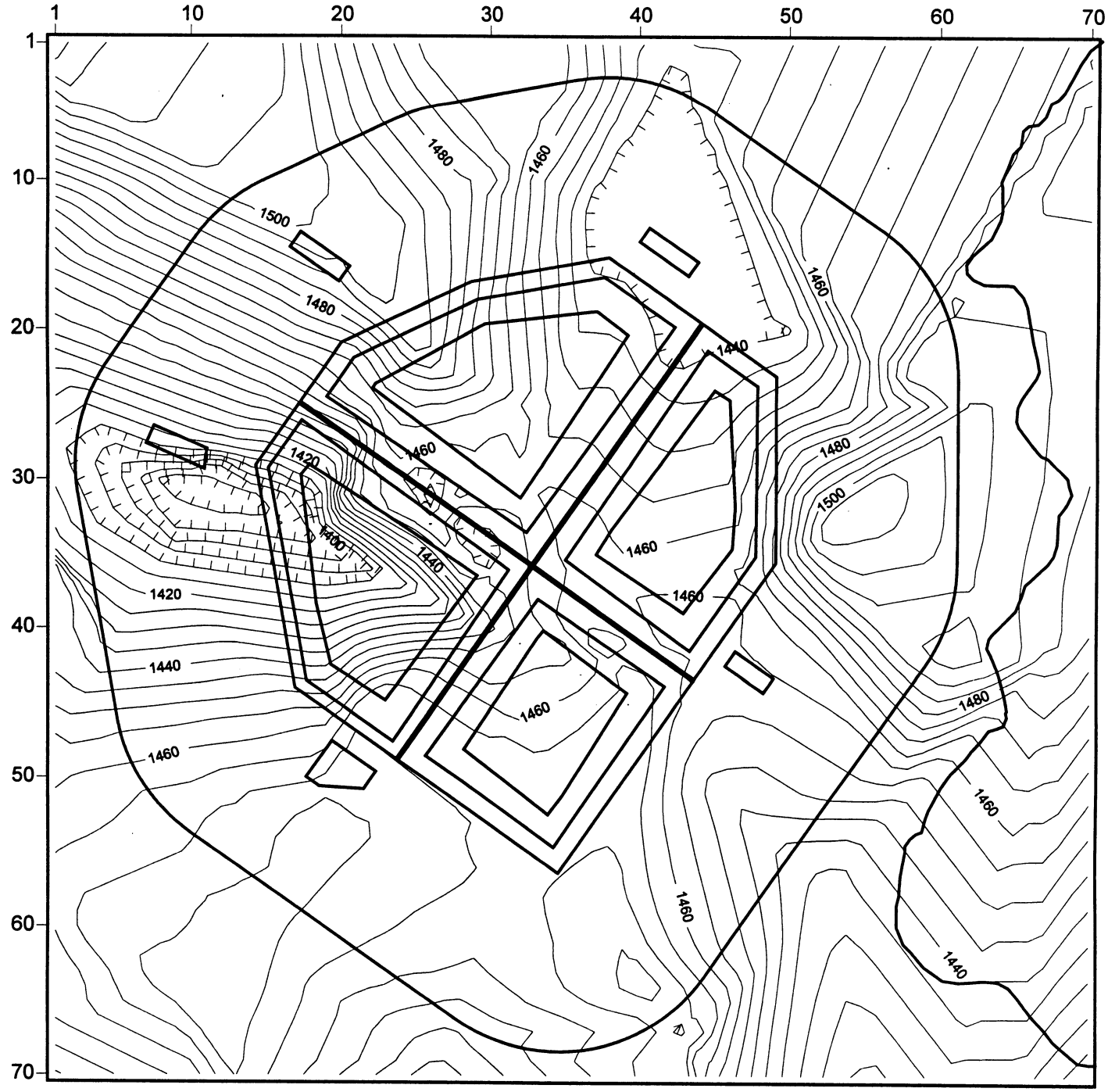

Notes:
Contour interval is 5 feet.
Elevation datum is mean sea level.

GeoTrans, inc.

REVISED	DATE	BY	DESCRIPTION

CHECKED BY: PV	DATE: NOV 96
APPROVED BY: RTH	DATE: NOV 96
APPROVED BY: PFA	DATE: NOV 96

Crandon Mining Company

Figure 2.11
Elevation of the bottom of model layer 6

Scale: 1" = 1000'	Date: Nov 1996
Prepared By: GeoTrans, Inc.	By: GWC

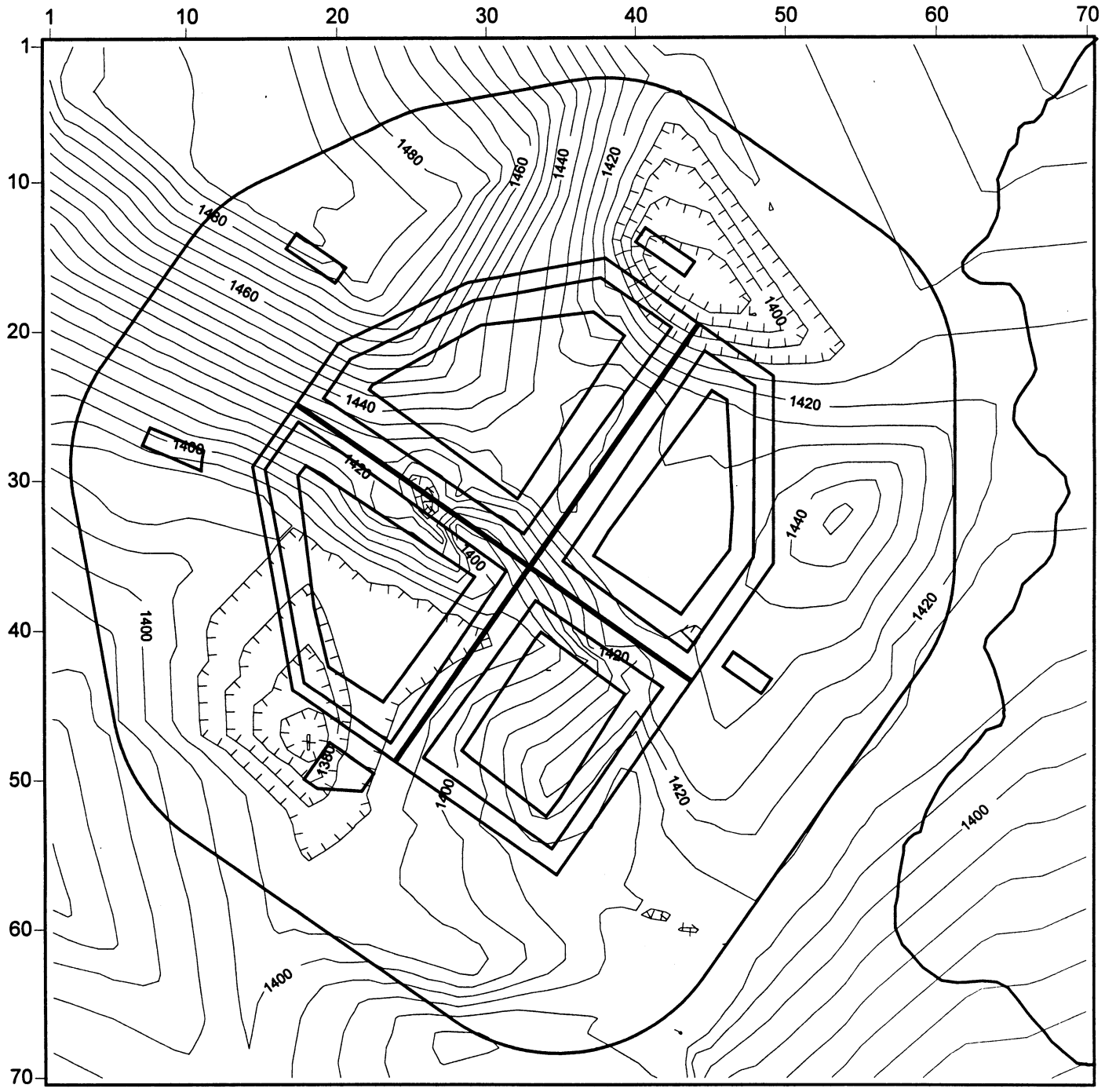

Notes:
Contour interval is 5 feet.
Elevation datum is mean sea level.

GeoTrans, inc.			
REVISED	DATE	BY	DESCRIPTION

CHECKED BY: PV	DATE: NOV 96
APPROVED BY: RTH	DATE: NOV 96
APPROVED BY: PFA	DATE: NOV 96

Crandon Mining Company

Figure 2.12
Elevation of the bottom of model layer 7

Scale: 1" = 1000'	Date: Nov 1996
Prepared By: GeoTrans, Inc.	By: GWC

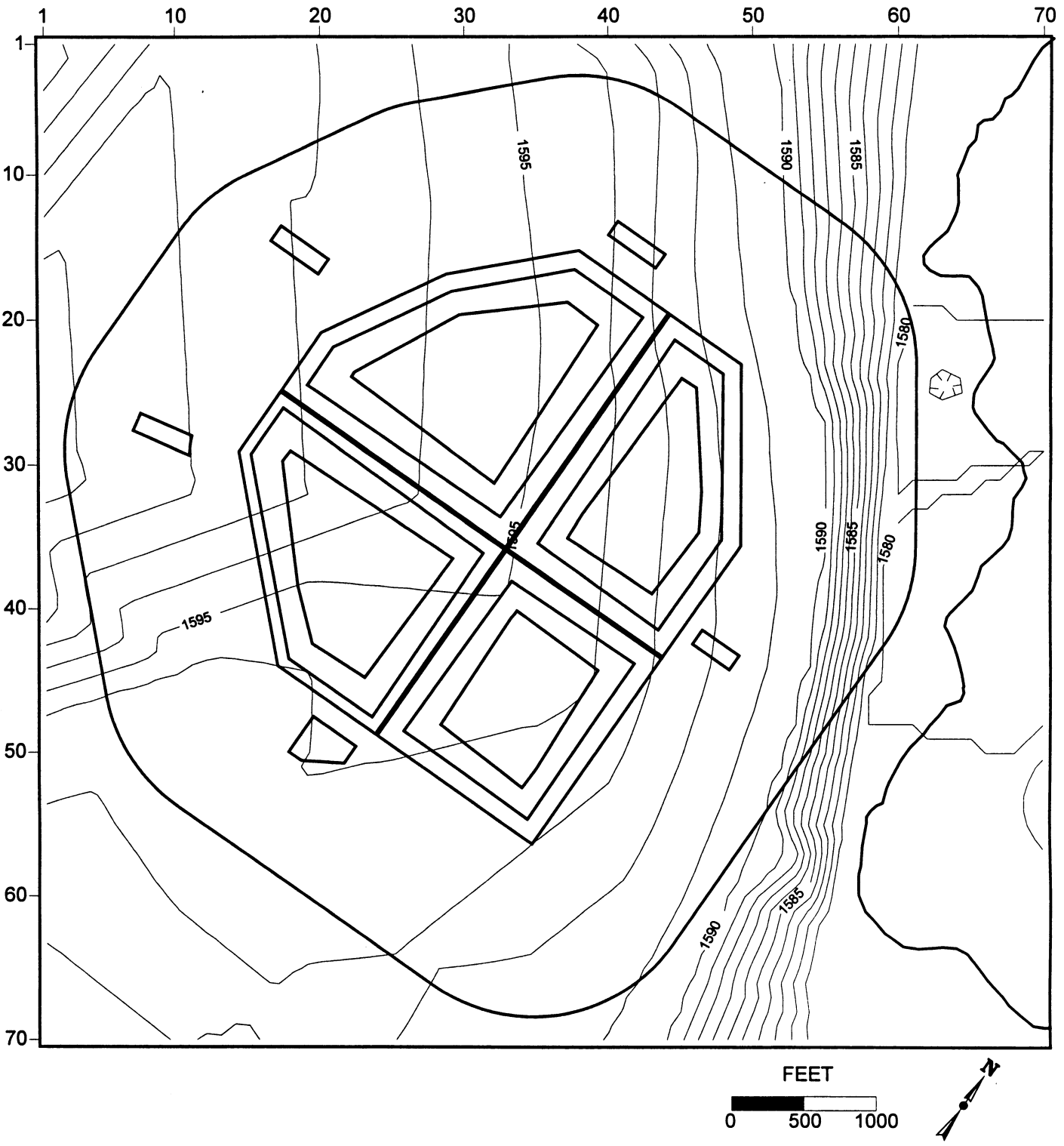

GeoTrans, inc.			
REVISED	DATE	BY	DESCRIPTION

CHECKED BY: PV	DATE: NOV 96
APPROVED BY: RTH	DATE: NOV 96
APPROVED BY: PFA	DATE: NOV 96

Crandon Mining Company

Figure 2.13
Water table elevation (ft)
from 1984 measurements

Scale: 1" = 1000'	Date: Nov 1996
Prepared By: GeoTrans, Inc.	By: GWC

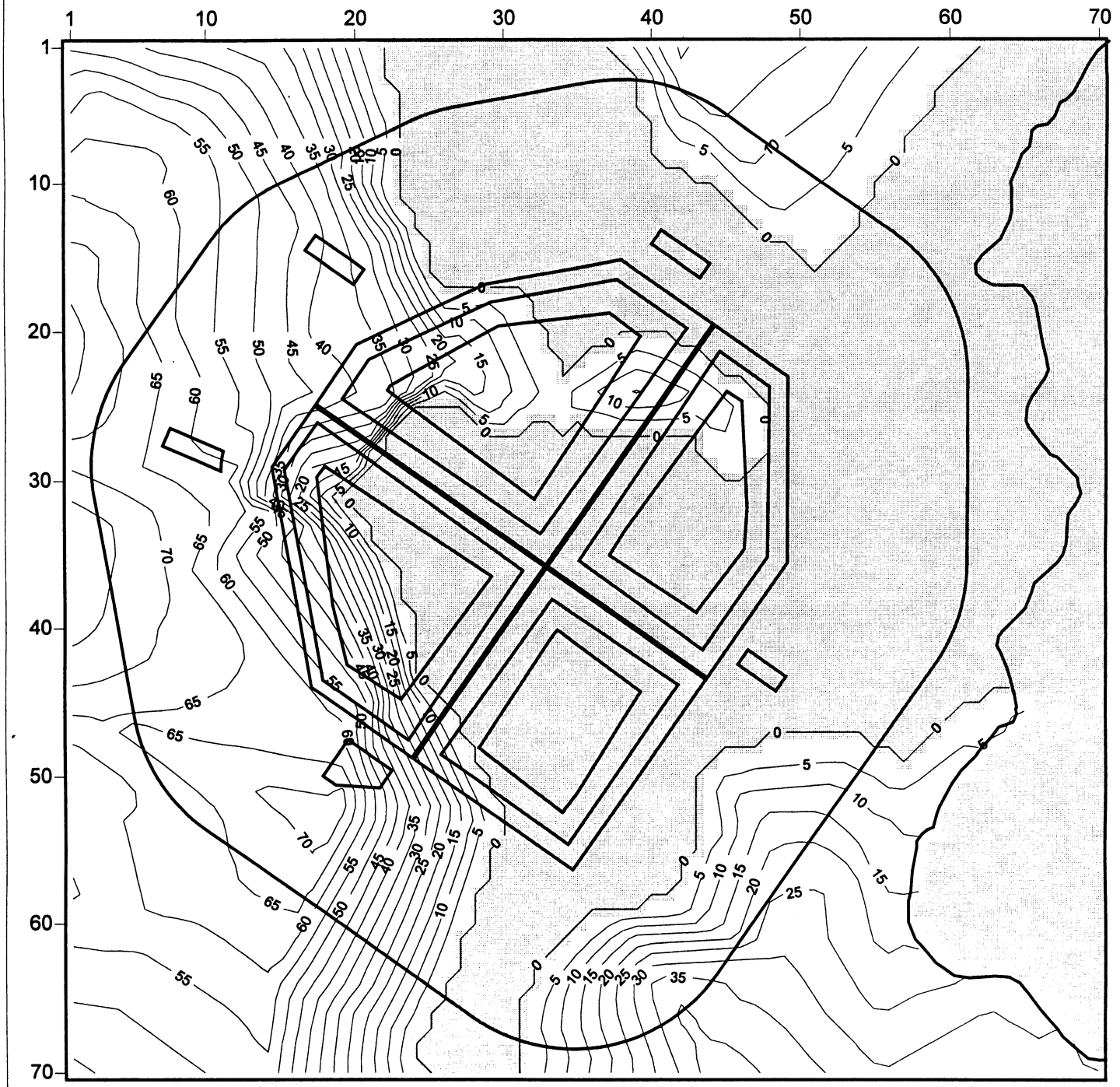

Note: contour interval is 5 feet.

GeoTrans, inc.			
REVISED	DATE	BY	DESCRIPTION

CHECKED BY: PV	DATE: NOV 96
APPROVED BY: RTH	DATE: NOV 96
APPROVED BY: PFA	DATE: NOV 96

Crandon Mining Company

Figure 2.14
Saturated thickness of model layer 1

Scale: 1" = 1000'	Date: Nov 1996
Prepared By: GeoTrans, Inc.	By: GWC

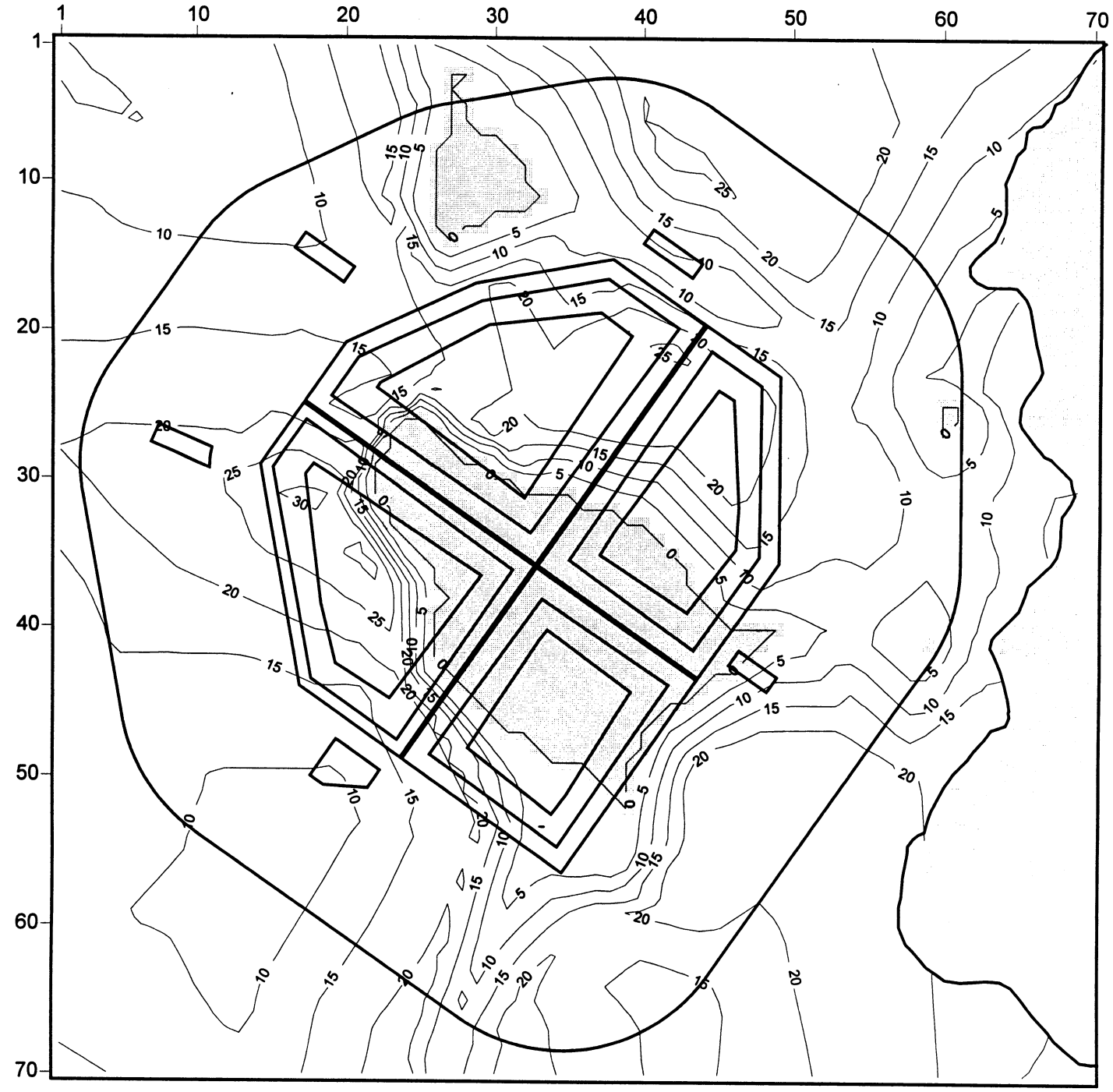

Note: contour interval is 5 feet.

GeoTrans, inc.

REVISED	DATE	BY	DESCRIPTION

CHECKED BY: PV	DATE: NOV 96
APPROVED BY: RTH	DATE: NOV 96
APPROVED BY: PFA	DATE: NOV 96

Crandon Mining Company

Figure 2.15
Saturated thickness of model layer 2

Scale: 1" = 1000'	Date: Nov 1996
Prepared By: GeoTrans, Inc.	By: GWC

Note: contour interval is 5 feet.

GeoTrans, inc.			
REVISED	DATE	BY	DESCRIPTION

CHECKED BY: PV	DATE: NOV 96
APPROVED BY: RTH	DATE: NOV 96
APPROVED BY: PFA	DATE: NOV 96

Crandon Mining Company

Figure 2.16
Saturated thickness of model layer 3

Scale: 1" = 1000'	Date: Nov 1996
Prepared By: GeoTrans, Inc.	By: GWC

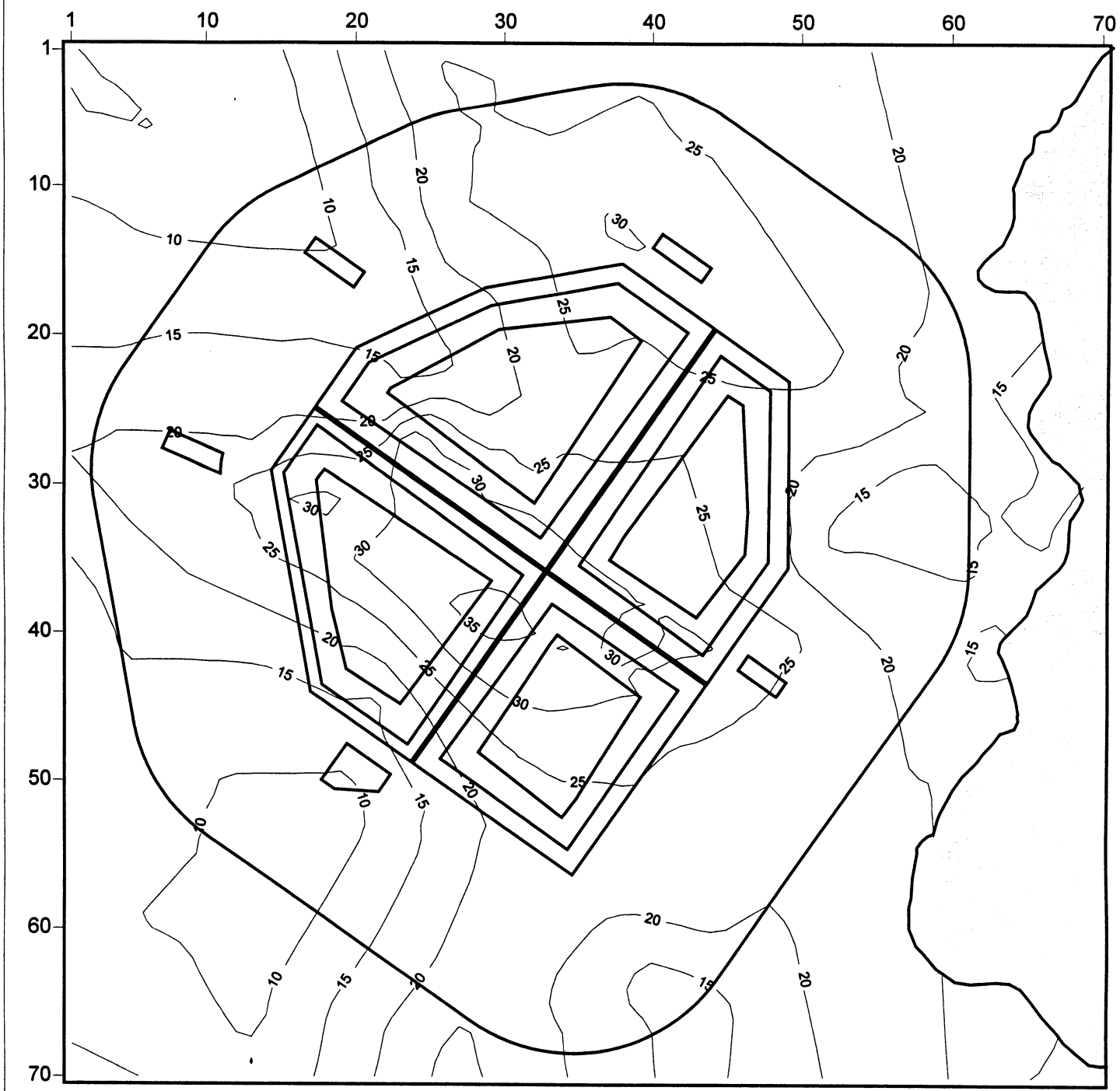

Note: contour interval is 5 feet.

GeoTrans, inc.

REVISED	DATE	BY	DESCRIPTION

CHECKED BY: PV	DATE: NOV 96
APPROVED BY: RTH	DATE: NOV 96
APPROVED BY: PFA	DATE: NOV 96

Crandon Mining Company

Figure 2.17
Saturated thickness of model layer 4

Scale: 1" = 1000'	Date: Nov 1996
Prepared By: GeoTrans, Inc.	By: GWC

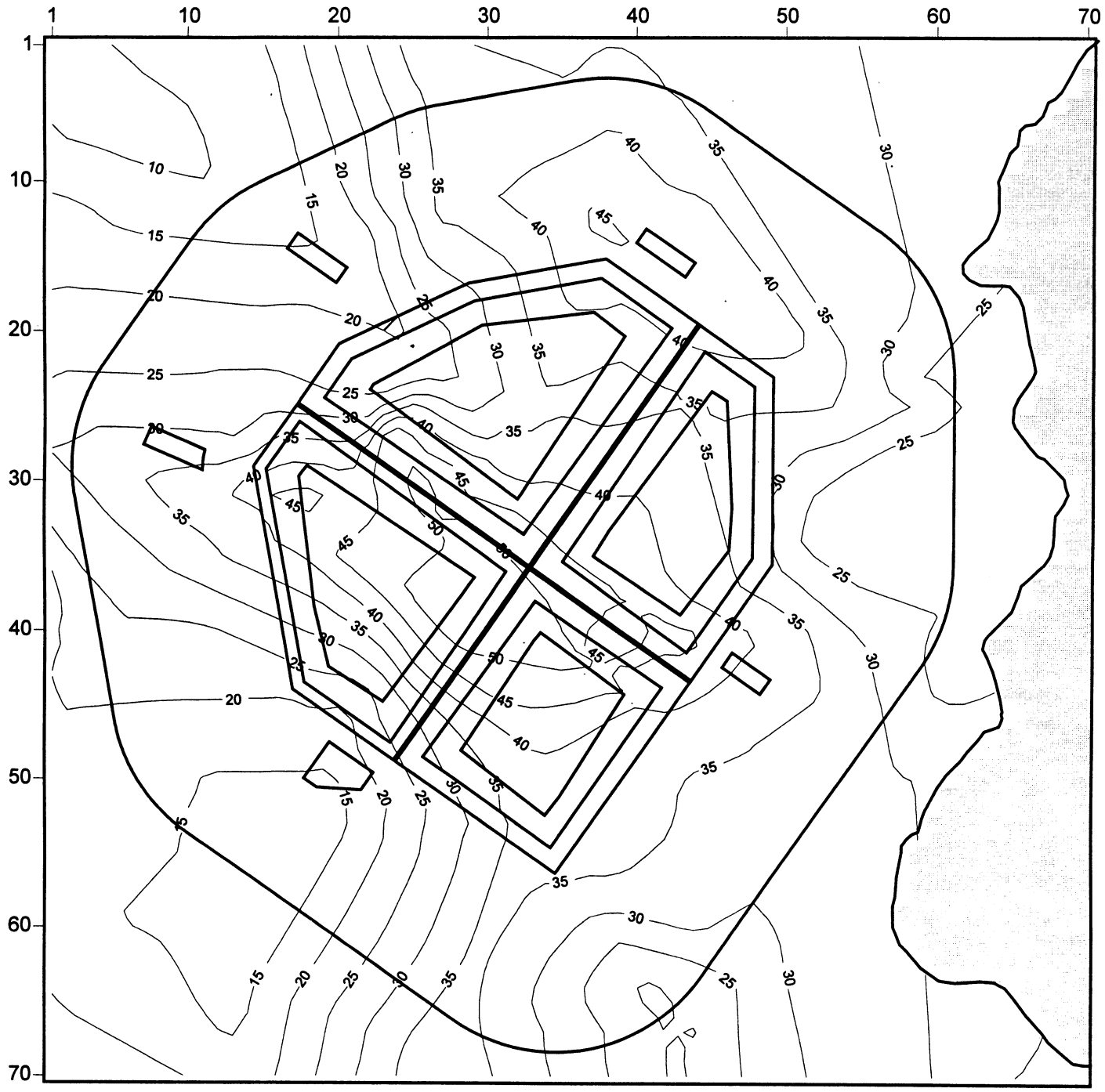

Note: contour interval is 5 feet.

GeoTrans, inc.			
REVISED	DATE	BY	DESCRIPTION

CHECKED BY: PV	DATE: NOV 96
APPROVED BY: RTH	DATE: NOV 96
APPROVED BY: PFA	DATE: NOV 96

Crandon Mining Company

Figure 2.18
Saturated thickness of model layer 5

Scale: 1" = 1000'	Date: Nov 1996
Prepared By: GeoTrans, Inc.	By: GWC

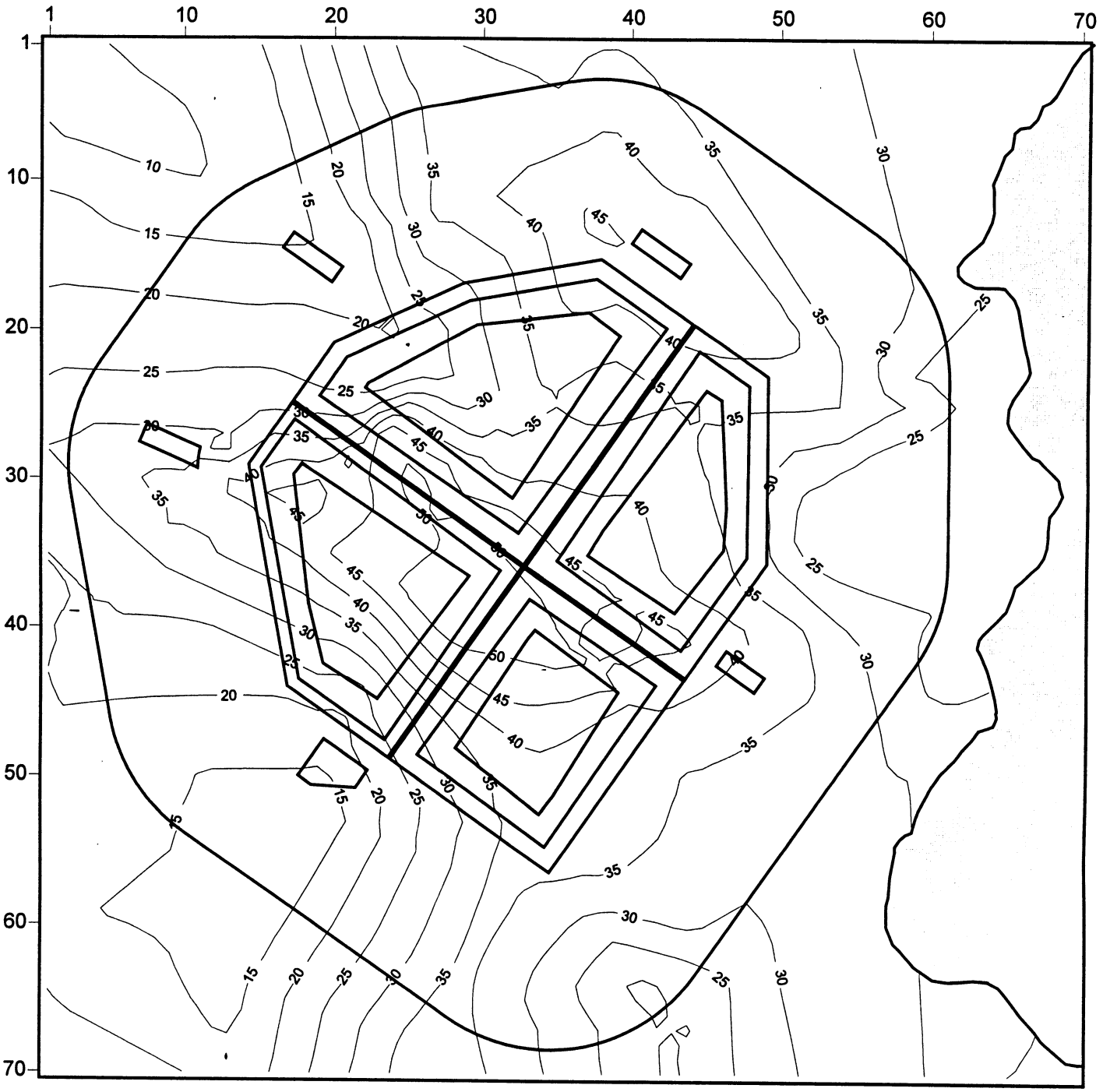

Note: contour interval is 5 feet.

GeoTrans, inc.

REVISED	DATE	BY	DESCRIPTION

CHECKED BY: PV	DATE: NOV 96
APPROVED BY: RTH	DATE: NOV 96
APPROVED BY: PFA	DATE: NOV 96

Crandon Mining Company

Figure 2.19
Saturated thickness of model layer 6

Scale: 1" = 1000'	Date: Nov 1996
Prepared By: GeoTrans, Inc.	By: GWC

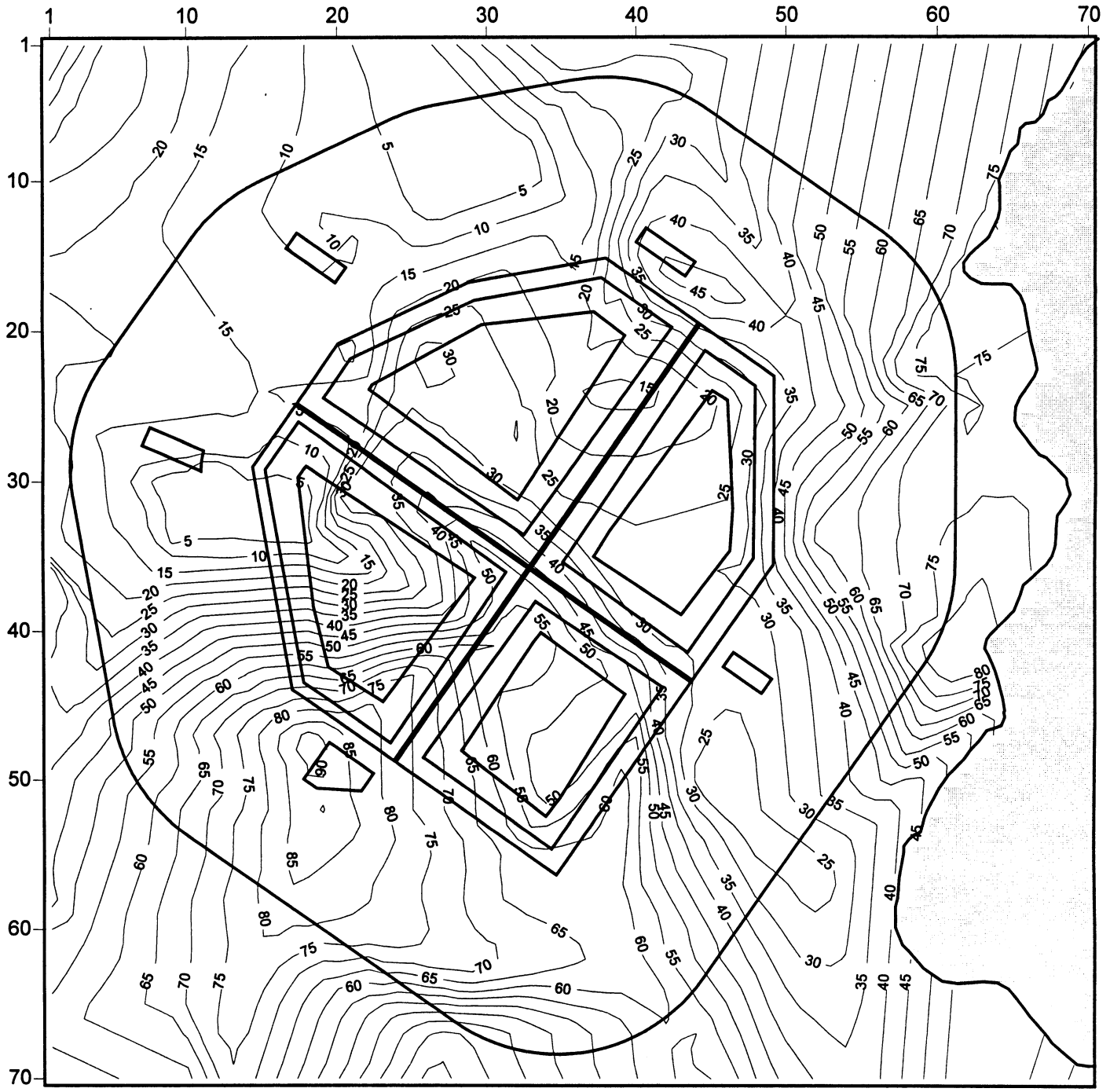

Note: contour interval is 5 feet.

GeoTrans, inc.			
REVISED	DATE	BY	DESCRIPTION

CHECKED BY: PV	DATE: NOV 96
APPROVED BY: RTH	DATE: NOV 96
APPROVED BY: PFA	DATE: NOV 96

Crandon Mining Company

Figure 2.20
Saturated thickness of model layer 7

Scale: 1" = 1000'	Date: Nov 1996
Prepared By: GeoTrans, Inc.	By: GWC

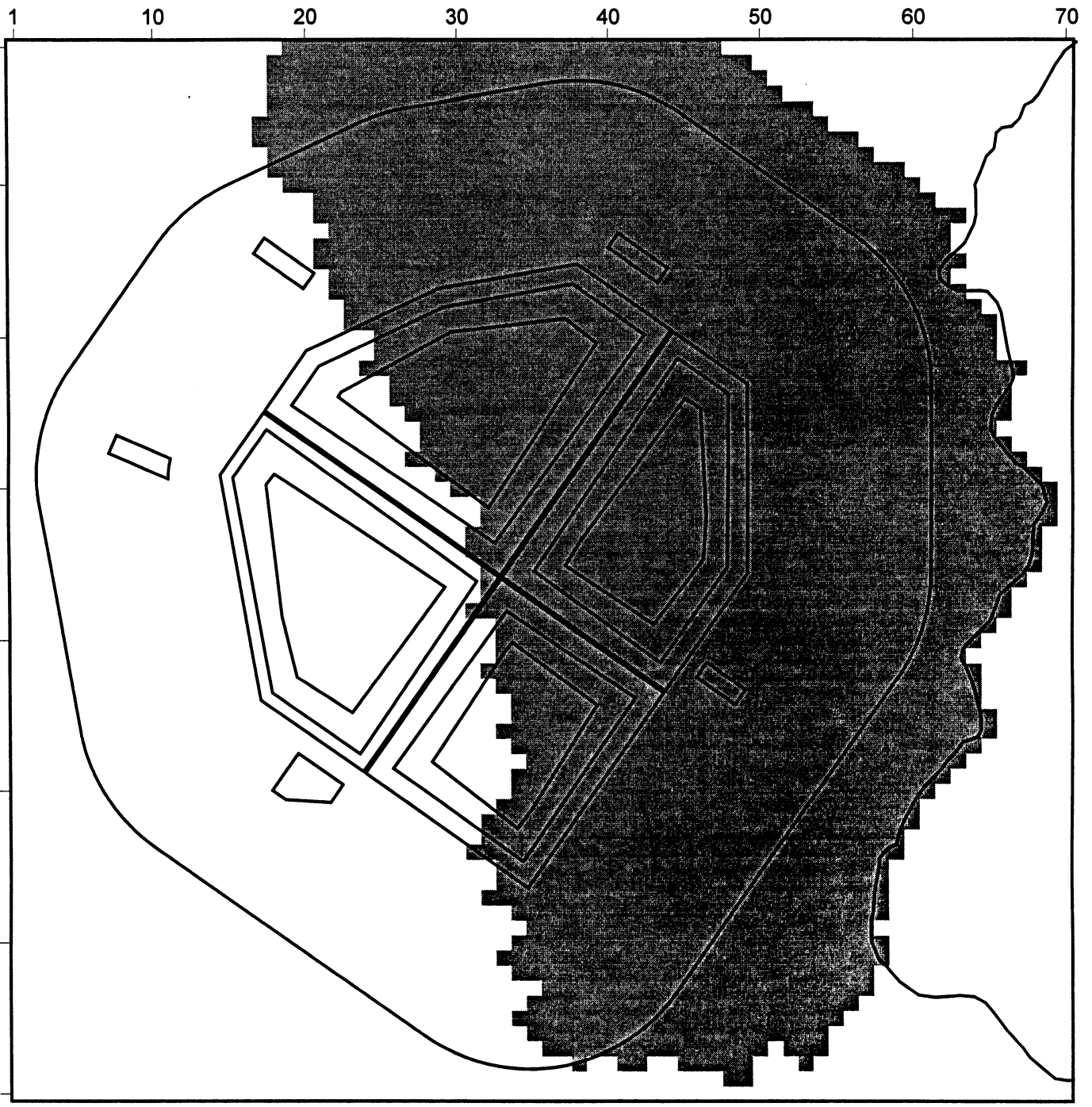

GeoTrans, inc.			
REVISED	DATE	BY	DESCRIPTION

CHECKED BY: PV	DATE: NOV 96
APPROVED BY: RTH	DATE: NOV 96
APPROVED BY: PFA	DATE: NOV 96

Crandon Mining Company

Figure 2.21
Coarse outwash conductivity zonation

Scale: 1" = 1000'	Date: Nov 1996
Prepared By: GeoTrans, Inc.	By: GWC

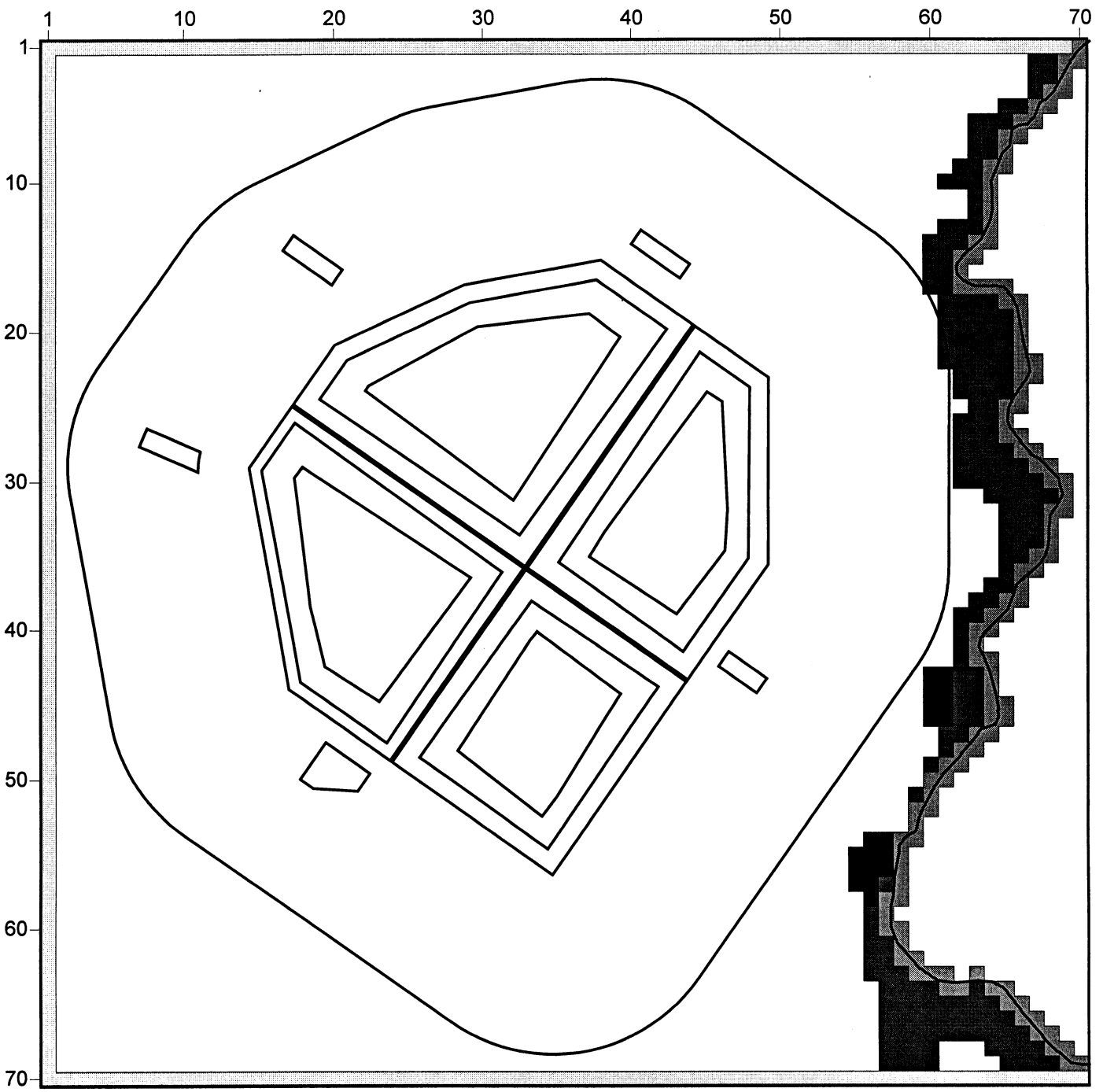

LEGEND

Boundary	MODFLOW Package	Model Layer(s)
Model Edge	General Head (GHB)	All Active Layers
Hemlock Creek	River (RIV)	Uppermost Active Layer
Discharge Wetlands	Drain (DRN)	Uppermost Active Layer
Seepage Wetlands	River (RIV)	Uppermost Active Layer

FEET

0 500 1000

N

GeoTrans, inc.

REVISED	DATE	BY	DESCRIPTION

CHECKED BY: PV	DATE: NOV 96
APPROVED BY: RTH	DATE: NOV 96
APPROVED BY: PFA	DATE: NOV 96

Crandon Mining Company

Figure 2.22
Flow boundary conditions

Scale: 1" = 1000'	Date: Nov 1996
Prepared By: GeoTrans, Inc.	By: GWC

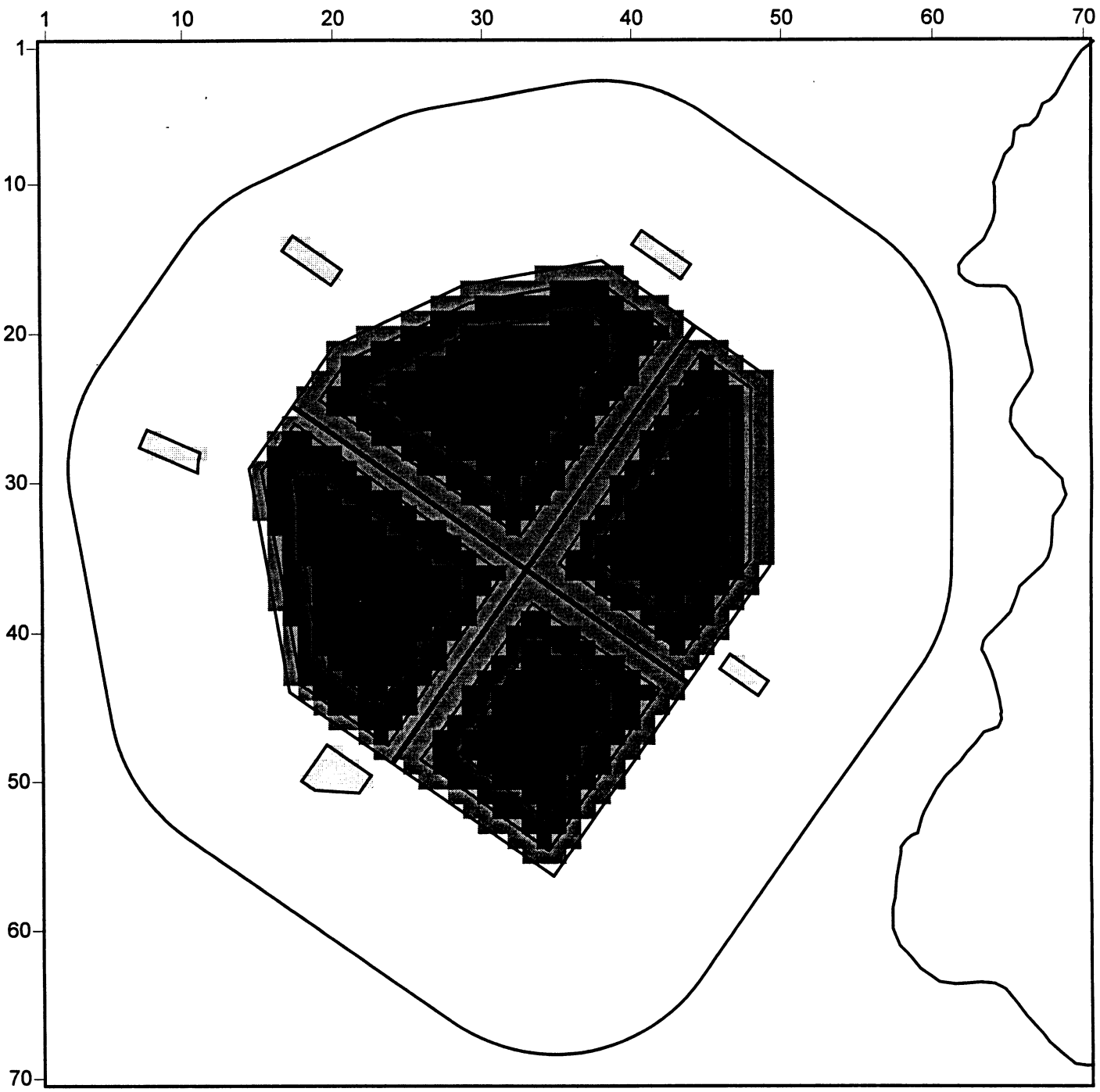

FEET

0 500 1000

N

TMA Basin

TMA Sideslope with Drainage

TMA Sideslope without Drainage

Runoff basin (zero concentration)

GeoTrans, inc.

REVISED	DATE	BY	DESCRIPTION

CHECKED BY: PV	DATE: NOV 96
APPROVED BY: RTH	DATE: NOV 96
APPROVED BY: PFA	DATE: NOV 96

Crandon Mining Company

Figure 2.23
TMA recharge zones

Scale: 1" = 1000'	Date: Nov 1996
Prepared By: GeoTrans, Inc.	By: GWC

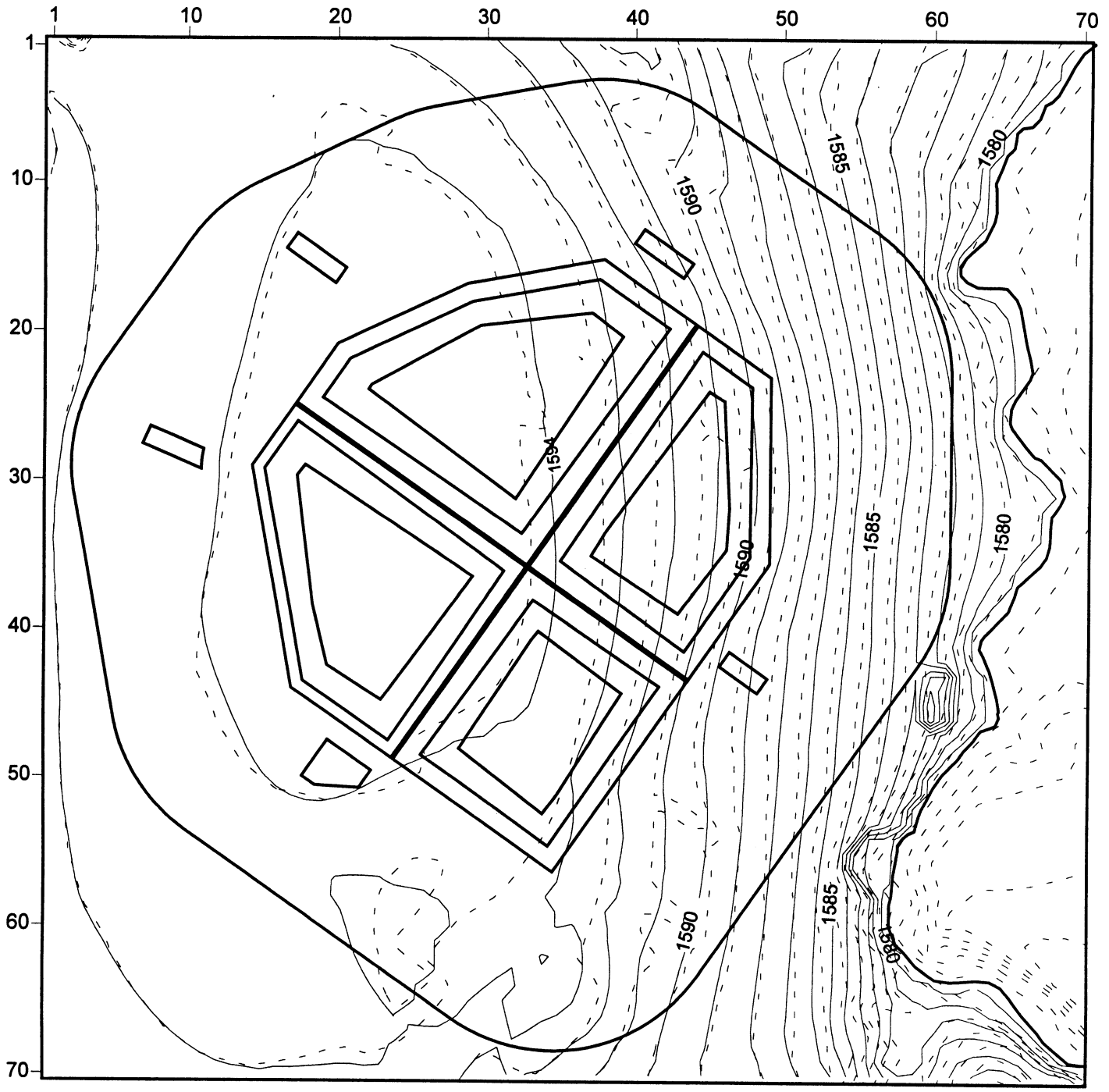

Notes:
Contour interval is 1 foot.
Elevation datum is mean sea level.

TMA sub-model
Regional model

GeoTrans, inc.			
REVISED	DATE	BY	DESCRIPTION

CHECKED BY: PV	DATE: NOV 96
APPROVED BY: RTH	DATE: NOV 96
APPROVED BY: PFA	DATE: NOV 96

Crandon Mining Company

Figure 2.24
Modeled water table for the TMA sub-model and the regional model

Scale: 1" = 1000'	Date: Nov 1996
Prepared By: GeoTrans, Inc.	By: GWC

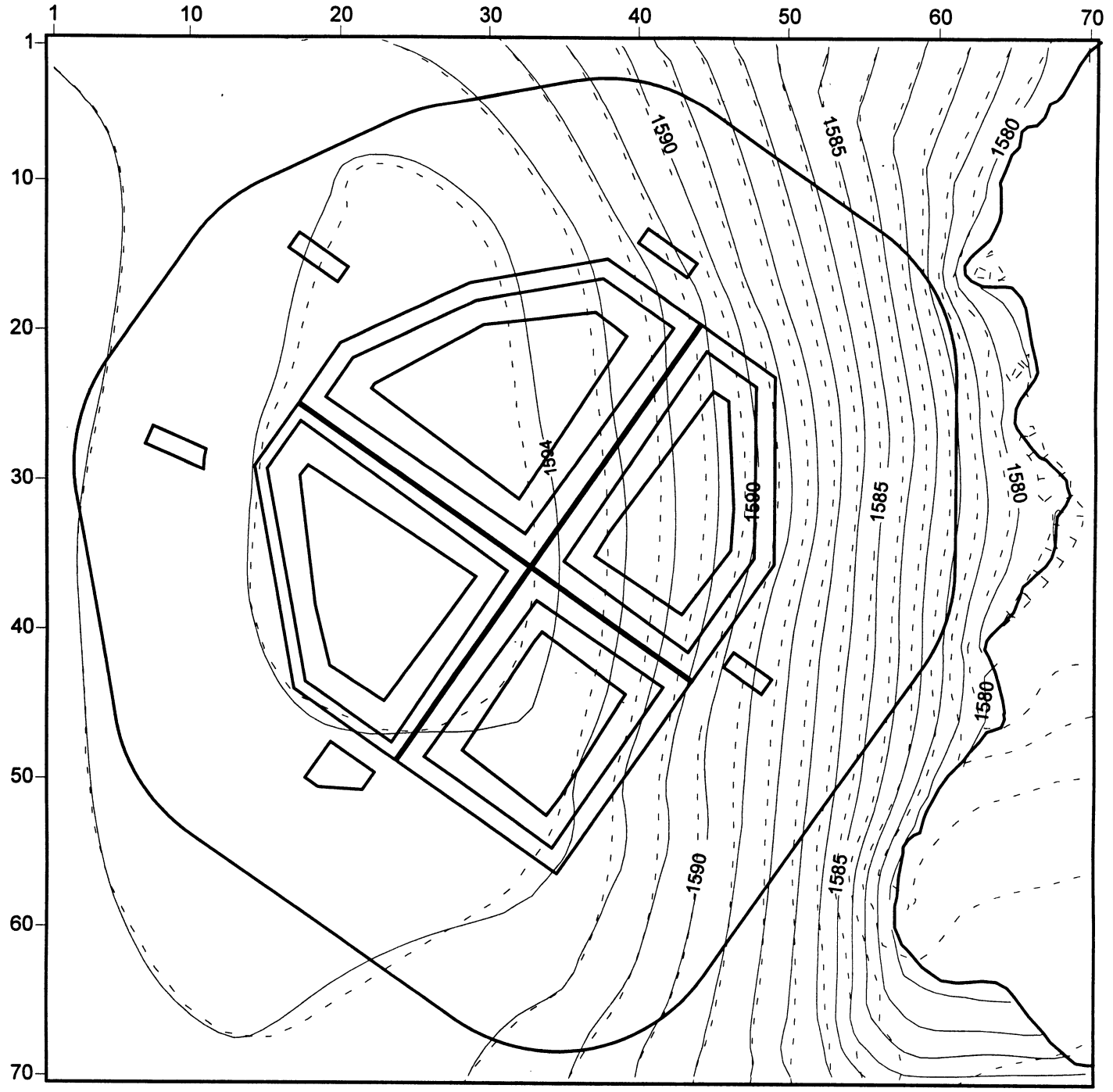

Notes:
Contour interval is 1 foot.
Elevation datum is mean sea level.

TMA sub-model
Regional model

GeoTrans, inc.			
REVISED	DATE	BY	DESCRIPTION

CHECKED BY: PV	DATE: NOV 96
APPROVED BY: RTH	DATE: NOV 96
APPROVED BY: PFA	DATE: NOV 96

Crandon Mining Company

Figure 2.25
Modeled head in TMA sub-model layer 3 and regional model layer 2

Scale: 1" = 1000'	Date: Nov 1996
Prepared By: GeoTrans, Inc.	By: GWC

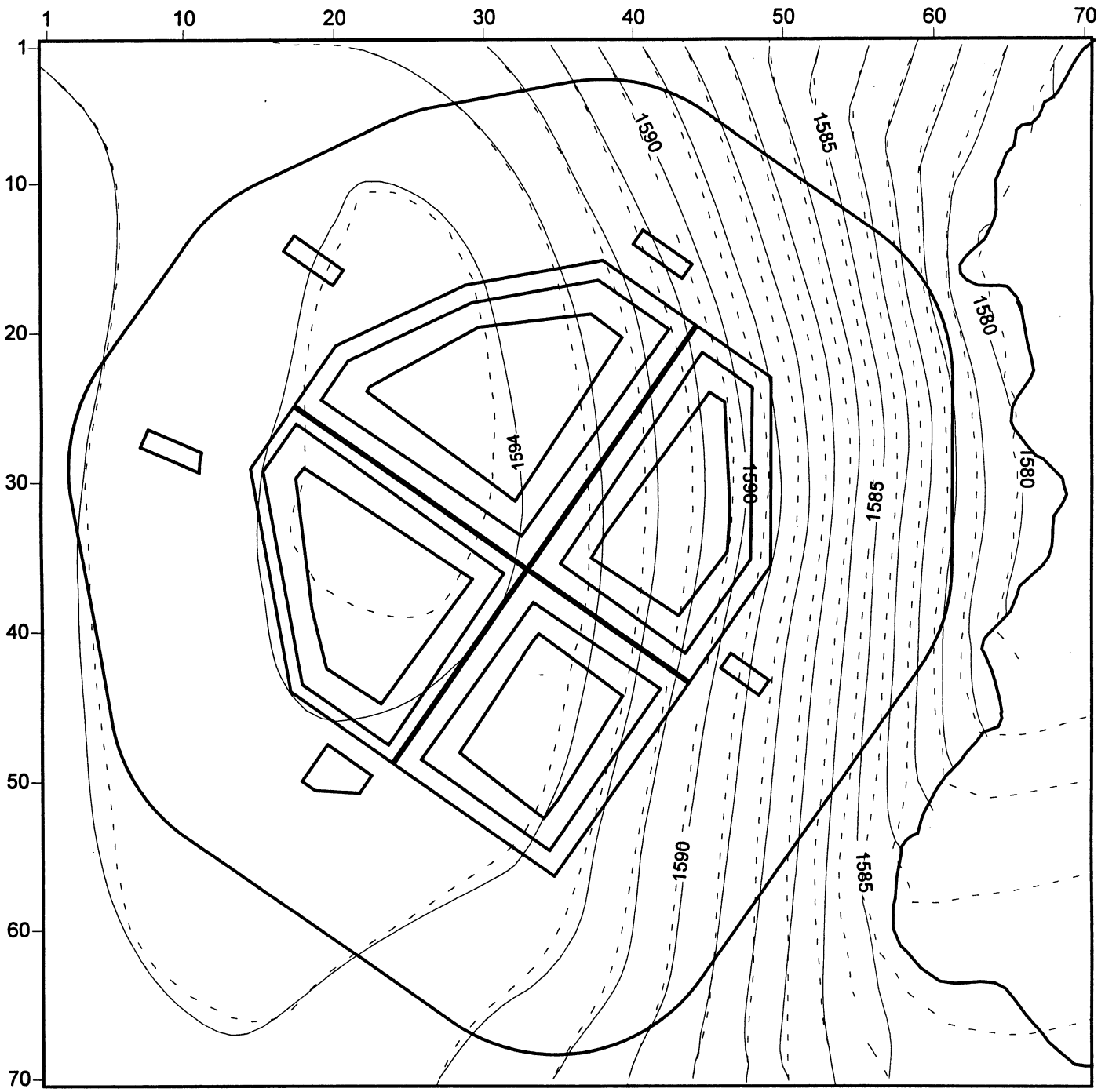

Notes:
Contour interval is 1 foot.
Elevation datum is mean sea level.

TMA sub-model
Regional model

GeoTrans, inc.			
REVISED	DATE	BY	DESCRIPTION

CHECKED BY: PV	DATE: NOV 96
APPROVED BY: RTH	DATE: NOV 96
APPROVED BY: PFA	DATE: NOV 96

Crandon Mining Company

Figure 2.26
Modeled head in TMA sub-model layer 7 and regional model layer 4

Scale: 1" = 1000'	Date: Nov 1996
Prepared By: GeoTrans, Inc.	By: GWC

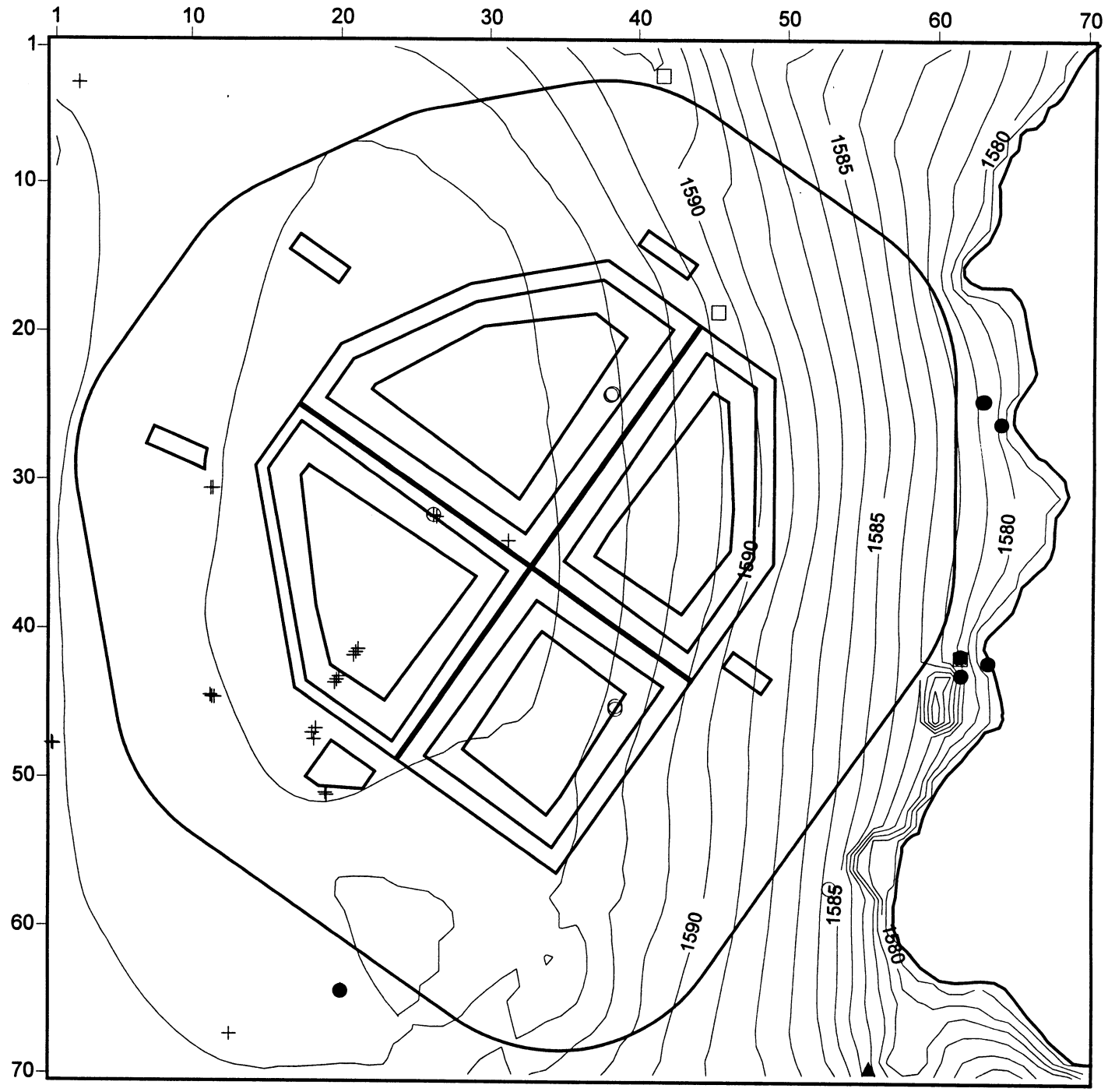

Residuals

- ▲ >5 ft
- ■ 3 to 5 ft
- ● 1 to 3 ft
- \+ -1 to 1 ft
- ○ -3 to -1 ft
- □ -5 to -3 ft
- △ <-5 ft

(Modeled Water Table Contours Shown)

FEET

0 500 1000

N

GeoTrans, inc.

REVISED	DATE	BY	DESCRIPTION

CHECKED BY: PV	DATE: NOV 96
APPROVED BY: RTH	DATE: NOV 96
APPROVED BY: PFA	DATE: NOV 96

Crandon Mining Company

Figure 2.27
Modeled steady-state head residuals in the TMA sub-model

Scale: 1" = 1000'	Date: Nov 1996
Prepared By: GeoTrans, Inc.	By: GWC

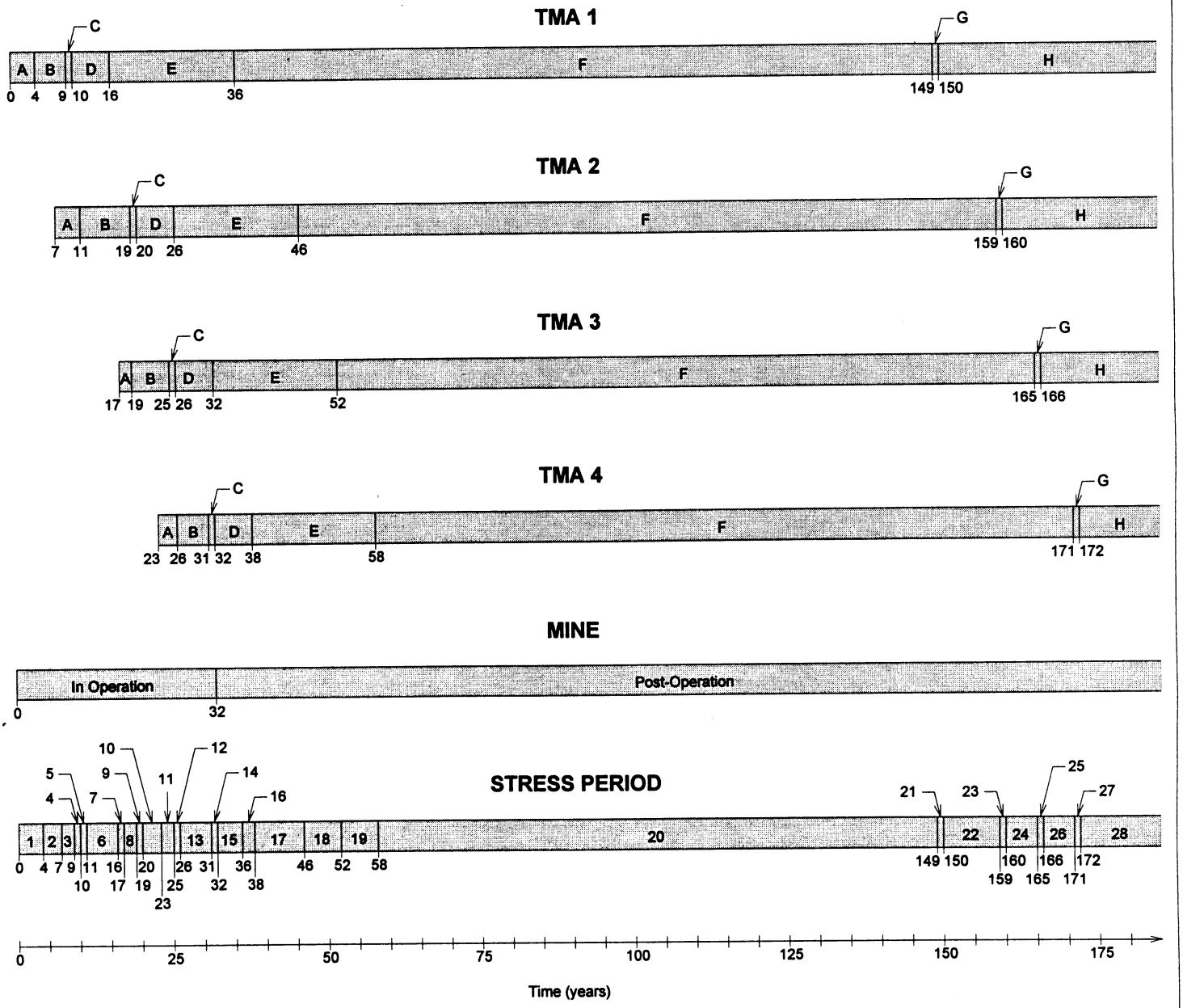

TMA Phases

A: First stage of operation
B: Second stage of operation
C: Cap in place, part 1
D: Cap in place, part 2
E: Cap in place, part 3
F: Cap in place, part 4
G: No liner, part 1
H: No liner, steady-state

GeoTrans, inc.

REVISED	DATE	BY	DESCRIPTION

CHECKED BY: PV	DATE: NOV 96
APPROVED BY: RTH	DATE: NOV 96
APPROVED BY: PFA	DATE: NOV 96

Crandon Mining Company

Figure 2.28
TMA sub-model time line

Scale: 1" = 25 years	Date: Nov 1996
Prepared By: GeoTrans, Inc.	By: GWC

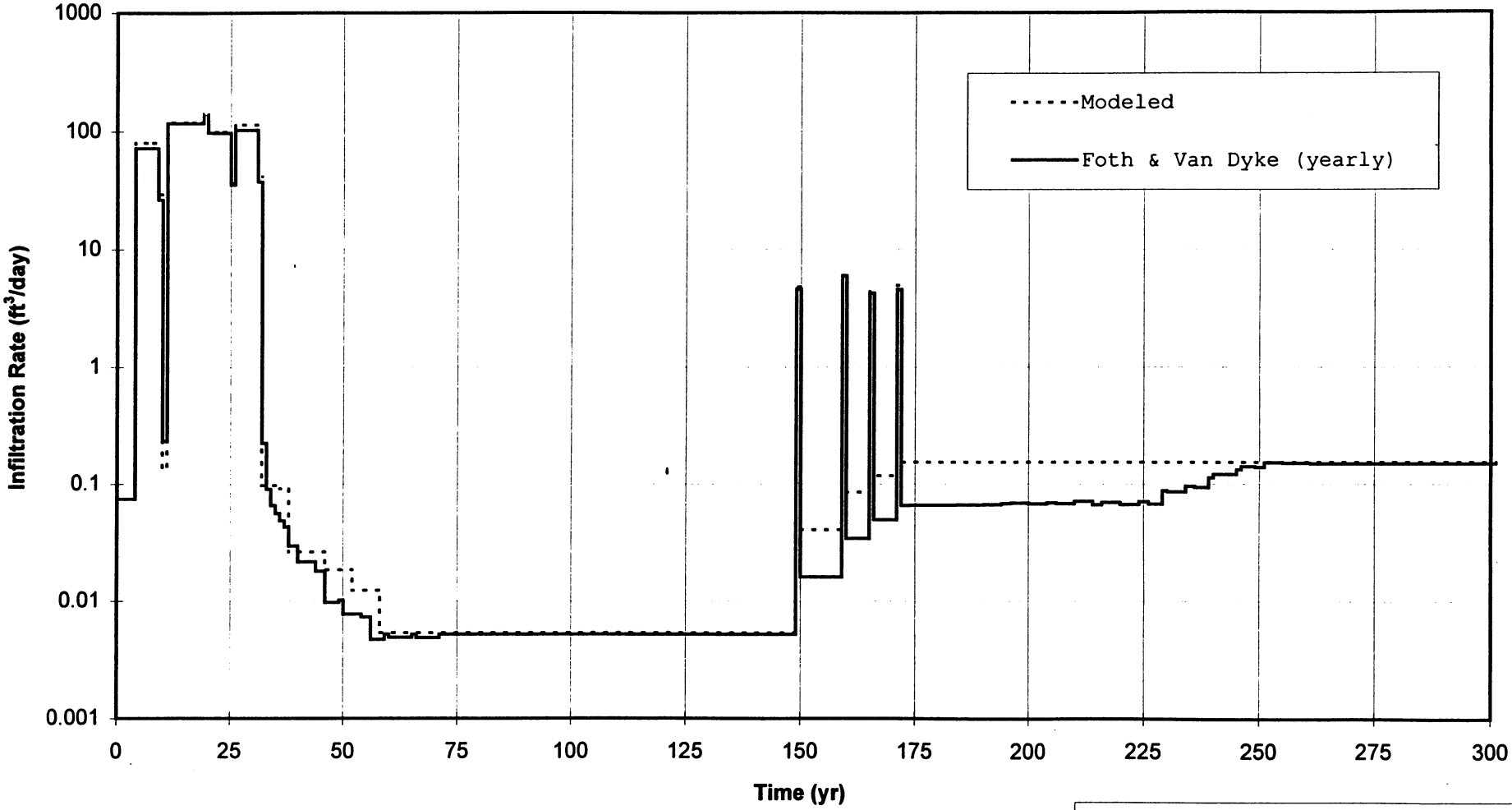

Note: Infiltration rate (Y-axis) is shown on a logarithmic scale.

GeoTrans, inc.			
REVISED	DATE	BY	DESCRIPTION

CHECKED BY: PV	DATE: OCT 96
APPROVED BY: RTH	DATE: OCT 96
APPROVED BY: PFA	DATE: OCT 96

Crandon Mining Company

Figure 2.29
TMA flux rate

Scale: None	Date: Oct 1996
Prepared By: GeoTrans, Inc.	By: GWC

4.2-10-69

Percrat3.xls

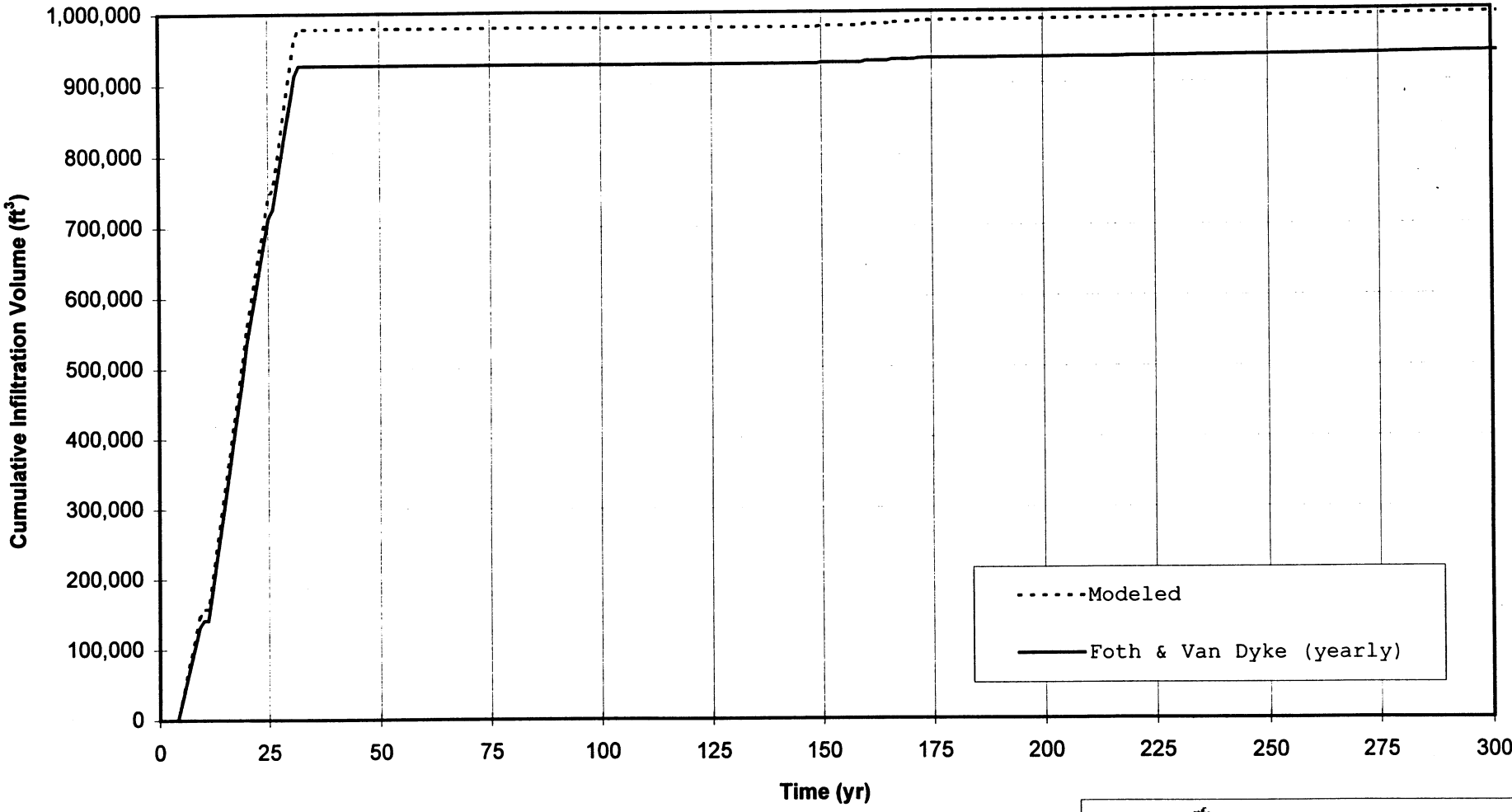

4.2-10-70

GeoTrans, inc.

REVISED	DATE	BY	DESCRIPTION

CHECKED BY: PV	DATE: OCT 96
APPROVED BY: RTH	DATE: OCT 96
APPROVED BY: PFA	DATE: OCT 96

Crandon Mining Company

Figure 2.30
TMA Cumulative Exfiltration Volume

Scale: None	Date: Oct 1996
Prepared By: GeoTrans, Inc.	By: GWC

Percrat2

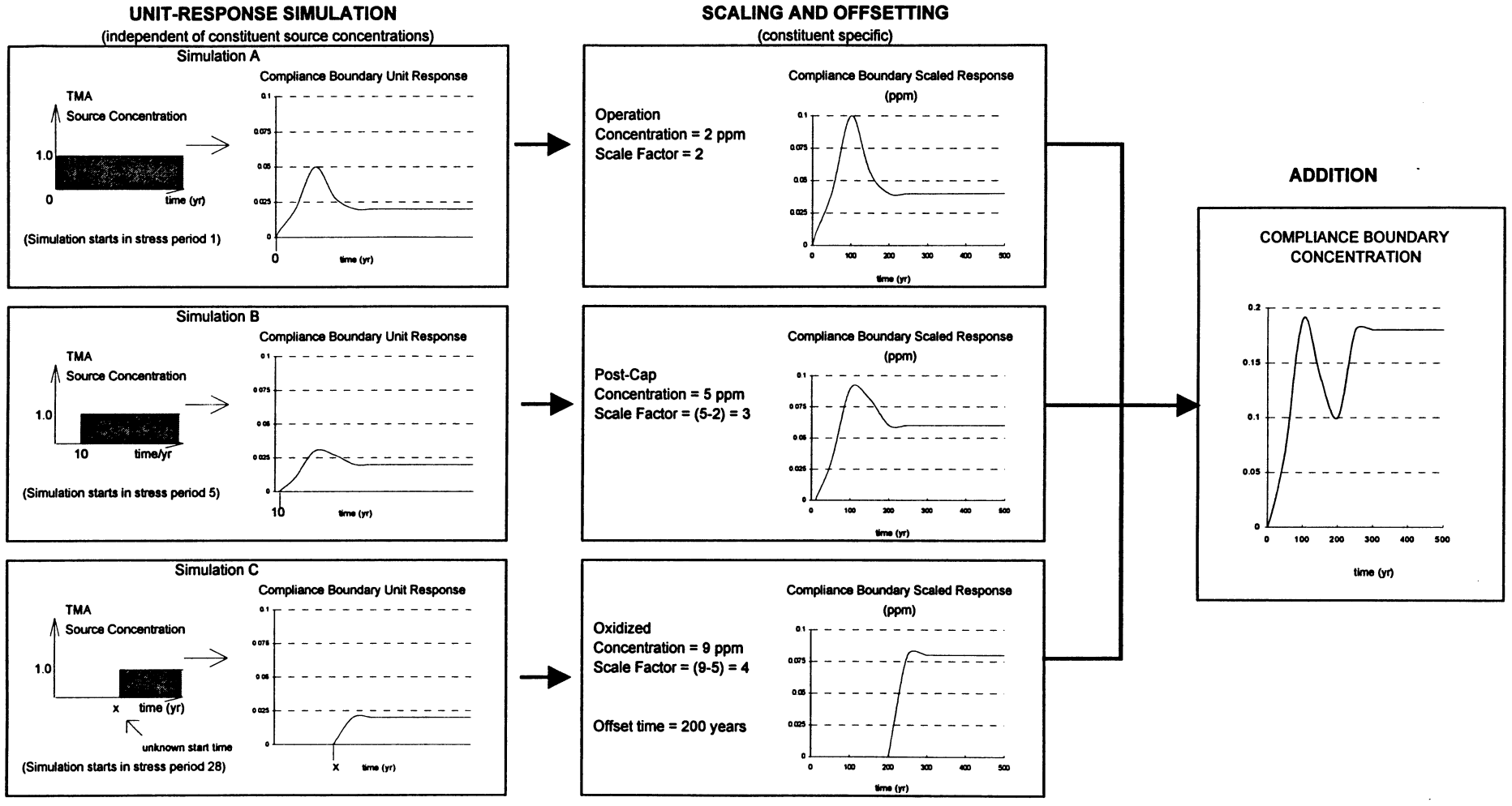

This hypothetical example shows the superposition method applied for a constituent with the following source concentrations:

Operation: 2 ppm
Post-cap: 5 ppm
Oxidized: 9 ppm

The Simulation C start time is set to 51 years after assumed degradation of the FML for this example (time = 200 years for TMA1).

GeoTrans, inc.

REVISED	DATE	BY	DESCRIPTION

CHECKED BY:	PV	DATE: NOV 96
APPROVED BY:	RTH	DATE: NOV 96
APPROVED BY:	PFA	DATE: NOV 96

Crandon Mining Company

Figure 2.31
Illustration of the superposition method

Scale: None	Date: Nov 1996
Prepared By: GeoTrans, Inc.	By: GWC

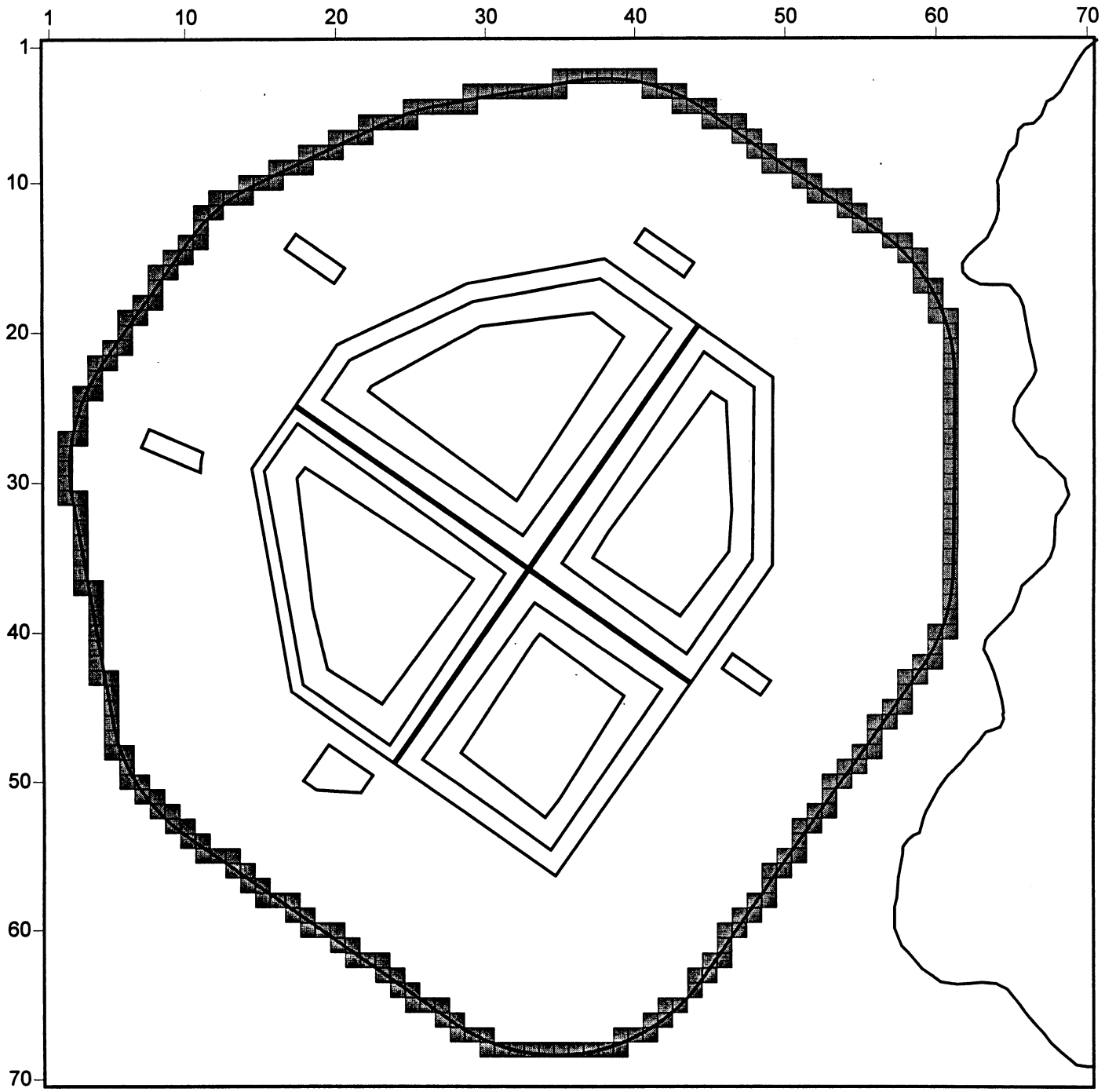

GeoTrans, inc.			
REVISED	DATE	BY	DESCRIPTION

CHECKED BY: PV	DATE: NOV 96
APPROVED BY: RTH	DATE: NOV 96
APPROVED BY: PFA	DATE: NOV 96

Crandon Mining Company

Figure 2.32
Location of compliance boundary observation cells

Scale: 1" = 1000'	Date: Nov 1996
Prepared By: GeoTrans, Inc.	By: GWC

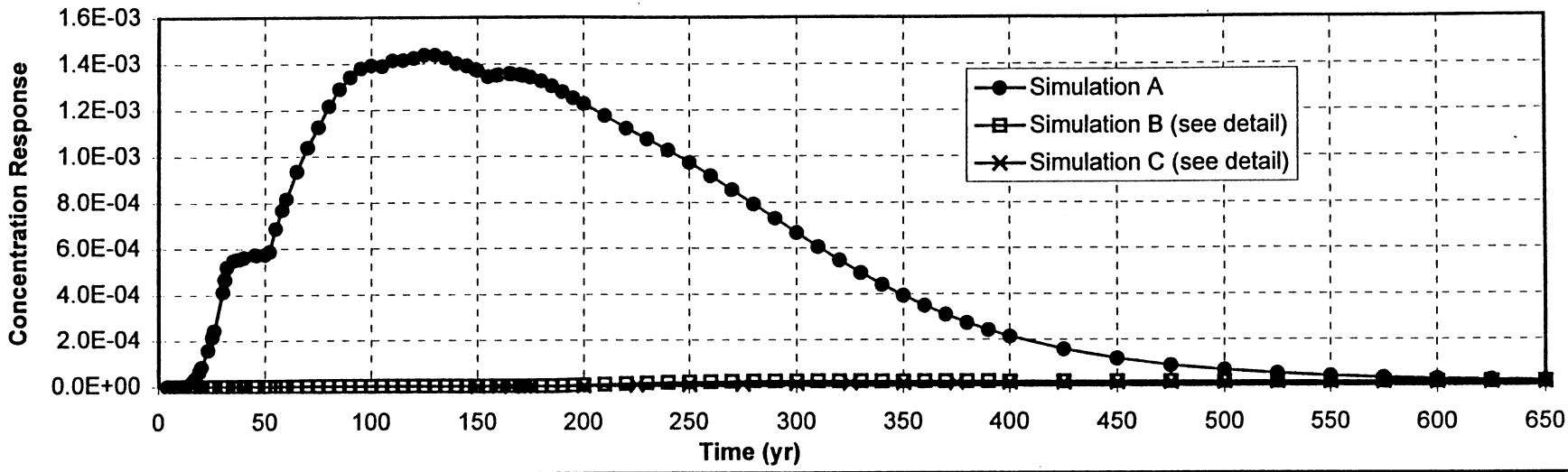

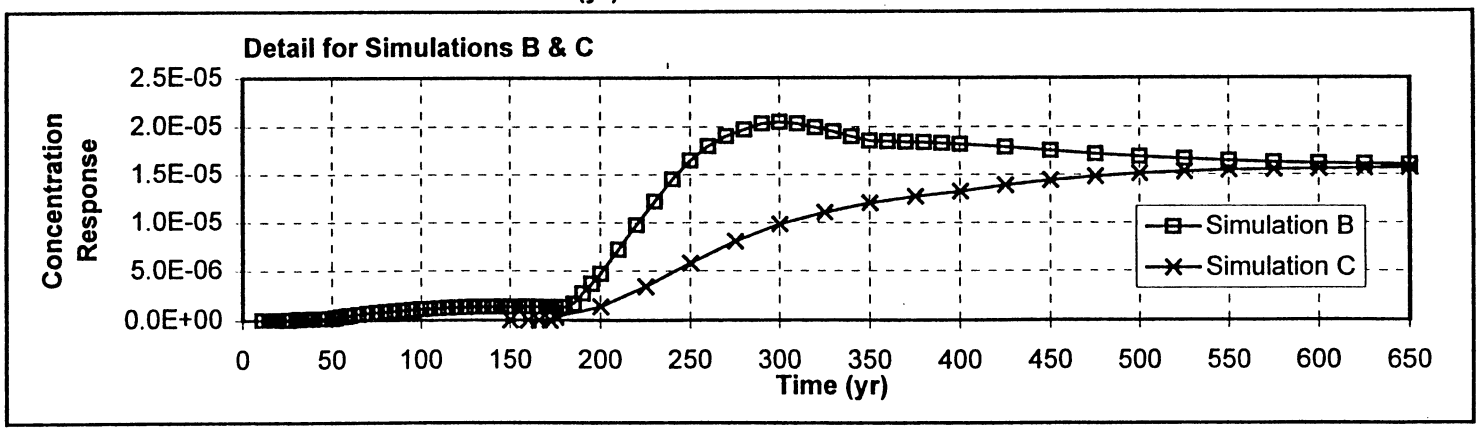

Note:
For these plots, the start time for Simulation C is set to 150 years.

GeoTrans, inc.			
REVISED	DATE	BY	DESCRIPTION

CHECKED BY: PV	DATE: NOV 96
APPROVED BY: RTH	DATE: NOV 96
APPROVED BY: PFA	DATE: NOV 96

Crandon Mining Company

Figure 2.33
BEJ Concentration response curves at the compliance boundary

Scale: None	Date: Nov 96
Prepared by: GeoTrans, Inc.	By: GWC

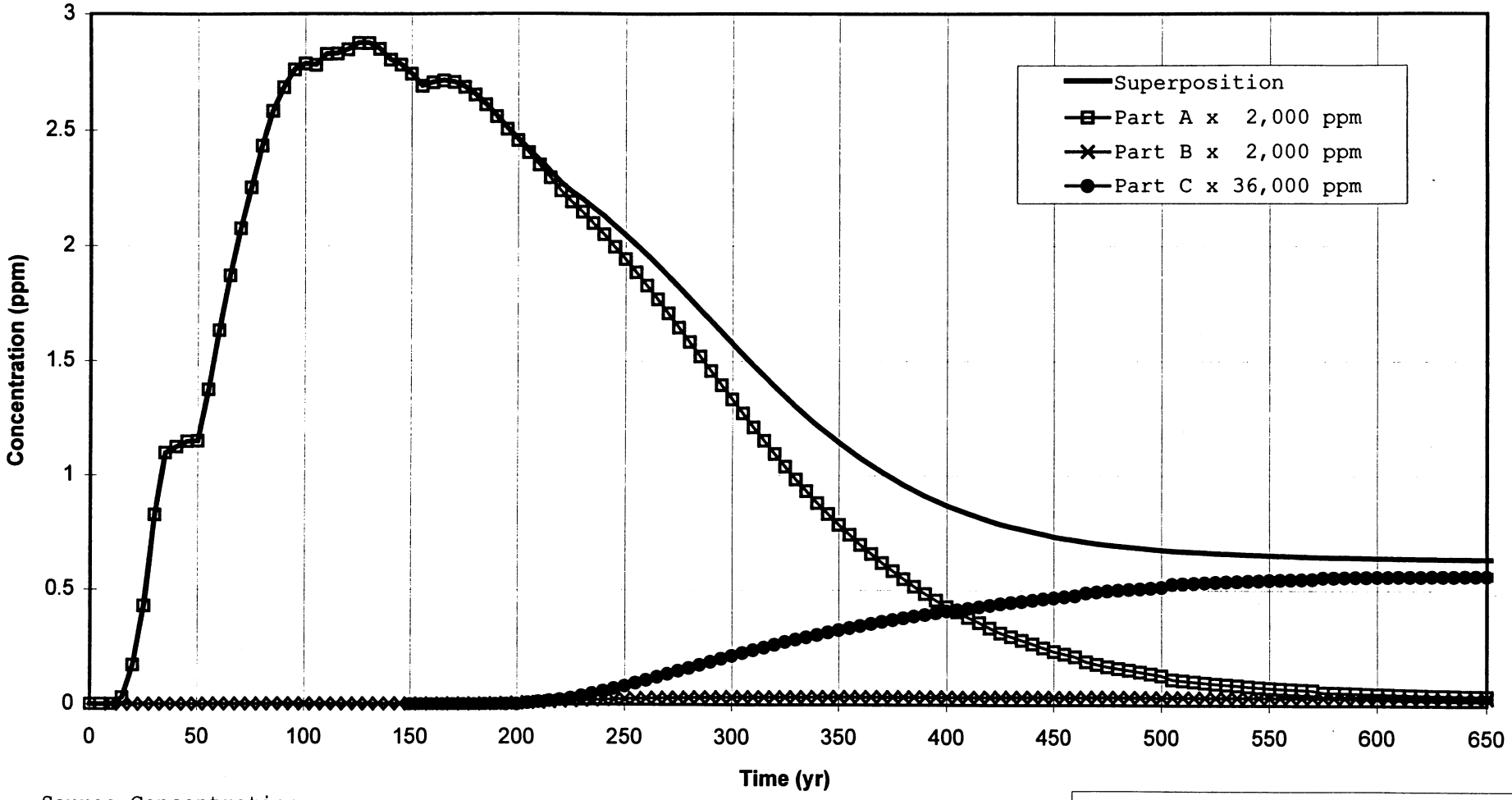

Source Concentration:
Operation: 2,000 ppm
Post-cap: 4,000 ppm
Oxidized: 40,000 ppm*

*As a conservative assumption, the oxidized concentration begins one year after assumed degradation of the flexible membrane liner.

GeoTrans, inc.

REVISED	DATE	BY	DESCRIPTION

CHECKED BY: PV	DATE: OCT 96
APPROVED BY: RTH	DATE: OCT 96
APPROVED BY: PFA	DATE: OCT 96

Crandon Mining Company

Figure 2.34
BEJ concentration at the compliance boundary (sulfate example)

Scale: None	Date: Oct 1996
Prepared By: GeoTrans, Inc.	By: GWC

4.2-10-74

Brkthru5.xl

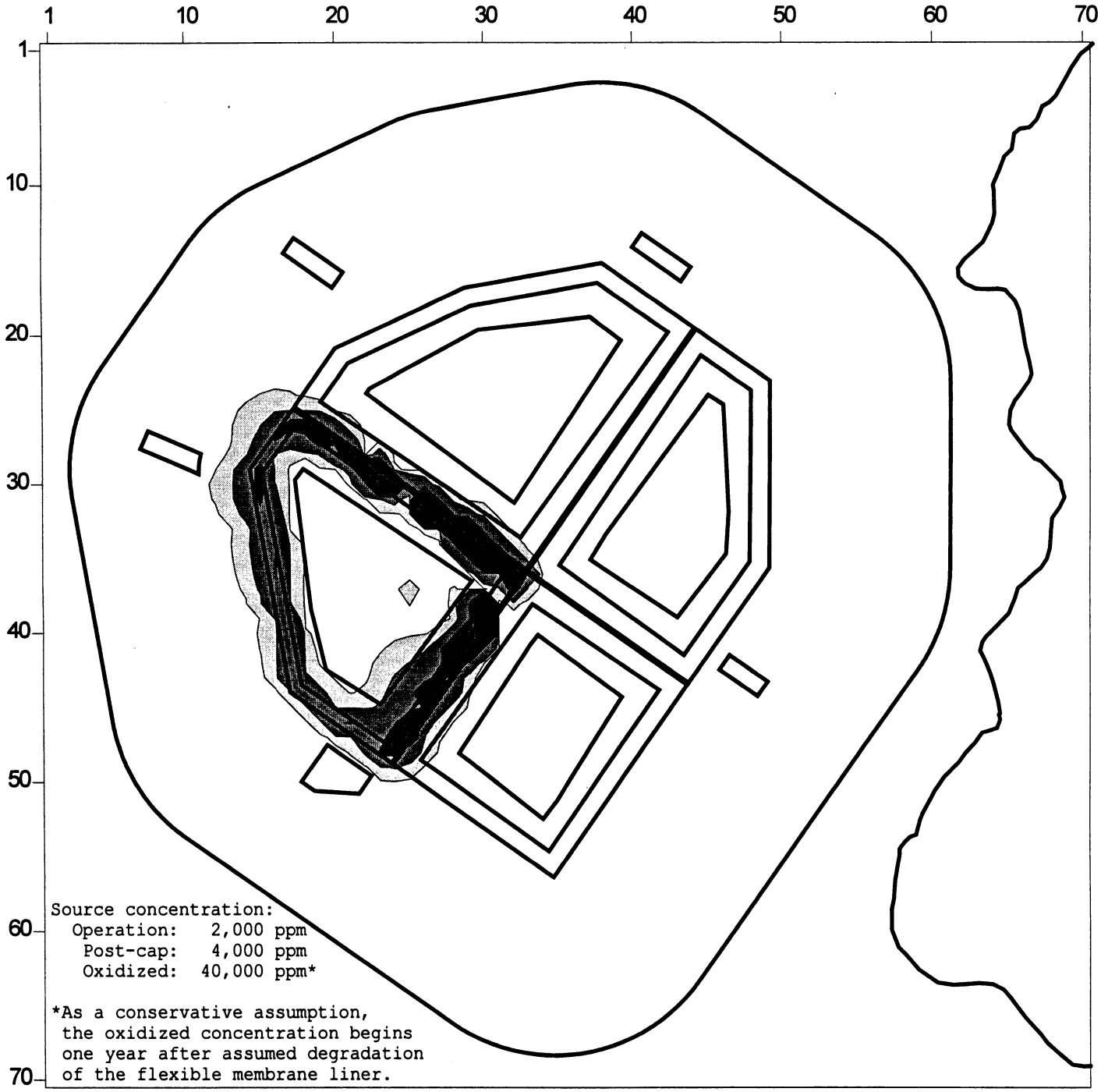

Concentration Scale

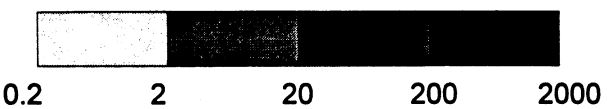

Note: This plot shows shaded contours of maximum concentration in any layer.

GeoTrans, inc.			
REVISED	DATE	BY	DESCRIPTION

CHECKED BY: PV	DATE: NOV 96
APPROVED BY: RTH	DATE: NOV 96
APPROVED BY: PFA	DATE: NOV 96

Crandon Mining Company

Figure 2.35
BEJ concentration after 7 years (sulfate example, plan view)

Scale 1" = 1000'	Date: Nov 1996
Prepared By: GeoTrans, Inc.	By: GWC

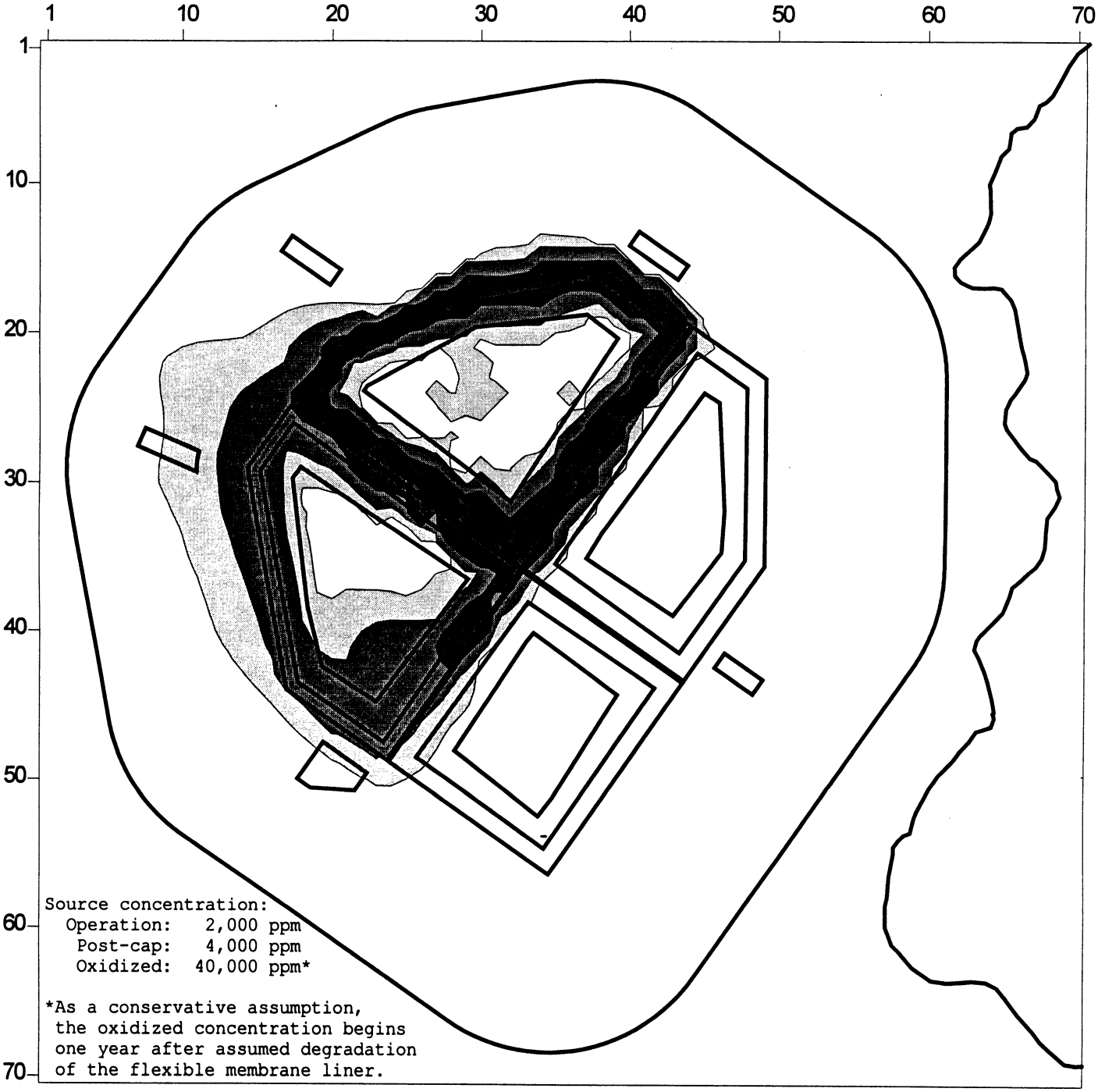

Concentration Scale

Note: This plot shows shaded contours of maximum concentration in any layer.

GeoTrans, inc.			
REVISED	DATE	BY	DESCRIPTION

CHECKED BY: PV	DATE: NOV 96
APPROVED BY: RTH	DATE: NOV 96
APPROVED BY: PFA	DATE: NOV 96

Crandon Mining Company

Figure 2.36
BEJ concentration after 17 years (sulfate example, plan view)

Scale 1" = 1000'	Date: Nov 1996
Prepared By: GeoTrans, Inc.	By: GWC

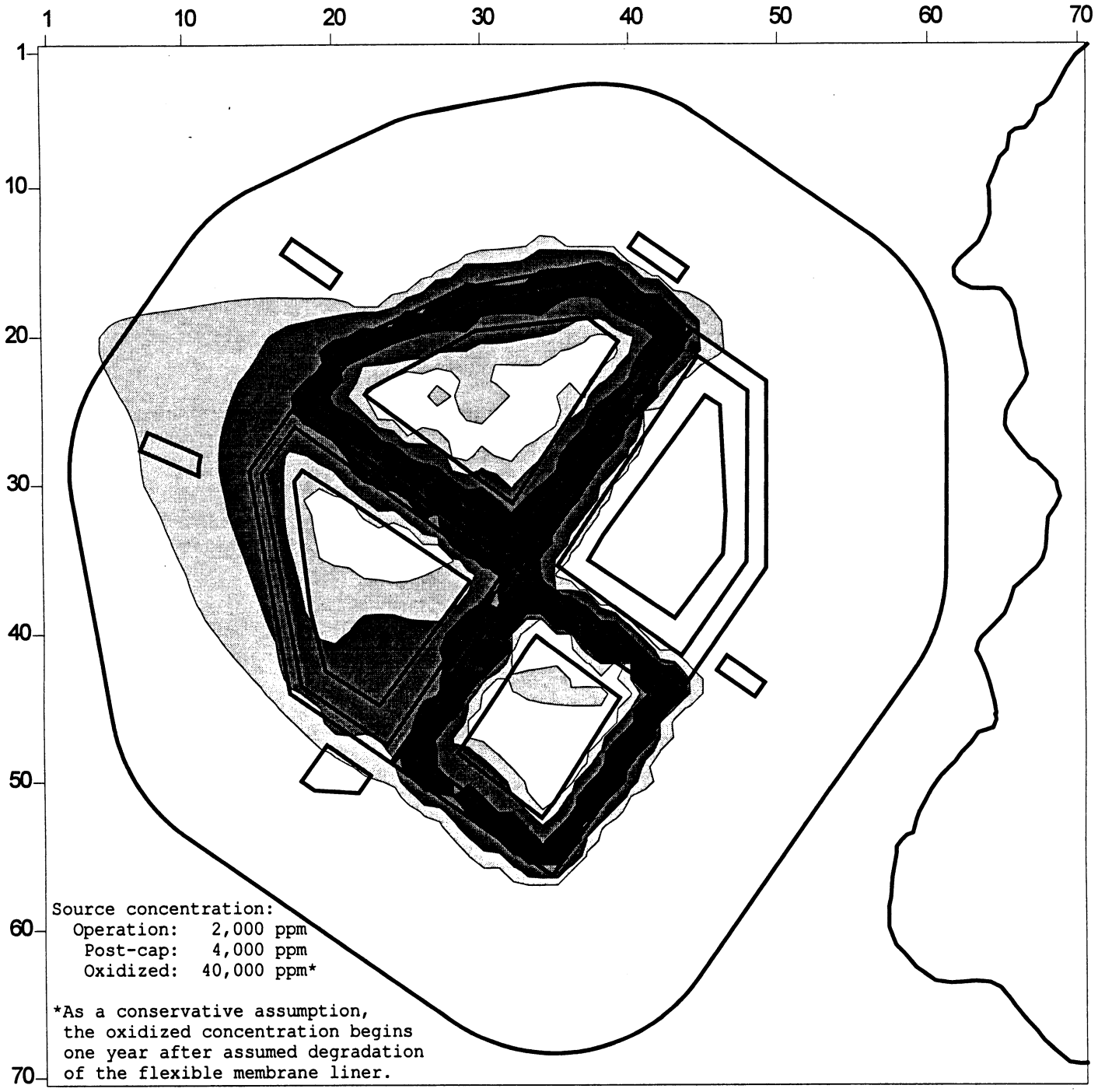

Concentration Scale

Note: This plot shows shaded contours of maximum concentration in any layer.

GeoTrans, inc.			
REVISED	DATE	BY	DESCRIPTION
CHECKED BY:	PV		DATE: NOV 96
APPROVED BY:	RTH		DATE: NOV 96
APPROVED BY:	PFA		DATE: NOV 96

Crandon Mining Company

Figure 2.37
BEJ concentration after 23 years (sulfate example, plan view)

Scale 1" = 1000'	Date: Nov 1996
Prepared By: GeoTrans, Inc.	By: GWC

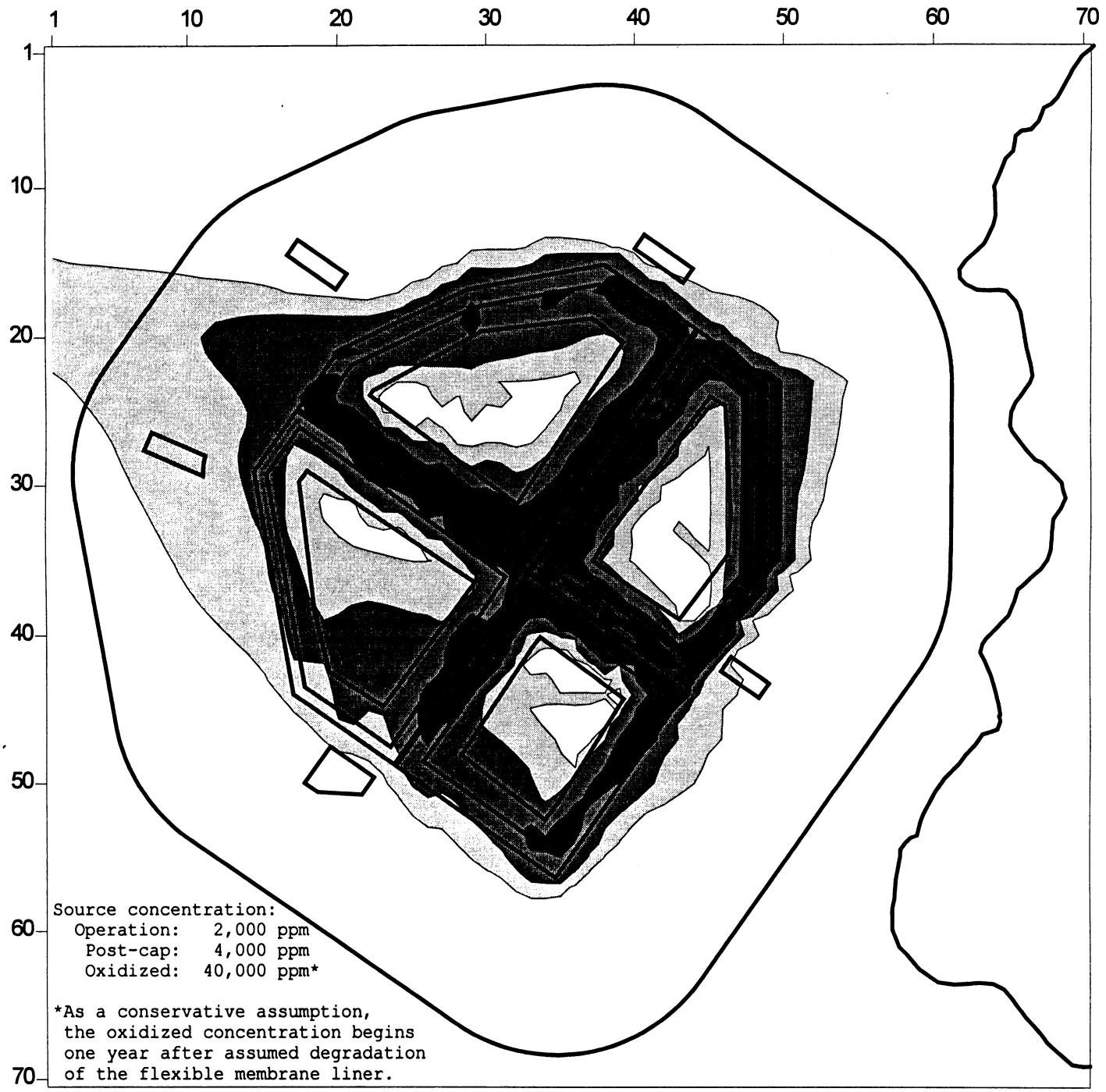

Concentration Scale

Note: This plot shows shaded contours of maximum concentration in any layer.

GeoTrans, inc.			
REVISED	DATE	BY	DESCRIPTION
CHECKED BY: PV			DATE: NOV 96
APPROVED BY: RTH			DATE: NOV 96
APPROVED BY: PFA			DATE: NOV 96

Crandon Mining Company

Figure 2.38
BEJ concentration after 32 years (sulfate example, plan view)

Scale 1" = 1000'	Date: Nov 1996
Prepared By: GeoTrans, Inc.	By: GWC

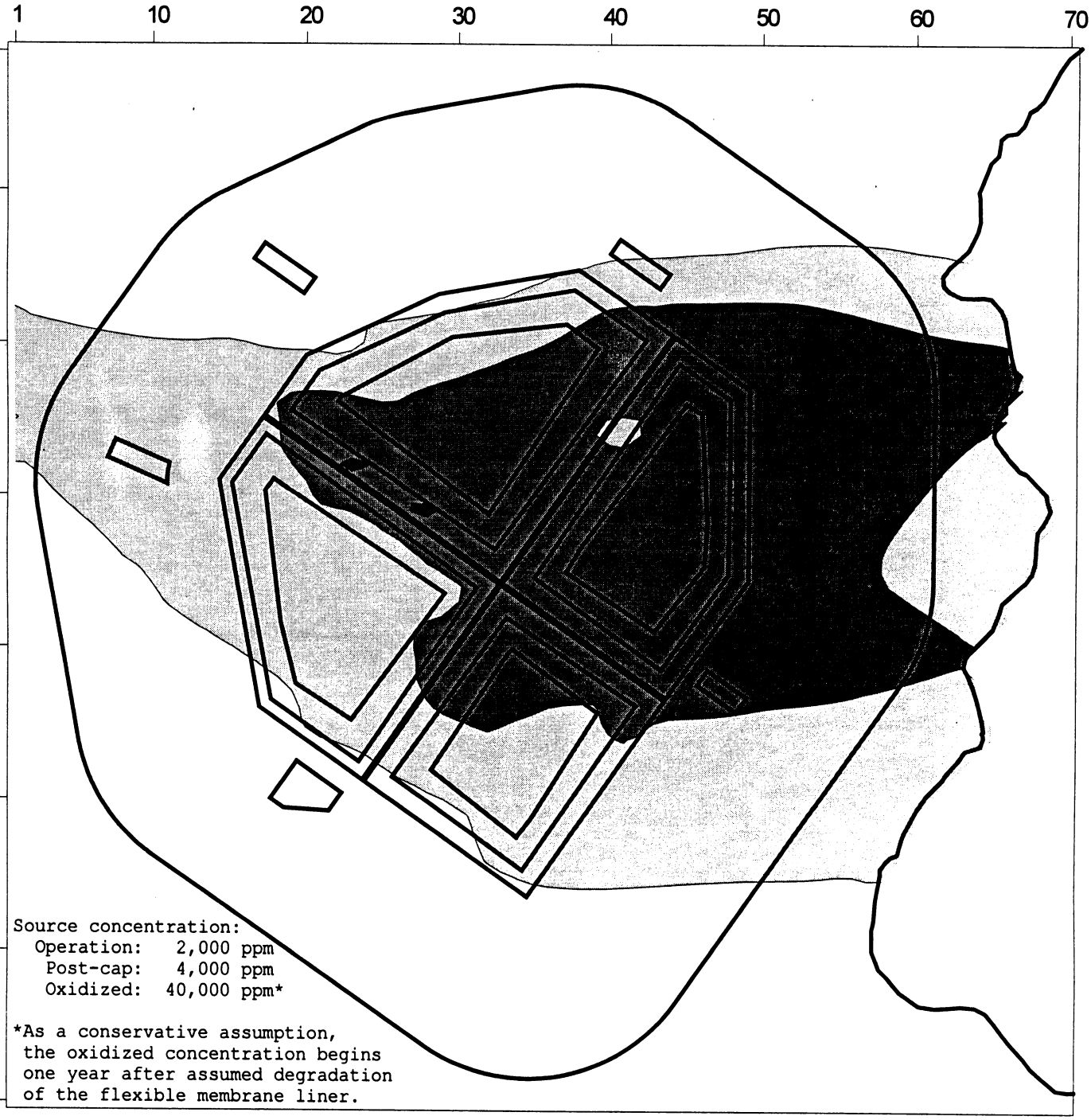

Concentration Scale

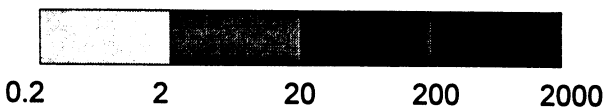

Note: This plot shows shaded contours of maximum concentration in any layer.

GeoTrans, inc.			
REVISED	DATE	BY	DESCRIPTION
CHECKED BY:	PV	DATE: NOV 96	
APPROVED BY:	RTH	DATE: NOV 96	
APPROVED BY:	PFA	DATE: NOV 96	

Crandon Mining Company

Figure 2.39
BEJ concentration after 100 years (sulfate example, plan view)

Scale 1" = 1000'	Date: Nov 1996
Prepared By: GeoTrans, Inc.	By: GWC

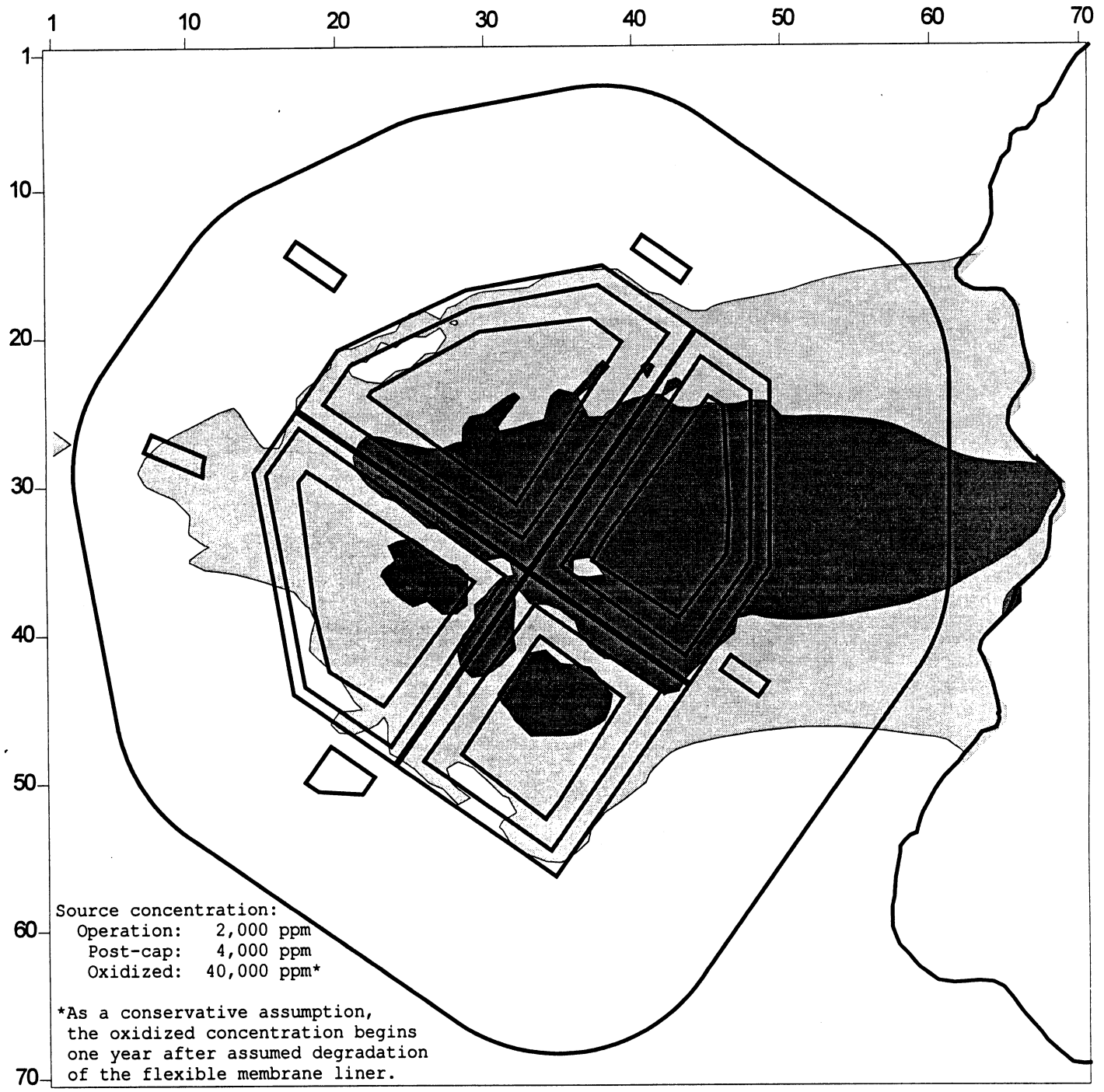

Concentration Scale

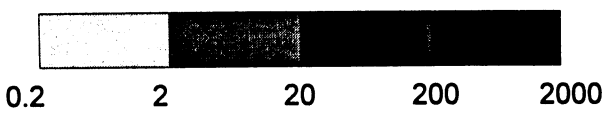

Note: This plot shows shaded contours of maximum concentration in any layer.

GeoTrans, inc.			
REVISED	DATE	BY	DESCRIPTION

CHECKED BY: PV	DATE: NOV 96
APPROVED BY: RTH	DATE: NOV 96
APPROVED BY: PFA	DATE: NOV 96

Crandon Mining Company

Figure 2.40
BEJ concentration after 200 years (sulfate example, plan view)

Scale 1" = 1000'	Date: Nov 1996
Prepared By: GeoTrans, Inc.	By: GWC

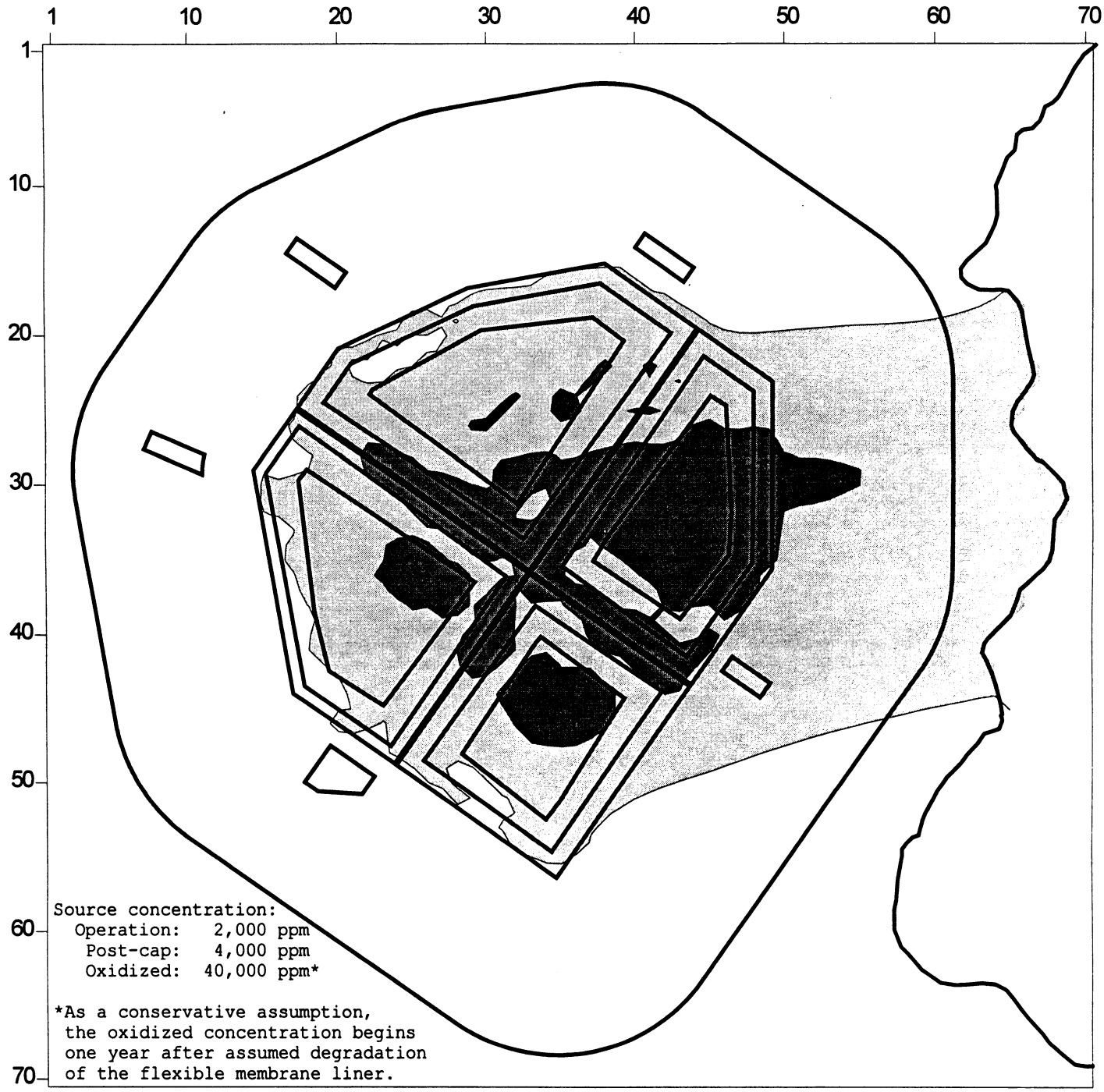

Concentration Scale

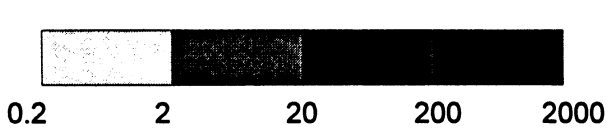

Note: This plot shows shaded contours of maximum concentration in any layer.

GeoTrans, inc.

REVISED	DATE	BY	DESCRIPTION

CHECKED BY:	PV	DATE: NOV 96
APPROVED BY:	RTH	DATE: NOV 96
APPROVED BY:	PFA	DATE: NOV 96

Crandon Mining Company

Figure 2.41
BEJ concentration after 300 years (sulfate example, plan view)

Scale 1" = 1000'	Date: Nov 1996
Prepared By: GeoTrans, Inc.	By: GWC

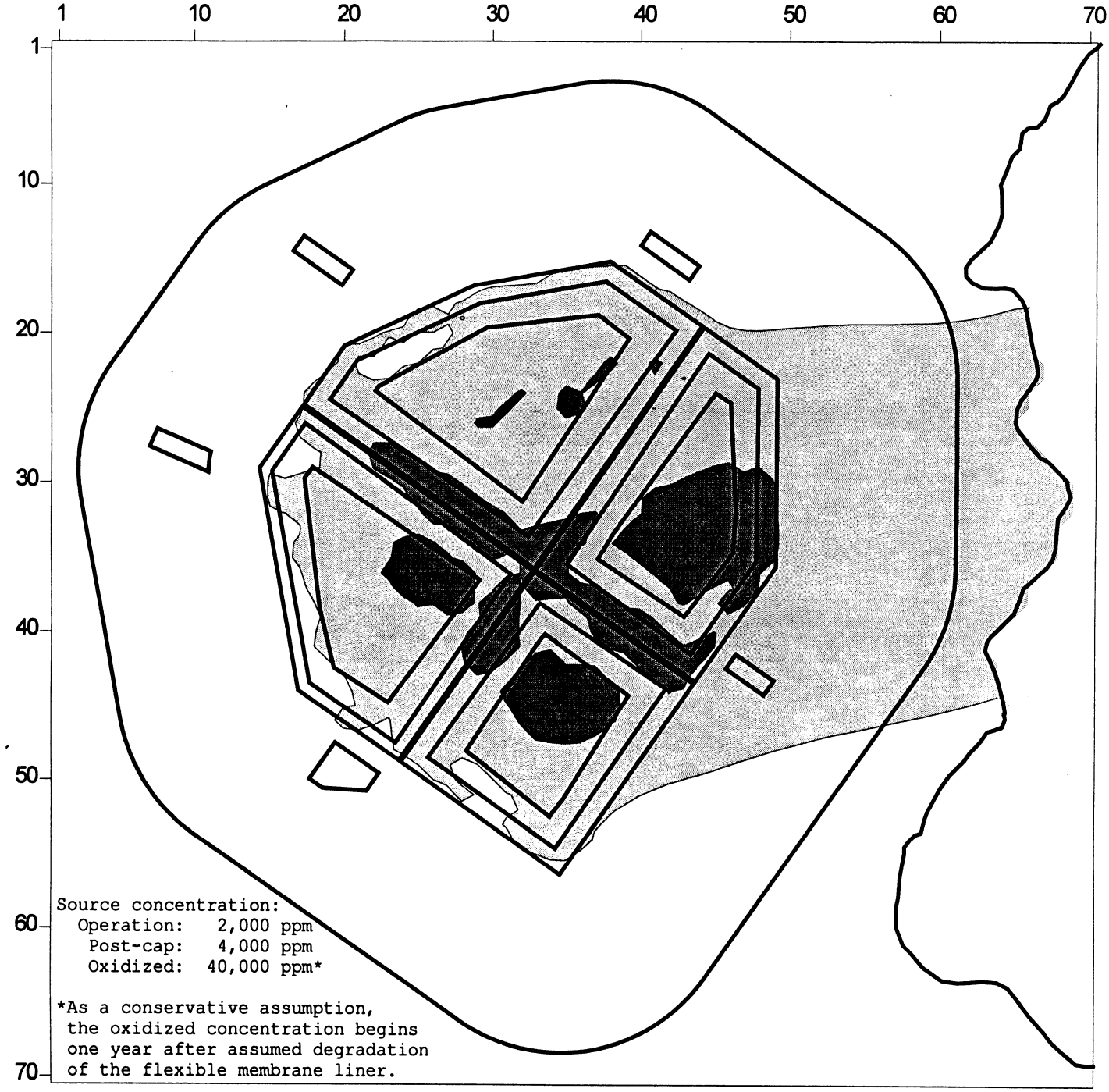

Concentration Scale

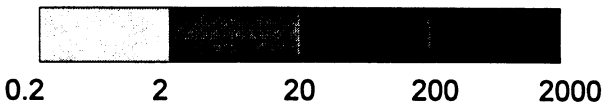

Note: This plot shows shaded contours of maximum concentration in any layer.

GeoTrans, inc.			
REVISED	DATE	BY	DESCRIPTION

CHECKED BY:	PV	DATE: NOV 96
APPROVED BY:	RTH	DATE: NOV 96
APPROVED BY:	PFA	DATE: NOV 96

Crandon Mining Company

Figure 2.42
BEJ concentration after 650 years (sulfate example, plan view)

Scale 1" = 1000'	Date: Nov 1996
Prepared By: GeoTrans, Inc.	By: GWC

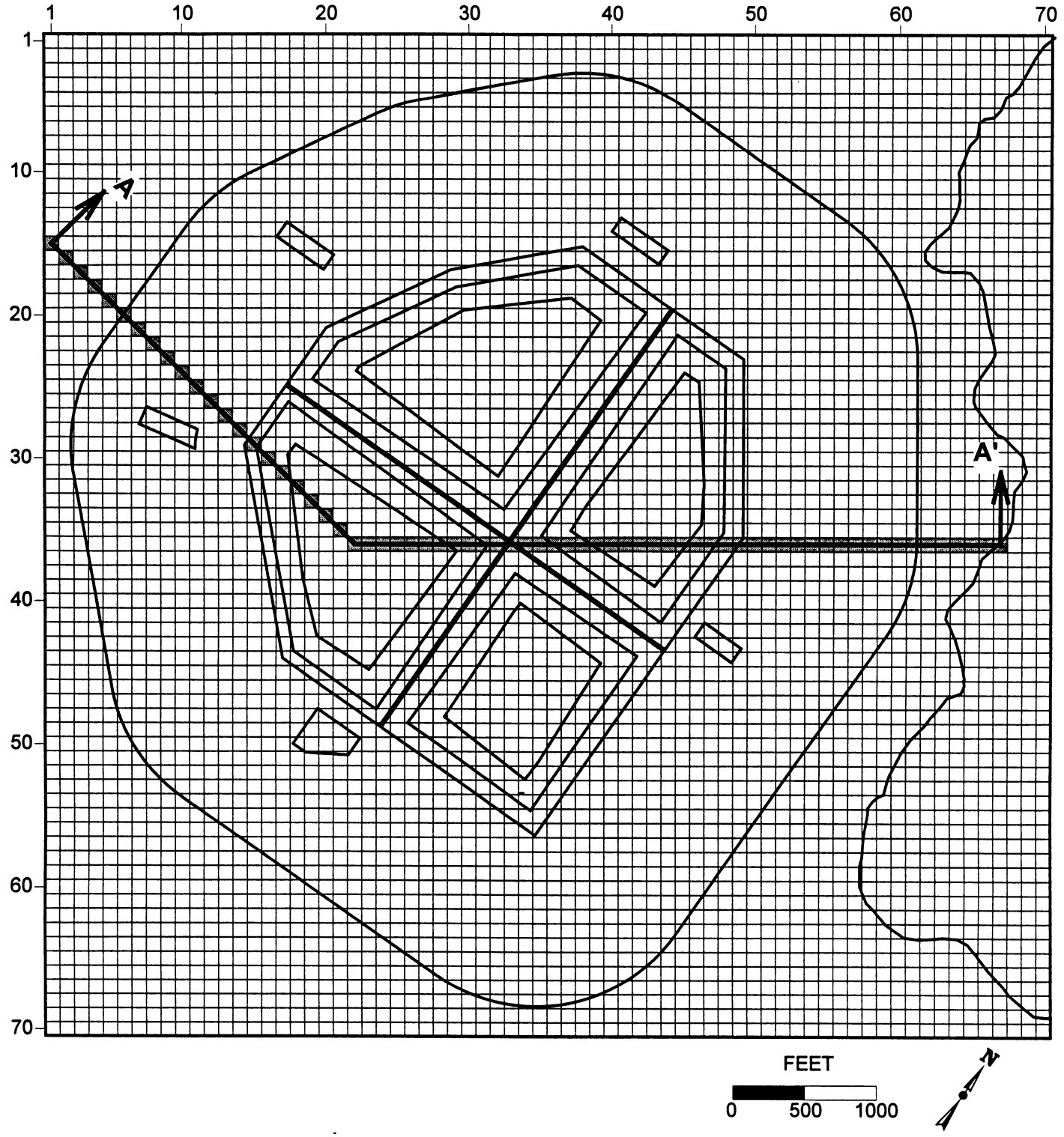

GeoTrans, inc.

REVISED	DATE	BY	DESCRIPTION

CHECKED BY: PV	DATE: NOV 96
APPROVED BY: RTH	DATE: NOV 96
APPROVED BY: PFA	DATE: NOV 96

Crandon Mining Company

Figure 2.43
Location of cross-section used for viewing concentration

Scale: 1" = 1000'	Date: Nov 1996
Prepared By: GeoTrans, Inc.	By: GWC

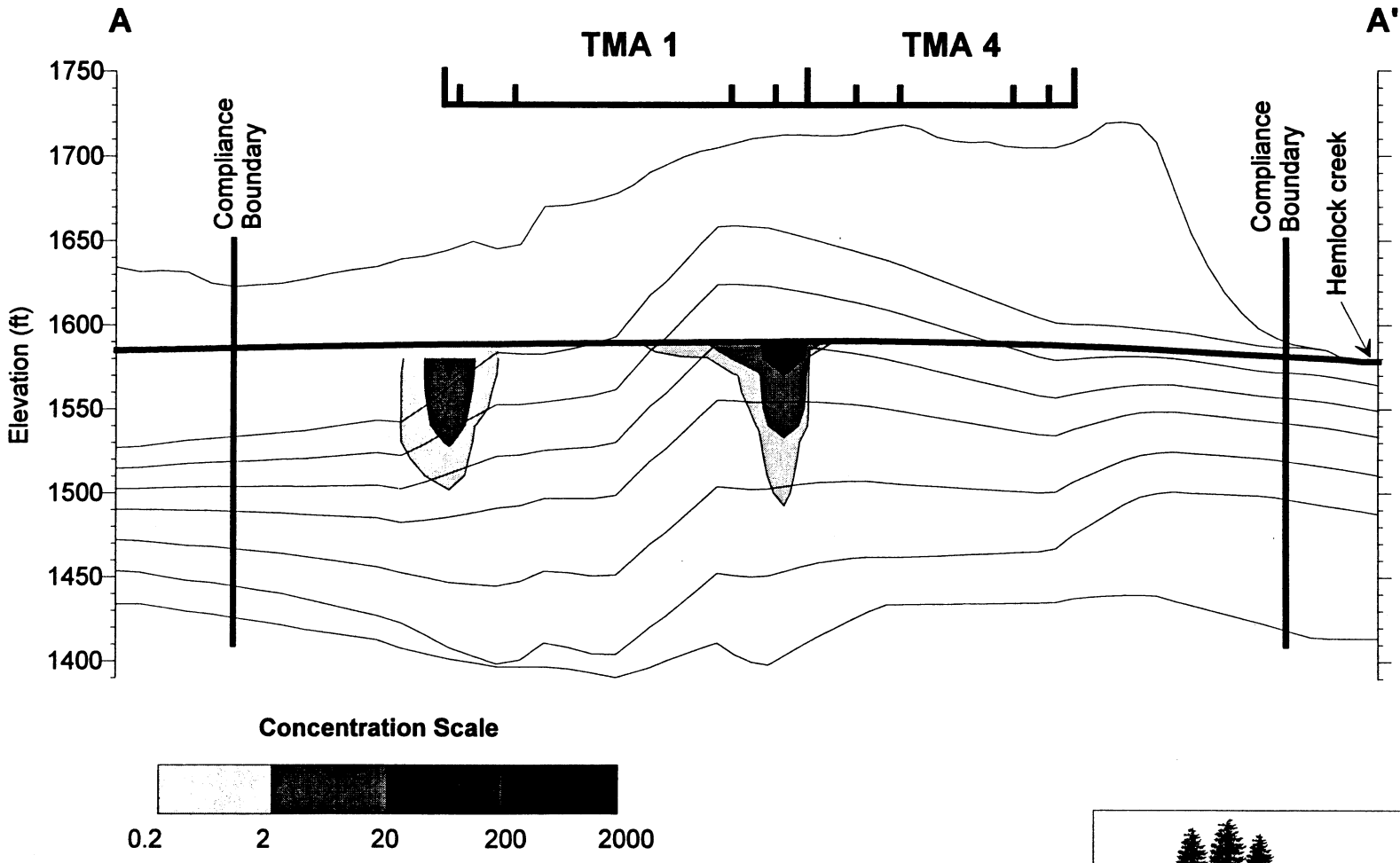

4.2-10-84

GeoTrans, inc.			
REVISED	DATE	BY	DESCRIPTION

CHECKED BY:	PV	DATE: NOV 96
APPROVED BY:	RTH	DATE: NOV 96
APPROVED BY:	PFA	DATE: NOV 96

Crandon Mining Company

Figure 2.44
BEJ concentration after 7 years
(sulfate example, cross section)

Scale: 1" = 1000' (h), 100' (v)	Date: Nov 1996
Prepared By: GeoTrans, GA	By: GWC

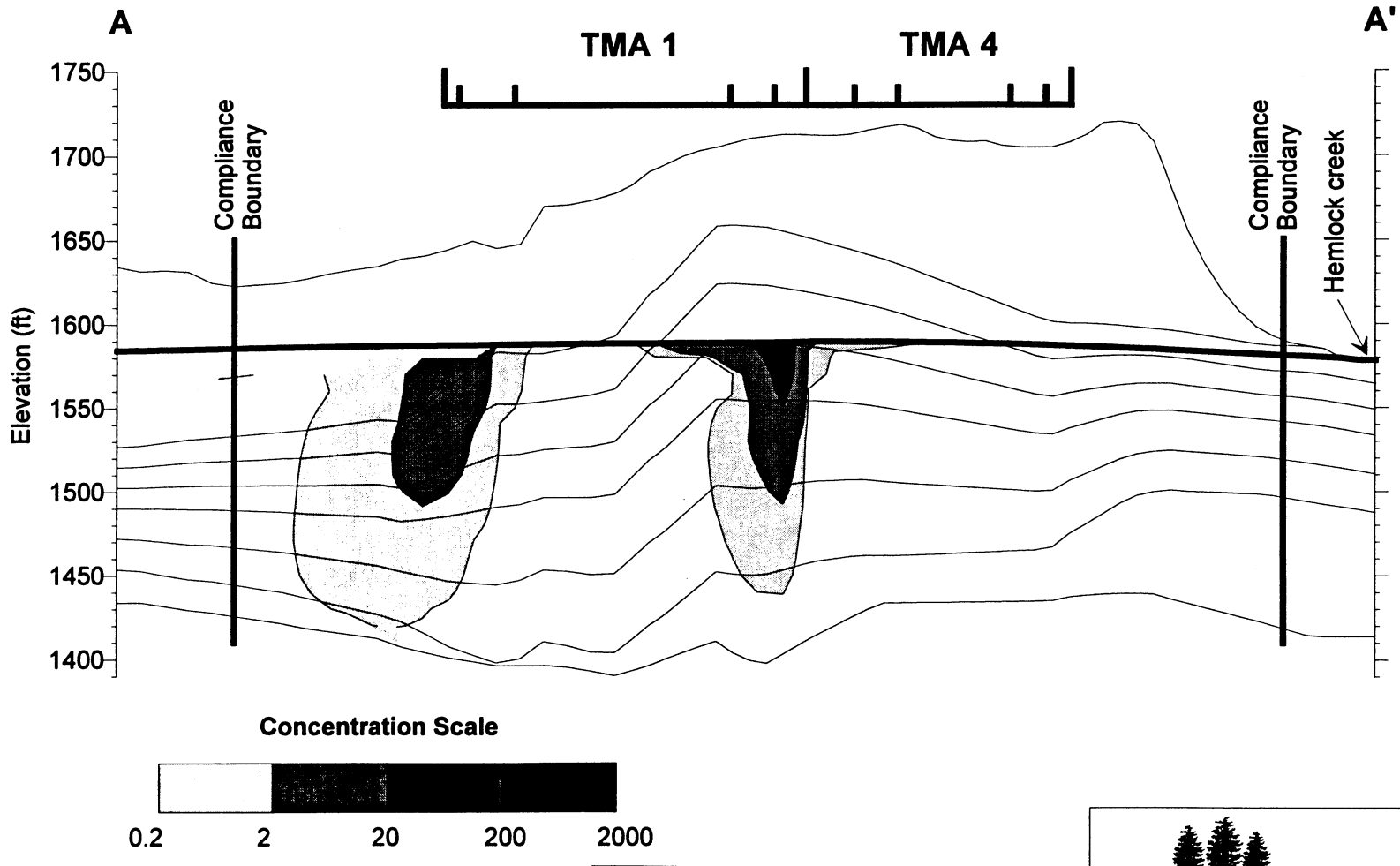

4.2-10-85

GeoTrans, inc.

REVISED	DATE	BY	DESCRIPTION

CHECKED BY:	PV	DATE: NOV 96
APPROVED BY:	RTH	DATE: NOV 96
APPROVED BY:	PFA	DATE: NOV 96

Crandon Mining Company

Figure 2.45
BEJ concentration after 17 years (sulfate example, cross section)

Scale: 1" = 1000' (h), 100' (v)	Date: Nov 1996
Prepared By: GeoTrans, GA	By: GWC

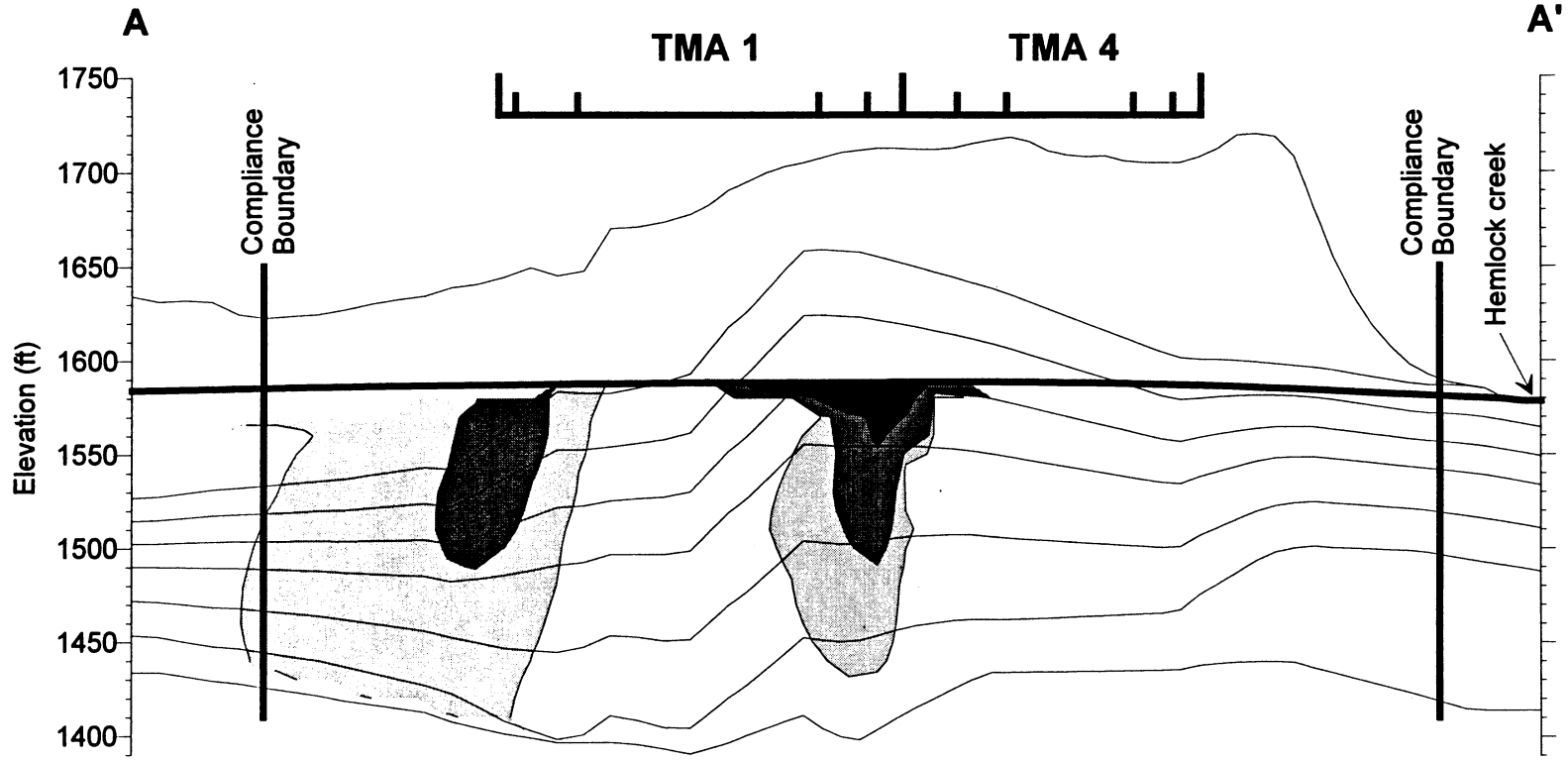

4.2-10-86

GeoTrans, inc.			
REVISED	DATE	BY	DESCRIPTION
CHECKED BY: PV			DATE: NOV 96
APPROVED BY: RTH			DATE: NOV 96
APPROVED BY: PFA			DATE: NOV 96

Crandon Mining Company

Figure 2.46
BEJ concentration after 23 years
(sulfate example, cross section)

Scale: 1" = 1000' (h), 100' (v) | Date: Nov 1996

Prepared By: GeoTrans, GA | By: GWC

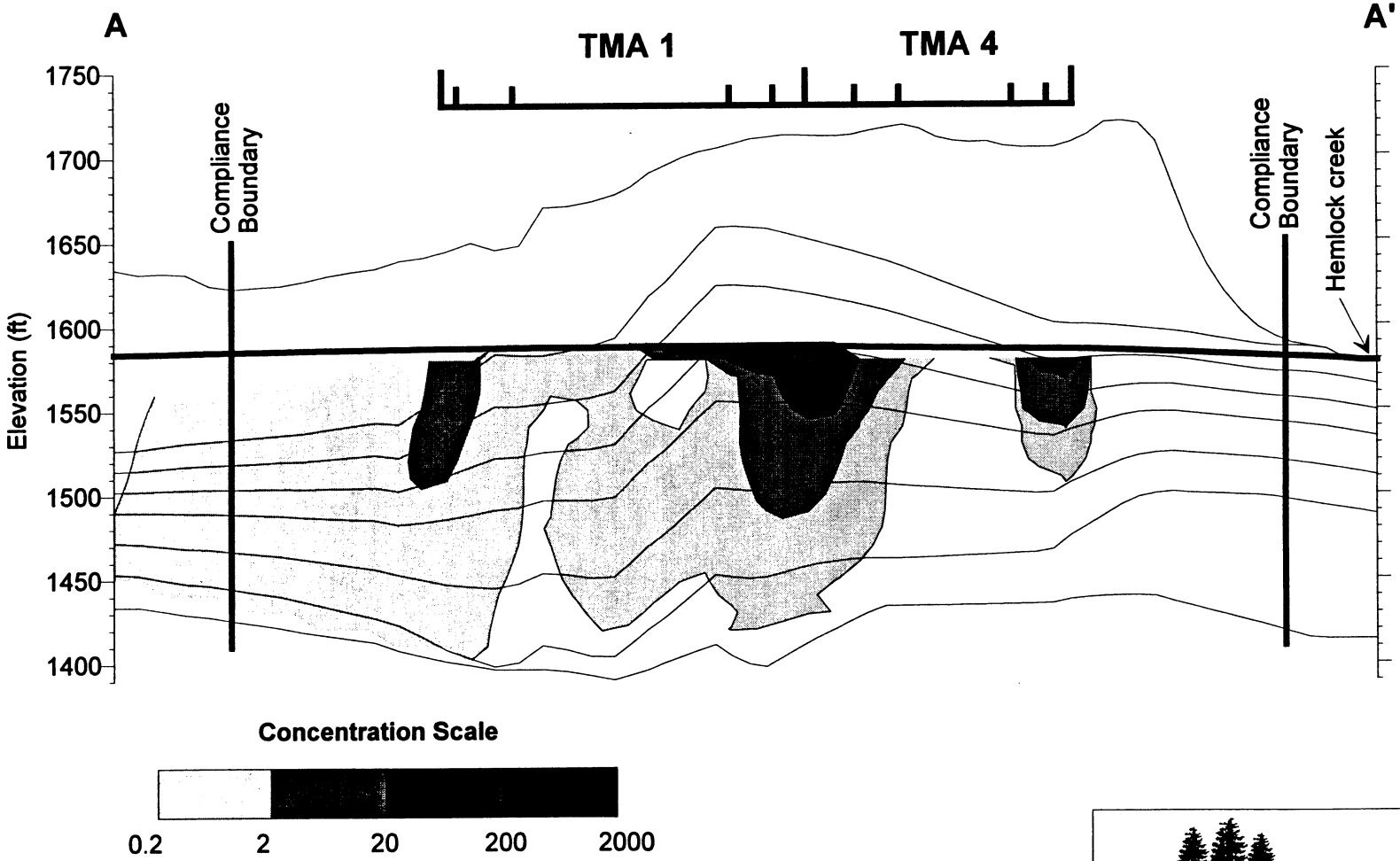

4.2-10-87

GeoTrans, inc.

REVISED	DATE	BY	DESCRIPTION

CHECKED BY:	PV	DATE: NOV 96
APPROVED BY:	RTH	DATE: NOV 96
APPROVED BY:	PFA	DATE: NOV 96

Crandon Mining Company

Figure 2.47
BEJ concentration after 32 years
(sulfate example, cross section)

Scale: 1" = 1000' (h), 100' (v)	Date: Nov 1996
Prepared By: GeoTrans, GA	By: GWC

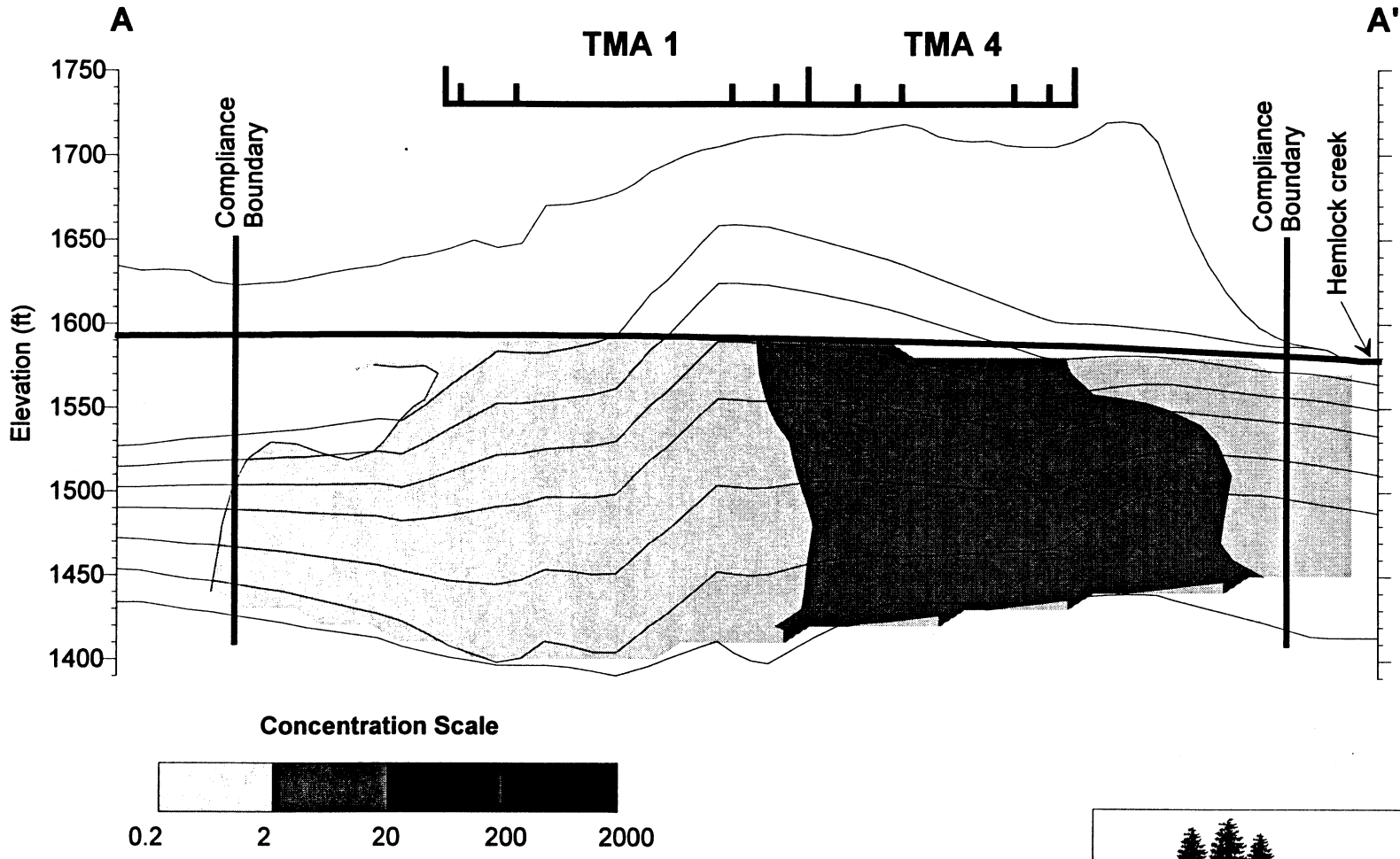

4.2-10-88

GeoTrans, inc.

REVISED	DATE	BY	DESCRIPTION

CHECKED BY:	PV	DATE: NOV 96
APPROVED BY:	RTH	DATE: NOV 96
APPROVED BY:	PFA	DATE: NOV 96

Crandon Mining Company

Figure 2.48
BEJ concentration after 100 years (sulfate example, cross section)

Scale: 1" = 1000' (h), 100' (v)	Date: Nov 1996
Prepared By: GeoTrans, GA	By: GWC

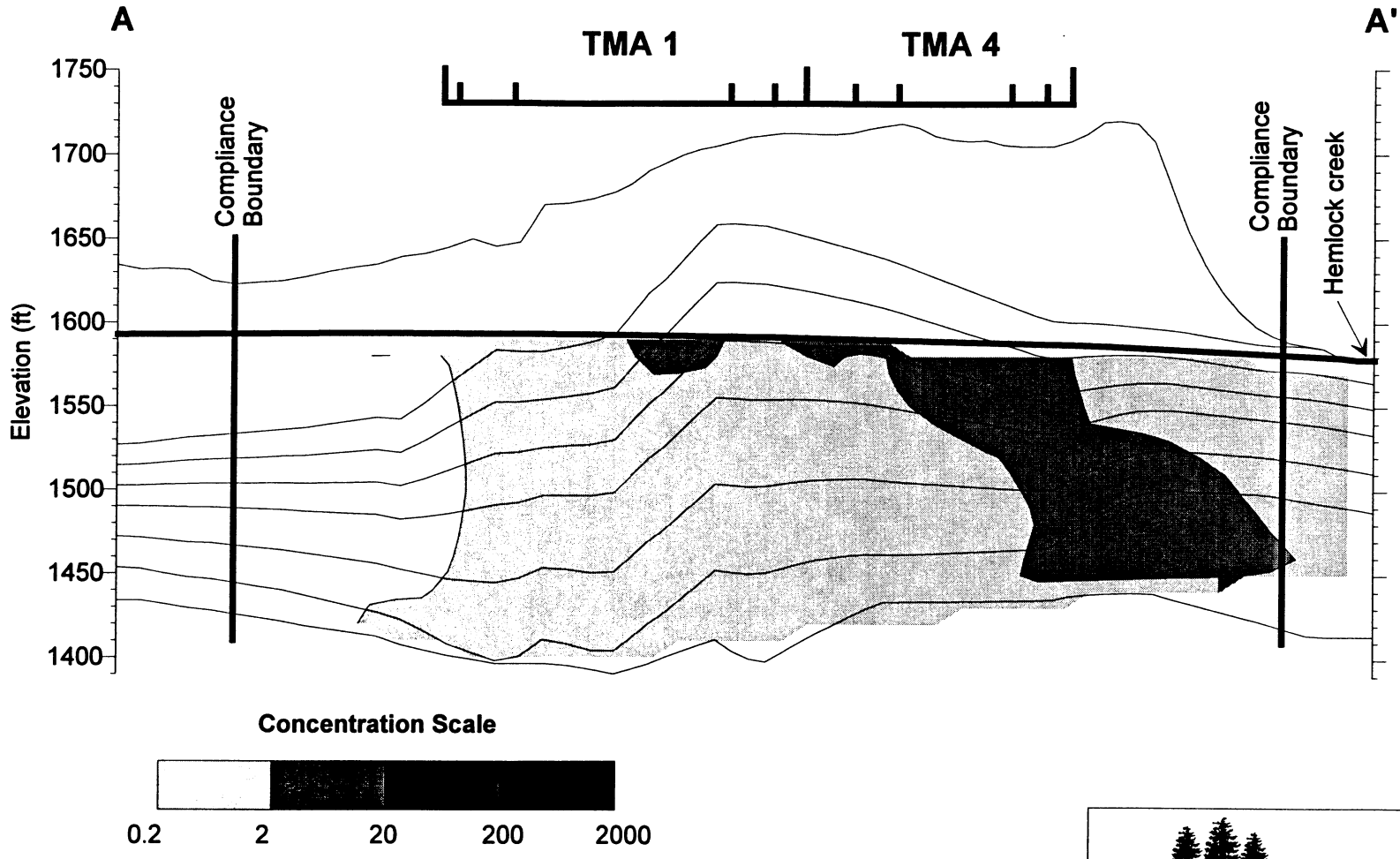

GeoTrans, inc.			
REVISED	DATE	BY	DESCRIPTION

CHECKED BY:	PV	DATE: NOV 96
APPROVED BY:	RTH	DATE: NOV 96
APPROVED BY:	PFA	DATE: NOV 96

Crandon Mining Company

Figure 2.49
BEJ concentration after 200 years (sulfate example, cross section)

Scale: 1" = 1000' (h), 100' (v)	Date: Nov 1996
Prepared By: GeoTrans, GA	By: GWC

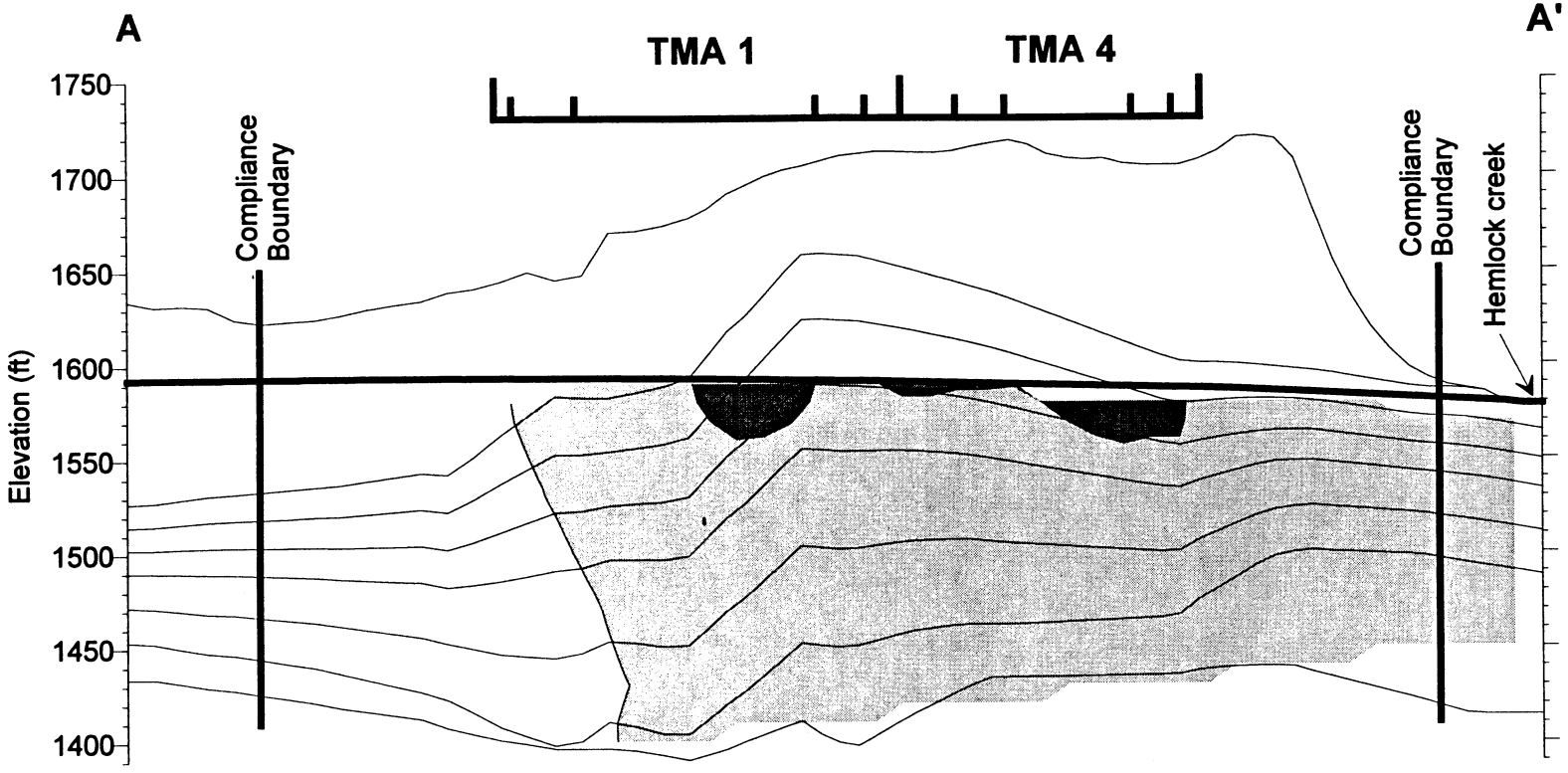

Concentration Scale

4.2-10-90

GeoTrans, inc.

REVISED	DATE	BY	DESCRIPTION

CHECKED BY:	PV	DATE: NOV 96
APPROVED BY:	RTH	DATE: NOV 96
APPROVED BY:	PFA	DATE: NOV 96

Crandon Mining Company

Figure 2.50
BEJ concentration after 300 years (sulfate example, cross section)

Scale: 1" = 1000' (h), 100' (v)	Date: Nov 1996
Prepared By: GeoTrans, GA	By: GWC

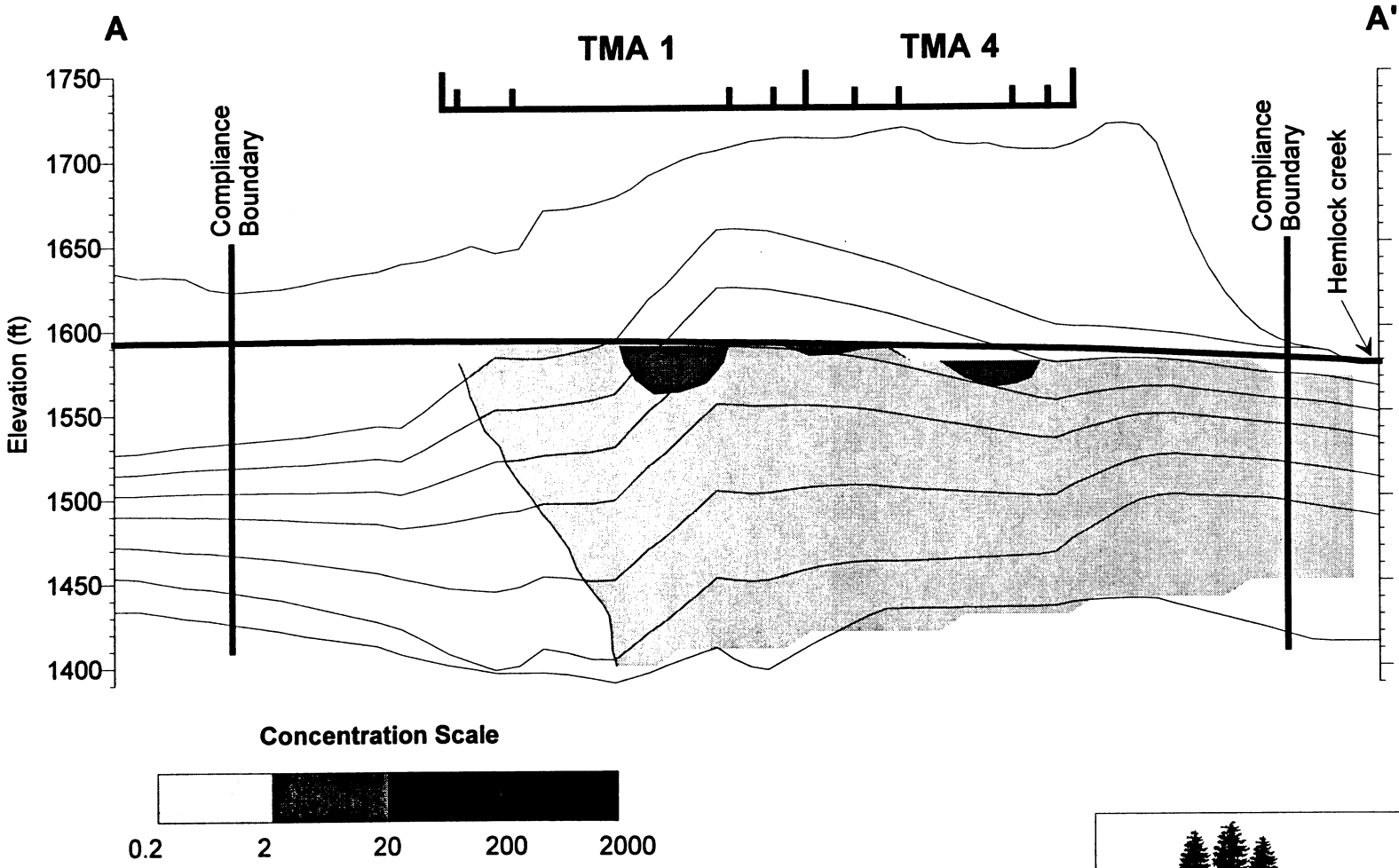

GeoTrans, inc.			
REVISED	DATE	BY	DESCRIPTION

CHECKED BY:	PV	DATE: NOV 96
APPROVED BY:	RTH	DATE: NOV 96
APPROVED BY:	PFA	DATE: NOV 96

Crandon Mining Company

Figure 2.51
BEJ concentration after 650 years
(sulfate example, cross section)

Scale: 1" = 1000' (h), 100' (v)	Date: Nov 1996
Prepared By: GeoTrans, GA	By: GWC

4.2-10-91

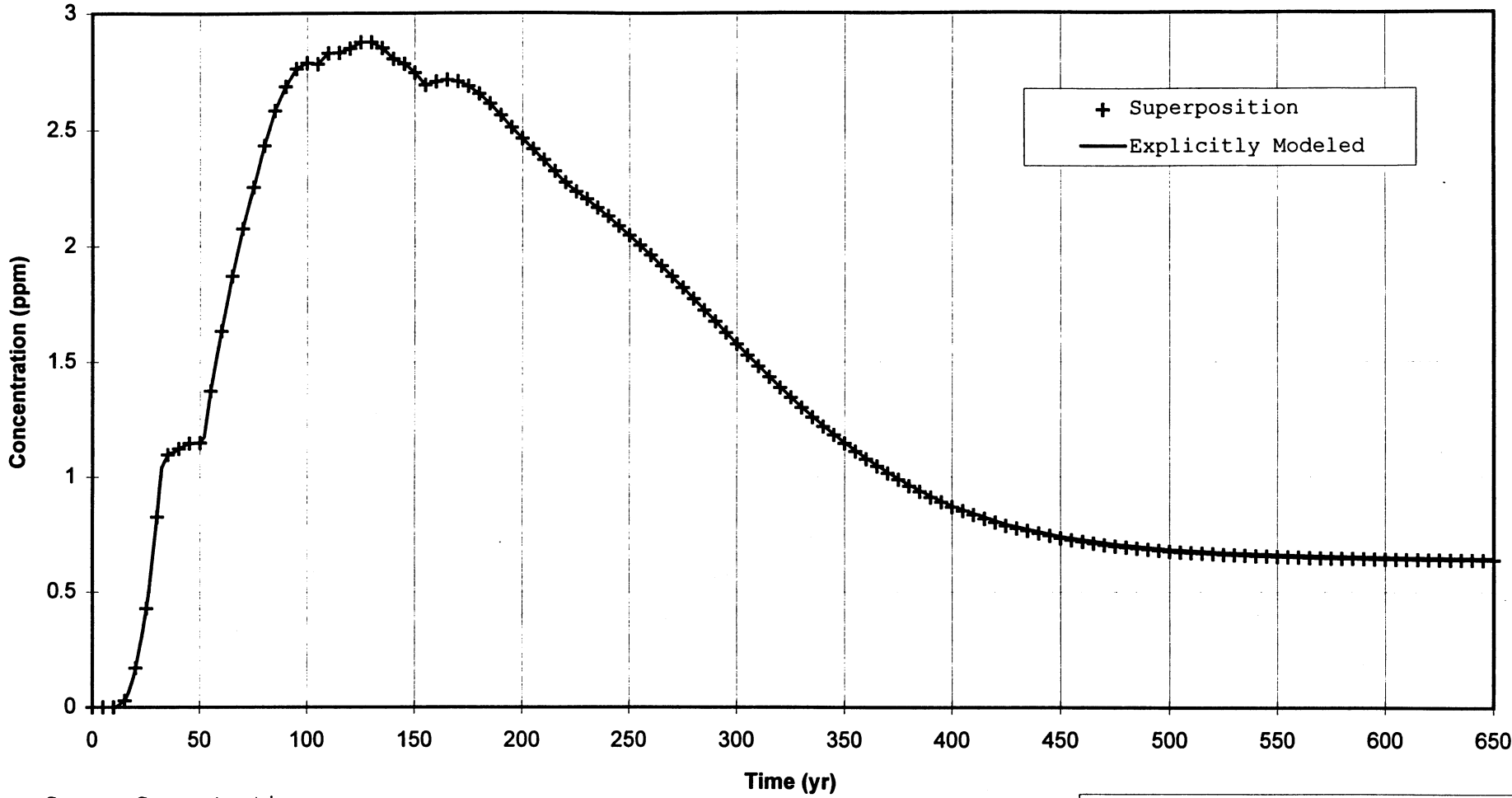

Source Concentration:
Operation: 2,000 ppm
Post-cap: 4,000 ppm
Oxidized: 40,000 ppm*

*As a conservative assumption, the oxidized concentration begins one year after assumed degradation of the flexible membrane liner.

GeoTrans, inc.

REVISED	DATE	BY	DESCRIPTION

CHECKED BY: PV	DATE: OCT 96
APPROVED BY: RTH	DATE: OCT 96
APPROVED BY: PFA	DATE: OCT 96

Crandon Mining Company

Figure 2.52
Verification of the superposition method for the BEJ sulfate example

Scale: None	Date: Oct 1996
Prepared By: GeoTrans, Inc.	By: GWC

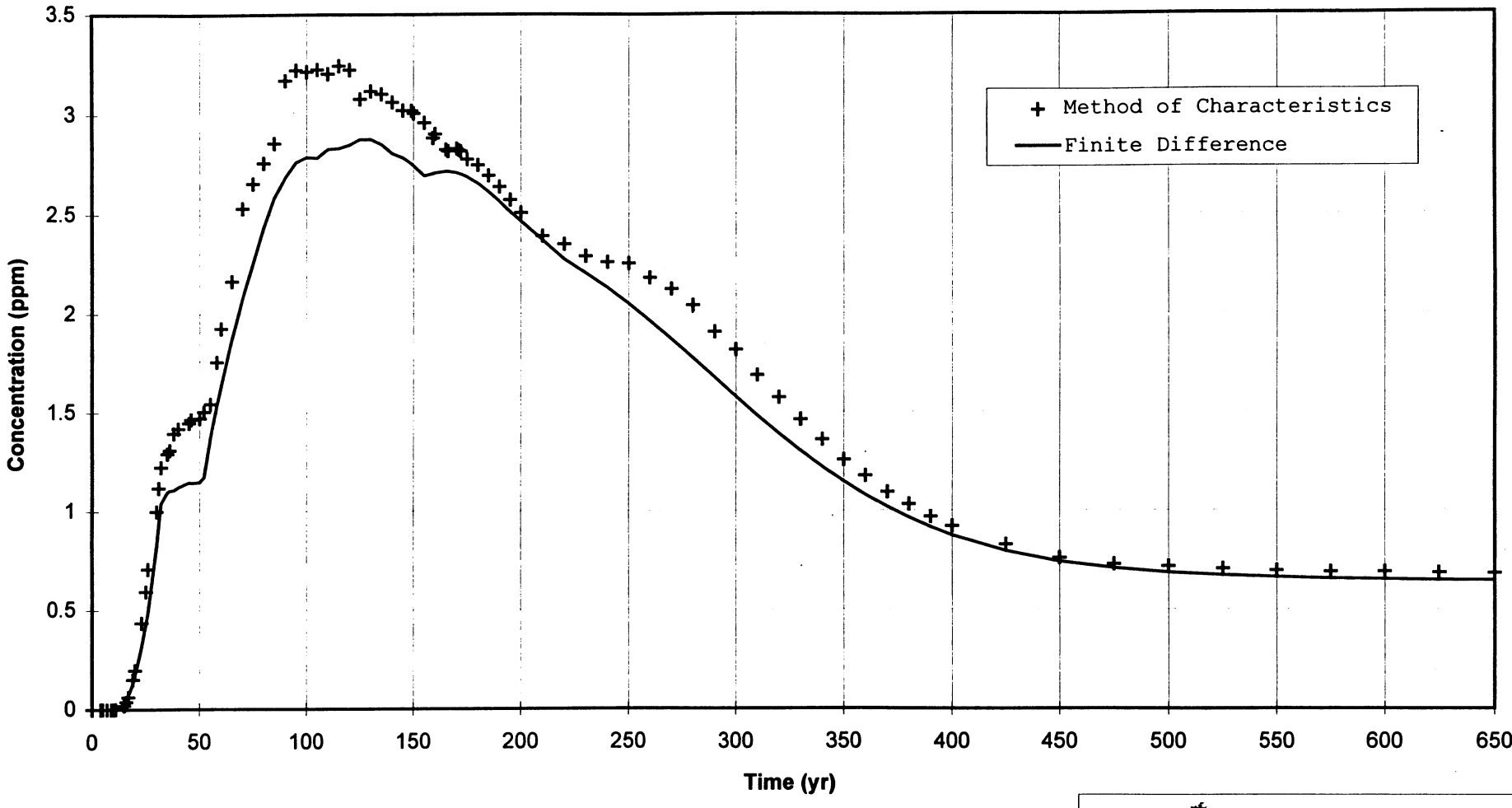

Source Concentration:
Operation: 2,000 ppm
Post-cap: 4,000 ppm
Oxidized: 40,000 ppm*

*As a conservative assumption, the oxidized concentration begins one year after assumed degradation of the flexible membrane liner.

GeoTrans, inc.

REVISED	DATE	BY	DESCRIPTION

CHECKED BY: PV	DATE: NOV 96
APPROVED BY: RTH	DATE: NOV 96
APPROVED BY: PFA	DATE: NOV 96

Crandon Mining Company

Figure 2.53
Comparison of finite-difference and method-of-characteristics techniques

Scale: None	Date: Nov 1996
Prepared By: GeoTrans, Inc.	By: GWC

4.2-10-93

Brkthru5.xls

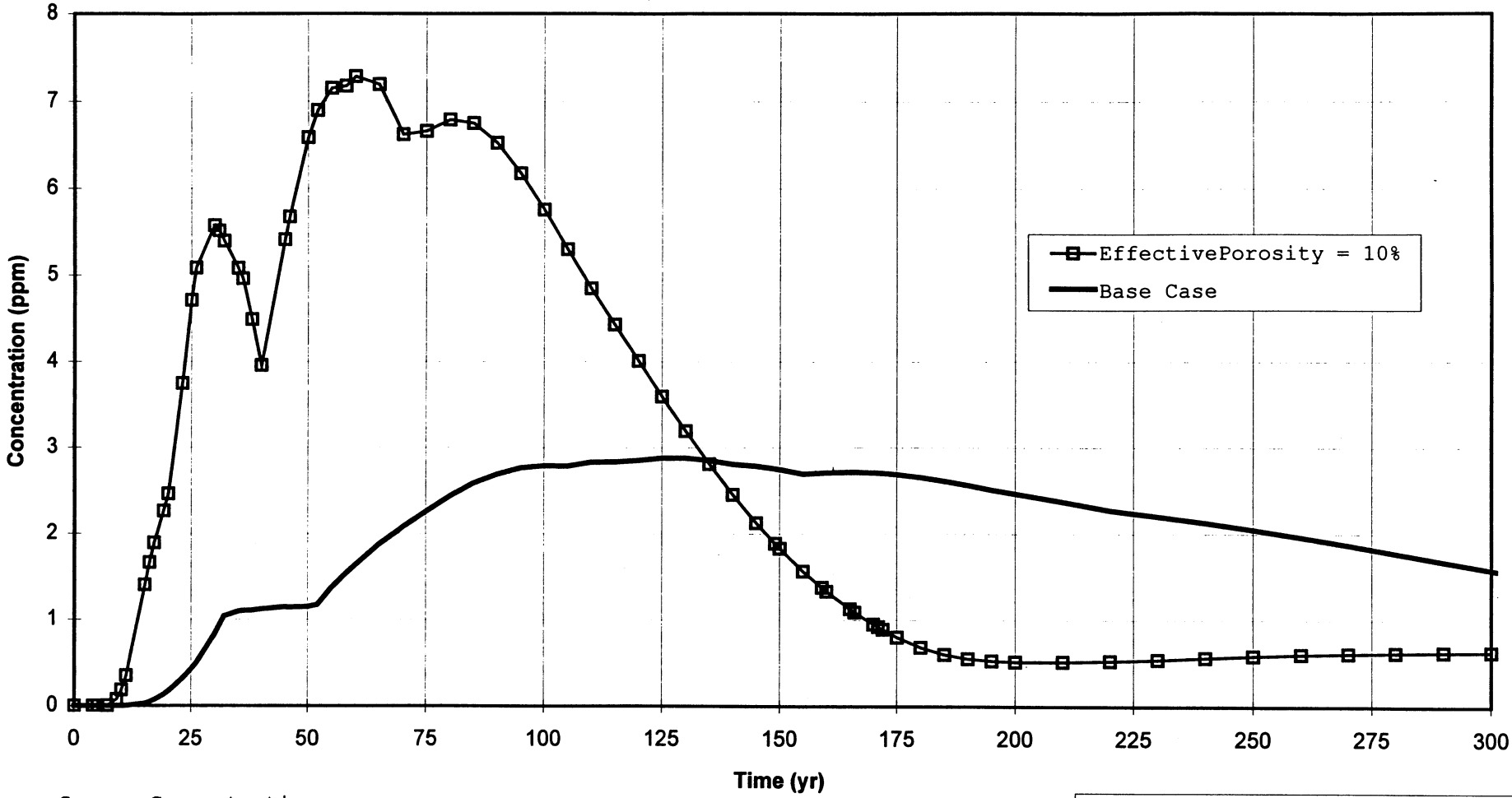

Source Concentration:
Operation: 2,000 ppm
Post-cap: 4,000 ppm
Oxidized: 40,000 ppm*

*As a conservative assumption, the oxidized concentration begins one year after assumed degradation of the flexible membrane liner.

GeoTrans, inc.

REVISED	DATE	BY	DESCRIPTION

CHECKED BY: PV	DATE: OCT 96
APPROVED BY: RTH	DATE: OCT 96
APPROVED BY: PFA	DATE: OCT 96

Crandon Mining Company

Figure 2.54
Sensitivity to variations in effective porosity

Scale: None	Date: Oct 1996
Prepared By: GeoTrans, Inc.	By: GWC

4.2-10-94

Brkthru7.*

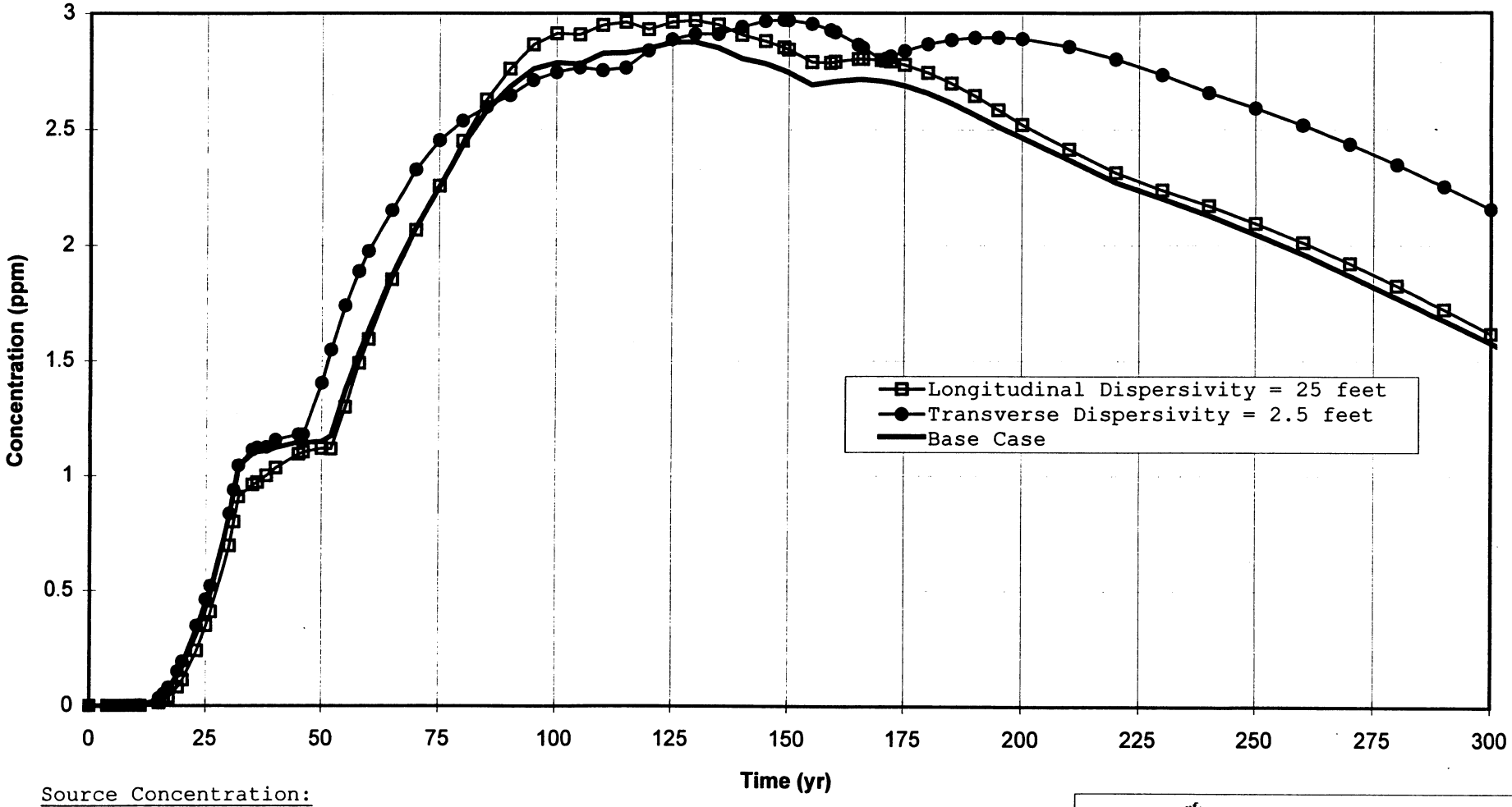

Source Concentration:

Operation:	2,000 ppm
Post-cap:	4,000 ppm
Oxidized:	40,000 ppm*

*As a conservative assumption, the oxidized concentration begins one year after assumed degradation of the flexible membrane liner.

GeoTrans, inc.

REVISED	DATE	BY	DESCRIPTION

CHECKED BY: PV	DATE: OCT 96
APPROVED BY: RTH	DATE: OCT 96
APPROVED BY: PFA	DATE: OCT 96

Crandon Mining Company

Figure 2.55
Sensitivity to variations in dispersivity

Scale: None	Date: Oct 1996
Prepared By: GeoTrans, Inc.	By: GWC

4.2-10-95

Brkthru7.xls

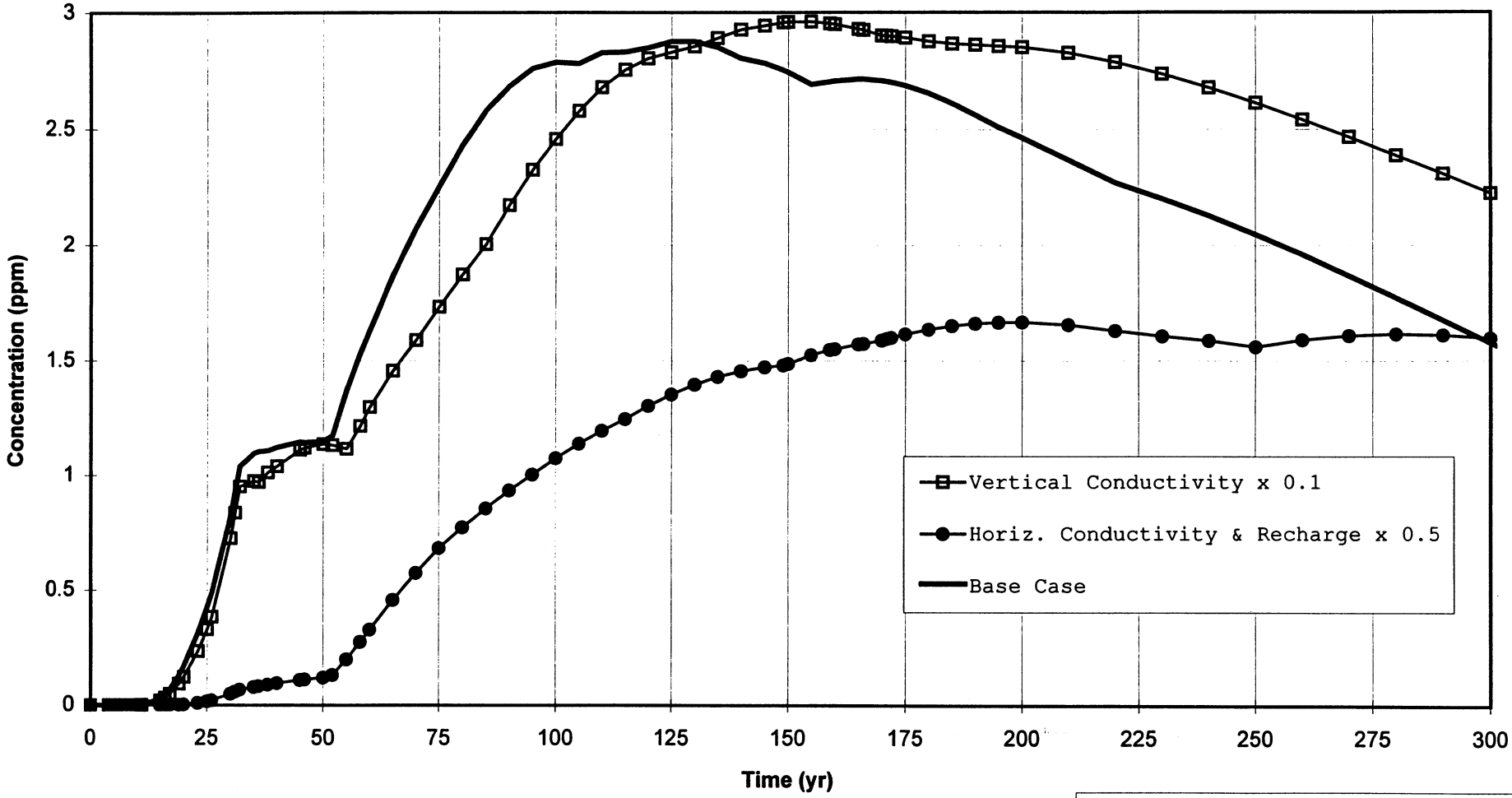

Source Concentration:
Operation: 2,000 ppm
Post-cap: 4,000 ppm
Oxidized: 40,000 ppm*

*As a conservative assumption, the oxidized concentration begins one year after assumed degradation of the flexible membrane liner.

GeoTrans, inc.

REVISED	DATE	BY	DESCRIPTION

CHECKED BY: PV	DATE: OCT 96
APPROVED BY: RTH	DATE: OCT 96
APPROVED BY: PFA	DATE: OCT 96

Crandon Mining Company

Figure 2.56
Sensitivity to variations in hydraulic conductivity and recharge

Scale: None	Date: Oct 1996
Prepared By: GeoTrans, Inc.	By: GWC

4.2-10-96

Brkthru7.xls

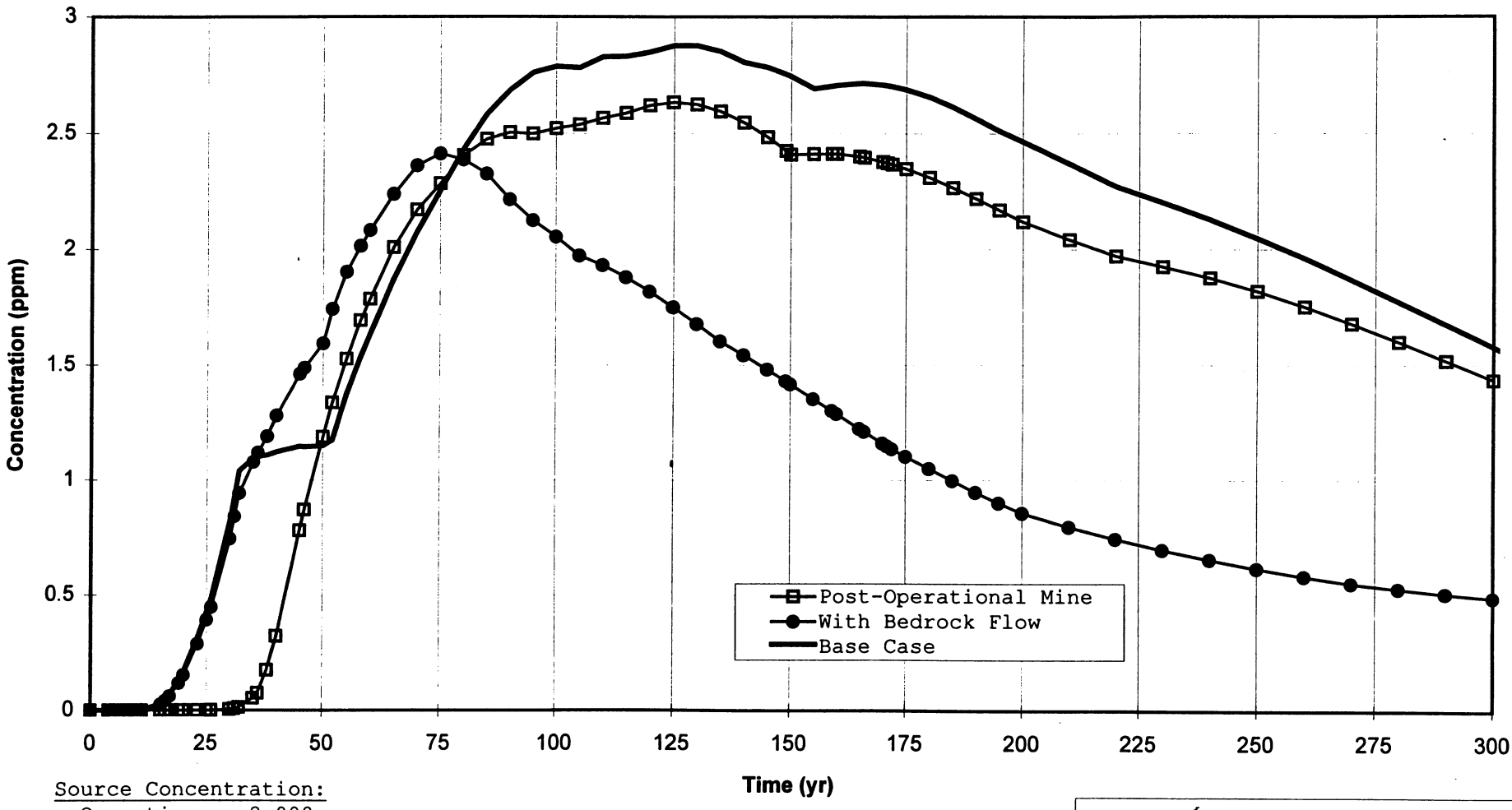

Source Concentration:
Operation: 2,000 ppm
Post-cap: 4,000 ppm
Oxidized: 40,000 ppm*

*As a conservative assumption, the oxidized concentration begins one year after assumed degradation of the flexible membrane liner.

GeoTrans, inc.			
REVISED	DATE	BY	DESCRIPTION

CHECKED BY: PV	DATE: OCT 96
APPROVED BY: RTH	DATE: OCT 96
APPROVED BY: PFA	DATE: OCT 96

Crandon Mining Company

Figure 2.57
Sensitivity to variations in flow boundary conditions

Scale: None	Date: Oct 1996
Prepared By: GeoTrans, Inc.	By: GWC

4.2-10-97

Brkthru7.xls

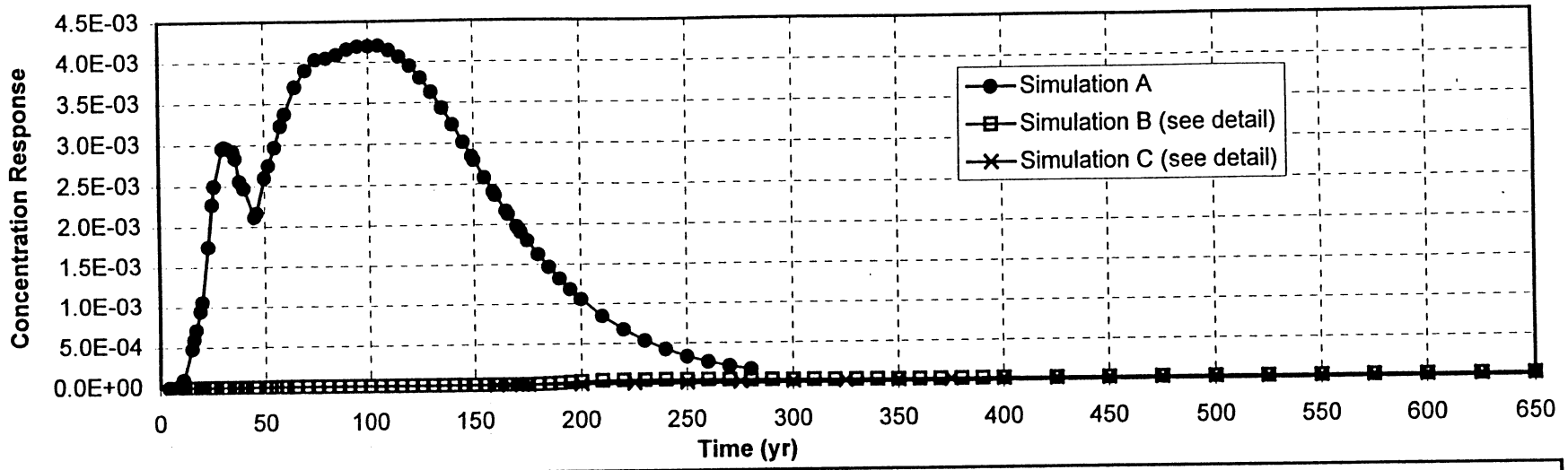

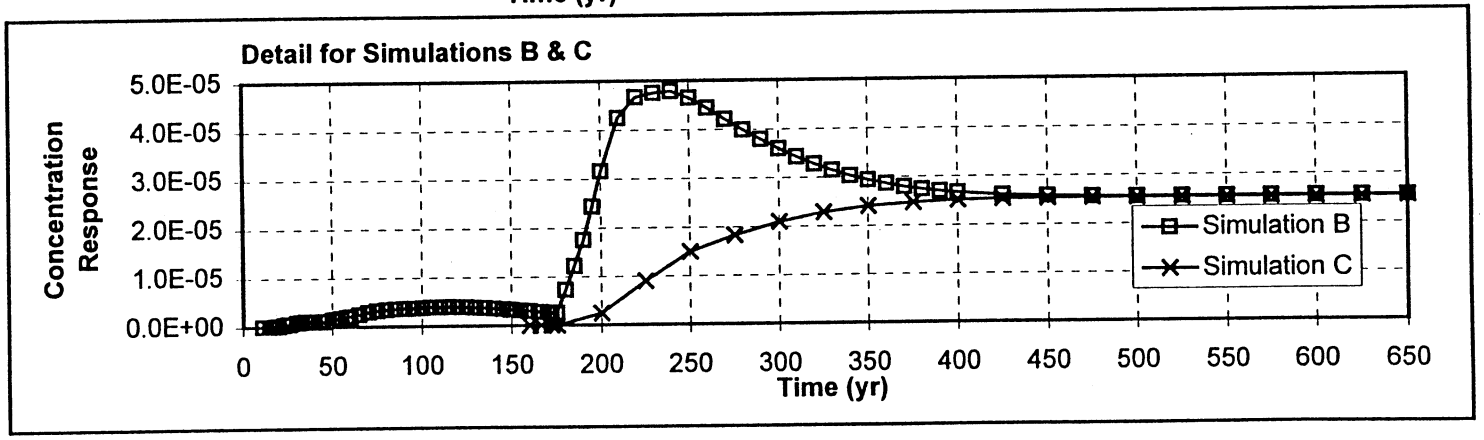

Note:
For these plots, the start time for Simulation C is set to 150 years.

GeoTrans, inc.			
REVISED	DATE	BY	DESCRIPTION
CHECKED BY: PV			DATE: NOV 96
APPROVED BY: RTH			DATE: NOV 96
APPROVED BY: PFA			DATE: NOV 96

Crandon Mining Company

Figure 2.58
PWC Concentration response curves at the compliance boundary

Scale: None	Date: Nov 96
Prepared by: GeoTrans, Inc.	By: GWC

4.2-10-98

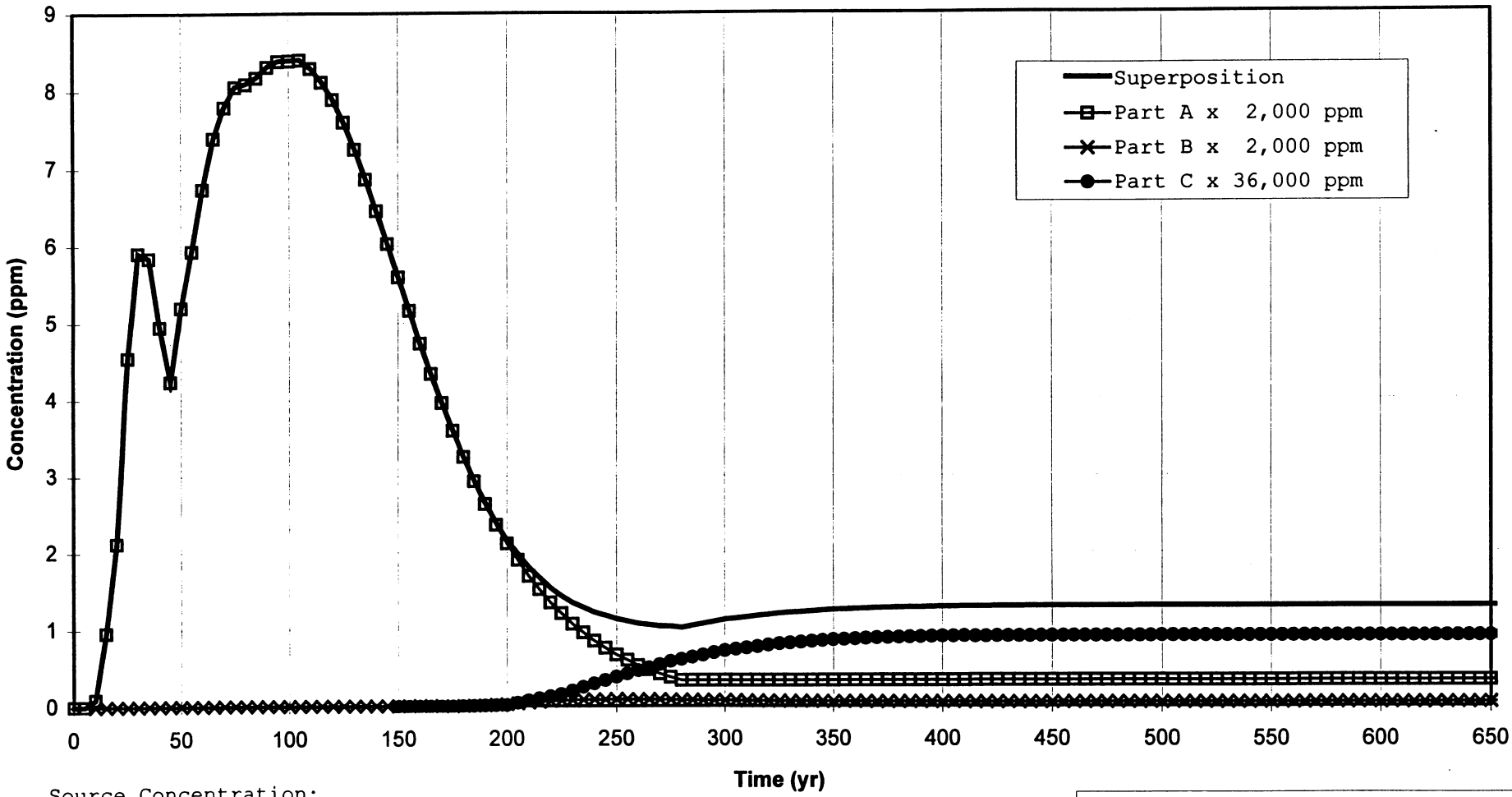

Source Concentration:
Operation: 2,000 ppm
Post-cap: 4,000 ppm
Oxidized: 40,000 ppm*

*As a conservative assumption, the oxidized concentration begins one year after assumed degradation of the flexible membrane liner.

GeoTrans, inc.

REVISED	DATE	BY	DESCRIPTION

CHECKED BY:	PV	DATE: OCT 96
APPROVED BY:	RTH	DATE: OCT 96
APPROVED BY:	PFA	DATE: OCT 96

Crandon Mining Company

Figure 2.59
PWC concentration at the compliance boundary (sulfate example)

Scale: None	Date: Oct 1996
Prepared By: GeoTrans, Inc.	By: GWC

4.2-10-99

Brkthru6.xls

Concentration Scale

Note: This plot shows shaded contours of maximum concentration in any layer.

GeoTrans, inc.

REVISED	DATE	BY	DESCRIPTION

CHECKED BY:	PV	DATE: OCT 96
APPROVED BY:	RTH	DATE: OCT 96
APPROVED BY:	PFA	DATE: OCT 96

Crandon Mining Company

Figure 2.60
PWC concentration after 7 years (sulfate example, plan view)

Scale 1" = 1000'	Date: Oct 1996
Prepared By: GeoTrans, Inc.	By: GWC

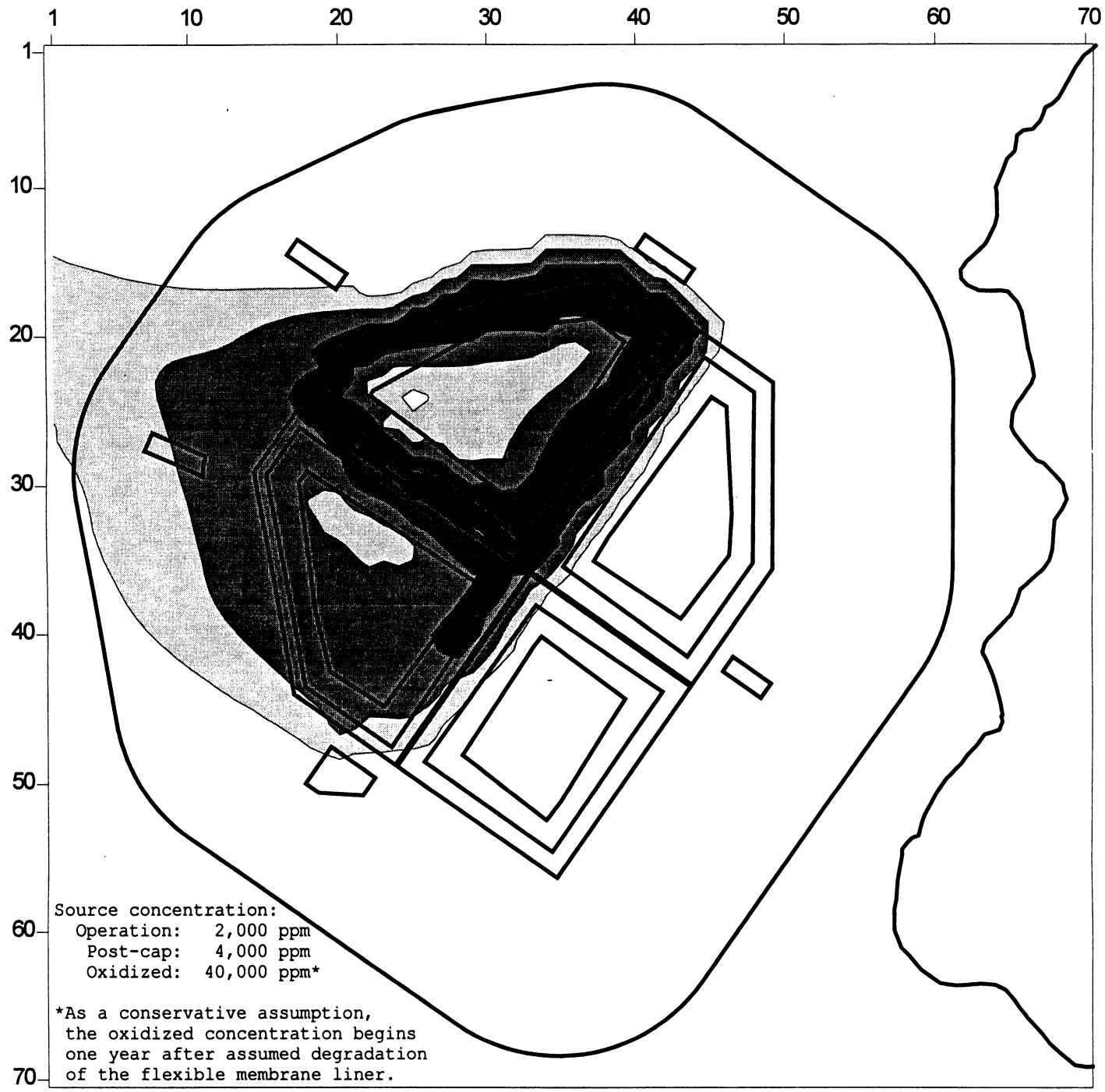

Concentration Scale

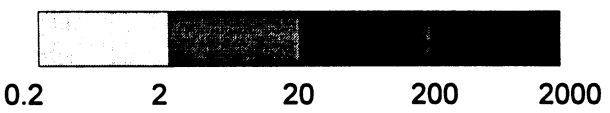

Note: This plot shows shaded contours of maximum concentration in any layer.

GeoTrans, inc.			
REVISED	DATE	BY	DESCRIPTION

CHECKED BY: PV	DATE: OCT 96
APPROVED BY: RTH	DATE: OCT 96
APPROVED BY: PFA	DATE: OCT 96

Crandon Mining Company

Figure 2.61
PWC concentration after 17 years (sulfate example, plan view)

Scale 1" = 1000'	Date: Oct 1996
Prepared By: GeoTrans, Inc.	By: GWC

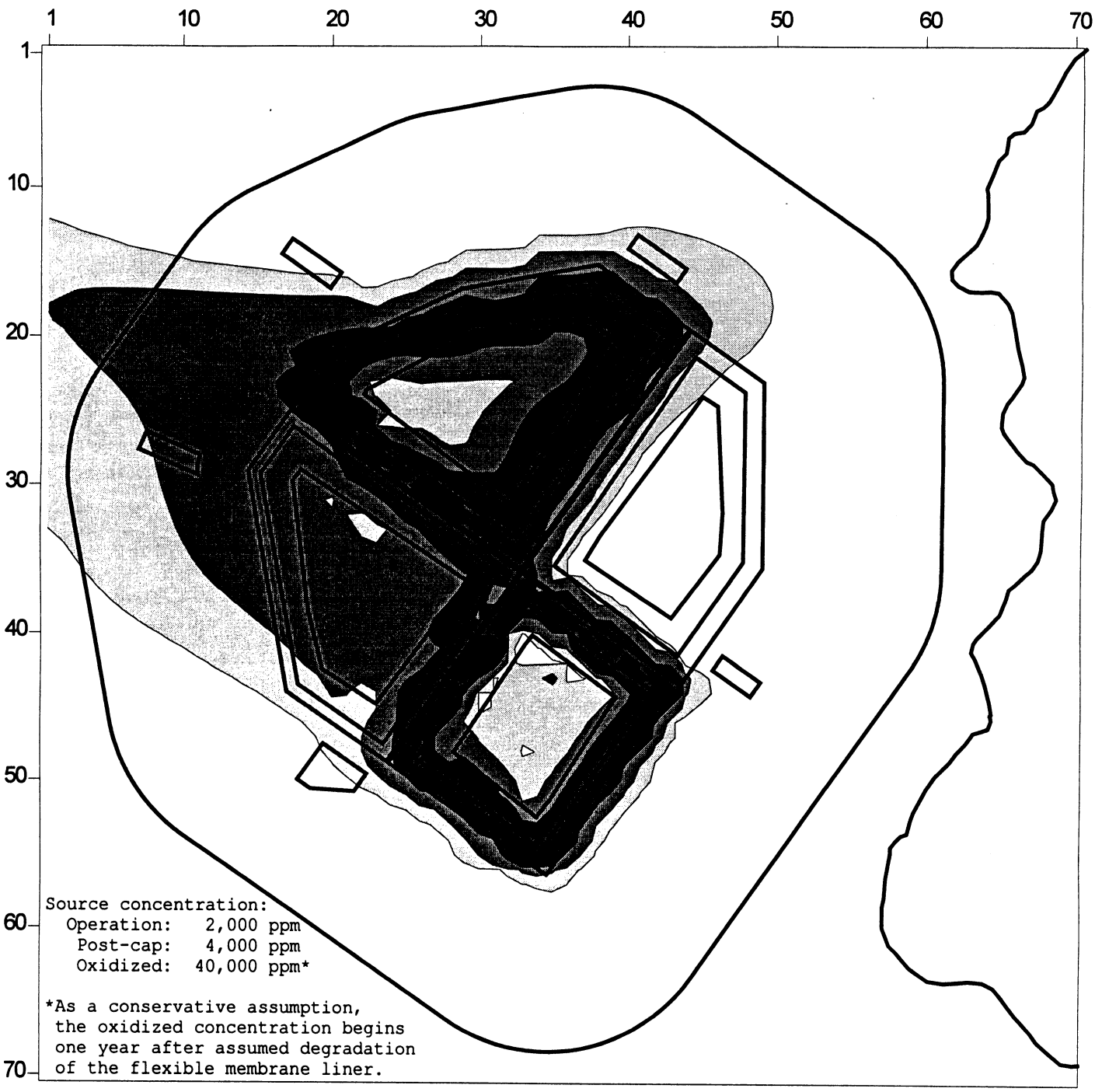

Concentration Scale

Note: This plot shows shaded contours of maximum concentration in any layer.

GeoTrans, inc.

REVISED	DATE	BY	DESCRIPTION

CHECKED BY:	PV	DATE: OCT 96
APPROVED BY:	RTH	DATE: OCT 96
APPROVED BY:	PFA	DATE: OCT 96

Crandon Mining Company

Figure 2.62
PWC concentration after 23 years (sulfate example, plan view)

Scale 1" = 1000'	Date: Oct 1996
Prepared By: GeoTrans, Inc.	By: GWC

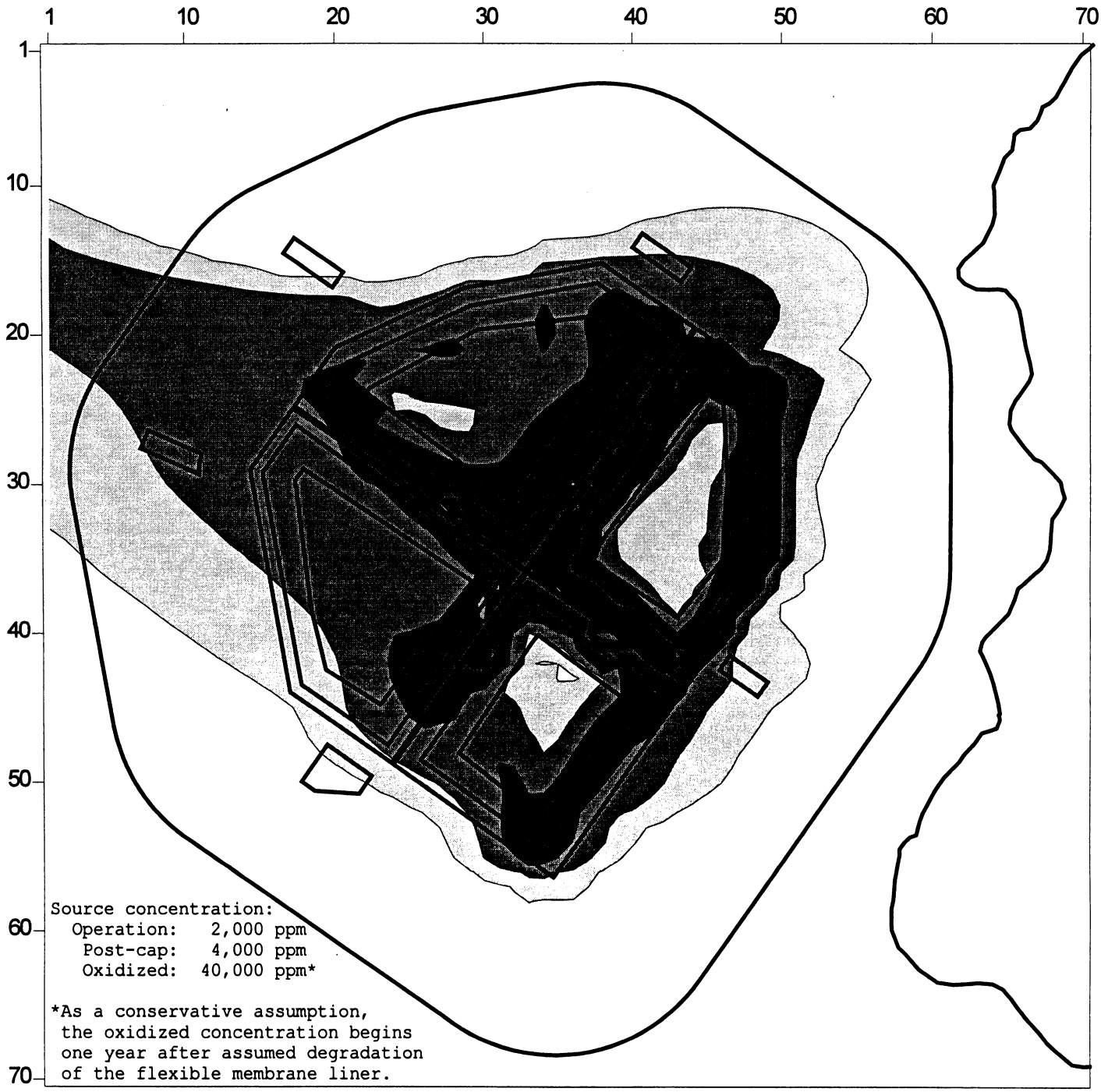

Concentration Scale

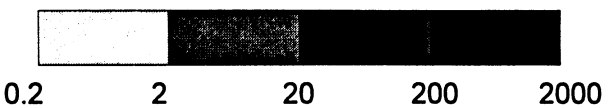

Note: This plot shows shaded contours of maximum concentration in any layer.

GeoTrans, inc.

REVISED	DATE	BY	DESCRIPTION

CHECKED BY:	PV	DATE: OCT 96
APPROVED BY:	RTH	DATE: OCT 96
APPROVED BY:	PFA	DATE: OCT 96

Crandon Mining Company

Figure 2.63
PWC concentration after 32 years (sulfate example, plan view)

Scale 1" = 1000'	Date: Oct 1996
Prepared By: GeoTrans, Inc.	By: GWC

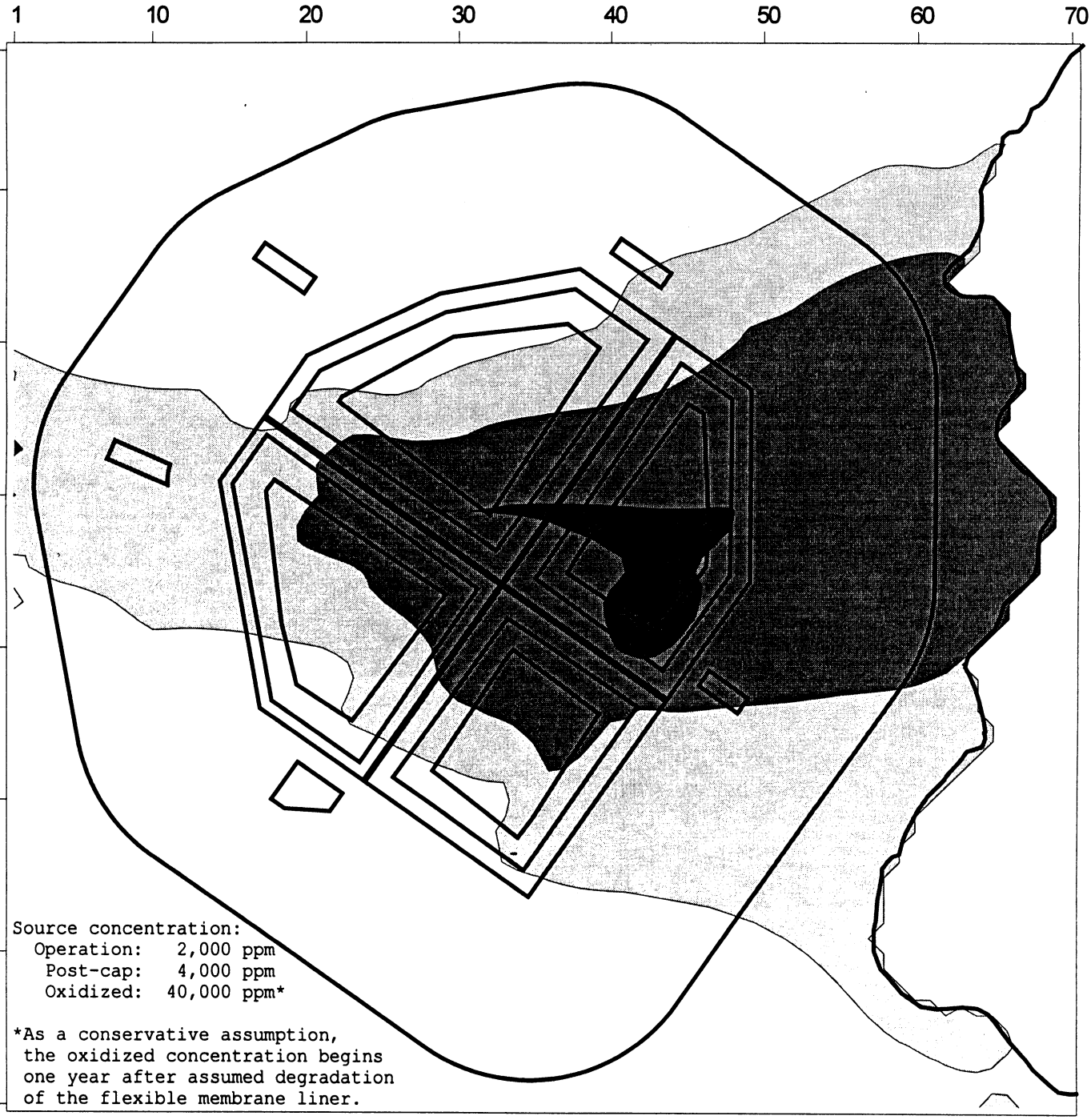

Concentration Scale

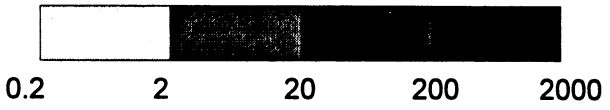

Note: This plot shows shaded contours of maximum concentration in any layer.

GeoTrans, inc.			
REVISED	DATE	BY	DESCRIPTION
CHECKED BY:	PV	DATE: OCT 96	
APPROVED BY:	RTH	DATE: OCT 96	
APPROVED BY:	PFA	DATE: OCT 96	

Crandon Mining Company

Figure 2.64
PWC concentration after 100 years (sulfate example, plan view)

Scale 1" = 1000'	Date: Oct 1996
Prepared By: GeoTrans, Inc.	By: GWC

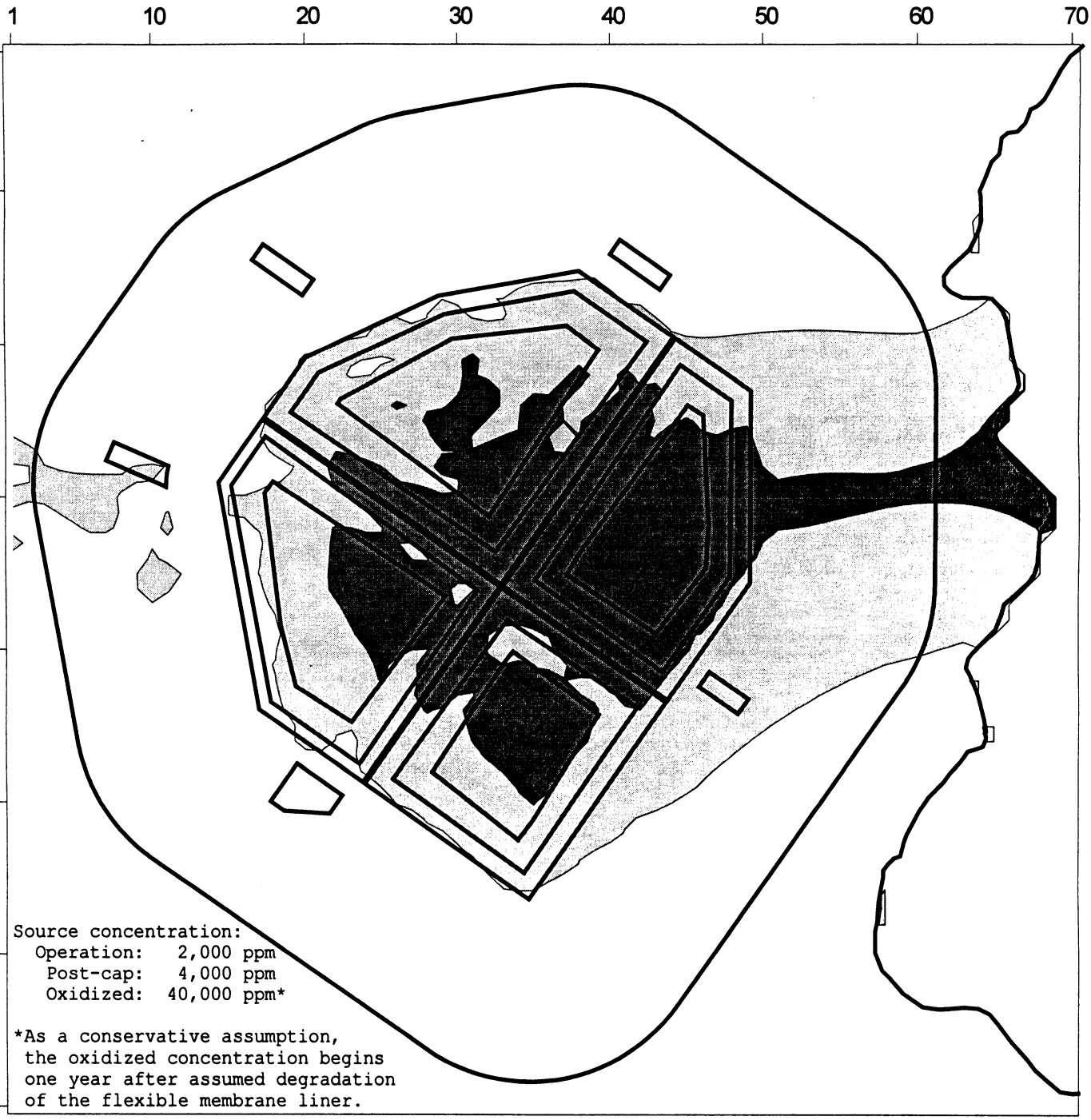

Concentration Scale

Note: This plot shows shaded contours of maximum concentration in any layer.

GeoTrans, inc.

REVISED	DATE	BY	DESCRIPTION

CHECKED BY:	PV	DATE: OCT 96
APPROVED BY:	RTH	DATE: OCT 96
APPROVED BY:	PFA	DATE: OCT 96

Crandon Mining Company

Figure 2.65
PWC concentration after 200 years (sulfate example, plan view)

Scale 1" = 1000'	Date: Oct 1996
Prepared By: GeoTrans, Inc.	By: GWC

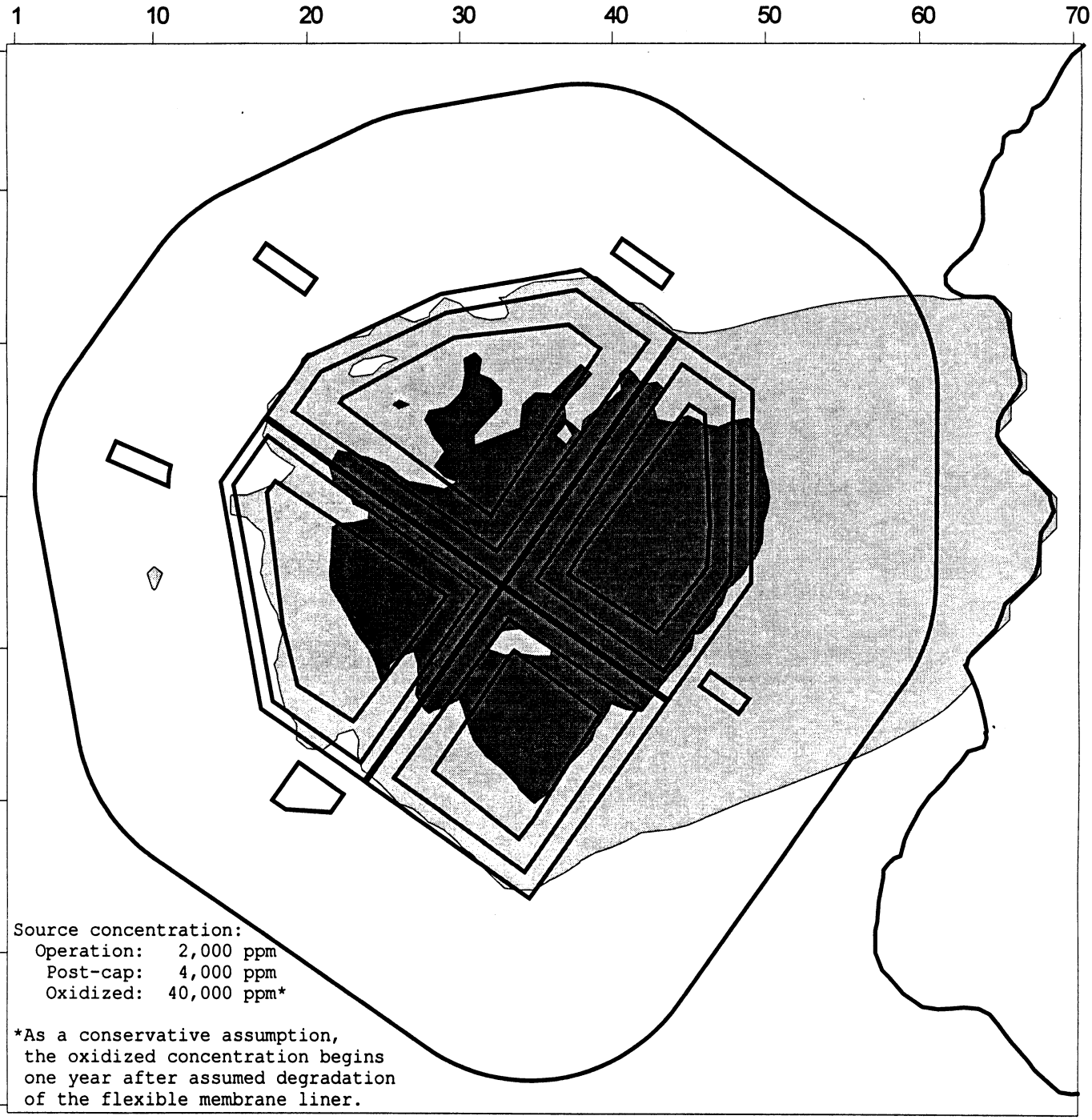

Concentration Scale

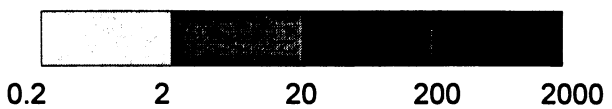

Note: This plot shows shaded contours of maximum concentration in any layer.

GeoTrans, inc.			
REVISED	DATE	BY	DESCRIPTION

CHECKED BY:	PV	DATE: OCT 96
APPROVED BY:	RTH	DATE: OCT 96
APPROVED BY:	PFA	DATE: OCT 96

Crandon Mining Company

Figure 2.66
PWC concentration after 300 years (sulfate example, plan view)

Scale 1" = 1000'	Date: Oct 1996
Prepared By: GeoTrans, Inc.	By: GWC

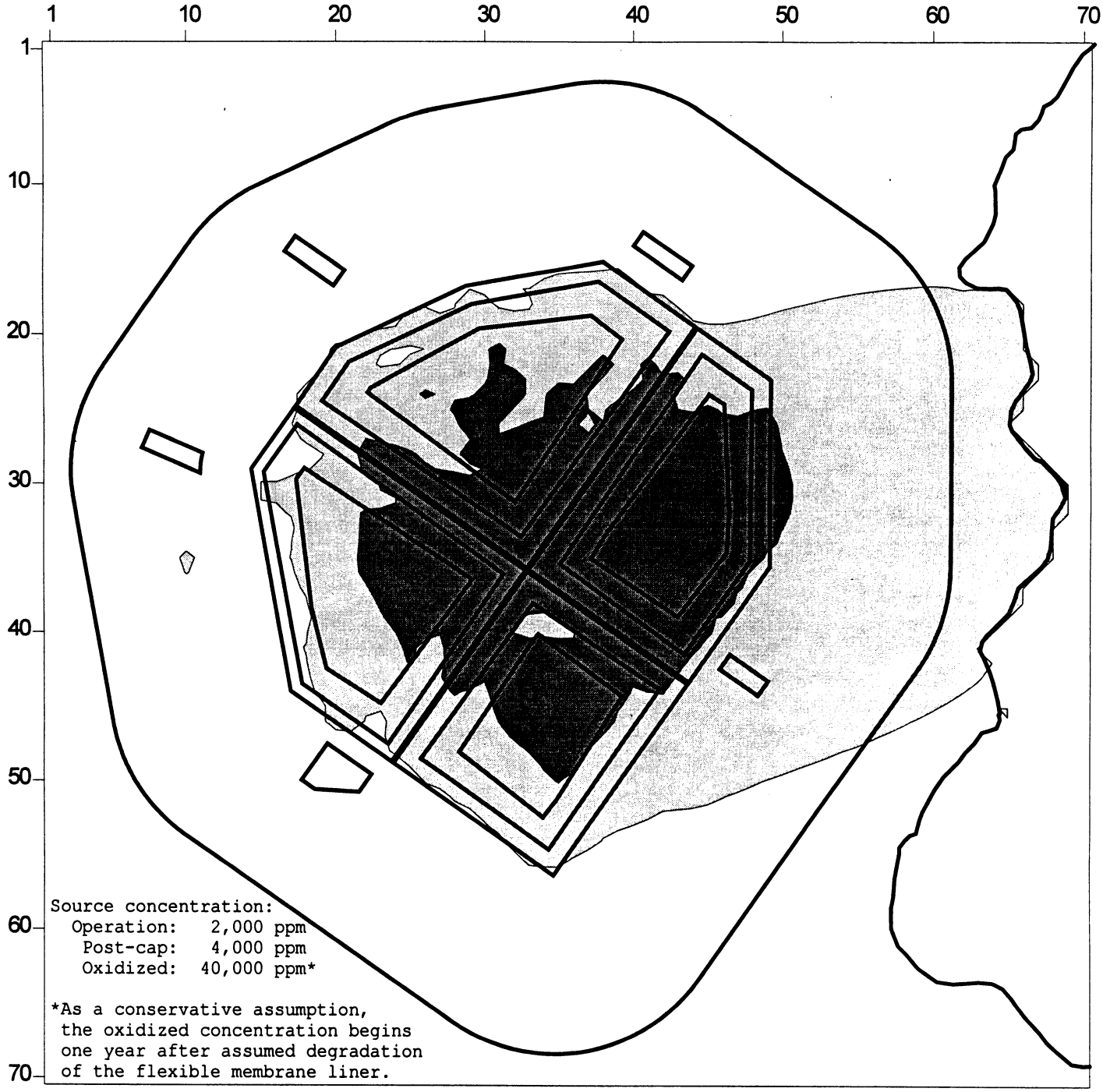

Concentration Scale

Note: This plot shows shaded contours of maximum concentration in any layer.

GeoTrans, inc.

REVISED	DATE	BY	DESCRIPTION

CHECKED BY:	PV	DATE: OCT 96
APPROVED BY:	RTH	DATE: OCT 96
APPROVED BY:	PFA	DATE: OCT 96

Crandon Mining Company

Figure 2.67
PWC concentration after 650 years (sulfate example, plan view)

Scale 1" = 1000'	Date: Oct 1996
Prepared By: GeoTrans, Inc.	By: GWC

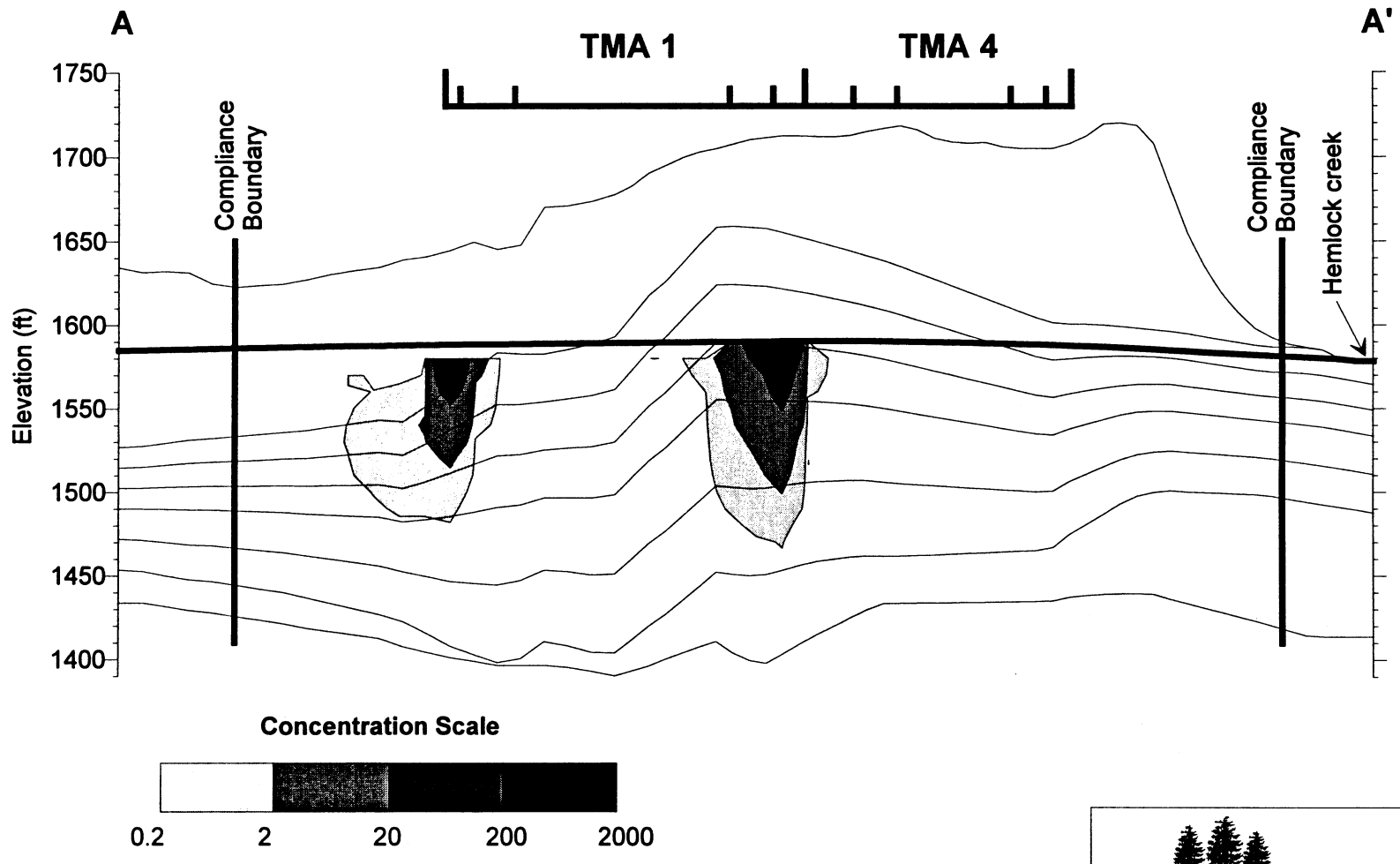

4.2-10-108

GeoTrans, inc.			
REVISED	DATE	BY	DESCRIPTION

CHECKED BY:	PV	DATE: NOV 96
APPROVED BY:	RTH	DATE: NOV 96
APPROVED BY:	PFA	DATE: NOV 96

Crandon Mining Company

Figure 2.68
PWC concentration after 7 years
(sulfate example, cross section)

Scale: 1" = 1000' (h), 100' (v)	Date: Nov 1996
Prepared By: GeoTrans, GA	By: GWC

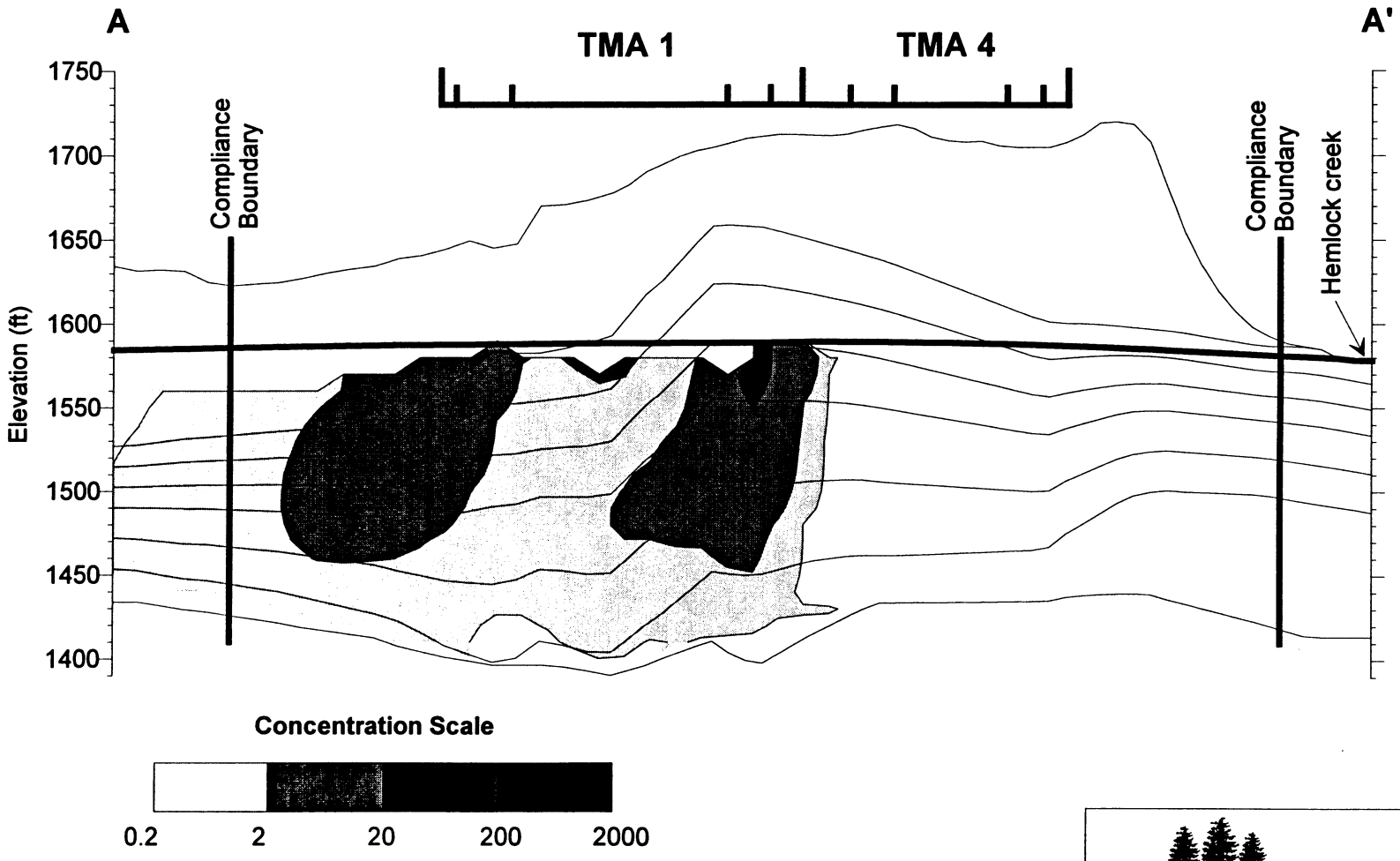

GeoTrans, inc.			
REVISED	DATE	BY	DESCRIPTION

CHECKED BY:	PV	DATE: NOV 96
APPROVED BY:	RTH	DATE: NOV 96
APPROVED BY:	PFA	DATE: NOV 96

Crandon Mining Company

Figure 2.69
PWC concentration after 17 years (sulfate example, cross section)

Scale: 1" = 1000' (h), 100' (v)	Date: Nov 1996
Prepared By: GeoTrans, GA	By: GWC

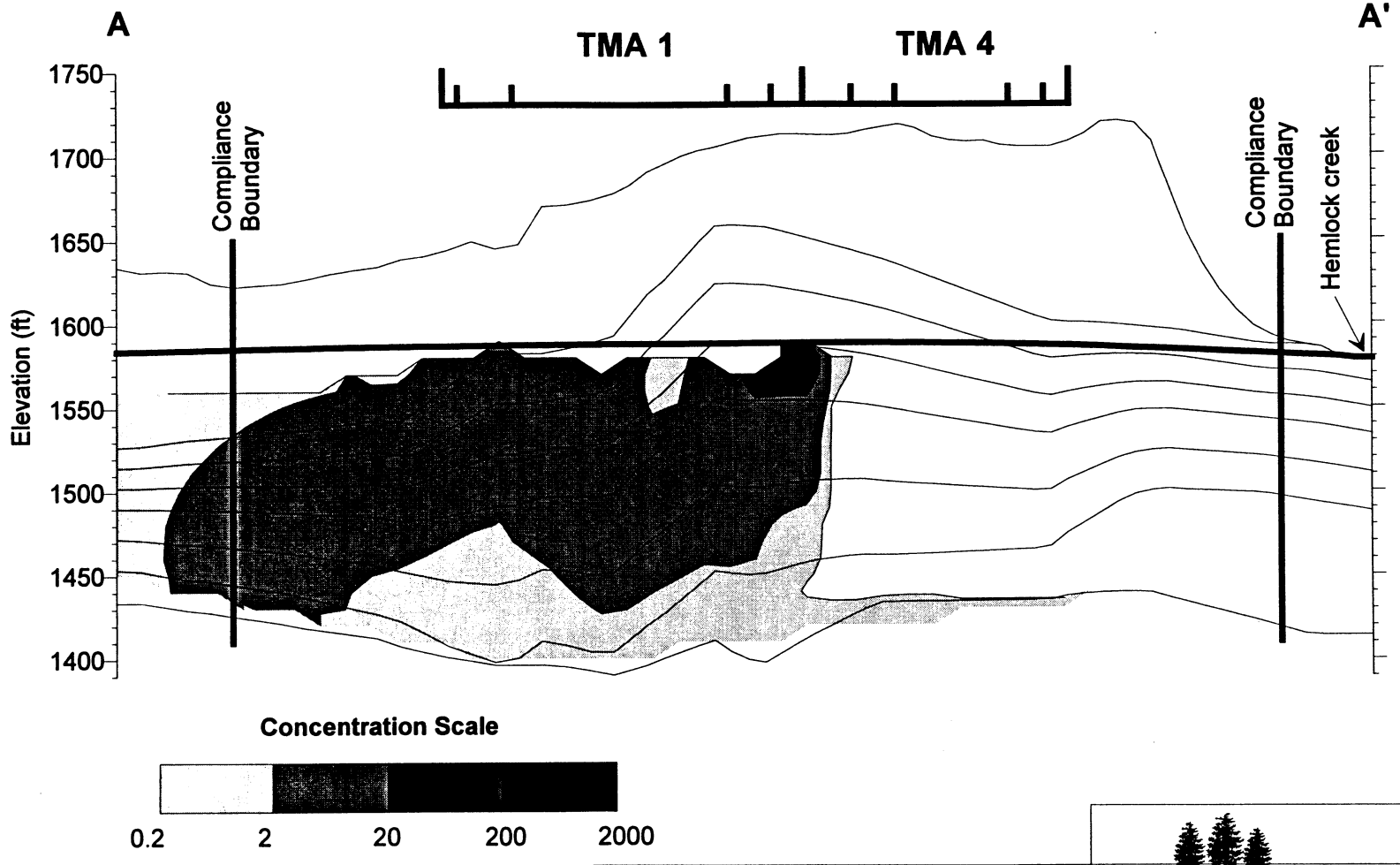

GeoTrans, inc.			
REVISED	DATE	BY	DESCRIPTION

CHECKED BY:	PV	DATE: NOV 96
APPROVED BY:	RTH	DATE: NOV 96
APPROVED BY:	PFA	DATE: NOV 96

Crandon Mining Company

Figure 2.70
PWC concentration after 23 years
(sulfate example, cross section)

Scale: 1" = 1000' (h), 100' (v)	Date: Nov 1996
Prepared By: GeoTrans, GA	By: GWC

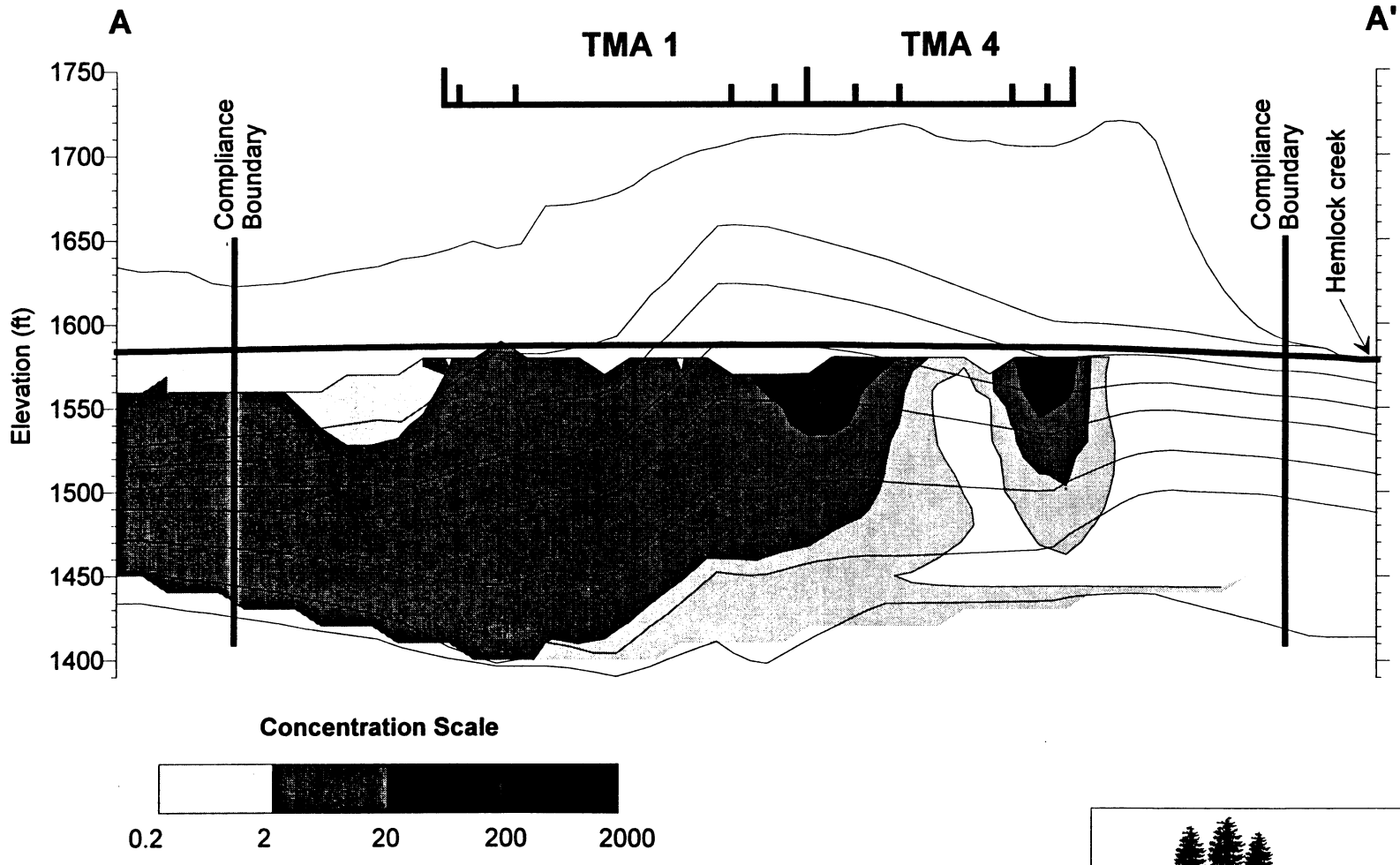

GeoTrans, inc.			
REVISED	DATE	BY	DESCRIPTION

CHECKED BY: PV	DATE: NOV 96
APPROVED BY: RTH	DATE: NOV 96
APPROVED BY: PFA	DATE: NOV 96

Crandon Mining Company

Figure 2.71
PWC concentration after 32 years
(sulfate example, cross section)

Scale: 1" = 1000' (h), 100' (v)	Date: Nov 1996
Prepared By: GeoTrans, GA	By: GWC

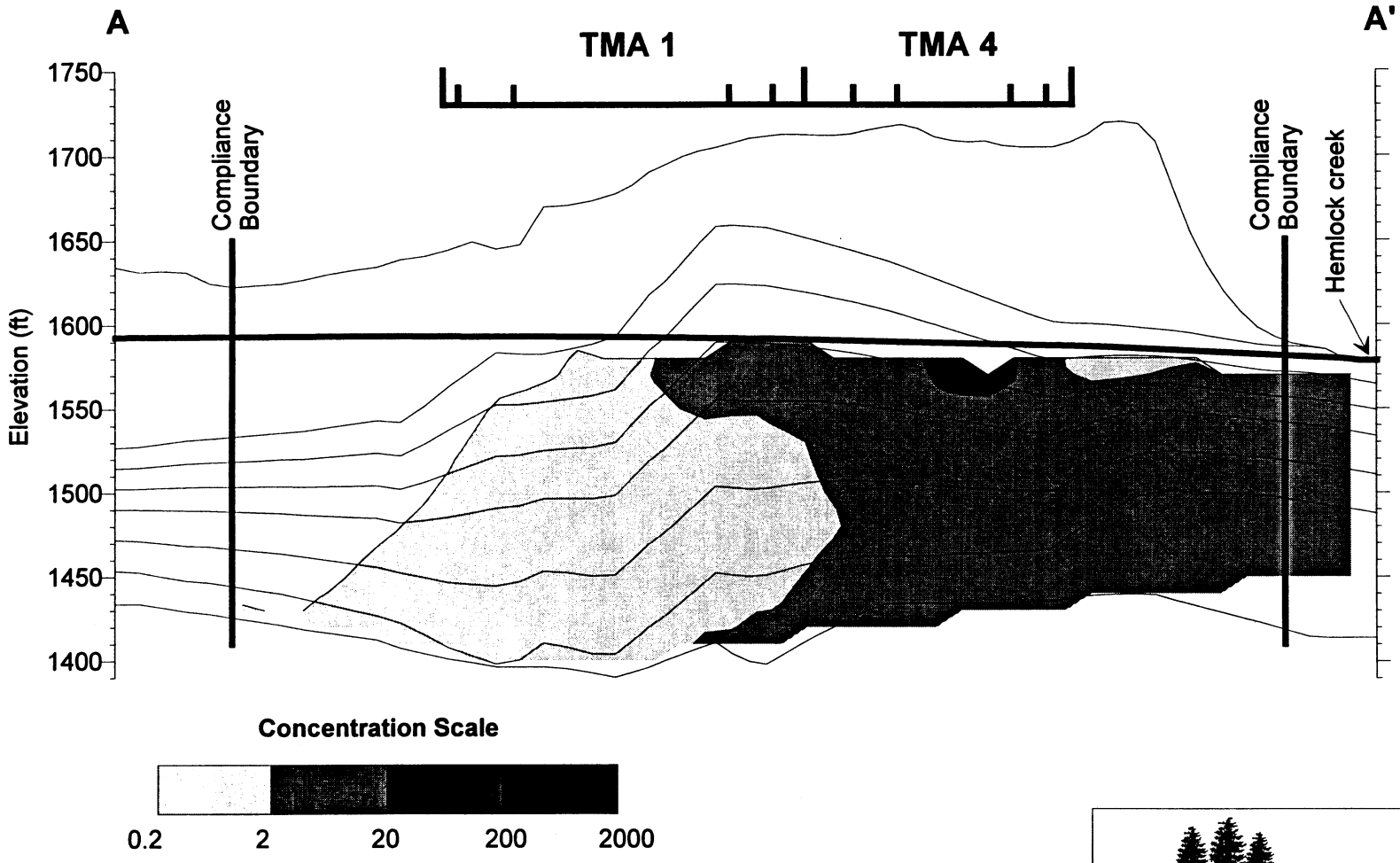

4.2-10-112

GeoTrans, inc.			
REVISED	DATE	BY	DESCRIPTION

CHECKED BY:	PV	DATE: NOV 96
APPROVED BY:	RTH	DATE: NOV 96
APPROVED BY:	PFA	DATE: NOV 96

Crandon Mining Company

Figure 2.72
PWC concentration after 100 years
(sulfate example, cross section)

Scale: 1" = 1000' (h), 100' (v)	Date: Nov 1996
Prepared By: GeoTrans, GA	By: GWC

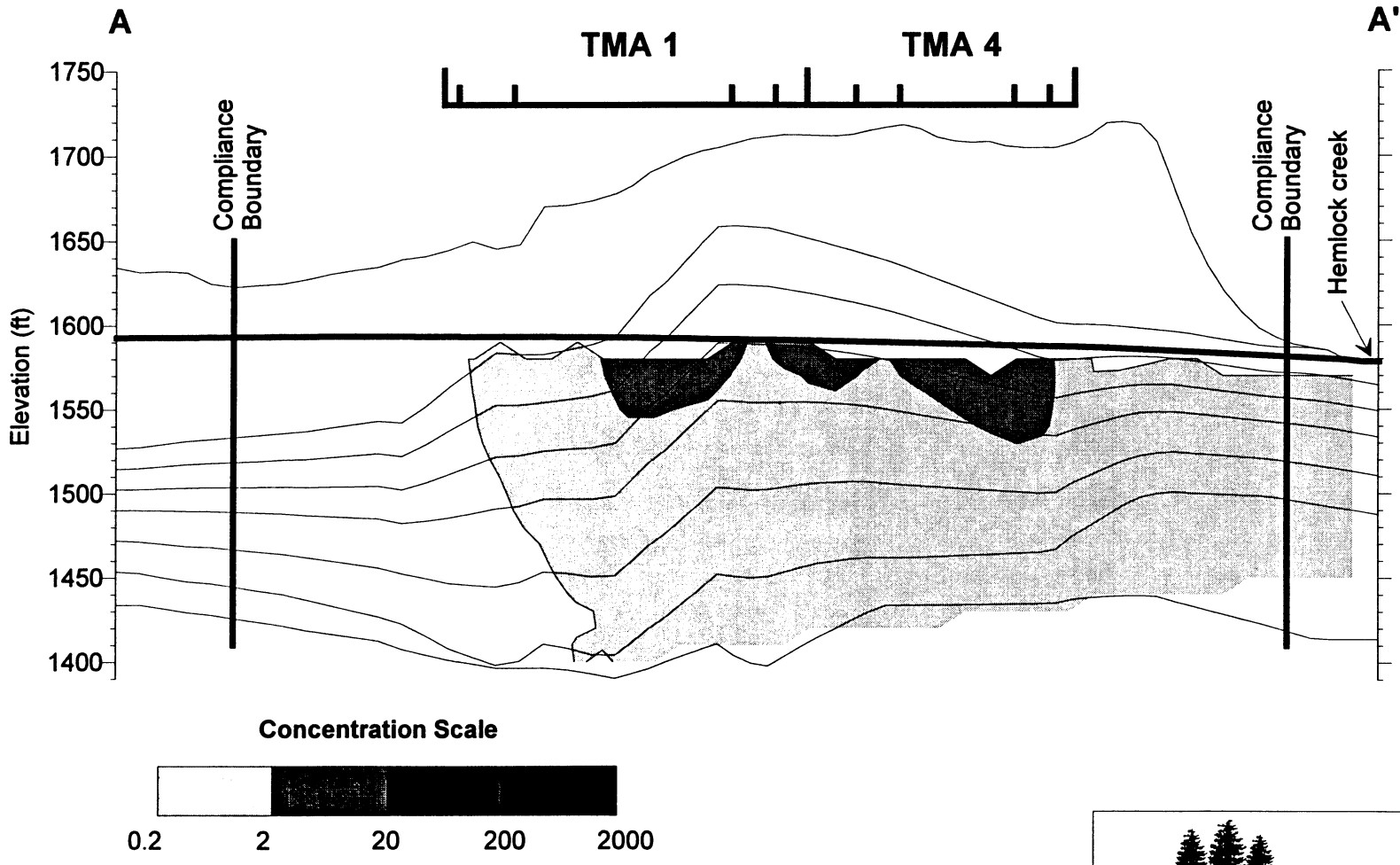

GeoTrans, inc.			
REVISED	DATE	BY	DESCRIPTION

CHECKED BY:	PV	DATE: NOV 96
APPROVED BY:	RTH	DATE: NOV 96
APPROVED BY:	PFA	DATE: NOV 96

Crandon Mining Company

Figure 2.73
PWC concentration after 200 years (sulfate example, cross section)

Scale: 1" = 1000' (h), 100' (v)	Date: Nov 1996
Prepared By: GeoTrans, GA	By: GWC

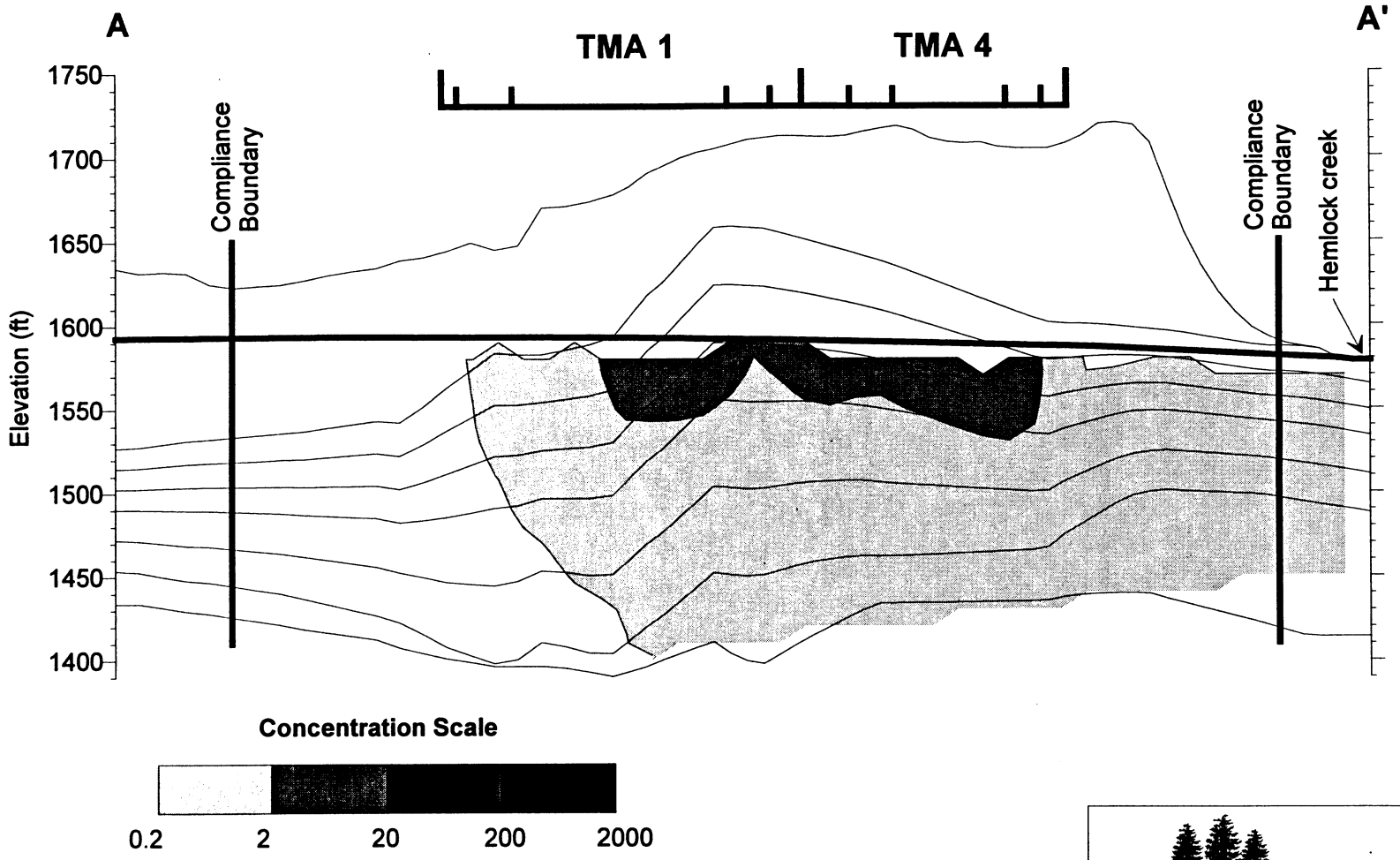

GeoTrans, inc.			
REVISED	DATE	BY	DESCRIPTION

CHECKED BY:	PV	DATE: NOV 96
APPROVED BY:	RTH	DATE: NOV 96
APPROVED BY:	PFA	DATE: NOV 96

Crandon Mining Company

Figure 2.74
PWC concentration after 300 years
(sulfate example, cross section)

Scale: 1" = 1000' (h), 100' (v)	Date: Nov 1996
Prepared By: GeoTrans, GA	By: GWC

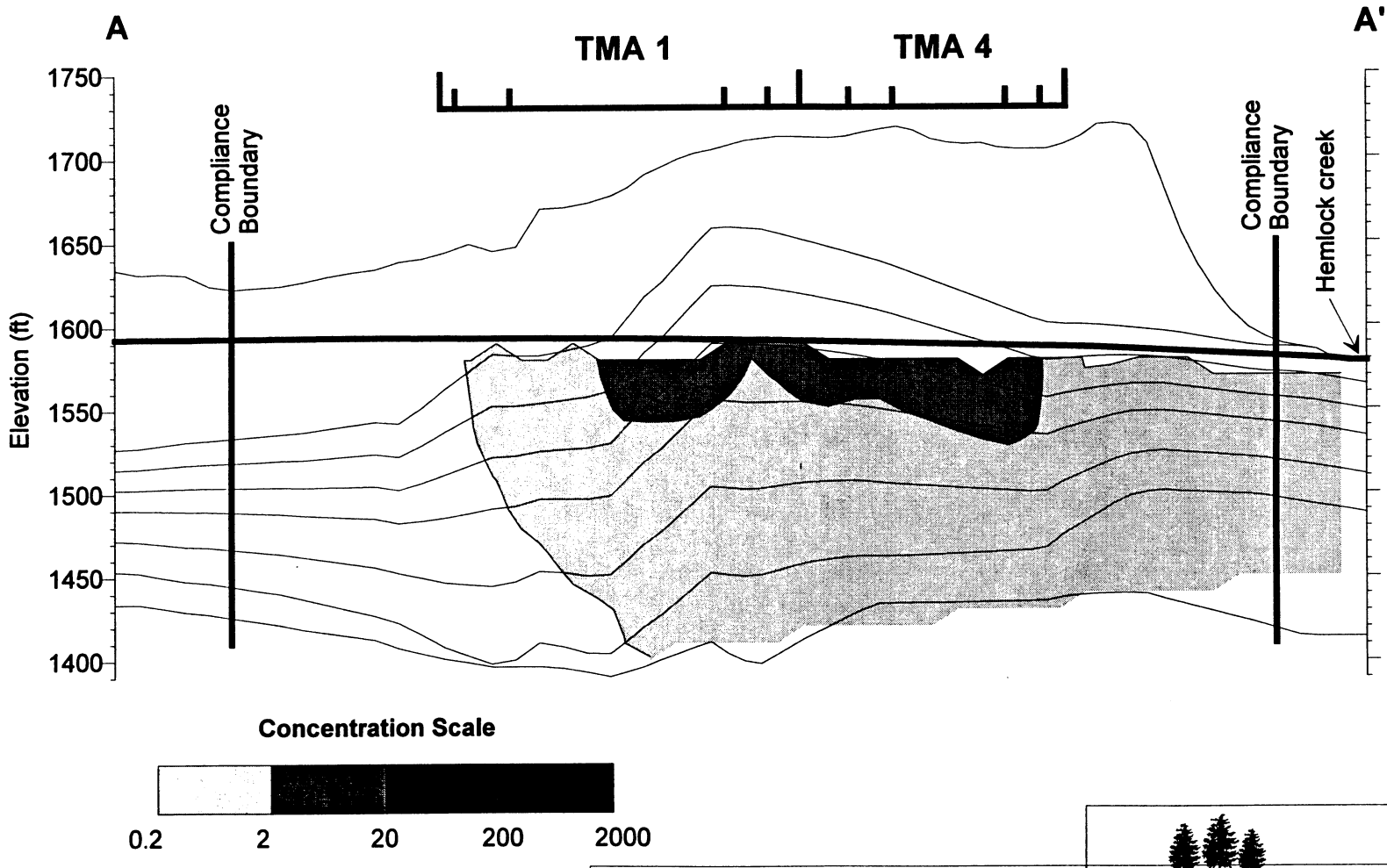

GeoTrans, inc.			
REVISED	DATE	BY	DESCRIPTION

CHECKED BY:	PV	DATE: NOV 96
APPROVED BY:	RTH	DATE: NOV 96
APPROVED BY:	PFA	DATE: NOV 96

Crandon Mining Company

Figure 2.75
PWC concentration after 650 years (sulfate example, cross section)

Scale: 1" = 1000' (h), 100' (v)	Date: Nov 1996
Prepared By: GeoTrans, GA	By: GWC

3 MINE REFLOODING MODEL

3.1 APPROACH

This section describes the analysis used to assess the potential for upward movement of solute from the backfilled mine into the glacial system following mine reflooding. Figure 3.1 shows limited regions of an upward hydraulic gradient from layer 6 to layer 4 in the steady-state regional groundwater flow model during post-mining conditions. These regions of upward gradient outline areas where solutes from the backfilled mine have the potential to travel upward to the glacial system.

The mine reflooding analysis was performed with the calibrated groundwater model and particle tracking using MODPATH (Pollack, 1990). Particle tracking is typically utilized in solute transport codes that use Method of Characteristic techniques (such as MT3D) to assess advective transport in the groundwater system. Particle tracking was selected as a scoping analysis to efficiently analyze advection travel paths and travel times in three dimensions. A solute transport model would only be necessary if the particle tracking indicated that advective flow to a compliance boundary set in the till 1200 feet from the ore body was significant. The particle tracking analysis uses the Best Engineering Judgement (BEJ) flow field with a porosity of 25 percent and a Practical Worst Case (PWC) flow field to assess the potential range of travel times from the mine to the glacial overburden.

The particle tracking assumes that the mine will be backfilled with cemented and uncemented tailings having a bulk hydraulic conductivity of 2.8E-3 ft/day (1.0E-6 cm/s). It is assumed that the Crandon Formation will be replaced with backfill material in layer 6 (moderately weathered bedrock) and layer 7 (low to weakly weathered bedrock). It is assumed that layer 5 will not be backfilled with tailings because it is comprised of strongly weathered bedrock which forms the crown pillar.

Particles were initiated within the mined, backfilled zone in layers 6 and 7 that had more than 10 percent Crandon Formation/backfill. The particles were placed at a density of one particle per model cell. For the BEJ, particles were placed in the middle of the mined zone. For the PWC, particles were placed in the upper 25 percent of the mined zone. The bottom of the mined zone was defined at an elevation of 1200 feet. The top elevation of the mined zone ranges from 1450 feet in the eastern portion of the orebody to 1250 feet in the western portion of the orebody. The particles typically started in a range between the upper portion of layer 7 to the middle of layer 6, though some particles started as high as the top of model layer 6 in the PWC.

3.2 MODEL PREDICTIONS

3.2.1 BEST ENGINEERING JUDGEMENT

The BEJ flow field uses the calibrated model parameters with a porosity of 25 percent. A total of 125 particles are initiated in the center of the mined portion of the ore body. Figure 3.2 shows the particle pathlines at 7,500 years for the BEJ. Dashed lines represent flow in the bedrock while solid lines represent flow in the glacial overburden. Figure 3.2 illustrates that at 7,500 years, two particles originating in the mine extend beyond the compliance boundary. The particles travel laterally and upward. The first particle reaches the compliance boundary after 6,200 years. This particle is within the bedrock when it crosses the compliance boundary. The first particle to enter the till beyond the compliance boundary does so after 7,300 years.

3.2.2 PRACTICAL WORST CASE

The PWC flow field uses the same hydraulic parameters as the PWC model used for flow modeling (described in the groundwater flow modeling report). This PWC model uses higher bedrock conductivities, a higher massive saprolite/till leakance, and higher lake bed conductivities. The PWC particle tracking model further assumes a lower porosity of 0.10 and initiates the particles in the upper 25 percent of the mined area. PWC simulations represent a combination of possible, but unlikely factors, that could cause advective transport in excess of the BEJ case. Figure 3.3 shows the particle pathlines at 600 years for the PWC. At 600 years, two of the particles extend beyond the compliance boundary. The first particle crosses the compliance boundary at 570 years. This particle is within the bedrock when it crosses the compliance boundary. The first particle to enter the till beyond the compliance boundary does so after 593 years.

3.3 SUMMARY OF MINE REFLOODING MODEL RESULTS

The particle tracking results show that advective travel times from the mine to the compliance boundary in the glacial overburden range from 600 years for the PWC to over 6,000 years for the BEJ. These excessively long travel times represent a low potential for solute to travel from the mine to the glacial overburden. Solute transport modeling of the reflooded mine would indicate an even longer time for the concentration to peak at the compliance boundary. The longer time is due to the inclusion of dispersion and mixing which would further reduce solute concentrations.

Solute transport modeling is not deemed necessary due to:

- the very low rate of solute movement from the backfilled mine upward through the crown pillar rock and massive saprolite,
- the long travel time for solute particles from the mined areas to the compliance boundary,
- the conservative nature of particle tracking which does not account for mixing and dispersion, and
- neglect of chemical precipitation and adsorption which would also increase travel times and reduce concentrations of a number of constituents in the reflooded mine water.

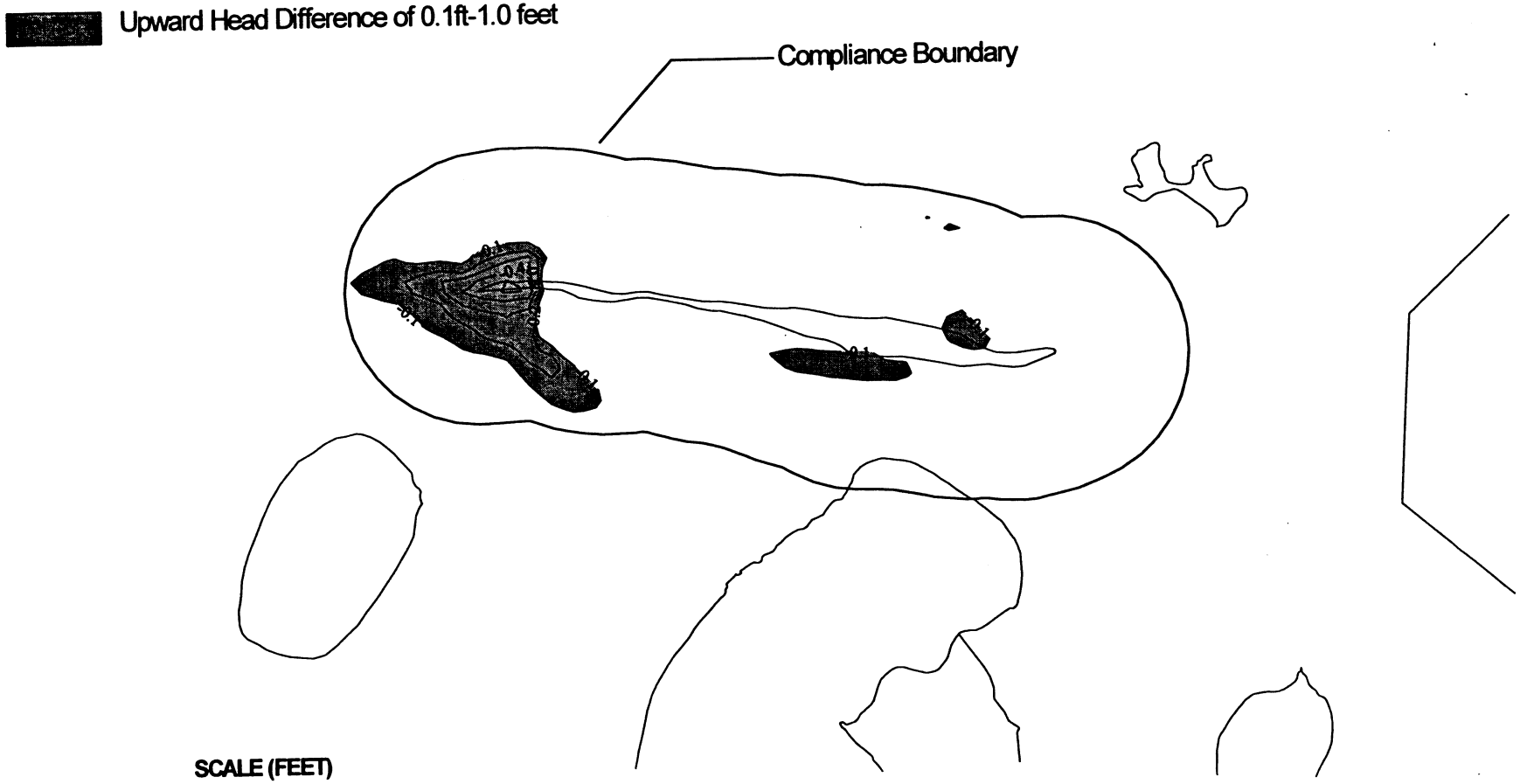

GeoTrans, inc.			
REVISED	DATE	BY	DESCRIPTION

CHECKED BY: PV	DATE: NOV 96
APPROVED BY: RTH	DATE: NOV 96
APPROVED BY: PFA	DATE: NOV 96

Crandon Mining Company

Figure 3.1
Area of upward vertical head difference between layers 4 and 6 in regional model

Scale: None	Date: Nov 96
Prepared by: GeoTrans, Inc.	By: GWC

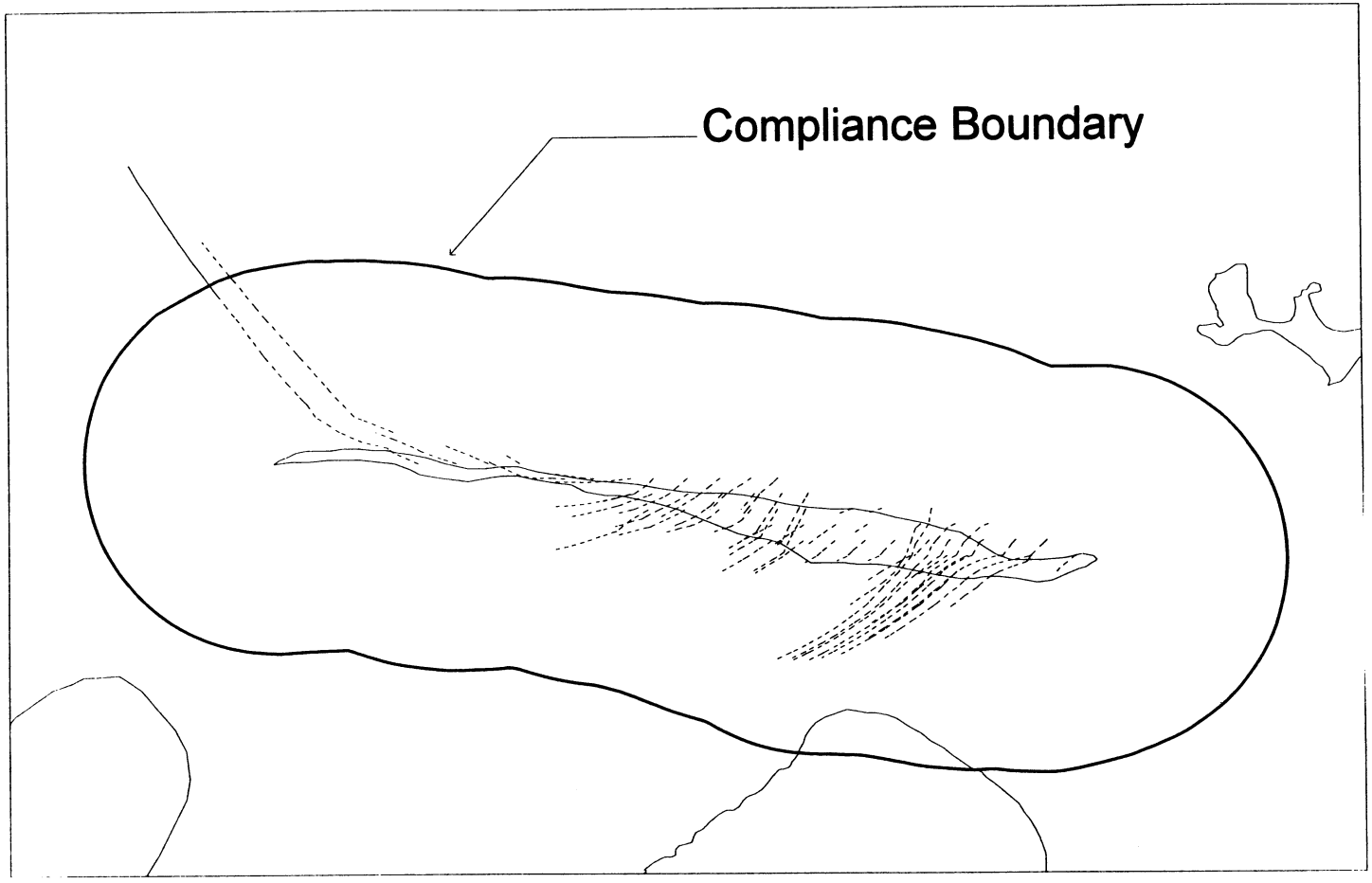

GeoTrans, inc.			
REVISED	DATE	BY	DESCRIPTION

CHECKED BY: PV	DATE: NOV 96
APPROVED BY: RTH	DATE: NOV 96
APPROVED BY: PFA	DATE: NOV 96

Crandon Mining Company

Figure 3.2
Particle pathlines at year 7500
for the BEJ model

Scale: None	Date: Nov 96
Prepared by: GeoTrans, Inc.	By: GWC

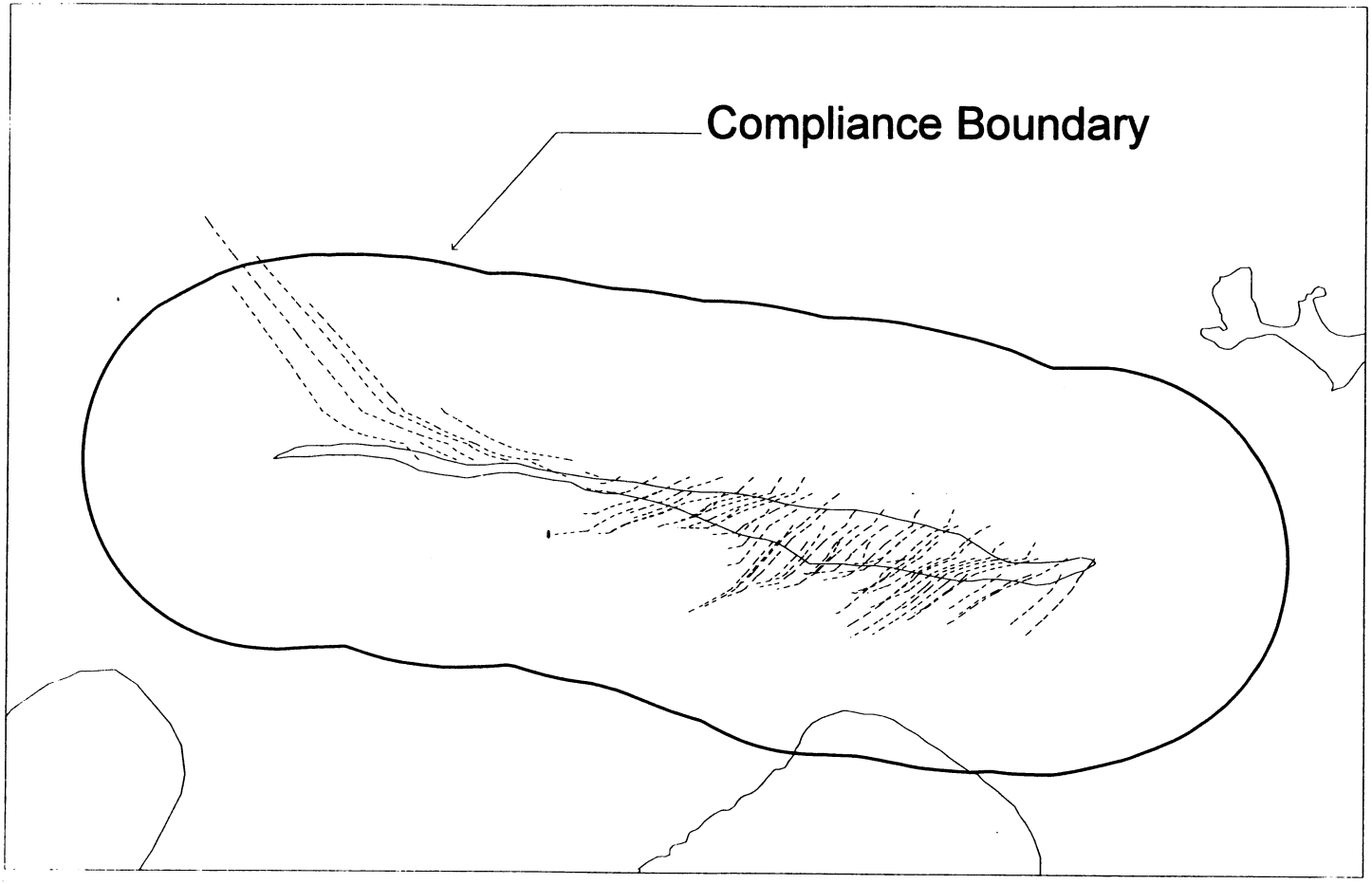

GeoTrans, inc.			
REVISED	DATE	BY	DESCRIPTION
CHECKED BY: PV			DATE: NOV 96
APPROVED BY: RTH			DATE: NOV 96
APPROVED BY: PFA			DATE: NOV 96

Crandon Mining Company

Figure 3.3
Particle pathlines at year 600
for the PWC model

Scale: None	Date: Nov 96
Prepared by: GeoTrans, Inc.	By: GWC

4 REFERENCES

Exxon Minerals Company, 1985. Environmental Impact Report.

Faust, C.R., D.N. Sims, C.P. Spalding, P.F. Andersen, and D.E. Stephenson, 1990. FTWORK: A three-dimensional groundwater flow and solute transport code. Westinghouse Savannah River Company Report WSRC-PR-89-1085.

Foth & Van Dyke, 1994. Notification of intent to collect data and detailed scope of study, Crandon Project, Crandon, Wisconsin, February, 1994.

Foth & Van Dyke, 1995a. Mine Permit Application, Crandon Project, Crandon, Wisconsin.

Foth & Van Dyke, 1995b. Environmental Impact Report, Crandon Project, Crandon, Wisconsin.

Foth & Van Dyke, 1995C. Tailings Management Area Feasibility Report/Plan of Operation. Crandon Project, Crandon, Wisconsin.

Gelhar, L.W., C. Welty, and K.R. Rehfeldt. A critical review of data on field-scale dispersion in aquifers, *Water Resour. Res.*, 28(7), 1955-1974, 1992.

GeoTrans, 1995. Numerical simulation of the effect on groundwater and surface water of the proposed zinc and copper mine near Crandon, Wisconsin (September, 1995).

GeoTrans, 1996. Numerical simulation of the effect on groundwater and surface water of the proposed zinc and copper mine near Crandon, Wisconsin (August, 1996).

McDonald, M.G., A.W. Harbaugh, 1988. A modular three-dimensional finite difference groundwater flow model: *U.S. Geological Survey Techniques of Water-Resources Investigations*, Book 6, Chapter A1.

Pollack, D.W., 1989. Documentation of computer programs to complete and display pathlines using results from the U.S. Geological Survey modular three-dimensional finite difference groundwater model, U.S.G.S. Open File Report 89-381, 81 pp.

Saad, D.A., 1996. Using chlorofluorocarbons to date groundwater and determine hydrologic properties of sediments near the proposed Crandon mine near Crandon, Wisconsin. Summary report, submitted to WDNR June 10, 1996, 16 pp.

Zheng, C., 1996. MT3D^{96}, Modular three-dimensional transport model. Version 2.0.

UPDATE TO:

NUMERICAL SIMULATION OF POTENTIAL SOLUTE TRANSPORT AT THE PROPOSED ZINC AND COPPER MINE NEAR CRANDON, WISCONSIN

April 28, 1998

TABLE OF CONTENTS

LIST OF FIGURES

LIST OF TABLES

1 INTRODUCTION

1.1 PROJECT DESCRIPTION

On February 15, 1994 Crandon Mining Company (CMC) issued to the Wisconsin Department of Natural Resources (WDNR) a Notice of Intent with a Detailed Scope of Study (NOI/SOS) informing the agency of its plan to seek permits and mine a zinc and copper deposit located in Forest County, Wisconsin, approximately five miles south of the City of Crandon (Foth & Van Dyke, 1994). The location of the Crandon ore body is shown in Figure 1.1. The ore body is long and tabular with an approximate width of 100 feet, north-south, and a strike length of 4900 feet, east-west. Based on the results of drilling, the mineable ore body extends to an approximate depth of 2200 feet.

The operating plan calls for mining the deposit via underground mining methods. This will involve both intercepting groundwater and removing it prior to entry into areas being mined and collecting and treating groundwater that bypasses the intercept system. Ore from the deposit will be physically concentrated on-site prior to shipment for further processing. Tailings from the processed ore will be used to backfill the mine workings, or will be pumped to an engineered tailings management area constructed with a composite base liner, a leachate collection system, and composite cap. The NOI/SOS described in detail the environmental studies that were conducted as part of the permitting process. An extensive description of the project is included in the Mine Permit Application (Foth & Van Dyke, 1995a).

As part of the project studies outlined in the NOI/SOS, a broad spectrum of environmental issues were studied, including archaeology, biology, blasting, geology and soils, groundwater, noise, topography, surface water, tailings management, waste characterization, water management, wetlands, etc. This report describes in detail the solute transport modeling that was performed as part of the environmental studies for the permit process. The solute transport model is a tool that was used to assess potential groundwater quality impacts of tailings management and mine closure activities. A separate groundwater flow modeling report provides estimates of mine water inflow and quantifies potential impacts of the mine water inflow on the overlying glacial aquifer and the subsequent impact on the lakes and streams.

1.2 OBJECTIVES OF STUDY

Solute transport modeling was performed to meet two primary objectives:

- to evaluate Tailings Management Area (TMA) compliance with groundwater standards,
- to evaluate groundwater quality in the glacial aquifer following mine reflooding.

Results from this solute transport modeling study are incorporated into related environmental studies. Results are also used in the impact section of the project's Environmental Impact Report (EIR) to evaluate compliance with groundwater standards and regulations.

This update builds on the analysis reported in the original report of November 20, 1996 (HSI GeoTrans, 1996a). At the request of the regulators, some minor changes have been made to model construction and some new sensitivity simulations have been conducted. However, the sensitivity results in the original report are still valid. As such, these sensitivities are not repeated in this update.

1.3 METHOD OF INVESTIGATION

The objectives described in Section 1.2 are accomplished through the development of a numerical model that is capable of simulating the transport of dissolved constituents in the groundwater and from evaluation of flow directions during and following mine operations. This type of an analysis integrates available data and allows a hydrogeologic evaluation with extensive physical complexities (e.g. heterogeneity and other non-uniform parameter distributions). Predictions of future hydrologic changes on the system can be made, as well as an assessment of the sensitivity of various parameters on model results. The TMA transport model differs from the previously documented flow model in that it computes concentrations at points within the model, instead of the hydraulic heads that were computed by the flow model.

The generalized modeling process begins with development of a conceptual hydrogeological model. The conceptual model includes definition of hydrostratigraphic units, boundary conditions, sources, and sinks. The conceptual model is transformed into a mathematical model, consisting of governing groundwater flow and solute transport equations, which is solved by a computer program. The numerical groundwater flow model is calibrated to observed conditions. Model calibration is an iterative process of adjusting and revising model features and/or parameters, within hydrogeological reason, in order to test the conceptual understanding of the system and to match modeled results to field measured values. After the model is calibrated, predictive simulations are performed.

The solute transport modeling for this study uses the results of a regional groundwater flow model as its basis for representing the hydrogeological system. Detailed descriptions of the conceptual model, model construction, calibration, sensitivity analysis, and predictions are contained in HSI GeoTrans (1998a) and HSI

GeoTrans (1998b). The three-dimensional solute transport modeling documented in this report expands upon a two-dimensional cross-sectional analysis that was documented in an earlier version of the groundwater modeling report (HSI GeoTrans, 1995) and updates a three-dimensional solute transport model documented in HSI GeoTrans (1996a). The earlier modeling report was completed in September 1995 and submitted to the WDNR, U.S. Army Corps of Engineers (COE), and other interested parties for review. That study and report (HSI GeoTrans, 1995) were the subject of several meetings with the regulators. The discussions from those meetings resulted in an expanded modeling effort. The primary change for the solute transport analysis was to extend the model to three dimensions. The three-dimensional model (HSI GeoTrans, 1996a) was based on a groundwater flow model (HSI GeoTrans, 1996b). Both of these models have also gone through a thorough review process by the regulators. Based on comments from the regulators, revisions to the groundwater flow model (HSI GeoTrans, 1998a and HSI GeoTrans, 1998b), and design changes to the TMA, the solute transport model has again been updated. The most significant changes to the solute transport model include:

- incorporation of all changes from the updated flow model (layering, hydraulic parameters, outwash pinchout zone) that affect the hydrogeologic representation in the vicinity of the TMA,
- lowering of effective porosity based on the flow model calibration,
- inclusion of the reclaim pond as a source of solute infiltration,
- increase in model size to accommodate the reclaim ponds, and
- decreased infiltration rates due to re-design of the liner system beneath the TMA.

The results of this most recent update are documented in this report. Because this report is an update, some elements of the prior report (HSI GeoTrans, 1996a) are not repeated. The most significant element, as discussed in Section 2.4.3, is the documentation of seven sensitivity simulations that are still pertinent.

Construction of the TMA solute transport model consisted of focusing the model domain used in the regional flow model on the vicinity of the TMA and it's proposed compliance boundary and increasing the resolution of computational points within that area. The stratigraphic layering and hydraulic parameters used in the solute transport model are therefore nearly identical to those used for the TMA area of the regional flow model. The construction of the solute transport model is discussed in detail in Section 2.1.

The solute transport model uses parameters and boundary conditions derived from the calibrated regional groundwater flow model. In this sense, the groundwater flow aspects of the solute transport model are calibrated. Comparison of the solute transport model flow field to the groundwater model flow field as well as to observed field data were made to verify calibration. The results of this comparison is provided in Section 2.2. Calibration of solute transport properties is not possible.

Groundwater quality in the glacial aquifer following mine reflooding was assessed by analyzing flow paths and velocities of particles originating in the mined ore body. This advective solute transport model used the calibrated regional groundwater flow model directly. Therefore, additional model construction and calibration were not necessary to evaluate groundwater quality in the glacial aquifer following mine reflooding.

Predictive simulations of the potential groundwater quality impacts of tailings management and mine closure activities were also made. The predictive simulations with parameters that were based on model calibration and best available data are referred to as the Best Engineering Judgement for Transport (BEJT) simulations. Confidence in the ability of the model to represent the natural system was obtained from the multiple calibrations and sensitivity analysis performed with the groundwater flow model. In addition, a series of sensitivity simulations were performed on the solute transport model predictions. Sensitivity analysis involved running the models with a range of parameter values in order to determine which parameters are most influential in the model and system. These sensitivity simulations formed the basis for the Practical Worst Case for Transport (PWCT) simulations. The PWCT simulations represents a combination of possible, but unlikely factors that could cause impacts to be in excess of those predicted by the BEJT simulation.

1.4 CONCEPTUAL MODEL

Separate conceptual models exist for each of the two objectives of the solute transport modeling study. The first deals with leakage of dissolved constituents from the engineered TMA facility. The second deals with water flowing upwards out of the ore body into the glacial aquifer system following mine closure.

The simulated mechanisms for solute transport from the TMA into the glacial system include movement of water through the lined facility during operation of each TMA basin, movement of water through the covered and lined facility following closure of each TMA basin, and postulated degradation of the Flexible Membrane Liner (FML) at some time in the future. These hypothetical events are assumed to be sequential. The first two events during which leakage is considered, operation and closure, are of known duration. Degradation of the FML, if it occurs, would happen at an unknown time in the future. A reasonable FML life was therefore assumed.

The conceptual model of leakage from the TMA involves water entering the TMA basins either by direct input during operation or through the composite liner (including FML and geosynthetic clay layer) following closure. Tailings water is assumed to bypass the leachate collection system and percolate through the composite liner (FML and geosynthetic clay layer). Percolation through the composite liner was based on HELP model calculations completed by Foth and Van Dyke as part of the development of the TMA Feasibility Report/Plan of Operation. These data are summarized in Appendix A. These calculations consider the amount of leakage that would result from a scenario involving an assumed number of holes in the FML and are standard for landfill design and assessment. The leakage through the FML is assumed to enter the unsaturated zone and travel vertically to the glacial aquifer system. The transit time in the unsaturated zone is likely on the order of many years or decades (EMC, 1985). For purposes of this analysis, two events were considered, entry of solute to the groundwater system on the first day of operation as the BEJ case and entry of solute to the groundwater system following cessation of mining activities as a sensitivity simulation. Once solute enters the groundwater system, it is assumed to be advected along groundwater flow paths toward groundwater discharge points. Along the route to discharge points, the solute mixes with resident groundwater and is dispersed through travel along tortuous paths in the saturated groundwater system. No geochemical reactions, such as adsorption or decay, are assumed to occur. Disregarding geochemical reactions is conservative with respect to travel time (adsorption) and with respect to concentrations at the compliance boundary (decay). As will be discussed in Nicolet Minerals Company's (NMC, formerly CMC) final Waste Characterization Report, concentrations within the source area are assumed to vary through time.

The conceptual model of flow through the mine workings is only possible after the mine has been reflooded following cessation of mining activities. Flow through the upper part of the mined workings into the glacial system is postulated to occur because there is a slight upward head gradient on the western end of the ore body under current conditions. The possibility therefore exists for flow passing through the upper mine workings, coming in contact with backfilled tailings and exiting the western part of the ore body. The analysis that was conducted assessed groundwater flowpaths resulting from post-mining conditions. This scenario involved assessment of flow through the mine, once the mined area had been backfilled with tailings.

1.5 NUMERICAL MODELING APPROACH

Waste characterization studies documented in the Environmental Impact Report (Foth & Van Dyke, 1995b) indicate that source term concentration of some constituents will be in excess of applicable groundwater standards if these concentrations were considered at a compliance boundary. However, scoping calculations documented in the TMA Feasibility Report (Foth & Van Dyke, 1995c and subsequent addenda) indicate that concentrations will be reduced at least ten-fold between the source term

and the proposed compliance boundary. Although the ten-fold reduction in concentration is sufficient for most constituents to comply with groundwater standards, a more sophisticated approach of computing concentrations at the compliance boundary and at points in between was desired. Numerical modeling was selected as the tool to address such complexities as a three-dimensional flow system, changing flow directions due to cessation of mining operations, a changing source term, and the need to efficiently assess parameter sensitivity and PWCT situations.

Two separate numerical analyses, one for the TMA leak scenario and one for the mine reflooding scenario were made. For the TMA leak scenario, the entire history of solute transport was simulated, from entry of solute to the groundwater flow system until occurrence of a steady-state concentration at the proposed compliance boundary. The model simulates flow in the saturated zone only, from point of entry to the glacial system to the proposed compliance boundary or nearby hydrologic boundary. Relative concentrations are used, such that concentrations at the proposed compliance boundary are expressed as a fraction of the input term. A superposition approach is used to account for time-variant changes in source concentrations. The advantage that this method has over using constituent specific concentrations is that a single simulation can be used for a variety of constituents. Actual concentrations can be calculated by multiplying the source concentration by the relative concentration computed by the model. A demonstration of the superposition and relative concentration method is provided in Section 2.3.

A three-dimensional model was used to evaluate groundwater flow in the vicinity of the TMA. The model uses a greater resolution of nodes, both vertically and horizontally, than the regional groundwater flow model. The model uses parameters and boundary conditions derived from the regional groundwater flow model. Solute transport properties were obtained from the technical literature. Determination of site specific solute transport properties such as dispersivity and retardation by field methods was not considered necessary or practical. Instead of conducting field tests, reasonable ranges of solute transport parameters were tested with the model in the sensitivity analysis. Reasonable ranges for dispersivity were based on Gelhar, et al (1992). Retardation was conservatively assumed to not occur. The possible ranges in concentrations and travel time were evaluated with the model and discussed as the PWCT.

The regional groundwater flow model was used to simulate the potential for upward flow, out of the ore body and into the glacial system, following mine closure and reflooding. This flowpath currently occurs and is the result of hydraulic conductivity differences between the ore body, bedrock, and glacial system. The model evaluated future flowpaths resulting from decreased hydraulic conductivities in the ore body caused by backfilling with coarse tailings. The model was based on site-specific conditions and how they would be altered as a part of mine backfilling operations.

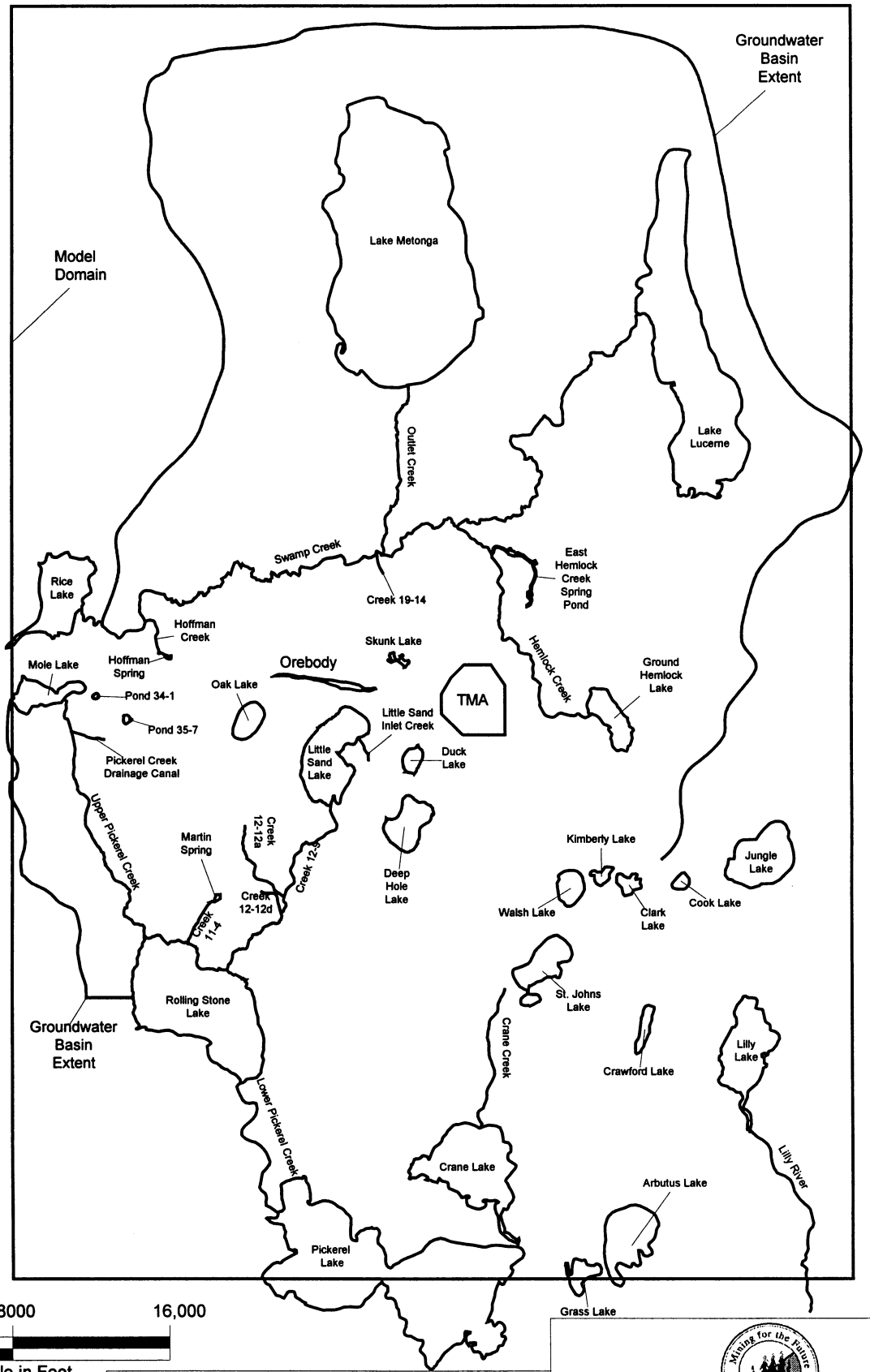

HSI GEOTRANS			
REVISED	DATE	BY	DESCRIPTION
CHECKED BY: PAW		DATE: April 1998	
APPROVED BY: PFA		DATE: April 1998	
APPROVED BY:		DATE:	

Nicolet Minerals COMPANY

Figure 1.1
Location Map

Scale: 1 in. = 8000 ft. | Date: April 1998

Prepared By: HSI GeoTrans | By: GWC

\Crandon\TmaMod3\G...\LocMap.wor

2 TAILINGS MANAGEMENT AREA MODEL

Groundwater transport of solutes originating at the Tailings Management Area (TMA) was simulated with a numerical model covering an area much smaller than that of the regional groundwater flow model (HSI GeoTrans, 1998a) (Figure 2.1). The TMA sub-model was built from the same data set used to construct the regional model, as explained in Section 2.1. Section 2.2 demonstrates that the sub-model produces results that are consistent with those of the regional model.

Full details of the TMA design appear in a separate report (Foth & Van Dyke, 1995c and subsequent adenda). As shown in Figure 2.2, the TMA will consist of cells TMA 1 through TMA 4, each with three regions: base, lower sideslope with drainage, and upper sideslope with drainage. The TMA cells will be operated on a phased schedule, with TMA 1 receiving the first mine tailings, TMA 2 beginning operations about seven years later, and so on. The exfiltration rate from the TMA to the groundwater will be much smaller than the natural precipitation recharge rate because of the engineered liner and drainage system (Foth & Van Dyke, 1995c and subsequent addenda). Within each cell, the exfiltration rate will vary depending on the region (base, lower sideslope, or upper sideslope). Modeled variations in the TMA exfiltration rate are explained in detail in Section 2.3.

The mine tailings in the TMA may contain many constituents to be monitored (e.g. sulfate, iron, manganese, etc.). The concentration of these constituents in the pore water of the tailings will depend on many factors, including the availability of air in the pores. A characterization of the pore water chemistry is currently being conducted as a separate study. To account for tailings concentrations that vary from constituent to constituent and that vary over the life of the TMA, this report presents a generalized approach to transport modeling that involves unit-response curves and superposition (Section 2.3.2). With this method, the results presented here will be applicable to a variety of constituents, even accounting for source concentration changes over time as the tailings chemistry changes. Thus, results from the ongoing tailings characterization study can be combined with the results here to evaluate regulatory compliance for a variety of constituents.

Uncertainty in model predictions is addressed with an approach analogous to the one used in the regional groundwater modeling report (HSI GeoTrans, 1996b) and subsequent updates and clarifications (HSI GeoTrans, 1998a and HSI GeoTrans, 1998b). First, reasonable flow and transport parameters were used to make Best Engineering Judgement for Transport (BEJT) predictions. Then, various sensitivity simulations were conducted to determine the sensitivity of the predictions to variations in the chosen parameters. Finally, a combination of conservative and unlikely

parameters were used to make Practical Worst Case for Transport (PWCT) predictions. In the regional groundwater flow model, the quantities of concern were mine inflow rate, lake level changes, streamflow changes, and the magnitude and extent of groundwater drawdown. For the TMA sub-model, the primary quantity of concern is the concentration of constituents at the proposed compliance boundary located 1200 feet from the edge of the TMA facility. Model predictions are presented in Section 2.4.

2.1 NUMERICAL MODEL DESIGN

This section describes the design and construction of the solute transport model. The computer code selected for use is described, along with the associated input data. Input data include grid location and spacing, boundary conditions, and aquifer parameters.

2.1.1 CODE SELECTION

MT3D^{96} (Zheng, 1996) was selected in consultation with WDNR for three-dimensional modeling of solute transport at the Crandon site. MT3D^{96} was originally developed as MT3D for the USEPA. MT3D^{96} is the first major upgrade of the code since 1992. It is commercially available through organizations such as the International Ground Water Modeling Center (IGWMC) and Scientific Software, Inc.

MT3D^{96} is a three-dimensional model for simulating solute transport processes in fully saturated porous media. The transport model is structured such that it can be used in conjunction with any block-centered finite-difference flow model such as the MODFLOW (McDonald and Harbaugh, 1988) model. MODFLOW was the groundwater flow model used for the regional model (HSI GeoTrans, 1998a). MT3D^{96} can be used to simulate changes in concentration of single species soluble constituents in groundwater considering advection, dispersion, and some simple chemical reactions. The chemical reactions include equilibrium controlled linear or non-linear adsorption and first-order irreversible decay or biodegradation.

Following solution of the flow field by MODFLOW, or another finite-difference code, MT3D^{96} uses one of four solution techniques to solve for concentrations. Three of the solution techniques, Method of Characteristics, Modified Method of Characteristics, and Hybrid Method of Characteristics, are particle based. An explicit finite-difference solution option is also offered. The finite difference solution was selected for application at the Crandon site because it is significantly more efficient than the particle based methods.

MT3D^{96} was developed for the USEPA for solute transport applications. It is generally accepted by state and federal regulators as a tool for solving solute transport problems. MT3D^{96} was used for verification of the cross-sectional solute transport modeling performed using FTWORK (Faust, et al, 1989) in the original Crandon

Project groundwater modeling report (HSI GeoTrans, 1995). MT3D[96] was selected in favor of FTWORK for this application because the conversion of data sets to MT3D[96] was more expeditious than to FTWORK.

2.1.2 GRID DESIGN AND DISCRETIZATION

The TMA sub-model covers a 7600-foot by 7300-foot square rotated 35 degrees west of north (Figure 2.1). The model extends a minimum of 400 feet past the proposed 1200-foot compliance boundary on the northwest, southwest, and southeast sides, and to Hemlock Creek on the northeast side (Figure 2.3). The model grid consists of 76 rows and 73 columns, with uniform 100-foot grid spacing in either direction. The orientation was chosen such that model rows approximately line up with the flow direction from the TMA to Hemlock Creek, increasing numerical accuracy. Since Hemlock Creek is a natural flow boundary, all cells on the far side of the stream (to the east and north of the stream) are inactive in the model.

Vertically, the glacial overburden in the subsurface is divided into seven layers based on stratigraphic changes interpreted from the hydrogeologic cross sections documented in HSI GeoTrans (1998a). These cross sections were based on observed data from geological drilling programs. The method for vertical discretization is the same as that used for the regional groundwater flow model, and is explained in that report (HSI GeoTrans, 1998a). However, regional model layers 2 and 3, which primarily represent the outwash strata, are sub-divided into 5 layers for the TMA sub-model to increase the resolution of flow and transport in these higher-conductivity layers. The conversion from regional model layering to TMA sub-model layering is depicted in Figure 2.4. Regional model layer 1 (primarily Late Wisconsinan Till) is the same as TMA sub-model layer 1. Regional model layer 2 is evenly divided into three parts, becoming TMA sub-model layers 2, 3 and 4. Similarly, regional model layer 3 is evenly divided into two parts, becoming TMA sub-model layers 5 and 6. Regional model layer 4 (primarily Pre- to Early- Wisconsinan Till and massive saprolite) is the same as TMA sub-model layer 7. Detailed cross-sections showing model layering superimposed on the hydrostratigraphy are shown in Figures 2.5 through 2.10. These figures may be compared to those shown in the regional groundwater flow modeling report (HSI GeoTrans, 1998a) as Figures 2.24, 2.25, 2.26, 2.28, 2.30, and 2.33. Bedrock layers 5, 6, and 7 of the regional flow model are not represented in the TMA sub-model because flow across the bedrock/glacial interface is very limited away from the mine. Note that it is conservative for concentrations computed at the proposed compliance boundary to assume that the solute plume does not spread vertically beyond the limits of the glacial overburden. The sensitivity of predictions to flow across the bedrock/glacial interface is addressed in Section 2.4.3. A contour map of topography is shown in Figure 2.11. The bottom elevations for all seven layers of the TMA sub-model are shown in Figures 2.12 through 2.18.

In order to calculate hydraulic conductivity in the model, the makeup of each model cell was calculated in terms of fractional content of each of the geological units present. For this purpose, only the saturated portion of the layers are considered (see HSI GeoTrans, 1998a for a more detailed description of the method). The water table elevation used to determine saturated thickness was derived from measurements made in 1984, and is shown in Figure 2.19. The saturated thicknesses of all seven model layers are shown in Figures 2.20 through 2.26. Note that zero-thickness cells, which represent areas above the water table, are inactive in the model.

2.1.3 Model Parameters and Boundary Conditions

The hydraulic conductivities for the geologic units (Table 2.1) were taken from the calibrated, BEJ regional groundwater model. As in the regional model, there are two zones of hydraulic conductivity for the coarse outwash (Figure 2.27). This zonation is based primarily on a conceptual model of the glacial depositional process developed by Dunning and Johnson (1997). A number of factors including grain size analyses, slug test results, potentiometry, model calibration, and chloroflourocarbon (CFC) travel time analysis conducted by the USGS (Saad, 1996) support the inclusion of this zone. The conductivity zonation is discussed in further detail in the regional groundwater flow report (GeoTrans, 1998a). The hydraulic conductivity at each cell is calculated from the conductivity values for each geologic material (Table 2.1) and each cell's fractional content. The cell-wide hydraulic conductivities are computed with the ACALC program, also described in the regional groundwater flow report (GeoTrans, 1998a).

Figure 2.28 through 2.34 show the proportions of each material (late Wiconsinan till, coarse outwash, fine outwash, pre- to early Wisconsinan Till/massive saprolite) present in each area of model layer. Note that these properties were determined for each model layer following subdivision of the layers based on elevation. In this manner, the solute transport model provides increased resolution over the regional groundwater of vertical hydraulic conductivity variations.

Five types of flow boundaries are used to model the area: 1) no-flow at the base of the model and on the far side of Hemlock Creek, 2) head-dependent flux to simulate fixed heads along the northwestern, southwestern, and southeastern edges of the model grid, 3) a head-dependent flux or river-type boundary for Hemlock Creek, 4) head dependent or river-type boundaries for the seepage wetlands in the eastern part of the model, and 5) specified flux to represent areal recharge derived from precipitation and infiltration from engineered facilities. The cell locations for fixed head and river-type boundaries are shown in Figure 2.35.

The no-flow boundary at the base of the model is valid because flow across the bedrock/glacial interface is very limited in this area. It was observed during model calibration (discussed in Section 2.4.3 of HSI GeoTrans, 1996a) that without mining,

the modeled groundwater head in the lowest glacial layer changes little when the bedrock is removed. When the mine is in operation, flow becomes less downward when the bedrock is removed, which would tend to limit spreading of the plume and raise the maximum concentration at the proposed compliance boundary. Therefore, not including the bedrock in the solute transport model is conservative with regard to computed concentrations at the proposed compliance boundary because the computed concentrations are higher than they would be had the bedrock been included. The appropriateness of this boundary was assessed in the prior solute transport report (HSI GeoTrans, 1996a) with a sensitivity simulation where flow and solute transport across the glacial bedrock interface was represented by a head-dependent flux boundary.

Since Hemlock Creek is a receiving stream with groundwater from both sides contributing to flow, it is a natural groundwater divide for the glacial aquifer. This is also evident from plots of modeled head in layers 1 through 4 of the regional flow model (HSI GeoTrans, 1998a, Figures 3.3 through 3.6, 4.1, 4.2, 5.5, and 5.6). Thus all cells to the northeast of Hemlock Creek were set inactive, effectively creating a no-flow boundary on the far side of the creek. This conceptualization means that all water flowing to the northeast from the TMA must exit through Hemlock Creek.

There are no natural groundwater boundaries along the northwest, southwest and southeast edges of the model. Therefore, heads along these boundaries were specified in the TMA sub-model. They were computed directly from the regional flow model using three-dimensional linear interpolation (from regional model cell-center-points to sub-model cell-center-points). The MODFLOW General-Head-Boundary (GHB) package was used to specify heads at these locations. To ensure that the head values in the cells along these edges is equal to the specified boundary head, the conductance used for each GHB cell is set to a sufficiently high value (1.0E6 ft^2/day). Using the GHB package for specified heads instead of setting the cells to constant-head in the MODFLOW Basic package makes it easy to change the value of the boundary heads from stress period to stress period during the simulation. The boundary heads change in response to cessation of mining and when TMA construction reduces areal recharge. Specified head boundaries were applied at all seven layers along the model edges (except layer 1 cells where the saturated thickness is zero). The GHB cells are placed at a minimum of 400 feet (over twice the aquifer thickness) from the compliance boundary so that the boundary conditions will not affect computed concentrations at the point of interest.

Hemlock Creek was modeled with the MODFLOW River package using parameters identical to those used in the regional flow model (Table 2.1). The stage in the stream was taken from topographic maps similar to the one shown in Figure 2.11, and varies from 1578.63 feet-msl in row 72 to 1578.20 feet-msl in row 4. The conductance at each river cell was calculated as the length of the creek (which varies from cell to cell) times the width of the creek (14.0 feet) times the hydraulic conductivity of the creekbed (1.0 ft/day, which is 3.5E-4 cm/sec) divided by the

thickness of the creekbed (1.0 foot). The river bottom elevation was set 2.0 feet below the river stage (representing a 1.0-foot water depth and a 1.0-foot thick creekbed). The river boundary that was used to represent Hemlock Creek was applied to the uppermost active layer (either layer 1 or layer 2). Application to only the uppermost layer is consistent with a conceptual model of a shallow, partially penetrating stream.

The small seepage wetlands adjacent to the streams were modeled with the MODFLOW River package using parameters identical to those used in the regional flow model (Table 2.1). The elevations and conductances were derived with a sediment hydraulic conductivity of 0.03 ft/day (1.06E-5 cm/sec) and a sediment thickness of 5.0 feet. The bottoms of the wetland sediments were set 7.0 feet below the wetland elevation (representing a 2.0-foot water depth and a 5.0-foot sediment thickness). Seepage wetland boundaries were applied to the uppermost active layer (either layer 1 or layer 2).

The discharge wetlands around Hemlock Creek were not modeled in this application in order to be consistent with the methodology used in the regional groundwater flow model (HSI GeoTrans, 1998a). This representation causes the same amount of flow that in reality discharges to the wetlands and creek to be diverted only to the creek in the model. Recharge was adjusted in the discharge area to account for a slight surplus in annual precipitation over evaporation. Recharge zones are described below in more detail.

Areal recharge is applied to the uppermost active layer using the MODFLOW Recharge package. The default recharge rate applied over most of the model is 8 in/yr (1.827E-3 ft/day). Recharge in the amount of 3 in/yr was specified in the area representing the discharge wetlands. This conceptual model causes groundwater discharge to be accounted for at the creeks, but recognizes that in northern Wisconsin, there is a slight surplus of precipitation over evaporation, which will be part of the near-stream water budget. The recharge rate was set to zero at Hemlock Creek and the seepage wetlands. Recharge to wetlands was initiated based on a 50 percent or greater coverage of the wetland in a cell. Recharge zones were identified for modeling the TMA exfiltration over time in the transport simulations. These zones, shown in Figure 2.36, are model representations of the four TMA cells, each with three regions. Additional zones represent the six runoff basins adjacent to the TMA and the reclaim pond. The TMA, reclaim basin, and runoff-basin zones were used in predictive simulations to model exfiltration rates that change over time. Further details on exfiltration rates are provided in Section 2.3.1.

Two additional parameters, effective porosity and dispersivity, are required when simulating solute transport. Effective porosity represents the portion of the soil/water medium that is available for transport, or the ratio of interconnected pore space to total volume of geologic material. As described in the regional flow model report (HSI GeoTrans, 1998a, Section 3.2), a specific yield of 0.10 was obtained for the

glacial sediments by model calibration. Because the specific yield closely approximates the effective porosity, the effective porosity was set at 0.10 for all sediments. This value is conservatively lower than the range of 0.15 to 0.35 originally established in Section 3.2.2.6 of HSI GeoTrans (1996b). Dispersivity is a length scale for spreading of solute. The solute disperses primarily because of the random, tortuous pathways of varying lengths and varying directions that are available for solute transport. Dispersivity is not a measurable quantity, but in many applications, the longitudinal dispersivity (that is, dispersivity in the direction of flow) is roughly one-tenth to one-hundredth of the model length scale (Gelhar, et al, 1992). It is often assumed that the transverse dispersivities (perpendicular to flow) in the horizontal and vertical directions are one-tenth of the longitudinal dispersivity. For the purpose of the BEJ simulation, the longitudinal dispersivity was set at 50 feet (roughly one-sixtieth of the distance from the center of the TMA to the proposed compliance boundary), and the transverse dispersivities were set at 5 feet. The length scale for molecular diffusion (on the order of microns) is insignificant compared to these dispersivity values, therefore molecular diffusion is not simulated. Dispersivity values were varied as a part of the sensitivity analysis documented in this report and the prior solute transport analysis (HSI GeoTrans, 1996a).

To be conservative and applicable to many constituents, retardation (sorption and desorption of solute to and from soil solids) and chemical decay were not considered in the model. This is equivalent to setting the retardation factor of the solute transport model to 1.0 and the first order decay constant to zero.

2.2 MODEL CALIBRATION

The TMA sub-model was constructed as a "zoomed-in" version of the regional groundwater flow model. As such, it should produce results that are consistent with those of the regional model. To verify this, the TMA sub-model was run with stresses that represent steady-state (October 1984) pre-mining conditions. The groundwater head field computed by the TMA sub-model was then compared to the head field computed by the regional model in the vicinity of the TMA. Head values at well locations were also compared to observed water levels to verify that the TMA sub-model is reasonably calibrated to field conditions. Finally, particle traces and travel times were compared to pre-established estimates. Travel time estimates were based on CFC analysis performed by the U.S.G.S. (Saad, 1996).

2.2.1 COMPARISON TO THE REGIONAL GROUNDWATER FLOW MODEL

In the steady-state, pre-mining simulation, the TMA sub-model produces a head field very similar to that produced by the regional flow model. Note that the specified heads along the northwestern, southwestern, and southeastern boundaries were interpolated from computed heads in the steady-state, pre-mining simulation of the regional flow model. Figure 2.37 demonstrates the similarity of the computed water

table elevations in the TMA submodel and the regional model. Noting that the center of TMA sub-model layer 3 is the same as the center of regional model layer 2, Figure 2.38 shows the similarity of computed head in the outwash for the two models. Similarly, noting that the center of TMA sub-model layer 7 is the same as the center of regional model layer 4, Figure 2.39 reveals the consistency of the models at the base of the glacial aquifer. The minor differences noted between the regional model and the TMA submodel may be related to finer discretization of the submodel or simplification of the submodel to not include bedrock.

2.2.2 COMPARISON TO FIELD DATA

Figure 2.40 shows the locations of water level measurements in the area, with symbols that indicate the magnitude of differences between modeled and observed values or residuals. As expected, the residuals at these wells are very similar to those of the regional model, as demonstrated in Table 2.2. The overall gradient from the TMA to Hemlock Creek is reasonably approximated. This gradient governs the movement of solute in transport simulations.

A particle tracking simulation was made to verify steady state flow paths under existing conditions and to approximate advective travel times. Comparison of modeled travel times to approximations based on analysis of Chlorofluorocarbon (CFC) data (Saad, 1996) was made to verify the calibration. Backtracking of particles from the EX-8/GEO25/GEO50 nest indicate flowpaths that are consistent with a flownet (Figures 2.41 and 2.42). Particles that are recovered in the shallow wells (GEO25 and GEO50) generally originate at relatively short distances from the discharge points. Particles recovered in the deeper portions of the aquifer (greater than 100 feet) originate at distances in excess of 3000 feet from the discharge point. Note that the flowpath for a particle recovered in EX8-AL, the deepest well in the nest, is nearly vertical at the entry point to the aquifer. This flowpath indicates that portions of solute exfiltrating from the TMA would follow a deep flowpath and cause a plume to spread across much of the depth of the glacial aquifer.

Modeled particle travel times from the TMA to the observation points are generally consistent with the CFC data, when a correction factor is applied to the modeled times to account for transit time in the unsaturated zone. The correction factor is the same as was used by Saad (1996) to compute CFC travel times. Table 2.3 compares travel times for particles in the model.

2.3 TRANSPORT SIMULATION METHODOLOGY

In order to simulate solute transport, sources must be specified in terms of flux rates and source concentrations. For the TMA sub-model, the source flux rate is a complicated function in space and time, and the source concentrations vary from constituent to constituent and are currently being estimated in another study. In this

subsection, the modeled representation of the source flux is discussed. Subsequently, a general approach for simulating an unknown and constituent-specific source concentration that varies over time is presented.

2.3.1 TMA EXFILTRATION RATES

When a TMA cell is active (that is, it is receiving or has already received tailings), the water exfiltrating through the engineered liner and drain system becomes the source infiltration flux for groundwater transport. Note that it is conservatively assumed that the entire amount of exfiltrated water travels immediately through the unsaturated zone beneath the TMA to reach the water table.

The complete design and operation of the TMA is presented in a separate report (Foth & Van Dyke, 1995c and subsequent addenda). Each TMA cell is designed to receive mine tailings for 7 to 12 years, after which a protective cap is placed over each cell. For the purposes of this study it was assumed that each TMA cell's FML remains intact for 140 years after the cell is capped, a 150 year life. At that time, it is assumed that the water within the tailings is released to the groundwater. Following this postulated FML degradation it was further assumed that a constant infiltration rate (equal to the amount of water entering the TMA through the cap) prevails. The exfiltration rate in each year of activity was derived in the TMA design report using the HELP model. The TMA reclaim pond is a 4.3 acre lined pond that is used to store recycled water from the TMA. During operations, the reclaim pond is assumed to operate with a water depth of 15 feet above the FML resulting in a percolation rate of 1.5E-5 ft/d. During the reclamation phase the reclaim pond is assumed to operate at a water depth of 7 feet, and a percolation rate of 4.0E-6 ft/d. These quantities are based on calculations using Giroud and Bonaparte (1989) shown in Appendix A.

In order to create a manageable number of stress periods for the transport model, the active period of a TMA cell was divided into 10 phases, labeled A through J in Table 2.4. These phases were designed to represent periods where the exfiltration rate is approximately constant for a unique TMA cell. Phases A through J are staggered for the four TMA cells, as each cell becomes active at a different elapsed time. Phases A and B represent operational phases of the TMA (unique to each cell), when tailings are being received. Phases C through F represent the period when the cap is on and the FML has not degraded. The exfiltration rate decreases during these phases due to cap placement. Phase G represents the first year after degradation of the FML, phases H and I present subsequent phases after degradation of the FML, and phase J represents the final, constant exfiltration rate resulting from a capped TMA with the FML degraded. It is important to note that phases G through J assume that the FML is no longer intact, and that this is a very conservative assumption. In Table 2.4, the exfiltration rates are listed for each TMA region (base, lower sideslope, and upper sideslope) for each phase.

The operation of the four TMA cells is staggered in time such that TMA cell 2 begins receiving tailings two years before the cap is in place over TMA cell 1, TMA cell 3 begins operation 2 years before TMA 2 is capped, and TMA 4 starts two years before TMA 3 is capped. A detailed time line of the phase sequence for each TMA cell is shown in Figure 2.43. Note that the duration of operational phases A and B is different for the different cells, because of different capacities. In order to properly simulate every phase change at every cell, the model is made up of 39 stress periods of varying lengths, as shown in Figure 2.43 and listed in Table 2.5. Tables 2.6 through 2.9 provide detailed lists of modeled exfiltration rates for each TMA cell by stress period. Using these rates, the total modeled flux is plotted versus time in Figure 2.44. Figure 2.45 shows the cumulative volume of water exfiltrated from the TMA over time, and demonstrates that the spatial and temporal discretization used for the TMA sub-model conservatively approximates the design specifications. Note that prior to operation, TMA cells 2, 3, and 4 receive the default recharge rate of 8 in/yr (1.827E-3 ft/day) containing no solute (phase X in Tables 2.4 and 2.6-2.9), and do not contribute to the total TMA flux reflected in Figures 2.44 and 2.45. Note, however, that the TMA reclaim pond does contribute a flux of 1.6E-5 ft/d and 4.0E-6 ft/d for the operational and reclamation phase, respectively, that is included in Figure 2.44 and 2.45.

Each stress period was simulated as steady-state for flow, meaning that flow field changes take effect immediately. This simplifies the modeling approach considerably and does not lead to any significant errors in the prediction of concentration.

2.3.2 SUPERPOSITION OF SOURCES

Simulation of multiple constituents could present several challenges from a practical standpoint. First, source term concentrations for each constituent are in the process of being developed in a separate study, and their absolute concentrations are not currently available. Second, the time varying nature of source term concentration is unique for each constituent. In order to overcome these potential challenges, a general approach using unit concentration sources is used in this report. Using the principal of superposition and scaleable unit concentration sources, it is possible to account for source concentrations that vary over the life of the TMA and constituent specific source concentrations. The process is explained here.

Consider a simulation that has a source concentration equal to 1.0 ppm over the entire life of each TMA cell (that is, starting at time zero for TMA 1, time 7 years for TMA 2, etc. and continuing indefinitely). The result of the simulation is a prediction of concentration at every cell in the model at all times resulting from the unit-concentration source. To then determine the concentration in groundwater at a specific time and place of a specific constituent that (hypothetically) has a constant concentration in the tailings, the modeled concentration at that time and place is multiplied (or scaled) by the actual source concentration of the constituent. Another

constituent, having a source concentration twice as large as the first would be scaled in the same way resulting in a modeled concentration also twice as large as that for the first constituent. Thus, using unit-concentration sources makes it easy to apply results from a single simulation to multiple constituents, after the simulation is complete.

Now consider a constituent that does *not* have a constant concentration over the life of the TMA. Instead, phases A-C are characterized by an "operational" source concentration, C_A, and phases D-G are characterized by another concentration "post cap" source concentration, C_B, (because the capping of the tailings has changed the chemistry in the pore water), and phases H-J are characterized by a third source "oxidized" concentration, C_C, (due to hypothesized oxidation of the tailings pore water after FML. To account for these hypothesized concentration changes, three simulations (Simulations A, B, and C) are performed. In simulation A, a source concentration of 1.0 ppm is applied only during phase A-C of each TMA, and during operational phase of the reclaim pond. In simulation B, the source concentration is again 1.0 ppm, but it is only applied during phases D-G at each TMA cell and during the reclamation phase of the reclaim pond. In simulation C, the source concentration of 1.0 ppm is applied during phases H-J.

Simulations A, B, and C can then be used to compute the concentration at any point, and at any time, regardless of the magnitude of the source concentrations C_A, C_B, and C_C. Once the source concentrations are known for a constituent the principle of superposition is used to compute the constituent-specific concentration in the groundwater. The process is illustrated in Figure 2.46. First the simulations are run to generate unit response functions. At a given model cell, the functions are curves of concentration versus time, or unit response curves as shown in Figure 2.46. The unit response curve for Simulation A is scaled by the constituent specific concentration C_A. The unit response curve for Simulation B is scaled by the constituent specific concentration C_B, and the unit response curve for Simulation C is scaled by the constituent specific concentration C_C. The three scaled response curves are then added (or superimposed) to yield the function of concentration versus time that is sought for the constituent. This process can be repeated for any number of constituents without need of re-executing the simulations.

The method of superposition applied in this manner is valid because of the linear nature of the underlying differential equations that govern solute transport. A validation of the method with actual simulation results is presented in Section 2.4.2.

2.3.3 Other Changing Boundary Conditions

In this configuration, model time zero is the beginning of TMA operation, which is approximately coincidental with the beginning of mining. Mine operation is modeled with the specified-head boundary conditions along the model edges. Allowing for 30 years of mine operation and 2 years for recovery, the mine is assumed to be in

post-operation mode after 32 years in the model. The specified heads used at the beginning of the simulation, for stress periods 1 and 2, were interpolated from a steady-state simulation with the regional model that had zero recharge in TMA 1 only (default recharge in the other three) and the mine in operation. In stress periods 3 through 7, specified heads were interpolated from a regional model simulation with the mine operating and TMA cells 1 and 2 receiving zero recharge. Specified heads for stress periods 8 through 10 were taken from a simulation with mine operation and zero recharge in TMA 1, 2 and 3. In stress periods 11 through 16, the specified heads were computed from a regional model simulation with zero recharge over the entire TMA and the mine in operation. Finally, in stress periods 17 through 39, the mine is no longer in operation, and the specified head values are interpolated from a regional model simulation made with a backfilled mine and zero recharge over the entire TMA. Assuming zero recharge for active TMA cells in the regional model, instead of using actual values derived in Section 2.3.1, is a good approximation for regional flow modeling, because the TMA exfiltration rates are orders of magnitude less than the default recharge of 8 in/yr (1.827E-3 ft/day). Because the discrepancy between recharge rates derived from the regional model and actual computed recharge rates is small, use of specified heads interpolated directly from the regional model is appropriate.

The runoff basins around the TMA do not receive tailings and thus have a source concentration of zero. They do, however contribute additional recharge to the groundwater due to the collection of water from the TMA cap. In the model, each runoff basin recharge zone (Figure 2.36) contributes 13 in/yr (2.97E-3 ft/day), beginning when the nearest TMA cell becomes active. The additional 5 in/yr over default recharge assumes an average 30-day period each year with 2 feet of standing water in the runoff basin which is underlain by 1 foot of fine grained (conductivity of 1.0E-6 cm/sec, or 2.8E-3 ft/day) sediment. Because the runoff basins are a small portion of the total model area, the transport results are not sensitive to the runoff basin recharge rate.

The TMA reclaim pond contributes fluxes of 1.6E-5 ft/d and 4.0E-6 ft/d during the operational and reclamation phases, respectively. Following these periods, the default recharge rate of 8 in/yr is used.

2.4 MODEL PREDICTIONS

Using MODFLOW with MT3D[96] in finite-difference mode, BEJT, sensitivity, and PWCT simulations were conducted. The results are BEJT and PWCT predictions of unit concentration response curves at the proposed compliance boundary. These curves will be used (in the EIR) to assess groundwater quality performance at the proposed compliance boundary concentrations for specific constituents of concern. In order to demonstrate the use of the unit response curves, a hypothetical example is used.

This example also provides the base simulation for verification and sensitivity simulations.

2.4.1 BEST ENGINEERING JUDGEMENT FOR TRANSPORT

Using the BEJT parameters listed in Table 2.1, and the methodology explained in Section 2.3, BEJT unit response functions were computed with the MT3D[96] transport modeling code. Focusing on the proposed compliance boundary, 1200 feet from the outer edge of the TMA facility, unit-response curves (normalized concentration versus time) were computed for each cell shown in Figure 2.47. These curves can be scaled with constituent-specific source concentrations and summed to produce a profile of concentration versus time at each proposed compliance cell for the constituent of concern.

Figure 2.48 shows the maximum concentration unit-response curves for all three BEJT superposition simulations. Note that different cells may contain the maximum concentration at different times during the simulations. Thus, the curves in Figure 2.48 represent the concentration at a point that moves with time, always at the point on the proposed compliance boundary with the maximum concentration.

To demonstrate the use of the unit-response curves produced by the three BEJT simulations, a hypothetical example was considered. Suppose a constituent of concern is sulfate, and that the initial source concentration is 2,000 ppm. During post-cap phases D-G, the concentration of sulfate hypothetically increases to 4,000 ppm in the tailings pore water. And starting in beginning of phase H, the concentration escalates to 40,000 ppm (see Table 2.10). In this example, to determine the sulfate concentration at the proposed compliance boundary, all of the unit-response curves (one for each proposed compliance boundary cell) for Simulation A are multiplied by 2,000. The unit-response curves for Simulation B are multiplied by 4,000. And the unit-response curves for Simulation C are multiplied by 40,000. At each proposed compliance cell, the scaled-response curves are summed to yield the modeled sulfate concentration versus time. Figure 2.49 shows how this superposition method works. Note that the curves in Figure 2.49 represent a moving point that is always at the point on the proposed compliance boundary with the maximum total sulfate concentration. Because of this, Figure 2.49 exhibits a slight increase at approximately 100 years as the point of maximum concentration shifts from a point on the western proposed compliance boundary to a point on the eastern proposed compliance boundary. In this example, it is evident that the initial source concentration, though the lowest of the three source concentrations, produces the greatest concentration at the proposed compliance boundary. This occurs because the infiltration rates from the source areas are much greater during the operational phases of the reclaim pond and TMA cells. Note that the source concentration is continuous in Simulation C, which causes the compliance

boundary response to asymptotically approach a non-zero steady-state concentration, as shown in Figures 2.48 and 2.49.

To better understand the movement of solute through the aquifer from the TMA cells to the proposed compliance boundary, several snapshots of the modeled concentration plumes (plan view) are shown for this example in Figures 2.50 through 2.58. These figures show the maximum modeled concentration in any cell, following scaling and superposition, regardless of layer. The figures show the TMA cells beginning operation in succession, the initial movement of the solute plume to the west and toward the mine, and the eventual movement of the plume to the northeast, toward Hemlock Creek. Using the cross-section line A-A' shown in Figure 2.59, the modeled plume is viewed in cross-section in Figures 2.60 through 2.67. Note that the reclaim pond (located to the north of Section A-A') causes higher concentration near the western compliance boundary. Also note that the discontinuity in the curves in Figures 2.48 and 2.49 at time 100 years occurs when the point of maximum concentration moves from a point on the proposed compliance boundary west of the TMA to a point on the proposed compliance boundary northeast of the TMA.

Figure 2.69 shows particle traces originating from various areas of each TMA cell. In general, the figure shows that the flow paths are horizontal immediately beneath the TMA basins, but become vertical outside the basins as precipitation recharge causes a vertical gradient to exist. These flow paths are consistent with the plumes shown in cross-section in Figures 2.60 through 2.68. The particle tracking results indicate that the deep migration of the plumes is largely due to advection, not dispersion.

2.4.2 VERIFICATION OF METHODOLOGY

A verification simulation was performed to demonstrate that the method of superposition, as used in the preceding sulfate example, is accurate. A single simulation was conducted with the source concentrations explicitly specified in the model. That is, the concentration for phases A through C was set to 2,000 ppm in the model input, the concentration for phases D through G was set to 4,000 ppm, and the concentration for phases H-J was set to 40,000 ppm. It is important to remember that these concentrations are hypothetical and are not the actual source concentrations for sulfate, and that the time of concentration increase to 40,000 ppm was arbitrarily set to the very beginning of phase H. The model was run once and concentration at the proposed compliance boundary cells was recorded. Figure 2.70 shows that the results of this model are practically identical to the results obtained with superposition, as expected.

In the prior solute transport model report (HSI GeoTrans, 1996a) a simulation was made to check the validity of the finite-difference method for solving the transport

problem. A hypothetical sulfate example was run with MT3D[96] using another solution technique called the Method Of Characteristics (MOC). The MOC technique solves the solute transport equation by moving and dispersing particles that represent solute. This is much more computationally intensive than the finite difference method, therefore causing excessively long simulation times. A single 650-year simulation takes about 11.5 days on a 166MHz pentium-processor computer. As with the previous verification simulation, all source concentrations were specified explicitly in the model input, eliminating the need to perform multiple simulations for superposition. The results of this simulation indicate that the MOC solution predicts concentrations that are similar, but slightly higher than the finite difference solution. The two solutions are as similar as other verifications presented for less complex problems. From a practical standpoint, the two solutions are similar and this exercise provides verification that the finite difference solution technique is working properly.

2.4.3 SENSITIVITY ANALYSIS

Seven sensitivity simulations were conducted with the prior solute transport model (HSI GeoTrans, 1996a) to assess the effect of parameter uncertainty on model predictions. These simulations helped to guide the selection of parameters used in a PWCT simulation. Four additional sensitivity simulations were made with the current model to further evaluate parameter uncertainty and to address questions raised by the regulators. It is assumed that model sensitivity to parameters has not changed sufficiently from the prior solute transport model to change decisions whether the parameter should be included in the PWCT simulation. Therefore, the four additional sensitivity simulations further our knowledge of the effect of parameter uncertainty and design specifications on modeled results.

The sensitivity simulations involved independent variations of key parameters in the model. Each simulation was based on the hypothetical sulfate example with concentrations explicitly specified (Figure 2.70, solid line). The sensitivity simulations were run to 300 years to compute the concentration peak. As in the flow model report, the sensitivity simulations that caused results that were less favorable than the BEJT simulation were considered for the PWCT. For the transport model, these simulations cause an increase in the peak concentration or decrease in the time to peak concentration.

The factors that were tested in the sensitivity analysis performed in HSI GeoTrans (1996a) were:

- effective porosity,
- longitudinal dispersivity,

- transverse dispersivity (horizontal and vertical)
- horizontal hydraulic conductivity of the outwash in conjunction with precipitation recharge,
- vertical hydraulic conductivity of the glacial deposits,
- introduction of solute to the aquifer following cessation of mining operations, and
- inclusion of flow to the bedrock as a boundary condition.

Of these factors, lowering the effective porosity to 0.1, lowering the longitudinal dispersivity from 50 feet to 25 feet, lowering the transverse dispersivity from 5 feet to 2.5 feet, and lowering the vertical hydraulic conductivity of the glacial deposits by a factor of ten caused results that were less favorable than the BEJT model. These factors were included in the prior PWCT simulation (HSI GeoTrans, 1996a).

The four additional factors that were assessed with the current model are:

- independent lowering of vertical transverse dispersivity,
- a global increase in horizontal hydraulic conductivity of the glacial deposits in conjunction with precipitation recharge,
- an additional period of leakage from the TMA to simulate a two-year hiatus in mining operations, and
- change in source term flux.

Of these factors, the first two quantify uncertainty in hydrologic system parameters while the latter two factors show the sensitivity to operational or design parameters.

Figure 2.71 shows that lowering the vertical dispersivity by a factor of 10 causes compliance boundary concentrations to peak slightly later than the BEJT simulation, but remain higher for times greater than 50 years. The higher concentrations are most significant in the time period 50 years to 200 years, where they reach a maximum of approximately double the BEJT concentrations. This result is most likely caused because the plume disperses less downward than under BEJT conditions.

Figure 2.71 shows that raising the hydraulic conductivity and recharge by a factor of 1.25 causes lower peak concentrations. This result is most likely caused by the additional recharge, which provides more dilution of solute.

The effect of a hiatus in mining was simulated by extending the time period where TMA basin 2 is in operation by two years. Stress period 7 was increased from one year to three years, and the starting and ending times for subsequent stress periods were shifted accordingly. Figure 2.72 shows that an operational change such as this has a minor effect on concentrations at the compliance boundary. Concentrations increase in years 30 to 60 by less than five percent. Note that the peak concentrations are essentially the same for the two simulations.

Concentrations at the compliance boundary are directly proportional to source flux, as shown in Figure 2.72. In this sensitivity simulation, all source term flux (TMA, runoff basins, reclaim pond) was doubled, resulting in a doubling of compliance boundary concentrations. This simulation demonstrates that compliance boundary concentrations can be scaled to determine the conservatism of the computed source flux term.

The results of the four sensitivity simulations described above are summarized in Table 2.11.

2.4.4 Practical Worst Case for Transport

The sensitivity simulations conducted with the prior model (HSI GeoTrans, 1996a) indicated that lower porosity, lower dispersivity, and lower vertical conductivity can all lead to higher concentrations at the proposed compliance boundary. In addition, the sensitivity simulations conducted as a part of the current analysis indicted that a lower vertical dispersivity and a higher source term flux rate can lead to higher concentrations at the proposed compliance boundary. The analysis also suggested that a lower hydraulic conductivity combined with a lower precipitation recharge rate can lead to higher concentrations. The effect of a hiatus in mining was minor.

In developing the PWCT, the following assumptions and considerations were made. The PWCT effective porosity was set at 0.10, which is the same as the BEJT value for the current model and the PWCT for the previous model (HSI GeoTrans, 1996a). Adjusting effective porosity downwards from 0.10 was not considered to be reasonable because this value is already below the practical range that was established prior to model calibration. This practical range was based on field data and published values for similar sediments. The source term flux was kept at the BEJT value because this is a design parameter. The purpose of the sensitivity simulation was to prove that permissable fluxes could be back-calculated based proportionality between flux and concentration, not for consideration as a PWCT variable. Precipitation recharge and hydraulic conductivity were kept at the BEJT values because a value lower than 8 in/yr could not be justified.

The sensitivity analysis conducted in the prior solute transport modeling study (HSI GeoTrans, 1996a) indicated that assuming the solute entered the system immediately was more conservative than assuming a delay due to unsaturated travel times. This is still believed to be the case because the peak concentration is attained on the western compliance boundary, which is closer to the TMA reclaim pond, which appears to be the primary source of the solute. Assuming that the solute entered the groundwater system following mine closure would shift the groundwater divide further west, causing less plume migration to the west (lower concentrations on the western boundary) and no opportunity to add more solute to a plume that had changed direction.

Therefore, the remaining parameters that caused a less favorable result than the BEJ simulation were combined to form the PWCT simulation. Combining the low-range of probable values for these parameters results in the following PWCT parameters (also listed in Table 2.12): 1) the longitudinal, horizontal transverse, and vertical transverse dispersivities are reduced to 25 feet, 2.5 feet, and 0.5 feet, respectively, 2) the vertical conductivity of all geological units is reduced by a factor of 10. All other parameters are the same as those listed in Table 2.1.

Three unit-concentration simulations were conducted with the PWCT parameters. The results from these simulations (Figure 2.73) can be combined using superposition. For the hypothetical sulfate example, the superposition method is illustrated in Figure 2.74. Comparison of Figures 2.74 and 2.49 shows that the peak concentration for this example is only slightly higher with PWCT parameters than with BEJT parameters. There is a second peak that occurs at approximately year 60, that is not present in the BEJT simulation. Apparently, the first peak occurs due to the reclaim pond while the second peak occurs due to the TMA. The higher concentrations of the second superposition simulation also contributes to the second peak. Note that PWCT concentrations after year 300 are approximately 50 percent higher than the BEJT concentrations. PWCT concentration plumes are shown in plan view in Figures 2.75 through 2.83, and in cross-sectional view in Figures 2.84 through 2.92.

2.5 SUMMARY OF TAILINGS MANAGEMENT AREA MODEL RESULTS

Transport in groundwater of solute originating from the Tailings Management Area was simulated using the MT3D^{96} model. The model was designed specifically to focus on the area near the TMA as defined by the regulatory proposed compliance boundaries. The TMA model was constructed based on input parameters and boundary conditions from the regional groundwater flow model. However, grid resolution was improved both vertically and horizontally over the regional model in order to accurately model the potential movement of solute.

A generalized analysis method was created that enabled simulation of multiple constituents and a changing source term concentration without having to make numerous simulations. This method was verified and described in detail in the report text. Data regarding TMA exfiltration rates versus time were based on HELP model calculations by Foth and Van Dyke (see Appendix A). The analysis described in this report developed response functions for three phases of TMA operation, corresponding to changes in source term concentration. Once source term concentrations are known for specific constituents, groundwater concentrations at the proposed compliance boundary can be computed by scaling and combining the response functions documented herein. A hypothetical set of source term concentrations for sulfate was used to demonstrate the applicability of the generalized simulation methodology. The sulfate example was also used in the sensitivity simulations.

Sensitivity analysis was performed by varying aquifer parameters and solute transport properties. Combinations of the most influential parameters in the sensitivity analysis constituted the PWCT simulation. Note that the BEJT and PWCT results are not markedly different, indicating that the computed concentrations are less a function of solute transport parameters (dispersivity, etc.) than the exfiltration rate and input concentration. The response functions presented in this report will be used to determine both the BEJT groundwater concentrations and PWCT groundwater concentrations at the proposed compliance boundary. These groundwater concentrations will be documented for specific constituents in an update to the impact section of the EIR.

Table 2.1 Best Engineering Judgement for Transport model parameters.

Geologic Unit or Boundary	Parameter	Value	1996 Model
All Geologic Units	Effective Porosity	0.10	0.25
	Longitudinal Dispersivity	50.0 ft	50.0 ft
	Horizontal Transverse Dispersivity	5.0 ft	5.0 ft
	Vertical Dispersivity	5.0 ft	5.0 ft
Late Wisconsinan Till	Horizontal Conductivity	0.80 ft/day	0.80 ft/day
	Vertical Conductivity	0.40 ft/day	0.40 ft/day
Coarse Outwash	Horizontal Conductivity	80.0 ft/day	60.2 ft/dy
	Vertical Conductivity	8.0 ft/day	6.02 ft/day
	Pinchout Zone Horizontal Conductivity	6.0 ft/day	7.3 ft/day
	Pinchout Zone Vertical Conductivity	0.6 ft/day	0.73 ft/day
Fine Outwash	Horizontal Conductivity	20.0 ft/day	15.0 ft/day
	Vertical Conductivity	2.0 ft/day	1.50 ft/day
	PInchout Zone Horizontal Conductivity	6.0 ft/day	15.0 ft/day
	Pinchout Zone Vertical Conductivity	0.6 ft/day	1.5 ft/day
Pre- to Early-Wisconsinan Till and Massive Saprolite	Horizontal Conductivity	2.00 ft/day	0.80 ft/day
	Vertical Conductivity	0.075 ft/day	0.10 ft/day
Ancient Lacustrine	Horizontal Conductivity	2.00 ft/day	0.80 ft/day
	Vertical Conductivity	0.075ft/day	0.16 ft/day
Hemlock Creek	Width	14.0	14.0 ft
	Creekbed Vertical Conductivity	1.0 ft/day	1.0 ft/day
	Creekbed Sediment Thickness	1.0 ft	1.0 ft
	Water Depth	1.0 ft	1.0 ft
Seepage Wetlands	Bottom Sediment Vertical Conductivity	0.03 ft/day	0.00318 ft/day
	Bottom Sediment Thickness	5.0 ft	5.0 ft
	Water Depth	2.0 ft	2.0 ft

Prepared by:KMR
Checked by: GWC
Approved by: PFA

April 1998
P:\CMC\TMAMOD3\BEJParam.wpd

Table 2.2 Modeled and observed water levels at wells.

Well ID	Observed[1] Water Level (feet, msl)	TMA Sub-Model[2] Water Level (feet, msl)	TMA Sub-Model[2] Residual[4] (feet)	Regional Flow Model[3] Water Level (feet, msl)	Regional Flow Model[3] Residual[4] (feet)
DMB-1A	1594.78	1593.50	-1.28	1593.57	-1.21
DMB-3	1580.22	1579.58	-0.64	1581.00	0.78
DMB-4	1593.73	1592.84	-0.89	1592.84	-0.89
DMB-5	1593.50	1593.14	-0.36	1593.16	-0.34
DMB-5A	1592.58	1593.14	0.56	1593.16	0.58
DMB-6	1593.80	1592.76	-1.04	1592.70	-1.10
DMB-8	1588.58	1583.66	-4.92	1585.53	-3.05
EX-10AL	1594.62	1593.59	-1.03	1593.66	-0.96
EX-10AU	1594.72	1593.73	-0.99	1593.69	-1.03
EX-10BL	1595.14	1593.73	-1.41	1593.69	-1.45
EX-10BU	1596.06	1594.00	-2.06	1593.93	-2.13
EX-11AL	1593.93	1593.26	-0.67	1593.23	-0.70
EX-11AU	1593.47	1593.26	-0.21	1593.23	-0.24
EX-11BL	1594.19	1593.29	-0.90	1593.32	-0.87
EX-11BU	1593.37	1593.48	0.11	1593.51	0.14
EX-11CL	1593.80	1593.46	-0.34	1593.44	-0.36
EX-12AL	1593.83	1593.31	-0.52	1593.33	-0.50
EX-12AU	1593.73	1593.37	-0.36	1593.40	-0.33
EX-12BL	1593.73	1593.38	-0.35	1593.41	-0.32
EX-12BU	1594.03	1593.54	-0.49	1593.58	-0.45
EX-13AL	1592.16	1592.36	0.20	1592.36	0.20
EX-13BL	1592.19	1592.36	0.17	1592.36	0.17
EX-13BU	1592.16	1592.36	0.20	1592.37	0.20
EX-13CL	1592.29	1592.50	0.21	1592.50	0.20
EX-13DL	1592.52	1592.50	-0.02	1592.50	-0.03
EX-16AL	1593.44	1592.57	-0.87	1592.61	-0.84
EX-16AU	1593.31	1592.58	-0.73	1592.61	-0.70
EX-16BL	1593.73	1592.85	-0.88	1592.73	-1.00
EX-7AL	1582.32	1580.56	-1.76	1581.56	-0.76
EX-7BL	1581.27	1580.56	-0.71	1581.56	0.29
EX-7BU	1579.66	1579.71	0.05	1580.62	0.95
EX-7CL	1578.61	1579.70	1.09	1580.44	1.83
EX-8AL	1584.68	1580.66	-4.02	1581.69	-3.00
EX-8AU	1582.97	1580.66	-2.31	1581.69	-1.29
EX-8BL	1579.85	1579.65	-0.20	1580.55	0.70
EX-8BU	1579.89	1579.51	-0.38	1580.32	0.43
EX-9AU	1594.32	1593.27	-1.05	1593.34	-0.98
EX-9BL	1594.52	1593.36	-1.16	1593.42	-1.10
EX-9BU	1594.62	1593.39	-1.23	1593.51	-1.11
G41-B12	1593.90	1593.67	-0.23	1593.67	-0.23
G41-C15	1593.11	1592.62	-0.49	1592.57	-0.54
G41-E13	1594.52	1593.40	-1.12	1593.37	-1.15
G41-E17	1592.78	1592.60	-0.18	1592.55	-0.23
G41-G13	1594.49	1593.46	-1.03	1593.53	-0.96
G41-G14A	1593.83	1593.55	-0.28	1593.57	-0.26
G41-G14B	1593.90	1593.49	-0.41	1593.52	-0.38
G41-G14C	1594.39	1593.66	-0.73	1593.71	-0.68
G41-G14D	1594.23	1593.51	-0.72	1593.53	-0.70
G41-G14E	1594.06	1593.65	-0.41	1593.70	-0.37
G41-G14F	1593.73	1593.46	-0.27	1593.50	-0.23
G41-G15	1593.90	1593.40	-0.50	1593.43	-0.47
G41-G15A	1593.70	1593.57	-0.13	1593.61	-0.09
G41-G15B	1593.73	1593.57	-0.16	1593.61	-0.12
G41-H18B	1592.52	1592.60	0.08	1592.54	0.02
G41-H9	1594.00	1592.81	-1.19	1592.64	-1.36
G41-K13	1593.37	1592.83	-0.54	1593.02	-0.35
G41-K13A	1594.09	1593.08	-1.01	1593.19	-0.90
G41-M11	1579.89	1579.65	-0.24	1580.76	0.87
G41-P16	1579.33	1583.72	4.39	1583.88	4.55
SG-WP-6	1577.20	1579.22	2.02	1580.98	3.78
SG-WP-7	1578.15	1579.23	1.08	1579.92	1.77

Notes:

[1] Observed water level in October 1984.

[2] Simulation T03A.

[3] Simulation 23A.

[4] Modeled - Observed.

Prepared by: GWC
Checked by: PAW
Approved by: PFA

April 1998
\Crandon\TmaMod3\Excel\Targets.xls, Compare

Table 2.3 Travel time for particles reaching well clusters CMC-02, EX-11, and EX-8.

Well ID	Travel Time from Water Table (Years)	Modeled Recharge Date	CFC-Derived Date
CMC-02P	13	1974	1978.0
CMC-02R	0.2	1987	1989.5
EX-11AL	41	1948	<1954.5
EX-11AU	26	1963	<1959.0
EX-11BL	12	1977	1955.0
EX-11BU	7	1982	<1966.0
EX-11CL	0.01	1989	1978.2
EX-8AL	111	1878	1975.0
EX-8AU	71	1917	<1954.5
EX-8BL	26	1961	<1958
EX-8BU	0.4	1996	1984.5
Geo25	8	1980	1977.0
Geo50	20	1967	1956.5

Prepared by: GWC
Checked by: PAW
Approved by: PFA

Simulation T03A-MP
April 1998
\Crandon\TMAmod3\Excel\T03a-mp.xls, RchDate

Table 2.4 Basis for TMA phases and flux rates[1]

Phase	Description	Duration (years)	Basis for Exfiltration Rate
X	Pre-construction	0-22[2]	Regional model calibrated value
A	First Phase of Operation	2-5[2]	Appendix A Table 1 average[3]
B	Second Phase of Operation plus two years of consolidation	5-7[2]	Appendix A Table 2 average
C	Cap in Place Part 1	1	Appendix A Table 3 Year 1
D	Cap in Place Part 2	6	Appendix A Table 3 Years 2-7
E	Cap in Place Part 3	20	Appendix A Table 3 Years 8-25
F	Cap in Place Part 4	113	Appendix A Table 3 Years 26-140
G	Degraded FML Part 1	1	Appendix A Table 3 Year 141
H	Degraded FML Part 2	49	Appendix A Table 3 Years 142-190
I	Degraded FML Part 3	50	Appendix A Table 3 Years 191-240
J	Degraded FML Steady-State	N/A	Appendix A Table 3 Years 241+

Phase	Base		Lower Sideslope		Upper Sideslope	
	Rate(in/yr)	Rate(ft/d)	Rate(in/yr)	Rate(ft/d)	Rate(in/yr)	Rate(ft/d)
X	8.00	1.825E-03	8.00	1.825E-03	8.00	1.825E-03
A	5.704E-03	1.301E-06	2.502E-07	5.708E-11	8.00	1.825E-03
B	5.704E-03	1.301E-06	2.502E-07	5.708E-11	2.502E-07	5.708E-11
C	4.684E-03	1.069E-06	2.502E-07	5.708E-11	2.502E-07	5.708E-11
D	9.463E-04	2.159E-07	2.502E-07	5.708E-11	2.502E-07	5.708E-11
E	2.067E-04	4.717E-08	2.502E-07	5.708E-11	2.502E-07	5.708E-11
F	3.012E-05	6.872E-09	2.502E-07	5.708E-11	2.502E-07	5.708E-11
G	8.763E-03	1.999E-06	3.879E-03	8.849E-07	1.377E-03	3.142E-07
H	2.502E-07	5.708E-11	2.502E-07	5.708E-11	2.502E-07	5.708E-11
I	2.502E-07	5.708E-11	2.502E-07	5.708E-11	3.002E-05	6.849E-09
J	3.002E-05	6.849E-09	3.002E-05	6.849E-09	3.002E-05	6.849E-09

Notes

[1] The TMA reclaim pond is active during years 2-32 during which its flux is 1.6E-5 ft/d, and years 33-42 (reclamation phase) during which its flux is 4.0E-6 ft/d. Thereafter a uniform 1.825E-3 ft/d is used to represent precipication recharge.

[2] Varies by TMA Cell

[3] During the first phase of operation, the TMA upper sideslope receives full recharge (from regional model) with a concentration of zero.

Prepared by: GWC
Checked by: PAW
Approved by: PFA

April 1998
\Crandon\TmaMod3\Excel\StresTab.xls, Basis

Table 2.5 TMA sub-model stress periods.

Stress Period	Time (years)			Time (days)		
	Start	Duration	End	Start	Duration	End
1	0	3	3	0.00	1095.75	1095.75
2	3	3	6	1095.75	1095.75	2191.50
3	6	2	8	2191.50	730.50	2922.00
4	8	1	9	2922.00	365.25	3287.25
5	9	2	11	3287.25	730.50	4017.75
6	11	4	15	4017.75	1461.00	5478.75
7	15	1	16	5478.75	365.25	5844.00
8	16	2	18	5844.00	730.50	6574.50
9	18	1	19	6574.50	365.25	6939.75
10	19	3	22	6939.75	1095.75	8035.50
11	22	2	24	8035.50	730.50	8766.00
12	24	1	25	8766.00	365.25	9131.25
13	25	1	26	9131.25	365.25	9496.50
14	26	4	30	9496.50	1461.00	10957.50
15	30	1	31	10957.50	365.25	11322.75
16	31	1	32	11322.75	365.25	11688.00
17	32	3	35	11688.00	1095.75	12783.75
18	35	2	37	12783.75	730.50	13514.25
19	37	5	42	13514.25	1826.25	15340.50
20	42	3	45	15340.50	1095.75	16436.25
21	45	6	51	16436.25	2191.50	18627.75
22	51	6	57	18627.75	2191.50	20819.25
23	57	91	148	20819.25	33237.75	54057.00
24	148	1	149	54057.00	365.25	54422.25
25	149	9	158	54422.25	3287.25	57709.50
26	158	1	159	57709.50	365.25	58074.75
27	159	5	164	58074.75	1826.25	59901.00
28	164	1	165	59901.00	365.25	60266.25
29	165	5	170	60266.25	1826.25	62092.50
30	170	1	171	62092.50	365.25	62457.75
31	171	27	198	62457.75	9861.75	72319.50
32	198	10	208	72319.50	3652.50	75972.00
33	208	6	214	75972.00	2191.50	78163.50
34	214	6	220	78163.50	2191.50	80355.00
35	220	28	248	80355.00	10227.00	90582.00
36	248	10	258	90582.00	3652.50	94234.50
37	258	6	264	94234.50	2191.50	96426.00
38	264	6	270	96426.00	2191.50	98617.50
39	270	380	650	98617.50	138795.00	237412.50

Prepared by: GWC
Checked by: PAW
Approved by: PFA

April 1998
\Crandon\TmaMod3\Excel\StresTab.xls, Stress

Table 2.6 TMA 1 exfiltration rates by stress period.

Stress Period	Phase	Exfiltration Rate (ft/day)		
		Base	Lower Sideslope	Upper Sideslope
1	A	1.30E-06	5.71E-11	1.83E-03 [1]
2	B	1.30E-06	5.71E-11	5.71E-11
3	B	1.30E-06	5.71E-11	5.71E-11
4	C	1.07E-06	5.71E-11	5.71E-11
5	D	2.16E-07	5.71E-11	5.71E-11
6	D	2.16E-07	5.71E-11	5.71E-11
7	E	4.72E-08	5.71E-11	5.71E-11
8	E	4.72E-08	5.71E-11	5.71E-11
9	E	4.72E-08	5.71E-11	5.71E-11
10	E	4.72E-08	5.71E-11	5.71E-11
11	E	4.72E-08	5.71E-11	5.71E-11
12	E	4.72E-08	5.71E-11	5.71E-11
13	E	4.72E-08	5.71E-11	5.71E-11
14	E	4.72E-08	5.71E-11	5.71E-11
15	E	4.72E-08	5.71E-11	5.71E-11
16	E	4.72E-08	5.71E-11	5.71E-11
17	E	4.72E-08	5.71E-11	5.71E-11
18	F	6.87E-09	5.71E-11	5.71E-11
19	F	6.87E-09	5.71E-11	5.71E-11
20	F	6.87E-09	5.71E-11	5.71E-11
21	F	6.87E-09	5.71E-11	5.71E-11
22	F	6.87E-09	5.71E-11	5.71E-11
23	F	6.87E-09	5.71E-11	5.71E-11
24	G	2.00E-06	8.85E-07	3.14E-07
25	H	5.71E-11	5.71E-11	5.71E-11
26	H	5.71E-11	5.71E-11	5.71E-11
27	H	5.71E-11	5.71E-11	5.71E-11
28	H	5.71E-11	5.71E-11	5.71E-11
29	H	5.71E-11	5.71E-11	5.71E-11
30	H	5.71E-11	5.71E-11	5.71E-11
31	H	5.71E-11	5.71E-11	5.71E-11
32	I	5.71E-11	5.71E-11	6.85E-09
33	I	5.71E-11	5.71E-11	6.85E-09
34	I	5.71E-11	5.71E-11	6.85E-09
35	I	5.71E-11	5.71E-11	6.85E-09
36	J	6.85E-09	6.85E-09	6.85E-09
37	J	6.85E-09	6.85E-09	6.85E-09
38	J	6.85E-09	6.85E-09	6.85E-09
39	J	6.85E-09	6.85E-09	6.85E-09

Note: [1] Equal to default recharge, no source applied.

Table 2.7 TMA 2 exfiltration rates by stress period.

Stress Period	Phase	Exfiltration Rate (ft/day)		
		Base	Lower Sideslope	Upper Sideslope
1	X	1.83E-03 [1]	1.83E-03 [1]	1.83E-03 [1]
2	X	1.83E-03 [1]	1.83E-03 [1]	1.83E-03 [1]
3	A	1.30E-06	5.71E-11	1.83E-03 [1]
4	A	1.30E-06	5.71E-11	1.83E-03 [1]
5	A	1.30E-06	5.71E-11	1.83E-03 [1]
6	B	1.30E-06	5.71E-11	5.71E-11
7	B	1.30E-06	5.71E-11	5.71E-11
8	B	1.30E-06	5.71E-11	5.71E-11
9	C	1.07E-06	5.71E-11	5.71E-11
10	D	2.16E-07	5.71E-11	5.71E-11
11	D	2.16E-07	5.71E-11	5.71E-11
12	D	2.16E-07	5.71E-11	5.71E-11
13	E	4.72E-08	5.71E-11	5.71E-11
14	E	4.72E-08	5.71E-11	5.71E-11
15	E	4.72E-08	5.71E-11	5.71E-11
16	E	4.72E-08	5.71E-11	5.71E-11
17	E	4.72E-08	5.71E-11	5.71E-11
18	E	4.72E-08	5.71E-11	5.71E-11
19	E	4.72E-08	5.71E-11	5.71E-11
20	E	4.72E-08	5.71E-11	5.71E-11
21	F	6.87E-09	5.71E-11	5.71E-11
22	F	6.87E-09	5.71E-11	5.71E-11
23	F	6.87E-09	5.71E-11	5.71E-11
24	F	6.87E-09	5.71E-11	5.71E-11
25	F	6.87E-09	5.71E-11	5.71E-11
26	G	2.00E-06	8.85E-07	3.14E-07
27	H	5.71E-11	5.71E-11	5.71E-11
28	H	5.71E-11	5.71E-11	5.71E-11
29	H	5.71E-11	5.71E-11	5.71E-11
30	H	5.71E-11	5.71E-11	5.71E-11
31	H	5.71E-11	5.71E-11	5.71E-11
32	H	5.71E-11	5.71E-11	5.71E-11
33	I	5.71E-11	5.71E-11	6.85E-09
34	I	5.71E-11	5.71E-11	6.85E-09
35	I	5.71E-11	5.71E-11	6.85E-09
36	I	5.71E-11	5.71E-11	6.85E-09
37	J	6.85E-09	6.85E-09	6.85E-09
38	J	6.85E-09	6.85E-09	6.85E-09
39	J	6.85E-09	6.85E-09	6.85E-09

Note: [1] Equal to default recharge, no source applied.

Table 2.8 TMA 3 exfiltration rates by stress period.

Stress Period	Phase	Exfiltration Rate (ft/day)		
		Base	Lower Sideslope	Upper Sideslope
1	X	1.83E-03 [1]	1.83E-03 [1]	1.83E-03 [1]
2	X	1.83E-03 [1]	1.83E-03 [1]	1.83E-03 [1]
3	X	1.83E-03 [1]	1.83E-03 [1]	1.83E-03 [1]
4	X	1.83E-03 [1]	1.83E-03 [1]	1.83E-03 [1]
5	X	1.83E-03 [1]	1.83E-03 [1]	1.83E-03 [1]
6	X	1.83E-03 [1]	1.83E-03 [1]	1.83E-03 [1]
7	X	1.83E-03 [1]	1.83E-03 [1]	1.83E-03 [1]
8	A	1.30E-06	5.71E-11	1.83E-03 [1]
9	B	1.30E-06	5.71E-11	5.71E-11
10	B	1.30E-06	5.71E-11	5.71E-11
11	B	1.30E-06	5.71E-11	5.71E-11
12	C	1.07E-06	5.71E-11	5.71E-11
13	D	2.16E-07	5.71E-11	5.71E-11
14	D	2.16E-07	5.71E-11	5.71E-11
15	D	2.16E-07	5.71E-11	5.71E-11
16	E	4.72E-08	5.71E-11	5.71E-11
17	E	4.72E-08	5.71E-11	5.71E-11
18	E	4.72E-08	5.71E-11	5.71E-11
19	E	4.72E-08	5.71E-11	5.71E-11
20	E	4.72E-08	5.71E-11	5.71E-11
21	E	4.72E-08	5.71E-11	5.71E-11
22	F	6.87E-09	5.71E-11	5.71E-11
23	F	6.87E-09	5.71E-11	5.71E-11
24	F	6.87E-09	5.71E-11	5.71E-11
25	F	6.87E-09	5.71E-11	5.71E-11
26	F	6.87E-09	5.71E-11	5.71E-11
27	F	6.87E-09	5.71E-11	5.71E-11
28	G	2.00E-06	8.85E-07	3.14E-07
29	H	5.71E-11	5.71E-11	5.71E-11
30	H	5.71E-11	5.71E-11	5.71E-11
31	H	5.71E-11	5.71E-11	5.71E-11
32	H	5.71E-11	5.71E-11	5.71E-11
33	H	5.71E-11	5.71E-11	5.71E-11
34	I	5.71E-11	5.71E-11	6.85E-09
35	I	5.71E-11	5.71E-11	6.85E-09
36	I	5.71E-11	5.71E-11	6.85E-09
37	I	5.71E-11	5.71E-11	6.85E-09
38	J	6.85E-09	6.85E-09	6.85E-09
39	J	6.85E-09	6.85E-09	6.85E-09

Note: [1] Equal to default recharge, no source applied.

Table 2.9 TMA 4 exfiltration rates by stress period.

Stress Period	Phase	Exfiltration Rate (ft/day)		
		Base	Lower Sideslope	Upper Sideslope
1	X	1.83E-03 [1]	1.83E-03 [1]	1.83E-03 [1]
2	X	1.83E-03 [1]	1.83E-03 [1]	1.83E-03 [1]
3	X	1.83E-03 [1]	1.83E-03 [1]	1.83E-03 [1]
4	X	1.83E-03 [1]	1.83E-03 [1]	1.83E-03 [1]
5	X	1.83E-03 [1]	1.83E-03 [1]	1.83E-03 [1]
6	X	1.83E-03 [1]	1.83E-03 [1]	1.83E-03 [1]
7	X	1.83E-03 [1]	1.83E-03 [1]	1.83E-03 [1]
8	X	1.83E-03 [1]	1.83E-03 [1]	1.83E-03 [1]
9	X	1.83E-03 [1]	1.83E-03 [1]	1.83E-03 [1]
10	X	1.83E-03 [1]	1.83E-03 [1]	1.83E-03 [1]
11	A	1.30E-06	5.71E-11	1.83E-03 [1]
12	A	1.30E-06	5.71E-11	1.83E-03 [1]
13	B	1.30E-06	5.71E-11	5.71E-11
14	B	1.30E-06	5.71E-11	5.71E-11
15	C	1.07E-06	5.71E-11	5.71E-11
16	D	2.16E-07	5.71E-11	5.71E-11
17	D	2.16E-07	5.71E-11	5.71E-11
18	D	2.16E-07	5.71E-11	5.71E-11
19	E	4.72E-08	5.71E-11	5.71E-11
20	E	4.72E-08	5.71E-11	5.71E-11
21	E	4.72E-08	5.71E-11	5.71E-11
22	E	4.72E-08	5.71E-11	5.71E-11
23	F	6.87E-09	5.71E-11	5.71E-11
24	F	6.87E-09	5.71E-11	5.71E-11
25	F	6.87E-09	5.71E-11	5.71E-11
26	F	6.87E-09	5.71E-11	5.71E-11
27	F	6.87E-09	5.71E-11	5.71E-11
28	F	6.87E-09	5.71E-11	5.71E-11
29	F	6.87E-09	5.71E-11	5.71E-11
30	G	2.00E-06	8.85E-07	3.14E-07
31	H	5.71E-11	5.71E-11	5.71E-11
32	H	5.71E-11	5.71E-11	5.71E-11
33	H	5.71E-11	5.71E-11	5.71E-11
34	H	5.71E-11	5.71E-11	5.71E-11
35	I	5.71E-11	5.71E-11	6.85E-09
36	I	5.71E-11	5.71E-11	6.85E-09
37	I	5.71E-11	5.71E-11	6.85E-09
38	I	5.71E-11	5.71E-11	6.85E-09
39	J	6.85E-09	6.85E-09	6.85E-09

Note: [1] Equal to default recharge, no source applied.

Table 2.10 Hypothetical concentration phases for sulfate.

Description	Source Concentration (ppm)	Beginning Time[1]
Operational	2,000	Start of flow phase A
Post-Cap	4,000	Start of flow phase D
Oxidized	40,000	Start of flow phase H[2]

Notes
[1] Varies by TMA Cell
[2] As a conservative assumption, the oxidized concentration begins one year after assumed degradation of the flexible membrane liner.

Prepared by: GWC
Checked by: PAW
Approved by: PFA

April 1998
\Crandon\TmaMod3\Excel\SulfSrc.xls

Table 2.11 Summary of Sensitivity Simulations.

Description of Simulation	Parameter Variation(s)	Peak Concentration (ppm)	Time to Peak (years)
Best Engineering Judgement for Transport (BEJT)	None	1.37	32
Lower Vertical Dispersivity	Vertical Dispersivity = 0.5 ft	1.33	32
Higher Transmissivity and Recharge	All Horizontal Conductivities x 1.25 Default Recharge Rate = 10 in/year	1.16	32
Two Year Mine Shutdown	Duration of Stress Period 7 = 3 years	1.39	34
Higher Source Flux	All Source Fluxes x 2	2.75	32

Table 2.12 Practical Worst Case for Transport model parameters.

Geologic Unit or Boundary	Parameter	Value[1]	1996 Model
All Geologic Units	Effective Porosity	0.10	0.10
	Longitudinal Dispersivity	**25 ft**	25.0 ft
	Horizontal Transverse Dispersivity	**2.5 ft**	2.5 ft
	Vertical Dispersivity	**0.5 ft**	2.5 ft
Late Wisconsinan Till	Horizontal Conductivity	0.8 ft/day	0.80 ft/day
	Vertical Conductivity	**0.040 ft/day**	0.040 ft/day
Coarse Outwash	Horizontal Conductivity	80.0 ft/day	60.2 ft/dy
	Vertical Conductivity	**0.8 ft/day**	0.602 ft/day
	Pinchout Zone Horizontal Conductivity	6.0 ft/day	7.3 ft/day
	Pinchout Zone Vertical Conductivity	**0.06 ft/day**	0.073 ft/day
Fine Outwash	Horizontal Conductivity	20.0 ft/day	15.0 ft/day
	Vertical Conductivity	**0.20 ft/day**	0.150 ft/day
	Pinchout Horizontal Conductivity	6.0 ft/day	15.0 ft/day
	Pinchout Vertical Conductivity	0.06 ft/day	0.15 ft/day
Pre- to Early-Wisconsinan Till and Massive Saprolite	Horizontal Conductivity	2 ft/day	0.80 ft/day
	Vertical Conductivity	**0.075 ft/day**	0.010 ft/day
Ancient Lacustrine	Horizontal Conductivity	2 ft/day	0.80 ft/day
	Vertical Conductivity	**0.0025 ft/day**	0.016 ft/day
Hemlock Creek	Width	14.0 ft	14.0 ft
	Creekbed Vertical Conductivity	1.0 ft/day	1.0 ft/day
	Creekbed Sediment Thickness	1.0 ft	1.0 ft
	Water Depth	1.0 ft	1.0 ft
Seepage Wetlands	Bottom Sediment Vertical Conductivity	0.03 ft/day	0.00318 ft/day
	Bottom Sediment Thickness	5.0 ft	5.0 ft
	Water Depth	2.0 ft	2.0 ft

[1] Bold values indicate changes from Best Engineering Judgement for Transport model parameters.

Prepared by:KMR
Checked by: GWC
Approved by: PFA

April 1998
P:\CMC\TMAMOD3\BEJParam.wpd

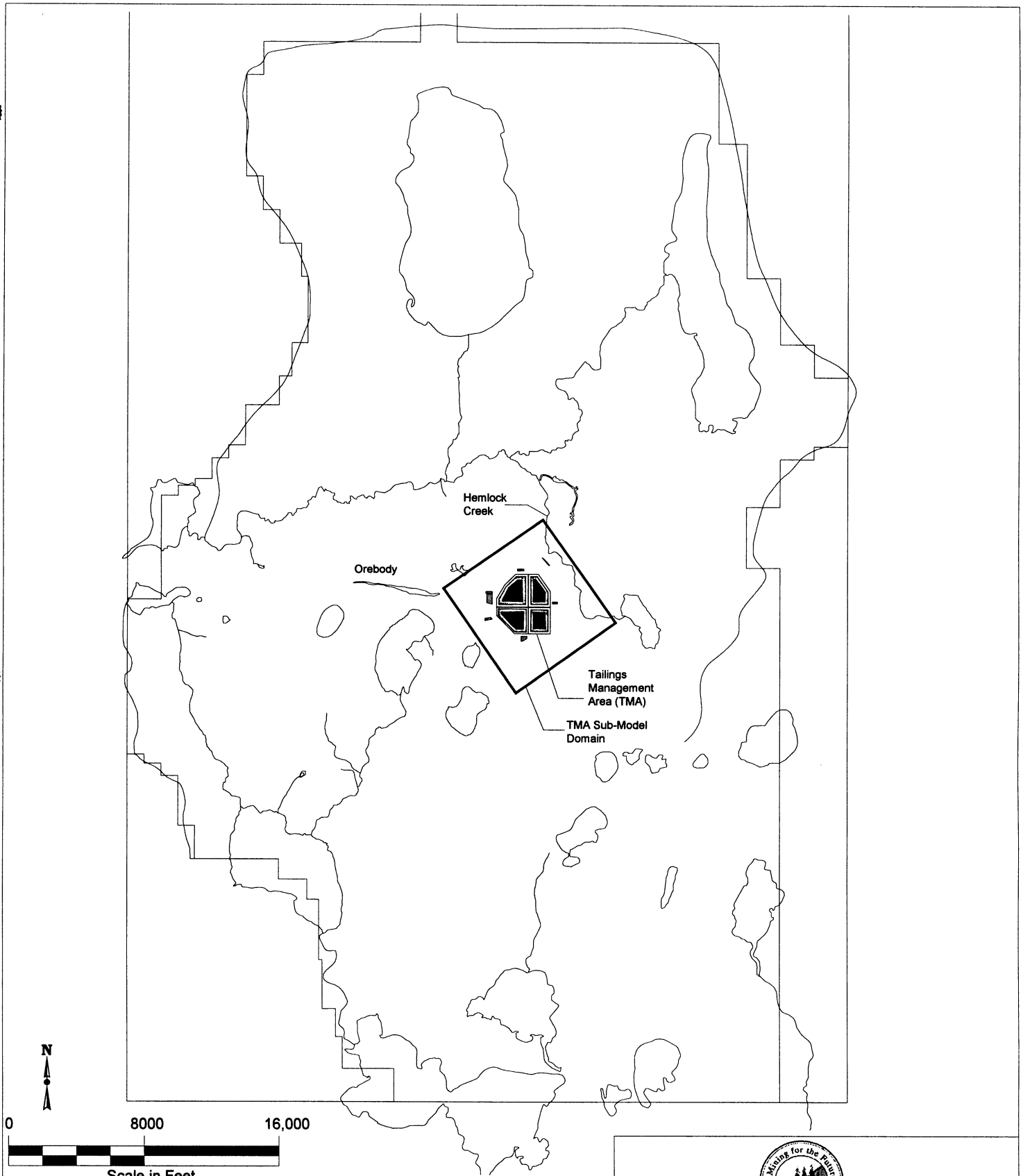

HSI GEOTRANS

REVISED	DATE	BY	DESCRIPTION

CHECKED BY: PAW	DATE: April 1998
APPROVED BY: PFA	DATE: April 1998
APPROVED BY:	DATE:

Nicolet Minerals COMPANY

Figure 2.1
TMA Sub-Model
Location Map

Scale: 1 in. = 8000 ft.	Date: April 1998
Prepared By: HSI GeoTrans	By: GWC

\Crandon\TmaMod3\GI...LocatMap.wor

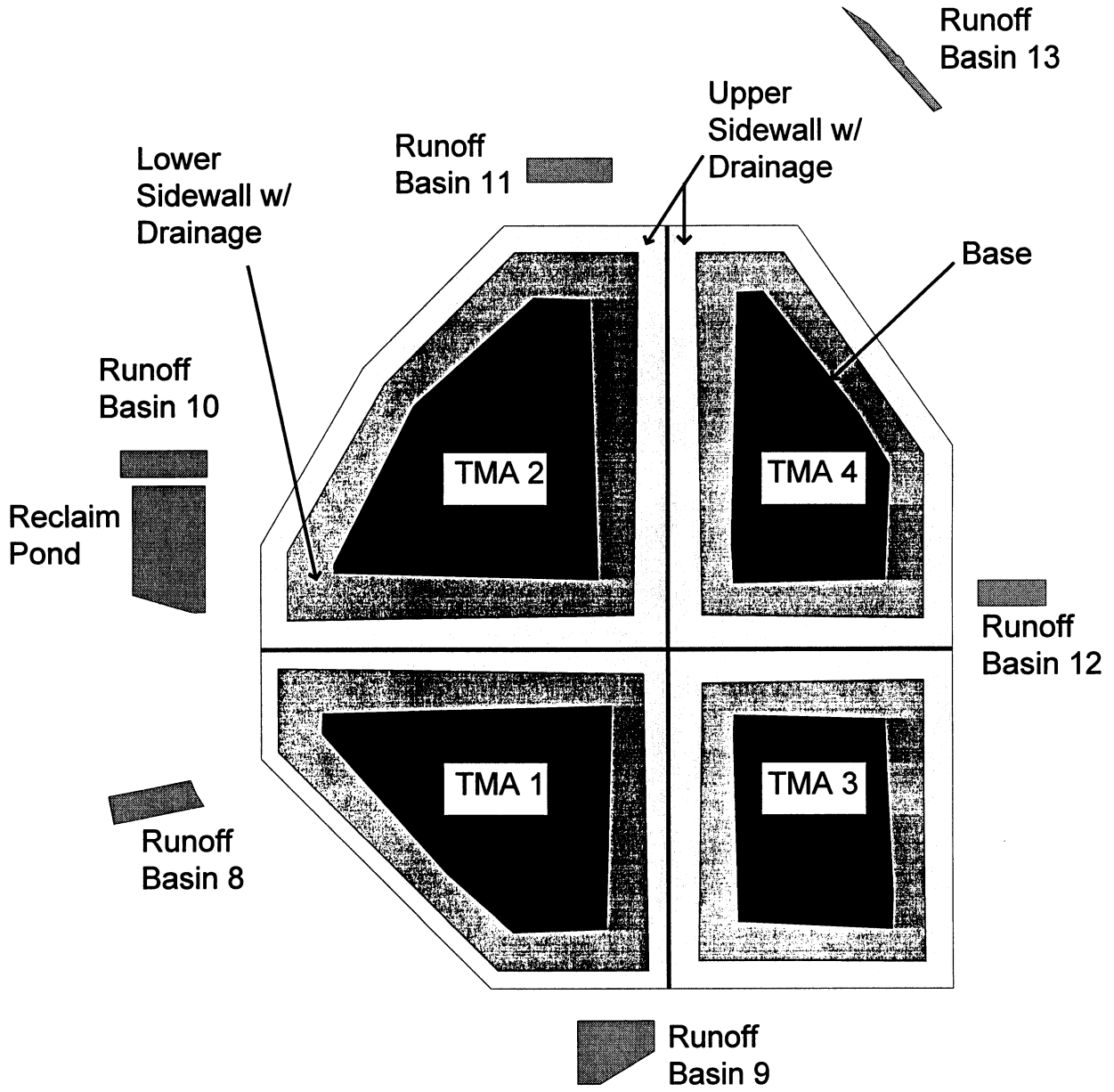

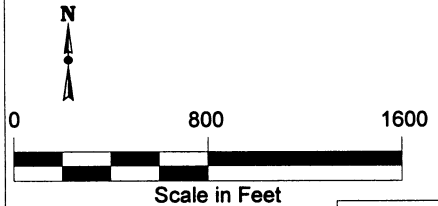

HSI GEOTRANS			
REVISED	DATE	BY	DESCRIPTION

CHECKED BY: PAW	DATE: April 1998
APPROVED BY: PFA	DATE: April 1998
APPROVED BY:	DATE:

Nicolet Minerals COMPANY

Figure 2.2
TMA Detail

Scale: 1 in. = 8000 ft.	Date: April 1998
Prepared By: HSI GeoTrans	By: GWC

\Crandon\TmaMod3\GIS_site\Detail.wor

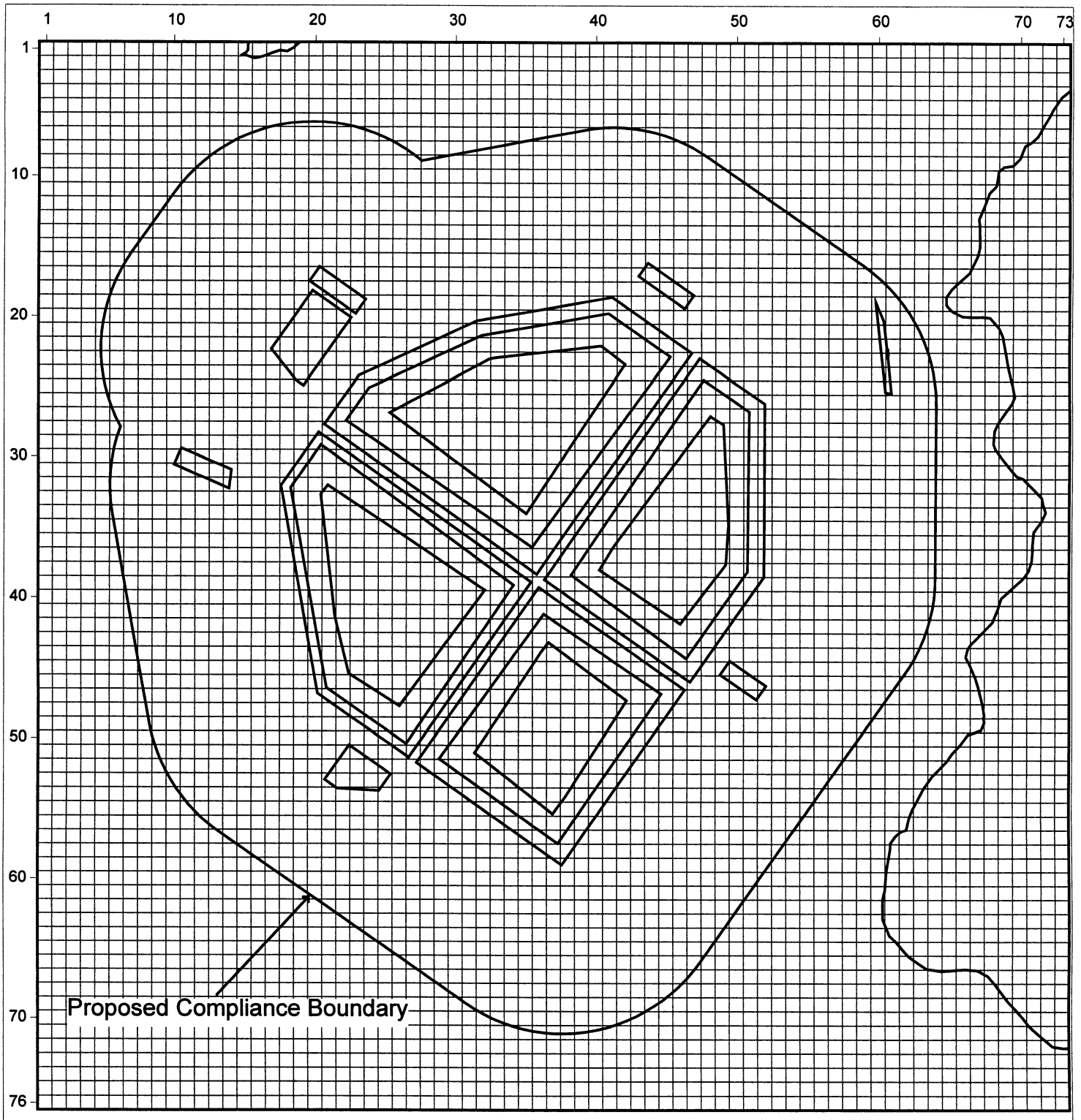

HSI GEOTRANS			
REVISED	DATE	BY	DESCRIPTION

CHECKED BY: PAW	DATE: April 1998
APPROVED BY: PFA	DATE: April 1998
APPROVED BY:	DATE:

Nicolet Minerals COMPANY

Figure 2.3
Model Grid

Scale: 1 in. = 1000 ft. | Date: April 1998

Prepared By: HSI GeoTrans | By: GWC

\Crandon\TmaMod3\Gr...\Grid.wor

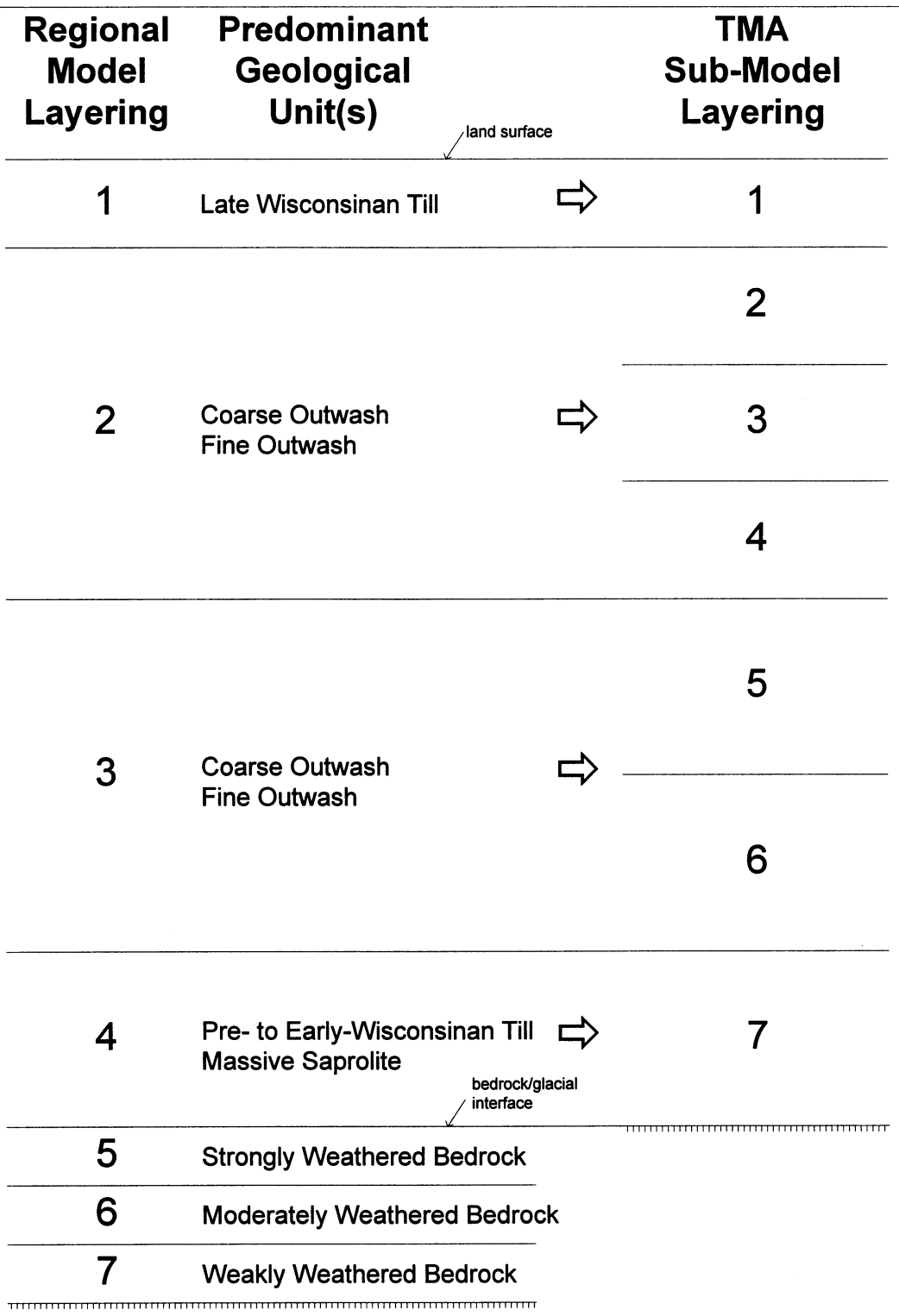

HSI GEOTRANS			
REVISED	DATE	BY	DESCRIPTION
CHECKED BY: PAW			DATE: April 1998
APPROVED BY: PFA			DATE: April 1998
APPROVED BY:			DATE:

Nicolet Minerals COMPANY

Figure 2.4
Model Layering

Scale: None	Date: April 1998
Prepared By: HSI GeoTrans	By: GWC

\CrandonITmaMod3\GIS_mod\Layering.wor

N015003A.DWG

SECTION F–F'

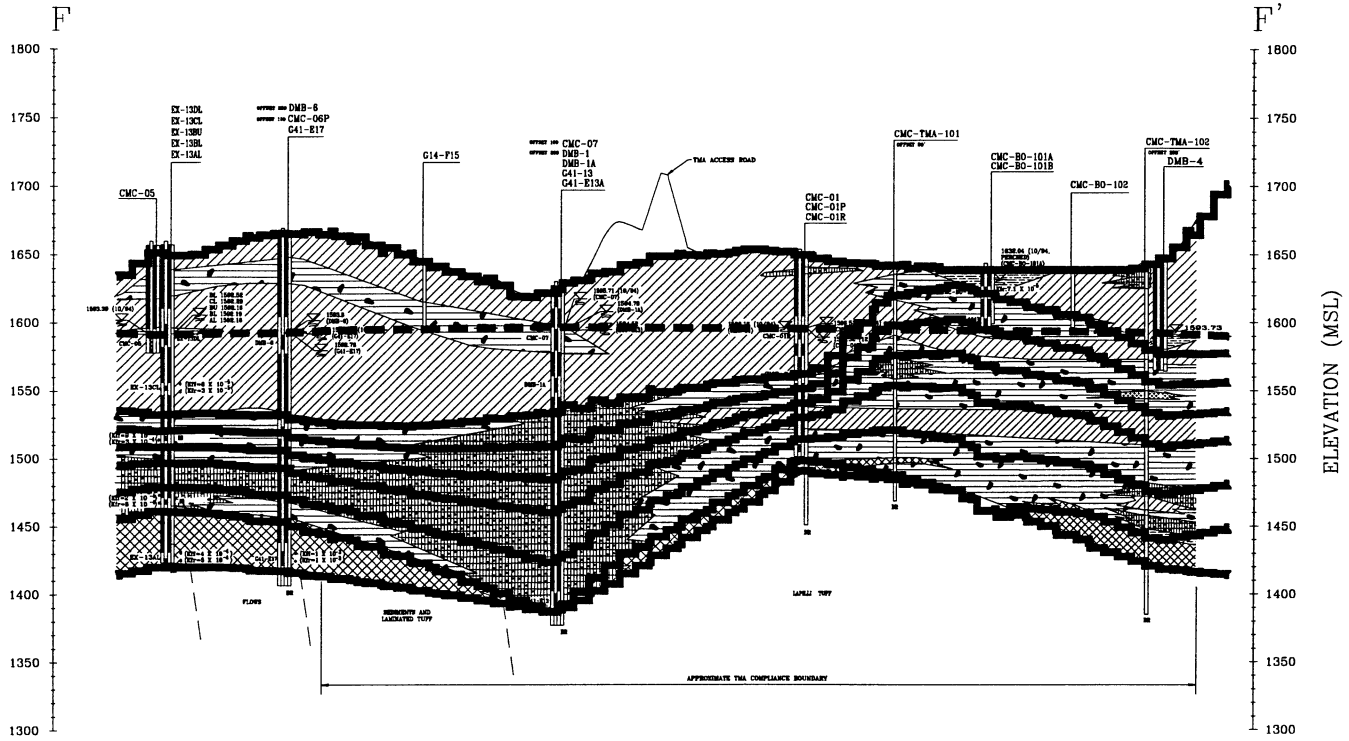

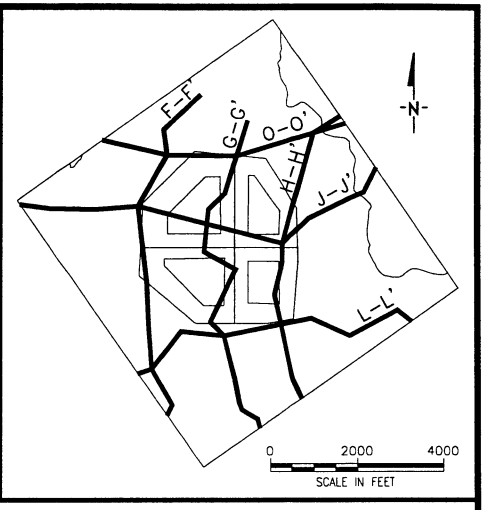

4.2-10-172

WELL CONSTRUCTION INFORMATION

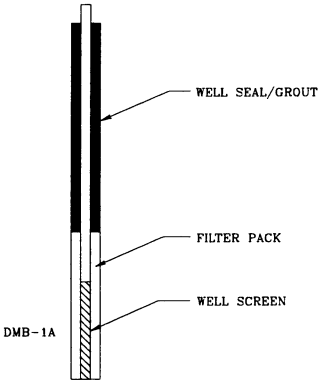

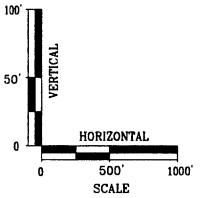

LEGEND

- LATE WISCONSIN TILL
- EARLY WISCONSIN TILL
- FINE OUTWASH
- COARSE OUTWASH
- GEOLOGIC CONTACT
- POTENTIOMETRIC SURFACE
- MODEL LAYER
- LACUSTRINE
- ICE MARGINAL SAND & GRAVEL AND LACUSTRINE CLAY
- MASSIVE SAPROLITE
- STRUCTURED SAPROLITE BEDROCK
- 1555.45 ▽ WATER LEVEL ON 10/84 UNLESS OTHERWISE NOTED
- BR UNDIFFERENTIATED BEDROCK
- ● BR INFERRED UNDIFFERENTIATED BEDROCK ELEVATION BASED UPON STS 1984 BEDROCK ELEVATION MAP
- • Kff FIELD PERMEABILITY – FALLING HEAD TEST IN CM/SEC.
- • Kfr FIELD PERMEABILITY – RISING HEAD TEST IN CM/SEC.

NOTE: GEOLOGIC CROSS SECTIONS OBTAINED FROM FOTH AND VAN DYKE'S REGIONAL, REVISED REGIONAL, AND REVISED TMA CROSS SECTIONS.

HSI GEOTRANS, INC.

REVISED	DATE	BY	DESCRIPTION

CHECKED BY: GWC	DATE: April 98
APPROVED BY: PFA	DATE: April 98
APPROVED BY:	DATE:

Nicolet Minerals COMPANY

Mining for the Future • Commitment

FIGURE 2.5
MODEL CROSS SECTION F–F'

Scale: AS SHOWN	Date: APRIL, 1998
Prepared By: HSI GEOTRANS, INC.	By: CMP

N015003B.DWG

SECTION G–G'

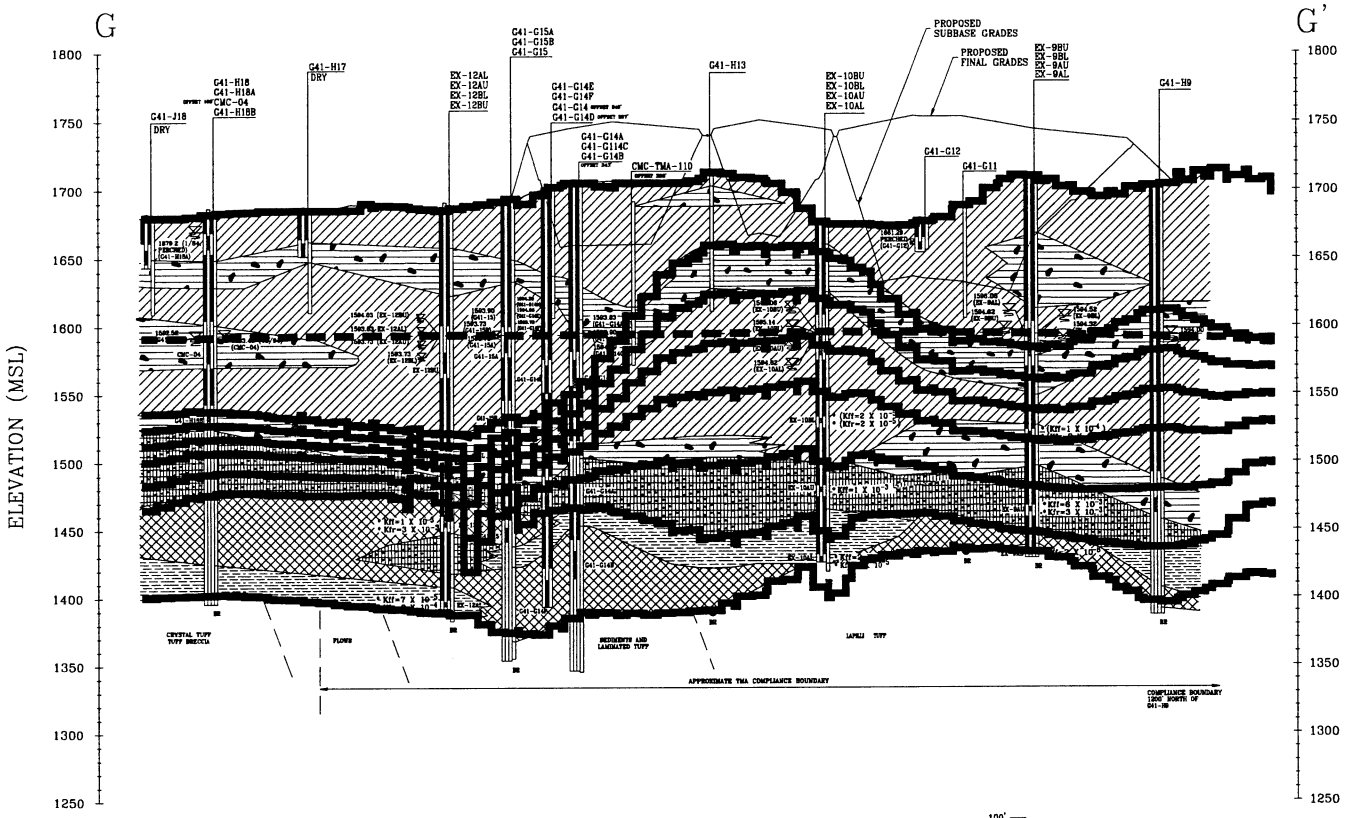

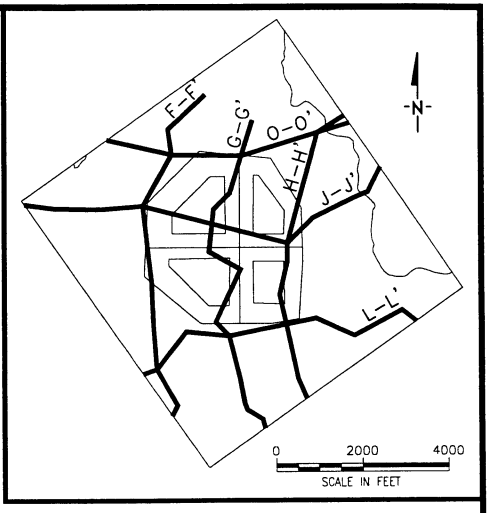

WELL CONSTRUCTION INFORMATION

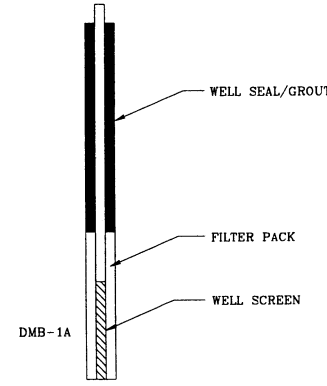

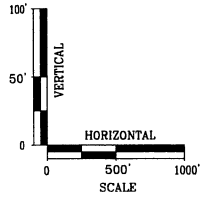

LEGEND

- LATE WISCONSIN TILL
- EARLY WISCONSIN TILL
- FINE OUTWASH
- COARSE OUTWASH
- GEOLOGIC CONTACT
- POTENTIOMETRIC SURFACE
- MODEL LAYER
- LACUSTRINE
- ICE MARGINAL SAND & GRAVEL AND LACUSTRINE CLAY
- MASSIVE SAPROLITE
- STRUCTURED SAPROLITE BEDROCK
- 1555.45 WATER LEVEL ON 10/84 UNLESS OTHERWISE NOTED
- BR UNDIFFERENTIATED BEDROCK
- ● BR INFERRED UNDIFFERENTIATED BEDROCK ELEVATION BASED UPON STS 1984 BEDROCK ELEVATION MAP
- * Kff FIELD PERMEABILITY – FALLING HEAD TEST IN CM/SEC.
- * Kfr FIELD PERMEABILITY – RISING HEAD TEST IN CM/SEC.

NOTE: GEOLOGIC CROSS SECTIONS OBTAINED FROM FOTH AND VAN DYKE'S REGIONAL, REVISED REGIONAL, AND REVISED TMA CROSS SECTIONS.

4.2-10-173

HSI GEOTRANS, INC.

REVISED	DATE	BY	DESCRIPTION

CHECKED BY: GWC	DATE: 4/98
APPROVED BY: PFA	DATE: 4/98
APPROVED BY:	DATE:

Nicolet Minerals COMPANY

FIGURE 2.6
MODEL CROSS SECTION G–G'

Scale: AS SHOWN	Date: APRIL, 1998
Prepared By: HSI GEOTRANS, INC.	By: CMP

N015003C.DWG

SECTION H–H'

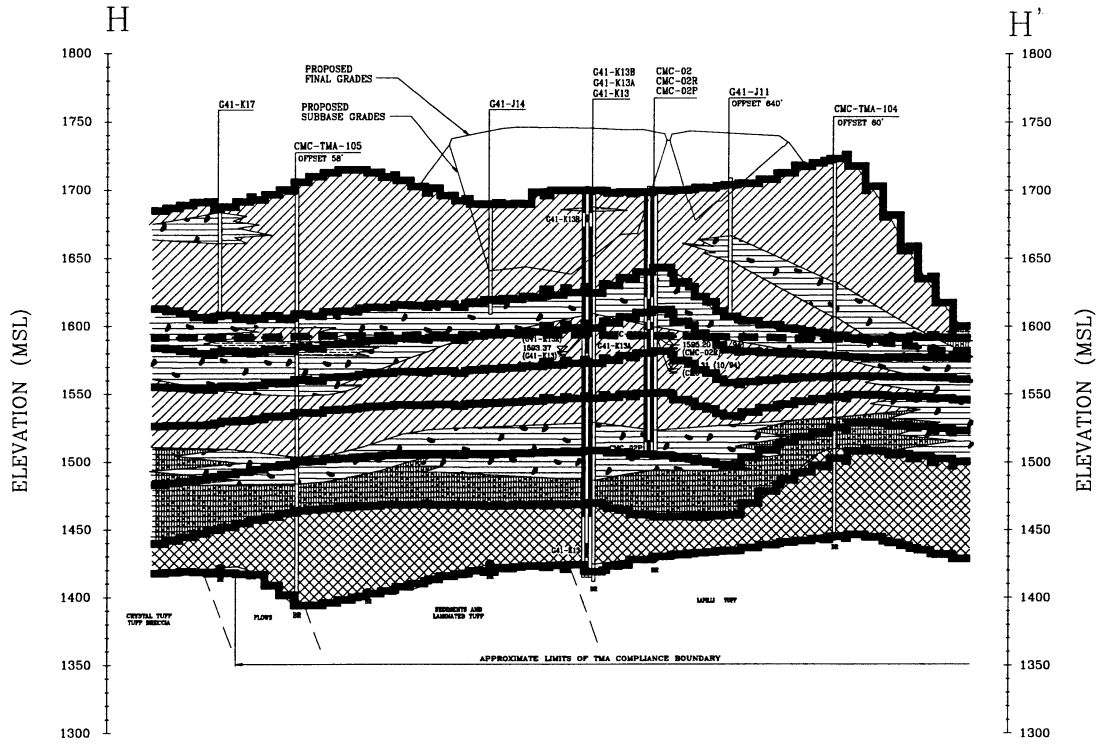

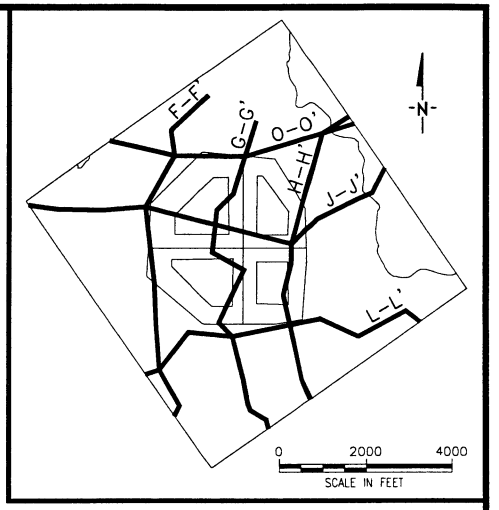

WELL CONSTRUCTION INFORMATION

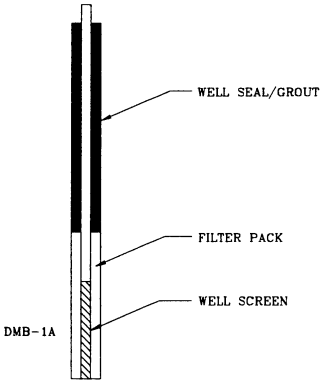

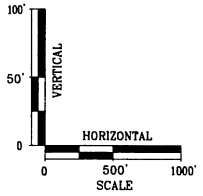

LEGEND

- LATE WISCONSIN TILL
- EARLY WISCONSIN TILL
- FINE OUTWASH
- COARSE OUTWASH
- GEOLOGIC CONTACT
- POTENTIOMETRIC SURFACE
- MODEL LAYER
- LACUSTRINE
- ICE MARGINAL SAND & GRAVEL AND LACUSTRINE CLAY
- MASSIVE SAPROLITE
- STRUCTURED SAPROLITE BEDROCK
- 1555.45 WATER LEVEL ON 10/84 UNLESS OTHERWISE NOTED
- BR UNDIFFERENTIATED BEDROCK
- ● BR INFERRED UNDIFFERENTIATED BEDROCK ELEVATION BASED UPON STS 1984 BEDROCK ELEVATION MAP
- • Kff FIELD PERMEABILITY – FALLING HEAD TEST IN CM/SEC.
- • Kfr FIELD PERMEABILITY – RISING HEAD TEST IN CM/SEC.

NOTE: GEOLOGIC CROSS SECTIONS OBTAINED FROM FOTH AND VAN DYKE'S REGIONAL, REVISED REGIONAL, AND REVISED TMA CROSS SECTIONS.

4.2-10-174

HSI GEOTRANS, INC.

REVISED	DATE	BY	DESCRIPTION

CHECKED BY: GWC	DATE: April 98
APPROVED BY: PFA	DATE: April 98
APPROVED BY:	DATE:

Nicolet Minerals COMPANY

Mining for the Future Commitment

FIGURE 2.7
MODEL CROSS SECTION H–H'

Scale: AS SHOWN	Date: APRIL, 1998
Prepared By: HSI GEOTRANS, INC.	By: CMP

NO15003D.DWG

SECTION 0–0'

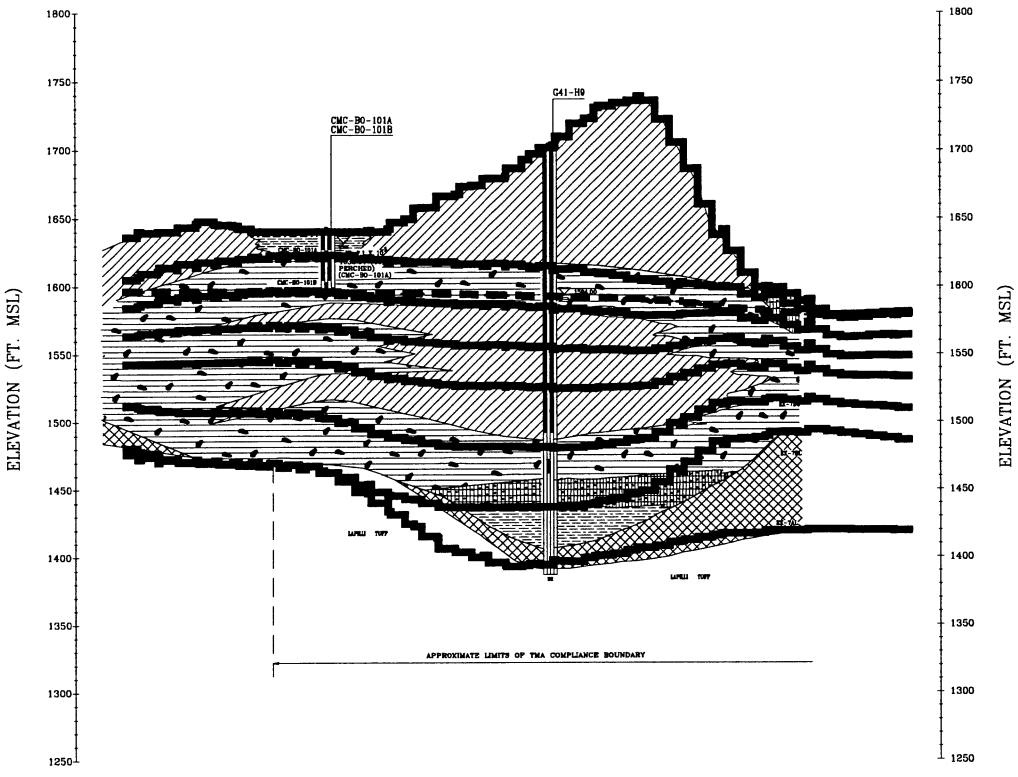

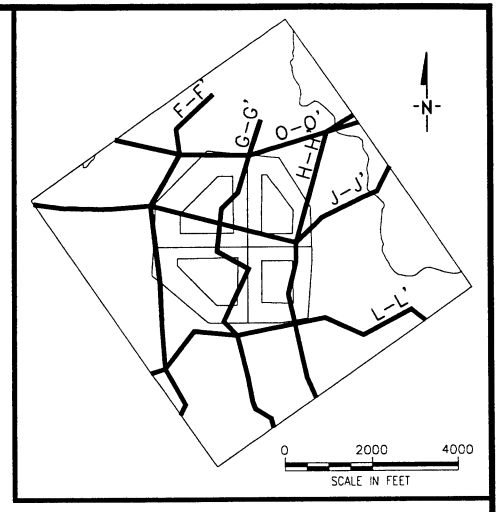

WELL CONSTRUCTION INFORMATION

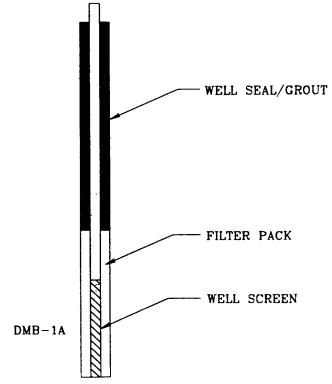

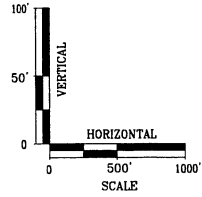

4.2-10-175

LEGEND

- LATE WISCONSIN TILL
- EARLY WISCONSIN TILL
- FINE OUTWASH
- COARSE OUTWASH
- GEOLOGIC CONTACT
- POTENTIOMETRIC SURFACE
- MODEL LAYER
- LACUSTRINE
- ICE MARGINAL SAND & GRAVEL AND LACUSTRINE CLAY
- MASSIVE SAPROLITE
- STRUCTURED SAPROLITE BEDROCK
- 1555.45 WATER LEVEL ON 10/84 UNLESS OTHERWISE NOTED
- BR UNDIFFERENTIATED BEDROCK
- ● BR INFERRED UNDIFFERENTIATED BEDROCK ELEVATION BASED UPON STS 1984 BEDROCK ELEVATION MAP
- * Kff FIELD PERMEABILITY – FALLING HEAD TEST IN CM/SEC.
- * Kfr FIELD PERMEABILITY – RISING HEAD TEST IN CM/SEC.

NOTE: GEOLOGIC CROSS SECTIONS OBTAINED FROM FOTH AND VAN DYKE'S REGIONAL, REVISED REGIONAL, AND REVISED TMA CROSS SECTIONS.

HSI GEOTRANS, INC.			
REVISED	DATE	BY	DESCRIPTION
CHECKED BY: GWC			DATE: April 98
APPROVED BY: PFA			DATE: April 98
APPROVED BY:			DATE:

Nicolet Minerals COMPANY

Mining for the Future • Commitment

FIGURE 2.8
MODEL CROSS SECTION 0–0'

Scale: AS SHOWN	Date: APRIL, 1998
Prepared By: HSI GEOTRANS, INC.	By: CMP

NO15003E.DWG

SECTION J–J'

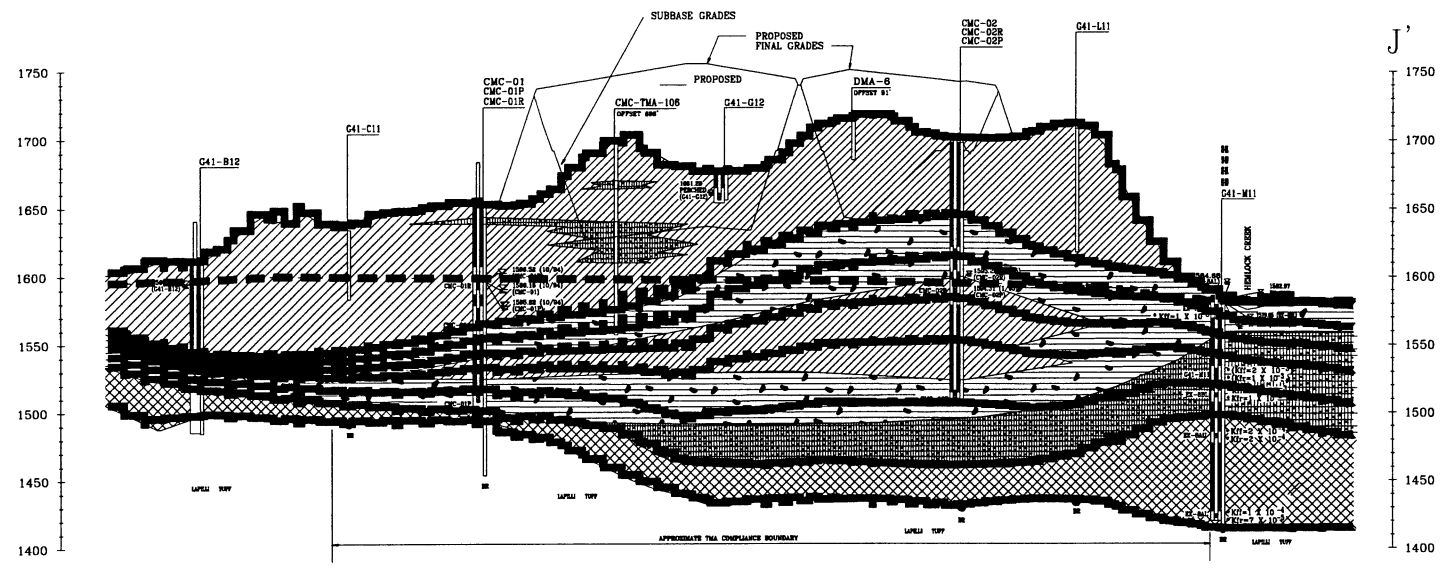

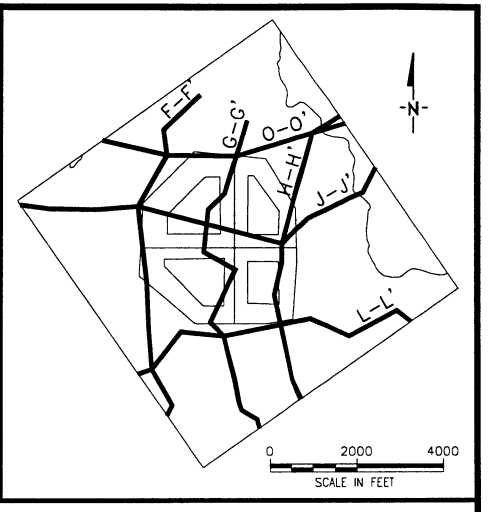

4.2-10-176

WELL CONSTRUCTION INFORMATION

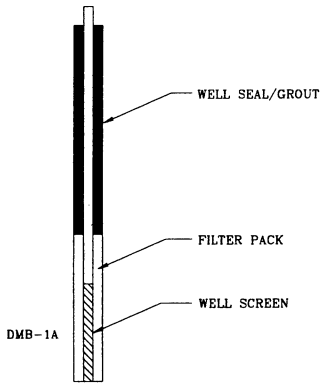

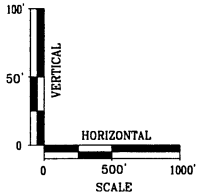

LEGEND

- LATE WISCONSIN TILL
- EARLY WISCONSIN TILL
- FINE OUTWASH
- COARSE OUTWASH
- GEOLOGIC CONTACT
- POTENTIOMETRIC SURFACE
- MODEL LAYER
- LACUSTRINE
- ICE MARGINAL SAND & GRAVEL AND LACUSTRINE CLAY
- MASSIVE SAPROLITE
- STRUCTURED SAPROLITE BEDROCK
- 1555.45 WATER LEVEL ON 10/84 UNLESS OTHERWISE NOTED
- BR UNDIFFERENTIATED BEDROCK
- BR INFERRED UNDIFFERENTIATED BEDROCK ELEVATION BASED UPON STS 1984 BEDROCK ELEVATION MAP
- • Kff FIELD PERMEABILITY – FALLING HEAD TEST IN CM/SEC.
- • Kfr FIELD PERMEABILITY – RISING HEAD TEST IN CM/SEC.

NOTE: GEOLOGIC CROSS SECTIONS OBTAINED FROM FOTH AND VAN DYKE'S REGIONAL, REVISED REGIONAL, AND REVISED TMA CROSS SECTIONS.

HSI GEOTRANS, INC.

REVISED	DATE	BY	DESCRIPTION

CHECKED BY: GWC	DATE: April 98
APPROVED BY: PFA	DATE: April 98
APPROVED BY:	DATE:

Nicolet Minerals COMPANY

FIGURE 2.9
MODEL CROSS SECTION J–J'

Scale: AS SHOWN	Date: APRIL, 1998
Prepared By: HSI GEOTRANS, INC.	By: CMP

N015003F.DWG

SECTION L-L'

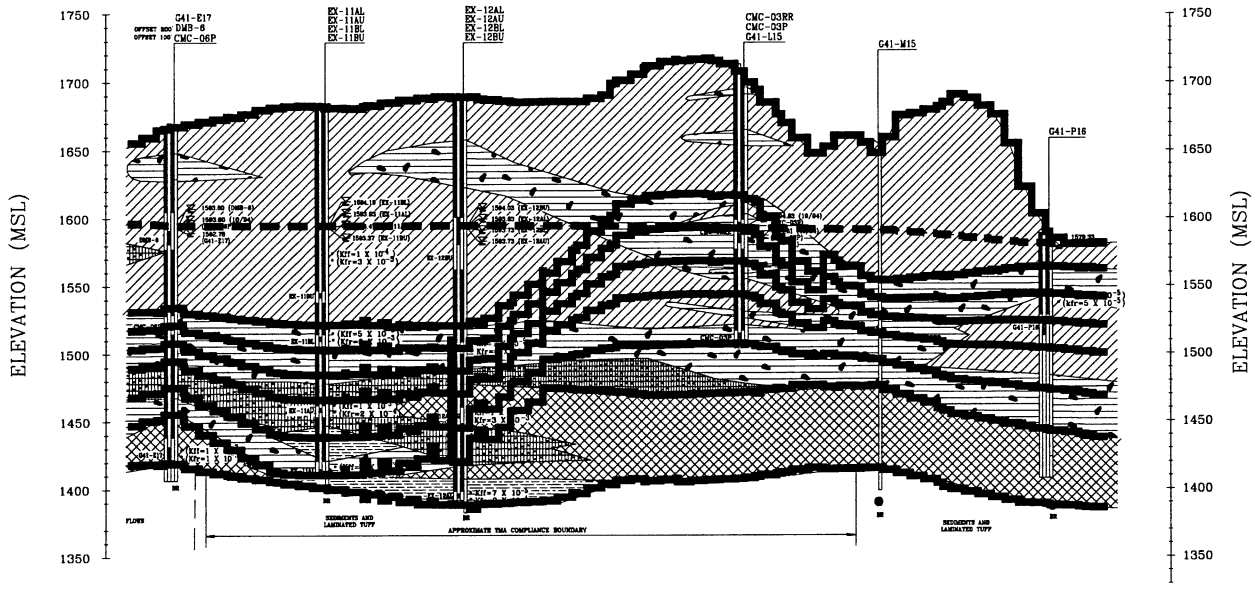

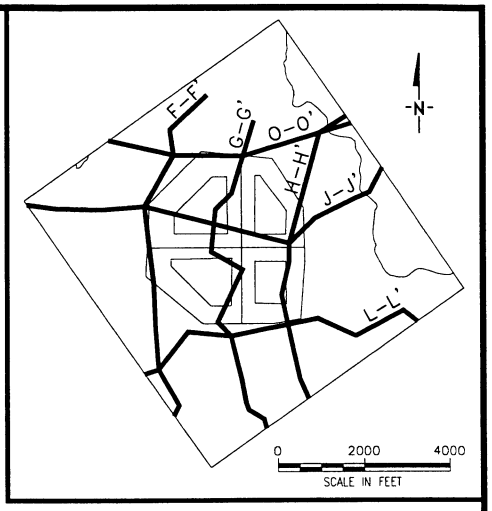

WELL CONSTRUCTION INFORMATION

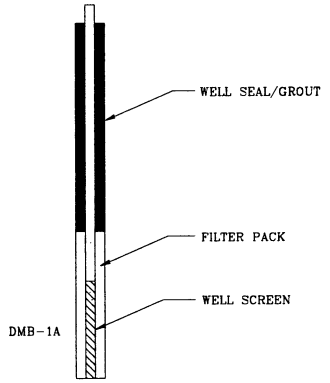

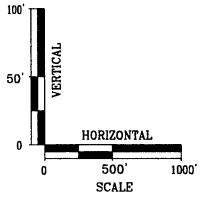

LEGEND

- LATE WISCONSIN TILL
- EARLY WISCONSIN TILL
- FINE OUTWASH
- COARSE OUTWASH
- GEOLOGIC CONTACT
- POTENTIOMETRIC SURFACE
- MODEL LAYER
- LACUSTRINE
- ICE MARGINAL SAND & GRAVEL AND LACUSTRINE CLAY
- MASSIVE SAPROLITE
- STRUCTURED SAPROLITE BEDROCK
- 1555.45 WATER LEVEL ON 10/84 UNLESS OTHERWISE NOTED
- BR UNDIFFERENTIATED BEDROCK
- BR INFERRED UNDIFFERENTIATED BEDROCK ELEVATION BASED UPON STS 1984 BEDROCK ELEVATION MAP
- • Kff FIELD PERMEABILITY - FALLING HEAD TEST IN CM/SEC.
- • Kfr FIELD PERMEABILITY - RISING HEAD TEST IN CM/SEC.

NOTE: GEOLOGIC CROSS SECTIONS OBTAINED FROM FOTH AND VAN DYKE'S REGIONAL, REVISED REGIONAL, AND REVISED TMA CROSS SECTIONS.

4.2-10-177

HSI GEOTRANS, INC.			
REVISED	DATE	BY	DESCRIPTION
CHECKED BY: GWC			DATE: April 98
APPROVED BY: PFA			DATE: April 98
APPROVED BY:			DATE:

Nicolet Minerals COMPANY

FIGURE 2.10
MODEL CROSS SECTION L-L'

Scale: AS SHOWN	Date: APRIL, 1998
Prepared By: HSI GEOTRANS, INC.	By: CMP

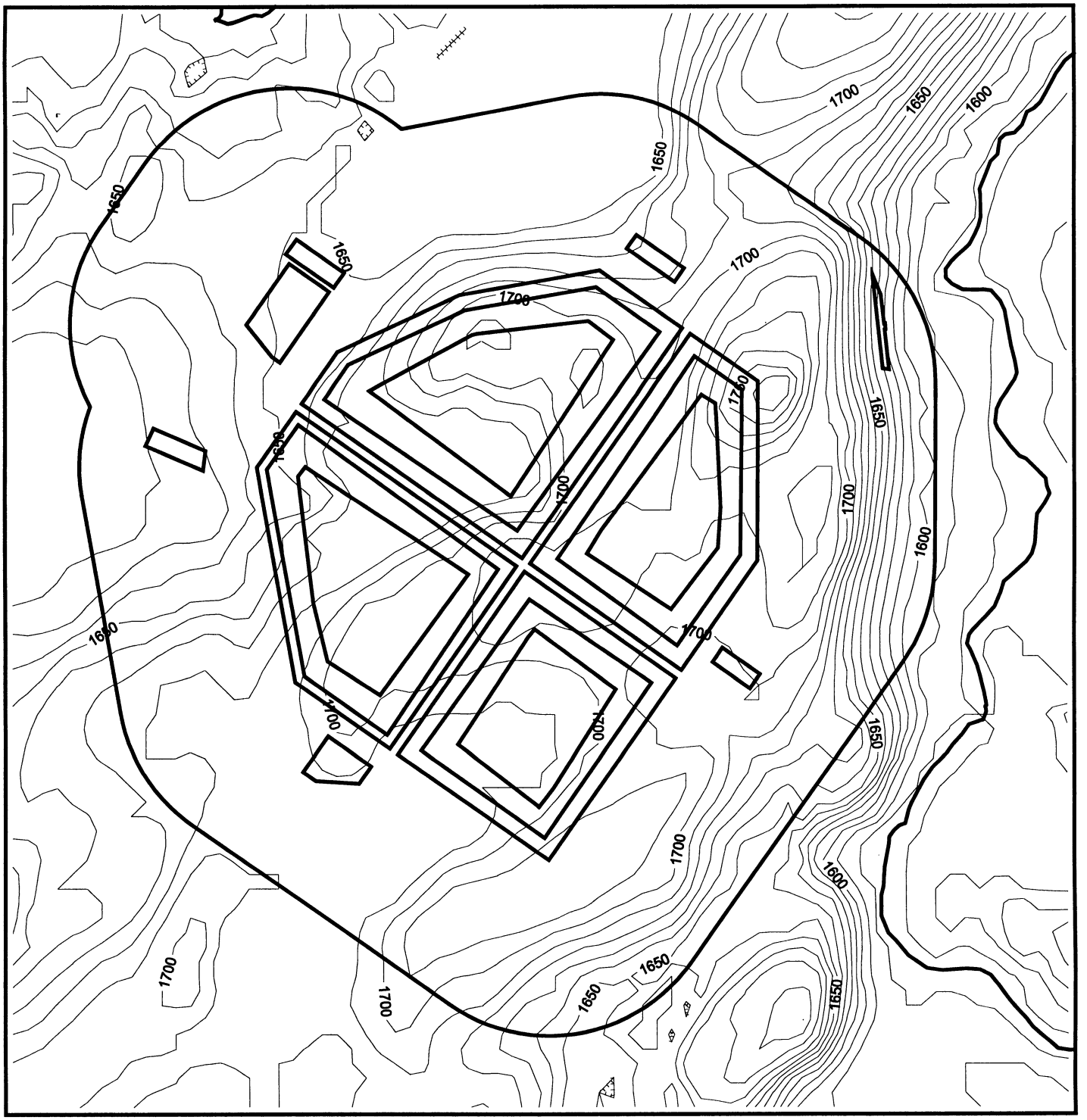

Notes:
1) Elevation in feet, msl.
2) Contour interval 10 feet.

0 1000 2000

Scale in Feet

HSI GEOTRANS			
REVISED	DATE	BY	DESCRIPTION

CHECKED BY: GWC	DATE: April 1998
APPROVED BY: PFA	DATE: April 1998
APPROVED BY:	DATE:

Nicolet Minerals COMPANY

Figure 2.11
Topographic Elevation in the TMA Sub-Model Domain

Scale: 1 in. = 1000 ft.	Date: April 1998
Prepared By: HSI GEOTRANS	By: RMD

\Crandon\TmaMod3\Surfer\wp0.srf

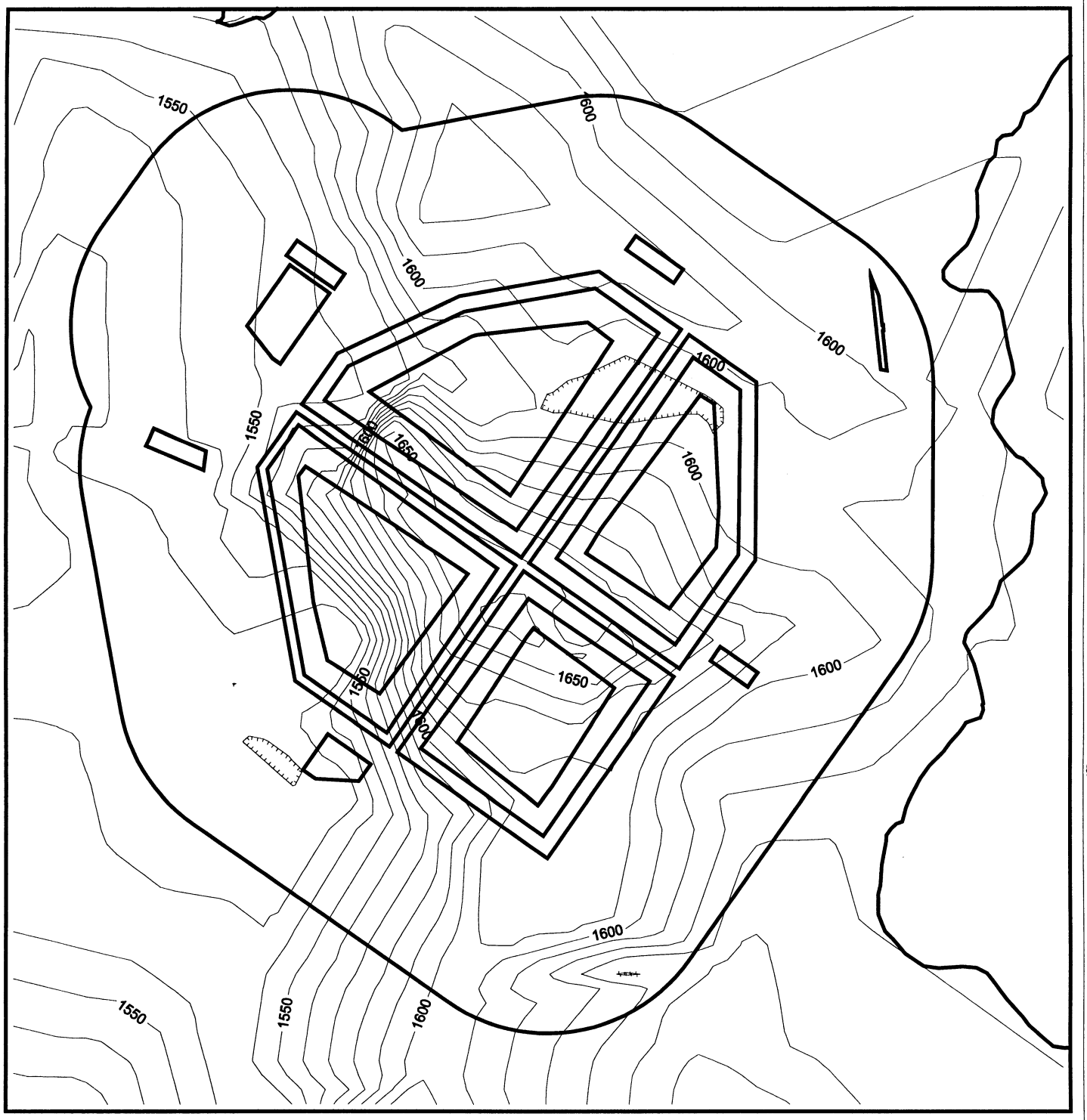

Notes:
1) Elevation in feet, msl.
2) Contour interval 10 feet.

N

0 1000 2000

Scale in Feet

HSI GEOTRANS			
REVISED	DATE	BY	DESCRIPTION

CHECKED BY: GWC	DATE: April 1998
APPROVED BY: PFA	DATE: April 1998
APPROVED BY:	DATE:

Nicolet Minerals COMPANY

Figure 2.12
Model Layer 1 Bottom Elevation

Scale: 1 in. = 1000 ft.	Date: April 1998
Prepared By: HSI GEOTRANS	By: RMD

\Crandon\Tmw\Mod3\Surfer\Bot1.srf

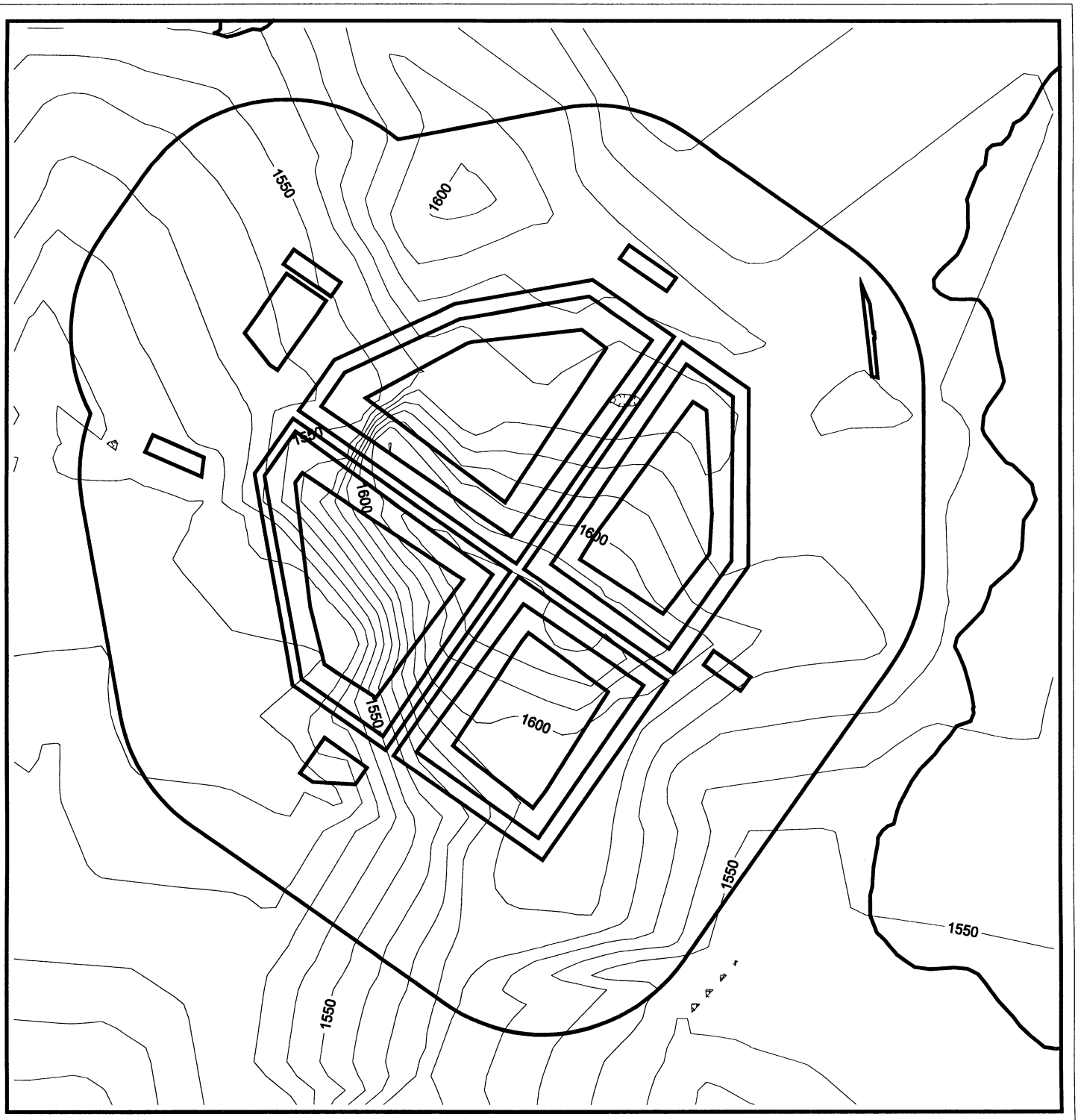

Notes:
1) Elevation in feet, msl.
2) Contour interval 10 feet.

0 1000 2000

Scale in Feet

HSI GEOTRANS			
REVISED	DATE	BY	DESCRIPTION

CHECKED BY: GWC	DATE: April 1998
APPROVED BY: PFA	DATE: April 1998
APPROVED BY:	DATE:

Nicolet Minerals COMPANY

Figure 2.13
Model Layer 2 Bottom Elevation

Scale: 1 in. = 1000 ft.	Date: April 1998
Prepared By: HSI GEOTRANS	By: RMD

\CrandonTmwMod3\Surfaces\Lay2.srf

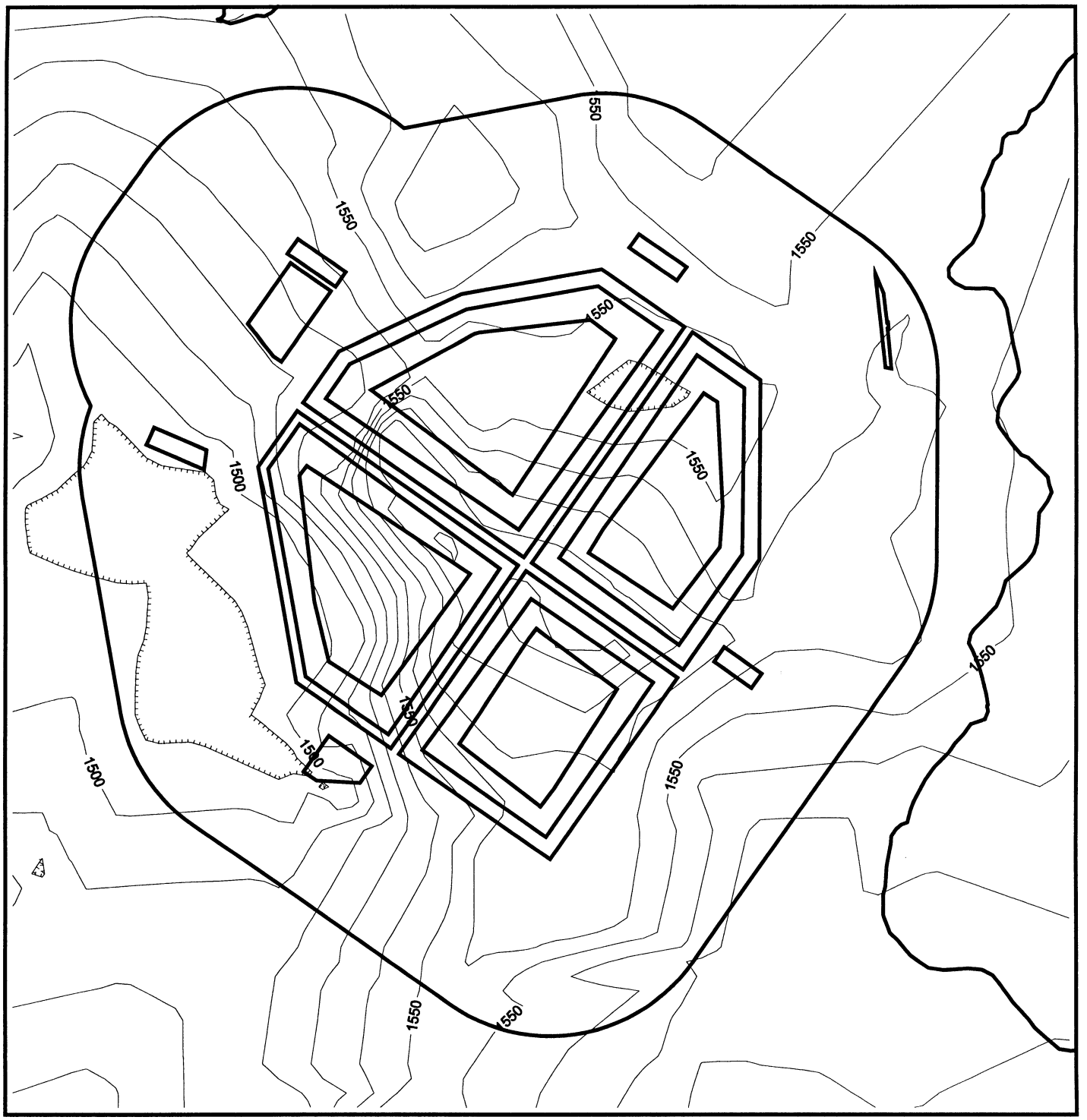

Notes:
1) Elevation in feet, msl.
2) Contour interval 10 feet.

N

0 1000 2000

Scale in Feet

HSI GEOTRANS			
REVISED	DATE	BY	DESCRIPTION

CHECKED BY: GWC	DATE: April 1998
APPROVED BY: PFA	DATE: April 1998
APPROVED BY:	DATE:

Nicolet Minerals COMPANY

Figure 2.14
Model Layer 3 Bottom Elevation

Scale: 1 in. = 1000 ft.	Date: April 1998
Prepared By: HSI GEOTRANS	By: RMD

\Crandon\Tma\Mod3\Surfer\Bot3.srf

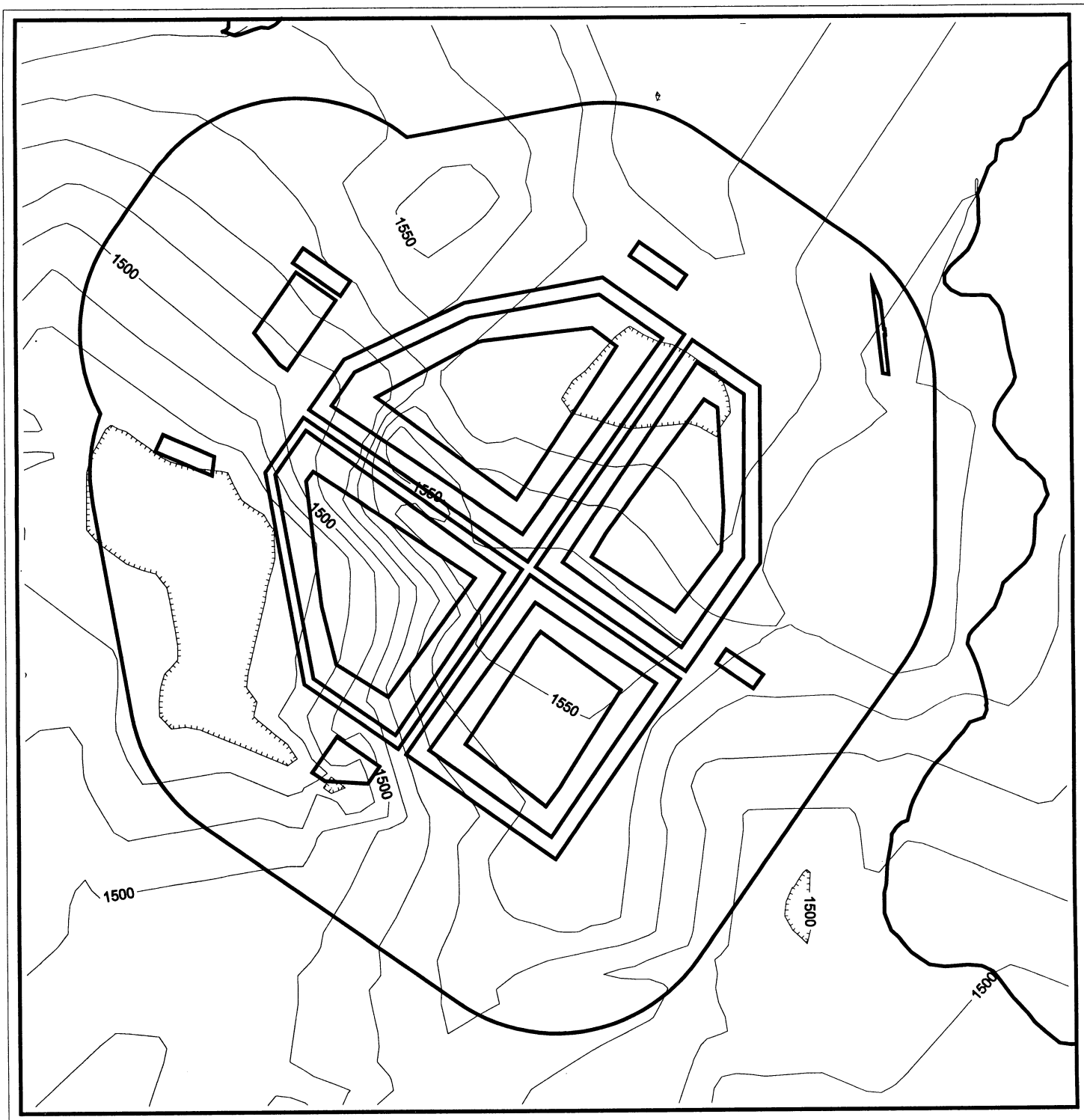

Notes:
1) Elevation in feet, msl.
2) Contour interval 10 feet.

N

0 1000 2000

Scale in Feet

HSI GEOTRANS			
REVISED	DATE	BY	DESCRIPTION
CHECKED BY: GWC			DATE: April 1998
APPROVED BY: PFA			DATE: April 1998
APPROVED BY:			DATE:

Nicolet Minerals COMPANY

Figure 2.15
Model Layer 4 Bottom Elevation

Scale: 1 in. = 1000 ft.	Date: April 1998
Prepared By: HSI GEOTRANS	By: RMD

\Crandon\Tmal\Mod3\Surfaces\lay4.srf

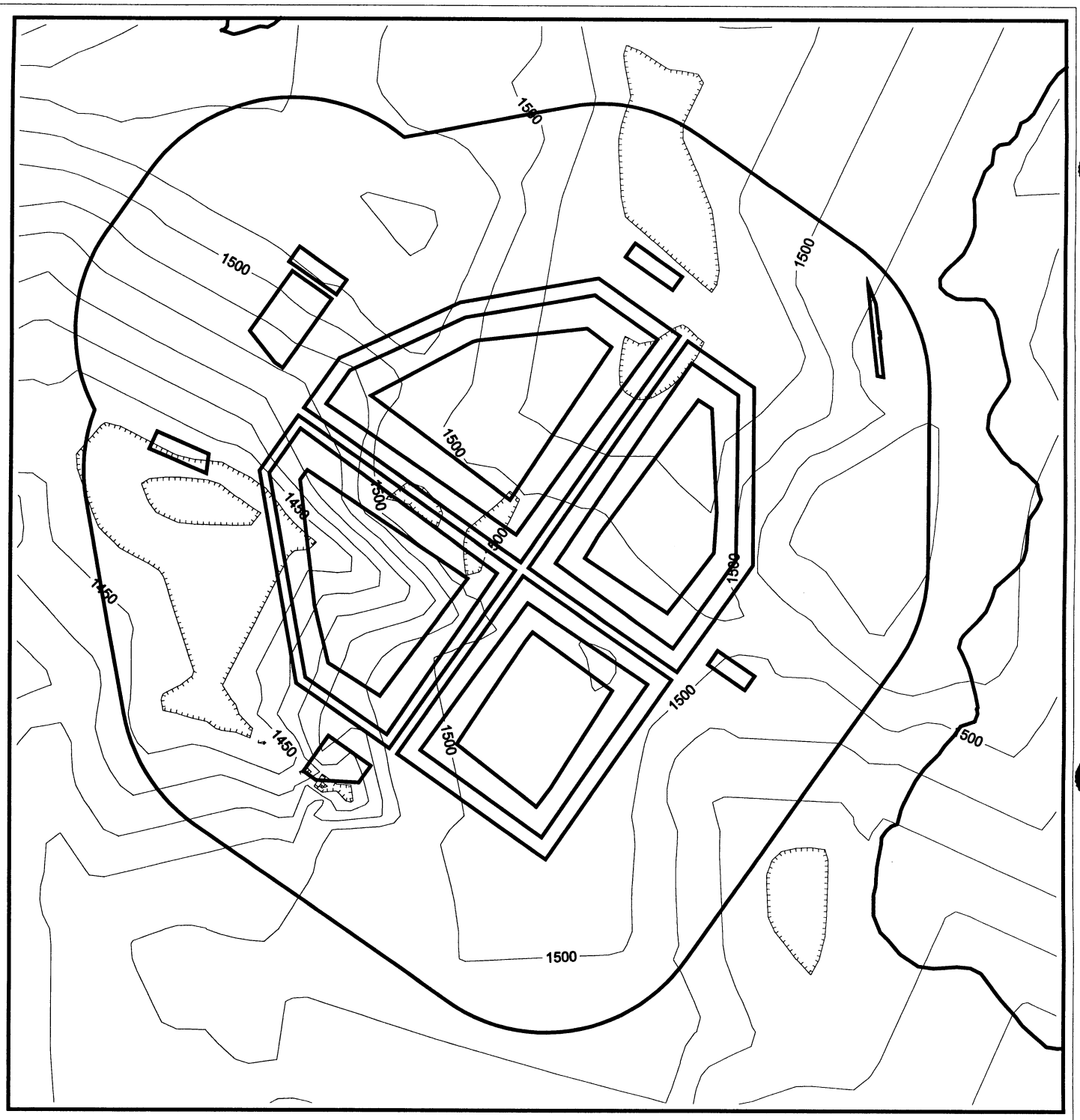

Notes:
1) Elevation in feet, msl.
2) Contour interval 10 feet.

N

0 1000 2000

Scale in Feet

HSI GEOTRANS			
REVISED	DATE	BY	DESCRIPTION

CHECKED BY: GWC	DATE: April 1998
APPROVED BY: PFA	DATE: April 1998
APPROVED BY:	DATE:

Nicolet Minerals COMPANY

Figure 2.16
Model Layer 5 Bottom Elevation

Scale: 1 in. = 1000 ft.	Date: April 1998
Prepared By: HSI GEOTRANS	By: RMD

\CrandonTmaMod3\Surfer\Bot5.srf

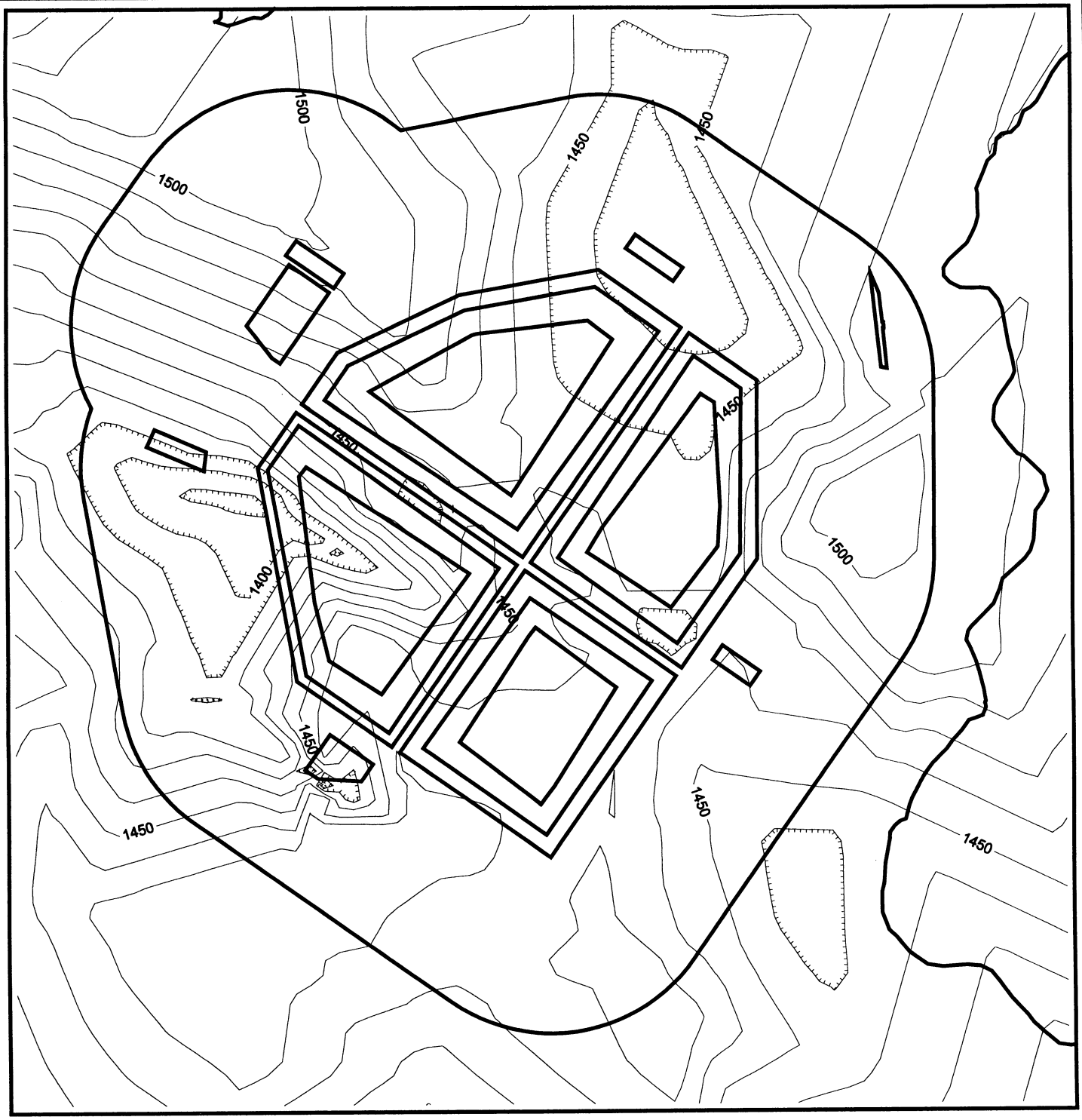

Notes:
1) Elevation in feet, msl.
2) Contour interval 10 feet.

0 1000 2000

Scale in Feet

HSI GEOTRANS			
REVISED	DATE	BY	DESCRIPTION

CHECKED BY: GWC	DATE: April 1998
APPROVED BY: PFA	DATE: April 1998
APPROVED BY:	DATE:

Nicolet Minerals COMPANY

Figure 2.17
Model Layer 6 Bottom Elevation

Scale: 1 in. = 1000 ft.	Date: April 1998
Prepared By: HSI GEOTRANS	By: RMD

\Crandon\Tmal\Mod3\Surfs\...srf

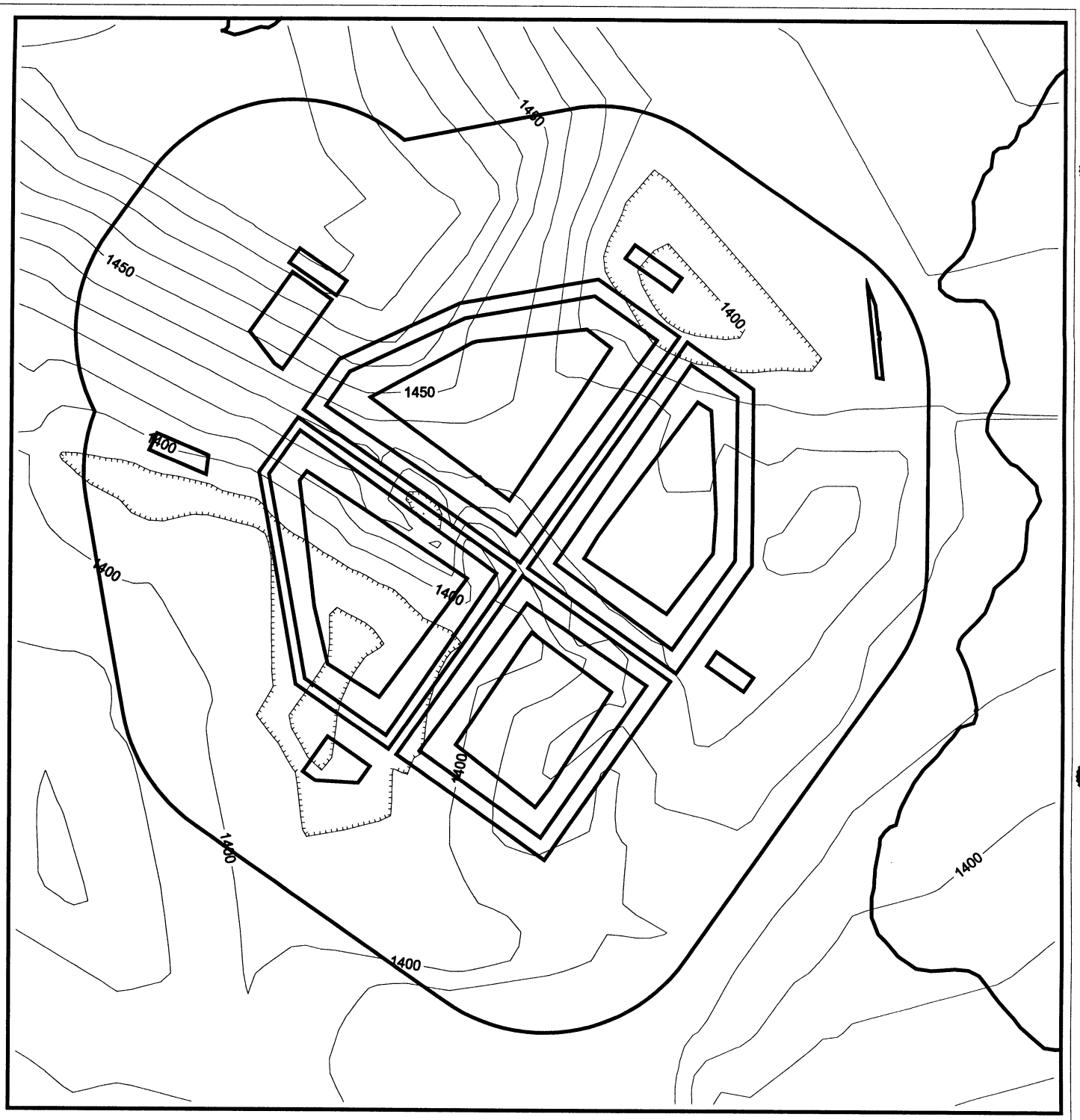

Notes:
1) Elevation in feet, msl.
2) Contour interval 10 feet.

N

0 1000 2000

Scale in Feet

HSI GEOTRANS			
REVISED	DATE	BY	DESCRIPTION

CHECKED BY: GWC	DATE: April 1998
APPROVED BY: PFA	DATE: April 1998
APPROVED BY:	DATE:

Nicolet Minerals COMPANY

Mining for the Future Commitment

Figure 2.18
Model Layer 7 Bottom Elevation

Scale: 1 in. = 1000 ft.	Date: April 1998
Prepared By: HSI GEOTRANS	By: RMD

\Crandon\Tma\Mod3\Surfer\Bot7.srf

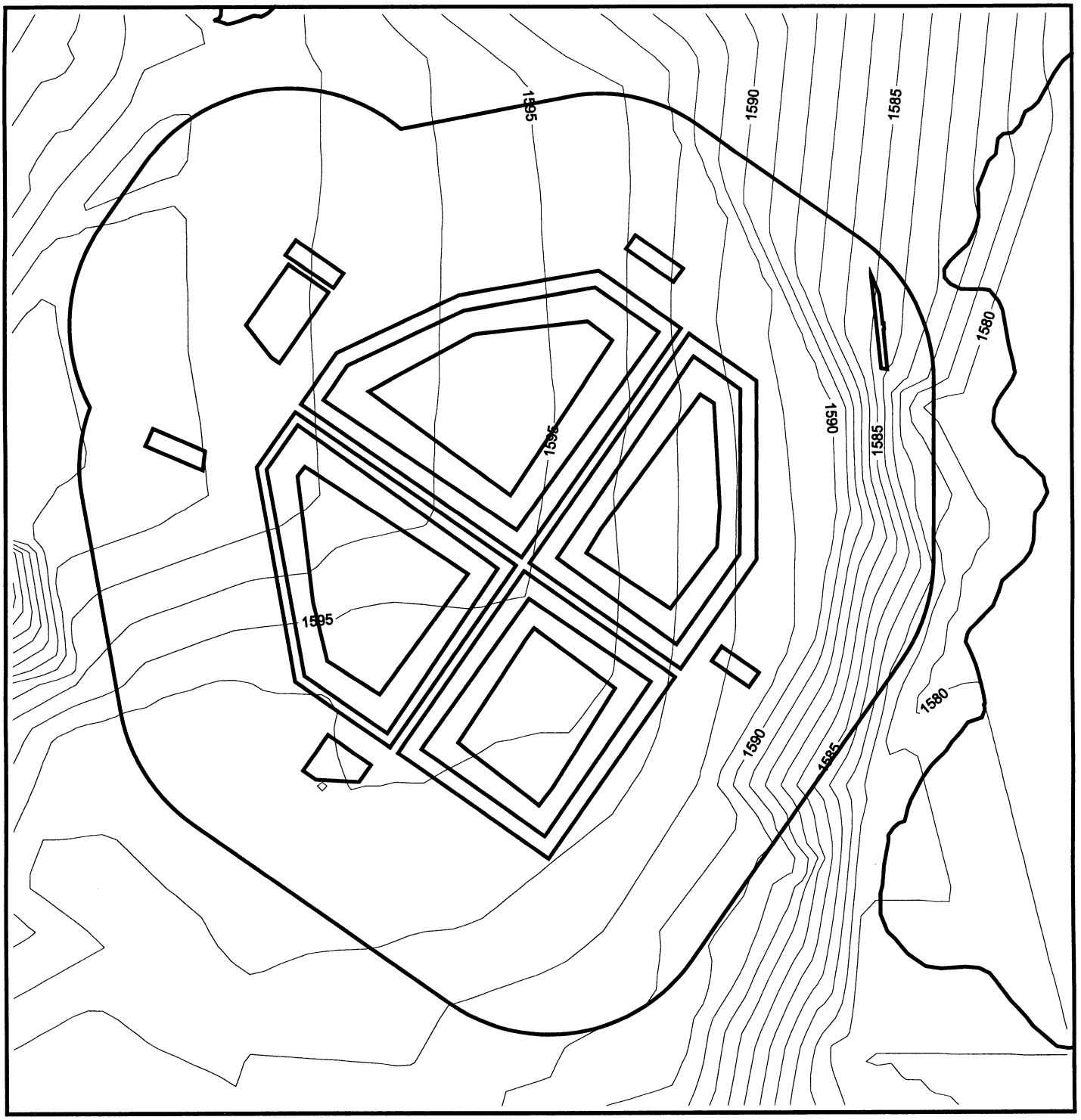

Notes:
1) Elevation in feet, msl.
2) Contour interval 1 foot.

0 1000 2000

Scale in Feet

HSI GEOTRANS			
REVISED	DATE	BY	DESCRIPTION
CHECKED BY: GWC			DATE: April 1998
APPROVED BY: PFA			DATE: April 1998
APPROVED BY:			DATE:

Nicolet Minerals COMPANY

Figure 2.19
1984 Observed Water Table

Scale: 1 in. = 1000 ft.	Date: April 1998
Prepared By: HSI GEOTRANS	By: RMD

\Crandon\TmaMod3\Surfa...srf

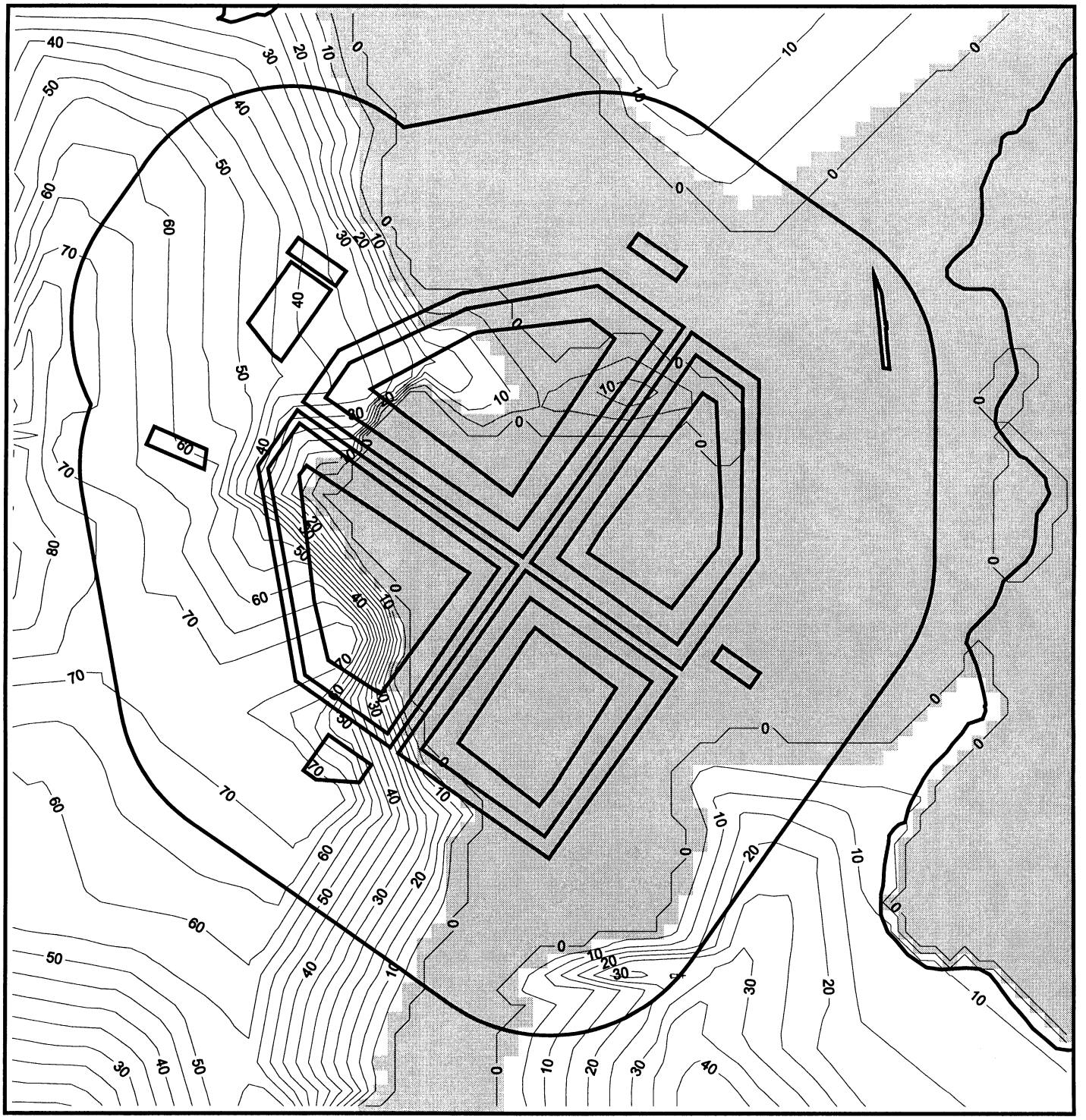

Inactive Area

Note:
Contour interval 5 feet.

N

0 1000 2000

Scale in Feet

HSI GEOTRANS			
REVISED	DATE	BY	DESCRIPTION

CHECKED BY: GWC	DATE: April 1998
APPROVED BY: PFA	DATE: April 1998
APPROVED BY:	DATE:

Nicolet Minerals COMPANY

Figure 2.20
Saturated Thickness of Model Layer 1

Scale: 1 in. = 1000 ft.	Date: April 1998
Prepared By: HSI GEOTRANS	By: RMD

\Crandon\Tma\Mod3\Surfer\Thk1.srf

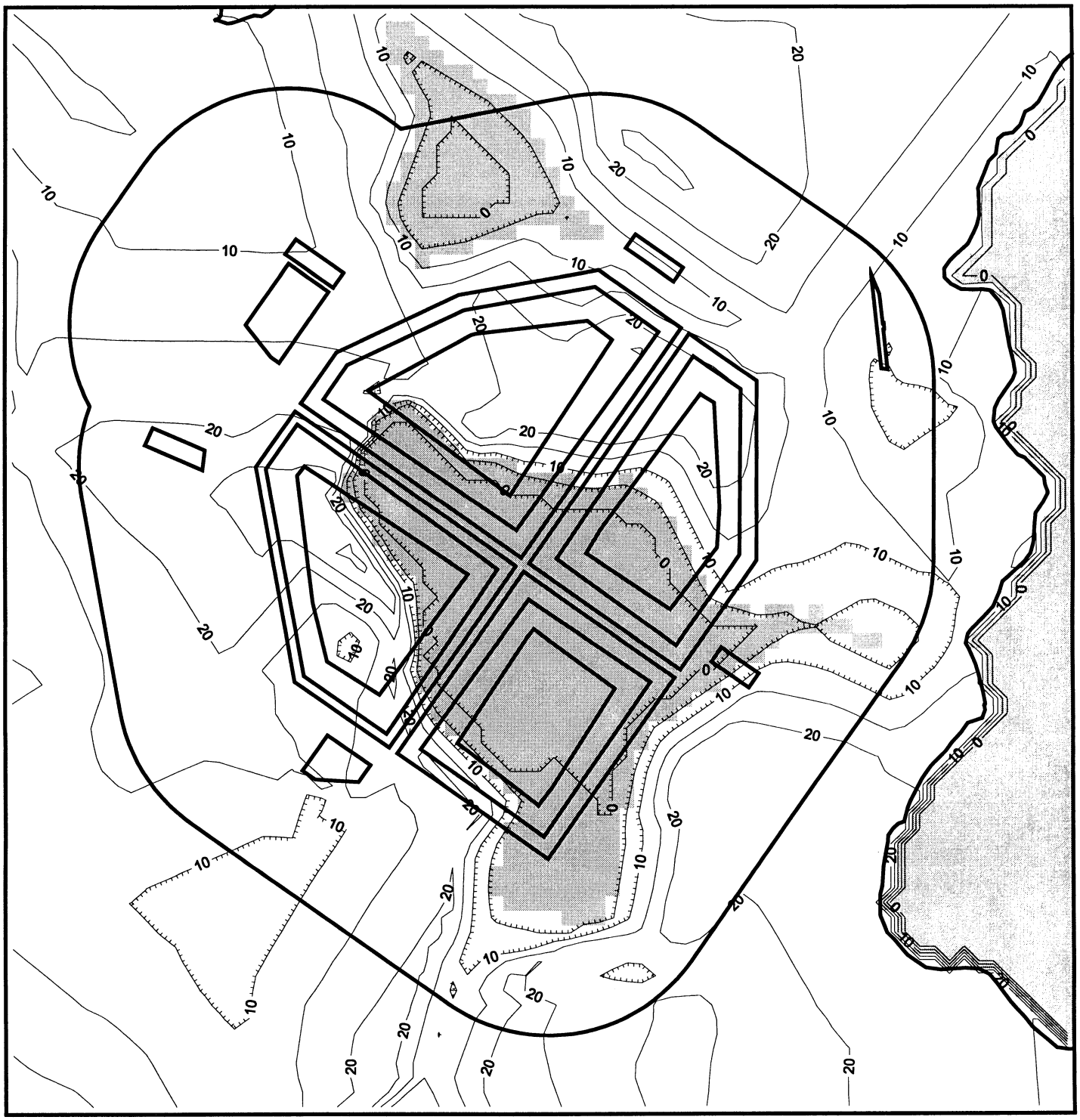

Inactive Area

Note:
Contour interval 5 feet.

N

0 1000 2000

Scale in Feet

HSI GEOTRANS			
REVISED	DATE	BY	DESCRIPTION

CHECKED BY: GWC	DATE: April 1998
APPROVED BY: PFA	DATE: April 1998
APPROVED BY:	DATE:

Nicolet Minerals COMPANY

Figure 2.21
Saturated Thickness of Model Layer 2

Scale: 1 in. = 1000 ft.	Date: April 1998
Prepared By: HSI GEOTRANS	By: RMD

\Crandon\Tma\Mod3\Surfc...srf

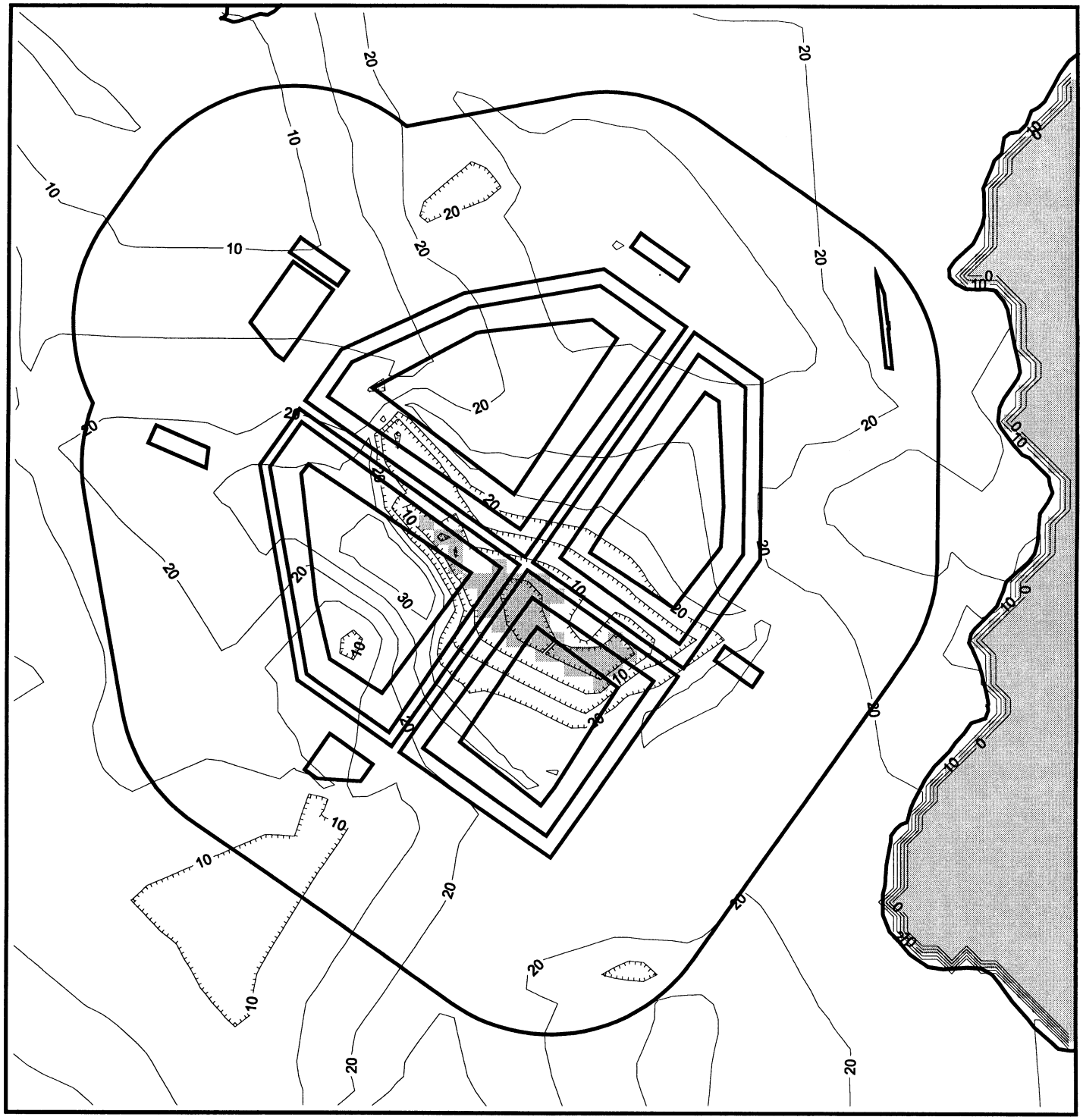

Inactive Area

Note:
Contour interval 5 feet.

N

0 1000 2000

Scale in Feet

HSI GEOTRANS			
REVISED	DATE	BY	DESCRIPTION

CHECKED BY: GWC	DATE: April 1998
APPROVED BY: PFA	DATE: April 1998
APPROVED BY:	DATE:

Nicolet Minerals COMPANY

Figure 2.22
Saturated Thickness of Model Layer 3

Scale: 1 in. = 1000 ft.	Date: April 1998
Prepared By: HSI GEOTRANS	By: RMD

\Crandon\Tmal\Mod3\Surfer\Thk3.srf

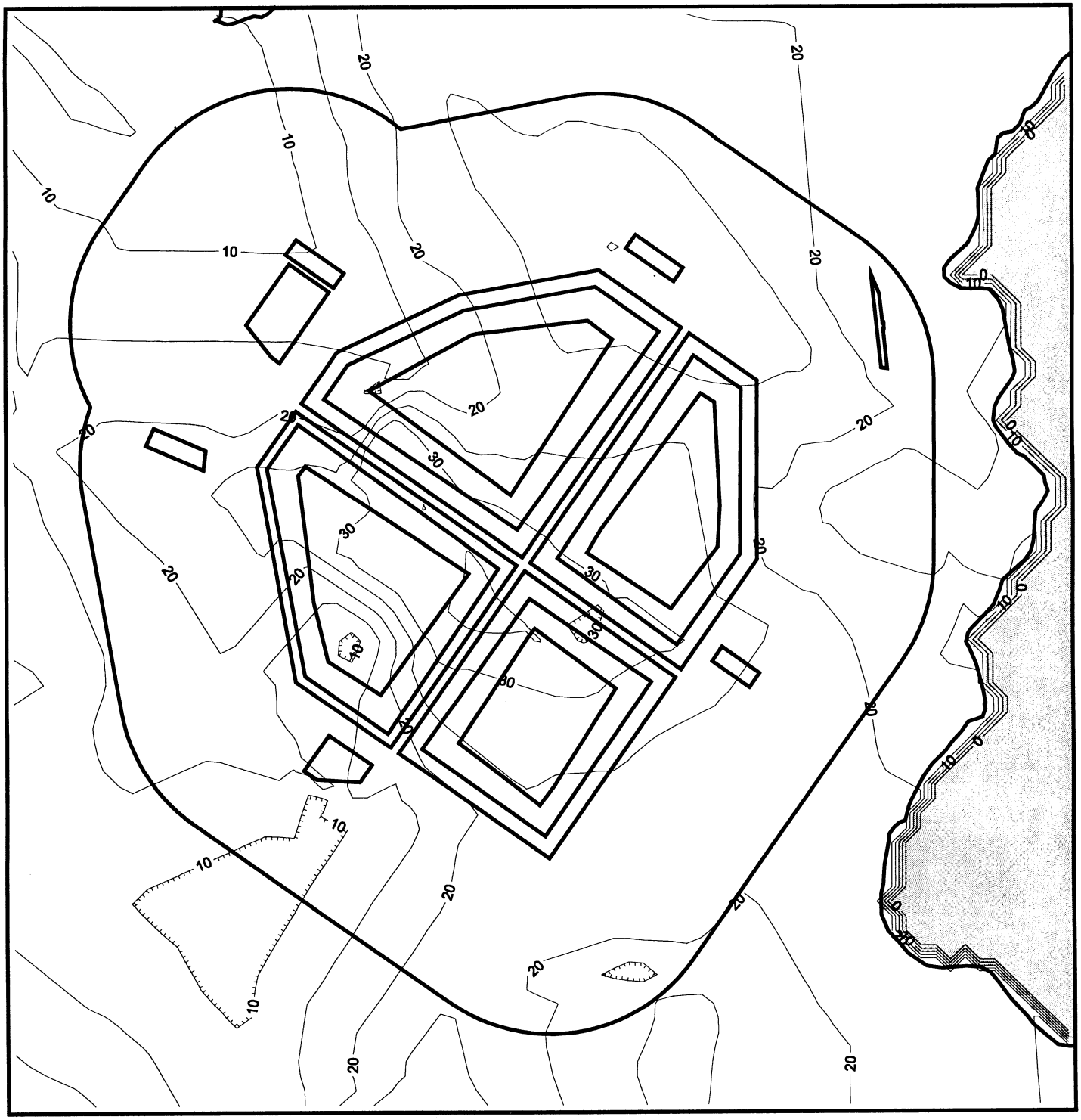

Inactive Area

Note:
Contour interval 5 feet.

0 1000 2000

Scale in Feet

HSI GEOTRANS			
REVISED	DATE	BY	DESCRIPTION

CHECKED BY: GWC	DATE: April 1998
APPROVED BY: PFA	DATE: April 1998
APPROVED BY:	DATE:

Nicolet Minerals COMPANY

Figure 2.23
Saturated Thickness of Model Layer 4

Scale: 1 in. = 1000 ft.	Date: April 1998
Prepared By: HSI GEOTRANS	By: RMD

\Crandon\Tma\Mod3\Surfer\wk4.srf

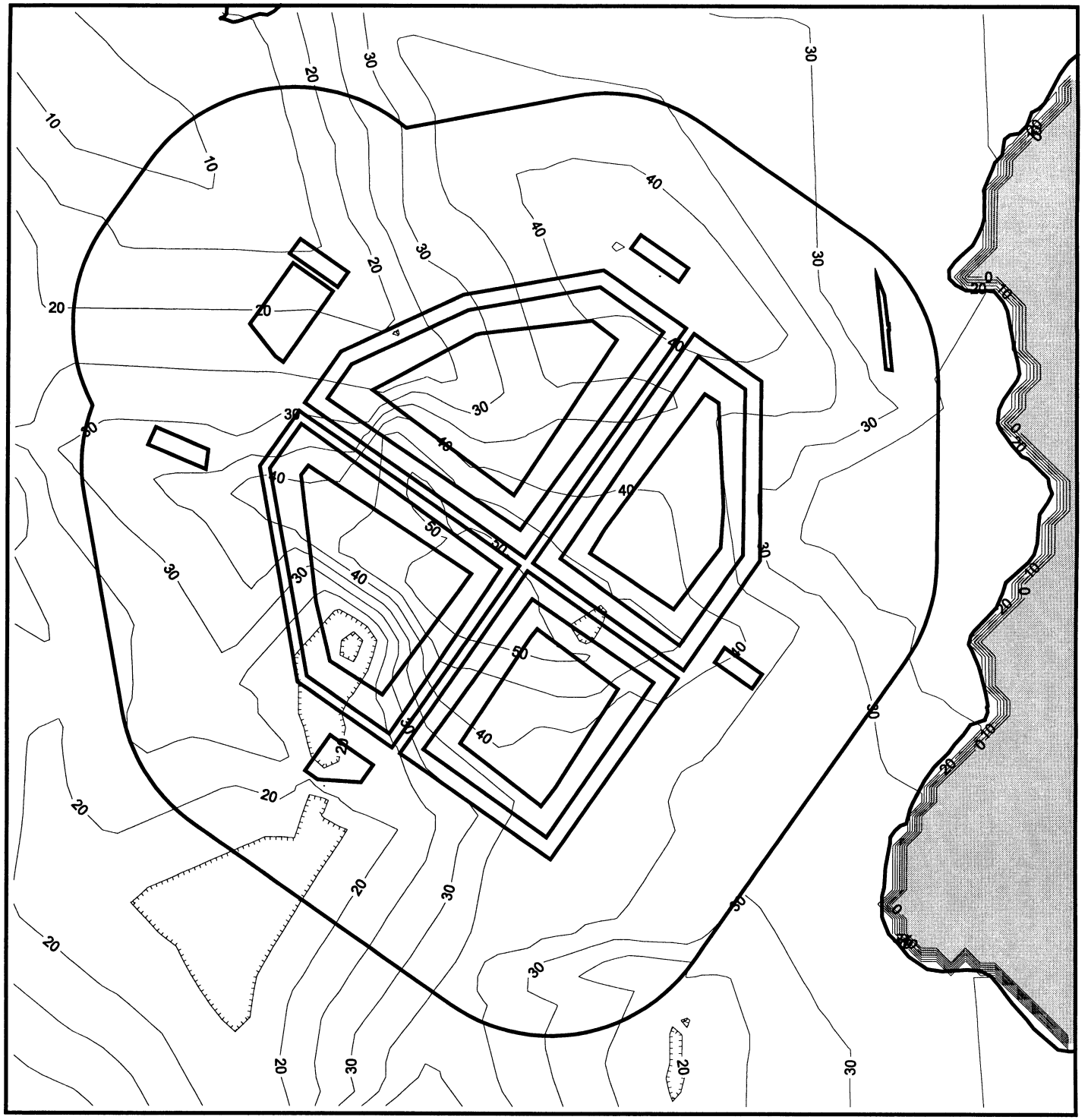

Inactive Area

Note:
Contour interval 5 feet.

N

0 1000 2000

Scale in Feet

HSI GEOTRANS			
REVISED	DATE	BY	DESCRIPTION
CHECKED BY: GWC			DATE: April 1998
APPROVED BY: PFA			DATE: April 1998
APPROVED BY:			DATE:

Nicolet Minerals COMPANY

Figure 2.24
Saturated Thickness of Model Layer 5

Scale: 1 in. = 1000 ft.	Date: April 1998
Prepared By: HSI GEOTRANS	By: RMD

\Crandon\Tmw\Mod3\Surfer\Thk5.srf

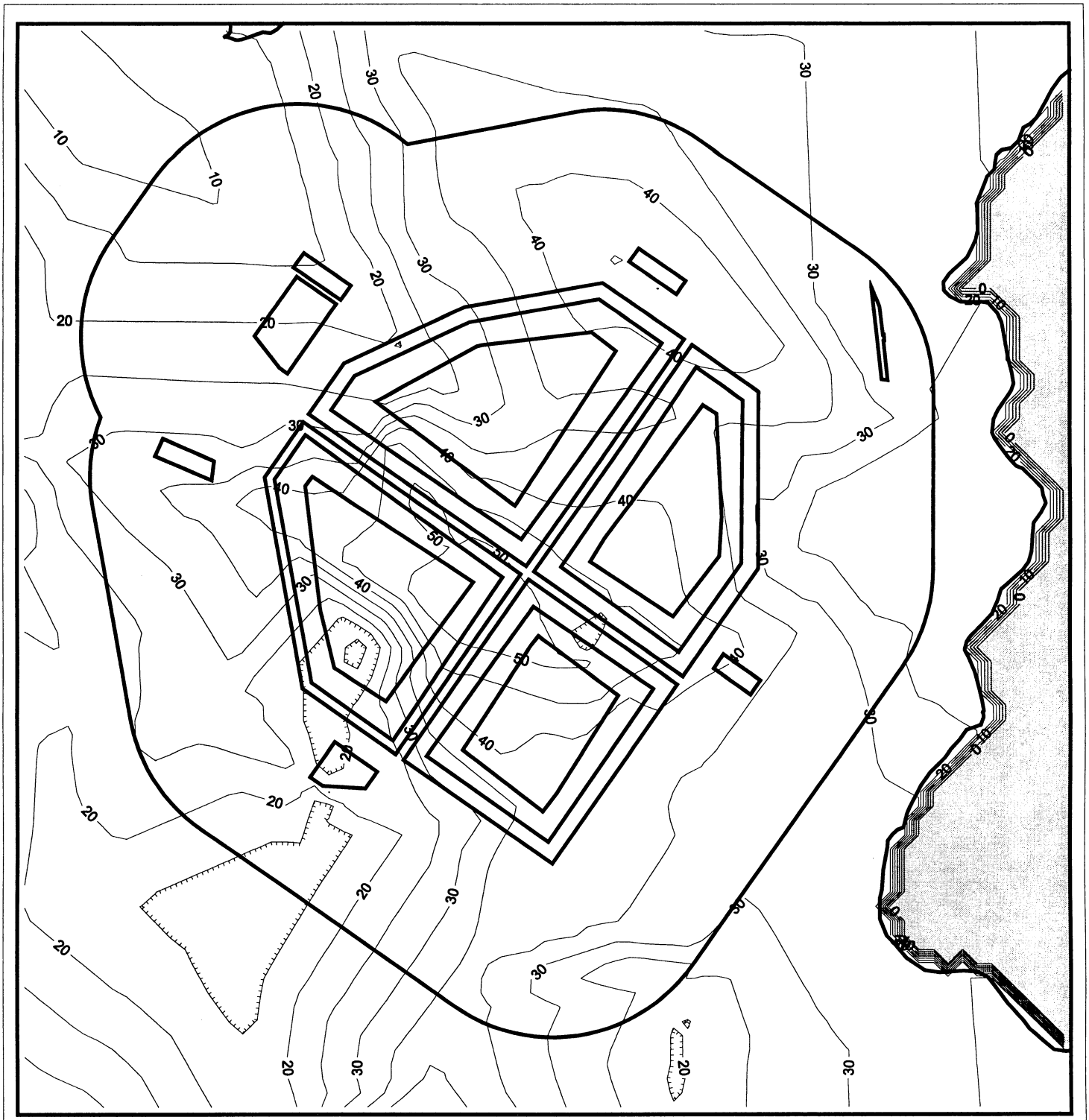

Inactive Area

Note:
Contour interval 5 feet.

0 1000 2000

Scale in Feet

HSI GEOTRANS			
REVISED	DATE	BY	DESCRIPTION

CHECKED BY: GWC	DATE: April 1998
APPROVED BY: PFA	DATE: Apil 1998
APPROVED BY:	DATE:

Nicolet Minerals COMPANY

Figure 2.25
Saturated Thickness of Model Layer 6

Scale: 1 in. = 1000 ft.	Date: April 1998
Prepared By: HSI GEOTRANS	By: RMD

\Crandon\Tmw\Mod3\Surfer\fm6.srf

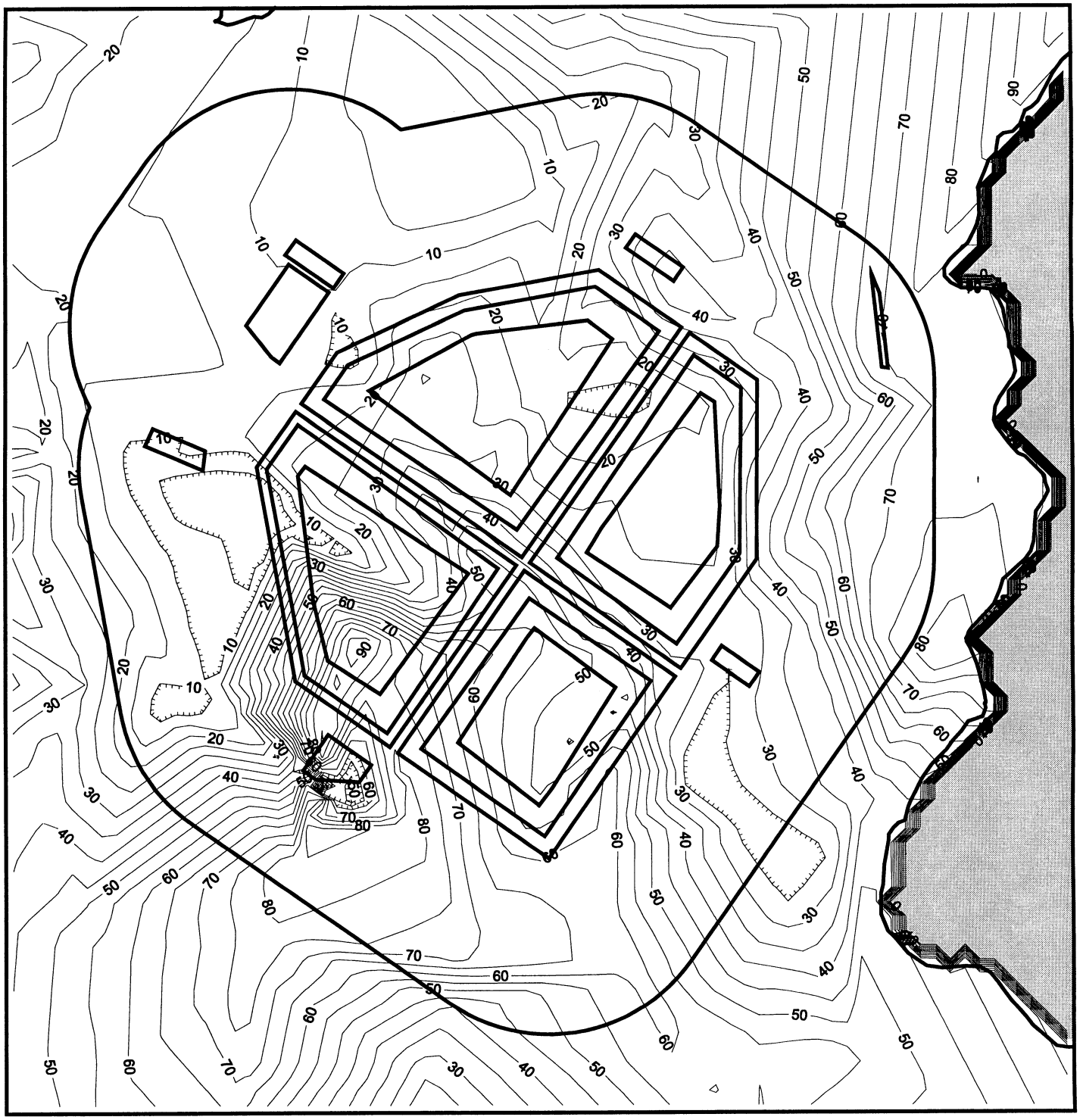

Inactive Area

Note:
Contour interval 5 feet.

0 1000 2000

Scale in Feet

HSI GEOTRANS			
REVISED	DATE	BY	DESCRIPTION

CHECKED BY: GWC	DATE: April 1998
APPROVED BY: PFA	DATE: April 1998
APPROVED BY:	DATE:

Nicolet Minerals COMPANY

Figure 2.26
Saturated Thickness of Model Layer 7

Scale: 1 in. = 1000 ft.	Date: April 1998
Prepared By: HSI GEOTRANS	By: RMD

\Crandon\Tma\Mod3\Surfer\Thk7.srf

Legend

Outwash Pinchout

N

0 1000 2000

Scale in Feet

HSI GEOTRANS			
REVISED	DATE	BY	DESCRIPTION
CHECKED BY: PAW			DATE: April 1998
APPROVED BY: PFA			DATE: April 1998
APPROVED BY:			DATE:

Nicolet Minerals COMPANY

Figure 2.27
Location of Modeled Outwash Pinchout

Scale: 1 in. = 1000 ft. | Date: April 1998

Prepared By: HSI GeoTrans | By: GWC

\Crandon\TmaMod3\...dlowkzone.wor

Coarse Outwash

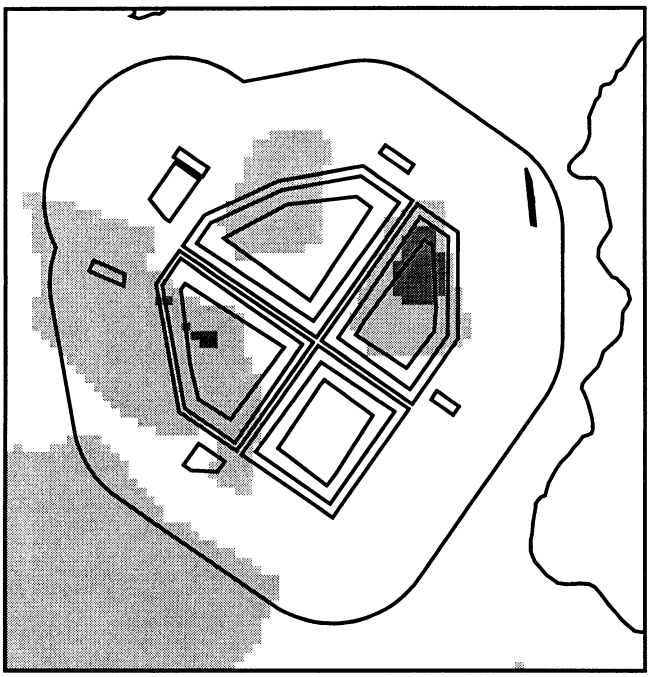

Fine Outwash

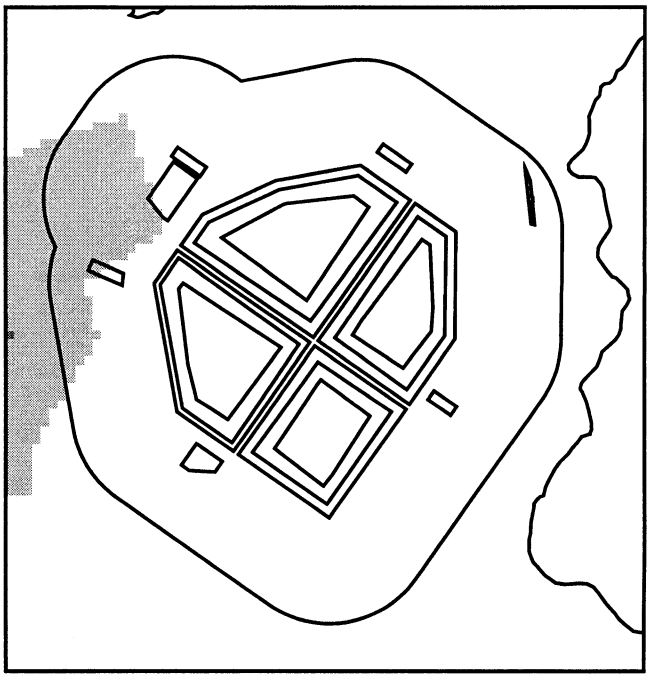

Late Wisconsinan Till

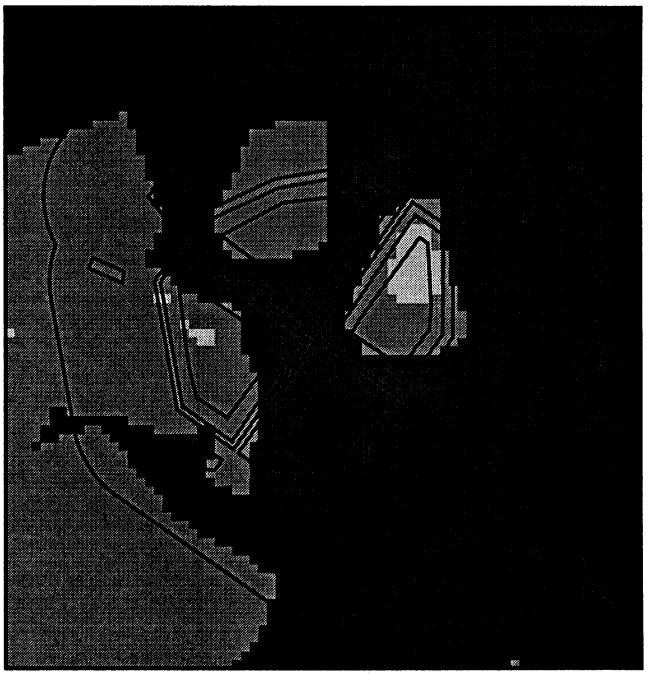

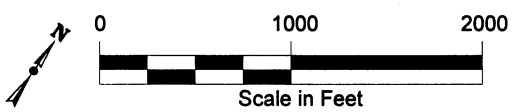

Legend

- None
- Less than 50%
- More than 50%
- All

HSI GEOTRANS			
REVISED	DATE	BY	DESCRIPTION

CHECKED BY: PAW	DATE: April 1998
APPROVED BY: PFA	DATE: APril 1998
APPROVED BY:	DATE:

Nicolet Minerals COMPANY

Figure 2.28
Hydrogeologic Compostition of Model Layer 1

Scale: 1 in. = 1000 ft.	Date: April 1998
Prepared By: HSI GeoTrans	By: GWC

\CrandonTmaMod3\GIS_modPCT1.wor

Coarse Outwash

Fine Outwash

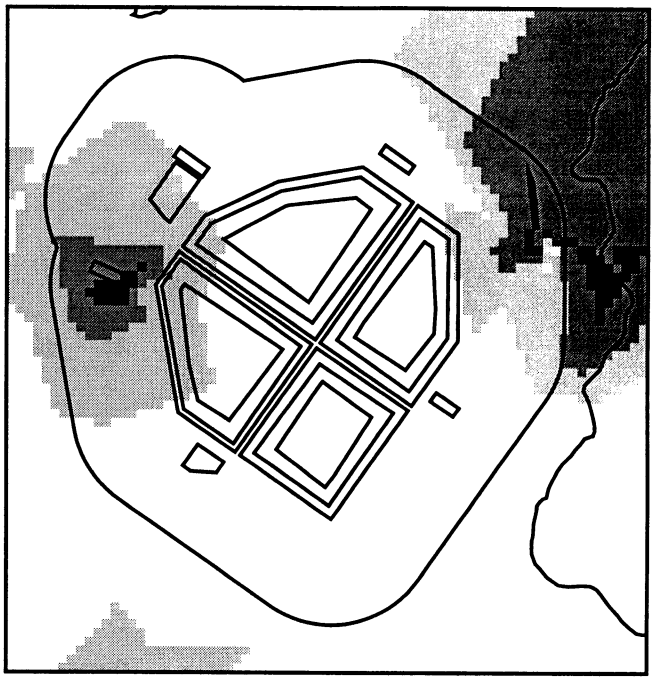

Late Wisconsinan Till

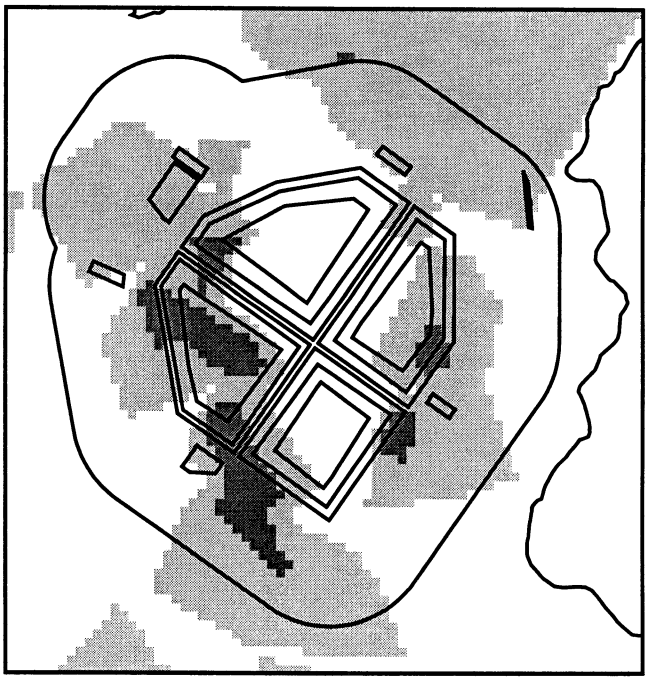

Legend

- None
- Less than 50%
- More than 50%
- All

HSI GEOTRANS			
REVISED	DATE	BY	DESCRIPTION

CHECKED BY: PAW	DATE: April 1998
APPROVED BY: PFA	DATE: April 1998
APPROVED BY:	DATE:

Nicolet Minerals COMPANY

Figure 2.29
Hydrogeologic Composition of Model Layer 2

Scale: 1 in. = 1000 ft.	Date: April 1998
Prepared By: HSI GeoTrans	By: GWC

\CrandonITmaMod3\GMS\Mod1PCT2.wor

Coarse Outwash

Fine Outwash

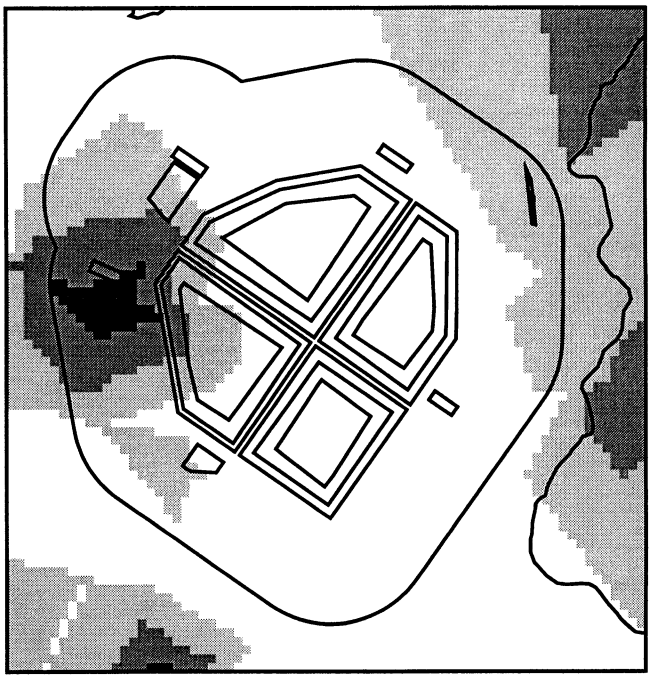

Late Wisconsinan Till

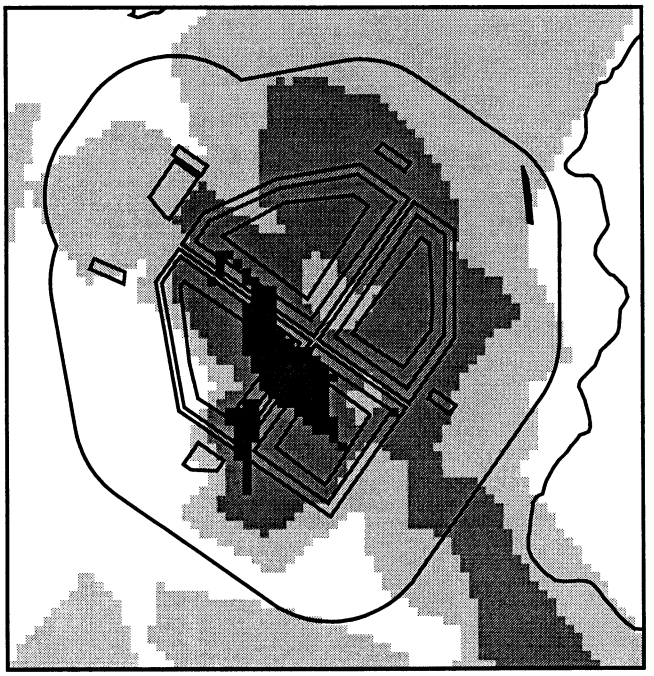

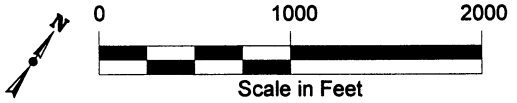

Legend

- None
- Less than 50%
- More than 50%
- All

HSI GEOTRANS

REVISED	DATE	BY	DESCRIPTION

CHECKED BY: PAW	DATE: April 1998
APPROVED BY: PFA	DATE: April 1998
APPROVED BY:	DATE:

Nicolet Minerals COMPANY

Figure 2.30
Hydrogeologic Composition of Model Layer 3

Scale: 1 in. = 1000 ft.	Date: April 1998
Prepared By: HSI GeoTrans	By: GWC

\Crandon\TmaMod3\GIS_mod\PCT3.wor

Coarse Outwash

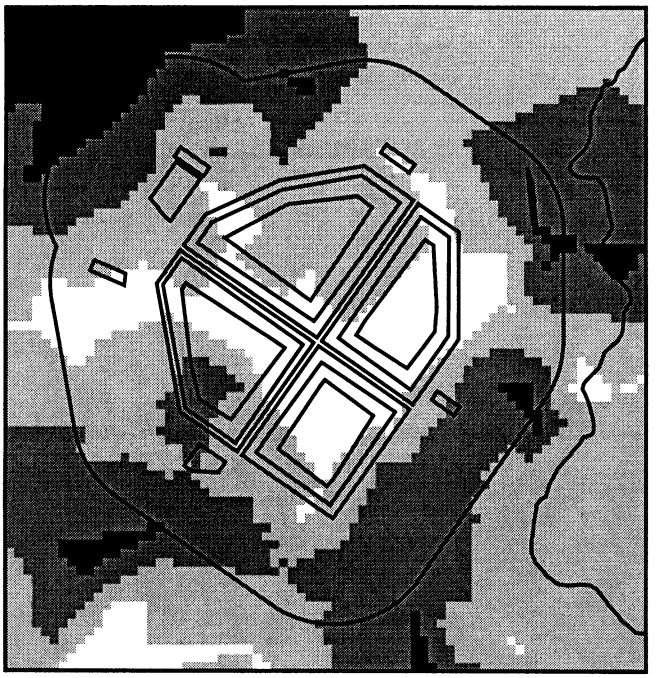

Fine Outwash

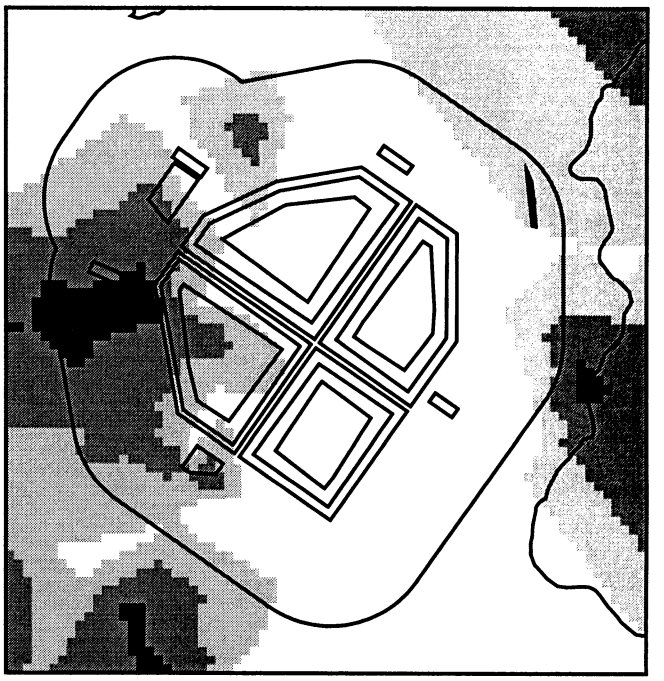

Late Wisconsinan Till

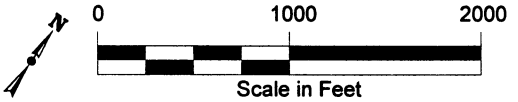

Legend

- None
- Less than 50%
- More than 50%
- All

HSI GEOTRANS			
REVISED	DATE	BY	DESCRIPTION

CHECKED BY: PAW	DATE: April 1998
APPROVED BY: PFA	DATE: April 1998
APPROVED BY:	DATE:

Nicolet Minerals COMPANY

Figure 2.31
Hydrogeologic Composition of Model Layer 4

Scale: 1 in. = 1000 ft.	Date: April 1998
Prepared By: HSI GeoTrans	By: GWC

\Crandon\TmaMod3\G...\PCT4.wor

Coarse Outwash

Fine Outwash

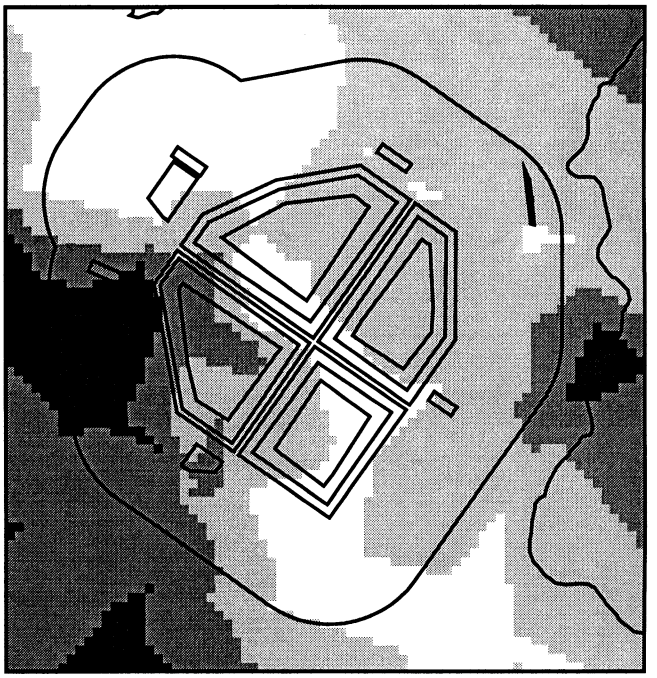

Late Wisconsinan Till

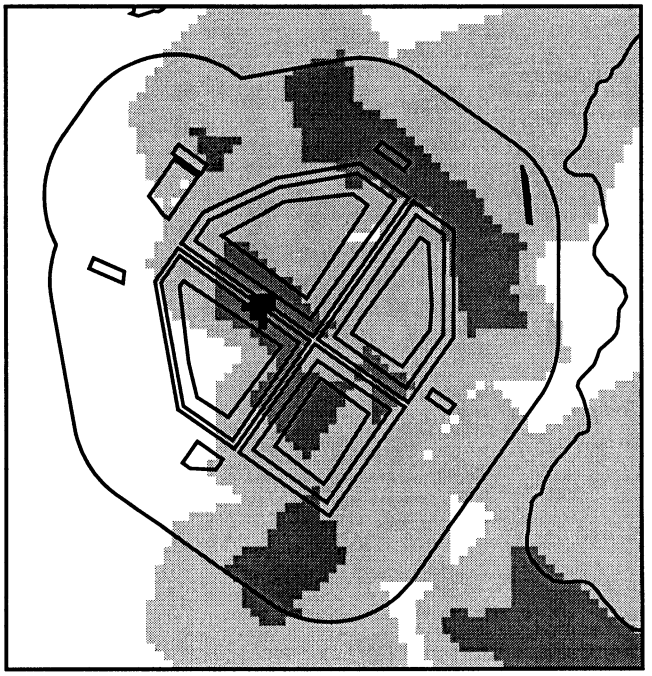

0 1000 2000

Scale in Feet

Legend

- None
- Less than 50%
- More than 50%
- All

HSI GEOTRANS			
REVISED	DATE	BY	DESCRIPTION

CHECKED BY: PAW	DATE: April 1998
APPROVED BY: PFA	DATE: April 1998
APPROVED BY:	DATE:

Nicolet Minerals COMPANY

Figure 2.32
Hydrogeologic Composition of Model Layer 5

Scale: 1 in. = 1000 ft.	Date: April 1998
Prepared By: HSI GeoTrans	By: GWC

\Crandon\TmaMod3\GIS_mod\PCT5.wor

Coarse Outwash

Fine Outwash

Late Wisconsinan Till

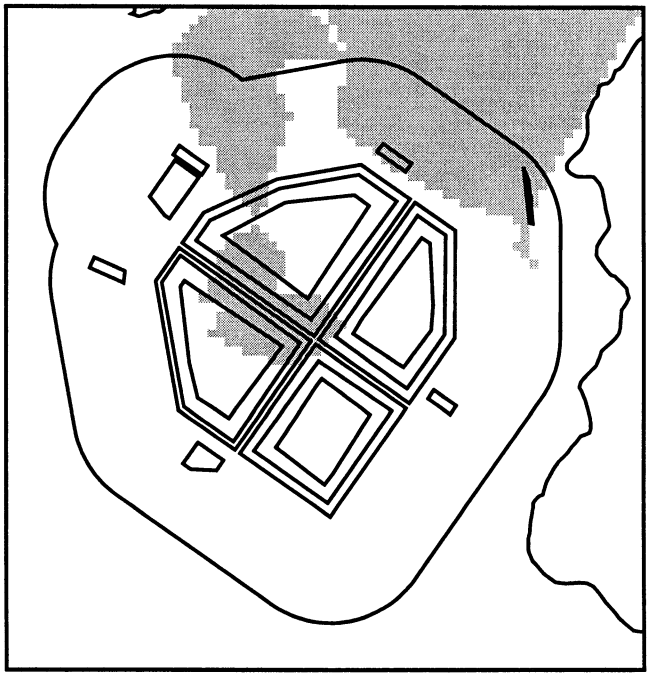

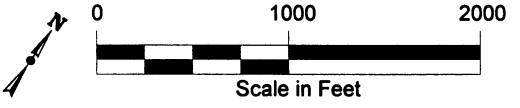

Legend

- None
- Less than 50%
- More than 50%
- All

HSI GEOTRANS			
REVISED	DATE	BY	DESCRIPTION

CHECKED BY: PAW	DATE: April 1998
APPROVED BY: PFA	DATE: April 1998
APPROVED BY:	DATE:

Nicolet Minerals COMPANY

Figure 2.33
Hydrogeologic Composition of Model Layer 6

Scale: 1 in. = 1000 ft. | Date: April 1998

Prepared By: HSI GeoTrans | By: GWC

\Crandon\TmaMod3\G...\PCT6.wor

Coarse Outwash

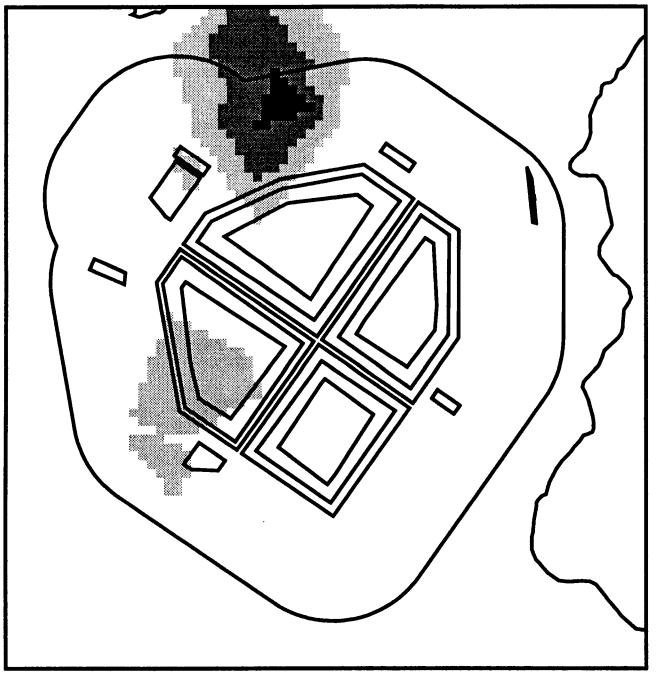

Fine Outwash

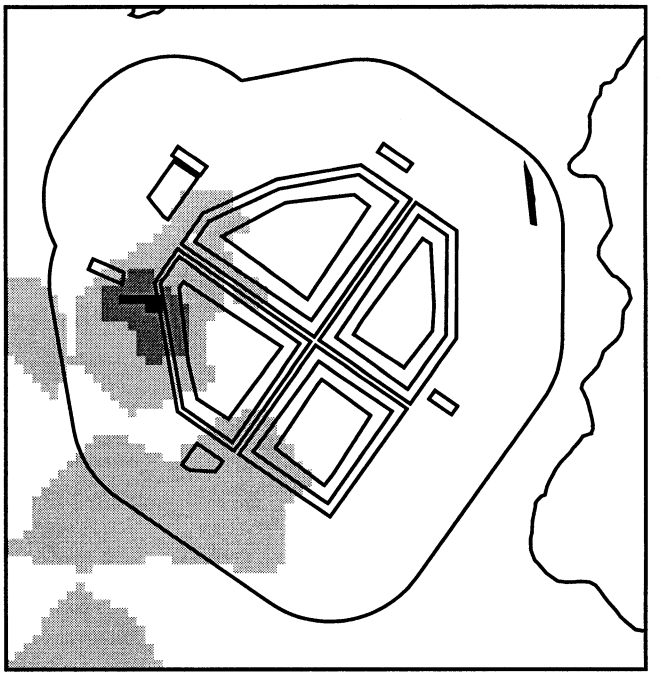

Early Wisconsinan Till

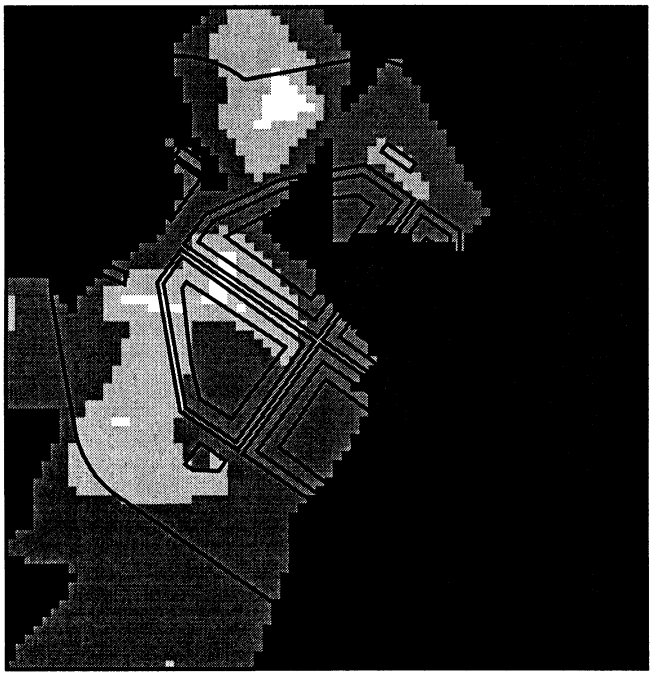

Ancient Lacustrine Deposits

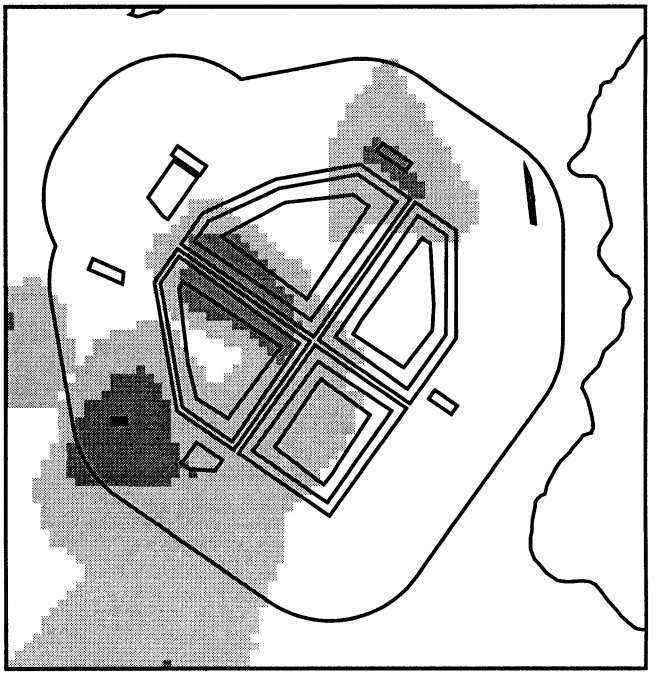

Legend

- None
- Less than 50%
- More than 50%
- All

HSI GEOTRANS			
REVISED	DATE	BY	DESCRIPTION

CHECKED BY: PAW	DATE: April 1998
APPROVED BY: PFA	DATE: April 1998
APPROVED BY:	DATE:

Nicolet Minerals COMPANY

Figure 2.34
Hydrologeologic Compostion of Model Layer 7

Scale: 1 in. = 1000 ft.	Date: April 1998
Prepared By: HSI GeoTrans	By: GWC

\Crandon\TmaMod3\GIS_mod\PCT7.wor

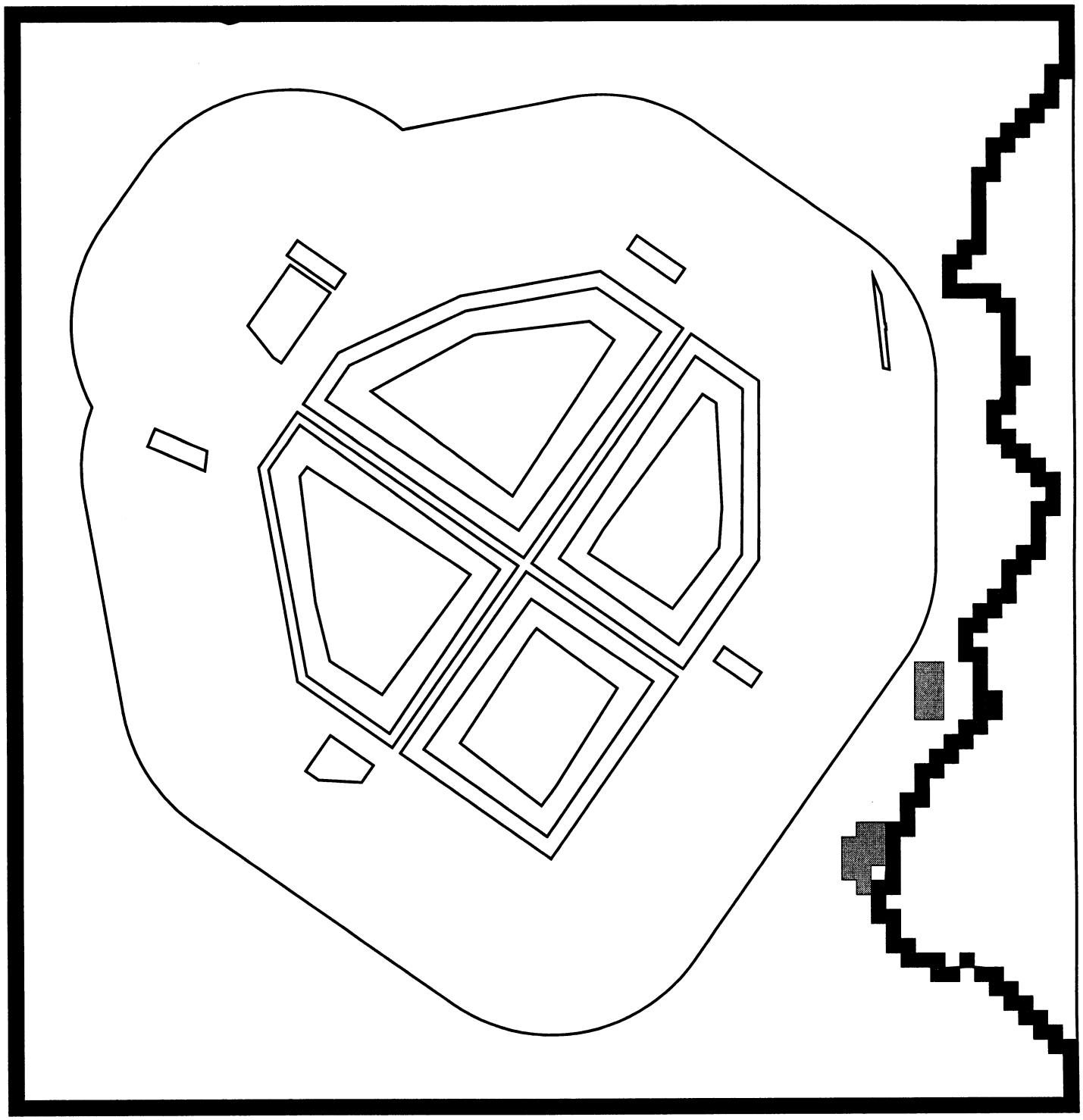

LEGEND

- Hemlock Creek (River Package, Top Active Layer
- Seepage Wetland (River Package, Top Active Layer)
- Fixed Head Boundary (GHB Package, All Active Layers)

N

0 1000 2000

Scale in Feet

HSI GEOTRANS			
REVISED	DATE	BY	DESCRIPTION
CHECKED BY: PAW			DATE: April 1998
APPROVED BY: PFA			DATE: April 1998
APPROVED BY:			DATE:

Nicolet Minerals COMPANY

Mining for the Future

Figure 2.35
TMA Sub-Model
Flow Boundary Conditions

Scale: 1 in. = 1000 ft. Date: April 1998

Prepared By: HSI GeoTrans By: GWC

\Crandon\TmaMod3\G...dBndry.wor

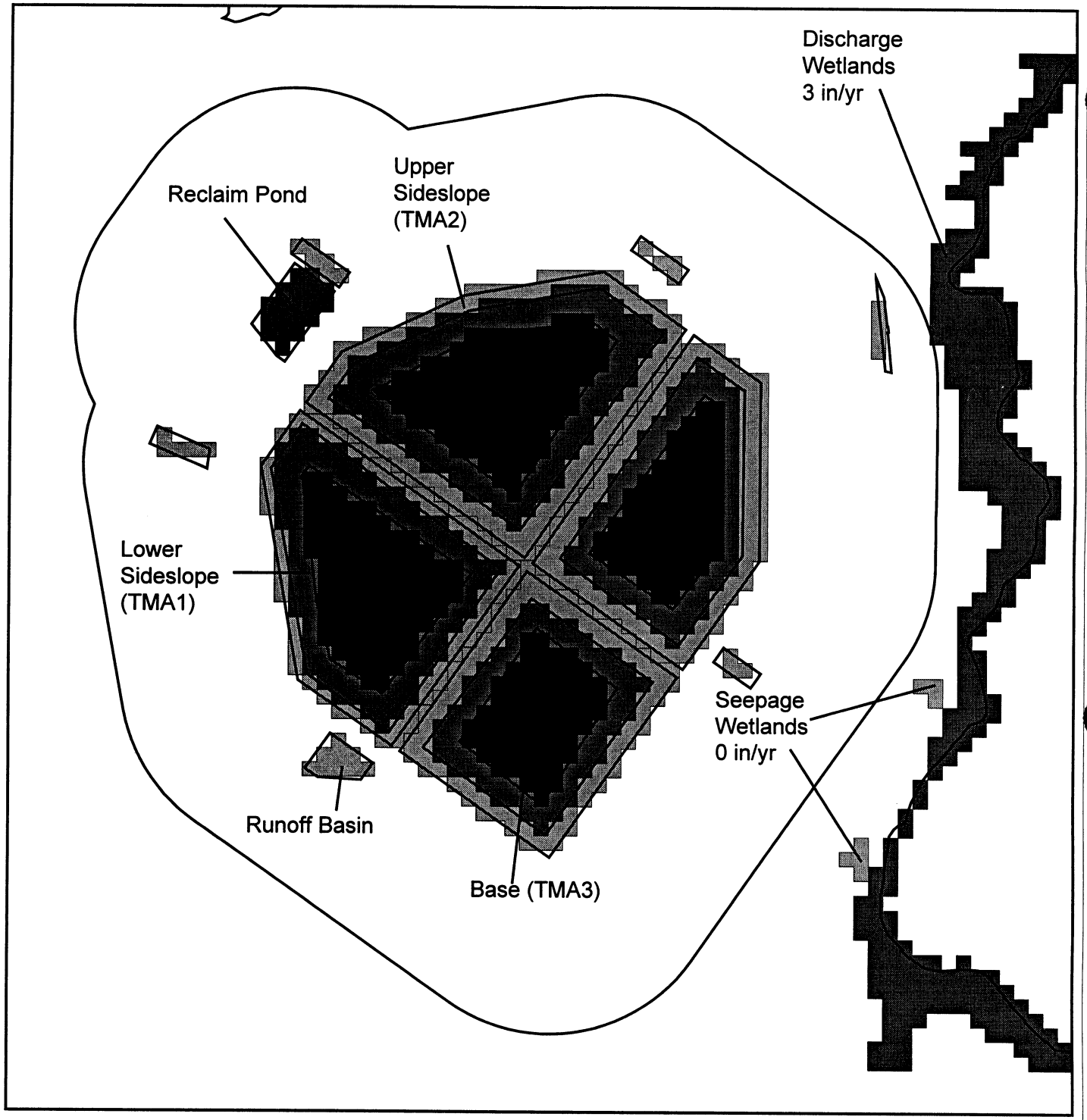

HSI GEOTRANS			
REVISED	DATE	BY	DESCRIPTION
CHECKED BY: PAW			DATE: April 1998
APPROVED BY: PFA			DATE: April 1998
APPROVED BY:			DATE:

Nicolet Minerals COMPANY

Figure 2.36
TMA Sub-Model
Recharge Zones

Scale: 1 in. = 1000 ft.	Date: April 1998
Prepared By: HSI GeoTrans	By: GWC

\Crandon\TmaMod3\GIS_mod\RchZone.wor

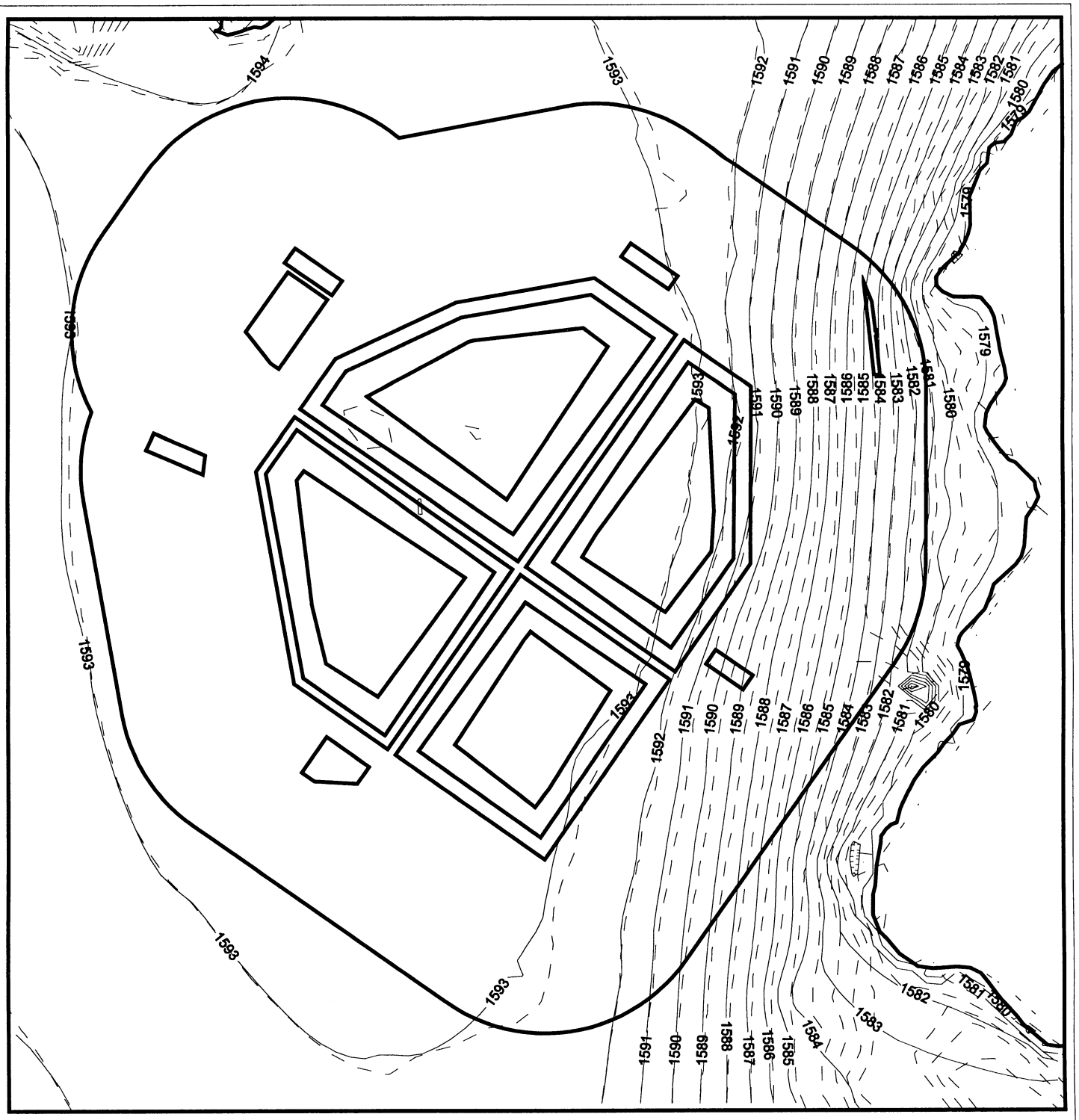

Notes:
1) Elevation in feet, msl.
2) Contour interval 1 foot.
3) TMA sub-model simulation T03A.
4) Regional model simulation 23A.

Legend
- TMA sub-model head contour
- Regional model head contour

0 1000 2000
Scale in Feet

HSI GEOTRANS

REVISED	DATE	BY	DESCRIPTION

CHECKED BY: GWC	DATE: April 1998
APPROVED BY: PFA	DATE: April 1998
APPROVED BY:	DATE:

Nicolet Minerals COMPANY

Figure 2.37
Modeled Water Table in the TMA Sub-Model and the Regional Model

Scale: 1 in. = 1000 ft.	Date: April 1998
Prepared By: HSI GEOTRANS	By: RMD

\CrandonTmaMod3\Surfer\tsss-wtb.srf

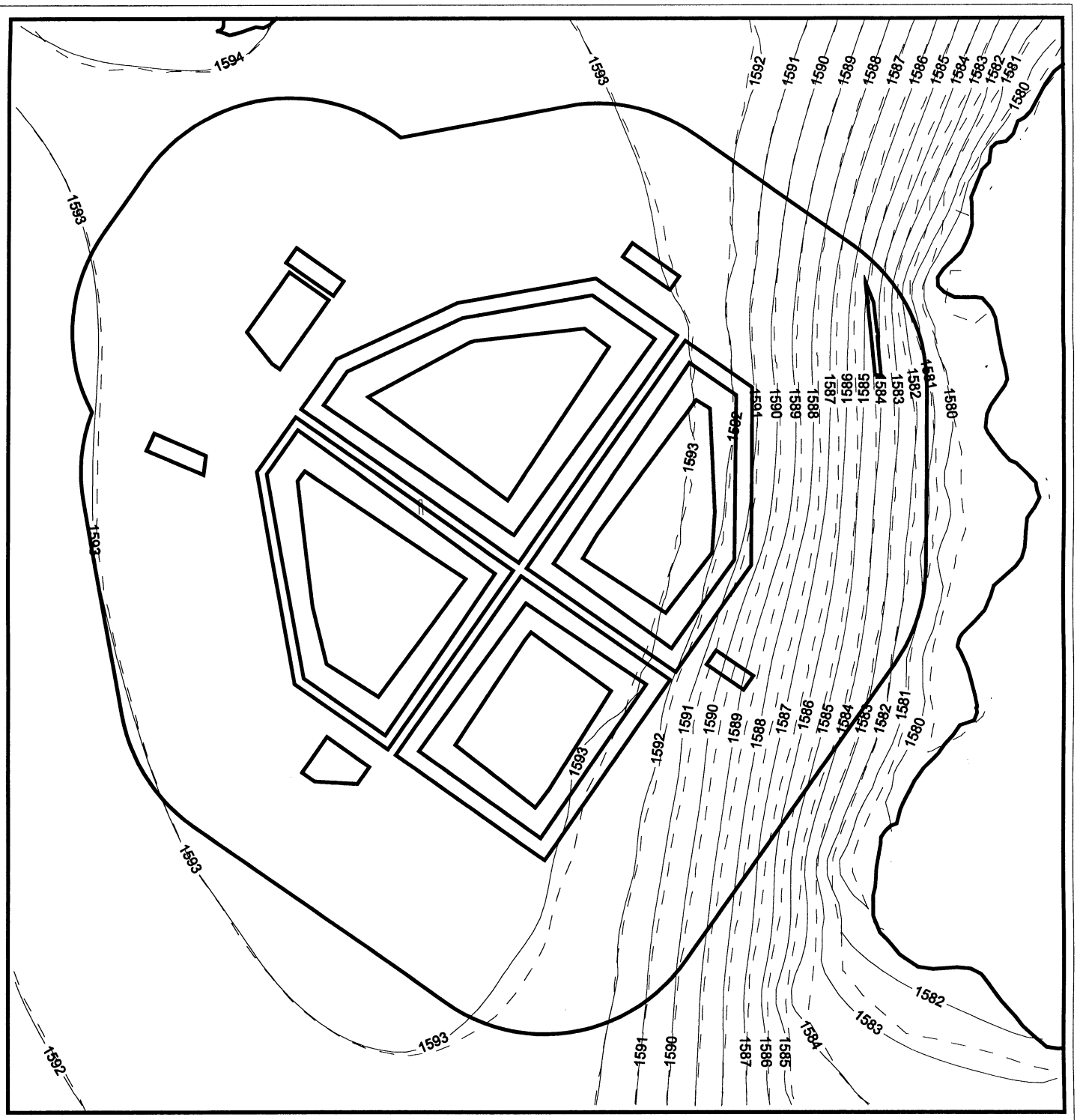

Notes:
1) Elevation in feet, msl.
2) Contour interval 1 foot.
3) TMA sub-model simulation T03A.
4) Regional model simulation 23A.

Legend
- TMA sub-model head contour
- Regional model head contour

N

0 1000 2000

Scale in Feet

HSI GEOTRANS			
REVISED	DATE	BY	DESCRIPTION
CHECKED BY: GWC			DATE: April 1998
APPROVED BY: PFA			DATE: April 1998
APPROVED BY:			DATE: April 1998

Nicolet Minerals COMPANY

Figure 2.38
Modeled Head in TMA Sub-Model Layer 3 and Regional Model Layer 2

Scale: 1 in. = 1000 ft. | Date: April 1998

Prepared By: HSI GEOTRANS | By: RMD

\Crandon\TmaMod3\Surfer\t03a-hd3.srf

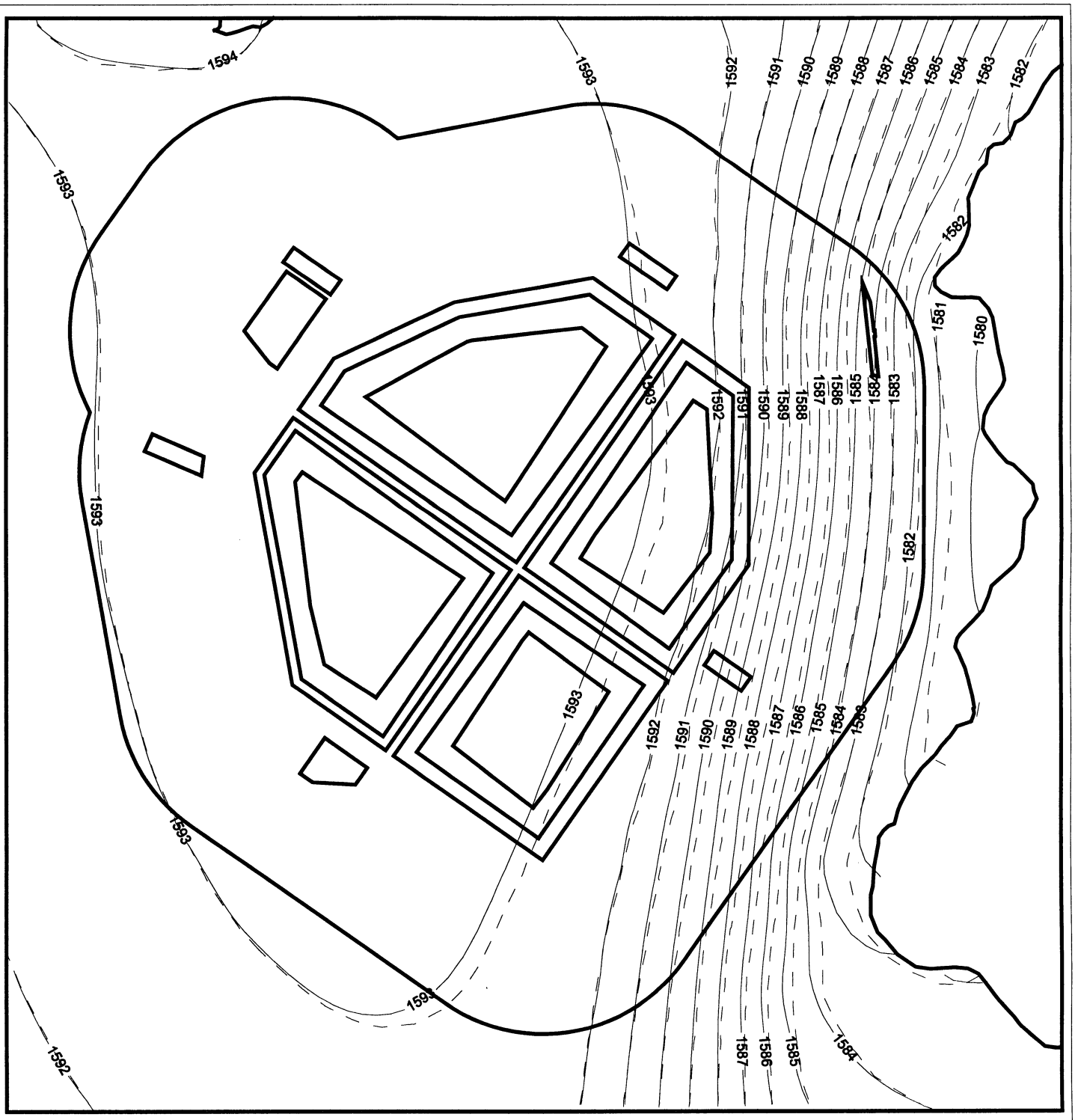

Notes:
1) Elevation in feet, msl.
2) Contour interval 1 foot.
3) TMA sub-model simulation T03A.
4) Regional model simulation 23A.

Legend
TMA sub-model head contour
Regional model head contour

N

0 1000 2000
Scale in Feet

HSI GEOTRANS			
REVISED	DATE	BY	DESCRIPTION

CHECKED BY: GWC	DATE: April 1998
APPROVED BY: PFA	DATE: April 1998
APPROVED BY:	DATE:

Nicolet Minerals COMPANY

Figure 2.39
Modeled Head in TMA Sub-Model Layer 7 and Regional Model Layer 4

Scale: 1 in. = 1000 ft.	Date: April 1998
Prepared By: HSI GEOTRANS	By: RMD

\Crandon\TmaMod3\Surfer\t03a-hd7.srf

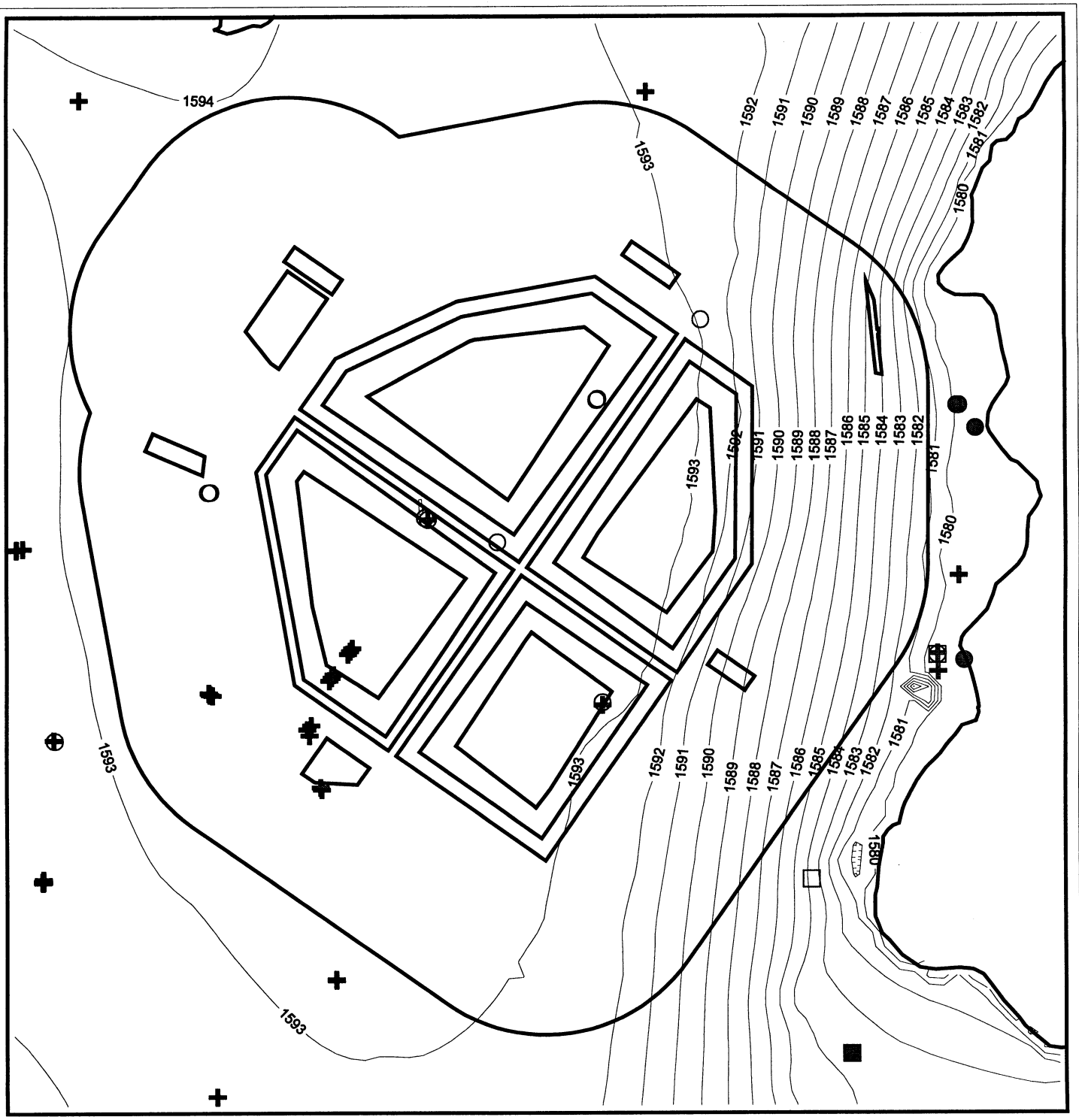

Residuals
(Modeled - Observed)

- Less than -5
- -5 to -3
- -3 to -1
- -1 to 1
- 1 to 3
- 3 to 5
- Greater than 5

N

0 1000 2000

Scale in Feet

Notes:
1) Elevation in feet, msl.
2) Contour interval 1 foot.
3) TMA sub-model simluation T03A.

HSI GEOTRANS

REVISED	DATE	BY	DESCRIPTION

CHECKED BY: GWC	DATE: April 1998
APPROVED BY: PFA	DATE: April 1998
APPROVED BY:	DATE:

Nicolet Minerals COMPANY

Figure 2.40
Modeled Steady-State Water Table and Water Level Residuals at Wells

Scale: 1 in. = 1000 ft.	Date: April 1998
Prepared By: HSI GEOTRANS	By: RMD

\Crandon\Tma\Mod3\Surfer\t03a-res.srf

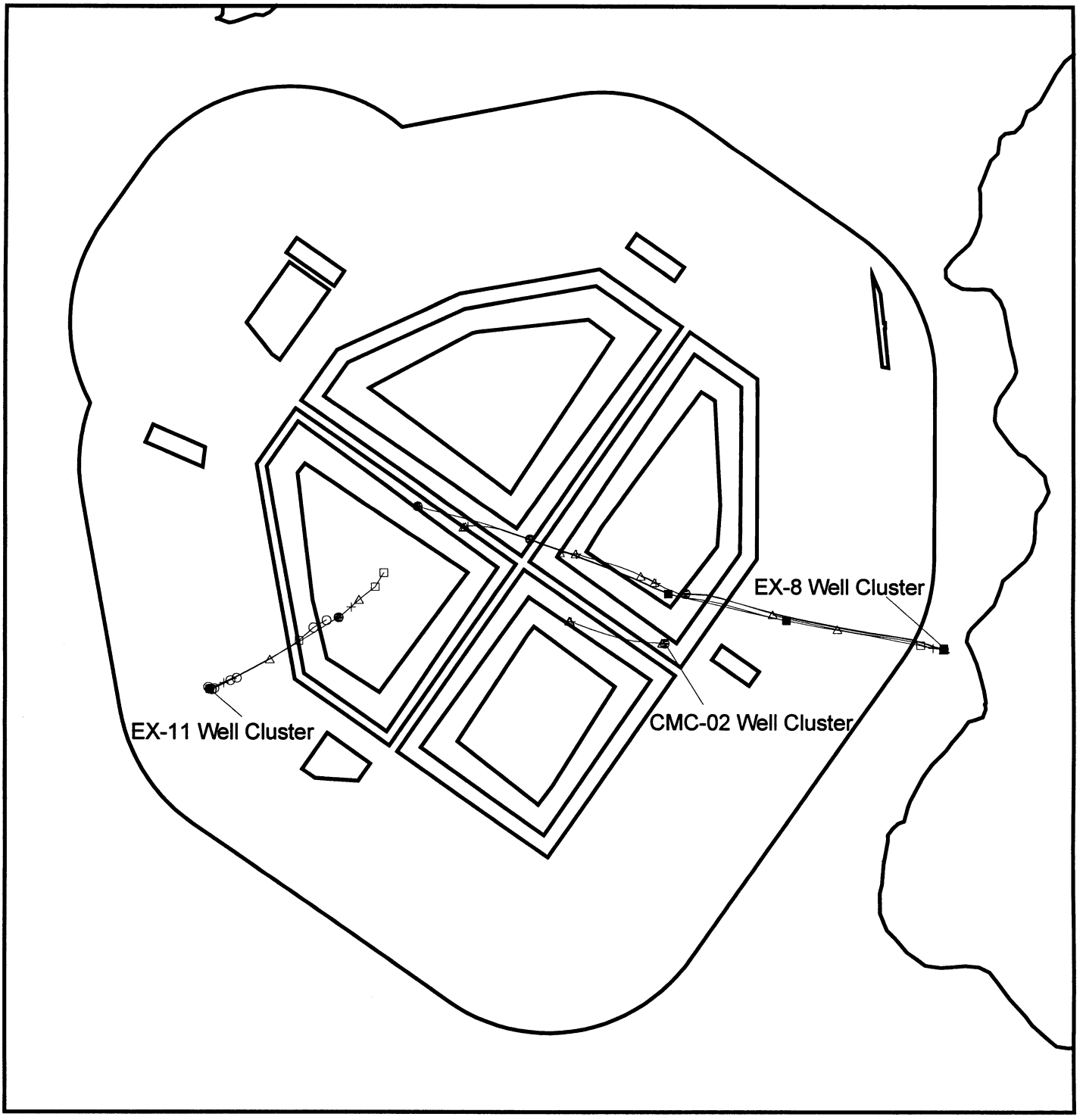

0 1000 2000

Scale in Feet

HSI GEOTRANS			
REVISED	DATE	BY	DESCRIPTION

CHECKED BY: GWC	DATE: April 1998
APPROVED BY: PFA	DATE: April 1998
APPROVED BY:	DATE:

Simulation T03A-MP

Nicolet Minerals COMPANY

Figure 2.41
Backwards Particle Traces
From EX-8, EX-11, and CMC-02

Scale: 1 in. = 1000 ft.	Date: April 1998
Prepared By: HSI GEOTRANS	By: RMD

\Crandon\Tmat\Mod3\Sunset\cca-mp.srf

\Crandon\TmaMod3\Excel\T03a-mp.xls, EX8Trace

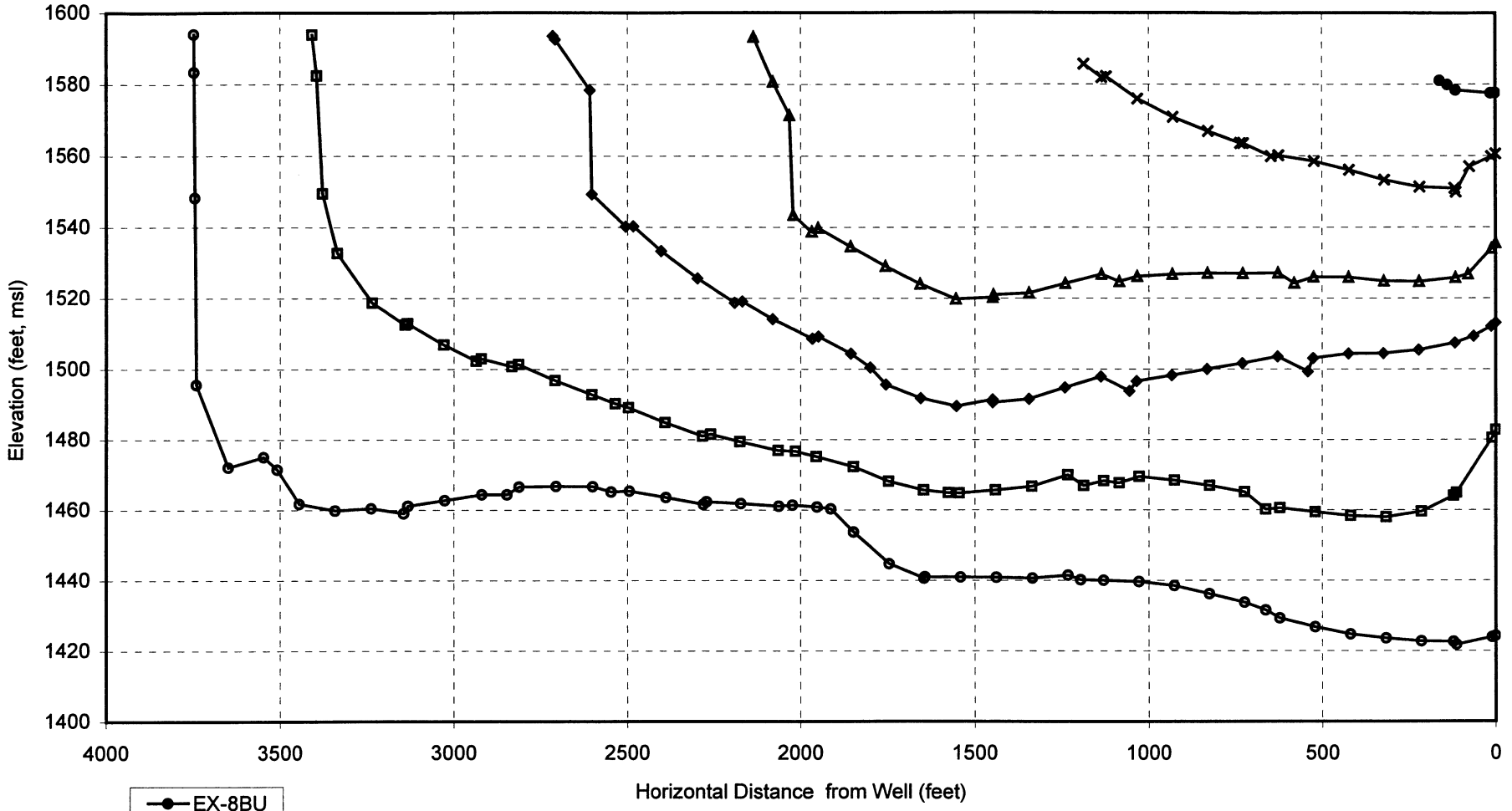

4.2-10-209

HSI GEOTRANS			
REVISED	DATE	BY	DESCRIPTION

CHECKED BY: PAW	DATE: April 1998
APPROVED BY: PFA	DATE: April 1998
APPROVED BY:	DATE:

Simulation T03A-MP

Nicolet Minerals COMPANY

Figure 2.42
Backwards Particle Traces from the EX-8 Well Cluster to the Water Table

Scale: None	Date: April 1998
Prepared By: HSI GEOTRANS	By: GWC

\Crandon\TmaMod3\Excel\TimeLine1.xls, Chart

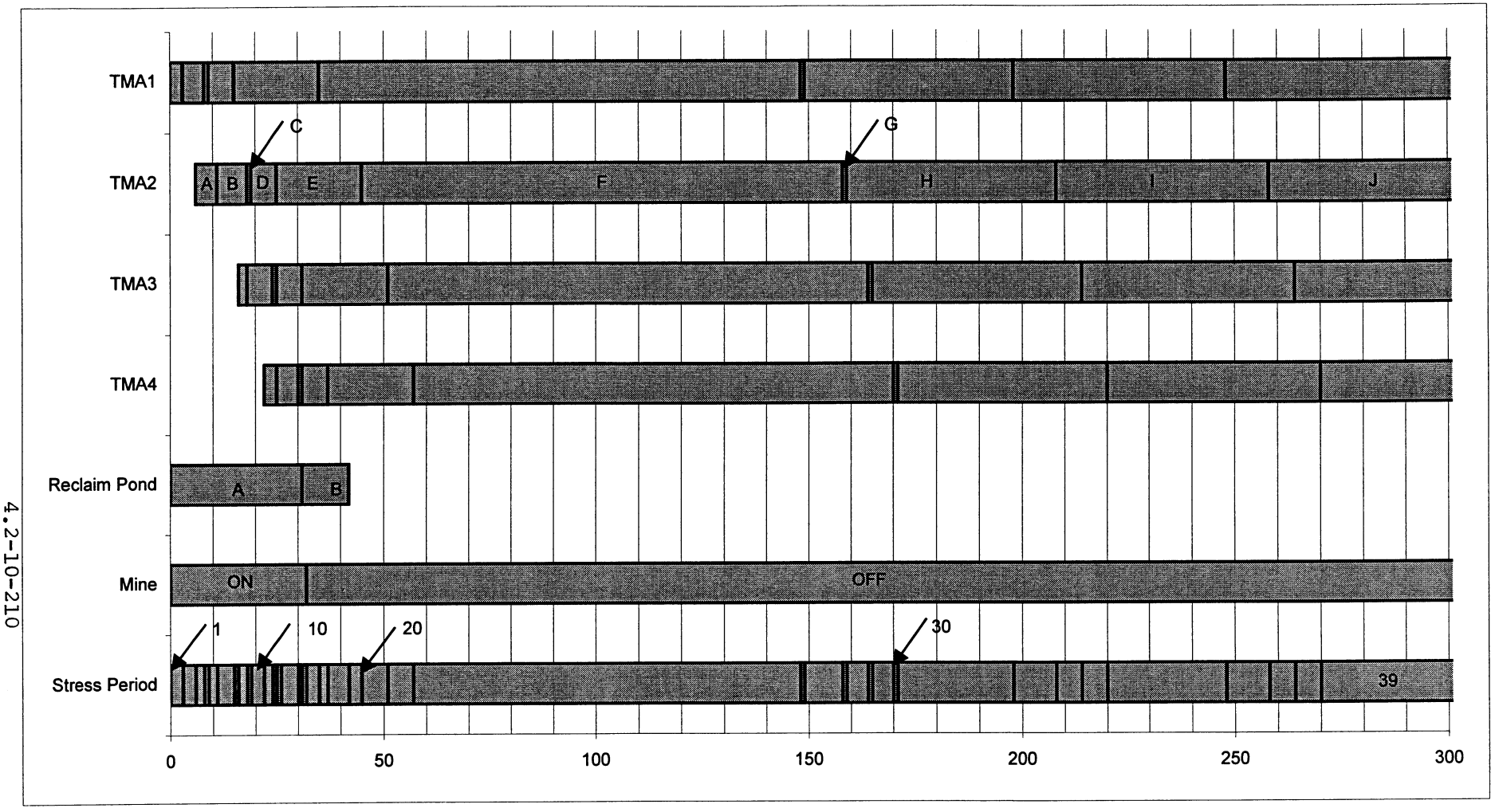

4.2-10-210

Notes:

1. TMA phases are labeled for TMA2 - others are similar
2. Reclaim Pond has the following phases:
   - A. Rate = 1.61E-5 ft/d, Conc. = Operational
   - B. Rate = 4.00E-6 ft/d, Conc. = Post-Cap

HSI GEOTRANS			
REVISED	DATE	BY	DESCRIPTION

CHECKED BY: PAW	DATE: April 1998
APPROVED BY: PFA	DATE: April 1998
APPROVED BY:	DATE:

Nicolet Minerals COMPANY

Figure 2.43
TMS Sub-Model Time Line

Scale: None	Date: April 1998
Prepared By: HSI GEOTRANS	By: GWC

\Crandon\TmaMod3\Excel\Rates1.xls, Flux

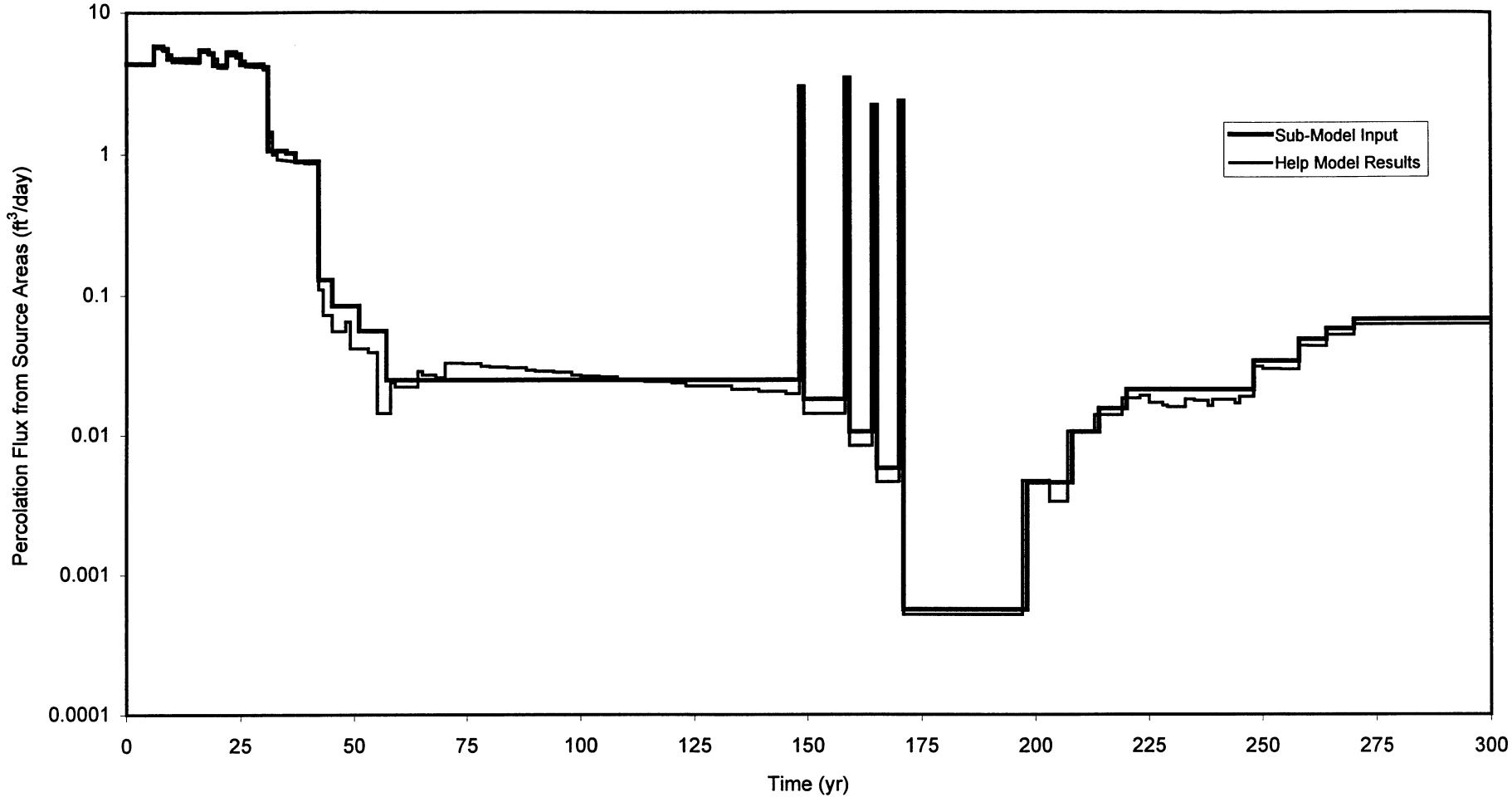

4.2-10-211

Note:
Percolation rate (Y-axis) is shown on a logarithmic scale.

HSI GEOTRANS			
REVISED	DATE	BY	DESCRIPTION

CHECKED BY: GWC	DATE: April 1998
APPROVED BY: PFA	DATE: April 1998
APPROVED BY:	DATE:

Nicolet Minerals COMPANY

Figure 2.44
Source Areas Percolation Flux Rate

Scale: None	Date: April 1998
Prepared By: HSI GEOTRANS	By: KMR

\Crandon\TmaMod3\Excel\Rates1.xls, CumVol

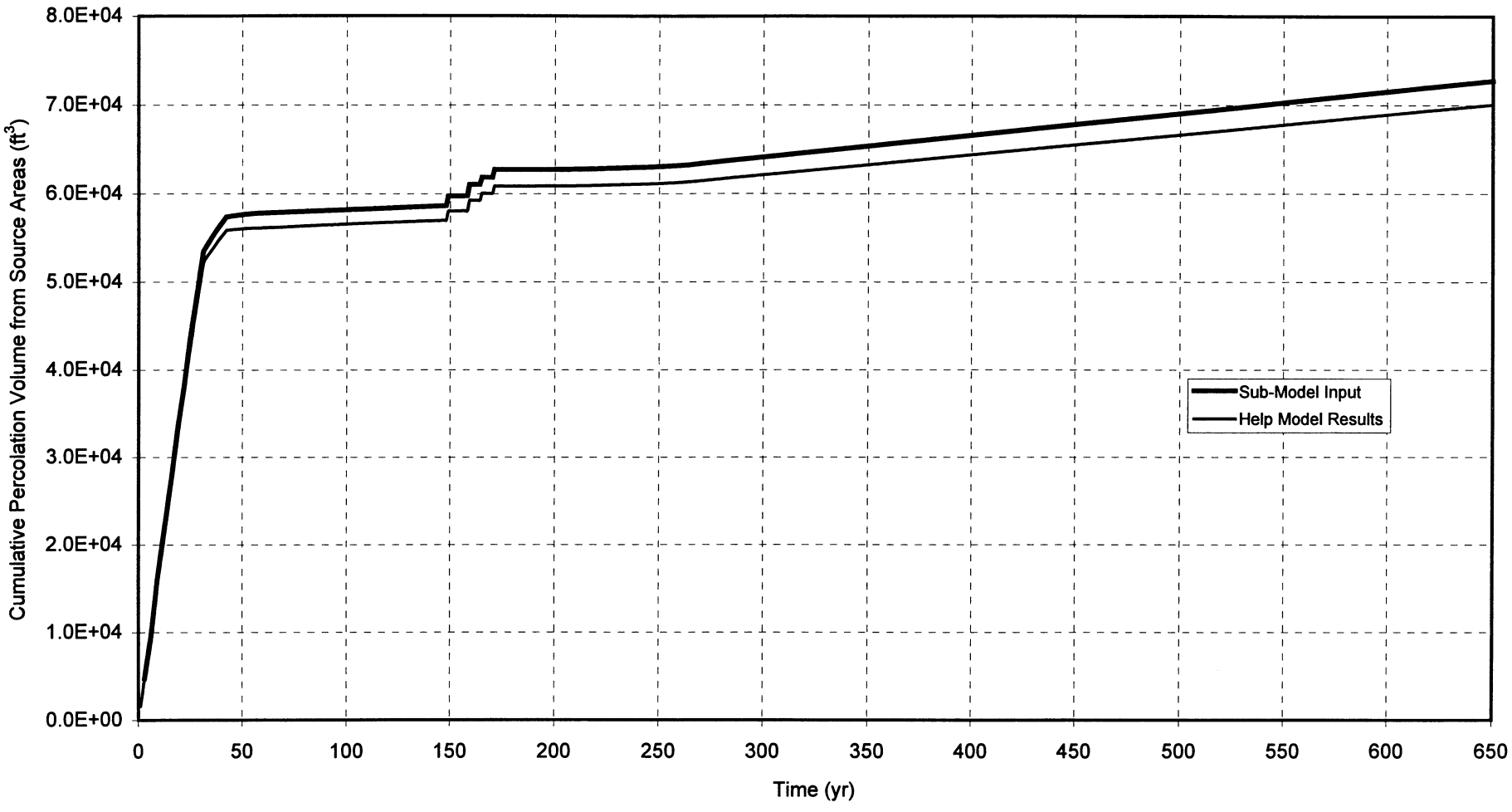

4.2-10-212

HSI GEOTRANS			
REVISED	DATE	BY	DESCRIPTION

CHECKED BY: PAW	DATE: April 1998
APPROVED BY: PFA	DATE: April 1998
APPROVED BY:	DATE:

Nicolet Minerals COMPANY

Figure 2.45
Source Areas Cumulative Percolation Volume

Scale: None	Date: April 1998
Prepared By: HSI GEOTRANS	By: GWC

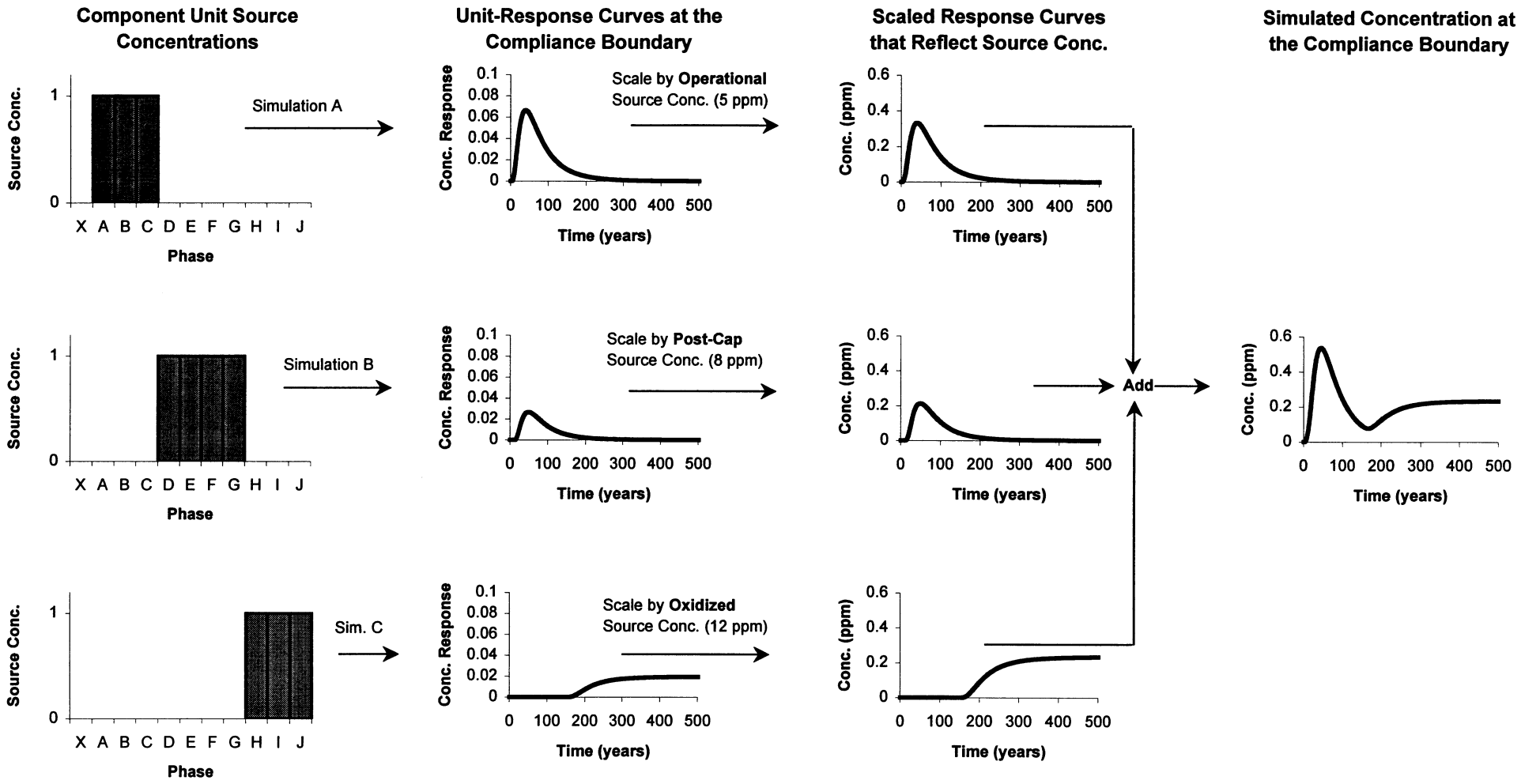

This hypothetical example shows the superposition method applied for a constituent with the following source concentrations:

Operation: 5 ppm
Post-Cap: 8 ppm
Oxidized: 12 ppm

4.2-10-213

HSI GEOTRANS			
REVISED	DATE	BY	DESCRIPTION

CHECKED BY: PAW	DATE: April 1998
APPROVED BY: PFA	DATE: April 1998
APPROVED BY:	DATE:

Nicolet Minerals COMPANY

Figure 2.46
Illustration of the Superposition Method

Scale: None	Date: April 1998
Prepared By: HSI GEOTRANS	By: GWC

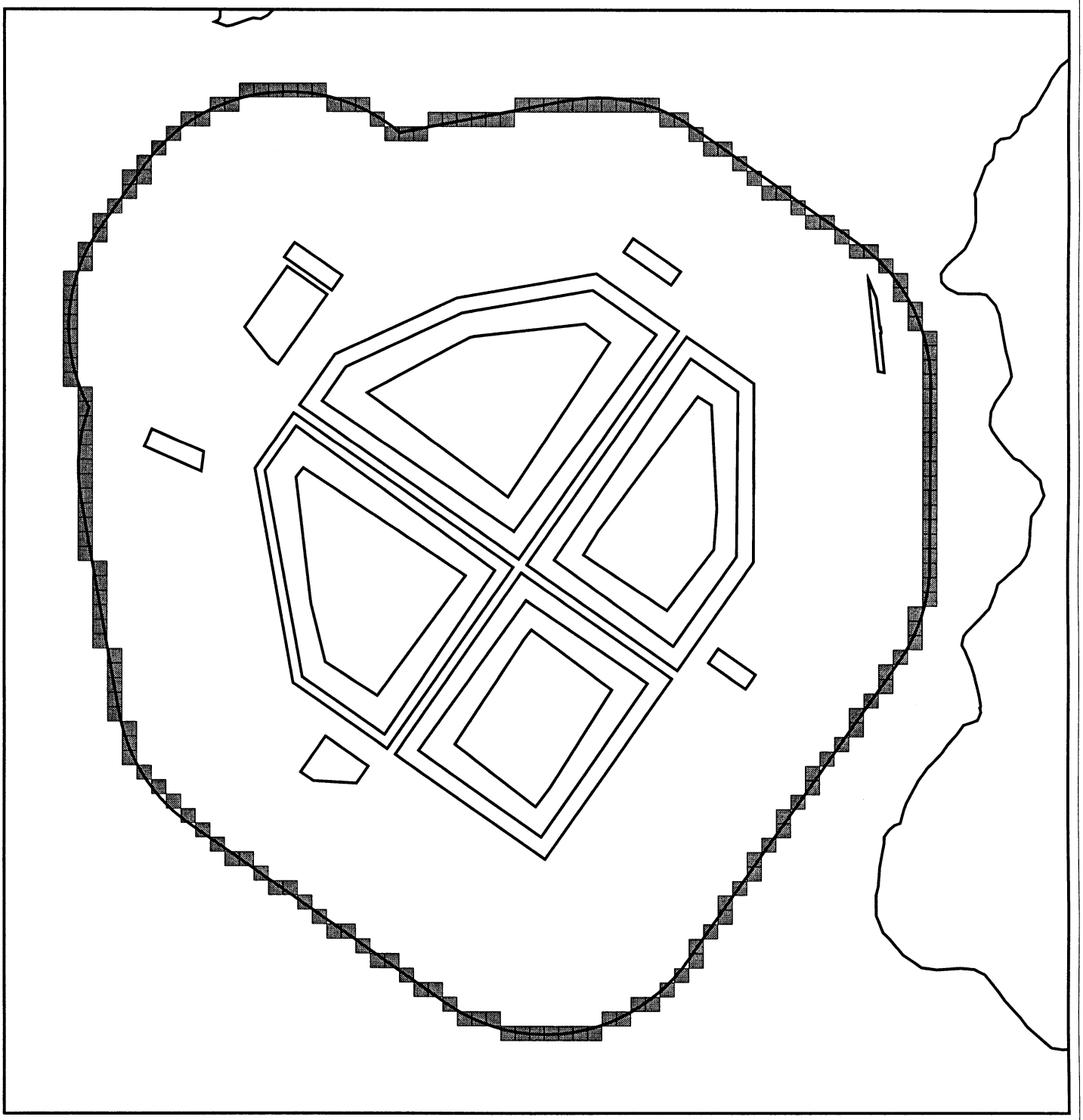

0 1000 2000

Scale in Feet

HSI GEOTRANS			
REVISED	DATE	BY	DESCRIPTION
CHECKED BY: PAW			DATE: April 1998
APPROVED BY: PFA			DATE: April 1998
APPROVED BY:			DATE:

Nicolet Minerals COMPANY

Figure 2.47
Observation Cells at the 1200-foot Compliance Boundary

Scale: 1 in. = 1000 ft. | Date: April 1998

Prepared By: HSI GeoTrans | By: GWC

\Crandon\TmaMod3\Ch...od\End1200.wor

\Crandon\TmaMod3\Excel\T03C.xls, Response

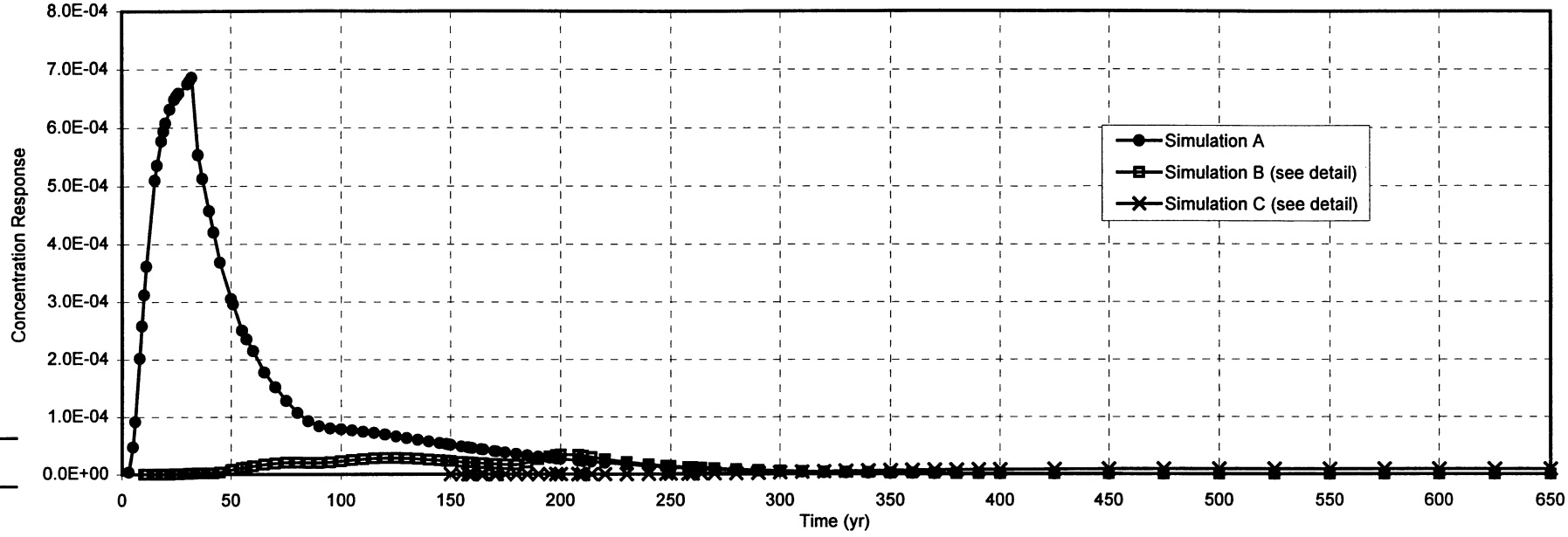

Detail for Simulations B & C

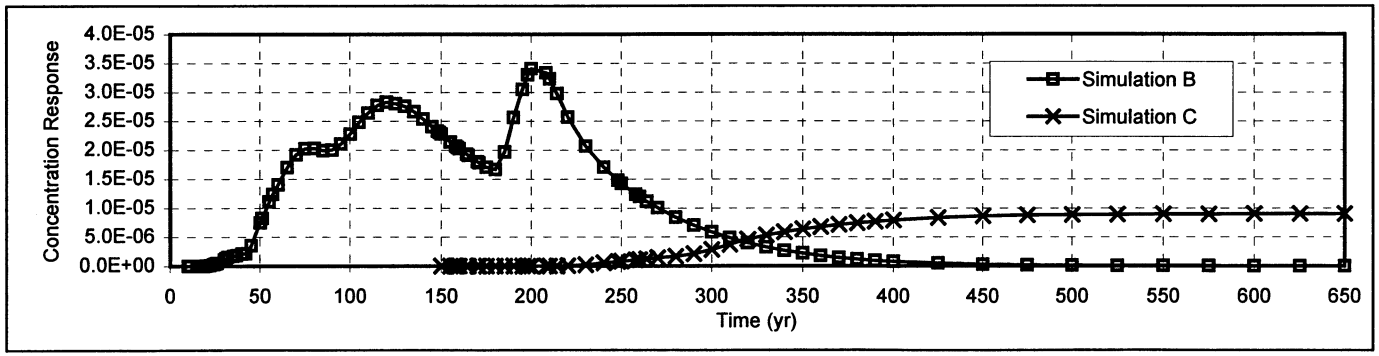

4.2-10-215

HSI GEOTRANS			
REVISED	DATE	BY	DESCRIPTION

CHECKED BY: PAW	DATE: April 1998
APPROVED BY: PFA	DATE: April 1998
APPROVED BY:	DATE:

Simulations T03C1,2,3

Nicolet Minerals COMPANY

Figure 2.48
BEJT Concentration Response Curves at the Compliance Boundary

Scale: None	Date: April 1998
Prepared By: HSI GEOTRANS	By: GWC

\Crandon\TmaMod3\Excel\T03C.xls, Super1

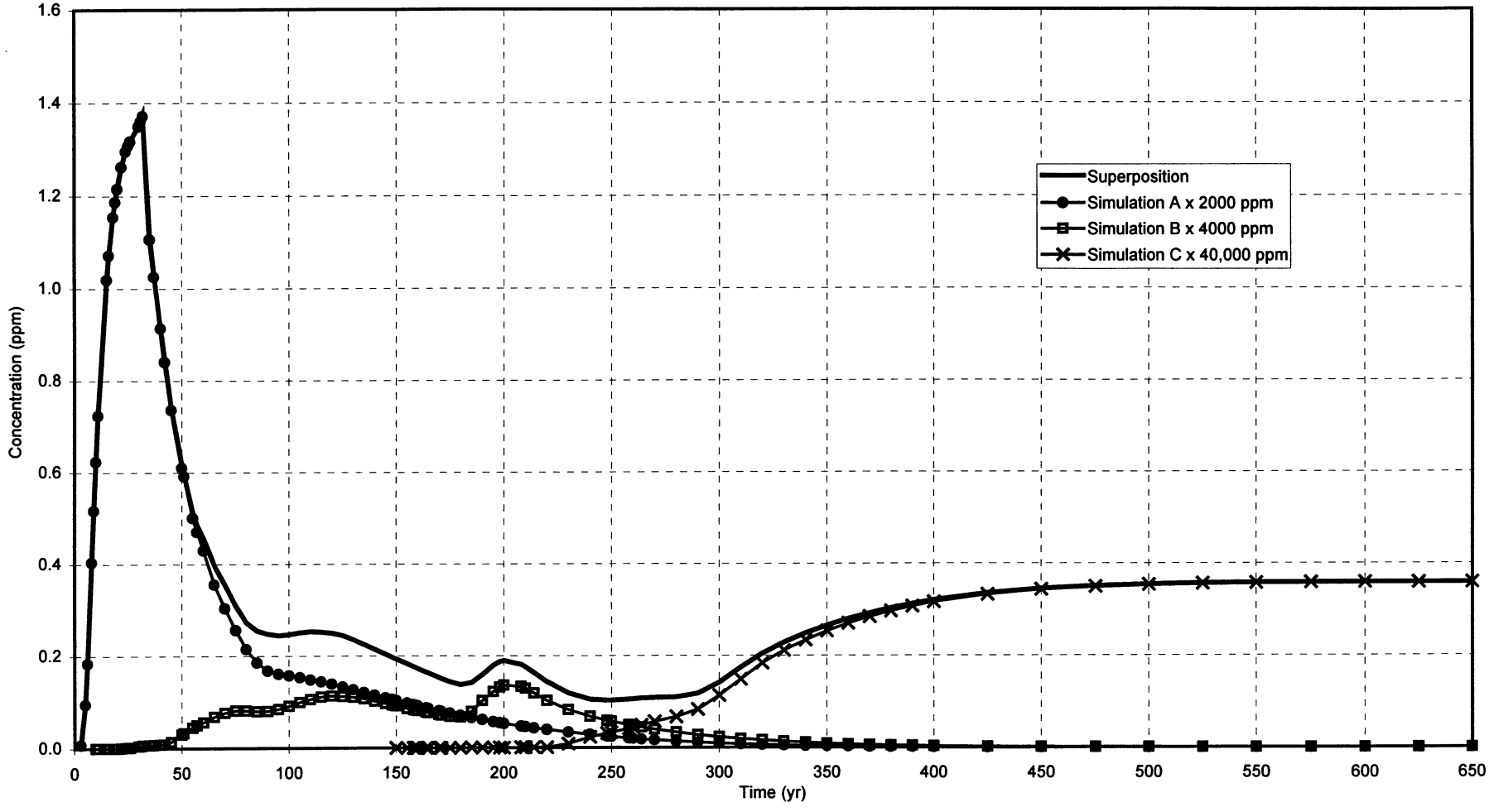

Source Concentration:
Operation: 2000 ppm
Post-Cap: 4000 ppm
Oxidized: 40,000 ppm*

* As a conservative assumption, the oxidized concentration begins one year after assumed degradation of the flexible membrane liner.

HSI GEOTRANS			
REVISED	DATE	BY	DESCRIPTION

CHECKED BY: PAW	DATE: April 1998
APPROVED BY: PFA	DATE: April 1998
APPROVED BY:	DATE:

Simulations T03C1,2,3

Nicolet Minerals COMPANY

Figure 2.49
BEJT Concentration at the Compliance Boundary (Example Constituent)

Scale: None	Date: April 1998
Prepared By: HSI GEOTRANS	By: GWC

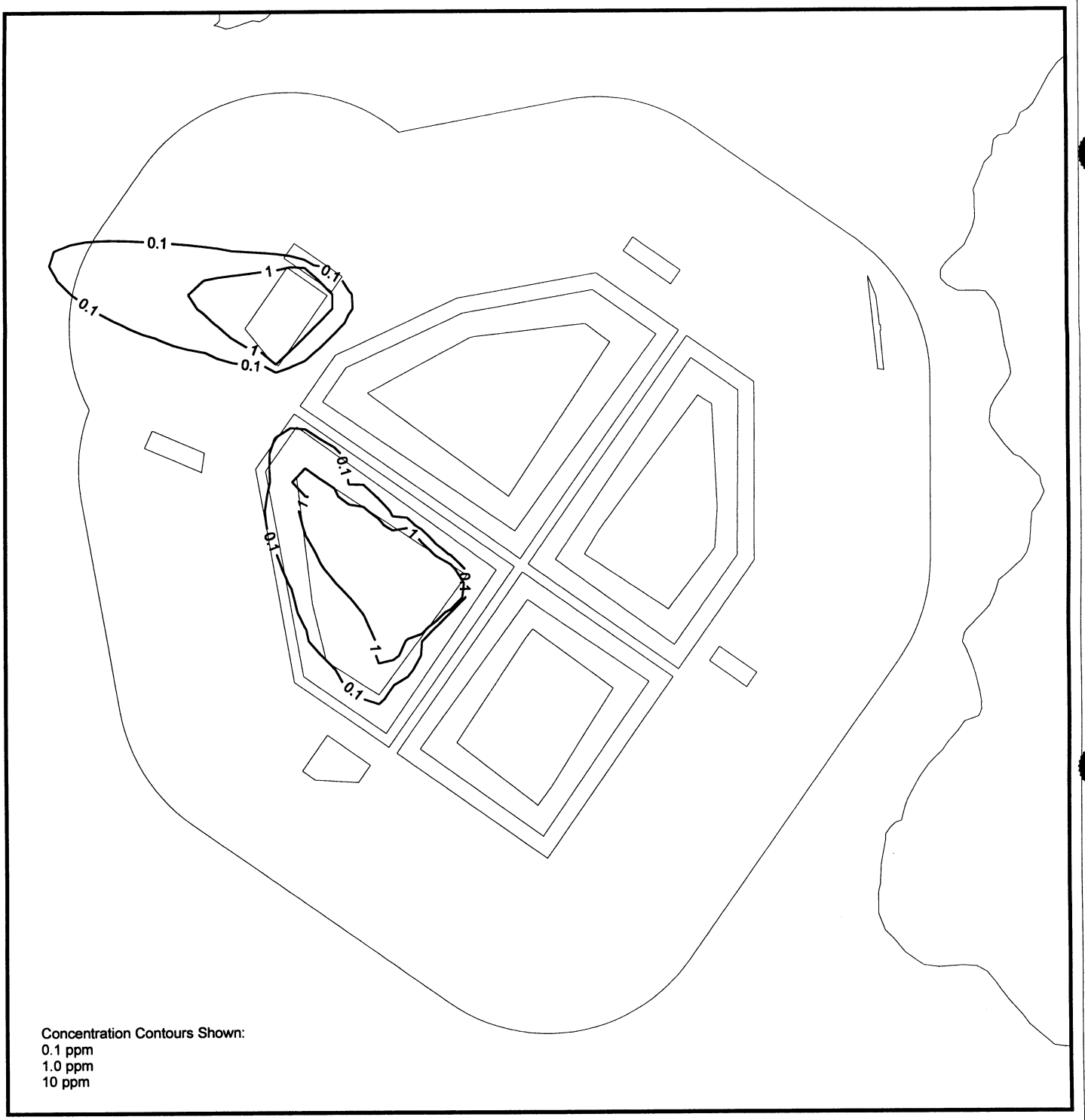

Source Concentration
Operation: 2000 ppm
Post-cap: 4000 ppm
Oxidized: 40,000 ppm*

* As a conservative assumption, the oxidized concentration begins one year after assumed degradation of the flexible membrane liner.

Note:
This plot shows contours of maximum concentratration in any layer.

0 1000 2000
Scale in Feet

HSI GEOTRANS

REVISED	DATE	BY	DESCRIPTION

CHECKED BY: GWC	DATE: April 1998
APPROVED BY: PFA	DATE: April 1998
APPROVED BY:	DATE:

Nicolet Minerals COMPANY

Figure 2.50
BEJT Concentration After 6 Years
(Example Constituent, Plan View)

Scale: 1 in. = 1000 ft.	Date: April 1998
Prepared By: HSI GEOTRANS	By: RMD

\Crandon\Tmal\Mod3\Surfer\Bejt00c.srf

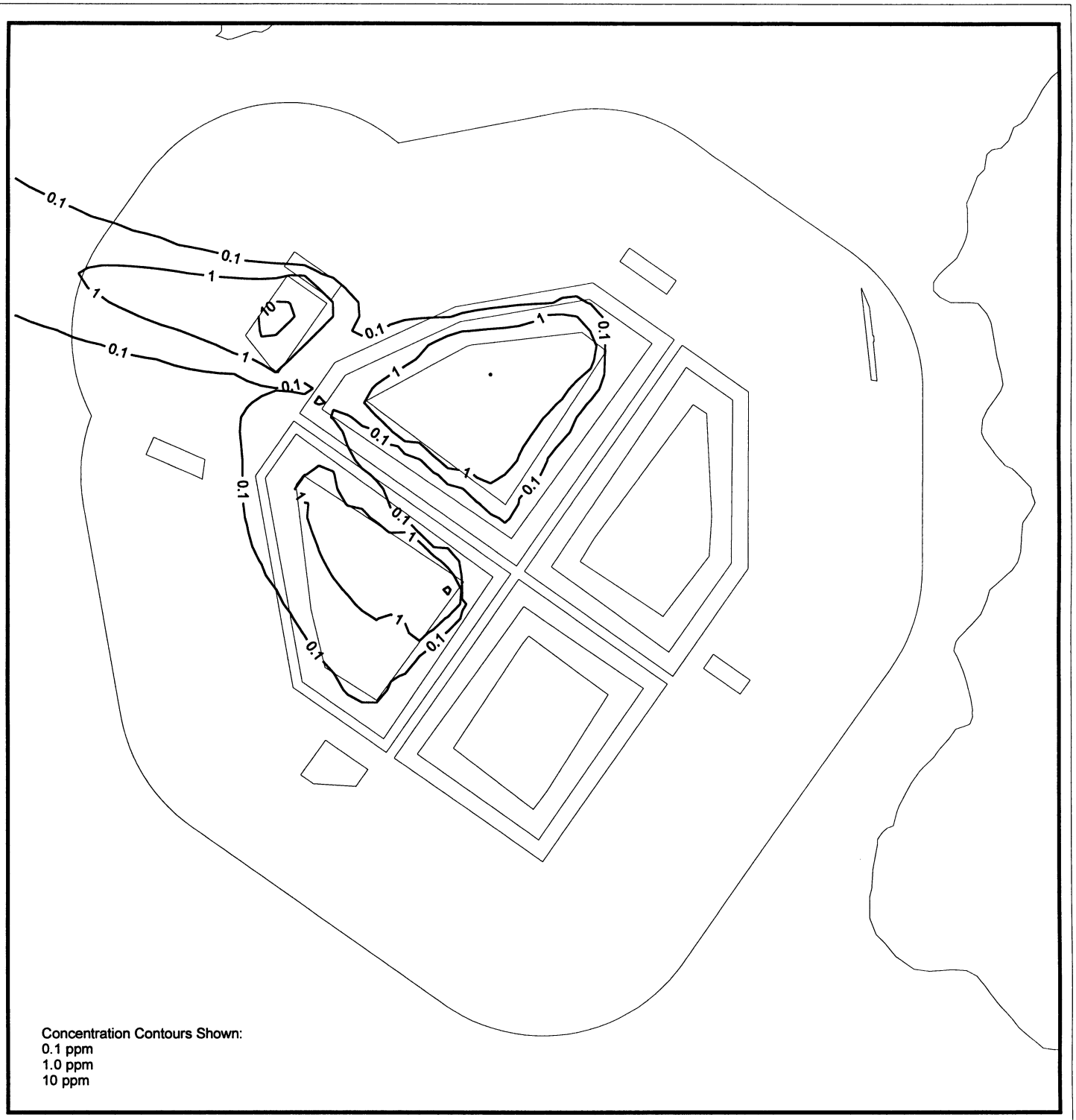

Source Concentration
Operation: 2000 ppm
Post-cap: 4000 ppm
Oxidized: 40,000 ppm*

* As a conservative assumption, the oxidized concentration begins one year after assumed degradation of the flexible membrane liner.

Note:
This plot shows contours of maximum concentratration in any layer.

N

0 1000 2000

Scale in Feet

HSI GEOTRANS

REVISED	DATE	BY	DESCRIPTION

CHECKED BY: GWC	DATE: April 98
APPROVED BY: PFA	DATE: April 1998
APPROVED BY:	DATE:

Nicolet Minerals COMPANY

Figure 2.51
BEJT Concentration After 16 Years
(Example Constituent, Plan View)

Scale: 1 in. = 1000 ft.	Date: April 1998
Prepared By: HSI GEOTRANS	By: RMD

\CrandonTmaMod3\Surfaces\016c.srf

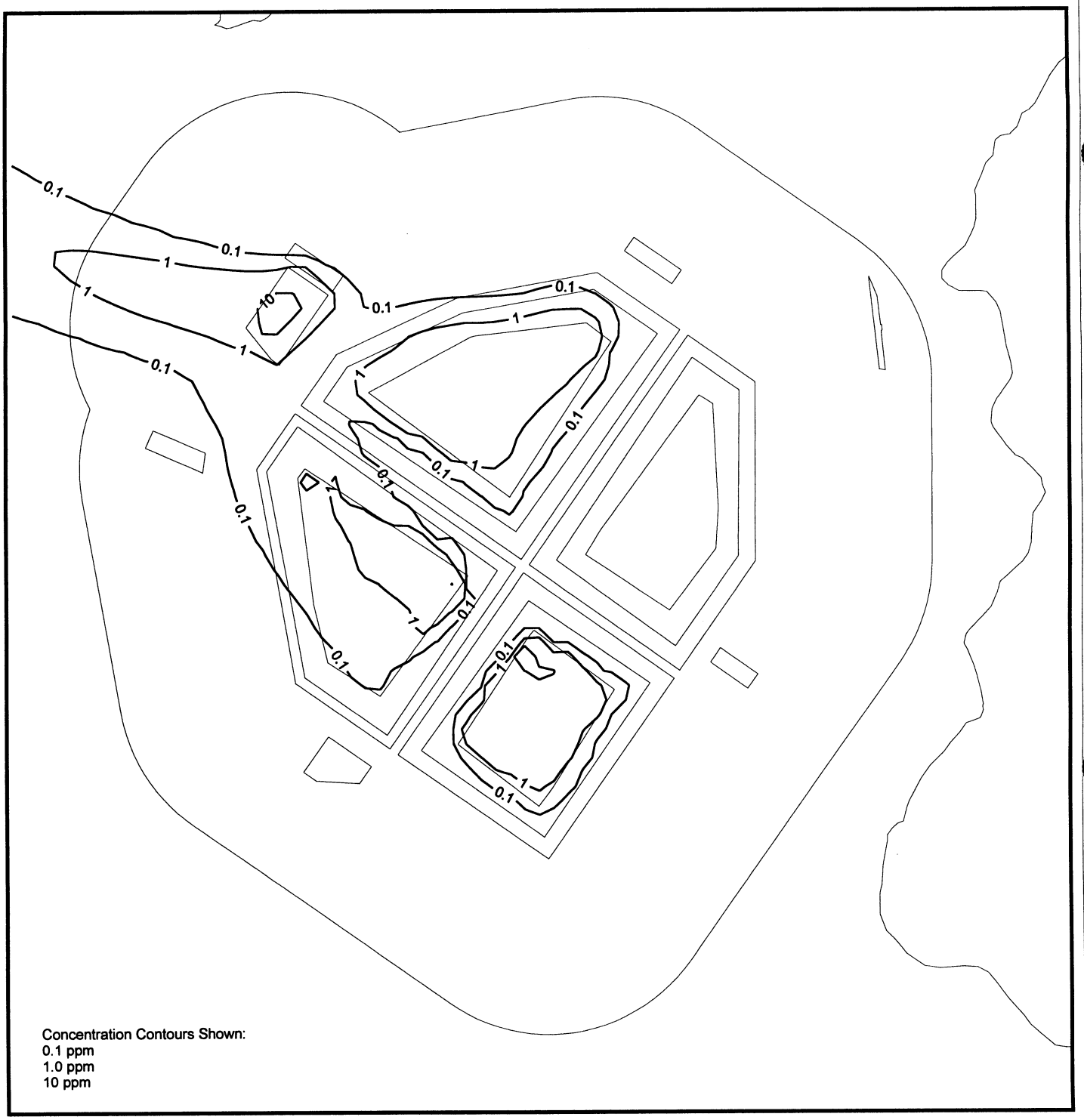

Source Concentration
Operation: 2000 ppm
Post-cap: 4000 ppm
Oxidized: 40,000 ppm*

* As a conservative assumption, the oxidized concentration begins one year after assumed degradation of the flexible membrane liner.

Note:
This plot shows contours of maximum concentratration in any layer.

N

0 1000 2000

Scale in Feet

HSI GEOTRANS

REVISED	DATE	BY	DESCRIPTION

CHECKED BY: GWC	DATE: April 98
APPROVED BY: PFA	DATE: April 1998
APPROVED BY:	DATE:

Nicolet Minerals COMPANY

Figure 2.52
BEJT Concentration After 22 Years (Example Constituent, Plan View)

Scale: 1 in. = 1000 ft.	Date: April 1998
Prepared By: HSI GEOTRANS	By: RMD

\Crandon\Tmat\Mod3\Surfer\Bej022c.srf

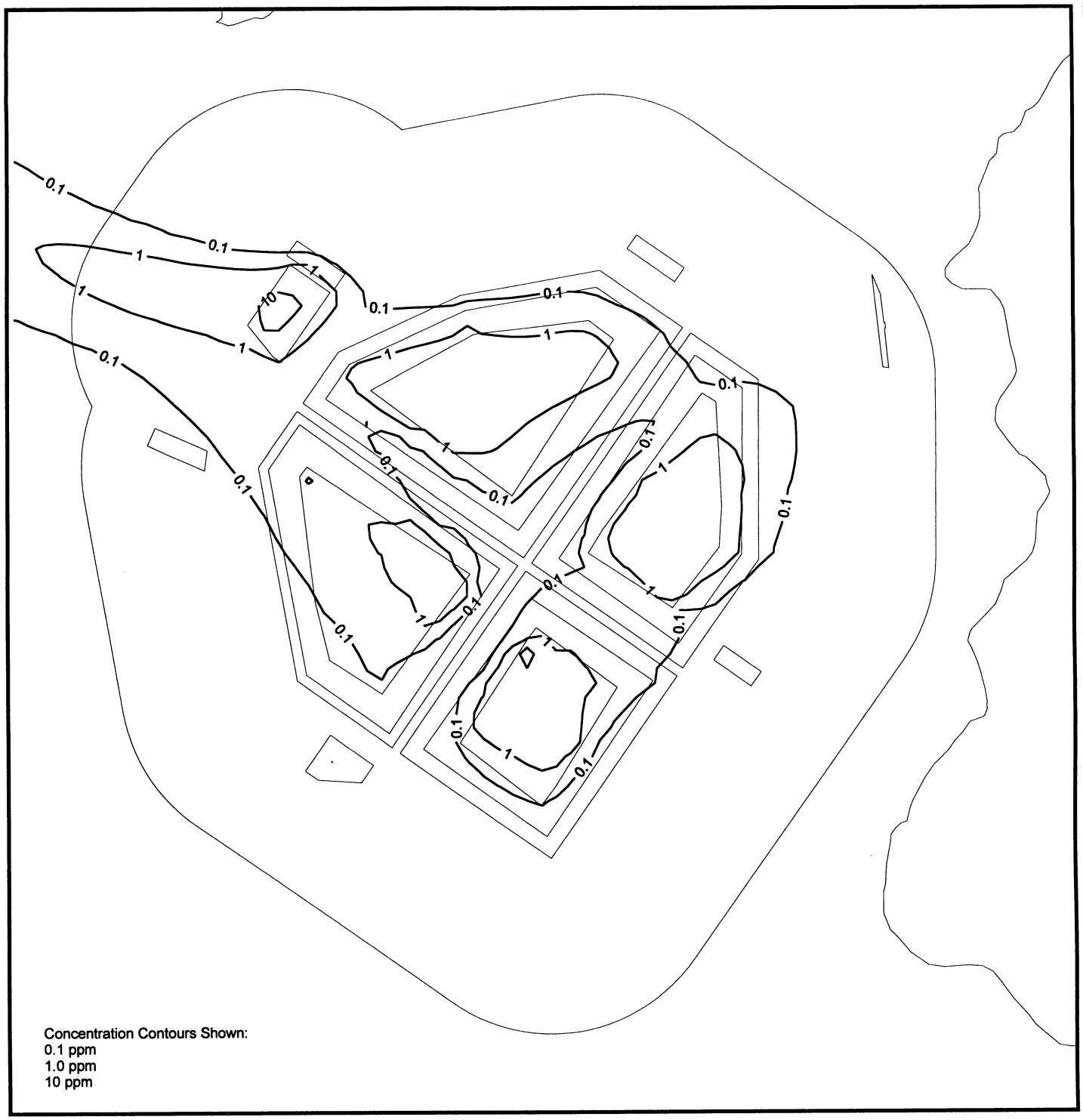

Source Concentration
Operation: 2000 ppm
Post-cap: 4000 ppm
Oxidized: 40,000 ppm*

* As a conservative assumption, the oxidized concentration begins one year after assumed degradation of the flexible membrane liner.

Note:
This plot shows contours of maximum concentratration in any layer.

N

0 1000 2000

Scale in Feet

HSI GEOTRANS

REVISED	DATE	BY	DESCRIPTION

CHECKED BY: GWC	DATE: April 98
APPROVED BY: PFA	DATE: April 1998
APPROVED BY:	DATE:

Nicolet Minerals COMPANY

Figure 2.53
BEJT Concentration After 32 Years
(Example Constituent, Plan View)

Scale: 1 in. = 1000 ft.	Date: April 1998
Prepared By: HSI GEOTRANS	By: RMD

\Crandon\Tmod3\Surfer\bejt032c.srf

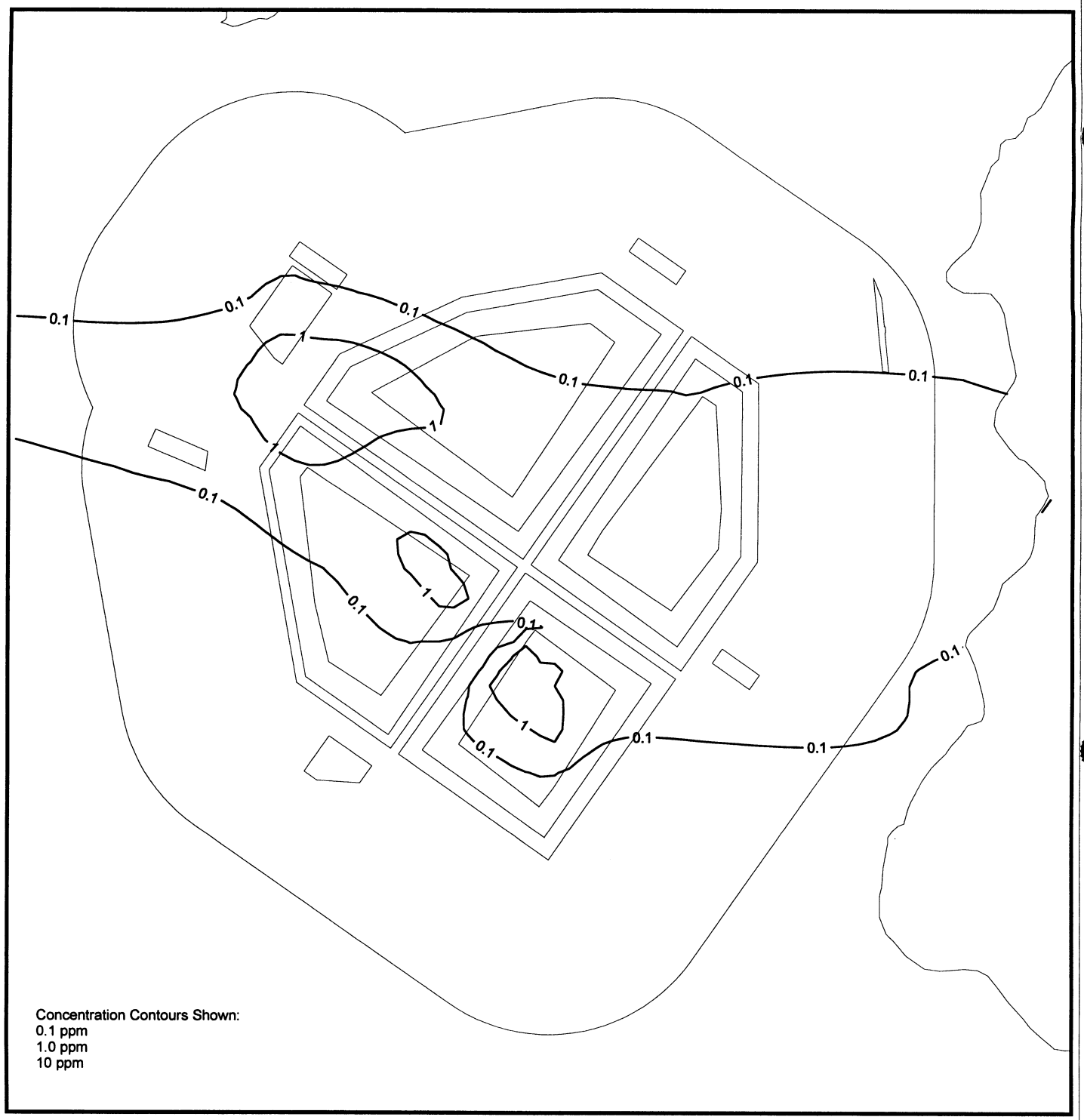

Source Concentration
Operation: 2000 ppm
Post-cap: 4000 ppm
Oxidized: 40,000 ppm*

* As a conservative assumption, the oxidized concentration begins one year after assumed degradation of the flexible membrane liner.

Note:
This plot shows contours of maximum concentratration in any layer.

N

0 1000 2000

Scale in Feet

HSI GEOTRANS

REVISED	DATE	BY	DESCRIPTION

CHECKED BY: GWC	DATE: April 98
APPROVED BY: PFA	DATE: April 1998
APPROVED BY:	DATE:

Nicolet Minerals COMPANY

Figure 2.54
BEJT Concentration After 60 Years
(Example Constituent, Plan View)

Scale: 1 in. = 1000 ft.	Date: April 1998
Prepared By: HSI GEOTRANS	By: RMD

\\Crandon\Tmal\Mod3\Surfer\Bejt060c.srf

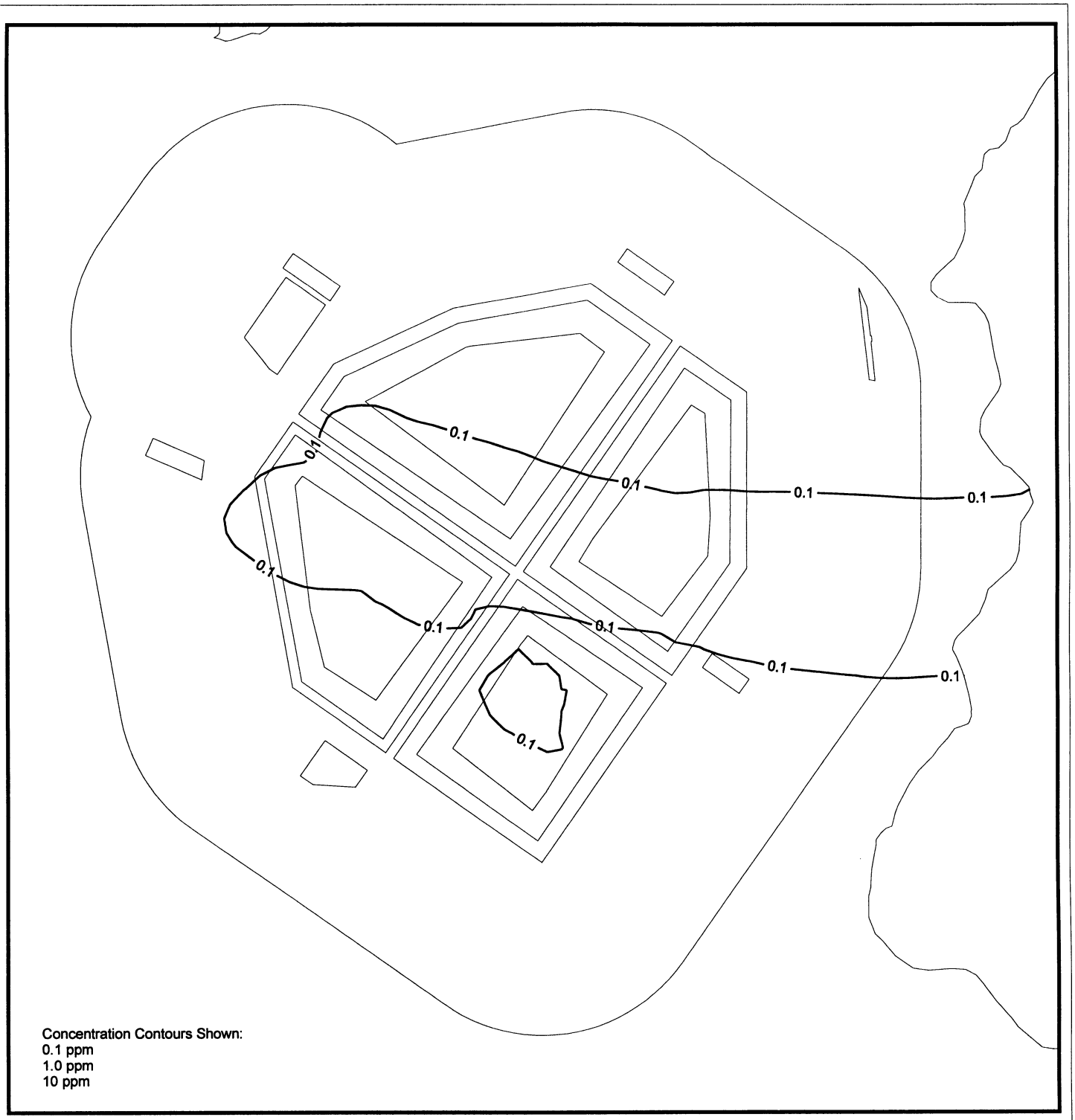

Concentration Contours Shown:
0.1 ppm
1.0 ppm
10 ppm

Source Concentration
Operation: 2000 ppm
Post-cap: 4000 ppm
Oxidized: 40,000 ppm*

* As a conservative assumption, the oxidized concentration begins one year after assumed degradation of the flexible membrane liner.

Note:
This plot shows contours of maximum concentratration in any layer.

0 1000 2000
Scale in Feet

HSI GEOTRANS

REVISED	DATE	BY	DESCRIPTION

CHECKED BY: GWC	DATE: April 98
APPROVED BY: PFA	DATE: April 1998
APPROVED BY:	DATE:

Nicolet Minerals COMPANY

Figure 2.55
BEJT Concentration After 125 Years
(Example Constituent, Plan View)

Scale: 1 in. = 1000 ft.	Date: April 1998
Prepared By: HSI GEOTRANS	By: RMD

\Crandon\Tmwmod3\Surfer\bej125c.srf

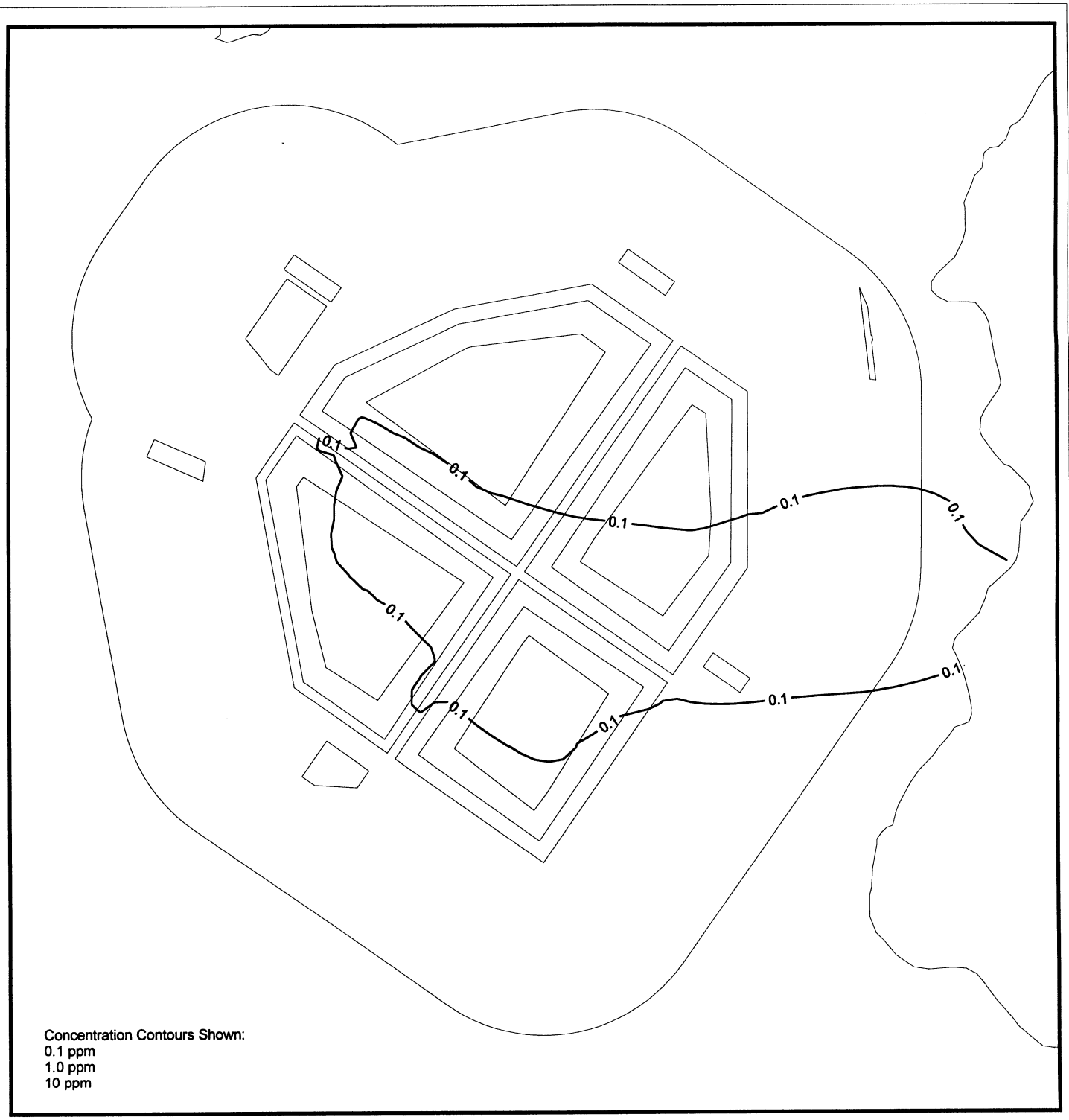

Source Concentration
Operation: 2000 ppm
Post-cap: 4000 ppm
Oxidized: 40,000 ppm*

* As a conservative assumption, the oxidized concentration begins one year after assumed degradation of the flexible membrane liner.

Note:
This plot shows contours of maximum concentratration in any layer.

N

0 1000 2000

Scale in Feet

HSI GEOTRANS

REVISED	DATE	BY	DESCRIPTION

CHECKED BY: GWC	DATE: April 98
APPROVED BY: PFA	DATE: April 1998
APPROVED BY:	DATE:

Nicolet Minerals COMPANY

Figure 2.56
BEJT Concentration After 200 Years (Example Constituent, Plan View)

Scale: 1 in. = 1000 ft.	Date: April 1998
Prepared By: HSI GEOTRANS	By: RMD

\Crandon\Tmat\Mod3\Surfer\Bej200c.srf

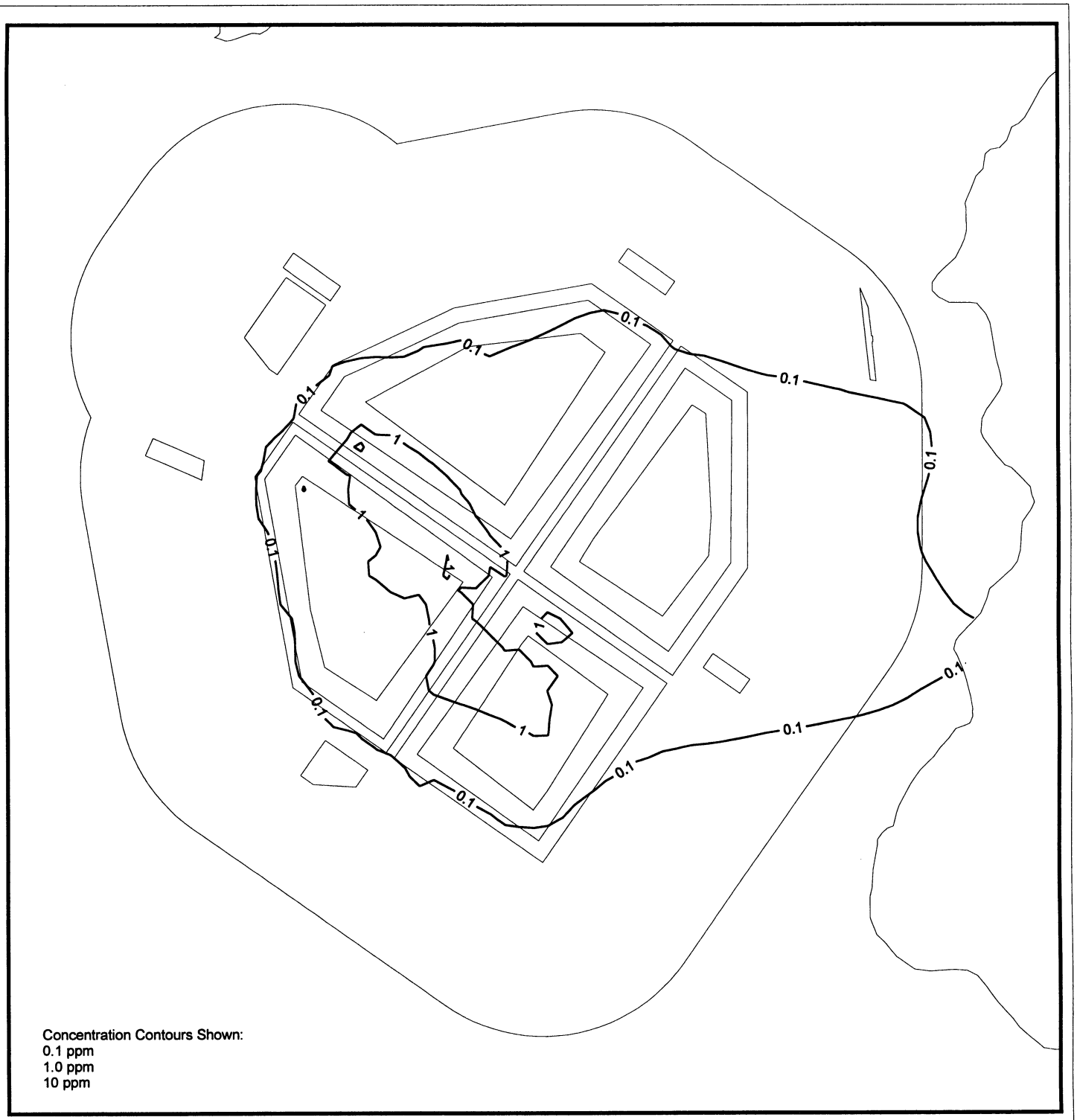

Source Concentration
Operation: 2000 ppm
Post-cap: 4000 ppm
Oxidized: 40,000 ppm*

* As a conservative assumption, the oxidized concentration begins one year after assumed degradation of the flexible membrane liner.

Note:
This plot shows contours of maximum concentratration in any layer.

N

0 1000 2000

Scale in Feet

HSI GEOTRANS

REVISED	DATE	BY	DESCRIPTION

CHECKED BY: GWC	DATE: April 98
APPROVED BY: PFA	DATE: April 1998
APPROVED BY:	DATE:

Nicolet Minerals COMPANY

Figure 2.57
BEJT Concentration After 300 Years (Example Constituent, Plan View)

Scale: 1 in. = 1000 ft.	Date: April 1998
Prepared By: HSI GEOTRANS	By: RMD

\Crandon\Tmwmod3\Surfer\bej300c.srf

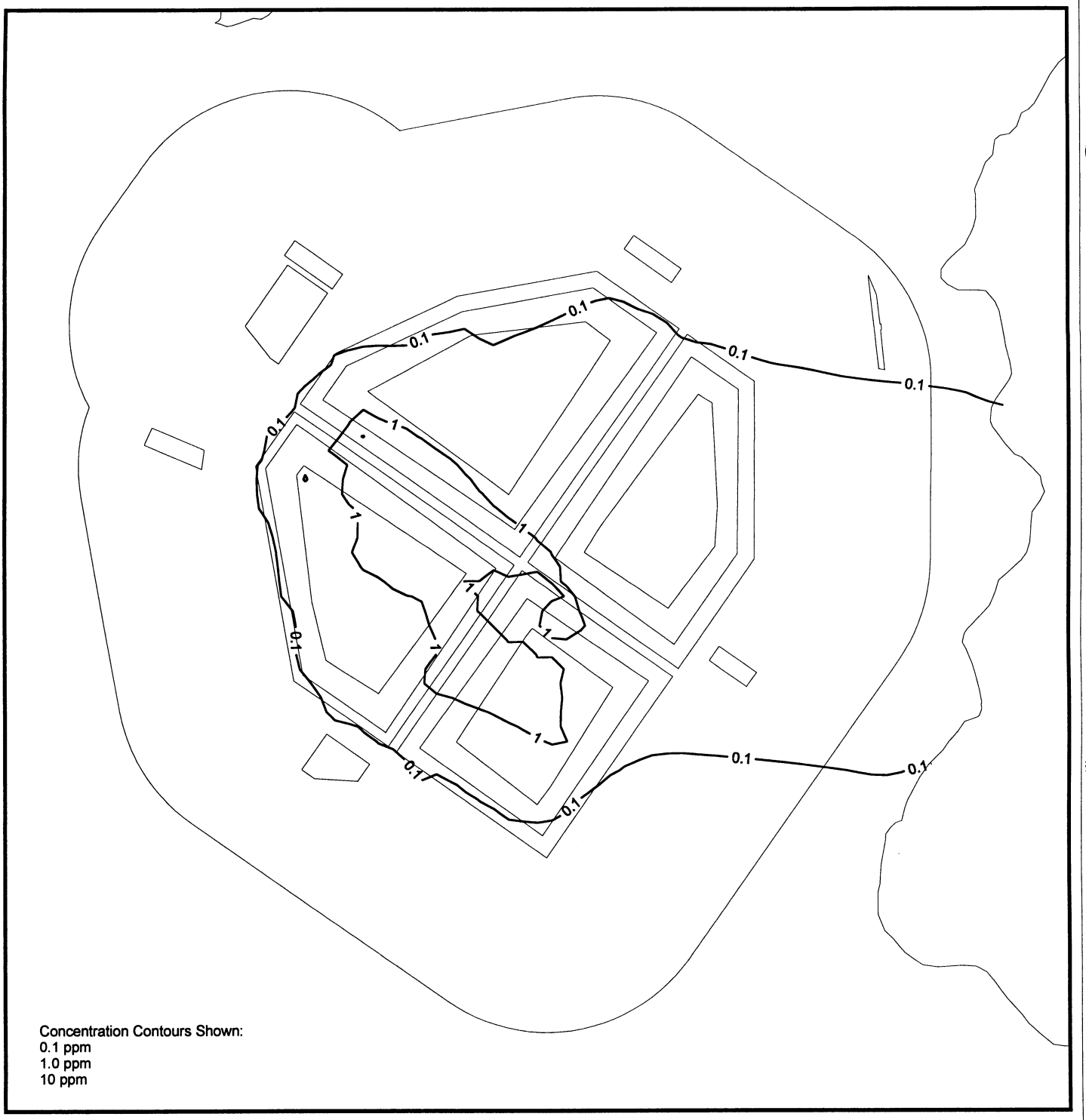

Source Concentration
Operation: 2000 ppm
Post-cap: 4000 ppm
Oxidized: 40,000 ppm*

* As a conservative assumption, the oxidized concentration begins one year after assumed degradation of the flexible membrane liner.

Note:
This plot shows contours of maximum concentratration in any layer.

N

0 1000 2000

Scale in Feet

HSI GEOTRANS

REVISED	DATE	BY	DESCRIPTION

CHECKED BY: GWC	DATE: April 98
APPROVED BY: PFA	DATE: April 1998
APPROVED BY:	DATE:

Nicolet Minerals COMPANY

Figure 2.58
BEJT Concentration After 650 Years
(Example Constituent, Plan View)

Scale: 1 in. = 1000 ft.	Date: April 1998
Prepared By: HSI GEOTRANS	By: RMD

\Crandon\Tma\Mod3\Surfer\Bej650c.srf

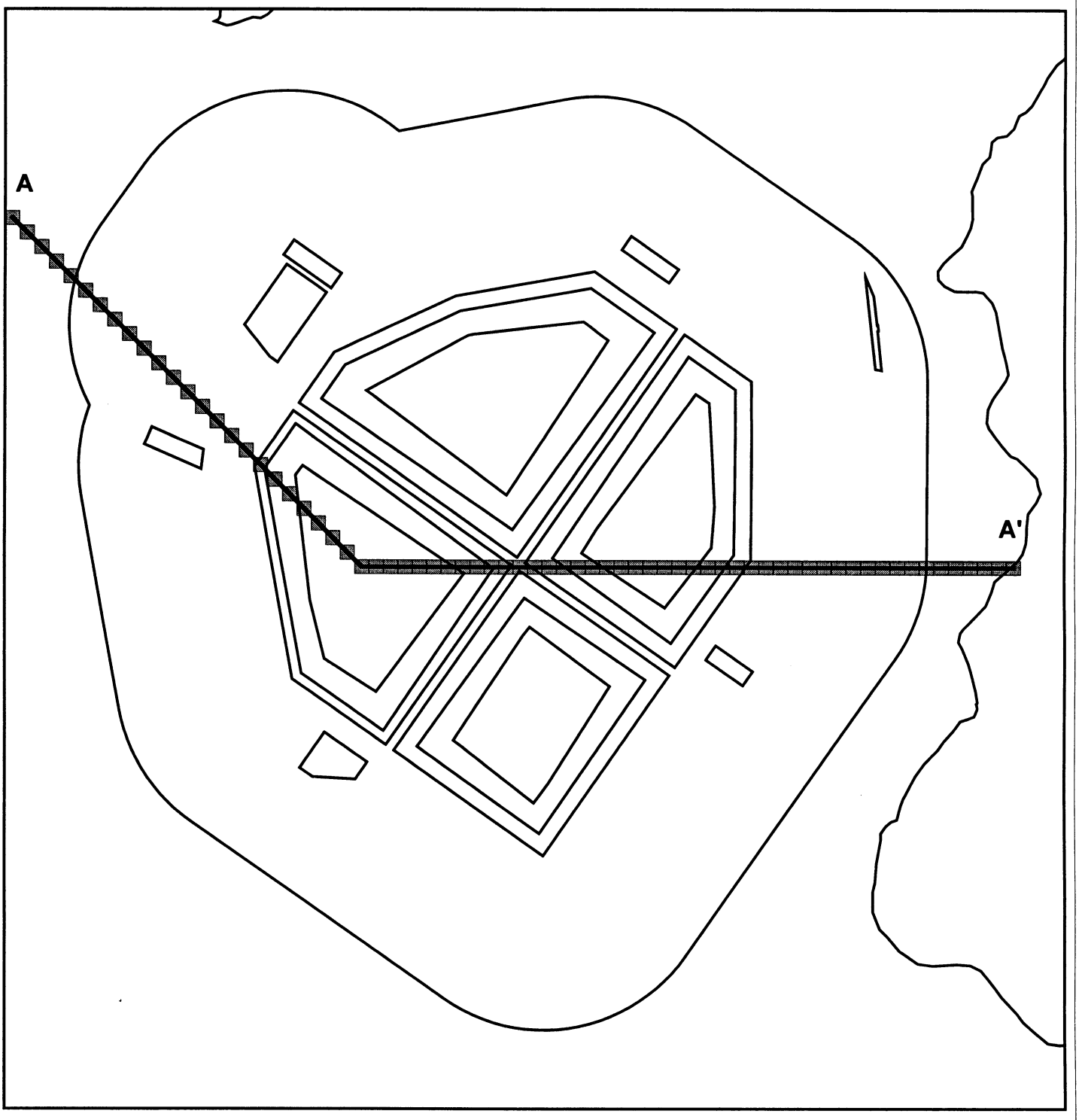

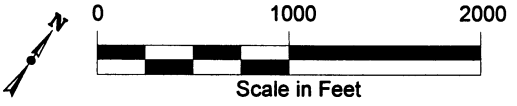

HSI GEOTRANS			
REVISED	DATE	BY	DESCRIPTION

CHECKED BY: PAW	DATE: April 1998
APPROVED BY: PFA	DATE: April 1998
APPROVED BY:	DATE:

Nicolet Minerals COMPANY

Figure 2.59
Location of Cross-Section Used for Viewing Plumes

Scale: 1 in. = 1000 ft.	Date: April 1998
Prepared By: HSI GeoTrans	By: GWC

\Crandon\TmaMod3\G...d\SecAA.wor

\Crandon\TmaMod3\Surfer\Bej006x.srf

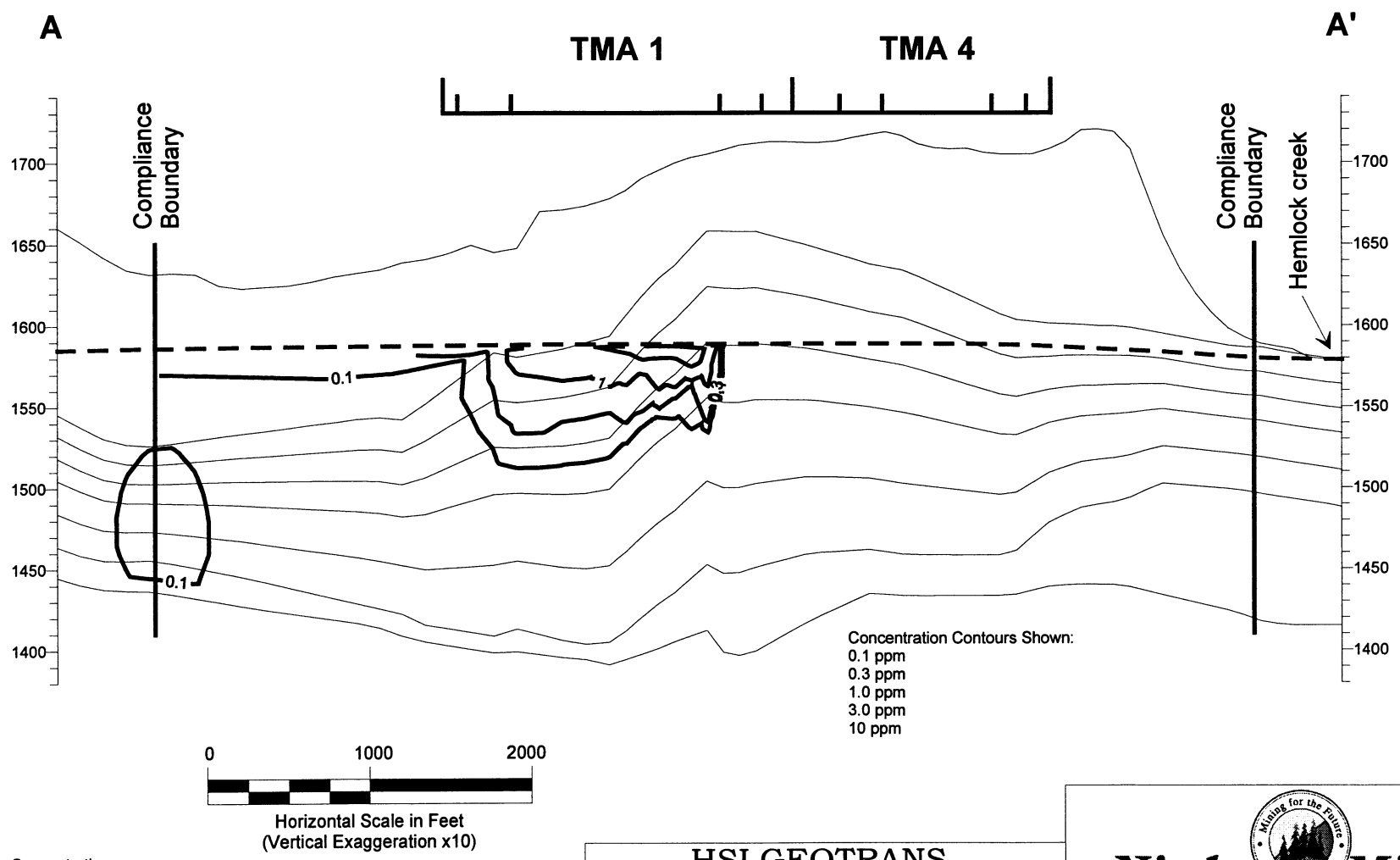

4.2-10-227

Source Concentration
Operation: 2000 ppm
Post-cap: 4000 ppm
Oxidized: 40,000 ppm*

* As a conservative assumption, the oxidized concentration begins one year after assumed degradation of the flexible membrane liner.

HSI GEOTRANS

REVISED	DATE	BY	DESCRIPTION

CHECKED BY: GWC	DATE: April 1998
APPROVED BY: PFA	DATE: April 1998
APPROVED BY:	DATE:

Nicolet Minerals COMPANY

Figure 2.60
BEJT Concentration After 6 Years (Example Constituent, Cross Section)

Scale: 1" = 1000' (h), 100' (v)	Date: April 1998
Prepared By: HSI GeoTrans	By: RMD

\Crandon\TmaMod3\Surfer\Bej016x.srf

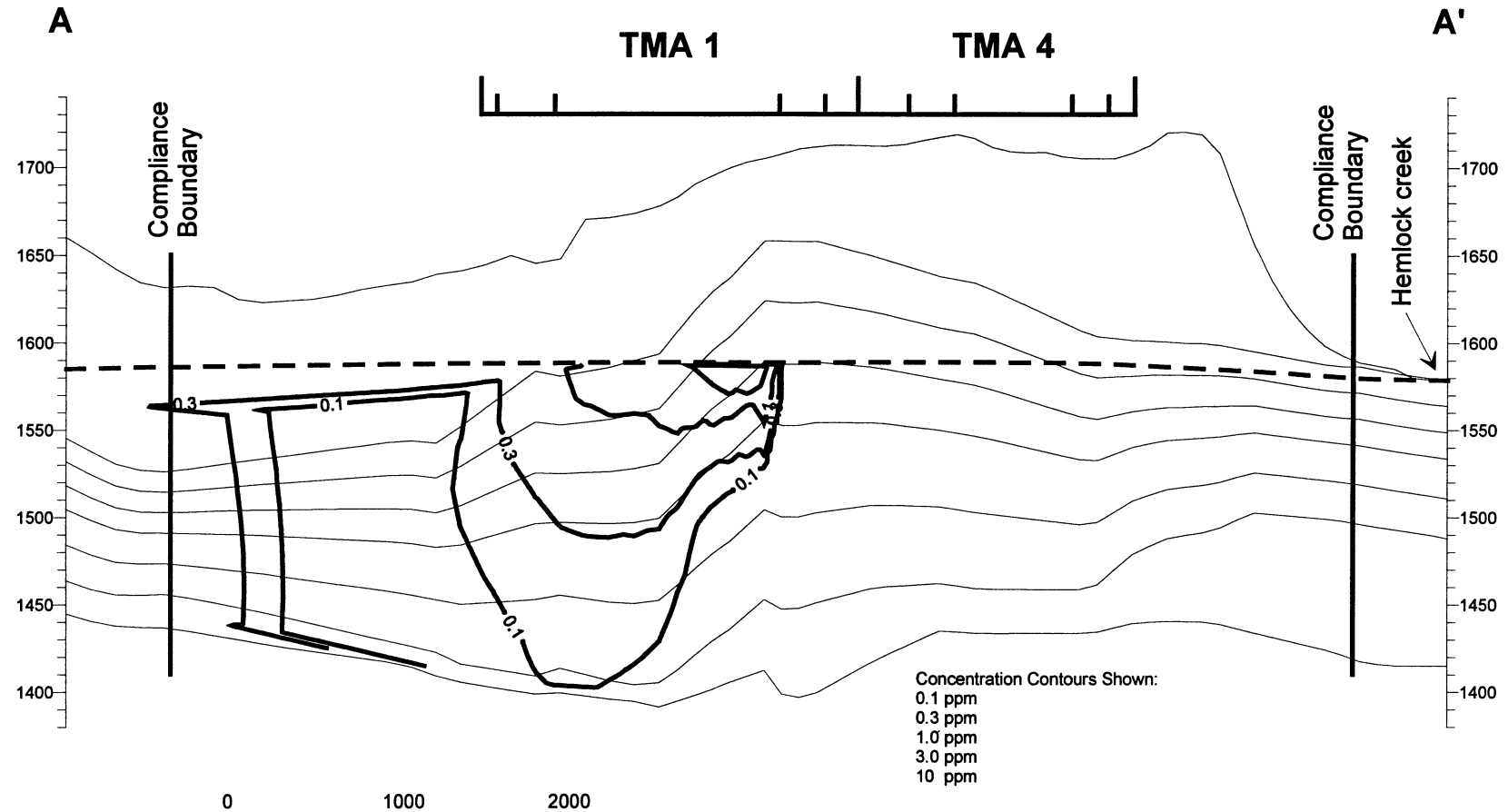

4.2-10-228

Source Concentration
Operation: 2000 ppm
Post-cap: 4000 ppm
Oxidized: 40,000 ppm*

* As a conservative assumption, the oxidized concentration begins one year after assumed degradation of the flexible membrane liner.

HSI GEOTRANS

REVISED	DATE	BY	DESCRIPTION

CHECKED BY: GWC	DATE: April 1998
APPROVED BY: PFA	DATE: April 1998
APPROVED BY:	DATE:

Nicolet Minerals COMPANY

Figure 2.61
BEJT Concentration After 16 Years (Example Constituent, Cross Section)

Scale: 1" = 1000' (h), 100' (v)	Date: April 1998
Prepared By: HSI GeoTrans	By: RMD

\Crandon\TmaMod3\Surfer\Bej022x.srf

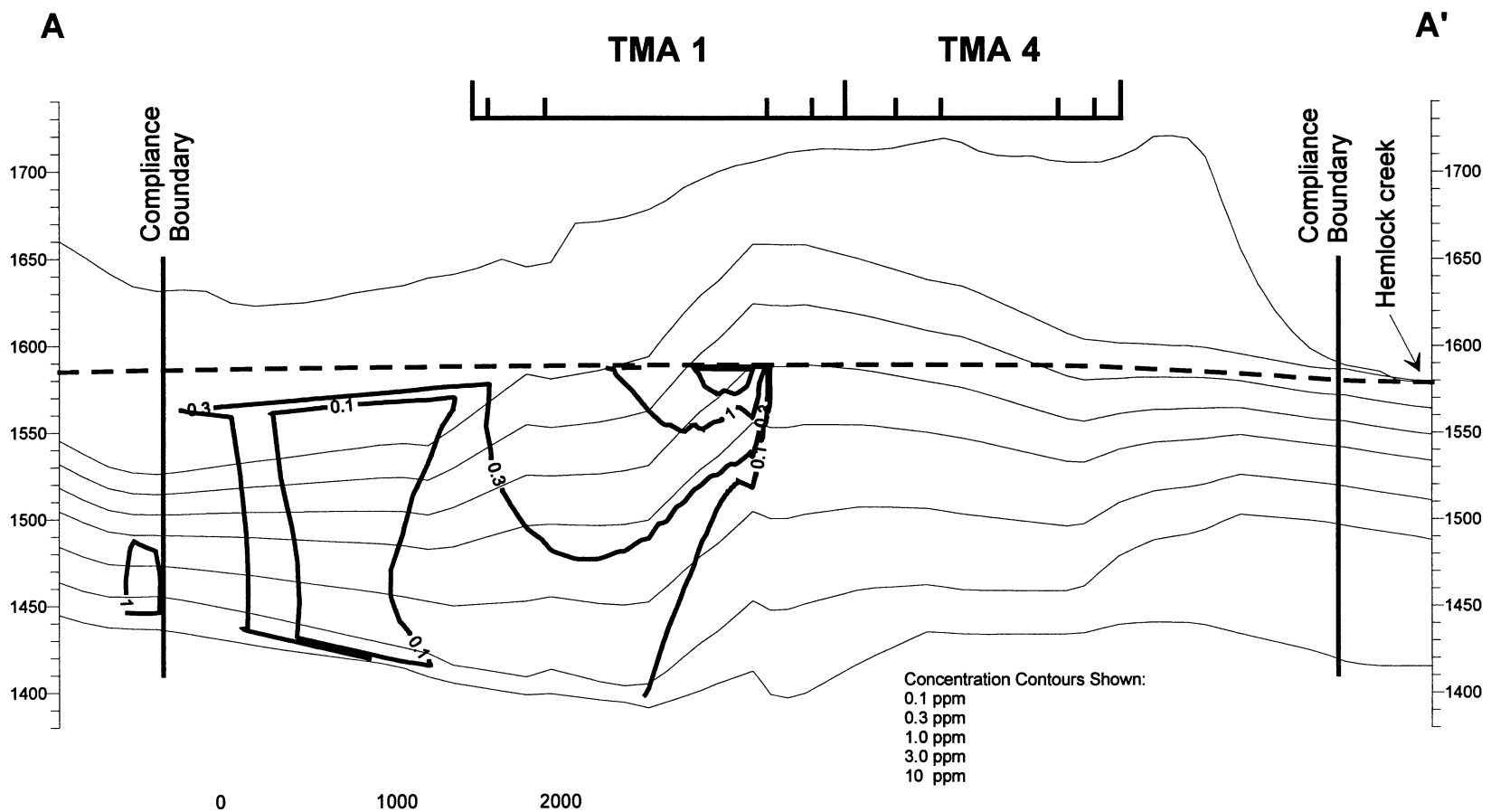

4.2-10-229

Source Concentration
Operation: 2000 ppm
Post-cap: 4000 ppm
Oxidized: 40,000 ppm*

* As a conservative assumption, the oxidized concentration begins one year after assumed degradation of the flexible membrane liner.

HSI GEOTRANS

REVISED	DATE	BY	DESCRIPTION

CHECKED BY: GWC	DATE: April 1998
APPROVED BY: PFA	DATE: April 1998
APPROVED BY:	DATE:

Nicolet Minerals COMPANY

Figure 2.62
BEJT Concentration After 22 Years (Example Constituent, Cross Section)

Scale: 1" = 1000' (h), 100' (v)	Date: April 1998
Prepared By: HSI GeoTrans	By: RMD

\Crandon\TmaMod3\Surfer\Bej032x.srf

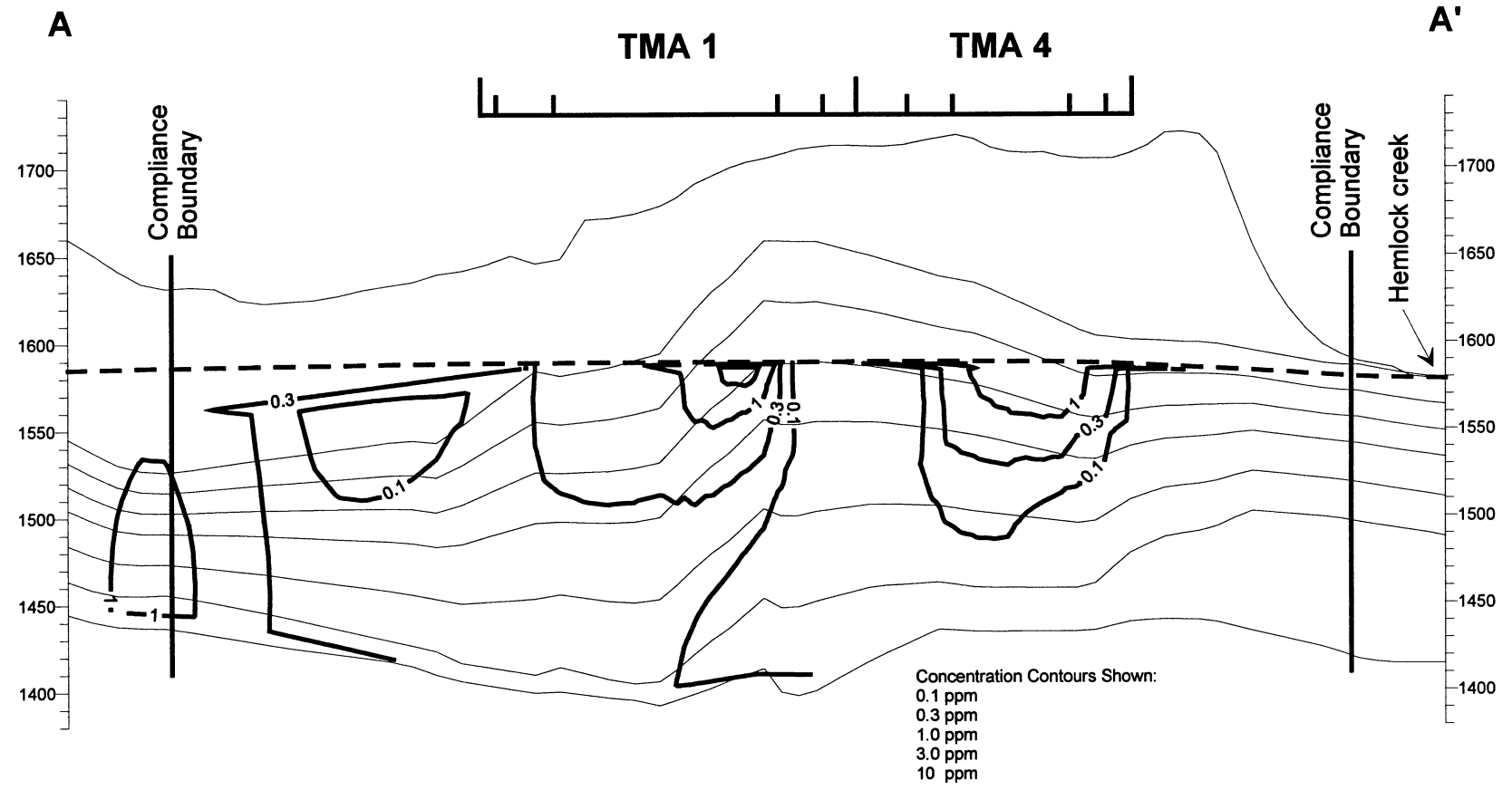

4.2-10-230

Source Concentration
Operation: 2000 ppm
Post-cap: 4000 ppm
Oxidized: 40,000 ppm*

* As a conservative assumption, the oxidized concentration begins one year after assumed degradation of the flexible membrane liner.

HSI GEOTRANS

REVISED	DATE	BY	DESCRIPTION

CHECKED BY: GWC	DATE: April 1998
APPROVED BY: PFA	DATE: April 1998
APPROVED BY:	DATE:

Nicolet Minerals COMPANY

Figure 2.63
BEJT Concentration After 32 Years (Example Constituent, Cross Section)

Scale: 1" = 1000' (h), 100' (v)	Date: April 1998
Prepared By: HSI GeoTrans	By: RMD

\Crandon\TmaMod3\Surfer\Bej060x.srf

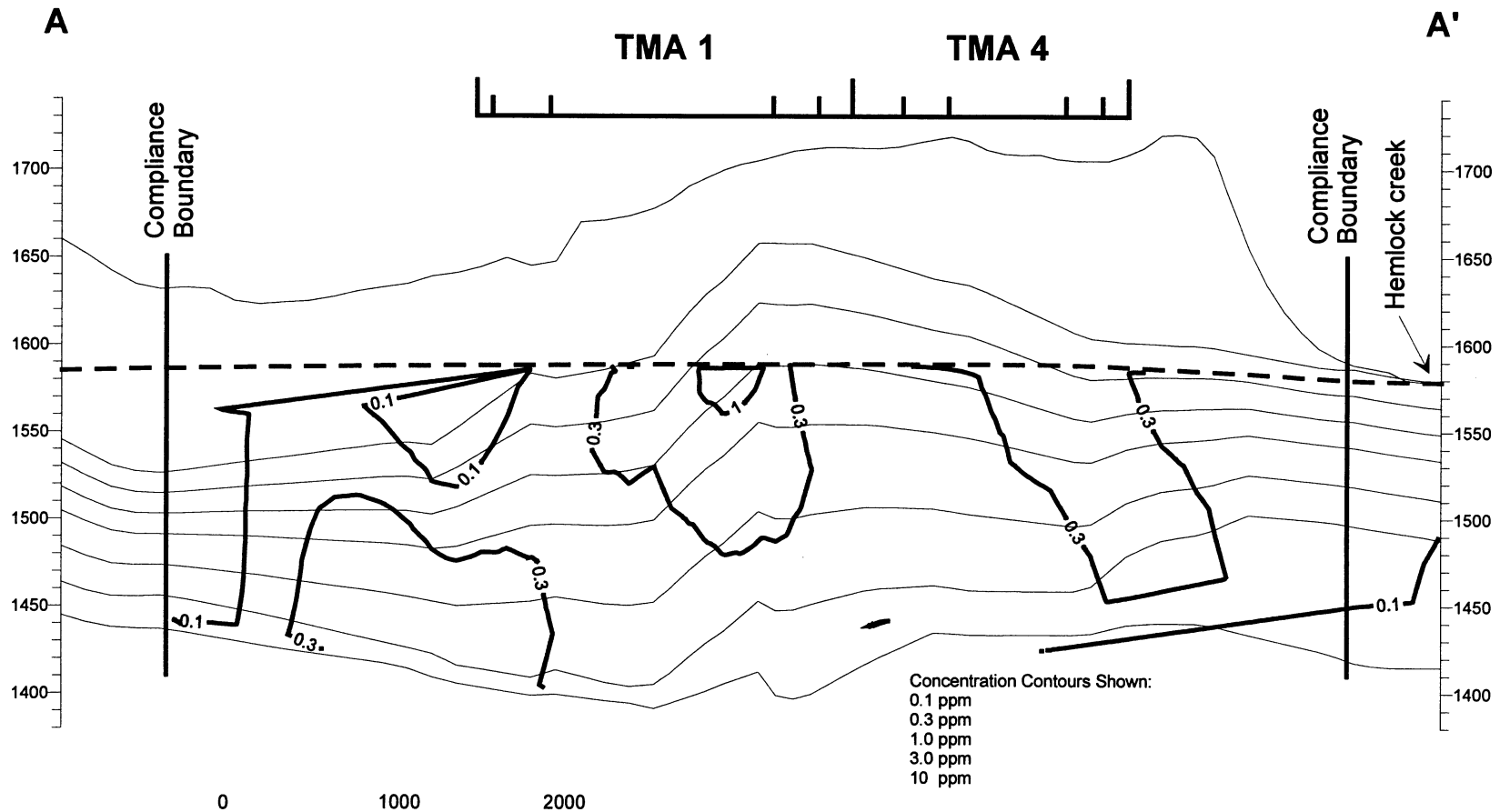

4.2-10-231

Source Concentration
Operation: 2000 ppm
Post-cap: 4000 ppm
Oxidized: 40,000 ppm*

* As a conservative assumption, the oxidized concentration begins one year after assumed degradation of the flexible membrane liner.

HSI GEOTRANS

REVISED	DATE	BY	DESCRIPTION

CHECKED BY: GWC	DATE: April 1998
APPROVED BY: PFA	DATE: April 1998
APPROVED BY:	DATE:

Nicolet Minerals COMPANY

Figure 2.64
BEJT Concentration After 60 Years (Example Constituent, Cross Section)

Scale: 1" = 1000' (h), 100' (v)	Date: April 1998
Prepared By: HSI GeoTrans	By: RMD

\Crandon\TmaMod3\Surfer\Bej125x.srf

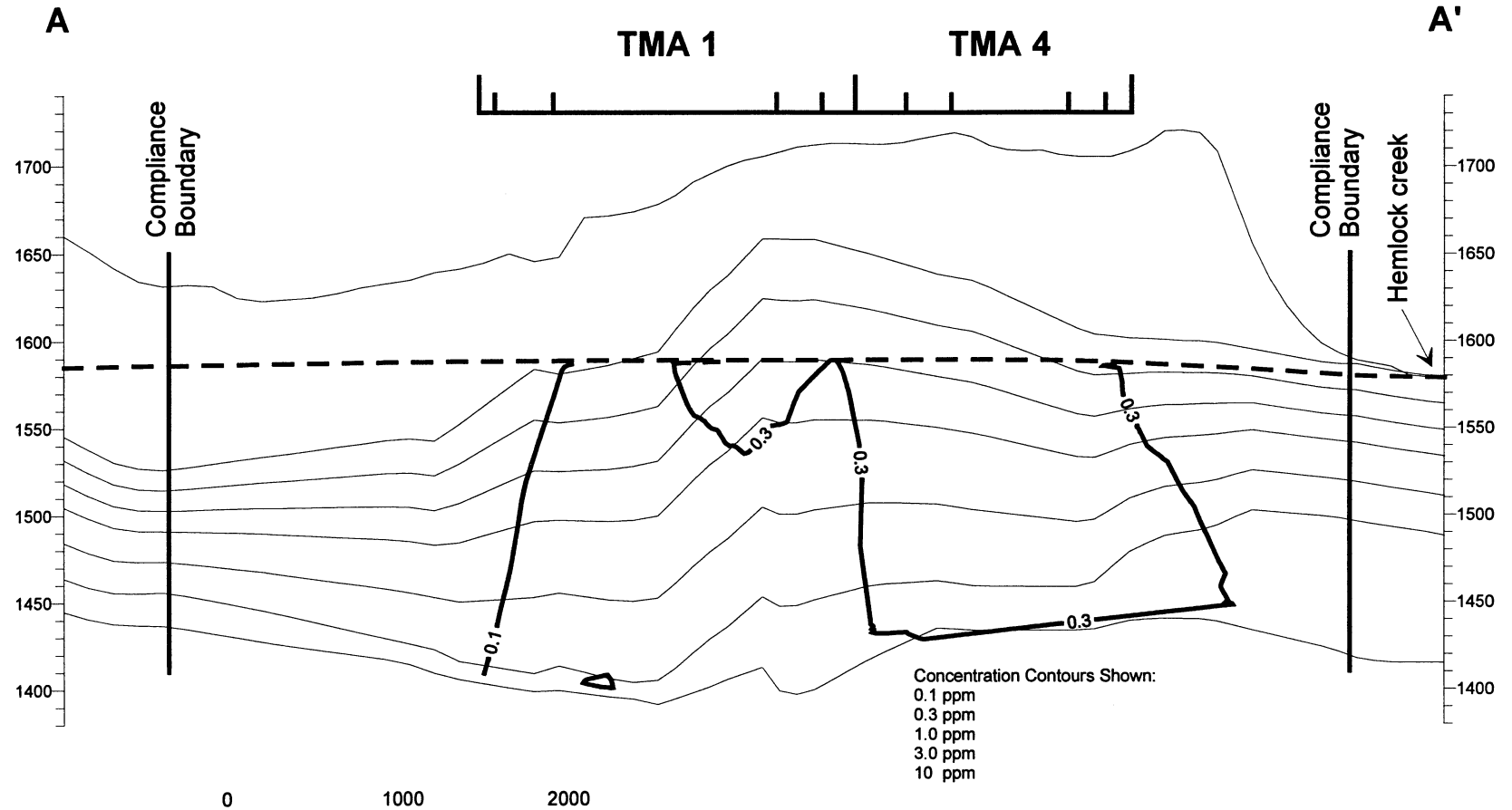

Source Concentration
Operation: 2000 ppm
Post-cap: 4000 ppm
Oxidized: 40,000 ppm*

* As a conservative assumption, the oxidized concentration begins one year after assumed degradation of the flexible membrane liner.

4.2-10-232

HSI GEOTRANS

REVISED	DATE	BY	DESCRIPTION

CHECKED BY: GWC	DATE: April 1998
APPROVED BY: PFA	DATE: April 1998
APPROVED BY:	DATE:

Nicolet Minerals COMPANY

Figure 2.65
BEJT Concentration After 125 Years
(Example Constituent, Cross Section)

Scale: 1" = 1000' (h), 100' (v)	Date: April 1998
Prepared By: HSI GeoTrans	By: RMD

\Crandon\TmaMod3\Surfer\Bej200x.srf

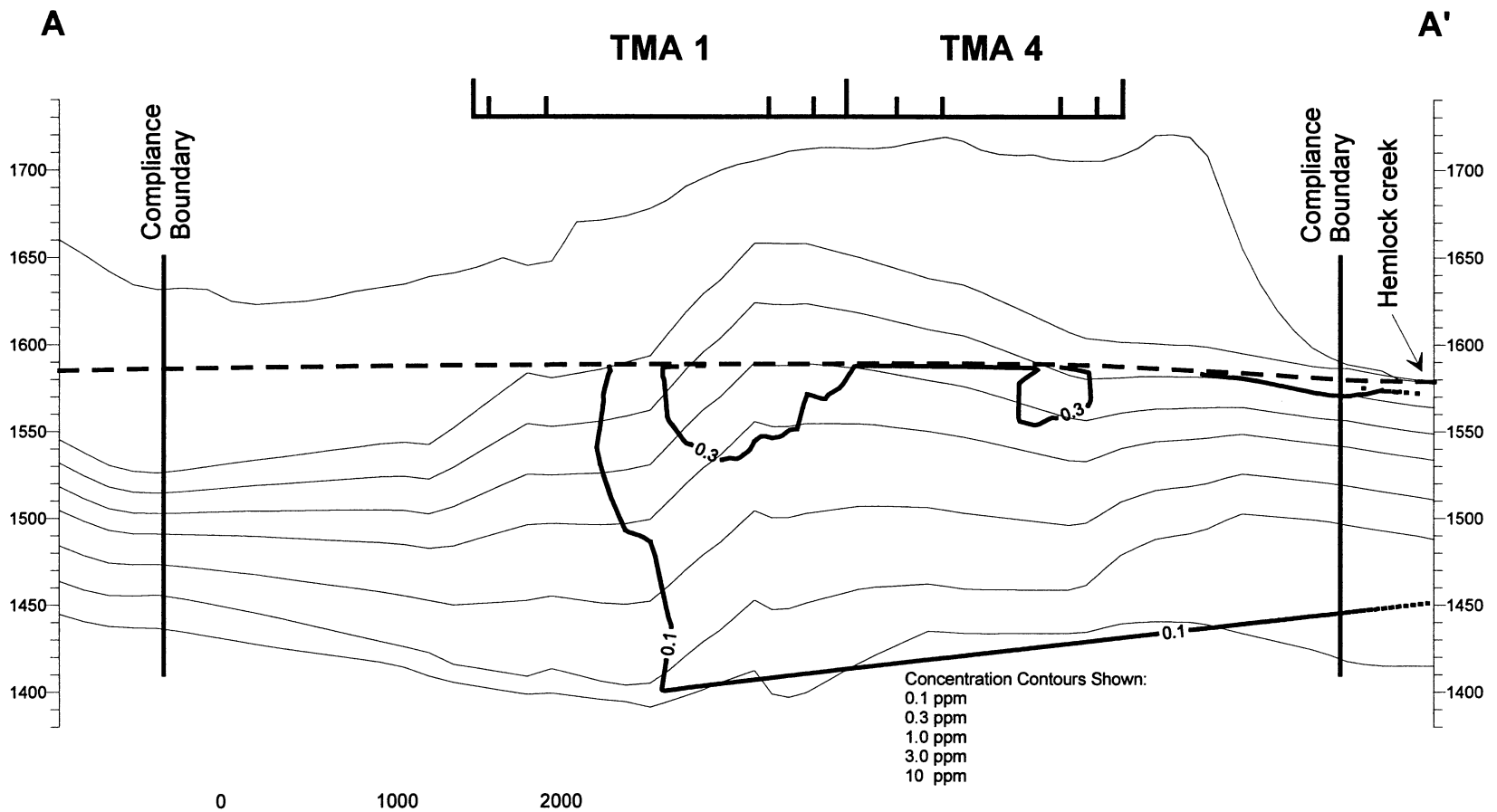

4.2-10-233

Source Concentration
Operation: 2000 ppm
Post-cap: 4000 ppm
Oxidized: 40,000 ppm*

* As a conservative assumption, the oxidized concentration begins one year after assumed degradation of the flexible membrane liner.

HSI GEOTRANS

REVISED	DATE	BY	DESCRIPTION

CHECKED BY: GWC	DATE: April 1998
APPROVED BY: PFA	DATE: April 1998
APPROVED BY:	DATE:

Nicolet Minerals COMPANY

Figure 2.66
BEJT Concentration After 200 Years (Example Constituent, Cross Section)

Scale: 1" = 1000' (h), 100' (v)	Date: April 1998
Prepared By: HSI GeoTrans	By: RMD

\Crandon\TmaMod3\Surfer\Bej300x.srf

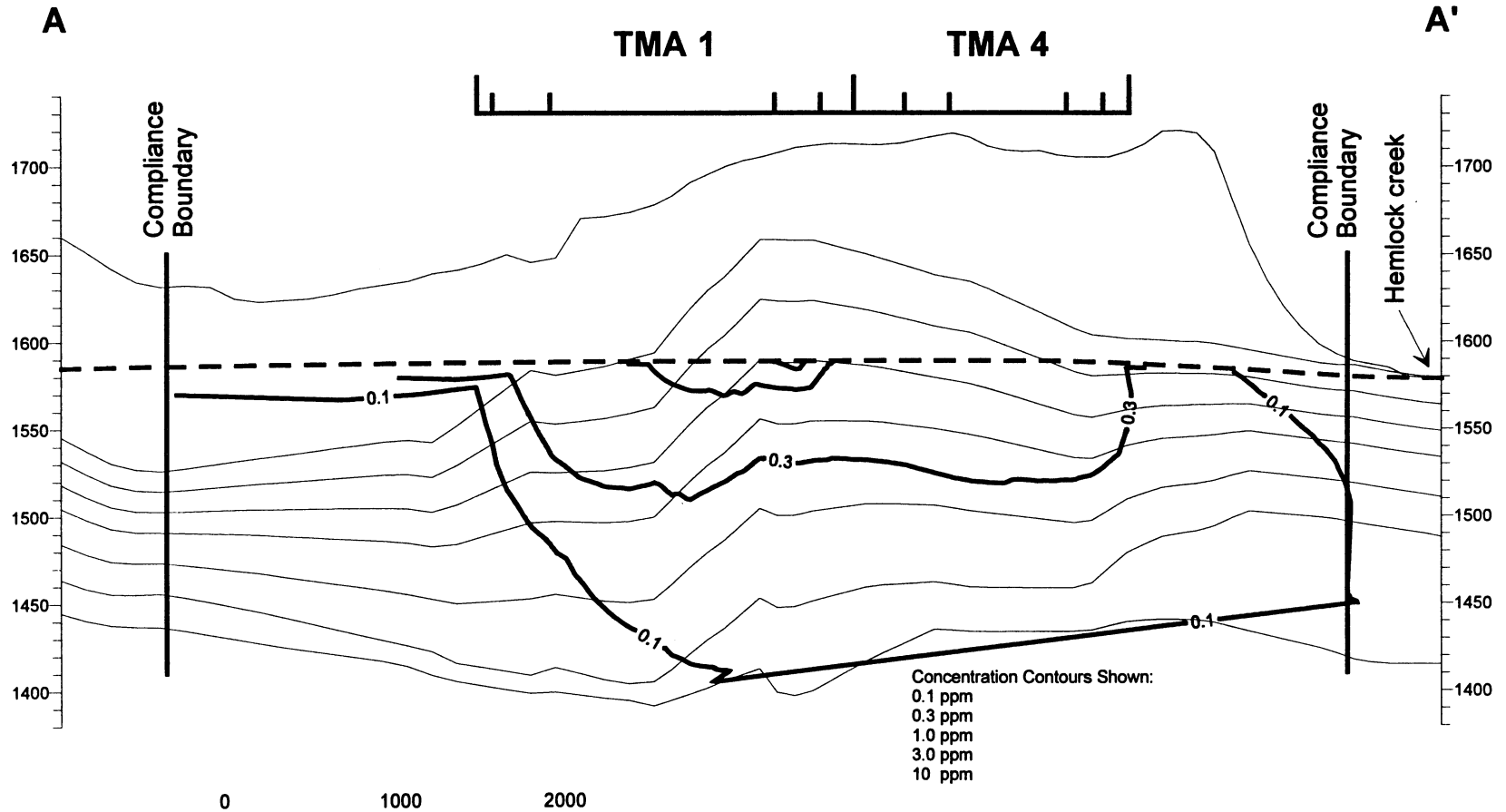

4.2-10-234

Source Concentration
Operation: 2000 ppm
Post-cap: 4000 ppm
Oxidized: 40,000 ppm*

* As a conservative assumption, the oxidized concentration begins one year after assumed degradation of the flexible membrane liner.

HSI GEOTRANS

REVISED	DATE	BY	DESCRIPTION

CHECKED BY: GWC	DATE: April 1998
APPROVED BY: PFA	DATE: April 1998
APPROVED BY:	DATE:

Nicolet Minerals COMPANY

Figure 2.67
BEJT Concentration After 300 Years (Example Constituent, Cross Section)

Scale: 1" = 1000' (h), 100' (v)	Date: April 1998
Prepared By: HSI GeoTrans	By: RMD

\Crandon\TmaMod3\Surfer\Bej650x.srf

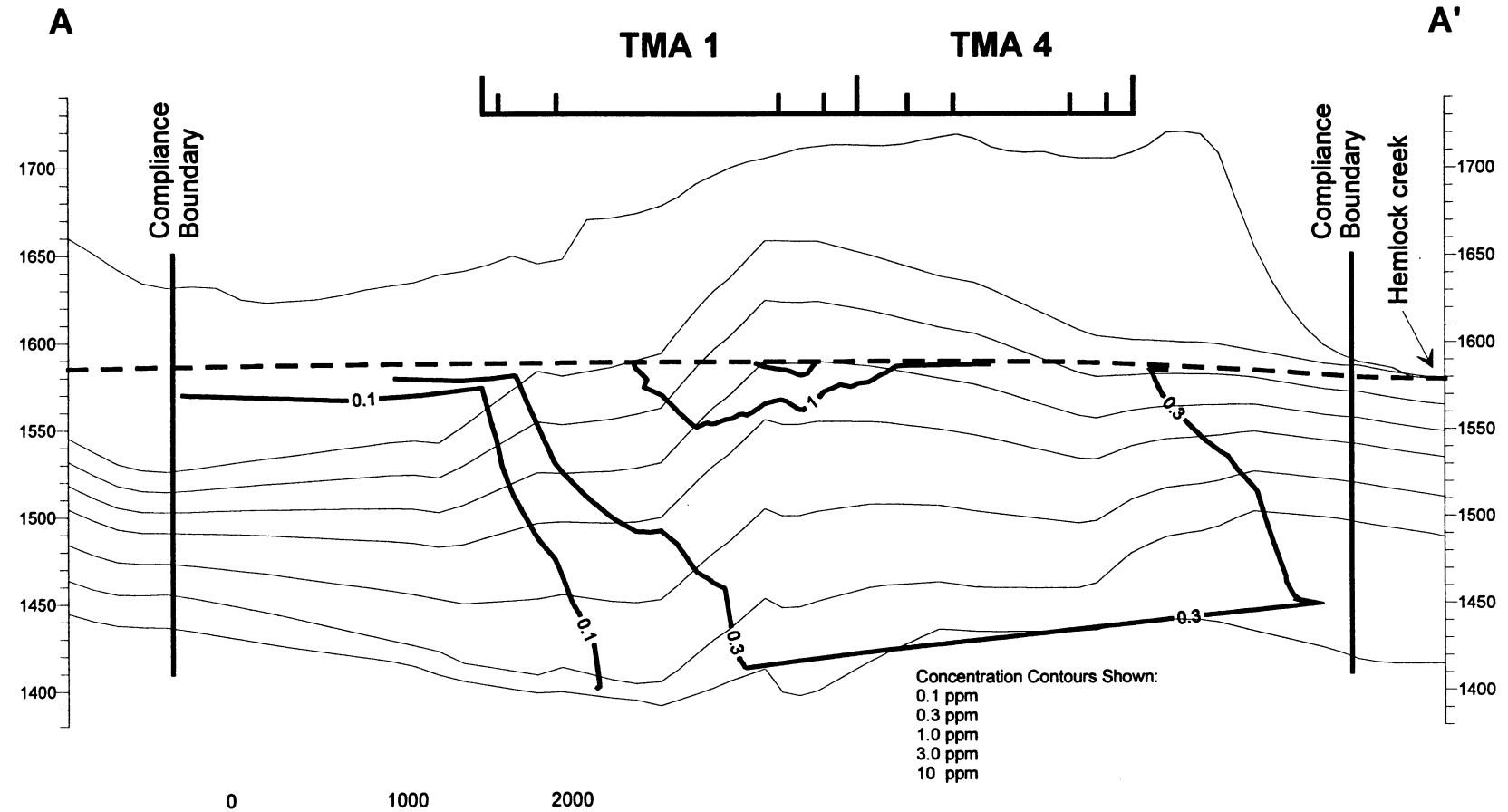

4.2-10-235

Source Concentration
Operation: 2000 ppm
Post-cap: 4000 ppm
Oxidized: 40,000 ppm*

* As a conservative assumption, the oxidized concentration begins one year after assumed degradation of the flexible membrane liner.

HSI GEOTRANS

REVISED	DATE	BY	DESCRIPTION

CHECKED BY: GWC	DATE: April 1998
APPROVED BY: PFA	DATE: April 1998
APPROVED BY:	DATE:

Nicolet Minerals COMPANY

Figure 2.68
BEJT Concentration After 650 Years
(Example Constituent, Cross Section)

Scale: 1" = 1000' (h), 100' (v)	Date: April 1998
Prepared By: HSI GeoTrans	By: RMD

\Crandon\TmaMod3\Excel\T03C-Mp1.xls, Fig

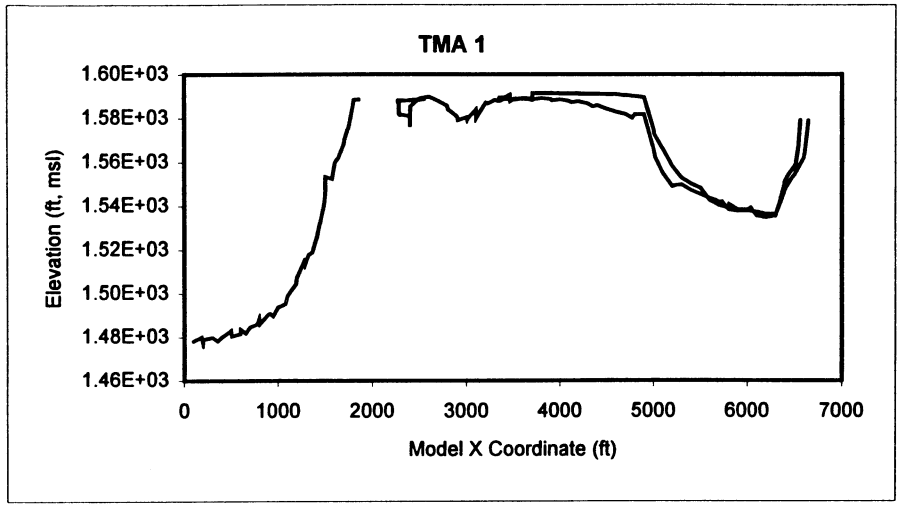

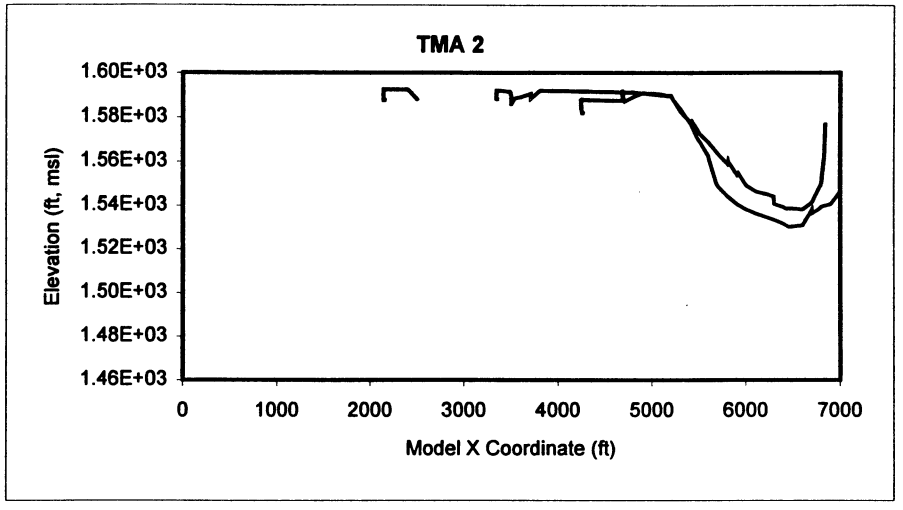

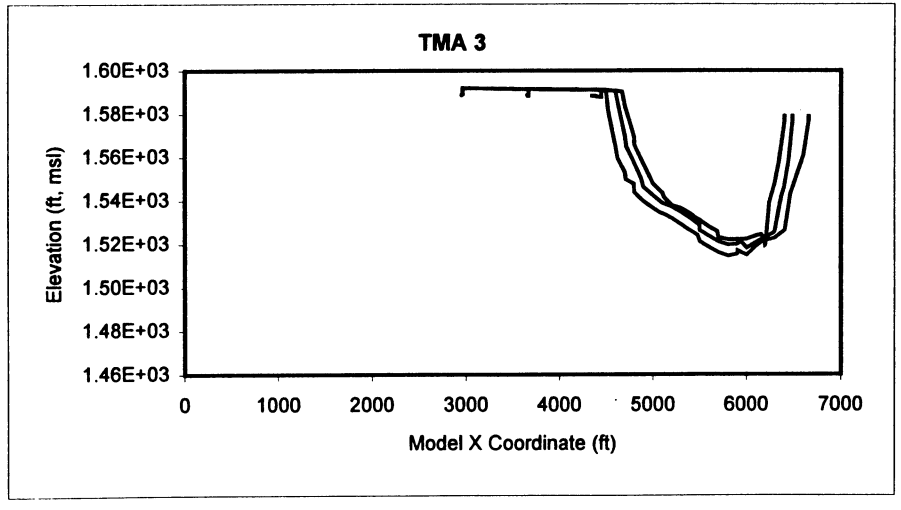

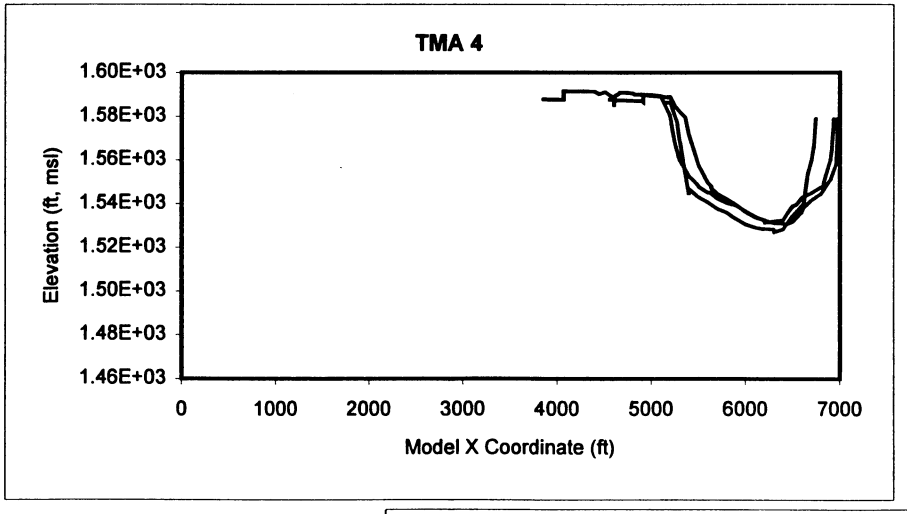

4.2-10-236

HSI GEOTRANS			
REVISED	DATE	BY	DESCRIPTION

CHECKED BY: PAW	DATE: April 1998
APPROVED BY: PFA	DATE: April 1998
APPROVED BY:	DATE:

Simulation T03C-MP

Nicolet Minerals COMPANY

Figure 2.69
Particle Traces From Each TMA Basin, Cross-Section

Scale: None	Date: April 1998
Prepared By: HSI GEOTRANS	By: GWC

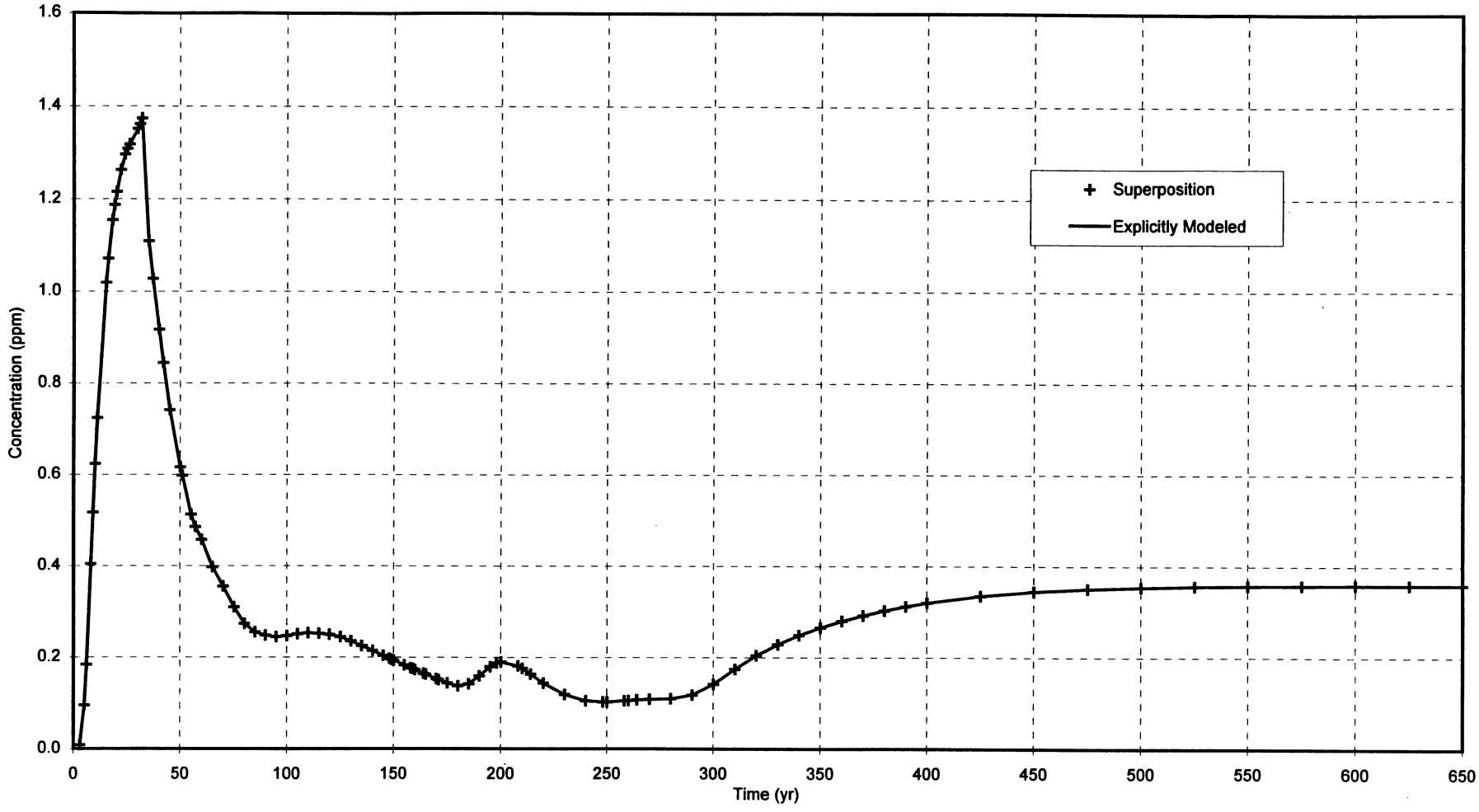

Source Concentration:
Operation: 2000 ppm
Post-Cap: 4000 ppm
Oxidized: 40,000 ppm*

* As a conservative assumption, the oxidized concentration begins one year after assumed degradation of the flexible membrane liner.

HSI GEOTRANS

REVISED	DATE	BY	DESCRIPTION

CHECKED BY: PAW	DATE: April 1998
APPROVED BY: PFA	DATE: April 1998
APPROVED BY:	DATE:

Simulations T03C1,2,3,4

Nicolet Minerals COMPANY

Figure 2.70
Verification of the Superposition Method for the Example Constituent, BEJT

Scale: None	Date: April 1998
Prepared By: HSI GEOTRANS	By: GWC

\Crandon\TmaMod3\Excel\T03c4a.xls, SensFig

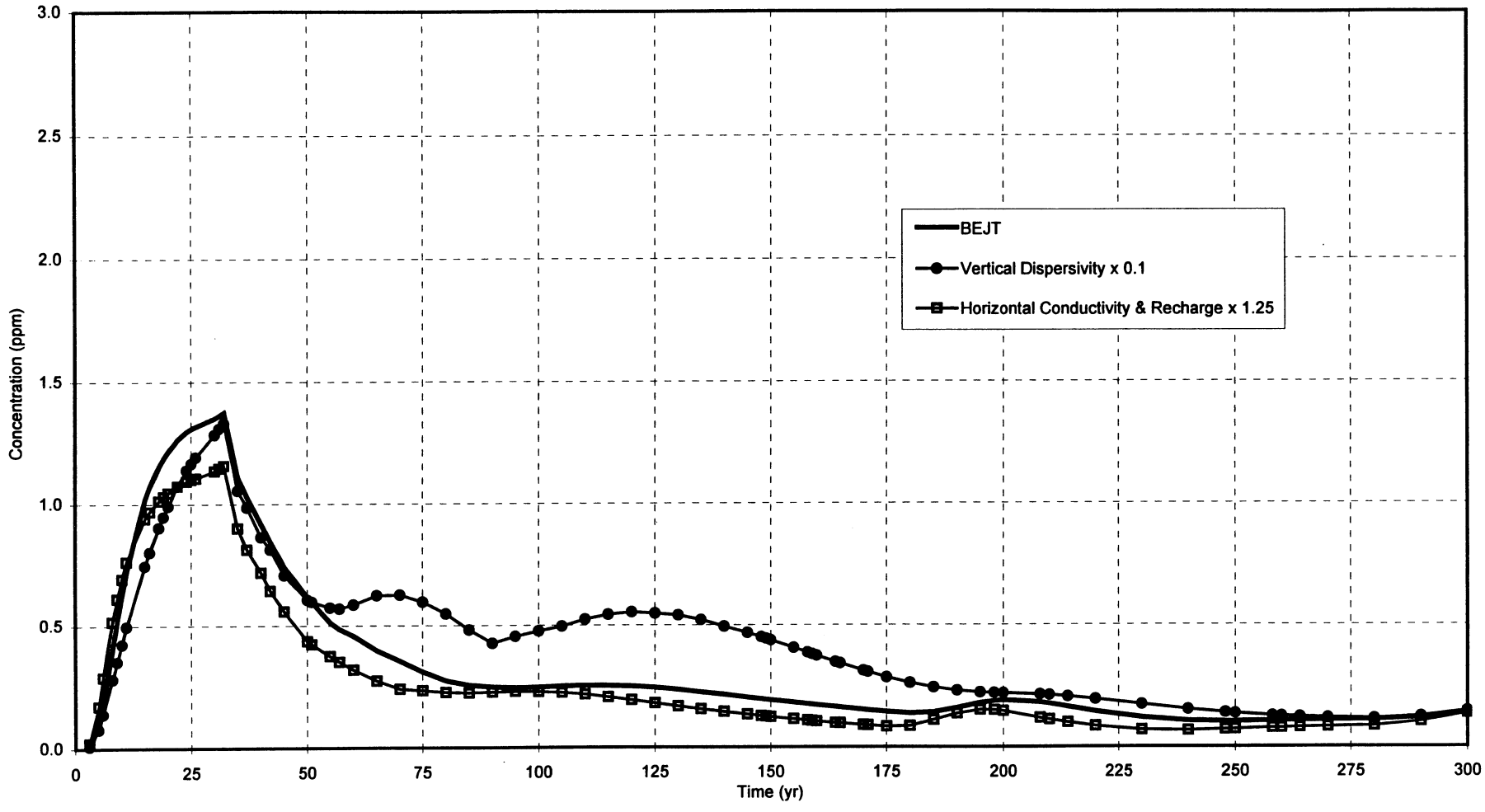

4.2-10-238

Source Concentration:
Operation: 2000 ppm
Post-Cap: 4000 ppm
Oxidized: 40,000 ppm*

* As a conservative assumption, the oxidized concentration begins one year after assumed degradation of the flexible membrane liner.

HSI GEOTRANS

REVISED	DATE	BY	DESCRIPTION

CHECKED BY: PAW		DATE: April 1998
APPROVED BY: PFA		DATE: April 1998
APPROVED BY:		DATE:

Simulations T03C4, T03C4A & T04C4

Nicolet Minerals COMPANY

Figure 2.71
Sensitivity of Compliance Boundary Concentrations to Aquifer Changes

Scale: None	Date: April 1998
Prepared By: HSI GEOTRANS	By: GWC

\Crandon\TmaMod3\Excel\T03c4a.xls, SensFig1

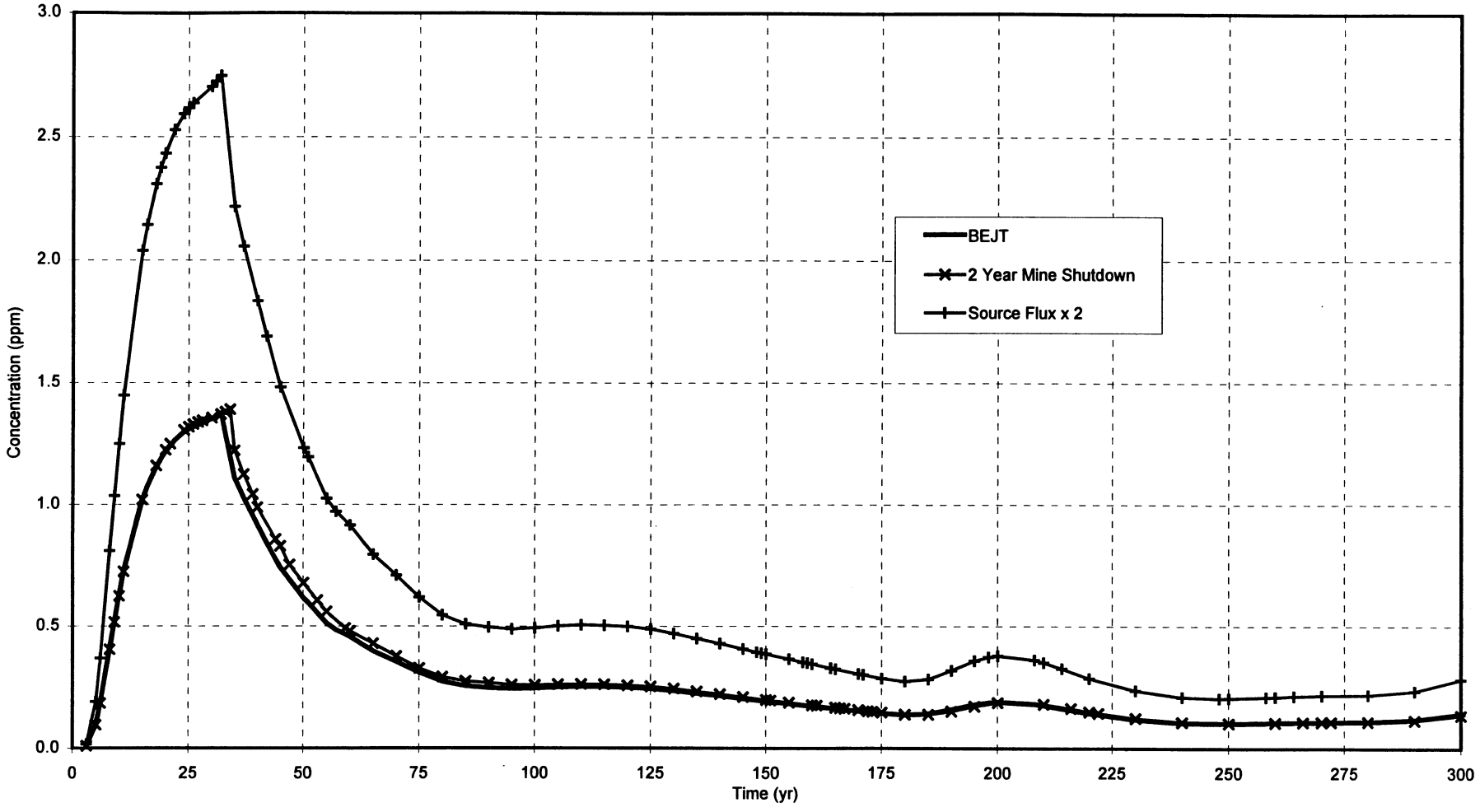

4.2-10-239

Source Concentration:
Operation: 2000 ppm
Post-Cap: 4000 ppm
Oxidized: 40,000 ppm*

* As a conservative assumption, the oxidized concentration begins one year after assumed degradation of the flexible membrane liner.

HSI GEOTRANS			
REVISED	DATE	BY	DESCRIPTION

Simulations T03C4, T03D4 & T06C4	CHECKED BY: PAW	DATE: April 1998
	APPROVED BY: PFA	DATE: April 1998
	APPROVED BY:	DATE:

Nicolet Minerals COMPANY

Figure 2.72
Sensitivity of Compliance Boundary Concentrations to Source Changes

Scale: None	Date: April 1998
Prepared By: HSI GEOTRANS	By: GWC

\Crandon\TmaMod3\Excel\T05C.xls, Response

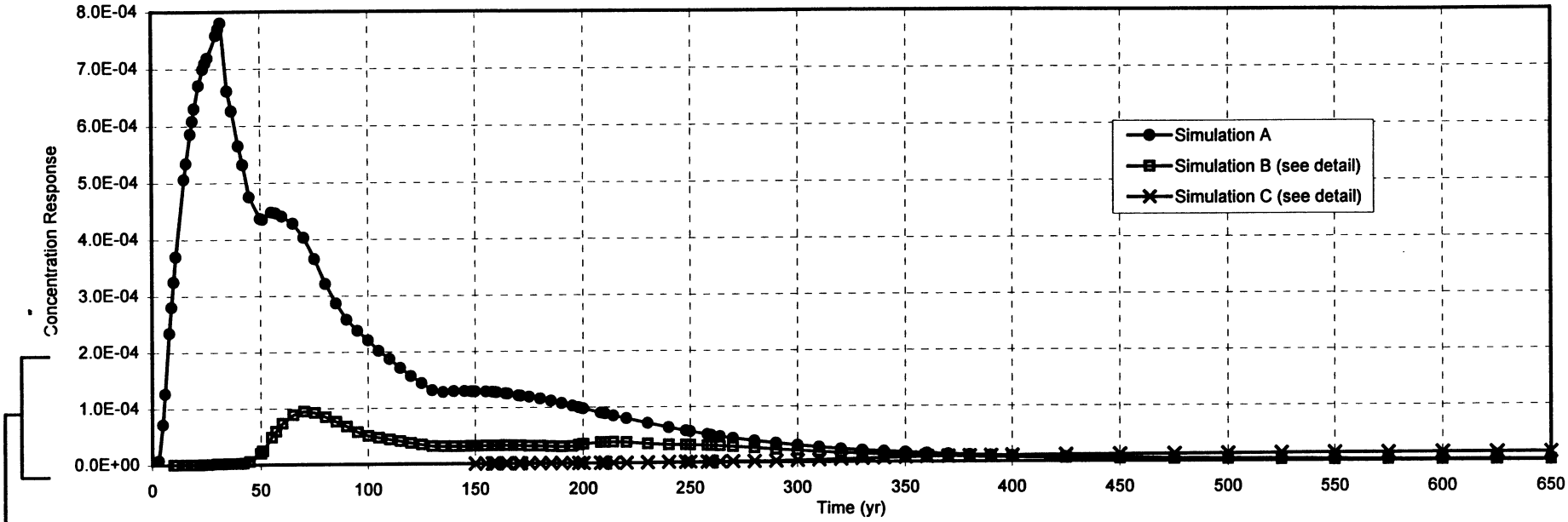

Detail for Simulations B & C

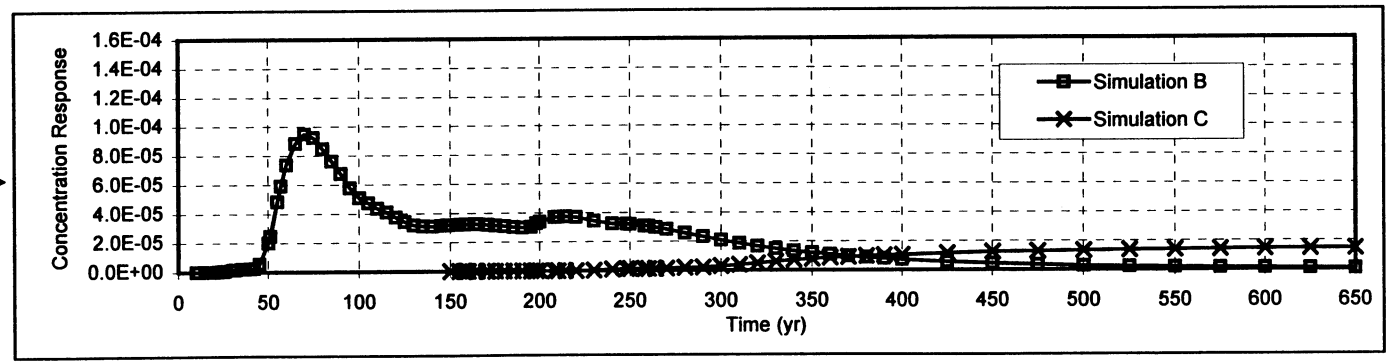

4.2-10-240

HSI GEOTRANS			
REVISED	DATE	BY	DESCRIPTION

CHECKED BY: PAW	DATE: April 1998
APPROVED BY: PFA	DATE: April 1998
APPROVED BY:	DATE:

Simulations T05C1,2,3

Nicolet Minerals COMPANY

Figure 2.73
PWCT Concentration Response Curves at the Compliance Boundary

Scale: None	Date: April 1998
Prepared By: HSI GEOTRANS	By: GWC

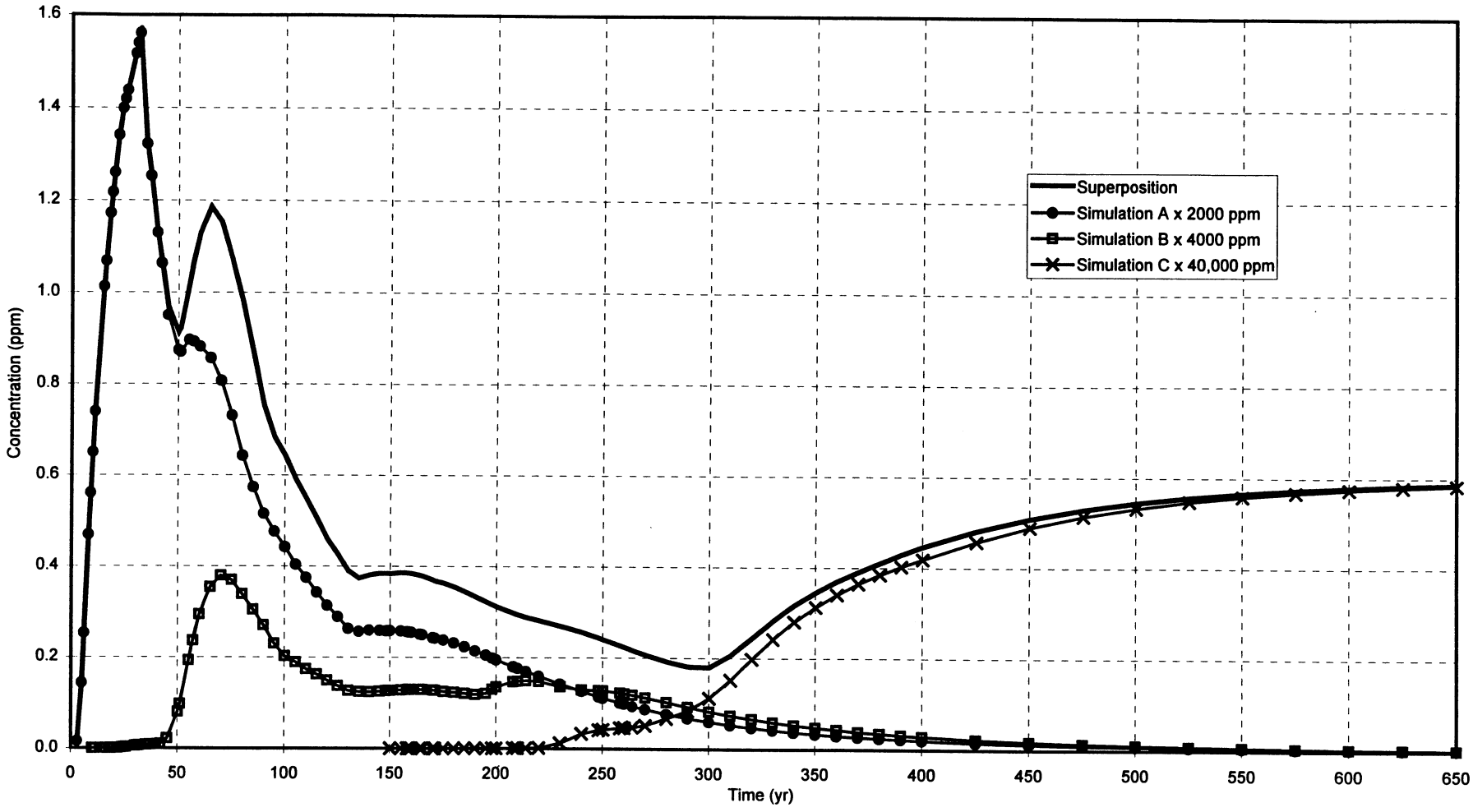

4.2-10-241

Source Concentration:
Operation: 2000 ppm
Post-Cap: 4000 ppm
Oxidized: 40,000 ppm*

* As a conservative assumption, the oxidized concentration begins one year after assumed degradation of the flexible membrane liner.

HSI GEOTRANS				
REVISED	DATE	BY	DESCRIPTION	
CHECKED BY: PAW				DATE: April 1998
APPROVED BY: PFA				DATE: April 1998
Simulations T05C1,2,3,4	APPROVED BY:			DATE:

Nicolet Minerals COMPANY

Figure 2.74
PWCT Concentration at the Compliance Boundary (Example Constituent)

Scale: None	Date: April 1998
Prepared By: HSI GEOTRANS	By: GWC

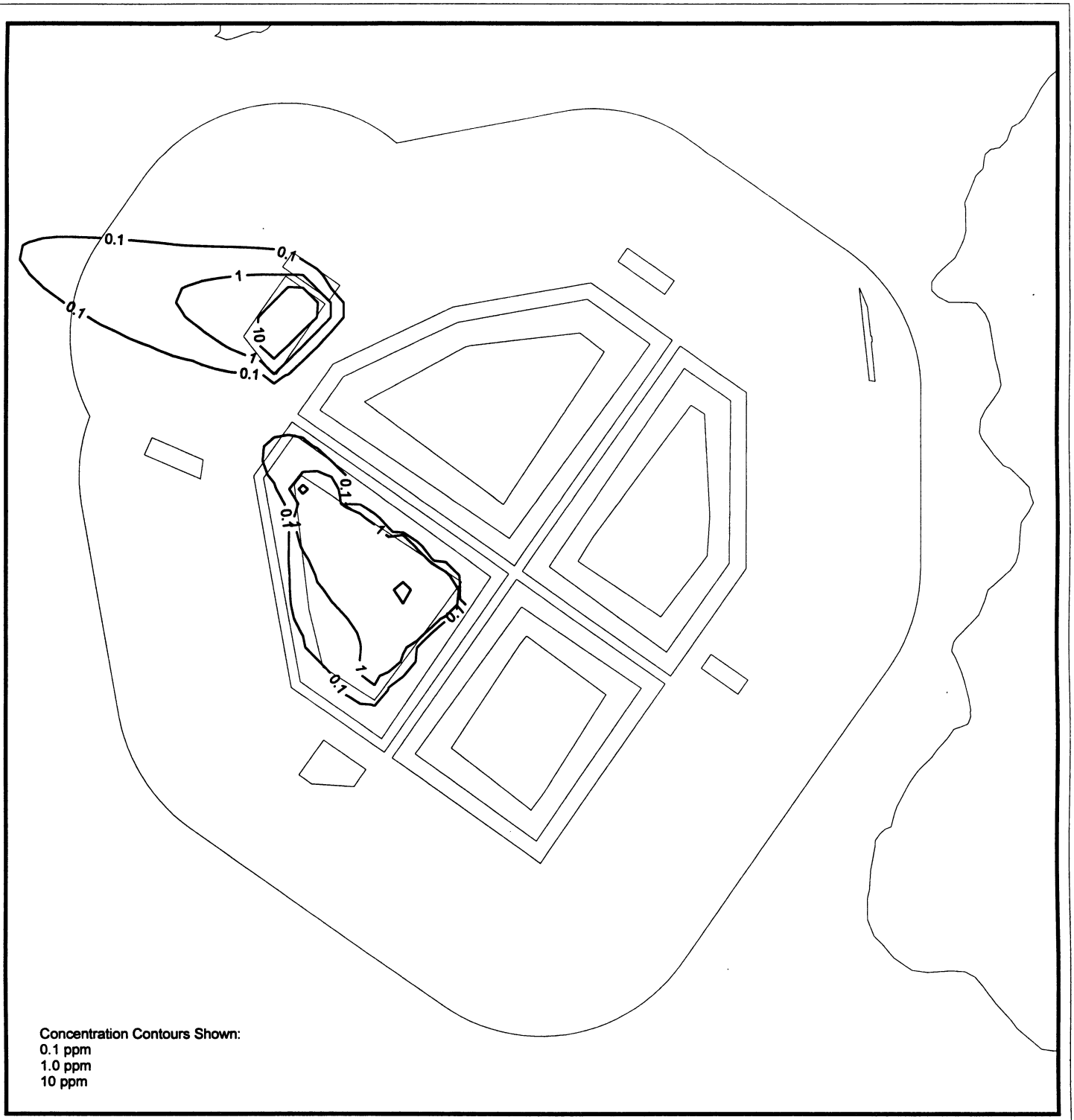

Source Concentration
Operation: 2000 ppm
Post-cap: 4000 ppm
Oxidized: 40,000 ppm*

* As a conservative assumption, the oxidized concentration begins one year after assumed degradation of the flexible membrane liner.

Note:
This plot shows contours of maximum concentratration in any layer.

N

0 1000 2000

Scale in Feet

HSI GEOTRANS

REVISED	DATE	BY	DESCRIPTION

CHECKED BY: GWC	DATE: April 98
APPROVED BY: PFA	DATE: April 1998
APPROVED BY:	DATE:

Nicolet Minerals COMPANY

Figure 2.75
PWCT Concentration After 6 Years (Example Constituent, Plan View)

Scale: 1 in. = 1000 ft.	Date: April 1998
Prepared By: HSI GEOTRANS	By: RMD

\Crandon\Tmal\Mod3\Surfer\Pwct06c.srf

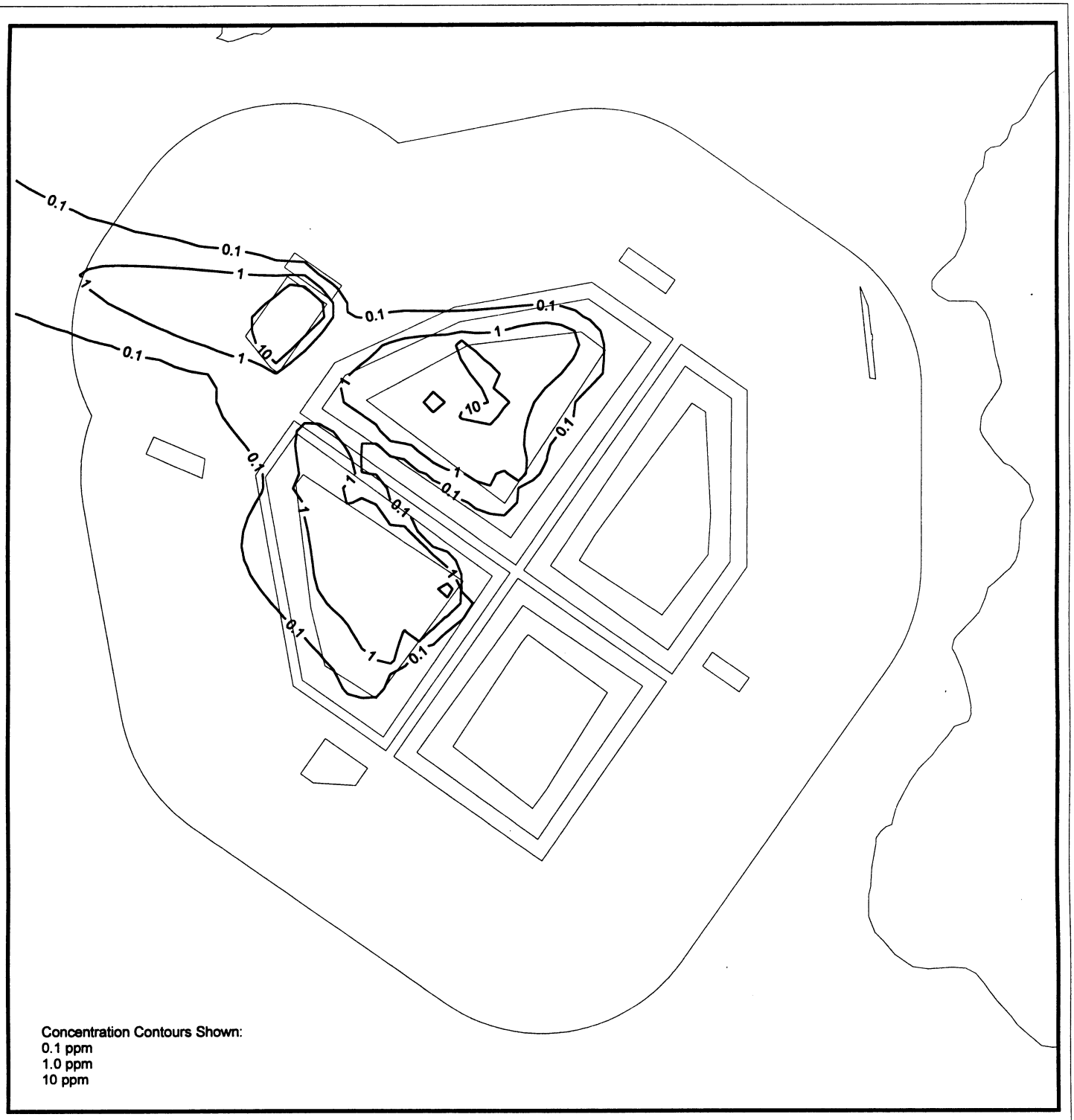

Source Concentration
Operation: 2000 ppm
Post-cap: 4000 ppm
Oxidized: 40,000 ppm*

* As a conservative assumption, the oxidized concentration begins one year after assumed degradation of the flexible membrane liner.

Note:
This plot shows contours of maximum concentratration in any layer.

N

0 1000 2000

Scale in Feet

HSI GEOTRANS

REVISED	DATE	BY	DESCRIPTION

CHECKED BY: GWC	DATE: April 98
APPROVED BY: PFA	DATE: April 1998
APPROVED BY:	DATE:

Nicolet Minerals COMPANY

Figure 2.76
PWCT Concentration After 16 Years (Example Constituent, Plan View)

Scale: 1 in. = 1000 ft.	Date: April 1998
Prepared By: HSI GEOTRANS	By: RMD

\Crandon\Tmwmod3\Surfer\Pwc016c.srf

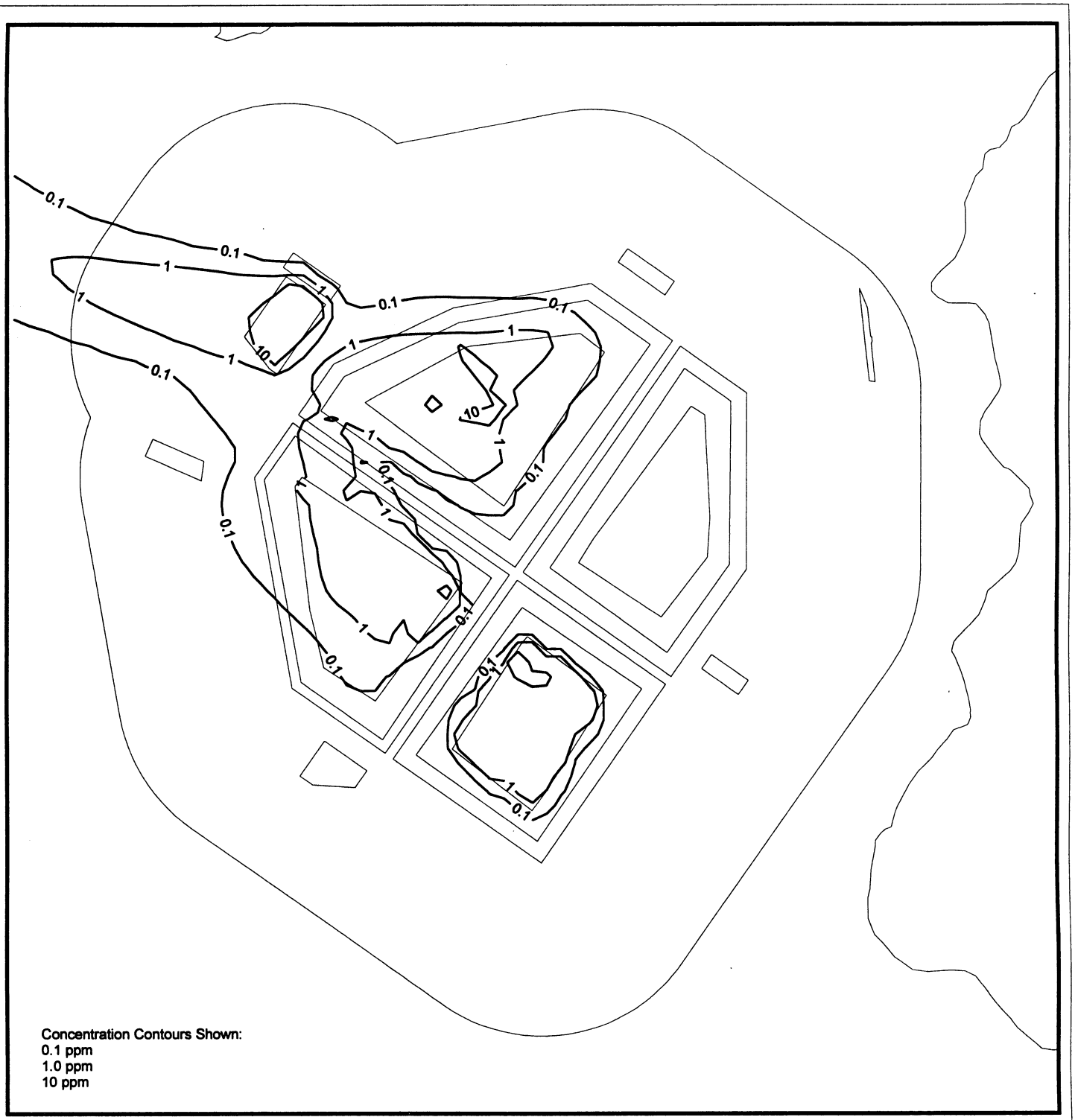

Source Concentration
Operation: 2000 ppm
Post-cap: 4000 ppm
Oxidized: 40,000 ppm*

* As a conservative assumption, the oxidized concentration begins one year after assumed degradation of the flexible membrane liner.

Note:
This plot shows contours of maximum concentratration in any layer.

N

0 1000 2000

Scale in Feet

HSI GEOTRANS

REVISED	DATE	BY	DESCRIPTION

CHECKED BY: GWC	DATE: April 98
APPROVED BY: PFA	DATE: April 1998
APPROVED BY:	DATE:

Nicolet Minerals COMPANY

Figure 2.77
PWCT Concentration After 22 Years (Example Constituent, Plan View)

Scale: 1 in. = 1000 ft.	Date: April 1998
Prepared By: HSI GEOTRANS	By: RMD

\Crandon\Tma\Mod3\Surfer\wc22c.srf

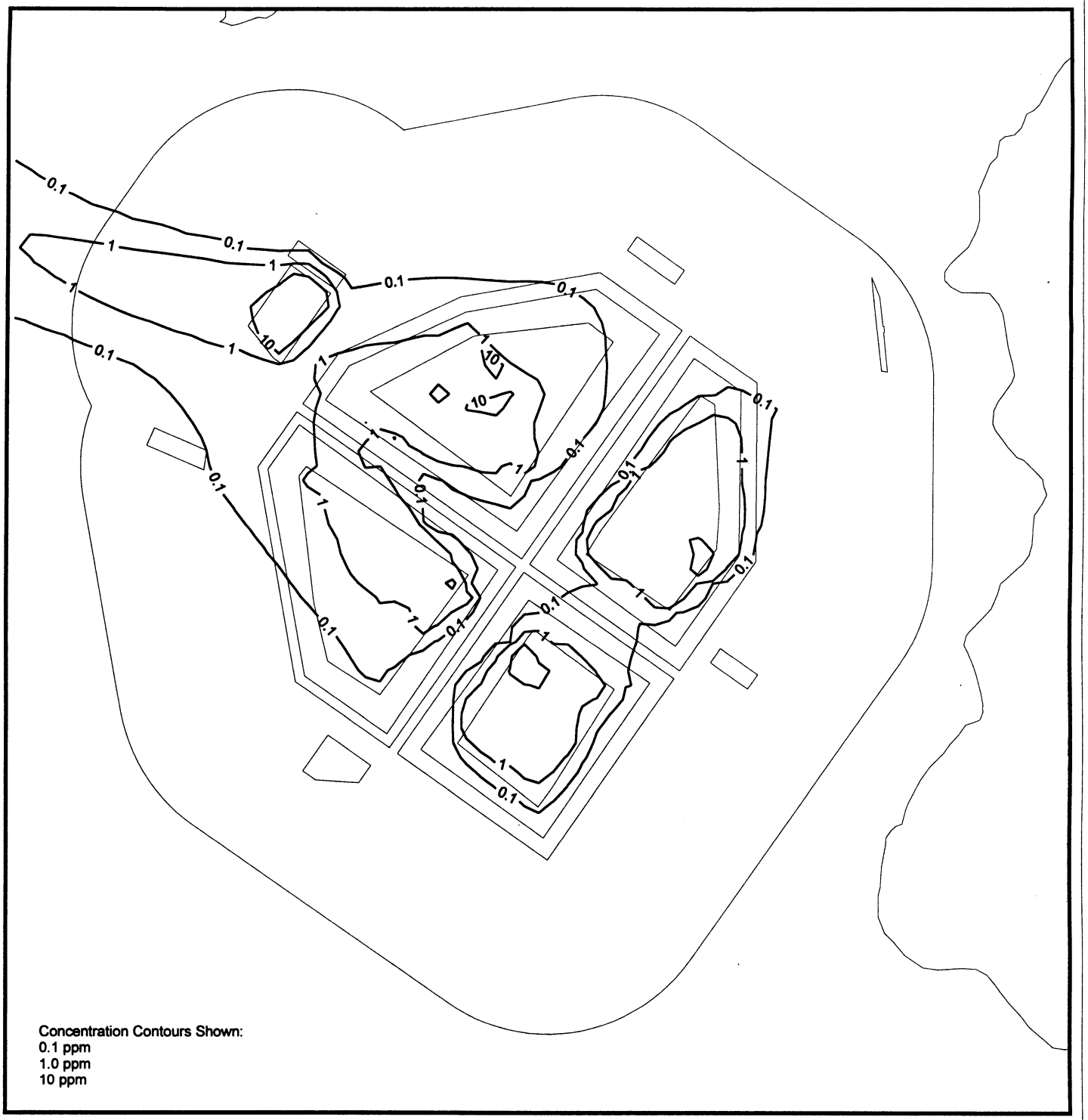

Source Concentration
Operation: 2000 ppm
Post-cap: 4000 ppm
Oxidized: 40,000 ppm*

* As a conservative assumption, the oxidized concentration begins one year after assumed degradation of the flexible membrane liner.

Note:
This plot shows contours of maximum concentratration in any layer.

N

0 1000 2000

Scale in Feet

HSI GEOTRANS

REVISED	DATE	BY	DESCRIPTION

CHECKED BY: GWC	DATE: April 98
APPROVED BY: PFA	DATE: April 1998
APPROVED BY:	DATE:

Nicolet Minerals COMPANY

Figure 2.78
PWCT Concentration After 32 Years (Example Constituent, Plan View)

Scale: 1 in. = 1000 ft.	Date: April 1998
Prepared By: HSI GEOTRANS	By: RMD

\Crandon\Tmal\Mod3\Surfer\Pwc032c.srf

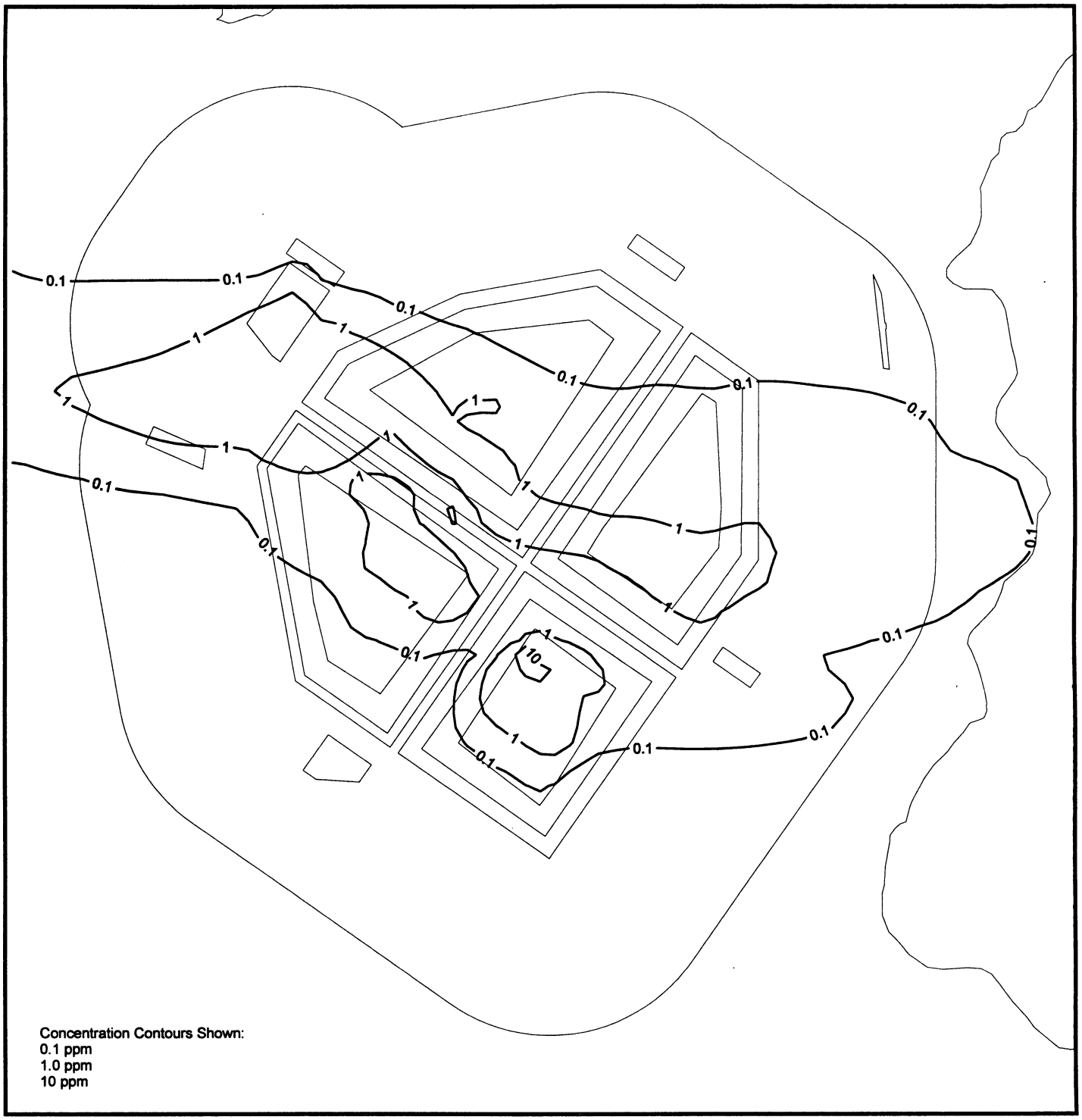

Source Concentration
Operation: 2000 ppm
Post-cap: 4000 ppm
Oxidized: 40,000 ppm*

* As a conservative assumption, the oxidized concentration begins one year after assumed degradation of the flexible membrane liner.

Note:
This plot shows contours of maximum concentratration in any layer.

0 1000 2000
Scale in Feet

HSI GEOTRANS

REVISED	DATE	BY	DESCRIPTION

CHECKED BY: GWC	DATE: April 98
APPROVED BY: PFA	DATE: April 1998
APPROVED BY:	DATE:

Nicolet Minerals COMPANY

Figure 2.79
BEJT Concentration After 60 Years (Example Constituent, Plan View)

Scale: 1 in. = 1000 ft.	Date: April 1998
Prepared By: HSI GEOTRANS	By: RMD

\Crandon\Tma\Mod3\Surfer\Bej060c.srf

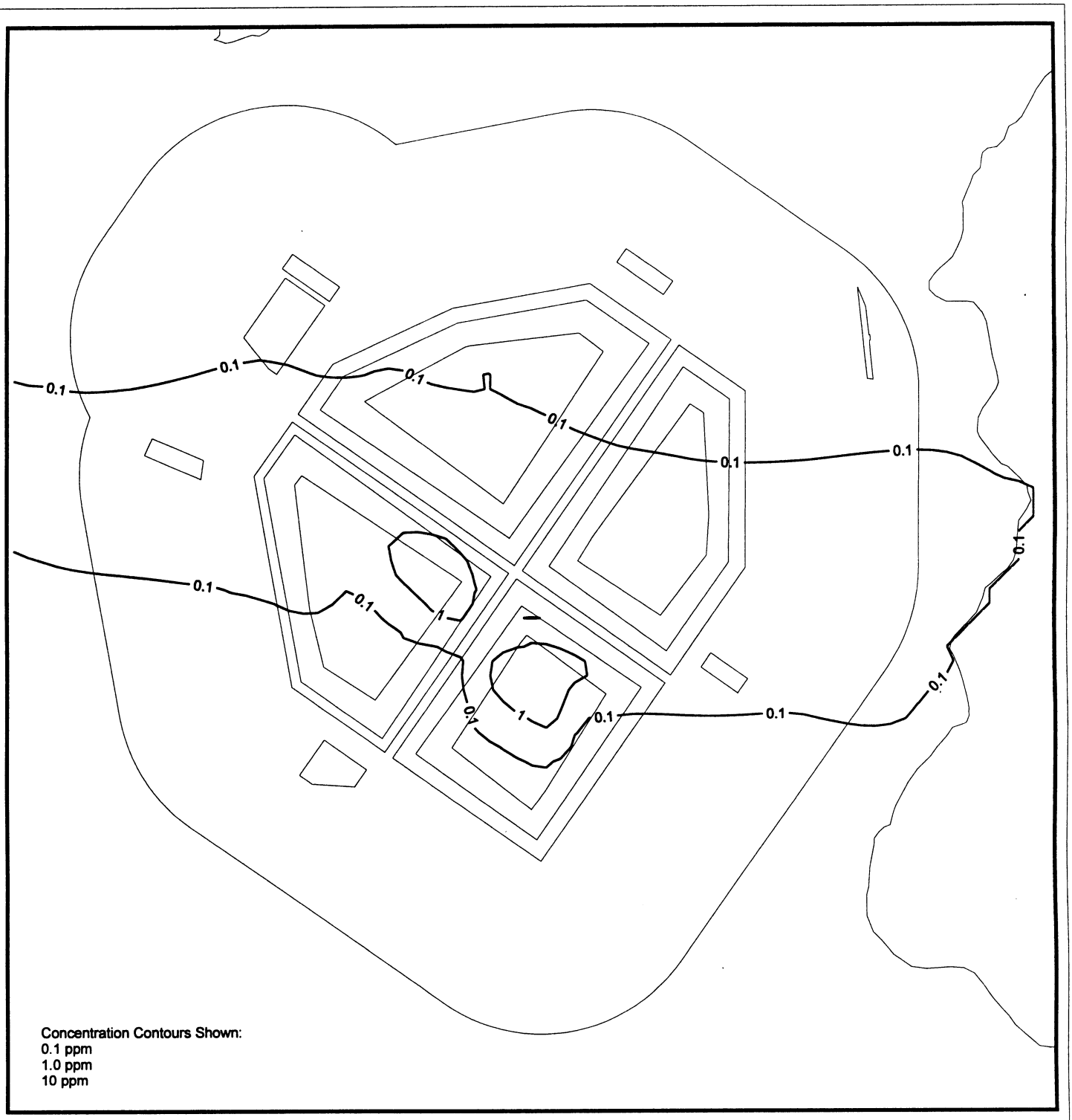

Source Concentration
Operation: 2000 ppm
Post-cap: 4000 ppm
Oxidized: 40,000 ppm*

* As a conservative assumption, the oxidized concentration begins one year after assumed degradation of the flexible membrane liner.

Note:
This plot shows contours of maximum concentratration in any layer.

N

0 1000 2000

Scale in Feet

HSI GEOTRANS

REVISED	DATE	BY	DESCRIPTION

CHECKED BY: GWC	DATE: April 98
APPROVED BY: PFA	DATE: April 1998
APPROVED BY:	DATE:

Nicolet Minerals COMPANY

Figure 2.80
PWCT Concentration After 125 Years (Example Constituent, Plan View)

Scale: 1 in. = 1000 ft.	Date: April 1998
Prepared By: HSI GEOTRANS	By: RMD

\Crandon\Tmal\Mod3\Surfer\Pwc125c.srf

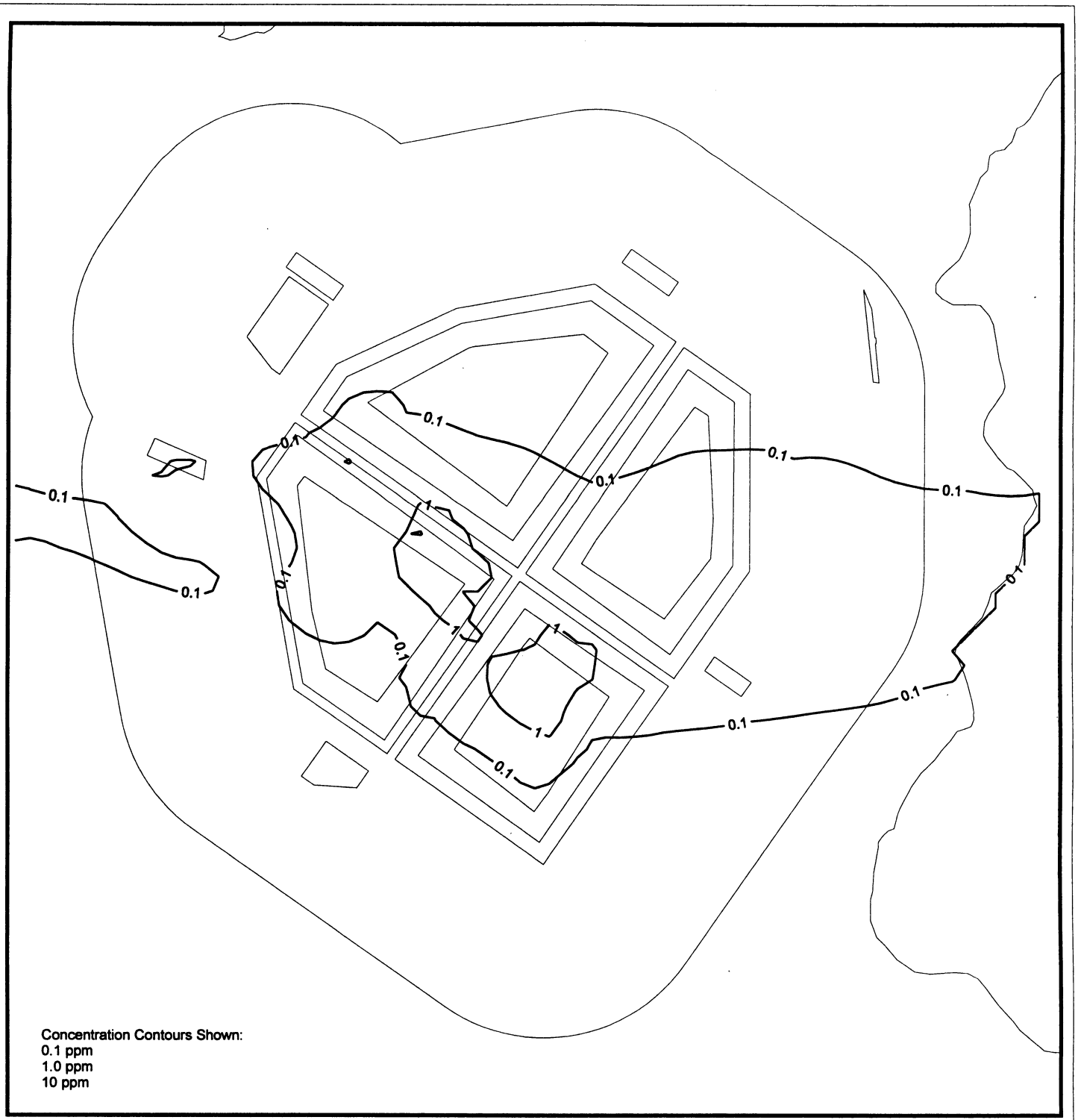

Source Concentration
Operation: 2000 ppm
Post-cap: 4000 ppm
Oxidized: 40,000 ppm*

* As a conservative assumption, the oxidized concentration begins one year after assumed degradation of the flexible membrane liner.

Note:
This plot shows contours of maximum concentratration in any layer.

0 1000 2000
Scale in Feet

HSI GEOTRANS

REVISED	DATE	BY	DESCRIPTION

CHECKED BY: GWC	DATE: April 98
APPROVED BY: PFA	DATE: April 1998
APPROVED BY:	DATE:

Nicolet Minerals COMPANY

Figure 2.81
PWCT Concentration After 200 Years (Example Constituent, Plan View)

Scale: 1 in. = 1000 ft.	Date: April 1998
Prepared By: HSI GEOTRANS	By: RMD

\Crandon\Tma\Mod3\Surfe 00c.srf

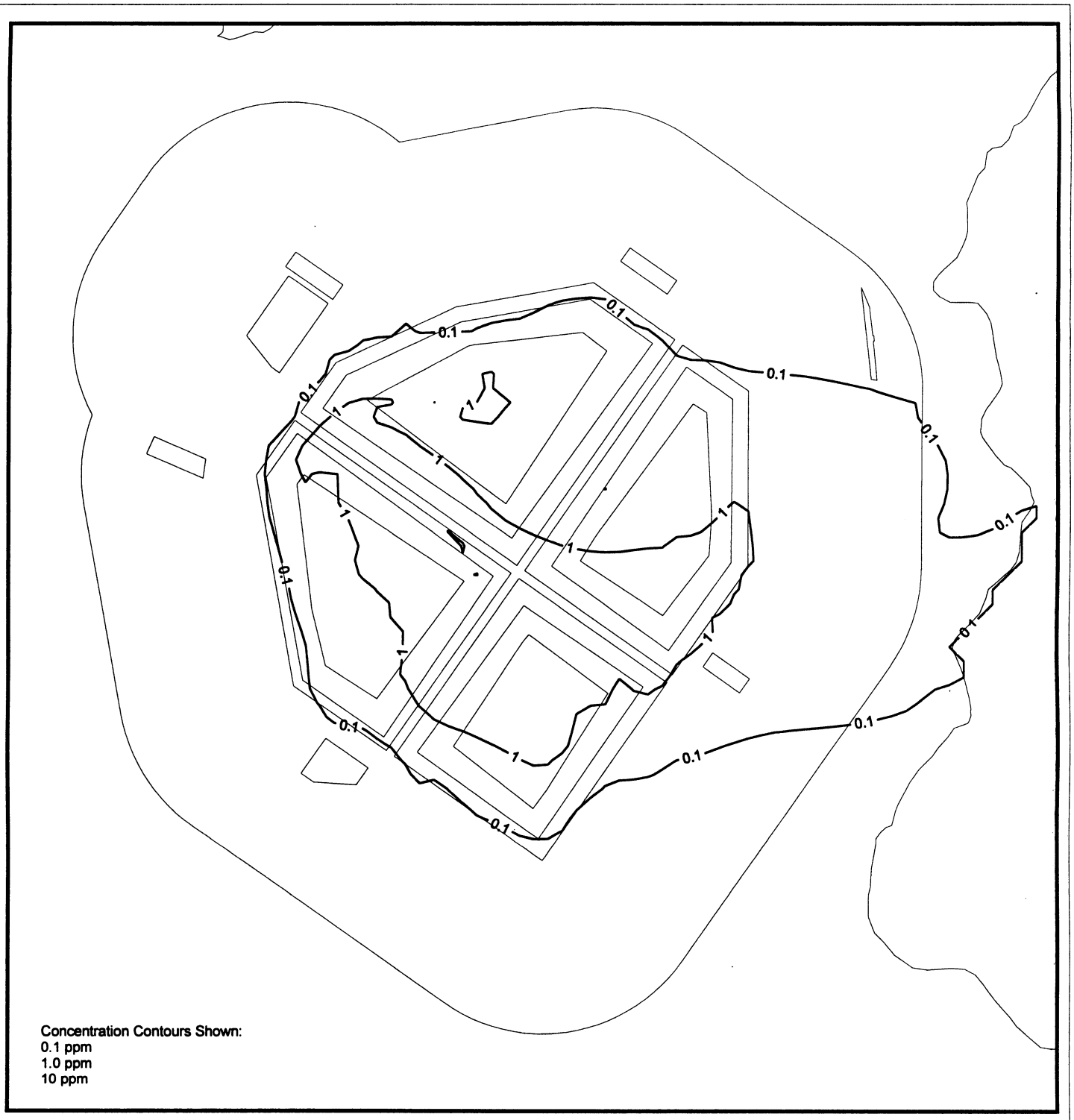

Source Concentration
Operation: 2000 ppm
Post-cap: 4000 ppm
Oxidized: 40,000 ppm*

* As a conservative assumption, the oxidized concentration begins one year after assumed degradation of the flexible membrane liner.

Note:
This plot shows contours of maximum concentratration in any layer.

N

0 1000 2000

Scale in Feet

HSI GEOTRANS

REVISED	DATE	BY	DESCRIPTION

CHECKED BY: GWC	DATE: April 98
APPROVED BY: PFA	DATE: April 1998
APPROVED BY:	DATE:

Nicolet Minerals COMPANY

Figure 2.82
PWCT Concentration After 300 Years (Example Constituent, Plan View)

Scale: 1 in. = 1000 ft.	Date: April 1998
Prepared By: HSI GEOTRANS	By: RMD

\Crandon\Tma\Mod3\Surfer\Pwc300c.srf

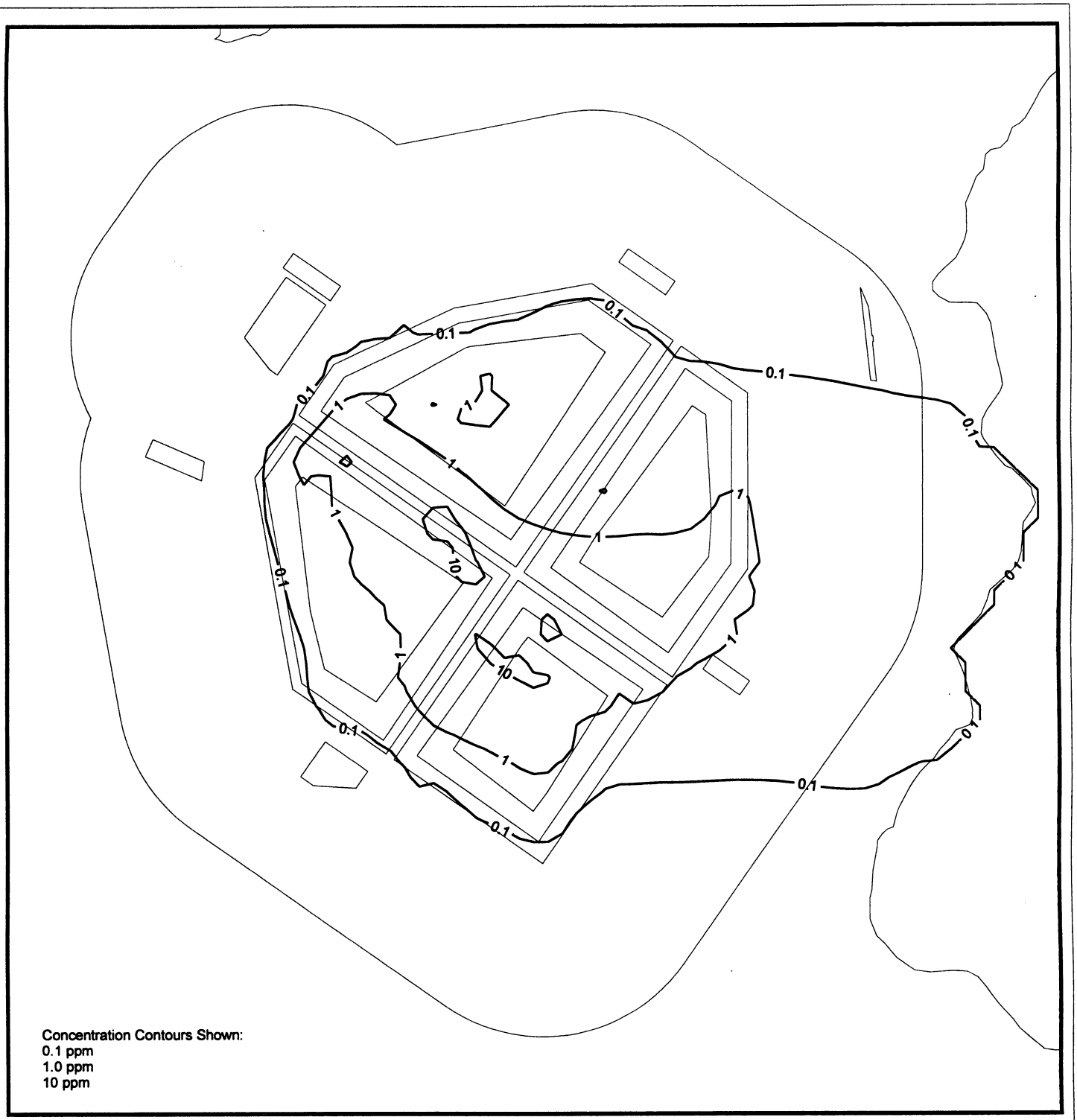

Source Concentration
Operation: 2000 ppm
Post-cap: 4000 ppm
Oxidized: 40,000 ppm*

* As a conservative assumption, the oxidized concentration begins one year after assumed degradation of the flexible membrane liner.

Note:
This plot shows contours of maximum concentratration in any layer.

N

0 1000 2000

Scale in Feet

HSI GEOTRANS

REVISED	DATE	BY	DESCRIPTION

CHECKED BY: GWC	DATE: April 98
APPROVED BY: PFA	DATE: April 1998
APPROVED BY:	DATE:

Nicolet Minerals COMPANY

Figure 2.83
PWCT Concentration After 650 Years (Example Constituent, Plan View)

Scale: 1 in. = 1000 ft.	Date: April 1998
Prepared By: HSI GEOTRANS	By: RMD

\Crandon\Tmal\Mod3\Surfer\pwc650c.srf

\Crandon\TmaMod3\Surfer\pwc006x.srf

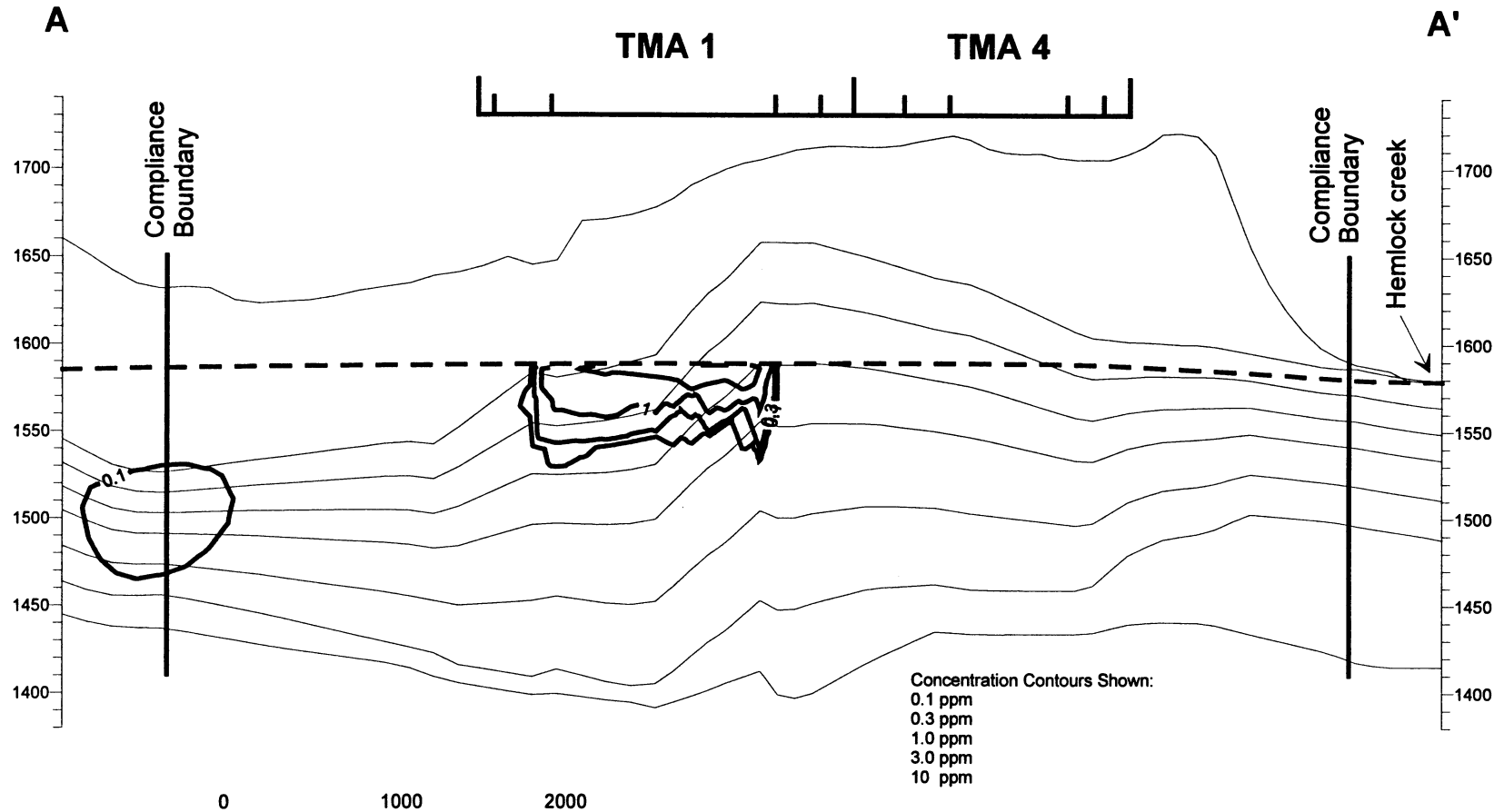

4.2-10-251

Source Concentration
Operation: 2000 ppm
Post-cap: 4000 ppm
Oxidized: 40,000 ppm*

* As a conservative assumption, the oxidized concentration begins one year after assumed degradation of the flexible membrane liner.

HSI GEOTRANS

REVISED	DATE	BY	DESCRIPTION

CHECKED BY: GWC	DATE: April 1998
APPROVED BY: PFA	DATE: April 1998
APPROVED BY:	DATE:

Nicolet Minerals COMPANY

Figure 2.84
PWCT Concentration After 6 Years (Example Constituent, Cross Section)

Scale: 1" = 1000' (h), 100' (v)	Date: April 1998
Prepared By: HSI GeoTrans	By: RMD

\Crandon\TmaMod3\Surfer\pwc016x.srf

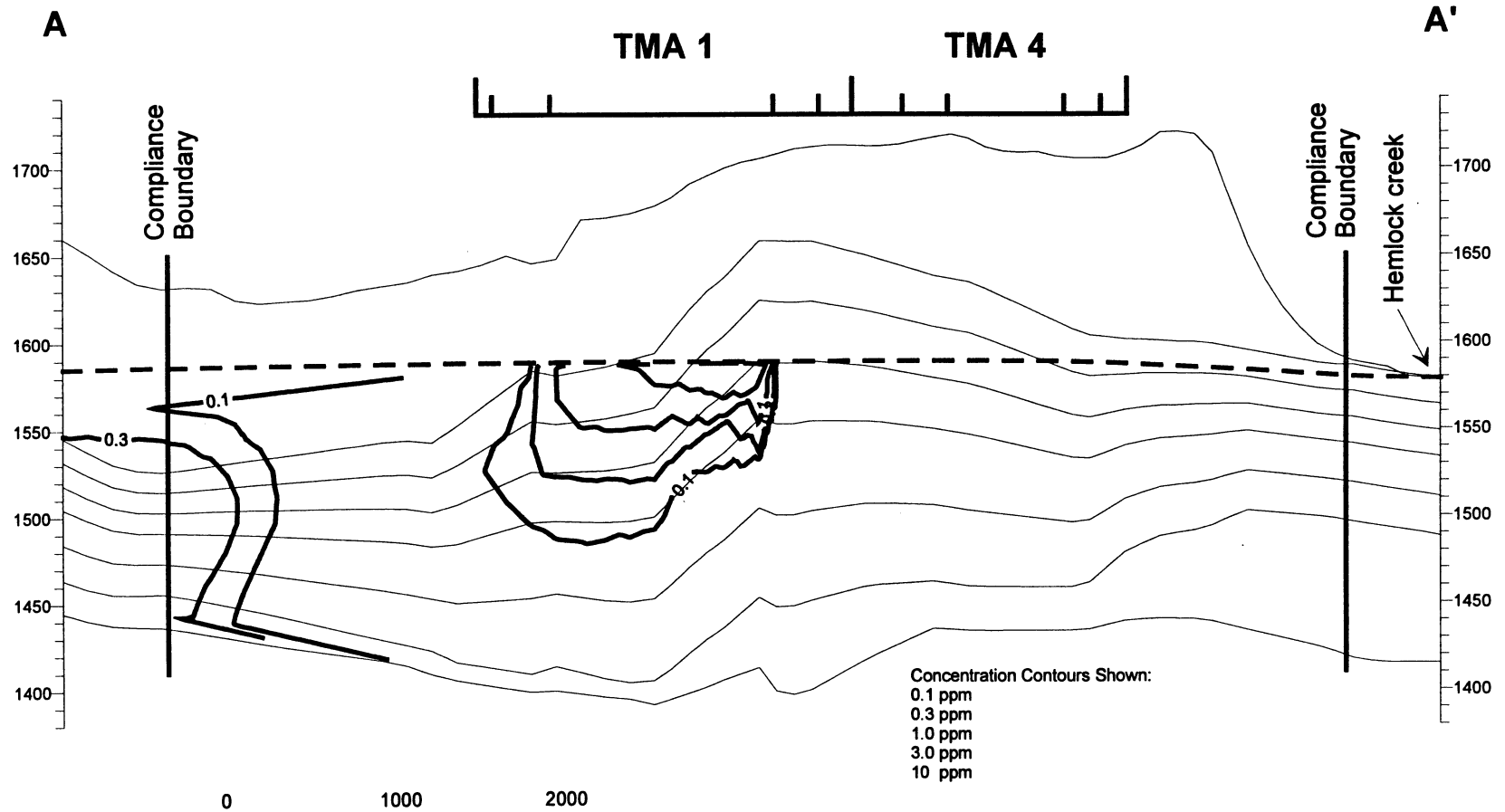

4.2-10-252

Source Concentration
Operation: 2000 ppm
Post-cap: 4000 ppm
Oxidized: 40,000 ppm*

* As a conservative assumption, the oxidized concentration begins one year after assumed degradation of the flexible membrane liner.

HSI GEOTRANS

REVISED	DATE	BY	DESCRIPTION

CHECKED BY: GWC	DATE: April 1998
APPROVED BY: PFA	DATE: April 1998
APPROVED BY:	DATE:

Nicolet Minerals COMPANY

Figure 2.85
PWCT Concentration After 16 Years (Example Constituent, Cross Section)

Scale: 1" = 1000' (h), 100' (v)	Date: April 1998
Prepared By: HSI GeoTrans	By: RMD

\Crandon\TmaMod3\Surfer\pwc022x.srf

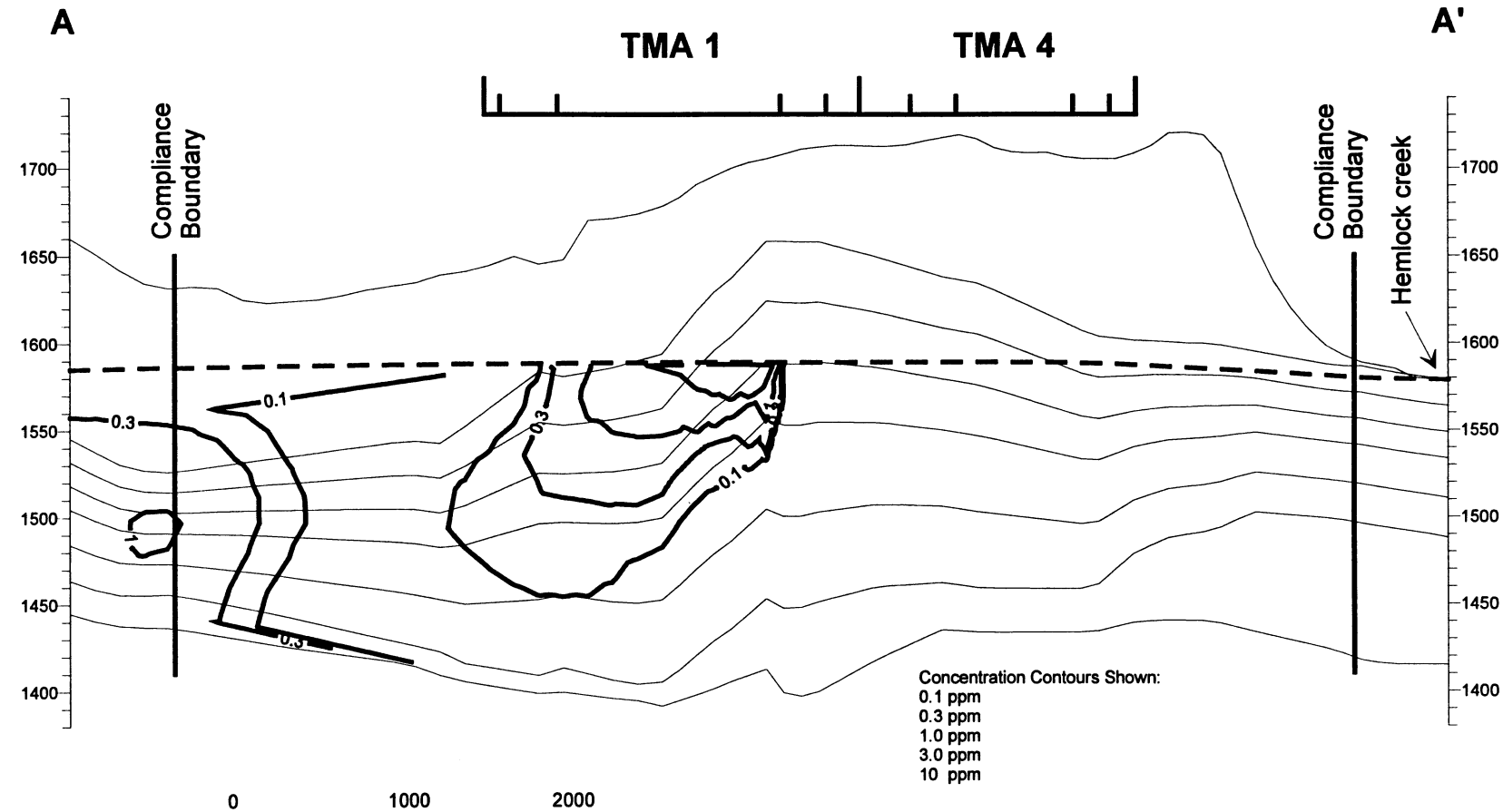

4.2-10-253

Source Concentration
Operation: 2000 ppm
Post-cap: 4000 ppm
Oxidized: 40,000 ppm*

* As a conservative assumption, the oxidized concentration begins one year after assumed degradation of the flexible membrane liner.

HSI GEOTRANS

REVISED	DATE	BY	DESCRIPTION

CHECKED BY: GWC	DATE: April 1998
APPROVED BY: PFA	DATE: April 1998
APPROVED BY:	DATE:

Nicolet Minerals COMPANY

Figure 2.86
PWCT Concentration After 22 Years (Example Constituent, Cross Section)

Scale: 1" = 1000' (h), 100' (v)	Date: April 1998
Prepared By: HSI GeoTrans	By: RMD

\Crandon\TmaMod3\Surfer\pwc032x.srf

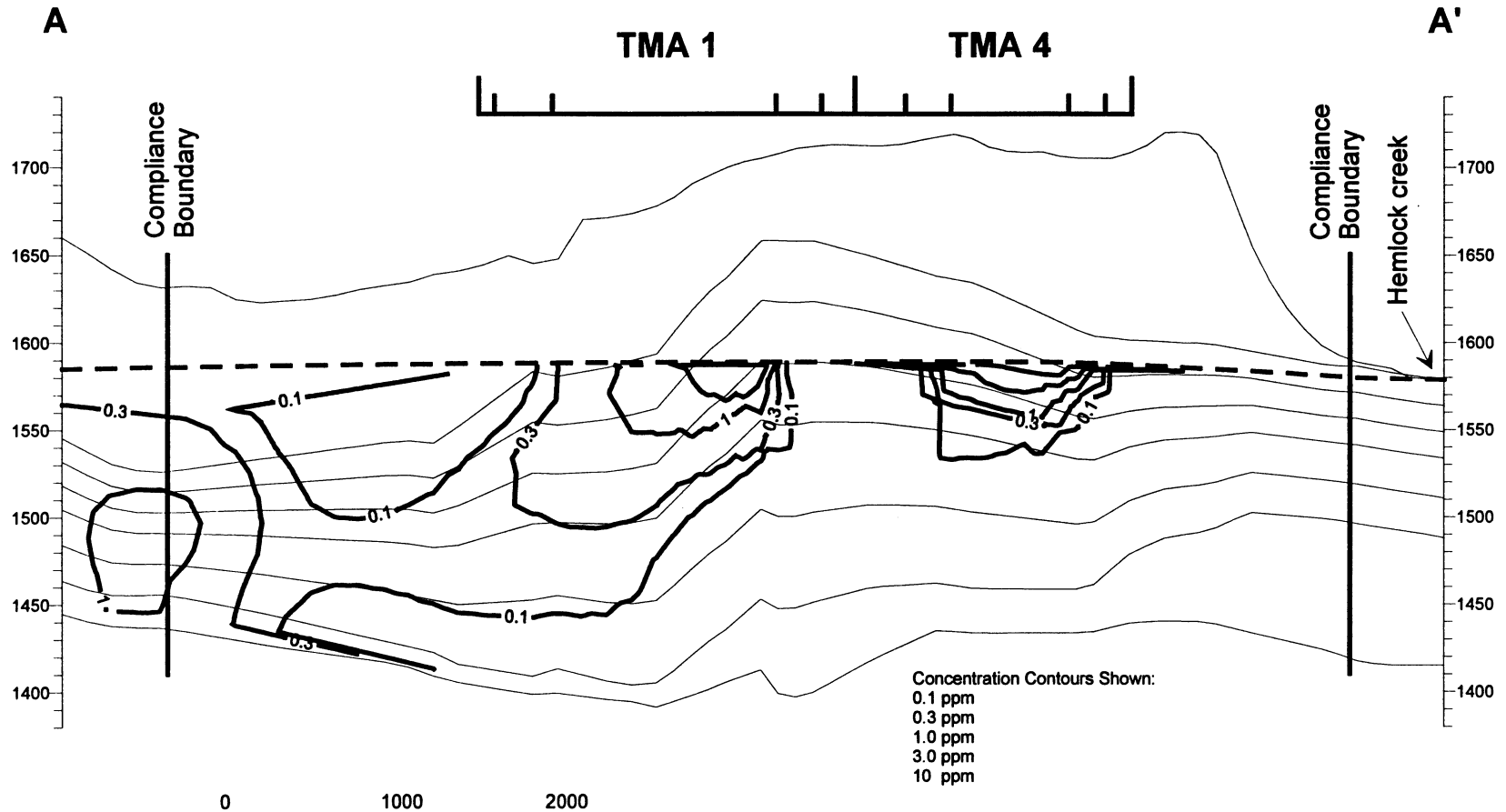

4.2-10-254

Source Concentration
Operation: 2000 ppm
Post-cap: 4000 ppm
Oxidized: 40,000 ppm*

* As a conservative assumption, the oxidized concentration begins one year after assumed degradation of the flexible membrane liner.

HSI GEOTRANS

REVISED	DATE	BY	DESCRIPTION

CHECKED BY: GWC	DATE: April 1998
APPROVED BY: PFA	DATE: April 1998
APPROVED BY:	DATE:

Nicolet Minerals COMPANY

Figure 2.87
PWCT Concentration After 32 Years (Example Constituent, Cross Section)

Scale: 1" = 1000' (h), 100' (v)	Date: April 1998
Prepared By: HSI GeoTrans	By: RMD

\Crandon\TmaMod3\Surfer\pwc060x.srf

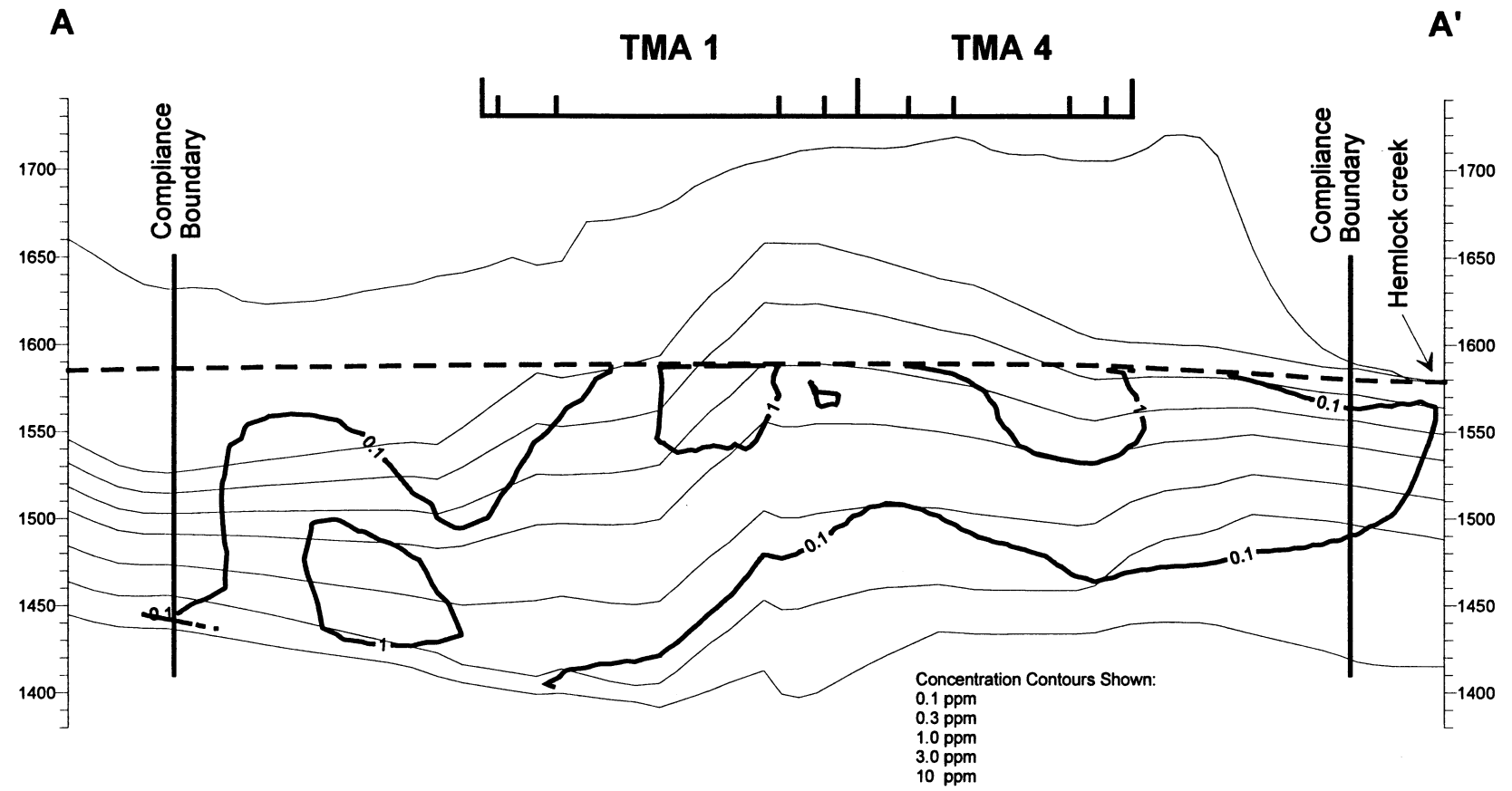

4.2-10-255

Source Concentration
Operation: 2000 ppm
Post-cap: 4000 ppm
Oxidized: 40,000 ppm*

* As a conservative assumption, the oxidized concentration begins one year after assumed degradation of the flexible membrane liner.

HSI GEOTRANS

REVISED	DATE	BY	DESCRIPTION

CHECKED BY: GWC	DATE: April 1998
APPROVED BY: PFA	DATE: April 1998
APPROVED BY:	DATE:

Nicolet Minerals COMPANY

Figure 2.88
PWCT Concentration After 60 Years (Example Constituent, Cross Section)

Scale: 1" = 1000' (h), 100' (v)	Date: April 1998
Prepared By: HSI GeoTrans	By: RMD

\Crandon\TmaMod3\Surfer\pwc125x.srf

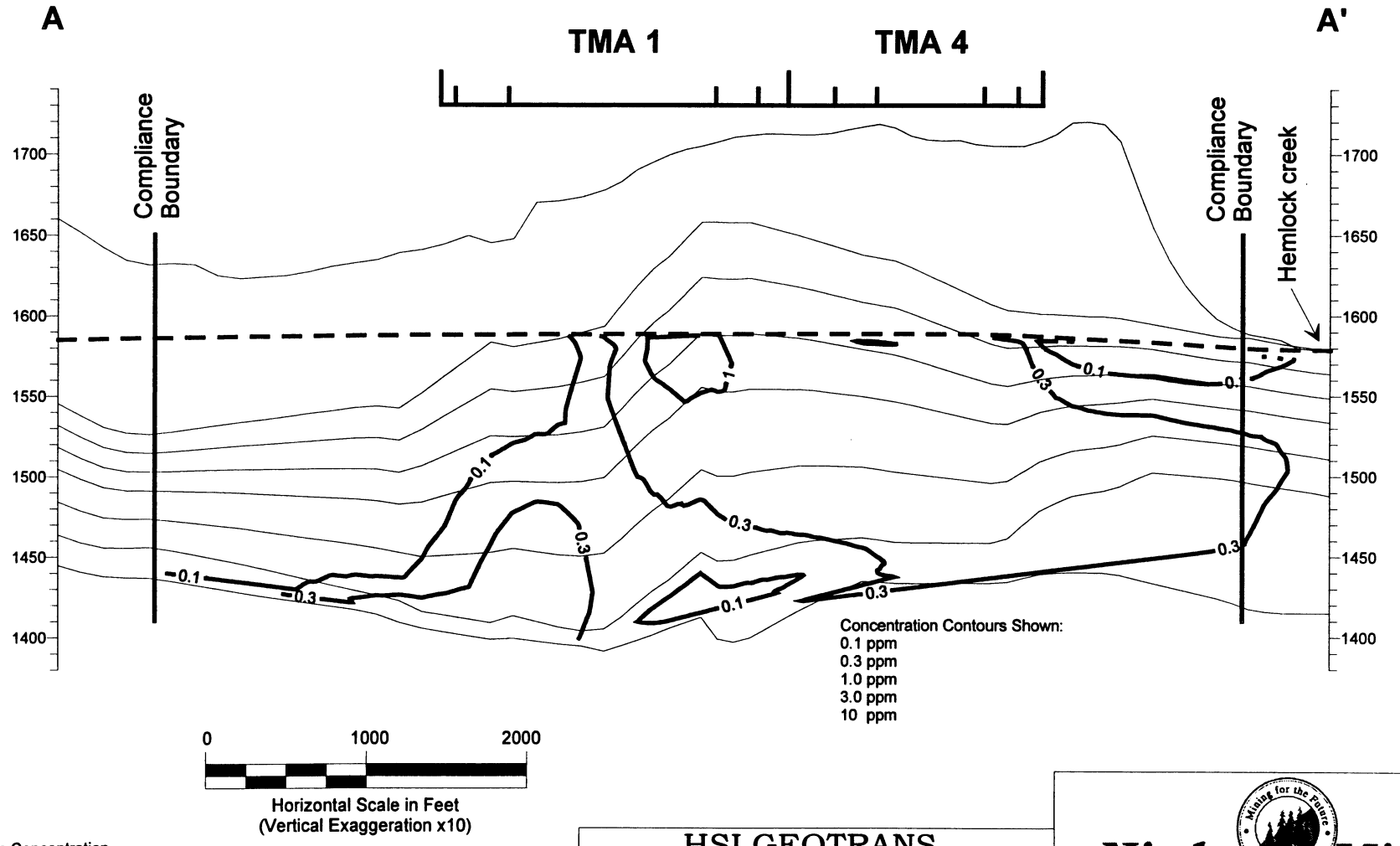

4.2-10-256

Source Concentration
Operation: 2000 ppm
Post-cap: 4000 ppm
Oxidized: 40,000 ppm*

* As a conservative assumption, the oxidized concentration begins one year after assumed degradation of the flexible membrane liner.

HSI GEOTRANS

REVISED	DATE	BY	DESCRIPTION

CHECKED BY: GWC	DATE: April 1998
APPROVED BY: PFA	DATE: April 1998
APPROVED BY:	DATE:

Nicolet Minerals COMPANY

Figure 2.89
PWCT Concentration After 125 Years (Example Constituent, Cross Section)

Scale: 1" = 1000' (h), 100' (v)	Date: April 1998
Prepared By: HSI GeoTrans	By: RMD

\Crandon\TmaMod3\Surfer\pwc200x.srf

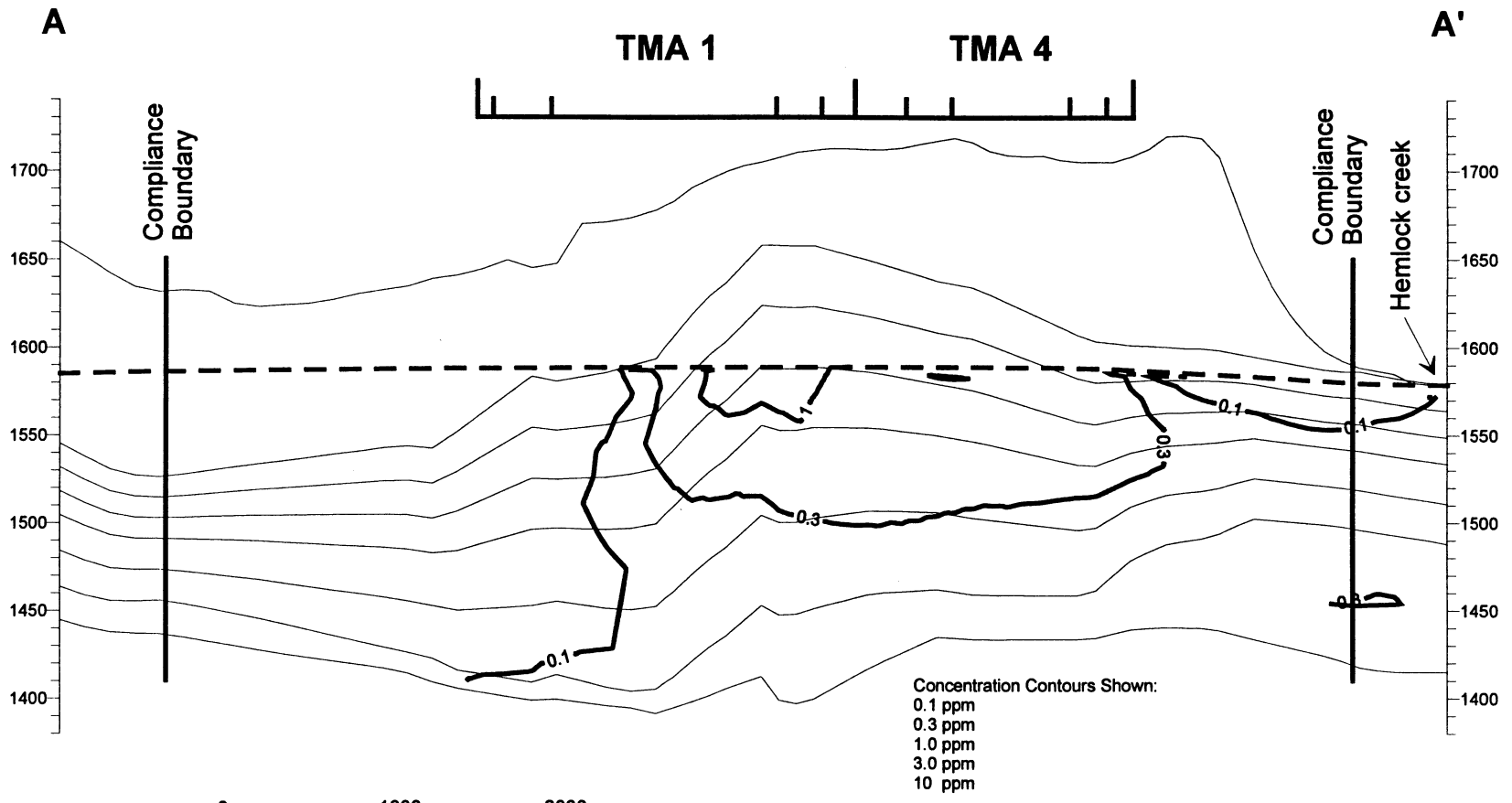

4.2-10-257

Source Concentration
Operation: 2000 ppm
Post-cap: 4000 ppm
Oxidized: 40,000 ppm*

* As a conservative assumption, the oxidized concentration begins one year after assumed degradation of the flexible membrane liner.

HSI GEOTRANS

REVISED	DATE	BY	DESCRIPTION

CHECKED BY: GWC	DATE: April 1998
APPROVED BY: PFA	DATE: April 1998
APPROVED BY:	DATE:

Nicolet Minerals COMPANY

Figure 2.90
PWCT Concentration After 200 Years (Example Constituent, Cross Section)

Scale: 1" = 1000' (h), 100' (v)	Date: April 1998
Prepared By: HSI GeoTrans	By: RMD

\Crandon\TmaMod3\Surfer\pwc300x.srf

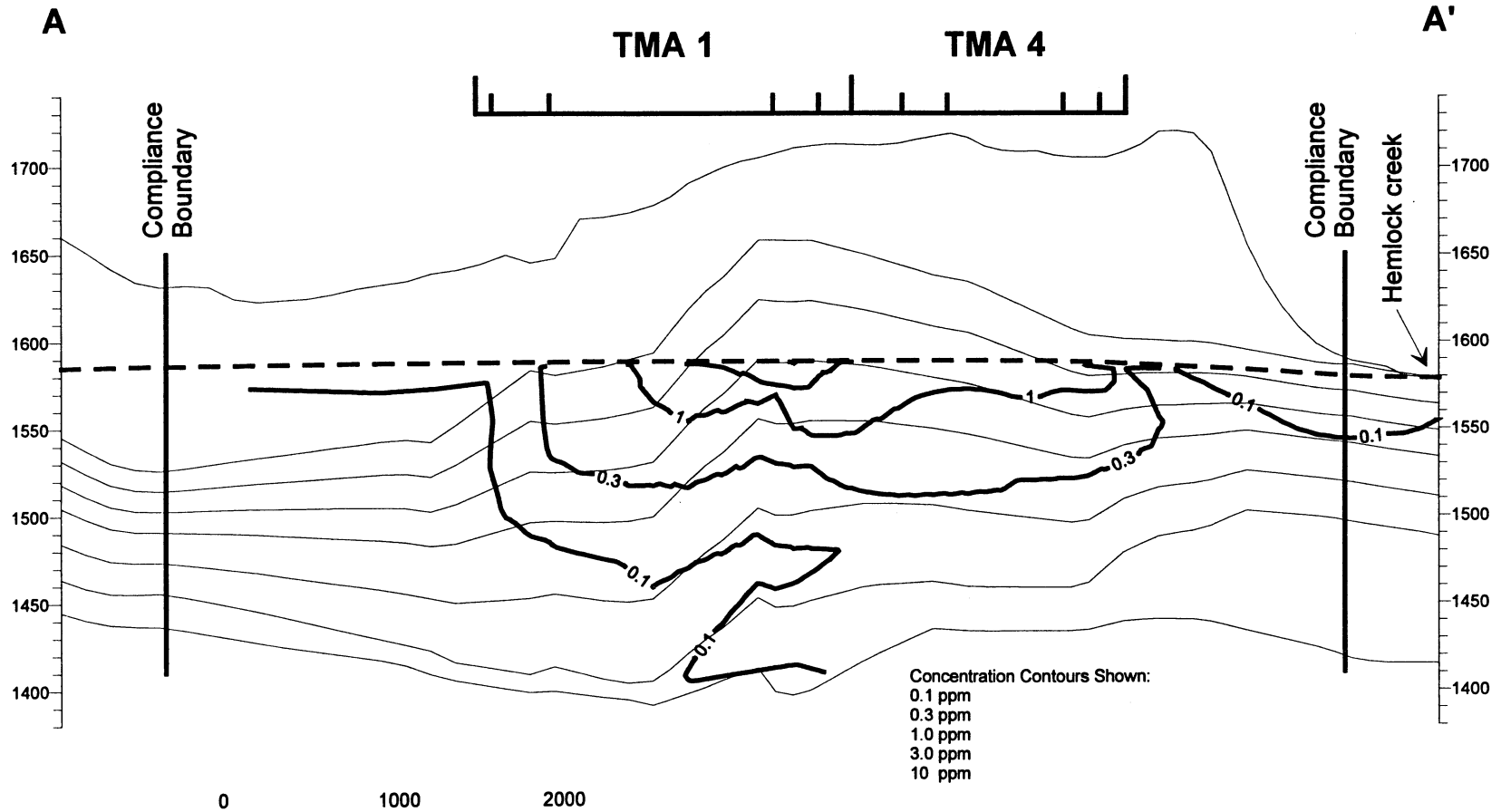

4.2-10-258

Source Concentration
Operation: 2000 ppm
Post-cap: 4000 ppm
Oxidized: 40,000 ppm*

* As a conservative assumption, the oxidized concentration begins one year after assumed degradation of the flexible membrane liner.

HSI GEOTRANS

REVISED	DATE	BY	DESCRIPTION

CHECKED BY: GWC	DATE: April 1998
APPROVED BY: PFA	DATE: April 1998
APPROVED BY:	DATE:

Nicolet Minerals COMPANY

Figure 2.91
PWCT Concentration After 300 Years (Example Constituent, Cross Section)

Scale: 1" = 1000' (h), 100' (v)	Date: April 1998
Prepared By: HSI GeoTrans	By: RMD

\Crandon\TmaMod3\Surfer\pwc650x.srf

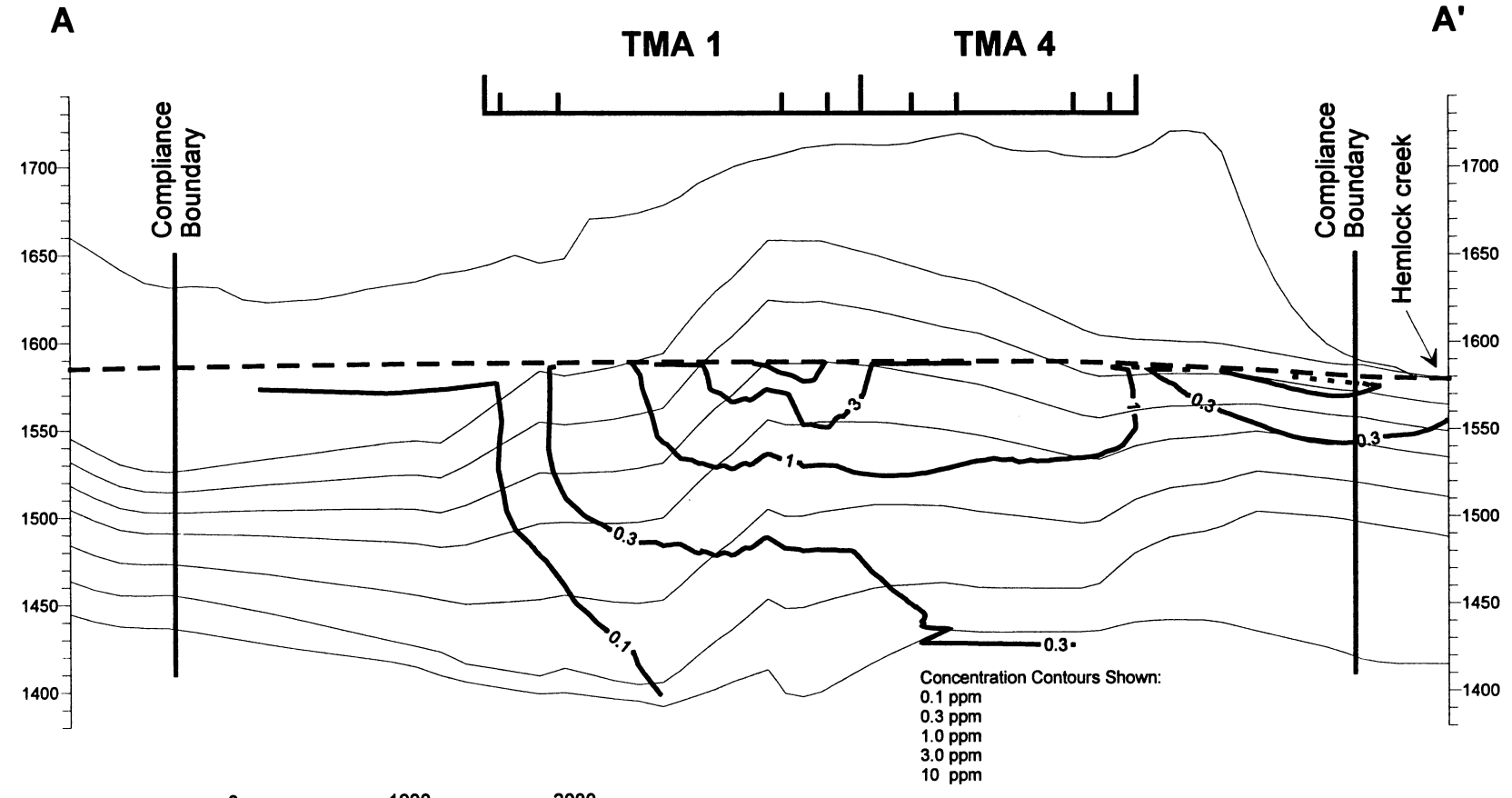

4.2-10-259

Source Concentration
Operation: 2000 ppm
Post-cap: 4000 ppm
Oxidized: 40,000 ppm*

* As a conservative assumption, the oxidized concentration begins one year after assumed degradation of the flexible membrane liner.

HSI GEOTRANS

REVISED	DATE	BY	DESCRIPTION

CHECKED BY: GWC	DATE: April 1998
APPROVED BY: PFA	DATE: April 1998
APPROVED BY:	DATE:

Nicolet Minerals COMPANY

Figure 2.92
PWCT Concentration After 650 Years (Example Constituent, Cross Section)

Scale: 1" = 1000' (h), 100' (v)	Date: April 1998
Prepared By: HSI GeoTrans	By: RMD

3 MINE REFLOODING MODEL

3.1 APPROACH

This section describes the analysis used to assess the potential for upward movement of solute from the backfilled mine into the glacial system following mine reflooding. Figure 3.1 shows limited regions of an upward hydraulic gradient from layer 6 to layer 4 in the steady-state regional groundwater flow model during post-mining conditions. These regions of upward gradient outline areas where solutes from the backfilled mine have the potential to travel upward to the glacial system.

The mine reflooding analysis was performed with the calibrated groundwater model (HSI GeoTrans, 1998a) and particle tracking using MODPATH (Pollack, 1990). Particle tracking is typically utilized in solute transport codes that use Method of Characteristic techniques (such as MT3D) to assess advective transport in the groundwater system. Particle tracking was selected as a scoping analysis to efficiently analyze advective travel paths and travel times in three dimensions. The particle tracking analysis uses the BEJ groundwater flow field and PWC groundwater flow field from HSI GeoTrans (1998a) to assess the potential range of travel times from the mine to the proposed compliance boundary 1200 feet from the orebody.

The particle tracking assumes that the mine will be backfilled with cemented and uncemented tailings having a bulk hydraulic conductivity of 2.8E-3 ft/day (1.0E-6 cm/s). It is assumed that the Crandon Formation will be replaced with backfill material in layer 6 (moderately weathered bedrock) and layer 7 (low to weakly weathered bedrock). Layer 5 will not be backfilled with tailings because this layer is comprised of strongly weathered bedrock which forms the crown pillar. As discussed below, a sensitivity analysis was performed to evaluate the effect of a higher bulk hydraulic conductivity of the tailings.

Particles were initiated within the mined, backfilled zone in layers 6 and 7 that had more than 10 percent Crandon Formation/backfill. The particles were placed at a density of one particle per model cell. Particles were placed at the vertical center of layers 6 and 7 as shown in Figure 3.2. A sensitivity simulation was performed to evaluate the effect of placing the particles at the top of layers 6 and 7, as shown in Figure 3.3.

3.2 MODEL PREDICTIONS

3.2.1 BEST ENGINEERING JUDGEMENT FOR TRANSPORT

The flow field uses the calibrated model parameters (HSI GeoTrans, 1998b) with a porosity of 10 percent. A total of 293 particles were initiated in the vertical centers of layers 6 and 7 in the mined portion of the ore body. The results of the particle tracking analysis are summarized in Table 3.1. Figure 3.4 shows a histogram of particle arrival times at the compliance boundary and a plot of percentage of particles reaching the compliance boundary versus time. The first particle reaches the compliance boundary at 927 years. However, after approximately 4,000 years only ten percent of the particles have reached the compliance boundary, while after 10,000 years fifty percent of the particles have reached the compliance boundary. Note that the histogram differentiates layers in which the particles originate. It is apparent that for the first 3000 years particles that cross the compliance boundary originate in Layer 6.

A sensitivity simulation was conducted to assess the significance of particle placement within a layer. In this simulation, particles were initiated at the top of layers 6 and 7. Particle placement at the top of layer 6 approximates the movement of solute from the base of the crown pillar. There are areas, particularly on the west side of the orebody, where the crown pillar extends into layer 7 (see Figures 3.2 and 3.3). Therefore, the particle placement used in this sensitivity simulation probably underestimates travel times, particularly for those particles on the west side of the orebody. All other features of the BEJT analysis were used. The histogram and plot of percentage of particles reaching the compliance boundary is shown in Figure 3.5. These plots show that the first particle reaches the compliance boundary at 591 years. However, after approximately 3,000 years, only ten percent of the particles have reached the compliance boundary while after 9,000 years fifty percent of the particles have reached the compliance boundary.

A sensitivity simulation was conducted to assess the significance of the bulk hydraulic conductivity of the cemented and uncemented tailings. In this simulation, the bulk hydraulic conductivity was increased one order of magnitude from 2.8E-3 ft/d to 2.8E-2 ft/d. All other features of the BEJT analysis were used. The histogram and plot of percentage of particles reaching the compliance boundary is shown in the Figure 3.6. These plots show that the first particle reaches the compliance boundary at 676 years. However, after approximately 3000 years only 10 percent of the particles have reached the compliance boundary while after 7000 years fifty percent of the particles have reached the compliance boundary.

3.2.2 PRACTICAL WORST CASE FOR TRANSPORT

The Practical Worst Case for Transport (PWCT) particle tracking simulations used the same parameters as the Practical Worst Case simulation documented in the groundwater flow modeling report (HSI GeoTrans, 1998a). The parameter changes included increasing the bedrock hydraulic conductivities.

The results of the simulation with particles originating at the vertical center of layers 6 and 7 are shown in Figure 3.7. The first particle reaches the compliance boundary at 393 years. A greater quantity of particles have reached the compliance boundary within the first 1000 years than in the BEJT simulation. Fifty percent of the particles have reached the compliance boundary by 3,000 years.

The results of a sensitivity simulation with particles originating at the top of layers 6 and 7 are shown in Figure 3.8. In this simulation, the first particle arrives at the compliance boundary at 159 years. Ten percent of the particles arrive by 1,000 years, while 50 percent arrive by 3,000 years.

3.3 SUMMARY OF MINE REFLOODING MODEL RESULTS

The particle tracking results show that the most rapid advective travel times from the mine to the compliance boundary range from 393 years for the PWCT simulation to 927 years for the BEJT simulation. These travel times are fairly long, particularly considering the implausibility of the PWCT, as was described in the prior section.

Of greater importance than the arrival time of the first particle, however, is the long time over which particles reach the compliance boundary for all cases. In the BEJT simulation, the standard deviation around the mean of arrival times is approximately 5,000 years. This means that it takes 10,000 years for 67 percent of the mass to cross the compliance boundary. This wide variation in arrival times corresponds to a very slow leach rate. In the PWCT simulation the standard deviation around the mean of arrival times is approximately 2,500 years.

The relatively long travel times suggest that the mined area has limited potential for affecting the glacial aquifer within a reasonable time frame. In addition, the slow release rate suggests that mixing with groundwater in the bedrock and glacial system will significantly reduce concentrations of any solute that does approach the compliance boundary. Solute transport modeling of the reflooded mine would likely indicate an even longer time for the concentration to peak at the compliance boundary. The longer time is due to the inclusion of dispersion and mixing which would further reduce solute concentrations.

Solute transport modeling is not deemed necessary due to:

- the very low rate of solute movement from the backfilled mine upward through the crown pillar rock and massive saprolite,
- the long travel time for solute particles from the mined areas to the compliance boundary,
- the large variation in travel times for solute particles from the mined areas to the compliance boundary,
- the conservative nature of particle tracking which does not account for mixing and dispersion, and
- the conservative nature of particle tracking which does not account for chemical precipitation and adsorption, which would also increase travel times and reduce concentrations of a number of constituents in the reflooded mine water.

Table 3.1 Summary of Particle Tracking Simulations.

Simulation/Particle Origination	Minimum Travel Time (years)	Average Travel Time (years)	Standard Deviation (years)
BEJT Center	927	10,398	5,193
BEJT Top	591	9,923	5,324
BEJT Center K (backfill) * 10	676	7,159	2,649
PWCT Center	393	3,694	2,461
PWCT Top	159	3,434	2,545

\Crandon\FlowMod2\Surfer\35i-h46.srf

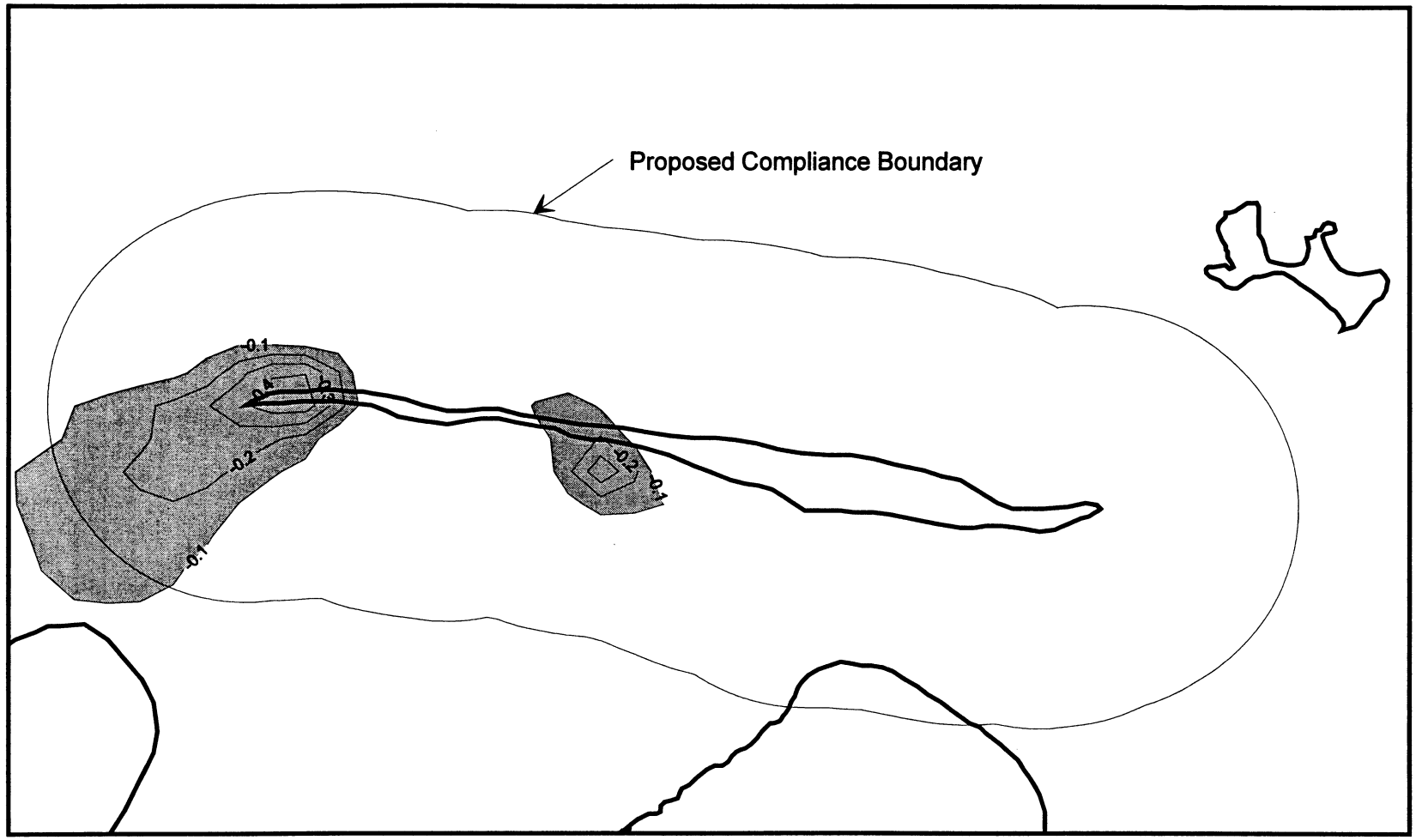

4.2-10-265

0 1000 2000

Horizontal Scale in Feet

Notes:
1. Contours of head difference between layers 4 and 6 are shown at 0.1 foot intervals.
2. Shaded areas indicate an upward head difference of at least 0.1 foot.
3. Only upward differences are contoured.

HSI GEOTRANS			
REVISED	DATE	BY	DESCRIPTION

CHECKED BY: PAW	DATE: April 1998
APPROVED BY: PFA	DATE: April 1998
APPROVED BY:	DATE:

Nicolet Minerals COMPANY

Figure 3.1
Areas of Upward Head Gradients Near the Backfilled Mine

Scale: 1" = 1000'	Date: April 1998
Prepared By: HSI GeoTrans	By: GWC

\Crandon\Flowmod2\Excel\x-sect.xls

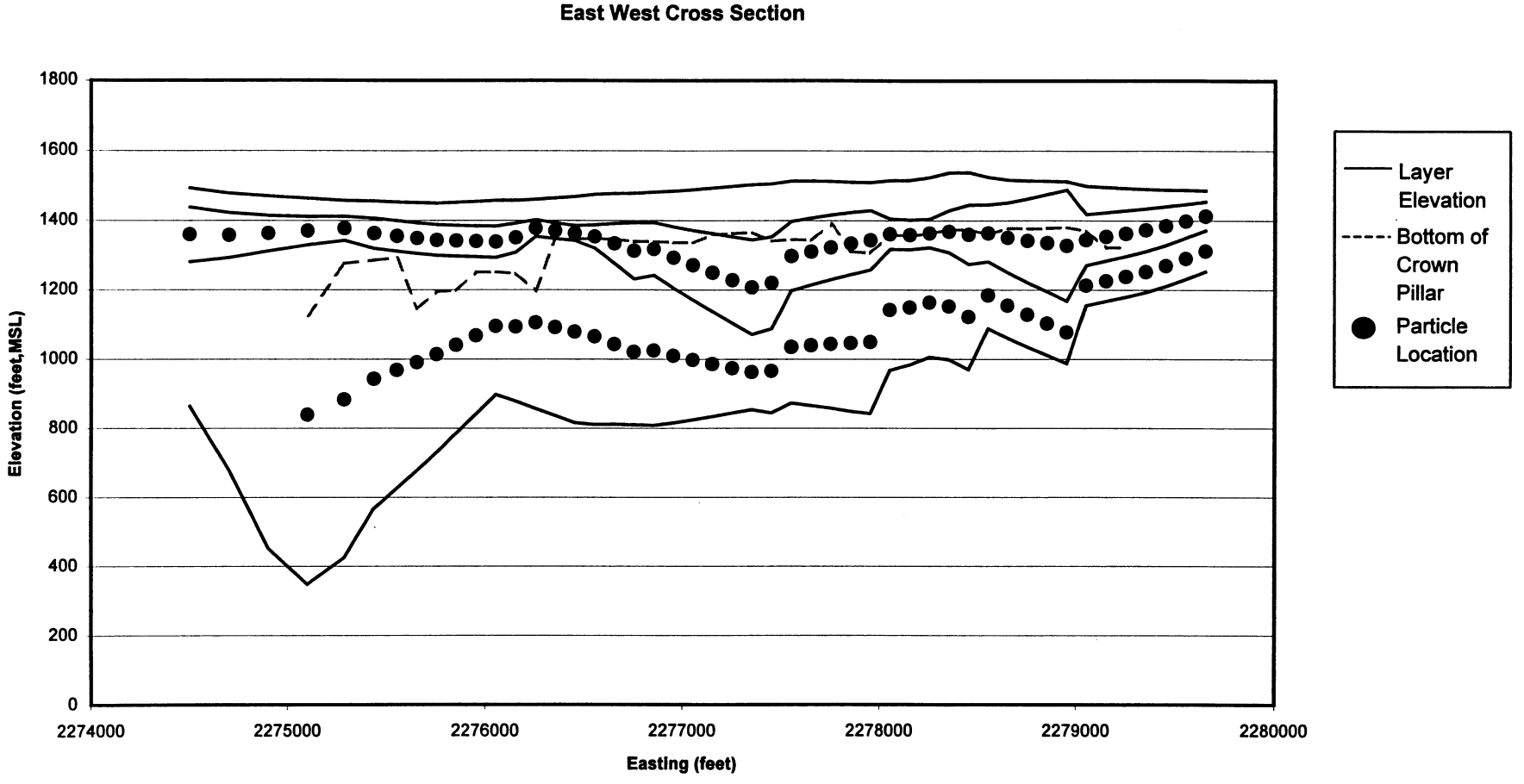

4.2-10-266

HSI GEOTRANS			
REVISED	DATE	BY	DESCRIPTION

CHECKED BY: GWC	DATE: April 1998
APPROVED BY: PFA	DATE: April 1998
APPROVED BY:	DATE:

Simulations 35i, 36i

Nicolet Minerals COMPANY

Figure 3.2
Particle Placement at Vertical Centers of Layers 6 and 7

Scale: None	Date: April 1998
Prepared By: HSI GEOTRANS	By: PAW

\Crandon\Flowmod2\Excel\x-sect.xls

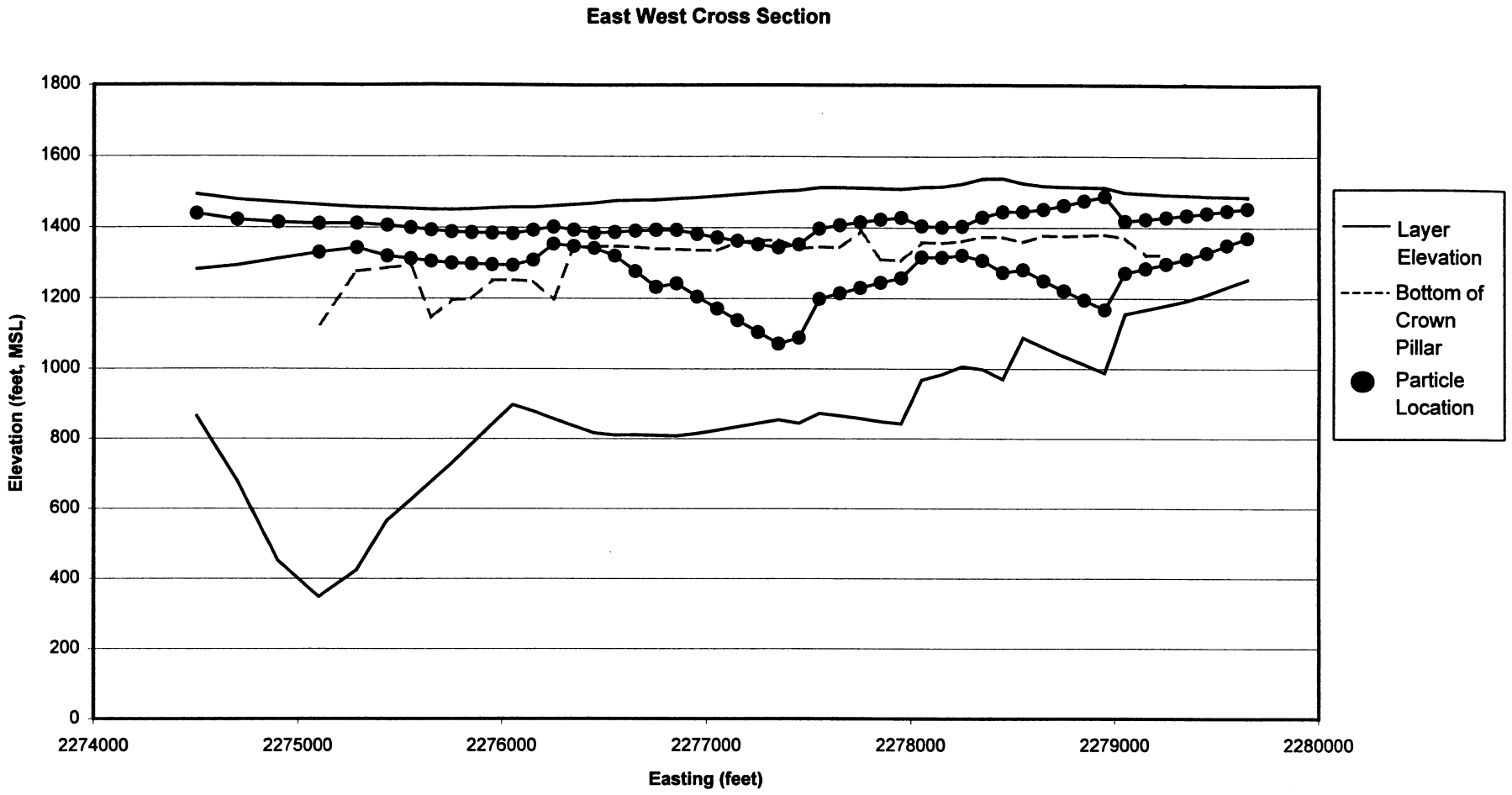

4.2-10-267

HSI GEOTRANS			
REVISED	DATE	BY	DESCRIPTION
CHECKED BY: GWC			DATE: April 1998
APPROVED BY: PFA			DATE: April 1998
APPROVED BY:			DATE:

Simulations 35i, 36i

Nicolet Minerals COMPANY

Figure 3.3
Particle Placement at Vertical Tops of Layers 6 and 7

Scale: None	Date: April 1998
Prepared By: HSI GEOTRANS	By: PAW

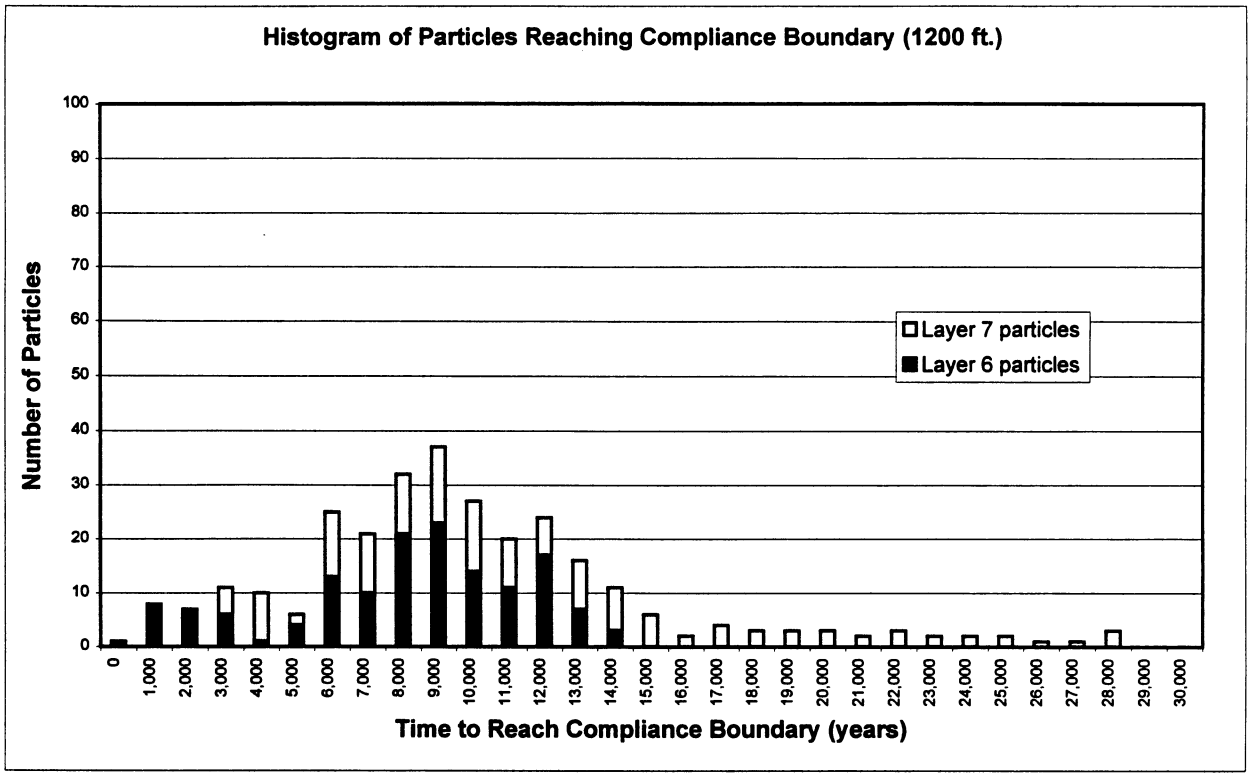

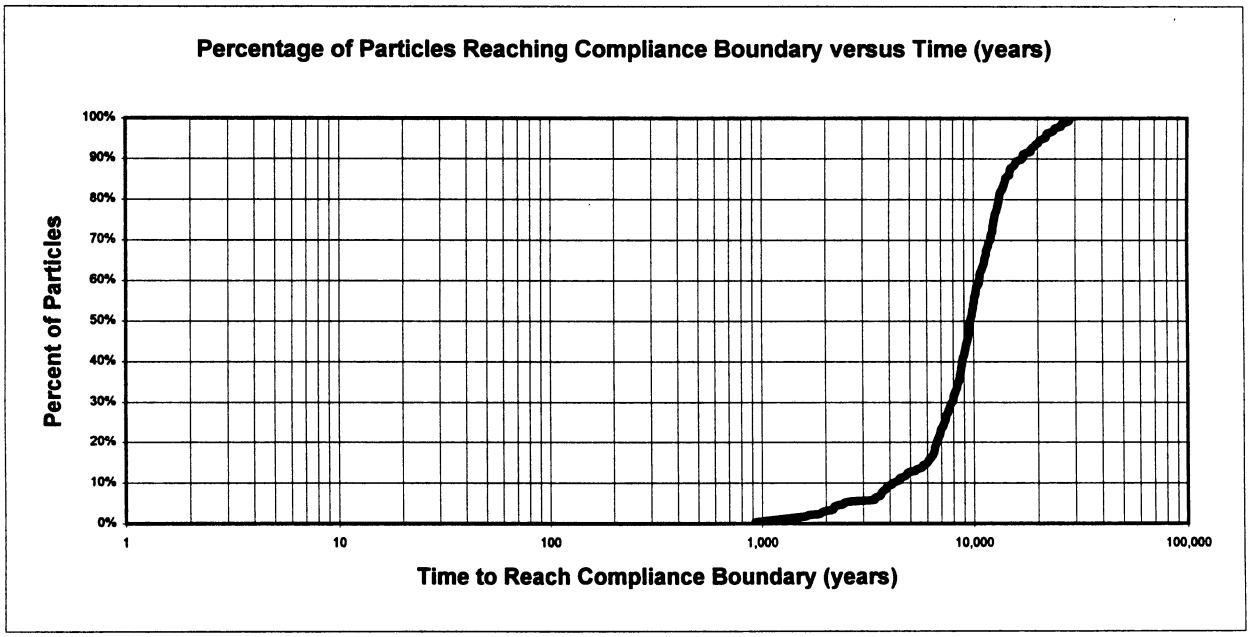

Particles begin in the center of cells in layers 6 and 7 for cells with >10% Crandon Formation

HSI GEOTRANS			
REVISED	DATE	BY	DESCRIPTION
CHECKED BY: GWC		DATE: Apr 98	
APPROVED BY: RTH		DATE: Apr 98	
APPROVED BY: PFA		DATE: Apr 98	

Nicolet Minerals COMPANY

Figure 3.4
Time (years) for Particles to Reach Compliance Boundary - BEJT

Scale: None	Date: Apr 1998
Prepared By: HSI GEOTRANS	By: PAW

Simulation 35i2

\Crandon\FlowMod2\Excel\35i3-end.xls

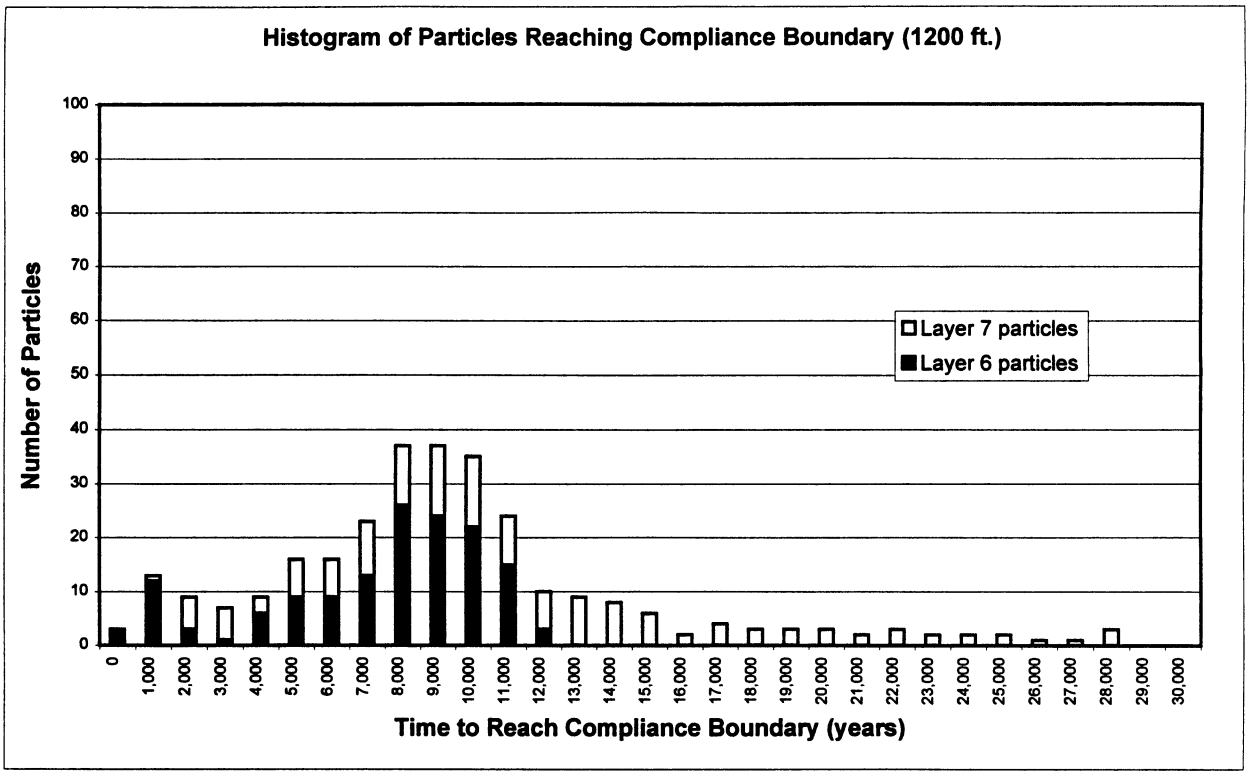

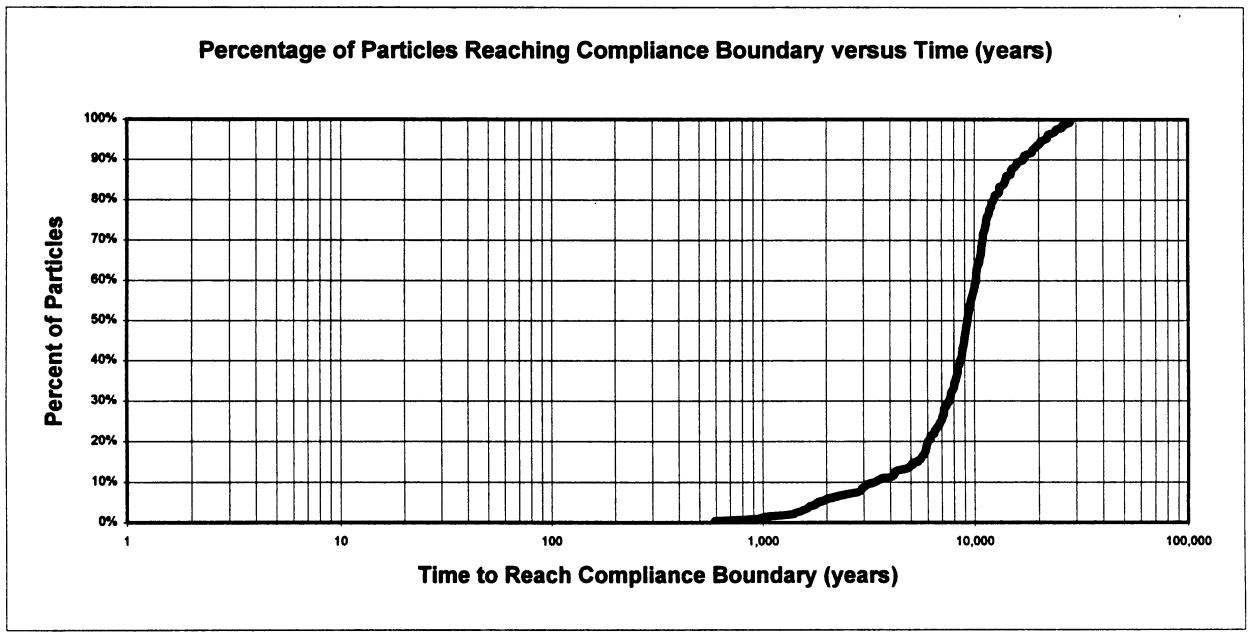

Particles begin at the top of cells in layers 6 and 7 for cells with >10% Crandon Formation

HSI GEOTRANS			
REVISED	DATE	BY	DESCRIPTION

CHECKED BY: GWC	DATE: Apr 98
APPROVED BY: RTH	DATE: Apr 98
APPROVED BY: PFA	DATE: Apr 98

Simulation 35i2

Nicolet Minerals COMPANY

Figure 3.5
Sensitivity Analysis - Time for Particles to Reach Compliance Boundary - BEJT

Scale: None	Date: Apr 1998
Prepared By: HSI GEOTRANS	By: PAW

\Crandon\FlowMod2\Excel\35i4-end.xls

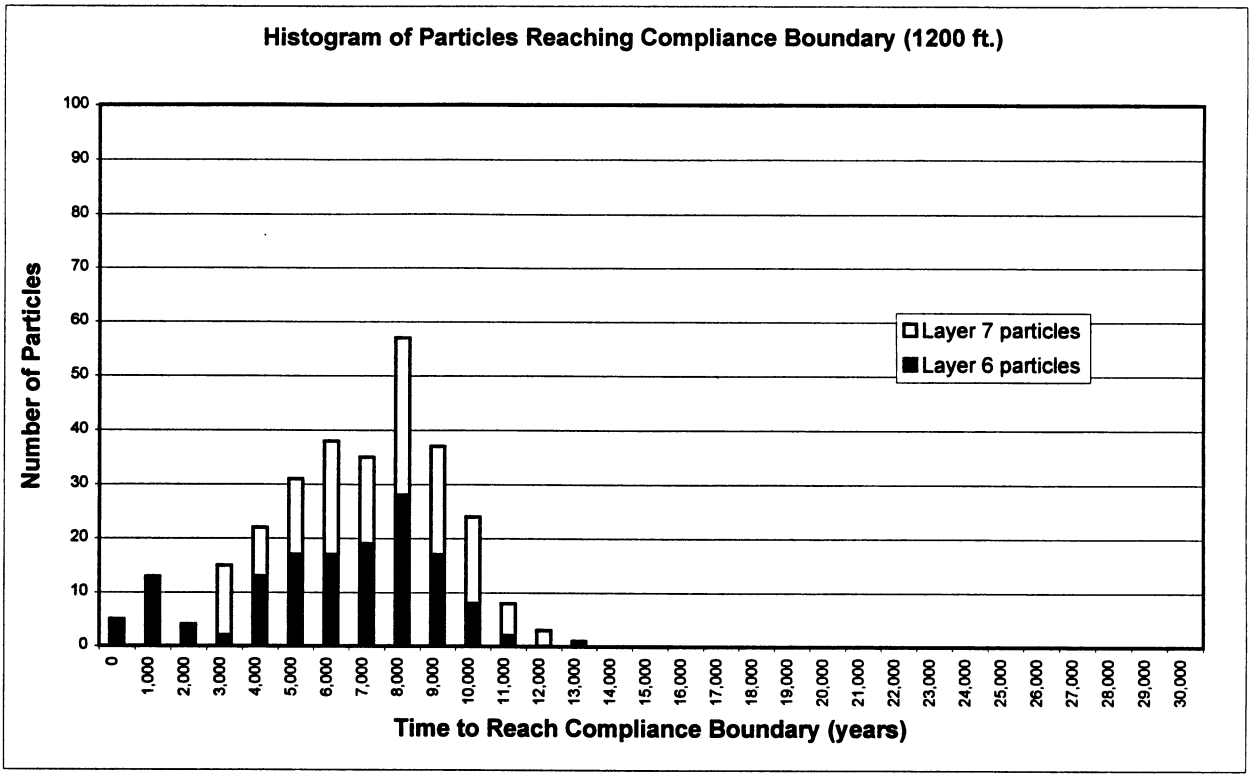

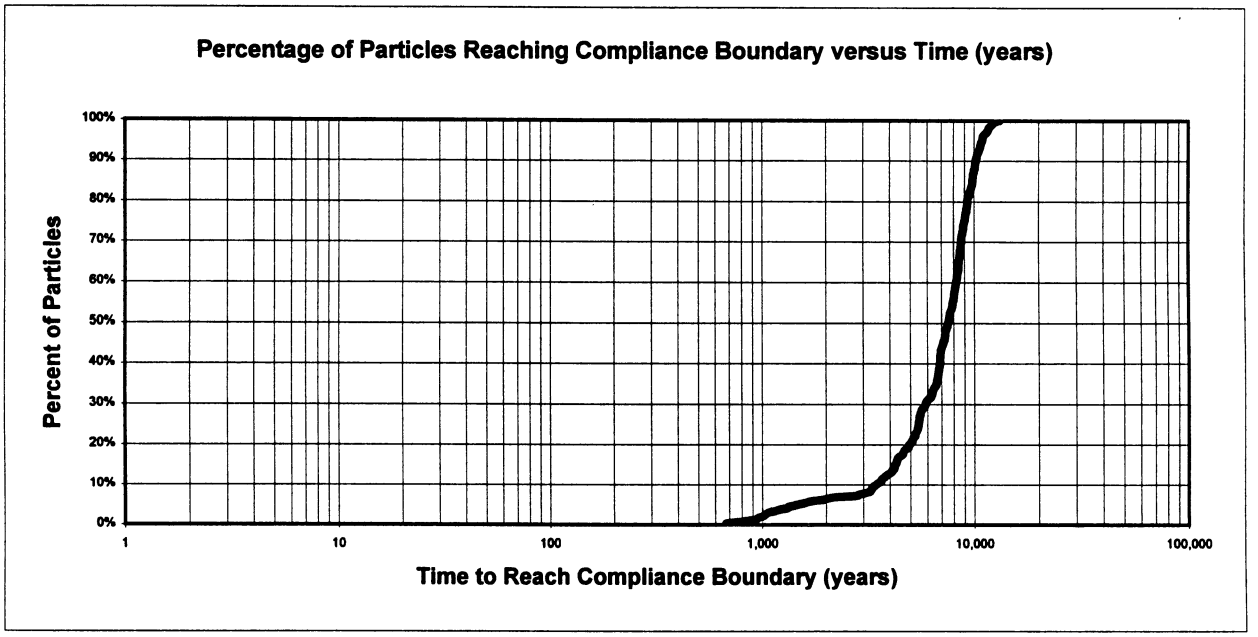

Particles begin in the center of cells in layers 6 and 7 for cells with >10% Crandon Formation

Sensitivity Simulation: K (backfill) * 10

HSI GEOTRANS			
REVISED	DATE	BY	DESCRIPTION
CHECKED BY: GWC			DATE: Apr 98
APPROVED BY: RTH			DATE: Apr 98
APPROVED BY: PFA			DATE: Apr 98

Simulation 35i6

Nicolet Minerals COMPANY

Figure 3.6
Backfill Sensitivity Analysis - Time for Particles to Reach Comp. Boundary - BEJT

Scale: None	Date: Apr 1998
Prepared By: HSI GEOTRANS	By: PAW

\Crandon\FlowMod2\Excel\35i6-end.xls

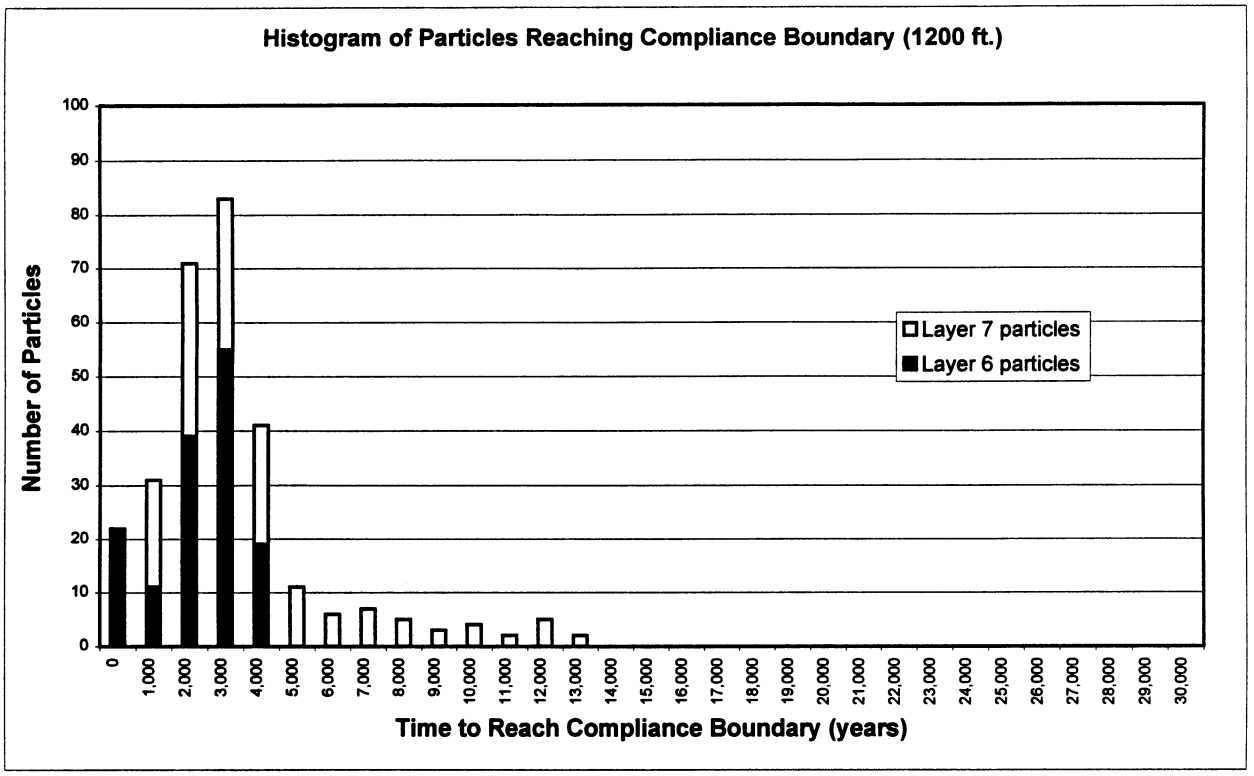

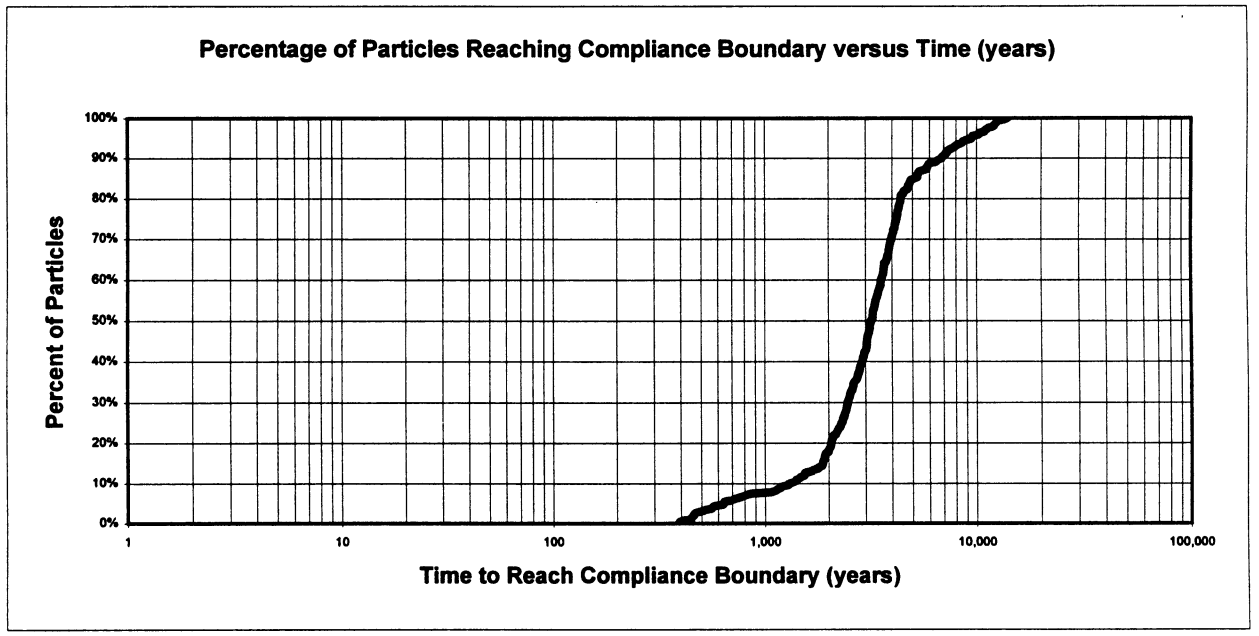

Particles begin in the center of cells in layers 6 and 7 for cells with >10% Crandon Formation

HSI GEOTRANS			
REVISED	DATE	BY	DESCRIPTION

CHECKED BY: GWC	DATE: Apr 98
APPROVED BY: RTH	DATE: Apr 98
APPROVED BY: PFA	DATE: Apr 98

Simulation 36i2

Nicolet Minerals COMPANY

Figure 3.7
Time (years) for Particles to Reach Compliance Boundary - PWCT

Scale: None	Date: Apr 1998
Prepared By: HSI GEOTRANS	By: PAW

\Crandon\FlowMod2\Excel\36i3-end.xls

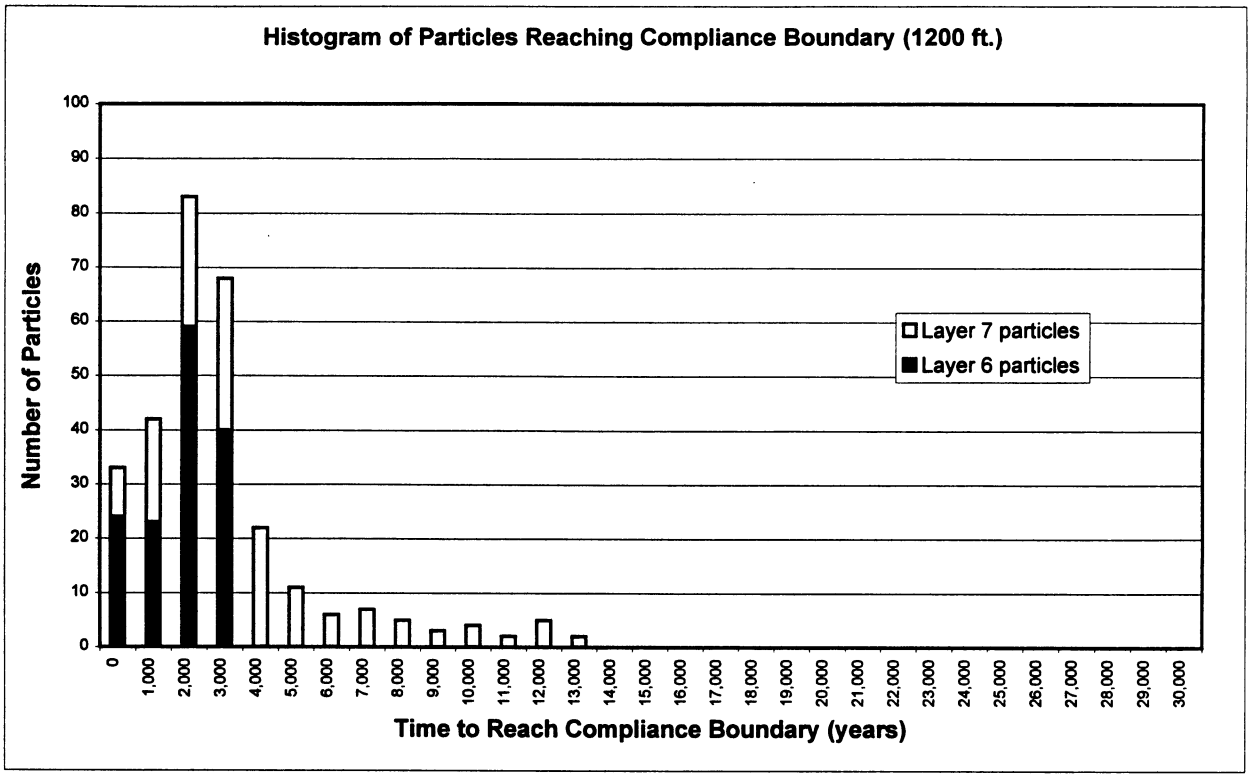

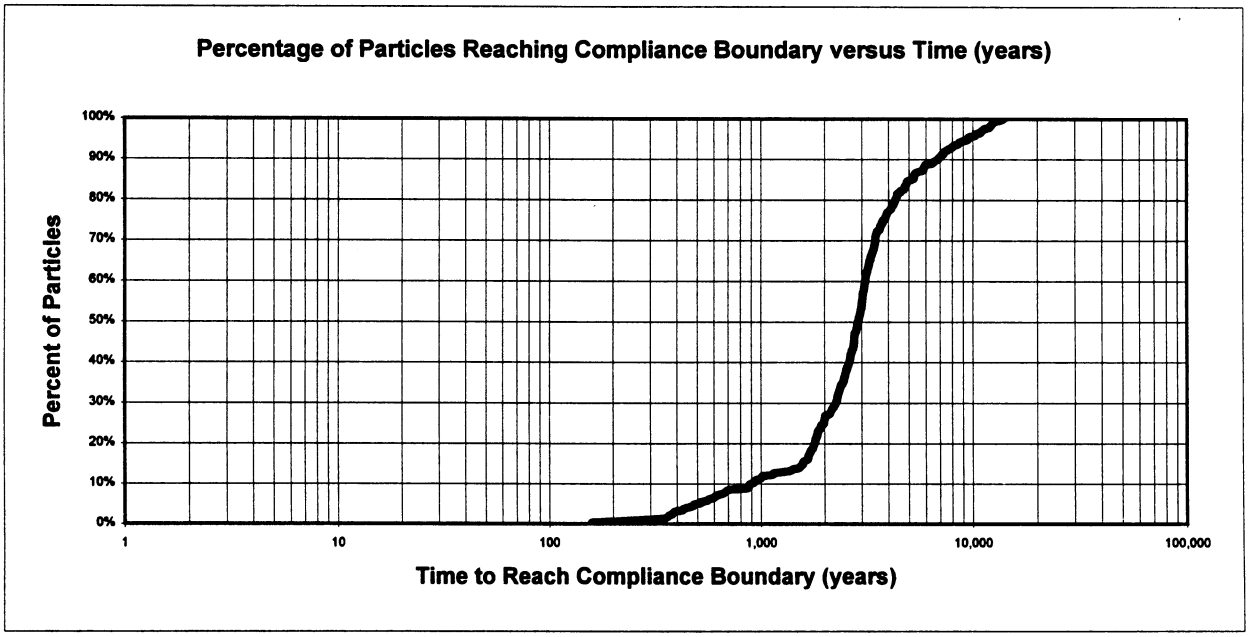

Particles begin at the top of cells in layers 6 and 7 for cells with >10% Crandon Formation

HSI GEOTRANS			
REVISED	DATE	BY	DESCRIPTION

CHECKED BY: GWC	DATE: Apr 98	
APPROVED BY: RTH	DATE: Apr 98	
APPROVED BY: PFA	DATE: Apr 98	

Simulation 36i2

Nicolet Minerals COMPANY

Figure 3.8
Sensitivity Analysis - Time for Particles to Reach Compliance Boundary - PWCT

Scale: None	Date: Apr 1998
Prepared By: HSI GEOTRANS	By: PAW

\Crandon\FlowMod2\Excel\36i4-end.xls

4 REFERENCES

Dunning, C., D. Johnson, and B. Batten, June 30, 1997. Review of Glacial Sediments in the Vicinity of the Proposed Crandon Mine. U.S. Geological Survey Memorandum.

Exxon Minerals Company, 1985. Environmental Impact Report.

Faust, C.R., P.N. Sims, C.P. Spalding, P.F. Andersen, and D.E. Stephenson, 1990. FTWORK: A three-dimensional groundwater flow and solute transport code. Westinghouse Savannah River Company Report WSRC-PR-89-1085.

Foth & Van Dyke, 1994. Notification of intent to collect data and detailed scope of study, Crandon Project, Crandon, Wisconsin, February 1994.

Foth & Van Dyke, 1995a. Mine Permit Application, Crandon Project, Crandon, Wisconsin.

Foth & Van Dyke, 1995b. Envrironmental Impact Report, Crandon Project, Crandon, Wisconsin.

Foth & Van Dyke, 1995c. Tailings Management Area Feasibility Report/Plan of Operation. Crandon Project, Crandon, Wisconsin.

Gelhar, L.W., C. Welty, and K.R. Rehfeldt. A critical review of data on field-scale dispersion in aquifers, *Water Resour. Res.*, 28(7), 1955-1974, 1992.

Giroud, J.P. and R. Bonaparte, 1989. Leakage through liners constructed with geomembranes. Part 1 - Geomembrane liners. Geotextiles and Geomembranes. Vol. 8, No 1.

HSI GeoTrans, 1995. Numerical Simulation of the effect on groundwater and surface water of the proposed zinc and copper mine near Crandon, Wisconsin (September, 1995).

HSI GeoTrans, 1996a. Numerical Simulation of Potential Solute Transport at the proposed zinc and copper mine near Crandon, Wisconsin (November, 1996)

HSI GeoTrans, 1996b. Numerical Simulation of the effect on groundwater and surface water of the proposed zinc and copper mine near Crandon, Wisconsin (August, 1996).

HSI GeoTrans, 1998a. Addendum No. 1 to Numerical Simulation of the effect on groundwater and surface water of the proposed zinc and copper mine near Crandon, Wisconsin (February, 1998).

HSI GeoTrans, 1998b. Errata and clarifications to Addendum No. 1 to Numerical Simulation of the effect on groundwater and surface water of the proposed zinc and copper mine near Crandon, Wisconsin (March 1998).

McDonald, M.G., A.W. Harbaugh, 1988. A modular three-dimensional finite difference groundwater flow model: *U.S. Geological Survey Techniques of Water-Resources Investigations*, Book 6, Chapter A1.

Pollack, D.W., 1989. Documentation of computer programs to complete and display pathlines using results results from the U.S. Geological Survey modular three-dimensional finite difference groundwater model, U.S.G.S. Open File Report 89-381, 81pp.

Saad, D.A., 1996. Using chlorofluorocarbons to date groundwater and determine hydrologic properties of sediments near the proposed Crandon mines near Crandon, Wisconsin. Summary report, submitted to WDNR June 10, 1996, 16 pp.

Zheng, C., 1996. MT3D^{96}, Modular three-dimensional transport model. Version 2.0.

APPENDIX A

Calculations of Leakage Rates used in the Solute Transport Model

Foth & Van Dyke
Memorandum

March 4, 1998

TO: Peter F. Andersen, HSI GeoTrans, Inc.

CC: Jerry Sevick, Foth & Van Dyke
Don Moe, Nicolet Minerals Company
Nandu Paruvakat, Foth & Van Dyke
Master File

FR: Steve Donohue, Foth & Van Dyke SVD

RE: Crandon Project - Solute Transport Model Update: Updated TMA Footprint Boundaries Leakage Rates

As part of the work on updating the solute transport model simulations for the Crandon Project TMA, several recent minor modifications to the TMA design need to be taken into account.

TMA Cell 2

Attachment 1 contains an updated table on the site life for the TMA cells and stages. Note that the site life/stages in TMA 2 have changed slightly from that used in the 1996 solute transport model. The first stage life of TMA 2 (Stage III) has been changed from approximately 4 yr to approximately 5 yr. The second stage life of TMA 2 (Stage IV) has been changed from approximately 6 yr to approximately 5 yr.

TMA Percolation Rates

HELP model simulations for a period of 10 yr were completed to estimate percolation rates during operations for the TMA base, TMA lower sideslope, and the redesigned TMA upper sideslope with drainage. The 1996 solute transport model used the maximum percolation rate from the 10-yr HELP model simulation. Given that the solute transport model is simulating a 30-yr period of operations, and each TMA cell is operated for a period of 6-10 yr, the 10-yr operational average as produced from the HELP model is a more representative number. The tables in Attachment 2 provide the most recent estimates of percolation from the TMA. For percolation values listed as <0.0000005 in/yr, the HELP model is predicting that for an area of 200 ac, between zero and 0.3 cu ft of leachate is percolating through the liner on an annual basis. This equates to a percolation rate of between 0 in/yr and <0.0000005 in/yr. Thus the median percolation rate for use in the solute transport model is 0.00000025 in/yr.

Source Area Footprint

Drawing 1 in Attachment 3 delineates the footprint for the TMA and related features. Note that also included on the drawing is the footprint for the TMA reclaim pond which needs to be represented as a source area during operations and reclamation. During operations, the reclaim pond is assumed to operate with a water depth of 15 ft above the FML resulting in a percolation rate of 1.92×10^{-4} in/day (1.6×10^{-5} ft/d). During the reclamation phase (years 1 through 11 of the TMA post-closure period), the reclaim pond is assumed to operate at a water depth of 7 ft, and a percolation rate of 4.79×10^{-5} in/day (4.0×10^{-6} ft/day). The supporting documentation on the percolation rates for the reclaim pond is provided in Attachment 4.

Attachment 1

Table 13
from the December 12, 1997, Letter from Don Moe, CMC, to Bill Tans, Christopher Carlson, and Bob Grefe, WDNR
Crandon Project - Response to WDNR September 26, 1997, Completeness Determination on the Feasibility Report for the Proposed Crandon Mine Tailings Management Area

Table 13

Estimated Volumes and Site Life for TMA Cells and Stages

(Updated Table 4.1-2 from May 1995 TMA Feasibility Report)

Tailings Cell	Stage	Tailings (x 10^6 cy)	Approximate Phase Life (yrs.)	Other Wastes (x 10^6 cy)	Contingencies (x 10^6 cy)	Calculated Need (x 10^6 cy)	Cell Design Total[4] (x 10^6 cy)	Capacity as Percent of Total
Zinc Ore Production								
TMA 1	I	1.83	3.0	0.66	--	2.49	2.48	
TMA 1	II	2.02	3.3	0.13	--	2.15	2.15	
Subtotal		3.85	6.3	0.79		4.64	4.63	39.5
TMA 2	III	3.11	5.1	0.09	--	3.2	3.2	
TMA 2[1]	IV	2.80	4.6	0.08	1.02	3.9	3.9	
Subtotal		5.91	9.7	0.17		7.1	7.1	60.5
Zinc Total Tailings		9.76	16.0	0.96	1.02	11.74	11.73	100.0
Copper Ore Production								
TMA 3	V	1.22	2.0	0.1[2,3]	--	1.32	1.61	
TMA 3	VI	2.44	4.0	0.1[2,3]	--	2.54	2.65	
Subtotal		3.66	6.0	0.2	--	3.86	4.26	48.2
TMA 4	VII	1.83	3.0	0.1[2,3]	--	1.93	1.73	
TMA 4[1]	VIII	1.83	3.0	0.1[2,3]	1.10	3.03[1]	2.85	
Subtotal		3.66	6.0	0.2		4.96	4.58	51.8
Copper Total Tailings		7.32	12.0	0.4	1.10	8.82	8.84	100.0
Total Zinc & Copper		17.08	28	1.36	2.12	20.56	20.57	

[1]Final zinc cell includes a 10.5% contingency calculated based on the total "expected" production of zinc tailings and waste rock. Final copper cell includes a 15% contingency calculated based on the total "expected" production of copper tailings and waste rock.
[2]Other materials for copper cells include 1/4 of 0.30 x 10^6 cy of WTPS + 1/4 of the estimate for other wastes (0.11 x 10^6 cy) for each cell or 0.075 + 0.0275 = 0.1025 million cy per stage.
[3]Other materials include all waste rock, wastewater treatment and reclaim pond solids, and laboratory wastes.
[4]Cell design total is the actual design volume based on model calculation performed by Foth and Van Dyke's Computer Aided Drafting and Design (CADD) system. The design total is within 0.5% of the required total.
cy - Cubic yards
yrs - years

Prepared by: REM/JKS1
Checked by: NXP/REM

4.2-10-279

Attachment 2

TMA Percolation Rates
Tables 1, 2, and 3
Revised Tables 7.3-5, 7.3-6, and 7.3-8
from the January 30, 1997
Addendum No. 3 to the May 1995 Crandon Project Tailings Management Area Feasibility Report/Plan of Operation

Table 1

Percolation from TMA Based on Doubled Precipitation Values During Operation of Initial Stages

Year	Sideslope		Base (in/yr)
	Lower Sideslope (in/yr)	Upper Sideslope (in/yr)	
1	<0.0000005	NA	0.010461
2	<0.0000005	NA	0.004917
3	<0.0000005	NA	0.003490
4	<0.0000005	NA	0.008997
5	<0.0000005	NA	0.005416
6	<0.0000005	NA	0.004207
7	<0.0000005	NA	0.006230
8	<0.0000005	NA	0.003004
9	<0.0000005	NA	0.001347
10	<0.0000005	NA	0.008891

NA = Not Applicable

Prepared by: MRS
Checked by: NXP

Table 2

Percolation from TMA Based on Doubled Precipitation Values During Operation of Second Stages

Year	Sideslope		Base (in/yr)
	Lower Sideslope (in/yr)	Upper Sideslope (in/yr)	
1	0.000001	<0.0000005	0.012519
2	<0.0000005	<0.0000005	0.006330
3	<0.0000005	<0.0000005	0.004707
4	<0.0000005	<0.0000005	0.007421
5	<0.0000005	<0.0000005	0.004741
6	<0.0000005	<0.0000005	0.004464
7	<0.0000005	<0.0000005	0.005390
8	<0.0000005	<0.0000005	0.003720
9	<0.0000005	<0.0000005	0.002812
10	<0.0000005	<0.0000005	0.004966

Prepared by: MRS
Checked by: NXP

Table 3

Post-Closure Percolation

Year from Placement of Cover	Sideslope: Lower Sideslope (in/yr)	Sideslope: Upper Sideslope (in/yr)	Base (in/yr)
1	<0.0000005	<0.0000005	0.004681
2	<0.0000005	<0.0000005	0.003328
3	<0.0000005	<0.0000005	0.000607
4	<0.0000005	<0.0000005	0.000512
5	<0.0000005	<0.0000005	0.000453
6	<0.0000005	<0.0000005	0.000406
7	<0.0000005	<0.0000005	0.000368
8-15	<0.0000005	<0.0000005	0.000264
16-25	<0.0000005	<0.0000005	0.000162
26-35	<0.0000005	<0.0000005	0.000012
36-40	<0.0000005	<0.0000005	0.000002
41-50	<0.0000005	<0.0000005	0.000044
51-60	<0.0000005	<0.0000005	0.000042
61-70	<0.0000005	<0.0000005	0.000039
71-80	<0.0000005	<0.0000005	0.000036
81-90	<0.0000005	<0.0000005	0.000034
91-115	<0.0000005	<0.0000005	0.000030
116-140	<0.0000005	<0.0000005	0.000025
141	0.003876	0.001376	0.008757
142-165	<0.0000005	<0.0000005	<0.0000005
166-175	<0.0000005	<0.0000005	<0.0000005
176-190	<0.0000005	<0.0000005	<0.0000005
190-195	<0.0000005	0.000043[1]	<0.0000005

Table 3 *(Continued)*

Year from Placement of Cover	Sideslope: Lower Sideslope (in/yr)	Sideslope: Upper Sideslope (in/yr)	Base (in/yr)
196-205	<0.0000005	0.000029[1]	<0.0000005
206-215	<0.0000005	0.000026[1]	<0.0000005
216-220	<0.0000005	0.000039[1]	<0.0000005
221-230	<0.0000005	0.000031[1]	<0.0000005
231-240	<0.0000005	0.000030[1]	<0.0000005
241+[2]	0.000030	0.000030	0.000030

[1]Percolation equal to infiltration through cover.
[2]Conservatively assumed to be equal to infiltration through cover. For base this will occur at >241 years and for lower sideslope >>241 years.

Prepared by: MRS
Checked by: NXP

Attachment 3

Drawing 1
TMA Surface Areas

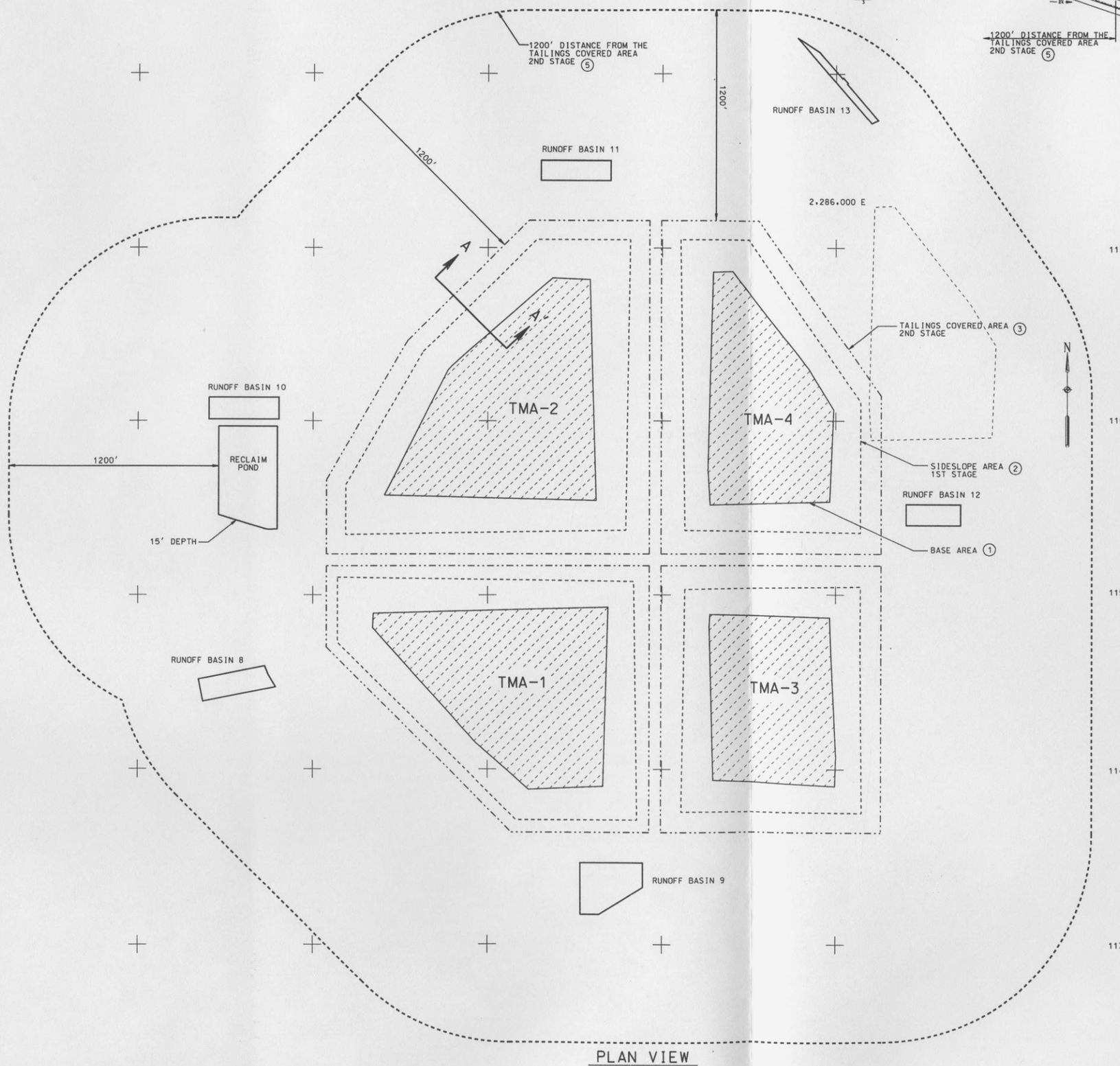

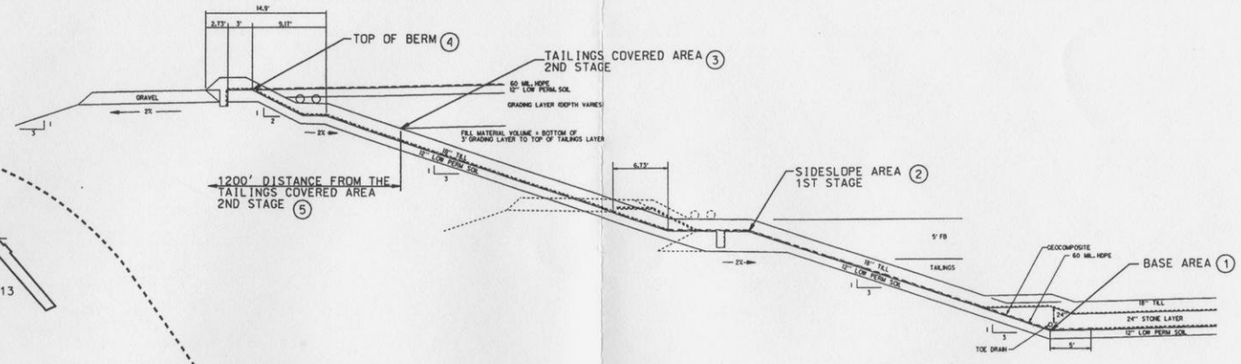

PLAN VIEW

LEGEND

- APPROXIMATE LIMITS OF TAILINGS COVERED AREA 2ND STAGE
- APPROXIMATE LIMITS OF SIDESLOPE AREA 1ST STAGE
- APPROXIMATE LIMITS OF BASE AREA

0 300' 600'
SCALE

Crandon Mining Company

Foth & Van Dyke

REVISED	DATE	BY	DESCRIPTION

TITLE
TMA SURFACE AREAS

SCALE AS SHOWN	STATE WISCONSIN		COUNTY FOREST		
DRAWN BY JOW	DATE 1/98	CHECKED BY JKS1	DATE 1/98		
APPROVED BY SVDI	DATE 1/98	APPROVED BY NXP	DATE 1/98		
APPROVED BY GWS	DATE 1/98	CRANDON MINING COMPANY DEM	DATE 1/98		
DRAWING NO. 1	SHEET ___ OF ___	REVISION NO.			

b:\94c067\4c67z51.3d
03/04/98 krb2

Attachment 4

Reclaim Pond Percolation Rates
Revised Attachment 5 from the April 1, 1997, Letter from Don Moe, CMC, to Ben Wopat, USCOE
Crandon Project - CMC Responses to the U.S. Army Corps of Engineers August 2, 1996 TMA Feasibility Report Review Letter

Foth & Van Dyke
consultants · engineers · scientists

Client:	Nicolet Minerals Company	Scope I.D.:	93C049
Project:	Pond Liner Percolation	Page:	1 of 4
Prepared by:	Nandu Paruvakat	Date:	3/26/97
Checked by:	Ron Meister	Date:	3/26/97
Revised by:	Nandu Paruvakat	Date:	2/26/98
Checked by:	Ron Meister	Date:	2/27/98

COPY IN M.F.

Determination of Percolation Through the Liners of the Process Water Reclaim Pond and Wastewater Basins

A. Purpose: To estimate the percolation quantities through the composite liners of the:

- Process water reclaim pond;
- Pipeline spill containment basin 4;
- Wastewater storage basin 5;
- Wastewater storage basin 6; and
- Wastewater storage basin 7.

B. Scope: Use Giroud and Bonaparte equations for leakage through composite liners of the basins with the following hydraulic heads:

Unit	Maximum Head (ft)	Average Head (ft)
Process water reclaim pond	19	15
Pipeline spill containment basin 4	12	3
Wastewater storage basin 5	8	2
Wastewater storage basin 6	19	7
Wastewater storage basin 7	19	7

C. Assumptions

1. The composite liner consists of a 60 mil HDPE geomembrane overlying a geosynthetic clay liner (GCL) which, in turn, overlies a compacted 1-ft lift of P40 till.

2. The geomembrane will be leak tested using leak location surveys or similar electrical methods and all installation defects located will be repaired. The only holes remaining during the operation period of the ponds will be the pinholes as a result of manufacturing processes.

3. For the analysis, pinhole density will be established at one per acre. The pinholes will have an area of 0.000000784 m^2 (similar to HELP model runs).

4. The GCL will be 0.24 in (6 mm) thick and have a design hydraulic conductivity of 6.9×10^{-9} cm/sec. The ponds and basin will be filled with clean water for a 2 day period prior to being put into service to allow GCL hydration through any remaining pinholes to occur with clean water.

5. The equivalent hydraulic conductivity of the HDPE equals 2×10^{-13} cm/sec.

6. Liner contact is good.

7. The till layer underlying the GCL does not have any effect on the leakage through the geomembrane defects.

D. Calculations

Total leakage through the liner

$$q = q_1 + q_2$$

where q = *total leakage*

q_1 = *leakage through diffusion*

q_2 = *leakage through pinholes*

$$q_1 = k_l i A \text{ or } k_l i \text{ per unit area}$$

where k_l = *equivalent hydraulic conductivity of HDPE, m/s*

$$i = \frac{h}{t}$$

h = *head on the liner, m*

t = *liner thickness, m*

$$q_2 = k_s i_a \pi R^2 \left(\frac{n_{20}}{n_{15}}\right) \ m^3/s/acre$$

$$= 0.8772\ k_s i_a \pi R^2 \ per\ pinhole$$

where $k_s = 6.9x10^{-9}\ cm/s = 6.9x10^{-11}\ m/s$

$$i_a = 1 + \left[\frac{h}{2t_s \ln\left(\frac{R}{r_o}\right)}\right]$$

h = *head on the liner, m*

t_s = *thickness of GCL* = 6 *mm* = 0.006 *m*

$R = 0.129\ h^{0.45}\ k_s^{-0.13}$, *m*

r_o = *radius of geomembrane pinhole* $= \sqrt{\frac{0.000000784}{\pi}} = 0.0005\ m$

Calculate q_1 and q_2 as functions of h

$$q_1 = 2x10^{-15} i\ m/s$$

$$i = \frac{h \times 1000}{60} \ where\ h\ is\ in\ inches = 16.67\ h$$

$$= 1.389\ h,\ where\ h\ is\ in\ ft$$

h	19 ft (5.79 m)	15 ft (4.57 m)	12 ft (3.66 m)	8 ft (2.44 m)	7 ft (2.13 m)	2 ft (0.61 m)
q_1 *m/s*	$5.28x10^{-14}$	$4.17x10^{-14}$	$3.33x10^{-14}$	$2.2x10^{-14}$	$1.94x10^{-14}$	$5.56x10^{-15}$

$$q_2 = (0.8772)(6.9x10^{-11})\pi R^2 i_a$$

$$= (1.9015x10^{-10}) R^2 i_a,\ m^3/sec/acre$$

h (m)	5.79	4.57	3.66	2.44	2.13	0.61	
R (m)	5.953	5.352	4.846	4.035	3.796	2.162	$R=0.129(6.9\times10^{-11})^{0.13}h^{0.45}$ $=2.701\ h^{0.45}$
$2t_s ln(R/r_o)$ (m)	0.113	0.111	0.110	0.108	0.107	0.100	2(0.006)ln(R/0.0005)
i_a	52.42	42.06	34.27	23.61	20.87	7.07	$1+\frac{h}{2t_s \ln(\frac{R}{r_o})}$
q_2 (m^3/s/acre)	3.53×10^{-7}	2.29×10^{-7}	1.53×10^{-7}	7.32×10^{-8}	5.72×10^{-8}	6.28×10^{-9}	$1.9015\times10^{-10}R^2i_a$

E. Summary of Results

h (ft)	19	15	12	8	7	2	
q_1 (m/s)	5.28×10^{-14}	4.17×10^{-14}	3.33×10^{-14}	2.2×10^{-14}	1.94×10^{-14}	5.56×10^{-15}	
q_2 (m^3/s/acre)	3.53×10^{-7}	2.29×10^{-7}	1.53×10^{-7}	7.32×10^{-8}	5.72×10^{-8}	6.28×10^{-9}	
q_2 (m/s)	8.72×10^{-11}	5.66×10^{-11}	3.78×10^{-11}	1.81×10^{-11}	1.41×10^{-11}	1.55×10^{-12}	1 acre = 4,047 m^2
Total (m/s)	8.73×10^{-11}	5.66×10^{-11}	3.78×10^{-11}	1.81×10^{-11}	1.41×10^{-11}	1.56×10^{-12}	
Total (in/day)	2.97×10^{-4}	1.92×10^{-4}	1.29×10^{-4}	6.15×10^{-5}	4.79×10^{-5}	5.3×10^{-6}	1 m/s = 3.4×10^{-6} in/day

HSI GEOTRANS
A TETRA TECH COMPANY

1080 Holcomb Bridge Road
Building 200, Suite 305
Roswell, Georgia
30076

770-642-1000 FAX 770-642-8808

MEMORANDUM

TO: Jerry Sevick, Foth and Van Dyke

FROM: Peter F. Andersen, HSI GeoTrans PFA

DATE: April 23, 1998

SUBJECT: Reflooded mine source term
HSI GeoTrans Project No. N015-020

INTRODUCTION

Groundwater modeling performed by HSI GeoTrans to assess the potential for solute transport from the orebody into the glacial system following mine reflooding consisted of evaluating:

- potential flow paths from the orebody past a compliance boundary, and;
- travel times from the orebody past a compliance boundary.

These factors were evaluated using the regional groundwater flow model documented in HSI GeoTrans (1998a) and were described in the solute transport model report (HSI GeoTrans, 1998b). The analysis used particle tracking techniques to determine flowpaths and travel times. The results of the analysis indicated that particles could migrate within the bedrock or upwards into the glacial system towards a compliance boundary 1200 feet from the orebody. Upwards migration into the glacial system was primarily restricted to the western side of the orebody following mine reflooding. Particle migration was found to be very slow, with transport times to the compliance boundary being on the order of hundreds to thousands of years. In addition to the slow migration, the arrival times at the compliance boundary of particles originating at various locations in the orebody were found to be quite variable. The arrival times at the compliance boundary for 67 percent of the particles ranged over 10,000 years for the Best Engineering Judgement for Transport (BEJT) simulation and 5000 years for the Practical Worst Case for Transport (PWCT) simulation.

Discussions with WDNR and USCOE indicated that they would reserve judgement as to whether the particle tracking simulations were a sufficient demonstration of compliance until they had reviewed data regarding the concentrations of source terms associated with the reflooded mine. I have reviewed the original and recently updated reports by SRK (1997 and 1998) and believe that the calculated source term concentrations are sufficiently low to preclude the necessity of additional analysis regarding attenuation between the orebody and the compliance boundary. Two primary reasons have led to this conclusion.

First, the concentrations of constituents *within the mine workings* will be further reduced as they migrate from the vicinity of the orebody and into the glacial system. I have calculated the expected concentration reduction factor under Best Engineering Judgement for Transport (BEJT) to be 0.00096 based on an analytical relationship that is shown below. This factor means that concentrations will be reduced by 1042 (1/0.00096) times from the original concentration. This factor results in the concentration of all constituents to be below standards at the compliance boundary. Under Practical Worst Case for Transport (PWCT) conditions, the concentration reduction factor is 0.0019, based on the same analytical relationship cited earlier. This factor means that concentrations will be reduced by 526 (1/0.0019) times from the original concentration. This factor also results in the concentrations of all constituents to be below standards at the compliance boundary.

Second, the analyses that are documented in this memorandum use conservative simplifying assumptions that tend to overstate the concentrations beyond those that would have been determined had a more detailed analysis been performed. Examples of key conservative assumptions include neglecting dispersion, adsorption, and precipitation and assuming mixing only in the lower ten feet of the outwash deposits. These assumptions are discussed further later in this memorandum.

The calculations that were made to determine the concentration reduction factors cited above are based on mixing water that has come in contact with the mine workings with water flowing in the glacial system. The flow rate across the compliance boundary of water from the orebody is computed by dividing the volumetric quantity of water within the orebody by the time period over which particles cross the compliance boundary as determined from the particle tracking analysis. The flow in the glacial system is determined with a simple Darcy evaluation of the flow in the glacial system in the vicinity of the orebody.

MIXING CALCULATION

The volume of water potentially containing water that has been in contact with the mine workings consists of the open space within the orebody in the weathered zones. This volume is:

Volume = Length x width x depth x porosity

= 4800 ft x 100 ft x 550 ft x 0.3

= 7.92 E 07 ft^3

Particles cross the compliance boundary over a 30,000 year period in the BEJT case (HSI GeoTrans, 1998b). Note that the distribution of particles crossing the compliance bondary versus time is normally distributed with a mean transit time of approximately 10,000 years. The standard deviation around the mean of particle transit times is approximately 5,000 years. This implies that 67% of particles cross the compliance boundary between years 5,000 and 15,000. Because one particle is used per cell, each particle represents a parcel of water. Therefore 67% of the water within the orebody crosses the compliance boundary in a 10,000 year period under the BEJT case:

Volume crossing in 10,000 year period = 0.67 x total volume

= 0.67 x 7.92 E 07 ft^3

= 5.28 E 07 ft^3

The daily flux crossing the boundary is given by:

Flux = 5.28 E07 ft^3 / 10,000 yr x yr / 365 d

Flux = 14.5 ft^3 / d

If we assume that this entire quantity exits upward into the overburden prior to crossing the compliance boundary, then it will mix with lateral flow in the glacial system. Lateral flow in the glacial system is governed by Darcy's Law:

$$Q = Kibw$$

where:			
	Q	=	volumetric flow rate [L^3]
	K	=	horizontal hydraulic conductivity [L/T]
	i	=	horizontal hydraulic gradient [L/L]
	b	=	thickness of flow regime
	w	=	width of flow regime

The flow regime in the glacial system consists of the Pre- to Early Wisconsinan Till/massive saprolite and the outwash deposits. Flow in the Pre-to Early Wisconsinan Till/massive saprolite is predominantly vertical because of the large contrast in hydraulic conductivities between these sediments (2.0 ft/d) and the outwash deposits (approximately 50 ft/d). Therefore, we assume that upward flow from the bedrock will mix with lateral flow in the Pre- to Early Wisconsinan Till/massive saprolite and the outwash deposits:

$$Q_{Total} = Q_{EWT} + Q_{OW}$$

where:			
	Q_{Total}	=	total lateral flow in glacial deposits
	Q_{EWT}	=	lateral flow in Pre- to Early Wisconsinan Till/massive saprolite
	Q_{OW}	=	lateral flow in outwash deposits

The lateral flow in the Pre- to Early Wisconsinan Till/massive saprolite may be approximated from Darcy's Law as:

$$Q_{EWT} = Kibw$$

where:			
	K	=	2.0 ft/d, from HSI GeoTrans (1998a),
	i	=	10 ft / 2000 ft, from potentiometric surface maps,
	b	=	100 feet, from geologic cross-sections, and
	w	=	4300 feet, from width of flow net in SRK (1998) (see Figure 1)

therefore:

$$Q_{EWT} = 2.0\ ft/d\ x\ \frac{10\ ft}{2000\ ft}\ x\ 100\ ft\ x\ 4300\ ft$$

$$Q_{EWT} = 4300\ ft^3/d$$

Some of the flow from the bedrock will continue to flow upwards into the outwash. If we assume that it will mix with flow in the lower 10 feet of the glacial system, then

$$Q_{OW} = Kibw$$

where:	K	=	50 ft/d, average value of coarse and fine outwash, from HSI GeoTrans (1998a),
	i	=	10 ft / 2000 ft, from potentiometric surface maps,
	b	=	10 feet, conservative assumption for mixing zone,
	w	=	4300 feet, from width of flow net in SRK (1998)

therefore:

$$Q_{OW} = 50\ ft/d\ x\ \frac{10\ ft}{2000\ ft}\ x\ 10\ ft\ x\ 4300\ ft$$

$$Q_{OW} = 10750\ ft^3/d$$

The ratio of upward flow from the bedrock to lateral flow in the glacial deposits within the compliance boundary is the concentration reduction factor.

$$Concentration\ reduction\ factor = \frac{Q_{Bedrock}}{Q_{EWT} + Q_{OW}}$$

Substituting the flow crossing the compliance boundary and flows computed above gives:

$$\frac{14.5\ ft^3/d}{4300\ ft^3/d\ +\ 10750\ ft^3/d} = 0.00096$$

Under PWCT conditions, particles cross the compliance boundary over a 11,000 year period. The mean transit time of particles to the compliance boundary is 3,500 years. The standard deviation around the mean of particle transit times is approximately 2,500 years. This implies that 67% of particles cross the compliance boundary between years 1,000 and 6,000. The daily flux crossing the boundary is given by:

Flux = 5.28 E07 ft^3 / 5,000 yr x yr / 365 d

Flux = 28.9 ft^3 / d

Using the same methodology as was used for the BEJT calculation, the concentration reduction factor under PWCT conditions is:

$$\frac{28.9\ ft^3/d}{4300\ ft^3/d\ +\ 10750\ ft^3/d} = 0.0019$$

Note that the flows through the Pre- to Early Wisconsinan Till/massive saprolite and outwash deposits are the same for the PWCT case and the BEJT case. This is because the PWCT case does not alter the outwash hydraulic conductivity or the horizontal Pre- to Early Wisconsinan Till/massive saprolite hydraulic conductivity.

These calculations contain several conservative assumptions that will tend to underestimate the amount of mixing that will occur. First, it is assumed that *all* flow through the orebody will mix with the glacial deposits. Therefore, the quantity used in the numerator of the concentration reduction factor calculation is conservatively high, resulting in less mixing in the glacial system than will actually occur. The second conservative assumption is that dispersion is neglected, which will tend to provide greater mixing and a reduction in concentration if included in the calculation. Third, adsorption and precipitation are not accounted for, which will tend to further increase the travel time, spread out the time over which the particles cross the compliance boundary, and reduce peak concentrations. Finally, only the lower ten feet of the outwash deposits are

considered in the mixing calculation. As illustrated in the Tailings Management Area (TMA) solute transport model, the vertical mixing zone is likely to be much larger, particularly in areas where there is a vertical gradient. A larger mixing zone would further reduce concentrations if included in the calculation.

CONCLUSIONS

In summary, we have reviewed the source term concentrations derived by SRK (1998) and have determined their significance relative to compliance with groundwater standards. We have made mixing calculations for the BEJT and PWCT cases to determine the concentration reduction due to mixing with water within the compliance boundary. These calculations are relatively simple and contain several assumptions that would tend to underestimate the amount of mixing and overestimate the concentrations.

The calculations show that expected concentration reduction factor for the BEJT case is 0.00096. This number represents the factor that concentrations in the mine workings should be multiplied by to determine the concentration at the compliance boundary. The calculations show that the concentration reduction factor for the PWCT is 0.0019.

When these factors are applied to the concentrations within the mine workings (flow weighted average) obtained by SRK (1998), the concentrations of all constituents at the proposed compliance boundary are below the currently anticipated groundwater standards (see Table 1).

Given the conservatism that has been built into these first order dilution calculations (including neglecting dispersion, adsorption, and precipitation), and the long travel times determined from particel tracking analysis described in the solute transport modeling report (HSI GeoTrans, 1998b), we do not believe that there is a reasonable expectation that the groundwater standards would be exceeded at the compliance boundary. Therefore, additional assessment is not necessary to further quantify concentration reductions between the orebody and the compliance boundary for the reflooded mine scenario.

REFERENCES

HSI GeoTrans, 1998a. Addendum No 1 to Numerical Simulation of the Effect on Groundwater and Surface Water of the Proposed Zinc and Copper Mine Near Crandon, Wisconsin. Consulting report prepared for Foth & Van Dyke. February 6, 1998.

HSI GeoTrans, 1998b. Update to: Numerical Simulation of Potential Solute Transport at the Proposed Zinc and Copper Mine Near Crandon, Wisconsin. Consulting report prepared for Foth & Van Dyke. April 27, 1998.

SRK, 1997. Reflooded Mine Source Term. Consulting report prepared for Foth & Van Dyke. March 1997.

SRK, 1998. Comments on Reflooded Mine Source Term for the Proposed Crandon Mine. Consulting report prepared for Foth & Van Dyke. April 1998.

Table 1. Estimated Concentration in the Glacial Overburden at the Proposed 1200 Foot Compliance Boundary for the Reflooded Mine

	Estimated Concentrations (mg/l)		Anticipated Groundwater Standard[1] (mg/l)
	Under Best Engineering Judgement Conditions	Under Practical Worst Case Conditions	
Sulfate	0.8	1.5	250[2]
Arsenic	0.0004	0.0008	0.05
Copper	0.0002	0.0004	1.3
Iron	0.009	0.02	0.3[2]
Manganese[3]	0.001	0.002	0.05[2]
Selenium	0.0001	0.0002	0.05
Zinc	0.01	0.02	5[2]

[1]NR 809 MCL.
[2]Secondary standard.
[3]Parameter likely to have an alternate concentration level due to background conditions above the standard.

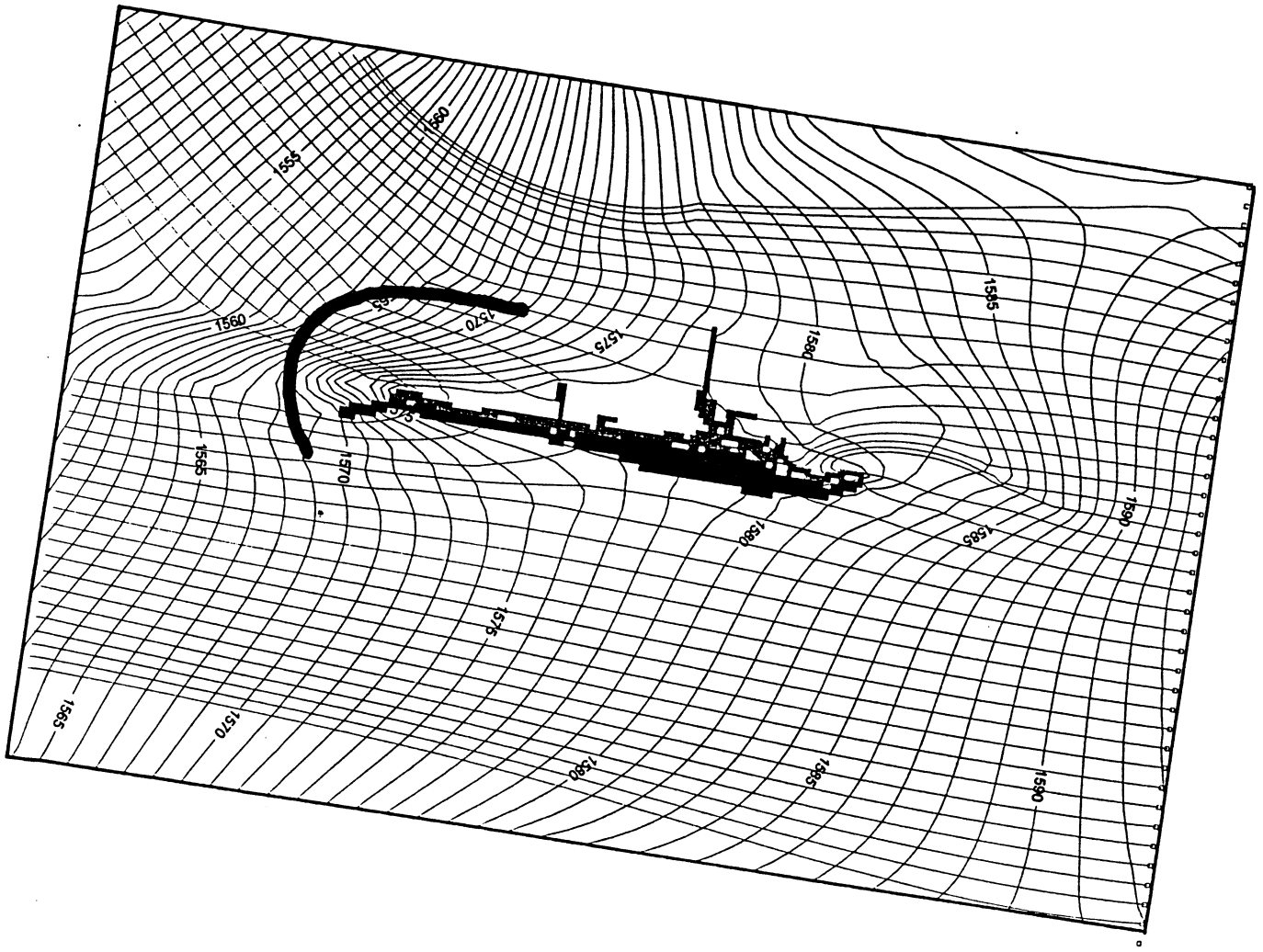

CONTOUR INTERVAL=1'

0 1000 2000 3000 4000 5000 FEET

1"=2000'

STEFFEN ROBERTSON AND KIRSTEN
Consulting Engineers

FOTH & VAN DYKE

REFLOODED MINE SOURCE TERM

GROUNDWATER FLOW MODEL
1350 FOOT ELEVATION

PROJECT NO.	DATE	APPROVED	FIGURE
F107107/2	APRIL 1998	MDR	

FILE REF: FIG-C-1

4.2-14-10

FIGURE 1 FLOW FIELD WIDTH

UPDATE NO. 2 TO:

NUMERICAL SIMULATION OF POTENTIAL SOLUTE TRANSPORT AT THE PROPOSED ZINC AND COPPER MINE NEAR CRANDON, WISCONSIN

January 19, 1999

Table of Contents

List of Figures

List of Tables

1 Introduction

As a part of the permitting process for the proposed Crandon mine, HSI GeoTrans has completed several reports that describe the simulation of groundwater flow and solute transport. The groundwater flow modeling reports describe current and future predicted groundwater levels, stream flows, and lake levels. The solute transport modeling reports describe the predicted movement of solute, either from the Tailings Management Area (TMA) or from the mine itself following closure and reflooding. Because solute transport is, in part, governed by groundwater levels, any updates to the groundwater flow system as described in the flow model must be reflected in the solute transport analysis.

Since submittal of the most recent solute transport modeling report (HSI GeoTrans, 1998a) a number of project design and operational changes have been proposed by the Nicolet Minerals Company (NMC). These changes necessitated revisions to the groundwater flow model, so it would account for the crown pillar, a proposed grout blanket in the crown pillar, and mine plan. In addition, the Wisconsin Department of Natural Resources requested that the groundwater flow model be recalibrated using some hydrologic parameters that it felt were more appropriate. The changes to the groundwater flow model (documented in HSI GeoTrans, 1998b), combined with design changes to the TMA and guidance regarding placement of a design management zone (DMZ) have necessitated changes to the solute transport analysis. This report documents the changes that have been made to the solute transport analysis and presents updated results.

As was the case for the prior solute transport studies, two analyses are conducted: one to evaluate TMA compliance with groundwater standards and one to assess the potential for movement of solute from the backfilled mine following mine reflooding. Separate models are used for each of these analyses.

Much of the information presented in the April 1998 solute transport modeling report is still pertinent. Rather than create an entirely new modeling report in the style of the April 1998 and previous reports, this report serves to update the prior reports. A complete revision to the 1998 solute transport modeling report was not undertaken because it is HSI GeoTrans' and NMC's understanding that the WDNR plans to use the model described herein as a general framework for their modeling, but may make additional modifications and present those results in their Environmental Impact Statement.

The changes to the TMA model and updated results are described in Section 2 of this report. The mine reflooding model is described in Section 3. Both Best Engineering Judgement for Transport (BEJT) and Practical Worst Case for Transport (PWCT) results are presented for each analysis.

2 Tailings Management Area Model

The Tailings Management Area (TMA) numerical model of groundwater flow and solute transport has been revised. The new model reflects changes in the TMA facilities design (Appendix A) and changes made to the regional model of groundwater flow (HSI GeoTrans, 1998b). The simulation codes MODFLOW (McDonald and Harbaugh, 1988) and MT3D^{96} (Zheng, 1996) are used to perform model simulations for groundwater flow and solute transport, respectively. The sub-model construction and modeling methodology are very similar to those previously reported (HSI GeoTrans, 1998a). The technical details already reported are not repeated in this document.

This section describes the specific modifications made to the TMA sub-model, provides a demonstration of model calibration, and presents predictive results with Best Engineering Judgement for Transport (BEJT) and Practical Worst Case for Transport (PWCT) parameter values. No sensitivity simulations are included for this model. The general results of previous sensitivity analyses (HSI GeoTrans, 1996, 1998a) are still valid for this modified model.

The primary results of the model simulations are BEJT and PWCT response functions that define the Design Management Zone (DMZ) concentration resulting from pulse-source inflows of unit concentration. Using superposition methodology, the response functions can later be scaled and combined to represent any constituent of interest for the TMA using estimates of source concentrations (from potentially uncollected leachate percolating from the base of the TMA composite liner) for that constituent.

2.1 Model construction

The TMA sub-model domain lies within the regional groundwater model (HSI GeoTrans, 1998b) domain as shown in Figure 2.1. The sub-model is more finely discretized than the regional model, having 100-foot grid spacing and 7 layers to represent the glacial overburden aquifer. The base of the model coincides with the top of bedrock. Details of model construction can be found in the previous solute transport document (HSI GeoTrans, 1998a).

The model has been updated to reflect design changes for the TMA facilities (Appendix A). The new design includes a smaller TMA footprint (Figure 2.2), which results in fewer model cells used to represent the TMA cell bases, upper sidewalls, and lower side walls (Figure 2.3).

As a result of TMA design changes, the estimated TMA percolation rates have also changed. The percolation rates used in the model are taken from updated HELP model runs (Appendix A). The estimated percolation rates, which vary over time, have been divided into 8 phases as described in Table 2.1. Because operations begin at different times for the various TMA cells and because all cells do not have the same operational life, the phases are staggered as

illustrated in Figure 2.4. In order to properly simulate every phase change for each TMA cell, the solute transport model is simulated in 22 stress periods as defined in Table 2.2. The percolation rates for each TMA cell are tabulated by stress periods in Tables 2.3-2.6. Figure 2.5 shows the total source area flux rate as a function of time, and Figure 2.6 shows the cumulative source-area percolation volume versus time. Each plot compares well with the raw HELP model results, indicating that the time (phase) discretization and space (model cell) discretization is appropriate for representing the solute transport source.

In the model, the percolation rates are entered as part of the recharge array in MODFLOW. In MT3D[96], the appropriate source concentration is assigned as a recharge source.

Recent changes that were made in the regional groundwater flow model (HSI GeoTrans, 1998b) were carried forward to the TMA sub-model: default recharge was raised to 9.7 in/yr (2.21e-3 ft/d), the seepage wetland bed hydraulic conductivity was lowered to 0.003 ft/d, and the heads used to define the perimeter constant head boundary conditions in the TMA sub-model were taken from updated BEJ simulations with the regional model.

2.2 Model Calibration

Modeled head output from the TMA sub-model was checked against head output from the regional model and 61 observed water levels to verify that calibration was maintained. The sub-model was set up for pre-development conditions as follows: the default recharge (9.7 in/yr) was used for all TMA, runoff basin, and reclaim pond zones in Figure 2.3, and perimeter constant heads were taken from the regional model BEJ calibration simulation (HSI GeoTrans, 1998b).

The TMA sub-model closely reproduced the head field generated by the regional groundwater model. A comparison of water table elevations is presented in Figure 2.7. Heads in the outwash (Figure 2.8) and in the Early Wisconsinan Till (Figure 2.9) also match closely in the two models.

Observed (October 1984) water levels are also generally well-matched in the TMA sub-model (Table 2.7). Figure 2.10 shows the modeled water table with residuals (modeled – observed head) posted. The residual root-mean square is 1.46 feet and the mean absolute residual is 0.97 feet. These statistics are lower than the residual statistics of the regional flow model (fewer wells are used), and indicate a very good calibration. Also, the overall gradient from the TMA to Hemlock Creek is well-approximated in the sub-model.

A particle tracking simulation was made to verify steady state flow paths under existing conditions and to approximate advective travel times. Comparison of modeled travel time to approximations based on analysis of Chlorofluorocarbon (CFC) data (Saad, 1996) was made to verify the calibration. Backtracking of particles from the EX-8/GEO25/GEO50 nest indicate flowpaths that are consistent with a flownet (Figures 2.11 and 2.12). Particles that are recovered

in the shallow wells (GEO25 and GEO50) generally originate at relatively short distances from the discharge points. Particles recovered in the deeper portions of the aquifer (greater than 100 feet) originate at distances in excess of 3000 feet from the discharge point. Note that the flowpath for a particle recovered in EX8-AL, the deepest well in the nest, is nearly vertical at the entry point to the aquifer.

When a correction factor is applied to the modeled times to account for transit time in the unsaturated zone, modeled particle travel times from the TMA to the observation points are generally consistent with the CFC data. The correction factor is the same as was used by Saad (1996) to compute CFC travel times. Table 2.8 compares travel times for particles in the model.

2.3 Model Predictions

For predictive simulations, the MODFLOW model was executed with 22 stress periods (Table 2.2, Figure 2.4). The different stress periods are characterized by slightly different recharge rates for the TMA zones, reclaim pond, and runoff basins (Figure 2.3, Tables 2.3-2.6). Also, the perimeter head boundary changes once during the simulation (at the beginning of stress period 13, after 32 years) to model the recovery of the regional heads following mine reflooding. In stress periods 1-12, the perimeter head values are taken from the regional flow model (HSI GeoTrans, 1998b) BEJ zinc mining simulation. The perimeter heads for stress periods 13-22 are taken from the regional model simulation of post-mining conditions.

Using the predictive flow model, particle traces were generated that started at the water table beneath each TMA cell (Figure 2.13). These particles show the expected advective flow paths for constituents in the TMA percolation water. Note that many of the particles travel to the lower portions of the glacial aquifer.

Using the MT3D[96] program, solute transport was simulated to predict how constituents would move in the groundwater. Three discrete concentration phases were assumed for the source: operation, post-cap, and oxidized. Thus, a given constituent would have one source concentration during operation, a second source concentration for percolation after cap placement, and a third source concentration after the postulated degradation of the flexible membrane liner (FML). Note that it is conservatively assumed that the FML is completely degraded 140 years after cap placement. Using the principle of superposition, it is possible to model many constituents with only three model simulations. The procedure is described in the previous solute transport document (HSI GeoTrans, 1998a) and is illustrated in Figure 2.14.

The model output consists of a concentration response function to a unit-concentration source during either the operations, post-cap, or oxidized concentration phase. By scaling and combining these response functions, the concentration of a specific constituent is determined (c(x,y,z,t)). Conservatively, sorption, chemical reactions, and decay are not considered. The concentrations at the regulatory DMZs are of particular interest. For this modeling, two DMZs are considered (Figure 2.15). The first is located 1200 feet from the limits of tailings placement

within the TMA cells, and the second is located 150 feet outside of the reclaim pond. Note that the reclaim pond is removed after approximately 46 years. Therefore, the reclaim pond DMZ is only considered for the first 60 years of simulation.

2.3.1 Best Engineering Judgement for Transport (BEJT)

The BEJT parameter values are listed in Table 2.9. The dispersivity values of 50 feet (longitudinal) and 5 feet (transverse) were selected to be consistent with previous BEJT transport simulations (HSI GeoTrans, 1996, 1998a). As explained in an earlier report (HSI GeoTrans, 1996), the dispersivity is a length scale for dispersion and has been shown to be dependent on the degree of geologic heterogeneity and the scale of the problem, or distance from the source to the measurement (Gelhar et al., 1992). Often for modeling purposes, the longitudinal dispersivity is taken as 1/10 of the problem's length scale, with lower values (perhaps 1/100 of the length scale) sometimes being used. Lower dispersivities are associated with less unmodeled variability in the flow field. For this model, the length scale is between 1200 feet (from TMA waste edge to DMZ) and 2500 feet (from TMA center to DMZ). The BEJT ratio of longitudinal dispersivity to problem scale is therefore between 1/20 and 1/50. As is customary, the transverse dispersivities are taken to be 1/10 of the longitudinal dispersivity. Note that the PWCT simulation (section 2.3.2) includes lower dispersivities.

Using BEJT parameter values (Table 2.9) response functions were generated by three MT3D^{96} simulations. The maximum concentration responses at the DMZs as a function of time are shown in Figure 2.16.

To demonstrate the patterns of solute migration from the TMA and reclaim pond, a hypothetical constituent is considered that has a percolation concentration of 2,000 ppm during operations, 4,000 ppm during the post-cap phase, and 40,000 ppm after oxidation (Table 2.10). Using superposition, this hypothetical constituent's maximum DMZ concentrations are plotted as a function of time (Figure 2.17). Note that in all graphs of DMZ concentration versus time, the maximum concentration at the DMZ is always plotted, and that this point of maximum concentration may move in time as the solute plume changes shape. Results for the reclaim pond DMZ are shown for the first 60 years of simulation, which includes approximately 14 years after the removal of the reclaim pond.

The BEJT solute plumes for the example constituent are plotted in plan view at different times in Figures 2.18 - 2.26. In these plots, the maximum concentration in any layer at a given x,y location is contoured. Using the section identified in Figure 2.27, the BEJT example constituent plumes are plotted in profile (Figures 2.28 - 2.36).

2.3.2 Practical Worst Case for Transport (PWCT)

Three more simulations were conducted using the PWCT parameter values listed in Table 2.9. The PWCT simulations include lower vertical hydraulic conductivities and lower dispersivities in the aquifer. PWCT response curves at the DMZs are shown in Figure 2.37.

Using the example constituent of Table 2.10, and the superposition method, the maximum DMZ concentrations are plotted as a function of time (Figure 2.38). The PWCT example constituent plumes are shown at select times in Figure 2.39-2.47 (plan view) and in Figure 2.48-2.56 (profile view).

2.4 Conclusions

The primary output from the TMA model is the set of response functions under BEJT and PWCT conditions. These response functions can be used to predict DMZ concentrations for any (conservative) constituent in the TMA leachate. The forthcoming Groundwater Quality Performance Evaluation (GWQPE) will present DMZ concentrations for individual constituents of interest at the TMA. The GWQPE results will be obtained by applying the superposition method described in Section 2.3.

The primary reasons for differences in simulated results in this report versus those in the previous solute transport report (HSI GeoTrans, 1998a) are:

1) the location of the DMZ closer to the reclaim pond,
2) new predictions of percolation rates from the HELP model, and
3) a revised TMA footprint.

Table 2.1 Basis for TMA phases and flux rates[1]

Phase	Description	Duration (years)	Basis for Percolation Rate
X	Pre-construction	0-22[2]	Regional model calibrated value
A	First Phase of Operation	2-7[2]	Appendix A Table 2 average[3]
B	Second Phase of Operation plus two years of consolidation	5-11[2]	Appendix A Table 3 average
C	Cap in Place Part 1	1	Appendix A Table 4 Year 1
D	Cap in Place Part 2	7	Appendix A Table 4 Years 2-7
E	Cap in Place Part 3	20	Appendix A Table 4 Years 8-25
F	Cap in Place Part 4	104-114[2]	Appendix A Table 4 Years 26-140
G	Degraded FML Steady-State	N/A	Appendix A Table 4 Years 241+

Phase	Base		Lower Sideslope		Upper Sideslope	
	Rate(in/yr)	Rate(ft/d)	Rate(in/yr)	Rate(ft/d)	Rate(in/yr)	Rate(ft/d)
X	9.70	2.21E-03	9.70	2.21E-03	9.70	2.21E-03
A	6.44E-03	1.47E-06	2.50E-07	5.71E-11	9.70E+00	2.21E-03
B	8.47E-03	1.93E-06	2.50E-07	5.71E-11	1.03E-06	2.34E-10
C	6.52E-01	1.49E-04	1.39E-02	3.17E-06	7.54E-03	1.72E-06
D	3.26E-03	7.45E-07	2.50E-07	5.71E-11	2.50E-07	5.71E-11
E	4.15E-04	9.47E-08	2.50E-07	5.71E-11	2.50E-07	5.71E-11
F	6.05E-05	1.38E-08	2.50E-07	5.71E-11	2.50E-07	5.71E-11
G	2.00E-05	4.57E-09	2.00E-05	4.57E-09	2.00E-05	4.57E-09

Notes

[1] The TMA reclaim pond is active during years 1-31 during which its flux is 1.6E-5 ft/d, and years 32-46 (reclamation phase) during which its flux is 4.0E-6 ft/d. Thereafter a uniform 2.214E-3 ft/d is used to represent precipitation recharge.

[2] Varies by TMA Cell

[3] During the first phase of operation, the TMA upper sideslope receives full recharge (from regional model) with a concentration of zero.

Prepared by: KMR
Checked by: GWC
Approved by: PFA

December 1998
P:\Crandon\TmaMod4\Excel\StresTab.xls, Basis

Table 2.2 TMA sub-model stress periods.

Stress Period	Time (years)			Time (days)		
	Start	Duration	End	Start	Duration	End
1	0	3	3	0.00	1095.75	1095.75
2	3	4	7	1095.75	1461.00	2556.75
3	7	9	16	2556.75	3287.25	5844.00
4	16	2	18	5844.00	730.50	6574.50
5	18	1	19	6574.50	365.25	6939.75
6	19	3	22	6939.75	1095.75	8035.50
7	22	2	24	8035.50	730.50	8766.00
8	24	1	25	8766.00	365.25	9131.25
9	25	1	26	9131.25	365.25	9496.50
10	26	4	30	9496.50	1461.00	10957.50
11	30	1	31	10957.50	365.25	11322.75
12	31	1	32	11322.75	365.25	11688.00
13	32	6	38	11688.00	2191.50	13879.50
14	38	6	44	13879.50	2191.50	16071.00
15	44	2	46	16071.00	730.50	16801.50
16	46	6	52	16801.50	2191.50	18993.00
17	52	6	58	18993.00	2191.50	21184.50
18	58	92	150	21184.50	33603.00	54787.50
19	150	3	153	54787.50	1095.75	55883.25
20	153	13	166	55883.25	4748.25	60631.50
21	166	6	172	60631.50	2191.50	62823.00
22	172	478	650	62823.00	174589.50	237412.50

Prepared by: KMR
Checked by: GWC
Approved by: PFA

December 1998
\Crandon\TmaMod3\Excel\StresTab.xls, Stress

Table 2.3 TMA 1A percolation rates by stress period.

Stress Period	Phase	Percolation Rate (ft/day)		
		Base	Lower Sideslope	Upper Sideslope
1	A	1.47E-06	5.71E-11	2.21E-03 [1]
2	A	1.47E-06	5.71E-11	2.21E-03 [1]
3	B	1.93E-06	5.71E-11	2.34E-10
4	B	1.93E-06	5.71E-11	2.34E-10
5	C	1.49E-04	3.17E-06	1.72E-06
6	D	7.45E-07	5.71E-11	5.71E-11
7	D	7.45E-07	5.71E-11	5.71E-11
8	D	7.45E-07	5.71E-11	5.71E-11
9	D	7.45E-07	5.71E-11	5.71E-11
10	E	9.47E-08	5.71E-11	5.71E-11
11	E	9.47E-08	5.71E-11	5.71E-11
12	E	9.47E-08	5.71E-11	5.71E-11
13	E	9.47E-08	5.71E-11	5.71E-11
14	E	9.47E-08	5.71E-11	5.71E-11
15	E	9.47E-08	5.71E-11	5.71E-11
16	F	1.38E-08	5.71E-11	5.71E-11
17	F	1.38E-08	5.71E-11	5.71E-11
18	F	1.38E-08	5.71E-11	5.71E-11
19	G	4.57E-09	4.57E-09	4.57E-09
20	G	4.57E-09	4.57E-09	4.57E-09
21	G	4.57E-09	4.57E-09	4.57E-09
22	G	4.57E-09	4.57E-09	4.57E-09

Note: [1] Equal to default recharge, no source applied.

Prepared by: KMR
Checked by: GWC
Approved by: PFA

December 1998
P:\CMC\TmaMod4\Excel\StresTab.xls, TMA1A

Table 2.4 TMA 1B percolation rates by stress period.

Stress Period	Phase	Percolation Rate (ft/day)		
		Base	Lower Sideslope	Upper Sideslope
1	X	2.21E-03 [1]	2.21E-03 [1]	2.21E-03 [1]
2	A	1.47E-06	5.71E-11	2.21E-03 [1]
3	B	1.93E-06	5.71E-11	2.34E-10
4	B	1.93E-06	5.71E-11	2.34E-10
5	C	1.49E-04	3.17E-06	1.72E-06
6	D	7.45E-07	5.71E-11	5.71E-11
7	D	7.45E-07	5.71E-11	5.71E-11
8	D	7.45E-07	5.71E-11	5.71E-11
9	D	7.45E-07	5.71E-11	5.71E-11
10	E	9.47E-08	5.71E-11	5.71E-11
11	E	9.47E-08	5.71E-11	5.71E-11
12	E	9.47E-08	5.71E-11	5.71E-11
13	E	9.47E-08	5.71E-11	5.71E-11
14	E	9.47E-08	5.71E-11	5.71E-11
15	E	9.47E-08	5.71E-11	5.71E-11
16	F	1.38E-08	5.71E-11	5.71E-11
17	F	1.38E-08	5.71E-11	5.71E-11
18	F	1.38E-08	5.71E-11	5.71E-11
19	F	1.38E-08	5.71E-11	5.71E-11
20	G	4.57E-09	4.57E-09	4.57E-09
21	G	4.57E-09	4.57E-09	4.57E-09
22	G	4.57E-09	4.57E-09	4.57E-09

Note: [1] Equal to default recharge, no source applied.

Prepared by: KMR
Checked by: GWC
Approved by: PFA

December 1998
P:\CMC\TmaMod4\Excel\StresTab.xls, TMA1B

Table 2.5 TMA 2 percolation rates by stress period.

Stress Period	Phase	Percolation Rate (ft/day)		
		Base	Lower Sideslope	Upper Sideslope
1	X	2.21E-03 [1]	2.21E-03 [1]	2.21E-03 [1]
2	X	2.21E-03 [1]	2.21E-03 [1]	2.21E-03 [1]
3	X	2.21E-03 [1]	2.21E-03 [1]	2.21E-03 [1]
4	A	1.47E-06	5.71E-11	2.21E-03 [1]
5	B	1.93E-06	5.71E-11	2.34E-10
6	B	1.93E-06	5.71E-11	2.34E-10
7	B	1.93E-06	5.71E-11	2.34E-10
8	C	1.49E-04	3.17E-06	1.72E-06
9	D	7.45E-07	5.71E-11	5.71E-11
10	D	7.45E-07	5.71E-11	5.71E-11
11	D	7.45E-07	5.71E-11	5.71E-11
12	D	7.45E-07	5.71E-11	5.71E-11
13	E	9.47E-08	5.71E-11	5.71E-11
14	E	9.47E-08	5.71E-11	5.71E-11
15	E	9.47E-08	5.71E-11	5.71E-11
16	E	9.47E-08	5.71E-11	5.71E-11
17	F	1.38E-08	5.71E-11	5.71E-11
18	F	1.38E-08	5.71E-11	5.71E-11
19	F	1.38E-08	5.71E-11	5.71E-11
20	F	1.38E-08	5.71E-11	5.71E-11
21	G	4.57E-09	4.57E-09	4.57E-09
22	G	4.57E-09	4.57E-09	4.57E-09

Note: [1] Equal to default recharge, no source applied.

Prepared by: KMR
Checked by: GWC
Approved by: PFA

December 1998
P:\CMC\TmaMod4\Excel\StresTab.xls, TMA2

Table 2.6 TMA 3 percolation rates by stress period.

Stress Period	Phase	Percolation Rate (ft/day)		
		Base	Lower Sideslope	Upper Sideslope
1	X	2.21E-03 [1]	2.21E-03 [1]	2.21E-03 [1]
2	X	2.21E-03 [1]	2.21E-03 [1]	2.21E-03 [1]
3	X	2.21E-03 [1]	2.21E-03 [1]	2.21E-03 [1]
4	X	2.21E-03 [1]	2.21E-03 [1]	2.21E-03 [1]
5	X	2.21E-03 [1]	2.21E-03 [1]	2.21E-03 [1]
6	X	2.21E-03 [1]	2.21E-03 [1]	2.21E-03 [1]
7	A	1.47E-06	5.71E-11	2.21E-03 [1]
8	B	1.93E-06	5.71E-11	2.34E-10
9	B	1.93E-06	5.71E-11	2.34E-10
10	B	1.93E-06	5.71E-11	2.34E-10
11	C	1.49E-04	3.17E-06	1.72E-06
12	D	7.45E-07	5.71E-11	5.71E-11
13	D	7.45E-07	5.71E-11	5.71E-11
14	E	9.47E-08	5.71E-11	5.71E-11
15	E	9.47E-08	5.71E-11	5.71E-11
16	E	9.47E-08	5.71E-11	5.71E-11
17	E	9.47E-08	5.71E-11	5.71E-11
18	F	1.38E-08	5.71E-11	5.71E-11
19	F	1.38E-08	5.71E-11	5.71E-11
20	F	1.38E-08	5.71E-11	5.71E-11
21	F	1.38E-08	5.71E-11	5.71E-11
22	G	4.57E-09	4.57E-09	4.57E-09

Note: [1] Equal to default recharge, no source applied.

Prepared by: KMR
Checked by: GWC
Approved by: PFA

December 1998
P:\CMC\TmaMod4\Excel\StresTab.xls, TMA3

Table 2.7 Modeled and observed water levels at wells.

Well ID	Observed[1] Water Level (feet, msl)	TMA Sub-Model[2] Water Level (feet, msl)	TMA Sub-Model[2] Residual[4] (feet)	Regional Flow Model[3] Water Level (feet, msl)	Regional Flow Model[3] Residual[4] (feet)
DMB-1A	1594.78	1593.06	-1.72	1593.19	-1.59
DMB-3	1580.22	1579.65	-0.57	1581.48	1.26
DMB-4	1593.73	1592.48	-1.25	1592.48	-1.25
DMB-5	1593.50	1593.86	0.36	1593.91	0.41
DMB-5A	1592.58	1593.86	1.28	1593.91	1.33
DMB-6	1593.80	1592.61	-1.19	1592.53	-1.27
DMB-8	1588.58	1584.53	-4.05	1586.99	-1.59
EX-10AL	1594.62	1593.57	-1.05	1593.63	-0.99
EX-10AU	1594.72	1593.74	-0.98	1593.67	-1.05
EX-10BL	1595.14	1593.74	-1.40	1593.67	-1.47
EX-10BU	1596.06	1594.07	-1.99	1593.96	-2.10
EX-11AL	1593.93	1593.24	-0.69	1593.19	-0.75
EX-11AU	1593.47	1593.24	-0.23	1593.19	-0.29
EX-11BL	1594.19	1593.32	-0.87	1593.37	-0.82
EX-11BU	1593.37	1593.53	0.16	1593.58	0.21
EX-11CL	1593.80	1593.47	-0.33	1593.42	-0.38
EX-12AL	1593.83	1593.68	-0.15	1593.73	-0.10
EX-12AU	1593.73	1593.70	-0.03	1593.76	0.03
EX-12BL	1593.73	1593.71	-0.02	1593.77	0.04
EX-12BU	1594.03	1593.91	-0.12	1593.98	-0.06
EX-13AL	1592.16	1592.43	0.27	1592.46	0.30
EX-13BL	1592.19	1592.42	0.23	1592.45	0.26
EX-13BU	1592.16	1592.43	0.27	1592.46	0.30
EX-13CL	1592.29	1592.59	0.30	1592.62	0.33
EX-13DL	1592.52	1592.59	0.07	1592.62	0.10
EX-16AL	1593.44	1591.83	-1.61	1591.90	-1.54
EX-16AU	1593.31	1591.85	-1.46	1591.90	-1.41
EX-16BL	1593.73	1592.20	-1.53	1592.04	-1.69
EX-7AL	1582.32	1580.65	-1.67	1581.93	-0.39
EX-7BL	1581.27	1580.65	-0.62	1581.93	0.66
EX-7BU	1579.66	1579.78	0.12	1580.91	1.25
EX-7CL	1578.61	1579.77	1.16	1580.71	2.10
EX-8AL	1584.68	1580.71	-3.97	1582.43	-2.25
EX-8AU	1582.97	1580.71	-2.26	1582.43	-0.54
EX-8BL	1579.85	1579.60	-0.25	1581.07	1.22
EX-8BU	1579.89	1579.44	-0.45	1580.78	0.89
EX-9AU	1594.32	1593.20	-1.12	1593.31	-1.01
EX-9BL	1594.52	1593.31	-1.21	1593.41	-1.11
EX-9BU	1594.62	1593.35	-1.27	1593.53	-1.09
G41-B12	1593.90	1591.72	-2.18	1591.70	-2.20
G41-C15	1593.11	1591.90	-1.21	1591.84	-1.27
G41-E13	1594.52	1592.95	-1.57	1592.88	-1.64
G41-E17	1592.78	1592.42	-0.36	1592.35	-0.43
G41-G13	1594.49	1593.60	-0.89	1593.70	-0.79
G41-G14A	1593.83	1593.64	-0.19	1593.72	-0.11
G41-G14B	1593.90	1593.59	-0.31	1593.67	-0.23
G41-G14C	1594.39	1593.76	-0.63	1593.83	-0.56
G41-G14D	1594.23	1593.63	-0.60	1593.71	-0.52
G41-G14E	1594.06	1593.75	-0.31	1593.85	-0.21
G41-G14F	1593.73	1593.59	-0.14	1593.67	-0.07
G41-G15	1593.90	1593.60	-0.30	1593.66	-0.24
G41-G15A	1593.70	1593.78	0.08	1593.85	0.15
G41-G15B	1593.73	1593.78	0.05	1593.85	0.12
G41-H18B	1592.52	1593.29	0.77	1593.25	0.73
G41-H9	1594.00	1592.73	-1.27	1592.61	-1.39
G41-K13	1593.37	1593.33	-0.04	1593.58	0.21
G41-K13A	1594.09	1593.64	-0.45	1593.80	-0.29
G41-M11	1579.89	1579.57	-0.32	1581.32	1.43
G41-P16	1579.33	1585.68	6.35	1585.93	6.60
SG-WP-6	1577.20	1579.27	2.07	1581.30	4.10
SG-WP-7	1578.15	1579.17	1.02	1580.30	2.15

Notes:

[1] Observed water level in October 1984.

[2] Simulation T07A.

[3] Simulation 49A.

[4] Modeled - Observed.

Prepared by: GWC
Checked by: KMR
Approved by: PFA

December 1998
\Crandon\TmaMod4\Excel\Targets.xls, Compare

Table 2.8 Travel time for particles reaching well clusters CMC-02, EX-11, and EX-8.

Well ID	Travel Time from Water Table (Years)	Unsaturated Zone Travel Time[1] (Years)	Modeled Recharge Date[2]	CFC-Derived Date
CMC-02P	10.6	8.5	1976.9	1978.0
CMC-02R	0.1	8.5	1987.4	1989.5
EX-11AL	42.1	7.0	1946.9	<1954.5
EX-11AU	19.7	7.0	1969.3	<1959.0
EX-11BL	10.0	7.0	1979.0	1955.0
EX-11BU	6.1	7.0	1982.9	<1966.0
EX-11CL	0.01	6.7	1989.3	1978.2
EX-8AL	96.9	7.0	1892.1	1975.0
EX-8AU	51.1	8.5	1936.4	<1954.5
EX-8BL	23.0	8.5	1964.5	<1958
EX-8BU	0.3	0.0	1995.7	1984.5
Geo25	6.0	8.5	1981.5	1977.0
Geo50	18.7	8.5	1968.8	1956.5

Notes:

[1] From Saad, 1996.

[2] Using 1996 as refernce date.

Prepared by: GWC
Checked by: KMR
Approved by: PFA

Simulation T07A-MP
December 1998
\Crandon\TMAmod4\Excel\T07a-mp.xls, RchDate

Table 2.9 BEJT and PWCT model parameter values.

Geologic Unit or Boundary	Parameter	BEJT Value	PWCT Value
All Geologic Units	Effective Porosity	0.10	0.10
	Longitudinal Dispersivity	50.0 ft	25.0 ft
	Horizontal Transverse Dispersivity	5.0 ft	2.5 ft
	Vertical Dispersivity	5.0 ft	2.5 ft
Late Wisconsinan Till	Horizontal Conductivity	0.80 ft/d	0.80 ft/d
	Vertical Conductivity	0.40 ft/d	0.04 ft/d
Coarse Outwash	Horizontal Conductivity	80.0 ft/d	80.0 ft/d
	Vertical Conductivity	8.0 ft/d	0.8 ft/d
	Pinchout Zone Horizontal Conductivity	6.0 ft/d	6.0 ft/d
	Pinchout Zone Vertical Conductivity	0.6 ft/d	0.06 ft/d
Fine Outwash	Horizontal Conductivity	20.0 ft/d	20.0 ft/d
	Vertical Conductivity	2.0 ft/d	0.2 ft/d
	Pinchout Zone Horizontal Conductivity	6.0 ft/d	6.0 ft/d
	Pinchout Zone Vertical Conductivity	0.6 ft/d	0.06 ft/d
Pre- to Early-Wisconsinan Till and Massive Saprolite	Horizontal Conductivity	2.00 ft/d	2.00 ft/d
	Vertical Conductivity	0.075 ft/d	0.0075 ft/d
Ancient Lacustrine	Horizontal Conductivity	2.00 ft/d	2.00 ft/d
	Vertical Conductivity	0.075ft/d	0.0075 ft/d
Hemlock Creek	Width	14.0	14.0 ft
	Creekbed Vertical Conductivity	1.0 ft/d	1.0 ft/d
	Creekbed Sediment Thickness	1.0 ft	1.0 ft
	Water Depth	1.0 ft	1.0 ft
Seepage Wetlands	Bottom Sediment Vertical Conductivity	0.003 ft/d	0.003 ft/d
	Bottom Sediment Thickness	5.0 ft	5.0 ft
	Water Depth	2.0 ft	2.0 ft

Table 2.10 Hypothetical concentration phases for sulfate.

Description	Source Concentration (ppm)	Beginning Time[1]
Operational	2,000	Start of flow phase A
Post-Cap	4,000	Start of flow phase D
Oxidized	40,000	Start of flow phase G[2]

Notes
[1] Varies by TMA Cell
[2] As a conservative assumption, the oxidized concentration begins immediately after assumed degradation of the flexible membrane liner.

Prepared by: GWC
Checked by: KMR
Approved by: PFA

December 1998
\Crandon\TmaMod4\Excel\SulfSrc.xls

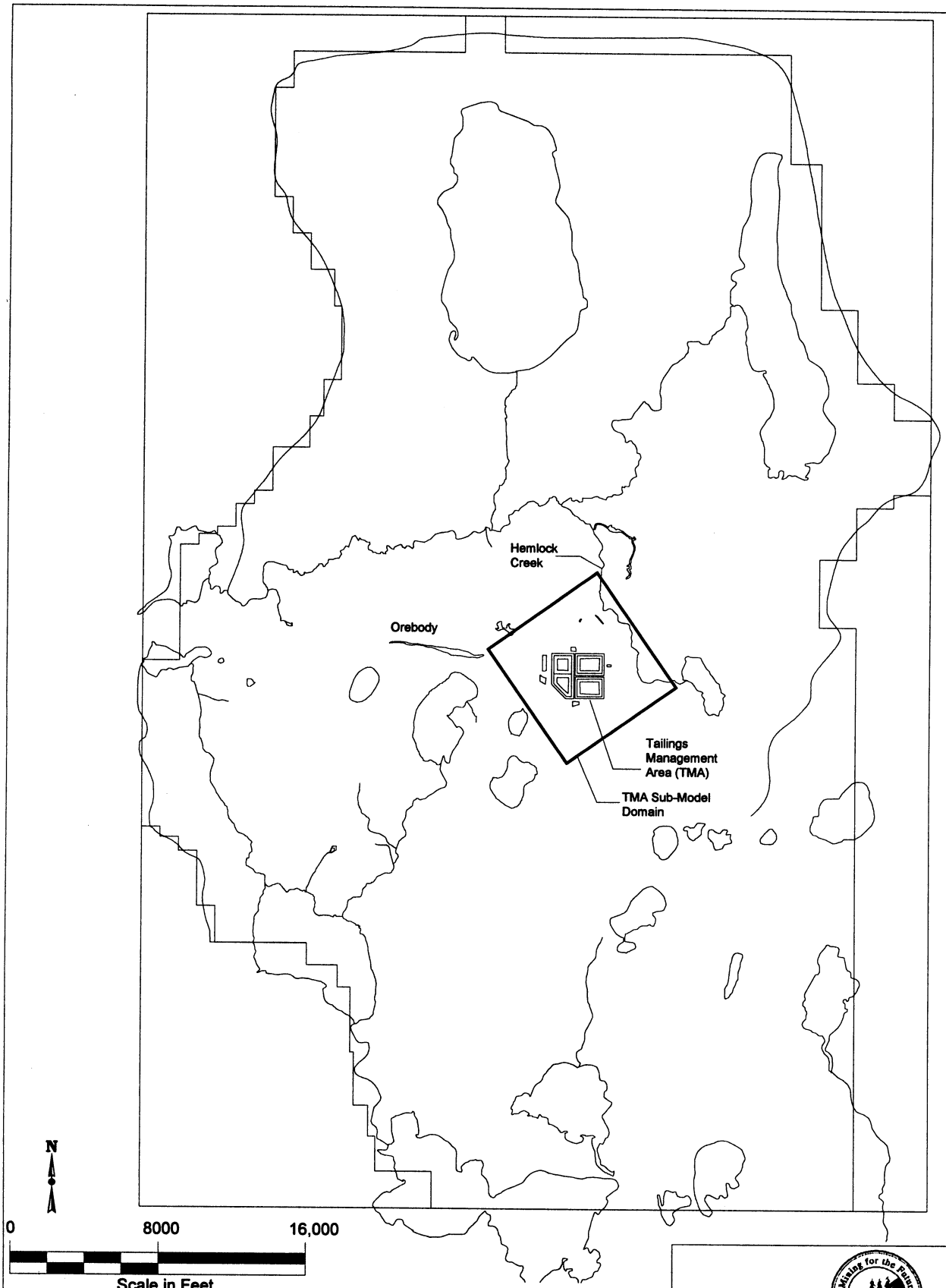

HSI GEOTRANS

REVISED	DATE	BY	DESCRIPTION

CHECKED BY: KMR	DATE: Dec 1998
APPROVED BY: PFA	DATE: Dec 1998
APPROVED BY:	DATE:

Nicolet Minerals COMPANY

Figure 2.1
TMA Sub-Model
Location Map

Scale: 1 in. = 8000 ft.	Date: Dec 1998
Prepared By: HSI GeoTrans	By: GWC

\Crandon\TmaMod4\GIS\LocatMap.wor

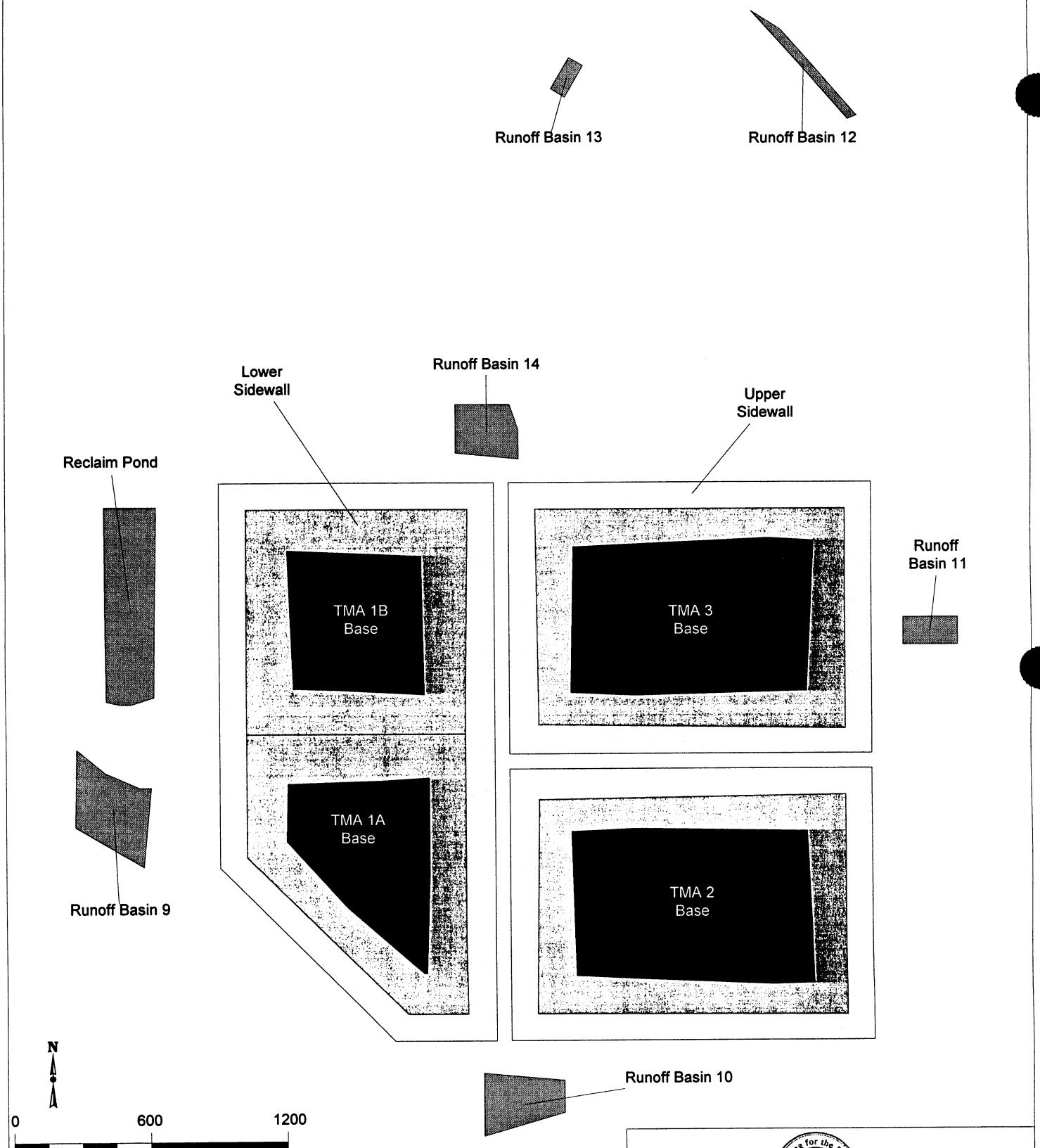

HSI GEOTRANS			
REVISED	DATE	BY	DESCRIPTION
CHECKED BY: KMR			DATE: Dec 1998
APPROVED BY: PFA			DATE: Dec 1998
APPROVED BY:			DATE:

Nicolet Minerals COMPANY

Figure 2.2
TMA Cell Configuration and Associated Facilities

Scale: 1 in. = 600 ft.	Date: Dec 1998
Prepared By: HSI GeoTrans	By: GWC

P:\GIS\maMod4\GIS\Detail.wor

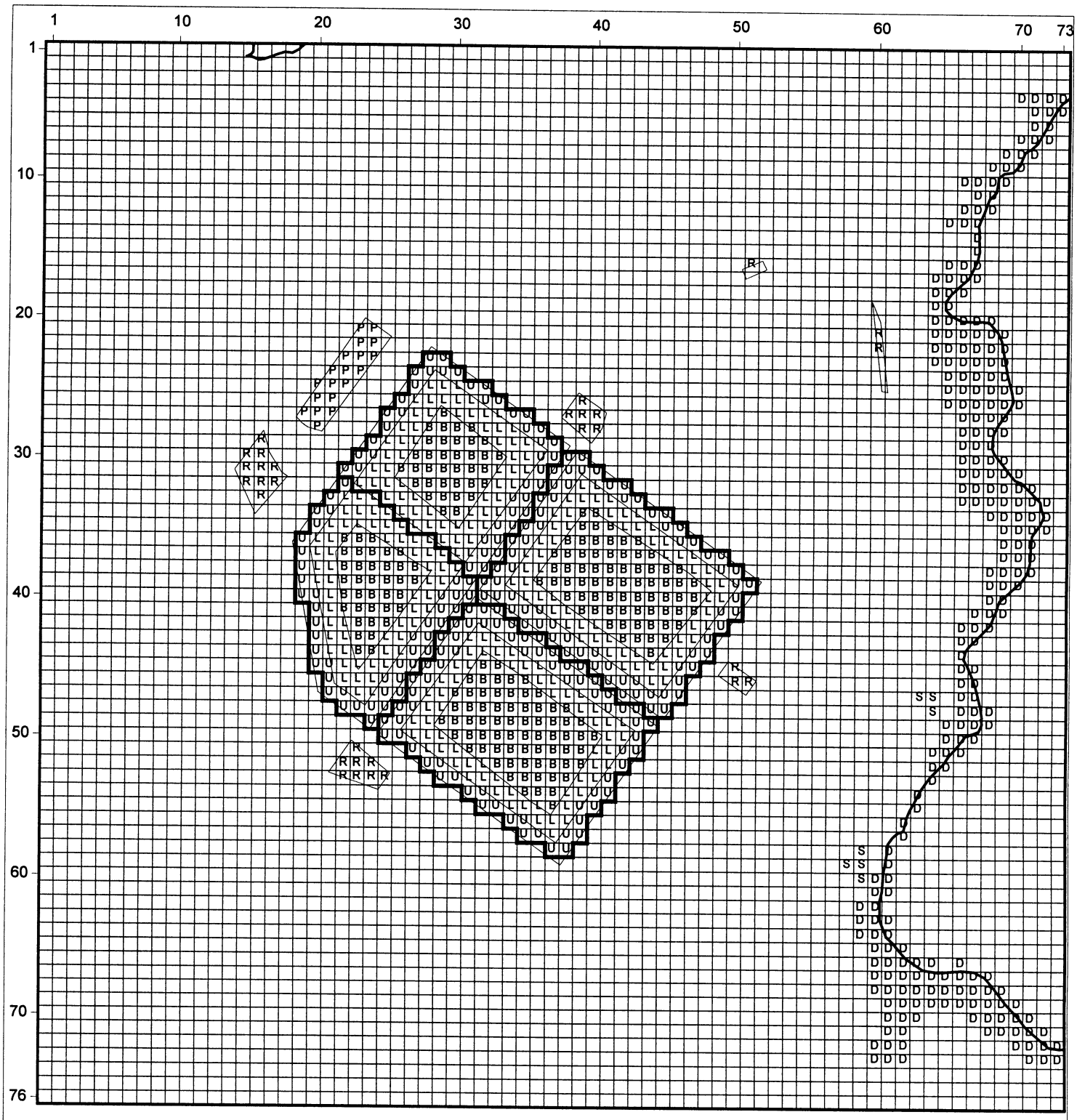

LEGEND

	Default Recharge (9.7 in/yr)
D	Discharge Wetland (3 in/yr)
S	Seepage Wetland (No Recharge)
B	TMA Base
L	TMA Lower Sidewall
U	TMA Upper Sidewall
P	Reclaim Pond
R	Runoff Basin

N

0 1000 2000

Scale in Feet

HSI GEOTRANS

REVISED	DATE	BY	DESCRIPTION

CHECKED BY: KMR	DATE: Dec 1998
APPROVED BY: PFA	DATE: Dec 1998
APPROVED BY:	DATE:

Nicolet Minerals COMPANY

Figure 2.3
Model Grid and Recharge Zones

Scale: 1 in. = 1000 ft. Date: Dec 1998

Prepared By: HSI GeoTrans By: GWC

\Crandon\TmaMod4\GIS\RechZon.wor

P:\CMC\TmaMod4\Excel\TimeLine.xls, Chart

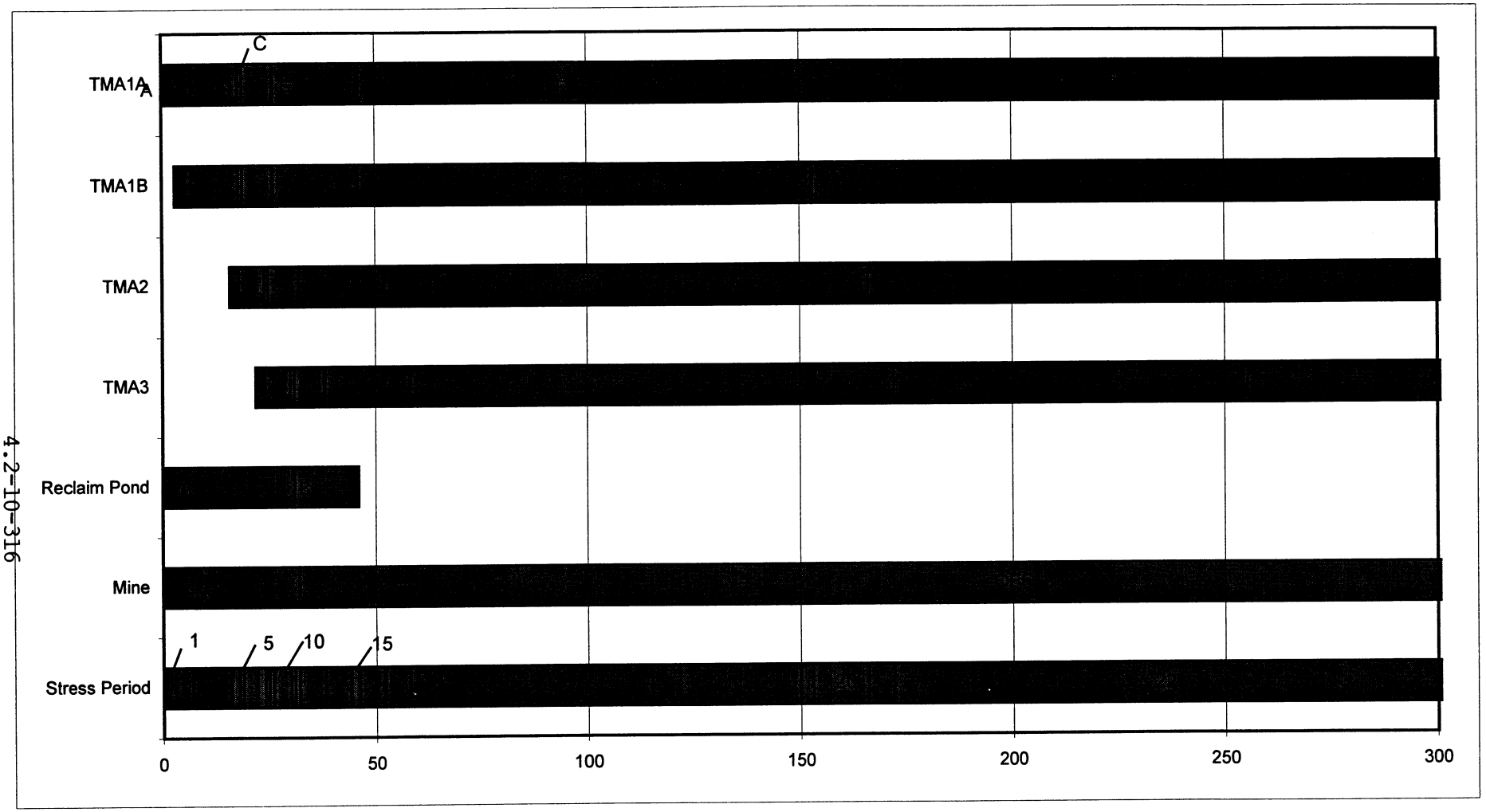

4.2-10-316

HSI GEOTRANS			
REVISED	DATE	BY	DESCRIPTION
CHECKED BY:GWC			DATE: Dec 98
APPROVED BY: PFA			DATE: Dec 98
APPROVED BY:			DATE:

Nicolet Minerals COMPANY

Figure 2.4
TMA Sub-Model Time Line

Scale: None	Date: December 1998
Prepared By: HSI GEOTRANS	By: KMR

\Crandon\TmaMod3\Excel\HelpComp.xls, Flux

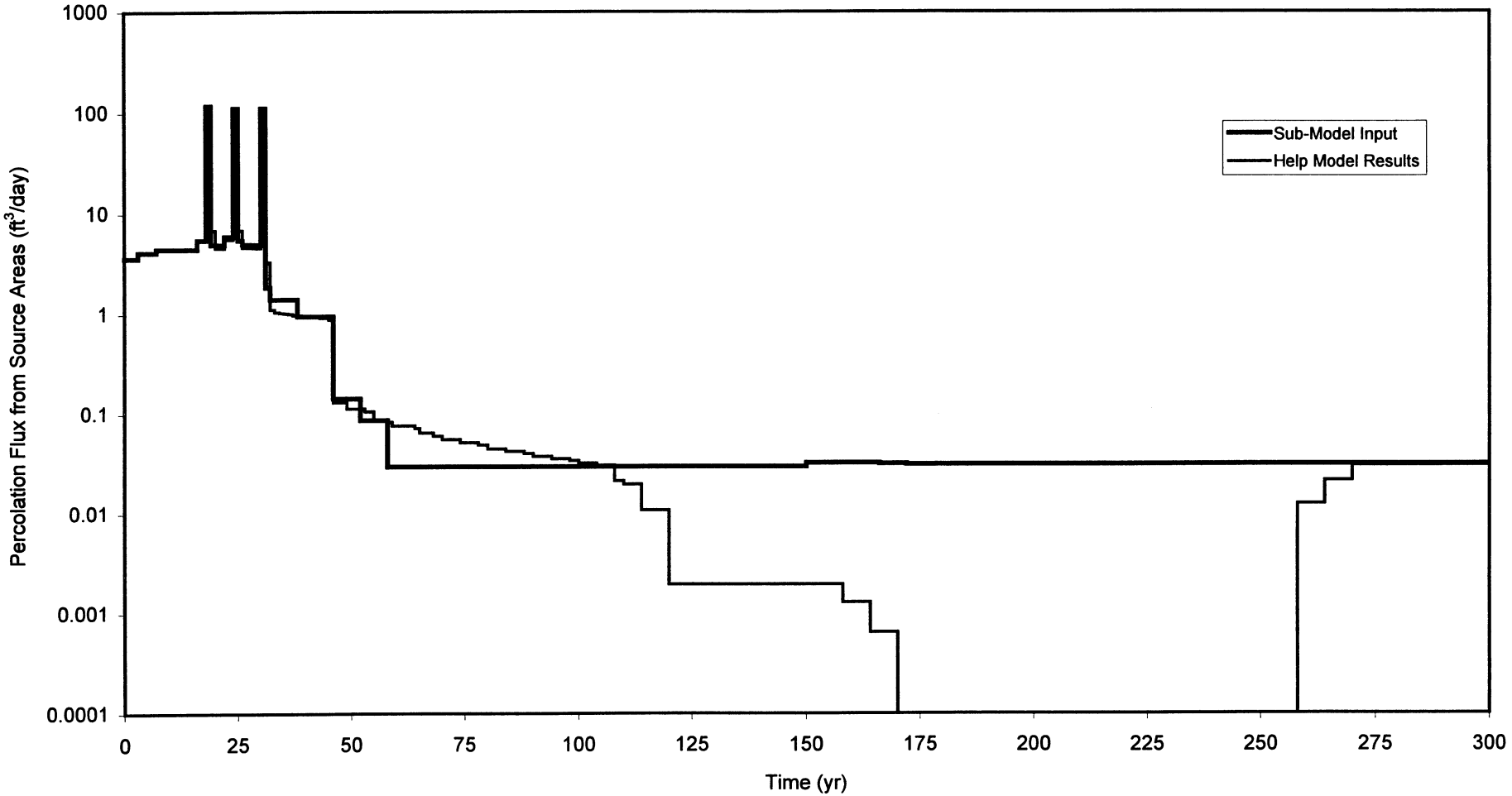

4.2-10-317

Note:
Percolation rate (Y-axis) is shown on a logarithmic scale.

HSI GEOTRANS			
REVISED	DATE	BY	DESCRIPTION
CHECKED BY: GWC			DATE: Dec 1998
APPROVED BY: PFA			DATE: Dec 1998
APPROVED BY:			DATE:

Nicolet Minerals COMPANY

Figure 2.5
Source Areas Percolation Flux Rate

Scale: None	Date: Dec 1998
Prepared By: HSI GEOTRANS	By: KMR

\Crandon\TmaMod4\Excel\HelpComp.xls, CumVol

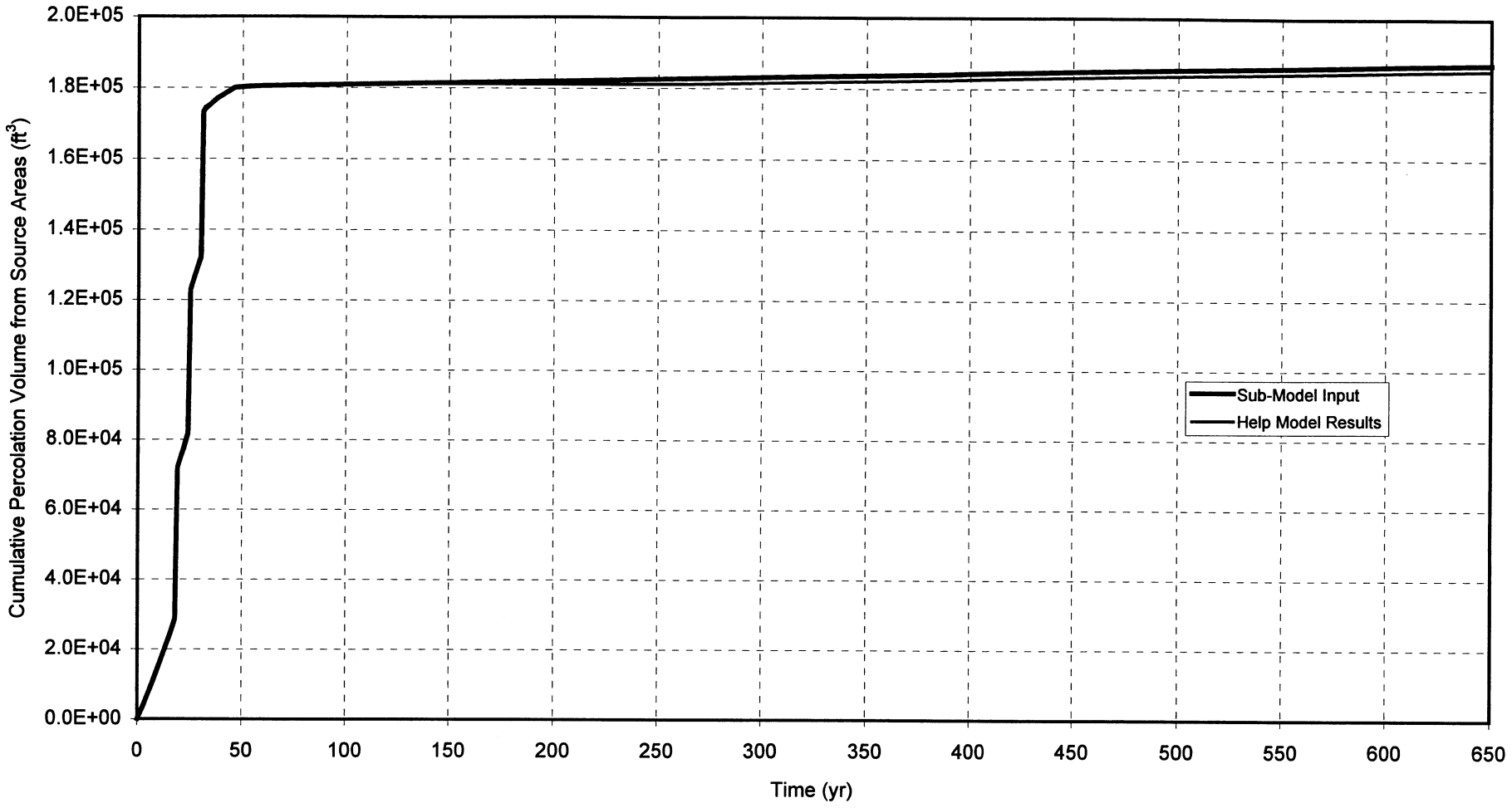

4.2-10-318

HSI GEOTRANS			
REVISED	DATE	BY	DESCRIPTION
CHECKED BY: PAW			DATE: Dec 1998
APPROVED BY: PFA			DATE: Dec 1998
APPROVED BY:			DATE:

Nicolet Minerals COMPANY

Figure 2.6
Source Areas Cumulative Percolation Volume

Scale: None	Date: Dec 1998
Prepared By: HSI GEOTRANS	By: GWC

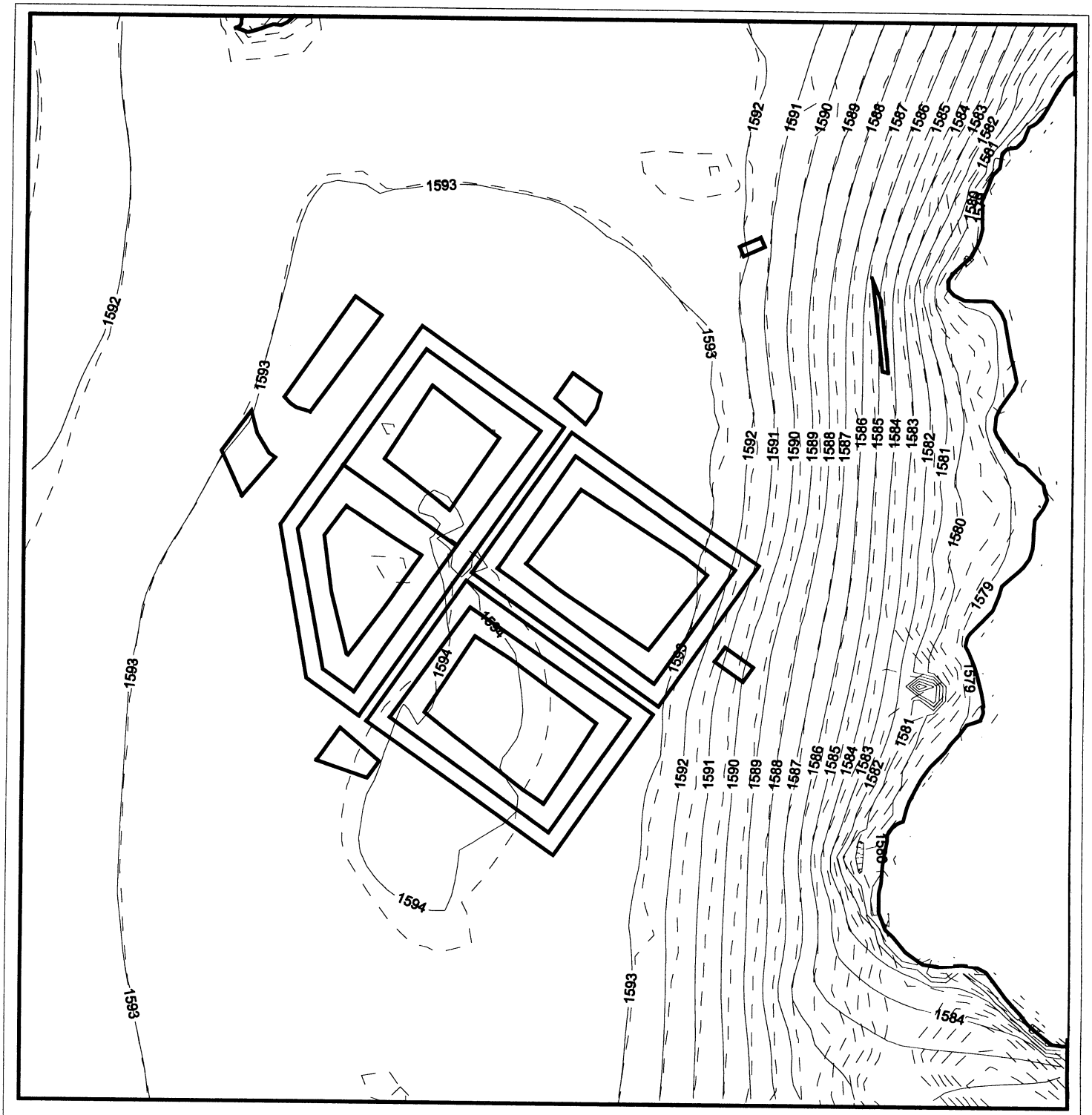

Notes:
1) Elevation in feet, msl.
2) Contour interval 1 foot.
3) TMA sub-model simulation T07A.
4) Regional model simulation 49A.

Legend
- TMA sub-model head contour
- Regional model head contour

0 1000 2000
Scale in Feet

HSI GEOTRANS			
REVISED	DATE	BY	DESCRIPTION
CHECKED BY: PAW			DATE: Dec 1998
APPROVED BY: PFA			DATE: Dec 1998
APPROVED BY:			DATE:

Nicolet Minerals COMPANY

Figure 2.7
Modeled Water Table in the TMA Sub-Model and Regional Model

Scale: 1 in. = 1000 ft.	Date: Dec 1998
Prepared By: HSI GEOTRANS	By: GWC

\Crandon\Tma\Mod4\Surfer\fig2-wtb.srf

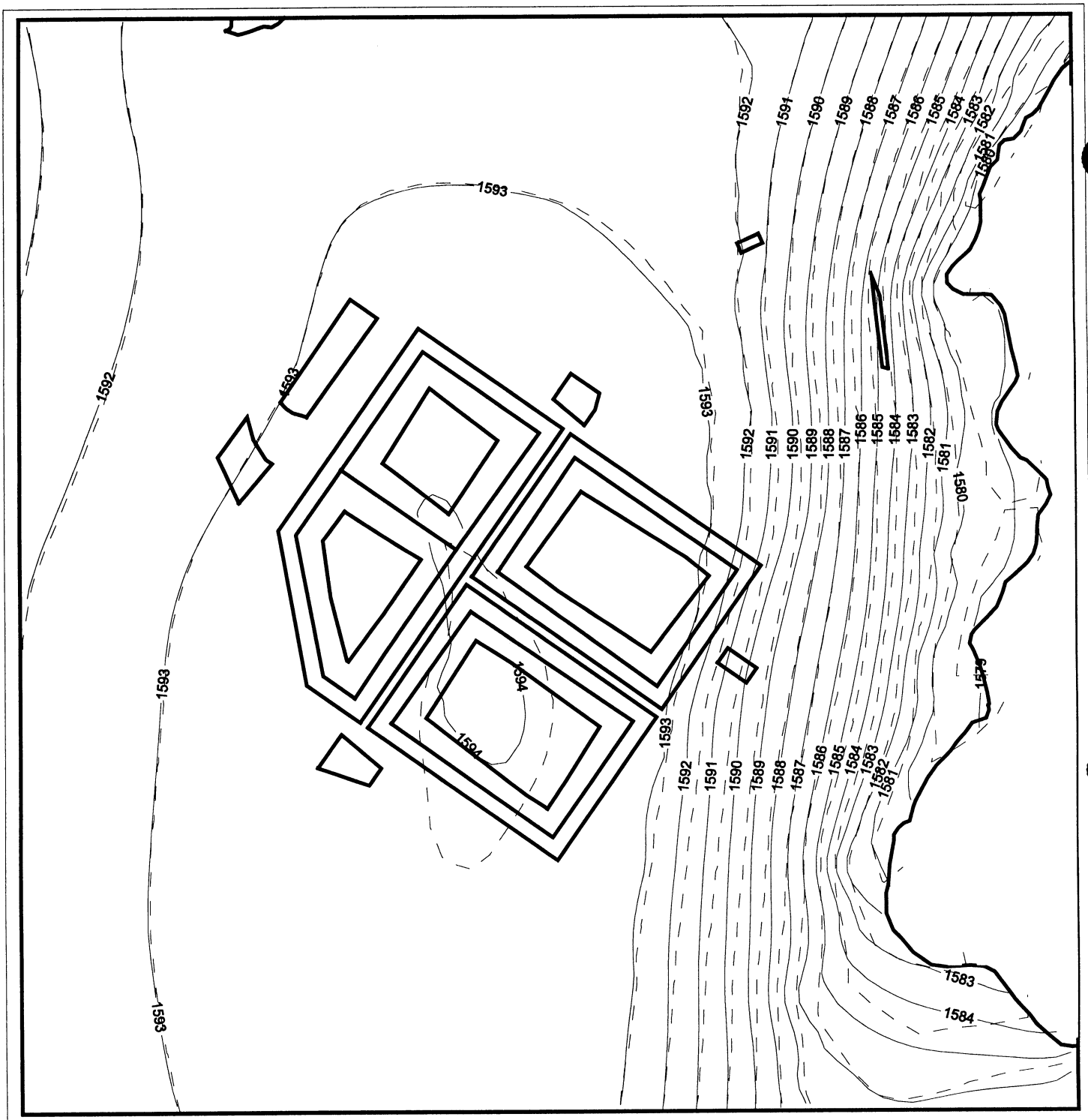

Notes:
1) Elevation in feet, msl.
2) Contour interval 1 foot.
3) TMA sub-model simulation T07A.
4) Regional model simulation 49A.

Legend
TMA sub-model head contour
Regional model head contour

0 1000 2000
Scale in Feet

HSI GEOTRANS

REVISED	DATE	BY	DESCRIPTION

CHECKED BY: PAW	DATE: Dec 1998
APPROVED BY: PFA	DATE: Dec 1998
APPROVED BY:	DATE:

Nicolet Minerals COMPANY

Figure 2.8
Modeled Head in TMA Sub-Model Layer 3 and Regional Model Layer 2

Scale: 1 in. = 1000 ft.	Date: Dec 1998
Prepared By: HSI GEOTRANS	By: GWC

\Crandon\Tma\Mod4\Surfer\t07a-hed3.srf

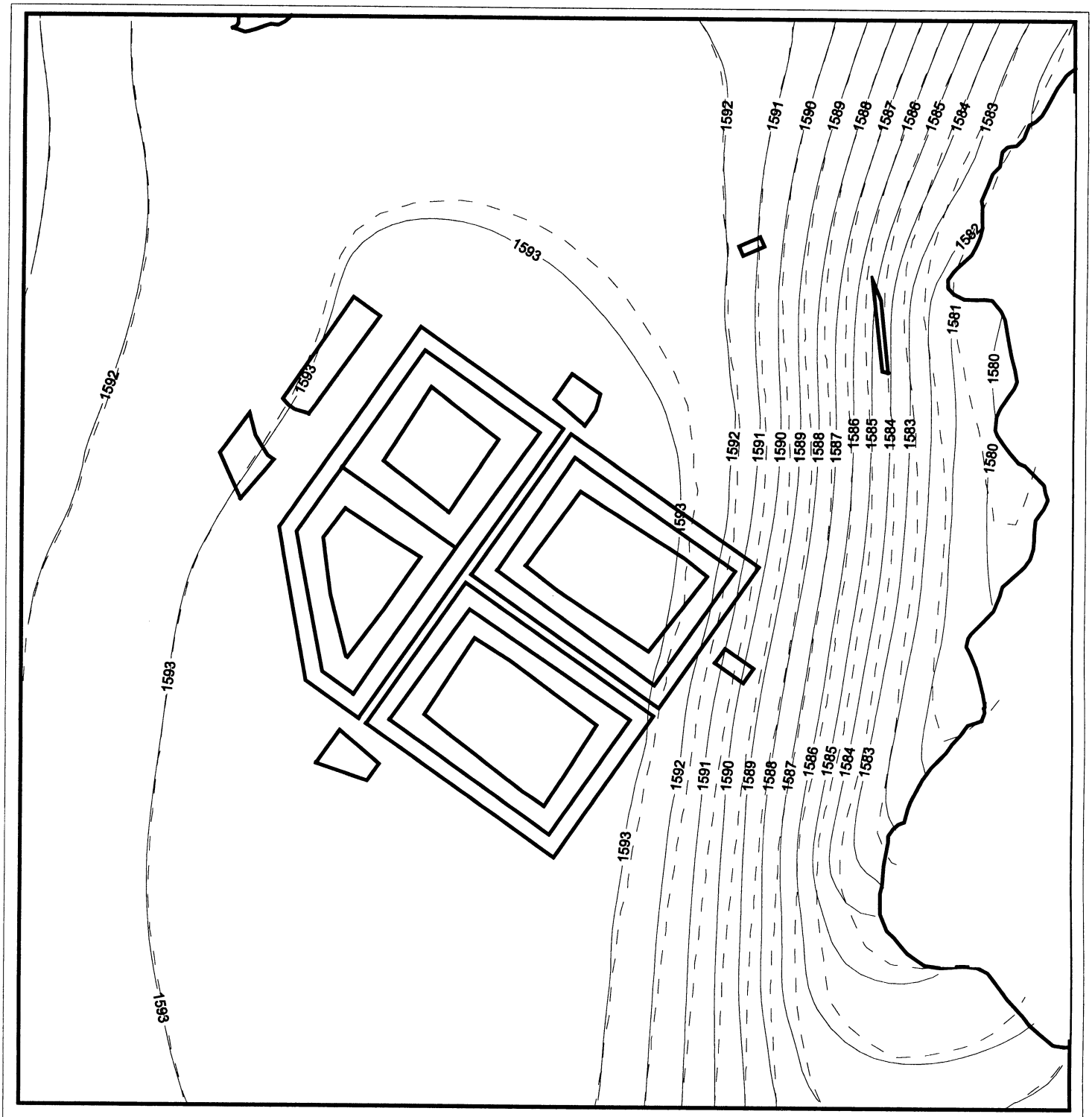

Notes:
1) Elevation in feet, msl.
2) Contour interval 1 foot.
3) TMA sub-model simulation T07A.
4) Regional model simulation 49A.

Legend
TMA sub-model head contour
Regional model head contour

0 1000 2000
Scale in Feet

HSI GEOTRANS			
REVISED	DATE	BY	DESCRIPTION
CHECKED BY: PAW			DATE: Dec 1998
APPROVED BY: PFA			DATE: Dec 1998
APPROVED BY:			DATE:

Nicolet Minerals COMPANY

Figure 2.9
Modeled Head in TMA Sub-Model Layer 7 and Regional Model Layer 4

Scale: 1 in. = 1000 ft. | Date: Dec 1998
Prepared By: HSI GEOTRANS | By: GWC

\Crandon\TmaMod4\Surfer\t07a-hed7.srf

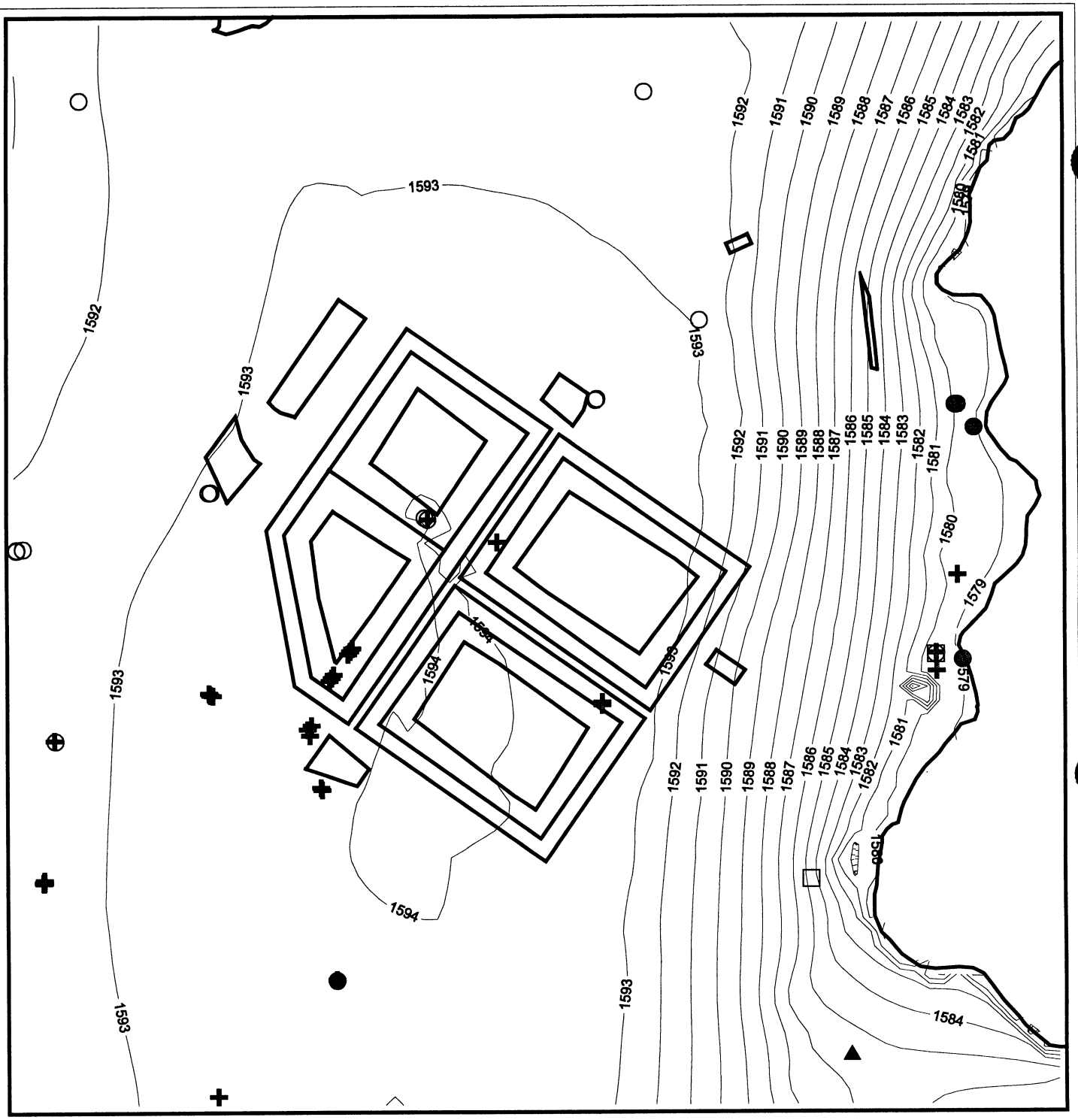

Residuals
(Modeled - Observed)

- Less than -5
- -5 to -3
- -3 to -1
- -1 to 1
- 1 to 3
- 3 to 5
- Greater than 5

N

0 1000 2000

Scale in Feet

Notes:
1) Elevation in feet, msl.
2) Contour interval 1 foot.
3) TMA sub-model simluation T07A.

HSI GEOTRANS

REVISED	DATE	BY	DESCRIPTION

CHECKED BY: PAW	DATE: Dec 1998
APPROVED BY: PFA	DATE: Dec 1998
APPROVED BY:	DATE:

Nicolet Minerals COMPANY

Figure 2.10
Modeled Steady-State Water Table and Water Level Residuals at Wells

Scale: 1 in. = 1000 ft.	Date: Dec 1998
Prepared By: HSI GEOTRANS	By: GWC

\Crandon\Tma\Mod4\Surfer\t07a-res.srf

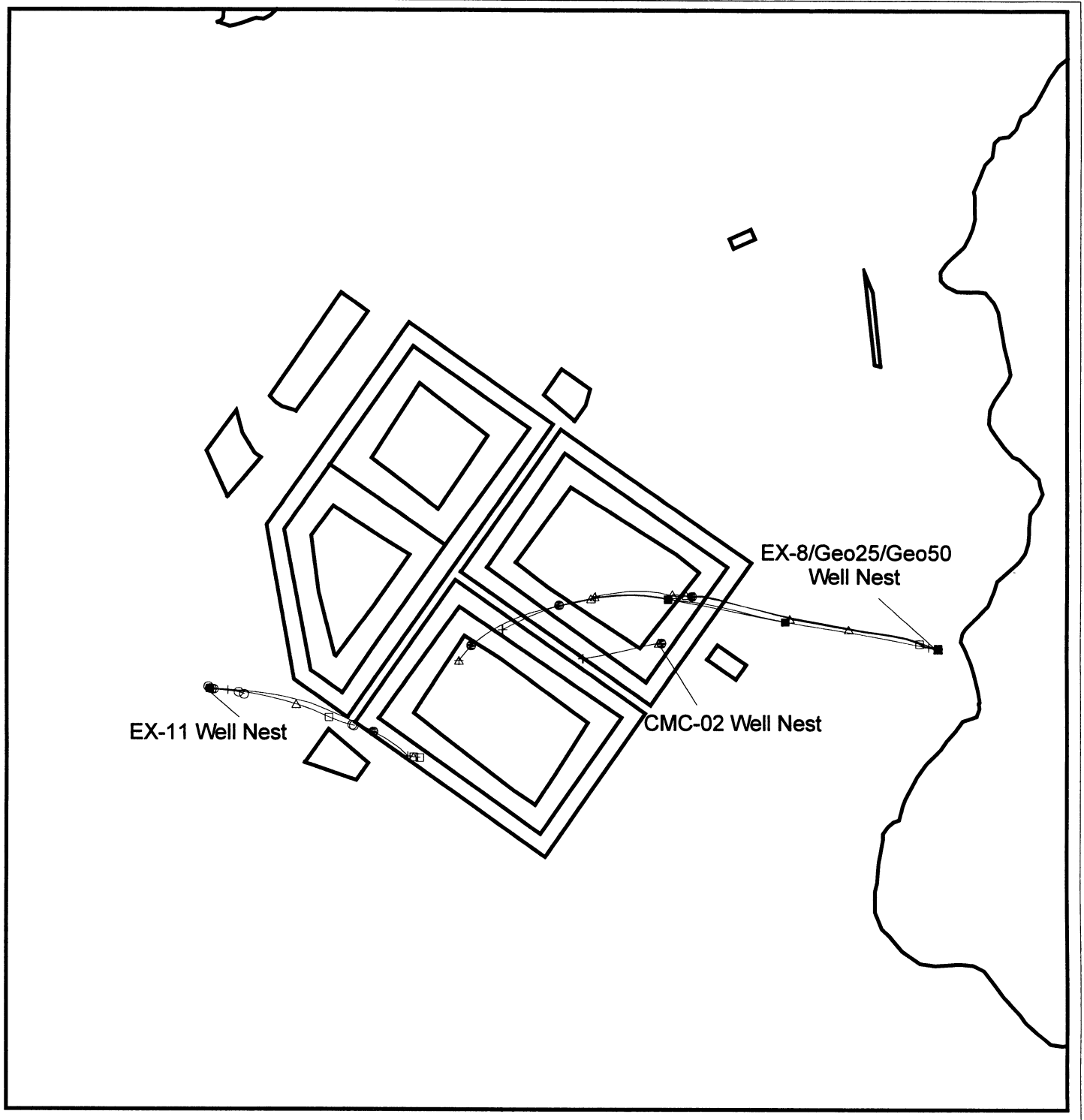

0 1000 2000

Scale in Feet

HSI GEOTRANS			
REVISED	DATE	BY	DESCRIPTION

CHECKED BY: PAW	DATE: Dec 1998
APPROVED BY: PFA	DATE: Dec 1998
APPROVED BY:	DATE:

Simulation T07A-MP

Nicolet Minerals COMPANY

Figure 2.11
Backwards Particle Traces From EX-8/Geo25/Geo50, EX-11, and CMC-02

Scale: 1 in. = 1000 ft.	Date: Dec 1998
Prepared By: HSI GEOTRANS	By: GWC

\Crandon\Tma\Mod4\Surfer\sav\ex11rp.srf

\Crandon\TmaMod4\Excel\T07a-mp.xls, EX8Trace

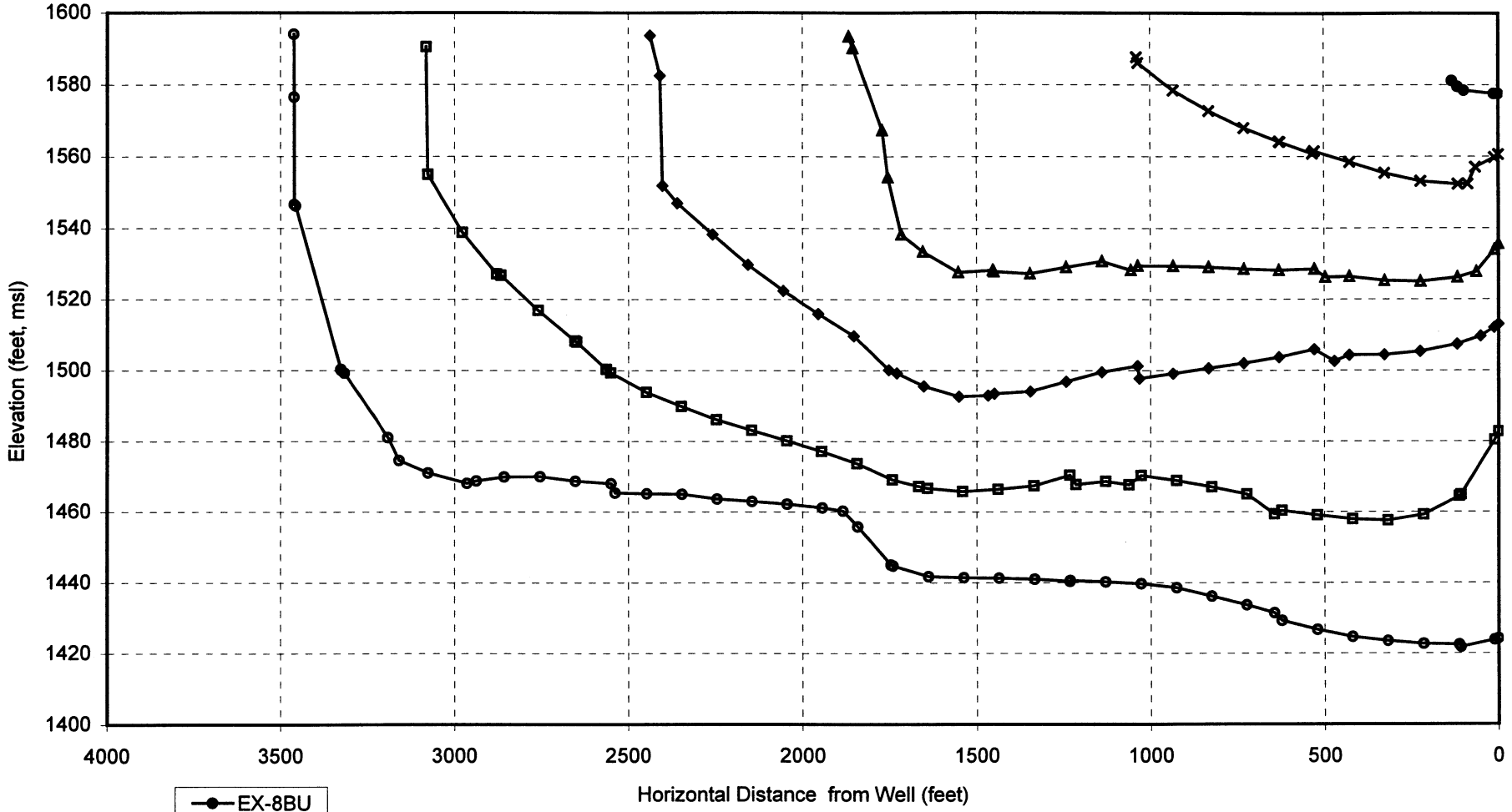

4.2-10-324

HSI GEOTRANS			
REVISED	DATE	BY	DESCRIPTION
CHECKED BY: PAW			DATE: Dec 1998
APPROVED BY: PFA			DATE: Dec 1998
Simulation T07A-MP	APPROVED BY:		DATE:

Nicolet Minerals COMPANY

Figure 2.12
Backwards Particle Traces from the EX-8/Geo25/Geo50 Well Cluster to the Water Table

Scale: None	Date: Dec 1998
Prepared By: HSI GEOTRANS	By: GWC

\Crandon\TmaMod4\Excel\T07C-Mp.xls, Fig

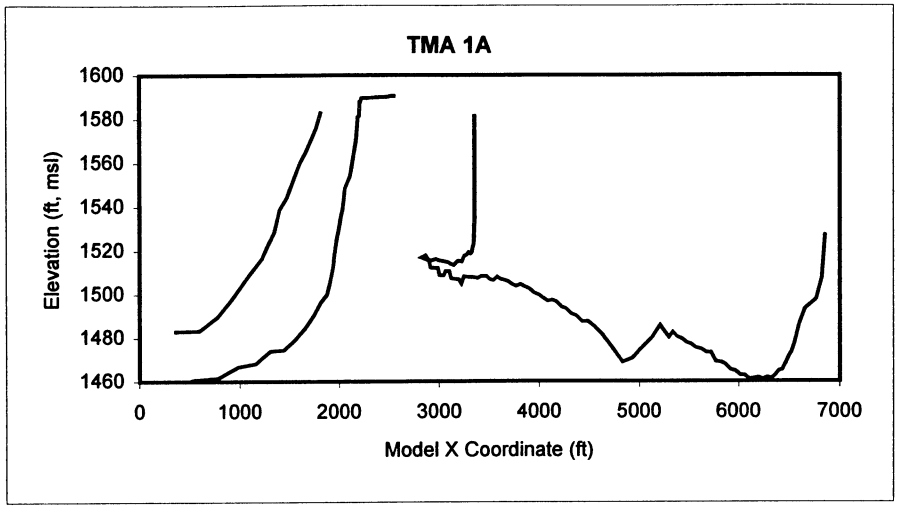

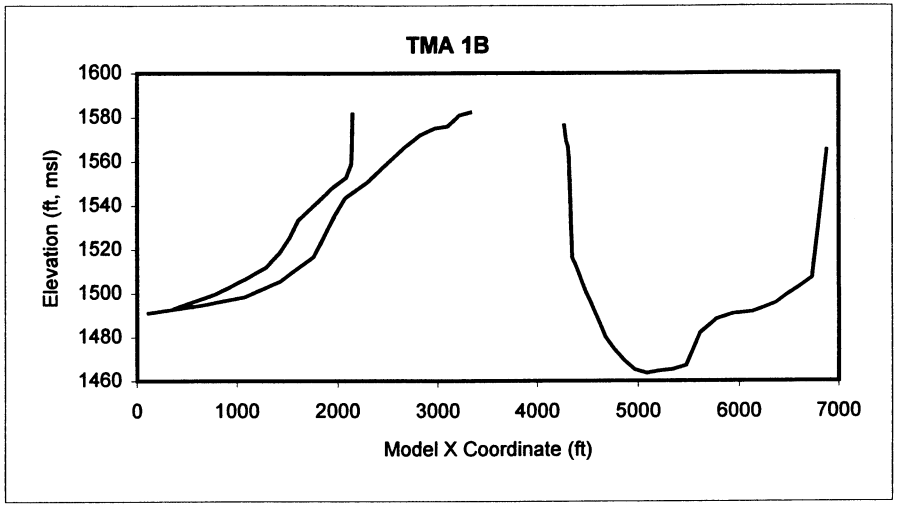

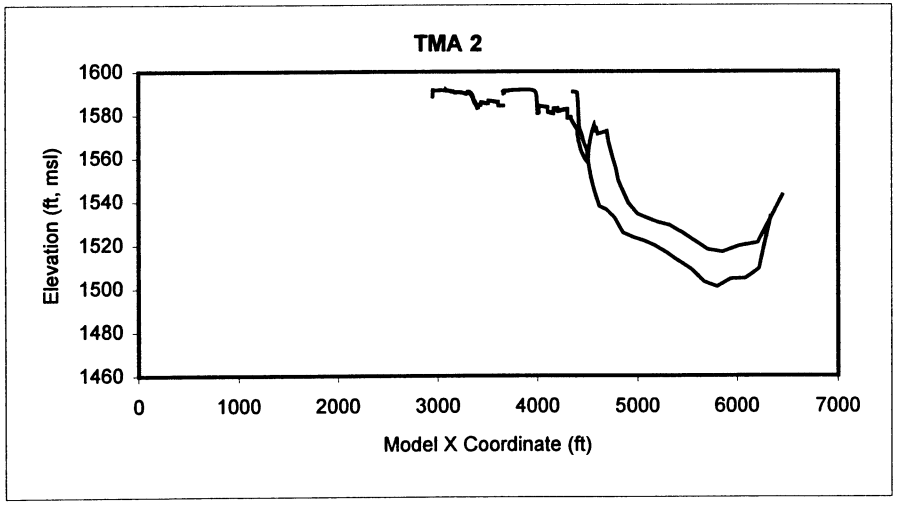

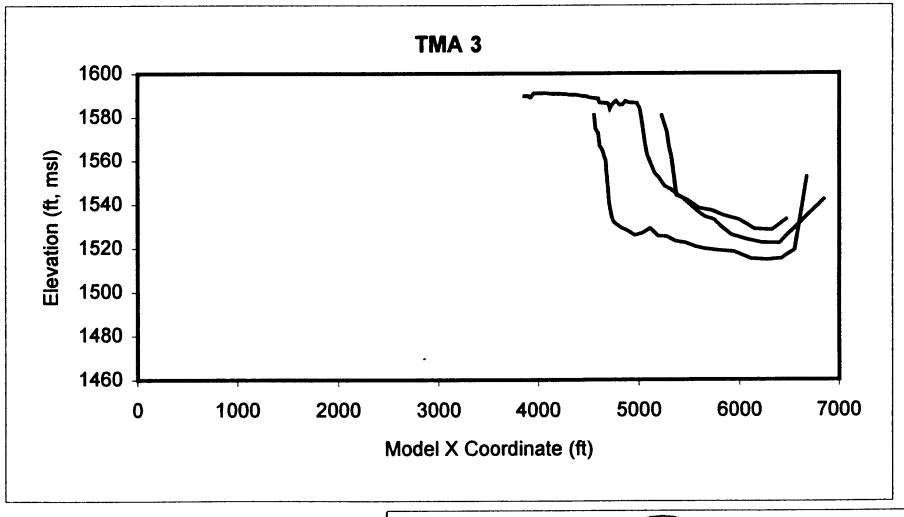

4.2-10-325

HSI GEOTRANS			
REVISED	DATE	BY	DESCRIPTION

CHECKED BY: PAW		DATE: Dec 1998
APPROVED BY: PFA		DATE: Dec 1998
Simulation T07C-MP	APPROVED BY:	DATE:

Nicolet Minerals COMPANY

Figure 2.13
Particle Traces From Each TMA Basin, Cross-Section

Scale: None	Date: Dec 1998
Prepared By: HSI GEOTRANS	By: GWC

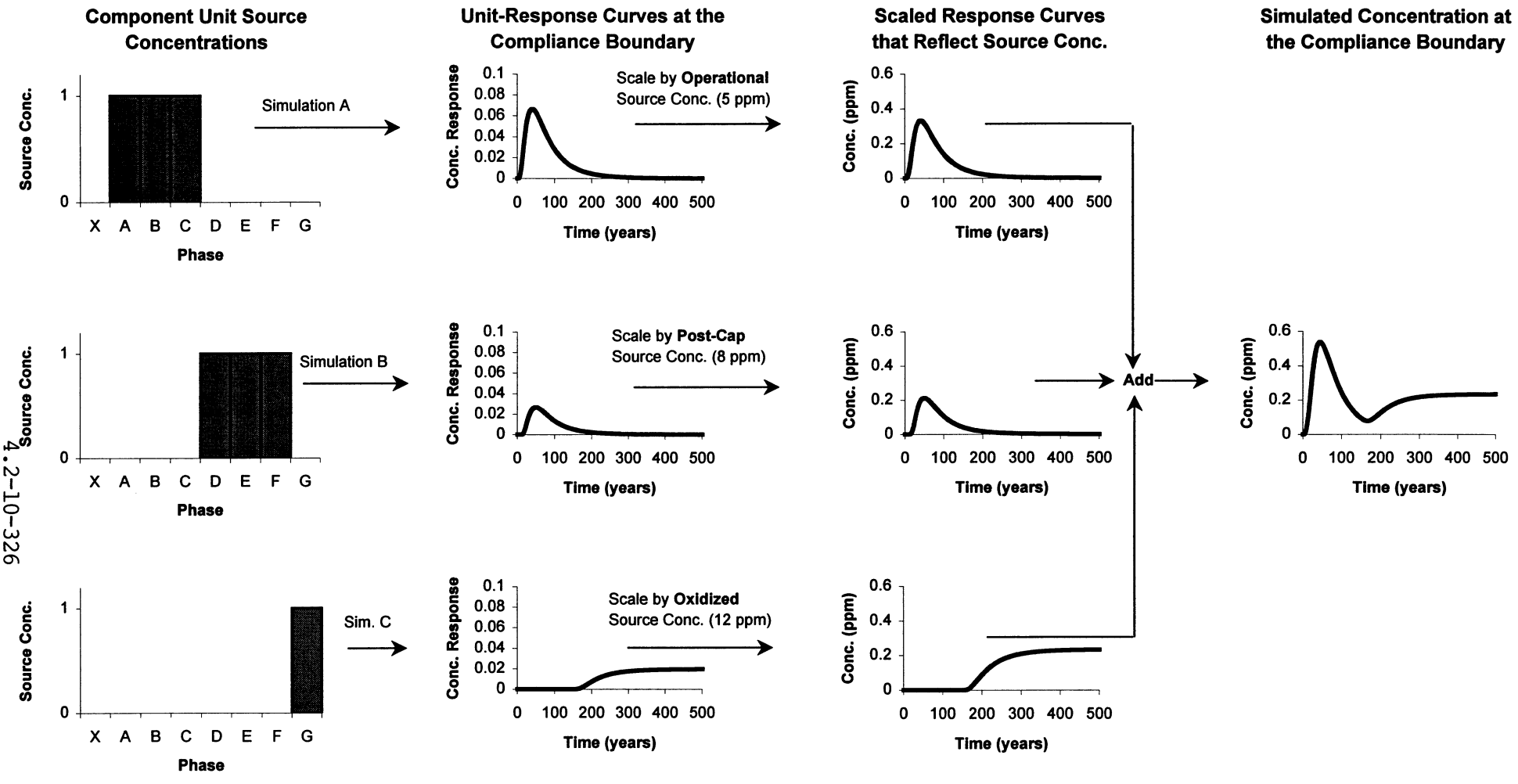

This hypothetical example shows the superposition method applied for a constituent with the following source concentrations:

Operation: 5 ppm
Post-Cap: 8 ppm
Oxidized: 12 ppm

HSI GEOTRANS			
REVISED	DATE	BY	DESCRIPTION
CHECKED BY: PAW			DATE: Dec 1998
APPROVED BY: PFA			DATE: Dec 1998
APPROVED BY:			DATE:

Nicolet Minerals COMPANY

Figure 2.14
Illustration of the Superposition Method

Scale: None	Date: Dec 1998
Prepared By: HSI GEOTRANS	By: GWC

4.2-10-326

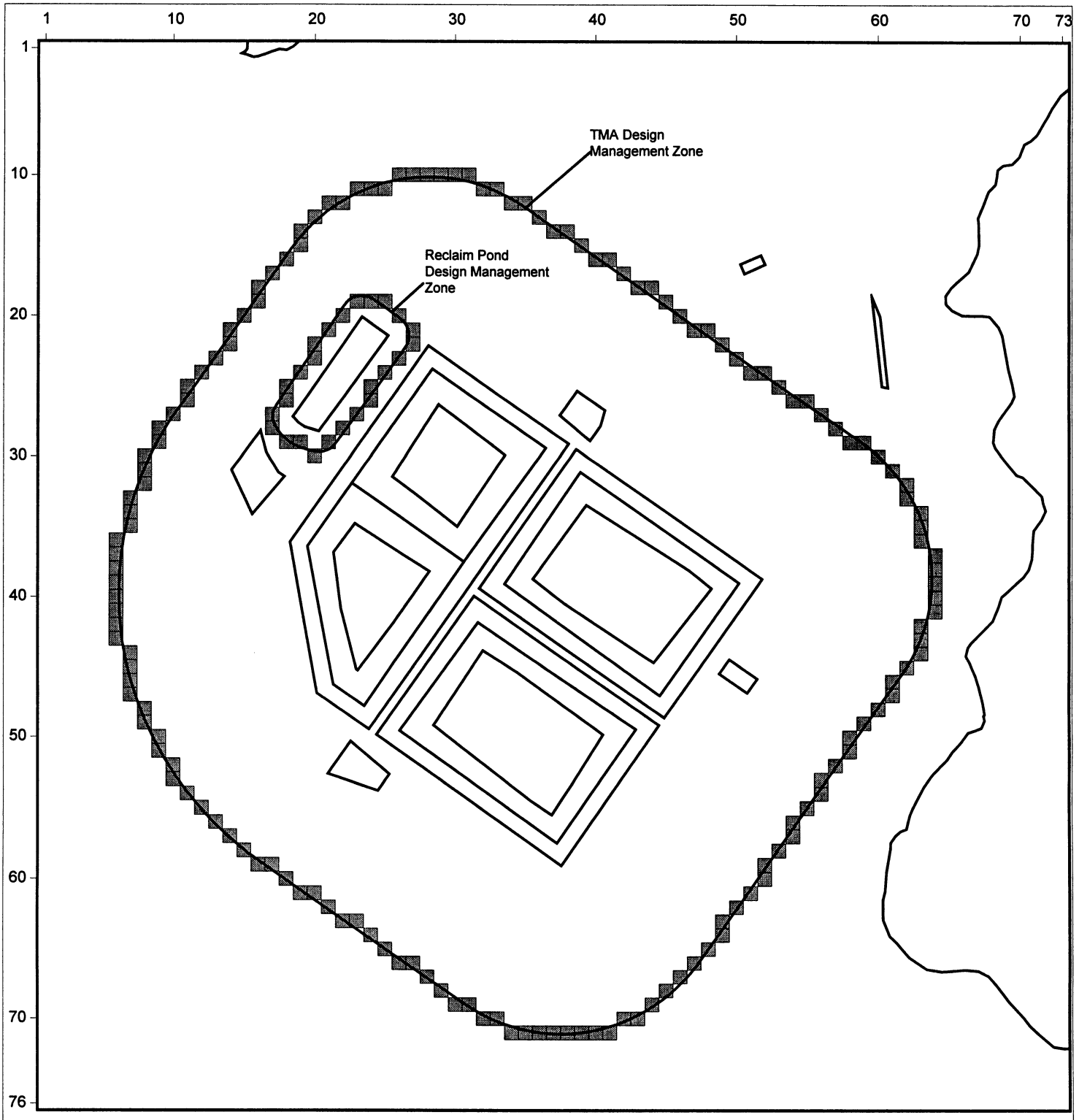

0 1000 2000

Scale in Feet

HSI GEOTRANS

REVISED	DATE	BY	DESCRIPTION

CHECKED BY: KMR	DATE: Dec 1998
APPROVED BY: PFA	DATE: Dec 1998
APPROVED BY:	DATE:

Nicolet Minerals COMPANY

Mining for the Future

Figure 2.15
Observation Cells at the design Management Zones

Scale: 1 in. = 1000 ft. | Date: Dec 1998

Prepared By: HSI GeoTrans | By: GWC

P:\CMC\TmaMod4\GIS\CmpBdry.wor

Tailings Management Area Design Management Zone

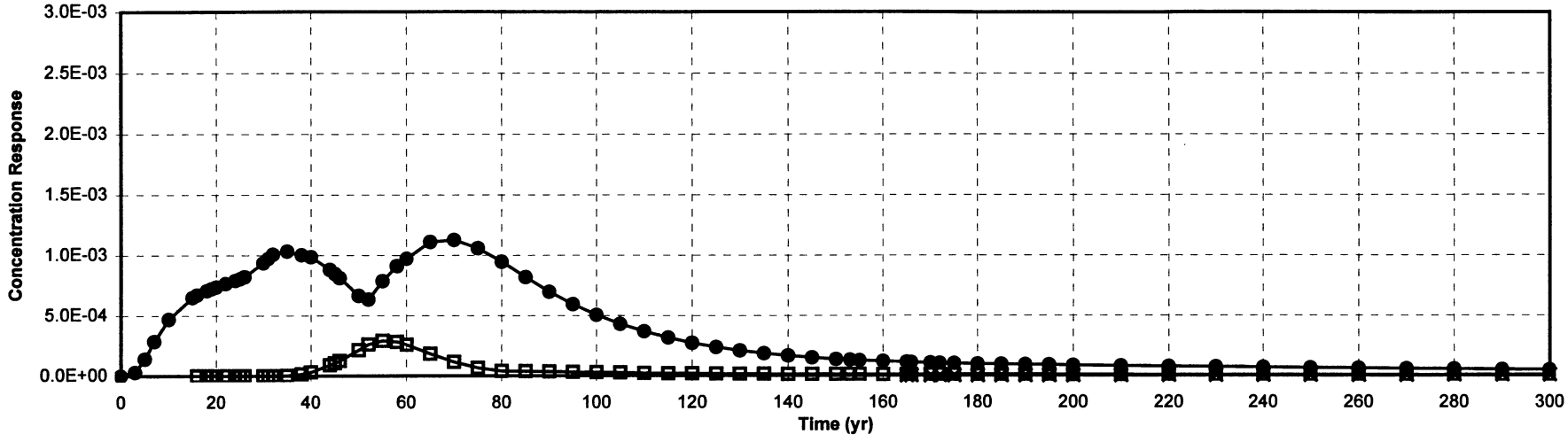

Reclaim Pond Design Management Zone

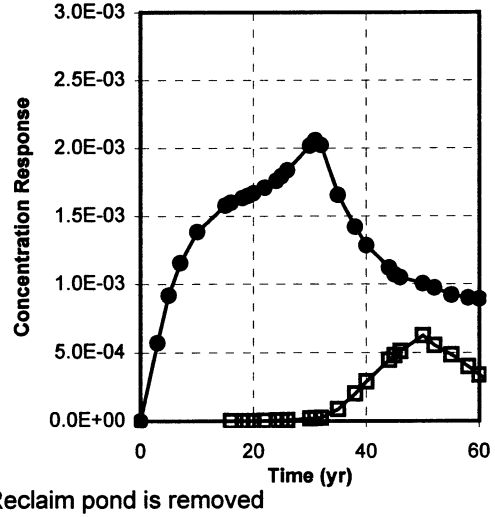

Note: Reclaim pond is removed at approximately year 46

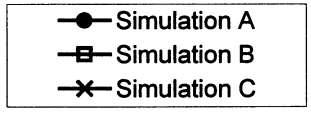

Note: The maximum concentration at any point on the Design Management Zone is plotted.

HSI GEOTRANS			
REVISED	DATE	BY	DESCRIPTION
CHECKED BY: GWC			DATE: Dec 1998
APPROVED BY: PFA			DATE: Dec 1998
Simulations T07C1,2,3	APPROVED BY:		DATE:

Nicolet Minerals COMPANY

Figure 2.16
BEJT Concentration Response Curves at the Design Management Zones

Scale: None | Date: Dec 1998

Prepared By: HSI GEOTRANS | By: RAK

\Crandon\TmaMod4\Excel\hypothet.xls, bej

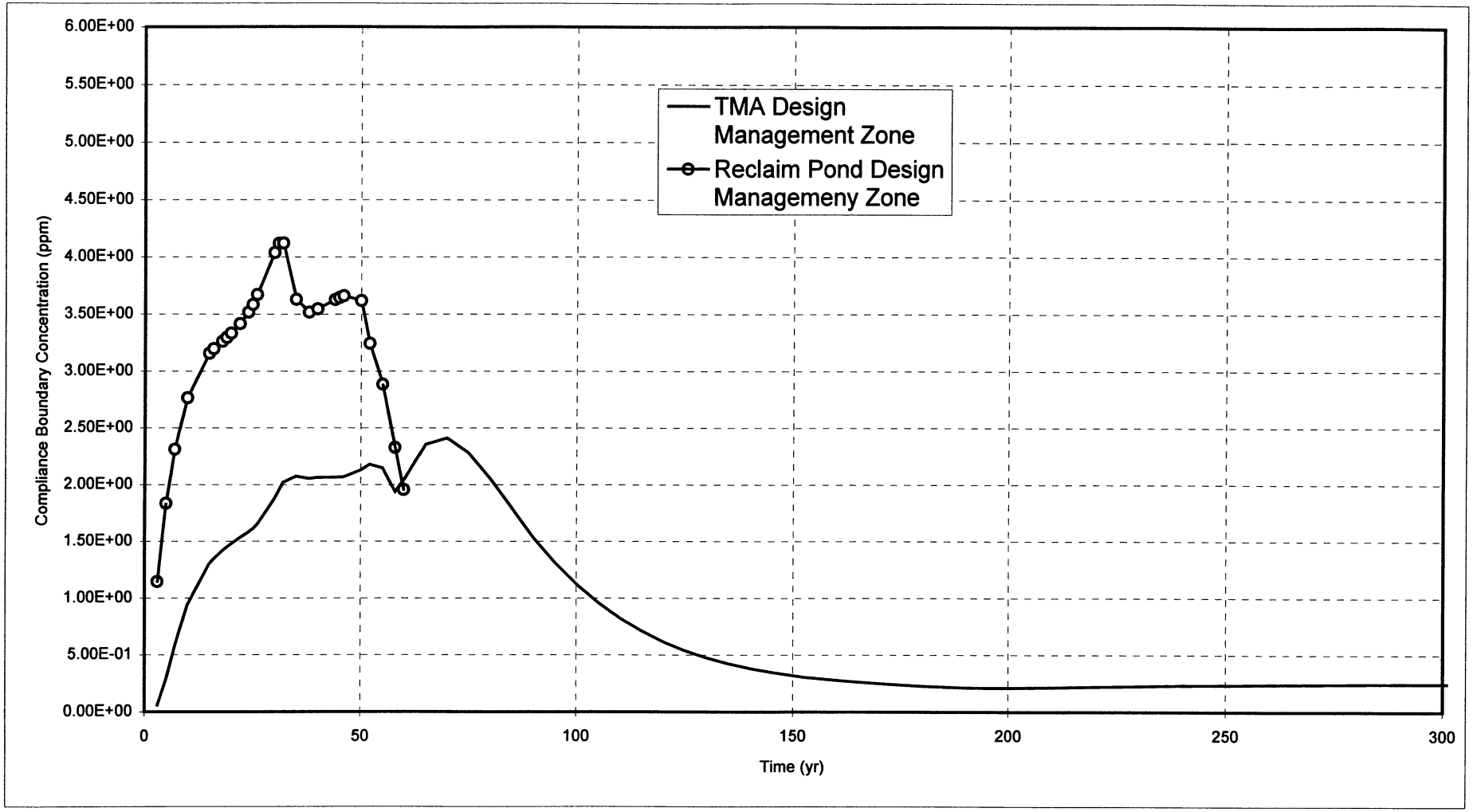

4.2-10-329

Source Concentration:
Operation: 2000 ppm
Post-Cap: 4000 ppm
Oxidized: 40000 ppm*

* As a conservative assumption, the oxidized concentration begins immediately after assumed degradation of the flexible membrane liner.

HSI GEOTRANS			
REVISED	DATE	BY	DESCRIPTION
CHECKED BY: GWC			DATE: Dec 1998
APPROVED BY: PFA			DATE: Dec 1998
APPROVED BY:			DATE:

Simulations T07C1, 2, 3

Nicolet Minerals COMPANY

Figure 2.17
BEJT Concentration at the Design Management Zones (Example Constituent)

Scale: None	Date: Dec 1998
Prepared By: HSI GEOTRANS	By: RAK

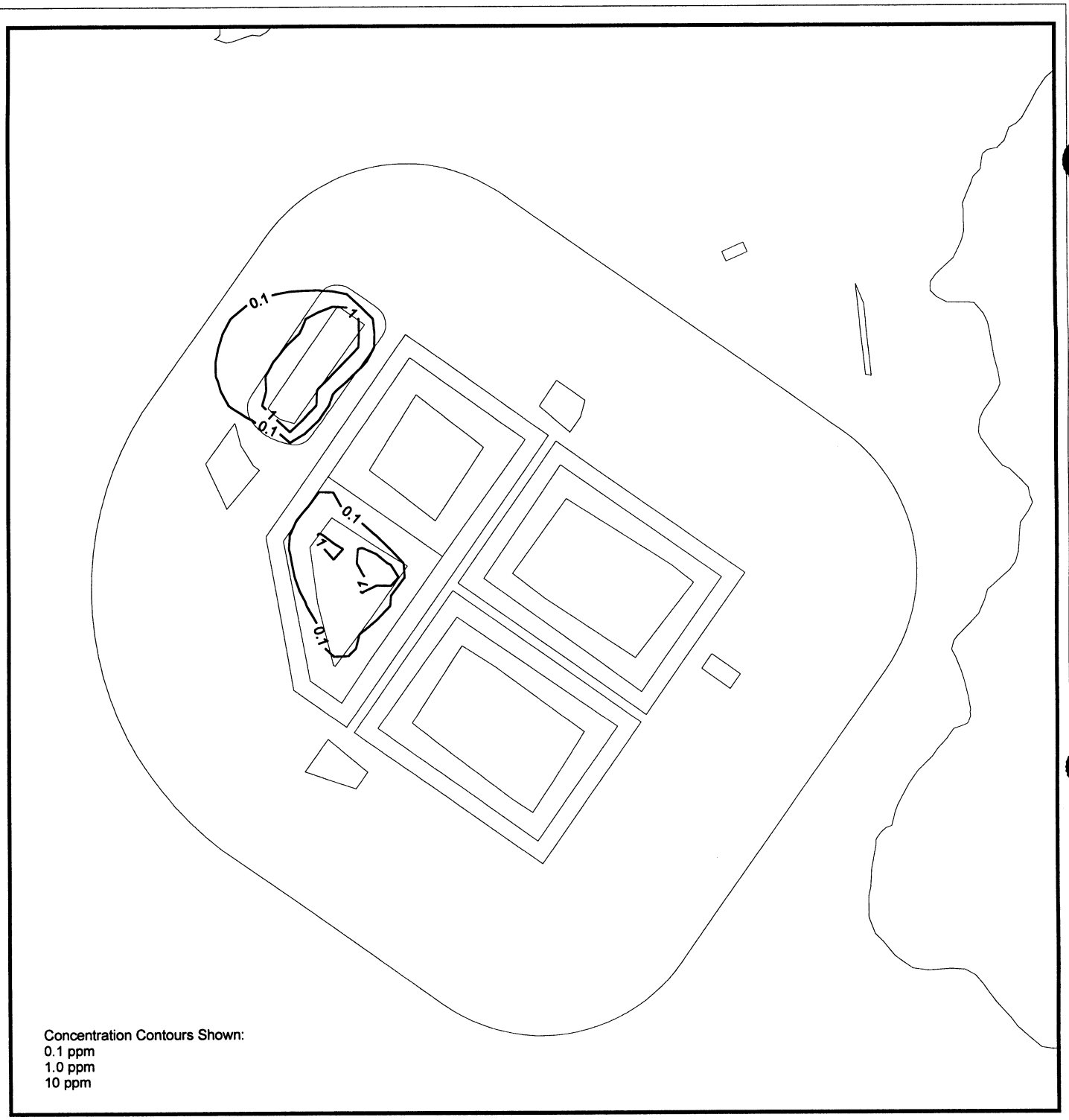

Concentration Contours Shown:
0.1 ppm
1.0 ppm
10 ppm

Source Concentration
Operation: 2000 ppm
Post-cap: 4000 ppm
Oxidized: 40,000 ppm*

* As a conservative assumption, the oxidized concentration begins immediately after assumed degradation of the flexible membrane liner.

Note:
This plot shows contours of maximum concentratration in any layer.

0 1000 2000
Scale in Feet

HSI GEOTRANS

REVISED	DATE	BY	DESCRIPTION

CHECKED BY: GWC	DATE: Dec 98
APPROVED BY: PFA	DATE: Dec 98
APPROVED BY:	DATE:

Nicolet Minerals COMPANY

Figure 2.18
BEJT Concentration After 3 Years
(Example Constituent, Plan View)

Scale: 1 in. = 1000 ft.	Date: November 1998
Prepared By: HSI GEOTRANS	By: KMR

\Crandon\Tmwmodfl\Surfer\Bej003.srf

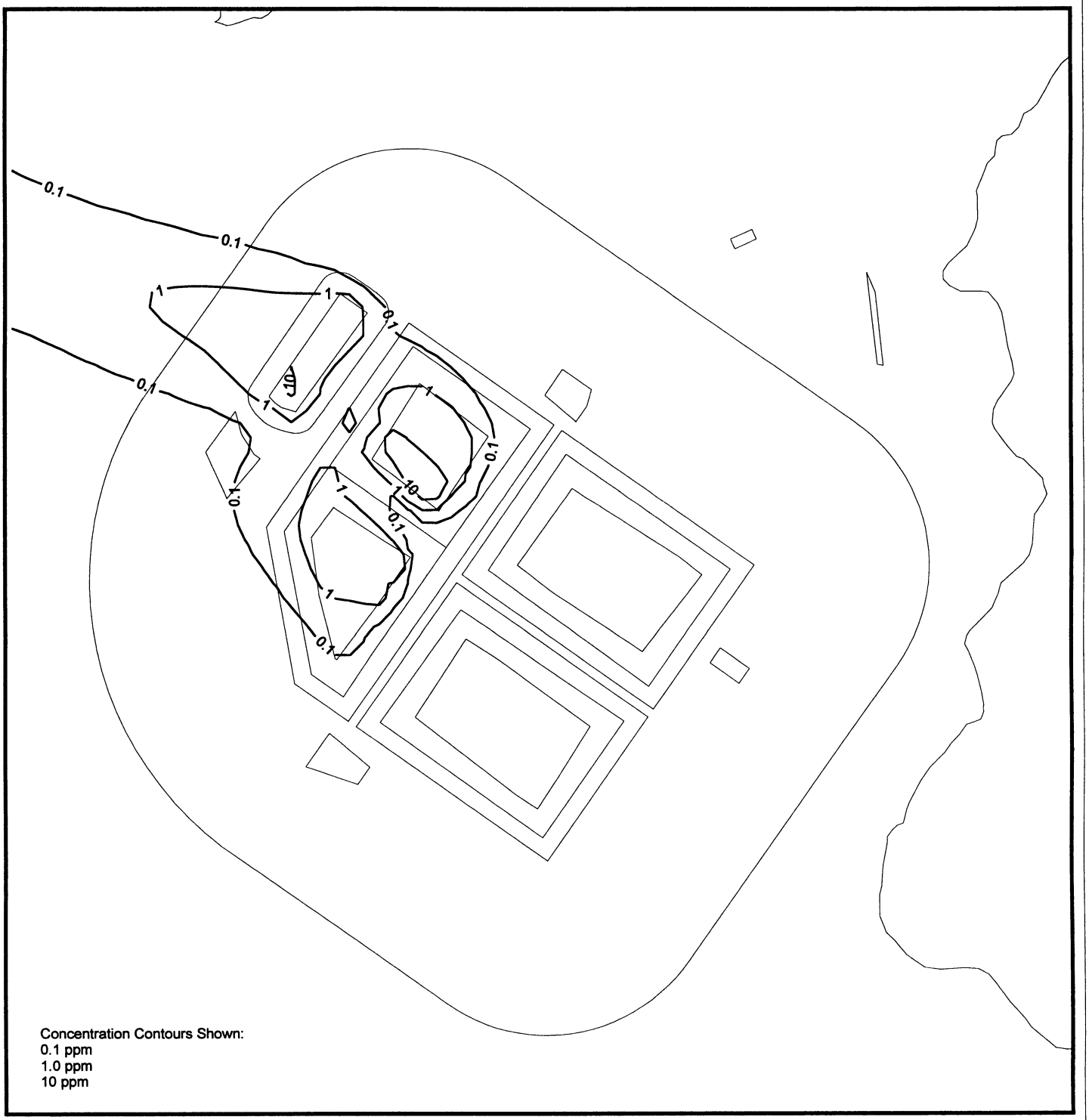

Concentration Contours Shown:
0.1 ppm
1.0 ppm
10 ppm

Source Concentration
Operation: 2000 ppm
Post-cap: 4000 ppm
Oxidized: 40,000 ppm*

* As a conservative assumption, the oxidized concentration begins immediately after assumed degradation of the flexible membrane liner.

Note:
This plot shows contours of maximum concentratration in any layer.

N

0 1000 2000

Scale in Feet

HSI GEOTRANS

REVISED	DATE	BY	DESCRIPTION

CHECKED BY: GWC	DATE: Dec 98
APPROVED BY: PFA	DATE: Dec 98
APPROVED BY:	DATE:

Nicolet Minerals COMPANY

Figure 2.19
BEJT Concentration After 16 Years (Example Constituent, Plan View)

Scale: 1 in. = 1000 ft.	Date: November 1998
Prepared By: HSI GEOTRANS	By: KMR

\CrandonTmal\Mod4\Surfer\Bejt016.srf

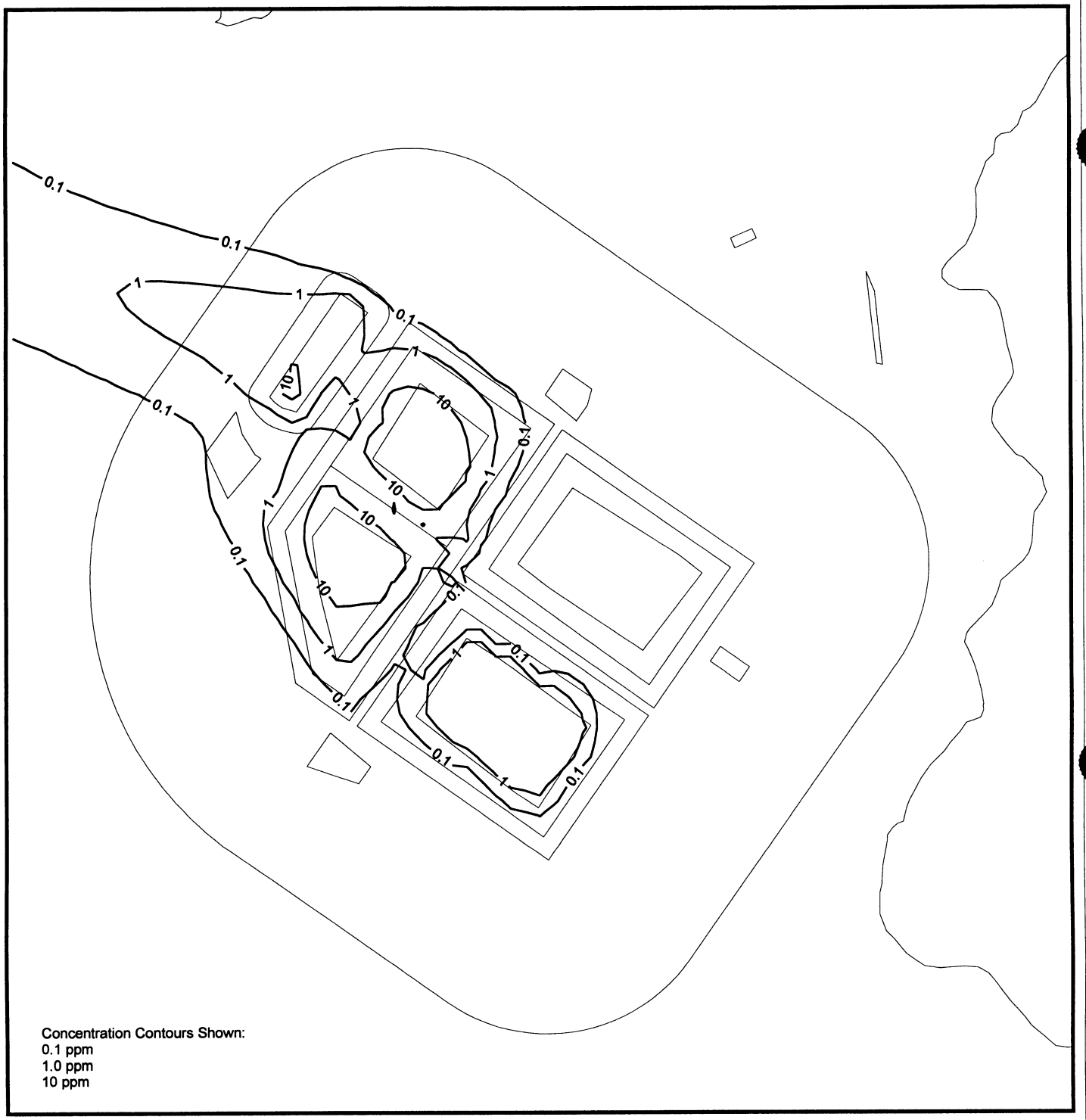

Source Concentration
Operation: 2000 ppm
Post-cap: 4000 ppm
Oxidized: 40,000 ppm*

* As a conservative assumption, the oxidized concentration begins immediately after assumed degradation of the flexible membrane liner.

Note:
This plot shows contours of maximum concentratration in any layer.

N

0 1000 2000

Scale in Feet

HSI GEOTRANS

REVISED	DATE	BY	DESCRIPTION

CHECKED BY: GWC	DATE: Dec 98
APPROVED BY: PFA	DATE: Dec 98
APPROVED BY:	DATE:

Nicolet Minerals COMPANY

Figure 2.20
BEJT Concentration After 22 Years
(Example Constituent, Plan View)

Scale: 1 in. = 1000 ft.	Date: November 1998
Prepared By: HSI GEOTRANS	By: KMR

\Crandon\Tmal\Mod4\Surfer\Bejt022.srf

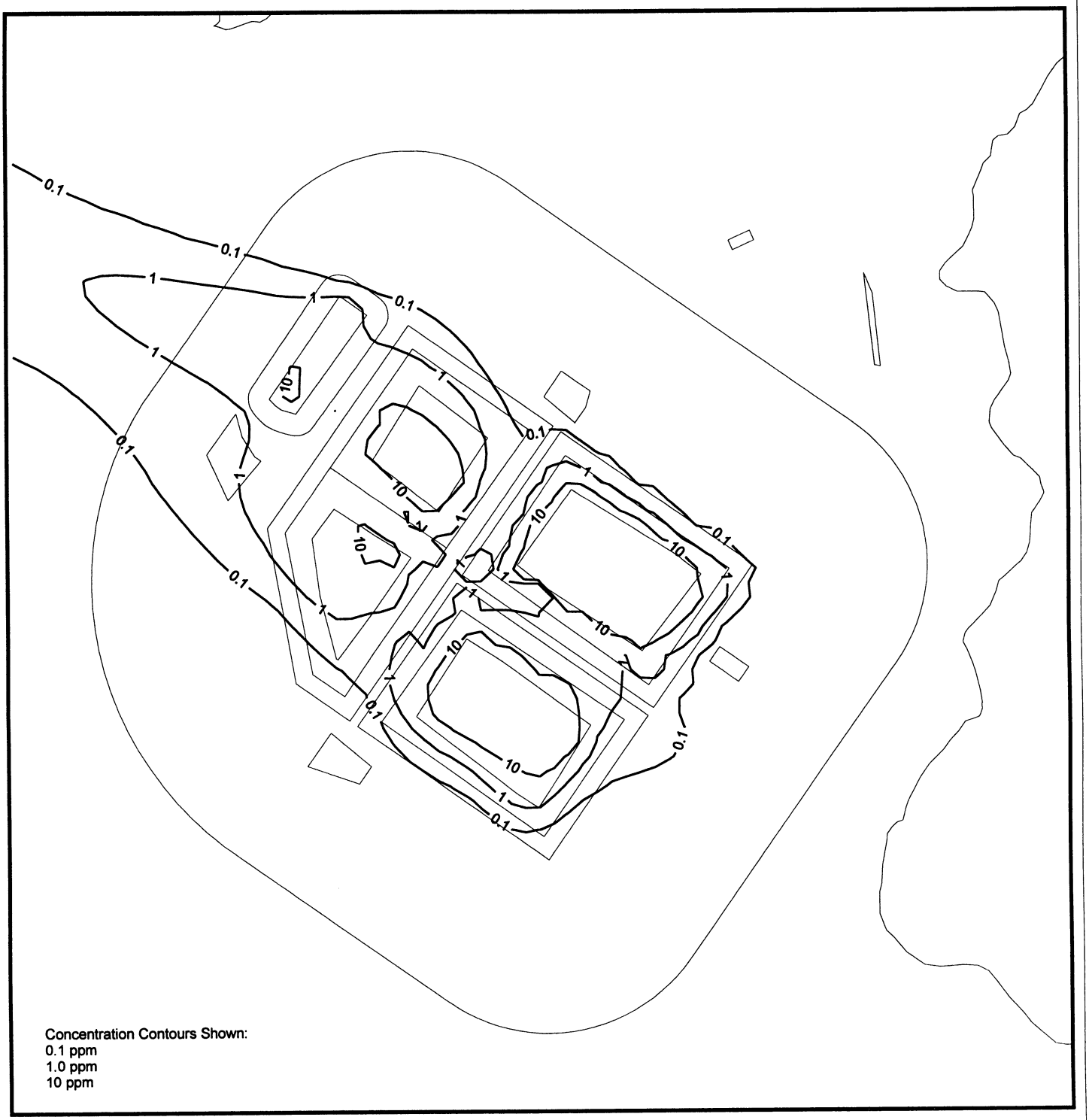

Concentration Contours Shown:
0.1 ppm
1.0 ppm
10 ppm

Source Concentration
Operation: 2000 ppm
Post-cap: 4000 ppm
Oxidized: 40,000 ppm*

* As a conservative assumption, the oxidized concentration begins immediately after assumed degradation of the flexible membrane liner.

Note:
This plot shows contours of maximum concentratration in any layer.

N

0 1000 2000

Scale in Feet

HSI GEOTRANS			
REVISED	DATE	BY	DESCRIPTION
CHECKED BY: GWC			DATE: Dec 98
APPROVED BY: PFA			DATE: Dec 98
APPROVED BY:			DATE:

Nicolet Minerals COMPANY

Figure 2.21
BEJT Concentration After 32 Years (Example Constituent, Plan View)

Scale: 1 in. = 1000 ft.	Date: November 1998
Prepared By: HSI GEOTRANS	By: KMR

\Crandon\Tmal\Mod4\Surfer\Bej032.srf

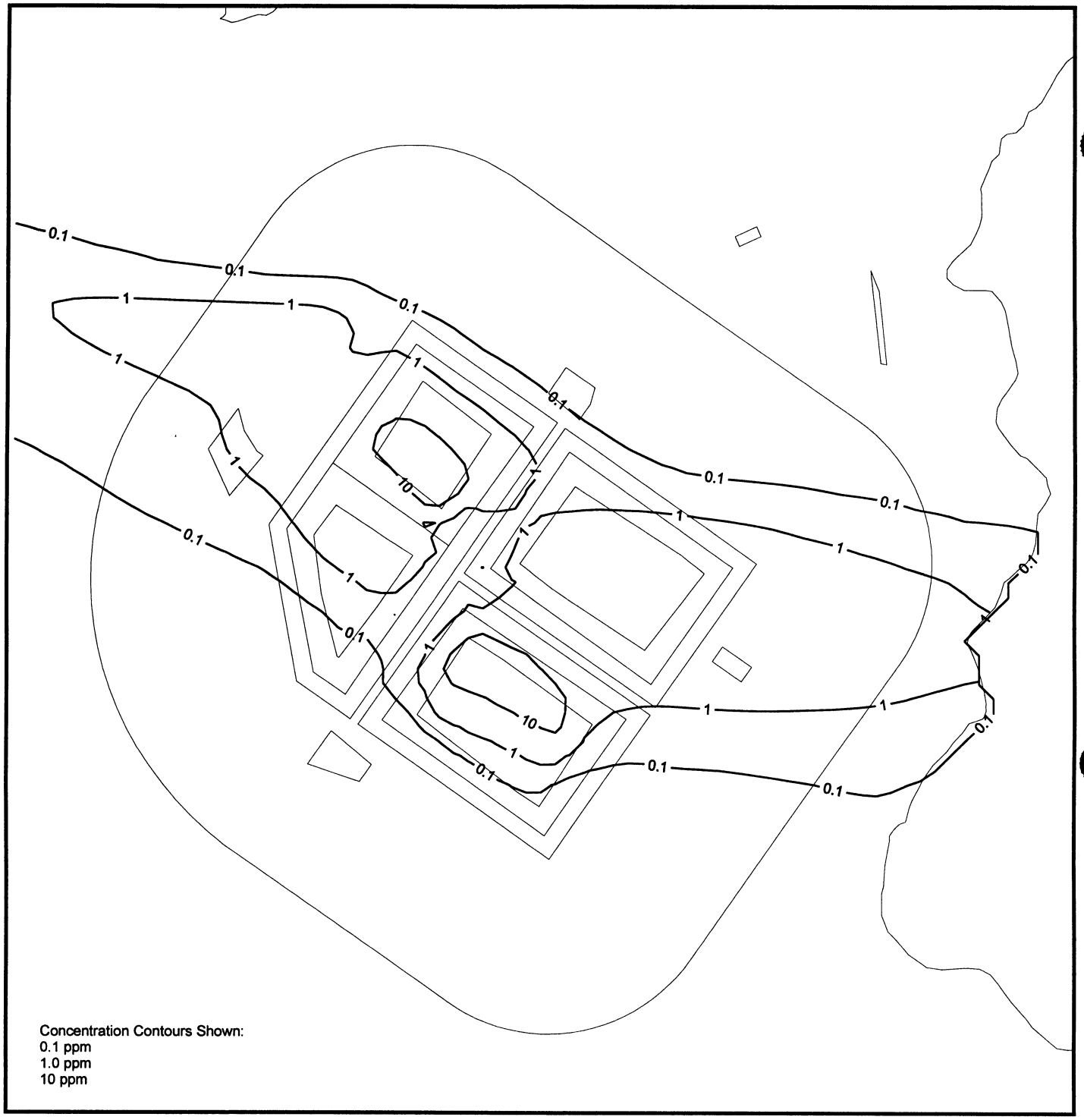

Source Concentration
Operation: 2000 ppm
Post-cap: 4000 ppm
Oxidized: 40,000 ppm*

* As a conservative assumption, the oxidized concentration begins immediately after assumed degradation of the flexible membrane liner.

Note:
This plot shows contours of maximum concentratration in any layer.

N

0 1000 2000

Scale in Feet

HSI GEOTRANS

REVISED	DATE	BY	DESCRIPTION

CHECKED BY: GWC	DATE: Dec 98
APPROVED BY: PFA	DATE: Dec 98
APPROVED BY:	DATE:

Nicolet Minerals COMPANY

Figure 2.22
BEJT Concentration After 60 Years
(Example Constituent, Plan View)

Scale: 1 in. = 1000 ft.	Date: November 1998
Prepared By: HSI GEOTRANS	By: KMR

\CrandonTmaMod4\Surfer\Bej060.srf

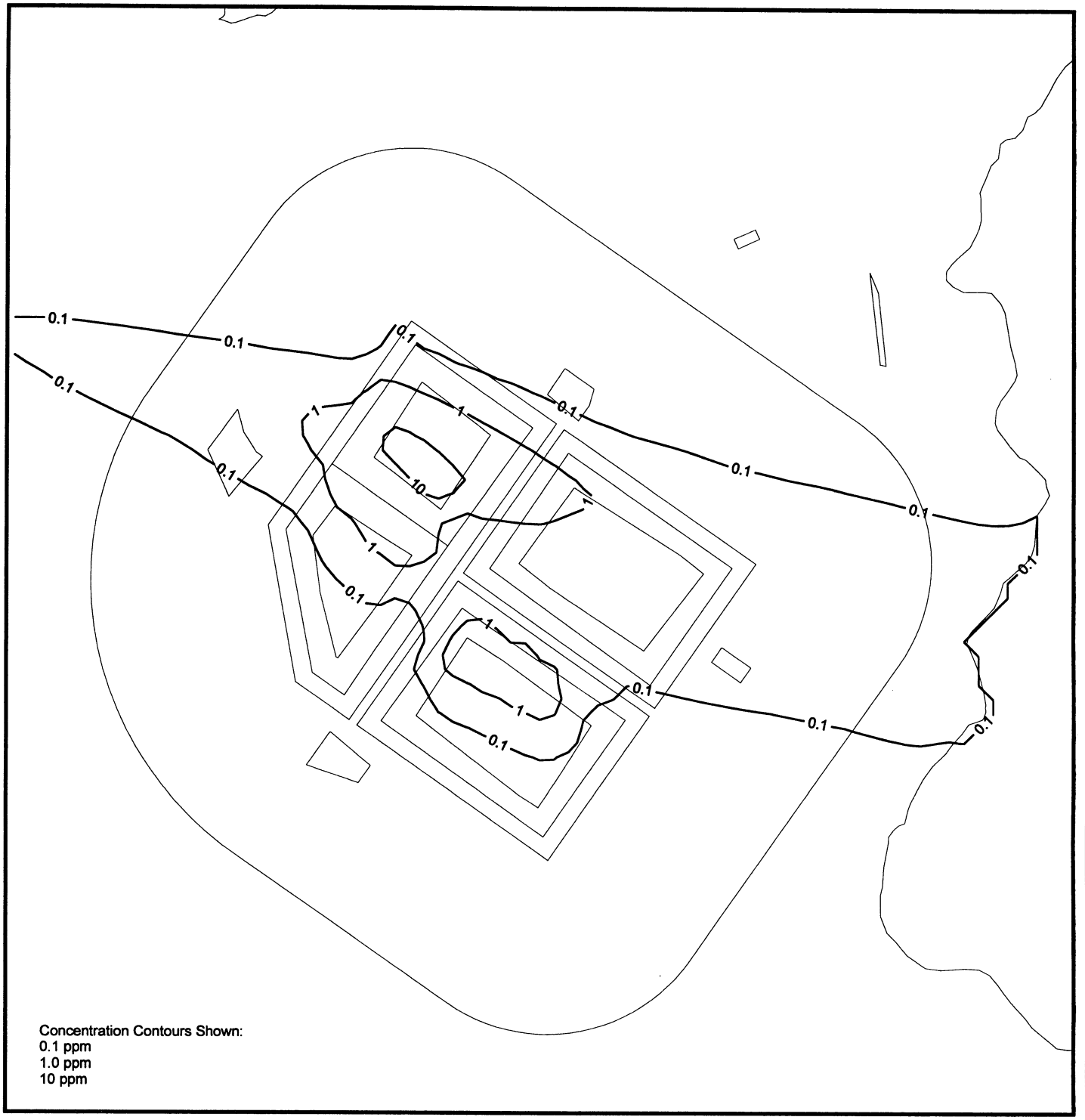

Source Concentration
Operation: 2000 ppm
Post-cap: 4000 ppm
Oxidized: 40,000 ppm*

* As a conservative assumption, the oxidized concentration begins immediately after assumed degradation of the flexible membrane liner.

Note:
This plot shows contours of maximum concentratration in any layer.

0 1000 2000
Scale in Feet

HSI GEOTRANS

REVISED	DATE	BY	DESCRIPTION

CHECKED BY: GWC	DATE: Dec 98
APPROVED BY: PFA	DATE: Dec 98
APPROVED BY:	DATE:

Nicolet Minerals COMPANY

Figure 2.23
BEJT Concentration After 125 Years (Example Constituent, Plan View)

Scale: 1 in. = 1000 ft.	Date: November 1998
Prepared By: HSI GEOTRANS	By: KMR

\Crandon\Tmwmod\Surfer\3dj125.srf

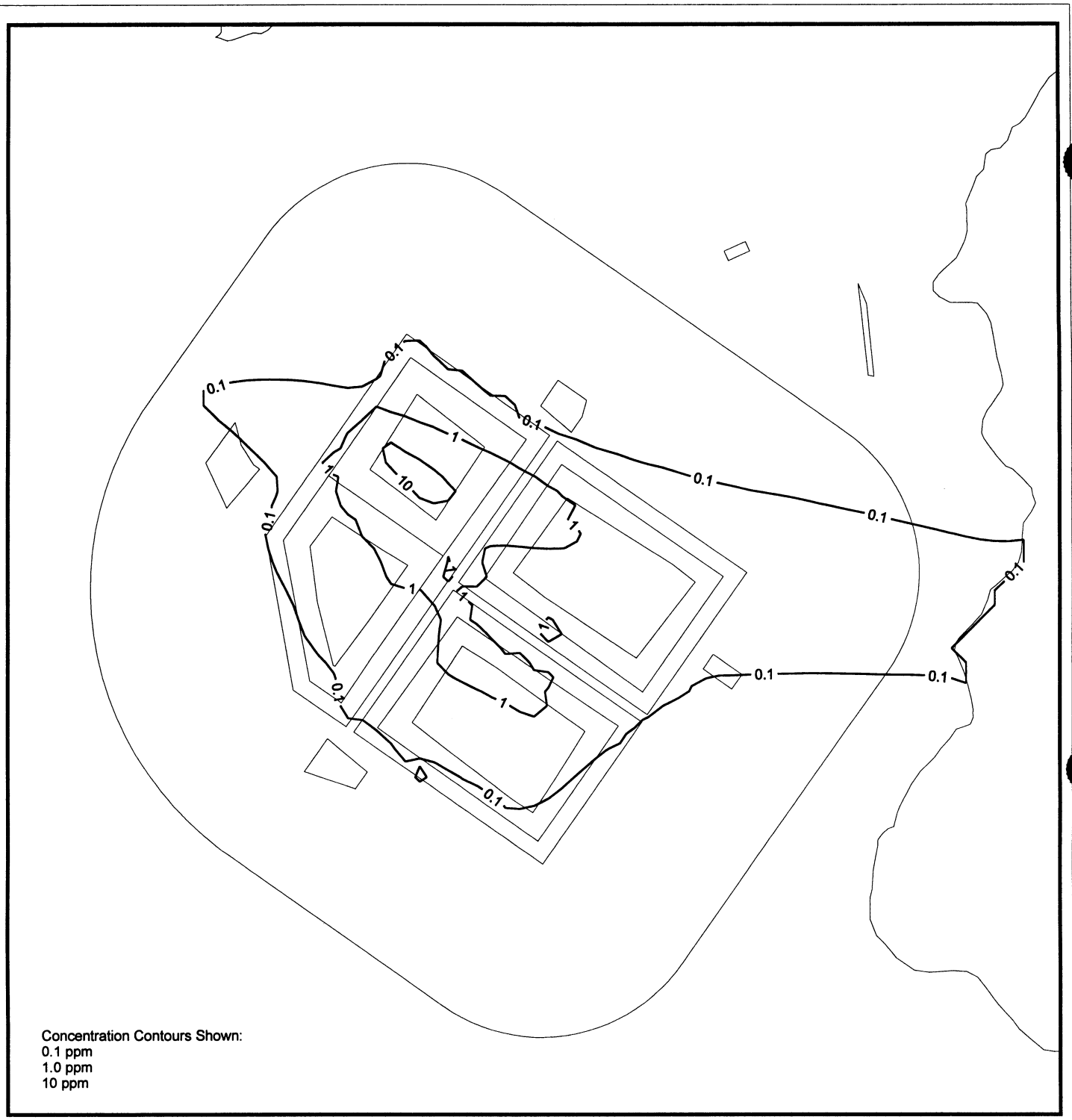

Source Concentration
Operation: 2000 ppm
Post-cap: 4000 ppm
Oxidized: 40,000 ppm*

* As a conservative assumption, the oxidized concentration begins immediately after assumed degradation of the flexible membrane liner.

Note:
This plot shows contours of maximum concentratration in any layer.

0 1000 2000
Scale in Feet

HSI GEOTRANS

REVISED	DATE	BY	DESCRIPTION

CHECKED BY: GWC	DATE: Dec 98
APPROVED BY: PFA	DATE: Dec 98
APPROVED BY:	DATE:

Nicolet Minerals COMPANY

Figure 2.24
BEJT Concentration After 200 Years (Example Constituent, Plan View)

Scale: 1 in. = 1000 ft.	Date: November 1998
Prepared By: HSI GEOTRANS	By: KMR

\Crandon\Tmwf\Mod4\Surfer\Beg200.srf

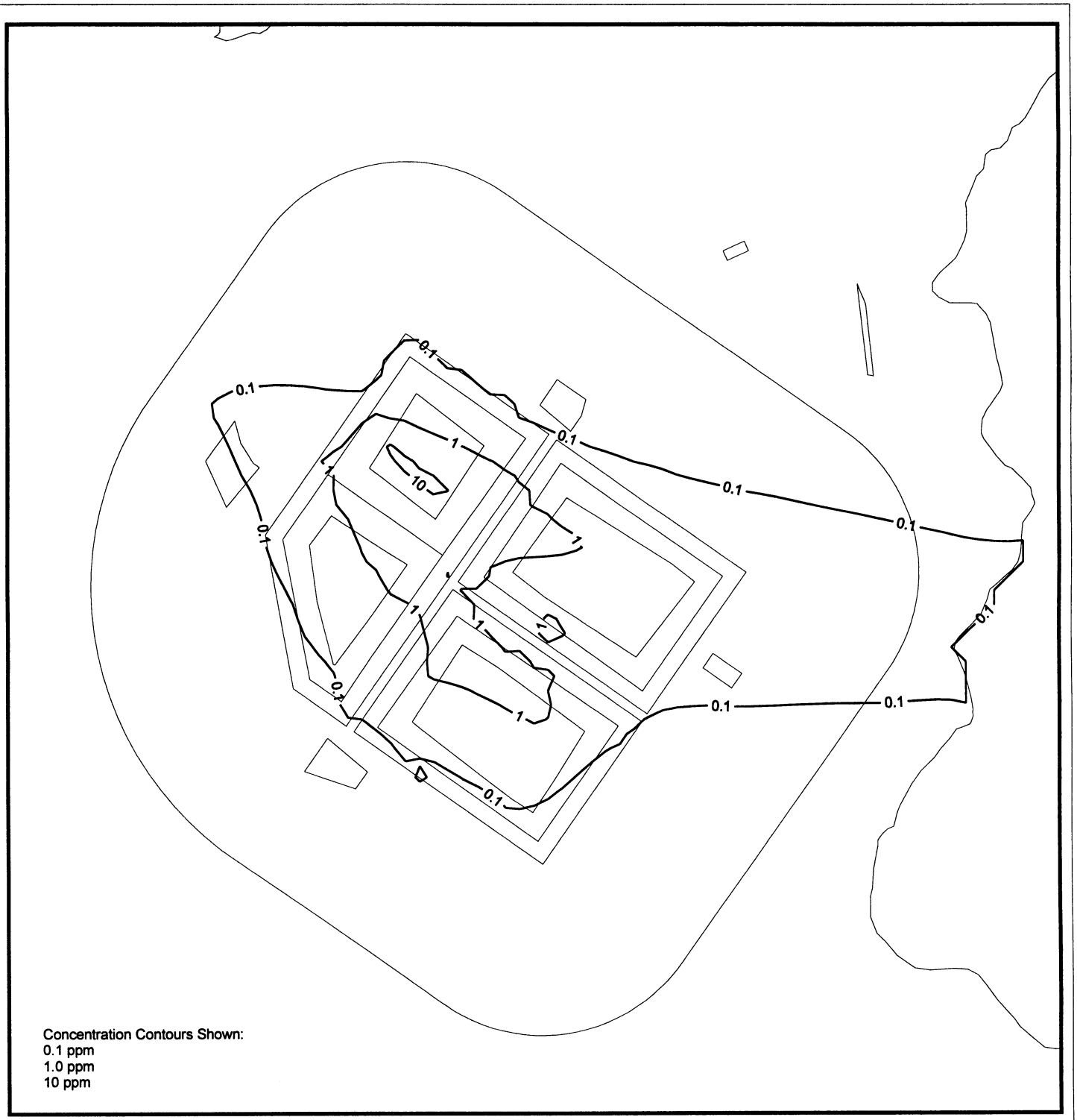

Source Concentration
Operation: 2000 ppm
Post-cap: 4000 ppm
Oxidized: 40,000 ppm*

* As a conservative assumption, the oxidized concentration begins immediately after assumed degradation of the flexible membrane liner.

Note:
This plot shows contours of maximum concentratration in any layer.

0 1000 2000
Scale in Feet

HSI GEOTRANS			
REVISED	DATE	BY	DESCRIPTION

CHECKED BY: GWC	DATE: Dec 98
APPROVED BY: PFA	DATE: Dec 98
APPROVED BY:	DATE:

Nicolet Minerals COMPANY

Figure 2.25
BEJT Concentration After 300 Years (Example Constituent, Plan View)

Scale: 1 in. = 1000 ft.	Date: November 1998
Prepared By: HSI GEOTRANS	By: KMR

\Crandon\TmaMod4\Surfer\Bej300.srf

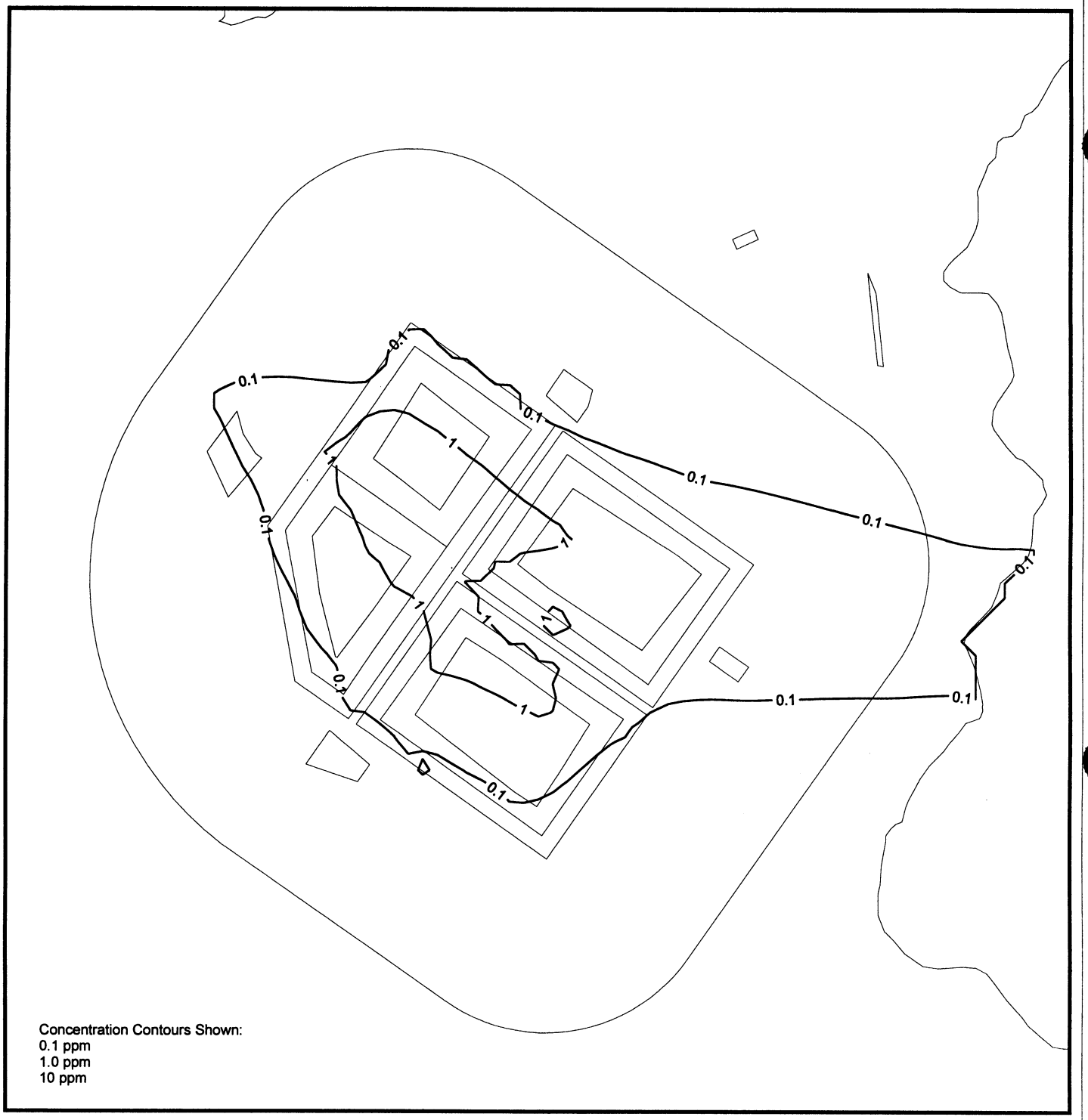

Source Concentration
Operation: 2000 ppm
Post-cap: 4000 ppm
Oxidized: 40,000 ppm*

* As a conservative assumption, the oxidized concentration begins immediately after assumed degradation of the flexible membrane liner.

Note:
This plot shows contours of maximum concentratration in any layer.

N

0 1000 2000

Scale in Feet

HSI GEOTRANS

REVISED	DATE	BY	DESCRIPTION

CHECKED BY: GWC	DATE: Dec 98
APPROVED BY: PFA	DATE: Dec 98
APPROVED BY:	DATE:

Nicolet Minerals COMPANY

Figure 2.26
BEJT Concentration After 650 Years
(Example Constituent, Plan View)

Scale: 1 in. = 1000 ft.	Date: November 1998
Prepared By: HSI GEOTRANS	By: KMR

\CrandonTmaMod4\Surfer\Bejt650.srf

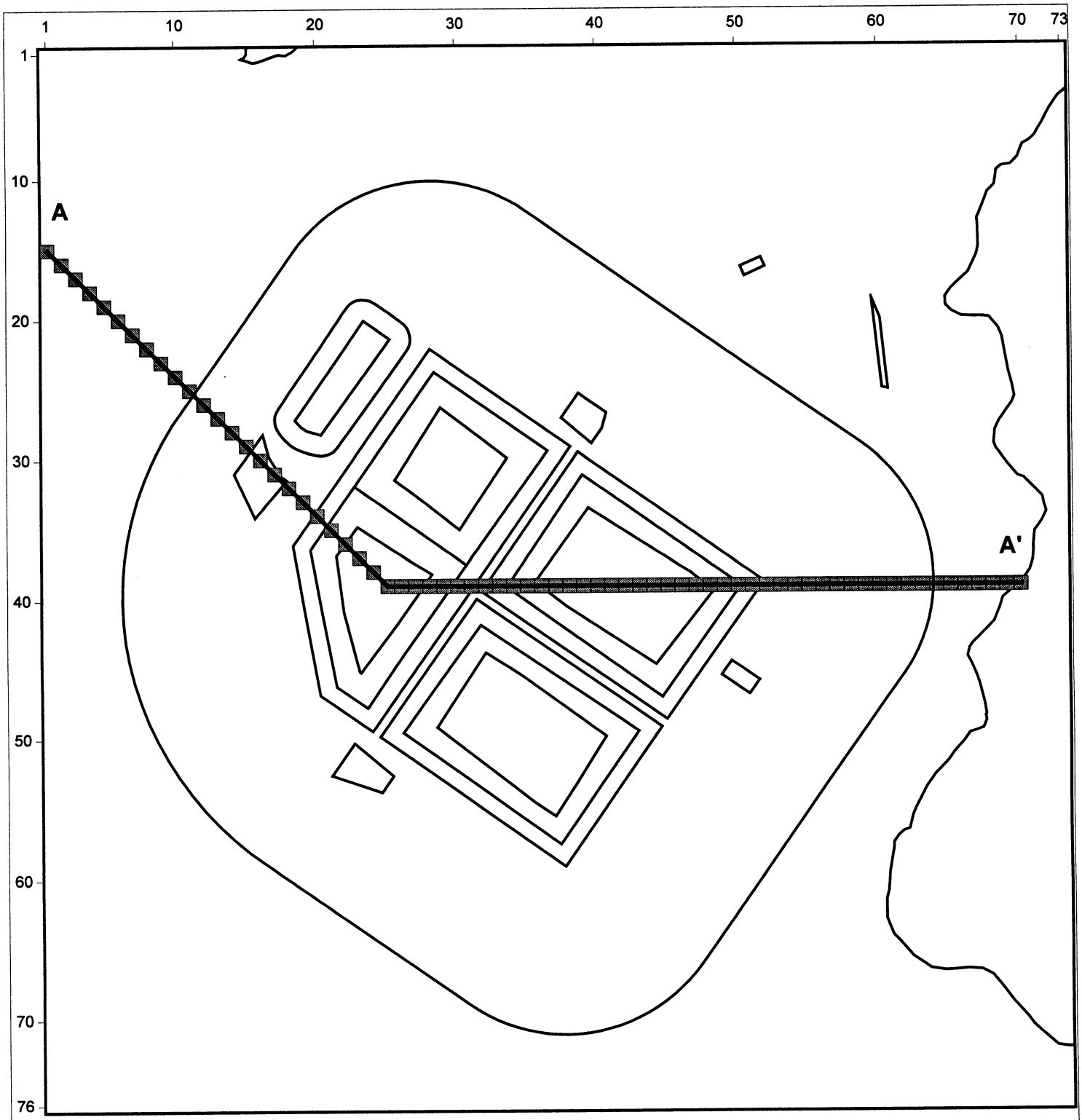

0 1000 2000

Scale in Feet

HSI GEOTRANS

REVISED	DATE	BY	DESCRIPTION

CHECKED BY: KMR	DATE: Dec 1998
APPROVED BY: PFA	DATE: Dec 1998
APPROVED BY:	DATE:

Nicolet Minerals COMPANY

Figure 2.27
Location of Cross-Section Used for Viewing Plumes

Scale: 1 in. = 1000 ft. | Date: Dec 1998

Prepared By: HSI GeoTrans | By: GWC

P:\CMC\TmaMod4\GIS\Section.wor

\Crandon\TmaMod4\Surfer\07c003x.srf

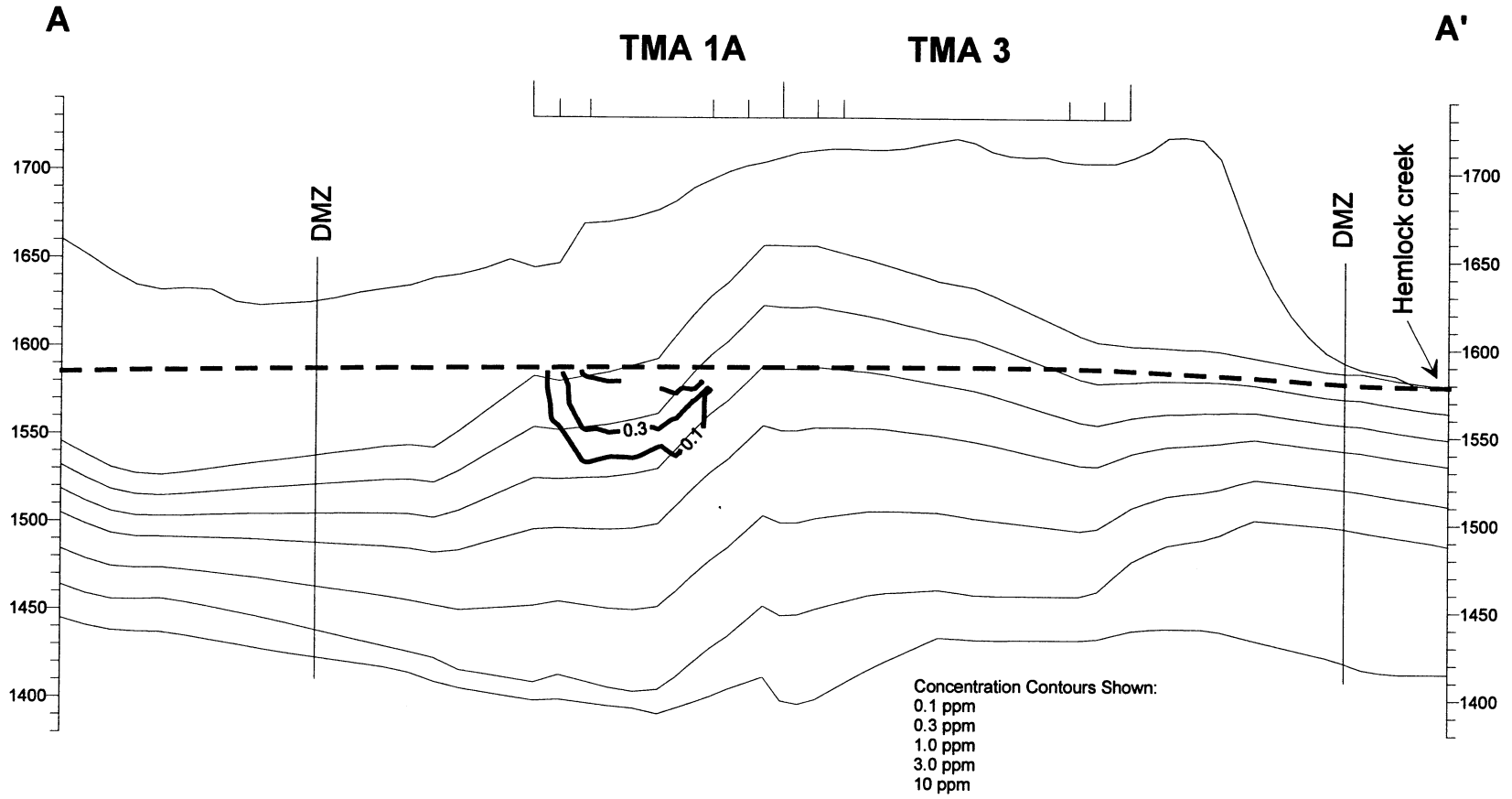

4.2-10-340

Source Concentration
Operation: 2000 ppm
Post-cap: 4000 ppm
Oxidized: 40,000 ppm*

* As a conservative assumption, the oxidized concentration begins immediately after assumed degradation of the flexible membrane liner.

HSI GEOTRANS

REVISED	DATE	BY	DESCRIPTION

CHECKED BY: RAK	DATE: Dec 98
APPROVED BY: PFA	DATE: Dec 98
APPROVED BY:	DATE:

Nicolet Minerals COMPANY

Figure 2.28
BEJT Concentration After 3 Years (Example Constituent, Cross Section)

Scale: 1" = 1000' (h), 100' (v)	Date: Dec 1998
Prepared By: HSI GeoTrans	By: GWC

\Crandon\TmaMod4\Surfer\07c016x.srf

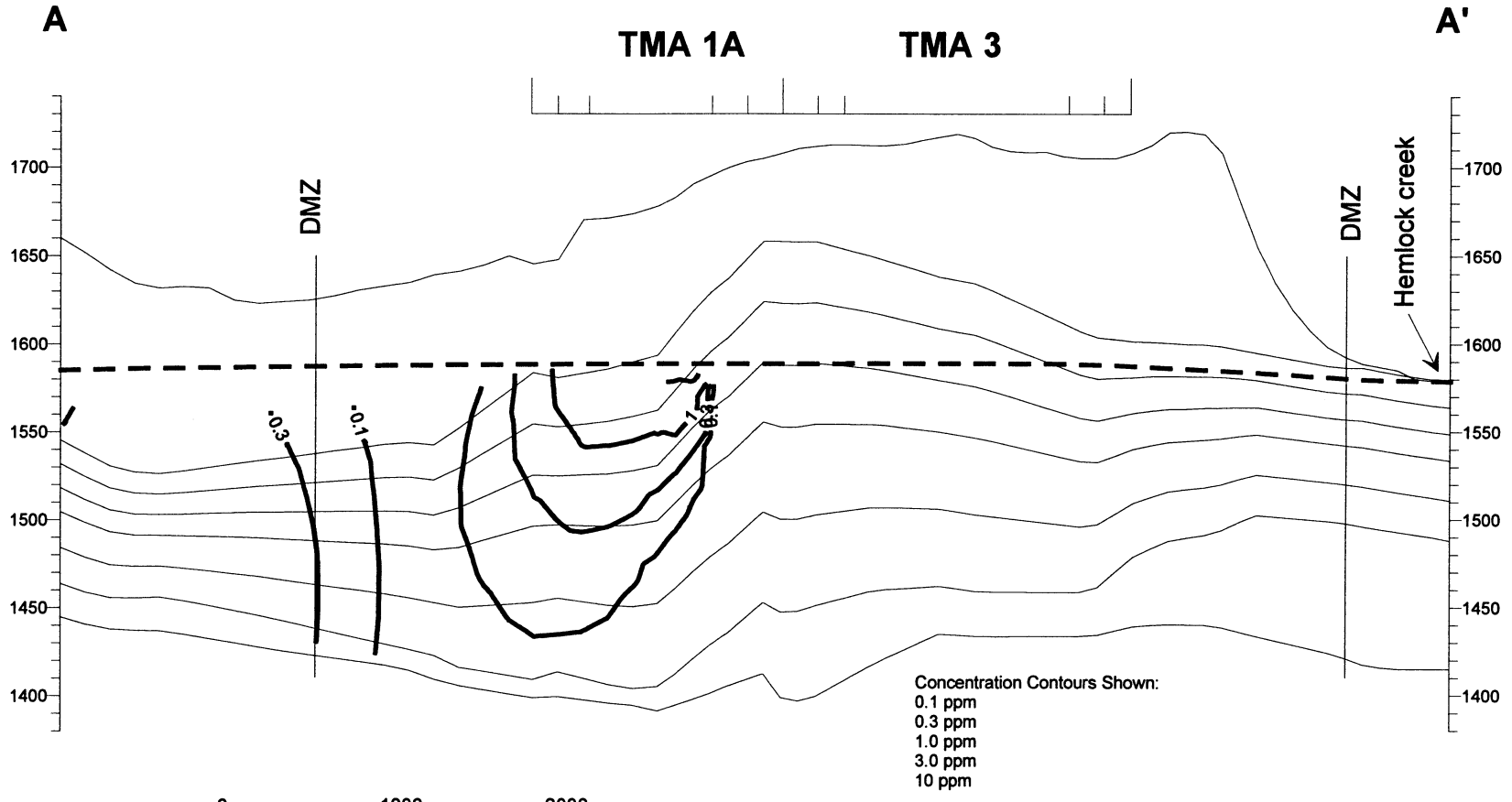

4.2-10-341

Source Concentration
Operation: 2000 ppm
Post-cap: 4000 ppm
Oxidized: 40,000 ppm*

* As a conservative assumption, the oxidized concentration begins immediately after assumed degradation of the flexible membrane liner.

HSI GEOTRANS

REVISED	DATE	BY	DESCRIPTION

CHECKED BY: GWC	DATE: Dec 98
APPROVED BY: PFA	DATE: Dec 98
APPROVED BY:	DATE:

Nicolet Minerals COMPANY

Figure 2.29
BEJT Concentration After 16 Years
(Example Constituent, Cross Section)

Scale: 1" = 1000' (h), 100' (v)	Date: Dec 1998
Prepared By: HSI GeoTrans	By: RAK

\Crandon\TmaMod4\Surfer\07c022x.srf

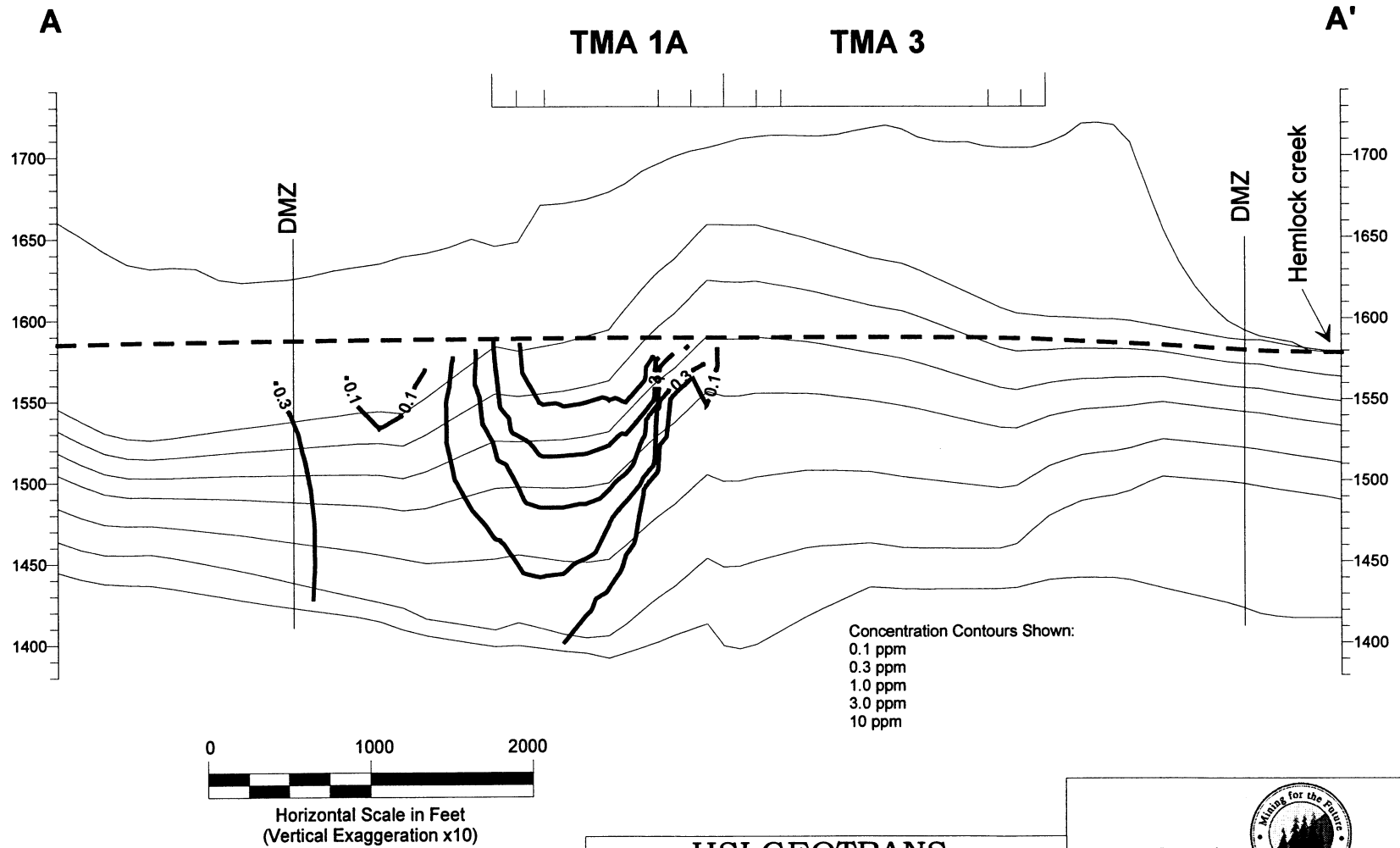

4.2-10-342

Source Concentration
Operation: 2000 ppm
Post-cap: 4000 ppm
Oxidized: 40,000 ppm*

* As a conservative assumption, the oxidized concentration begins immediately after assumed degradation of the flexible membrane liner.

HSI GEOTRANS

REVISED	DATE	BY	DESCRIPTION

CHECKED BY: GWC	DATE: Dec 98
APPROVED BY: PFA	DATE: Dec 98
APPROVED BY:	DATE:

Nicolet Minerals COMPANY

Mining for the Future

Figure 2.30
BEJT Concentration After 22 Years (Example Constituent, Cross Section)

Scale: 1" = 1000' (h), 100' (v)	Date: Dec 1998
Prepared By: HSI GeoTrans	By: RAK

\Crandon\TmaMod4\Surfer\07c032x.srf

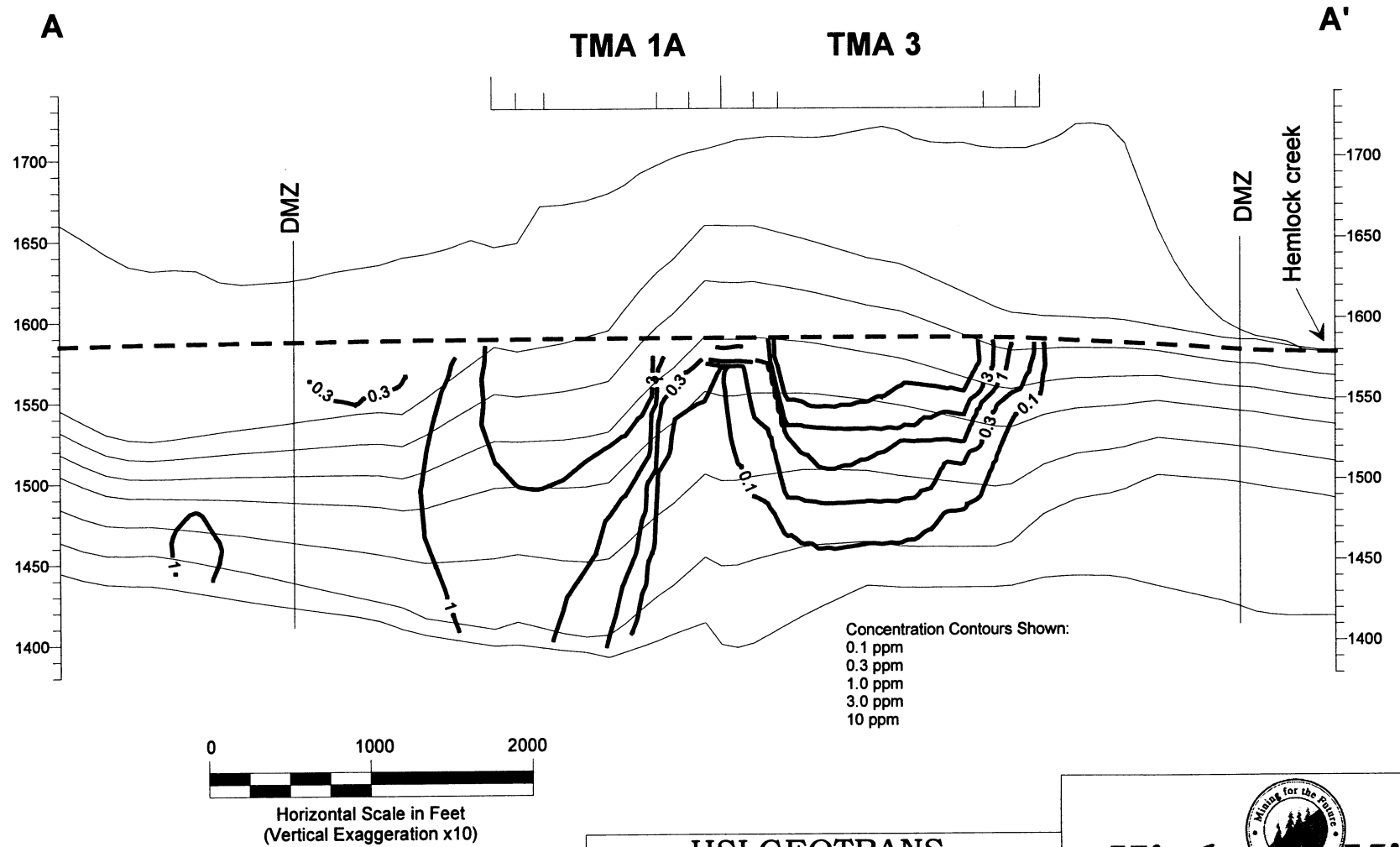

4.2-10-343

Source Concentration
Operation: 2000 ppm
Post-cap: 4000 ppm
Oxidized: 40,000 ppm*

* As a conservative assumption, the oxidized concentration begins immediately after assumed degradation of the flexible membrane liner.

HSI GEOTRANS

REVISED	DATE	BY	DESCRIPTION

CHECKED BY: GWC	DATE: Dec 98
APPROVED BY: PFA	DATE: Dec 98
APPROVED BY:	DATE:

Nicolet Minerals COMPANY

Figure 2.31
BEJT Concentration After 32 Years (Example Constituent, Cross Section)

Scale: 1" = 1000' (h), 100' (v)	Date: Dec 1998
Prepared By: HSI GeoTrans	By: RAK

\Crandon\TmaMod4\Surfer\07c060x.srf

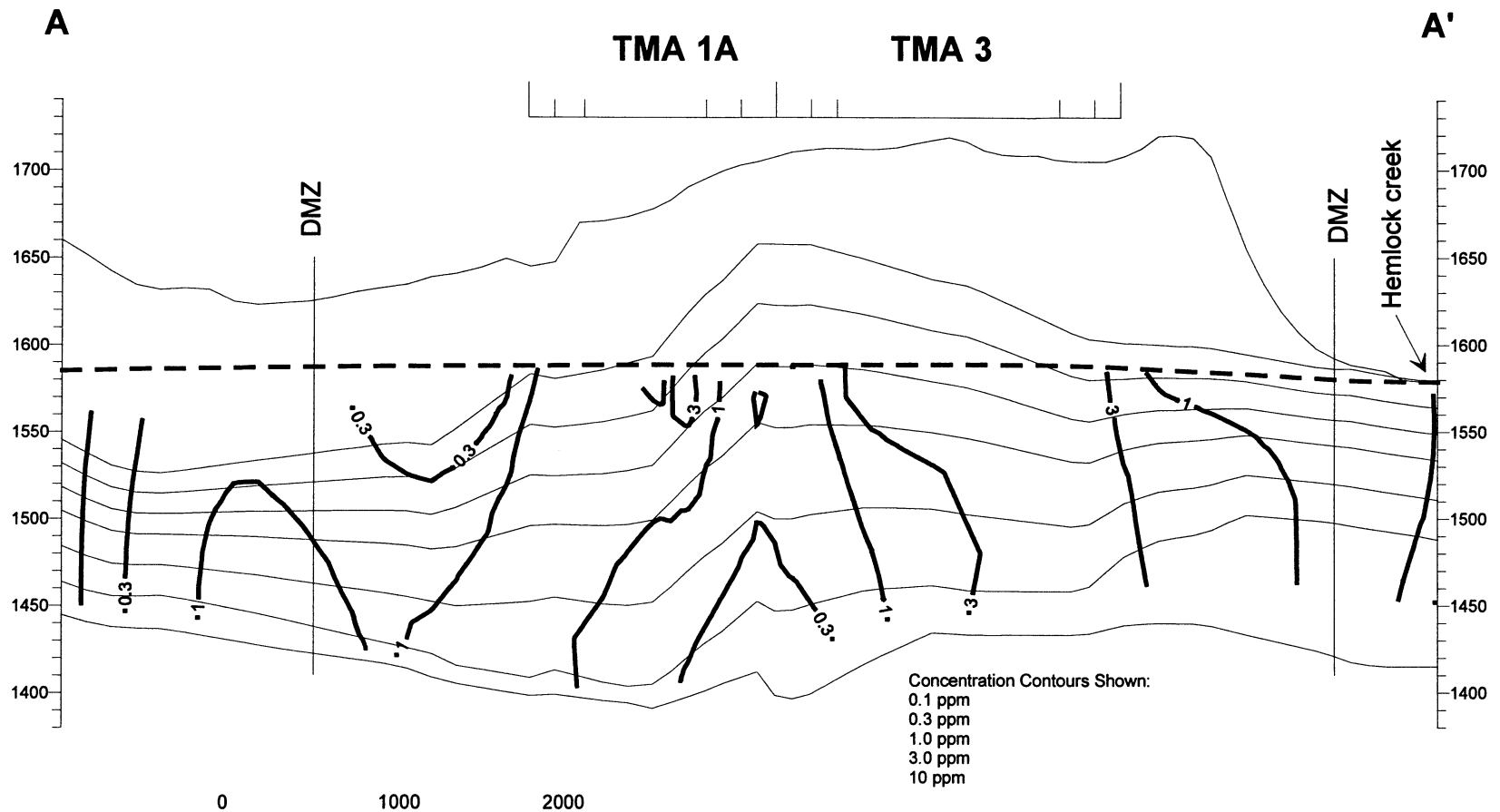

Concentration Contours Shown:
0.1 ppm
0.3 ppm
1.0 ppm
3.0 ppm
10 ppm

0 1000 2000

Horizontal Scale in Feet
(Vertical Exaggeration x10)

Source Concentration
Operation: 2000 ppm
Post-cap: 4000 ppm
Oxidized: 40,000 ppm*

* As a conservative assumption, the oxidized concentration begins immediately after assumed degradation of the flexible membrane liner.

4.2-10-344

HSI GEOTRANS

REVISED	DATE	BY	DESCRIPTION

CHECKED BY: GWC	DATE: Dec 98
APPROVED BY: PFA	DATE: Dec 98
APPROVED BY:	DATE:

Nicolet Minerals COMPANY

Figure 2.32
BEJT Concentration After 60 Years (Example Constituent, Cross Section)

Scale: 1" = 1000' (h), 100' (v)	Date: Dec 1998
Prepared By: HSI GeoTrans	By: RAK

\Crandon\TmaMod4\Surfer\07c125x.srf

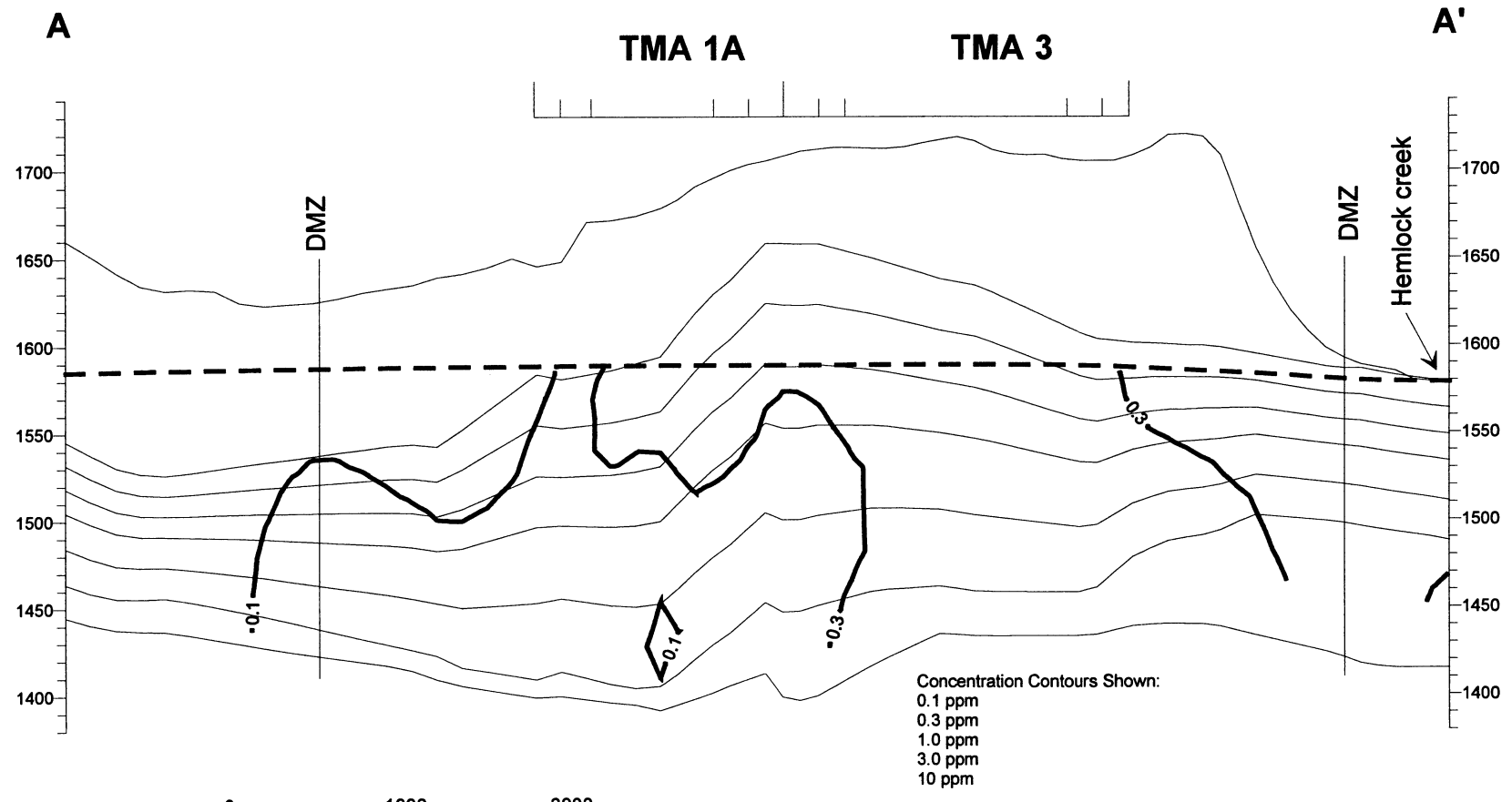

4.2-10-345

Source Concentration
Operation: 2000 ppm
Post-cap: 4000 ppm
Oxidized: 40,000 ppm*

* As a conservative assumption, the oxidized concentration begins immediately after assumed degradation of the flexible membrane liner.

HSI GEOTRANS

REVISED	DATE	BY	DESCRIPTION

CHECKED BY: GWC	DATE: Dec 98
APPROVED BY: PFA	DATE: Dec 98
APPROVED BY:	DATE:

Nicolet Minerals COMPANY

Figure 2.33
BEJT Concentration After 125 Years (Example Constituent, Cross Section)

Scale: 1" = 1000' (h), 100' (v)	Date: Dec 1998
Prepared By: HSI GeoTrans	By: RAK

\Crandon\TmaMod4\Surfer\07c200x.srf

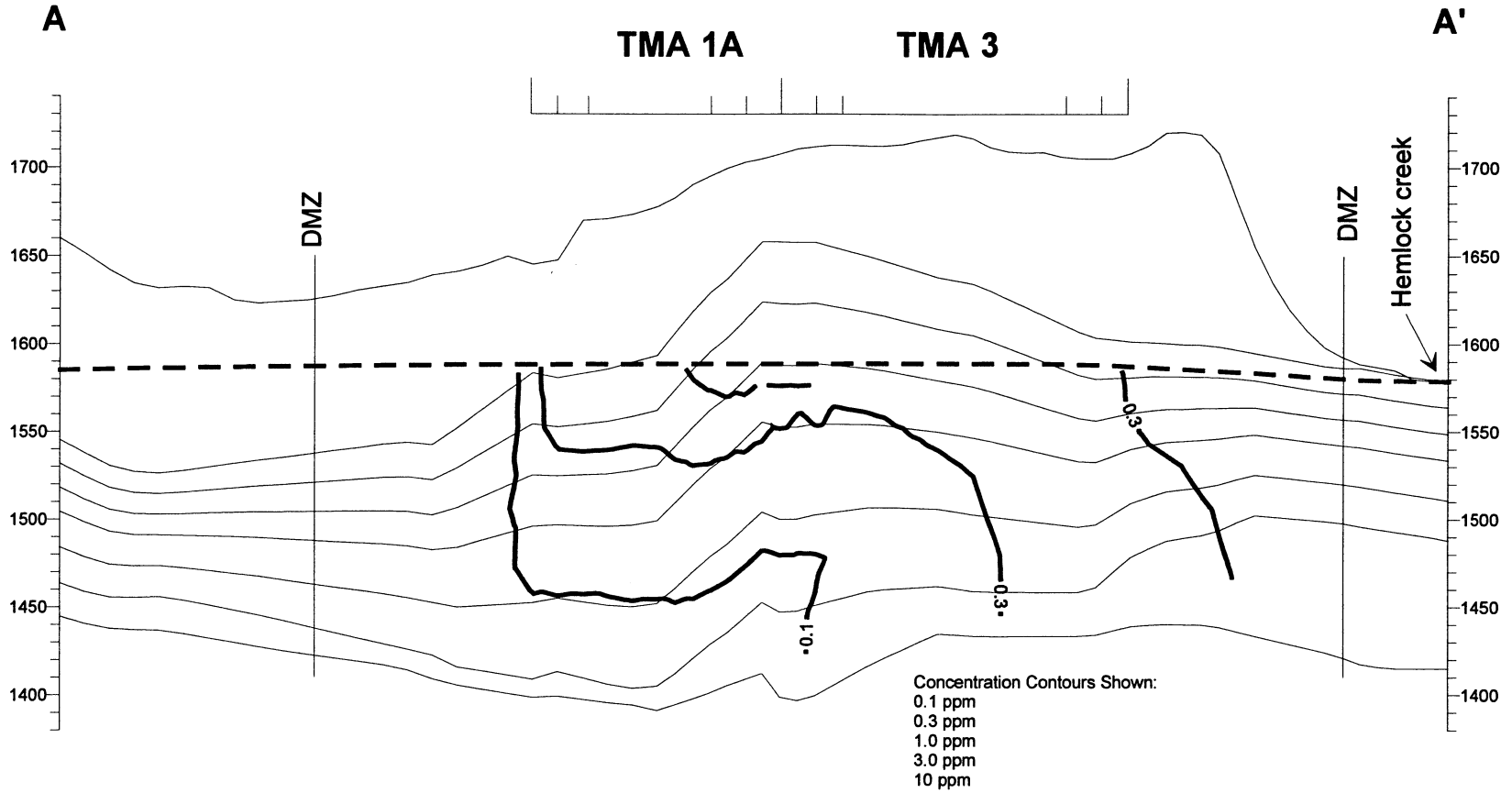

4.2-10-346

Source Concentration
Operation: 2000 ppm
Post-cap: 4000 ppm
Oxidized: 40,000 ppm*

* As a conservative assumption, the oxidized concentration begins immediately after assumed degradation of the flexible membrane liner.

HSI GEOTRANS

REVISED	DATE	BY	DESCRIPTION

CHECKED BY: GWC	DATE: Dec 98
APPROVED BY: PFA	DATE: Dec 98
APPROVED BY:	DATE:

Nicolet Minerals COMPANY

Figure 2.34
BEJT Concentration After 200 Years (Example Constituent, Cross Section)

Scale: 1" = 1000' (h), 100' (v)	Date: Dec 1998
Prepared By: HSI GeoTrans	By: RAK

\Crandon\TmaMod4\Surfer\07c300x.srf

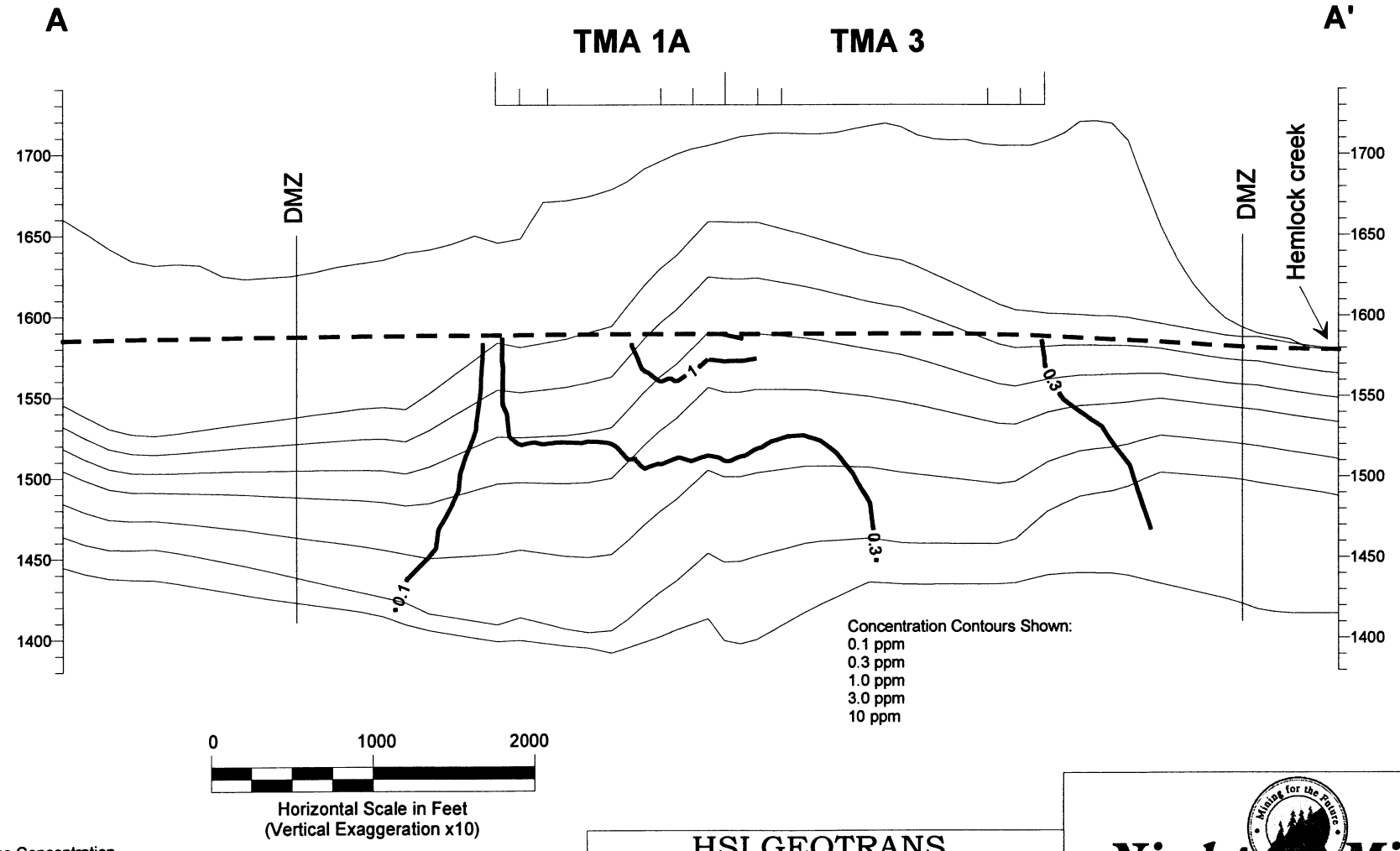

4.2-10-347

Source Concentration
Operation: 2000 ppm
Post-cap: 4000 ppm
Oxidized: 40,000 ppm*

* As a conservative assumption, the oxidized concentration begins immediately after assumed degradation of the flexible membrane liner.

HSI GEOTRANS			
REVISED	DATE	BY	DESCRIPTION

CHECKED BY: GWC	DATE: Dec 98
APPROVED BY: PFA	DATE: Dec 98
APPROVED BY:	DATE:

Nicolet Minerals COMPANY

Figure 2.35
BEJT Concentration After 300 Years (Example Constituent, Cross Section)

Scale: 1" = 1000' (h), 100' (v)	Date: Dec 1998
Prepared By: HSI GeoTrans	By: RAK

\Crandon\TmaMod4\Surfer\07c650x.srf

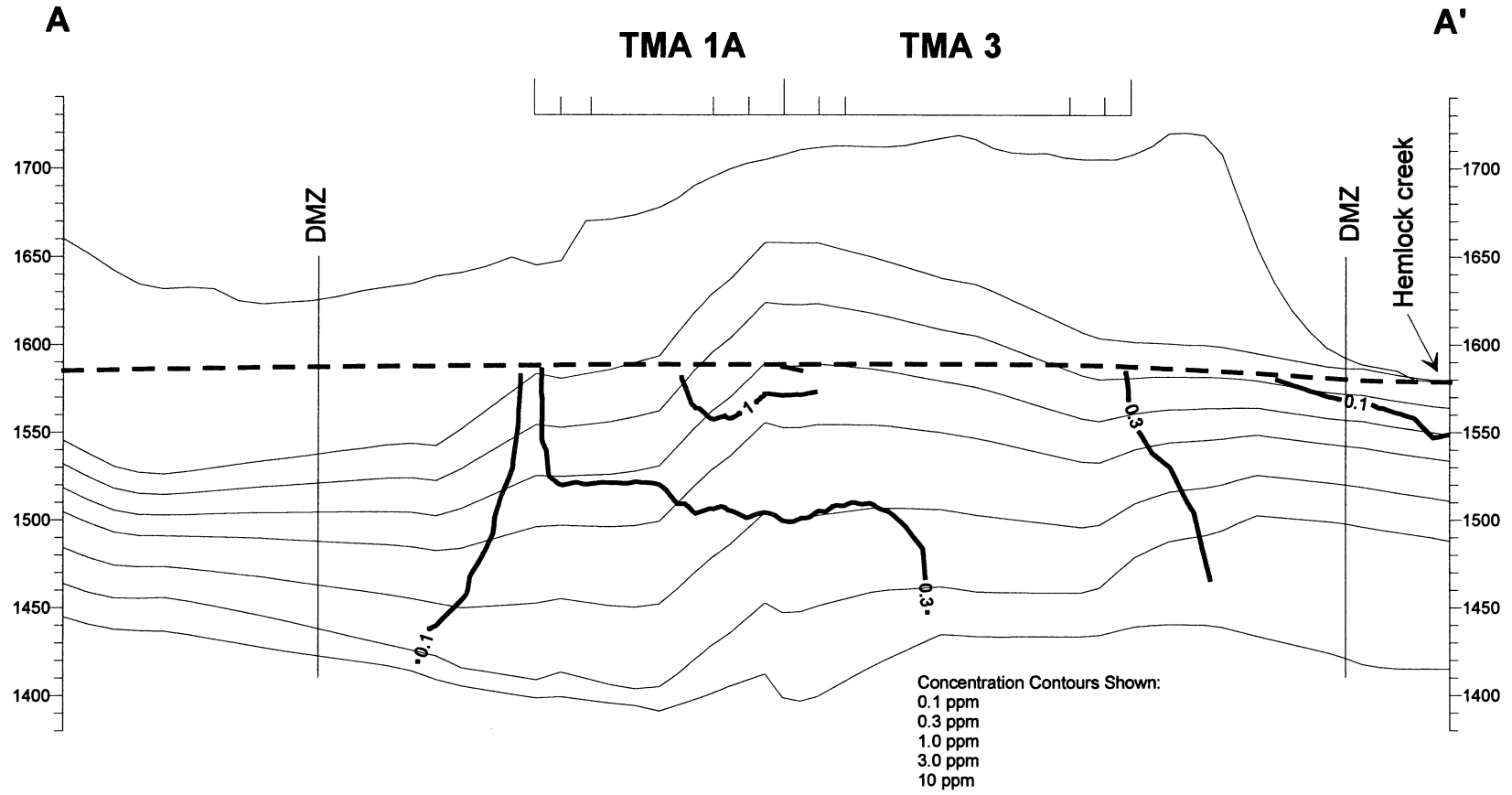

4.2-10-348

Source Concentration
Operation: 2000 ppm
Post-cap: 4000 ppm
Oxidized: 40,000 ppm*

* As a conservative assumption, the oxidized concentration begins immeditately after assumed degradation of the flexible membrane liner.

HSI GEOTRANS

REVISED	DATE	BY	DESCRIPTION

CHECKED BY: GWC	DATE: Dec 98
APPROVED BY: PFA	DATE: Dec 98
APPROVED BY:	DATE:

Nicolet Minerals COMPANY

Figure 2.36
BEJT Concentration After 650 Years (Example Constituent, Cross Section)

Scale: 1" = 1000' (h), 100' (v)	Date: Dec 1998
Prepared By: HSI GeoTrans	By: RAK

\Crandon\TmaMod4\Excel\PwcRsp.xls, Response

Tailings Management Area Design Management Zone

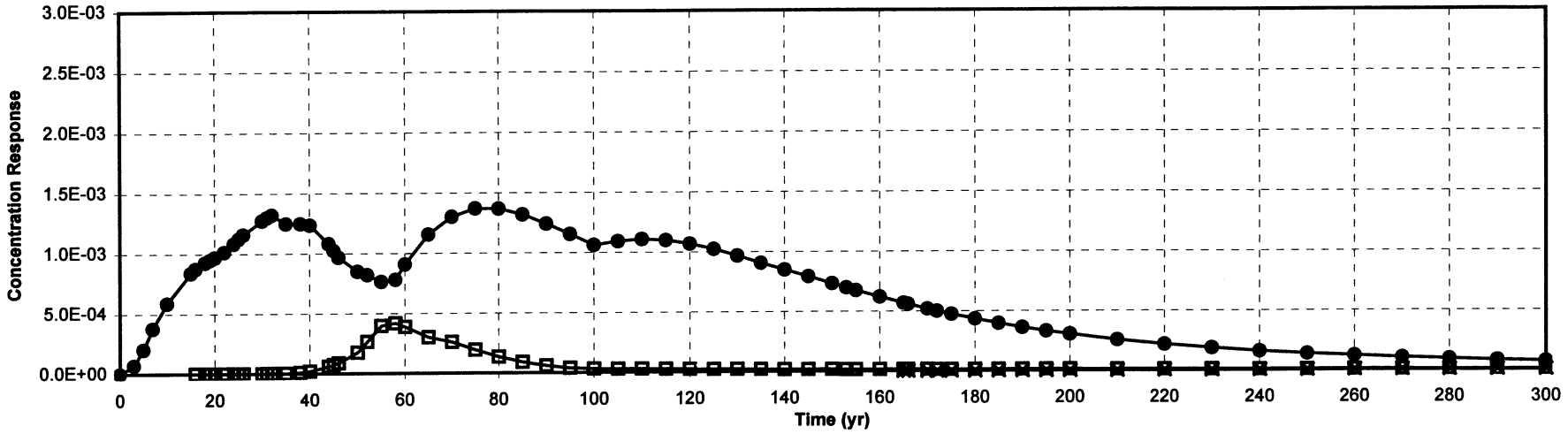

Reclaim Pond Design Management Zone

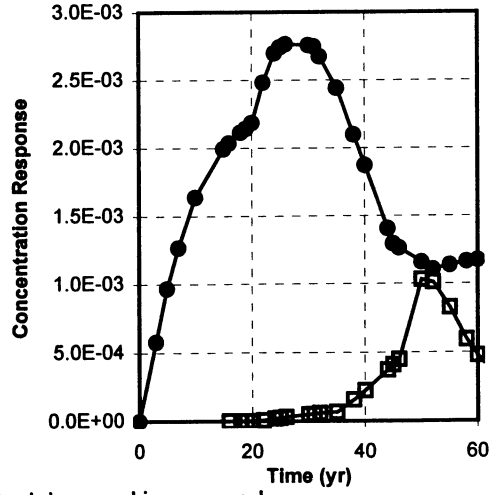

Note: Reclaim pond is removed at approximately year 46

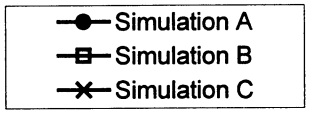

Note: The maximum concentration at any point on the Design Management Zone is plotted.

HSI GEOTRANS			
REVISED	DATE	BY	DESCRIPTION
CHECKED BY: GWC			DATE: Dec 1998
APPROVED BY: PFA			DATE: Dec 1998
Simulations T08C1,2,3	APPROVED BY:		DATE:

Nicolet Minerals COMPANY

Figure 2.37
PWCT Concentration Response Curves at the Design Management Zones

Scale: None	Date: Dec 1998
Prepared By: HSI GEOTRANS	By: RAK

\Crandon\TmaMod4\Excel\hypothet.xls.pwc

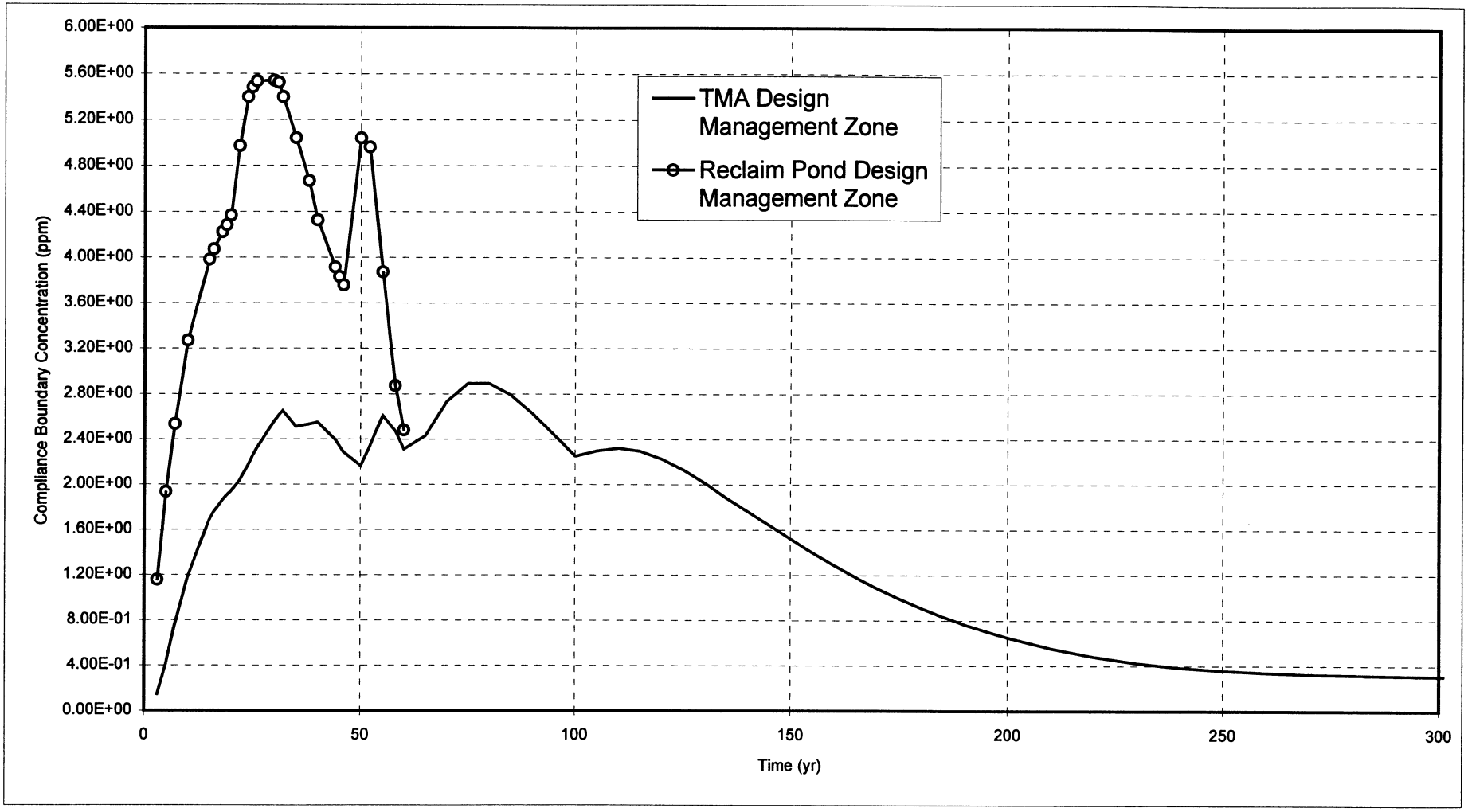

4.2-10-350

Source Concentration:
Operation: 2000 ppm
Post-Cap: 4000 ppm
Oxidized: 40000 ppm*

* As a conservative assumption, the oxidized concentration begins immediately after assumed degradation of the flexible membrane liner.

HSI GEOTRANS

REVISED	DATE	BY	DESCRIPTION

CHECKED BY: GWC	DATE: Dec 1998
APPROVED BY: PFA	DATE: Dec 1998
APPROVED BY:	DATE:

Simulations T08C1, 2, 3

Nicolet Minerals COMPANY

Figure 2.38
PWCT Concentration at the Design Management Zones (Example Constituent)

Scale: None	Date: Dec 1998
Prepared By: HSI GEOTRANS	By: RAK

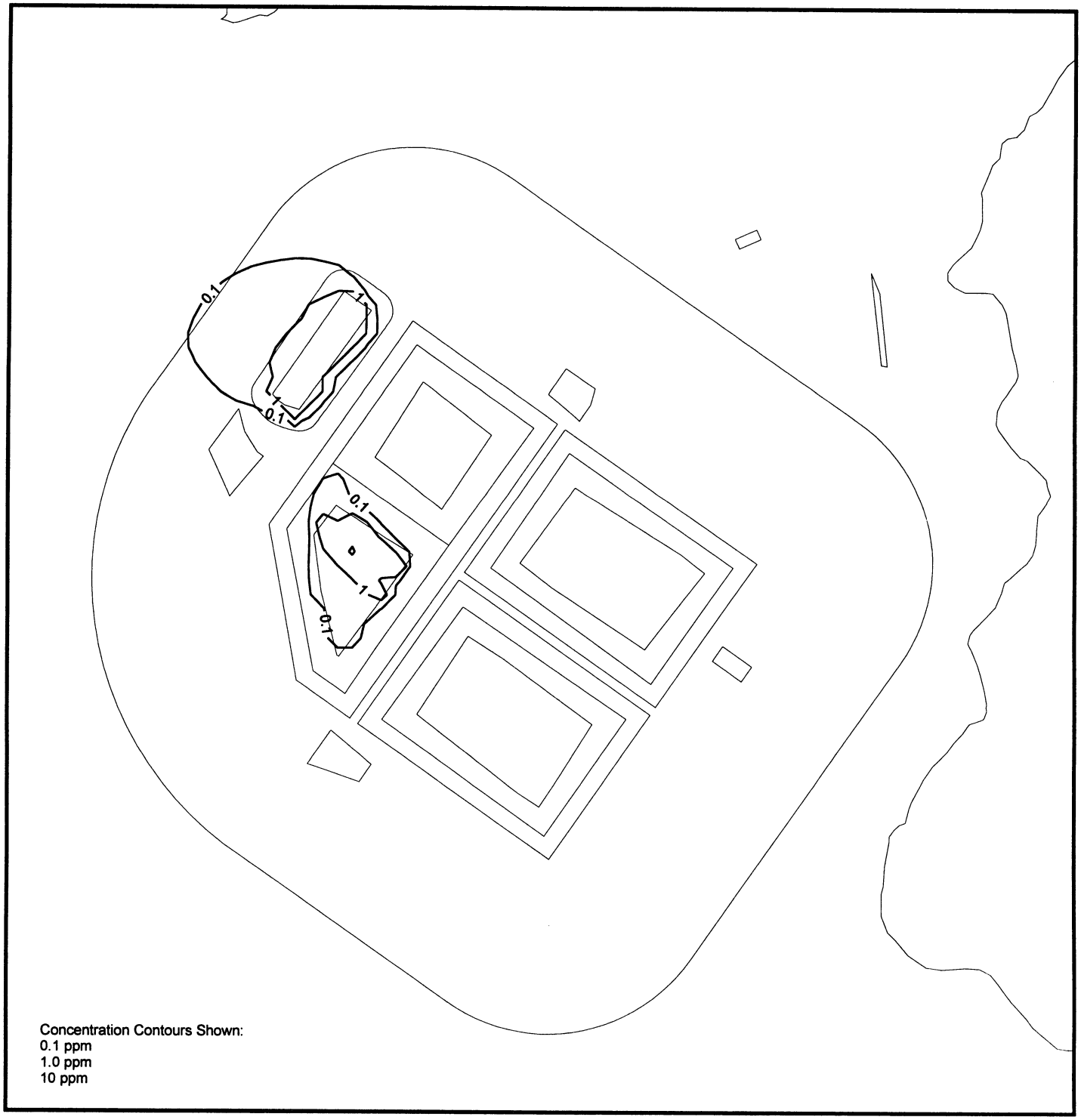

Concentration Contours Shown:
0.1 ppm
1.0 ppm
10 ppm

Source Concentration
Operation: 2000 ppm
Post-cap: 4000 ppm
Oxidized: 40,000 ppm*

* As a conservative assumption, the oxidized concentration begins immediately after assumed degradation of the flexible membrane liner.

Note:
This plot shows contours of maximum concentratration in any layer.

0 1000 2000
Scale in Feet

HSI GEOTRANS			
REVISED	DATE	BY	DESCRIPTION

CHECKED BY: GWC	DATE: Dec 98
APPROVED BY: PFA	DATE: Dec 98
APPROVED BY:	DATE:

Nicolet Minerals COMPANY

Figure 2.39
PWCT Concentration After 3 Years (Example Constituent, Plan View)

Scale: 1 in. = 1000 ft.	Date: December 1998
Prepared By: HSI GEOTRANS	By: KMR

\Crandon\Tmwmod4\Surfer\PWC003.srf

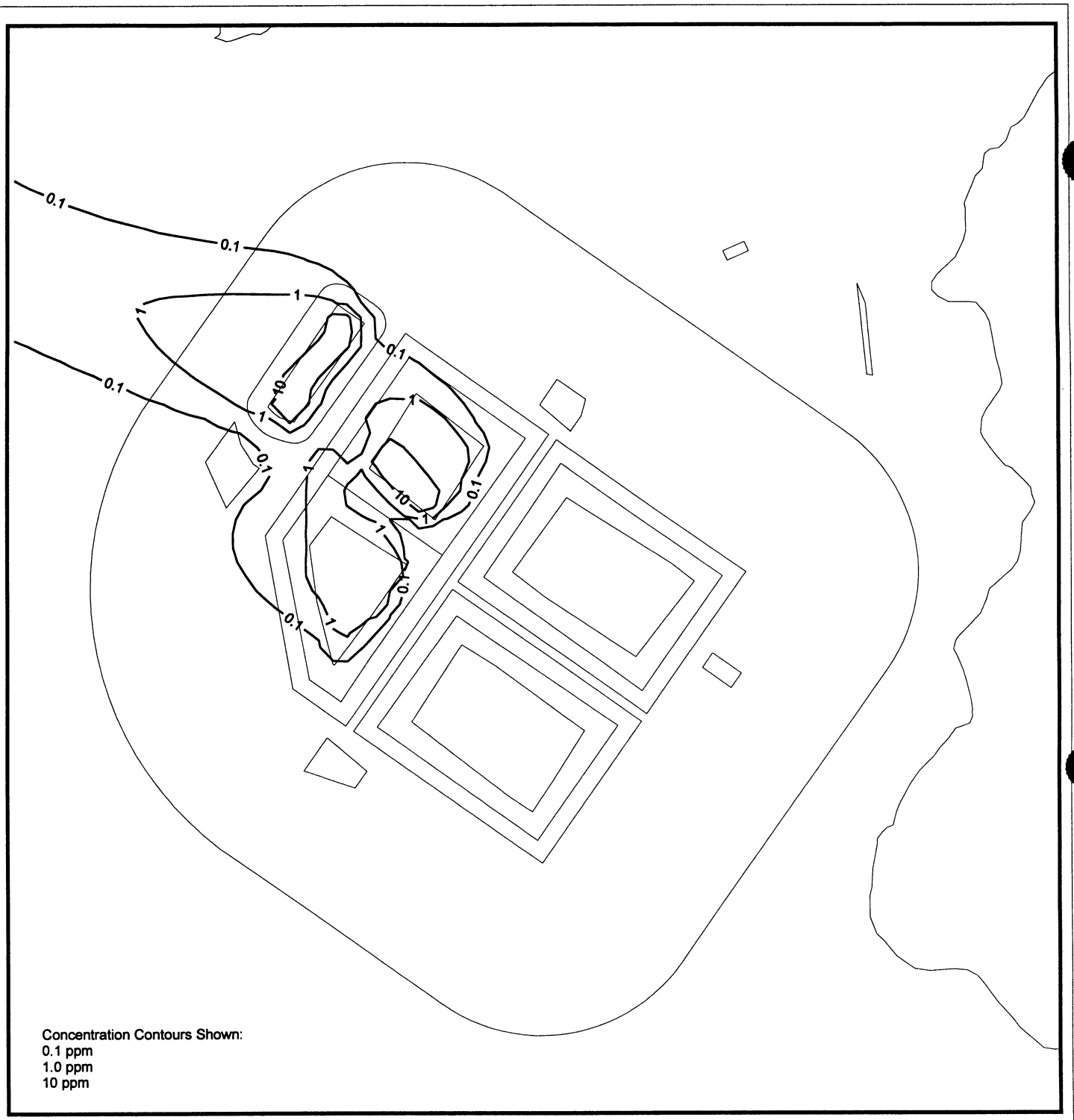

Source Concentration
Operation: 2000 ppm
Post-cap: 4000 ppm
Oxidized: 40,000 ppm*

* As a conservative assumption, the oxidized concentration begins immediately after assumed degradation of the flexible membrane liner.

Note:
This plot shows contours of maximum concentratration in any layer.

0 1000 2000
Scale in Feet

HSI GEOTRANS

REVISED	DATE	BY	DESCRIPTION

CHECKED BY: GWC	DATE: Dec 98
APPROVED BY: PFA	DATE: Dec 98
APPROVED BY:	DATE:

Nicolet Minerals COMPANY

Figure 2.40
PWCT Concentration After 16 Years
(Example Constituent, Plan View)

Scale: 1 in. = 1000 ft.	Date: December 1998
Prepared By: HSI GEOTRANS	By: KMR

\Crandon\Tmat\Mod4\Surfer\PWC016.srf

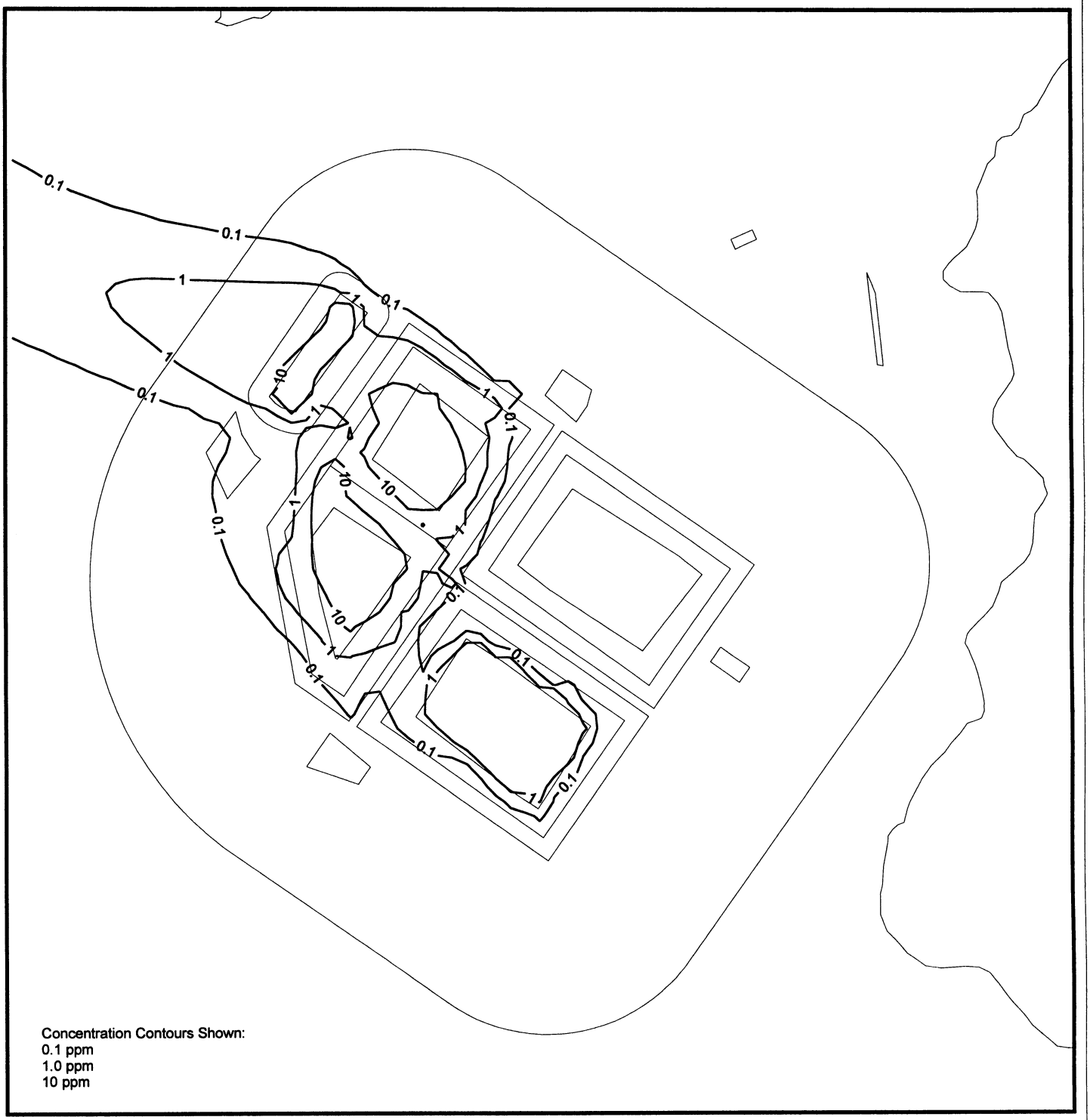

Source Concentration
Operation: 2000 ppm
Post-cap: 4000 ppm
Oxidized: 40,000 ppm*

* As a conservative assumption, the oxidized concentration begins immediately after assumed degradation of the flexible membrane liner.

Note:
This plot shows contours of maximum concentratration in any layer.

0 1000 2000
Scale in Feet

HSI GEOTRANS			
REVISED	DATE	BY	DESCRIPTION

CHECKED BY: GWC	DATE: Dec 98
APPROVED BY: PFA	DATE: Dec 98
APPROVED BY:	DATE:

Nicolet Minerals COMPANY

Figure 2.41
PWCT Concentration After 22 Years (Example Constituent, Plan View)

Scale: 1 in. = 1000 ft.	Date: December 1998
Prepared By: HSI GEOTRANS	By: KMR

\Crandon\Tmal\Mod4\Surfer\PWC022.srf

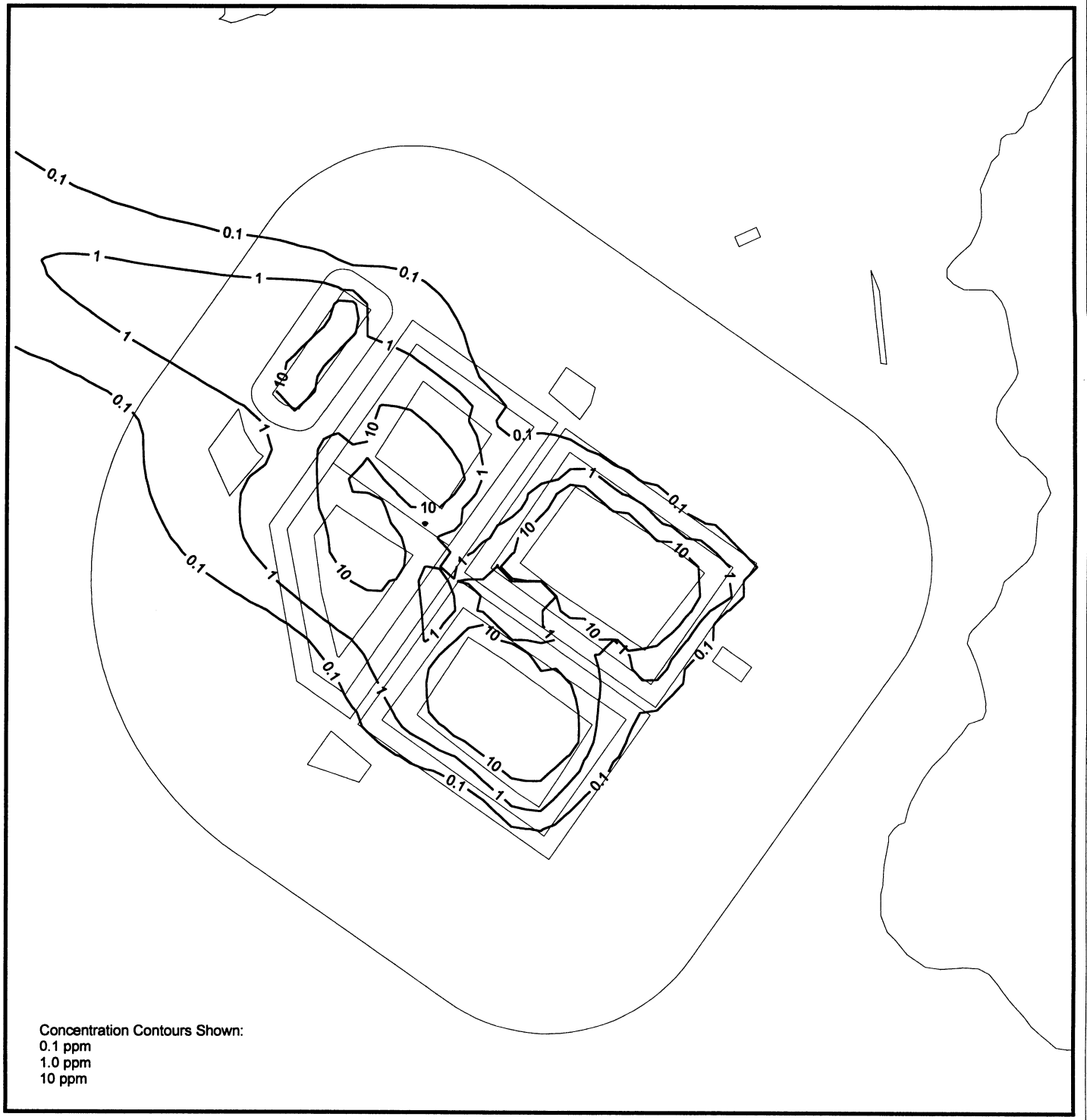

Source Concentration
Operation: 2000 ppm
Post-cap: 4000 ppm
Oxidized: 40,000 ppm*

* As a conservative assumption, the oxidized concentration begins immediately after assumed degradation of the flexible membrane liner.

Note:
This plot shows contours of maximum concentratration in any layer.

0 1000 2000
Scale in Feet

HSI GEOTRANS

REVISED	DATE	BY	DESCRIPTION

CHECKED BY: GWC	DATE: Dec 98
APPROVED BY: PFA	DATE: Dec 98
APPROVED BY:	DATE:

Nicolet Minerals COMPANY

Figure 2.42
PWCT Concentration After 32 Years (Example Constituent, Plan View)

Scale: 1 in. = 1000 ft.	Date: December 1998
Prepared By: HSI GEOTRANS	By: KMR

\Crandon\Tmal\Mod4\Surfer\PWCC02.srf

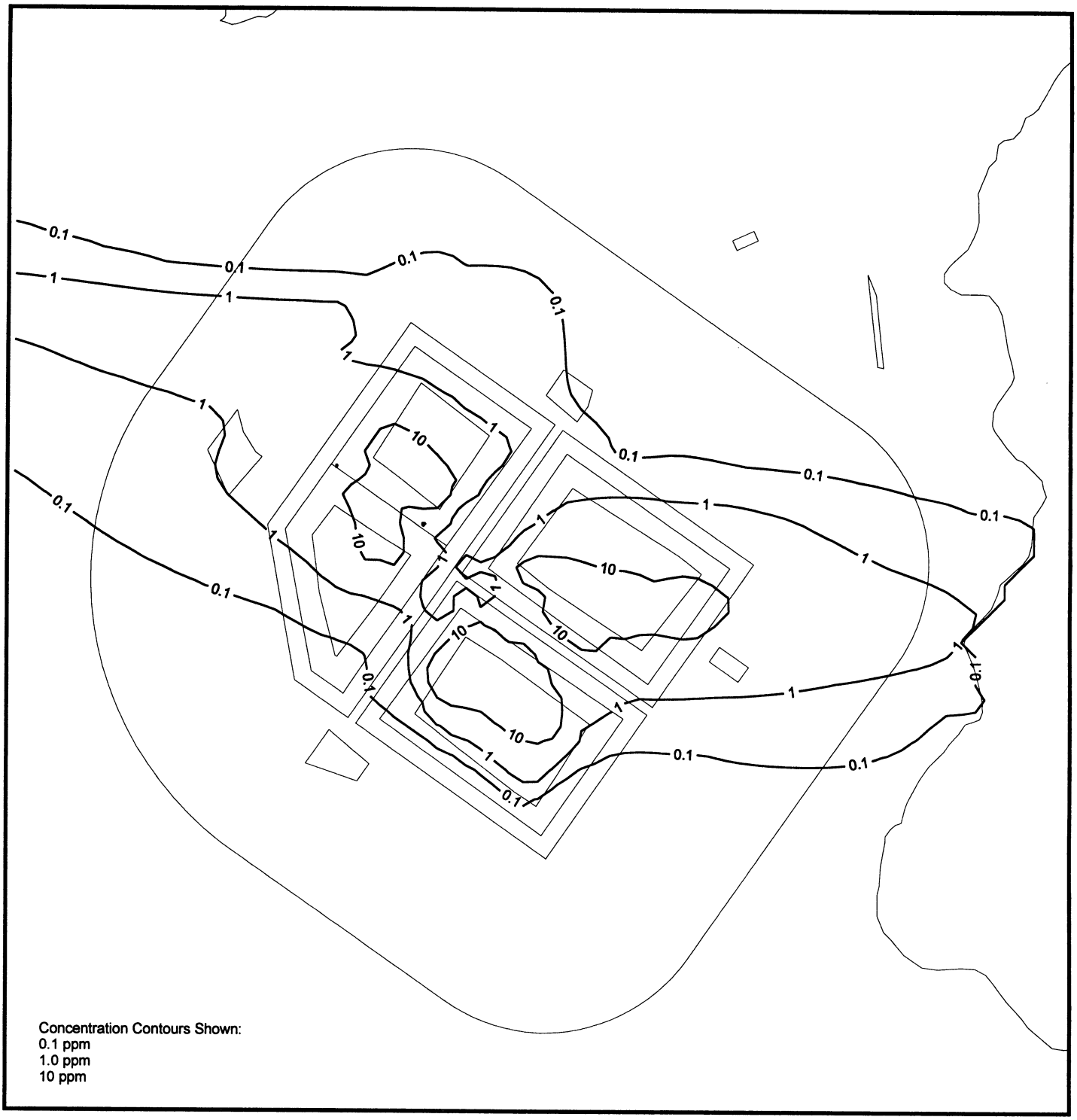

Source Concentration
Operation: 2000 ppm
Post-cap: 4000 ppm
Oxidized: 40,000 ppm*

* As a conservative assumption, the oxidized concentration begins immediately after assumed degradation of the flexible membrane liner.

Note:
This plot shows contours of maximum concentratration in any layer.

0 1000 2000
Scale in Feet

HSI GEOTRANS			
REVISED	DATE	BY	DESCRIPTION

CHECKED BY: GWC	DATE: Dec 98
APPROVED BY: PFA	DATE: Dec 98
APPROVED BY:	DATE:

Nicolet Minerals COMPANY

Figure 2.43
PWCT Concentration After 60 Years (Example Constituent, Plan View)

Scale: 1 in. = 1000 ft.	Date: December 1998
Prepared By: HSI GEOTRANS	By: KMR

\Crandon\TimeModel\Surfer\PWC060.srf

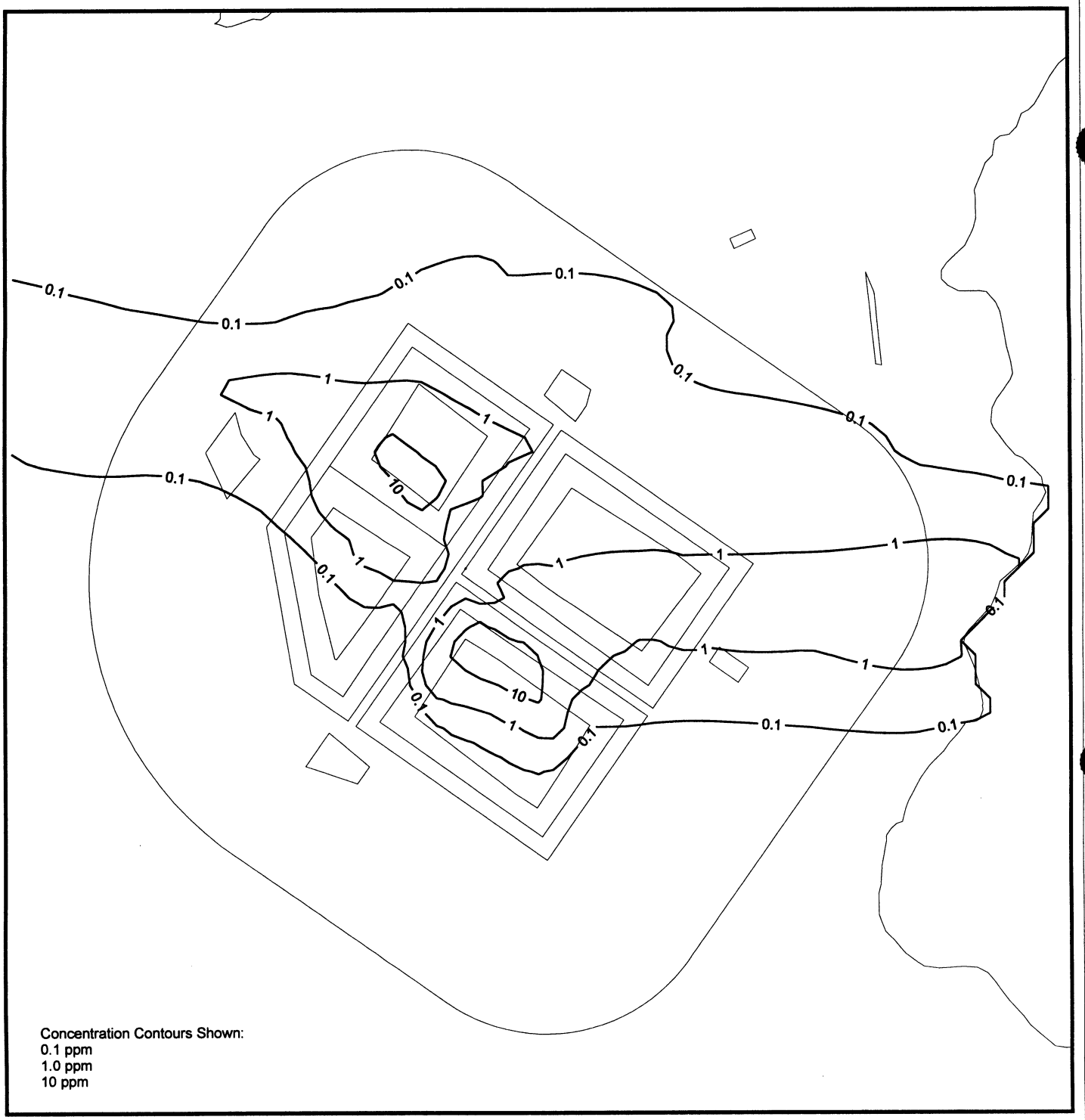

Source Concentration
Operation: 2000 ppm
Post-cap: 4000 ppm
Oxidized: 40,000 ppm*

* As a conservative assumption, the oxidized concentration begins immediately after assumed degradation of the flexible membrane liner.

Note:
This plot shows contours of maximum concentratration in any layer.

N

0 1000 2000

Scale in Feet

HSI GEOTRANS

REVISED	DATE	BY	DESCRIPTION

CHECKED BY: GWC	DATE: Dec 98
APPROVED BY: PFA	DATE: Dec 98
APPROVED BY:	DATE:

Nicolet Minerals COMPANY

Figure 2.44
PWCT Concentration After 125 Years (Example Constituent, Plan View)

Scale: 1 in. = 1000 ft.	Date: December 1998
Prepared By: HSI GEOTRANS	By: KMR

\Crandon\Tmx\Mod4\Surfer\PWC125.srf

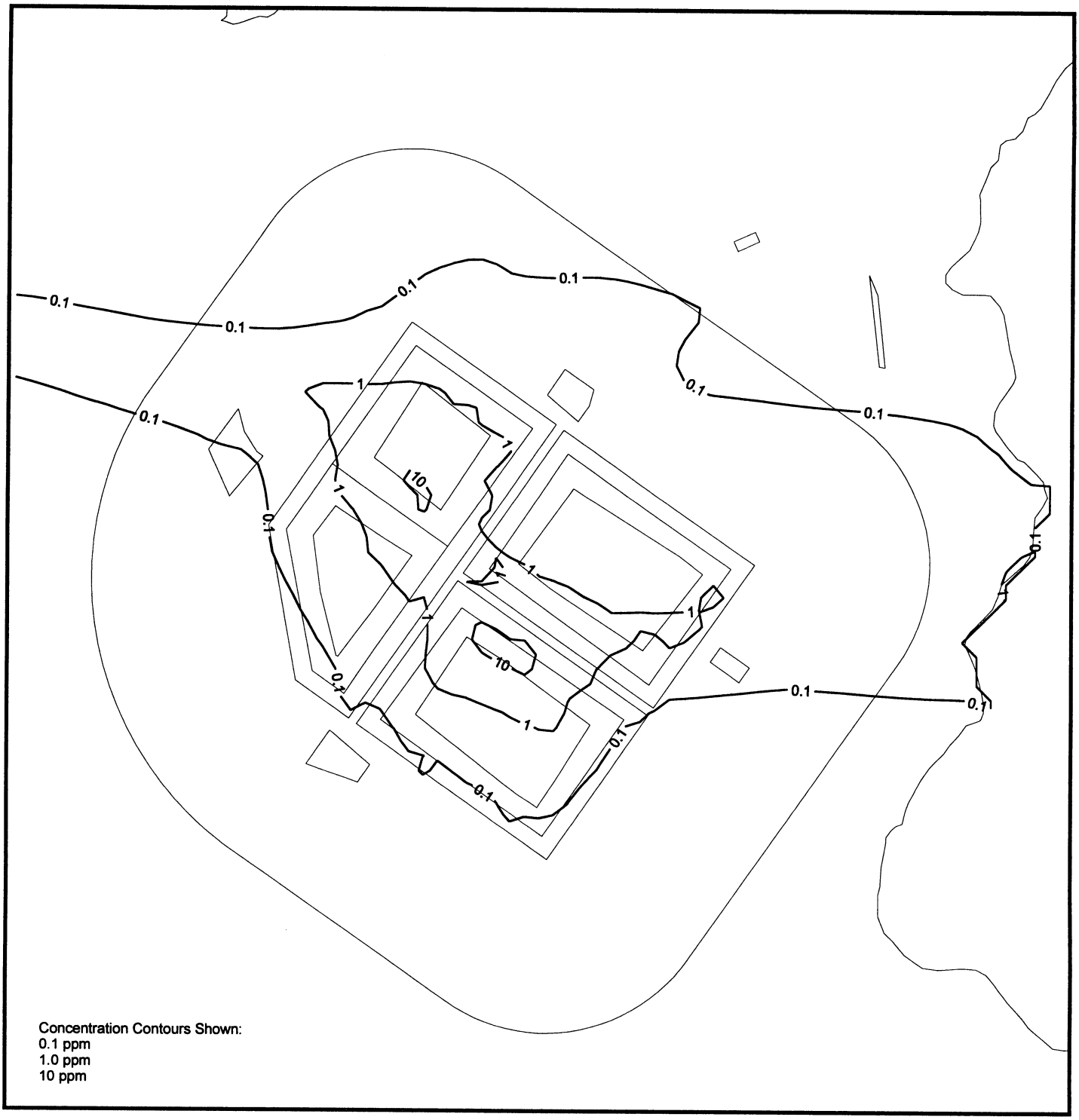

Source Concentration
Operation: 2000 ppm
Post-cap: 4000 ppm
Oxidized: 40,000 ppm*

* As a conservative assumption, the oxidized concentration begins immediately after assumed degradation of the flexible membrane liner.

Note:
This plot shows contours of maximum concentratration in any layer.

0 1000 2000
Scale in Feet

HSI GEOTRANS			
REVISED	DATE	BY	DESCRIPTION

CHECKED BY: GWC	DATE: Dec 98
APPROVED BY: PFA	DATE: Dec 98
APPROVED BY:	DATE:

Nicolet Minerals COMPANY

Figure 2.45
PWCT Concentration After 200 Years (Example Constituent, Plan View)

Scale: 1 in. = 1000 ft.	Date: December 1998
Prepared By: HSI GEOTRANS	By: KMR

\Crandon\Tmal\Model\Surfer\PWC200.srf

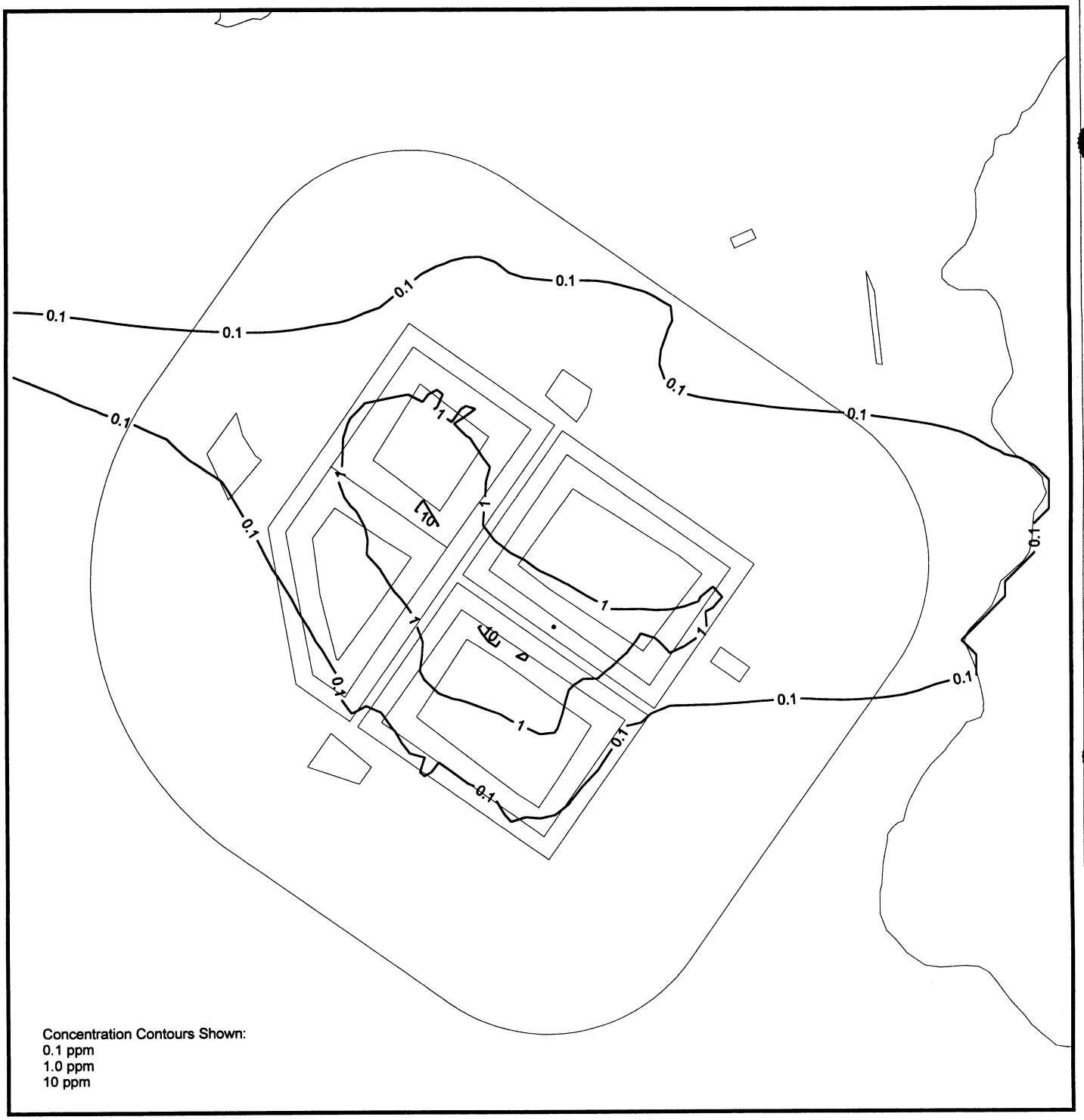

Source Concentration
Operation: 2000 ppm
Post-cap: 4000 ppm
Oxidized: 40,000 ppm*

* As a conservative assumption, the oxidized concentration begins immediately after assumed degradation of the flexible membrane liner.

Note:
This plot shows contours of maximum concentratration in any layer.

N

0 1000 2000

Scale in Feet

HSI GEOTRANS

REVISED	DATE	BY	DESCRIPTION

CHECKED BY: GWC	DATE: Dec 98
APPROVED BY: PFA	DATE: Dec 98
APPROVED BY:	DATE:

Nicolet Minerals COMPANY

Figure 2.46
PWCT Concentration After 300 Years (Example Constituent, Plan View)

Scale: 1 in. = 1000 ft.	Date: December 1998
Prepared By: HSI GEOTRANS	By: KMR

\Crandon\Tmal\Mod4\Surfer\PWC300.srf

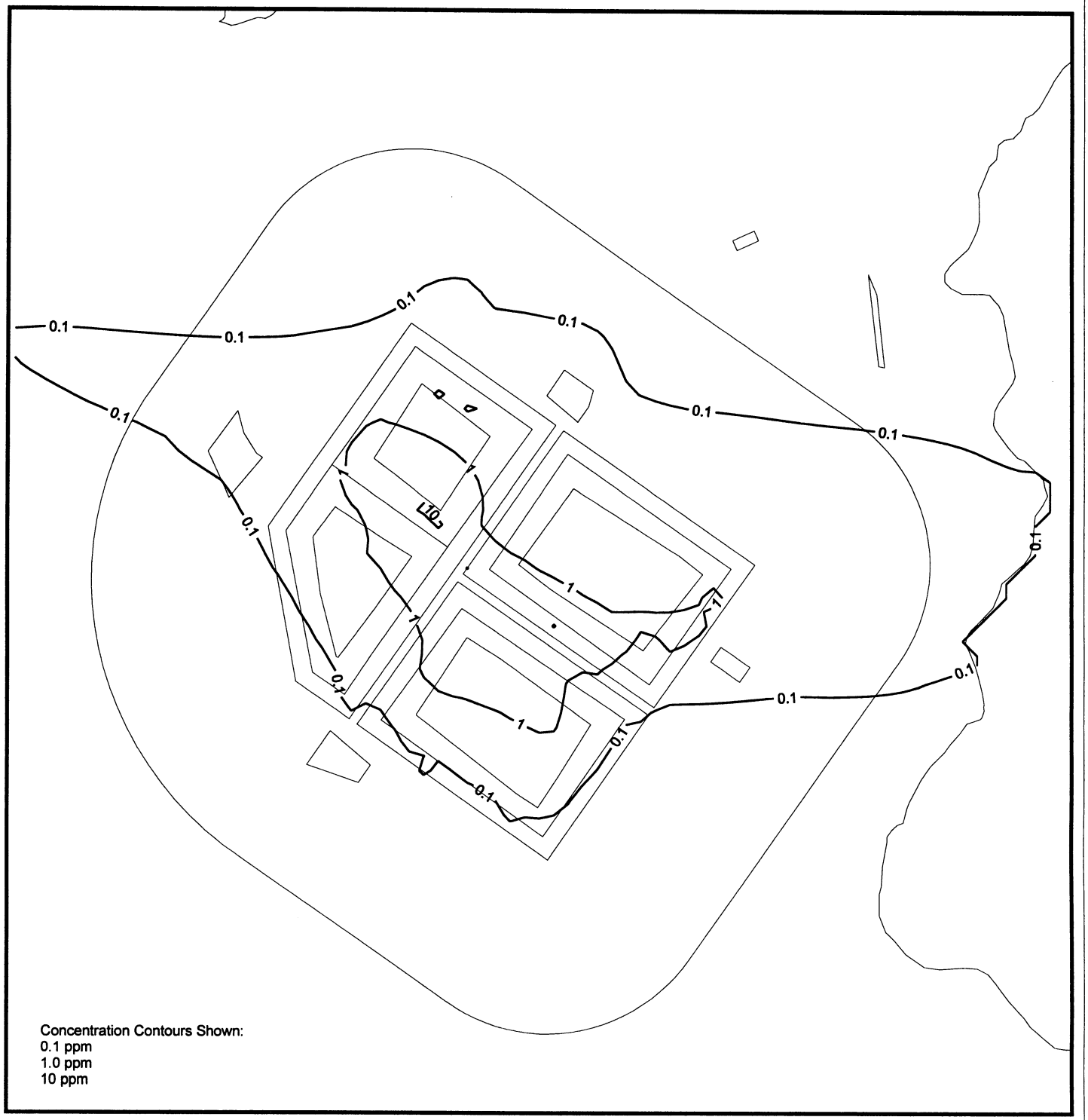

Source Concentration
Operation: 2000 ppm
Post-cap: 4000 ppm
Oxidized: 40,000 ppm*

* As a conservative assumption, the oxidized concentration begins immediately after assumed degradation of the flexible membrane liner.

Note:
This plot shows contours of maximum concentratration in any layer.

0 1000 2000
Scale in Feet

HSI GEOTRANS

REVISED	DATE	BY	DESCRIPTION

CHECKED BY: GWC	DATE: Dec 98
APPROVED BY: PFA	DATE: Dec 98
APPROVED BY:	DATE:

Nicolet Minerals COMPANY

Figure 2.47
PWCT Concentration After 650 Years (Example Constituent, Plan View)

Scale: 1 in. = 1000 ft.	Date: December 1998
Prepared By: HSI GEOTRANS	By: KMR

\CrandonTmaMod4\Surfer\PWC650.srf

\Crandon\TmaMod4\Surfer\08c003x.srf

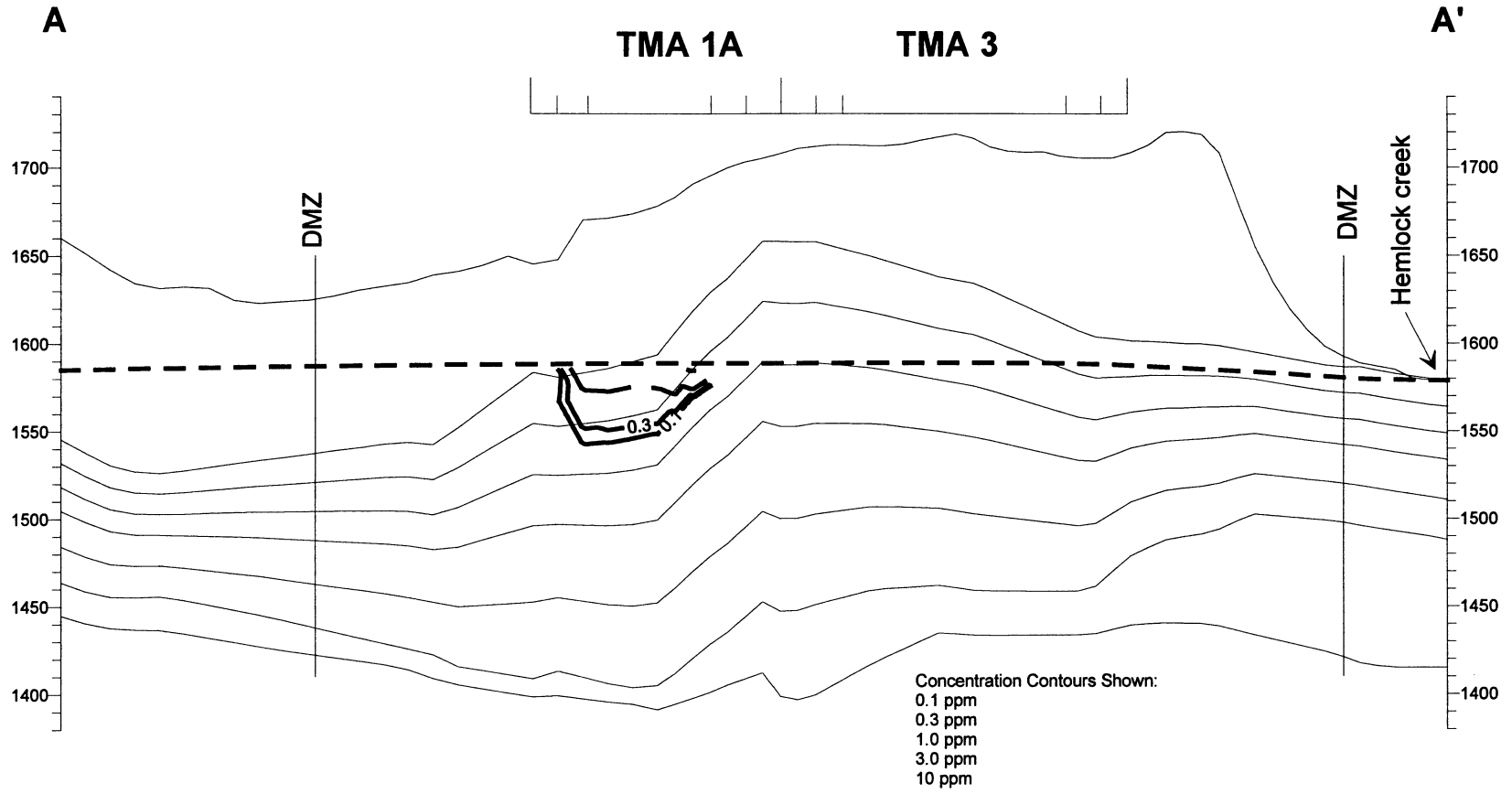

4.2-10-360

Source Concentration
Operation: 2000 ppm
Post-cap: 4000 ppm
Oxidized: 40,000 ppm*

* As a conservative assumption, the oxidized concentration begins immediately after assumed degradation of the flexible membrane liner.

HSI GEOTRANS

REVISED	DATE	BY	DESCRIPTION

CHECKED BY: GWC	DATE: Dec 98
APPROVED BY: PFA	DATE: Dec 98
APPROVED BY:	DATE:

Nicolet Minerals COMPANY

Figure 2.48
PWCT Concentration After 3 Years (Example Constituent, Cross Section)

Scale: 1" = 1000' (h), 100' (v)	Date: Dec 1998
Prepared By: HSI GeoTrans	By: RAK

\Crandon\TmaMod4\Surfer\08c016x.srf

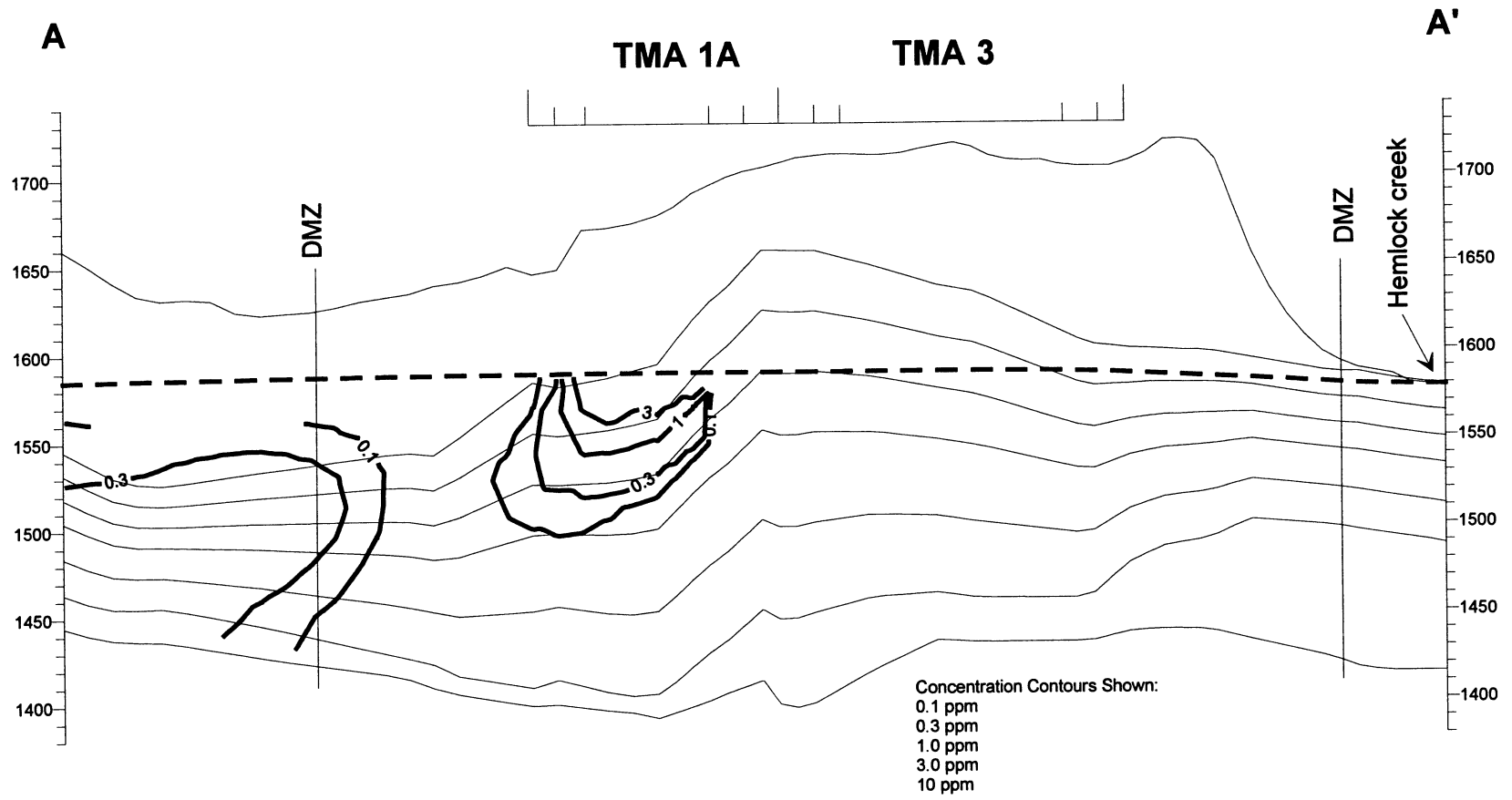

4.2-10-361

Source Concentration
Operation: 2000 ppm
Post-cap: 4000 ppm
Oxidized: 40,000 ppm*

* As a conservative assumption, the oxidized concentration begins immediately after assumed degradation of the flexible membrane liner.

HSI GEOTRANS

REVISED	DATE	BY	DESCRIPTION

CHECKED BY: GWC	DATE: Dec 98
APPROVED BY: PFA	DATE: Dec 98
APPROVED BY:	DATE:

Nicolet Minerals COMPANY

Figure 2.49
PWCT Concentration After 16 Years (Example Constituent, Cross Section)

Scale: 1" = 1000' (h), 100' (v)	Date: Dec 1998
Prepared By: HSI GeoTrans	By: RAK

\Crandon\TmaMod4\Surfer\08c022x.srf

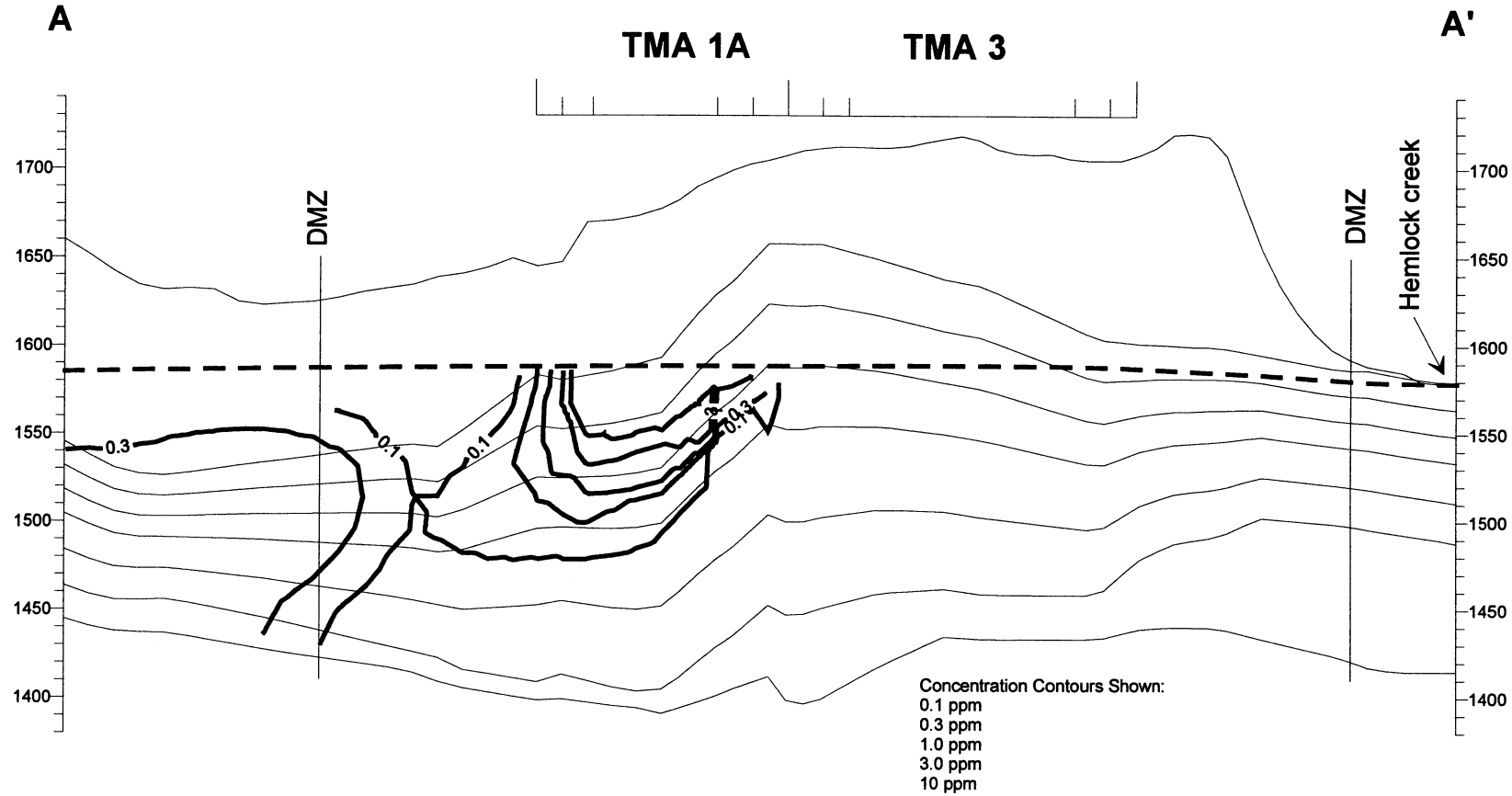

4.2-10-362

Source Concentration
Operation: 2000 ppm
Post-cap: 4000 ppm
Oxidized: 40,000 ppm*

* As a conservative assumption, the oxidized concentration begins immediately after assumed degradation of the flexible membrane liner.

HSI GEOTRANS

REVISED	DATE	BY	DESCRIPTION

CHECKED BY: GWC	DATE: Dec 98
APPROVED BY: PFA	DATE: Dec 98
APPROVED BY:	DATE:

Nicolet Minerals COMPANY

Figure 2.50
PWCT Concentration After 22 Years (Example Constituent, Cross Section)

Scale: 1" = 1000' (h), 100' (v)	Date: Dec 1998
Prepared By: HSI GeoTrans	By: RAK

\Crandon\TmaMod4\Surfer\08c032x.srf

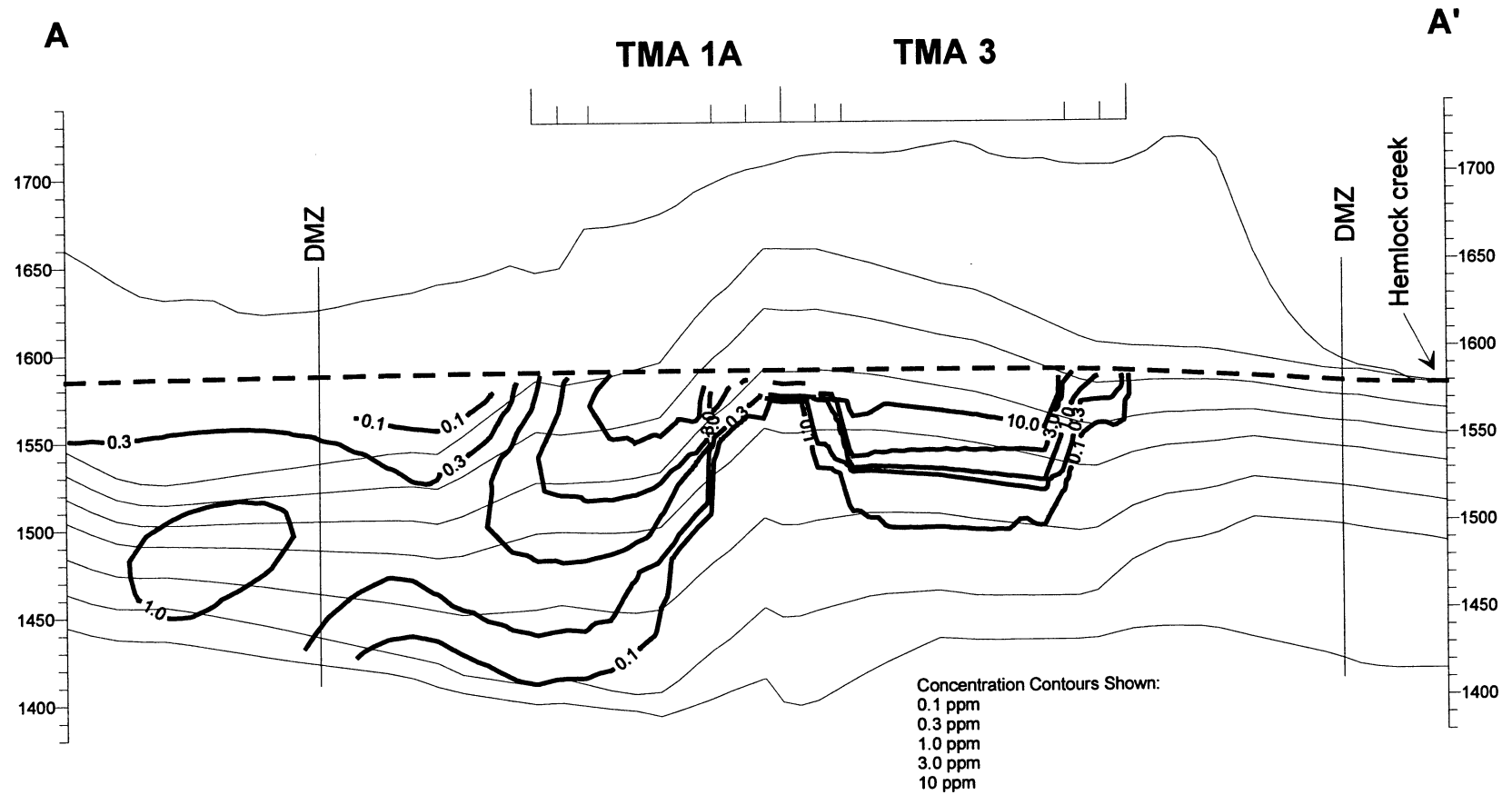

4.2-10-363

Source Concentration
Operation: 2000 ppm
Post-cap: 4000 ppm
Oxidized: 40,000 ppm*

* As a conservative assumption, the oxidized concentration begins immediately after assumed degradation of the flexible membrane liner.

HSI GEOTRANS

REVISED	DATE	BY	DESCRIPTION

CHECKED BY: GWC	DATE: Dec 98
APPROVED BY: PFA	DATE: Dec 98
APPROVED BY:	DATE:

Nicolet Minerals COMPANY

Mining for the Future

Figure 2.51
PWCT Concentration After 32 Years (Example Constituent, Cross Section)

Scale: 1" = 1000' (h), 100' (v)	Date: Dec 1998
Prepared By: HSI GeoTrans	By: RAK

\Crandon\TmaMod4\Surfer\08c060x.srf

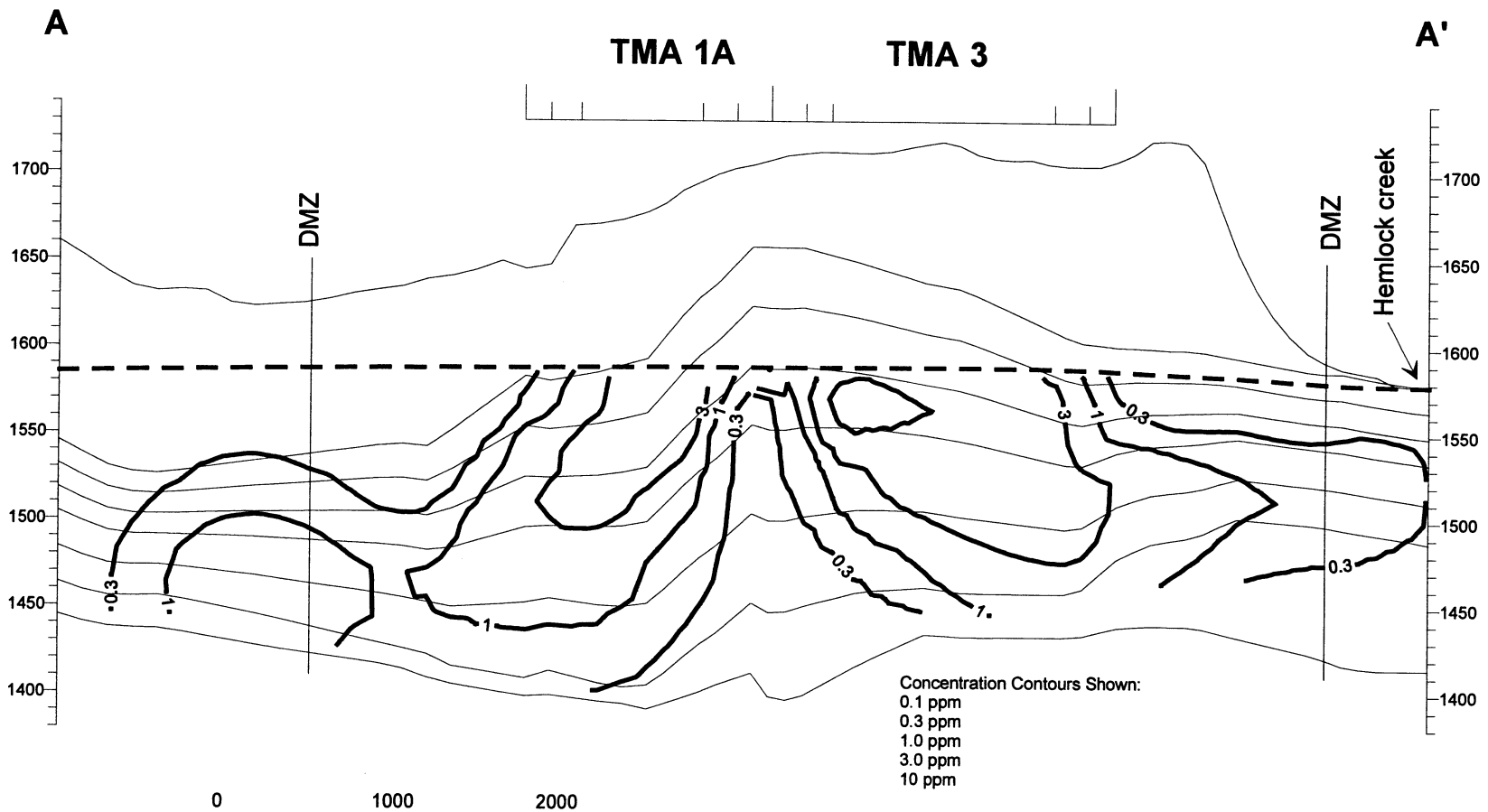

4.2-10-364

Source Concentration
Operation: 2000 ppm
Post-cap: 4000 ppm
Oxidized: 40,000 ppm*

* As a conservative assumption, the oxidized concentration begins immediately after assumed degradation of the flexible membrane liner.

HSI GEOTRANS

REVISED	DATE	BY	DESCRIPTION

CHECKED BY: GWC	DATE: Dec 98
APPROVED BY: PFA	DATE: Dec 98
APPROVED BY:	DATE:

Nicolet Minerals COMPANY

Figure 2.52
PWCT Concentration After 60 Years (Example Constituent, Cross Section)

Scale: 1" = 1000' (h), 100' (v)	Date: Dec 1998
Prepared By: HSI GeoTrans	By: RAK

\Crandon\TmaMod4\Surfer\08c125x.srf

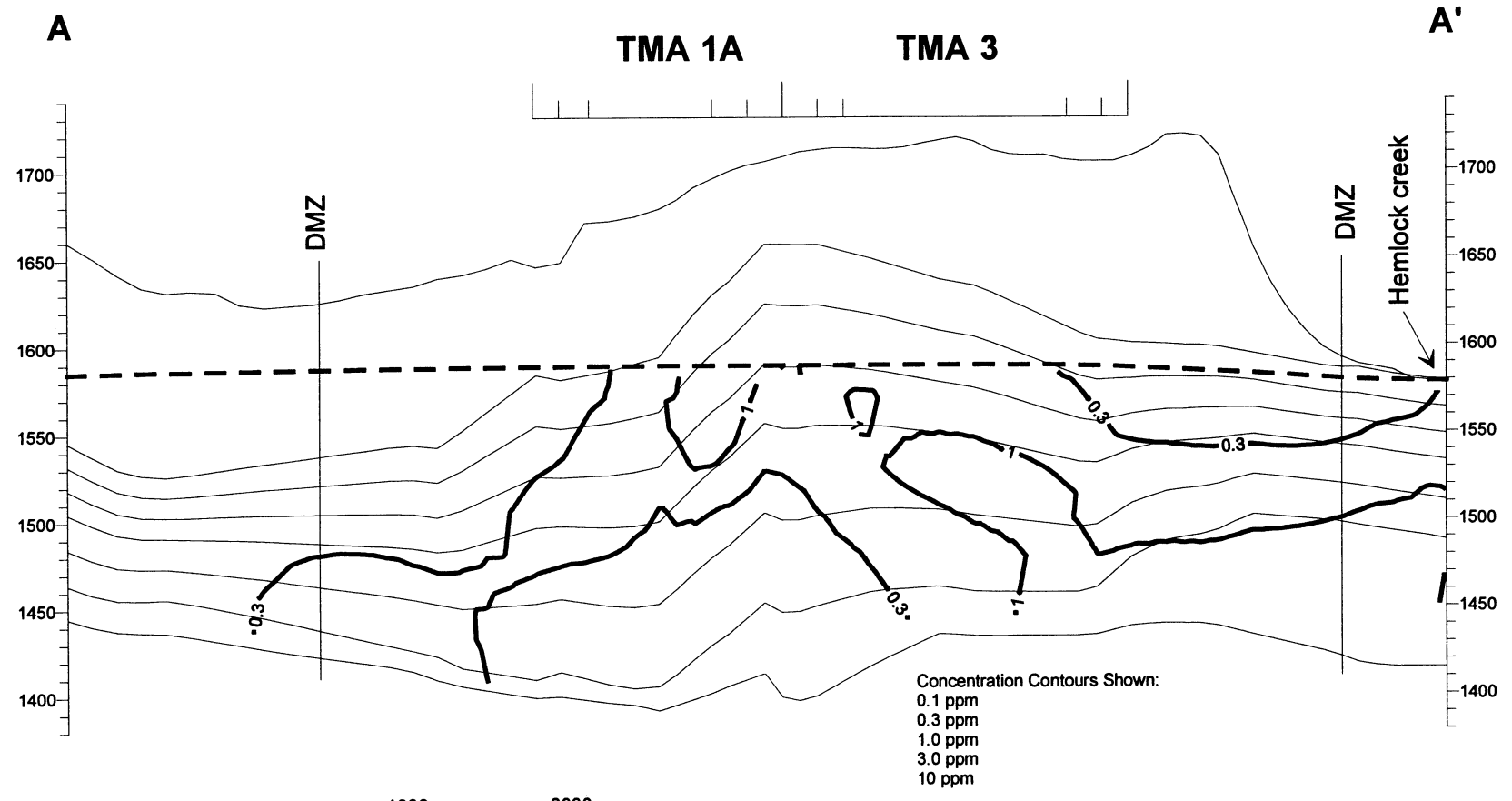

4.2-10-365

Source Concentration
Operation: 2000 ppm
Post-cap: 4000 ppm
Oxidized: 40,000 ppm*

* As a conservative assumption, the oxidized concentration begins immediately after assumed degradation of the flexible membrane liner.

HSI GEOTRANS

REVISED	DATE	BY	DESCRIPTION

CHECKED BY: GWC	DATE: Dec 98
APPROVED BY: PFA	DATE: Dec 98
APPROVED BY:	DATE:

Nicolet Minerals COMPANY

Figure 2.53
PWCT Concentration After 125 Years (Example Constituent, Cross Section)

Scale: 1" = 1000' (h), 100' (v)	Date: Dec 1998
Prepared By: HSI GeoTrans	By: RAK

\Crandon\TmaMod4\Surfer\08c200x.srf

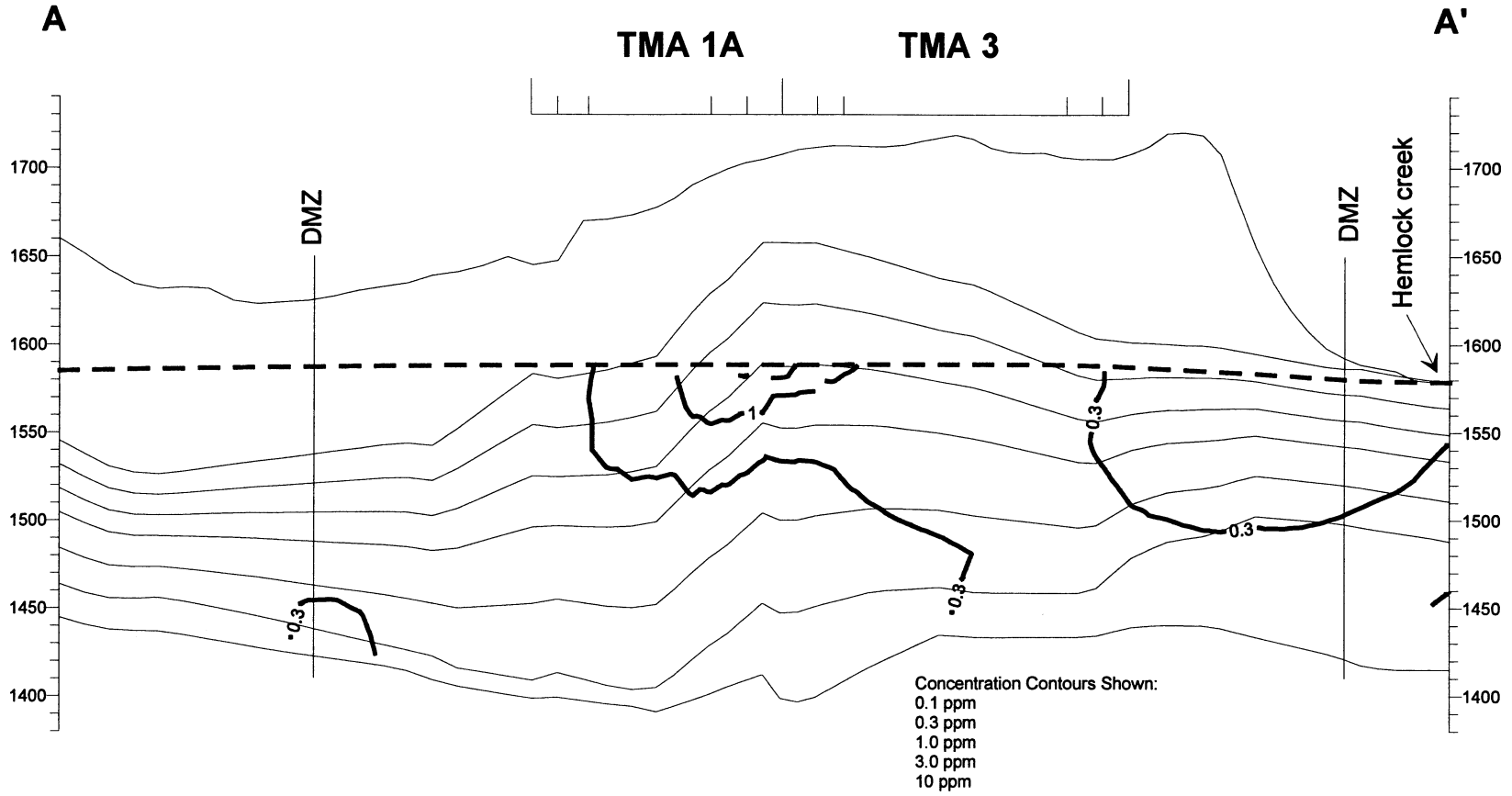

4.2-10-366

Source Concentration
Operation: 2000 ppm
Post-cap: 4000 ppm
Oxidized: 40,000 ppm*

* As a conservative assumption, the oxidized concentration begins immediately after assumed degradation of the flexible membrane liner.

HSI GEOTRANS

REVISED	DATE	BY	DESCRIPTION

CHECKED BY: GWC	DATE: Dec 98
APPROVED BY: PFA	DATE: Dec 98
APPROVED BY:	DATE:

Nicolet Minerals COMPANY

Figure 2.54
PWCT Concentration After 200 Years (Example Constituent, Cross Section)

Scale: 1" = 1000' (h), 100' (v)	Date: Dec 1998
Prepared By: HSI GeoTrans	By: RAK

\Crandon\TmaMod4\Surfer\08c300x.srf

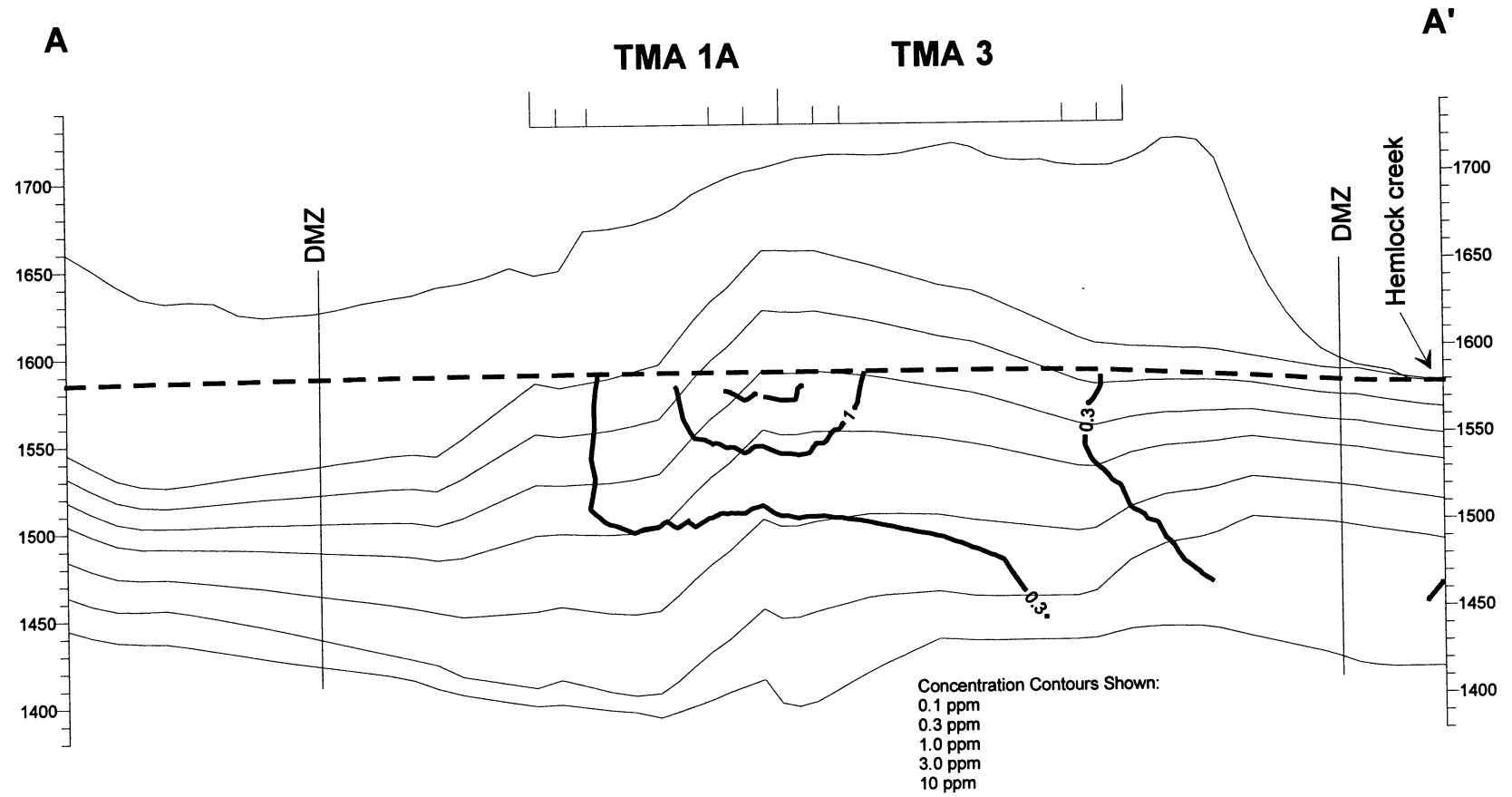

4.2-10-367

Source Concentration
Operation: 2000 ppm
Post-cap: 4000 ppm
Oxidized: 40,000 ppm*

* As a conservative assumption, the oxidized concentration begins immediately after assumed degradation of the flexible membrane liner.

HSI GEOTRANS

REVISED	DATE	BY	DESCRIPTION

CHECKED BY: GWC	DATE: Dec 98
APPROVED BY: PFA	DATE: Dec 98
APPROVED BY:	DATE:

Nicolet Minerals COMPANY

Figure 2.55
PWCT Concentration After 300 Years (Example Constituent, Cross Section)

Scale: 1" = 1000' (h), 100' (v)	Date: Dec 1998
Prepared By: HSI GeoTrans	By: RAK

\Crandon\TmaMod4\Surfer\08c650x.srf

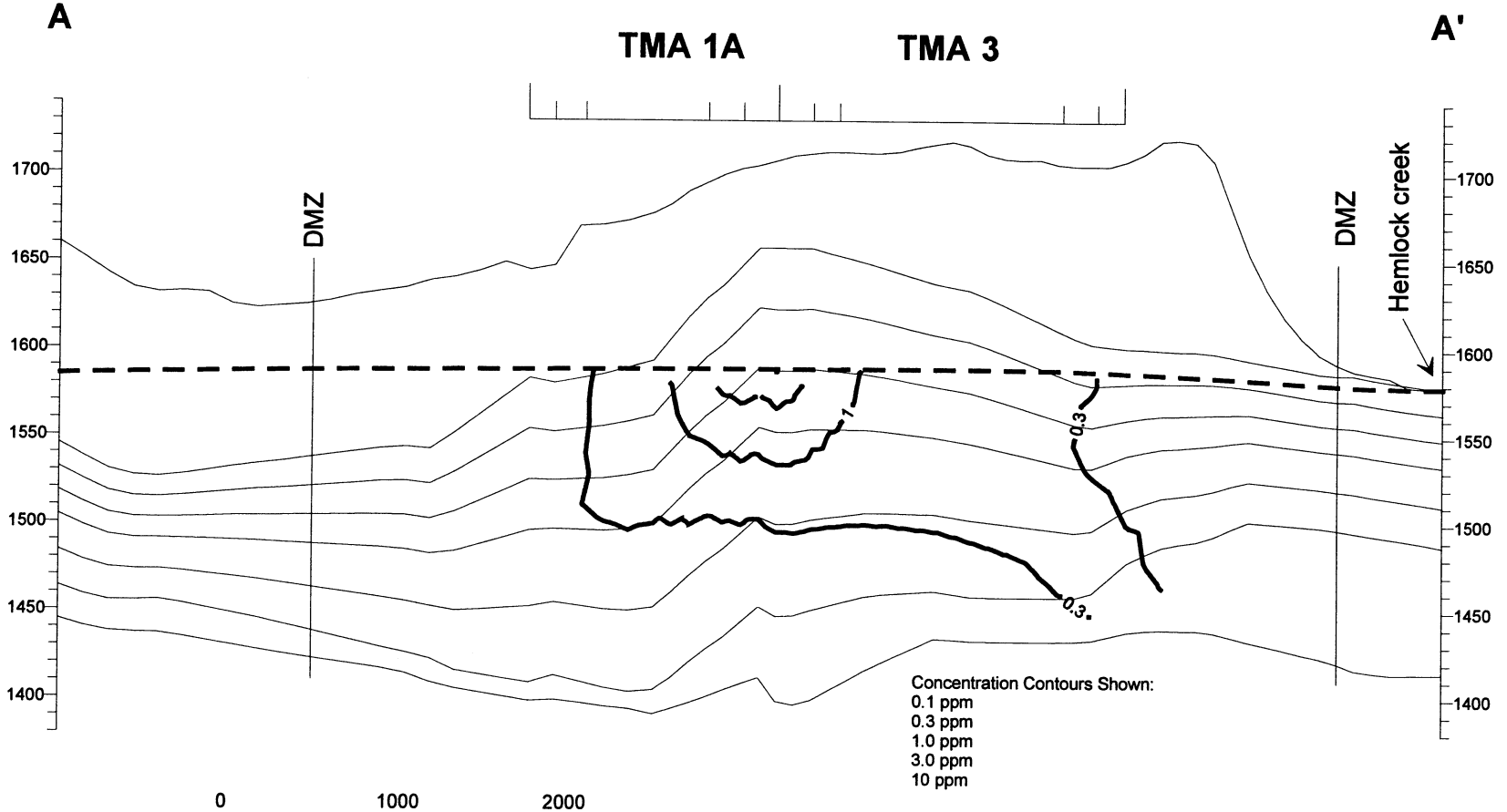

4.2-10-368

Source Concentration
Operation: 2000 ppm
Post-cap: 4000 ppm
Oxidized: 40,000 ppm*

* As a conservative assumption, the oxidized concentration begins immediately after assumed degradation of the flexible membrane liner.

HSI GEOTRANS

REVISED	DATE	BY	DESCRIPTION

CHECKED BY: GWC	DATE: Dec 98
APPROVED BY: PFA	DATE: Dec 98
APPROVED BY:	DATE:

Nicolet Minerals COMPANY

Figure 2.56
PWCT Concentration After 650 Years (Example Constituent, Cross Section)

Scale: 1" = 1000' (h), 100' (v)	Date: Dec 1998
Prepared By: HSI GeoTrans	By: RAK

3 Mine Reflooding Model

3.1 Approach

This section describes the analysis used to assess the potential for upward movement of solute from the backfilled mine following mine reflooding. Figure 3.1 shows limited regions of an upward hydraulic gradient from layer 7 to layer 4 in the steady-state regional groundwater flow model during post-mining conditions. These regions of upward gradient outline areas where solutes from the backfilled mine have the potential to travel upward to the glacial system.

The mine reflooding analysis was performed with the calibrated regional groundwater model (HSI GeoTrans, 1998b) and particle tracking using MODPATH (Pollack, 1990). Particle tracking is typically utilized in solute transport codes that use Method of Characteristic techniques (such as MT3D[96]) to assess advective transport in the groundwater system. Particle tracking was selected as a scoping analysis to efficiently analyze advective travel paths and travel times in three dimensions. The particle tracking analysis uses the BEJ groundwater flow field and PWC groundwater flow field from HSI GeoTrans (1998b) to assess the potential range of travel times from the mine to the proposed DMZ 1200 feet from the orebody.

The particle tracking assumes that the mine will be backfilled with cemented tailings. All mined bedrock cells below the crown pillar are assigned a hydraulic conductivity typical of the backfill in this analysis. As discussed below, a sensitivity analysis was performed to evaluate the effect of a higher bulk hydraulic conductivity of the cemented tailings. It is conservatively assumed that the proposed grouting in the crown pillar will not remain stable indefinitely after mining. Therefore, the low-conductivity grout layer is not included in this analysis.

Particles were initiated within the mined, backfilled zinc and copper ore cells. The particles were placed at a density of one particle per model cell. Particles were placed at the vertical center of the cells as shown in Figure 3.2. Sensitivity simulations were performed to evaluate the effect of placing the particles at the top of these cells, as shown in Figure 3.3.

3.2 Model Predictions

3.2.1 Best Engineering Judgement for Transport

The flow field uses the calibrated model parameters (HSI GeoTrans, 1998b) with a porosity of 10 percent. All mined bedrock cells below the crown pillar are assigned a hydraulic conductivity of 2.8E-4 ft/d (1.0E-7 cm/s) to represent the backfill. A total of 467 particles were initiated at the vertical centers of the mined cells in the ore body. The results of the particle

tracking analysis are summarized in Table 3.1. Figure 3.4 shows the cumulative percentage of particles reaching the DMZ versus time. The first particle reaches the DMZ at 4,594 years. However, only two percent of the particles have reached the DMZ after 10,000 years, while after 106,000 years fifty percent of the particles have reached the DMZ. The earliest-arriving particles originate in the upper part of the mine (just below the crown pillar), while the latest-arriving particles originate in the bottom model layer.

A sensitivity simulation was conducted to assess the significance of particle placement within a layer. In this simulation, particles were initiated at the top of the mined cells. This placement puts some particles directly beneath the crown pillar and minimizes their travel time to the DMZ. All other features of the BEJT analysis were used. The cumulative percentage plot of particles reaching the DMZ is shown in Figure 3.5. These plots show that the first particle reaches the DMZ at 1,488 years. However, after 10,000 years, only three percent of the particles have reached the DMZ while after 94,000 years fifty percent of the particles have reached the DMZ.

3.2.2 Practical Worst Case for Transport

The Practical Worst Case for Transport (PWCT) particle tracking simulations used the same parameters as the Practical Worst Case simulation documented in the groundwater flow modeling report (HSI GeoTrans, 1998b). The parameter changes included increasing the bedrock hydraulic conductivities and increasing the backfill hydraulic conductivity to 5×10^{-7} cm/s.

The results of the simulation with particles originating at the vertical center of mined cells are shown in Figure 3.6. The first particle reaches the DMZ at 1,206 years. Approximately 18 percent of the particles have reached the DMZ within the first 10,000 years. Fifty percent of the particles have reached the DMZ by 25,000 years.

The results of a sensitivity simulation with particles originating at the top of mine cells are shown in Figure 3.7. In this simulation, the first particle arrives at the DMZ at 457 years. Twenty two percent of the particles arrive by 10,000 years, while 50 percent arrive by 23,000 years.

3.3 Summary of Mine Reflooding Model Results

The particle tracking results show that the most rapid advective travel times from the mine to the DMZ range from 1,206 years for the PWCT simulation to 4,594 years for the BEJT simulation. These travel times are long, particularly considering the implausibility of the PWCT, as was described in HSI GeoTrans (1998b).

Of greater importance than the arrival time of the first particle, however, is the long time over which particles reach the DMZ for all cases. As shown in Figure 3.4, it takes about one million years for 90% of the particles to cross the DMZ. This wide variation in arrival times corresponds to a very slow leach rate. In the PWCT simulation (Figure 3.7), it takes about 200,000 years for 90% of the particles to cross the DMZ.

The relatively long travel times show that the mined area has limited potential for affecting groundwater. In addition, the slow release rate suggests that mixing with groundwater in the bedrock and glacial system will significantly reduce concentrations of any solute that does approach the DMZ. Solute transport modeling of the reflooded mine would likely indicate an even longer time for the concentration to peak at the DMZ. The longer time is due to the inclusion of dispersion and mixing which would further reduce solute concentrations.

Solute transport modeling is not deemed necessary due to:

- the very low rate of solute movement from the backfilled mine upward through the crown pillar rock and massive saprolite,
- the long travel time for solute particles from the mined areas to the DMZ,
- the large variation in travel times for solute particles from the mined areas to the DMZ,
- the conservative nature of particle tracking which does not account for mixing and dispersion, and
- the conservative nature of particle tracking which does not account for chemical precipitation and adsorption, which would also increase travel times and reduce concentrations of a number of constituents in the reflooded mine water.

Table 3.1 Summary of Particle Tracking Simulations.

Simulation/Particle Origination	Minimum Travel Time (years)	Average Travel Times (years)
BEJT Center	4,594	458,948
BEJT Top	1,488	383,062
PWCT Center	1,206	97,230
PWCT Top	457	78,370

\Crandon\FlowMod2\Surfer\49t-h47.srf

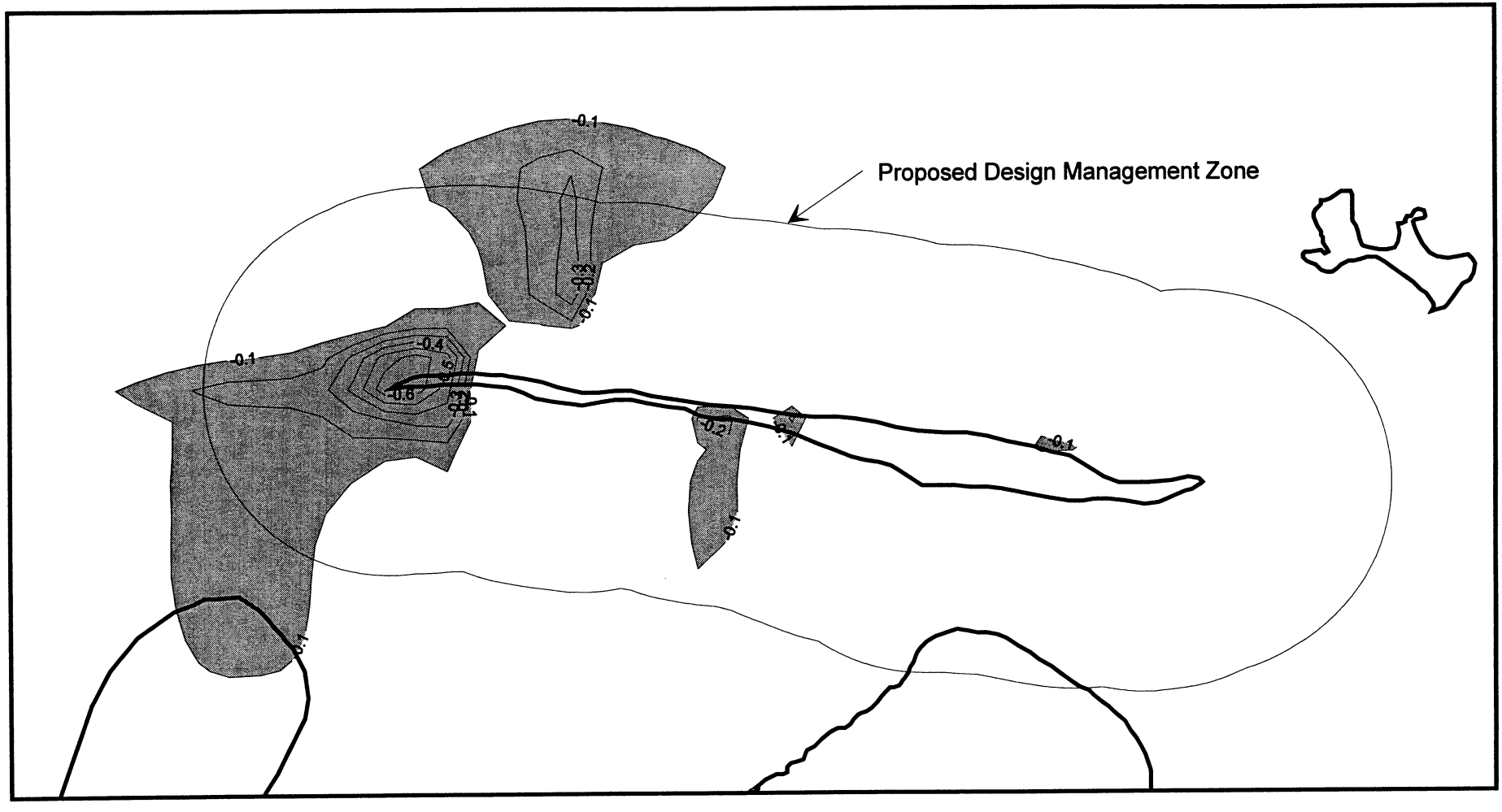

4.2-10-373

0 1000 2000

Horizontal Scale in Feet

Notes:
1. Contours of head difference between layers 4 and 7 are shown at 0.1 foot intervals.
2. Shaded areas indicate an upward head difference of at least 0.1 foot.
3. Only upward differences are contoured.

HSI GEOTRANS

REVISED	DATE	BY	DESCRIPTION

CHECKED BY: KMR	DATE: Dec 98
APPROVED BY: PFA	DATE: Dec 98
APPROVED BY:	DATE:

Nicolet Minerals COMPANY

Mining for the Future

Figure 3.1
Areas of Upward Head Gradients Near the Backfilled Mine

Scale: 1" = 1000'	Date: Oct. 1998
Prepared By: HSI GeoTrans	By: GWC

\Crandon\FlowMod2\GIS\PartCent.wor

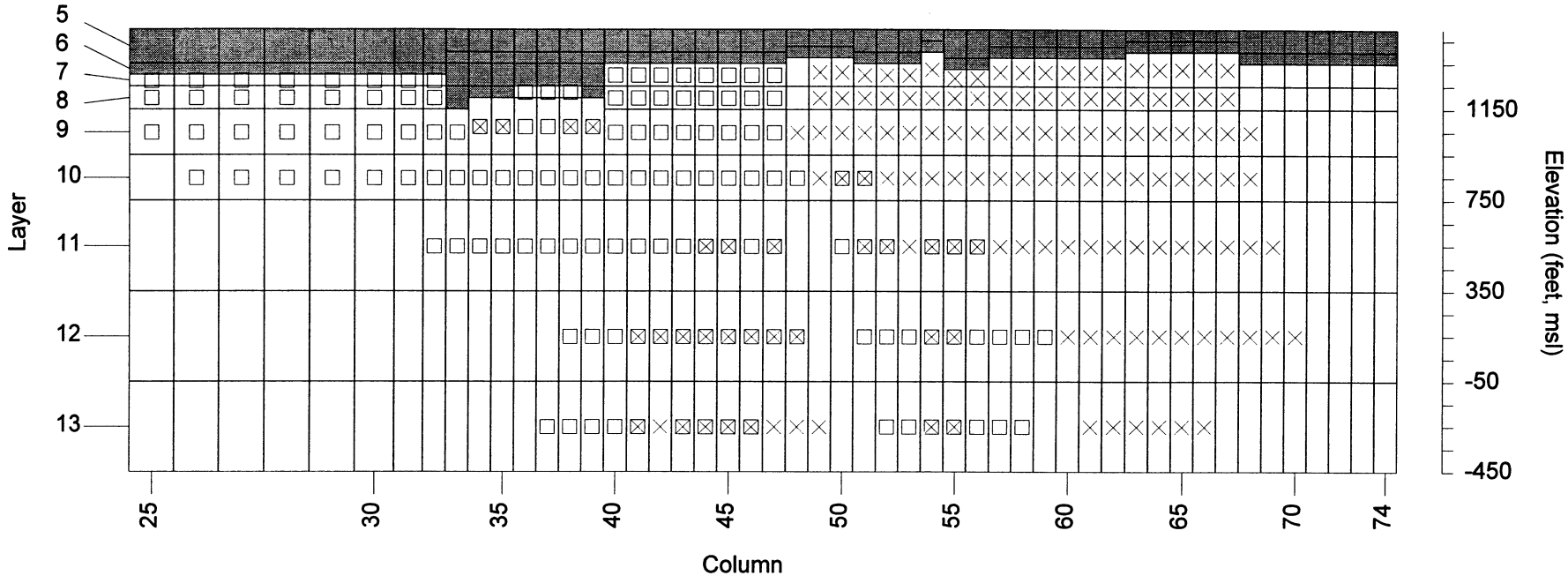

4.2-10-374

Legend

- Crown Pillar
- Zinc Ore Particle
- Copper Ore Particle

0 700 1400

Scale in Feet

HSI GEOTRANS			
REVISED	DATE	BY	DESCRIPTION
CHECKED BY: KMR			DATE: Dec 98
APPROVED BY: PFA			DATE: Dec 98
APPROVED BY:			DATE:

Nicolet Minerals COMPANY

Figure 3.2
Particle Placement at Vertical Centers of Backfilled Mine Cells

Scale: 1 in. = 700 ft. | Date: Oct 1998

Prepared By: HSI GeoTrans | By: GWC

\Crandon\FlowMod2\GIS\PartTop.wor

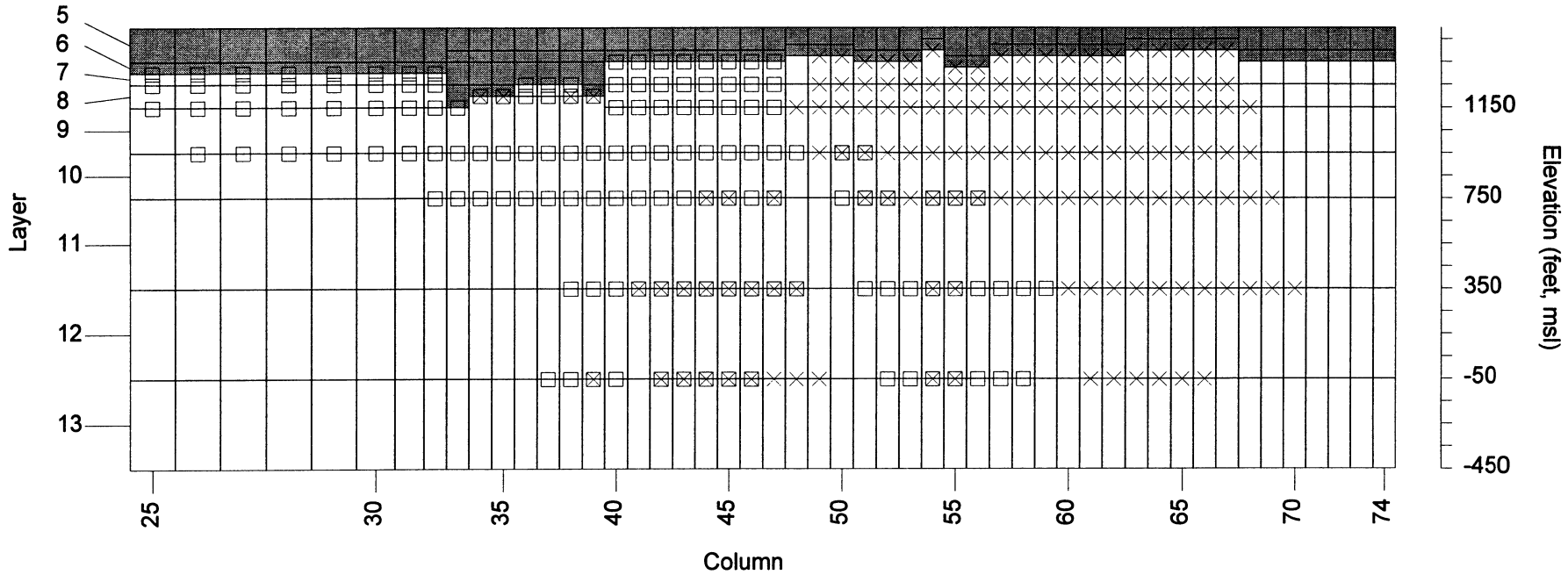

4.2-10-375

Legend

- Crown Pillar
- Zinc Ore Particle
- Copper Ore Particle

0 700 1400

Scale in Feet

HSI GEOTRANS			
REVISED	DATE	BY	DESCRIPTION
CHECKED BY: KMR			DATE: Dec 98
APPROVED BY: PFA			DATE: Dec 98
APPROVED BY:			DATE:

Nicolet Minerals COMPANY

Figure 3.3
Particle Placement at Vertical Tops of Backfilled Mine Cells

Scale: 1 in. = 700 ft. | Date: Oct 1998

Prepared By: HSI GeoTrans | By: GWC

\Crandon\Flowmod2\Excel\49t1.xls

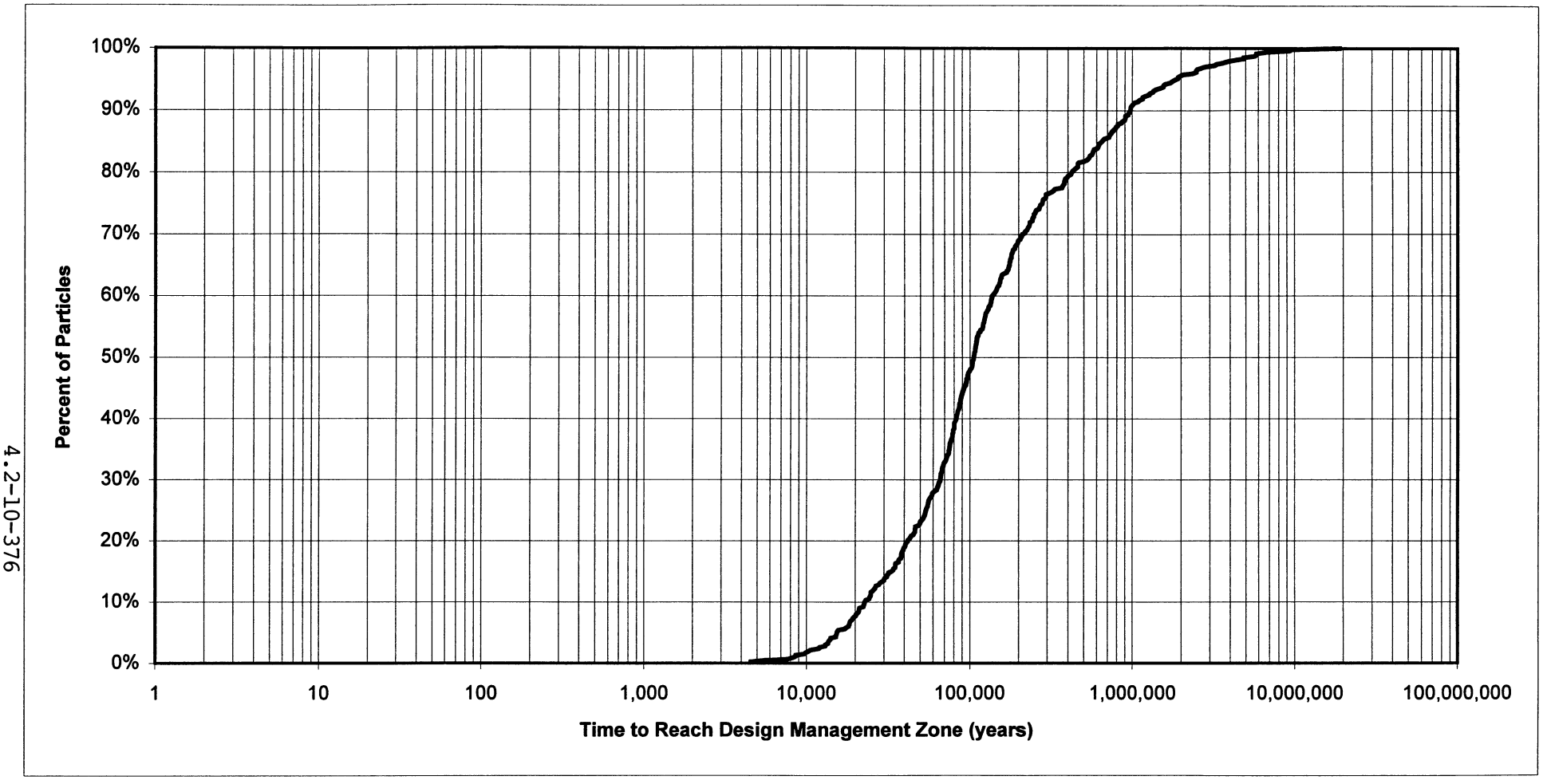

4.2-10-376

Travel Time (years)	
Minimum	4,594
Maximum	18,879,589
Mean	458,948
Median	105,570
Std. Dev.	1,328,151

Note: Particles originate at mine cell centers.

HSI GEOTRANS

REVISED	DATE	BY	DESCRIPTION

CHECKED BY: KMR	DATE: Dec 98
APPROVED BY: PFA	DATE: Dec 98
APPROVED BY:	DATE:

Simulation 49T1

Nicolet Minerals COMPANY

Figure 3.4
Particle Travel Times to Design Management Zone BEJT Center

Scale: None	Date: Oct 1998
Prepared By: HSI GEOTRANS	By: GWC

\Crandon\Flowmod2\Excel\49t2.xls

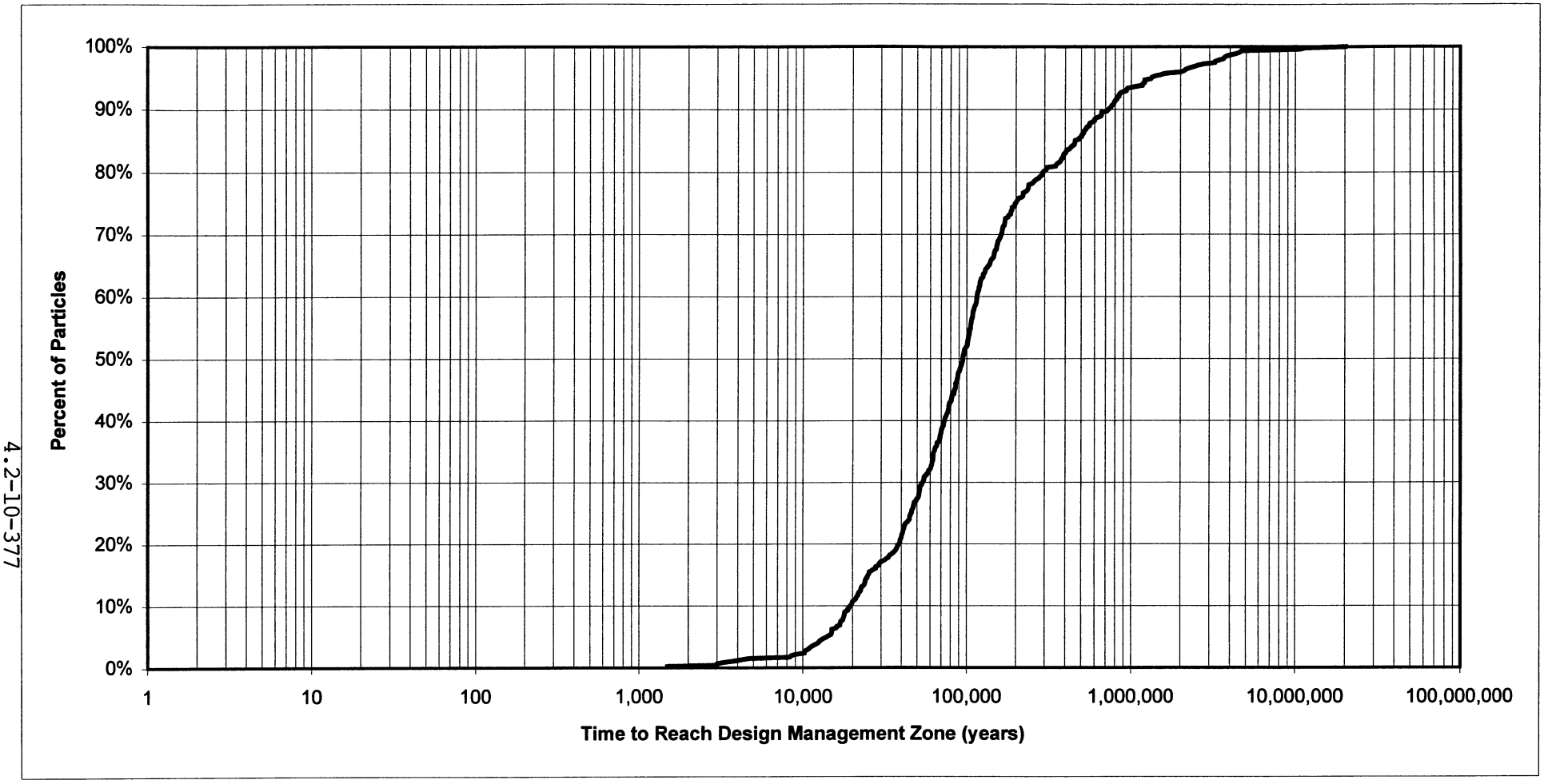

4.2-10-377

Travel Time (years)	
Minimum	1,488
Maximum	20,068,282
Mean	383,062
Median	94,492
Std. Dev.	1,319,837

Note: Particles originate at mine cell tops.

HSI GEOTRANS

REVISED	DATE	BY	DESCRIPTION

CHECKED BY: KMR	DATE: Dec 98
APPROVED BY: PFA	DATE: Dec 98
APPROVED BY:	DATE:

Simulation 49T2

Nicolet Minerals COMPANY

Figure 3.5
Particle Travel Times to Design Management Zone BEJT Top

Scale: None	Date: Oct 1998
Prepared By: HSI GEOTRANS	By: GWC

\Crandon\Flowmod2\Excel\50t4.xls

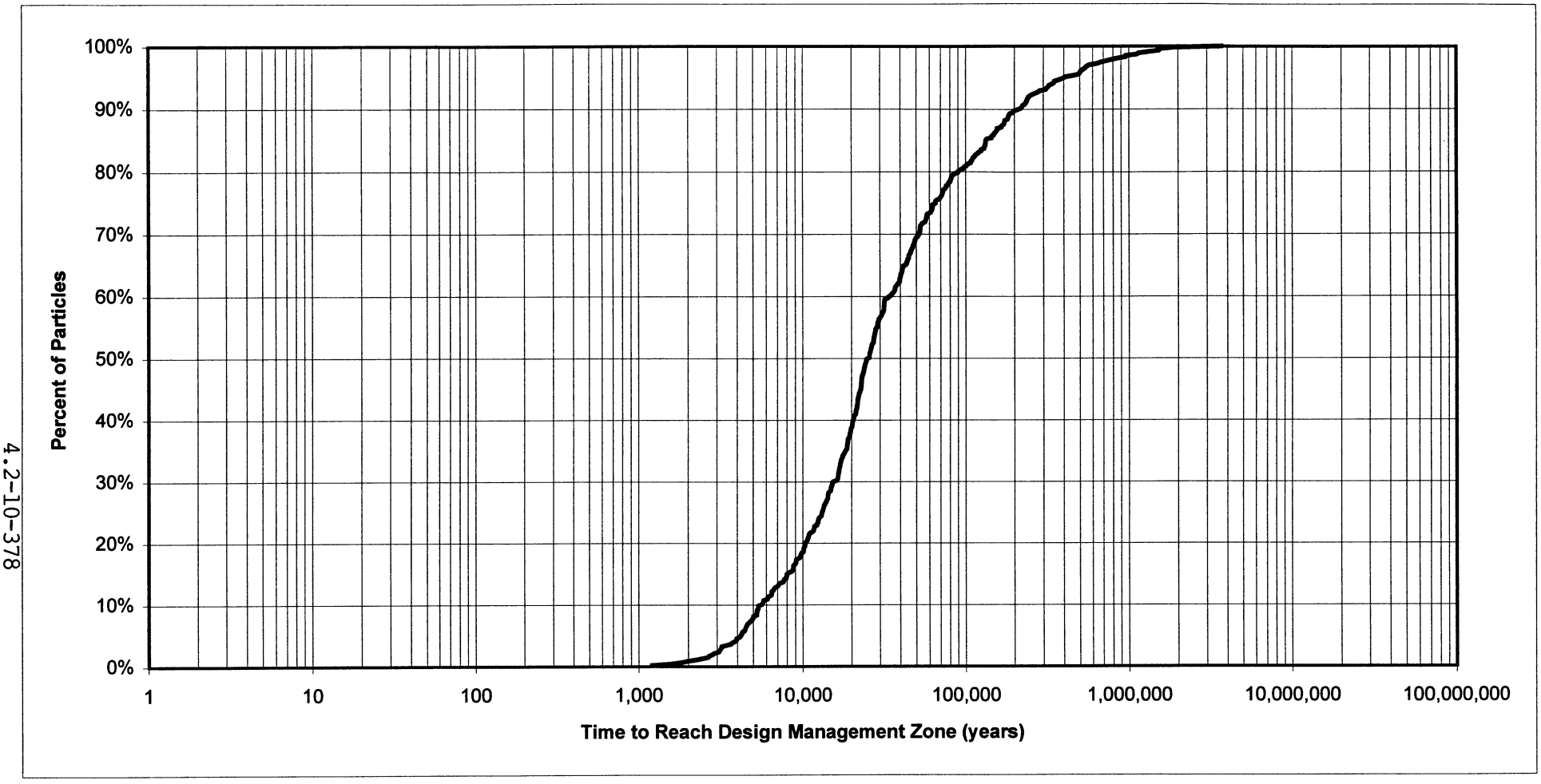

4.2-10-378

Travel Time (years)	
Minimum	1,206
Maximum	3,653,196
Mean	97,230
Median	25,248
Std. Dev.	260,992

Note: Particles originate at mine cell centers.

HSI GEOTRANS

REVISED	DATE	BY	DESCRIPTION

CHECKED BY: KMR	DATE: Dec 98
APPROVED BY: PFA	DATE: Dec 98
APPROVED BY:	DATE:

Simulation 50T4

Nicolet Minerals COMPANY

Figure 3.6
Particle Travel Times to Design Management Zone PWCT Center

Scale: None	Date: Nov 1998
Prepared By: HSI GEOTRANS	By: GWC

\Crandon\Flowmod2\Excel\50t5.xls

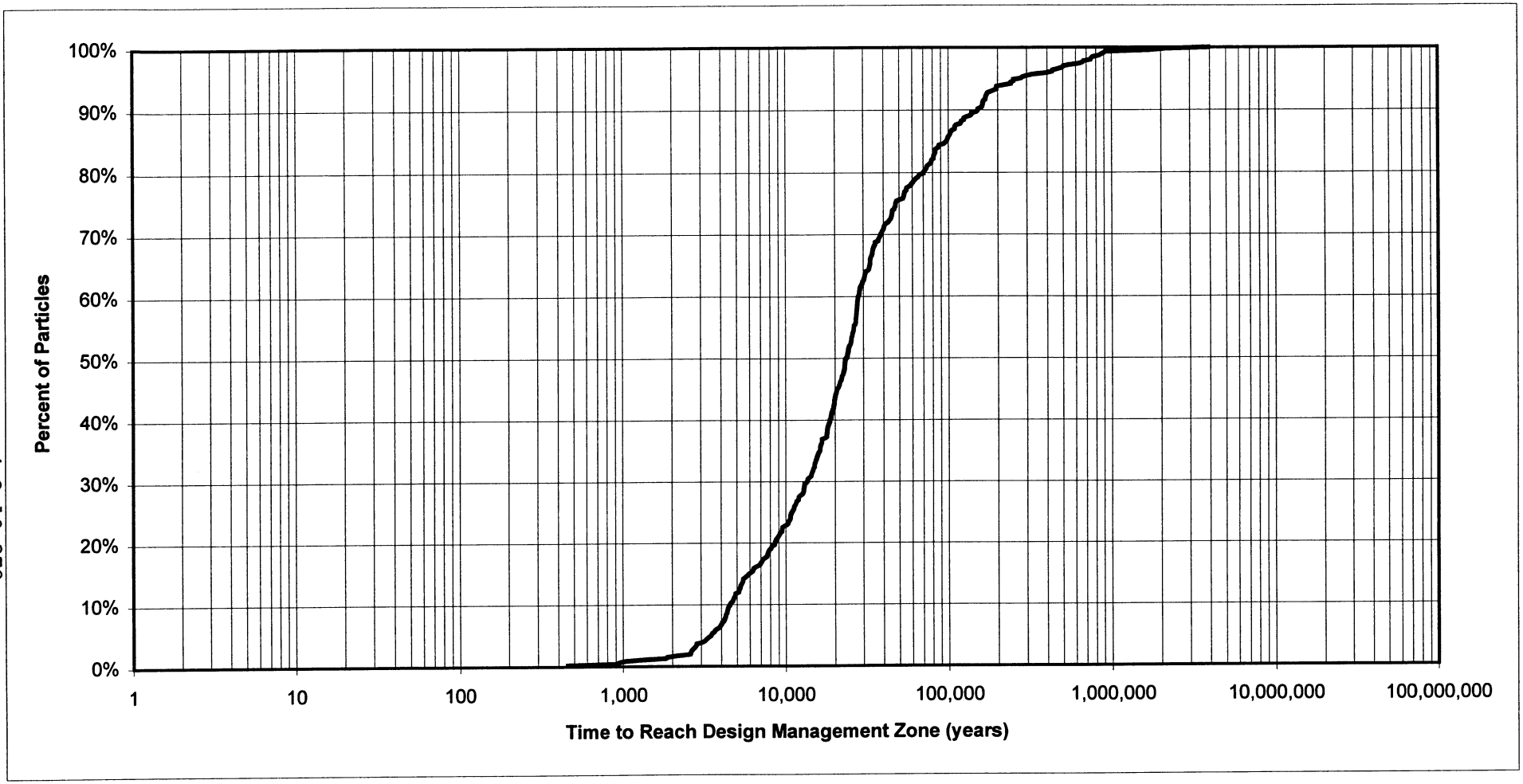

Travel Time (years)	
Minimum	457
Maximum	3,908,090
Mean	78,370
Median	23,468
Std. Dev.	250,982

Note: Particles originate at mine cell tops.

HSI GEOTRANS

REVISED	DATE	BY	DESCRIPTION

CHECKED BY: KMR DATE: Dec 98

APPROVED BY: PFA DATE: Dec 98

Simulation 50T5 APPROVED BY: DATE:

Nicolet Minerals COMPANY

Figure 3.7
Particle Travel Times to Design Management Zone PWCT Top

Scale: None Date: Nov 1998

Prepared By: HSI GEOTRANS By: GWC

4 References

Gelhar, L.W., C. Welty, and K.R. Rehfeldt. A critical review of data on field-scale dispersion in aquifers, *Water Resour. Res.*, 28(7), 1955-1974, 1992.

HSI GeoTrans, 1996. Numerical Simulation of Potential Solute Transport at the proposed zinc and copper mine near Crandon, Wisconsin (November, 1996)

HSI GeoTrans, 1998a. Update to Numerical Simulation of potential solute transport at the proposed zinc and copper mine near Crandon, Wisconsin (April 1998).

HSI GeoTrans, 1998b. Addendum No.2 to Numerical Simulation of the effect on groundwater and surface water of the proposed zinc and copper mine near Crandon, Wisconsin (August, 1998).

McDonald, M.G., A.W. Harbaugh, 1988. A modular three-dimensional finite difference groundwater flow model: *U.S. Geological Survey Techniques of Water-Resources Investigations*, Book 6, Chapter A1.

Pollack, D.W., 1989. Documentation of computer programs to complete and display pathlines using results results from the U.S. Geological Survey modular three-dimensional finite difference groundwater model, U.S.G.S. Open File Report 89-381, 81pp.

Saad, D.A., 1996. Using chlorofluorocarbons to date groundwater and determine hydrologic properties of sediments near the proposed Crandon mines near Crandon, Wisconsin. Summary report, submitted to WDNR June 10, 1996, 16 pp.

Zheng, C., 1996. MT3D^{96}, Modular three-dimensional transport model. Version 2.0.

APPENDIX A

Update No. 2 to the TMA Footprint Boundaries
and Percolation Rates

Foth & Van Dyke
Memorandum

November 10, 1998

TO: Pete Andersen, HSI GeoTrans, Inc.

CC: Jerry Sevick, Foth & Van Dyke
Ken Black, Nicolet Minerals Company
Steve Dischler, Foth & Van Dyke
Denis Roznowski, Foth & Van Dyke
Master File

FR: Steve Donohue, Foth & Van Dyke SVD

RE: Crandon Project - Solute Transport Model: Update No. 2 to the TMA Footprint Boundaries and Percolation Rates

As part of the work on updating the solute transport model simulations for the Crandon Project TMA, several recent modifications to the TMA design need to be taken into account.

TMA Footprint

Due to the pyrite removal process, the volume of tailings placed in the TMA will be reduced. As such, the footprint of the facility will be smaller than previously simulated. Figure 1 shows the revised TMA layout and revised reclaim pond. Based on a letter to NMC from the WDNR dated July 15, 1998, the design management zone (DMZ) for the reclaim pond will be 150 ft during the operational life of the pond. The DMZ for the TMA will be 1,200 ft. Accordingly, Figure 1 shows the location of both DMZs.

TMA Percolation Rates & Site Life

Table 1 summarizes the site life for each TMA cell. Tables 2 - 4 summarize the revised percolation rates for the TMA. The incorporation of these numbers into the solute transport model should be consistent with the methodology described in the March 4, 1998, memorandum which was included in the 1998 solute transport model report (HSI GeoTrans, Inc., 1998).

Reclaim Pond

The reclaim pond percolation rates remain unchanged from what was used in the 1998 solute transport model report (HSI, GeoTrans, Inc., 1998). However, the operation life of the reclaim pond will be extended. Based on the HELP Model analysis, it is now estimated that the reclaim pond will be utilized until the 16th year after closure of the TMA facility. Thus, at approximately 46 years, percolation from the reclaim pond will be terminated.

References

HSI GeoTrans, Inc. 1998. *Update to: Numerical Simulation of Potential Solute Transport at the Proposed Zinc and Copper Mine Near Crandon, Wisconsin.*

Table 1

Estimated Volumes and Site Life for TMA Cells and Stages

Tailings Cell	Stage	Tailings (cy)	Approximate Phase Life (yrs.)
Zinc Ore Production			
TMA 1A	I	987,500	3.2
TMA 1B	I	1,203,500	3.9
TMA 1A & 1B	II	2,746,500	8.9
Zinc Total Tailings		4,937,500	16.0
Copper Ore Production			
TMA 2	I	1,366,600	2.4
TMA 2	II	2,049,800	3.6
Subtotal		3,985,800	6.0
TMA 3	I	1,366,600	2.4
TMA 3[1]	II	2,049,800	3.6
Subtotal		3,985,800	6.0
Copper Total Tailings		6,832,800	12.0
Total Zinc & Copper		11,770,300	28

cy = Cubic yards
yrs = Years

Prepared by: MRS
Checked by: SAD2

Table 2

Percolation from TMA Based on Doubled Precipitation Values During Operation of Initial Stages

Year	Sideslope (in/yr)	Base (in/yr)
1	0.000001	0.024968
2	<0.0000005	0.003517
3	<0.0000005	0.004562
4	<0.0000005	0.008642
5	<0.0000005	0.003126
6	<0.0000005	0.004671
7	<0.0000005	0.005429
8	<0.0000005	0.001883
9	<0.0000005	0.001380
10	<0.0000005	0.006263
Average	<0.0000005	0.006440

Note: HELP model output rounds off to six digits.

Prepared by: MRS
Checked by: NXP

Table 3

Percolation from TMA Based on Doubled Precipitation Values During Operation of Second Stages

Year	Lower Sideslope (in/yr)	Upper Sideslope (in/yr)	Base (in/yr)
1	0.000001	0.000002	0.034353
2	0.000001	0.000001	0.016261
3	<0.0000005	0.000001	0.005851
4	<0.0000005	0.000001	0.004205
5	<0.0000005	0.000001	0.007981
6	<0.0000005	0.000001	0.003110
7	<0.0000005	0.000001	0.004669
8	<0.0000005	<0.0000005	0.004549
9	<0.0000005	0.000001	0.001967
10	<0.0000005	0.000001	0.001725
Average	<0.0000005	0.000001	0.008470

Note: HELP model output rounds off to six digits.

Prepared by: MRS
Checked by: NXP

Table 4

Post-Closure Percolation

Year from Placement of Cover	Lower Sideslope (in/yr)	Upper Sideslope (in/yr)	Base (in/yr)
1	0.013885	0.007540	0.652038
2	<0.0000005	<0.0000005	0.014870
3	<0.0000005	<0.0000005	0.001169
4	<0.0000005	<0.0000005	0.001021
5	<0.0000005	<0.0000005	0.000916
6	<0.0000005	<0.0000005	0.000835
7	<0.0000005	<0.0000005	0.000763
8-15	<0.0000005	<0.0000005	0.000552
16-25	<0.0000005	<0.0000005	0.000308
26-35	<0.0000005	<0.0000005	0.000195
36-40	<0.0000005	<0.0000005	0.000151
41-50	<0.0000005	0	0.000123
51-60	<0.0000005	0	0.000097
61-70	<0.0000005	0	0.000081
71-80	<0.0000005	0	0.000069
81-90	<0.0000005	0	0.000059
91-115	0	0	0.000004
116-140	0	0	0.000004
141-165	0	0	0
166-175	0	0	0
176-185	0	0	0
186-195	0	0	0
196-205	0	0	0
206-215	0	0	0

Table 4 *(Continued)*

Year from Placement of Cover	Lower Sideslope (in/yr)	Upper Sideslope (in/yr)	Base (in/yr)
216-220	0	0	0
221-230	0	0	0
231-240	0	0	0
241 plus[1]	0.00002	0.00002	0.00002

Note: HELP Model output rounds to off to six digits.

[1] Percolation is conservatively assumed at this time period to be equal to infiltration through cover, even though the HELP Model indicates it will take longer to achieve this equilibrium.

Prepared by: MRS
Checked by: NXP

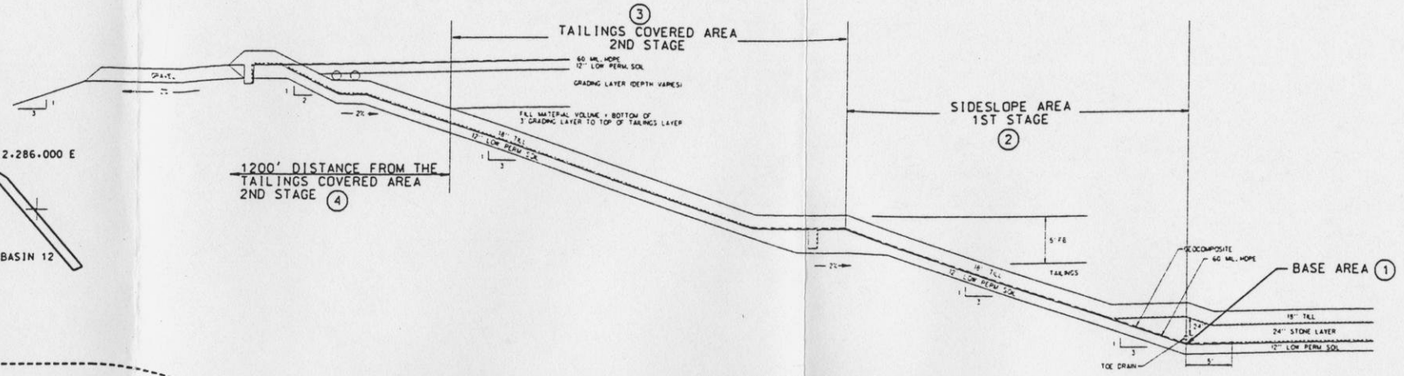

SECTION A-A'

NOT TO SCALE

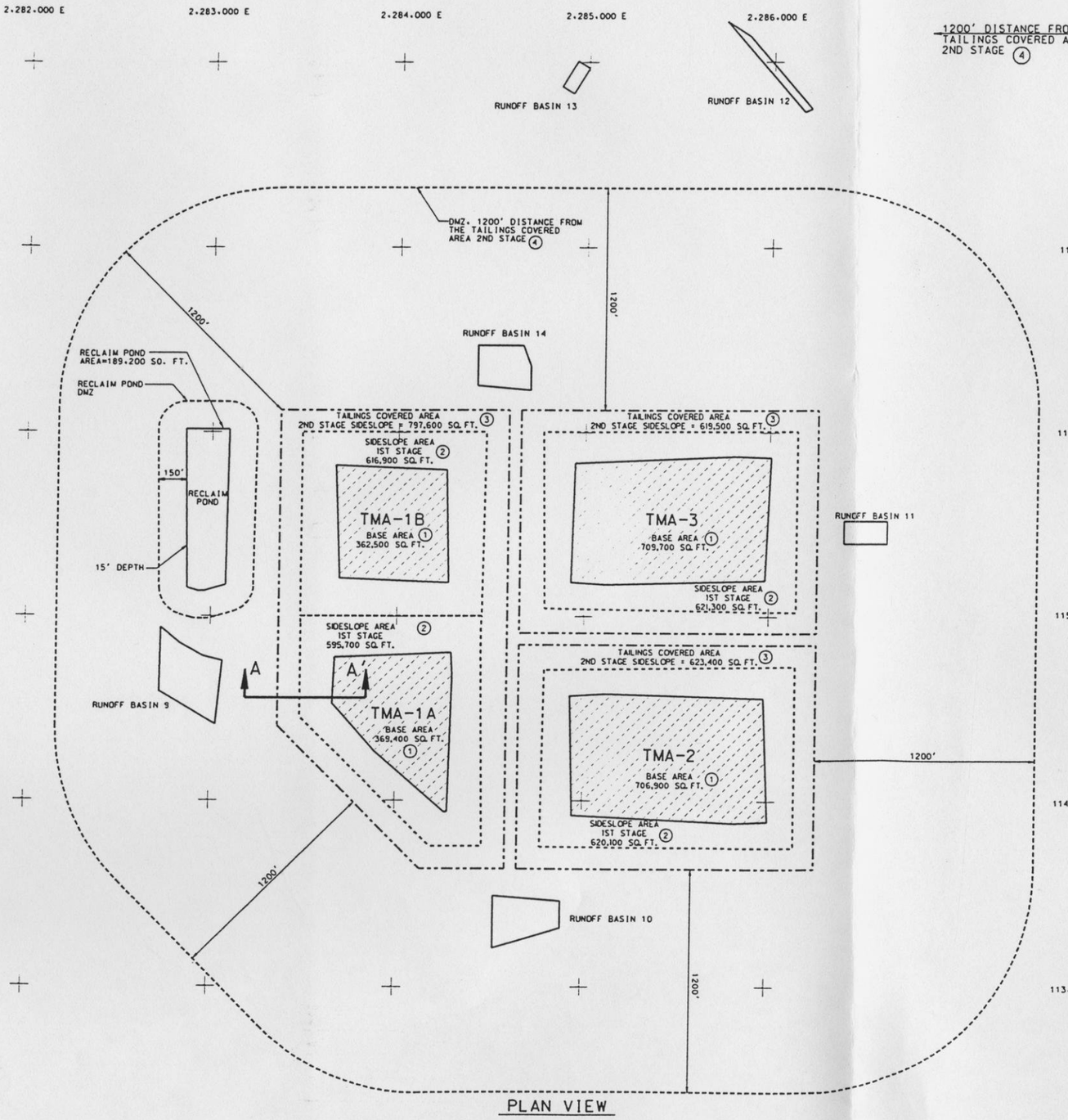

PLAN VIEW

LEGEND

- APPROXIMATE LIMITS OF TAILINGS COVERED AREA 2ND STAGE
- APPROXIMATE LIMITS OF SIDESLOPE AREA 1ST STAGE
- APPROXIMATE LIMITS OF BASE AREA

0 350' 700'

SCALE

Foth & Van Dyke				
REVISED	DATE	BY	DESCRIPTION	
CHECKED BY:		MRS		DATE: OCT '98
APPROVED BY:		SAD2		DATE: OCT '98
APPROVED BY:		---		DATE: OCT '98

Nicolet Minerals COMPANY

Mining for the Future Commitment

FIGURE 1

TMA SURFACE AREAS

Scale: 0 350' 700' | Date: NOVEMBER, 1998

Prepared By: Foth & Van Dyke | By: JRB2 | 93C049

I:\93c049\98c03818c38f50.3d Nov. 06, 1998 14:06:13

Addendum No. 1 to:
Update No. 2 to:
Numerical Simulation of Potential Solute Transport at the Proposed Zinc And Copper Mine Near Crandon, Wisconsin

June 21, 1999

This report presents an updated modeling analysis of solute transport from the proposed Tailings Management Area (TMA) at the Crandon mine site. The most recent report on the TMA modeling was completed in January 1999 (HSI GeoTrans 1999, section 2). Since that time, the project's HELP model results that are used as an input to the numerical transport model (Foth & Van Dyke, 1999a included as Appendix A) have been updated to correct a discrepancy in the input parameters. As a consequence, the affected solute transport model simulations were re-executed and the results regenerated.

The HELP model results (Appendix A) are the predicted water percolation rates from the bottom of the TMA cells to the groundwater over the life of the facility. The modeled concentrations of solutes in the groundwater are dependent on the predicted percolation rates. Therefore, it was necessary to update the simulations which were affected by the recent revision to percolation rates. However, it was not necessary to re-evaluate the calibration of the model (HSI GeoTrans, 1999), which is not dependent on the HELP results. Also, the qualitative results of the sensitivity analyses presented in earlier reports (HSI GeoTrans, 1998 and GeoTrans, 1996) still remain valid.

This report is an addendum to the most recent transport modeling analysis (HSI GeoTrans, 1999). The tables, figures, and text presented herein are revisions to some (but not all) of those in the prior report. This report documents 1) the specific revisions to model input as a consequence of the changes in the HELP model analysis, and 2) the updated results (concentration contour plots and concentration response vs. time plots) for the Best Engineering Judgement for Transport (BEJT) and the Practical Worst Case for Transport (PWCT) scenarios. For more information on the construction of the numerical model, simulation procedures, model calibration, and the method of combining simulation results using superposition, please refer to section 2 of the prior report (HSI GeoTrans, 1999).

Changes to Model Input

The TMA percolation rates, determined from the recently-updated HELP model analysis, are used to assign aquifer recharge rates (in the MODFLOW recharge array) for the model cells beneath the TMA cells. In the transport model simulations, these recharge rates are presumed to have associated non-zero concentrations (in the MT3D recharge concentration array) forming a solute source for the model.

The predictive solute transport model is comprised of 22 stress periods (HSI GeoTrans, 1999). During the stress periods, each TMA cell (TMA 1A, TMA 1B, TMA 2, TMA 3) goes through a series of 7 percolation "phases" during and after operation. These phases are referenced using the letters A through G. An additional percolation phase (X) is included to represent pre-construction conditions (no tailings or percolation barrier present). The water percolation rates for each phase, and the basis for these rates are presented in Table 1. Note that the percolation rate is different for the three components of the TMA cells: base, lower sideslope, and upper sideslope. The rates for Phases A-G are based on values obtained by the HELP analysis. For Phase X, the percolation rate is equivalent to the default (calibrated) recharge rate of 9.7 in/yr (2.21×10^{-3} ft/d). Also, because of the manner of operation during the first phase of operation, the Phase A percolation rate for the upper sideslope is also equal to the default recharge rate, and there is no simulated source for that part of the cell.

Tables 2 through 5 list the percolation rates for the individual TMA cells by stress period. The different TMA cells begin operations at staggered times according to the designed use of the facility. Note, in Tables 1-5, that the percolation rates for all phases except C and D are unchanged from the prior analysis (HSI GeoTrans, 1999, Tables 2.1, 2.3-2.6). As a result, only stress periods 5-13 have revised percolation rates in the model.

Because the yearly rates produced by the HELP model were grouped into rates for 7 percolation phases for the numerical model, and because the discretized representation of the TMA cells results in source surface areas that differ slightly from the designed areas, the total percolation flux input to the numerical model is not exactly the same as the HELP-predicted percolation flux, as shown in Figure 1 (compare to Figure 2.5 in HSI GeoTrans, 1999). However, as shown in Figure 2 (compare to Figure 2.6 in HSI GeoTrans, 1999) the approximations tend to overestimate the cumulative amount of source percolation to the aquifer, relative to the HELP analysis, which is a small deviation on the conservative side.

Model Predictions

Prior to running the transport model, two groundwater flow simulations were made using the percolation rates defined for the 22 stress periods (one for BEJT and one for PWCT). The two simulations differed only in that the PWCT simulation used one-tenth of the vertical conductivities (MODFLOW Vcont arrays) of the BEJT simulation. As in the prior analysis (HSI

GeoTrans, 1999), the flow simulations were executed in quasi-steady mode. The resulting heads and cell-to-cell flows were needed to make the required transport model runs.

Before making simulations with MT3D, a simpler simulation was made using MODPATH and the results of the BEJT flow model to confirm the direction in which solute from the TMA would travel. In this simulation, a few particles were released from the various TMA cells as they began operation. The resulting pathways are shown in cross-section in Figure 3. These results, which are nearly identical to those in the prior report (HSI GeoTrans, 1999, Figure 2.13), indicate solute pathways deep into the glacial aquifer — to depths of 100 feet or more for some particles.

As noted in the prior modeling reports (HSI GeoTrans, 1999, 1998, and GeoTrans, 1996), three MT3D solute transport simulations are used to define "unit-response functions" that are used as building blocks to quantify the concentration of any constituent of interest (COI) for the TMA (see Figure 2.14 in HSI GeoTrans, 1999). In the first simulation the concentration is set to 1.0 when and where a TMA cell is in Phase A (base and lower sideslope only), B, or C (these phases are characterized by an "operation" source concentration). In the second simulation, a unit-concentration is applied for Phase D, E, and F only (representing the "post-cap" concentration). At the end of Phase F, it is conservatively assumed that the flexible membrane liner (FML) of the TMA cell is completely degraded, and that the final phase, Phase G, is characterized by a third source concentration — the "oxidized" concentration. Therefore, the third simulation has a unit-concentration source for TMA cells during only phase G.

Once the three MT3D simulations are complete, results for individual COIs are easily obtained from its characteristic "operation", "post-cap", and "oxidized" concentrations by applying the principle of superposition. The results for individual COIs are presented in the project's Groundwater Quality Performance Evaluation (Foth & Van Dyke, 1999b). In this report, the concentration-response vs. time at the Design Management Zones (DMZs) are shown for each of the three simulations (for both BEJT and PWCT). Also, an example constituent is used to illustrate the types of results that could be produced for any given COI. The hypothetical example constituent has an operation concentration of 2000 ppm (or mg/L), a post-cap concentration of 4000 ppm, and an oxidized concentration of 40,000 ppm. Note that these concentrations refer to the concentration in the percolate that is a source to the groundwater aquifer (just below the TMA). It is conservatively assumed that the percolate immediately reaches the water table, ignoring dispersion in the vadose zone. Furthermore, it is conservatively assumed in all of the transport modeling analyses that the modeled solute is non-decaying, non-reactive, non-volatile, and non-retarded in the aquifer.

BEJT Results

The first and second BEJT MT3D simulations (Simulations A and B) were re-executed with the new flow model results generated using the updated HELP-based percolation rates. The

third simulation (which has no source until stress period 20) was unchanged from the prior analysis (HSI GeoTrans, 1999) because there were no revisions made to percolation rates in stress periods 20-22.

The modeled concentration at each aquifer cell was saved at many times during the 650-year simulations. Subsequently, a post-processing utility was used to determine the maximum concentration along the two DMZ boundaries at each saved time. One DMZ extends 1200 feet from the edge of the TMA footprint, and the other DMZ extends 150 feet from the edge of the Reclaim Pond. The concentration response curves are shown in Figure 4 for both DMZs for each of the three BEJT transport simulations (the two new simulations plus the prior Simulation C). Compared with the results of the last analysis (HSI GeoTrans, 1999, Figure 2.16), the Simulation A response at the TMA DMZ does not have a second peak, and the maximum concentration at both DMZs is slightly reduced. This is attributable to a significant reduction in the Phase C percolation rate, which lowers the solute mass influx to the aquifer. The response curves for Simulation B are also slightly modified from their prior shapes due to changes in the Phase D percolation rates. As in the prior analysis, the early-time (prior to about 50 years) concentration responses at both DMZs are largely the result of the source at the Reclaim Pond, which has a relatively high percolation rate, is closer to the DMZ boundaries, and is unaffected by recent updates to the HELP analysis.

Using the example constituent (2000/4000/40,000 ppm source), the concentration fields for the three BEJT simulations were scaled and summed using superposition. The resulting fields were processed to determine the maximum concentration at the DMZ boundaries through time, shown in Figure 5. For the traces on this figure, the second peaks are largely due to the higher post-cap concentration (relative to the operation concentration) that is multiplied by the Simulation B response. The traces have similar shapes to those generated in the prior analysis (HSI GeoTrans, 1999, Figure 2.17), but have slightly lower concentrations.

For the example constituent, concentration plumes are contoured in plan view at various times in Figures 6 through 14 (compare to Figures 2.18 through 2.26 in HSI GeoTrans 1999). In these figures, the maximum concentration in any of the seven modeled layers is taken as the value to be contoured. The figures clearly show the important influence of the Reclaim Pond source on the concentration plume in the western portion of the model. Also evident from these contour plots is the direction change, from westward flow to eastward flow, after 32 years due to mine recovery.

Using the cross-section defined in the prior report (HSI GeoTrans, 1999, Figure 2.27), profile views of the BEJT example constituent plume are shown in Figures 15 through 23. Like the corresponding figures in the prior report (HSI GeoTrans, 1999, Figures 2.28 through 2.36), these plots show the vertical movement of the plume, due in large part to downward gradients beneath and near the TMA (as indicated by Figure 3).

PWCT Results

The PWCT results were also regenerated using the updated percolation rates. Again, only Simulations A and B were re-executed; Simulation C was unchanged. As with the prior analysis (HSI GeoTrans, 1999) the PWCT scenario uses lower dispersivity values (25 ft longitudinal, 2.5 ft transverse, as compared to the BEJT values of 50 ft longitudinal, 5 ft transverse) along with lower vertical hydraulic conductivities. These changes decrease the spreading of the plume, both vertically and laterally, which leads to increased concentrations relative to the BEJT scenario.

Figure 24 shows the predicted PWCT concentration response curves for the three transport simulations at both DMZs. Again, compared to the previous analysis (HSI GeoTrans 1999, Figure 2.37), the second peak for Simulation A at the TMA DMZ is absent and the peak concentrations are slightly reduced. For the example constituent, the DMZ concentration vs. time traces are shown in Figure 25. The shapes of these curves are somewhat modified from the prior analysis (HSI GeoTrans 1999, Figure 2.38), and the peak concentrations are lowered, due to the revised percolation rates.

Plan-view PWCT concentration plumes for the example constituent are shown at various times in Figures 26 through 34 (compare to Figures 2.39 through 2.47 in HSI GeoTrans, 1999). Cross-sectional views of the plume are shown at the same times in Figures 35 through 43 (compare to Figures 2.48 through 2.56 in HSI GeoTrans, 1999). These figures show that the plume behaves similarly in the current and prior analyses.

Summary

As a result of a recent update to the HELP model analysis of the TMA, the solute transport modeling of the TMA was revisited. Revised percolation rates were entered into the model and revised results were obtained. The results are similar to those presented in the previous report (HSI GeoTrans, 1999), which this report updates. Because percolation rates were, on average, reduced in the updated HELP analysis, the predicted aquifer concentrations have been reduced slightly.

References

GeoTrans, 1996. Numerical Simulation of Potential Solute Transport at the Proposed Zinc and Copper Mine Near Crandon, Wisconsin. Consulting report prepared for Foth & Van Dyke, November 20, 1996.

HSI GeoTrans, 1998. Update to: Numerical Simulation of Potential Solute Transport at the Proposed Zinc And Copper Mine Near Crandon, Wisconsin. Consulting report prepared for Foth & Van Dyke, April 28, 1998.

HSI GeoTrans, 1999. Update No. 2 to: Numerical Simulation of Potential Solute Transport at the Proposed Zinc And Copper Mine Near Crandon, Wisconsin. Consulting report prepared for Foth & Van Dyke, January 19, 1999.

Foth & Van Dyke, 1999a. Memorandum from Steve Donohue to Pete Anderson of HSI GeoTrans regarding "Crandon Project — Solute Transport Model: Update No. 3 to the TMA Percolation Rates." May 25, 1999. (Included as Appendix A)

Foth & Van Dyke, 1999b. Crandon Project Tailings Management Area Groundwater Quality Performance Evaluation (Depyritized Tailings). June 4, 1999.

Appendix A

Memorandum regarding:
"Crandon Project — Solute Transport Model: Update No. 3 to the TMA Percolation Rates."

Table 1 Basis for TMA phases and flux rates[1]

Phase	Description	Duration (years)	Basis for Percolation Rate
X	Pre-construction	0-22[2]	Regional model calibrated value
A	First Phase of Operation	2-7[2]	Appendix A Table 2 average[3]
B	Second Phase of Operation plus two years of consolidation	5-11[2]	Appendix A Table 3 average
C	Cap in Place Part 1	1	Appendix A Table 4 Year 1
D	Cap in Place Part 2	7	Appendix A Table 4 Years 2-7
E	Cap in Place Part 3	20	Appendix A Table 4 Years 8-25
F	Cap in Place Part 4	104-114[2]	Appendix A Table 4 Years 26-140
G	Degraded FML Steady-State	N/A	Appendix A Table 4 Years 241+

Phase	Base		Lower Sideslope		Upper Sideslope	
	Rate(in/yr)	Rate(ft/d)	Rate(in/yr)	Rate(ft/d)	Rate(in/yr)	Rate(ft/d)
X	9.70	2.21E-03	9.70	2.21E-03	9.70	2.21E-03
A	6.44E-03	1.47E-06	2.50E-07	5.71E-11	9.70E+00	2.21E-03
B	8.47E-03	1.93E-06	2.50E-07	5.71E-11	1.03E-06	2.34E-10
C	3.88E-02	8.86E-06	1.00E-06	2.28E-10	2.00E-06	4.57E-10
D	3.26E-03	7.45E-07	1.00E-06	2.28E-10	2.50E-07	5.71E-11
E	4.15E-04	9.47E-08	2.50E-07	5.71E-11	2.50E-07	5.71E-11
F	6.05E-05	1.38E-08	2.50E-07	5.71E-11	2.50E-07	5.71E-11
G	2.00E-05	4.57E-09	2.00E-05	4.57E-09	2.00E-05	4.57E-09

Notes

Shaded cells indicate values that have changed since the prior report (HSI GeoTrans 1999).

[1] The TMA reclaim pond is active during years 1-31 during which its flux is 1.6E-5 ft/d, and years 32-46 (reclamation phase) during which its flux is 4.0E-6 ft/d. Thereafter a uniform 2.214E-3 ft/d is used to represent precipitation recharge.

[2] Varies by TMA Cell.

[3] During the first phase of operation, the TMA upper sideslope receives full recharge (from regional model) with a concentration of zero.

Prepared by: KMR
Checked by: GWC
Approved by: PFA

December 1998
Revised 6/99 (GWC, Updated STM)
P:\Crandon\TmaMod4\Excel\StresTab1.xls, Basis

Table 2 TMA 1A percolation rates by stress period.

Stress Period	Phase	Percolation Rate (ft/day)		
		Base	Lower Sideslope	Upper Sideslope
1	A	1.47E-06	5.71E-11	2.21E-03 [1]
2	A	1.47E-06	5.71E-11	2.21E-03 [1]
3	B	1.93E-06	5.71E-11	2.34E-10
4	B	1.93E-06	5.71E-11	2.34E-10
5	C	8.86E-06	2.28E-10	4.57E-10
6	D	7.45E-07	2.28E-10	5.71E-11
7	D	7.45E-07	2.28E-10	5.71E-11
8	D	7.45E-07	2.28E-10	5.71E-11
9	D	7.45E-07	2.28E-10	5.71E-11
10	E	9.47E-08	5.71E-11	5.71E-11
11	E	9.47E-08	5.71E-11	5.71E-11
12	E	9.47E-08	5.71E-11	5.71E-11
13	E	9.47E-08	5.71E-11	5.71E-11
14	E	9.47E-08	5.71E-11	5.71E-11
15	E	9.47E-08	5.71E-11	5.71E-11
16	F	1.38E-08	5.71E-11	5.71E-11
17	F	1.38E-08	5.71E-11	5.71E-11
18	F	1.38E-08	5.71E-11	5.71E-11
19	G	4.57E-09	4.57E-09	4.57E-09
20	G	4.57E-09	4.57E-09	4.57E-09
21	G	4.57E-09	4.57E-09	4.57E-09
22	G	4.57E-09	4.57E-09	4.57E-09

Notes: Shaded cells indicate values that have changed since the prior report (HSI GeoTrans 1999).
[1] Equal to default recharge, no source applied.

Prepared by: KMR
Checked by: GWC
Approved by: PFA

December 1998
Revised 6/99 (GWC, Updated STM)
P:\Crandon\TmaMod4\Excel\StresTab1.xls, TMA1A

Table 3 TMA 1B percolation rates by stress period.

Stress Period	Phase	Percolation Rate (ft/day)		
		Base	Lower Sideslope	Upper Sideslope
1	X	2.21E-03 [1]	2.21E-03 [1]	2.21E-03 [1]
2	A	1.47E-06	5.71E-11	2.21E-03 [1]
3	B	1.93E-06	5.71E-11	2.34E-10
4	B	1.93E-06	5.71E-11	2.34E-10
5	C	8.86E-06	2.28E-10	4.57E-10
6	D	7.45E-07	2.28E-10	5.71E-11
7	D	7.45E-07	2.28E-10	5.71E-11
8	D	7.45E-07	2.28E-10	5.71E-11
9	D	7.45E-07	2.28E-10	5.71E-11
10	E	9.47E-08	5.71E-11	5.71E-11
11	E	9.47E-08	5.71E-11	5.71E-11
12	E	9.47E-08	5.71E-11	5.71E-11
13	E	9.47E-08	5.71E-11	5.71E-11
14	E	9.47E-08	5.71E-11	5.71E-11
15	E	9.47E-08	5.71E-11	5.71E-11
16	F	1.38E-08	5.71E-11	5.71E-11
17	F	1.38E-08	5.71E-11	5.71E-11
18	F	1.38E-08	5.71E-11	5.71E-11
19	F	1.38E-08	5.71E-11	5.71E-11
20	G	4.57E-09	4.57E-09	4.57E-09
21	G	4.57E-09	4.57E-09	4.57E-09
22	G	4.57E-09	4.57E-09	4.57E-09

Notes: Shaded cells indicate values that have changed since the prior report (HSI GeoTrans 1999).
[1] Equal to default recharge, no source applied.

Prepared by: KMR
Checked by: GWC
Approved by: PFA

December 1998
Revised 6/99 (GWC, Updated STM)
P:\Crandon\TmaMod4\Excel\StresTab1.xls, TMA1B

Table 4 TMA 2 percolation rates by stress period.

Stress Period	Phase	Percolation Rate (ft/day)		
		Base	Lower Sideslope	Upper Sideslope
1	X	2.21E-03 [1]	2.21E-03 [1]	2.21E-03 [1]
2	X	2.21E-03 [1]	2.21E-03 [1]	2.21E-03 [1]
3	X	2.21E-03 [1]	2.21E-03 [1]	2.21E-03 [1]
4	A	1.47E-06	5.71E-11	2.21E-03 [1]
5	B	1.93E-06	5.71E-11	2.34E-10
6	B	1.93E-06	5.71E-11	2.34E-10
7	B	1.93E-06	5.71E-11	2.34E-10
8	C	8.86E-06	2.28E-10	4.57E-10
9	D	7.45E-07	2.28E-10	5.71E-11
10	D	7.45E-07	2.28E-10	5.71E-11
11	D	7.45E-07	2.28E-10	5.71E-11
12	D	7.45E-07	2.28E-10	5.71E-11
13	E	9.47E-08	5.71E-11	5.71E-11
14	E	9.47E-08	5.71E-11	5.71E-11
15	E	9.47E-08	5.71E-11	5.71E-11
16	E	9.47E-08	5.71E-11	5.71E-11
17	F	1.38E-08	5.71E-11	5.71E-11
18	F	1.38E-08	5.71E-11	5.71E-11
19	F	1.38E-08	5.71E-11	5.71E-11
20	F	1.38E-08	5.71E-11	5.71E-11
21	G	4.57E-09	4.57E-09	4.57E-09
22	G	4.57E-09	4.57E-09	4.57E-09

Notes: Shaded cells indicate values that have changed since the prior report (HSI GeoTrans 1999).
[1] Equal to default recharge, no source applied.

Prepared by: KMR
Checked by: GWC
Approved by: PFA

December 1998
Revised 6/99 (GWC, Updated STM)
P:\Crandon\TmaMod4\Excel\StresTab1.xls, TMA2

Table 5 TMA 3 percolation rates by stress period.

Stress Period	Phase	Percolation Rate (ft/day)		
		Base	Lower Sideslope	Upper Sideslope
1	X	2.21E-03 [1]	2.21E-03 [1]	2.21E-03 [1]
2	X	2.21E-03 [1]	2.21E-03 [1]	2.21E-03 [1]
3	X	2.21E-03 [1]	2.21E-03 [1]	2.21E-03 [1]
4	X	2.21E-03 [1]	2.21E-03 [1]	2.21E-03 [1]
5	X	2.21E-03 [1]	2.21E-03 [1]	2.21E-03 [1]
6	X	2.21E-03 [1]	2.21E-03 [1]	2.21E-03 [1]
7	A	1.47E-06	5.71E-11	2.21E-03 [1]
8	B	1.93E-06	5.71E-11	2.34E-10
9	B	1.93E-06	5.71E-11	2.34E-10
10	B	1.93E-06	5.71E-11	2.34E-10
11	C	8.86E-06	2.28E-10	4.57E-10
12	D	7.45E-07	2.28E-10	5.71E-11
13	D	7.45E-07	2.28E-10	5.71E-11
14	E	9.47E-08	5.71E-11	5.71E-11
15	E	9.47E-08	5.71E-11	5.71E-11
16	E	9.47E-08	5.71E-11	5.71E-11
17	E	9.47E-08	5.71E-11	5.71E-11
18	F	1.38E-08	5.71E-11	5.71E-11
19	F	1.38E-08	5.71E-11	5.71E-11
20	F	1.38E-08	5.71E-11	5.71E-11
21	F	1.38E-08	5.71E-11	5.71E-11
22	G	4.57E-09	4.57E-09	4.57E-09

Notes: Shaded cells indicate values that have changed since the prior report (HSI GeoTrans 1999).
[1] Equal to default recharge, no source applied.

Prepared by: KMR
Checked by: GWC
Approved by: PFA

December 1998
Revised 6/99 (GWC, Updated STM)
P:\Crandon\TmaMod4\Excel\StresTab1.xls, TMA3

\Crandon\TmaMod3\Excel\HelpComp2.xls, Flux (2)

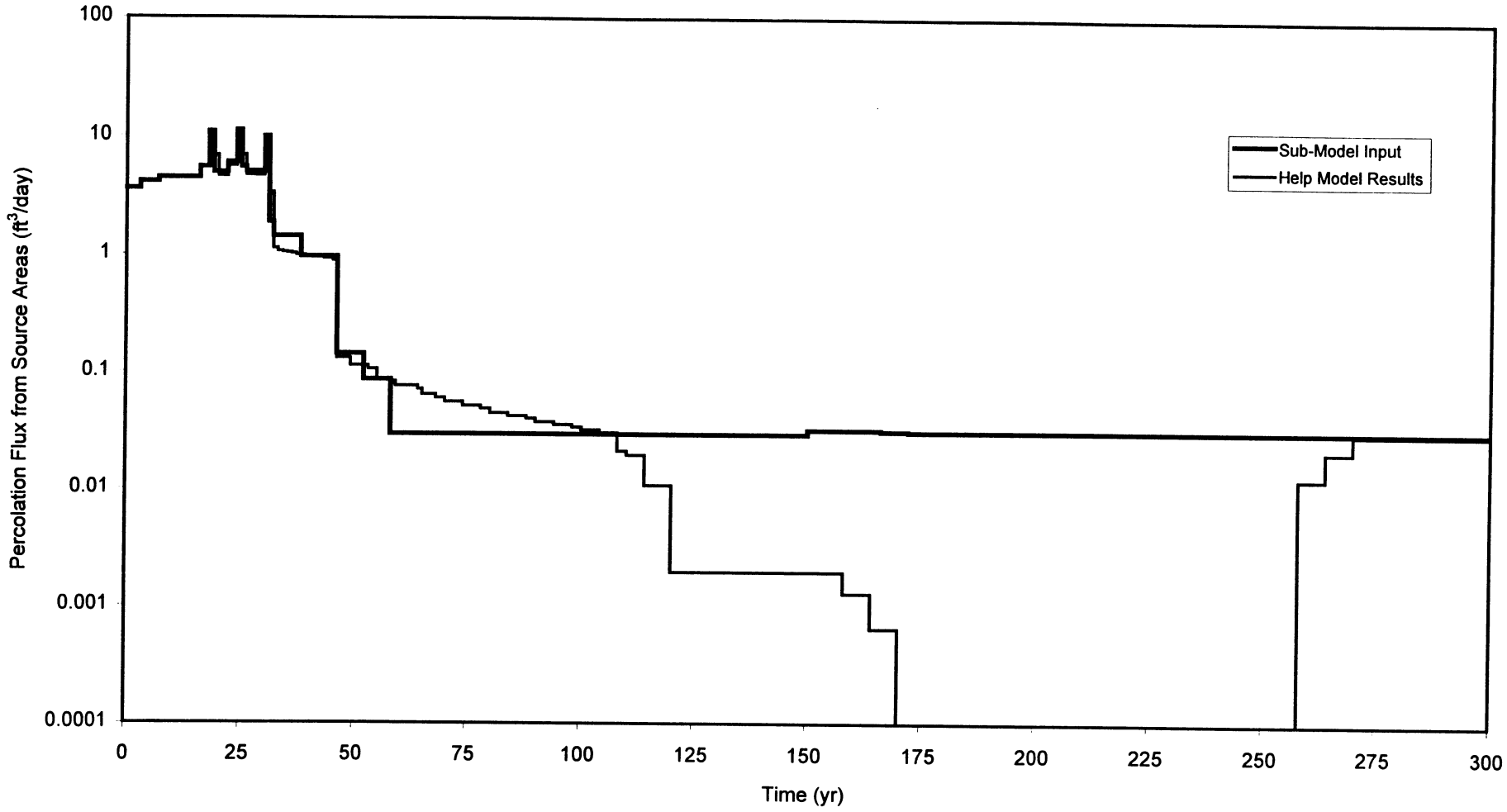

4.2-10-402

Note:
Percolation rate (Y-axis) is shown on a logarithmic scale.

HSI GEOTRANS			
REVISED	DATE	BY	DESCRIPTION
1	6/99	GWC	Updated STM

CHECKED BY: GWC	DATE: Apr 1998
APPROVED BY: PFA	DATE: Apr 1998
APPROVED BY:	DATE:

Nicolet Minerals COMPANY

Figure 1
Source Areas Percolation Flux Rate

Scale: None	Date: April 1998
Prepared By: HSI GEOTRANS	By: KMR

\Crandon\TmaMod4\Excel\HelpCom2.xls, CumVol

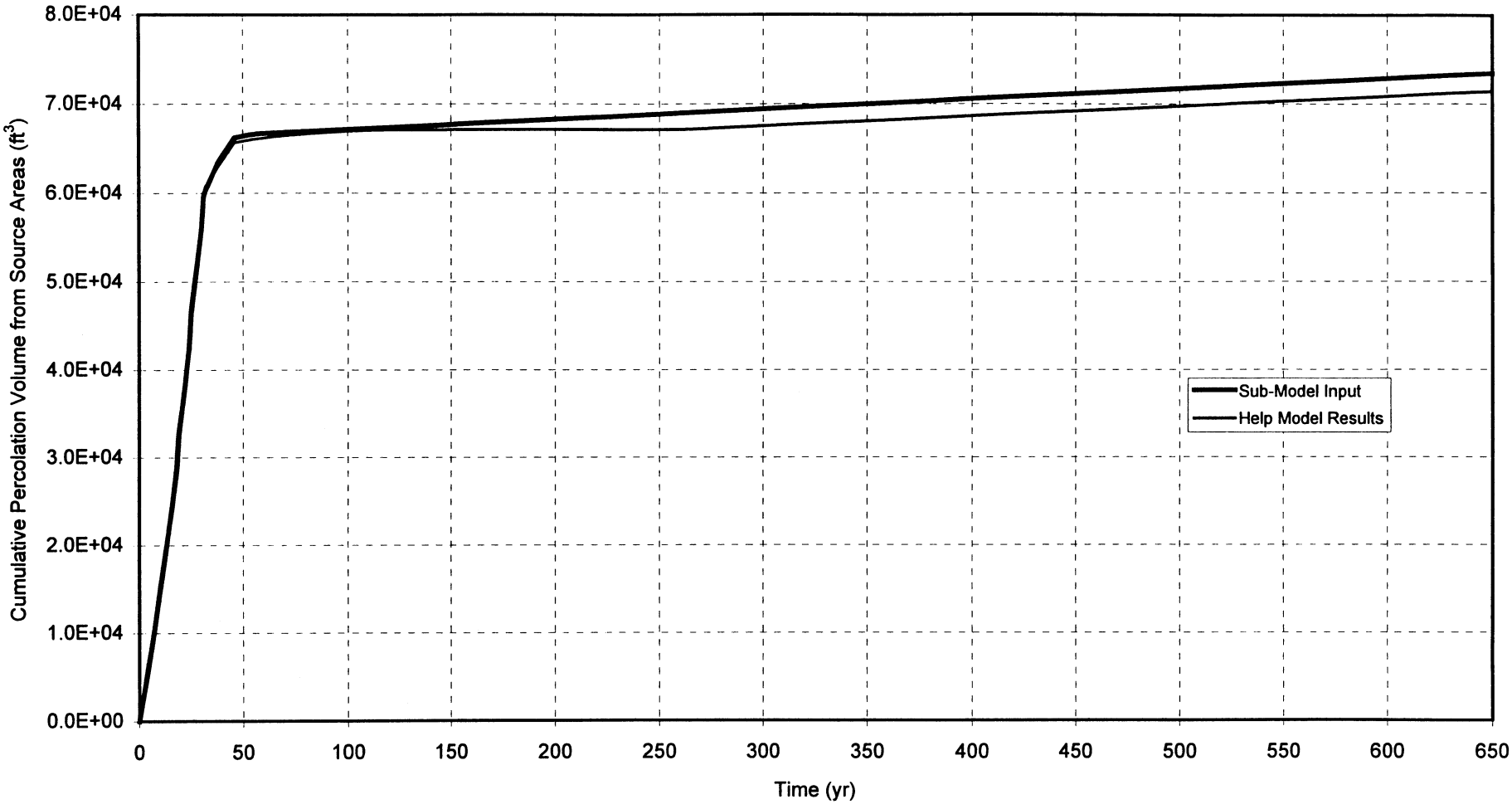

4.2-10-403

HSI GEOTRANS			
REVISED	DATE	BY	DESCRIPTION

CHECKED BY: PAW	DATE: Dec 1998
APPROVED BY: PFA	DATE: Dec 1998
APPROVED BY:	DATE:

Nicolet Minerals COMPANY

Figure 2
Source Areas Cumulative Percolation Volume

Scale: None	Date: Dec 1998
Prepared By: HSI GEOTRANS	By: GWC

\Crandon\TmaMod4\Excel\T09C-Mp.xls, Fig

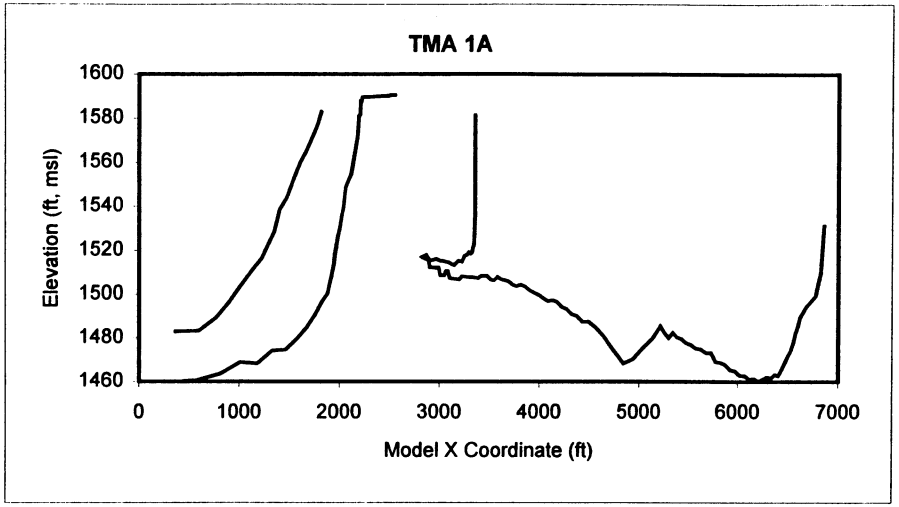

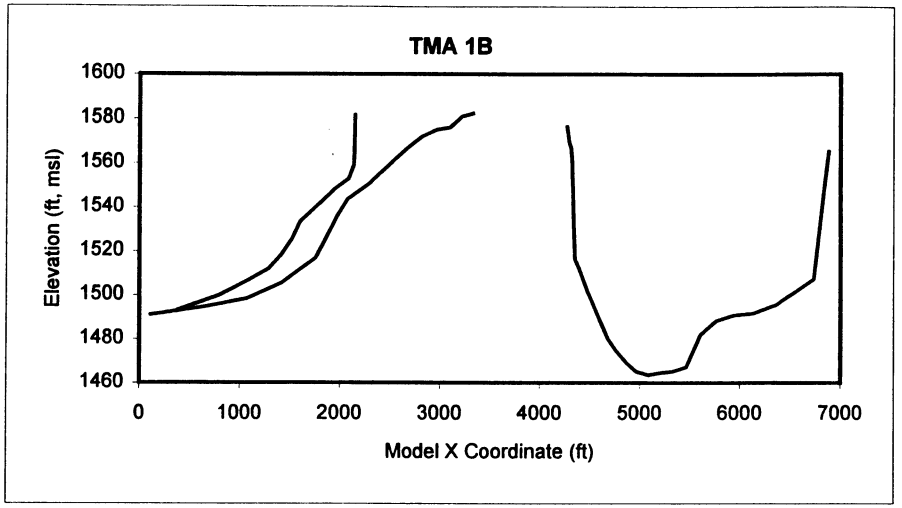

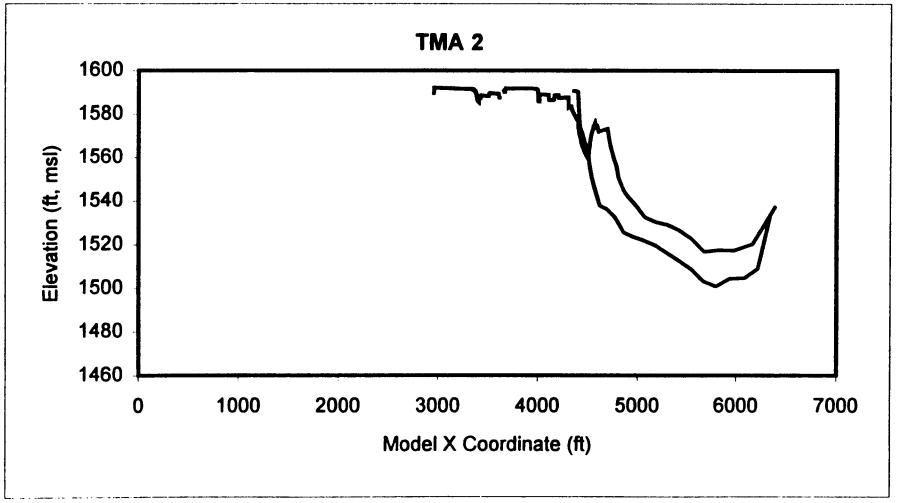

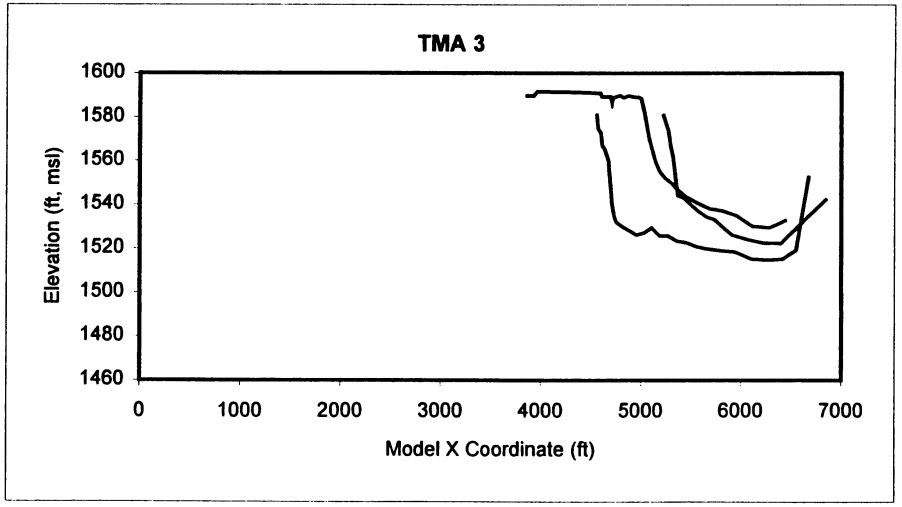

4.2-10-404

HSI GEOTRANS			
REVISED	DATE	BY	DESCRIPTION
1	6/99	GWC	Updated STM

CHECKED BY: PAW		DATE: Dec 1998
APPROVED BY: PFA		DATE: Dec 1998
Simulation T09C-MP	APPROVED BY:	DATE:

Nicolet Minerals COMPANY

Figure 3
Particle Traces From Each TMA Basin, Cross-Section

Scale: None	Date: Dec 1998
Prepared By: HSI GEOTRANS	By: GWC

Tailings Management Area Design Management Zone

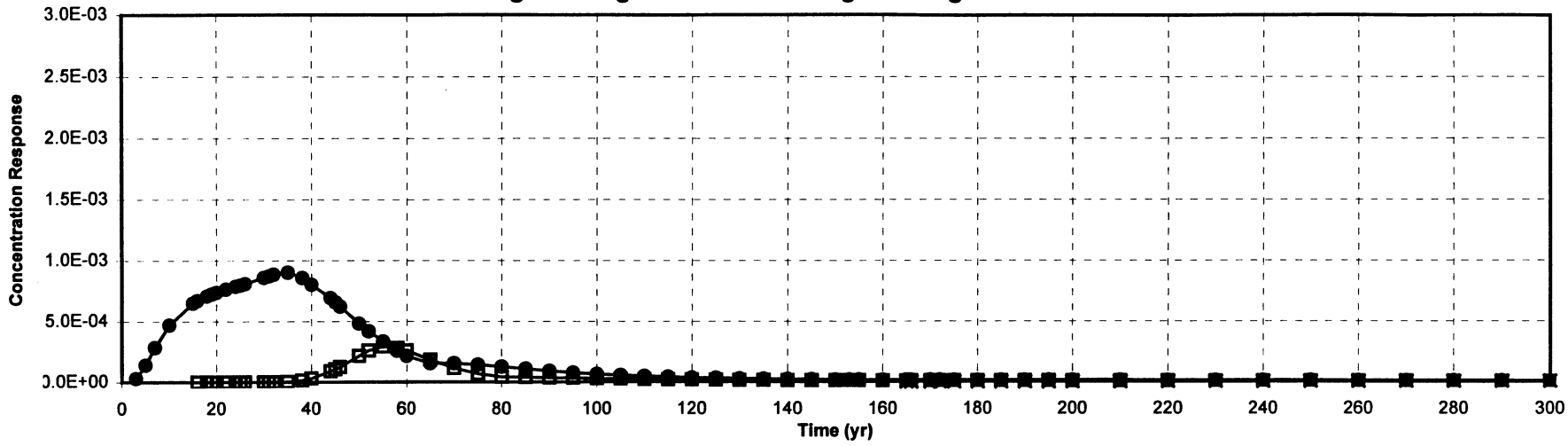

Reclaim Pond Design Management Zone

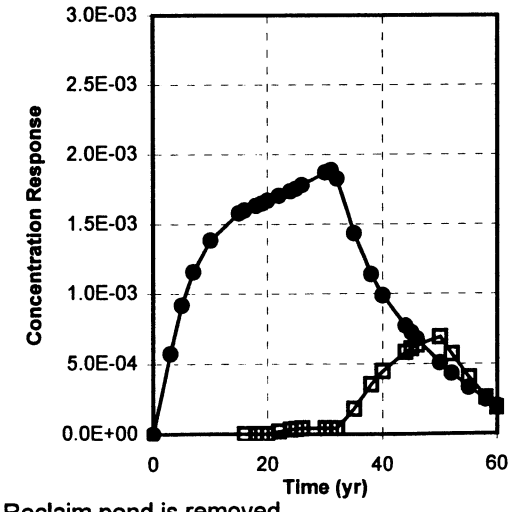

Note: Reclaim pond is removed at approximately year 46

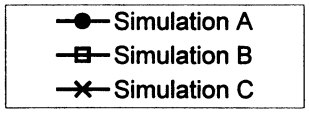

Note: The maximum concentration at any point on the Design Management Zone is plotted.

Simulations T09C1,2,T07C3

HSI GEOTRANS			
REVISED	DATE	BY	DESCRIPTION
1	5/99	RAK	Updated STM

CHECKED BY: PAW	DATE: Dec 1998
APPROVED BY: PFA	DATE: Dec 1998
APPROVED BY:	DATE:

Nicolet Minerals COMPANY

Figure 4
BEJT Concentration Response Curves for the Design Management Zones

Scale: None	Date: December 1998
Prepared By: HSI GEOTRANS	By: GWC

\Crandon\TmaMod4\Excel\Examp1.xls, BEJ

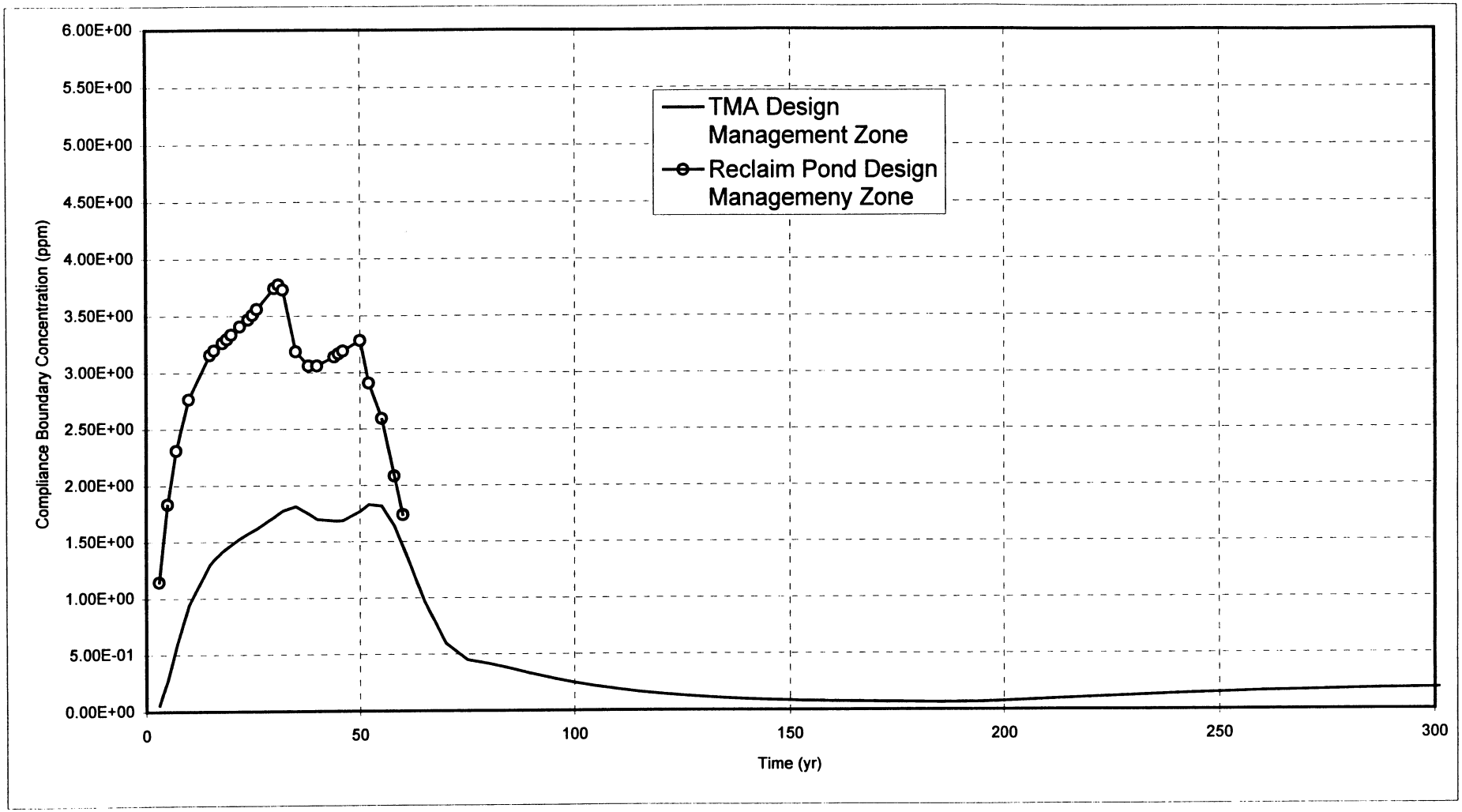

4.2-10-406

Source Concentration:
Operation: 2000 ppm
Post-Cap: 4000 ppm
Oxidized: 40000 ppm*

* As a conservative assumption, the oxidized concentration begins immediately after assumed degradation of the flexible membrane liner.

HSI GEOTRANS

REVISED	DATE	BY	DESCRIPTION
1	6/99	GWC	Updated STM

CHECKED BY: GWC	DATE: Dec 1998
APPROVED BY: PFA	DATE: Dec 1998
APPROVED BY:	DATE:

Simulations T07C1, 2, 3

Nicolet Minerals COMPANY

Figure 5
BEJT Concentration at the Design Management Zones (Example Constituent)

Scale: None	Date: Dec 1998
Prepared By: HSI GEOTRANS	By: RAK

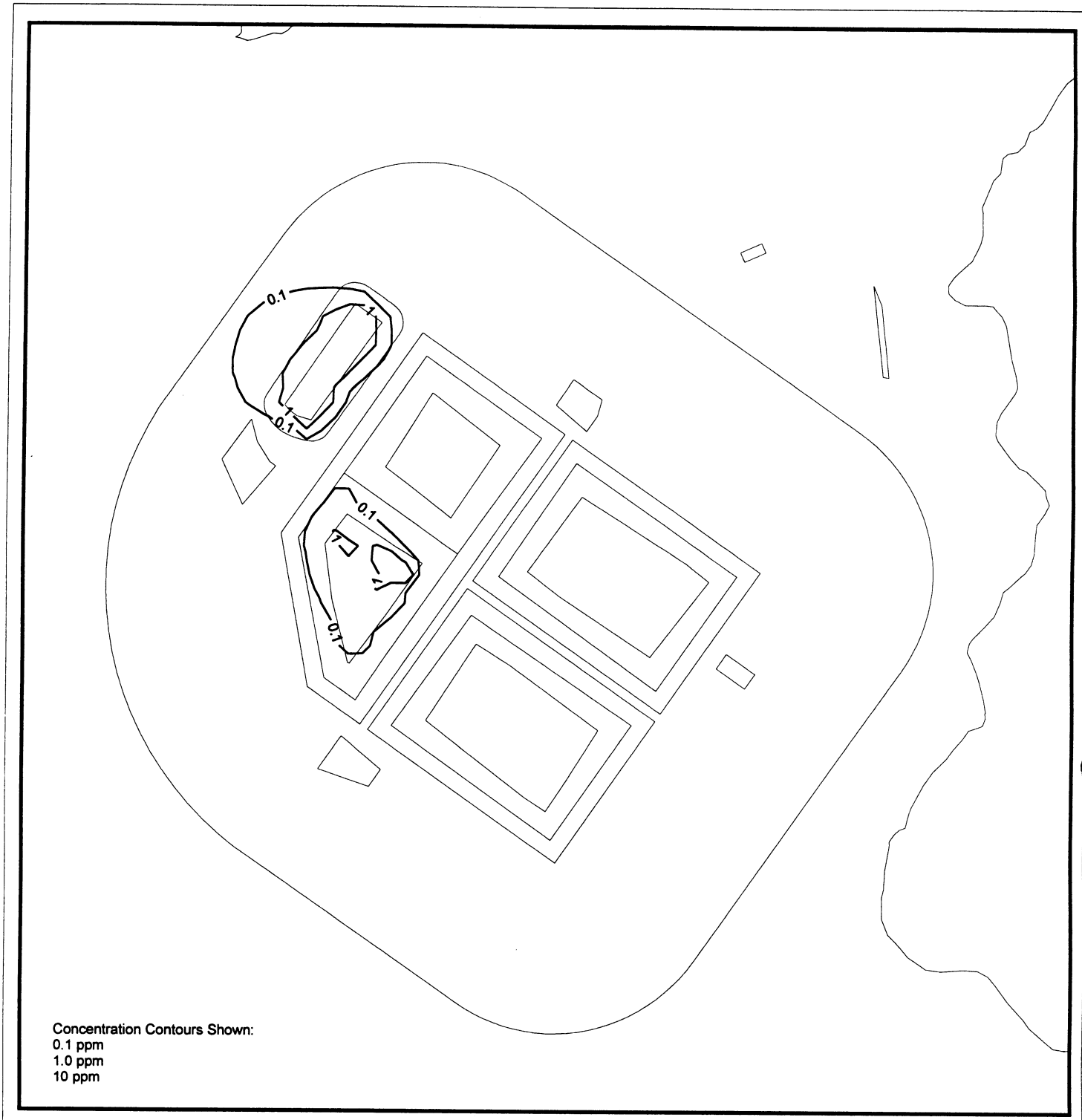

Concentration Contours Shown:
0.1 ppm
1.0 ppm
10 ppm

Source Concentration
Operation: 2000 ppm
Post-cap: 4000 ppm
Oxidized: 40,000 ppm*

* As a conservative assumption, the oxidized concentration begins immediately after assumed degradation of the flexible membrane liner.

Note:
This plot shows contours of maximum concentratration in any layer.

Simulations
T09C1, T09C2, T07C3

0 1000 2000
Scale in Feet

HSI GEOTRANS

REVISED	DATE	BY	DESCRIPTION
1	6/99	RAK	Updated STM

CHECKED BY: GWC	DATE: Dec 98
APPROVED BY: PFA	DATE: Dec 98
APPROVED BY:	DATE:

Nicolet Minerals COMPANY

Figure 6
BEJT Concentration After 3 Years
(Example Constituent, Plan View)

Scale: 1 in. = 1000 ft. | Date: November 1998
Prepared By: HSI GEOTRANS | By: KMR

\Crandon\Tmat\Mod4\Surfer2\Bejt003.srf

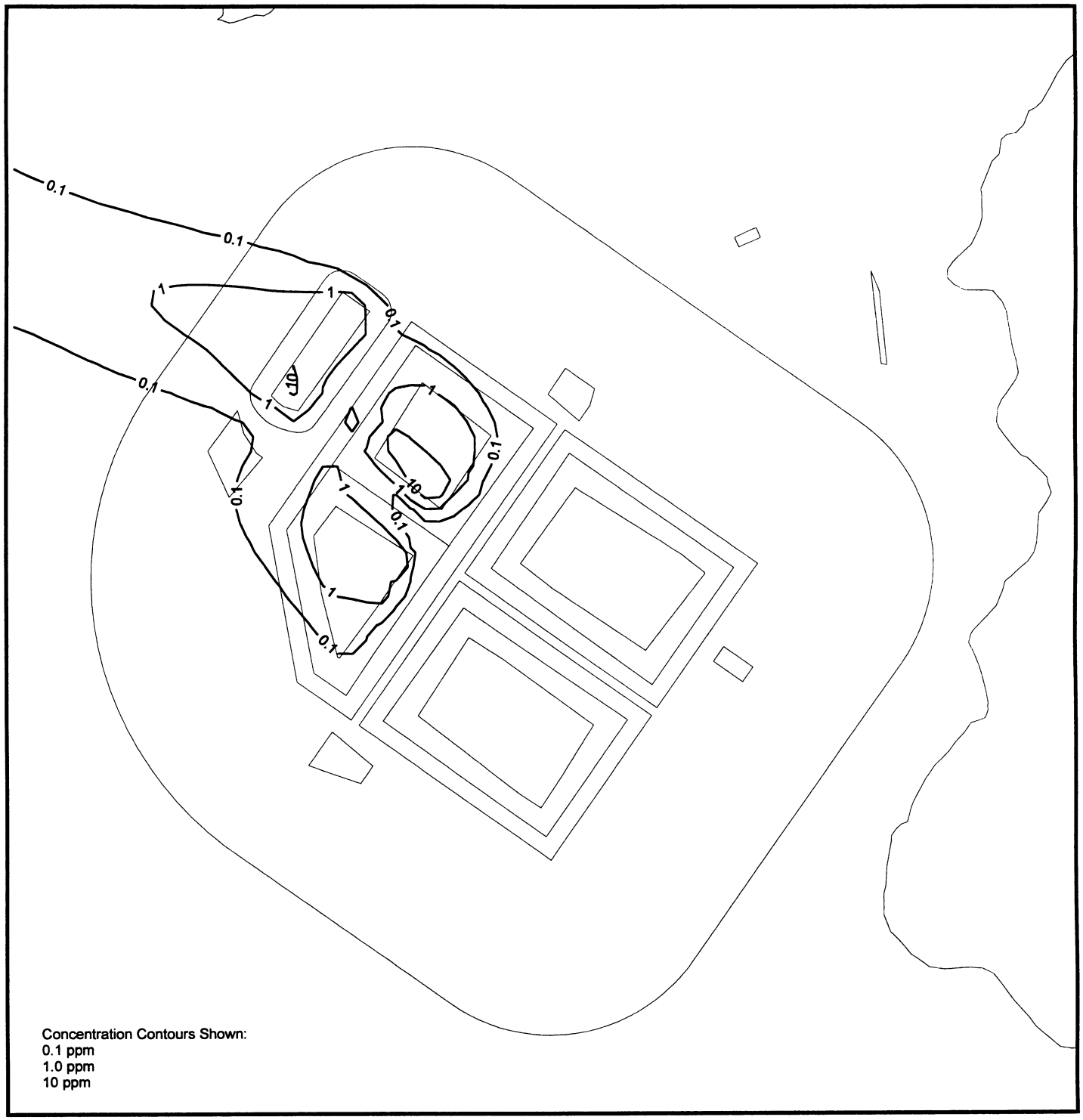

Source Concentration
Operation: 2000 ppm
Post-cap: 4000 ppm
Oxidized: 40,000 ppm*

* As a conservative assumption, the oxidized concentration begins immediately after assumed degradation of the flexible membrane liner.

Note:
This plot shows contours of maximum concentratration in any layer.

Simulations
T09C1, T09C2, T07C3

N

0 1000 2000

Scale in Feet

HSI GEOTRANS

REVISED	DATE	BY	DESCRIPTION
1	6/99	RAK	Updated STM

CHECKED BY: GWC	DATE: Dec 98
APPROVED BY: PFA	DATE: Dec 98
APPROVED BY:	DATE:

Nicolet Minerals COMPANY

Figure 7
BEJT Concentration After 16 Years
(Example Constituent, Plan View)

Scale: 1 in. = 1000 ft.	Date: November 1998
Prepared By: HSI GEOTRANS	By: KMR

\Crandon\Tmal\Mod4\Surfer2\Beg016.srf

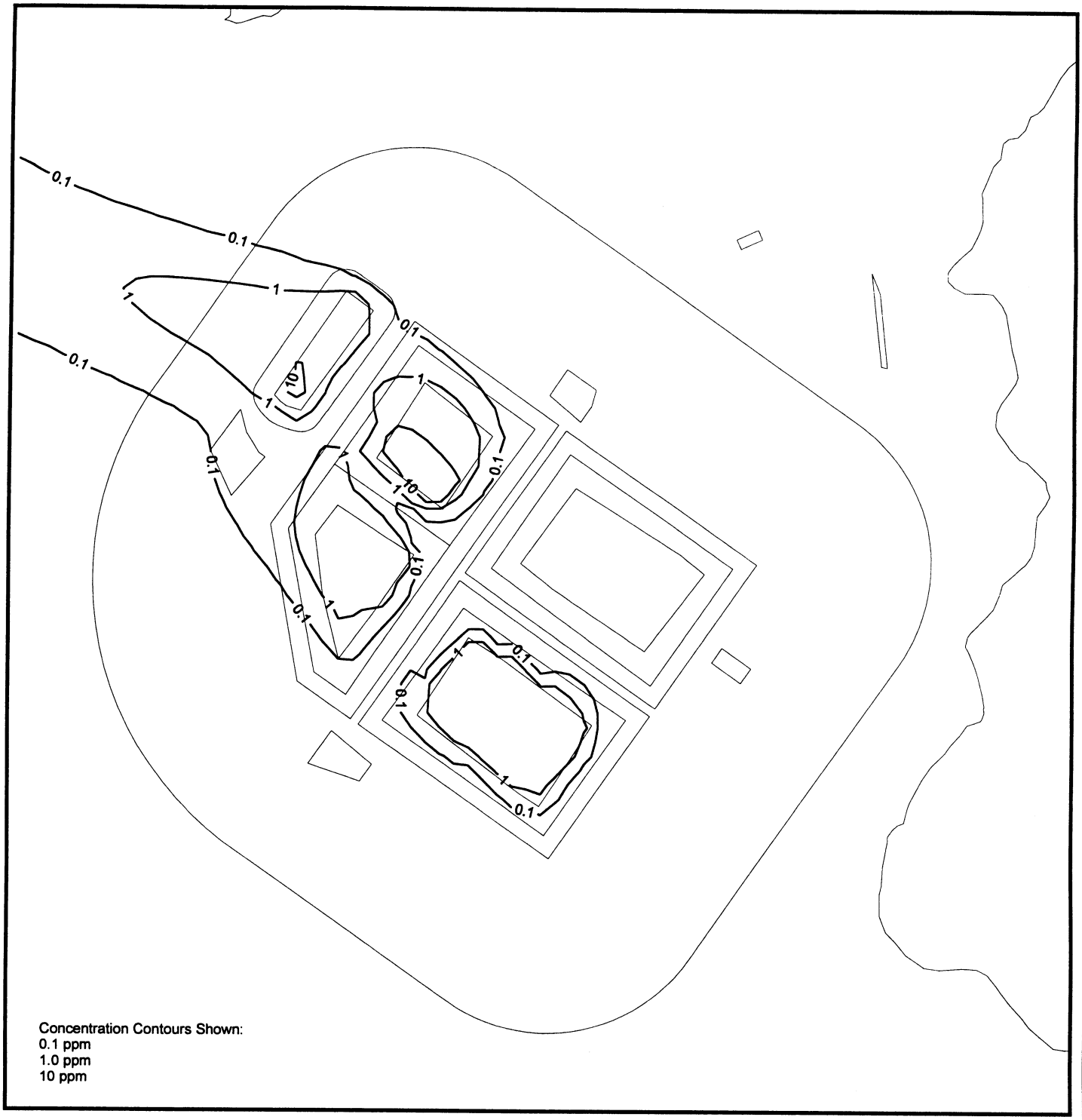

Concentration Contours Shown:
0.1 ppm
1.0 ppm
10 ppm

Source Concentration
Operation: 2000 ppm
Post-cap: 4000 ppm
Oxidized: 40,000 ppm*

* As a conservative assumption, the oxidized concentration begins immediately after assumed degradation of the flexible membrane liner.

Note:
This plot shows contours of maximum concentratration in any layer.

Simulations
T09C1, T09C2, T07C3

N

0 1000 2000

Scale in Feet

HSI GEOTRANS

REVISED	DATE	BY	DESCRIPTION
1	6/99	RAK	Updated STM

CHECKED BY: GWC	DATE: Dec 98
APPROVED BY: PFA	DATE: Dec 98
APPROVED BY:	DATE:

Nicolet Minerals COMPANY

Figure 8
BEJT Concentration After 22 Years
(Example Constituent, Plan View)

Scale: 1 in. = 1000 ft. | Date: November 1998
Prepared By: HSI GEOTRANS | By: KMR

\Crandon\Tmat\Mod4\Surfer2\Bejt022.srf

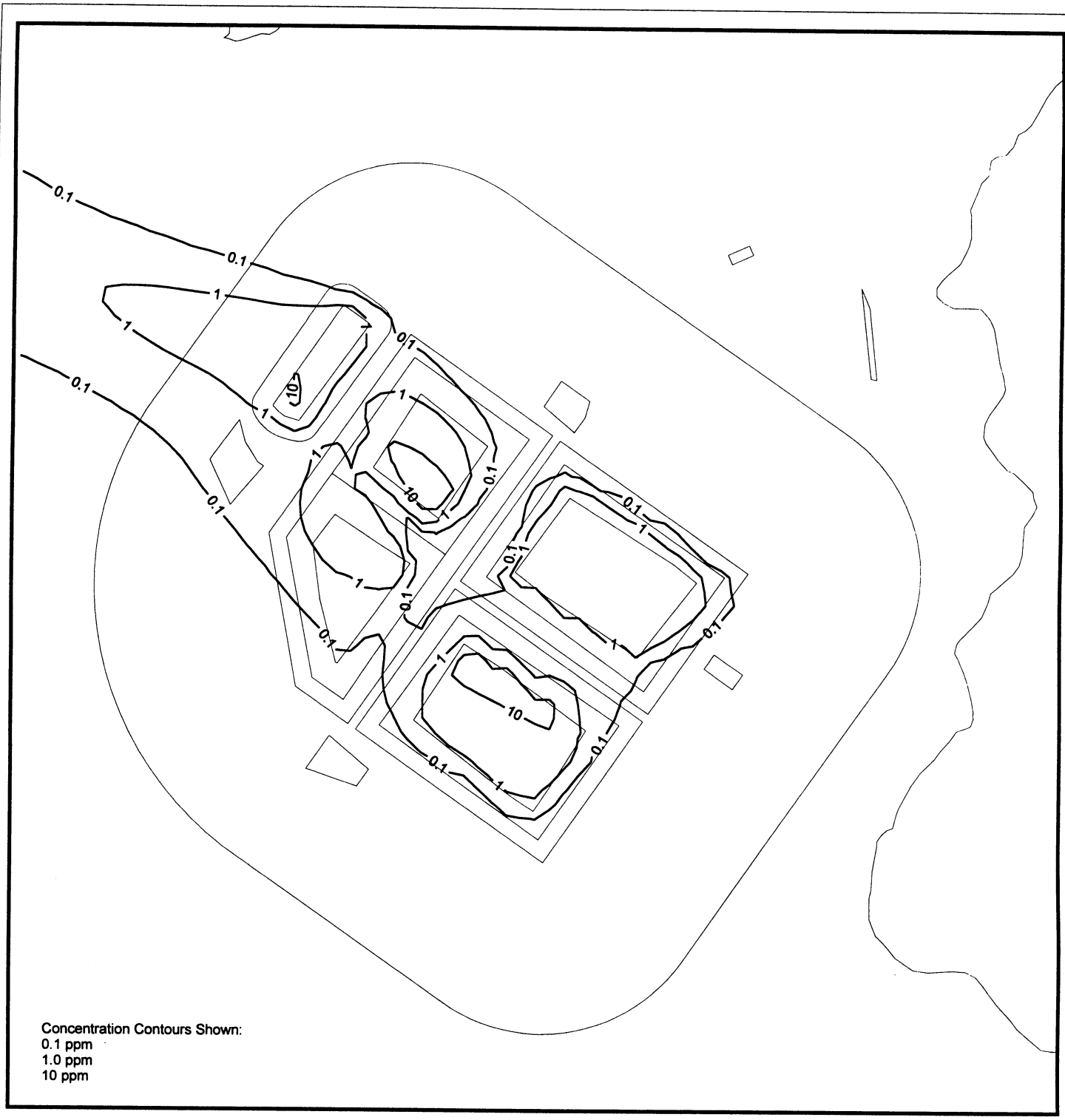

Source Concentration
Operation: 2000 ppm
Post-cap: 4000 ppm
Oxidized: 40,000 ppm*

* As a conservative assumption, the oxidized concentration begins immediately after assumed degradation of the flexible membrane liner.

Note:
This plot shows contours of maximum concentratration in any layer.

Simulations
T09C1, T09C2, T07C3

0 1000 2000
Scale in Feet

HSI GEOTRANS

REVISED	DATE	BY	DESCRIPTION
1	6/99	RAK	Updated STM

CHECKED BY: GWC	DATE: Dec 98
APPROVED BY: PFA	DATE: Dec 98
APPROVED BY:	DATE:

Nicolet Minerals COMPANY

Figure 9
BEJT Concentration After 32 Years (Example Constituent, Plan View)

Scale: 1 in. = 1000 ft. | Date: November 1998
Prepared By: HSI GEOTRANS | By: KMR

\Crandon\Tmal\Mod4\Surfer2\Bejt032.srf

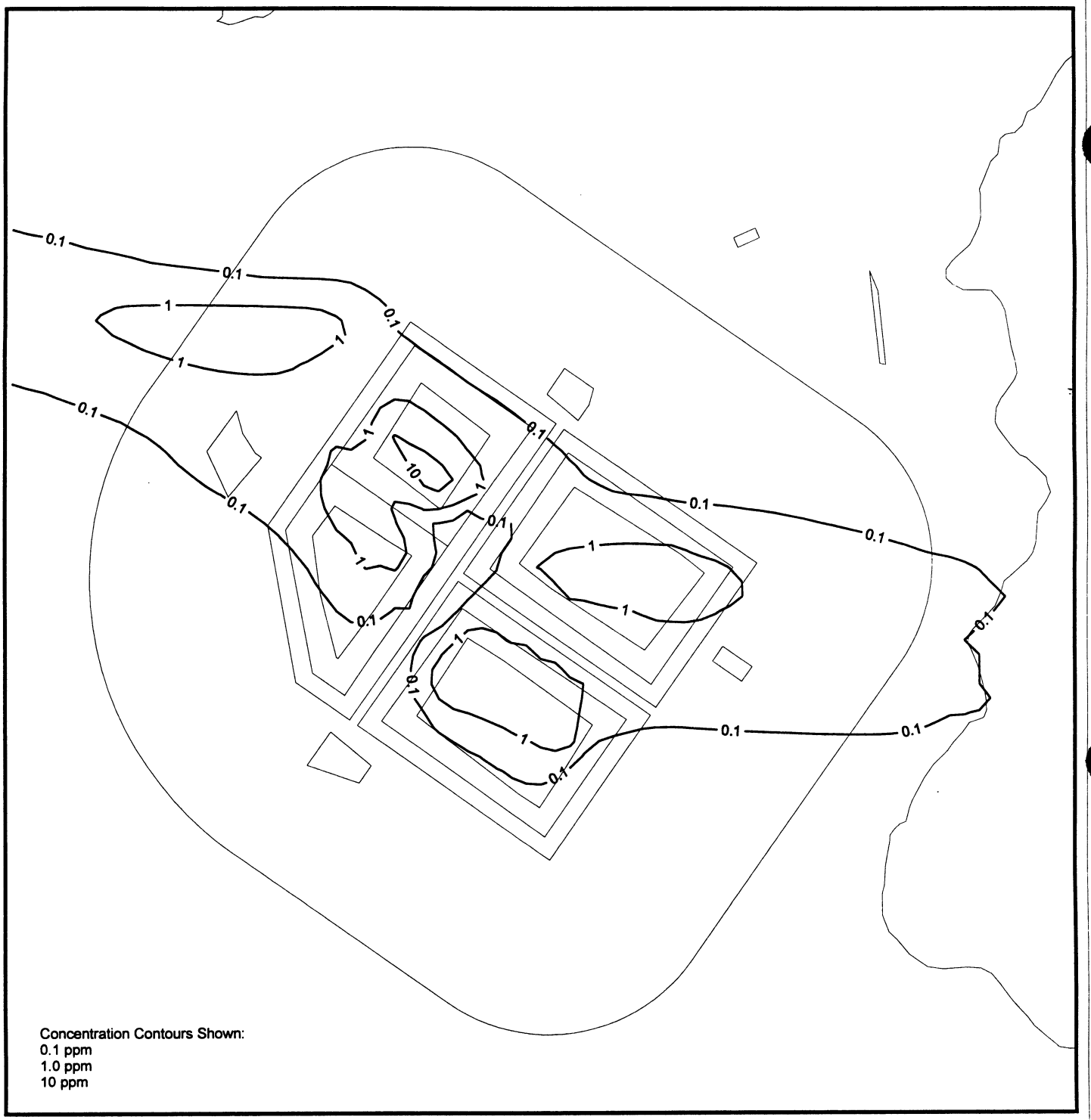

Source Concentration
Operation: 2000 ppm
Post-cap: 4000 ppm
Oxidized: 40,000 ppm*

* As a conservative assumption, the oxidized concentration begins immediately after assumed degradation of the flexible membrane liner.

Note:
This plot shows contours of maximum concentratration in any layer.

Simulations
T09C1, T09C2, T07C3

0 1000 2000
Scale in Feet

HSI GEOTRANS

REVISED	DATE	BY	DESCRIPTION
1	6/99	RAK	Updated STM

CHECKED BY: GWC	DATE: Dec 98
APPROVED BY: PFA	DATE: Dec 98
APPROVED BY:	DATE:

Nicolet Minerals COMPANY

Figure 10
BEJT Concentration After 60 Years
(Example Constituent, Plan View)

Scale: 1 in. = 1000 ft. | Date: November 1998
Prepared By: HSI GEOTRANS | By: KMR

\Crandon\Tma\Mod\4\Surfer2\Bej060.srf

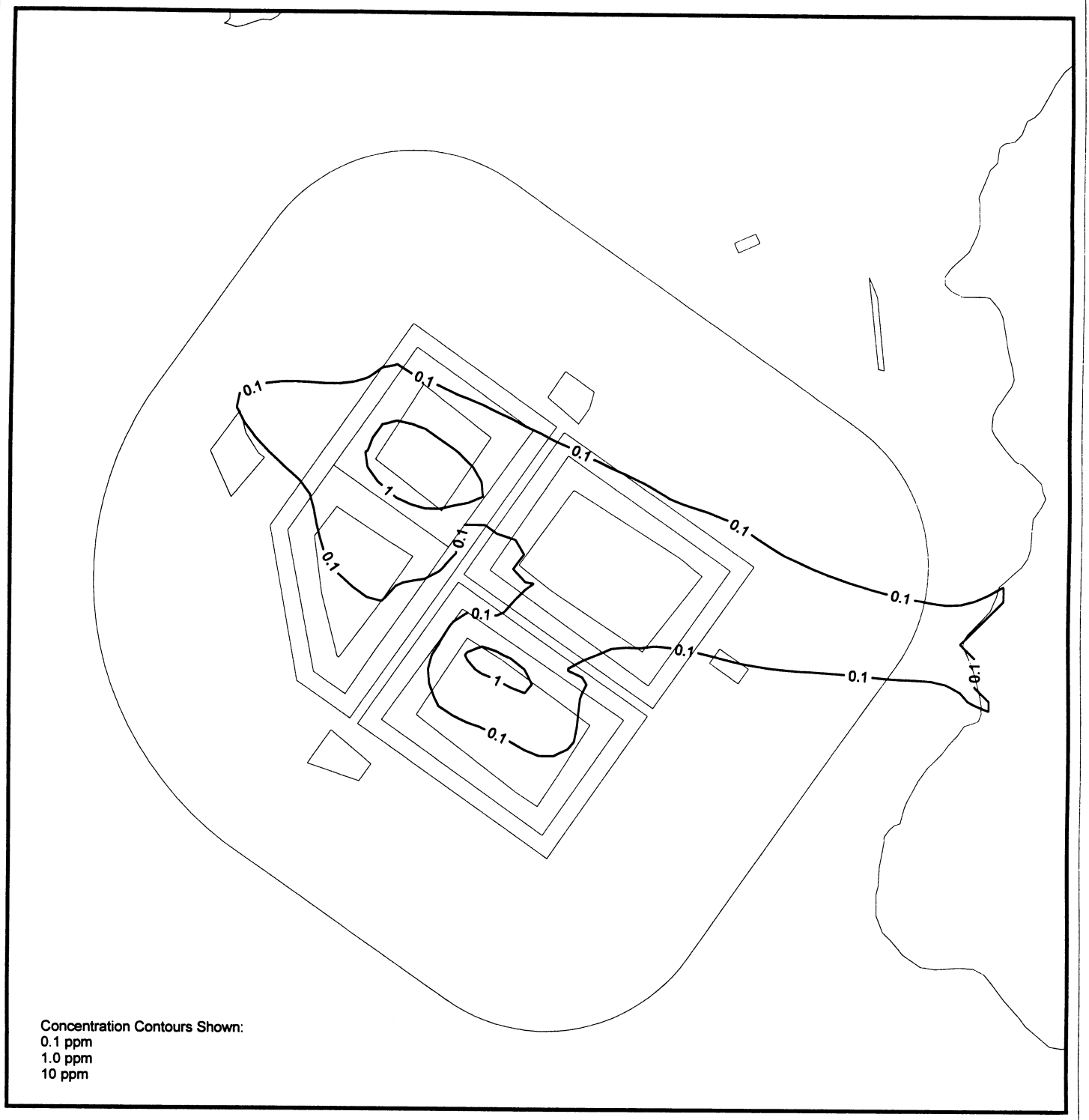

Concentration Contours Shown:
0.1 ppm
1.0 ppm
10 ppm

Source Concentration
Operation: 2000 ppm
Post-cap: 4000 ppm
Oxidized: 40,000 ppm*

* As a conservative assumption, the oxidized concentration begins immediately after assumed degradation of the flexible membrane liner.

Note:
This plot shows contours of maximum concentratration in any layer.

Simulations
T09C1, T09C2, T07C3

0 1000 2000
Scale in Feet

HSI GEOTRANS

REVISED	DATE	BY	DESCRIPTION
1	6/99	RAK	Updated STM

CHECKED BY: GWC	DATE: Dec 98
APPROVED BY: PFA	DATE: Dec 98
APPROVED BY:	DATE:

Nicolet Minerals COMPANY

Figure 11
BEJT Concentration After 125 Years
(Example Constituent, Plan View)

Scale: 1 in. = 1000 ft.	Date: November 1998
Prepared By: HSI GEOTRANS	By: KMR

\Crandon\Tma\Mod4\Surfer2\bej125.srf

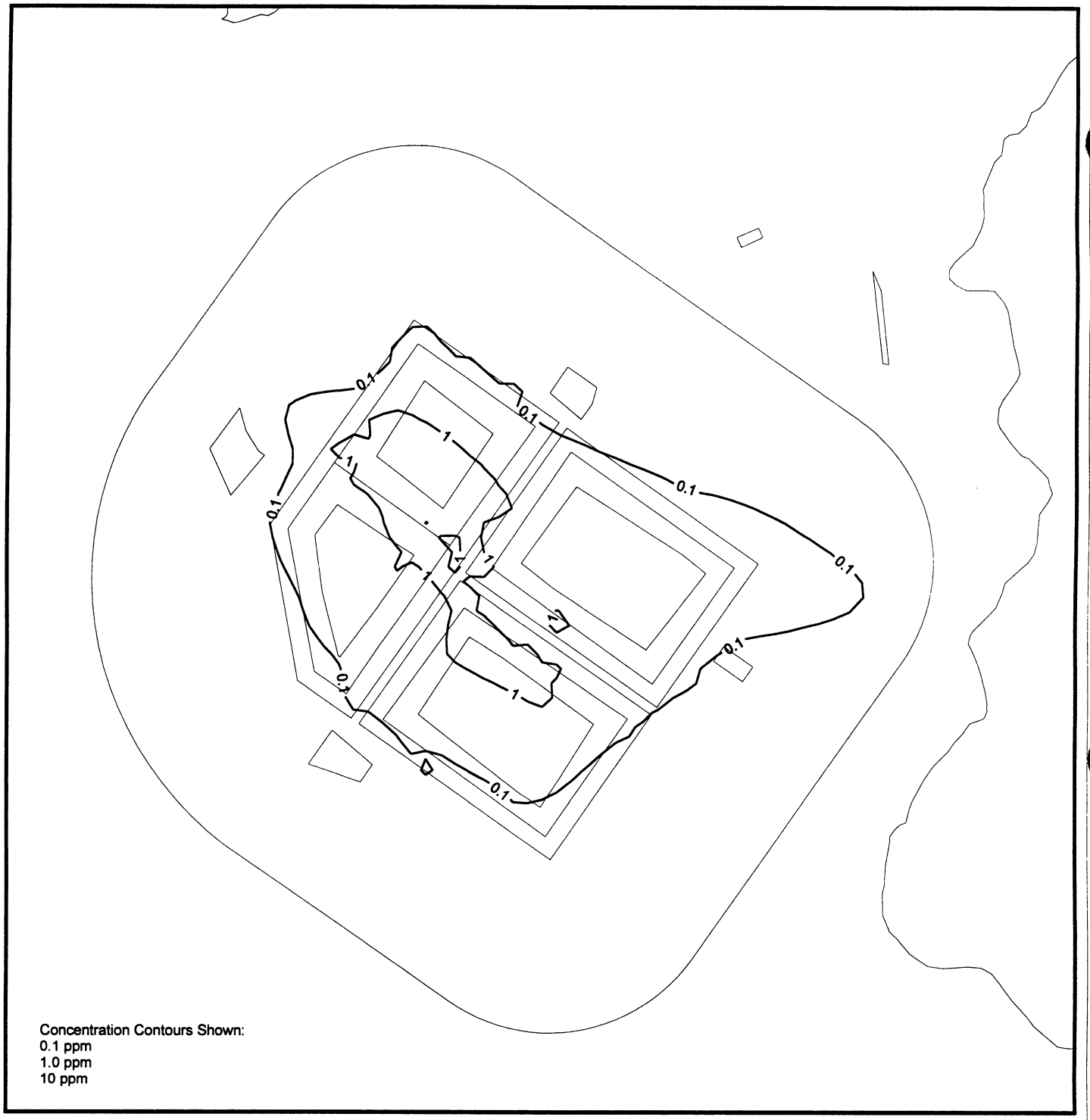

Concentration Contours Shown:
0.1 ppm
1.0 ppm
10 ppm

Source Concentration
Operation: 2000 ppm
Post-cap: 4000 ppm
Oxidized: 40,000 ppm*

* As a conservative assumption, the oxidized concentration begins immediately after assumed degradation of the flexible membrane liner.

Note:
This plot shows contours of maximum concentratration in any layer.

Simulations
T09C1, T09C2, T07C3

N

0 1000 2000

Scale in Feet

HSI GEOTRANS

REVISED	DATE	BY	DESCRIPTION
1	6/99	RAK	Updated STM

CHECKED BY: GWC	DATE: Dec 98
APPROVED BY: PFA	DATE: Dec 98
APPROVED BY:	DATE:

Nicolet Minerals COMPANY

Figure 12
BEJT Concentration After 200 Years
(Example Constituent, Plan View)

Scale: 1 in. = 1000 ft. | Date: November 1998
Prepared By: HSI GEOTRANS | By: KMR

\Crandon\Tmwfmod4\Surfer2\Bejt200.srf

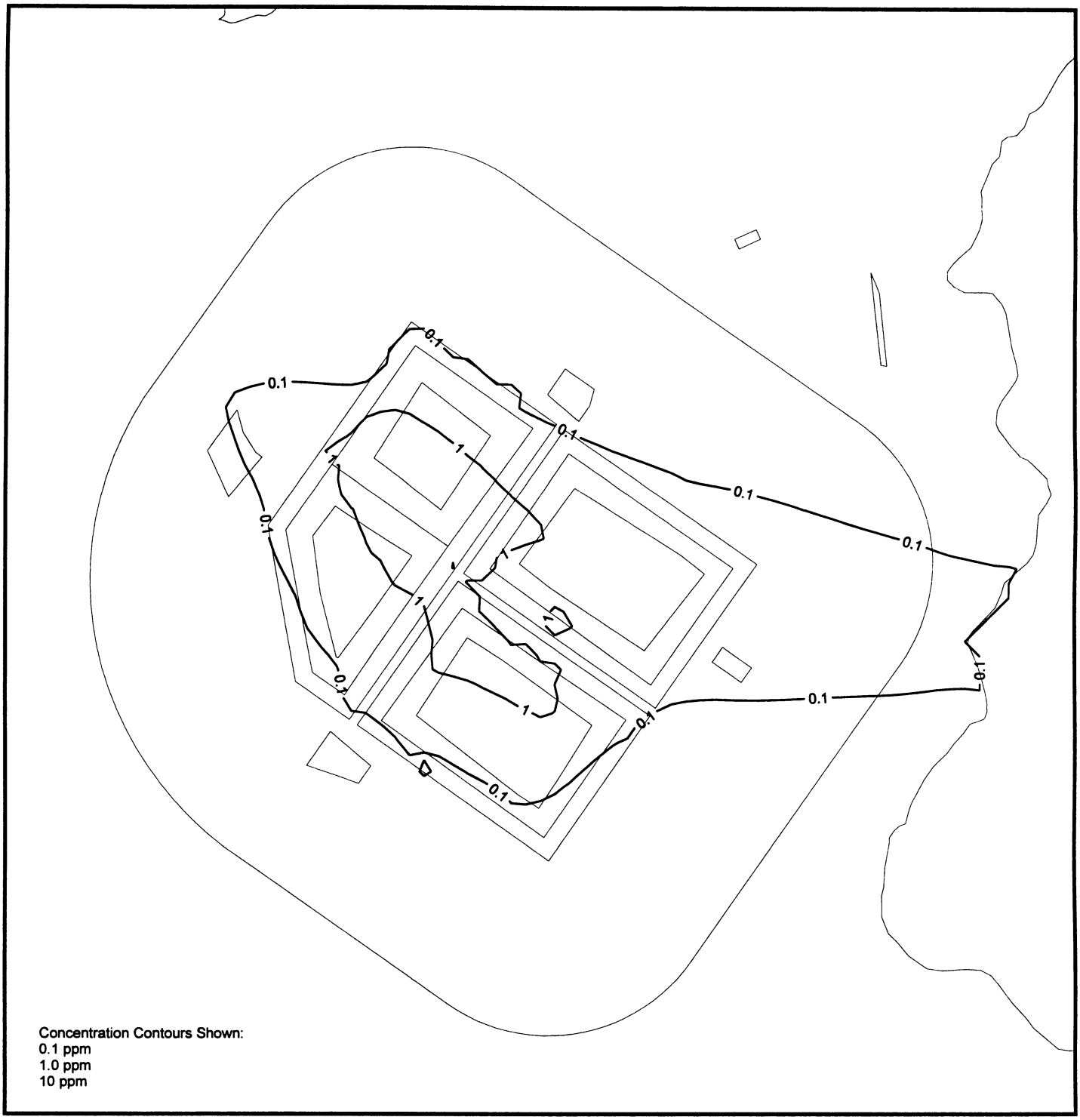

Concentration Contours Shown:
0.1 ppm
1.0 ppm
10 ppm

Source Concentration
Operation: 2000 ppm
Post-cap: 4000 ppm
Oxidized: 40,000 ppm*

* As a conservative assumption, the oxidized concentration begins immediately after assumed degradation of the flexible membrane liner.

Note:
This plot shows contours of maximum concentratration in any layer.

Simulations
T09C1, T09C2, T07C3

0 1000 2000
Scale in Feet

HSI GEOTRANS

REVISED	DATE	BY	DESCRIPTION
1	6/99	RAK	Updated STM

CHECKED BY: GWC	DATE: Dec 98
APPROVED BY: PFA	DATE: Dec 98
APPROVED BY:	DATE:

Nicolet Minerals COMPANY

Figure 13
BEJT Concentration After 300 Years
(Example Constituent, Plan View)

Scale: 1 in. = 1000 ft. | Date: November 1998
Prepared By: HSI GEOTRANS | By: KMR

\Crandon\Tmwmod4\Surfer2\Bej300.srf

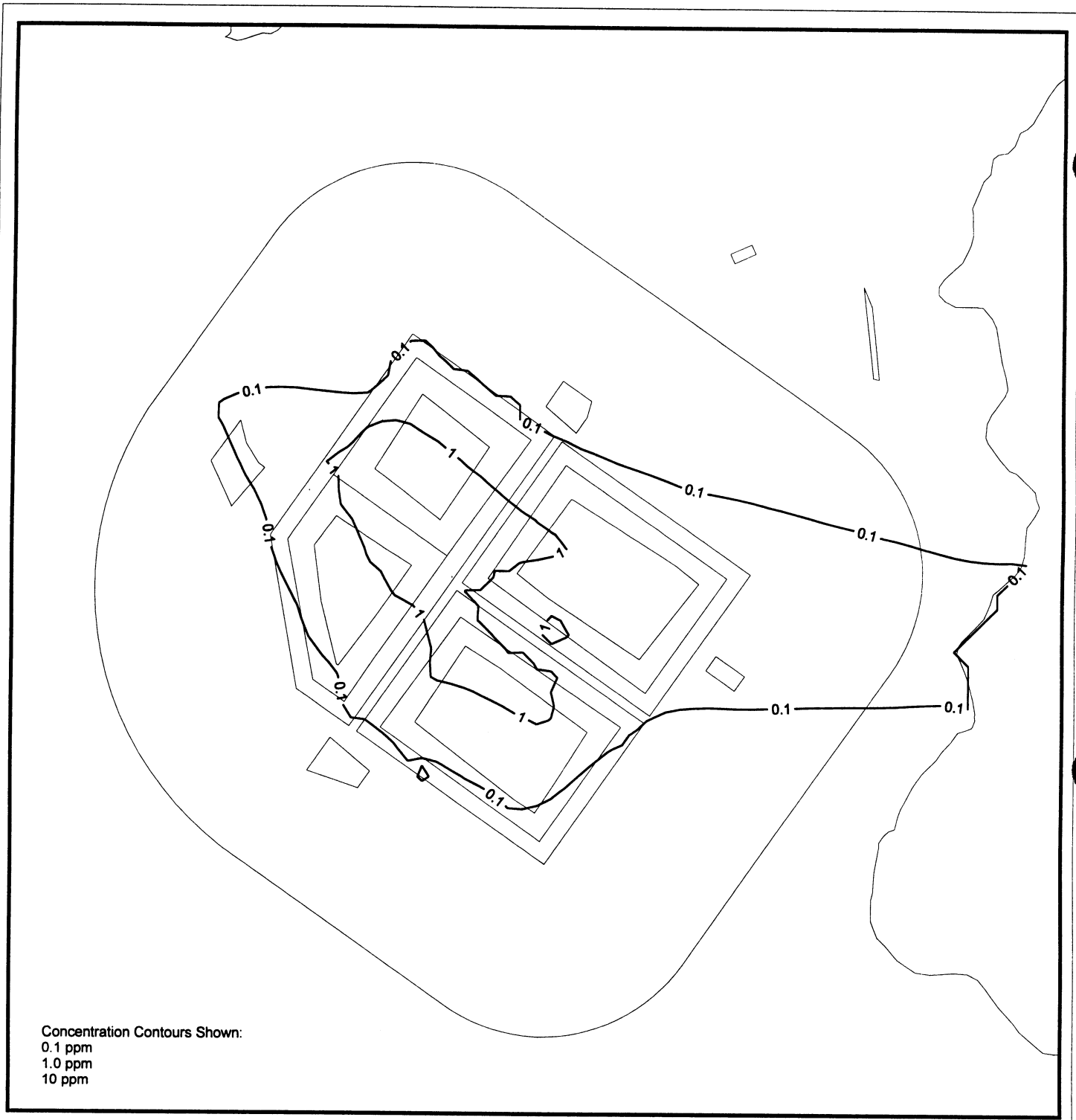

Concentration Contours Shown:
0.1 ppm
1.0 ppm
10 ppm

Source Concentration
Operation: 2000 ppm
Post-cap: 4000 ppm
Oxidized: 40,000 ppm*

* As a conservative assumption, the oxidized concentration begins immediately after assumed degradation of the flexible membrane liner.

Note:
This plot shows contours of maximum concentratration in any layer.

Simulations
T09C1, T09C2, T07C3

0 1000 2000
Scale in Feet

HSI GEOTRANS

REVISED	DATE	BY	DESCRIPTION
1	6/99	RAK	Updated STM

CHECKED BY: GWC	DATE: Dec 98
APPROVED BY: PFA	DATE: Dec 98
APPROVED BY:	DATE:

Nicolet Minerals COMPANY

Figure 14
BEJT Concentration After 650 Years
(Example Constituent, Plan View)

Scale: 1 in. = 1000 ft.	Date: November 1998
Prepared By: HSI GEOTRANS	By: KMR

\Crandon\TmaModl\Surfer2\Bej650.srf

\Crandon\TmaMod4\Surfer2\XBEJ003.srf

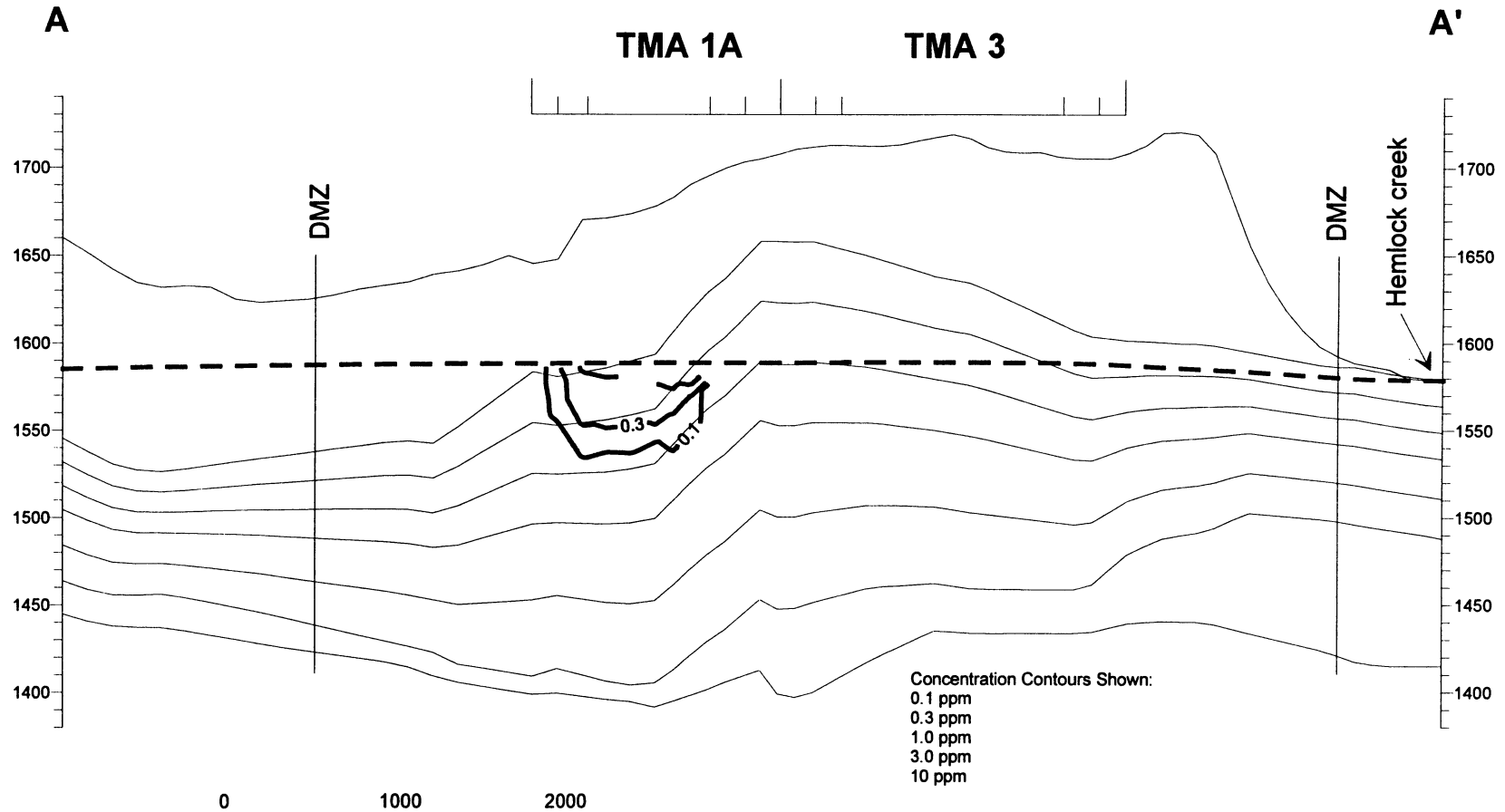

4.2-10-416

Source Concentration
Operation: 2000 ppm
Post-cap: 4000 ppm
Oxidized: 40,000 ppm*

* As a conservative assumption, the oxidized concentration begins immediately after assumed degradation of the flexible membrane liner.

Simulations
T09C1, T09C2, T07C3

HSI GEOTRANS

REVISED	DATE	BY	DESCRIPTION
1	6/99	JDC	Updated STM

CHECKED BY: RAK	DATE: Dec 98
APPROVED BY: PFA	DATE: Dec 98
APPROVED BY:	DATE:

Nicolet Minerals COMPANY

Figure 15
BEJT Concentration After 3 Years
(Example Constituent, Cross-Section)

Scale: 1" = 1000' (h), 100' (v) | Date: Dec 1998

Prepared By: HSI GeoTrans | By: GWC

\Crandon\TmaMod4\Surfer2\XBEJ016.srf

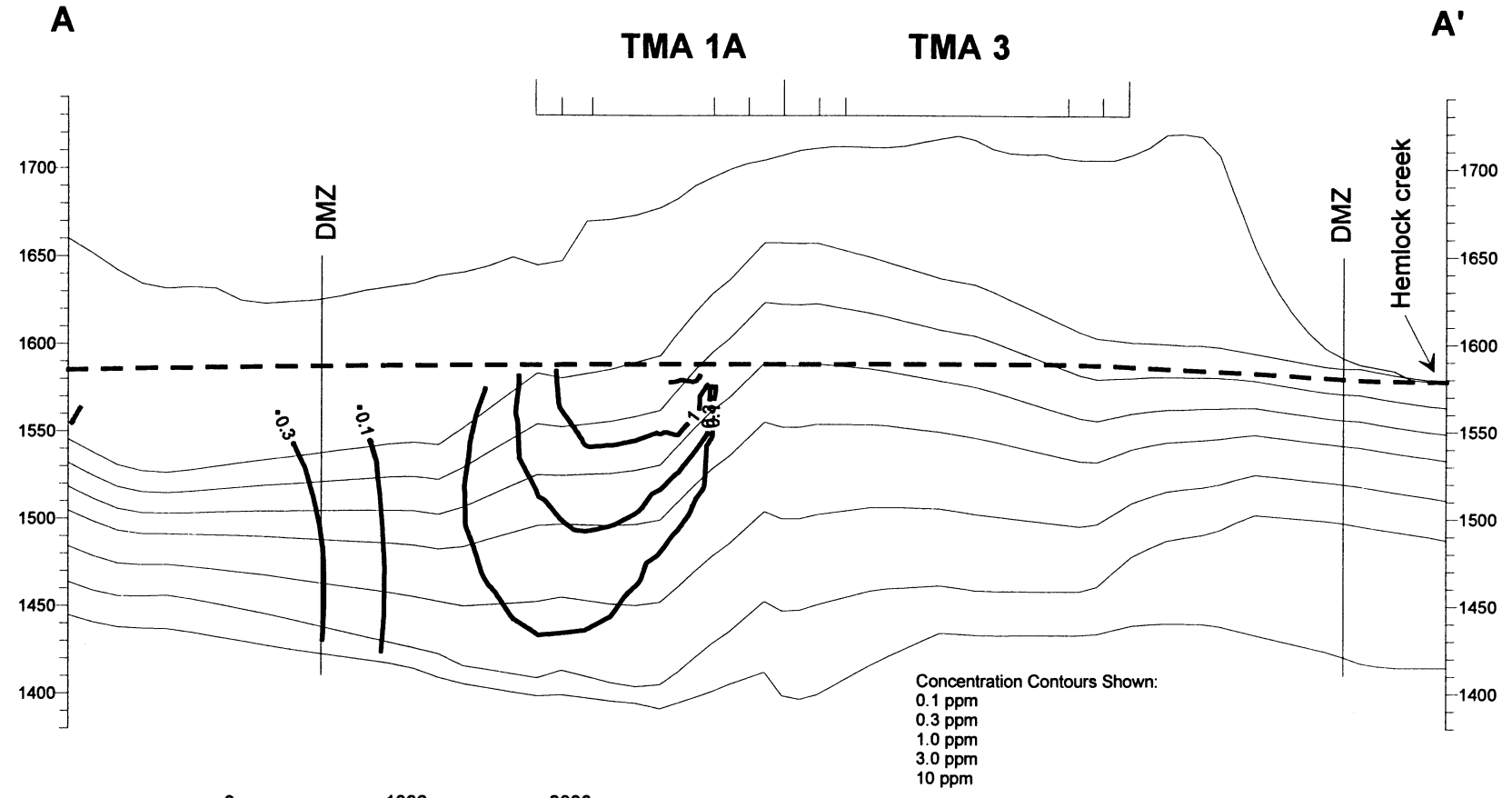

4.2-10-417

Source Concentration
Operation: 2000 ppm
Post-cap: 4000 ppm
Oxidized: 40,000 ppm*

* As a conservative assumption, the oxidized concentration begins immediately after assumed degradation of the flexible membrane liner.

Simulations
T09C1, T09C2, T07C3

HSI GEOTRANS

REVISED	DATE	BY	DESCRIPTION
1	6/99	JDC	Updated STM

CHECKED BY: RAK	DATE: Dec 98
APPROVED BY: PFA	DATE: Dec 98
APPROVED BY:	DATE:

Nicolet Minerals COMPANY

Figure 16
BEJT Concentration After 16 Years
(Example Constituent, Cross-Section)

Scale: 1" = 1000' (h), 100' (v)	Date: Dec 1998
Prepared By: HSI GeoTrans	By: GWC

\Crandon\TmaMod4\Surfer2\XBEJ022.srf

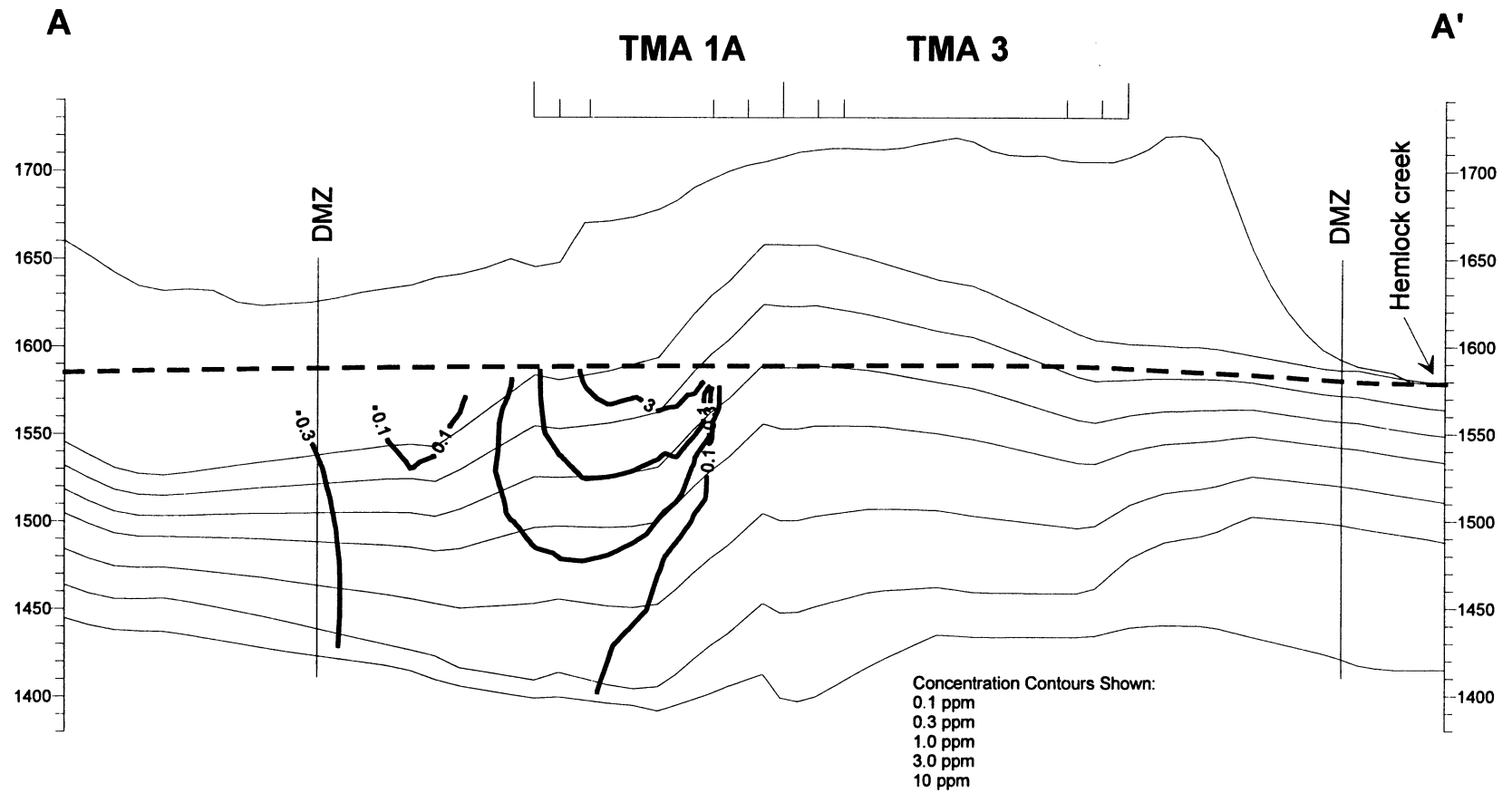

4.2-10-418

Source Concentration
Operation: 2000 ppm
Post-cap: 4000 ppm
Oxidized: 40,000 ppm*

* As a conservative assumption, the oxidized concentration begins immediately after assumed degradation of the flexible membrane liner.

Simulations
T09C1, T09C2, T07C3

HSI GEOTRANS

REVISED	DATE	BY	DESCRIPTION
1	6/99	JDC	Updated STM

CHECKED BY: RAK	DATE: Dec 98
APPROVED BY: PFA	DATE: Dec 98
APPROVED BY:	DATE:

Nicolet Minerals COMPANY

Figure 17
BEJT Concentration After 22 Years (Example Constituent, Cross-Section)

Scale: 1" = 1000' (h), 100' (v)	Date: Dec 1998
Prepared By: HSI GeoTrans	By: GWC

\Crandon\TmaMod4\Surfer2\XBEJ032.srf

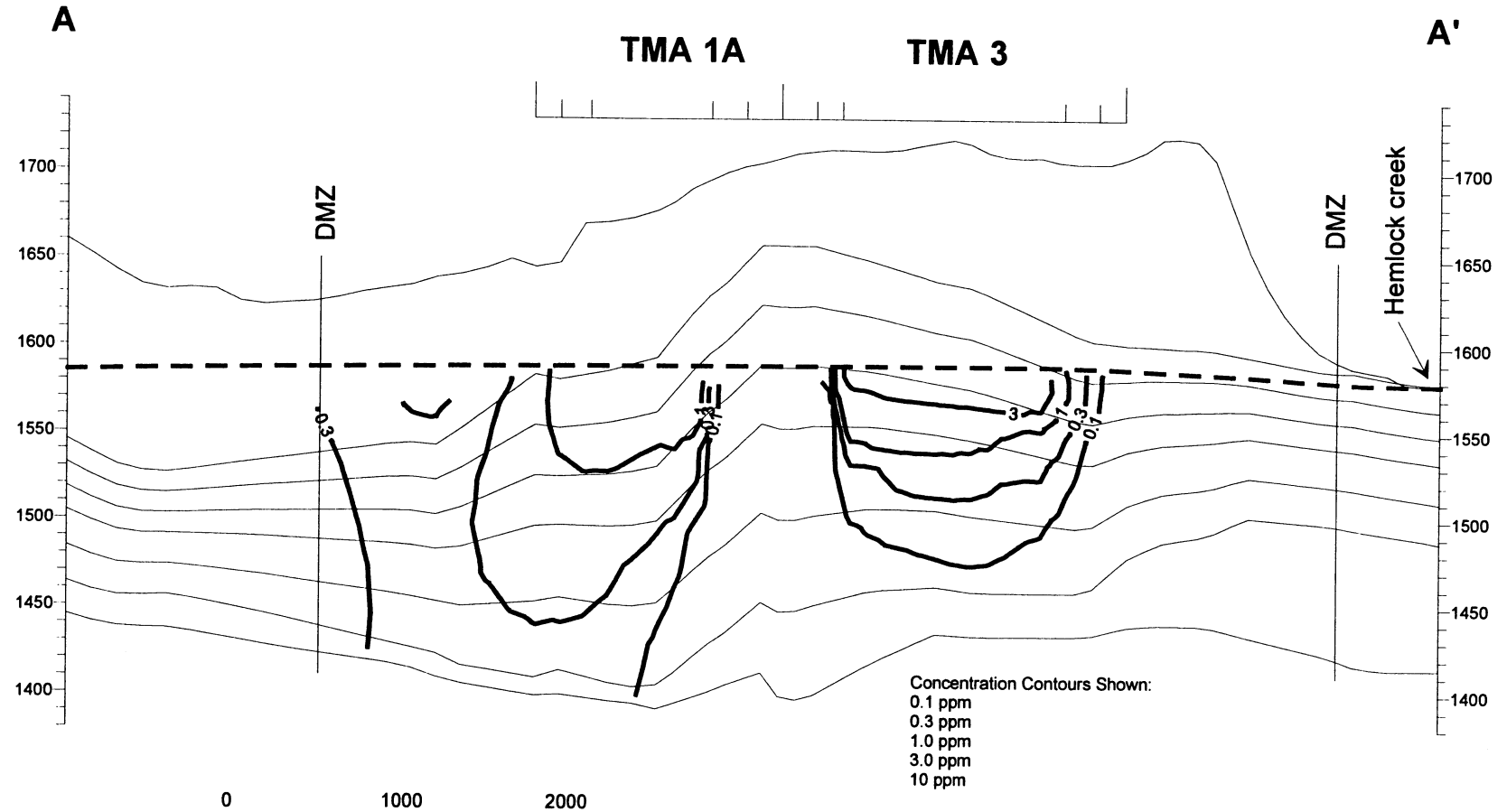

4.2-10-419

Source Concentration
Operation: 2000 ppm
Post-cap: 4000 ppm
Oxidized: 40,000 ppm*

* As a conservative assumption, the oxidized concentration begins immediately after assumed degradation of the flexible membrane liner.

Simulations
T09C1, T07C3, T09C2

HSI GEOTRANS

REVISED	DATE	BY	DESCRIPTION
1	6/99	JDC	Updated STM

CHECKED BY: RAK	DATE: Dec 98
APPROVED BY: PFA	DATE: Dec 98
APPROVED BY:	DATE:

Nicolet Minerals COMPANY

Figure 18
BEJT Concentration After 32 Years (Example Constituent, Cross-Section)

Scale: 1" = 1000' (h), 100' (v) | Date: Dec 1998

Prepared By: HSI GeoTrans | By: GWC

\Crandon\TmaMod4\Surfer2\XBEJ060.srf

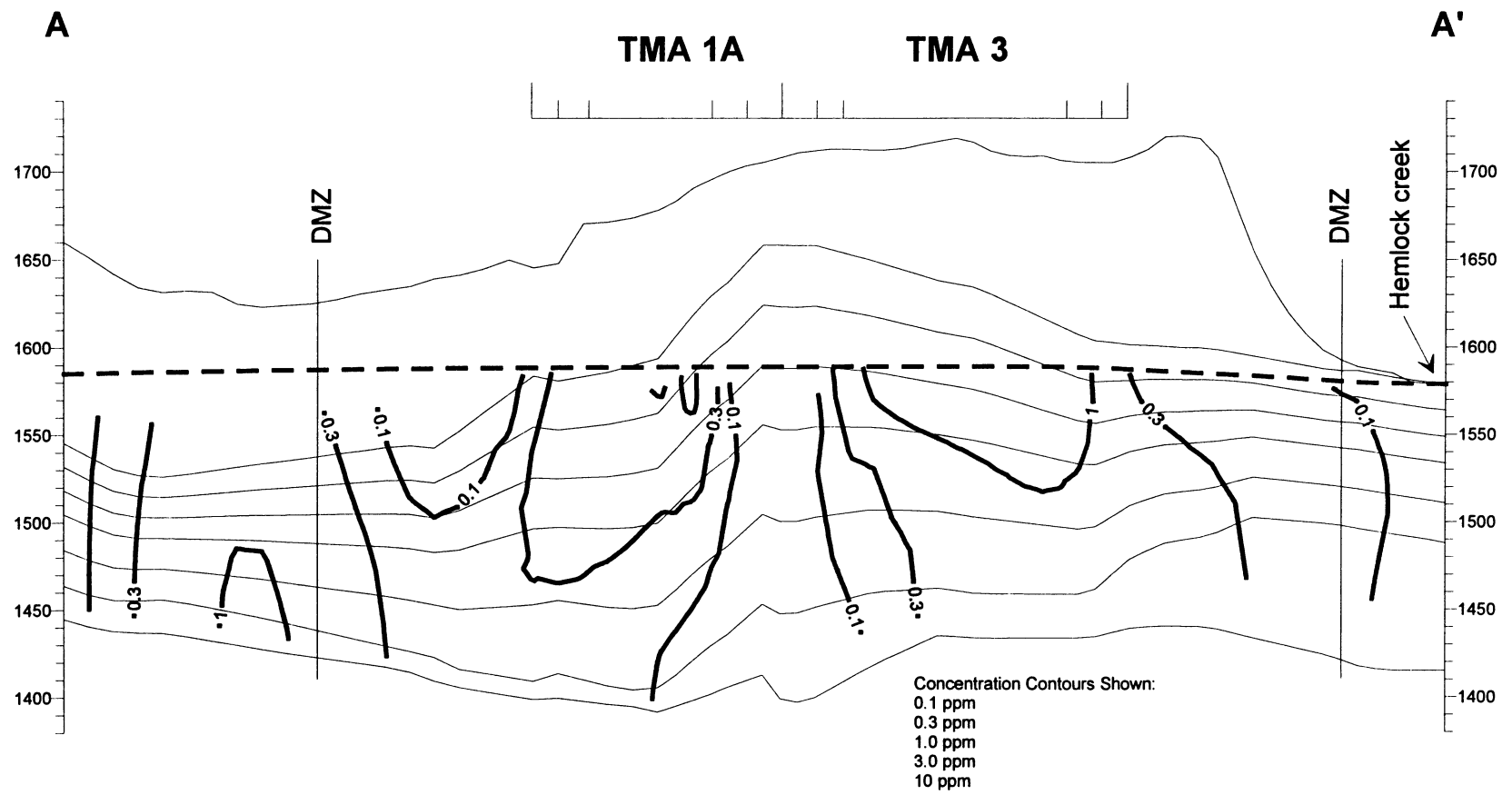

4.2-10-420

Source Concentration
Operation: 2000 ppm
Post-cap: 4000 ppm
Oxidized: 40,000 ppm*

* As a conservative assumption, the oxidized concentration begins immediately after assumed degradation of the flexible membrane liner.

Simulations
T09C1, T09C2, T07C3

HSI GEOTRANS

REVISED	DATE	BY	DESCRIPTION
1	6/99	JDC	Updated STM

CHECKED BY: RAK	DATE: Dec 98
APPROVED BY: PFA	DATE: Dec 98
APPROVED BY:	DATE:

Nicolet Minerals COMPANY

Figure 19
BEJT Concentration After 60 Years (Example Constituent, Cross-Section)

Scale: 1" = 1000' (h), 100' (v)	Date: Dec 1998
Prepared By: HSI GeoTrans	By: GWC

\Crandon\TmaMod4\Surfer2\XBEJ125.srf

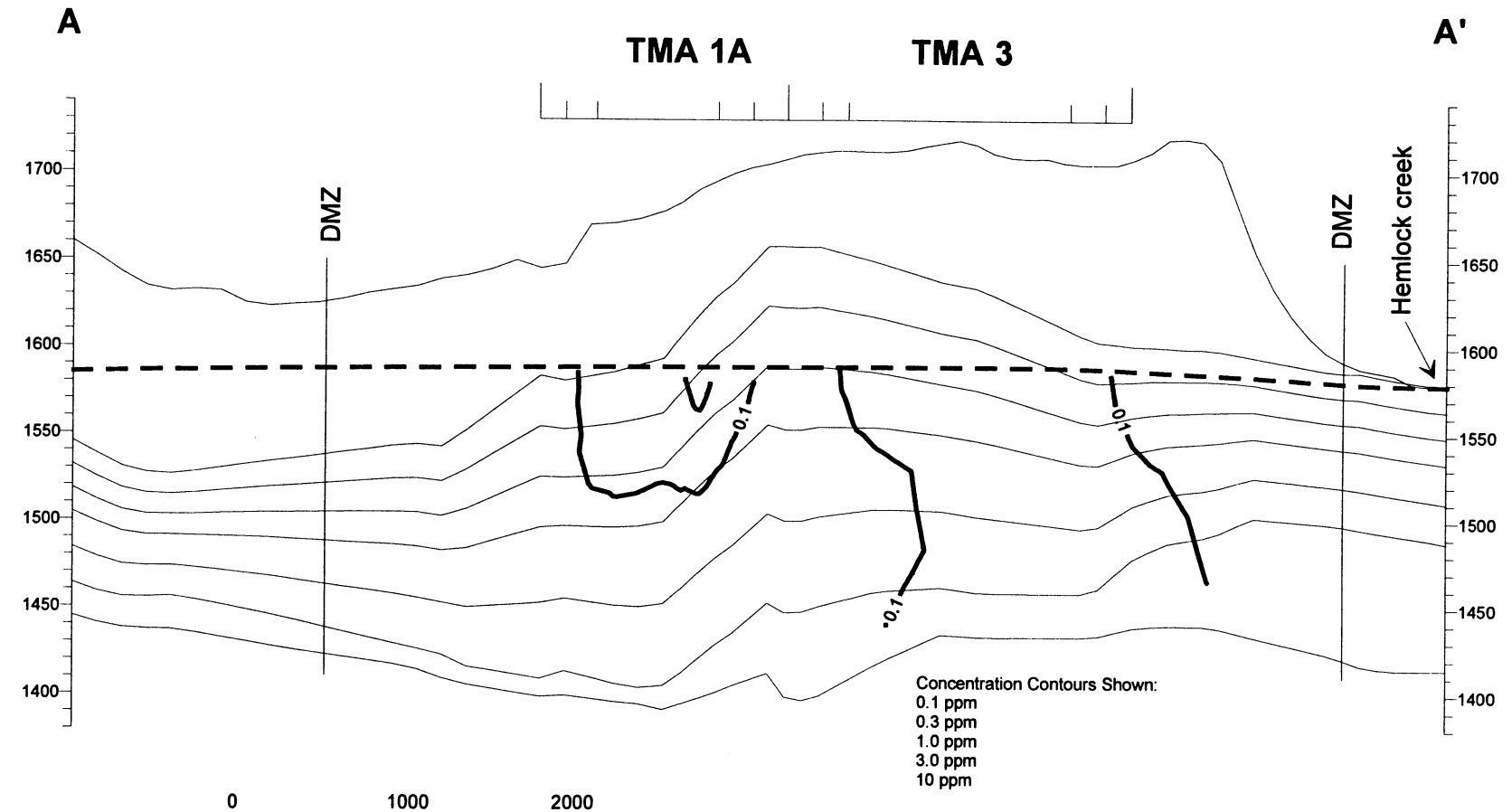

4.2-10-421

Source Concentration
Operation: 2000 ppm
Post-cap: 4000 ppm
Oxidized: 40,000 ppm*

* As a conservative assumption, the oxidized concentration begins immediately after assumed degradation of the flexible membrane liner.

Simulations
T09C1, T07C3

HSI GEOTRANS

REVISED	DATE	BY	DESCRIPTION
1	6/99	JDC	Updated STM

CHECKED BY: RAK	DATE: Dec 98
APPROVED BY: PFA	DATE: Dec 98
APPROVED BY:	DATE:

Nicolet Minerals COMPANY

Figure 20
BEJT Concentration After 125 Years
(Example Constituent, Cross-Section)

Scale: 1" = 1000' (h), 100' (v) | Date: Dec 1998

Prepared By: HSI GeoTrans | By: GWC

\Crandon\TmaMod4\Surfer2\XBEJ200.srf

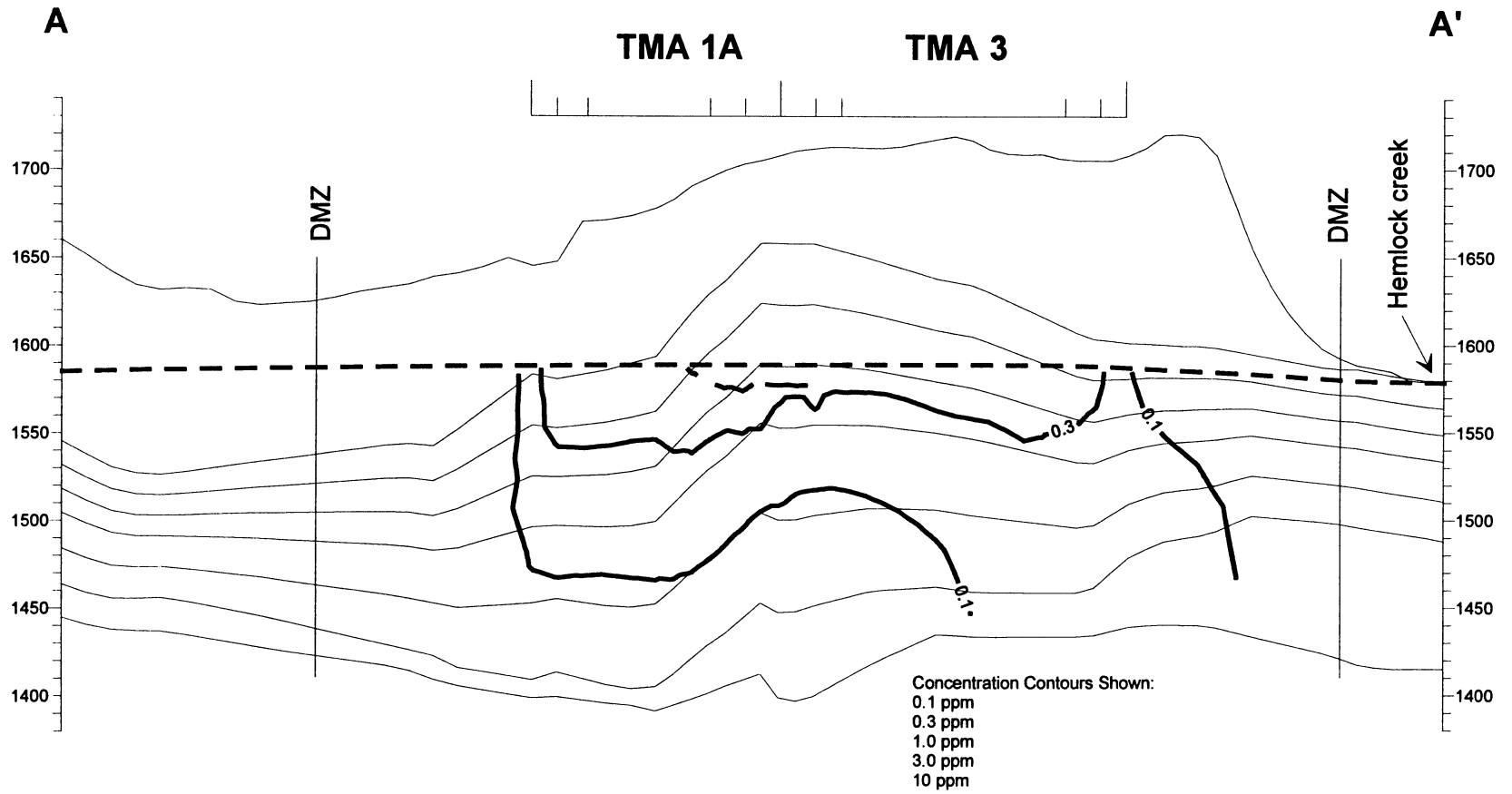

4.2-10-422

Source Concentration
Operation: 2000 ppm
Post-cap: 4000 ppm
Oxidized: 40,000 ppm*

* As a conservative assumption, the oxidized concentration begins immediately after assumed degradation of the flexible membrane liner.

Simulations
T09C1, T09C2, T07C3

HSI GEOTRANS

REVISED	DATE	BY	DESCRIPTION
1	6/99	JDC	Updated STM

CHECKED BY: RAK	DATE: Dec 98
APPROVED BY: PFA	DATE: Dec 98
APPROVED BY:	DATE:

Nicolet Minerals COMPANY

Figure 21
BEJT Concentration After 200 Years
(Example Constituent, Cross-Section)

Scale: 1" = 1000' (h), 100' (v) | Date: Dec 1998

Prepared By: HSI GeoTrans | By: GWC

\Crandon\TmaMod4\Surfer2\XBEJ300.srf

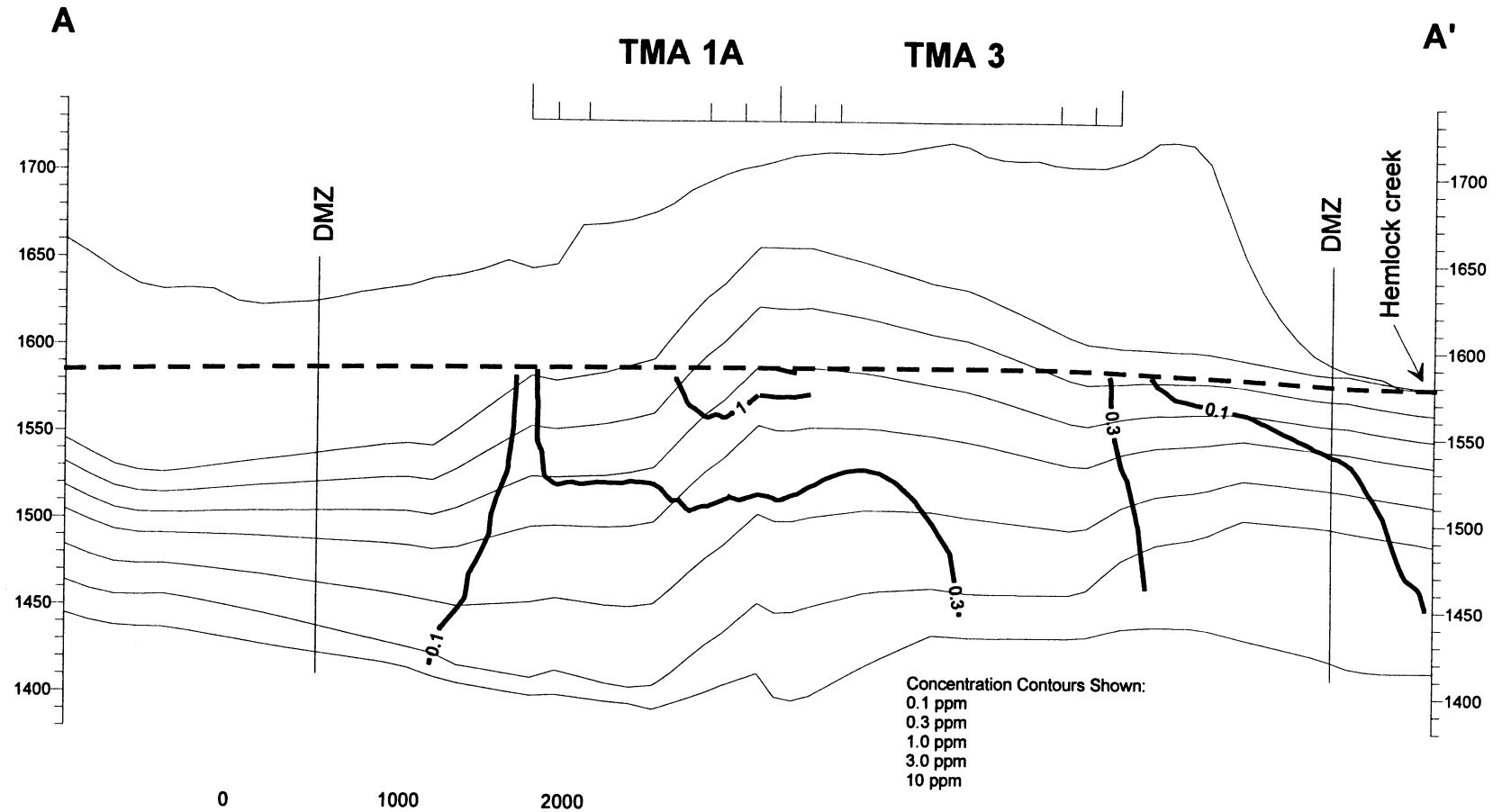

4.2-10-423

Source Concentration
Operation: 2000 ppm
Post-cap: 4000 ppm
Oxidized: 40,000 ppm*

* As a conservative assumption, the oxidized concentration begins immediately after assumed degradation of the flexible membrane liner.

Simulations
T09C1, T09C2, T07C3

HSI GEOTRANS

REVISED	DATE	BY	DESCRIPTION
1	6/99	JDC	Updated STM

CHECKED BY: RAK	DATE: Dec 98
APPROVED BY: PFA	DATE: Dec 98
APPROVED BY:	DATE:

Nicolet Minerals COMPANY

Figure 22
BEJT Concentration After 300 Years (Example Constituent, Cross-Section)

Scale: 1" = 1000' (h), 100' (v)	Date: Dec 1998
Prepared By: HSI GeoTrans	By: GWC

\Crandon\TmaMod4\Surfer2\XBEJ650.srf

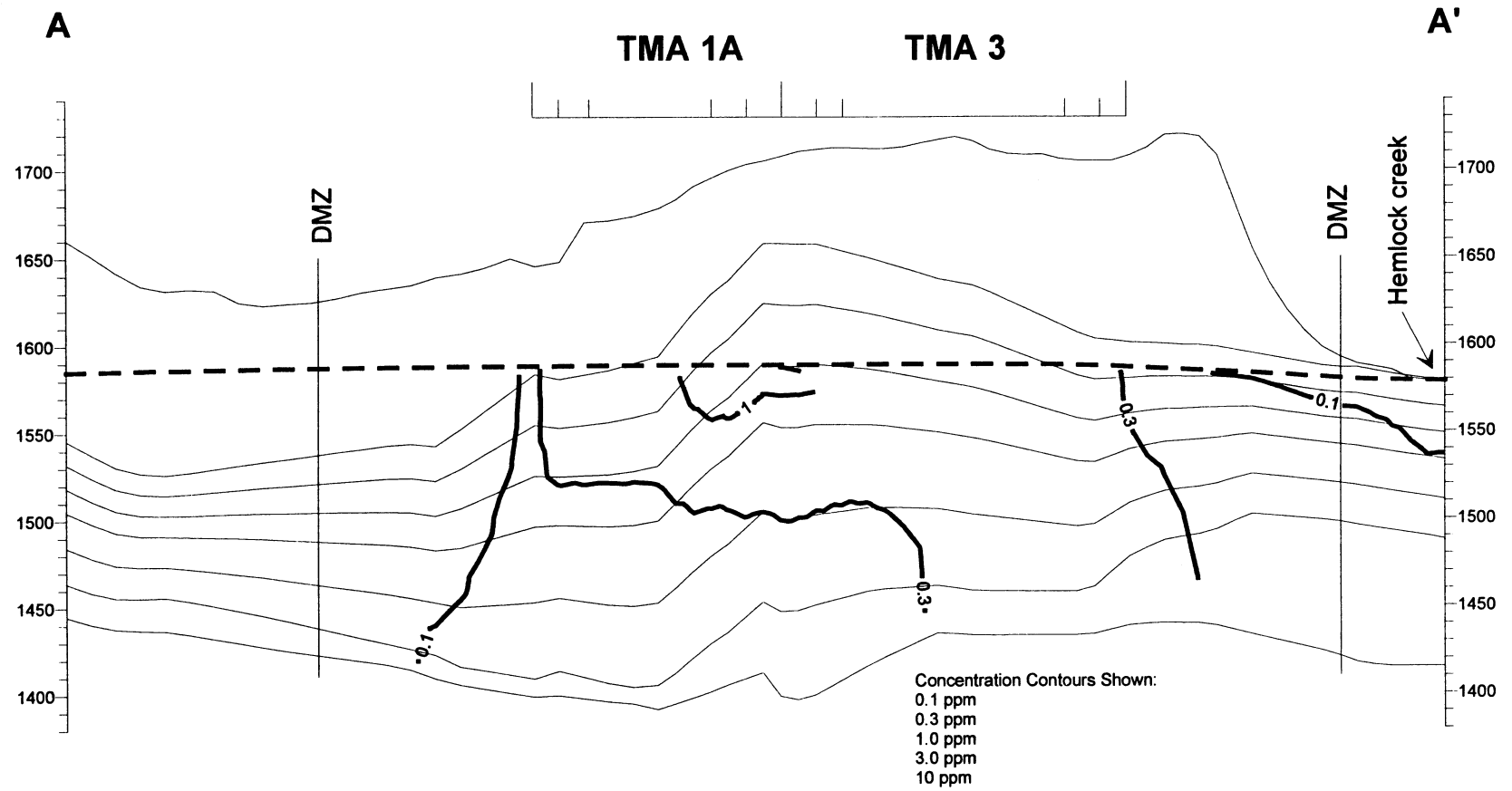

4.2-10-424

Source Concentration
Operation: 2000 ppm
Post-cap: 4000 ppm
Oxidized: 40,000 ppm*

* As a conservative assumption, the oxidized concentration begins immediately after assumed degradation of the flexible membrane liner.

Simulations
T09C1, T09C2, T07C3

HSI GEOTRANS

REVISED	DATE	BY	DESCRIPTION
1	6/99	JDC	Updated STM

CHECKED BY: RAK	DATE: Dec 98
APPROVED BY: PFA	DATE: Dec 98
APPROVED BY:	DATE:

Nicolet Minerals COMPANY

Figure 23
BEJT Concentration After 650 Years (Example Constituent, Cross-Section)

Scale: 1" = 1000' (h), 100' (v) | Date: Dec 1998

Prepared By: HSI GeoTrans | By: GWC

Tailings Management Area Design Management Zone

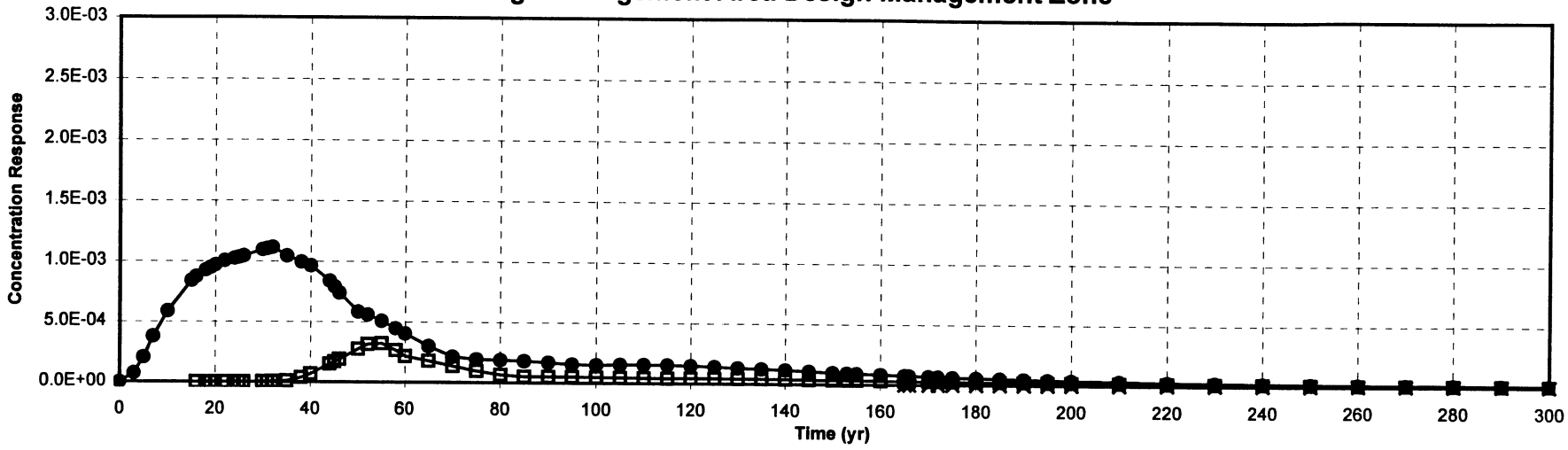

Reclaim Pond Design Management Zone

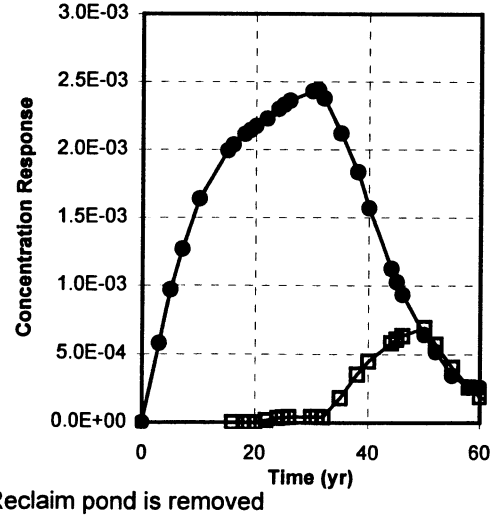

Note: Reclaim pond is removed at approximately year 46

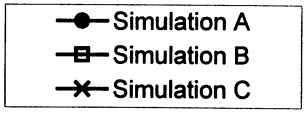

Note: The maximum concentration at any point on the Design Management Zone is plotted.

HSI GEOTRANS			
REVISED	DATE	BY	DESCRIPTION
1	5/99	RAK	Updated STM

CHECKED BY: PAW		DATE: Dec 1998
APPROVED BY: PFA		DATE: Dec 1998
APPROVED BY:		DATE:

Simulations
T10C1,2,T08C3

Nicolet Minerals COMPANY

Figure 24
PWCT Concentration Response Curves for the Design Management Zones

Scale: None	Date: December 1998
Prepared By: HSI GEOTRANS	By: GWC

\Crandon\TmaMod4\Excel\Examp1.xls.PWC

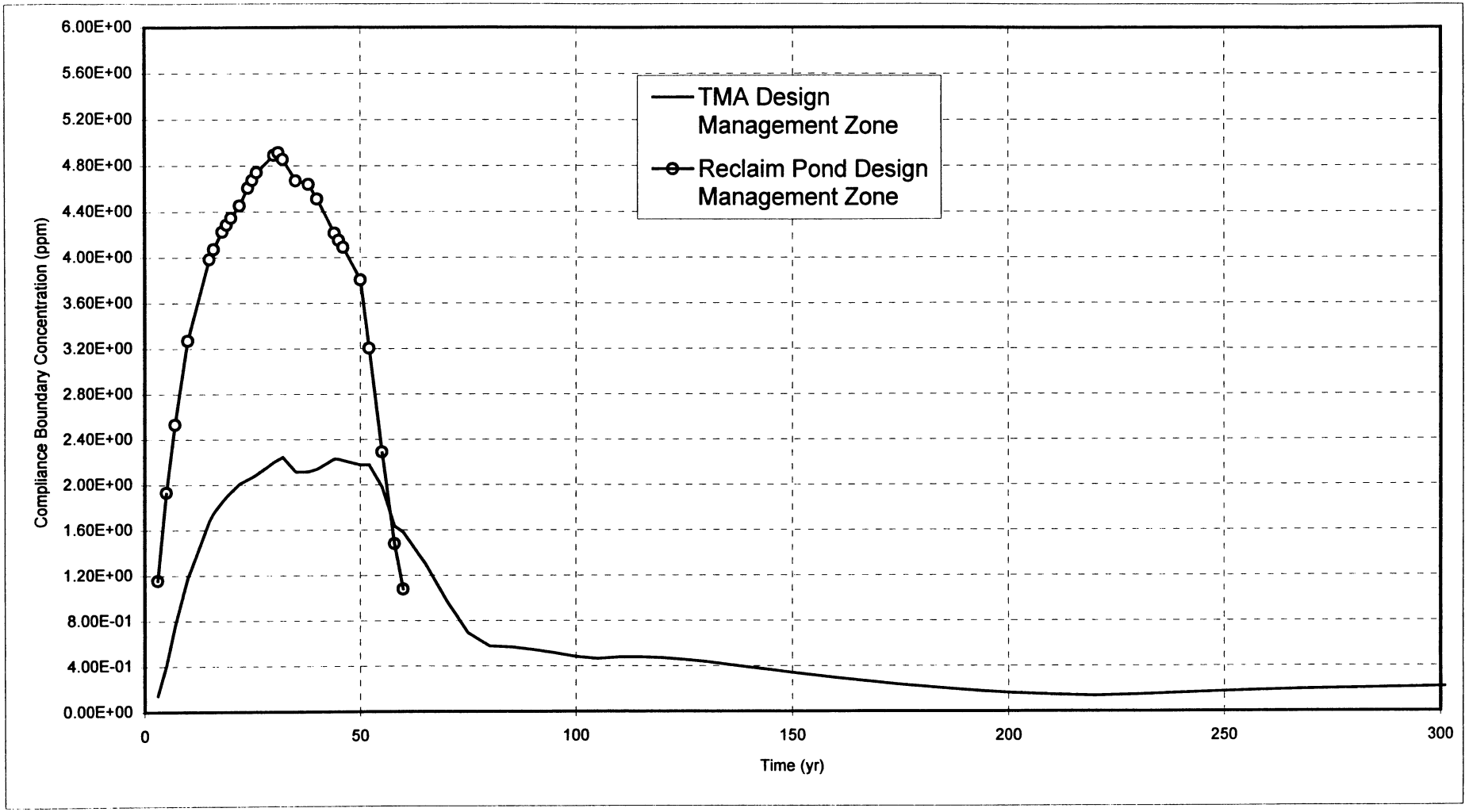

4.2-10-426

Source Concentration:
Operation: 2000 ppm
Post-Cap: 4000 ppm
Oxidized: 40000 ppm*

* As a conservative assumption, the oxidized concentration begins immediately after assumed degradation of the flexible membrane liner.

HSI GEOTRANS

REVISED	DATE	BY	DESCRIPTION
1	6/99	GWC	Updated STM

CHECKED BY: GWC	DATE: Dec 1998
APPROVED BY: PFA	DATE: Dec 1998
APPROVED BY:	DATE:

Simulations T08C1, 2, 3

Nicolet Minerals COMPANY

Figure 25
PWCT Concentration at the Design Management Zones (Example Constituent)

Scale: None	Date: Dec 1998
Prepared By: HSI GEOTRANS	By: RAK

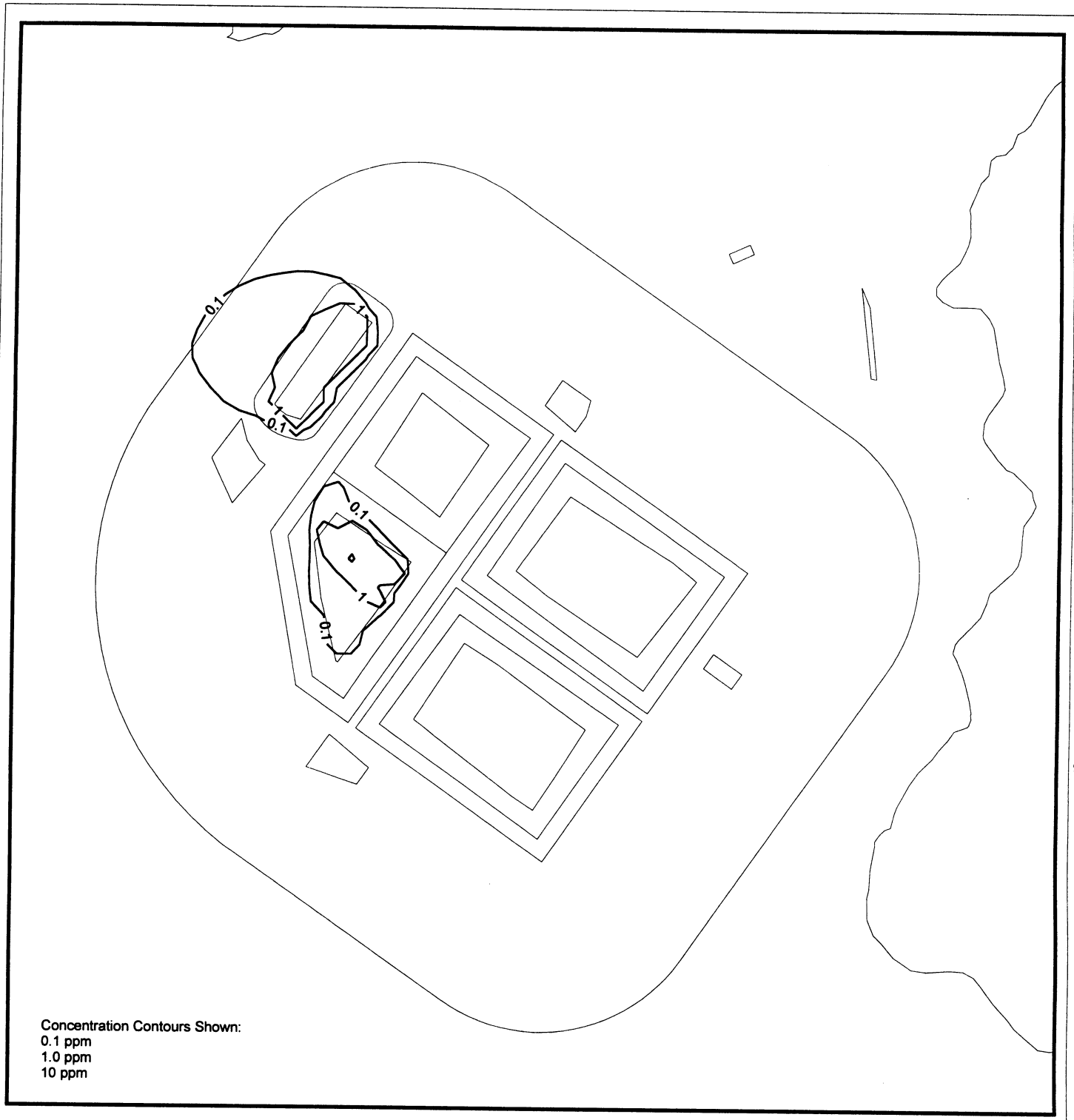

Concentration Contours Shown:
0.1 ppm
1.0 ppm
10 ppm

Source Concentration
Operation: 2000 ppm
Post-cap: 4000 ppm
Oxidized: 40,000 ppm*

* As a conservative assumption, the oxidized concentration begins immediately after assumed degradation of the flexible membrane liner.

Note:
This plot shows contours of maximum concentratration in any layer.

Simulations
T10C1, T10C2, T08C3

N

0 1000 2000

Scale in Feet

HSI GEOTRANS

REVISED	DATE	BY	DESCRIPTION
1	6/99	RAK	Updated STM

CHECKED BY: GWC	DATE: Dec 98
APPROVED BY: PFA	DATE: Dec 98
APPROVED BY:	DATE:

Nicolet Minerals COMPANY

Figure 26
PWCT Concentration After 3 Years
(Example Constituent, Plan View)

Scale: 1 in. = 1000 ft.	Date: December 1998
Prepared By: HSI GEOTRANS	By: KMR

\Crandon\Tmal\Mod4\Surfer2\PWC0003.srf

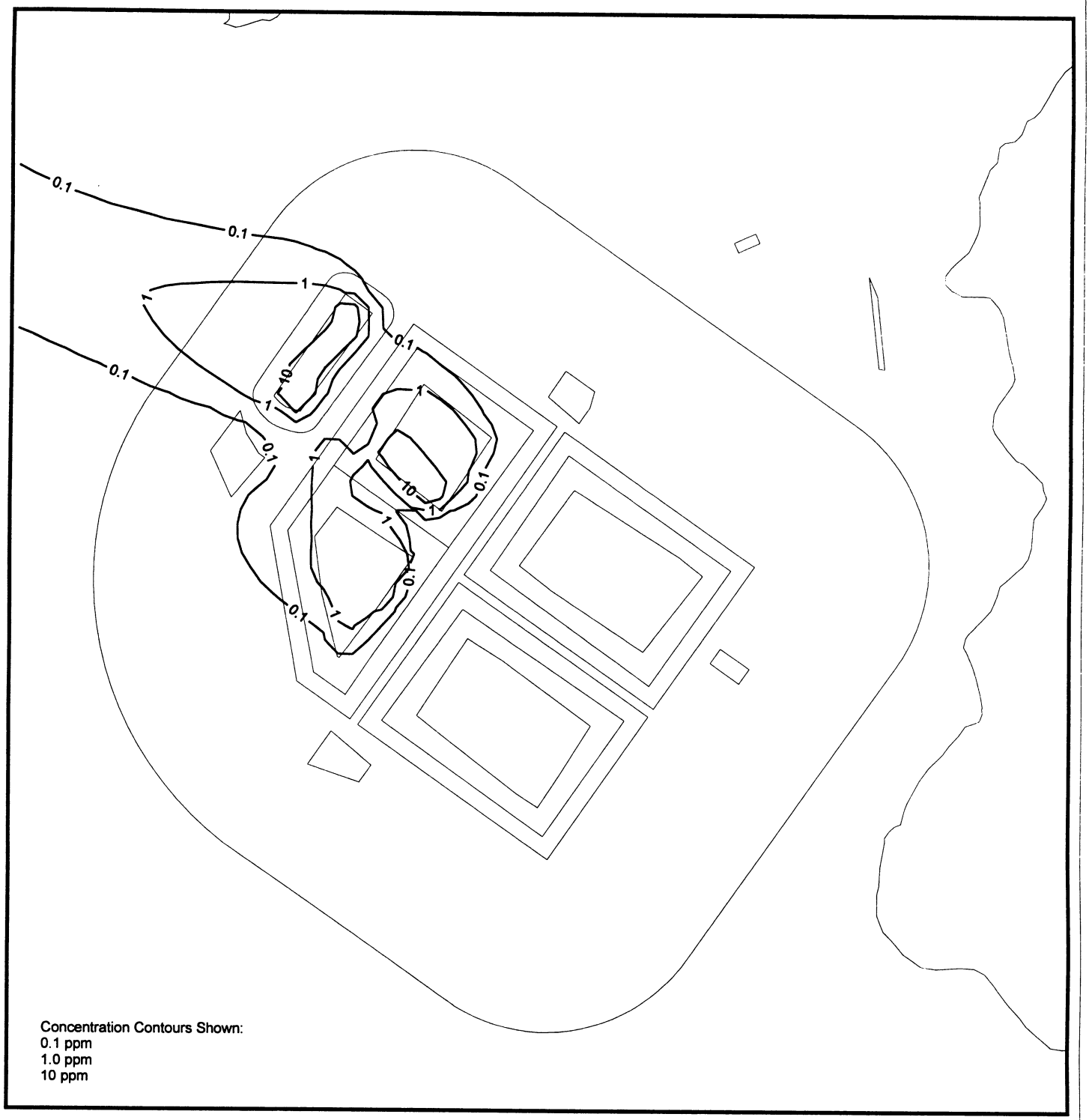

Source Concentration
Operation: 2000 ppm
Post-cap: 4000 ppm
Oxidized: 40,000 ppm*

* As a conservative assumption, the oxidized concentration begins immediately after assumed degradation of the flexible membrane liner.

Note:
This plot shows contours of maximum concentratration in any layer.

Simulations
T10C1, T10C2, T08C3

0 1000 2000
Scale in Feet

HSI GEOTRANS

REVISED	DATE	BY	DESCRIPTION
1	6/99	RAK	Updated STM

CHECKED BY: GWC	DATE: Dec 98
APPROVED BY: PFA	DATE: Dec 98
APPROVED BY:	DATE:

Nicolet Minerals COMPANY

Figure 27
PWCT Concentration After 16 Years
(Example Constituent, Plan View)

Scale: 1 in. = 1000 ft. | Date: December 1998
Prepared By: HSI GEOTRANS | By: KMR

\Crandon\Tma\Mod\Surfer2\PWC016.srf

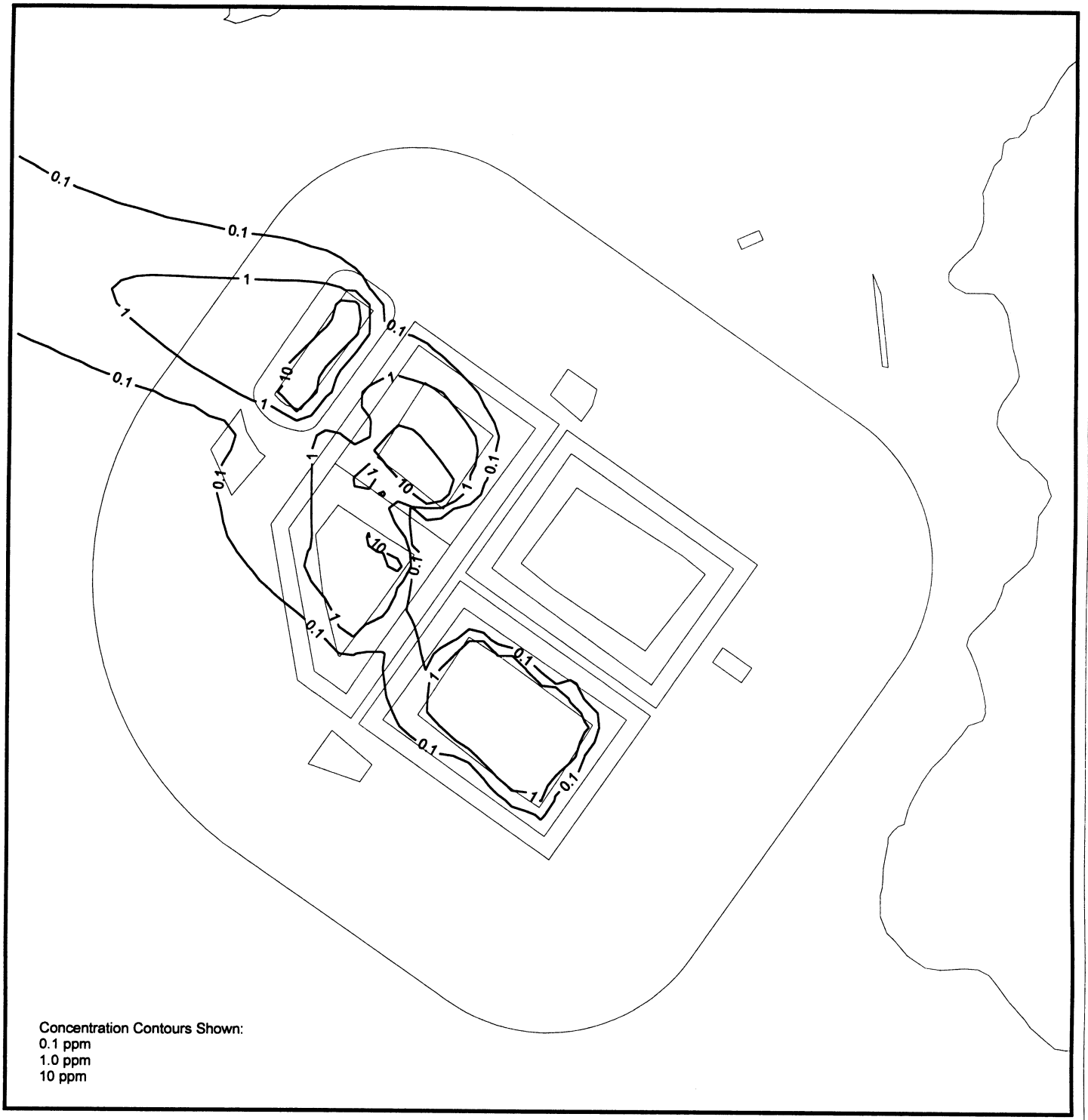

Concentration Contours Shown:
0.1 ppm
1.0 ppm
10 ppm

Source Concentration
Operation: 2000 ppm
Post-cap: 4000 ppm
Oxidized: 40,000 ppm*

* As a conservative assumption, the oxidized concentration begins immediately after assumed degradation of the flexible membrane liner.

Note:
This plot shows contours of maximum concentratration in any layer.

Simulations
T10C1, T10C2, T08C3

N

0 1000 2000

Scale in Feet

HSI GEOTRANS

REVISED	DATE	BY	DESCRIPTION
1	6/99	RAK	Updated STM

CHECKED BY: GWC	DATE: Dec 98
APPROVED BY: PFA	DATE: Dec 98
APPROVED BY:	DATE:

Nicolet Minerals COMPANY

Figure 28
PWCT Concentration After 22 Years (Example Constituent, Plan View)

Scale: 1 in. = 1000 ft.	Date: December 1998
Prepared By: HSI GEOTRANS	By: KMR

\Crandon\TmaModl\Surfer2\PWC022.srf

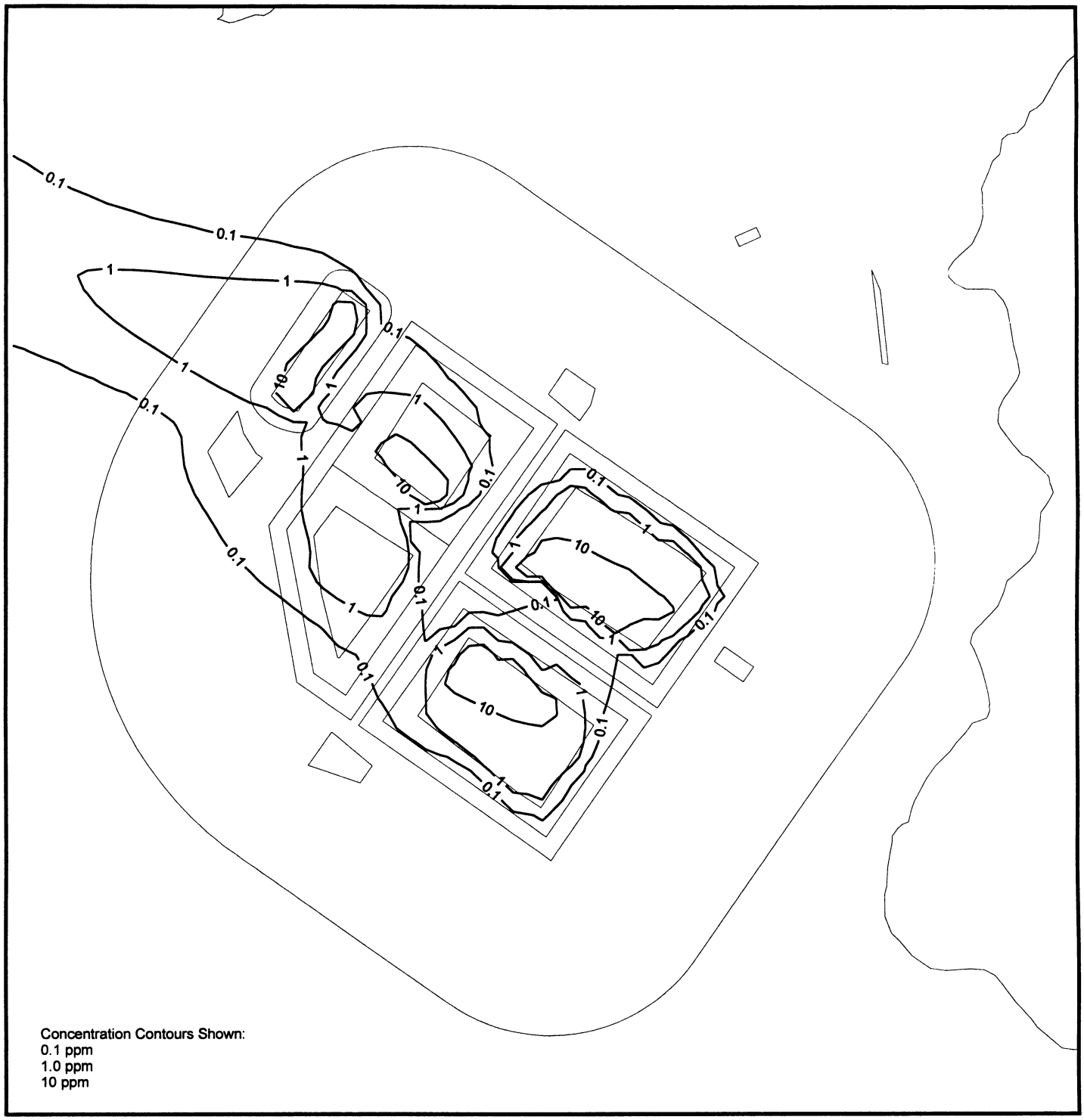

Source Concentration
Operation: 2000 ppm
Post-cap: 4000 ppm
Oxidized: 40,000 ppm*

* As a conservative assumption, the oxidized concentration begins immediately after assumed degradation of the flexible membrane liner.

Note:
This plot shows contours of maximum concentratration in any layer.

Simulations
T10C1, T10C2, T08C3

0 1000 2000
Scale in Feet

HSI GEOTRANS

REVISED	DATE	BY	DESCRIPTION
1	6/99	RAK	Updated STM

CHECKED BY: GWC	DATE: Dec 98
APPROVED BY: PFA	DATE: Dec 98
APPROVED BY:	DATE:

Nicolet Minerals COMPANY

Figure 29
PWCT Concentration After 32 Years (Example Constituent, Plan View)

Scale: 1 in. = 1000 ft.	Date: December 1998
Prepared By: HSI GEOTRANS	By: KMR

\Crandon\Tma\Mod4\Surfer2\PWC032.srf

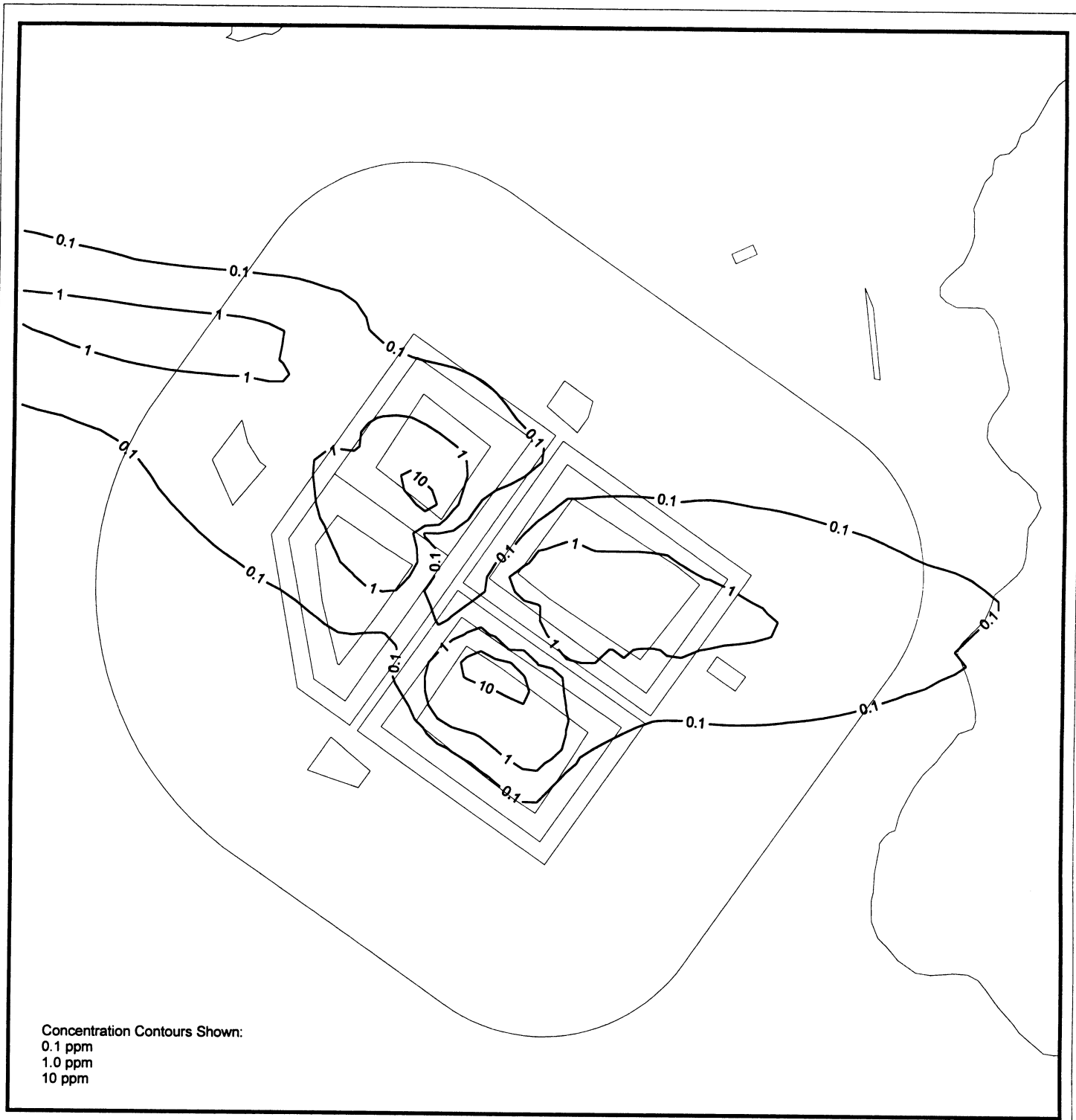

Source Concentration
Operation: 2000 ppm
Post-cap: 4000 ppm
Oxidized: 40,000 ppm*

* As a conservative assumption, the oxidized concentration begins immediately after assumed degradation of the flexible membrane liner.

Note:
This plot shows contours of maximum concentratration in any layer.

Simulations
T10C1, T10C2, T08C3

N

0 1000 2000

Scale in Feet

HSI GEOTRANS

REVISED	DATE	BY	DESCRIPTION
1	6/99	RAK	Updated STM

CHECKED BY: GWC	DATE: Dec 98
APPROVED BY: PFA	DATE: Dec 98
APPROVED BY:	DATE:

Nicolet Minerals COMPANY

Figure 30
PWCT Concentration After 60 Years
(Example Constituent, Plan View)

Scale: 1 in. = 1000 ft.	Date: November 1998
Prepared By: HSI GEOTRANS	By: KMR

\Crandon\Tmal\Mod\Surfer2\Pwc030.srf

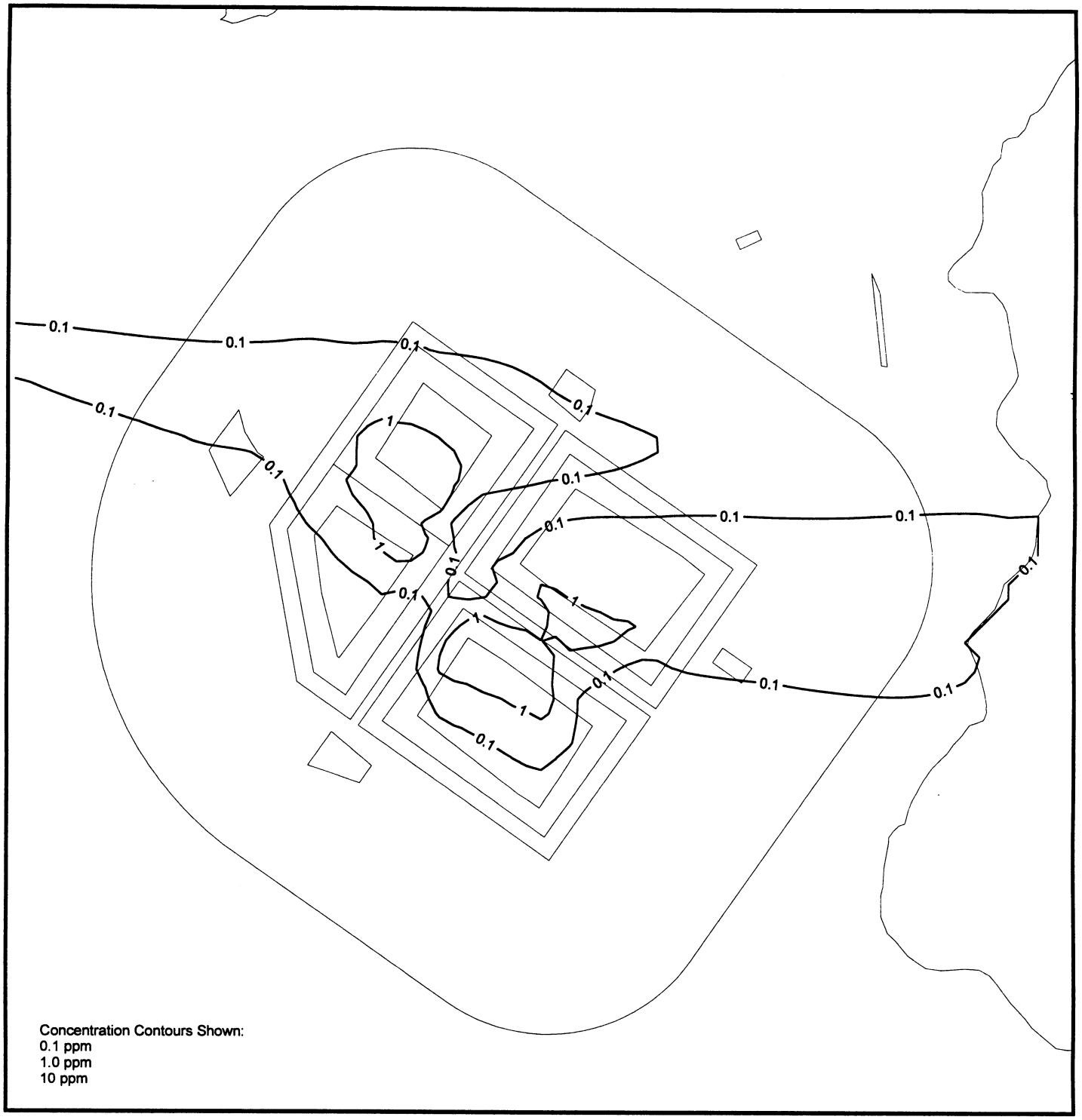

Source Concentration
Operation: 2000 ppm
Post-cap: 4000 ppm
Oxidized: 40,000 ppm*

* As a conservative assumption, the oxidized concentration begins immediately after assumed degradation of the flexible membrane liner.

Note:
This plot shows contours of maximum concentratration in any layer.

Simulations
T10C1, T10C2, T08C3

N

0 1000 2000

Scale in Feet

HSI GEOTRANS

REVISED	DATE	BY	DESCRIPTION
1	6/99	RAK	Updated STM

CHECKED BY: GWC	DATE: Dec 98
APPROVED BY: PFA	DATE: Dec 98
APPROVED BY:	DATE:

Nicolet Minerals COMPANY

Figure 31
PWCT Concentration After 125 Years
(Example Constituent, Plan View)

Scale: 1 in. = 1000 ft. | Date: November 1998

Prepared By: HSI GEOTRANS | By: KMR

\Crandon\Tmal\Mod4\Surfer2\Pwc125.srf

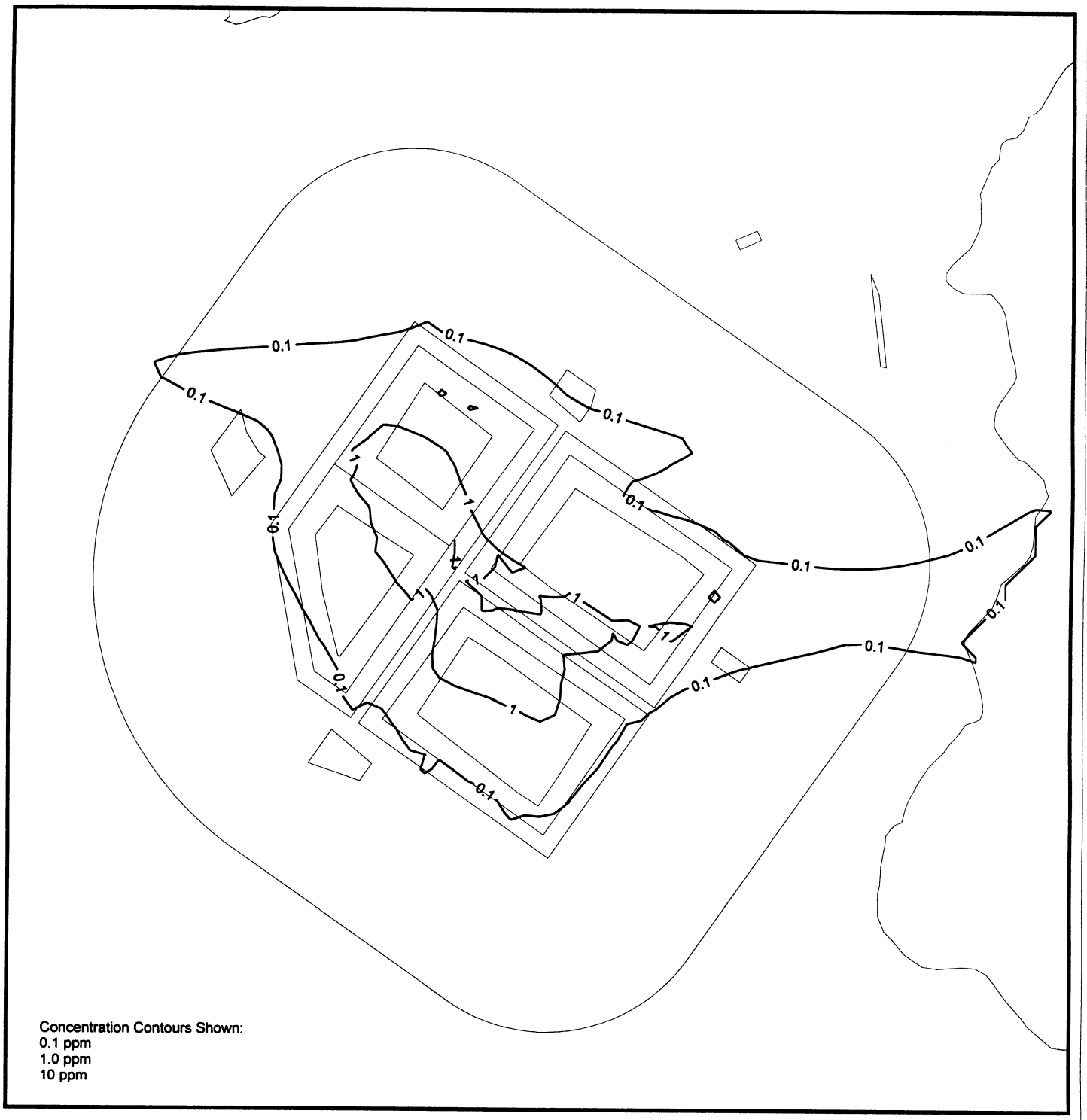

Source Concentration
Operation: 2000 ppm
Post-cap: 4000 ppm
Oxidized: 40,000 ppm*

* As a conservative assumption, the oxidized concentration begins immediately after assumed degradation of the flexible membrane liner.

Note:
This plot shows contours of maximum concentratration in any layer.

Simulations
T10C1, T10C2, T08C3

N

0 1000 2000

Scale in Feet

HSI GEOTRANS

REVISED	DATE	BY	DESCRIPTION
1	6/99	RAK	Updated STM

CHECKED BY: GWC	DATE: Dec 98
APPROVED BY: PFA	DATE: Dec 98
APPROVED BY:	DATE:

Nicolet Minerals COMPANY

Figure 32
PWCT Concentration After 200 Years
(Example Constituent, Plan View)

Scale: 1 in. = 1000 ft.	Date: November 1998
Prepared By: HSI GEOTRANS	By: KMR

\Crandon\TmaMod4\Surfer2\Pwc200.srf

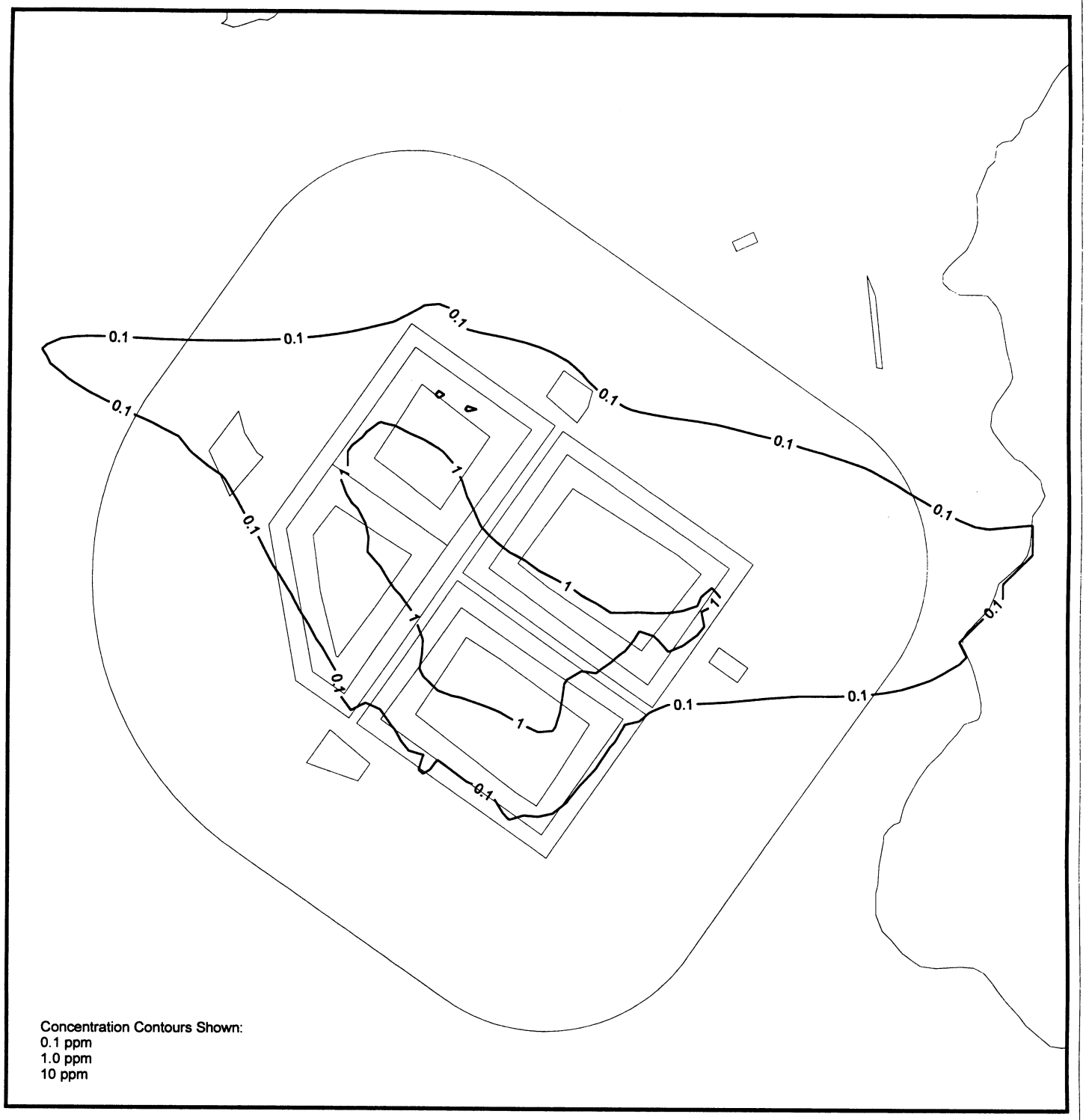

Source Concentration
Operation: 2000 ppm
Post-cap: 4000 ppm
Oxidized: 40,000 ppm*

* As a conservative assumption, the oxidized concentration begins immediately after assumed degradation of the flexible membrane liner.

Note:
This plot shows contours of maximum concentratration in any layer.

Simulations
T10C1, T10C2, T08C3

0 1000 2000
Scale in Feet

HSI GEOTRANS

REVISED	DATE	BY	DESCRIPTION
1	6/99	RAK	Updated STM

CHECKED BY: GWC	DATE: Dec 98
APPROVED BY: PFA	DATE: Dec 98
APPROVED BY:	DATE:

Nicolet Minerals COMPANY

Figure 33
PWCT Concentration After 300 Years
(Example Constituent, Plan View)

Scale: 1 in. = 1000 ft. | Date: November 1998
Prepared By: HSI GEOTRANS | By: KMR

\Crandon\Tma\Mod4\Surfer2\Pwc300.srf

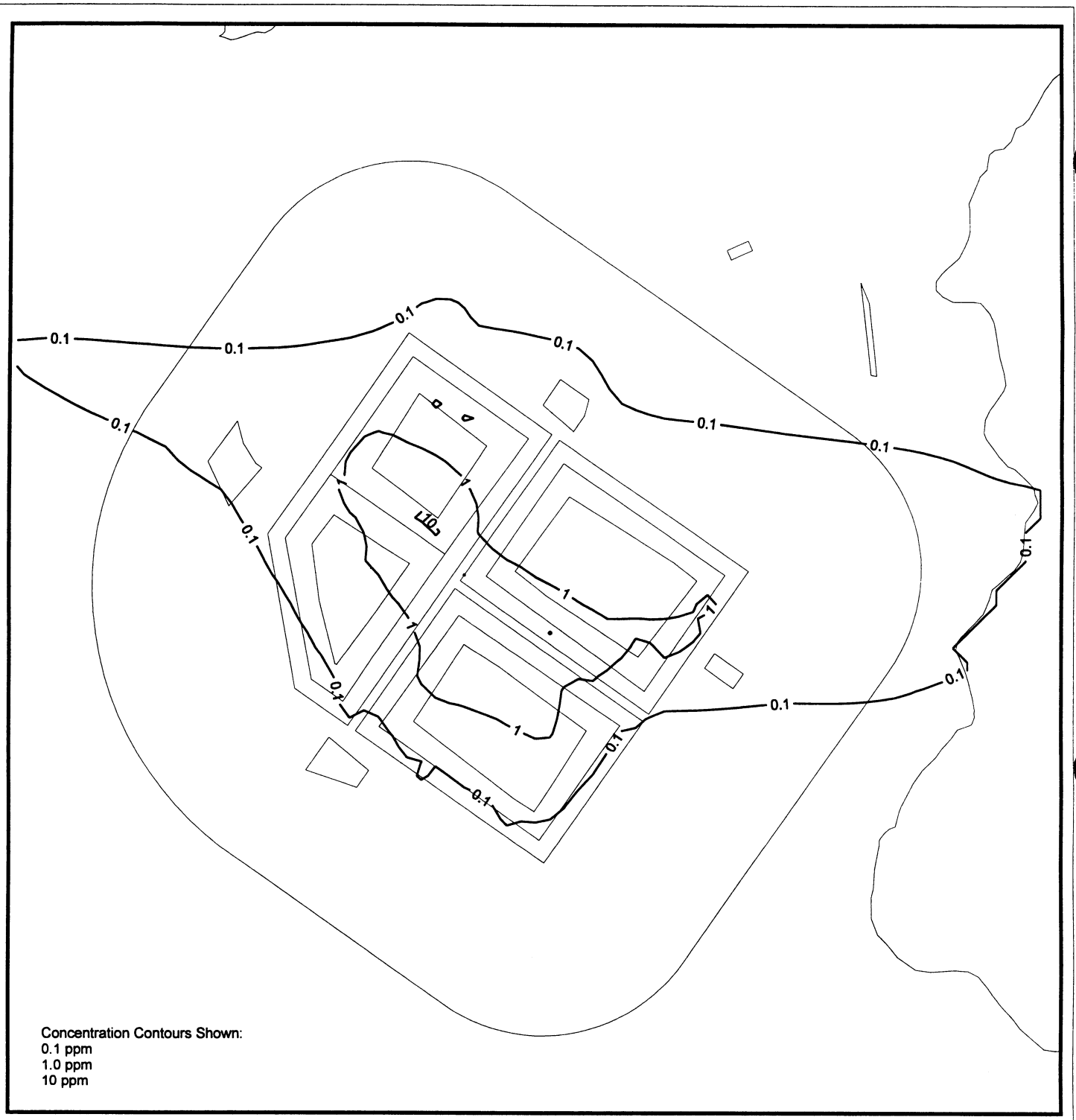

Source Concentration
Operation: 2000 ppm
Post-cap: 4000 ppm
Oxidized: 40,000 ppm*

* As a conservative assumption, the oxidized concentration begins immediately after assumed degradation of the flexible membrane liner.

Note:
This plot shows contours of maximum concentratration in any layer.

Simulations
T10C1, T10C2, T08C3

N

0 1000 2000

Scale in Feet

HSI GEOTRANS			
REVISED	DATE	BY	DESCRIPTION
1	6/99	RAK	Updated STM

CHECKED BY: GWC	DATE: Dec 98
APPROVED BY: PFA	DATE: Dec 98
APPROVED BY:	DATE:

Nicolet Minerals COMPANY

Mining for the Future

Figure 34
PWCT Concentration After 650 Years
(Example Constituent, Plan View)

Scale: 1 in. = 1000 ft.	Date: November 1998
Prepared By: HSI GEOTRANS	By: KMR

\Crandon\TmaMod4\Surfer2\Pwc650.srf

\Crandon\TmaMod4\Surfer2\XPWC003.srf

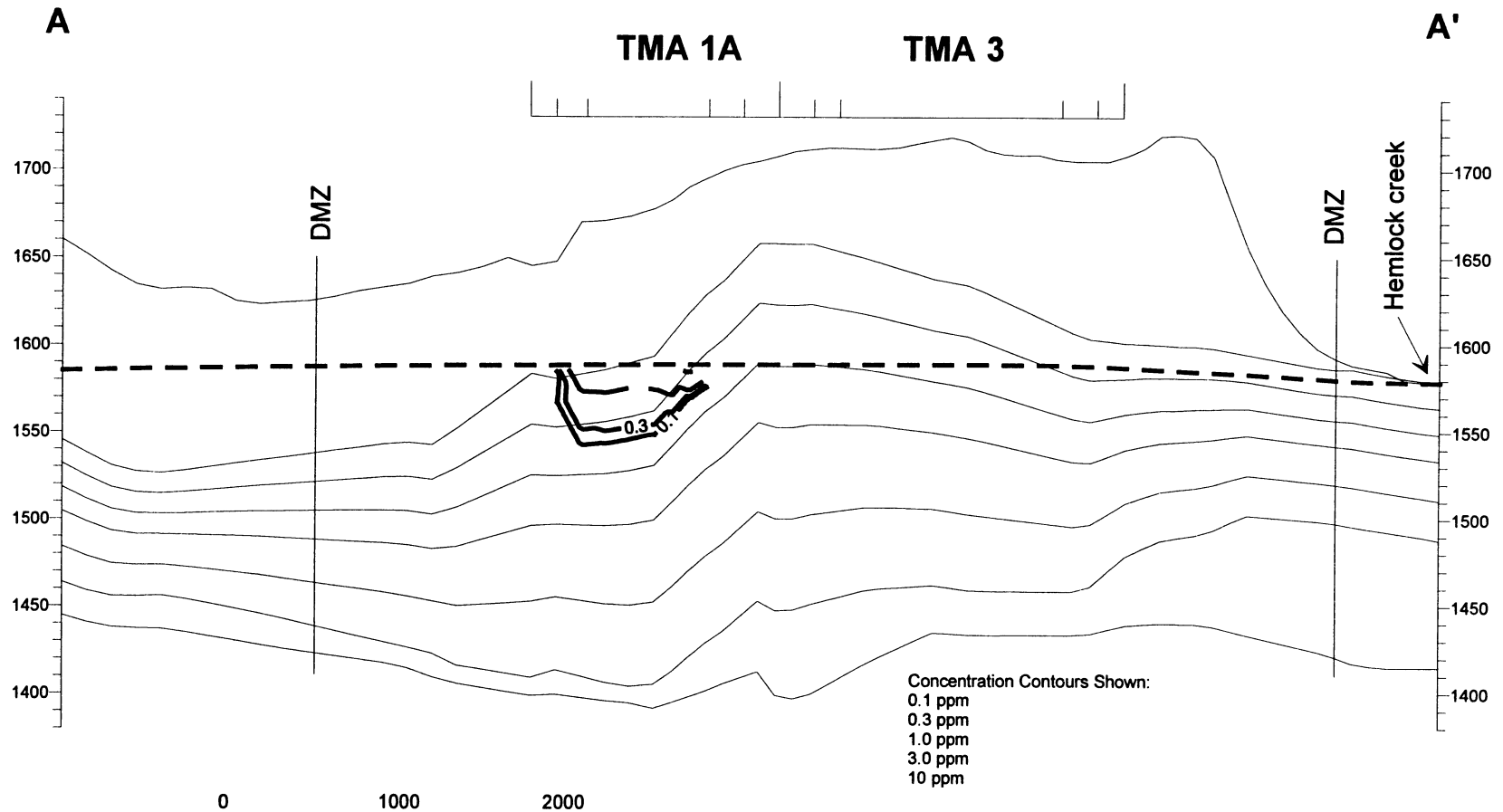

4.2-10-436

Source Concentration
Operation: 2000 ppm
Post-cap: 4000 ppm
Oxidized: 40,000 ppm*

* As a conservative assumption, the oxidized concentration begins immediately after assumed degradation of the flexible membrane liner.

Simulations
T10C1, T10C2, T08C3

HSI GEOTRANS

REVISED	DATE	BY	DESCRIPTION
1	6/99	JDC	Updated STM

CHECKED BY: RAK	DATE: Dec 98
APPROVED BY: PFA	DATE: Dec 98
APPROVED BY:	DATE:

Nicolet Minerals COMPANY

Figure 35
PWCT Concentration After 3 Years (Example Constituent, Cross-Section)

Scale: 1" = 1000' (h), 100' (v) | Date: Dec 1998

Prepared By: HSI GeoTrans | By: GWC

\Crandon\TmaMod4\Surfer2\XPWC016.srf

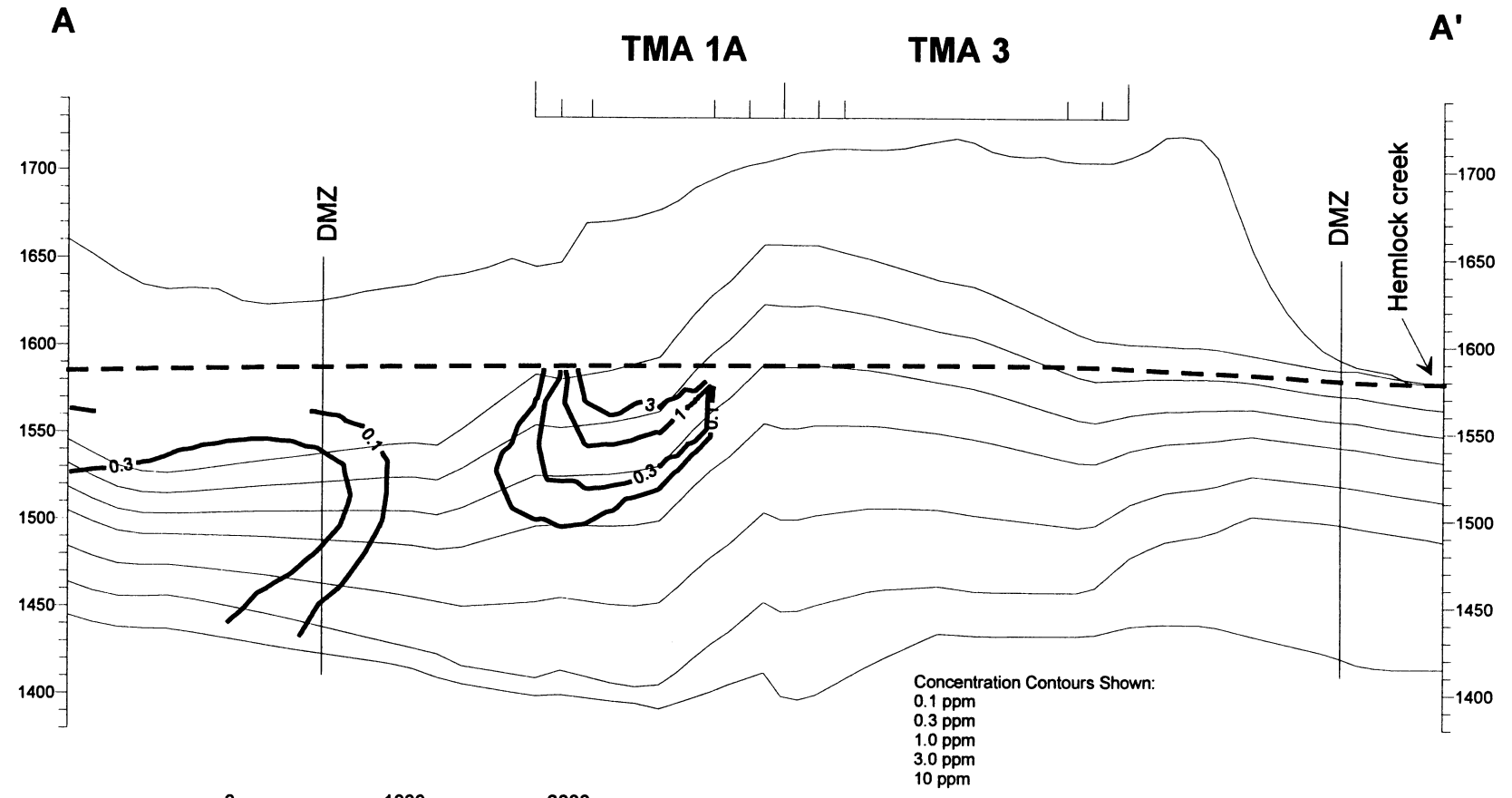

Concentration Contours Shown:
0.1 ppm
0.3 ppm
1.0 ppm
3.0 ppm
10 ppm

0 1000 2000

Horizontal Scale in Feet
(Vertical Exaggeration x10)

4.2-10-437

Source Concentration
Operation: 2000 ppm
Post-cap: 4000 ppm
Oxidized: 40,000 ppm*

* As a conservative assumption, the oxidized concentration begins immediately after assumed degradation of the flexible membrane liner.

Simulations
T10C1, T10C2, T08C3

HSI GEOTRANS

REVISED	DATE	BY	DESCRIPTION
1	6/99	JDC	Updated STM

CHECKED BY: RAK	DATE: Dec 98
APPROVED BY: PFA	DATE: Dec 98
APPROVED BY:	DATE:

Nicolet Minerals COMPANY

Mining for the Future

Figure 36
PWCT Concentration After 16 Years
(Example Constituent, Cross-Section)

Scale: 1" = 1000' (h), 100' (v)	Date: Dec 1998
Prepared By: HSI GeoTrans	By: GWC

\Crandon\TmaMod4\Surfer2\XPWC022.srf

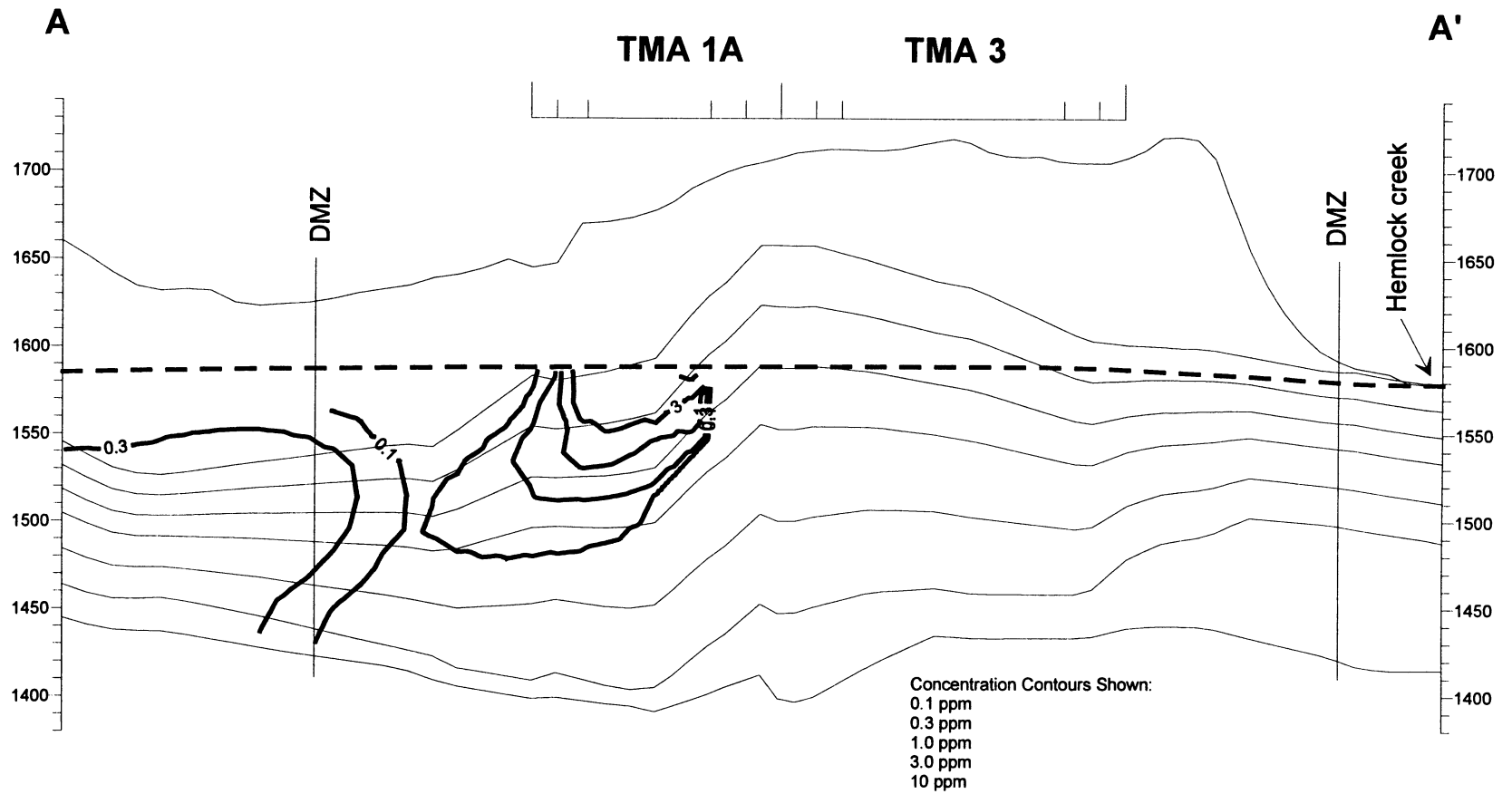

4.2-10-438

Source Concentration
Operation: 2000 ppm
Post-cap: 4000 ppm
Oxidized: 40,000 ppm*

* As a conservative assumption, the oxidized concentration begins immediately after assumed degradation of the flexible membrane liner.

Simulations
T10C1, T10C2, T08C3

HSI GEOTRANS

REVISED	DATE	BY	DESCRIPTION
1	6/99	JDC	Updated STM

CHECKED BY: RAK	DATE: Dec 98
APPROVED BY: PFA	DATE: Dec 98
APPROVED BY:	DATE:

Nicolet Minerals COMPANY

Figure 37
PWCT Concentration After 22 Years (Example Constituent, Cross-Section)

Scale: 1" = 1000' (h), 100' (v) | Date: Dec 1998

Prepared By: HSI GeoTrans | By: GWC

\Crandon\TmaMod4\Surfer2\XPWC032.srf

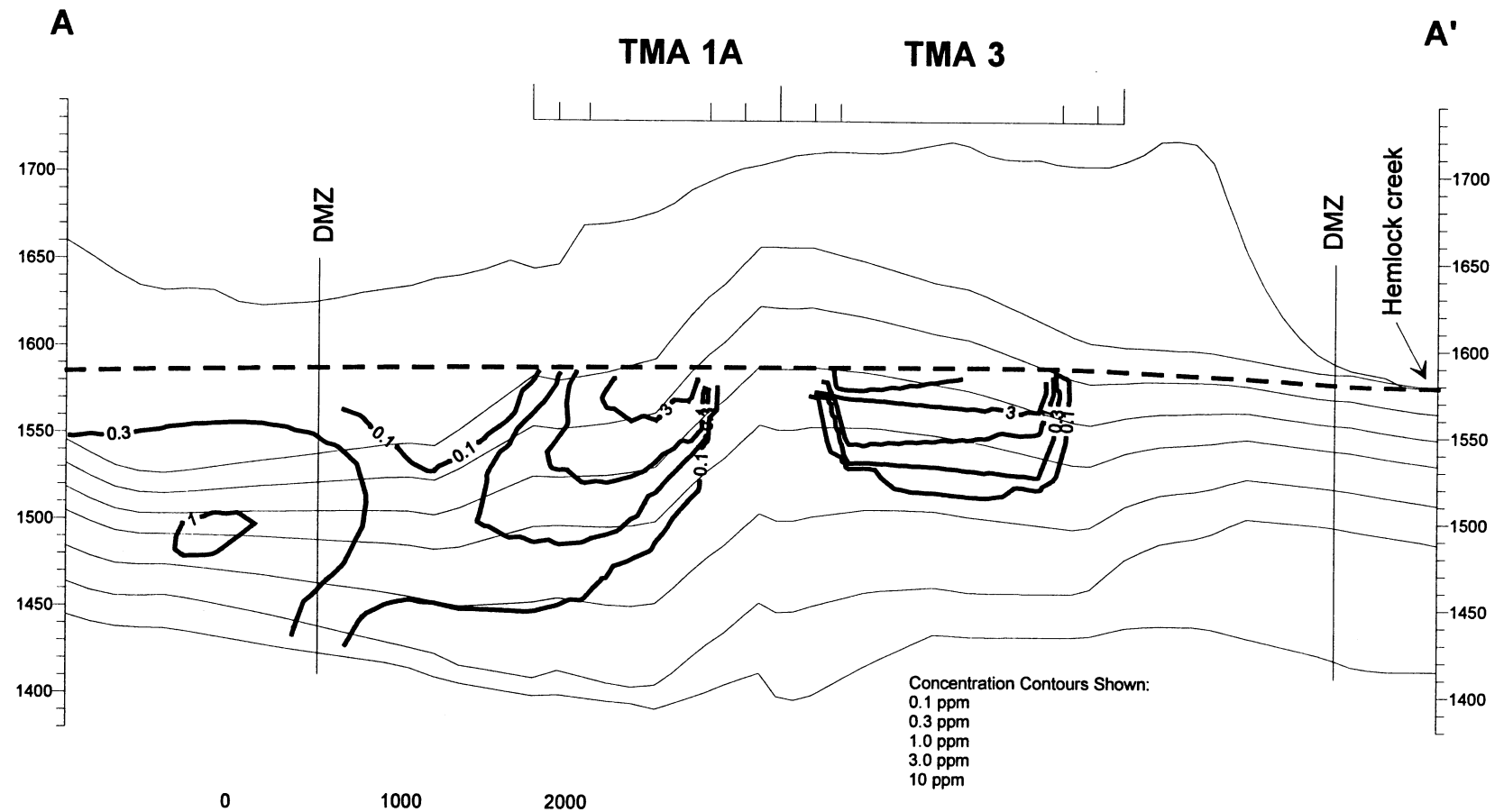

4.2-10-439

Source Concentration
Operation: 2000 ppm
Post-cap: 4000 ppm
Oxidized: 40,000 ppm*

* As a conservative assumption, the oxidized concentration begins immediately after assumed degradation of the flexible membrane liner.

Simulations
T10C1, T10C2, T08C3

HSI GEOTRANS

REVISED	DATE	BY	DESCRIPTION
1	6/99	JDC	Updated STM

CHECKED BY: RAK	DATE: Dec 98
APPROVED BY: PFA	DATE: Dec 98
APPROVED BY:	DATE:

Nicolet Minerals COMPANY

Figure 38
PWCT Concentration After 32 Years (Example Constituent, Cross-Section)

Scale: 1" = 1000' (h), 100' (v) | Date: Dec 1998

Prepared By: HSI GeoTrans | By: GWC

\Crandon\TmaMod4\Surfer2\XPWC060.srf

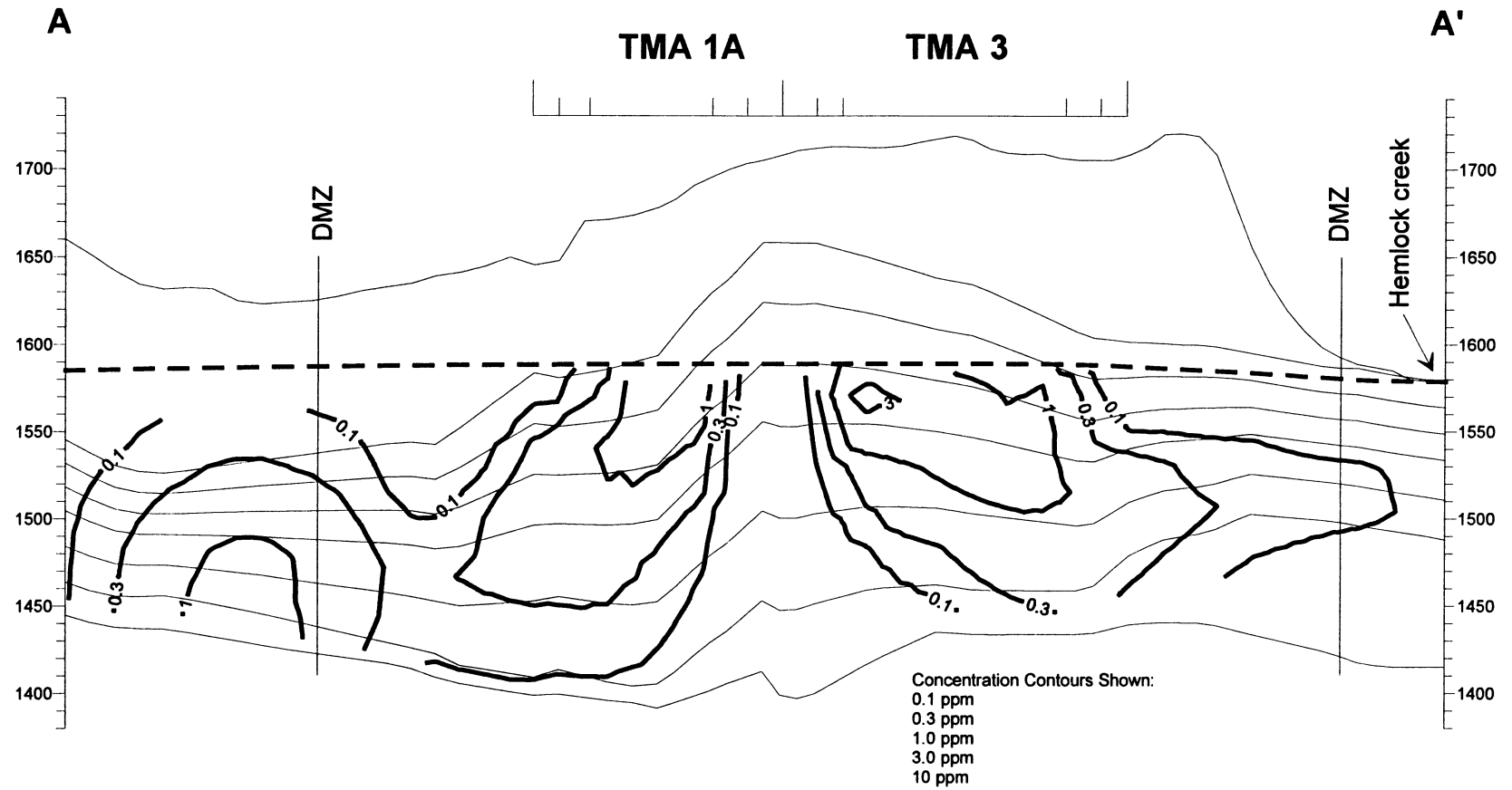

4.2-10-440

Source Concentration
Operation: 2000 ppm
Post-cap: 4000 ppm
Oxidized: 40,000 ppm*

* As a conservative assumption, the oxidized concentration begins immediately after assumed degradation of the flexible membrane liner.

Simulations
T10C1, T10C2, T08C3

HSI GEOTRANS

REVISED	DATE	BY	DESCRIPTION
1	6/99	JDC	Updated STM

CHECKED BY: RAK	DATE: Dec 98
APPROVED BY: PFA	DATE: Dec 98
APPROVED BY:	DATE:

Nicolet Minerals COMPANY

Figure 39
PWCT Concentration After 60 Years
(Example Constituent, Cross-Section)

Scale: 1" = 1000' (h), 100' (v) | Date: Dec 1998

Prepared By: HSI GeoTrans | By: GWC

\Crandon\TmaMod4\Surfer2\XPWC125.srf

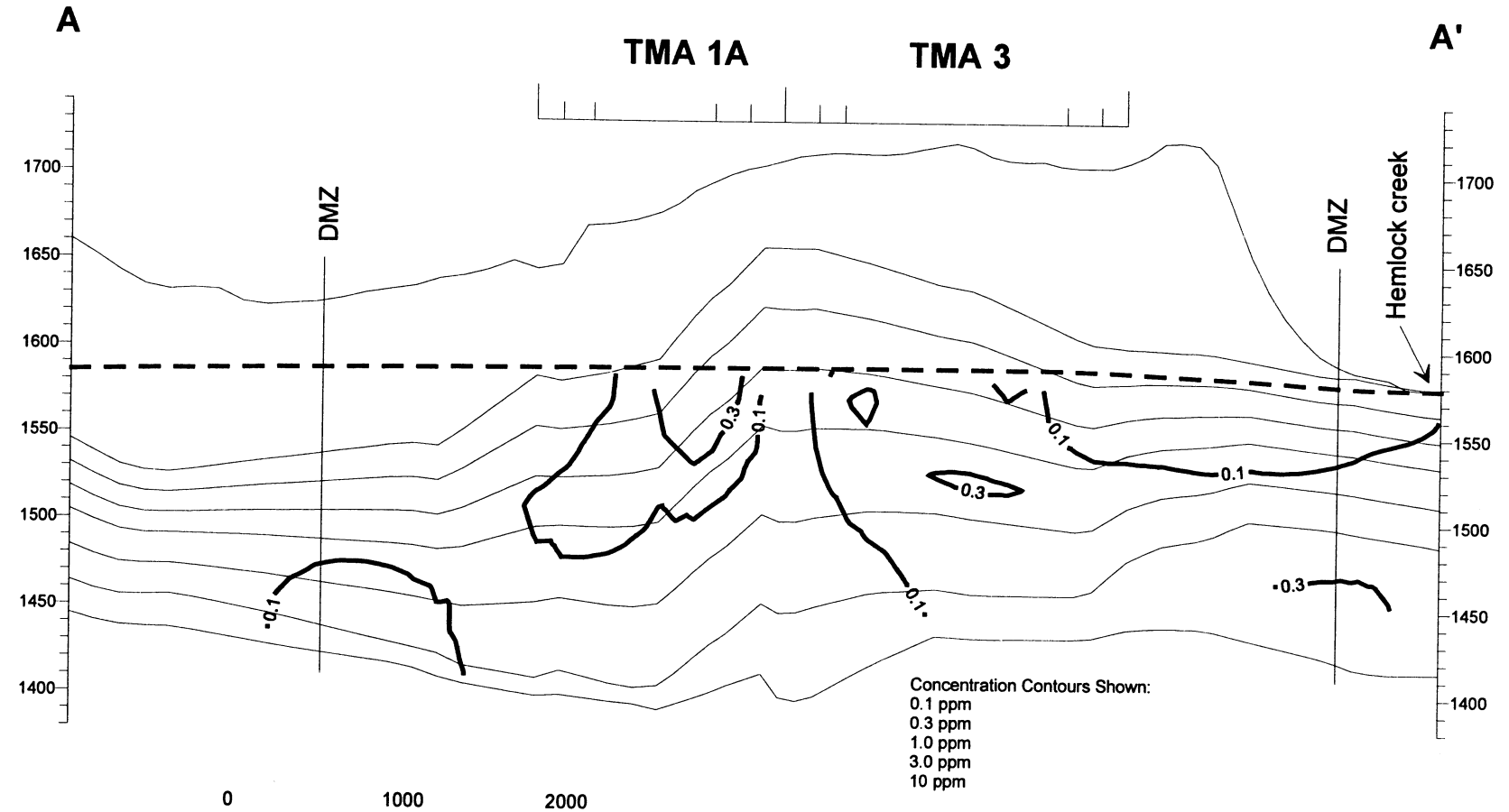

4.2-10-441

Source Concentration
Operation: 2000 ppm
Post-cap: 4000 ppm
Oxidized: 40,000 ppm*

* As a conservative assumption, the oxidized concentration begins immediately after assumed degradation of the flexible membrane liner.

Simulations
T10C1, T10C2, T08C3

HSI GEOTRANS

REVISED	DATE	BY	DESCRIPTION
1	6/99	JDC	Updated STM

CHECKED BY: RAK	DATE: Dec 98
APPROVED BY: PFA	DATE: Dec 98
APPROVED BY:	DATE:

Nicolet Minerals COMPANY

Figure 40
PWCT Concentration After 125 Years (Example Constituent, Cross-Section)

Scale: 1" = 1000' (h), 100' (v) | Date: Dec 1998

Prepared By: HSI GeoTrans | By: GWC

\Crandon\TmaMod4\Surfer2\XPWC200.srf

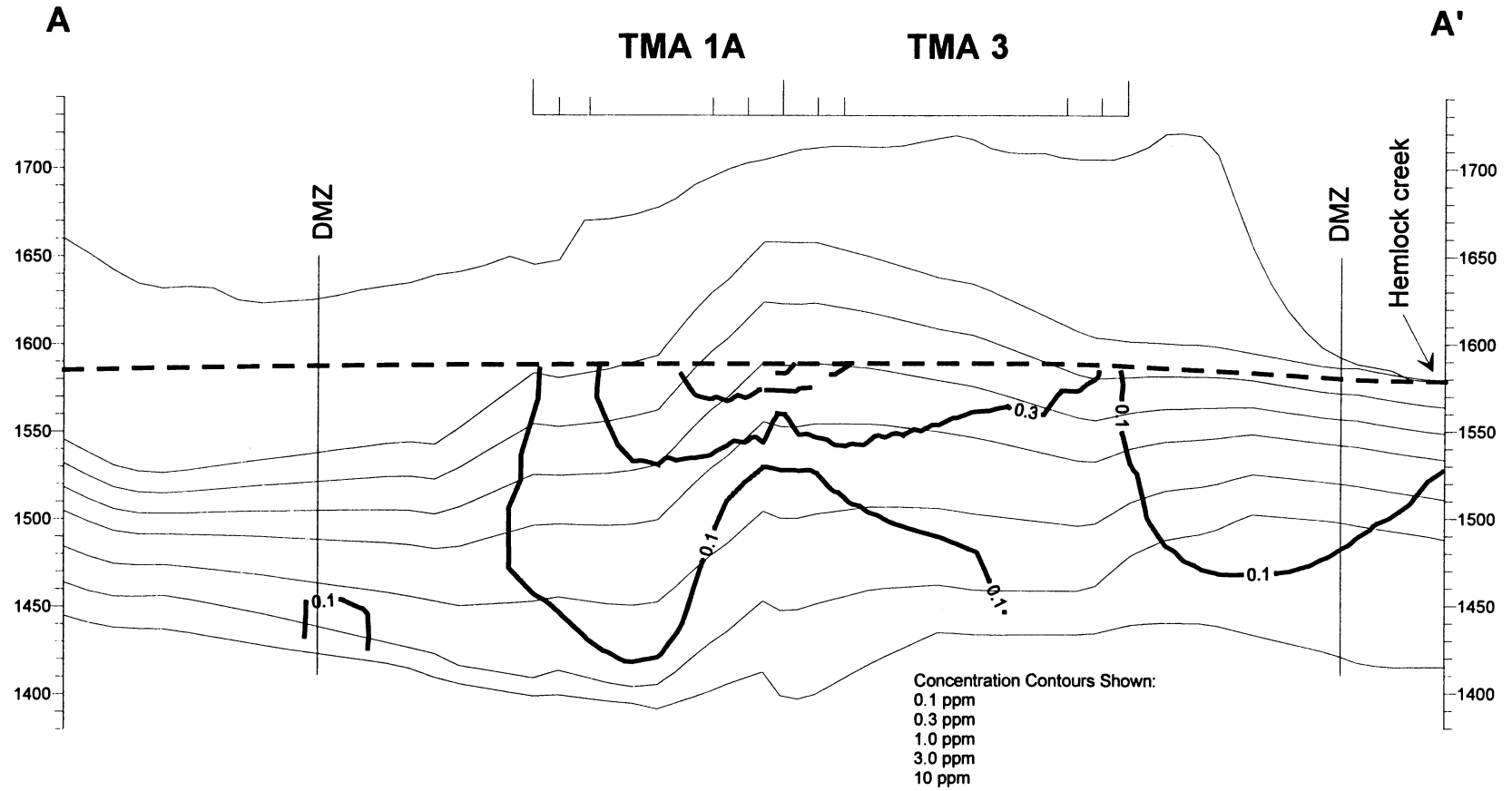

4.2-10-442

Source Concentration
Operation: 2000 ppm
Post-cap: 4000 ppm
Oxidized: 40,000 ppm*

* As a conservative assumption, the oxidized concentration begins immediately after assumed degradation of the flexible membrane liner.

Simulations
T10C1, T10C2, T08C3

HSI GEOTRANS

REVISED	DATE	BY	DESCRIPTION
1	6/99	JDC	Updated STM

CHECKED BY: RAK	DATE: Dec 98
APPROVED BY: PFA	DATE: Dec 98
APPROVED BY:	DATE:

Nicolet Minerals COMPANY

Figure 41
PWCT Concentration After 200 Years (Example Constituent, Cross-Section)

Scale: 1" = 1000' (h), 100' (v) | Date: Dec 1998

Prepared By: HSI GeoTrans | By: GWC

\Crandon\TmaMod4\Surfer2\XPWC300.srf

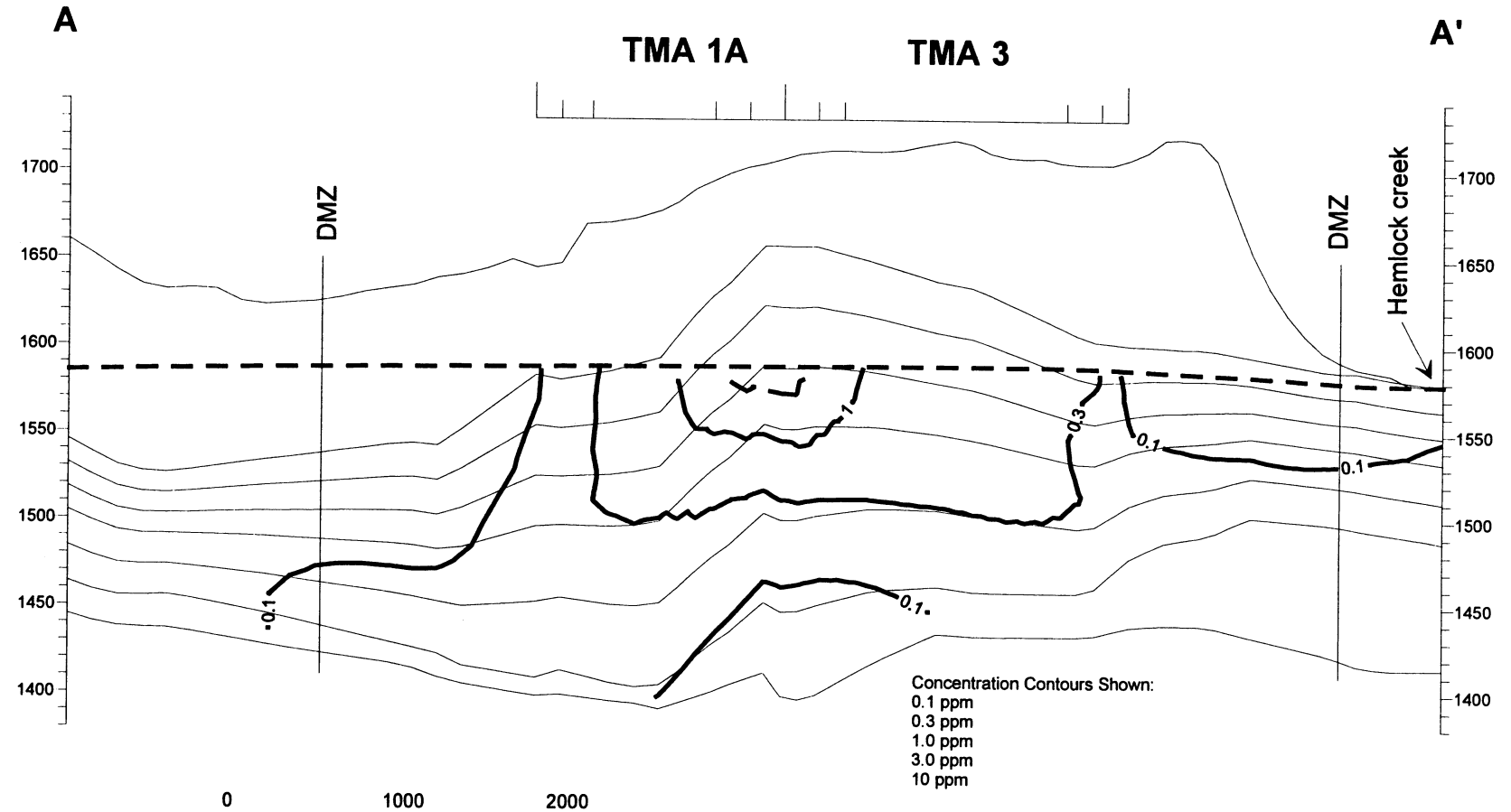

4.2-10-443

Source Concentration
Operation: 2000 ppm
Post-cap: 4000 ppm
Oxidized: 40,000 ppm*

* As a conservative assumption, the oxidized concentration begins immediately after assumed degradation of the flexible membrane liner.

Simulations
T10C1, T10C2, T08C3

HSI GEOTRANS

REVISED	DATE	BY	DESCRIPTION
1	6/99	JDC	Updated STM

CHECKED BY: RAK	DATE: Dec 98
APPROVED BY: PFA	DATE: Dec 98
APPROVED BY:	DATE:

Nicolet Minerals COMPANY

Figure 42
PWCT Concentration After 300 Years (Example Constituent, Cross-Section)

Scale: 1" = 1000' (h), 100' (v)	Date: Dec 1998
Prepared By: HSI GeoTrans	By: GWC

\Crandon\TmaMod4\Surfer2\XPWC650.srf

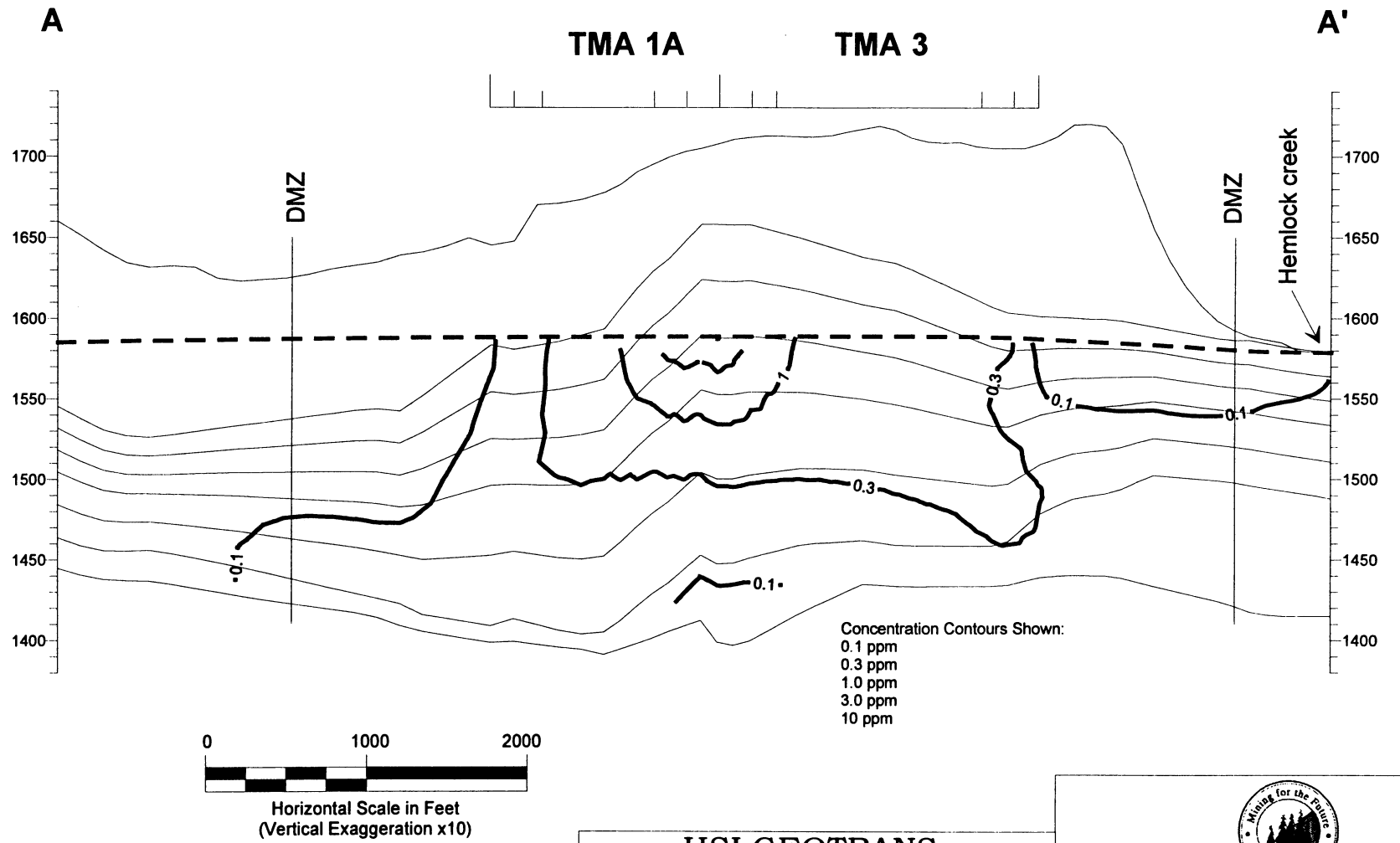

4.2-10-444

Source Concentration
Operation: 2000 ppm
Post-cap: 4000 ppm
Oxidized: 40,000 ppm*

* As a conservative assumption, the oxidized concentration begins immediately after assumed degradation of the flexible membrane liner.

Simulations
T10C1, T10C2, T08C3

HSI GEOTRANS

REVISED	DATE	BY	DESCRIPTION
1	6/99	JDC	Updated STM

CHECKED BY: RAK	DATE: Dec 98
APPROVED BY: PFA	DATE: Dec 98
APPROVED BY:	DATE:

Nicolet Minerals COMPANY

Figure 43
PWCT Concentration After 650 Years (Example Constituent, Cross-Section)

Scale: 1" = 1000' (h), 100' (v) | Date: Dec 1998

Prepared By: HSI GeoTrans | By: GWC

Appendix A

Memorandum regarding:
"Crandon Project — Solute Transport Model: Update No. 3 to the TMA Percolation Rates."

Foth & Van Dyke
Memorandum

May 25, 1999

TO: Pete Andersen, HSI GeoTrans, Inc.

CC: Jerry Sevick, Foth & Van Dyke
Ken Black, Nicolet Minerals Company
Steve Dischler, Foth & Van Dyke
Denis Roznowski, Foth & Van Dyke
Master File

FR: Steve Donohue, Foth & Van Dyke SVD

RE: Crandon Project - Solute Transport Model: Update No. 3 to the TMA Percolation Rates

TMA percolation rates for Update No. 2 to the TMA Solute Transport Model for the Crandon Project were documented in a memorandum dated November 10, 1998. Upon further analysis of the HELP Model output, a discrepancy was noted in the first and second year post-closure percolation rates. The attached tables from the November 10, 1998 memorandum provide the updated percolation tables. Please note that the updated percolation rates pertain only to years 1 and 2 in Table 4.

SVD1:cer1
Attachments

Table 2

Percolation from TMA Based on Doubled Precipitation Values During Operation of Initial Stages

Year	Sideslope (in/yr)	Base (in/yr)
1	0.000001	0.024968
2	<0.0000005	0.003517
3	<0.0000005	0.004562
4	<0.0000005	0.008642
5	<0.0000005	0.003126
6	<0.0000005	0.004671
7	<0.0000005	0.005429
8	<0.0000005	0.001883
9	<0.0000005	0.001380
10	<0.0000005	0.006263
Average	<0.0000005	0.006440

Note: HELP model output rounds off to six digits.

Prepared by: MRS
Checked by: NXP

Table 3

Percolation from TMA Based on Doubled Precipitation Values During Operation of Second Stages

Year	Lower Sideslope (in/yr)	Upper Sideslope (in/yr)	Base (in/yr)
1	0.000001	0.000002	0.034353
2	0.000001	0.000001	0.016261
3	<0.0000005	0.000001	0.005851
4	<0.0000005	0.000001	0.004205
5	<0.0000005	0.000001	0.007981
6	<0.0000005	0.000001	0.003110
7	<0.0000005	0.000001	0.004669
8	<0.0000005	<0.0000005	0.004549
9	<0.0000005	0.000001	0.001967
10	<0.0000005	0.000001	0.001725
Average	<0.0000005	0.000001	0.008470

Note: HELP model output rounds off to six digits.

Prepared by: MRS
Checked by: NXP

Table 4

Post-Closure Percolation

Year from Placement of Cover	Lower Sideslope (in/yr)	Upper Sideslope (in/yr)	Base (in/yr)
1	0.000001	0.000002	0.038786
2	0.000001	<0.0000005	0.014870
3	<0.0000005	<0.0000005	0.001169
4	<0.0000005	<0.0000005	0.001021
5	<0.0000005	<0.0000005	0.000916
6	<0.0000005	<0.0000005	0.000835
7	<0.0000005	<0.0000005	0.000763
8-15	<0.0000005	<0.0000005	0.000552
16-25	<0.0000005	<0.0000005	0.000308
26-35	<0.0000005	<0.0000005	0.000195
36-40	<0.0000005	<0.0000005	0.000151
41-50	<0.0000005	0	0.000123
51-60	<0.0000005	0	0.000097
61-70	<0.0000005	0	0.000081
71-80	<0.0000005	0	0.000069
81-90	<0.0000005	0	0.000059
91-115	0	0	0.000004
116-140	0	0	0.000004
141-165	0	0	0
166-175	0	0	0
176-185	0	0	0
186-195	0	0	0
196-205	0	0	0
206-215	0	0	0

Table 4 *(Continued)*

Year from Placement of Cover	Lower Sideslope (in/yr)	Upper Sideslope (in/yr)	Base (in/yr)
216-220	0	0	0
221-230	0	0	0
231-240	0	0	0
241 plus[1]	0.00002	0.00002	0.00002

Note: HELP Model output rounds to off to six digits.

[1] Percolation is conservatively assumed at this time period to be equal to infiltration through cover, even though the HELP Model indicates it will take longer to achieve this equilibrium.

Prepared by: MRS
Checked by: NXP
Revised by: NXP
Checked by: SVD1

UPDATE NO. 3 TO:

NUMERICAL SIMULATION OF POTENTIAL SOLUTE TRANSPORT AT THE PROPOSED ZINC AND COPPER MINE NEAR CRANDON, WISCONSIN

March 27, 2000

Update No. 3 to:
Numerical Simulation of Potential Solute Transport at the Proposed Zinc And Copper Mine Near Crandon, Wisconsin

March 27, 2000

This report presents an updated modeling analysis of solute transport from the proposed Tailings Management Area (TMA) at the Crandon mine site. The modeling has been updated in this report to consider additional variation over time of the source concentration from the TMA and associated reclaim pond. Prior analyses represented the TMA source concentrations as three discrete phases: during operation, following cap emplacement, and after the hypothetical FML degradation. The current analysis allows consideration of the 2-year period where the TMA is undergoing consolidation as a fourth concentration phase. This phase falls between the operational phase and the post-cap emplacement phase. Prior analyses also represented the reclaim pond as having the same source concentration as the TMA. The current analysis allows consideration of source concentrations for two phases of reclaim pond operation that are independent of the TMA concentrations. The two changes in this update offer more flexibility in evaluating TMA compliance with groundwater standards and present a more accurate representation of the TMA and reclaim pond sources.

The most recent reports on the TMA modeling were completed in January of 1999 (HSI GeoTrans, 1999a) and in June of 1999 (HSI GeoTrans, 1999b). The June report was an addendum to the January report and corrected a discrepancy that was present in the HELP model results that were used as input to the modeling reported in the earlier report. Another report, HSI GeoTrans (1998a) presented a comprehensive documentation of the solute transport modeling process. Much of the information presented in the 1998 solute transport modeling report is still pertinent. Rather than create an entirely new modeling report in the style of the 1998 and previous reports, this report serves to update the prior reports. A complete revision to the 1998 solute transport modeling report was not undertaken because it is HSI GeoTrans' and NMC's understanding that the WDNR plans to use the model described herein as a general framework for their modeling, but may make additional modifications and present those results in their Environmental Impact Statement.

This report describes the specific modifications made to the TMA sub-model and presents predictive results with Best Engineering Judgement for Transport (BEJT) and Practical Worst Case for Transport (PWCT) parameter values. The primary results of the model simulations are BEJT and PWCT response functions that define the Design Management Zone (DMZ)

concentration resulting from specified-source inflows of unit concentration. Using superposition methodology, the response functions can later be scaled and combined to represent any constituent of interest for the TMA using estimates of source concentrations (from potentially uncollected leachate percolating from the base of the TMA composite liner) for that constituent. The superposition methodology is also applied to constituents of interest that may seep from the reclaim pond. For illustrative purposes, results of superpositioning of the response functions for a hypothetical example constituent are presented.

Model Construction

The TMA sub-model domain lies within the regional groundwater model (HSI GeoTrans, 1998b) domain as shown in Figure 1. The sub-model is more finely discretized than the regional model, having 100-foot grid spacing and 7 layers to represent the glacial overburden aquifer. The base of the model coincides with the top of bedrock. Details of model construction can be found in a previous solute transport document (HSI GeoTrans, 1998a). For reference, the TMA footprint is shown in Figure 2. This footprint was revised in HSI GeoTrans (1999a) to reflect design changes for the TMA facilities. The model representation of TMA cell bases, upper sidewalls, lower side walls, reclaim ponds, and runoff basins are shown in Figure 3. These features are modeled as recharge zones in the numerical flow and transport model, with source areas (TMA, reclaim pond) having an assigned concentration of 1.0.

The current analysis considers additional variation over time of the source concentration from the TMA. A separate concentration phase during the two-year consolidation phase prior to cap emplacement has been added. The flexibility exists to retain the previous concentration phases or to apply separate concentration phases during operation, consolidation, following cap emplacement, and after the hypothetical FML degradation. The percolation rates used in the model are taken from the HELP model runs used in HSI GeoTrans (1999b). However, percolation rates for input to the model have been re-computed to account for the additional phase that is modeled. The estimated percolation rates, which vary over time, have been divided into 8 phases as described in Table 1. Appendix A provides the basis for the averaged rates shown in Table 1. Because operations begin at different times for the various TMA cells and because all cells do not have the same operational life, the phases are staggered as illustrated in Figure 4. In order to properly simulate every phase change for each TMA cell, the solute transport model is simulated in 20 stress periods as defined in Table 2. The percolation rates for each TMA cell are tabulated by stress periods in Tables 3 through 6. Figure 5 shows the total source-area flux rate as a function of time, and Figure 6 shows the cumulative source-area percolation volume versus time. Each plot compares well with the raw HELP model results, indicating that the time (phase) discretization and space (model cell) discretization is appropriate for representing the solute source. In the model, the percolation rates are entered as part of the recharge array in MODFLOW. In MT3D[96], the appropriate source concentration is assigned as a recharge source.

Model Calibration and Sensitivity Analysis

The changes that were made to the model only affect percolation rates and concentrations during the predictive phase of the modeling. The calibration results presented in HSI GeoTrans (1999a) are therefore still valid and it is unnecessary to report calibration results in this update. No sensitivity simulations are included for this model. The general results of previous sensitivity analyses (HSI GeoTrans, 1996, 1998a) are still valid for this modified model.

Model Predictions

For predictive simulations, the MODFLOW model was executed with 20 stress periods (Table 2, Figure 4). The different stress periods are characterized by slightly different recharge rates for the TMA zones, reclaim pond, and runoff basins (Tables 3 though 6, Figure 3). Also, the perimeter head boundary changes once during the simulation (at the beginning of stress period 11, after 32 years) to model the recovery of the regional heads following mine reflooding. In stress periods 1-10, the perimeter head values are taken from the regional flow model (HSI GeoTrans, 1998b) BEJ zinc mining simulation. The perimeter heads for stress periods 11-20 are taken from the regional model simulation of post-mining conditions.

Using the predictive flow model, particle traces were generated that started at the water table beneath each TMA cell (Figure 7). These particles show the expected advective flow paths for constituents in the TMA percolation water. Note that many of the particles travel to the lower portions of the glacial aquifer (60 feet deep for most particles).

Using the MT3D^{96} program, solute transport was simulated to predict how constituents would move in the groundwater. Four discrete concentration phases were assumed for the TMA source: operation, consolidation, post-cap, and post-FML-degradation. Thus, a given constituent could have one source concentration during operation, a second source concentration during consolidation, a third source concentration for percolation after cap placement, and a fourth source concentration after the postulated degradation of the flexible membrane liner (FML). Note that it is conservatively assumed that the FML is completely degraded 150 years after the start of operations. In addition, two discrete concentration phases were assumed for the reclaim pond source: during TMA operations and after TMA operations. Note that the same concentration value may be used for multiple concentration phases. Using the principle of superposition, it is possible to model many constituents with only six model simulations (four for the TMA and two for the reclaim pond). The superpositioning procedure is described in a previous solute transport document (HSI GeoTrans, 1998a) and is illustrated in Figure 8.

The model output consists of a concentration response function to a unit-concentration source at the TMA during either the operation, consolidation, post-cap, or post-FML-degradation concentration phase. A concentration response function to a unit-concentration source is also generated for each of the two phases of operation of the reclaim pond. By scaling and combining these response functions, the concentration of a specific constituent is determined (c(x,y,z,t)).

Separate treatment of the TMA and reclaim ponds allows specification of different source concentrations in each of these areas. Conservatively, sorption, chemical reactions, and decay are not considered. The concentrations at the regulatory DMZs are of particular interest. For this modeling, two DMZs are considered (Figure 9). The first is located 1200 feet from the limits of tailings placement within the TMA cells, and the second is located 150 feet outside of the reclaim pond. Note that the reclaim pond is removed after approximately 46 years. Therefore, the reclaim pond DMZ is only considered for the first 60 years of simulation.

Note that the DMZ for the TMA is slightly different (and more accurate) than that shown in previous reports (HSI GeoTrans, 1999a, 1999b). The difference results from a greater number of points used to define the 1200 foot distance from the TMA.

Best Engineering Judgement for Transport (BEJT)

Using the BEJT parameter values from the prior modeling, response functions were generated by six MT3D^{96} simulations (four for the TMA source and two for the reclaim pond source). The maximum concentration responses due to the TMA and reclaim pond at the DMZs as a function of time are shown in Figure 10. Note that the concentration response for the reclaim ponds (Simulations E, F) is larger than the response for the TMA (Simulations A-D). This difference results from the comparatively larger water flux from the reclaim ponds. The larger concentration response due to the reclaim ponds indicates that they are of primary importance in the solute transport calculation.

To demonstrate the patterns of solute migration from the TMA and reclaim ponds, a hypothetical constituent is considered that has a percolation concentration from the TMA of 2,000 ppm during operations, 2,500 ppm during the consolidation phase, 4,000 ppm during the post-cap phase, and 4,000 ppm after postulated degradation of the FML (Table 7). The hypothetical constituent also has a percolation concentration from the reclaim ponds of 1,000 ppm during operation and 4,000 ppm in the post-cap phase. Using superposition, this hypothetical constituent's maximum DMZ concentrations are plotted as a function of time (Figure 11). Note that in all graphs of DMZ concentration versus time, the maximum concentration at the DMZ is always plotted, and that this point of maximum concentration may move in time as the solute plume changes shape. Results at the reclaim pond DMZ are shown for the first 60 years of simulation, which includes approximately 14 years after the removal of the reclaim pond.

The BEJT solute plumes for the example constituent are plotted in plan view at different times in Figures 12 through 20. In these plots, the maximum concentration in any layer at a given x,y location is contoured. Using the section identified in Figure 21, the BEJT example constituent plumes are plotted in profile (Figures 22 through 30).

Practical Worst Case for Transport (PWCT)

Six more simulations were conducted using the PWCT parameter values from the prior modeling (HSI GeoTrans, 1999a, 1999b). The PWCT simulations include lower vertical hydraulic conductivities and lower dispersivities in the aquifer. These changes lead to less mixing with ambient (clean) water and therefore higher concentration predictions. PWCT response curves at the DMZs due to the TMA source and the reclaim pond source are shown in Figure 31.

Using the example constituent of Table 7, and the superposition method, the maximum DMZ concentrations are plotted as a function of time (Figure 32). The PWCT example constituent plumes are shown at select times in Figures 33 though 41 (plan view) and in Figure 42 through 50 (profile view).

Summary

The primary output from the TMA model is the set of response functions under BEJT and PWCT conditions. These response functions can be used to predict concentrations at the limits of the DMZ for any (conservative) constituent in the TMA leachate and water percolating from the reclaim pond. The forthcoming update to the Groundwater Quality Performance Evaluation (GWQPE) will present DMZ concentrations for individual constituents of interest at the TMA. The GWQPE results will be obtained by applying the superposition method.

The primary reasons for differences in simulated results in this report from those in the previous solute transport report (HSI GeoTrans, 1999b) are: 1) the representation of the consolidation phase as a separate source concentration and percolation rate, and 2) the use of different source concentrations for the example constituent.

References

HSI GeoTrans, 1996. Numerical Simulation of Potential Solute Transport at the Proposed Zinc and Copper Mine near Crandon, Wisconsin (November, 1996).

HSI GeoTrans, 1998a. Update to Numerical Simulation of Potential Solute Transport at the Proposed Zinc and Copper Mine near Crandon, Wisconsin (April 1998).

HSI GeoTrans, 1998b. Addendum No. 2 to Numerical Simulation of the Effect on Groundwater and Surface Water of the Proposed Zinc and Copper Mine near Crandon, Wisconsin (August, 1998).

HSI GeoTrans, 1999a. Update No. 2 to Numerical Simulation of Potential Solute Transport at the Proposed Zinc and Copper Mine near Crandon, Wisconsin (January 1999).

HSI GeoTrans, 1999b. Addendum No. 2 Update No. 1 to Numerical Simulation of Potential Solute Transport at the Proposed Zinc and Copper Mine near Crandon, Wisconsin (July 1999).

Table 1 Basis for TMA phases and flux rates[1]

Phase	Description	Duration (years)	Basis for Percolation Rate
X	Pre-construction	0-22[2]	Regional model calibrated value
A	First Phase of Operation	2-4[2]	Appendix A Table 2 average[3]
B	Second Phase of Operation	4-10[2]	Appendix A Table 3 average
C	Consolidation	2	Appendix A Table 3 average
D	Cap in Place Part 1	8	Appendix A Table 4 Years 1-7
E	Cap in Place Part 2	20	Appendix A Table 4 Years 8-25
F	Cap in Place Part 3	104-114[2]	Appendix A Table 4 Years 26-140
G	Degraded FML Steady-State	N/A	Appendix A Table 4 Years 241+

Phase	Base		Lower Sideslope		Upper Sideslope	
	Rate(in/yr)	Rate(ft/d)	Rate(in/yr)	Rate(ft/d)	Rate(in/yr)	Rate(ft/d)
X	9.70	2.21E-03	9.70	2.21E-03	9.70	2.21E-03
A	6.44E-03	1.47E-06	2.50E-07	5.71E-11	9.70[3]	2.21E-03
B	8.47E-03	1.93E-06	2.50E-07	5.71E-11	1.03E-06	2.34E-10
C	8.47E-03	1.93E-06	2.50E-07	5.71E-11	1.03E-06	2.34E-10
D	8.34E-03	1.90E-06	4.60E-07	1.05E-10	5.00E-07	1.14E-10
E	4.15E-04	9.47E-08	2.50E-07	5.71E-11	2.50E-07	5.71E-11
F	6.05E-05	1.38E-08	2.50E-07	5.71E-11	2.50E-07	5.71E-11
G	2.00E-05	4.57E-09	2.00E-05	4.57E-09	2.00E-05	4.57E-09

Notes

[1] The TMA reclaim pond is active during years 1-28 during which its flux is 1.6E-5 ft/d, and years 29-46 (after the TMA is capped) during which its flux is 4.0E-6 ft/d. Thereafter a uniform 2.21E-3 ft/d is used to represent precipitation recharge.

[2] Varies by TMA Cell

[3] During the first phase of operation, the TMA upper sideslope receives full recharge (from regional model) with a concentration of zero.

Prepared by: LMG
Checked by: GWC
Approved by: PFA

March 2000
P:\Crandon\TmaMod4\Excel\StresTab2.xls, Basis

Table 2 TMA sub-model stress periods.

Stress Period	Time (years)			Time (days)		
	Start	Duration	End	Start	Duration	End
1	0	2	2	0.0	730.5	730.5
2	2	4	6	730.5	1461.0	2191.5
3	6	10	16	2191.5	3652.5	5844.0
4	16	2	18	5844.0	730.5	6574.5
5	18	4	22	6574.5	1461.0	8035.5
6	22	2	24	8035.5	730.5	8766.0
7	24	2	26	8766.0	730.5	9496.5
8	26	2	28	9496.5	730.5	10227.0
9	28	2	30	10227.0	730.5	10957.5
10	30	2	32	10957.5	730.5	11688.0
11	32	6	38	11688.0	2191.5	13879.5
12	38	6	44	13879.5	2191.5	16071.0
13	44	2	46	16071.0	730.5	16801.5
14	46	6	52	16801.5	2191.5	18993.0
15	52	6	58	18993.0	2191.5	21184.5
16	58	92	150	21184.5	33603.0	54787.5
17	150	2	152	54787.5	730.5	55518.0
18	152	14	166	55518.0	5113.5	60631.5
19	166	6	172	60631.5	2191.5	62823.0
20	172	478	650	62823.0	174589.5	237412.5

Prepared by: LMG
Checked by: GWC
Approved by: PFA

March 2000
\Crandon\TmaMod4\Excel\StresTab2.xls, Stress

Table 3 TMA 1A percolation rates by stress period.

Stress Period	Phase	Percolation Rate (ft/day)		
		Base	Lower Sideslope	Upper Sideslope
1	A	1.47E-06	5.71E-11	2.21E-03 [1]
2	A	1.47E-06	5.71E-11	2.21E-03 [1]
3	B	1.93E-06	5.71E-11	5.71E-11
4	C	1.93E-06	5.71E-11	5.71E-11
5	D	1.90E-06	1.05E-10	1.05E-10
6	D	1.90E-06	1.05E-10	1.05E-10
7	D	1.90E-06	1.05E-10	1.05E-10
8	E	9.47E-08	5.71E-11	5.71E-11
9	E	9.47E-08	5.71E-11	5.71E-11
10	E	9.47E-08	5.71E-11	5.71E-11
11	E	9.47E-08	5.71E-11	5.71E-11
12	E	9.47E-08	5.71E-11	5.71E-11
13	E	9.47E-08	5.71E-11	5.71E-11
14	F	1.38E-08	5.71E-11	5.71E-11
15	F	1.38E-08	5.71E-11	5.71E-11
16	F	1.38E-08	5.71E-11	5.71E-11
17	G	4.57E-09	4.57E-09	4.57E-09
18	G	4.57E-09	4.57E-09	4.57E-09
19	G	4.57E-09	4.57E-09	4.57E-09
20	G	4.57E-09	4.57E-09	4.57E-09

Note: [1] Equal to default recharge, no source applied.

Prepared by: LMG
Checked by: GWC
Approved by: PFA

March 2000
P:\CMC\TmaMod4\Excel\StresTab.xls, TMA1A

Table 4 TMA 1B percolation rates by stress period.

Stress Period	Phase	Percolation Rate (ft/day)		
		Base	Lower Sideslope	Upper Sideslope
1	X	2.21E-03 [1]	2.21E-03 [1]	2.21E-03 [1]
2	A	1.47E-06	5.71E-11	2.21E-03 [1]
3	B	1.93E-06	5.71E-11	5.71E-11
4	C	1.93E-06	5.71E-11	5.71E-11
5	D	1.90E-06	1.05E-10	1.05E-10
6	D	1.90E-06	1.05E-10	1.05E-10
7	D	1.90E-06	1.05E-10	1.05E-10
8	E	9.47E-08	5.71E-11	5.71E-11
9	E	9.47E-08	5.71E-11	5.71E-11
10	E	9.47E-08	5.71E-11	5.71E-11
11	E	9.47E-08	5.71E-11	5.71E-11
12	E	9.47E-08	5.71E-11	5.71E-11
13	E	9.47E-08	5.71E-11	5.71E-11
14	F	1.38E-08	5.71E-11	5.71E-11
15	F	1.38E-08	5.71E-11	5.71E-11
16	F	1.38E-08	5.71E-11	5.71E-11
17	F	1.38E-08	5.71E-11	5.71E-11
18	G	4.57E-09	4.57E-09	4.57E-09
19	G	4.57E-09	4.57E-09	4.57E-09
20	G	4.57E-09	4.57E-09	4.57E-09

Note: [1] Equal to default recharge, no source applied.

Prepared by: LMG
Checked by: GWC
Approved by: PFA

March 2000
P:\Crandon\TmaMod4\Excel\StresTab.xls, TMA1B

Table 5 TMA 2 percolation rates by stress period.

Stress Period	Phase	Percolation Rate (ft/day)		
		Base	Lower Sideslope	Upper Sideslope
1	X	2.21E-03 [1]	2.21E-03 [1]	2.21E-03 [1]
2	X	2.21E-03 [1]	2.21E-03 [1]	2.21E-03 [1]
3	X	2.21E-03 [1]	2.21E-03 [1]	2.21E-03 [1]
4	A	1.47E-06	5.71E-11	2.21E-03 [1]
5	B	1.93E-06	5.71E-11	5.71E-11
6	C	1.93E-06	5.71E-11	5.71E-11
7	D	1.90E-06	1.05E-10	1.05E-10
8	D	1.90E-06	1.05E-10	1.05E-10
9	D	1.90E-06	1.05E-10	1.05E-10
10	D	1.90E-06	1.05E-10	1.05E-10
11	E	9.47E-08	5.71E-11	5.71E-11
12	E	9.47E-08	5.71E-11	5.71E-11
13	E	9.47E-08	5.71E-11	5.71E-11
14	E	9.47E-08	5.71E-11	5.71E-11
15	F	1.38E-08	5.71E-11	5.71E-11
16	F	1.38E-08	5.71E-11	5.71E-11
17	F	1.38E-08	5.71E-11	5.71E-11
18	F	1.38E-08	5.71E-11	5.71E-11
19	G	4.57E-09	4.57E-09	4.57E-09
20	G	4.57E-09	4.57E-09	4.57E-09

Note: [1] Equal to default recharge, no source applied.

Prepared by: LMG
Checked by: GWC
Approved by: PFA

March 2000
P:\CMC\TmaMod4\Excel\StresTab.xls, TMA2

Table 6 TMA 3 percolation rates by stress period.

Stress Period	Phase	Percolation Rate (ft/day)		
		Base	Lower Sideslope	Upper Sideslope
1	X	2.21E-03 [1]	2.21E-03 [1]	2.21E-03 [1]
2	X	2.21E-03 [1]	2.21E-03 [1]	2.21E-03 [1]
3	X	2.21E-03 [1]	2.21E-03 [1]	2.21E-03 [1]
4	X	2.21E-03 [1]	2.21E-03 [1]	2.21E-03 [1]
5	X	2.21E-03 [1]	2.21E-03 [1]	2.21E-03 [1]
6	A	2.21E-03 [1]	2.21E-03 [1]	2.21E-03 [1]
7	B	1.93E-06	5.71E-11	2.21E-03 [1]
8	B	1.93E-06	5.71E-11	5.71E-11
9	C	1.93E-06	5.71E-11	5.71E-11
10	D	1.90E-06	1.05E-10	1.05E-10
11	D	1.90E-06	1.05E-10	1.05E-10
12	E	9.47E-08	5.71E-11	5.71E-11
13	E	9.47E-08	5.71E-11	5.71E-11
14	E	9.47E-08	5.71E-11	5.71E-11
15	E	9.47E-08	5.71E-11	5.71E-11
16	F	1.38E-08	5.71E-11	5.71E-11
17	F	1.38E-08	5.71E-11	5.71E-11
18	F	1.38E-08	5.71E-11	5.71E-11
19	F	1.38E-08	5.71E-11	5.71E-11
20	G	4.57E-09	4.57E-09	4.57E-09

Note: [1] Equal to default recharge, no source applied.

Prepared by: LMG
Checked by: GWC
Approved by: PFA

March 2000
P:\Crandon\TmaMod4\Excel\StresTab.xls, TMA3

Table 7 Source concentration for the example constituent.

Description	Source Concentration (ppm)	Active Time[1]
(A) TMA Operational	2,000	Flow phases A & B
(B) TMA Consolidation	2,500	Flow phase C
(C) TMA Post-Cap	4,000	Flow phases D, E, & F
(D) TMA Post-FML-Degradation	4,000	Flow phase G
(E) Reclaim Pond Operation	1,000	Years 1-28
(F) Reclaim Pond After TMA Capping	4,000	Year 29-46

Notes
[1] Varies by TMA Cell

Prepared by: LMG
Checked by: GWC
Approved by: PFA

March 2000
\Crandon\TmaMod4\Excel\SulfSrc.xls

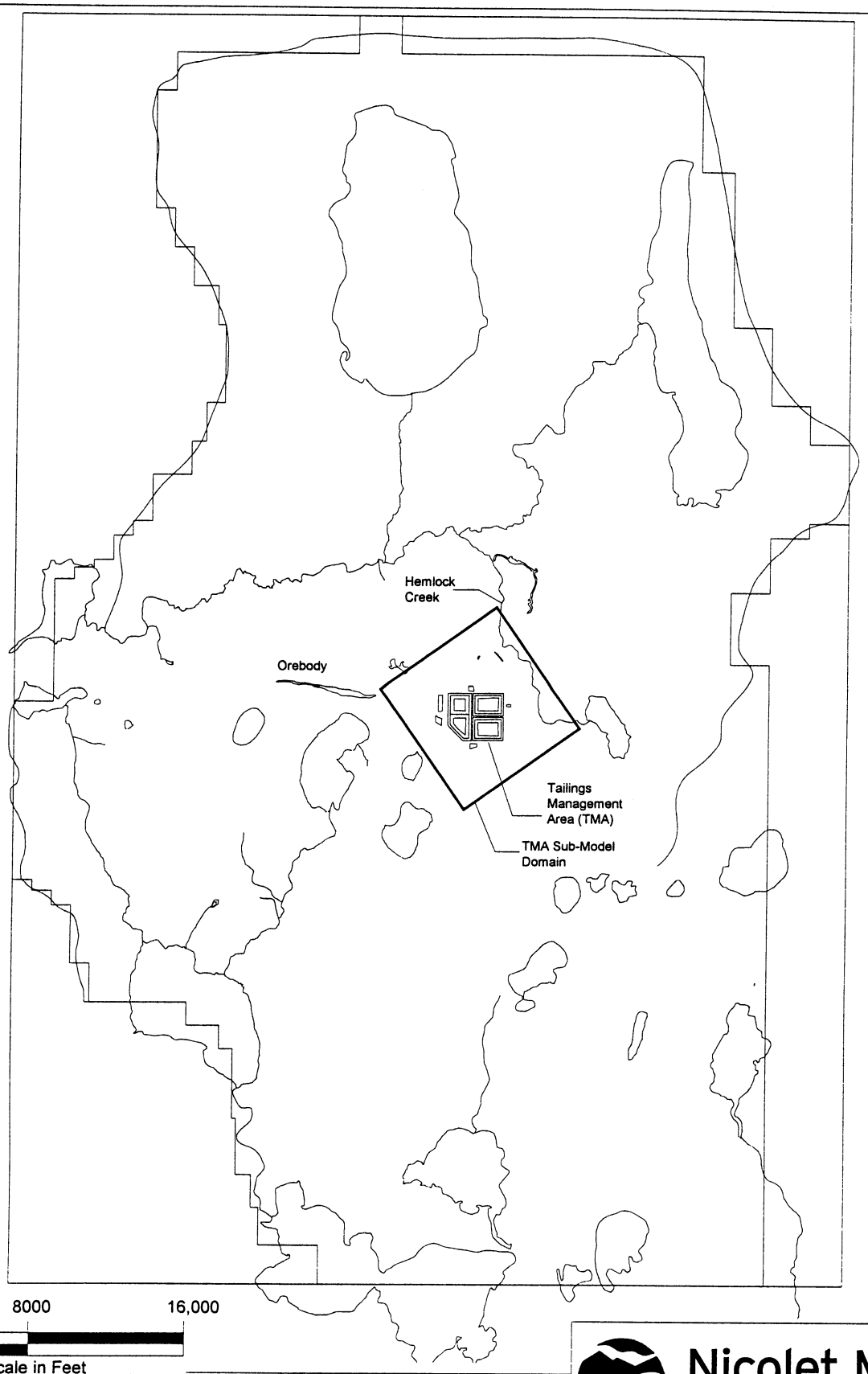

HSI GEOTRANS

REVISED	DATE	BY	DESCRIPTION

CHECKED BY: KMR	DATE: Dec 1998
APPROVED BY: PFA	DATE: Dec 1998
APPROVED BY:	DATE:

Nicolet Minerals
a Rio Algom company

Figure 1
TMA Sub-Model
Location Map

Scale: 1 in. = 8000 ft. Date: Dec 1998
Prepared By: HSI GeoTrans By: GWC

4.2-10-465

\Crandon\TmaMod4\GIS\LocatMap2.wor

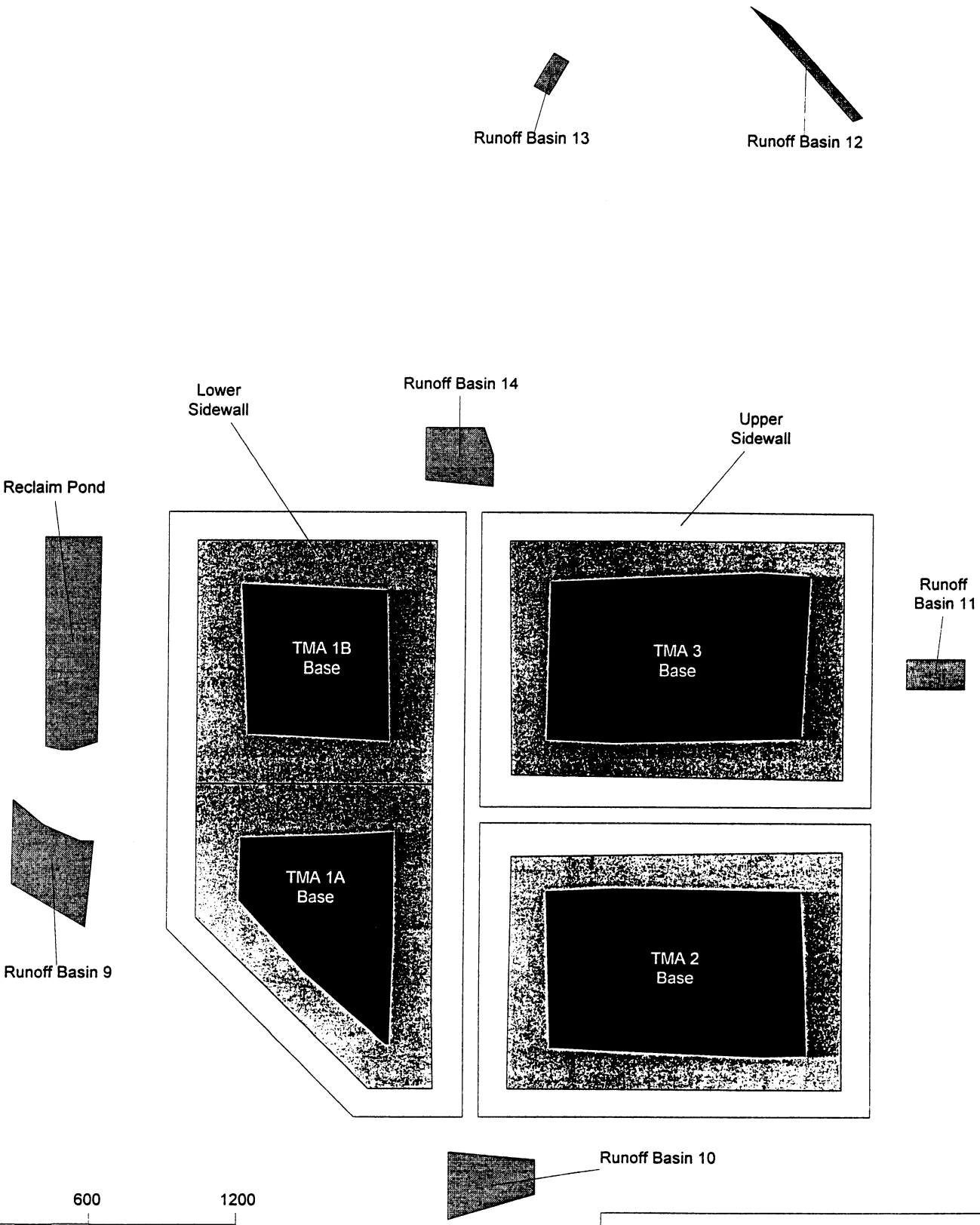

HSI GEOTRANS

REVISED	DATE	BY	DESCRIPTION

CHECKED BY: KMR	DATE: Dec 1998
APPROVED BY: PFA	DATE: Dec 1998
APPROVED BY:	DATE:

4.2-10-466

Nicolet Minerals
a Rio Algom company

Figure 2
TMA Cell Configuration and Associated Facilities

Scale: 1 in. = 600 ft. | Date: Dec 1998
Prepared By: HSI GeoTrans | By: GWC

P:\CMC\TmaMod4\GIS\DeTail.wor

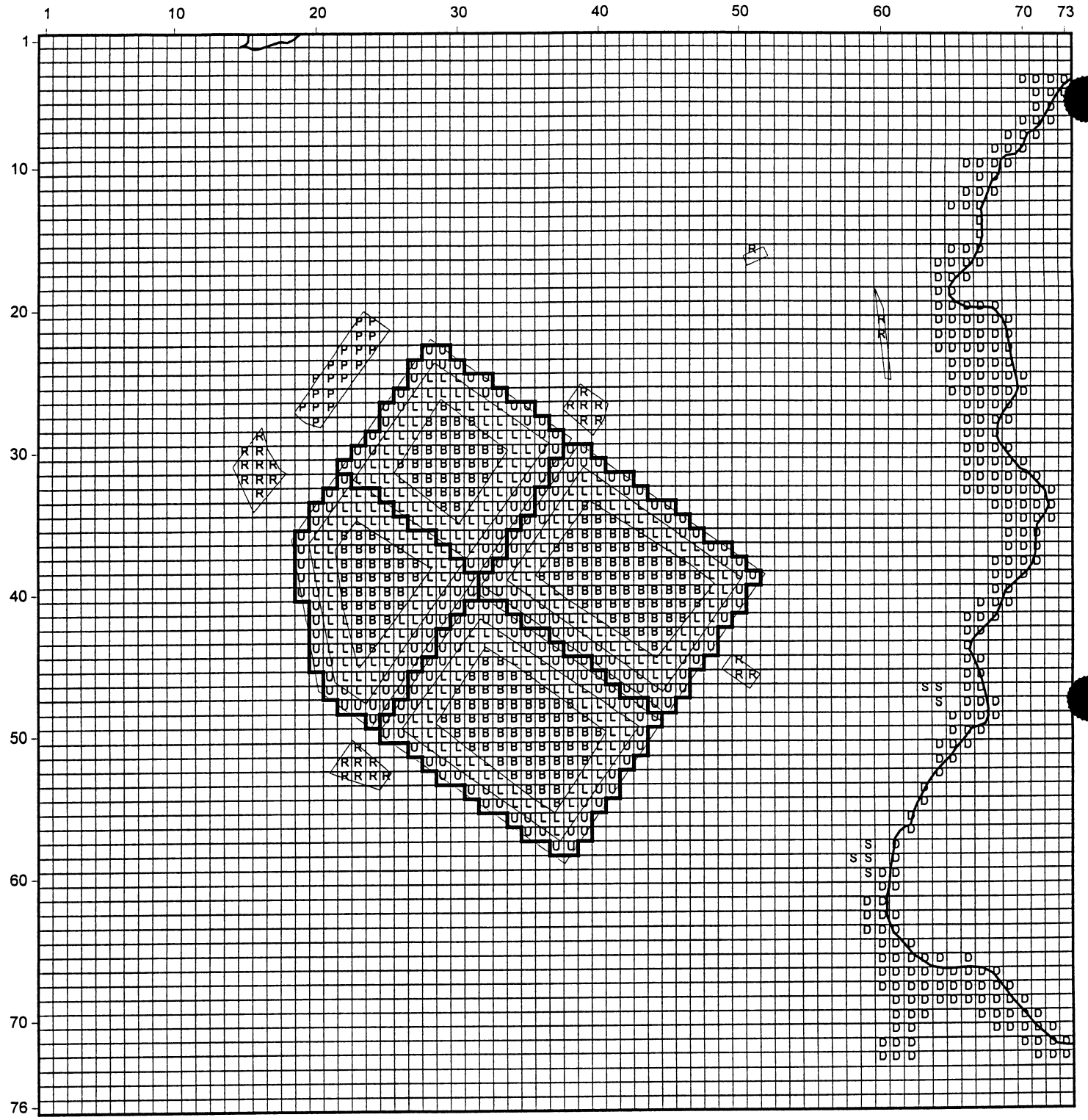

LEGEND

	Default Recharge (9.7 in/yr)
D	Discharge Wetland (3 in/yr)
S	Seepage Wetland (No Recharge)
B	TMA Base
L	TMA Lower Sidewall
U	TMA Upper Sidewall
P	Reclaim Pond
R	Runoff Basin

N

0 1000 2000

Scale in Feet

HSI GEOTRANS

REVISED	DATE	BY	DESCRIPTION

CHECKED BY: KMR	DATE: Dec 1998
APPROVED BY: PFA	DATE: Dec 1998
APPROVED BY:	DATE:

4.2-10-467

Nicolet Minerals
a Rio Algom company

Figure 3
Model Grid and Recharge Zones

Scale: 1 in. = 1000 ft. Date: Dec 1998

Prepared By: HSI GeoTrans By: GWC

\Crandon\TmaMod4\GIS\RchZon2.wor

P:\Crandon\TmaMod4\Excel\TimeLine2.xls, Chart

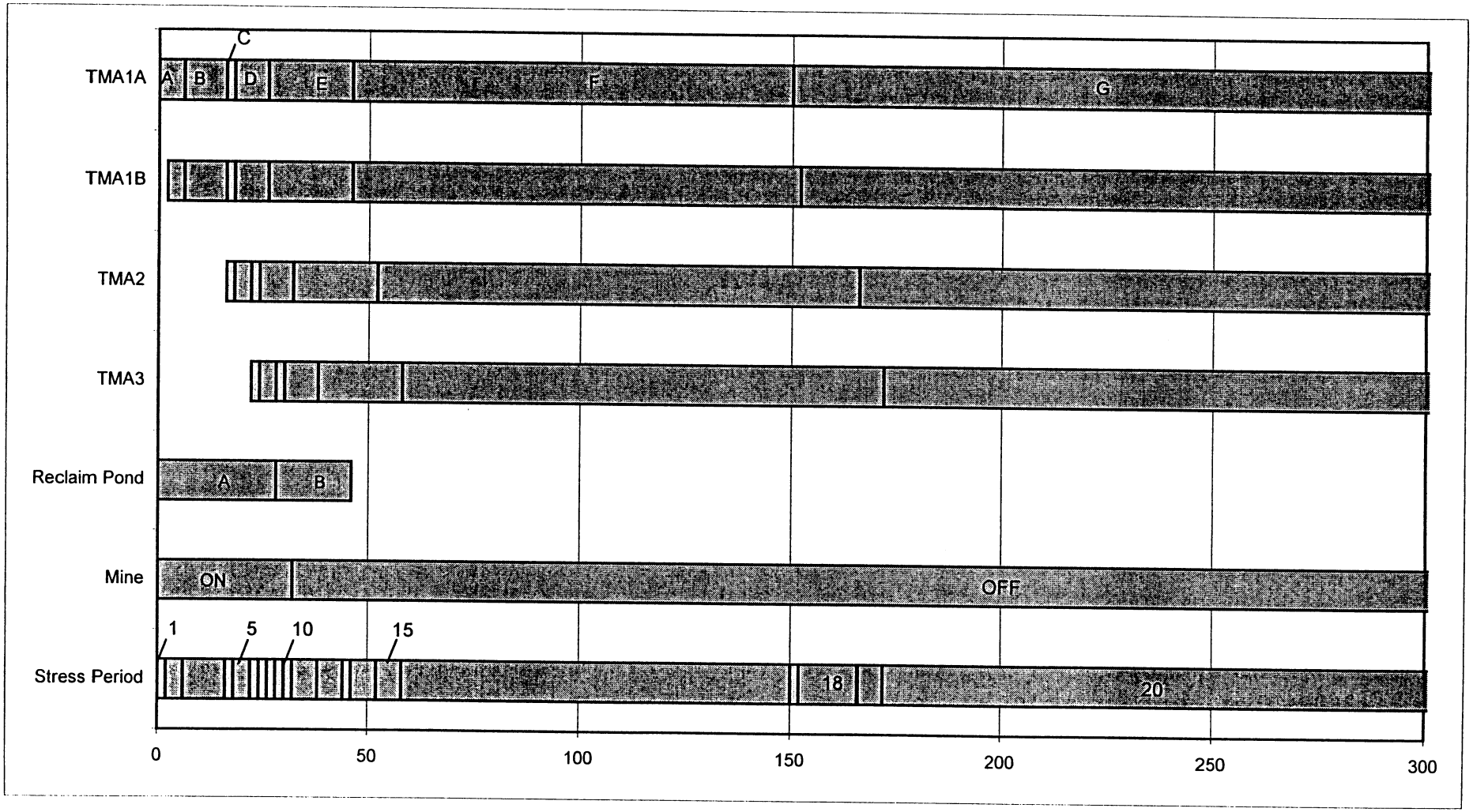

4.2-10-468

HSI GEOTRANS			
REVISED	DATE	BY	DESCRIPTION
CHECKED BY:GWC			DATE: Mar 2000
APPROVED BY: PFA			DATE: Mar 2000
APPROVED BY:			DATE:

Nicolet Minerals
a Rio Algom company

Figure 4
TMA Sub-Model Time Line

Scale: None	Date: March 2000
Prepared By: HSI GEOTRANS	By: LMG

\Crandon\TmaMod3\Excel\HelpComp3.xls, Flux

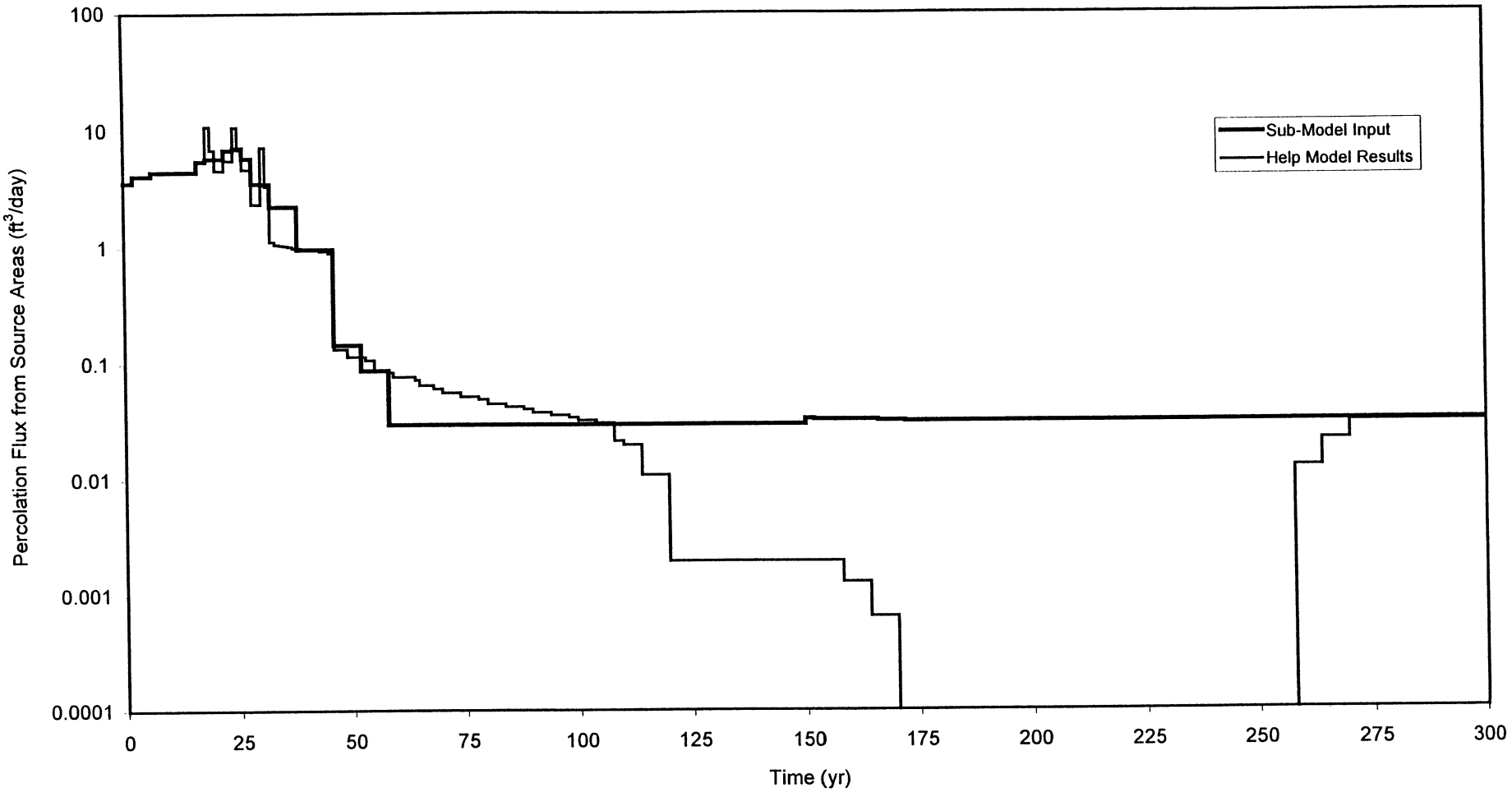

4.2-10-469

Note:
Percolation rate (Y-axis) is shown on a logarithmic scale.

HSI GEOTRANS			
REVISED	DATE	BY	DESCRIPTION
CHECKED BY: GWC			DATE: Mar 2000
APPROVED BY: PFA			DATE: Mar 2000
APPROVED BY:			DATE:

Nicolet Minerals
a Rio Algom company

Figure 5
Source Areas Percolation Flux Rate

Scale: None	Date: March 2000
Prepared By: HSI GEOTRANS	By: LMG

\Crandon\TmaMod4\Excel\HelpCom3.xls, CumVol

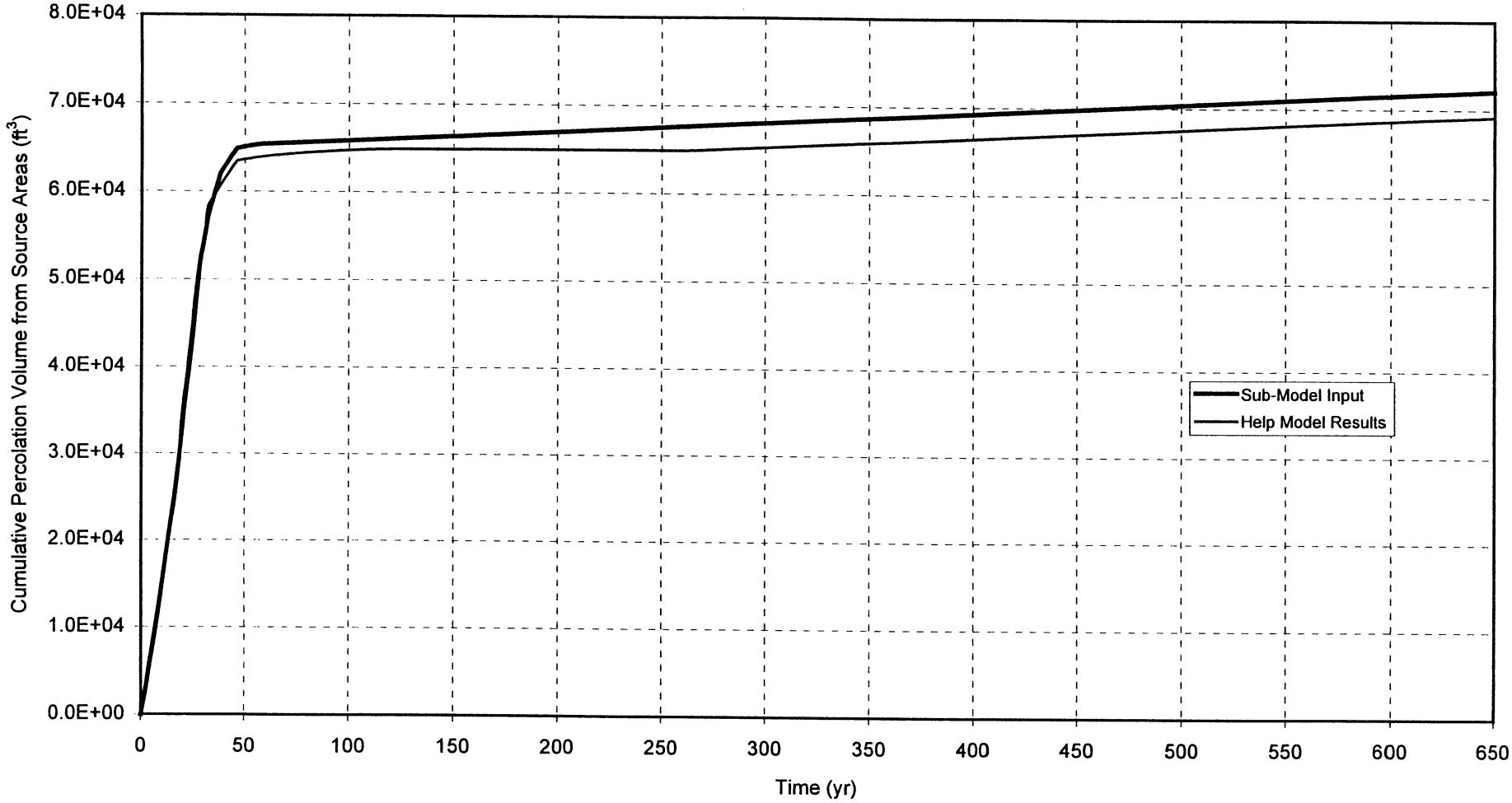

4.2-10-470

HSI GEOTRANS			
REVISED	DATE	BY	DESCRIPTION
CHECKED BY: GWC			DATE: Mar 2000
APPROVED BY: PFA			DATE: Mar 2000
APPROVED BY:			DATE:

Nicolet Minerals
a Rio Algom company

Figure 6
Source Areas Cumulative Percolation Volume

Scale: None	Date: March 2000
Prepared By: HSI GEOTRANS	By: LMG

\Crandon\TmaMod4\Excel\T13C-Mp.xls, Fig

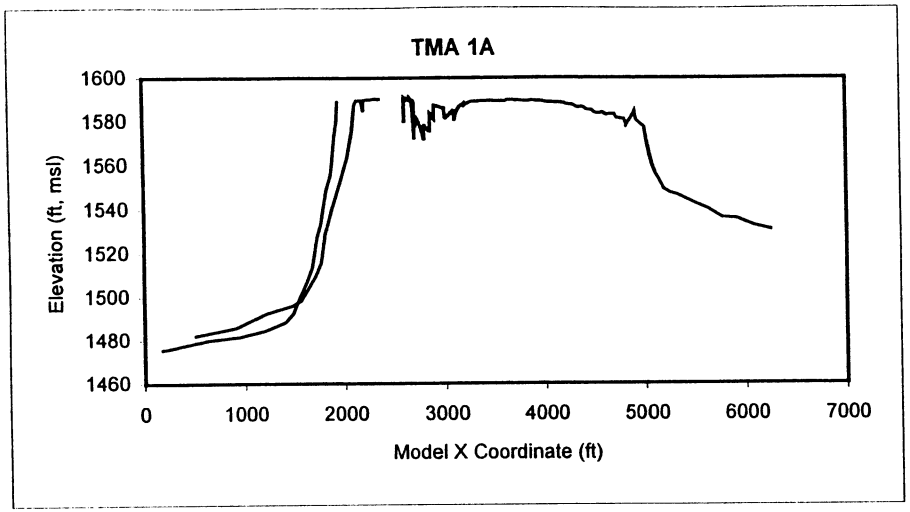

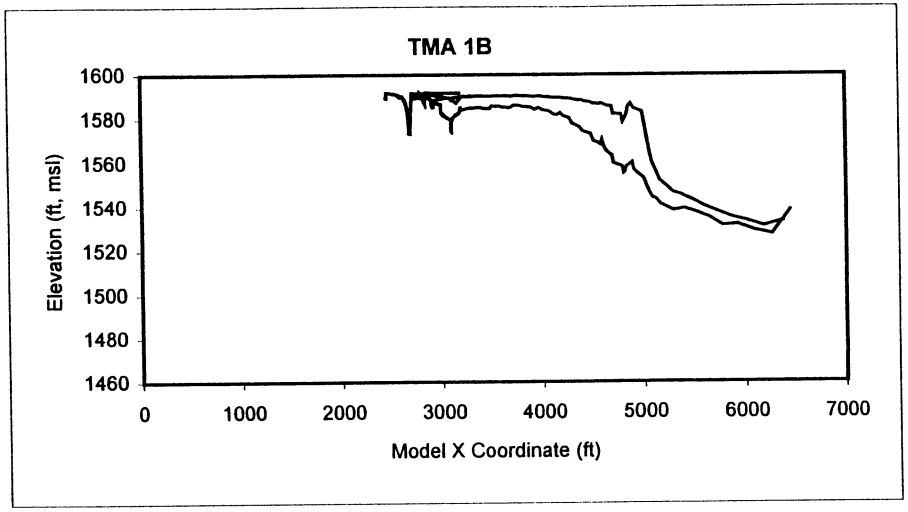

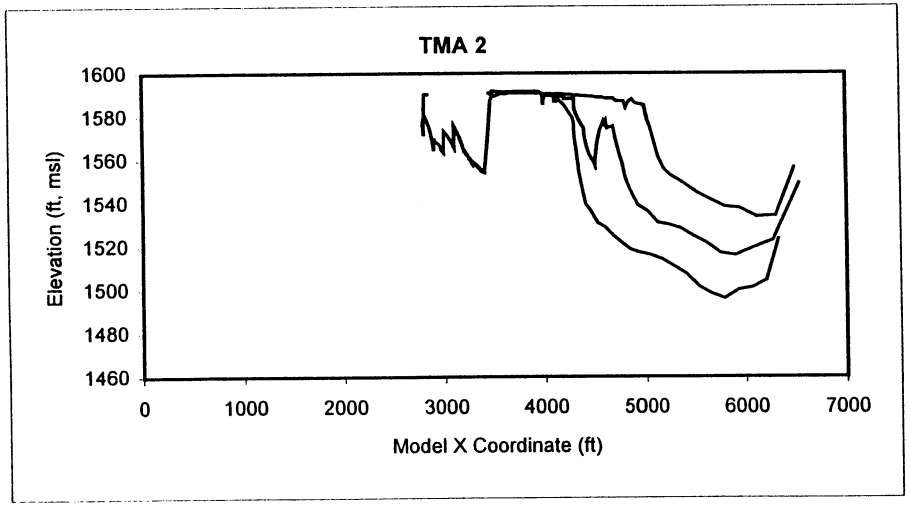

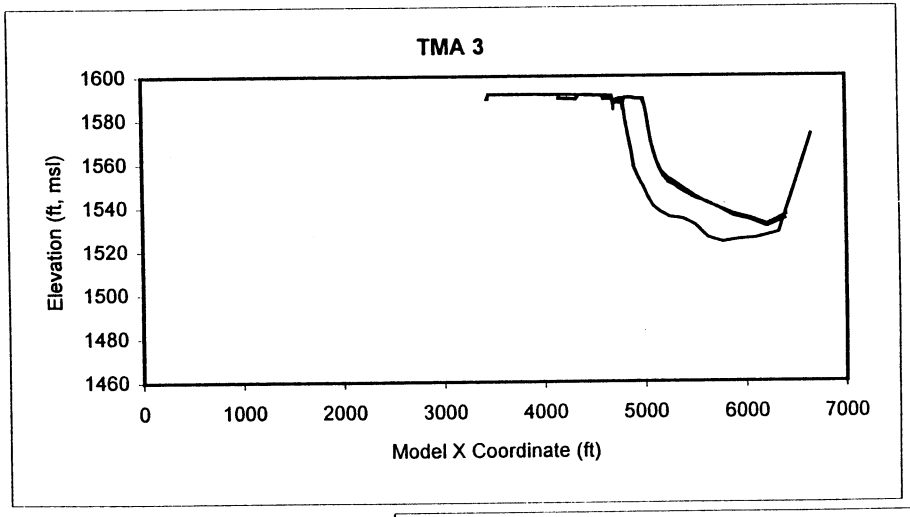

4.2-10-471

HSI GEOTRANS			
REVISED	DATE	BY	DESCRIPTION
CHECKED BY: JDC			DATE: 3/00
APPROVED BY: PFA			DATE: 3/00
APPROVED BY:			DATE:

Simulation T13C-MP

Nicolet Minerals
a Rio Algom company

Figure 7
Particle Traces From Each TMA Basin, Cross-Section

Scale: None	Date: March 2000
Prepared By: HSI GEOTRANS	By: GWC

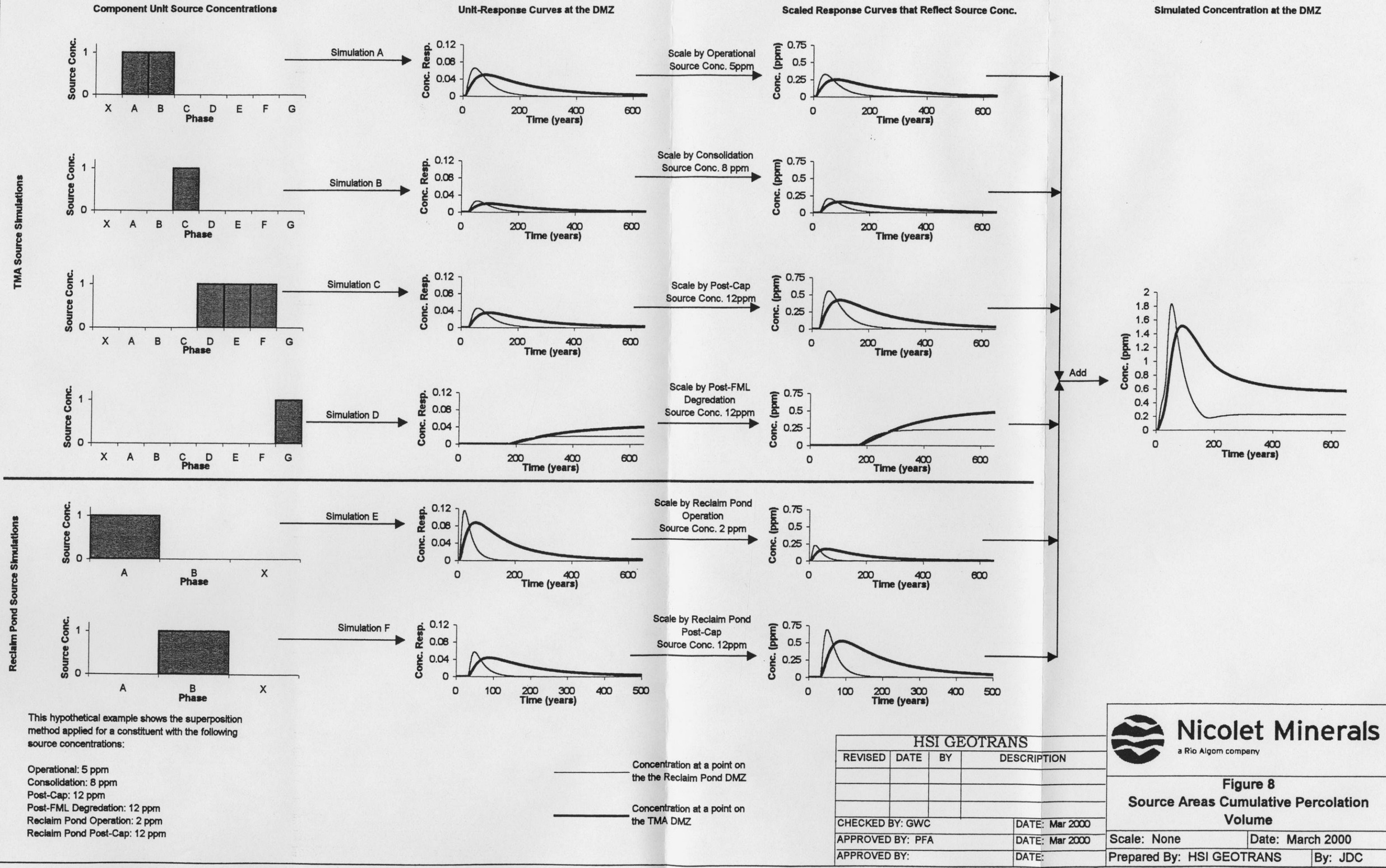

This hypothetical example shows the superposition method applied for a constituent with the following source concentrations:

Operational: 5 ppm
Consolidation: 8 ppm
Post-Cap: 12 ppm
Post-FML Degredation: 12 ppm
Reclaim Pond Operation: 2 ppm
Reclaim Pond Post-Cap: 12 ppm

Concentration at a point on the the Reclaim Pond DMZ

Concentration at a point on the TMA DMZ

HSI GEOTRANS			
REVISED	DATE	BY	DESCRIPTION
CHECKED BY: GWC			DATE: Mar 2000
APPROVED BY: PFA			DATE: Mar 2000
APPROVED BY:			DATE:

Nicolet Minerals
a Rio Algom company

Figure 8
Source Areas Cumulative Percolation Volume

Scale: None	Date: March 2000
Prepared By: HSI GEOTRANS	By: JDC

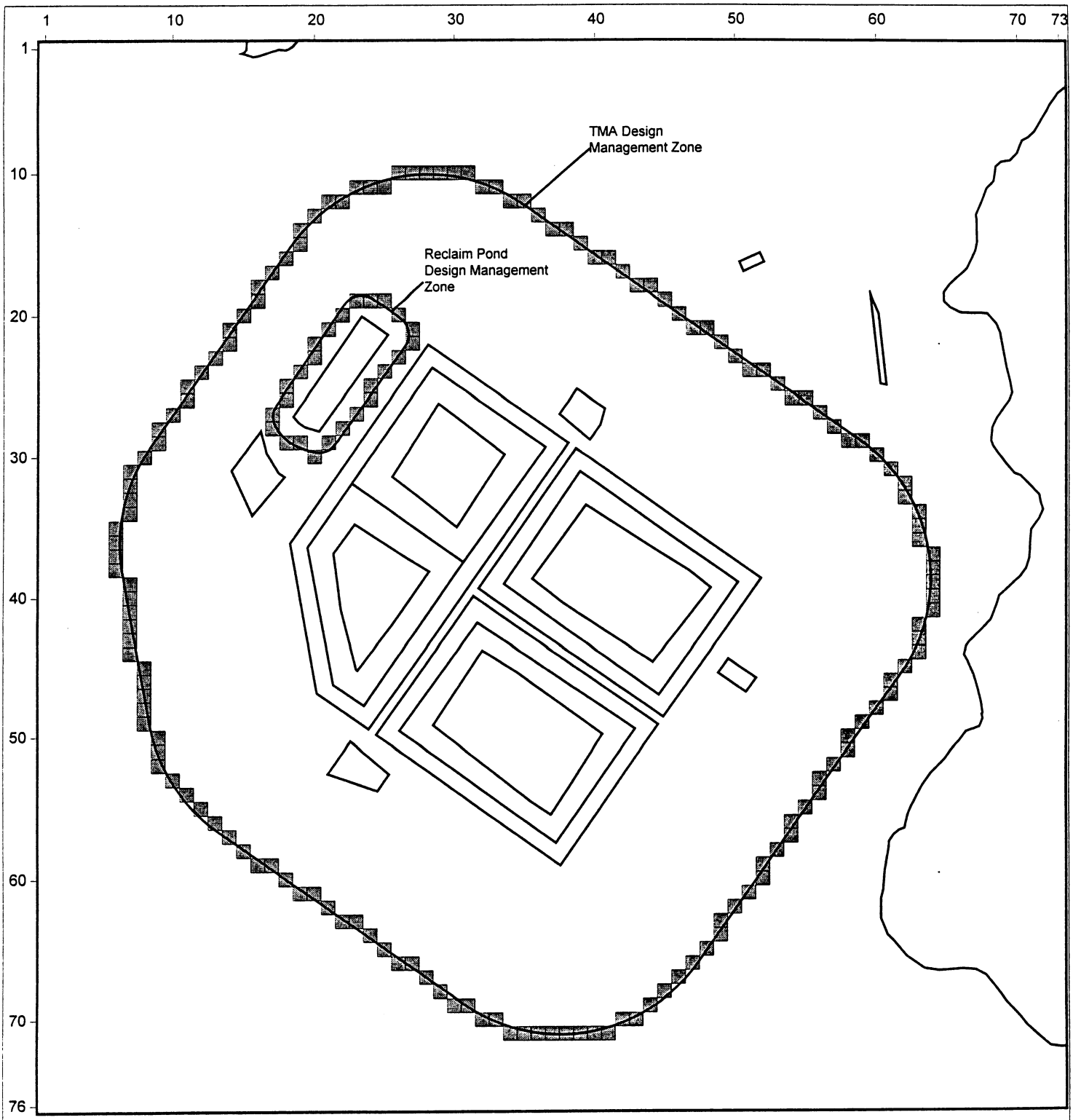

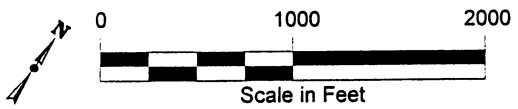

HSI GEOTRANS

REVISED	DATE	BY	DESCRIPTION
1	1/00	GWC	Mod. SW side TMA DMZ

CHECKED BY: KMR	DATE: Dec 1998
APPROVED BY: PFA	DATE: Dec 1998
APPROVED BY:	DATE:

Nicolet Minerals
a Rio Algom company

Figure 9
Observation Cells at the
Design Management Zones

Scale: 1 in. = 1000 ft. | Date: Dec 1998
Prepared By: HSI GeoTrans | By: GWC

P:\Crandon\GIS\RevisedDMZ.wor

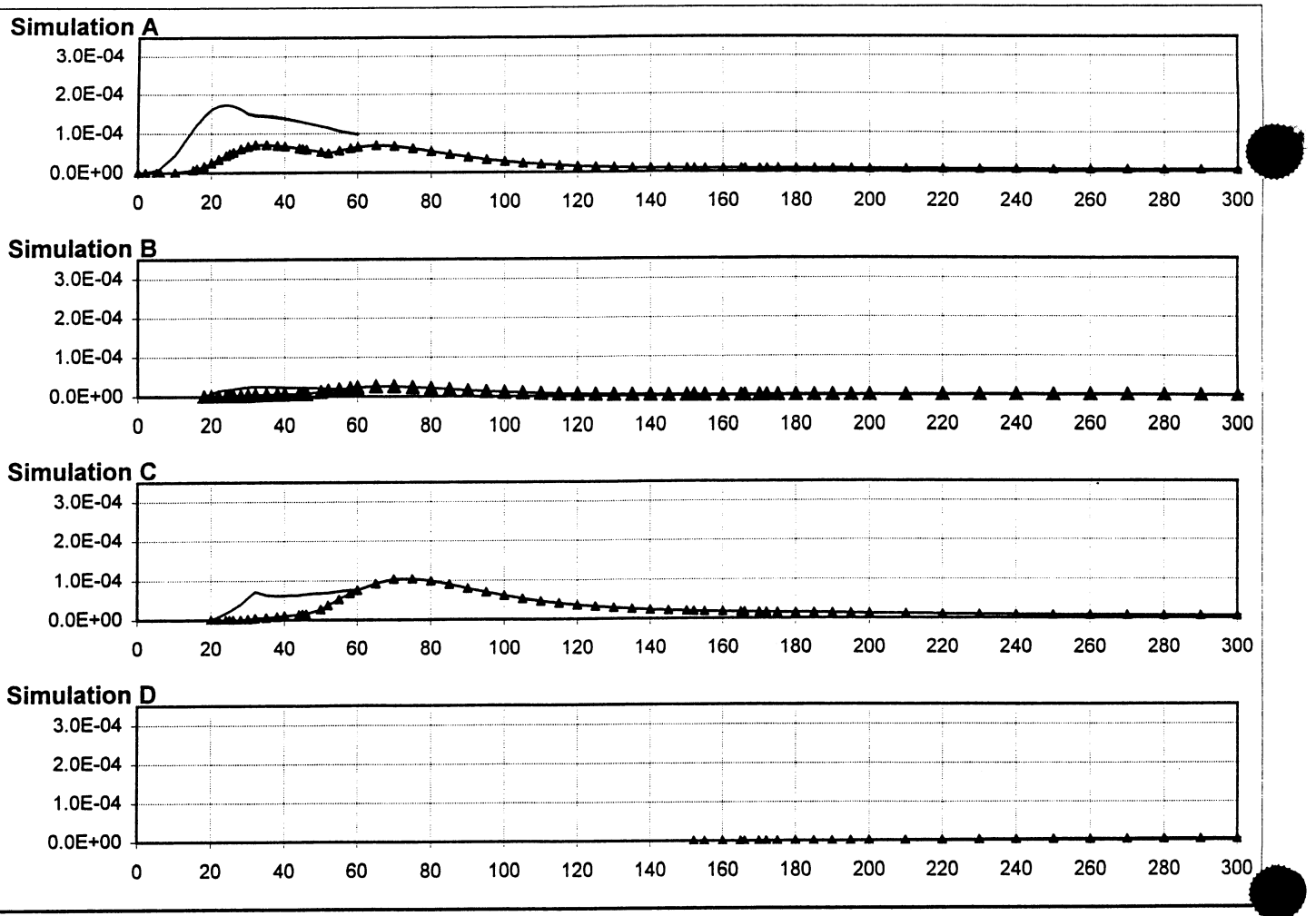

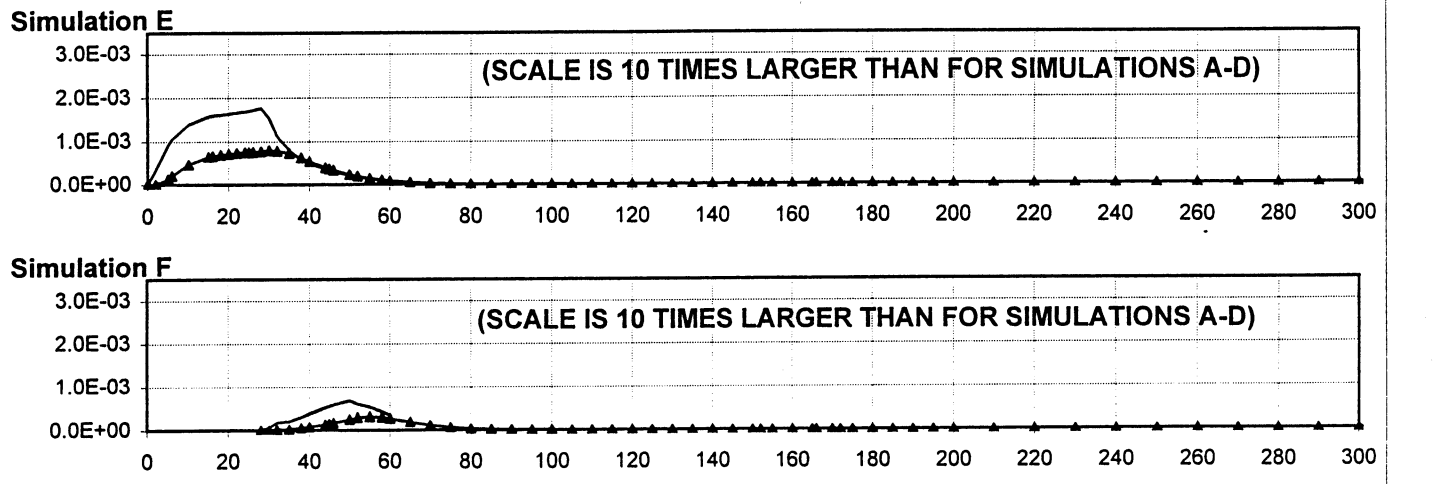

Note:

Maximum concentration at any cell on the DMZ is plotted

Y axis is concentration response (unitless)

X axis is time in years

TMA DMZ

Rec Pond DMZ

HSI GEOTRANS			
REVISED	DATE	BY	DESCRIPTION
CHECKED BY:GWC			DATE:3/00
APPROVED BY:PFA			DATE:3/00
APPROVED BY:			DATE:

Nicolet Minerals

a Rio Algom company

Figure 10

BEJT Concentration Response Curves at the Design Management Zones (DMZs)

Scale: None	Date:March 2000
Prepared By: HSI GEOTRANS	By:LMG

Simulation T13c

4.2-10-474

\Crandon\Flowmod2\Excel\M49a-Res.xls

\Crandon\TmaMod4\Excel\hypothet2.xls, bej

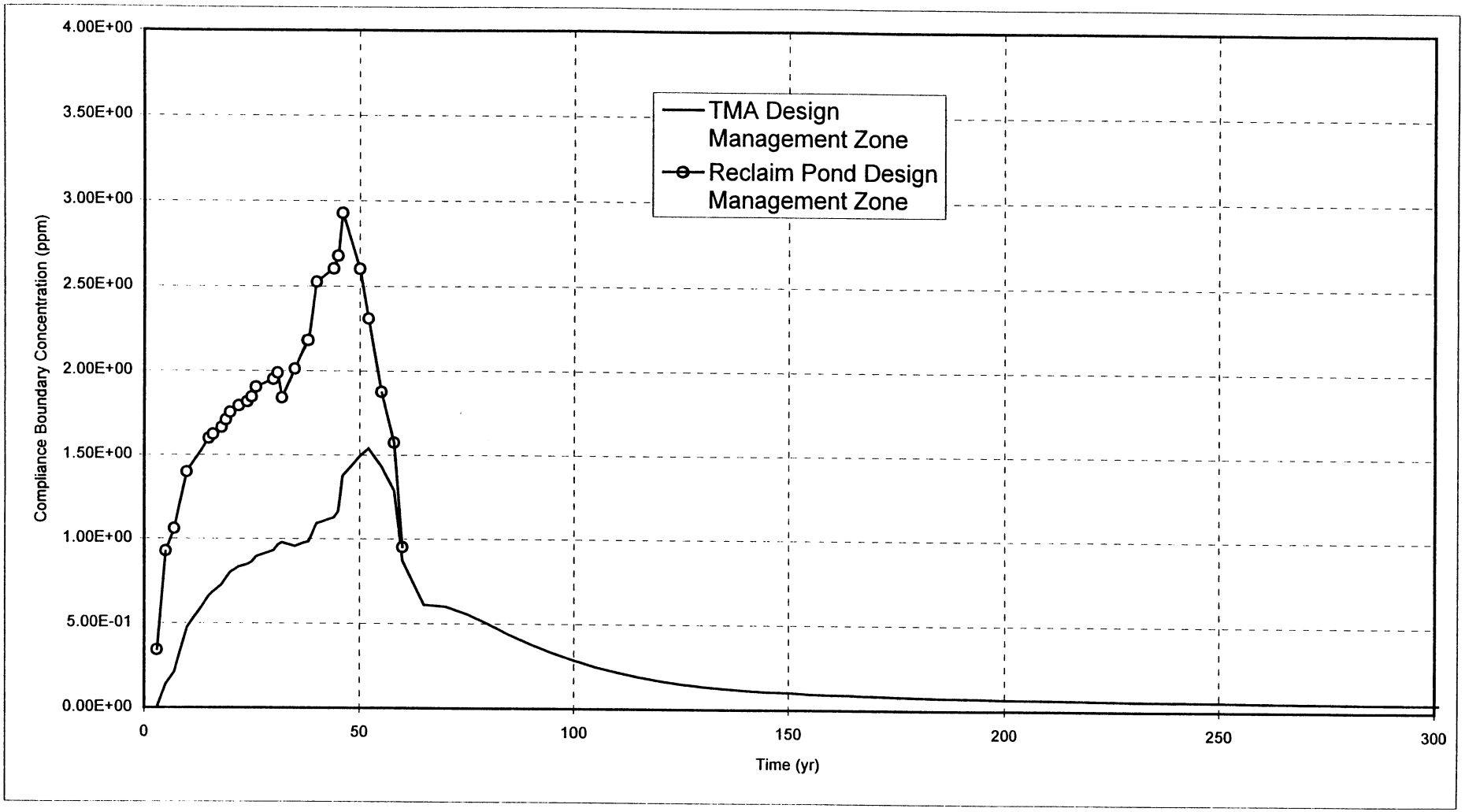

4.2-10-475

Source Concentration:

Operation:	2000 ppm
Consolidation:	2500 ppm
Post-Cap:	4000 ppm
Post-FML-Degradation:	4000 ppm
Reclaim Pond Operation:	1000 ppm
Reclaim Pond Post-Cap:	4000 ppm

HSI GEOTRANS

REVISED	DATE	BY	DESCRIPTION

CHECKED BY: GWC		DATE: Mar 2000
APPROVED BY: PFA		DATE: Mar 2000
Simulations T13C*	APPROVED BY:	DATE:

Nicolet Minerals
a Rio Algom company

Figure 11
BEJT Concentration at the Design Management Zones (Example Constituent)

Scale: None	Date: Mar 2000
Prepared By: HSI GEOTRANS	By: LMG

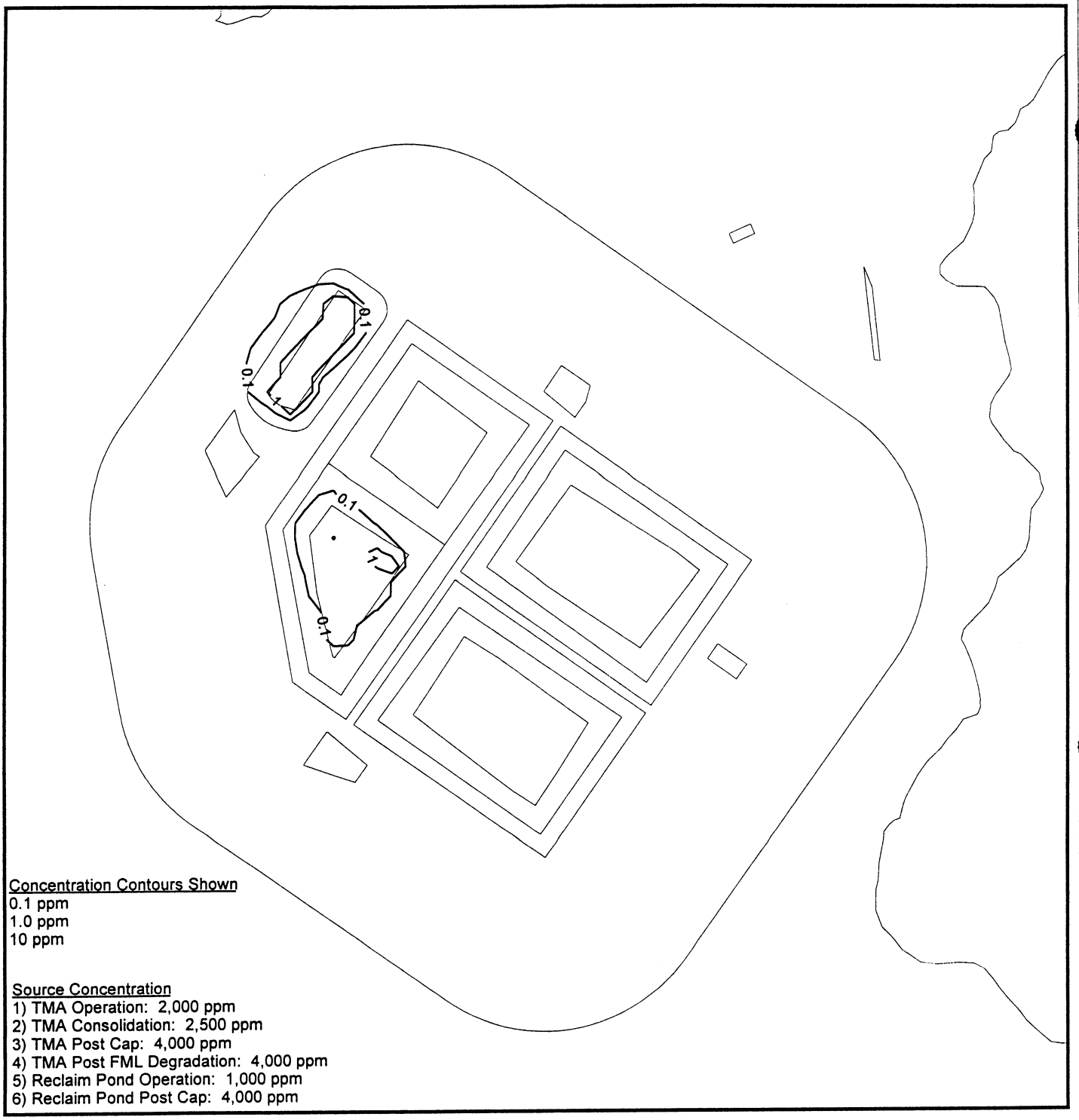

Concentration Contours Shown
0.1 ppm
1.0 ppm
10 ppm

Source Concentration
1) TMA Operation: 2,000 ppm
2) TMA Consolidation: 2,500 ppm
3) TMA Post Cap: 4,000 ppm
4) TMA Post FML Degradation: 4,000 ppm
5) Reclaim Pond Operation: 1,000 ppm
6) Reclaim Pond Post Cap: 4,000 ppm

Note:
This plot shows
contours of maximum
concentratration in any layer.

0 1000 2000
Scale in Feet

HSI GEOTRANS

REVISED	DATE	BY	DESCRIPTION

CHECKED BY: GWC		DATE: 3/00
APPROVED BY: PFA		DATE: 3/00
APPROVED BY:		DATE:

Simulations
T13C1 - T13C6

4.2-10-476

Nicolet Minerals
a Rio Algom company

Figure 12
BEJT Concentration After 2 Years
(Example Constituent, Plan View)

Scale: 1 in. = 1000 ft.	Date: March 2000
Prepared By: HSI GEOTRANS	By:JDC

P:\Crandon\Tma\Mod4\Surfer\P13by002.srf

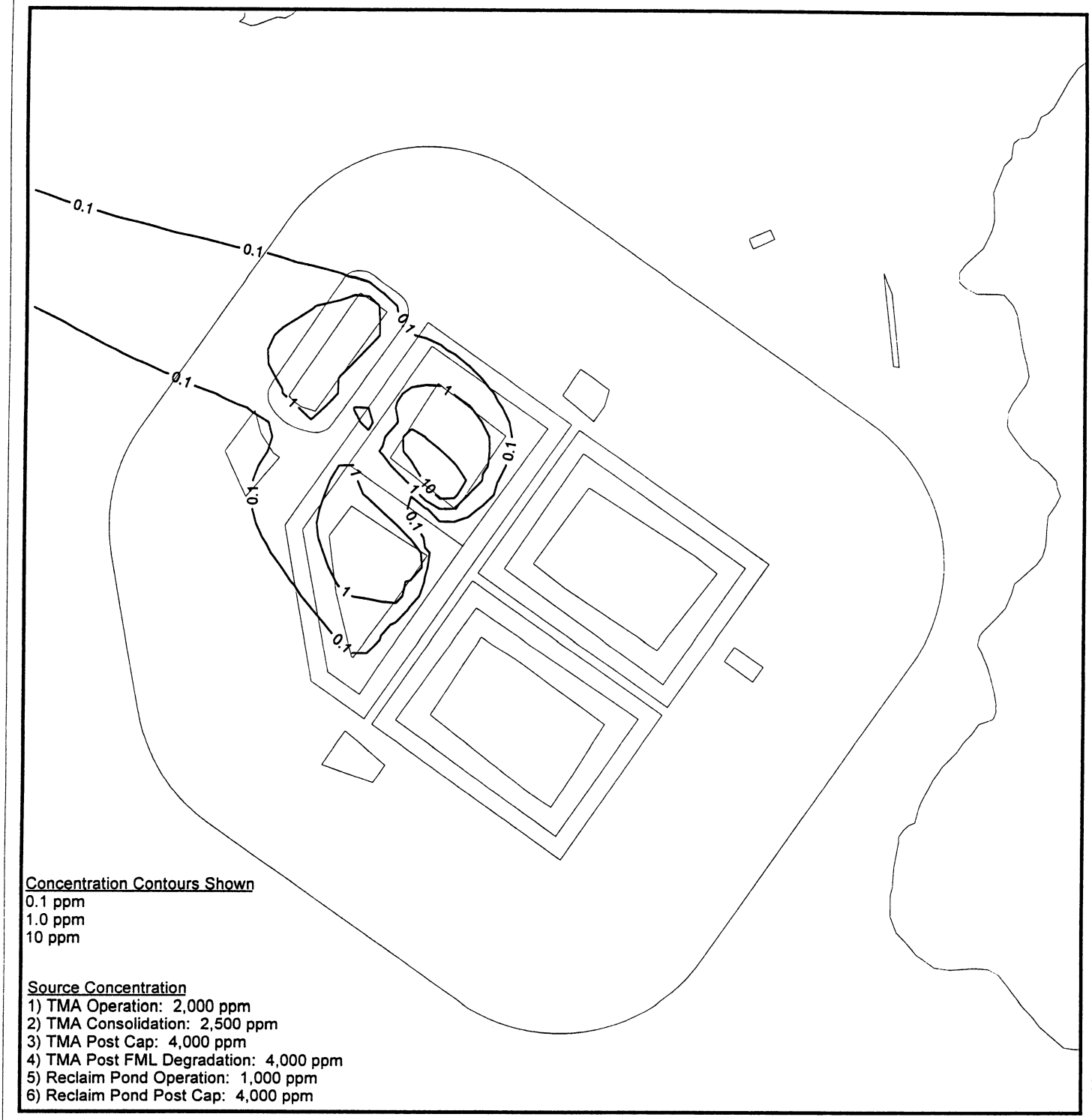

Concentration Contours Shown
0.1 ppm
1.0 ppm
10 ppm

Source Concentration
1) TMA Operation: 2,000 ppm
2) TMA Consolidation: 2,500 ppm
3) TMA Post Cap: 4,000 ppm
4) TMA Post FML Degradation: 4,000 ppm
5) Reclaim Pond Operation: 1,000 ppm
6) Reclaim Pond Post Cap: 4,000 ppm

Note:
This plot shows
contours of maximum
concentratration in any layer.

N

0 1000 2000

Scale in Feet

HSI GEOTRANS

REVISED	DATE	BY	DESCRIPTION

CHECKED BY: GWC		DATE: 3/00
APPROVED BY: PFA		DATE: 3/00
APPROVED BY:		DATE:

Simulations
T13C1 - T13C6

4-2-10-477

Nicolet Minerals
a Rio Algom company

Figure 13
BEJT Concentration After 16 Years
(Example Constituent, Plan View)

Scale: 1 in. = 1000 ft. | Date: March 2000

Prepared By: HSI GEOTRANS | By: JDC

P:\Crandon\Tma\Mod4\Surfer\PT13fy016.srf

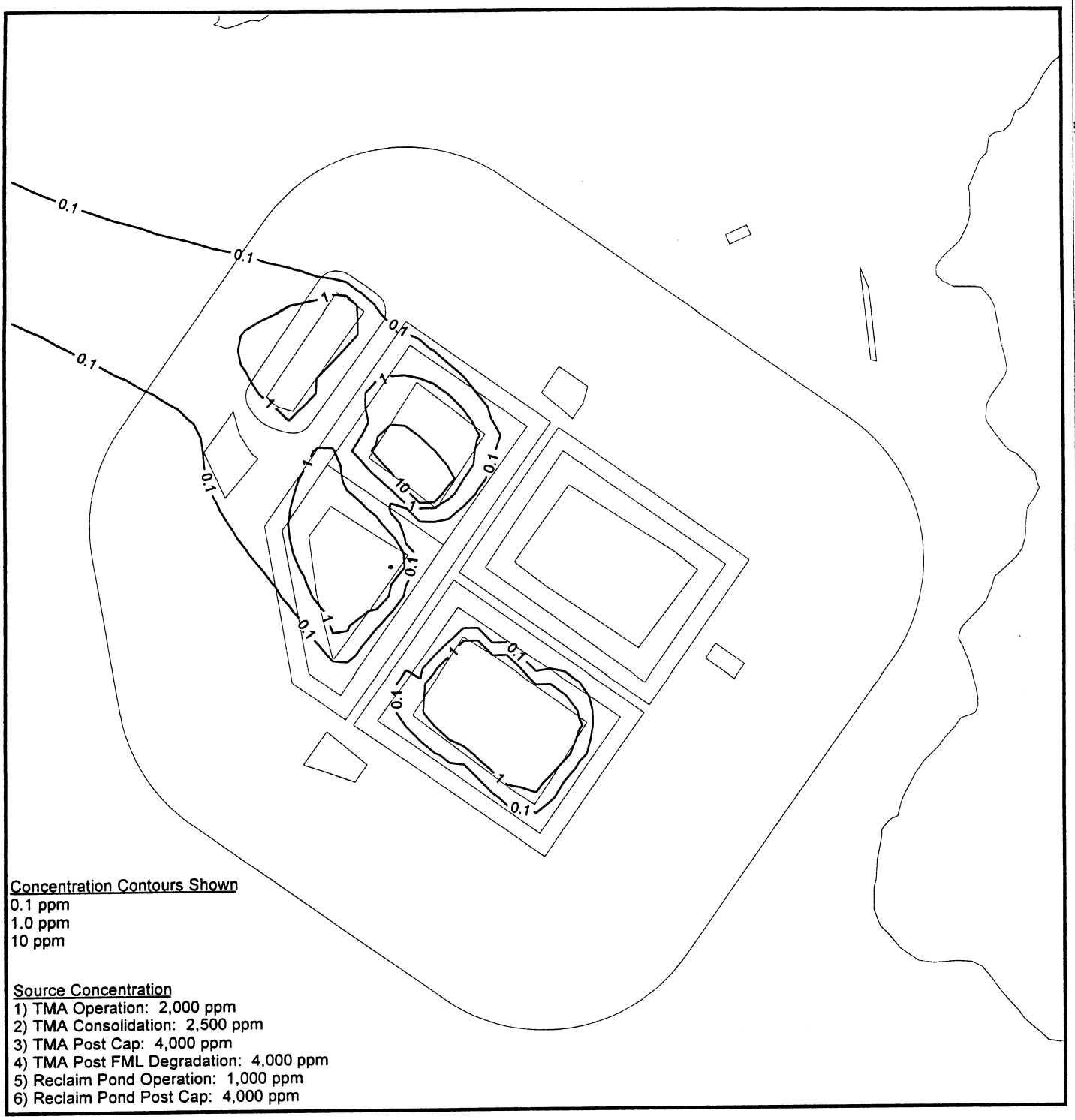

Concentration Contours Shown
0.1 ppm
1.0 ppm
10 ppm

Source Concentration
1) TMA Operation: 2,000 ppm
2) TMA Consolidation: 2,500 ppm
3) TMA Post Cap: 4,000 ppm
4) TMA Post FML Degradation: 4,000 ppm
5) Reclaim Pond Operation: 1,000 ppm
6) Reclaim Pond Post Cap: 4,000 ppm

Note:
This plot shows
contours of maximum
concentratration in any layer.

N

0 1000 2000

Scale in Feet

HSI GEOTRANS

REVISED	DATE	BY	DESCRIPTION

CHECKED BY: GWC		DATE: 3/00
APPROVED BY: PFA		DATE: 3/00
APPROVED BY:		DATE:

Simulations
T13C1 - T13C6

4.2-10-478

Nicolet Minerals
a Rio Algom company

Figure 14
BEJT Concentration After 22 Years
(Example Constituent, Plan View)

Scale: 1 in. = 1000 ft.	Date: March 2000
Prepared By: HSI GEOTRANS	By:JDC

P:\Crandon\TmaMod4\Surfer\P13hy022.srf

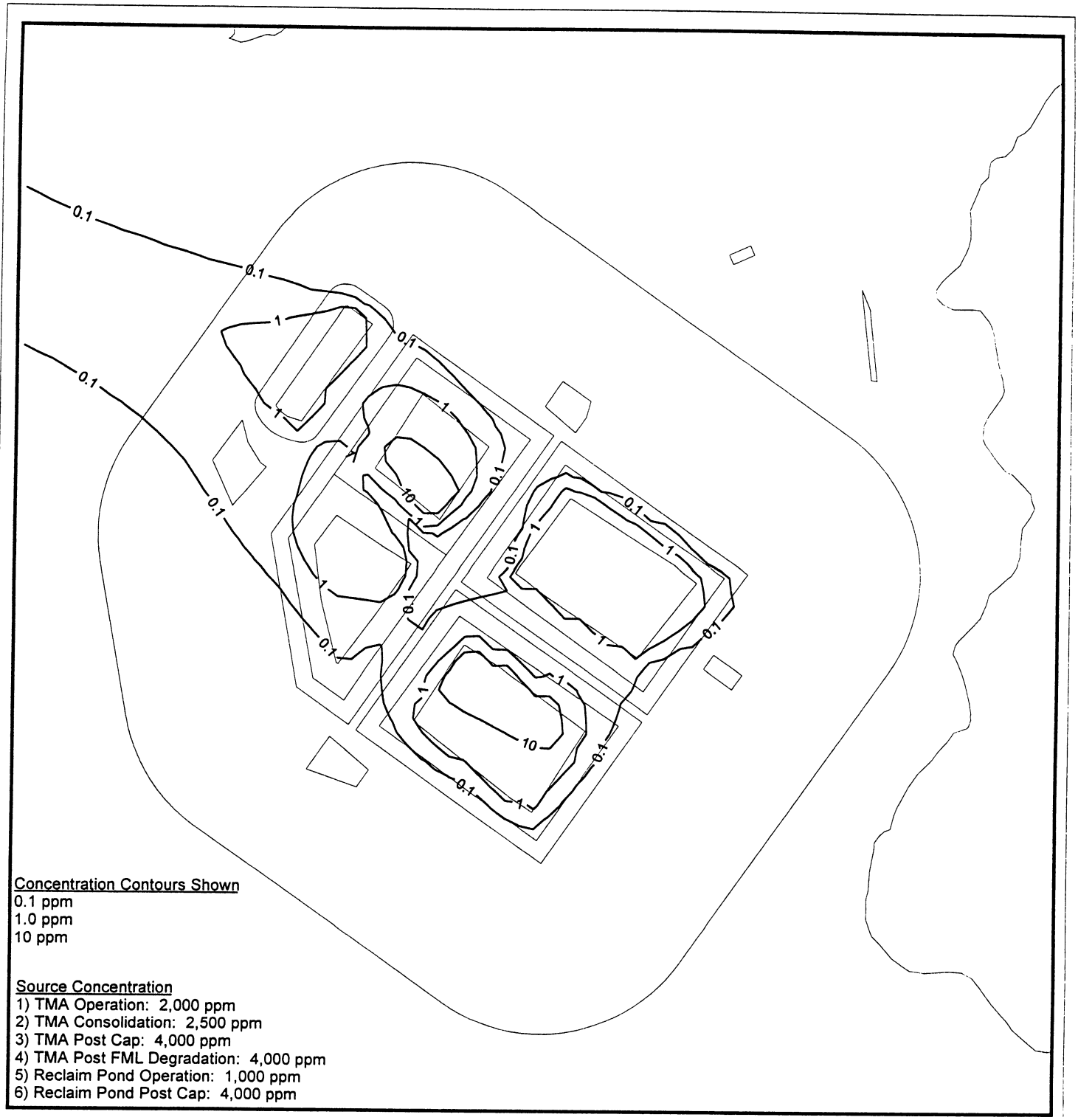

Note:
This plot shows
contours of maximum
concentratration in any layer.

N

0 1000 2000

Scale in Feet

HSI GEOTRANS

REVISED	DATE	BY	DESCRIPTION

	CHECKED BY: GWC	DATE: 3/00
Simulations T13C1 - T13C6	APPROVED BY: PFA	DATE: 3/00
	APPROVED BY:	DATE:

Nicolet Minerals
a Rio Algom company

Figure 15
BEJT Concentration After 32 Years
(Example Constituent, Plan View)

Scale: 1 in. = 1000 ft.	Date: March 2000
Prepared By: HSI GEOTRANS	By: JDC

P:\Crandon\TmaModel\Surfer\...032.srf

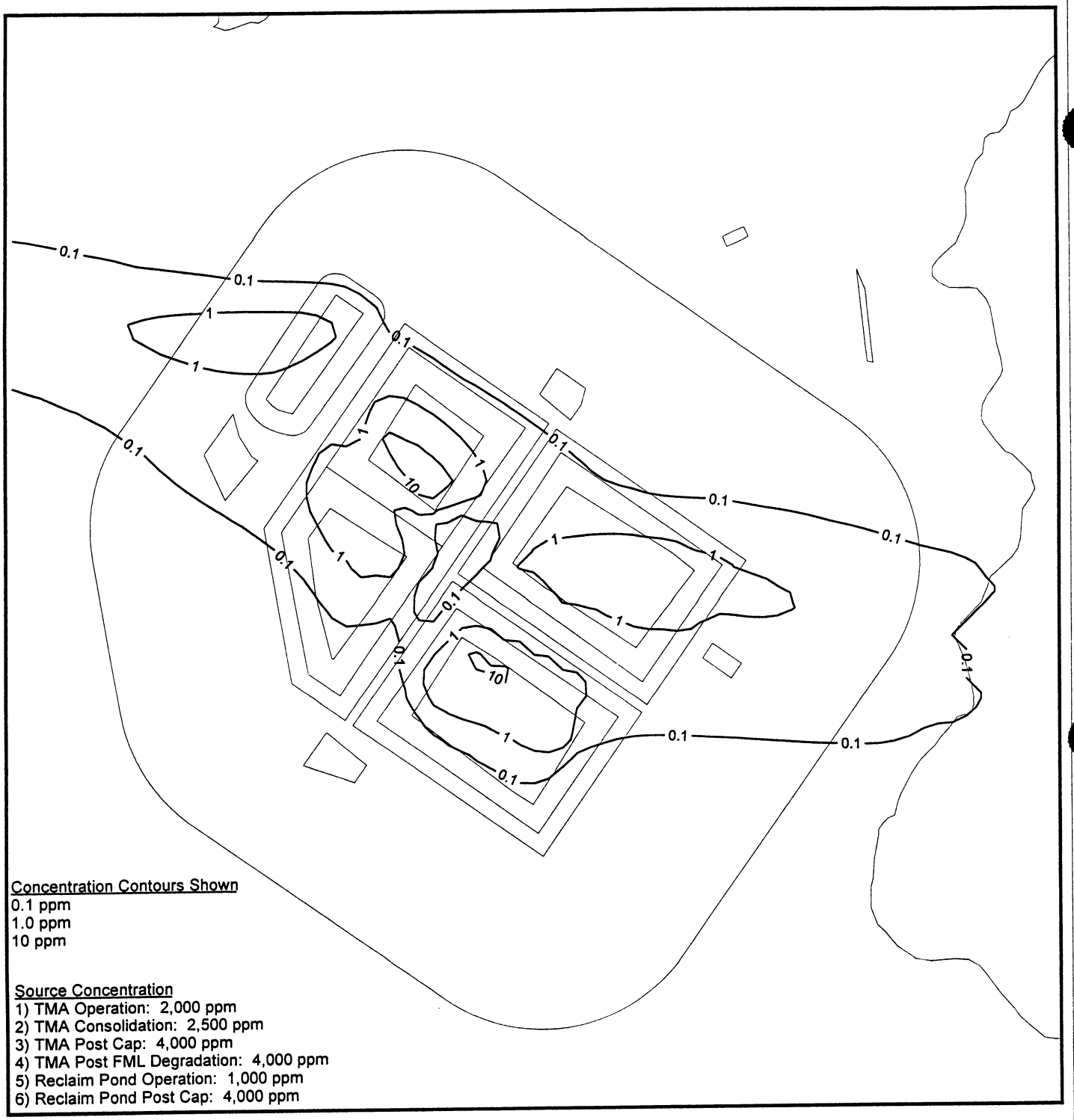

Note:
This plot shows contours of maximum concentratration in any layer.

0 1000 2000

Scale in Feet

HSI GEOTRANS

REVISED	DATE	BY	DESCRIPTION

CHECKED BY: GWC	DATE: 3/00	
APPROVED BY: PFA	DATE: 3/00	
APPROVED BY:	DATE:	

Simulations T13C1 - T13C6

4.2-10-480

Nicolet Minerals
a Rio Algom company

Figure 16
BEJT Concentration After 60 Years
(Example Constituent, Plan View)

Scale: 1 in. = 1000 ft. | Date: March 2000

Prepared By: HSI GEOTRANS | By: JDC

P:\Crandon\Tmamod4\Surfer\P13hy060.srf

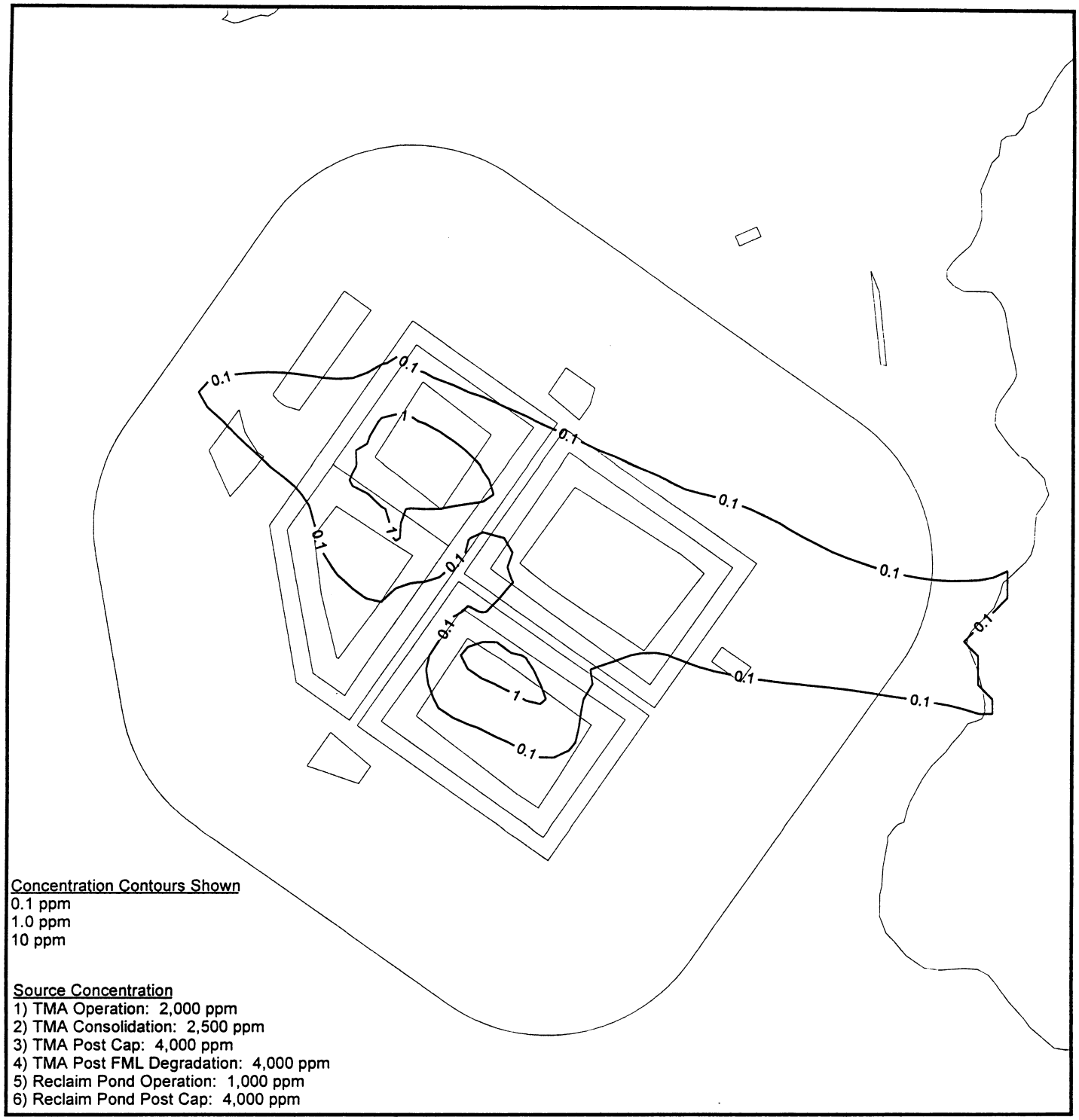

Concentration Contours Shown
0.1 ppm
1.0 ppm
10 ppm

Source Concentration
1) TMA Operation: 2,000 ppm
2) TMA Consolidation: 2,500 ppm
3) TMA Post Cap: 4,000 ppm
4) TMA Post FML Degradation: 4,000 ppm
5) Reclaim Pond Operation: 1,000 ppm
6) Reclaim Pond Post Cap: 4,000 ppm

Note:
This plot shows
contours of maximum
concentratration in any layer.

0 1000 2000
Scale in Feet

HSI GEOTRANS

REVISED	DATE	BY	DESCRIPTION

Simulations T13C1 - T13C6	CHECKED BY: GWC	DATE: 3/00
	APPROVED BY: PFA	DATE: 3/00
	APPROVED BY:	DATE:

Nicolet Minerals
a Rio Algom company

Figure 17
BEJT Concentration After 125 Years
(Example Constituent, Plan View)

Scale: 1 in. = 1000 ft. | Date: March 2000
Prepared By: HSI GEOTRANS | By: JDC

4.2-10-481

P:\Crandon\Tma\Mod4\Surfer7\3dy125.srf

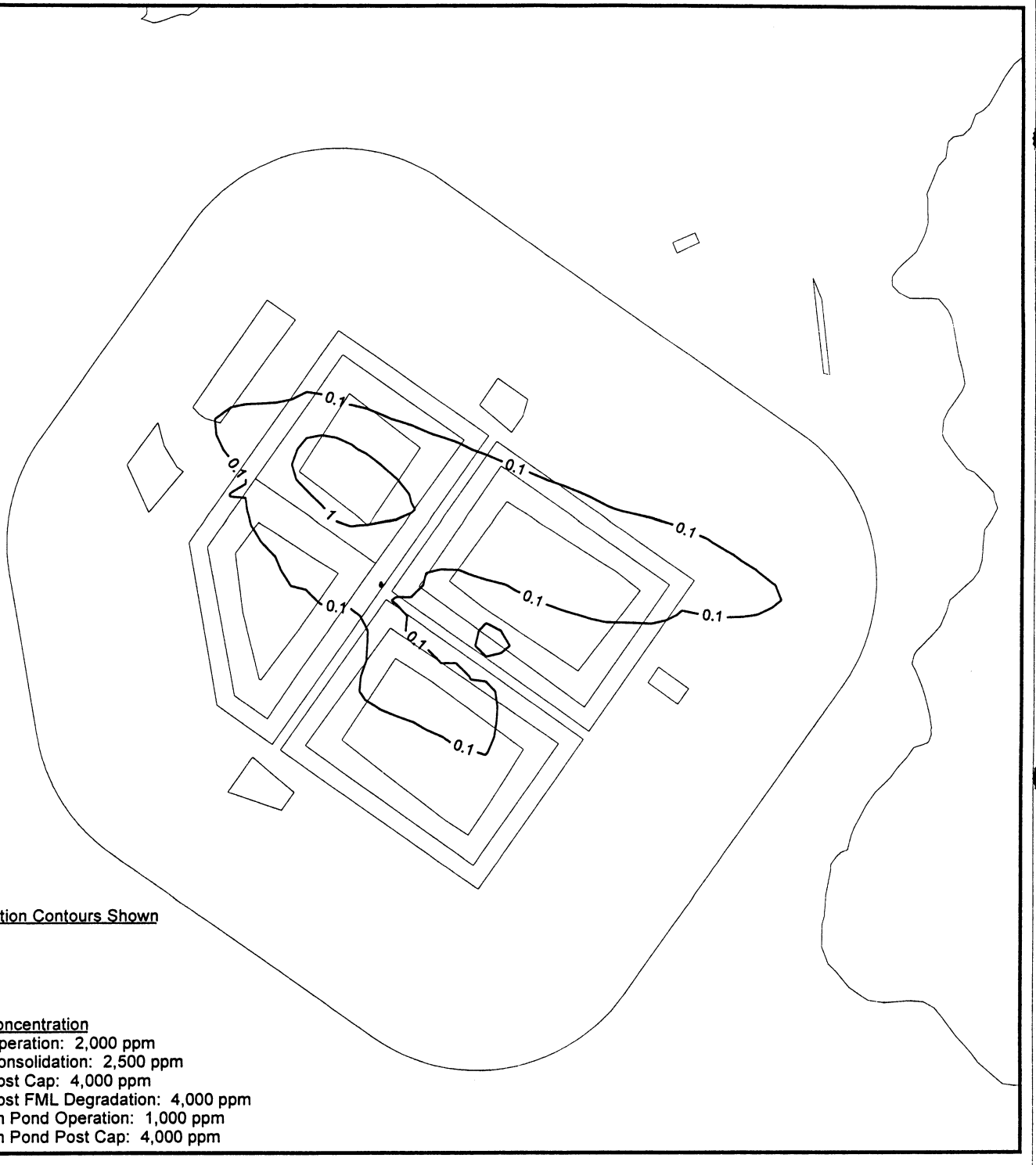

Concentration Contours Shown
0.1 ppm
1.0 ppm
10 ppm

Source Concentration
1) TMA Operation: 2,000 ppm
2) TMA Consolidation: 2,500 ppm
3) TMA Post Cap: 4,000 ppm
4) TMA Post FML Degradation: 4,000 ppm
5) Reclaim Pond Operation: 1,000 ppm
6) Reclaim Pond Post Cap: 4,000 ppm

Note:
This plot shows
contours of maximum
concentratration in any layer.

0 1000 2000
Scale in Feet

HSI GEOTRANS

REVISED	DATE	BY	DESCRIPTION

CHECKED BY: GWC DATE: 3/00
APPROVED BY: PFA DATE: 3/00
APPROVED BY: DATE:

Simulations
T13C1 - T13C6

4.2-10-482

Nicolet Minerals
a Rio Algom company

Figure 18
BEJT Concentration After 200 Years
(Example Constituent, Plan View)

Scale: 1 in. = 1000 ft. Date: March 2000
Prepared By: HSI GEOTRANS By: JDC

P:\Crandon\Tmamod4\Surfer\P13hy200.srf

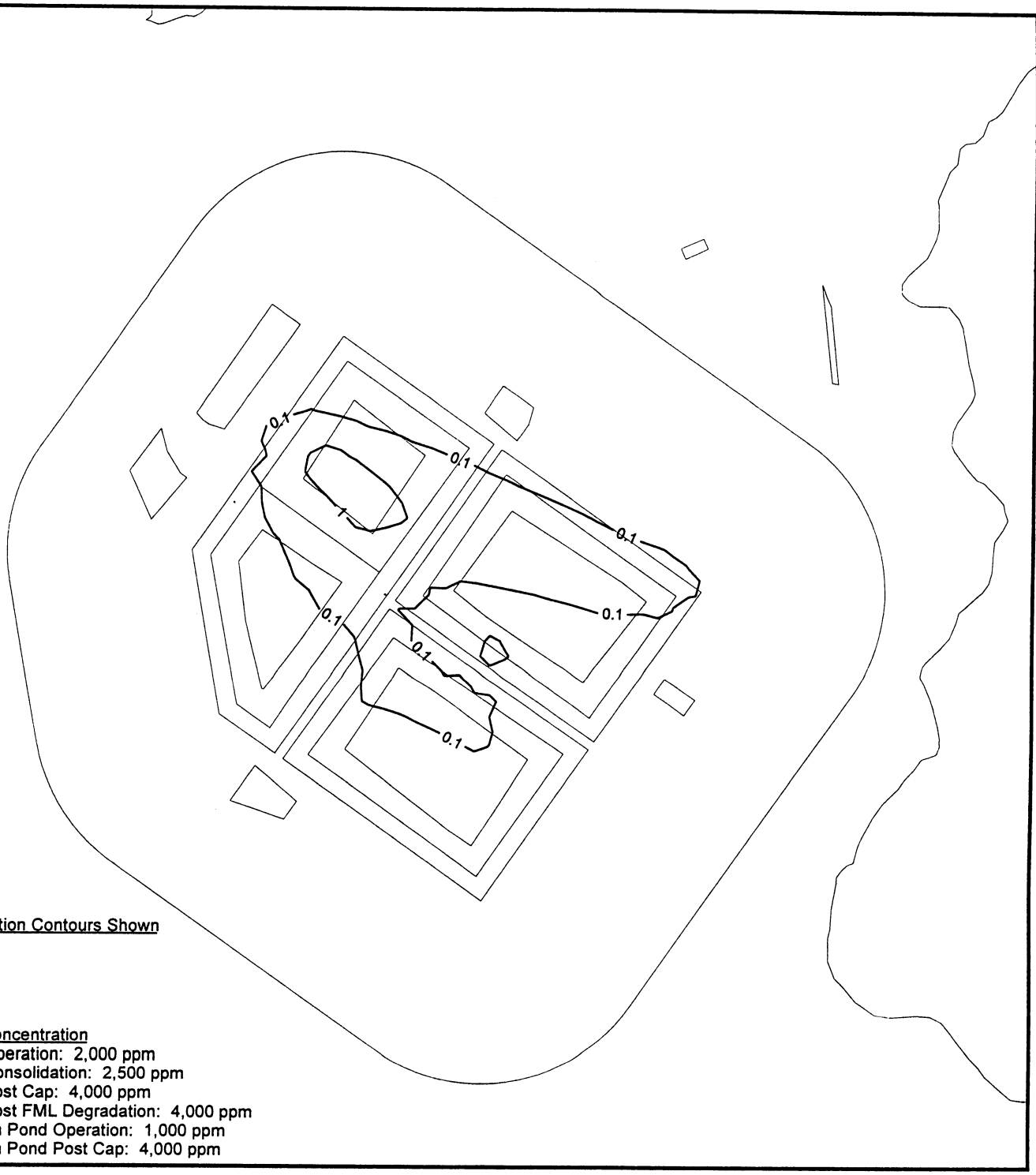

Concentration Contours Shown
0.1 ppm
1.0 ppm
10 ppm

Source Concentration
1) TMA Operation: 2,000 ppm
2) TMA Consolidation: 2,500 ppm
3) TMA Post Cap: 4,000 ppm
4) TMA Post FML Degradation: 4,000 ppm
5) Reclaim Pond Operation: 1,000 ppm
6) Reclaim Pond Post Cap: 4,000 ppm

Note:
This plot shows
contours of maximum
concentratration in any layer.

0 1000 2000
Scale in Feet

HSI GEOTRANS

REVISED	DATE	BY	DESCRIPTION

CHECKED BY: GWC		DATE: 3/00
APPROVED BY: PFA		DATE: 3/00
APPROVED BY:		DATE:

Simulations
T13C1 - T13C6

4.2-10-483

Nicolet Minerals
a Rio Algom company

Figure 19
BEJT Concentration After 300 Years
(Example Constituent, Plan View)

Scale: 1 in. = 1000 ft. | Date: March 2000
Prepared By: HSI GEOTRANS | By: JDC

P:\Crandon\Tma\Mod4\Surfer\P13by300.srf

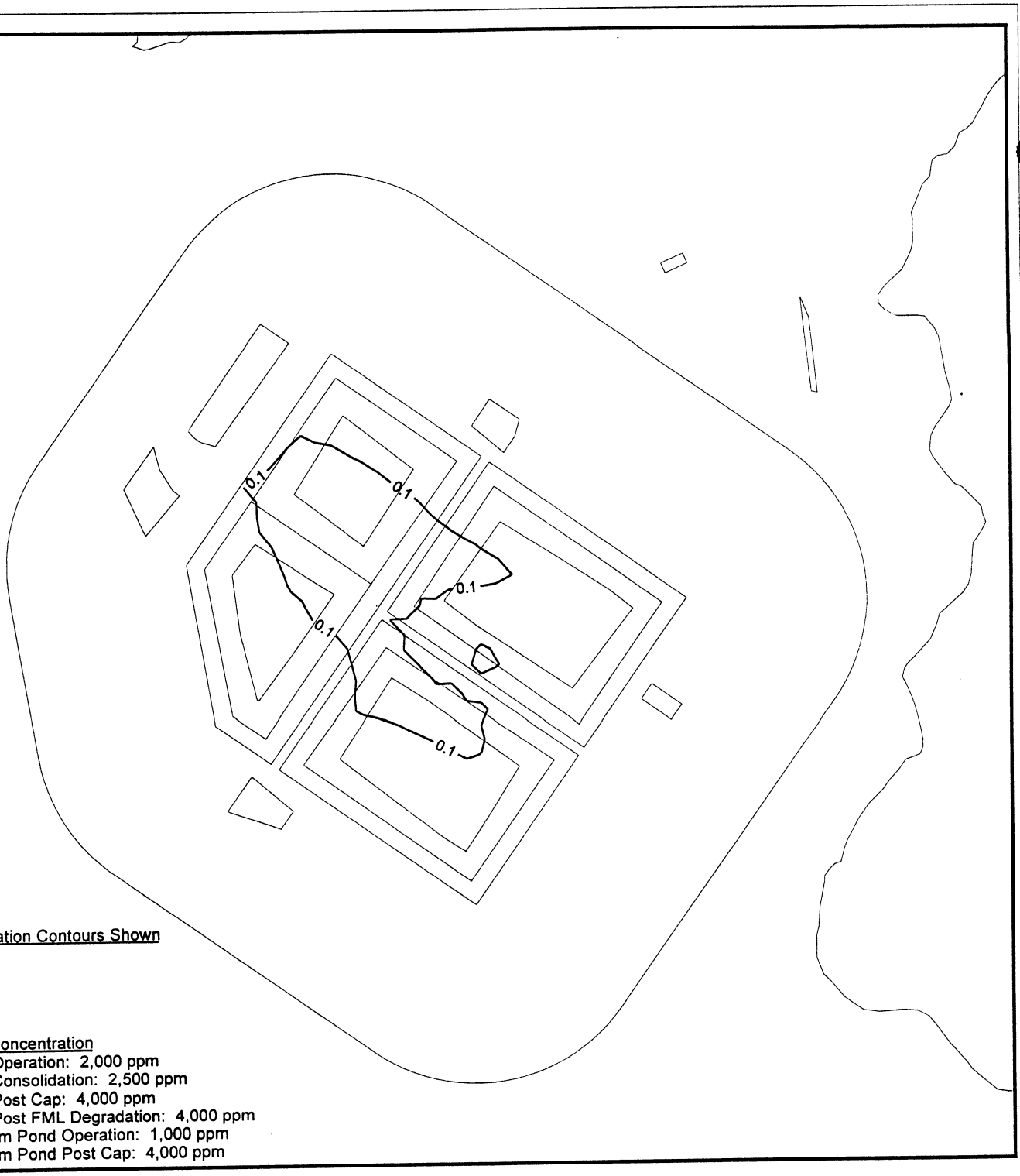

Concentration Contours Shown
0.1 ppm
1.0 ppm
10 ppm

Source Concentration
1) TMA Operation: 2,000 ppm
2) TMA Consolidation: 2,500 ppm
3) TMA Post Cap: 4,000 ppm
4) TMA Post FML Degradation: 4,000 ppm
5) Reclaim Pond Operation: 1,000 ppm
6) Reclaim Pond Post Cap: 4,000 ppm

Note:
This plot shows contours of maximum concentratration in any layer.

N

0 1000 2000
Scale in Feet

HSI GEOTRANS

REVISED	DATE	BY	DESCRIPTION

Simulations T13C1 - T13C6	CHECKED BY: GWC	DATE: 3/00
	APPROVED BY: PFA	DATE: 3/00
	APPROVED BY:	DATE:

4.2-10-484

Nicolet Minerals
a Rio Algom company

Figure 20
BEJT Concentration After 650 Years
(Example Constituent, Plan View)

Scale: 1 in. = 1000 ft.	Date: March 2000
Prepared By: HSI GEOTRANS	By: JDC

P:\Crandon\Tmwl\Mod4\Surfer\P13\hy650.srf

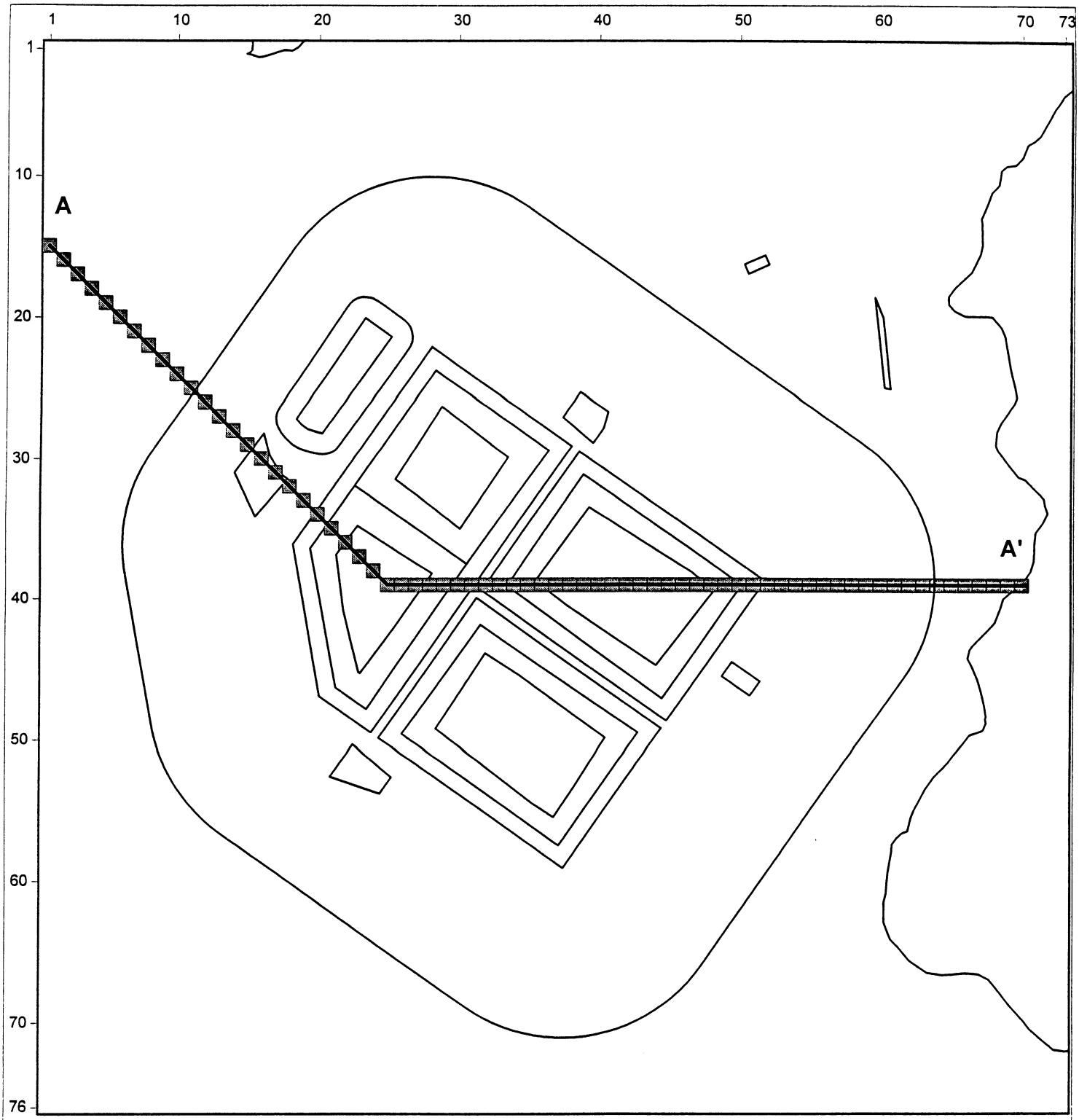

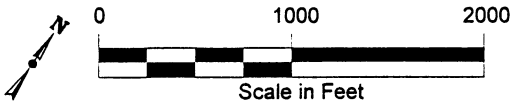

HSI GEOTRANS

REVISED	DATE	BY	DESCRIPTION

CHECKED BY: KMR	DATE: Dec 1998
APPROVED BY: PFA	DATE: Dec 1998
APPROVED BY:	DATE:

Nicolet Minerals COMPANY

Figure 21
Location of Cross-Section Used for Viewing Plumes

Scale: 1 in. = 1000 ft. | Date: Dec 1998

Prepared By: HSI GeoTrans | By: GWC

P:\CMC\TmalMod4\GIS\Section.wor

P:\Crandon\TmaMod4\Surfer\X13hy002.srf

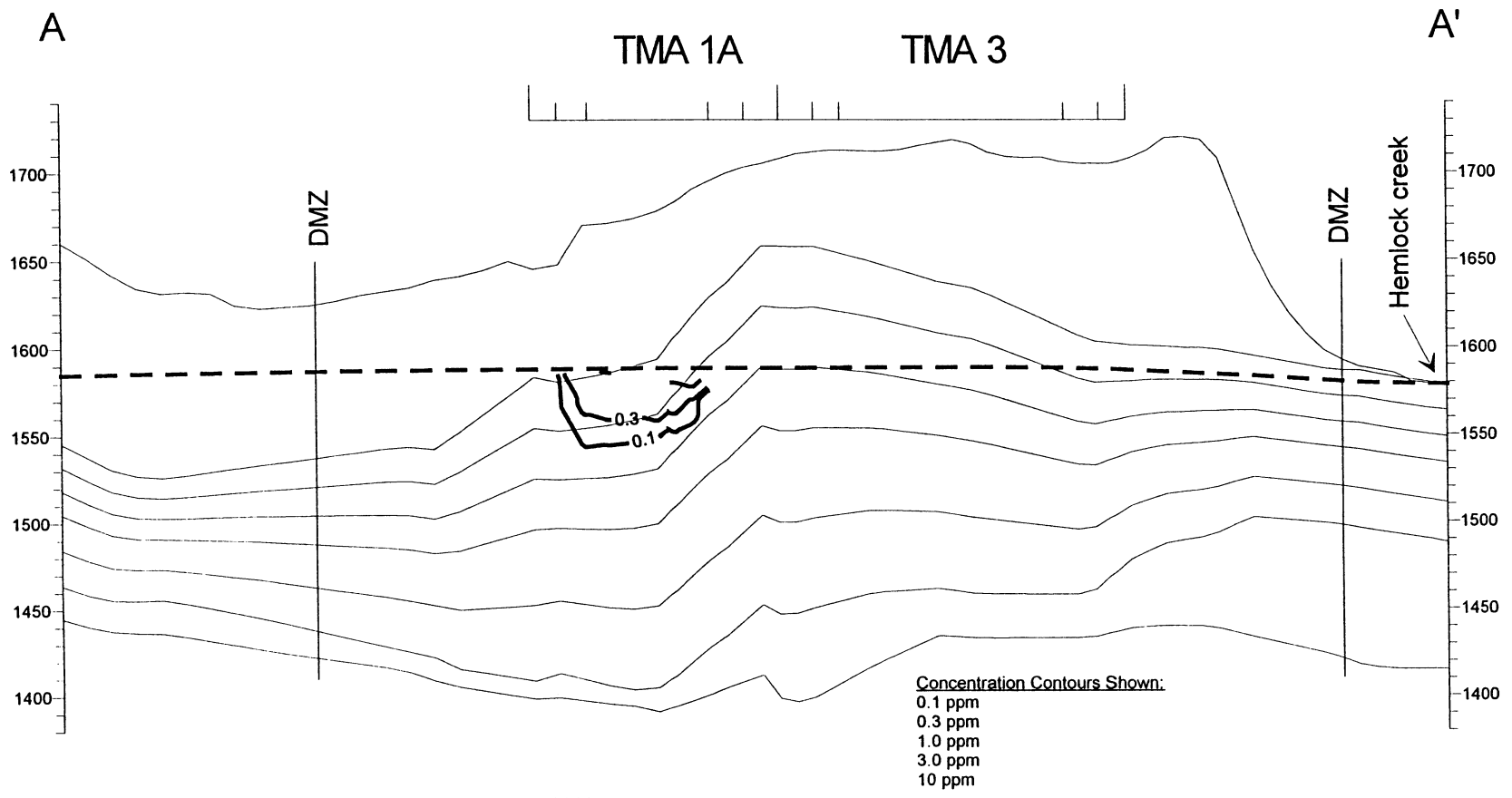

4.2-10-486

Source Concentration
1) TMA Operation: 2,000 ppm
2) TMA Consolidation: 2,500 ppm
3) TMA Post Cap: 4,000 ppm
4) TMA Post FML Degradation: 4,000 ppm
5) Reclaim Pond Operation: 1,000 ppm
6) Reclaim Pond Post Cap: 4,000 ppm

Simulations
T13C1 - T13C6

HSI GEOTRANS

REVISED	DATE	BY	DESCRIPTION

CHECKED BY: GWC	DATE: 3/00
APPROVED BY: PFA	DATE: 3/00
APPROVED BY:	DATE:

Nicolet Minerals
a Rio Algom company

Figure 22
BEJT Concentration After 2 Years
(Example Constituent, Cross-Section)

Scale: 1" = 1000' (h), 100' (v)	Date: March 2000
Prepared By: HSI GeoTrans	By: JDC

P:\Crandon\TmaMod4\Surfer\X13hy016.srf

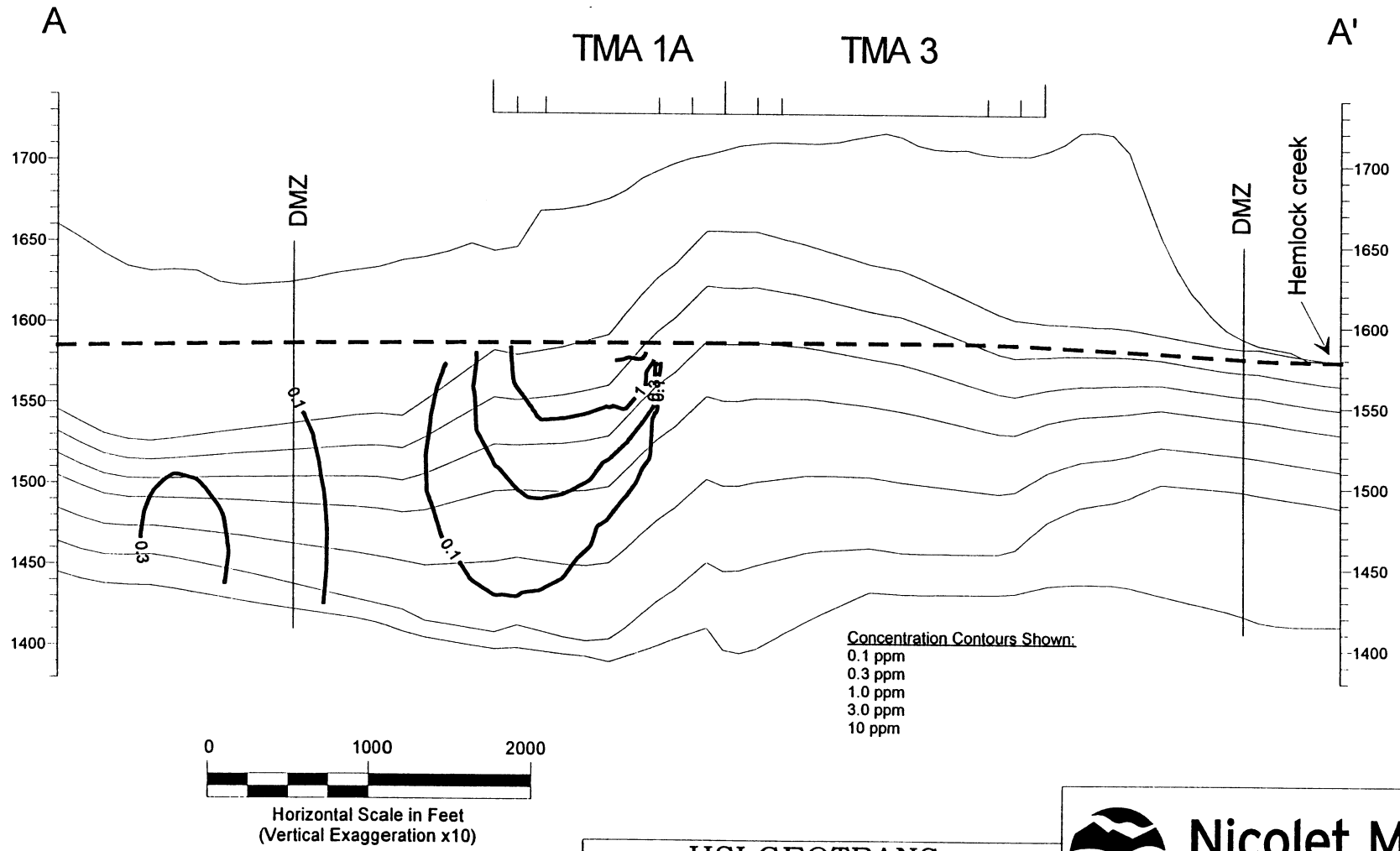

4.2-10-487

Source Concentration
1) TMA Operation: 2,000 ppm
2) TMA Consolidation: 2,500 ppm
3) TMA Post Cap: 4,000 ppm
4) TMA Post FML Degradation: 4,000 ppm
5) Reclaim Pond Operation: 1,000 ppm
6) Reclaim Pond Post Cap: 4,000 ppm

Simulations
T13C1 - T13C6

HSI GEOTRANS

REVISED	DATE	BY	DESCRIPTION

CHECKED BY: GWC	DATE: 3/00
APPROVED BY: PFA	DATE: 3/00
APPROVED BY:	DATE:

Nicolet Minerals
a Rio Algom company

Figure 23
BEJT Concentration After 16 Years
(Example Constituent, Cross-Section)

Scale: 1" = 1000' (h), 100' (v)	Date: March 2000
Prepared By: HSI GeoTrans	By: JDC

P:\Crandon\TmaMod4\Surfer\X13hy022.srf

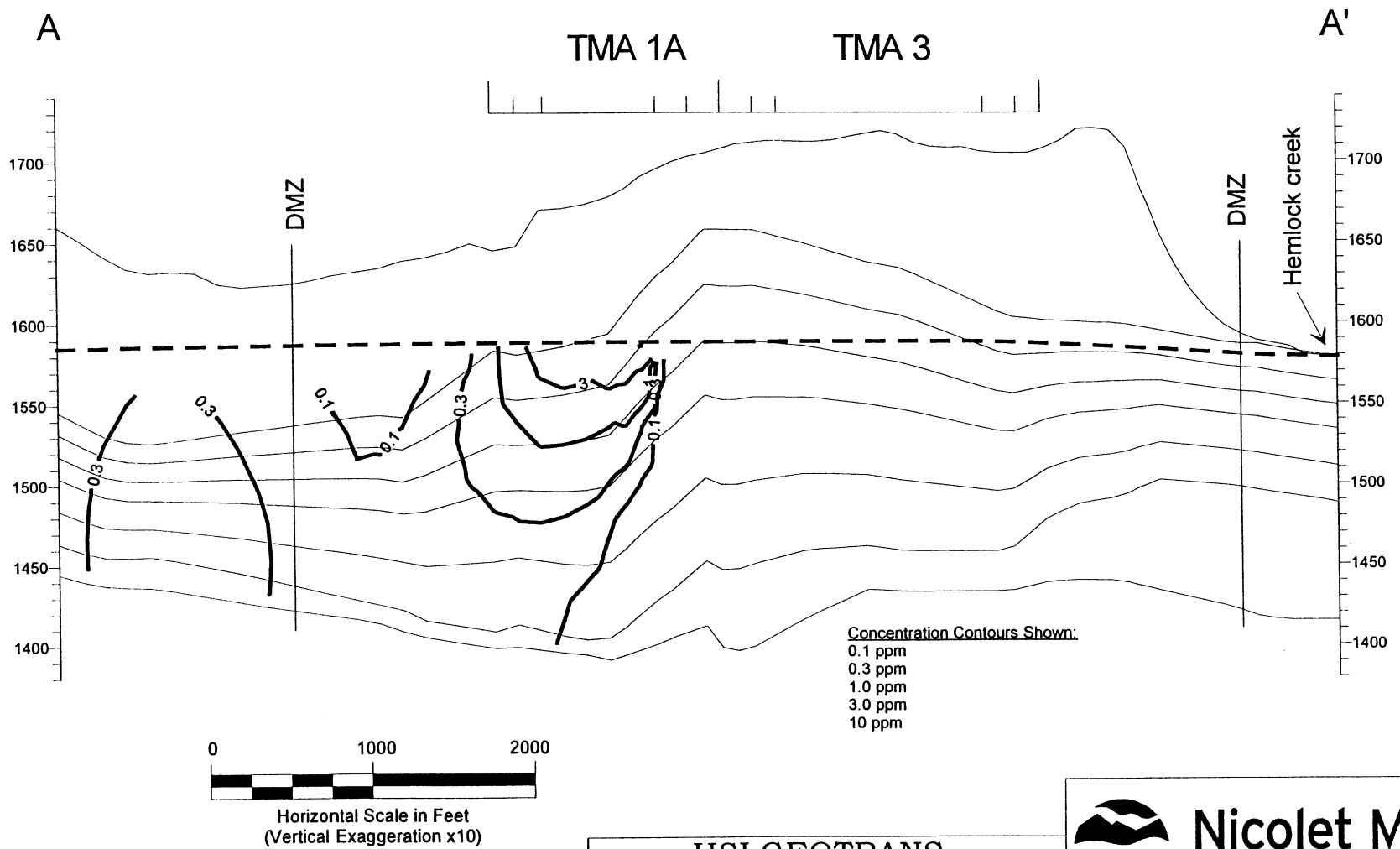

4.2-10-488

Source Concentration
1) TMA Operation: 2,000 ppm
2) TMA Consolidation: 2,500 ppm
3) TMA Post Cap: 4,000 ppm
4) TMA Post FML Degradation: 4,000 ppm
5) Reclaim Pond Operation: 1,000 ppm
6) Reclaim Pond Post Cap: 4,000 ppm

Simulations
T13C1 - T13C6

HSI GEOTRANS

REVISED	DATE	BY	DESCRIPTION

CHECKED BY: GWC	DATE: 3/00
APPROVED BY: PFA	DATE: 3/00
APPROVED BY:	DATE:

Nicolet Minerals
a Rio Algom company

Figure 24
BEJT Concentration After 22 Years
(Example Constituent, Cross-Section)

Scale: 1" = 1000' (h), 100' (v)	Date: March 2000
Prepared By: HSI GeoTrans	By: JDC

P:\Crandon\TmaMod4\Surfer\X13hy032.srf

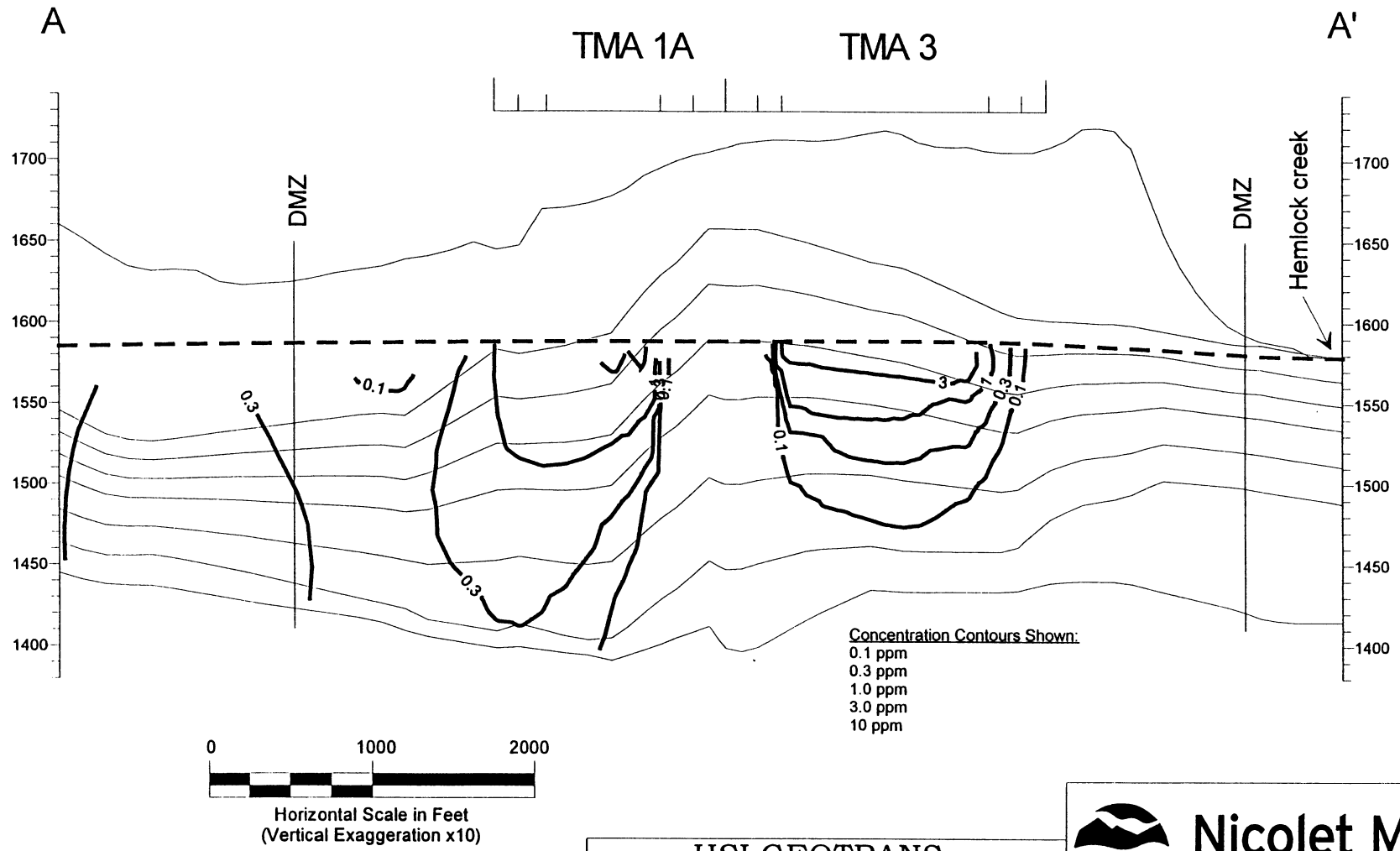

4.2-10-489

Source Concentration
1) TMA Operation: 2,000 ppm
2) TMA Consolidation: 2,500 ppm
3) TMA Post Cap: 4,000 ppm
4) TMA Post FML Degradation: 4,000 ppm
5) Reclaim Pond Operation: 1,000 ppm
6) Reclaim Pond Post Cap: 4,000 ppm

Simulations
T13C1 - T13C6

HSI GEOTRANS

REVISED	DATE	BY	DESCRIPTION

CHECKED BY: GWC	DATE: 3/00
APPROVED BY: PFA	DATE: 3/00
APPROVED BY:	DATE:

Nicolet Minerals
a Rio Algom company

Figure 25
BEJT Concentration After 32 Years
(Example Constituent, Cross-Section)

Scale: 1" = 1000' (h), 100' (v)	Date: March 2000
Prepared By: HSI GeoTrans	By: JDC

P:\Crandon\TmaMod4\Surfer\X13hy060.srf

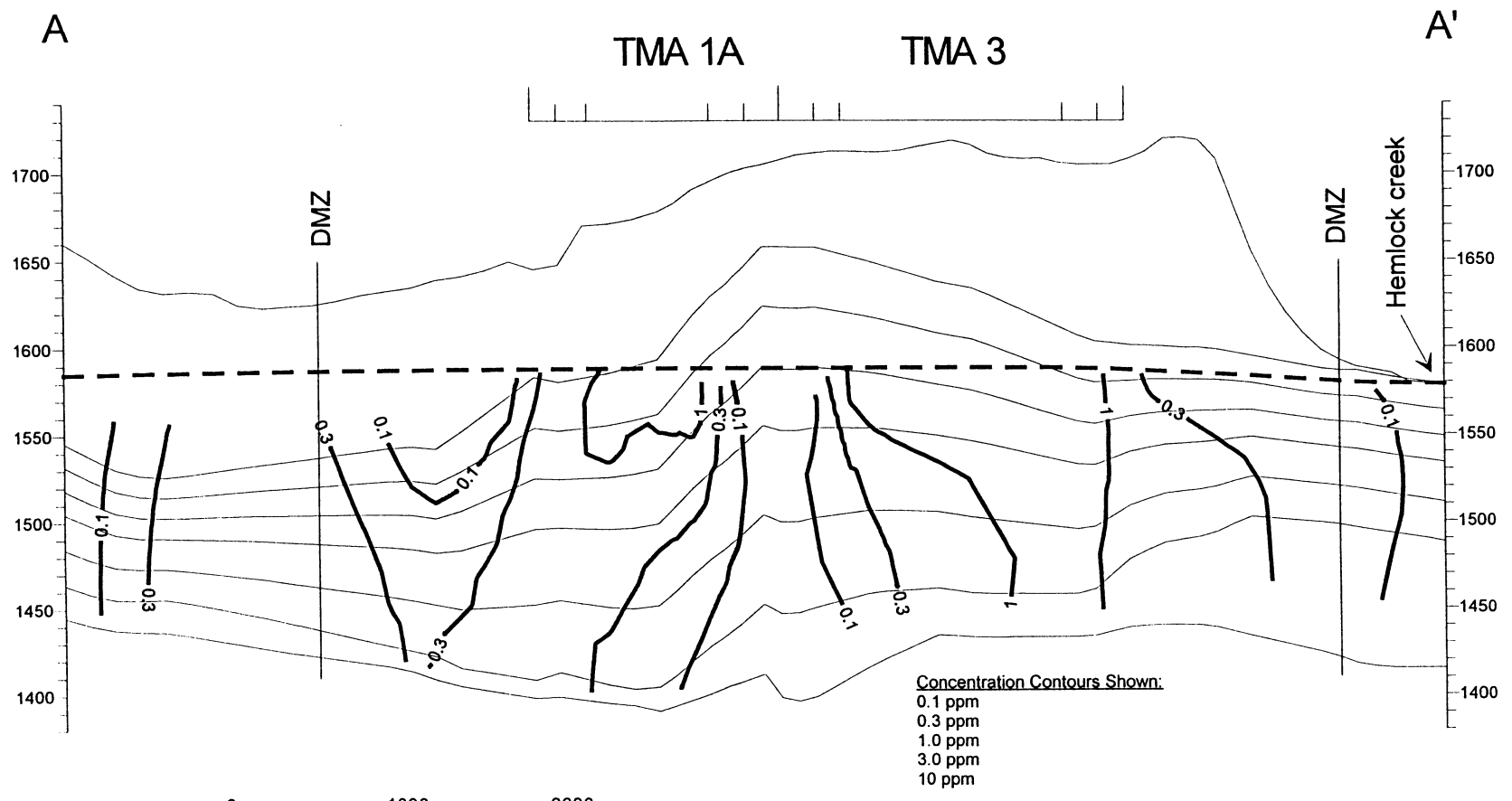

4.2-10-490

Source Concentration
1) TMA Operation: 2,000 ppm
2) TMA Consolidation: 2,500 ppm
3) TMA Post Cap: 4,000 ppm
4) TMA Post FML Degradation: 4,000 ppm
5) Reclaim Pond Operation: 1,000 ppm
6) Reclaim Pond Post Cap: 4,000 ppm

Simulations
T13C1 - T13C6

HSI GEOTRANS

REVISED	DATE	BY	DESCRIPTION

CHECKED BY: GWC	DATE: 3/00
APPROVED BY: PFA	DATE: 3/00
APPROVED BY:	DATE:

Nicolet Minerals
a Rio Algom company

Figure 26
BEJT Concentration After 60 Years
(Example Constituent, Cross-Section)

Scale: 1" = 1000' (h), 100' (v)	Date: March 2000
Prepared By: HSI GeoTrans	By: JDC

P:\Crandon\TmaMod4\Surfer\X13hy125.srf

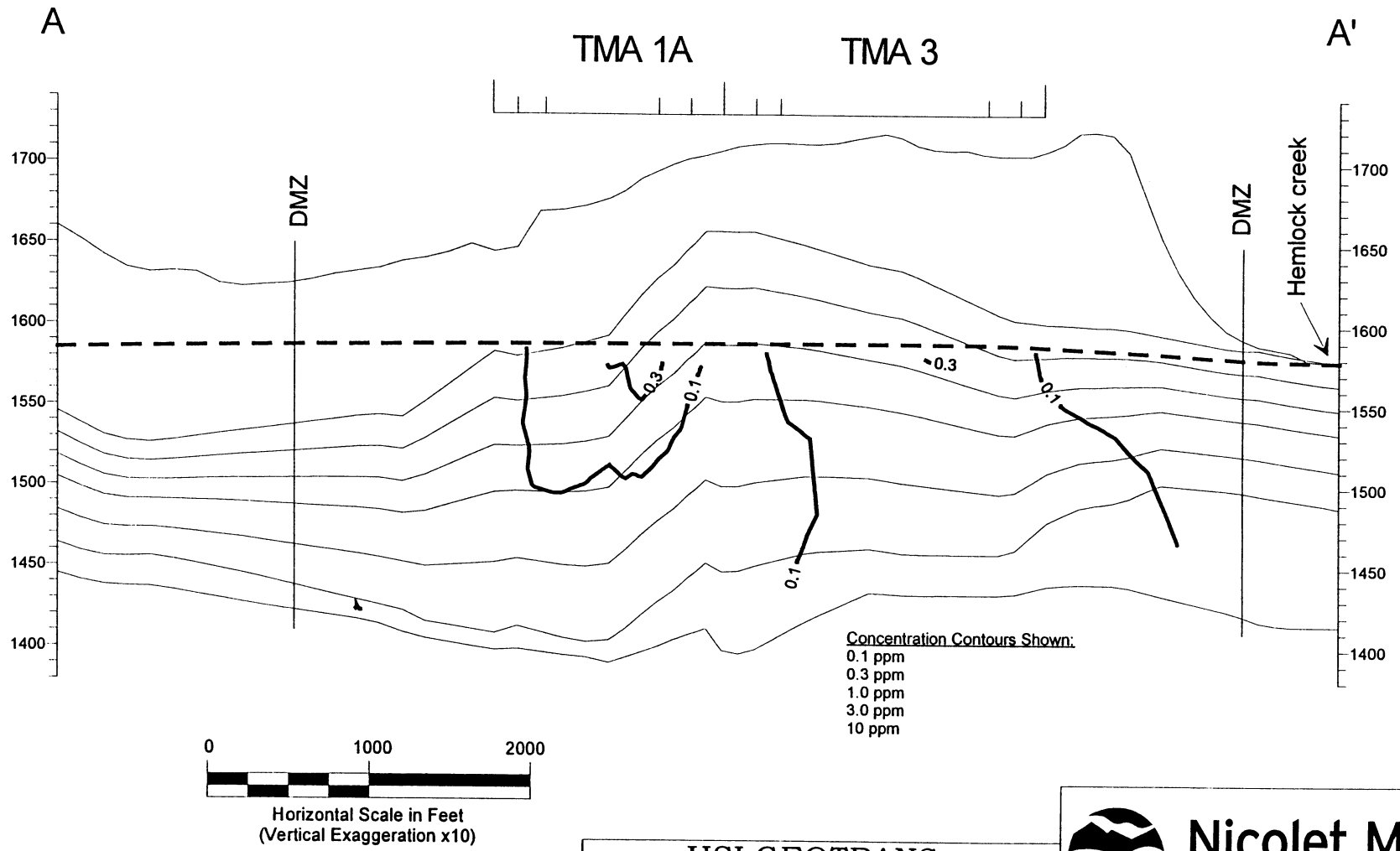

4.2-10-491

Source Concentration
1) TMA Operation: 2,000 ppm
2) TMA Consolidation: 2,500 ppm
3) TMA Post Cap: 4,000 ppm
4) TMA Post FML Degradation: 4,000 ppm
5) Reclaim Pond Operation: 1,000 ppm
6) Reclaim Pond Post Cap: 4,000 ppm

Simulations
T13C1 - T13C6

HSI GEOTRANS

REVISED	DATE	BY	DESCRIPTION

CHECKED BY: GWC	DATE: 3/00
APPROVED BY: PFA	DATE: 3/00
APPROVED BY:	DATE:

Nicolet Minerals
a Rio Algom company

Figure 27
BEJT Concentration After 125 Years
(Example Constituent, Cross-Section)

Scale: 1" = 1000' (h), 100' (v)	Date: March 2000
Prepared By: HSI GeoTrans	By: JDC

P:\Crandon\TmaMod4\Surfer\X13hy200.srf

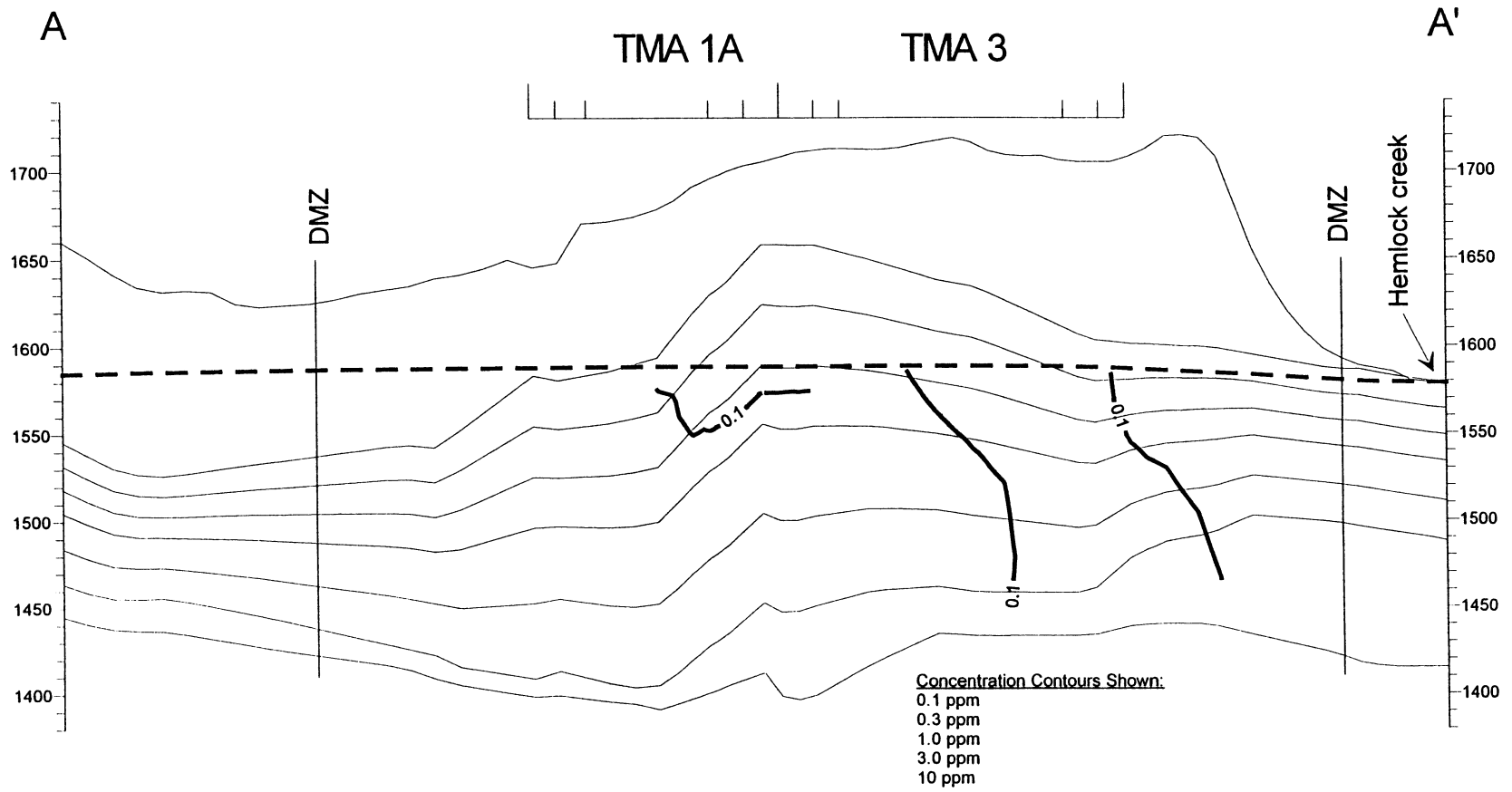

4.2-10-492

Source Concentration
1) TMA Operation: 2,000 ppm
2) TMA Consolidation: 2,500 ppm
3) TMA Post Cap: 4,000 ppm
4) TMA Post FML Degradation: 4,000 ppm
5) Reclaim Pond Operation: 1,000 ppm
6) Reclaim Pond Post Cap: 4,000 ppm

Simulations
T13C1 - T13C6

HSI GEOTRANS

REVISED	DATE	BY	DESCRIPTION

CHECKED BY: GWC	DATE: 3/00
APPROVED BY: PFA	DATE: 3/00
APPROVED BY:	DATE:

Nicolet Minerals
a Rio Algom company

Figure 28
BEJT Concentration After 200 Years
(Example Constituent, Cross-Section)

Scale: 1" = 1000' (h), 100' (v)	Date: March 2000
Prepared By: HSI GeoTrans	By: JDC

P:\Crandon\TmaMod4\Surfer\X13hy300.srf

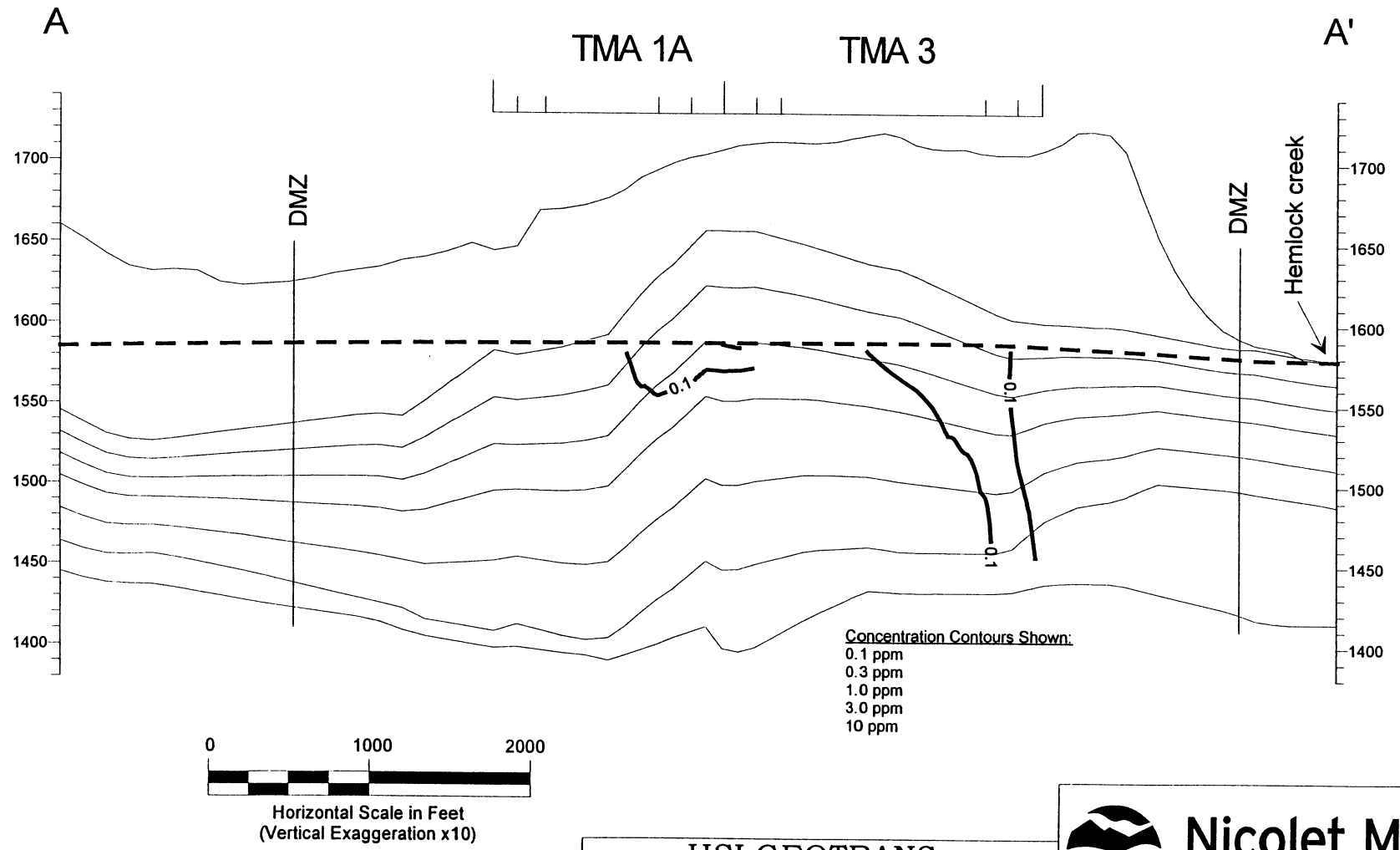

4.2-10-493

Source Concentration
1) TMA Operation: 2,000 ppm
2) TMA Consolidation: 2,500 ppm
3) TMA Post Cap: 4,000 ppm
4) TMA Post FML Degradation: 4,000 ppm
5) Reclaim Pond Operation: 1,000 ppm
6) Reclaim Pond Post Cap: 4,000 ppm

Simulations
T13C1 - T13C6

HSI GEOTRANS

REVISED	DATE	BY	DESCRIPTION

CHECKED BY: GWC	DATE: 3/00
APPROVED BY: PFA	DATE: 3/00
APPROVED BY:	DATE:

Nicolet Minerals
a Rio Algom company

Figure 29
BEJT Concentration After 300 Years
(Example Constituent, Cross-Section)

Scale: 1" = 1000' (h), 100' (v)	Date: March 2000
Prepared By: HSI GeoTrans	By: JDC

P:\Crandon\TmaMod4\Surfer\X13hy650.srf

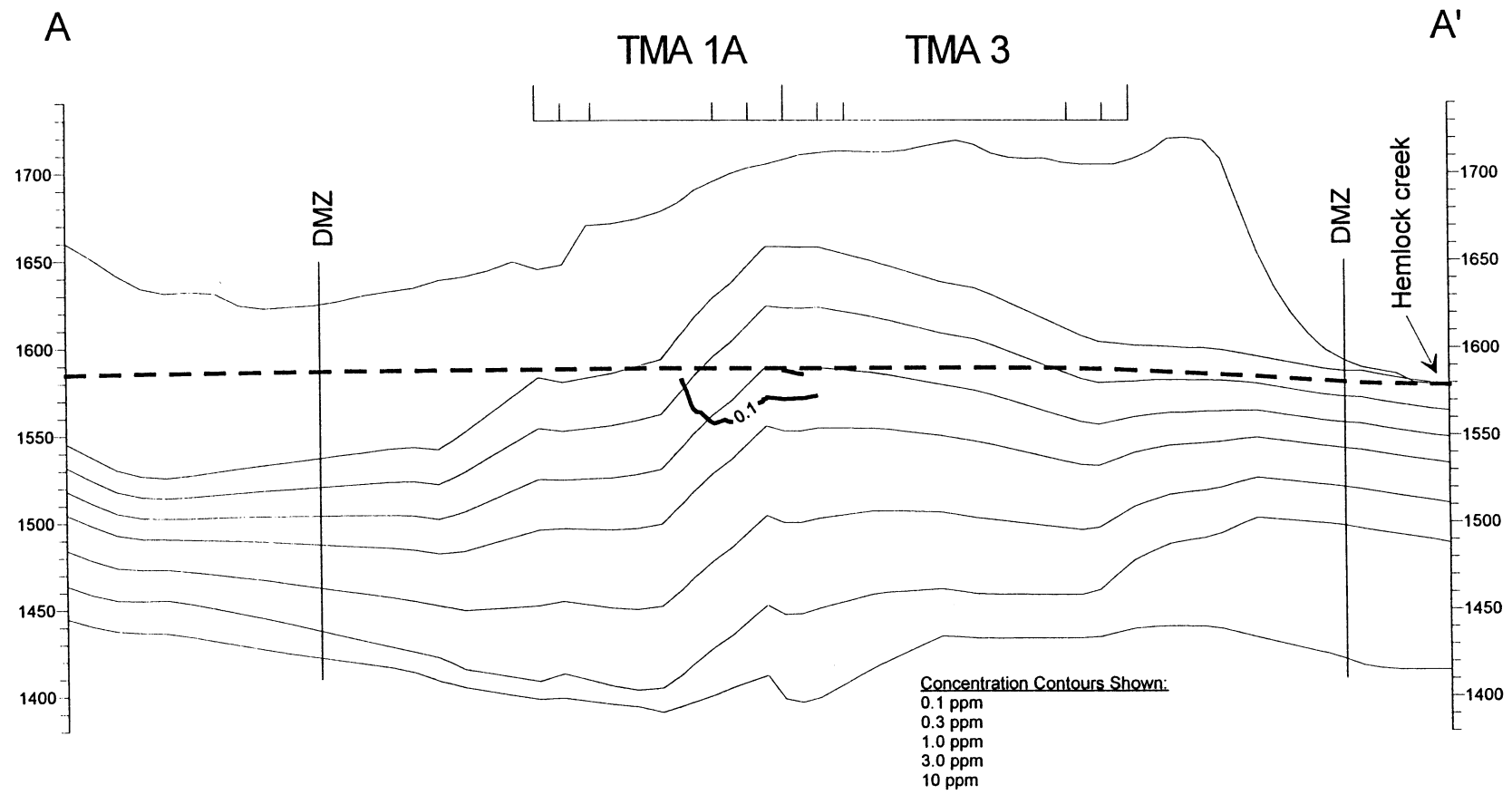

4.2-10-494

Source Concentration
1) TMA Operation: 2,000 ppm
2) TMA Consolidation: 2,500 ppm
3) TMA Post Cap: 4,000 ppm
4) TMA Post FML Degradation: 4,000 ppm
5) Reclaim Pond Operation: 1,000 ppm
6) Reclaim Pond Post Cap: 4,000 ppm

Simulations
T13C1 - T13C6

HSI GEOTRANS

REVISED	DATE	BY	DESCRIPTION

CHECKED BY: GWC	DATE: 3/00
APPROVED BY: PFA	DATE: 3/00
APPROVED BY:	DATE:

Nicolet Minerals
a Rio Algom company

Figure 30
BEJT Concentration After 650 Years
(Example Constituent, Cross-Section)

Scale: 1" = 1000' (h), 100' (v)	Date: March 2000
Prepared By: HSI GeoTrans	By: JDC

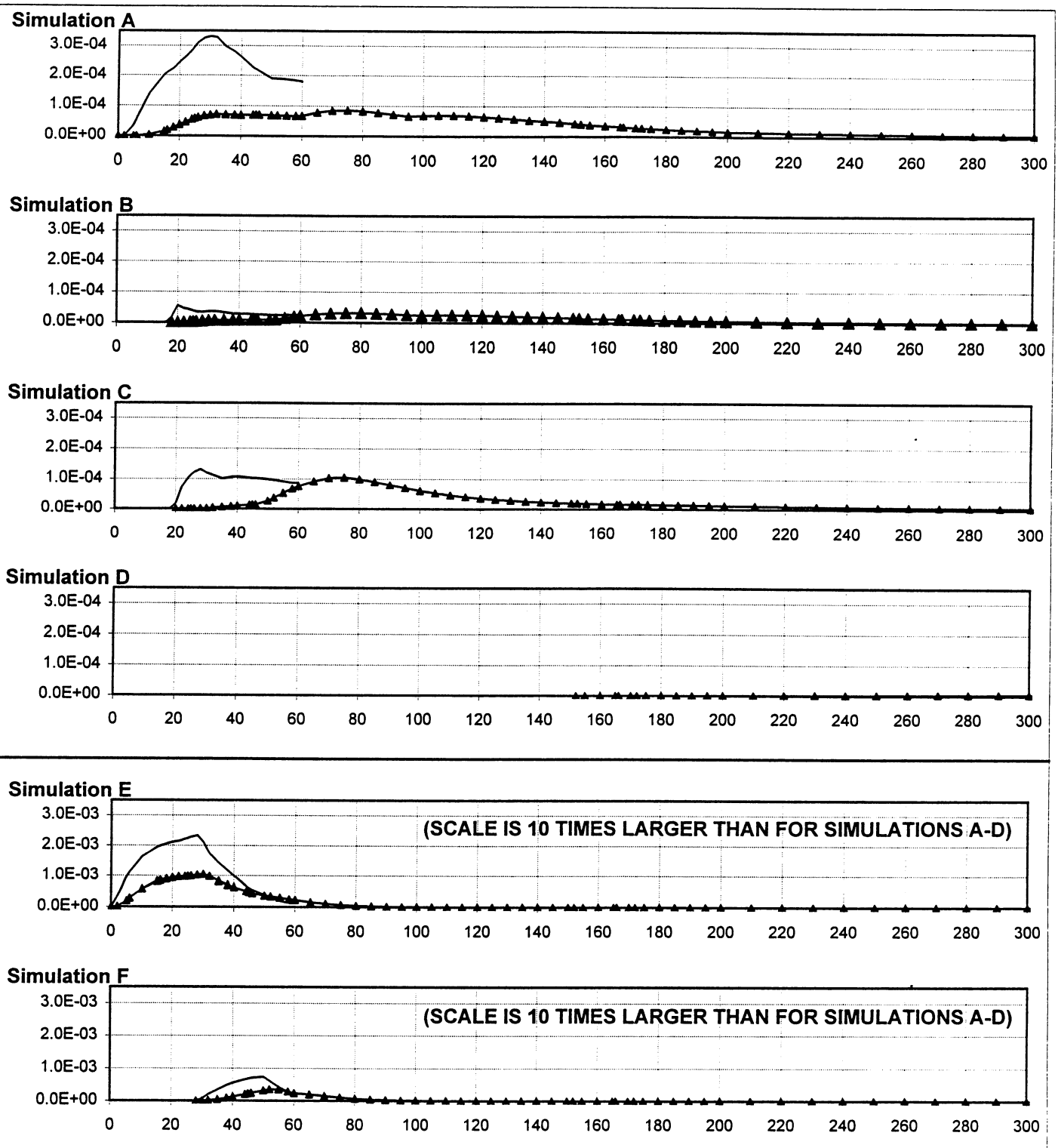

Note:

Maximum concentration at any cell on the DMZ is plotted
Y axis is concentration response (unitless)
X axis is time in years

TMA DMZ
Rec Pond DMZ

HSI GEOTRANS

REVISED	DATE	BY	DESCRIPTION

CHECKED BY:GWC	DATE:3/00
APPROVED BY:PFA	DATE:3/00
APPROVED BY:	DATE:

Simulation T14c

Nicolet Minerals
a Rio Algom company

Figure 31
PWCT Concentration Response Curves at the Design Management Zones (DMZs)

Scale: None	Date:March 2000
Prepared By: HSI GEOTRANS	By:LMG

4.2-10-495

\Crandon\Flowmod2\Excel\49a-Res.xls

\Crandon\TmaMod4\Excel\hypothet2.xls.pwc

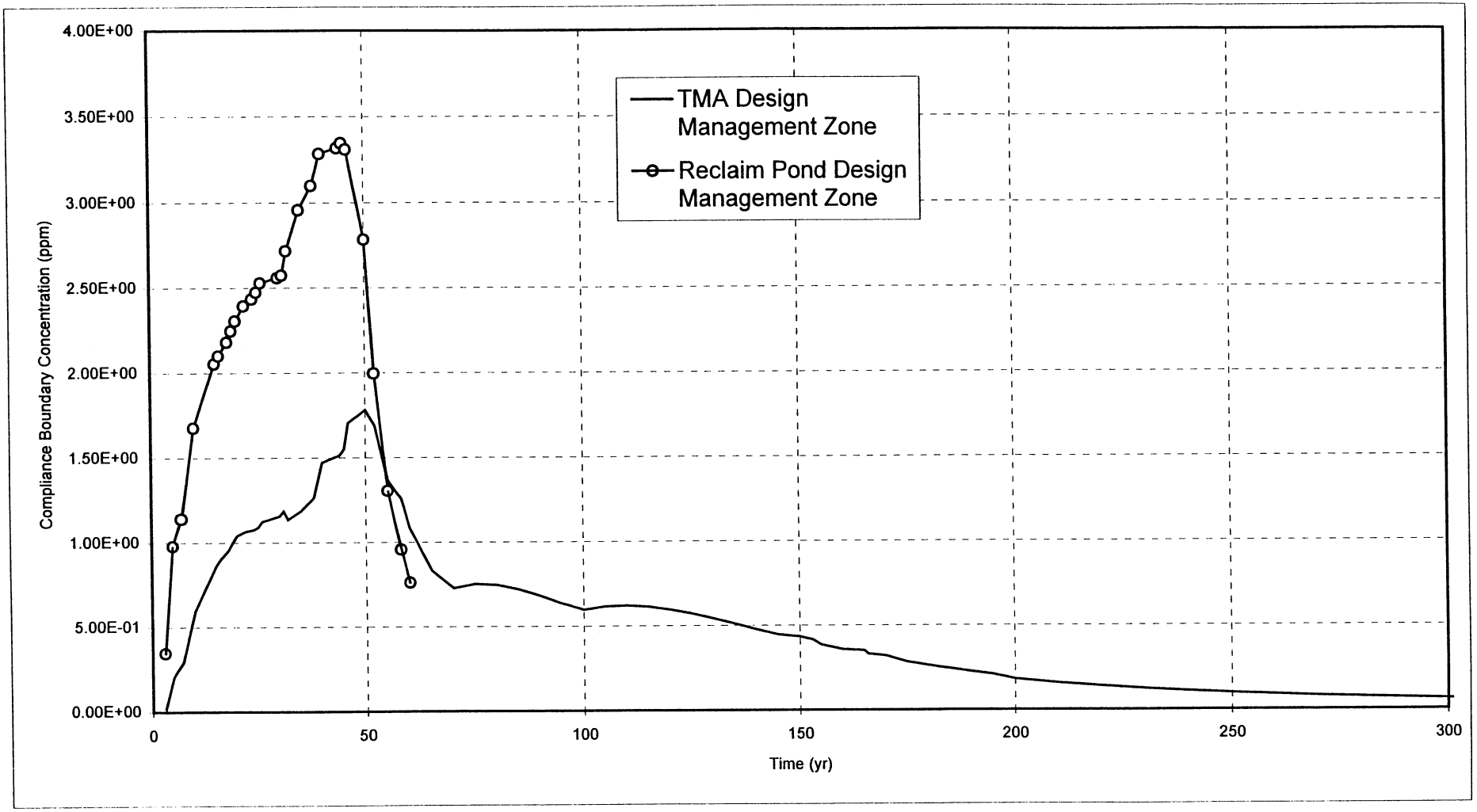

4.2-10-496

Source Concentration:

Operation:	2000 ppm
Consolidation:	2500 ppm
Post-Cap:	4000 ppm
Post-FML-Degradation:	4000 ppm
Reclaim Pond Operation:	1000 ppm
Reclaim Pond Post-Cap:	4000 ppm

HSI GEOTRANS			
REVISED	DATE	BY	DESCRIPTION

CHECKED BY: GWC	DATE: Mar 2000
APPROVED BY: PFA	DATE: Mar 2000
APPROVED BY:	DATE:

Simulations T14C*

Nicolet Minerals
a Rio Algom company

Figure 32
PWCT Concentration at the Design Management Zones (Example Constituent)

Scale: None	Date: Mar 2000
Prepared By: HSI GEOTRANS	By: LMG

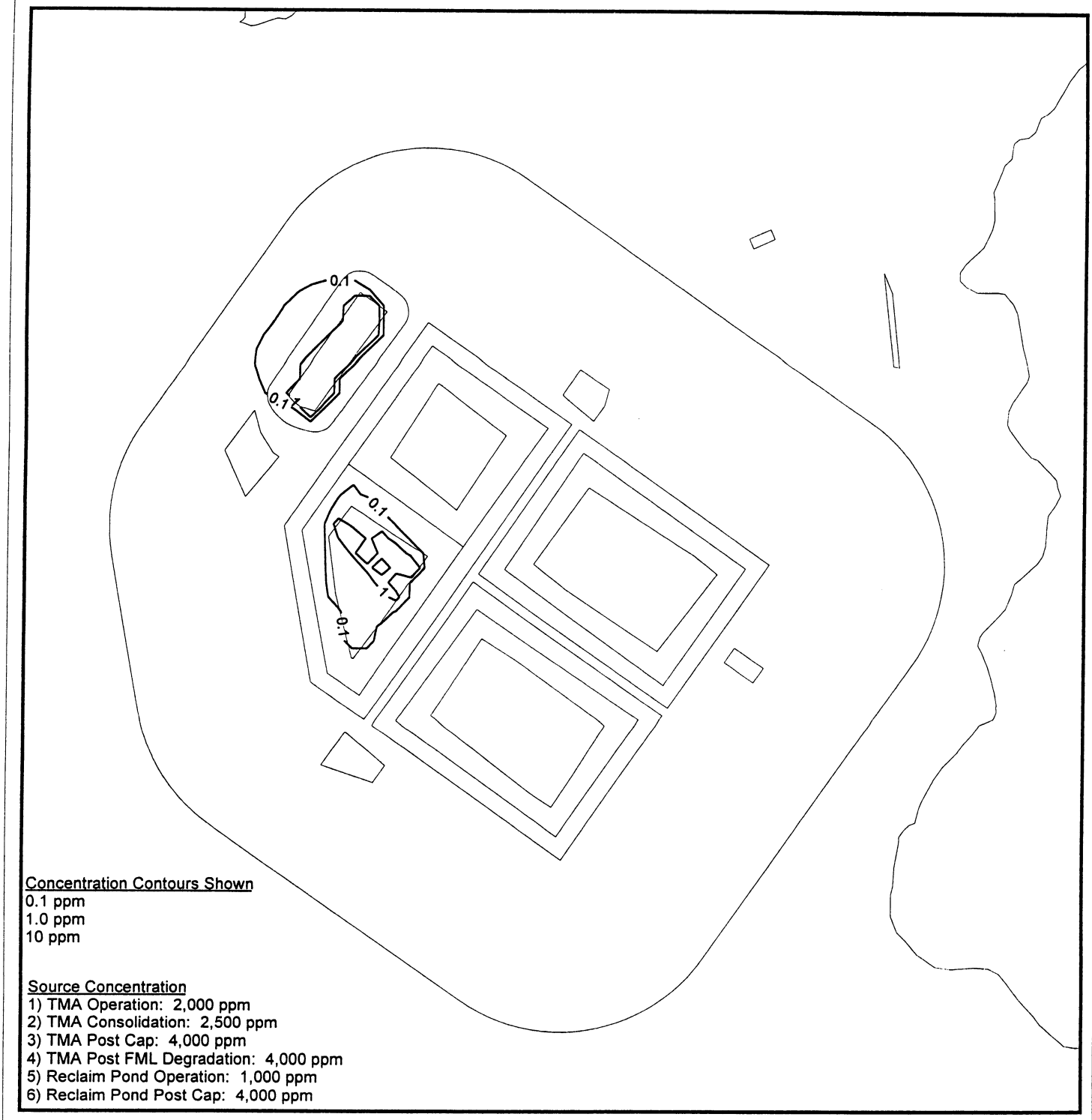

Concentration Contours Shown
0.1 ppm
1.0 ppm
10 ppm

Source Concentration
1) TMA Operation: 2,000 ppm
2) TMA Consolidation: 2,500 ppm
3) TMA Post Cap: 4,000 ppm
4) TMA Post FML Degradation: 4,000 ppm
5) Reclaim Pond Operation: 1,000 ppm
6) Reclaim Pond Post Cap: 4,000 ppm

Note:
This plot shows
contours of maximum
concentratration in any layer.

N

0 1000 2000

Scale in Feet

HSI GEOTRANS

REVISED	DATE	BY	DESCRIPTION

CHECKED BY: GWC		DATE: 3/00
APPROVED BY: PFA		DATE: 3/00
APPROVED BY:		DATE:

Simulations
T14C1 - T14C6

4.2-10-497

Nicolet Minerals
a Rio Algom company

Figure 33
PWCT Concentration After 2 Years
(Example Constituent, Plan View)

Scale: 1 in. = 1000 ft.	Date: March 2000
Prepared By: HSI GEOTRANS	By: JDC

P:\Crandon\Tma\Mod4\Surfer\P14fy002.srf

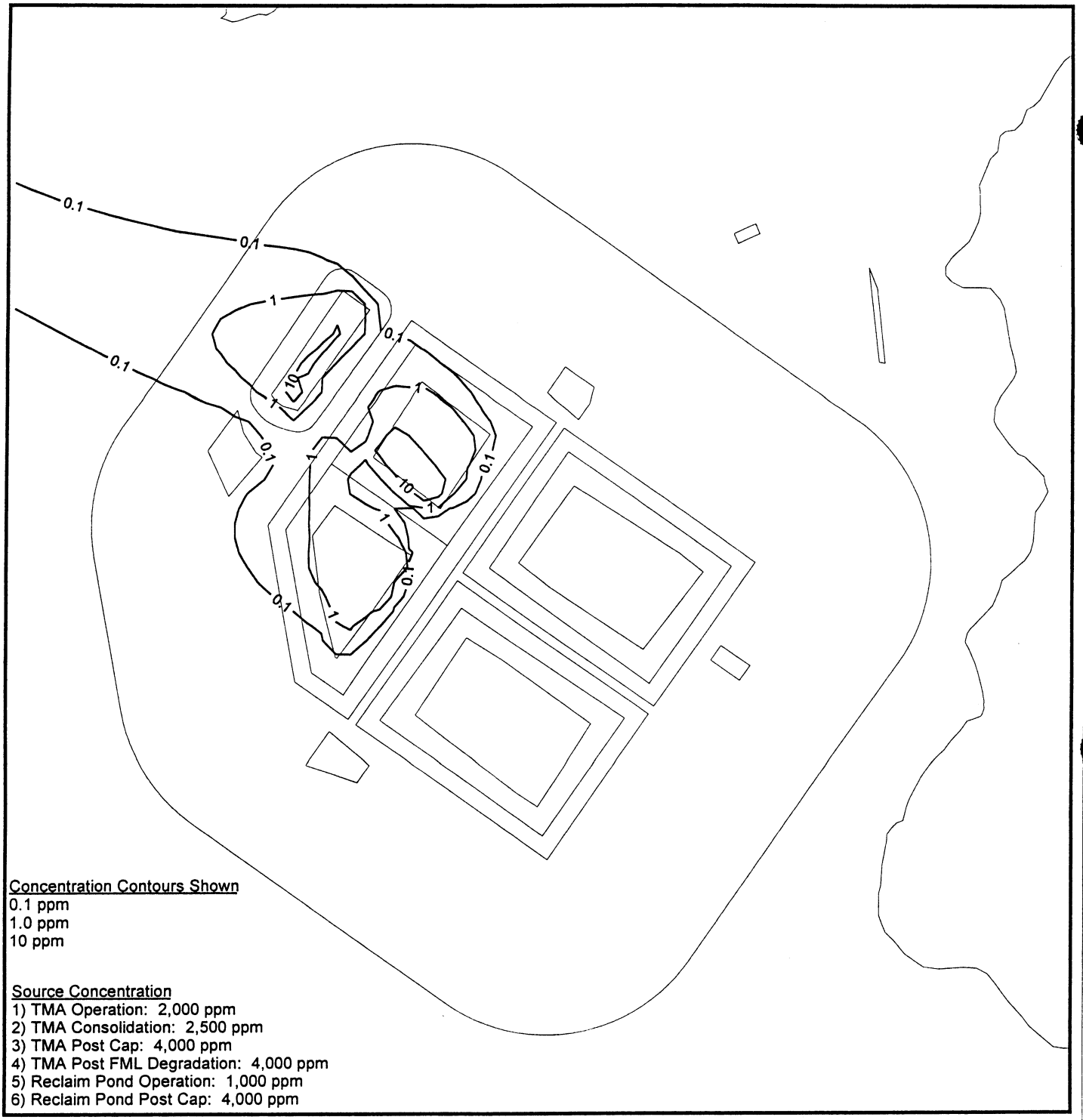

Concentration Contours Shown
0.1 ppm
1.0 ppm
10 ppm

Source Concentration
1) TMA Operation: 2,000 ppm
2) TMA Consolidation: 2,500 ppm
3) TMA Post Cap: 4,000 ppm
4) TMA Post FML Degradation: 4,000 ppm
5) Reclaim Pond Operation: 1,000 ppm
6) Reclaim Pond Post Cap: 4,000 ppm

Note:
This plot shows
contours of maximum
concentratration in any layer.

N

0 1000 2000

Scale in Feet

HSI GEOTRANS

REVISED	DATE	BY	DESCRIPTION

CHECKED BY: GWC DATE: 3/00

APPROVED BY: PFA DATE: 3/00

APPROVED BY: DATE:

Simulations
T14C1 - T14C6

4.2-10-498

Nicolet Minerals
a Rio Algom company

Figure 34
PWCT Concentration After 16 Years
(Example Constituent, Plan View)

Scale: 1 in. = 1000 ft. Date: March 2000

Prepared By: HSI GEOTRANS By: JDC

P:\Crandon\Tma\Mod4\Surfer\P14fy016.srf

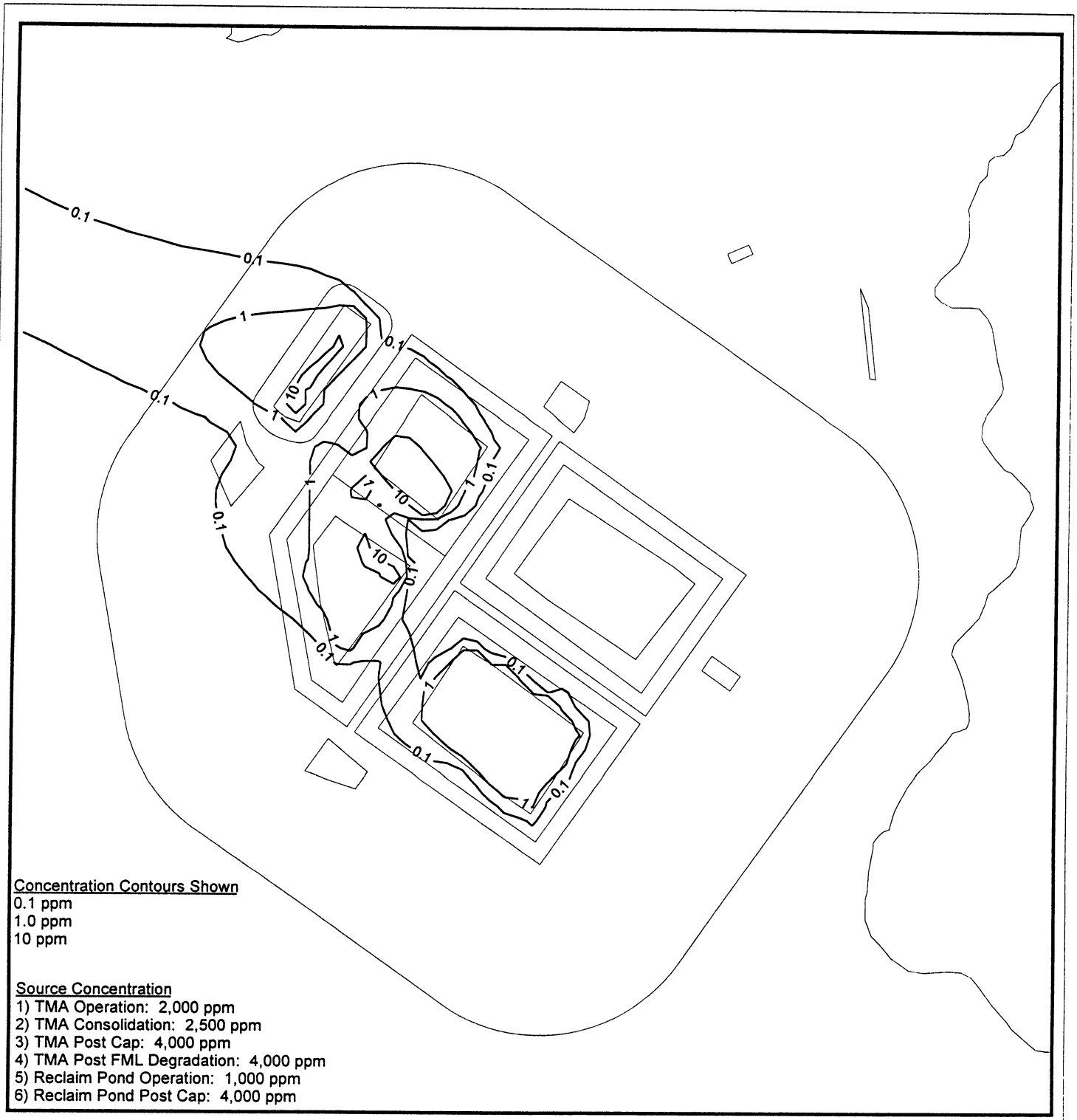

Concentration Contours Shown
0.1 ppm
1.0 ppm
10 ppm

Source Concentration
1) TMA Operation: 2,000 ppm
2) TMA Consolidation: 2,500 ppm
3) TMA Post Cap: 4,000 ppm
4) TMA Post FML Degradation: 4,000 ppm
5) Reclaim Pond Operation: 1,000 ppm
6) Reclaim Pond Post Cap: 4,000 ppm

Note:
This plot shows
contours of maximum
concentratration in any layer.

N

0 1000 2000

Scale in Feet

HSI GEOTRANS

REVISED	DATE	BY	DESCRIPTION

CHECKED BY: GWC		DATE: 3/00
APPROVED BY: PFA		DATE: 3/00
APPROVED BY:		DATE:

Simulations
T14C1 - T14C6

4.2-10-499

Nicolet Minerals
a Rio Algom company

Figure 35
PWCT Concentration After 22 Years
(Example Constituent, Plan View)

Scale: 1 in. = 1000 ft. | Date: March 2000

Prepared By: HSI GEOTRANS | By: JDC

P:\Crandon\TimeMod4\Surfer\Plan022.srf

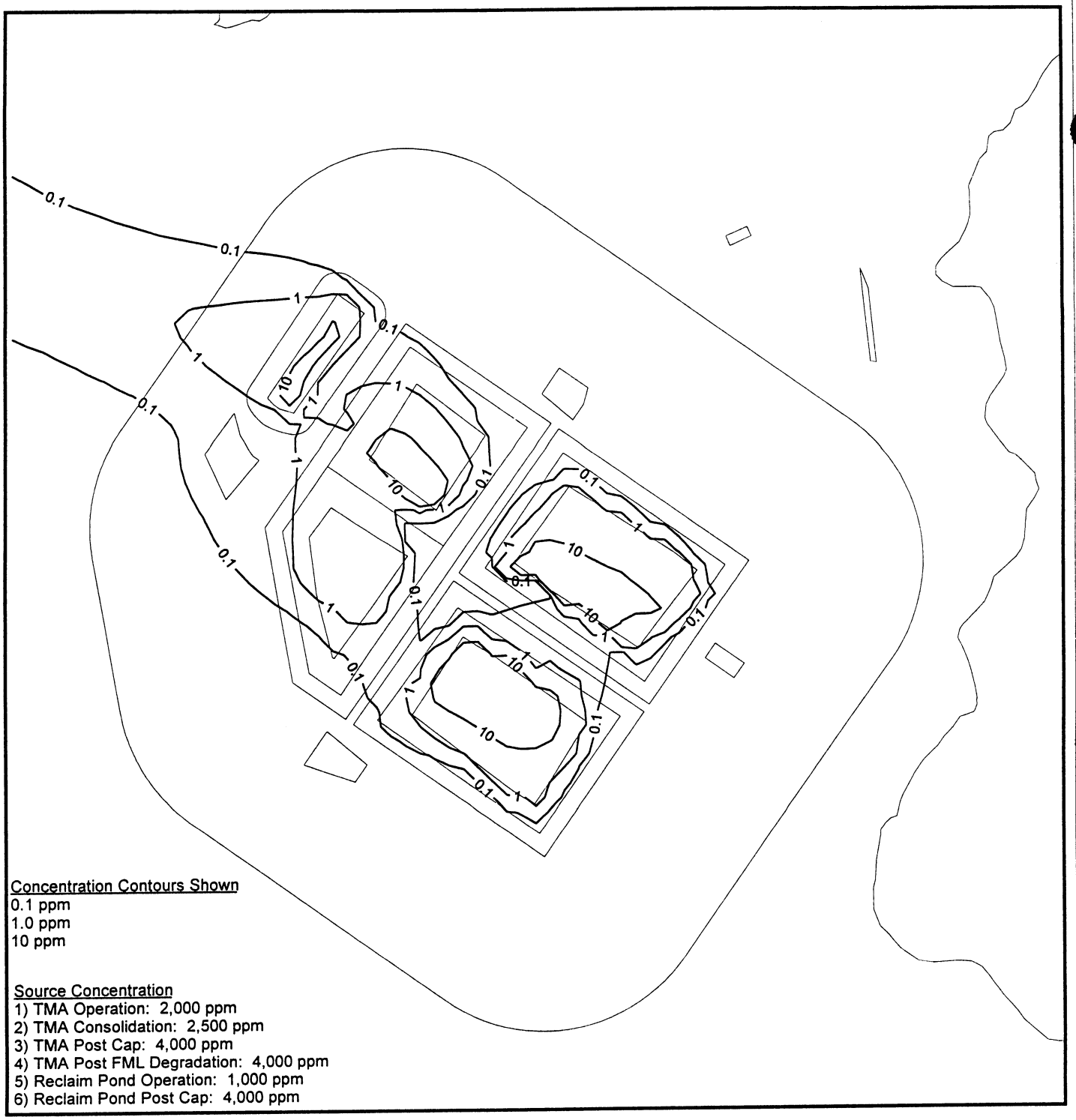

Note:
This plot shows
contours of maximum
concentratration in any layer.

N

0 1000 2000

Scale in Feet

HSI GEOTRANS

REVISED	DATE	BY	DESCRIPTION

CHECKED BY: GWC		DATE: 3/00
APPROVED BY: PFA		DATE: 3/00
APPROVED BY:		DATE:

Simulations
T14C1 - T14C6

4.2-10-500

Nicolet Minerals
a Rio Algom company

Figure 36
PWCT Concentration After 32 Years
(Example Constituent, Plan View)

Scale: 1 in. = 1000 ft. | Date: March 2000

Prepared By: HSI GEOTRANS | By: JDC

P:\Crandon\Tmal\Mod4\Surfer\P14hy032.srf

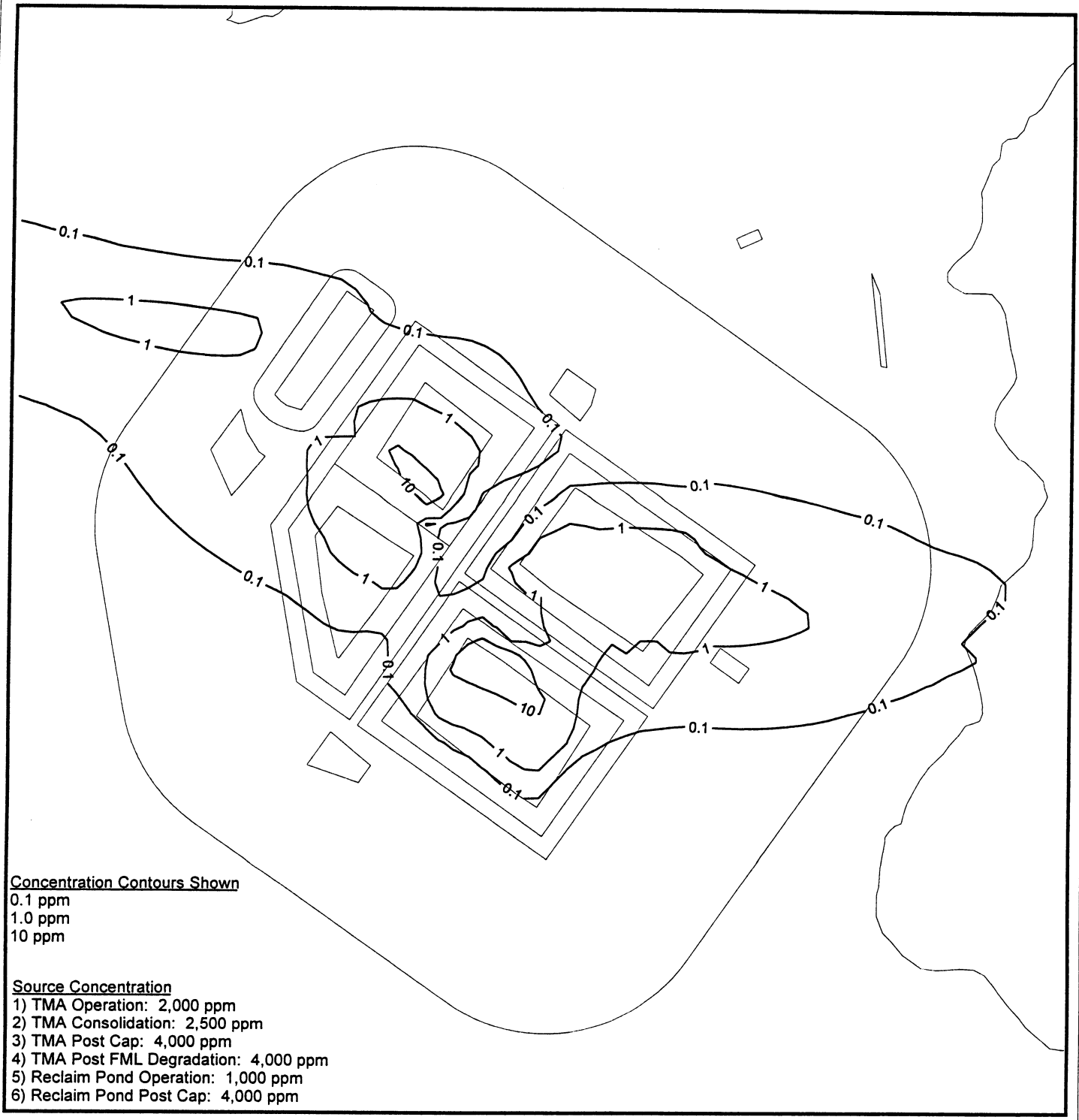

Concentration Contours Shown
0.1 ppm
1.0 ppm
10 ppm

Source Concentration
1) TMA Operation: 2,000 ppm
2) TMA Consolidation: 2,500 ppm
3) TMA Post Cap: 4,000 ppm
4) TMA Post FML Degradation: 4,000 ppm
5) Reclaim Pond Operation: 1,000 ppm
6) Reclaim Pond Post Cap: 4,000 ppm

Note:
This plot shows
contours of maximum
concentratration in any layer.

N

0 1000 2000

Scale in Feet

HSI GEOTRANS

REVISED	DATE	BY	DESCRIPTION

CHECKED BY: GWC		DATE: 3/00
APPROVED BY: PFA		DATE: 3/00
APPROVED BY:		DATE:

Simulations
T14C1 - T14C6

4.2-10-501

Nicolet Minerals
a Rio Algom company

Figure 37
PWCT Concentration After 60 Years
(Example Constituent, Plan View)

Scale: 1 in. = 1000 ft. | Date: March 2000

Prepared By: HSI GEOTRANS | By: JDC

P:\Crandon\TmaMod4\Surfer\P14fy060.srf

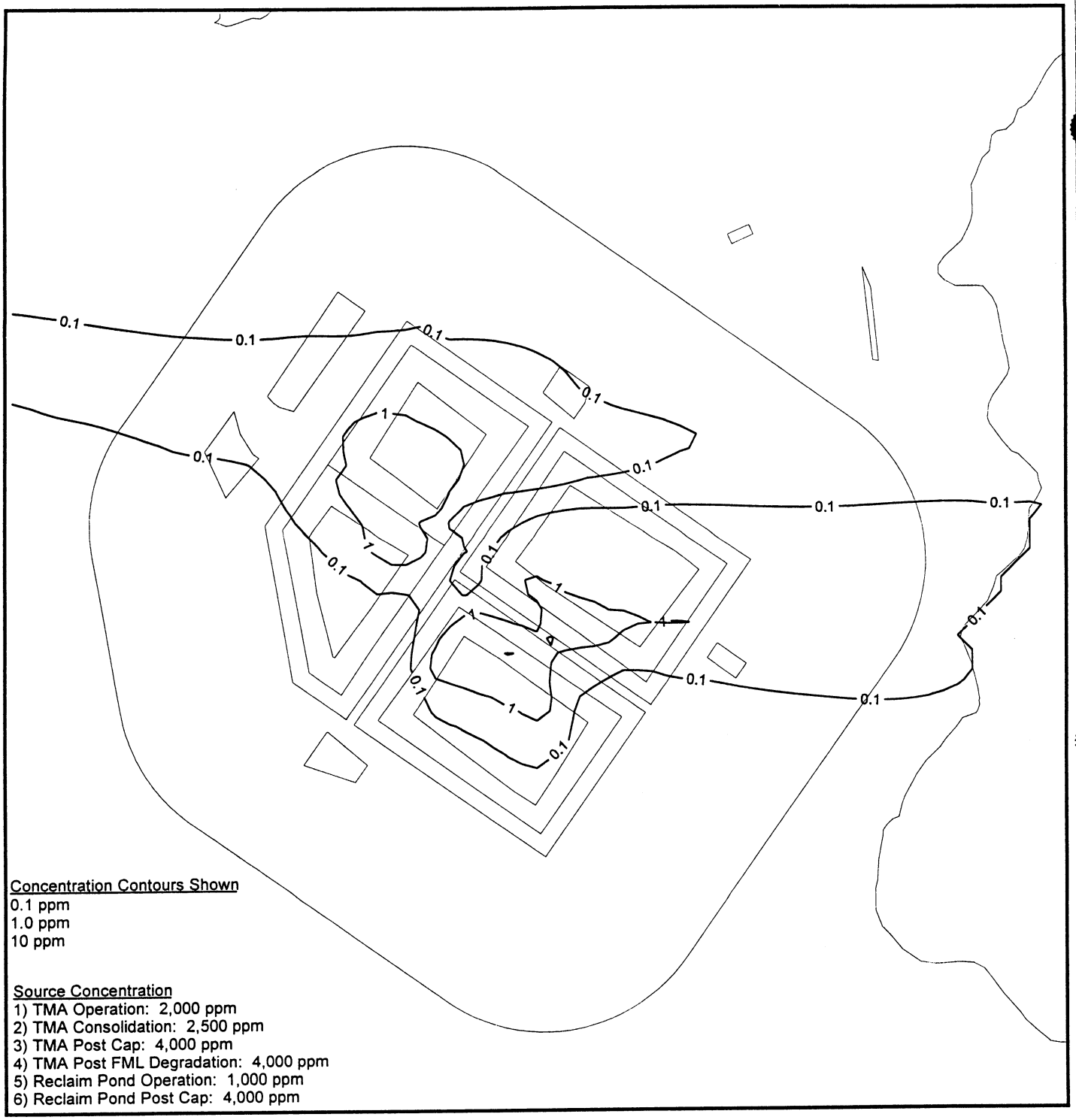

Note:
This plot shows
contours of maximum
concentratration in any layer.

N

0 1000 2000

Scale in Feet

HSI GEOTRANS

REVISED	DATE	BY	DESCRIPTION

	CHECKED BY: GWC	DATE: 3/00
Simulations T14C1 - T14C6	APPROVED BY: PFA	DATE: 3/00
	APPROVED BY:	DATE:

4.2-10-502

Nicolet Minerals
a Rio Algom company

Figure 38
PWCT Concentration After 125 Years
(Example Constituent, Plan View)

Scale: 1 in. = 1000 ft. | Date: March 2000

Prepared By: HSI GEOTRANS | By: JDC

P:\Crandon\Tmwlod4\Surfer\P14hy125.srf

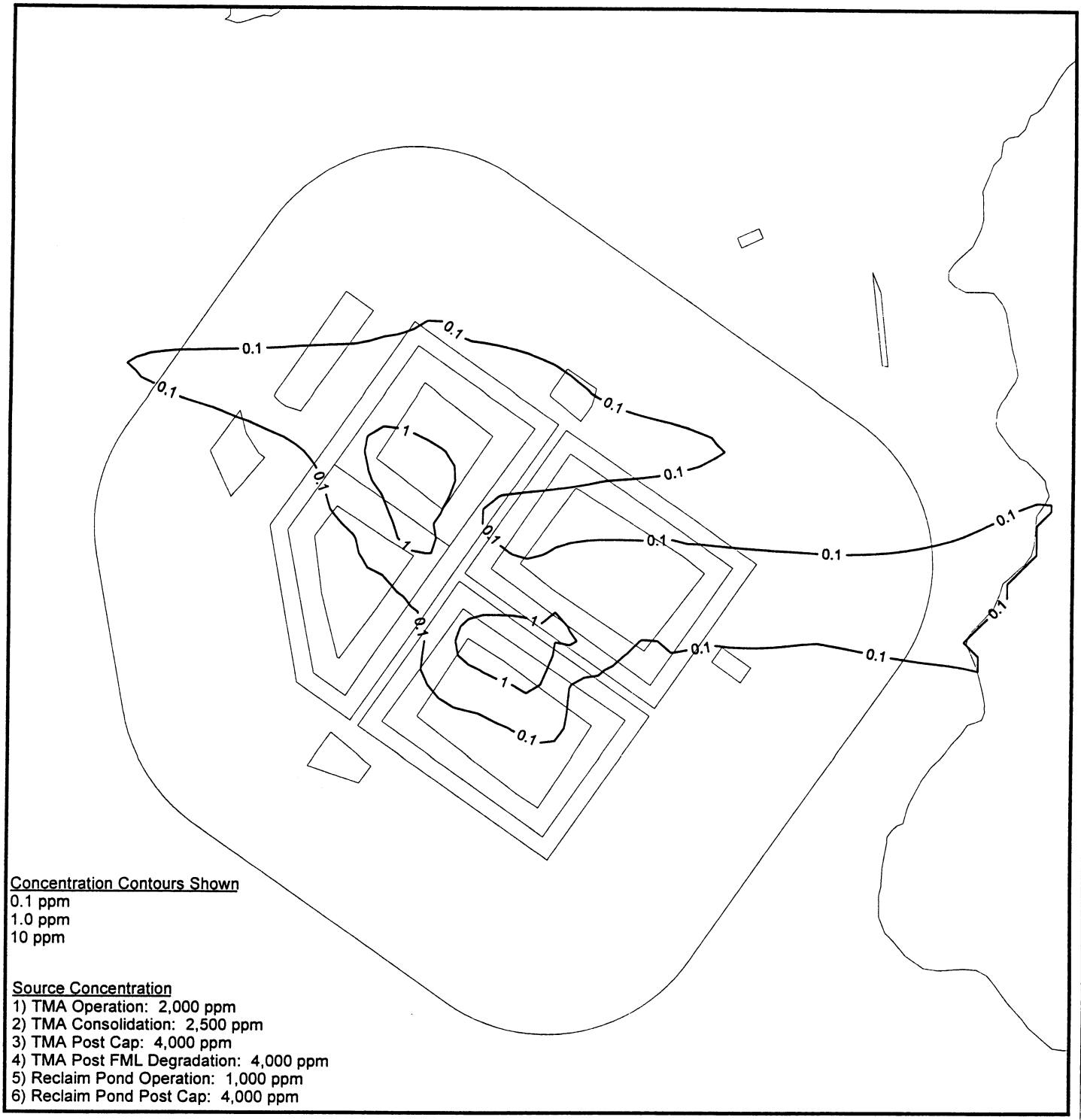

Concentration Contours Shown
0.1 ppm
1.0 ppm
10 ppm

Source Concentration
1) TMA Operation: 2,000 ppm
2) TMA Consolidation: 2,500 ppm
3) TMA Post Cap: 4,000 ppm
4) TMA Post FML Degradation: 4,000 ppm
5) Reclaim Pond Operation: 1,000 ppm
6) Reclaim Pond Post Cap: 4,000 ppm

Note:
This plot shows
contours of maximum
concentratration in any layer.

0 1000 2000
Scale in Feet

HSI GEOTRANS

REVISED	DATE	BY	DESCRIPTION

	CHECKED BY: GWC	DATE: 3/00
Simulations T14C1 - T14C6	APPROVED BY: PFA	DATE: 3/00
	APPROVED BY:	DATE:

4.2-10-503

Nicolet Minerals
a Rio Algom company

Figure 39
PWCT Concentration After 200 Years
(Example Constituent, Plan View)

Scale: 1 in. = 1000 ft.	Date: March 2000
Prepared By: HSI GEOTRANS	By: JDC

P:\Crandon\Tma\Mod4\Surfer\P14y200.srf

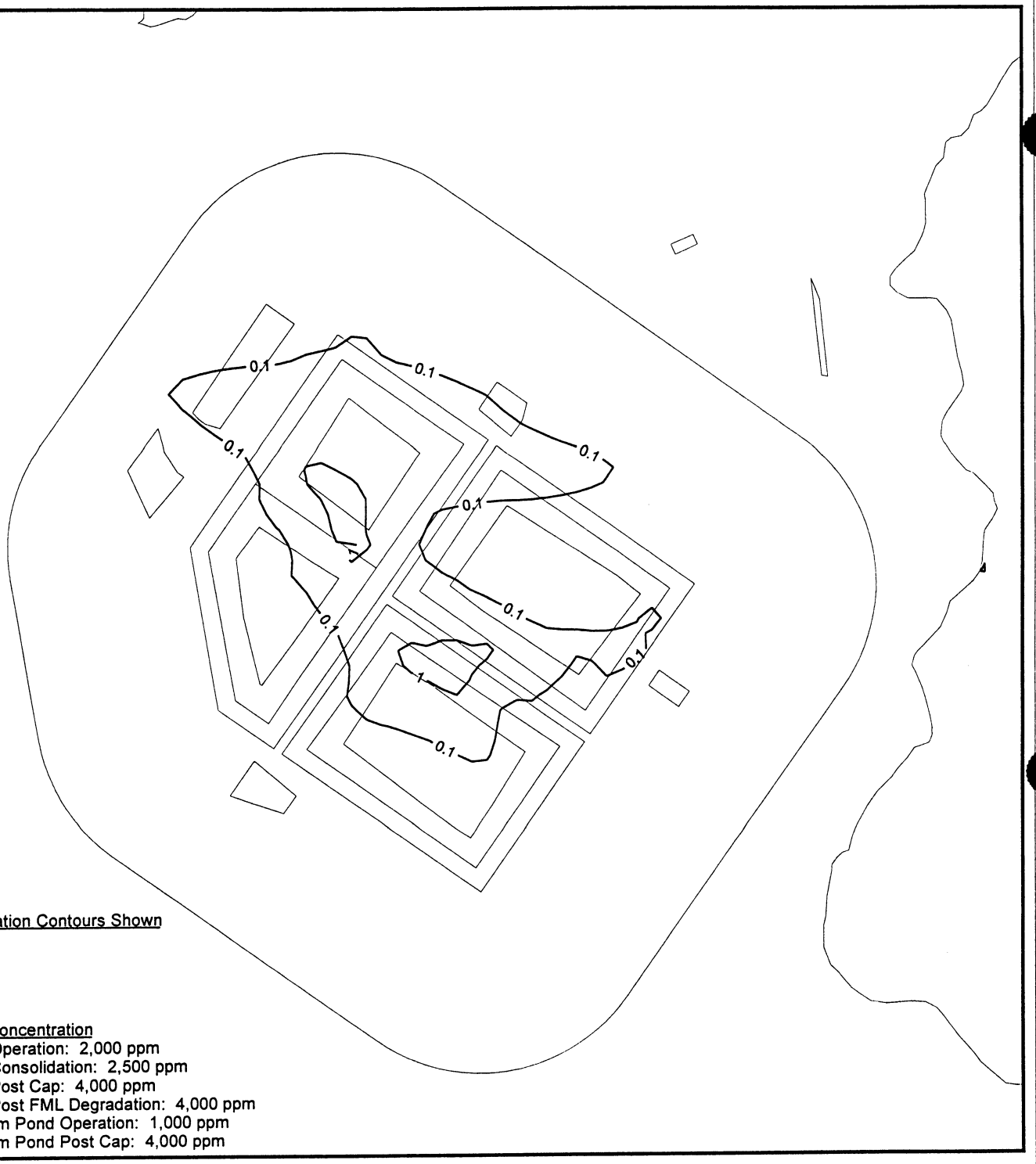

Concentration Contours Shown
0.1 ppm
1.0 ppm
10 ppm

Source Concentration
1) TMA Operation: 2,000 ppm
2) TMA Consolidation: 2,500 ppm
3) TMA Post Cap: 4,000 ppm
4) TMA Post FML Degradation: 4,000 ppm
5) Reclaim Pond Operation: 1,000 ppm
6) Reclaim Pond Post Cap: 4,000 ppm

Note:
This plot shows
contours of maximum
concentratration in any layer.

N

0 1000 2000

Scale in Feet

HSI GEOTRANS

REVISED	DATE	BY	DESCRIPTION

CHECKED BY: GWC		DATE: 3/00
APPROVED BY: PFA		DATE: 3/00
APPROVED BY:		DATE:

Simulations
T14C1 - T14C6

4.2-10-504

Nicolet Minerals
a Rio Algom company

Figure 40
PWCT Concentration After 300 Years
(Example Constituent, Plan View)

Scale: 1 in. = 1000 ft. | Date: March 2000

Prepared By: HSI GEOTRANS | By: JDC

P:\Crandon\Tmawod4\Surfer\P14hy300.srf

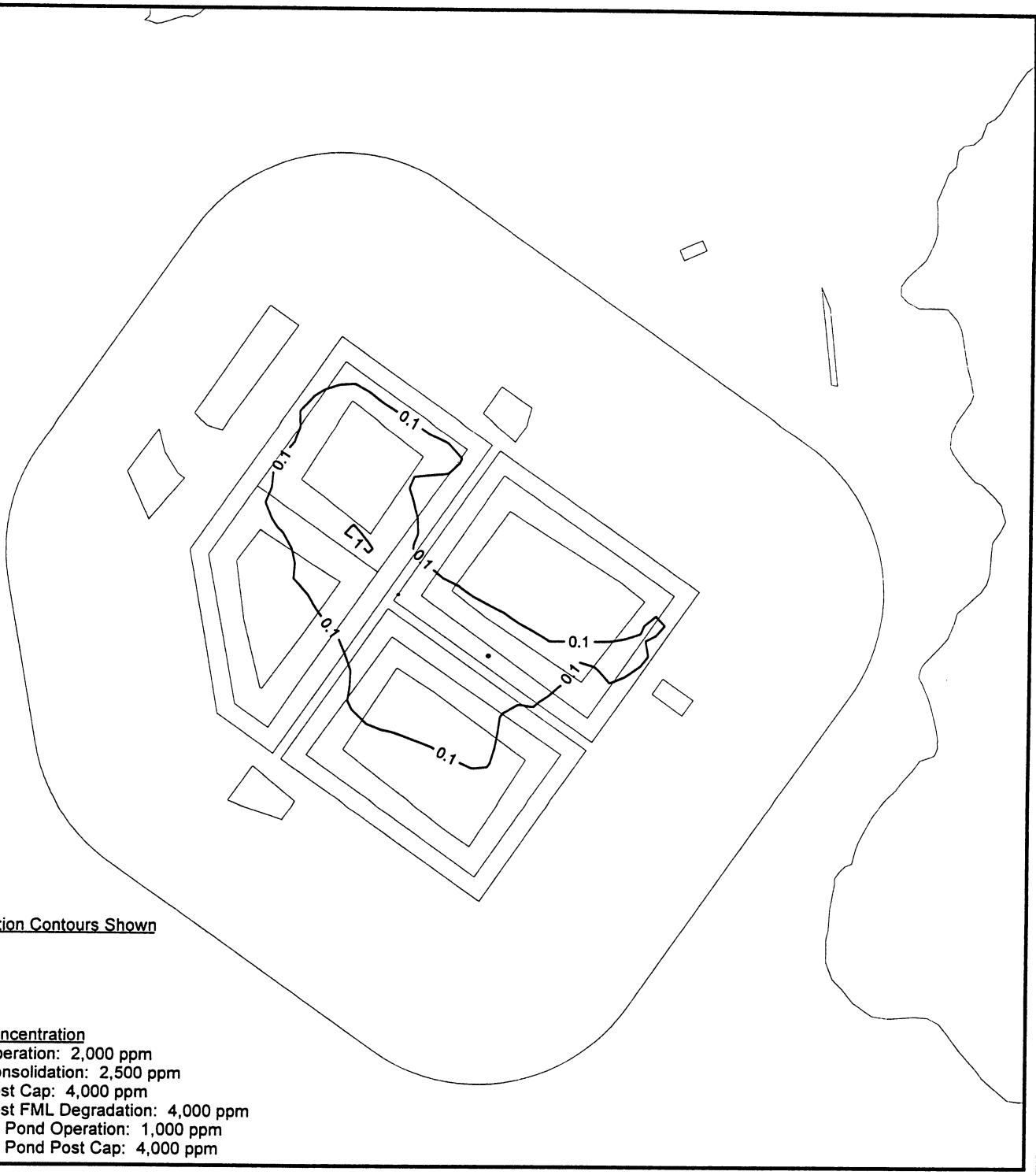

Concentration Contours Shown
0.1 ppm
1.0 ppm
10 ppm

Source Concentration
1) TMA Operation: 2,000 ppm
2) TMA Consolidation: 2,500 ppm
3) TMA Post Cap: 4,000 ppm
4) TMA Post FML Degradation: 4,000 ppm
5) Reclaim Pond Operation: 1,000 ppm
6) Reclaim Pond Post Cap: 4,000 ppm

Note:
This plot shows
contours of maximum
concentratration in any layer.

0 1000 2000
Scale in Feet

HSI GEOTRANS

REVISED	DATE	BY	DESCRIPTION

CHECKED BY: GWC DATE: 3/00
APPROVED BY: PFA DATE: 3/00
APPROVED BY: DATE:

Simulations
T14C1 - T14C6

4.2-10-505

Nicolet Minerals
a Rio Algom company

Figure 41
PWCT Concentration After 650 Years
(Example Constituent, Plan View)

Scale: 1 in. = 1000 ft. Date: March 2000
Prepared By: HSI GEOTRANS By: JDC

P:\Crandon\Tmal\Mod4\Surfer\Pmfy650.srf

P:\Crandon\TmaMod4\Surfer\X14hy002.srf

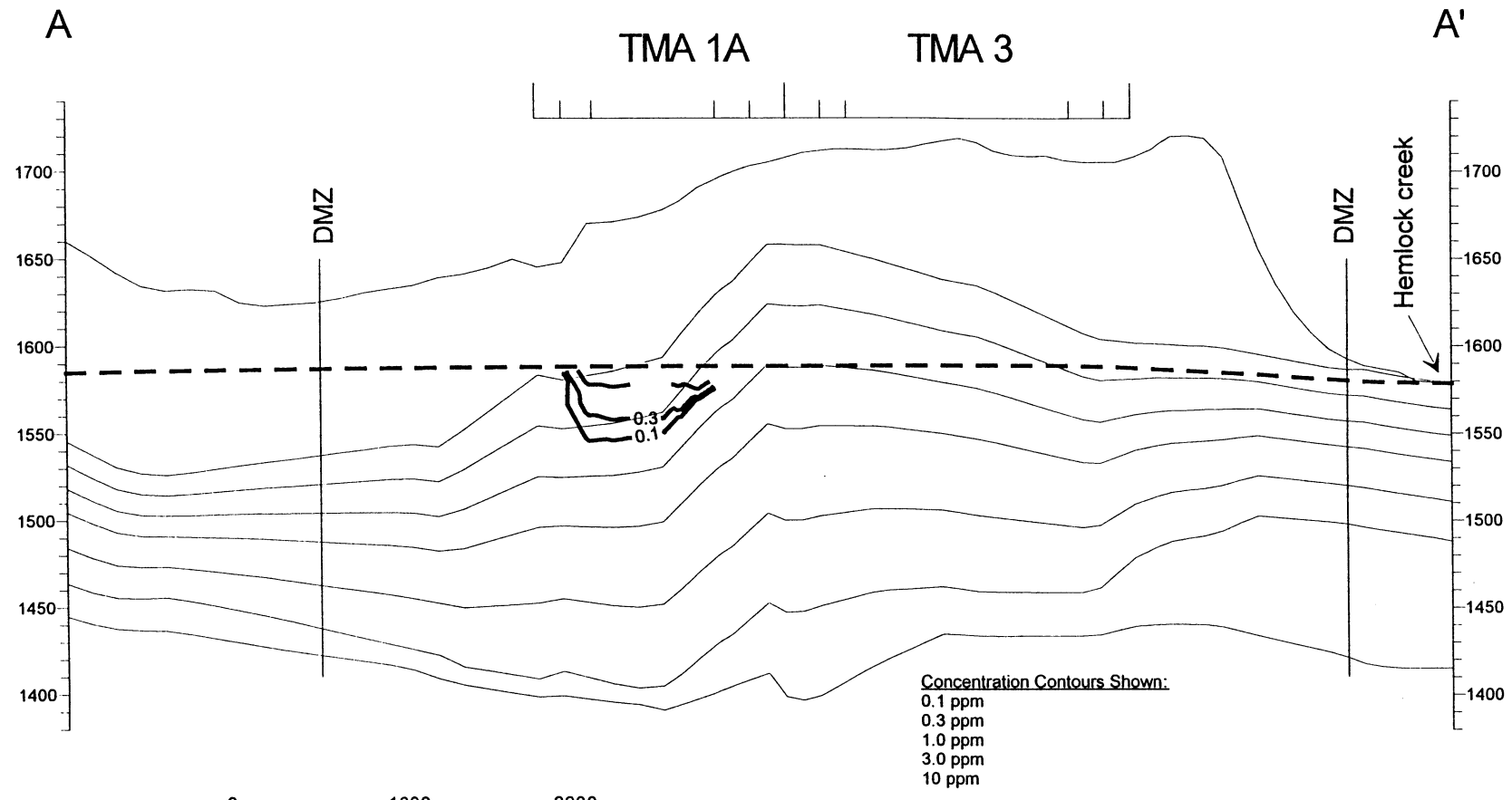

4.2-10-506

Source Concentration
1) TMA Operation: 2,000 ppm
2) TMA Consolidation: 2,500 ppm
3) TMA Post Cap: 4,000 ppm
4) TMA Post FML Degradation: 4,000 ppm
5) Reclaim Pond Operation: 1,000 ppm
6) Reclaim Pond Post Cap: 4,000 ppm

Simulations
T14C1 - T14C6

HSI GEOTRANS

REVISED	DATE	BY	DESCRIPTION

CHECKED BY: GWC	DATE: 3/00
APPROVED BY: PFA	DATE: 3/00
APPROVED BY:	DATE:

Nicolet Minerals
a Rio Algom company

Figure 42
PWCT Concentration After 2 Years
(Example Constituent, Cross-Section)

Scale: 1" = 1000' (h), 100' (v)	Date: March 2000
Prepared By: HSI GeoTrans	By: JDC

P:\Crandon\TmaMod4\Surfer\X14hy016.srf

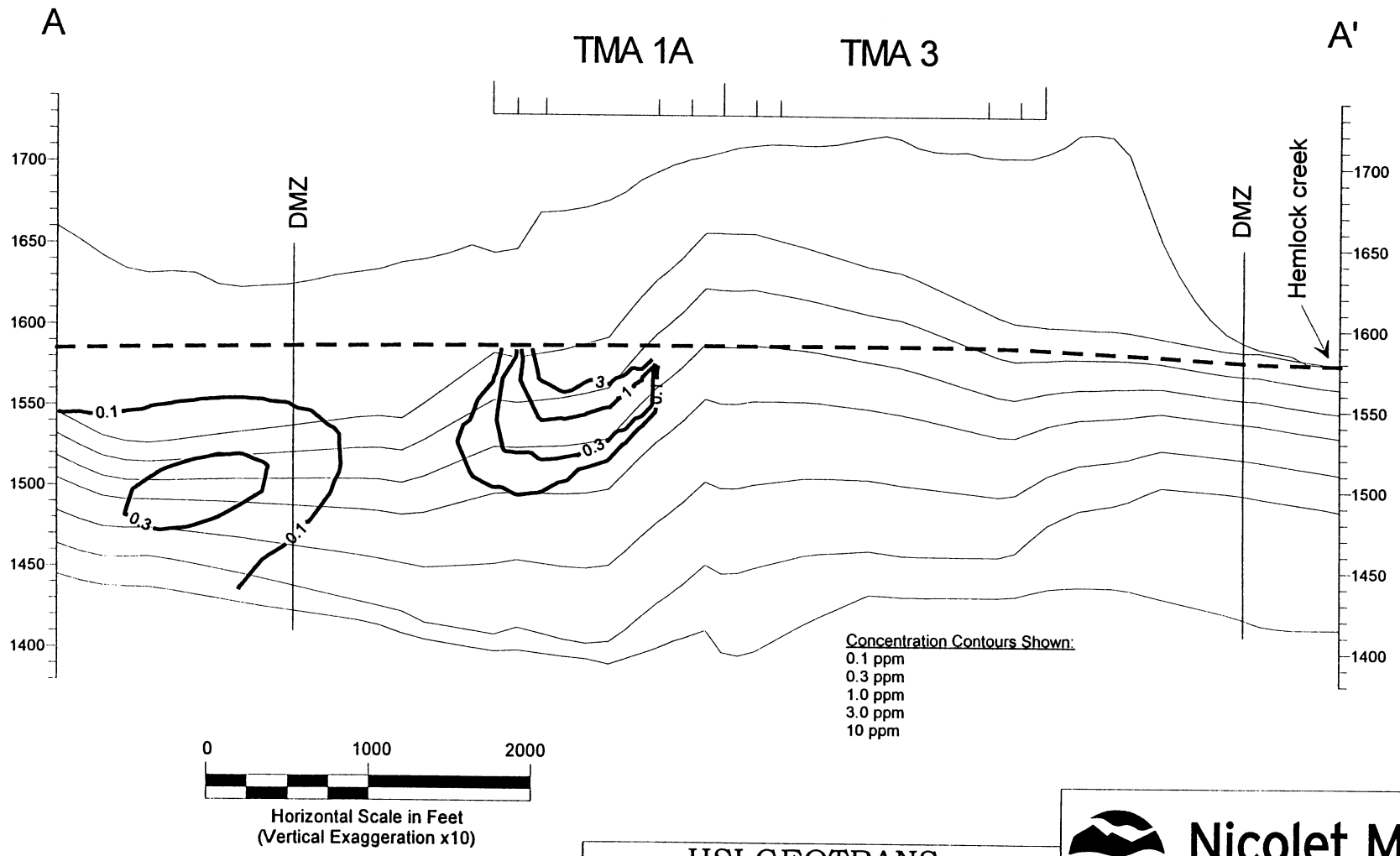

4.2-10-507

Source Concentration
1) TMA Operation: 2,000 ppm
2) TMA Consolidation: 2,500 ppm
3) TMA Post Cap: 4,000 ppm
4) TMA Post FML Degradation: 4,000 ppm
5) Reclaim Pond Operation: 1,000 ppm
6) Reclaim Pond Post Cap: 4,000 ppm

Simulations
T14C1 - T14C6

HSI GEOTRANS

REVISED	DATE	BY	DESCRIPTION

CHECKED BY: GWC	DATE: 3/00
APPROVED BY: PFA	DATE: 3/00
APPROVED BY:	DATE:

Nicolet Minerals
a Rio Algom company

Figure 43
PWCT Concentration After 16 Years
(Example Constituent, Cross-Section)

Scale: 1" = 1000' (h), 100' (v)	Date: March 2000
Prepared By: HSI GeoTrans	By: JDC

P:\Crandon\TmaMod41\Surfer\X14hy022.srf

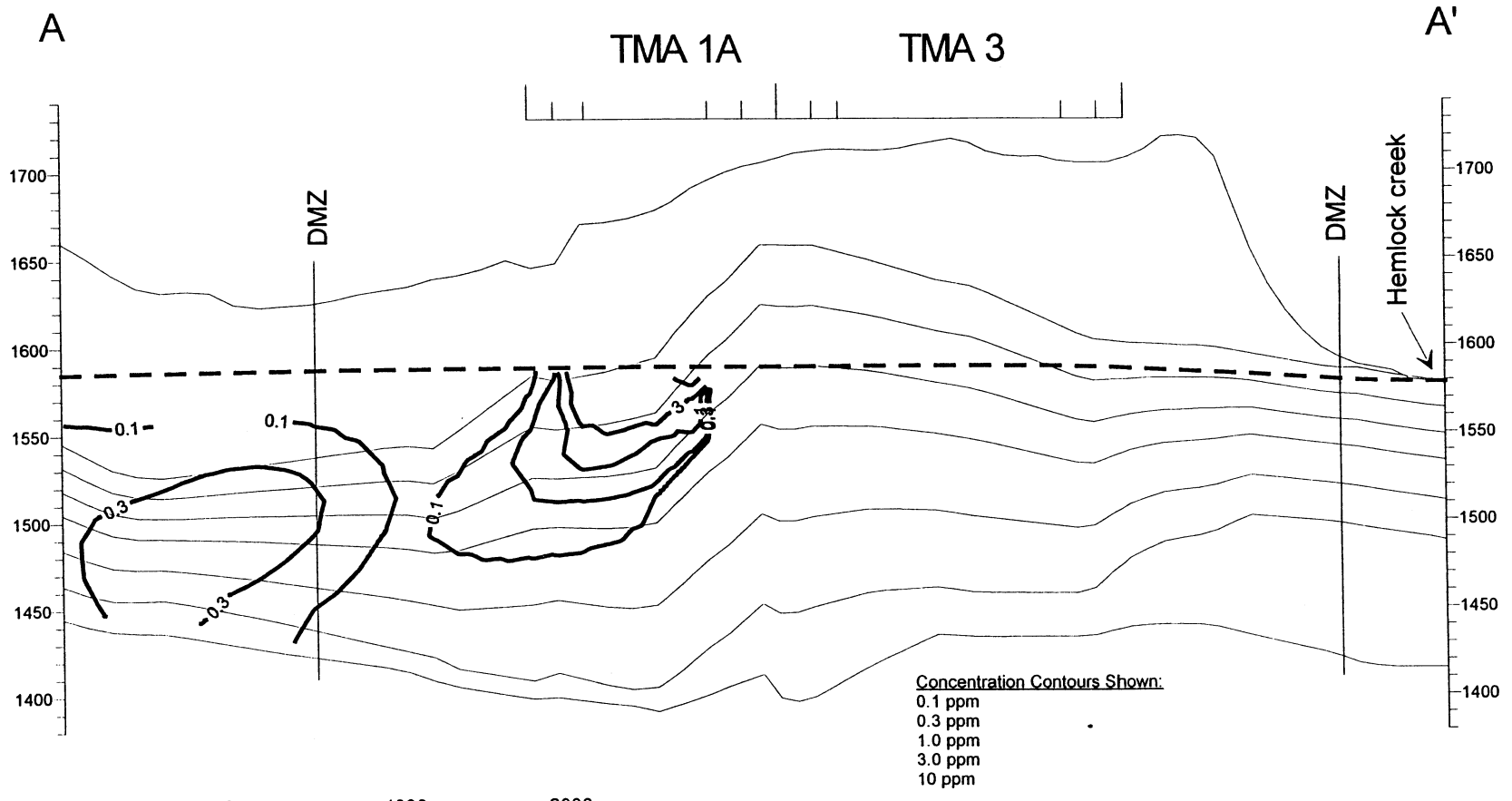

4.2-10-508

Source Concentration
1) TMA Operation: 2,000 ppm
2) TMA Consolidation: 2,500 ppm
3) TMA Post Cap: 4,000 ppm
4) TMA Post FML Degradation: 4,000 ppm
5) Reclaim Pond Operation: 1,000 ppm
6) Reclaim Pond Post Cap: 4,000 ppm

Simulations
T14C1 - T14C6

HSI GEOTRANS

REVISED	DATE	BY	DESCRIPTION

CHECKED BY: GWC	DATE: 3/00
APPROVED BY: PFA	DATE: 3/00
APPROVED BY:	DATE:

Nicolet Minerals
a Rio Algom company

Figure 44
PWCT Concentration After 22 Years
(Example Constituent, Cross-Section)

Scale: 1" = 1000' (h), 100' (v)	Date: March 2000
Prepared By: HSI GeoTrans	By: JDC

P:\Crandon\TmaMod4\Surfer\X14hy032.srf

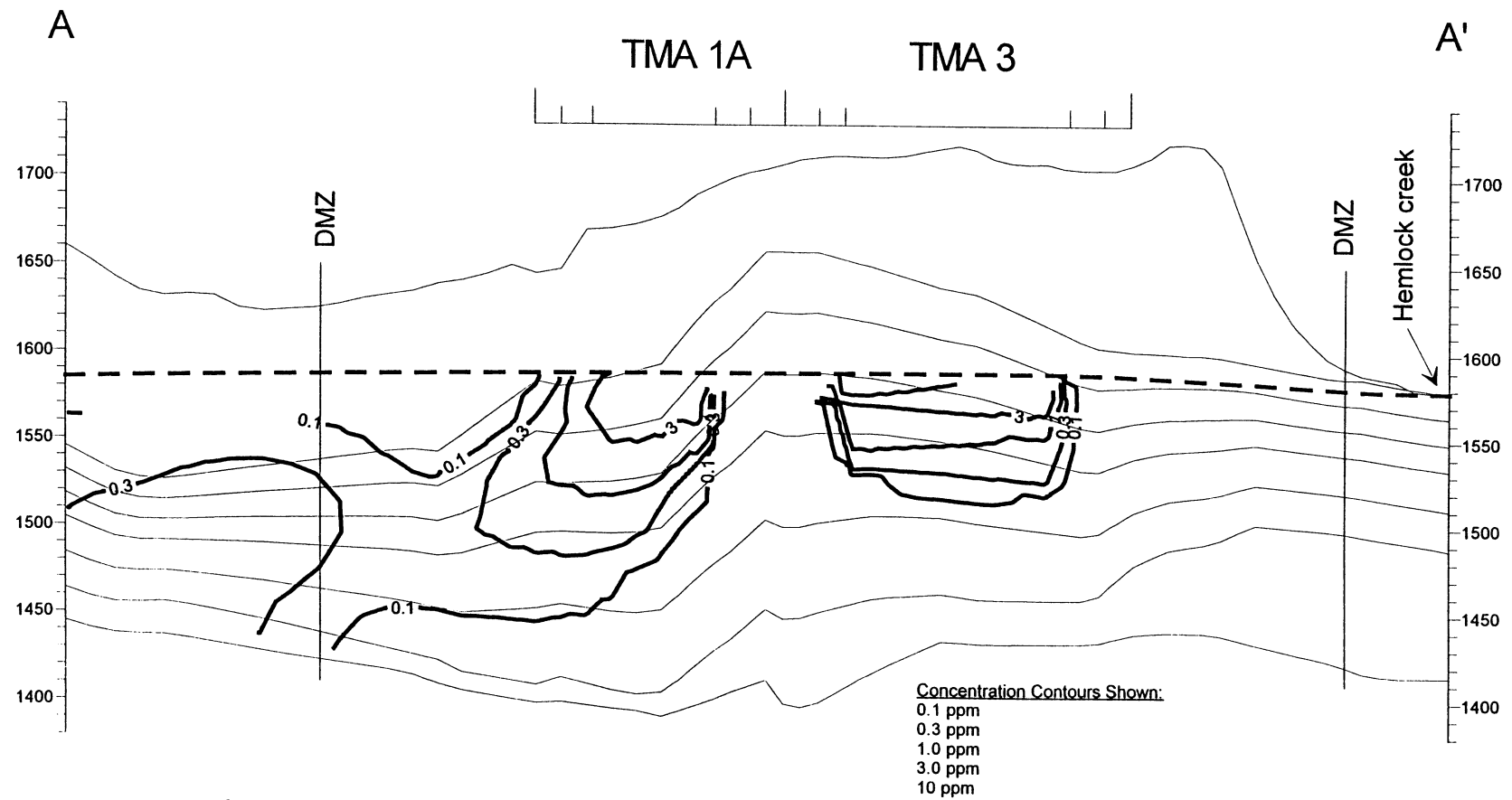

4.2-10-509

Source Concentration
1) TMA Operation: 2,000 ppm
2) TMA Consolidation: 2,500 ppm
3) TMA Post Cap: 4,000 ppm
4) TMA Post FML Degradation: 4,000 ppm
5) Reclaim Pond Operation: 1,000 ppm
6) Reclaim Pond Post Cap: 4,000 ppm

Simulations
T14C1 - T14C6

HSI GEOTRANS

REVISED	DATE	BY	DESCRIPTION

CHECKED BY: GWC	DATE: 3/00
APPROVED BY: PFA	DATE: 3/00
APPROVED BY:	DATE:

Nicolet Minerals
a Rio Algom company

Figure 45
PWCT Concentration After 32 Years
(Example Constituent, Cross-Section)

Scale: 1" = 1000' (h), 100' (v)	Date: March 2000
Prepared By: HSI GeoTrans	By: JDC

P:\Crandon\TmaMod4\Surfer\X14hy060.srf

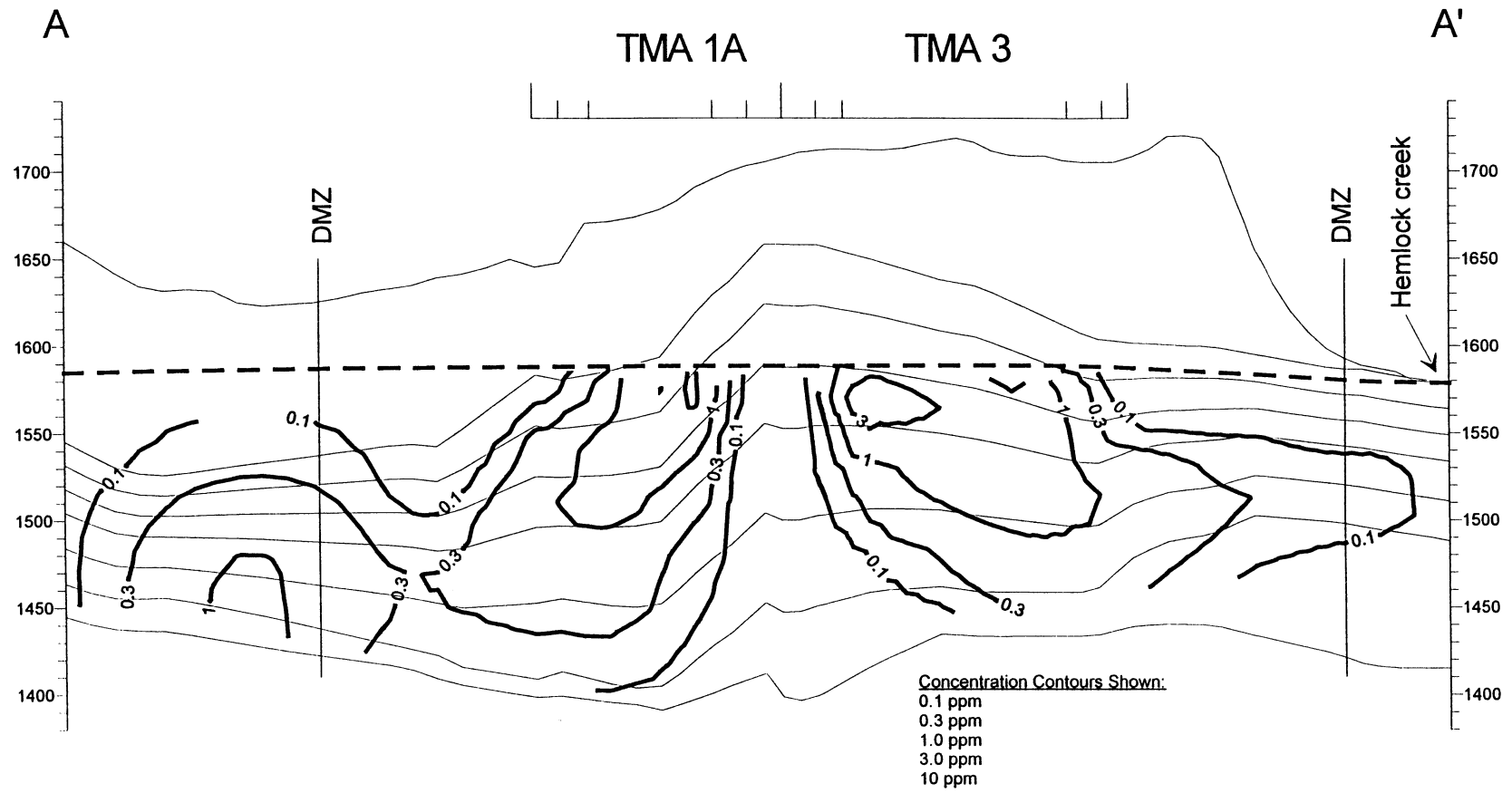

4.2-10-510

Source Concentration
1) TMA Operation: 2,000 ppm
2) TMA Consolidation: 2,500 ppm
3) TMA Post Cap: 4,000 ppm
4) TMA Post FML Degradation: 4,000 ppm
5) Reclaim Pond Operation: 1,000 ppm
6) Reclaim Pond Post Cap: 4,000 ppm

Simulations
T14C1 - T14C6

HSI GEOTRANS

REVISED	DATE	BY	DESCRIPTION

CHECKED BY: GWC	DATE: 3/00
APPROVED BY: PFA	DATE: 3/00
APPROVED BY:	DATE:

Nicolet Minerals
a Rio Algom company

Figure 46
PWCT Concentration After 60 Years
(Example Constituent, Cross-Section)

Scale: 1" = 1000' (h), 100' (v)	Date: March 2000
Prepared By: HSI GeoTrans	By: JDC

P:\Crandon\TmaMod4\Surfer\X14hy0125.srf

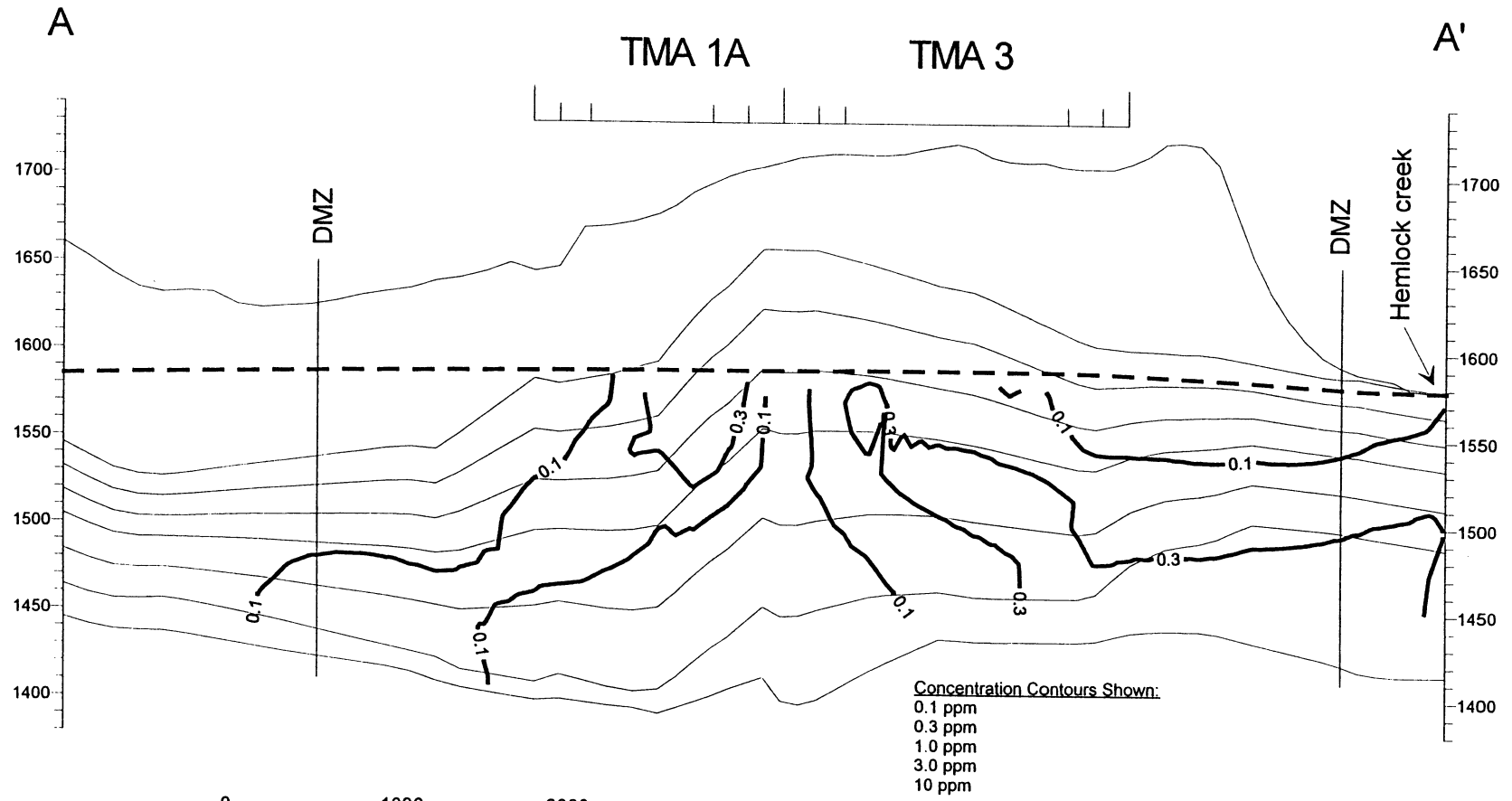

4.2-10-511

Source Concentration
1) TMA Operation: 2,000 ppm
2) TMA Consolidation: 2,500 ppm
3) TMA Post Cap: 4,000 ppm
4) TMA Post FML Degradation: 4,000 ppm
5) Reclaim Pond Operation: 1,000 ppm
6) Reclaim Pond Post Cap: 4,000 ppm

Simulations
T14C1 - T14C6

HSI GEOTRANS

REVISED	DATE	BY	DESCRIPTION

CHECKED BY: GWC	DATE: 3/00
APPROVED BY: PFA	DATE: 3/00
APPROVED BY:	DATE:

Nicolet Minerals
a Rio Algom company

Figure 47
PWCT Concentration After 125 Years
(Example Constituent, Cross-Section)

Scale: 1" = 1000' (h), 100' (v)	Date: March 2000
Prepared By: HSI GeoTrans	By: JDC

P:\Crandon\TmaMod4\Surfer\X14hy200.srf

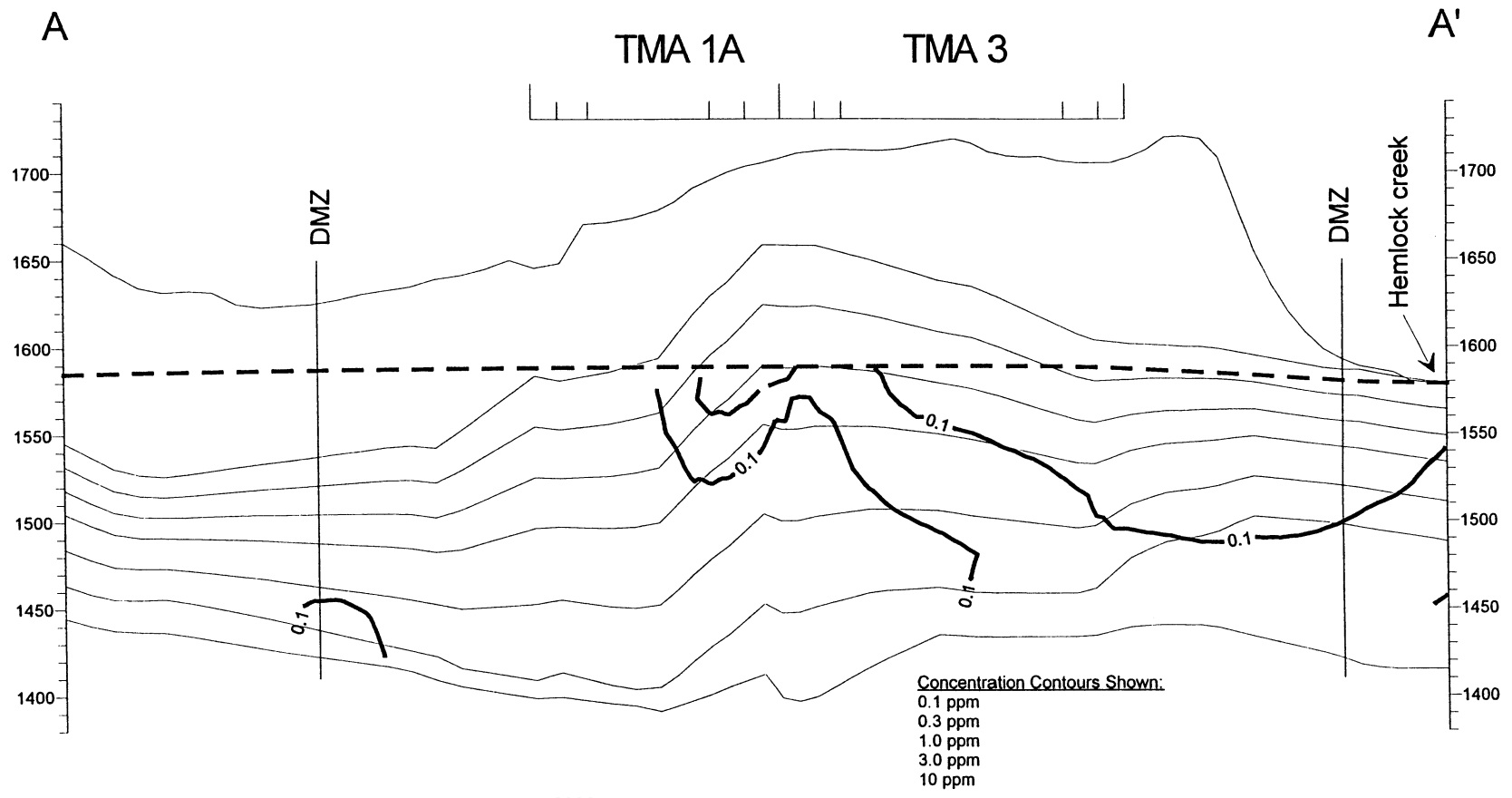

4.2-10-512

Source Concentration
1) TMA Operation: 2,000 ppm
2) TMA Consolidation: 2,500 ppm
3) TMA Post Cap: 4,000 ppm
4) TMA Post FML Degradation: 4,000 ppm
5) Reclaim Pond Operation: 1,000 ppm
6) Reclaim Pond Post Cap: 4,000 ppm

Simulations
T14C1 - T14C6

HSI GEOTRANS

REVISED	DATE	BY	DESCRIPTION

CHECKED BY: GWC	DATE: 3/00
APPROVED BY: PFA	DATE: 3/00
APPROVED BY:	DATE:

Nicolet Minerals
a Rio Algom company

Figure 48
PWCT Concentration After 200 Years
(Example Constituent, Cross-Section)

Scale: 1" = 1000' (h), 100' (v)	Date: March 2000
Prepared By: HSI GeoTrans	By: JDC

P:\Crandon\TmaMod4\Surfer\X14hy300.srf

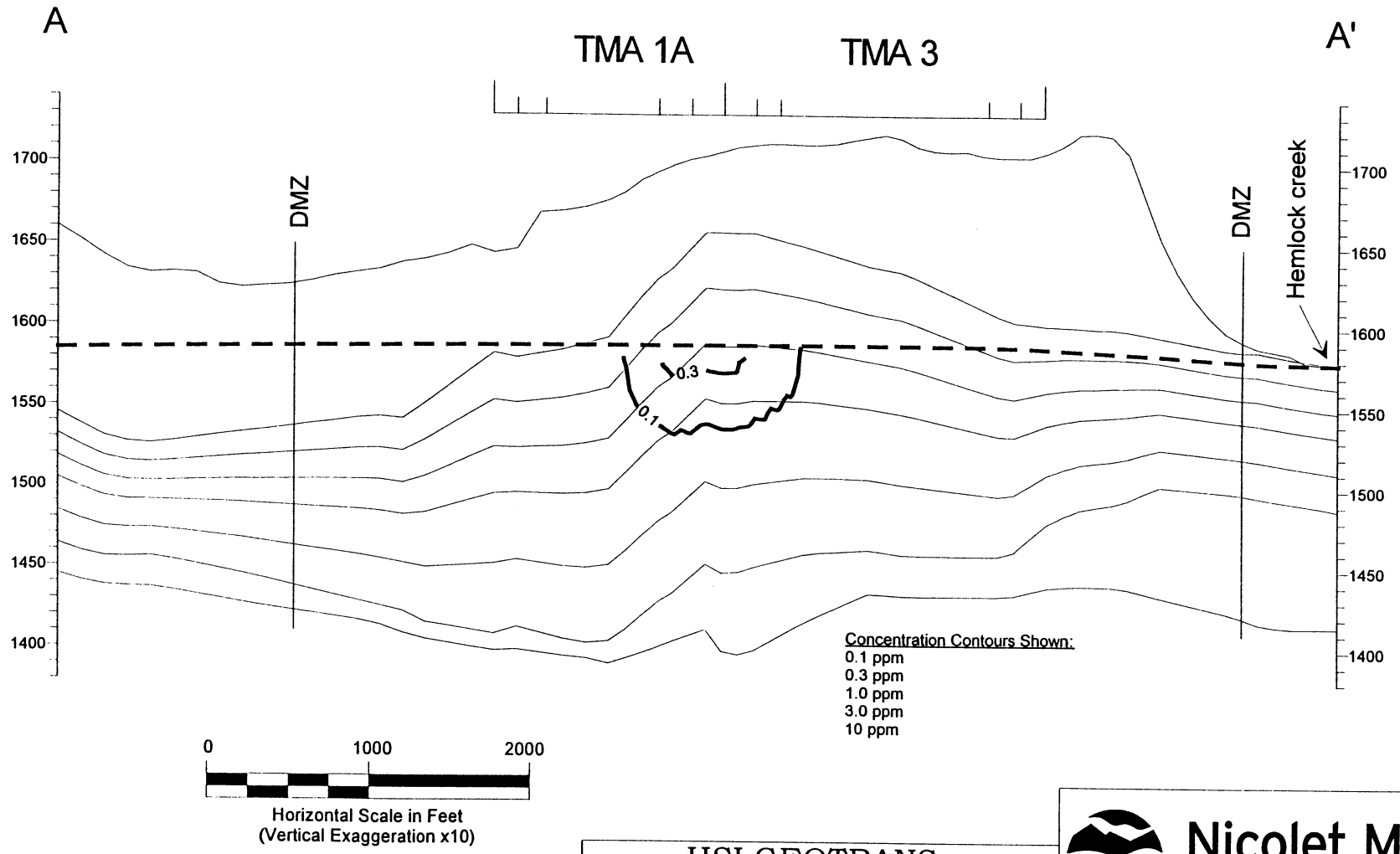

4.2-10-513

Source Concentration
1) TMA Operation: 2,000 ppm
2) TMA Consolidation: 2,500 ppm
3) TMA Post Cap: 4,000 ppm
4) TMA Post FML Degradation: 4,000 ppm
5) Reclaim Pond Operation: 1,000 ppm
6) Reclaim Pond Post Cap: 4,000 ppm

Simulations
T14C1 - T14C6

HSI GEOTRANS

REVISED	DATE	BY	DESCRIPTION

CHECKED BY: GWC	DATE: 3/00
APPROVED BY: PFA	DATE: 3/00
APPROVED BY:	DATE:

Nicolet Minerals
a Rio Algom company

Figure 49
PWCT Concentration After 300 Years
(Example Constituent, Cross-Section)

Scale: 1" = 1000' (h), 100' (v)	Date: March 2000
Prepared By: HSI GeoTrans	By: JDC

P:\Crandon\TmaMod4\Surfer\X14hy650.srf

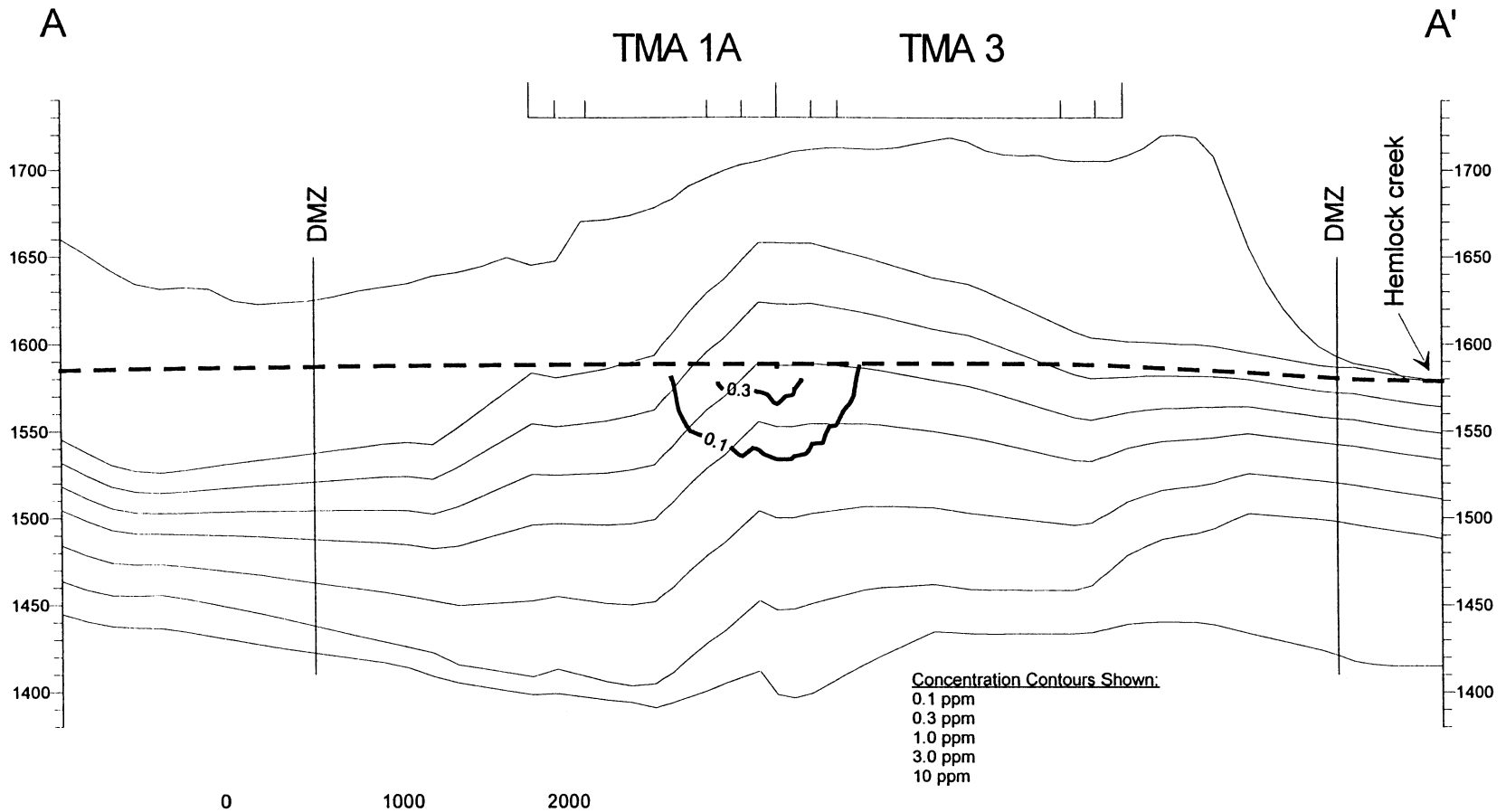

4.2-10-514

Source Concentration
1) TMA Operation: 2,000 ppm
2) TMA Consolidation: 2,500 ppm
3) TMA Post Cap: 4,000 ppm
4) TMA Post FML Degradation: 4,000 ppm
5) Reclaim Pond Operation: 1,000 ppm
6) Reclaim Pond Post Cap: 4,000 ppm

Simulations
T14C1 - T14C6

HSI GEOTRANS

REVISED	DATE	BY	DESCRIPTION

CHECKED BY: GWC	DATE: 3/00
APPROVED BY: PFA	DATE: 3/00
APPROVED BY:	DATE:

Nicolet Minerals
a Rio Algom company

Figure 50
PWCT Concentration After 650 Years
(Example Constituent, Cross-Section)

Scale: 1" = 1000' (h), 100' (v) | Date: March 2000

Prepared By: HSI GeoTrans | By: JDC

APPENDIX A

HELP Model Results

Foth & Van Dyke
Memorandum

March 20, 2000

TO: Greg Council, HSI GeoTrans, Inc.

CC: Master File

FR: Steve Donohue, Foth & Van Dyke SVD

RE: Crandon Project - TMA Help Model Results and Construction Phases

TMA percolation rates for *Addendum No. 1 to Update No. 2 to the TMA Solute Transport Model for the Crandon Project* were documented in a memorandum dated May 25, 1999. For *Update No. 3 to the TMA Solute Transport Model*, the same percolation rates will be used. For completeness purposes, the same percolation tables are attached to this memorandum. Also included is Table 4.3-1 from *Addendum No. 5 to the TMA Feasibility Report* (Foth & Van Dyke, 1998). The phase life of TMA 1A and 1B are slightly different from what was used in the prior STM reports. Specifically, it was assumed that TMA 1A and TMA 1B had a phase life of 3 and 4 years, respectively. The actual phase life of each of these subcells should be simulated as 2 years for TMA 1A and 4 years for TMA 1B. The second stage of TMA 1A and 1 B was simulated as 9 years. Based on Table 4.3-1, the actual phase life for the second stage of TMA 1A and 1B should be 10 years.

Several other modifications will also be included in the updated STM. Specifically, the 2 year consolidation period, previously included in Flow Phase B, will now be simulated as a separate flow phase. This change has been requested by the WDNR to account for a change in the source term due to the development of the oxidation zone in the tailings during the consolidation period. This two year consolidation period will now be called Flow Phase C. As a result of these changes, what was simulated as Flow Phase C (the first year after cap placement) will now be included in Flow Phase D. There will be one other change to the STM. Previously, the reclaim pond used the same source term as the TMA. In the updated model, the reclaim pond will have a separate source term during operations. After filling of TMA 3, the reclaim pond will receive the same source term as is applied to the TMA after capping has taken place.

SVD1:cer1
Attachments

References

Foth & Van Dyke, 1998. *Addendum No. 5 to the May 1995 Tailings Management Area Feasibility Report/Plan of Operation.* December 1998.

Table 2

Percolation from TMA Based on Doubled Precipitation Values During Operation of Initial Stages

Year	Sideslope (in/yr)	Base (in/yr)
1	0.000001	0.024968
2	<0.0000005	0.003517
3	<0.0000005	0.004562
4	<0.0000005	0.008642
5	<0.0000005	0.003126
6	<0.0000005	0.004671
7	<0.0000005	0.005429
8	<0.0000005	0.001883
9	<0.0000005	0.001380
10	<0.0000005	0.006263
Average	<0.0000005	0.006440

Note: HELP model output rounds off to six digits.

Prepared by: MRS
Checked by: NXP

Table 3

Percolation from TMA Based on Doubled Precipitation Values During Operation of Second Stages

Year	Lower Sideslope (in/yr)	Upper Sideslope (in/yr)	Base (in/yr)
1	0.000001	0.000002	0.034353
2	0.000001	0.000001	0.016261
3	<0.0000005	0.000001	0.005851
4	<0.0000005	0.000001	0.004205
5	<0.0000005	0.000001	0.007981
6	<0.0000005	0.000001	0.003110
7	<0.0000005	0.000001	0.004669
8	<0.0000005	<0.0000005	0.004549
9	<0.0000005	0.000001	0.001967
10	<0.0000005	0.000001	0.001725
Average	<0.0000005	0.000001	0.008470

Note: HELP model output rounds off to six digits.

Prepared by: MRS
Checked by: NAP

Table 4

Post-Closure Percolation

Year from Placement of Cover	Lower Sideslope (in/yr)	Upper Sideslope (in/yr)	Base (in/yr)
1	0.000001	0.000002	0.038786
2	0.000001	<0.0000005	0.014870
3	<0.0000005	<0.0000005	0.001169
4	<0.0000005	<0.0000005	0.001021
5	<0.0000005	<0.0000005	0.000916
6	<0.0000005	<0.0000005	0.000835
7	<0.0000005	<0.0000005	0.000763
8-15	<0.0000005	<0.0000005	0.000552
16-25	<0.0000005	<0.0000005	0.000308
26-35	<0.0000005	<0.0000005	0.000195
36-40	<0.0000005	<0.0000005	0.000151
41-50	<0.0000005	0	0.000123
51-60	<0.0000005	0	0.000097
61-70	<0.0000005	0	0.000081
71-80	<0.0000005	0	0.000069
81-90	<0.0000005	0	0.000059
91-115	0	0	0.000004
116-140	0	0	0.000004
141-165	0	0	0
166-175	0	0	0
176-185	0	0	0
186-195	0	0	0
196-205	0	0	0
206-215	0	0	0

Table 4 *(Continued)*

Year from Placement of Cover	Lower Sideslope (in/yr)	Upper Sideslope (in/yr)	Base (in/yr)
216-220	0	0	0
221-230	0	0	0
231-240	0	0	0
241 plus[1]	0.00002	0.00002	0.00002

Note: HELP Model output rounds to off to six digits.

[1] Percolation is conservatively assumed at this time period to be equal to infiltration through cover, even though the HELP Model indicates it will take longer to achieve this equilibrium.

Prepared by: MRS
Checked by: NXP
Revised by: NXP
Checked by: SVD1

Table 4.3-1

Estimated Volumes and Site Life for TMA Cells and Stages

(Updated Table 13 from December 1997 Completeness Determination Response)

Tailings Cell	Stage	Tailings[1] (cy)	Approximate Phase Life (yrs.)	Other Wastes[2] (cy)	Contingency[3] (cy)	Calculated Need (cy)	Cell Design Total[4] (cy)	Capacity as Percent of Total
Zinc Ore Production								
TMA 1A	I	648,000	2.1	361,000	—	1,009,000	1,000,000	
TMA 1B	II	1,173,000	3.8	61,000	—	1,234,000	1,220,000	
TMA 1	III	3,117,000	10.1	59,000	641,000	3,817,000	3,840,000	
Zinc Total Tailings		4,938,000	16.0	481,000	641,000	6,060,000	6,060,000	100.0
Copper Ore Production								
TMA 2	IV	1,367,000	2.4	41,000	—	1,408,000	1,390,000	
TMA 2	V	2,050,000	3.6	31,000	531,000	2,612,000	2,630,000	
Subtotal		3,417,000	6.0	72,000	531,000	4,020,000	4,020,000	50.0
TMA 3	VI	1,367,000	2.4	41,000	—	1,408,000	1,400,000	
TMA 3	VII	2,050,000	3.6	183,000	379,000	2,612,000	2,620,000	
Subtotal		3,417,000	6.0	224,000	379,000	4,020,000	4,020,000	50.0
Copper Total Tailings		6,834,000	12.0	296,000	910,000	8,040,000	8,040,000	100.0
Total Zinc & Copper		11,772,000	28	777,000	1,551,000	14,100,000	14,100,000	

4.2-10-521

[1] Zinc ore production tailings generation rate is 308,600 cy/yr; copper ore production tailings generation rate is 569,400 cy/yr.

[2] Other wastes include waste rock, wastewater treatment solids, laboratory wastes, and demolition wastes. Demolition wastes estimated at 150,000 cy will be placed in TMA 3 Stage VII.

[3] The zinc and copper cells include an approximate 12% and 13% contingency respectively, based on the total expected production of tailings and other wastes.

[4] Cell design total is the actual design volume based on model calculation performed by Computer Aided Drafting and Design (CADD). The design total is within 0.5% of the required total.

cy = Cubic yards

yrs = Years

Prepared by: SAD2

Checked by: DMR

Appendix 4.2-11

Crown Pillar Studies

- **Hydrologic Stability of the Crown Pillar, Crandon Deposit**
- **Numerical Analysis Results for Evaluation of the Influence of Mining on the Crown Pillar, Crandon Deposit**

HYDROLOGIC STABILITY OF THE CROWN PILLAR

CRANDON DEPOSIT

A report submitted to
Crandon Mining Company
Rhinelander, Wisconsin

May 7, 1996

Distribution:	**1 copy**	—	**Crandon Mining Co.** **Rhinelander, Wisconsin**
	1 copy	—	**Agapito Associates, Inc.** **Las Vegas, Nevada**
	1 copy	—	**Agapito Associates, Inc.** **Grand Junction, Colorado**

AGAPITO ASSOCIATES, INC.
3841 W. Charleston, Suite 203, Las Vegas, NV 89102
TEL. (702) 258-7046 FAX (702) 258-7418

FILE MAIN EM-1
Sub GE
Sub 1A
Keywords

AGAPITO ASSOCIATES, INC.
CONSULTING ENGINEERS

LAS VEGAS OFFICE

May 7, 1996

235-2

Mr. Ken Black
Crandon Mining Company
7 N. Brown St. 3rd Floor
Rhinelander, WI 54501-3161

RE: "Hydrologic stability of the Crown Pillar, Crandon Deposit".

Dear Ken:

The above mentioned final report has been sent to you under separate cover. The report presents the results of the Agapito Associates, Inc. (AAI) evaluation of the hydrologic stability of the crown pillar that will remain after extraction of the zinc and copper ores at the Crandon deposit.

The report presents the results of the 3-D boundary element and 2-D finite difference analyses of crown pillar stress changes that have led us to conclude that the mining activities planned at the Crandon deposit will not change the permeability of the crown pillar. We believe that the approach used in the analyses produced a conservative estimate of the stress transfer to the crown pillar and that the resulting assessment, that there will be no impact on hydrologic stability, is therefore accurate. We believe that the stress modeling was conservative for the following reasons:

- The 3-D boundary element analysis of the stress transferred to the crown pillar was based on the ore outline along the entire strike length. The mining process was simulated at 100% extraction to the 1200 ft. elevation without taking credit for the load that would be carried by backfill in the secondary stopes. The predicted crown pillar stress was therefore higher than would be predicted by a more detailed analysis that considered the backfill in the secondary stopes.

- The 2-D finite difference analysis used the results of the 3-D analysis as the initial stress state.

- The 2-D analysis was a plane strain simulation that assumed that the crown pillar was the minimum thickness. It therefore overestimated the load transfer because it did not consider the variation in thickness of the crown pillar along strike. The 2-D simulation produced elastic stresses that were 122% of those projected by the 3-D analysis.

- The 2-D analysis was based on a Mohr-Coulomb material model that could yield due to overstress. This allowed concentration of deformation into a zone of shear. The concentrated deformations could then be compared to strain limit criteria developed to provide guidance for protecting aquitard layers from disruption by mining induced deformations.

- Mechanical properties used in the analysis were derived from correlations with rock mass quality published in the technical literature. Use of those correlations allowed us to account for the effects of weathering and fracturing characteristics that are observed in the Crandon core data.

Maximum strain criteria recommended by the SME Mining Engineers Handbook published by the Society for Mining, Metallurgy and Exploration then provided a realistic basis to evaluate the results of the stress analyses.

You can reach me at (702) 258-7046 if there are any details of the report that require clarification.

Sincerely yours,

Carl E. Brechtel
Principal

CEB.rms(ceb1596.doc)#235-2

Table of Contents

List of Figures

List of Tables

1. INTRODUCTION

1.1. Background

This report presents the results of an assessment of the hydrologic stability of the crown pillar that will remain after extraction of zinc and copper ores at the Crandon deposit in Forest County, Wisconsin. For the purpose of this report, hydrologic stability refers to the integrity of the crown pillar with regard to fracture frequency, aperture and interconnectedness that control vertical hydraulic conductivity and that could be impacted by mining. The crown pillar is the rock remaining between the uppermost extent of mining and the base of surficial glacial deposits, that is to be left in place to protect the surface and the glacial aquifer system. Earlier mining plans for Crandon ores proposed the leaving of a crown pillar with thickness varying between 70 and 310 ft along the 4900-ft strike length of the orebody. Along this strike length individual zones of ore may be mined with north-south (N-S) widths varying from 10 to 130 ft.

Work, under a contract, was authorized by the agreement for services between Crandon Mining Company (CMC) and Agapito Associates, Inc. (AAI) dated December 20, 1995.

The issue of hydrologic stability of the crown pillar has been raised by the Department of Natural Resources, State of Wisconsin, as a potential concern because of the implication for mine inflow and mine reflooding[1]. Groundwater modeling studies suggest that mine reflooding poses little to no risk of adversely impacting the glacial aquifer system at the mine surface. These models assume that vertical hydraulic conductivity of the crown pillar will not be altered by the mining.

Mine planning at the Crandon project has been based upon the recognized need to protect the glacial aquifer system. The need to use alternate mining techniques in the area immediately beneath the crown pillar in the upper part of the mine was recognized early in the mine planning, and a preliminary assessment of mining methods suitable for this area was performed based upon rock mechanics and geotechnical criteria by Smith (1982). Using the rock mechanics criteria, early plans for mining beneath the crown pillar area were developed by DYNATEC (1982) based

---

[1]Carlson, C.P. (1995, November 28). [Personal Letter. Hydrogeologist, Solid Waste Management Section, Bureau of Solid and Hazardous Waste Management, Department of Natural Resources, State of Wisconsin to D. Moe, Crandon Mining Company (see Appendix D)].

upon different variations of mechanized cut-and-fill mining. The cut-and-fill mining systems that have been identified as applicable to the Crandon project include specific mining criteria that prevent instability of the rock during the mining process by:

- limiting the amount of open underground stoping excavation at any given time thereby eliminating the potential of excavation failure;
- providing partial support to the crown pillar rock by leaving small but intact pillars to support the back (ceiling) of stopes; and
- providing access for personnel to identify potentially unstable conditions and, if present, allowing access of equipment to install local, remedial rock support that will prevent instability.

1.2. Approach to Crown Pillar Evaluation

The early mining plans for the area beneath the crown pillar by DYNATEC (1982) were used to establish the general mining parameters and the range of crown pillar thickness. These plans were reevaluated based upon the most recent geologic and ore reserve cross sections developed by CMC that form the preliminary mine plan.

The ratio of the width of the mining to the thickness of the crown pillar in the preliminary plan provided an index to compare the potential for mining impacts at the various locations along the strike length of the orebody. Higher values of this ratio indicate that the crown pillar is thinner with respect to the width of ore to be mined beneath the crown pillar.

Detailed geologic cross sections that showed both the location of the crown pillar with respect to the projected preliminary mining geometry and the patterns of weathering in the crown pillar were used to establish the basis for the analyses. The cross sections were analyzed to establish the width of mining and thickness of the crown pillar. The variation of these two parameters along strike, in conjunction with the geology were used to define the projected worst-case condition for analysis and more typical conditions for comparison to the analysis.

The global stress concentration due to mining of the entire orebody along the length of the crown pillar was simulated to provide input for a more specific two-dimensional analysis of a cross section selected to investigate the potential worst-case geometry (e.g. minimum crown pillar thickness to mining width). The material properties utilized for the analysis were based upon evaluation of the rock conditions in the crown pillar area. Analysis of the geotechnical data

was needed to make certain that the input parameters used in the modeling were representative of the rock mass at the scale of mining excavation.

Rock quality data from core and photographs of core taken in holes drilled through or just below the crown pillar were correlated with the detailed geology and weathering descriptions. These data consisted of Rock Quality Designation (RQD), total fracture frequency, and rock strength testing data, and were used to define the rock mass quality using the Rock Mass Rating index (RMR) of the commonly used Geomechanics Classification System (Bieniawski 1976).

Rock mechanical properties used in the modeling simulation of stress and deformation were estimated using correlations with the rock mass quality index. These correlations, published in the literature, were developed using field measurements and observations of rock mechanical properties at large (excavation) scale. Properties measured on core samples have been shown to overestimate those at the excavation scale because they do not consider inhomogeneities in the rock mass (joints, vugs, weathering, etc.). The rock mass quality-rock mass mechanical properties correlations have been observed to produce generally conservative results when utilized for geoengineering design.

Several criteria have been adopted in this study to assure that the final design of the crown pillar provides very high levels of confidence that there will be no hydrologic impacts. These criteria are:

- Specifications for minimum crown pillar thickness would be based on model results for the projected worst-case geometry such that horizontal strains are $< \pm 5.0 \times 10^{-3}$. This strain limit criteria was recommended based on mining case history data by the SME Mining Engineers Handbook published by the Society for Mining, Metallurgy and Exploration (SME 1992) as a suggested criteria for the preservation of the effectiveness of existing aquitards. In coal mining, which produces much greater surface disturbance than the mining of volcanogenic sulfide deposits such as Crandon, strains below $\pm 5.0 \times 10^{-3}$ have been sufficiently low to prevent the draining of surface water bodies into mining excavations passing underneath. The more extensive nature of coal mining disturbance makes this a very conservative criteria for application to the Crandon crown pillar, thereby assuring very high levels of confidence.

- The stress changes projected to occur in the crown pillar due to mining have been used to project the change in hydraulic conductivity that could occur on identified fracture sets for the upper bedrock in the crown pillar. The changes in crown pillar stresses should not result in fracture hydraulic conductivity increases that would increase crown pillar permeability.
- The planned tight filling at the base of the crown pillar after mining of the final stopes is based on case history data for the occurrence of surface chimney type subsidence over unfilled coal mines. This provides a method to assure high levels of confidence that in the long-term no voids could migrate through the crown pillar to create flow paths to the surface glacial aquifers.

1.3. Report Organization

Following this introduction, Section 2 of the report presents a summary of the investigations and the resulting conclusions, and is organized to specifically address requests for information in the Wisconsin Department of Natural Resources query of November 28, 1995. Those topics include:

- analysis of mining impacts on hydrologic stability of the crown pillar,
- mining plans for the crown pillar area, and
- geology and geotechnical characteristics of the crown pillar area.

The geology and rock mass characteristics that form the basis of the analysis are presented in Section 3 and the appendices. Section 4 describes the general mining geometry that provided the basis of the numerical simulations of stress change and displacement. Section 5 presents the results of the numerical simulations of the stress and strain changes. Strain changes for elastic and elastic-plastic analyses were compared to published criteria on disruption of aquitards (geologic layers that resist or retard groundwater flow) from mining case history. Projected changes to hydraulic conductivity of single fractures, due to the modeled stress changes, are also presented.

Appendix A presents some general information on the geology of the glacial overburden. The geotechnical data and derived rock mass properties are presented in Appendix B. Modeling assumptions are presented in Appendix C.

2. CONCLUSIONS AND RECOMMENDATIONS

2.1. Mining Impacts on Crown Pillar Hydrologic Stability

AAI believes that mining activities at the Crandon deposit will not change the permeability of the crown pillar during mining or after reflooding. It is believed:

- the existing mining plans to utilize mechanized cut-and-fill mining techniques beneath the crown pillar will be effective in preventing any instability during mining that could impact the crown pillar permeability,
- the final configuration of stopes with the placement of backfill close to the back (ceiling) will prevent any long-term movement of the crown pillar rocks that would adversely impact the permeability, and
- the analysis of stress and strain changes in the crown pillar provides a basis to verify that the planned thickness of the crown pillar is sufficient to preserve the rock mass integrity and thereby prevent changes of the crown pillar permeability.

Two-dimensional analyses performed by AAI indicate that, as currently planned, the extent of mining at the base of the crown pillar will preserve hydrologic stability along 88% of the orebody strike length. AAI's analyses indicate that in the remaining 12%, the crown pillar thickness should be increased from the current range (72–92 ft) to a minimum of 100 ft based on two-dimensional stress analysis and comparison to the strain limitation criteria ($< \pm 5.0 \times 10^{-3}$) suggested by SME (1992) to preserve aquitards.

The two-dimensional stress analysis was considered a realistic and conservative assessment of the crown pillar stress and deformation changes due to mining because:

- it simulated the crown pillar at its thinnest location where weathering impacts had reduced the rock strength and rock mass quality,
- it utilized elastic-plastic material properties which allow rock failure (yield), and
- it utilized initial stresses that reflected the stress concentration due to extraction of the entire orebody below the 1200-ft elevation.

Evaluation of factors of safety for shear movement along fracture orientations identified as the five dominant trends in the upper bedrock region indicated that the four most predominant fracture sets (Nos. 1, 2, 3 and 4) would not undergo shear movement. The stress change on the four sets (Nos. 1, 2, 3 and 4) suggested either fracture closure or very little change. Fracture flow

rates would be reduced or remain the same in Sets 1–4. Factors of safety for fracture Set 5, the least frequent, were less than 1.0 indicating that it could undergo shear movement. Fracture Set 5 could open during shear movement and its flow rate could increase.

Simplified evaluations of fracture deformations due to stress changes in the middle of the crown pillar were performed for the fracture sets projected to occur in the upper bedrock regions, and indicated that the most predominate fractures, east-west (E-W) trending fractures with near-vertical dip, would close due to stress changes in the crown pillar thereby reducing the fracture conductivity. The E-W trending fractures have been observed to be weathered and are suspected to be the most likely to transmit water (Foth & Van Dyke 1995b). The less dominant inclined fractures of Set 5 were projected to undergo shear failure and open (dilate), thereby increasing hydraulic conductivity. However, when the pressure gradient on the individual fracture sets and the relative numerical occurrence are considered, the results of the analysis indicate there will be no increase in the net permeability of the crown pillar due to changes in fracture conductivity that result from mining-induced stress change.

2.2. Mine Plans for the Crown Pillar Area

Mine plans for the crown pillar area specify the use of mechanized cut-and-fill mining techniques that ensure a high degree of stability during mining. Stability is required because men and equipment must access the stoping areas regularly to perform the mining and backfilling operations. Specification of these mining techniques will act to eliminate the potential of a major instability that could impact hydrologic stability of the crown pillar. Specific conclusions and recommendations with respect to the mining plans are:

- Early mining plans for the crown pillar area were based upon mining techniques that would minimize the potential to impact the hydrology of the crown pillar. Mining plans developed by DYNATEC (1982) provided acceptable general mining criteria for the crown pillar area.
- Modifications to the early planning for crown pillar mining, based on the most recent ore reserve cross sections, have reduced the mining dimensions assumed in the DYNATEC study, thereby reducing the potential for hydrologic impacts in the crown pillar.

- Based on analysis of the current cross sections for the preliminary plan, the crown pillar would be sufficiently thick at all locations, using the recommended minimum thickness of 100 ft, to prevent hydrologic changes. The crown pillar thickness distribution along the orebody strike as a cumulative percent would be:
  - — greater than 100 feet = 100%,
  - — greater than 150 feet = 48%,
  - — greater than 200 feet = 21%, or
  - — greater than 250 feet = 3%.
- Pillar thickness was the definitive parameter effecting the results of the analyses because it controlled the magnitude of the stress concentration. The cross section selected for the analysis had the thinnest crown pillar (72 ft) in all the preliminary cross sections. It also had a relatively wide ore section (90 ft).
- The N-S width of individual mining zones at the base of the crown pillar varies between 10 and 120 ft. Multiple mining zones separated by waste intervals of varying thickness occur at 45% of the cross sections. As many as three zones are present at 9% of the cross sections.
- The current state of mining plans for the area beneath the crown pillar is consistent with the level of geologic and resource definition. The existing data is sufficient to predict hydrologic stability.

2.3. Geology and Geotechnical Character of the Crown Pillar Area

Available data reviewed to provide input for this evaluation included geologic cross sections, descriptions of the hydrogeology and hydrologic modeling, rock mechanics testing data, and earlier core review and RQD determination in other studies. Photographs of core from the crown pillar area along the entire strike of the orebody were evaluated to estimate RQD and fracture frequency in areas where this data had not been previously collected. These data were processed to estimate rock mass quality using the RMR index. Specific conclusions are:

- The existing geotechnical data was sufficient to support the crown pillar evaluation at this stage of mine design. The data will be verified as underground access allows

more detailed geologic, mine planning and rock mechanics information to be developed.

- The physical character of the ore and adjacent hanging wall and footwall rocks has been altered by weathering effects in the crown pillar area.
- These weathering effects, subdivided into the categories of strongly, moderately, and weakly weathered in previous work, provide a consistent basis to describe the geotechnical characteristics of the rocks in the crown pillar area.
- The crown pillar will be comprised of substantial portions of moderately and weakly weathered rock to the west where copper ore predominates. Rock strengths in this area will be higher than in the area of zinc mining and, therefore, there will be less potential to impact hydrologic stability.
- The crown pillar will be mostly comprised of strongly and moderately weathered rock to the east where the zinc ore of the Crandon Formation is predominant. Crown pillar rocks will be weaker and there will be more potential for hydrologic impacts.
- Areas of gossan in the Crandon Formation zinc ore with an RQD of 2% were photographed in only two holes. RQD in moderately weathered ore has an average value of 37%, and averaged 68% in weakly weathered ore.
- RQD in the hanging wall unit correlated with the weathering intensity and had average values of 41%, 54% and 66% for strongly, moderately and weakly weathered descriptions, respectively.
- RQD in the footwall rocks was generally higher and less impacted by weathering and averaged 86% and 72% for moderately and weakly weathered categories.
- Average fracture frequency, as measured in core runs in core photographs, ranged from 2.2–6.3 fractures/foot. No correlation was apparent with weathering intensity.
- Estimated values of RMR correlated well with weathering intensity. RMR was approximately 40 for strongly weathered rock or gossan, which indicates poor ground conditions in excavations. Moderately weathered rocks had average values ranging from 48–61 (fair) indicating improved conditions in excavation and less ground support requirements. Weakly weathered rock had average values ranging from 48–78 (fair–good) suggesting less ground support in excavations.

- Rock strength based on core samples in strongly weathered rock were estimated to have as little as 52% and 30% of the strength of weakly weathered rock in the hanging wall and zinc ore, respectively. These effects were included in the analysis by using empirical correlations with rock quality.
- Glacial aquifers overlie the crown pillar in glacial overburden that ranges in thickness from 75–250 ft. A glacial till at the base of the overburden forms a portion of the aquitard separating the bedrock and glacial hydrologic system. The crown pillar will be sufficiently thick to prevent disruption of this aquitard.
- Strongly weathered bedrock at the top of the crown pillar/base glacial overburden also contributes to the aquitard separating the glacial and bedrock hydrologic system. This rock has been weathered to a clay-rich massive saprolite that is typically 20-ft thick over the Crandon orebody. This clay rock layer is expected to be undisturbed during mining due to its relatively soft nature.

2.4. Summary and Recommendations

This evaluation suggests that the preliminary mining plans developed for the crown pillar are consistent with requirements for hydrologic stability in almost all areas. Localized exceptions were indicated by the analysis at four cross sections where the preliminary plans indicate a crown pillar thickness less than 100 ft. These exceptions were eliminated by the adoption of a 100-ft minimum crown pillar thickness. It is recommended that specific criteria be developed to guide final design of the mining extraction. These criteria are listed below and will provide additional assurance that vertical conductivity of the crown pillar will not be increased by mining in the crown pillar area:

- Minimum crown pillar thickness should be 100 ft.
- Maximum open void height in post-pillar mining at the top lift (where cable bolts are not installed) should be 8 ft.
- Final stope backfilling at the base of the crown pillar should use tight filling techniques.

Additional data collected from underground excavations during mine-level development will be used to verify the conclusion about hydrologic stability and, if required, will provide the basis to refine the mining criteria.

3. CROWN PILLAR GEOLOGY, GEOTECHNICAL CHARACTER AND HYDROLOGY

3.1. Introduction

This section of the report presents a summary of the geology of the ore deposit and of the surface overburden in the vicinity of the crown pillar. The geotechnical data from boreholes drilled through the crown pillar are summarized in this section and are presented in more detail in Appendix B. Finally, the glacial aquifers at the surface are briefly described to provide background for assessment of the impacts of the planned mining on the crown pillar hydrology.

3.2. Crown Pillar Description

The crown pillar refers to the bedrock left between the top mining horizon and the glacial overburden. It will be left unmined to protect the surface and the near-surface groundwater aquifers from the impacts of mining. The extent of the crown pillar[2] and it's currently planned base elevation are illustrated in the long section shown as Figure 3-1, which shows the extent of the zinc and copper zones. Mining extraction may extend for a distance of approximately 4900 ft between 2,274,575 E and 2,279,450 E. Zinc ore will be mined first and extends for approximately 4275 ft between 2,275,175 E and 2,279,450 E. The copper ore extends for approximately 2400 ft between 2,274,575 E and 2,276,975 E. The glacial overburden thickness varies between 75 and 250 ft, thickening to the west. The planned thickness of the crown pillar varies along strike from 330 to 70 ft.

3.3. Crown Pillar Geology

Bedrock units of the Crandon orebody are subdivided into three major rock types:

- Hanging wall rocks (Mole Lake Formation) — north of the orebody.
- Zinc ore (Crandon Formation) and footwall copper ore beneath the Crandon formation.
- Footwall rocks — south of the zinc orebody.

---

[2]Moe, D. (1995, December 19). [Personal Communication. Crandon Mining Company, Rhinelander, WI.]

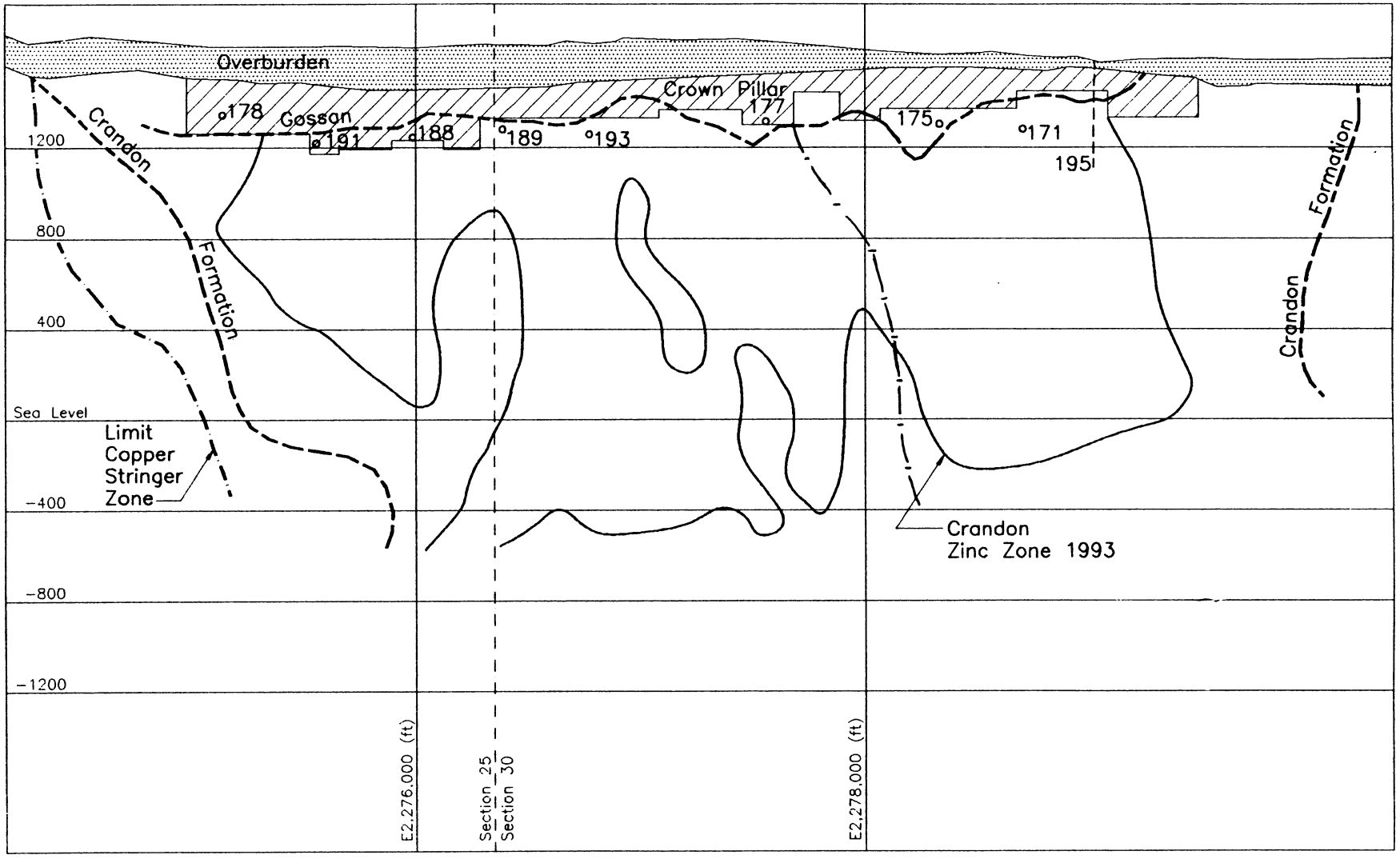

Figure 3-1. Longitudinal projection looking North through the Crandon Formation showing extent of the zinc and copper zones and the currently planned thickness of the crown pillar (thickness will be increased locally where required).

The host rocks and associated sulfide mineralization which forms the orebody were deposited on the ocean floor by a submarine volcanic system during the middle Precambrian. Through geologic time, the deposit has been buried, lithified, metamorphosed, and tilted into its present nearly vertical position. Much of the original sulfide mineralization and its host rock have been eroded away. What remains has been covered by unconsolidated sediments of glacial origin. The general structural relationship of the mineralization, bedrock and overburden are shown in the cross section in Figure 3-2.

Near-surface, the orebody and bedrock have been subjected to chemical and physical weathering processes that include one or more of the following: oxidation and leaching, argillization, and fracturing. The type and weathering intensity has been subdivided into categories of:

- Strong (S) — strong weathering intensity, includes gossan (G);
- Moderate (M) — moderate weathering intensity; and
- Weak (W) — weak weathering intensity, includes low (L) weathering intensity.

The bedrock weathering has been most intense near-surface within and along specific horizons in the orebody and along it's northern, hanging wall boundary. These weathering intensities have been the basis for grouping geotechnical data to provide mechanical properties estimates for analysis.

The crown pillar typically includes rocks that are strongly to moderately weathered, because they are directly below the surficial glacial deposits and have been exposed to surface effects prior to burial by the glacial overburden. Immediately below the glacial overburden the bedrock has been weathered into a saprolite of variable thickness that is subdivided into two subunits;

- a lower, structured saprolite, and
- an upper, massive saprolite.

The structured saprolite preserves the original rock structure but has been largely altered to clay and iron oxides. The structured saprolite is typically 20–100 ft thick (GeoTrans 1995). The massive saprolite has similar composition but the original rock structure has undergone chemical and physical alteration of the rock mass, obliterating primary rock features.

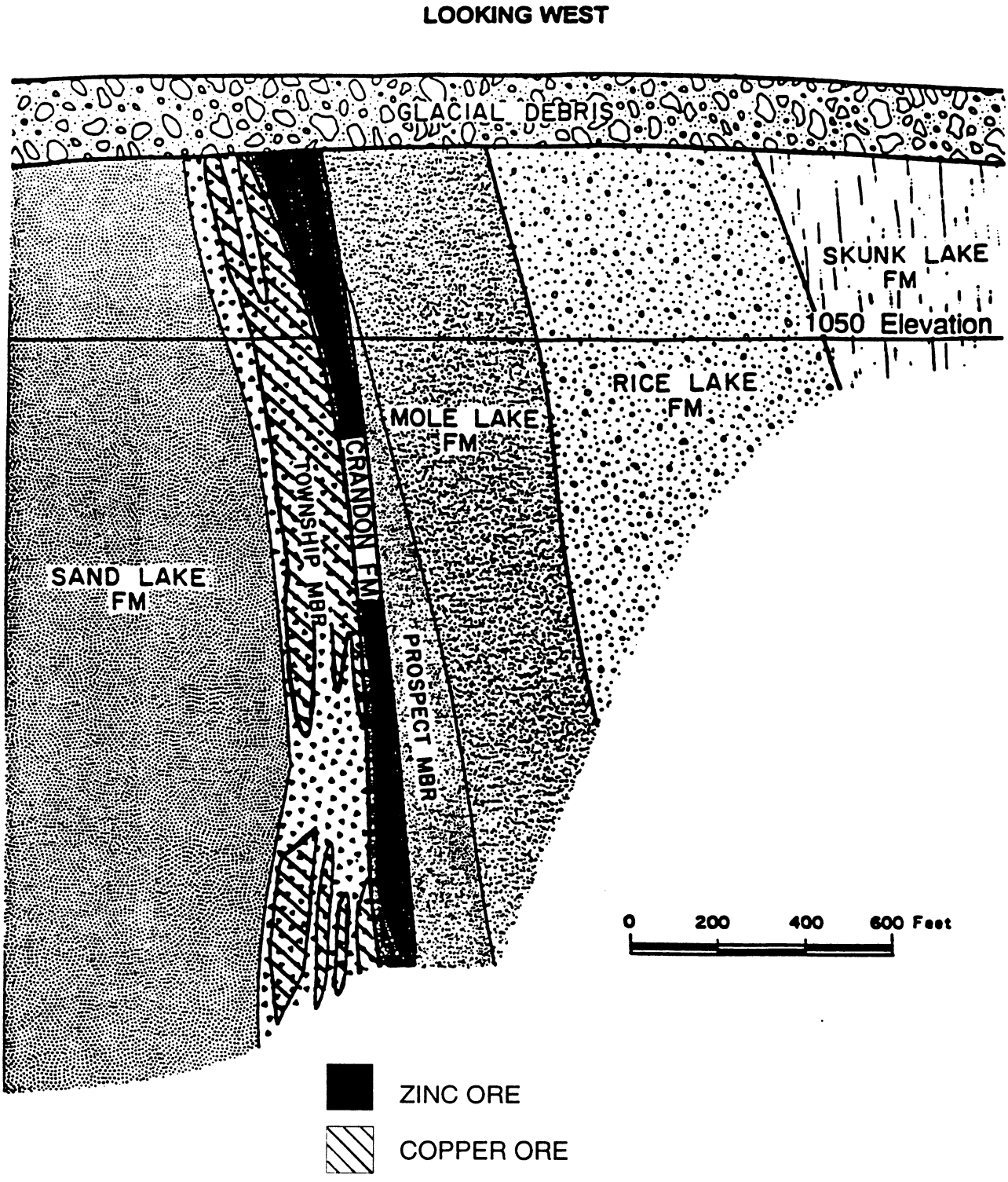

Figure 3-2. **Generalized geologic cross section through the Crandon orebody (adapted from Foth & Van Dyke 1995a).**

The massive saprolite has been studied extensively because, together with glacial till deposits immediately on top of the bedrock, it forms a layer of low permeability material between the bedrock and the overlying course-grained outwash contained in the glacial aquifer system. Isopach maps[3] indicate that the massive saprolite is typically 20 ft-thick over the orebody and thins to the 1-ft range within 1000 ft to the north and south of the orebody.

Five cross sections along the strike length of the orebody are presented as Figures 3-3, 3-4, 3-5, 3-6, and 3-7 to illustrate the relationship of the zinc and copper ore zones, the variation of weathering intensity and the thickness of the massive saprolite in the crown pillar. The figures also show the currently planned extent of mining beneath the crown pillar area (above 1200-ft elevation) which is discussed in Section 4. The sections show that the weathering extends deeper into the zinc ore than into copper ore areas. Crown pillar rocks in the eastern portion of the orebody are typically strongly weathered down to the top of mining. In contrast, crown pillar rocks above the top of mining of the copper ores are typically moderately or weakly weathered.

3.4. Crown Pillar Geotechnical Data

Geotechnical data from Crandon boreholes that sampled the rock in the crown pillar have been compiled to estimate the geotechnical character of the rock. The data are presented in Appendix B. RQD and fracture frequency were estimated using photographs of core from eight holes that pass through or just below the base of the crown pillar. These estimates are conservative and indicate lower rock quality than actual because they include all damage from boxing and handling the core. The locations of these holes along the orebody strike are illustrated in Figure 3-1, an E-W projection that shows where angle holes pierce the hanging wall/Crandon Formation contact. Figure 3-8 presents a composite N-S projection that illustrates the location of the ore zone at two cross sections along strike and shows the relative position of the core holes for which the core photographs were available. The range in the base of the crown pillar along the orebody is also plotted to show that the holes sample rock that is typically included in the crown pillar.

---

[3]GeoTrans, Inc. (1995). *Numerical simulation of the effect on groundwater and surface water on the proposed zinc and copper mine near Crandon, Wisconsin.* Prepared for Foth & Van Dyke, Green Bay, WI. Roswell, GA:Author (Project No. 7702-003) (Figure 2-3, a copy is presented in Appendix A).

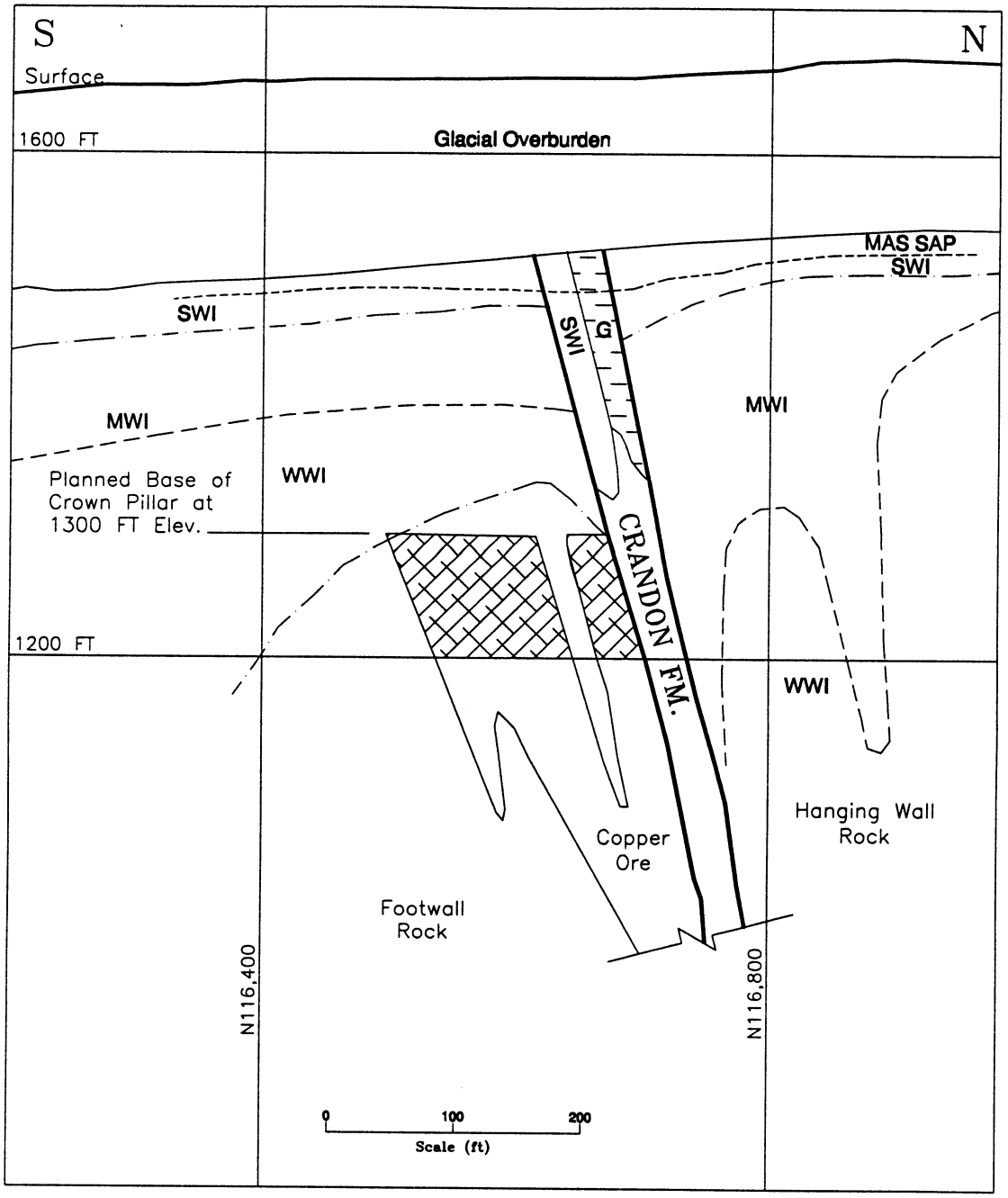

N-S Section
2,275,025

Figure 3-3. Projection along 2,275,025 E showing geology, weathering intensity, and top of mining forming crown pillar.

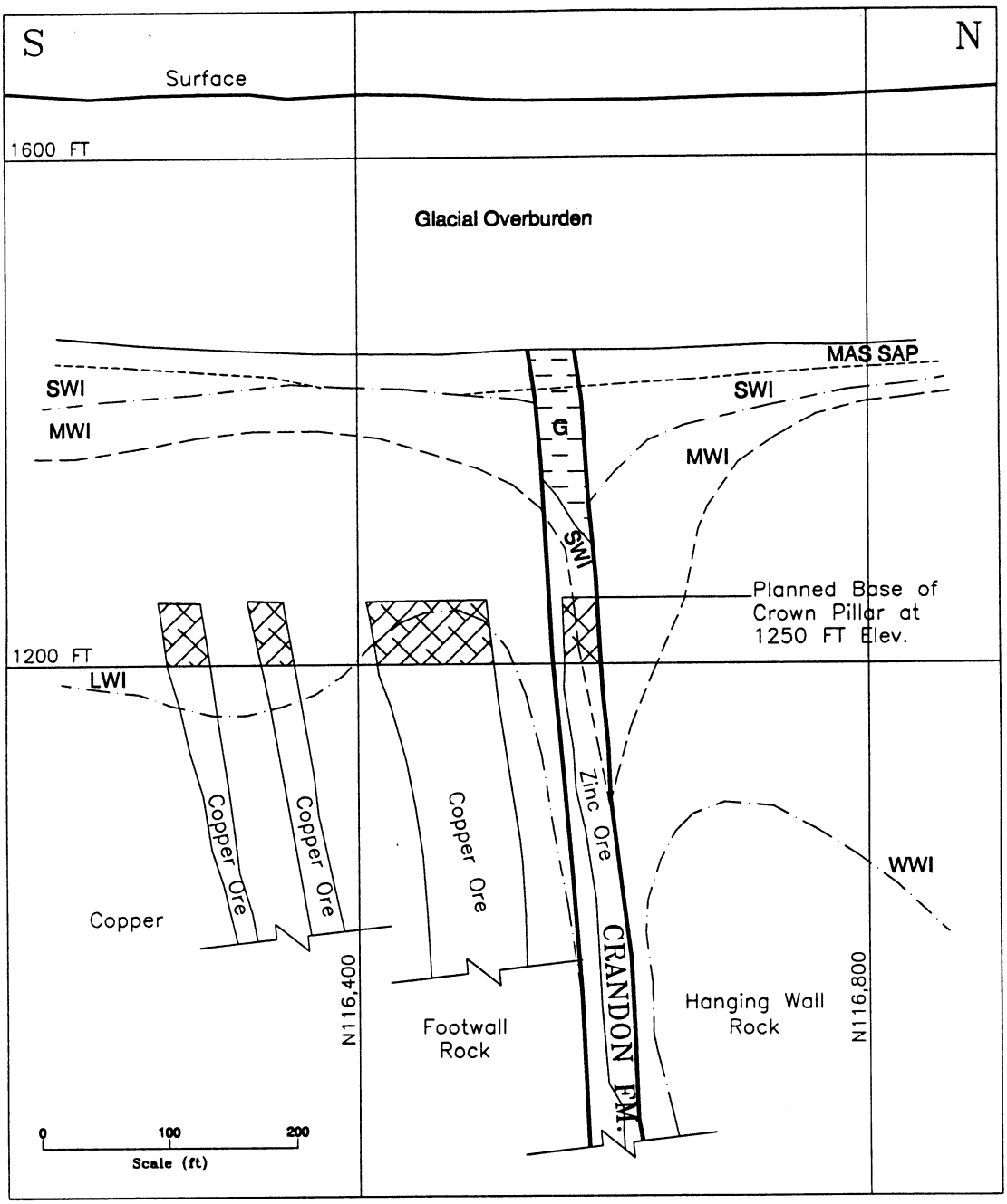

N-S Section
2,275,925

Figure 3-4. Projection along 2,275,925 E showing geology, weathering intensity, and top of mining forming crown pillar.

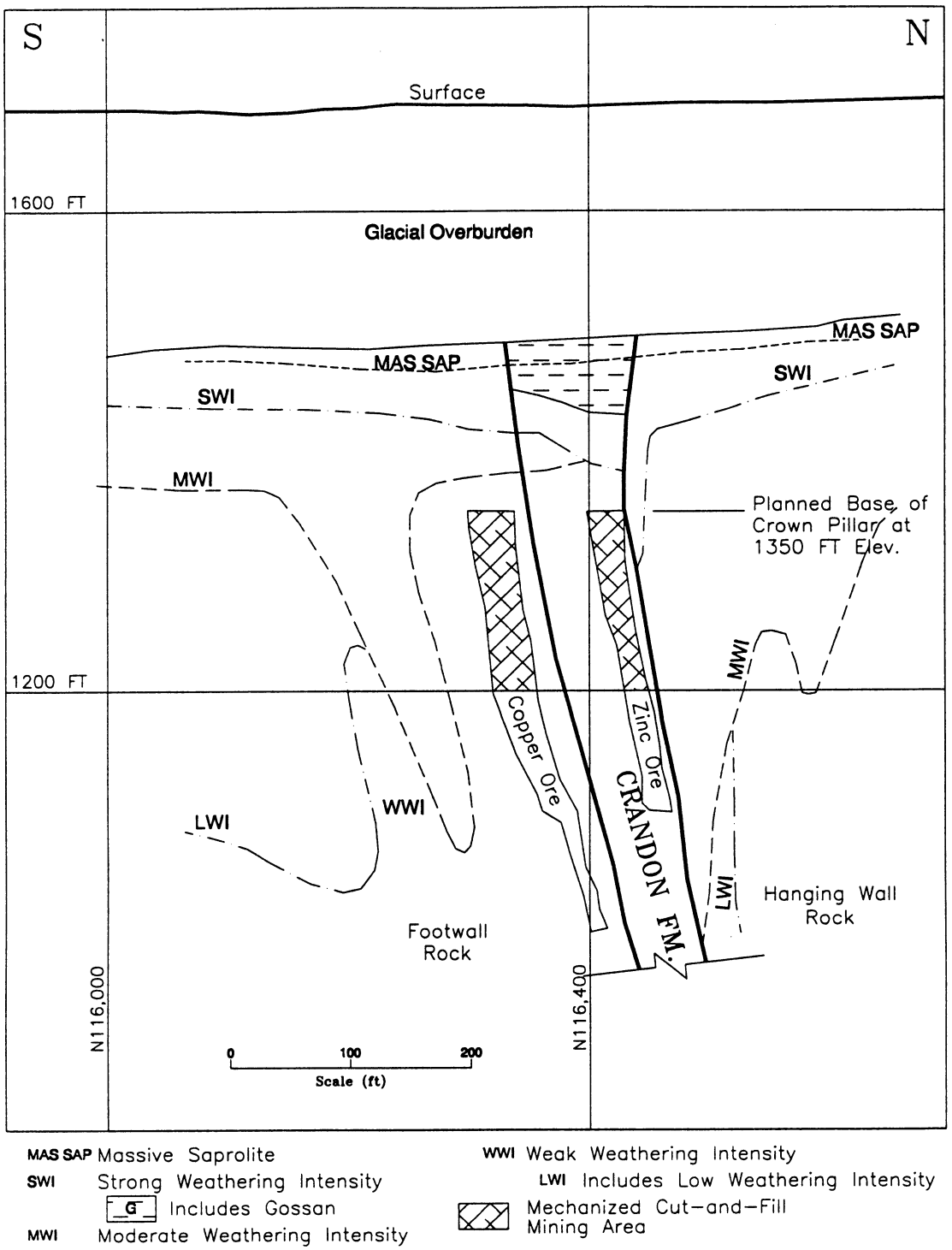

N-S Section
2,276,975

Figure 3-5. Projection along 2,276,975 E showing geology, weathering intensity, and top of mining forming crown pillar.

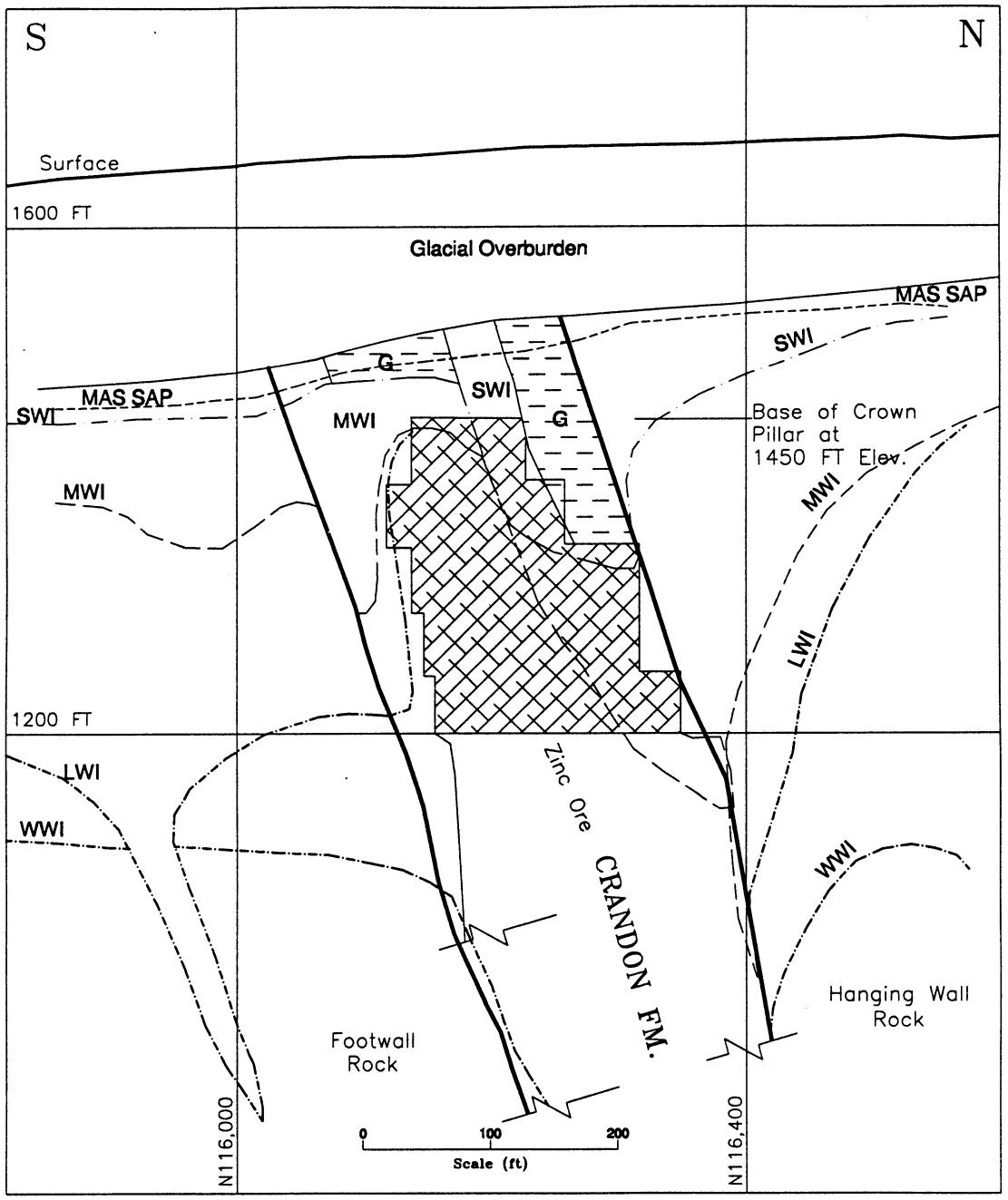

N-S Section
2,277,800

Figure 3-6. Projection along 2,277,800 E showing geology, weathering intensity, and top of mining forming crown pillar.

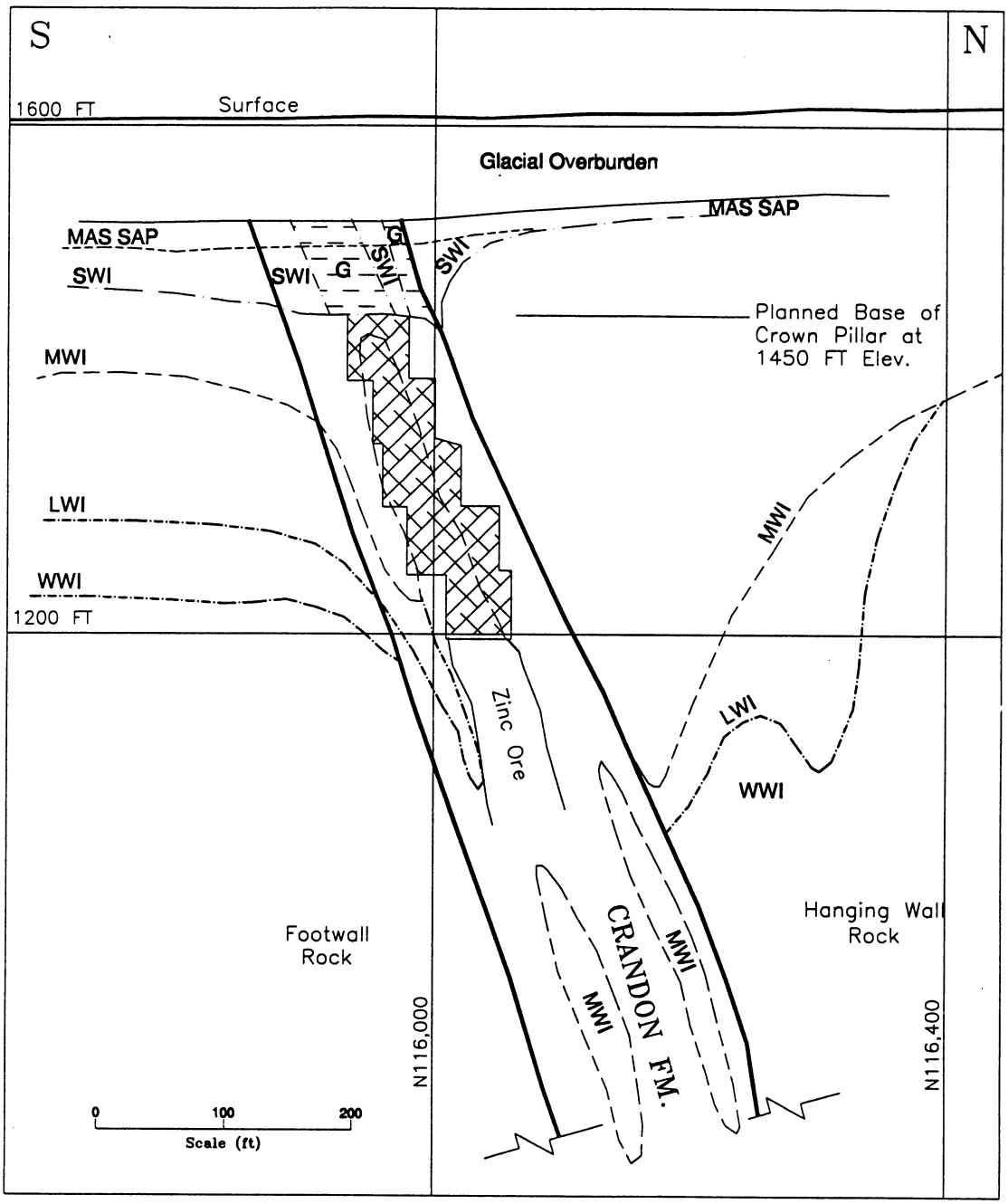

N-S Section
2,279,000

Figure 3-7. Projection along 2,279,000 E showing geology, weathering intensity, and top of mining forming crown pillar.

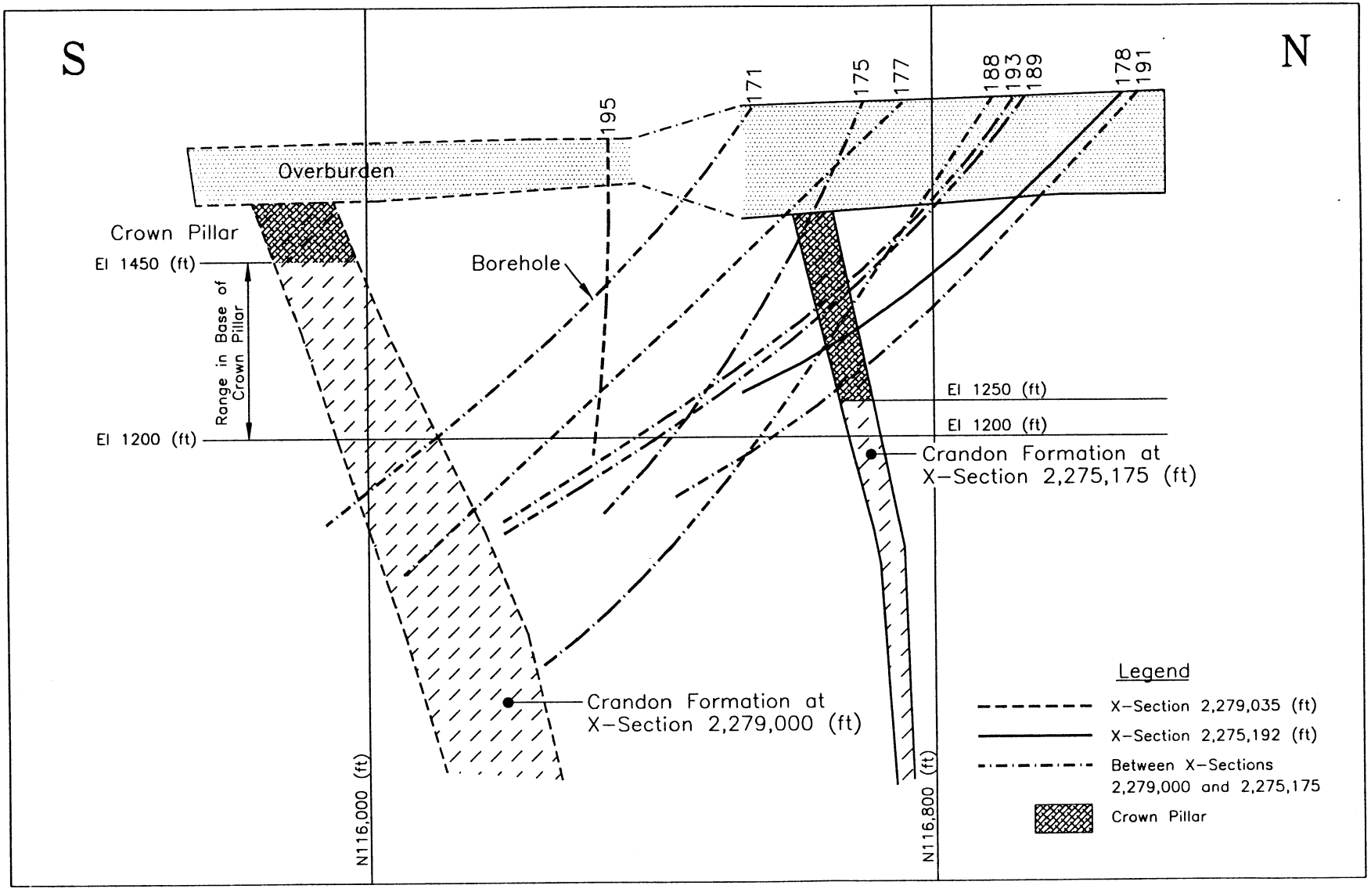

Figure 3-8. Composite projection of the Crandon Formation and the locations of boreholes 175, 177, 178, 188, 189, 191, 193 and 195 with respect to the range in the base of the crown pillar.

The geotechnical data were grouped into the categories of weathering intensity for each of the three units of hanging wall rocks, footwall rocks, and zinc ore (Crandon Formation). The cross sections in Figures 3-3 through 3-7 show that the zones of weathering intensity are consistent along the orebody strike. This grouping was used to define the characteristics of the rock and the data were then used to estimate rock mass quality and rock mass properties for the analysis.

Modeling and analysis of the potential impacts of mining below the crown pillar on hydrologic stability required mechanical properties of rock strength and deformation modulus that account for scale effects between the laboratory and field. Rock strength and deformation moduli are generally much lower at the excavation scale than measurements on core samples from the same location. This reduction in strength/modulus at the larger scale is due to fractures, weathering, and other inhomogeneities.

Geotechnical design analysis therefore uses mechanical properties that compensate for scale effects between laboratory and field-scale measurements. This is generally done by empirical correlations between rock mass quality, a relative index that accounts for rock characteristics that effect excavation stability, and mechanical properties that average the effects of inhomogeneities. The rock mass quality index used is an industry-wide standard called the "Geomechanics Index" or Rock Mass Rating—RMR (Bieniawski 1976).

The process and data used to evaluate the rock mass quality—RMR and to estimate mechanical properties for the analysis is described in Appendix B. The derived average parameters are listed in Table 3-1, to illustrate the characteristics of the rocks in the crown pillar area. Rock quality designation (RQD) is an index that describes the portion of core in a given run interval that is produced in pieces of 4 inches or greater in length. Fractures, rubble zones and lost core effect the piece length. The values derived by photographic analysis underestimate the actual RQD because all fractures are counted, regardless of the source and, therefore, provide a conservative estimate. The values in Table 3-1 indicate that the rock quality in the crown pillar area is lower than in the deep parts of the orebody where the RQD averages 86–93%. The RQD values tend to increase as weathering intensity decreases in the hanging wall and Crandon Formation. The footwall rocks appear to be less impacted by the weathering intensity.

Table 3-1. Summary of geotechnical parameters derived from data from the crown pillar area.

Parameter	Rock Unit	Weathering Intensity				
		Gossan	Strongly	Moderately	Low/Weakly	Unweathered
RQD (%)	HW	NA	41	54	66	63
	CF	2	ND	37	68	ND
	FW	NA	ND	86	72	82
Uniaxial Compressive Strength (psi)	HW	NA	5,030	5,995	3,720	9,690
	CF	ND	12,860	11,680	42,770	ND
	FW	NA	ND	16,940	21,110	22,870
Fracture Frequency (fractures/ft)	HW	NA	3.9	3.5	6.3	3.9
	CF	2.2	ND	2.8	1.5	ND
	FW	NA	ND	2.2	3.5	2.3
RMR	HW	NA	39	48	48	51
	CF	38	ND	52	78	ND
	FW	NA	ND	61	61	64
Estimated Rock Mass Uniaxial Strength (psi)	HW	NA	600	820	820	NR
	CF	ND	730	1,980	13,500	NR
	FW	NA	ND	3,240	3,240	NR

HW—*hanging wall*, CF—*Crandon Formation*, FW—*footwall*, NA—*not applicable*, ND—*no data*, NR—*not required for analysis*.

The uniaxial compressive strengths in Table 3-1 are estimates derived from point load test measurements on core and correlation between point load tests and compressive strength. Spot values of laboratory uniaxial strength tests were consistent with the range of point load predictions. The values in Table 3-1 indicate that the hanging wall and Crandon Formation (zinc ore) rocks in the crown pillar have lower strength due to the weathering when compared to the results from holes below the weathering depth. However, the intact rock strengths indicated for the strong weathering intensity are still relatively high when compared to the stresses at the shallow depth of the crown pillar, a condition that is positive for stability.

The estimation of RMR from the core data is a typical procedure for developing a basis for underground design prior to actual underground excavations. On a comparative basis, the strong weathering (and gossan) has resulted in relatively low rock quality. The planned mechanized cut-and-fill mining methods are appropriate for the RMR values that were determined for the strongly weathered rocks in the hanging wall and Crandon formation (zinc ore).

The RMR values resulted in estimates of low rock mass strength when compared to the core data, as indicated in Table 3-1. The strongly weathered portions of the hanging wall and Crandon Formation were modeled as having 6–12% of the intact strength. No strength data was available for the gossan material in the Crandon Formation, it was therefore estimated to have a rock mass strength sufficient to support the assumed in situ stress state.

This approach to the estimation of mechanical properties at the rock mass scale generally produces very conservative values. In this respect, it is a method to account for the uncertainties that exist due to the lack of underground access typical at this stage in the project. The lack of data for some of the weathering intensities would not adversely effect the modeling results because the crown pillar, in its projected worst-case geometry and geology, is comprised of strongly weathered Crandon Formation and gossan for which a sufficient understanding of the geotechnical character exists.

4. CROWN PILLAR MINING LAYOUTS

4.1. Introduction

This section describes plans for mining immediately below the crown pillar to provide the basis for developing the analysis in Section 5. Mechanized cut-and-fill mining methods are identified for the interval along the 1200-ft elevation to assure a high degree of stability during mining. These methods incorporate incremental backfilling after mining to minimize the extent of open voids.

The individual variations of the cut-and-fill mining methods are described briefly with respect to the potential impact on hydrologic stability of the crown pillar. Cross sections showing the projected mining geometry at different locations along the orebody strike were previously presented in Section 3. Variations of crown pillar thickness, mining width and the ratio of pillar thickness to mining width are presented to provide a basis for selecting the cross section to be analyzed.

Mining plans for the extraction of ore in the interval of lower rock quality immediately below the crown pillar were initially developed in the Crown Pillar Area Mining Methods Study (DYNATEC 1982). Ore included in this study was primarily above 1200-ft elevation where stability concerns due to lower rock quality were judged to require methods other than the blasthole open stoping with delayed backfill method to be used in the majority of the orebody. The DYNATEC study established the general criteria for mining immediately below the crown pillar to preserve the surface and to avoid potential impacts to the glacial aquifers. Preliminary planning for the extent of mining immediately below the crown pillar has been based on the most recent ore reserve cross sections (Geosolutions Resources, Inc. 1995).

4.2. Geometry of the Crown Pillar

The variations in thickness of the crown pillar, width of the mining beneath the crown pillar and the resulting ratio are illustrated in Figures 4-1 and 4-2 for copper ore and zinc ore along the strike of the orebody for preliminary mine plans. In the western end of the deposit, copper ore is predominant. Both copper and zinc ore occur between 2,275,175 E and 2,276,975 E, and zinc ore is predominant in the eastern part of the orebody.

Count	X-Section (ft)	Base of Crown Pillar Elevation (ft)	Crown Pillar Width at Base Ore Zone 1 (ft)	Ore Zone 2 (ft)	Ore Zone 3 (ft)	Width of Waste Between Ore Zones (ft)	Crown Pillar Thickness (ft)	Maximum Ore Width/ Pillar Thickness
1	2,274,283	1320	10	10	—	95	160	0.06
2	2,274,431	1400	10	10	—	95	40	0.25
3	2,274,575	1350	10	10	15	95	180	0.08
4	2,274,725	1350	30	10	58	77	180	0.32
5	2,274,875	1350	113	35	—	22	180	0.63
6	2,275,025	1300	108	35	—	20	220	0.49
7	2,275,175	1250	74	25	—	65	250	0.30
8	2,275,325	1300	110	—	—	0	180	0.61
9	2,275,475	1300	40	—	—	0	170	0.24
10	2,275,625	1150	30	48	—	35	310	0.15
11	2,275,775	1200	42	—	—	0	247	0.17
12	2,275,925	1250	32	24	92	107	200	0.46
13	2,276,075	1250	25	84	—	153	200	0.42
14	2,276,225	1200	110	—	—	0	247	0.45
15	2,276,375	1350	62	—	—	0	110	0.56
16	2,276,525	1350	17	—	—	0	110	0.15
17	2,276,675	1350	10	—	—	0	122	0.08
18	2,276,825	1350	28	—	—	0	120	0.23
19	2,276,975	1350	30	—	—	0	140	0.21

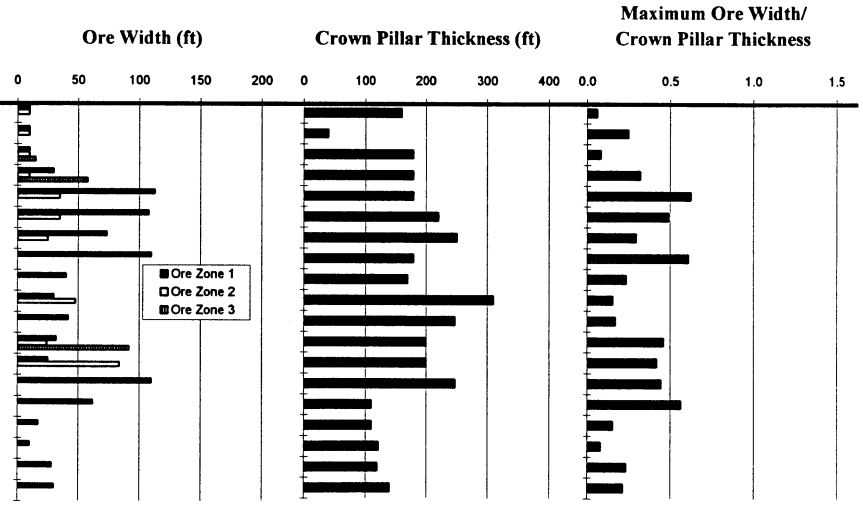

Figure 4-1. Variation of preliminary crown pillar thickness, mining width in ore zones and thickness-mining width ratio for cross sections containing copper ore.

Count	X-Section (ft)	Base of Crown Pillar Elevation (ft)	Crown Pillar Width at Base Ore Zone 1 (ft)	Ore Zone 2 (ft)	Ore Zone 3 (ft)	Width of Waste Between Ore Zones (ft)	Crown Pillar Thickness (ft)	Maximum Ore Width/ Pillar Thickness
1	2,275,175	1250	10	—	—	0	250	0.04
2	2,275,325	1300	20	—	—	0	180	0.11
3	2,275,475	1300	30	—	—	0	170	0.18
4	2,275,625	1150	10	—	—	0	310	0.03
5	2,275,775	1200	10	—	—	0	247	0.04
6	2,275,925	1250	30	—	—	0	200	0.15
7	2,276,075	1250	30	—	—	0	200	0.15
8	2,276,225	1200	30	—	—	0	247	0.12
9	2,276,375	1350	20	—	—	0	110	0.18
10	2,276,525	1350	20	—	—	0	110	0.18
11	2,276,675	1350	10	—	—	0	122	0.08
12	2,276,825	1350	10	—	—	0	120	0.08
13	2,276,975	1350	30	—	—	0	140	0.21
14	2,277,200	1400	30	—	—	0	100	0.30
15	2,277,350	1400	20	30	—	30	110	0.27
16	2,277,500	1350	120	—	—	0	160	0.75
17	2,277,650	1350	130	—	—	0	160	0.81
18	2,277,800	1450	90	—	—	0	72	1.25
19	2,277,950	1350	120	60	—	50	180	0.67
20	2,278,100	1400	20	—	—	0	138	0.14
21	2,278,250	1400	30	—	—	0	140	0.21
22	2,278,400	1400	10	20	—	160	135	0.15
23	2,278,550	1400	90	—	—	0	145	0.62
24	2,278,700	1450	10	50	—	90	92	0.54
25	2,278,850	1450	40	30	—	60	80	0.50
26	2,279,000	1450	50	—	—	0	75	0.67
27	2,279,150	1350	10	—	—	0	170	0.06

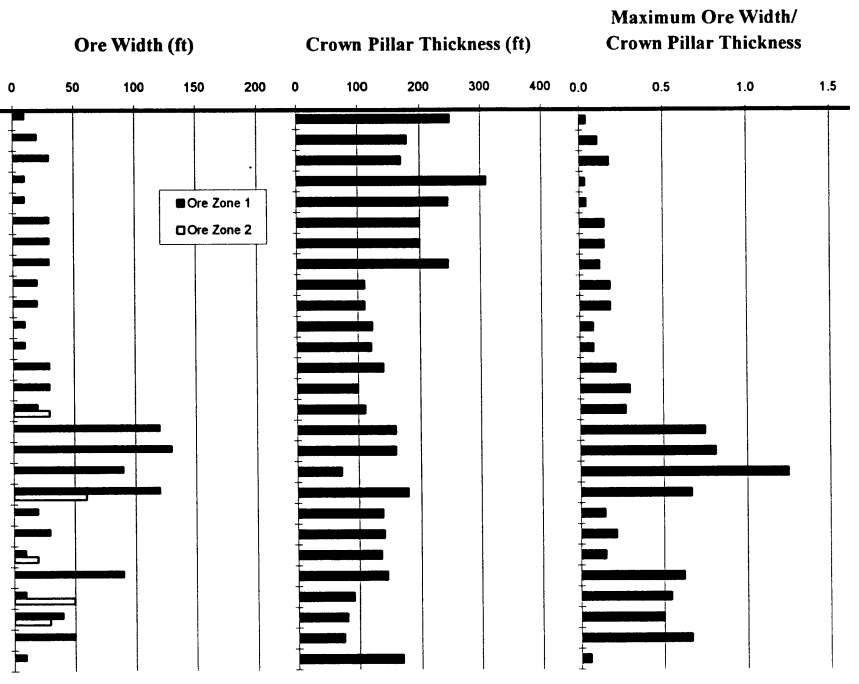

Figure 4-2. Variation of preliminary crown pillar thickness, mining width in ore zones and thickness-mining width ratio for cross sections containing zinc ore.

Figures 4-1 and 4-2 list the elevation of the base of the crown pillar and the width of mining at the pillar base. As illustrated in Figures 3-3, 3-4, and 3-5, some cross sections have several mining zones separated by intervals of waste. The width of the waste zone is listed and would be sufficient to act to isolate the potential impacts of each mining zone. The thickness of the crown pillar between the base of the glacial overburden and the top of mining is also listed in Figures 4-1 and 4-2.

The ratio of mining width to preliminary crown pillar thickness was used to compare the potential for mining impacts to crown pillar hydrology along the strike of the ore. The ratio incorporates two considerations:

- larger mining widths indicate a larger area over which potential impacts can occur, and
- thinner crown pillars have higher stress concentrations which has increased potential to impact hydraulic conductivity.

The variations in the ratio, along with variations in preliminary crown pillar thickness and mining width are shown in Figures 4-1 and 4-2 for copper ore and zinc ore, respectively. The largest values of the ratio occur in the zinc ore between sections 2,277,650 E and 2,279,000 E. The cross sections in this area were characterized by ore widths as great as 130 ft and crown pillar thicknesses as small as 72 ft. The worst case occurred at section 2,277,800 E, where the ore width was 90 ft and crown pillar thickness was 72 ft, giving a ratio of 1.3.

Analytically, the crown pillar thickness was the definitive parameter because it directly controls the magnitude of the stress concentration. The stress analysis presented in Section 5 indicated that crown pillar thicknesses should be 100 ft or greater. On this basis, the preliminary plan for crown pillar thickness meets the thickness requirement established in Section 5 in 88% of the cross sections. The crown pillar thickness needs to be increased at four cross sections: 2,277,800 E; 2,278,700 E; 2,278,850 E and 2,279,000 E.

When the minimum pillar thickness is increased to 100 ft, the maximum value of width-thickness ratio would be 0.9. In the copper ore, all cross sections have width-thickness ratios of 0.6 or less, indicating less potential for adverse impacts. In the zinc ore, 85% of the cross sections would have width-thickness ratios of 0.6 or less.

4.3. Mining Methods

4.3.1. Blasthole Open Stope Mining with Delayed Backfill

The majority of the Crandon deposit will be mined using blasthole open stoping with delayed backfill. In this method, illustrated by Figure 4-3, approximately 50% of the ore would be extracted in primary stopes between pillars that are designed to support the concentrated stresses. The primary stopes would then be backfilled with hydraulic fill stabilized with cement as a binder. After the backfill has cured, the pillars would be extracted as secondary stopes and then backfilled with uncemented tailings. The blasthole mining would be employed in ore up to the 1200-ft elevation, above which mechanized cut-and-fill methods would be used.

4.3.2. Mining Methods for the Crown Pillar Area (above 1200-ft elevation)

The DYNATEC study identified three cut-and-fill mining methods that limit the open void, which exists at anytime in the mining operation, by close cycling of mining and backfilling. Minimizing the open void eliminates the possibility of a large-scale instability near the crown pillar, thereby removing the potential for major hydrologic impacts.

These cut-and-fill mining methods require personnel and equipment to have repeated access into the stopes which requires a high degree of rock stability. In order to assure a safe working environment, stability must be monitored and maintained by the installation of rock support, for example rock bolts or long cable bolts. Each method is described briefly in the following sections.

Vertical Crater Retreat (VCR) Mining

The VCR mining method, illustrated in Figure 4-4, is similar to blasthole open stoping with the exception that spherical charge blasting is used to break rock to a horizontal free face rather than a vertical free face. However, the stope remains full of broken ore until it has been blasted through to the upper (drilling) level. The ore can then be rapidly mucked from drawpoints at the stope bottom, and the stope backfilled immediately which minimizes the time that a large void is present.

Post-Pillar Cut-and-Fill (PCF) Mining

Post-pillar cut-and-fill, a variation of room-and-pillar mining, was specified by DYNATEC (1982) for mining above 1350-ft elevation. In this method, illustrated by Figure 4-5, the ore is extracted in horizontal slices approximately 15 ft-high. Small pillars (15-ft square post

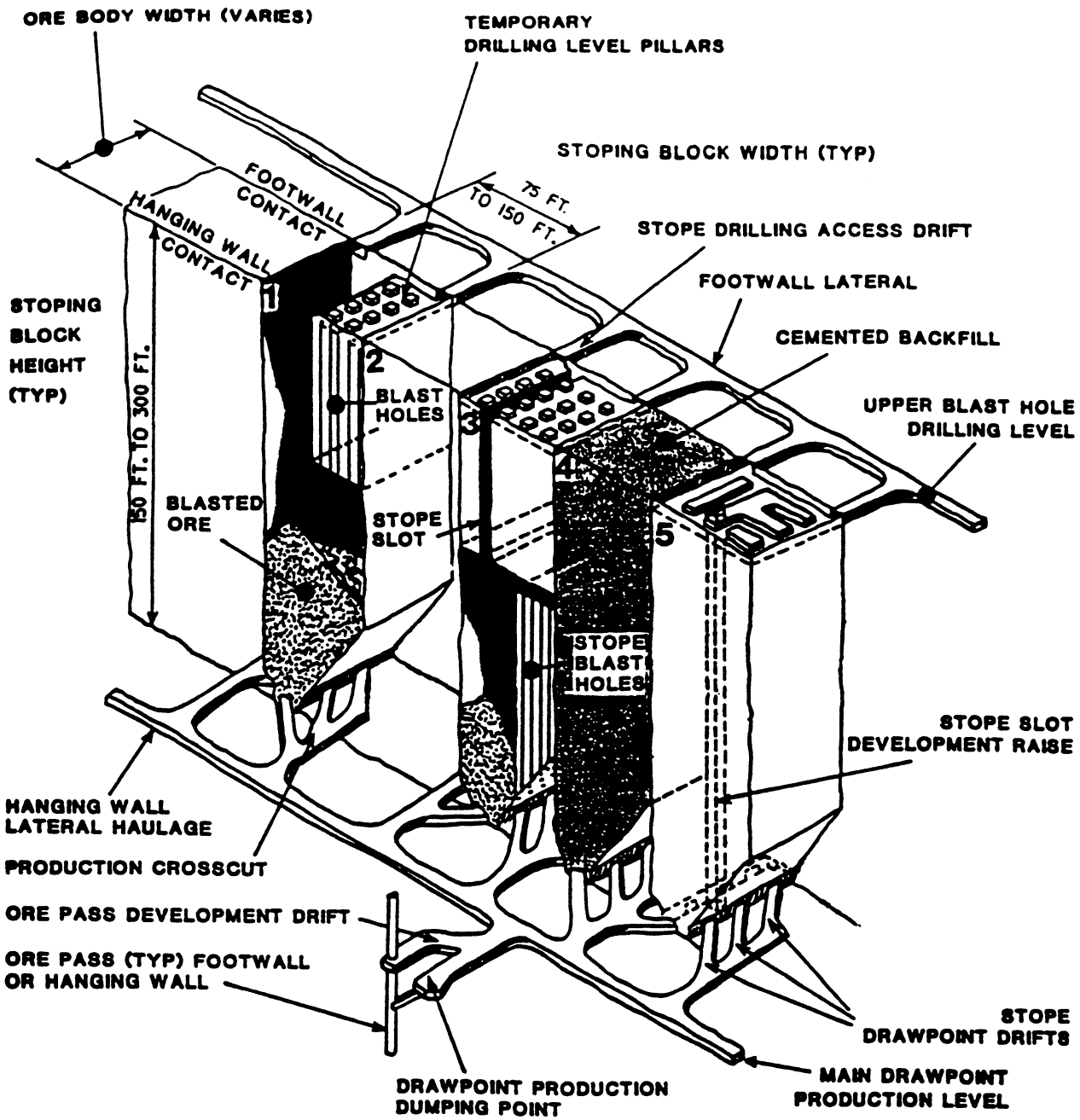

Figure 4-3. Schematic of blasthole open stoping with delayed backfill (Foth & Van Dyke 1995a).

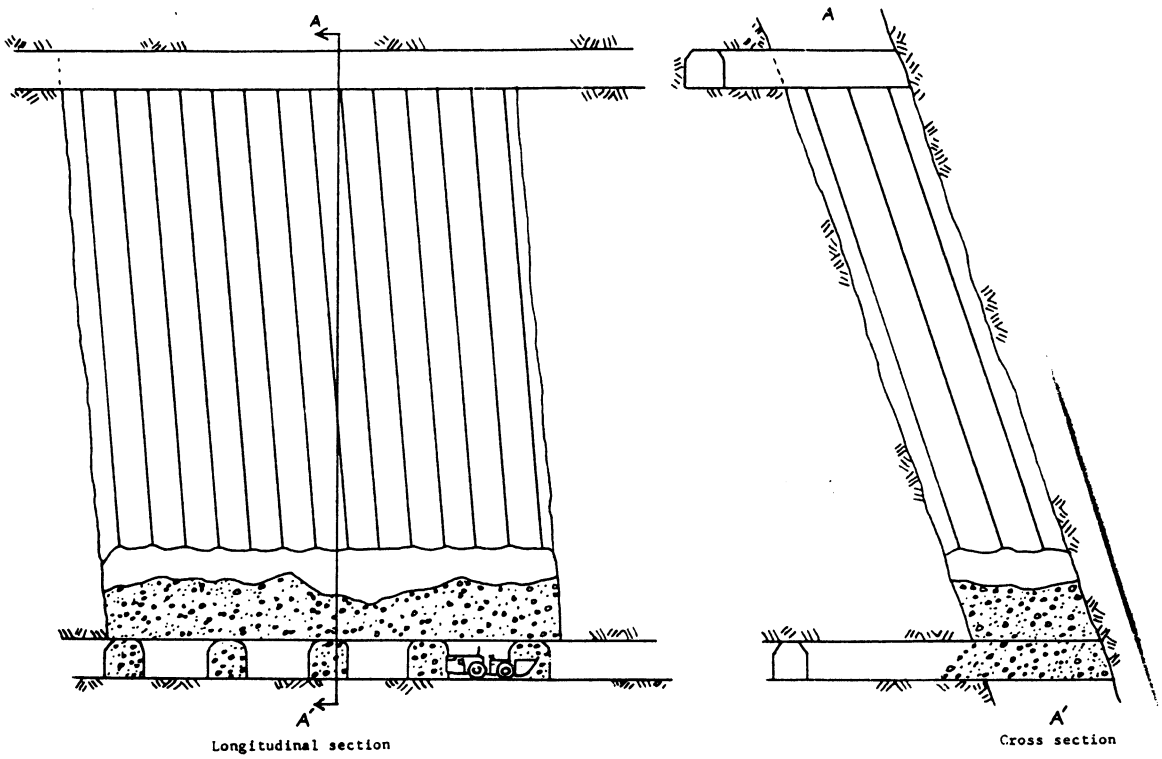

Figure 4-4. Schematic illustrating vertical crater retreat stoping.

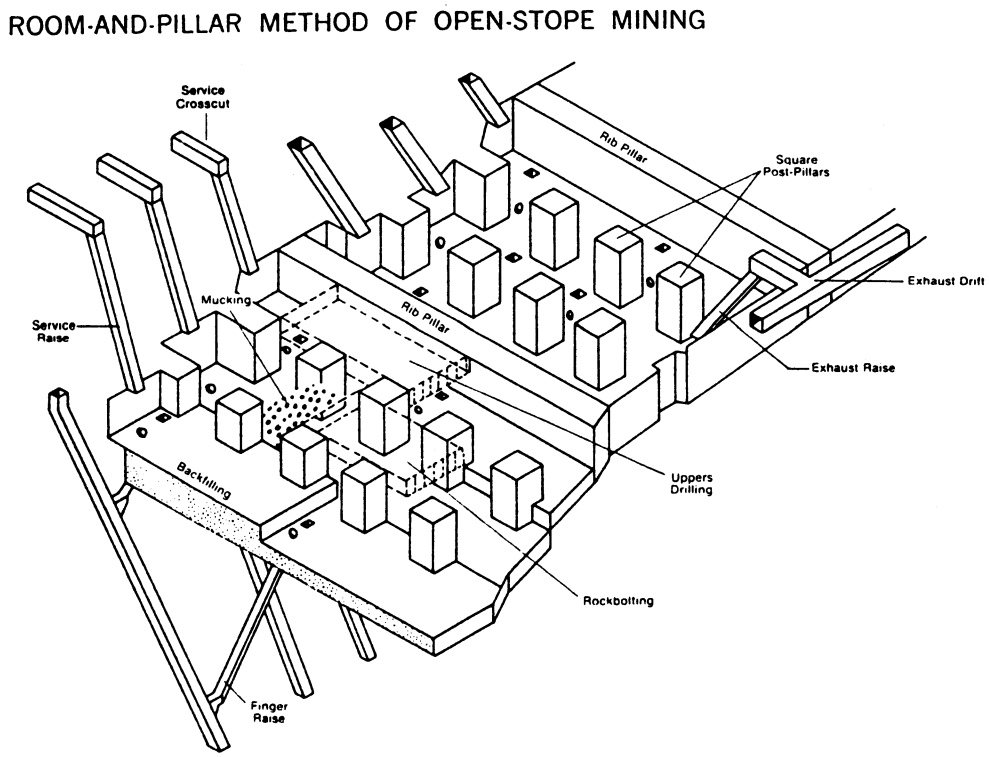

Figure 4-5. General schematic illustrating post-pillar cut-and-fill mining.

pillars) are left on a regular pattern to provide local roof support. The ore is extracted from rooms between pillars with spans of approximately 23–32 ft. The DYNATEC study estimated an extraction ratio between 82–88%.

Each horizontal level is backfilled which provides the floor to access the next ore above. Backfill can be cemented or uncemented hydraulic fill and acts to limit the open void as well as provide horizontal constraint to the post pillars. The DYNATEC study called for the installation of vertical cable bolts from the level at the base of the crown pillar down to the bottom of post-pillar mining at 1350-ft elevation. The cable bolts would support the roof as the mining advanced vertically upward.

Undercut-and-Fill Mining (UCF)

Longitudinal undercut-and-fill mining was identified for a small part of the planned production immediately below the crown pillar. This method would only be used where ore grades were sufficiently high to justify its additional cost. In this method, mining would be initiated from the base of the crown pillar and would proceed downward in successive horizontal levels 11-ft high. On each horizontal level, individual excavations would be driven approximately 14-ft wide for a distance of 150 ft along strike. After the excavation is complete, it will be backfilled with cement stabilized hydraulic fill. Rock bolts can be placed on the floor and then immersed in hydraulic fill as illustrated in Figure 4-6. After excavation and backfilling of the top slice, excavation would take place underneath backfill as shown in Figure 4-6.

4.4 Extent of Mining Extraction

Modeling of the mining extraction has been based on the full outline of zinc ore in Figure 3-1 to be conservative. As is typical in underground mining, the layout of the Crandon orebody has been developed at a level of detail consistent with the existing resource definition. Details about the areal extent of mining, regional pillars between stoping areas and transition between the mining methods cannot be established until the mine is developed and additional ore grade definition and geotechnical/rock mechanics data is collected. However, the inclusion of the details would tend to reduce the estimated stress concentration in the crown pillar. General

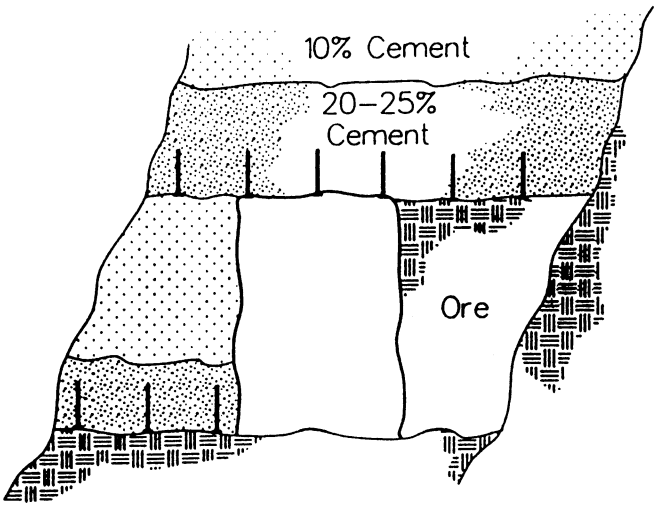

Figure 4-6. Schematic illustrating undercut-and-fill mining.

descriptions of the mining system[4] state that between 5 and 10% of the minable ore below the crown pillar will be left in place as pillars. The longitudinal projection shown in Figure 3-1 illustrates the potential areal extent of mining extraction with the outline of ore.

Approximately 90% of all ore will be extracted by blasthole open stope mining with delayed backfill[5]. At the currently planned production rate, approximately eight blasthole stopes would be mined out and backfilled each year exposing less than 5% of the total hanging wall of the orebody at any one time[6]. This incremental mining and backfilling distributes the open voids into different areas of the orebody and therefore removes the potential of large impacts to the crown pillar area.

As mining proceeds, the horizontal stresses normal to the hanging wall would be gradually redistributed. The backfill prevents large displacements of the hanging wall and horizontal stresses would be gradually transferred to the regional pillars and abutment zones around the excavation, and to the backfill. The crown pillar will be one area where the horizontal

---

[4]Foth & Van Dyke (1995a). *Summary: Project Description and Environmental Baseline Data, Crandon Project, Crandon, Wisconsin.* Prepared for Crandon Mining Company. Green Bay, WI:Author.

[5]Ibid.

[6]Ibid.

stresses are concentrated and the full extent of mining has therefore been modeled without regional pillars to evaluate the projected worst-case loading in the crown pillar area.

4.5. Final Backfilling of Stopes at the Base of the Crown Pillar

Final backfilling of the stopes at the base of the crown pillar will be performed to eliminate the potential for long-term subsidence impacts on the hydrologic stability. Case history data from near surface coal mining provides a basis to establish criteria that will produce very high levels of confidence that such subsidence will not propagate to the glacial aquifers in the overburden. These coal mining data are collected from unfilled excavations that cover much greater areal extent than the Crandon mining and are excavated in much weaker sedimentary rocks. They, therefore, provide a conservative basis to show that the backfilling will eliminate potential subsidence events.

Empirical data from near surface coal mining in Colorado was evaluated by Matheson and Eckert-Clift (1986) to assemble a probabilistic measure of the likelihood of an unfilled mine opening at a given depth propagating to the surface. The surface above near-surface room-and-pillar coal mines in Colorado was surveyed to locate sinkholes that had formed as rock collapsed into unfilled mine openings over a period of 20–30 yrs after mining was completed. It was found that for the same unfilled height of mine opening, fewer sinkholes would form at the surface if the overburden depth was greater. These data were compiled graphically in Figure 4-7 which shows the number of openings that formed sinkholes at the surface as a percentage of the number of existing mine openings at a particular location. This was plotted versus the overburden thickness divided by the mine opening height to account for the depth of the mine.

The stopes at the base of the crown pillar will be backfilled to prevent the possibility of long-term subsidence. Figure 4-7 indicates that to achieve a 98% confidence that no subsidence event could reach the surficial glacial alluvium, the ratio of the crown pillar thickness to any unfilled height that might remain at the top of the stope should be 16. The minimum crown pillar thickness (100 ft) has been adjusted to 80 ft to be more conservative. The criteria would then be that no subsidence event could reach the approximate based of the massive saprolite. According to Figure 4-7, unfilled voids less than 5-ft high would have a very low probability (2%) of reaching the massive saprolite. Stopes at the base of the crown pillar will be tight filled in 15-ft high increments. Tight filling of stopes at Crandon will leave unfilled voids that are

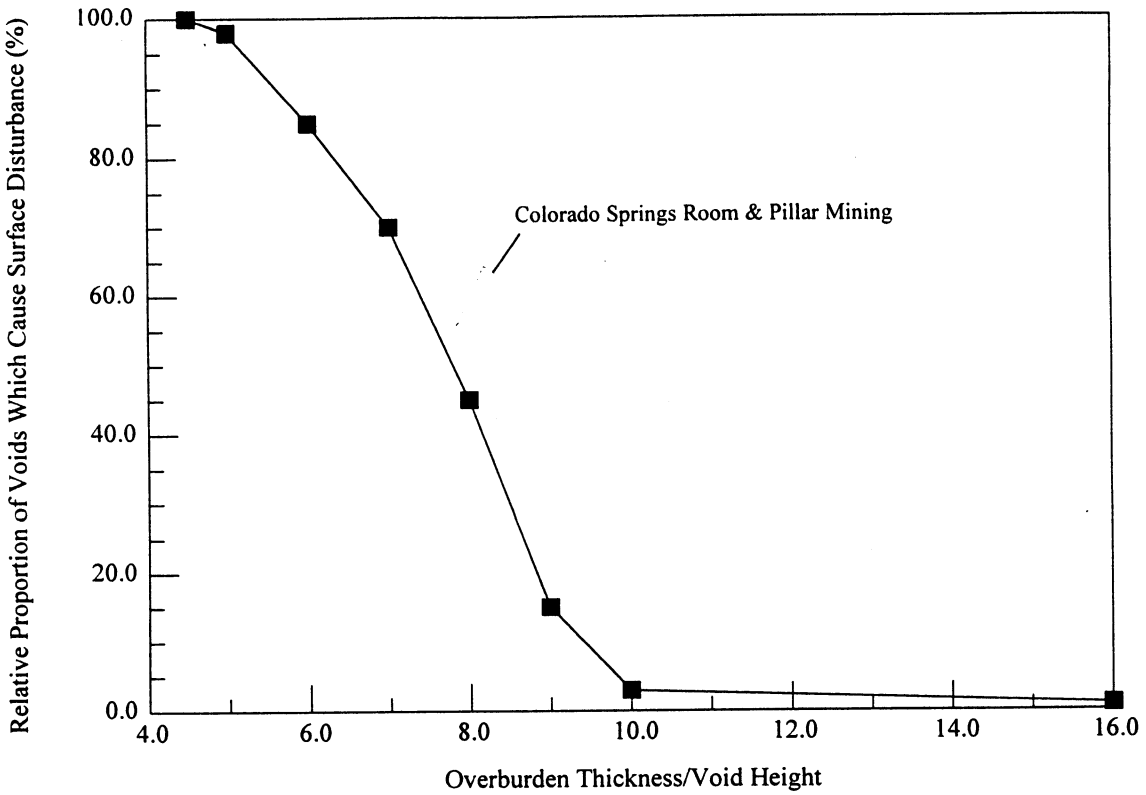

Figure 4-7. Relative portion of voids which cause surface disturbance versus the ratio of overburden thickness/mined height (adapted from Matheson and Eckert-Clift 1986).

on the order of 2 ft, which will produce minimum values of overburden thickness/void height of greater than 40. Values of 40 would give 100% confidence of no subsidence event reaching the glacial alluvium.

5. EVALUATION OF CROWN PILLAR HYDROLOGIC STABILITY

This section presents the results of the evaluation of the crown pillar hydrologic stability.

5.1. Modeling Approach

The modeling approach used to assess the potential impacts on hydrologic stability consisted of three separate analyses, the first two of which provided input to the succeeding evaluation. The three analyses were:

- Three-Dimensional Simulation of the Mining of the Entire Crandon Orebody: This simulation was performed to provide the initial stress state for the subsequent detailed two-dimensional analysis of the projected worst-case geometry of the crown pillar and to verify that the crown pillar stresses produced in the two-dimensional analysis were realistic. The computer code MULSIM was used.
- Two-Dimensional Simulation of Stress and Strain Changes at the Projected Worst-Case Crown Pillar Geometry Developed from the Cross Section at 2,277,800 E: This simulation was performed to estimate the magnitude of strain changes that could occur in the crown pillar if rock mass strength was exceeded by the changes in stress. Exceeding the rock mass strength would cause highly localized deformation that could exceed the strain criteria ($> \pm 5 \times 10^{-3}$) for protection of the integrity of aquitards. The computer code FLAC was used.
- Analysis of Potential for Shear Dilation (opening) on Existing Fractures: Stress changes that were projected to occur in the crown pillar could cause opening or closing of fracture apertures which would impact the vertical conductivity of the fracture network. The potential for changes in aperture for the predominant fractures reported for the upper bedrock region were evaluated. The computer code UDEC was used.

The results of each analysis are presented in the following sections.

5.2. Three-Dimensional Simulation of Crown Pillar Stress Change

The boundary-element program MULSIM, provided by the U.S. Bureau of Mines, was used to simulate the crown pillar stress change due to complete extraction of the Crandon ore. The mining process was simulated in three steps:

- Step 1—Mine all primary stopes (50% extraction ratio) and backfill from the bottom of the ore up to the 1200-ft elevation.
- Step 2—Mine all secondary stopes (rib pillars) up to the 1200-ft elevation.
- Step 3—Extend all mining from the 1200-ft elevation to the base of the crown pillar.

The extent of the mining simulation was developed from the zinc ore outline in Figure 3-1. The resulting model of the mine at the completion of Step 3 is shown in Figure 5-1 where each alphanumeric character represents a plane area 40 ft × 40 ft square on a seam inclined at 75° to the north. In the simulation, 100% of all the ore has been extracted and 50% of the ore has been replaced with cemented backfill. Backfilling of the secondary stope was not simulated which adds some conservatism to the model. Material properties and in situ stress assumptions are presented in Appendix C.

The stress change perpendicular (normal) to the crown pillar (N-S) is shown in Figure 5-2 as a function of depth below the glacial overburden at cross section 2,277,800 E. Figure 5-2 shows that the magnitude of the stress change that is projected to occur is relatively small throughout most of the crown pillar. The largest changes in stress are focused at the base of the crown pillar. The pattern of stress change is similar in both cases, even though the thickness of the crown pillar has decreased from 320 to 80 ft. The normal stress change in most of the 80-ft crown pillar is limited to the 500–750 psi range.

The stresses calculated at the point when the crown pillar was 320-ft thick represents mining up to the 1200-ft elevation. Those stress levels were used as the initial stress state for the two-dimensional simulation to assure that the results reflected the full mining of the orebody.

5.3. Two-Dimensional Analysis of Crown Pillar Stress and Strain

Mining extraction will produce increasing stress and deformation in the crown pillar as the excavation progresses upward and the thickness of the crown pillar is reduced. Deformation of the crown pillar will be induced due to the mining of the ore and the concentration of horizontal stress. A criteria developed from coal mining experience, where total extraction of the coal seams can produce very large deformations, has been adopted as the limit criteria for this analysis. This quantitative criteria for the preservation of aquifers and aquitards is that horizontal strain should be less than $\pm 5.0 \times 10^{-3}$ inch/inch (SME 1992).

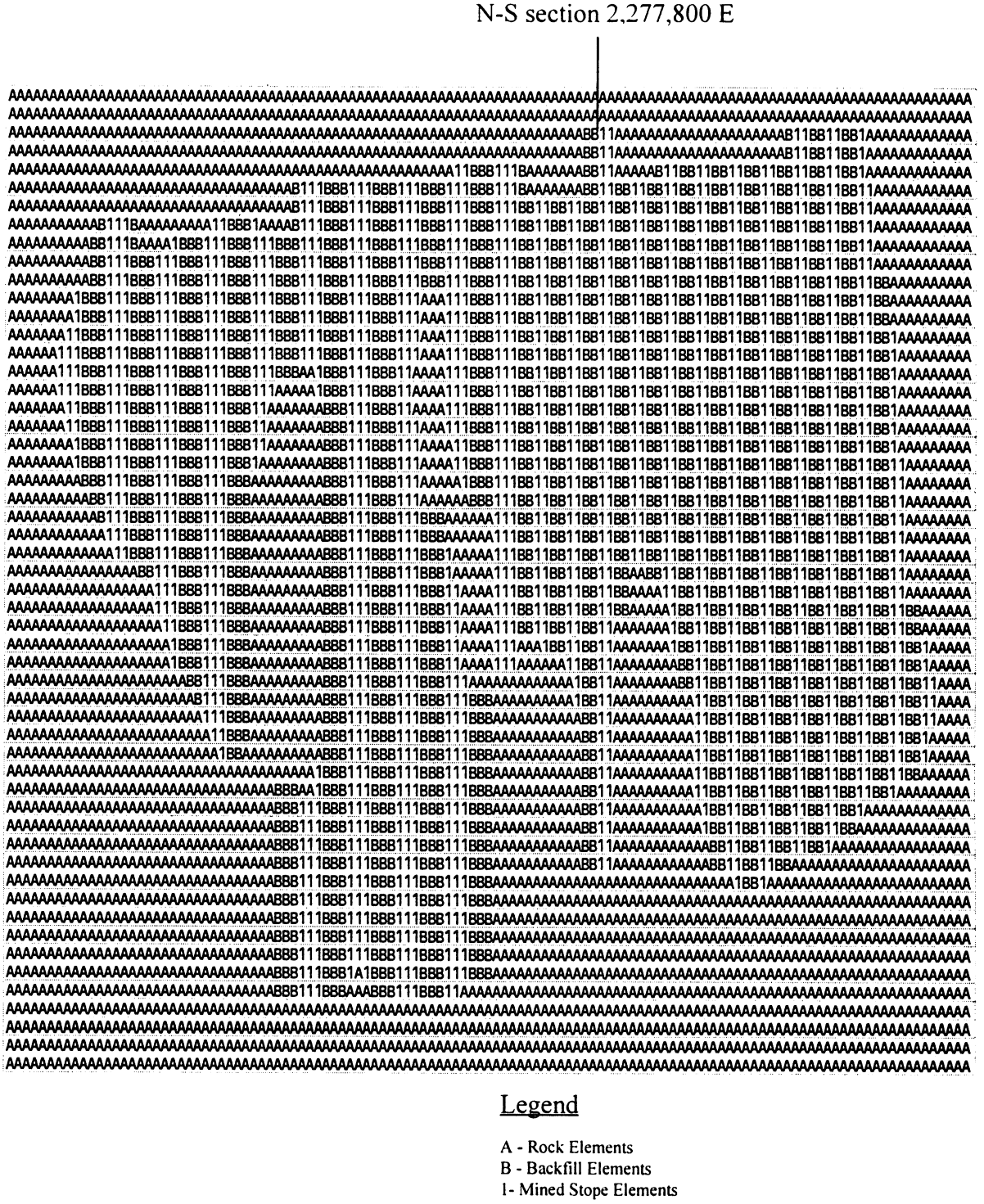

Figure 5-1. Three-dimensional boundary-element mesh simulating mining extraction to the base of the crown pillar.

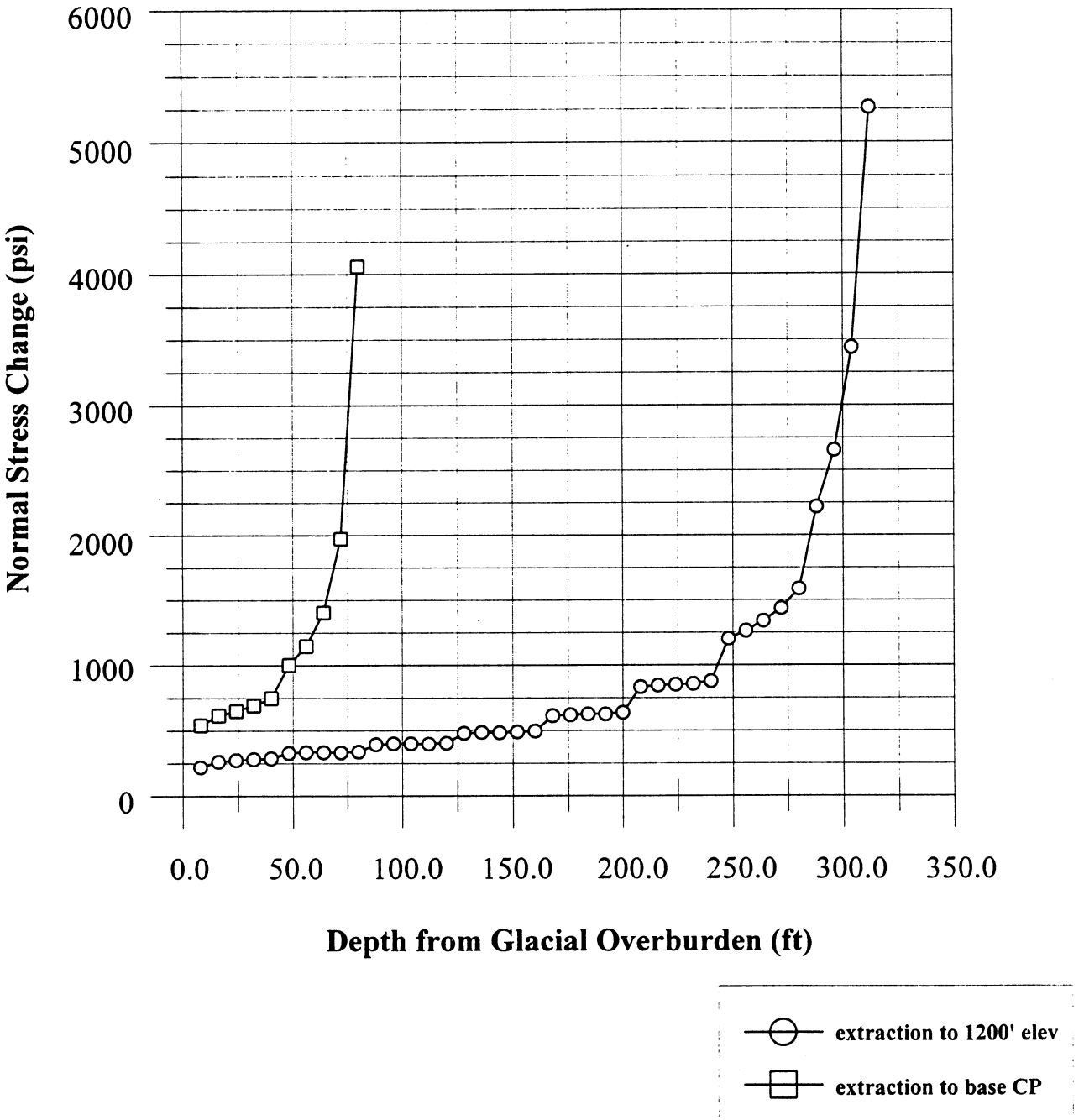

Figure 5-2. **Projected normal stress changes at 2,277,800 E due to extraction up to 1200-ft elevation compared to extraction to the base of the crown pillar.**

The strain criteria is based upon case history experience from longwall coal mines below surface waters or near-surface aquifers. These case studies show that strains (change in length ÷ original length) calculated from the observed subsidence are less than 5×10^{-3} inches/inch. It provided a conservative approach because it is based on observations of surface disturbance caused by undermining much larger areas without backfilling. Surface deformations are typically on the order of several feet over some coal mines. The limited width of extraction at Crandon and the backfilling will limit any potential for surface deformation to much smaller values.

The two-dimensional finite-difference code FLAC was used to analyze the cross section where the crown pillar geometry (mining width:crown pillar thickness is a maximum) represents a projected worst case. This condition occurs at 2,277,800 E. At this section, strong weathering intensity and gossan have affected a large part of the crown pillar above the final mining horizon.

The analyses were conducted using elastic-plastic material property assumptions that allow failure or yielding of the rock. The elastic-plastic assumptions were developed to produce yield or shear failure which allows deformation to be concentrated in weaker materials in the model. This would result in the formation of bands of shear failure where volume expansion could create paths with increased vertical hydraulic conductivity.

The mesh developed to simulate Section 2,277,800 E is shown in Figure 5-3, where the different weathering intensities and rocks are shaded for the values of shear modulus (PSF). Mining near the crown pillar was simulated as eight steps of extraction followed by backfilling. The mesh in Figure 5-3 shows the configuration at Step 6. Figures 5-4a, b, and c show an expanded view of the mesh in Steps 6, 7, and 8. In the final configuration at Step 8, the top lift is shown as excavated before backfilling.

Mining extraction concentrates the horizontal stresses in the crown pillar above the top of the mining. The concentration of horizontal stress for elastic (no rock failure) analysis is shown in Figure 5-5 as the principal stress vectors. The magnitude of the horizontal stress at the center of the crown pillar in elastic analysis at Step 8 is approximately 1880 psi or 122% of the stress predicted by the three-dimensional analysis. This confirms that the two-dimensional analysis gives a conservative assessment of the crown pillar loading.

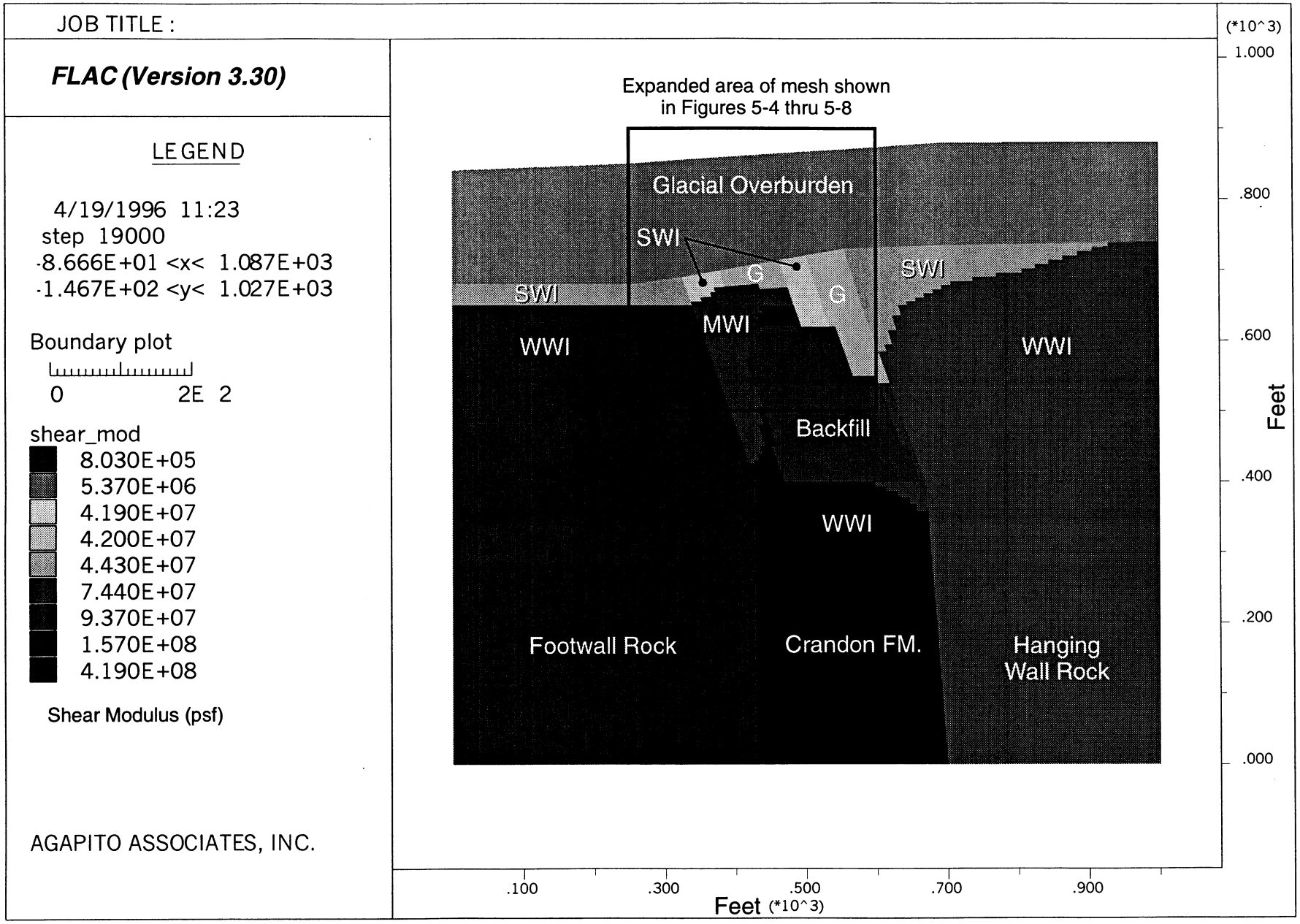

SWI-Strong Weathering Intensity, MWI-Moderate Weathering Intensity, WWI-Weak Weathering Intensity, G-Gossan

Figure 5-3. Color coded material types (shear modulus) in two-dimensional analysis at Step 6.

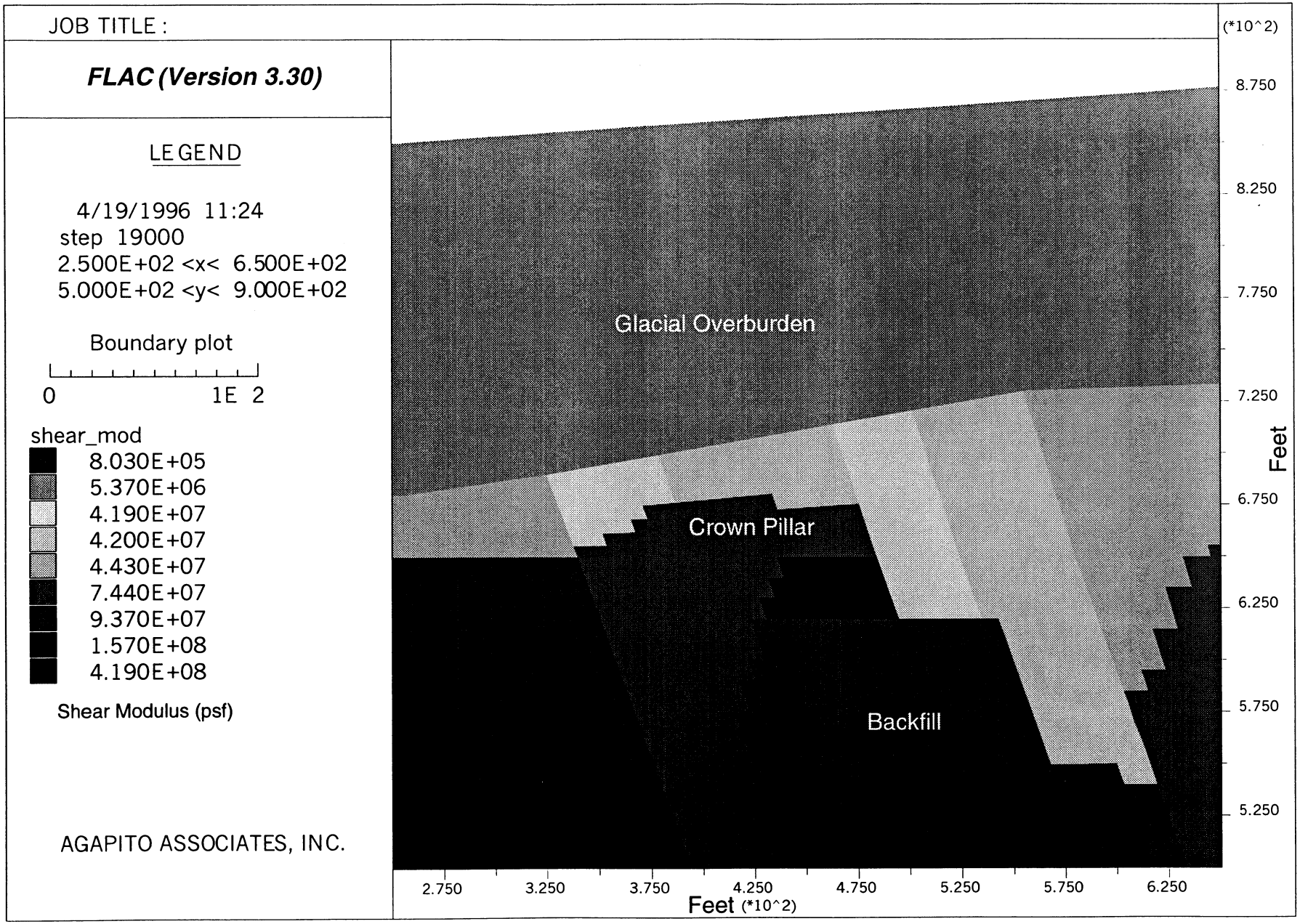

Figure 5-4a. Expanded area showing color coded material types (shear modulus) in two-dimensional analysis at Step 6.

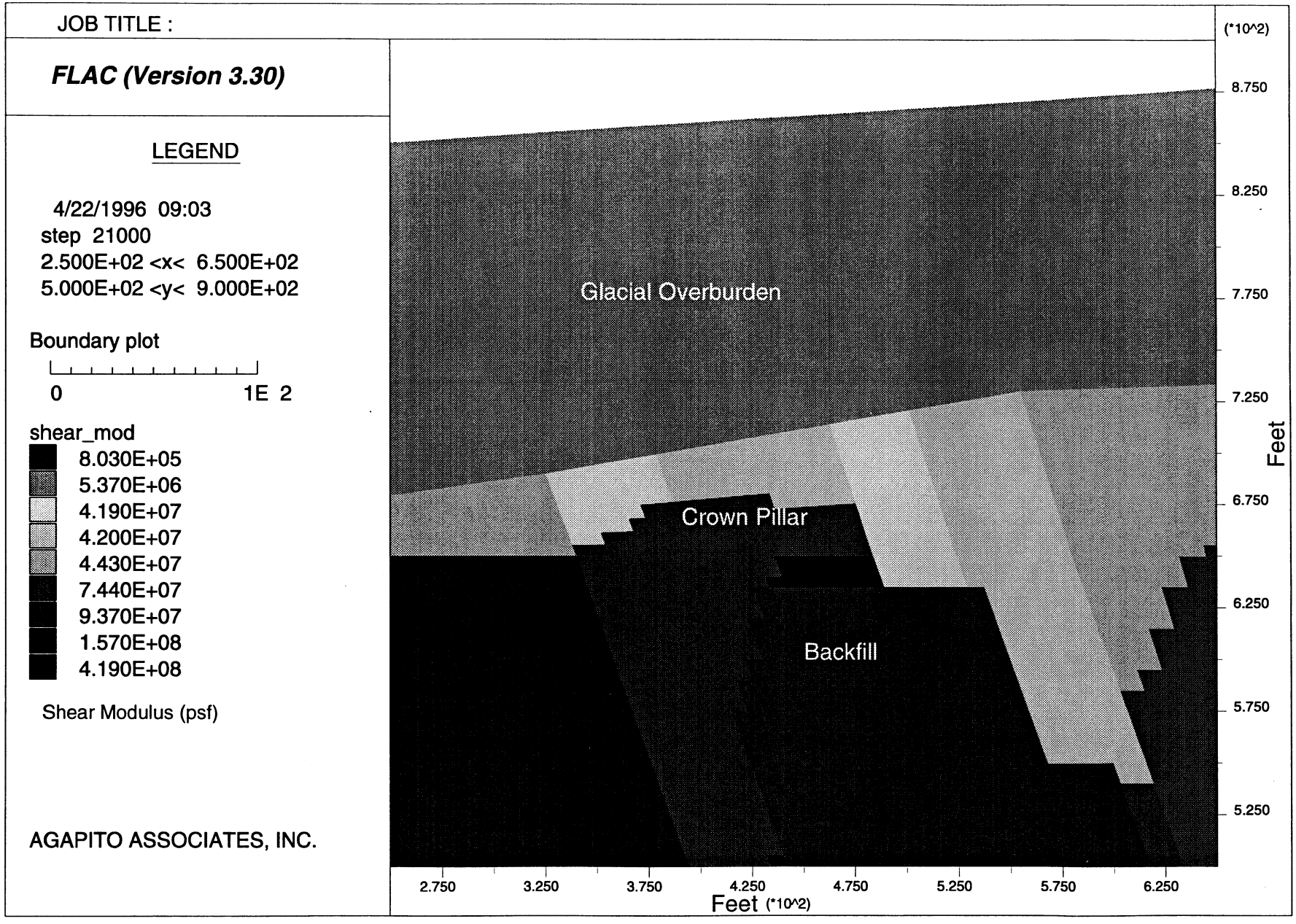

Figure 5-4b. Expanded area showing color coded material types (shear modulus) in two-dimensional analysis at Step 7.

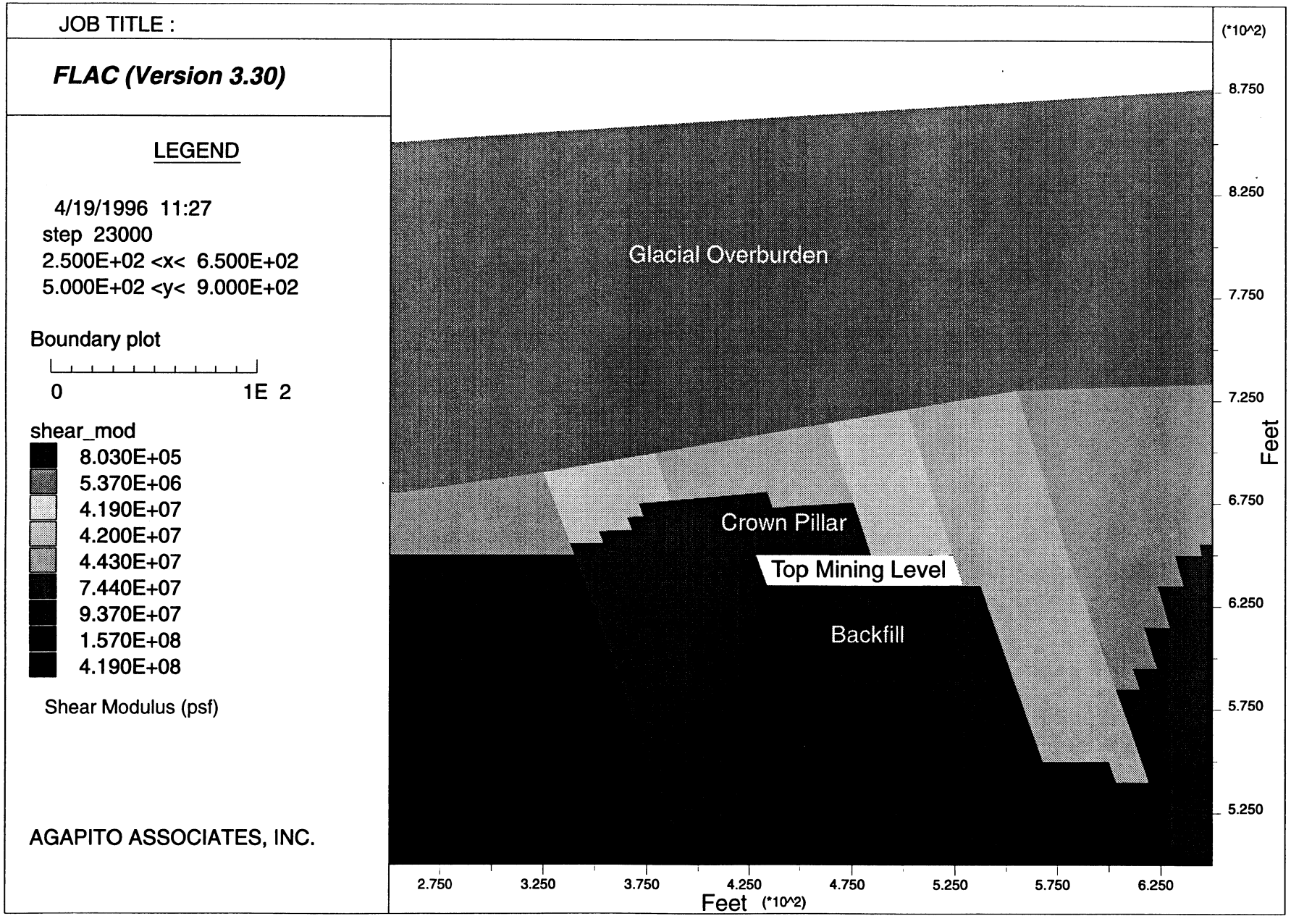

Figure 5-4c. Expanded area showing color coded material types (shear modulus) in two-dimensional analysis at Step 8.

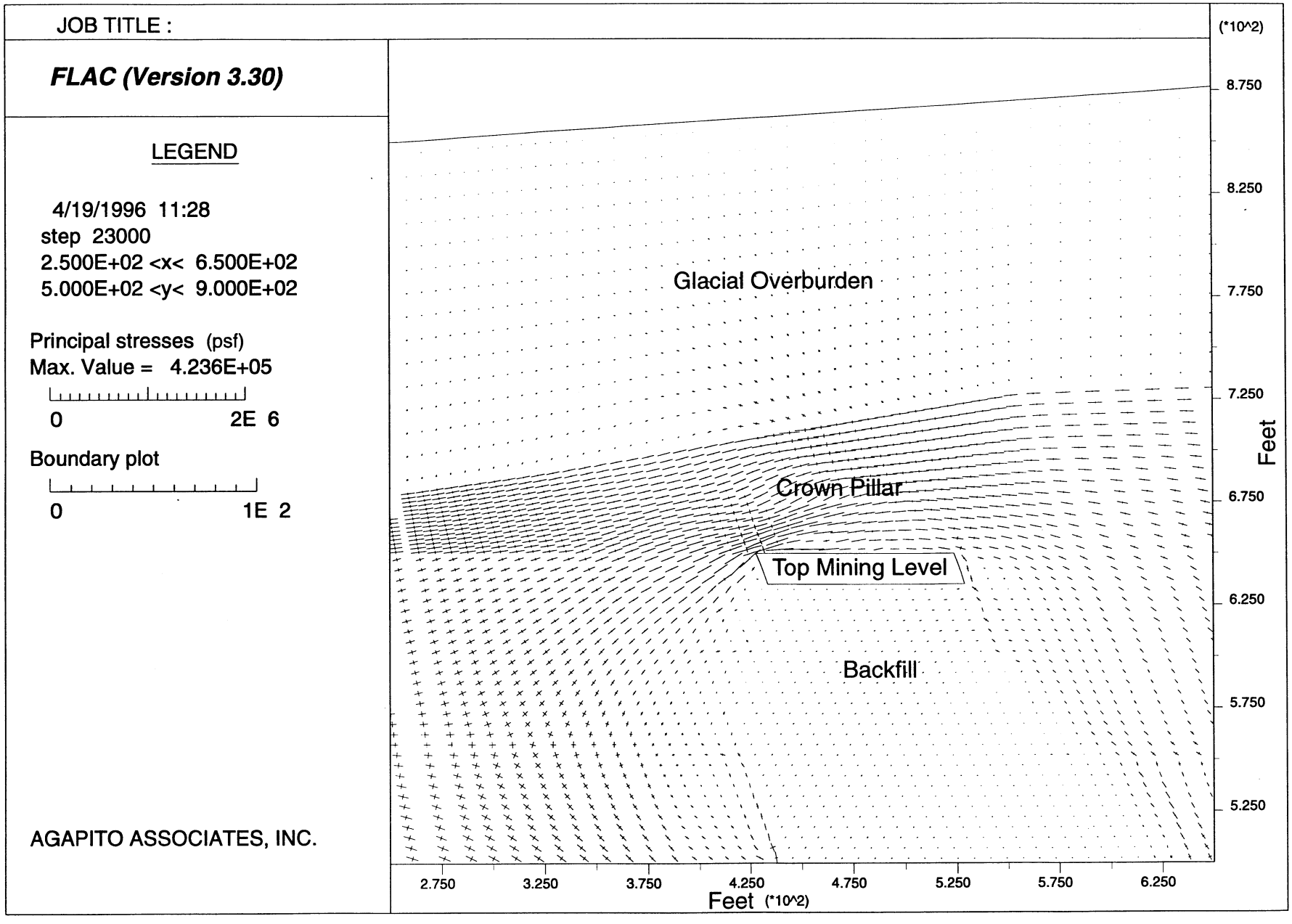

Figure 5-5. Principal stress vectors showing concentration of stress in crown pillar at Step 8 (elastic case—no rock failure).

Elastic-plastic analysis predicts greater strains because yield or rock failure can occur, concentrating the strain in the weaker materials. This is indicated in Figures 5-6, 5-7, and 5-8 as the thickness of the crown pillar is reduced by 15 ft for each of Steps 6, 7, and 8. In this analysis, the strength of the gossan material was back calculated to satisfy the condition of stress equilibrium prior to mining. This back analysis predicted a rock mass cohesion of 305 psi (2.1 MPa). A low value of angle of internal friction was assumed ($\phi = 22°$) so that any increase in stress would cause rock yield. This was a conservative approach that would produce strain concentration in the weaker materials.

The growth of the yield zone was utilized to provide a conservative criteria for the minimum thickness of the crown pillar. Figures 5-6, 5-7 and 5-8 show the formation of a zone of yield inclined from horizontal within the crown pillar. This zone corresponds to rock where the stress has exceeded the strength and the rock exhibits shear failure or yield. In this process, rock volume increases locally by the formation of small cracks and fractures. The cracks and fractures could form a conduit with increased hydraulic conductivity if the strain magnitudes are allowed to exceed the strain criteria.

The Steps 6, 7 and 8 in the model correspond to the reduction in crown pillar thickness from 100 to70 ft, which results in the increase of stress in the remaining rock. The increased stress cannot be supported and the rock deforms, with deformation concentrated in the shear zone. The maximum strain magnitudes are listed in Table 5-1 for each of Steps 6, 7 and 8. The maximum strain magnitude for Step 6 was -3×10^{-3}, well below the limit criteria of -5×10^{-3}. The peak values occur in very small areas of the zone of strain concentration. As the crown pillar thickness is decreased to 85 ft in Step 7, the maximum strain reached -5×10^{-3} in very small areas within the crown pillar.

The occurrence of the small zone of strain that reaches the limit criteria of -5×10^{-3} has been used to establish the minimum crown pillar thickness of 100 ft. This is a conservative approach because the strain limit was reached only in a small area in Step 7 and did not form a continuous zone that could connect the glacial overburden to the top of mining.

The strain contours in Figure 5-6 show levels of elevated strain that occur at the base of the glacial alluvium along the zone of yield. The magnitude of these strains are well below the limit criteria and no impact on hydraulic conductivity is projected to occur. The existence of the

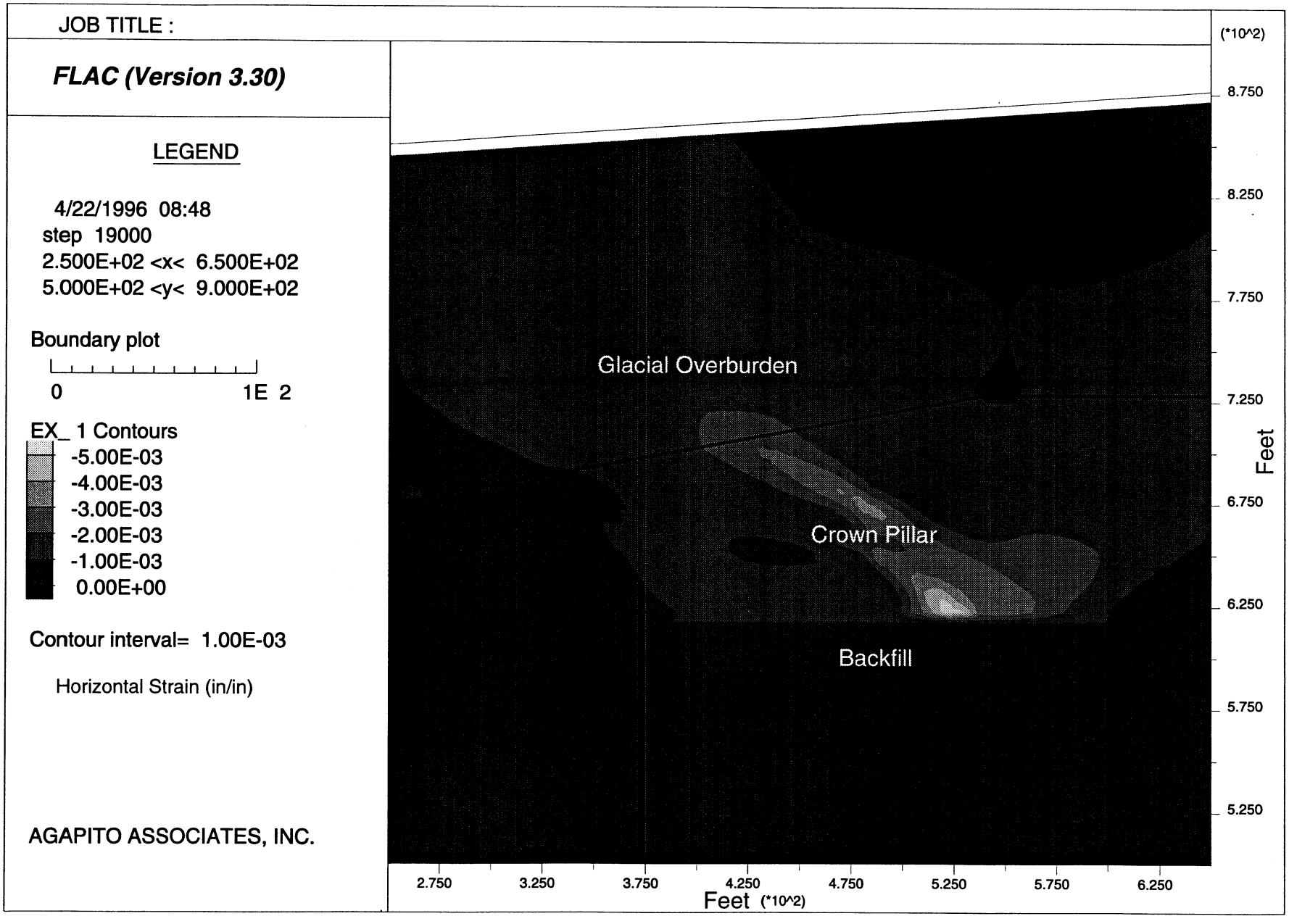

Figure 5-6. Color contours of strain magnitude at Step 6 of the two-dimensional analysis.

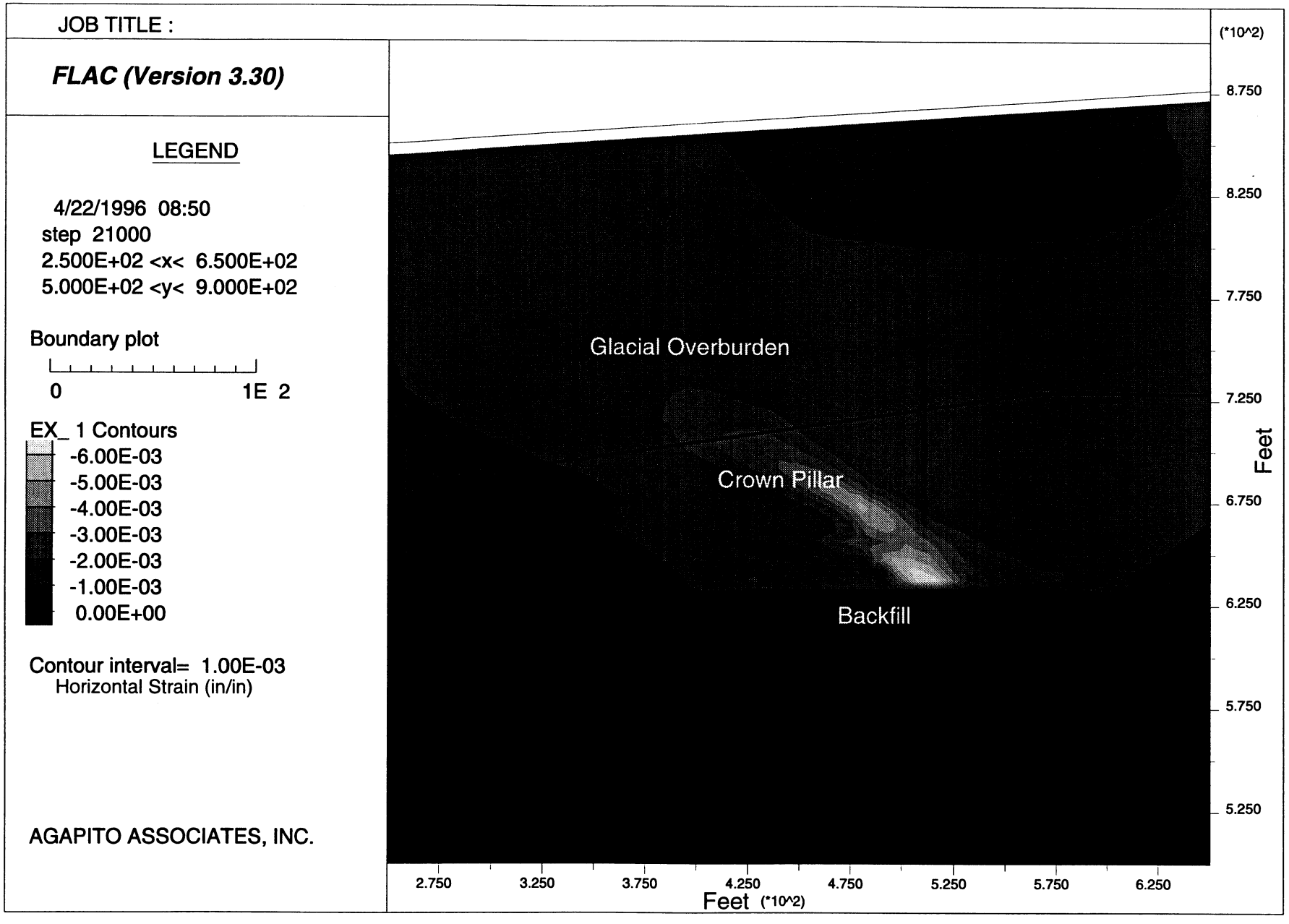

Figure 5-7. Color contours of strain magnitude at Step 7 of the two-dimensional analysis.

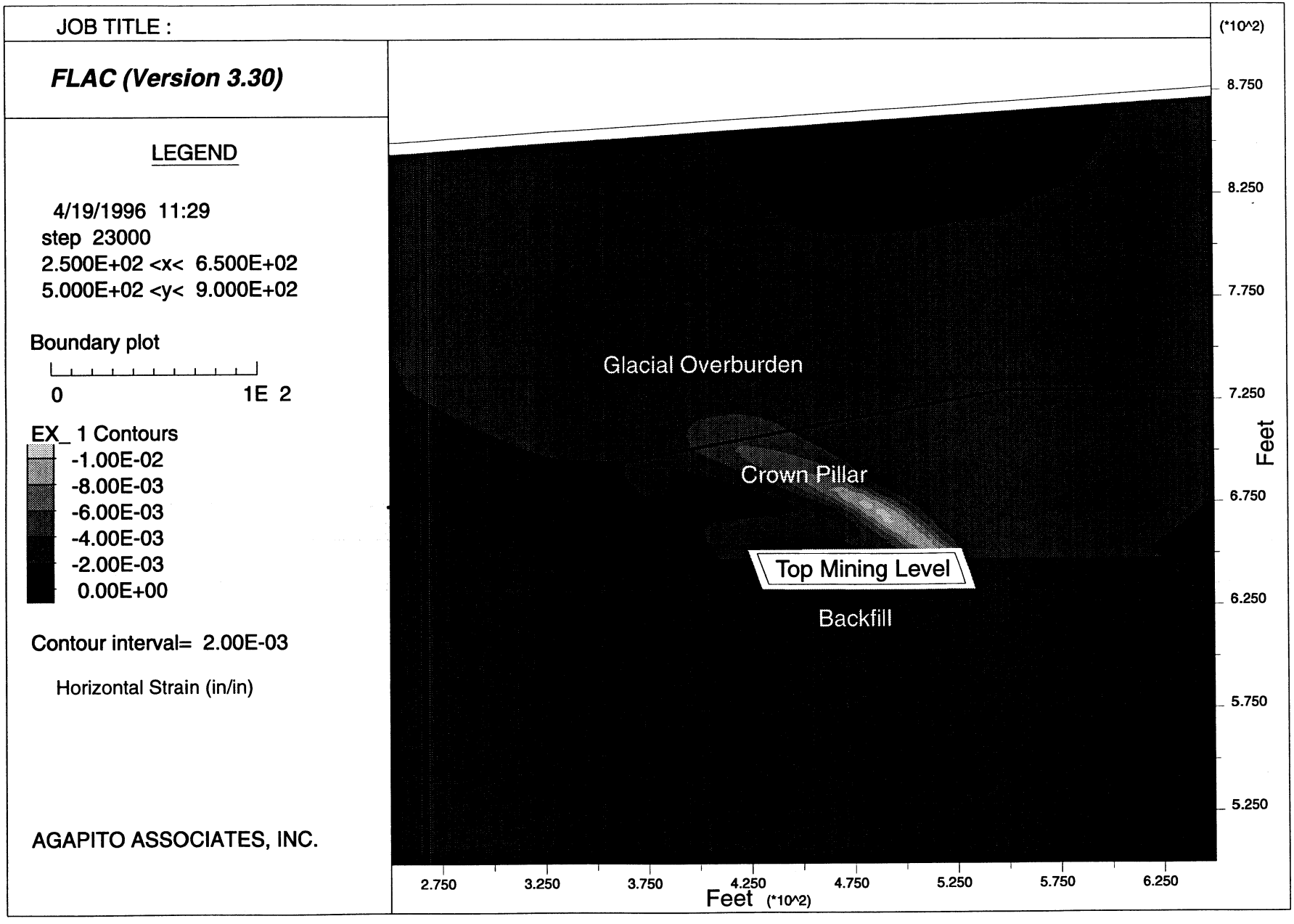

Figure 5-8. Color contours of strain magnitude at Step 8 of the two-dimensional analysis.

Table 5-1. Comparison of horizontal strain magnitude to the mining width-crown pillar thickness ratio for Steps 6, 7, and 8 of the two-dimensional analysis.

Analysis Step	Mining Width (ft)	Crown Pillar Thickness (ft)	Mining Width-Crown Pillar Thickness Ratio	Maximum Horizontal Strain in Middle of Crown Pillar
6	121	100	1.20	-3×10^{-3}
7	114	85	1.34	-5×10^{-3}
8	90	70	1.30	-1×10^{-2}

clay-rich massive saprolite immediately below the glacial overburden will act to limit the effects of any strain changes. Peng (1992) reports that the presence of impermeable strata such as clay or clayey mudstone below an aquifer will limit the effects of fractures that penetrate the aquifer as a result of mining underneath.

Table 5-1 indicates that the mining width-crown pillar thickness ratio was fairly constant in the analysis through Steps 6, 7, and 8 because of the shape of the ore zone. The maximum strain magnitude was correlated with crown pillar thickness and dropped below the criteria for preservation of aquitards as the crown pillar thickness increased from 85 to 100 ft. This trend indicates that the magnitude of the stress concentration is a function of the thickness of the crown pillar, with little sensitivity to the mining width. Review of the variation in currently planned crown pillar geometry presented in Figures 4-1 and 4-2 indicates that there are only four cross sections where the crown pillar indicated in the ore reserve model would be less that 100-ft thick (2,277,800 E; 2,278,700 E; 2,278,850 E; and 2,279,000 E). Adopting a minimum crown pillar thickness specification of 100 ft would increase confidence that there would be no impact on the hydrologic stability.

5.4. Projected Changes of Fracture Hydraulic Conductivity

In this section, potential changes in fracture aperture (open width) that could result from the projected changes in horizontal stress caused by mining underneath the crown pillar are examined as a mechanism for changes in vertical hydraulic conductivity. The permeability of the bedrock at the Crandon site, as described by Foth & Van Dyke (1995b), is attributed to

fracture and secondary permeability. Porosity of the crystalline and metamorphic rocks is typically low and not interconnected, however, this has probably been modified in the crown pillar by leaching of sulfides. Hydraulic conductivity in the crown pillar is attributed to the existing fractures, vugs and leached zones.

The hydraulic conductivity of the existing fractures could be changed by stress redistribution in the crown pillar as a result of mining. Depending on the orientation of fractures, the increase in horizontal stress could act to either reduce or increase the hydraulic conductivity. For example, vertical fracture surfaces would close with increases in the horizontal stress, thereby reducing the fracture conductivity. Other fractures that are inclined from the direction of horizontal stress change could undergo shear movement where the opposite surfaces slide past each other. During shearing of existing fractures, the fracture undulations may cause the fractures to open thereby increasing their hydraulic conductivity.

Foth & Van Dyke (1995b) presented a detailed discussion of fracture characterization at Crandon and the projected impact on the bedrock hydrogeology. The reported five fracture trends within the upper bedrock region, to depth of 1000 ft below surface, are listed in Table 5-2. Sets labeled 1 and 2 in Table 5-2 are the predominant fractures and are oriented generally E-W. They are reported to exhibit weathering with iron oxide coatings, and therefore are suggested to be most likely to transmit water. Fractures in Sets 3, 4, and 5 were reported to be tighter and show less evidence of weathering.

The fracture directions presented in Table 5-2 were used as the basis to evaluate the potential impact of mining on fracture conductivity in the crown pillar. The maximum stress change would occur in the horizontal plane in the N-S direction. Stress in the vertical direction could decrease near the base of the crown pillar but generally would remain unchanged through much of the crown pillar. The E-W stress would undergo a small increase. The orientation of the fracture sets relative to the direction of maximum stress change (N-S) are listed in Table 5-2 as the apparent dip in the N-S direction.

The projected stress changes for the elastic loading in the two-dimensional analysis presented in Section 5.2 were used to evaluate the potential for shear movement. Fracture properties were estimated using empirical methods developed by Barton and Choubey (1977) and Bandis et al. (1983) that are based upon rock strength, joint roughness and infilling. The

Table 5-2. Summary of fracture orientations—shallow hanging wall/orebody/footwall units (adapted from Foth & Van Dyke, 1995b, p. 20).

Set Number	Strike Azimuth	Dip	Apparent N-S Dip
1	85°E	85°SE	85°S
2	62°NE	8°SE	7°S
3	151°SE	81°SW	72°S
4	140°SE	39°SW	27°S
5	116°SE	25°NE	23°N

estimated joint fracture strength properties were a friction angle, 38.9°; and cohesion, 15 psi. The fracture strength estimation methodology of Barton and Choubey (1977) and Bandis et al. (1983) was developed by analysis of fractures in open pit or highway slope environments. The resulting estimates are conservative when applied to underground assessments where in situ stresses compress the fracture surfaces and restrict dilation (opening) of the fractures. In the underground environment, the fracture cohesion would be higher due to the inherent compressed state of the joint.

Factors of safety defined as joint shear strength divided by joint shear stress were calculated for the projected (three-dimensional) stress change results from the crown pillar mining and fracture orientations listed in Table 5-2. The results are listed in Table 5-3. The analysis indicated that fracture sets 1, 2, 3 and 4 have factors of safety greater than 1.0 for stress changes associated with a crown pillar thickness of 100 ft. This indicates that the fractures will not undergo shear slip and that the fracture aperture will close or remain nearly the same depending on the orientation. Only fracture Set 5, with the least frequency of occurrence, had a factor of safety less than 1.0 indicating the potential for shear movement and fracture opening.

The deformation behaviors of the fractures under the projected stress change in the crown pillar were grouped according to the factor of safety analysis. Sets 1, 3 and 4 are inclined and the projected stress changes indicate the fractures would close. Set 2 will not undergo shear movement but has some potential to open because of the small reduction in vertical stress caused by mining under the crown pillar. Set 5 has a factor of safety less than 1.0 indicating potential for shear movement.

Table 5-3. Fracture factors of safety for joint slip.

Crown Pillar Thickness	Set 1	Set 2	Set 3	Set 4	Set 5
100	1.91	2.64	1.86	1.13	0.92
85	1.98	1.54	1.78	1.05	0.82
70	2.11	1.01	1.70	0.98	0.74

Simple UDEC models containing a single fracture oriented with the apparent dip listed in Table 5-2 were loaded with the change in stress projected in the crown pillar to evaluate the affects of the projected stress change on the different fracture orientations. Three geometries representing fracture Sets 1, 3 and 4; Set 2; and Set 5 were analyzed. Figure 5-9 shows the model of the inclined joint for Set 5 to illustrate the approach. Horizontal stresses equivalent to the elastic loads resulting from mining were imposed on the two blocks in eight steps.

The fracture surfaces were assigned properties that would allow the fracture to open or close in response to changes in stress. Increases of normal stress (perpendicular to the fracture) would cause closure. Shear displacement would cause the fracture to open or dilate to simulate rough surfaces moving past each other. Fracture deformation properties were derived from observations of joint roughness in Crandon core, reported by AAI (1996), and rock compressive strength using empirical approaches developed by Barton and Choubey (1977) and Bandis et al. (1981). A peak friction angle of 49° was calculated to produce a factor of safety of 1.0 for Set 5 in Table 5-3 for the 100-ft crown pillar case. This assumption, which is greater than the estimated friction angle of 38.9°, produced the maximum fracture opening during shear displacement that could occur. Fracture opening in shear movement is controlled by the difference in peak friction angle and the residual friction angle which has a value of 30° for most rocks. If a peak friction angle greater than 49° is assumed, no shear movement would occur because the fracture shear strength would be greater than the shear stress.

The models indicated the following behaviors:

- Predominant Fracture Set 1 — Fracture closes -6×10^{-4} ft (–0.0072 inches) due to the increase in horizontal stress which is nearly perpendicular to the fracture. No shear failure or shear displacement. Vertical hydraulic conductivity will decrease.

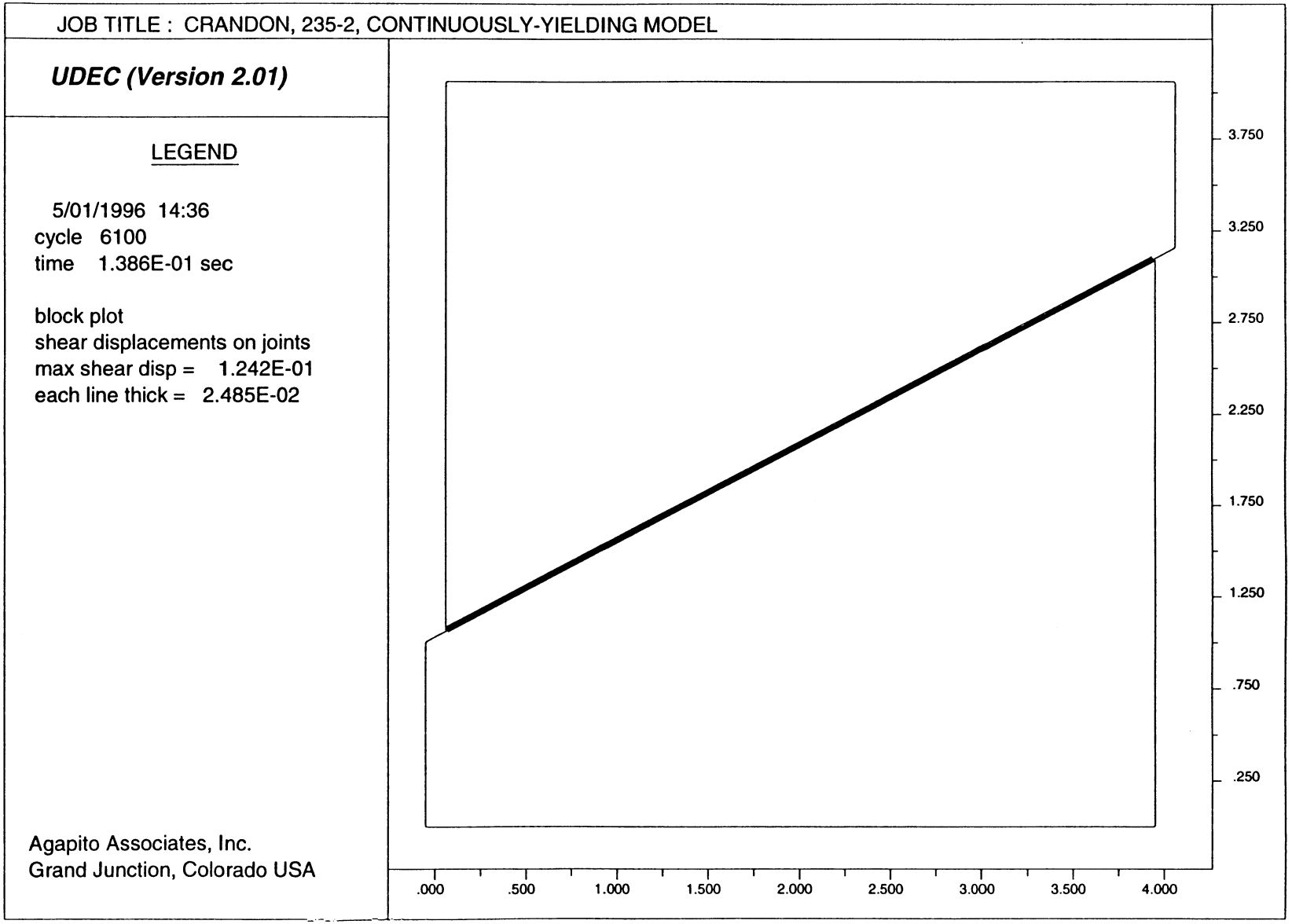

Figure 5-9. Example of simple block model of Set 5 fractures analyzed by the UDEC code.

- Predominant Fracture Set 2 — Fracture opens 4.5×10^{-5} ft (0.00054 inches) due to a small decrease in vertical stress due to the proximity of the mining roof which is nearly parallel to the fracture. No shear displacement occurs. Vertical hydraulic conductivity would not be changed.
- Minor Fracture Set 5 — Fracture opens 0.85×10^{-3} ft (0.010 inches) due to shear displacement caused by the increase in horizontal stress. The shear strength of the fracture was exceeded causing the fracture to dilate (open). Fracture hydraulic conductivity would increase.

Fracture hydraulic conductivity to water is a function of the fracture width (aperture or separation of the fracture surface) and pressure gradient. The fracture flow rate is calculated by equation 5-1 (Snow 1965):

$$Q = \frac{a^3}{12\mu}\frac{dp}{dx} \qquad (5\text{-}1)$$

where Q = flow rate (inches^3/sec),
a = effective fracture width or aperture,
μ = dynamic viscosity and
$\frac{dp}{dx}$ = pressure gradient.

The hydraulic equivalent fracture widths for crystalline and metamorphic rocks are typically in the range of 0.0394 inches (1 mm) according to Freeze and Cherry (1979). For water flowing in fractures at a constant pressure gradient, the flow rate can be calculated for a given fracture aperture or width.

Table 5-4 lists the ratio of final to original flow rate, assuming original fracture widths of 0.0394 inches (1 mm) and a constant pressure gradient of 1.0. The final fracture flow rate is the flow calculated after taking into account the stress change that is projected to occur in the crown pillar. The flow rates are also impacted by the pressure gradient along the fracture which is listed in Table 5-4. Table 5-4 indicates that the flow rate in the Set 1 fractures would be reduced. Most of the fracture flow would be expected to occur in the Set 1 type fractures. Rowe (1985) reported that near-vertical fractures in holes 214 and 155 were approximately half of the total fractures between 100- and 200-ft depth. Table 5-4 indicates little change in the Set 2 flow rate and a very

Table 5-4. Projected increase or decrease in flow rate along a fracture for changes in the fracture aperture due to projected horizontal stress changes in the crown pillar.

Fracture Set	Original Fracture Width (inches)	Final Fracture Width (inches)	Q_{Final}[1] / $Q_{ORIGINAL}$	$\frac{dp}{dx}$[2]
1	0.03940	0.03220	0.54	1.00
2	0.03940	0.03994	1.04	0.14
5	0.03940	0.04940	1.97	0.42

[1] *at dp/dx = constant*
[2] *based on dip of fracture set*

low pressure gradient. Set 2 is projected to include the second highest number of fractures after Set 1 but would contribute little to vertical water flow because of its near-horizontal orientation.

The inclined fractures in Set 5 could open (dilate) as they shear and their flow rate would increase. However, the contribution of the Set 5 fractures to total flow is projected to be low due to the low pressure gradient and to the low frequency of occurrence within the fracture population. The existing observations suggest that these inclined fractures may not be well connected as indicated by their less weathered appearance. The change in flow rate is also a function of the initial fracture aperture (width).

The interaction of the projected fracture set orientations with the estimated stress changes indicate that the near-vertical fractures would close resulting in lower vertical flow rates. This reduction may be offset partially or totally by opening of some of the inclined fractures due to shear. However, the magnitude of projected changes in hydraulic conductivity are not high when compared to the range in fracture orientation, fracture connectivity, and the initial conditions of the aperture width and presence of clay infillings. The fact that the predominant set is projected to experience a reduction in hydraulic conductivity with only a single minor set indicating a modest increase in conductivity suggests that the 100-ft crown pillar will not exhibit a measurable change in hydraulic properties due to mining.

6. REFERENCES

Agapito Associates, Inc. (1996 April 29). [Letter to Ken Black, Crandon Mining Co. *Fracture Descriptions for Boreholes 139, 151, 234, 262, 263, 264, 265, 266, 267, 268, 270, 271 and 272.*]

Arjang, B. (1991). Pre-Mining Stresses at Some Hard Rock Mines in the Canadian Shield. CIM Bulletin, 84 (945):80–96.

Bandis, S., A.C. Lumsden and N.R. Barton (1981). Experimental Studies of Scale Effects on the Shear Behavior of Rock Joints. International Journal of Rock Mechanics and Mining Sciences & Geomechanics Abstracts, 18,1–21.

Bandis, S., A.C. Lumsden and N.R. Barton (1983). Fundamentals of Rock Joint Deformation. International Journal of Rock Mechanics and Mining Sciences & Geomechanics Abstracts, 20 (6):249–268.

Barton, N., R. Lien and J. Lunde (1974). Engineering Classification of Rock Masses for Design of Tunnel Support. Rock Mechanics, 6 (4):189–236, Springer-Verlag.

Barton, N. and V. Choubey (1977). The Shear Strength of Rock Joints in Theory and Practice, Rock Mechanics, 10:1–54, Springer-Verlag

Barton, N. (1991). "Scale Effects or Sampling Biar?" *Scale Effects in Rock Masses.* Brookfield, MA: A.A. Balkema.

Bieniawski, Z.T. (1976). "Rock Mass Classification in Rock Engineering." *Proceedings Symposium on Exploration for Rock Engineering*, Johannesburg, South Africa, pp. 97–106,. Rotterdam: A. A. Balkema.

DYNATEC (1982). *Crown Pillar Area Mining Methods Study.* A Report prepared for Exxon Minerals Company, Richmond Hill, Ontario, Canada: Author

Foth & Van Dyke (1995a). *Summary: Project Description and Environmental Baseline Data, Crandon Project, Crandon, Wisconsin.* A Report prepared for Crandon Mining Company by Foth & Van Dyke and Associates, Inc., Green Bay, WI.

Foth & Van Dyke (1995b). *Bedrock Hydrogeology at the Crandon Site, Crandon Project, Crandon, Wisconsin.* A Report prepared for Crandon Mining Company by Foth & VanDyke and Associates, Inc., Green Bay, WI.

Freeze, R.A. and J.A. Cherry (1979). *Groundwater.* Englewood Cliffs, NJ: Prentice-Hall, Inc.

Geosolutions Resources, Inc. (1995). *Ore Reserve Cross Sections, Crandon Orebody.* Report prepared for Crandon Mining Company: Author.

GeoTrans, Inc. (1995). *Numerical Simulation of the Effect on Groundwater and Surface Water of the Proposed Zinc and Copper Mine Near Crandon, Wisconsin.* A Report prepared for Foth & Van Dyke and Associates, Inc., Green Bay, WI. Roswell, GA: Author.

Haimson, B.C. (1982). "Deep Stress Measurements in Three Ohio Quarries and Their Comparison to Near-Surface Tests." *23rd U.S. Symposium on Rock Mechanics*, Berkeley, CA.

Hoek, E., and E.T. Brown (1988). "The Hoek-Brown Failure Criterion — A 1988 Update." *Canadian Rock Mechanics Symposium.*

Laubscher, D. H. (1990). A Geomechanics Classification System for the Rating of Rock Mass in Mine Design. Journal of the South African Institute of Mining and Metallurgy, 90 (10):257–271.

Matheson, G.M. and A.D. Eckert-Clift (1986). "Characteristics of Chimney Subsidence Development from Abandoned Underground Coal Mines along the Colorado Front Range." *Proceedings, 2nd Workshop on Surface Subsidence Due to Underground Mining,* West Virginia University, Morgantown, VA. S. Peng, ed.

Milne, D. (1991). "Standardized Joint Descriptions for Improved Rock Classification." *Proceedings 31st U.S. Symposium on Rock Mechanics*, pp. 35–41.

Peng, S. S. (1992). *Subsurface Subsidence Engineering.* Littleton, CO: Society for Mining, Metallurgy and Exploration, Inc.

Rowe, R.G. (1985). *Bedrock Permeability.* Exxon Minerals Company, CMC-NOI-39.

Serafim, J.L. and J.P. Pereira (1983). "Consideration of the Geomechanical Classification of Bieniawski." *Proceedings, International Symposium on Engineering Geology and Underground Construction*, pp. 1133–1144.

SME (1992). *Mining Engineering Handbook.* Littleton, CO: Society of Mining Engineers of AIME.

Smith, J.D. (1982). *Selection of Mining Methods for the Crandon Crown Pillar Based on Rock Mechanics Considerations.* A Report prepared for DYNATEC Mining, Ltd. Kingston, Ontario, Canada: John D. Smith Engineering Associates, Ltd.

Snow, D.T. (1965). *A Parallel Plate Model of Permeable Fractured Media.* Berkley, CA: University of California. PHd. Thesis.

APPENDIX A — CROSS SECTION SHOWING GEOLOGY OF GLACIAL OVERBURDEN. CONTOUR MAP SHOWING THICKNESS OF MASSIVE SAPROLITE LAYER.

SECTION C-C'

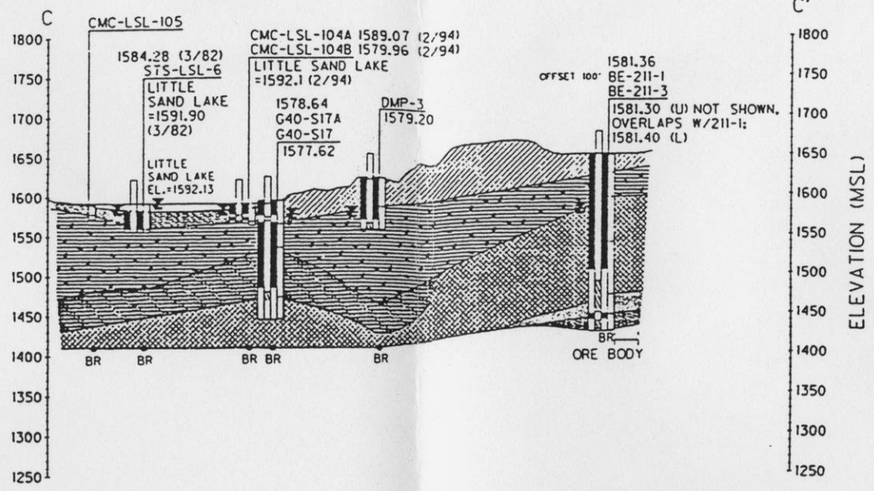

SECTION D-D'

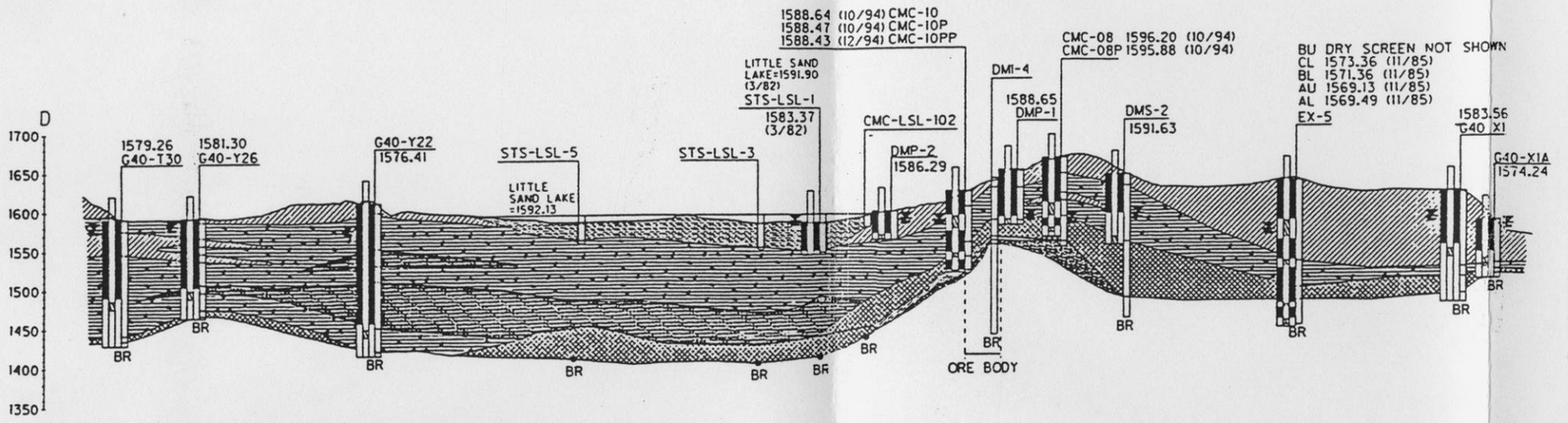

LEGEND

- Qtl UNDIFFERENTIATED LATE WISCONSINAN TILL — NASHVILLE MEMBER, COPPER FALLS FORMATION AND THE MAPLEVILLE MEMBER, HORICON FORMATION
- Qte UNDIFFERENTIATED EARLY-WISCONSINAN-TILL AND PRE-WISCONSIN TILL — MARATHON AND LINCOLN FORMATIONS, MAY INCLUDE MASSIVE SAPROLITE
- Qowf FINE-GRAINED OUTWASH DEPOSITS — GLACIAL FLUVIAL STRATIFIED SAND AND SILT OF WISCONSINAN AGE
- Qowl COARSE-GRAINED OUTWASH DEPOSITS — GLACIAL FLUVIAL STRATIFIED SAND AND GRAVEL OF WISCONSINAN AGE
- INFERRED GEOLOGIC CONTACT
- Ql LACUSTRINE DEPOSITS — GLACIO-LACUSTRINE, RHYMETRICALLY BEDDED, SILT AND CLAY WITH MINOR AMOUNTS OF SAND OF WISCONSINAN, HOLOCENC AND RECENT AGE.
- Qhlc ICE-CONTACT DEPOSITS — ABLATION TILL, FLOW TILL, GLACIO-FLUVIAL SILT, CLAY AND SAND OF WISCONSINAN AGE
- Ms MASSIVE SAPROLITE — UNSTRUCTURED CLAY, SILT AND SAND, HIGHLY WEATHERED BEDROCK
- Ss STRUCTURED SAPROLITE BEDROCK — CLAY, SILT AND SAND WITH RELIC BEDROCK STRUCTURES, PARTLY WEATHERED BEDROCK
- PCu UNDIFFERENTIATED BEDROCK — PRECAMBRIAN METAVOLCANIC BEDROCK, MAY INCLUDE STRUCTURED SAPROLITE
- INFERRED UNDIFFERENTIATED BEDROCK ELEVATION BASED UPON STS 1984 BEDROCK ELEVATION MAP

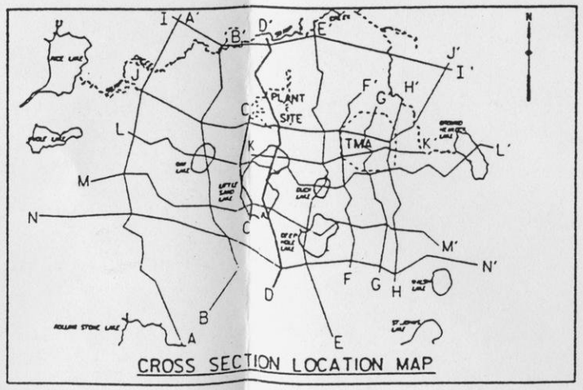

WELL CONSTRUCTION DIAGRAM

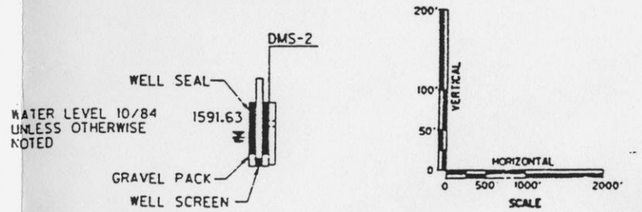

Foth & Van Dyke

REVISED	DATE	BY	DESCRIPTION

CHECKED BY:	JKSI	DATE: MAY '95
APPROVED BY:	SVDI	DATE: MAY '95
APPROVED BY:	GWS	DATE: MAY '95

Crandon Mining Company

FIGURE 2.6
GEOLOGIC CROSS SECTIONS
C-C' AND D-D'

Scale:	AS SHOWN	Date:	MAY, 1995
Prepared By:	Foth & Van Dyke	By:	BSH

930049

4.2-11-65

2274000 E 2275000 E 2276000 E 2277000 E 2278000 E 2279000 E 2280000 E

118000 N 117000 N 116000 N 115000 N

N

X 1692.0 X 1637.0 X 1621.0 X 1602.0 X 1597.0

LITTLE SAND LAKE

LEGEND

- LAKES
- STREAMS
- EXISTING ROAD
- —1675— EXISTING CONTOUR
- 1637.0 X SPOT ELEVATION
- ORE BODY OUTLINE
- —30— ISOPACH CONTOUR (MASSIVE SAPROLITE THICKNESS IN FEET BASED ON DATA POINTS REPRESENTING COMPLETE RECORDS)
- X-155 ● 1 EXPLORATORY DRILL HOLE, TOTAL SAMPLE RECORD AVAILABLE
- DMI-3 ● 10 DMI-3, BE-211-2, ALL CMC WELLS TOTAL SAMPLE RECORD AVAILABLE FROM ENVIRONMENTAL STUDIES
- X-111 ◉ 22 EXPLORATORY DRILL HOLE, PARTIAL SAMPLE RECORD AND GEOLOGIC LOG DATA
- CDM-1 ◉ 30 PARTIAL SAMPLE RECORD AND GEOLOGIC LOG DATA FROM ENVIRONMENTAL STUDIES

NOTES:

1. APPROXIMATE SITE AREA: PART OF SECTION 25, T35N, R12E, TOWN OF NASHVILLE AND PART OF SECTIONS 29, 30 AND 32, T35N, R13E, TOWN OF LINCOLN, FOREST COUNTY, WISCONSIN.
2. TOPOGRAPHIC BASE MAP DIGITIZED FROM 1"=1000' SCALE, 5' CONTOUR INTERVAL MAP PREPARED BY AERO-METRIC ENGINEERING, INC., SHEBOYGAN, WISCONSIN. DATE OF PHOTOGRAPHY APRIL 28, 1976.
3. HORIZONTAL DATUM BASED ON WISCONSIN STATE PLANE COORDINATE SYSTEM - NORTH ZONE.
4. VERTICAL DATUM BASED ON MEAN SEA LEVEL DATUM. CONTOUR INTERVAL IS FIVE FEET.
5. COUNTY AND TOWNSHIP LINES DIGITIZED FROM 7.5' SERIES USGS MAPS.
6. ORE BODY OUTLINE REPRESENTIVE OF THE SUBCROP AT THE BASE OF THE OVERBURDEN.

/d3/d1/users/jpr1/3c49f150.dgn

Foth & Van Dyke

REVISED	DATE	BY	DESCRIPTION
CHECKED BY:		JKS1	DATE: JULY '95
APPROVED BY:		SVD1	DATE: JULY '95
APPROVED BY:		GWS	DATE: JULY '95

Crandon Mining Company

FIGURE 2.3

DRILL HOLE LOCATIONS AND REVISED MASSIVE SAPROLITE ISOPACH

Scale: 0 200' 400' Date: JULY, 1995

Prepared By: Foth & Van Dyke By: JPR1

4.2-11-66

93C049

APPENDIX B — CROWN PILLAR GEOTECHNICAL DATA

B-1 RQD ESTIMATES FROM CORE PHOTOGRAPHS

Rock quality designation RQD was estimated from photographs of the core by using a scale correlated with the length of the core box. RQD was calculated for core runs indicated in each box using equation B-1, which is the same procedure used throughout the Crandon drilling data:

$$RQD(\%) = \frac{\sum CoreLengths \geq 4inches}{CoreRunLengths} \qquad \text{(B-1)}$$

All fractures apparent in the photographs were included in the piece length measurements which produces a lower RQD than actual, giving a conservative assessment.

The average RQD correlated with weathering intensity as indicated by the average values which are listed in Table B-1 according to the rock unit and weathering intensity. The table also lists the number of core runs in each hole, the length weighted average in each hole and the average for all holes in each zone. Very limited data were available for the gossan in the zinc ore, and no data were available for the strongly weathered zinc ore or footwall rocks. RQD estimates for each run in individual holes are presented in Table B-2.

B-2 COMPRESSIVE STRENGTH MEASUREMENTS

Compressive strength data, compiled by CMC in Microsoft EXCEL™ spreadsheets, were sorted into weathering intensity zones according to the cross sections and weighted averages were listed in Table B-3. The majority of the test results were point load measurements on core used to estimate strength. Point load measurements parallel to the foliation planes typically produced the lowest strength and were therefore utilized here. Some uniaxial compressive strength measurements were also available for the crown pillar area and were in the range of strength predicted by the point load measurement. Individual data are presented in Table B-4.

The trends in the average values from Table B-3 generally correlate well with the weathering intensity and indicate that weathering has reduced compressive strength by 50–70%, compared to the same rock types from deeper, unweathered areas.

Table B-1. Length-weighted average RQD for boreholes in the crown pillar area.

		Rock Quality Designation (RQD)									
Stratigraphy	Borehole Number	No. of Core Runs	Gossan	No. of Core Runs	Strongly Weathered	No. of Core Runs	Moderately Weathered	No. of Core Runs	Weakly Weathered	No. of Core Runs	Unweathered
Hangiing Wall	175					18	67				
	177			11	43	10	35				
	178			7	42	31	48	5	77		
	188			10	50	30	66				
	189			4	20	6	45	29	61		
	191					63	49				
	193			14	28	19	41	12	75		
	195			5	71	31	64			2	63
Weighted Average			—		**41**		**54**		**66**		**63**
Crandon Formation	177	2	2					4	66		
(Zinc Ore)	178	4	2			3	33				
	188					7	45				
	189					3	79	1	78		
	191					9	17				
Weighted Average			**2**		—		**37**		**68**		—
Footwall	178					1	67			4	82
	188					3	92	1	72		
Weighted Average			—		—		**86**		**72**		**82**

Table B-2. Summary of Rock Quality Designation (RQD) data.

Borehole Number	Lithology[1]	Weathering[1]	Core Run Interval Start (ft)	Core Run Interval End (ft)	RQD (%)
175	HW	M	293	307	57
	HW	M	307	313	58
	HW	M	313	323	60
	HW	M	323	333	71
	HW	M	333	343	70
	HW	M	343	353	82
	HW	M	353	363	70
	HW	M	363	373	93
	HW	M	373	383	80
	HW	M	383	413	90
	HW	M	413	423	94
	HW	M	423	433	78
	HW	M	433	443	53
	HW	M	443	453	49
	HW	M	453	473	59
	HW	M	473	483	43
	HW	M	483	493	46
	HW	M	493	503	60
177	HW	S	302	307	35
	HW	S	307	317	63
	HW	S	317	333	52
	HW	S	333	348	22
	HW	S	348	357	26
	HW	S	357	361	50
	HW	S	361	371	43
	HW	S	371	383	45
	HW	S	383	393	46
	HW	S	393	400	62
	HW	S	400	405	33
	HW	M	405	423	69
	HW	M	423	433	71
	HW	M	433	463	21
	HW	M	463	473	37
	HW	M	473	493	54
	HW	M	493	503	53
	HW	M	503	518	26
	HW	M	518	532	16
	HW	M	532	533	0
	HW	M	533	543	3
	CF	G	543	553	0
	CF	G	553	563	3
	CF	W	563	573	38
	CF	W	573	583	81
	CF	W	583	592	60
	CF	W	592	633	86

Table B-2. Summary of Rock Quality Designation (RQD) data (continued).

Borehole Number	Lithology[1]	Weathering[1]	Core Run Interval Start (ft)	Core Run Interval End (ft)	RQD (%)
178	HW	S	210	215	47
	HW	S	215	222	50
	HW	S	222	226	46
	HW	S	226	233	82
	HW	S	233	241	0
	HW	S	241	246	20
	HW	S	246	252	49
	HW	W	252	256	98
	HW	W	256	273	74
	HW	W	273	283	84
	HW	W	283	288	75
	HW	W	288	294	53
	HW	M	294	310	83
	HW	M	310	315	58
	HW	M	315	324	75
	HW	M	324	330	35
	HW	M	330	338	58
	HW	M	338	346	36
	HW	M	346	353	55
	HW	M	353	359	58
	HW	M	359	364	52
	HW	M	364	374	64
	HW	M	374	383	76
	HW	M	383	389	54
	HW	M	389	396	56
	HW	M	396	401	57
	HW	M	401	408	40
	HW	M	408	415	54
	HW	M	415	422	60
	HW	M	422	427	13
	HW	M	427	438	35
	HW	M	438	448	87
	HW	M	448	455	61
	HW	M	455	464	71
	HW	M	464	469	78
	HW	M	469	474	65
	HW	M	474	477	11
	HW	M	477	483	39
	HW	M	483	486	11
	HW	M	486	489	11
	HW	M	489	494	31
	HW	M	494	497	0
	HW	M	497	502	0
	CF	G	502	507	0
	CF	G	507	508	0
	CF	G	508	518	8
	CF	G	518	524	0
	CF	M	524	531	5
	CF	M	531	544	43
	CF	M	544	553	53
	FW	M	553	560	67
	FW	U	560	570	69
	FW	U	570	586	84
	FW	U	586	592	97
	FW	U	592	602	78

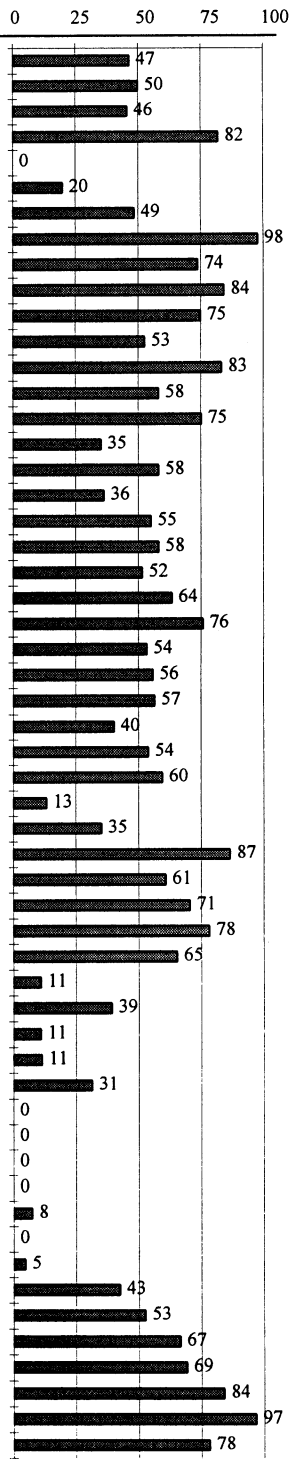

Table B-2. Summary of Rock Quality Designation (RQD) data (continued).

Borehole Number	Lithology[1]	Weathering[1]	Core Run Interval Start (ft)	Core Run Interval End (ft)	RQD (%)
188	HW	S	268	272	38
	HW	S	272	276	38
	HW	S	276	281	80
	HW	S	281	286	45
	HW	S	286	290	46
	HW	S	290	293	86
	HW	S	293	298	53
	HW	S	298	302	29
	HW	S	302	308	46
	HW	S	308	312	40
	HW	M	312	315	33
	HW	M	315	320	70
	HW	M	320	326	74
	HW	M	326	329	53
	HW	M	329	334	37
	HW	M	334	336	67
	HW	M	336	341	69
	HW	M	341	346	67
	HW	M	346	354	88
	HW	M	354	360	88
	HW	M	360	366	57
	HW	M	366	372	49
	HW	M	372	376	70
	HW	M	376	390	65
	HW	M	390	393	39
	HW	M	393	403	81
	HW	M	403	409	69
	HW	M	409	415	92
	HW	M	415	422	73
	HW	M	422	427	78
	HW	M	427	432	65
	HW	M	432	440	68
	HW	M	440	444	65
	HW	M	444	454	83
	HW	M	454	457	56
	HW	M	457	467	86
	HW	M	467	478	0
	HW	M	478	482	81
	HW	M	482	490	61
	HW	M	490	495	52
	HW	M	495	505	50
	CF	M	505	518	10
	CF	M	518	524	0
	CF	M	524	528	10
	CF	M	528	534	47
	CF	M	534	544	78
	CF	M	544	550	88
	CF	M	550	560	84
	FW	M	560	570	100
	FW	M	570	580	91
	FW	M	580	590	84
	FW	W	590	598	72

Table B-2. Summary of Rock Quality Designation (RQD) data (continued).

Borehole Number	Lithology[1]	Weathering[1]	Core Run Interval Start (ft)	Core Run Interval End (ft)	RQD (%)
189	HW	S	247	249	0
	HW	S	249	253	9
	HW	S	253	257	48
	HW	S	257	260	25
	HW	W	260	267	46
	HW	W	267	274	39
	HW	W	274	283	65
	HW	W	283	290	62
	HW	W	290	298	52
	HW	W	298	308	26
	HW	W	308	318	62
	HW	W	318	328	70
	HW	W	328	336	68
	HW	W	336	346	71
	HW	W	346	354	47
	HW	W	354	364	66
	HW	W	364	372	59
	HW	W	372	382	82
	HW	W	382	398	76
	HW	W	398	405	67
	HW	W	405	414	59
	HW	W	414	424	84
	HW	W	424	434	67
	HW	W	434	442	50
	HW	W	442	449	56
	HW	W	449	469	83
	HW	W	469	474	67
	HW	W	474	479	17
	HW	W	479	484	27
	HW	W	484	501	100
	HW	W	501	511	89
	HW	W	511	520	81
	HW	W	520	525	31
	HW	M	525	530	9
	HW	M	530	536	51
	HW	M	536	539	58
	HW	M	539	545	44
	HW	M	545	556	39
	HW	M	556	565	67
	CF	M	565	572	54
	CF	M	572	578	65
	CF	M	578	596	79
	CF	W	596	606	78

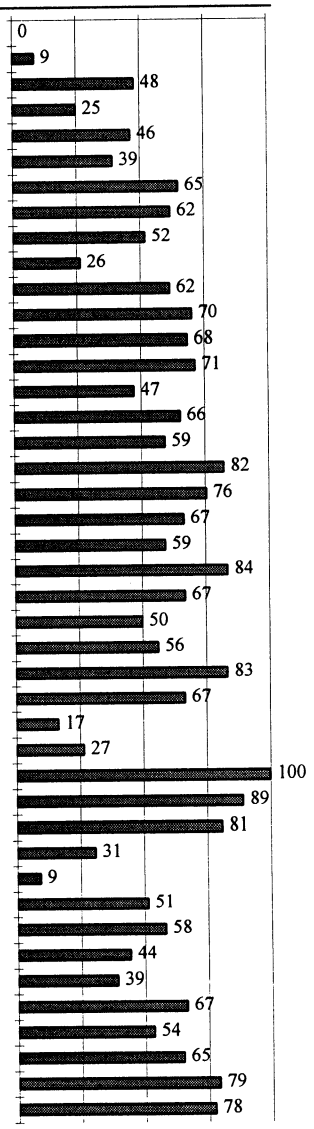

Table B-2. Summary of Rock Quality Designation (RQD) data (continued).

Borehole Number	Lithology[1]	Weathering[1]	Core Run Interval Start (ft)	Core Run Interval End (ft)	RQD (%)
191	HW	M	279	280	42
	HW	M	280	282	21
	HW	M	282	284	0
	HW	M	284	286	17
	HW	M	286	289	22
	HW	M	289	293	19
	HW	M	293	295	23
	HW	M	295	299	23
	HW	M	299	302	44
	HW	M	302	304	0
	HW	M	304	305	33
	HW	M	305	309	25
	HW	M	309	311	0
	HW	M	311	321	81
	HW	M	321	326	82
	HW	M	326	333	69
	HW	M	333	336	64
	HW	M	336	343	49
	HW	M	343	347	25
	HW	M	347	357	80
	HW	M	357	360	89
	HW	M	360	365	45
	HW	M	365	367	71
	HW	M	367	385	65
	HW	M	385	393	86
	HW	M	393	400	69
	HW	M	400	410	78
	HW	M	410	419	74
	HW	M	419	439	73
	HW	M	439	444	37
	HW	M	444	454	78
	HW	M	454	458	50
	HW	M	458	461	0
	HW	M	461	462	50
	HW	M	462	463	0
	HW	M	463	470	70
	HW	M	470	479	73
	HW	M	479	486	79
	HW	M	486	493	60
	HW	M	493	503	84
	HW	M	503	509	57
	HW	M	509	519	70
	HW	M	519	526	38
	HW	M	526	530	77
	HW	M	530	537	90
	HW	M	537	551	70
	HW	M	551	553	29
	HW	M	553	556	44
	HW	M	556	558	38
	HW	M	558	562	35
	HW	M	562	564	29
	HW	M	564	567	11
	HW	M	567	573	59
	HW	M	573	579	53
	HW	M	579	584	42
	HW	M	584	589	43
	HW	M	589	596	57
	HW	M	596	606	59

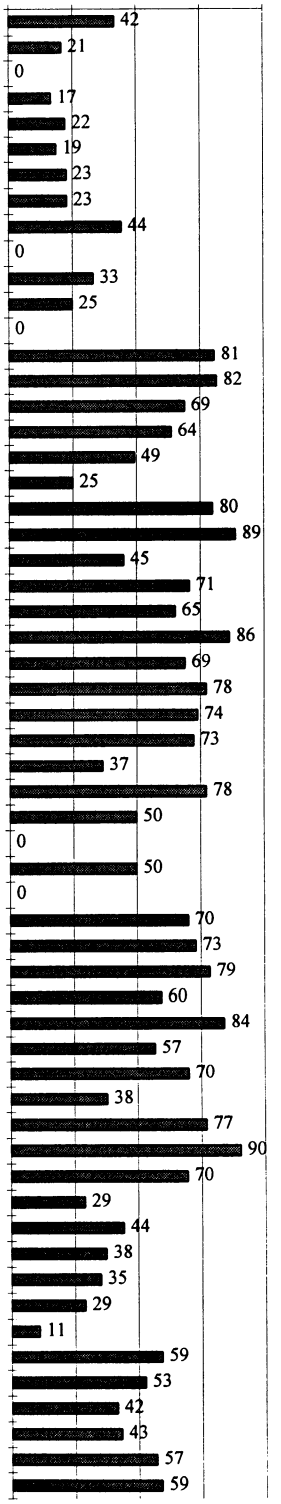

Table B-2. Summary of Rock Quality Designation (RQD) data (continued).

Borehole Number	Lithology[1]	Weathering[1]	Core Run Interval Start (ft)	Core Run Interval End (ft)	RQD (%)
191	HW	M	606	611	16
	HW	M	611	619	27
	HW	M	619	623	80
	HW	M	623	628	18
	HW	M	628	634	7
	CF	M	634	639	33
	CF	M	639	640	16
	CF	M	640	649	43
	CF	M	649	655	18
	CF	M	655	665	0
	CF	M	665	675	7
	CF	M	675	685	21
	CF	M	685	695	11
	CF	M	695	705	
193	HW	S	244	248	0
	HW	S	248	251	22
	HW	S	251	253	58
	HW	S	253	254	0
	HW	S	254	256	0
	HW	S	256	258	25
	HW	S	258	260	46
	HW	S	260	262	17
	HW	S	262	265	47
	HW	S	265	271	39
	HW	S	271	274	19
	HW	S	274	278	69
	HW	S	278	282	54
	HW	S	282	289	0
	HW	M	289	294	0
	HW	M	294	298	33
	HW	M	298	302	83
	HW	M	302	309	58
	HW	M	309	315	21
	HW	M	315	319	19
	HW	M	319	324	35
	HW	M	324	325	42
	HW	M	325	327	17
	HW	M	327	332	38
	HW	M	332	336	44
	HW	M	336	338	33
	HW	M	338	343	28
	HW	M	343	348	77
	HW	M	348	350	33
	HW	M	350	351	0
	HW	M	351	354	47
	HW	M	354	358	94
	HW	M	358	368	80
	HW	W	368	381	80
	HW	W	381	388	64
	HW	W	388	398	87
	HW	W	398	408	93
	HW	W	408	413	80
	HW	W	413	423	68
	HW	W	423	432	71
	HW	W	432	441	82
	HW	W	441	451	67
	HW	W	451	458	49
	HW	W	458	468	81
	HW	W	468	478	80

Table B-2. Summary of Rock Quality Designation (RQD) data (continued).

Borehole Number	Lithology[1]	Weathering[1]	Core Run Interval Start (ft)	Core Run Interval End (ft)	RQD (%)
195	HW	S	77	81	96
	HW	S	81	86	64
	HW	S	86	91	65
	HW	S	91	101	72
	HW	S	101	102	58
	HW	M	102	107	53
	HW	M	107	112	68
	HW	M	112	117	55
	HW	M	117	122	76
	HW	M	122	127	78
	HW	M	127	137	53
	HW	M	137	142	73
	HW	M	142	147	37
	HW	M	147	152	82
	HW	M	152	157	73
	HW	M	157	162	43
	HW	M	162	167	55
	HW	M	167	172	40
	HW	M	172	177	75
	HW	M	177	182	72
	HW	M	182	187	75
	HW	M	187	192	65
	HW	M	192	197	67
	HW	M	197	202	35
	HW	M	202	207	58
	HW	M	207	212	58
	HW	M	212	217	62
	HW	M	217	222	73
	HW	M	222	227	78
	HW	M	227	232	80
	HW	M	232	237	75
	HW	M	237	242	62
	HW	M	242	247	78
	HW	M	247	252	77
	HW	M	252	257	45
	HW	M	257	262	60
	HW	U	262	267	58
	HW	U	267	272	67

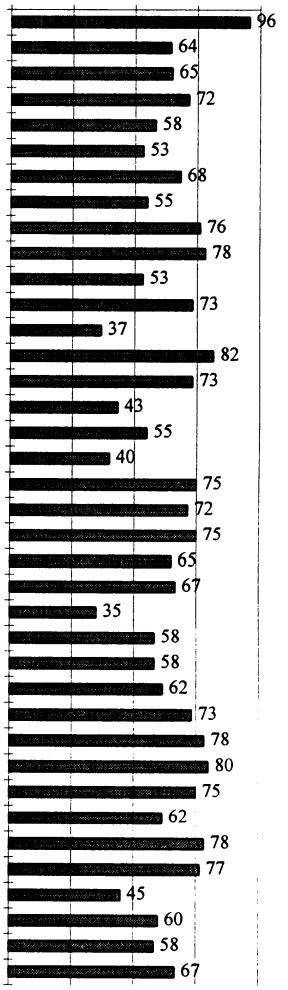

[1] HW—*hanging wall*, CF—*Crandon Formation*, FW—*footwall*, G—gossan, S—*strongly weathered*, M—*moderately weathered* W—*weakly weathered*, U—*unweathered*

Table B-3. Compressive strength-measurements for the crown pillar area.

		Compressive Strength (psi)									
Stratigraphy	Borehole Number	No. of Core Runs	Gossan	No. of Core Runs	Strongly Weathered	No. of Core Runs	Moderately Weathered	No. of Core Runs	Weakly Weathered	No. of Core Runs	Unweathered
Hanging Wall	177			3	3621	2	4839				
	178					4	4436	1	3764		
	188			1	3539	10	9072				
	189			2	977	2	12024	25	4121		
	191					33	3782				
	193					5	1140	15	3039		
	195			3	9629	13	10842			15	9689
Weighted Average			—		**5027**		**5995**		**3716**		**9689**
Crandon Formation	175					4	15638				
(Zinc Ore)	177					2	14383	7	42769		
	178					1	6066				
	188					5	8259				
	189					5	21485				
	191					3	644				
	193			3	12857	4	8072				
Weighted Average			**1000***		**12857**		**11680**		**42769**		—
Footwall	177							5	14065		
	178									8	24714
	188					3	31863	32	26012	8	21034
	189					9	23807	26	21379		
	191					8	14791	16	20241		
	193					13	10053	12	11531		
Weighted Average			—		—		**16935**		**21108**		**22874**

** Assumed value; no data*

Table B-4. Summary of strength data.

Summary Statistics	Borehole Number	Downhole Distance (ft)	Lithology[1]	Weathering[1]	Uniaxial Compressive Strength (psi)	Broch Parallel Compressive Strength (psi)	Broch Perpendicular Compressive Strength (psi)	Hassani Parallel Compressive Strength (psi)	Hassani Perpendicular Compressive Strength (psi)
	171	296.9	HW	M	9748				
	171	349.1	HW	M	1865				
	171	401.9	HW	M	5509				
	171	455.1	HW	M	5217				
	177	455.1	HW	M		5772	28315	6452	28543
	177	508.9	HW	M		2886	11506	3226	10875
	178	348.1	HW	M		5291	30059	5915	20159
	178	414.0	HW	M		4570	22331	5108	17644
	178	461.9	HW	M		4570	24209	5108	19498
	178	492.1	HW	M		1443	5413	1613	4863
	188	323.2	HW	M	2945				
	188	350.1	HW	M		11362	52122	12523	28370
	188	370.1	HW	M					
	188	415.0	HW	M		3705	18696	4084	11731
	188	430.1	HW	M	3220				
	188	440.0	HW	M		3552	20081	3860	12600
	188	450.1	HW	M		11926	30601	12958	21874
	188	453.1	HW	M		7866	39508	8547	22039
	188	460.0	HW	M		11419	91276	12407	43710
	188	469.2	HW	M					
	188	470.1	HW	M		19792	112330	21505	68256
	188	480.0	HW	M		10657	73263	11580	33246
	188	490.2	HW	M		1976	66991	2178	37370
	188	500.0	HW	M		962	28342	1075	15810
	189	540.0	HW	M		8547	15626	8884	13066
	189	549.9	HW	M		13956	33488	15164	23442
	191	307.1	HW	M		481	1924	538	1669
	191	316.9	HW	M		2405	19838	2688	20933
	191	327.1	HW	M		4089	16949	4570	15755

Table B-4. Summary of strength data (continued).

Summary Statistics	Borehole Number	Downhole Distance (ft)	Lithology[1]	Weathering[1]	Uniaxial Compressive Strength (psi)	Broch Parallel Compressive Strength (psi)	Broch Perpendicular Compressive Strength (psi)	Hassani Parallel Compressive Strength (psi)	Hassani Perpendicular Compressive Strength (psi)
	191	336.9	HW	M		2646	18572	2957	18137
	191	347.1	HW	M		1924	34049	2151	33252
	191	357.0	HW	M		1203	24326	1344	22993
	191	367.1	HW	M		44012	51068	49198	57882
	191	377.0	HW	M		241	19285	269	20954
	191	387.1	HW	M		3608	28551	4033	28332
	191	397.0	HW	M		3367	39448	3764	37286
	191	407.2	HW	M		3367	24229	3764	24423
	191	417.0	HW	M		5051	21309	5646	21481
	191	430.1	HW	M		8177	36563	9141	31706
	191	440.0	HW	M		3127	12589	3495	11505
	191	450.1	HW	M		2405	36563	2688	31706
	191	460.0	HW	M		782	1857	838	1814
	191	470.1	HW	M		722	18519	807	20701
	191	480.0	HW	M		4089	19395	4570	18332
	191	490.2	HW	M		1443	18883	1613	17257
	191	500.0	HW	M		2886	9830	3226	9138
	191	511.2	HW	M	4670	1924	15450	2151	14604
	191	520.0	HW	M		1684	6597	1882	7168
	191	529.9	HW	M		1522		1654	
	191	540.0	HW	M		494	2386	544	2032
	191	287.1	HW	M		962	5003	1075	4339
	191	296.9	HW	M		1776	6644	1930	6072
	191	549.9	HW	M			1444		1297
	191	560.0	HW	M		722	8043	807	8486
	191	567.9	HW	M	2379	494	1548	544	1511
	191	567.9	HW	M	7859				
	191	579.1	HW	M		241	6543	269	5674
	191	588.9	HW	M			1320		1064

Table B-4. Summary of strength data (continued).

Summary Statistics	Borehole Number	Downhole Distance (ft)	Lithology[1]	Weathering[1]	Uniaxial Compressive Strength (psi)	Broch Parallel Compressive Strength (psi)	Broch Perpendicular Compressive Strength (psi)	Hassani Parallel Compressive Strength (psi)	Hassani Perpendicular Compressive Strength (psi)
	191	589.9	HW	M		522	470	559	653
	191	600.1	HW	M		507	1193	551	1016
	191	623.0	HW	M		2347	4773	2513	4065
	191	629.9	HW	M		3095	3952	3023	4356
	193	490.2	HW	M		1482	2949	1633	3112
	193	497.0	HW	M		494	9791	544	8948
	193	509.8	HW	M		1203	10194	1344	12029
	193	605.0	HW	M			3508		3371
	193	520.0	HW	M		1235	11385	1361	11476
	193	529.9	HW	M		741	7304	817	8392
	195	109.9	HW	M		3745		5882	
	195	125.0	HW	M	11857	7928	13000	12135	15741
	195	140.1	HW	M		9604		13214	
	195	149.9	HW	M		5663		8818	
	195	160.1	HW	M		7017		10927	
	195	178.1	HW	M	8673	5717		8594	
	195	190.0	HW	M		8083		12262	
	195	200.1	HW	M		9079		13896	
	195	210.0	HW	M		5085		7713	
	195	226.0	HW	M		9268		13677	
	195	240.2	HW	M		12703		18569	
	195	250.0	HW	M		604		949	
	195	259.8	HW	M		10404		14315	
Samples	**81**	**81.0**			**11**	**69**	**59**	**69**	**59**
Min		**109.9**			**1865**	**241**	**470**	**269**	**653**
Max		**629.9**			**11857**	**44012**	**112330**	**49198**	**68256**
Average		**414.5**			**5813**	**4966**	**21719**	**5995**	**17013**

Table B-4. Summary of strength data (continued).

Summary Statistics	Borehole Number	Downhole Distance (ft)	Lithology[1]	Weathering[1]	Uniaxial Compressive Strength (psi)	Broch Parallel Compressive Strength (psi)	Broch Perpendicular Compressive Strength (psi)	Hassani Parallel Compressive Strength (psi)	Hassani Perpendicular Compressive Strength (psi)
	171	546.9	CF	M	43056				
	171	691.9	CF	M	3228				
	171	504.9	CF	M	34410				
	175	539.0	CF	M		1924	24876	2151	23903
	175	562.0	CF	M		1203	14209	1344	14993
	175	569.9	CF	M		1443	10477	1613	10890
	175	597.1	CF	M		52116	89743	57443	84826
	177	720.1	CF	M		14671	20748	16399	22868
	177	748.0	CF	M		11063	15386	12367	16476
	178	534.1	CF	M		5582	7213	6066	7157
	188	529.9	CF	M		8627	7946	9374	5562
	188	540.0	CF	M		241	5871	269	4461
	188	549.9	CF	M		25253	48512	28228	31831
	188	554.1	CF	M					
	188	509.8	CF	M		2145	102965	2263	33793
	188	520.0	CF	M		1135	6587	1162	3497
	189	565.9	CF	M		3127	12765	3495	10281
	189	569.9	CF	M		18031	27573	19874	24338
	189	573.2	CF	M	3452				
	189	580.1	CF	M		16690	28384	17872	27274
	189	589.9	CF	M		32075	40171	34349	34211
	189	600.1	CF	M	29460	29728	25480	31835	33933
	191	640.1	CF	M		481	3211	538	3539
	191	649.9	CF	M			183		236
	191	662.1	CF	M		761		827	
	191	687.0	CF	M	1842	536		566	
	193	660.1	CF	M		5051	12434	5646	13510

Table B-4. Summary of strength data (continued).

Summary Statistics	Borehole Number	Downhole Distance (ft)	Lithology[1]	Weathering[1]	Uniaxial Compressive Strength (psi)	Broch Parallel Compressive Strength (psi)	Broch Perpendicular Compressive Strength (psi)	Hassani Parallel Compressive Strength (psi)	Hassani Perpendicular Compressive Strength (psi)
	193	669.9	CF	M		14634	4988	11341	5887
	193	687.0	CF	M		5074	9372	3778	11920
	193	691.9	CF	M	15448	15167	11548	11524	10374
Samples	**30**	**30.0**			**7**	**24**	**23**	**24**	**23**
Min		**504.9**			**1842**	**241**	**183**	**269**	**236**
Max		**748.0**			**43056**	**52116**	**102965**	**57443**	**84826**
Average		**601.5**			**18699**	**11115**	**23071**	**11680**	**18946**
	188	560.0	FW	M		20737	58333	20578	46091
	188	569.9	FW	M		39838	47637	43287	39099
	188	577.1	FW	M					
	188	580.1	FW	M		28379	122392	31723	57066
	189	799.9	FW	M		7937	21998	8872	26298
	189	810.0	FW	M		17509	19539	19024	21230
	189	819.9	FW	M		25687	10363	28313	16545
	189	830.1	FW	M		16835	26477	18819	30422
	189	839.9	FW	M		32257	12282	33531	15435
	189	850.1	FW	M		19240	26091	21507	35898
	189	859.9	FW	M		25734	31090	28766	39071
	189	870.1	FW	M		26338	19478	28205	28472
	189	877.0	FW	M		24699	18955	27224	26356
	191	712.9	FW	M		2284	358	2481	466
	191	720.1	FW	M		1015	481	1103	538
	191	736.9	FW	M	1261	1924	890	2151	1036
	191	736.9	FW	M	1309				
	191	745.1	FW	M		30562	31098	32248	32814
	191	750.0	FW	M		17537	21038	19329	24826
	191	763.1	FW	M	19002	18031	21889	19874	29151

Table B-4. Summary of strength data (continued).

Summary Statistics	Borehole Number	Downhole Distance (ft)	Lithology[1]	Weathering[1]	Uniaxial Compressive Strength (psi)	Broch Parallel Compressive Strength (psi)	Broch Perpendicular Compressive Strength (psi)	Hassani Parallel Compressive Strength (psi)	Hassani Perpendicular Compressive Strength (psi)
	191	770.0	FW	M		16835	17211	18819	18431
	191	779.9	FW	M	24490	20254	29753	22324	29524
	193	700.1	FW	M		8970	10060	6951	8880
	193	710.0	FW	M		27381	34037	21218	39637
	193	720.1	FW	M	15543	40127	34604	31095	35426
	193	799.9	FW	M		22188	43491	17194	37713
	193	810.0	FW	M		2832	23698	2195	18724
	193	819.9	FW	M		23132	15461	17925	17524
	193	830.1	FW	M		12746	30685	9877	23779
	193	839.9	FW	M		6137	14109	4756	9462
	193	850.1	FW	M		2360	25931	1829	19702
	193	859.9	FW	M		4721	16743	3658	12468
	193	870.1	FW	M			42943		23955
	193	879.9	FW	M		3305	21938	2561	19023
	193	890.1	FW	M		7828	24153	5948	19085
	193	899.9	FW	M	20518	7081	27140	5487	22693
Samples	**36**	**36.0**			**6**	**33**	**34**	**33**	**34**
Min		**560.0**			**1261**	**1015**	**358**	**1103**	**466**
Max		**899.9**			**24490**	**40127**	**122392**	**43287**	**57066**
Average		**778.9**			**13687**	**17044**	**26540**	**16936**	**24319**
	177	298.9	HW	S		1571	26706	2467	23989
	177	357.9	HW	S		6603	2214	7996	3834
	177	404.9	HW	S		266	3145	400	3904
	188	270.0	HW	S		3211	31901	3539	20472
	189	245.1	HW	S		722	1017	807	945
	189	254.9	HW	S		1103	3290	1146	2751
	195	79.1	HW	S	5755	7545		11547	

Table B-4. Summary of strength data (continued).

Summary Statistics	Borehole Number	Downhole Distance (ft)	Lithology[1]	Weathering[1]	Uniaxial Compressive Strength (psi)	Broch Parallel Compressive Strength (psi)	Broch Perpendicular Compressive Strength (psi)	Hassani Parallel Compressive Strength (psi)	Hassani Perpendicular Compressive Strength (psi)
	195	89.9	HW	S		6771		10544	
	195	100.1	HW	S		4520		6795	
Samples	**9**	**9.0**			**1**	**9**	**6**	**9**	**6**
Min		**79.1**			**5755**	**266**	**1017**	**400**	**945**
Max		**404.9**			**5755**	**7545**	**31901**	**11547**	**23989**
Average		**233.4**			**5755**	**3590**	**11379**	**5027**	**9316**
	193	631.9	CF	S					
	193	644.0	CF	S		10582	30957	11829	33637
	193	652.9	CF	S		12597	16167	13884	16552
Samples	**3**	**3.0**			**0**	**2**	**2**	**2**	**2**
Min		**631.9**			**0**	**10582**	**16167**	**11829**	**16552**
Max		**652.9**			**0**	**12597**	**30957**	**13884**	**33637**
Average		**642.9**			**0**	**11590**	**23562**	**12857**	**25095**
	195	274.9	HW	U	3979	10486	38886	16049	44076
	195	290.0	HW	U		7685	1745	9774	3662
	195	299.9	HW	U		5293		8243	
	195	310.0	HW	U		6524		10160	
	195	323.2	HW	U	5469	5646		8253	
	195	339.9	HW	U		9444		12994	
	195	350.1	HW	U		10602		14120	
	195	359.9	HW	U		6650		10177	
	195	375.0	HW	U		12231	14995	18387	19071
	195	390.1	HW	U		2393	2394	3597	3188
	195	399.9	HW	U		6640		9798	
	195	410.1	HW	U		8469	10122	12379	12873

Table B-4. Summary of strength data (continued).

Summary Statistics	Borehole Number	Downhole Distance (ft)	Lithology[1]	Weathering[1]	Uniaxial Compressive Strength (psi)	Broch Parallel Compressive Strength (psi)	Broch Perpendicular Compressive Strength (psi)	Hassani Parallel Compressive Strength (psi)	Hassani Perpendicular Compressive Strength (psi)
	195	425.9	HW	U	4183	3650		5538	
	195	440.0	HW	U		128		196	
	195	452.1	HW	U		3708	1799	5676	2450
Samples	**15**	**15.0**			**3**	**15**	**6**	**15**	**6**
Min		**274.9**			**3979**	**128**	**1745**	**196**	**2450**
Max		**452.1**			**5469**	**12231**	**38886**	**18387**	**44076**
Average		**362.7**			**4544**	**6637**	**11657**	**9689**	**14220**
	178	561.0	FW	U		1684	4566	1882	3400
	178	586.9	FW	U		30544	58044	34143	55775
	178	607.9	FW	U		17797	61301	19894	61794
	178	630.9	FW	U		37999	79986	42477	81887
	178	657.2	FW	U		28139	45080	31455	44734
	178	681.1	FW	U		21886	69362	24465	65562
	178	706.0	FW	U		15633	63293	17475	57843
	178	732.9	FW	U		23852	96614	25917	76338
	188	930.1	FW	U		17316	82412	19357	52887
	188	940.0	FW	U		20443	71138	22852	59484
	188	954.1	FW	U	17174	23810	51054	26615	46658
	188	960.0	FW	U		18278	28253	20432	32901
	188	970.1	FW	U		25193	77411	27768	63536
	188	980.0	FW	U		18759	61251	20970	52163
	188	990.2	FW	U		12103	60640	13340	39789
	188	999.0	FW	U		15152	58271	16937	47827
Samples	**16**	**16.0**			**1**	**16**	**16**	**16**	**16**
Min		**561.0**			**17174**	**1684**	**4566**	**1882**	**3400**
Max		**999.0**			**17174**	**37999**	**96614**	**42477**	**81887**
Average		**805.5**			**17174**	**20537**	**60542**	**22874**	**52661**

Table B-4. Summary of strength data (continued).

Summary Statistics	Borehole Number	Downhole Distance (ft)	Lithology[1]	Weathering[1]	Uniaxial Compressive Strength (psi)	Broch Parallel Compressive Strength (psi)	Broch Perpendicular Compressive Strength (psi)	Hassani Parallel Compressive Strength (psi)	Hassani Perpendicular Compressive Strength (psi)
	178	296.9	HW	W		3367	22888	3764	18435
	189	265.1	HW	W		241	4465	269	4290
	189	274.9	HW	W		4810	10170	5377	10891
	189	285.1	HW	W		7456	15593	8334	14494
	189	294.9	HW	W		962	5250	1075	6032
	189	305.1	HW	W		962	3145	1075	3904
	189	315.0	HW	W		1924	6090	2151	6617
	189	325.1	HW	W		1443	14182	1613	14519
	189	335.0	HW	W		1203	7760	1344	8917
	189	345.1	HW	W		241	7141	269	9191
	189	355.0	HW	W		2405	5856	2688	6638
	189	365.2	HW	W		962	4465	1075	4290
	189	377.0	HW	W		3458	15763	3811	15890
	189	391.1	HW	W		3608	16114	4033	18012
	189	399.9	HW	W		2405	14315	2688	16892
	189	410.1	HW	W		2165	21611	2420	19076
	189	425.9	HW	W	1334	4089	17423	4570	16468
	189	440.0	HW	W		3608	33220	4033	30879
	189	450.1	HW	W		722	14435	807	12967
	189	460.0	HW	W		1443	18184	1613	16618
	189	473.1	HW	W	5991	3367	7615	3764	9103
	189	480.0	HW	W		4810	11913	5377	12196
	189	490.2	HW	W		9380	17541	10485	16855
	189	500.0	HW	W		16835	37772	18819	39263
	189	509.8	HW	W		6494	26428	7259	29130
	189	525.9	HW	W		7215	25402	8065	22027
	193	399.9	HW	W		3848	26001	4301	25392
	193	410.1	HW	W		2886	11880	3226	14568

Table B-4. Summary of strength data (continued).

Summary Statistics	Borehole Number	Downhole Distance (ft)	Lithology[1]	Weathering[1]	Uniaxial Compressive Strength (psi)	Broch Parallel Compressive Strength (psi)	Broch Perpendicular Compressive Strength (psi)	Hassani Parallel Compressive Strength (psi)	Hassani Perpendicular Compressive Strength (psi)
	193	419.9	HW	W		4810	22708	5377	19691
	193	430.1	HW	W		1443	33220	1613	30879
	193	440.0	HW	W		3458	27200	3811	24009
	193	449.1	HW	W		722	18983	807	17645
	193	460.0	HW	W		4446	26620	4900	25997
	193	470.1	HW	W		1976	23937	2178	24129
	193	480.0	HW	W		241	9156	269	11783
	193	540.0	HW	W		3127	28787	3495	28113
	193	549.9	HW	W	7187	8899	20126	9947	20921
	193	560.0	HW	W		3608	16434	4033	18883
	193	569.9	HW	W		988	10089	1089	13437
	193	580.1	HW	W		241	11481	269	11032
	193	589.9	HW	W		241	9644	269	9873
Samples	**41**	**41.0**			**3**	**41**	**41**	**41**	**41**
Min		**265.1**			**1334**	**241**	**3145**	**269**	**3904**
Max		**589.9**			**7187**	**16835**	**37772**	**18819**	**39263**
Average		**425.5**			**4837**	**3329**	**16610**	**3716**	**16584**
	171	521.0	CF	W	42726				
	171	577.1	CF	W	30564				
	171	600.1	CF	W	62738				
	171	631.9	CF	W	16398				
	171	637.1	CF	W	3994				
	177	576.1	CF	W		33911		37907	
	177	592.8	CF	W		42376	28594	46044	35061
	177	618.1	CF	W		45455	37792	50811	50331
	177	631.9	CF	W		54834	61399	61296	71502
	177	655.8	CF	W		41126	52304	45972	50258

Table B-4. Summary of strength data (continued).

Summary Statistics	Borehole Number	Downhole Distance (ft)	Lithology[1]	Weathering[1]	Uniaxial Compressive Strength (psi)	Broch Parallel Compressive Strength (psi)	Broch Perpendicular Compressive Strength (psi)	Hassani Parallel Compressive Strength (psi)	Hassani Perpendicular Compressive Strength (psi)
	177	681.1	CF	W		24050	42767	26884	45798
	177	778.9	CF	W		26696	33670	29842	37638
Samples	**12**	**12.0**			**5**	**7**	**6**	**7**	**6**
Min		**521.0**			**3994**	**24050**	**28594**	**26884**	**35061**
Max		**778.9**			**62738**	**54834**	**61399**	**61296**	**71502**
Average		**625.2**			**31284**	**38350**	**42754**	**42679**	**48431**
	177	804.1	FW	W		4693	21667	5173	21160
	177	850.1	FW	W		21039	87514	15985	46464
	177	900.9	FW	W		28867	58471	21932	41796
	177	950.1	FW	W		22324	126096	16625	66948
	177	999.0	FW	W		13690	121124	10609	53476
	188	589.9	FW	W		14430	64972	16131	39846
	188	600.1	FW	W		32109	58223	35391	44237
	188	605.0	FW	W					
	188	609.9	FW	W		28898	151746	31852	72667
	188	620.1	FW	W		26468	37461	27512	26223
	188	629.9	FW	W		29392	66277	32397	39715
	188	630.9	FW	W	18682				
	188	640.1	FW	W		27910	68938	30763	45233
	188	649.9	FW	W		26897	63556	29225	35454
	188	655.8	FW	W					
	188	660.1	FW	W		25012	145955	27960	75559
	188	669.9	FW	W		44332	54895	47474	36019
	188	680.1	FW	W		40754	76821	44920	46033
	188	690.0	FW	W		32850	101674	36208	60926
	188	700.1	FW	W		8418	42767	9409	28062
	188	701.1	FW	W					

Table B-4. Summary of strength data (continued).

Summary Statistics	Borehole Number	Downhole Distance (ft)	Lithology[1]	Weathering[1]	Uniaxial Compressive Strength (psi)	Broch Parallel Compressive Strength (psi)	Broch Perpendicular Compressive Strength (psi)	Hassani Parallel Compressive Strength (psi)	Hassani Perpendicular Compressive Strength (psi)
	188	710.0	FW	W		20107	56486	21216	33848
	188	720.1	FW	W		18759	15986	20970	17370
	188	730.0	FW	W		28651	97953	31580	53317
	188	740.2	FW	W		30957	85105	33637	50997
	188	750.0	FW	W		25974	117942	29035	69031
	188	752.0	FW	W	11053				
	188	759.8	FW	W		21164	61809	23658	39665
	188	770.0	FW	W		22607	94143	25271	56413
	188	779.9	FW	W		22367	123273	25002	65449
	188	790.0	FW	W		19721	157149	22045	83435
	188	799.9	FW	W		11419	10217	12407	7152
	188	810.0	FW	W		19513	131991	21507	61541
	188	819.9	FW	W		31506	86810	35218	56961
	188	830.1	FW	W		22229	122660	24502	71792
	188	839.9	FW	W		21886	81406	24465	55786
	188	850.1	FW	W		10101	49163	11291	30848
	188	854.0	FW	W					
	188	859.9	FW	W		18038	61979	20163	48972
	188	870.1	FW	W		24291	167224	27153	82217
	188	879.9	FW	W		20924	55810	23389	41562
	188	890.1	FW	W		15633	104326	17475	59622
	188	919.9	FW	W		11785	44781	13173	30033
	189	609.9	FW	W		25734	23111	28766	27984
	189	623.0	FW	W	17957	27177	27714	30379	34406
	189	629.9	FW	W		30874	32226	34030	35015
	189	640.1	FW	W		48164	44150	53087	59451
	189	649.9	FW	W		29435	31015	31982	36599
	189	660.1	FW	W		23464	19304	25863	26278
	189	672.9	FW	W		28139	27642	31455	31331

Table B-4. Summary of strength data (continued).

Summary Statistics	Borehole Number	Downhole Distance (ft)	Lithology[1]	Weathering[1]	Uniaxial Compressive Strength (psi)	Broch Parallel Compressive Strength (psi)	Broch Perpendicular Compressive Strength (psi)	Hassani Parallel Compressive Strength (psi)	Hassani Perpendicular Compressive Strength (psi)
	189	680.1	FW	W		8899	5882	9947	9003
	189	690.0	FW	W		26455	28846	29573	34039
	189	699.1	FW	W	13301	23711	38240	26135	42746
	189	710.0	FW	W		31718	39766	34464	43831
	189	720.1	FW	W		34256	16284	37221	26416
	189	727.0	FW	W		28651	27124	31580	33674
	189	741.1	FW	W		10127	23435	11162	24360
	189	750.0	FW	W		4570	6442	5108	8387
	189	759.8	FW	W		9683	4402	7799	3545
	189	773.0	FW	W		3608	10307	4033	11683
	189	776.9	FW	W	13809	24867	26461	27020	31224
	189	790.0	FW	W		8658	23111	9678	27984
	189	890.1	FW	W		21315	14526	23160	22621
	189	899.9	FW	W		9620	13468	10754	15055
	189	910.1	FW	W		13949	26956	15593	25479
	189	919.9	FW	W		17043	13295	18785	19986
	189	930.1	FW	W	1378	6734	21601	7528	21775
	189	940.0	FW	W		4570	22883	5108	23787
	189	950.1	FW	W		5051	20989	5646	21488
	191	788.1	FW	W	24490	23464	30927	25863	39335
	191	799.9	FW	W		19266	46915	21235	49504
	191	813.0	FW	W	14243	30703	33324	33361	38290
	191	813.0	FW	W	8594				
	191	819.9	FW	W		34151	22737	38176	29943
	191	830.1	FW	W		26922	21241	29674	23413
	191	836.9	FW	W	8050	21644	34683	23178	37141
	191	850.1	FW	W		17316	32850	19357	36208
	191	860.9	FW	W		20924	29810	23389	34715
	191	870.1	FW	W		18759	24176	20970	30014

Table B-4. Summary of strength data (continued).

Summary Statistics	Borehole Number	Downhole Distance (ft)	Lithology[1]	Weathering[1]	Uniaxial Compressive Strength (psi)	Broch Parallel Compressive Strength (psi)	Broch Perpendicular Compressive Strength (psi)	Hassani Parallel Compressive Strength (psi)	Hassani Perpendicular Compressive Strength (psi)
	191	879.9	FW	W		16114	34436	18012	39031
	191	890.1	FW	W		10582	16967	11829	23345
	191	898.9	FW	W		6253	25934	6990	28585
	191	913.1	FW	W	9312	14573	38590	16062	37081
	191	913.1	FW	W	9546				
	191	919.9	FW	W		8658	23645	9678	23835
	191	930.1	FW	W		17316	37287	19357	34660
	191	940.0	FW	W		6013	31234	6721	31485
	193	720.2	FW	W	18227				
	193	730.0	FW	W		24548	19819	19023	21223
	193	740.2	FW	W		33518	35388	25974	37340
	193	744.1	FW	W	18454	26436	29593	20486	26582
	193	745.1	FW	W	18664				
	193	750.0	FW	W		29741	37453	23047	36577
	193	759.8	FW	W		12274	20107	9511	21216
	193	772.0	FW	W	18690	11802	35878	9146	27803
	193	772.0	FW	W	21805				
	193	779.9	FW	W		6609	7076	5122	8130
	193	910.1	FW	W		9442	20866	7316	18418
	193	919.9	FW	W		9914	102490	7682	45249
	193	930.1	FW	W		7828	35515	5948	26448
	193	940.0	FW	W		1416	18883	1097	14633
	193	950.1	FW	W		5193	21716	4024	16828
Samples	**102**	**102.0**			**17**	**91**	**91**	**91**	**91**
Min		**589.9**			**1378**	**1416**	**4402**	**1097**	**3545**
Max		**999.0**			**24490**	**48164**	**167224**	**53087**	**83435**
Average		**784.7**			**14486**	**20039**	**49814**	**21108**	**36604**

[1] HW—*hanging wall*, CF—*Crandon Formation*, FW—*footwall*, S—*strongly weathered*, M—*moderately weathered*, W—*weakly weathered*, U—*unweathered*

B-3 FRACTURE FREQUENCY

Fracture frequency was measured by normalizing the number of fractures observed in core photographs to the core run length. Table B-5 lists the results as averages in each hole and averages for the different weathering intensities.

B-4 ESTIMATES OF ROCK MASS QUALITY INDEX — RMR

The rock mass quality has been estimated for each of the weathering intensity zones using the geomechanics index—RMR to provide a basis for determining material properties for the computer analyses. RMR is usually based on data collected by mapping underground excavations but was estimated here based on core data using procedures suggested by Laubscher (1990), Barton et al. (1974), and Milne (1991). RMR is a relative index of rock mass quality that ranges from 0–100 (very poor–very good) and is calculated by considering impacts of different rock characteristics that affect stability of excavations in rock. The parameters considered are:

- RQD index (IRQD),
- rock compressive strength index (C),
- fracture frequency index (IF),
- joint condition index (JCD) (roughness, infilling, waviness, weathering), and
- hydrologic conditions index (Jw).

The index is calculated by equation (B-2).

$$RMR = IRQD + C + IF + JCD + Jw \qquad \text{(B-2)}$$

The resulting average values for the different weathering intensities are listed in Table B-6. The range in relative rock quality generally correlates with the weathering intensity. Gossan and strongly weathered portions of the hanging wall had RMR values of 38–39 for a poor rating. Moderately weathered portions of the three rock units (hanging wall, Crandon Formation, footwall) were fair rock quality.

The modified rock mass rating (RMR) value (Laubscher 1990) was calculated for each rock unit and weathering intensity in the crown pillar area using borehole data. The rock was categorized according to rock units of hanging wall, Crandon Formation (zinc ore), and footwall with grouping by weathering intensity. Data for each category was collected and entered into a

Table B-5. Fracture frequencies for the crown pillar area.

Stratigraphy	Borehole Number	Fracture Frequency (fractures per foot) Gossan	Strongly Weathered	Moderately Weathered	Weakly Weathered	Unweathered
Hanging Wall	177		4.1	3.0		
	178		4.2	4.0	12.8	
	188		3.4	2.9		
	189		5.9	4.7	3.7	
	193		4.0	3.8	2.5	
	195		2.0	2.4		3.9
Average		—	**3.9**	**3.5**	**6.3**	**3.9**
Crandon Formation	177	2.4			1.5	
(Zinc Ore)	178	2.0		3.4		
	188			2.2		
	189			2.9		
Average		**2.2**	—	**2.8**	**1.5**	—
Footwall						
	178			3.0		2.3
	188			1.4	3.5	
Average		—	—	**2.2**	**3.5**	**2.3**

Table B-6. Estimated RMR data for the crown pillar area.

		RMR Values				
Stratigraphy	**Borehole Number**	**Gossan**	**Strongly Weathered**	**Moderately Weathered**	**Weakly Weathered**	**Unweathered**
Hanging Wall	177		38.4	45.2	45.2	
	178		38.2	52.8		
	188		40.1	49.3		
	189		34.4	44.9	47.6	
	193		36.4	46.0	50.6	
	195		45.1	49.9		51.1
Average		—	**39**	**48**	**48**	**51**
Crandon Formation	177	35.4			78.1	
(Zinc Ore)	178	40.6		48.6		
	188			51.6		
	189			54.5		
Average		**38**	—	**52**	**78**	—
Footwall+A5	178			57.7		64.2
	188			63.7	60.8	
Average		—	—	**61**	**61**	**64**

spreadsheet for assessing rock mass quality based on borehole data. The input required for each rock unit, or interval of core of similar rock quality, includes the following:

- length of recovered core,
- length or rubble zone,
- total length of core pieces > 4 inches,
- number of fractures,
- small-scale joint roughness (JRC),
- joint aperture (thickness of mineral infill),
- large-scale joint amplitude,
- description of joint condition, and
- rock strength.

Photographs of core used to assess the crown pillar included holes 171, 177, 178, 188, 189, 191, 193, and 195. The length of recovered core, length of rubble zones, total length of core pieces greater than 4 inches, and the total number of fractures were measured by scaling the dimensions from core photography. Small-scale joint roughness and joint aperture width were estimated visually from the core photographs. A JRC value of 7 was selected as representative of each interval based on the typical joint roughness profiles (Barton and Choubey 1977). A joint aperture of 1 mm was used for each interval based on the minimal infill observed in the core photographs. The large-scale joint amplitude was assumed to be 150 mm. The joint condition was described as *weathered* for the strongly weathered category. For all other categories, a joint description of *open* was used based on typical core photographs. RMR and parameter assessments are presented in Table B-7. RQD estimates for individual core runs in each hole are listed in Table B-2.

Strength data was compiled for each of the boreholes based on available rock mechanics testing data supplied in spreadsheets by CMC. Strength data was generated by uniaxial compressive strength testing and by point load testing. Two methods were used to relate point load data to compressive strength for parallel and perpendicular to the plane of the foliation. This data is summarized in Table B-4, which indicates a wide range of compressive strength values for each rock unit and weathering intensity. The data labeled Hassani parallel point load

Table B-7. Summary of rock mass rating (RMR) parameters.

Interval													RMR Components								Rock Mass Quality Rating
Borehole Number	Interval Ending Footage	Lithology[1]	Recovered Core (ft)	Length of Rubble (ft)	Total Length of Pieces > 4 in. (ft)	Fracture Count	JRC_s	JRC_L	AW (mm)	Aa (mm)	Infill Type	Estimated Strength (MPa)	RQD	SI (Rock Strength)	S2 (Fracture Frequency)	A	B	C	D	S3 (Joint Condition)	RMR[2]
177	405	HW/S	101.3	14.6	43.4	355	7	4	1	150	Weathered	35	27	4	15.6	0.80	0.69	0.75	1.00	16.6	36
	543	HW/M	135.9	8.1	51.0	381	7	4	1	150	Open	41	37	5	18.1	0.80	0.69	1.00	1.00	22.1	45
	563	CF/G	20.0	3.2	0.3	41	7	4	1	150	Weathered	20	10	3	14.7	0.80	0.69	0.75	1.00	16.6	34
	633	CF/W	70.0	1.8	52.6	104	7	4	1	150	Open	294	75	30	26.0	0.80	0.69	1.00	1.00	22.1	78
178	252	HW/S	42.0	6.4	17.3	150	7	4	1	150	Weathered	35	10	4	12.9	0.80	0.69	0.75	1.00	16.6	34
	294	HW/W	11.7	0.5	31.6	143	7	4	1	150	Open	26	75	4	19.1	0.80	0.69	1.00	1.00	22.1	45
	502	HW/M	202.0	2.9	140.8	798	7	4	1	150	Open	41	68	5	21.7	0.80	0.69	1.00	1.00	22.1	49
	524	CF/G	22.0	2.4	9.0	39	7	4	1	150	Weathered	20	41	3	20.0	0.80	0.69	0.75	1.00	16.6	40
	553	CF/M	28.3	0.7	10.3	94	7	4	1	150	Open	81	36	9	17.4	0.80	0.69	1.00	1.00	22.1	49
	560	FW/M	7.0	0.1	4.7	21	7	4	1	150	Open	117	67	13	22.5	0.80	0.69	1.00	1.00	22.1	58
	602	FW/U	40.3	0.0	32.7	91	7	4	1	150	Open	158	78	17	25.1	0.80	0.69	1.00	1.00	22.1	64
188	312	HW/S	44.0	0.5	21.8	150	7	4	1	150	Weathered	35	10	4	13.6	0.80	0.69	0.75	1.00	16.6	34
	505	HW/M	192.3	1.5	124.0	560	7	4	1	150	Open	41	64	5	22.2	0.80	0.69	1.00	1.00	22.1	49
	560	CF/M	54.8	2.4	25.7	115	7	4	1	150	Open	81	47	9	20.5	0.80	0.69	1.00	1.00	22.1	52
	590	FW/M	30.0	0.0	27.4	43	7	4	1	150	Open	117	91	13	28.6	0.80	0.69	1.00	1.00	22.1	64
	598	FW/W	7.8	0.0	5.7	27	7	4	1	150	Open	146	71	16	22.7	0.80	0.69	1.00	1.00	22.1	61
189	260	HW/S	12.8	1.5	3.0	67	7	4	1	150	Weathered	35	23	4	13.8	0.80	0.69	0.75	1.00	16.6	34
	525	HW/W	259.6	3.5	171.4	950	7	4	1	150	Open	26	65	4	21.5	0.80	0.69	1.00	1.00	22.1	48
	565	HW/M	39.2	0.8	18.1	182	7	4	1	150	Open	41	45	5	17.8	0.80	0.69	1.00	1.00	22.1	45
	606	CF/M	40.8	0.3	29.5	119	7	4	1	150	Open	81	72	9	23.4	0.80	0.69	1.00	1.00	22.1	54
193	289	HW/S	45.0	1.6	12.8	175	7	4	1	150	Weathered	35	10	4	13.1	0.80	0.69	0.75	1.00	16.6	34
	368	HW/M	79.0	2.0	37.5	290	7	4	1	150	Open	41	47	5	18.9	0.80	0.69	1.00	1.00	22.1	46
	478	HW/W	110.0	0.1	83.5	272	7	4	1	150	Open	26	76	4	24.5	0.80	0.69	1.00	1.00	22.1	51
195	102	HW/S	24.7	0.0	17.8	49	7	4	1	150	Weathered	35	17	4	16.5	0.80	0.69	0.75	1.00	16.6	37
	262	HW/M	160.0	1.5	101.8	385	7	4	1	150	Open	41	64	5	22.7	0.80	0.69	1.00	1.00	22.1	50
	272	HW/U	10.0	0.0	6.2	39	7	4	1	150	Open	67	62	8	21.0	0.80	0.69	1.00	1.00	22.1	51

[1] HW—*hanging wall*, CF—*Crandon Formation*, FW—*footwall*, G—*gossan*, S—*strongly weathered*, M—*moderately weathered*, W—*weakly weathered*, U—*unweathered*

[2] RMR = S1+S2+S3; S3 = 40 x (AxBxCxD)

compressive strength in Table B-4, was selected for use in the RMR assessment because it falls in the low end of the range of strength values.

B-5 ROCK MASS MECHANICAL PROPERTIES ESTIMATES

Mechanical properties at the scale of excavations (rock mass scale) differ strongly from laboratory measurements on core samples because the inhomogeneities at the larger scale (fractures, weathering, etc.) weaken the rock. Rock mass properties for analysis of mining impacts on the crown pillar stress and deformation have therefore been estimated using published correlations between strength and the rock mass quality RMR. These correlations produce generally conservative estimates of the properties required for modeling and analysis and are therefore used in design.

Rock mass elastic modulus was estimated using a correlation published by Serafim and Pereira (1983), shown as equation B-3:

$$E = 10^{\left(\frac{RMR-10}{40}\right)} \qquad \text{(B-3)}$$

where E = elastic modulus (GPa) and 1 Gpa = 145,000 psi.

The resulting values for the two-dimensional analysis are listed in Table B-8.

Rock mass strength was estimated using an approach suggested by Hoek and Brown (1988) who proposed equation B-4:

$$\sigma_1 = \sigma_3 + \sqrt{m\sigma_c\sigma_3 + s\sigma_c^2} \qquad \text{(B-4)}$$

where σ_1 = rock mass strength,

σ_3 = minimum principal stress,

σ_c = uniaxial compressive strength at the intact (laboratory) scale,

m = $m_i e^{(RMR-28)}$,

m_i = a constant, and

s = $e^{(RMR-100)/9}$.

Values for constants m_i were selected from charts based on comparative rock types such that:

- gossan m_i = 18.8 similar to sandstone and
- other rock and weathering units m_i = 29.2 similar to gneiss.

Table B-8. Estimated rock mass elastic moduli for the crown pillar area.

Stratigraphy	Parameter[1]	Weathering Intensity: Strongly Weathered	Moderately Weathered	Weakly Weathered	Unweathered
Hanging Wall	RMR	39	48	48	51
	E (GPa)[2]	5.31	8.91	8.91	10.59
	ν	0.25	0.25	0.25	0.25
	G (GPa)	2.12	3.57	3.57	4.24
	K (GPa)	3.54	5.94	5.94	7.06
Crandon Formation (zinc ore)	RMR	38	52	78	
	E (GPa)	5.01	11.22	50.12	
	ν	0.25	0.25	0.25	
	G (GPa)	2.00	4.49	20.05	
	K (GPa)	3.34	7.48	33.41	
Footwall	RMR	39	61	61	64
	E (GPa)[2]	5.31	18.84	18.84	22.39
	ν	0.25	0.25	0.25	0.25
	G (GPa)	2.12	7.53	7.53	8.95
	K (GPa)	3.54	12.56	12.56	14.92

[1] E—*elastic modulus*, G—*shear modulus*, K—*bulk modulus*, ν—*Poisson's ratio*.

[2] GPa–*gigapascals* (10^9Pa) 1 GPa = 145,000 psi.

Using these assumption and average values for uniaxial compressive strength from Table B-3, rock mass strength criteria were derived using equation B-4. The numerical model utilized for the two-dimensional analysis of the crown pillar (FLAC) has the capability to simulate yield (elastic–plastic behavior) using a Mohr-Coulomb failure criteria. The rock mass strength criteria defined by equation B-4 were therefore converted to Mohr-Coulomb criteria by fitting a linear equation to data pairs calculated using equation B-4. Table B-9 lists the resulting rock mass uniaxial compressive strength (σ_{RM} at σ_3=0) and equation constants for both the Hoek-Brown and linear criteria. Table B-9 lists the uniaxial compressive strength at the intact (laboratory) scale and compares it to the estimated uniaxial strength at the rock mass scale (σ_{RM}). The rock mass uniaxial strength for the linear criteria used in the two-dimensional analysis were between 6% and 31% of the estimated intact strength based upon the point load testing.

Table B-9. Estimated rock mass strength (psi) criteria.

Rock Unit	Weathering Intensity	Hoek-Brown $\sigma_1 = \sigma_3 + \sqrt{m\sigma_c\sigma_3 + s\sigma_c^2}$				Linear Criteria [1] $\sigma_1 = \sigma_{RM} + N\sigma_3$	
		σ_c	σ_{RM}^2	m	s	σ_{RM}	N
Hanging Wall	Strong	5027	170	1.29	0.001	598	3.14
	Moderate	5995	333	1.78	0.003	822	3.68
	Low/Weak	5995	333	1.78	0.003	822	3.68
Crandon Formation (zinc ore)	Gossan	1000[3]	32	2.05	0.001	312	2.23
	Strong	5000	160	2.05	0.001	731	3.72
	Moderate	11,680	812	5.26	0.005	1979	7.43
	Low/Weak	42,680	12,572	13.31	0.087	13,491	15.10
Footwall	Moderate	16,936	1940	7.25	0.013	3239	9.67
	Low/Weak	16,936	1940	7.25	0.013	3239	9.67

[1] Basis for Mohr-Coulomb failure criteria $\tau = c + \sigma_3 \tan \phi$

where cohesion $c_o = \sigma_{RM}/2\sqrt{N}$; angle of internal friction $\phi_{RM} = 2(\tan^{-1}\sqrt{N} - 45°)$

[2] $\sigma_{RM} = \sigma_1$ at $\sigma_3 = 0$

[3] No data, assigned intact uniaxial strength of 20% of strongly weathered zinc ore.

B-6 GLACIAL OVERBURDEN

The weathered bedrock and/or massive saprolite is overlain by 75–250 ft of overburden containing deposits of sand, silt, gravel, and clay. This overburden has been subdivided into six geologic units[7] based on geologic composition, geologic age, and depositional history. From the bedrock upward these six units are:

- pre- to early Wisconsinan till,
- coarse-grained outwash,
- fine-grained outwash,
- late Wisconsinan till,
- lacustrine deposits, and
- ice margin contact deposits.

[7]Ibid. Page 3-5.

The overburden units are illustrated in Appendix A, a cross section developed from soil borings (Foth & Van Dyke 1995b) and reproduced from Figure 2-3 by GeoTrans, Inc. (1995).

The pre- to early Wisconsinan till varies in thickness from 0–120 ft and consists of poorly sorted silt, sand, gravel, and clay with a high percentage of –200 mesh material. In conjunction with the massive saprolite bedrock, this till forms a hydrologically, resistive layer below glacial aquifers that occur in the outwash units.

APPENDIX C — MODELING ASSUMPTIONS

Model assumptions govern the degree to which the numerical simulations are representative of the potential range of behavior of the crown pillar. The important model assumptions are described below.

C-1 THREE-DIMENSIONAL MODELING EXTRACTION RATIO

Mining of the Crandon deposit is planned to proceed vertically upward with 50% primary extraction between rock pillars followed by backfilling of the primary stopes using cement stabilized hydraulic fill. Pillars are then extracted between the backfill and the secondary stopes filled with uncemented hydraulic fill. This produces a relaxation of the hanging wall where the horizontal stresses are gradually transmitted to the backfill and abutment zones both within and at the periphery of the extracted zone. The use of boundary-element methods allows the entire mine pattern to be simulated. All materials were assumed to be linear elastic with values as listed in Table B-8 for the rock materials and in Section C-3 for the backfill.

C-2 PLANE STRAIN

The two-dimensional analyses assume plane strain where the excavation is very long in the direction normal to the cross section (EW). This can produce very conservative loading because the mining shape is generally more complex with local abutments moderating the stresses. This is a conservative assumption since the initial stress state was derived from three-dimensional simulation of the full mining pattern.

C-3 SEQUENTIAL MINING/BACKFILLING

Both three- and two-dimensional analyses simulate the extraction of the stopes followed by backfilling. Backfill material properties were based on published data on hydraulic fill:

- elastic modulus $E = 0.10$ GPa (14,500 psi),
- shear modulus $G = 0.04$ GPa (5,800 psi), and
- Poisson's ratio $\nu = 0.3$.

C-4 IN SITU STRESSES

In situ stresses for rock were assumed to be similar to published data for the Canadian Shield (Arjang 1991) and data for Wisconsin (Haimson 1982). Principal stresses were assumed to be:

- maximum horizontal stress $\sigma_{HMAX} = 8.1 + 0.03$ D,
- minimum horizontal stress $\sigma_{HMIN} = 4.5 + 0.02$ D and
- vertical stress $\sigma_v = 0.025$ D,

where D = depth (m) and

σ = MPa (1 MPa = 145 psi).

This stress field was applied to the models beginning at the base of the glacial overburden. Stresses were rotated into the N-S direction for use in the analysis.

Stresses in the alluvium were assumed to be due to gravity loading using a density of 2039 kg/m^3, a soil grain specific gravity of 2.67 and a water content of 18.1%.

C-5 MATERIAL PROPERTIES

Material properties for rock were developed in Appendix B, Tables B-8 and B-9. The two-dimensional meshes were designed to simulate the different rock units and weathering intensities as shown in the cross section in Figure 3-6.

The glacial alluvium was assumed to have the following properties:

- elastic modulus E = 0.72 GPa (104,000 psi),
- shear modulus G = 0.26 GPa (37,700 psi) and
- Poisson's ratio ν = 0.40.

C-6 FRACTURE MECHANICAL PROPERTIES

Fracture mechanical properties were estimated based on the parameters of joint roughness coefficient (JRC) and joint compressive strength (JCS) using approaches proposed by Barton and Choubey (1977), Bandis et al. (1983) and Barton (1991). A JRC value of 7 and JCS value of 12,500 psi were used for the analysis. Inputs derived for the continuously-yielding joint model in the UDEC program were:

- joint normal stiffness = 21.687 MPa/mm $\sigma^{1.0332}$ and
- joint shear stiffness = 4.7519 MPa/mm $\sigma^{0.8924}$,

where σ = joint normal stress,

joint initial friction angle = 38.9° and

joint final friction = 30°.

The joint initial friction angle of 38.9° had a factor of safety for fracture slip of less than 1.0 for the Set 5 fractures. An initial friction angle of 49° was required to produce a factor of safety of

1.0. This value was judged to be conservative because it results in larger fracture dilation than use of a 38.9° angle. In the joint model, the magnitude of dilation is a function of the difference between the initial and final values of the friction angle. The use of 49° is an upper bound, in this case, because a higher value would prevent fracture shear movement. The fracture dilation occurs during shear movement.

APPENDIX D — LETTER TO MR. DON MOE, CRANDON MINING COMPANY FROM CHRISTOPHER P. CARLSON, HYDROLOGIST, SOLID WASTE MANAGEMENT SECTION, BUREAU OF SOLID AND HAZARDOUS WASTE MANAGEMENT, DEPARTMENT OF NATURAL RESOURCES, STATE OF WISCONSIN, NOVEMBER 28, 1995

WISCONSIN
DEPT. OF NATURAL RESOURCES

George E. Meyer
Secretary

State of Wisconsin \ DEPARTMENT OF NATURAL RESOURCES

101 South Webster Street
Box 7921
Madison, Wisconsin 53707
DNR TELEPHONE 608-266-2621
DNR TELEFAX 608-267-3579
DNR TDD 608-267-6897
SOLID WASTE MGMT 608-266-2111
SOLID WASTE TELEFAX 608-267-2768

November 28, 1995

Mr. Don Moe
Crandon Mining Company
7 North Brown Street, 3rd Floor
Rhinelander, WI 54501

SUBJECT: Crown Pillar Hydrology

Dear Mr. Moe:

The issue of the ***hydrologic*** stability of the crown pillar has been raised at each of the last two groundwater meetings. This is an issue of potential concern due to the implications for mine inflow and for mine reflooding. Crandon Mining Company presented an analysis in the groundwater modeling addendum to the Environmental Impact Report that the mine reflooding posed little to no risk of contaminating the glacial aquifer system. This was based on an assumption that the crown pillar hydraulic conductivity would remain unchanged through mining, even though the crown pillar would be experiencing significantly altered stress regimes.

In order to better understand the crown pillar system and the potential for changes through mining, the Department requests the additional information detailed below be submitted in one distinct package.

- Detailed geology of the crown pillar, including cross sections drawn both perpendicular and parallel to structure illustrating the crown pillar and surrounding materials.
- Specific tabulation of all RQD and percent recovery data from the crown pillar.
- Detailed description of existing joint and fracture frequency and orientation in the crown pillar and adjacent areas of the hanging wall and footwall.
- Detailed mine plan for ore body and adjacent structures directly beneath the crown pillar, including cross sections and scale drawings as needed.
- Results from any stress modeling conducted to determine the dimensions and stability of the crown pillar, including appropriate graphics depicting the stress field within the crown pillar and adjacent portions of the hanging wall and footwall through mining and reflooding.
- References to data and reports used to compile/prepare the above information.

Please feel free to contact me at 608/267-0856 if you wish to discuss this further.

Sincerely,

Christopher P. Carlson, P.G., Hydrogeologist
Solid Waste Management Section
Bureau of Solid & Hazardous Waste Management

cc: Bill Tans - EA/6
Larry Lynch - SW/3
Paul Huebner - SW/3
Dave Johnson - WR/2
Archie Wilson/Ken Markart - NCD
Ken Bradbury - WGNHS
Jim Krohelski/Randy Hunt/Chuck Dunning - USGS-Madison
Dan Cozza - US EPA Region V
Bill Ryan - US EPA Region V
Margaret Thielke - US EPA Region V
Dave Ballman - US Army COE
Mark Myers - US Army COE
Earl Edris - US Army COE - Waterways Experiment Station
Robert Jaeger - BIA
John Coleman - UW-Madison (GLIFWC)
Peter Andersen - GeoTrans
Jerry Sevick - Foth & Van Dyke
Mark Nelson/Daniel Santos - Horsley & Witten
Doug Cherkauer - UW-Milwaukee
Arlyn Ackley - Mole Lake Chippewa
John Teller - Menominee Nation
Al Milham - Forest County Potawatomi
Rudolfo de la Cruz - UW-Madison
Dave Blouin - Sierra Club

Hydrologic Stability of the Crown Pillar, Crandon Deposit

Numerical Analysis Results for Evaluation of the Influence of Mining on the Crown Pillar, Crandon Deposit

NUMERICAL ANALYSIS RESULTS FOR EVALUATION OF THE INFLUENCE OF MINING ON THE CROWN PILLAR, CRANDON DEPOSIT

A report submitted to
Crandon Mining Company
Rhinelander, Wisconsin

July 1997

AGAPITO ASSOCIATES, INC.
715 Horizon Dr., Ste. 340, Grand Junction, CO 81506
970/242-4220 • FAX 970/245-9234 • e-mail:agapito@gj.net

Crandon Mining Company

July 15, 1997

Mr. Christopher P. Carlson
Wisconsin Department of Natural Resources
Bureau of Waste Management
101 South Webster Street
P. O. Box 7921
Madison, WI, 53707-7921

Dear Mr. Carlson:

The attached report was prepared by Agapito Associates Inc. to address specific questions that the department and its consultant, Dr. S.L. Crouch had on the two dimensional Crown Pillar analysis dated June 13, 1996.

The department in consultation with Dr. Crouch recommended that the model be expanded to a three dimensional analysis to look at resulting impacts to the hangingwall and footwall areas of the mine. A preliminary draft of the FLAC3D analysis was completed and forwarded for comments to the department and Dr. Crouch on April 24, 1997. This review by DNR resulted in a request that CMC conduct an additional two dimensional analysis to assess the interaction of the two principal joint sets.

Enclosed is the final report on the FLAC3D and the 2D - UDEC analysis on the "Hydrologic Stability of the Crown Pillar." This report, combined with the prior report, was prepared to address your November 28,1995 letter to Crandon Mining Company regarding crown pillar hydrology.

Should you have any questions regarding the enclosed report, please call me at (715)-365-1450.

Sincerely,

D.E. Moe

Don Moe
Technical/Permitting Manager
Crandon Mining Company

Enclosure

RHINELANDER BUSINESS OFFICE
7 N. BROWN STREET, 3RD FLOOR
RHINELANDER, WI 54501-3161
TEL.: (715) 365-1450 FAX: (715) 365-1457

ENVIRONMENTALLY RESPONSIBLE

CRANDON FIELD OFFICE
104 W. MADISON P.O. BOX 336
CRANDON, WI 54520-0336
TEL.: (715) 478-3393 FAX: (715) 478-3641

cc: Mr. Bill Tans, Wisconsin Department of Natural Resources (2 copies)
Mr. Larry Lynch, Wisconsin Department of Natural Resources
Mr. Archie Wilson, Wisconsin Department of Natural Resources (2 copies)
Mr. Steven L. Crouch, St. Paul, MN (2 copies)
Mr. Kenneth Bradbury, Wisconsin Geological and natural History Survey
Mr. James Krohelski, U.S. Geological Survey
Mr. Robert Jaeger, U.S. Department of the Interior
Mr. Philip Shopodock, Forest County Potawatomi
Mr. Arlyn Ackley, Sokaogon Chippewa Community
Apesanahkwat, Menominee Indian Tribe of Wisconsin
Ms. M. Catherine Condon, Greene, Meyer & McElroy
Mr. John Coleman, Great Lakes Indian Fish & Wildlife Commission
Mr. Dan Cozza, USEPA
Mr. David Ballman, U.S. Army Corp of Engineers
Mr. Mark Meyers, U.S. Army Corp of Engineers
Mr. John Barko, U.S. Army Corp of Engineers
Mr. Mark Nelson, Horsley & Witten
Mr. Douglas Cherkauer, University of Wisconsin-Milwaukee
Mr. David Blowes, University of Waterloo
Mr. Jerry Sevick, Foth & Van Dyke
Mr. Stephen Donohue, Foth & Van Dyke
Mr. Peter Andersen, GeoTrans, Inc.
Mr. Michael Hardy, Agapito Associates Inc. (letter only)

Numerical Analysis Results for Evaluation of the Influence of Mining on the Crown Pillar, Crandon Deposit

Table of Contents

List of Tables

List of Figures

Numerical Analysis Results for Evaluation of the Influence of Mining on the Crown Pillar, Crandon Deposit

1. Introduction

This report summarizes the results of the numerical analysis conducted for the evaluation of the potential influence of mining on the hydrologic characteristics of the crown pillar at the Crandon deposit. The report is based on data and properties presented in the report entitled *Hydrologic Stability of the Crown Pillar, Crandon Deposit* (Agapito Associates, Inc. 1996) and results from the technical review of that report by the Wisconsin Department of Natural Resources (DNR). The Wisconsin DNR consultant, Dr. S.L. Crouch, suggested that three-dimensional analysis should be completed to resolve the questions and concerns arising from his review (Crouch 1997). Dr. Crouch proposed a two-phased approach involving regional scale, three-dimensional elastic analysis followed by local analysis of joints. The protocol established for conducting the first phase three-dimensional analysis using FLAC3D was proposed by Agapito Associates, Inc. (AAI) and Crandon Mining Company (CMC). The protocol, attached as Appendix A, was agreed upon by the Wisconsin DNR during a conference call on February 12, 1997. Subsequently, a draft of the FLAC3D analysis was completed and forwarded for comments to the Wisconsin DNR on April 24, 1997.

Review of the FLAC3D analysis by Wisconsin DNR resulted in a request that CMC conduct an additional two-dimensional UDEC analysis to assess the interaction of the predominant vertical joint set (set 1) and horizontal joint set (set 2). In the UDEC analysis, the joints with nonlinear behavior were explicitly simulated to allow the direct investigation of the potential interaction of joint sets 1 and 2. This report includes the results from the FLAC3D analysis with the UDEC analysis presented in Appendix B.

2. FLAC3D Analysis Background

The FLAC3D analysis assumed linear-elastic behavior for the alluvium and bedrock, and provided the stress redistribution due to mining in the crown pillar, hanging wall, and footwall. The stress results were then transformed to the planes of the five joint sets identified by Foth & Van Dyke (1995). Normal stresses and maximum shear stresses on the joint planes for the five joint sets were calculated to determine the safety factors (SFs) based on estimated strength of each joint set.

The safety factor (SF) is used as an indicator of potential change in hydraulic response of the joints. If the joints have a SF greater than one, the joint will respond elastically to the stress changes induced by mining with little to no change in hydraulic conductivity of the joints. If the SF is less than 1.0, nonlinear deformation or slip may occur along the joint to relieve stresses projected to be greater than the joint strength. At low stresses normal to the joint, this slip can result in dilation of the joint and enhancement of the hydraulic conductivity of the joints.

The computations to get these results have been extensive using a 128-megabyte RAM G6-200 Gateway Pentium-Pro 200 computer with a 5.8-gigabyte hard disk. Each run takes approximately 90 hours to complete and generates a file of approximately 85 megabytes. The mesh has approximately 54,000 elements. We have reviewed these data, but present here only the results on four cross sections and two plan views. The results presented in the form of SF contours represent a synthesis of the results.

3. Model Geometry

The FLAC3D mesh constructed for the analysis is shown in Figure 1. The coordinate system adopted in the mesh is Easting as X axis, Northing as Y axis, and vertical upward as Z axis. The dimensions of the mesh are 8350 ft in the X direction (from E273,425 to E281,775), 6000 ft in the Y direction (from N113,300 to N119,300), and 3210 ft in the Z direction (elevation –1550 ft to 1660 ft). Test runs were conducted to examine the extent of the region required to ensure minimum boundary effect to the stress results. The resulting mesh was considerably larger than that proposed in the protocol document (see discussion on the boundary conditions below). The mesh consists of 53,856 elements with element sizes ranging from 15 ft to approximately 400 ft.

The mining geometry modeled along the strike direction of the deposit is shown in Figure 2. The mining geometry was derived from the Zones 2011/2021/2511 Long Section Map (Geosolution Resources 1996) with the exception of the elevations of the crown pillar base. The elevations for the base of the crown pillar were directly measured from the section maps and are consistent with the geometry used in AAI (1996). The highest elevation of the base of the crown pillar is set at 1420 ft so that the crown pillar thickness is greater than 100 ft. Ore thickness, as shown in Figure 2, was generalized to either 20 or 40 ft in the western portion of the orebody and 30, 60, 90, and 120 ft in the east. The surface was modeled as a horizontal plane at elevation 1660 ft. The dip of the ore

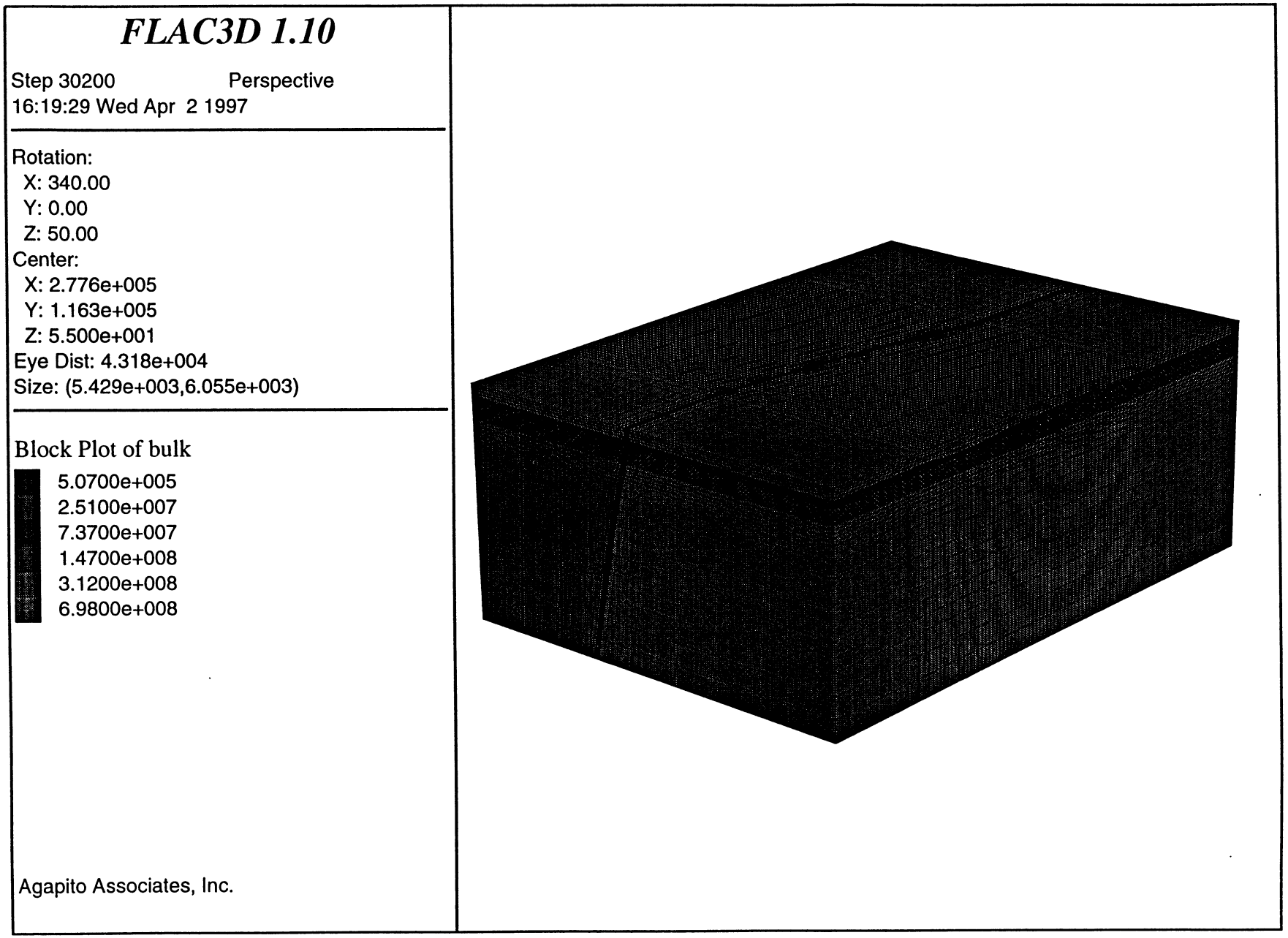

Figure 1. FLAC3D Mesh

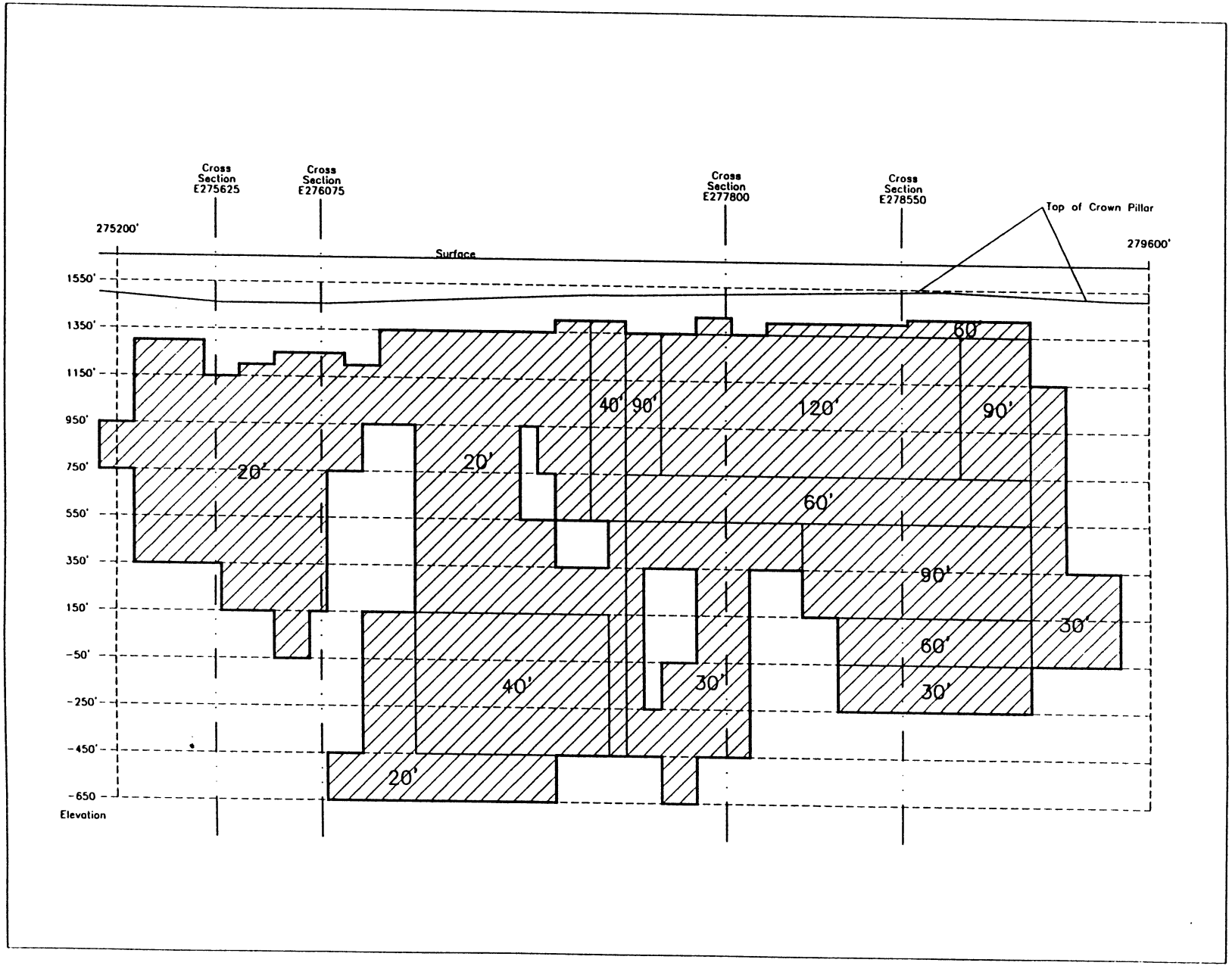

Figure 2. Mining Geometry and Thickness as Modeled in FLAC3D Along Ore Strike Direction

was simplified and modeled as 75° above the 400-ft elevation and 79° below the 400-ft elevation. The strikes of the ore were also simplified. A strike azimuth of 96.8°SE was used in the model for the section between E275,125 and E277,825, and strike azimuth of 101.6°SE was adopted for the section between E277,825 and E279,475.

4. Model Boundary Conditions

Fixed-displacement boundary conditions were used at the edges of the FLAC3D mesh to simulate the effect of the surrounding rock mass. Vertical planes at the north, south, east, and west edges of the model were fixed in both the X and Y directions. The horizontal plane at the bottom of the mesh was fixed in the Z direction. The mesh size used in the model has been examined to ensure minimum effect from the fixed boundary conditions to the stress results at areas of interest. Test runs with different mesh sizes were conducted to examine the effect of the fixed boundary conditions to the stress results at areas of interest. The results from the test runs indicated that a distance of 2500 ft from the location of the crown pillar to the model boundary was needed to minimize edge effects. The mesh was then constructed following this guideline to ensure minimum impact of the model boundaries to the stress results.

5. In Situ Stresses

The in situ stresses (psi) used in the model were:

In alluvium $\sigma_H = 0.59 \times D_1$
$\sigma_V = 0.88 \times D_1$, where D_1 (ft) is the depth measured from the surface.

In rock $\sigma_{H1} = 1175 + 1.33 \times D_2$, N63°E
$\sigma_{H2} = 653 + 0.88 \times D_2$, N27°W
$\sigma_V = 176 + 1.1 \times D_2$, where D_2 (ft) is the depth measured from the top of bedrock.

These are the same initial in situ stresses as adopted in AAI (1996).

6. Material Elastic Properties

As outlined in the protocol, seven different materials were used to represent the alluvium and the bedrock in the analysis. Young's modulus and Poisson's ratios for these materials are presented in Table 1. The crown pillar horizon in the footwall, hanging wall, and zone immediately above the mined areas is modeled as strongly weathered. The values of the Young's modulus for the strongly

Table 1. Material Elastic Properties

Material	Young's Modulus (psi)	Poisson's Ratio
Alluvium	1.04E + 05	0.40
Crown pillar horizon (weathered footwall, hanging wall, and Crandon Formation.)	7.70E + 05	0.25
Hanging wall	1.54E + 06	0.25
Crandon Formation	7.27E + 06	0.25
Footwall	3.25E + 06	0.25
Backfill, 20-ft thickness	7.95E + 03	0.30
Backfill, 30-ft thickness	6.66E + 03	0.30
Backfill, 60-ft thickness	4.22E + 03	0.30
Backfill, 90-ft thickness	3.73E + 03	0.30
Backfill, 120-ft thickness	2.24E + 03	0.30

weathered hanging wall, footwall, and Crandon Formation are similar, differing within 5%. The Young's modulus of 7.7×10^5 psi of strongly weathered hanging wall was used to represent all strongly weathered material.

Backfill properties used in these analyses were conservatively derived from the uncemented backfill laboratory data reported by Briggs (1988). Laboratory tests and field monitoring of hydraulically placed backfill for blasthole open-stope mining have indicated highly nonlinear behavior with substantial strain hardening with increasing applied stress. Direct simulation of the nonlinear backfill stress-strain curve was not a standard option in FLAC3D, therefore, an equivalent linear model was used. The linear model was based on calculated elastic closure between the hanging wall and footwall for each zone of the orebody with different thickness.

The equivalent modulus of the backfill is defined for each section of the orebody with the same orebody thickness. The elastic backfill modulus is estimated based upon a projected average rock unloading path and its intersection with the backfill loading path as illustrated in Figure 3. The average rock unloading stress-deformation path was calculated based on the analogy of a three-dimensional penny-shaped slit using the solution derived by Sneddon (1946). The backfill modulus used (Table 1) is very low relative to the rock properties and is lower than the 0.1 GPa (14,500 psi) used in the earlier AAI (1996) analysis. The soft backfill inclusion in a stiff bedrock results in low

stress loading in the backfill. The backfill stresses predicted by the FLAC3D analysis are, in general, less than 100 psi. A degree of conservatism is added to the simulation by using the low stiffness uncemented hydraulic backfill in the model. The backfill modulus is likely to be stiffer due to the use of cemented fill in the primary stopes, compaction during placement, and the sequencing of backfilling immediately after mining. Stiffer backfill material will tend to carry more load and therefore reduce the loading from the crown pillar. Unmined portions of the orebody, or remnants, will also add to the effective stiffness of the backfill.

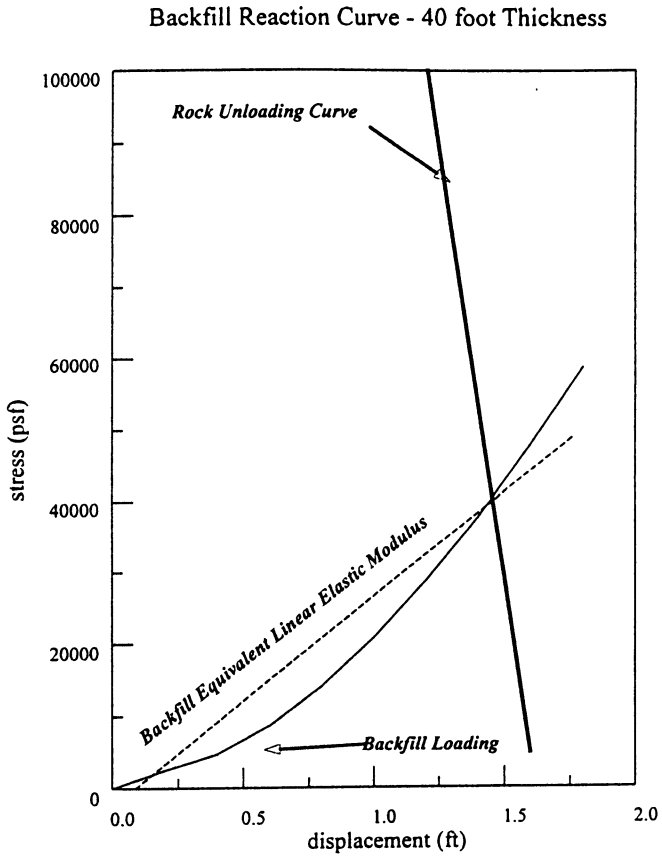

Figure 3. An Example of the Graphical Method to Define Equivalent Linear Elastic Module

7. Mining Process Simulation

The mining and backfill processes were simulated in eight steps. The sequence is illustrated in Figure 4. The simulation is not exactly the same as the current mine plan. However, the simplification is designed to be conservative and capture the mechanism of load transferring to the crown pillar for the mine plan. The first step is to mine all primary stopes (50% extraction ratio) from the bottom of the ore up to the 1150-ft elevation. The second step is to backfill the primary stopes and mine all secondary stopes (rib pillars) up to the 1150-ft elevation. The third thru sixth steps simulate cut-and-fill mining below the crown pillar with a 50- or 60-ft lift per step. The seventh and eighth steps are restricted to mining in between 1380- and 1420-ft elevations with a 20-ft lift per step.

8. Joint Orientations and Mechanical Properties

Foth & Van Dyke (1995) presented a detailed discussion of fracture characterization at Crandon. The reported five fracture trends within the upper bedrock region, to depth of 1000 ft

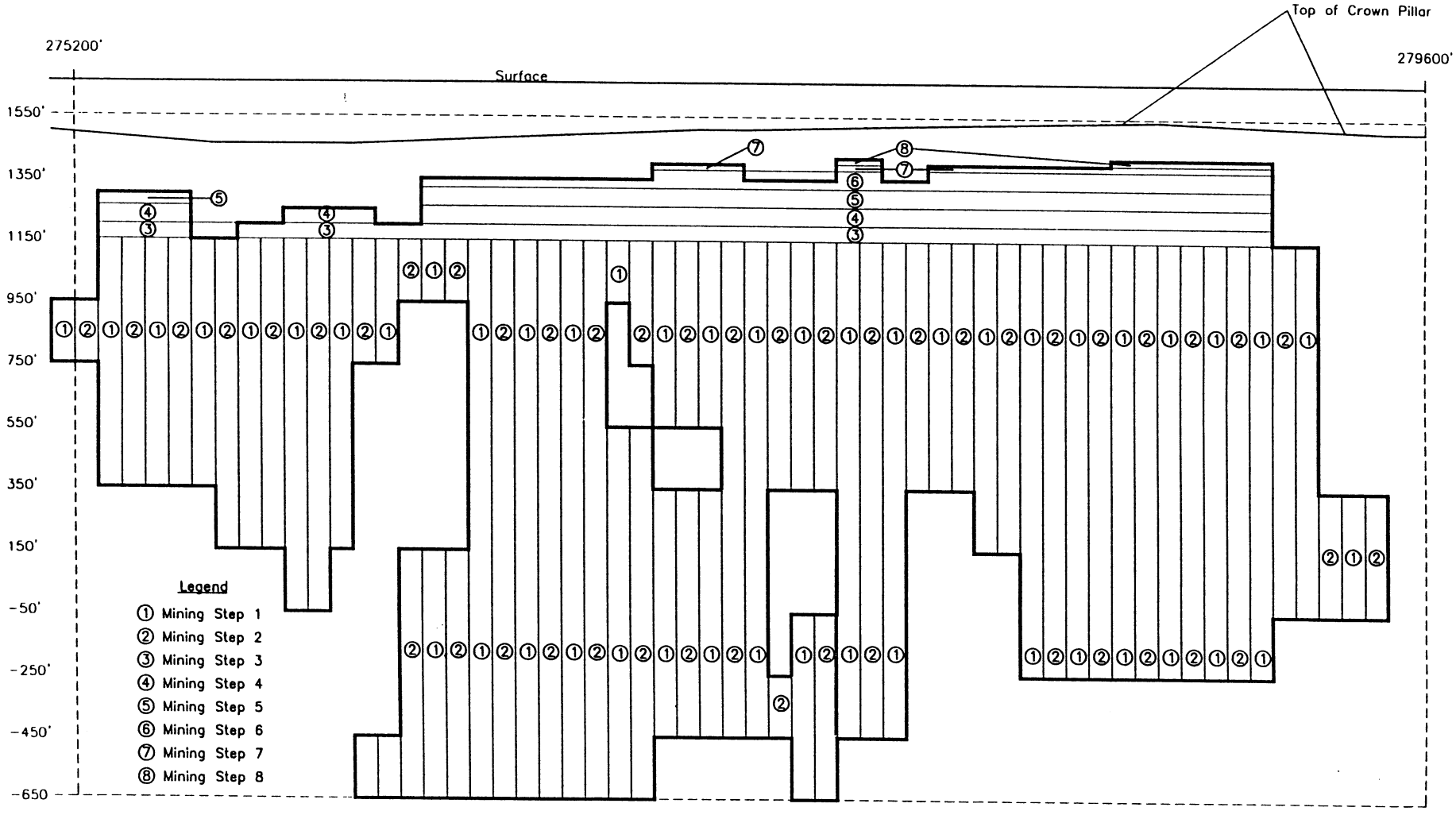

Figure 4. Mining Process Simulation in FLAC3D Model

below surface, are listed in Table 2. The most prominent is listed as one, with the least prominent listed as five. Sets 1 and 2 were orientated east-west and were reported to exhibit weathering with iron-oxide coatings. Fractures in sets 3, 4, and 5 were reported to be tight and show less evidence of weathering.

Table 2. Joint Orientation (Foth & Van Dyke 1995)

Joint Set Number	Strike Azimuth	Dip	Comment
1	85°E	85°SE	WWIC, parallel to the orebody, near vertical
2	62°NE	8°SE	WWIC, near horizontal
3	151°SE	81°SW	Tight, near vertical
4	140°SE	39°SW	Tight, inclined
5	116°SE	25°NE	Tight, inclined

WWIC = *Weathering with iron-oxide coating.*

Strength parameters for the fractures were conservatively estimated using empirical methods developed by Barton and Choubey (1977) and Bandis et al. (1983) that are based upon rock strength, joint roughness, and infilling. The Mohr-Coulomb strength parameters, including cohesion and friction angle, were derived by linear curve fit of the shear strength envelope from empirical methods (Barton and Choubey 1977, Bandis et al. 1983). The Mohr-Coulomb SF is calculated based on the following equation:

$$SF = \frac{C + \sigma_n \tan\phi}{\tau}$$

where C is the cohesion,

ϕ is the friction angle,

σ_n is the normal stress loaded on the joint, and

τ is the maximum shear stress in the joint plane.

The Mohr-Coulomb envelope consists of the stress states with SFs equal to 1.0. Plastic yield is indicated when the SF predicted in the analysis is equal to or less than 1.0. The amount of plastic deformation is not determined in elastic analysis.

The strength parameters were developed for two groups of joints: the first group contains joints of sets 1 and 2 with weathering and iron-oxide coating; the second group includes tighter joints of sets 3, 4, and 5 with little to no evidence of weathering. A friction angle of 39° and cohesion of 15 psi were estimated to represent the Mohr-Coulomb joint strength parameters for sets 1 and 2. These are the joint properties assumed in AAI (1996) for all joint sets.

The values for the joint strength parameters for sets 3, 4 and 5 were examined for compatibility with the in situ stress prior to mining. In AAI (1996), it was noted that the joint strength properties used for sets 4 and 5 were incompatible with the assumed pre-mining in situ stresses. For this three-dimensional analysis, we have re-estimated the strength properties and assigned a friction angle of 49° and cohesion of 67 psi to represent the strength parameters for sets 3, 4, and 5 based on the description of the joint characteristics. The calculated SFs at several elevations based on the revised joint strength properties are presented in Table 3. For the in situ pre-mining condition, no SF was less than 1.0. SFs for sets 4 and 5 prior to mining were calculated to be in the range of 1.3 to 2.0 over the crown pillar horizon (approximately in the elevation of 1300 to 1500 ft).

Table 3. Mohr-Coulomb Safety Factors in the Bedrock Prior to Mining

Elevation (ft)	Joint Set Number									
	1		2		3		4		5	
	C	ϕ	C	ϕ	C	ϕ	C	ϕ	C	ϕ
	15	39	15	39	67	49	67	49	67	49
1500*	3.2		2.5		9.0		1.5		1.3	
1300	3.5		5.7		10.4		2.0		2.0	
1100	3.7		9.7		11.8		2.4		2.7	
900	3.8		14.8		13.0		2.8		3.3	
700	3.9		21.3		14.1		3.2		3.9	
500	4.0		30.1		15.2		3.5		4.4	
300	4.1		42.8		16.1		3.8		4.9	
100	4.2		62.3		17.0		4.1		5.4	
–100	4.2		96.2		17.9		4.4		5.8	
–300	4.3		169.9		18.6		4.7		6.2	
–500	4.3		435.1		19.3		4.9		6.6	
–700	4.4		745.9		20.0		5.1		6.9	

**Top of the bedrock*
C = *cohesion (psi)*
ϕ = *friction angle (degrees)*

9. Analysis Results

Four north-south cross sections and two plan elevations were selected to best present the three-dimensional analysis results. The north-south cross sections—E275,625; E276,075; E277,800; and E278,550 (located in Figure 2)—represent a variation of crown pillar thickness from 100 to

300 ft. The plane elevation 1480 ft was selected as the elevation in the mid-height of the crown pillar at cross section E277,800. The plane elevation 1200 ft was selected to represent the elevation with maximum extraction.

Comparison of the normal stress results in the crown pillar area for cross section E277,800 from FLAC3D and MULSIM (from AAI 1996) is presented in Figure 5. The magnitude of normal stresses in the vicinity of mining predicted from MULSIM appears to be higher than those from FLAC3D. The geometry, material properties, and mining and backfill sequence simulated in the FLAC3D model are more sophisticated than what were used in the MULSIM analysis. We conclude that the results from FLAC3D and MULSIM simulations are similar in the immediate crown pillar area.

The calculated SFs based on Mohr-Coulomb criterion for the five joint sets are presented and discussed in two groups: Group I with predominant joint sets of 1 and 2, and Group II with less prominent sets of 3, 4 and 5.

The SF contours for joint sets 1 and 2 are presented in Figures 6 to 9 for the four north-south cross sections, respectively. In general, regions with SFs less than 1.0 are restricted in the footwall and hanging wall areas with minor exclusions into the lower portions of the crown pillar horizon, except for joint set 2 in cross section E278,550. As shown in Figure 9, the area with SF less than 1.0 for joint set 2 extends to the crown pillar horizon where part of the area extends up to two-thirds through the crown pillar horizon in both the hanging wall and footwall.

Joint set 2, which is near horizontal, will have only a secondary effect on vertical hydraulic conductivity and, hence, likely limited impact on vertical movement of water in the vicinity of the mined areas. Joint set 1—the most dominant set which is parallel to the orebody, near vertical, and potentially could influence vertical hydraulic conductivity—shows no zones where the SF is less than 1.0 in the crown pillar horizon. Joint set 1 will be subject to higher horizontal stresses in the crown pillar. This change in stress will tend to close the joints and reduce vertical hydraulic conductivity.

The SF contours for sets 3, 4, and 5 are presented in Figures 10 to 13. Joint set 3 has no areas of SF less than 1.0 either in the crown pillar or in the hanging wall and footwall areas. As shown in Figures 10 and 11, regions with SF less than 1.0 for sets 4 and 5 are restricted to the footwall for cross sections E275,625 and E276,075. At cross sections E277,800 and E278,550 (Figures 11 and 13), regions with SF less than 1.0 for set 4 are also restricted to the footwall. For

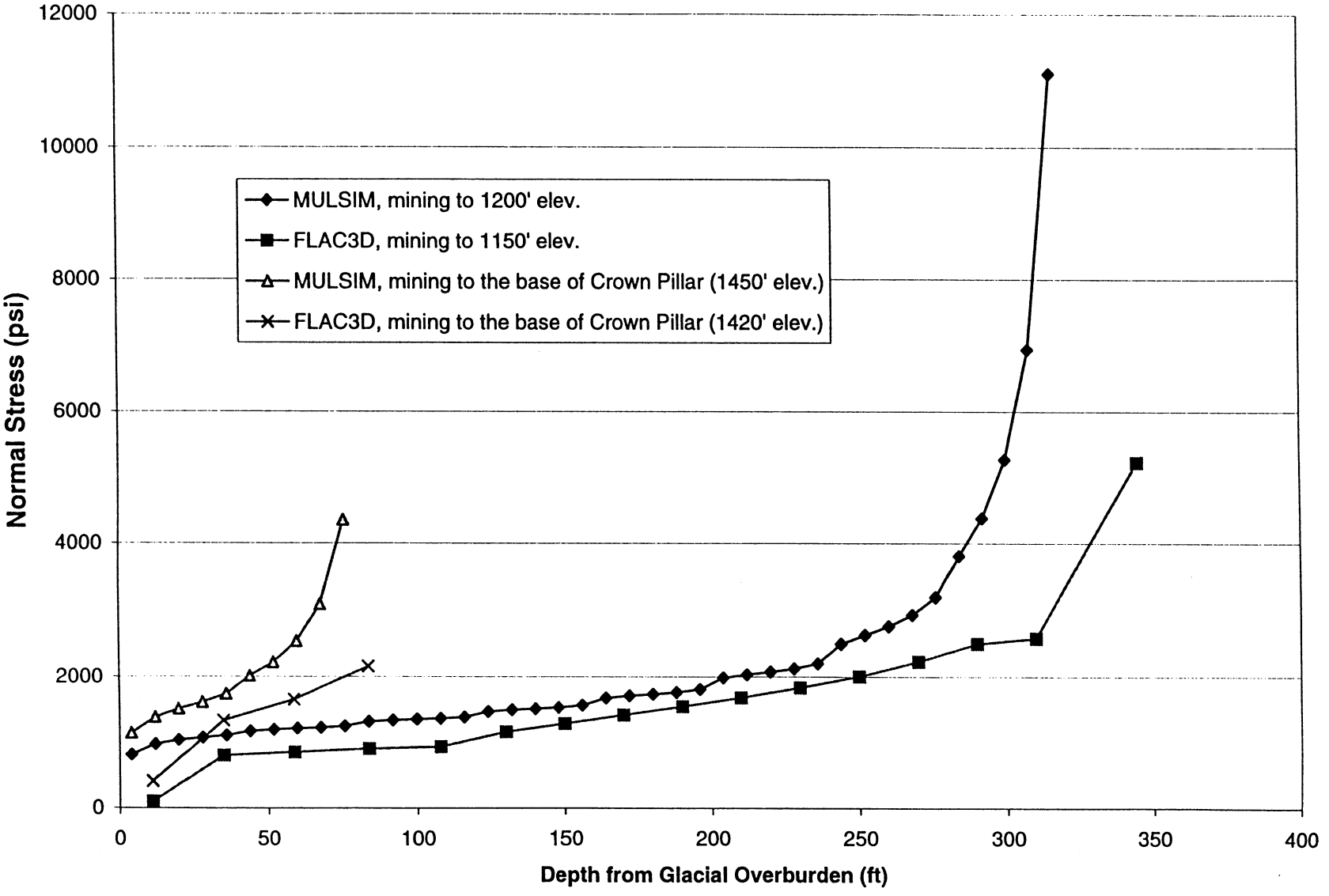

Figure 5. Comparison of FLAC3D and MULSIM Analyses Results at the Crown Pillar Along Section E277,800

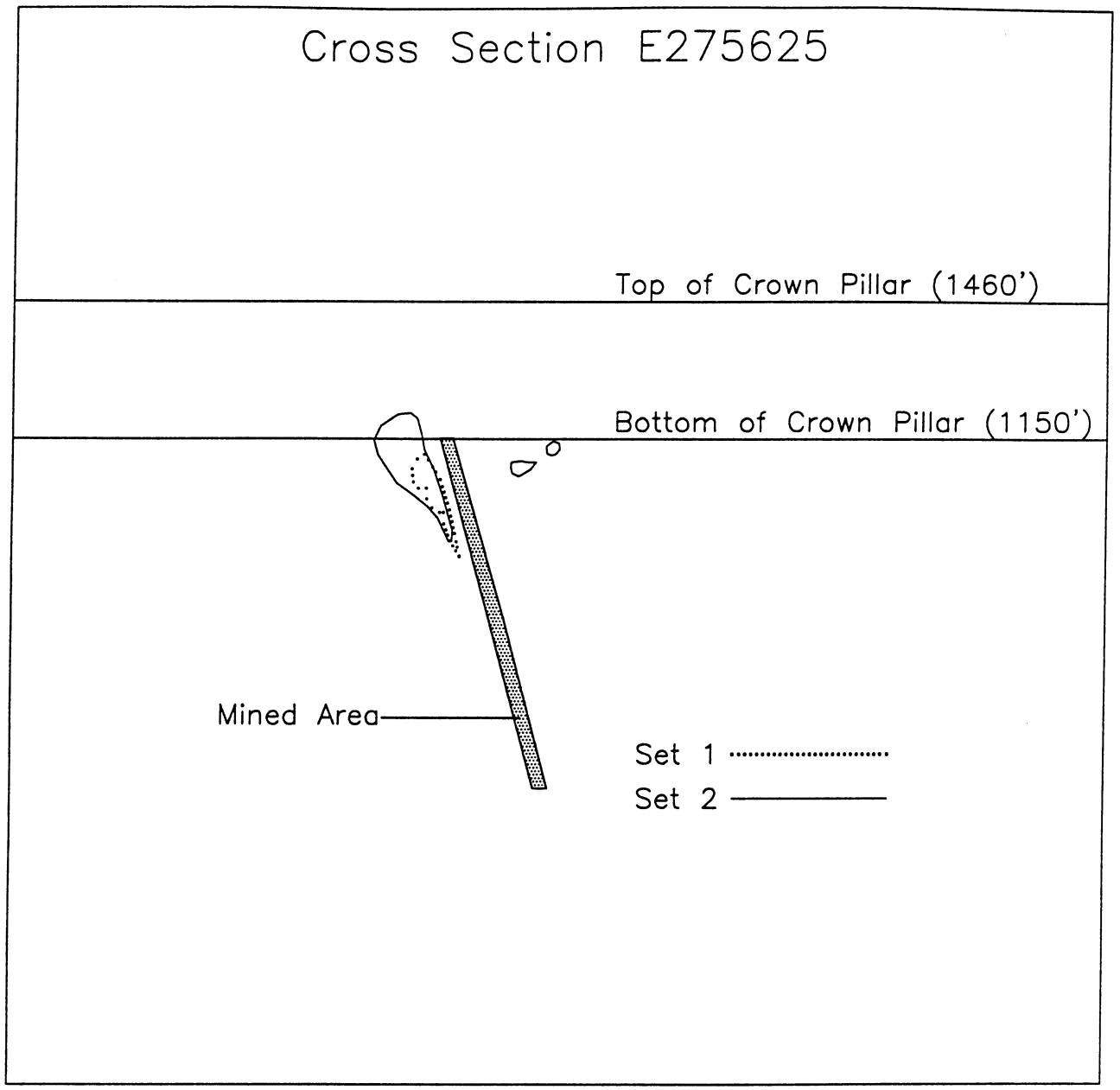

Figure 6. **Safety Factor 1.0 Contours for Joint Sets 1 and 2 at North-South Cross Section E275,625**

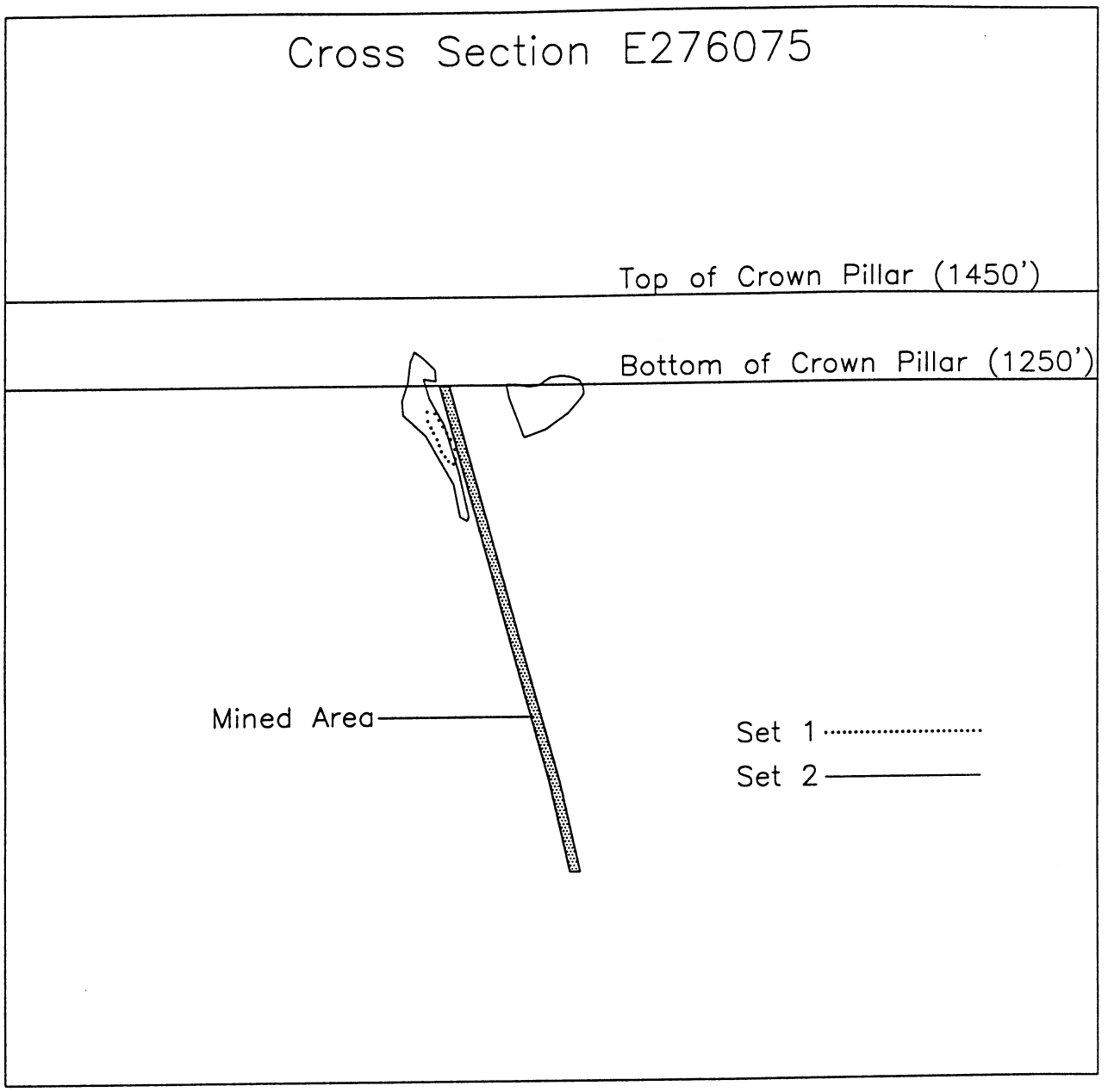

Figure 7. **Safety Factor 1.0 Contours for Joint Sets 1 and 2 at North-South Cross Section E276,075**

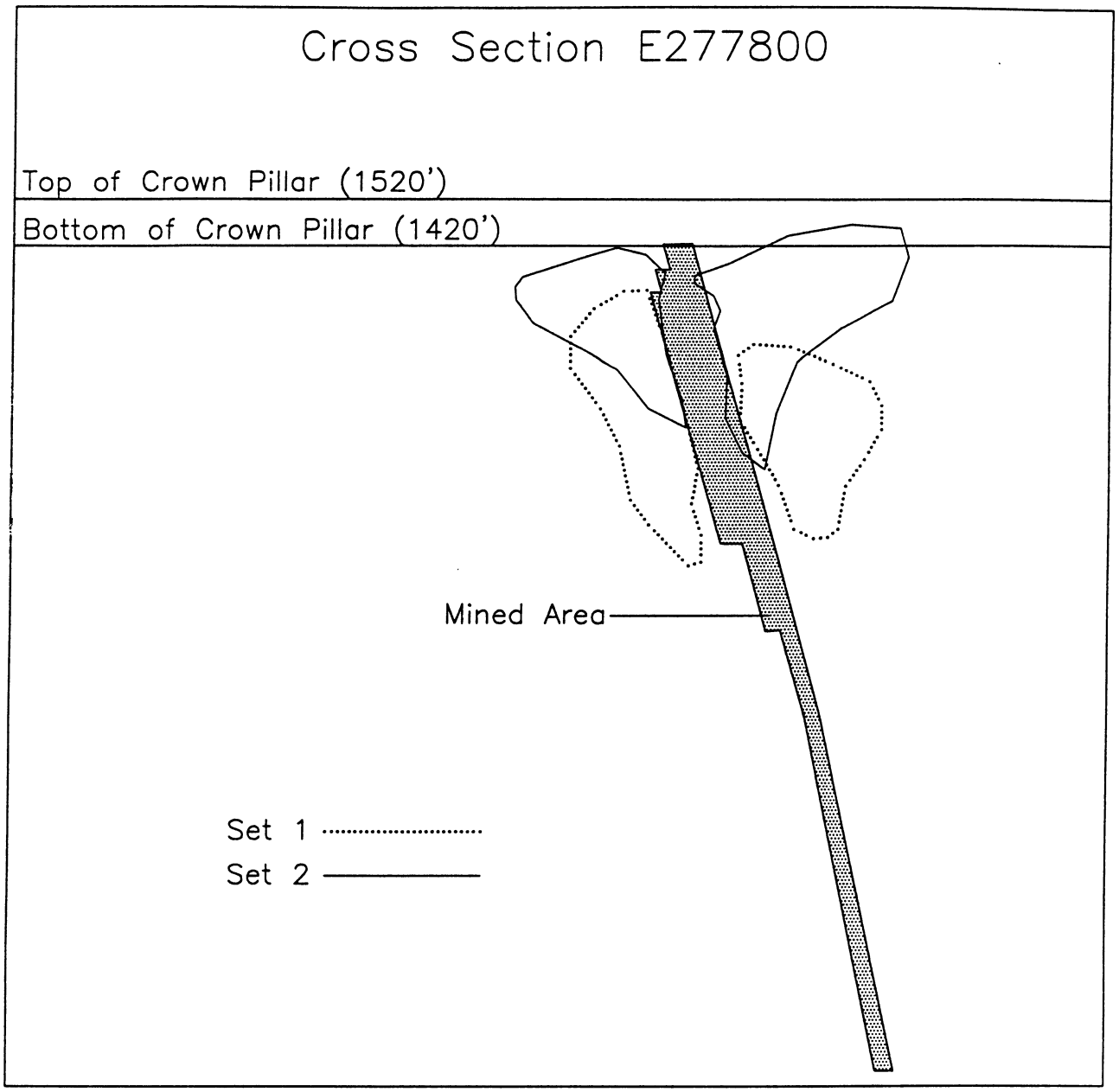

Figure 8. **Safety Factor 1.0 Contours for Joint Sets 1 and 2 at North-South Cross Section E277,800**

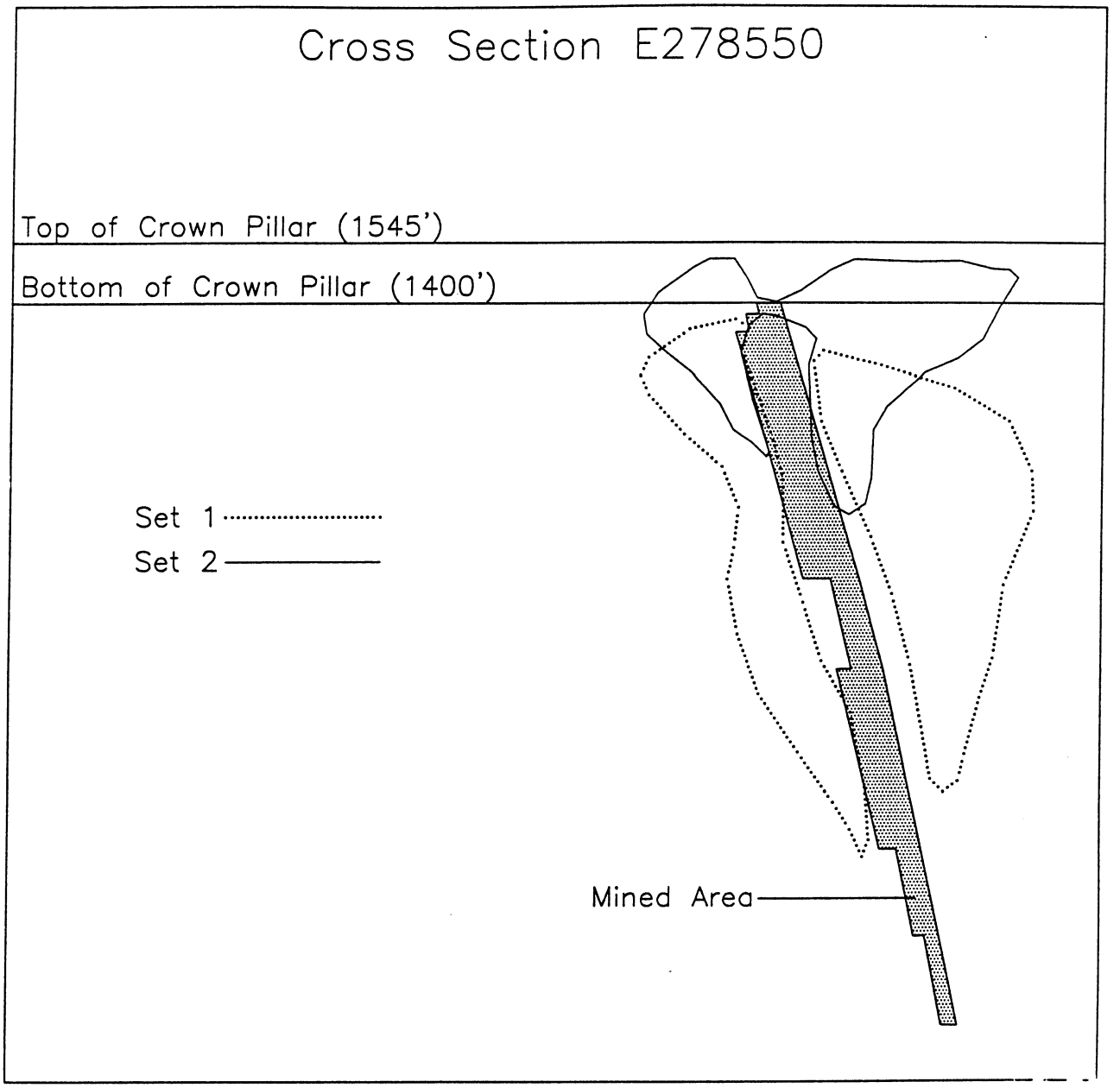

Figure 9. **Safety Factor 1.0 Contours for Joint Sets 1 and 2 at North-South Cross Section E278,550**

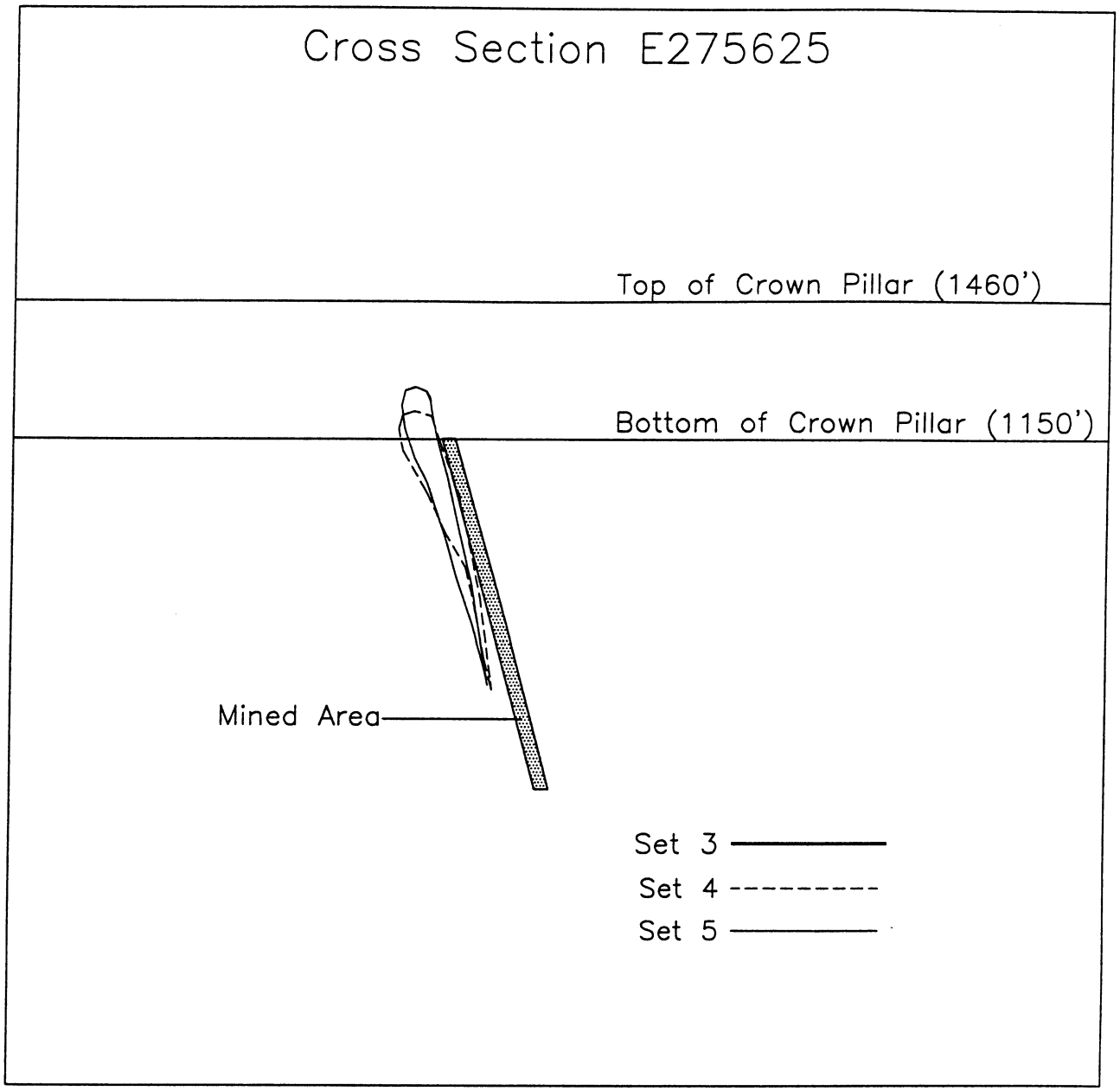

Figure 10. **Safety Factor 1.0 Contours for Joint Sets 3, 4 and 5 at North-South Cross Section E275,625**

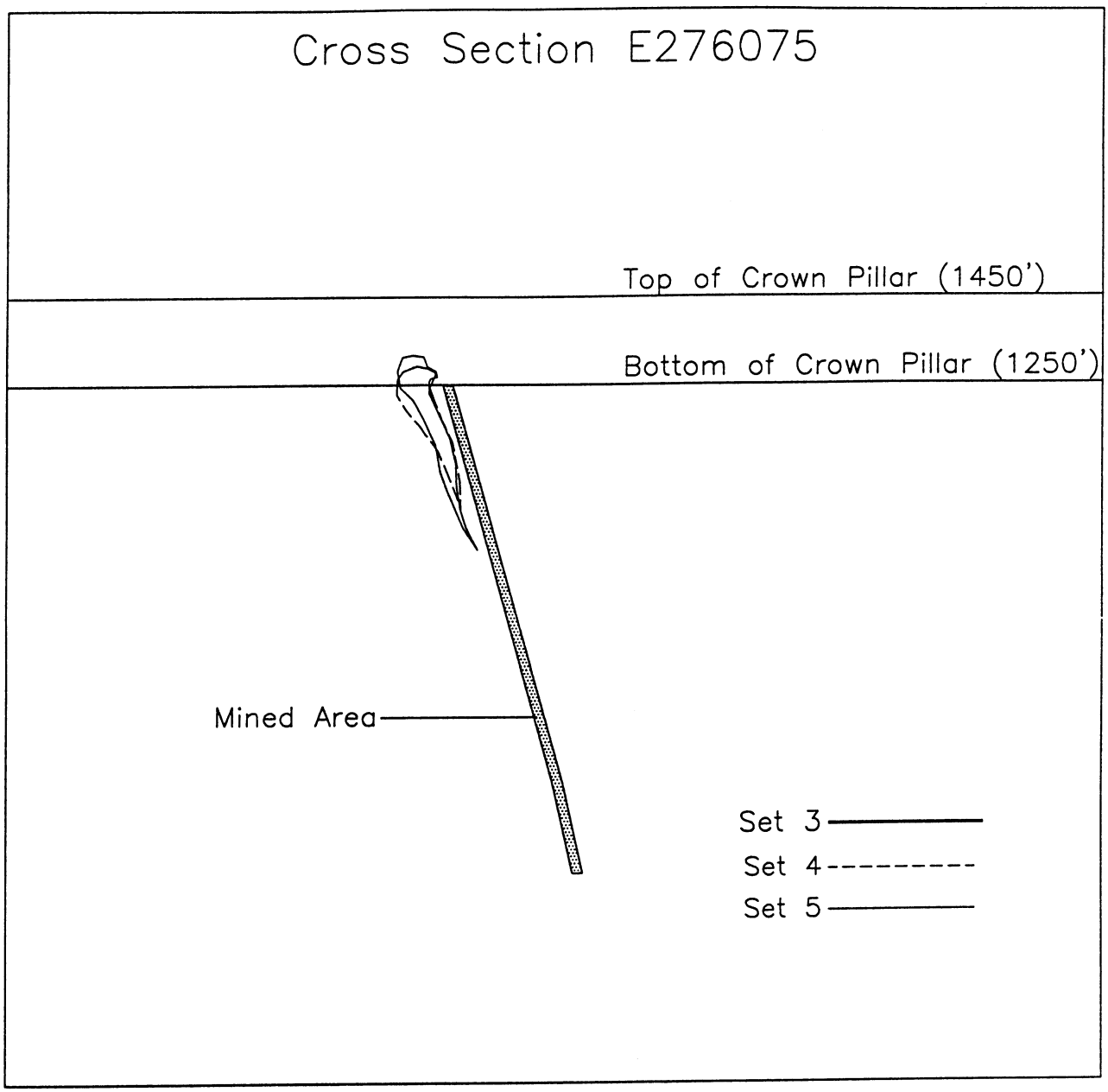

Figure 11. **Safety Factor 1.0 Contours for Joint Sets 3, 4 and 5 at North-South Cross Section E276,075**

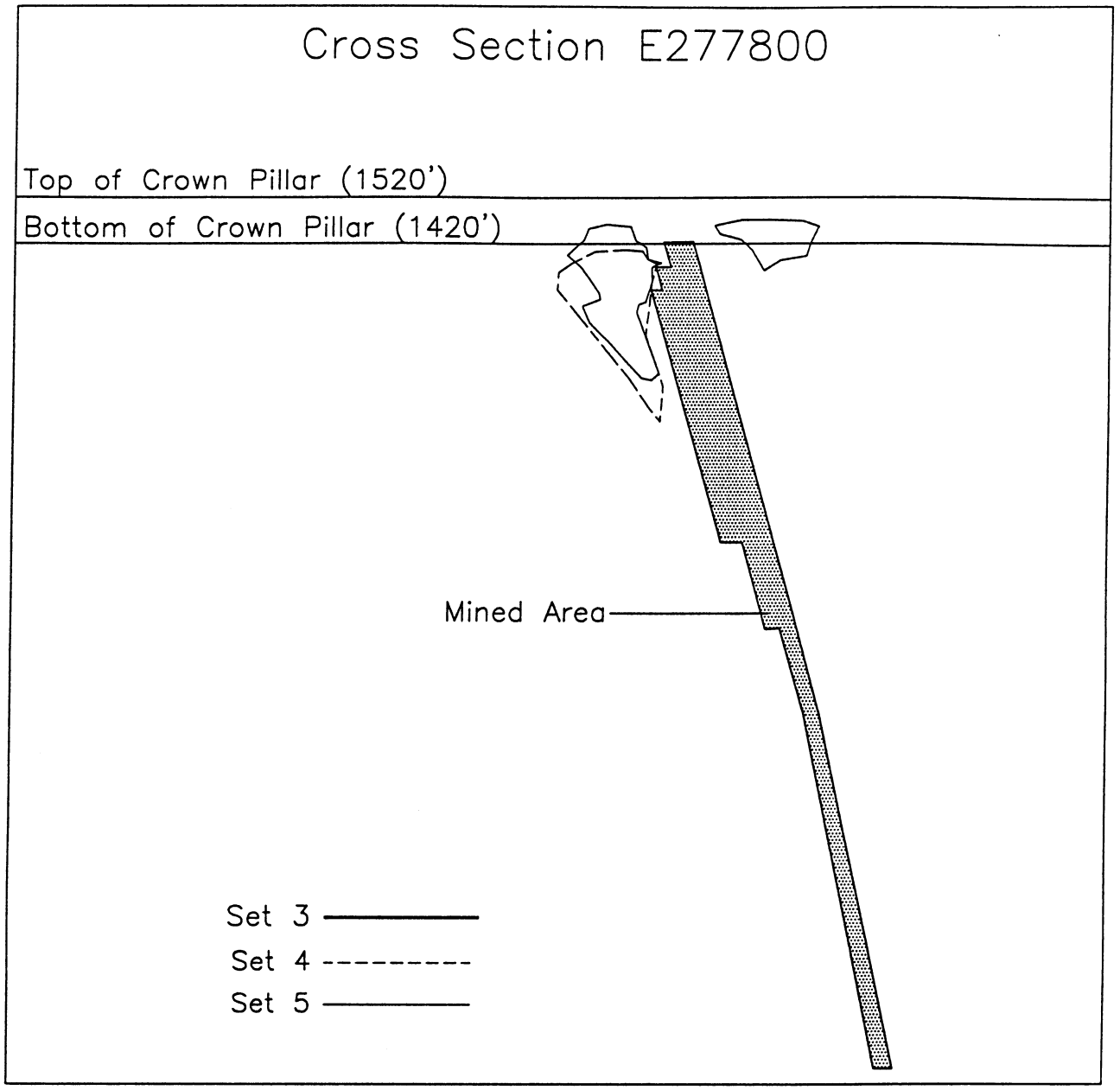

Figure 12. Safety Factor 1.0 Contours for Joint Sets 3, 4 and 5 at North-South Cross Section E277,800

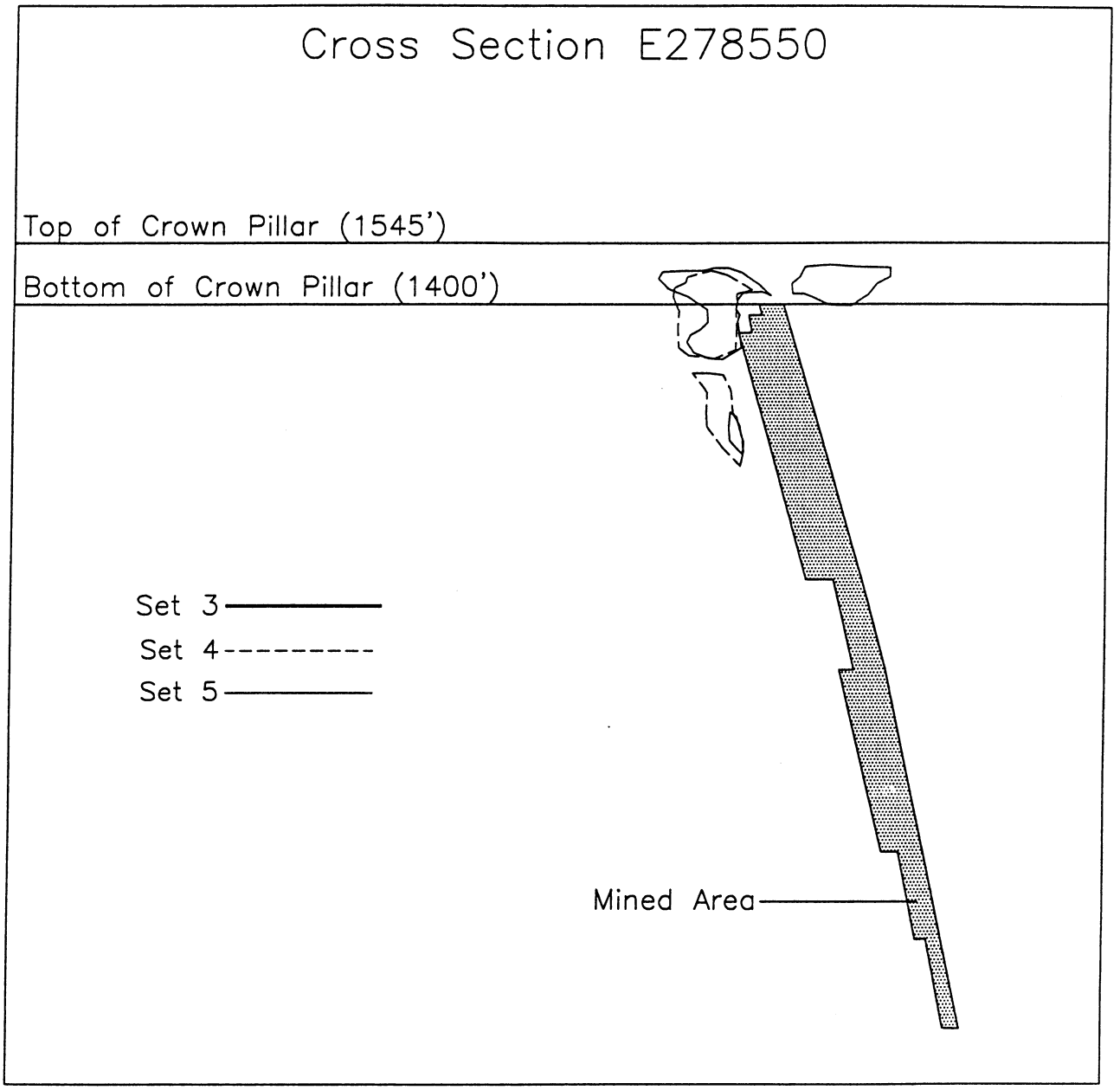

Figure 13. Safety Factor 1.0 Contours for Joint Sets 3, 4 and 5 at North-South Cross Section E278,550

set 5 at cross section E277,800, the region with SF less than 1.0 exists in the footwall, the hanging wall, and extends to the crown pillar horizon. The immediate roof of the mining area, however, shows no area with SF less than 1.0. Regions with SFs less than 1.0 are more extensive in the crown pillar horizon at E278,550 compared to those shown in section E277,800. The immediate crown pillar directly above the mining area has SF greater than 1.0.

The SF contours for the plane elevations are presented in Figures 14 to 17. The results, shown in plane elevations, conclude that regions with SF less than 1.0 are mainly in the eastern part of the ore where mined areas are largest.

10. Discussion of Hydrologic Significance of FLAC3D Results

The hydrologic significance of the stress redistribution in the immediate crown pillar area and the crown pillar horizon can be assessed qualitatively based on the following:

- The most dominant joint set (set 1), which is perhaps the most significant contributor to the vertical hydraulic conductivity because of its orientation (near vertical) and the characterization as having weathered surfaces and iron-oxide coating, will most likely see a decrease in hydraulic conductivity resulting from increased horizontal stresses normal to the joints. This increase in horizontal stress will result in joint closure and hence the reduction in joint hydraulic conductivity.
- Joint set 2, the second most frequent joint set, is near horizontal and should have little if any influence on the vertical hydraulic conductivity.
- Joint set 3 is apparently unaffected by the stress redistribution in the crown pillar horizon.
- Joint sets 4 and 5 are both characterized as tight with no weathering or water staining so can be assumed to contribute very little to the hydraulic conductivity prior to mining. Both these joint sets show areas where the SF is less than 1.0 in the crown pillar horizon, but not in the immediate area above the mining. In areas where the SF is less than 1.0, some further stress redistribution may occur resulting in limited slip along the joints. This slip can result in changes in the hydraulic conductivity of those joints. However, these regions of changes in hydraulic conductivity are projected to be in the lower portion of the crown pillar horizon. The hydraulic conductivity of the upper portion of the crown pillar horizon essentially will be unaffected.

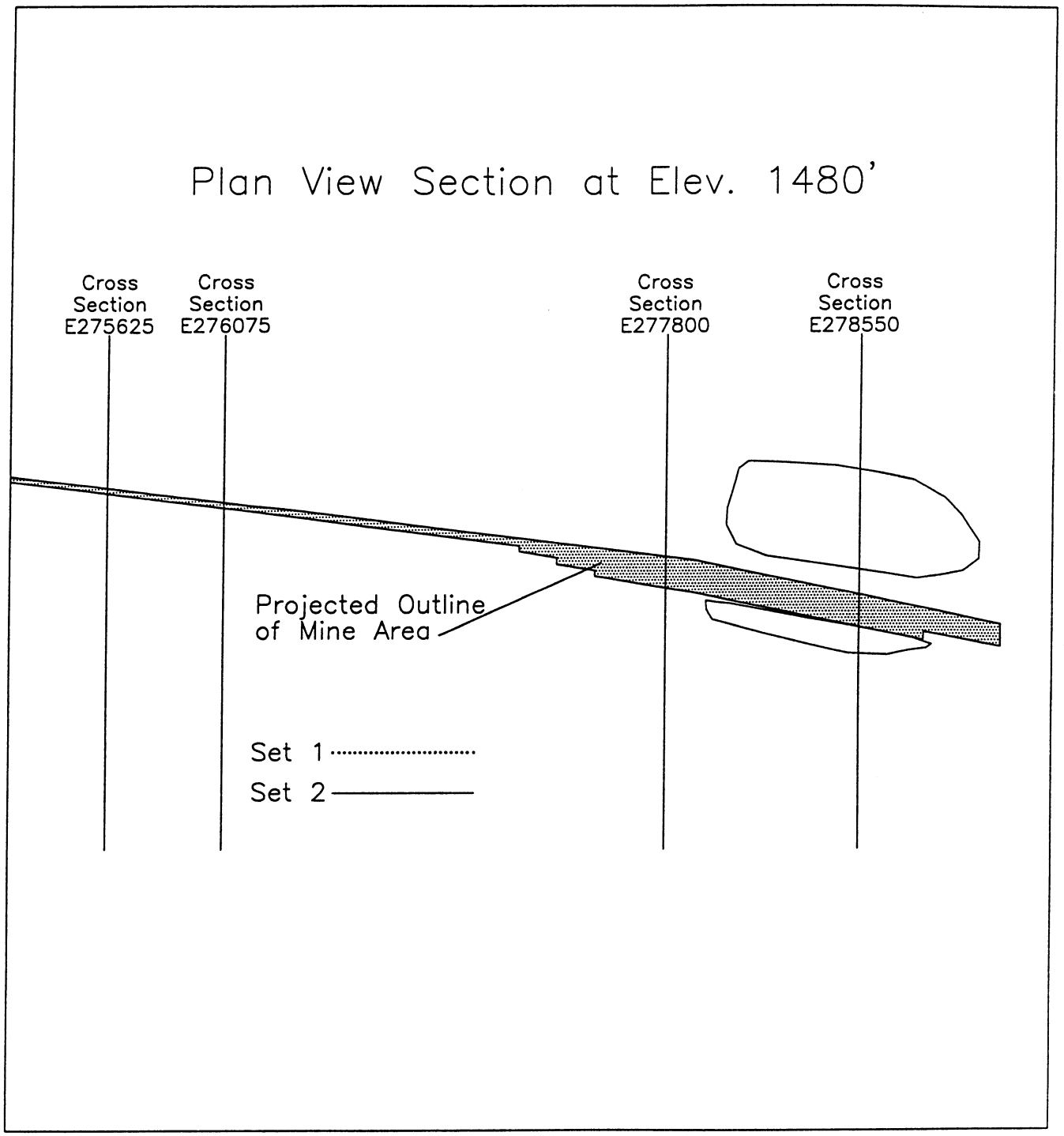

Figure 14. Safety Factor 1.0 Contours for Joint Sets 1 and 2 at Plane Elevation 1480 ft

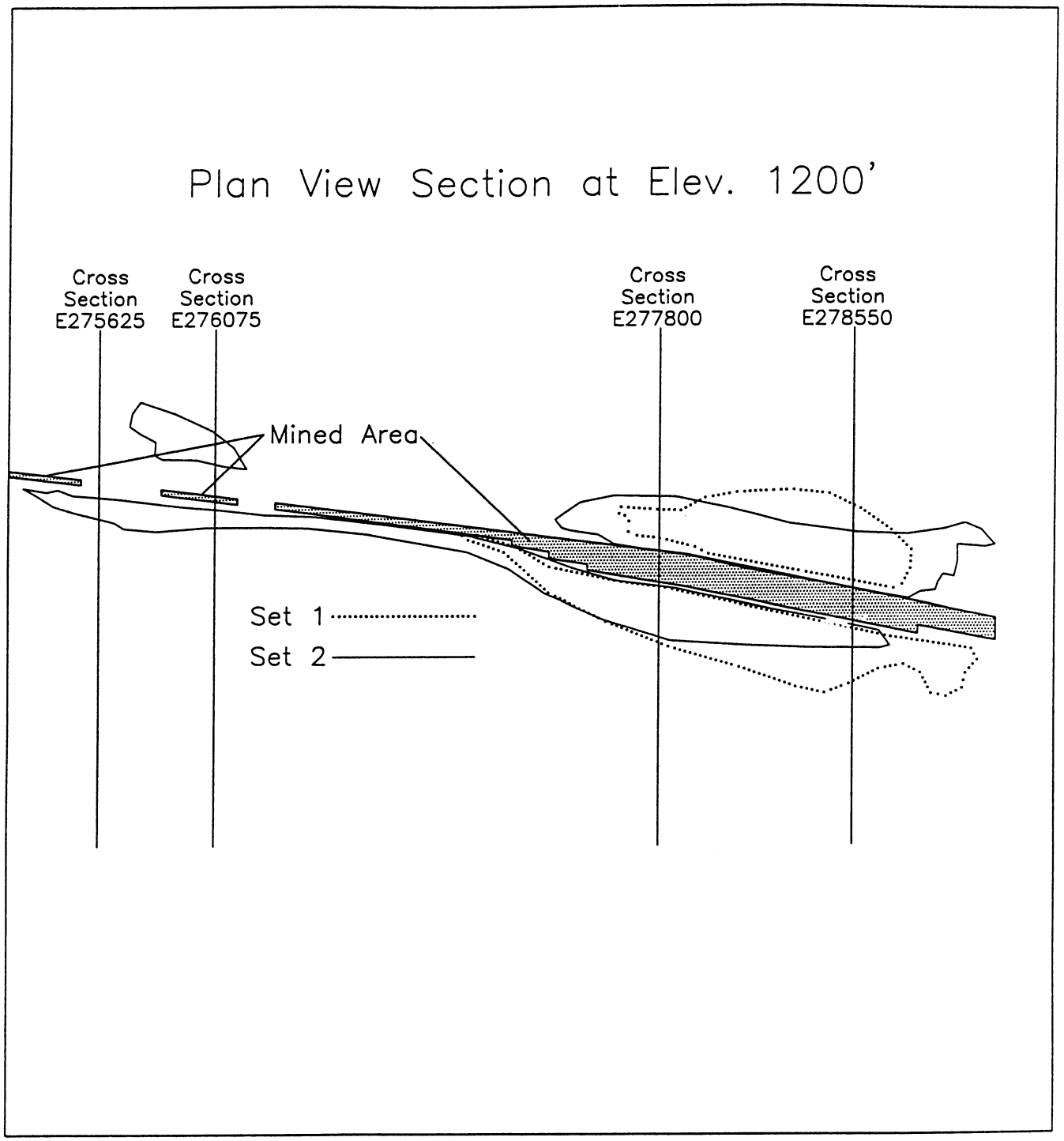

Figure 15. Safety Factor 1.0 Contours for Joint Sets 1 and 2 at Plane Elevation 1200 ft

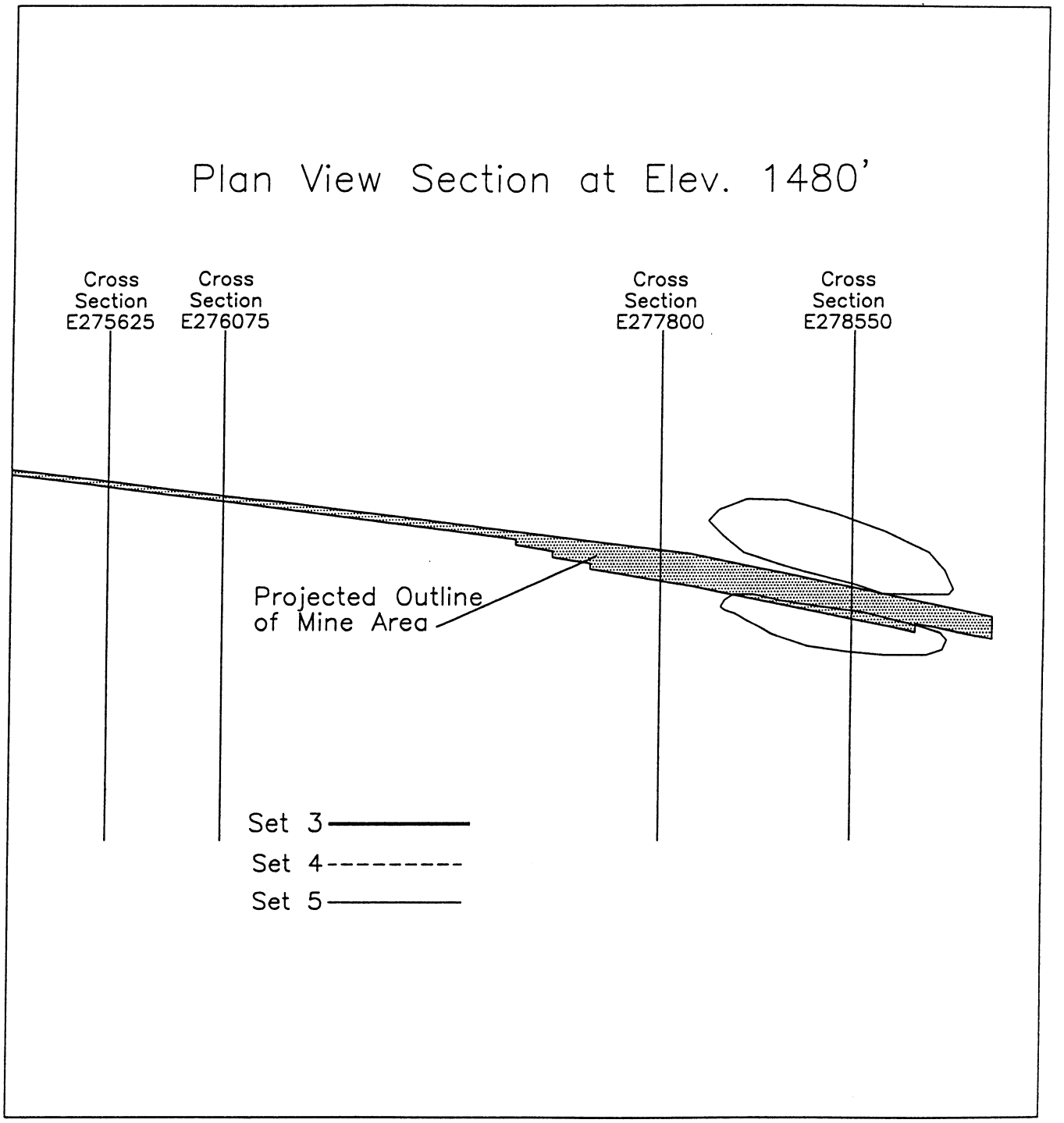

Figure 16. Safety Factor 1.0 Contours for Joint Sets 3, 4 and 5 at Plane Elevation 1480 ft

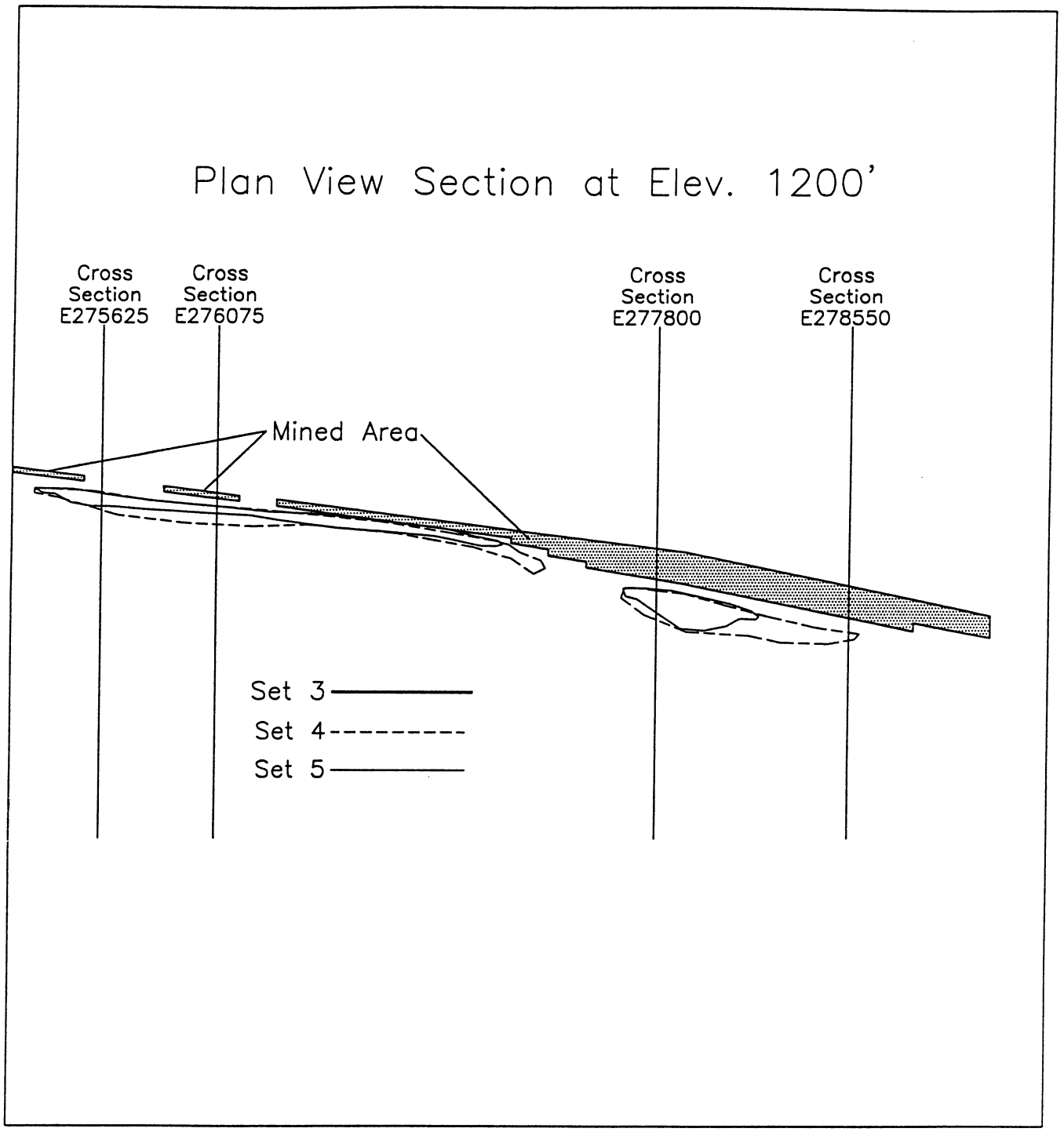

Figure 17. Safety Factor Contours for Joint Sets 3, 4 and 5 at Plane Elevation 1200 ft

Some insight as to the potential impact of changes in hydraulic conductivity in the crown pillar horizon can be gained by reviewing the regional hydrologic studies completed for the Crandon Project.

Significant hydraulic characterization and modeling of the proposed Crandon Mine have been completed in support of permitting. Recent analysis by GeoTrans (1996) provided some insight into the influence of changes in hydraulic conductivity on projected mine water inflow, change in water level in lakes, and the effect of mining on stream flows. This analysis used three-dimensional characterization of the hydrological system, and historical and field test data to calibrate the model. Table 4 lists the two set values of hydraulic conductivity used in the model. The first set termed "Best Engineering Judgment (BEJ) Case" results from calibration of the model to fit the historical and field test data. The second set "Practical Worst (PW) Case" includes a combination of material properties selected from within the range of each individual property to represent the practical worst expected conditions.

Table 4. Summary of Parameter Ranges for Site Data and Groundwater Flow Model

Parameter	Units	BEJ Case	PW Case	Ratio PW/BEJ
Strongly Weathered Bedrock				
k_h and k_v Hanging wall	ft/day	0.048	0.24	5
k_h and k_v Footwall	ft/day	0.23	1.1	4.78
k_h and k_v Orebody	ft/day	0.45	2.6	5.78
Moderately Weathered Bedrock				
k_h and k_v Hanging wall	ft/day	0.014	0.091	6.5
k_h and k_v Footwall	ft/day	0.028	0.091	3.36
k_h and k_v Orebody	ft/day	1.7	8.5	5
Low/Weakly Weathered Bedrock				
k_h and k_v Hanging wall	ft/day	0.00094	0.0034	3.6
k_h and k_v Footwall	ft/day	0.012	0.04	3.3
k_h and k_v Orebody	ft/day	0.012	0.06	5

k_h — hydraulic conductivity in horizontal direction
k_v — hydraulic conductivity in vertical direction

From sensitivity studies, it was shown that the hydraulic conductivity of the weathered bedrock material had a significant impact on the hydrological outputs (mine water inflow, stream flows, and lake water levels). So in the practical worst case, that parameter was varied to the highest expected. Listed in Table 5 is the ratio of the parameter for the "Practical Worst (PW) Case" and

"Best Engineering Judgment (BEJ) Case"; the average ratio is 4.7. The average ratio of the hydraulic conductivity in the strongly weathered bedrock, the material in the crown pillar horizon, was 5.18.

In AAI (1996), the effect of the stress changes in the crown pillar on the hydraulic conductivity of the joints was estimated. Flow in joint set 1 was projected to decrease by about 50%, set 2 would increase by 4%, and the inclined sets (4 and 5) would increase by 97%. In aggregate this would suggest a modest, if any, change in joint hydraulic conductivity and hence no significant change in hydraulic flow through the crown pillar horizon. It appears that the projected changes in hydraulic conductivity are within the range analyzed by GeoTrans (1996).

11. Subsidence

Another output from FLAC3D is the estimated surface subsidence as a result of mining. The prediction of surface subsidence from the FLAC3D model is presented in Figure 18. Based on the analysis results, the subsidence is likely to occur only in the hanging wall side. The maximum subsidence is predicted to be approximately 0.5 ft. The prediction is consistent with a prior assessment by Smith et al. (1982) dealing with surface effects of underground mining.

The maximum subsidence of 0.5 ft is a conservative estimate, the actual subsidence could be substantially less. The estimate was based on conservative assumptions such as 100% extraction of ore and the use of low stiffness uncemented backfill.

12. Summary and Conclusions

The FLAC3D analysis is considered a conservative assessment of the stress redistribution due to mining because:

- The low stiffness backfill material used in the model results in higher crown pillar loading than if a stiffer backfill were used. A cemented fill will be used in the primary stopes, and the range of actual in-place backfill stiffness is likely to be high.
- The current mine plan calls for 80% extraction of ore above elevation 1200 ft and 90% extraction of ore below elevation 1200 ft. A 100% extraction was used for all mining areas in the simulation. The remnants should act to stiffen the response of the fill.

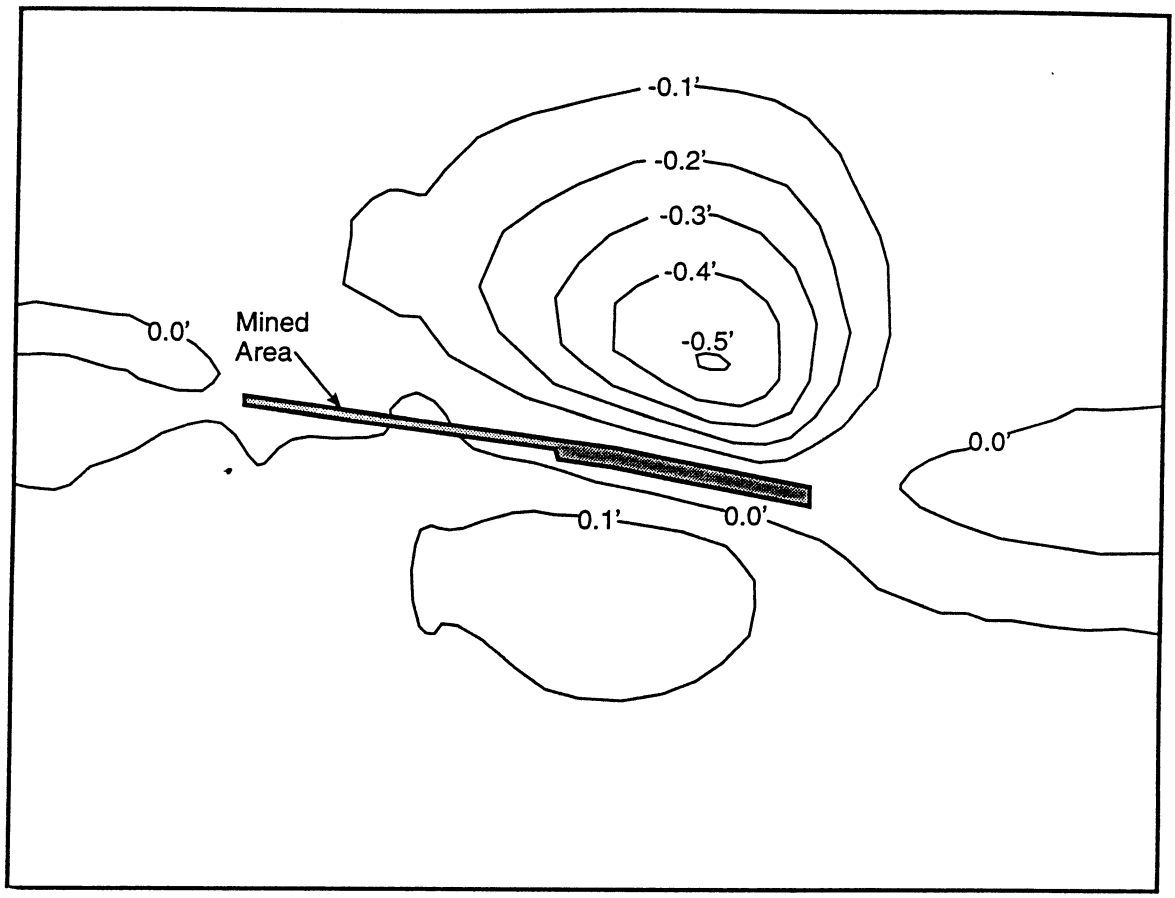

Figure 18. Predicted Surface Subsidence from FLAC3D Elastic Analysis

- The less prominent joint sets, such as sets 4 and 5, are estimated to be less frequent with low persistence. This was not included in the estimation of strength parameters for these joint sets.

The conclusions drawn from FLAC3D analysis are:

- SFs for the crown pillar immediately above the mine workings are all greater than 1.0. This suggests that the 100-ft crown pillar will not exhibit a measurable change in hydraulic properties due to mining.
- In the hanging wall and footwall, regions exist where the SF is less than 1.0 for all joints. However, zones with SF less than 1.0 in the crown pillar horizon are limited to joint sets 2, 4 and 5. Joint set 2 is near horizontal and has only a secondary effect on vertical hydraulic conductivity. At no location does the zone of SF less than 1.0 for joint sets 4

and 5 extend beyond the lower two-thirds of the crown pillar horizon. The "reduced stress conduits" between the mine workings and the glacial aquifer discussed by Dr. Crouch (1997) in his review letter are not indicated by the FLAC3D analysis.

- Comparison of the new FLAC3D results with analysis completed earlier (AAI 1996), suggest that the hydrologic impacts of the stress changes in the crown pillar horizon will be small. The hydraulic conductivity of the predominant hydraulic conduit, joint set 1, will decrease because of joint closure. The hydraulic conductivity of joint sets 4 and 5 may increase over the lower portion of the crown pillar horizon. Estimates of changes in joint aperture and hydraulic conductivity in AAI (1996) suggest that the changes in flow through the crown pillar will be very small. Sensitivity studies by GeoTrans (1996) vary these properties by a factor of 5. We conclude that there will be no measurable impact to the hydrologic regime due to stress redistribution in the crown pillar or crown pillar horizon.
- Calculation of the vertical displacement along the surface was included in the FLAC3D analysis. The maximum surface subsidence of 0.5 ft is predicted from the FLAC3D model. This is considered conservative since the estimate was based on assumptions such as 100% extraction of the ore and the use of low stiffness uncemented backfill.

The UDEC analysis, presented in Appendix B, included both a footwall (FW) block and a hanging wall (HW) block and covered the scenario for both increase and decrease of stresses due to mining. The effect of joint interaction was examined qualitatively by comparing the areas with predicted joint opening/dilation and by quantitatively calculating the effective vertical hydraulic conductivities through the joint rock. The analysis results indicate that interaction of joint sets 1 and 2 is not significant.

13. Recommendations

The results from the FLAC3D analysis indicate an insignificant impact of the crown pillar and crown pillar horizon stress changes due to mining on the overall hydrologic response of the area. The results of FLAC3D analysis, although more extensive and complete, are comparable to the results presented in the earlier AAI (1996) report. Changes in hydraulic characteristics of the joints in the earlier AAI (1996) report were projected to be small. Further analysis of specific joint

combinations using 3DEC as suggested by Dr. Crouch (1997) may be of limited use, particularly given that many more assumptions of joint characteristics (persistence, aperture, spacings, etc.) will have to be made.

14. References

Agapito Associates, Inc. (1996). "Hydrologic Stability of the Crown Pillar, Crandon Deposit," report to Crandon Mining Company.

Bandis, S., A.C. Lumsden, and N.R. Barton (1983). "Fundamentals of Rock Joint Deformation," *International Journal of Rock Mechanics & Mining Sciences & Geomechanics Abstracts*, 20(6):249–268.

Barton, N. and V. Choubey (1977). "The Shear Strength of Rock Joints in Theory and Practice," *Rock Mechanics*, Springer-Verlag, 10:1–54.

Briggs, D.J. (1988). "The Load-Bearing Properties of Fill Materials (Uncemented Fills)," *Backfill in South African Mines*, Johannesburg, SAIMM, 35–60.

Crouch, S.L. (1997). "Comments on May 7, 1996 Report by Agapito Associates, Inc: Hydrologic Stability of the Crown Pillar, Crandon Deposit," prepared for the Wisconsin Department of Natural Resources.

Foth & Van Dyke (1995). "Bedrock Hydrology at the Crandon Site, Crandon Project, Crandon, Wisconsin," report prepared for Crandon Mining Company by Foth & Van Dyke and Associates, Inc., Green Bay, Wisconsin.

Geosolution Resources (1996). Zone 2011/2021/2511 Long Section Map, Geosolution Resources, Inc.

GeoTrans (1996). "Final Report on the Numerical Simulation of the Effect on Groundwater and Surface Water of the Proposed Zinc and Copper Mine Near Crandon, Wisconsin," Environmental Impact Statement, Appendix 4.2–3.

Smith, J.D., R.J. Mitchell and R. Olsen (1982). "Evaluation of Surface Effects, Crandon Project, Exxon Minerals Company, USA," John D. Smith, Engineering Associates, Ltd., Ontario, Canada.

Sneddon, I.N. (1946). "The Distribution of Stress in the Neighborhood of a Crack in an Elastic Solid," *Proceedings of the Royal Society of London.*

APPENDIX A

PROTOCOL—Three-Dimensional Stress Analysis, Crandon Crown Pillar

PROTOCOL—Three-Dimensional Stress Analysis, Crandon Crown Pillar

1. A fully three-dimensional simulation of stress changes due to mining extraction of the Crandon orebody will be performed using the FLAC^{3D} explicit finite-difference program.

Characteristics of the Crandon Model

- Elastic analysis
- Initial stress field
  - — Rock Principal Stresses[1,2]
    $\sigma_1 = 8.1 + 0.03D$ N63°W, horizontal
    $\sigma_2 = 4.5 + 0.02D$ N27°W, horizontal
    $\sigma_3 = 0.025D$ vertical
    where σ = MPa,
    D = depth (meters).
  - — Glacial Overburden
    $\sigma_V = 0.020D$
    $\sigma_H = k\sigma_V$
    where $k = 0.67$.
- Eight different materials:
  - — glacial overburden
  - — crown pillar
  - — weathered hanging wall
  - — weathered footwall
  - — hanging wall
  - — footwall
  - — Crandon Formation (orebody)
  - — backfill
- Model dimensions are illustrated in Figure 1 8800 ft along strike, 1725-ft wide and 2860-ft deep.
- Crandon orebody along strike, illustrated in Figure 2, as per ore blocks defined in the zone 2011/2021/2511 long section by Geosolution Resources, Inc., February 27, 1996.
  - — Ore thicknesses averaged into four areas with approximate thickness ranges
    <30 ft
    30–60 ft
    60–90 ft
    >100 ft
- Model steps are
  - — Step 1: 50% extraction using primary ore blocks 75-ft wide up to 1200-ft elevation.
  - — Step 2: Backfill primary ore blocks.
  - — Step 3: Extract secondary ore blocks up to 1200-ft elevation.
  - — Step 4: Backfill secondary ore blocks.

---

[1]Haimson (1982). "Deep Stress Measurements in Three Ohio Quarries and Their Comparison to Near Surface Tests," 23rd U.S. Symposium on Rock Mechanics, Berkeley, CA.

[2]Haimson (1978). "The Hydrofracturing Stress Measuring Method and Recent Field Results," International Journal of Rock Mechanics, Mining Sciences & Geomechanics Abstracts, 15:167–178.

— Step 5: Extraction and backfill of ore blocks between 1200-ft elevation and base of crown pillar in 60-ft vertical increments, with last two increments in critical locations limited to 30 ft.

— Planned element dimensions are illustrated in Figure 3. Total elements are estimated to be 40,000. Planned grid size in the crown pillar area is 30-ft wide by 20-ft deep by 75-ft long. Planned grid size in the glacial overburden is 30-ft wide by 40-ft deep by 75-ft long.

Analysis of Results

- Contours of principal stresses at four north-south cross sections with varying crown pillar thickness.
- Contours of principal stresses in a vertical long section through center of the crown pillar.
- Contours of joint factors of safety for defined joint sets in:
  — four north-south cross sections with varying crown pillar thickness,
  — one east-west long section at the center of crown pillar,
  — two plan elevations within crown pillar, and
  — east-west long sections in both hanging wall and footwall.
- Comparison to previous two-dimensional results.
- Identify location for 3DEC analysis.

2. Perform three-dimensional simulations of potential joint shear using the 3DEC distinct-element program for cubical blocks located in the crown pillar, hanging wall and footwall.

Characteristics of the Models

- Final stresses derived from FLAC^{3D} analysis for locations in the crown pillar, hanging wall, and footwall that represent the most adverse and typical stress changes.
- Initial stresses identical to FLAC^{3D} simulations at the appropriate depth.
- Model dimensions up to 100 ft by 100 ft by 100 ft.
- Joint populations simulated using 3DEC fracture generation routines for orientation, spacing and persistence assumptions about defined Crandon joint sets.
- Joints simulated using 3DEC continuously yielding model.
- Joint strength parameters as defined in the previous report and satisfying equilibrium requirements for initial stress state.

Evaluation of Results

- Identification zones where joint opening/dilation is possible.
- Contours of joint normal displacement in the joint plane.
- Contours of joint shear displacement in the joint plane.
- Impact of changes in aperture on hydraulic conductivity (parallel plate model).

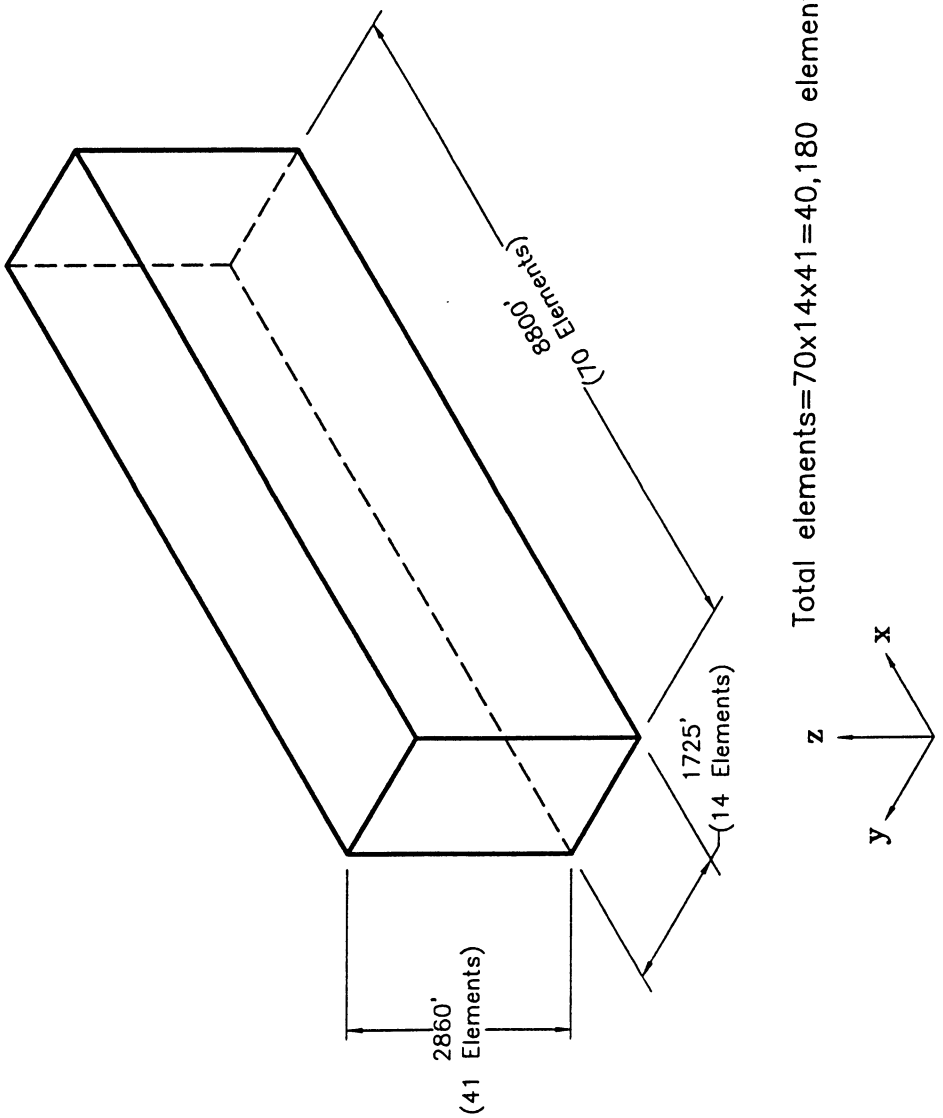

Figure 1. FLAC^{3D} Modeling Geometry

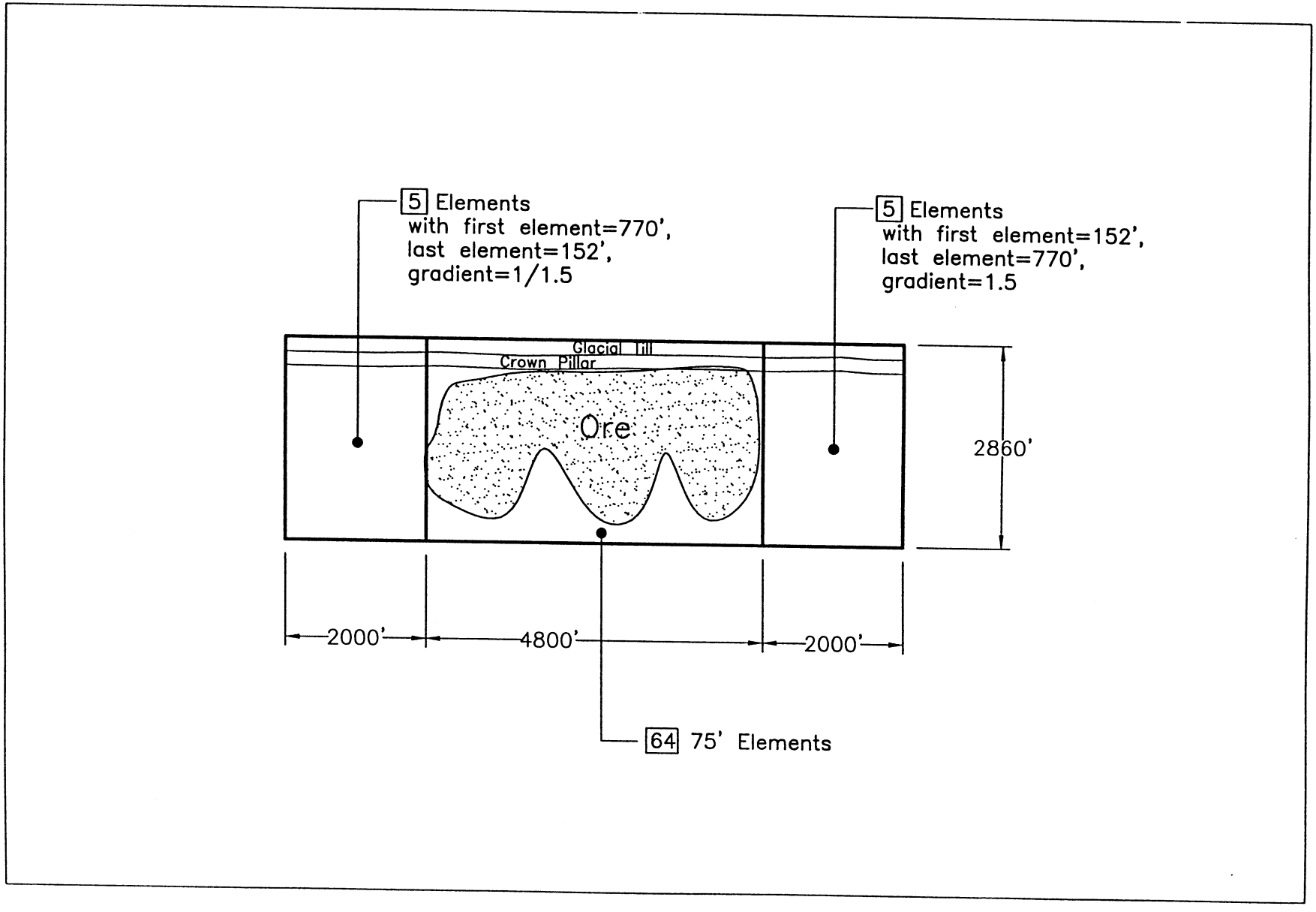

Figure 2. Long Section (orebody strike) Illustrating General FLAC^{3D} Model in the X-Z Plane

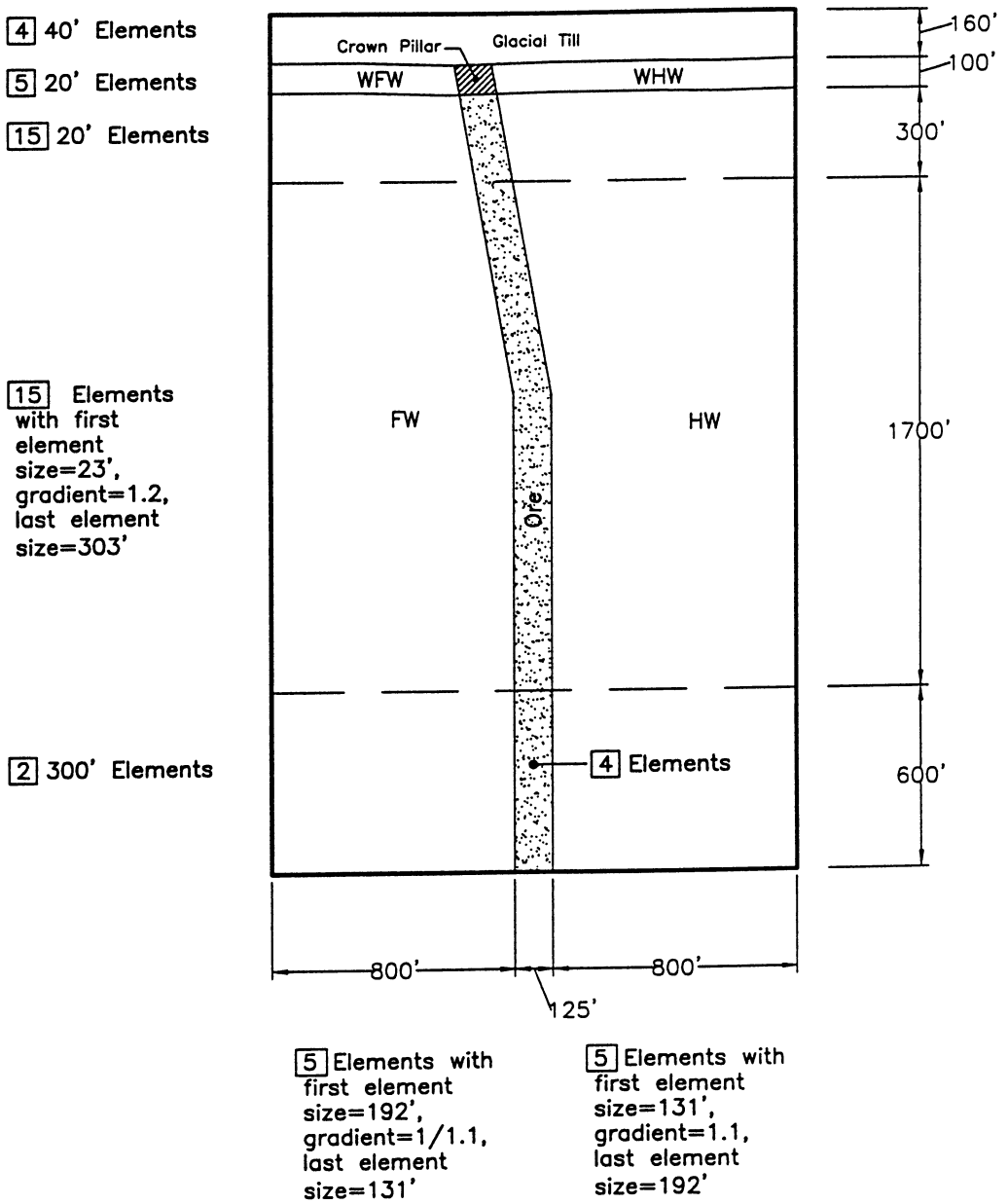

Figure 3. Cross Section Through Orebody Illustrating General FLAC^{3D} Model in the Y-Z Plane

Errata Sheet

PROTOCOL—Three-Dimensional Stress Analysis, Crandon Crown Pillar

- Initial stress field
  - — Rock Principal Stresses[3,4]

    $\sigma_1 = 8.1 + 0.03D_1$ — N63°E, horizontal

    $\sigma_2 = 4.5 + 0.02D_1$ — N27°W, horizontal

    $\sigma_3 = 0.025D_1$ + glacial overburden load — vertical

  - — Glacial Overburden

    $\sigma_V = 0.020D_2$

    $\sigma_H = k\sigma_V$

    where $k = 0.67$.

    where σ = MPa,

    D_1 = depth (meters) measured from the top of the bedrock, and

    D_2 = depth (meters) measured from the surface.

---

[3]Haimson (1982). "Deep Stress Measurements in Three Ohio Quarries and Their Comparison to Near Surface Tests," 23rd U.S. Symposium on Rock Mechanics, Berkeley, CA.

[4]Haimson (1978). "The Hydrofracturing Stress Measuring Method and Recent Field Results," International Journal of Rock Mechanics, Mining Sciences & Geomechanics Abstracts, 15:167–178.

APPENDIX B

UDEC Analysis Results for Evaluation of the Joint Interaction

UDEC Analysis Results for Evaluation of the Joint Interaction

B-1. Introduction

This appendix summarizes the results of the UDEC analysis conducted for the evaluation of the potential joint interaction of the predominant vertical joint set (set 1) and horizontal joint set (set 2). The study is part of the effort to evaluate the influence of mining on the crown pillar of the Crandon deposit. Previously, a draft FLAC3D elastic analysis was completed and reviewed by the Wisconsin DNR. It was suggested by the Wisconsin DNR consultant, Dr. S.L. Crouch, that a follow-up two-dimensional UDEC analysis be conducted to evaluate joint interaction in regions where the SF was predicted to be less than 1 for the predominant horizontal and vertical sets. A protocol established for conducting the UDEC analysis was proposed by AAI and CMC, and was subsequently finalized in consultation with Dr. Crouch. The protocol is attached to this report as Attachment B-1.

UDEC (Itasca 1996) is a two-dimensional numerical program based on the distinct-element method for discontinuum modeling. The discontinuous medium is represented as an assemblage of discrete blocks. The discontinuities (joints) are treated as boundary conditions between blocks; individual blocks are elastically deformable. The relative motion of the discontinuities (joints) is governed by linear or nonlinear force displacement relations for movements in both the normal and shear directions. The constitutive models for simulation of joint mechanical behavior in UDEC include the Mohr-Coulomb, Continuously-Yielding (Cundall and Hart 1984), and Barton-Bandis (Bandis et al. 1983) models. In this analysis, both the Mohr-Coulomb and Continuously-Yielding models were used for joint simulation.

UDEC has the capability to assess fluid flow through the fractures of a system of impermeable blocks. A fully coupled mechanical-hydraulic model was implemented in which fracture conductivity was dependent on mechanical deformation. In this analysis, the cubic law for flow in fractures (Witherspoon et al. 1980) was applied in the hydraulic calculation.

The locations for UDEC analysis, shown in Figure B-1, were selected at cross section E278,500 which provided among the highest after-mining stresses predicted in FLAC3D analysis. The first block is located partly in the crown pillar horizon and partly in the footwall (FW block), whereas the second block is located in the hanging wall (HW block). These locations include regions with SF less than 1 for the horizontal and vertical joint sets.

The joint hydraulic, mechanical, and geometrical properties were derived using conservative assumptions and best engineering judgement and were calibrated quantitatively versus field tests and regional hydraulic models. Joint hydraulic properties were calibrated so that the equivalent hydraulic conductivities in the footwall/crown pillar areas are similar to hydraulic properties interpreted from the field pump tests and calibrated regional hydraulic models in the footwall and ore areas (GeoTrans 1996). To be conservative, the values for these properties were also adopted for the joints in the HW block. The analysis does not intend to simulate the absolute amount of groundwater flow in the bedrock. Rather, the flow of groundwater calculated in the analysis and the changes in equivalent hydraulic conductivities of the blocks serve only as an indicator for the effect of joint interaction, in the comparative sense. This is especially true for the HW block where the emphasis of the analysis is on the comparison of results for the two cases where either both joint sets are present or only the vertical set is modeled.

B-2. Intact and Joint Properties

The intact rock and joint properties used in the UDEC analysis are presented in Table B-1. The intact properties are consistent with the properties used in the FLAC3D analysis.

The joint properties are categorized into three groups in Table B-1: joint mechanical properties, joint geometrical properties, and joint hydraulic properties. Joint properties are assigned the same values for the vertical and horizontal sets if not specified otherwise in Table B-1. Both the Mohr-Coulomb and Continuously-Yielding models were used as joint mechanical properties. Constant normal and shear stiffnesses of 0.4 million psi/in. were used in the analysis. The values for the normal and shear stiffnesses were revised from 0.04 million psi/in. in the protocol. The revision was made to better model the joint hydraulic behavior. The details will be explained in the discussion of joint hydraulic properties below. Joint tensile strength was conservatively set as zero for both mechanical models; cohesion and friction angles are consistent with previous analyses. The dilation angle, intrinsic friction angle (or residual friction angle), and joint roughness parameters were obtained or derived from literature sources (Bandis et al. 1983, Barton and Choubey 1977) or with best engineering judgement.

Table B-1. Intact and Joint Properties Proposed for UDEC Model

Intact Properties		
Crown Pillar Horizon	Elastic Modulus (psi)	7.70E+05
	Poisson's Ratio	0.25
Hanging Wall	Elastic Modulus (psi)	1.54E+06
	Poisson's Ratio	0.25
Footwall	Elastic Modulus (psi)	3.25E+06
	Poisson's Ratio	0.25
Joint Mechanical Properties		
Mohr-Coulomb Model	Normal Stiffness (psi/in)	4.00E+05
	Shear Stiffness (psi/in)	4.00E+05
	Tensile Strength (psi)	0
	Cohesion (psi)	15
	Friction Angle (degree)	39
	Dilation Angle (degree)	9
Continuously Yielding Model	Normal Stiffness (psi/in)	4.00E+05
	Shear Stiffness (psi/in)	4.00E+05
	Tensile Strength (psi)	0
	Cohesion (psi)	15
	Initial Friction Angle (degree)	39
	Intrinsic Friction Angle (degree)	30
	Roughness Parameter (mm)	0.1
Joint Geometrical Properties		
	Spacing for Set 1 (ft)	4
	Spacing for Set 2 (ft)	10
	Persistence for Set 1 (%)	100
	Persistence for Set 2 (%)	50
Joint Hydrologic Properties		
	Aperture for Zero Normal Stress (mm)	0.2
	Residual Aperture at High Stress (mm)	0.005
	Joint Permeability Constant (1/psi/sec)	5.7×10^5

Joint geometrical properties consist of spacing and persistence. Joint spacing provides the measurement of frequency along the direction perpendicular to the joint orientation. Joint persistence is the indicator of the degree of continuity along the trace of joints. Joint spacings in the Crandon deposit were determined based on the fracture data collected by logging core from thirteen boreholes (139, 151, 234, 262, 263, 264, 265, 266, 267, 268, 270, 271 and 272). Site-specific joint persistence data is not available. By considering the nature of the vertical joints as the bedding planes, a 100% persistence was assigned for the vertical set. The horizontal set is created mainly due to the relief of glacial overburden. Persistence for this set was conservatively assigned to be 50% to 100% in the protocol. Convergence could not be obtained during test analyses with 100%

persistence for the two joint sets. In consultation with Dr. Crouch, 50% persistence was agreed upon as adequate to address joint interaction.

Joint hydraulic properties include the joint permeability constant, aperture for zero normal stress, residual aperture at high stress, and joint normal stiffness (k_n). The joint permeability constant is a function of the dynamic viscosity of fluid in fractures. The value for the joint permeability constant listed in Table B-1 was calculated using the dynamic viscosity of water. The other hydraulic properties define the relation between hydraulic aperture and joint normal stress as shown in Figure B-2.

The hydraulic aperture at the base of the crown pillar before mining is approximately 4.8×10^{-4} ft (or 0.15 mm); the equivalent hydraulic conductivity for these joints spaced at 4 ft was calculated as 0.58 ft/day. This conductivity is consistent with values for strongly weathered bedrock in the groundwater flow modeling studies (GeoTrans 1996). In these studies, GeoTrans selected hydraulic properties to be consistent with field test data. The hydraulic aperture at the base of the crown pillar is based on normal stiffness of 0.4 million psi/in., which is different from the normal stiffness of 0.04 million psi/in. as proposed in the protocol. The aperture for a normal stiffness of 0.04 million psi/in. would be 1.6×10^{-5} ft (or 0.005 mm) for joints in the HW and FW blocks before mining, and this magnitude would remain the same for most areas in the blocks after mining (see Figure B-2). This magnitude of aperture would result in an equivalent hydraulic conductivity of 2.35×10^{-5} ft/day, which is not appropriate for this analysis. It is not appropriate because the conductivity is significantly lower than the GeoTrans (1996) values and also the conductivity would undergo little change before and after mining. Therefore, for this analysis, the normal stiffness of 0.04 million psi/in. was revised to 0.4 million psi/in.

B-3. Model Geometry and Boundary Condition

The UDEC block systems constructed for the analysis are shown in Figure B-3. Finite-difference zones within the deformable blocks are not shown in the figure. A total of 1,112 deformable blocks and 37,140 finite-difference zones are created for the first block system. For the second block system, 76 deformable blocks and 98,802 finite-difference zones are included. The dimension for the block systems is 300 ft by 300 ft. The coordinate system in UDEC is horizontal as the X direction, vertical as the Y direction, and out-of-plane as the Z direction. The first block system consists of both the horizontal and vertical joint sets; the second block system includes only

the vertical set. The first block system was constructed based on the joint geometrical properties of 100% persistence for the vertical set and 50% persistence for the horizontal set. This block system was used to model two cases: the first one with both horizontal and vertical sets, and the second with only the horizontal set. For the horizontal set only case, high-strength parameters were assigned for the vertical joints to substantiate the block system as a horizontal jointing system.

The traction boundary conditions for the UDEC analysis were calculated from FLAC3D at locations shown in Figure B-1 and were used as the traction boundary for the UDEC analysis. Fixed vertical displacement and shear tractions were applied to the lower boundary. Figures B-4 and B-5 show the magnitude of the stresses obtained from FLAC3D for the FW and HW blocks, respectively. The out-of-plane shear stresses were neglected as required in a two-dimensional plane-strain analysis. A fixed pore pressure of 300 psf was applied at the top and bottom boundaries to saturate the fractures and initiate the water inflow. Lateral boundaries were assumed impermeable. With the fixed pore pressure, the hydraulic gradient in the vertical direction was set as 1.

B-4. Analyses Results

Three sets of analyses were conducted based on the Mohr-Coulomb joint mechanical model: the first with only the vertical set, and the second with only the horizontal set. The third analysis included both the horizontal and vertical sets. The areas where joint slip occurs and the flow through the block are presented for each set of analysis. The hydraulic calculations were not conducted for the case with horizontal joints only because, in this case, hydraulic conductivity along the vertical direction was approaching zero for the block system.

Figures B-6 to B-8 present the analysis results identifying regions where opening/dilation occurs for the FW block. Also included in the figures are the predicted SF equal to 1 contours from the FLAC3D analysis results. In general, UDEC analyses results tend to show fewer areas where opening/dilation occurs. This is considered reasonable judging that out-of-plane shear stresses were neglected in the UDEC analyses. Interaction of joint sets 1 and 2 does not appear to be significant after comparing the results in Figure B-8 (two joint sets case) to Figure B-6 (vertical joints only case) and Figure B-7 (horizontal joints only case).

The same set of analyses results for the HW block, with the same sequence, are presented in Figures B-9 to B-11. As was observed in the FW block, UDEC analyses results tended to show fewer areas where opening/dilation occurred than predicted by the FLAC3D analysis. For the analysis

including both the horizontal and vertical joints, stress concentration and localization were observed in blocks at the right-hand boundary, as shown in Figure B-11. The block system undergoes redistribution of stresses such that the regions where opening/dilation occurs are now concentrated over the area close to the right-hand boundary. This is shown in the block displacement vectors plot in Figure B-12.

The vertical flow through the block system was calculated to assess the effect of joint interaction to the flow rate. The equivalent hydraulic conductivity of the block system can be calculated from the total vertical flow based on Darcy's law:

$$k_v = Q/A/I$$

where k_v is the equivalent hydraulic conductivity in the vertical direction,

Q is the total flow,

A is the area of flow, and

I is the hydraulic gradient.

The total flow and the equivalent hydraulic conductivities calculated based on UDEC analyses results are presented in Table B-2. For the FW block, equivalent hydraulic conductivity for the in-situ state is approximately 0.55 ft/day, and is predicted to reduce to 0.37 ft/day for the vertical joint set only case and 0.42 ft/day for the horizontal and vertical joint sets case. The increase of normal stresses over the crown pillar horizon (see Figure B-4) has contributed to the closing of the aperture and, hence, the reduction of the hydraulic conductivities. Inclusion of the second joint set accounts for the 16% increase in the predicted flow through the block.

Table B-2. Calculated Total Flow and Equivalent Hydraulic Conductivities from UDEC Mohr-Coulomb Analyses

	FW, 1st Set Only		FW, 1st and 2nd Sets		HW, 1st Set Only		HW, 1st and 2nd Sets	
	Before Mining*	After Mining	Before Mining	After Mining	Before Mining	After Mining	Before Mining	After Mining
Total Flow (ft^2/sec)	0.00191	0.00127	0.00191	0.00147	0.00146	0.00359	0.00145	0.00269
Conductivity** (ft/day)	0.55	0.37	0.55	0.42	0.42	1.03	0.42	0.77

*Before Mining *is equivalent to the in situ state.*

***Note: Conductivity specific to this analysis only.*

For the HW block, equivalent hydraulic conductivity for the in-situ state is approximately 0.42 ft/day and is predicted to increase to 1.03 ft/day for the vertical set only case and 0.77 ft/day for the horizontal and vertical joint sets case. The increase in hydraulic conductivity is due to mining-induced stress relief over the hanging wall area (see Figure B-5).

The UDEC hydraulic results for the HW block are not considered to be significant with regard to the effectiveness of the crown pillar hydrologic model. The HW block is located below the crown pillar horizon near the stoped areas. The block was selected for analysis to evaluate the effect of interaction between the horizontal and vertical sets. With both sets included in the analysis, the equivalent hydraulic conductivity and the vertical flow through the block was reduced, indicating that interaction of the joint sets is not adverse.

Analyses based on the Continuously-Yielding model were conducted only for the case with both horizontal and vertical joints. The total flow and equivalent hydraulic conductivity calculated from the UDEC analyses results are presented in Table B-3. Table B-3 also includes the results based on the Mohr-Coulomb model. Comparison of these results indicates that the Mohr-Coulomb model results are relatively conservative.

Table B-3. Calculated Total Flow and Equivalent Hydraulic Conductivities from UDEC Analyses with Horizontal and Vertical Joints

	Footwall				Hanging Wall			
	Continuously Yielding Model		Mohr-Coulomb Model		Continuously Yielding Model		Mohr-Coulomb Model	
	Before Mining*	After Mining	Before Mining	After Mining	Before Mining	After Mining	Before Mining	After Mining
Total Flow (ft^2/sec)	0.00191	0.00115	0.00191	0.00147	0.00145	0.00181	0.00145	0.00269
Conductivity** (ft/day)	0.55	0.33	0.55	0.42	0.42	0.52	0.42	0.77

*Before Mining *is equivalent to the in situ state.*
** *Note: See Table B-2.*

B-5. Conclusion

Based on the results of the coupled mechanical-hydraulic UDEC analyses, the interaction of joint sets 1 and 2 is not significant. The analyses included both FW and HW blocks and covered the scenario for both increase and decrease of stresses due to mining. The effect of joint interaction was examined by qualitatively comparing the areas with predicted joint opening/dilation and by

quantitatively calculating the equivalent vertical hydraulic conductivities through the blocks. The analyses results confirm the conclusion provided in the report for the FLAC3D analysis..

B-6. References

Bandis, S., A.C. Lumsden, and N.R. Barton (1983). "Fundamentals of Rock Joint Deformation," *International Journal of Rock Mechanics & Mining Sciences & Geomechanics Abstracts*, 20(6):249–268.

Barton, N., and V. Choubey (1977). "The Shear Strength of Rock Joints in Theory and Practice," *Rock Mechanics*, Springer-Verlag, 10:1–54.

Cundall, P.A. and R.D. Hart (1984). "Analysis of Bock Test No. 1 Inelastic Rock Mass Behavior: Phase 2 — A Characterization of Joint Behavior (Final Report)." Itasca Consulting Group Report, Rockwell Hanford Operations, Subcontract SA-957.

GeoTrans (1996). "Final Report on the Numerical Simulation of the Effect on Groundwater and Surface Water of the Proposed Zinc and Copper Mine Near Crandon, Wisconsin," Environmental Impact Statement, Appendix 4.2–3.

Itasca (1996). "UDEC, Version 3.0, User's Manual. Itasca Consulting Group, Inc.", Minneapolis, MN.

Witherspoon, P.A., J.S.Y. Wang, K. Iawi and J. E. Gale (1980). "Validity of Cubic Law for Fluid Flow in a Deformable Rock Fracture." *Water Resources Research*, 16(6):1016–1024.

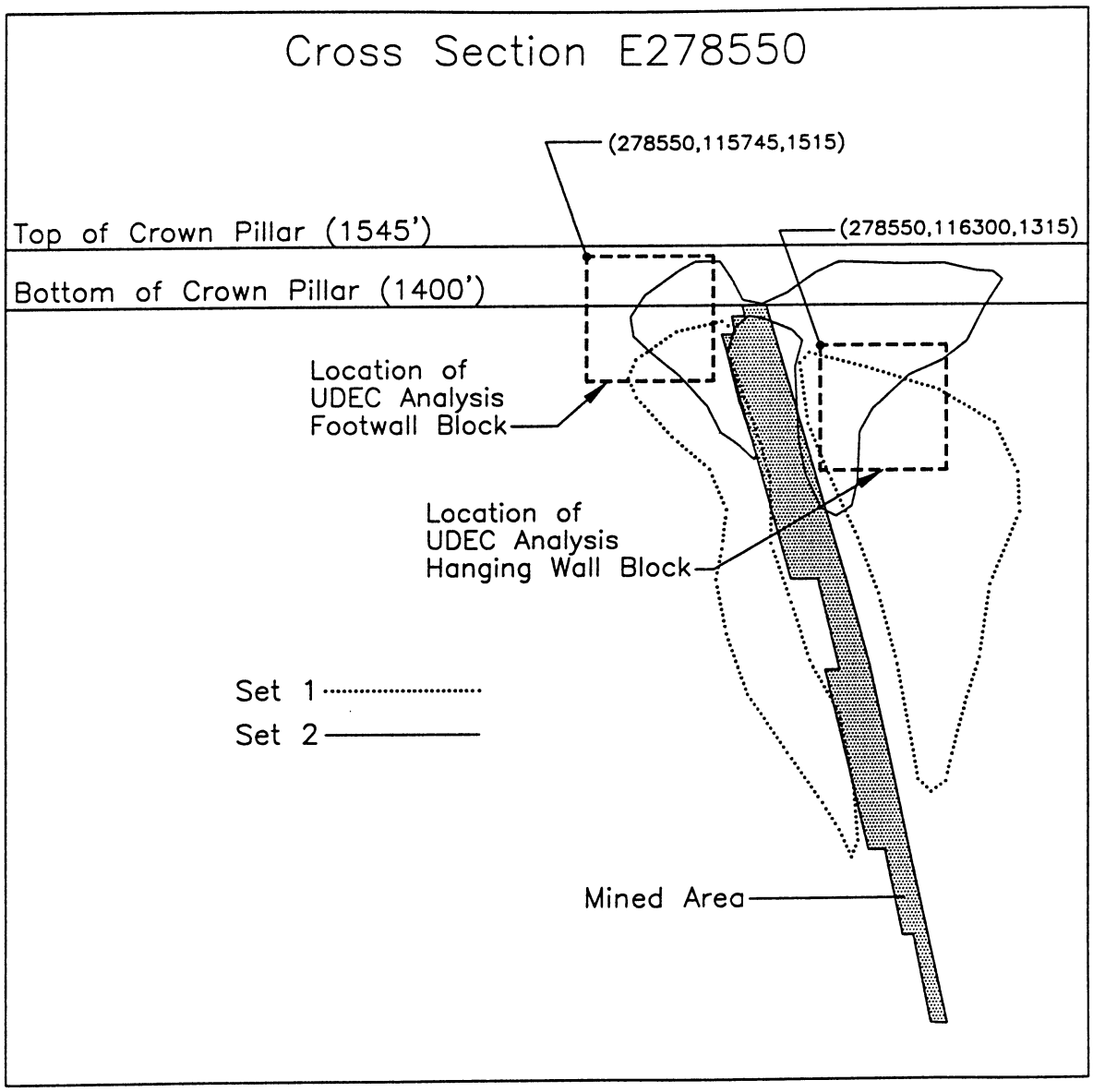

Figure B-1. Locations of the Blocks for the UDEC Analysis and Safety Factor 1.0 Contours for Joint Sets 1 and 2 Predicted with FLAC3D Analysis

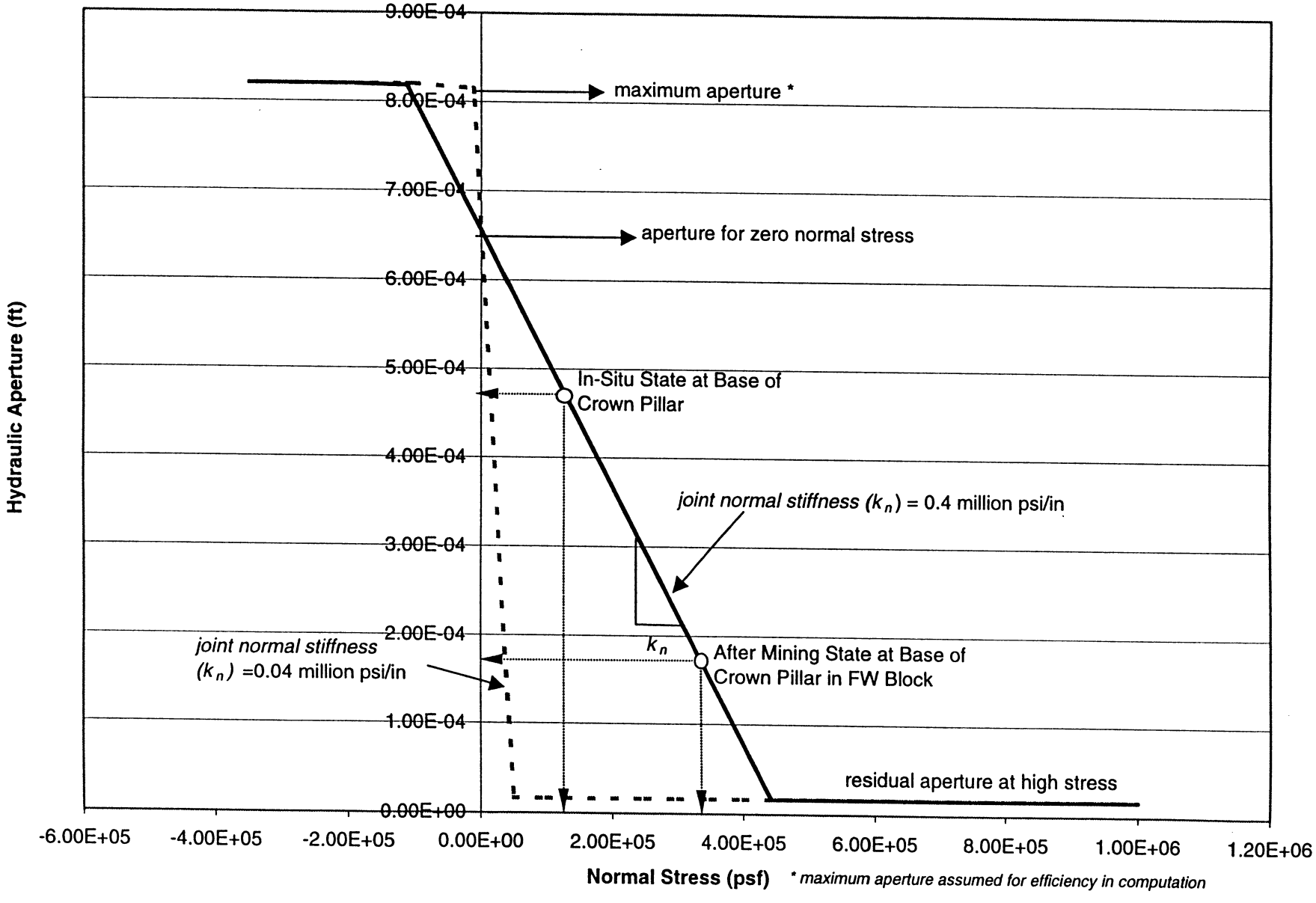

Figure B-2. Relationship Between Hydraulic Aperture and Joint Normal Stress in UDEC

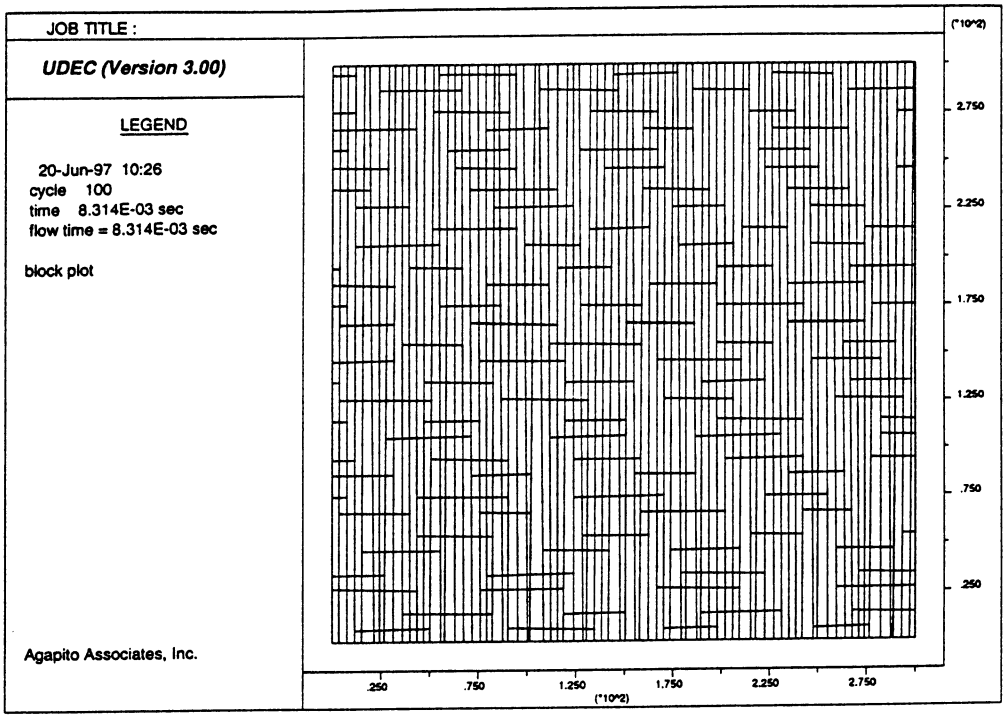

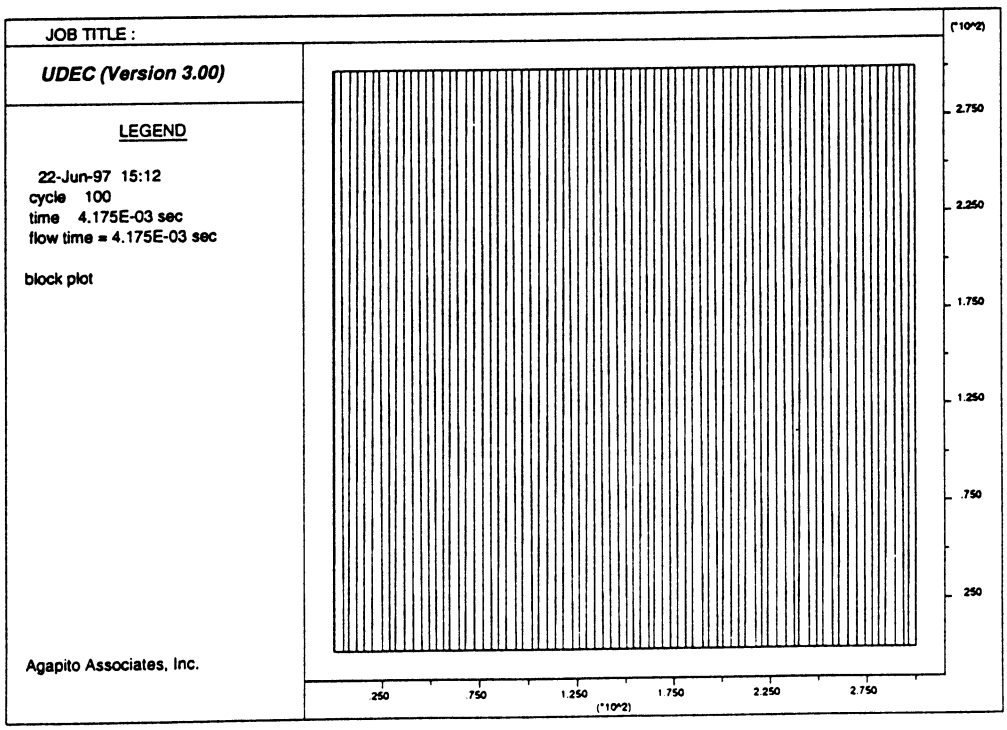

Figure B-3. UDEC Block Systems

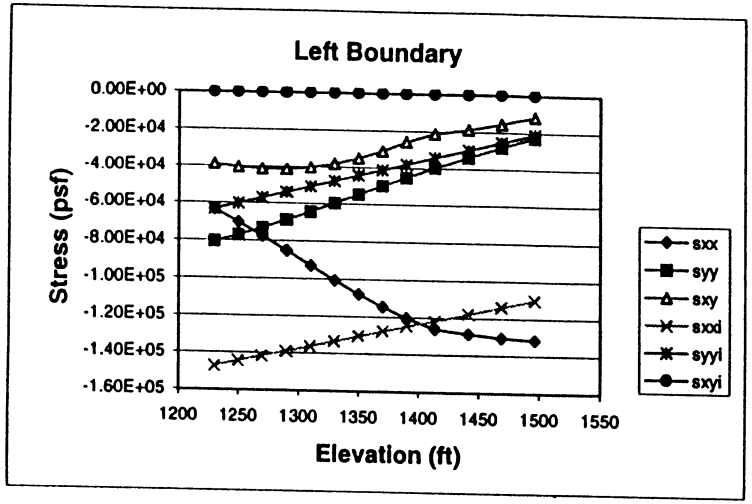

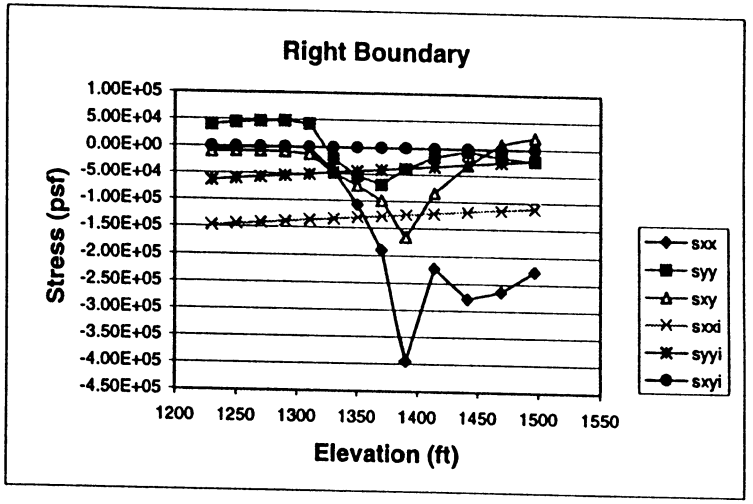

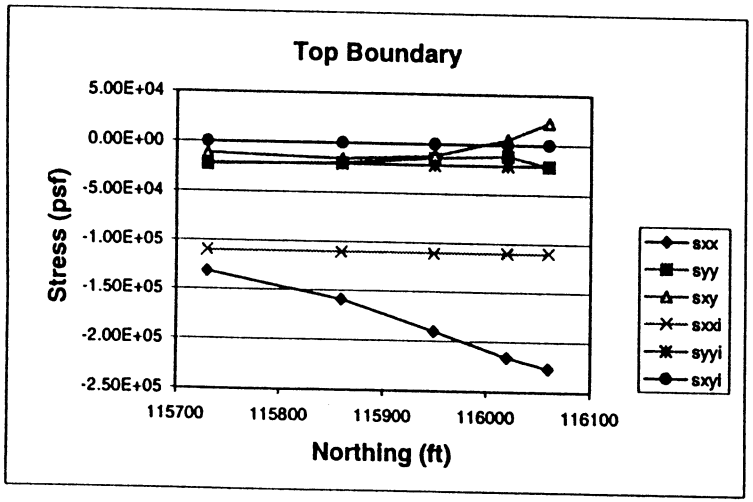

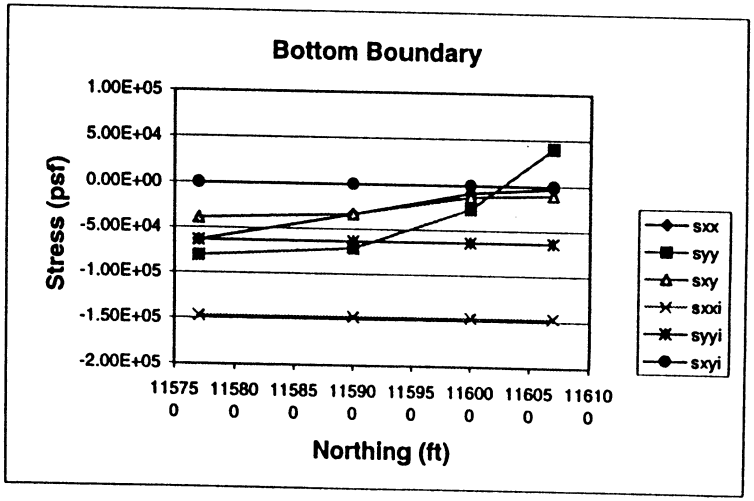

sxxi = in-situ horizontal stress
syyi = in-situ vertical stress
sxyi = in-situ shear stress

sxx = after-mining horizontal stress
syy = after-mining vertical stress
sxy = after-mining shear stress

Figure B-4. Stresses Along the FW Block from FLAC3D Analysis

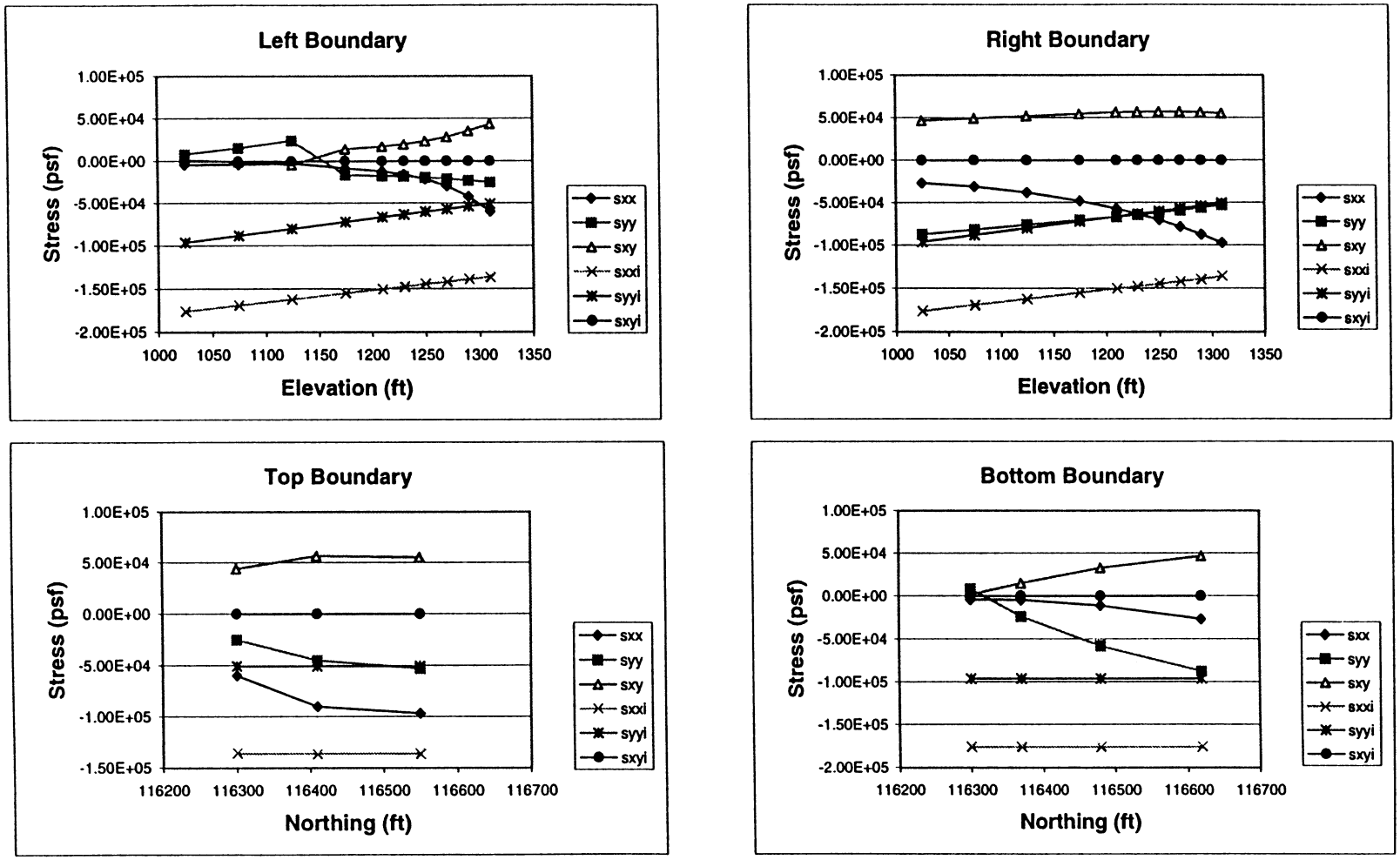

sxxi = in-situ horizontal stress
syyi = in-situ vertical stress
sxyi = in-situ shear stress

sxx = after-mining horizontal stress
syy = after-mining vertical stress
sxy = after-mining shear stress

Figure B-5. Stresses Along the HW Block from FLAC3D Analysis

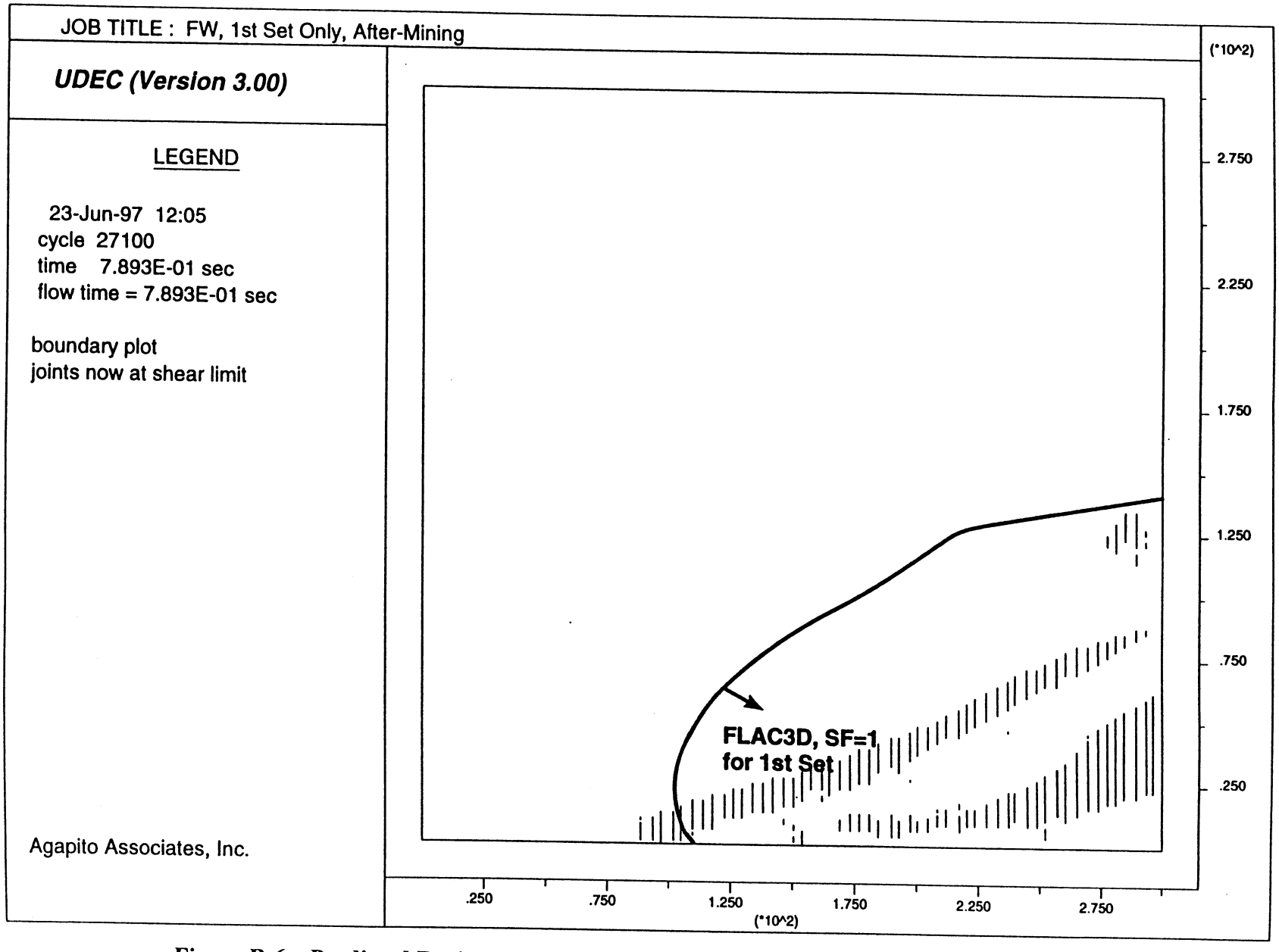

Figure B-6. Predicted Regions of Joint Opening/Dilation, FW Block, Vertical Set Only

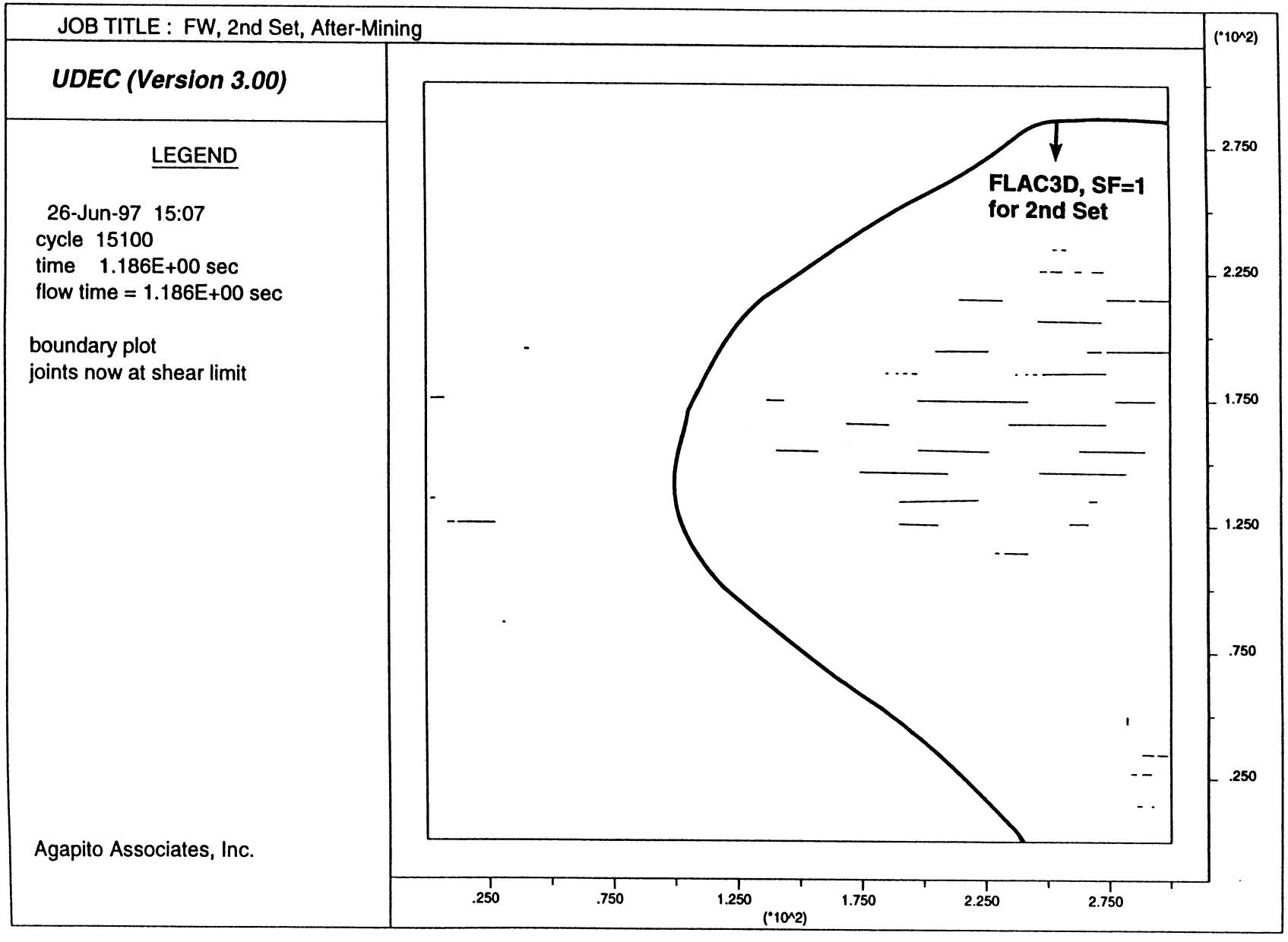

Figure B-7. Predicted Regions of Joint Opening/Dilation, FW Block, Horizontal Set Only

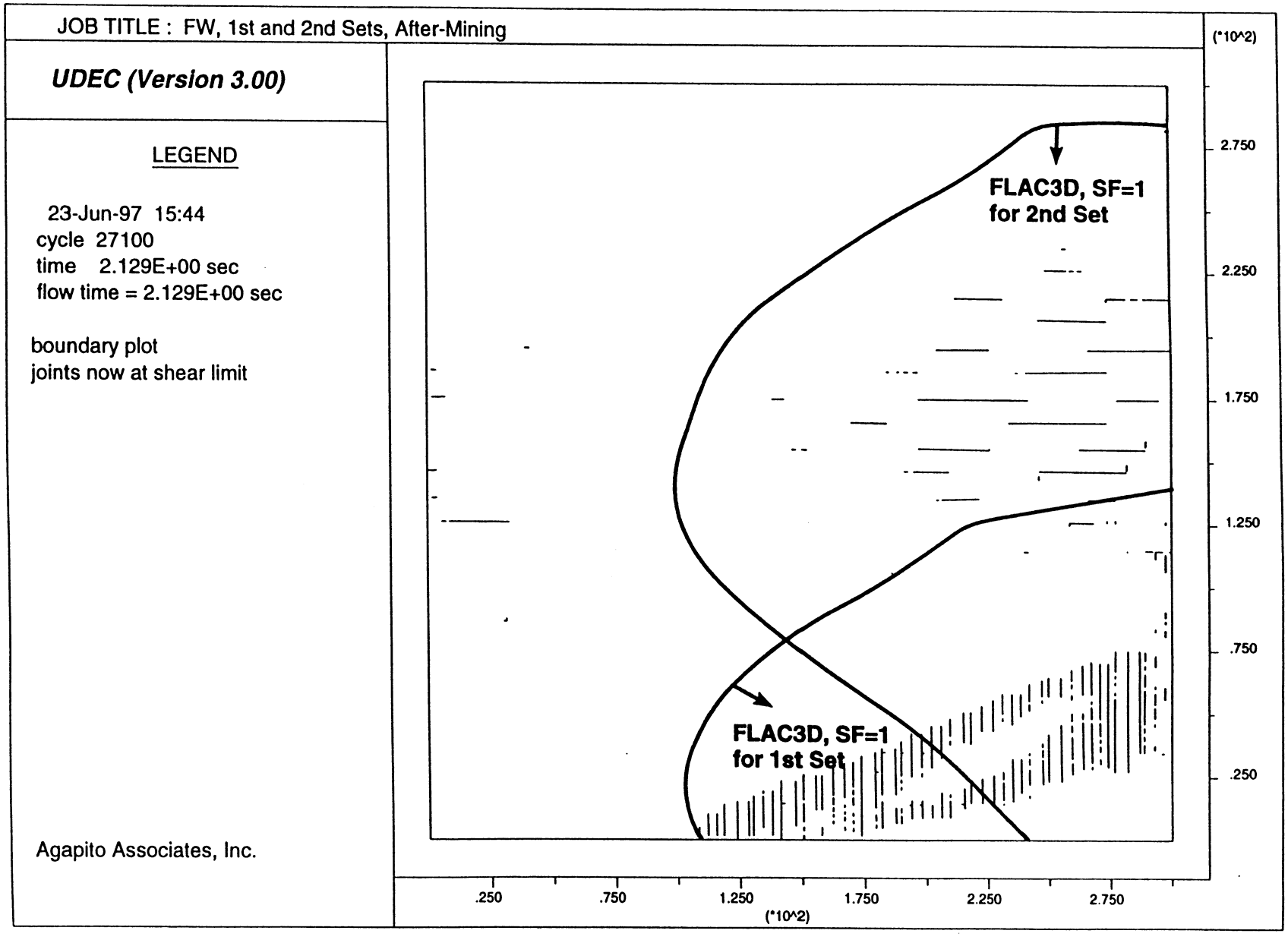

Figure B-8. Predicted Regions of Joint Opening/Dilation, FW Block, Two Joint Sets

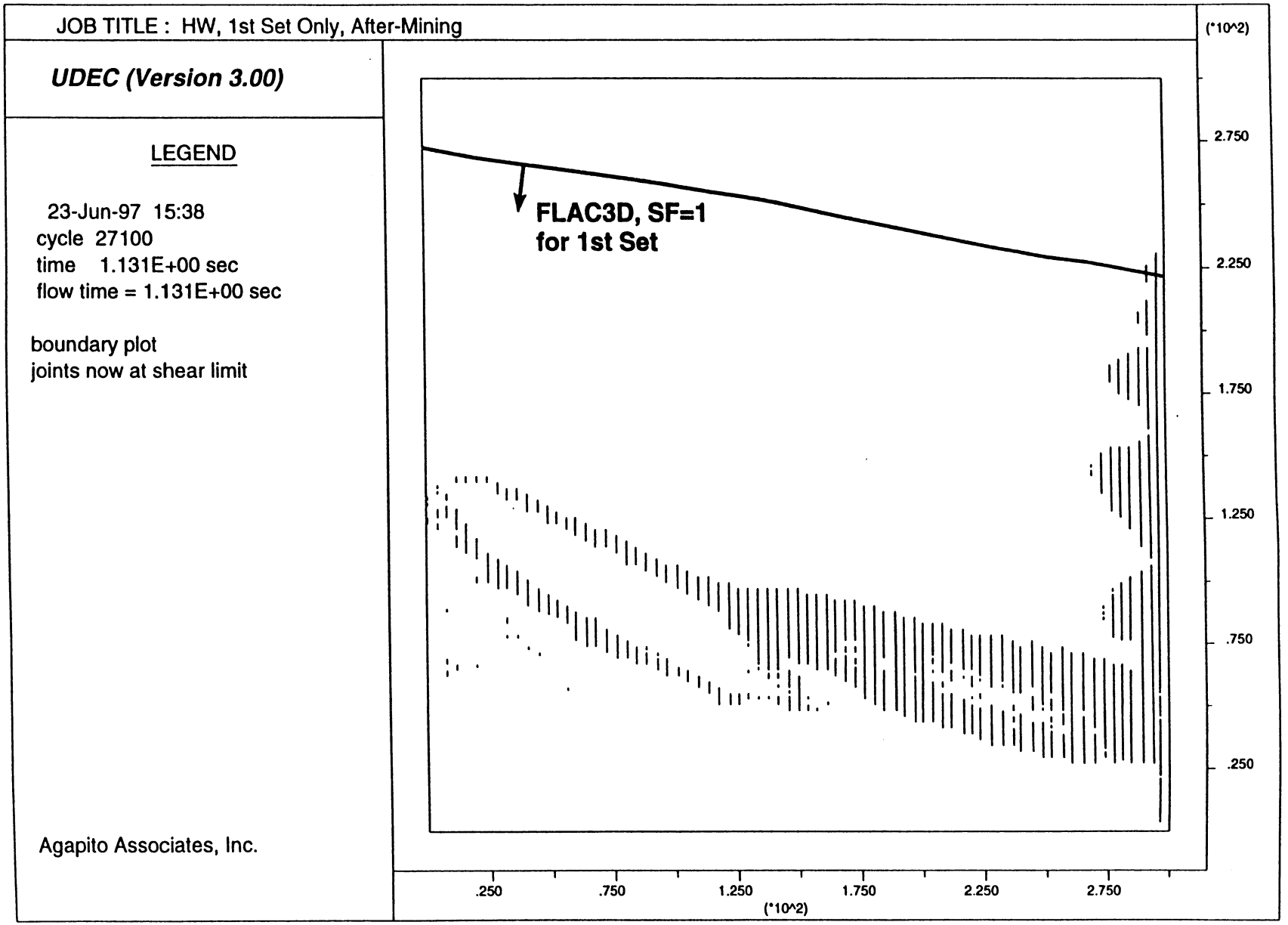

Figure B-9. Predicted Regions of Joint Opening/Dilation, HW Block, Vertical Set Only

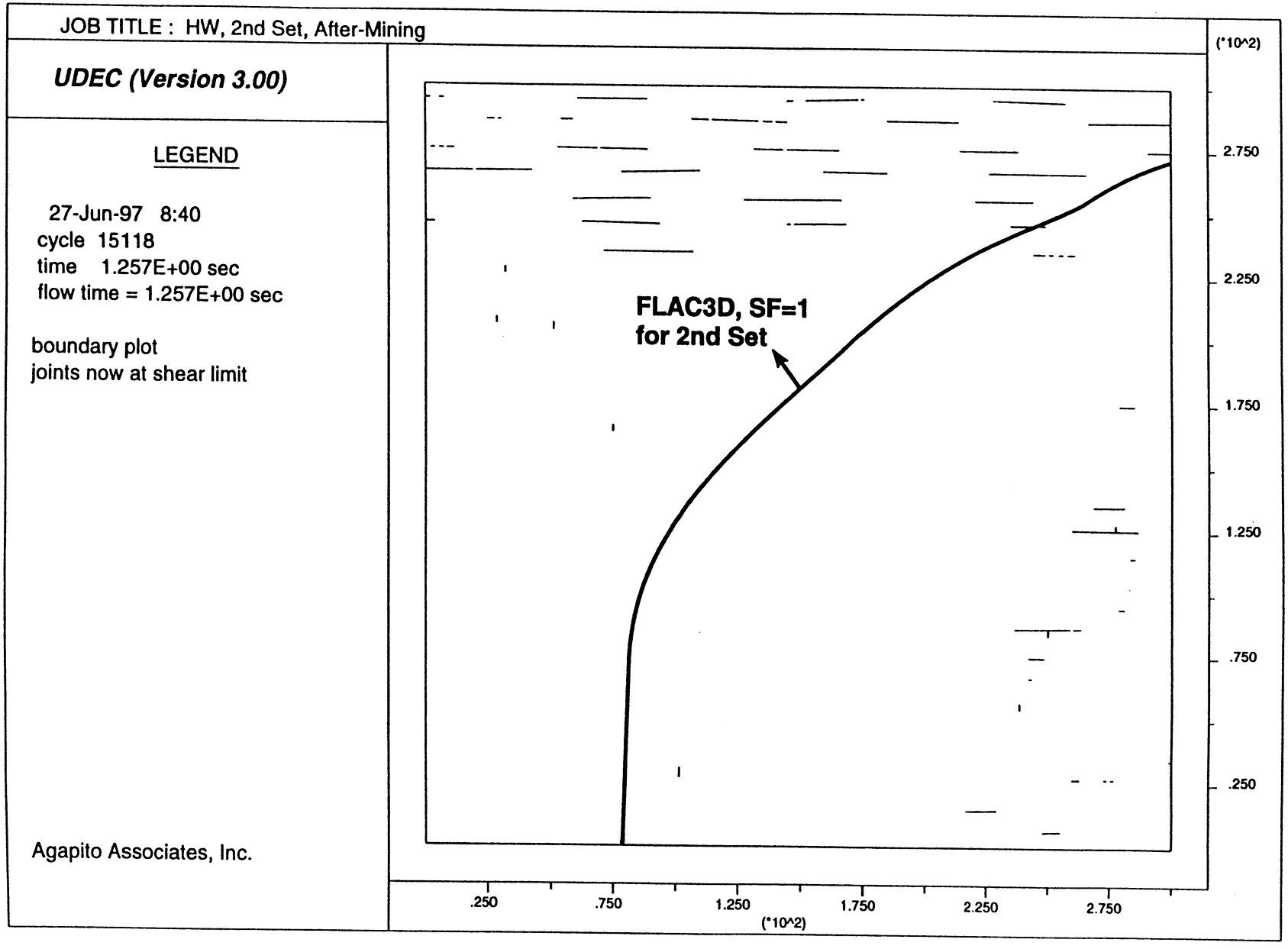

Figure B-10. Predicted Regions of Joint Opening/Dilation, HW Block, Horizontal Set Only

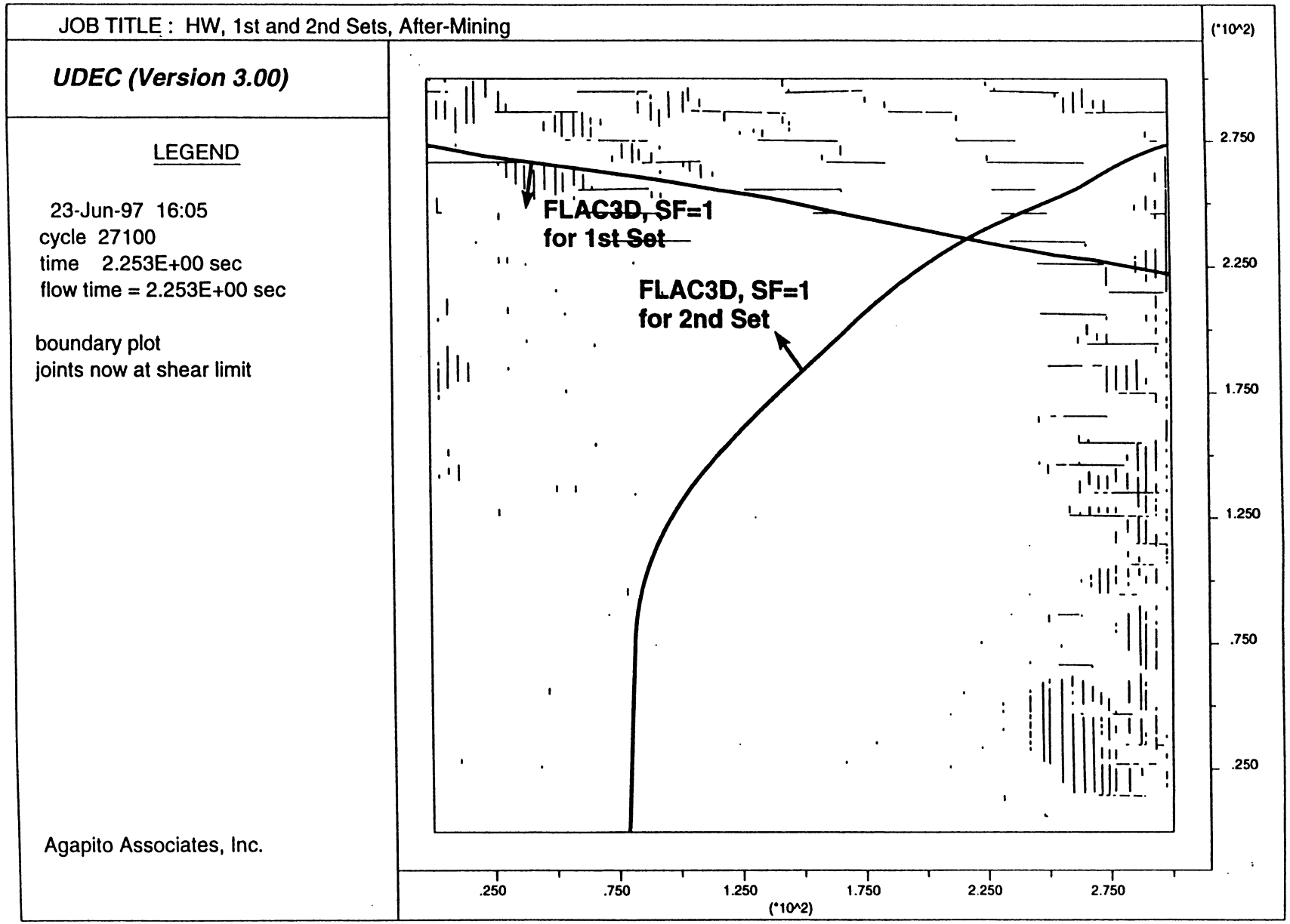

Figure B-11. Predicted Regions of Joint Opening/Dilation, HW Block, Two Joint Sets

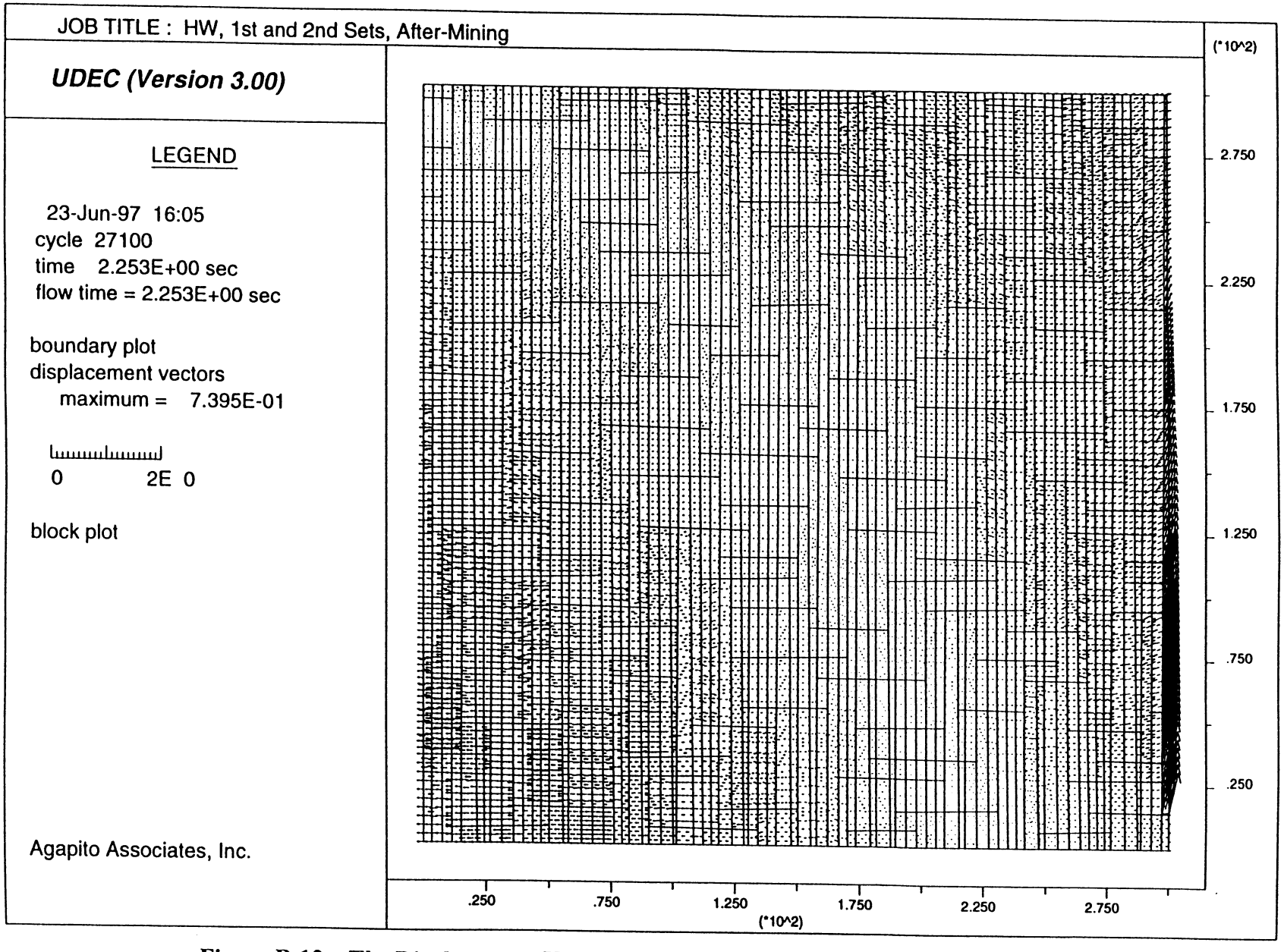

Figure B-12. The Displacement Vectors for the HW Block, Two Joint Sets Case

ATTACHMENT B-1

PROTOCOL—UDEC Joint Interaction Analysis

PROTOCOL - UDEC Joints Interaction Analysis

Objective

Perform two-dimensional UDEC simulations of potential joint shear for the 1st and 2nd sets and investigate the effect of the joints interaction between sets 1 and 2.

Characteristics of the Analysis

1. Fully coupled mechanical-hydrological model. A fixed head difference between the top and bottom of the model will be assumed to initiate the water inflow.

2. Model dimensions up to 300 ft by 300 ft. The location for the analysis is selected in the cross section E278,500 as shown in Figure 1. The location is selected to include regions with safety factor less than 1 for joint sets 1 and 2.

3. The intact and joint properties proposed for the UDEC model are listed in Table 1. Both the Mohr-Coulomb model and the continuously yielding model (CYM) will be used to simulate joint mechanical behavior. Elastic properties for the hanging wall defined in FLAC3D analysis are used as intact rock properties in the model. Joint strength parameters derived previously will be used in Mohr-Coulomb model. Joint mechanical properties, including normal stiffness, shear stiffness, joint tensile strength, joint dilation angle, joint initial friction angle (for CYM), and joint roughness parameter (for CYM) are derived based on best available data. Joint geometrical properties, including joint spacings and joint persistences are derived based on site specific core hole data. Typical values for joint hydrological properties, including aperture for zero normal stress, residual aperture at high stress, and joint permeability constant, are adopted in this model. Statistical joint-set generator will be used for joint generation. Random fluctuation about the mean geometrical properties will be modeled. A 10% standard deviation of random fluctuation is planned for the model.

4. Three analyses will be conducted, the first with only the horizontal set (set 2) and the second with only the vertical set (set 1). The third analysis will include both the horizontal and vertical sets. For each analysis, both the premining stress condition (base case) and mining-induced stress condition will be completed. The results from the first and second analyses will be used to compare with the third analysis to quantify the possible interaction of the sets 1 and 2.

5. Stresses calculated from FLAC3D at location shown in Figure 1 will be used as the traction boundary conditions for UDEC analysis. Traction boundary condition will be used for the upper and lateral boundaries. Both displacement and traction boundaries will be applied to the lower boundary. The lower boundary will be fixed in the vertical direction and with imposed shear stress in the horizontal direction. The out of plane shear stresses will be neglected as required in a plane-strain UDEC analysis.

Evaluation of Results

1. Identify regions where opening/dilation is possible for base case and post-mining case in all three analyses and comparing the extent of results from the third analysis to those from the first and second analyses.

2. Calculate the vertical flow through the modeled block and assess the effect of joint interaction to the flow rate. Discuss the effect of the mining-induced stress changes on the effective hydraulic conductivity of the block.

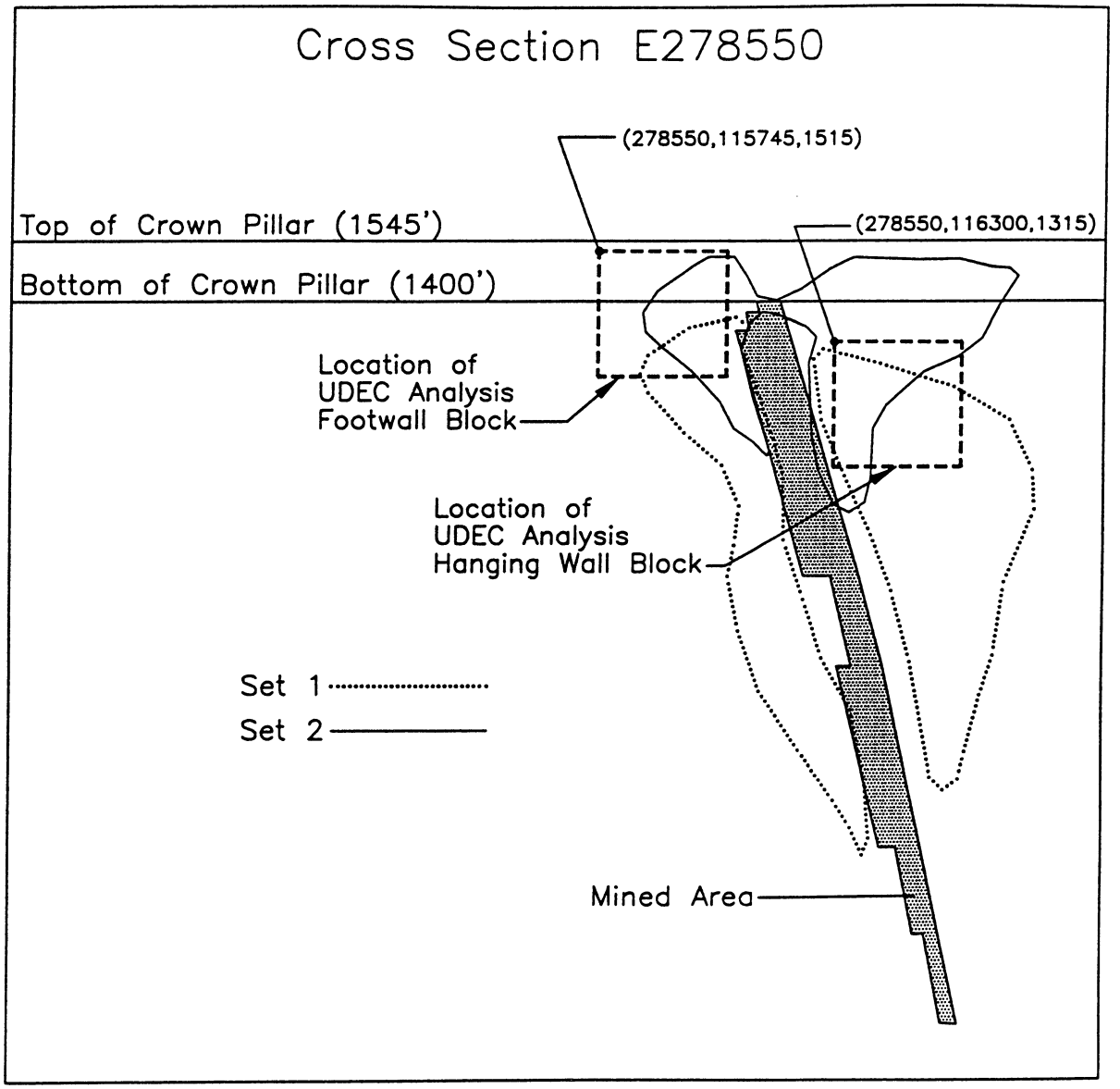

Figure 1 Proposed Location for UDEC Analysis

Table 1 Intact and Joint Properties Proposed for UDEC Model

Intact Properties		
Crown Pillar Horizon	Elastic Modulus (psi)	7.70E+05
	Poisson's Ratio	0.25
Hanging Wall	Elastic Modulus (psi)	1.54E+06
	Poisson's Ratio	0.25
Footwall	Elastic Modulus (psi)	3.25E+06
	Poisson's Ratio	0.25
Joint Mechanical Properties		
Mohr-Coulomb Model	Normal Stiffness (psi/in)	4.00E+04
	Shear Stiffness (psi/in)	4.00E+04
	Tensile Strength (psi)	0
	Cohesion (psi)	15
	Friction Angle (degree)	39
	Dilation Angle (degree)	9
Continuously Yielding Model	Normal Stiffness (psi/in)	4.00E+04
	Shear Stiffness (psi/in)	4.00E+04
	Tensile Strength (psi)	0
	Cohesion (psi)	15
	Initial Friction Angle (degree)	39
	Intrinsic Friction Angle (degree)	30
	Roughness Parameter (mm)	0.1
Joint Geometrical Properties		
	Spacing for Set 1 (ft)	4
	Spacing for Set 2 (ft)	10
	Persistence for Set 1 (%)	100
	Persistence for Set 2 (%)	50–100
Joint Hydrologic Properties		
	Aperture for Zero Normal Stress (mm)	0.2
	Residual Aperture at High Stress (mm)	0.005
	Joint Permeability Constant (1/psi/sec)	5.7×10^5

Appendix 4.2-12

Crandon Project Tailings Management Area
Groundwater Quality Performance Evaluation (Depyritized Tailings)

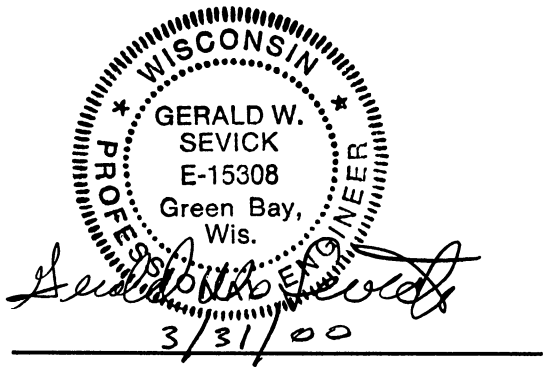

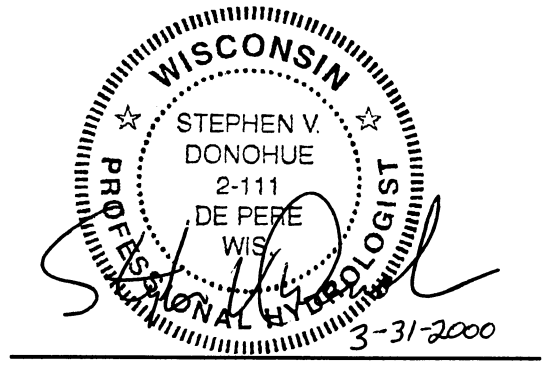

Crandon Project Tailings Management Area Groundwater Quality Performance Evaluation (Depyritized Tailings)

Scope ID: 00C002

Prepared for
Nicolet Minerals Company
7 North Brown Street, 3rd Floor
Rhinelander, WI 54501-3161

Prepared by
Foth & Van Dyke and Associates Inc.

June 1999
Updated March 2000

Foth & Van Dyke 2000
2737 S. Ridge Road, P.O. Box19012, Green Bay, Wisconsin 54304, 920/497-2500, FAX: 920/497-8516

Crandon Project Tailings Management Area
Groundwater Quality Performance Evaluation (Depyritized Tailings)

Executive Summary

Introduction

As part of the permitting process for the Crandon Project tailings management area (TMA and reclaim pond), Nicolet Minerals Company (NMC) must demonstrate that the facilities will not cause concentrations of substances in the groundwater at or beyond the DMZ that exceed groundwater quality standards by a statistically significant amount. The *Crandon Project Tailings Management Area Groundwater Quality Performance Evaluation (Depyritized Tailings)* report documents the methodology used by NMC to complete this demonstration. The evaluation concluded that in all cases, the predicted concentrations for all parameters for both the best engineering judgement and practical worst case scenarios fall below the groundwater standards and that the facilities will not cause an exceedance of groundwater standards at the DMZ boundary.

Methodology

The method used to perform the assessment consisted of the following four steps:

- Defining the quality (source concentrations) of water that might percolate from the facilities.

- Calculating the estimated incremental groundwater changes at the DMZ boundary due to the facilities without considering baseline groundwater concentrations.

- Evaluating existing groundwater quality data to define baseline conditions and to determine if any baseline concentrations exceed the groundwater standards for the facilities, and if required, establishing alternative concentration limits for those parameters that do.

- Combining the baseline concentrations and estimated incremental groundwater changes due to the facilities, and comparing the resulting estimated parameter concentrations at the DMZ boundary to groundwater standards, to determine if the facilities as designed will meet those standards.

Water flow patterns in the TMA, tailings mineralogy and geochemistry and the sequence of reactions or "reaction path" that the tailings will follow if they are exposed to oxygen, and rates of oxygen supply to the tailings were all considered in characterizing the quality of the water that might percolate from the TMA. Both an expected and an upper bound concentration was determined for the potential solutes of interest in the tailings pore water. The source

concentrations were estimated for the operations period and post-closure period. Source concentrations were also estimated for the reclaim pond during TMA operations and following TMA closure, when the reclaim pond is used to store leachate collected from the TMA.

The resulting source concentrations for TMA percolate and reclaim pond were used as inputs to the project's solute transport model to produce predictions of the incremental groundwater changes at the DMZ boundaries. A superpositioning and scaling technique was used to estimate these changes considering the potential variation in source concentration over time.

An evaluation of current groundwater regulations applicable to the facilities was done to define groundwater standards. The analytical results from the monitoring of groundwater in the vicinity of the facilities were analyzed statistically to define current groundwater quality in the area. The statistical analysis resulted in the establishment of alternative concentration limits for a number of parameters. The baseline groundwater quality was added to the estimated incremental changes at the DMZ boundaries to generate an estimate of parameter concentrations at the DMZ boundaries.

Results

The estimated parameter concentrations at the DMZ boundaries for both the best engineering judgement and practical worst case scenarios were compared to the groundwater standards and the alternative concentration limits. In all cases, the predicted concentration for all parameters fell below the standard or alternative concentration limit. Therefore, it was concluded that the TMA and reclaim pond as designed will not cause an exceedance of groundwater standards at the DMZ boundaries. This conclusion is further supported by the conservative assumptions used in completing each individual element of the evaluation. A synopsis of the most significant of these assumptions follows:

- The practical worst-case analysis is based on a combination of both conservative and unlikely parameters.
- An assumed instantaneous degradation of the HDPE geomembrane in the composite liner system.
- For the modeling of oxygen transport into the uncovered tailings, the assumption that the tailings will begin to drain immediately after deposition ceases.
- Use of conservatively high estimates of oxidation rates for all oxygen transport modeling.
- In the geochemical equilibrium modeling, the assumption of low redox potential, no co-precipitation or sorption, high carbon dioxide, and no siderite formation which lead to high estimates, in particular, of iron and arsenic concentrations in the oxidation zone.

- Neglecting the potential effect of oxidation reactions on percolation rates.

- The assumption that solute released from the TMA will be transported as a nonreactive material whose concentration will be controlled only by advection and dispersion processes. No chemical reactions, such as adsorption, chemical precipitation, or decay, were assumed to occur. Disregarding geochemical reactions is conservative with respect to travel time (adsorption) and with respect to maximum concentrations at the DMZ boundaries (decay and precipitation) as these reactions would tend to reduce the number of constituents in the solute thus reducing concentrations at the DMZ boundaries.

- Disregarding adsorption, chemical precipitation, decay and dilution in the unsaturated zone.

Crandon Project Tailings Management Area
Groundwater Quality Performance Evaluation (Depyritized Tailings)

Contents

Page

Tables

Figures

(Note: Figures for the Crandon Project Tailings Management Area Groundwater Quality Performance Evaluation are located at the end of the text, following page 51)

Page

Page

Appendices

1 Introduction

Since the fall of 1993, Nicolet Minerals Company (NMC) has been working to obtain permits to mine a zinc and copper deposit located near Crandon, Wisconsin. The permitting process has included baseline data collection, the preparation of an Environmental Impact Report (EIR), and the preparation of numerous permit applications. The operating plan for the proposed project includes underground mining, ore beneficiation on the surface, and the return of about 75% of the tailings underground as cemented paste backfill in the mined-out stopes. The remaining depyritized tailings will be placed in the tailings management area (TMA) which is to be located approximately 1 mile to the east of the plant site. The characterization of the TMA site and a presentation of its proposed design are discussed in the May 1995 *Tailings Management Area Feasibility Report/Plan of Operation* (Foth & Van Dyke, 1995a) and Addenda No. 1, 2, 3, 4, and 5 (Foth & Van Dyke, 1996a, 1996b, 1997, 1998a, 1998b, and 1999). The TMA design includes a composite liner, a leachate collection system located above the liner, and composite cover to minimize infiltration into and percolation from the facility.

A major consideration in the design of the TMA and its adjacent water reclaim pond was the development of facilities that will be in compliance with groundwater regulations. The objective of this report is to provide the documentation of the methodology used by NMC to evaluate the performance of the TMA and reclaim pond in relation to groundwater standards. The method used to perform the assessment consisted of the following four steps:

- Define the solute concentrations in water that could percolate from the facilities.
- Calculate the estimated incremental groundwater changes at the DMZ boundary due to the facilities without considering baseline groundwater concentrations.
- Evaluate existing groundwater quality data to define baseline conditions and to determine if any baseline concentrations exceed the groundwater standards for the facility, and if required, establish alternative concentration limits (ACLs) for those parameters that do.
- Combining the baseline concentrations and estimated incremental groundwater changes due to the facilities and comparing the resulting estimated parameter concentrations at the TMA and reclaim pond design management zones (DMZ) to groundwater standards, and ACLs where appropriate, to determine if the facilities as designed will meet the standards.

The derivation of the TMA source concentrations is discussed in Section 2 of this report. The derivation work was performed by Steffen Robertson and Kirsten (Canada), Inc. (SRK). The SRK analysis includes:

- An evaluation of the patterns of water flow into, within and out of the TMA.

- Characterization of the mineralogical and geochemical properties of the tailings, and the sequence of reactions or "reaction path" that the tailings will follow if they are exposed to oxygen.

- Estimation of the rates of oxygen supply to the tailings at different stages in the TMA life.

- Characterization of the solute concentrations at different stages of the TMA life that will result from the combined effects of water flow, oxygen supply, and geochemical reactions.

The determination of the estimated incremental groundwater changes at the DMZ boundary due to the TMA and reclaim pond (Section 3) was performed by HSI GeoTrans, Inc., based on the work presented in their report *Update No. 3 to: Numerical Simulation of Potential Solute Transport at the Proposed Zinc and Copper Mine Near Crandon, Wisconsin* (HSI GeoTrans, 2000). This updated report is included in Appendix 4.2-10 of the Crandon Project EIR (Foth & Van Dyke, 1995/1998c). The work by HSI GeoTrans involved taking the source concentrations derived from the SRK analysis and integrating these concentrations with the solute transport model to develop estimated groundwater concentrations at the DMZ boundaries without considering baseline conditions. Model predictions include a best engineering judgement for transport (BEJT) case, which uses reasonable flow and solute transport parameters, and a practical worst case for transport (PWCT) which uses a combination of conservative and unlikely parameters. Concentration versus time graphs and figures showing the areal distribution of concentrations for the BEJT and PWCT scenarios were developed by HSI GeoTrans for selected parameters.

The evaluation of existing groundwater quality data and the TMA performance assessment presented in Section 4 of this report were completed by Foth & Van Dyke. The assessment concluded that in all cases, the predicted concentration for all parameters for both the BEJT and the PWCT scenarios falls below the groundwater standards and ACLs. Therefore it is concluded that the TMA will not cause an increase in groundwater concentrations harmful to public health, safety or welfare.

Section 5 of this report discusses conclusions of the work performed and describes the conservative nature of many of the inputs and analyses. Finally, a series of appendices are also included with the report. Appendix A contains a series of reports relating to the project's waste characterization work. Appendix B contains a description of, and the results from geochemical equilibrium modeling. Appendix C consists of a series of reports describing the oxygen transport modeling completed for the TMA. Appendices D and E contain additional information in relation to the methods used to define the TMA source concentrations. Appendix F includes calculations to establish baseline concentrations and ACLs.

This document dated March 2000 supersedes both the original *Crandon Project Tailings Management Area Groundwater Quality Performance Evaluation* issued in 1997 and the updated reports issued in April 1998 and June 1999. This report was prepared to incorporate TMA design modifications (Foth & Van Dyke, 1998b), the review and comments of the WDNR and its consultants, and revisions to the project's solute transport model (HSI GeoTrans, 2000).

2 TMA Source Concentrations

2.1 Introduction

In order to estimate solute concentrations in water that could percolate from the TMA, NMC and its consultants applied a combination of mathematical models, literature review, and laboratory waste characterization studies. The overall approach consisted of first defining the key processes that will influence solute concentrations, and then investigating each process and describing it by either a detailed sub-model or a conservative assumption derived from laboratory or literature data. The use of detailed modeling only when required, in combination with conservative assumptions, is intended to produce conclusions that are as clear as possible.

Figure 2-1 summarizes the steps involved in estimating solute concentrations in the water that could percolate from the TMA. The figure clarifies the logic used in the investigation. A description of the key elements in that logic follows:

- The pattern of water flow into, within, and out of the TMA influences all of the processes listed below. Flow patterns were characterized through the HELP modeling that was carried out during the TMA design and reported by Foth & Van Dyke (1998b) (see Section 2.2 below).

- The geochemical properties of the tailings were characterized as the sequence of reactions or "reaction path" that the tailings will follow as they come into equilibrium with the TMA environment. The reaction path is in turn a consequence of the inherent mineralogical and geochemical properties of the tailings (see Section 2.3 and Appendices A and B).

- To characterize the rate of oxygen supply to the tailings, the processes of oxygen transport into the TMA were modeled (see Section 2.4 and Appendix C). Since oxygen transport is much faster in unsaturated than in saturated porous media, the oxygen transport modeling required an understanding of water flow patterns within the TMA. The oxygen consuming reactions of the tailings were also required as inputs to the oxygen transport models.

- Leachate solute concentrations were determined based on expected geochemical reactions within the TMA (see Section 2.5), which are in turn influenced by the three factors listed above.

Throughout the investigation, two sets of estimates were carried forward. The best engineering judgement or BEJT estimates were based on moderately conservative assumptions. As a form of sensitivity analysis, more conservative assumptions were applied and used to derive "upper bound" or UB estimates.

2.2 Water Flow Patterns

2.2.1 Results of HELP Modeling

HELP model calculations were conducted to support the design of the TMA composite liner, leachate collection system, and cover systems. Model runs were completed for the upper sidewall, the lower sidewall and the base of a representative TMA cell, as shown in Figure 2-2. The design calls for three TMA cells to be sequentially constructed, operated, and then closed. The operating life of each cell will last from 6 to 16 years, depending on the size of the TMA cell in question. *Addendum No. 5 to the Tailings Management Area Feasibility Report*, (Foth & Van Dyke, 1998b), reports the results of HELP modeling, including estimates of the rates of infiltration into the TMA, flow rates in the leachate collection system, and the rates of percolation through the composite liner system into the underlying soil.

The flow patterns apparent from the HELP modeling can be summarized as follows:

- The maximum flows into the TMA, the maximum leachate collection, and the maximum percolation rates from the TMA will occur during the period of active tailings deposition.

- After a cell's cover is in place, infiltration will drop to very low levels estimated at 0.00002 in/yr. As a result, both leachate collection and percolation rates will diminish rapidly. Leachate collection rates will be dependent on the amount of freely drainable water within the TMA. Leachate collection rates will decrease as freely drainable water is removed by the leachate collection system. In contrast, percolation rates are dependent on the head across the composite liner and the hydraulic conductivity of the drainage layer. At the base of the TMA, the leachate collection system will limit the head on the liner, and thereby limit percolation rates. Along the sidewall, the 3:1 slope and the efficiency of the geocomposite drainage layer will result in very small heads on the liner, and percolation rates will be negligible.

- Drainage of freely drainable water within the tailings mass will continue to diminish for a period of up to 125 years after cell closure. Due to the fine grained nature of the tailings, approximately 70% of the water will be retained by capillary suction.

- After drainage of freely drainable water ceases, the TMA will reach a near steady state condition in which the maximum rate at which water can percolate through the composite liner will be limited by the rate of infiltration through the cover.

- The high density polyethylene (HDPE) geomembrane included in the TMA composite liner and cover system is expected to function as designed for a very long time (e.g., hundreds of years) without deterioration in performance (GeoSyntec, 1996). For the HELP Model analysis, NMC postulated that the HDPE in the composite liner would deteriorate instantaneously 150 years after installation. This assumption is very

conservative since the HDPE specified for the TMA composite liner system should not degrade for hundreds of years and, if it does, the degradation process will be very slow, not instantaneous (GeoSyntec, 1996).

2.2.2 Percolation Rates

Table 2-1 summarizes the percolation rates estimated from the HELP modeling. The results are grouped into seven flow phases, each of which represents a period of similar percolation rates. Such grouping produces a manageable number of inputs into the subsequent calculations of solute load and transport, as described in more detail in HSI GeoTrans (2000). The average percolation rate within each operational phase was assumed to represent the percolation for the entire phase. Figure 2-3 shows the cumulative percolation rates from all three cells.

The HELP modeling did not consider the effect of geochemical reactions on water flow patterns within the TMA. The oxidation of sulfide minerals consumes water, as does the subsequent precipitation of secondary minerals. Although these effects are unlikely to alter flow patterns in the short term, they may be very influential once the TMA cover limits infiltration, and drainage of freely drainable water ceases. Under those conditions, oxidation reactions could cause a significant reduction in the water content of the surrounding tailings. The resulting water content and salinity gradients would tend to draw water into and toward the oxidation zone. Calculations presented in Appendix E show that the net consumption of water in reactions within the TMA will significantly exceed the long term rate of infiltration through the cover. The implication of this is that long-term percolation from the TMA will be less than the already very low rate predicted by the HELP modeling, or will even be eliminated altogether.

2.2.3 Water Content Estimates

The HELP model runs were conducted under the assumption that the tailings will remain saturated during deposition. The operating plan calls for regular rotation of the tailings deposition points around the circumference of each TMA cell. At any point on the circumference, the maximum time between deposition events will be about three months. In such a short period, the phreatic surface is unlikely to fall even a few feet below the surface. Hence, the assumption that the tailings surface will remain largely saturated during deposition is appropriate.

Figure 2-4 shows the water content profiles predicted by the HELP model after one year and two years of drainage during the consolidation period. The HELP modeling disregarded the effects of consolidation, and assumed that the tailings begin to drain (downward) immediately after deposition ceases. This assumption is conservative in that it leads to a higher estimate of oxygen transport rates.

Table 2-1

Percolation Rates from HELP Model Results

Flow Phase	Description	Assumed Duration (years)	Percolation Rates (in/yr)		
			Base	Lower Sidewall	Upper Sidewall
A	Lower Stage Operations	2-4	0.00644	2.5×10^{-7}	NA
B	Upper Stage Operations	4-10	0.00847	2.5×10^{-7}	1×10^{-6}
C	2 Year Consolidation Period	2	0.00847	2.5×10^{-7}	1.0×10^{-6}
D	Cap in Place - Part 1	8	0.00834	4.6×10^{-7}	5.0×10^{-7}
E	Cap in Place - Part 2	20	0.00042	2.5×10^{-7}	2.5×10^{-7}
F	Cap in Place - Part 3	104-114	6.1×10^{-5}	2.5×10^{-7}	2.5×10^{-7}
G	Assumed Degraded Geomembrane - Steady State	Indefinite	2.0×10^{-5}	2.0×10^{-5}	2.0×10^{-5}

NA = Not Applicable

Prepared by: DH
Checked by: SVD1/NXP
Revised by: SVD1
Checked by: NXP

Table 2-2

Tailings Water Contents from HELP Model Results

Flow Phase	Description	Assumed Duration (years)	Water Content Assumed in Oxygen Transport Modeling
A	Lower Stage Operations	2-4	Saturated
B	Upper Stage Operations	4-10	Saturated
C	2 Year Consolidation Period	2	Partially Drained - see Figure 2-4
D	Cap in Place - Part 1	8	Field Capacity
E	Cap in Place - Part 2	20	Field Capacity
F	Cap in Place - Part 3	104-114	Field Capacity
G	Assumed Degraded Geomembrane - Steady State	Indefinite	Field Capacity

Prepared by: DH
Checked by: JWS
Revised by: SVD1
Checked by: NXP

The HELP model predicts that, after the TMA cover is in place, the tailings will continue to drain pore water until 125 years after closure. Table 2-2 summarizes the water content values used in the oxygen transport modeling that correspond to the flow phases introduced in Section 2.2.2.

2.3 Depyritized Tailings Geochemistry and Reaction Path

2.3.1 Depyritized Tailings Composition

The laboratory investigations carried out to characterize the geochemistry of the depyritized tailings are discussed in Appendix A1. Appendix A2 discusses other solids, namely waste rock and wastewater treatment solids, that will also be placed in the TMA, and shows that they will not significantly alter the geochemical properties of the depyritized tailings. Results of additional laboratory tests, including humidity cell tests of the depyritized tailings, are provided in Appendix A3.

Characterization of the depyritized tailings composition included bulk chemical analyses, acid base accounting, and mineralogical examinations. The key results are summarized in Tables 2-3 to 2-5. Table 2-3 summarizes the results of bulk chemical analyses. Table 2-4 shows the results of acid base accounting.

Table 2-5 shows the primary mineral phases identified in the mineralogical examinations completed for the project. The abundance of each phase was estimated using optical microscope point counts (Appendix A1). Microprobe analysis of the carbonate minerals (Appendix A4) indicated that the tailings are dominated by ferroan dolomites (90 percent of the carbonates), which contain trace amounts of iron and manganese. Correcting the composition of the carbonates for the iron and manganese content in the ferroan dolomites, as well as the portion of the carbonates that are present as siderite, indicates 84 percent of the carbonate in the tailings is associated with calcium or magnesium, and, therefore, has the potential to neutralize acidity (i.e., 84 percent of the CO_3-NP value in Table 2-4). Appendix A5 discusses the representativeness of the samples used in this and other tailings characterization work.

NMC has committed to a detailed tailings monitoring plan and to adding additional limestone to the tailings, if necessary, to maintain neutral conditions. The NP addition, control, and monitoring program is described in Appendix A6.

2.3.2 Reaction Path

As the depyritized tailings are placed in the TMA, they will begin to undergo a series of reactions that will result in modifications to the chemical composition of the tailings pore water. The series of reactions, or reaction path, has been determined from the geochemical characterization (Appendix A1), the short term humidity cell tests (Appendix A3), and geochemical equilibrium modeling described in Appendix B.

Table 2-3

Summary of Bulk Chemical Analysis of Depyritized Tailings Samples

Parameter	Units	Depyritized Tailings	Depyritized Tailings (duplicate)	Average
Aluminum	mg/kg	37,500	37,500	37,500
Antimony	mg/kg	20	20	20
Arsenic	mg/kg	100	100	100
Barium	mg/kg	70	100	85
Beryllium	mg/kg	<10	<10	<10
Cadmium	mg/kg	<5.0	<5.0	<5
Chromium	mg/kg	24	23	23.5
Copper	mg/kg	89	89	89
Iron (total)	mg/kg	38,200	38,700	38,450
Fluoride	mg/kg	1,000	1,000	1,000
Lead	mg/kg	<500	600	<550
Manganese	mg/kg	1100	1100	1100
Mercury	mg/kg	<0.3	<0.3	<0.3
Nickel	mg/kg	11	9.3	10.15
Potassium	mg/kg	15,000	15,000	15,000
Selenium	mg/kg	<3	<3	<3
Silver	mg/kg	2.5	2.0	2.25
Sulfur (T)	mg/kg	7,600	7,500	7,550
Zinc	mg/kg	1,200	1,300	1,250

Prepared by: JTC
Checked by: DEH

Table 2-4

Summary of Acid Base Accounting Tests of Depyritized Tailings Samples

Sample ID	Paste pH s.u.	Sulfur (T) %	Sulfur (Sulfide) %	Sulfur (Sulfate) %	CO_3 %	CO_3-NP[1]	Sobek NP[1]	AP[1,2]	NNP[1]	Sobek NP/AP	CO_3-NP/AP
Depyritized Tailings	6.73	0.82	0.72	<0.4	5.37	89.5	76.1	25.6	50.5	3.0	3.5
Depyritized Tailings (dup.)	6.75	0.75	0.54	<0.4	5.38	89.7	74.4	23.4	51.0	3.2	3.8

[1]Units for all NP, AP and NNP are kg $CaCO_3$ eq/tonne.
[2]AP calculated from total sulfur.

Prepared by: JTC
Checked by: DDS

Table 2-5

Estimated Mineral Abundance in Depyritized Tailings Samples

Mineral	Depyritized Tailings[1,2,3]
Opaques:	
Pyrite	trace
Other Sulfides	trace
Sphalerite	trace
Arsenopyrite	trace
Galena	trace
Chalcopyrite	trace
Pyrrhotite	trace
Iron Oxyhyroxides	trace
Hematite	trace
Non Opaques	
Quartz	72
Muscovite/Illite	6.9
Chlorite	3.4
Carbonates	17

[1]Units are in percent abundance.
[2]Trace indicates <0.2%
[3]Results are based on point counts of 500 mineral grains and are semi-quantitative.

Prepared by: KSS
Checked by: DDS

The reaction path expected for the Crandon tailings is graphically depicted in Figure 2-5(a), and summarized below:

1. During tailings deposition, the pore water in the TMA will be refreshed continually and flushed through the tailings. Solute concentrations in the pore water will be determined largely by the composition of the water that is used to transport tailings from the mill to the TMA. Section 2 of Appendix B discusses the sources and composition of the "process water".

2. Over time, as the flow of process water through the tailings slows, the pore water will equilibrate with the tailings. Solute concentrations will then be determined by a combination of the initial process water concentrations and by secondary equilibration with the tailings solids (under anoxic conditions).

3. Assuming that the tailings are subsequently exposed to oxygen, the sulfide minerals in the tailings will begin to oxidize and initiate a series of reactions. The acidity released by the oxidation reactions will be neutralized by reactions with carbonate minerals also present in the tailings. The carbonate minerals will buffer the pore water to approximately neutral pH, which in turn will lead to the precipitation of some metals as hydroxide or carbonate phases. Other reactions expected to be associated with the oxidation are precipitation of calcium and sulfate as gypsum, and co-precipitation of anionic solutes, such as arsenic, with iron and aluminum hydroxides.

The depyritized tailings characterization program (Appendix A1), and the humidity cell tests (Appendix A3) represent investigations of the above reaction path. Results to date indicate that the depyritized tailings will remain at neutral pH. As mentioned, NMC is committed to adding limestone to the tailings, if necessary, to maintain neutral conditions.

Another significant result of the testing to date is a quantification of the rates at which solutes will be released by oxidation of the depyritized tailings. As discussed in Appendix A3, the depyritized tailings oxidize relatively slowly, even in the presence of abundant oxygen. Oxidation rates of 5.6×10^{-10} to 3×10^{-9} moles O_2 kg^{-1} s^{-1} have been estimated from the humidity cell tests. The oxidation and subsequent reactions will result in the release of solutes from mineral phases in the depyritized tailings. Table 2-6 shows the rates at which solutes were released (relative to sulfur), in the short term humidity cell tests.

Figure 2-5(b) shows how the steps in the reaction path would translate into two zones in a hypothetical TMA cell subjected to continuing oxidation at the surface (e.g., during the final stages of consolidation). In the figure, the oxidation zone near the surface is well developed. However, neutral pH conditions are maintained by the carbonate minerals present in the oxidation zone. Below the oxidation zone is the area within which conditions are still dominated by the equilibrated process water.

Table 2-6

Relative Solute Release Rates Under Oxidizing Conditions

Parameter	Relative Release Rate (mole solute / mole S)
Al	3.2E-03
Sb	1.7E-04
As	5.5E-03
Ba	3.8E-05
Be	1.0E-03
Cd	1.9E-05
Cr	7.2E-05
Cu	1.4E-04
F	2.0E-02
Pb	5.8E-03
Mn	4.0E-02
Hg	4.5E-06
Ni	2.03-04
K	2.9E-02
Se	5.3E-04
Ag	2.4E-05
Na	4.3E-02
SO_4	1.0E+00
Zn	2.0E-02

Prepared by: DEH
Checked by: KSS

2.4 Oxygen Transport into TMA

The reaction path presented in the preceding section is a useful tool to summarize many results of the geochemical characterization. However, the reaction path only defines the sequence of reactions, not the rate at which they will occur. In the TMA, progress along the reaction path will be limited by the supply of oxygen.

The supply of oxygen into the TMA was initially investigated by the oxygen transport modeling for pyritic tailings presented in a report contained in Appendix C1. Also included in that appendix is a March 7, 1998, letter (SRK, 1998) providing responses to the requests from the WDNR for clarification and additional information pertaining to the oxygen transport modeling report. Appendix C1 shows that by far the greatest oxygen fluxes into the TMA will occur during the tailings consolidation period.

The depyritized tailings to be placed in the TMA will have lower oxidation rates and different moisture retention properties than the tailings modeled in Appendix C1. Appendix C2 provides an update, based on depyritized tailings, to the earlier estimates of oxygen transport for the consolidation period.

Figure 2-6 presents the results of the updated oxygen transport modeling for the depyritized tailings in schematic form. The following are the most important conclusions from the work:

- The low rates of oxygen transport into saturated tailings will limit oxidation to a negligible minimum during tailings deposition.

- During the consolidation period, the surface of the tailings is assumed to become unsaturated (see Section 2.2.3). Oxygen will diffuse rapidly through the unsaturated pore space. Using conservatively high estimates of oxidation rates and diffusion coefficients, it was estimated that approximately 76 to 147 moles of O_2 gas will penetrate each square meter of the tailings surface in each year that the surface is unsaturated. The resulting oxidation will generate enough acidity to consume 4.1 to 7.8 kg $CaCO_3$ per square meter of tailings surface per year. Using the most conservative reaction model, the oxygen was estimated to penetrate 3 to 6 feet into the tailings.

- After the cover is in place, oxygen transport into the TMA through the tailings surface will be reduced to less than 0.2 kg $CaCO_3$ equivalent per square meter per year.

- Oxygen transport into the TMA through the intact composite liner will be insignificant. However, if it is assumed that the HDPE in the liner degrades, oxygen transport through the liner will increase. Near the point where the upper sidewall liner approaches the ground surface, oxygen transport through an assumed degraded liner is estimated to be as high as 10 kg $CaCO_3$ equivalent per square meter of liner per year. The rate of oxygen penetration through the liner will drop off sharply with depth, and

will be much lower at the middle of the lower phase sidewall. Oxygen penetration through the base will be limited to less than $1x10^{-4}$ kg $CaCO_3$ equivalent per square meter per year.

Appendix C3 presents a similar modeling effort to estimate the concentrations of carbon dioxide that will develop within the pores of the oxidation zone. As discussed in Appendix B, carbon dioxide accumulation can influence pore water chemistry.

2.5 Solute Concentrations in TMA Pore Water

Estimates of solute concentrations in the tailings pore water were obtained through geochemical equilibrium modeling, literature review, the depyritized tailings characterization, and review of water quality measurements from humidity cell tests. A complete discussion of the geochemical equilibrium modeling is provided in Appendix B.

2.5.1 During Tailings Deposition

As noted in Section 2.4, the rate of oxygen transport into the tailings during deposition, and hence the rate of oxidation, are predicted to be negligible. The only reactions that will occur will be continuing equilibration between the tailings and the pore water, with significant dilution by the continual influx of process water.

Table 2-7 summarizes the estimates of solute concentrations in the tailings pore water during tailings deposition. The first column shows estimates of solute concentrations in the process water as it enters the TMA. As discussed in Appendix B, the process water will be a mixture of streams from several sources. The values in the first column of Table 2-7 represent a weighted average of the composition of each source stream with an adjustment to the calcium and sulfate concentrations to account for buildup of sulfate in the mill (Appendix B, Section 2.1).

The geochemical equilibrium model MINTEQA2 was used to define solubility controls on some elements at neutral pH. The results are also listed in the second column of Table 2-7. Comparison of the solubility limits with the measured values indicates that the process water is supersaturated with respect to some of the expected secondary mineral phases. Over time, the process water that remains in the tailings pores would be expected to come into equilibrium with these phases.

The last two columns of Table 2-7 show the BEJ and UB estimates of solute concentrations in the portion of the tailings that is dominated by process water which has equilibrated with the tailings solids. Where the equilibrium modeling indicated supersaturation of a secondary mineral, the equilibrium concentration was used as the BEJ estimate. The maximum value from the process water and the MINTEQA2 modeling was used as the UB estimate. Note that this approach leads to some of the BEJ estimates being as high as the UB estimate.

Table 2-7

Pore Water Quality in Process Water Dominated Zone[1]

	Average of Inputs (mg/L)	MINTEQA2 (mg/L)	BEJ Estimate (mg/L)	UB Estimate (mg/L)
Al	0.94	0.0050	0.0050	0.94
Sb	0.071	0.012	0.012	0.071
As	0.069	—	0.069	0.069
Ba	0.035	0.0033	0.0033	0.035
Be	0.00045	—	0.00045	0.00045
Cd	0.0061	—	0.0061	0.0061
Ca	549	624	549	624
Cr	0.038	—	0.038	0.038
Cu	0.047	—	0.047	0.047
F	0.38	—	0.38	0.38
Fe	0.33	2.9	0.33	2.9
Pb	0.19	—	0.19	0.19
Mg	5.1	326	5.1	326
Mn	0.68	—	0.68	0.68
Hg	0.00018	—	0.00018	0.00018
Ni	0.045	—	0.045	0.045
K	15	—	15	15
Se	0.20	—	0.20	0.20
Ag	0.066	—	0.066	0.066
Na	27	—	27	27
SO_4	1599	2714	1599	2714
Zn	6.9	40	6.9	40

[1]Table 4 from Geochemical Modeling report contained in Appendix B.

Prepared by: KSS
Checked by: DEH
Revised by: KSS
Checked by: JTC

2.5.2 During Consolidation

2.5.2.1 Oxidation Zone

During the latter part of the consolidation period, when the tailings surface becomes unsaturated, oxygen transport through the unsaturated pore space will cause oxidation of the near surface tailings. To estimate solute concentrations within the oxidized zone, the following assumptions were made:

- An oxygen transport rate of 4.0 kg $CaCO_3$ equivalent per square meter per year was assumed to be maintained for one year.
- The oxygen input was assumed to be consumed within the first 2.0 m (6.6 feet) of tailings, as indicated by the oxygen transport modeling.

The steps involved in translating these assumptions to BEJ estimates of solute concentrations in the oxidation zone pore water were as follows (example calculations are given in Appendix D):

1. The amount of sulfide that could be oxidized below each square meter of tailings surface was calculated, and the relative release rates in Table 2-6 were used to estimate the resulting release of each solute during one year of oxidation.
2. The mass of each solute released was divided by the amount of water flowing through the oxidation zone to estimate the contribution of oxidation and neutralization reactions to each solute's concentration.
3. The concentrations contributed by the reactions were then added to the concentrations initially present in the pore water to obtain preliminary estimates of each solute's concentration in the oxidation zone.
4. The estimates were compared to solubility maxima derived from geochemical equilibrium modeling. The modeling, described in detail in Appendix B, assumed a redox potential of (200 mV) and carbon dioxide concentrations of 12.7 percent. Solid phases allowed to precipitate in the model were selected from literature and laboratory observations. For elements where the initial estimate exceeded the solubility maximum predicted by geochemical equilibrium modeling, the equilibrium model prediction was used.
5. Concentration estimates obtained from either of the preliminary calculations for the equilibrium modeling were then compared to maximum concentrations measured in the humidity cell tests. If a higher concentration was measured in any of the humidity cell tests, it was used as the concentration estimate. (This last step is very conservative for some elements, due to anomolously high concentrations measured in one cycle of one humidity cell.)

To arrive at the UB estimates, the above calculations were repeated with an assumed oxygen flux equivalent to 7.8 kg $CaCO_3$ equivalent per square meter per year, and an oxygen penetration of 1.04 m (3.4 feet). Narrowing the oxidation zone results in all of the oxygen being consumed in a smaller volume of tailings, hence releasing higher concentrations of solutes. To be further conservative, the oxidation period was extended to two years. Geochemical equilibrium modeling results were also used to represent solubility limitations on the UB estimate. However, a lower redox value of 0 mV was used.

Results of the initial estimates of solute concentrations corrected for the solubility maxima, the humidity cell results, and the resulting BEJ and UB estimates are provided in Table 2-8.

2.5.2.2 Process Water Dominated Zone

Below the depth of penetration of water from the oxidized zone, the pore water in the TMA will remain dominated by the characteristics of the equilibrated process water. The estimated solute concentrations provided in Table 2-7 were used as the BEJ and UB estimates for this zone.

2.5.3 After Assumed Degradation of the Geomembrane

The oxygen transport modeling indicates that, if the geomembrane in the composite liner is assumed to be degraded, oxygen penetration through the liner will increase. Since there will be very little water flow, the tailings would essentially be oxidized in place.

As discussed in Section 2.6.3, the oxidized zones are not expected to contribute to percolation from the TMA.

2.6 Solute Concentrations in TMA Percolate

Free draining pore water within the TMA will tend to migrate downward to the leachate collection system. The majority of the free draining water will be collected in sumps, pumped to surface, and treated. A small amount could percolate through the TMA composite liner. Solute concentrations in this percolate will be determined by the pore water concentrations, as estimated in the previous section, and by flow patterns within the TMA.

2.6.1 During Tailings Deposition

During tailings deposition, solute concentrations will be similar throughout the TMA, and dominated by the equilibrated process water. Estimates of the solute concentrations during deposition are shown in Table 2-9. The estimates were taken from the last two columns of Table 2-7. The same concentration estimates apply to any percolate from the TMA during this period.

Table 2-8

Concentrations in Oxidation Zone During Consolidation

Parameter	BEJ after Equilibrium Modeling (mg/L)	UB after Equilibrium Modeling (mg/L)	Humidity Cell (mg/L)	BEJ Estimate (mg/L)	UB Estimate (mg/L)
Al	0.00025	0.0011	0.067	0.067	0.067
Sb	0.012	5.2	0.0047	0.012	5.2
As	23	106	0.033	23	106
Ba	0.0034	0.0020	0.017	0.017	0.017
Be	0.52	2.4	0.0021	0.52	2.4
Cd	0.12	0.56	0.34	0.34	0.56
Ca	559	400	210	559	400
Cr	0.24	0.98	0.0026	0.24	0.98
Cu	0.51	2.2	0.56	0.56	2.2
F	1.9	4.1	0.71	1.9	4.1
Fe	5.6	410	0.069	5.6	410
Pb	9.0	4.8	6.1	9.0	6.1
Mg	931	3,349	89	931	3,349
Mn	16	22	6.6	16	22
Hg	0.050	0.23	0.000016	0.050	0.23
Ni	0.69	3.1	0.36	0.69	3.1
K	75	302	2.80	75	302
Se	2.5	11	0.058	2.5	11
Ag	0.032	0.037	0.0016	0.032	0.037
Na	76	268	3.2	76	268
SO_4	4,224	13,958	1,420	4,224	13,958
Zn	71	350	98[1]	98[1]	350

Notes: underlined values were limited by solubility constraints.

[1] The 98 mg/L value is an extreme outlier in the humidity cell data base. The duplicate cell (HC DPT-IT1) and the other short and long term humidity cell results were all below 5 mg/L. The outlier also affects all other estimates.

Prepared by: KSS
Checked by: DEH
Revised by: KSS
Checked by: JTC

Table 2-9

Estimated Solute Concentrations in Percolate During Operations

Parameter	BEJ Estimate (mg/L)	UB Estimate (mg/L)
Al	0.0050	0.94
Sb	0.012	0.071
As	0.069	0.069
Ba	0.0033	0.035
Be	0.00045	0.00045
Cd	0.0061	0.0061
Ca	549	624
Cr	0.038	0.038
Cu	0.047	0.047
F	0.38	0.38
Fe	0.33	2.9
Pb	0.19	0.19
Mg	5.1	326
Mn	0.68	0.68
Hg	0.00018	0.00018
Ni	0.045	0.045
K	15	15
Se	0.20	0.20
Ag	0.066	0.066
Na	27	27
SO_4	1,599	2,714
Zn	6.9	40
CN	0.30	0.30

Note: cyanide (CN) is discussed in Appendix B.

Prepared by: DEH
Checked by: KSS
Revised by: KSS
Checked by: JTC

2.6.2 During Consolidation

During the two year consolidation period, TMA percolate solute concentrations will be composed of a portion of the solutes contained in the equilibrated process water, as shown in Table 2-9; and those contained in water from the oxidation zone, as shown in Table 2-10. The methodology used to define solute concentrations for the consolidation period for use in solute transport modeling is described in Section 3.2 of this report.

2.6.3 After Consolidation Period

As discussed in Section 2.5.2, the oxygen entry projected to occur during the consolidation period will create an oxidation zone across the surface of the TMA. The process water dominated zone will underly the oxidation zone. The pore water from each zone will migrate downward to the leachate collection system.

As a conservative simplifying assumption, solute concentrations in TMA percolate after the consolidation period were estimated by taking the volume-weighted average of concentrations in the oxidation and process water dominated zones. The volume weighting was based on the total volumes of each water type over the entire TMA. Details of the calculation are provided in Appendix D. The resulting estimates of volume-averaged solute concentrations are shown in Table 2-10.

The fact that this assumption is conservative has been demonstrated by modeling of the flow patterns within the TMA. The modeling indicates that the proportion of water arriving at the leachate collection system from the process water dominated zone will significantly exceed the proportion estimated by the simple volume weighting (Attachment 1 of NMC, 1999). Furthermore, the bulk of the water from the oxidation zone arrives at the sideslope of the TMA, and the HELP model calculations show that by far the majority of percolation occurs through the TMA base.

2.6.4 After Degradation of the Geomembrane

As discussed in Section 2.4, if it is assumed that the geomembrane in the composite liner degrades, oxygen transport modeling predicts that the sulfides in the tailings just inside the liner will begin to oxidize. Current estimates are that degradation of the base HDPE will not occur until hundreds of years after operations cease (GeoSyntec, 1996), i.e., long after the 125 year period required to drain freely drainable water from the TMA. Calculations provided in Appendix E indicate that oxidation at the predicted rates would consume far more water than would be supplied by the limited infiltration through the TMA cover. In fact, the calculations show that even the relatively slow oxidation and secondary mineralization processes directly below the TMA cover will be sufficient to consume any infiltrating water. The result will be a localized water deficit that will draw water into any oxidation zones.

Table 2-10

Estimated Average Solute Concentrations in TMA Percolate After Consolidation

Parameter	BEJ Estimate (mg/L)	UB Estimate (mg/L)
Al	0.014	0.84
Sb	0.012	0.67
As	3.3	12
Ba	0.0052	0.033
Be	0.072	0.28
Cd	0.053	0.070
Ca	550	598
Cr	0.066	0.15
Cu	0.12	0.30
F	0.59	0.81
Fe	1.1	50
Pb	1.4	0.87
Mg	134	674
Mn	2.8	3.2
Hg	0.0071	0.027
Ni	0.14	0.40
K	23	48
Se	0.52	1.4
Ag	0.062	0.063
Na	34	55
SO_4	1965	4010
Zn	20	76
CN	0.30	0.30

Note: Cyanide (CN) is discussed in Appendix B.

Prepared by: KSS
Checked by: DEH
Revised by: KSS
Checked by: JTC

As a conservative assumption, the potential effect of the oxidation reactions on long term percolation rates was neglected. However, a postulated geomembrane degradation of the base liner would not occur until well after freely drainable water has been removed from the TMA. As explained in Appendix E, any oxidation zones that may develop will consume far more water than will infiltrate through the cover. Therefore, the oxidation zones are not expected to contribute to water percolating from the TMA. Solute concentrations in the TMA percolate were therefore assumed to remain similar to the estimates given in Table 2-10.

2.7 Estimated Solute Concentrations in the Reclaim Pond

A reclaim pond is located adjacent to the TMA and may be an additional source of solutes. The reclaim pond will receive water from both the TMA drainage collection system and the TMA pond decant system. Estimates from the TMA water balance and the HELP modeling indicate that, during tailings deposition, approximately 15 percent of the water in the reclaim pond will come from the drainage collection system and 85 percent from the pond decant. Solute concentrations in the reclaim pond were therefore estimated as an 15/85 combination of solute concentrations in equilibrated process water and solute concentrations in the water delivered to the TMA with the tailings slurry. The latter concentrations are provided in the first column of Table 2-7, and the former in the respective BEJ and UB columns of the same table.

After tailings deposition ceases, the reclaim pond will continue to receive water, but only from the TMA drainage collection system. Solute concentrations for that period were therefore assumed to be equal to those in Table 2-10.

Table 2-11 summarizes the solute concentration estimates for the reclaim pond. Both sets of estimates are likely to be conservative with respect to elements such as iron and arsenic, which would be expected to oxidize and be removed from solution in the reclaim pond.

Table 2-11

Reclaim Pond Water Quality

Parameter	Operations		Post Capping	
	BEJ (mg/L)	UB (mg/L)	BEJ (mg/L)	UB (mg/L)
Al	0.80	0.94	0.014	0.84
Sb	0.062	0.071	0.012	0.67
As	0.069	0.069	3.3	12
Ba	0.030	0.035	0.0052	0.033
Be	0.00045	0.00045	0.072	0.28
Cd	0.0061	0.0061	0.053	0.070
Ca	549	560	550	598
Cr	0.038	0.038	0.066	0.15
Cu	0.047	0.047	0.12	0.30
F	0.38	0.38	0.59	0.81
Fe	0.33	0.72	1.1	50
Pb	0.19	0.19	1.4	0.87
Mg	5.1	53	134	674
Mn	0.68	0.68	2.8	3.2
Hg	0.00018	0.00018	0.0071	0.027
Ni	0.045	0.045	0.14	0.40
K	15	15	23	48
Se	0.20	0.20	0.52	1.4
Ag	0.066	0.066	0.062	0.063
Na	27	27	34	55
SO_4	1599	1768	1965	4010
Zn	6.9	12	20	76
CN	0.30	0.30	0.30	0.30

Note: Cyanide (CN) is discussed in Appendix B.

Prepared by: JTC
Checked by: DEH
Revised by: KSS
Checked by: JTC

3 TMA Solute Transport Analysis

3.1 Introduction

A solute transport model was developed to provide information to be used to evaluate tailings management area (TMA) compliance with groundwater standards. The model simulates transport of dissolved constituents in the groundwater from the point where the constituents enter the water table past the limits of the design management zones for the TMA and reclaim pond. The modeling approach, assumptions, and framework are described in several solute transport modeling reports prepared by HSI GeoTrans (GeoTrans, 1996; HSI GeoTrans, 1998c; HSI GeoTrans, 1999a; HSI GeoTrans, 1999b; and HSI GeoTrans, 2000). These reports have been submitted to the WDNR and U.S. Army Corps of Engineers for review. These reports are contained in Appendix 4.2-10 of the project's *Environmental Impact Report* (Foth & Van Dyke, 1995/1998c). The solute transport modeling results that are discussed in this report are presented in HSI GeoTrans (2000).

Section 3.2 of this report summarizes the solute transport modeling process. The conceptual model of solute transport from the TMA is presented, followed by a discussion of the construction and operation of the model. A description of a superpositioning and scaling technique for computing actual concentrations of specific constituents is also presented. The technique accounts for source concentrations that change with time and are unique to each constituent.

Section 3.3 presents the results of the solute transport modeling work. The source concentrations derived from the waste characterization studies are integrated with the solute transport model to develop estimates of the incremental changes in groundwater concentrations at the DMZ boundaries. Model predictions include a best engineering judgement transport (BEJT) case, which uses reasonable flow and solute transport parameters, and a practical worst-case transport (PWCT) case which uses a combination of conservative and unlikely parameters. Concentration versus time graphs and figures showing the areal distribution of concentrations for BEJT and PWCT are presented.

3.2 Solute Transport Modeling Process

The primary solute transport modeling objective related to the TMA as stated in HSI GeoTrans (1998c) is to evaluate Tailings Management Area (TMA) compliance with groundwater standards. This objective was accomplished through the development of a numerical model that is capable of modeling the transport of dissolved constituents in the groundwater in the vicinity of the TMA. The transport model differs from the flow model (HSI GeoTrans, 1998a, 1998b, and 1998d) in that it computes concentrations of solute at points within the modeled glacial overburden, instead of the hydraulic heads that were computed in the flow modeling.

The simulated mechanisms for representing solute transport from the TMA into the glacial system include movement of water through the lined facility during operation and consolidation

period of each TMA cell, movement of water through the covered and lined facility following closure of each TMA cell, and a postulated deterioration of the geomembrane composite liner at some time in the future. These events are assumed to be sequential. The first three events, operation, consolidation, and closure, are of known duration. An assumed deterioration of the geomembrane, if it occurs, would happen at an unknown time in the distant future and would occur gradually. To provide a conservative modeling approach, the geomembrane in the composite liner is assumed to completely deteriorate at approximately 150 years after installation. The postulated degradation scenario is very conservative and is included in the analysis to assess the performance of the TMA if such an unlikely condition were to occur. In fact, based on the December 1996 report prepared by GeoSyntec Consultants of Boca Raton, Florida, titled *Assessment of Long-Term Performance of the Proposed HDPE Geomembrane Liner and Cap at the Crandon Project TMA Facility* (GeoSyntec, 1996), ". . . the HDPE geomembrane liner and cap at the TMA facility should function as designed for a very long time (e.g., hundreds of years) without deterioration in performance." The GeoSyntec report is reproduced in Appendix F of *Addendum No. 3 to the Tailings Management Area Feasibility Report/Plan of Operation* (Foth & Van Dyke, 1997).

The conceptual model of solute transport from the TMA is as follows. Water will enter the TMA cells during operation either with the tailings slurry as process water, or by direct precipitation, or through the composite geomembrane/geosynthetic clay liner (GCL) final cover system following cell closure. A portion of the tailings pore water is then assumed to bypass the leachate collection system and percolate through the composite liner. Water can also enter the groundwater flow system from the TMA reclaim pond, which will be lined with a geomembrane and a geosynthetic clay liner. The reclaim pond will be used to store recycled water from the TMA. The percolated water from either source is assumed to enter the unsaturated zone and move vertically to the glacial aquifer system. Once solute enters the groundwater system, it is assumed to be advected along groundwater flow paths toward groundwater discharge points. Along the route to the discharge points, the solute mixes with resident groundwater and is dispersed through travel along tortuous paths in the saturated groundwater system. No chemical reactions, such as adsorption, chemical precipitation, or decay, are assumed to occur. Disregarding chemical reactions is conservative with respect to travel time (adsorption) and with respect to concentrations at the DMZ boundaries (decay and precipitation) as these reactions tend to reduce the number of constituents in the groundwater and thus reduce the concentrations at the DMZ boundaries.

Numerical modeling was selected as the tool to address complexities such as changing flow directions due to cessation of mining operations, a changing percolation rate from the TMA, changing concentrations in the TMA source term, and the need to efficiently assess parameter sensitivity and practical worst-case scenarios. Numerical modeling will also provide the entire history of solute transport from entry of solute to the groundwater system until occurrence of a significant decline in concentration at the DMZ boundaries.

MT3D[96] (Zheng, 1996) was selected for three-dimensional modeling of solute transport at the Crandon site. It is a three-dimensional model for simulating solute transport processes in fully

saturated porous media. The transport model is structured such that it can be used in conjunction with other finite difference groundwater flow models, such as the MODFLOW model that was used in the regional groundwater flow modeling. MT3D[96] can be used to simulate changes in concentration of single species soluble constituents in groundwater considering advection, dispersion, and some simple chemical reactions. MT3D[96] was developed for the USEPA for solute transport applications. It is generally accepted by state and federal regulatory agencies as a tool for completing solute transport work.

The TMA solute transport model referenced in this report uses the results of a regional groundwater flow model (HSI GeoTrans, 1998d) as its basis for representing the hydrogeological system. The TMA solute transport model was built from the same data set used to construct the regional model. However, the TMA solute transport model covers a smaller area and offers greater computational resolution than the regional model. The TMA solute transport model also differs from the regional model in that it computes concentrations at points within the glacial overburden within the model area, instead of the hydraulic heads that were computed by the flow model.

The TMA solute transport model covers a 7,600 foot by 7,300 foot square rotated 35 degrees west of north. The model extends a minimum of about 500 feet beyond the 1,200 foot TMA DMZ boundary. The model grid consists of 76 rows by 73 columns, with uniform 100 foot grid spacing in both directions. Vertically the model extends from the water table to the base of the Pre- to Early Wisconsinan Till. The bedrock is not represented in this model because flow across the bedrock/glacial interface is very limited away from the mine. The model consists of seven layers, which were subdivided from the four layers used in the regional groundwater flow model to represent the glacial system.

Five types of flow boundaries are used to model the area: 1) no-flow at the base of the model and on the far side of Hemlock Creek; 2) head-dependent flux to simulate fixed heads along the northwest, southwest, and southeast edges of the model grid; 3) head-dependent flux (river-type) for Hemlock Creek; 4) head-dependent flux (river-type) for the seepage wetlands on the eastern part of the model, and 5) specified flux to represent precipitation recharge or infiltration into and percolation from the TMA. Precipitation recharge rates were based on those used in the regional groundwater flow model. TMA percolation rates were derived from HELP Model calculations presented in *Addendum No. 5 to the TMA Feasibility Report/Plan of Operation* for the Crandon Project (Foth and Van Dyke, 1998b). Values of hydraulic head used on the perimeter boundary were interpolated from the regional groundwater flow model.

Most of the hydrologic parameters used in the solute transport model were derived from the regional groundwater flow model (HSI GeoTrans, 1998d). Those specific to solute transport, effective porosity and dispersivity, were based on field data and on values typical for similar scales of analysis and geologic environments.

Calibration of the solute transport model involved verifying that the flow field from the regional model and from observed data matched the flow field modeled with the solute transport model.

In addition, modeled flow paths and travel times were compared to pre-established estimates (Saad, 1996). Calibration of the transport portion of the model is not possible because solute transport is essentially a prediction.

The predicted flux to the groundwater system varies considerably with time, as various cells of the TMA come on-line and are closed. In the model, there are 20 stress periods, or changes in boundary conditions during the simulation. Most of the stress periods are concentrated in early time to accommodate the approximate 10-year cycle of first and second stage operation and closure of each TMA cell. For modeling purposes, an assumed conservative complete degradation of the geomembrane in each cell's composite liner is modeled at approximately 140 years after cell closure or approximately 150 years after cell start-up.

The modeling presented by HSI GeoTrans (2000) was done to enable groundwater concentrations to be predicted for various constituents that could potentially percolate from the TMA cells or the nearby reclaim pond (RP). The Solute Transport Model (STM) simulations were specifically designed so that the principle of superposition could be easily applied to give predicted constituent concentrations at the TMA and RP Design Management Zone (DMZ) boundaries.

As described by HSI GeoTrans (2000), six Best Engineering Judgement for Transport (BEJT) simulations and six Practical Worst Case for Transport (PWCT) simulations were completed. In each case, six simulations were made to represent six potentially distinct "concentration phases" of source characteristics, with each phase being represented by a (potentially) different source concentration. These concentration phases are distinct from, and overlap with, the flow phases discussed in Section 2.2.2. The following discussion describes the correlation between the concentration phases and flow phases.

As described in the report (HSI GeoTrans, 2000), nominal source concentrations of 1.0 were used in each simulation to facilitate the use of superposition for calculating the groundwater concentrations of any constituent, which could have a variable source concentration represented by six concentration phases, labeled A-F: A) the concentration of the TMA percolate (potentially uncollected leachate) during cell operation, B) the concentration of TMA percolate during the 2-year period of consolidation prior to cell capping, C) the TMA percolate concentration after cap placement, D) the TMA percolate concentration after a postulated complete degradation of the geomembrane component of the TMA composite liner (which is conservatively assumed to happen 150 years after the beginning of operation), E) the RP percolate concentration during the TMA operational period, and F) the RP percolate concentration after the entire TMA is capped, prior to removal of the RP. The six simulations correspond to the six concentration phases, such that, during simulation A, for instance, each TMA cell has a source concentration equal to 1.0 for only those years when the cell is operational (the concentration is zero at other times, and zero at the RP). Note that, because different cells of the TMA begin operations at different times, different portions of the TMA change source concentrations at different times. For instance, during the 23rd year of TMA operation, cell TMA 1 is in concentration phase C (post-cap), TMA 2 is in concentration phase B

(consolidation), TMA 3 is in concentration phase A (operation), and the RP is in concentration phase E (RP operation). The details of the model timing and construction can be found in the STM report (HSI GeoTrans, 2000).

Also in the STM report (HSI GeoTrans, 2000), the principle of superposition is applied to an example (hypothetical) constituent for illustrative purposes. Figure 3-1 illustrates the concepts behind the application of superposition to transform model results into a constituent-specific concentration prediction. Note that the phases listed along the x-axes of the first column of graphs are *flow* phases, which are distinct from the six potential *concentration* phases that correspond to the six STM simulations. This is because the volumetric flux of water from the TMA is assumed to have greater variability with time than does the concentration of the percolate. Thus, TMA flow phases A and B correspond with the operational source concentration (STM simulation A), TMA flow phase C corresponds with the consolidation period source concentration (STM simulation B), TMA flow phases D, E, and F represent different volumetric percolation rates during the post-cap period (STM simulation C), and TMA flow phase G represents the final, steady-state percolation from the TMA after the postulated geomembrane degradation (STM simulation D). Similarly, RP flow phase A corresponds to the period of TMA operation, or concentration phase E (STM simulation E), and RP flow phase B corresponds with the RP source after TMA capping in STM simulation F. Note that flow phase X in this figure indicates that no constituent source is present.

When the six simulations are run, the results are six concentration response functions (second column of Figure 3-1), which describe the concentration at each model cell, at all simulated times, as a fraction of the source concentration. Mathematically, these results can be written:

$$c'_A(x,y,z,t)$$
$$c'_B(x,y,z,t)$$
$$c'_C(x,y,z,t)$$
$$c'_D(x,y,z,t)$$
$$c'_E(x,y,z,t)$$
$$c'_F(x,y,z,t)$$

where each c' represents the groundwater response to a unit concentration source applied during a specific concentration phase.

Each constituent is assumed to have known source concentrations in each concentration phase, which are represented here as A_i, B_i, C_i, D_i, E_i, and F_i, for the i^{th} constituent. The six concentration response functions, c', are scaled (multiplied) by these source concentrations to yield six constituent-specific scaled response functions (third column in Figure 3-1) defined at all cells and all simulated times. Finally, the six scaled response functions are summed (fourth column) to yield the predicted groundwater concentration, $c_i(x, y, z, t)$, for the i^{th} constituent:

$$c_i(x,y,z,t) = A_i c'_A + B_i c'_B + C_i c'_C + D_i c'_D + E_i c'_E + F_i c'_F$$

This equation of superposition, and this overall method, is valid because of the linearity of the partial differential equation that describes advective-dispersive transport of dissolved solutes in groundwater. For a given constituent (i), the above equation is calculated from the six unit-response functions (the simulation output) and the six known source concentrations using a FORTRAN utility program called "Superpo2". This program is executed twice for each constituent (once for BEJT and once for PWCT).

At any particular cell in the model, which has a prescribed (x, y, z) location, the concentration response functions, and final concentration can be depicted as concentration versus time curves. Sets of two such curves are shown in the plots of Figure 3-1. While the resulting concentration is defined for all model cells, the cells along the boundaries of the DMZs are of particular interest for compliance demonstration. A second FORTRAN utility program, called "Ecurve", is used to extract the maximum concentration for a constituent at the DMZ boundaries at each simulated time. The input to Ecurve consists of the predicted constituent concentration at all cells at all times (the output from Superpo2), and a list of the cells along a DMZ boundary (Ecurve is executed separately for each DMZ). For each simulated time, Ecurve determines the DMZ boundary cell that has the highest concentration and outputs that location and predicted concentration. Ecurve is executed four times per constituent to give maximum concentrations at both the TMA and RP DMZ boundaries under both BEJT and PWCT conditions.

The BEJ and upper bound (UB) source concentrations have been presented for concentration phases A, C, E, and F in Tables 2-9, 2-10, and 2-11, respectively. Concentration phase D has the same source concentrations as phase C, according to SRK, while phase B represents a period of change from the concentration in phase A to that of phase C. For BEJT, SRK has suggested applying the phase A concentration for phase B also. Under PWCT, the upper-bound source concentrations are used, and the higher concentration of phases A and C is applied for phase B. Eighteen constituents are analyzed, with BEJT and PWCT source concentrations for each concentration phase listed in Table 3-1. Note that, in addition to higher source concentrations, the PWCT scenario is simulated with lower dispersivities and lower vertical hydraulic conductivities to limit mixing.

Table 3-1

Solute Transport Model Source Concentrations (mg/L) for Each Constituent

	BEJT Simulations						PWCT Simulations					
Constituent	Sim A[1]	Sim B[1]	Sim C[2]	Sim D[2]	Sim E[3]	Sim F[4]	Sim A[5]	Sim B[6]	Sim C[7]	Sim D[7]	Sim E[8]	Sim F[9]
Antimony	0.012	0.012	0.012	0.012	0.062	0.012	0.071	0.67	0.67	0.67	0.071	0.67
Arsenic	0.069	0.069	3.3	3.3	0.069	3.3	0.069	12	12	12	0.069	12
Barium	0.0033	0.0033	0.0052	0.0052	0.03	0.0052	0.035	0.035	0.033	0.033	0.035	0.033
Beryllium	0.00045	0.00045	0.072	0.072	0.00045	0.072	0.00045	0.28	0.28	0.28	0.00045	0.28
Cadmium	0.0061	0.0061	0.053	0.053	0.0061	0.053	0.0061	0.07	0.07	0.07	0.0061	0.07
Chromium	0.038	0.038	0.066	0.066	0.038	0.066	0.038	0.15	0.15	0.15	0.038	0.15
Copper	0.047	0.047	0.12	0.12	0.047	0.12	0.047	0.3	0.3	0.3	0.047	0.3
Fluoride	0.38	0.38	0.59	0.59	0.38	0.59	0.38	0.81	0.81	0.81	0.38	0.81
Iron	0.33	0.33	1.1	1.1	0.33	1.1	2.9	50	50	50	0.72	50
Lead	0.19	0.19	1.4	1.4	0.19	1.4	0.19	0.87	0.87	0.87	0.19	0.87
Manganese	0.68	0.68	2.8	2.8	0.68	2.8	0.68	3.2	3.2	3.2	0.68	3.2
Mercury	0.00018	0.00018	0.0071	0.0071	0.00018	0.0071	0.00018	0.027	0.027	0.027	0.00018	0.027
Nickel	0.045	0.045	0.14	0.14	0.045	0.14	0.045	0.4	0.4	0.4	0.045	0.4
Selenium	0.2	0.2	0.52	0.52	0.2	0.52	0.2	1.4	1.4	1.4	0.2	1.4
Silver	0.066	0.066	0.062	0.062	0.066	0.062	0.066	0.066	0.063	0.063	0.066	0.063

4.2-12-39

Table 3-1 *(Continued)*

Constituent	BEJT Simulations						PWCT Simulations					
	Sim A[1]	Sim B[1]	Sim C[2]	Sim D[2]	Sim E[3]	Sim F[4]	Sim A[5]	Sim B[6]	Sim C[7]	Sim D[7]	Sim E[8]	Sim F[9]
Sulfate	1599	1599	1965	1965	1599	1965	2714	4010	4010	4010	1768	4010
Zinc	6.9	6.9	20	20	6.9	20	40	76	76	76	12	76
Cyanide	0.3	0.3	0.3	0.3	0.3	0.3	0.3	0.3	0.3	0.3	0.3	0.3

Sim = Solute transport simulation (see Figure 3-1).
Sim A = TMA operations.
Sim B = TMA consolidation.
Sim C = TMA after consolidation, with cap in place.
Sim D = TMA with cap in place after hypothetical degradation of geomembrane in liner.
Sim E = Reclaim pond during TMA operations.
Sim F = Reclaim pond post capping.

Prepared by: GC
Checked by: SVD1
Revised by: GC
Checked by: SVD1

4.2-12-40

[1] Table 2-9: Estimated Solute Concentrations in Percolate During Operations (also applied during consolidation). BEJ Estimate.
[2] Table 2-10: Estimated Solute Concentrations in TMA Percolate After Consolidation. BEJ Estimate.
[3] Table 2-11: Reclaim Pond Water Quality During Operations. BEJ Estimate.
[4] Table 2-11: Reclaim Pond Water Quality Post Capping. BEJ Estimate.
[5] Table 2-9: Estimated Solute Concentrations in Percolate During Operations. UB Estimate.
[6] Table 2-9 or Table 2-10: Highest UB Estimate from Table 2-9 or Table 2-10 is applied.
[7] Table 2-10: Estimated solute Concentrations in TMA Percolate After Consolidation. UB Estimate.
[8] Table 2-11: Reclaim Pond Water Quality During Operations. UB Operations.
[9] Table 2-11: Reclaim Pond Water Quality Post Capping. UB Estimate.

3.3 Solute Transport Modeling Results

The source concentration derivation work discussed in Section 2 above identified constituents expected to be present in the tailings pore water in the TMA. Source concentrations have been developed in Tables 2-9, 2-10, and 2-11 for each of these constituents for the TMA percolate during operations, TMA percolate after consolidation, reclaim pond percolate during operations, and reclaim pond percolate after TMA capping. The source concentrations from Tables 2-9, 2-10, and 2-11 for those constituents identified in Section 4 of this report for which NR 140 Wis. Admin. Code preventative action limits (PALs) and enforcement standards (ESs) exist were applied to the DMZ concentration-versus-time unit response curves derived from the solute transport model to develop groundwater concentration versus time data specific to each constituent. It should be noted that the unit response curves following postulated geomembrane degradation (superpositioning concentration Phase D) are based on percolation rates calculated by the HELP model (Foth & Van Dyke, 1998b). Since, as discussed in Section 2.6.3 above, the actual amount of water that will percolate from the TMA will likely be less than that predicted by the HELP model, the unit response curve for this period is conservative.

Table 3-2 shows the differences in assumptions between the BEJT and the PWCT solute transport models. For each of the 18 constituents, Superpo2 is executed twice (BEJT, PWCT), and for each Superpo2 result, Ecurve is executed twice (TMA DMZ, RP DMZ). All of the Ecurve results are analyzed to determine the maximum concentration on each DMZ boundary for BEJT and PWCT at any time. Table 3-3 shows the maximum incremental groundwater concentration change (i.e., maximum predicted concentration above baseline) due to TMA and reclaim pond operations at the TMA and reclaim pond DMZ boundaries based on the source concentration data presented in Tables 2-9, 2-10, and 2-11. Further details regarding temporal and spatial aspects of the incremental groundwater concentration changes are presented in graphs of concentration versus time and figures showing the predicted spatial extent of constituent concentration in the groundwater. It is noted again that these concentration plots are conservative in that the solute transport modeling does not consider concentration reductions due to chemical reactions such as adsorption, precipitation, or decay.

Figures 3-2 through 3-13 are plots of BEJT concentration versus time for 12 constituents: antimony, arsenic, barium, beryllium, cadmium, chromium, iron, lead, manganese, mercury, selenium, and sulfate. These twelve were selected to provide a representative sampling of parameters showing a range of changes at the TMA and reclaim pond DMZ boundaries. The maximum incremental concentration change anywhere along the DMZ boundaries are shown in these figures. The extent of the y-axis is based on one-tenth of the PAL or alternative concentration limit (ACL), as discussed in Section 4 below. These figures demonstrate that the incremental change in concentration of some constituents is small relative to the PAL or ACL. Note that different model cells may contain the maximum concentration at different times during the simulation. Thus, the curves in Figures 3-2 through 3-13 represent the concentration at a point that moves with time, always at the point at the DMZ boundaries with the maximum concentration. For all constituents, the peak concentration is driven largely by the TMA reclaim pond.

Table 3-2

Differences Between BEJT and PWCT Model Assumptions

Parameter	BEJT	PWCT
Effective Porosity	0.10	0.10
Longitudinal Dispersivity	50 ft	25 ft
Horizontal Transverse Dispersivity	5 ft	2.5 ft
Vertical Transverse Dispersivity	5 ft	0.5 ft
Vertical Hydraulic Conductivity	From BEJT Regional Flow Model	0.10 x BEJT Values
Source Concentration	BEJT Simulation (see Table 3-1)	PWCT Simulation (see Table 3-1)

Prepared by: GWC
Checked by: PFA

Table 3-3

Maximum Modeled Incremental Design Management Zone Concentrations by Parameter

	Maximum Incremental Concentration Change at the DMZ Boundary (mg/l)			
	Best Engineering Judgement Transport		Practical Worst Case Transport	
Parameter	TMA DMZ	Reclaim Pond DMZ	TMA DMZ	Reclaim Pond DMZ
Antimony	0.00005	0.00011	0.00027	0.00052
Arsenic	0.0011	0.0022	0.0045	0.009
Barium	0.000024	0.000053	0.000038	0.000084
Beryllium	0.000024	0.000049	0.0001	0.00021
Cadmium	0.000019	0.000037	0.000028	0.000054
Chromium	0.000033	0.00007	0.000066	0.00013
Copper	0.000048	0.00009	0.00012	0.00024
Fluoride	0.00033	0.0007	0.00042	0.00093
Iron	0.00042	0.00081	0.019	0.038
Lead	0.00050	0.00098	0.00038	0.00071
Manganese	0.001	0.002	0.0014	0.0026
Mercury	0.0000024	0.0000048	0.00001	0.00002
Nickel	0.000054	0.0001	0.00016	0.00031
Selenium	0.00021	0.00039	0.00057	0.0011
Silver	0.000057	0.00012	0.000072	0.00016
Sulfate	1.4	2.9	2.0	4.4
Zinc	0.0079	0.015	0.032	0.061
Cyanide	0.00026	0.00055	0.00033	0.00072

Prepared by: GC
Checked by: SVD1
Revised by: GC
Checked by: SVD1

Figures 3-14 through 3-20 show plan view snapshots through time of the modeled lead concentrations under BEJT conditions. These figures show the maximum modeled concentration in any cell, following scaling and superposition, regardless of layer. The time intervals used, 2, 16, 22, 32, 60, 125, and 300 years, correspond to key points in the life of the TMA. The figures show the TMA cells operating in succession, the operation of the reclaim pond, the initial movement of the solute to the west and toward the mine, and the eventual movement of the solute to the northeast, toward Hemlock Creek. The contour plots show that the concentrations are a function of the percolation from the reclaim pond and percolation from the TMA cells during operation. By the year 300, the solute has receded to concentrations that are more than two orders of magnitude below the ACL. Note that the figures are contoured using a logarithmic interval. The lowest concentration contour that is shown corresponds to a value that is 100 times below the groundwater standard. If no contour interval is displayed, it is because the predicted concentrations at all nodes within the model domain are more than 100 times below the groundwater standard.

Figures 3-21 through 3-27 show plan view snapshots through time for sulfate and Figures 3-28 through 3-34 show plan view snapshots through time for arsenic. The assumptions used to develop these figures are similar to those used for lead. The time response of sulfate and arsenic concentrations are also similar to that of lead.

Figures 3-35 through 3-46 are plots of PWCT concentration versus time for the same 12 constituents that were discussed previously. Many of the assumptions that were used to develop Figures 3-2 through 3-13 were also used to develop these figures. In general, the PWCT peak groundwater concentrations are approximately 1 to 54 times higher than they were under BEJT conditions. The exception is lead, which has a lower PWCT maximum concentration due to a lower upper bound source concentration for lead. For the other constituents, the higher concentrations are related to hydraulic changes (porosity, dispersivity) and to higher upper bound source concentrations. The peak groundwater concentrations at the limits of the DMZ occur between 28 and 55 years, depending on the constituent and its related concentration characteristics.
Figures 3-47 through 3-53 show plan view snapshots through time of modeled lead PWCT concentrations. These figures are similar to those presented in Figures 3-14 through 3-20.

Figure 3-54 through 3-60 and Figures 3-61 through 3-67 show plan view snapshots through time for sulfate and arsenic, respectively, under PWCT conditions. The assumptions used to develop these figures are similar to those used for lead. The time response for sulfate is also similar to that of lead.

4 Groundwater Criteria Performance Evaluation

4.1 Introduction

The objective of this section of the report is to compare the expected performance of the TMA as designed to groundwater quality standards. This comparison has been completed based on:

- The data and descriptive materials related to the TMA design and background water quality that are available in project documents issued to date. The pertinent information in these documents is incorporated into this report by reference, and therefore will not be repeated here.

- The results of the evaluation presented in Section 2 of this report establishing the source concentrations for the TMA. The source concentrations represent the quality of the small amount of leachate that will potentially percolate from the TMA and reach the groundwater system and reclaim pond.

- The results of the project's solute transport modeling analysis presented in Section 3 of this report, which takes into consideration the characteristics, volume, and timing of leachate percolating from the TMA.

- A review of groundwater quality regulations that will be applied to the TMA.

- Appropriate statistical calculations.

4.2 Regulatory Background

Groundwater quality associated with the TMA is regulated under Chapter NR 182, Wis. Adm. Code. According to this code, groundwater quality standards at the DMZ boundary are to be based on three key criteria:

- Preventative action limits (PALs) and enforcement standards (ESs) as specified in NR 140;

- The baseline concentration where that concentration exceeds the PAL or ES; and

- The need to protect public health, safety and welfare.

The term "baseline concentration" is defined in NR 182 as "the concentration of a substance in groundwater . . . as determined by monitoring before mining operations." The same regulation defines the term "background concentration" as "the concentration of a substance in groundwater . . . as determined by monitoring at locations which are not to be affected by the mining site."

Given the above considerations, in order to accomplish the groundwater compliance assessment for the TMA, the following four steps had to be completed. The first was to define the source concentrations for the TMA. The second was to calculate estimated incremental groundwater changes at the DMZ boundaries due to the TMA and reclaim pond without considering baseline groundwater concentrations. The TMA DMZ is expected to encompass the facility at a distance of 1,200 feet from the limit of the tailings placement. The reclaim pond DMZ is expected to encompass the reclaim pond at a distance of 150 feet from the reclaim pond water level. These first two items were the topic of Sections 2 and 3 of this report, respectively.

The third step was to evaluate existing groundwater quality data within the vicinity of the TMA. This analysis was performed to define baseline conditions and to determine if any baseline concentrations exceed NR 140 PALs and/or ESs, which would then require the establishment of an alternative concentration limit (ACL) for those parameters per the WDNR guidance document "PAL/ACL Calculations Guidance for Solid Waste Facilities" (WDNR, 1994).

The fourth step of the analysis involved combining the baseline concentrations and estimated incremental groundwater changes due to the TMA and reclaim pond and comparing the resulting estimated parameter concentrations at the TMA and reclaim pond DMZ boundaries to the NR 140 PALs and ESs, and ACLs where appropriate, to determine if the TMA and reclaim pond as designed will meet groundwater standards.

It should be noted that baseline water quality for the wells to be used for compliance monitoring of the TMA is planned to be completed prior to the initiation of construction. Upon the completion of this work it will be necessary to statistically evaluate the data to determine if individual ACLs will need to be established for any of the individual wells to be used in the future monitoring system.

4.3 Performance Evaluation

As discussed in Section 2 of this report, the short and long-term quality of the TMA leachate has been estimated by Steffen Robertson and Kirsten (Canada), Inc. TMA solute transport modeling has been simulated by HSI GeoTrans, Inc. as part of the project's regional groundwater modeling work and is discussed in Section 3 of this report. It has been conservatively assumed that upon release of a source to the groundwater system it will be transported as a nonreactive solute whose concentration is only controlled by advection and dispersion processes. No chemical reactions, such as adsorption, chemical precipitation, or decay, are assumed to occur. Disregarding geochemical reactions is conservative with respect to travel time (adsorption) and with respect to concentrations at the DMZ boundaries (decay and precipitation) as these reactions tend to reduce a number of constituents in the solute thus reducing concentrations at the DMZ boundaries. The analysis was also conservative since adsorption and dilution in the unsaturated zone were not considered. If the above factors were incorporated into the analysis they would be expected to result in lower concentrations at the DMZ boundary.

4.3.1 Existing Baseline Water Quality

The 16 groundwater monitoring wells used for TMA groundwater quality validation in 1994 and 1995 as described in Section 3.6 of the EIR (Foth & Van Dyke, 1995/1998c) were used to define current groundwater quality in the area. It should be noted that a different set of wells will be used to establish baseline groundwater quality conditions at the TMA prior to construction and for monitoring of groundwater quality once mining begins. An analysis similar to that described below or one for each parameter for each well will need to be completed once baseline data is collected to determine if ACLs are needed for these new wells.

The process used to determine whether baseline water quality in the vicinity of the TMA exceeds NR 140 public health and welfare standards based on the data for the 16 wells referenced above is that given in the Wisconsin Department of Natural Resources guidance document "PAL/ACL Calculations Guidance for Solid Waste Facilities" (WDNR, 1994). According to the guidance document, if one NR 140 enforcement standard or two NR 140 Preventative Action Limit exceedances are observed in the baseline data, or if the average of the baseline data exceeds the NR 140 PAL, an alternative concentration limit is calculated for that parameter. The alternative concentration limit is calculated as the average baseline groundwater quality plus two standard deviations. All non-detections are replaced with one-half the detection limit. The WDNR guidance document is included as Attachment 1 to the memorandum contained in Appendix F.

The data and documentation used for calculating ACLs and the calculated ACLs for the TMA based on the WDNR guidance document are presented in Appendix F, Table 1. Based on an analysis of the data derived from the monitoring program described above, ACLs were calculated for antimony, arsenic, cadmium, chromium, iron, lead, manganese, mercury, and nickel.

4.3.2 Compliance Demonstration

In order to assess if the TMA meets water quality standards at the TMA and reclaim pond DMZ boundaries it was necessary to add the incremental source concentrations at the boundaries estimated in Section 3 of this report to the baseline groundwater quality and compare the result to the NR 140 PALs and ESs and, where appropriate, to the calculated ACLs. The average baseline groundwater quality was conservatively calculated as the upper 95% confidence limit of the mean for each parameter. As with the calculation of the ACLs, the guidance given in USEPA (1989) was used to determine the appropriate type of confidence limit to use. This criteria is outlined in the documentation provided in Appendix F and briefly described below:

- If at least 85% of the baseline data are above detection, all non-detects are replaced with one-half the detection limit and an upper confidence limit based on the normal distribution is calculated.

- If at least 50% but less than 85% of the baseline data are above the detection limit, the mean and standard deviation are adjusted using Cohen's adjustment and an upper confidence limit based on the normal distribution is calculated.

- If less than 50% of the baseline data are above the detection limit, a non-parametric upper confidence limit on the median is used.

Since all parameters have at least thirty results, the data sets were considered to be large samples and a test for normality was unnecessary. This is due to the fact that the mean of a large sample is a normally distributed variable.

Tables 4-1 and 4-2 compare the estimated parameter concentrations at the TMA and reclaim pond DMZ boundaries under BEJT and PWCT conditions to the NR 140 PALs and ESs, or ACLs, where appropriate. In all cases, the predicted concentration for all parameters for both the best engineering judgement transport and the practical worst-case transport scenarios fall below the standard or ACL. Therefore it can be concluded that the TMA and reclaim pond as designed will not cause an exceedance of groundwater standards at the DMZ boundaries.

4.3.3 Sensitivity to TMA Facility Percolation Rates

Results from sensitivity analysis with the solute transport model (HSI GeoTrans, 1998c) indicate that the predicted concentration increases at the DMZ boundaries are proportional to the percolation rate from the TMA and reclaim pond. This indicates that if the percolation rate from the facilities were to double, the predicted concentration increase at the DMZ boundaries would double. For example, as summarized in Table 4-1, the model indicates that for sulfate the incremental increase at the reclaim pond DMZ under BEJT conditions is approximately 2.9 mg/l. Increasing the percolation rate by a factor of 2 would result in an incremental increase at the reclaim pond DMZ of 5.8 mg/l. The linearity between the percolation rate and incremental increase at the DMZ boundaries provides a means of assessing how high the percolation rate would have to be in order to attain a PAL or ACL at the DMZ of the reclaim pond. Note that since the reclaim pond DMZ is within the TMA DMZ, the reclaim pond DMZ boundary is the controlling point with regard to the compliance demonstration.

Using sulfate as an example, under BEJT conditions, approximately 109 mg/l can be added to the groundwater before reaching the PAL at the reclaim pond DMZ boundary. This is defined as the concentration capacity. Dividing the concentration capacity by the incremental increase at the DMZ boundary (109÷2.9 = 38) provides an estimate of how much TMA percolation would have to increase to reach the sulfate standard at the reclaim pond DMZ. In the case of sulfate, the net percolation rate from the TMA and reclaim pond would have to increase by a factor of 38 under BEJT conditions to reach the standard at the reclaim pond DMZ boundary. Following this methodology, it is possible to calculate for each parameter the factor that the net percolation rate would have to increase by in order to exceed standards. Table 4-3 provides a summary of the concentration capacity for each parameter and the corresponding estimated factor that the percolation rate would have to increase by in order to exceed standards. Under BEJT conditions, lead is controlling and the percolation rate would have to increase by a factor of 3.3 to exceed standards. Under PWCT conditions, beryllium is controlling and the percolation rate would have to increase by a factor of 0.9 to exceed standards.

Table 4-1

Best Engineering Judgement Compliance Performance Assessment

Parameter	Units	Incremental Concentration Change at TMA or Reclaim Pond DMZ Boundary Due to Source Term[1]		Average Baseline Groundwater Quality[2]	Estimated Parameter Concentration at TMA or Reclaim Pond DMZ Boundary [3]		NR 140 Groundwater Quality Standards		
		TMA	Reclaim Pond		TMA	Reclaim Pond	PAL[4]	ES[5]	ACL[6]
Antimony	mg/l	0.00005	0.00011	<0.05	<0.05	<0.05	0.0012	0.006	0.12
Arsenic	mg/l	0.0011	0.0022	<0.005	<0.005	<0.005	<0.005	0.05	0.025
Barium	mg/l	0.000024	0.000053	0.025	0.025	0.025	0.4	2	
Beryllium	mg/l	0.000024	0.000049	—[7]	—	—	0.0004	0.004	
Cadmium	mg/l	0.000019	0.000037	<0.001	<0.001	<0.001	0.0005	0.005	0.0007
Chromium	mg/l	0.000033	0.00007	<0.005	<0.005	<0.005	0.01	0.1	0.026
Copper	mg/l	0.000048	0.00009	<0.03	<0.03	<0.03	0.13	1.3	
Fluoride	mg/l	0.00033	0.0007	0.098	0.098	0.099	0.8	4	
Iron	mg/l	0.00042	0.00081	<0.1	<0.1	<0.1	0.15	0.3	0.18
Lead	mg/l	0.00050	0.00098	<0.002	<0.002	0.002	0.0015	0.015	0.0052
Manganese	mg/l	0.001	0.002	0.011	0.012	0.013	0.025	0.05	0.73
Mercury	μg/l	0.0024	0.0048	<0.2	<0.2	<0.2	0.2	2	0.46
Nickel	mg/l	0.000054	0.0001	<0.03	<0.03	<0.03	0.02	0.1	0.037
Selenium	mg/l	0.00021	0.00039	<0.005	<0.005	<0.005	0.01	0.05	

4.2-12-49

Table 4-1 *(Continued)*

Parameter	Units	Incremental Concentration Change at TMA or Reclaim Pond DMZ Boundary Due to Source Term[1]		Average Baseline Groundwater Quality[2]	Estimated Parameter Concentration at TMA or Reclaim Pond DMZ Boundary [3]		NR 140 Groundwater Quality Standards		
		TMA	Reclaim Pond		TMA	Reclaim Pond	PAL[4]	ES[5]	ACL[6]
Silver	mg/l	0.000057	0.00012	<0.01	<0.01	<0.01	0.01	0.05	
Sulfate	mg/l	1.4	2.9	13	14.4	15.9	125	250	
Zinc	mg/l	0.0079	0.015	<0.02	<0.02	0.025	2.5	5	
Cyanide	mg/l	0.00026	0.00055	<0.02	<0.02	<0.02	0.04	0.2	

42-12-50

[1] From Table 3-3 of this report.
[2] Value is upper 95% confidence limit of the mean.
[3] Equals the incremental source concentration at the DMZ plus the upper 95% confidence limits of the mean. For confidence limits below detection the incremental source concentration was added to one-half the detection limit. For those cases where the estimated parameter concentration was still less than the detection limit, the estimated parameter concentration was set at the detection limit.
[4] NR 140 Preventive Action Limit
[5] NR 140 Enforcement Standard
[6] Alternative Concentration Level calculated statistically using baseline water quality data. Where ACL is between PAL and ES, ACL replaces NR 140 PAL only. Where ACL is greater than ES, ACL replaces PAL and ES.
[7] No baseline data available.

Prepared by: SVD1
Checked by: JWS
Revised by: KWC
Checked by: SVD1

Table 4-2

Practical Worst Case Compliance Performance Assessment

Parameter	Units	Incremental Concentration Change at TMA or Reclaim Pond DMZ Boundary Due to Source Term[1]		Average Baseline Groundwater Quality[2]	Estimated Parameter Concentration at TMA or Reclaim Pond DMZ Boundary [3]		NR 140 Groundwater Quality Standards		
		TMA	Reclaim Pond		TMA	Reclaim Pond	PAL[4]	ES[5]	ACL[6]
Antimony	mg/l	0.00027	0.00052	<0.05	<0.05	<0.05	0.0012	0.006	0.12
Arsenic	mg/l	0.0045	0.009	<0.005	0.0070	0.0115	0.005	0.05	0.025
Barium	mg/l	0.000038	0.000084	0.025	0.025	0.025	0.4	2	
Beryllium	mg/l	0.0001	0.00021	—[7]	—	—	0.0004	0.004	
Cadmium	mg/l	0.000028	0.000054	<0.001	<0.001	<0.001	0.0005	0.005	0.0007
Chromium	mg/l	0.000066	0.00013	<0.005	<0.005	<0.005	0.01	0.1	0.026
Copper	mg/l	0.00012	0.00024	<0.03	<0.03	<0.03	0.13	1.3	
Fluoride	mg/l	0.00042	0.00093	0.098	0.098	0.099	0.8	4	
Iron	mg/l	0.019	0.038	<0.1	<0.1	<0.1	0.15	0.3	0.18
Lead	mg/l	0.00038	0.00071	<0.002	<0.002	<0.002	0.0015	0.015	0.0052
Manganese	mg/l	0.0014	0.0026	0.011	0.012	0.014	0.025	0.05	0.73
Mercury	µg/l	0.01	0.02	<0.2	<0.2	<0.2	0.2	2	0.46
Nickel	mg/l	0.00016	0.00031	<0.03	<0.03	<0.03	0.02	0.1	0.037
Selenium	mg/l	0.00057	0.0011	<0.005	<0.005	<0.005	0.01	0.05	

4.2-12-51

Table 4-2 *(Continued)*

Parameter	Units	Incremental Concentration Change at TMA or Reclaim Pond DMZ Boundary Due to Source Term[1]		Average Baseline Groundwater Quality[2]	Estimated Parameter Concentration at TMA or Reclaim Pond DMZ Boundary [3]		NR 140 Groundwater Quality Standards		
		TMA	Reclaim Pond		TMA	Reclaim Pond	PAL[4]	ES[5]	ACL[6]
Silver	mg/l	0.000072	0.00016	<0.01	<0.01	<0.01	0.01	0.05	
Sulfate	mg/l	2.0	4.4	13	15	17.4	125	250	
Zinc	mg/l	0.032	0.061	<0.02	0.042	0.071	2.5	5	
Cyanide[8]	mg/l	0.00033	0.00072	<0.02	<0.02	<0.02	0.04	0.2	

[1] From Table 3-3 of this report.
[2] Value is upper 95% confidence limit of the mean.
[3] Equals the incremental source concentration at the DMZ plus the upper 95% confidence limits of the mean. For confidence limits below detection the incremental source concentration was added to one-half the detection limit. For those cases where the estimated parameter concentration was still less than the detection limit, the estimated parameter concentration was set at the detection limit.
[4] NR 140 Preventive Action Limit
[5] NR 140 Enforcement Standard
[6] Alternative Concentration Level calculated statistically using baseline water quality data. Where ACL is between PAL and ES, ACL replaces NR 140 PAL only. Where ACL is greater than ES, ACL replaces PAL and ES.
[7] No baseline data available.

Prepared by: SVD1
Checked by: JWS
Revised by: KWC
Checked by: SVD1

4.2-12-52

Table 4-3

Estimated Required Increase in Net TMA/Reclaim Pond Percolation Rates to Exceed Standards at Reclaim Pond DMZ Boundary

		NR 140 PAL/ACL - Predicted Concentration (Concentration Capacity)[1]		Estimated Allowable Increase in TMA Facility Percolation Rates[2]	
Parameter	Units	BEJT	PWCT	BEJT	PWCT
Antimony	mg/l	0.095	0.094	864	181
Arsenic	mg/l	0.02	0.014	9.1	1.6
Barium	mg/l	0.38	0.38	7,170	4,524
Beryllium	mg/l	0.00035	0.00019	7.1	0.9
Cadmium	mg/l	0.00016	0.00015	4.3	2.8
Chromium	mg/l	0.023	0.023	329	177
Copper	mg/l	0.11	0.11	1,222	458
Fluoride	mg/l	0.7	0.7	1,000	753
Iron	mg/l	0.13	0.092	160	2.4
Lead	mg/l	0.0032	0.0035	3.3	4.9
Manganese	mg/l	0.72	0.72	360	277
Mercury	μg/l	0.36	0.34	75	17
Nickel	mg/l	0.022	0.022	220	71
Selenium	mg/l	0.0071	0.0064	18	5.8
Silver	mg/l	0.0049	0.0048	41	30
Sulfate	mg/l	109.1	107.6	38	24
Zinc	mg/l	2.48	2.43	165	40
Cyanide	mg/l	0.029	0.029	53	40

[1] Concentration capacity was estimated by subtracting from the PAL or ACL the estimated parameter concentration at the DMZ boundary. If the estimated concentration at the DMZ boundary was less than the detection limit, the incremental increase at the DMZ boundary plus half the detection limit was subtracted from the PAL or ACL.

[2] Estimated allowable increase was calculated by dividing the concentration capacity by the estimated incremental increase. This procedure is valid since the solute transport model has shown that the incremental increase at the DMZ boundary is proportional to the percolation rate.

Prepared by: SVD1
Checked by: KWC
Revised by: KWC
Checked by: SVD1

5 Summary and Conclusions

The TMA groundwater quality performance evaluation presented in this report documents the methodology used by NMC to evaluate the performance of the Crandon Project TMA with respect to groundwater standards. As a result of the evaluation, it has been concluded that the Crandon Project TMA will not cause an exceedance of groundwater standards at the boundary of the TMA or reclaim pond DMZ. This conclusion is based on:

- The predicted characteristics of the small amounts of leachate that could potentially percolate from the facilities over their life.
- The predictions, based on 3D solute transport modeling, of the incremental change in groundwater concentrations at the boundary of the DMZs as a result of potential leachate percolation from the facilities.
- A statistical analysis of baseline groundwater quality in the vicinity of the facilities.
- The establishment of estimated parameter concentrations at the boundary of the DMZs as derived by adding average baseline groundwater quality to the solute transport model derived incremental concentration changes.
- A comparison of the estimated parameter concentrations at the boundary of the DMZs to groundwater standards.
- Under BEJT and PWCT conditions, the percolation rate from the facilities would have to increase by a factor of at least 3.3 to 0.9, respectively, in order to exceed standards at the boundary of the DMZs. Note that this is primarily attributed to the reclaim pond.

The above analysis was performed for both a BEJT and PWCT scenario. Water flow patterns within the TMA, tailings mineralogy and geochemistry and the sequence of reactions or "reaction path" that the tailings will follow if they are exposed to oxygen; and rates of oxygen supply to the tailings were all considered in predicting the quality of the TMA percolate. Both an expected and an upper bound concentration was determined for the potential solutes of interest in the tailings pore water. The source concentrations were estimated for the operations period, the TMA post-closure period, and the reclaim pond operations period.

The simulated mechanisms for representing solute transport from the TMA into the glacial system include the movement of water through the lined facility during operation of each TMA cell, movement of water through the covered and lined facility following closure of each TMA cell, and a postulated deterioration of the geomembrane in the composite liner at some time in the future. The events were assumed to be sequential.

Estimates of the potential percolation from the TMA were derived from HELP model analyses. A method of superpositioning and scaling was developed to predict concentrations of specific constituents at the boundary of the DMZs using the predicted source concentrations.

The statistical analysis of baseline groundwater characteristics was completed to define baseline characteristics and to determine if any baseline concentrations exceed a groundwater standard, which would then require the establishment of an alternative concentration limit (ACL) for that parameter. The statistical analysis resulted in the calculation of an ACL for several solute parameters.

The comparison of the estimated parameter concentrations at the boundary of the DMZs to the groundwater standards and ACLs showed no exceedances for either the BEJT or PWCT scenario. Furthermore, the analysis indicates that the percolation rate would have to increase by a factor of 3.3 under BEJT conditions or a factor of 0.9 under PWCT conditions in order to exceed standards. In essence, a safety factor that assumes no attenuation processes is built into facility design as it relates to groundwater quality, such that percolation rates could increase by 90 percent (under PWCT conditions) to 330 percent (under BEJT conditions) before exceeding NR 140 PALs and ACLs.

As noted throughout the report, conservative assumptions were used in completing each individual element of the evaluation. A synopsis of the most significant of these assumptions follows:

- The practical worst-case analysis is based on a combination of both conservative and unlikely parameters.

- An assumed instantaneous degradation of the HDPE geomembrane in the composite liner system.

- For the modeling of oxygen transport into the uncovered tailings, the assumption that the tailings will begin to drain immediately after deposition ceases.

- Use of conservatively high estimates of oxidation rates for all oxygen transport modeling.

- In the geochemical equilibrium modeling, the assumption of low redox potential, no co-precipitation or sorption, high carbon dioxide, and no siderite formation which lead to high estimates, in particular, of iron and arsenic concentrations in the oxidation zone.

- The derivation of solute concentrations in TMA percolate after the consolidation period, using the volume-weighted average of concentrations in the oxidation and process water dominated zones, even though modeling indicates that the proportion of water arriving at the leachate collection system from the process water dominated zone will significantly exceed the proportion estimated by the simple volume weighting (Attachment 1 of NMC, 1999).

- The use of conservative solute concentration estimates for the reclaim pond water with respect to elements such as iron and arsenic, which would be expected to oxidize and be removed from solution as water ages in the reclaim pond.

- Neglecting the potential effect of oxidation reactions on percolation rates.

- The assumption that solute released from the TMA will be transported as a nonreactive material whose concentration will be controlled only by advection and dispersion processes. No chemical reactions, such as adsorption, chemical precipitation, or decay, were assumed to occur. Disregarding geochemical reactions is conservative with respect to travel time (adsorption) and with respect to maximum concentrations at the DMZ boundaries (decay and precipitation) as these reactions would tend to reduce the number of constituents in the solute thus reducing concentrations at the DMZ boundaries.

- Disregarding adsorption, chemical precipitation, decay and dilution in the unsaturated zone.

6 References

Foth & Van Dyke, May 1995a. *Tailings Management Area Feasibility Report/Plan of Operation for the Crandon Project.*

Foth & Van Dyke, May 1995/1998c. *Environmental Impact Report for the Crandon Project.* Originally issued May 1995. Updated December 1998.

Foth & Van Dyke, February 1996a. *Addendum No. 1 to the Tailings Management Area Feasibility Report/Plan of Operation for the Crandon Project.*

Foth & Van Dyke, March 1996b. *Addendum No. 2 to the Tailings Management Area Feasibility Report/Plan of Operation for the Crandon Project.*

Foth & Van Dyke, January 1997. *Addendum No. 3 to the Tailings Management Area Feasibility Report/Plan of Operation for the Crandon Project.*

Foth & Van Dyke, May 1998a. *Addendum No. 4 to the Tailings Management Area Feasibility Report/Plan of Operation for the Crandon Project.*

Foth & Van Dyke, December 1998b. *Addendum No. 5 to the Tailings Management Area Feasibility Report/Plan of Operation for the Crandon Project.*

Foth & Van Dyke, November 1999. *Addendum No. 6 to the May 1995 Crandon Project Tailings Management Area Feasibility Report/Plan of Operation.*

GeoSyntec Consultants, December 1996. *Assessment of Long-Term Performance of the Proposed HDPE Geomembrane Liner and Cap at the Crandon Project TMA Facility.*

GeoTrans, Inc., 1996. *Numerical Simulation of Potential Solute Transport at the Proposed Zinc and Copper Mine Near Crandon, Wisconsin.*

HSI GeoTrans, Inc., 1998a. *Addendum No. 1 to Numerical Simulation of the Effect on Groundwater and Surface Water of the Proposed Zinc and Copper Mine Near Crandon, Wisconsin.*

HSI GeoTrans, Inc., 1998b. *Errata and Clarifications to: Addendum No. 1 to Numerical Simulation of the Effect on Groundwater and Surface Water of the Proposed Zinc and Copper Mine Near Crandon, Wisconsin.*

HSI GeoTrans, Inc., 1998c. *Update to Numerical Simulation of Potential Solute Transport at the Proposed Zinc and Copper Mine Near Crandon, Wisconsin.*

HSI GeoTrans, Inc., 1998d. *Addendum No. 2 to Numerical Simulation of the Effect on Groundwater and Surface Water of the Proposed Zinc and Copper Mine Near Crandon, Wisconsin.*

HSI GeoTrans, Inc., 1999a. *Update No. 2 to: Numerical Simulation of Potential Solute Transport at the Proposed Zinc and Copper Mine Near Crandon, Wisconsin.*

HSI GeoTrans, Inc., 1999b. *Addendum No. 1 to Update No. 2 to: Numerical Simulation of Potential Solute Transport at the Proposed Zinc and Copper Mine Near Crandon, Wisconsin.*

HSI GeoTrans, Inc., 2000. *Update No. 3 to: Numerical Simulation of Potential Solute Transport at the Proposed Zinc and Copper Mine Near Crandon, Wisconsin.* March, 2000.

Nicolet Minerals Company, 1999. Letter Response to WDNR's March 16, 1999 Comment Letter on Environmental Impact Report Appendix 4.2-12 (Groundwater Quality Performance Evaluation and Associated Documents). August 12, 1999.

Saad, D.A., 1996. *Using Chlorofluorocarbons to Date Groundwater and Determine Hydrologic Properties of Sediments Near the Proposed Crandon Mines Near Crandon, Wisconsin.* Summary report, submitted to the WDNR June 10, 1996.

Steffen Robertson and Kirsten (Canada), Inc., 1998. Letter to Gerald Sevick of Foth & Van Dyke Re: Crandon Project - Addendum 1 to the April 1997 TMA Oxygen Transport Modeling Report. March 7, 1998.

USEPA, 1989. Statistical Analysis of Ground-Water Monitoring Data at RCRA Facilities - Interim Final Guidance. Office of Solid Waste, Washington, D.C.

Wisconsin Department of Natural Resources, 1994. *PAL/ACL Calculations Guidance for Solid Waste Facilities*. May 6, 1994.

Zheng, C., 1996. MT3D^{96}, Modular Three-Dimensional Transport Model. Version 2.0.

Figures for the *Crandon Project Tailings Management Area Groundwater Quality Performance Evaluation (Depyritized Tailings)*

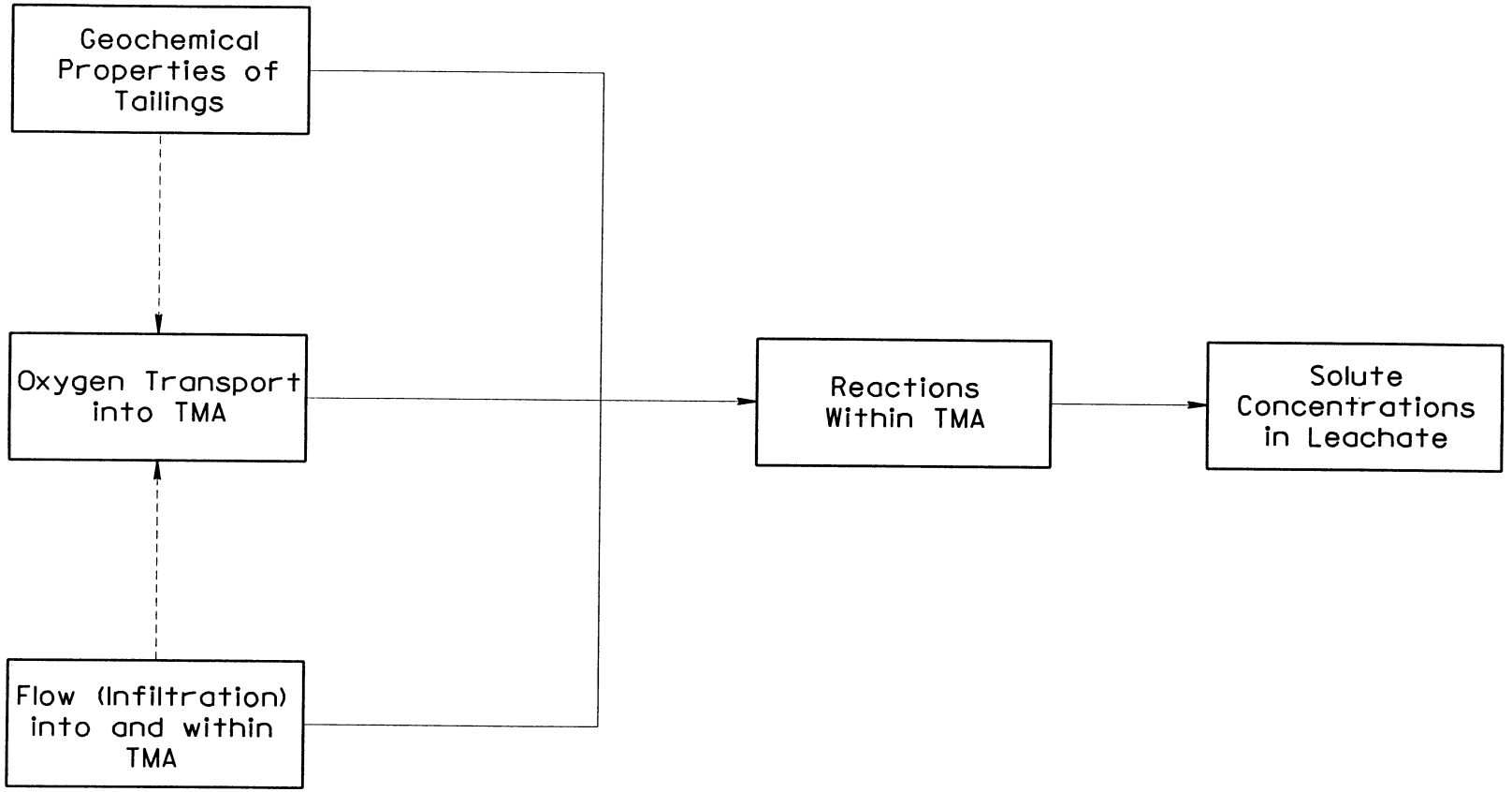

Foth & Van Dyke			
REVISED	DATE	BY	DESCRIPTION
1	4/2/98 3/27/00	MLD2	REVISED TITLE BLOCK

CHECKED BY:	JKSI	DATE:	MAY '97
APPROVED BY:	DH	DATE:	MAY '97
APPROVED BY:	GWS	DATE:	MAY '97

Nicolet Minerals
a Rio Algom company

FIGURE 2-1

TMA SOURCE TERM COMPONENTS

Scale: NOT TO SCALE		Date:	MAY, 1997
Prepared By: Foth & Van Dyke	By: JRB2		00C002

4.2-12-60

L:\00c002\3c49f228d.dgn 03/28/00 04:13:02

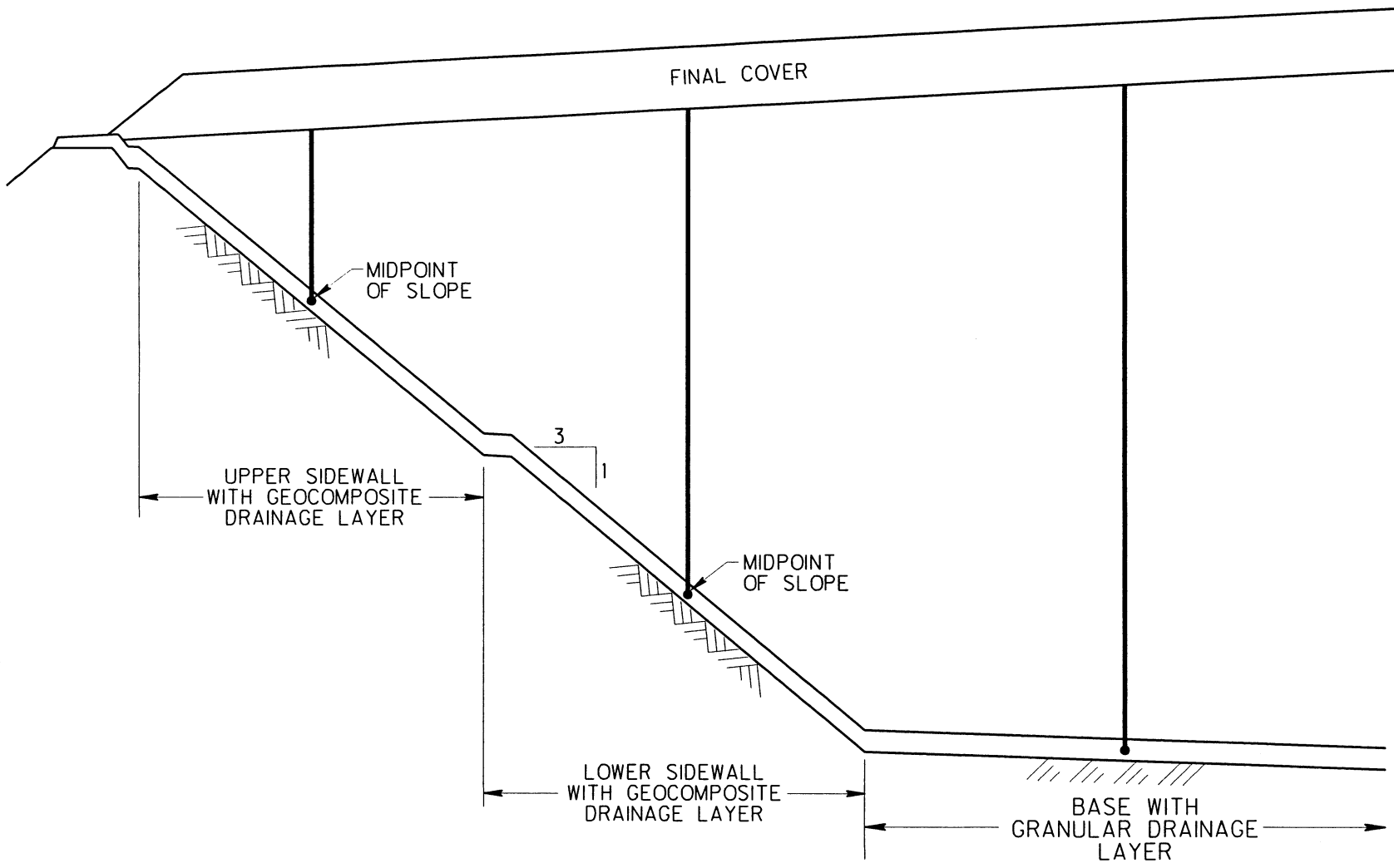

NOTE:

VERTICAL SCALE EXAGGERATED.

1

Foth & Van Dyke

REVISED	DATE	BY	DESCRIPTION
1	4/2/98 3/27/00	MLD2	REVISED TITLE BLOCK

CHECKED BY:	JKS1	DATE:	MAY '97
APPROVED BY:	NXP	DATE:	MAY '97
APPROVED BY:	GWS	DATE:	MAY '97

Nicolet Minerals
a Rio Algom company

FIGURE 2-2

AVERAGE CONDITIONS REPRESENTED IN THE THREE PRIMARY HELP MODELS

Scale: NOT TO SCALE		Date:	MAY, 1997
Prepared By: Foth & Van Dyke	By: JRB2		00C002

\Crandon\TmaMod3\Excel\HelpComp3.xls, Flux

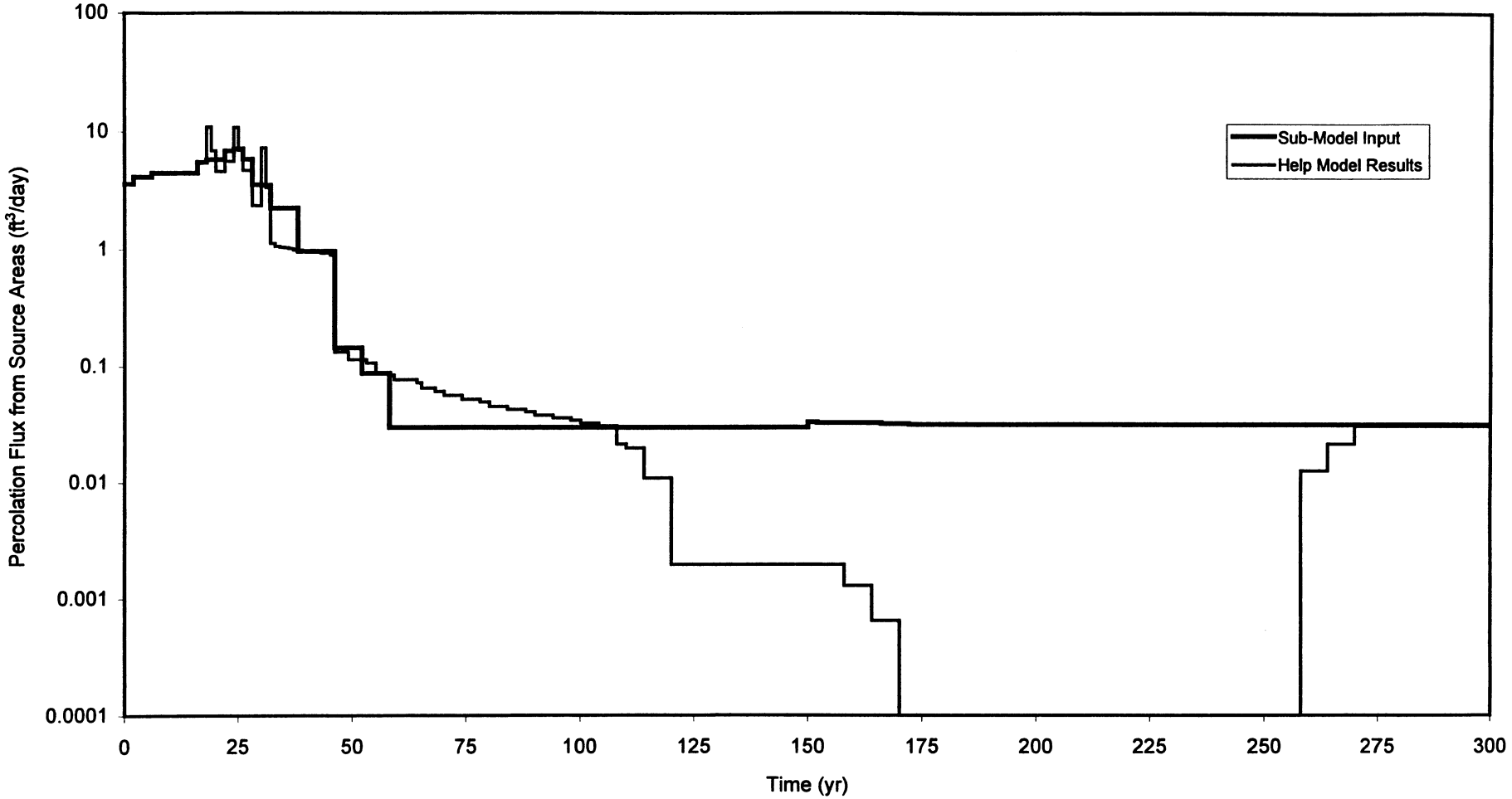

Note:
Percolation rate (Y-axis) is shown on a logarithmic scale.

HSI GEOTRANS			
REVISED	DATE	BY	DESCRIPTION

CHECKED BY: GWC	DATE: Mar 2000
APPROVED BY: PFA	DATE: Mar 2000
APPROVED BY:	DATE:

Nicolet Minerals
a Rio Algom company

Figure 2-3
Source Areas Percolation Flux Rate

Scale: None	Date: March 2000
Prepared By: HSI GEOTRANS	By: LMG

4.2-12-62

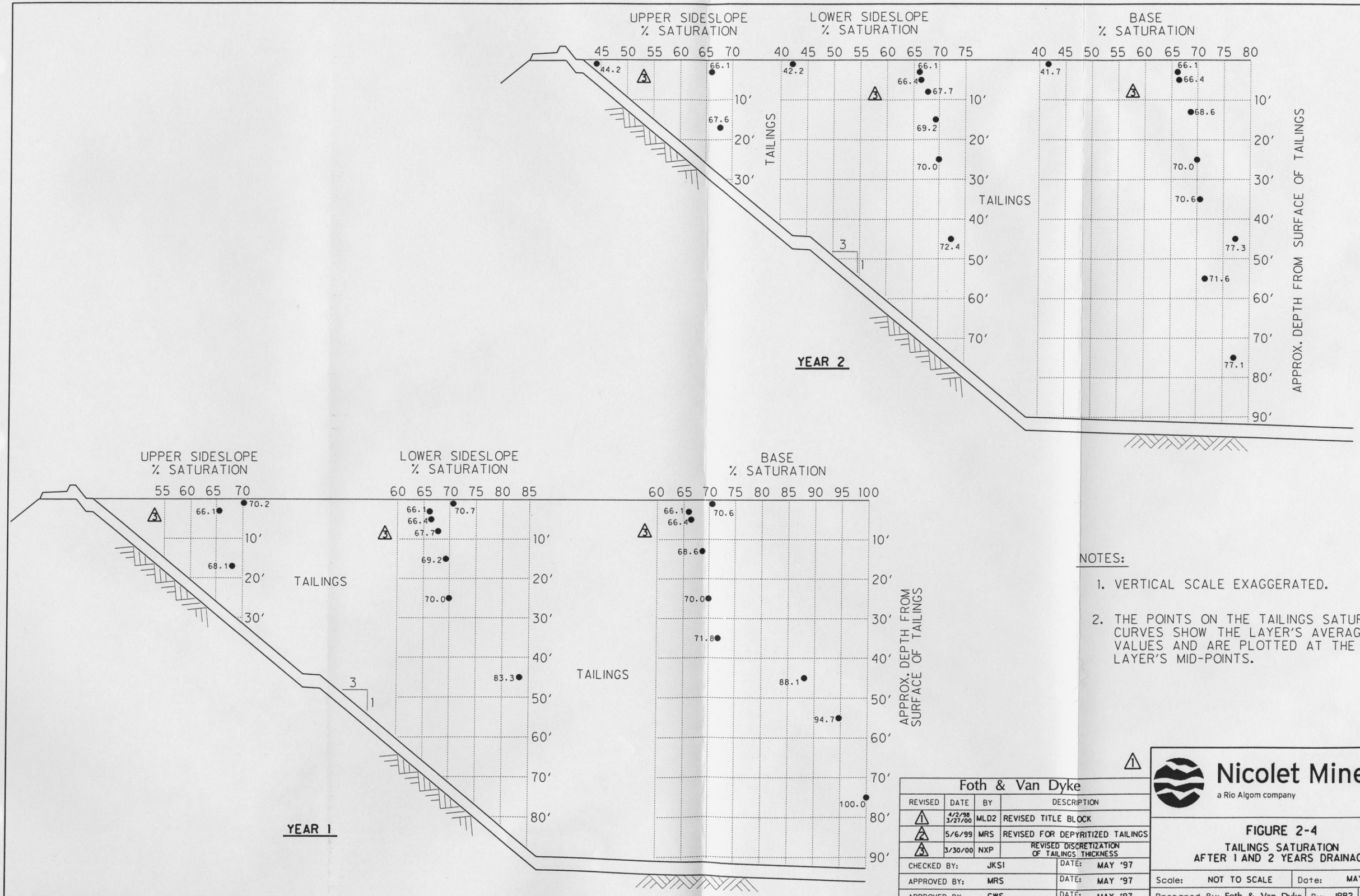

NOTES:

1. VERTICAL SCALE EXAGGERATED.
2. THE POINTS ON THE TAILINGS SATURATION CURVES SHOW THE LAYER'S AVERAGE VALUES AND ARE PLOTTED AT THE LAYER'S MID-POINTS.

Foth & Van Dyke			
REVISED	DATE	BY	DESCRIPTION
1	4/2/98 3/27/00	MLD2	REVISED TITLE BLOCK
2	5/6/99	MRS	REVISED FOR DEPYRITIZED TAILINGS
3	3/30/00	NXP	REVISED DISCRETIZATION OF TAILINGS THICKNESS
CHECKED BY:	JKSI	DATE:	MAY '97
APPROVED BY:	MRS	DATE:	MAY '97
APPROVED BY:	GWS	DATE:	MAY '97

Nicolet Minerals
a Rio Algom company

FIGURE 2-4
TAILINGS SATURATION AFTER 1 AND 2 YEARS DRAINAGE

Scale: NOT TO SCALE	Date: MAY, 1997		
Prepared By: Foth & Van Dyke	By: JRB2	00C002	

L:\00c002\3c49f228b.dgn 03/29/00 04:08:44

(a) REACTION PATH VS TIME (ASSUMING CONTINUING OXIDATION AT ONE LOCATION)

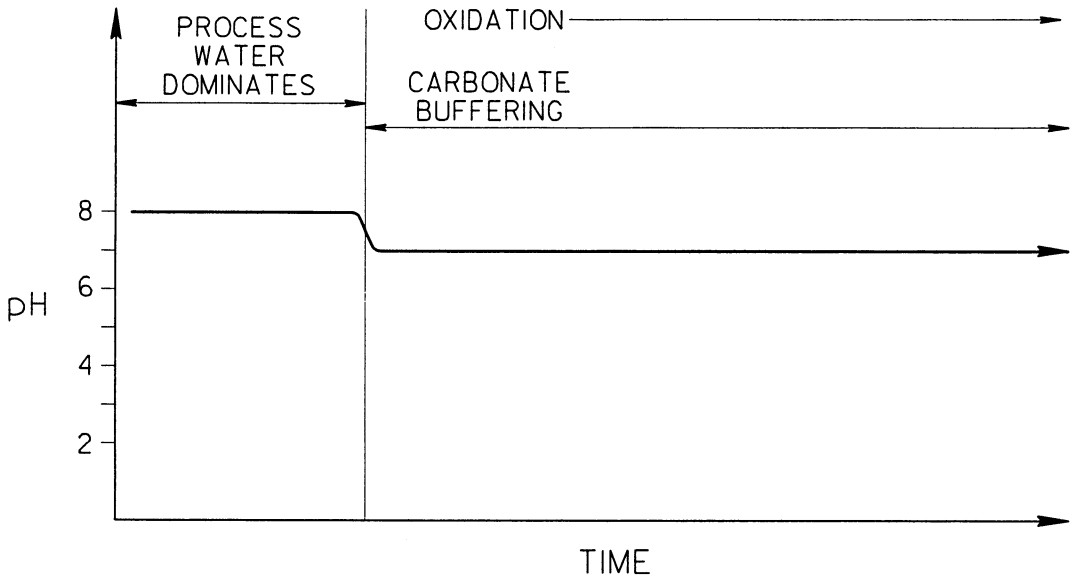

(b) REACTION PATH VS. DEPTH IN TAILINGS
(ASSUMING OXYGEN ENTERS FROM SURFACE AND REACTION PRODUCTS ARE CARRIED DOWNWARDS IN INFILTRATION)

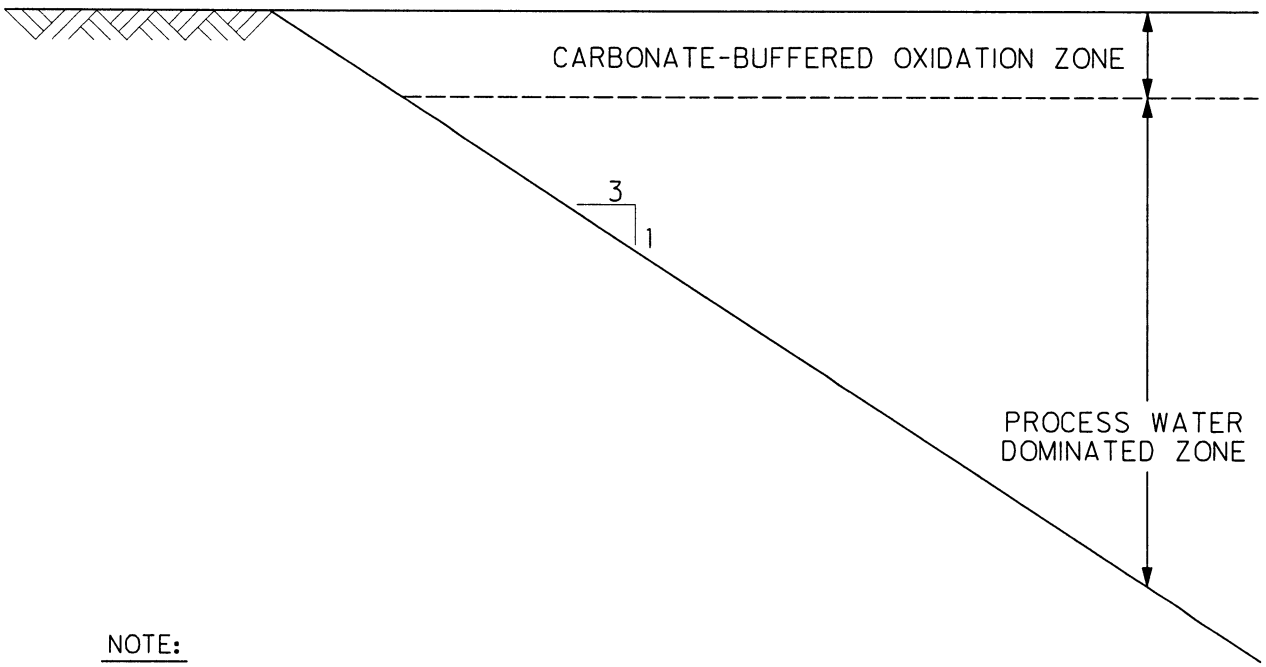

NOTE:
VERTICAL SCALE EXAGGERATED.

Foth & Van Dyke			
REVISED	DATE	BY	DESCRIPTION
1	4/2/98 3/27/00	MLD2	REVISED TITLE BLOCK
2	6/1/99	GWS	REVISED FOR DEPYRITIZED TAILINGS
CHECKED BY:	JKS1	DATE:	MAY '97
APPROVED BY:	DH	DATE:	MAY '97
APPROVED BY:	GWS	DATE:	MAY '97

Nicolet Minerals
a Rio Algom company

FIGURE 2-5
REACTION PATH

Scale: NOT TO SCALE	Date: MAY, 1997
Prepared By: Foth & Van Dyke	By: JRB2	00C002

L:\00c002\3c49f228c.dgn 03/28/00 04:28:57

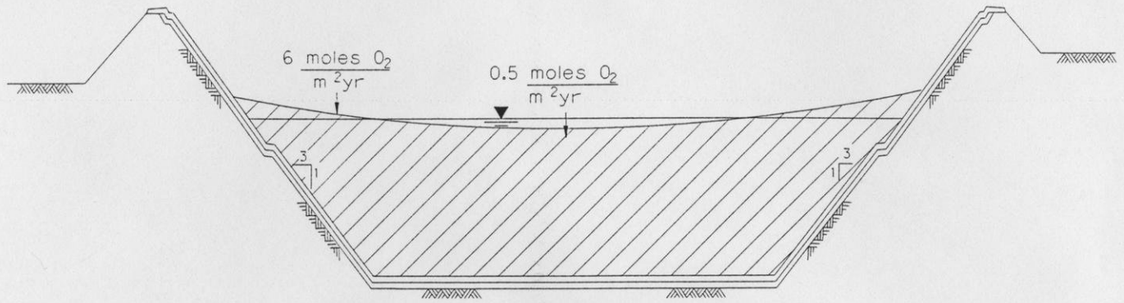

A) DURING TAILINGS DEPOSITION

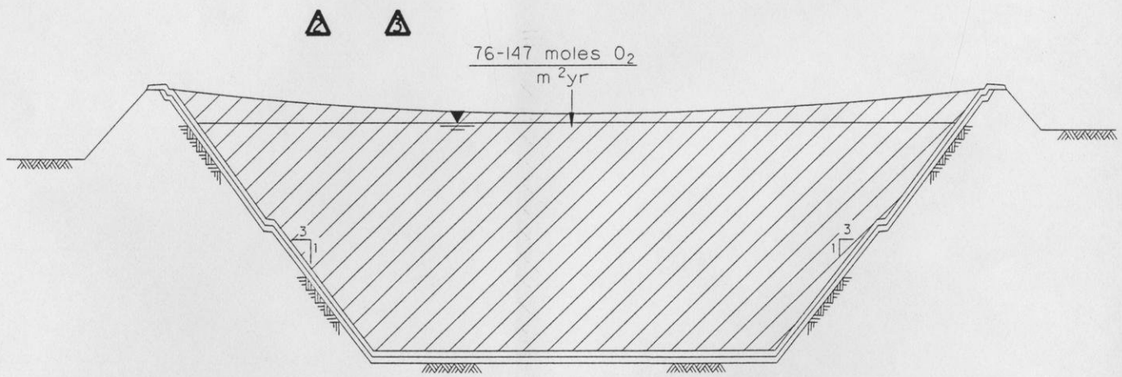

B) AT END OF CONSOLIDATION PERIOD

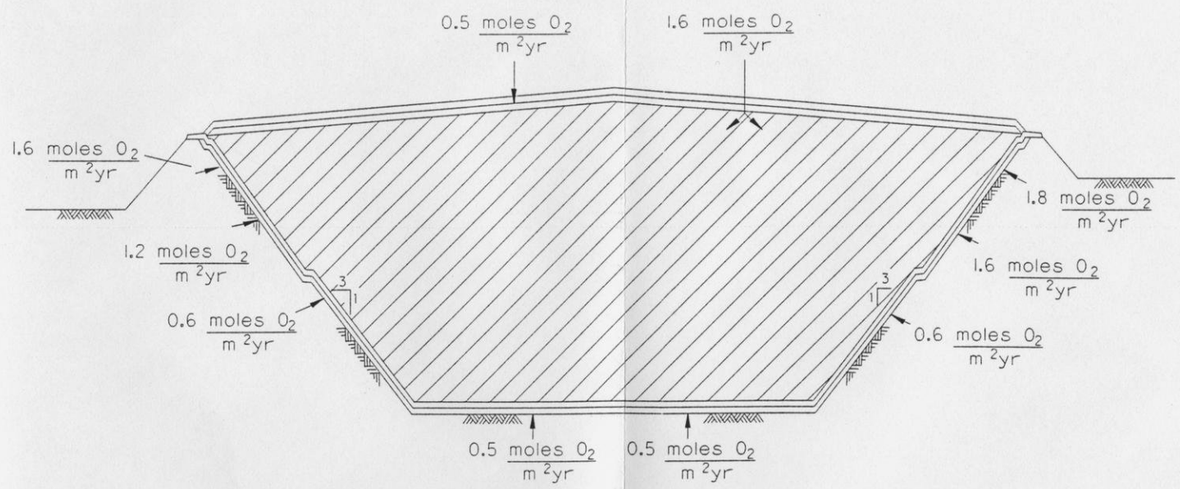

C) AFTER COVER IN PLACE

D) AFTER ASSUMED DEGRADATION OF HDPE IN LINER

NOTE:
VERTICAL SCALE EXAGGERATED

Foth & Van Dyke					
REVISED	DATE	BY	DESCRIPTION		
1	4/2/98 3/27/00	MLD2	REVISED TITLE BLOCK		
2	6/1/99	GWS	REVISED FOR DEPYRITIZED TAILINGS		
3	3/27/00	GWS	REVISED O_2 TRANSPORT ASSESSMENT		
CHECKED	BY:		JKS1	DATE:	MAY '97
APPROVED BY:			DH	DATE:	MAY '97
APPROVED BY:			GWS	DATE:	MAY '97

Nicolet Minerals
a Rio Algom company

FIGURE 2-6
ESTIMATED RATES OF OXYGEN TRANSPORTED INTO TMA

Scale:	NOT TO SCALE	Date:	MAY, 1997
Prepared By: Foth & Van Dyke		By: JRB2	00C002

L:\00c002\3c49f202a.dgn 03/30/00 01:35:09

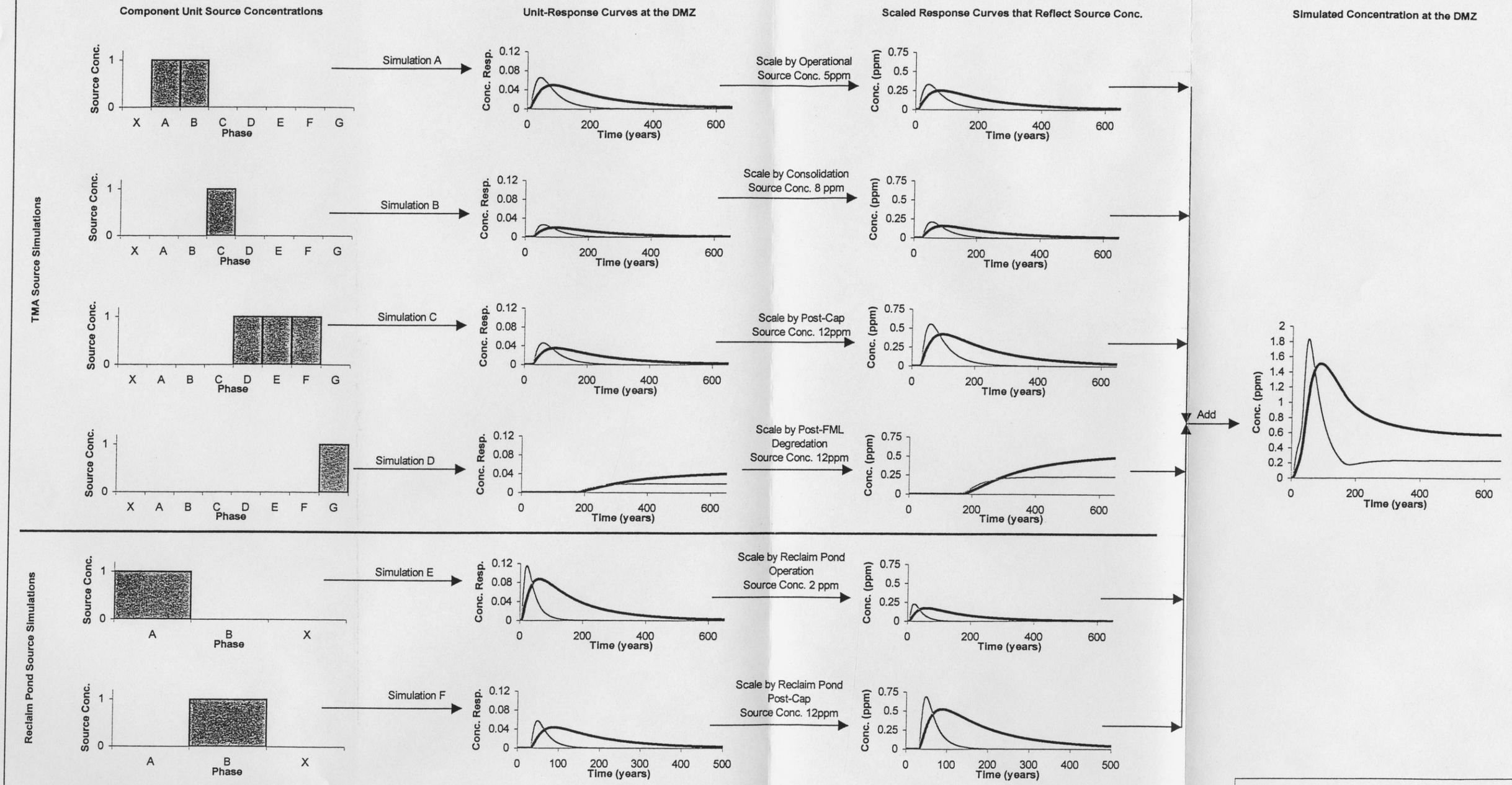

This hypothetical example shows the superposition method applied for a constituent with the following source concentrations:

Operational: 5 ppm
Consolidation: 8 ppm
Post-Cap: 12 ppm
Post-FML Degredation: 12 ppm
Reclaim Pond Operation: 2 ppm
Reclaim Pond Post-Cap: 12 ppm

HSI GEOTRANS			
REVISED	DATE	BY	DESCRIPTION
CHECKED BY: GWC			DATE: Mar 2000
APPROVED BY: PFA			DATE: Mar 2000
APPROVED BY:			DATE:

Nicolet Minerals
a Rio Algom company

Figure 3-1
Source Areas Cumulative Percolation Volume

Scale: None	Date: March 2000
Prepared By: HSI GEOTRANS	By: JDC

\Crandon\TMAMod4\Response\T13gwqpe.xls, Sb

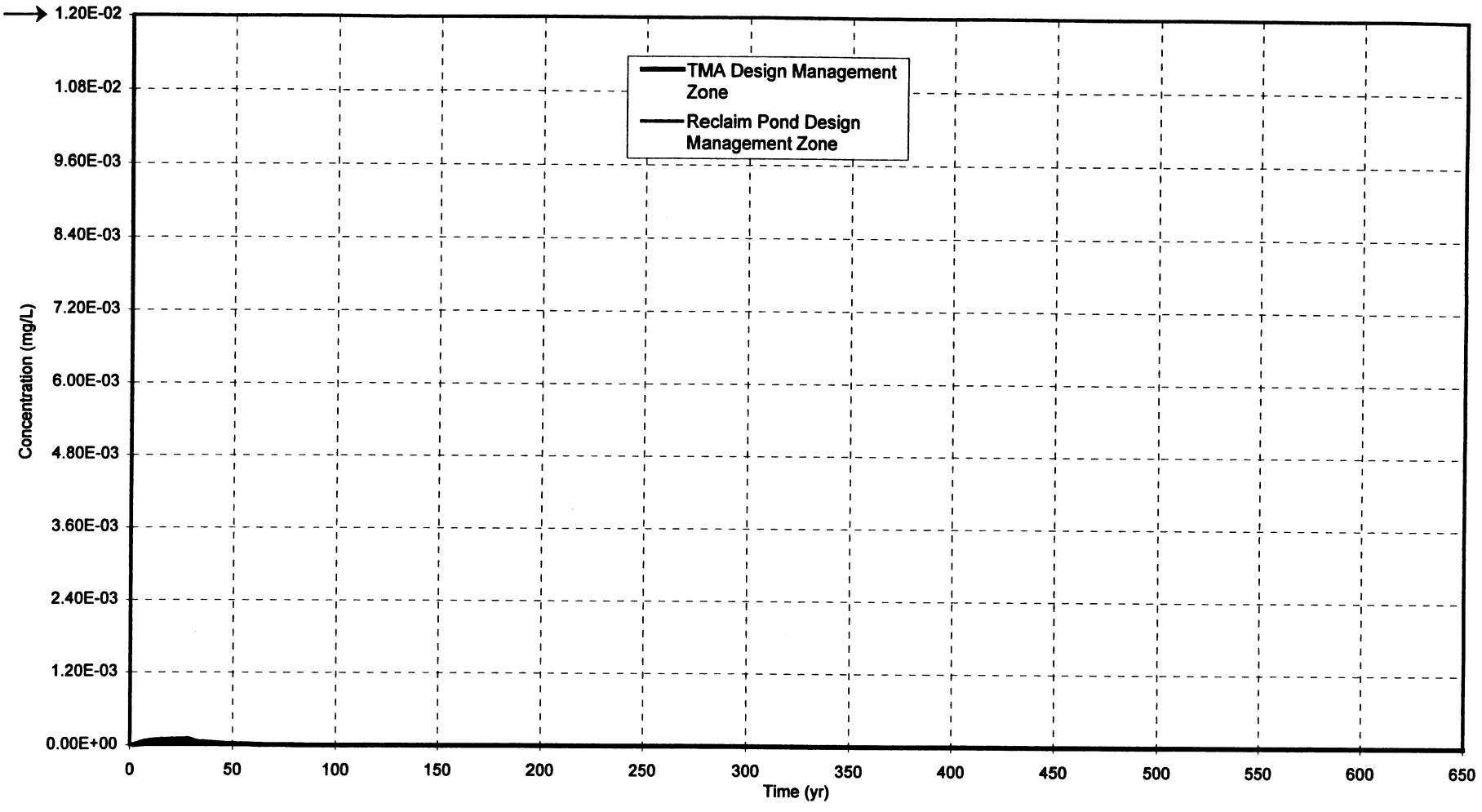

Source Concentration:

TMA Operation:	0.012 (mg/L)
TMA Consolidation:	0.012 (mg/L)
TMA Post-Cap:	0.012 (mg/L)
TMA Post-FML-Degradation:	0.012 (mg/L)
Reclaim Pond Operation:	0.062 (mg/L)
Reclaim Pond After TMA Capping:	0.012 (mg/L)

Simulations T13C1-T13C6

HSI GEOTRANS

REVISED	DATE	BY	DESCRIPTION
1	6/99	JDC	Updated STM
2	3/00	JDC	Updated STM

CHECKED BY: GWC	DATE: April 1998
APPROVED BY: PFA	DATE: April 1998
APPROVED BY:	DATE:

Nicolet Minerals
a Rio Algom company

Figure 3-2
Maximum Concentration at the Compliance Boundary for Antimony, BEJT

Scale: None	Date: April 1998
Prepared By: HSI GEOTRANS	By: JDC

\Crandon\TMAMod4\Response\T13gwqpe.xls, As

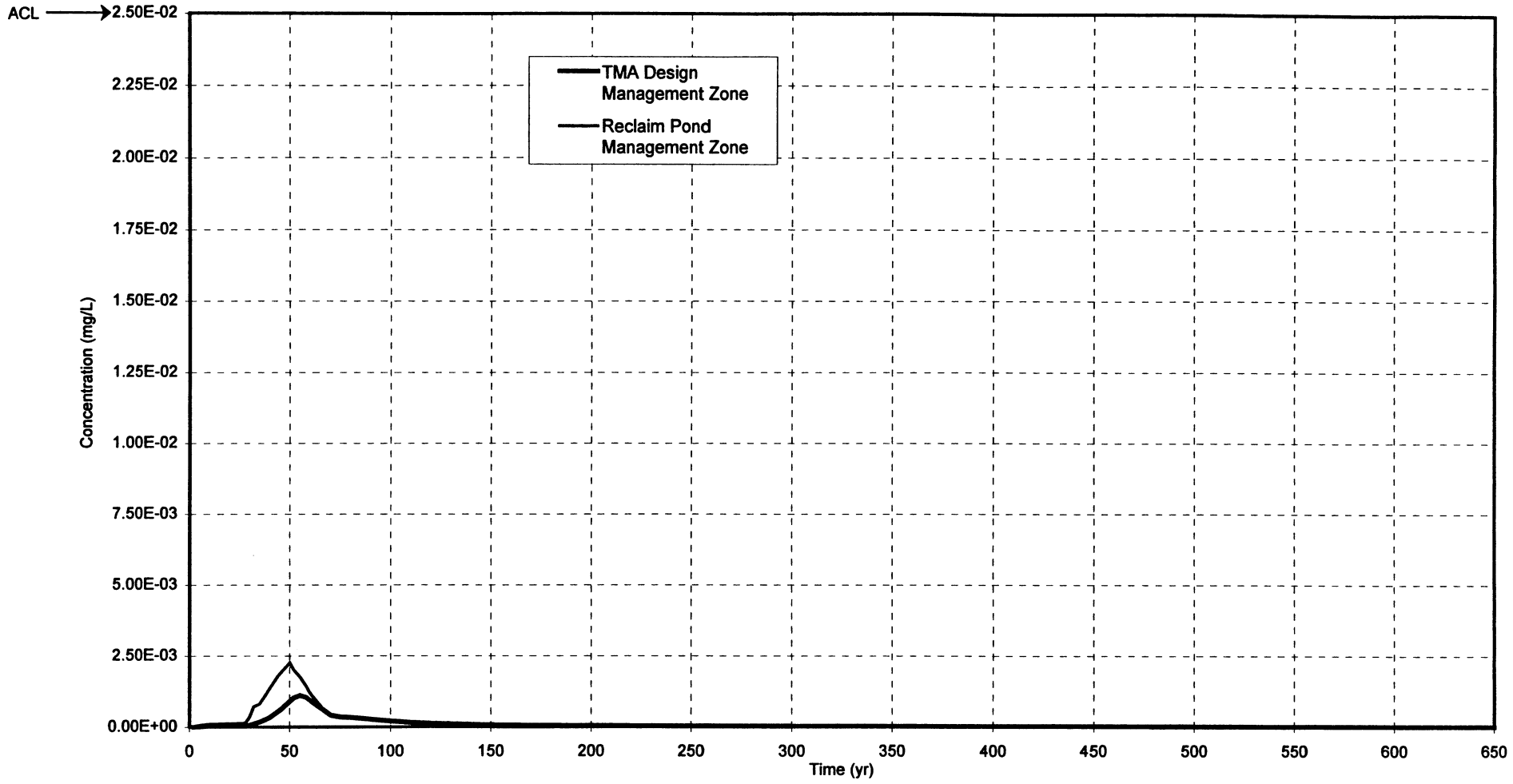

Source Concentration:

TMA Operation:	0.069 (mg/L)
TMA Consolidation:	0.069 (mg/L)
TMA Post-Cap:	3.3 (mg/L)
TMA Post-FML-Degradation:	3.3 (mg/L)
Reclaim Pond Operation:	0.069 (mg/L)
Reclaim Pond After TMA Capping:	3.3 (mg/L)

Simulations T13C1-T13C6

HSI GEOTRANS

REVISED	DATE	BY	DESCRIPTION
1	6/99	JDC	Updated STM
2	3/00	JDC	Updated STM

CHECKED BY: GWC	DATE: April 1998
APPROVED BY: PFA	DATE: April 1998
APPROVED BY:	DATE:

Nicolet Minerals
a Rio Algom company

Figure 3-3
Maximum Concentration at the Compliance Boundary for Arsenic, BEJT

Scale: None	Date: April 1998
Prepared By: HSI GEOTRANS	By: KMR

\Crandon\TMAMod4\Response\T13gwqpe.xls, Ba

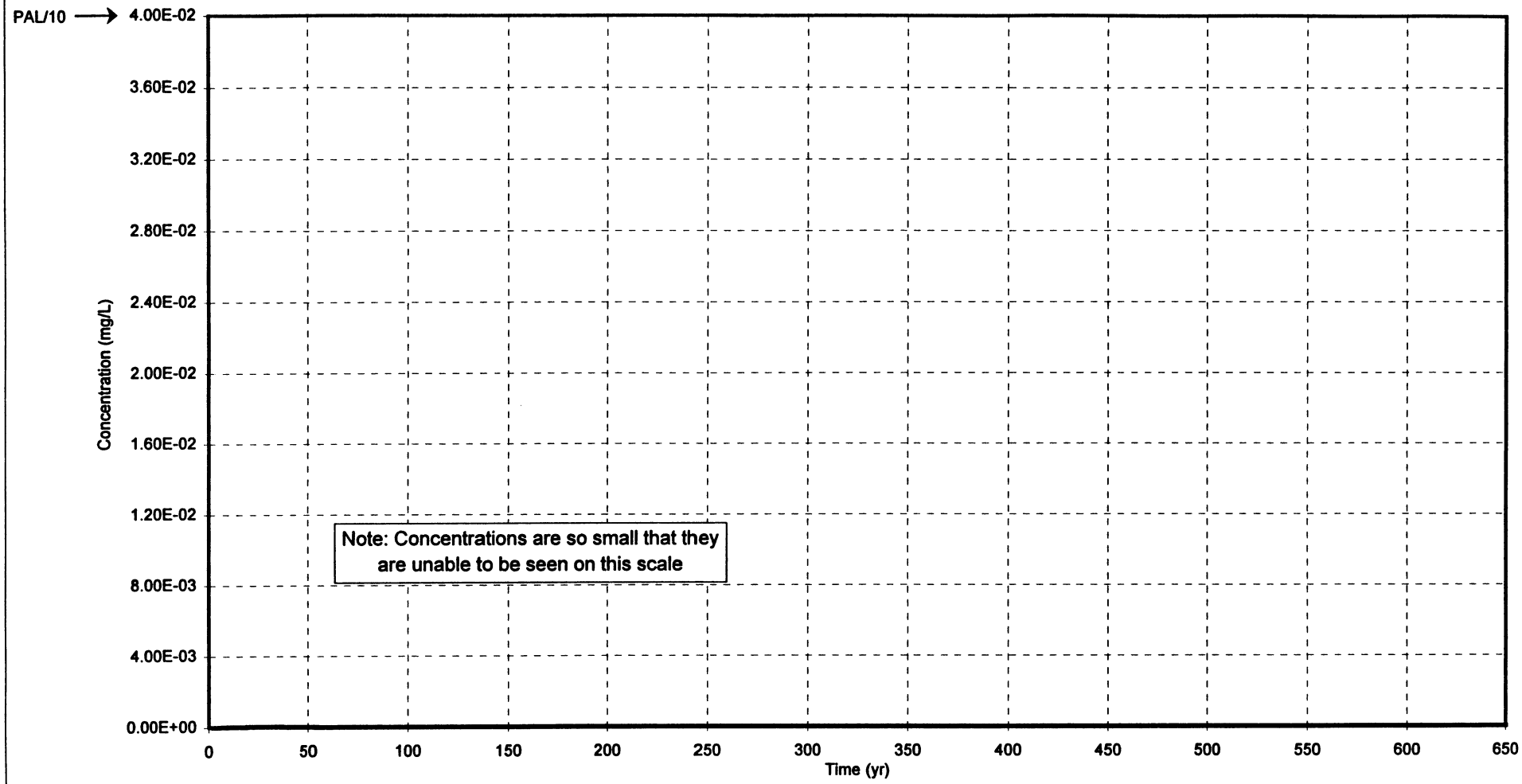

Source Concentration:

TMA Operation:	0.0033 (mg/L)
TMA Consolidation:	0.0033 (mg/L)
TMA Post-Cap:	0.0052 (mg/L)
TMA Post-FML-Degradation:	0.0052 (mg/L)
Reclaim Pond Operation:	0.03 (mg/L)
Reclaim Pond After TMA Capping:	0.0052 (mg/L)

Simulations T13C1-T13C6

HSI GEOTRANS

REVISED	DATE	BY	DESCRIPTION
1	6/99	JDC	Updated STM
2	3/00	JDC	Updated STM

CHECKED BY: GWC	DATE: April 1998
APPROVED BY: PFA	DATE: April 1998
APPROVED BY:	DATE:

Nicolet Minerals
a Rio Algom company

Figure 3-4
Maximum Concentration at the Compliance Boundary for Barium, BEJT

Scale: None	Date: April 1998
Prepared By: HSI GEOTRANS	By: KMR

\Crandon\TMAMod4\Response\T13gwqpe.xls, Be

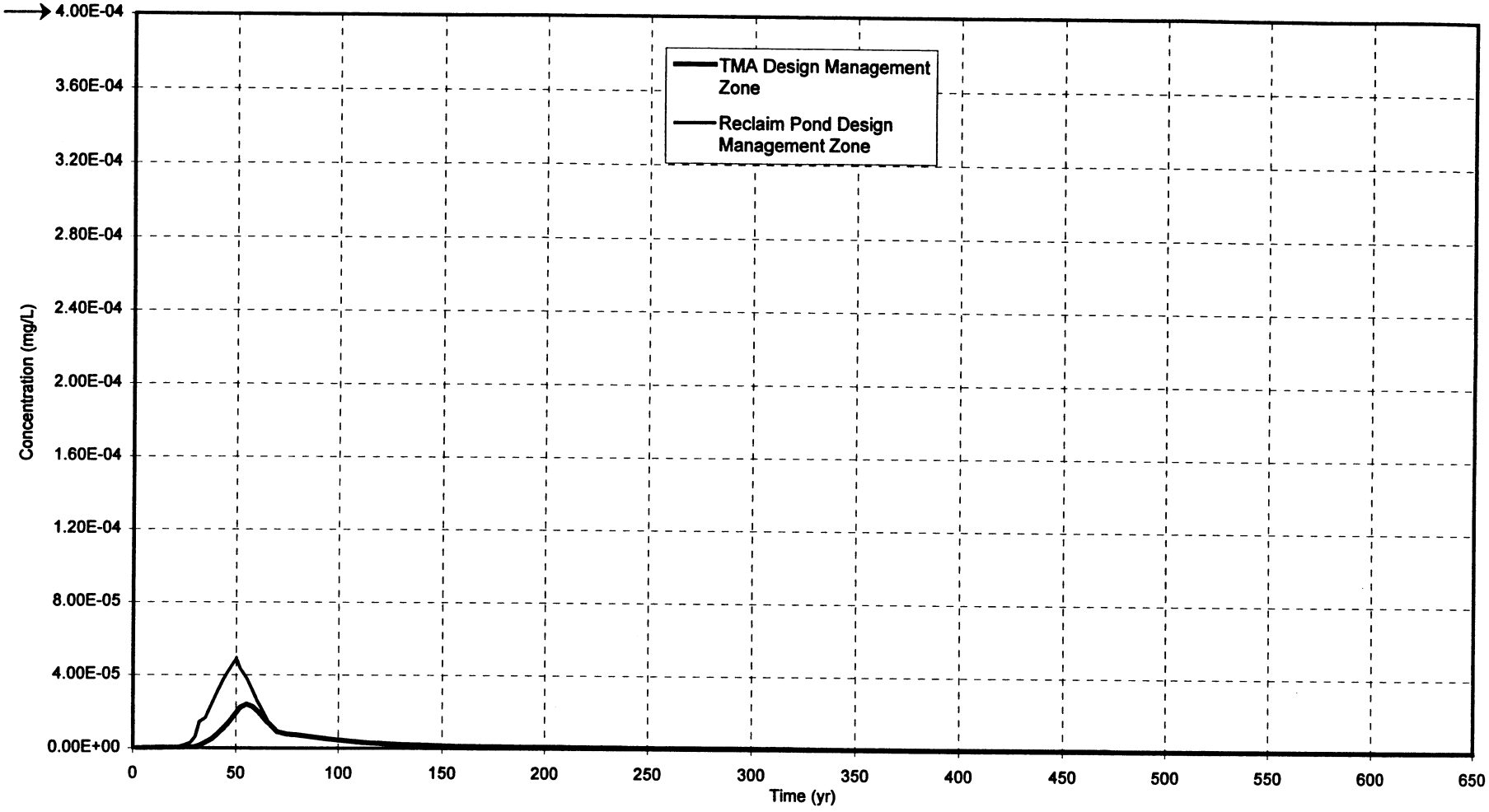

Source Concentration:

TMA Operation:	0.00045 (mg/L)
TMA Consolidation:	0.00045 (mg/L)
TMA Post-Cap:	0.072 (mg/L)
TMA Post-FML-Degradation:	0.072 (mg/L)
Reclaim Pond Operation:	0.00045 (mg/L)
Reclaim Pond After TMA Capping:	0.072 (mg/L)

Simulations T13C1-T13C6

HSI GEOTRANS

REVISED	DATE	BY	DESCRIPTION
1	6/99	JDC	Updated STM
2	3/00	JDC	Updated STM

CHECKED BY: GWC	DATE: April 1998
APPROVED BY: PFA	DATE: April 1998
APPROVED BY:	DATE:

Nicolet Minerals
a Rio Algom company

Figure 3-5
Maximum Concentration at the Compliance Boundary for Beryllium, BEJT

Scale: None	Date: April 1998
Prepared By: HSI GEOTRANS	By:KMR

\Crandon\TMAMod4\Response\T13gwqpe.xls, Cd

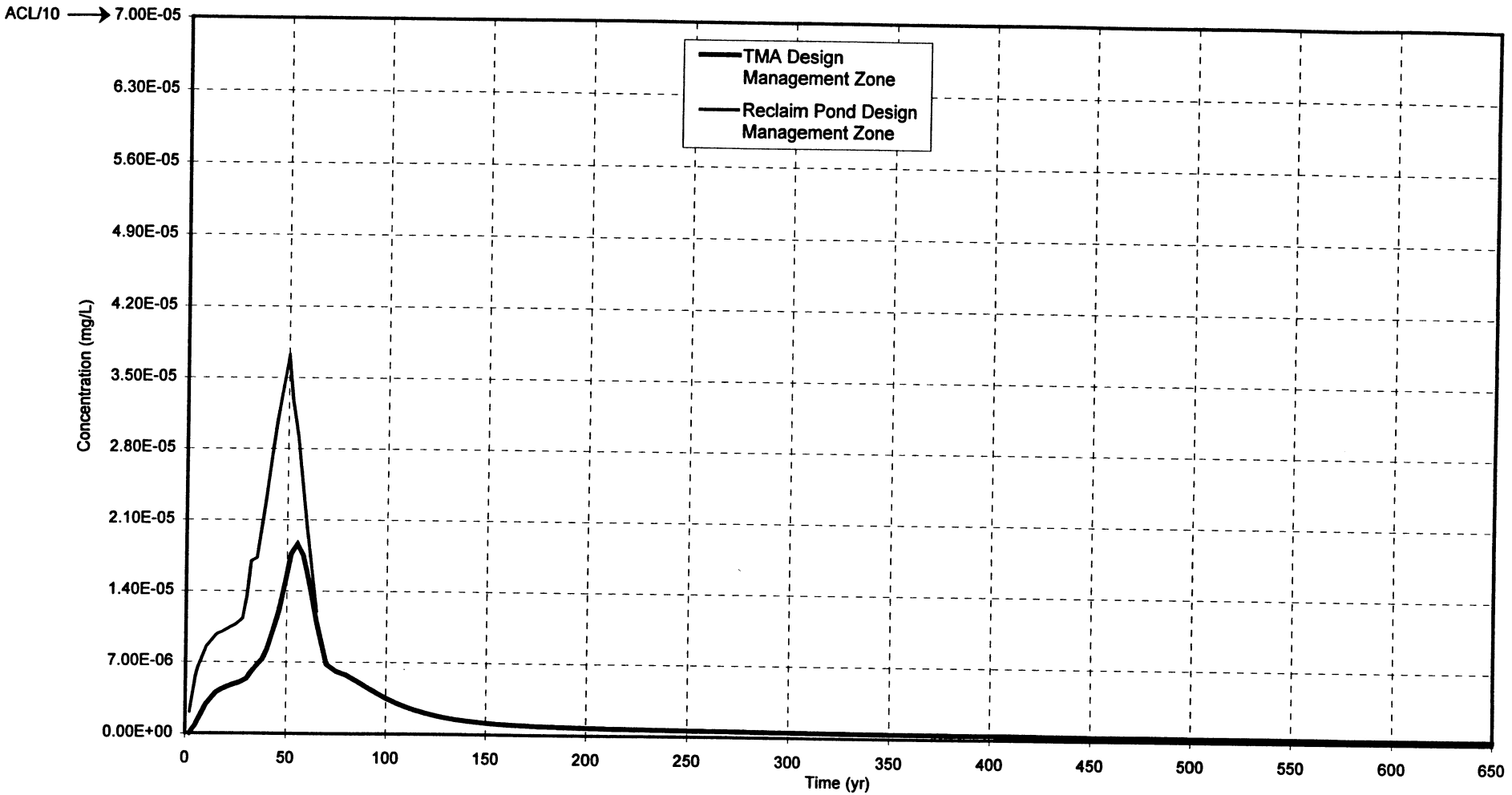

Source Concentration:

TMA Operation:	0.0061 (mg/L)
TMA Consolidation:	0.0061 (mg/L)
TMA Post-Cap:	0.053 (mg/L)
TMA Post-FML-Degradation:	0.053 (mg/L)
Reclaim Pond Operation:	0.0061 (mg/L)
Reclaim Pond After TMA Capping:	0.053 (mg/L)

Simulations T13C1-T13C6

HSI GEOTRANS

REVISED	DATE	BY	DESCRIPTION
1	6/99	JDC	Updated STM
2	3/00	JDC	Updated STM

CHECKED BY: GWC	DATE: April 1998
APPROVED BY: PFA	DATE: April 1998
APPROVED BY:	DATE:

Nicolet Minerals
a Rio Algom company

Figure 3-6
Maximum Concentration at the Compliance Boundary for Cadmium, BEJT

Scale: None	Date: April 1998
Prepared By: HSI GEOTRANS	By: KMR

4-2-12-71

\Crandon\TMAMod4\Response\T13gwqpe.xls, Cr

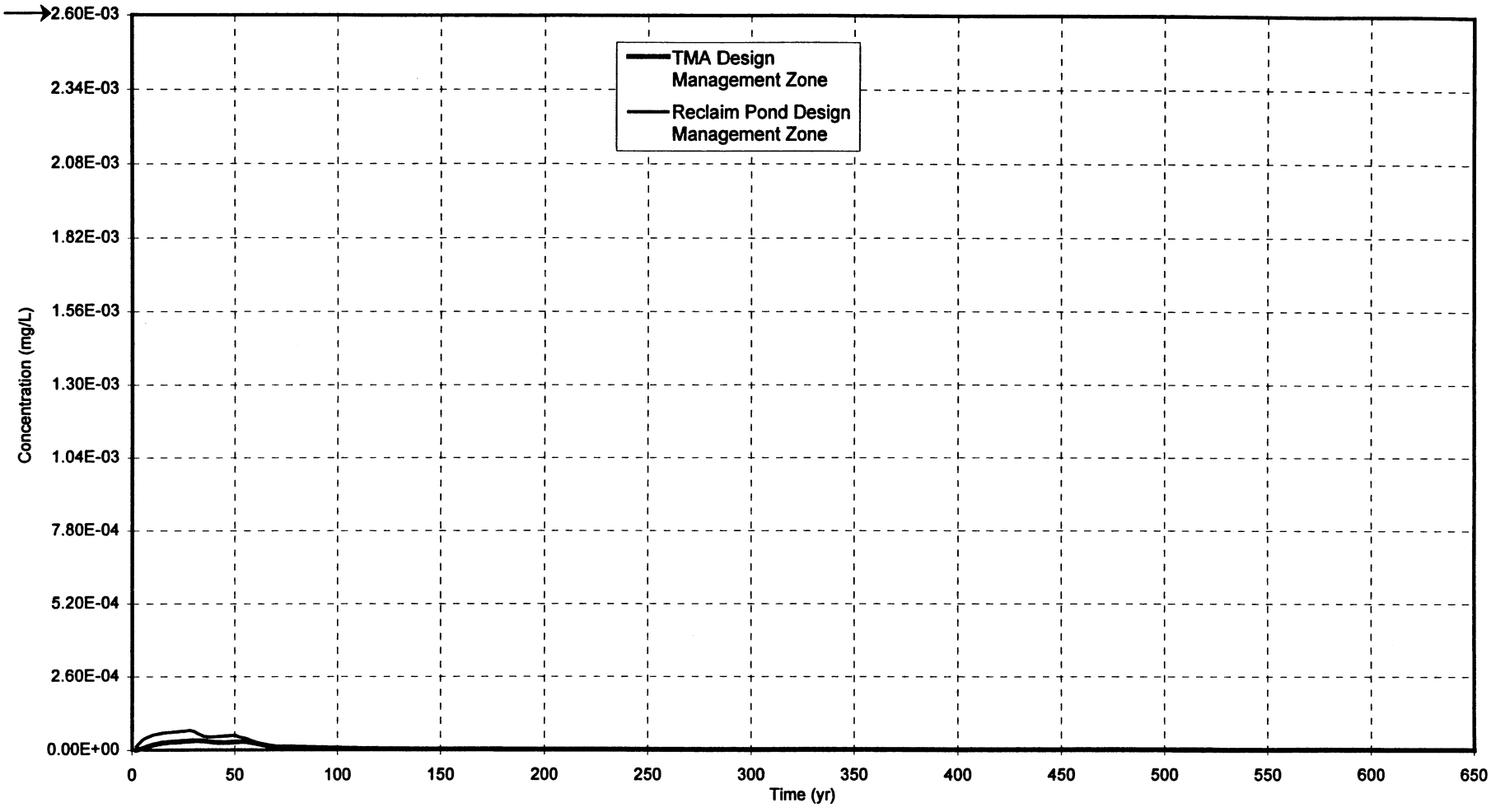

Source Concentration:

TMA Operation:	0.038 (mg/L)
TMA Consolidation:	0.038 (mg/L)
TMA Post-Cap:	0.066 (mg/L)
TMA Post-FML-Degradation:	0.066 (mg/L)
Reclaim Pond Operation:	0.038 (mg/L)
Reclaim Pond After TMA Capping:	0.066 (mg/L)

Simulations T13C1-T13C6

HSI GEOTRANS

REVISED	DATE	BY	DESCRIPTION
1	6/99	JDC	Updated STM
2	3/00	JDC	Updated STM

CHECKED BY: GWC	DATE: April 1998
APPROVED BY: PFA	DATE: April 1998
APPROVED BY:	DATE:

Nicolet Minerals
a Rio Algom company

Figure 3-7
Maximum Concentration at the Compliance Boundary for Chromium, BEJT

Scale: None	Date: April 1998
Prepared By: HSI GEOTRANS	By: KMR

\Crandon\TMAMod4\Response\T13gwqpe.xls, Fe

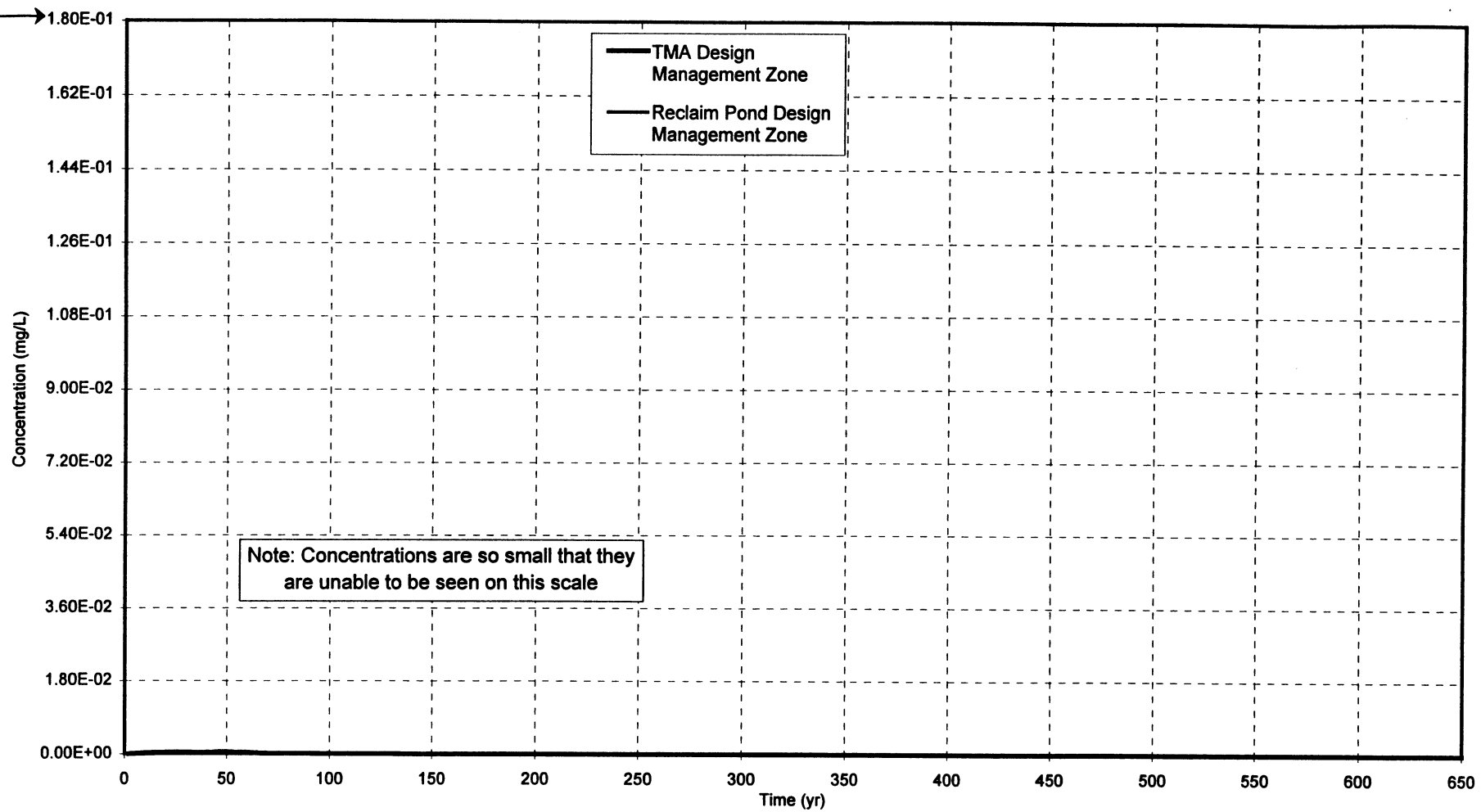

Source Concentration:

TMA Operation:	0.33 (mg/L)
TMA Consolidation:	0.33 (mg/L)
TMA Post-Cap:	1.0 (mg/L)
TMA Post-FML-Degradation:	1.0 (mg/L)
Reclaim Pond Operation:	0.33 (mg/L)
Reclaim Pond After TMA Capping:	1.0 (mg/L)

Simulations T13C1-T13C6

HSI GEOTRANS

REVISED	DATE	BY	DESCRIPTION
1	6/99	JDC	Updated STM
2	3/00	JDC	Updated STM

CHECKED BY: GWC	DATE: April 1998
APPROVED BY: PFA	DATE: April 1998
APPROVED BY:	DATE:

Nicolet Minerals
a Rio Algom company

Figure 3-8
Maximum Concentration at the Compliance Boundary for Iron, BEJT

Scale: None	Date: April 1998
Prepared By: HSI GEOTRANS	By: KMR

4.2-12-73

\Crandon\TMAMod4\Response\T13gwqpe.xls, Pb

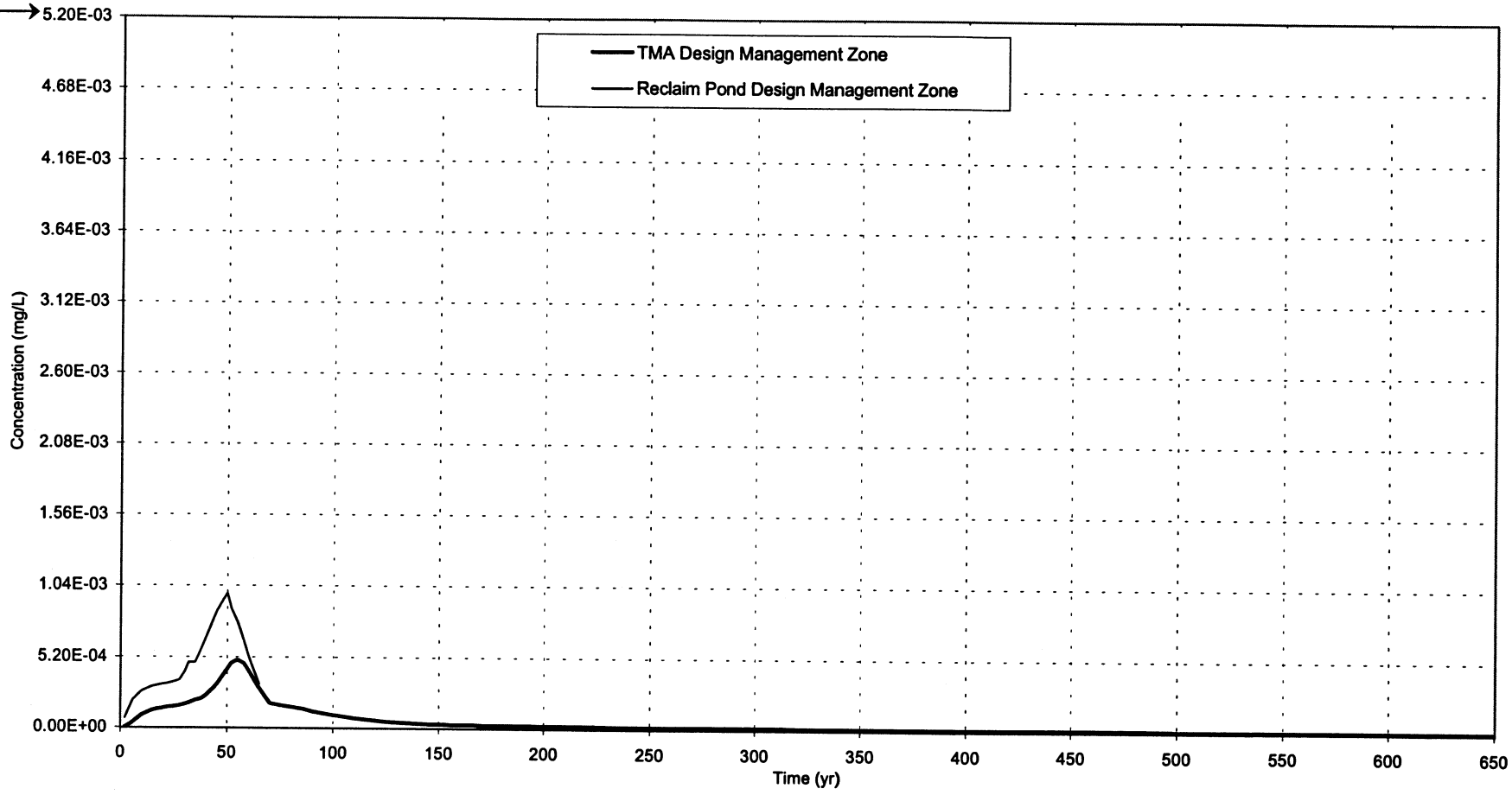

Source Concentration:

TMA Operation:	0.19 (mg/L)
TMA Consolidation:	0.19 (mg/L)
TMA Post-Cap:	1.4 (mg/L)
TMA Post-FML-Degradation:	1.4 (mg/L)
Reclaim Pond Operation:	0.19 (mg/L)
Reclaim Pond After TMA Capping:	1.4 (mg/L)

REVISED	DATE	BY	DESCRIPTION
1	6/99	JDC	Updated STM
2	3/00	JDC	Updated STM
3	8/00	GWC	Revised Source Conc

CHECKED BY: GWC	DATE: April 1998
APPROVED BY: PFA	DATE: April 1998
APPROVED BY:	DATE:

Simulations T13C1-T13C6

Nicolet Minerals
a Rio Algom company

Figure 3-9
Maximum Concentration at the Compliance Boundary for Lead, BEJT

Scale: None	Date: April 1998
Prepared By: HSI GEOTRANS	By: KMR

4.2-12-74

\Crandon\TMAMod4\Response\T13gwqpe.xls, Mn

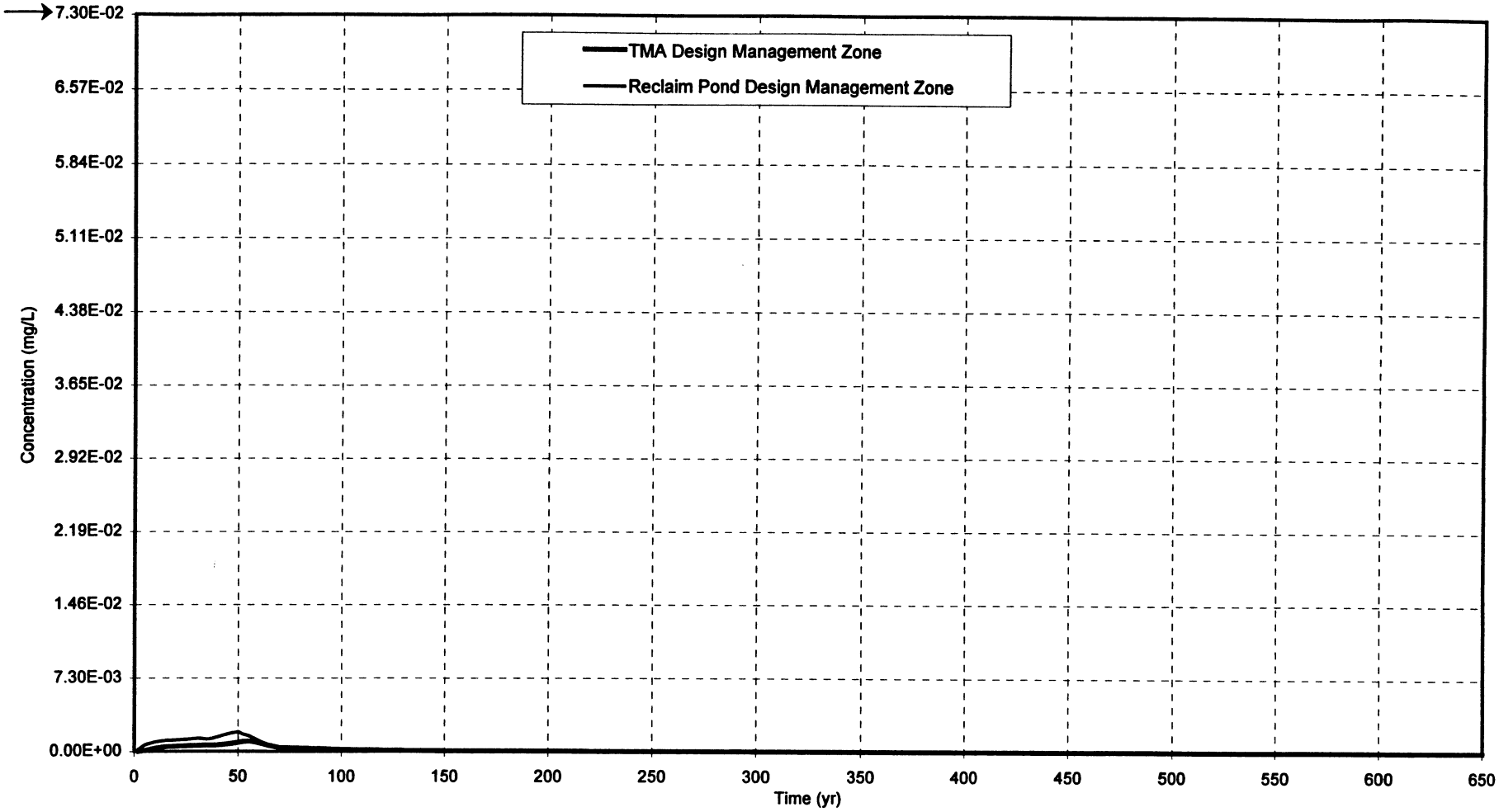

Source Concentration:

TMA Operation:	0.68 (mg/L)
TMA Consolidation:	0.68 (mg/L)
TMA Post-Cap:	2.7 (mg/L)
TMA Post-FML-Degradation:	2.7 (mg/L)
Reclaim Pond Operation:	0.68 (mg/L)
Reclaim Pond After TMA Capping:	2.7 (mg/L)

HSI GEOTRANS

REVISED	DATE	BY	DESCRIPTION
1	6/99	JDC	Updated STM
2	3/00	JDC	Updated STM

CHECKED BY: GWC	DATE: April 1998
APPROVED BY: PFA	DATE: April 1998
APPROVED BY:	DATE:

Simulations T13C1-T13C6

Nicolet Minerals
a Rio Algom company

Figure 3-10
Maximum Concentration at the Compliance Boundary for Manganese, BEJT

Scale: None	Date: April 1998
Prepared By: HSI GEOTRANS	By: KMR

\Crandon\TMAMod4\Response\T13gwqpe.xls, Hg

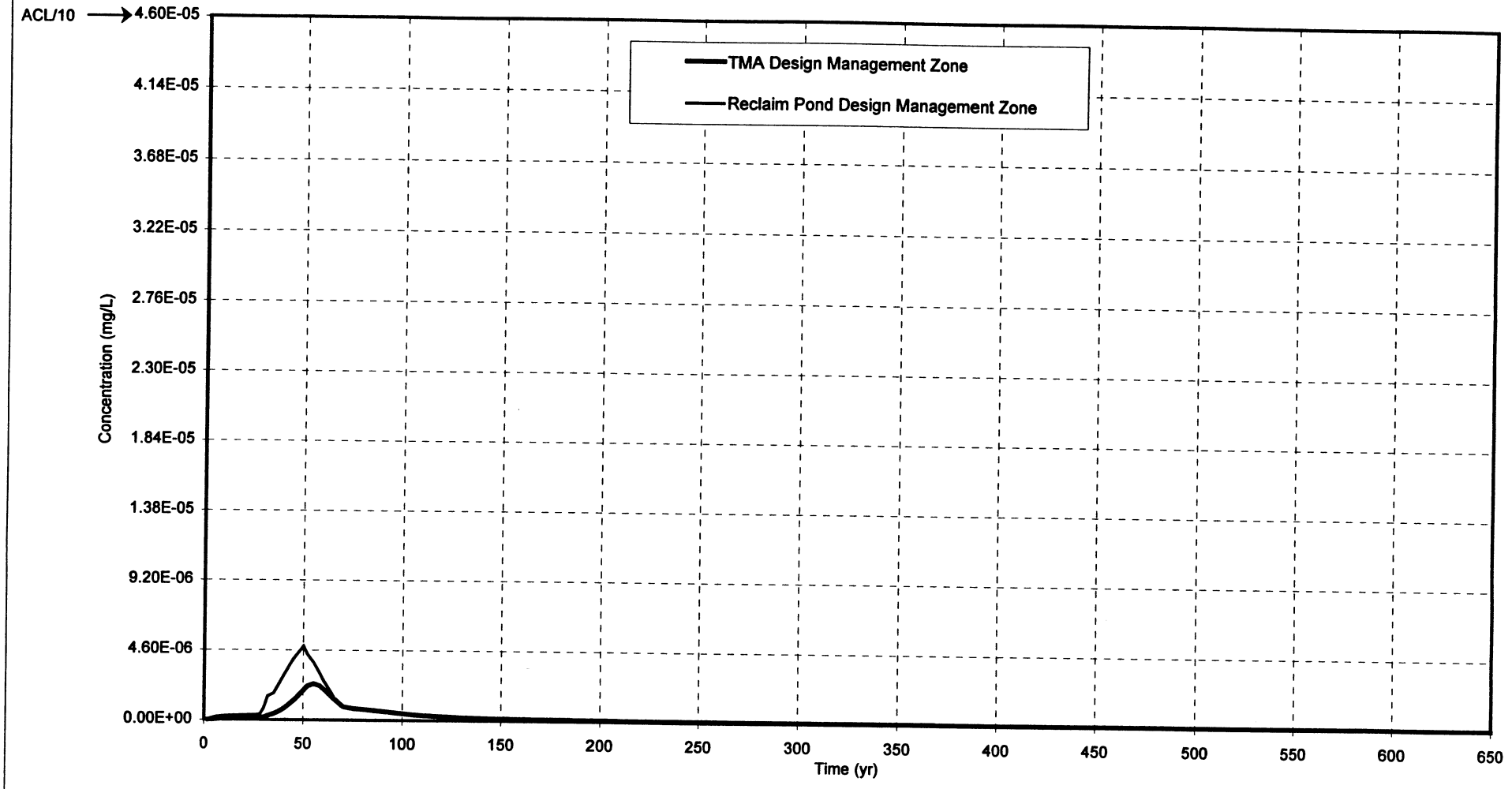

Source Concentration:

TMA Operation:	0.00018 (mg/L)
TMA Consolidation:	0.00018 (mg/L)
TMA Post-Cap:	0.0071 (mg/L)
TMA Post-FML-Degradation:	0.0071 (mg/L)
Reclaim Pond Operation:	0.00018 (mg/L)
Reclaim Pond After TMA Capping:	0.0071 (mg/L)

Simulations T13C1-T13C6

HSI GEOTRANS

REVISED	DATE	BY	DESCRIPTION
1	6/99	JDC	Updated STM
2	3/00	JDC	Updated STM

CHECKED BY: GWC	DATE: April 1998
APPROVED BY: PFA	DATE: April 1998
APPROVED BY:	DATE:

Nicolet Minerals
a Rio Algom company

Figure 3-11
Maximum Concentration at the Compliance Boundary for Mercury, BEJT

Scale: None	Date: April 1998
Prepared By: HSI GEOTRANS	By: KMR

\Crandon\TMAMod4\Response\T13gwqpe.xls, Se

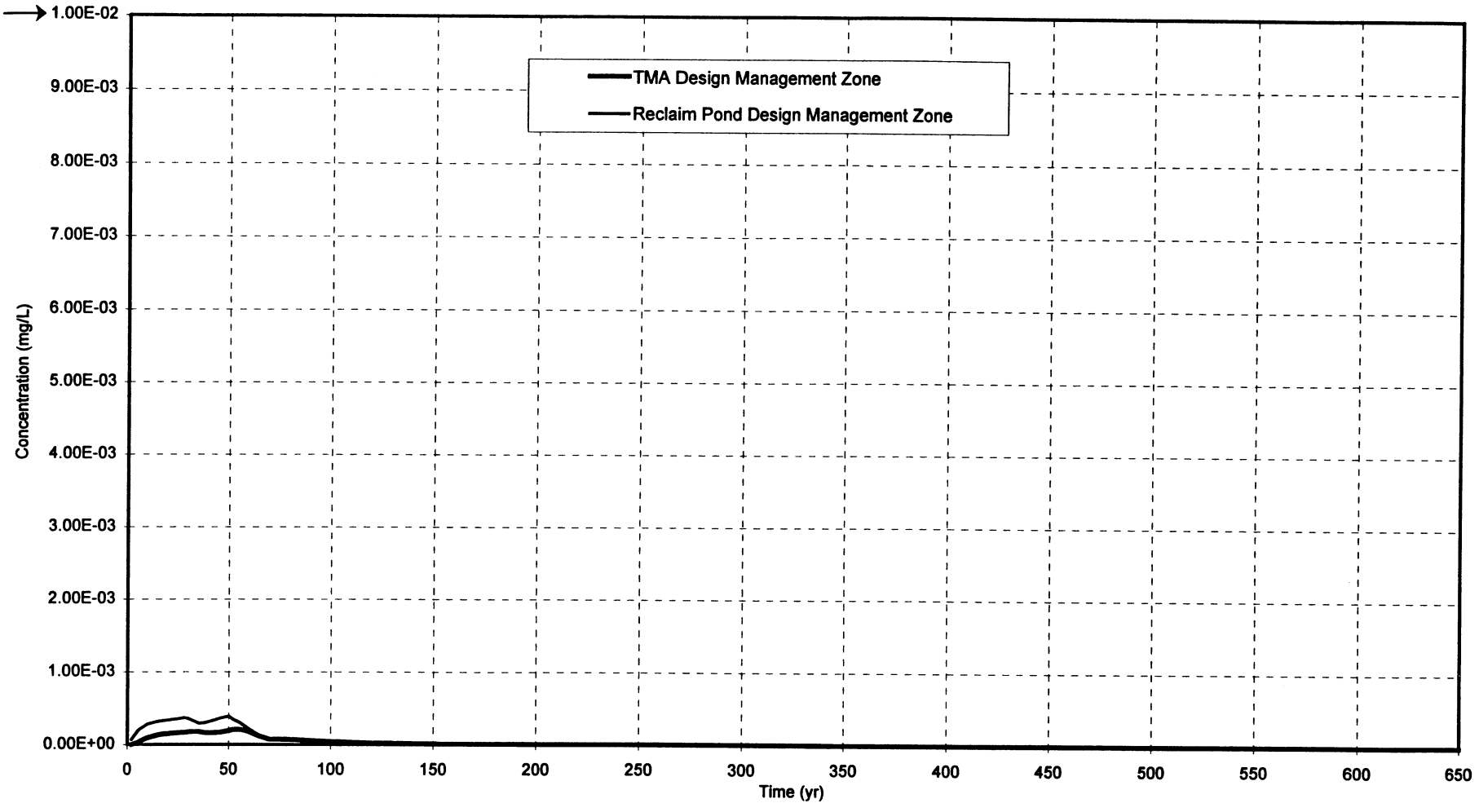

Source Concentration:

TMA Operation:	0.2 (mg/L)
TMA Consolidation:	0.2 (mg/L)
TMA Post-Cap:	0.52 (mg/L)
TMA Post-FML-Degradation:	0.52 (mg/L)
Reclaim Pond Operation:	0.2 (mg/L)
Reclaim Pond After TMA Capping:	0.52 (mg/L)

Simulations T13C1-T13C6

HSI GEOTRANS

REVISED	DATE	BY	DESCRIPTION
1	6/99	JDC	Updated STM
2	3/00	JDC	Updated STM

CHECKED BY: GWC	DATE: April 1998
APPROVED BY: PFA	DATE: April 1998
APPROVED BY:	DATE:

Nicolet Minerals
a Rio Algom company

Figure 3-12
Maximum Concentration at the Compliance Boundary for Selenium, BEJT

Scale: None	Date: April 1998
Prepared By: HSI GEOTRANS	By: KMR

4.2-12-77

\Crandon\TMAMod4\Response\T13gwqpe1.xls, SO4

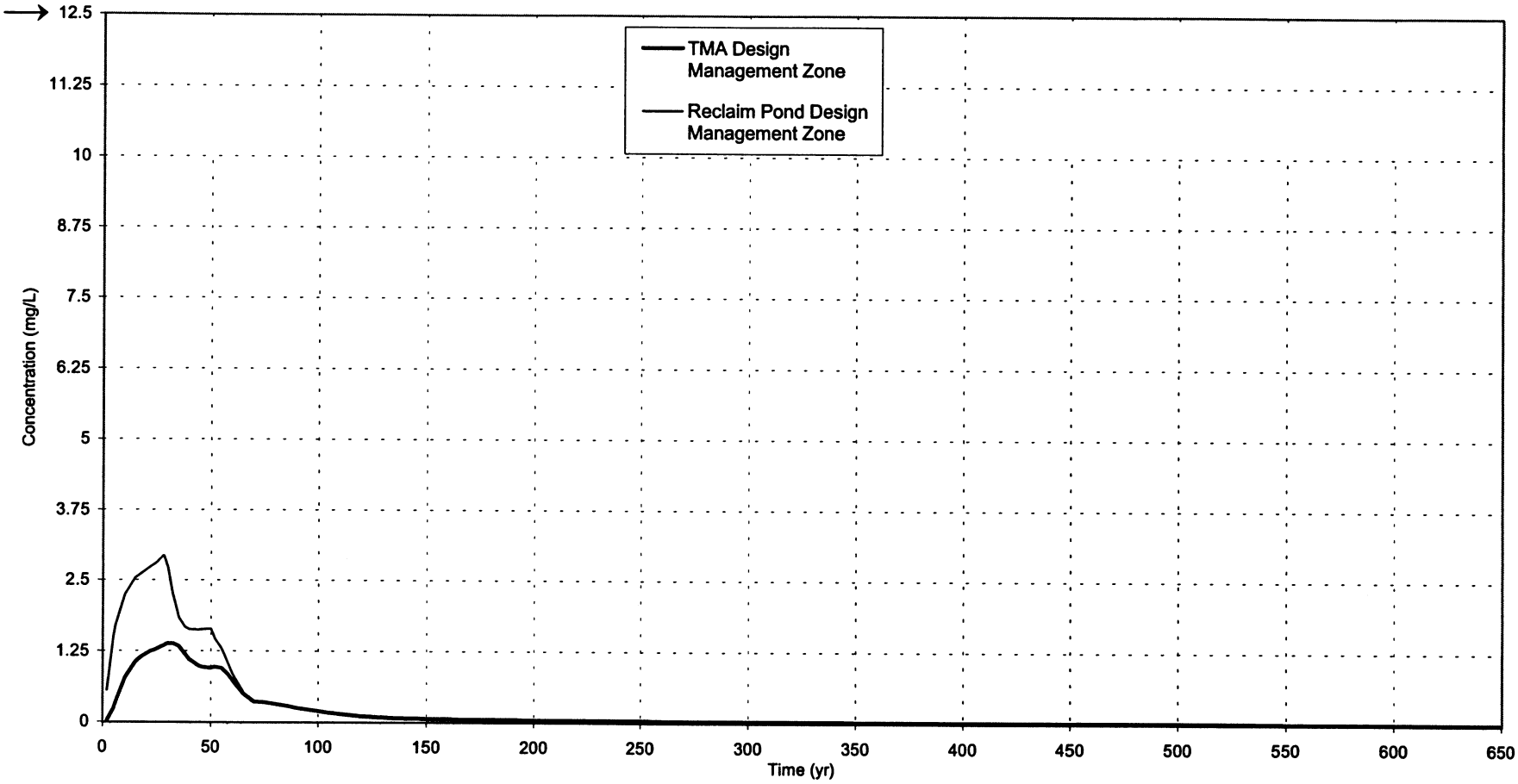

Source Concentration:

TMA Operation:	1599	(mg/L)
TMA Consolidation:	1599	(mg/L)
TMA Post-Cap:	1965	(mg/L)
TMA Post-FML-Degradation:	1965	(mg/L)
Reclaim Pond Operation:	1599	(mg/L)
Reclaim Pond After TMA Capping:	1965	(mg/L)

REVISED	DATE	BY	DESCRIPTION
1	6/99	JDC	Updated STM
2	3/00	JDC	Updated STM
3	8/00	GWC	Revised Source Conc

CHECKED BY: GWC	DATE: April 1998
APPROVED BY: PFA	DATE: April 1998
APPROVED BY:	DATE:

Simulations T13C1-T13C6

Nicolet Minerals
a Rio Algom company

Figure 3-13
Maximum Concentration at the Compliance Boundary for Sulfate, BEJT

Scale: None	Date: April 1998
Prepared By: HSI GEOTRANS	By: KMR

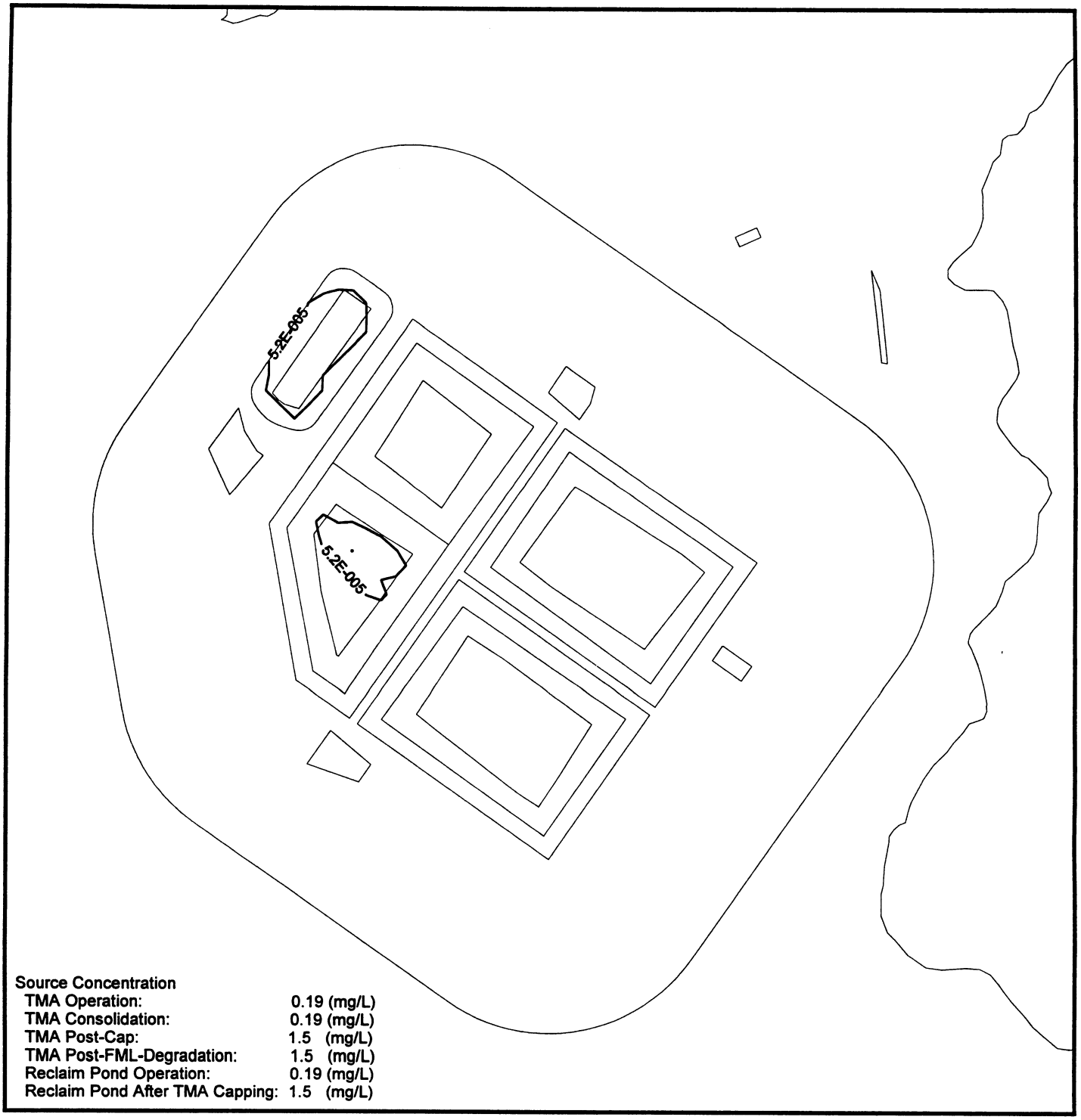

Source Concentration

TMA Operation:	0.19 (mg/L)
TMA Consolidation:	0.19 (mg/L)
TMA Post-Cap:	1.5 (mg/L)
TMA Post-FML-Degradation:	1.5 (mg/L)
Reclaim Pond Operation:	0.19 (mg/L)
Reclaim Pond After TMA Capping:	1.5 (mg/L)

Concentration Contours Shown
0.0052 mg/L (ACL)
0.00052 mg/L
0.000052 mg/L

N

0 1000 2000

Scale in Feet

HSI GEOTRANS

REVISED	DATE	BY	DESCRIPTION
1	6/99	RAK	Updated STM
2	3/00	JDC	Updated STM

CHECKED BY: GWC		DATE: April 1998
APPROVED BY: PFA		DATE: April 1998
APPROVED BY:		DATE:

Simulations T13C1 - T13C6

Nicolet Minerals
a Rio Algom company

Figure 3-14
Lead Concentration After 2 Years, BEJT
(Example Constituent, Plan View)

Scale: 1 in. = 1000 ft. | Date: April 1998

Prepared By: HSI GEOTRANS | By: RMD

P:\Crandon\Tma\Mod4\Sum...pb002.srf

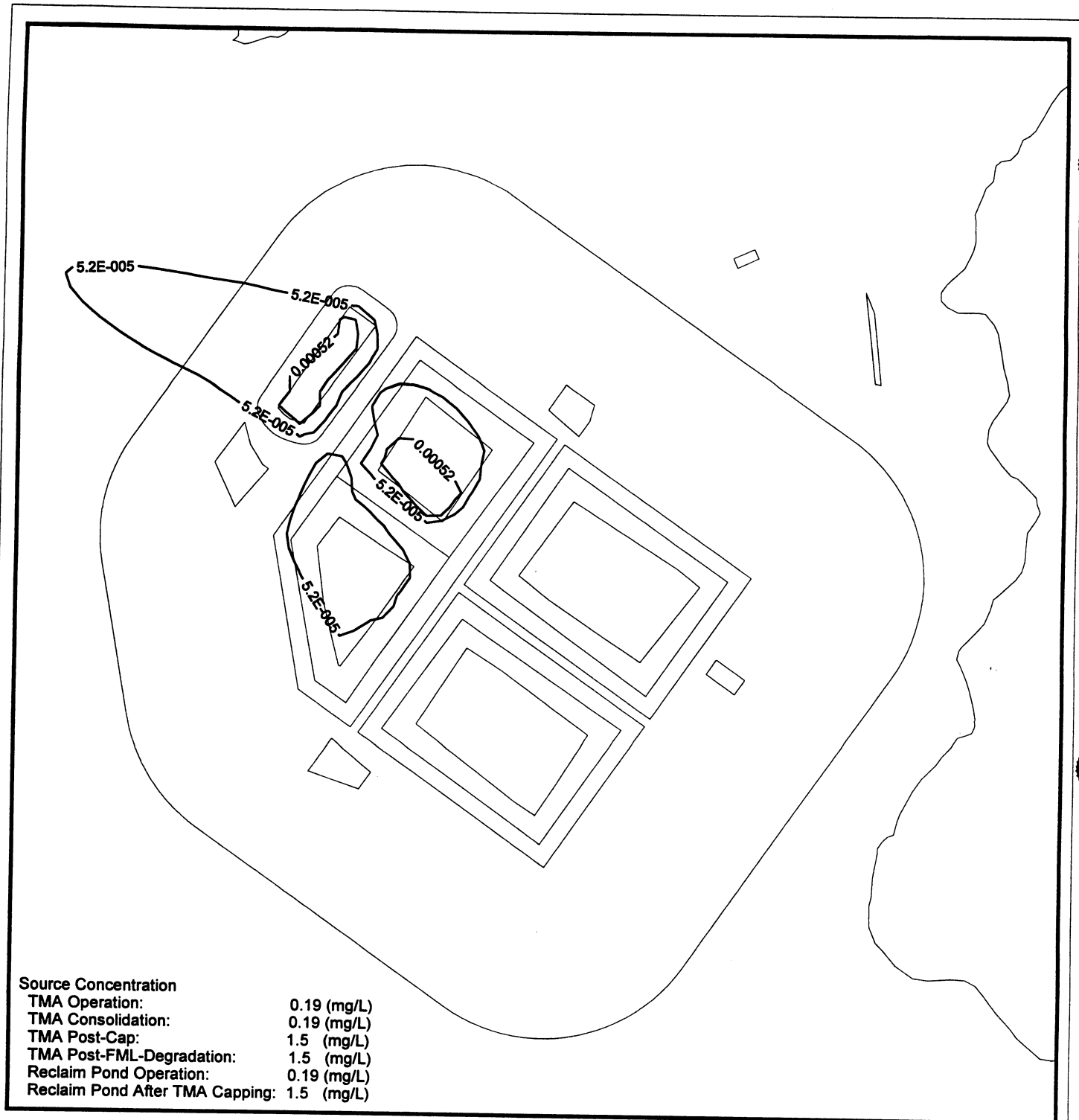

Source Concentration

TMA Operation:	0.19 (mg/L)
TMA Consolidation:	0.19 (mg/L)
TMA Post-Cap:	1.5 (mg/L)
TMA Post-FML-Degradation:	1.5 (mg/L)
Reclaim Pond Operation:	0.19 (mg/L)
Reclaim Pond After TMA Capping:	1.5 (mg/L)

Concentration Contours Shown
0.0052 mg/L (ACL)
0.00052 mg/L
0.000052 mg/L

N

0 1000 2000

Scale in Feet

HSI GEOTRANS

REVISED	DATE	BY	DESCRIPTION
1	6/99	RAK	Updated STM
2	3/00	JDC	Updated STM

CHECKED BY: GWC		DATE: April 1998
APPROVED BY: PFA		DATE: April 1998
APPROVED BY:		DATE:

Simulations T13C1 - T13C6

Nicolet Minerals
a Rio Algom company

Figure 3-15
Lead Concentration After 16 Years, BEJT
(Example Constituent, Plan View)

Scale: 1 in. = 1000 ft. | Date: April 1998

Prepared By: HSI GEOTRANS | By: RMD

P:\Crandon\Tma\Mod4\Surfer\P13pb016.srf

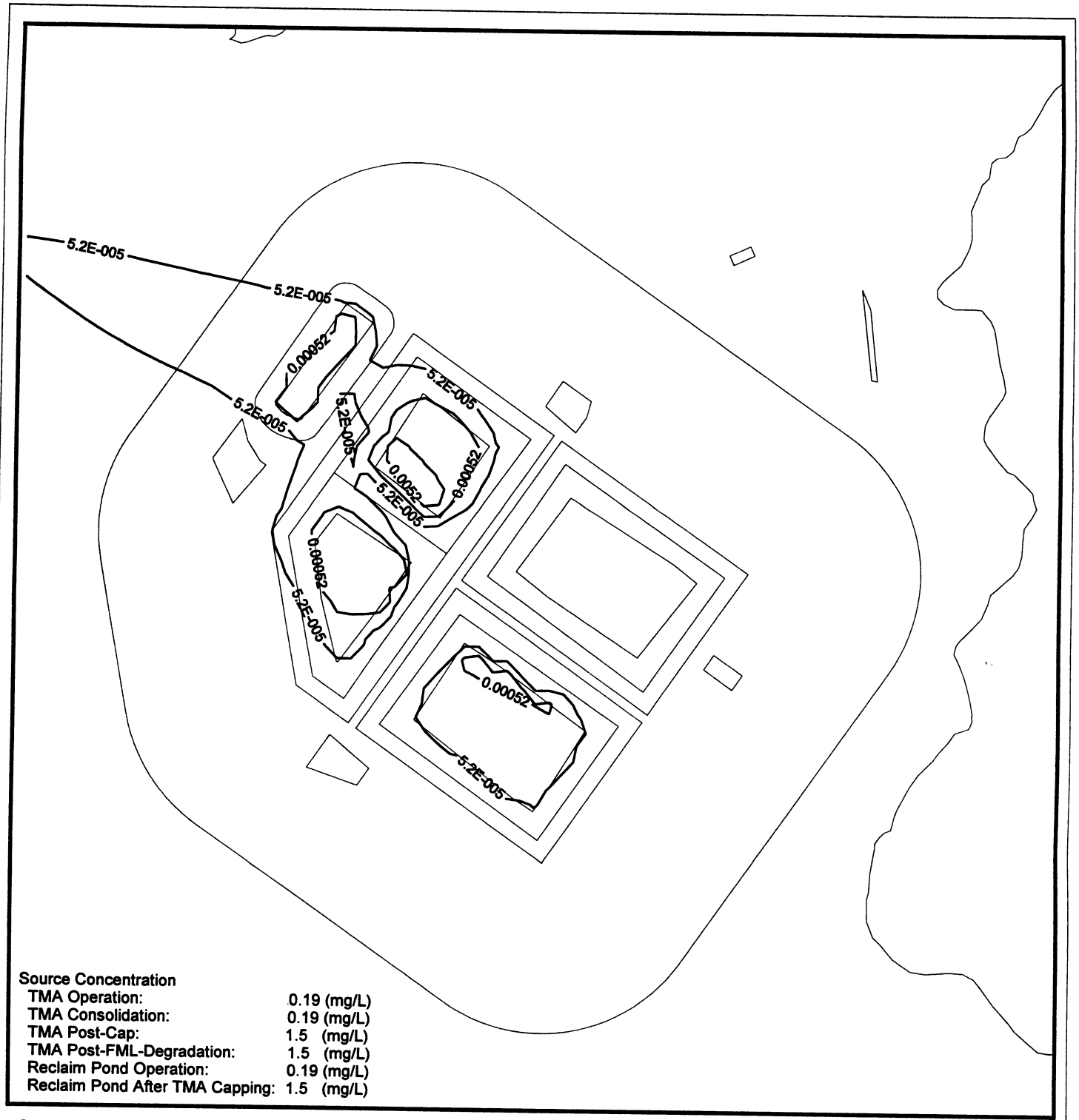

Source Concentration

TMA Operation:	0.19 (mg/L)
TMA Consolidation:	0.19 (mg/L)
TMA Post-Cap:	1.5 (mg/L)
TMA Post-FML-Degradation:	1.5 (mg/L)
Reclaim Pond Operation:	0.19 (mg/L)
Reclaim Pond After TMA Capping:	1.5 (mg/L)

Concentration Contours Shown
0.0052 mg/L (ACL)
0.00052 mg/L
0.000052 mg/L

N

0 1000 2000

Scale in Feet

HSI GEOTRANS

REVISED	DATE	BY	DESCRIPTION
1	6/99	RAK	Updated STM
2	3/00	JDC	Updated STM

CHECKED BY: GWC DATE: April 1998

APPROVED BY: PFA DATE: April 1998

APPROVED BY: DATE:

Simulations T13C1 - T13C6

Nicolet Minerals
a Rio Algom company

Figure 3-16
Lead Concentration After 22 Years, BEJT
(Example Constituent, Plan View)

Scale: 1 in. = 1000 ft. Date: April 1998

Prepared By: HSI GEOTRANS By: RMD

P:\Crandon\Tmalvod4\S\...p022.srf

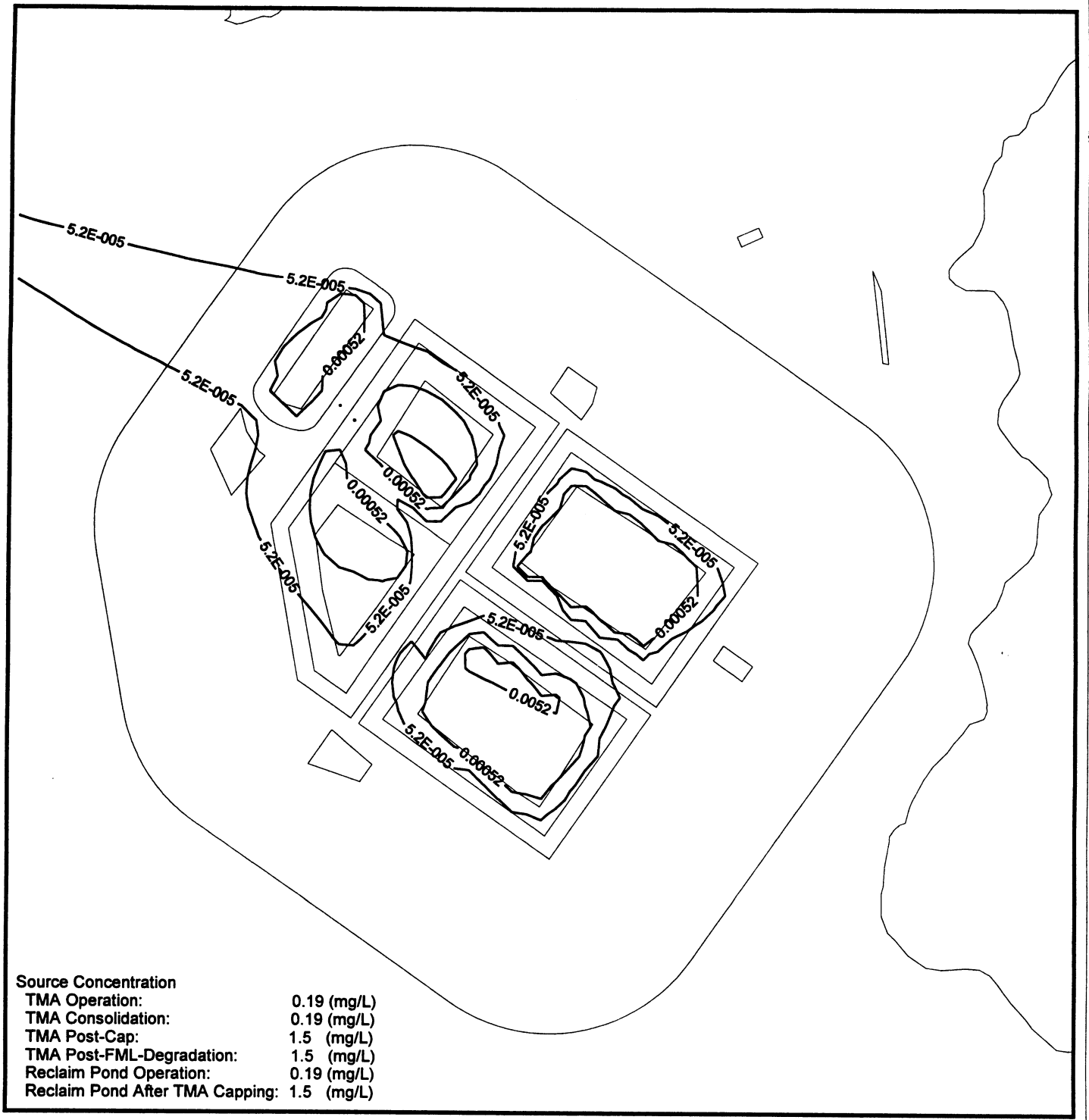

Source Concentration

TMA Operation:	0.19 (mg/L)
TMA Consolidation:	0.19 (mg/L)
TMA Post-Cap:	1.5 (mg/L)
TMA Post-FML-Degradation:	1.5 (mg/L)
Reclaim Pond Operation:	0.19 (mg/L)
Reclaim Pond After TMA Capping:	1.5 (mg/L)

Concentration Contours Shown
0.0052 mg/L (ACL)
0.00052 mg/L
0.000052 mg/L

N

0 1000 2000

Scale in Feet

HSI GEOTRANS

REVISED	DATE	BY	DESCRIPTION
1	6/99	RAK	Updated STM
2	3/00	JDC	Updated STM

CHECKED BY: GWC DATE: April 1998

APPROVED BY: PFA DATE: April 1998

APPROVED BY: DATE:

Simulations T13C1 - T13C6

Nicolet Minerals
a Rio Algom company

Figure 3-17
Lead Concentration After 32 Years, BEJT
(Example Constituent, Plan View)

Scale: 1 in. = 1000 ft. Date: April 1998

Prepared By: HSI GEOTRANS By: RMD

P:\Crandon\Tmwf\Mod4fSurfer\P13pb032.srf

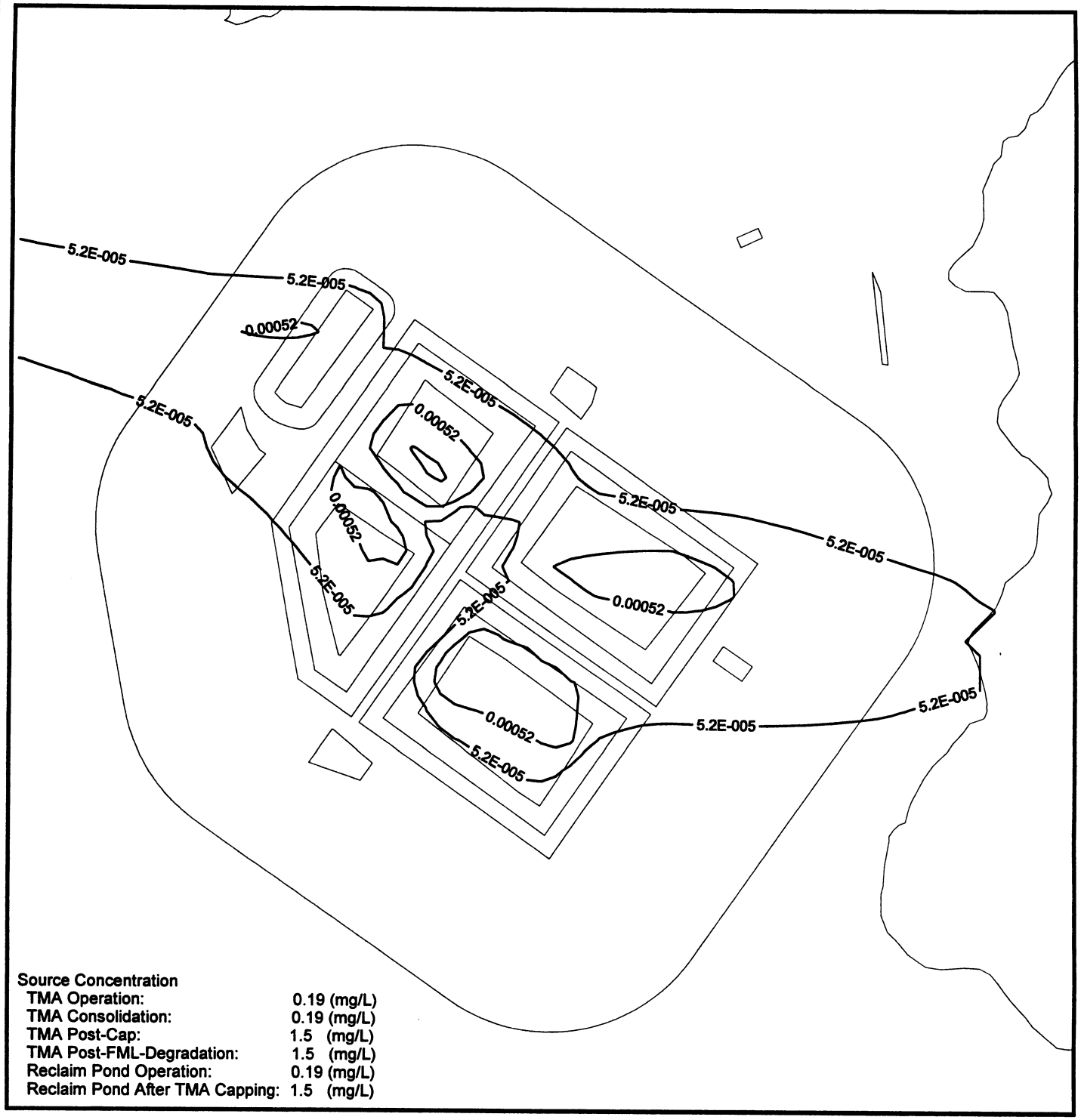

Source Concentration

TMA Operation:	0.19 (mg/L)
TMA Consolidation:	0.19 (mg/L)
TMA Post-Cap:	1.5 (mg/L)
TMA Post-FML-Degradation:	1.5 (mg/L)
Reclaim Pond Operation:	0.19 (mg/L)
Reclaim Pond After TMA Capping:	1.5 (mg/L)

Concentration Contours Shown
0.0052 mg/L (ACL)
0.00052 mg/L
0.000052 mg/L

N

0 1000 2000

Scale in Feet

HSI GEOTRANS

REVISED	DATE	BY	DESCRIPTION
1	6/99	RAK	Updated STM
2	3/00	JDC	Updated STM

	CHECKED BY: GWC	DATE: April 1998
Simulations T13C1 - T13C6	APPROVED BY: PFA	DATE: April 1998
	APPROVED BY:	DATE:

Nicolet Minerals
a Rio Algom company

Figure 3-18
Lead Concentration After 60 Years, BEJT
(Example Constituent, Plan View)

Scale: 1 in. = 1000 ft.	Date: April 1998
Prepared By: HSI GEOTRANS	By: RMD

P:\Crandon\Tma\Mod4\S...cpb090.srf

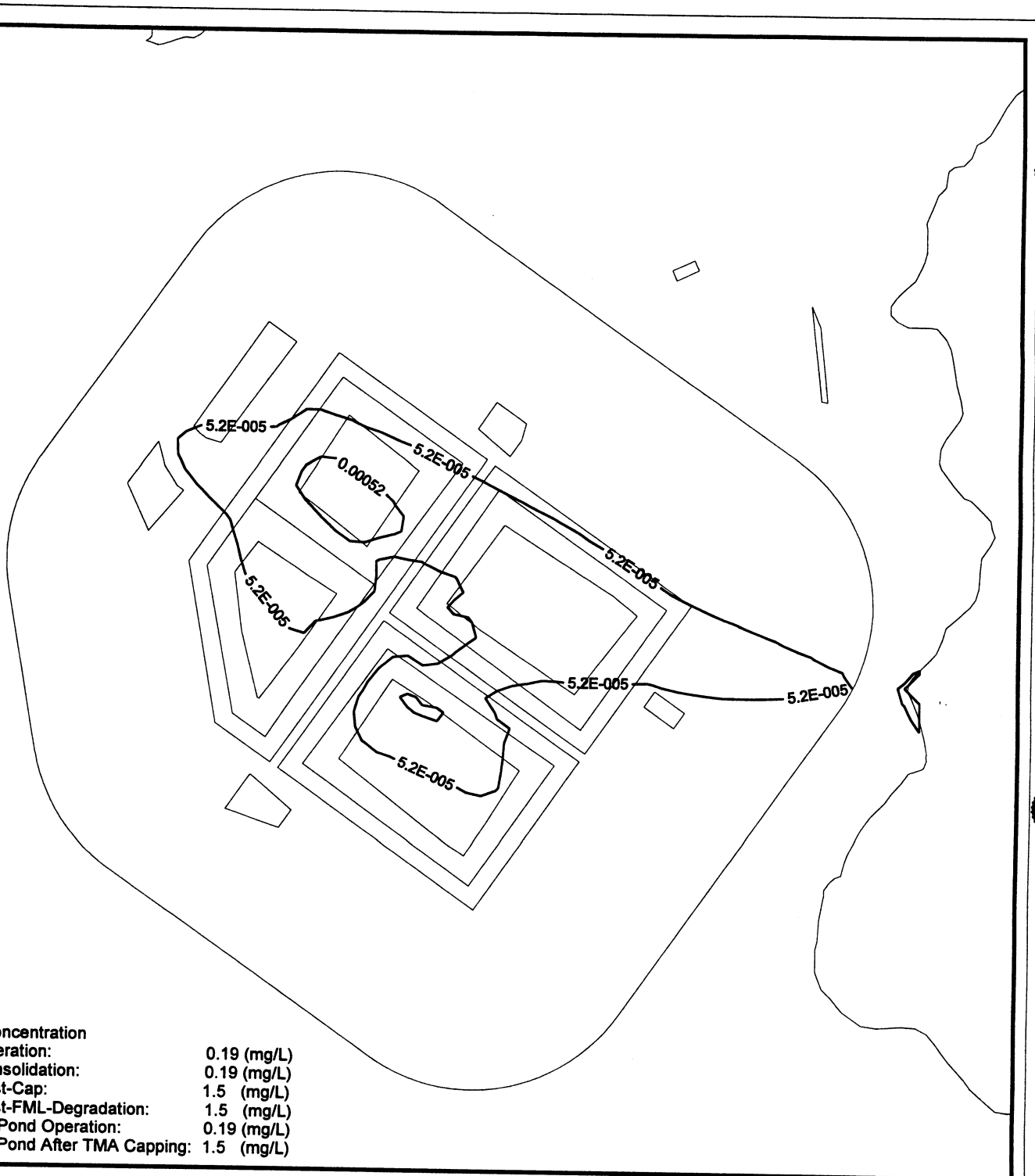

Source Concentration

TMA Operation:	0.19 (mg/L)
TMA Consolidation:	0.19 (mg/L)
TMA Post-Cap:	1.5 (mg/L)
TMA Post-FML-Degradation:	1.5 (mg/L)
Reclaim Pond Operation:	0.19 (mg/L)
Reclaim Pond After TMA Capping:	1.5 (mg/L)

Concentration Contours Shown
0.0052 mg/L (ACL)
0.00052 mg/L
0.000052 mg/L

N

0 1000 2000

Scale in Feet

HSI GEOTRANS

REVISED	DATE	BY	DESCRIPTION
1	6/99	RAK	Updated STM
2	3/00	JDC	Updated STM

Simulations T13C1 - T13C6	CHECKED BY: GWC	DATE: April 1998
	APPROVED BY: PFA	DATE: April 1998
	APPROVED BY:	DATE:

Nicolet Minerals
a Rio Algom company

Figure 3-19
Lead Concentration After 125 Years, BEJT
(Example Constituent, Plan View)

Scale: 1 in. = 1000 ft.	Date: April 1998
Prepared By: HSI GEOTRANS	By: RMD

P:\Crandon\Tma\Mod4\Surfer\P13pb125.srf

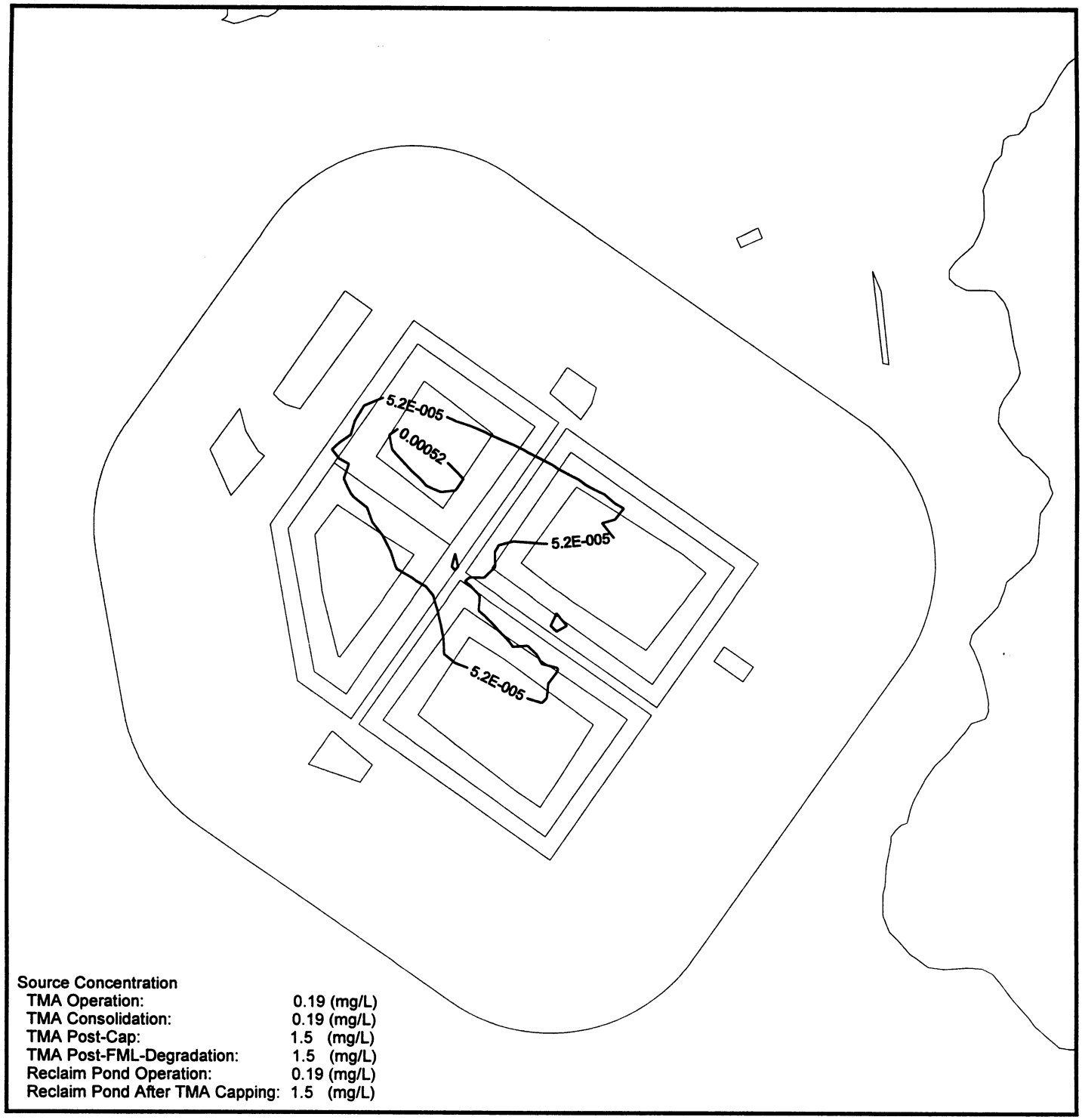

Source Concentration

TMA Operation:	0.19 (mg/L)
TMA Consolidation:	0.19 (mg/L)
TMA Post-Cap:	1.5 (mg/L)
TMA Post-FML-Degradation:	1.5 (mg/L)
Reclaim Pond Operation:	0.19 (mg/L)
Reclaim Pond After TMA Capping:	1.5 (mg/L)

Concentration Contours Shown
0.0052 mg/L (ACL)
0.00052 mg/L
0.000052 mg/L

N

0 1000 2000

Scale in Feet

HSI GEOTRANS

REVISED	DATE	BY	DESCRIPTION
1	6/99	RAK	Updated STM
2	3/00	JDC	Updated STM

Simulations T13C1 - T13C6	CHECKED BY: GWC	DATE: April 1998
	APPROVED BY: PFA	DATE: April 1998
	APPROVED BY:	DATE:

Nicolet Minerals
a Rio Algom company

Figure 3-20
Lead Concentration After 300 Years, BEJT
(Example Constituent, Plan View)

Scale: 1 in. = 1000 ft.	Date: April 1998
Prepared By: HSI GEOTRANS	By: RMD

P:\Crandon\Tmel\Mod4\Surfer\P13cb300.srf

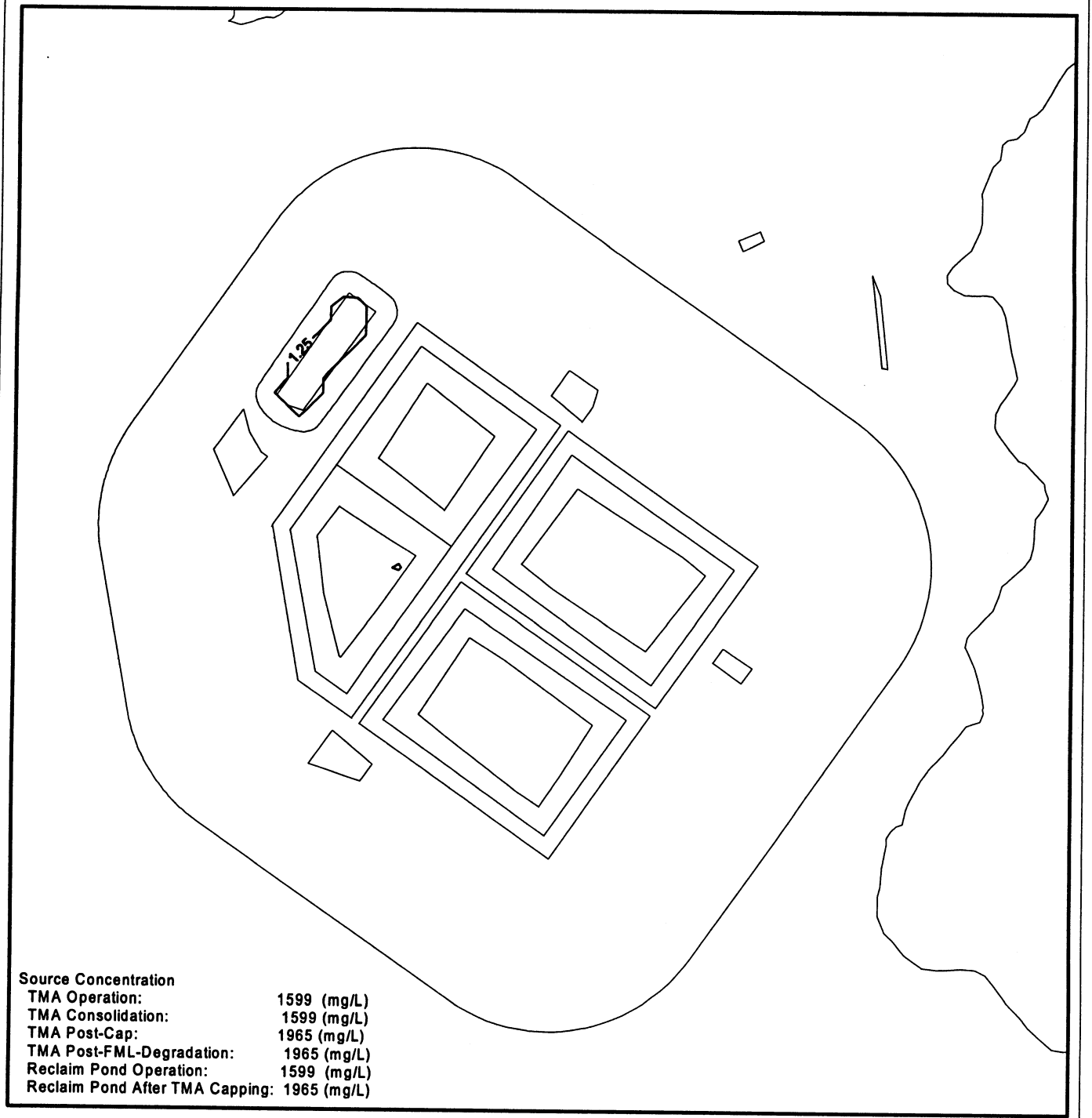

Source Concentration

TMA Operation:	1599 (mg/L)
TMA Consolidation:	1599 (mg/L)
TMA Post-Cap:	1965 (mg/L)
TMA Post-FML-Degradation:	1965 (mg/L)
Reclaim Pond Operation:	1599 (mg/L)
Reclaim Pond After TMA Capping:	1965 (mg/L)

Concentration Contours Shown
- 125 mg/L (ACL)
- 12.5 mg/L
- 1.25 mg/L

0 1000 2000

Scale in Feet

HSI GEOTRANS

REVISED	DATE	BY	DESCRIPTION
1	6/99	RAK	Updated STM
2	3/00	JDC	Updated STM
3	8/00	GWC	Updated Source Conc.

CHECKED BY: GWC DATE: April 1998

APPROVED BY: PFA DATE: April 1998

APPROVED BY: DATE:

Simulations T13C1 - T13C6

Nicolet Minerals
a Rio Algom company

Figure 3-21
Sulfate Concentration After 2 Years, BEJT

Scale: 1 in. = 1000 ft. Date: April 1998

Prepared By: HSI GEOTRANS By: RMD

P:\Crandon\TmaMod4\Surfer\P13so002a.srf

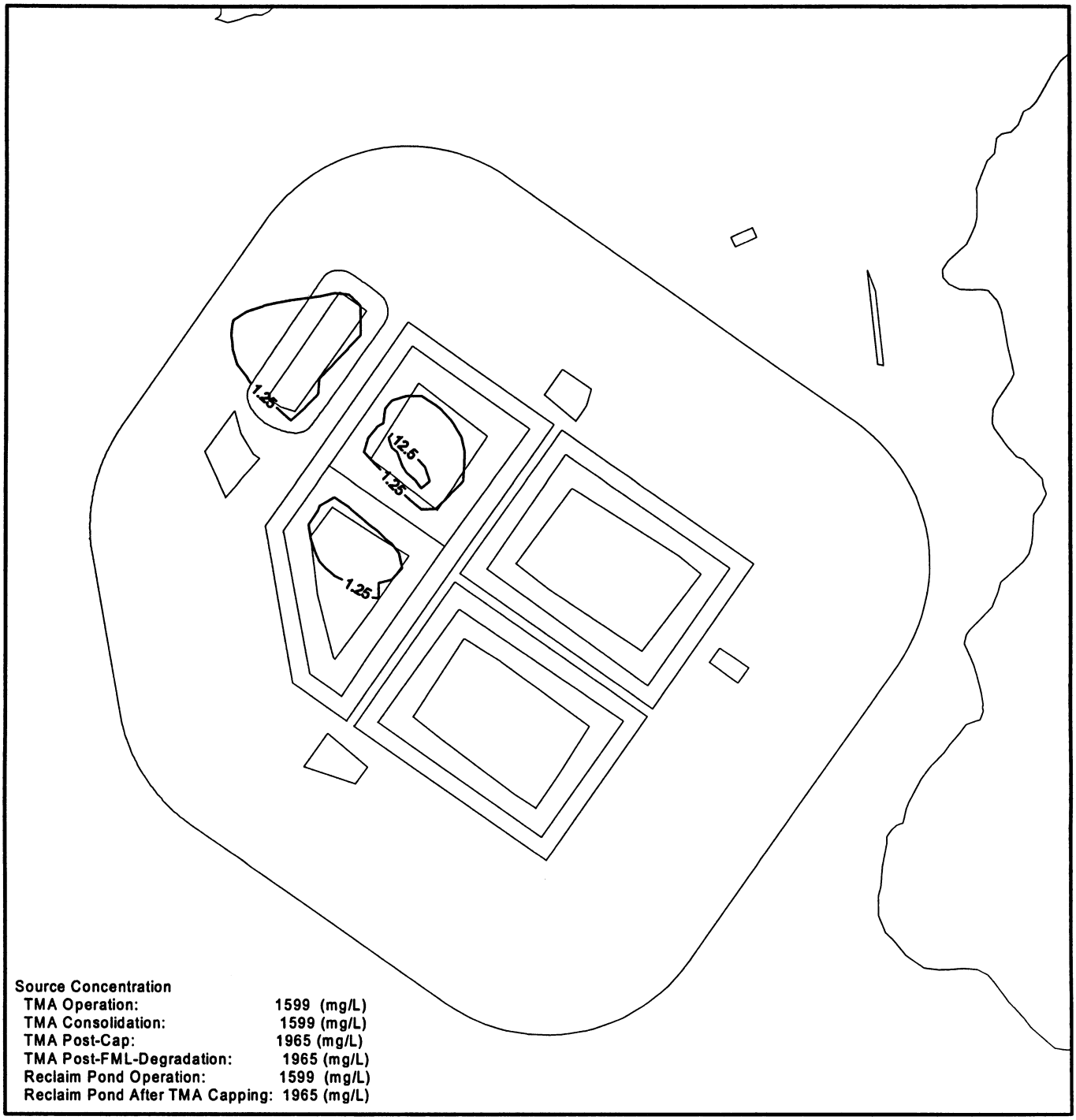

Source Concentration

TMA Operation:	1599 (mg/L)
TMA Consolidation:	1599 (mg/L)
TMA Post-Cap:	1965 (mg/L)
TMA Post-FML-Degradation:	1965 (mg/L)
Reclaim Pond Operation:	1599 (mg/L)
Reclaim Pond After TMA Capping:	1965 (mg/L)

Concentration Contours Shown
- 125 mg/L (ACL)
- 12.5 mg/L
- 1.25 mg/L

N

0 1000 2000

Scale in Feet

HSI GEOTRANS

REVISED	DATE	BY	DESCRIPTION
1	6/99	RAK	Updated STM
2	3/00	JDC	Updated STM
3	8/00	GWC	Updated Source Conc.

CHECKED BY: GWC		DATE: April 1998
APPROVED BY: PFA		DATE: April 1998
APPROVED BY:		DATE:

Simulations T13C1 - T13C6

Nicolet Minerals
a Rio Algom company

Figure 3-22
Sulfate Concentration After 16 Years, BEJT

Scale: 1 in. = 1000 ft.	Date: April 1998
Prepared By: HSI GEOTRANS	By: RMD

P:\Crandon\Tma\Mod4\Surfer\P13so016a.srf

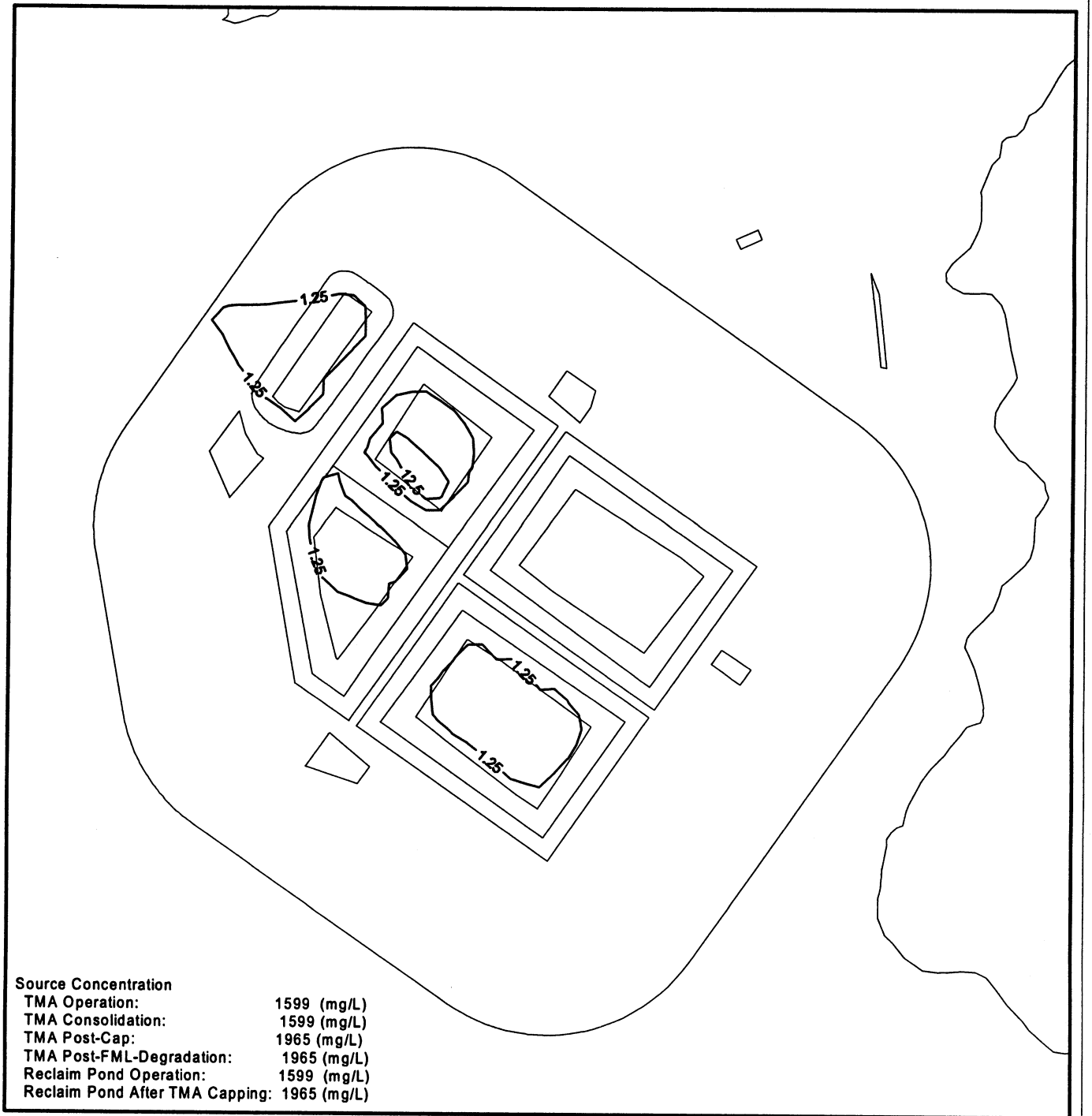

Source Concentration

TMA Operation:	1599 (mg/L)
TMA Consolidation:	1599 (mg/L)
TMA Post-Cap:	1965 (mg/L)
TMA Post-FML-Degradation:	1965 (mg/L)
Reclaim Pond Operation:	1599 (mg/L)
Reclaim Pond After TMA Capping:	1965 (mg/L)

Concentration Contours Shown
- 125 mg/L (ACL)
- 12.5 mg/L
- 1.25 mg/L

N

0 1000 2000

Scale in Feet

HSI GEOTRANS

REVISED	DATE	BY	DESCRIPTION
1	6/99	RAK	Updated STM
2	3/00	JDC	Updated STM
3	8/00	GWC	Updated Source Conc.

CHECKED BY: GWC DATE: April 1998

APPROVED BY: PFA DATE: April 1998

APPROVED BY: DATE:

Simulations T13C1 - T13C6

Nicolet Minerals
a Rio Algom company

Figure 3-23
Sulfate Concentration After 22 Years, BEJT

Scale: 1 in. = 1000 ft. Date: April 1998

Prepared By: HSI GEOTRANS By: RMD

P:\Crandon\Tma\Mod4\Surfer\P13so022a.srf

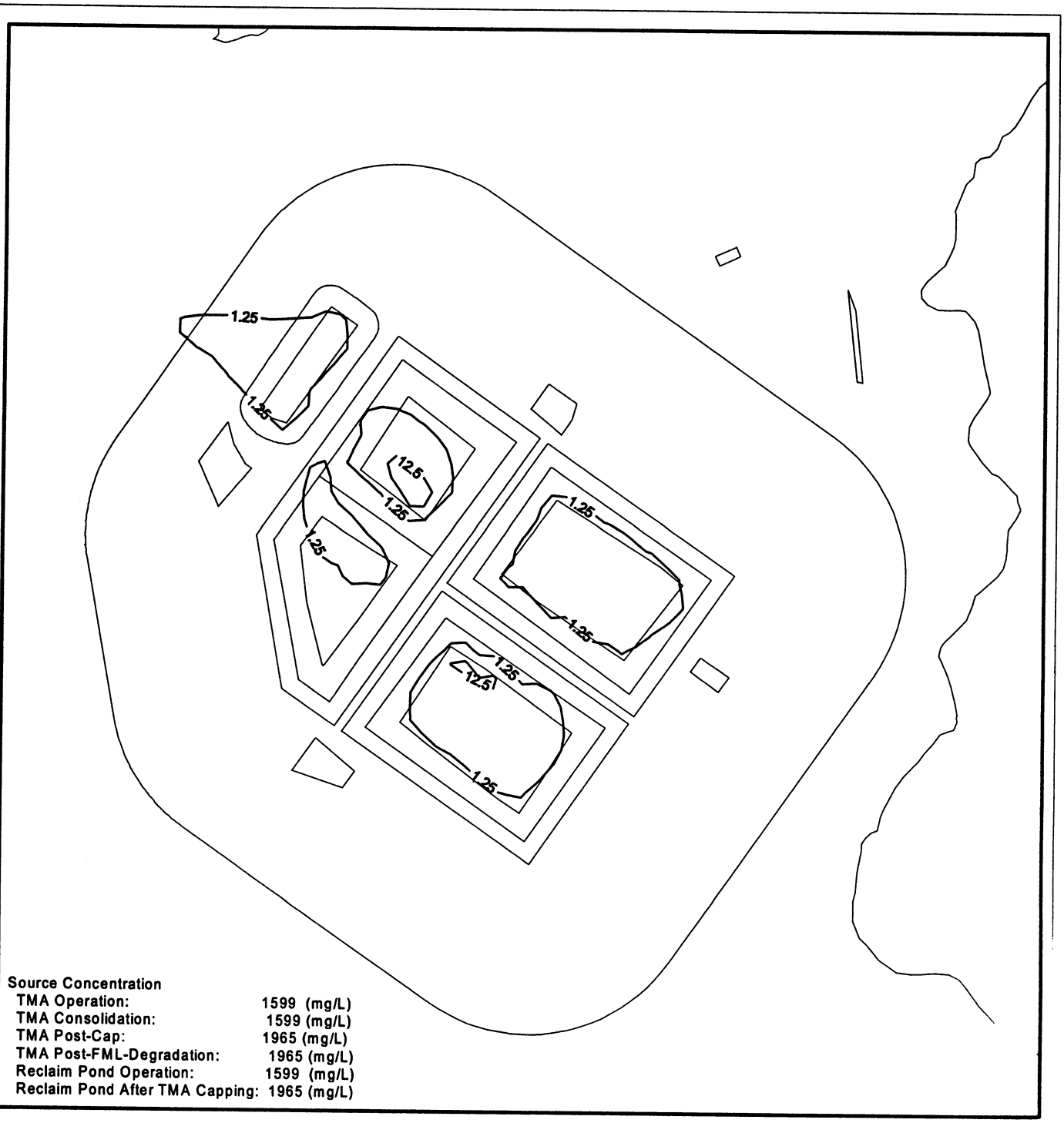

Source Concentration

TMA Operation:	1599 (mg/L)
TMA Consolidation:	1599 (mg/L)
TMA Post-Cap:	1965 (mg/L)
TMA Post-FML-Degradation:	1965 (mg/L)
Reclaim Pond Operation:	1599 (mg/L)
Reclaim Pond After TMA Capping:	1965 (mg/L)

Concentration Contours Shown
- 125 mg/L (ACL)
- 12.5 mg/L
- 1.25 mg/L

0 1000 2000

Scale in Feet

HSI GEOTRANS

REVISED	DATE	BY	DESCRIPTION
1	6/99	RAK	Updated STM
2	3/00	JDC	Updated STM
3	8/00	GWC	Updated Source Conc.

CHECKED BY: GWC		DATE: April 1998
APPROVED BY: PFA		DATE: April 1998
APPROVED BY:		DATE:

Simulations T13C1 - T13C6

Nicolet Minerals
a Rio Algom company

Figure 3-24
Sulfate Concentration After 32 Years, BEJT

Scale: 1 in. = 1000 ft. | Date: April 1998

Prepared By: HSI GEOTRANS | By: RMD

P:\Crandon\TmaMod4\Surfer\P13so032a.srf

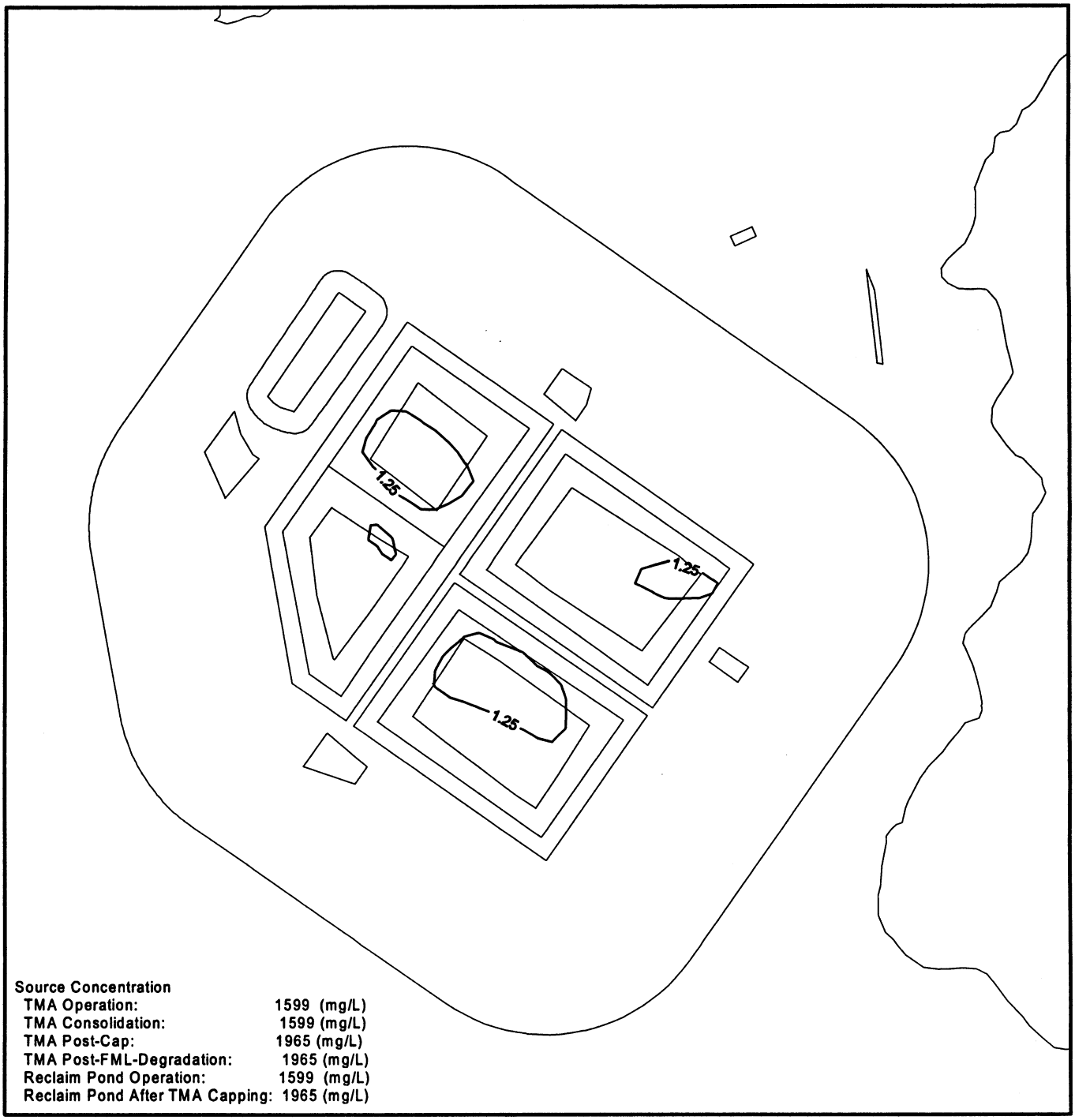

Source Concentration

TMA Operation:	1599 (mg/L)
TMA Consolidation:	1599 (mg/L)
TMA Post-Cap:	1965 (mg/L)
TMA Post-FML-Degradation:	1965 (mg/L)
Reclaim Pond Operation:	1599 (mg/L)
Reclaim Pond After TMA Capping:	1965 (mg/L)

Concentration Contours Shown

125 mg/L (ACL)
12.5 mg/L
1.25 mg/L

0 1000 2000

Scale in Feet

HSI GEOTRANS

REVISED	DATE	BY	DESCRIPTION
1	6/99	RAK	Updated STM
2	3/00	JDC	Updated STM
3	8/00	GWC	Updated Source Conc.

CHECKED BY: GWC DATE: April 1998

APPROVED BY: PFA DATE: April 1998

APPROVED BY: DATE:

Simulations T13C1 - T13C6

Nicolet Minerals
a Rio Algom company

Figure 3-25
Sulfate Concentration After 60 Years, BEJT

Scale: 1 in. = 1000 ft. Date: April 1998

Prepared By: HSI GEOTRANS By: RMD

P:\Crandon\TmeMod4\Surfer\P13sc060a.srf

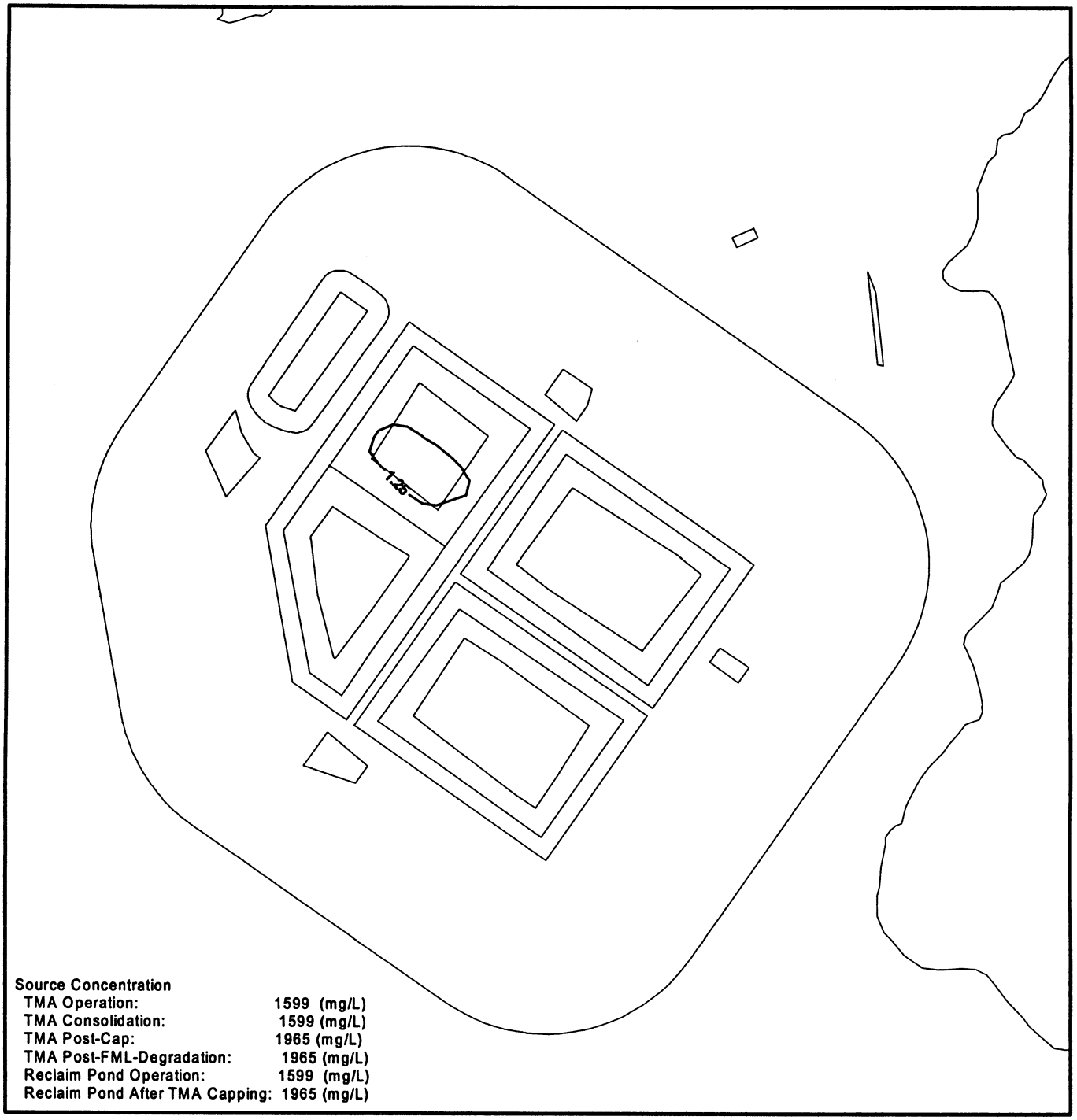

Source Concentration

TMA Operation:	1599 (mg/L)
TMA Consolidation:	1599 (mg/L)
TMA Post-Cap:	1965 (mg/L)
TMA Post-FML-Degradation:	1965 (mg/L)
Reclaim Pond Operation:	1599 (mg/L)
Reclaim Pond After TMA Capping:	1965 (mg/L)

Concentration Contours Shown
- 125 mg/L (ACL)
- 12.5 mg/L
- 1.25 mg/L

0 1000 2000

Scale in Feet

HSI GEOTRANS

REVISED	DATE	BY	DESCRIPTION
1	6/99	RAK	Updated STM
2	3/00	JDC	Updated STM
3	8/00	GWC	Updated Source Conc.

CHECKED BY: GWC		DATE: April 1998
APPROVED BY: PFA		DATE: April 1998
APPROVED BY:		DATE:

Simulations T13C1 - T13C6

Nicolet Minerals
a Rio Algom company

Figure 3-26
Sulfate Concentration After 125 Years, BEJT

Scale: 1 in. = 1000 ft. | Date: April 1998

Prepared By: HSI GEOTRANS | By: RMD

P:\Crandon\Tma\Mod4\Surfer\P13so125a.srf

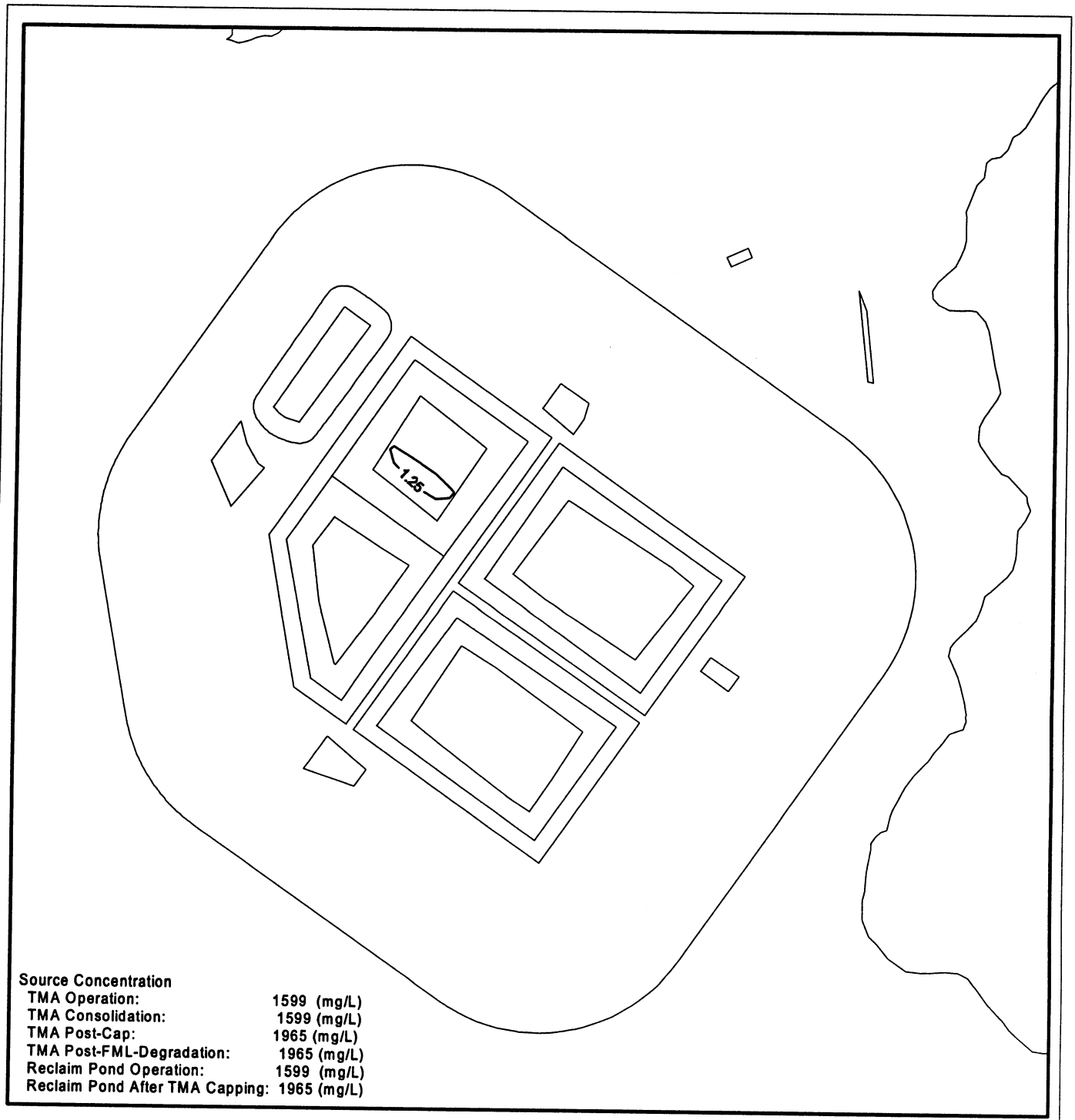

Source Concentration

TMA Operation:	1599 (mg/L)
TMA Consolidation:	1599 (mg/L)
TMA Post-Cap:	1965 (mg/L)
TMA Post-FML-Degradation:	1965 (mg/L)
Reclaim Pond Operation:	1599 (mg/L)
Reclaim Pond After TMA Capping:	1965 (mg/L)

Concentration Contours Shown
- 125 mg/L (ACL)
- 12.5 mg/L
- 1.25 mg/L

0 1000 2000

Scale in Feet

HSI GEOTRANS

REVISED	DATE	BY	DESCRIPTION
1	6/99	RAK	Updated STM
2	3/00	JDC	Updated STM
3	8/00	GWC	Updated Source Conc.

CHECKED BY: GWC	DATE: April 1998	
APPROVED BY: PFA	DATE: April 1998	
APPROVED BY:	DATE:	

Simulations T13C1 - T13C6

Nicolet Minerals
a Rio Algom company

Figure 3-27
Sulfate Concentration After 300 Years, BEJT

Scale: 1 in. = 1000 ft. | Date: April 1998

Prepared By: HSI GEOTRANS | By: RMD

P:\Crandon\TmaMod4\Surfer\P13so300a.srf

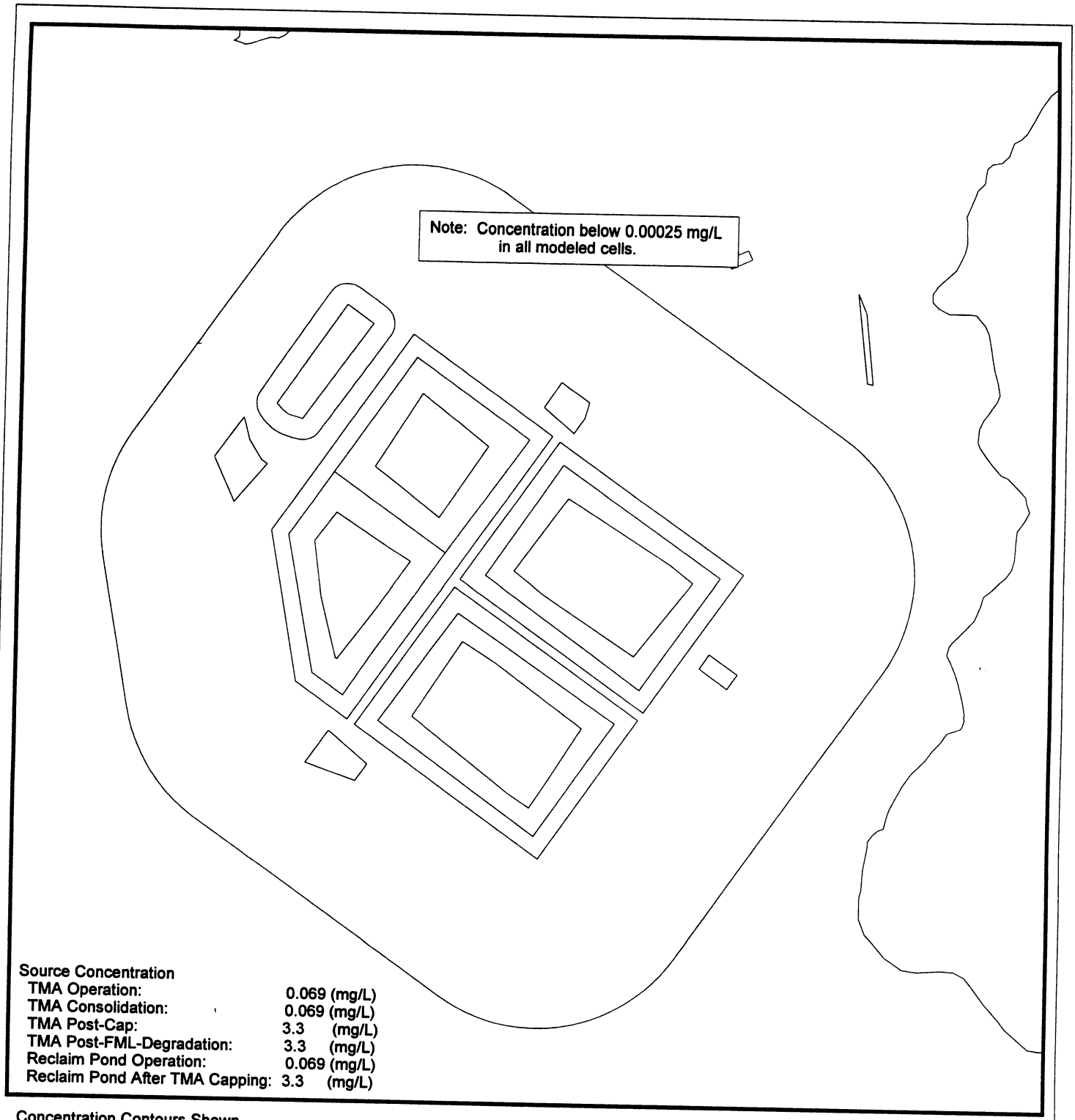

Source Concentration

TMA Operation:	0.069 (mg/L)
TMA Consolidation:	0.069 (mg/L)
TMA Post-Cap:	3.3 (mg/L)
TMA Post-FML-Degradation:	3.3 (mg/L)
Reclaim Pond Operation:	0.069 (mg/L)
Reclaim Pond After TMA Capping:	3.3 (mg/L)

Concentration Contours Shown
0.025 mg/L (ACL)
0.0025 mg/L
0.00025 mg/L

0 1000 2000
Scale in Feet

HSI GEOTRANS

REVISED	DATE	BY	DESCRIPTION
1	6/99	RAK	Updated STM
2	3/00	JDC	Updated STM

Simulations T13C1 - T13C6	CHECKED BY: GWC	DATE: April 1998
	APPROVED BY: PFA	DATE: April 1998
	APPROVED BY:	DATE:

Nicolet Minerals
a Rio Algom company

Figure 3-28
Arsenic Concentration After 2 Years, BEJT
(Example Constituent, Plan View)

Scale: 1 in. = 1000 ft.	Date: April 1998
Prepared By: HSI GEOTRANS	By: RMD

P:\Crandon\Tma\Mod4\S...s002.srf

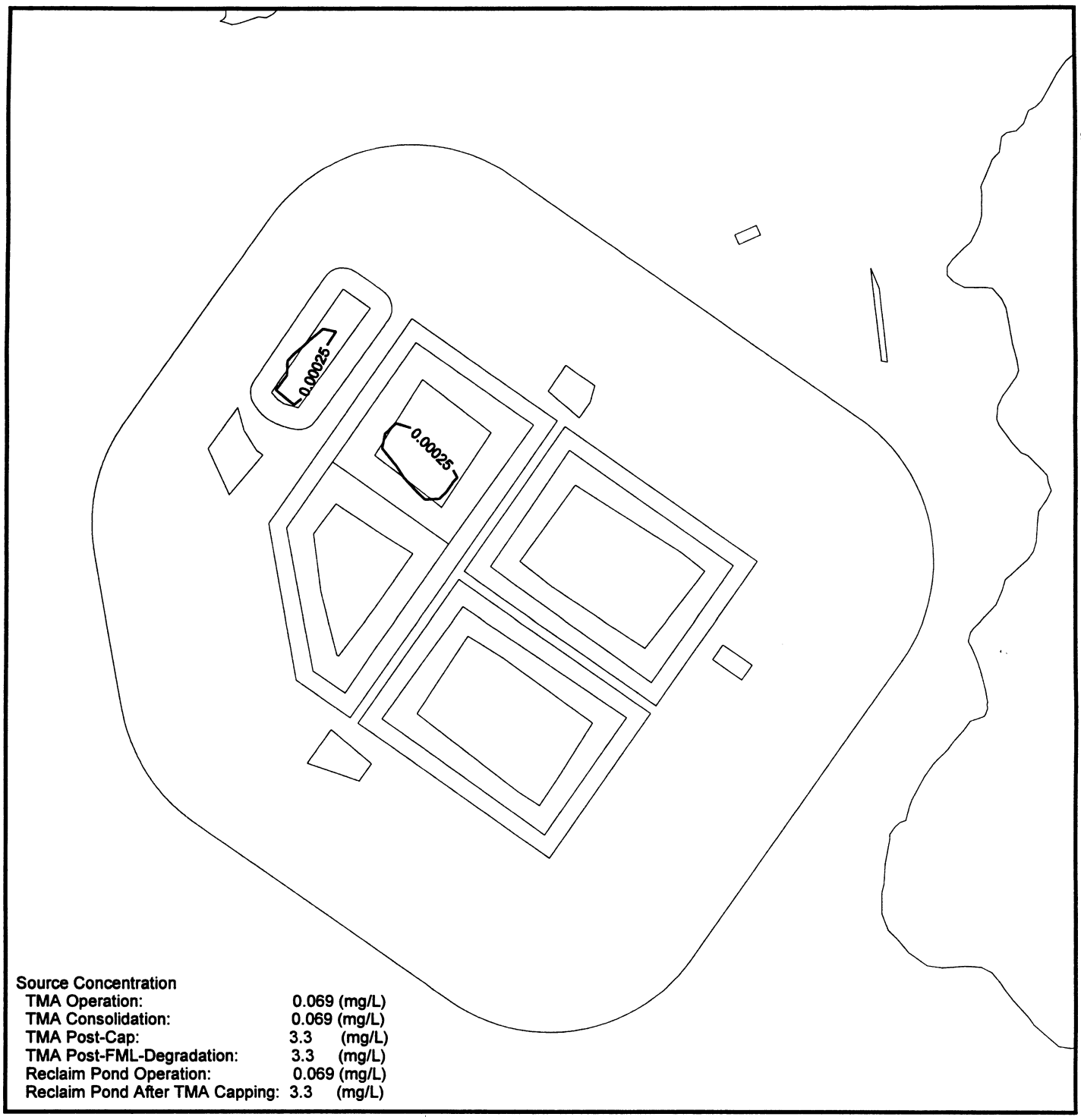

Source Concentration

TMA Operation:	0.069	(mg/L)
TMA Consolidation:	0.069	(mg/L)
TMA Post-Cap:	3.3	(mg/L)
TMA Post-FML-Degradation:	3.3	(mg/L)
Reclaim Pond Operation:	0.069	(mg/L)
Reclaim Pond After TMA Capping:	3.3	(mg/L)

Concentration Contours Shown
0.025 mg/L (ACL)
0.0025 mg/L
0.00025 mg/L

N

0 1000 2000

Scale in Feet

HSI GEOTRANS

REVISED	DATE	BY	DESCRIPTION
1	6/99	RAK	Updated STM
2	3/00	JDC	Updated STM

CHECKED BY: GWC		DATE: April 1998
APPROVED BY: PFA		DATE: April 1998
APPROVED BY:		DATE:

Simulations T13C1 - T13C6

Nicolet Minerals
a Rio Algom company

Figure 3-29
Arsenic Concentration After 16 Years, BEJT
(Example Constituent, Plan View)

Scale: 1 in. = 1000 ft.	Date: April 1998
Prepared By: HSI GEOTRANS	By: RMD

P:\Crandon\Tmat\Mod4\Surfer\P13as016.srf

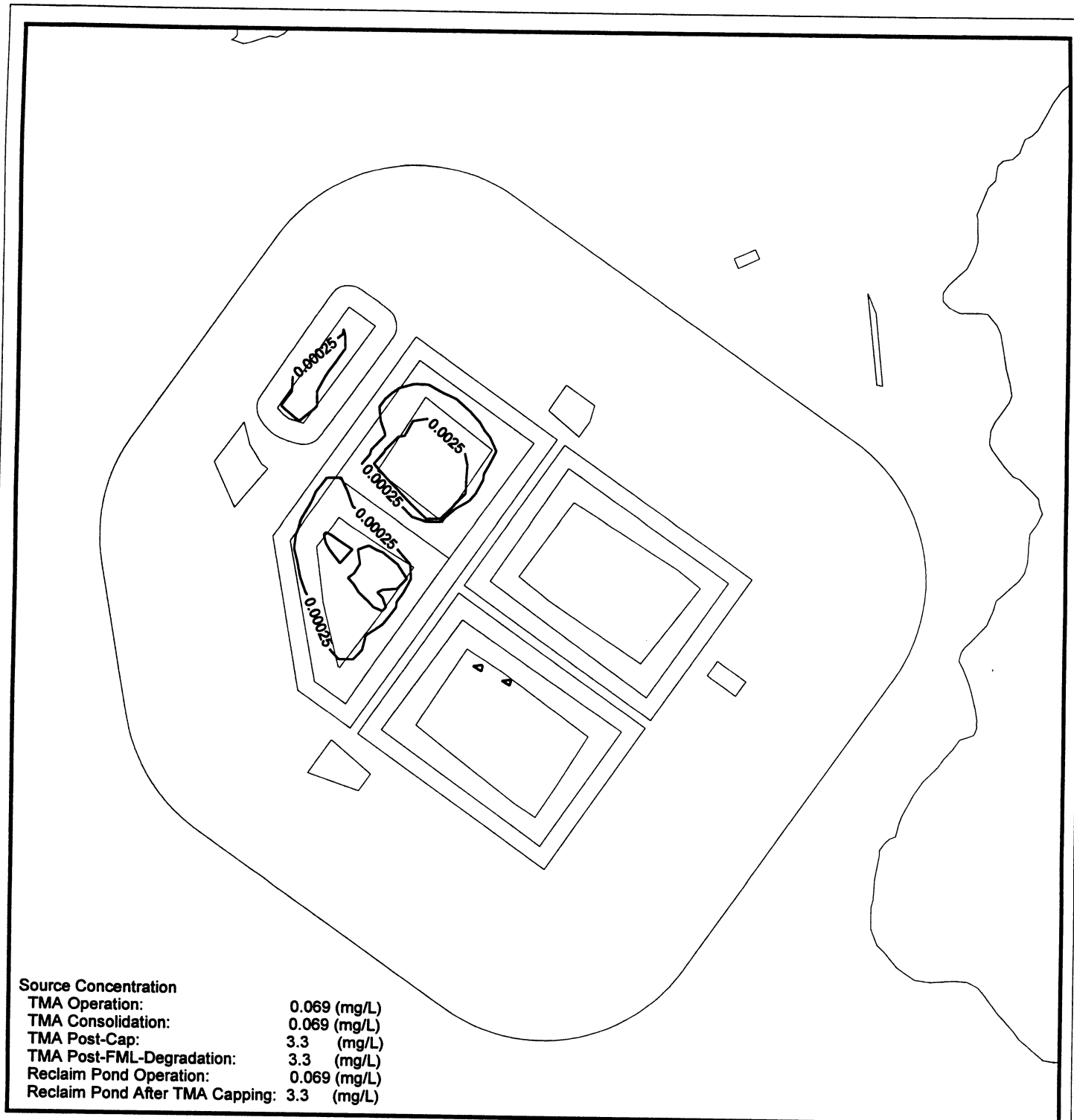

Source Concentration

TMA Operation:	0.069 (mg/L)
TMA Consolidation:	0.069 (mg/L)
TMA Post-Cap:	3.3 (mg/L)
TMA Post-FML-Degradation:	3.3 (mg/L)
Reclaim Pond Operation:	0.069 (mg/L)
Reclaim Pond After TMA Capping:	3.3 (mg/L)

Concentration Contours Shown
0.025 mg/L (ACL)
0.0025 mg/L
0.00025 mg/L

N

0 1000 2000

Scale in Feet

HSI GEOTRANS

REVISED	DATE	BY	DESCRIPTION
1	6/99	RAK	Updated STM
2	3/00	JDC	Updated STM

CHECKED BY: GWC DATE: April 1998

APPROVED BY: PFA DATE: April 1998

APPROVED BY: DATE:

Simulations T13C1 - T13C6

Nicolet Minerals
a Rio Algom company

Figure 3-30
Arsenic Concentration After 22 Years, BEJT
(Example Constituent, Plan View)

Scale: 1 in. = 1000 ft. Date: April 1998

Prepared By: HSI GEOTRANS By: RMD

P:\Crandon\Tma\Mod4\S...ase022.srf

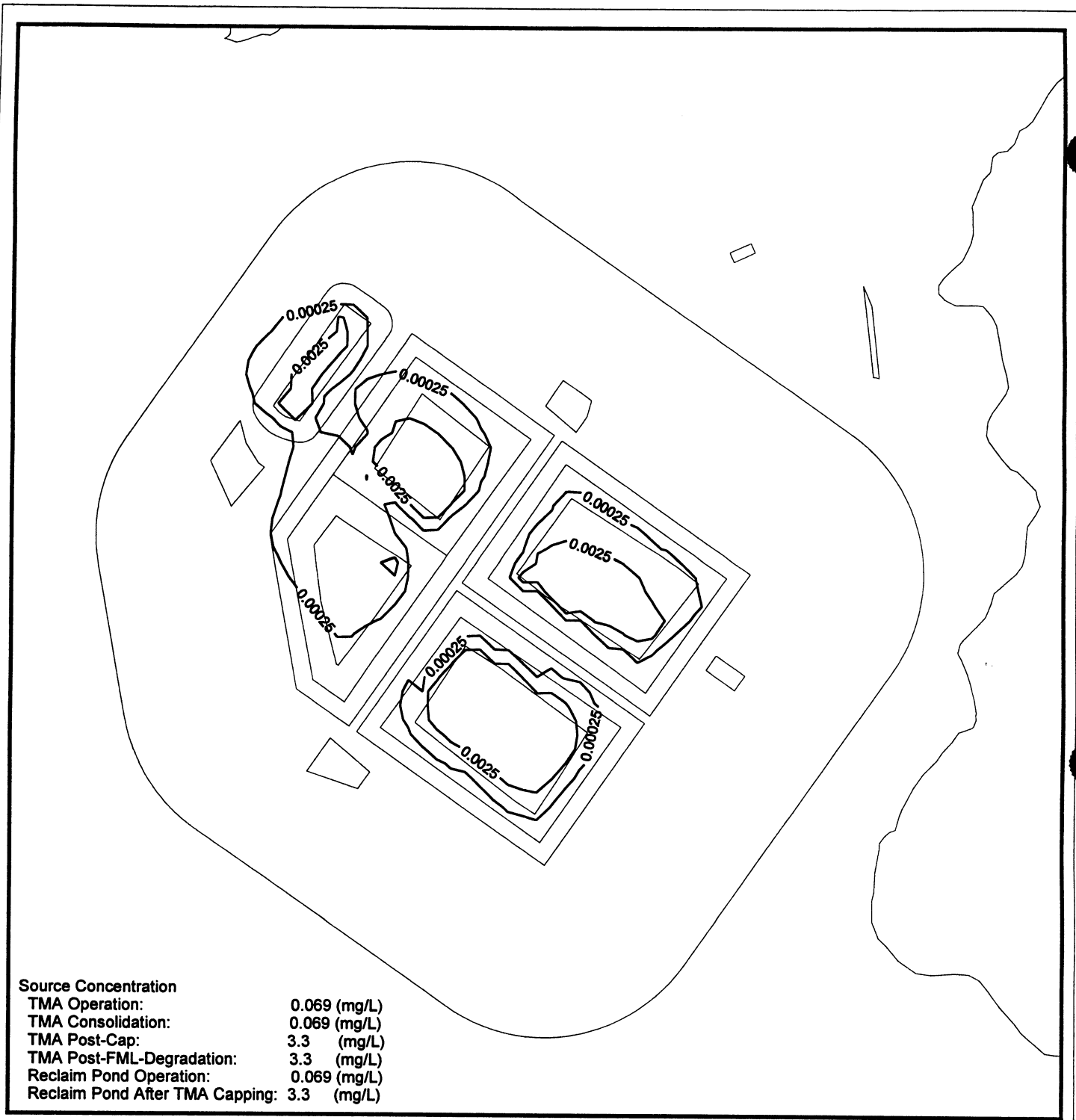

Source Concentration

TMA Operation:	0.069 (mg/L)
TMA Consolidation:	0.069 (mg/L)
TMA Post-Cap:	3.3 (mg/L)
TMA Post-FML-Degradation:	3.3 (mg/L)
Reclaim Pond Operation:	0.069 (mg/L)
Reclaim Pond After TMA Capping:	3.3 (mg/L)

Concentration Contours Shown
0.025 mg/L (ACL)
0.0025 mg/L
0.00025 mg/L

0 1000 2000
Scale in Feet

HSI GEOTRANS

REVISED	DATE	BY	DESCRIPTION
1	6/99	RAK	Updated STM
2	3/00	JDC	Updated STM

CHECKED BY: GWC		DATE: April 1998
APPROVED BY: PFA		DATE: April 1998
APPROVED BY:		DATE:

Simulations T13C1 - T13C6

Nicolet Minerals
a Rio Algom company

Figure 3-31
Arsenic Concentration After 32 Years, BEJT
(Example Constituent, Plan View)

Scale: 1 in. = 1000 ft. | Date: April 1998
Prepared By: HSI GEOTRANS | By: RMD

P:\Crandon\Tma\Mod4Surfer\P13as032.srf

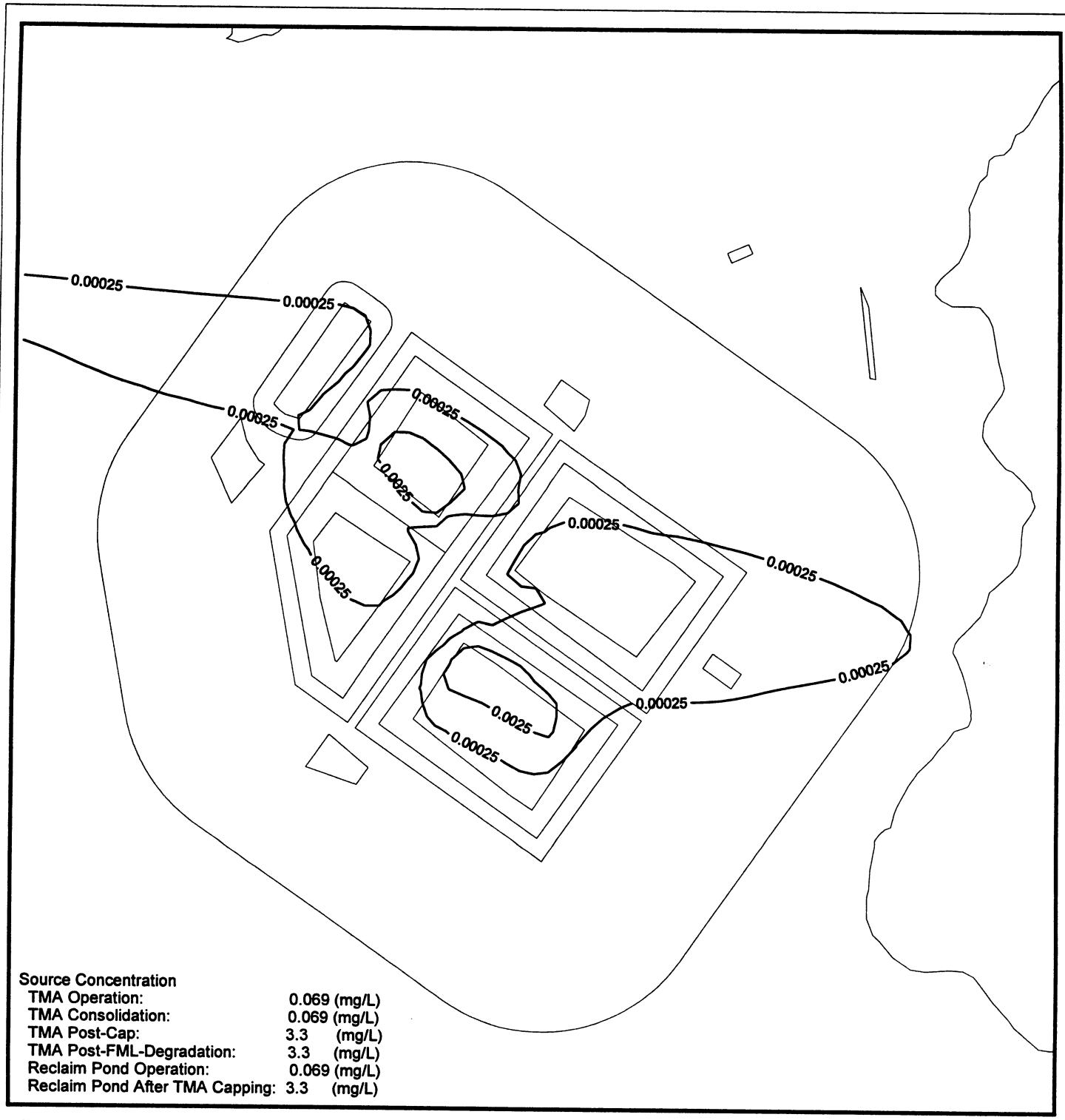

Source Concentration

TMA Operation:	0.069	(mg/L)
TMA Consolidation:	0.069	(mg/L)
TMA Post-Cap:	3.3	(mg/L)
TMA Post-FML-Degradation:	3.3	(mg/L)
Reclaim Pond Operation:	0.069	(mg/L)
Reclaim Pond After TMA Capping:	3.3	(mg/L)

Concentration Contours Shown
0.025 mg/L (ACL)
0.0025 mg/L
0.00025 mg/L

N

0 1000 2000

Scale in Feet

HSI GEOTRANS			
REVISED	DATE	BY	DESCRIPTION
1	6/99	RAK	Updated STM
2	3/00	JDC	Updated STM
CHECKED BY: GWC			DATE: April 1998
APPROVED BY: PFA			DATE: April 1998
APPROVED BY:			DATE:

Simulations T13C1 - T13C6

Nicolet Minerals
a Rio Algom company

Figure 3-32
Arsenic Concentration After 60 Years, BEJT
(Example Constituent, Plan View)

Scale: 1 in. = 1000 ft. | Date: April 1998

Prepared By: HSI GEOTRANS | By: RMD

P:\Crandon\Tma\Mod4\Sim...es060.srf

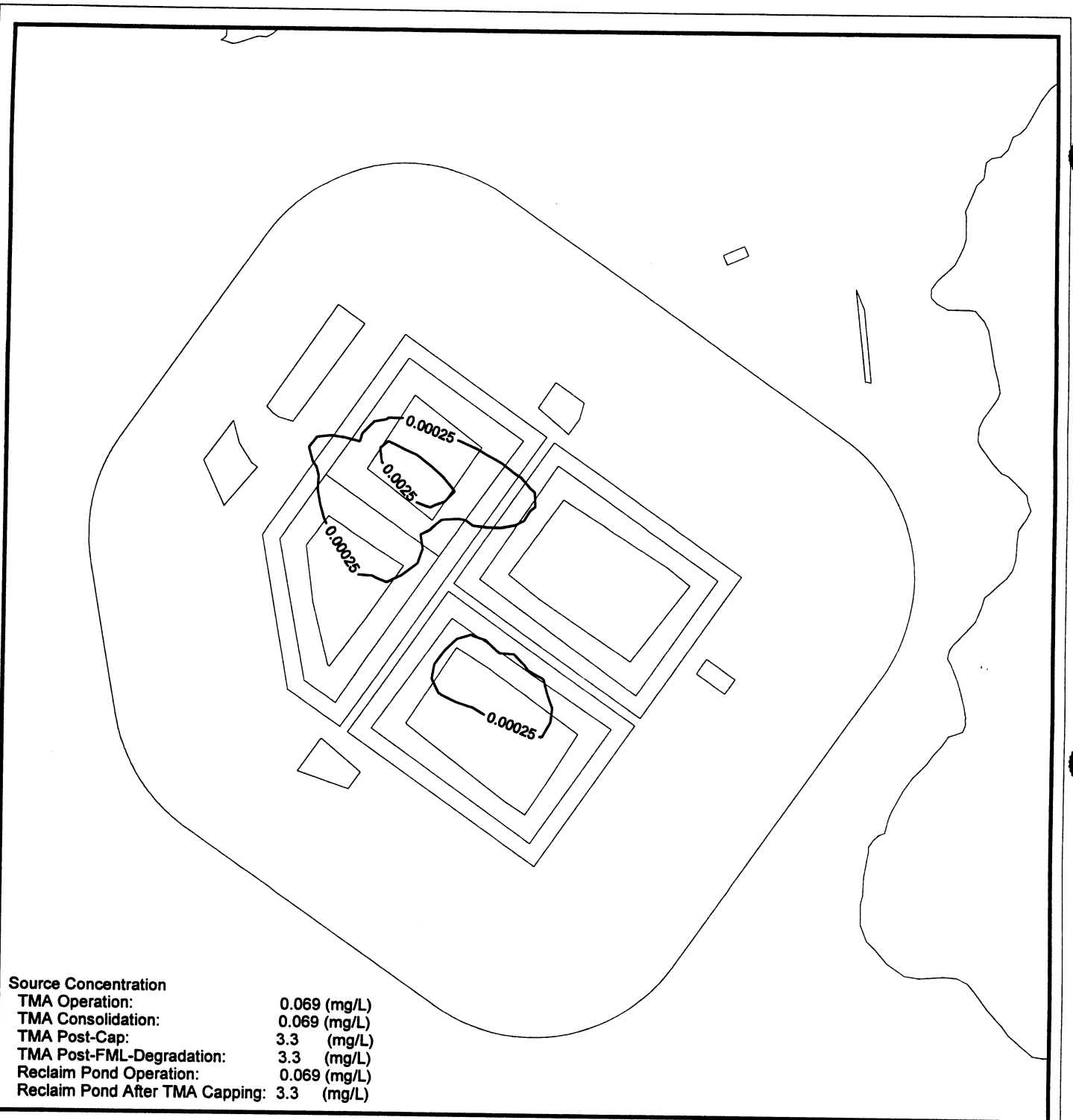

Source Concentration

TMA Operation:	0.069 (mg/L)
TMA Consolidation:	0.069 (mg/L)
TMA Post-Cap:	3.3 (mg/L)
TMA Post-FML-Degradation:	3.3 (mg/L)
Reclaim Pond Operation:	0.069 (mg/L)
Reclaim Pond After TMA Capping:	3.3 (mg/L)

Concentration Contours Shown
0.025 mg/L (ACL)
0.0025 mg/L
0.00025 mg/L

N

0 1000 2000

Scale in Feet

HSI GEOTRANS

REVISED	DATE	BY	DESCRIPTION
1	6/99	RAK	Updated STM
2	3/00	JDC	Updated STM

CHECKED BY: GWC DATE: April 1998

APPROVED BY: PFA DATE: April 1998

APPROVED BY: DATE:

Simulations T13C1 - T13C6

Nicolet Minerals
a Rio Algom company

Figure 3-33
Arsenic Concentration After 125 Years, BEJT
(Example Constituent, Plan View)

Scale: 1 in. = 1000 ft. Date: April 1998

Prepared By: HSI GEOTRANS By: RMD

P:\Crandon\Tma\Mod4\Surfer\P13as125.srf

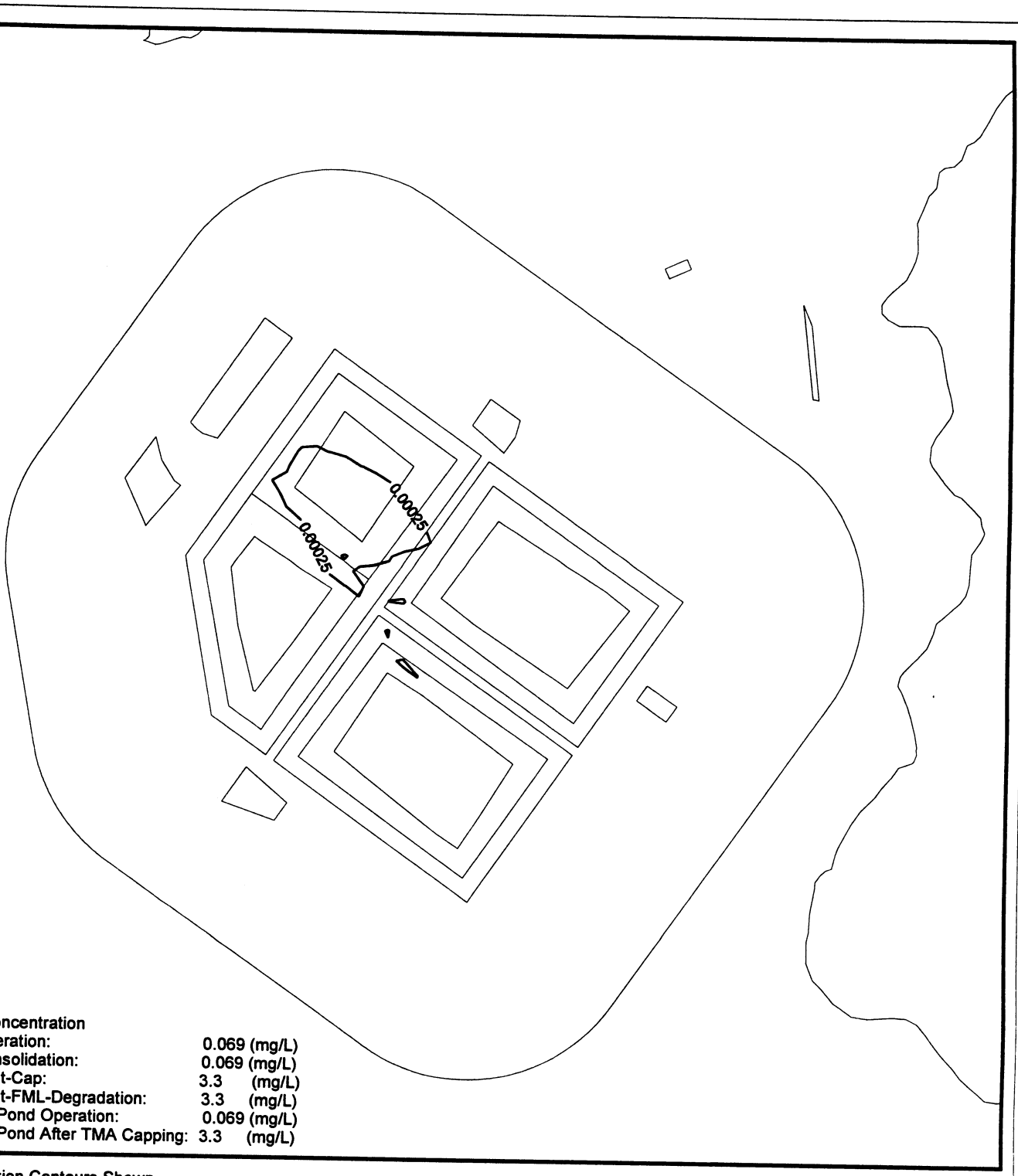

Source Concentration

TMA Operation:	0.069 (mg/L)
TMA Consolidation:	0.069 (mg/L)
TMA Post-Cap:	3.3 (mg/L)
TMA Post-FML-Degradation:	3.3 (mg/L)
Reclaim Pond Operation:	0.069 (mg/L)
Reclaim Pond After TMA Capping:	3.3 (mg/L)

Concentration Contours Shown
0.025 mg/L (ACL)
0.0025 mg/L
0.00025 mg/L

0 1000 2000
Scale in Feet

HSI GEOTRANS

REVISED	DATE	BY	DESCRIPTION
1	6/99	RAK	Updated STM
2	3/00	JDC	Updated STM

CHECKED BY: GWC DATE: April 1998
APPROVED BY: PFA DATE: April 1998
APPROVED BY: DATE:

Simulations T13C1 - T13C6

Nicolet Minerals
a Rio Algom company

Figure 3-34
Arsenic Concentration After 300 Years, BEJT
(Example Constituent, Plan View)

Scale: 1 in. = 1000 ft. Date: April 1998
Prepared By: HSI GEOTRANS By: RMD

P:\Crandon\Tmsmod4\S...se300.srf

\Crandon\TMAMod4\Response\T14gwqpe.xls, Sb

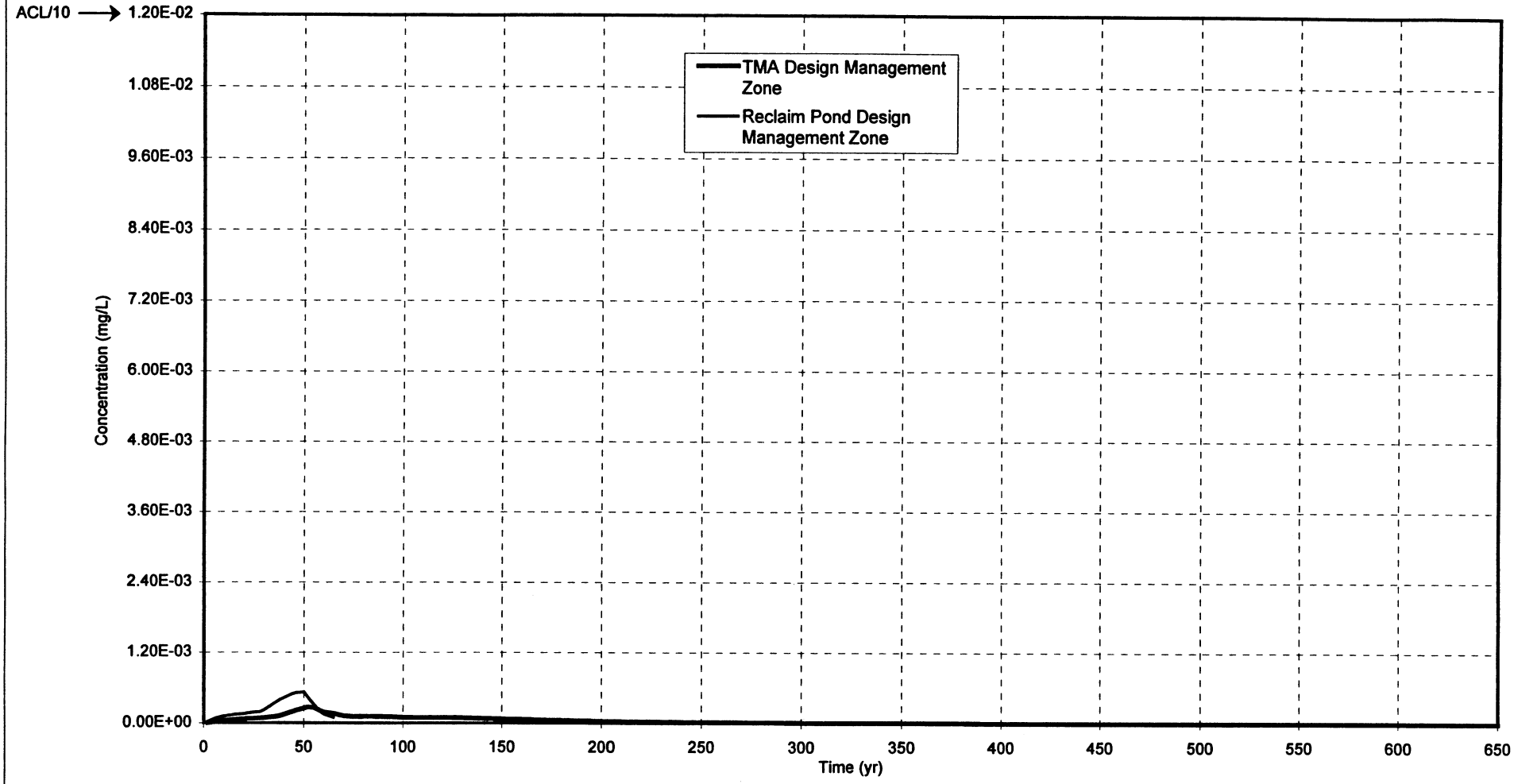

4.2-12-100

Source Concentration:

TMA Operation:	0.071 (mg/L)
TMA Consolidation:	0.67 (mg/L)
TMA Post-Cap:	0.67 (mg/L)
TMA Post-FML-Degradation:	0.67 (mg/L)
Reclaim Pond Operation:	0.071 (mg/L)
Reclaim Pond After TMA Capping:	0.67 (mg/L)

Simulations T14C1-T14C6

HSI GEOTRANS

REVISED	DATE	BY	DESCRIPTION
1	6/99	JDC	Updated STM
2	3/00	JDC	Updated STM

CHECKED BY: GWC	DATE: April 1998
APPROVED BY: PFA	DATE: April 1998
APPROVED BY:	DATE:

Nicolet Minerals
a Rio Algom company

Figure 3-35
Maximum Concentration at the Compliance Boundary for Antimony, PWCT

Scale: None	Date: April 1998
Prepared By: HSI GEOTRANS	By: JDC

\Crandon\TMAMod4\Response\T14gwqpe.xls, As

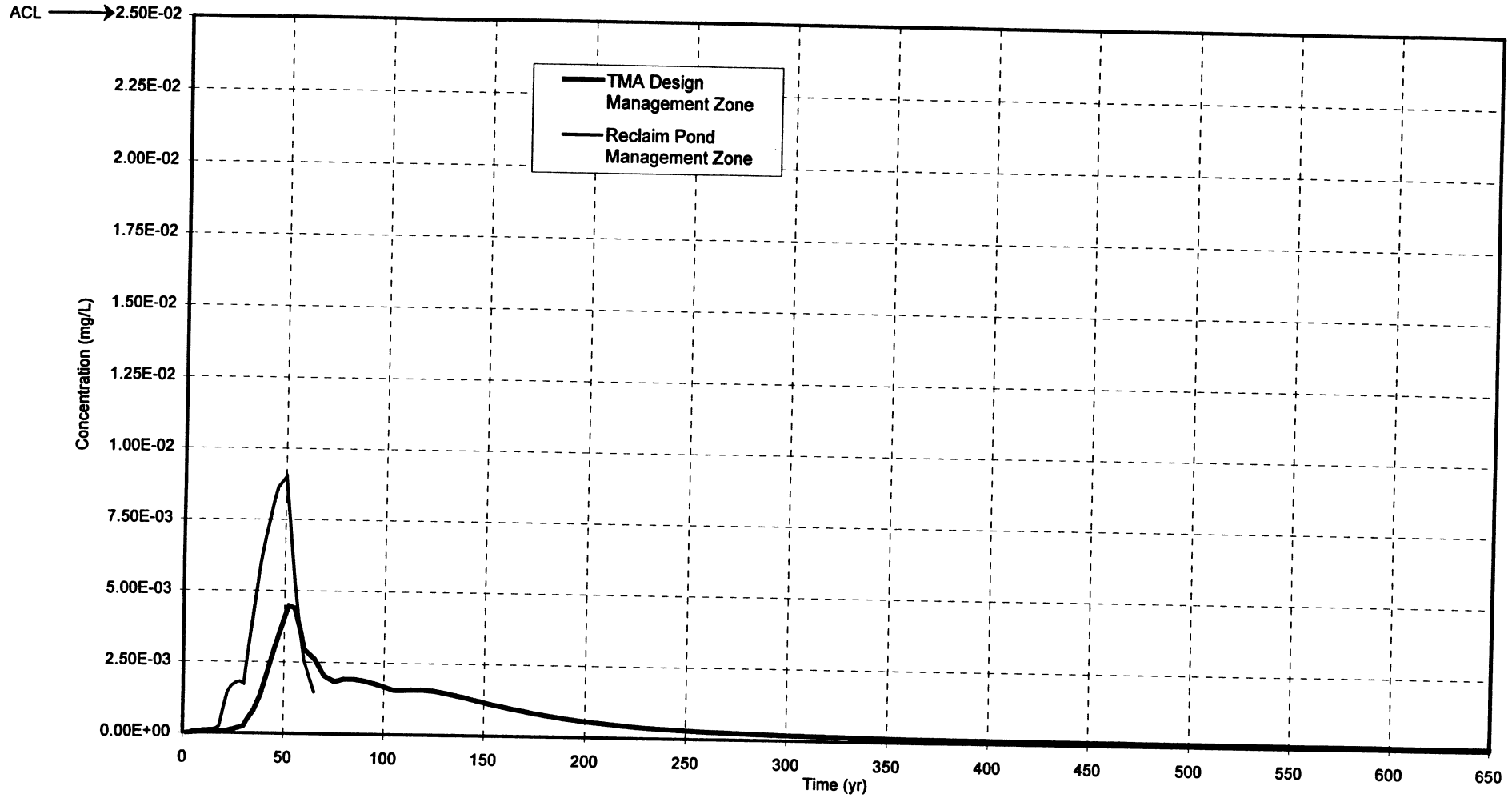

4.2-12-101

Source Concentration:

TMA Operation:	0.069	(mg/L)
TMA Consolidation:	12.0	(mg/L)
TMA Post-Cap:	12.0	(mg/L)
TMA Post-FML-Degradation:	12.0	(mg/L)
Reclaim Pond Operation:	0.069	(mg/L)
Reclaim Pond After TMA Capping:	12.0	(mg/L)

Simulations T14C1-T14C6

HSI GEOTRANS

REVISED	DATE	BY	DESCRIPTION
1	6/99	JDC	Updated STM
2	3/00	JDC	Updated STM

CHECKED BY: GWC	DATE: April 1998
APPROVED BY: PFA	DATE: April 1998
APPROVED BY:	DATE:

Nicolet Minerals
a Rio Algom company

Figure 3-36
Maximum Concentration at the Compliance Boundary for Arsenic, PWCT

Scale: None	Date: April 1998
Prepared By: HSI GEOTRANS	By: KMR

\Crandon\TMAMod4\Response\T14gwqpe.xls, Ba

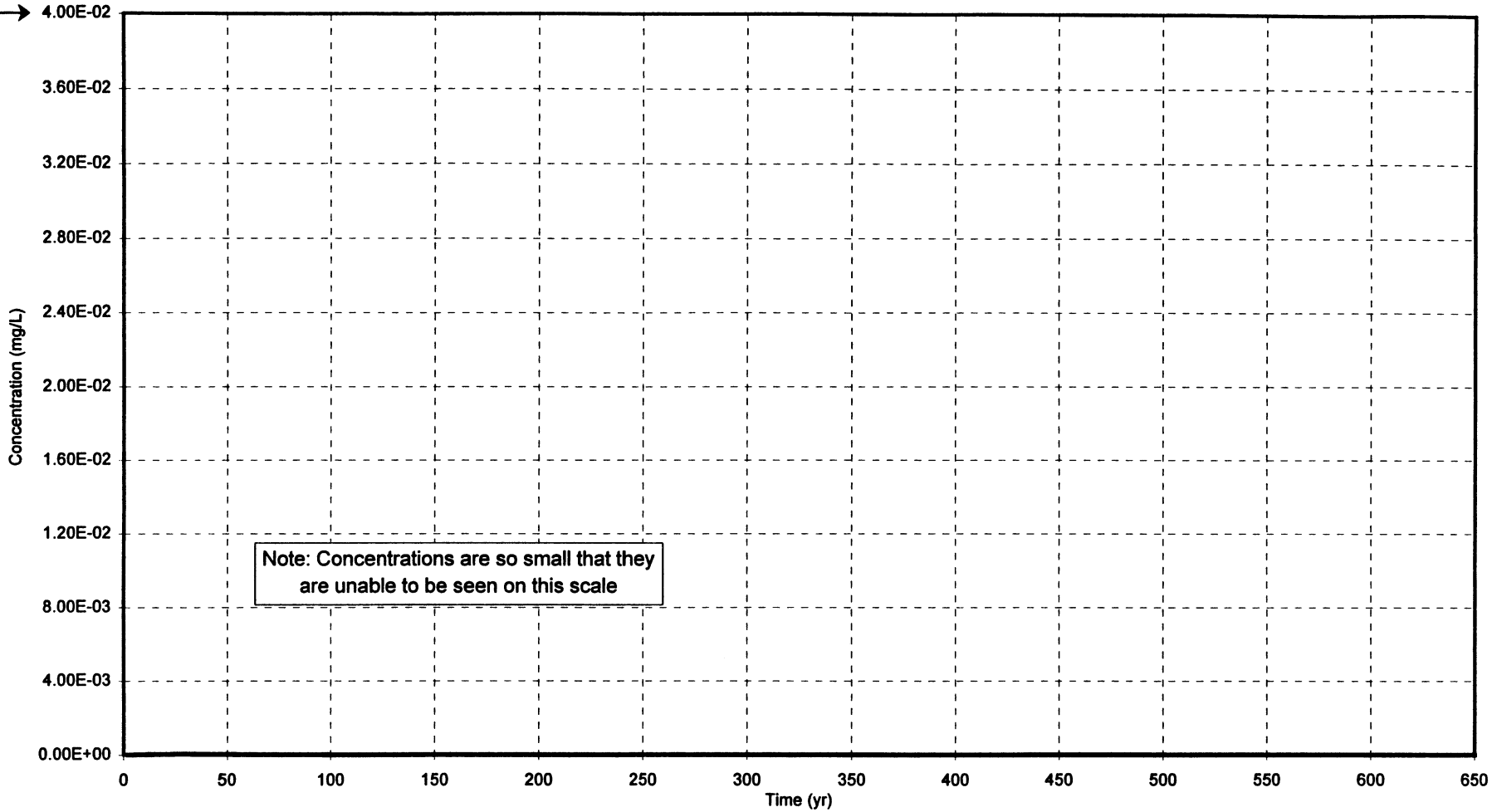

Source Concentration:

TMA Operation:	0.035 (mg/L)
TMA Consolidation:	0.035 (mg/L)
TMA Post-Cap:	0.033 (mg/L)
TMA Post-FML-Degradation:	0.033 (mg/L)
Reclaim Pond Operation:	0.035 (mg/L)
Reclaim Pond After TMA Capping:	0.033 (mg/L)

Simulations T14C1-T14C6

HSI GEOTRANS

REVISED	DATE	BY	DESCRIPTION
1	6/99	JDC	Updated STM
2	3/00	JDC	Updated STM

CHECKED BY: GWC	DATE: April 1998
APPROVED BY: PFA	DATE: April 1998
APPROVED BY:	DATE:

Nicolet Minerals
a Rio Algom company

Figure 3-37
Maximum Concentration at the Compliance Boundary for Barium, PWCT

Scale: None	Date: April 1998
Prepared By: HSI GEOTRANS	By: KMR

\Crandon\TMAMod4\Response\T14gwqpe.xls, Be

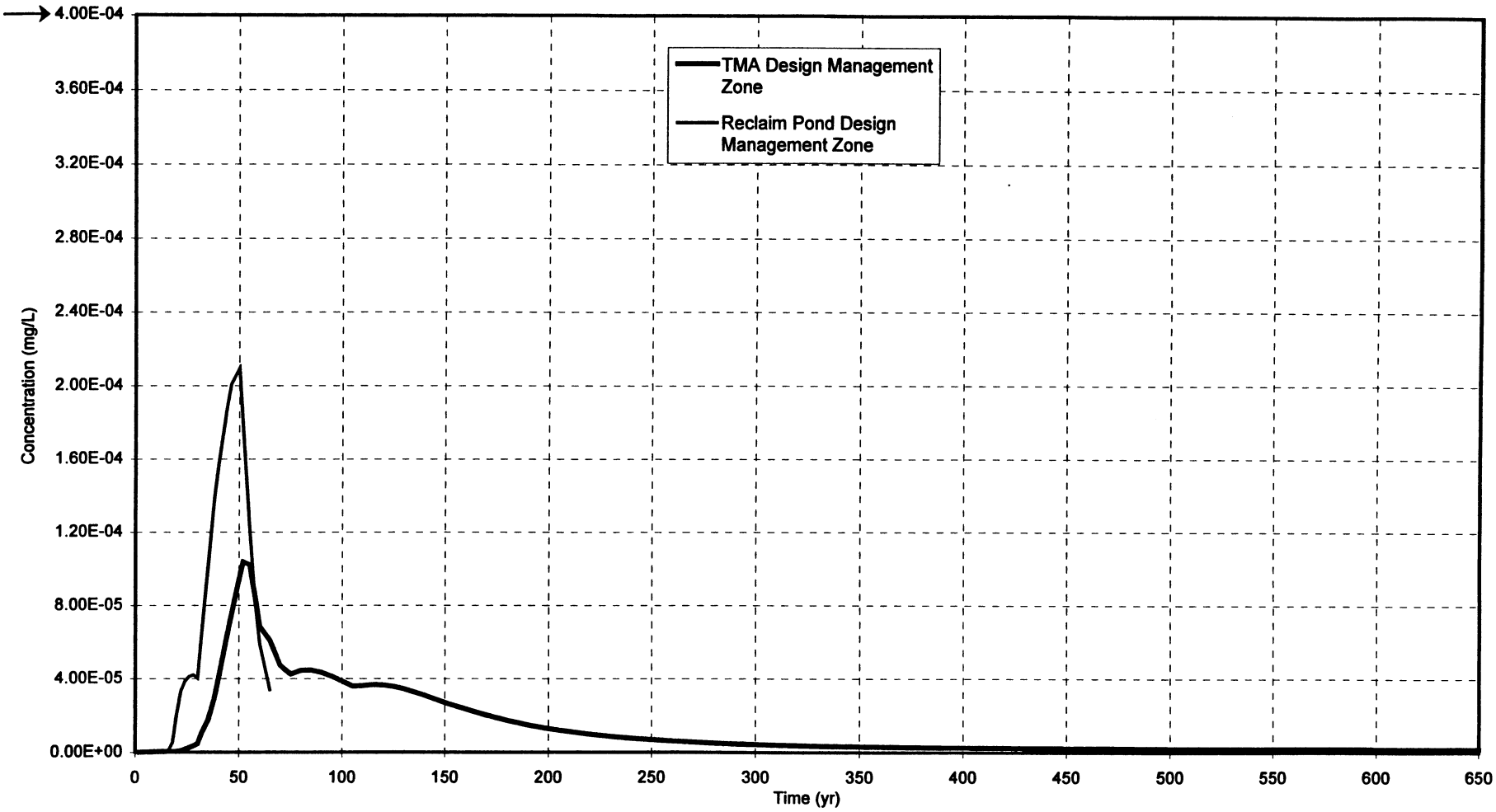

Source Concentration:

TMA Operation:	0.00045	(mg/L)
TMA Consolidation:	0.28	(mg/L)
TMA Post-Cap:	0.28	(mg/L)
TMA Post-FML-Degradation:	0.28	(mg/L)
Reclaim Pond Operation:	0.00045	(mg/L)
Reclaim Pond After TMA Capping:	0.28	(mg/L)

Simulations T14C1-T14C6

HSI GEOTRANS

REVISED	DATE	BY	DESCRIPTION
1	6/99	JDC	Updated STM
2	3/00	JDC	Updated STM

CHECKED BY: GWC	DATE: April 1998
APPROVED BY: PFA	DATE: April 1998
APPROVED BY:	DATE:

Nicolet Minerals
a Rio Algom company

Figure 3-38
Maximum Concentration at the Compliance Boundary for Beryllium, PWCT

Scale: None	Date: April 1998
Prepared By: HSI GEOTRANS	By:KMR

\Crandon\TMAMod4\Response\T14gwqpe.xls, Cd

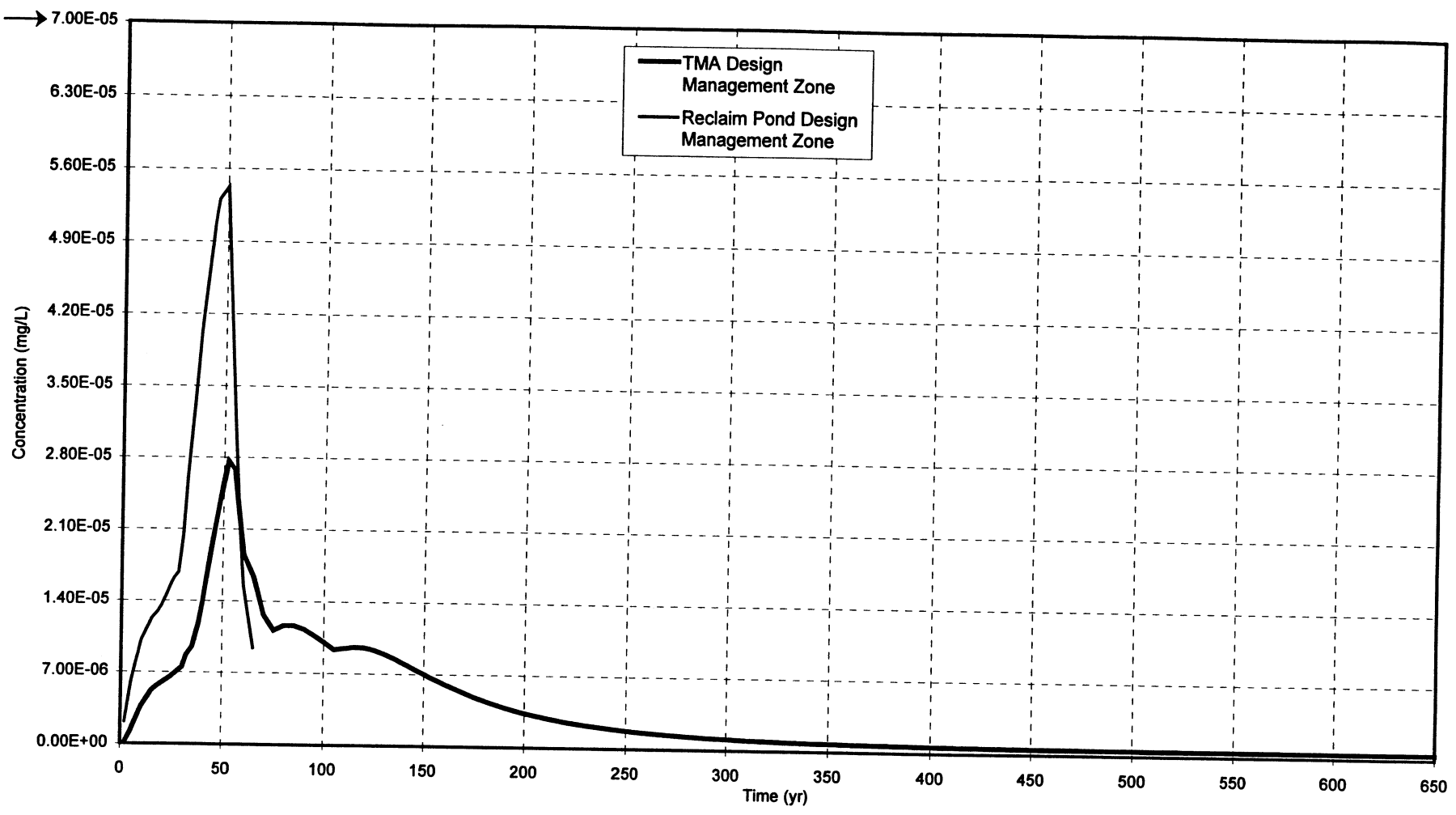

Source Concentration:

TMA Operation:	0.0061	(mg/L)
TMA Consolidation:	0.07	(mg/L)
TMA Post-Cap:	0.07	(mg/L)
TMA Post-FML-Degradation:	0.07	(mg/L)
Reclaim Pond Operation:	0.0061	(mg/L)
Reclaim Pond After TMA Capping:	0.07	(mg/L)

Simulations T14C1-T14C6

HSI GEOTRANS

REVISED	DATE	BY	DESCRIPTION
1	6/99	JDC	Updated STM
2	3/00	JDC	Updated STM

CHECKED BY: GWC	DATE: April 1998
APPROVED BY: PFA	DATE: April 1998
APPROVED BY:	DATE:

Nicolet Minerals
a Rio Algom company

Figure 3-39
Maximum Concentration at the Compliance Boundary for Cadmium, PWCT

Scale: None	Date: April 1998
Prepared By: HSI GEOTRANS	By: KMR

\Crandon\TMAMod4\Response\T14gwqpe.xls, Cr

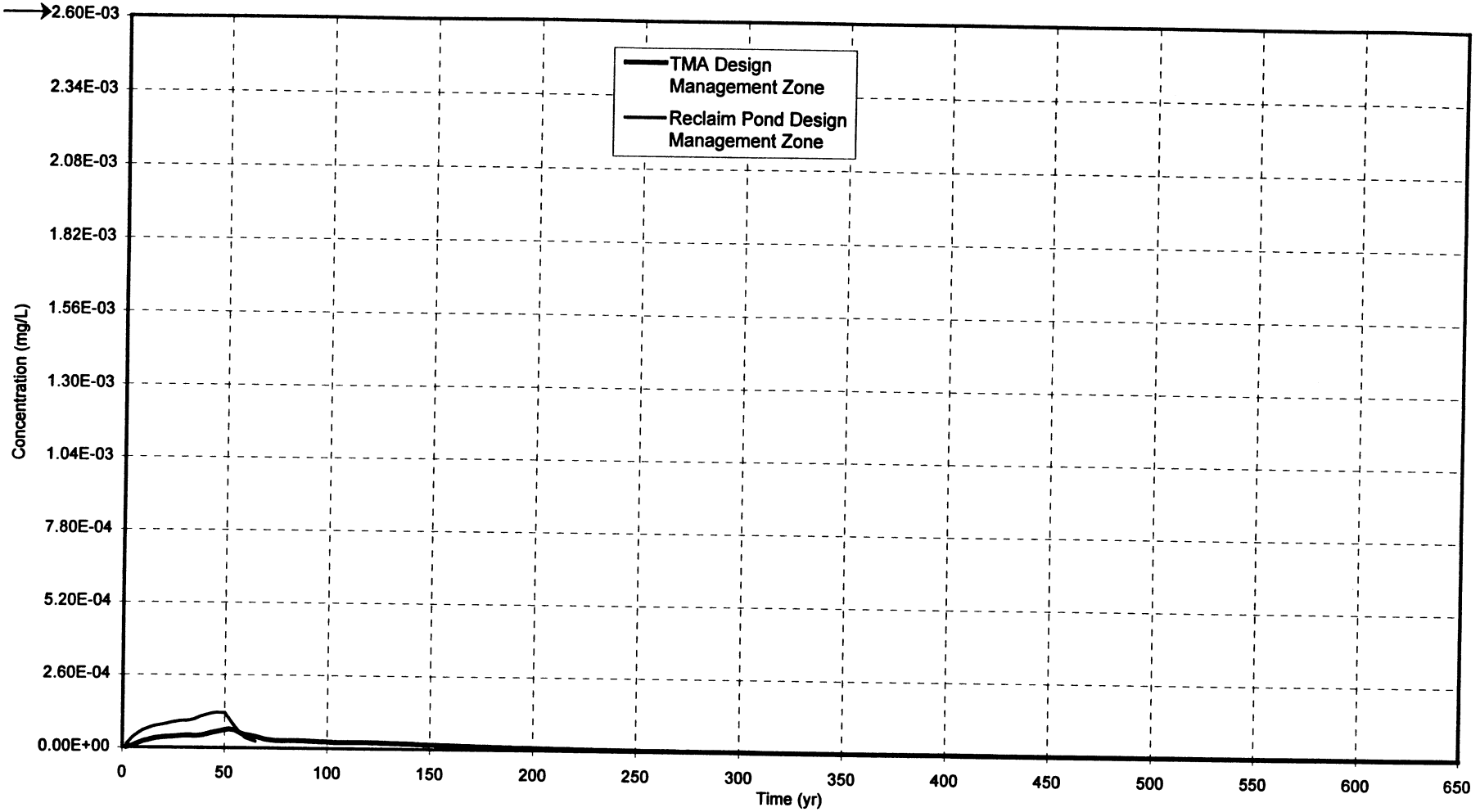

Source Concentration:

TMA Operation:	0.038 (mg/L)
TMA Consolidation:	0.15 (mg/L)
TMA Post-Cap:	0.15 (mg/L)
TMA Post-FML-Degradation:	0.15 (mg/L)
Reclaim Pond Operation:	0.038 (mg/L)
Reclaim Pond After TMA Capping:	0.15 (mg/L)

Simulations T14C1-T14C6

HSI GEOTRANS

REVISED	DATE	BY	DESCRIPTION
1	6/99	JDC	Updated STM
2	3/00	JDC	Updated STM

CHECKED BY: GWC	DATE: April 1998
APPROVED BY: PFA	DATE: April 1998
APPROVED BY:	DATE:

Nicolet Minerals
a Rio Algom company

Figure 3-40
Maximum Concentration at the Compliance Boundary for Chromium, PWCT

Scale: None	Date: April 1998
Prepared By: HSI GEOTRANS	By: KMR

\Crandon\TMAMod4\Response\T14gwqpe.xls, Fe

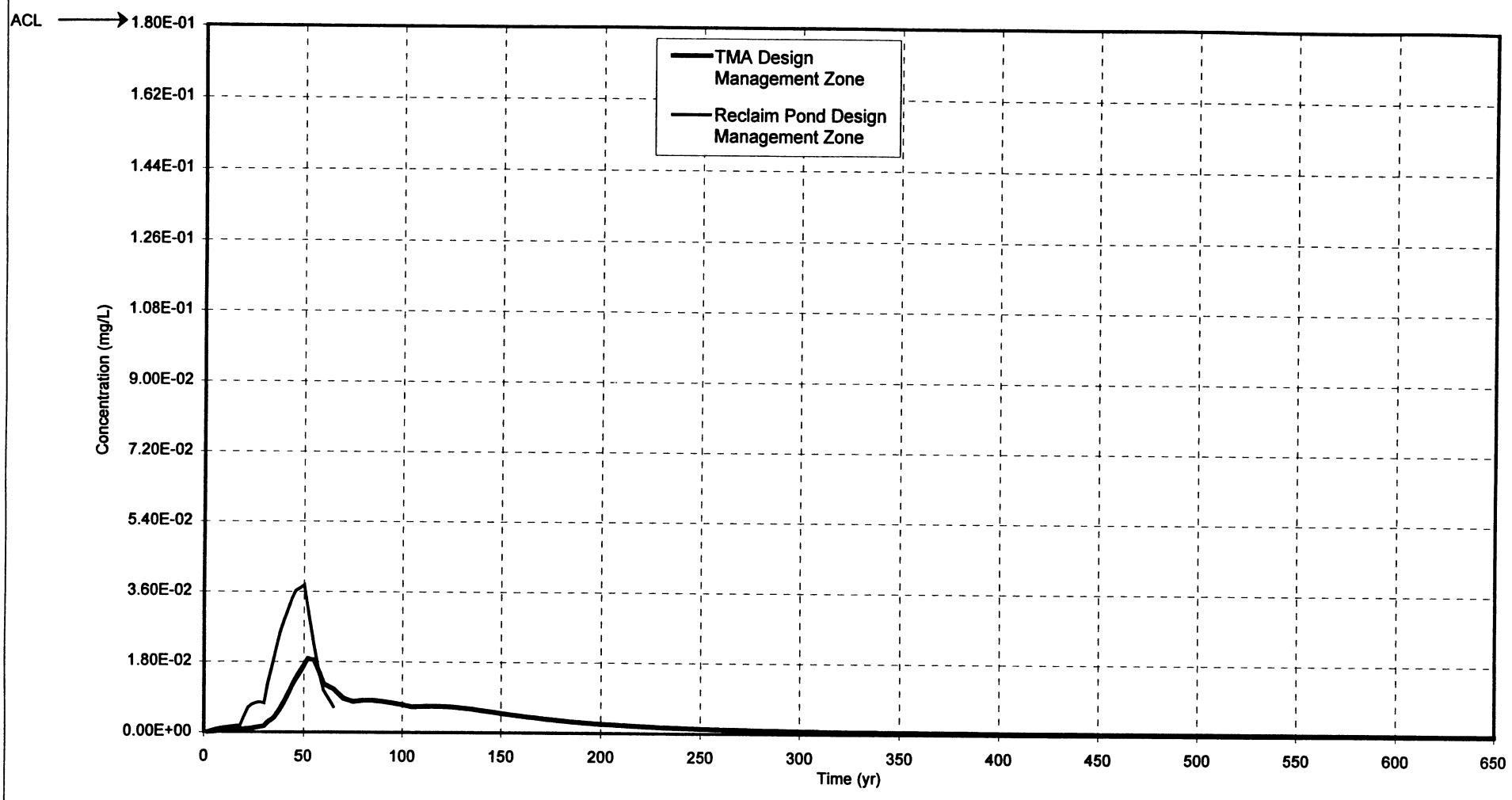

4.2-12-106

Source Concentration:

TMA Operation:	2.9 (mg/L)
TMA Consolidation:	50.0 (mg/L)
TMA Post-Cap:	50.0 (mg/L)
TMA Post-FML-Degradation:	50.0 (mg/L)
Reclaim Pond Operation:	0.72 (mg/L)
Reclaim Pond After TMA Capping:	50.0 (mg/L)

Simulations T14C1-T14C6

HSI GEOTRANS

REVISED	DATE	BY	DESCRIPTION
1	6/99	JDC	Updated STM
2	3/00	JDC	Updated STM

CHECKED BY: GWC	DATE: April 1998
APPROVED BY: PFA	DATE: April 1998
APPROVED BY:	DATE:

Nicolet Minerals
a Rio Algom company

Figure 3-41
Maximum Concentration at the Compliance Boundary for Iron, PWCT

Scale: None	Date: April 1998
Prepared By: HSI GEOTRANS	By: KMR

\Crandon\TMAMod4\Response\T14gwqpe.xls, Pb

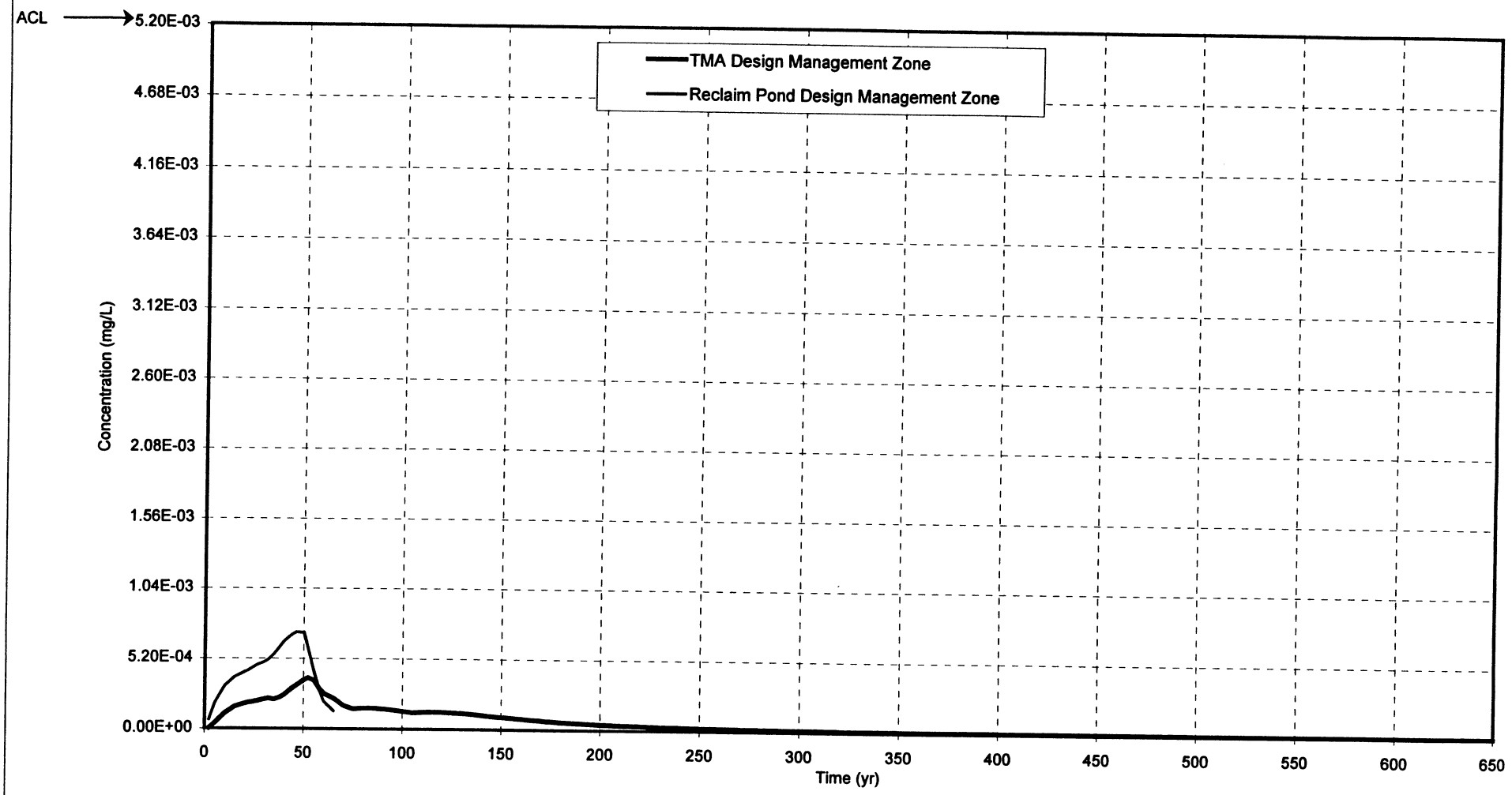

Source Concentration:

TMA Operation:	0.19 (mg/L)
TMA Consolidation:	0.87 (mg/L)
TMA Post-Cap:	0.87 (mg/L)
TMA Post-FML-Degradation:	0.87 (mg/L)
Reclaim Pond Operation:	0.19 (mg/L)
Reclaim Pond After TMA Capping:	0.87 (mg/L)

Simulations T14C1-T14C6

HSI GEOTRANS

REVISED	DATE	BY	DESCRIPTION
1	6/99	JDC	Updated STM
2	3/00	JDC	Updated STM

CHECKED BY: GWC	DATE: April 1998
APPROVED BY: PFA	DATE: April 1998
APPROVED BY:	DATE:

Nicolet Minerals
a Rio Algom company

Figure 3-42
Maximum Concentration at the Compliance Boundary for Lead, PWCT

Scale: None	Date: April 1998
Prepared By: HSI GEOTRANS	By: KMR

\Crandon\TMAMod4\Response\T14gwqpe.xls, Mn

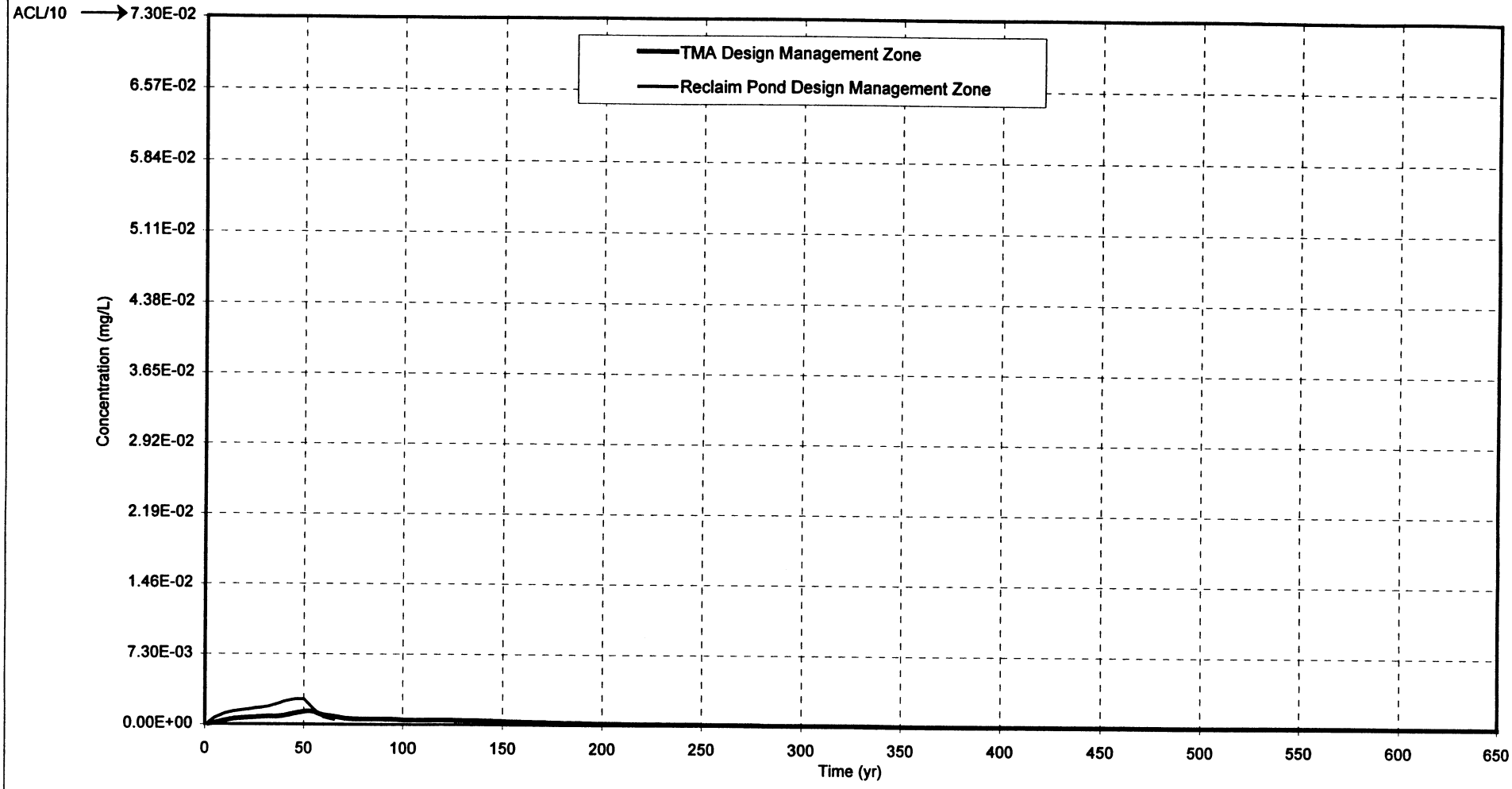

Source Concentration:

TMA Operation:	0.68 (mg/L)
TMA Consolidation:	3.2 (mg/L)
TMA Post-Cap:	3.2 (mg/L)
TMA Post-FML-Degradation:	3.2 (mg/L)
Reclaim Pond Operation:	0.68 (mg/L)
Reclaim Pond After TMA Capping:	3.2 (mg/L)

Simulations T14C1-T14C6

HSI GEOTRANS

REVISED	DATE	BY	DESCRIPTION
1	6/99	JDC	Updated STM
2	3/00	JDC	Updated STM

CHECKED BY: GWC	DATE: April 1998
APPROVED BY: PFA	DATE: April 1998
APPROVED BY:	DATE:

Nicolet Minerals
a Rio Algom company

Figure-43
Maximum Concentration at the Compliance Boundary for Manganese, PWCT

Scale: None	Date: April 1998
Prepared By: HSI GEOTRANS	By: KMR

\Crandon\TMAMod4\Response\T14gwqpe.xls, Hg

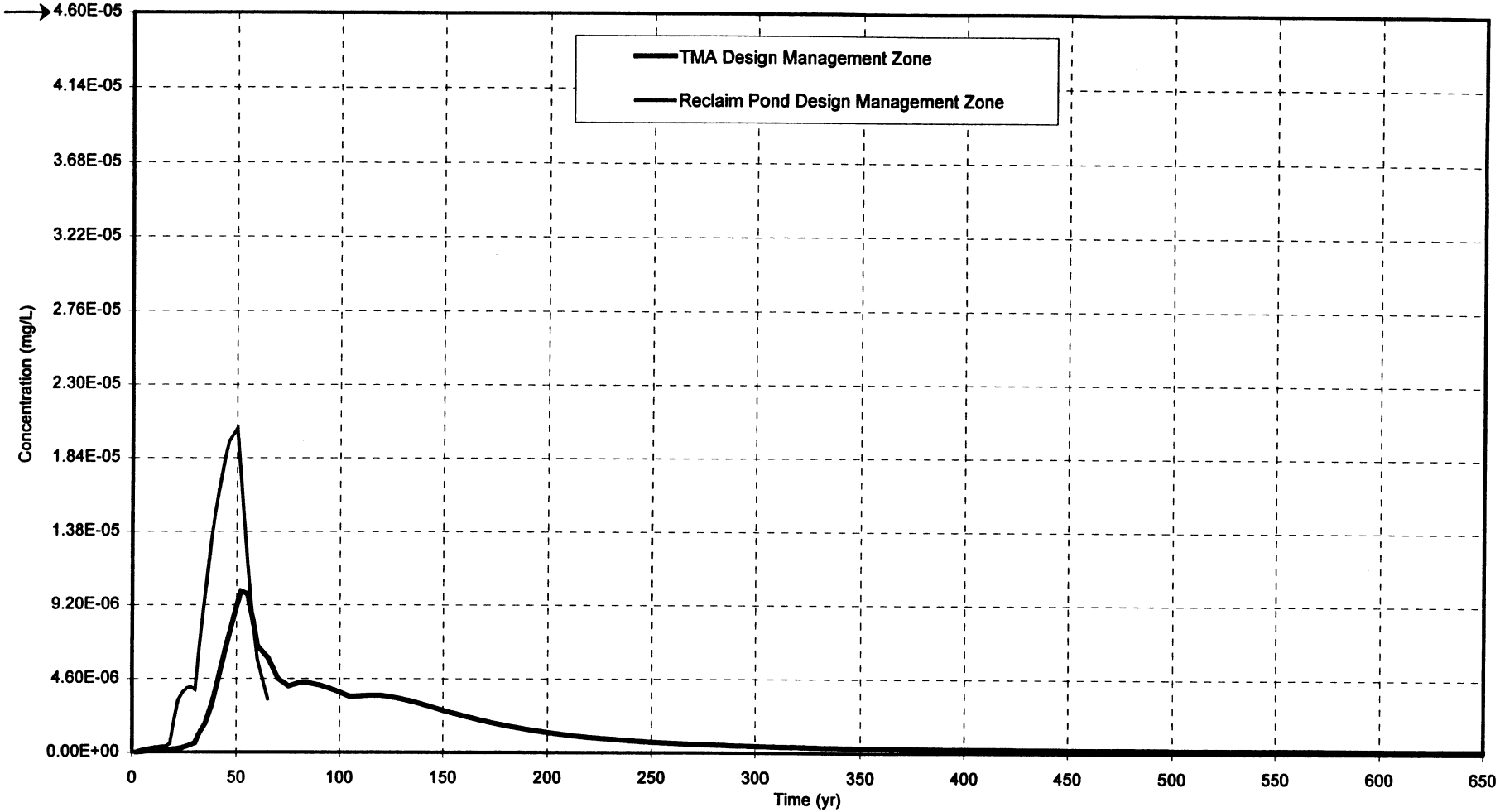

Source Concentration:

TMA Operation:	0.00018	(mg/L)
TMA Consolidation:	0.027	(mg/L)
TMA Post-Cap:	0.027	(mg/L)
TMA Post-FML-Degradation:	0.027	(mg/L)
Reclaim Pond Operation:	0.00018	(mg/L)
Reclaim Pond After TMA Capping:	0.027	(mg/L)

Simulations T14C1-T14C6

HSI GEOTRANS

REVISED	DATE	BY	DESCRIPTION
1	6/99	JDC	Updated STM
2	3/00	JDC	Updated STM

CHECKED BY: GWC	DATE: April 1998
APPROVED BY: PFA	DATE: April 1998
APPROVED BY:	DATE:

Nicolet Minerals
a Rio Algom company

Figure 3-44
Maximum Concentration at the Compliance Boundary for Mercury, PWCT

Scale: None	Date: April 1998
Prepared By: HSI GEOTRANS	By: KMR

\Crandon\TMAMod4\Response\T14gwqpe.xls, Se

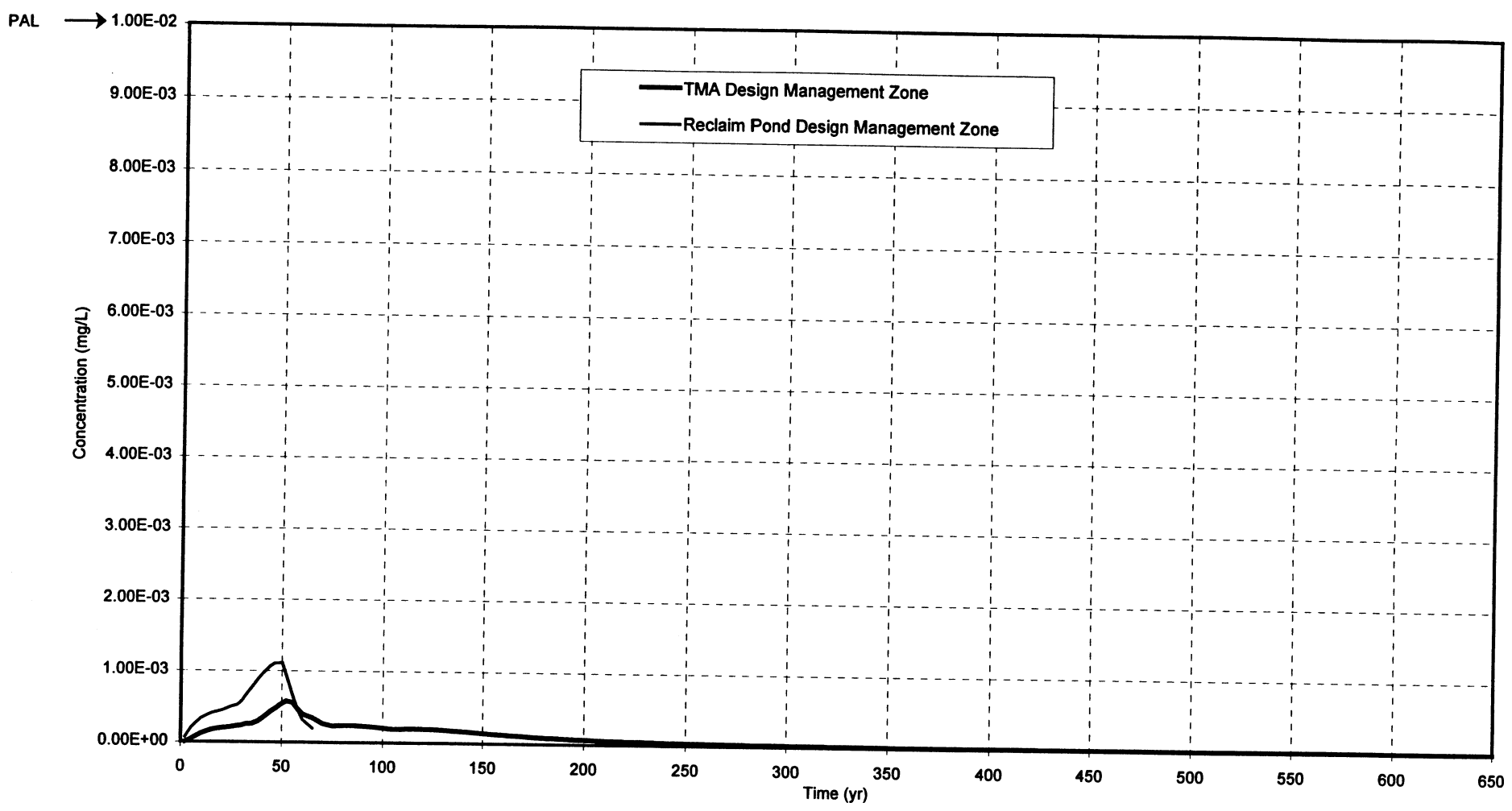

4.2-12-110

Source Concentration:

TMA Operation:	0.2 (mg/L)
TMA Consolidation:	1.4 (mg/L)
TMA Post-Cap:	1.4 (mg/L)
TMA Post-FML-Degradation:	1.4 (mg/L)
Reclaim Pond Operation:	0.2 (mg/L)
Reclaim Pond After TMA Capping:	1.4 (mg/L)

Simulations T14C1-T14C6

HSI GEOTRANS

REVISED	DATE	BY	DESCRIPTION
1	6/99	JDC	Updated STM
2	3/00	JDC	Updated STM

CHECKED BY: GWC	DATE: April 1998
APPROVED BY: PFA	DATE: April 1998
APPROVED BY:	DATE:

Nicolet Minerals
a Rio Algom company

Figure 3-45
Maximum Concentration at the Compliance Boundary for Selenium, PWCT

Scale: None	Date: April 1998
Prepared By: HSI GEOTRANS	By: KMR

\Crandon\TMAMod4\Response\T14gwqpe1.xls, SO4

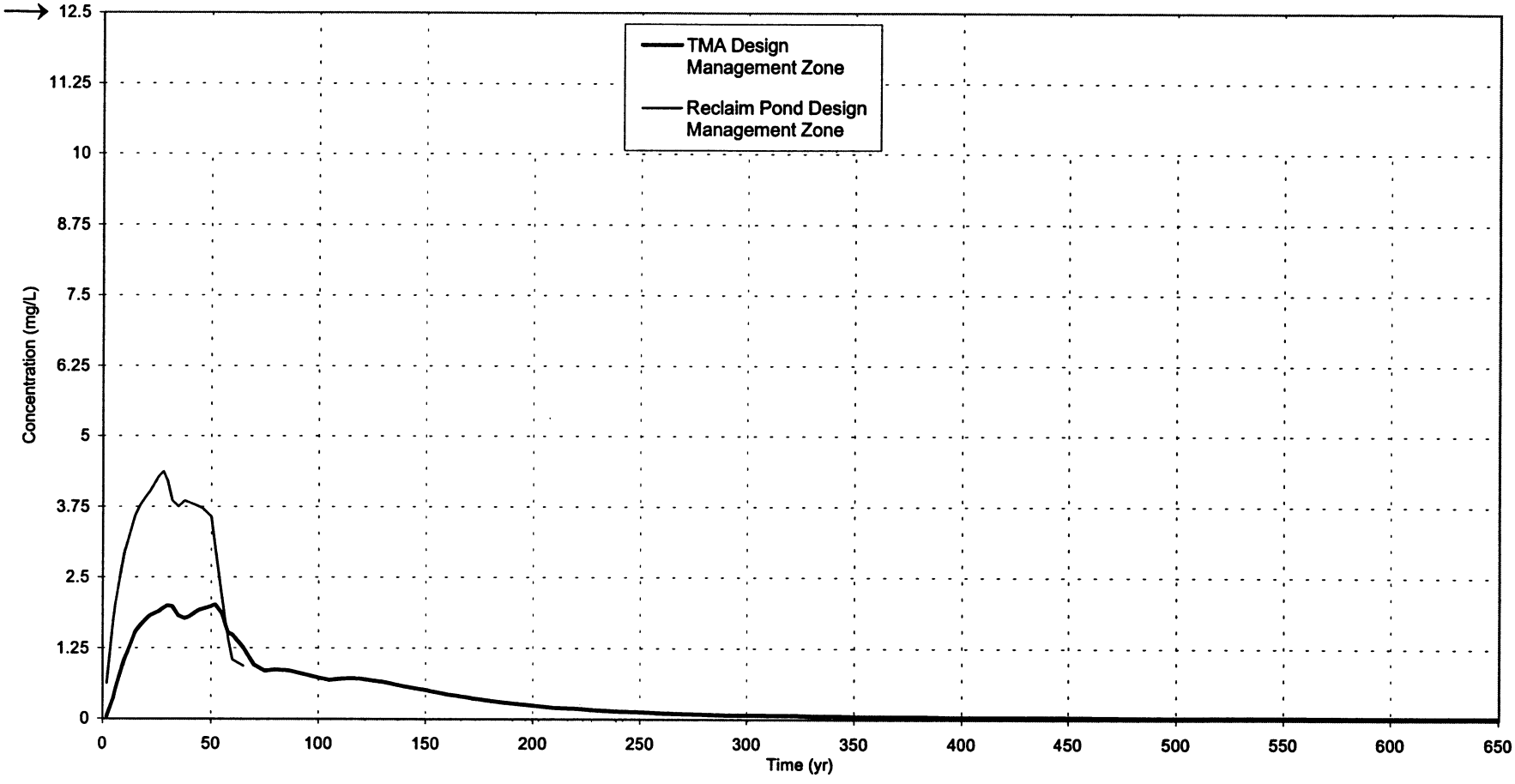

4.2-12-111

Source Concentration:

TMA Operation:	2714 (mg/L)
TMA Consolidation:	4010 (mg/L)
TMA Post-Cap:	4010 (mg/L)
TMA Post-FML-Degradation:	4010 (mg/L)
Reclaim Pond Operation:	1768 (mg/L)
Reclaim Pond After TMA Capping:	4010 (mg/L)

Simulations T14C1-T14C6

REVISED	DATE	BY	DESCRIPTION
1	6/99	JDC	Updated STM
2	3/00	JDC	Updated STM
3	8/00	GWC	Revised Source Conc

CHECKED BY: GWC	DATE: April 1998
APPROVED BY: PFA	DATE: April 1998
APPROVED BY:	DATE:

Nicolet Minerals
a Rio Algom company

Figure 3-46
Maximum Concentration at the Compliance Boundary for Sulfate, PWCT

Scale: None	Date: April 1998
Prepared By: HSI GEOTRANS	By: KMR

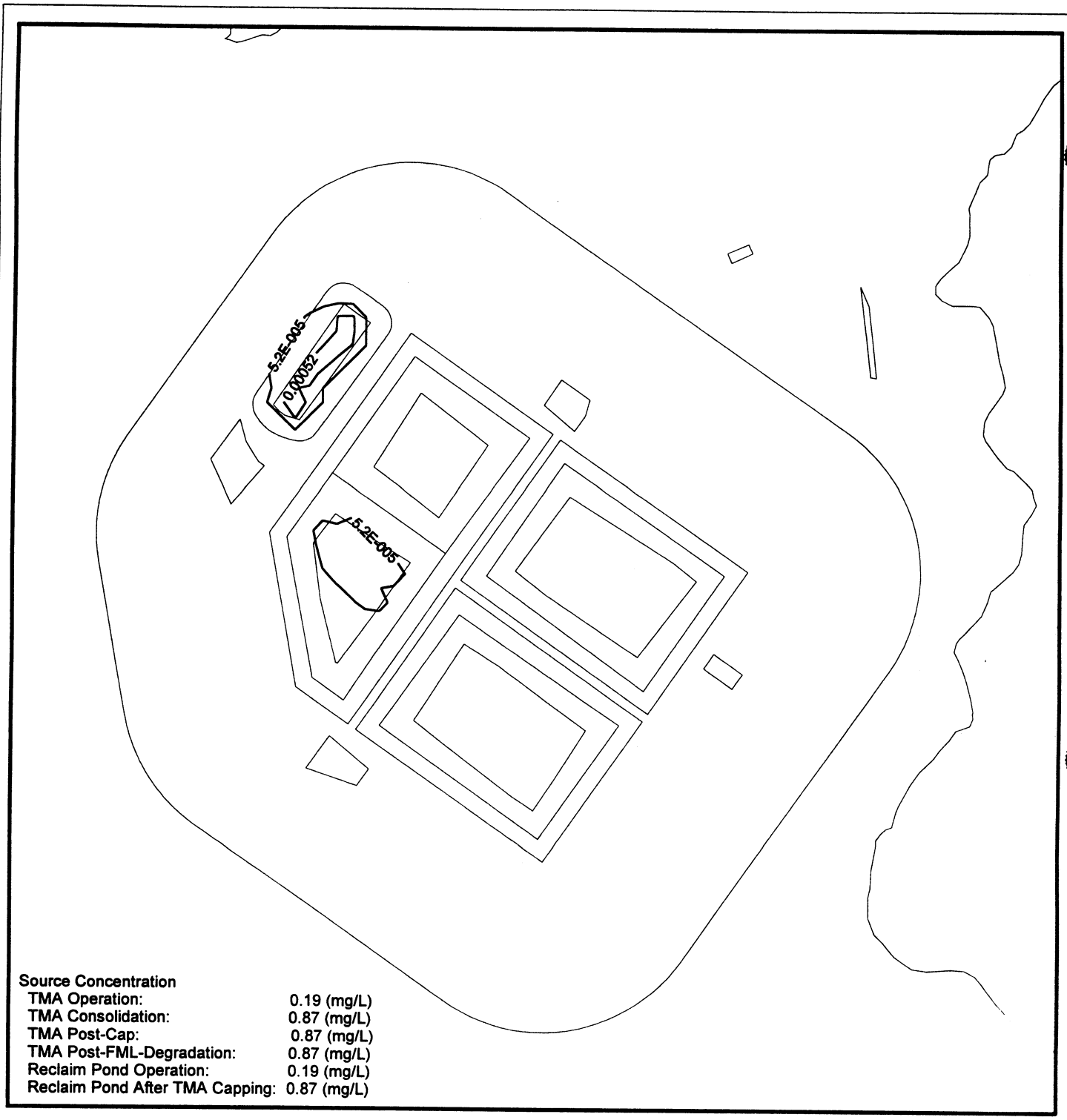

Source Concentration

TMA Operation:	0.19 (mg/L)
TMA Consolidation:	0.87 (mg/L)
TMA Post-Cap:	0.87 (mg/L)
TMA Post-FML-Degradation:	0.87 (mg/L)
Reclaim Pond Operation:	0.19 (mg/L)
Reclaim Pond After TMA Capping:	0.87 (mg/L)

Concentration Contours Shown
0.0052 mg/L (ACL)
0.00052 mg/L
0.000052 mg/L

N

0 1000 2000

Scale in Feet

HSI GEOTRANS

REVISED	DATE	BY	DESCRIPTION
1	6/99	RAK	Updated STM
2	3/00	JDC	Updated STM

CHECKED BY: GWC	DATE: April 1998	
APPROVED BY: PFA	DATE: April 1998	
APPROVED BY:	DATE:	

Simulations T14C1 - T14C6

Nicolet Minerals
a Rio Algom company

Figure 3-47
Lead Concentration After 2 Years, PWCT
(Example Constituent, Plan View)

Scale: 1 in. = 1000 ft. | Date: April 1998

Prepared By: HSI GEOTRANS | By: RMD

P:\Crandon\Tmalvod4\Surfer\P14pb002.srf

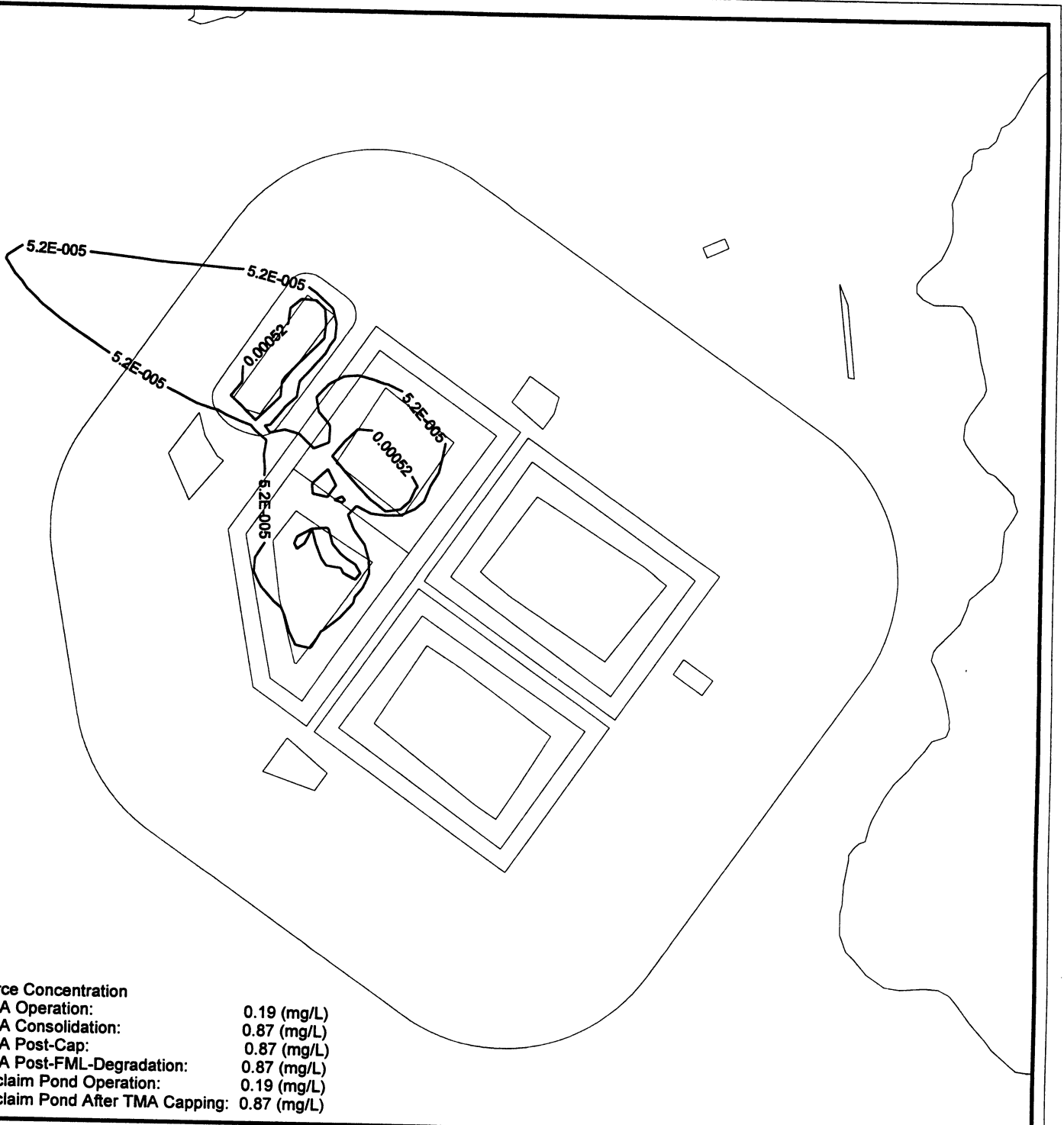

Source Concentration

TMA Operation:	0.19 (mg/L)
TMA Consolidation:	0.87 (mg/L)
TMA Post-Cap:	0.87 (mg/L)
TMA Post-FML-Degradation:	0.87 (mg/L)
Reclaim Pond Operation:	0.19 (mg/L)
Reclaim Pond After TMA Capping:	0.87 (mg/L)

Concentration Contours Shown
0.0052 mg/L (ACL)
0.00052 mg/L
0.000052 mg/L

N

0 1000 2000

Scale in Feet

HSI GEOTRANS

REVISED	DATE	BY	DESCRIPTION
1	6/99	RAK	Updated STM
2	3/00	JDC	Updated STM

CHECKED BY: GWC DATE: April 1998

APPROVED BY: PFA DATE: April 1998

APPROVED BY: DATE:

Simulations T14C1 - T14C6

Nicolet Minerals
a Rio Algom company

Figure 3-48
Lead Concentration After 16 Years, PWCT
(Example Constituent, Plan View)

Scale: 1 in. = 1000 ft. Date: April 1998

Prepared By: HSI GEOTRANS By: RMD

P:\Crandon\Tma\Mod4\Sb\...tb016.srf

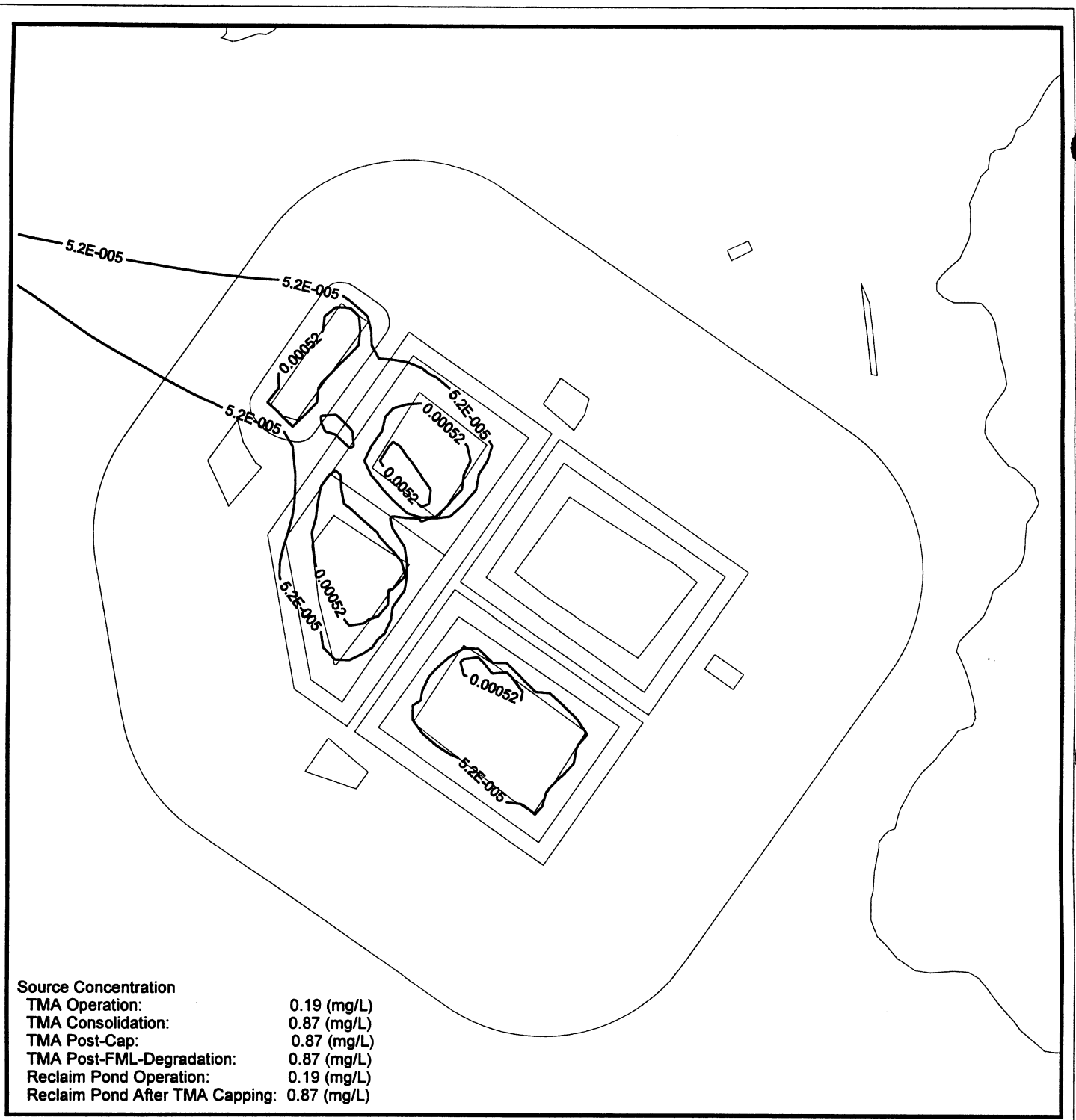

Source Concentration

TMA Operation:	0.19 (mg/L)
TMA Consolidation:	0.87 (mg/L)
TMA Post-Cap:	0.87 (mg/L)
TMA Post-FML-Degradation:	0.87 (mg/L)
Reclaim Pond Operation:	0.19 (mg/L)
Reclaim Pond After TMA Capping:	0.87 (mg/L)

Concentration Contours Shown
0.0052 mg/L (ACL)
0.00052 mg/L
0.000052 mg/L

0 1000 2000
Scale in Feet

HSI GEOTRANS

REVISED	DATE	BY	DESCRIPTION
1	6/99	RAK	Updated STM
2	3/00	JDC	Updated STM

CHECKED BY: GWC		DATE: April 1998
APPROVED BY: PFA		DATE: April 1998
APPROVED BY:		DATE:

Simulations T14C1 - T14C6

Nicolet Minerals
a Rio Algom company

Figure 3-49
Lead Concentration After 22 Years, PWCT
(Example Constituent, Plan View)

Scale: 1 in. = 1000 ft. | Date: April 1998
Prepared By: HSI GEOTRANS | By: RMD

P:\Crandon\Tmal\Mod4\Surfer\P14p022.srf

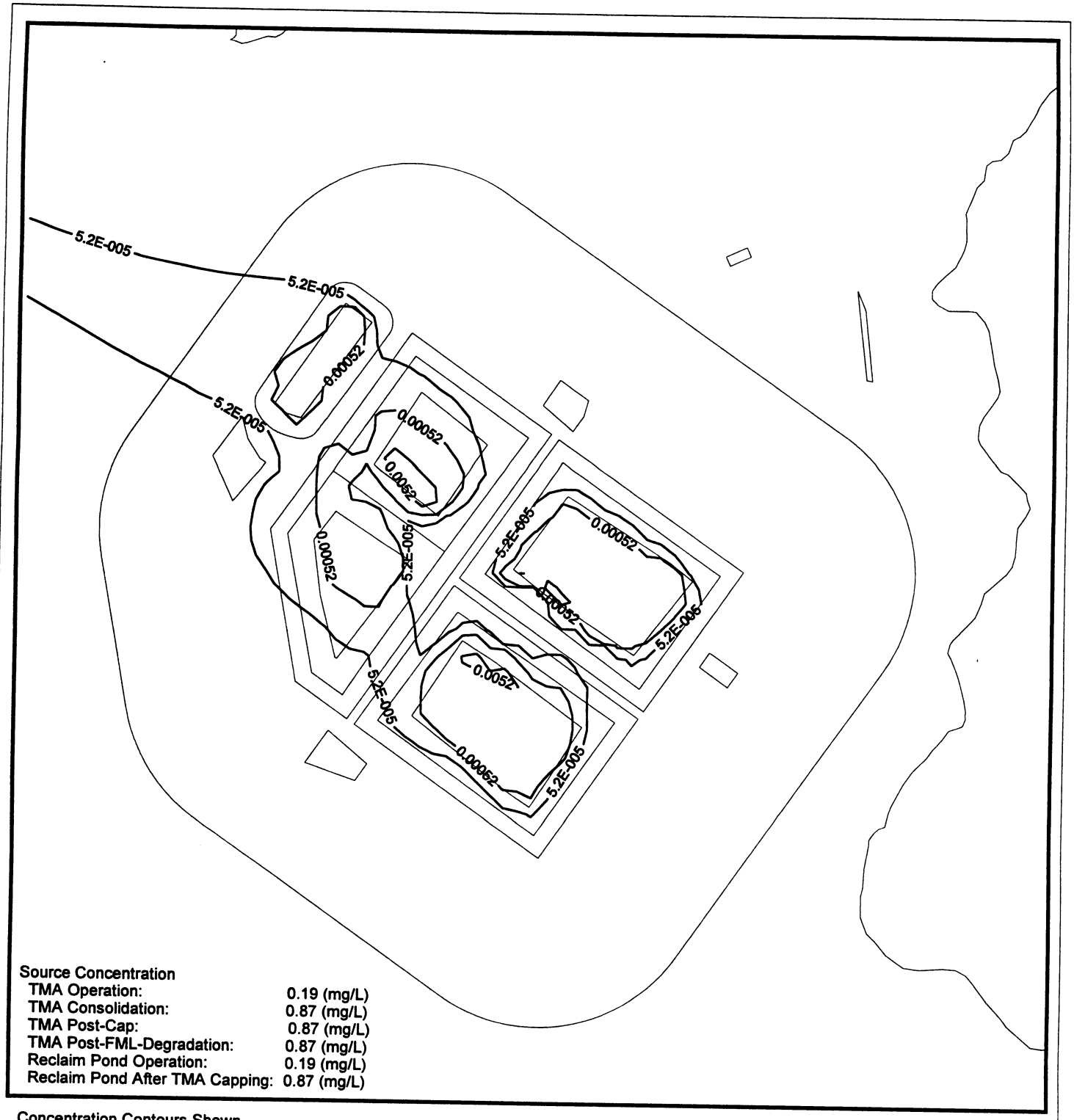

Source Concentration

TMA Operation:	0.19 (mg/L)
TMA Consolidation:	0.87 (mg/L)
TMA Post-Cap:	0.87 (mg/L)
TMA Post-FML-Degradation:	0.87 (mg/L)
Reclaim Pond Operation:	0.19 (mg/L)
Reclaim Pond After TMA Capping:	0.87 (mg/L)

Concentration Contours Shown
0.0052 mg/L (ACL)
0.00052 mg/L
0.000052 mg/L

N

0 1000 2000

Scale in Feet

HSI GEOTRANS

REVISED	DATE	BY	DESCRIPTION
1	6/99	RAK	Updated STM
2	3/00	JDC	Updated STM

CHECKED BY: GWC		DATE: April 1998
APPROVED BY: PFA		DATE: April 1998
APPROVED BY:		DATE:

Simulations T14C1 - T14C6

Nicolet Minerals
a Rio Algom company

Figure 3-50
Lead Concentration After 32 Years, PWCT
(Example Constituent, Plan View)

Scale: 1 in. = 1000 ft. | Date: April 1998

Prepared By: HSI GEOTRANS | By: RMD

P:\Crandon\Tma\Mod4\Sur\...\ppt032.srf

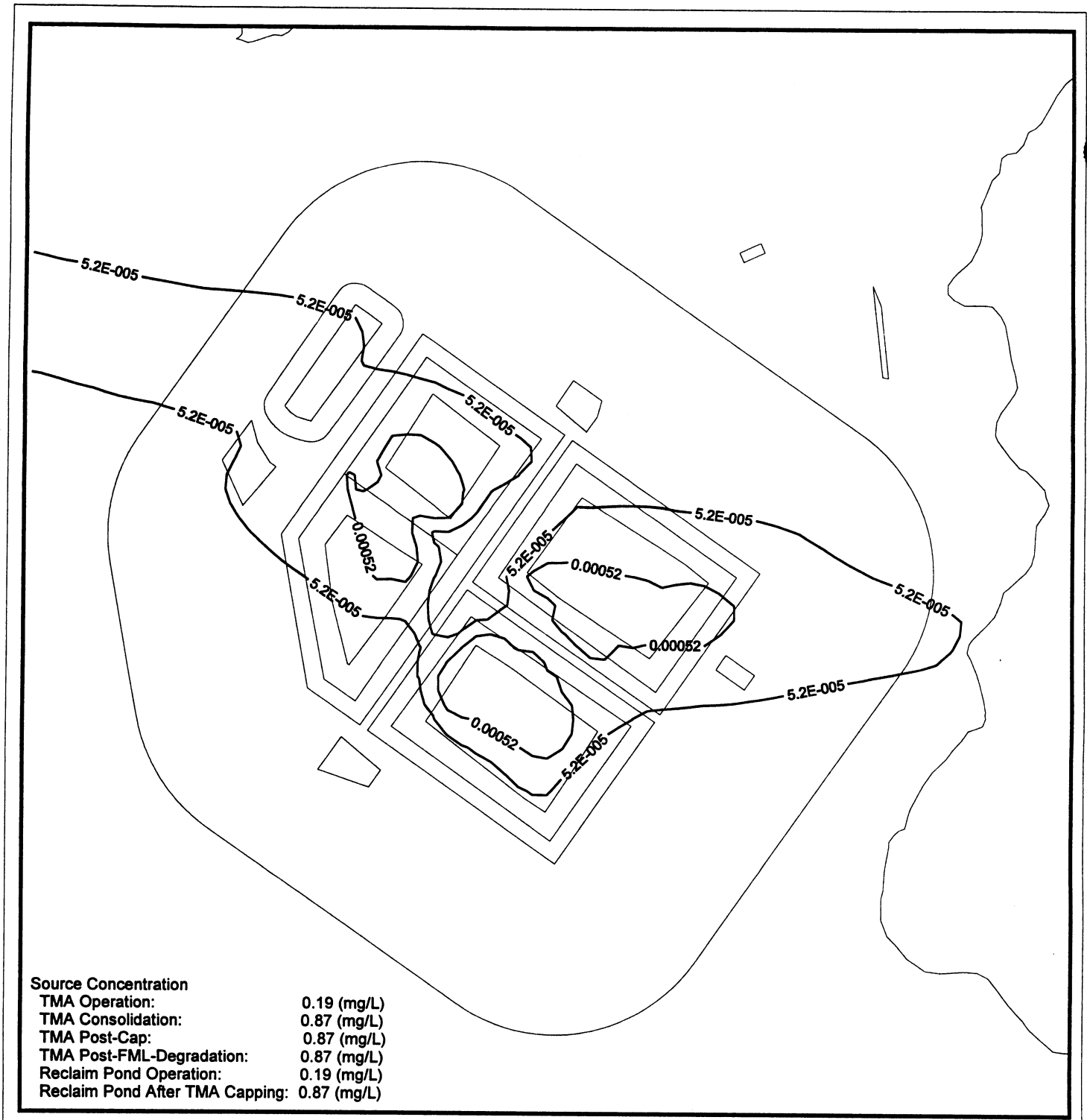

Source Concentration

TMA Operation:	0.19 (mg/L)
TMA Consolidation:	0.87 (mg/L)
TMA Post-Cap:	0.87 (mg/L)
TMA Post-FML-Degradation:	0.87 (mg/L)
Reclaim Pond Operation:	0.19 (mg/L)
Reclaim Pond After TMA Capping:	0.87 (mg/L)

Concentration Contours Shown
0.0052 mg/L (ACL)
0.00052 mg/L
0.000052 mg/L

N

0 1000 2000

Scale in Feet

HSI GEOTRANS

REVISED	DATE	BY	DESCRIPTION
1	6/99	RAK	Updated STM
2	3/00	JDC	Updated STM

CHECKED BY: GWC DATE: April 1998
APPROVED BY: PFA DATE: April 1998
APPROVED BY: DATE:

Simulations T14C1 - T14C6

Nicolet Minerals
a Rio Algom company

Figure 3-51
Lead Concentration After 60 Years, PWCT
(Example Constituent, Plan View)

Scale: 1 in. = 1000 ft. Date: April 1998
Prepared By: HSI GEOTRANS By: RMD

P:\Crandon\Tmwf\Mod4\Surfer\P14pb060.srf

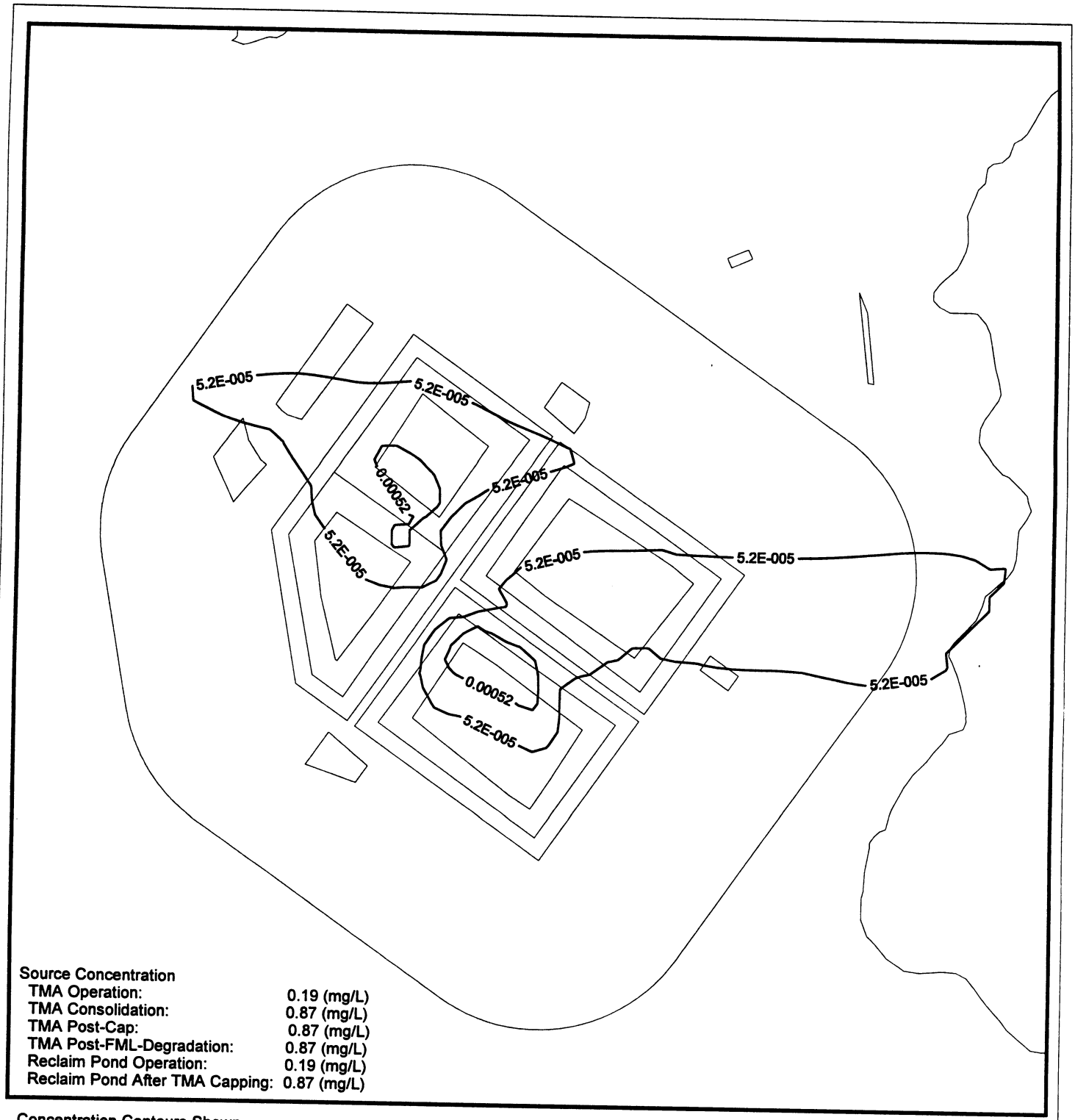

Source Concentration

TMA Operation:	0.19 (mg/L)
TMA Consolidation:	0.87 (mg/L)
TMA Post-Cap:	0.87 (mg/L)
TMA Post-FML-Degradation:	0.87 (mg/L)
Reclaim Pond Operation:	0.19 (mg/L)
Reclaim Pond After TMA Capping:	0.87 (mg/L)

Concentration Contours Shown
0.0052 mg/L (ACL)
0.00052 mg/L
0.000052 mg/L

0 1000 2000
Scale in Feet

HSI GEOTRANS

REVISED	DATE	BY	DESCRIPTION
1	6/99	RAK	Updated STM
2	3/00	JDC	Updated STM

Simulations T14C1 - T14C6	CHECKED BY: GWC	DATE: April 1998
	APPROVED BY: PFA	DATE: April 1998
	APPROVED BY:	DATE:

Nicolet Minerals
a Rio Algom company

Figure 3-52
Lead Concentration After 125 Years, PWCT
(Example Constituent, Plan View)

Scale: 1 in. = 1000 ft.	Date: April 1998
Prepared By: HSI GEOTRANS	By: RMD

P:\Crandon\Tmal\Mod4\Sumeasu\pb125.srf

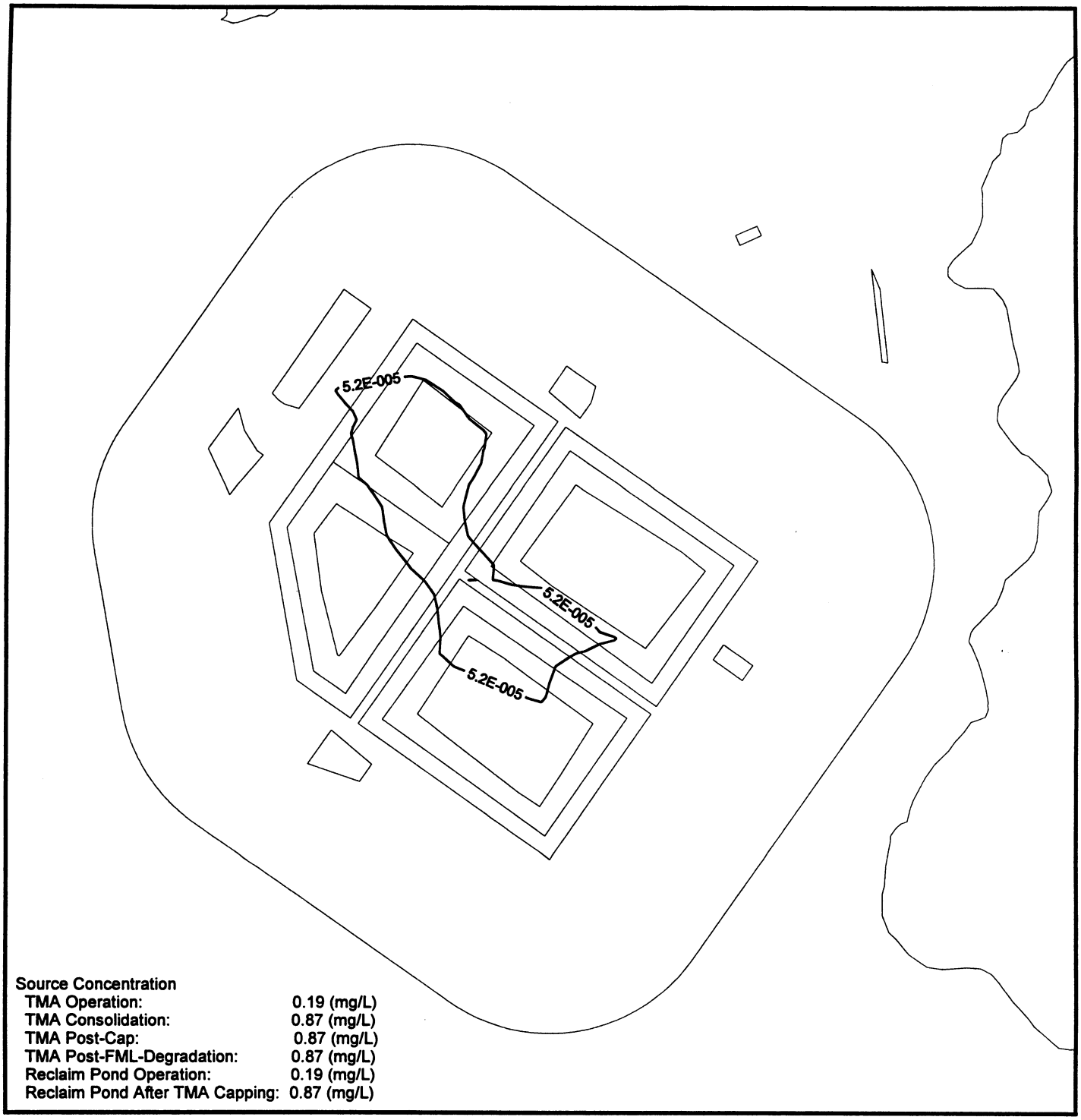

Source Concentration

TMA Operation:	0.19 (mg/L)
TMA Consolidation:	0.87 (mg/L)
TMA Post-Cap:	0.87 (mg/L)
TMA Post-FML-Degradation:	0.87 (mg/L)
Reclaim Pond Operation:	0.19 (mg/L)
Reclaim Pond After TMA Capping:	0.87 (mg/L)

Concentration Contours Shown
0.0052 mg/L (ACL)
0.00052 mg/L
0.000052 mg/L

N

0 1000 2000

Scale in Feet

HSI GEOTRANS

REVISED	DATE	BY	DESCRIPTION
1	6/99	RAK	Updated STM
2	3/00	JDC	Updated STM

CHECKED BY: GWC		DATE: April 1998
APPROVED BY: PFA		DATE: April 1998
APPROVED BY:		DATE:

Simulations T14C1 - T14C6

Nicolet Minerals
a Rio Algom company

Figure 3-53
Lead Concentration After 300 Years, PWCT
(Example Constituent, Plan View)

Scale: 1 in. = 1000 ft. | Date: April 1998

Prepared By: HSI GEOTRANS | By: RMD

P:\Chandon\Tma\Mod4\Surfer\P14pb300.srf

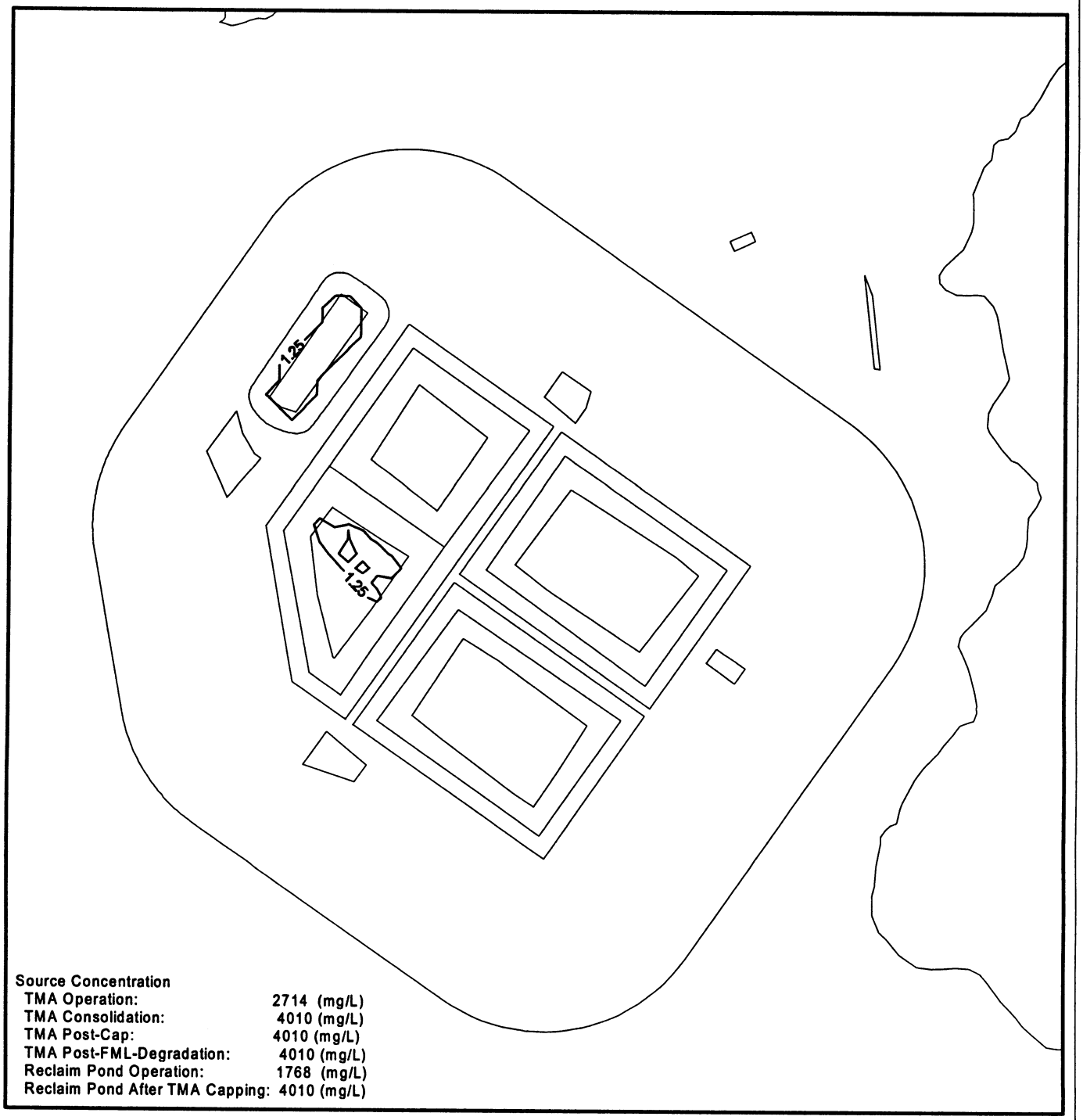

Source Concentration

TMA Operation:	2714 (mg/L)
TMA Consolidation:	4010 (mg/L)
TMA Post-Cap:	4010 (mg/L)
TMA Post-FML-Degradation:	4010 (mg/L)
Reclaim Pond Operation:	1768 (mg/L)
Reclaim Pond After TMA Capping:	4010 (mg/L)

Concentration Contours Shown
- 125 mg/L (ACL)
- 12.5 mg/L
- 1.25 mg/L

0 1000 2000

Scale in Feet

HSI GEOTRANS

REVISED	DATE	BY	DESCRIPTION
1	6/99	RAK	Updated STM
2	3/00	JDC	Updated STM
3	8/00	GWC	Updated Source Conc.

CHECKED BY: GWC		DATE: April 1998
APPROVED BY: PFA		DATE: April 1998
APPROVED BY:		DATE:

Simulations T14C1 - T14C6

Nicolet Minerals
a Rio Algom company

Figure 3-54
Sulfate Concentration After 2 Years, PWCT

Scale: 1 in. = 1000 ft.	Date: April 1998
Prepared By: HSI GEOTRANS	By: RMD

P:\Crandon\Tma\Mod4\Surfer\P14so002a.srf

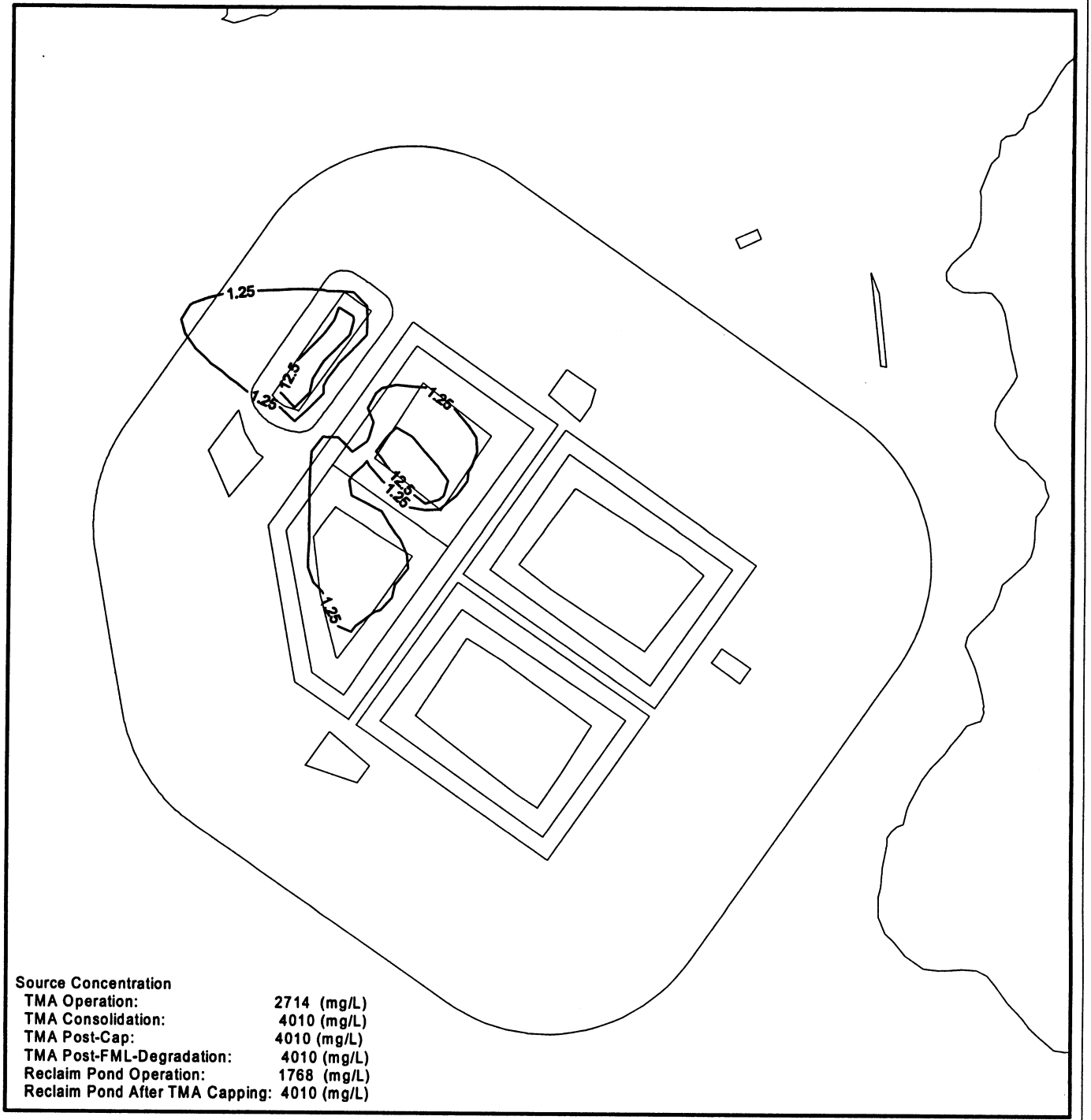

Source Concentration

TMA Operation:	2714 (mg/L)
TMA Consolidation:	4010 (mg/L)
TMA Post-Cap:	4010 (mg/L)
TMA Post-FML-Degradation:	4010 (mg/L)
Reclaim Pond Operation:	1768 (mg/L)
Reclaim Pond After TMA Capping:	4010 (mg/L)

Concentration Contours Shown
125 mg/L (ACL)
12.5 mg/L
1.25 mg/L

N

0 1000 2000

Scale in Feet

HSI GEOTRANS

REVISED	DATE	BY	DESCRIPTION
1	6/99	RAK	Updated STM
2	3/00	JDC	Updated STM
3	8/00	GWC	Updated Source Conc.

CHECKED BY: GWC DATE: April 1998

APPROVED BY: PFA DATE: April 1998

APPROVED BY: DATE:

Simulations T14C1 - T14C6

Nicolet Minerals
a Rio Algom company

Figure 3-55
Sulfate Concentration After 16 Years, PWCT

Scale: 1 in. = 1000 ft. Date: April 1998

Prepared By: HSI GEOTRANS By: RMD

P:\Crandon\TmaMod4\Surfer\P14so016a.srf

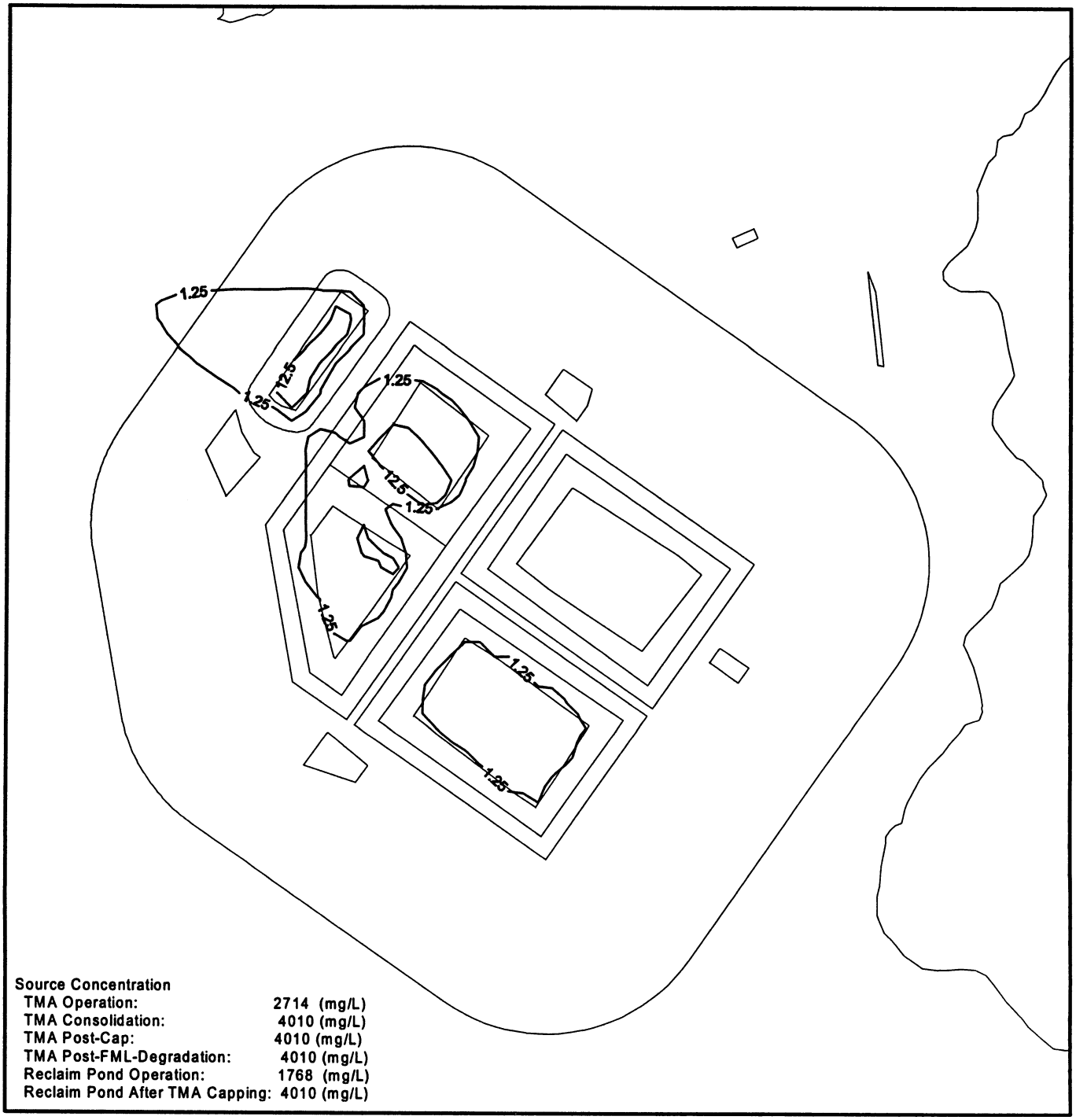

Source Concentration

TMA Operation:	2714 (mg/L)
TMA Consolidation:	4010 (mg/L)
TMA Post-Cap:	4010 (mg/L)
TMA Post-FML-Degradation:	4010 (mg/L)
Reclaim Pond Operation:	1768 (mg/L)
Reclaim Pond After TMA Capping:	4010 (mg/L)

Concentration Contours Shown
- 125 mg/L (ACL)
- 12.5 mg/L
- 1.25 mg/L

0 1000 2000

Scale in Feet

HSI GEOTRANS

REVISED	DATE	BY	DESCRIPTION
1	6/99	RAK	Updated STM
2	3/00	JDC	Updated STM
3	8/00	GWC	Updated Source Conc.

CHECKED BY: GWC		DATE: April 1998
APPROVED BY: PFA		DATE: April 1998
APPROVED BY:		DATE:

Simulations T14C1 - T14C6

Nicolet Minerals
a Rio Algom company

Figure 3-56
Sulfate Concentration After 22 Years, PWCT

Scale: 1 in. = 1000 ft. | Date: April 1998

Prepared By: HSI GEOTRANS | By: RMD

P:\Crandon\TmaMod4\Surfer\P14so022a.srf

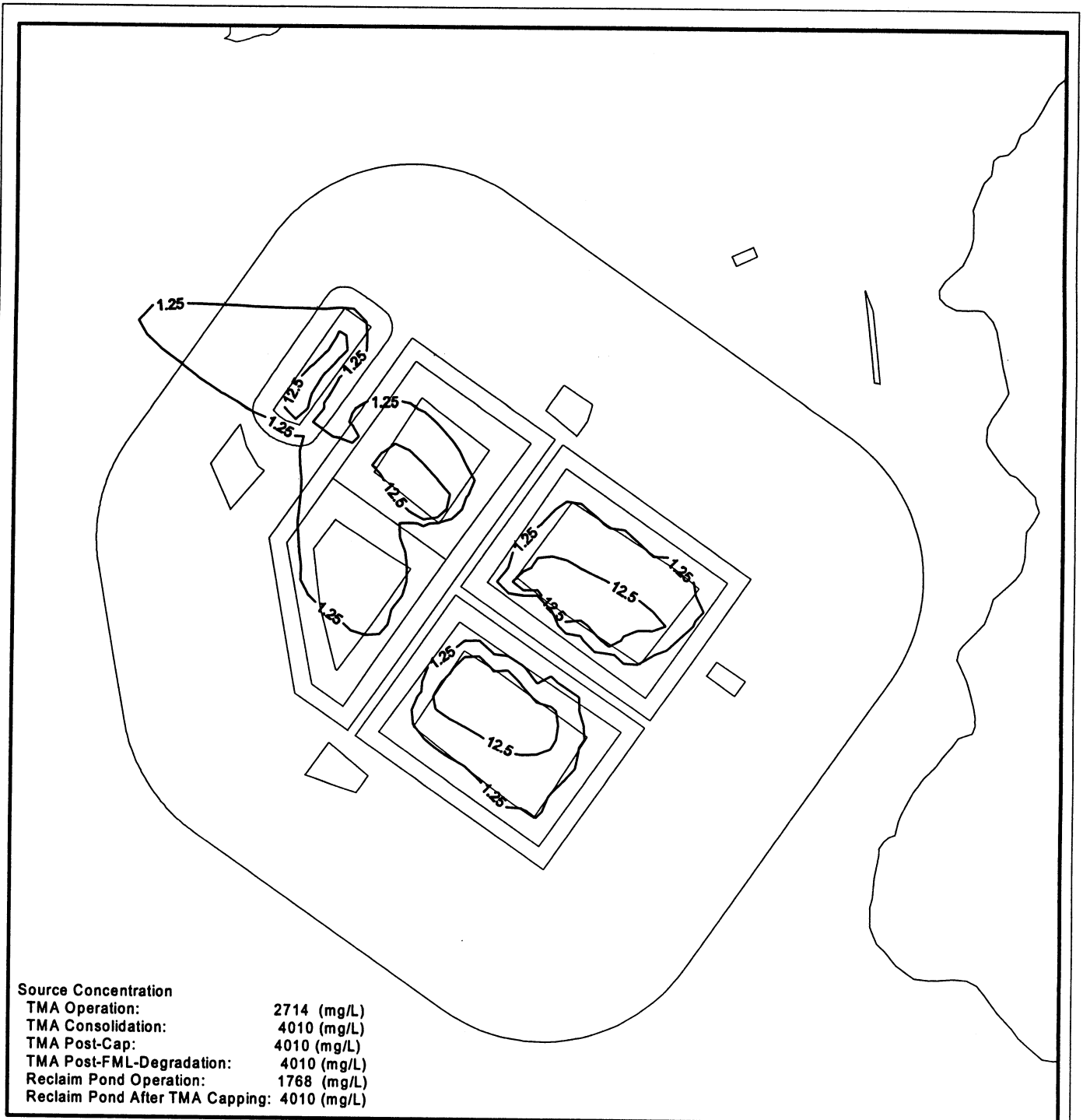

Source Concentration

TMA Operation:	2714 (mg/L)
TMA Consolidation:	4010 (mg/L)
TMA Post-Cap:	4010 (mg/L)
TMA Post-FML-Degradation:	4010 (mg/L)
Reclaim Pond Operation:	1768 (mg/L)
Reclaim Pond After TMA Capping:	4010 (mg/L)

Concentration Contours Shown
- 125 mg/L (ACL)
- 12.5 mg/L
- 1.25 mg/L

N

0 1000 2000

Scale in Feet

HSI GEOTRANS

REVISED	DATE	BY	DESCRIPTION
1	6/99	RAK	Updated STM
2	3/00	JDC	Updated STM
3	8/00	GWC	Updated Source Conc.

CHECKED BY: GWC DATE: April 1998

APPROVED BY: PFA DATE: April 1998

APPROVED BY: DATE:

Simulations T14C1 - T14C6

Nicolet Minerals
a Rio Algom company

Figure 3-57
Sulfate Concentration After 32 Years, PWCT

Scale: 1 in. = 1000 ft. Date: April 1998

Prepared By: HSI GEOTRANS By: RMD

P:\Crandon\TmaMod4\Surfer\P14so032a.srf

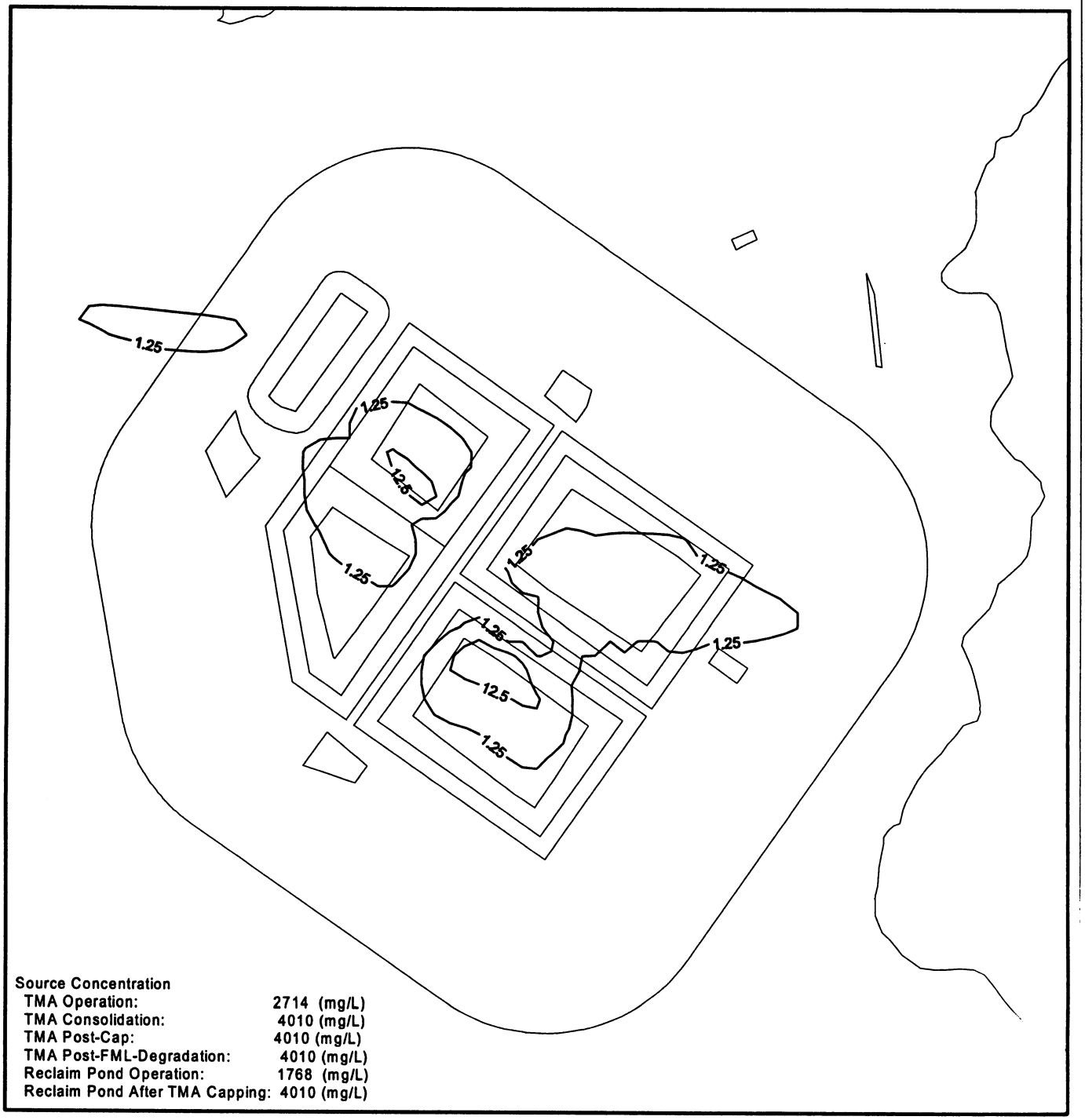

Source Concentration

TMA Operation:	2714 (mg/L)
TMA Consolidation:	4010 (mg/L)
TMA Post-Cap:	4010 (mg/L)
TMA Post-FML-Degradation:	4010 (mg/L)
Reclaim Pond Operation:	1768 (mg/L)
Reclaim Pond After TMA Capping:	4010 (mg/L)

Concentration Contours Shown
- 125 mg/L (ACL)
- 12.5 mg/L
- 1.25 mg/L

N

0 1000 2000

Scale in Feet

HSI GEOTRANS

REVISED	DATE	BY	DESCRIPTION
1	6/99	RAK	Updated STM
2	3/00	JDC	Updated STM
3	8/00	GWC	Updated Source Conc.

CHECKED BY: GWC		DATE: April 1998
APPROVED BY: PFA		DATE: April 1998
APPROVED BY:		DATE:

Simulations T14C1 - T14C6

Nicolet Minerals
a Rio Algom company

Figure 3-58
Sulfate Concentration After 60 Years, PWCT

Scale: 1 in. = 1000 ft.	Date: April 1998
Prepared By: HSI GEOTRANS	By: RMD

P:\Crandon\TmaMod4\Surfer\P14so060a.srf

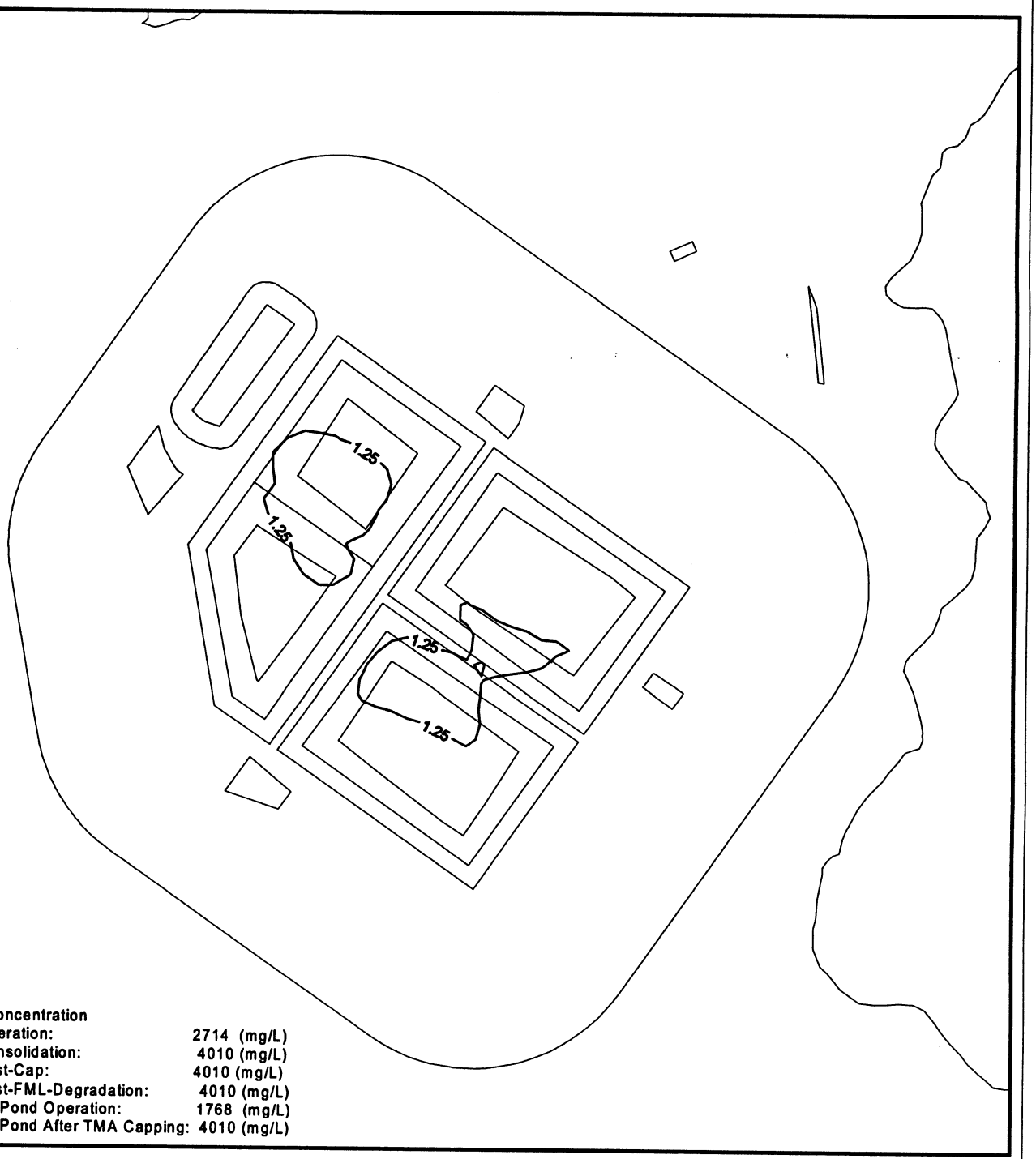

Source Concentration

TMA Operation:	2714 (mg/L)
TMA Consolidation:	4010 (mg/L)
TMA Post-Cap:	4010 (mg/L)
TMA Post-FML-Degradation:	4010 (mg/L)
Reclaim Pond Operation:	1768 (mg/L)
Reclaim Pond After TMA Capping:	4010 (mg/L)

Concentration Contours Shown
125 mg/L (ACL)
12.5 mg/L
1.25 mg/L

N

0 1000 2000

Scale in Feet

HSI GEOTRANS

REVISED	DATE	BY	DESCRIPTION
1	6/99	RAK	Updated STM
2	3/00	JDC	Updated STM
3	8/00	GWC	Updated Source Conc.

CHECKED BY: GWC DATE: April 1998
APPROVED BY: PFA DATE: April 1998
APPROVED BY: DATE:

Simulations T14C1 - T14C6

Nicolet Minerals
a Rio Algom company

Figure 3-59
Sulfate Concentration After 125 Years, PWCT

Scale: 1 in. = 1000 ft. Date: April 1998
Prepared By: HSI GEOTRANS By: RMD

P:\Crandon\Tma\Mod4\Surfer\P14so125a.srf

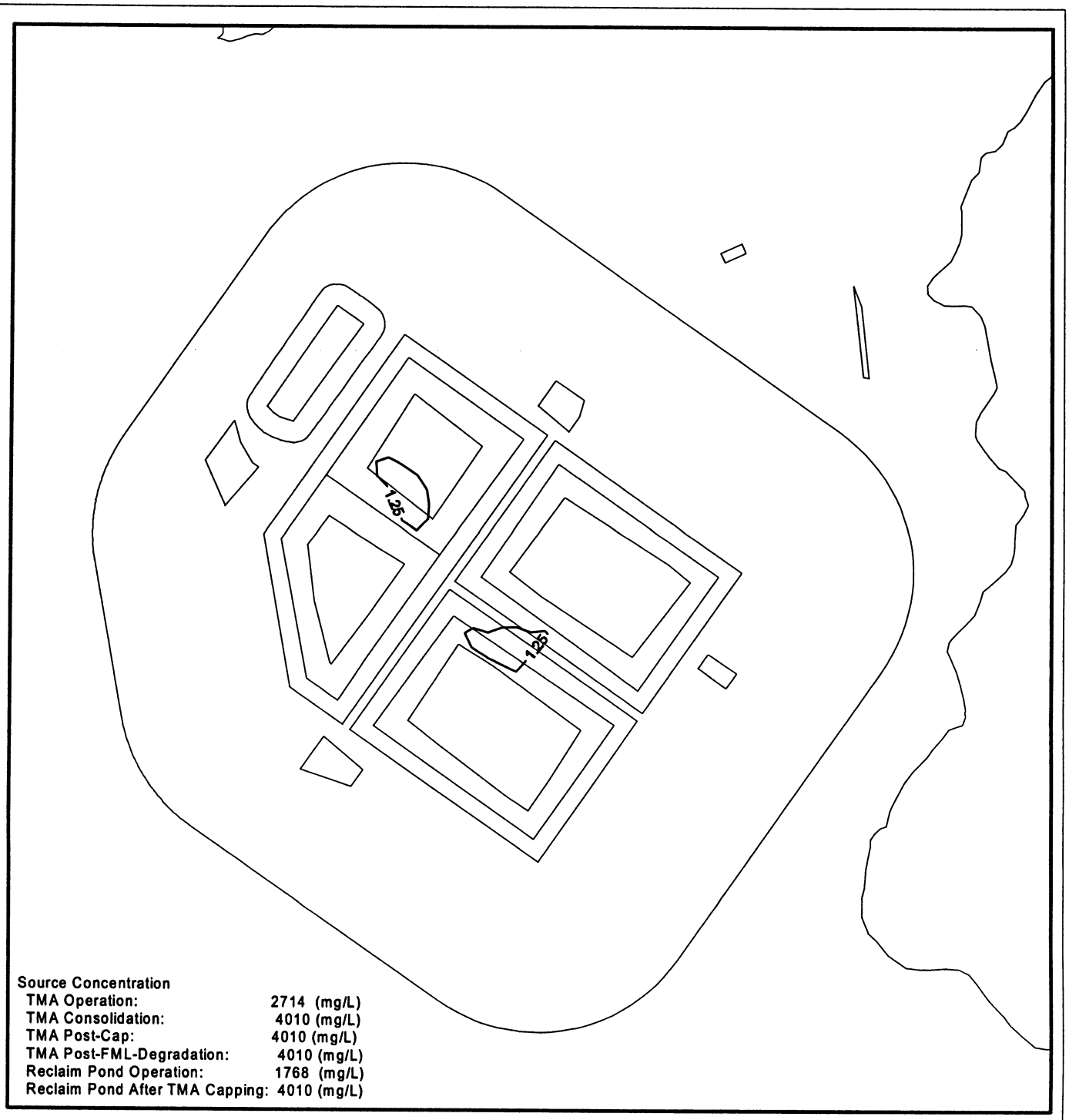

Source Concentration

TMA Operation:	2714 (mg/L)
TMA Consolidation:	4010 (mg/L)
TMA Post-Cap:	4010 (mg/L)
TMA Post-FML-Degradation:	4010 (mg/L)
Reclaim Pond Operation:	1768 (mg/L)
Reclaim Pond After TMA Capping:	4010 (mg/L)

Concentration Contours Shown
125 mg/L (ACL)
12.5 mg/L
1.25 mg/L

0 1000 2000

Scale in Feet

HSI GEOTRANS

REVISED	DATE	BY	DESCRIPTION
1	6/99	RAK	Updated STM
2	3/00	JDC	Updated STM
3	8/00	GWC	Updated Source Conc.

CHECKED BY: GWC		DATE: April 1998
APPROVED BY: PFA		DATE: April 1998
APPROVED BY:		DATE:

Simulations T14C1 - T14C6

Nicolet Minerals
a Rio Algom company

Figure 3-60
Sulfate Concentration After 300 Years, PWCT

Scale: 1 in. = 1000 ft.	Date: April 1998
Prepared By: HSI GEOTRANS	By: RMD

P:\Crandon\Tmas\Mod4\Surfer\P14so300a.srf

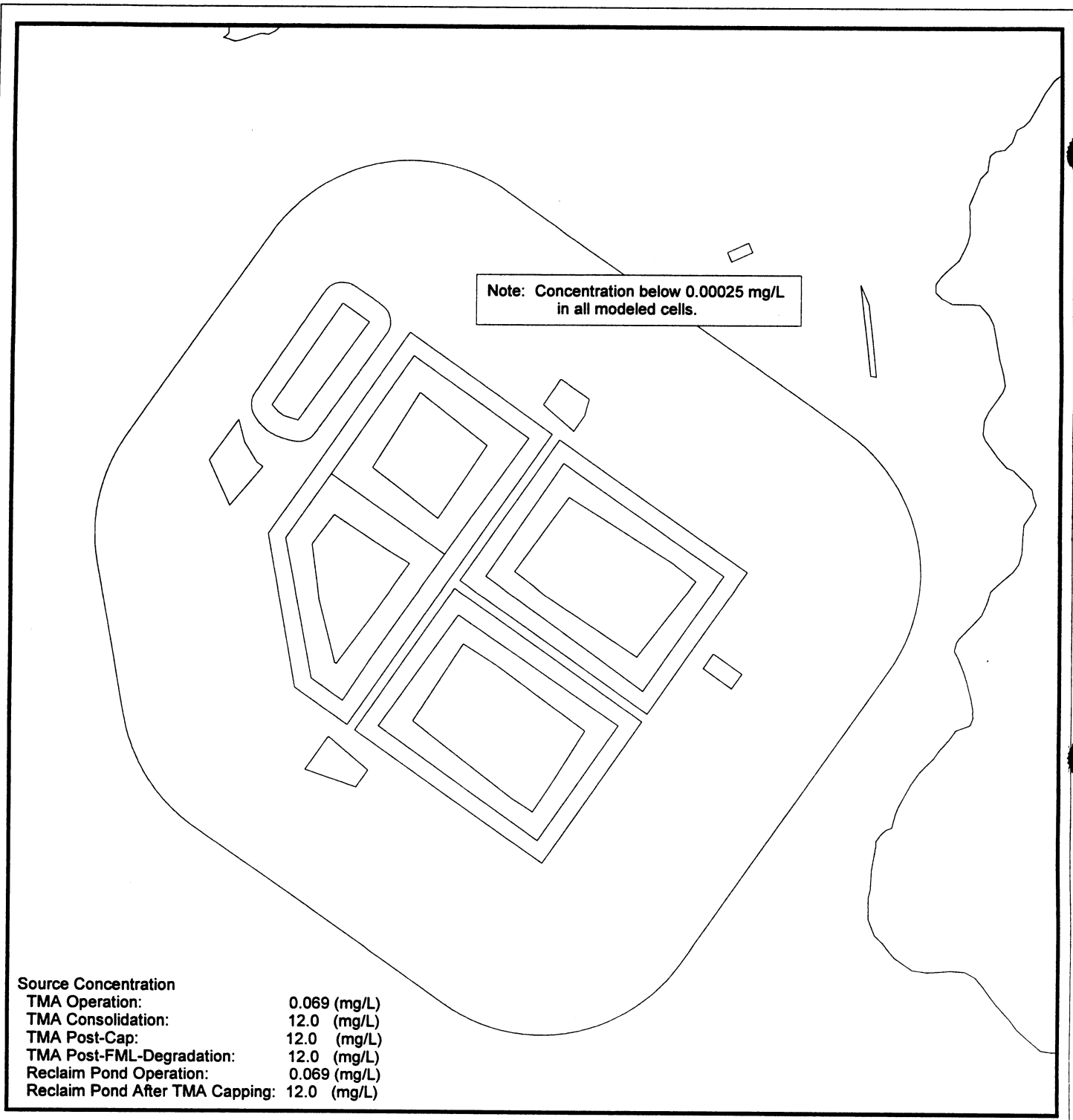

Source Concentration

TMA Operation:	0.069 (mg/L)
TMA Consolidation:	12.0 (mg/L)
TMA Post-Cap:	12.0 (mg/L)
TMA Post-FML-Degradation:	12.0 (mg/L)
Reclaim Pond Operation:	0.069 (mg/L)
Reclaim Pond After TMA Capping:	12.0 (mg/L)

Concentration Contours Shown
0.025 mg/L (ACL)
0.0025 mg/L
0.00025 mg/L

0 1000 2000
Scale in Feet

HSI GEOTRANS

REVISED	DATE	BY	DESCRIPTION
1	6/99	RAK	Updated STM
2	3/00	JDC	Updated STM

CHECKED BY: GWC	DATE: April 1998	
APPROVED BY: PFA	DATE: April 1998	
APPROVED BY:	DATE:	

Simulations T14C1 - T14C6

Nicolet Minerals
a Rio Algom company

Figure 3-61
Arsenic Concentration After 2 Years, PWCT
(Example Constituent, Plan View)

Scale: 1 in. = 1000 ft. | Date: April 1998
Prepared By: HSI GEOTRANS | By: RMD

P:\Crandon\Tma\Mod4\Surfer\P14as002.srf

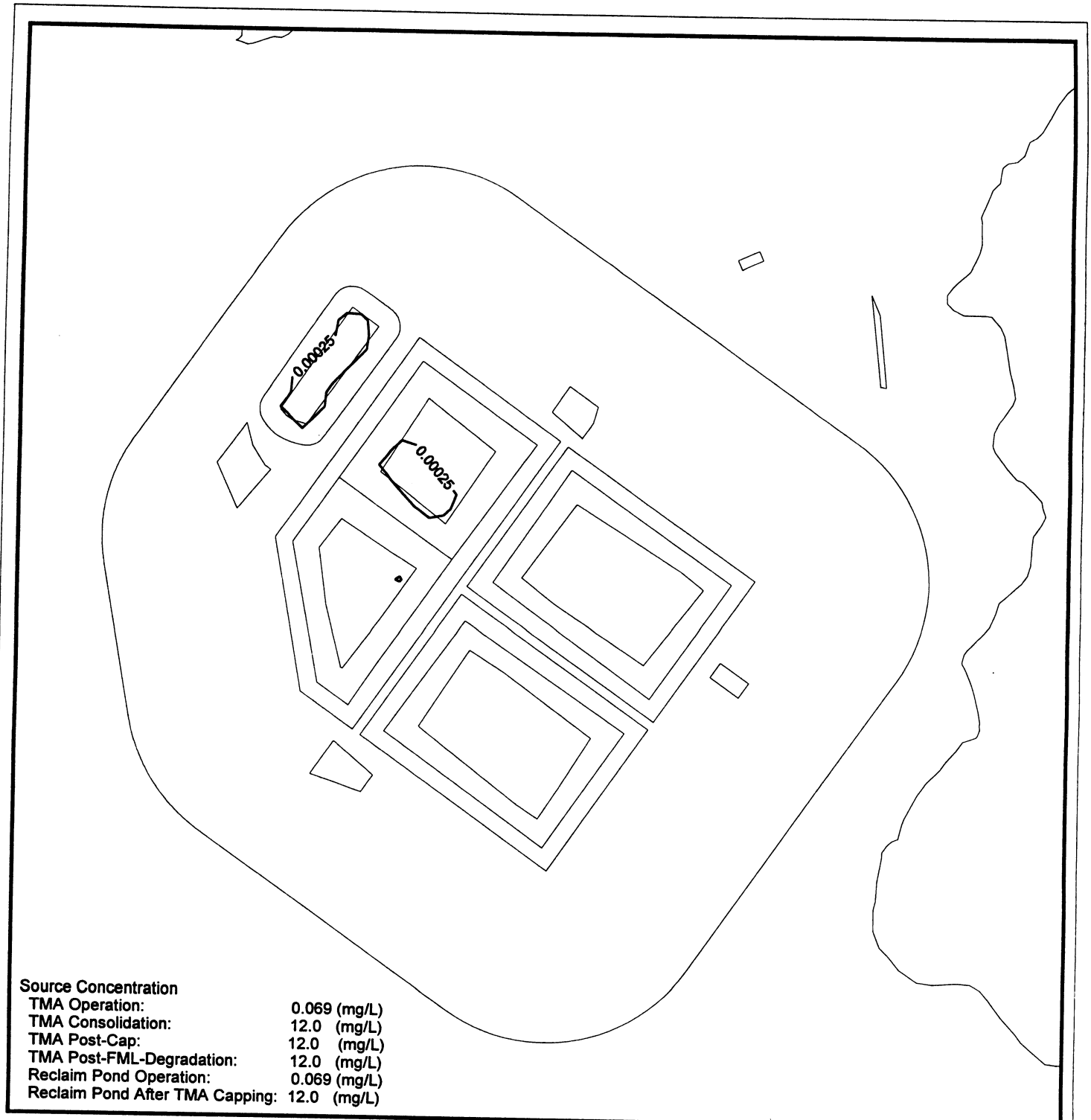

Source Concentration

TMA Operation:	0.069 (mg/L)
TMA Consolidation:	12.0 (mg/L)
TMA Post-Cap:	12.0 (mg/L)
TMA Post-FML-Degradation:	12.0 (mg/L)
Reclaim Pond Operation:	0.069 (mg/L)
Reclaim Pond After TMA Capping:	12.0 (mg/L)

Concentration Contours Shown
0.025 mg/L (ACL)
0.0025 mg/L
0.00025 mg/L

N

0 1000 2000

Scale in Feet

HSI GEOTRANS

REVISED	DATE	BY	DESCRIPTION
1	6/99	RAK	Updated STM
2	3/00	JDC	Updated STM

CHECKED BY: GWC DATE: April 1998

APPROVED BY: PFA DATE: April 1998

APPROVED BY: DATE:

Simulations T14C1 - T14C6

Nicolet Minerals
a Rio Algom company

Figure 3-62
Arsenic Concentration After 16 Years, PWCT
(Example Constituent, Plan View)

Scale: 1 in. = 1000 ft. Date: April 1998

Prepared By: HSI GEOTRANS By: RMD

P:\Crandon\TimeMod\ASU...ss016.srf

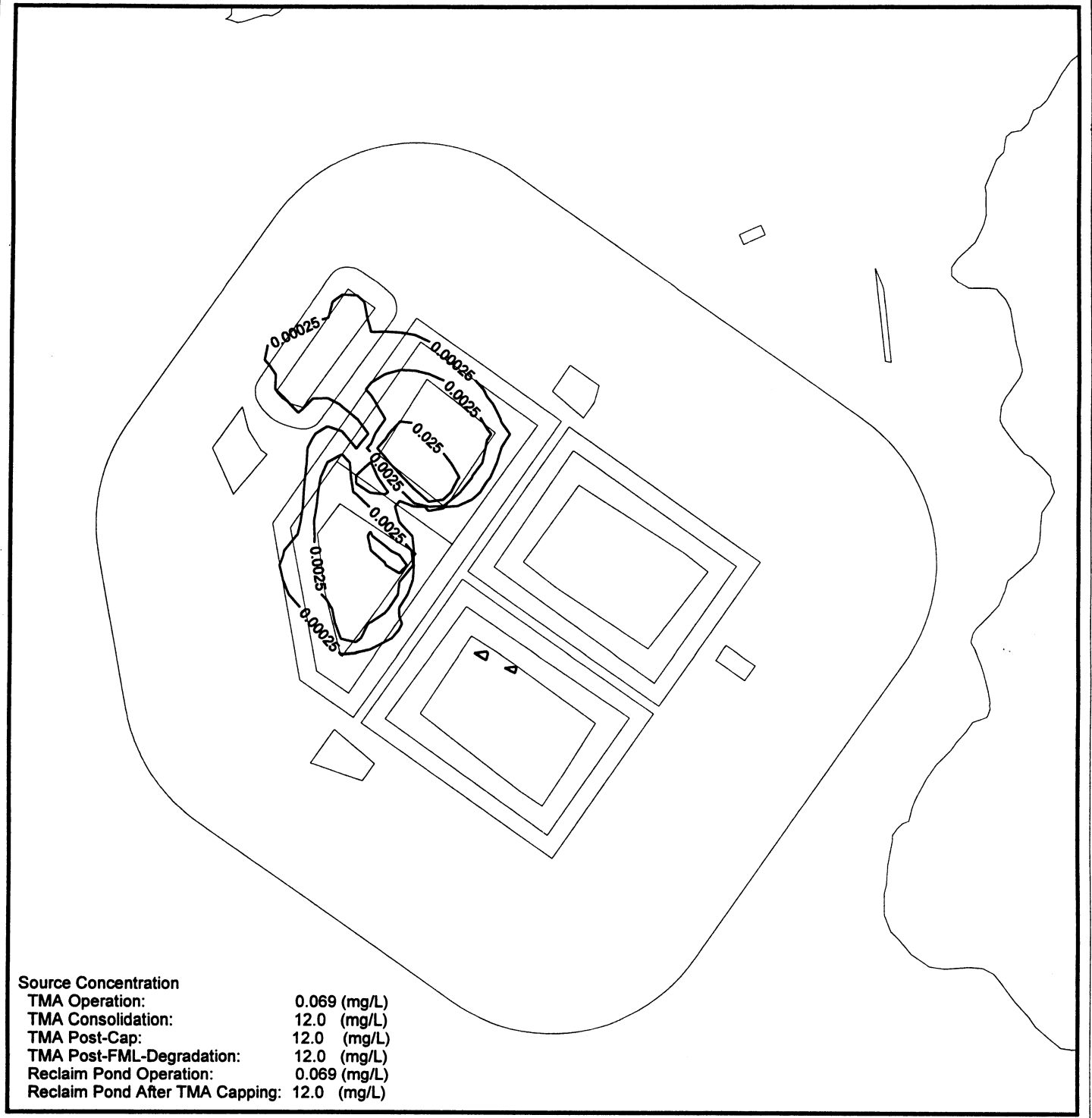

Source Concentration

TMA Operation:	0.069 (mg/L)
TMA Consolidation:	12.0 (mg/L)
TMA Post-Cap:	12.0 (mg/L)
TMA Post-FML-Degradation:	12.0 (mg/L)
Reclaim Pond Operation:	0.069 (mg/L)
Reclaim Pond After TMA Capping:	12.0 (mg/L)

Concentration Contours Shown
- 0.025 mg/L (ACL)
- 0.0025 mg/L
- 0.00025 mg/L

N

0 1000 2000

Scale in Feet

HSI GEOTRANS			
REVISED	DATE	BY	DESCRIPTION
1	6/99	RAK	Updated STM
2	3/00	JDC	Updated STM
CHECKED BY: GWC			DATE: April 1998
APPROVED BY: PFA			DATE: April 1998
APPROVED BY:			DATE:

Simulations T14C1 - T14C6

Nicolet Minerals
a Rio Algom company

Figure 3-63
Arsenic Concentration After 22 Years, PWCT
(Example Constituent, Plan View)

Scale: 1 in. = 1000 ft. | Date: April 1998

Prepared By: HSI GEOTRANS | By: RMD

P:\Crandon\Tmwfmod4\Surfer\P14es022.srf

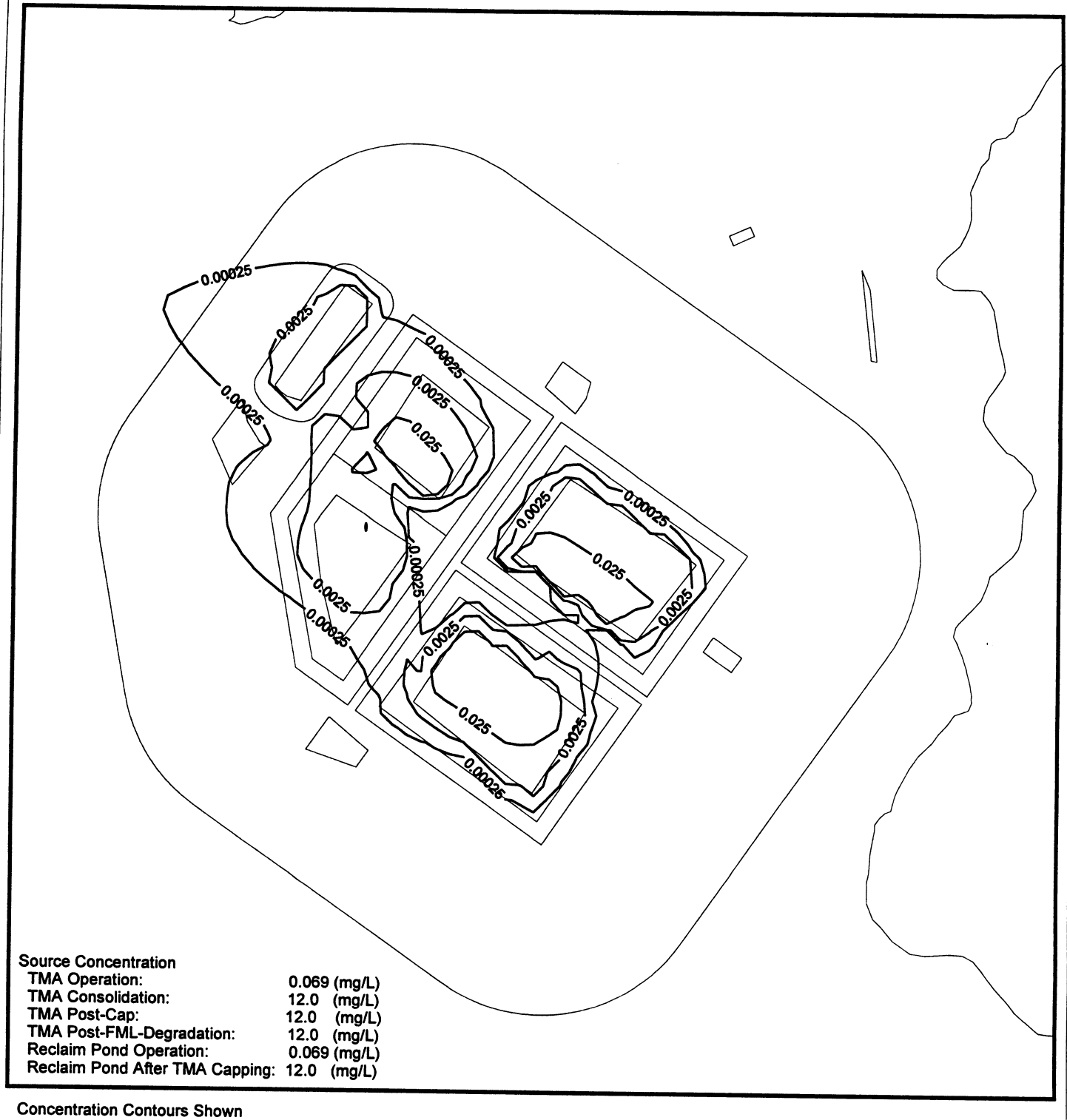

Source Concentration

TMA Operation:	0.069 (mg/L)
TMA Consolidation:	12.0 (mg/L)
TMA Post-Cap:	12.0 (mg/L)
TMA Post-FML-Degradation:	12.0 (mg/L)
Reclaim Pond Operation:	0.069 (mg/L)
Reclaim Pond After TMA Capping:	12.0 (mg/L)

Concentration Contours Shown
0.025 mg/L (ACL)
0.0025 mg/L
0.00025 mg/L

N

0 1000 2000

Scale in Feet

HSI GEOTRANS

REVISED	DATE	BY	DESCRIPTION
1	6/99	RAK	Updated STM
2	3/00	JDC	Updated STM

CHECKED BY: GWC DATE: April 1998

Simulations T14C1 - T14C6

APPROVED BY: PFA DATE: April 1998

APPROVED BY: DATE:

Nicolet Minerals
a Rio Algom company

Figure 3-64
Arsenic Concentration After 32 Years, PWCT
(Example Constituent, Plan View)

Scale: 1 in. = 1000 ft. Date: April 1998

Prepared By: HSI GEOTRANS By: RMD

P:\Crandon\Tmat\Mod4\Su...st032.srf

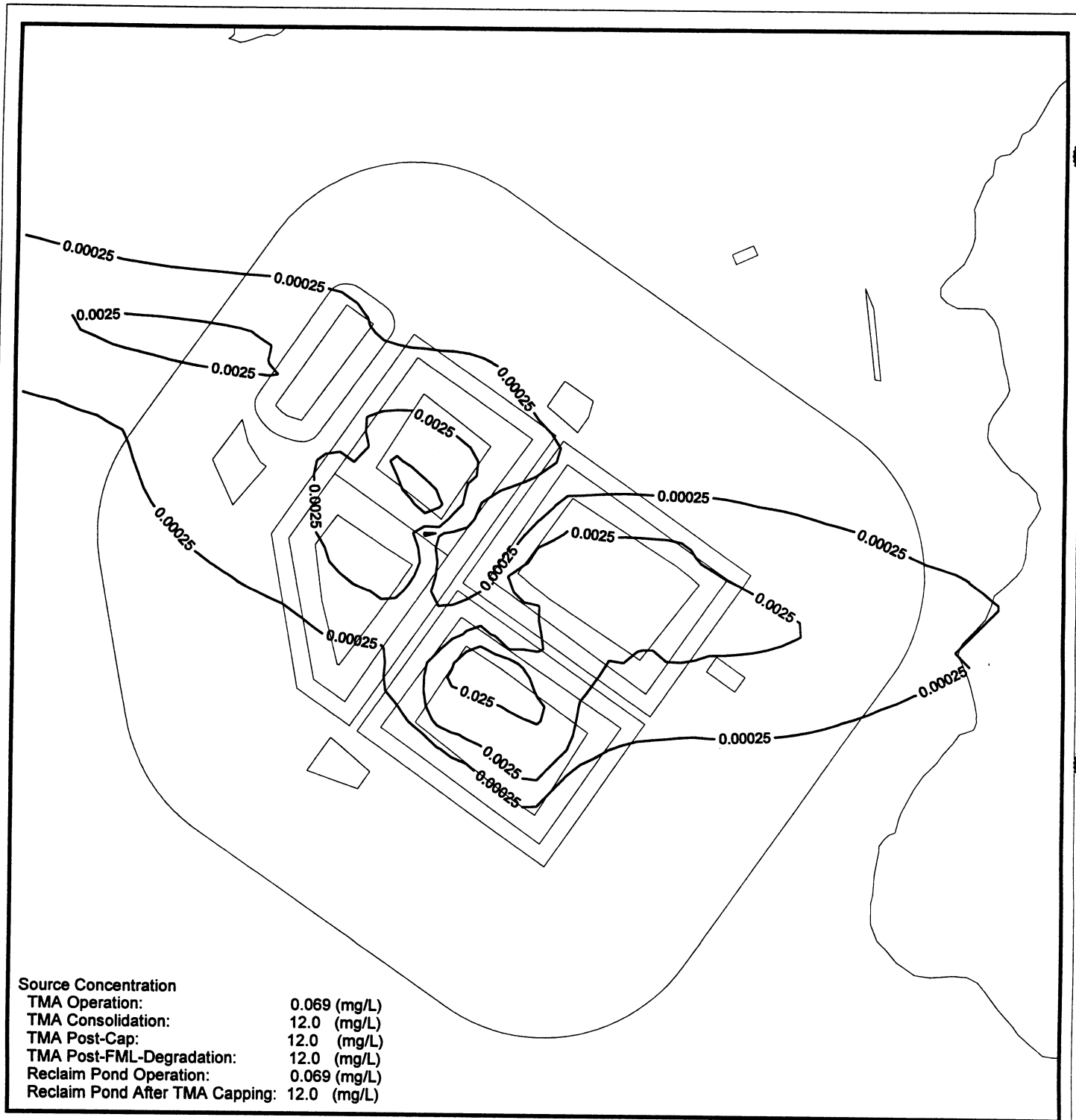

Source Concentration

TMA Operation:	0.069 (mg/L)
TMA Consolidation:	12.0 (mg/L)
TMA Post-Cap:	12.0 (mg/L)
TMA Post-FML-Degradation:	12.0 (mg/L)
Reclaim Pond Operation:	0.069 (mg/L)
Reclaim Pond After TMA Capping:	12.0 (mg/L)

Concentration Contours Shown
0.025 mg/L (ACL)
0.0025 mg/L
0.00025 mg/L

N

0 1000 2000

Scale in Feet

HSI GEOTRANS

REVISED	DATE	BY	DESCRIPTION
1	6/99	RAK	Updated STM
2	3/00	JDC	Updated STM

CHECKED BY: GWC		DATE: April 1998
APPROVED BY: PFA		DATE: April 1998
APPROVED BY:		DATE:

Simulations T14C1 - T14C6

Nicolet Minerals
a Rio Algom company

Figure 3-65
Arsenic Concentration After 60 Years, PWCT
(Example Constituent, Plan View)

Scale: 1 in. = 1000 ft.	Date: April 1998
Prepared By: HSI GEOTRANS	By: RMD

P:\Crandon\Tmal\Mod4\Surfer\P14se030.srf

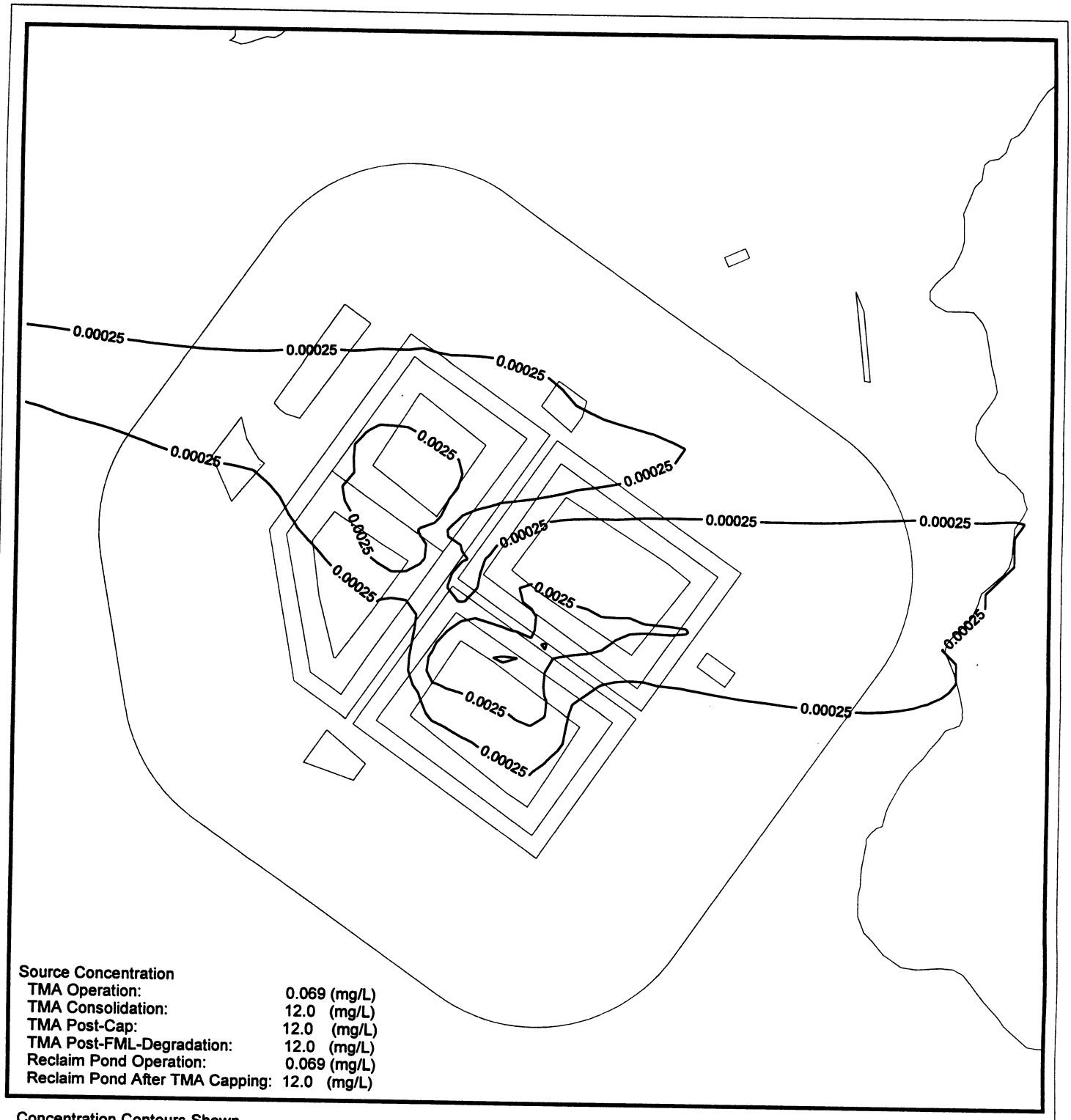

Source Concentration

TMA Operation:	0.069 (mg/L)
TMA Consolidation:	12.0 (mg/L)
TMA Post-Cap:	12.0 (mg/L)
TMA Post-FML-Degradation:	12.0 (mg/L)
Reclaim Pond Operation:	0.069 (mg/L)
Reclaim Pond After TMA Capping:	12.0 (mg/L)

Concentration Contours Shown
0.025 mg/L (ACL)
0.0025 mg/L
0.00025 mg/L

N

0 1000 2000

Scale in Feet

HSI GEOTRANS

REVISED	DATE	BY	DESCRIPTION
1	6/99	RAK	Updated STM
2	3/00	JDC	Updated STM

CHECKED BY: GWC DATE: April 1998

Simulations T14C1 - T14C6

APPROVED BY: PFA DATE: April 1998

APPROVED BY: DATE:

Nicolet Minerals
a Rio Algom company

Figure 3-66
Arsenic Concentration After 125 Years, PWCT
(Example Constituent, Plan View)

Scale: 1 in. = 1000 ft. Date: April 1998

Prepared By: HSI GEOTRANS By: RMD

P:\Crandon\Tma\Mod4\S...as125.srf

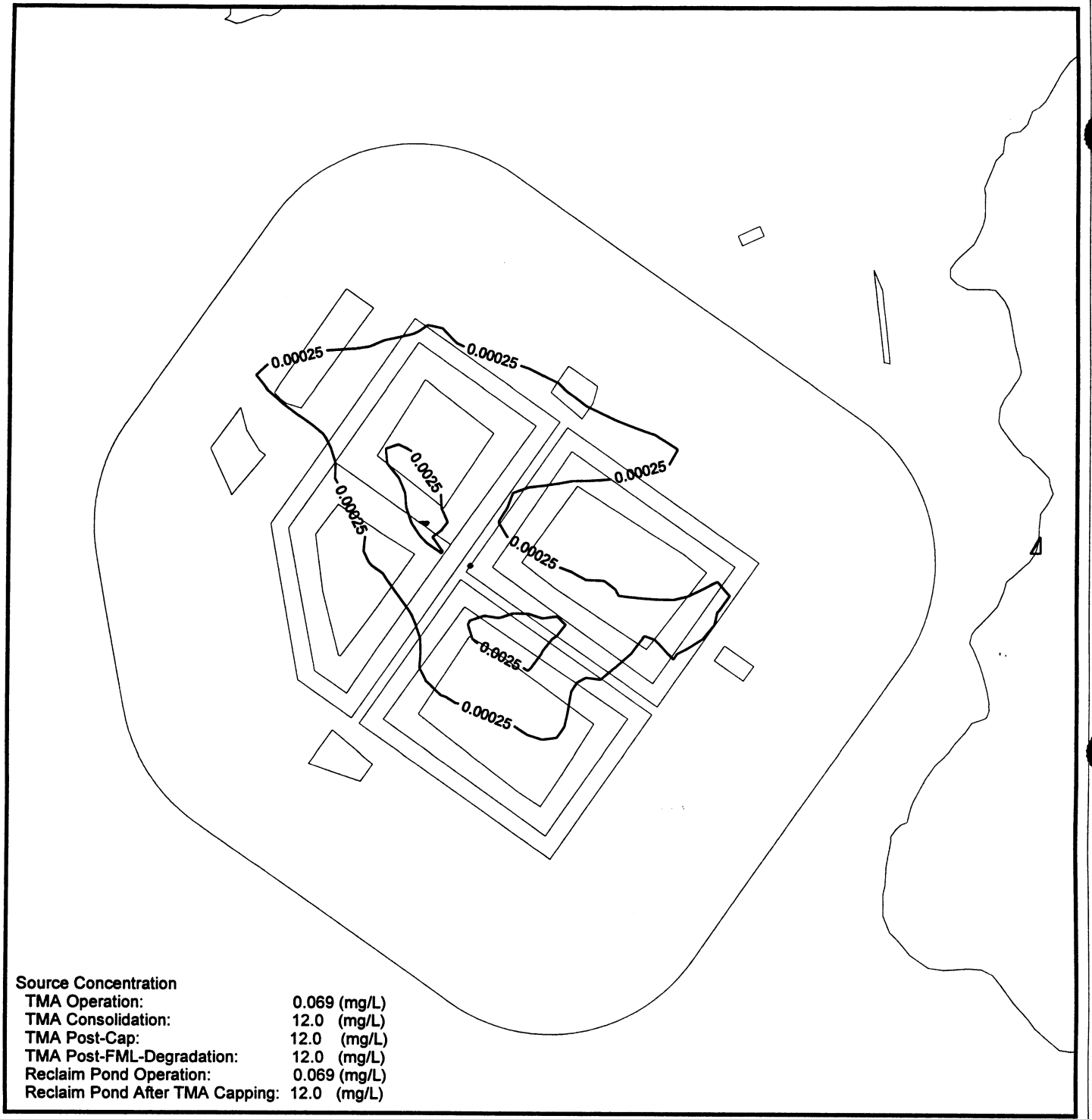

Source Concentration

TMA Operation:	0.069 (mg/L)
TMA Consolidation:	12.0 (mg/L)
TMA Post-Cap:	12.0 (mg/L)
TMA Post-FML-Degradation:	12.0 (mg/L)
Reclaim Pond Operation:	0.069 (mg/L)
Reclaim Pond After TMA Capping:	12.0 (mg/L)

Concentration Contours Shown
0.025 mg/L (ACL)
0.0025 mg/L
0.00025 mg/L

N

0 1000 2000

Scale in Feet

HSI GEOTRANS

REVISED	DATE	BY	DESCRIPTION
1	6/99	RAK	Updated STM
2	3/00	JDC	Updated STM

CHECKED BY: GWC		DATE: April 1998
APPROVED BY: PFA		DATE: April 1998
APPROVED BY:		DATE:

Simulations T14C1 - T14C6

Nicolet Minerals
a Rio Algom company

Figure 3-67
Arsenic Concentration After 300 Years, PWCT
(Example Constituent, Plan View)

Scale: 1 in. = 1000 ft. | Date: April 1998

Prepared By: HSI GEOTRANS | By: RMD

P:\Crandon\Tmwmod4\Surfer\P14as300.srf

Appendix A1

Geochemical Characterization of Depyritized Tailings, Pyrite Concentrate and Pyritic Paste Backfill

Note: The referenced document can be found in Appendix 4.2-15 of the Crandon Project's *Environmental Impact Report*.

Appendix A2

Waste Rock and Wastewater Treatment Solids in the Crandon TMA

Note: The referenced document can be found in Appendix 4.2-15a of the Crandon Project's *Environmental Impact Report.*

Appendix A3

Corroborative Testing of the Depyritized Tailings, Pyrite Concentrate and Pyritic Paste Backfill

Results to November 1999

Note: The referenced document can be found in Appendix 4.2-16 of the Crandon Project's *Environmental Impact Report*.

Appendix A4

Electron Microprobe Analysis of Carbonates in the Depyritized Tailings and Pyrite Concentrate

Note: The referenced document can be found in Appendix 4.2-16a of the Crandon Project's *Environmental Impact Report*.

Appendix A5

Representativeness of Ore and Tailings Samples from the Crandon Deposit

Note: The referenced document can be found in Appendix 4.2-16b of the Crandon Project's *Environmental Impact Report*.

Appendix A6

NP Addition Control and Monitoring Program

Note: The referenced document can be found in Appendix 4.2-16c of the Crandon Project's *Environmental Impact Report.*

Appendix B

Geochemical Modeling

APPENDIX B

GEOCHEMICAL MODELING

Prepared for:

FOTH AND VAN DYKE
2737 South Ridge Road
Green Bay, WI, 54307-9012

Prepared by:

STEFFEN ROBERTSON AND KIRSTEN (CANADA) INC.
Suite 800, 580 Hornby Street
Vancouver, B.C. V6C 3B6
Tel: (604) 681-4196 • Fax: (604) 687-5532
E-mail: vancouver@srk.com Web site: www.srk.com

Originally Issued MAY, 1999
Updated MARCH, 2000
Revised AUGUST 2000

APPENDIX B

GEOCHEMICAL MODELING

TABLE OF CONTENTS

LIST OF TABLES

LIST OF ATTACHMENTS

APPENDIX B

TMA SOURCE CONCENTRATIONS
GEOCHEMICAL MODELING

1. INTRODUCTION

This appendix describes the geochemical equilibrium modeling carried out to support TMA water quality predictions. Results of the geochemcial equilibrium modeling are referred to in Section 2 of the GWQPE. Appendix D provides further information on other calculations used in the water quality predictions.

The objective of the geochemical equilibrium modeling was to determine solubility controls on solute concentrations in the pore water of the depyritized tailings. The modeling simulated conditions in:

- Process water that equilibrates with the tailings in the absence of oxidation; and,

- The oxidation zone that will be generated near the surface of the tailings during the consolidation period

Sections 2 and 3 below discuss the geochemical modeling undertaken for each of the above conditions. The geochemical modeling was undertaken with MINTEQA2 (Allison et al., 1991) updated with the thermodynamic database from WATEQ4F (Ball and Nordstrom, 1991). Where appropriate, the sensitivity of the MINTEQA2 results to assumed redox potentials, carbon dioxide levels, and the presence or absence of calcite, dolomite, smithsonite, antimony hydroxide and siderite were considered. Best Engineering Judgement (BEJ) and Upper Bound (UB) estimates were then selected from the base case and sensitivity runs.

2. PROCESS WATER DOMINATED ZONE

2.1 Process Water Discharged to TMA

The process water discharged to the TMA during operations will comprise flows from various milling processes. Table 1 presents the process streams and flow rates that will contribute to flows into the TMA. As shown, the highest proportion of the total discharge will originate from the zinc tailings thickener.

TABLE 1
Summary of Process Streams Discharging to TMA

Stream	Stream ID	Flow (gpm)	Flow (%)
Zinc Tails Thickener Overflow	ZTTO	1328	56.1
Depyritized Tailings Process Water	DTPW	475	20.1
Pyrite Backfill PPSM[1] Overflow	PBPO	197	8.3
Zinc Concentrate Thickener Overflow	ZCTO	240	10.1
Lead Hydroseparator Overflow	LHSO	55	2.3
Lead Concentrate Thickener Overflow	LCTO	30	1.3
Copper Concentrate Thickener Overflow	CCTO	42	1.8

Notes: 1. PPSM denotes Paste Production Storage Mechanism

Prepared by: JTC
Checked by: DBA

Solute concentrations in the different flows entering the TMA were estimated as follows:

- Solute concentrations in the zinc tailings thickener overflow (ZTTO) were assumed to be the same as in the zinc tailings process water that was investigated in the 1994 locked cycle testing program completed by Lakefield (Appendix 3.5-32 of the EIR, FVD 1995/1998).

- Solute concentrations in the depyritized tailings process water (DTPW) were as measured by Lakefield during locked cycle testing (Appendix A1).

- Solute concentrations in the pyritic paste backfill PPSM overflow (PBPO) were obtained by conservatively selecting the higher solute concentrations from the process water quality measured for Pyrite Concentrate 1 and 2 (Appendix A1).

- Zinc concentrate thickener overflow (ZCTO) was assumed to be similar to the zinc tailings process water (ZTTO) on the basis of the high pH.

- The pH values of the remainder of the process water flows ranged from 7.2 to 8.5; therefore the depyritized tailings pore water (Appendix A1) was assumed to be representative of these flows. The contribution of these overflow streams is very small by comparison to total tailings flow. Therefore, the calculation of the composite water is less sensitive to the assumed solute concentrations for these flow components.

The estimated solute concentrations are presented in the final column of Table 2. It should be noted that sulfate concentrations in the mixed process water are below saturation with respect to gypsum. However, addition of reagents during milling is expected to lead to a build-up of sulfate, with maximum concentrations controlled by equilibrium with gypsum. To simulate build-up of sulfate in the mill, MINTEQA2 was used to equilibrate gypsum with the mixed process water. The resulting calcium and sulfate concentrations (TMA_PWS.out) are shown in brackets in the final column of Table 2. These concentrations are used in subsequent calculation steps.

TABLE 2
Summary of Solute Concentration Estimates and Calculated Discharge to TMA

Parameter	Units	STREAM ID (See Table 1 for Descriptions)							Process Water Discharge To TMA
		ZTTO	DTPW	PBPO	ZCTO	LHSO	LCTO	CCTO	
Operating flow	**gpm**	1328	475	197	240	55	30	42	2367
Operating pH	**s.u.**	11.2	6	6	11.8	8.5	8.5	7.2	11.1
Acidity as $CaCO_3$	eq.		34	60		< 0.0002			12
Aluminum	mg/L	1.4	< 0.018	0.043	1.4	< 0.022			0.94
Antimony	mg/L	0.1	0.017	0.014	0.1	0.0061			0.071
Arsenic	mg/L	0.1	0.0048	0.022	0.1	0.0025			0.069
Barium	mg/L	0.0196	0.063	0.091	0.0196	0.028			0.035
Beryllium	mg/L	0.0006	< 0.00012	< 0.00012	0.0006	< 0.00033			0.0004
Boron	mg/L		0.021	0.021		0.022			0.021
Cadmium	mg/L	0.0002	0.018	0.027	0.0002	0.0018			0.0061
Calcium	mg/L	299	210	270	299	300			279 (624)**
Chloride	mg/L		36	36		33			36
Chromium	mg/L	0.056	0.0022	0.0042	0.056	< 0.00053			0.038
Cobalt	mg/L	0.041	0.037	0.038	0.041	0.030			0.039
Copper	mg/L	0.063	0.0081	0.039	0.063	0.0017			0.047
Cyanide, total	mg/L		< 0.0034	< 0.0034		< 0.0034			< 0.0034
Cyanide, WAD	mg/L		< 0.0029	< 0.0029		< 0.0029			< 0.0029
Fluoride	mg/L		0.28	0.22		1			0.38
Iron	mg/L	0.41	0.049	0.6	0.41	< 0.0023			0.33
Lead	mg/L	0.27	0.017	0.091	0.27	0.0044			0.19
Magnesium	mg/L	0.15	12	14	0.15	27			5.1
Manganese	mg/L	0.0046	2	2.5	0.0046	1.2			0.68
Mercury	mg/L	0.0002	0.00018	< 0.00008	0.0002	< 0.00008			0.0002
Nickel	mg/L	0.006	0.12	0.2	0.006	0.016			0.045
Potassium	mg/L	10.3	24	21	10.3	27			14.8
Selenium	mg/L	0.29	0.032	0.041	0.29	0.024			0.20
Silver	mg/L	0.1	< 0.0003	0.00067	0.1	0.00028			0.066
Sodium	mg/L	30	20	20	30	26			27
Sulfate	mg/L	868*	490	620	868*	901			773 (1599)**
Zinc	mg/L	0.455	19	33	0.455	1.3			6.9

Note: eq = mg$CaCO_3$ eq/L

Prepared by: JTC
Checked by: KSS

* Sulfate data was not available for this tests, and was therefore calculated based on the ion balance.

** Numbers in brackets are from the MINTEQA2 run TMA_PWS.out

2.2 Cyanide in the Process Water

Based on an average NaCN addition of 69 grams per metric ton of ore in the milling circuit, and an average water flow rate of 2,367 gpm, an average concentration of 14 mg/L total cyanide could result in the process water within the mill.

Sodium cyanide is widely used in the selective flotation of lead-copper-zinc ores as a depressant for pyrite and to a lesser extent, sphalerite. Cyanide depresses pyrite flotation by reacting with the pyrite surface and inhibiting the binding of floatation reagents.

The pyrite surfaces are re-activated for the pyritic flotation (depyritization) process by decreasing the pH from above 10 s.u. (where cyanide species are stable) to a pH of about 6 s.u. At this pH cyanide is readily volatilized.

$$H^+ + CN^- \leftrightarrow HCN\,(g)$$

Volatilization of HCN (g) reduces free cyanide concentrations in the porewater to very low levels. Actual measured cyanide concentrations were <0.0034 mg/L in the depyritized tailings samples, and about 0.011 mg/L in the pyrite concentrate samples (see Attachment D of Appendix A1).

Any residual cyanide that may enter the TMA will degrade rapidly as a result of oxidation and volatilization (Smith and Mudder, 1991). Data provided in USEPA (1992) indicates that a total cyanide dosage in the range of 14 mg/L results in a total cyanide concentration of less than 0.3 mg/L in process water. It is therefore conservative to assume that the average total cyanide concentration in the process water discharged to the TMA will be less than 0.3 mg/L.

2.3 Geochemical Modeling of Equilibrated Process Water

The Process Water Discharge to TMA column in Table 2 shows the weighted average solute concentrations calculated from the input flows. These solute concentrations were input to MINTEQA2 to simulate the reactions that will occur as the process water equilibrates with tailings solids. The MINTEQA2 input and output files are provided in Attachment A, and summarized in Table 3.

TABLE 3
MINTEQA2 Simulations of the Process Water Dominated Zone of the TMA

Parameter	Units	TMA_PW1.out (Initial Step)	TMA_PW4.out (Dolomite)	TMA_PW5.out (Calcite)	TMA_PW6.out (Dolomite)*
Aluminum	mg/L	0.94	0.0073	0.0052	0.0050
Antimony	mg/L	0.071	0.012	0.012	0.012
Arsenic	mg/L	0.069	0.069	0.069	0.069
Barium	mg/L	0.035	0.0034	0.0041	0.0033
Beryllium	mg/L	na	na	na	na
Cadmium	mg/L	0.0061	0.0061	0.0061	0.0061
Calcium	mg/L	632	551	626	549
Chromium	mg/L	na	na	na	na
Cobalt	mg/L	na	na	na	na
Copper (Cu^{+}/ Cu^{2+})	mg/L	0.019/0.028	0.043/0.0046	0.042/0.0052	0.022/0.0249
Cyanide	mg/L	0.0011	na	na	na
Fluoride	mg/L	0.38	0.38	0.38	na
Iron (Fe^{2+}/Fe^{3+})	mg/L	0.31/0.017	0.29/0.00035	0.29/0.00034	2.8/0.019
Lead	mg/L	0.19	0.19	0.19	0.19
Magnesium	mg/L	8.9	327	5	326
Manganese (Mn^{2+}/Mn^{3+})	mg/L	0.68/9.8e-28	0.68/na	0.68/na	0.68/na
Mercury	mg/L	na	na	na	na
Nickel	mg/L	0.045	0.045	0.045	0.045
Potassium	mg/L	15	15	15	15
Selenium	mg/L	na	na	na	na
Silver	mg/L	na	na	na	na
Sodium	mg/L	27	27	27	27
Sulfate	mg/L	1602	2679	1590	2714
Zinc	mg/L	6.9	6.9	6.9	40
Ionic Difference	%	1.8	1.2	1.8	0.24
Ionic Strength	Molar	0.05	0.07	0.05	0.07
Equilibrium pH	s.u.	8.8	8.4	8.3	8.25
Equilibrium Eh	mV	-52	-71	-54	0.2
Saturation Indices					
Gibbsite (C)		1.73	0*	0*	0*
Ferrihydrite		1.62	0*	0*	1.75
$Pb(OH)_2$ (C)		1.04	0.79	0.66	0.49
Barite		0.94	0*	0*	0*
$Sb(OH)_3$ (s)		0.76	0*	0*	0*
CuCN		0.64	na	na	na
Calcite		0.81	0*	0*	0*
$Zn(OH)_2$ (A)		0.18	-0.33	-0.47	0.14
Dolomite		0*	0*	-1.86	0*
Cerrusite		-0.14	-0.27	-0.27	-0.23
$Ni(OH)_2$		-0.12	-0.36	-0.51	-0.70
Rhodochrosite		-0.39	-1.09	-1.15	-1.09
Smithsonite		-0.41	-0.81	-0.83	0*
Gypsum		-0.003	0*	0*	0*
Siderite (D)		-0.75	-1.50	-1.56	-0.51
Siderite (C)		-0.24	-0.99	-1.05	0*
Otavite		-1.07	-1.84	-1.87	-1.83
Anglesite		-2.51	-1.83	-1.83	-1.80

Notes: * Allowed to precipitate or dissolve
** Includes smithsonite and siderite dissolution
na = not applicable (parameter not included in the model run)

Prepared by: JTC
Checked by: KSS

The initial MINTEQA2 run (TMA_PW1r) simulated equilibrium with dolomite, and was used to identify minerals that were likely to be at saturation. The results indicated that there would be a very slight increase in calcium and magnesium concentrations resulting from equilibration with the dolomite, and that gypsum, gibbsite, ferrihydrite, $Pb(OH)_2$, barite, $Sb(OH)_3$, CuCN, calcite, and $Zn(OH)_2$ were at saturation. The initial run (TMA PW1r) was also used to refine the inputs of subsequent runs, and allow for more rapid conversion of the model. The following adjustments were made as a result:

- Mn was entered as Mn^{2+}, and the Mn redox couple was dropped from the subsequent runs because manganese was found to be predominantly Mn^{2+} (with Mn^{3+} about 10^{-27} mole/L).

- Cyanide was not considered in subsequent runs because it was present at a very low initial concentration (0.003 mg/L), and was supersaturated with respect to CuCN.

Arsenic speciation was not considered in any of the runs due to its low concentration. Since MINTEQA2 predicts no secondary mineral controls on arsenic solubility at these concentrations, its speciation is of little consequence to the current modeling.

In the second and third runs (TMA_PW4r and TMA_PW5r), gibbsite, ferrihydrite, calcite, barite, and $Sb(OH)_3$, were allowed to form if they reached saturation.In TMA_PW4r, the porewater was equilibrated with dolomite and gypsum, and in TMA_PW5r, the porewater was equilibrated with calcite and gypsum.

The results of the two runs (TMA_PW4r and TMA_PW5r) are similar, indicating there would be little difference in equilibrium concentrations of the trace metals in contact with the different carbonate minerals. However, the dolomite equilibrated pore water had a substantially higher sulfate and magnesium concentration than that predicted for calcite. Therefore, the dolomite equilibrated pore water was used in subsequent predictions of water quality.

Electron microprobe analyses of the carbonate grains (Appendix A4) indicate that the carbonate minerals present in the depyritized tailings occur predominantly as ferroan dolomites. Some magnesian siderite and trace amounts of ferroan magnesite are also present. Zinc was detected as a trace component (average of 0.01 wt.%, and maximum of 0.08 wt.%) in some of the carbonate grains. To evaluate the potential for

dissolution of iron and zinc from these phases, an additional MINTEQA2 run (file: TMA_PW6) was completed. The model conditions were the same as for TMA_PW4 (equilibrium pH and Eh calculated), with the addition of siderite and smithsonite as finite solids. Ferrihydrite was not allowed to form in this run. A phase corresponding to a log K_{sp} of –10.89 was used to establish the dissolution of siderite.

The results for TMA_PW6r (Table 3) indicate dissolution of siderite and smithsonite would result in substantial increases in dissolved iron and zinc concentrations. The dissolution of siderite is reasonable given that siderite is present in the depyritized tailings. However, because ferrihydrite was not allowed to form in the modeling runs, the resulting iron concentrations are considered to be an upper bound estimate. Similarly, dissolution of smithsonite provides very conservative estimates of zinc concentrations for the following reasons:

- Zinc concentrations in the depyritized tailings process water (Appendix A1) decreased from 19 mg/L to 1.3 mg/L over a two month period, suggesting that zinc was precipitating, rather than dissolving as the tailings solids reached equilibrium with the tailings process water;
- Smithsonite was not identified as a distinct phase in the depyritized tailings samples; and,
- The zinc content of the carbonates is very low.

It is concluded that iron and zinc concentrations determined in TMA_PW6 should be used only as upper bound estimates.

2.4 Recommendations for BEJ and UB Concentration Estimates

Table 4 summarizes the best engineering judgement (BEJ) and upper bound (UB) estimates of solute concentrations in the tailings process water. The second column shows estimated solute concentrations in the process water that will be discharged to the TMA (Table 2). The third column shows the equilibrium concentrations taken from TMA_PW6r (Table 3).

Where the equilibrium modeling indicated supersaturation of a secondary mineral, the equilibrium concentration was used for the BEJ estimate. Where no solubility controlling phase was identified, or where the equilibrated value exceeded the process water concentration, the estimated process water concentration was used for the BEJ estimate. The UB estimates were based on the highest concentrations observed in

either the process water or the equilibrium concentrations. Note that this approach leads to some of the BEJ estimates being as high as the UB estimate.

TABLE 4
Estimates of Porewater Quality in Process Water Dominated Zone

	Process Water mg/L	Equilibrated Process Water* mg/L	BEJ Estimate mg/L	UB Estimate mg/L
Al	0.94	0.0050	0.0050	0.94
Sb	0.071	0.012	0.012	0.071
As	0.069		0.069	0.069
Ba	0.035	0.0033	0.0033	0.035
Be	0.00045		0.00045	0.00045
Cd	0.0061		0.0061	0.0061
Ca	624	549	549	624
Cr	0.038		0.038	0.038
Cu	0.047		0.047	0.047
F	0.38		0.38	0.38
Fe	0.33	2.9	0.33	2.9
Pb	0.19		0.19	0.19
Mg	5.1	326	5.1	326
Mn	0.68		0.68	0.68
Hg	0.00018		0.00018	0.00018
Ni	0.045		0.045	0.045
K	15		15	15
Se	0.20		0.20	0.20
Ag	0.066		0.066	0.066
Na	27		27	27
SO_4	1599	2,714	1599	2,714
Zn	6.9	40	6.9	40

Notes: * From the MINTEQA2 run: TMA_PW6.out

Prepared by: KSS
Checked by: JTC

3. OXIDATION ZONE

The oxygen transport modeling (Appendices C1 and C2) predicts that the most significant tailings oxidation will occur in the unsaturated tailings during the consolidation period. Acidity generated from oxidation will be neutralized by the available excess carbonate neutralization potential, resulting in neutral pH porewater. The following sections describe the geochemical equilibrium modeling that was undertaken to establish solute concentrations in the oxidation zone.

3.1 Procedure

The geochemical equilibrium modeling of the oxidation zone included five steps:

- Obtain initial concentration estimates from the rates of oxidation predicted by the oxygen transport modeling and the relative solute release rates measured in humidity cell tests.

- Obtain initial estimates major solute concentrations (Fe, CO_3, Ca, Mg) by their stoichiometric relationship to sulfate release and by preliminary MINETQA2 modeling of major phases (dolomite, gypsum, ferrihyrite).

- Define the secondary minerals that will be allowed to precipitate in subsequent runs.

- Apply equilibrium conditions to the initial concentration estimates over various CO_2 partial pressures and redox conditions.

- Select appropriate runs for use in BEJ and UB predictions.

3.2 Input Parameters

3.2.1 Initial Concentration Estimates

Initial estimates of other solute concentrations in the oxidation zone were calculated as follows:

1. The amount of sulfide oxidized below each square meter of tailings surface was estimated from the rate of oxygen entry, as determined by the oxygen transport modeling (Appendix C2).

2. The mass of each solute released during the oxidation period was estimated by multiplying the mass of sulfide oxidized by the relative release rates measured in the humidity cell tests (Appendix A3).

3. Initial estimates of concentrations were obtained by first adding the mass of solute released to the mass contained in the initial porewater (i.e. equilibrated process water) then dividing by the sum of the initial volume of porewater and the volume that flows through the oxidation zone during the oxidation period. (Equations are provided in Appendix D).

The resulting initial estimates are presented in Table 5. The following comments apply:

- Due to high release rates observed in the humidity cells for more soluble phases, the estimated release of some solutes exceeded the amount present in the solid phase. Estimates underlined in the table were corrected to not exceed the amount initially present in the tailings.

- Zinc release was obtained from the relative release rates observed in the humidity cell tests. The release of zinc from dissolution of carbonates was also calculated, but was less than the amount accounted for by the relative release calculations. The difference is due to the oxidation of zinc sulfides.

- Manganese release was derived directly from the relative release rates observed in the humidity cell tests. The calculated release of manganese is what would be expected from dissolution of manganese-bearing carbonates.

Initial estimates of calcium, magnesium, carbonate and iron concentrations were obtained as described in the following section. Therefore, they are not included in Table 5.

TABLE 5
Estimated Solute Release to Porewater in Oxidation Zone

Parameter	Oxidation Release	
	BEJ (mg/L)	UB (mg/L)
Aluminum	4.8	23
Antimony	1.1	5.2
Arsenic	23	106
Barium	0.29	1.4
Beryllium	0.52	2.4
Cadmium	0.12	0.56
Chloride	41	36
Chromium	0.24	1.0
Cobalt	1.0	4.4
Copper	0.51	2.2
Fluoride	21	98
Lead	67	312
Manganese	121	561
Mercury	0.050	0.23
Nickel	0.69	3.1
Potassium	75	302
Selenium	2.5	11
Silver	0.19	0.69
Sodium	76	268
Sulfate	5,937	26,132
Zinc	76	350

Notes: 1. Underlined values represent maximum concentrations possible for complete dissolution of the solids.

Prepared by: JTC
Checked by: KSS

3.2.2 Estimates of Major Solute Concentrations

An initial MINTEQA2 run was completed to estimate the starting concentrations for each of the major solutes (calcium, magnesium, iron, carbonate and sulfate). This initial run was based on the stoichiometry of the following reaction for pyrite oxidation and carbonate neutralization under oxidizing conditions:

$$FeS_2 + 15/4O_2 + 21/2H_2O + 2Ca_{0.5}Mg_{0.5}CO_3 \rightarrow CaSO_4.2H_2O + MgSO_4 7H_2O + Fe(OH)_3 + 2CO_2(g)$$

Carbonates in the depyritized tailings contain approximately 14% iron (atomic %). Therefore, a small amount of $FeCO_3$ is also added to the reaction. The reaction for iron carbonate dissolution is written as follows:

$$FeCO_3 + 1/4O_2 + 5/2H_2O \rightarrow Fe(OH)_3 + H_2CO_3$$

Adding the above two reactions, assuming there is 14% iron in the dolomite (Appendix A4), and normalizing to the production of 1 mole of sulfate gives the following:

$$1/2FeS_2 + 15/8O_2 + 21/4H_2O + Ca_{0.5}Mg_{0.5}CO_3 + 1/2(0.16)FeCO_3 + 1/8(0.16)O_2 + 5/4(0.16)H_2O \rightarrow$$
$$1/2CaSO_4{\cdot}2H_2O + 1/2MgSO_4{\cdot}7H_2O + 1/2Fe(OH)_3 + CO_2(g) + 1/2(0.16)Fe(OH)_3 + 1/2(0.16)H_2CO_3$$

The initial MINTEQA2 runs for the BEJ and UB case were completed as follows:

1. Solids products from the above reaction were entered as finite solid phases, and allowed to equilibrate with water and excess dolomite. The amount of each solid was based on the total sulfate release in Table 5: i.e., for every mole of sulfate released during oxidation, 0.5 moles of $CaSO_4{\cdot}2H_2O$, 0.5 moles of $MgSO_4{\cdot}7H_2O$, and 0.5+0.5(0.16) moles of $Fe(OH)_3$ were added to the MINTEQA2 inputs.

2. CO_2 was entered as a gas at a fixed partial pressures of 0.00035 atm in the first BEJ run (BEJ-1ca.in), 0.127 atm in the second BEJ run (BEJ-1c12.in), and 0.127 atm in the UB run (UB-c12). The carbon dioxide modeling (Appendix C3) has shown that the carbon dioxide concentrations would be in the range of 0.00035 atm to 0.127 atm.

3. The redox couple for iron was also included in the initial model runs.

The resulting estimates of calcium, magnesium, iron, carbonate and sulfate concentrations were used as inputs for each series of subsequent runs.

3.2.3 Secondary Minerals

Short term humidity cell tests have been completed on the depyritized tailings, with the tests on the intermediate and long term cells continuing. At the low oxidation rates and high dilution from flushing, secondary mineral accumulation has been minimal. In fact, the tests are designed to limit the build-up of secondary mineral phases. Only iron oxy-hydroxides (predominantly ferrihydrite) have been detected in the humidity cell residues. This, however, does not mean that other secondary mineral phases have not formed, or are not likely to form. Secondary mineral phases allowed to form in the equilibrium modeling were therefore selected from previous investigations on tailings from the Crandon Project, and from phases reported in the literature. The following summarizes the reasons for which each of the phases was selected.

Barite ($BaSO_4$) is a common, well known, insoluble secondary mineral that is known to occur in many environments (Hem, 1989).

Cerargyrite (AgCl). Cerargyrite is readily formed under natural conditions and is the phase that is used in wet chemistry methods to identify the presence of silver in solutions. Cerargyrite occurs in upper parts of silver veins in silver ore deposits and is one of the few insoluble halides (Wills, 1981)

Fluorite (CaF_2). Fluorite is a common fluoride mineral. Potentially, there are several controls that can limit the solubility of fluoride. However, with respect to waters that contain high concentrations of calcium, such as predicted for the Crandon tailings percolate, fluorite is the likely controlling phase (Hem, 1989)

Anglesite ($PbSO_4$). Anglesite has been identified in tailings impoundments (Jambor, 1994). In particular, lead concentrations in tailings pore water appear to be controlled at relatively low concentrations by anglesite (e.g. Blowes and Jambor, 1990).

Gibbsite ($Al(OH)_3$) has been demonstrated by Nordstrom and Alpers (1998) to be a probable controlling phase limiting the solubility of aluminum.

Gypsum ($CaSO_4 \cdot 2H_2O$) was not observed in the current testing however it was identified in earlier investigations (SRK, 1998). It is also commonly observed to form in tailings environments where it is generally associated with the neutralization of sulfide derived acidity.

Smithsonite ($ZnCO_3$) was not identified in the current testing. A zinc carbonate phase was identified in earlier investigations on Crandon Tailings (Thresher, 1998), however, it was not possible to establish whether it was a primary or secondary phase. MINTEQA2 runs were therefore completed with and without smithsonite to indicate the potential influence this phase may have on dissolved zinc concentrations. Smithsonite was selected in preference to $ZnCO_3.H_2O$ as it is slightly more soluble than $ZnCO_3 \cdot H_2O$.

Ferrihydrite ($Fe(OH)_3$). Iron oxy-hydroxides have been identified in the residues from the short term humidity cell tests. Ferrihydrite was selected conservatively as this meta-stable mineral has a higher solubility than most other iron oxy-hydroxides, and is prone to dissolution at lower redox conditions.

Rhodochrosite ($MnCO_3$). The adsorption of Mn^{2+} onto alkaline surfaces, such as those of calcite and dolomite, with equivalent release of either Ca or Mg has been reported elsewhere (Stumm and Morgan, 1970; Garrels and Christ, 1965). In addition, Evangelou et al (1991) showed that at high concentrations of Mn^{2+} in solution, and after saturation of the surface sites, nucleation at $CaCO_3$ surfaces was followed by $MnCO_3$ precipitation. The conditions in the TMA are expected to be similar to the test conditions under which these observations were made.

$Sb(OH)_3$. The relatively low abundance of antimony precludes the potential for identifying any secondary mineral phase. Rai et al. (1984) indicate that the species $Sb(OH)_3$ is predominant for pH conditions between 1.5 and 12 s.u., and for pE+pH < 11.4, i.e. for Eh < 300 mV for circum neutral pH conditions, which corresponds to the anticipated TMA conditions. They suggest that the solubility of antimony would be controlled by this phase at pH values below about 8 s.u. Comparison runs were completed in MINTEQA2 to demonstrate the potential influence on dissolved antimony concentrations in the oxidation zone.

Siderite ($FeCO_3$). The formation of siderite as a secondary mineral that limits dissolved iron concentrations has been inferred at various tailings sites (e.g. Morin and Cherry, 1986; Blowes and Ptacek, 1994) on the basis of saturation conditions. While these investigations did not isolate secondary siderite, the precipitation of ferrous iron carbonates (calcium siderite and siderite) has been shown to control ferrous iron to low concentrations under natural, anoxic conditions (Ho, et al. 1984; Wajon et al., 1984). Experimental work carried out under a carbon dioxide atmosphere further indicated that ferrous iron removal was readily effected by dolomite, while reagent grade calcite was ineffective. The dominant carbonate phase in the Crandon depyritized tailings is dolomite. Two siderite phases are used in the geochemical modelling described in this report. Thermodynamic data for siderite (C), (a crystalline phase formed under high temperature conditions, Smith, 1918), is used to assess the effects of dissolution of siderite in process water modeling (Section 2), while thermodyanamic data for siderite (D), (a disordered or precipitate phase formed at low temperature conditions, Singer and Stumm, 1970), is used to assess the potential effects of siderite precipitation in the TMA.

The mineralogical investigation completed on the humidity cell residues (Appendix A3) showed that the iron oxy-hydroxides were enriched with zinc. This is consistent with the earlier investigations (Thresher, 1998) which also showed enrichment of other elements, in particular arsenic. These observations are attributable to co-precipitation and adsorption of ions with iron oxy-hydroxides. Although co-precipitation and adsorption reactions can have a significant influence on solute concentrations (again particularly for arsenic), they are not easily modeled in MINTEQA2. They were therefore not included in the geochemical modeling undertaken herein. The result is that concentrations of some solutes will be over-estimated.

3.2.4 Other Inputs

Runs were completed to show the sensitivity of equilibrium concentrations to the presence or absence of siderite, to redox conditions, and to CO_2 partial pressure, as discussed below:

- Two sets of MINTEQA2 runs were completed to estimate the solute concentrations in the BEJ case. In both sets, gypsum and ferrihydrite were

entered as finite phases, with abundances as determined from the initial (Section 3.2.2) output. In the first set, ferrihydrite was retained as the only controlling phase on the solubility of iron. In addition, smithsonite and $Sb(OH)_3$ were not allowed to precipitate, therefore there were no controls on zinc or antimony concentrations. In the second set, siderite, $Sb(OH)_3$ and smithsonite were allowed to precipitate. In this second set, chloride and fluoride were omitted from the input to accelerate convergence.

- In each set of model runs, equilibrium concentrations were calculated over a range of redox conditions from 0 mV to + 300 mV, representing the range typical of systems dominated by ferric hydroxide and neutral pH conditions. The low Eh values were intended to result in high estimates of the concentration of ferrous iron. In reality, the conversion of ferric hydroxide to the more soluble ferrous form will be kinetically limited, and is unlikely to occur until long after the consolidation phase. Furthermore, redox conditions are unlikely to reach the lower end of this range during the consolidation period.

- Carbonate concentrations determined in the initial runs at atmospheric CO_2 (BEJ-1ca) or 12.7% CO_2 (BEJ-1c12 and UB-1c12) were used to define the total carbonate content in the subsequent runs. (12.7% CO_2 represents the steady state CO_2 concentrations that could develop in the tailings during consolidation and following capping, as described in Appendix C3). The CO_2 gas phase used in the initial runs was then removed to allow for convergence, therefore, the system was effectively "closed" with respect to CO_2 loss or gain in these final runs.

- Beryllium, chromium, cobalt, mercury, nickel and selenium were not included in the geochemical modeling because they were either present at very low initial concentrations, or are not contained in the MINTEQA2 database. These metals are however included in the TMA source concentration predictions (Chapter 2) at the concentrations shown in Table 6.

3.3 Results

The MINTEQA2 input and output files for the BEJ and UB runs are provided in Attachments B and C, respectively. Summaries of the outputs are provided in Tables 6 to 8. The modeling results can be summarized as follows.

3.3.1 BEJ Runs

Results for the modeling runs with the BEJ starting concentrations are summarized in Tables 6 and 7. As discussed previously, the first model runs (BEJx1ca and BEJx1c12) established the major solute concentrations for use in the second and third model runs.

The second runs (BEJx2ca and BEJx2c12) established equilibrium conditions for a range of redox conditions, with ferrihydrite as the controlling phase for iron. The results indicate that many of the secondary minerals described in Section 3.2.3 are at saturation. They include: barite, cerargyrite, dolomite, ferrihydrite, fluorite, gibbsite, gypsum and rhodochrosite. Smithsonite and $Sb(OH)_3$, were supersaturated, but were not allowed to form. It should be noted that phases other than those selected remain supersaturated with respect to the predicted concentrations for iron, copper, zinc and lead, which suggest that the predicted concentrations are likely to be conservative.

Redox has a significant influence on the solubility of ferrihydrite, with higher iron concentrations observed under low Eh conditions. The redox also has a small influence on the pH, with higher pH's observed under low Eh conditions. The increase in pH causes a small decrease in the solubility of zinc. Redox potential also influences the speciation of arsenic, copper and manganese.

The third runs (BEJx3ca and BEJx3c12) include ferrihydrite as a finite solid, and siderite as an allowable solid. Therefore, the initial controlling phase on iron solubility is ferrihydrite, but as the redox decreases siderite becomes the controlling phase. Smithsonite and $Sb(OH)_3$ are also present as allowable solids. As a result, the predicted iron, zinc and antimony concentrations in the BEJ-3 runs are lower than those predicted in the BEJ-2 runs.

A comparison of the results in Tables 6 and 7 indicates that pH, and iron concentrations are strongly influenced by CO_2, with lower pH's, and higher iron concentrations observed in the 12.7% CO_2 runs.

TABLE 6
Solute Concentrations for BEJ - System with Atmospheric CO_2
MINTEQA2 Modeling Results

Parameter	BEJx1ca	BEJx2ca				BEJx3ca			
		Sweep 1	Sweep 2	Sweep 3	Sweep 4	Sweep 1	Sweep 2	Sweep 3	Sweep 4
Equilibrium Concentrations (mg/L)									
Ag^{+1}		0.032	0.032	0.032	0.032	0.19	0.19	0.19	0.19
Al^{+3}		0.00059	0.00059	0.00060	0.00082	0.00049	0.00049	0.00050	0.00085
H_3AsO_3		1.4E-10	4.3E-07	0.0012	0.57	1.5E-10	4.6E-07	0.0013	0.45
H_3AsO_4		23	23	23	22	23	23	23	22
Ba^{+2}		0.0031	0.0031	0.0031	0.0031	0.0031	0.0031	0.0031	0.0031
Ca^{+2}	494	527	527	527	523	527	527	527	522
Cd^{+2}		0.12	0.12	0.12	0.12	0.12	0.12	0.12	0.12
Cl^{-1}		41	41	41	41				
Cu^{+1}		0.00015	0.0084	0.25	0.50	0.00012	0.0068	0.22	0.49
Cu^{+2}		0.51	0.51	0.27	0.016	0.51	0.51	0.30	0.021
F^{-1}		1.9	1.9	1.9	1.9				
Fe^{+2}	0.000009	0.00049	0.027	1.4	18	0.00050	0.028	1.4	15
Fe^{+3}	0.00036	0.00055	0.00055	0.00055	0.00044	0.00056	0.00056	0.00055	0.00043
K^{+1}		75	75	75	75				
Mg^{+2}	837	881	881	880	870	883	884	883	873
Mn^{+2}		14	14	14	13	14	14	14	13
Mn^{+3}		4.1E-20	7.3E-22	1.3E-23	2.3E-25	4.1E-20	7.3E-22	1.3E-23	2.3E-25
Na^{+1}		76	76	76	76				
Pb^{+2}		7.5	7.5	7.5	7.5	7.5	7.5	7.5	7.4
SO_4^{-2}	4466	4395	4395	4398	4427	4334	4335	4337	4365
$Sb(OH)_3$		1.1	1.1	1.1	1.1	0.012	0.012	0.012	0.012
Zn^{+2}		76	76	76	76	61	61	61	60
Equilibrium conditions									
Percent Difference	0.00	9.0	9.0	9.0	8.8	8.6	8.6	8.6	8.3
Ionic Strength (m)	0.11	0.12	0.12	0.12	0.12	0.12	0.12	0.12	0.12
Equilibrium pH	7.78	7.21	7.21	7.22	7.43	7.20	7.20	7.21	7.46
Equilibrium Eh (mV)	300	300	200	100	0	300	200	100	0
Saturation Indices									
Barite		0.00	0.00	0.00	0.00	0.00	0.00	0.00	0.00
Cerargyrite		0.00	0.00	0.00	0.00	-	-	-	-
Gibbsite (C)		0.00	0.00	0.00	0.00	0.00	0.00	0.00	0.00
Gypsum	0.00	0.00	0.00	0.00	0.00	0.00	0.00	0.00	0.00
Smithsonite		0.10	0.10	0.10	0.11	0.00	0.00	0.00	0.00
Ferrihydrite	0.00	0.00	0.00	0.00	0.00	0.00	0.00	0.00	0.00
Rhodochrosite		0.00	0.00	0.00	0.00	0.00	0.00	0.00	0.00
$Sb(OH)_3$ (S)		1.98	1.98	1.98	1.98	0.00	0.00	0.00	0.00
Fluorite		0.00	0.00	0.00	0.00	-	-	-	-
Dolomite	0.00	0.00	0.00	0.00	0.00	0.00	0.00	0.00	0.00
Anglesite		0.00	0.00	0.00	0.00	0.00	0.00	0.00	0.00
Siderite (C)	-5.67	-3.98	-2.23	-0.52	0.60	-3.97	-2.22	-0.51	0.51
Siderite (D)	-6.18	-4.49	-2.75	-1.03	0.09	-4.48	-2.74	-1.02	0.00
Goethite	5.52	5.52	5.52	5.52	5.52	5.52	5.52	5.52	5.52
Lepidocrocite	3.52	3.52	3.52	3.52	3.52	3.52	3.52	3.52	3.52
Cerrusite		1.34	1.34	1.34	1.34	1.34	1.34	1.34	1.34
$ZnCO_3$, $1H_2O$		0.47	0.47	0.47	0.48	0.37	0.37	0.37	0.37
Hydcerrusite		2.22	2.22	2.25	2.67	2.21	2.21	2.24	2.72
Calcite	-0.23	-0.23	-0.23	-0.23	-0.22	-0.23	-0.23	-0.23	-0.23
Otavite		-0.76	-0.76	-0.76	-0.76	-0.75	-0.75	-0.75	-0.75
Malachite		0.46	0.44	-0.10	-2.55	0.46	0.44	-0.02	-2.32
$Pb(OH)_2$ (C)		0.09	0.09	0.12	0.53	0.08	0.08	0.11	0.59
$Fe_3(OH)_8$	-5.31	-4.74	-2.99	-1.25	0.29	-4.73	-2.98	-1.25	0.26

Prepared by: DDS
Checked by: KSS

TABLE 7
Solute Concentrations for BEJ System, with 12.7% CO_2
MINTEQA2 Modeling Results

Parameter	BEJx1c12	BEJx2c12				BEJx3c12			
		Sweep 1	Sweep 2	Sweep 3	Sweep 4	Sweep 1	Sweep 2	Sweep 3	Sweep 4
Equilibrium Concentrations (mg/L)									
Ag^{+1}		0.032	0.032	0.032	0.032				
Al^{+3}		0.017	0.017	0.0071	0.00070	0.00026	0.00025	0.00028	0.00086
H_3AsO_3		8.7E-08	0.00026	0.28	11	8.9E-08	0.00027	0.024	0.42
H_3AsO_4		23	23	23	12	23	23	23	22
Ba^{+2}		0.0034	0.0034	0.0032	0.0029	0.0034	0.0034	0.0031	0.0029
Ca^{+2}	528	559	558	540	508	560	559	521	507
Cd^{+2}		0.12	0.12	0.12	0.12	0.12	0.12	0.12	0.12
Cl^{-1}		41	41	41	41				
Cu^{+1}		0.00019	0.010	0.28	0.51	0.00015	0.0083	0.25	0.49
Cu^{+2}		0.51	0.50	0.24	0.0084	0.51	0.51	0.26	0.022
F^{-1}		1.9	1.9	1.9	1.9				
Fe^{+2}	0.080	0.103	5.5	123	299	0.10	5.6	15	14
Fe^{+3}	0.0017	0.0019	0.0019	0.0014	0.00069	0.0019	0.0019	0.00087	0.00043
K^{+1}		75	75	75	75	75	75	75	75
Mg^{+2}	895	933	930	880	790	933	931	863	836
Mn^{+2}		16	16	15	13	16	16	14	13
Mn^{+3}		4.5E-20	8.0E-22	1.3E-23	2.1E-25	4.4E-20	7.9E-22	1.3E-23	2.1E-25
Na^{+1}		76	76	76	76				
Pb^{+2}		9.0	9.0	8.5	7.8	9.0	9.0	7.8	7.4
SO_4^{-2}	4318	4269	4276	4431	4711	4217	4224	4402	4473
$Sb(OH)_3$		1.1	1.1	1.1	1.1	0.012	0.012	0.012	0.012
Zn^{+2}		76	76	76	76	71	71	62	58
Equilibrium conditions									
Percent Difference	0.0	8.3	8.2	6.8	4.4	7.9	7.8	4.4	3.2
Ionic Strength (m)	0.12	0.13	0.13	0.13	0.13	0.13	0.13	0.12	0.12
Equilibrium pH	6.5	6.5	6.5	6.59	7.03	6.4	6.5	6.9	7.5
Equilibrium Eh (mV)	300	300	200	100	0	300	200	100	0
Saturation Indices									
Barite		0.00	0.00	0.00	0.00	0.00	0.00	0.00	0.00
Cerargyrite		0.00	0.00	0.00	0.00				
Gibbsite (C)		0.00	0.00	0.00	0.00	0.00	0.00	0.00	0.00
Gypsum	0.00	0.00	0.00	0.00	0.00	0.00	0.00	0.00	0.00
Smithsonite		0.03	0.04	0.06	0.12	0.00	0.00	0.00	0.00
Ferrihydrite	0.00	0.00	0.00	0.00	0.00	0.00	0.00	0.00	0.00
Rhodochrosite		0.00	0.00	0.00	0.00	0.00	0.00	0.00	0.00
$Sb(OH)_3$ (S)		1.98	1.98	1.98	1.98	0.00	0.00	0.00	0.00
Fluorite		0.00	0.00	0.00	0.00				
Dolomite	0.00	0.00	0.00	0.00	0.00	0.00	0.00	0.00	0.00
Anglesite		0.00	0.00	0.00	0.00	0.00	0.00	0.00	0.00
Siderite (C)	-2.33	-2.24	-0.51	0.87	1.32	-2.24	-0.51	0.00	0.00
Siderite (D)	-1.82	-1.73	0.00	1.38	1.83	-1.73	0.01	0.51	0.51
Goethite	5.52	5.52	5.52	5.52	5.52	5.52	5.52	5.52	5.52
Lepidocrocite	3.52	3.52	3.52	3.52	3.52	3.52	3.52	3.52	3.52
Cerrusite		1.34	1.34	1.34	1.35	1.34	1.34	1.34	1.34
$ZnCO_3$, $1H_2O$		0.40	0.40	0.43	0.49	0.37	0.37	0.37	0.37
Hydcerrusite		0.73	0.74	1.00	1.87	0.73	0.74	1.56	2.72
Calcite	-0.23	-0.22	-0.22	-0.22	-0.21	-0.22	-0.22	-0.22	-0.22
Otavite		-0.79	-0.79	-0.77	-0.74	-0.78	-0.78	-0.75	-0.74
Malachite		-0.91	-0.91	-1.26	-3.29	-0.91	-0.91	-0.55	-2.28
$Pb(OH)_2$ (C)		-1.40	-1.39	-1.15	-0.29	-1.40	-1.39	-0.58	0.59
$Fe_3(OH)_8$	-4.02	-3.98	-2.24	-0.62	0.69	-3.98	-2.23	-0.91	0.25

Prepared by: KSS
Checked by: JTC

3.3.2 UB Runs

The results of the modeling runs completed for the UB concentrations are summarized in Table 8. All of the UB runs assumed a carbon dioxide partial pressure of 12.7% to reflect the upper limit indicated by the CO_2 modeling (Appendix C3). The range of redox conditions was the same as in the BEJ runs.

The results indicate that even though the initial solute concentrations input to MINTEQA2 were significantly higher, general trends in pH and solubilities of controlling secondary mineral phases were similar to those observed for the BEJ runs. Sulfate is higher due to the magnesium provided by higher initial dissolution of dolomite. The higher sulfate results in increased precipitation of anglesite ($PbSO_4$).

TABLE 8
Solute Concentrations for UB - System with 12.7% CO_2, MINTEQA2 Modeling Results

Parameter	UB-1c12	UB-2c12				UB-3c12			
		Sweep 1	Sweep 2	Sweep 3	Sweep 4	Sweep 1	Sweep 2	Sweep 3	Sweep 4
Equilibrium Concentrations (mg/L)									
Ag^{+1}		0.037	0.037	0.037	0.037				
Al^{+3}		0.077	0.072	0.021	0.0011	0.00043	0.00041	0.00028	0.00086
H_3AsO_3		7.5E-07	2.2E-03	1.5	42	8.1E-07	2.3E-03	0.11	1.9
H_3AsO_4		106	106	105	65	106	106	106	104
Ba^{+2}		0.0021	0.0021	0.0021	0.0020	0.0022	0.0022	0.0021	0.0020
Ca^{+2}	387	421	420	411	400	425	424	410	406
Cd^{+2}		0.56	0.56	0.56	0.56	0.56	0.56	0.56	0.56
Cl^{-1}		36	36	36	36				
Cu^{+1}		0.00069	0.038	1.1	2.2	0.00060	0.033	1.08	2.2
Cu^{+2}		2.2	2.2	1.1	0.040	2.2	2.2	1.16	0.083
F^{-1}		4.2	4.2	4.2	4.1				
Fe^{+2}	0.13	0.29	15	230	410	0.31	16	26	25
Fe^{+3}	0.0019	0.0024	0.0024	0.0016	0.00070	0.0025	0.0024	0.00093	0.00044
K^{+1}									
Mg^{+2}	3376	3558	3551	3456	3349	3595	3590	3493	3463
Mn^{+2}		26	26	24	22	26	26	24	23
Mn^{+3}		8.7E-20	1.6E-21	2.7E-23	4.6E-25	8.8E-20	1.6E-21	2.7E-23	4.7E-25
Na^{+1}									
Pb^{+2}		5.7	5.6	5.3	4.8	5.7	5.7	4.9	4.7
SO_4^{-2}	13718	13170	13199	13555	13958	12805	12824	13170	13276
$Sb(OH)_3$		5.2	5.2	5.2	5.2	0.011	0.011	0.011	0.011
Zn^{+2}		350	350	350	350	137	137	127	125
Equilibrium conditions									
Percent Difference	0.001	10	10	9	8	12	12	10	10
Ionic Strength (m)	0.31	0.32	0.32	0.32	0.32	0.32	0.32	0.31	0.31
Equilibrium pH	6.47	6.35	6.36	6.54	7.04	6.34	6.35	6.85	7.44
Equilibrium Eh (mV)	300	300	200	100	0	300	200	100	0
Saturation Indices									
Barite		0	0	0	0	0	0	0	0
Cerargyrite		0	0	0	0	-	-	-	-
Gibbsite (C)		0	0	0	0	0	0	0	0
Gypsum	0.0	0	0	0	0	0	0	0	0
Smithsonite		0.41	0.41	0.43	0.45	0	0	0	0
Ferrihydrite	0.0	0	0	0	0	0	0	0	0
Rhodochrosite		0	0	0	0	0	0	0	0
$Sb(OH)_3$ (S)		2.7	2.7	2.7	2.7	0	0	0	0
Fluorite		0	0	0	0	-	-	-	-
Dolomite	0.0	0	0	0	0	0	0	0	0
Anglesite		0	0	0	0	0	0	0	0
Siderite (C)	-1.80	-1.5	0.23	1.4	1.7	-1.5	0.25	0.51	0.51
Siderite (D)	-2.31	-2.0	-0.28	0.93	1.2	-2.0	-0.26	0	0
Goethite	5.5	5.5	5.5	5.5	5.5	5.5	5.5	5.5	5.5
Lepidocrocite	3.5	3.5	3.5	3.5	3.5	3.5	3.5	3.5	3.5
Cerrusite		1.0	1.0	1.0	1.0	1.0	1.0	1.0	1.0
$ZnCO_3$, $1H_2O$		0.78	0.78	0.80	0.82	0.37	0.37	0.37	0.37
Hydcerrusite		-0.48	-0.46	-0.10	0.87	-0.49	-0.47	0.51	1.7
Calcite	-0.58	-0.58	-0.58	-0.58	-0.58	-0.58	-0.58	-0.58	-0.58
Otavite		-0.47	-0.47	-0.47	-0.46	-0.47	-0.47	-0.46	-0.46
Malachite		0.0	0.0	-0.18	-2.1	-0.046	-0.034	0.52	-1.2
$Pb(OH)_2$ (C)		-1.9	-1.9	-1.5	-0.56	-1.9	-1.9	-0.91	0.26
$Fe_3(OH)_8$	-4.0	-3.9	-2.1	-0.57	0.68	-3.9	-2.1	-0.88	0.28

Prepared by: JTC
Checked by: KSS

3.4 Recommendation for BEJ and UB Concentration Estimates

Table 9 summarizes the BEJ and UB estimates of solubility-controlled concentrations in the oxidation zone.

Sweep 2 from the run BEJ-3c12 is recommended for the BEJ estimates for the following reasons:

- The transport calculations in Appendix C3 show that a carbon dioxide partial pressure in the range of 0.00035 to 0.127 atm is anticipated for the consolidation period. The more conservative value of 0.127 atm was selected;
- Iron solubility in the humidity cells is limited by oxy-hydroxides, therefore, iron solubility in the oxidation zone is likely to be limited by oxy-hydroxides; and,
- An Eh of 200 mV was selected to be most representative of the anticipated redox conditions within the oxidation zone.

(Note: Since chloride and fluoride were not included in the selected sweep, equilibrium concentrations for these species, and silver, were obtained from Sweep 2 of BEJ-2c12.)

Sweep 4 from the run UB-2c12 is recommended for the UB estimates for the following reasons:

- The carbon dioxide partial pressure of 0.127 atm is the maximum concentration expected in the tailings (Appendix C3).
- Although siderite is predicted to form under these conditions, this run did not allow siderite precipitation. The combination of low Eh and no siderite leads to very conservative estimates of soluble iron concentrations.
- An Eh of 0 mV was selected to reflect the trend towards lower Eh conditions that could occur over time. However, redox conditions are unlikely to reach this low value during the consolidation period. As a result, the Eh used is considered to be very conservative.

Both the BEJ and UB estimates assume acid neutralization by dolomite dissolution. The humidity cell tests indicate an overall Ca:Mg molar ratio of about 1.4:1, rather than the 1:1 ratio normally found in dolomite. Therefore, both sets of estimates conservatively over estimate magnesium and sulfate concentrations.

As indicated by the summaries of the equilibrated solute concentrations, no solubility controlling phases were included in the modeling for arsenic. However, humidity cell testing provides evidence that arsenic released from its primary sulfide mineral phase is in fact retained in the tailings, and is likely associated with the iron oxy-hydroxides. The approach taken with respect to arsenic is therefore conservative.

TABLE 9
BEJ and UB Solubility Controls in Oxidation Zone

Parameter	Units	File BEJ-3c12 Sweep 2 (Eh = 200 mV)		File UB-2c12 Sweep 4 (Eh = 0 mV)	
		Conc.	Controlling Phase	Conc.	Controlling Phase
Ag	mg/L	0.032	Cerargyrite	0.037	Cerargyrite
Al	mg/L	0.00025	Gibbsite (C)	0.0011	Gibbsite (C)
Ba	mg/L	0.0034	Barite	0.0020	Barite
Ca	mg/L	559	Gypsum	400	Gypsum
F	mg/L	1.9	Fluorite	4.1	Fluorite
Fe	mg/L	5.6	Ferrihydrite**	410	Ferrihydrite
Mg	mg/L	931	Dolomite	3,349	Dolomite
Mn	mg/L	16	Rhodochrosite	22	Rhodochrosite
Pb	mg/L	9.0	Anglesite	4.8	Anglesite
SO_4	mg/L	4224	Gypsum	13,958	Gypsum
$Sb(OH)_3$	mg/L	0.012	$Sb(OH)_3$ (s)		n/a*
Zn	mg/L	71	Smithsonite		n/a*

Notes: *n/a indicates no solubility control allowed
** siderite was allowed, but was not saturated in this sweep.

Prepared by: JTC
Checked by: KSS

4. REFERENCES

Allison, J.D., Brown, D.S., and Novo-Gradac, K.J. (1991), MINTEQA2/PRODEFA2, A Geochemical Assessment Model for Environmental Systems: Version 3.0 User's Manual, EPA/600/3-91/021. U.S. Environmental Protection Agency, Environ. Res. Lab., Athens, Ga.

Ball, J.W. and D.K. Nordstrom (1991), User's manual for WATEQ4F, with revised thermodynamic data base and test cases for calculating speciation of major, trace, and redox elements in natural waters. Open-File Report 91-183, U.S. Geological Survey, July, 1991.

Blowes, D.W., and Jambor, J.L. (1990), The pore-water geochemistry and the mineralogy of the vadose zone of sulfide tailings, Waite Amulet, Quebec, Canada. Applied Geochem. Vol. 5, pp. 327-346.

Blowes, D.W. and Ptacek, C.J. (1994) Acid-neutralization Mechanisms in Inactive Mine Tailings. In J.L. Jambor and D.W. Blowes, Eds., "Short Course Handbook on Environmental Geochemistry of Sulfide Mine-Wastes", Waterloo Ontario, May 1994.

Blowes, D.L., Reardon, E.J., Jambor, J.L. and Cherry, J.A. (1991), The formation and potential importance of cemented layers in inactive sulfide mine tailings. Geochim. Cosmochim. Acta vol. 55, pp. 965-978.

Evangelou, V.P., U.M. Sainju and Hiao Huang (1991), Evaluation and Quantification of Armoring Mechanisms of Calcite, Dolomite and Rock Phosphate, In proceedings of Second International Conference on Abatement of Acidic Drainage, Montreal, Sept. 16-18, 1991, pp. 363-381.

Foth and Van Dyke (1995/1998), Environmental Impact Report for the Crandon Project.

Garrels R.M. and Christ C.L. (1965), Solutions, Minerals and Equilibria. Freeman Cooper Co., San Francisco, Calif. ISBN 0-87735-333-6

Hem, J. D. (1989), Study and Interpretation of the Chemical Characteristics of Natural Water, Third Edition, USGS Water Supply Paper 2254. Libr. of Congress Catalog- Card No. 85-600603.

Ho, G. E., Murphy, P. J., Platell, N., and Wajon, J. E. (1984), Iron Removal from TiO, Plant Acidic Wastewater, Journal of Environmental Engineering, Vol. 110, No. 4. ISBN 0733/9372/84/0004-0828.

Jambor, J.L. (1994), Mineralogy of Sulfide-Rich Tailings and Their Oxidation Products" in J.L. Jambor & D.W. Blowes, Eds. "Short Course Handbook on Environmental Geochemistry of Sulfide Mine-Wastes", Mineralogical Association of Canada, Waterloo Ontario, May 1994.

Morin, K.A., and Cherry, J.A. (1986), Trace Amounts of Siderite Near a Tailings Impoundment, Elliot Lake, Ontario, and Its Implication in Controlling Contaminant Migration in a Sand Aquifer. Chem. Geol., Vol. 56, pp. 117-134.

Nordstrom, D.K., Robertson, C.E., Ball J.W., and Hanshaw B.B. (1984), The Effect of Sulfate Concentrations in Natural Waters: II. Field Occurrences and Identification of Aluminum Hydroxysulfate Precipitates. Abstracts Program of the Geological Society. (Ref. No. 43634).

Nordstrom D.K. and Alpers C,N. (1998), Geochemistry of Acid Mine Waters. In Reviews in Economic Geology Vol.7A, Editor C.M, Lesher, (in print).

Rai, D and Zachara J.M. (1984), Chemical Attenuation Rates, Coefficients and Constants in Leachate Migration, Volume 1: A Critical Review. Prepared by Batelle, Pacific North West Laboratories, Batelle Boulevard, Richland, Washington.

Singer, P.C. and Stumm, W. (1970) Journal of American Water Works Association, Volume 22, pp. 198-202.

Smith, H.J. (1918) Journal of the American Chemical Society, Volume 40, pp. 879-883.

Smith A. and T. Mudder (1991), The Chemistry and Treatment of Cyanidation Wastes. *Publ. Mining Journal Books, London.*

Steffen, Robertson and Kirsten, 1998. Crandon TMA - Supplementary Waste Characterization Program, Final Report. April 1998.

Stumm W. and Morgan, J.J. (1970), Aquatic Chemistry, Wiley Interscience, New York, NY.

Thresher and Son, Inc. (1998), Mineralogical Evaluation of the Crandon Deposit, Tailings and Waste Characterization Test Products.

United States Environmental Protection Agency (1982), Final Development Document for Effluent Limitations Guidelines and Standards for the Ore Mining & Dressing Point Source Category, U.S. EPA 440/1-82/061

Wajon, J.E., Ho, G.E., and Murphy, P,J. (1984), Rate of Precipitation of Ferrous Iron and Formation of Mixed Iron-Calcium Carbonates by Naturally Occurring Carbonate Materials. In Water Resources, Vol. 19, No. 7. Pergamon Press Ltd.

Wills, B.A. (1981) Mineral Processing Technology. Second Edition, Editor D.W. Hopkins, Pergamon Press. ISBN 0-08-027322-8

Attachment A

MINTEQA2 Runs to Simulate Equilibration of Tailings Process Water

(Files provided on compact disk to selected reviewers)

ATTACHMENT A

Geochemical Modeling of Process Water Discharged to TMA

MINTEQA2 Files:

TMA_pws.in TMA pws.out	Simulated equilibrium with gypsum
TMA_pw1r.in TMA_pw1r.out	Simulated equilibrium with dolomite
TMA_pw4r.in TMA_pw4r.out	Simulated equilibrium with dolomite and gypsum
TMA_pw5r.in TMA_pw5r.out	Simulated equilibrium with calcite and gypsum
TMA_pw6r.in TMA_pw6r.out	Simulated equilibrium with dolomite, gypsum siderite (C), and smithsonite

Attachment B

MINTEQA2 Runs to Establish Equilibrium Concentrations for Solutes Released During Consolidation (Best Engineering Judgement Runs)

(Files provided on compact disk to selected reviewers)

ATTACHMENT B

MINTEQA2 Runs to Establish Equilibrium Concentrations for Solutes Released During Consolidation (Best Engineering Judgement Runs)

MINTEQA2 Files:

BEJ under atmospheric CO_2 Conditions:

BEJx1ca.in BEJx1ca.out	Estimate starting concentrations for each major element under atmospheric CO_2 concentrations.
BEJx2ca.in BEJx2ca.out	Estimate solute concentrations with ferrihydrite as the only controlling phase for iron.
BEJx3ca.in BEJx3ca.out	Estimate solute concentrations with siderite allowed to precipitate, and gypsum and ferrihydrite present in the amount determined in the first run.

BEJ under 0.127 atm partial pressure of CO_2:

BEJx1c12.in BEJx1c12.out	Estimate starting concentrations for each major element under a CO_2 partial pressure of 0.127 atm.
BEJx2c12.in BEJx2c12.out	Estimate solute concentrations with ferrihydrite the only controlling phase for iron.
BEJx3c12.in BEJx3c12.out	Estimate solute concentrations with siderite allowed to precipitate, and gypsum and ferrihydrite present in the amount determined in the first run.

Attachment C

MINTEQA2 Runs to Establish Equilibrium Concentrations for Solutes Released During Consolidation (Upper Bound Runs)

(Files provided on compact disk to selected reviewers)

ATTACHMENT C

MINTEQA2 Runs to Establish Equilibrium Concentrations for Solutes Released During Consolidation (Upper Bound Runs)

MINTEQA2 Files:

Runs completed at 12.7% CO_2:

UB-1c12.in UB-1c12.out	Estimate starting concentrations for each major element under a CO_2 partial pressure of 0.127 atm.
UB-2c12.in UB-2c12.out	Estimate solute concentrations with ferrihydrite as the only controlling phase for iron.
UB-3c12.in UB-3c12.out	Estimate solute concentrations with siderite allowed to precipitate and gypsum and ferrihydrite present in the amount determined in the first run.

Appendix C1

Crandon Project TMA
Oxygen Transport Modeling

Appendix C1

Crandon Project TMA
Oxygen Transport Modeling Report

Note: On September 26, 1997, the WDNR issued a letter to NMC regarding its Completeness Determination of the Crandon Project Tailings Management Area Feasibility Report. Comment 30 of that letter related to the oxygen transport modeling report contained in the Groundwater Quality Performance Evaluation. NMC provided an initial response to WDNR's comment in a letter dated December 12, 1997. During a conference call held after the issuance of the December 12, 1997, letter, the WDNR further clarified their needs regarding the oxygen transport model comment. Following this discussion, Steffen Robertson and Kirsten (Canada), Inc. (SRK) issued a letter to Foth & Van Dyke, dated March 7, 1998, which completed the response to Comment 30 of the WDNR's September 26, 1997, TMA Completeness Determination letter. SRK's letter has been incorporated into this appendix.

STEFFEN, ROBERTSON AND KIRSTEN (CANADA) INC.
Consulting Engineers and Scientists

Suite 800
580 Hornby Street
Vancouver, B.C.
Canada
V6C 3B6

Tel: (604) 681-4196
Fax: (604) 687-5532

March 7, 1998
Project F107107

Foth and Van Dyke
2737 S. Ridge Road
P.O. Box 19012
Green Bay, WI
54307-9012

Attention: Mr. Gerald Sevick

Dear Mr. Sevick:

RE: CRANDON PROJECT - ADDENDUM 1 TO THE APRIL 1997 TMA OXYGEN TRANSPORT MODELING REPORT

As part of its Tailings Management Area Feasibility Report Completeness Determination letter, dated September 26, 1997, the Wisconsin Department of Natural Resources (WDNR) forwarded the following request to Nicolet Minerals Company (NMC).

> **Comment 30:** Please revise the Oxygen Transport Modeling portions of the TMA Groundwater Quality Performance Evaluation (EIR Appendix 4.2-12) to include the following:
>
> a. A more complete sensitivity analysis for all significant parameters, including (but not limited to) varying the diffusion coefficient by up to a factor of 3.

b. A revised estimation of the expected moisture content profile in the tailings using an unsaturated zone model of the tailings facility. Accurate determination of moisture content in individual layers for the purpose of estimating other soil parameters is outside the intended use of the HELP Model and is likely beyond its reasonable application.

c. Documentation of the initial conditions and boundary conditions used to solve the differential equations describing transport.

d. An additional set of model runs that provide worst-case assessments of transport. The characteristics of the worst cases should include, but not necessarily be limited to, the following: 1) the proposed cover system without the geomembrane (the barrier portion of the cover consisting of only the GCL and P40 till); and 2) input parameters based on the scale at which the facility monitoring program will be able to detect increases in oxygen concentration and moisture content.

In preparing a response, NMC, Foth & Van Dyke (FVD), and Steffen Robertson and Kirsten (SRK) participated in telephone conversations with representatives of the WDNR and U.S. Army Corps of Engineers (USCOE) to more clearly define the requested information. An initial response to Comment 30 was prepared by SRK, with input from NMC and FVD, and provided to WDNR in a letter dated December 12, 1997. The initial response was discussed with representatives of the WDNR on December 19, 1997, resulting in further clarification of the WDNR's information needs. SRK then carried out additional model runs.

This letter represents our update to the letter dated December 12, 1997. It incorporates the pertinent information from the original response to Comment 30, and additional clarification requested by WDNR.

The following is our completed response to Comment 30.

a. In carrying out the oxygen transport modeling reported in Appendix C of the TMA Groundwater Quality Performance Evaluation (i.e. the "Oxygen Transport Modeling Report"), input parameters were selected so as to result in conservatively high estimates of oxygen transport into the tailings. Arbitrarily varying all of the previously selected parameters by a factor of 3 could lead to results that are overly conservative, to the point of being misleading.

Despite this concern, SRK has completed additional runs to demonstrate the sensitivity of each transport model's output to the assumed input parameters. Two sensitivity runs were completed for each transport model: one using the combination of inputs that lead to the minimum oxygen flux, and one using the combination of inputs that lead to the maximum flux. In general, the input values for each parameter were obtained by doubling or halving the value used in the predictive run.

The sensitivity runs are presented in Attachment 1. The results show that all of the oxygen transport models respond in a predictable manner to changes in the inputs. The predicted oxygen fluxes vary linearly or less strongly with the inputs. For many of the models, including the model of oxygen diffusion through tailings pore air (which leads to by far the highest predicted oxidation rates), the model outputs vary with the square root of the key input parameters. For example, in the air phase diffusion model, doubling both the diffusion coefficient and the reaction rate constant only increases the predicted oxygen flux by a factor of two.

b. The importance of the expected moisture content profile is that it influences the predicted rate of oxygen diffusion into the tailings surface. As discussed in Section 3.3.3 of the Oxygen Transport Modeling Report, a diffusion coefficient of $1x10^{-8}$ m^2/sec was selected for simulations of (air phase) diffusion of oxygen into the tailings surface . This value

was obtained from two literature equations that relate tailings water content to oxygen diffusion coefficients. Both equations predict diffusion coefficients of less than $1x10^{-8}$ m^2/sec for water contents above approximately 85% of saturation.

There are several reasons why it is conservative to assume, for the purpose of oxygen transport modeling, that moisture contents in the tailings will be 85% of saturation or greater.

First, NMC has committed to a tailings deposition plan that would result in the tailings deposition points being moved regularly. As a result, the maximum period that a tailings surface will be exposed is about 2 months (during deposition). The analysis below indicates that drying of the tailings during the 2-month deposition cycle will be very limited. Furthermore, any oxidation products that could accumulate during that period would be flushed out during the subsequent flooding with process water.

Second, results from the HELP model simulations of the consolidation period predict that the uppermost layer of tailings (between 7.5 and 20 feet in thickness) would be 88% saturated after two years of vertical drainage. For drainage times less than two years, and for tailings further below the surface, predicted moisture contents were consistently higher.

Third, the phreatic surface in the tailings mass will remain very near the surface throughout operations, and for much of the consolidation period. Figure 1 shows a profile of the tailings surface after deposition ceases in Cell 2. The difference in elevation between the highest and lowest points on the tailings surface is only 10 feet. Initially, a pond will cover about half of the profile. The phreatic surface within tailings that are not covered by the pond will initially be at the tailings surface. Water will drain sideways through the tailings, gradually lowering the phreatic surface until it comes into equilibrium with the pond. If the same process were seen in plan view, it would show

that, initially, only the perimeter of the tailings beach would have a moisture content below saturation. The line demarcating saturated and partially unsaturated tailings would move concentrically towards the pond, at a rate controlled by the slow process of lateral drainge.

Fourth, laboratory tests of the tailings have shown that moisture contents remain at 85% of saturation or greater at heights of up to 35 feet above a phreatic surface. In other words, even as the water table within a TMA cell drops, which will only happen after tailings deposition ceases and consolidation rates slow, capillary forces will hold water within the tailings. Figure 2 shows the test results referred to. Note that the tailings remain essentially completely saturated up to 10 feet above the phreatic surface.

Fifth, not shown in Figures 1 and 2 are the effects of consolidation. As the tailings consolidate, the tailings surface will drop slightly. Water forced out of the tailings will exit to the nearest boundary, meaning it will flow upwards and/or horizontally to the surface. The overall effect will be to keep the phreatic surface even closer to the tailings surface than it would otherwise be.

Finally, the estimated oxygen transport rates are in fact not that sensitive to the assumed moisture content. As discussed above, the oxygen transport rate due to air phase diffusion varies with the square root of the diffusion coefficient. To increase the estimated oxygen flux by a factor of 10 would require that the oxygen diffusion coefficient be 100 times greater than estimated, or $1x10^{-6}$ m^2/sec. As shown by Figure 3.2 of the Oxygen Transport Modeling Report, that oxygen diffusion coefficient would correspond to a moisture content of from 40% to 55% of saturation. For comparison, the HELP model predicts that the tailings will be at 88 % of saturation even 50 years after the TMA cover is in place.

Hence it is our opinion that it is conservative to assume, for the oxygen transport modeling, that moisture contents in the tailings will be 85% or more of saturation, and consequently that oxygen diffusion coefficients in the tailings will be $1x10^{-8}$ m^2/sec or less.

In the discussions with WDNR, further information was requested on the potential for evaporation to affect the moisture content of the tailings surface. To illustrate that evaporation would not significantly affect the moisture content of the tailings surface, a simple one-dimensional simulation was completed. A discussion of the simulation follows.

The simulation used the numerical code SWMS-2D (Simunek, et al., 1994). The code solves the modified form of Richard's equation (see Attachment 2) using the method of finite elements. For a given set of initial and boundary conditions the code solves for pressure head, water content and flux at every node of the model domain.

SWMS-2D uses a set of closed form equations (van Genuchten, 1980) to approximate the unsaturated flow characteristics of soil. The functions were fitted to the measured water content vs. pressure head curve for the -10/-30 micron tailings. This fit is shown in Figure 3. The input parameters used in the simulation are shown in Table 1.

TABLE 1

Input Parameters to SWMS-2D

Parameter	Symbol	Value
Saturated water content	s	0.580 vol/vol
Residual water content	r	0.015 vol/vol
Saturated hydraulic conductivity	K_s	$1.05x10^{-3}$ ft/day
Fitting parameter	n	5.7896
Fitting parameter	α	0.02333

Prepared by: JS
Checked by: DH

The initial conditions for the tailings were set as saturated throughout the column. In mathematical terms this is expressed as:

$$q(x) = q_s \quad \text{for } 0 \leq x \leq 90$$

A net potential evaporation rate of 5.9 inches/year was applied to the upper boundary. Precipitation and pan evaporation data from a measuring station near the project site are presented in Table 2, and show how conservative the above assumption is. A net potential evaporation rate of 5.9 inches/year is equivalent to assuming that the maximum net monthly evaporation (i.e., pan evaporation minus precipitation for the month of July) could be sustained for ten months of the year. In mathematical terms the upper boundary condition is expressed as:

$$q \leq \text{Potential Evaporation}$$

TABLE 2
Monthly Precipitation and Evaporation[1]

Month	Average Monthly Precipitation (inches)	Average Monthly Lake Evaporation (inches)	Monthly Net Precipitation (inches)	Monthly Net Evaporation (inches)
Jan	0.94	0.29	0.65	
Feb	0.57	0.37	0.20	
Mar	1.90	0.94	0.96	
Apr	2.73	2.31	0.42	
May	3.23	3.73		0.50
Jun	3.84	4.30		0.46
Jul	3.58	4.15		0.57
Aug	3.30	3.61		0.31
Sep	3.96	2.31	1.65	
Oct	2.98	1.89	1.09	
Nov	2.67	0.88	1.79	
Dec	1.21	0.33	0.88	

Prepared by: JK
Checked by: DH

[1] Source is USACE database, Rainbow Reservoir

Averages taken over years 1984-1996

A pressure head of zero was applied to the lower boundary. This boundary condition represents the lower drains. In mathematical terms this is expressed as:

$$h = 0$$

In the first simulation, no precipitation was allowed. Figure 4 shows the predicted water content profiles for 1 day, 10 days, 20 days, 30 days, 60 days and one year. The saturation profile after 60 days shows that tailings remain at 98% saturation at the surface. The one year profile shows that the tailings remain 93% saturated at the surface. Note that these results do not account for water inputs from precipitation or sprinkling, nor for the insulating effects of winter snow and ice cover.

In the second simulation, the calculated average monthly precipitation and potential evaporation values shown in Table 2 were applied as the upper boundary condition. In this case, the tailings were predicted to remain completely saturated throughout the year.

The modeling illustrates that it is unlikely that evaporation will result in tailings moisture saturation less than the value of 85% assumed in the oxygen transport modeling. These results further support the conclusion that the oxygen diffusion coefficients used in the Oxygen Transport Modeling Report are conservatively high.

c. The initial and boundary conditions for each simulation reported in the Oxygen Transport Modeling Report are provided in Attachment 3.

d. NMC has committed to replacing the geomembrane in the final cover system in the future, if necessary. As part of the previously referenced discussions with the WDNR and USCOE, it was agreed that the additional information provided for this response

should be focused on illustrating the effects of the geomembrane included in the final cover design from the standpoint of oxygen transport.

HELP model simulations were re-run without a geomembrane in the final cover system. The resulting estimates of water content and porosity in each layer are shown in Table 3. To predict oxygen flux through the cover, the estimates of water content were then input to the oxygen transport model described in the TMA Groundwater Quality Performance Evaluation. The model predicted an oxygen flux of 2×10^{-6} mol O_2 m^{-2} s^{-1}, or 63 mol O_2 m^{-2} yr^{-1}. The analysis shows that the oxygen flux for the final cover with the geomembrane is approximately 100 times less than that predicted for a hypothetical cover without the geomembrane.

The conditions described in part 2 of comment 30d fall somewhere between the above extreme and the cases presented in Sections 3.4 and 3.5 of the Oxygen Transport Modeling Report.

TABLE 3

Water Contents in TMA Cover Materials
Without a Geomembrane in the Final Cover System

Layer	Thickness (inches)	Water Content (vol/vol)	Total Porosity (vol/vol)
Topsoil	6	0.3328	*0.463*
Rooting layer	36	0.2469	*0.398*
Drainage layer	12	.0396	*0.397*
GCL	0.5	0.75	0.75
Low permeability soil	12	0.284	*0.501*
Grading layer	36	0.244	*0.398*
Tailings[1]	n/a	0.06	*0.580*

n/a = not applicable

Prepared by: JPS
Checked by: DH

[1] Water content in the tailings layer was assumed to be very low in order to provide a conservative estimate of flux through the cover.

In conclusion, the above responses and following attachments address issues raised in Comment 30 of WDNR's letter of Septembter 26, 1997, and in subsequent telephone communications with NMC, FVD, WDNR and USCOE. This memorandum should be considered an addendum to the April 1997 Crandon Project TMA Oxygen Transport Modeling Report.

Yours truly,

STEFFEN ROBERTSON AND KIRSTEN (CANADA) INC.

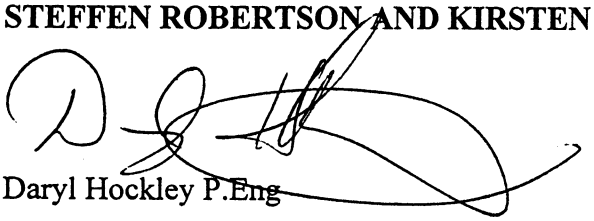

Daryl Hockley P.Eng
Principal Engineer

References

Foth & Van Dyke; Steffen Robertson and Kirsten (Canada), Inc.; HSI GeoTrans, Inc.; May 1997. *Crandon Project Tailings Management Area Groundwater Quality Performance Evaluation.*

HSI GeoTrans, Inc., August 1996. *Numerical Simulation of the Effect on Groundwater and Surface Water of the Proposed Zinc and Copper Mine Near Crandon, Wisconsin.*

Simunek, J., T. Vogel, and M.T.H. Van Genuchten, 1994. *The SWMS2D Code for Simulating Water Flow and Solute Transport in 2-Dimensional Variably Unsaturated Media.* Ver. 1.2, Research Report 132, February 1994. U.S. Salinity Laboratory, Dept. of Agricultural Research Service, U.S. Dept. of Agriculture, Riverside, California.

Van Genuchten, M.T.H., 1980. "A Closed Form Equation for Predicting the Hydraulic Conductivity of Unsaturated Soils". *Soil Sci. Soc. Am. J.*, 44, pp. 892–898.

FIGURES

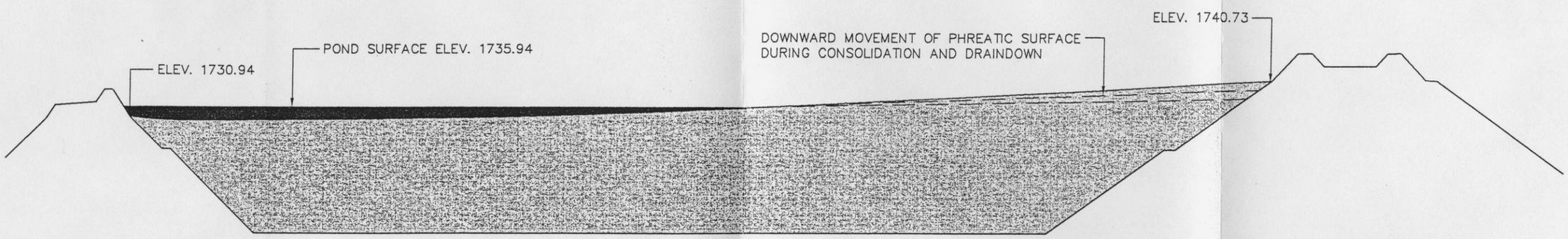

SECTION A–A THROUGH CELL TMA–2

VERTICAL SCALE EXAGGERATED

FILE REF: SECTION.DWG

STEFFEN ROBERTSON AND KIRSTEN
Consulting Engineers

FOTH & VAN DYKE

OXYGEN TRANSPORT ADDENDUM

SECTION A–A
(THROUGH TMA–2)

PROJECT NO.	DATE	APPROVED	FIGURE
F107107	FEB. 1998		1

4.2-12-188

FILE REF: f107_fig2.xls

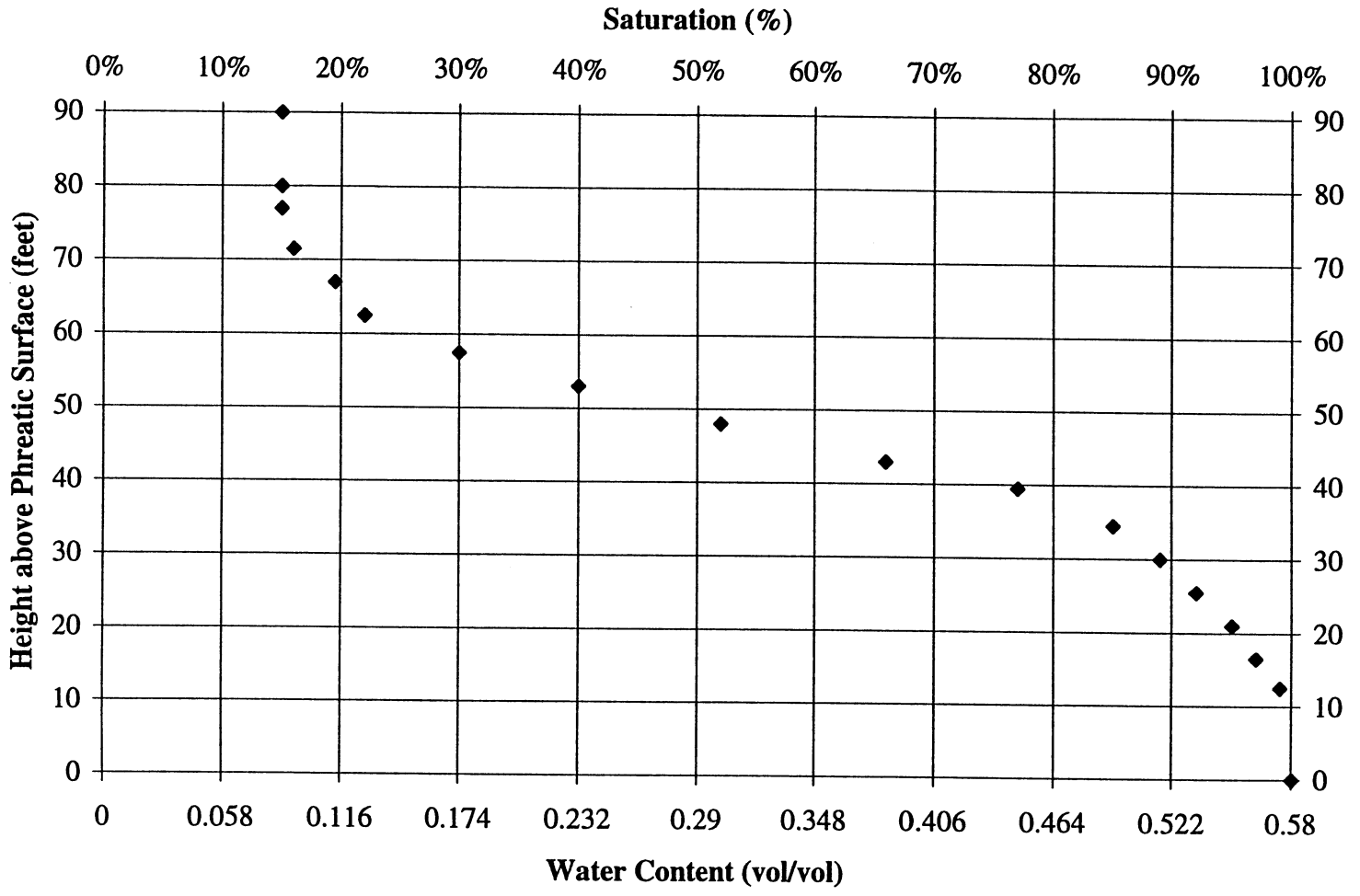

STEFFEN ROBERTSON AND KIRSTEN *Consulting Engineers and Geoscientists*				OXYGEN TRANSPORT ADDENDUM
				EXPERIMENTAL SOIL WATER RETENTION CURVE
FOTH & VAN DYKE	PROJECT F107107	DATE Feb. 1998	APPROVED DH	FIGURE **2**

FILE REF: f107_fig3.xls

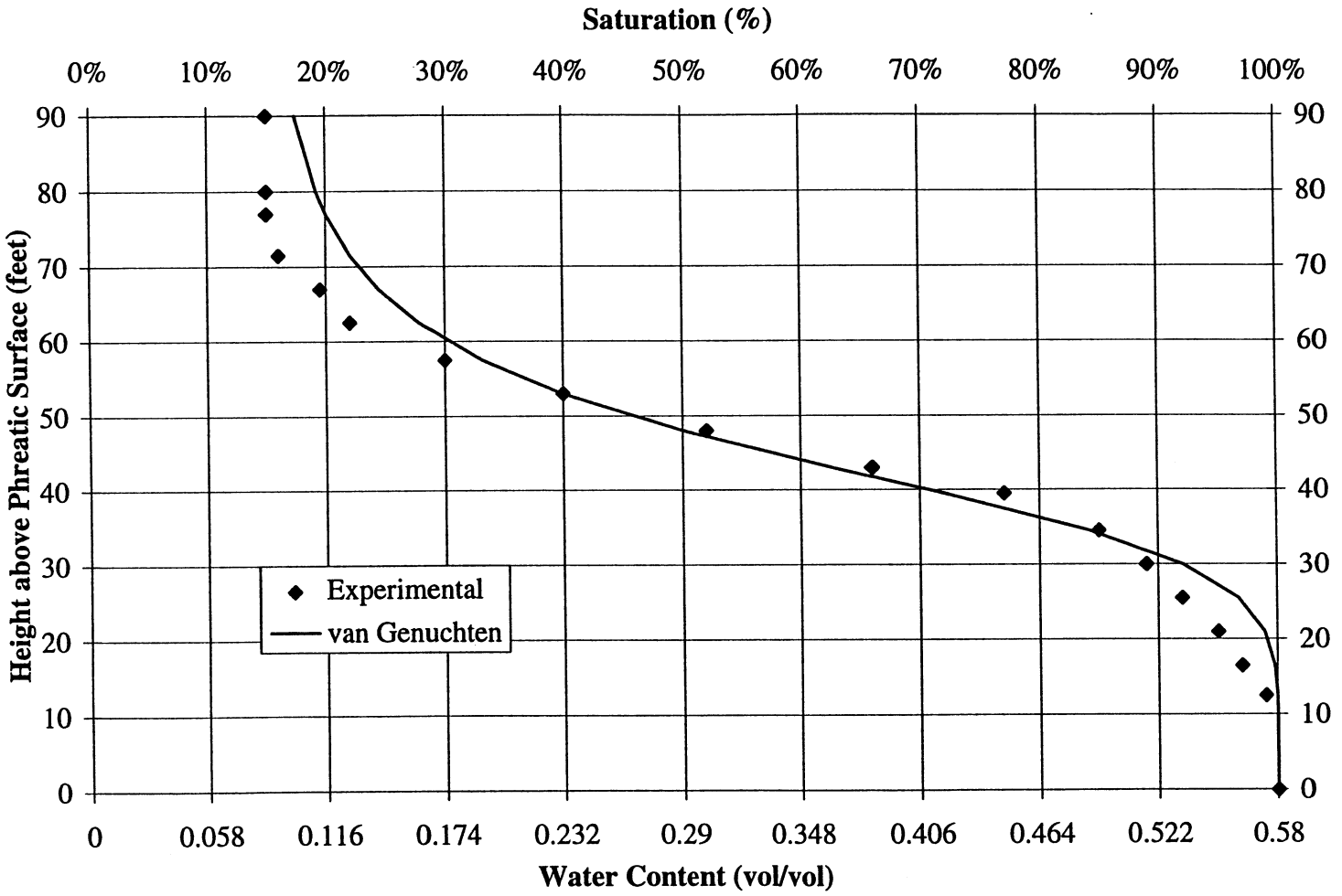

STEFFEN ROBERTSON AND KIRSTEN *Consulting Engineers and Geoscientists*				OXYGEN TRANSPORT ADDENDUM
				MODEL SOIL WATER RETENTION CURVE
FOTH & VAN DYKE	PROJECT F107107	DATE Feb. 1998	APPROVED DH	FIGURE 3

FILE REF: f107_fig4.xls

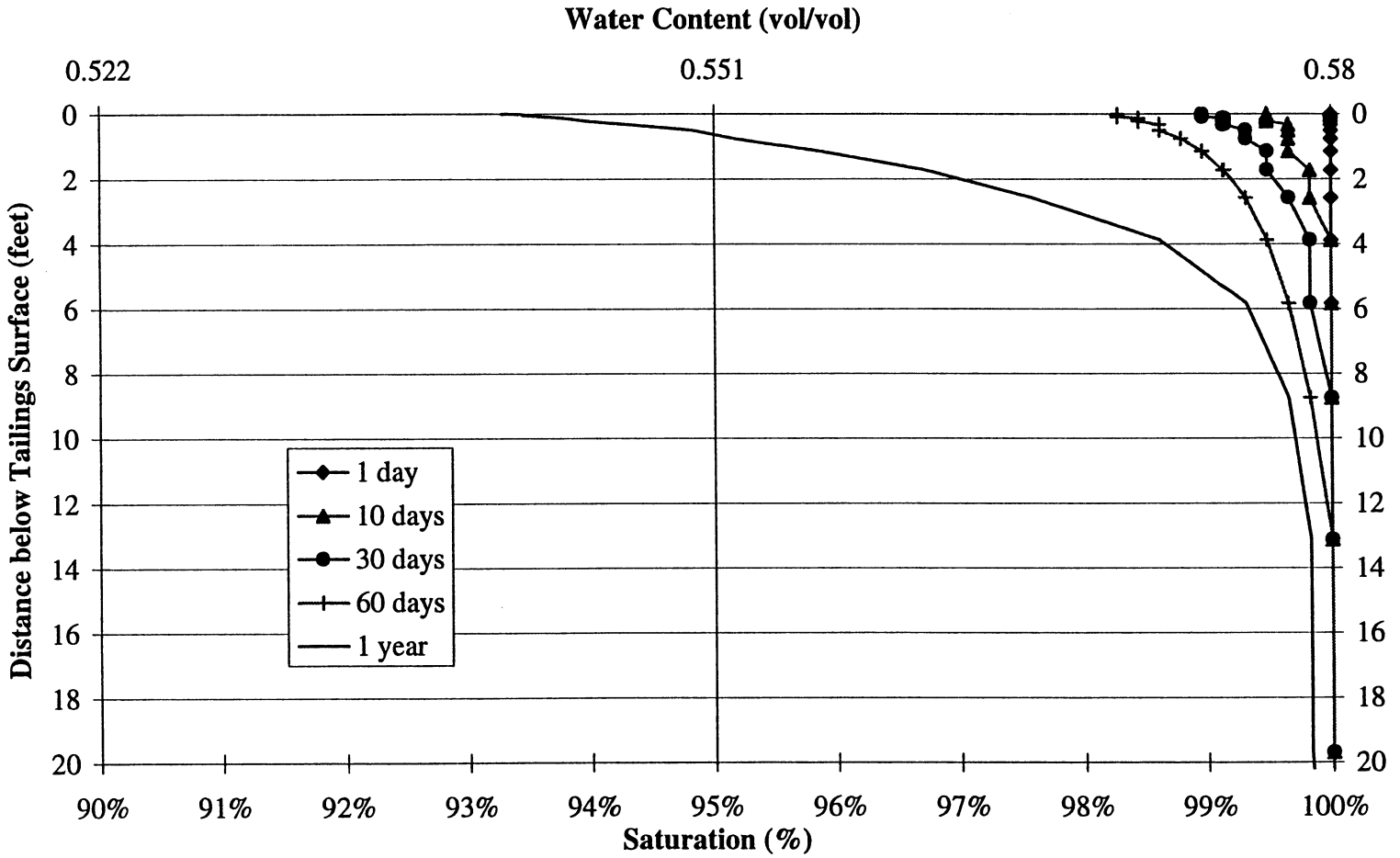

STEFFEN ROBERTSON AND KIRSTEN *Consulting Engineers and Geoscientists*	OXYGEN TRANSPORT ADDENDUM			
	RESULTS OF SWMS-2D SIMULATION WITH HIGH EVAPORATION RATE			
FOTH & VAN DYKE	PROJECT F107107	DATE Feb. 1998	APPROVED DH	FIGURE 4

Attachment 1

Sensitivity Analyses of Oxygen Transport Models

ATTACHMENT 1
SENSITIVITY ANALYSES OF OXYGEN TRANSPORT MODELS

In completing the model runs reported in the Oxygen Transport Model Report, input parameters were selected to give conservatively high estimates of oxygen flux. Nonetheless it is informative to further vary input parameters in order to illustrate the sensitivity of the predictions to each input.

Sensitivity analyses were conducted on all significant variables in each transport model. Two sensitivity runs were completed for each transport model: one using the combination of inputs that lead to the minimum oxygen flux, and one using the combination of inputs that lead to the maximum flux. In general, the input values for each parameter were obtained by doubling or halving the value used in the predictive run. The results should therefore not be interpreted as representing reasonable predictions.

1. Advection in water (Section 3.1)

The flux of oxygen associated with advection is given by:

Flux (mol O_2 m^{-2} yr^{-1}) = *Concentration* (mol O_2 L^{-1}) * *Flowrate* (m yr^{-1}) * 1000 (L m^{-3}) (1-1)

Advection in water was considered in cases 1a, 1b and 2/3. Both O_2 concentration and flowrate were varied for the sensitivity runs.

The maximum O_2 solubility in water is limited by temperature. Appelo and Postma (1994) list a range from 8.26 mg/L (2.6 x 10^{-4} mol O_2 L^{-1}) at 25 °C to12.8 mg/L (4 x 10^{-4} mol O_2 L^{-1}) at 5 °C. This range was used for the sensitivity analyses.

For Case 1a the flowrate was 4 x 10^{-8} m/s, based on a hydraulic conductivity of 4 x 10^{-8} m/s and a vertical gradient of 1 for gravity drainage. For the sensitivity analysis the range of hydraulic conductivities used was 2 x 10^{-8} m/s to 8 x 10^{-8} m/s.

For Case 1b the flowrate was 15 in./yr (1.21 x 10^{-8} m/s), based on the range 12.5 to16.2 in/yr (1 x 10^{-8} to1.31 x 10^{-8} m/s) predicted by the HELP modeling reported by Foth & Van Dyke (1997). This original range was used for the sensitivity analysis.

For Cases 2 & 3 the flowrate was 0.0001 in/yr (8.0×10^{-14} m/s) based on the above referenced HELP modelling. The range 5×10^{-5} to 2×10^{-4} in/yr (4.0×10^{-14}-1.6×10^{-13} m/s) was used for the sensitivity analysis.

Table 1 displays the variables used and results obtained for the advection through water sensitivities.

TABLE 1
Advection in Water - Sensitivity Analyses

	Case 1a Process Water		Case 1b Uncovered Surface		Case4 2 & 3 Through Holes	
Parameter	min	max	min	max	min	max
O_2 Concentration ($molO_2 m^{-3}$)	0.26	0.40	0.26	0.40	0.26	0.40
Flow Rate (m/s)	2.00E-08	8.00E-08	1.00E-08	1.31E-08	4.00E-14	1.60E-13
O_2 Flux (mol $m^{-2}s^{-1}$)	5.20E-09	3.20E-08	2.62E-09	5.22E-09	1.05E-14	6.44E-14

2. Diffusion in tailings pore water (Section 3.2)

Diffusion of oxygen in tailings pore water was predicted from:

$$j_0 = C_0\sqrt{rD} \qquad (2\text{-}1)$$

All three variables (C_0, D and r) were varied for the sensitivity runs.

- The oxygen concentration range for the sensitivity runs was the same as in Section 1 above.
- The diffusion coefficient used in the predictive run was 2.1×10^{-9} m^2/s. A range of 1.05×10^{-9} m^2/s to 4.2×10^{-9} m^2/s was used for the sensitivity runs.
- The first order reaction rate constant used in the predictive run was 1.07×10^{-4} s^{-1}. A range of 5.35×10^{-5} s^{-1} to 2.14×10^{-4} s^{-1} was used for the sensitivity runs.

Table 2 summarizes the results of the sensitivity runs for diffusion in tailings pore water.

TABLE 2
Diffusion in Water - Sensitivity Analyses

Parameter	Half Orig Values Minimum Flux	Double Orig Values Maximum Flux
D (m^2/s)	1.05E-09	4.20E-09
r (s^{-1})	5.35E-05	2.14E-04
Co (mol m^{-3})	0.26	0.40
Flux (mol O_2 m^{-2} s^{-1})	6.16E-08	3.79E-07

3. Diffusion in tailings pore air (Section 3.3)

One-dimensional diffusion of oxygen into unsaturated tailings was estimated using the governing equation for oxygen diffusion:

$$\frac{dC}{dt} = \frac{\partial}{\partial x}\left(D\frac{\partial C}{\partial x}\right) - rC^n \qquad (3\text{-}1)$$

For n=1 (i.e. first order reaction), flux is obtained analytically using equation 3-1. For n <>1 the finite difference model was used to estimate the oxygen flux.

The concentration of oxygen in air does not vary significantly. The other variables (D and r) were varied by halving and doubling the values used in the predictive runs. Table 3 summarizes the input parameters and the results of these sensitivity runs.

TABLE 3

Sensitivity Analyses for Diffusion in Air

First Order Model		
	Half Original Values	Double Original Values
	Minimum Flux	Max Flux
D (m^2/s)	5.00E-09	2.00E-08
r (s^{-1})	2.35E-04	9.40E-04
Flux (mol m^2 s^{-1})	9.65E-06	3.86E-05

Zero Order Model		
	Half Original Values	Double Original Values
	Minimum Flux	Max Flux
D (m^2/s)	5.00E-09	2.00E-08
r (mol m^3 s^{-1})	2.10E-03	8.40E-03
Flux (mol m^2 s^{-1})	1.12E-05	5.08E-05

Half Order Model		
	Half Original Values	Double Original Values
	Minimum Flux	Max Flux
D (m^2/s)	5.00E-09	2.00E-08
r (mol $m^{0.5}m^{-1.5}$ s^{-1})	5.70E-04	2.28E-03
Flux (mol m^2 s^{-1})	7.97E-06	2.88E-05

Mixed Model		
	Half Original Values	Double Original Values
	Minimum Flux	Max Flux
D (m^2/s)	5.00E-09	2.00E-08
r	9.90E-04	3.96E-03
Flux (mol m^2 s^{-1})	9.98E-06	3.05E-05

4. Diffusion through intact cover (Section 3.4)

The flux of oxygen through a cover was predicted from:

$$j = \frac{C_0\sqrt{r_t D_t}\cdot EXP}{\frac{1}{H_m}\sqrt{r_t D_t}\cdot EXP + 1} \qquad (4\text{-}1)$$

where:

$$EXP = \frac{\exp\left[l_t\sqrt{\frac{r}{D_t}}\right] - \exp\left[-l_t\sqrt{\frac{r}{D_t}}\right]}{\exp\left[l_t\sqrt{\frac{r}{D_t}}\right] + \exp\left[-l_t\sqrt{\frac{r}{D_t}}\right]} \qquad (4\text{-}2)$$

$$H_m = \frac{1}{\frac{l_1}{D_1} + \frac{l_2}{D_2} + \frac{l_3}{D_3} + \cdots} \qquad (4\text{-}3)$$

where:

j - molar flux (mol m^{-2} s^{-1})

l_1, l_2, l_3 - thickness of non-consuming cover layers (m);

D_1, D_2, D_3 - diffusivities for cover layers (m^2 s^{-1});

D_t - diffusivity for reactive tailings (m^2 s^{-1});

r_t - first-order rate constant for reactive tailings (s^{-1})

H_m - mass transfer coefficient (m s^{-1})

Inspection of the equation shows that low diffusion layers will control flux through the system. In the predictive run, the diffusion coefficient of the HDPE was estimated to be $3x10^{-12}$ m^2s^{-1}, about six orders of magnitude lower than the soil layers. The sensitivity analyses for this process were therefore based on doubling and halving of this parameter. Table 4 summarizes the results of this sensitivity analysis.

TABLE 4
Diffusion Through Intact Cover

	Half Original Values	Double Original Values
	Minimum Flux	**Max Flux**
D_{HDPE} (m^2/s	1.50E-12	6.00E-12
Flux (mol m^{-2} s^{-1})	8.46E-09	3.38E-08

5. Diffusion Through Defects in Cover (Section 3.5)

The governing equation for oxygen diffusion in two dimensions is

$$\frac{dc}{dt} = \frac{d}{dx} D \frac{dc}{dx} + \frac{d}{dy} D \frac{dc}{dy} - rC^n \qquad (5\text{-}1)$$

Diffusive fluxes through defects were calculated from the two-dimensional finite-difference diffusion model. Previous one-dimensional analyses showed that flux was not sensitive to rate order (n), therefore these analyses were only carried out for a rate order of n=1.

Defect width (w), the tailings diffusion constant (D) and the first order reaction rate (r) were varied for the sensitivity runs:

- The defect width assumed for the predictive run was 1 cm. The widths used for the sensitivity analysis were 0.5 cm and 2 cm.

- The predictive model used a tailings diffusion coefficient of 3.0 x 10^{-6} m^2s^{-1}. For this sensitivity analysis, 1.5 x 10^{-6} m^2s^{-1} and 6.0 x 10^{-6} m^2s^{-1} were used.

- The first order reaction rate constant was varied as in Section 2 above.

Table 5 summarizes the results of the sensitivity runs for diffusion through holes in the cover.

TABLE 5
Diffusion through holes in cover

	Half Original Values	Double Original Values
	Minimum Flux	Max Flux
width (m)	5.00E-03	2.00E-02
r (s^{-1})	5.35E-05	2.14E-04
Dtail m^2/s	1.50E-06	6.00E-06
Flux (mol O2 m^{-2} s^{-1})	2.49E-08	9.96E-08

6. Barometric pumping through defects in cover (Section 3.6)

The equation for two dimensional air advection through a heterogeneous domain is given by:

$$n\frac{dP}{dt} = \frac{\partial}{\partial x}(\alpha\frac{\partial P}{\partial x}) \qquad (6\text{-}1)$$

where:

$$\alpha = \frac{\rho R T k_a}{m\mu} \qquad (6\text{-}2)$$

Barometric pumping through defects in the cover was calculated using the two-dimensional finite-difference barometric pumping model.

Air permeabilities for the cover, tailings and till were varied for the sensitivity runs.

- The predictive run used a defective cover permeability of 3.5×10^{-12} m^2. For this analysis, a range of 1.75×10^{-12} m^2 to 7.0×10^{-12} m^2 was used.

- The predictive run model used a tailings permeability of 2.0×10^{-14} m^2. For this analysis, a range of 1.0×10^{-14} m^2 to 4.0×10^{-14} m^2 was used.

- The predictive run used a till permeability of 3.5×10^{-12} m^2. For this analysis, a range of 1.75×10^{-12} m^2 to 7.0×10^{-12} m^2 was used.

Table 6 summarizes the results of this sensitivity analysis.

TABLE 6
Barometric Pumping through Cover Holes

	Half Original Values	Double Original Values
	Minimum Flux	Max Flux
Kcov (m^2)	1.75E-12	7.00E-12
Ktail (m^2)	1.00E-14	4.00E-14
Ktill (m^2)	1.75E-12	7.00E-12
Flux (mol m^{-2} s^{-1})	1.52E-08	3.53E-08

7. Diffusion through embankments (Section 3.7)

Oxygen diffusion through the TMA sidewalls is governed by equation 5-1 above. Fluxes were calculated from the two-dimensional finite-difference diffusion model:

Air diffusion coefficients for the cover, embankment soil and liner were varied for the sensitivity runs.

- The original model used a till diffusion coefficient of 3.0×10^{-6} m^2s^{-1}. For this analysis, a range of 1.5×10^{-6} m^2 s^{-1} to 6.0×10^{-6} m^2 s^{-1} was used.

- The original model used a liner diffusion coefficient of 3.0×10^{-9} m^2s^{-1}. For this analysis, a range of 1.5×10^{-9} m^2 s^{-1} to 6.0×10^{-9} m^2 s^{-1} was used.

Table 7 summarizes the results of this sensitivity analysis

TABLE 7
Diffusion through TMA Embankment

	Half Original Values	Double Original Values
	Minimum Flux	Maximum Flux
Dliner m^2/s	1.50E-09	6.00E-09
Dtill m^2/s	1.50E-06	6.00E-06
Top (mol O2 m^{-2} s^{-1})	2.60E-08	1.05E-07
Mid Phase 2 (mol O2 m^{-2} s^{-1})	1.86E-08	7.48E-08
Mid Phase 1 (mol O2 m^{-2} s^{-1})	8.97E-08	3.61E-08
Base (mol O2 m^{-2} s^{-1})	3.36E-10	1.35E-09

8. Barometric pumping through embankments (Section 3.8)

Barometric pumping through the TMA sidewalls was predicted using equation 6-1 above. Fluxes were calculated from the two-dimensional finite-difference barometric pumping model.

Air permeability coefficients for the cover, embankment soil and tailings were varied for the sensitivity runs. The ranges were the same as in Section 6 above.

Table 8 summarizes the results of this sensitivity analysis

TABLE 8
Barometric Pumping through Embankments

	Half Orig Values Minimum Flux	Double Orig Values Maximum Flux
ktail (m/s)	1.00E-14	4.00E-14
ktill (m/s)	1.75E-12	7.00E-12
Flux (mol O2 m^{-2} s^{-1})	7.71E-09	2.29E-08

9. References

Appelo, C.A.J. and Postma, D. *Geochemistry, Groundwater and Pollution.* A.A. Balkema, Rotterdam, 1994.

Attachment 2

Equations Solved by SWMS-2D

ATTACHMENT 2
EQUATIONS SOLVED BY SWMS-2D

The governing equation for two dimensional isothermal Darcian flow of water in a variably saturated rigid porous medium, where the air phase plays an insignificant role in the liquid flow process, is given by the following modified form of the Richard's equation:

$$\frac{\partial \theta}{\partial t} = \frac{\partial}{\partial x_i}\left[K(h)\left(K_{ij}^{A} \frac{\partial h}{\partial x_j} + K_{ij}^{A} \right)\right] - S \quad (1)$$

where θ the volumetric water content [L^3L^{-3}], h is the pressure head [L], S is a sink term [T^{-1}], x_i (I=1,2) are the spatial coordinates [L], t is time [T], K_{ij}^{A} are components of a dimensionless anisotropy tensor K^A and K is the unsaturated hydraulic conductivity function [LT^{-1}] The anisotropy tensor K_{ij}^{A} in (1) is used to account for an anisotropic medium. The diagonal entries of K_{ij}^{A} equal one and the off-diagonal entries zero for an isotropic medium.

The soil water retention θ (h), and hydraulic conductivity, $K(h)$, functions in SWMS_2D are given by:

$$\theta(h) == \begin{cases} \theta_r + \dfrac{\theta_s - \theta_r}{\left[1 + |\alpha h|^n\right]^m} & h < 0 \\ \theta_s & h \geq 0 \end{cases} \quad (2)$$

$$m = 1 - \frac{1}{n} \quad n > 1 \quad (3)$$

$$S_e = \frac{\theta - \theta_r}{\theta_s - \theta_r} \quad (4)$$

$$K_r = S_e^{1/2}\left[1-\left(1-S_e^{1/m}\right)^m\right]^2 \quad (5)$$

$$K(h) = \begin{cases} K_s K_r(h) & h < 0 \\ K_s & h \geq 0 \end{cases} \quad (6)$$

in which θ_r and θ_s denote the residual and saturated water contents, respectively: K_s is the saturated hydraulic conductivity k_r is the relative hydraulic conductivity function; α and n are fitting parameters; and S_e is the saturated fraction.

Attachment 3

Initial and Boundary Conditions

ATTACHMENT 3
INITIAL AND BOUNDARY CONDITIONS

The following sections provide initial and boundary conditions for each model used in the report.

1. Advection in Water (section 3.1)

The steady-state boundary condition at the tailings surface was:

$$C(x=0,t)=C_0$$

where:

$C_0=4x10^{-1}$ mol O_2 m^{-3} (the upper limit of oxygen solubility in water at 5 ^{0}C).

2. Diffusion in tailings pore water (section 3.2)

Steady state boundary conditions were:

$$C(0,t)=C_0$$

$$C(\infty,t)=0.0$$

where:

$C_0=4x10^{-1}$ mol O_2 m^{-3} (the upper limit of oxygen solubility in water at 5 ^{0}C).

3. Diffusion in tailings pore air (Section 3.3)

A diagram of the one-dimensional modeling domain with boundary conditions is shown in Figure 3.1 of the report. Boundary conditions were:

$$\frac{dC}{dx}(L,t)=0$$

$$C(0,t)=C_0$$

where:

C_0=8.9 mol O_2 m^{-3} (concentration oxygen in the atmosphere at 15 ^{0}C).
L=30 m (length of modeling domain)

Concentrations through the column were intentionally set to C_o but the model was run to obtain the reported results.

4. Diffusion through intact cover (Section 3.4)

Steady state boundary conditions were:

$C(0,t)=C_0$
$C(\infty,t)=0.0$

where:
C_0=8.9 mol O_2 m^{-3} (concentration oxygen in the atmosphere at 15 ^{0}C).

5. Diffusion through defects in cover (Section 3.5)

A diagram of the two-dimensional modeling domain with boundary conditions is shown in Figure 3.3 of the report. Boundary conditions were as follows:

At holes in the cover:

$C(t)=C_0$

Everywhere else:

$$\frac{dC}{dx}(t) = 0$$

where x is a vector orthogonal to the modeling domain.

6. Barometric pumping through defects in cover (Section 3.6)

Again, a diagram of the two-dimensional modeling domain with boundary conditions is shown in Figure 3.3 of the report.

At defects in the cover, the boundary condition was:

$$P(t)=P_0$$

where P_0 was input as the hourly atmospheric pressure readings from a 26-day pressure cycle extracted from the 1995 barometric data collected at a Green Bay weather station.

Everywhere else:

$$\frac{dP}{dx}(t) = 0$$

Where x is a vector orthogonal to the modeling domain.

7. Diffusion through embankments (Section 3.7)

A diagram of the two-dimensional modeling domain with boundary conditions is shown in Figures 3.6 and 3.7 of the report for the large and small embankments, respectively.

At the soil-air interface, the boundary condition was:

$$C(t)=C_0$$

At the tailings-soil interface, the boundary condition was:

$$C(t)=0$$

Concentrations were initially set to C_0 but the model was run to steady state to obtain the reported results.

8. Barometric Pumping (Section 3.8)

A diagram of the two-dimensional modeling domain with boundary conditions is shown in Figures 3.8 and 3.9 of the report for the large and small embankments, respectively.

At the soil-air interface, the boundary condition was:

$$P(t)=P_0$$

where P_0 was input as the hourly atmospheric pressure readings from a 26-day pressure cycle extracted from the 1995 barometric data collected at a Green Bay weather station.

Along all other model boundaries (i.e., cover, interior of pile), the boundary condition was:

$$\frac{dP}{dx}(t) = 0$$

F107107/1

CRANDON PROJECT TMA
OXYGEN TRANSPORT MODELING

Prepared for:

FOTH & VAN DYKE
2737 S. Ridge Road
P.O. Box 19012
Green Bay, Wisconsin
54307-9012

Prepared by:

STEFFEN ROBERTSON AND KIRSTEN (CANADA) INC.
Suite 800, 580 Hornby Street
Vancouver, B.C. V6C 3B6
Tel: (604) 681-4196 • Fax: (604) 687-5532

APRIL, 1997

F107107/1

CRANDON PROJECT TMA
OXYGEN TRANSPORT MODELING

TABLE OF CONTENTS

LIST OF TABLES

LIST OF FIGURES

LIST OF ATTACHMENTS

F107107/1

CRANDON PROJECT TMA
OXYGEN TRANSPORT MODELING

1.0 INTRODUCTION

The oxygen transport modeling reported herein is part of a larger investigation to characterize the geochemical processes that will occur in the Tailings Management Area (TMA) of the proposed Crandon Project. Other components of the investigation include:

- Laboratory tests of the tailings under oxidizing conditions, and tests of the response of limestone amended tailings to inputs of acidity;
- Mineralogical characterization of the tailings before and after the above tests;
- Modeling of the geochemical reactions within the TMA; and,
- Modeling of solute transport in groundwater down-gradient of the TMA.

The objective of the oxygen transport modeling is to estimate the rate at which oxygen could enter the Crandon TMA at various stages in its operation, closure and long term management. Oxygen is the primary oxidant of the sulfide minerals that occur in the Crandon tailings. The sulfide oxidation reactions are in turn the primary sources of soluble metals, sulfate, and acidity. Quantifying the rate at which oxygen can enter the system provides an upper bound on the rate at which sulfide oxidation and the subsequent reactions can take place.

The report is organized in five sections. Section 2 describes the cases and oxygen transport mechanisms that were considered. Section 3 presents the equations, inputs and outputs for models of each transport mechanism. Section 4 presents the results of the modeling by case, in terms of alkalinity requirements. Section 5 summarizes the major conclusions of the study.

Steffen, Robertson and Kirsten
April, 1997

2.0 DESCRIPTION OF CASES

The dominant mechanisms of oxygen transport to the tailings will change during the operation, closure, and long term management of the TMA. To represent the different conditions that will arise, the oxygen transport modeling considered the following four cases:

- Case 1a, During tailings deposition;
- Case 1b, During the tailings consolidation period, (after deposition and prior to cover construction);
- Case 2, After construction of the cover; and,
- Case 3, After an assumed degradation of the flexible geomembrane liner (HDPE) in the composite liner beneath the tailings.

The four cases are depicted schematically in Figures 2.1 to 2.4, and discussed in the following sections.

2.1 Case 1a: During Tailings Deposition

Case 1a represents the period in which tailings will be deposited into a cell. The tailings will be transported to the TMA in a slurry, and deposited from a series of spigots located around the perimeter of each cell. The spigots will be activated in sequence so that the deposition point will move around the cell. It is expected to take approximately two months for one complete circuit of a cell.

The sequence of events that follow tailings deposition is well established by experience at other impoundments. After the tailings slurry leaves the spigots, it will begin to separate. Coarser grained tailings will settle nearer the spigots, forming a "beach". Finer grained tailings and the remaining slurry water will flow towards the center of the impoundment, forming a pond. The fine-grained tailings will settle in the pond area, and the slurry water will be largely recovered directly from the central pond. A small amount of water will percolate through the tailings and be recovered by the underdrain system. As a result of the continual movement of the deposition points,

tailings beaches are expected be localized and small, and the tailings and pond will form a uniform concentric pattern within each cell.

The mechanisms with a potential to transport oxygen into the tailings during the deposition period will be:

- Advection of oxygen as process water percolates through the tailings to the drainage layer;
- Diffusion of oxygen through the water-saturated pore space in areas where the pore water is stagnant; and,
- Diffusion of oxygen through any unsaturated pore space in the beach area.

Given the rapid deposition cycle and the water retention capacity of the tailings, it is expected that the tailings beaches will remain saturated throughout the deposition period. The third mechanism above is therefore not expected to be active except for very short periods in localized areas.

2.2 Case 1b: During Tailings Consolidation

Case 1b represents the period after tailings deposition is complete, and prior to construction of the cover. After deposition of tailings to a cell is completed, the tailings will be allowed to consolidate. During the consolidation period, the weight of overlying tailings will drive water out of the tailings pore space, resulting in an increase in both the overall density and strength of the tailings mass. After one to two years, the tailings will have gained sufficient strength to support construction of the cover.

During the consolidation period, the mechanisms with a potential to transport oxygen into the tailings will be:

- Advection of oxygen in water that infiltrates into the tailings surface;
- Diffusion of oxygen in water, through the tailings pore space that remains water-saturated; and,
- Diffusion of oxygen in air, through the tailings pore space that becomes unsaturated.

Experience at other tailings impoundments shows that tailings consolidation will follow a well defined sequence of steps. Initially, water being driven out of the tailings pores will take the shortest path to a drainage boundary. Water in the upper portions of the tailings will move upwards to the tailings surface, while water in the lower half of the tailings will move downwards to the drainage system. As a result of the upward flow, the tailings surface will initially remain water saturated. As the excess pore pressure in the tailings is dissipated, flow will become dominated by gravity, and will be predominantly downwards throughout the tailings. At that time, the upper layers of tailings will begin to become unsaturated. As the downward drainage continues, the tailings would eventually reach an equilibrium water content. The water content at each depth in the tailings would then be determined by the equilibrium between elevation head and capillary suction, which has been characterized in earlier work (Colorado School of Mines Research Institute, 1982).

The patterns of water flow will exert a strong influence on oxygen transport during the consolidation period. As long as water is flowing upwards to the surface of the tailings mass, it cannot be bringing oxygen into the tailings. However, once flow becomes predominantly downwards, input of oxygen carried by the water becomes possible. As the upper layers of tailings start to become unsaturated, oxygen can be transported by diffusion through the air in the unsaturated pores. The HELP modeling presented by Foth & Van Dyke (1997) indicates that after two years of (downwards) drainage, the tailings will remain more than 90% saturated. The same modeling indicates that it will be approximately 40 years after the TMA closure before drainage ceases.

2.3 Case 2: After Cover Construction

Case 2 represents the period after construction of the cover, and prior to any potential degradation of the flexible geomembrane liner (HDPE) included in the composite liner system of the TMA. The cover constructed over the tailings will consist of the layers shown in Figure 2.5. The cover also includes a geomembrane, which CMC has committed to maintaining in perpetuity.

The mechanisms with a potential to transport oxygen through the cover will be:

- Advection of oxygen in water that infiltrates through defects in the geomembrane;
- Diffusion of oxygen through the cover and directly through the geomembrane;
- Diffusion of oxygen through defects in the geomembrane; and,
- Advection of oxygen in air that is "pumped" through defects in the geomembrane by changes in barometric pressure.

The cover is expected to limit the rate at which oxygen enters the tailings surface. In relative terms, oxygen transport through the underside of the TMA may then become more significant. Mechanisms with a potential to transport oxygen to the underside of the TMA will be:

- Diffusion and/or advection of oxygen into the TMA via the drainage system;
- Diffusion of oxygen to and through the sidewalls and base of the TMA; and,
- Advection of oxygen by barometric pumping to the sidewalls and base of the TMA, followed by diffusion directly through the intact liner.

2.4 Case 3: After an Assumed Degradation of the Geomembrane in the Liner

Case 3 considers oxygen transport after an assumed complete degradation of the geomembrane in the liner (under the tailings). As noted in the May 1995 TMA Feasibility Report (Foth & Van Dyke, 1995a), the design for the TMA includes a composite liner, with an HDPE geomembrane. Case 3 is intended to address the question of what would occur if the geomembrane in the liner were to degrade. The current TMA liner design specifies high density polyethylene (HDPE) as the geomembrane of choice. CMC has estimated that the geomembrane will have a design life of hundreds of years. To address the question of what would occur in the TMA if the geomembrane were to degrade, CMC has conservatively chosen to complete its TMA impact analysis under two scenarios: 1) with the geomembrane intact in both the cap and liner; and 2) assuming the geomembrane were to degrade after 150 years in the liner. CMC has committed to maintaining the TMA final cover in perpetuity, therefore, the second analysis does not consider geomembrane degradation in the cap. It should be noted that the assumption of geomembrane

degradation after 150 years is very conservative. To assess the longevity of the HDPE geomembrane proposed for use in the TMA, CMC commissioned GeoSyntec Consultants, Inc. of Boca Raton, Florida, to identify and evaluate the mechanisms of degradation that could affect longevity of the HDPE as applied to the Crandon Project. In its report, GeoSyntec (1996) concluded "that the proposed HDPE geomembrane can be expected to be used under conditions that should not adversely impact its long term performance." GeoSyntec also concluded that "the HDPE geomembrane liner and cap at the TMA facility should function as designed for a very long time (e.g., hundreds of years) without deterioration in performance." Also, in the unlikely event degradation were to take place, it would not happen instantaneously as CMC's analysis assumes. Rather, degradation would likely occur slowly over hundreds of years.

Figure 2.6 shows a section through the liner (with the geomembrane intact). If the geomembrane is assumed to be completely degraded, the mechanisms with a potential to transport oxygen to the underside of the tailings would be:

- Diffusion of oxygen to the sidewalls and base of the TMA, followed by diffusion through the remaining liner components; and,
- Advection of oxygen by barometric pumping to the sidewalls and base of the TMA, followed by diffusion through the remaining liner components.

Oxygen transport mechanisms through the cover in Case 3 will be exactly the same as those in Case 2.

2.5 Summary

Table 2.1 lists the oxygen transport mechanisms and shows which mechanisms will have the most significant potential to transport oxygen into the tailings in each of Cases 1a, 1b, 2 and 3.

TABLE 2.1
Summary of Cases and Oxygen Transport Mechanisms

Oxygen Transport Mechanism	Case 1a	Case 1b	Case 2	Case 3
Advection in water				
process water	✓			
infiltration		✓		
through defects in cover			✓	✓
Diffusion in uncovered tailings pore water	✓	✓		
Diffusion in uncovered tailings pore air		✓		
Diffusion through intact cover			✓	✓
Diffusion through defects in cover			✓	✓
Barometric pumping through defects in cover			✓	✓
Diffusion through embankment				
and intact liner			✓	
and liner with no geomembrane				✓
Barometric pumping through embankments				
and intact liner			✓	
and liner with no geomembrane				✓

3.0 MODEL EQUATIONS, INPUTS AND OUTPUTS

The mathematical models used to estimate oxygen fluxes associated with each oxygen transport mechanism are described in the following sections.

3.1 Advection in Water

3.1.1 Description of Transport Mechanism

Advection in water is the process by which a substance, in this case oxygen, that is dissolved or suspended in water, is transported along with the water. In Case 1a an overwhelming majority of the water entering the tailings is process water. In Case 1b precipitation that falls on the tailings surface is assumed to infiltrate. In Cases 2 and 3 water will only flow into the tailings through defects in the cover.

3.1.2 Model Equation and Solution Method

The flux of oxygen associated with advection is given by the multiple of the flow rate and the oxygen concentration *i.e.*:

$$\textit{Flux}\ (\text{mol } O_2\ m^{-2}\ yr^{-1}) = \textit{Concentration}\ (\text{mol } O_2\ L^{-1}) * \textit{Flowrate}\ (\text{m } yr^{-1}) * 1000\ (\text{L } m^{-3})$$

The simple equation can be solved directly, and the sensitivity of the predicted flux to the input variables is clear.

3.1.3 Model Inputs

Oxygen concentrations in process water, precipitation, and seepage through defects in the cover will vary. However, the maximum solubility of oxygen in water is limited, ranging from only 8.26 mg/L at 25°C, to 12.8 mg/L at 5°C (Appelo & Postma, 1994). The upper number (12.8 mg/L = 4×10^{-4} mol O_2 L^{-1}) was used in this analysis as a conservative estimate.

Flowrates for each case were estimated from data presented by Foth & Van Dyke (1997).

- During tailings deposition, the rate of water flow into the tailings was estimated by assuming the tailings would have a saturated hydraulic conductivity of 4×10^{-6} cm/s and a unit hydraulic gradient.

- During the consolidation period, infiltration into the tailings was estimated to be 15 in/yr (1.21×10^{-8} ms^{-1}), in the middle of the range 12.5-16.2 in/yr predicted by the HELP modeling reported by Foth & Van Dyke (1997).

- Infiltration into the tailings through the cover was estimated to be 0.0001 in/yr (8.0×10^{-14} ms^{-1}), as predicted by the HELP modeling reported by Foth & Van Dyke (1997).

3.1.4 Model Outputs

Table 3.1 summarises the estimated oxygen fluxes due to advection in water.

TABLE 3.1
Model Inputs and Outputs - Advection in Water

Case	Mechanism	Flow rate ($m\ s^{-1}$)	O_2 Conc. ($mol\ L^{-1}$)	Estimated O_2 Flux ($mol\ O_2\ m^2\ s^{-1}$)
1a	Advection in process water	$4x10^{-8}$	$4.0x10^{-4}$	$1.6x10^{-8}$
1b	Advection in infiltration through uncovered surface	$1.21x10^{-8}$	$4.0x10^{-4}$	$4.8x10^{-9}$
2 and 3	Advection in infiltration through defects in cover	$8.0x10^{-14}$	$4.0x10^{-4}$	$3.2x10^{-14}$

3.2 Diffusion Through Tailings Water

3.2.1 Description of Transport Mechanism

Molecular diffusion is the movement of a substance in response to a concentration gradient. As long as the surface of the tailings remains wet, the only significant diffusion of oxygen will be through the pore water.

3.2.2 Model Equations and Solution Method

Transport by diffusion is governed by Fick's Law. Integrating the one-dimensional form of Fick's Law over an elemental volume, and incorporating oxygen consuming reactions leads to the conservation equation:

$$\frac{dC}{dt} = \frac{\partial}{\partial x}\left(D\frac{\partial C}{\partial x}\right) - r * C^n$$

where: C is oxygen concentration (mol m^{-3}); t is time (s); D is the effective diffusion coefficient (m^2s^{-1}); n is the rate order; and r is a reaction constant which depends upon the rate order. For $n = 1$, r has the units s^{-1}. The steady-state analytical solution for this is given by:

$$C = C_0 e^{-\sqrt{\frac{r}{D}}x}$$

flux is given by:

$$j = C_0 \sqrt{rD} \cdot e^{-\sqrt{\frac{r}{D}}x}$$

the flux of oxygen into the system is given by:

$$j_0 = C_0 \sqrt{rD}$$

The oxygen consumption reaction is here assumed to be first order with respect to oxygen concentration. Section 3.3 below considers other reaction orders and shows that the effect of this assumption is negligible.

3.2.3 Model Inputs

The concentration of oxygen at the upper boundary of the tailings was assumed to be in equilibrium with the atmosphere. As discussed in Section 3.1.3, the maximum oxygen concentration in water that is in equilibrium with air is of 12.8 mg/L or 0.0004 mol O_2 L^{-1} (0.4 mol O_2m^{-3}).

The diffusion coefficient for oxygen in water is 2.10 x 10^{-9} m^2/s (Cussler, 1984) at 25°C. Diffusion in water filled pores of a porous medium is typically 2-3 times slower than in open water, due to the tortuous path that diffusing molecules must take through the pores. Lower temperatures also tend to reduce diffusion coefficients. The above value is therefore a conservative estimate of the effective diffusion coefficient in water saturated tailings.

Sensitivity analyses with the air phase diffusion model, (see Section 3.3), indicated that the oxygen transport predictions were relatively insensitive to reaction order, with

a first order model predicting the deepest penetration of oxygen into the tailings. The oxygen consumption reaction was therefore assumed to be first order (n=1). The rate constant was conservatively assumed to be 1.07×10^{-4} s^{-1}, derived from the oxidation rates estimated in the laboratory tests.

3.2.4 Model Outputs

The diffusion model predicted a total oxygen flux into the tailings of 1.9×10^{-7} mol O_2 $m^{-2}s^{-1}$. Input and output parameters are summarized in Table 3.2.

TABLE 3.2
Model Inputs and Outputs - Oxygen Diffusion in Tailings Water

Reaction model	Rate constant (s^{-1})	Diffusion Coefficient (m^2 s^{-1})	Predicted Flux (mol O_2 m^{-2} s^{-1})
First order	1.07×10^{-4}	2.1×10^{-9}	1.9×10^{-7}

3.3 Diffusion Through Tailings Pore Air

3.3.1 Description of Transport Mechanism

Like diffusion in water, diffusion in air occurs in response to a concentration gradient. As a rough rule of thumb, diffusion in air is 3-4 orders of magnitude faster than diffusion in water. However, air phase diffusion is not significant until the water content drops below the air entry value, i.e. when unsaturated pores become interconnected.

.3.2 Model Equations and Solution Method

Diffusion through the tailings pore air at equilibrium water content was modeled using the equation for one-dimensional diffusion with reaction, given by:

$$\frac{dC}{dt} = \frac{\partial}{\partial x}\left(D\frac{\partial C}{\partial x}\right) - r * C^n$$

where: C is oxygen concentration (mol m^{-3}); t is time (s); D is the effective diffusion coefficient (m^2s^{-1}); n is the rate order; and **r** is a reaction constant which depends upon the rate order. For $n = 1$, r has the units s^{-1}. The solution to this equation was obtained using the alternating difference implicit (ADI) finite difference code described in Attachment A.

The modeling domain consisted of a column of variably spaced grid blocks. A fine grid block spacing was used at the top of the model where oxygen concentration changes most rapidly with depth. A coarser spacing was used deeper into the column. A constant concentration source of C = 8.9 mol m^{-3} was applied to the top of the column and a no flux boundary was applied to the bottom. The simulations were run until a steady-state oxygen concentration profile was achieved. Although this condition depends upon the diffusion coefficient, reaction rate and reaction rate order, all simulations attained steady-state conditions within the first year.

3.3.3 Input Parameters

The air phase diffusion coefficient in tailings depends upon the moisture content. As discussed in Section 2.2, tailings are expected to remain saturated with water for at least part of the consolidation period. HELP modeling (Foth & Van Dyke, 1997) indicates that the tailings will remain approximately 90% saturated with water, even after two full years of (downwards) drainage. The uppermost tailings will be slightly drier, but still over 87% saturated.

Two of the most commonly cited water content vs. diffusion coefficient relationships for fine tailings from the literature are compared in Figure 3.2. Elberling et al. (1993) reported a relationship given by:

$$D = \tau D_a^0 (1 - S)^{\alpha} + \frac{\tau S D_w^0}{H}$$

where: D is effective diffusion coefficient (m^2s^{-1}); S is degree of saturation; D_a^0 is the effective diffusion coefficient for oxygen in air (m^2s^{-1}); D_w^0 is the effective diffusion coefficient for oxygen in water (m^2s^{-1}); H is the unitless modified Henry's Law constant defined as the concentration of oxygen in the water phase divided by the concentration of oxygen in the gas phase at equilibrium; and, τ and α are fitting parameters from non-linear regression analysis, equal to 0.273 +/- 0.08 and 3.28 +/- 0.4 respectively.

Reardon and Moddle (1985) determined a relationship of:

$$D = 3.98 \cdot 10^{-5} \left[\frac{\varepsilon - 0.05}{0.95} \right]^{1.7} T^{\frac{3}{2}}$$

where ε is air filled porosity, and T is temperature (Kelvin).

As shown in Figure 3.2, the difference in diffusion coefficients predicted by these two methods is small. The second relationship does not consider diffusion in water, and is therefore inaccurate at high water contents. The first relationship is more reliable at high water contents, and estimates that diffusion coefficients in tailings that are 90% saturated will be less than 10^{-9} m^2/s. A conservative estimate of $D=10^{-8}$ m^2/s was used in the modeling.

Several reaction rate models for tailings oxidation have been reported in the literature (Nicholson et al., 1988, McKibben & Barnes, 1986). A sensitivity analysis was carried out to compare four reaction rate models: zero-order, half-order, first-order and a mixed first-order zero-order model. The input parameters for these simulations are reported in Table 3.3. In all cases, the reaction rate constants were back calculated to provide an overall oxidation rate of 1.0×10^{-7} mol O_2 $kg^{-1}s^{-1}$ under atmospheric oxygen concentrations, as estimated from the laboratory testing.

Results of the sensitivity runs are summarised in Table 3.3. The zero-order model predicted the highest flux, but comparison with the results of the other models showed that flux is relatively insensitive to rate order. On the other hand, the penetration depth did vary between the models. The first order model predicted the largest depth of penetration and was therefore selected as the most conservative model for subsequent simulations.

More complex reaction models in the literature also consider a reduction in the oxidation rate with time, as the pyrite is depleted or encapsulated in reaction products, and as pH varies. The relative insensitivity of the model outputs to changes in the reaction order indicated that further complexity was not warranted. Instead, the conservative assumption of a high reaction rate, constant over time, was adopted.

TABLE 3.3
Model Inputs and Outputs - Air Phase Diffusion

Reaction Model	Input Parameters			Output Results	
	Equation for *D*	*n*	*r* (units vary)	Depth of Penetration (in)	Steady State Flux (mol m^{-2} s^{-1})
zero order	Elberling *et al.* (1993)	0	$4.2x10^{-3}$	<1	$2.35x10^{-5}$
half order	Elberling *et al.* (1993)	0.5	$1.4x10^{-3}$	<1	$1.94x10^{-5}$
first order	Elberling *et al.* (1993)	1	$4.7x10^{-4}$	1.5	$1.93x10^{-5}$
mixed first- and zero-order	Elberling *et al.* (1993)	0/1	$r_0 = 4.2x10^{-3}$ $r_1 = 2.0x10^{-3}$	1	$2.25x10^{-5}$

3.3.4 Model Outputs

Outputs from the sensitivity analyses are given in Table 3.3. The run with the first order reaction model provides the most conservative estimate of the depth of penetration. Changing the reaction order has very little influence on the estimated oxygen flux into the tailings. The zero order reaction model provides the most conservative estimate of flux.

3.4 Diffusion Through the Intact Cover

3.4.1 Description of the Transport Mechanism

As shown in Figure 2.5, the TMA cover will consist of several layers, one of which will be an HDPE geomembrane. Literature data show that oxygen can permeate through plastic liners by a diffusion process. Although the local flux due to such a process will be very small, it was necessary to consider the large surface area of the TMA cover, and the fact that this process will continue in perpetuity, in order to evaluate its overall significance.

3.4.2 Model Equation and Solution Method

The steady-state diffusional flux through the intact cover was determined by solving the governing equation for one-dimensional diffusion with reaction for a layered system:

$$\frac{dC}{dt} = \frac{\partial}{\partial x}\left(D\frac{\partial C}{\partial x}\right) - r * C^n$$

where: C is oxygen concentration (mol m^{-3}); t is time (s); D is the effective diffusion coefficient (m^2s^{-1}); n is the rate order; and r is a reaction constant which depends upon the rate order. For n = 1, r has the units s^{-1}. Colin (1987) presents an analytical solution to the above differential equation for n=1:

$$j = \frac{C_0\sqrt{r_t D_t}\cdot EXP}{\frac{1}{H_m}\sqrt{r_t D_t}\cdot EXP + 1}$$

where:

$$EXP = \frac{\exp\left[l_t\sqrt{\frac{r}{D_t}}\right] - \exp\left[-l_t\sqrt{\frac{r}{D_t}}\right]}{\exp\left[l_t\sqrt{\frac{r}{D_t}}\right] + \exp\left[-l_t\sqrt{\frac{r}{D_t}}\right]}$$

$$H_m = \frac{1}{\frac{l_1}{D_1} + \frac{l_2}{D_2} + \frac{l_3}{D_3} + \cdots}$$

where:

j - molar flux (mol m^{-2} s^{-1})

l_1, l_2, l_3 - thickness of non-consuming cover layers (m);

D_1, D_2, D_3 - diffusivities for cover layers (m^2 s^{-1});

D_t - diffusivity for reactive tailings (m^2 s^{-1});

r_t - first-order rate constant for reactive tailings (s^{-1})

H_m - mass transfer coefficient (m s^{-1})

3.4.3 Model Inputs

The above model requires estimates of diffusion coefficients for each of the soil layers and the geomembrane.

Rogers (1985) reports the results of experiments of oxygen permeation through various geosynthetic liner materials. The fluxes reported range from 0.6 to 45 g O_2 m^{-2} d^{-1}. These values translate into diffusion coefficients ranging from 3.5×10^{-14} to 2.9×10^{-12} m^2 s^{-1}. The upper end of this range compares with diffusion coefficients of around 3×10^{-12} m^2 s^{-1} reported by Lord et al. (1988) for water vapour in HDPE. The value of 3×10^{-12} m^2 s^{-1}, was adopted for the modeling herein.

Three alternative methods to estimate diffusion coefficients through the soil, rock and tailings layers were tested. The first method was to apply an empirical relationship developed by the U.S. Nuclear Regulatory Commission (1984) to estimate radon diffusion coefficients in soil covers over uranium tailings piles. The equation is:

$$D\ (cm^2/s) = 0.07\ exp\ (-4\ (m - mn^2 + m^5))$$

where *m* is the moisture saturation factor (i.e. the volumetric water content divided by the volumetric porosity) and *n* is the volumetric porosity. Estimates of porosity and water content were obtained from the HELP modeling reported by Foth & Van Dyke (1997).

In the second method, the diffusion coefficients in all soil, rock and tailings layers were assumed to be $1x10^{-8}$ m^2 s^{-1}, equivalent to values measured in laboratory tests on compacted, moist till (Senes, 1991). In the third method, a hypothetical maximum diffusion coefficient of $1x10^{-5}$ m^2 s^{-1}, equal to the diffusion coefficient for oxygen in open air, was assumed for all soil, rock and tailings layers.

3.4.4 Model Outputs

Model inputs and outputs are summarized in Table 3.4. The table shows that the model predicts similar oxygen fluxes regardless of the method used to calculate diffusion coefficients in the soil, rock and tailings layers. The reason is that the geomembrane represents a far more significant barrier to oxygen than any of the other layers.

The last column of Table 3.4 reports the predicted concentration of oxygen at the interface between the geomembrane and the underlying layers. Oxygen concentrations are very low in all cases, because the limited amount of oxygen that passes through the geomembrane is readily consumed by oxidation of the tailings. These results support the assumption, used in Section 3.7 and 3.8, that the interface with the tailings can be modeled as a zero concentration boundary.

TABLE 3.4
Model Inputs And Outputs - Diffusion Through Intact Cover

Model Inputs			Model Outputs	
Geomembrane D (m^2s^{-1})	Soil D (m^2s^{-1})	Reaction rate constant, r (s^{-1})	O_2 Flux into tailings (mol O_2 m^{-2} s^{-1})	O_2 concentration at interface (mol O_2 m^{-3})
$3x10^{-12}$	U.S. NRC equation	$1.07x10^{-4}$	$1.7x10^{-8}$	$3.4x10^{-9}$
$3x10^{-12}$	$1x10^{-8}$	$1.07x10^{-4}$	$1.1x10^{-8}$	$3.4x10^{-11}$
$3x10^{-12}$	$1X10^{-5}$	$1.07x10^{-4}$	$1.7x10^{-8}$	$5.2x10^{-9}$

3.5 Diffusion Through Defects in Cover

3.5.1 Description of the Transport Mechanism

The geomembrane in the cover is predicted to have on average five defects per acre, with each defect approximately 1 cm^2 (Foth & Van Dyke, 1997). Oxygen will diffuse through the soil layers above the defects, through the defects, through the underlying layers and into the tailings.

3.5.2 Model Equations and Solution Method

Diffusion through defects in the tailings cover was modeled using the equation for two-dimensional diffusion with first-order reaction:

$$\frac{dC}{dt} = \frac{\partial}{\partial x}\left(D\frac{\partial C}{\partial x}\right) + \frac{\partial}{\partial y}\left(D\frac{\partial C}{\partial y}\right) - r * C$$

The solution to this equation was obtained using the alternating difference implicit (ADI) finite difference code described in Attachment A.

3.5.3 Model Inputs

To determine whether the diffusive flux through a single defect would be independent and thus could be treated separately from adjacent defects, two different model geometries were compared (Figure 3.3). The first geometry consisted of a rectangular grid 200 ft. long by 140 ft. high with a single 1 cm defect through the geomembrane located in the center of the grid. The second geometry consisted of a rectangular grid 300 ft. long by 140 ft. high with three 1 cm defects spaced evenly across the width of the grid. Both geometries were based on an average defect spacing across the tailings cover of 5 defects per acre (Foth and Van Dyke, 1997). The geometries were obtained from taking two hypothetical cross sections, one diagonal and one longitudinal, through a one square acre section of tailings cover with five evenly spaced defects distributed across it (Figure 3.4). In both cases a finer discretization of grid blocks was used in the vicinity of the grid block defects.

Each defect was represented as a constant atmospheric concentration boundary condition of 8.9 mol m^{-3}. All other points along the domain boundary were treated as no flux boundaries. A diffusion coefficient of $3x10^{-6}$ m^2s^{-1}, selected from Figure 3.2 as representative of dry tailings, was used throughout. The first-order reaction rate constant of $1.07x10^{-4}$ s^{-1} was used to represent reactive tailings with a low moisture content. Simulations were run until steady-state profiles were established.

3.5.4 Model Outputs

A summary of results for the runs is provided in Table 3.5. Flux into the three defect domain was approximately three times the flux into the one defect domain. This indicates that the diffusive flux through one defect is independent of the flux through adjacent defects and the per defect flux may be multiplied by the estimated number of defects to arrive at a flux through the cover.

TABLE 3.5
Model Inputs and Outputs - Diffusion through Defects

Run	Input Parameters		Output Results
	D $m^2 s^{-1}$	$r_{tailings}$ s^{-1}	Steady State Flux* mol $m^{-2} s^{-1}$
one-defect section	3.00E-06	1.07E-04	$4.9x10^{-8}$
three-defect section	3.00E-06	1.07E-04	$4.9x10^{-8}$

*Average flux assuming five defects per acre of cover

3.6 Barometric Pumping Through Defects in Cover

3.6.1 Description of the Transport Mechanism

Fluctuations in barometric pressure above the TMA will lead to pressure difference between the atmosphere and air in the pore space within the TMA. The pressure differences will cause air to flow into or out of the TMA through defects in the cover. This phenomenon is known as "barometric pumping" (Massman & Farrier, 1992).

3.6.2 Model Equations and Solution Method

Barometric pumping through defects in the tailings cover was modeled using the equation for two-dimensional air advection:

$$n\frac{dP}{dt} = \frac{\partial}{\partial x}(\alpha\frac{\partial P}{\partial x}) + \frac{\partial}{\partial y}(\alpha\frac{\partial P}{\partial y})$$

$$\alpha = \frac{\rho R T k_a}{m\mu}$$

where P is air pressure (Pa); t is time (s); n is the effective porosity (m^3pores/m^3rock); ρ is the air density (kg/m^3); m is the molar mass of air (0.0289 kg/mol); μ is the

kinematic viscosity (Ns/m^2); T is temperature (K); and R is the universal gas constant (joules/K·mol), and k_a is the air permeability (m^2).

The solution to this equation was obtained using the alternating difference implicit (ADI) finite difference code described in Attachment A.

3.6.3 Model Inputs

The same two model geometries and discretizations as used for the diffusion modeling through the tailings cover (Figure 3.3 and 3.4) were used. Again, a sensitivity analysis was carried out to determine whether the advective flux through a single defect would be independent from adjacent defects.

Defects were represented as fixed atmospheric pressure sources which varied with time. All other points along the domain boundary were treated as no flux boundaries. A twenty-six day pressure cycle extracted from the hourly barometric pressure data for 1995 from a Green Bay weather station was used as input to the model. This cycle represents a large barometric pressure fluctuation for the year and therefore provides a conservative (i.e. high) estimate of the average yearly flux into the tailings. To speed up simulation time, the average daily values were input to the model rather than the raw hourly values. (Sensitivity runs were completed to compare results using hourly and daily pressures. The differences in outputs were negligible).

Air permeabilities for the soil and tailings layers within the TMA have not been measured. Values were estimated by back-calculation from measured saturated hydraulic conductivities (Foth and Van Dyke, 1997) according to the equation:

$$k_a = \frac{K\mu}{\rho g}$$

where k_a is air permeability (m^2); K is saturated hydraulic conductivity ($m\ s^{-1}$); μ is the kinematic viscosity (Ns/m^2); ρ is the air density (kg/m^3). Air permeability values are presented in Table 3.6. For comparison, Table 3.6 also presents air permeabilities for unconsolidated soils from a number of other sites (U.S. EPA, 1995).

TABLE 3.6
Air Permeability Estimates Used In Barometric Pumping Models

Unit	Air Permeability (m^2)	Basis/Reference
tailings cover (dry)	$3.5x10^{-12}$	back calculated
foundation soil (till)	$3.5x10^{-12}$	back calculated
tailings (at field capacity)	$2.0x10^{-14}$	back calculated
typical high value	$1x10^{-10}$	U.S. EPA, 1995
typical low value	$1x10^{-14}$	U.S. EPA, 1995

3.6.4 Model Outputs

The model predicted the movement of air into and out of the defects. To convert to oxygen fluxes, it was conservatively assumed that air going into the defects would contain 21% oxygen, but air leaving through the defects would contain no oxygen. The results of the simulations (Table 3.7) show that more oxygen flux is contributed per defect for the one defect geometry than for the three defect geometry. This indicates that the effects of barometric pumping through adjacent defects are not independent. Using the one defect geometry leads to a conservative (i.e. high) estimate of flux into the TMA.

TABLE 3.7
Model Inputs and Outputs - Barometric Pumping through Defects in the TMA Cover

Run	Input Parameters			Output Results
	k_{cover}	$k_{tailings}$	k_{till}	Estimated Flux*
	(m^2)	(m^2)	(m^2)	(mol m^{-2} s^{-1})
one-defect section	3.50E-12	2.00E-14	3.50E-12	$2.4x10^{-8}$
three-defect section	3.50E-12	2.00E-14	3.50E-12	$1.31x10^{-8}$

* Assuming five defects per acre

These results show that the oxygen flux from the barometric pumping simulation is similar in magnitude to the oxygen flux from diffusion. This pattern is consistent with similar modeling studies from other sites (SRK, 1995).

3.7 Diffusion Through Embankments

3.7.1 Description of the Transport Mechanism

Monitoring at the site of the TMA shows that oxygen concentrations at depths of up to 110 ft. are at or near equilibrium with the atmosphere (see Attachment B). The diffusion processes that transport oxygen to these depths will also be capable of transporting oxygen through the embankment and foundation soils to the underside of the TMA.

3.7.2 Model Equations and Solution Method

Diffusion through the foundation (embankment) soils into the sides of the TMA was modeled using the equation for two-dimensional diffusion:

$$\frac{dC}{dt} = \frac{\partial}{\partial x}\left(D\frac{\partial C}{\partial x}\right) + \frac{\partial}{\partial y}\left(D\frac{\partial C}{\partial y}\right)$$

The solution to this equation was obtained using the alternating difference implicit (ADI) finite difference code described in Attachment A.

3.7.3 Model Inputs

To account for the size variation of the embankments surrounding the TMA, two representative model geometries were used: a typical large embankment and a typical small embankment. As shown in Figure 3.5, both geometries were discretized from cross-section A-A' of the TMA Feasibility Report (Foth & Van Dyke, 1995a). For both discretizations, a finer grid spacing was used in the top 30 ft. of tailings, where oxygen flux to the sides of the TMA will be greatest.

A fixed atmospheric oxygen concentration 8.9 mol m^{-3} was applied to nodes representing the outside of the embankment exposed to the atmosphere. To represent reactive tailings, a fixed concentration boundary of 0.0 mol m^{-3} was applied at interior nodes representing the embankment-tailings interface. The latter boundary condition assumes complete reaction of oxygen with the tailings and thus gives a conservative (i.e. high) estimation of oxygen flux into the tailings. Because the reaction is assumed to be instantaneous, no assumptions regarding reaction rate order and reaction rate constants were required. The models were run until steady-state conditions were achieved.

Boundary conditions are shown in Figures 3.6 and 3.7. Diffusion coefficients of $3x10^{-6}$ m^2s^{-1} were used for both the till soil and tailings based on empirical relationships for dry soil (Elberling et al., 1993; Reardon and Moddle, 1985). A diffusion coefficient of $3x10^{-9}$ m^2s^{-1} was estimated for the liner using the model presented in Section 3.4. The diffusion coefficient for the cover was set to $1x10^{-20}$ m^2s^{-1} to effectively create a no flux boundary along the top of the model. Oxygen transport through the cover is treated separately in sections 3.5 and 3.6.

3.7.4 Model Outputs

For each geometry two simulations were conducted. Before and after an assumed degradation of the geomembrane. The results for these simulations are summarised in Table 3.8.

TABLE 3.8
Model Inputs and Outputs -
Diffusion through Embankments and TMA Liner

Run	Input Parameters			Steady State Fluxes (mol m^{-2} s^{-1})			
	D_{liner} m^2s^{-1}	D_{cover} m^2s^{-1}	D_{till} m^2s^{-1}	top of sidewall	middle of Phase 2 sidewall	middle of Phase 1 sidewall	base of TMA
Diffusion through large embankment (intact liner)	$3x10^{-9}$	$1x10^{-20}$	$3x10^{-6}$	$5.2x10^{-8}$	$3.9x10^{-8}$	$1.8x10^{-8}$	$1.6x10^{-8}$
Diffusion through small embankment (intact liner)	$3x10^{-9}$	$1x10^{-20}$	$3x10^{-6}$	$5.6x10^{-8}$	$5.0x10^{-8}$	$1.9x10^{-8}$	$1.6x10^{-8}$
Diffusion through large embankment (degraded liner)	$3x10^{-6}$	$1x10^{-20}$	$3x10^{-6}$	$2.6x10^{-6}$	$1.4x10^{-7}$	$1.7x10^{-8}$	$4.8x10^{-11}$
Diffusion through small embankment (degraded liner)	$3x10^{-6}$	$1x10^{-20}$	$3x10^{-6}$	$5.9x10^{-6}$	$3.4x10^{-6}$	$5.0x10^{-9}$	$2.0x10^{-11}$
Diffusion through large embankment (degraded liner) Sensitivity to Diffusion Coefficient	$6x10^{-9}$	$1x10^{-20}$	$6x10^{-6}$	$5.2x10^{-6}$	$4.0x10^{-6}$	$6.3x10^{-9}$	$3.0x10^{-11}$

The results show that, in all cases, oxygen fluxes are greatest near the top of the sidewall, and decrease with depth. The oxygen fluxes into the base of the TMA are predicted to be small, apparently because oxygen is consumed by reactions along the sidewall before it can reach the base of the TMA. Comparison of results for the cases with and without the geomembrane shows that oxygen fluxes are much greater when the geomembrane is not present, particularly near the top of the sidewalls.

3.8 Barometric Pumping Through Foundation Soil

3.8.1 Description of the Transport Mechanism

Changes in barometric pressure can lead to barometric pumping of oxygen into and out of soil (e.g. Massman & Farrier, 1992), and may be capable of transporting oxygen to the underside of the TMA. When the HDPE geomembrane is present in the TMA liner, barometric pressure changes would not be sufficient to push oxygen into the

TMA. However, if it is assumed that the geomembrane is degraded, barometric pumping of oxygen unto the tailings through the liner becomes possible.

3.8.2 Model Equations and Solution Method

Barometric pumping through the foundation soil and the degraded liner was modeled using the equations and solution methods presented in Section 3.6.

3.8.3 Model Inputs

The two model geometries and discretizations used for the diffusion modeling through large and small embankments were also used for the barometric pumping simulations. Boundary conditions are shown in Figures 3.8 and 3.9.

A time varying pressure was applied at the boundary representing the outside of the embankment. The pressure record consisted of twenty-six daily average values obtained from 1995 barometric data. The 26 day period used represents a typical large barometric cycle from the 1995 year and thus provides a conservative (i.e. high) estimation of average annual flux due to barometric pumping. As mentioned in Section 3.6, a sensitivity analysis showed that daily averages adequately represent the hourly pressure data.

Air permeabilities for the till foundation soil, embankments and grading layer were assumed to be as presented in Table 3.6.

3.8.4 Model Outputs

As discussed in Section 3.6, the barometric pumping model outputs the total flux of air into the TMA. The average oxygen flux into the TMA was calculated by multiplying the air flux by the average concentration of oxygen in the air in contact with the TMA sidewall and base as estimated from the diffusion model (Section 3.7). Table 3.9 presents the results. Comparison of Tables 3.8 and 3.9 shows that barometric pumping through the foundation soils is a minor process compared to diffusion through foundation soils.

TABLE 3.9
Model Inputs and Outputs -
Barometric Pumping through Embankment

Run	Input Parameters			Average Flux into TMA (mol m^{-2} s^{-1})
	k_{cover} (m^2)	$k_{tailings}$ (m^2)	k_{till} (m^2)	
Barometric pumping through large embankment	$3.50x10^{-12}$	$2.00x10^{-14}$	$3.50x10^{-12}$	$1.2x10^{-8}$
Barometric pumping through small embankment	$3.50x10^{-12}$	$2.00x10^{-14}$	$3.50x10^{-12}$	$1.4x10^{-8}$
Barometric pumping through large embankment (hourly fluctuations)	$3.50x10^{-12}$	$2.00x10^{-14}$	$3.50x10^{-12}$	$1.2x10^{-8}$

4.0 MODEL RESULTS BY CASE

4.1 Summary of Model Results

Table 4.1 summarizes the results of the oxygen transport modeling in terms that can be related to Cases 1-4. The first column in the table identifies the oxygen transport mechanism. For each transport mechanism, the next two columns list the oxygen flux in units of moles per m^2 per second, and moles per m^2 per year. The latter represents the total number of moles of oxygen that the transport mechanism would push through a square metre of the tailings surface each year. (Note that the surface is not the same for each mechanism. While most of the mechanisms act on the top surface of the TMA the mechanisms in the lower rows of the table act on the sidewalls or base).

The rate of oxygen transport into the tailings will limit the potential for acid generation. If the oxygen that enters the tailings is assumed to react with pyrite, producing sulfuric acid and ferric hydroxide, then each mole of oxygen will produce sufficient oxidation products to consume 8/15 moles of alkalinity. The last two columns of Table 4.1 quantify each transport mechanism in terms of "oxygen limited acid generation rates". The oxygen limited acid generation rate can be thought of as the maximum amount of acidity that can be produced below each square meter of tailings surface for each year that the transport mechanism will be active.

TABLE 4.1
Summary of Oxygen Transport Modeling

Transport mechanism	Oxygen Flux		Oxygen-limited Acid Generation Rate	
	mol m^{-2} s^{-1}	mol m^{-2} yr^{-1}	mol m^{-2} yr^{-1}	kg $CaCO_3$ eq. m^{-2} yr^{-1}
Diffusion through pore air at equilibrium water content				
zero order reaction	2.35×10^{-5}	742	396	40
first order reaction	1.93×10^{-5}	609	325	32
half order reaction	1.94×10^{-5}	612	327	33
mixed zero & first order reaction	2.25×10^{-5}	710	379	38
Diffusion in pore water	1.9×10^{-7}	6.0	3.2	0.32
Advection in infiltrating water				
during deposition	1.6×10^{-8}	0.50	0.27	0.03
during consolidation	4.8×10^{-9}	0.15	0.08	0.008
through cover	3.2×10^{-14}	1.0×10^{-6}	5.4×10^{-7}	5.4×10^{-8}
Diffusion through intact cover				
with soil at wilting point	1.70×10^{-8}	0.54	0.29	0.029
with moisture retaining soil	1.10×10^{-8}	0.35	0.18	0.019
with dry soil	1.70×10^{-8}	0.54	0.29	0.029
Diffusion through defects in cover				
5 defects/acre, each 1 sq. cm.	4.9×10^{-8}	1.55	0.82	0.082
Barometric Pumping through defects in cover				
5 defects/acre, each 1 sq. cm.	2.4×10^{-8}	0.75	0.40	0.040
Diffusion through large embankment (intact liner)				
top of sidewall	5.2×10^{-8}	1.6	0.87	0.088
middle of Phase 2 sidewall	3.9×10^{-8}	1.2	0.62	0.062
middle of Phase 1 sidewall	1.8×10^{-8}	0.57	0.30	0.030
base of TMA	1.6×10^{-8}	0.50	0.01	0.001
Diffusion through small embankment (intact liner)				
top of sidewall	5.6×10^{-8}	1.77	0.94	0.094
middle of Phase 2 sidewall	5.0×10^{-8}	1.58	0.84	0.084
middle of Phase 1 sidewall	1.9×10^{-8}	0.60	0.32	0.032
base of TMA	1.6×10^{-8}	0.50	0.27	0.027
Diffusion through large embankment (degraded liner)				
top of sidewall	2.6×10^{-6}	82	44	4.4
middle of Phase 2 sidewall	1.4×10^{-7}	4.4	2.4	0.24
middle of Phase 1 sidewall	1.7×10^{-8}	0.54	0.29	0.029
base of TMA	4.8×10^{-11}	1.5×10^{-3}	8.1×10^{-4}	8.1×10^{-5}
Diffusion through small embankment (degraded liner)				
top of sidewall	5.9×10^{-6}	187	99	9.9
middle of Phase 2 sidewall	3.4×10^{-6}	107	57	5.7
middle of Phase 1 sidewall	5.0×10^{-9}	0.16	0.08	0.008
base of TMA	2.0×10^{-11}	6.3×10^{-4}	3.4×10^{-4}	3.4×10^{-5}

F1071071.rep 4/28/97

Steffen, Robertson and Kirsten
April, 1997

4.2 Oxygen Limited Acid Generation Rates by Case

Table 4.2 presents the same information arranged by the cases introduced in Section 2. As discussed in Section 2, only certain transport mechanisms are active within each of the cases (see Table 2.1 for a summary). Only the relevant oxygen limited AP's are shown in Table 4.2.

Looking down each column of Table 4.2, it is possible to identify the dominant transport mechanisms in each case.

- During tailings deposition (Case 1a), the dominant oxygen transport mechanism is advection in the infiltrating water.

- During the tailings consolidation period (Case 1b), the dominant oxygen transport mechanism is diffusion through the unsaturated tailings pores.

- After the tailings cover is in place (Case 2), diffusion through the intact cover, diffusion through defects in the cover, and barometric pumping through the cover contribute nearly equally to transport to the tailings surface. Diffusion through the embankment dominates oxygen transport to the sidewalls and base of the TMA.

- After an assumed complete degradation of the geomembrane in the liner (Case 3), oxygen diffusion through the base and sidewalls increases. The range of acid generation rates due to diffusion through the embankments reflects the much higher rate of oxygen transport to the upper sidewall of the TMA.

4.3 Acid Generation Potentials

For Cases 1a and 1b, which have a well-defined duration, it is possible to translate the oxygen limited acid generation rates of Table 4.2 to oxygen limited acid generation potentials ("oxygen limited AP"). For Cases 2 and 3, where the duration is undefined, the oxygen limited acid generation rates will need to be taken into the water quality models.

TABLE 4.2
Oxygen Limited Acid Generation Rates (kg $CaCO_3$ eq. m^{-2} yr^{-1})
Resulting from each Transport Mechanism

Oxygen Transport Mechanism	Case 1a	Case 1b	Case 2	Case 3
Advection in water				
process water	0.027			
infiltration		0.008		
through defects in cover			$5.4x10^{-8}$	$5.4x10^{-8}$
Diffusion in tailings pore water	0.32	0.32		
Diffusion in tailings pore air		40		
Diffusion through intact cover			0.029	0.029
Diffusion through defects in cover			0.082	0.082
Barometric pumping through defects in cover			0.040	0.040
Diffusion through embankment				
and intact liner			0.03 - 0.09	
and liner with no geomembrane				$3x10^{-5}$ - 9.9
Barometric pumping through embankments				
and liner with no geomembrane				<0.020

4.3.1 Case 1a: During Tailings Deposition

Case 1a represents the period during which tailings are deposited into a cell. The maximum deposition period is nine years, for cell TMA 2. Making the conservative assumption that the Case 1a oxygen transport mechanisms are active for nine years leads to an oxygen limited AP of approximately 3 kg $CaCO_3/m^2$.

As discussed in Section 2.1, the process of tailings deposition will continually bury tailings and generate a fresh surface. As a result, the acid generation will be distributed throughout the tailings column. In other words, alkalinity of 4 kg $CaCO_3$ will need to be distributed uniformly throughout each 1 m^2 vertical column of tailings. Based on waste characterization work completed for the project (Foth & Van Dyke, 1995b), there is sufficient neutralizing potential in the tailings to counteract the Case 1 oxygen limited AP.

TABLE 4.3
Alkalinity Requirement (kg $CaCO_3$ m^{-2}) to Neutralize Oxidation Products resulting from each Transport Mechanism over Design Period

Oxygen Transport Mechanism	Case 1a 9 years	Case 1b 1 year
Advection in water process water infiltration through defects in cover	0.27	-
Diffusion in tailings pore water	2.7	-
Diffusion in tailings pore air		40

4.3.2 Case 1b: During Tailings Consolidation

Diffusion through unsaturated tailings pores will be by far the dominant transport mechanism during the tailings consolidation period, which is expected to last up to two years. However, as discussed in Section 2.2, the tailings pores will not be unsaturated for the entire two years. In fact, water will flow upwards out of the tailings for some time.

Under the conservative assumption that oxygen will diffuse through the unsaturated tailings pores for one full year, the oxygen limited AP would be 40 kg $CaCO_3/m^2$, as shown in Table 4.3. Note that this estimate also incorporates the conservative assumptions that oxygen consumption will be by a zero order reaction, and that the reaction rate will be constant and at the high end of values reported in the literature.

The acid generation in Case 1b will not be distributed uniformly throughout the tailings column. As discussed in Section 3.3, they oxygen is entirely consumed within the upper few inches of the tailings.

5.0 CONCLUSIONS

The oxygen transport modeling presented herein allows identification of the dominant oxygen transport mechanisms within each stage of the TMA operation, closure, and long term management, as well as estimation of the rates at which oxygen will enter the tailings.

The predictions of oxygen transport presented herein are based on the following conservative assumptions:

- Use of a 12.8 mg/l dissolved O_2 at 5°C vs. 8.26 at 25°C (p. 8).
- Diffusion coefficient at 25°C water vs. 2-3 less for porous media at lower temperature (p. 10).
- Assumed $D=10^{-8}$ m^2/s for diffusion modeling (p. 13).
- Use of a first order reaction model with greatest depth of oxygen penetration (p. 13).
- Use of a highest value of $3x10^{-12}$ m^2/s for oxygen diffusion through geomembrane vs. $3x10^{-14}$ (p. 16).
- Assumed 100% O_2 consumption in barometric pumping (p. 22).
- Assumed one defect geometry for flux of $2.4x10^{-8}$ vs. $1.3x10^{-8}$ for multiple defects (p. 22).
- Assumed 100% transfer of O_2 to tailings (p. 23).
- Use of extreme barometric cycles to represent annual average (p. 21 and 25).

The effect of these assumptions is to produce conservatively high estimates of oxygen transport into the TMA. In cases where even these high estimates lead to relatively

insignificant oxygen fluxes, the transport mechanisms need not be considered in further analyses.

Under the assumption that the oxygen will oxidize pyrite in the tailings to sulfuric acid and ferric hydroxide, the oxygen transport rates can be used to estimate the potential acid generation rates. The resulting estimates show the following:

- The neutralization potential contained within the tailings will be more than adequate to neutralize any oxidation products that might be generated during tailings deposition.

- Using conservative assumptions with respect to tailings water content, oxygen entry during the consolidation period is estimated to be sufficient to consume the alkalinity available at the tailings surface.

- Over the long term, the TMA cover system will constrain oxygen access to the upper surface of the tailings.

- Over the very long term, i.e. hundreds of years, degradation of the geomembrane in the TMA liner could lead to increased penetration of oxygen, particularly along the upper sidewall nearest the ground surface.

REFERENCES

Appelo, C.A.J., Postma, D., 1994. Geochemistry, groundwater and pollution. A.A.Balkema/Rotterdam/Brookfield, 536 pp.

Colin, M., 1987. Mathematical Modeling of Water and Oxygen Transport in Layered Soil Covers for Deposition of Pyritic Mine Tailings, Licentiate Treatise, Royal Institute of Technology, Department of Chemical Engineering, Stockholm, Sweden.

Colorado School of Mines Research Institute, 1982. Characterization of Crandon Mill Tailings. Golden, Colorado, CMC-NOI-149.

Cussler, E.L., 1984. Diffusion: Mass Transfer in Fluid Systems. Cambridge University Press, 525 pp.

Elberling, B., Nicholson, R.V., and David, D.J., 1993. Field Evaluation of Sulphide Oxidation Rates. Nordic Hydrology, vol.24, p.323-338.

Foth & Van Dyke, 1997. Addendum No. 3 to the TMA Feasibility Report/Plan of Operation.

Foth & Van Dyke, 1995a. Tailings Management Area Feasibility Report/Plan of Operation.

Foth & Van Dyke, 1995b. Waste Characterization Update Report - Crandon Project, Crandon, Wisconsin.

GeoSyntec Consultants, December 1996. Assessment of Long-Term Performance of the Proposed HDPE Geomembrane Liner and Cap at the Crandon Project TMA Facility.

Lord, A.E. Jr., R.M. Koerner, & R.H. Swan Jr., Chemical mass transport measurements to determine flexible membrane liner lifetimes. Geotechnical Testing Journal, vol. 11, no. 2, June 1988, pp. 83-91.

Massman, J. and Farrier, D.F., 1992. Effects of Atmospheric Pressures on Gas Transport in the Vadose Zone. Water Resources Research, vol.28, no.3, p.777-791.

McKibben M.A. and H.L. Barnes, 1986. "Oxidation of Pyrite in Low Temperature Acidic Solutions: Rate Laws and Surface Textures" Geochim. Cosmochim. Acta Vol. 51, p 793-801.

Nicholson, R.V., Gillham R.W. and Reardon E.J., 1988 "Pyrite Oxidation in Carbonate-Buffered Solutions: 1. Experimental Kinetics" Geochim. Cosmochim. Acta Vol. 52 p. 1077-1085

Reardon, E.J. and Moddle, P.M., 1985. Gas Diffusion Coefficient Measurements On Uranium Mill Tailings: Implications to Cover Layer Design. Uranium, vol.2, p.111-131.

Rogers, C.E., 1985. "Permeation of Gases and Vapours in Polymers". In *Polymer Permeability*, J. Comyn, ed. Elsevier Applied Science Publishers, London.

Senes 1991 Acid Generation Modeling, Equity Silver Waste Rock Dumps". Report to Equity Silver Mines Ltd. December, 1991.

Steffen, Robertson and Kirsten, 1995. Interim Report on Investigation of Methods For In Situ remediation of Nordhalde and Innenkippe. SRK Report W104203/1 prepared for WISMUT GmbH, May, 1995.

United States Environmental Protection Agency Manual, 1995. Bioventing Principles and Practice, Volume 1: Bioventing Principles. EPA/540/R-95/534a, September, 1995, 80 pp.

United States Nuclear Regulatory Commission, 1984. Radon Attenuation Handbook for Uranium Mill Tailings Cover Design. Report NUREG / CR-3533, prepared by Rogers & Associates Engineering Corporation under contract to Pacific Northwest Laboratory.

FIGURES

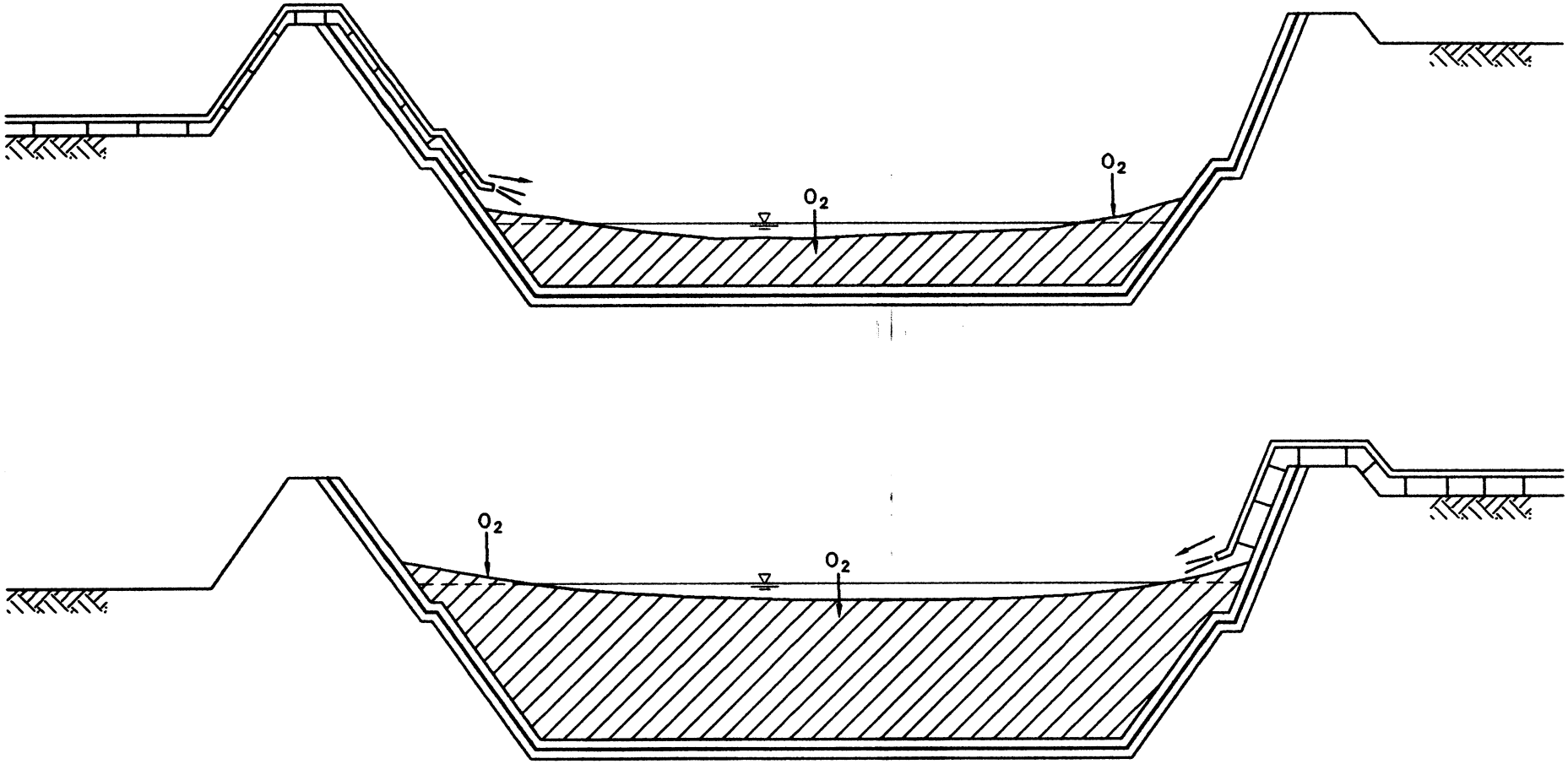

VERTICAL SCALE EXAGGERATED

STEFFEN ROBERTSON AND KIRSTEN
Consulting Engineers

FOTH & VAN DYKE

CRANDON TMA SOURCE TERM

O_2 TRANSPORT
CASE 1A – DURING TAILINGS DEPOSITION

PROJECT NO.	DATE	APPROVED	FIGURE
F107107/1	APRIL 1997		2.1

4.2-12-251

FILE REF: FIG-2-1

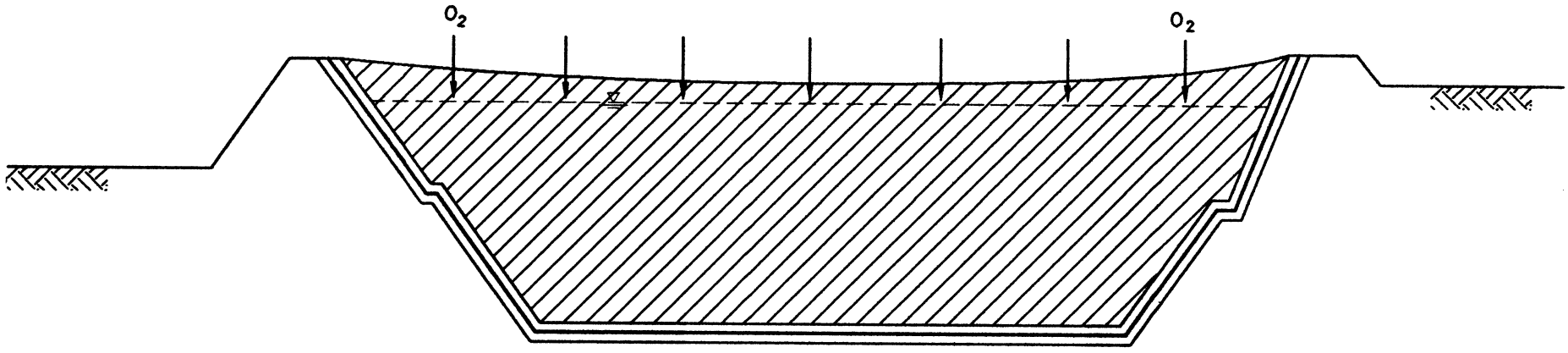

VERTICAL SCALE EXAGGERATED

STEFFEN ROBERTSON AND KIRSTEN
Consulting Engineers

FOTH & VAN DYKE

CRANDON TMA SOURCE TERM

O_2 TRANSPORT
CASE 1B – DURING TAILINGS CONSOLIDATION

PROJECT NO.	DATE	APPROVED	FIGURE
F107107/1	APRIL 1997		2.2

FILE REF:FIG-2-2

C:\cadwork\3c49f200.dgn

4.2-12-253

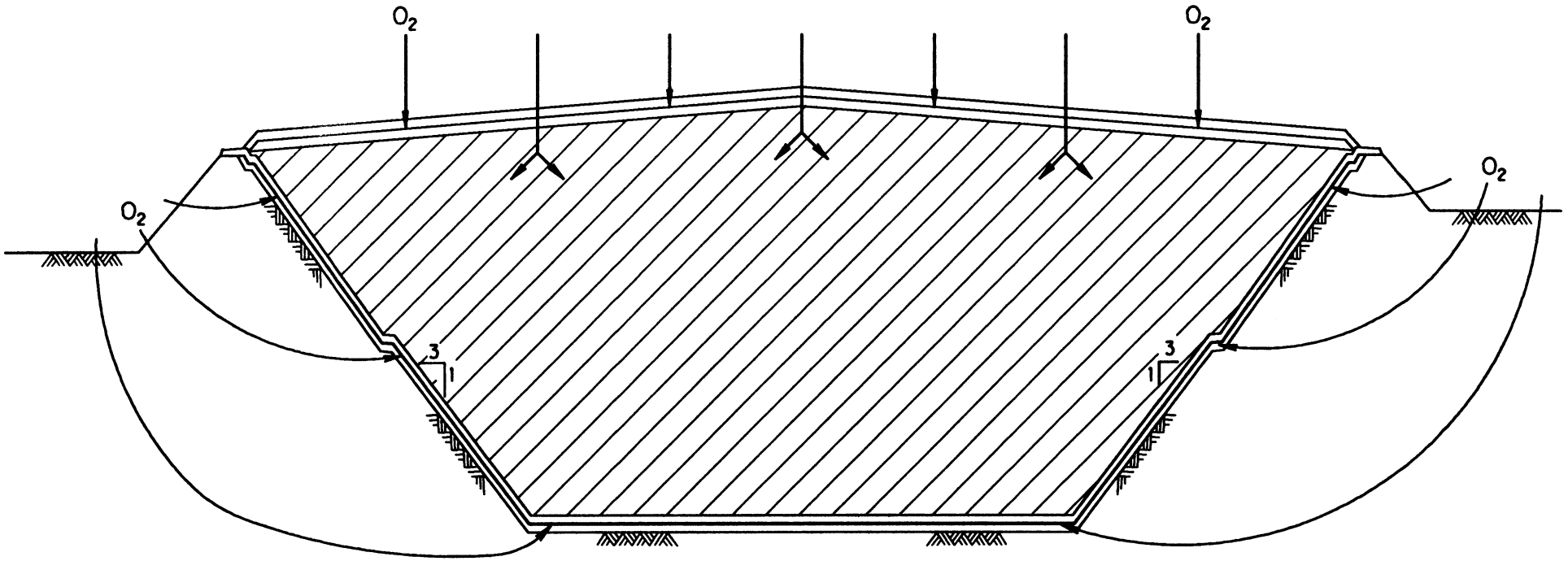

VERTICAL SCALE EXAGGERATED

STEFFEN ROBERTSON AND KIRSTEN
Consulting Engineers

Foth & Van Dyke

CRANDON TMA SOURCE TERM

O_2 TRANSPORT
CASE 2 - AFTER COVER CONSTRUCTION

PROJECT NO.	DATE	APPROVED	FIGURE
F107107/1	APRIL 1997	JTC	2.3

93C049

C:\cadwork\3c49f200.dgn

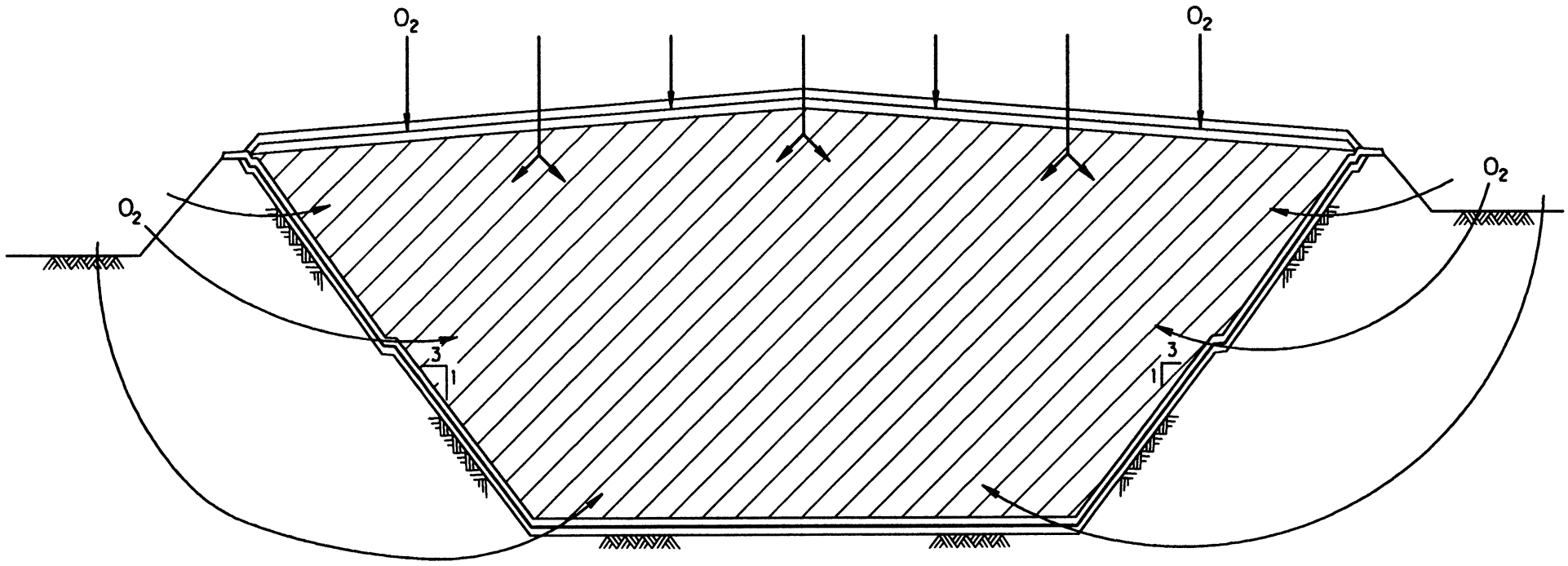

4.2-12-254

VERTICAL SCALE EXAGGERATED

STEFFEN ROBERTSON AND KIRSTEN
Consulting Engineers

Foth & Van Dyke

CRANDON TMA SOURCE TERM

O_2 TRANSPORT
CASE 3 - AFTER ASSUMED DEGRADATION OF GEOMEMBRANE IN LINER

PROJECT NO.	DATE	APPROVED	FIGURE
F107107/1	APRIL 1997	JTC	2.4

93C049

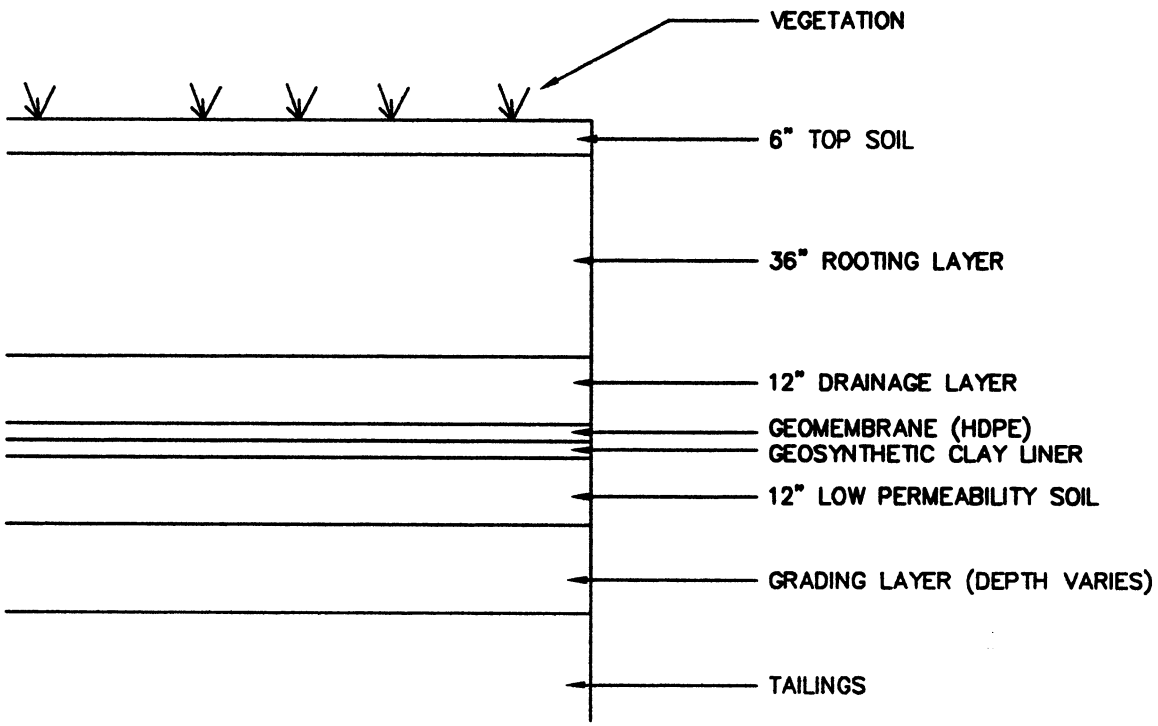

STEFFEN ROBERTSON AND KIRSTEN
Consulting Engineers

FOTH & VAN DYKE

CRANDON TMA SOURCE TERM

SECTION THROUGH TMA COVER

PROJECT NO.	DATE	APPROVED	FIGURE
F107107/1	APRIL 1997		2.5

FILE REF: DG-2-5

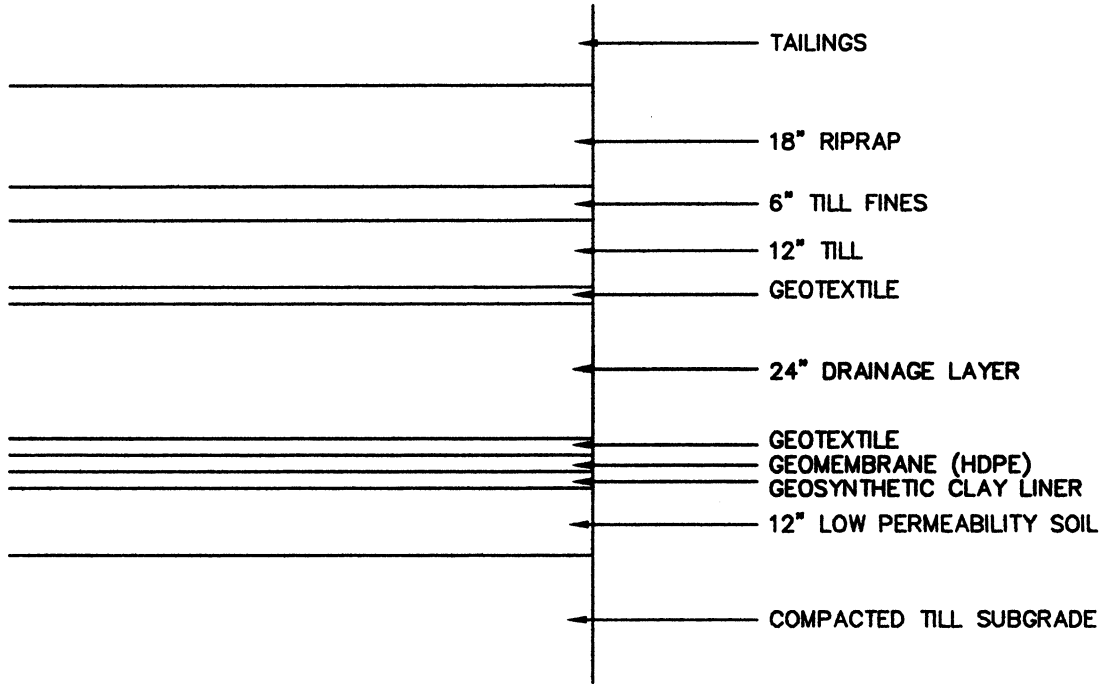

STEFFEN ROBERTSON AND KIRSTEN
Consulting Engineers

FOTH & VAN DYKE

CRANDON TMA SOURCE TERM

SECTION THROUGH TMA BASE LINER

PROJECT NO.	DATE	APPROVED	FIGURE
F107107/1	APRIL 1997		2.6

FILE REF: FIG-2-6

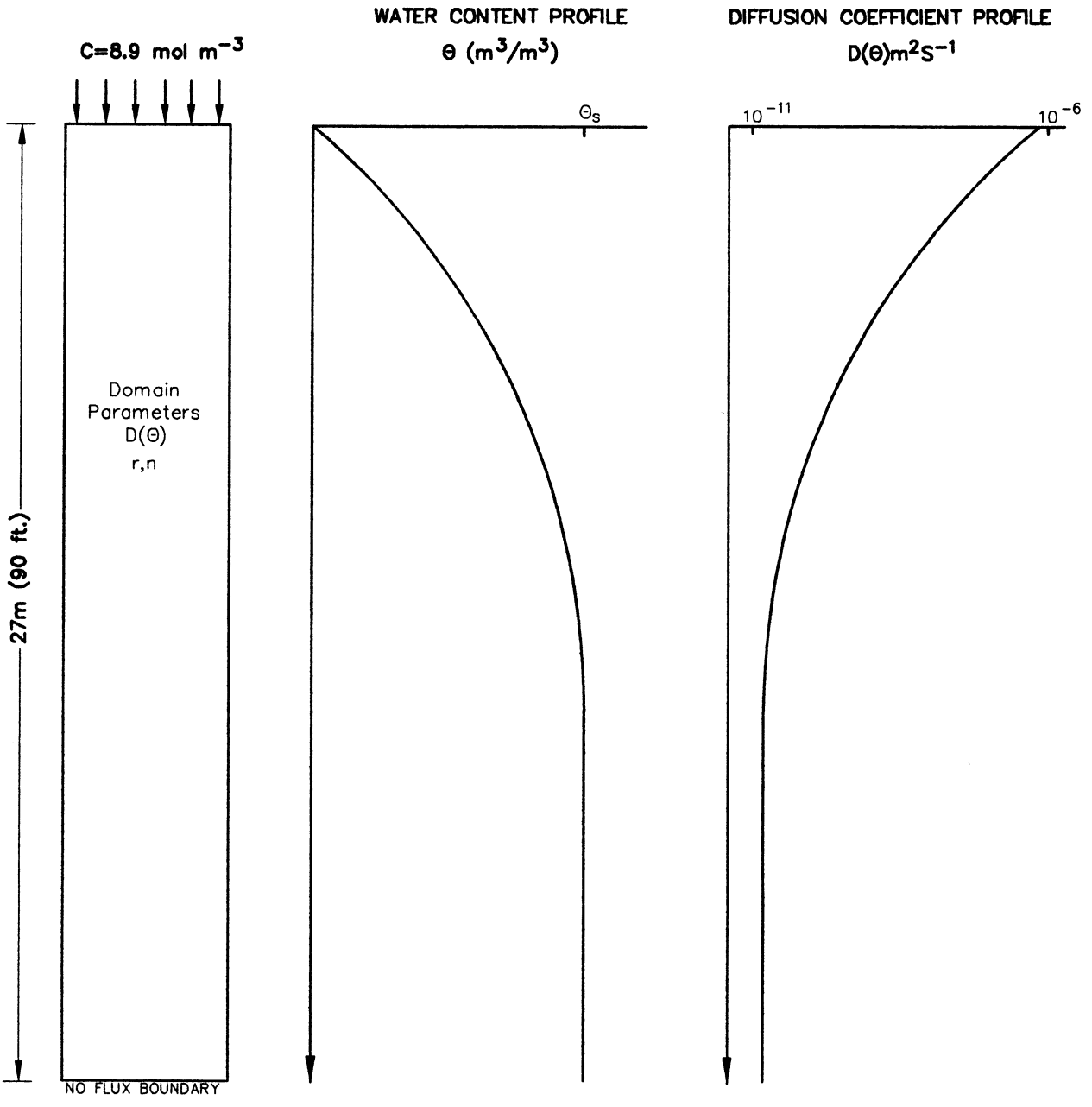

STEFFEN ROBERTSON AND KIRSTEN
Consulting Engineers

FOTH & VAN DYKE

CRANDON TMA SOURCE TERM

INPUTS TO 1-D DIFFUSION MODEL OF PORE AIR AT EQUILIBRIUM WATER CONTENT

PROJECT NO.	DATE	APPROVED	FIGURE
F107107/1	APRIL 1997		3.1

FILE REF: SKETCH-2

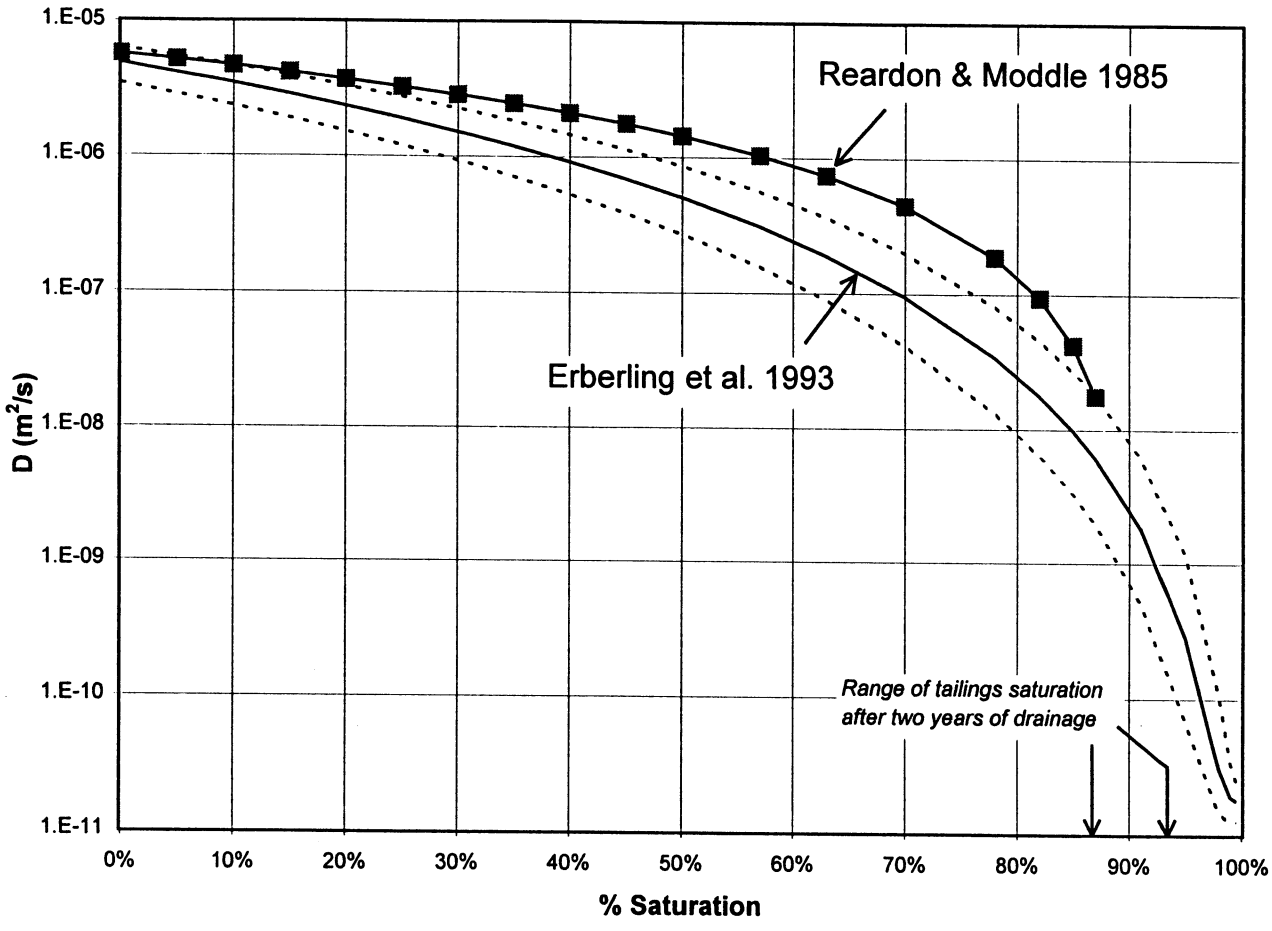

4.2-12-258

FILE REF: TITLE

STEFFEN ROBERTSON AND KIRSTEN
Consulting Engineers

FOTH & VAN DYKE

CRANDON TMA SOURCE TERM

COMPARISON OF DIFFUSION COEFFICIENT RELATIONSHIPS

PROJECT NO.	DATE	APPROVED	FIGURE
F107107/1	APRIL 1997		3.2

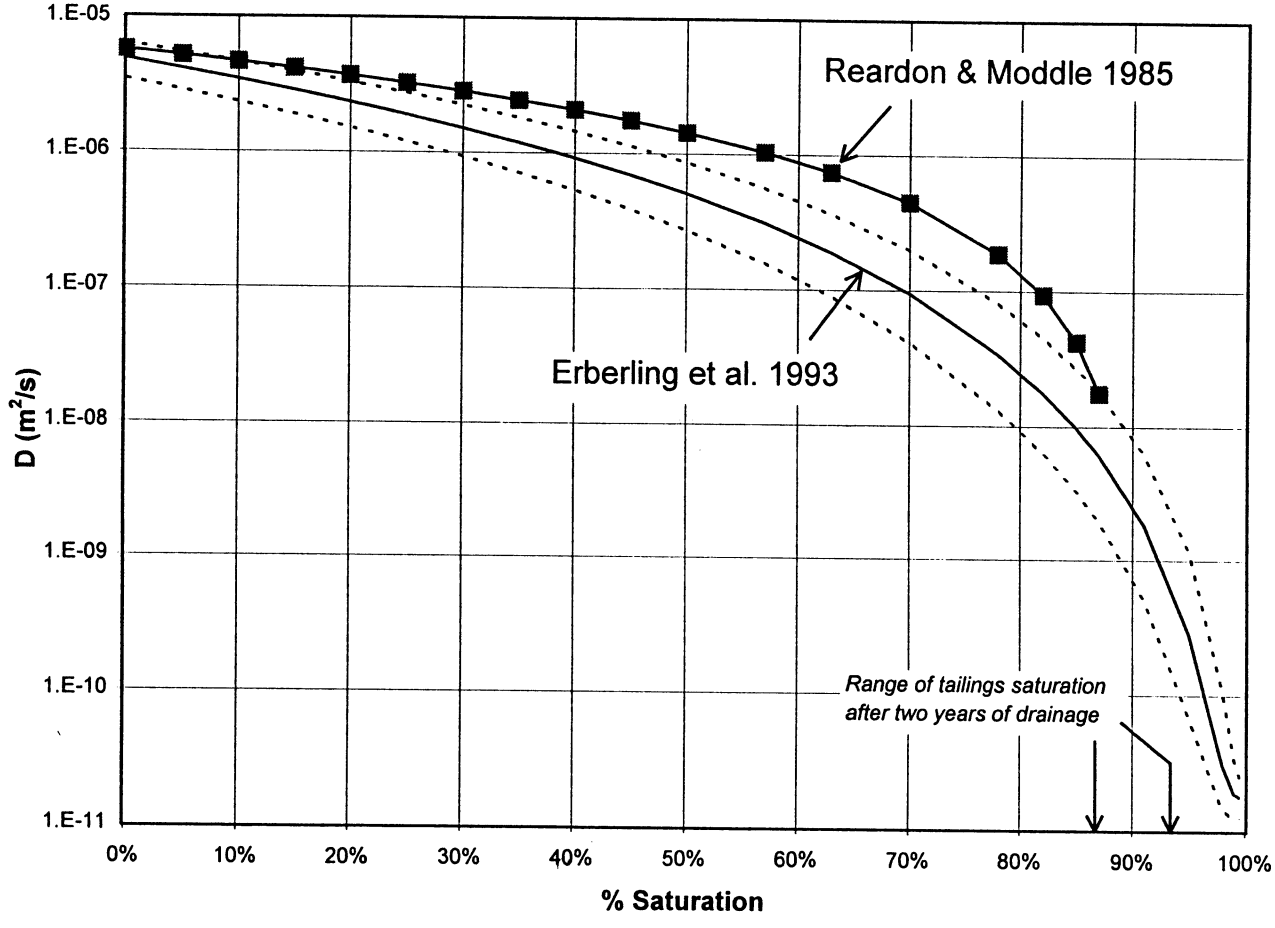

STEFFEN ROBERTSON AND KIRSTEN Consulting Engineers	CRANDON TMA SOURCE TERM		
FOTH & VAN DYKE	COMPARISON OF DIFFUSION COEFFICIENT RELATIONSHIPS		
	PROJECT NO. F107107/1	DATE APRIL 1997	APPROVED	FIGURE 3.2

4.2-12-259

FILE REF: TITLE

a) SECTION 1

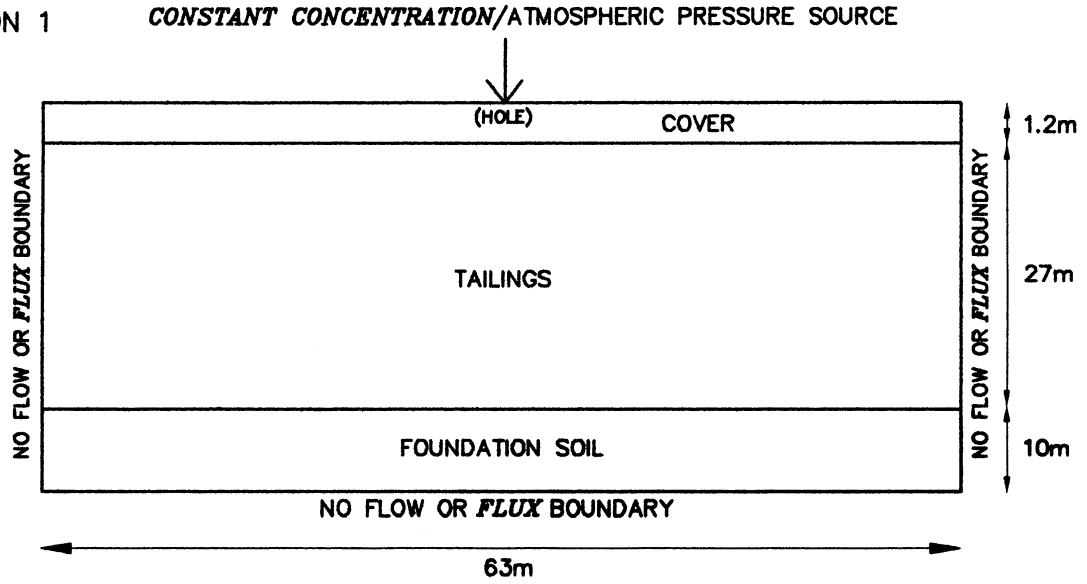

b) SECTION 2

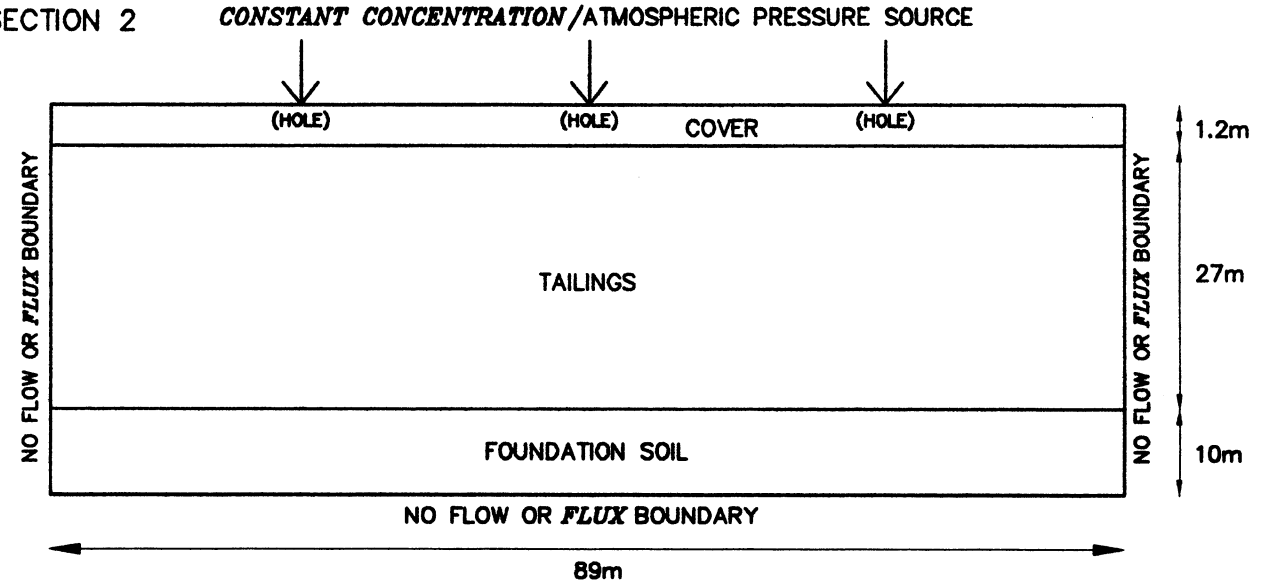

c) MODELLING PARAMETERS

DIFFUSION

$D_{COVER} = 3 \times 10^{-6} m^2 s^{-1}$ $r_{COVER} = 0$

$D_{TAILINGS} = 3 \times 10^{-6} m^2 s^{-1}$ $r_{TAILINGS} = 1.07 \times 10^{-4} S^{-1}$

$D_{SOIL} = 3 \times 10^{-6} m^2 s^{-1}$ $r_{SOIL} = 0$

BAROMETRIC PUMPING

$k_{COVER} = 3.5 \times 10^{-12} m^2$

$k_{TAILINGS} = 2 \times 10^{-14} m^2$

$k_{SOIL} = 3.5 \times 10^{-12} m^2$

STEFFEN ROBERTSON AND KIRSTEN Consulting Engineers	CRANDON TMA SOURCE TERM		
FOTH & VAN DYKE	DIFFUSION AND BAROMETRIC PUMPING THROUGH DEFECTS IN COVER		
	PROJECT NO. F107107/1	DATE APRIL 1997	APPROVED	FIGURE 3.3

FILE REF: SKETCH-1

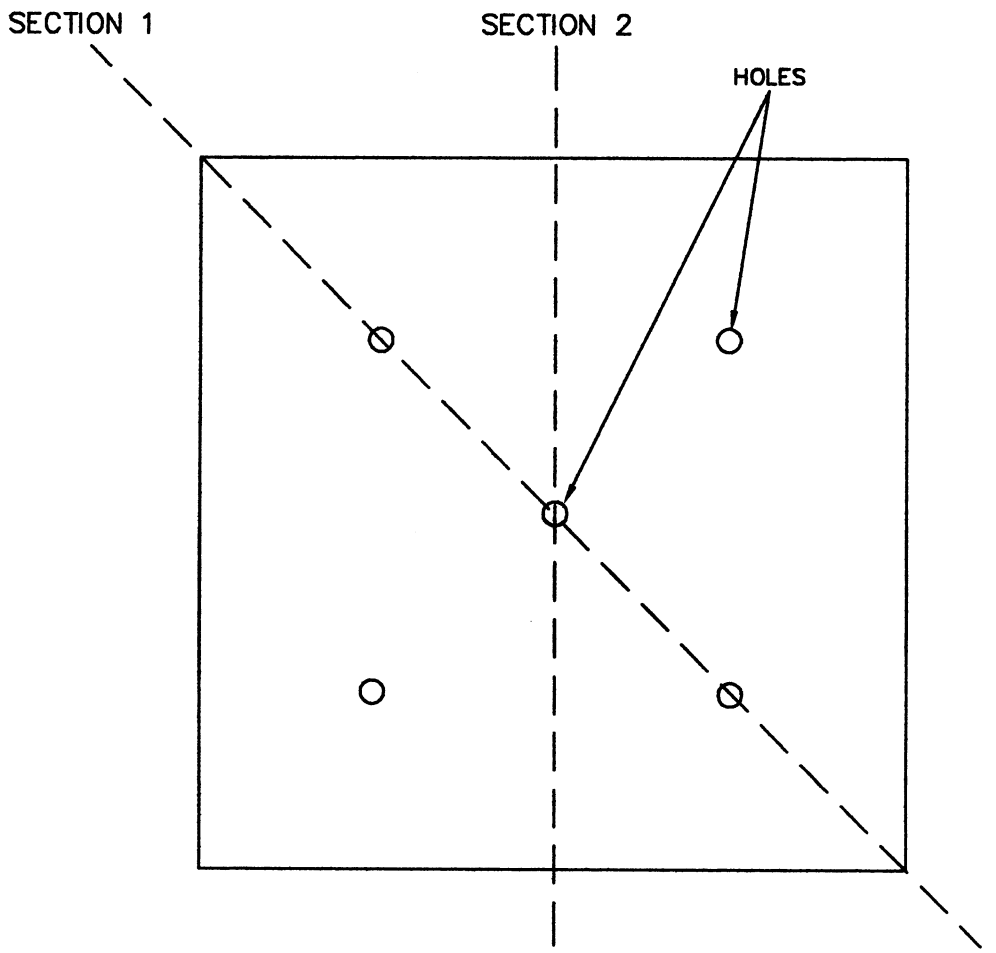

STEFFEN ROBERTSON AND KIRSTEN
Consulting Engineers

FOTH & VAN DYKE

CRANDON TMA SOURCE TERM

PLAN VIEW OF DEFECTS
IN 1 ACRE OF COVER

PROJECT NO.	DATE	APPROVED	FIGURE
F1071071/1	APRIL 1997		3.4

FILE REF:SKETCH-3

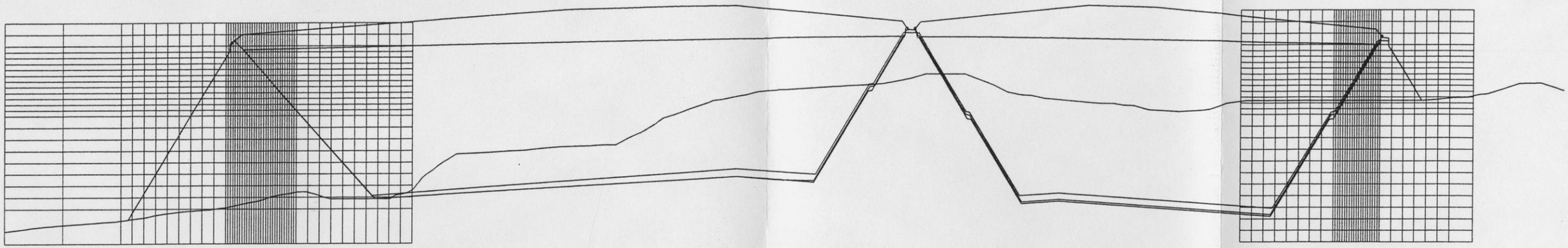

VERTICAL SCALE
EXAGGERATED

HORIZONTAL SCALE

0 150 300 450 600 750 FEET

1"=300'

FILE REF: JASON.DWG

STEFFEN ROBERTSON AND KIRSTEN
Consulting Engineers

FOTH & VAN DYKE

CRANDON TMA SOURCE TERM

CROSS SECTION THROUGH TMA SHOWING DISCRETIZATIONS FOR DIFFUSION AND BAROMETRIC PUMPING MODELLING

PROJECT NO.	DATE	APPROVED	FIGURE
F107107/1	APRIL 1997		3.5

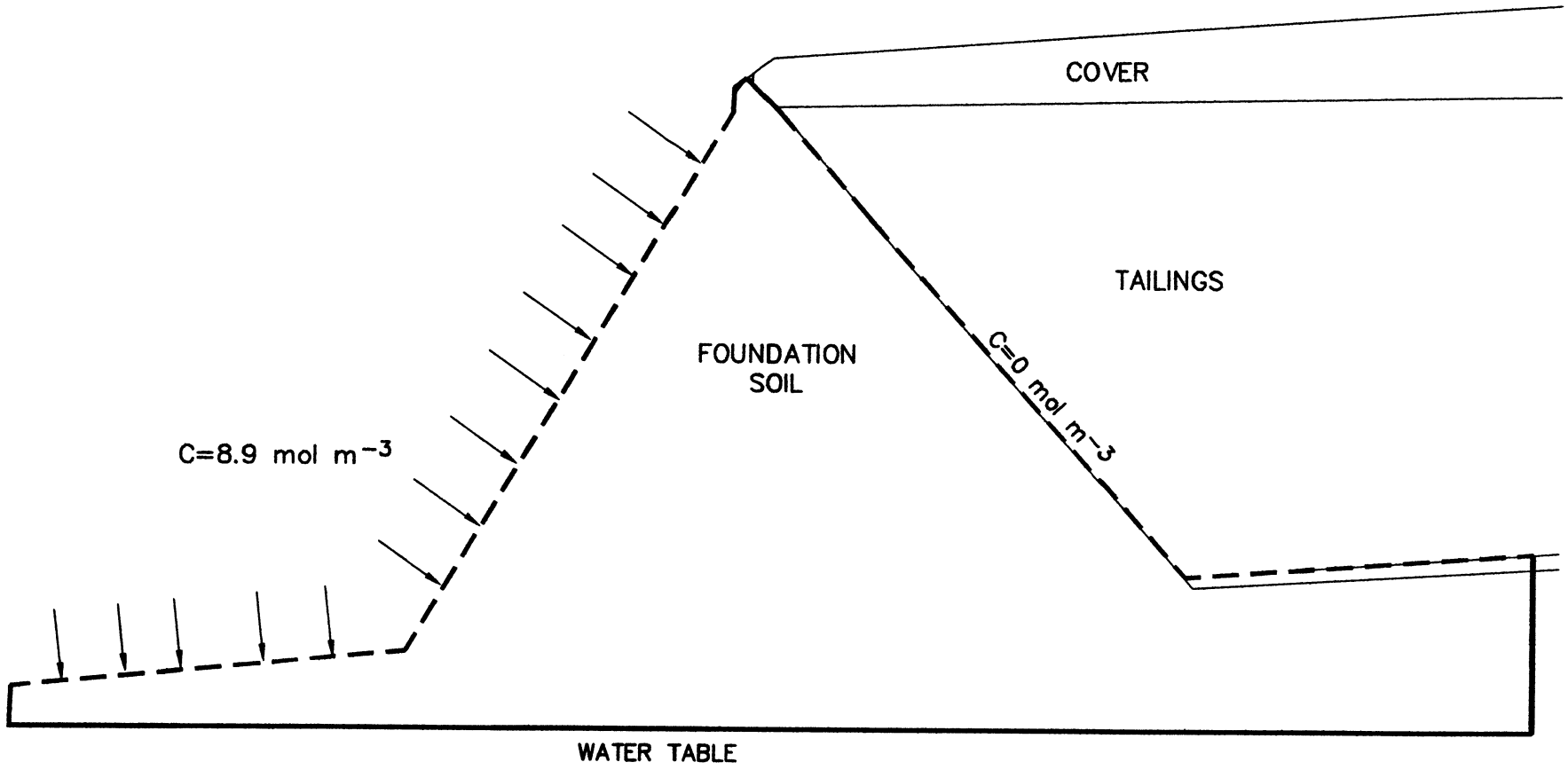

NO FLUX BOUNDARY

CONSTANT CONCENTRATION BOUNDARY

VERTICAL SCALE EXAGGERATED

STEFFEN ROBERTSON AND KIRSTEN
Consulting Engineers

FOTH & VAN DYKE

CRANDON TMA SOURCE TERM

CONCEPTUAL MODEL FOR DIFFUSION THROUGH LARGE EMBANKMENT

PROJECT NO.	DATE	APPROVED	FIGURE
F107107/1	APRIL 1997		3.6

4.2-12-263

FILE REF: JASON-3b.DWG

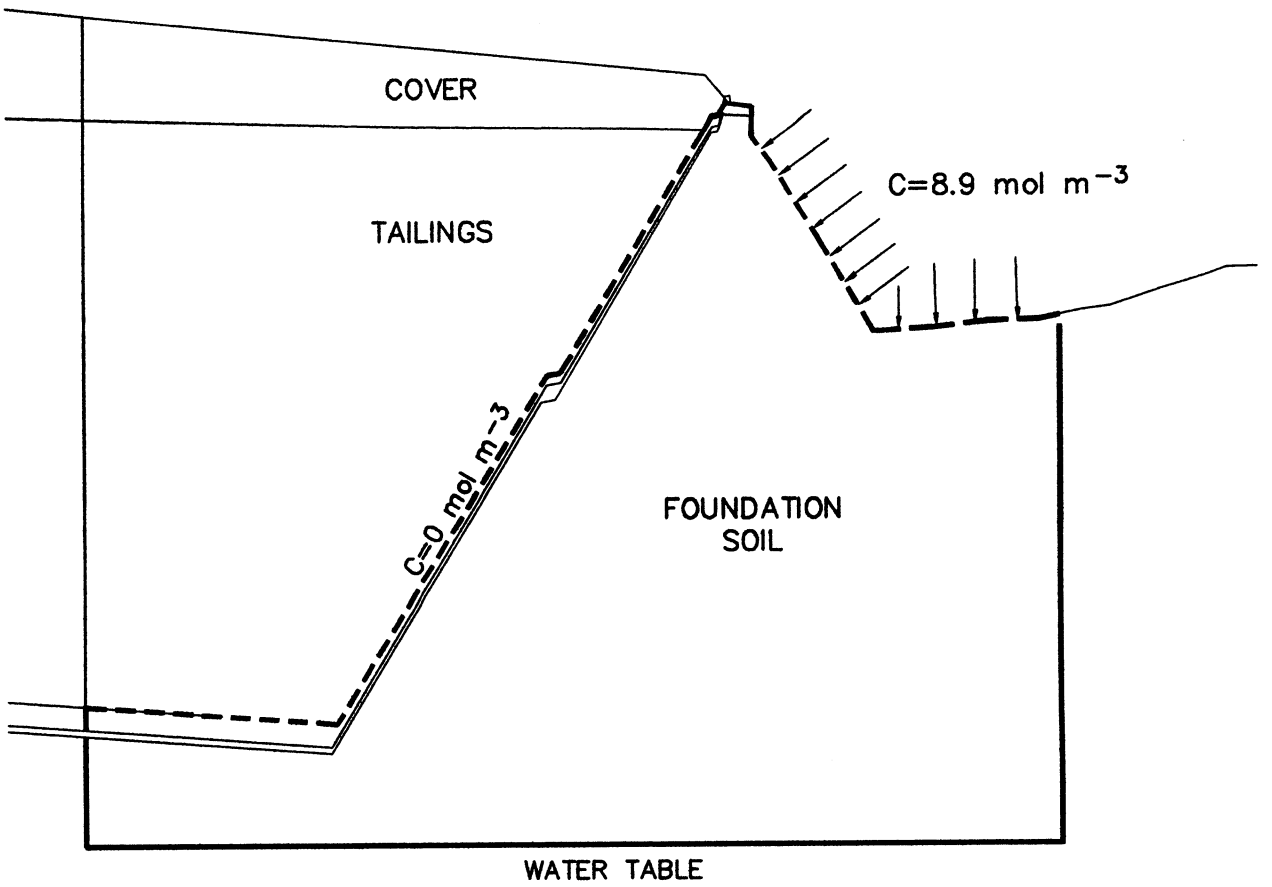

CONSTANT CONCENTRATION BOUNDARY

NO FLUX BOUNDARY

VERTICAL SCALE EXAGGERATED

STEFFEN ROBERTSON AND KIRSTEN
Consulting Engineers

FOTH & VAN DYKE

4.2-12-264

CRANDON TMA SOURCE TERM

CONCEPTUAL MODEL FOR DIFFUSION THROUGH SMALL EMBANKMENT

PROJECT NO.	DATE	APPROVED	FIGURE
F107107/1	APRIL 1997		3.7

FILE REF: JASON-2b.DWG

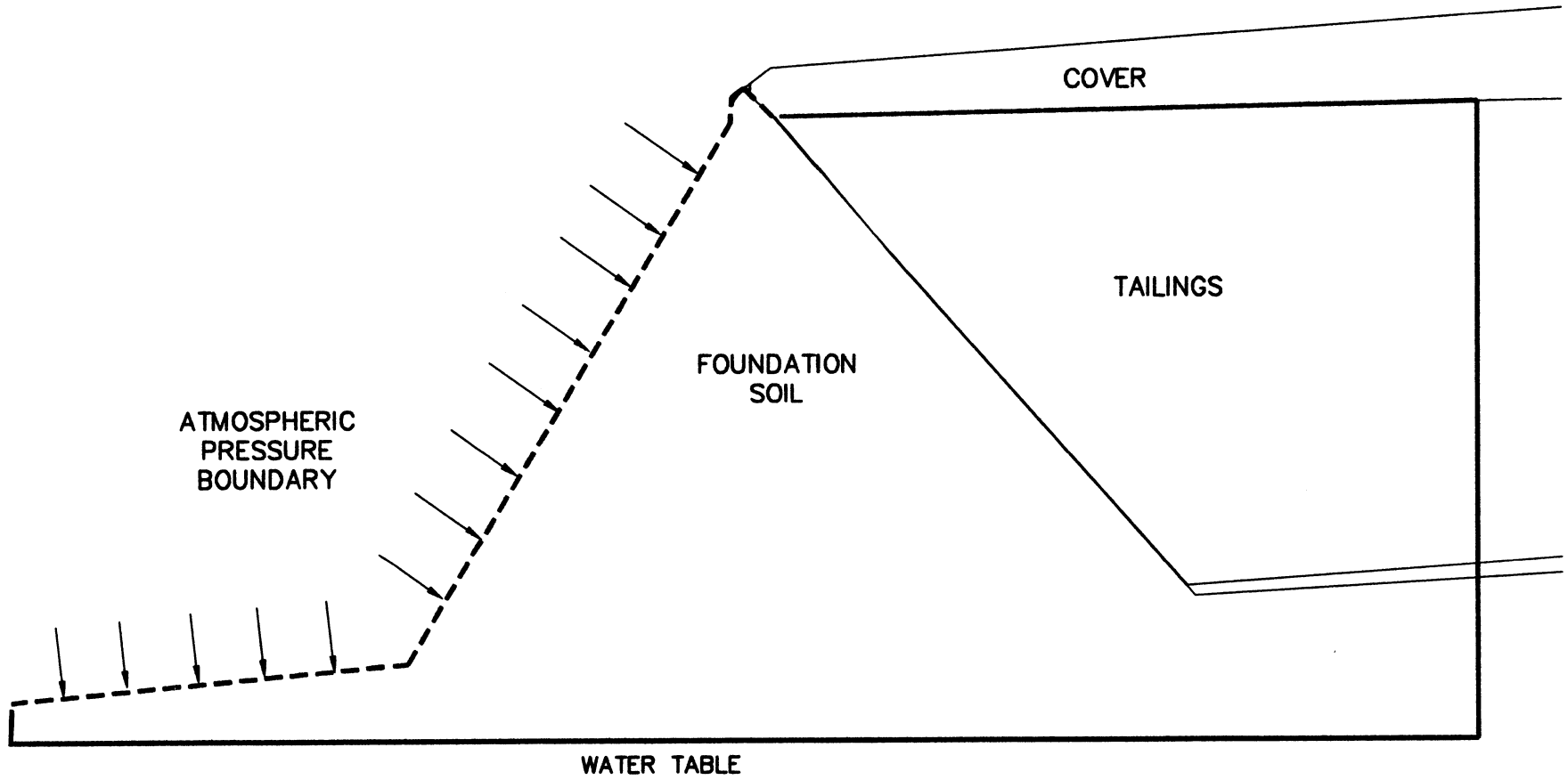

STEFFEN ROBERTSON AND KIRSTEN
Consulting Engineers

FOTH & VAN DYKE

CRANDON TMA SOURCE TERM

CONCEPTUAL MODEL FOR BAROMETRIC PUMPING THROUGH LARGE EMBANKMENT

PROJECT NO.	DATE	APPROVED	FIGURE
F107107/1	APRIL 1997		3.8

4.2-12-265

FILE REF: JASON-3a.DWG

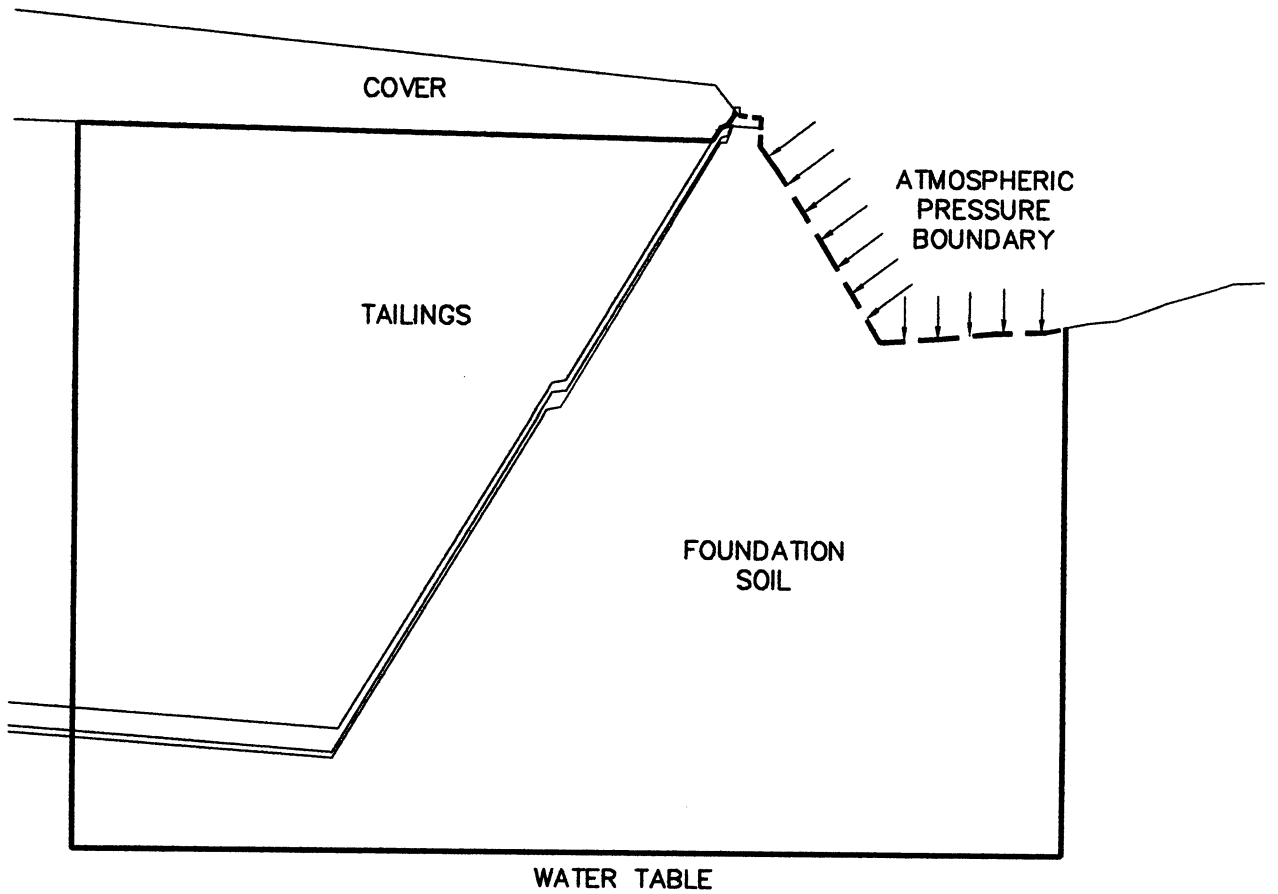

ATMOSPHERIC PRESSURE BOUNDARY

NO FLOW BOUNDARY

VERTICAL SCALE EXAGGERATED

STEFFEN ROBERTSON AND KIRSTEN
Consulting Engineers

FOTH & VAN DYKE

4.2-12-266

CRANDON TMA SOURCE TERM

CONCEPTUAL MODEL FOR BAROMETRIC PUMPING THROUGH SMALL EMBANMKMENT

PROJECT NO.	DATE	APPROVED	FIGURE
F107107/1	APRIL 1997		3.9

FILE REF: JASON-2a.DWG

ATTACHMENT A

ATTACHMENT A
DESCRIPTION OF FINITE-DIFFERENCE MODELS FOR OXYGEN TRANSPORT

A1.0 INTRODUCTION

This attachment summarizes the two-dimensional finite-difference models used to simulate oxygen diffusion and barometric pumping into the TMA for the cases of transport through the foundation soils (Sections 3.5 and 3.6) and transport through holes in the cover (Sections 3.7 and 3.8).

A2.0 TWO-DIMENSIONAL DIFFUSION AND REACTION

A2.1 Model Description Governing Equation

The equation for two dimensional diffusion with reaction through a heterogeneous domain is given by:

$$\frac{dC}{dt} = \frac{\partial}{\partial x}\left(D\frac{\partial C}{\partial x}\right) + \frac{\partial}{\partial y}\left(D\frac{\partial C}{\partial y}\right) - r * C^n$$

Where:

C is oxygen concentration (mol/m^3); **t** is time (s); **D** is the effective diffusion coefficient (m^2/s); **n** is the rate order; and **r** is a reaction constant. The units of **r** depends upon the rate order. For **n** = 1, **r** has the units s^{-1}.

This equation has been solved using finite-differences programmed in the Visual Basic language provided with Microsoft Excel 5.0. The code uses an alternating direction implicit (ADI) scheme to solve the set of finite-difference equations. This solution scheme is memory efficient and unconditionally stable. Model parameters, boundary conditions and model results are all contained within an Excel workbook; Each simulation run is saved as a separate Excel file.

A2.2 Finite Difference Equations

The Alternating Implicit Direction Method (ADI) solves the diffusion equation by alternately treating the spatial derivatives in one direction explicitly (i.e. concentration at present time) and the other direction implicitly (i.e. concentration at the future time).

For the first half of the time step horizontal nodes are treated implicitly and vertical nodes are treated explicitly. The finite difference equations are given by:

$$C_{ij-1}^{\,t+\Delta t/2}\frac{L_w}{\Delta x_{ij}} - C_{ij}^{\,t+\Delta t/2}\left[\frac{(L_e+L_w)}{\Delta x_{ij}}+\frac{2}{\Delta t}\right] + C_{ij+1}^{\,t+\Delta t/2}\frac{L_e}{\Delta x_{ij}} =$$

$$\frac{-2C_{ij}^{\,t}}{\Delta t} - \left[C_{i+1j}^{\,t}\frac{L_n}{\Delta y_{ij}} - C_{ij}^{\,t}\left[\frac{(L_n+L_s)}{\Delta y_{ij}}\right] - r\left(C_{ij}^{\,t}\right)^n + C_{i-1j}^{\,t}\frac{L_s}{\Delta y_{ij}}\right]$$

where $C_{xx}^{\,t}$ are nodal concentrations at the present time (known) and $C_{xx}^{\,t+\Delta t/2}$ are nodal concentrations at the future time and are unknown. The unknown future concentrations form a system of equations which are solved with tridiagonal matrix solver routine. After the first half of the time step is solved, a second sweep is conducted where the vertical nodes are treated implicitly and the horizontal nodes are treated explicitly.

The finite difference equation for the second half of the time step are given by:

$$C_{i+1j}^{\,t+\Delta t}\frac{L_n}{\Delta y_{ij}} - C_{ij}^{\,t+\Delta t}\left[\frac{(L_n+L_s)}{\Delta y_{ij}}+\frac{2}{\Delta t}\right] + C_{i-1j}^{\,t+\Delta t}\frac{L_s}{\Delta y_{ij}} =$$

$$\frac{-2C_{ij}^{\,t+\Delta t/2}}{\Delta t} - \left[C_{ij-1}^{\,t+\Delta t/2}\frac{L_w}{\Delta x_{ij}} - C_{ij}^{\,t+\Delta t/2}\left[\frac{(L_w+L_e)}{\Delta x_{ij}}\right] - r\left(C_{ij}^{\,t+\Delta t/2}\right)^n + C_{ij+1}^{\,t+\Delta t/2}\frac{L_e}{\Delta x_{ij}}\right]$$

Ln, Ls, Le and Lw are harmonically averaged transport coefficients which account for differences in diffusion coefficient between gridblocks:

$$L_w = \frac{2D_{ij}D_{ij-1}}{D_{ij}\Delta x_{ij-1} + D_{ij-1}\Delta x_{ij}}$$

$$L_e = \frac{2D_{ij}D_{ij+1}}{D_{ij}\Delta x_{ij+1} + D_{ij+1}\Delta x_{ij}}$$

$$L_n = \frac{2D_{ij}D_{i+1j}}{D_{ij}\Delta x_{i+1j} + D_{i+1j}\Delta x_{ij}}$$

$$L_s = \frac{2D_{ij}D_{i-1j}}{D_{ij}\Delta x_{i-1j} + D_{i-1j}\Delta x_{ij}}$$

A2.3 BOUNDARY CONDITIONS

Two boundary conditions may be specified at the model boundaries: specified concentration and specified flux. The first boundary condition is applied by replacing the equations at the boundary nodes with a constant value:

$$C_{ij}^{t+\Delta t} = C_{boundary}.$$

The second boundary condition is applied by adding an extra source term to the explicit (right hand side) of the finite difference equation, i.e.

IMPLICIT TERMS = EXPLICIT TERMS + FLUX.

A3.0 BAROMETRIC PUMPING

A3.1 Governing Equation

The equation for two dimensional air advection through a heterogeneous domain is given by:

$$n\frac{dP}{dt} = \frac{\partial}{\partial x}(\alpha\frac{\partial P}{\partial x}) + \frac{\partial}{\partial y}(\alpha\frac{\partial P}{\partial y})$$

$$\alpha = \frac{\rho R T k_a}{m\mu}$$

Where:

P is air pressure (Pa); **t** is time (s); **n** is the effective porosity (m^3pores/m^3rock); ρ is the air density (kg/m^3); **m** is the molar mass of air (0.0289 kg/mol); μ is the viscosity (Ns/m^2); **T** is temperature (K); **R** is the universal gas constant (joules/K·mol) and k_a is the air permeability (m^2).

This equation has been solved using a similar finite-difference program as described above in section A2.1. Again, all code, model parameters, boundary conditions and model results for a barometric pumping simulation are contained within a single Excel file.

A3.2 Finite Difference Equations

A more detailed description of the ADI method is provided in A2.2.

The finite-difference equations for the first half of a time step are given by:

$$P_{ij-1}^{t+\Delta t/2}\frac{C_w}{\Delta x_{ij}} - P_{ij}^{t+\Delta t/2}\left[\frac{(C_e + C_w)}{\Delta x_{ij}} + \frac{2n}{\Delta t}\right] + P_{ij+1}^{t+\Delta t/2}\frac{C_e}{\Delta x_{ij}} =$$
$$\frac{-2nP_{ij}^{t}}{\Delta t} - \left[P_{i+1j}^{t}\frac{C_n}{\Delta y_{ij}} - P_{ij}^{t}\left[\frac{(C_n + C_s)}{\Delta y_{ij}}\right] + P_{i-1j}^{t}\frac{C_s}{\Delta y_{ij}}\right]$$

The finite-difference equations for the second half of a time step are given by:

$$P_{i+1j}^{t+\Delta t}\frac{C_n}{\Delta y_{ij}} - P_{ij}^{t+\Delta t}\left[\frac{(C_n + C_s)}{\Delta y_{ij}} + \frac{2n}{\Delta t}\right] + P_{i-1j}^{t+\Delta t}\frac{C_s}{\Delta y_{ij}} =$$
$$\frac{-2P_{ij}^{t+\Delta t/2}}{\Delta t} - \left[P_{ij-1}^{t+\Delta t/2}\frac{C_w}{\Delta x_{ij}} - P_{ij}^{t+\Delta t/2}\left[\frac{(C_w + C_e)}{\Delta x_{ij}}\right] + P_{ij+1}^{t+\Delta t/2}\frac{C_e}{\Delta x_{ij}}\right]$$

where C_n, C_s, C_e, and C_w are harmonically averaged conductances:

$$C_w = \frac{2\alpha_{ij}\alpha_{ij-1}}{\alpha_{ij}\Delta x_{ij-1} + \alpha_{ij-1}\Delta x_{ij}}$$

$$C_e = \frac{2\alpha_{ij}\alpha_{ij+1}}{\alpha_{ij}\Delta x_{ij+1} + \alpha_{ij+1}\Delta x_{ij}}$$

$$C_n = \frac{2\alpha_{ij}\alpha_{i+1j}}{\alpha_{ij}\Delta x_{i+1j} + \alpha_{i+1j}\Delta x_{ij}}$$

$$C_s = \frac{2\alpha_{ij}\alpha_{i-1j}}{\alpha_{ij}\Delta x_{i-1j} + \alpha_{i-1j}\Delta x_{ij}}$$

A3.3 Boundary Conditions

Two boundary conditions may be specified at the model boundaries: specified pressure and specified flow. The first boundary condition is applied by replacing the equations at the boundary nodes with a constant value:

$$P_{ij}^{t+\Delta t} = P_{boundary}.$$

The second boundary condition is applied by adding an extra source term to the explicit (right hand side) of the finite difference equation, i.e.

$$\text{IMPLICIT TERMS} = \text{EXPLICIT TERMS} + \underline{\underline{\text{FLOW.}}}$$

ATTACHMENT B

Foth & Van Dyke
Memorandum

October 9, 1996

TO: Jerry Sevick, Foth & Van Dyke

CC: Don Moe, Crandon Mining Company
Daryl Hockley, SRK
Master File

FR: Steve Donohue, Foth & Van Dyke SVD
Fred Anderson, Foth & Van Dyke

RE: Crandon Project - Soil Gas Probe Installation and Soil Gas Data

Two multi-level soil gas monitoring probes were installed in the vicinity of the proposed TMA facility during the week of July 29 to August 2, 1996. The location of the probes are shown on Figure 1. Probe CMC-O2-SE was installed approximately 100 ft west of soil boring CMC-TMA-107. Probe CMC-O2-NW was installed approximately 100 ft south of monitoring well nest EX-9.

The first multi-level probe (CMC-O2-SE) borehole was drilled to a total depth of approximately 115 ft. The initial borehole diameter was 8 in with casing driven to a depth of 75 ft to maintain the integrity of the borehole. The remainder of the boring was advanced as a 6-in borehole. Adherence to dry drilling conditions was observed when feasible. However, water was used to advance the borehole when resistant materials were encountered such as boulders. No drilling mud or additives were used. Ten individual probes were installed at predetermined elevations. One probe was adjusted slightly in depth from 44 ft to 50 ft to intersect the targeted fine outwash layer. The casing was withdrawn as the probes were constructed. The boring log and construction details for probe CMC-O2-SE are provided in Attachment 1.

The second multi-level probe (CMC-O2-NW) borehole was drilled to a total depth of 104 ft. Casing was driven to a depth of 95 ft to maintain the integrity of the 8-in borehole. The remainder of the borehole was advanced as a 6-in borehole. Water was used to advance the borehole only when resistant materials were encountered. No drilling mud or additives were used. Nine individual probes were installed at predetermined depths. The casing was withdrawn as the probes were constructed. The boring log and construction details for probe CMC-O2-NW are provided in Attachment 2.

For each probe, an individual custom slotted, 6-in long screen was installed at a predetermined interval attached to a flush threaded, ⅝-in (i.d) schedule 40 PVC riser. Each probe was finished in red flint sand #30 filter pack material sealed from above with a 6-in clean fine sand seal. One to two-and-one-half feet of granular bentonite was placed on top of the fine sand. For probes installed at a depth greater than 15 ft below land surface, chipped bentonite (⅜-in) was placed above the hydrated granular bentonite in 1- to 3-ft lifts. The bentonite was hydrated as it was placed in the hole at a ratio of 1 gal per 10 lbs of bentonite. Completed probes were finished

with top valves sealed with PVC glue. A locked protective casing was installed over the top of the probes at both locations for protection and security.

Soil gas measurements for percent oxygen, carbon dioxide, and pressure were recorded on August 2, 9, 23, and 29. Barometric pressure at the site was recorded each day that measurements were acquired. The procedure for measuring the soil gas content from each multi-level probe was as follows:

1. Calibrate the Landtec GA-90L gas analyzer.

2. Attach pressure gage to each probe, open probe valve and measure and record the pressure difference (inches of water) relative to surface barometric pressure.

3. Measure and record soil gas sampling rate (cc/min) of the Landtec GA-90L gas analyzer.

4. Purge three probe volumes of gas from each individual multi-level probe.

5. After purging was complete, measure and record the soil gas concentrations of oxygen and carbon dioxide.

On August 2, 1996, each nest of probes at each location was purged and sampled starting with the deepest probe first. The remaining probes in each nest were purged and sampled in ascending order so that the shallow 3-ft probe was purged and sampled last. On August 9, 1996, the order was reversed. The shallow 3-ft probe was purged and sampled first. The remaining probes were purged and sampled in descending order, so that the deepest probe was purged and sampled last.

On August 23 and 29, 1996, an alternative sampling sequence was used. At each probe nest, every other probe was purged and sampled in descending order. Approximately 3 hr later the remaining probes were sampled, also in descending order. This methodology was used to verify that the probes were isolated from each other by the installed seals.

In addition to measuring the soil gas content via the newly installed oxygen probes, the soil gas was also measured from well CMC-BO-101B. This well is located in the Bur Oak Swamp and is screened in the unsaturated outwash sands beneath the perched wetland at a depth of about 39 ft. The well head was outfitted with an adapter that was glued to the PVC riser to seal the well from the atmosphere. Soil gas from CMC-BO-101B was sampled according to the procedure described above.

The results from the soil gas sampling are summarized in Table 1.

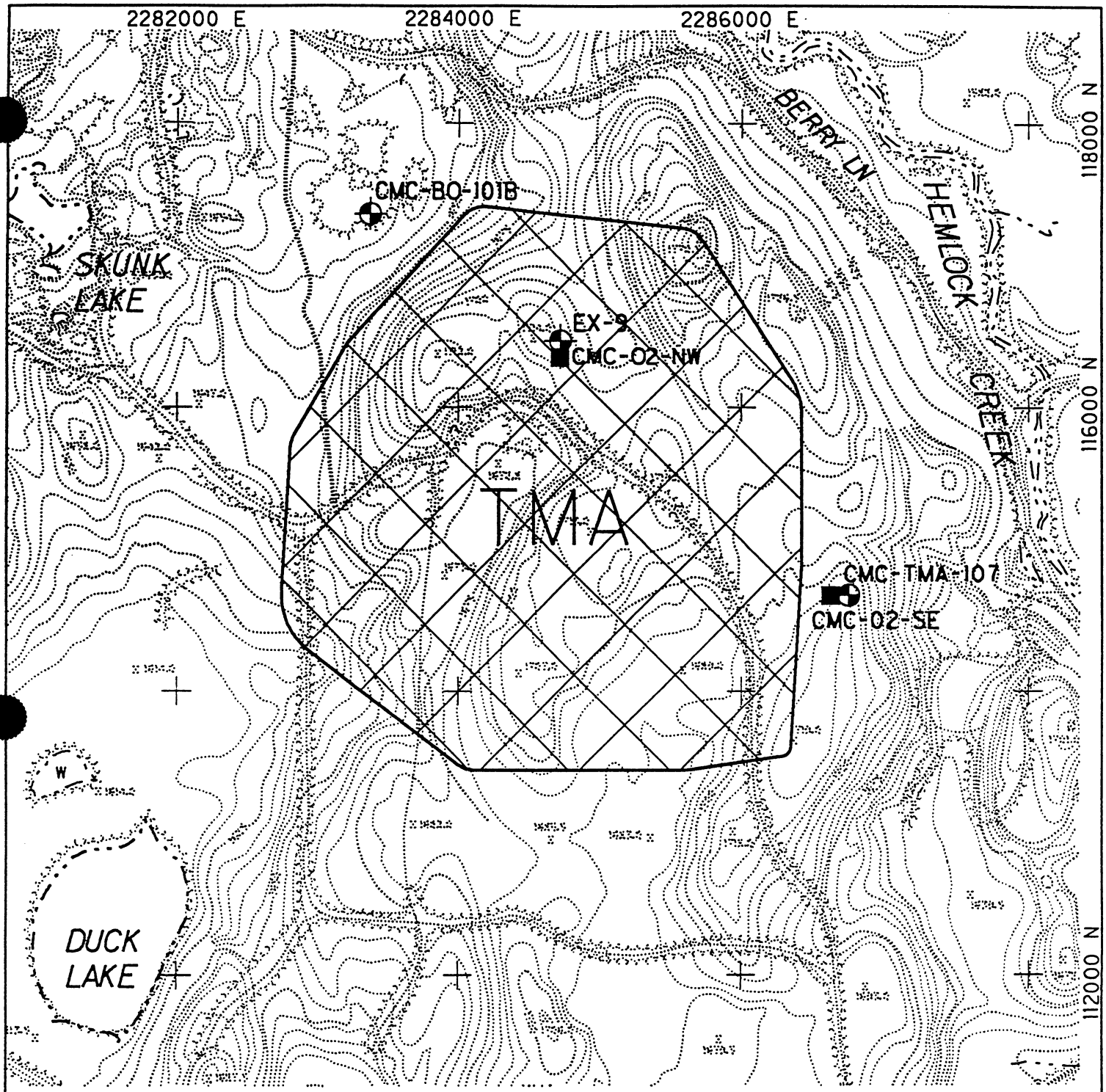

LEGEND

CMC-02-SE ■	OXYGEN PROBE LOCATION AND NUMBER
CMC-TMA-107 ⊕	BORING LOCATION AND NUMBER
EX-9 ⊕	MONITORING WELL LOCATION AND NUMBER

0 1000' 2000'

BAR SCALE

N

Foth & Van Dyke

REVISED	DATE	BY	DESCRIPTION

CHECKED BY:	JKS1	DATE: SEPT.'96
APPROVED BY:	SVD1	DATE: SEPT.'96
APPROVED BY:	GWS	DATE: SEPT.'96

Crandon Mining Company

FIGURE 1

OXYGEN PROBE LOCATION MAP

Scale:	SEE BAR SCALE	Date:	SEPTEMBER, 1996
Prepared By:	Foth & Van Dyke	By:	JRB2

C:\cadwork\3c49f185.dgn

93C049

Table 1

Summary of Soil Gas Data

Probe	Depth (ft)	August 2, 1996			August 9, 1996			August 23, 1996			August 29, 1996		
		Pressure (in. water)	Percent Oxygen	Percent Carbon Dioxide	Pressure (in. water)	Percent Oxygen	Percent Carbon Dioxide	Pressure (in. water)	Percent Oxygen	Percent Carbon Dioxide	Pressure (in. water)	Percent Oxygen	Percent Carbon Dioxide
CMC-O2-SE	3	0.2	17.8	3	0	13.4	1.1	-0.1	12.5	4.2	-0.1	11.9	6
	6	0	15	4.4	0	13.6	0.6	0	13.4	2.8	-0.1	12	4.9
	10	-0.18	14.8	3.7	0	12.5	0.2	0	15.7	0.3	-0.1	16.6	0.4
	15	0	15.6	4.4	0	16.3	0.3	0	17.4	0.3	-0.15	18.5	0.4
	25	0.02	13.9	0.3	-0.5	13.7	0.3	-0.5	15.5	0.1	-0.2	17.4	0
	50	0	14.6	4.6	-1.55	16.5	0	-1.8	18.2	0	-0.6	20.6	0
	60	0	19.9	0.2	-1.85	16.8	0	-2.1	19	0	-0.75	20.8	0
	80	0	20.8	0	-1.45	18.4	0	-1.8	20.4	0	-0.6	20.6	0.3
	100	0	12.9	4.1	-1.65	18.8	0	-2	17.5	0	-0.7	18.8	0
	115	0	16.2	3.9	-1.75	12.4	0.1	-2	16.9	0	-0.7	17.2	0
CMC-O2-NW	3	0	19.5	0	0	15	2	-0.1	14.6	5.7	-0.25	14.6	5.2
	6	0	17.1	1.8	0	15.2	3	-0.05	14.7	5.8	-0.6	14.8	5.9
	10	0	17.7	0	-0.9	18.2	0.2	-1.35	19.2	1.2	-0.6	18.7	1.4
	15	0	19.1	0	-1.1	17.9	0	-1.7	19	0	-0.65	18.8	0
	30	0	19.5	0	-1	19.2	0	-1.7	20.2	0.3	-0.45	19.2	0.9
	50	0	19.8	0	-1.1	19.3	0	-1.9	19.4	0	-0.55	19.7	0.2
	65	0	20.2	0	-1.25	18.5	0	-2	20.2	0	-0.5	19.4	0
	80	0	20.5	0.2	-1.25	18.3	0	-2.1	19.7	0.5	-0.55	19.1	1.1
	103	0	18.5	0.2	-1.25	18.1	0.2	-2.1	18.9	0	-0.45	19.2	0
CMC-BO-101B	39	0	20.2	0	-0.75	20.1	0	-1.8	20.8	0	-0.4	20.4	0

Barometric Pressure (in of Hg):

August 2, 1996 = 30.11 (rising)
August 9, 1996 = 30.16 (steady)
August 23, 1996 = 30.22 (rising)
August 29, 1996 = 30.17 (steady)

MI D2\93C049\GBAPP\37068\6000

Prepared by: SVD1
Checked by: JFS

Attachment 1

Boring Log and Construction Details for Probe CMC-O2-SE

State of Wisconsin
Department of Natural Resources

Route to:
☐ Solid Waste ☐ Haz. Waste
☐ Emergency Response ☐ Underground Tanks
☐ Wastewater ☐ Water Resources
☐ Other

SOIL BORING LOG INFORMATION
Form 4400-122 7-91

Facility/Project Name	License/Permit/Monitoring Number	Boring Number
Crandon Mining Company - TMA 93C049		CMC-02-SE

Boring Drilled by (Firm name and name of crew chief)	Date Started MM/DD/YY	Date Completed MM/DD/YY	Drilling Method
Boart Longyear Mike Nelson	07/29/96	07/31/96	Rotosonic

DNR Facility Well No.	WI Unique Well No.	Common Well Name	Final Static Water Level	Surface Elevation	Borehole Diameter
				1,705'	8" (0'-75') 6" (75'-115')

Boring Location	Local Grid Location (if applicable)
State Plane ____ N, ____ E S/C/N Lat 1/4 of 1/4 of Section , T N, R E Long	____ N ____ E Feet ____ S Feet ____ W

County	DNR County Code	Civil Town/City/or Village
Forest	21	

SAMPLE No.	SAMPLE Rec (in)	Blow Counts	Depth in Feet	Soil/Rock description and geologic origin for each major unit	USCS	Graph Log	Well Diag	PID/FID	Soil Properties: Std Pntr	Mst Cont	Liq Lim	Plas Lim	P 200	RQD/Comm
C1	60	1	0	0-5 Red brown (7.5YR5/4) SAND w/angular gravel, moist.	SP									1254 Blow counts= rate of drill string approx. min/5' penetration
		1	5	5-10 Red brown (7.5YR5/4) fine sand w/gravel, moist, subangular to subrounded.	SP/GW									1305
C2	120	1	10	10-15 As above w/coarse gravel to fine cobbles, subrounded - subangular 1-3".	GW									
C3	60	1	15	15-20 Red brown (7.5YR5/4) silty fine sand w/10% 10mm subrounded gravel. Till.	SM/SP									1312
	60	1	20	20-25 Red brown (7.5YR5/4) silty fine sand (subrounded to subangular). 15%. Dry. Till. 10-25 mm gravel.	SM/GM									1330
C4	48	2	25	25-30 Red brown (7.5YR5/4) silty fine sand w/ gravel. Minor subrounded fine cobbles. Till.	SM/GM									Snapped drill rod
C5	60	2	30	30-35 As above, increasing fine subrounded cobbles 40-50mm till. Coarsening w/depth silty matrix.	GM/SM									1535
C6	60	10	35	35-40 Brown (10YR6/4) SILT w/trace subrounded gravel, matrix, very fine sand. Fine cobbles @ 40' outwash gray staining.	SM									1550
C7	60	10	40	40-45 Red brown (2.5YR5/4) silty sand, very fine-grained w/trace 5 mm subangular-subrounded medium sand 5% cobbles at 44.5'. Fine outwash. 44.5-45 Coarse granitic cobbles encountered.	SM									1637
C8	60	10	45	45-50 Red brown (5YR5/4) silty very fine-grained sand w/trace 5-10 mm subrounded gravel.	SM									1710

I hereby certify that the information on this form is true and correct to the best of my knowledge.

Signature Fred Anderson
Firm Foth & Van Dyke

This form is authorized by Chapters 114.147 and 162, Wis. Stats. Completion of this report is mandatory.
Penalties: Forfeit not less than $10 nor more then $5,000 for each violation. Fined not less than $10 or more than $100 or imprisoned not less than 30 days, or both for each violation. Each day of continued violation is a separate offense, pursuant to ss 114.06, Wis. Stats.

State of Wisconsin
Department of Natural Resources
BORING NUMBER: CMC-02-SE

Route to:

SOIL BORING LOG INFORMATION
Form 4400-122 7-91

SAMPLE No.	Rec (in)	Blow Counts	Depth in Feet	Soil/Rock description and geologic origin for each major unit	USCS	Graph Log	Well Diag	PID/ FID	Soil Properties: Std Pntr	Mst Cont	Liq Lim	Plas Lim	P 200	RQD/ Comm
				Red brown (5YR5/4) silt lens at 48'. Till.										
C9	60	10	50	50-55 Red brown (7.5YR5/6) sandy gravel, very fine-grained sand w/subrounded, coarse gravel, cobbles @ 55', well rounded, 15 cm, 5% gravel.	SP									1830
C10	60	5												1950
			55	55-60 Red brown (7.5YR5/6) vfg SAND w/silt, well sorted, trace 5 mm subrounded gravel grading down into red brown (7.5YR5/6) very	SM/ SW									
C11	60	5		fine-grained sand w/fine to medium gravel, subrounded, loose outwash.										0750
			60	60-65 Lt. brown (10YR6/4) vfg SAND w/trace subrounded, 2 cm gravel and cobbles 4-6 cm, loose, outwash as above, little fines <5%.	SP/ SM									
C12	60	5												0810
			65	65-69.5 Same as above. Fine outwash.										
C13	60	10		69.5-70 Brown (10YR4/4) SAND. Medium to coarse grained moderately well sorted. Sub-rounded-subangular grains. Wet.	SW									0825
			70	70-74 Lt. brown (10YR6/4) - grey (10YR2/1) well graded SAND and GRAVEL. Subrounded gravel w/subangular sand. Trace well rounded	SW/ GW									
C14	60	10		cobbles, loose. Till.										0850
			75	74-75 Red (2.5YR4/4) well graded GRAVEL with silt. Angular gravel. Weathering halo around granite. Cobbles (local). FeO_2.	GM									
15	84	10		75-83 Red brown (7.5YR5/6) very fine-grained SAND w/medium to coarse subangular gravel. Grey (10YR6/1) zones at 80'. Trace rounded	SP/ GM									0930
			80	cobbles. Till. Increasing fines to 83'. 0-5%.										
				83-90 Same as above.										
C16	84	10	85		SP/ SM									0950
			90	90-95 Same as above w/moderate density increasing w/depth w/increasing medium subangular gravel.	SP/ SM									
C17	60	10												1020 Drilled hard.
			95	95-96 Same as above.	SM									1140 Snapped hub support chain.
				96-97 Light grey (10YR2/1) to pale brown silty sand w/angular gravel. Trace biotite granite, well rounded cobbles.										
				97-100 Same as above.										1430
C18	24	15	100	100-105 Red brown (5YR5/4) coarse to very fine-grained subangular sand w/silt, trace subrounded gravel with well rounded and angular cobbles. Till. Loose.	SM/ GM									
C19	96	5	105	105-110 Same as above.	SM									1600
			110	110-111 Gray (10YR2/1) very fine-grained coarse, subangular sand w/fine subrounded gravel, Outwash.	SW									
20	84	10		111-112 Red brown (7YR4/6) silty very fine-grained-coarse grained angular sand w/med angular gravel, tr. well rounded cobbles. Till.	SM/ GM									1640
C21	48	5	115	112-115 Same as above. Moist. Capillary fringe.										1657
				E.O.B. @ 115'										▽ Capillary fringe

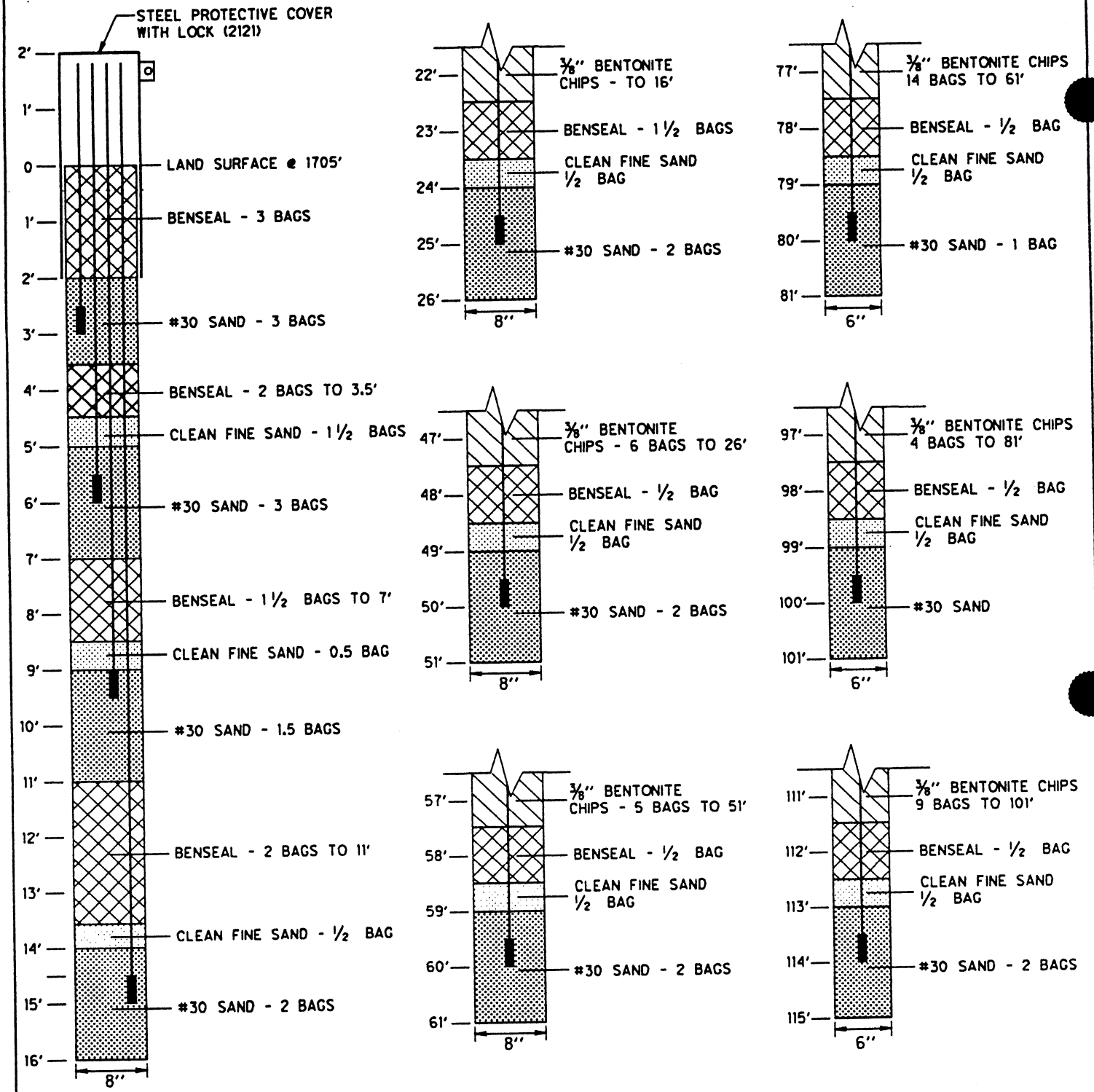

SEALING PROCEDURES

1. BENSEAL PLACED VIA GRAVITY ABOVE CLEAN FINE SAND.
2. BENSEAL HYDRATED, WATER ADDITION @ 1 GAL./10 LBS.
3. 3/8" BENTONITE CHIPS ADDED THROUGH WATER IN 1' TO 3' LIFTS TO NEXT SCREENED INTERVAL.

Foth & Van Dyke

REVISED	DATE	BY	DESCRIPTION

CHECKED BY:	JKS1	DATE: SEPT.'96
APPROVED BY:	SVD1	DATE: SEPT.'96
APPROVED BY:	GWS	DATE: SEPT.'96

Crandon Mining Company

CONSTRUCTION DIAGRAM FOR CMC-02-SE
(5/8" I.D. SCH 40 PVC RISER
1.5MM HAND SLOT 6" SCREEN)

Scale:	NOT TO SCALE	Date:	SEPTEMBER, 1996
Prepared By:	Foth & Van Dyke	By:	JRB2

93C049

C:\cadwork\3c49f187.dgn

Attachment 2

Boring Log and Construction Details for Probe CMC-O2-NW

State of Wisconsin
Department of Natural Resources

Route to:
☐ Solid Waste ☐ Haz. Waste
☐ Emergency Response ☐ Underground Tanks
☐ Wastewater ☐ Water Resources
☐ Other

SOIL BORING LOG INFORMATION
Form 4400-122 7-91

Facility/Project Name	License/Permit/Monitoring Number	Boring Number
Crandon Mining Company - TMA 93C049		CMC-02-NW

Boring Drilled by (Firm name and name of crew chief)	Date Started	Date Completed	Drilling Method
Boart Longyear Mike Nelson	MM/DD/YY 08/01/96	MM/DD/YY 08/02/96	Rotosonic

DNR Facility Well No.	WI Unique Well No.	Common Well Name	Final Static Water Level	Surface Elevation	Borehole Diameter
				1,709'	8" (0'-95') 6" (95'-104')

Boring Location
State Plane ____ N, ____ E S/C/N Lat
1/4 of 1/4 of Section , T N, R E Long

Local Grid Location (if applicable)
____ N ____ E
Feet ____ S Feet ____ W

County	DNR County Code	Civil Town/City/or Village
Forest	21	

SAMPLE No.	SAMPLE Rec (in)	Blow Counts	Depth in Feet	Soil/Rock description and geologic origin for each major unit	USCS	Graph Log	Well Diag	PID/ FID	Soil Properties: Std Pntr	Mst Cont	Liq Lim	Plas Lim	P 200	RQD/ Comm
			0	0-2.5 Brown (10YR4/6) silty CLAY. Trace well-rounded cobbles.	CL									
C1	60	1		2.5-5 Brown (10YR4/6) SAND fine-grained to medium, angular, well sorted, outwash, moist, 10% coarse at 4-5'.	SP									0840
			5	5-15 Brown (10YR4/6) silty SAND w/gravel, fine-grained, angular sand w/subangular medium gravel w/10% subrounded cobbles. Till.										
C2	120	2.5	10											0900
			15	15-20 Red brown (7.5YR5/4) silty fine-grained, angular, SAND w/20% subangular medium gravel. Trace well-rounded cobbles. Till.	SM									
			20	20-25 Brown (10YR4/4) fine-grained well-sorted subangular SAND with medium to coarse sub-rounded, trace well-rounded cobbles. Till.	SP									
C3	60													0935
			25	25-33 Red brown (7.5YR5/4) silty, fine-grained well-sorted, angular sand with medium sub-angular gravel. Trace cobbles, well rounded, till.	SM									
C4	60	5												0945
			30		SM									
				33-35 Brown (10YR4/4) silty fine-grained angular SAND w/10% well rounded to subrounded med. gravel, grading to 95% sand as above. Till.										
C5	60	5	35	35-40 Red brown (7.5YR5/4) fine-grained, well-sorted, angular sand w/med, subangular gravel w/trace well rounded cobbles. Till. 5% silt.	SM/ SP									1015
			40	40-45 Red brown (7.5YR5/4) fine-coarse-grained angular sand w/fine to med. subangular gravel. Trace cobbles well rounded 5% silt. Till.	SP/ SM									Replace bit. 1020
C6	60	3		Coarse outwash at 44.5'.										
			45	45-50 Brown (10YR4/4) fine-med angular sand w/med subangular-subrounded gravel. Coarse outwash.										

I hereby certify that the information on this form is true and correct to the best of my knowledge.

Signature	Firm
Fred Anderson	Foth & Van Dyke

This form is authorized by Chapters 114.147 and 162, Wis. Stats. Completion of this report is mandatory.
Penalties: Forfeit not less than $10 nor more then $5,000 for each violation. Fined not less than $10 or more than $100 or imprisoned not less than 30 days, or both for each violation. Each day of continued violation is a separate offense, pursuant to ss 114.06, Wis. Stats.

State of Wisconsin
Department of Natural Resources
BORING NUMBER: CMC-02-NW

Route to:

SOIL BORING LOG INFORMATION
Form 4400-122 7-91

SAMPLE No.	SAMPLE Rec (in)	Blow Counts	Depth in Feet	Soil/Rock description and geologic origin for each major unit	USCS	Graph Log	Well Diag	PID/ FID	Soil Properties: Std Pntr	Mst Cont	Liq Lim	Plas Lim	P 200	RQD/ Comm
C7	60	5	50	50-53 Brown (10YR4/4) silty, fine, well-sorted angular SAND w/medium to coarse subrounded gravel. Coarse outwash to fine outwash.	SM/ SP									1100
C8		2		53-55 Same as above w/increased silt 5% fine subrounded gravel.	SM									1115
C9		1	55	55-57 Brown (10YR4/4) coarse angular SAND w/ medium subangular gravel outwash.	SP									1130
C10	60	5		57-60 Brown (10YR6/4) silty, fine to medium SAND w/coarse subrounded gravel. Trace cobbles, subrounded, coarse outwash.	SM/ SP									1210 Replace breaker jaws.
C11	60	1	60	60-62 Same as above. Coarse outwash.	SP/ SM									
				62-63.5 Same as above.	SP									
				63.5-64.5 Red-brown (5.5YR4/4) very fine-grained SAND, well sorted, loose.	SP									
C12	60	1	65	64.5-64.7 Black (10YR6/1) coarse SAND, angular, well sorted.	SP/ SM									1450
				64.7-67 Red-brown (5YR5/4) silty very fine-grained, angular SAND w/angular gravel, angular, coarse outwash.										
			70	67-75 Same as above w/5% well rounded cobbles.										
C13	108	5	75	75-76 Lt. brown (7.5YR4/4) very fine-grained, well sorted, angular SAND, loose. Outwash. 10% fine subrounded gravel.	SP									1500
				76-78 Same as above.	SW									
C14	108	5	80	78-84 Red brown (5YR5/4) medium-coarse, subangular SAND w/med to coarse subrounded gravel coarsening w/depth. Very fine-grained, well-sorted subangular SAND. Lt. brown @ 89'. Coarse outwash. Glaciofluvial.										1530
				84-90 Brown (10YR5/4) fine-medium sub-angular SAND w/medium subrounded gravel coarsening to 86'. Coarse outwash. Fluriostratified.	SW									
C15	72	5	85											1600
			90	90-95 Brown (10YR5/4) fine to med. SAND w/subrounded medium gravel cobbles at 93'. Fluriostratified coarse outwash.	SW/ GP									
			95	95-96 Same as above w/increasing silt.	SW/ SM									
C16	48	5		96-98 Red brown (5YR4/6) silty, very fine-grained angular-coarse grained SAND w/coarse sub-rounded gravel. Till.										1640
C17	36	5	100	98-101 Brown (10YR4/6) fine to coarse subangular SAND w/medium subrounded gravel. Outwash 5-10% gravel.	SP									1705
				101-104 Red brown (5YR4/6) silty angular fine-grained coarse SAND w/medium subrounded gravel. Till.										
C18	12	6	105	E.O.B. @ 104'.										2023

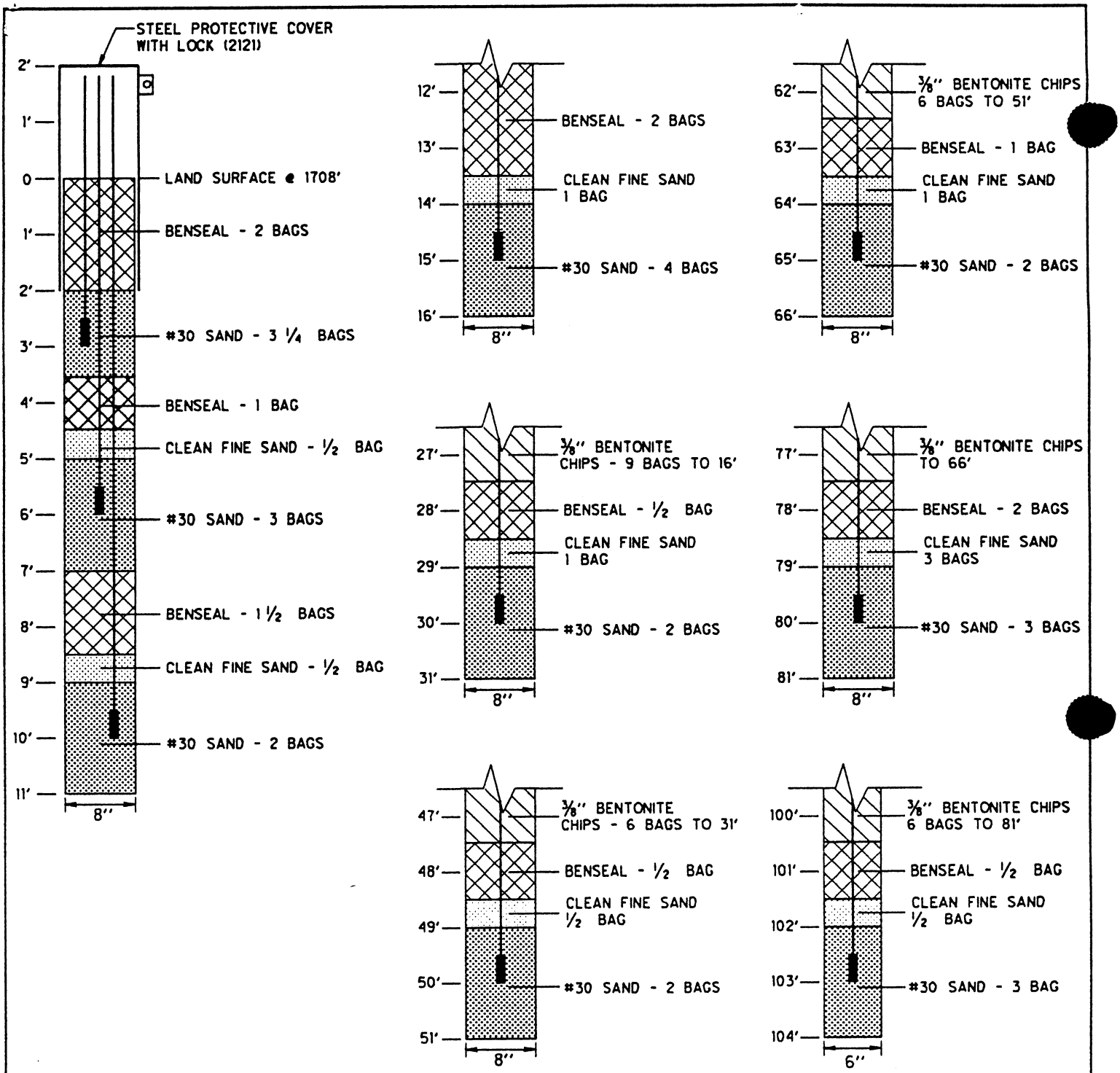

SEALING PROCEDURES

1. BENSEAL PLACED VIA GRAVITY ABOVE CLEAN FINE SAND.
2. BENSEAL HYDRATED, WATER ADDITION @ 1 GAL./10 LBS.
3. 3/8" BENTONITE CHIPS ADDED THROUGH WATER IN 1' TO 3' LIFTS TO NEXT SCREENED INTERVAL.

Foth & Van Dyke

REVISED	DATE	BY	DESCRIPTION

CHECKED BY:	JKS1	DATE: SEPT.'96
APPROVED BY:	SVD1	DATE: SEPT.'96
APPROVED BY:	GWS	DATE: SEPT.'96

Crandon Mining Company

CONSTRUCTION DIAGRAM FOR CMC-02-NW
(5/8" I.D. SCH 40 PVC RISER
1.5MM HAND SLOT 6" SCREEN)

Scale:	NOT TO SCALE	Date:	SEPTEMBER, 1996
Prepared By:	Foth & Van Dyke	By:	JRB2

C:\cadwork\3c49f187.dgn

4.2-12-286

93C049

Appendix C2

Update to Oxygen Transport Estimates

APPENDIX C2

UPDATE TO OXYGEN TRANSPORT ESTIMATES

Prepared for:

FOTH AND VAN DYKE
2737 South Ridge Road
Green Bay, WI, 54307-9012

Prepared by:

STEFFEN ROBERTSON AND KIRSTEN (CANADA) INC.
Suite 800, 580 Hornby Street
Vancouver, B.C. V6C 3B6
Tel: (604) 681-4196 • Fax: (604) 687-5532
E-mail: vancouver@srk.com Web site: www.srk.com

Originally Issued MAY, 1999
Updated MARCH, 2000

APPENDIX C2

UPDATE TO OXYGEN TRANSPORT ESTIMATES

TABLE OF CONTENTS

LIST OF TABLES

LIST OF FIGURES

LIST OF ATTACHMENTS

APPENDIX C2

UPDATE TO OXYGEN TRANSPORT ESTIMATES

1. INTRODUCTION

After the original oxygen transport modeling (Appendix C1) was completed, Nicolet Minerals Company introduced pyrite removal to the proposed tailings processing system. This appendix updates the earlier oxygen transport modeling for the case where the TMA contains depyritized tailings. Pressure membrane tests (FVD, 1998) indicated that the depyritized tailings will have different moisture retention properties than the previously tested pyritic tailings. Since the moisture content of unsaturated tailings strongly influences the effective oxygen diffusion coefficient (***D***), the new moisture retention properties will affect the rate at which oxygen will enter the Tailings Management Area (TMA). In addition, the latest round of humidity cell testing showed depyritized tailings to be less reactive to oxygen than the pyritic tailings. This will result in a lower value for the oxygen consumption rate constant (***r***), which will also affect the rate of oxygen transport into the TMA.

This appendix provides revised estimates of oxygen transport into the TMA. The earlier modeling (see Appendix C1) showed that the most significant oxygen transport into the TMA will be via diffusion through the unsaturated tailings pores during the tailings consolidation phase. Total oxygen transport due to that mechanism was orders of magnitude greater than that due to other mechanisms. Therefore, only oxygen diffusion through the unsaturated tailings pores during the consolidation phase is considered herein.

The revised estimates were obtained using a steady-state analytical equation for oxygen diffusion into a porous medium. Section 2 below presents the derivation of the equations used to estimate oxygen flux and the depth of oxygen penetration. Section 3 presents the derivation of the revised oxygen transport parameters (***D*** and ***r***) from the latest pressure membrane and kinetic testing. And Section 4 presents the results and conclusions of the analysis.

2. MODEL DESCRIPTION

2.1 Oxygen Flux

The continuity relationship describing oxygen diffusion through tailings pore air coupled with first-order oxygen consumption, is given by:

$$\frac{\partial}{\partial x}\left(D\frac{\partial C}{\partial x}\right) - rC = n\frac{dC}{dt} \qquad (1)$$

Where C is the concentration of oxygen in pore air (mol m^{-3} air), r is the first-order rate constant (s^{-1}), D is the effective diffusion coefficient for a porous media (m^2s^{-1}), x is distance (m), n is air porosity (m^3 pores m^{-3} tailings) and t is time (s). (Note: this form of the equation assumes that both D and r include corrections for air porosity n.)

For the case of one-dimensional steady-state diffusion, with boundary conditions shown in Figure C2-1, equation (1) may be re-written as:

$$\begin{aligned} D\frac{\partial^2 C}{\partial x^2} &= rC \\ C(x=0) &= C_0 \\ C(x=\infty) &= 0 \end{aligned} \qquad (2)$$

Where C_0 is the concentration of oxygen in atmosphere (8.9 mol m^{-3} or 21% by volume). The solution to (2) is:

$$C = C_0 e^{-x\sqrt{\frac{r}{D}}} \qquad (3)$$

The flux of oxygen through the tailings surface j (mol O_2 m^{-2} tailings s^{-1}) is given by Fick's first law:

$$j = -D\frac{\partial C}{\partial x} \qquad (4)$$

The flux through the upper surface of the tailings (x=0) is obtained by taking the derivative of (3) and plugging into (4), to give:

$$j = C_0\sqrt{rD} \qquad (5)$$

2.2 Minimum Depth of Oxidation Zone

The minimum depth of the oxidation zone is calculated by the relationship:

$$d = \frac{j}{Q_v} \qquad (6)$$

where d (m) is depth, j (mol O_2 m^{-2} tailings s^{-1}) is flux of oxygen through the upper surface of the tailings, and Q_v (mol O_2 m^{-3} tailings s^{-1}) is the maximum (volumetric) oxygen consumption rate.

The volumetric oxygen consumption rate is given by:

$$Q_v = k\rho \qquad (7)$$

Where k (mol O_2 kg^{-1} tailings s^{-1}) is the lab measured oxygen consumption rate and ρ (kg tailings / m^3 tailings) is the bulk density.

Substitution of (5) and (7) into (6) gives:

$$d = \frac{C_0\sqrt{rD}}{k\rho} \qquad (8)$$

For the purpose of geochemical modeling, this calculation returns a conservative (minimum) estimate of the depth of the oxidation zone because it assumes that oxygen consumption occurs at a uniform rate. Equation 3 shows that oxygen concentrations and hence oxidation rates will in fact decrease exponentially with depth. Solute release will therefore be distributed over a greater depth, and the actual solute concentration will be lower than estimated using equation 8.

3. MODEL PARAMETERS

3.1 Oxidation Rate Constant

The oxidation rate constant was calculated from reaction rates estimated from the humidity cell tests on the depyritized tailings. The available results for the short, intermediate and long-term humidity cell tests, are reported in Appendix A3.

Oxidation or oxygen consumption rates were calculated from steady state sulfate release rates for all humidity cell tests, and overall mass balance calculations for the short term tests that have been terminated. Oxidation rates calculated from steady state sulfate release rates for the short term tests are reported in Table 3.1 of Appendix A3, and in Table 3.13 of Appendix A3 for the longer term tests. The estimates derived from the overall mass balance calculations for the short-term tests are reported in Table 3.5 of Appendix A3. Exact calculation methods are provided in Appendix A3, Section 2.3.2. For convenience, calculated oxidation rates are summarized in the following table.

TABLE 1
Summary of Oxidation Rates Observed for Depyritized Tailings
(Extracted from Appendix A3)

Test	Oxidation Rate (mol O_2 kg^{-1} s^{-1})	
	From SO_4 Release Rate	From Overall Mass Balance
HC DPT-ST1	9.9×10^{-10}	2.6×10^{-9}
HC DPT-ST2	1.2×10^{-9}	3.0×10^{-9}
HC DPT-IT1	5.6×10^{-10}	na
HC DPT-IT2	7.6×10^{-10}	na
HC DPT-LT1	7.0×10^{-10}	na
HC DPT-LT2	6.2×10^{-10}	na

Prepared by: JTC
Checked by: KSS

As shown in the table, the oxidation rates estimated from sulfate release rates vary little, ranging from 5.6×10^{-10} to 1.2×10^{-9} with an average of 8.1×10^{-10} mole O_2/kg/s. The rates estimated from the overall mass balances are slightly higher than those estimated from the steady state sulfate release, probably because of the error

introduced by the aggressive leach extraction tests (see Appendix A3 Section 2.3.2). However, the estimates derived from the overall mass balance calculations are less reliable because they depend on the accuracy with which the hydroxylamine hydrochloride leach extractions can quantify the net accumulation of sulfate during the humidity cell test, which is discussed in Appendix A3, Section 3.1.2.4.

Based on the range of results presented in Table 1, an oxidation rate (oxygen consumption rate) of 8.1×10^{-10} mole O_2/kg tailings/s (equal to the average for all tests based on the steady state leachate sulfate generation rates) was selected as the Best Engineering Judgement (BEJ) estimate. A value of 3×10^{-9} mole O_2/kg tailings/ (the maximum rate) was selected for the Upper Bound (UB) estimate.

Corresponding estimates of the first order reaction rate constant, r (s^{-1}), appropriate for use in equations (1) to (8), were derived from:

$$r = (k \rho)/(C_0) \qquad (9)$$

Where r is the first order rate constant (s^{-1}), k is the measured oxygen consumption rate (mole O_2 / kg tailings / s), ρ is the dry bulk density of the tailings (1,490 kg tailings / m^3 tailings), and C_0 is the atmospheric concentration of oxygen (8.9 mole m^{-3}). Note that the first order rate constant determined from the above formula is in terms of the bulk tailings volume.

The calculations result in first order rate constants of 1.36×10^{-7} and 5.02×10^{-7} s^{-1} for the BEJ and UB respectively.

3.2 Saturation and Effective Diffusion Coefficient

Estimates of the porosity and water saturation of the tailings during of the consolidation period were obtained from HELP modeling (Foth and Van Dyke, 1998). Results of the HELP modeling are shown in Figure 2.4 of the main report. One year after tailings deposition ceases, the moisture content in the upper few feet of the tailings is predicted to range from 67-71%. Two years after tailings deposition ceases, the uppermost 2 feet of tailings are predicted to be at 42-44% saturation, and tailings from 2-6 feet deep are predicted to be 67-69% saturated. (For comparison, the equilibrium saturation curves measured in pressure plate tests of the depyritized tailings are summarized in Figure C2-2. The data in these curves were used as a basis for the HELP modeling.) The HELP model does not consider the effects of

consolidation, which is expected to drive additional water to the tailings surface and thereby increase saturation.

Two published empirical relationships were used to relate moisture saturation to the effective diffusion coefficient. Using the formula developed by Elberling et. al. (1994), and assuming an average moisture saturation of 66%, an effective diffusion coefficient of 1.43×10^{-7} m^2s^{-1} was obtained. A value of 5.44×10^{-7} m^2s^{-1} was obtained using the formula developed by Reardon and Moddle (1985).

4. RESULTS AND CONCLUSIONS

Equation (5) above was used to generate plots of oxygen concentrations versus tailings depth (Figure C2-3) for the four possible combinations of input parameters (***D*** and ***r***) reported in Section 3. Equation (8) above was used to calculate depth of oxygen penetration into the tailings. These results are also presented in the attached spreadsheet (Attachment 1) and summarized in Table 2.

From these results we recommend a revised BEJ flux of 2.42×10^{-6} mol O_2 m^{-2} tailings s^{-1} (Case 2) and a revised UB flux of 4.65×10^{-6} mol O_2 m^{-2} tailings s^{-1} (Case 4) be used in subsequent geochemical modeling runs. For depth of penetration we recommend a value of 2.00 m for the BEJ case and 1.04 m for the UB case.

TABLE 2
Model Results

Case	Description	*D* (m^2s^{-1})	*r* (s^{-1})	Flux (eq.5) (mol O_2 $m^{-2}s^{-1}$)	Depth of Penetration (eq.8) (m)
1	Elberling et al *D*, BEJ *r*	1.43×10^{-7}	1.36×10^{-7}	1.24×10^{-6}	1.03
2	Reardon & Moddle *D*, BEJ *r*	5.44×10^{-7}	1.36×10^{-7}	2.42×10^{-6}	2.00
3	Elberling et al *D*, UB *r*	1.43×10^{-7}	5.02×10^{-7}	2.38×10^{-6}	0.53
4	Reardon & Moddle *D*, UB *r*	5.44×10^{-7}	5.02×10^{-7}	4.65×10^{-6}	1.04

Prepared by: DH
Checked by: JTC

5. REFERENCES

Elberling, B., Nicholson, R.V., and Scharer, J.M., 1994. A combined kinetic and diffusion model for pyrite oxidation in tailings: a change in controls with time. Journal of Hydrology, v.157, p.47-60.

Foth and Van Dyke (1998). Addendum No. 5 to the May 1995 Crandon Project Tailings Management Area Feasibility Report / Plan of Operation, December 1998.

Reardon, E.J. and Moddle, P.M., 1985. Gas diffusion coefficient measurements on uranium mill tailings: implications to cover layer design. Uranium, v.2, p.111-131.

FIGURES

Boundary Conditions:

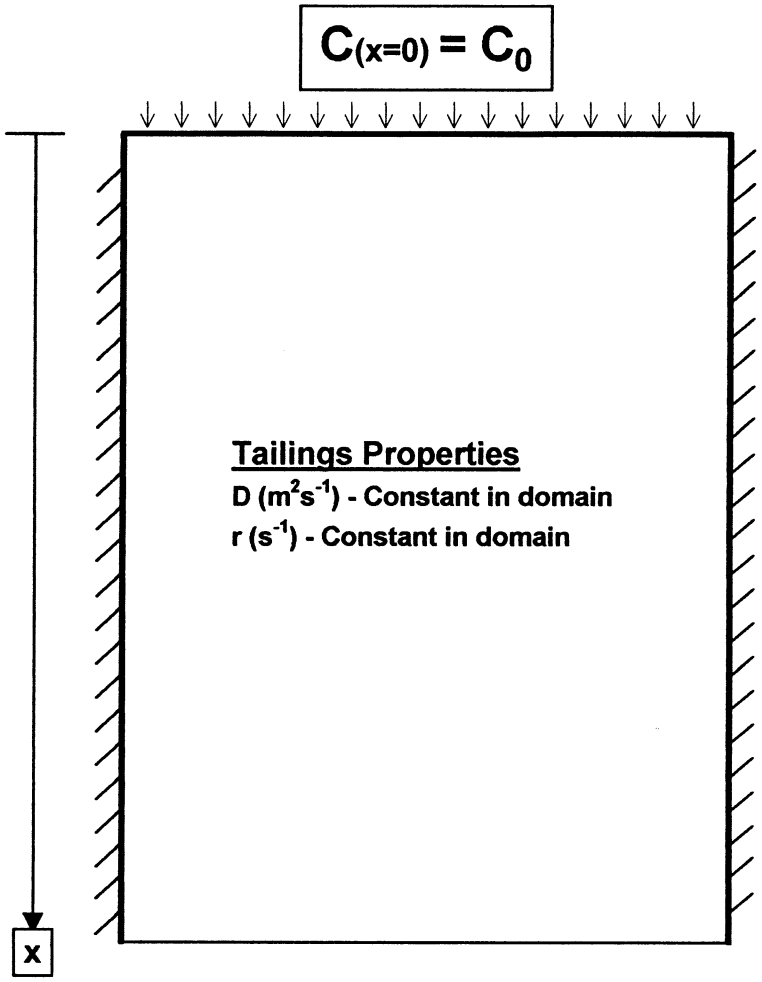

Governing Equation:

$$D\frac{\partial^2 C}{\partial x^2} = rC$$

SRK Consulting Engineers and Scientists		Appendix C2 - Oxygen Transport Update		
		Model Boundary Conditions (Steady-State)		
Foth and Van Dyke	Project 1US004.08	Date Jan-00	Approved	Figure C2-1

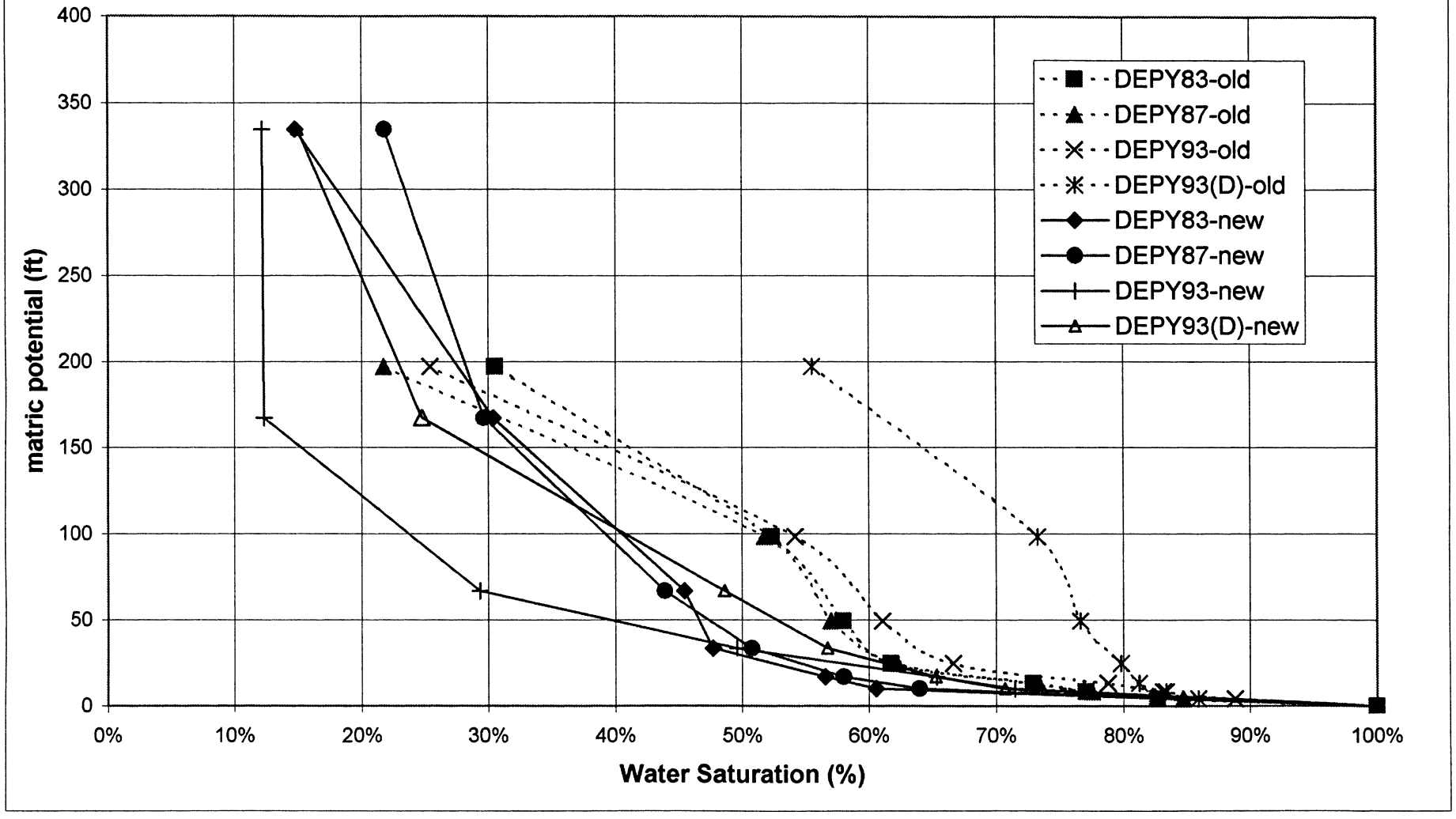

SRK Consulting
Engineers and Scientists

Foth and Van Dyke

Appendix C2 - Oxygen Transport Update

Equilibrium Saturation Curves

Project	Date	Approved	Figure
1US004.08	Mar-00		C2-2

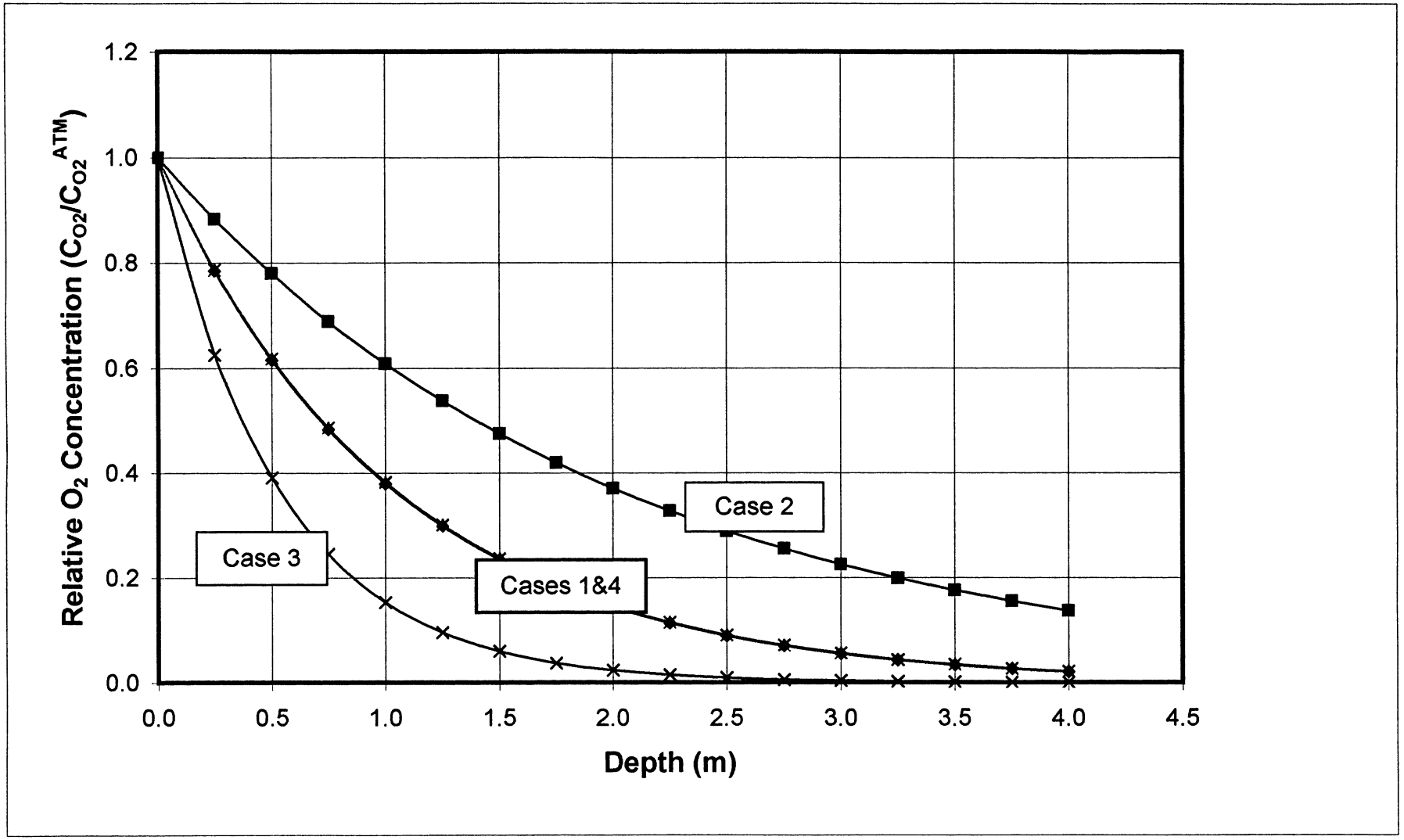

SRK Consulting
Engineers and Scientists

Foth and Van Dyke

Appendix C2 - Oxygen Transport Update

Model Results

Project	Date	Approved	Figure
1US004.08	Jan-00		C2-3

4.2-12-300

ATTACHMENT 1
Model Calculations

Attachment 1
Model Calculations

Laboratory oxygen consumption rate			
Parameter	**BEJ Calculation**	**UB Calculation**	**Units**
lab k	8.10E-10	3.00E-09	mol O_2 / kg tailings / s
	8.10E-07	3.00E-06	mol O_2 / tonne tailings / s
density	1.49	1.49	tonne tailings / m^3 tailings
	1.21E-06	4.47E-06	mol O_2 / m^3 tailings / s

Model first order rate constant			
Parameter	**BEJ Calculation**	**UB Calculation**	**Units**
O_2 conc	8.90	8.90	mol O_2 / m^3 tailings / s^{-1}
r =	1.36E-07	5.02E-07	

Diffusion coefficient					
Parameter	**BEJ Calculation**		**UB Calculation**		**Units**
Dw (m^2/s)	2.20E-09		2.20E-09		
Da (m^2/s)	1.80E-05		1.80E-05		
t	0.273		0.273		
a	3.28		3.28		
H	33.9		33.9		
saturation	66%		66%		
D(Erberling)	1.43E-07		1.43E-07		m^2 s^{-1}
D (R&M)		5.44E-07		5.44E-07	m^2 s^{-1}

O_2 flux into surface					
Parameter	**BEJ Calculation**		**UB Calculation**		**Units**
	D(Erberling)	**D (R&M)**	**D(Erberling)**	**D (R&M)**	
r	1.36E-07	1.36E-07	5.02E-07	5.02E-07	s^{-1}
D	1.43E-07	5.44E-07	1.43E-07	5.44E-07	M^2/s
					Mol/L
Co	8.90	8.90	8.90	8.90	mol O_2 m^{-3}
j (O_2)	1.24E-06	2.42E-06	2.38E-06	4.65E-06	mol O_2 m^{-2} s^{-1}

Minimum depth of oxidation zone					
Parameter	**BEJ Calculation**		**UB Calculation**		**Units**
k	8.10E-10	8.10E-10	3.00E-09	3.00E-09	mol O_2 kg^{-1} s^{-1}
density	1490	1490	1490	1490	kg m^{-3}
Qv	1.21E-06	1.21E-06	4.47E-06	4.47E-06	mol O_2 m^{-3} s^{-1}
j	1.24E-06	2.42E-06	2.38E-06	4.65E-06	mol O_2 m^{-2} s^{-1}
depth	1.03	2.00	0.53	1.04	m

Appendix C3

CO_2 Transport Modeling

APPENDIX C3

CO_2 TRANSPORT MODELING

Prepared for:

FOTH AND VAN DYKE
2737 South Ridge Road
Green Bay, WI, 54307-9012

Prepared by:

STEFFEN ROBERTSON AND KIRSTEN (CANADA) INC.
Suite 800, 580 Hornby Street
Vancouver, B.C. V6C 3B6
Tel: (604) 681-4196 • Fax: (604) 687-5532
E-mail: vancouver@srk.com Web site: www.srk.com

Originally Issued MAY, 1999
Updated MARCH, 2000

APPENDIX C3

CO_2 TRANSPORT MODELING

TABLE OF CONTENTS

LIST OF TABLES

LIST OF FIGURES

APPENDIX C3

CO_2 TRANSPORT MODELING

1. INTRODUCTION

Neutralization of acidity by carbonate minerals in the TMA could result in high concentrations (i.e. partial pressures) of carbon dioxide in tailings pore gas. To determine the potential for development of high concentrations, and the rate at which they could occur, one-dimensional gas diffusion modeling was carried out. The modeling considers the coupled processes of oxygen diffusion, pyrite oxidation, acidity generation and carbonate neutralization.

Carbon dioxide generation in the tailings will be a direct result of oxygen ingress, sulfide oxidation and subsequent carbonate neutralization. As discussed in Appendix C1, earlier modeling showed that oxygen fluxes into the TMA during the consolidation period were orders of magnitude higher than at other times. Therefore, only the consolidation period has been considered herein.

2. MODEL DESCRIPTION

The numerical model solves the coupled partial differential equations of oxygen and carbon dioxide diffusion in the pore gas phase.

The partial differential equation for oxygen diffusion is given by:

$$n\frac{dC_{O_2}}{dt} = \frac{\partial}{\partial x}\left(D\frac{\partial C_{O_2}}{\partial x}\right) - Q_{O_2} \qquad (1)$$

Where C_{O2} (mol m^{-3}), is the concentration of oxygen in the gaseous phase, n (m^3 pore space m^{-3} tailings) is the air porosity, t (s) is time and D (m^2 s^{-1}) is the effective diffusion coefficient for oxygen in tailings. Q_{O2} is the sink term that relates oxygen consumption to pyrite oxidation. For this model a first order relationship was assumed, i.e.:

$$Q_{O_2} = rC_{O_2} \qquad (2)$$

Where r (s^{-1}) is a first order rate constant.

Consumption of 1 mole of oxygen results in the liberation of 8/15 moles of carbon dioxide. Therefore, the partial differential equation for carbon dioxide diffusion may be written as:

$$n\frac{dC_{CO_2}}{dt} = \frac{\partial}{\partial x}\left(D\frac{\partial C_{CO_2}}{\partial x}\right) + \frac{8}{15}Q_{O_2} \qquad (3)$$

Where, C_{CO2} (mol m^{-3}) is the concentration of carbon dioxide.

The solution of equations (1) to (3) was obtained using a modified version of the Alternating Difference Implicit (ADI) finite difference code described in Attachment A of the April 1997 modeling report (Appendix C1). The initial and boundary conditions for the simulations are displayed in Figure C3-1.

The model neglects carbon dioxide uptake by the water phase and secondary mineralization. Thus, all carbon dioxide generated by the neutralization of carbonate is assumed to go only to the pore gas phase. As discussed further in Section 4 below, the result is that the model will approach a steady-state carbon dioxide profile more rapidly than if the sinks had been incorporated, which provides a more conservative result in terms of predicting partial pressure of carbon dioxide during the consolidation phase.

3. MODEL INPUTS

The model geometry consisted of a one-dimensional column 30 m in height (Figure C3-1). The upper boundary condition was assigned as a constant concentration boundary to represent atmospheric conditions. The lower boundary condition was assigned as zero flux. Homogeneous values of effective diffusion (***D***) and first order pyrite oxidation reaction rate (***r***) were assigned throughout the model domain.

Four cases were simulated to consider a range of ***D*** and ***r*** as shown in Table 1. These cases represent the four possible combinations of BEJ and UB parameters that were derived for depyritized tailings (discussed in Appendix C2). Runs were carried out for a total simulation period of 100 years. To determine how quickly the system reached steady state, output was generated at 3 months, 6 months, 1 year, 2 years and 100 years.

TABLE 1
Cases Considered For Coupled Oxygen and Carbon Dioxide Diffusion Simulations

Case	Description	*D* ($m^2 s^{-1}$)	*r* (s^{-1})
1	Elberling et al *D*, BEJ *r*	$1.43x10^{-7}$	$1.36x10^{-7}$
2	Reardon & Moddle *D*, BEJ *r*	$5.44x10^{-7}$	$1.36x10^{-7}$
3	Elberling et al *D*, UB *r*	$1.43x10^{-7}$	$5.02x10^{-7}$
4	Reardon & Moddle *D*, UB *r*	$5.44x10^{-7}$	$5.02x10^{-7}$

Prepared by: JS
Checked by: JTC

4. RESULTS AND CONCLUSIONS

All of the simulations reached near steady-state conditions by the end of year 1. Figure C3-2 shows the resulting oxygen and concentration profiles in the tailings at the end of year 2. Oxygen flux into the tailings and maximum carbon dioxide concentration within the tailings are summarized in Table 2.

TABLE 2
Model Results At Steady-state

Case	Description	D ($m^2 s^{-1}$)	r (s^{-1})	Max CO_2 (mol m^{-3})	Max CO_2 (Pa CO_2/Pa Air)
1	Elberling et al *D*, BEJ *r*	$1.43x10^{-7}$	$1.36x10^{-7}$	4.74	0.115
2	Reardon & Moddle *D*, BEJ *r*	$5.44x10^{-7}$	$1.36x10^{-7}$	4.74	0.115
3	Elberling et al *D*, UB *r*	$1.43x10^{-7}$	$5.02x10^{-7}$	4.74	0.115
4	Reardon & Moddle *D*, UB *r*	$5.44x10^{-7}$	$5.02x10^{-7}$	4.74	0.115

Prepared by: JS
Checked by: JTC

As discussed in Section 1, the model does not account for carbon dioxide uptake by solution and secondary mineralization. Therefore, the only removal of CO_2 in the model is upwards diffusion through the tailings surface. This assumption contributes to the rapid attainment for the steady state CO_2 profile.

A second factor that causes the model to reach steady state rapidly is the assumed initial condition of atmospheric O_2 concentration throughout the profile. An alternative assumption would have been to assume the pore air of the tailings to initially have low oxygen saturation, because the tailings will be deposited wet, and de-saturate slowly. To show that this assumption results in a less conservative result, the four cases were rerun with this modified initial condition. The resulting profiles after two years are shown in Figure C3-3. The figure shows a carbon dioxide profile that peaks at the oxidation front and then diminishes with depth. As shown in Table 3, this results in lower peak concentrations of carbon dioxide within the profile, although the oxygen flux into the profile remains unchanged. The long-term profiles from the revised simulations are the same as the earlier simulations i.e. high concentrations of CO_2 with depth.

TABLE 3
Summary of Coupled O_2/CO_2 Simulations for TMA
(For the Initial Condition of CO_2 (x)=0; simulation period 2 years)

Case	Description	D ($m^2 s^{-1}$)	r (s^{-1})	Max CO_2 (mol m^{-3} air)	Max CO_2 (Pa CO_2/Pa Air))
1	Elberling et al *D*, BEJ *r*	1.43E-07	1.36E-07	2.97	0.073
2	Reardon & Moddle *D*, BEJ *r*	5.44E-07	1.36E-07	2.97	0.073
3	Elberling et al *D*, UB *r*	1.43E-07	5.02E-07	3.52	0.086
4	Reardon & Moddle *D*, UB *r*	5.44E-07	5.02E-07	3.62	0.089

Prepared by: JS
Checked by: JTC

In all simulations the maximum carbon dioxide concentration increased to a steady-state concentration of 4.74 mole m^{-3} (0.115 Pa CO_2/Pa Air). This number corresponds to 8/15 of the atmospheric concentration of oxygen, which makes sense given the stoichiometric relationship between carbon dioxide production and oxygen consumption.

The above calculations do not consider the correction for the change in volume resulting from the consumption of oxygen. The highest estimate of carbon dioxide concentration is obtained by conservatively assuming that oxygen in the pore air is completely depleted, i.e.:

$$\text{Max } CO_2 = 11.5\% / (100\% - 21\% + 11.5\%)$$
$$= 12.7\%$$

A volume corrected gaseous carbon dioxide concentration of 12.7 % should be assumed as an upper bound estimate for models of geochemical equilibrium.

5. REFERENCES

Elberling, B., Nicholson, R.V., and David, D.J. (1993) Field Evaluation of Sulfide Oxidation Rates. Nordic Hydrology, vol.24, p.323-338.

Reardon, E.J. and Moddle, P.M. (1985) Gas Diffusion Coefficient Measurements On Uranium Mill Tailings: Implications to Cover Layer Design. Uranium, vol.2, P.111-131.

FIGURES

Boundary Conditions:

$C = C_0$ $C_{O2} = 8.9$ mol m^{-3} (0.21 atm)
$C_{CO2} = 0.0148$ mol m^{-3} (3.5×10^{-4} atm)

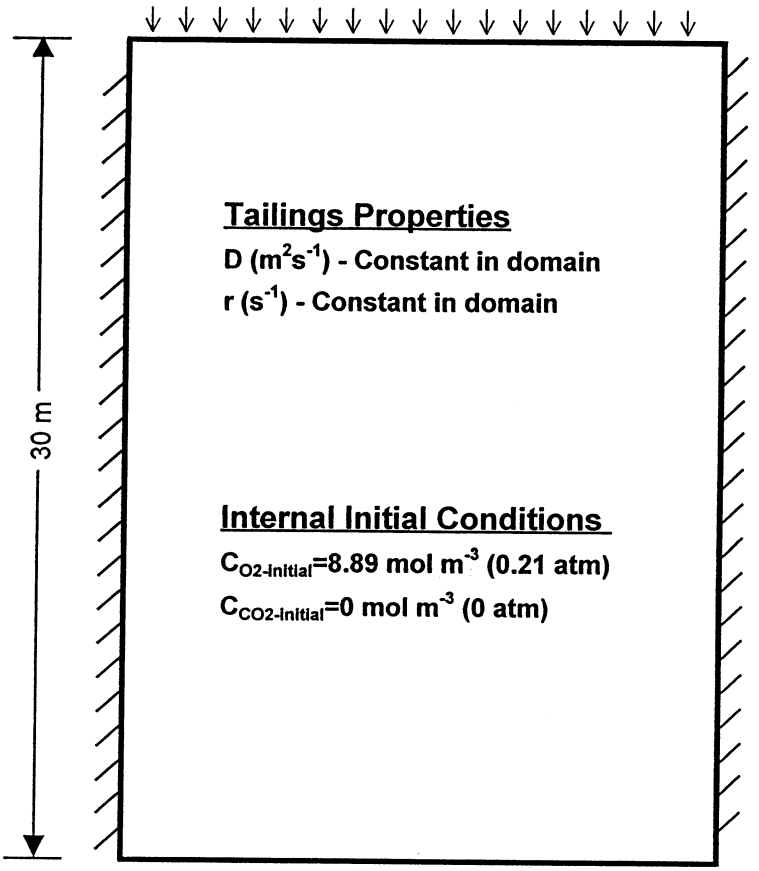

$$\partial C / \partial x = 0$$

Governing Equations:

$$\frac{dC_{O_2}}{dt} = \frac{\partial}{\partial x}\left(D\frac{\partial C_{O_2}}{\partial x}\right) - Q_{O_2}$$

$$\frac{dC_{CO_2}}{dt} = \frac{\partial}{\partial x}\left(D\frac{\partial C_{CO_2}}{\partial x}\right) + \frac{8}{15}Q_{O_2}$$

$$Q_{O_2} = rC_{O_2}$$

SRK Consulting Engineers and Scientists		Appendix C3 - CO_2 Modelling		
		Model Boundary Conditions		
Foth and Van Dyke	Project 1US004.08	Date Jan-00	Approved	Figure C3-1

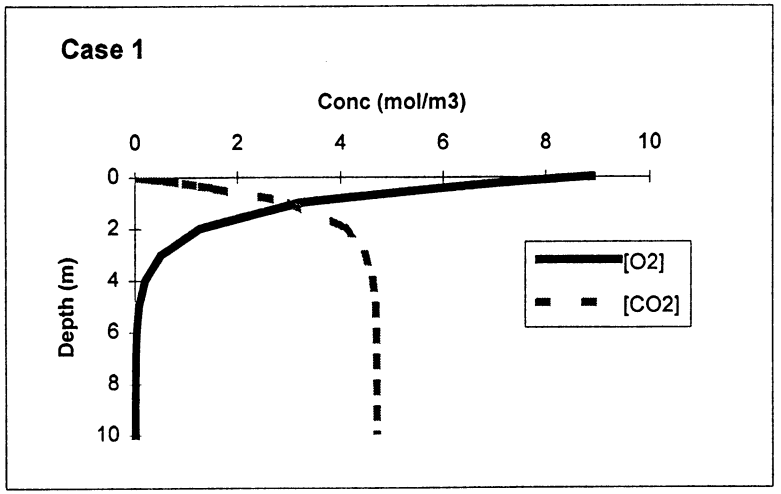

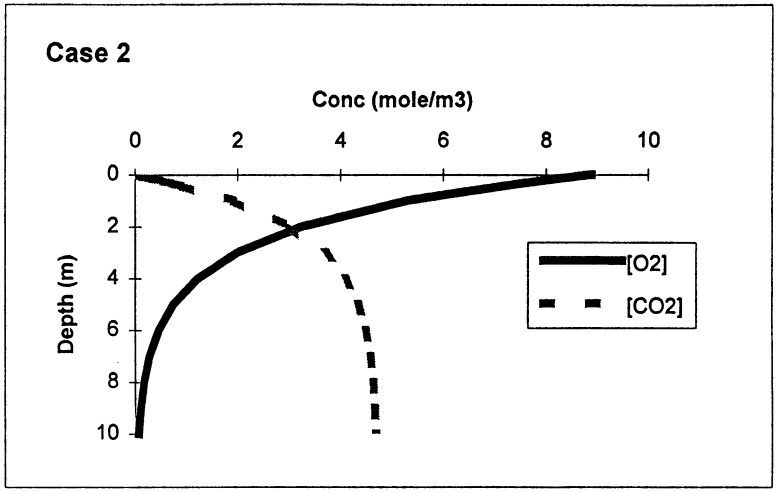

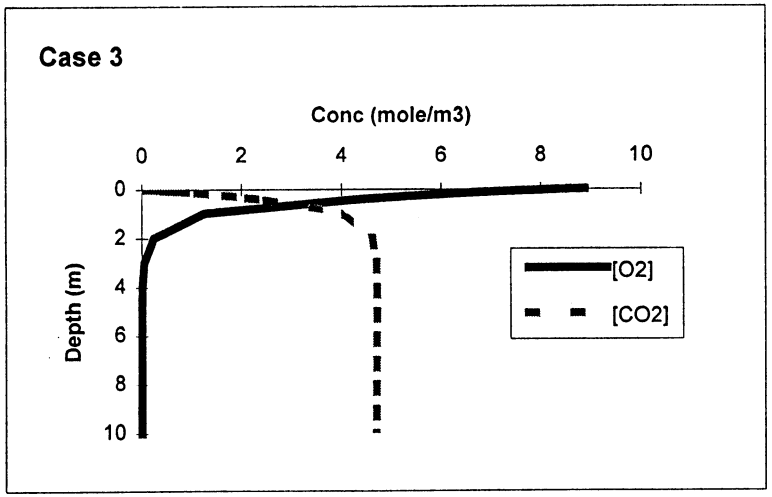

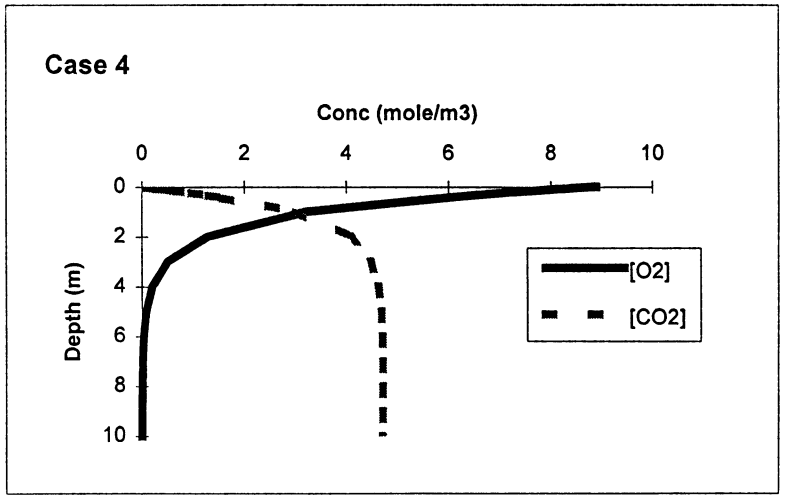

4.2-12-314

SRK Consulting
Engineers and Scientists

Foth and Van Dyke

Appendix C3 - CO_2 Modeling

Results of oxygen-carbon dioxide diffusion simulations after 2 years

Project	Date	Approved	Figure
1US004.08	Jan-00		C3-2

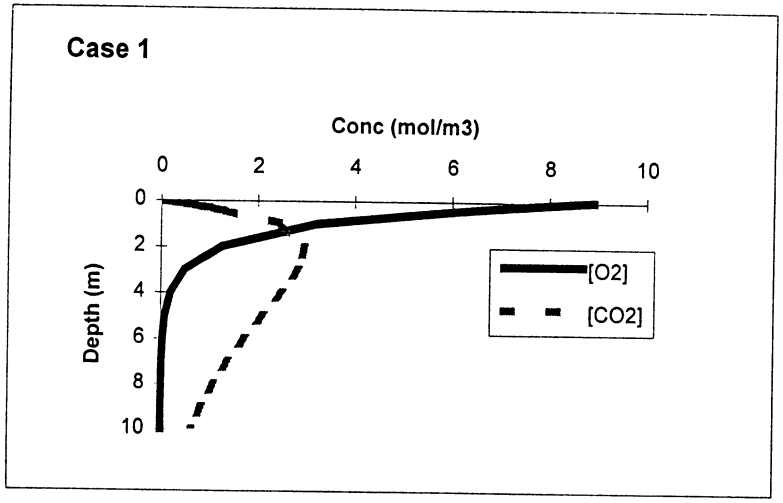

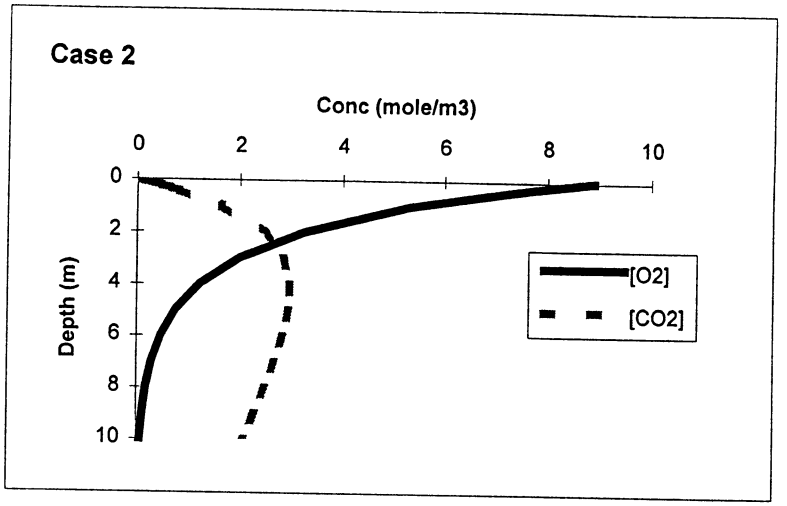

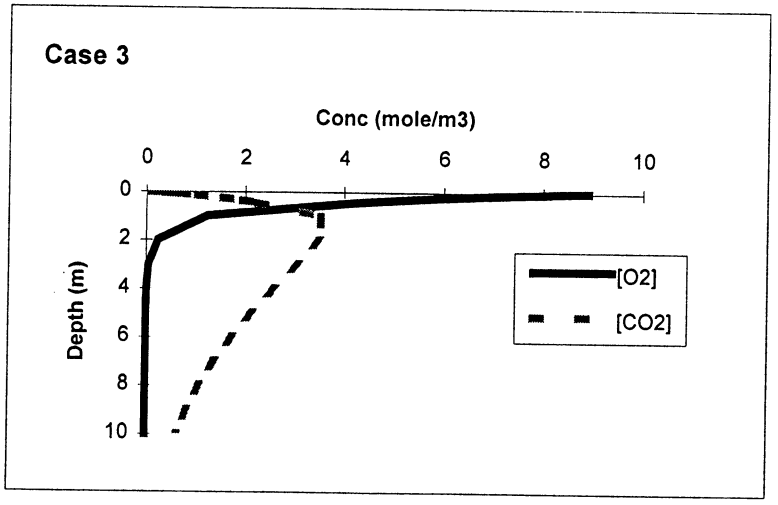

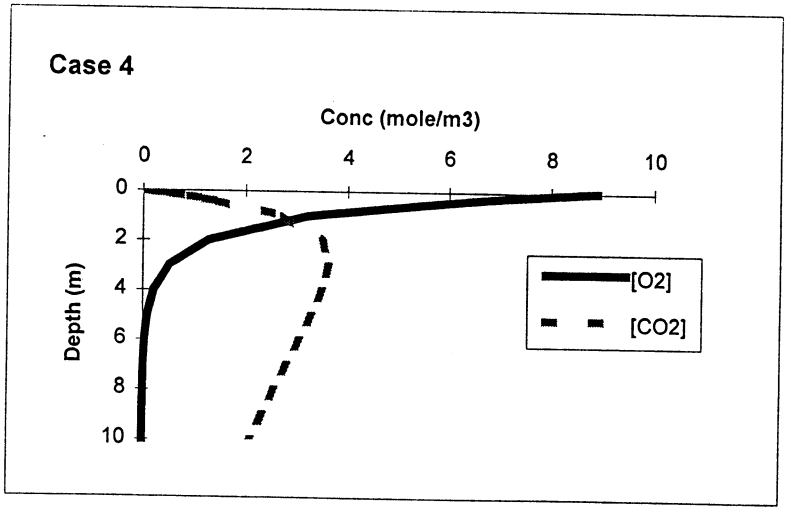

4.2-12-315

SRK Consulting
Engineers and Scientists

Foth and Van Dyke

Appendix C3 - CO_2 Modeling

Results with modified initial condition after 2 years

Project	Date	Approved	Figure
1US004.08	Jan-00		C3-3

Appendix D

Supporting Calculations for Water Quality Predictions

APPENDIX D

SUPPORTING CALCULATIONS FOR WATER QUALITY PREDICTIONS

Prepared for:

FOTH AND VAN DYKE
2737 S. Ridge Road, P.O Box 19012
Green Bay, WI 54307-9012

Prepared by:

STEFFEN ROBERTSON AND KIRSTEN (CANADA) INC.
Suite 800, 580 Hornby Street
Vancouver, B.C. V6C 3B6
Tel: (604) 681-4196 • Fax: (604) 687-5532
E-mail: vancouver@srk.com Web site: www.srk.com

Originally Issued MAY, 1999
Updated, MARCH, 2000

APPENDIX D

SUPPORTING CALCULATIONS FOR WATER QUALITY PREDICTIONS

TABLE OF CONTENTS

LIST OF TABLES

APPENDIX D

SUPPORTING CALCULATIONS FOR WATER QUALITY PREDICTIONS

1. INTRODUCTION

This appendix describes supporting calculations used to derive estimates of solute concentrations in pore water within and percolation from the TMA.

2. SOLUTE CONCENTRATIONS IN TAILINGS WATER AND IN PROCESS WATER DOMINATED ZONE

Solute concentrations in the water entering the TMA were estimated by taking a flow-weighted average of the solute concentrations in each of the seven streams that will contribute to the tailings slurry water:

- Zinc tails thickener overflow (ZTTO) at 1328 gpm;
- Depyritized tailings process water (DTPW) at 475 gpm;
- Pyrite backfill PPSM overflow (PBPO) at 197 gpm;
- Zinc concentrate thickener overflow (ZCTO) at 240 gpm;
- Lead hydroseparator overflow (LHSO) at 55 gpm;
- Lead concentrate thickener overflow (LCTO) at 30 gpm; and,
- Copper concentrate thickener overflow (CCTO) at 42 gpm.

Concentration estimates for each solute in each stream, and the flow-weighted averages, are provided in Section 2.2 of Appendix B. Those estimates represent the water that enters the TMA along with the tailings, and the water that is decanted from the pond without further equilibration with the tailings solids.

The flow-weighted average concentrations were then input to MINTEQA2 to determine the effects of equilibration within the pore water of the TMA. The geochemical equilibrium modeling and estimates of solute concentrations in "equilibrated" process water are provided in Sections 2.3 and 2.4 of Appendix B. As discussed in Section 2.5.1 and 2.5.2.2 of the main report, those concentrations represent pore water in the "process water dominated" zone of the TMA.

3. SOLUTE CONCENTRATIONS IN OXIDATION ZONE

Estimates of solute release from tailings oxidation during the consolidation period were obtained by calculating:

$$(1) \qquad C_1 = \left(\frac{R\left(\frac{kg\ CaCO_3 eq}{m^2\ yr}\right) \times t(yr)}{\left(\frac{0.1\ kg\ CaCO_3}{mol\ MeS}\right)} \right) \times \left(\frac{f_1\left(\frac{molMe}{molMeS}\right) \times \left(\frac{mgMe}{molMe}\right)}{\left[P\left(\frac{L}{m^2\ yr}\right) t(yr) + \theta d_1(m) \frac{1000L}{m^3}\right]} \right)$$

where: C_1 is the concentration contributed by solute release;

R is the rate of oxygen entry;

t is the time over which oxygen enters;

f_1 is the relative rate of solute release, obtained from the laboratory studies described in Appendix A3 relating the rate of release of the solute to the rate of sulfide oxidation;

P is the rate of infiltration into the tailings surface during the oxidation;

θ is the volumetric water content

d_1 is the depth of the oxidation zone;

the factor 0.1 converts kg $CaCO_3$ to moles of sulfide; and

Me and MeS are the metal and metal sulfide, respectively.

The calculation can be explained as follows:

- The term with Rt in the numerator estimates the amount of sulfide mineral that can be oxidized during the consolidation period.

- The term f_1 converts the amount of sulfide oxidized to the release of the solute *Me*.

- The term ($Pt + \theta d$) estimates the amount of water that contacts the oxidation zone, i.e. infiltration during the consolidation period plus the entrained water in the oxidation zone.

Parameters used in the BEJ and UB estimates are provided in Table 1 and Table 2 respectively. Values of f_1 are provided in Table 2-6 of the main report and Appendix A3.

To account for solutes that would be present in the tailings pore water prior to oxidation, the estimated concentrations were then adjusted upwards following:

$$(2) \qquad C_2 = \frac{C_1 (Pt + \theta d) + C_P \theta d}{(Pt + \theta d)}$$

where: C_2 is the initial estimate of concentrations in the oxidation zone;
C_1 is the estimate from equation (1):
C_p is the concentration in the process water dominated zone; and
all other variables are as above.

As discussed in Appendix B, the initial estimates of solute concentration in the oxidation zone were then input to the geochemical equilibrium model MINTEQA2.

The final estimates of concentrations in the oxidation zone of the TMA were then selected from the geochemical modeling, the initial estimates of solute concentrations and the results of humidity cell tests (see Section 2.5.2.1). The logic used to select the final estimate for each parameter was as follows:

- Where no solubility control was indicated by the MINTEQA2 modeling, the final estimate was the higher of the initial concentration estimate (C_2) and the highest concentration measured in leachate from the humidity cell tests.

- For solutes where the MINTEQA2 modeling showed that the initial concentration estimate (C_2) exceeded a solubility control, the final estimate was selected as the higher of the solubility-controlled value (from MINTEQA2) and the highest concentration measured in leachate from the humidity cell tests.

4. SOLUTE CONCENTRATIONS IN TMA PERCOLATE AFTER CONSOLIDATION PERIOD

After the oxidation that will occur during the consolidation period, the percolate from the TMA will consist of variable proportions of water that has contacted the oxidation zone and process water that has equilibrated with the tailings in the absence of

oxidation. Leachate from the oxidation and process water dominated zones will then be mixed in the drainage system, leading to intermediate concentrations in the percolate.

As a conservative simplification, it was assumed that the solute concentrations in the percolate would be simple volume averages of the concentrations in the oxidation and process water dominated zones:

$$C_D = (V_{ox}\, C_{ox} + V_p C_p\,) / (V_{ox} + V_p)$$

where:

C_D is the average concentration of the solute in the TMA during the drainage (post-consolidation) periods;

C_{ox} and C_p are the concentrations of the solute in oxidation zone and the process water zone, respectively; and

V_{ox}, and V_p are the volumes of water that contacts the oxidation zone and process water, respectively.

The volume of V_{ox} was estimated from:

$$V_{ox} = \textit{Surface Area} \times (Pt + \theta\, d_{ox})$$

The volume V_p was the remainder of the water in the TMA cell:

$$V_p = \textit{Total Volume} - V_{ox}$$

Input parameters and the resulting volumes for the BEJ and UB estimates are shown in Table 1 and Table 2 of Section 5.

5. INPUTS TO TMA WATER QUALITY CALCULATIONS

Values of the parameters defined above are summarized in Tables 1 and 2.

TABLE 1
Inputs to Water Quality Calculations - BEJ Estimates

	Value	Units	Source
Oxidation rate (R)	4.07	kg $CaCO_3$ m^{-2} yr^{-1}	O_2 transport model (see Appendix C2)
Oxidation time (t)	1.0	years	Half of consolidation period
($R\,t$ / 0.1)	41	mol MeS m^{-2}	Calculated
Infiltration rate (P)	6	inches	Conservatively assumed equal to annual net precipitation
Infiltration time (t)	1.0	years	Half of consolidation period
Oxidation Zone Depth (d_{ox})	6.6	ft	O_2 transport model (see Appendix C2)
Volumetric water content (θ)	0.2904		Porosity of 0.48 at 60% Saturation
($Pt + \theta\, d_{ox}$)	2.4	ft	Calculated
Plan area (A)	6,643,000	ft^2	November 10, 1988 Memo (FVD to Pete Anderson)
Oxidation Zone Volume (V_{ox})	15,994,000	ft^3	Calculated
Total Water Volume	114,793,000	ft^3	Calculated from volume of wastes (Addendum 5, pg. 104) at 70% saturation
Process Water Volume (V_p)	98,799,000	ft^3	Calculated

Prepared by: DEH
Checked by: KSS

TABLE 2
Inputs to Water Quality Calculations - UB Estimates

	Value	Units	Source
Oxidation rate (R)	7.83	kg $CaCO_3$ m^{-2} yr^{-1}	O_2 transport model (see Appendix C2)
Oxidation time (t)	2.0	years	Half of consolidation period
($R\ t$ / 0.1)	157	mol MeS m^{-2}	Calculated
Infiltration rate (P)	6	inches	Conservatively assumed equal to annual net precipitation
Infiltration time (t)	2.0	years	Half of consolidation period
Oxidation Zone Depth (d_{ox})	3.4	ft	O_2 transport model (see Appendix C2)
Volumetric water content (θ)	0.2904		Porosity of 0.48 at 60% Saturation
($Pt + \theta\ d_{ox}$)	1.99	ft	Calculated
Plan area (A)	6,643,000	ft^2	November 10, 1988 Memo (FVD to Pete Anderson)
Oxidation Zone Volume (V_{ox})	13,227,000	ft^3	Calculated
Total Water Volume	114,793,000	ft^3	Calculated from volume of wastes (Addendum 5, pg. 104) at 70% saturation
Process Water Volume (V_p)	101,567,000	ft^3	Calculated

Prepared by: DEH
Checked by: KSS

Appendix E

Consumption of Water in Reactions

APPENDIX E

CONSUMPTION OF WATER IN REACTIONS

Prepared for:

FOTH AND VAN DYKE
2737 S. Ridge Road, P.O Box 19012
Green Bay, WI 54307-9012

Prepared by:

STEFFEN ROBERTSON AND KIRSTEN (CANADA) INC.
Suite 800, 580 Hornby Street
Vancouver, B.C. V6C 3B6
Tel: (604) 681-4196 • Fax: (604) 687-5532
E-mail: vancouver@srk.com Web site: www.srk.com

MAY, 1999

APPENDIX E

CONSUMPTION OF WATER IN REACTIONS

TABLE OF CONTENTS

LIST OF TABLES

APPENDIX E

CONSUMPTION OF WATER IN REACTIONS

1 INTRODUCTION

Many of the oxidation, acid neutralization and secondary precipitation reactions that will occur in the tailings consume water. Normally, the amount of water consumed is not significant enough to affect flow patterns. However, once the TMA cover is in place and the tailings are fully drained, infiltration into the TMA will be very limited. Under those conditions, the consumption of water in reactions may be significant enough to affect flow patterns.

2 LONG TERM INFILTRATION RATE

The HELP modeling by Foth and Van Dyke (1998) predicts an infiltration rate of 0.00002 inches per year through the cover. That rate is equivalent to approximately $5.08*10^{-4}$ litres of water per square meter of surface per year.

For comparison to reaction rates, it is necessary to convert that rate to units of moles H_2O. Since each litre of water contains 55.5 moles of H_2O, the rate of water supply is:

$$5.08*10^{-4} \times 55.5 = 0.0282 \text{ mol } H_2O \cdot m^{-2} \cdot yr^{-1}$$

3 OXYGEN CONSUMPTION BY REACTIONS

Tables 1 and 2 present the reaction stoichiometry for the oxidation of pyrite and the formation of various secondary minerals. The tables also show the ratio of water consumption to oxygen consumption for each reaction.

Table 1 presents oxidation reactions that would occur under conditions that are sufficiently oxidizing to allow ferric iron to be produced. These reactions are presented for completeness and include:

- oxidation of pyrite to ferric iron, which rarely occurs in isolation;

- oxidation of pyrite, dissolution of calcite, and precipitation of gypsum and iron hydroxide, which is the sequence of reactions expected under oxidizing conditions in the oxidation zone of the depyritized tailings.

TABLE 1
Water Consumption in Reactions Producing Ferric Iron

Reaction	Water Consumption (moles H_2O / mole O_2)
Pyrite oxidation under oxidizing conditions $2FeS_2 + 15/2O_2 + H_2O \rightarrow 2Fe^{3+} + 4SO_4^{2-} + 2H^+$	1/(15/2)= 0.133
Pyrite oxidation, calcite dissolution, gypsum and iron hydroxide formation $2FeS_2 + 15/2O_2 + 11H_2O + 4CaCO_3 \rightarrow$ $2Fe(OH)_3 + 4CaSO_4.2H_2O + 4CO_2(g)$	11/(15/2) = 1.467

Prepared by: JTC
Checked by: KSS

Table 2 presents reactions that would occur under conditions that are not sufficiently oxidizing to form ferric iron, i.e. where ferrous iron is dominant. The reactions are:

- oxidation of pyrite to ferrous iron and sulfate, which rarely occurs in isolation;

- oxidation of pyrite, dissolution of calcite, and precipitation of gypsum and siderite (ferrous carbonate), which is the sequence of reactions expected under mildly reducing conditions when carbonate minerals are present; and,

- oxidation of pyrite and formation of melanterite (a ferrous sulfate), which occurs under mildly reducing conditions when siderite is not formed and iron and sulfate concentrations are high.

TABLE 2
Water Consumption in Reactions That Produce Ferrous Iron

Reaction	Water Consumption (moles H_2O / mole O_2)
Pyrite oxidation under low oxygen partial pressure conditions $FeS_2 + 7/2O_2 + H_2O \rightarrow Fe^{2+} + 2SO_4^{2-} + 2H^+$	1/(7/2) = 0.286
Pyrite oxidation under low oxygen partial pressure, calcite dissolution, gypsum and siderite formation $FeS_2 + 7/2O_2 + 4H_2O + 2CaCO_3 \rightarrow FeCO_3 + 2CaSO_4.2H_2O + CO_2(g)$	4/(7/2) = 1.143
Pyrite oxidation, calcite dissolution and gypsum and melanterite formation $FeS_2 + 7/2O_2 + 9H_2O + CaCO_3 \rightarrow FeSO_4{\cdot}7H_2O + CaSO_4.2H_2O + CO_2(g)$	9/(7/2) = 2.571

Prepared by: JTC
Checked by: KSS

The first reactions in each table are presented for completeness only. In most circumstances, the oxidation of pyrite will lead to formation of secondary minerals, as shown in the other reactions.

The reactions in Table 1 would occur only near the uncovered tailings surface during the consolidation period. In saturated or covered tailings, the reactions in Table 2 would predominate.

Table 3 summarizes the reaction information by presenting the rates that would be required for each reaction to consume all of the water supplied by infiltration. The units of mol O_2 m^{-2} yr^{-1} are used to characterize the reaction rates, in order to facilitate comparison with the long term rates predicted from the oxygen transport modeling.

TABLE 3
Oxygen Consumption Rates Expressed as Oxygen Requirement to Consume Long Term Infiltration

Reaction product	Oxygen Supply required to consume all of infiltration (mol O_2 m^{-2} yr^{-1})
Pyrite oxidation to ferric	0.212
Gypsum and iron hydroxide	0.019
Pyrite oxidation to ferrous	0.099
Gypsum and siderite	0.025
Gypsum and melanterite	0.011

Prepared by: JTC
Checked by: KSS

Table 4 summarizes the reaction rates predicted from the oxygen transport modeling. Comparing the rates in Table 4 with the minimum rates required to consume infiltration in Table 3, the following conclusions are reached:

- The reactions that occur directly below the cover will be sufficient to consume most, if not all, of the water that infiltrates the cover;

- The reactions that are predicted to occur along the base and sideslope of the TMA, with an intact geomembrane in the composite liner, are also sufficient to consume all of the water that infiltrates the cover;

- The reactions that are predicted to occur along the sideslope if it is assumed that the HDPE geomembrane degrades are capable of consuming water at rates that significantly exceed rates of infiltration through the cover.

TABLE 4
Summary of Long Term Reaction Rates Predicted By Oxygen Transport Modeling

Mechanism	Oxygen Supply (mol O_2 m^{-2} yr^{-1})
Through Cover	
diffusion with soil at wilting point	0.54
diffusion through holes	1.6
barometric pumping through holes	0.75
sum	2.89
Through Base	
intact liner – upper	1.77
intact liner – base	0.50
degraded liner – upper	187
degraded liner – base	0.0015

Notes: 1. Oxygen supply estimates are from Appendix C1

Prepared by: JTC
Checked by: KSS

4 CONSEQUENCES FOR FLOW PATTERNS AND DISCHARGES

The comparison of reaction and infiltration rates shows that there is a potential for the consumption of water in reactions to significantly affect long term water flow patterns in the TMA.

In nature, when the water required by a reaction exceeds the supply, the reaction ceases. Examples include the formation of evaporites, where the secondary phases listed in Tables 1 and 2 are replaced by less hydrated minerals. In the TMA however, there will be a substantial amount of water trapped in the pore space. The water in the pore space is enough to sustain the reactions rates listed in Table 4 for many years.

In the TMA, the consumption of water will cause only localized changes in the water content. Localized decreases in water content will cause a capillary gradient towards the reaction site, drawing water from the surroundings to sustain the reaction. Where the requirement for water even marginally exceeds the infiltration rate, the result will be a net deficit near the reaction site. In theory, even the reaction rates directly under the cover would be sufficient to consume all of the infiltrating water, thereby stopping the long term percolation from the TMA. However, the exact location of the infiltration and reaction points may not coincide. It may therefore be prudent to

conclude that water consumption will not completely stop percolation from the TMA.

In contrast, if it is assumed that the HDPE geomembrane in the composite base liner degrades, higher rates of oxidation will result. The rates predicted will be sufficient to cause a significant local water deficit. Once again, the question of location makes it difficult to conclude that the reactions would completely prevent percolation. However, it is conservative to conclude that the areas where reactions are occurring would not contribute to the percolation from the TMA.

The implications for the water quality modeling are:

- Long term percolation rates predicted by the HELP modeling are likely to be conservative, because much of the infiltrating water will be consumed by reactions.

- The higher oxidation rate predicted after an assumed degradation of the HDPE geomembrane in the composite base liner will lead to local water deficits, and therefore a net flow of water to any oxidation zones. The net flow to the oxidation zone will cause there to be little or no release of water from the oxidation zones.

As a result, the only water that is likely to percolate from the TMA over the long term will be water that does not contact any oxidation zone.

5. REFERENCES

Foth & Van Dyke, 1998. Addendum No. 5 to the May 1995 Crandon Project Tailings Management Area Feasibility Report/Plan of Operation.

Appendix F

Groundwater Quality Statistical Analysis

(Note: Table 1 and Attachment 2 have been updated as part of the June 1999 GWQPE update for depyritized tailings.)

Foth & Van Dyke
Memorandum

December 23, 1998

TO: Jerry W. Sevick, Foth & Van Dyke

CC: Steve Donohue, Foth & Van Dyke
Master File

FR: Stephen G Lehrke, Foth & Van Dyke SGL

RE: Crandon Project - Tailings Management Area and Reflooded Mine Area ACLs

TMA

The 16 groundwater monitoring wells used for TMA groundwater quality validation in 1994 and 1995, as described in Section 3.6 of the EIR (Foth & Van Dyke, 1995/1998), were used to define current groundwater quality in the area. It should be noted that a different set of wells will be used to establish baseline groundwater quality conditions at the TMA prior to construction and for monitoring of groundwater quality once mining begins. An analysis similar to that described below for each new well and chemical parameter will need to be completed once the additional baseline data is collected.

The process used to determine whether baseline water quality in the vicinity of the TMA exceeds Wisconsin State NR 140 public health and welfare standards based on the data for the 16 wells referenced above is that given in the Wisconsin Department of Natural Resources (WDNR) guidance document "PAL/ACL Calculations Guidance for Solid Waste Facilities" (WDNR, 1994). According to the guidance document, if one NR 140 Enforcement Standard (ES) or two NR 140 Preventative Action Limit (PAL) exceedances are observed in the baseline data, or if the average of the baseline data exceeds the NR 140 PAL, an alternative concentration limit is calculated for that parameter. The alternative concentration limit is calculated as the average baseline groundwater quality plus two standard deviations. All non-detections are replaced with one-half the detection limit. The WDNR guidance document is included as Attachment 1.

If the parameter under consideration is an indicator parameter (such as TDS), no NR 140 PAL or ES exists. In this instance, a PAL is calculated as the average plus three standard deviations, or the average plus the NR 140 minimum increase, whichever is greater.

The calculated ACLs for the TMA based on the WDNR guidance document are presented in Table 1. The baseline data used in the calculations, and the calculations themselves, are given in Attachment 2.

Reflooded Mine

The six groundwater monitoring wells used for the reflooded mine groundwater quality validation in 1994 and 1995 were used to define current groundwater quality in the area. The process used to determine whether baseline water quality in the vicinity of the mine exceeds NR 140 public health and welfare standards was also that given in WDNR (1994). The calculated ACLs for the reflooded mine based on this procedure are presented in Table 2. The baseline data used, along with the calculations, are given in Attachment 3.

Baseline Groundwater Conditions

The average baseline groundwater quality for both the TMA and reflooded mine areas was conservatively calculated as the upper 95% confidence limit of the mean for each parameter. Calculation of the upper 95% confidence limits followed the guidance given in USEPA (1989). This criteria is outlined in the flowchart illustrated on Figure 1, and is briefly described below:

- If at least 85% of the baseline data are above detection, all non-detects are replaced with one-half the detection limit and an upper confidence limit based on the normal distribution is calculated.

- If at least 50% but less than 85% of the baseline data are above the detection limit, the mean and standard deviation are adjusted using Cohen's adjustment and an upper confidence limit based on the normal distribution is calculated.

- If less than 50% of the baseline data are above the detection limit, a non-parametric upper confidence limit on the median is used.

Since all parameters have at least thirty results, the data sets were considered to be large samples and a test for normality was unnecessary. This is due to the fact that the mean of a large sample is a normally distributed variable. The results of the baseline calculations are provided on the summary tables in Attachments 2 and 3.

SGL:cer1
Attachments

References

Foth & Van Dyke, 1995/1998. *Environmental Impact Report for the Crandon Project.* Originally issued May 1995. Updated December 1998.

United States Environmental Protection Agency, 1989. *Analysis of Groundwater Monitoring Data at RCRA Facilities - Interim Final Guidance.* Office of Solid Waste, Washington D.C. February 1989.

Wisconsin Department of Natural Resources, 1994. *PAL/ACL Calculations Guidance for Solid Waste Facilities.* May 6, 1994.

Table 1

Tailings Management Area
Alternative Concentration Limits

Parameter	Units	NR 140 PAL	NR 140 ES	ACL[1]
Antimony	mg/l	0.0012	0.006	0.12
Arsenic	mg/l	0.005	0.05	0.025[2]
Barium	mg/l	0.4	2	—
Beryllium	mg/l	0.0004	0.004	—
Cadmium	mg/l	0.0005	0.005	0.0007[2]
Chromium	mg/l	0.01	0.1	0.026
Copper	mg/l	0.13	1.3	—
Cyanide	ug/l	40	200	—
Fluoride	mg/l	0.8	4	—
Iron	mg/l	0.15	0.3	0.18[2]
Lead	mg/l	0.0015	0.015	0.0052[2]
Manganese	mg/l	0.025	0.05	0.73
Mercury	ug/l	0.2	2	0.46
Nickel	mg/l	0.02	0.1	0.037[2]
Selenium	mg/l	0.01	0.05	—
Silver	mg/l	0.01	0.05	—
Sulfate	mg/l	125	250	—
Thallium	mg/l	0.0004	0.002	—
TDS	mg/l			370[3]
Zinc	mg/l	2.5	5	—

[1] Calculated as per the May 6, 1994, WDNR guidance document "PAL/ACL Calculations Guidance for Solid Waste Facilities".

[2] Replaces NR 140 PAL only.

[3] Represents PAL Calculation.

Prepared by: SGL
Checked by: SVD1

Table 2

Reflooded Mine
Alternative Concentration Limits

Parameter	Units	NR 140 PAL	NR 140 ES	ACL[1]
Antimony	mg/l	0.0012	0.006	0.12
Arsenic	mg/l	0.005	0.05	0.0042[2]
Barium	mg/l	0.4	2	—
Beryllium	mg/l	0.0004	0.004	—
Cadmium	mg/l	0.0005	0.005	0.00088[2]
Chromium	mg/l	0.01	0.1	—
Copper	mg/l	0.13	1.3	—
Cyanide	ug/l	0.040	200	—
Fluoride	mg/l	0.8	4	—
Iron	mg/l	0.15	0.3	0.21[2]
Lead	mg/l	0.0015	0.015	0.0034[2]
Manganese	mg/l	0.025	0.05	0.33
Mercury	ug/l	0.2	2	0.50
Nickel	mg/l	0.02	0.1	—
Selenium	mg/l	0.01	0.05	—
Silver	mg/l	0.01	0.05	0.015[2]
Sulfate	mg/l	125	250	160[2]
Thallium	mg/l	0.0004	0.002	—
TDS	mg/l	—	—	630[2]
Zinc	mg/l	2.5	5	—

[1] Calculated as per the May 6, 1994, WDNR guidance document "PAL/ACL Calculations Guidance for Solid Waste Facilities".

[2] Replaces NR 140 PAL only.

Prepared by: SGL
Checked by: SVD1

Statistical Confidence Limit Decision Flow Chart

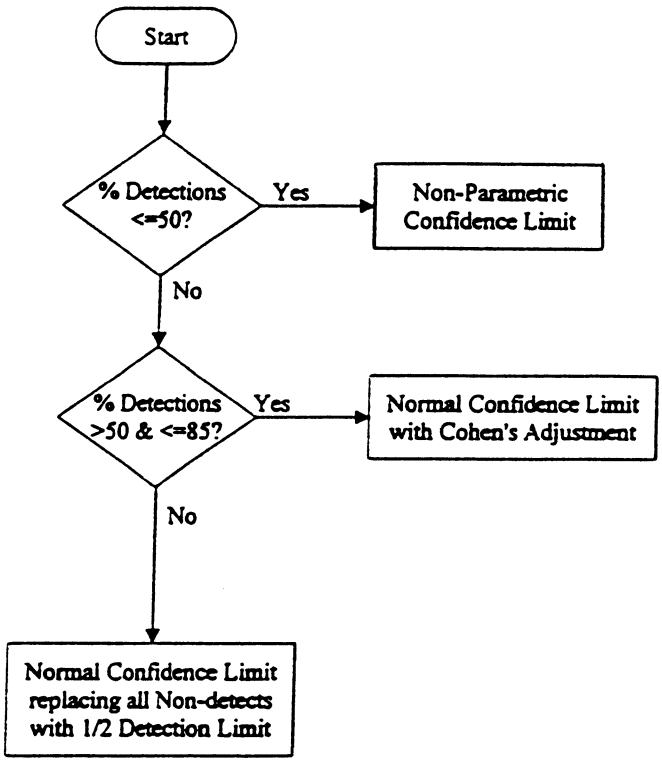

Foth & Van Dyke			
REVISED	DATE	BY	DESCRIPTION
1	12/98	MLD2	REVISED FOR 1998 UPDATE

CHECKED BY:	JKSI	DATE:	MAY '97
APPROVED BY:	SGL	DATE:	MAY '97
APPROVED BY:	GWS	DATE:	MAY '97

Nicolet Minerals COMPANY

FIGURE 1

STATISTICAL CONFIDENCE LIMIT DECISION FLOW CHART

Scale: NOT TO SCALE		Date:	MAY, 1997
Prepared By: Foth & Van Dyke		By: JRB2	93C049

I:\93c049\3c49f200.dgn Dec. 23, 1998 08:19:08

Attachment 1

WDNR Guidance Document for Calculating PALs/ACLs

PAL/ACL CALCULATIONS GUIDANCE FOR SOLID WASTE FACILITIES

May 6, 1994

Solid Waste Management Section
Bureau of Solid and Hazardous Waste Management
Wisconsin Department of Natural Resources

I. INTRODUCTION

A Preventive Action Limit (PAL) or Alternative Concentration Limit (ACL) for a specific parameter is the concentration above which a ground water monitoring well is flagged as possibly being impacted by a release. At ground water monitoring wells designated as Subtitle D wells (Sub-D), we will use PALs and/or ACLs to trigger assessment monitoring (as defined in Subtitle D) in addition to their current function(s) in ch. NR 140, Wis. Adm. Code. Definitions of terms used in this document are given in the last section of this guidance. Although this guidance is written specifically to fulfill the Subtitle D monitoring requirements, the guidance can be used by solid waste facility personnel for general PAL/ACL calculations.

Federal Subtitle-D requires analysis of groundwater samples from designated Sub-D wells for indicator parameters, 15 metals, and VOCs. (Note: Wisconsin does not require routine metals monitoring since EPA's approval of Wisconsin's program allows for the indicator parameters to be monitored regularly instead of the metals). The trigger level for beginning Sub-D assessment monitoring is the exceedance of the PAL or ACL of a routinely monitored parameter.

PALs for **Public Health** parameters are specified in Table 1 of s. NR 140.10, Wis. Adm. Code. PALs for **Public Welfare** parameters are specified in Table 2 of s. NR 140.12. PALs for **Indicator** parameters are calculated as the greater of either: 1) the mean of at least 8 values plus 3 standard deviations, or 2) the mean of at least 8 values plus the increment in s. NR 140.20, Table 3. NR 140 Tables 1 through 3 are provided as an attachment to this guidance.

INDICATOR PARAMETERS

The Solid Waste Management Program uses the following as indicator parameters for landfills accepting primarily municipal solid waste:

Indicator Parameters*	PAL calculation required?
39036 Alkalinity, filtered	Yes, at all wells
00341 COD, filtered	Yes, at all wells
00872 Field Conductivity (@25°C)	Yes, at all wells
22413 Total Hardness, filtered	Yes, at all wells
00400 Field pH	No
00010 Field Temperature	No

00842 Groundwater Elevation	No
00307 Chloride	No, PAL is in Table 2
01046 Iron	No, PAL is in Table 2

* NOTE: If you have special wastes such as papermill sludge, flyash or foundry sand, additional parameters may be required.

You need to submit background water quality information on all these indicator parameters. However, you need to calculate PALs (or ACLs) for only the first 4 indicator parameters in the table above according to the following instructions. Field pH, temperature and groundwater elevation will be used by the Department to establish trends but will not be used to trigger assessment monitoring, therefore, PAL calculations are not required for those 3 parameters.

PALs for iron and chloride are listed in Table 2 of s. NR 140.12, therefore, PAL calculations are not required for those parameters. However, you may request an exemption from the PAL for iron and/or chloride showing that your facility meets the criteria listed in s. NR 140.28 (3) or (4), Wis. Adm. Code if the background groundwater concentrations at the well are greater than the established PAL or Enforcement Standard (ES). An approved exemption means that you must calculate an ACL, according to the following instructions, for the parameter(s) in question. To avoid duplication of work and to reduce paper work, you can include both the exemption request and calculated ACLs in the same submittal.

PUBLIC WELFARE PARAMETERS

You must submit at least 4 background groundwater concentrations for the following parameters listed in s. NR 140.12, Wis. Adm. Code:

Welfare Parameters	Which wells?	PAL Calculation Required?
00277 Copper	All	No
00316 Manganese	All	No
00946 Sulfate	All	No
00275 Zinc	All	No

If background concentrations for any of the above parameters are greater than the established PAL and you wish to establish an ACL, you may submit both an exemption request meeting the criteria in NR 140.28 and the appropriate ACL calculations for which you need at least 8 background values. Exemptions may be granted if the background is unaffected by a release from the facility and 4 representative monitoring results meet the following criteria:

1. any of the values exceeds an ES, or
2. 2 or more of the values exceeds a PAL, or
3. the average of the values is greater than the PAL.

PUBLIC HEALTH PARAMETERS

To meet Sub-D and NR 508.14 (2) requirements, you must provide at least 4 rounds of background groundwater concentrations at all wells for all the public health parameters listed in Table 1 of s. NR 140.10, Wis. Adm. Code and the last 6 metals in the following table. The Department is using the proposed NR 140 PALs and Department of Health and Social Services advice to establish PALs for cobalt and vanadium. In particular, Sub-D requires analysis of the following 15 metals:

Metals	Which wells?	PAL Calculations Required?
01000 Arsenic	All	No, listed in Table 1
01005 Barium	All	No, listed in Table 1
00312 Cadmium	All	No, listed in Table 1
00273 Chromium	All	No, listed in Table 1
00240 Lead	All	No, listed in Table 1
71890 Mercury	All	No, listed in Table 1
01145 Selenium	All	No, listed in Table 1
01075 Silver	All	No, listed in Table 1
00950 Fluoride	All	No, listed in Table 1
01095 Antimony	Sub-D only	No, proposed PAL is 1.2 µg/ℓ
01010 Beryllium	Sub-D only	No, proposed PAL is 0.4 µg/ℓ
01035 Cobalt	Sub-D only	No, pending from DHSS
00276 Nickel	Sub-D only	No, proposed PAL is 20 µg/ℓ
01057 Thallium	Sub-D only	No, proposed PAL is 0.4 µg/ℓ
01085 Vanadium	Sub-D only	No, pending from DHSS

If background concentrations for any of the non-volatile public health parameters are greater than the established PAL and you wish to establish an ACL, you must submit both an exemption request meeting the criteria in NR 140.28 and the appropriate ACL calculations for which you need at least 8 background values.

You are also required to provide background groundwater monitoring data for Parameter 00631, **Nitrate + Nitrite (as N)**. The PAL of 2 mg/l is listed in Table 1, therefore, no PAL calculations are required. However, you may request a grant of exemption to the PAL and calculate an ACL using at least 8 background results.

VOLATILE ORGANIC COMPOUNDS (VOCs)

The Sub-D VOCs required in Wisconsin, group A on Form 4400-107A, also have PALs listed in Table 1 of NR 140. PALS of 1 µg/ℓ and 0.3 µg/ℓ have been proposed for bromomethane and chloromethane, respectively. The Department may, using professional judgement, establish an ACL for specific VOCs if your NR 140.28 exemption request is granted. If there is an ACL exceedance, the Department will use professional judgement to decide what action is appropriate for that exceedance. The Department will not accept either PAL or ACL calculations for Volatile Organic Compounds (VOCs).

The following instructions are designed to guide solid waste facility personnel through the PAL/ACL calculation process.

II. CALCULATIONS

STEPS TO CALCULATE PAL/ACLs

1. Assemble the complete data set for relevant parameters at all wells. Use the entire set of analyses available for a given well and parameter. The larger the data set, the more accurate predictor the PAL will be. Under state law (ch. NR 140, Wis. Adm. Code) you must have at least 8 background values to calculate PALs or ACLs. DO NOT submit calculations with less than 8 background values. If less than 8 are submitted, the entire report will be returned to you and you will be asked to provide complete information with

the next submittal unless you have made special arrangements with the Department.

NOTE: *Data used in the PAL/ACL calculations must have been generated at a DNR certified lab using an acceptable method and published sampling procedures.*

- Values reported as "less than" a detection limit must be used in the calculations and assigned a value of 1/2 (one-half) the detection limit.

- NR 140.16(2), Wis. Adm. Code, regarding limits of detection and limits of quantitation, is reprinted as a note at the end of Section IV.

- Values must be rounded "up" to 2 (two) significant figures following completion of the PAL calculation. For example, a value of 123.49 would be rounded to 130.

2. **Present** in <u>tabular form all</u> background **groundwater quality monitoring results** and any other relevant groundwater monitoring data in your submittal. Include the concentration, date of sampling and an indication of whether that value has been eliminated from the calculations such as shown in Figure 1. DO NOT use a computer program which rejects outliers.

3. **Determine valid justification** for the elimination of any background data which were not used in the PAL calculations. For example, "Contamination due to well construction" is valid whereas "Value is too high" is not acceptable. Other valid reasons could include lab error, reporting error, method interference or high blank reading. You must document why any data are eliminated. Figure 2 illustrates one possible way to present the documentation.

4. **Construct time vs concentration graphs** (see Figure 3 and Section III) for relevant parameters at all wells, using the monitoring results which you will use for the PAL calculations. For each parameter, the X-axis must have a uniform time scale and the Y-axis must have a uniform concentration scale. To avoid clutter, include no more than 3 downgradient and 1 upgradient wells per graph.

   NOTE: *These graphs will be used to compare your data set with that of the Department. You may call the Department hydrogeologist assigned to your site for approval of an alternate method of data presentation. Such an approval should be noted in your plan modification submittal to the Department.*

5. **Calculate the PAL**

   NOTE: *Using your professional judgement, determine if any wells at the site are impacted, and if so, use the guidance presented in Section III to calculate PALs at those impacted wells. Explain in your submittal how you handled those wells and provide the appropriate data.*

a. **Calculate** the mean (average) concentration plus 3 standard deviations for each indicator parameter.

b. Calculate the mean plus the NR 140.20 Table 3 increment.

c. **Choose** the greater of either (a) or (b) for the selected parameter; remember to round "up".

d. **Present information** pertaining to all wells for a given parameter in a table or chart that includes the mean, standard deviation, PAL using the standard deviation, PAL using the NR 140 Table 3 increment and the selected PAL (see Figure 4).

6. **Calculate ACLs** where appropriate, using the guidance in Steps 1 through 5.

a. For each parameter, **calculate** the mean concentration of at least 8 sampling events plus 2 standard deviations.

b. **Present information** pertaining to all wells for a given parameter in a table or chart that includes the mean, standard deviation and ACL.

c. **Include** an exemption request which contains the ACL calculations and fully explains the origin of the high value and why the appropriate criteria of s. NR 140.28 are met.

7. **Submit a groundwater monitoring plan modification** approval request to the Department addressed to Ms. Lakshmi Sridharan, DNR Bureau of Solid and Hazardous Waste Management, Solid Waste Management Section. The submittal must include <u>completed</u> PAL and ACL calculations under the signature of a hydrogeologist. Upon receipt of your submittal, the Department will send an invoice for the appropriate review fee. The DNR hydrogeologist assigned to your facility will review the submittal and decide whether to approve the PAL/ACLs. If they are approvable, the Department will send you a plan modification approval and enter the approved PAL/ACL values onto the Department's computer system. These values will be used as triggers in reports that are generated using the system. Future turnaround documents (TADs) for these wells will then include the PAL/ACLs.

III. IMPACTED WELLS

IDENTIFICATION OF IMPACTED WELLS

An impacted well will have high concentrations of one or more substances when compared to other wells screened in the same geologic formation and/or to the groundwater standards in ch. NR 140, Wis. Adm. Code.

Some facilities, particularly those located in a fine-grained soil environment, may decide to calculate ACLs rather than use the established PALs for public health and welfare parameters because of high background levels reflecting natural impacts. Those facilities must provide adequate justification for an NR 140.28 exemption when requesting the ACLs so that the Department can determine whether the high levels are natural background or the result of a release.

One or more of any of the following methods or tools may be used to identify impacted wells. The Department is willing to review other valid means of identification which you provide.

1. **Prior Investigation**

A well may have been identified as impacted during an investigation. Again, be sure to check if the well has been impacted for all parameters from the time of installation or if at least 8 rounds of "clean" data are available to calculate a PAL or ACL.

2. **Box Plots**

You may construct nonparametric box plots using all data for each parameter at each well; see Figure 7 for further information about box plots. For easy comparison with a "clean" well, include a background well on each chart of box plots. Past experience has shown us that the "clean" range is generally within ±5NP (Nonparametric) units of the median of data from all wells on site, where the site-wide median is shown as "0" on the horizontal axis of the box plots.

If box plots indicate that the well appears impacted, you can inspect the time vs concentration charts, determine if there is a period of time for which you have at least 8 rounds of "clean" data available and decide whether those values represent the background.

Figure 8 shows both the time vs concentration chart and box plots for field conductivity data at 4 wells. Used together, box plots and time vs concentration charts aid in the interpretation of water quality data. Figure 9 illustrates how an impacted well (MW-2) appears on both a box plot and time vs concentration chart. Note that the box plot for well MW-2 is greater than 5 NP units from the median.

3. **Time vs Concentration Charts**

Construct time vs concentration charts as shown in the attached examples using all data for each parameter at each well. Use no more than 3 downgradient and 1 upgradient well on each chart to avoid clutter. The upgradient well will most likely be a flat line representing a low concentration through time. The side- or downgradient wells might be any combination of flat and/or positive or negative slopes. You may note the dates of significant events such as cover placement or the opening of a new phase on the chart. Use the charts to find the period of time during which the samples most representative of background were collected. Calculate the PAL and/or ACL using those representative values, of which there must be at least 8.

Use professional judgement to decide whether a well is so impacted that PALs cannot be calculated. Figure 9 illustrates data for well MW-2 which appears to be impacted by a release(s) from the facility. If you have such wells, submit a brief justification for the way you established the PAL.

4. **Linear Regression**

Linear regression, a parametric statistic, can help you decide whether there is an increasing concentration with time; however, it assumes a normal distribution for

the data set. That assumption is usually not valid for groundwater samples. The Department will accept use of linear regression as evidence of impacted groundwater only if there is a normal distribution as determined by using a skewness test. (See "Methods for Determining Compliance with Groundwater Quality Regulations at Waste Disposal Facilities" dated January, 1989, by S. Fisher and K. Potter for skewness methodology.)

5. **Maps**

Plan view maps of the facility with the concentration of the parameter of interest noted next to the well will provide locational information which may help you decide how to handle an apparently impacted well. Be sure to include only wells which terminate in the same geologic formation or at the same elevation. Note, too, the well locations in respect to any possible contamination sources other than the waste mass itself. Contouring and color coding the concentration ranges can be a good visual tool. Preparation of such maps at several elevations, along with flow nets, cross sections, and fence diagrams will provide 3-dimensional insight to any impacts.

HOW TO CALCULATE PAL/ACLs FOR IMPACTED WELLS

NOTE: *A well may be impacted for one parameter and not for others. Be sure to check all parameters. In Figure 6, the time vs concentration chart shows high specific conductance, which may be due to well construction, during the first 3 quarters. The chart for total alkalinity, however, does not have the same trend. In this case, you would use all the sample results to calculate the PAL for alkalinity but only the results that are not impacted when calculating the PAL for specific conductance.*

1. Calculate the PAL using both the first 8 (unimpacted) points representative of background and the entire data set. Compare the results and use the smaller of the two numbers as the PAL.

2. If all data for a parameter, not just recent data, are impacted (and since by definition a PAL cannot be calculated at such a well):

   a. Use the PAL calculated at an upgradient well which is screened in the same formation, or

   b. If an upgradient well is not screened in the same formation:

      i. find another uncontaminated well which is appropriately screened, as it will probably have similar water quality, and use the PAL for that well, or

      ii. use the PAL for a well with similar water quality, as indicated by box plots with similar medians and confidence intervals for other parameters.

      NOTES: *You may use a well that is part of an adjacent facility's monitoring system only if it meets the above criteria better than any of the subject facility's wells.*

DO NOT merge data from monitoring wells and private wells because these well types are constructed and sampled so differently.

c. Calculate an indicator PAL using the impacted data and provide adequate justification for its use (i.e. an upgradient well is downgradient of an adjacent unlined facility).

IV. DEFINITIONS

An **Alternative Concentration Limit** (ACL) is defined in s. NR 140.05 (1m), Wis. Adm. Code, as the concentration of a substance in groundwater established by the department for a site to replace a preventive action limit or enforcement standard or both, from Table 1 or 2, when an exemption is granted in accordance with s. NR 140.28.

Background groundwater quality is defined in s. NR 140.05(3), Wis. Adm. Code, as groundwater quality at or near a facility, practice or activity which has not been affected by that facility, practice or activity.

An **Enforcement Standard** (ES) is defined as a numerical value expressing the concentration of a substance in groundwater which is adopted under s. 160.07, Stats. (establishment of enforcement standards; substances of public health concern), and s. NR 140.10, Wis. Adm. Code, (public health related groundwater standards) or s. 160.09, Stats. (establishment of enforcement standards; substances of public welfare concern), and s. NR 140.12, Wis. Adm. Code, (public welfare related groundwater standards).

An **error log** identifies data points which are eliminated because of a sampling error such as a defective conductivity meter. It may be combined with the nullify log if points are identified by an "e" or "n".

The **limit of detection** is the lowest concentration for an analytical test method and sample matrix at which the presence of a substance can be identified in an analytical sample, with a stated degree of confidence, regardless of whether the concentration of the substance in the sample can be quantified.

The arithmetic **mean** for a parameter at one well is the sum of the concentrations divided by the number of values used.

A **nonparametric statistic** is based on the order in which information is gathered rather than assuming a normal distribution of data.

A **nullify log** identifies data points which are eliminated for a reason other than sampling error, such as high concentration due to well construction. It may be combined with the error log if points are identified by an "e" or "n".

A **Preventive Action Limit** (PAL) is defined in s. NR 140.05(17), Wis. Adm. Code, as a numerical value expressing the concentration of a substance in groundwater which is adopted under s. 160.15, Stats. (establishment of PALs), and either listed in s. NR 140.10 (public health related groundwater standards), or s. NR 140.12 (public welfare related groundwater standards), or calculated under s. NR 140.20 (indicator parameter groundwater standards).

The **standard deviation** for a group of samples is defined in ch. NR 140.20(2), Wis. Adm. Code, as the square root of the value of the sum of the square of the difference between each sample in the sample group and the mean for that sample group divided by the number of samples in the sample group where the sample group has 30 or more samples and by one less than the number of samples in the sample group where the sample group has less than 30 samples.

A **uniform scale** is one which has consistent, non-logarithmic increments.

NOTE: **NR 140.16(2), Wis. Adm Code,** states "The laboratory shall select the analytical methodology which:

(a) Is specified in rules or approved by the regulatory agency, and
(b) Is appropriate for the concentration of the sample, and
(c) Is one of the following:

1. Has a limit of detection and limit of quantitation below the preventive action limit,

or

2. Produces the lowest available limit of detection and limit of quantitation if the limit of detection and limit of quantitation are above the preventive action limit.

Attachments: Figures 1 - 9
PAL/ACL Calculations Checklist
NR 140.10 Table 1, NR 140.12 Table 2, NR 140.20 Table 3

BH: PALACL\Facpal2.doc May 6, 1994

N59212A

WISCONSIN DEPARTMENT OF NATURAL RESOURCES
SUMMARY/EXCEEDANCE REPORT

03/02/94 08:25:42 PAGE 1

BARB HENNINGS

DISTRICT: AREA:

REPORTING PERIOD: 10/14/81 THRU 06/24/87

FACILITY-NAME: LICENSE-NUMBER: FACILITY-ID:

WELL	COMMON WELL NAME		COD FILTERED MG/L (00341)	COND(FIELD) @25C MICROMHO (00872)	TOT HARD, FILT MG/L (22413)	TOT ALK, FILTRD MG/L (39036)
002	W-2 PAL ES GRADIENT-NOT ENTRD	10/14/81	94 N	700 N	254 N	253 N
		12/11/81	110 N	625 N	240 N	278 N
		03/18/82	101 N	775 N	272 N	242 N
		06/08/82	59	600 N	194	198
		09/13/82	67	475	78	24
		12/22/82	32	450	80	36
		03/10/83	28	445	208	210
		06/09/83	50	370	148	152
		09/22/83	56	410	170	170
		12/13/83	54	390	160	164
		03/23/84	55	250	156	156
		06/18/84	38	260	144	142
		10/16/84	84	180	104	102
		12/28/84	33	155	104	96
		03/20/85	32	260	132	110
		06/28/85	39	310	140	140
		09/26/85	46	240	94	88
		12/13/85	16	255	110	110
		03/24/86	23	195	88	82
		06/30/86	49	360	170	160
		09/24/86	42	240	96	98
		12/18/86	25	310	130	140
		03/18/87	25	275	130	120
		06/24/87	27	350	180	170

N = Nullify

FIGURE 1

Example of data presentation showing dates and concentrations for parameters at one well. Note the Nullify flags which correspond to the log in Figure 2.

ERROR LOG (E)
+Nullify LOG (N)

ne of
cility _____ p.1 of 2

cense No. _____

Today's Date	Initials	Point ID	Common Name	Parameter	Value/Date Printed As (E) (N)	Comments	SMS USE F/M C/LTG
8/6/87	BBG	002	W-2	COD	94.0 81-10-14 (N)	initial value high, due to well construction	
8/6/87	BBG	002	W-2	COD	110.0 81-12-11 (N)	Initial value high, due to well construction	
8/6/87	BBG	002	W-2	COD	101.0 82-03-18 (N)	Initial value high, due to well construction	
8/6/87	BBG	001	W-1	pH	8.20 84-10-16 (E)	pH meter error	
8/6/87	BBG	002	W-2	pH	8.4 84-10-16 (E)	pH meter error	
8/6/87	BBG	003	W-3	pH	8.20 84-10-16 (E)	pH meter error	
8/6/87	BBG	002	W-2	Alk.	253 81-10-14 (N)	Initial high value, due to well construction	
8/6/87	BBG	002	W-2	Alk.	278 81-12-11 (N)	initial high value, due to well construction	
8/6/87	BBG	002	W-2	Alk.	242 82-03-18 (N)	Initial high value, due to well construction	
8/6/87	BBG	003	W-3	Spec. Cond	1425 82-06-08 (N)	well near salt storage area, Cl^- flushed out	
8/6/87	BBG	003	W-3	Spec. Cond	2100 87-03-18 (N)	well near salt storage area, Cl^- flushed out	
8/6/87	BBG	002	W-2	Hardness	253 81-10-14 (N)	Initial high value due to well construction	
8/6/87	BBG	002	W-2	Hdnss	278 81-12-11 (N)	initial high value due to well construction	
8/6/87	BBG	002	W-2	Hdnss	242 82-03-18 (N)	Initial high value due to well construction	

FIGURE 2

Example of an error and nullify log. Note that each line is identified whether it is an error or nullify condition.

FIGURE 3
PARAMETER #872, SPECIFIC CONDUCTANCE

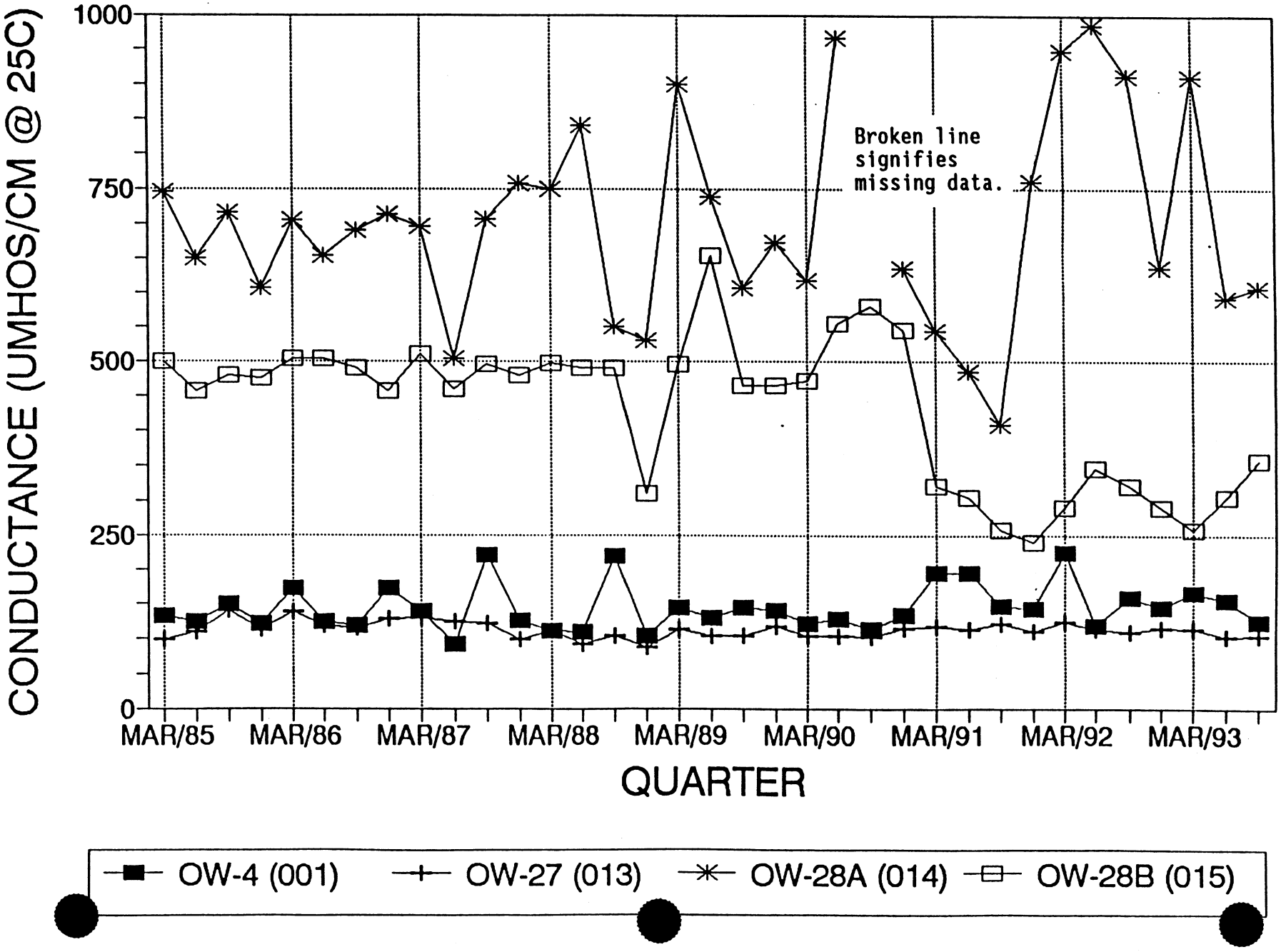

FIGURE 4

Chart showing the number of sample results used, mean, standard deviation, PAL values, and the selected PAL for a single parameter at all wells.

Parameter: Total Alkalinity, Filtered
NR 140 Minimum Increase: 100 mg/l*

Well (DNR #)	Number	Mean	Std Dev (σ)	3 x σ	(a) Mean + 3 σ	(b) Mean + Inc*	PAL
MW 1 (001)	8	257	51	152	409	357	410
MW 1P (002)	8	117	18	54	171	217	220
MW 2 (003)	8	139	19	58	197	239	240
MW 2P (004)	8	116	23	70	186	216	220
MW 3 (005)	8	187	33	99	286	287	290
MW 3P (006)	8	121	25	74	194	221	230
MW 6 (009)	8	124	16	48	172	224	230
MW 6P (010)	8	189	30	91	279	289	290
MW 7 (011)	8	190	15	45	235	290	290
MW 7P (012)	8	147	16	47	194	247	250
MW 16 (041)	8	212	22	65	277	312	320
MW 17 (042)	8	143	18	55	198	243	250
MW 17P (043)	8	96.4	51	153	249	196	250
MW 18 (044)	8	235	21	62	297	335	340
MW 18P (045)	8	152	20	59	211	252	260
MW 19 (046)	8	196	15	46	242	296	300
MW 19P (047)	8	134	27	80	214	234	240
MW 20 (048)	8	187	8	24	211	287	290
MW-21 (049)	8	214	10	31	245	314	320
MW 22 (050)	8	237	27	82	319	337	340
MW 25 (055)	8	198	13	40	238	298	300
MW 26 (056)	8	205	19	56	261	305	310
MW 27 (057)	8	94.1	12	37	131	194	200
MW 28 (058)	8	117	17	52	169	217	220

FIGURE 5

This chart of sample results used is incomplete. Note the blank data points and lack of sampling dates. Such submittals will be returned to the facility.

Parameter: Hardness

NR 1.40 Minimum Increas .100 mg/l

Well	Sample results, mg/l 1	2	3	4	5	6	7	8	Mea	DEV	3DEV	Mean + 3D	Mean + inc	PAL
mw1	320	240	440	230	250	343	361	368	319	74	222	541	419	541
mw1p	210	120	250	130	120	153	146	149	160	46	139	299	260	299
mw2	270	150	270	140	140	167	150	152	180	56	169	349	280	349
mw2p	230	140	240	120	120	143	123	125	155	50	150	306	255	306
mw3	320	230	310	190	200	235	216	207	239	50	149	387	339	387
mw3p	190	210	250	110	100	128	118	146	157	54	162	319	257	319
mw6	210	140	210	150	130	172	147	145	163	31	94	257	263	263
mw6p	320	230	300	200	200	231	210	206	237	47	141	378	337	378
mw7	320	210	270	200	190	235	204	207	230	44	133	363	330	363
mw7p	230	170	240	150	140	159	152	151	174	39	116	290	274	290
mw16	310	230	280	200	200	252	207	220	237	40	121	358	337	358
mw17	240	160	310	140	150	181	154	165	188	58	175	363	288	363
mw17p	160	150	230	80	75	84	76	76	116	58	173	289	216	289
mw18	340	240	350	240	240	282	269	277	280	44	131	411	380	411
mw18p	240	180	250	170	160	175	178	162	189	35	105	295	289	295
mw19	290	220	220	210	220	266	221	219	233	29	86	319	333	333
mw19p	210	200	250	120	120	137	130	131	162	50	151	313	262	313
mw20		271							271	0	0	271	371	371
mw21		229							229	0	0	229	329	329
mw22		329							329	0	0	329	429	429
mw25	221	245							233	17	51	284	333	333
mw26	230	256							243	18	55	298	343	343
mw27	115	129							122	10	30	152	222	222
mw28	139	154							147	11	32	178	247	247

This is unacceptable.
You must have at least
8 values.

FIGURE 6

Illustration of specific conductance which has apparently been affected by well construction compared to alkalinity which has not been affected.

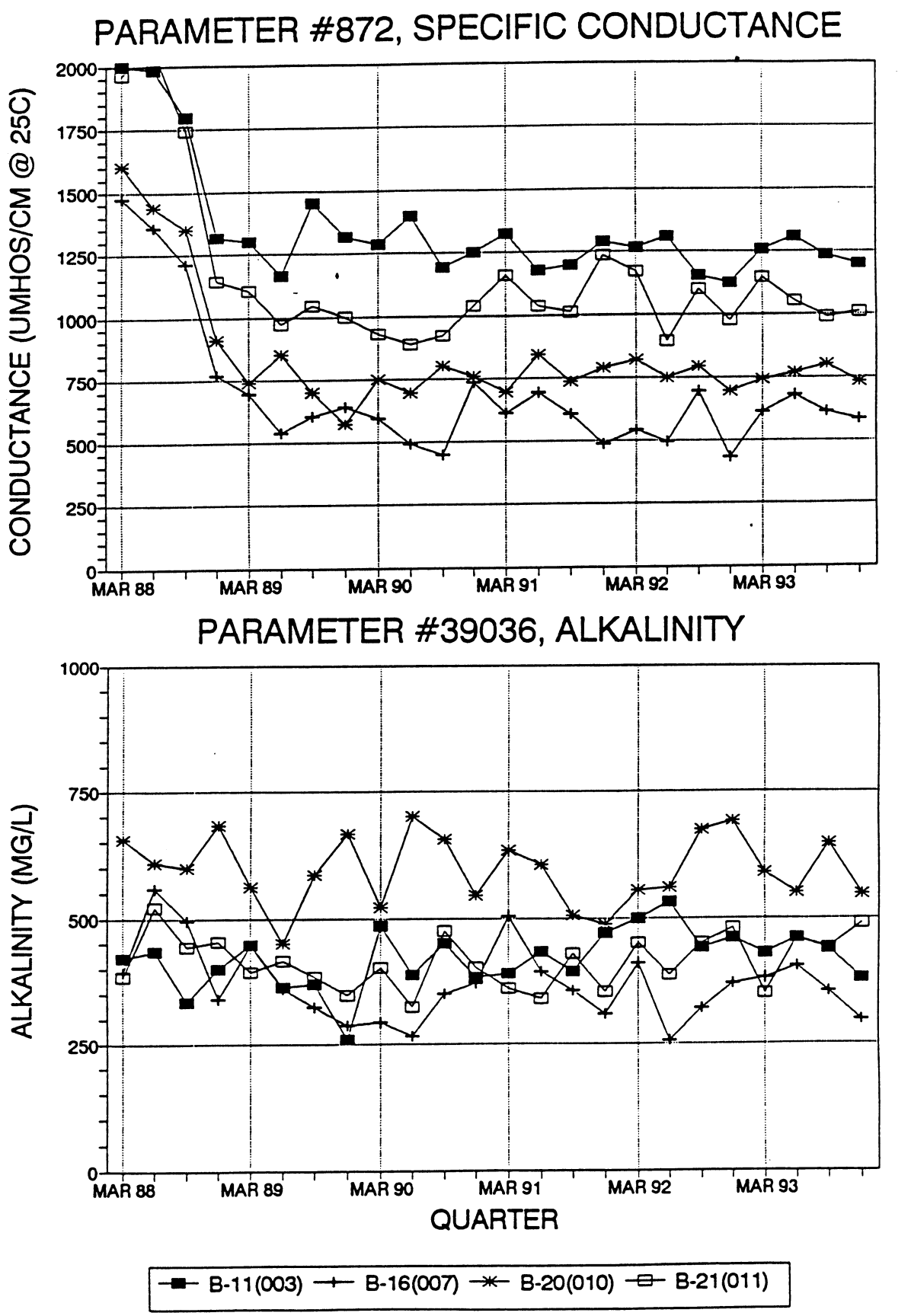

FIGURE 7

Description of Box Plots

Box plots can be an effective way to transmit a large amount of information in a small amount of space. At least five sample data are required to produce a box plot. A box plot consists of a median value for the set of information, the box containing 50% of the data values with the top line at 75% of the data and the bottom line at 25%. The notch in the side of the box indicates the 95% confidence interval for the median. If this interval is greater than the top or bottom of the interquartile range, it will extend outside the box. Box plots whose confidence intervals overlap statistically share a similar median. The whiskers are drawn to data points within 3/2 of the interquartile range and the outlier stars represent data outside of this distance.

The Department uses a nonparametric scale that allows different parameters to be compared with each other, even though their units might not be the same. This system puts zero NP (nonparametric) value as the site median for the parameter and adjusts the values of the parameter to a nonparametric value. The site median is a rough indicator of the site background for the parameter, although be aware that the whole site could be above the NR 140 PAL. The "clean" range is considered to be 0 ± 5 NP units, although if individual box plots deviate from the majority they should be investigated. Deviations greater than 5 NP units indicate serious contamination. Large interquartile (box) sizes mean that there is a lot of variation in the data for the well. If the box extends beyond 5 NP units, that well should also be investigated. Box plots of wells with similar water quality have overlapping confidence intervals. That is, the medians and 95% confidence intervals of these wells are usually similar to one another.

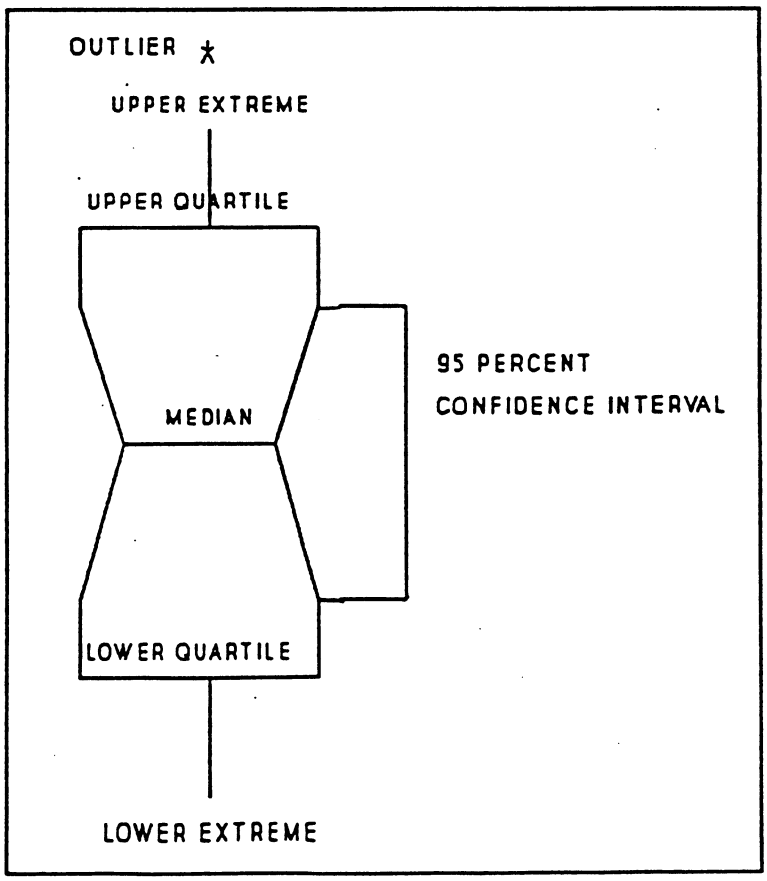

FIGURE 8

Illustration of 4 wells both as a time vs concentration chart and as box plots for the parameter specific conductance @ 25°C.

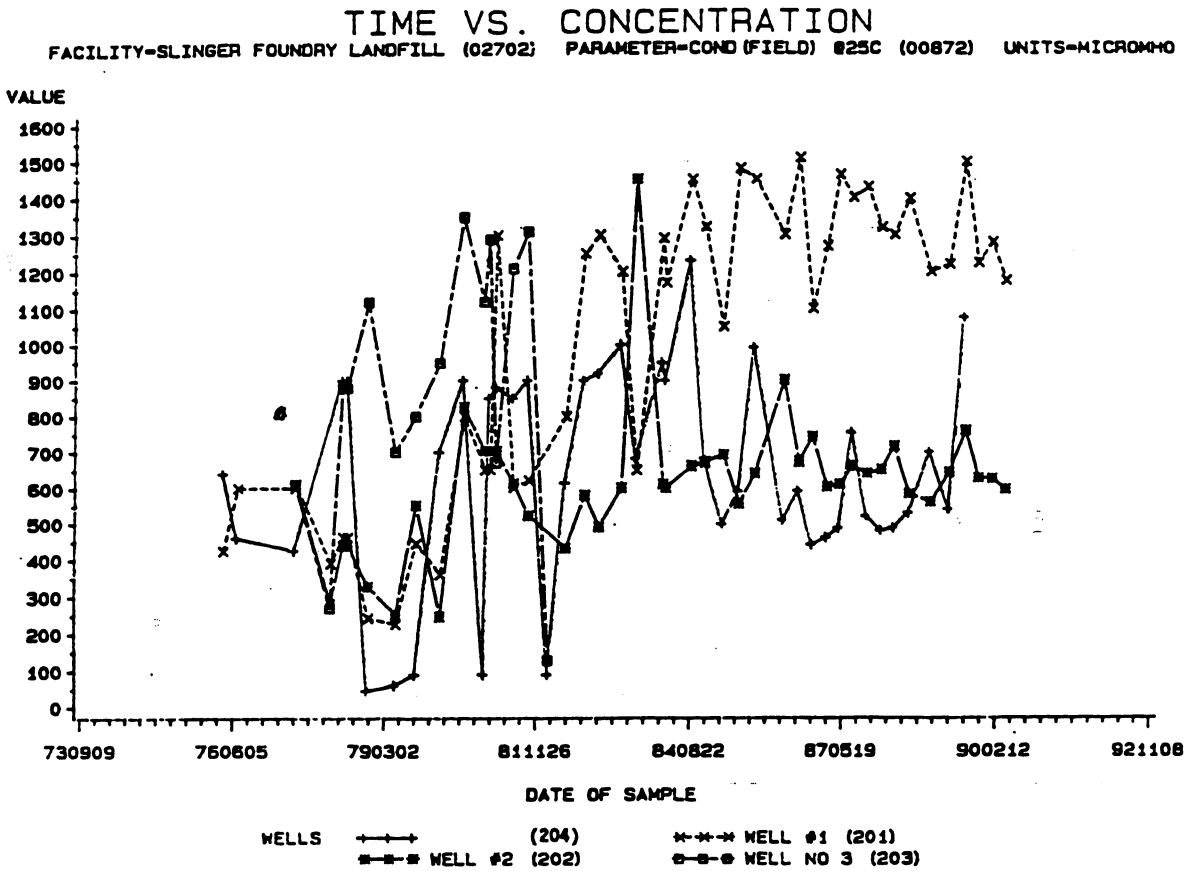

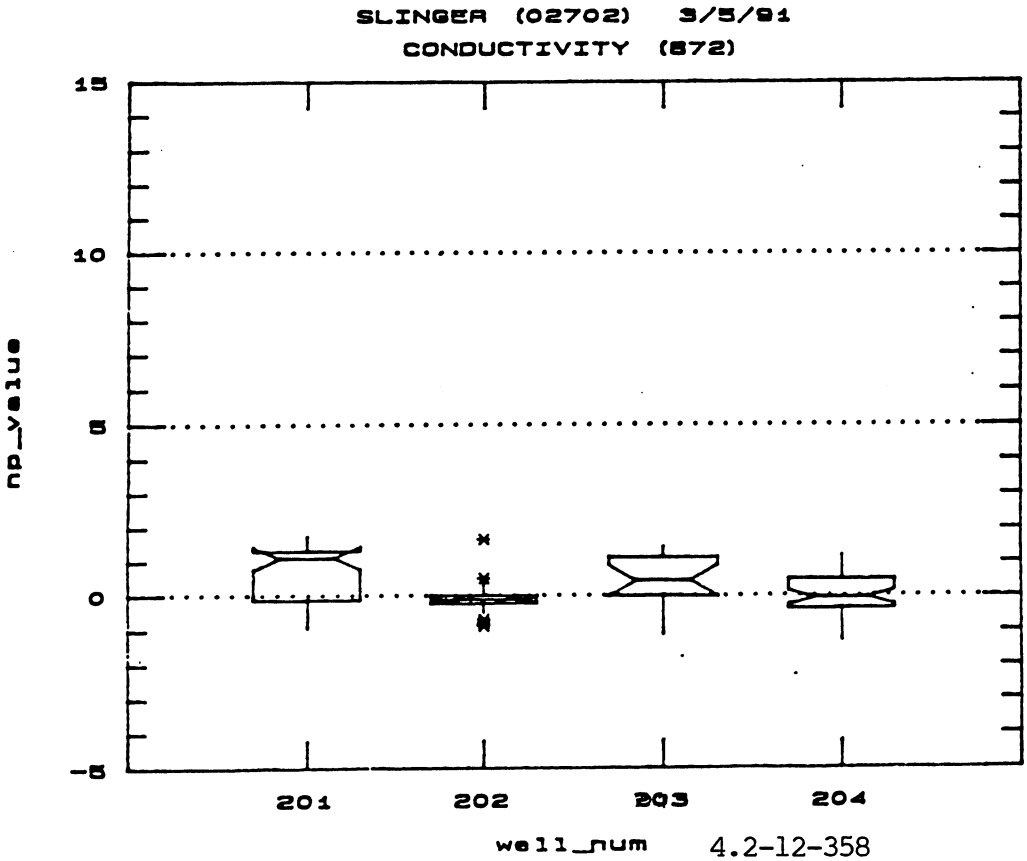

FIGURE 9

Illustration of how an impacted well, MW-2, might appear both on a time vs concentration chart and a box plot for specific conductance.

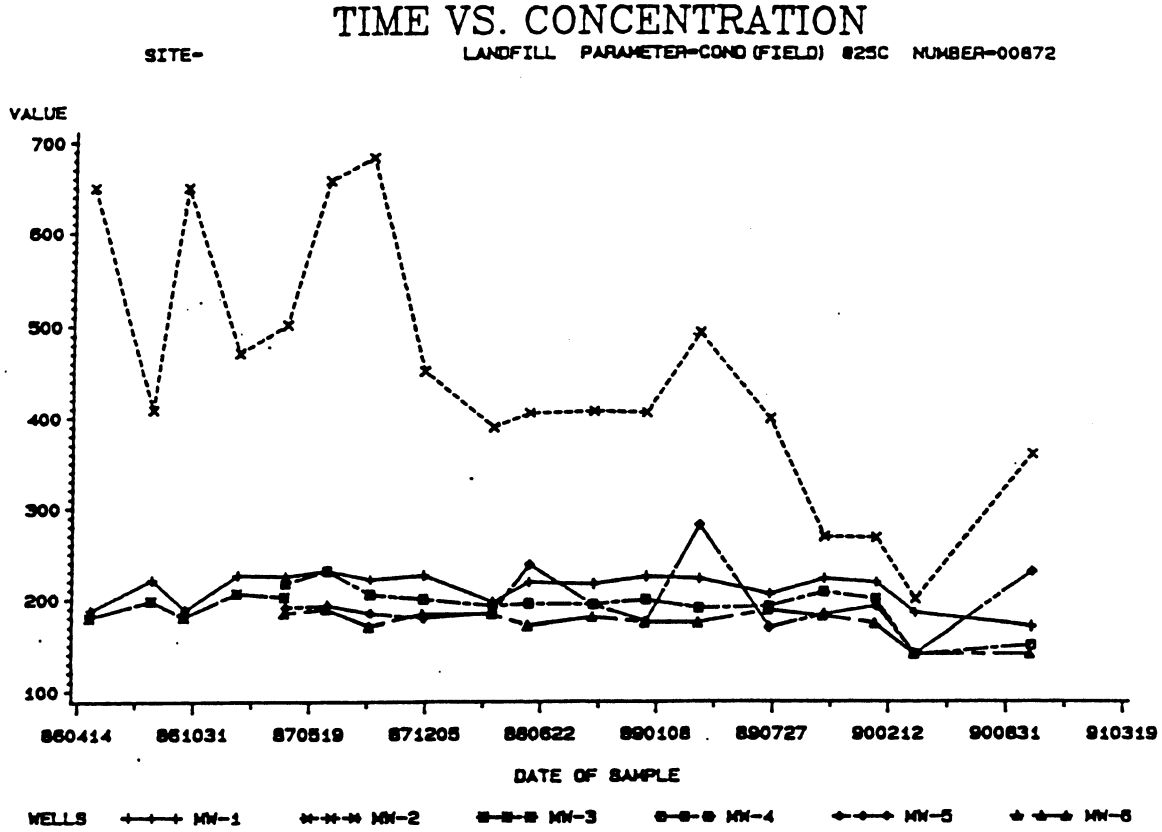

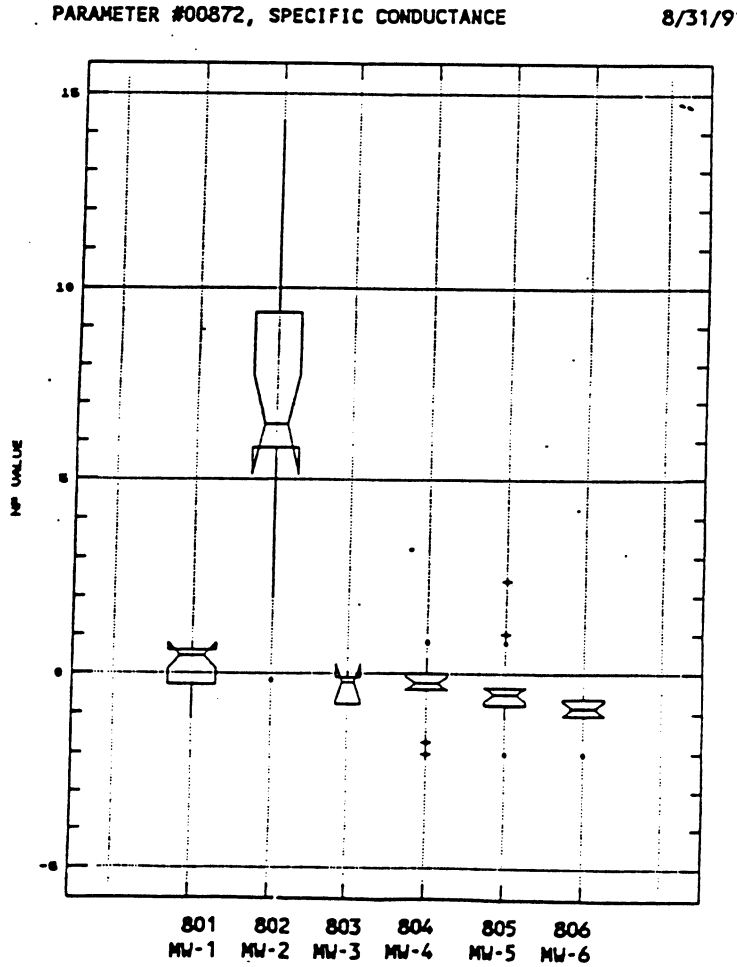

Attachment 2

TMA Baseline Results and PAL/ACL Calculations

Tailings Management Area
Groundwater Quality Statistical Analysis

Monitoring Well	Date	Aluminum mg/L	Antimony mg/L	Arsenic mg/L	Barium mg/L	Beryllium mg/L (1)	Cadmium mg/L	Chromium mg/L	Copper mg/L	Cyanide ug/L	Fluoride mg/L	Iron mg/L	Lead mg/L	Manganese mg/L	Mercury ug/L	Nickel mg/L	Selenium mg/L	Silver mg/L	Sulfate mg/L	Thallium mg/L (1)	TDS mg/L	Zinc mg/L
CMC-01P	May-94	< 0.200	< 0.050	< 0.005	0.012		< 0.001	< 0.005	< 0.030	< 20	< 0.100	< 0.100	< 0.001	0.031	< 0.2	< 0.030	< 0.005	< 0.010	12.0		139	< 0.020
CMC-01P	Jun-94	< 0.200	< 0.050	< 0.005	0.015		< 0.001	< 0.005	< 0.030	< 20	0.111	< 0.100	0.002	0.029	0.2	< 0.030	< 0.005	< 0.010	10.0		139	< 0.020
CMC-01P	Jul-94	< 0.200	< 0.050	< 0.005	0.015		< 0.001	< 0.005	< 0.030	< 20	< 0.100	< 0.100	< 0.001	0.031	0.3	< 0.030	< 0.005	< 0.010	10.0		128	< 0.020
CMC-01P	Aug-94	0.227	< 0.050	< 0.005	0.014		< 0.001	< 0.005	< 0.030	< 20	0.101	< 0.100	< 0.001	0.023	< 0.2	< 0.030	< 0.005	< 0.010	13.0		140	< 0.020
CMC-01P	Sep-94	< 0.050	< 0.20	< 0.0050	0.013		< 0.0001	< 0.005	< 0.030	< 20	0.1	< 0.050	< 0.0020	0.025	< 0.2	< 0.030	< 0.0050	< 0.010	13		150	< 0.020
CMC-01P	Oct-94	< 0.050	< 0.20	< 0.0050	0.011		< 0.0001	< 0.0050	< 0.030	< 20	0.1	< 0.050	< 0.0020	0.012	< 0.2	< 0.030	< 0.0050	< 0.010	15		170	< 0.020
CMC-01P	Nov-94	< 0.050	< 0.0050	< 0.0050	0.013		< 0.0001	< 0.0050	< 0.030	< 20	0.1	< 0.050	< 0.0030	0.016	< 0.20	< 0.030	< 0.0050	< 0.010	13		180	< 0.020
CMC-01P	Dec-94	< 0.050	< 0.0050	< 0.0050	0.012		< 0.0001	< 0.0050	< 0.030	< 20	< 0.1	< 0.050	< 0.0020	< 0.010	< 0.20	< 0.030	< 0.0050	< 0.010	12		170	< 0.020
CMC-01R	May-94	< 0.200	< 0.050	< 0.005	< 0.010		< 0.001	< 0.005	< 0.030	< 20	0.235	< 0.100	< 0.001	0.022	< 0.2	< 0.030	< 0.005	< 0.010	70.0		339	< 0.020
CMC-01R	Jun-94	< 0.200	< 0.050	< 0.005	0.030		0.001	< 0.005	< 0.030	< 20	0.248	< 0.100	0.017	0.035	0.3	< 0.030	< 0.005	< 0.010	35.0		258	< 0.020
CMC-01R	Jul-94	< 0.200	< 0.050	< 0.005	0.026		< 0.001	< 0.005	< 0.030	< 20	0.207	< 0.100	0.001	0.023	0.4	< 0.030	< 0.005	< 0.010	23.0		202	< 0.020
CMC-01R	Aug-94	0.274	< 0.050	< 0.005	0.026		< 0.001	< 0.005	< 0.030	< 20	0.173	< 0.100	< 0.001	< 0.010	0.2	< 0.030	< 0.005	< 0.010	21.0		170	< 0.020
CMC-01R	Sep-94	< 0.050	< 0.20	< 0.0050	0.028		0.0005	< 0.005	< 0.030	< 20	0.2	< 0.050	< 0.0020	< 0.010	< 0.2	< 0.030	< 0.0050	< 0.010	19		180	0.021
CMC-01R	Oct-94	< 0.050	< 0.20	< 0.0050	0.027		0.00032	< 0.0050	< 0.030	< 20	0.1	< 0.050	< 0.0020	< 0.010	< 0.2	< 0.030	< 0.0050	< 0.010	21		180	< 0.020
CMC-01R	Nov-94	< 0.050	< 0.0050	< 0.0050	0.027		< 0.0001	< 0.0050	< 0.030	< 20	0.1	< 0.050	< 0.0030	< 0.010	< 0.20	< 0.030	< 0.0050	< 0.010	19		190	< 0.020
CMC-01R	Dec-94	< 0.050	< 0.0050	< 0.0050	0.028		< 0.0001	< 0.0050	< 0.030	< 20	0.1	< 0.050	< 0.0020	< 0.010	< 0.20	< 0.030	< 0.0050	< 0.010	16		150	< 0.020
CMC-02P	May-94	< 0.200	< 0.050	< 0.005	0.011		< 0.001	< 0.005	< 0.030	< 20	< 0.100	< 0.100	< 0.001	< 0.010	< 0.2	< 0.030	< 0.005	< 0.010	13.0		150	< 0.020
CMC-02P	Jun-94	< 0.200	< 0.050	< 0.005	0.015		< 0.001	< 0.005	< 0.030	< 20	< 0.100	< 0.100	0.002	< 0.010	0.2	< 0.030	< 0.005	< 0.010	11.0		139	< 0.020
CMC-02P	Jul-94	< 0.200	< 0.050	< 0.005	0.010		< 0.001	< 0.005	< 0.030	< 20	< 0.100	< 0.100	0.003	< 0.010	0.7	< 0.030	< 0.005	< 0.010	13.0		130	< 0.020
CMC-02P	Aug-94	< 0.200	< 0.050	< 0.005	0.011		< 0.001	< 0.005	< 0.030	< 20	< 0.100	< 0.100	< 0.001	< 0.010	0.8	< 0.030	< 0.005	< 0.010	14.0		141	< 0.020
CMC-02P	Sep-94	< 0.050	< 0.20	< 0.0050	0.011		< 0.0001	< 0.005	< 0.030	< 20	0.1	< 0.050	< 0.0020	< 0.010	< 0.2	< 0.030	< 0.0050	< 0.010	14		150	< 0.020
CMC-02P	Oct-94	< 0.050	< 0.20	< 0.0050	0.0093		< 0.0001	< 0.0050	< 0.030	< 20	0.1	< 0.050	< 0.0020	< 0.010	< 0.2	< 0.030	< 0.0050	< 0.010	20		180	< 0.020
CMC-02P	Nov-94	< 0.050	< 0.0050	0.0055	0.012		< 0.0001	< 0.0050	< 0.030	< 20	0.1	< 0.050	< 0.0030	0.016	< 0.20	< 0.030	< 0.0050	< 0.010	14		150	< 0.020
CMC-02P	Dec-94	< 0.050	< 0.0050	0.0064	0.012		< 0.0001	< 0.0050	< 0.030	< 20	< 0.1	< 0.050	< 0.0020	< 0.010	< 0.20	< 0.030	< 0.0050	< 0.010	13		160	< 0.020
CMC-02R	Oct-94	< 0.050	< 0.20	< 0.0050	0.032		< 0.0001	< 0.0050	< 0.030	< 20	0.2	< 0.050	< 0.0020	0.14	< 0.2	< 0.030	< 0.0050	< 0.010	17		160	< 0.020
CMC-02R	Nov-94	< 0.050	< 0.0050	< 0.0050	0.040		< 0.0001	< 0.0050	< 0.030	< 20	0.2	< 0.050	< 0.0030	0.050	< 0.20	< 0.030	< 0.0050	< 0.010	17		160	< 0.020
CMC-02R	Dec-94	< 0.050	< 0.0050	< 0.0050	0.041		< 0.0001	< 0.0050	< 0.030	< 20	0.2	< 0.050	< 0.0020	0.33	< 0.20	< 0.030	< 0.0050	< 0.010	12		160	< 0.020
CMC-02R	Jan-95	< 0.050	< 0.0050	0.085	0.040		< 0.0001	< 0.0050	< 0.030	< 20	0.2	< 0.050	< 0.0020	0.042	< 0.20	< 0.030	< 0.0050	< 0.010	12		140	< 0.020
CMC-02R	Feb-95	< 0.050	< 0.005	< 0.0050	0.034		0.00031	< 0.0050	< 0.030	< 20	0.2	< 0.050	< 0.0020	0.065	< 0.20	< 0.030	< 0.0050	< 0.010	10		150	< 0.020
CMC-02R	Mar-95	< 0.050	< 0.0050	< 0.0050	0.037		0.0003	< 0.0050	< 0.030	< 20	0.1	< 0.050	< 0.0020	0.042	< 0.20	< 0.030	< 0.0050	< 0.010	11		180	< 0.020
CMC-02R	Apr-95	< 0.050	< 0.0050	< 0.0050	0.036		0.0001	< 0.0050	< 0.030	< 20	0.2	< 0.050	< 0.0020	0.022	< 0.20	< 0.030	< 0.0050	< 0.010	10		160	< 0.020
CMC-02R	May-95	< 0.050	< 0.0050	< 0.0050	0.038		0.00013	< 0.0050	< 0.030	< 20	0.2	< 0.050	< 0.0020	0.020	< 0.20	< 0.030	< 0.0050	< 0.010	13		180	< 0.020
CMC-03P	May-94	< 0.200	< 0.050	< 0.005	0.022		< 0.001	< 0.005	< 0.030	< 20	0.119	< 0.100	< 0.001	0.047	< 0.2	< 0.030	< 0.005	< 0.010	3.00		125	< 0.020
CMC-03P	Jun-94	< 0.200	< 0.050	< 0.005	0.023		< 0.001	< 0.005	< 0.030	< 20	0.118	< 0.100	< 0.001	0.030	0.2	< 0.030	< 0.005	< 0.010	< 2.00		122	< 0.020
CMC-03P	Jul-94	< 0.200	< 0.050	< 0.005	0.002		< 0.001	< 0.005	< 0.030	< 20	0.114	< 0.100	0.002	0.020	< 0.2	< 0.030	< 0.005	< 0.010	2.00		123	< 0.020
CMC-03P	Aug-94	< 0.200	< 0.050	< 0.005	0.021		< 0.001	< 0.005	< 0.030	< 20	0.116	< 0.100	< 0.001	0.011	< 0.2	< 0.030	< 0.005	< 0.010	3.00		118	< 0.020
CMC-03P	Sep-94	< 0.050	< 0.20	< 0.0050	0.020		< 0.0001	< 0.005	< 0.030	< 20	0.1	< 0.050	< 0.0020	0.011	< 0.2	< 0.030	< 0.0050	< 0.010	6.0		130	< 0.020
CMC-03P	Oct-94	< 0.050	< 0.20	< 0.0050	0.018		< 0.0001	< 0.0050	< 0.030	< 20	0.1	< 0.050	< 0.0020	< 0.010	< 0.2	< 0.030	< 0.0050	< 0.010	5.4		130	< 0.020
CMC-03P	Nov-94	< 0.050	< 0.0050	< 0.0050	0.021		< 0.0001	< 0.0050	< 0.030	< 20	0.1	< 0.050	< 0.0030	< 0.010	< 0.20	< 0.030	< 0.0050	< 0.010	5.7		180	< 0.020
CMC-03P	Dec-94	< 0.050	< 0.0050	< 0.0050	0.023		< 0.0001	< 0.0050	< 0.030	< 20	0.1	< 0.050	< 0.0020	0.034	< 0.20	< 0.030	< 0.0050	< 0.010	2.3		130	< 0.020
CMC-03RR	May-94	< 0.200	< 0.050	< 0.005	0.027		< 0.001	< 0.005	< 0.030	< 20	< 0.100	< 0.100	< 0.001	0.016	< 0.2	< 0.030	< 0.005	< 0.010	15.0		129	< 0.020
CMC-03RR	Jun-94	< 0.200	< 0.050	< 0.005	0.024		< 0.001	< 0.005	< 0.030	< 20	< 0.100	< 0.100	< 0.001	0.011	< 0.2	< 0.030	< 0.005	< 0.010	11.0		193	< 0.020
CMC-03RR	Jul-94	< 0.200	< 0.050	< 0.005	0.023		< 0.001	< 0.005	< 0.030	< 20	< 0.100	< 0.100	0.002	< 0.010	< 0.2	< 0.030	< 0.005	< 0.010	12.0		125	< 0.020
CMC-03RR	Aug-94	0.206	< 0.050	< 0.005	0.021		< 0.001	< 0.005	< 0.030	< 20	< 0.100	< 0.100	0.001	< 0.010	0.3	< 0.030	< 0.005	< 0.010	11.0		120	< 0.020
CMC-03RR	Sep-94	< 0.050	< 0.20	< 0.0050	0.022		< 0.0001	< 0.005	< 0.030	< 20	< 0.1	0.058	< 0.0020	< 0.010	< 0.2	< 0.030	< 0.0050	< 0.010	14		130	< 0.020
CMC-03RR	Oct-94	< 0.050	< 0.20	< 0.0050	0.020		< 0.0001	< 0.0050	< 0.030	< 20	0.1	< 0.050	< 0.0020	< 0.010	< 0.2	< 0.030	< 0.0050	< 0.010	17		130	< 0.020
CMC-03RR	Nov-94	< 0.050	< 0.0050	< 0.0050	0.020		< 0.0001	< 0.0050	< 0.030	< 20	0.1	< 0.050	< 0.0030	< 0.010	< 0.20	< 0.030	< 0.0050	< 0.010	14		110	< 0.020
CMC-03RR	Dec-94	< 0.050	< 0.0050	< 0.0050	0.021		< 0.0001	< 0.0050	< 0.030	< 20	< 0.1	< 0.050	< 0.0020	< 0.010	< 0.20	< 0.030	< 0.0050	< 0.010	13		110	< 0.020
CMC-04	Jun-94	< 0.200	< 0.050	< 0.005	0.023		< 0.001	< 0.005	< 0.030	< 20	0.110	< 0.100	0.004	0.227	0.2	< 0.030	< 0.005	< 0.010	10.0		205	< 0.020
CMC-04	Jul-94	< 0.200	< 0.050	< 0.005	0.045		< 0.001	< 0.005	< 0.030	< 20	< 0.100	< 0.100	0.003	0.116	< 0.2	< 0.030	< 0.005	< 0.010	8.80		208	< 0.020
CMC-04	Aug-94	< 0.200	< 0.050	< 0.005	0.046		< 0.001	< 0.005	< 0.030	< 20	< 0.100	< 0.100	< 0.001	0.024	< 0.2	< 0.030	< 0.005	< 0.010	10.0		184	< 0.020
CMC-04	Sep-94	< 0.050	< 0.20	< 0.0050	0.048		< 0.0001	< 0.005	< 0.030	< 200	< 0.1	< 0.050	< 0.0020	0.031	< 0.2	< 0.030	< 0.0050	< 0.010	9.7		200	< 0.020
CMC-04	Oct-94	< 0.050	< 0.20	< 0.0050	0.019		< 0.0001	< 0.0050	< 0.030	< 20	0.1	< 0.050	< 0.0020	1.1	0.3	< 0.030	< 0.0050	< 0.010	9.8		240	< 0.020
CMC-04	Nov-94	0.13	0.0068	0.0058	0.11		0.00015	0.13	0.11	< 20	0.1	0.15	< 0.0030	0.14	< 0.20	0.13	< 0.0050	< 0.010	11		280	0.15
CMC-04	Dec-94	< 0.050	< 0.0050	< 0.0050	0.048		0.0002	< 0.0050	< 0.030	< 20	< 0.1	0.064	< 0.0020	0.032	0.7	< 0.030	< 0.0050	< 0.010	8.1		190	< 0.020
CMC-04	Jan-95	< 0.050	0.0064	0.0055	0.044		0.00015	< 0.0050	< 0.030	< 20	< 0.1	< 0.050	< 0.0020	0.040	< 0.20	< 0.030	< 0.0050	< 0.010	6.3		190	< 0.020
CMC-04	Feb-95														< 0.20							
CMC-05	May-94	< 0.200	< 0.050	< 0.005	0.025		< 0.001	< 0.005	< 0.030	< 20	0.156	< 0.100	< 0.001	0.171	< 0.2	< 0.030	< 0.005	< 0.010	18.0		221	< 0.020
CMC-05	Jun-94	0.347	< 0.050	< 0.005	0.042		< 0.001	< 0.005	< 0.030	< 20	0.132	0.292	0.004	0.117	0.3	< 0.030	< 0.005	< 0.010	11.0		203	< 0.020
CMC-05	Jul-94	< 0.200	< 0.050	< 0.005	0.044		< 0.001	< 0.005	< 0.030	< 20	0.106	< 0.100	0.003	0.020	< 0.2	< 0.030	< 0.005	< 0.010	8.40		183	< 0.020
CMC-05	Aug-94	< 0.200	< 0.050	< 0.005	0.040		< 0.001	< 0.005	< 0.030	< 20	0.112	< 0.100	< 0.001	0.012	0.2	< 0.030	< 0.005	< 0.010	10.0		175	< 0.020
CMC-05	Sep-94	< 0.050	< 0.20	< 0.0050	0.040		0.0001	< 0.005	< 0.030	< 20	0.1	0.059	< 0.0020	< 0.010	< 0.2	0.037	< 0.0050	< 0.010	11		200	< 0.020
CMC-05	Oct-94	< 0.050	< 0.20	< 0.0050	0.037		< 0.0001	< 0.0050	< 0.030	< 20	0.1	< 0.050	< 0.0020	< 0.010	< 0.2	< 0.030	< 0.0050	< 0.010	11		240	< 0.020
CMC-05	Nov-94	< 0.050	0.0050	< 0.0050	0.039		< 0.0001	< 0.0050	< 0.030	< 20	0.2	< 0.050	< 0.0030	< 0.010	< 0.20	< 0.030	< 0.0050	< 0.010	10		230	< 0.020
CMC-05	Dec-94	< 0.050	< 0.0050	< 0.0050	0.038		< 0.0001	< 0.0050	< 0.030	< 20	0.1	< 0.050	< 0.0020	< 0.010	< 0.20	< 0.030	< 0.0050	< 0.010	7.7		150	< 0.020

4.2-12-361

Monitoring Well	Date	Aluminum mg/L	Antimony mg/L	Arsenic mg/L	Barium mg/L	Beryllium mg/L (1)	Cadmium mg/L	Chromium mg/L	Copper mg/L	Cyanide ug/L	Fluoride mg/L	Iron mg/L	Lead mg/L	Manganese mg/L	Mercury ug/L	Nickel mg/L	Selenium mg/L	Silver mg/L	Sulfate mg/L	Thallium mg/L (1)	TDS mg/L	Zinc mg/L
CMC-05	Feb-95														< 0.20							
CMC-06P	May-94	< 0.200	< 0.050	< 0.005	0.014		< 0.001	< 0.005	< 0.030	< 20	0.130	< 0.100	< 0.001	0.038	< 0.2	< 0.030	< 0.005	< 0.010	9.00		100	< 0.020
CMC-06P	Jun-94	< 0.200	< 0.050	< 0.005	0.015		< 0.001	< 0.005	< 0.030	< 20	0.121	< 0.100	< 0.001	0.024	< 0.2	< 0.030	< 0.005	< 0.010	8.00		83.0	< 0.020
CMC-06P	Jul-94	< 0.200	< 0.050	< 0.005	0.015		< 0.001	< 0.005	< 0.030	< 20	0.120	< 0.100	0.002	0.015	0.3	< 0.030	< 0.005	< 0.010	9.40		85.0	< 0.020
CMC-06P	Aug-94	0.231	< 0.050	< 0.005	0.012		< 0.001	< 0.005	< 0.030	< 20	0.123	< 0.100	< 0.001	0.014	< 0.2	< 0.030	< 0.005	< 0.010	8.00		83.0	< 0.020
CMC-06P	Sep-94	< 0.050	< 0.20	< 0.0050	0.013		< 0.0001	< 0.005	< 0.030	< 20	0.1	0.11	< 0.0020	0.011	< 0.2	< 0.030	< 0.0050	< 0.010	9.6		100	< 0.020
CMC-06P	Oct-94	< 0.050	< 0.20	< 0.0050	0.012		< 0.0001	< 0.0050	< 0.030	< 20	0.1	< 0.050	< 0.0020	< 0.010	< 0.2	< 0.030	< 0.0050	< 0.010	10		99	< 0.020
CMC-06P	Nov-94	< 0.050	< 0.0050	0.006	0.014		< 0.0001	< 0.0050	< 0.030	< 20	0.2	< 0.050	< 0.0030	0.016	< 0.20	< 0.030	< 0.0050	< 0.010	10		130	< 0.020
CMC-06P	Dec-94	< 0.050	< 0.0050	< 0.0050	0.015		< 0.0001	< 0.0050	< 0.030	< 20	0.1	< 0.050	< 0.0020	0.010	< 0.20	< 0.030	< 0.0050	< 0.010	8.8		81	< 0.020
CMC-07	May-94	< 0.200	< 0.050	< 0.005	0.012		< 0.001	< 0.005	< 0.030	< 20	0.174	< 0.100	< 0.001	0.012	< 0.2	< 0.030	< 0.005	< 0.010	20.0		219	< 0.020
CMC-07	Jun-94	< 0.200	< 0.050	< 0.005	0.041		< 0.001	< 0.005	< 0.030	< 20	0.155	< 0.100	0.002	< 0.010	< 0.2	< 0.030	< 0.005	< 0.010	13.0		185	< 0.020
CMC-07	Jul-94	< 0.200	< 0.050	< 0.005	0.033		< 0.001	< 0.005	< 0.030	< 20	< 0.100	< 0.100	0.002	< 0.010	0.4	< 0.030	< 0.005	< 0.010	11.0		180	< 0.020
CMC-07	Aug-94	< 0.200	< 0.050	< 0.005	0.036		< 0.001	< 0.005	< 0.030	< 20	< 0.100	< 0.100	0.001	< 0.010	< 0.2	< 0.030	< 0.005	< 0.010	13.0		166	< 0.020
CMC-07	Sep-94	< 0.050	< 0.20	< 0.0050	0.030		< 0.0001	< 0.005	< 0.030	< 20	< 0.1	< 0.050	< 0.0020	< 0.010	< 0.2	< 0.030	< 0.0050	< 0.010	13		180	< 0.020
CMC-07	Oct-94	< 0.050	< 0.20	< 0.0050	0.032		< 0.0001	< 0.0050	< 0.030	< 20	0.1	< 0.050	< 0.0020	< 0.010	< 0.2	< 0.030	< 0.0050	< 0.010	14		220	< 0.020
CMC-07	Nov-94	< 0.050	< 0.0050	< 0.0050	0.027		0.00014	< 0.0050	< 0.030	< 20	0.1	< 0.050	< 0.0030	< 0.010	< 0.20	< 0.030	< 0.0050	< 0.010	12		180	0.021
CMC-07	Dec-94	< 0.050	< 0.0050	< 0.0050	0.026		< 0.0001	< 0.0050	< 0.030	< 20	< 0.1	< 0.050	< 0.0020	< 0.010	< 0.20	< 0.030	< 0.0050	< 0.010	11		180	< 0.020
CMC-07	Feb-95														< 0.20							
DMB-1A	Jun-94	< 0.200	< 0.050	< 0.005	0.025		< 0.001	< 0.005	< 0.030	< 20	< 0.100	< 0.100	0.003	< 0.010	< 0.2	< 0.030	< 0.005	< 0.010	9.00		171	< 0.020
DMB-1A	Jul-94	< 0.200	< 0.050	< 0.005	0.021		< 0.001	< 0.005	< 0.030	< 20	< 0.100	< 0.100	0.002	< 0.010	< 0.2	< 0.030	< 0.005	< 0.010	9.70		186	< 0.020
DMB-1A	Aug-94	0.203	< 0.050	< 0.005	0.020		< 0.001	< 0.005	< 0.030	< 20	< 0.100	< 0.100	< 0.001	< 0.010	< 0.2	< 0.030	< 0.005	< 0.010	12.0		167	< 0.020
DMB-1A	Sep-94	< 0.050	< 0.20	< 0.0050	0.019		< 0.0001	< 0.005	< 0.030	< 20	< 0.1	< 0.050	< 0.0020	< 0.010	< 0.2	< 0.030	< 0.0050	< 0.010	12		180	< 0.020
DMB-1A	Oct-94	< 0.050	< 0.20	< 0.0050	0.019		< 0.0001	< 0.0050	< 0.030	< 20	0.1	< 0.050	< 0.0020	< 0.010	< 0.2	< 0.030	< 0.0050	< 0.010	13		200	< 0.020
DMB-1A	Nov-94	< 0.050	< 0.0050	< 0.0050	0.019		< 0.0001	< 0.0050	< 0.030	< 20	0.1	< 0.050	< 0.0030	< 0.010	< 0.20	< 0.030	< 0.0050	< 0.010	12		230	< 0.020
DMB-1A	Dec-94	< 0.050	< 0.0050	< 0.0050	0.020		< 0.0001	< 0.0050	< 0.030	< 20	< 0.1	< 0.050	< 0.0020	< 0.010	< 0.20	< 0.030	< 0.0050	< 0.010	11		240	< 0.020
DMB-1A	Jan-95	< 0.050	< 0.0050	0.086	0.019		< 0.0001	< 0.0050	< 0.030	< 20	< 0.1	< 0.050	< 0.0020	< 0.010	< 0.20	< 0.030	< 0.0050	< 0.010	10		200	< 0.020
DMB-1A	Feb-95														< 0.20							
DMB-6	May-94	< 0.200	< 0.050	< 0.005	0.018		< 0.001	< 0.005	< 0.030	< 20	0.736	< 0.100	0.001	< 0.010	< 0.2	< 0.030	< 0.005	< 0.010	16.0		200	< 0.020
DMB-6	Jun-94	< 0.200	< 0.050	< 0.005	0.026		< 0.001	< 0.005	< 0.030	< 20	< 0.100	< 0.100	0.003	0.072	0.3	< 0.030	< 0.005	< 0.010	14.0		175	< 0.020
DMB-6	Jul-94	< 0.200	< 0.050	< 0.005	0.025		< 0.001	< 0.005	< 0.030	< 20	< 0.100	< 0.100	0.002	< 0.010	< 0.2	< 0.030	< 0.005	< 0.010	16.0		178	< 0.020
DMB-6	Aug-94	< 0.200	< 0.050	< 0.005	0.023		< 0.001	< 0.005	< 0.030	< 20	< 0.100	< 0.100	< 0.001	< 0.010	0.3	< 0.030	< 0.005	< 0.010	19.0		167	< 0.020
DMB-6	Sep-94	< 0.050	< 0.20	< 0.0050	0.023		0.0010	< 0.005	< 0.030	< 20	< 0.1	< 0.050	< 0.0020	< 0.010	< 0.2	< 0.030	< 0.0050	< 0.010	18		190	< 0.020
DMB-6	Oct-94	< 0.050	< 0.20	< 0.0050	0.022		0.00033	< 0.0050	< 0.030	< 20	0.1	< 0.050	< 0.0020	< 0.010	< 0.2	< 0.030	< 0.0050	< 0.010	22		200	< 0.020
DMB-6	Nov-94	< 0.050	< 0.0050	< 0.0050	0.024		0.00021	< 0.0050	< 0.030	< 20	0.1	< 0.050	< 0.0030	< 0.010	< 0.20	< 0.030	< 0.0050	< 0.010	21		250	< 0.020
DMB-6	Dec-94	< 0.050	< 0.0050	0.0051	0.023		0.00013	< 0.0050	< 0.030	< 20	0.1	< 0.050	< 0.0020	< 0.010	< 0.20	< 0.030	< 0.0050	< 0.010	15		160	< 0.020
EX-13BU	May-94	< 0.200	< 0.050	< 0.005	0.012		< 0.001	< 0.005	< 0.030	< 20	< 0.100	< 0.100	< 0.001	< 0.010	0.2	< 0.030	< 0.005	< 0.010	4.00		141	< 0.020
EX-13BU	Jun-94	< 0.200	< 0.050	< 0.005	0.032		< 0.001	< 0.005	< 0.030	< 20	< 0.100	0.143	0.002	< 0.010	< 0.2	< 0.030	< 0.005	< 0.010	< 2.00		138	< 0.020
EX-13BU	Jul-94	< 0.200	< 0.050	< 0.005	0.014		< 0.001	< 0.005	< 0.030	< 20	< 0.100	< 0.100	0.013	< 0.010	< 0.2	< 0.030	< 0.005	< 0.010	3.80		143	< 0.020
EX-13BU	Aug-94	0.226	< 0.050	< 0.005	0.011		< 0.001	< 0.005	< 0.030	< 20	< 0.100	< 0.100	0.001	< 0.010	< 0.2	< 0.030	< 0.005	< 0.010	6.00		127	< 0.020
EX-13BU	Sep-94	< 0.050	< 0.20	< 0.0050	0.012		< 0.0001	< 0.005	< 0.030	< 20	0.1	0.21	< 0.0020	< 0.010	< 0.2	< 0.030	< 0.0050	< 0.010	7.3		140	< 0.020
EX-13BU	Oct-94	< 0.050	< 0.20	< 0.0050	0.012		< 0.0001	< 0.0050	< 0.030	< 20	0.1	< 0.050	< 0.0020	< 0.010	< 0.2	< 0.030	< 0.0050	< 0.010	7.1		160	< 0.020
EX-13BU	Nov-94	< 0.050	< 0.0050	< 0.0050	0.012		0.00018	< 0.0050	< 0.030	< 20	0.1	< 0.050	< 0.0030	< 0.010	< 0.20	< 0.030	< 0.0050	< 0.010	7.7		160	< 0.020
EX-13BU	Dec-94	< 0.050	< 0.0050	< 0.0050	0.014		< 0.0001	< 0.0050	< 0.030	< 20	< 0.1	< 0.050	< 0.0020	< 0.010	< 0.20	< 0.030	< 0.0050	< 0.010	6.3		180	< 0.020
EX-9BL	May-94	< 0.200	0.052	< 0.005	0.019		< 0.001	< 0.005	< 0.030	< 20	< 0.100	< 0.100	< 0.001	< 0.010	< 0.2	< 0.030	< 0.005	< 0.010	10.0		139	< 0.020
EX-9BL	Jun-94	< 0.200	< 0.050	< 0.005	0.021		< 0.001	< 0.005	< 0.030	< 20	< 0.100	< 0.100	< 0.001	< 0.010	< 0.2	< 0.030	< 0.005	< 0.010	8.00		126	< 0.020
EX-9BL	Jul-94	< 0.200	< 0.050	< 0.005	0.023		< 0.001	< 0.005	< 0.030	< 20	< 0.100	< 0.100	0.001	< 0.010	1	< 0.030	< 0.005	< 0.010	9.20		141	< 0.020
EX-9BL	Aug-94	< 0.200	< 0.050	< 0.005	0.018		< 0.001	< 0.005	< 0.030	< 20	< 0.100	< 0.100	< 0.001	< 0.010	< 0.2	< 0.030	< 0.005	< 0.010	10.0		142	< 0.020
EX-9BL	Sep-94	< 0.050	< 0.20	< 0.0050	0.019		< 0.0001	< 0.005	< 0.030	< 20	< 0.1	< 0.050	< 0.0020	< 0.010	< 0.2	< 0.030	< 0.0050	< 0.010	14		130	< 0.020
EX-9BL	Oct-94	< 0.050	< 0.20	< 0.0050	0.019		< 0.0001	< 0.0050	< 0.030	< 20	0.1	< 0.050	< 0.0020	< 0.010	< 0.2	< 0.030	< 0.0050	< 0.010	13		170	< 0.020
EX-9BL	Nov-94	< 0.050	< 0.0050	< 0.0050	0.020		< 0.0001	< 0.0050	< 0.030	< 20	0.1	< 0.050	< 0.0030	< 0.010	< 0.20	< 0.030	< 0.0050	< 0.010	12		170	< 0.020
EX-9BL	Dec-94	< 0.050	< 0.0050	< 0.0050	0.020		< 0.0001	< 0.0050	< 0.030	< 20	< 0.1	< 0.050	< 0.0020	< 0.010	< 0.20	< 0.030	< 0.0050	< 0.010	11		150	< 0.020
EX-9BU	May-94	< 0.200	< 0.050	< 0.005	0.011		< 0.001	< 0.005	< 0.030	< 20	< 0.100	< 0.100	< 0.001	< 0.010	0.2	< 0.030	< 0.005	< 0.010	12.0		129	< 0.020
EX-9BU	Jun-94	< 0.200	< 0.050	< 0.005	0.014		< 0.001	< 0.005	< 0.030	< 20	< 0.100	< 0.100	0.001	< 0.010	< 0.2	< 0.030	< 0.005	< 0.010	10.0		115	< 0.020
EX-9BU	Jul-94	< 0.200	< 0.050	< 0.005	0.011		< 0.001	< 0.005	< 0.030	< 20	< 0.100	< 0.100	0.003	< 0.010	0.3	< 0.030	< 0.005	< 0.010	11.0		128	< 0.020
EX-9BU	Aug-94	< 0.200	< 0.050	< 0.005	0.012			< 0.005	< 0.030	< 20	< 0.100	< 0.100	< 0.001	< 0.010	< 0.2	< 0.030	< 0.005	< 0.010	12.0		134	< 0.020
EX-9BU	Sep-94	< 0.050	< 0.20	< 0.0050	0.011		< 0.0001	< 0.005	< 0.030	< 20	< 0.1	< 0.050	< 0.0020	< 0.010	< 0.2	< 0.030	< 0.0050	< 0.010	17		140	< 0.020
EX-9BU	Oct-94	< 0.050	< 0.20	< 0.0050	0.010		< 0.0001	< 0.0050	< 0.030	< 20	0.1	< 0.050	< 0.0020	< 0.010	< 0.2	< 0.030	< 0.0050	< 0.010	15		160	< 0.020
EX-9BU	Nov-94	< 0.050	< 0.0050	< 0.0050	0.012		< 0.0001	< 0.0050	< 0.030	< 20	0.1	< 0.050	< 0.0030	< 0.010	< 0.20	< 0.030	< 0.0050	< 0.010	13		150	< 0.020
EX-9BU	Dec-94	< 0.050	< 0.0050	< 0.0050	0.012		< 0.0001	< 0.0050	< 0.030	< 20	< 0.1	< 0.050	< 0.0020	< 0.010	< 0.20	< 0.030	< 0.0050	< 0.010	12		130	< 0.020
G41-H18B	Jun-94	< 0.200	< 0.050	< 0.005	0.023		< 0.001	< 0.005	< 0.030	< 20	< 0.100	< 0.100	0.003	1.08	< 0.2	< 0.030	< 0.005	< 0.010	4.00		150	< 0.020
G41-H18B	Jul-94	< 0.200	< 0.050	< 0.005	0.021		< 0.001	< 0.005	< 0.030	< 20	< 0.100	< 0.100	0.003	0.918	1	< 0.030	< 0.005	< 0.010	5.10		161	< 0.020
G41-H18B	Aug-94	< 0.200	< 0.050	< 0.005	0.019		< 0.001	< 0.005	< 0.030	< 20	< 0.100	< 0.100	0.001	0.890	< 0.2	< 0.030	< 0.005	< 0.010	10.0		131	< 0.020
G41-H18B	Sep-94	< 0.050	< 0.20	< 0.0050	0.020		< 0.0001	< 0.005	< 0.030	< 200	< 0.1	0.63	< 0.0020	1.1	< 0.2	< 0.030	< 0.0050	< 0.010	7.7		160	< 0.020
G41-H18B	Oct-94	< 0.050	< 0.20	< 0.0050	0.049		< 0.0001	< 0.0050	< 0.030	< 20	0.1	< 0.050	< 0.0020	0.031	< 0.2	< 0.030	< 0.0050	< 0.010	9.3		170	< 0.020
G41-H18B	Nov-94	< 0.050	< 0.0050	< 0.0050	0.019		< 0.0001	< 0.0050	< 0.030	< 20	0.1	< 0.050	< 0.0030	1.5	< 0.20	< 0.030	< 0.0050	< 0.010	8.8		110	0.024

Updated June 4, 1999

Tailings Management Area
Groundwater Quality Statistical Analysis

Monitoring Well Date	Aluminum mg/L	Antimony mg/L	Arsenic mg/L	Barium mg/L	Beryllium mg/L (1)	Cadmium mg/L	Chromium mg/L	Copper mg/L	Cyanide ug/L	Fluoride mg/L	Iron mg/L	Lead mg/L	Manganese mg/L	Mercury ug/L	Nickel mg/L	Selenium mg/L	Silver mg/L	Sulfate mg/L	Thallium mg/L (1)	TDS mg/L	Zinc mg/L
G41-H18BDec-94	< 0.050	< 0.0050	< 0.0050	0.020		< 0.0001	< 0.0050	< 0.030	< 20	< 0.1	0.092	< 0.0020	1.9	< 0.20	< 0.030	< 0.0050	< 0.010	6.0		180	< 0.020
G41-H18BJan-95	< 0.050	< 0.0050	< 0.0050	0.021		< 0.0001	< 0.0050	< 0.030	< 20	< 0.1	< 0.050	< 0.0020	1.5	< 0.20	< 0.030	< 0.0050	< 0.010	4.4		130	< 0.020
# Samples	128	128	128	128	-	127	128	128	128	128	128	128	128	132	128	128	128	128	-	128	128
% Detections	6.3%	3.1%	6.3%	99.2%	-	13.4%	0.8%	0.8%	0.0%	56.3%	7.8%	23.4%	43.8%	18.2%	1.6%	0.0%	0.0%	98.4%	-	100%	3.1%
Minimum	< 0.05	< 0.005	< 0.005	< 0.01	-	< 0.0001	< 0.005	< 0.03	< 20	< 0.1	< 0.05	< 0.001	< 0.01	< 0.2	< 0.03	< 0.005	< 0.010	< 2	-	81	< 0.02
Maximum	0.347	0.052	0.086	0.11	-	0.001	0.13	0.11	< 200	0.736	0.63	0.017	1.9	1	0.13	< 0.005	< 0.010	70	-	339	0.15
Average (2)	0.067	0.036	0.004	0.023		0.000	0.0035	0.016	11.4	0.098	0.048	0.001	0.099	0.152	0.016	0.003	0.005	11.948		162.34	0.011
St. Dev.(2)	0.0574	0.0375	0.0103	0.013		0.0002	0.0113	0.0084	11.2	0.0752	0.0617	0.0019	0.3121	0.1536	0.0103			7.1161		40.779	0.012485
NR 140 Min. Inc.																				200	
NR 140 PAL	-	0.0012	0.005	0.4	0.0004	0.0005	0.01	0.13	40	0.8	0.15	0.0015	0.025	0.0002	0.02	0.01	0.01	125	0.0004		2.5
# PAL Exceedances	-	4	8	0		3	1	0	0	0	4	22	33	24	2	0	0	0		128	0
NR 140 ES	-	0.006	0.05	2	0.004	0.005	0.1	1.3	200	4	0.3	0.015	0.05	0.002	0.1	0.05	0.05	250	0.002		5
# ES Exceedances	-	3	2	0		0	1	0	0	0	1	1	18	24	1	0	0	0		128	0
PAL (3)																				362.34	
ACL (3)	-	0.1113	0.0246	-	-	0.0007	0.026	-	-	-	0.1713	0.0052	0.7232	0.4594	0.0367	-	-	-	-		-
Upper 95% Confidence Limit On Mean (4)	< 0.200 Non-Parametric	< 0.050 Non-Parametric	< 0.005 Non-Parametric	0.025 Normal	-	< 0.001 Non-Parametric	< 0.005 Non-Parametric	< 0.030 Non-Parametric	< 20 Non-Parametric	0.098 Normal (Cohen's Adjustment)	< 0.100 Non-Parametric	< 0.0020 Non-Parametric	0.011 Non-Parametric	< 0.2 Non-Parametric	< 0.030 Non-Parametric	< 0.005 Non-Parametric	< 0.010 Non-Parametric	13 Normal	-	168 Normal	< 0.020 Non-Parametric

(1) No baseline data exists for beryllium or thallium.

(2) All non-detected values replaced with one-half the detection limit as per the May 6, 1994 WDNR guidance document "PAL/ACL Calculations Guidance For Solid Waste Facilities"

(3) Calculated as per the May 6, 1994 WDNR guidance document "PAL/ACL Calculations Guidance For Solid Waste Facilities"

(4) If at least 85% values were above detection limit, average was calculated replacing non-detects with one-half the detection limit. If between 50% and 85% of the values were detected, the average was calculated using Cohen's adjustment. If less than 50% of the values were detected, the median is given rather than the average.

4.2-12-363

Attachment 3

Reflooded Mine Baseline Results and ACL Calculations

Crandon Mining Company
Baseline Monitoring
Reflooded Mine

Monitoring Well	Date	Aluminum mg/L	Antimony mg/L	Arsenic mg/L	Barium mg/L	Beryllium mg/L (1)	Cadmium mg/L	Chromium mg/L	Copper mg/L	Cyanide ug/L	Fluoride mg/L	Iron mg/L	Lead mg/L	Manganese mg/L	Mercury ug/L	Nickel mg/L	Selenium mg/L	Silver mg/L	Sulfate mg/L	Thallium mg/L (1)
CMC-08	May-94	< 0.200	< 0.050	< 0.005	0.050	-	< 0.001	< 0.005	< 0.030	< 20	0.121	< 0.100	< 0.001	< 0.010	0.4	< 0.030	< 0.005	< 0.010	34.0	-
CMC-08	Jun-94	< 0.200	< 0.050	< 0.005	0.076	-	< 0.001	< 0.005	< 0.030	< 20	0.136	< 0.100	0.002	0.054	0.3	< 0.030	< 0.005	< 0.010	28.0	-
CMC-08	Jul-94	< 0.200	< 0.050	< 0.005	0.079	-	< 0.001	< 0.005	< 0.030	< 20	0.123	< 0.100	0.006	0.011	0.2	< 0.030	< 0.005	< 0.010	28.0	-
CMC-08	Aug-94	0.249	< 0.050	< 0.005	0.065	-	< 0.001	< 0.005	< 0.030	< 20	0.120	< 0.100	< 0.001	< 0.010	< 0.2	< 0.030	< 0.005	< 0.010	38.0	-
CMC-08	Sep-94	< 0.050	< 0.20	< 0.0050	0.068	-	0.0005	< 0.005	< 0.030	< 20	0.1	< 0.050	< 0.0020	< 0.010	< 0.2	< 0.030	< 0.0050	< 0.010	30	-
CMC-08	Oct-94	< 0.050	< 0.20	< 0.0050	0.065	-	0.00010	< 0.0050	< 0.030	< 20	0.1	< 0.050	< 0.0020	< 0.010	< 0.2	< 0.030	< 0.0050	< 0.010	35	-
CMC-08	Dec-94	< 0.050	< 0.0050	< 0.0050	0.066	-	0.00010	< 0.0050	< 0.030	< 20	0.1	< 0.050	< 0.0020	< 0.010	< 0.20	< 0.030	< 0.0050	< 0.010	30	-
CMC-08	Jan-95	< 0.050	< 0.0050	< 0.0050	0.074	-	< 0.0001	0.014	< 0.030	< 20	0.1	< 0.050	< 0.0020	< 0.010	< 0.20	< 0.030	< 0.0050	0.016	31	-
CMC-08P	May-94	< 0.200	< 0.050	< 0.005	0.030	-	< 0.001	< 0.005	< 0.030	< 20	0.134	< 0.100	< 0.001	0.043	0.3	< 0.030	< 0.005	< 0.010	53.0	-
CMC-08P	Jun-94	< 0.200	< 0.050	< 0.005	0.065	-	< 0.001	< 0.005	< 0.030	< 20	0.156	< 0.100	0.005	0.046	0.7	< 0.030	< 0.005	< 0.010	48.0	-
CMC-08P	Jul-94	< 0.200	< 0.050	< 0.005	0.081	-	< 0.001	< 0.005	< 0.030	< 20	0.139	< 0.100	0.002	0.030	0.4	< 0.030	< 0.005	< 0.010	43.0	-
CMC-08P	Aug-94	< 0.200	< 0.050	< 0.005	0.071	-	< 0.001	< 0.005	< 0.030	< 20	0.144	< 0.100	< 0.001	< 0.010	< 0.2	< 0.030	< 0.005	< 0.010	43.0	-
CMC-08P	Sep-94	< 0.050	< 0.20	< 0.0050	0.080	-	0.0002	< 0.005	< 0.030	< 20	0.2	0.11	< 0.0020	0.011	< 0.2	< 0.030	< 0.005	< 0.010	43.0	-
CMC-08P	Oct-94	< 0.050	< 0.20	< 0.0050	0.077	-	0.00038	< 0.0050	< 0.030	< 20	0.1	< 0.050	< 0.0020	< 0.010	< 0.2	< 0.030	< 0.0050	< 0.010	35	-
CMC-08P	Dec-94	< 0.050	< 0.0050	< 0.0050	0.076	-	0.00042	< 0.0050	< 0.030	< 20	0.1	< 0.050	< 0.0020	< 0.010	< 0.2	< 0.030	< 0.0050	< 0.010	41	-
CMC-08P	Jan-95	< 0.050	< 0.0050	< 0.0050	0.077	-	0.00038	< 0.0050	< 0.030	< 20	0.1	< 0.050	< 0.0020	< 0.010	< 0.20	< 0.030	< 0.0050	< 0.010	30	-
CMC-09	May-94	< 0.200	< 0.050	< 0.005	0.037	-	< 0.001	< 0.005	< 0.030	< 20	< 0.100	< 0.100	< 0.001	0.015	0.6	< 0.030	< 0.005	< 0.010	31	-
CMC-09	Jun-94	< 0.200	< 0.050	< 0.005	0.038	-	< 0.001	< 0.005	< 0.030	< 20	< 0.100	0.120	< 0.001	0.011	0.3	< 0.030	< 0.005	< 0.010	11.0	-
CMC-09	Jul-94	< 0.200	< 0.050	< 0.005	0.031	-	< 0.001	< 0.005	< 0.030	< 20	< 0.100	< 0.100	0.002	< 0.010	0.5	< 0.030	< 0.005	< 0.010	9.00	-
CMC-09	Aug-94	< 0.200	< 0.050	< 0.005	0.026	-	< 0.001	< 0.005	< 0.030	< 20	< 0.100	< 0.100	0.001	< 0.010	< 0.2	< 0.030	< 0.005	< 0.010	10.0	-
CMC-09	Sep-94	< 0.050	< 0.20	< 0.0050	0.033	-	< 0.0001	< 0.005	< 0.030	< 20	< 0.1	< 0.050	< 0.0020	< 0.010	< 0.2	< 0.030	< 0.005	< 0.010	13.0	-
CMC-09	Oct-94	< 0.050	< 0.20	< 0.0050	0.032	-	< 0.0001	< 0.0050	< 0.030	< 20	0.1	< 0.050	< 0.0020	< 0.010	< 0.2	< 0.030	< 0.0050	< 0.010	13	-
CMC-09	Dec-94	< 0.050	< 0.0050	0.0050	0.026	-	< 0.0001	< 0.0050	< 0.030	< 20	1.0	< 0.050	< 0.0020	< 0.010	< 0.2	< 0.030	< 0.0050	< 0.010	16	-
CMC-09	Jan-95	< 0.050	< 0.0050	< 0.0050	0.025	-	< 0.0001	< 0.0050	< 0.030	< 20	< 0.1	< 0.050	< 0.0020	< 0.010	< 0.20	< 0.030	< 0.0050	0.032	12	-
CMC-09P	Jun-94	< 0.200	< 0.050	< 0.005	0.028	-	< 0.001	< 0.005	< 0.030	< 20	0.302	< 0.100	< 0.001	0.294	0.2	< 0.030	< 0.005	< 0.010	51.0	-
CMC-09P	Jul-94	< 0.200	< 0.050	< 0.005	0.028	-	< 0.001	< 0.005	< 0.030	< 20	0.290	< 0.100	0.003	0.261	0.3	< 0.030	< 0.005	< 0.010	38.0	-
CMC-09P	Aug-94	0.218	< 0.050	< 0.005	0.027	-	< 0.001	< 0.005	< 0.030	< 20	0.257	0.100	< 0.001	0.256	< 0.2	< 0.030	< 0.005	< 0.010	31.0	-
CMC-09P	Sep-94	0.083	< 0.20	< 0.0050	0.031	-	< 0.0001	< 0.005	< 0.030	< 20	0.3	0.32	< 0.0020	0.24	< 0.2	< 0.030	< 0.0050	< 0.010	25	-
CMC-09P	Oct-94	< 0.050	< 0.20	< 0.0050	0.031	-	< 0.0001	< 0.0050	< 0.030	< 20	0.2	0.21	< 0.0020	0.22	< 0.2	< 0.030	< 0.0050	< 0.010	28	-
CMC-09P	Dec-94	< 0.050	< 0.0050	0.0053	0.030	-	0.00030	< 0.0050	< 0.030	< 20	0.3	0.38	< 0.0020	0.22	< 0.20	< 0.030	< 0.0050	< 0.010	18	-
CMC-09P	Jan-95	< 0.050	< 0.0050	< 0.0050	0.029	-	0.00027	< 0.0050	< 0.030	< 20	0.2	< 0.050	< 0.0020	0.22	< 0.20	< 0.030	< 0.0050	< 0.010	17	-
CMC-09P	Feb-95	< 0.050	< 0.005	0.0062	0.027	-	0.0015	< 0.0050	< 0.030	< 20	0.2	< 0.050	< 0.0020	0.18	< 0.20	0.016	< 0.0050	< 0.010	12	-
CMC-10	May-94	< 0.200	< 0.050	< 0.005	0.039	-	< 0.001	< 0.005	< 0.030	< 20	< 0.100	< 0.100	< 0.001	< 0.010	0.4	< 0.030	< 0.005	< 0.010	200	-
CMC-10	Jun-94	< 0.200	< 0.050	< 0.005	0.034	-	< 0.001	< 0.005	< 0.030	< 20	< 0.100	< 0.100	< 0.001	< 0.010	0.4	< 0.030	< 0.005	< 0.010	93.0	-
CMC-10	Jul-94	< 0.200	< 0.050	< 0.005	0.026	-	< 0.001	< 0.005	< 0.030	< 20	< 0.100	< 0.100	0.001	< 0.010	< 0.2	< 0.030	< 0.005	< 0.010	170	-
CMC-10	Aug-94	0.236	< 0.050	< 0.005	0.023	-	< 0.001	< 0.005	< 0.030	< 20	< 0.100	< 0.100	< 0.001	< 0.010	< 0.2	< 0.030	< 0.005	< 0.010	160	-
CMC-10	Sep-94	< 0.050	< 0.20	< 0.0050	0.021	-	< 0.0001	< 0.005	< 0.030	< 20	< 0.1	0.14	< 0.0020	< 0.010	< 0.2	< 0.030	< 0.0050	< 0.010	120	-
CMC-10	Oct-94	< 0.050	< 0.20	< 0.0050	0.018	-	< 0.0001	< 0.0050	< 0.030	< 20	0.1	< 0.050	< 0.0020	< 0.010	< 0.2	< 0.030	< 0.0050	< 0.010	150	-
CMC-10	Dec-94	< 0.050	< 0.0050	< 0.0050	0.023	-	< 0.0001	< 0.0050	< 0.030	< 20	< 0.1	< 0.050	< 0.0020	< 0.010	< 0.20	< 0.030	< 0.0050	< 0.010	160	-
CMC-10	Jan-95	< 0.050	< 0.0050	< 0.0050	0.022	-	< 0.0001	< 0.0050	< 0.030	< 20	< 0.1	< 0.050	< 0.0020	< 0.010	< 0.20	< 0.030	< 0.0050	< 0.010	200	-
CMC-10P	May-94	< 0.200	< 0.050	< 0.005	0.032	-	< 0.001	< 0.005	< 0.030	< 20	< 0.100	< 0.100	< 0.001	0.182	< 0.2	< 0.030	< 0.005	< 0.010	8.00	-
CMC-10P	Jun-94	< 0.200	< 0.050	< 0.005	0.032	-	< 0.001	< 0.005	< 0.030	< 20	0.105	< 0.100	< 0.001	0.189	0.4	< 0.030	< 0.005	< 0.010	7.00	-
CMC-10P	Jul-94	< 0.200	< 0.050	< 0.005	0.030	-	< 0.001	< 0.005	< 0.030	< 20	0.102	< 0.100	0.003	0.172	0.4	< 0.030	< 0.005	< 0.010	5.40	-
CMC-10P	Aug-94	0.258	< 0.050	< 0.005	0.030	-	< 0.001	< 0.005	< 0.030	< 20	0.109	< 0.100	< 0.001	0.189	< 0.2	< 0.030	< 0.005	< 0.010	10.0	-
CMC-10P	Sep-94	< 0.050	< 0.20	< 0.0050	0.030	-	0.0003	< 0.005	< 0.030	< 20	0.1	< 0.050	< 0.0020	0.19	< 0.2	< 0.030	< 0.0050	< 0.010	11	-
CMC-10P	Oct-94	< 0.050	< 0.20	< 0.0050	0.027	-	< 0.0010	< 0.0050	< 0.030	< 20	0.1	< 0.050	< 0.0020	0.17	< 0.2	< 0.030	< 0.0050	< 0.010	9.7	-
CMC-10P	Dec-94	< 0.050	< 0.0050	< 0.0050	0.032	-	< 0.0001	< 0.0050	< 0.030	< 20	< 0.1	< 0.050	< 0.0020	0.48	< 0.20	< 0.030	< 0.0050	< 0.010	6.6	-
CMC-10P	Jan-95	< 0.050	< 0.0050	< 0.0050	0.031	-	< 0.0001	< 0.0050	< 0.030	< 20	0.1	< 0.050	< 0.0020	0.40	< 0.20	< 0.030	< 0.0050	< 0.010	6.4	-

4.2-12-365

Crandon Mining Company
Baseline Monitoring
Reflooded Mine

Monitoring Well	Date	TDS mg/L	Zinc mg/L
CMC-08	May-94	342	< 0.020
CMC-08	Jun-94	318	< 0.020
CMC-08	Jul-94	316	< 0.020
CMC-08	Aug-94	294	< 0.020
CMC-08	Sep-94	390	< 0.020
CMC-08	Oct-94	390	< 0.020
CMC-08	Dec-94	410	< 0.020
CMC-08	Jan-95	380	0.038
CMC-08P	May-94	332	< 0.020
CMC-08P	Jun-94	335	< 0.020
CMC-08P	Jul-94	334	< 0.020
CMC-08P	Aug-94	316	< 0.020
CMC-08P	Sep-94	370	< 0.020
CMC-08P	Oct-94	400	< 0.020
CMC-08P	Dec-94	390	< 0.020
CMC-08P	Jan-95	420	< 0.020
CMC-09	May-94	218	< 0.020
CMC-09	Jun-94	211	< 0.020
CMC-09	Jul-94	208	< 0.020
CMC-09	Aug-94	212	< 0.020
CMC-09	Sep-94	240	< 0.020
CMC-09	Oct-94	270	< 0.020
CMC-09	Dec-94	260	0.023
CMC-09	Jan-95	230	< 0.020
CMC-09P	Jun-94	282	< 0.020
CMC-09P	Jul-94	277	< 0.020
CMC-09P	Aug-94	211	< 0.020
CMC-09P	Sep-94	220	0.032
CMC-09P	Oct-94	250	0.025
CMC-09P	Dec-94	230	0.021
CMC-09P	Jan-95	220	0.021
CMC-09P	Feb-95	240	0.025
CMC-10	May-94	544	< 0.020
CMC-10	Jun-94	504	< 0.020
CMC-10	Jul-94	467	< 0.020
CMC-10	Aug-94	411	< 0.020
CMC-10	Sep-94	410	< 0.020
CMC-10	Oct-94	520	< 0.020
CMC-10	Dec-94	520	< 0.020
CMC-10	Jan-95	450	< 0.020
CMC-10P	May-94	181	< 0.020
CMC-10P	Jun-94	176	< 0.020
CMC-10P	Jul-94	164	< 0.020
CMC-10P	Aug-94	169	< 0.020
CMC-10P	Sep-94	180	< 0.020
CMC-10P	Oct-94	220	< 0.020
CMC-10P	Dec-94	170	< 0.020
CMC-10P	Jan-95	200	0.031

Crandon Mining Company
Baseline Monitoring
Reflooded Mine

Monitoring Well Date	Aluminum mg/L	Antimony mg/L	Arsenic mg/L	Barium mg/L	Beryllium mg/L (1)	Cadmium mg/L	Chromium mg/L	Copper mg/L	Cyanide ug/L	Fluoride mg/L	Iron mg/L	Lead mg/L	Manganese mg/L	Mercury ug/L	Nickel mg/L	Selenium mg/L	Silver mg/L	Sulfate mg/L	Thallium mg/L (1)
# Samples	48	48	48	48	-	48	48	48	48	48	48	48	48	48	48	48	48	48	-
% Detections	10.4%	0.0%	6.3%	100.0%	-	22.9%	2.1%	0.0%	0.0%	68.8%	14.6%	18.8%	52.1%	31.3%	2.1%	0.0%	4.2%	100.0%	-
Minimum	< 0.05	< 0.005	< 0.005	0.018	-	< 0.0001	< 0.005	< 0.03	< 20	< 0.1	< 0.05	< 0.001	< 0.01	< 0.2	< 0.03	< 0.005	< 0.01	5.4	-
Maximum	0.258	< 0.2	0.0062	0.081	-	0.0015	0.014	< 0.03	< 20	1	0.38	0.006	0.48	0.7	0.016	< 0.005	0.032	200	-
Average (2)	0.074	0.038	0.003	0.042	-	0.000	0.003	0.015	10.000	0.137	0.061	0.001	0.088	0.190	0.015	0.003	0.006	46.065	-
St. Dev.(2)	0.06223	0.03758	0.00075	0.02068	-	0.00026	0.00166	7.4E-12	0	0.14681	0.07043	0.00107	0.12038	0.15332	0.00014	1.5E-12	0.00418	53.48	-
NR 140 PAL	-	0.0012	0.005	0.4	-	0.0005	0.01	0.13	40	0.8	0.15	0.0015	0.025	0.2	0.02	0.01	0.01	125	-
# PAL Exceedances	-	0	3	0	-	2	1	0	0	1	3	7	21	15	0	0	2	6	-
NR 140 ES	-	0.006	0.05	2	-	0.005	0.1	1.3	200	4	0.3	0.015	0.05	2	0.1	0.05	0.05	250	-
# ES Exceedances	-	0	0	0	-	0	0	0	0	0	2	0	17	0	0	0	0	0	-
Min. Increase	-	-	-	-	-	-	-	-	-	-	-	-	-	-	-	-	-	-	-
Calculated PAL (3)	-	-	-	-	-	-	-	-	-	-	-	-	-	-	-	-	-	-	-
ACL (3)	-	0.11283	0.00418	-	-	0.00088	-	-	-	-	0.2019	0.00333	0.32906	0.49622	-	-	0.01415	153.025	-
Upper 95% C.L. On Mean (4)	< 0.2 Non-Parametric	< 0.05 Non-Parametric	< 0.005 Non-Parametric	0.047 Normal	-	< 0.001 Non-Parametric	< 0.005 Non-Parametric	< 0.03 Non-Parametric	< 20 Non-Parametric	0.16581 Normal (Cohen's)	< 0.1 Non-Parametric	< 0.002 Non-Parametric	0.1 Normal (Cohen's)	< 0.2 Non-Parametric	< 0.03 Non-Parametric	< 0.005 Non-Parametric	< 0.01 Non-Parametric	58.8 Normal	-

(1) No baseline data exists for beryllium or thallium.

(2) All non-detected values replaced with one-half the detection limit as per the May 6, 1994 WDNR guidance document "PAL/ACL Calculations Guidance For Solid Waste Facilities"

(3) Calculated as per the May 6, 1994 WDNR guidance document "PAL/ACL Calculations Guidance For Solid Waste Facilities"

(4) If at least 85% values were above detection limit, average was calculated replacing non-detects with one-half the detection limit. If less than 50% of values were detected, the median is given
If at least 50% values were above detection limit, average was calculated using Cohen's adjustment
If less than 50% of values were detected, the median is given rather than the average.

Crandon Mining Company
Baseline Monitoring
Reflooded Mine

Monitoring Well Date	TDS mg/L		Zinc mg/L
# Samples	48		48
% Detections	100.0%		16.7%
Minimum	164	<	0.02
Maximum	544		0.038
Average (2)	308.375		0.013
St. Dev.(2)	106.677		0.00681779
NR 140 PAL	-		2.5
# PAL Exceedances	-		0
NR 140 ES	-		5
# ES Exceedances	-		0
Min. Increase	200		-
Calculated			
PAL (3)	628.405		-
ACL (3)	-		-
Upper 95% C.L.	333.7	<	0.02
On Mean (4)	Normal		Non-Parametric

Appendix 4.2-13

Reflooded Mine Source Term
Crandon Mine

Note: In March 1997 NMC submitted the above titled report to the WDNR and USCOE for review. The WDNR issued a letter dated January 13, 1998, to NMC containing comments on the report. To respond to those comments, SRK issued a letter to Foth & Van Dyke dated April 23, 1998. This letter immediately follows this title page. As part of SRK's response, Chapters 2, 6, 7, and 8 of the report were updated. These updated chapters have been incorporated into the report, which follows the April 23, 1998, letter.

STEFFEN, ROBERTSON AND KIRSTEN (CANADA) INC.
Consulting Engineers and Scientists

Suite 800
580 Hornby Street
Vancouver, B.C.
Canada
V6C 3B6

Tel: (604) 681-4196
Fax: (604) 687-5532

April 23, 1998
Project Number F107107

Foth & Van Dyke
2737 S. Ridge Road, 54304
P.O. Box 19012
Green Bay, WI 54307-9012

Attention: Gerald W. Sevick, P.E.

Dear Mr. Sevick:

RE: COMMENTS ON THE REFLOODED MINE SOURCE TERM FOR THE PROPOSED CRANDON MINE

Per your request, Steffen Robertson and Kirsten (Canada) Inc. (SRK) has prepared a response to the January 13, 1998, Wisconsin Department of Natural Resources letter commenting on the March 1997 report titled *Reflooded Mine Source Term - Crandon Mine, Final Report*. Our response consists of updates to Chapters 2, 6, 7, and 8 of the March 1997 report and the series of remarks below.

Comments 1-8 Regarding Tailings Backfill

SRK has updated Chapter 2 of the underground source term report. The derivation of the contaminant concentrations associated with the backfilled tailings has been changed to provide consistency with results from the supplementary geochemical testing documented in Appendix A of the "TMA Groundwater Quality Performance Evaluation" (Foth and Van Dyke, 1998) and to simplify the presentation of calculations. The revisions address most of Comments 1 to 8. Those portions of the comments not addressed in the revisions are discussed below.

Comment 1

Clearly document the potential for advective transport of oxygen in the backfill (tails and waste rock). The analysis assumes only diffusive transport, but provides no substantive information to back up that assumption. For example, the potential for advective transport would appear to be quite high in the waste rock portions of the backfill (see Figures 2.1 and 2.2 of the report).

Response

Advective transport of oxygen into the backfilled stopes is unlikely to occur, primarily because the backfilled stopes will effectively seal off one end of the access cross-cuts. The other end of the access cross-cut will also be sealed with a bulkhead. Although the bulkheads will not necessarily be constructed as air-tight barriers, they will be a barrier to ventilation drafts. In other mines, it has been observed that oxygen concentrations do diminish in stopes behind bulkheads, supporting the contention that the bulkhead is at least a partial barrier to air flow.

Comments 2, 3, and 5

The results from the 1-D simulations that are presented in this section were developed from spreadsheet models of the three cases discussed. Include illustrations showing schematics of each modeled case with the boundary conditions and parameters used clearly presented. Also, please include copies of the spreadsheet models and the input spreadsheets for all significant runs in digital form.

Provide more information on how the parameters used in the simulations were selected. In particular, it is unclear how the rate constants cited were converted for this analysis.

Provide a figure or set of figures to document the calculations presented in Section 2.4. The illustration(s) should clearly indicate the procedures used and the assumptions made in generating the information presented. As an example, the spatial basis for the numbers used in the calculation at the bottom of page 12 is unclear.

Response

Comments 2, 3, and 5 relate to calculation methods and assumptions. All calculations are now shown in Appendix A and Chapter 2 of the revised report. A diskette copy of the Microsoft Excel worksheet can be provided upon request.

Comment 4

Address the potential for reaction in the waste rock portions of the backfill (see Figures 2.1 and 2.2 of the report). Much of the waste rock used in the backfill will be potentially reactive. Therefore, it would appear that oxygen consumption and subsequently generated reaction products should be included in the analysis. In addition, include more details on oxygen transport in the waste rock.

Response

The revised derivation of water quality associated with the backfilled stope openings presented in the updated Chapter 2 conservatively assumes that all oxygen entering the backfilled stope will be converted to acidity. This assumption means that it is not necessary to distinguish between oxidation of the waste rock and oxidation of the tailings.

Comments 6, 7, and 8

Comparison of oxygen-limited AP with NP does not account for potential incomplete availability of NP or potential spatial variability in acid neutralization which may result from uneven utilization of NP (either through more complete consumption at the exposed edge of the material or uneven distribution of consumption throughout the material). Therefore, revise your analysis to address these limitations.

Document the applicability of the very short-term humidity cell data used in Section 2.4 to estimate constituent concentrations. Those tests exposed tails to wet-dry cycles for only two weeks. Data from longer-term tests seem more applicable in this instance. Clarify what was involved in extrapolating the data used to the estimated average oxidation time of fifteen years. Provide more documentation on the use of a fifteen-year average oxidation time for the backfill.

Provide more information on the reasonableness of the phases used in the geochemical modeling. In particular, the use of $Ba(AsO_4)_2$, tenorite, and siderite is questionable.

Response

Comments 6, 7 and 8 refer to assumptions that are not used in the revised derivation. The revised derivation is now consistent with results from the supplementary geochemical testing program (which were not available when the initial report was submitted) and the subsequent geochemical equilibrium modeling.

Comments 9-11 Regarding Wall Rock

Comment 9

The analysis presented assumes that the foot wall rock exposed by the mining will contribute no contaminants. Provide more justification that the foot wall will not contribute to the overall contaminant loading. This should include, at a minimum, more details on the mineralogical composition of the exposed foot wall rock, more information on the proportion of foot wall exposed to hanging wall exposed, and more information on the time of foot wall exposure.

Response

Access to the zinc ore stopes will be through the hanging wall. The only workings in the footwall will be cross-cuts through the zinc ore to portions of the copper stringer ore. As a result, there will be no significant exposure of wall rock in the footwall. The confusion about this issue may have arisen because schematic pictures of blasthole open stoping presented in earlier reports (e.g. Foth & Van Dyke 1995, "Summary: Project Description and Environmental Baseline Data") incorrectly showed extensive lateral drifts and cross-cuts located in the footwall.

Comment 10

The analysis assumes a reactive surface to mine wall surface ratio of 30:1. Provide more justification for the selection of that value. Presentation of a rock quality analysis of the exposed mine wall areas could be of assistance. Provide a sensitivity analysis for this ratio.

Response

The attached report by Agapito Associates Inc. estimates the number of fractures that will result from blasting, and the resulting ratio of reactive surface to mine wall surface. The report presents literature data that indicate the assumption of a reactive surface to mine wall surface ratio of 30:1 to be conservative.

Table 1 below shows that the predicted concentrations of constituents after reflooding is insensitive to the assumed ratio of reactive surface to mine wall area. Although the concentrations in the wall rock affected groundwater increase linearly with the increase in reactive surface area, the effects on weighted average concentrations are small. The reasons are that the wall rock contributes relatively low concentrations, and that the volume of groundwater influenced by the wall rock is much less than the volume influenced by the backfilled tailings.

TABLE 1
Effect of Assumed Ratio of Crown Pillar
Reactive Surface to Nominal Surface Area

Source	Estimated Volume (ft^3)	Parameter Concentrations (mg/L)							
		SO_4	As	Ca	Cu	Fe	Mn	Se	Zn
Backfilled Tailings	1.1E+08	1021	0.58	404	0.26	13	1.5	0.12	15
Total Wall Rock	1.3E+07	17	0.016	10	0.078	2.6	0.12	0.004	0.12
Crown Pillar at 30:1 ratio	9.5E+05	35	0.001	2.8	1.5	0.8	0.06	0.004	13
Over Vol.-Weight Avg.(mg/L)	1.2E+08	907	0.515	359	0.25	11.9	1.35	0.108	13.7
Crown Pillar at 10:1 ratio	9.5E+05	12	0.0003	0.93	0.5	0.3	0.02	0.001	4.3
Over Vol.-Weight Avg.(mg/L)	1.2E+08	907	0.515	359	0.25	11.9	1.35	0.108	13.6
Crown Pillar at 100:1 ratio	9.5E+05	350	0.010	28	15	8	0.6	0.040	130
Over Vol.-Weight Avg.(mg/L)	1.2E+08	910	0.515	360	0.36	11.9	1.36	0.109	14.6

Comment 11

Provide more information justifying the selection of a 15-year average exposure period for the wall rock.

Response

The 15-year average exposure period was estimated from the fact that mining will occur over 28 years, and reflooding will take another 2 years. Mine development will continue throughout the mine life. If we assume that mine development roughly coincides with ore removal from each area, an average wall rock exposure time of 30 years / 2 = 15 years is obtained.

The estimates of constituent concentrations in the wall rock affected groundwater are linearly dependent on the assumed exposure time. For example, increasing the assumed average exposure time to 20 years would increase the predicted concentrations by (20-15) / 15 = 1/3. As discussed in the response to Comment 10, the weighted average concentrations are insensitive to changes in the wall rock affected groundwater. Hence changes in the average wall rock exposure time will not significantly influence the predicted weighted average concentrations.

Comments 12-16 Regarding Crown Pillar

Comment 12

Provide an illustration that shows how the gossan, supergene enriched, and sulfide zones of the crown pillar relate to the massive saprolite, structured saprolite, and moderately weathered bedrock designations.

Response

Figures 3-3 to 3-8 of Appendix 4.2-11 of "Crandon Project Environmental Impact Report" (Foth and Van Dyke, 1995) provide simplified north – south cross sections of the zinc ore zone which delineates the massive saprolite, the base of the crown pillar, the ore zone that will be mined by cut-and-fill mining methods, and the different weathering zones.

Comment 13

Provide more information on the effects of blasting on the potential for leaching from the crown pillar.

Response

There are two mechanisms by which leaching from the crown pillar might be enhanced by blasting:

- *Exposure to groundwater of new surfaces containing readily soluble minerals;*
- *Exposure to oxidation of new surfaces containing sulfide phases.*

The attached report by Agapito Associates Inc. discusses the effects of blasting on the crown pillar, and concludes that sound blasting procedures will keep the zone of blast damage at the base of the crown pillar to less than 5 feet in thickness. The same report presents logs of drillholes in rock excavated by conventional blasting methods. The drillholes exhibit from 3 to 9 fractures within the first five feet of core. However, two of the holes had rubble zones. Assigning 10 fractures to each rubble zone leads to an average of 15 fractures in the first five feet of core, or roughly three per foot. Comparing that number to the current average of 2 fractures per foot, (reference), it is clear that the blasting will not significantly increase the exposure of new surfaces to groundwater. The effect on oxidation has been accounted for by assuming that the reactive surface will be greater than the nominal surface (see response to Comments 10 and 15).

It is noteworthy that other blasting methods provided lower fracture densities, and that the mining methods proposed for the ore below the crown pillar will minimize the amount of rubble left behind. Hence, the above number seems conservative.

Comment 14

Provide more justification for the assumption that the gossan and supergene enriched zones would not contribute contaminants. Migration of pre-existing or newly-produced oxidized materials could add contaminants. As a part of this response, please provide

information on the mineralogical/chemical composition of the three identified zones within the crown pillar.

Response

Earlier reports by Agapito Associates Inc. ("Hydrologic Stability of the Crown Pillar, Crandon Deposit" (May 1996) and "Numeral Analysis Results for Evaluation of the Influence of Mining of the Crown Pillar, Crandon Deposit" (July 1997)) discuss the effects of mining on the crown pillar's hydraulic conductivity. The reports conclude that, of the five identified fracture sets, one will be closed and two will be dilated by the stress relief that will result from mining below the crown pillar. Flow in joint set 1 was predicted to be reduced by about half, flow in joint set 2 was predicted to increase by about 4%, and flow in joint set 5 was predicted to roughly double. Since joints sets 1 and 2 are more abundant than joint set 5, the overall effect is expected to be either no change or a slight reduction in groundwater flow through the crown pillar.

As discussed in "Bedrock Hydrology at the Crandon Site, Crandon Project, Crandon Wisconsin" (Foth and Van Dyke 1995), fracture sets 1 and 2 showed clear evidence of weathering and iron hydroxide coatings, whereas joint sets 3, 4 and 5 were tighter and showed little to no evidence of weathering. The shift of flow from the weathered joint set 1 to the unweathered joint set 5 will mean that groundwater is exposed to less of the soluble minerals that could cause an increase in contaminant concentrations.

Since total groundwater flows through the crown pillar are not expected to increases, and the exposure of the groundwater to soluble contaminants is expected to decrease, we conclude that the contribution of new contaminants from the bulk of the gossan and supergene enriched zones is likely to be insignificant. (The contribution associated with increased oxidation near the base of the crown pillar was included in the previous analysis.)

Comment 15

The analysis assumes a reactive surface to exposed surface ratio of 30:1. Provide more justification for the selection of that value. Presentation of a rock quality analysis of the exposed crown pillar areas could be of assistance. Provide a sensitivity analysis for this ratio.

Response

See the above response to Comment 10.

Comment 16

The analysis assumes an exposure period of 6 weeks. Estimates for the reflooding of the mine are about 2 years. Provide justification for the selection of the exposure period used for the crown pillar.

Response

The exposure period referred to in the analysis is the exposure to oxygen, which will be determined not by the reflooding schedule but rather by the mining sequence.

The bottom of the crown pillar will be exposed to oxygen by the blasting of ore from the back (roof) of the uppermost stopes. After the ore is removed, the stopes will be backfilled with cemented coarse tailings. As discussed in a letter from Mr. Don Moe to Mr. Christopher Carlson, WDNR (CMC, 1996), the uppermost stopes will be "tight-filled", i.e. the cemented tailings will be placed as near as possible to the stope roof. The access of oxygen into the void between the top of the cemented tailings and the base of the crown pillar will be cut off once the tailings block the stope access cross cut.
The estimated time required to complete ore removal from each stope is only five weeks. Assuming the tight filling will require one additional week leads to the conclusion that the total exposure period will be six weeks.

Comment 17 Regarding Underground Emissions

Comment 17

Nitrate, nitrite, and ammonia have the potential to be present in significant quantities in the mine as it refloods. Provide a more detailed analysis on the possibility of nitrogen compounds being significant contaminants.

Response

Section 3.2.1 of the Crandon Project September 1995 Preliminary Engineering Report for Wastewater Treatment Facilities (PER) addresses the issue of estimated ammonia and nitrate concentrations in the mine drainage water. While nitrite is not specifically addressed in that discussion, the reference to nitrates includes the combination of nitrites plus nitrates.

Table 3-4 of the PER, reproduced below as Table 2, provides specific estimates of ammonia and nitrate concentrations in mine drainage water. The estimates include an average value and a range of values for the low range, best engineering judgement (BEJ), and practical worst case (PWC) mine inflow estimates. The actual concentrations of ammonia and nitrate in the reflooded mine are expected to be less than those in the mine drainage water for the following reasons:

- *Ammonia and nitrate will principally result from blasting operations in the mine.*

- *Blasted ore and the majority of waste rock which will come into contact with the planned blasting agent (ANFO) will be removed from the mine, also resulting in the removal of residual ammonia and nitrate.*

- *As shown in Table 3-5 of the PER, the concentration of ammonia and nitrate in the TMA reclaim pond effluent water is expected to be 0.03 mg/l and 0.08 mg/l, respectively. Since the backfill pore water and reclaim pond effluent will have the same characteristics, the ammonia and nitrate concentrations in the backfill pore water will be insignificant.*

TABLE 2
Estimated Ammonia and Nitrate Concentrations in Mine Drainage Water for LR[1], BEJ[2] and PWC[3] Mine Inflow

	Concentrations[4]			
	Ammonia (as N)		Nitrate (as N)	
	Average	Range	Average	Range
LR[1]	4.4	1 to 9	10.9	2 to 22
BEJ[2]	3.3	<1 to 7	8.2	2 to 17
PWC[3]	2.2	<1 to 5	5.6	1 to 12

[1] Based on a Low Range Mine Inflow Estimate of 400 gpm.
[2] Based on a Best Engineering Judgement Mine Inflow Estimate of 700 gpm.
[3] Based on a Practical Worst Case Mine Inflow Estimate of 1,270 gpm.
[4] All concentrations are mg/L. Concentrations calculated by using ratio of the total mine drainage flow rate from PER Table 3-2, divided into 200 gpm times 10 mg/L for ammonia (as N) and 25 mg/L for nitrate (as N), respectively. Calculation assumes that mining and blasting rates are similar for the average mine generating 200 gpm of mine water and the Crandon mine.

While it is difficult to specifically predict the concentration of ammonia and nitrate in the reflooded mine, a conservative analysis to determine the possibility that these constituents would be significant contaminants can be completed using the result of the mixing calculations presented in the April 23, 1998, HSI GeoTrans memorandum titled "Reflooded Mine Source Term, HSI GeoTrans Project N015-020". The analysis, shown in Table 3 below, has been completed by conservatively assuming that the concentration of ammonia and nitrate in the reflooded mine would be equal to the high end of the ranges shown in Table 2 above and then applying the BEJ and PWC concentration reduction factors as derived in the HSI GeoTrans memorandum.

TABLE 3
Effect of Ammonia and Nitrate in the Reflooded Mine on the Glacial System

Constituent[1]	Assumed Maximum Concentration[2] (mg/l)	Concentration Reduction Factor[3]		Concentration In Glacial System (mg/l)	
		BEJ	PWC	BEJ	PWC
Ammonia	9	0.00096	0.0019	0.0086	0.017
Nitrates	22	0.00096	0.0019	0.021	0.04

[1] As N.
[2] From Table 3-4 of the September 1995 Preliminary Engineering Report for Wastewater Treatment Facilities.
[3] From the April 23, 1998, HSI GeoTrans memorandum, subject: Reflooded Mine Source Term.

As Table 3 shows, the concentration of nitrogen series compounds in the glacial system based on the conservative analysis would be well below the maximum NR 809, Wis. Admin. Code, drinking water standard of 10 mg/l. Therefore, it is concluded that ammonia and nitrates would not be significant contaminants in the reflooded mine.

Comments 18-20 Regarding Groundwater Modeling

Comment 18

Provide a justification for the assumption that moderately weathered zones terminate near the ends of the orebody. This does not appear to be consistent with the conceptualization in the regional flow model. In addition, clarify the need for and significance of this assumption for the inset model.

Response

As shown by Figure 3.31 in GeoTrans (1996), the weathering zone at the depth of the mine is associated with the ore deposit, but does not extend laterally to any significant distance at the specific depths of the inset model layers. The models presented in the revised Chapter 6 use a more accurate delineation of all of the weathering zone.

Comment 19

Since this model was submitted, the regional flow model has been revised. Several of the changes involved the bedrock. The current inset model is based on the BEJ/PWC from the 1996 regional flow model. Revise the inset model and this section of the report to account for the changes in the revised 1997/8 regional flow model.

Response

SRK has completed several new runs using the updated representation of the weathering zones at each level, including the effects of anisotropy. The runs are described and the resulting estimates of flow presented in the update to Chapter 6 of the report.

Comment 20

Revise Table 6.2 to be more consistent with the information presented in the regional flow model reports by using hydraulic conductivity instead of transmissivity.

Response

Since the model thickness is 10 feet, the reported transmissivity values (in ft^2/day) were simply ten times the hydraulic conductivies (in ft/day). For clarity, the updated Chapter 6 presents both transmissivity and conductivity values.

Yours truly,

STEFFEN ROBERTSON AND KIRSTEN (CANADA) INC.

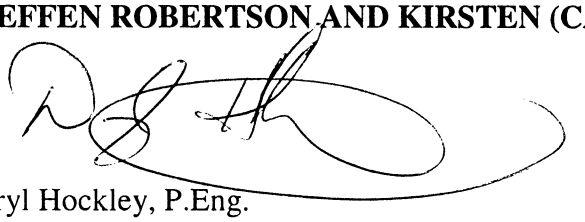

Daryl Hockley, P.Eng.
Principal Engineer

Attachment A: Agapito Letter Report (January 30, 1998)

ATTACHMENT A

Agapito Letter Report
(January 30, 1998)

RECEIVED
FEB - 2 1998

AGAPITO ASSOCIATES, INC.
CONSULTING ENGINEERS

GRAND JUNCTION OFFICE

January 30, 1998

235-4

Ken Black and Don Moe
Crandon Mining Company
7 N. Brown Street, 3rd Floor
Rhinelander, WI 54501-3161

RE: **Comments on the Reflooded Mine Source Term for the Proposed Crandon Mine**

Dear Ken and Don:

Following please find the responses prepared for Questions 10 and 13 for the above topic. Also included are papers by Agapito *et al* (1984) and Kelsall *et al* (1984) pertaining to these issues. We have prepared the response based on general conventional blasting practice. It is difficult to be more specific than this at this stage of the project. We could add that during cut-and-fill mining small diameter blast holes (less than three inches) are typically used. The small holes limit the explosive per hole, and the explosive per blast/delay can also be very limited. We could mention smooth wall blasting or perimeter blasting, but I don't think we want to be committed to restrictive blasting procedure.

To measure or estimate the extent of the blast damage we need to know the weight of the explosive per delay and the weight/ft of explosive. Peak particle velocity of less than 28 in/sec are associated with no cracking in the rock (see Figure 10 in Kelsall *et al* 1984). However, velocity of as little as 0.7 in/sec from a nearby blast can cause small roof falls and fine cracks in an adjacent opening (Diehl and Sariola 1977). Hence it is nearly impossible to estimate the extent of blast damage in the crown pillar without a blast pattern and some knowledge of the sequence of mining. Please feel free to call us if you have any questions.

Sincerely,

Michael P. Hardy
President

MPH/pg
Attachments (2)

Question 10: The analysis assumes a reactive surface to mine wall surface ratio of 30:1. Provide more justification for the selection of the value. Presentation of a rock quality analysis of the exposed mine wall areas could be of assistance. Provide a sensitivity analysis for this ratio.

Response: (The following is the material we found from oil shale mining to support the assumption of the ratio of a reactive surface to mine wall surface. We have done an extensive literature search on this subject, but were not able to find results that directly related to hard rock metal mining.)

Agapito *et al* (1984) conducted a study to investigate the zone of damage of oil shale pillars excavated by conventional blasting (CB), pre-split blasting (PS), and mechanical mining (MM).

The study was based on a comparison of *in situ* vertical stresses and fractures obtained from overcoring horizontal holes in the Colony Mine, Piceance Creek Basin, Colorado. Fracture Logs for these core holes are presented in Figure 1. Table 1 summarizes the number of fractures logged in the first 15 ft of core holes.

Table 1. The Number of Fractures Observed in the First 15 ft of Core Holes and the Ratio of Fracture Counts for Different Mining Method

	Area 1*	Area 2**	Area 3***	Area 4****
Fracture Counts from MM	3	7	NA	NA
Fracture Counts from PS	NA	NA	3	6
Fracture Counts from CB	14	NA	16	17
Ratio of CB/MM	4.7	NA	NA	NA
Ratio of CB/PS	NA	NA	5.3	2.8

* Area 1 includes core holes 1 and 2.
** Area 2 includes core holes 3 West and 3 East.
*** Area 3 includes core holes 4 and 5.
**** Area 4 includes core holes 6 and 7.

The locations of Areas 1, 2, 3, and 4 are presented in Figure 2. Rubble zones occurred at core holes 5 and 7. Ten fractures was assigned as the representative number for each rubble zone. The ratio of fracture counts from different mining methods are also presented in Table 1. The fractures observed in the cores with MM and PS mining appeared to be natural fractures. With conservative assumptions that all fractures observed in CB mining are blast-induced fractures, the ratio of blast-induced fractures to natural fractures are in the range of 2.8 to 5.3. The data set indicates that the assumption of a reactive surface to mine wall surface ratio of 30:1 is very conservative.

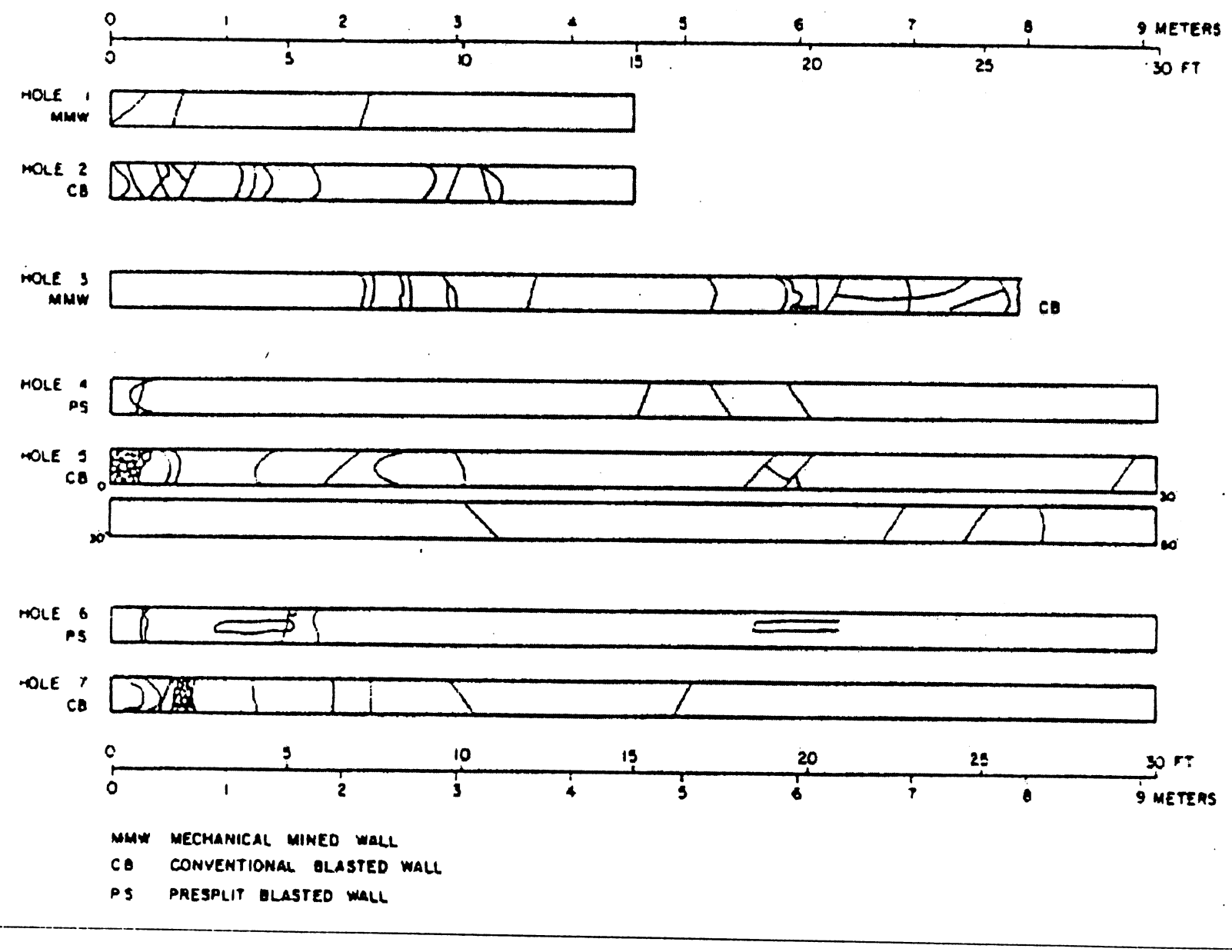

Figure 1. Fracture Logs of 15-1/4 cm (6 in) Holes (after Agapito *et al* 1984)

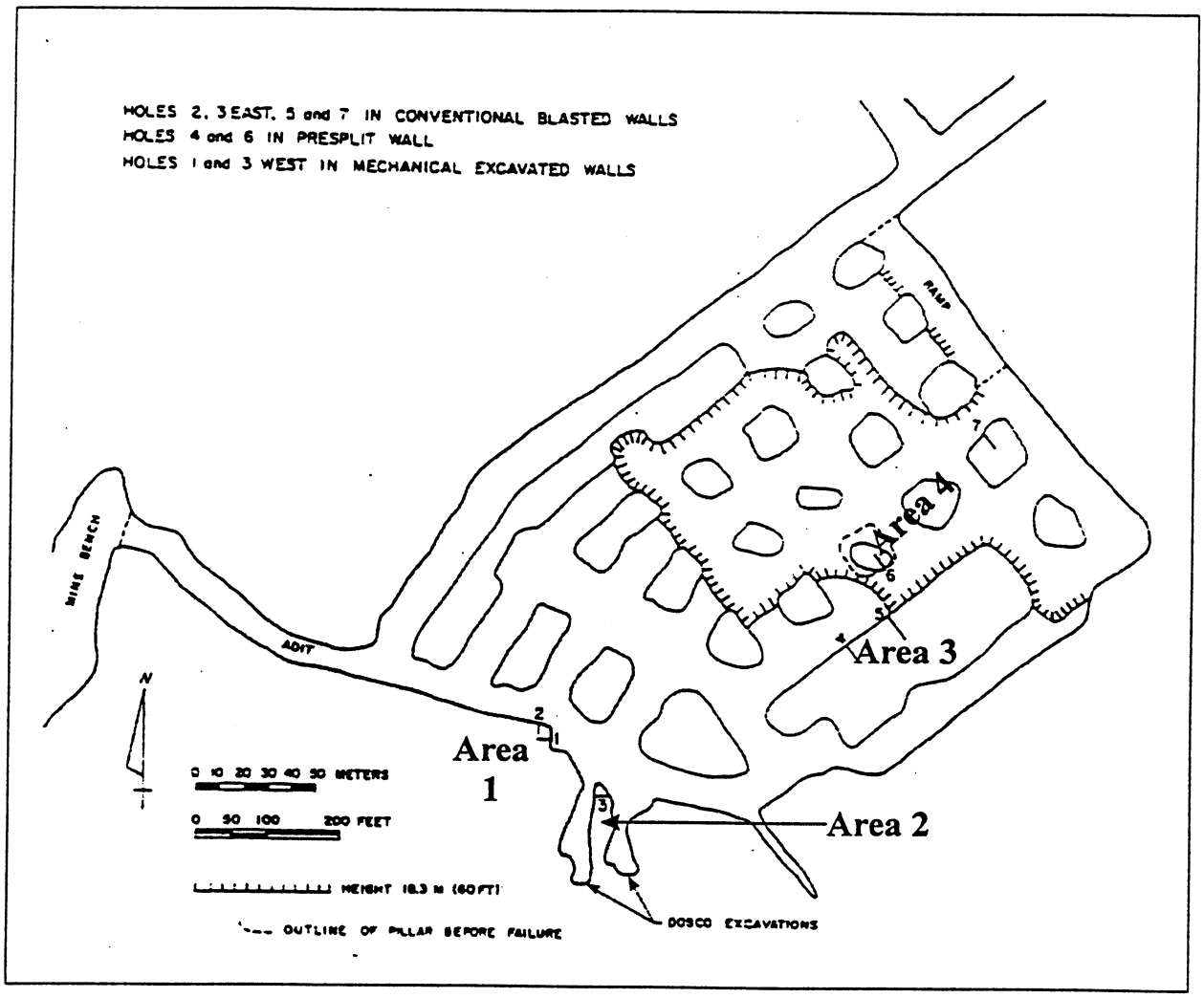

Figure 2. Mine Map and Hole Locations (after Agapito *et al* 1984)

Question 13: Provide more information on the effects of blasting on the potential for leaching from the crown pillar.

Response: Although blasthole open-stoping mining method is planned for the majority of the Crandon deposit, this method will only be employed in ore below 1200-ft elevation. Cut-and-fill mining methods that limit the open void with close cycling of mining and backfilling will be utilized for mining above 1200-ft elevation. The cut-and-fill methods employ relatively small blasts with low energy release to ensure minimum blast damage. Blast damage in the crown pillar will be controlled by engineered blasting, roof bolting, and placement of backfill. The extent of blast damage reported in the literatures are in the range of 1.0 to 4.3 ft (Kelsall *et al* 1984). Therefore, the extent of measurable blast damage at the base of the crown pillar is expected to be less than 5 ft when employing sound blasting procedure. Studies by Agapito Associates, Inc. (1996, 1997) have shown that no measurable change in hydraulic conductivity due to mining is expected for the crown pillar. Although stress relief and blast damage will cause a change in hydraulic conductivity/permeability at the bottom 5 to 10 ft of the crown pillar, this extent is considered inconsequential when compared with the minimum crown pillar thickness of 100 ft. Therefore, the potential for leaching from the crown pillar due to blasting is concluded to be very low.

REFERENCES

Agapito, J.F.T., H.N. Maleki, and J.R. Aggson (1984), "Impact of Excavation Technique on Strength of Oil Shale Pillars," Society of Mining Engineers of AIME, Called No. D, Littleton, Colorado.

Brechtel, C.E. (1996), "Hydrologic Stability of the Crown Pillar, Crandon Deposit," Report submitted to Crandon Mining Company, May.

Diehl, G.W. and P.J. Sariola (1977), "The Small-Hole Drilling Method in Rock Store Excavations", Proc. 1st Int'l Symp. on Storage in Excavated Rock Caverns, Stockholm, Vol. 3, pp. 23-27.

Hardy, M.P. and M. Lin (1997), "Numerical Analysis Results for Evaluation of the Influence of Mining on the Crown Pillar, Crandon Deposit," Report submitted to Crandon Mining Company, July.

Kelsall, P.C., J.B. Case, and C.R. Chabannes (1984), "Evaluation of Excavation-Induced Changes in Rock Permeability," Int'l J. Rock Mech. Min. Sci. & Geomech. Abstr., Vol. 21, No. 3, pp. 123-135.

Int. J. Rock Mech. Min. Sci. & Geomech. Abstr. Vol. 21, No. 3, pp. 123–135, 1984
Printed in Great Britain.

0148-9062/84 $3.00 + 0.00

Evaluation of Excavation-induced Changes in Rock Permeability

P. C. KELSALL*
J. B. CASE†
C. R. CHABANNES‡

The nature of the changes in permeability around an underground opening induced by blast-damage or stress-relief is an important factor in the design of nuclear waste repositories in rocks such as granite or basalt. Changes in stress and corresponding changes in rock mass hydraulic conductivity are analyzed for a circular shaft using simplifying assumptions regarding fracture geometry and initial stress state. Stress distributions around the shaft are calculated using closed-form solutions and are related to changes in hydraulic conductivity using a form of the cubic law for flow through fractured media. The analysis predicts that hydraulic conductivity may be increased, close to the wall of the opening, by two to three orders of magnitude over the far-field value solely in response to stress relief. The zone in which hydraulic conductivity is increased by at least one order of magnitude over the far-field value is limited to within one to two radii from the opening. Blasting may result in large increases in hydraulic conductivity immediately adjacent to an opening but blast damage may be limited to within 0.3 m of the opening using controlled blasting techniques with low perimeter charge weights.

LIST OF SYMBOLS

- σ_y = Maximum far-field horizontal stress.
- σ_x = Minimum far-field horizontal stress.
- σ_t = Tangential stress.
- σ_r = Radial stress.
- $R = \sigma_y/\sigma_x$.
- b = Fracture aperture.
- Q = Flow rate (L^3T^{-1}).
- Δh = Head difference.
- A, t, ζ = Empirical constants obtained from fracture deformability test.
- σ_e = Effective stress.
- b_e = Fracture aperture at normal stress, σ_e.
- b_0 = Fracture aperture at zero normal stress.
- K = Rock mass hydraulic conductivity (LT^{-1}).
- K_e = Hydraulic conductivity of a fracture system at normal stress, σ_e.
- K_0 = Hydraulic conductivity of a fracture system at zero normal stress.
- g = Acceleration constant.
- ν = Kinematic viscosity.
- s = Fracture spacing.

INTRODUCTION

The isolation of nuclear wastes in a deep, mined repository will require the sealing of shafts and tunnels which connect the repository to the surface. Seal design must address the possibility that the permeability of the rock mass adjacent to the wall of the shaft or tunnel might be increased as a result of blast-induced damage or stress relief [1, 2]. This paper provides a preliminary evaluation of the changes in permeability likely to occur in the "disturbed zone" based on analytical assessments and literature review. The results are applicable to other problems in shaft or tunnel design where the degree and depth of disturbance resulting from the excavation process must be known. Recently, Brown and Bray [3] have discussed the problem with regard to the design of pressure tunnels.

With regard to repository design, the properties of the disturbed zone will be characterized eventually by site-specific *in situ* testing. Meanwhile, information is required for use in conceptual design, performance assessment, and planning of field tests. A few investigations of the permeability of the disturbed zone have been described in the literature [e.g. 4–6] but these are not directly relevant to a deep, geologic repository in granite or basalt. At present, therefore, it is necessary to develop an analytical model for disturbed zone characteristics. The model described in this paper is considered to be preliminary in that it considers only circular openings in an isotropic virgin stress field and it is based partly on stress–hydraulic conductivity relations obtained in the laboratory. More rigorous solutions for non-circular openings and non-isotropic stress fields could be developed using, for example, the finite element method, but these solutions may not be justified at present because rock properties at candidate repository sites are not well known.

* Project Manager and †Project Engineer, D'Appolonia Consulting Engineers Inc., 2340 Alamo S.E., Suite 306, Albuquerque, NM 87106, U.S.A.
‡PB/KBB Inc., New Orleans, Louisiana; formerly with D'Appolonia Consulting Engineers Inc., Albuquerque, New Mexico.

DISTURBANCE MECHANISMS

Three processes may contribute to formation of a disturbed zone around an underground opening: stress redistribution, damage by the excavation process—especially if blasting is used, and weathering or interaction between the rock and groundwater. Of the three processes, only one is directly related to the excavation method. Also, the effects of stress redistribution apply to all openings and excavation methods although the magnitude of the effects depends greatly on site-specific conditions. Accordingly, it is not appropriate to consider the disturbed zone solely as a blast-damaged zone that does not exist if mechanical excavation methods are used.

The evaluation presented in this paper refers to a fractured rock with high intact strength, such as basalt or granite. In these rocks, the major mechanisms for disturbance are blasting and stress relief along fractures existing prior to excavation. In weaker rocks, the same mechanisms would apply but fracturing of intact rock in response to stress redistribution might also be important. Weathering and rock–groundwater interaction are considered to be relatively insignificant mechanisms for disturbance in granite and basalt provided that fractures do not contain soluble or erodable infillings.

The redistribution of stresses around an opening following excavation might affect the permeability of the rock mass in one of three ways:

(1) by fracturing of originally intact rock due to excessive compressive or tensile stresses;

(2) by opening or closing of pre-existing fractures due to changes in the normal stresses acting across the fractures or to shearing along the fractures; and

(3) by loosening of the crystal structure in response to reduced confining stresses.

The relative influence of these three processes on disturbed zone permeability will vary according to parameters such as the size of the opening relative to the fracture spacing, the strength of the intact rock, the *in situ* stress field, and the shape of the opening. Loosening of the crystal structure applies only to weak rocks such as salt. In hard rocks, such as basalt or granite, the relevant processes to consider are fracturing of intact rock and effects on pre-existing fractures.

The stress conditions under which fracturing of intact rock might occur around a circular opening can be examined using closed-form solutions. For example, the maximum elastic tangential stress (σ_t) on the surface of a circular shaft is given by a special case of the Kirsch solution:

$$\sigma_t = 3\sigma_y - \sigma_x \qquad (1)$$

where:

σ_y = maximum far-field horizontal stress;

σ_x = minimum far-field horizontal stress.

This solution can be re-expressed in terms of a factor (R), the ratio of the maximum and minimum far-field stresses:

$$\sigma_t = (3R - 1)\sigma_x \qquad (2)$$

The possibility for failure of intact rock at some point on the shaft perimeter due to stress redistribution can now be evaluated by comparing the maximum boundary stress—for various depths and values of R—against the unconfined compressive strength of the rock. Considering candidate repository sites in basalt or granite, the depth is likely to be 1000 m or less, intact rock compressive strengths are likely to exceed 150 MPa, and the *in situ* stresses are not expected to be highly anisotropic. With these conditions, fracturing of intact rock should not occur. Moreover, considering the effects of confinement in the rock mass away from the shaft wall, any fracturing that did occur would be limited, at least initially, to a thin zone locally developed around the wall.

By the reasoning presented above, it is concluded that fracturing of intact rock around circular openings is unlikely at proposed repository depths ($\leqslant$1000 m) in basalt or granite. In these same rock types, however, fracture permeability is known to be highly stress-dependent so that rock mass permeability is expected to increase in zones around a tunnel or shaft where stresses are relieved and to decrease in zones where stresses are increased. The following section describes an analytical approach for predicting the changes in rock mass permeability that might result from changes in the stresses acting across fractures. The degree to which blasting might increase the degree of disturbance, over and above that resulting from stress relief, is considered separately largely on the basis of case histories.

DISTURBANCE DUE TO STRESS REDISTRIBUTION

Consideration is given to the effects of stress changes around a circular shaft on the hydraulic conductivity of pre-existing fractures. Specifically, consideration is given to an *equivalent porous medium rock mass hydraulic conductivity* as would be applicable for cases where the fracture spacing is small (e.g. 10–50 cm) relative to the diameter of a shaft. A comparable approach could be developed for consideration of discrete fractures in cases where the fracture spacing is larger relative to the shaft diameter.

Effects of stress on rock mass hydraulic conductivity

Laminar flow through a single smooth-walled fracture is described by the "cubic law" which relates flow rate to the fracture aperture raised to the third power [7]:

$$\frac{Q}{\Delta h} = C(2b)^3 \qquad (3$$

where:

Q = flow rate;
Δh = head difference;
b = fracture aperture;
C = constant.

The degree to which flow through a fracture will be influenced by stresses acting on the fracture is determined by how the fracture aperture is influenced by stress or, in other words, by the deformability of the fracture. Iwai [8] proposed the following model for the influence of effective normal stress on flow rate, based on a model for non-linear deformability of a fracture originally proposed by Goodman [9]:

$$\frac{(Q/\Delta h)}{(Q/\Delta h)_0} = \frac{1}{\left[A\left(\frac{\sigma_e}{\zeta}\right)^t + 1\right]^3} \tag{4}$$

where:

$(Q/\Delta h)$ = flow rate divided by head difference at an effective stress, σ_e;
$(Q/\Delta h)_0$ = flow rate divided by head difference at zero effective stress;
A, ζ, t = empirical constants.

Substitution of (3) into (4) provides a relation between the effective aperture which determines flow through a fracture and parameters describing joint deformability (A, ζ, t) which can be obtained from laboratory testing:

$$b_e = \frac{b_0}{\left[A\left(\frac{\sigma_e}{\zeta}\right)^t + 1\right]} \tag{5}$$

where:

b_e = fracture aperture at effective normal stress, σ_e;
b_0 = fracture aperture at zero effective normal stress.

This relation can now be used to derive a relation between rock mass hydraulic conductivity and stress. Considering a single set of parallel fractures, the rock mass hydraulic conductivity (K) in the direction of the fractures is given by [10]:

$$K = \frac{g b^3}{12 \nu s} \tag{6}$$

where:

g = acceleration constant;
ν = kinematic viscosity;
s = fracture spacing.

Substitution of (5) into (6) provides the following relation between the rock mass hydraulic conductivity (K_e) at a specified effective normal stress (σ_e) and the rock mass hydraulic conductivity (K_0) at zero effective normal stress:

$$\frac{K_e}{K_0} = \frac{1}{\left[A\left(\frac{\sigma_e}{\zeta}\right)^t + 1\right]^3} \tag{7}$$

The similarity between equations (7) and (4) suggests that the relation K_e/K_0 for the hydraulic conductivity of a system of parallel fractures may be obtained from laboratory tests on a single fracture (assuming that all the fractures have the same deformability).

The validity of equation (4) to flow in rock fractures was tested in the laboratory by Iwai [8] using induced fractures in 15 cm dia samples of granite, basalt and marble. Figure 1 shows the comparison between test results obtained by Iwai for a basalt sample and the results predicted from equation (4) using constants for fracture deformability obtained from the same basalt fracture. The predicted relation is normalized ($Q/\Delta h = 1$) to an effective normal stress of 28 MPa (the assumed lithostatic stress at a depth of 1000 m in basalt). It can be seen that the predicted relation obtained from deformability data is more conservative (for purposes of the present study) in that it predicts a higher flow rate or hydraulic conductivity at any specified stress below the 28 MPa reference value. Also, the relation obtained from deformability data predicts that flow rate should be further reduced at stresses above 28 MPa; by comparison, the flow tests indicate that there is effectively no further reduction in flow above a stress of about 20 MPa.

The validity of the cubic law to natural, non-planar fractures is the subject of much continuing research. This research has included laboratory testing [8, 11, 12], field testing of jointed blocks [13, 14], and phenomenological modeling [15, 16]. Recent reviews of the subject are given by Witherspoon *et al.* [7] and Witherspoon [17]. Generally, this work has suggested that the cubic law is valid provided that it is based on a real aperture which takes into account the roughness and tortuosity of the fracture. The permeability-stress relation is then determined by a number of factors which influence the fracture stiffness, including fracture roughness, fracture wall compressive strength, and the initial aperture. It follows that the relation will differ according to the rock type, roughness, and weathering of the fracture surface, and any infillings that are present. The relation may also depend on the stress history of the fracture, and on whether displacements are purely normal or whether shearing occurs. There may be a scale effect, also, related to the fracture roughness.

It is not the purpose of this paper to present a detailed evaluation of the validity of the cubic law. For purposes of the analyses presented below, it is proposed that the approach described above is a reasonable approximation allowing the effects of stress on rock mass hydraulic conductivity to be estimated from fracture deformability as measured in the laboratory. The solid curve in Fig. 1 is used in subsequent analyses to determine relative rock mass hydraulic conductivities for fractures in basalt for any effective stress normal to the fractures in the range 0–60 MPa. A similar relation can be used for granite using different values for A and t also obtained from Iwai.

Stress distribution around a circular opening

The response of a rock mass to stress changes around an underground opening is determined by the properties of the rock mass and by the magnitudes of the induced stresses. Relatively strong rocks at shallow depths behave essentially elastically whereby deformations are theoretically reversible and there is no failure of the rock

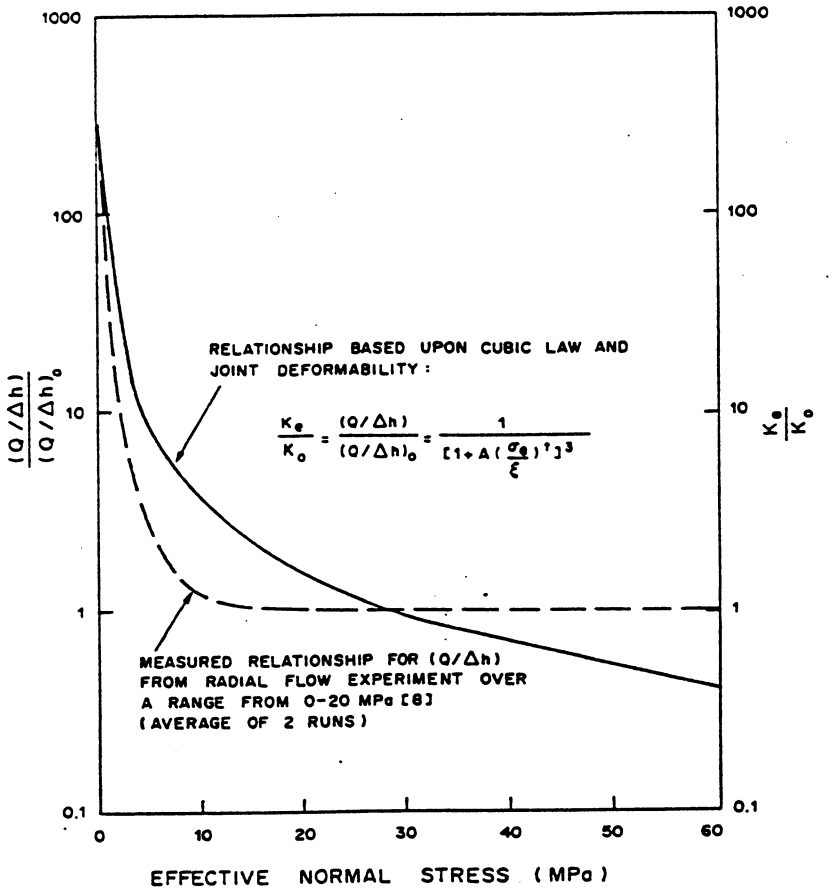

Fig. 1. Equivalent rock mass hydraulic conductivity and flow through a single fracture related to effective normal stress.

material. At greater depths, the same rock might respond with disproportionately greater deformations due to slippage along fractures. In this case, there is again no significant failure of intact rock material but deformations in the inelastic or "plastic" zone adjacent to the opening may be non-reversible.

The distinction between the elastic and plastic zones around an underground opening is important with respect to stress distributions and the resultant effects on fracture permeability. In the case of elastic deformations adjacent to an opening, the radial stress is reduced close to the shaft of tunnel wall whereas the tangential stress is increased. In this case, it is expected that the permeability of fractures tangential to the opening (perpendicular to the radial stress) should be increased, whereas the permeability of radial fractures should be reduced. In the case of plastic deformations adjacent to an opening, both the radial and tangential stresses are reduced close to the wall in the plastic zone [10] so that the permeability of both tangential and radial fractures should be increased.

The depth (stress level) at which inelastic or plastic behaviour is first observed and, at progressively greater stress levels, the extent of the plastic zone depend on the rock mass strength. At even greater depths, the stresses may be high enough to induce failure of the intact rock. Simple calculations using an analytical solution presented by Hoek and Brown [10] can be performed to estimate the depths in a circular shaft at which the plastic and fracture zones will be first observed for given rock

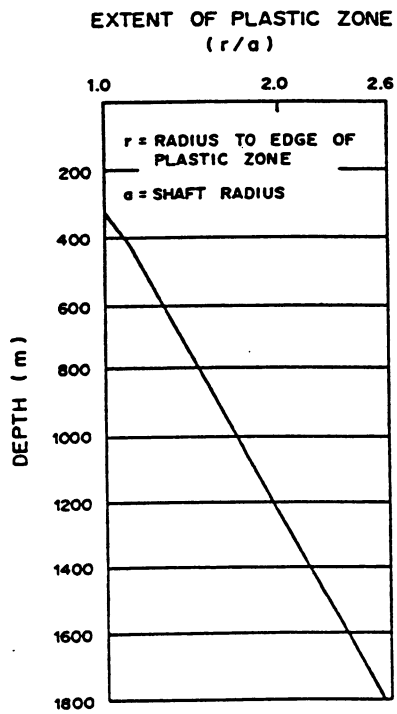

Fig. 2. Extent of plastic zone for a shaft in basalt with isotropic initial stress condition.

conditions. For example, for basalt with typical rock mass properties (Unconfined Compressive Strength (UCS) = 276 MPa; Rock Mass Rating (RMR) = 65) and an isotropic initial stress condition, plastic behaviour would be observed at depths below about 300 m (Fig. 2). Fracture of intact rock would not occur above a depth of about 2500 m for the isotropic initial stress condition. Stress distributions within the plastic zone are described in the following section. Essentially the same distributions are observed using solutions presented by Bray [18] and Jaeger and Cook [19] as obtained using Hoek and Brown's solution.

Predicted changes in rock mass hydraulic conductivity

Changes in rock mass hydraulic conductivity occurring in response to stress relief are predicted by calculating the changes in stress and then relating the stress changes to changes in hydraulic conductivity using the relation (solid curve) shown in Fig. 1. A number of simplifying assumptions are made:

(1) fracture aperture and spacing are statistically uniform through the rock mass prior to excavation;

(2) there is no change in fracture spacing or continuity in response to excavation;

(3) stress changes can be calculated using elastic or elasto-plastic, closed-form solutions for circular openings;

(4) hydraulic conductivity is determined by fractures perpendicular to specified stress orientations; and

(5) changes in hydraulic conductivity result from normal displacements across fractures (representing both true normal displacement and dilation during shearing).

In the analyses presented in this section, the initial stress condition is defined by two equal principal stresses acting in a plane normal to the penetration axis. In a sense this isotropic model is a hydrostatic stress condition although the stress in the direction of the penetration axis is ignored. Figure 3 shows the stress distributions in the radial and tangential directions around a circular opening for the elastic case. Corresponding hydraulic conductivities are obtained from Fig. 1 with K_e established at a stress of 28 MPa. Close to the excavation, the rock mass hydraulic conductivity in the axial

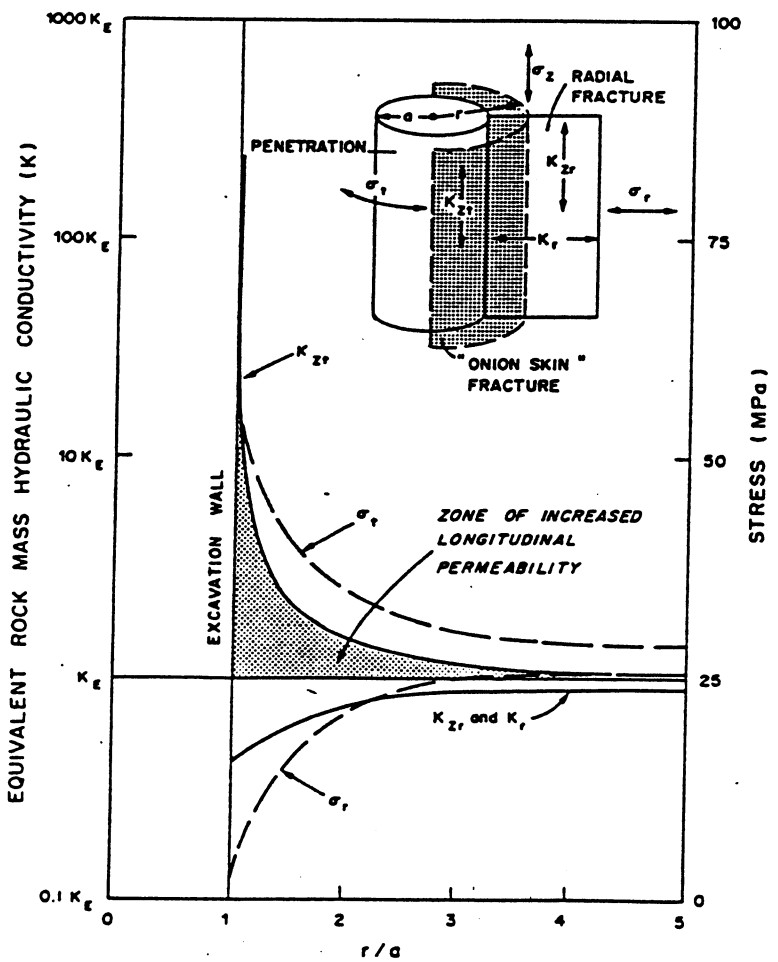

K_{Zr} = HYDRAULIC CONDUCTIVITY OF A SET OF RADIAL FRACTURES IN THE VERTICAL DIRECTION
K_{Zt} = HYDRAULIC CONDUCTIVITY OF A SET OF ONION SKIN FRACTURES IN THE VERTICAL DIRECTION
K_r = HYDRAULIC CONDUCTIVITY OF A SET OF RADIAL FRACTURES IN THE RADIAL DIRECTION
K_E = UNDISTURBED ROCK MASS HYDRAULIC CONDUCTIVITY (ISOTROPIC)

Fig. 3. Predicted effects of stress changes on rock mass hydraulic conductivity (elastic stress analysis for fractured basalt—isotropic initial stress condition).

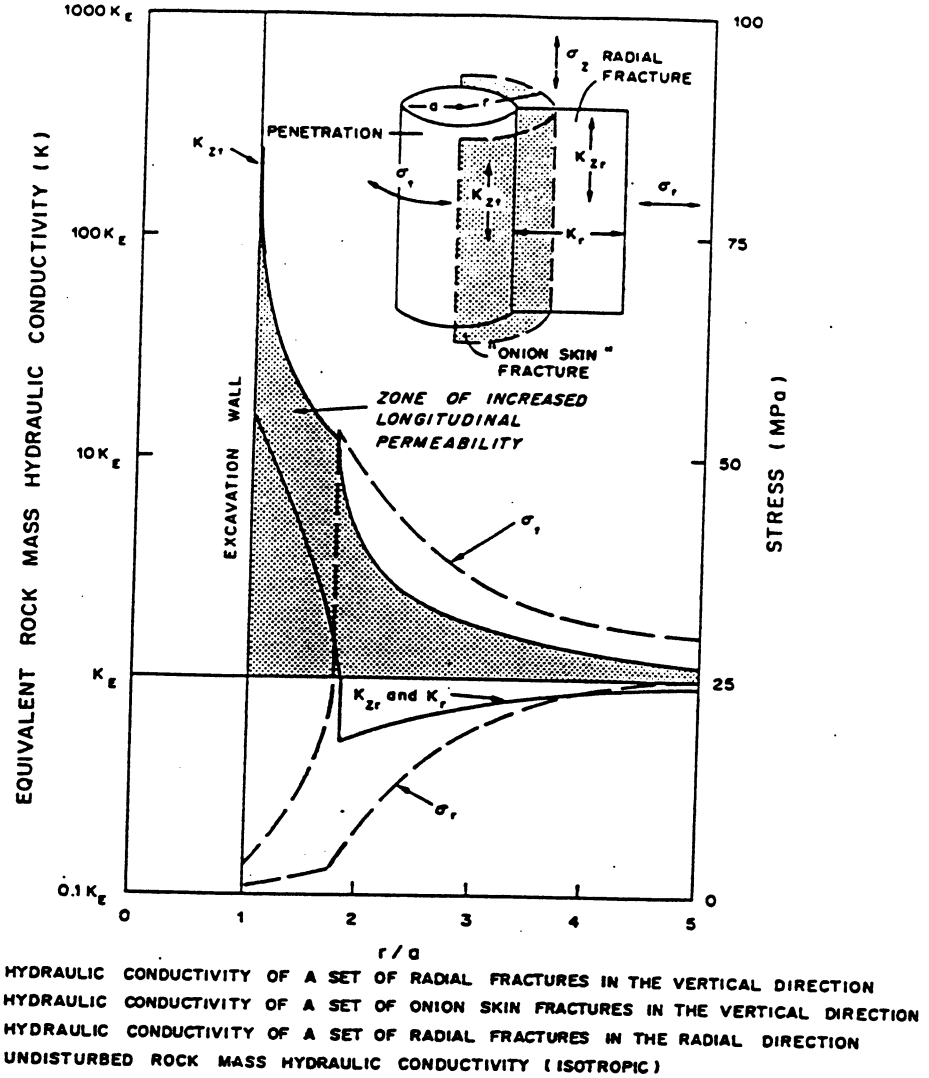

Fig. 4. Predicted effects of stress changes on rock mass hydraulic conductivity (elasto-plastic stress analysis for fractured basalt—isotropic initial stress condition).

direction (K_{zt}), determined by circumferential ("onion skin") or tangential fractures, is increased whereas the hydraulic conductivity of radial fractures (K_r or K_{zr}) is reduced. Figure 4 shows the same analysis for the elasto-plastic case again assuming hydrostatic *in situ* stresses. In this case, both the tangential and radial stresses are reduced in the plastic zone close to the excavation so that the hydraulic conductivities of all fractures within the plastic zone are increased. The maximum value of the axial hydraulic conductivity, corresponding to complete stress relief, is the same as for the elastic case but the thickness of the disturbed zone is greater.

Figures 3 and 4 show somewhat idealized fracture patterns around the opening. In reality, the changes in rock mass hydraulic conductivity will be determined in part by the orientation of the pre-existing fractures with respect to the opening and the principal stress directions. Actual fracture patterns may be complex but, as a first approximation, real cases can be modelled reasonably well as idealized radial or circumferential sets. Figure 5 illustrates the effect of fracture orientation on the extent of the zone in which the original, undisturbed hydraulic conductivity in the axial direction around a circular opening is increased by a factor of 10 or more. The extent of the disturbed zone with radial and tangential fractures, as considered previously, is compared against the extent of the disturbed zone for cases with orthogonal fractures oriented parallel to the far-field *in situ* stresses or with a single fracture set oriented parallel to one of the far-field stresses. With an elastic stress distribution, it is anticipated that axial hydraulic conductivity will be increased only where fractures are tangential to the surface of the opening. With an elasto-plastic stress distribution, hydraulic conductivity is increased all around the opening with the disturbed zone more extensive where there are fractures tangential to the surface of the opening. With the elasto-plastic stress distribution, there is little difference between the case with radial fractures and the case with tangential fractures and orthogonal fractures.

The significance of the hydraulic conductivity results obtained with either the elastic or elasto-plastic analyses is that the hydraulic conductivity reduces rapidly away from the excavation. With the more conservative elasto-plastic case, the hydraulic conductivity is 5 to 10 times greater than the undisturbed hydraulic conductivity at a distance of about one radius from the excavation and

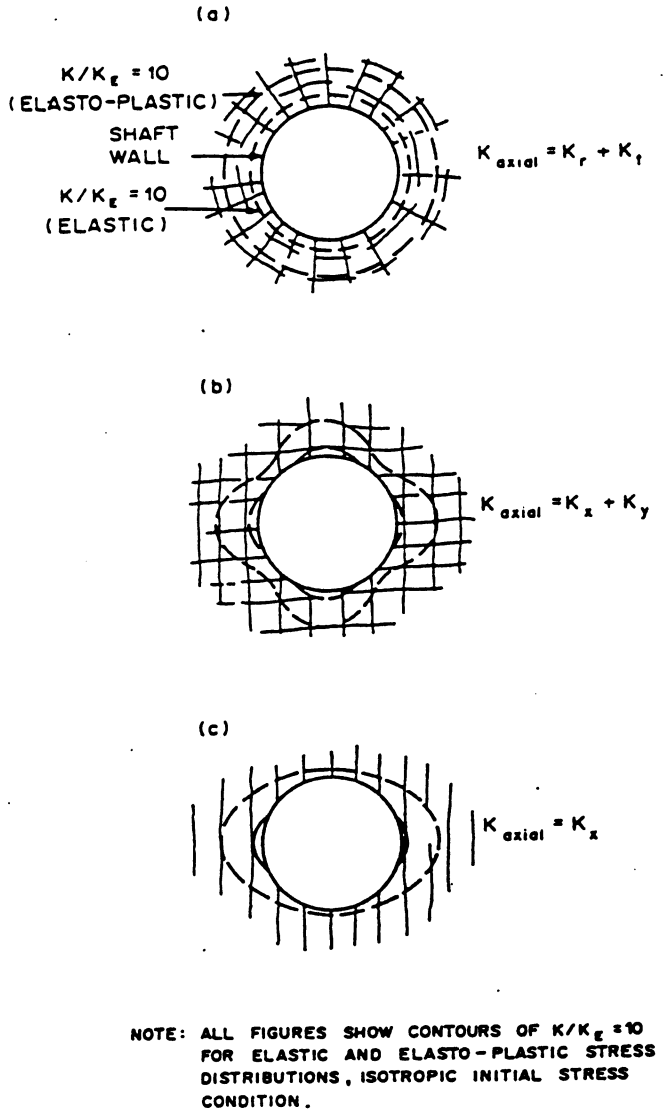

Fig. 5. Effect of fracture orientation on extent of disturbed zone. (a) Radial and tangential fractures. (b) Orthogonal fractures. (c) Single fracture set.

only two times greater at two radii. In a locally variable, fractured rock mass, differences in hydraulic conductivity of less than one order of magnitude are not considered to be highly significant. As noted previously, the analyses are conservative in that conducting fractures are assumed to occur in the direction normal to the minimum stress. On the other hand, there is no allowance for any increases in fracture frequency or continuity close to the opening. On balance, the analyses may offer a reasonable approximation of actual disturbed zone characteristics.

The analyses described above have not taken into account the effects of pore pressures. Conceptually, pore pressures might influence disturbed zone characteristics in two ways. First, pore pressures acting in fractures will increase the hydraulic conductivity by reducing the effective normal stress acting across the fractures. This effect should be minor assuming that the pore pressures dissipate due to drainage. Second, pore pressures will reduce the rock mass strength (in response to reduced effective stresses) so that the extent of the plastic zone may be greater than that shown in Fig. 4. In a worst case, assuming no dissipation of the pore pressures, the extent of the plastic zone would be increased to approximately 2.0 radii as compared with 0.8 radii shown in Fig. 4. The distribution of hydraulic conductivity within the plastic zone would have the same general shape as shown in Fig. 4, and the maximum hydraulic conductivity would be the same.

CASE HISTORIES

Edgar Mine, Colorado

Tests to evaluate the degree of disturbance associated with various types of blasting (e.g. smooth-wall; conventional) are in progress at the Colorado School of Mines mining research facility in the Edgar Mine in Colorado [20–22]. The principal rock type in the test area is a banded biotite-gneiss which contains two major fracture sets as well as several other subsidiary fracture trends. Fracture spacing varies from 60 to 100 cm.

The damage zone experiments are conducted in an experimental horizontal tunnel 5 m wide by 3 m high at a depth below ground surface of 100 m. Three 30 m long

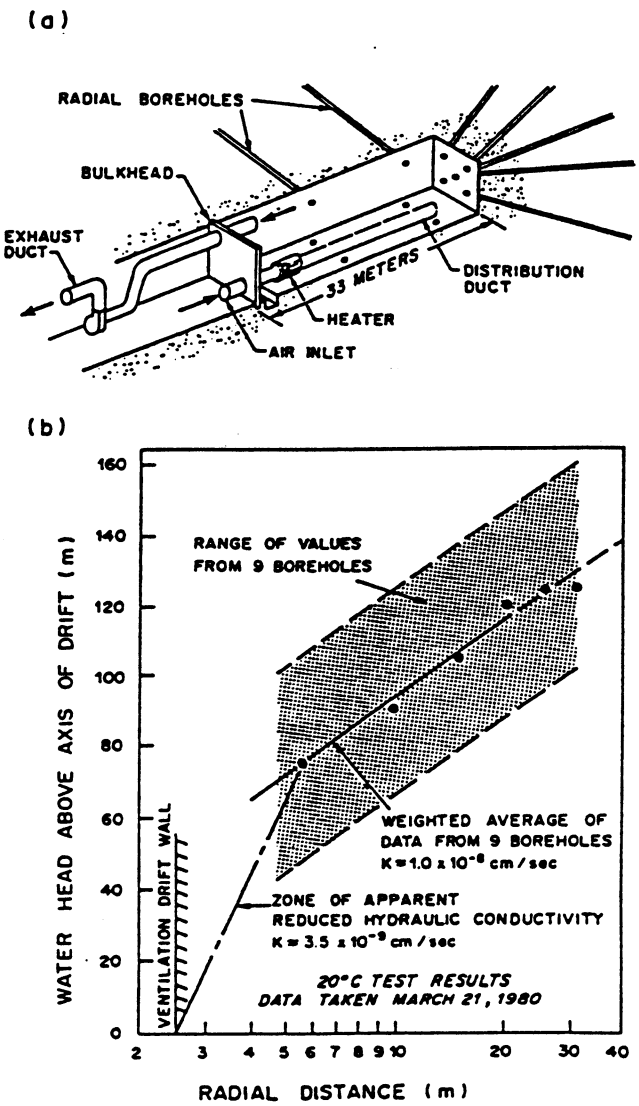

Fig. 6. Macropermeability test, Stripa (Nelson and Wilson [24]). (a) Test arrangement. (b) Distance-drawn on plot at end of 20°C temperature experiment.

holes were drilled parallel to the tunnel axis, and a pattern of 6.5 and 7.0 m long radial holes was drilled at each of six different blast round locations. A transient air injection method was used to measure permeability at intervals in each of these holes. Because the air injection tests were conducted in a partly saturated medium, and because the boundary conditions for the tests are poorly defined, the "permeabilities" obtained are better regarded as trend indicators than as accurate values. Acknowledging these limitations, the permeability of specific fractures oriented approximately perpendicular to the tunnel axis (as measured in the holes drilled parallel to the tunnel axis) was found to decrease by about one order of magnitude toward the tunnel face. In the radial boreholes, permeability was found to be higher (relative to far-field values) within 0.5–1.0 m of the face. These results appear to confirm the trends predicted by Fig. 3 for elastic behaviour in a shallow rock mass, in that the permeability of radial fractures tends to be reduced close to the tunnel wall, whereas the permeability of fractures oriented parallel to the tunnel axis tends to be increased close to the wall.

Stripa Mine, Sweden

Evidence regarding changes in permeability around a tunnel in granitic rock was obtained from the macropermeability test conducted at Stripa, Sweden [23, 24]. This test was designed to measure the permeability of a large volume of low-permeability, fractured rock by monitoring water inflow into a 33 m long section of a tunnel. Water inflow was monitored as the net moisture pick-up of the ventilation system inside a sealed portion of the tunnel. Hydraulic gradients around the tunnel were determined by monitoring groundwater pressures in piezometers installed in a total of 90 isolated intervals in 15 radial boreholes drilled from the tunnel. The tunnel was excavated using smooth-blasting techniques [25] at a depth of about 340 m. The major rock type in the tunnel is a medium-grained granite which is intruded by pegmatite and aplite dykes. Two major joint sets strike obliquely to the tunnel axis. Fracture frequency measured in holes drilled from the tunnel was on average 4.5 joints/m in inclined holes and 2.9 joints/m in vertical holes [26].

Figure 6 shows the hydraulic heads measured in the boreholes plotted vs radial distance from the wall of the tunnel. Using this plot, Nelson and Wilson [24] calculated an average rock mass hydraulic conductivity from the observed gradient (the slope of the head-distance plot) and the water inflow monitored in the tunnel. If the weighted average line shown in Fig. 6 is projected to the drift wall, it indicates a higher water head than can exist in practice. This indicates that there is a zone, approximately 2.5 m thick adjacent to the walls of the drift, in which the hydraulic conductivity is reduced by a factor of approximately three relative to the far-field value.

Nelson and Wilson [24] suggested that this permeability reduction might be related to thermal expansion of the rock or to chemical precipitation as the water evaporates into the tunnel. Although these explanations may be at least partly valid, an alternative explanation is that the permeability is reduced in response to the tangential stress concentration around the opening. This hypothesis is tested by comparing the observed changes with those predicted using the analytical approach described earlier. The predicted hydraulic conductivity is derived from equation (7) using empirical data for fracture deformability obtained by Iwai [8] from an induced fracture in a laboratory specimen (not Stripa granite). The far-field hydraulic conductivity away from the influence of the room is set as 1×10^{-8} cm/sec, the value inferred from the 20°C macropermeability test (Fig. 6). Assumptions made are that the flow to the tunnel is determined largely by radial fractures, and that the rock behaves essentially elastically. These assumptions are considered reasonable given that the dominant fractures strike obliquely to the tunnel and that the tunnel is located in good quality rock at relatively shallow depth (i.e. above the depth at which plastic behaviour would be anticipated).

Figure 7 shows that the predicted reduction in radial hydraulic conductivity close to the tunnel wall is consistent with the reduction inferred from the macropermeability test. The results apparently validate the hypothesis that increased tangential stresses may reduce hydraulic conductivities in the radial direction, although it is noted that the analysis involved several assumptions.

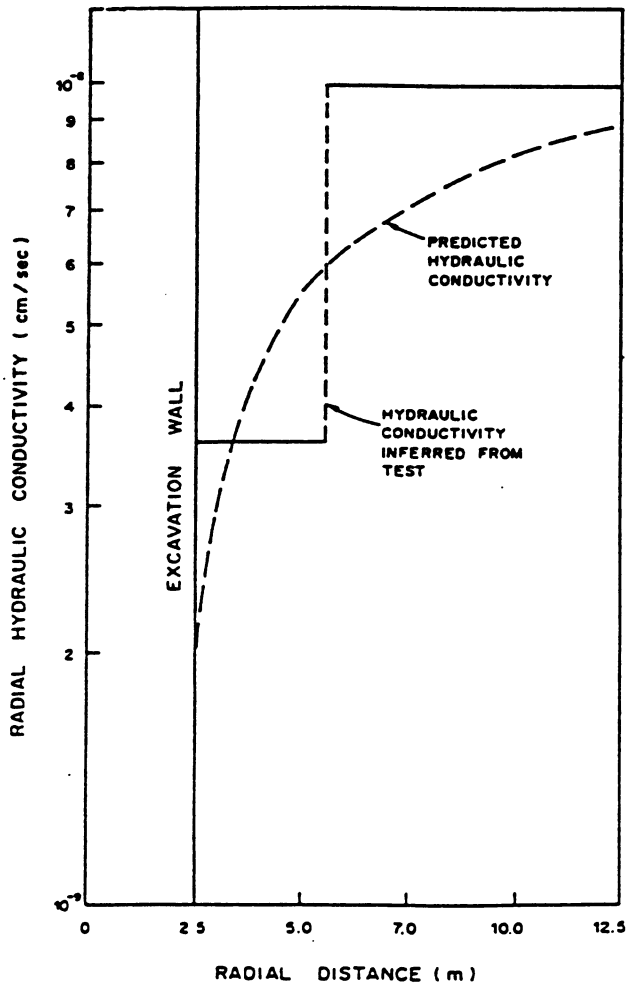

Fig. 7. Comparison of hydraulic conductivities predicted by analysis and inferred from field measurements, Stripa macropermeability test

The analysis may be extended to predict the increase in permeability that should occur in the disturbed zone in the axial direction.

Further confirmation of the influence of the tangential stress around the opening is obtained by considering the effects of temperature on flow rate into the tunnel. Theoretically, the effect of heating the tunnel should be to increase the tangential stress and, thereby, to reduce the rate of inflow. A simple analysis of thermal stresses around a tunnel was performed to demonstrate this effect. Temperature distributions around the tunnel were calculated using a closed-formed solution for transient heat conduction through a region bounded internally by a cylinder given by Carslaw and Jaeger [27]. Thermoelastic stresses were then calculated using relations developed by Carlsson [28] and the changes in stress were related to changes in rock mass hydraulic conductivity using equation (3) and data for fracture deformability obtained from Iwai [8]. The results showed that the flow rate for a test at 30°C should be approximately 30% lower than the flow rate at 20°C. The observed flow rates [24] were 50 ml/min at 20°C and 42 ml/min at 30°C, a difference of 16%.

Other disturbed zone assessments at Stripa were made by direct inspection of fractures produced by blasting and by borehole logging. A detailed inspection of the smooth-blasted tunnel walls showed that 10% of the outer ring holes had wavy fractures along their length [25]. The fractures were caused by blasting and their length ranged from 0.1 to 1.0 m. The extent of these fractures perpendicular to the tunnel walls was investigated by drilling a number of short core holes each intended to follow a particular fracture. The average extent of fractures was found to be about 0.3 m.

Other investigations

There are many case histories in the literature where the extent of the disturbed zone—but generally not the permeability—has been measured in tunnels or shafts. Methods used have included air-injection permeability tests in boreholes [4–6, 29, 30], seismic refraction or petite sismique [31–35], cross-hole seismic [36, 37], electrical resistivity [35], extensometers [35, 38], borehole deformation jacks [39], and plate-loading tests [40]. These investigations have generally shown that the major disturbance effects are limited to within one radius or less of the shaft or tunnel wall. Often, the results are indicative of a stress-relieved zone immediately adjacent to the face and a surrounding abutment zone with increased stresses.

Few of the investigations noted above have measured permeability in the disturbed zone. Fisekci and Barron [5] measured permeability as a function of depth in coal pillars at mines in Canada and Australia. The investigations were related to methane-inflow problems and permeability was evaluated from the rate of pressure increase due to methane inflow in packed-off sections of boreholes. Figure 8 shows permeability as a function of depth into the pillar face at the two sites. In one case, the permeability increases by nearly three orders of magnitude near to the edge of the rib, but in the other case the increase is much less dramatic. This difference may be attributed to differences in the properties of the coal or, possibly, to the greater depth of cover, and correspondingly lower undisturbed permeability, at the site displaying the greater change in permeability.

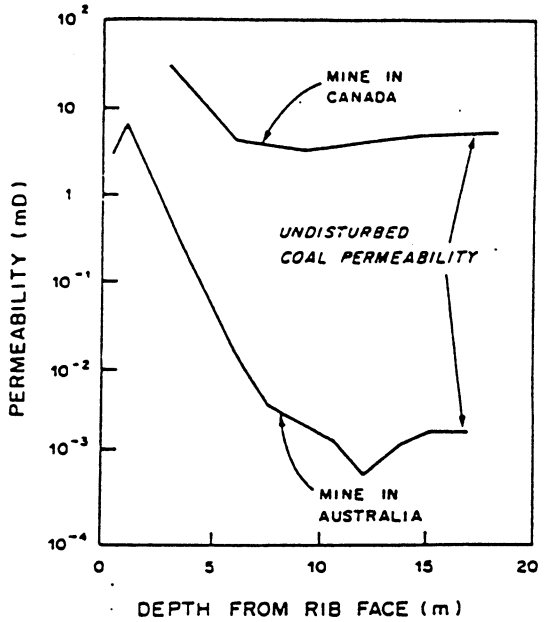

Fig. 8. Disturbed zone permeability in coal pillars measured by methane inflow between packers (Fisekci and Barron [5]).

Barron [4] used an air-injection method to investigate the degree of fracturing in coal pillars. In this case the air inflow in a packed-off section of a borehole was related to a fracture index which is inversely proportional to permeability. Figure 9 shows the variation in permeability observed across the complete width of a pillar. These results are interesting in that the variation in permeability closely matches the theoretical stress distribution across the pillar. Higher permeabilities close to the pillar edge correspond to a destressed zone, whereas lower permeabilities within the pillar correspond to increased stresses in abutment zones.

An air-injection method was also used to study the intensity of fracturing around a 3 m dia tunnel in volcanic rocks at the Nevada Test Site [6]. Injection tests were run at 0.3 m intervals in 17 boreholes drilled from

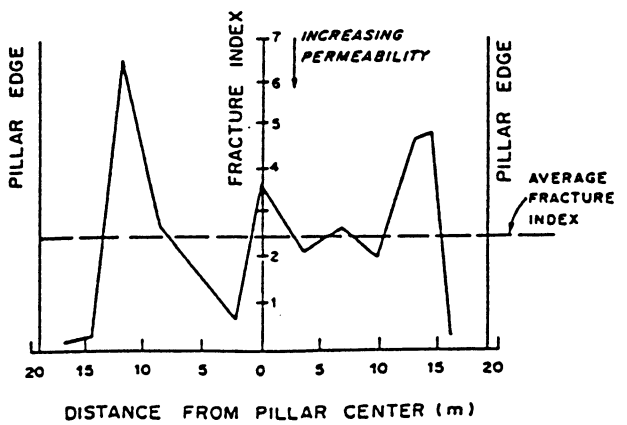

Fig. 9. Fracture index in a coal pillar measured by air-injection (Barron [4]).

the tunnel. Characteristically, the flow rates obtained were either very low (indicating no fractures present) or relatively high (indicating fractures present in the test interval), with 90% of the high flow rates recorded within 1.7 m of the tunnel face. Observations in the tunnel revealed many induced fractures attributed to blasting or stresses exceeding the rock strength. These induced fractures are probably responsible for the marked increase in permeability close to the tunnel face. The opening of pre-existing fractures in response to stress relief might be expected to produce a more gradational increase in permeability. The same air injection method was used to investigate fracturing around a shaft in the Coeur d'Alene mining district [30]. As at the Nevada Test Site, the flow rates obtained were typically very low away from the opening and much higher (6 orders of magnitude) in a surface zone extending 0.6–1.2 m from the shaft wall. Again, as at the Nevada Test Site, the marked increase in permeability results from the creation of fractures by blasting and stress relief.

DAMAGE DUE TO BLASTING

There are several case histories in the literature of investigations of the thickness of the zone damaged directly by blasting. Typical reported depths are 0.3 m for a 4 m wide tunnel in granite at Stripa [25], 0.3–0.6 m for a 2.4 m wide tunnel in gneiss at Churchill Falls [40], 0.5 m for the 5 m wide Edgar tunnel in gneiss [22], and "a few feet" for the 4 m dia Straight Creek pilot bore [35]. Nishida *et al.* [41] present an interesting example where the thickness of the "loosened zone" was compared for tunnel sections excavated in the same rock type (sandstone) using conventional blasting and tunnel-boring methods. In the section mined with a tunnel boring machine, the thickness of the loosened zone, measured by seismic refraction, was about 0.3 m. In sections mined by drill and blast, the thickness of the loosened zone was 0.6–1.3 m for sections lined with steel, and 0.3–0.7 m for sections supported at the face by bolts and shotcrete.

A general relation between blast damage and charge density for tunnel blasting conditions has been developed from Swedish experience in granitic rocks [42]. Figure 10 shows a series of correlations between peak particle velocity and radial distance from the charge for varying charge densities normalized for explosives with the weight strength of ANFO. The potential extent of the damage zone is indicated by the range of peak particle velocity associated with incipient rock fracture. This shows that a charge density of 1.5 kg/m ANFO should produce a damaged zone of about 1.5 m thickness. If the charge density (in the perimeter holes) is reduced to 0.2 kg/m, the damaged zone extent should be reduced to about 0.3 m. This reduced charge density can be achieved using an explosive with a lower linear charge density than ANFO. For example, GURIT, a special explosive used for smooth blasting in Sweden, has a linear charge density equivalent to 0.2 kg/m ANFO.

Figure 10 provides a general guideline for estimating the extent of the damage zone in hard, competent rocks when blasting parameters are known. The data suggest that blast effects are largely independent of excavation size. In practice, the extent of damage, relative to the size of the excavation, may be greater for smaller openings because of the effects of additional confinement. Also, the extent of the damage zone will be influenced by other parameters such as control of blasting procedures and rock conditions.

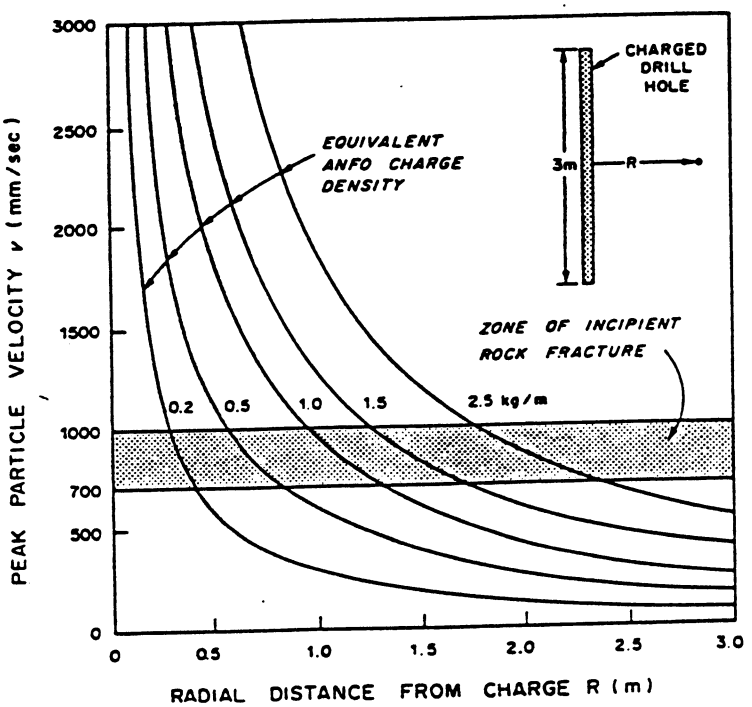

Fig. 10. Method for estimating thickness of blast-damaged zone in relation to explosive charge density (Holmberg and Persson [42]).

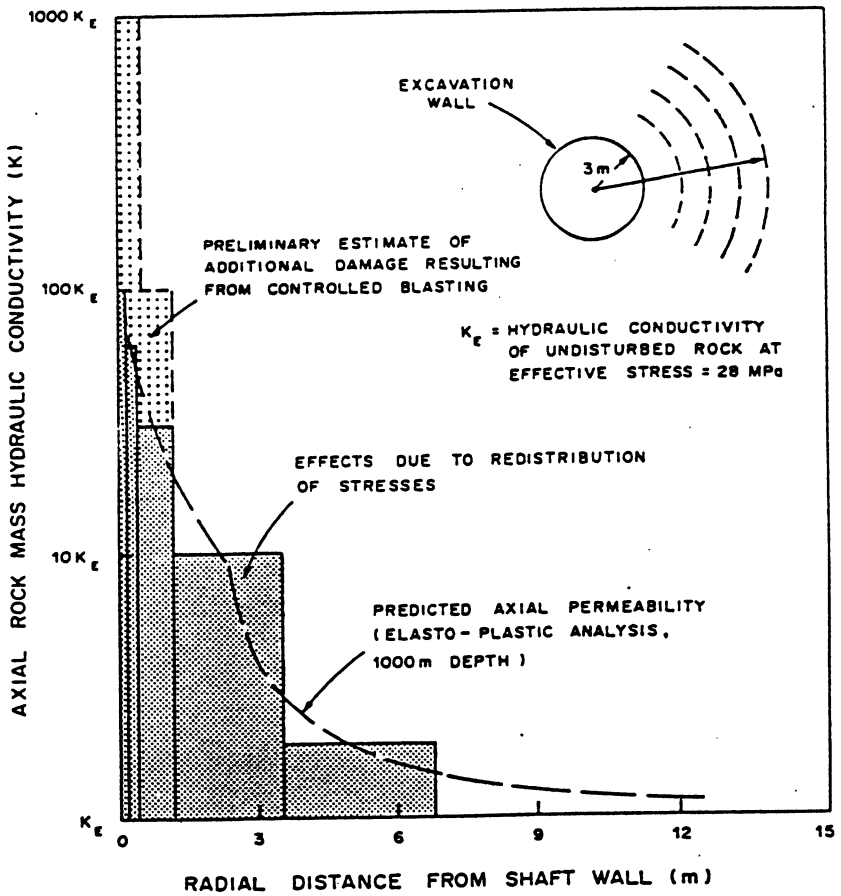

Fig. 11. Preliminary disturbed zone permeability model for a 3 m radius shaft in basalt at 1000 m depth (elasto-plastic analysis and isotropic initial stress condition).

Permeability changes associated with blast damage may be estimated from the increase in fracture frequency that is anticipated within the damaged zone. For example, consider a rock mass in which the natural fracture frequency is 10 fractures/m. Blasting is then assumed to create new fractures such that the frequency increases to 100 fractures/m within 0.3 m of the opening and to 30 fractures/m between 0.3 m and the edge of the blast-damaged zone at 1.0 m depth from the opening. (As a conservative assumption, this increase in fracture frequency is greater than has been observed at Stripa and other sites where controlled blasting has been used.) If the newly-created fractures have similar characteristics to the pre-existing fractures, the increase in permeability due to blasting (from equation 3) will be about 10 times in the outer zone and 5 times in the inner blast-damaged zone. These effects would be additional to the effects due to stress relief. Very highly-disturbed (shattered) material might occur in a thin skin adjacent to an opening wall, but this would usually be removed by scaling.

SUMMARY AND CONCLUSIONS REGARDING DISTURBED ZONE EXTENT AND PERMEABILITY IN FRACTURED ROCK

Data from field tests, supplemented by analytical evaluations, indicate a number of general trends regarding disturbed zone characteristics. 4.2-13-xxx

(1) There have been few measurements of disturbed zone permeability. Existing measurements show that disturbance may be obscured on a small scale (in borehole tests) by the variability of the undisturbed rock and that permeability may vary in the radial and longitudinal directions (as predicted by analysis).

(2) Theoretically, the effects of stress redistribution on fracture permeability are influenced by the orientation of the fractures relative to the axis of the opening and by the nature of deformations. In the case of essentially elastic behaviour (in competent rock at shallow depths), the permeability of fractures aligned parallel to the axis should be increased in the disturbed zone whereas the permeability of fractures aligned radially should be reduced in the disturbed zone. In deeper excavations where the rock exhibits inelastic deformation, the permeability of all fractures in the disturbed zone should be increased.

(3) An analytical approach has been presented for estimating the effects of stress changes on rock mass hydraulic conductivity in closely-fractured competent rock. This analysis suggests that hydraulic conductivities parallel to the axis of an opening may be increased relative to the undisturbed condition by two to three orders of magnitude. For a circular opening in basalt, in an isotropic initial stress field at a depth of 1000 m, the zone in which the axial hydraulic conductivity is increased by at least one order of magnitude may extend one to two radii from the wall. Highly anisotropic initial

stresses could result in more extensive disturbance, particularly if a major principal stress is parallel to a major fracture set.

(4) In practice, the effects of stress changes on hydraulic conductivity will depend on many factors related to site geology (especially fracture characteristics), excavation method, depth and penetration geometry. Provided that rock properties are well known, the simple analytical method described herein could be adapted for a wider range of geological conditions examining, for example, effects on discrete fractures or specific fracture systems.

(5) Few disturbed zone studies specifically distinguish blast-damage and stress relaxation effects. Available data indicate that significant blast-damage (creation of new fractures) may be limited to a zone 1 m or less thick. The extent of blast-damage will be greatly influenced by blasting technique but may be more or less independent of excavation size within the probable limits for repository shafts and tunnels. More severe disturbance may occur in a thin zone immediately adjacent to the face.

These preliminary conclusions are illustrated as a disturbed zone model for a 3 m dia shaft in basalt (Fig. 11). Although this model is tentative, it is more realistic than a model which assumes a uniform permeability across the disturbed zone. The model used to predict the effects of a stress redistribution was developed for basalt at a depth of 1000 m based on an elasto-plastic stress distribution and an isotropic initial stress condition. The model is probably conservative for shallower depths. As noted previously, the effects attributed to blast damage are derived from a preliminary estimate and require field confirmation.

Using the model in Fig. 11, it can be shown that blasting accounts for approximately 50–70% of the increased flow potential through the disturbed zone caused by blasting and stress relief combined. (The proportion due to blasting reduces as the penetration diameter increases because the blast-damaged zone is assumed to have the same depth regardless of the penetration size.) All of the blast damage occurs within 1 m of the penetration face with a substantial proportion within 0.3 m of the face. With regard to repository sealing, this damaged "skin" could be removed in critical seal zones by machine excavation.

FIELD INVESTIGATION OF DISTURBED ZONE PERMEABILITY

Additional field data are required to confirm the disturbed zone model presented in this paper. Possibly no one single technique is completely suitable for measuring disturbed zone permeability, and a combination of methods may be required. Test methods that might be considered include:

- macropermeability (similar to the Stripa test);
- piezometers installed in boreholes at varying distance from excavation;
- injection tests in boreholes;
- cross-hole tracer flow;
- integral sampling in boreholes, and borescope or impression packer logging;
- resistivity and radar profiling;
- seismic refraction (petite sismique) surveys;
- cross-hole acoustic surveys;
- borehole deformation jack;
- plate loading;
- multiple-point borehole extensometers.

Air-injection tests in boreholes drilled radially from an opening or parallel to the opening have been used as indices of disturbance in previous disturbed zone investigations. Although there are problems related to interpretation of these tests, they are relatively inexpensive and easy to perform and can be adapted to a wide range of *in situ* permeabilities. A shortcoming of all tests conducted in boreholes in fractured rock, however, is that only a very small volume of the rock mass is sampled by each test interval. Results will be strongly influenced by localized fracture frequency and disturbance may be obscured by pre-existing variations in the rock mass.

Seismic refraction surveys overcome the disadvantages of borehole surveys by sampling a much larger volume of the rock mass. Many case histories [e.g. 32–35] have demonstrated that seismic refraction can be used to delineate the extent of the disturbed zone in a variety of rock conditions. Also, laboratory studies [43, 44] have demonstrated that the relation between stress and seismic parameters is similar in form to the relation between stress and permeability shown in Fig. 1. It appears promising that good correlations between permeability and seismic parameters might be established for a particular rock type, and that seismic surveys could be used to estimate disturbed zone permeability *in situ*.

Acknowledgements—The work described in this paper was supported by the U.S. Department of Energy through the Office of Nuclear Waste Isolation, Battelle Memorial Institute, Columbus, Ohio, U.S.A.

Received 4 *March* 1983; *revised* 17 *November* 1983.

REFERENCES

1. U.S. Nuclear Regulatory Commission. Disposal of high-level radioactive wastes in geologic repositories: technical criteria (10 CFR 60). *Fedl Register* 48(120), 28194–28229 (1983).
2. Kelsall P. C., Case J. B. and Chabannes C. R. A preliminary evaluation of the rock mass disturbance resulting from shaft, tunnel, or borehole excavation. ONWI-411. Office of Nuclear Waste Isolation, Battelle Memorial Institute, Columbus, OH (1982).
3. Brown E. T. and Bray J. W. Rock-support interaction calculations for pressure shafts and tunnels. *Proc. ISRM Symp.*, Aachen, pp. 555–565 (1982).
4. Barron K. An air injection technique for investigating the integrity of pillars or ribs in coal mines. *Int. J. Rock Mech. Min. Sci. & Geomech. Abstr.* 15, 69–76 (1978).
5. Fisekci M. Y. and Barron K. Methane pressure and flow measurements in coal and surrounding strata. *Can. Min. metall. Bull.* 68, 91–98 (1975).
6. Miller C. H., Cunningham D. R. and Cunningham M. J. An air-injection technique to study intensity of fractures around a

tunnel in volcanic rock. *Bull. Ass. Engng Geol.* XI(3), 203–217 (1974).
7. Witherspoon P. A., Wang J. S. Y. and Gale J. E. Validity of cubic law for fluid flow in a deformable rock fracture. *Wat. Resour. Res.* 16(6), 1016–1024 (1980).
8. Iwai K. Fundamental studies of fluid flow through a single fracture. Ph.D. Dissertation, Univ. of California, Berkeley (1976).
9. Goodman R. E. *Methods of Geological Engineering in Discontinuous Rocks*. West, St Paul, MN (1976).
0. Hoek E. and Brown E. T. *Underground Excavations in Rock*. IMM. London (1980).
1. Kranz R. L., Frankel A. D., Engelder T. and Scholz C. H. The permeability of whole and jointed Barre granite. *Int. J. Rock Mech. Min. Sci. & Geomech. Abstr.* 16, 225–234 (1979).
2. Gale J. E. The effects of fracture type (induced versus natural) on the stress-fracture closure-fracture permeability relationships. *Proc. 23rd Symp. on Rock Mechanics*, Berkeley, pp. 290–298 (1982).
3. Pratt H. R., Swolfs H. S., Brace W. F., Black A. D. and Handin J. W. Elastic and transport properties of an *in situ* jointed granite. *Int. J. Rock Mech. Min. Sci. & Geomech. Abstr.* 14, 35–45 (1977).
4. Voegele M., Hardin E., Lingle D., Board M. and Barton N. Site characterization of joint permeability using the heated block test. *Proc. 22nd U.S. Symp. on Rock Mechanics*, MIT, pp. 120–128 (1981).
5. Gangi A. F. Variation of whole and fractured porous rock permeability with confining pressure. *Int. J. Rock Mech. Min. Sci. & Geomech. Abstr.* 15, 249–257 (1978).
6. Tsang Y. W. and Witherspoon P. A. Hydromechanical behavior of a deformable fracture subject to normal stress. *J. geophys. Res.* 86, 9287–9298 (1981).
7. Witherspoon P. A. Effect of size on fluid movement in rock fractures. *Geophys. Res. Lett.* 8(7), 659–661 (1981).
8. Bray J. W. A study of jointed and fractured rock—part II: theory of limiting equilibrium. *Rock Mech.* 4, 197–216.
9. Jaeger J. C. and Cook N. G. W. *Fundamentals of Rock Mechanics*. Methuen, London (1969).
0. Hustrulid W., Cudnik R., Trents R., Holmberg R., Sperry P. E., Hutchinson R. and Rosasco P. Mining technology development for hard rock excavation. *Proc. Rockstore 80 Symp.*, Stockholm, Sweden, Vol. 2, pp. 919–926. Pergamon Press, Oxford (1980).
1. El Rabaa A. W., Hustrulid W. A. and Ubbes W. F. Spatial distribution of deformation moduli around the CSM/ONWI room, Edgar Mine, Idaho Springs, Colorado. *Proc. 23rd Symp. on Rock Mechanics*, Berkeley, pp. 790–801 (1982).
2. Montazer P., Chitombo G., King R. and Ubbes W. F. Spatial distribution of permeability around CSM/ONWI room, Edgar Mine, Idaho Springs, Colorado. *Proc. 23rd Symp. on Rock Mechanics*, Berkeley, pp. 47–56 (1982).
3. Witherspoon P. A., Cook N. G. W. and Gale J. E. Geologic storage of radioactive waste: field studies in Sweden. *Science* 211, 894–900 (1981).
4. Nelson P. and Wilson C. Thermomechanical and macropermeability experiments in the Stripa granite—status report. *Proc. Workshop on Thermomechanical-Hydrochemical Modeling for a Hardrock Waste Repository*, LBL-11204, Lawrence Berkeley Laboratory (1980).
5. Andersson B. and Halen P. A. Mining methods used in the underground tunnels and test rooms at Stripa. Lawrence Berkeley Laboratory, Report 7081 (1978).
6. Olkiewicz A., Gale J. E., Thorpe R. and Paulsson B. Geology and fracture system at Stripa. Lawrence Berkeley Laboratory, Report LBL-8907 (1979).
7. Carslaw H. S. and Jaeger J. C. *Conduction of Heat in Solids*. Clarendon Press, Oxford (1959).
8. Carlsson H. A pilot heater test in the Stripa granite. Lawrence Berkeley Laboratory, Report LBL-7086 (1978).
9. Chan S. S. M., Thomas H. E. and Bada N. Air injection and hot-film flow logging for evaluation of roof cracks in White Pine mine. *Trans. Soc. min. Engrs, Am. Soc. min. Engrs* 256, 131–137 (1974).
0. Miller C. H. and Skinner E. H. The nature of fracturing and stress distribution in quartzite around the 1128 m (3700 ft.) level of the Crescent mine, Coeur de Alene Mining District, Idaho. *Engng Geol.* 16, 321–338 (1980).
1. Bieniawski Z. T. The 'petite sismique' technique—a review of current developments. *Proc. 2nd Conf. on Acoustic Emission/Microseismic Activity in Geologic Structures and Materials*, Pennsylvania State Univ. (Edited by Hardy H. R. and Leighton F. W.). Trans. Tech., Clausthal, West Germany (1980).
2. Plichon J. N. Measurement of the thickness of the decompressed zone in an excavation under high overburden cover, in Analysis of Tunnel Stability by the Convergence-Confinement Method. *Undergr. Space* 4(6), 361–402 (1980).
3. Murphy V. J. Seismic velocity measurements for moduli determinations in tunnels. *Proc. 1st North American Rapid Excavation and Tunneling Conf.*, Chicago, Vol. 1, pp. 209–216 (1972).
4. Brizzolari E. Miniseismic investigations in tunnels: methodology and results. *Geoexploration* 18, 259–267 (1981).
5. Scott J. H., Lee F. T., Carroll R. D. and Robinson C. S. The relationship of geophysical measurements to engineering and construction parameters in the Straight Creek Tunnel pilot bore, Colorado. *Int. J. Rock Mech. Min. Sci. Geomech. Abstr.* 5, 1–30 (1968).
6. O'Donogue J. B. and O'Flaherty R. M. The underground works in Turlough Hill; part I. *Wat. Pwr*, January, pp. 5–12 (1974).
7. Kujundzic B., Joranovic L. and Radosavljevic Z. A pressure tunnel lining using high-pressure grouting (in French). *Proc. 2nd Congr. ISRM*, Belgrade, pp. 4–66 and 867–881 (1970).
8. Cording E. J., Hendron A. J. and Deere D. U. Rock engineering for underground caverns. *Undergr. Rock Chambers*, pp. 567–600, ASCE, New York (1971).
9. Heuze F. E. Geomechanics of the Climax "mine-by", Nevada Test Site. *Proc. 22nd U.S. Symp. on Rock Mechanics*, MIT, pp. 428–434 (1981).
0. Benson R. P., Murphy D. K. and McCreath D. R. Modulus testing of rock at the Churchill Falls underground powerhouse, Labrador. In *Determination of the* In Situ *Modulus of Deformation of Rock*, American Society for Testing and Materials, ASTM STP 77, pp. 89–116 (1970).
1. Nishida T., Matsumura Y., Miyanga Y. and Hori M. Rock mechanical viewpoint on excavation of pressure tunnel by tunnel boring machine. *Proc. IRSM Symp.*, Aachen, pp. 815–826 (1982).
2. Holmberg R. and Persson P. A. Design of tunnel perimeter blasthole patterns to prevent rock damage. *Trans. Instn Min. Metall.* 89, A37–40 (1980).
3. New B. M. and West G. The transmission of compressional waves in jointed rock. *Engng Geol.* 15, 151–161 (1980).
4. Stacy T. R. Seismic assessment of rock masses. *Proc. Symp. on Exploration for Rock Engineering*. Johannesburg, South Africa, Vol. 2, pp. 113–117 (1976).

SOCIETY OF MINING ENGINEERS OF AIME

CALLER NO. D, LITTLETON, COLORADO 80127

PREPRINT NUMBER

84-28

IMPACT OF EXCAVATION TECHNIQUE ON STRENGTH OF OIL SHALE PILLARS

J. F. T. Agapito

H. N. Maleki

J. R. Aggson

J. F. T. Agapito and Associates, Inc.
Grand Junction, Colorado

L. A. Weakly

Exxon, Company, U. S. A.
Grand Junction, Colorado

For presentation at the SME-AIME Annual Meeting
Los Angeles, California - February 26-March 1, 1984

Abstract. The load carrying capacity of oil shale pillars excavated by conventional blasting, presplit blasting, and mechanical mining is evaluated. The study was based on a comparison of in-situ vertical stresses and fractures obtained from overcoring horizontal holes in the Colony Mine, Piceance Creek Basin, Colorado. Results indicate that conventional blasting causes a zone of damage approximately 3 m (10 ft) thick with low stress distributions. Presplit blasting reduces damage significantly, and increases the load carrying capacity in the 3 m (10 ft) thick zone by 5.93 MPa (860 psi). Mechanical mining causes little or no rock damage, and an increase of 9.83 MPa (1425 psi) in strength in the same 3 m (10 ft) thick zone. An example of pillar design is given showing that the use of presplit blasting and mechanical mining techniques can increase the extraction ratio by at least three and five percent, respectively, as compared to conventional blasting. It is speculated that comparable increases in extraction should also occur due to increases in span dimensions.

Introduction

In excavating large underground openings, the question often arises as to how much structural damage is caused by the use of explosives. Conventional blasting usually destroys the rock quality near underground openings by producing fractures that can penetrate several feet into the rock mass. The resulting damage reduces rock strength and increases the possibility of rib and roof failures. Controlled blasting techniques have been used successfully during the last 20 years for reducing vibration and overbreak. The introduction of these techniques has reduced the incidence of rock failure, which is one of the greatest of all mining hazards. The development of mechanical excavators has further enhanced the rock quality around mine openings by eliminating blasting damage altogether.

This paper evaluates the strength of oil shale pillars excavated by conventional and presplit blasting techniques, and by mechanical mining. The study was based on a comparison of the rock quality and vertical stress profiles obtained in pillars and rib walls formed by these three excavation techniques. The evaluation was greatly enhanced because some of the stress determinations were made very near the ultimate load carrying capacity of two pillars. Thus, in-situ strength criteria was available, which formed a basis for the analysis presented in this paper. The work was conducted at the Colony Pilot Mine located in the Piceance Creek Basin of northwestern Colorado. The Colony property is owned by Exxon Company.

Mine Structure and Pillar Strength

The Colony Pilot Mine has been used for conducting numerous mine studies on oil shale during the past 18 years. Room and pillar mining with an upper heading and benching was used to form 18.3 m (60 ft) cube pillars, and rooms 16.8 m (55 ft) wide by 18.3 m (60 ft) high. The upper heading and benching heights were 9.5 and 8.8 m (31 and 29 ft), respectively. Mining was performed at depths of 183 to 259 m (600 to 850 ft) in the Mahogany zone - a high kerogen content horizon located in the Parachute Creek Member of the Green River Formation. The geologic mine structure is characterized by a well-defined system of joints and bedding planes. Joint inclinations may vary from vertical to 45° and more, with spacing from a few centimeters to three or more meters. There are two major joint sets in the property, one system oriented at N 65° E, and the other at N 73°W. The in-situ rock mass strength is greatly dependent on these systems of joints and bedding planes. Small specimens of oil shale from the mining horizons without joints have a laboratory uniaxial compressive strength of 89.7 MPa (13,000 psi), but mine pillars have been monitored to fail at approximately 21.4 MPa (3,100 psi) (Agapito, 1974). Nevertheless, the rock mass is quite strong compared to many other rock materials, as shown by the large opening sizes in oil shale mines.

Blasting Effects On Mine Structure

Blasting impacted the pillars more than the roof. The roof follows a consistent bedding plane which separates easily, helping dampen blasting vibrations. However, three out of four major rock falls in the mine were triggered by blasting.

The upper bench openings were excavated with a 9.1 m (30 ft) deep V-cut round using 10.8 cm (4-1/4 in.) diameter holes. The holes were loaded with ANFO, with a maximum charge weight of 97.5 kg (215 lbs) in a single delay, and a total charge for the round of 805 kg (1775 lbs). The 8.8 m (29 ft) high bench was excavated by using three rows of vertical 10.8 cm (4-1/4 in.) holes spaced at 3 m (10 ft). The amount of explosive used in benching was less than that used in the upper heading.

Conventional blasting techniques impacted mostly the pillar corners, causing relatively large slabs to fall out. This caused, in some intersections, an increase in roof spans of 1.5 to 3 m (5 to 10 ft), and a comparable reduction in pillar sizes. Presplit blasting was done in a few rounds to determine the degree of wall rock quality improvement that could be obtained. The presplit was obtained by an outer row of 10.8 cm (4-1/4 in.) holes spaced approximately at 1.2 m (4 ft), both for the V-cut and bench rounds. These rows of holes were timed to fire first and simultaneously followed by the normal round. By locating the perimeter holes near each other, a fracture was obtained between the holes, which protected the walls by reflecting the shock waves from the main blast.

Mechanical Miner Test

In 1981 a Dosco TB 600 Twin Boom Miner was tested at the Colony Pilot Mine to determine the feasibility of the machine excavating key areas requiring long-term stability, such as the underground shop, warehouse, portals, etc. Another objective of the testing was to develop basic information to design a production-size mechanical miner. A total advance of 153 m (501 ft), equivalent to 5,972 tons (6,358 short

tons), of oil shale was mined. Details regarding some of this work have been given by Crookston, et al. (1983). Stress determinations were conducted as part of the test program to compare the support capacity of walls formed by blasting and mechanical mining.

Comparison of Rock Quality

Visual observations indicate that the wall rock formed by presplit blasting and mechanical mining has significantly less fractures than that formed by conventional blasting. Figures 1 and 2 show the contrast in rock quality between mechanical mining and conventional blasting, and between presplit and conventional blasting, respectively.

Seven drill holes, cored for stress determinations, were used for evaluating the degree of fracturing in the wall rock. These holes were 15.25 cm (6 in.) in diameter, and varied in length from 4.5 to 18.3 m (15 to 60 ft). All holes were drilled horizontally approximately at the mid mining horizon. Figure 3 shows the plan view of the mine with the location of the holes. Holes 2, the east half of 3, 5 and 7 were drilled in conventionally blasted walls; holes 1 and the west half of 3 in walls excavated by the Dosco Miner; and holes 4 and 6 in walls formed by presplitting.

The following should be noted concerning the hole locations:

- Hole 3 was drilled all the way through a stub pillar. The west side was excavated by the Dosco Miner, and the east side by conventional drilling and blasting.
- Approximately identical loading conditions should exist between holes 1 and 2, the east and west sides of hole 3, holes 4 and 5, and holes 6 and 7.
- Both pillars in which holes 6 and 7 were located failed. These failures have been described in previous papers (Agapito, 1974; Agapito and Page, 1976). The pillar in which hole 6 was located failed quite extensively. The outline of the pillar when the hole was drilled is shown as a dotted line in Figure 3.
- The barrier pillar in which holes 4 and 5 are located has an abutment load due to pillar failure in the center of the mine. Both holes in this pillar were drilled after the pillars failed.

Figure 4 shows the log of the 15.25 cm(6 in.) diameter cores obtained from the above holes. All fractures and open joints were logged. The approximate depth of induced damage seems quite consistent for the different excavation techniques. A significantly higher number of fractures occur to a depth of 3 m (10 ft) in the conventionally blasted walls. This depth confirms previous observations from other holes (Agapito, 1974). Presplit walls showed a fracture depth of 0.6 to 1.8 m (2 to 6 ft), and the mechanically mined walls, for practical purposes, have no visible damage. Figure 5 is a photograph of the core obtained from hole 3. The top of the photograph shows the good quality rock obtained near the machine-mined wall. The bottom of the photograph shows the poor rock quality obtained near the conventionally blasted wall. The blasting fractures usually can be differentiated from existing geological joints, since they tend to be more random and closely spaced.

Comparison of Vertical Stress Distributions

Stress determinations using the overcoring technique and the USBM deformation gage were made to determine the vertical load distribution perpendicular to the holes. Previous measurements indicated that this technique is very reliable for determining pillar loads at the Colony Pilot Mine (Agapito, 1974). Comparison of average stresses, obtained by dividing the area of the stress profiles by the length overcored, were found to be particularly useful in evaluating pillar loads, since irregularities in stresses caused by fractures and joints were evened out.

The increase in strength caused by reducing or eliminating blasting vibrations is shown as higher stress distributions near the openings created by presplit blasting and mechanical mining. Figures 6 through 9 compare the vertical stress distribution and fracture logs between holes located in areas of similar loading conditions (Figure 3). Table 1 summarizes the comparisons in terms of depth and load carrying capacity.

The stress profiles indicate the following:

- Depth of increased load carrying capacity varied from 2.1 to 4.5 m (7 to 15 ft), with an average of approximately 3 m (10 ft). The improvement in load carrying capacity varied from 1.54 to 2.36 MPa/m (68 to 104 psi/ft) for presplit walls to 3.23 MPa/m (142.5 psi/ft) for mechanically mined walls.
- Mechanically mined walls can carry high loads very near the openings (Figures 6 and 7); the contrast in stress distributions with conventionally blasted walls is well illustrated in Figure 7. The mechanically mined walls carry a high stress near the opening, which decreases rapidly to a nearly flat profile at 1.5 m (5 ft). The stresses remain approximately constant to a depth of 5 m (16.5 ft), and then decrease abruptly. Stress determinations were not possible from 5.5 m (18 ft) to the end of the hole at 7.9 m (26 ft) because of the blasting-induced fractures shown in the log. The depth of blast damage is approximately 3 m (10 ft) - the distance to the background stress level at 12.4 to 13.8 MPa (1800 to 2000 psi).
- The increase in load carrying capacity of the presplit walls is shown in Figures 8 and 9. The holes in Figure 8 are located in a barrier pillar subjected to abutment pressures transferred from the center of the mine (Figure 3). The abutment is shown as a double peak in the presplit wall at 0.6 and 4.6 m (2 and 15 ft), and as a single peak in the conventionally blasted wall at 6.4 m (21 ft). Overcoring measurements were made to a depth of 9.1 m (30 ft) in the presplit wall, and 18.2 m (60 ft) in the conventionally blasted wall. The increase in

load carrying capacity in the presplit wall occurs in the first 4.6 m (15 ft). Both profiles have identical average stresses from 4.6 to 9.1 m (15 to 30 ft). The average stresses beyond 9.1 m (30 ft) are assumed identical in both holes. The decay in abutment stress is very noticeable in both profiles.

- Holes 6 and 7 (Figure 9), completed just before pillar failure, show a significant difference in load carrying capacity in the first 3 m (10 ft). However, both profiles become very similar from 3 to 9.1 m (10 to 30 ft), the center of the pillar. They also indicate that a stress level of approximately 27.6 MPa (4000 psi) may be the maximum average load carrying capacity of rock unaffected by blast damage in 18.2 m (60 ft) cube pillars.

Pillar Strength Estimates

Strength of conventionally blasted pillars at the Colony Mine has been estimated at 21.4 MPa (3100 psi) (Agapito, 1974). Data from five pillars was used in this evaluation, including the profile of hole 6 (Figure 9). The strength profile for the 18.3 m by 18.3 m (60 ft by 60 ft) pillars may be conceptualized as: (1) a 3 m (10 ft) thick blast damage zone with a load carrying capacity of 16.6 MPa (2400 psi), and (2) an inner "intact" core from 3 m (10 ft) to the center of the pillar, with a load carrying capacity of 27.6 MPa (4000 psi) (Figure 10a).

In comparison to the above, the strength profile of a presplit pillar has an average additional 1.95 MPa/m (86 psi/ft) (Table 1) in the first 3 m (10 ft). This is equivalent to an additional load carrying capacity of 3.5 MPa (500 psi) in an 18.3 m by 18.3 m (60 ft by 60 ft) pillar, or a pillar strength of 24.8 MPa (3600 psi). The profile may be visualized as: (1) a 1.5 m (5 ft) thick blast damage zone with a load carrying capacity of 16.6 MPa (2400 psi), and (2) an "intact" core from 1.5 m (5 ft) to the center of the pillar, with a load carrying capacity of 27.6 MPa (4000 psi) (Figure 10b).

The mechanically mined pillar has an additional load carrying capacity of 3.23 MPa/m (142.5 psi/ft) (Table 1), as compared to pillars formed by conventional blasting. In an 18.3 m by 18.3 m (60 ft by 60 ft) pillar, this is equivalent to an additional load carrying capacity of 5.5 MPa (800 psi), or a pillar strength of 26.9 MPa (3900 psi). This value is very close to the 27.6 MPa (4000 psi) maximum average load carrying capacity of rock unaffected by blast damage mentioned previously. The strength profile in this case consists of a flat line at 27.6 MPa (4000 psi) with a few centimeters of mechanically-induced damage (Figure 10c).

Figure 11 shows the relation between the improvement in pillar strength and size of square pillars. This strength improvement is much more significant in narrow pillars than in wide pillars because of the higher proportion of the total pillar area affected by blasting.

Pillar design calculations were made to illustrate the pillar size reductions and extraction ratio increase that may be obtained by using presplit or mechanical mining techniques. The induced horizontal stress method of pillar design was used to obtain the pillar sizes (Agapito and Hardy, 1982). A room and pillar layout at a depth of 244 m (800 ft) with square pillars, 15.2 m (50 ft) mining height, and 16.8 m (55 ft) spans was assumed. In addition, a pillar safety factor of 1.5, a lithostatic stress field, and a vertical stress gradient of 22.7 kPa (1 psi/ft) were used in the calculations. Figure 12 shows both the relationship between the strength and width, and the stress and width. The ascending strength curves for the three excavation techniques show how the pillars' width for a given strength may be reduced. The pillar size is obtained at the intersection of the strength at stress curves. Table 2 summarizes the results obtained.

Table 2 shows improvements in extraction ratios of three and five percent for presplit and mechanically mined pillars, respectively. This improvement in resource recovery seems small at first, but can be significant because of accompanying span increases which may possibly contribute another three to five percent in extraction ratio. It should be noted that a one percent improvement in resource recovery represents several millions of barrels of oil. In addition, there are two other major advantages in reducing or eliminating blasting vibrations. First, there is improved safety because of a reduction in rock falls; and secondly, there is improved productivity because of less time needed for scaling and installing remedial support.

Conclusions

Stress determinations and observations indicate that improved rock quality and pillar strength will result as blasting vibrations are reduced or eliminated. Increases in strength are significant mostly in narrow pillars. Reductions in pillar size can bring improvements in resource recovery of at least three to five percent.

Economic and technical feasibility of mechanical excavators in oil shale has not yet been proven. There is a good possibility, however, that if the oil shale industry becomes viable, so will the application of mechanical excavators. The use of controlled blasting techniques to reduce blasting damage is well developed, and can be applied directly to oil shale mining with concrete benefits in the areas of safety, productivity and resource recovery.

References

Agapito, J. F. T., 1974, "Rock Mechanics Applications to the Design of Oil Shale Pillars," Mining Engineering, May, pp. 20-25.

Agapito, J. F. T. and Hardy, M. P., 1982, "Induced Horizontal Stress Method of Pillar Design in Oil Shale," Proceedings, 15th Oil Shale Symposium, Colorado School of Mines, Golden, Colorado, pp. 179-191.

Agapito, J. F. T. and Page, J. B., 1976, "A Case Study of Long-Term Stability in the Colony Oil Shale Mine, Piceance Creek Basin,

Colorado," Proceedings, 17th U. S. Symposium on Rock Mechanics, Snowbird, Utah, p. 3A4-1-G.

Crookston, R. B., Weiss, D. A. and Weakly, L. A., 1983, "Mechanical and Conventional Excavating Experience in Oil Shale Shafts and Tunnels," Proceedings, Rapid Excavation and Tunneling Conference, Chicago, Illinois.

Table 1. Comparison of Depth and Load Carrying Capacity

Comparison of Holes (Numbers)	Figure Number	Comparison of Excavation Techniques	Depth of Improved Load Carrying Capacity (m)	(ft)	Improvement in Load Carrying Capacity (MPa/m)	(psi/ft)
1 and 2	6	Mechanical mining and conventional blasting	2.1	(7)	3.27	(144)
3 West and 3 East	7	Mechanical mining and conventional blasting	3.0	(10)	3.20	(141)
4 and 5	8	Presplit and conventional blasting	4.6	(15)	1.54	(68)
6 and 7	9	Presplit and conventional blasting	3.0	(10)	2.36	(104)

Table 2. Example of Pillar Sizes and Extraction Ratios

Excavation Technique	Pillar Size (m by m)	(ft by ft)	Extraction Ratio (%)
Conventional blasting	21.9	(72)	68
Presplit blasting	19.8	(65)	71
Mechanical mining	18.3	(60)	73

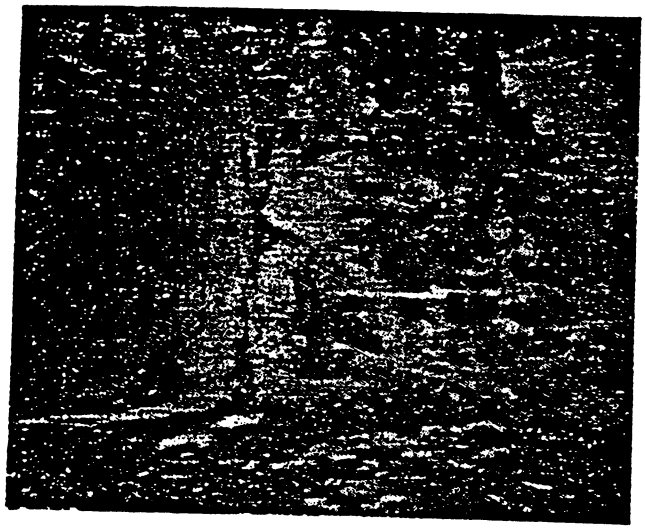

Figure 1. Wall Rock Quality Produced by Mechanical Mining in the Left and Conventional Blasting in the Right

Figure 2. Wall Rock Quality Produced by Presplit Blasting in the Right and Conventional Blasting in the Center

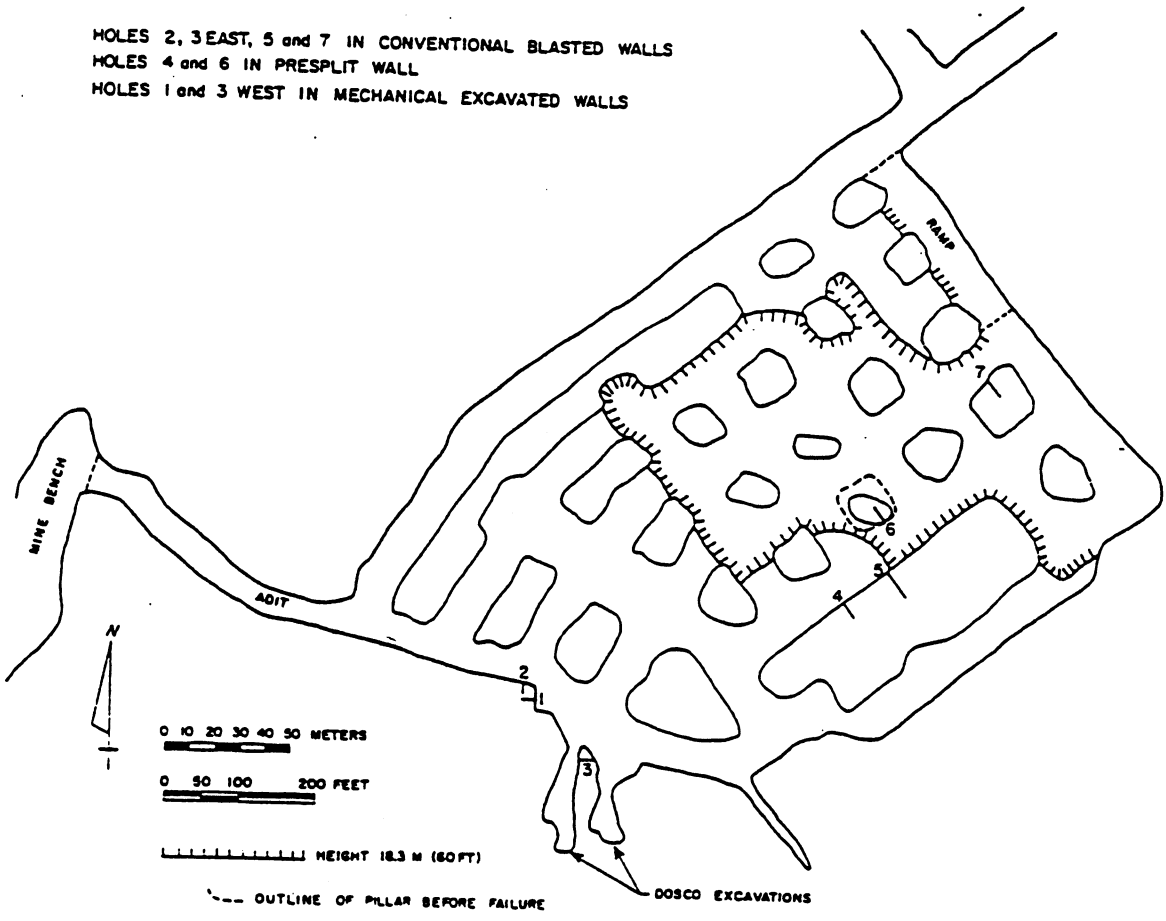

Figure 3. Mine Map and Hole Locations

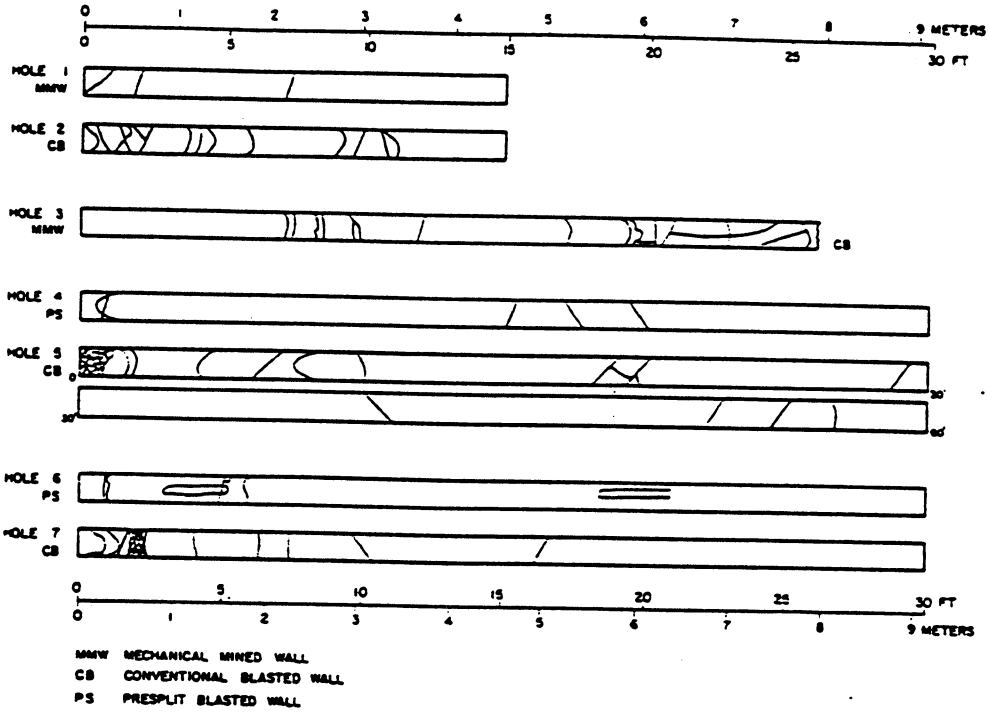

Figure 4. Fracture Logs of 15-1/4 cm (6 In.) Holes

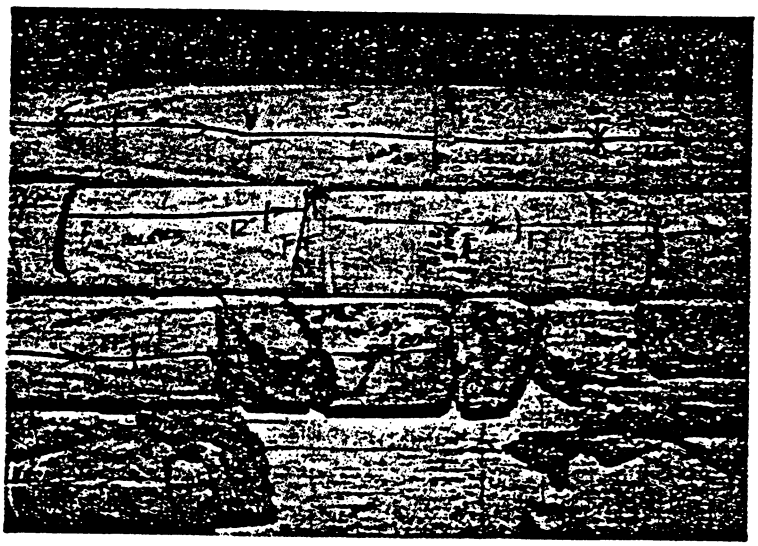

Figure 5. Core Obtained from Hole 3

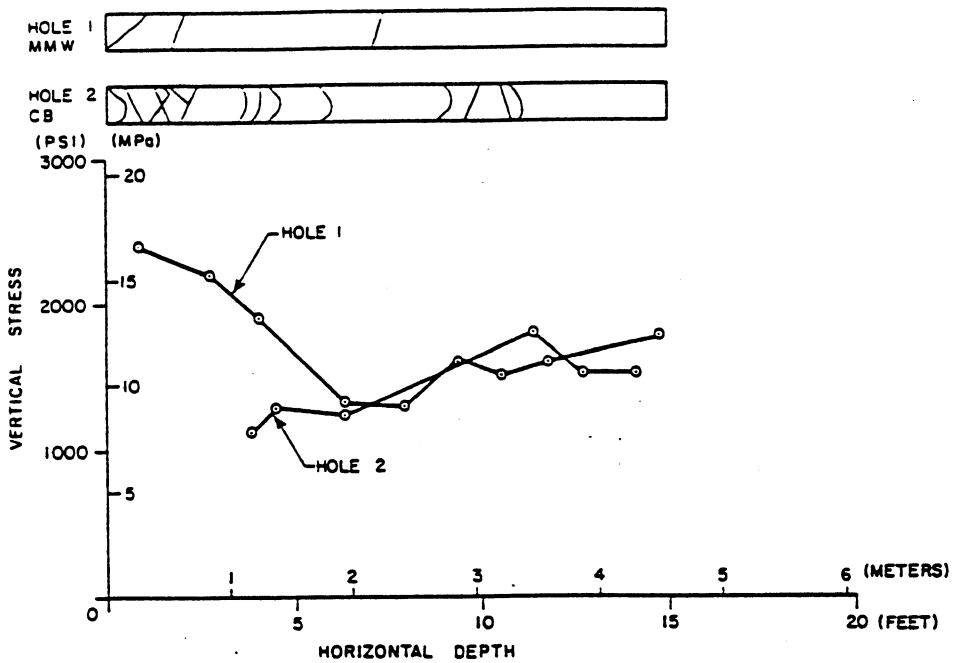

Figure 6. Comparison of Stress Distributions and Fracture Logs Between Holes 1 and 2

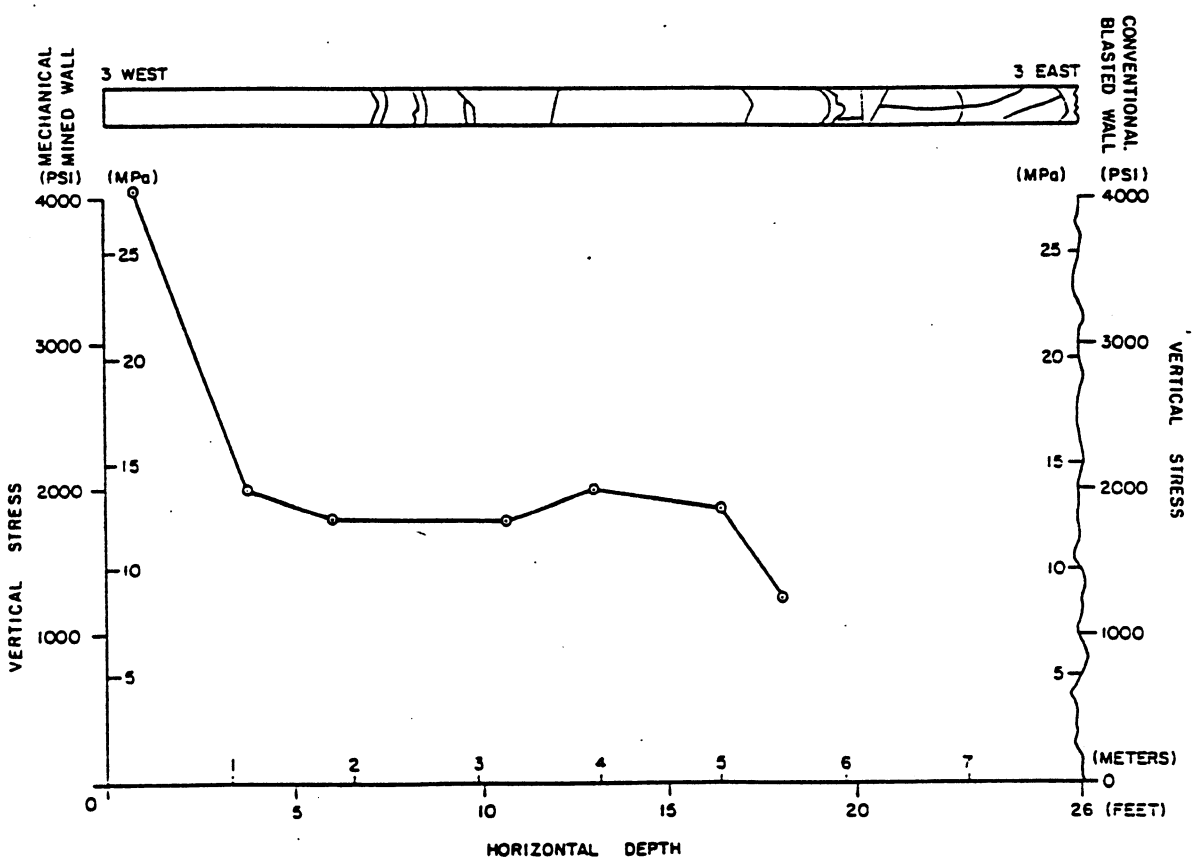

Figure 7. Comparison of Stress Distributions and Fracture Logs Between 3 West and 3 East

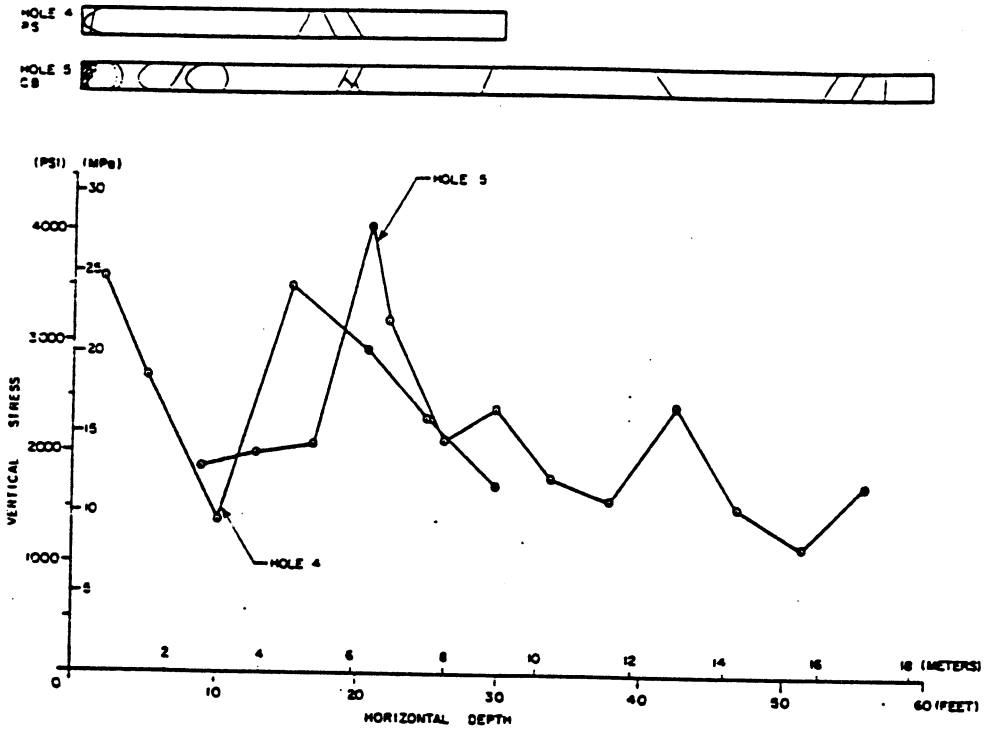

Figure 8. Comparison of Stress Distribution and Fracture Logs Between Holes 4 and 5

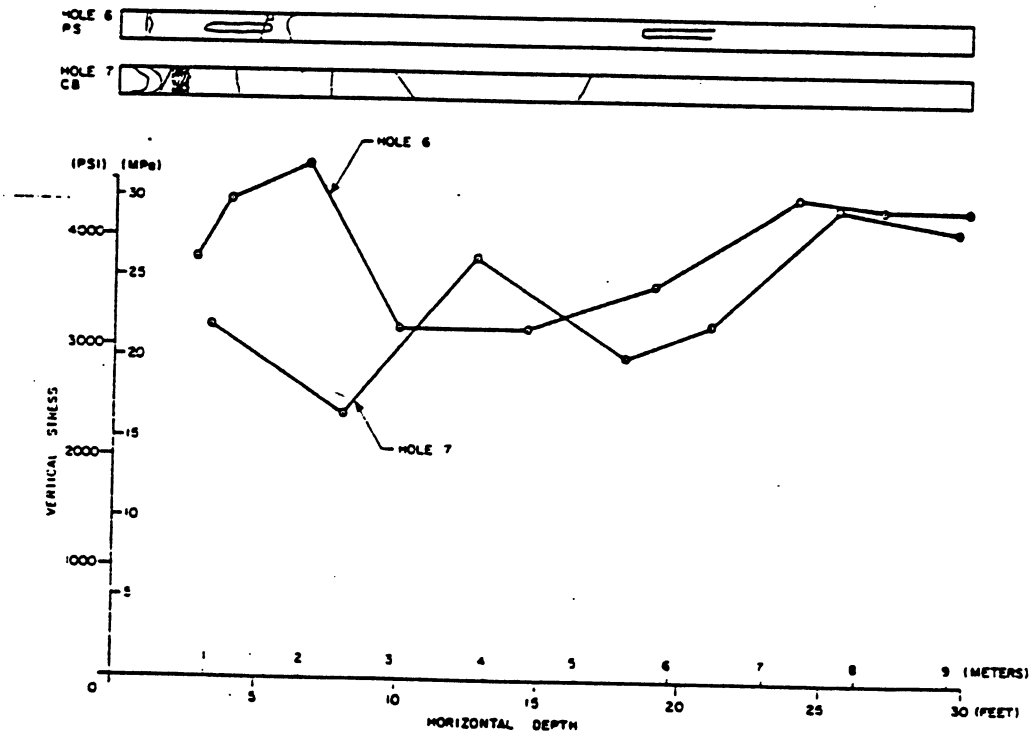

Figure 9. Comparison of Stress Distribution and Fracture Logs Between Holes 6 and 7

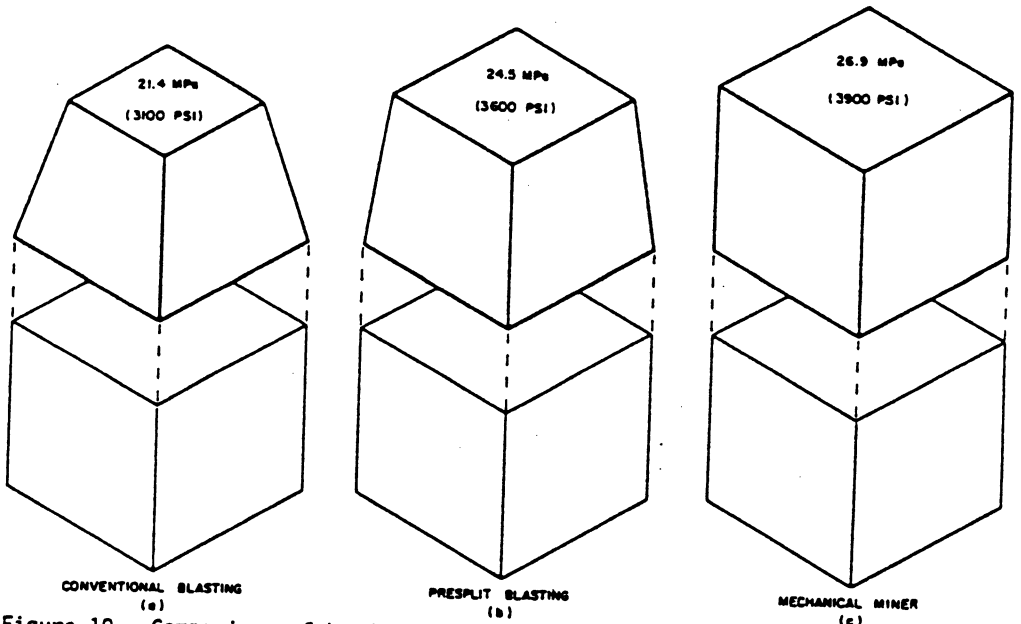

Figure 10. Comparison of Load-Carrying Capacity of 18.3 Meters (60 Ft) Cube Pillars

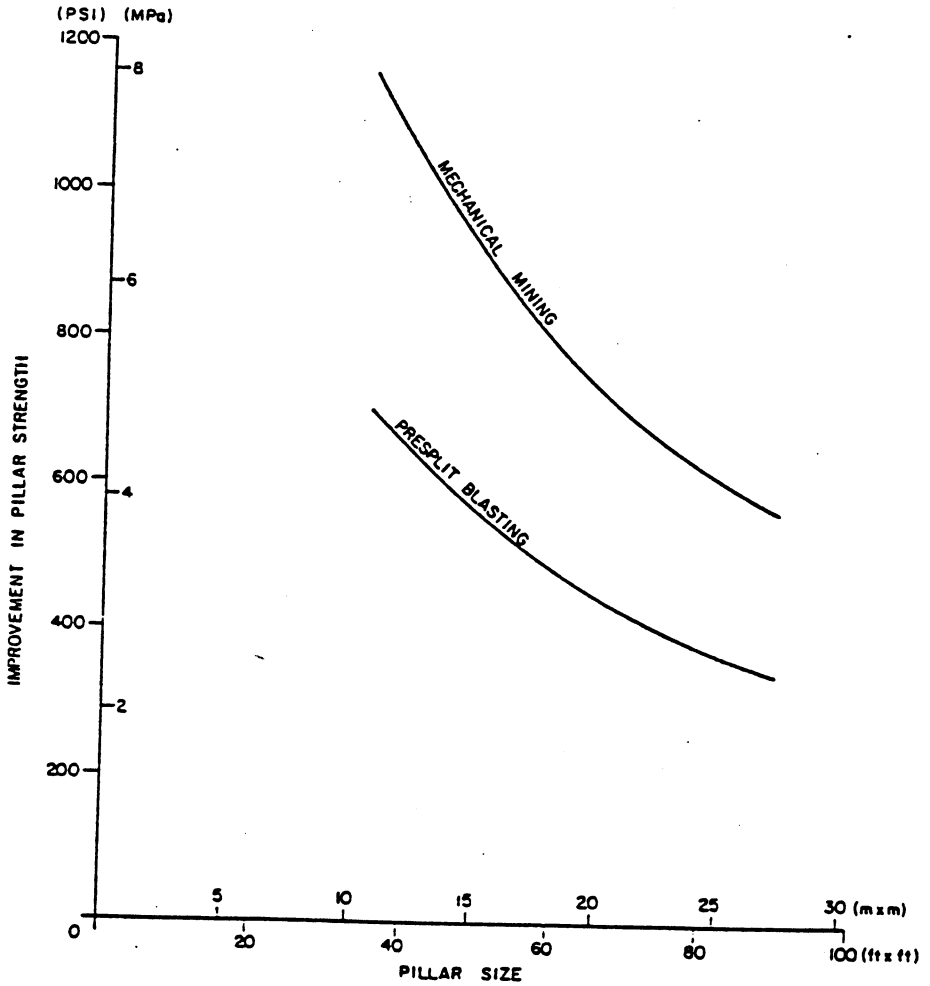

Figure 11. Relation Between Improvement in Pillar Strength and Pillar Size as Compared to Conventional Blasted Pillar

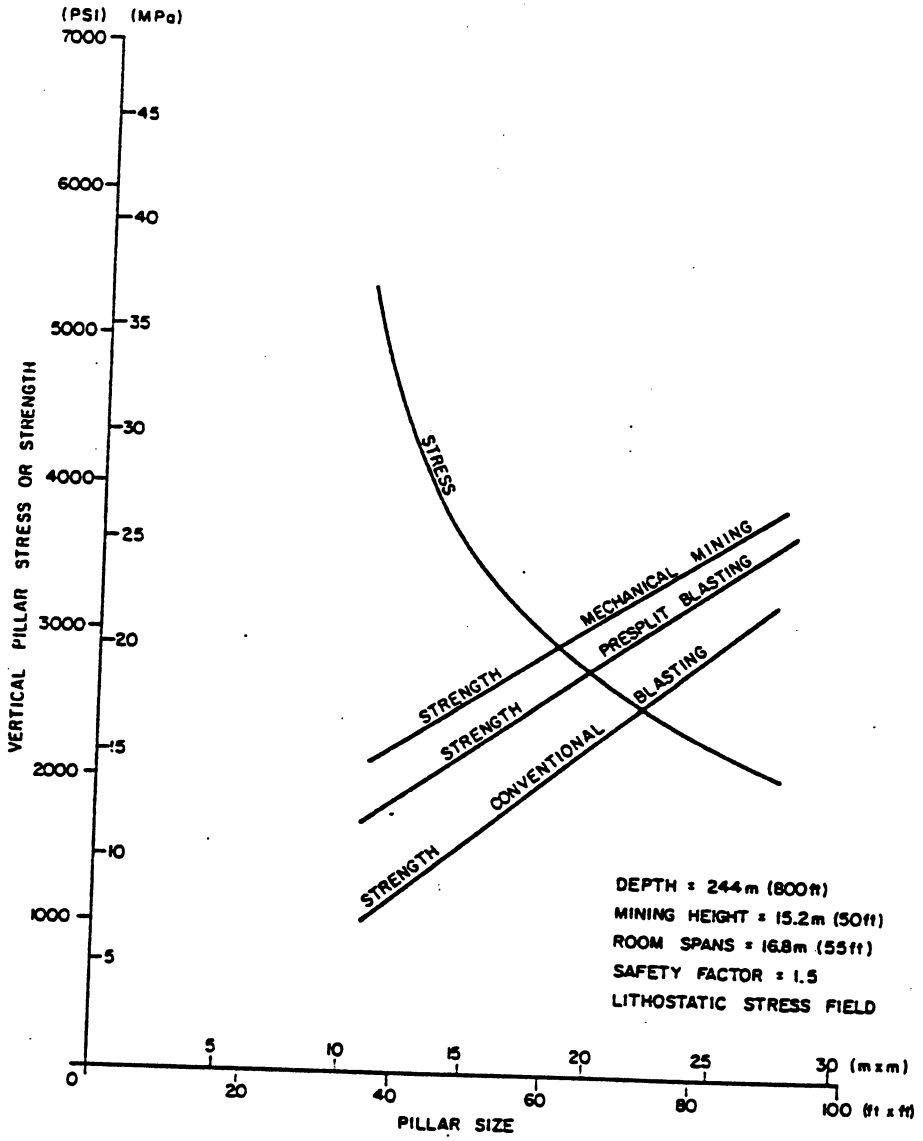

Figure 12. Example Showing Relation Between Pillar Stress, Strength and Size

F107107/2

REFLOODED MINE SOURCE TERM
CRANDON MINE

FINAL REPORT

Prepared for:

FOTH & VAN DYKE
2737 South Ridge Road
Green Bay, WI, 54307-9012

Prepared by:

STEFFEN ROBERTSON AND KIRSTEN (CANADA) INC.
Suite 800, 580 Hornby Street
Vancouver, B.C. V6C 3B6
Tel: (604) 681-4196 • Fax: (604) 687-5532

MARCH, 1997

F107107/2

REFLOODED MINE SOURCE TERM
CRANDON MINE

FINAL REPORT

TABLE OF CONTENTS

LIST OF TABLES

LIST OF FIGURES

LIST OF APPENDICES

F107107/2

REFLOODED MINE SOURCE TERM
CRANDON MINE

FINAL REPORT

1.0 INTRODUCTION

This report describes investigations directed towards characterizing the potential for the underground workings of the proposed Crandon Mine to release constituents to the groundwater. Four potential sources were investigated:

- backfilled tailings;
- wall rock;
- crown pillar; and,
- underground emissions.

The overall objective of the investigation was to identify the most significant sources and to obtain conservative estimates of their influence on future groundwater quality.

The initial plan for the investigation reported herein was developed by Crandon Mining Company (CMC) and its engineers and consultants, and communicated to the Wisconsin Department of Natural Resources and the U.S. Army Corps of Engineers (Letter from Don Moe to Mr. Christopher P. Carlson and Mr. David L. Ballman, dated July 24, 1996). Upon receipt of comments from the Wisconsin Department of Natural Resources and after telephone conversations to clarify the commentary, CMC submitted a letter outlining several clarifications and revisions to the initial plan (Letter from Don Moe to Mr. Christopher P. Carlson, dated October 14, 1996). The investigation reported herein generally followed the revised plan. Exceptions are noted in the text.

The investigation followed a "top down" approach, in order to identify and focus effort on the most important sources. When calculations were required, the simplest reasonable models were used, supported when necessary by conservative assumptions.

Chapters 2-5 report the investigations of the four sources listed above.

Although the details varied from one source to another, the investigation of each source included the following steps.

- First, the geochemical potential for the source to release constituents to groundwater was characterized, especially the potential for metals, sulfate and acidity to be released by the oxidation of sulfide minerals.

- When a significant geochemical potential for constituent release was indicated, calculations were carried out to quantify the potential. The calculations took two forms. In cases where the access of oxygen to the source would be limited, oxygen transport calculations were completed to determine an upper limit on oxidation rates. In cases where oxygen supply to the source would not be limited, constituent release was estimated by extrapolation from laboratory data.

- The estimated constituent releases were then divided by appropriate groundwater volumes to estimate the incremental contribution of the source to constituent concentrations in the groundwater that would fill the mine workings upon reflooding.

Chapter 6 describes the investigation of groundwater flow patterns in and around the reflooded mine. The groundwater flow patterns were examined with a simple groundwater model. The results were used to characterize the interaction of the constituent sources, and their cumulative effect on concentrations in the reflooding groundwater.

Chapter 7 summarizes the estimates of constituent concentrations in the groundwater that will re-flood the underground mine. Assumptions used in deriving the estimates are reviewed, and the resulting uncertainty in the estimates is characterized.

2.0 TAILINGS BACKFILL

2.1 Approach

Nicolet Mining Company (NMC) has proposed to use cemented and uncemented tailings to backfill mined-out stopes. The use of tailings as mine backfill is a common practice. In addition to enhancing the stability of the underground workings, the backfilling reduces the volume of tailings that need to be stored on surface and results in favorable conditions for the long term stability of sulfide minerals. In essence, the sulfide minerals are returned to the underground and submerged environment in which they have remained stable for millions of years.

However, tailings that are returned underground in the early years of mining may remain above the water table for up to thirty years. During this period there is a potential that sulfide minerals in the backfilled tailings may oxidize. After the groundwater table is allowed to recover, oxidation products stored in the backfill could be released.

It is clear from the acid base accounting tests reported by Foth and Van Dyke (December 1995) that the tailings have the geochemical potential to generate oxidation products and acidic conditions. However, the nature of the backfilling process, and the resulting geometry of the backfilled stopes, will lead to the isolation of the tailings from the ventilation system that will be supplying air to the remainder of the underground workings. The limitations on oxygen access will place a limit on the rate and extent of oxidation and acid generation within the backfilled tailings.

The approach used in this investigation was to analyze the backfilling methods to clarify the restrictions on oxygen transport, then to use simple mathematical models to estimate the rate of oxygen transport to the tailings, then to compare the oxygen limited oxidation rates to the amount of alkalinity and neutralizing minerals available within the tailings, and finally to use the conclusions as a basis for predicting water quality within the backfilled and reflooded tailings.

2.2 Description of Backfilling Methods

Oxygen transport into the tailings backfill will be dependent on the geometry of the backfilled workings, which will in turn depend on the mining method. Two mining methods will be used: blasthole open stoping methods below the 1,200 feet elevation and cut and fill methods above the 1,200 feet elevation.

The mining and backfilling methods were described in the Mine Permit Application and in a letter from CMC to Wisconsin Department of Natural Resources (Don Moe to Mr. Christopher P. Carlson, WDNR, October 14, 1996, Re: Crandon Project - Backfilled Mine Source Term Derivation). The following sections highlight aspects of the two backfilling methods that may influence the transport of oxygen and hence the potential for sulfide oxidation.

2.2.1 Blasthole Open Stoping

For blasthole open stoping, ore body entries will be driven at 200 to 300 foot vertical intervals to coincide with stope development. The nominal dimensions of the stopes will be 75 feet along strike, 200 to 300 feet in height, and 40 to 100 feet in ore body width. A typical stope will contain between 100,000 and 250,000 tons of ore. At the annual production rate of 2,000,000 tons of ore, about eight to twelve stopes will be mined out each year.

Mined out stopes will be backfilled with mill tailings and mine development waste rock. Primary stopes will be backfilled with cemented coarse tailings. After the cemented backfill has cured, the remaining stopes will be mined, and then backfilled with uncemented coarse mill tailings. Coarse or crushed waste rock may be co-deposited with the tailings backfill.

In preparation for backfilling, the stope entries will be sealed with timber and shotcrete bulkheads. Waste rock will be deposited at the base of the stope to provide a fill retaining bulkhead in the stope undercut throat, and to prevent tailings movement to the decant bulkheads at the stope entries. Similar fill retaining bulkheads will be placed in crosscuts to the stope.

The tailings will be transported and placed hydraulically as a slurry with a solids content of approximately 60 percent. The uncemented coarse tailings will drain rapidly after placement, precluding the build-up of hydrostatic heads. The cemented tailings will not be free draining, but the decant system will remove excess surface water.

Approximately 60% of the stopes will be backfilled with cemented tailings; the other 40% with uncemented tailings. Cemented tailings will be placed at the bottom of all stopes, nominally the lower 20 feet, to help ensure fill stability in stopes that remain largely uncemented. Higher strength cemented fill caps will also be placed at the top of otherwise uncemented backfilled stopes to provide for subsequent equipment re-entry for continued vertical stope development.

2.2.2 Cut and Fill Method

In the cut and fill method, each stope will be mined along strike at a vertical height of up to 14 feet. The width of the cut will be limited by the width of the ore (40 to 100 feet) and the distance between the rib pillars (approximately 120 feet). Once the ore is removed, the cut will then be backfilled with cemented tailings. The top surface of the backfill then becomes the floor for the next cut. Preparation for backfilling is similar to that described above. A bulkhead is installed and the cross cut entry to each level is backfilled with waste rock.

The primary difference between the two methods is that in the open stoping method, the entire stope is mined out before the stope is backfilled. In the cut and fill method, the stope is mined and backfilled in horizontal lifts. Up to three lifts will be accessed from each cross cut entry.

At the top of each stope, void space between the backfilled tailings and crown pillar or sill will be minimized through *tight filling* of tailings. Tight filling may be accomplished, for example, by extending tailings backfill supply pipes to high points within the stope. Return pipes are extended back to the supply point from each of the high points in the stope. A bulkhead is subsequently constructed across the open end of the stope, with allowance for the tailings supply and return pipes, and waste rock placed against the bulkhead for support. Tailings are then hydraulically placed as a

slurry. Each of the return pipes are shut off as slurry begins to return, until slurry is obtained from the last return pipe, at which point the tailings backfill supply is shut off. This method will result in less than two feet of void space between the top of the backfilled material and the stope back (or roof).

Another means of tight filling is to take down the back, to obtain a relatively even grade from the ends of the stope to a high point within the stope. A bulkhead is constructed across the open end of the stope and supported by waste rock. Tailings are then emplaced hydraulically as a slurry via an access raise to the high point in the stope.

2.3 Oxygen Transport Modeling

2.3.1 Objective

The oxidation of sulfide minerals in the backfilled tailings will only take place where oxygen is available. Oxygen transport modeling was carried out to estimate the rate of oxygen supply, and thereby the maximum extent of oxidation in the backfilled tailings.

The blasthole stope and cut and fill mining procedures will result in different mechanisms for oxygen entry into the tailings. To represent the different conditions that will arise, oxygen transport modeling considered the following cases.

2.3.2 Case 1, Oxygen Transport into Blasthole Open Stopes

Figure 2.1 shows a schematic of the backfilled tailings in an area mined by blasthole open stoping. The plugging of the access cross-cut will result in a conical layer of waste rock sandwiched between layers of cemented tailings. In secondary stopes, the cemented layers will be approximately 20 feet in thickness (cap and base), with uncemented tailings above and below. In the primary stopes, all of the backfilled

tailings will be cemented. Case 3 considers the transport of oxygen from the bulkhead, through the waste rock, and into the cemented cap and base.

Figure 2.1 shows that the tailings will completely seal the stope, so that circulation of air through the waste rock to the tailings surface will be impossible. As a result, oxygen transport to the tailings surface will be limited by the rate of diffusion through the bulkhead and waste rock.

Diffusion through the bulkhead and the waste rock will be three-dimensional. As a conservative simplification, the maximum flux of oxygen into the stope was estimated by assuming the maximum oxygen gradient through the crosscut. The resulting flux is given by Fick's Law:

$$\text{Flux} = D\, C_o\, L^{-1}$$

where D is the diffusion coefficient (m2 s-1), C_o is the concentration (mol O_2 m^{-3}) at the bulkhead, L is the length (m) of the crosscut behind the bulkhead, and the flux has units of mol O_2 m^{-2} s^{-1}. The oxygen concentration behind the bulkhead was conservatively assumed to be in equilibrium with the atmosphere (i.e. C_o=8.9 mol m^{-3}). The diffusion coefficient through the waste rock was estimated to be $6x10^{-6}$ m^2 s^{-1}, equivalent to the upper end of the range of oxygen diffusion coefficients measured in waste rock and reported by Ritchie (1994). The length of the crosscut behind the bulkhead was estimated to be 20 feet, or 6.1 m. The resulting estimate of the maximum oxygen flux was 8.76×10^{-6} mol O_2 m^{-2} s^{-1}. For a crosscut with nominal dimensions of 13 feet by 16 feet, or 19.3 m^2, the maximum rate of oxygen diffusion into the stope is 1.69×10^{-4} mol O_2 s^{-1}.

Mining will proceed for an estimated period of 28 years. After mining is complete, the underground openings are expected to be flooded after approximately two years. In an average stope, i.e. one mined halfway through the life of mine, the oxygen transport would continue for 15 years, resulting in a total oxygen input of approximately 80,000 mol O_2.

2.3.3 Case 2, Oxygen Entry through Backfilled Cross-cuts in Cut and Fill Stopes

The cross-cuts that provide access to cut and fill stopes will be backfilled with coarse waste rock prior to deposition of the tailings. The rock will remain relatively permeable, and provide a connection between the backfilled tailings and remaining development openings. The end result will be a number of oxygen entry points along one side of the stope, as depicted schematically in Figure 2.2. Case 2 considers oxygen diffusion through the backfilled access workings to the cemented tailings.

The geometry of Case 2 is very similar to that in Case 1. In both cases, blockage of the stope end of the crosscut will effectively prevent advection, and limit oxygen transport to diffusion. Using the same conservative assumptions that were applied for Case 1, the maximum rate of oxygen diffusion into the stope is 1.69×10^{-4} mol O_2 s^{-1}. However, unlike the blasthole stopes, the cut and fill stopes will be opened only in the last five years of mining. Again assuming a two year period for the groundwater table to recover, the cut and fill stopes will be exposed to oxidation for an average of 3.5 years. In an average cut and fill stope, the total oxygen input would be approximately 19,000 mol O_2.

2.3.4 Case 3, Oxygen Entry Between Cut and Fill Layers

Backfilling with the cut and fill method will result in a horizontal layering of the cemented tailings. The top surface of each layer will be exposed to aeration during the time that it takes to mine and backfill the next layer. Case 3 considers oxygen diffusion into the exposed surface.

The diffusion of oxygen into the cemented tailings surface was modeled using a one-dimensional diffusion - reaction equation:

$$\frac{dC}{dt} = \frac{\partial}{\partial x}\left(D\frac{\partial C}{\partial x}\right) - r * C^n$$

where: C is oxygen concentration, t is time, D is the effective diffusion coefficient; n is the rate order; and r is a reaction constant which depends upon the rate order.

For a constant concentration $C=C_o$ at the surface, the steady state flux (mol O_2 m^{-2} s^{-1}) of oxygen into the surface is given by:

$$\text{Flux} = C_o (r D)^{0.5},$$

and the concentration of oxygen at any depth z below the surface is given by:

$$C = C_o \exp\{-z (r D)^{0.5}\}$$

Oxygen concentrations at the surface were assumed to be in equilibrium with the atmosphere (i.e. C_o=8.9 mol O_2 m^{-3}). Oxygen was assumed to be consumed within the tailings by a first order reaction (n=1) with a rate constant of $r=1.18 \times 10^{-4}$ s^{-1}. Diffusion coefficients were estimated to be 5.06×10^{-7} m^2/s in uncemented tailings and 10 to 100 times lower in the cemented tailings. The former value was estimated by assuming that the tailings were at 50% water saturation, and applying the relationship derived by Reardon and Moddle (1985). Gas phase diffusion coefficients were estimated to be reduced by a factor of 100 in a study of tailings cemented by gypsum precipitation (Blowes et. al., 1990). Studies by Archibald and Nantel (1984) found that radon diffusion coefficients in cemented uranium tailings were 6-100 times less than in uncemented tailings.

The resulting estimates of oxygen flux into the cemented tailings are shown in Table 2.1. Also shown in the table is the depth of oxygen penetration. Because the oxygen consumption reaction is assumed to be first order, oxygen concentrations diminish logarithmically with depth and theoretically never reach zero. The values shown in Table 2.1 are the depths at which oxygen concentrations are 100 times lower than atmospheric concentrations.

The time required to mine one level of a cut and fill stope is expected to be approximately 10 weeks. For much of that time, the cemented tailings floor will be covered with ore muck. Assuming that oxygen diffusion into the cemented tailings continues for half of the mining period, (5 weeks), and using the higher of the two

estimates of flux, the total entry of oxygen into the cemented tailings surface will be approximately 31 mol m^{-2}.

TABLE 2.1

Estimated Oxygen Transport into Surface of Cut and Fill Stopes (Case 3)

	High D	Low D
Model Inputs		
r (s^{-1})	1.18×10^{-4}	1.18×10^{-4}
D (m^2 s^{-1})	5.06×10^{-8}	5.06×10^{-9}
Model Outputs		
O2 Flux (mol O2 m-2 s-1)	2.07×10^{-5}	6.55×10^{-6}
O2 Penetration (m)	0.10	0.03
O2 Penetration (ft)	0.33	0.099

2.4 Contribution to Groundwater Quality

2.4.1 Acidic Tailings

The oxygen transport modeling in the previous section estimated that 80,000 moles of O_2 would enter each of the backfilled blasthole stopes, and 19,000 moles of O_2 would enter each of the backfilled cut and fill stopes. In order to obtain a conservative prediction of the resulting effect on water quality, it is necessary to determine how much of the backfilled tailings could potentially be acidified by those amounts of oxygen.

A summary of the acid base account results for the cemented tailings backfill is provided in Table 2.2. The table also shows the carbonate analysis for the duplicate samples tested. Comparison of overall NP with the NP calculated from carbonate analyses indicates that approximately 60 percent of the total neutralization potential is carbonate based. The remainder is probably in the form of unreacted calcium oxide.

TABLE 2.2

Acid Base Account Results for Cemented Tailings Backfill

Sample	Paste pH (s.u.)	S(total) (%)	SO_4 (%)	S^{2-} (%)	CO_3 (%)	NP	$NP(CO_3)$	AP
CMC-CTC	12.0	25.9	<0.4	25.9	4.4	129.1	73.3	809.4
CMC-CTC	12.0	26.1	<0.4	26.1	4.5	127.8	75.0	815.6

Note: NP, $NP(CO_3)$, and AP in units of kg $CaCO_3$ eq./tonne material

The process of pyrite oxidation converts one mole of O_2 into 8/15 moles of $CaCO_3$ equivalent of acidity. Using that relationship, it is possible to convert the amount of oxygen transported into each stope into a maximum NP consumption, as shown in Table 2.3.

The spatial distribution of the oxidation reactions will determine the volume of tailings that actually becomes acidic. Oxidation rates are likely to be highest along the tailings surfaces nearest to the cross-cut openings, and slower elsewhere. The result will be that acidic conditions are limited to a thin layer of tailings very near the cross cut openings. However, to obtain a conservative estimate of the amount of tailings that could become acidic, it was assumed that the oxidation reactions would be distributed so as to just consume the NP in the cemented tailings, i.e.

Maximum NP consumption / Tailings NP = Maximum amount of tailings that can be acidified.

Table 2.3 also shows these calculations, and the subsequent conversions from mass units to volume units. The last two rows of Table 2.3 show the estimated number of stopes of each type, and the resulting estimates of the total volume of tailings that could become acidic during mine operations.

TABLE 2.3
Calculations of Acidic Tailings Volume

	Blasthole Stope	Cut and Fill Stope
O_2 transport (mol O_2)	80,129	18,697
Maximum acid production (mol $CaCO_3$ equivalent)	42,736	9,971
Maximum NP consumption (kg $CaCO_3$ equivalent)	4,274	997
Cemented tailings NP (kg $CaCO_3$ equivalent/tonne)	128	128
Maximum mass of tailings that can be acidified (tonne)	33.4	7.8
Assumed density of cemented tailings (tonne/m^3)	2.0	2.0
Maximum volume of tailings that can be acidified (m^3)	16.7	3.9
Maximum volume of tailings that can be acidified (ft^3)	590	138
Estimated number of stopes	212	50
Estimated total maximum volume of acidic tailings (ft^3)	124,900	6,878

In order to estimate solute concentrations in the water that will fill the pores within the acidified tailings, a series of calculations were completed. The calculations were similar to those presented in the TMA Groundwater Quality Performance Evaluation (FVD, 1998). In brief, the steps were:

1. Adopt the above assumption that 128 kg CaCO3 equivalent/tonne of oxidation products were created throughout the acidic tailings.

2. Convert the above value to moles of sulfide (S_2) oxidized.

3. Use the values derived in the TMA Groundwater Quality Performance Evaluation, Appendix A, to relate the mass of sulfide oxidized to estimates of the mass of each constituent released.

1. Compare the estimated mass of each constituent released to the mass of each constituent initially present in the tailings, and adopt the lower of the two in subsequent calculations.

2. Divide the estimated mass of each constituent by the amount of water that will fill the pore space, to obtain an initial estimate of each constituent's concentration in the acidic porewater.

3. Compare the initial estimate of each contaminant's concentration in the acidic porewater to solubility constraints, as derived from MINTEQA2 geochemical equilibrium modeling presented in Appendix A2.

4. Accept the lower of the initial estimate and the solubility constraint as the final estimate.

All steps in the calculations are shown in Appendix A1 of this report. The results are summarized in Table 2.4.

TABLE 2.4

Contribution of Acidic Cemented Tailings to Reflooding Groundwater

	Parameter							
	SO_4	As	Ca	Cu	Fe	Mn	Se	Zn
Estimated Total Release (mg/kg)[1]	120,080	159	3,510	95	26,900	618	1.7	6,540
Sample Content (mg/kg)[2]	608,000	2,670	9,330	500	271,00	605	92.9	6,100
Max Total Release(mg/kg)[3]	120,080	159	3,510	95	26,900	605	1.7	6,100
Maximum Concentration (mg/L)[4]	600,400	796	17,500	477	134,400	3,025	8.6	30,500
MINTEQA2 Conc. (mg/L)[5]	200,000	na	1,347	na	26,000	na	na	na
Estimated Concentration (mg/L)[6]	200,000	796	1,347	477	26,000	3,025	8.6	30,500

Footnotes to Table 2.4

1. Steps 1-3 in text, See Appendix A1 for details
2. From TMA GWQPE Appendix A
3. Step 4 in text
4. Step 5 in text
5. Step 6 in text, see Appendix A2 for MINTEQA2 results
6. Step 7 in text.

2.4.2 Oxidized Neutral Tailings

The results presented for Case 3 of the oxygen transport modeling indicate that the upper surface of the cemented tailings placed in each lift in the cut and fill stopes will be exposed to oxidation. However, the amount of oxidation that can occur in the limited time that each lift surface is exposed will be insufficient to create acidic conditions. Furthermore, the placement of the next lift will flush the oxidized surface with alkaline water, neutralizing any acidity that could be present. As a result, the tailings on the surface of each cut and fill lift will be oxidized but neutral.

Assuming that there will be approximately 50 cut and fill stopes, with average dimensions of 45 ft. x 120 ft. x100 ft., that each stope will be mined in three lifts, and that the depth of oxidation will be 0.1 m, the total volume of tailings that will be oxidized, but neutral, will be 591,000 ft^3.

Estimates of the constituent concentrations within the porewater of the oxidized neutral tailings were obtained by a series of calculations analogous to those described in the Section 2.4.1 The relevant data and the resulting concentration estimates are shown in Table 2.5. Detailed calculations are provided in Appendix A. As shown in the table footnote 5, the solubility constraints were obtained from geochemical equilibrium modeling reported in the TMA Groundwater Quality Performance Evaluation, Appendix B. Secondary mineral phases identified by MINTEQA2 modeling indicated solubility controls for Ca, SO4, Cu, Fe, Mn, and Zn.

TABLE 2.5
Contribution of Oxidized/Neutral Cemented Tailings to Reflooding Groundwater

	Parameter							
	SO_4	As	Ca	Cu	Fe	Mn	Se	Zn
Estimated Total Release (mg/kg)[1]	8,451	11	247	6.7	1,891	43	0.12	460
Sample Content (mg/kg)[2]	60,800	2.670	9,330	500	271,00	605	92.9	6,100
Max Total Release(mg/kg)[3]	8,451	11	247	6.7	1,891	43	0.12	460
Maximum Concentration (mg/L)[4]	42,257	56	1234	34	9,459	217	0.61	2300
MINTEQA2 Conc. (mg/L)[5]	12,200	na	203	0.01	5.2	3	na	8.7
Estimated Concentration (mg/L)[6]	12,200	56	203	0.01	5.2	3	0.61	8.7

Footnotes to Table 2.5

1. Steps 1-3 in text, See Appendix A1 for details
2. From TMA GWQPE Appendix A
3. Step 4 in text
4. Step 5 in text
5. Step 6 in text, see TMA GWQPE Appendix B
6. Step 7 in text.

2.4.3 Unoxidized Cemented Tailings

The majority of the cemented tailings will not be exposed to oxidation. Approximately 60% of the blasthole stopes and all of the cut and fill stopes will be filled with cemented tailings. Assuming as above that there will be 212 blasthole stopes with average dimensions 75 ft. x 250 ft. x 60 ft., and 50 cut and fill stopes with average dimensions 45 ft. x 120 ft. x 100 ft., the total volume of cemented tailings is estimated at 170,000,000 ft^3.

Estimates of the constituent concentrations in the water that will fill pores within the unoxidized cemented tailings were obtained from the latter cycles of the large scale column test completed on cemented tailings and described in Foth and Van Dyke (1995). The latter cycles were chosen to minimize the influence of the initial unsaturated cycles. A simple average of the concentrations measured over the last three analyzed cycles was calculated. The relevant data and the resulting estimates are shown in Table 2.6. As can be seen from the last row of Table 2.6, none of the average concentrations exceeded solubility constraints.

TABLE 2.6

Contribution of Unoxidized Cemented Tailings to Reflooding Groundwater

	Parameter							
	SO_4	As	Ca	Cu	Fe	Mn	Se	Zn
Cycle 10 (mg/L)*	260	0.003	290	0.006	0.020	0.005	0.020	0.020
Cycle 18 (mg/L)*	330	0.003	290	0.003	0.12	0.003	0.016	0.029
Cycle 34 (mg/L)*	400	0.110	320	0.003	0.010	nv	0.021	0.010
Average Concentration	330	0.038	300	0.004	0.050	0.003	0.019	0.020
MINTEQA2 Conc. (mg/L)	330	0.038	300	0.004	0.050	0.003	0.019	0.020

* from Foth and Van Dyke, December, 1995, Appendix 4.15, Tables 2 and 3, last three analyses; where parameter reported as "<", 1/2 value used in calculations

nv = no value

2.4.4 Unoxidized Uncemented Tailings

Approximately 40% of the blasthole stopes will be backfilled with uncemented tailings, the majority of which will also not be exposed to oxidation. Using the above assumptions, the volume of unoxidized uncemented tailings will be 95,300,000 ft^3 since they will be capped and sealed with cemented tailings.

Constituent concentrations in the pores of the uncemented tailings, which are not exposed to oxidation, are expected to remain similar to those in the process water. The values shown in Table 2.7 are taken from the TMA Groundwater Quality Performance Evaluation. The PWC values were used in subsequent calculations.

TABLE 2.7

Contribution of Unoxidized Uncemented Tailings to Reflooding Groundwater

	Parameter							
	SO_4	As	Ca	Cu	Fe	Mn	Se	Zn
Best Engineering Judgement Concentration (mg/L)	1634	0.10	273	0.070	0.0006	0.0046	0.29	0.46
Practical Worst Case Concentration (mg/L)	1908	0.10	589	0.070	0.41	0.0046	0.29	0.46

2.4.5 Water Quality Estimate

Table 2.8 summarizes the constituent concentrations predicted for the groundwater in each portion of the backfilled tailings. The fifth row of the table presents a volume-weighted average. (The lower table presents results for several other parameters that were also carried through the calculations.) Use of the volume-weighted concentrations to approximate average water quality within the backfilled tailings is conservative, because it neglects the neutralizing effect that will be provided by the large portion of alkaline water held within the cemented tailings.

TABLE 2.8
Overall Contribution of Tailings to Pore Water after Reflooding

Tailings Component	Volume (ft^3)	Porosity	Pore Volume (ft^3)	Parameter							
				SO_4	As	Ca	Cu	Fe	Mn	Se	Zn
Cemented Acidic	2.0E+05	0.40	8.1E+04	200000	796	1347	477	26000	3025	9	30500
Cemented Oxidized/Neutral	1.1E+06	0.40	4.2E+05	12200	56.0	203.0	0.010	5.2	3.00	0.61	8.7
Cemented Unoxidized	3.1E+08	0.40	1.2E+08	330	0.038	300	0.004	0.05	0.003	0.019	0.020
Uncemented Unoxidized	1.7E+08	0.40	7.0E+07	1908	0.100	589	0.070	0.41	0.0046	0.290	0.460
Over Vol.-Weight Avg.(mg/L)*	4.9E+08	0.40	1.9E+08	1006	0.51	404	0.227	11.0	1.273	0.121	12.93

Tailings Component	Volume (ft^3)	Porosity	Pore Volume (ft^3)	Parameter							
				Al	Ba	Cd	Cr	Pb	Mg	Ni	Ag
Cemented Acidic	2.0E+05	0.40	8.1E+04	4470	0.010	20.7	66	4.6	14431	8.4	0.0040
Cemented Oxidized/Neutral	1.1E+06	0.40	4.2E+05	0.010	0.010	0.0060	13	3.3	1016	0.59	0.0040
Cemented Unoxidized	3.1E+08	0.40	1.2E+08	0.080	0.001	0.001	0.003	0.03	0.020	0.010	0.000
Uncemented Unoxidized	1.7E+08	0.40	7.0E+07	1.4	0.0196	0.0002	0.400	0.27	4.300	0.006	0.100
Over Vol.-Weight Avg.(mg/L)*	4.9E+08	0.40	1.9E+08	2.420	0.0074	0.009	0.201	0.13	9.8	0.013	0.036

*Overall averages do not account for precipitation reaction that could occur as waters from the individual sources are mixed

4.2-13-23

Note: As a result of the April 1998 update to the Reflooded Mine Source Term - Crandon Project report, page 19 of the report has been deleted.

3.0 WALL ROCK

3.1 Approach

In order to characterize the geochemical potential for the wall rock to release constituents to the reflooding groundwater, geological information was compared to the proposed mine plan. The geological information was obtained from the following sources:

- Geological Summary, Crandon Deposit by A.J. Erickson, Jr. and R. Cote, dated January 24, 1996.

- Crandon Project Mine Permit Application, pages 35 to 49, 63, 81 to 84, dated September 29, 1995 and May 30, 1995.

- Memo Re: Hanging Wall Sulfide Content Review, Crandon Deposit Updated, from A.J. Erickson, Jr. to Mr. D.E. Moe, CMC, dated July 10, 1996.

- Memo Re: Hanging Wall Sulfide Estimates, from A.J. Erickson, Jr. to Mr. K. Black, CMC, dated February 6, 1997 (See Appendix B).

When the geological review indicated a potential for sulfide oxidation and constituent release, results from laboratory investigations of waste rock (Foth & Van Dyke, December 1995) were used to quantify that potential.

3.2 Access Development in the Hanging Wall

Proposed access developments include shafts, vent raises, drifts, cross-cuts and ramps. Details are provided below:

- The main production shaft will be 22 feet to 26 feet in diameter and approximately 2,200 feet deep.

- A second shaft, 16 to 19 feet in diameter, will be sunk on the eastern end of the orebody to a depth of 1,100 to 1,500 feet.

- A third shaft, or vent raise, approximately 16 to 19 feet in diameter, will be excavated in the western horizon of the orebody to provide ventilation.

- A ramp, development crosscuts and drifts will be excavated to access the orebody. They will have a nominal cross section of 16 feet by 13 feet.

- An underground maintenance shop and refueling station will be excavated adjacent to the ramp.

Most of the access development will be contained in the stratigraphic hanging wall rocks to the north of the orebody. These rocks include the Mole Lake, Rice Lake and Skunk Lake Formations, in order of sequence away from the orebody.

The Mole Lake Formation is adjacent to the zinc-rich Crandon Formation. It is a chloritic tuff that contains minor coarse pyroclastics. The eastern half of the formation is a fine chlorite tuff that contains little sulfide. The western half is a sericite-chlorite tuff with chert interbeds that contains veins with up to 4% pyrite.

The Rice Lake Formation is a thick series of volcanic debris and banded pumice flows. These flows typically contain angular chloritic fragments in a light-colored matrix, and little sulfide.

The Skunk Lake Formation is the most distant from the orebody. It consists of chert, cherty tuff and tuff, and contains zones of up to 10% sulfide in some near-surface areas of stringer mineralization.

Estimates of the surface area of wall rock that will be exposed in the access developments are summarized in Table 3.1. The surface area estimates were derived from waste rock volume estimates that were provided by CMC. The acid base accounting of the waste rock samples tested in the laboratory investigation (Foth and Van Dyke, December 1995) are also provided in Table 3.1. The S (%) and NNP values, and the fact that the wall rock in the access developments will remain exposed

to ventilation air throughout the life of mine, indicate a potential for oxidation during mining that would result in release of constituents to the reflooding groundwater.

TABLE 3.1
Estimated Development Wall Rock Exposure Surface Area and Waste Rock Acid Base Accounting

			ABA			
Formation	**Exposed Wall Rock**	**Composite**	**Sulfide (%)**	**AP**	**NP**	**NNP**
Lower Mole Lake	1,300,000 ft^2	Master	0.27	8.4	46	38
		High Sulfur	3.5	110	21	-89
Upper Mole Lake	160,000 ft^2	Master	0.1	3.1	48	45
		High Sulfur	3.8	120	6.8	-110
Rice Lake	1,400,000 ft^2	Master	0.05	1.6	1.6	0.0
		High Sulfur	3.2	100	0.5	-100
Skunk Lake	600,000 ft^2	Master	0.14	4.4	1	-3.4
		High Sulfur	3.6	110	12	-100

3.3 Ore Zone and Foot Wall

Blasthole open stoping will be the mining method used in ore horizons below 1,200 feet. Above that elevation cut and fill mining methods (post cut and fill or undercut fill mining) will be used in the ore below the crown pillar. With these methods, unmineable sill and rib pillars, low grade zones and other unrecoverable ore will be left in place.

The Crandon volcanogenic zinc-copper sulfide deposit consists of two main types of mineralization:

- Conformable, locally laminated, syngenetic, zinc-rich pyritic sulfide lenses within interbedded tuffs, ash, cherts and argillite of the Crandon Formation; and,

- Cross-cutting, epigenetic copper-bearing stringer sulfides, contained within fine grained tuffs, debris and lava flows of the foot wall Sand Lake Formation and within the lower portion of the Crandon Formation.

The estimated average mine wall surface area that will be exposed, at any given time during mining, is:

- 268,800 square feet, with an average sulfide content of 72%, within the zinc ore; and,

- 197,040 square feet, with an average sulfide content of 17%, within the copper ore.

These active surfaces will remain exposed to mine air for a relatively short period (weeks) prior to backfilling. Significant oxidation and metal release in the long term is therefore not anticipated. All surfaces within the orebody (with the exception of the crown pillar back discussed in the next chapter) will be flushed with alkaline water during backfilling. Any metals released in the short term will be washed into the mine drainage water, collected and pumped to the mine water treatment system. It was therefore concluded that wall rock in the ore zone and foot wall are unlikely to be significant sources of constituent release to the reflooding groundwater.

3.4 Constituent Release from Wall Rock in Access Developments

3.4.1 Constituent Release Model

The potential for sulfide oxidation and accumulation of soluble constituents within the access development wall rock was investigated using a simple calculation method:

Constituent release (mg) = Σ specific release (mg ft^{-2} yr^{-1}) x exposed surface (ft^2) x time (yr),

where the summation indicates that both the high sulfide and low sulfide rock were considered.

This method is similar to that used in studies of contaminant release from pit walls (e.g. Morin & Hutt, 1995). Although the method is quite simple, it does allow the importance of surface area, time, and material properties (as represented by the specific release) to be simulated.

3.4.2 Specific Release Rates

The rates of release of soluble constituents from a unit surface area of wall rock were estimated using the results of the humidity column tests completed on waste rock samples (Foth and Van Dyke, May and September, 1995). The masses of each constituent leached from the waste rock columns over a period of 54 weeks are summarized in Table 3.2.

TABLE 3.2
Column Test Results - Specific Mass Leached

Description		Time	Column Tests - Mass Leached (mg/kg)								
Formation	Composite	(Wks)	pH	SO4	As	Ca	Cu	Fe	Mn	Se	Zn
Lower Mole	Master	54	7.3	88	0.098	60	0.083	6.0	0.28	0.030	0.12
Lake	High Sulfur	54	2.9	4,300	0.053	790	75	55	49	0.54	160
Upper Mole	Master	54	7.6	41	0.044	34	0.078	7.7	0.22	0.018	0.61
Lake	High Sulfur	54	2.8	2,100	0.021	310	4.2	19	17	0.046	10
Rice Lake	Master	54	7.5	28	0.058	32	0.22	18	0.46	0.000	0.16
	High Sulfur	54	2.6	2,100	na	100	26	63	5.8	0.062	20
Skunk Lake	Master	54	6.5	90	0.031	28	0.17	4.1	0.46	0.032	0.14
	High Sulfur	54	7.0	670	0.018	150	0.078	2.2	2.2	0.044	2.5
Crandon Ore		6	---	910	0.013	72	39	21	1.5	0.095	330

The column testing was completed on rock samples characteristic of each formation, and of high-sulfur (sulfide) zones within each formation. The samples had a size distribution of less than 1.5 inches diameter, and were tested in 18 inch diameter columns with a rock column height ranging from about 10 to 20 inches. Based on the size gradation analyses, the specific surface area for the rock samples tested is in the order of 14 to 25 m^2/kg. The rate of constituent leaching is expressed on a surface area basis in Table 3.3.

TABLE 3.3
Column Test Results - Mass Leached/Surface Area

Description		Time	S.A./Mass	Specific Release Rate (mg/(ft^2/year))							
Formation	Composite	(Wks)	(ft^2/kg)	SO4	As	Ca	Cu	Fe	Mn	Se	Zn
Lower Mole	Master	54	19	4.6	0.005	3.2	0.004	0.32	0.003	0.002	0.006
Lake	High Sulfur	54	24	180	0.002	32	3.8	2.2	2.0	0.022	6.5
Upper Mole	Master	54	19	2.2	0.002	1.8	0.004	0.40	0.011	0.001	0.032
Lake	High Sulfur	54	19	120	0.001	16	0.23	1.0	0.90	0.002	0.56
Rice	Master	54	18	1.6	0.003	1.8	0.012	0.99	0.026	0.000	0.009
Lake	High Sulfur	54	21	97	na	4.9	1.3	3.0	0.28	0.003	0.97
Skunk	Master	54	20	4.4	0.002	1.4	0.008	0.20	.023	0.002	0.007
Lake	High Sulfur	54	14	47	0.001	11	0.005	0.15	0.16	0.003	0.18
Crandon Ore		6	14	66	0.001	5.2	2.8	1.5	0.11	0.007	24

3.4.3 Surface Area Estimates

Initial estimates of the wall rock surface area within each formation were provided by CMC (calculated from waste rock volumes and nominal mine working dimensions of 16' x 13'). However, blasting associated with mine development and operation will

fracture the wall rock immediately surrounding mine openings. The effect will be to expose additional surface area to oxidation. The amount of additional surface area will depend on the:

- structural characteristics of the wall rock and mineralization;
- degree of weathering;
- confining pressures;
- explosive charge and characteristics;
- blasting pattern employed;
- mining/ground support methods; and,
- size and orientation of mine working relative to the primary structural planes of the wall rock.

A study carried out in three open pits measured reactive surface/mine wall surface ratios ranging from 27:1 to 161:1 (Morin and Hutt, 1995). Because the lateral extent of mine wall fracturing associated with underground workings is generally less than that of surface workings (Morin, 1990), it is reasonable to assume that the reactive surface/mine wall surface ratio for underground mine operations should lie near or below the lower end of the published data for open pit operations. For the constituent release calculations, it was assumed that the reactive surface/mine wall surface ratio for the Crandon mine will be 30:1.

3.4.4 Proportions of High and Low Sulfide Surfaces

Estimates of the proportion of high sulfur rocks to be encountered by mine workings within a formation were derived from drillhole data summarized by Erickson (July 10, 1996 and February 6, 1997) (see Appendix B). Drillhole logs from each formation were examined and the length of high sulfur intercepts was estimated. The remainder of the rock in each case was assumed to be represented by the respective master composite samples. The proportion of high sulfur to master composite rock in each formation was then calculated.

3.4.5 Oxidation Time

An average oxidation period of 15 years was used in the calculation, based on the consideration that mine development is ongoing during the life of the mine operation. Therefore, some openings will be exposed for 30 years, while others will be exposed for only a few years or less.

3.4.6 Results

Table 3.4 shows, for each formation intersected by access developments, the nominal surface area, total exposed surface area, the proportion of high sulfide rock, and the resulting estimates of constituent release.

3.5 Constituent Concentrations in Groundwater

To characterize the contribution of the access development wall rock to constituent concentrations in the reflooding groundwater, it was assumed that the accumulated mass of each constituent (as shown in Table 3.4) will completely dissolve. The resulting concentrations were estimated by dividing the masses accumulated in each formation by the volume of the access development in that formation. The estimates are summarized in Table 3.5.

This approach is conservative for the following reasons:

- Solubility of secondary mineral phases may limit maximum constituent concentrations, depending on the final pH and redox potential;
- Some of the released constituents will have accumulated within fractures, and displacement of the fracture pore water, or diffusion, may be required to release them;
- Some of the constituents that are assumed to be "accumulated" will in fact have been washed away by water infiltrating during operations, and will have been pumped to the water treatment system; and,
- The reflooding groundwater will also fill porosity in the rock surrounding the workings, so the total volume of water will exceed the volume of the workings.

TABLE 3.4
Estimated Constituent Release from Wall Rock in Access Developments

Description				Est. Distr.**	Constituent Accumulation (kg)							
Formation	**Area (ft^2)**	**Eff. Area* (ft^2)**	**Composite**	**%**	**SO4**	**As**	**Ca**	**Cu**	**Fe**	**Mn**	**Se**	**Zn**
Lower Mole Lake	1,300,000	39,000,000	Master	99.25	2700	3.0	1900	2.6	190	8.6	0.93	3.7
			High Sulfur	0.75	780	0.01	140	14	10	8.9	0.098	29
Upper Mole Lake	160,000	4,700,000	Master	99.5	150	0.16	125	0.29	29	0.80	0.07	2.3
			High Sulfur	0.5	40	0.0004	5	0.1	0.4	0.3	0.001	0.20
O/A Mole Lake	1,500,000	44,000,000	Cumulative		3700	3.2	2100	17	230	19	1.1	35
Rice Lake	1,400,000	42,000,000	Master	99.9	1000	2.1	1200	7.9	630	17	0.000	5.6
			High Sulfur	0.1	61	na	3.1	0.80	1.9	0.18	0.002	0.61
			Cumulative		1100	2.1	1200	8.7	630	17	0.002	6.2
Skunk Lake	610,000	18,000,000	Master	100.	1200	0.42	380	2.3	55	6.2	0.43	1.9
			High Sulfur	-	-	-	-	-	-	-	-	-
			Cumulative		1200	0.42	380	2.3	55	6.2	0.43	1.9
Total Wall Rock	3,500,000	100,000,000			6000	5.7	3700	28	910	42	1.5	43

4.2-13-33

* Effective Area = Wall Rock Surface Area X Reactive Surface Area/Wall Rock Surface Area Ratio (30:1)

** Estimated Distribution (See Appendix B)

TABLE 3.5
Estimated Contribution to Development Openings
Groundwater After Reflooding

Description	Est. Volume*	Estimated Concentrations on Reflooding (mg/L)							
	(ft^3)	SO_4	As	Ca	Cu	Fe	Mn	Se	Zn
Mole Lake	5,300,000	24	0.021	14	0.11	1.5	0.12	0.007	0.23
Rice Lake	5,100,000	7.5	0.015	8.1	0.061	4.4	0.12	0.000	0.043
Skunk Lake	2,200,000	20	0.007	6.1	0.037	0.90	0.10	0.007	0.031
Total Wall Rock*	13,000,000	17	0.016	10	0.08	2.6	0.12	0.004	0.12

* Total concentration based on weighted average and assumes complete mixing

4.0 CROWN PILLAR

4.1 Approach

In order to characterize the geochemical potential for the crown pillar to release constituents to the reflooding groundwater, geological information was obtained from the following sources:

- Geological Summary, Crandon Deposit by A.J. Erickson, Jr. and R. Cote, dated January 24, 1996.
- Crandon Project Mine Permit Application, pages 35 to 49, 63, 81 to 84, dated September 29, 1995 and May 30, 1995.
- Crandon Mining Company Internal Memo Re: Reserves / Permanent Crown Pillar from A.J. Erickson, Jr. to File, dated November 8, 1996.

When the geological review indicated a potential for sulfide oxidation and constituent, results from laboratory investigations of ore and simple oxygen transport calculations were used to quantify that potential.

4.1 Crown Pillar Geology

The crown pillar will vary in thickness from a minimum of about 100 feet to greater than 310 feet (Erickson, January, 1996). The highest point of the top of the crown pillar is about 100 feet below ground level.

The crown pillar is predominantly composed of:

- an upper iron oxide, silica-rich, gossan;
- a limited zone of supergene sulfide mineralization lying below the gossan; and,
- a lower, unmined sulfide zone.

The gossan has resulted from weathering of the sulfide mineralization, and it contains only trace quantities of residual sulfides. The gossan generally extends less than 100 feet below the subcrop, and is commonly only a few tens of feet thick. Very locally it extends in excess of 400 feet below the subcrop along subvertical lithologic horizons, or along subvertical contacts within and along the margin of the Crandon Formation. After mining, it is estimated that approximately 2.3 M tons of the oxidized zinc ore gossan and approximately 0.7 M tons of the oxidized copper ore gossan will remain. The very limited amount of sulfide mineral in the gossan zone, and the extensive weathering that has already occurred, suggest that the gossan is unlikely to be a significant source of constituent release to the reflooding groundwater.

A limited amount of supergene copper sulfide mineralization, including chalcocite, covellite, and minor bornite, is present beneath the gossan. Minor amounts of copper oxides have also been noted in the saprolite, located over the orebody and within the upper, strongly weathered foot wall and hanging wall rocks. The supergene copper enriched zone is, however, small, in part due to the low amount of copper in the primary mineralization and in part to copper removal through weathering and surface erosion.

Sulfide ore is encountered below the gossan zone and saprolite. The upper limit of mining will be in the sulfide zone. The unmineable sulfide ores vary from approximately 10 to 180 feet thick. The estimated quantities are:

- 2.1 million tons of zinc ore, with an average sulfur content of 36% (sulfide mineral content of 72%); and,
- 1.9 million tons of copper ore, with an average sulfur content of 9% (sulfide mineral content of 17%).

The sulfide ores represent a potential source for constituent release to the reflooding groundwater.

4.2 Oxygen Transport and Surface Oxidation of the Crown Pillar

4.2.1 Constituent Release Model

The crown pillar area is covered by glacial overburden, which varies in thickness from 75 feet to over 250 feet. The overburden cover is expected to minimize the direct access of oxygen to the sulfidic parts of the crown pillar.

- Under the conservative assumptions that the entire mean annual infiltration of 10 inches (GeoTrans, 1996) percolates through the glacial overburden to the crown pillar, and maintains an oxygen concentration at the theoretical maximum solubility of 12.8 mg/L (at sea level), the flux of oxygen to the crown pillar will be approximately $3x10^{-9}$ mol O_2 m^{-2} s^{-1}. For comparison, this flux is four orders of magnitude less than the oxygen fluxes estimated in Chapter 2 for direct contact of ventilation air with the backfilled tailings (Case 1).

- Similarly, air phase diffusion of oxygen through an average 150 feet of overburden at a diffusion coefficient of $3 \times 10^{-6} m^2/s$ (which assumes uniformly unsaturated conditions), would supply only 5×10^{-7} mol $O_2 m^{-2} s^{-1}$ to the *top* of the crown pillar. Diffusion rates through the gossan zone are likely to be at least one order of magnitude less, implying that the diffusive flux to the sulfidic portions of the crown pillar will also be insignificant.

Clearly, areas where ventilation air is in direct contact with the crown pillar, i.e. the stope backs, will see the most significant oxidation. The model used in Chapter 3 to estimate constituent release in the wall rock was therefore also applied to the crown pillar.

4.2.2 Specific Release Rates

The rates of release of constituents associated with the crown pillar were estimated using the results of humidity column tests conducted on a representative sample of Crandon high-grade zinc ore (Foth and Van Dyke, May, 1995). The masses of each

constituent leached from the waste rock columns over an initial period of 6 weeks are shown in Table 4.1.

4.2.3 Surface Area Estimates

The surface area of copper sulfide ore and zinc sulfide ore that would be exposed at the base of the crown pillar was estimated from the sections provided by Erickson (1996). The ratio of reactive surface area to wall area was assumed to be 30:1, for the reasons provided in Section 3.3.

4.2.4 Oxidation Time

Mining directly below the crown pillar will be by cut and fill methods, and the tailings backfill will be cemented. Tight-filling methods will be used to minimize the void space between the top of the backfill and the stope backs. The backfill will seal off the stope access point, and prevent subsequent access of ventilation air to the stope back. The oxidation will therefore be limited to the period from end of mining to backfilling, estimated to be approximately six weeks.

4.2.5 Results

Table 4.1 shows the nominal surface area, total exposed surface area, and the resulting estimates of constituent release for both the zinc ore and copper ore portions of the crown pillar.

4.3 Constituent Concentrations in Groundwater

To estimate the influence of the crown pillar oxidation on the quality of the reflooding groundwater, it was conservatively assumed that all of the accumulated soluble constituents would be released to the volume of water that would fill the void between the stope backs and the backfill. The void was assumed to be uniformly 2 ft. high across the entire area of stope backs in the crown pillar. The resulting concentrations estimates are shown in Table 4.2.

The results shown in Table 4.2 are conservatively high estimates of constituent concentrations, for all of the reasons provided in Section 3.5. Furthermore, the cemented tailings are expected to act as a source of alkalinity that would neutralize much of the oxidation products from the adjacent crown pillar. Neglecting this effect makes the concentration estimates more conservative.

TABLE 4.1
Estimated Constituent Release from Crown Pillar

Description	Area	Eff. Area	Constituent Accumulation (kg)							
Formation	(ft^2)	(ft^2)	SO_4	As	Ca	Cu	Fe	Mn	Se	Zn
Zinc Ore	210,000	6,300,000	410	0.006	33	18	9.5	0.70	0.043	150
Copper Ore	270,000	8,000,000	520	0.008	41	22	12	0.89	0.054	190
Total	480,000	14,000,000	930	0.014	74	40	21	1.6	0.097	340

Crown Pillar Exposure Period: 0.115 years (6 weeks)

TABLE 4.2
Estimated Contribution to Crown Pillar Head Space Groundwater After Reflooding

Description	Est. Volume	Estimated Concentration on Reflooding (mg/L)							
	(ft^3)	SO_4	As	Ca	Cu	Fe	Mn	Se	Zn
Crown Pillar	950,000	35	0.001	2.7	1.5	0.80	0.059	0.004	13

5.0 COMBUSTION BY-PRODUCTS

5.1 Approach

During operation of the mine three sources of air emissions will occur underground. They are as follows:

- Combustion of natural gas for mine air heating;
- Combustion of fuel oil for mobile equipment use; and,
- Blasting operations.

The potential for these emissions to influence the quality of the reflooded groundwater was evaluated using simple mass balance calculations and a consideration of the geochemical and physical properties of the emission constituents.

5.2 Constituent Release and Accumulation

The primary emissions from the above sources are delineated in Table 5.1. The fate of these emissions is a function of the geochemical and physical properties of the constituents and the underground mine environment which includes an air flow rate of 700,000 scfm and relatively high levels of humidity. It is expected that gaseous emissions such as sulfur dioxide, volatile organic compounds, carbon monoxide, and nitrogen oxides will be completely removed from the underground mine by the large air flow discussed above. Volatile aerosols including formaldehyde and any unburned fuel oil are also expected to be removed from the mine by the large air flow. As a result, only particulate matter emissions will be addressed in the evaluation of emissions from combustion processes.

Particulate matter with adsorbed constituents, e.g., metals and polycyclic aromatic hydrocarbons (PAHs), will be largely exhausted from the mine, however, a portion will remain. Based on combustion of 1,979,760 gal of fuel oil by the underground equipment over the mine life, an assumed composition of the fuel (Appendix C) and a 66% particle settling rate in the vertical rise, the annual accumulation of particulate

matter that will remain in the mine and metals adsorbed on the particulates are as shown in Table 5.2.

The particulate matter value in the table also includes the contribution of particulate matter from natural gas mine air heating.

The trace metals found in No. 2 fuel oil will vaporize in the high temperature combustion zone of the mobile equipment engines and will eventually condense as the flue gas temperature decreases. During this condensing phase, most of the metals will condense onto existing particulate matter emitted as part of the diesel exhaust. This occurs uniformly on all available particulate surface area. Studies have shown that a majority of the particles emitted from the combustion of fuel oil are in the submicron size category (Watts and Wayfulonis, 1991). Since submicron particles contribute most of the available surface area, these particles will have a high concentration of volatile metals. This process is known as fine-particle enrichment (USEPA, April 1989; USEPA, 1993). As a result of the fine-particle enrichment process, most of the trace metal emissions will be attached to submicron particles.

The very small submicron particles will not settle out in the horizontal passageways within the mine as a result of gravity, but instead will remain suspended in the air stream and be transported to the vertical exhaust shaft (west raise). As the particles rise, significant deposition will occur as a result of adiabatic air expansion and the condensation of moisture. This deposition process is discussed in "The Phenomenon of Dust Deposition in Exhaust Ventilation Shafts at Inco Mines" (Stachulak, et al., 1991). Therefore, a majority of the trace metals will ultimately end up at the bottom of the west raise, with a portion of these metals likely transported to the project's wastewater treatment system with the mine drainage water that originates from the west raise.

Polycyclic aromatic hydrocarbons (PAH) that result from incomplete combustion are assumed to remain in the underground mine since they are not readily biodegradable or volatile. The resulting annual accumulation of PAHs from both mine air heating and mobile equipment use is 6.16 lb/yr. This is a very conservative estimate since some percentage of the PAHs will be exhausted by the large air flow through the mine.

TABLE 5.1
Primary Combustion By-Product Emissions

Source	Primary Emissions
Mine Air Heating	Particulate Matter Sulfur Dioxide Carbon Monoxide Nitrogen Oxides Formaldehyde Volatile Organic Compounds Polycyclic Aromatic Hydrocarbons
Mobile Equipment	Particulate Matter Sulfur Dioxide Carbon Monoxide Nitrogen Oxides Formaldehyde Volatile Organic Compounds Polycyclic Aromatic Hydrocarbons Metals (Arsenic, Beryllium, Cadmium, Chromium, Copper, Lead, Manganese, Mercury, and Nickel)
Blasting	Sulfur Dioxide Carbon Monoxide Nitrogen Oxides

TABLE 5.2
Annual Particulate Matter and Metal Accumulation

Particulate Matter	**2.43 ton/yr**
Arsenic	0.75 lb/yr
Beryllium	0.45 lb/yr
Cadmium	1.88 lb/yr
Chromium	8.59 lb/yr
Copper	50.12 lb/yr
Lead	1.59 lb/yr
Manganese	2.51 lb/yr
Mercury	0.54 lb/yr
Nickel	30.4 lb/yr

5.3 Relative Source Contribution

In Table 5.3 the total masses of metal constituents, estimated to accumulate in the mine from combustion over a 28 year mining period, are compared to the estimated total mass of metals to be contained in the backfilled tailings. This comparison demonstrates the relatively small potential contribution from the combustion source, compared to the backfilled tailings source, when the data are viewed on a total mass basis. As shown in Table 5.3, the potential contribution of any metal from combustion is orders-of-magnitude less than the backfilled tailings source. The combustion by-products not removed during the active years of mining by ventilation, flushing by mine drainage water, transportation to the surface with waste rock, ore, etc., or those not encapsulated in backfilled stopes will occupy the same underground mine environment as the backfilled tailings during mine closure, further underscoring the small potential constituent contribution from combustion by-products.

TABLE 5.3
Comparison of Total Metal Mass in
Backfilled Tailings vs. Accumulated Combustion By-Product Emissions

Metal	Backfilled Tailings ($kg \times 10^6$)	Combustion By-Products ($kg \times 10^6$)
Arsenic	52	0.000008
Beryllium	0.02	0.000002
Cadmium	0.4	0.00002
Chromium	0.6	0.0001
Copper	10	0.0006
Lead	58	0.00002
Manganese	10	0.00003
Mercury	0.04	0.000006
Nickel	0.4	0.0004

Note: Only a small fraction of total mass will dissolute and contribute to groundwater quality.

5.4 Potential Contribution to Groundwater Quality

The total metal mass estimates presented in Table 5.3 do not represent the readily available mass of metals to groundwater. Section 2 discussed the geochemical potential for the backfilled tailings to release constituents to groundwater. Oxygen transport modeling, tailings neutralization potentials and mixing of alkalinity from neutral tailings were all evaluated in Section 2 for their influence in controlling the release of tailing metals to groundwater.

Similarly, the total mass of DPM constituents presented in Section 5.3 also does not represent the readily available mass to groundwater. Geochemical and physical properties controlling the potential release of combustion constituents to groundwater include:

- DPM is comprised of submicron to micron sized particles with elemental carbon as a primary constituent (Watts and Waytulonis, 1991). As a result, DPM can be characterized as high surface area particles with good constituent adsorption potential. The good adsorption potential reduces the likelihood that constituents will appreciably partition into solution in sufficient quantities to elicit a water quality concern.

- Combustion metal constituents represent a very small potential source of metals to the reflooded mine, especially when compared to other potential sources of metals on a mass basis, e.g., backfilled tailings.

- Specific DPM metal adsorption coefficients are not available in the literature as industry and academic experts have viewed the metal DPM fraction to be a negligible environmental concern (Johnson and Gangal, personal communication).

- A large percentage of DPM will be transported to the vertical exhaust shaft and be subsequently removed over time with the mine drainage water.

- High mine air flow will promote ongoing removal of DPM.

- Reflooded mine groundwater will be high to neutral in pH with an elevated alkalinity, thereby dissolved metal concentrations will be further controlled by hydroxide secondary mineral phases.

The small potential contribution of constituents from combustion processes, combined with their geochemical and physical properties inhibiting or preventing releases to groundwater, suggest that combustion be viewed as a de minimus source, warranting no additional consideration.

6.0 GROUNDWATER MODELING

6.1 Approach

In order to understand how the source term components could release constituents to the groundwater, groundwater modeling of horizontal flow through various elevations of the mine was undertaken. The modeling was intended to provide a qualitative illustration of flow patterns surrounding the open and backfilled mine workings, and to provide order-of-magnitude estimates of flux through the backfilled tailings, open workings and wall rock. The model was based on the regional three-dimensional groundwater flow model documented in GeoTrans (1996), and was constructed using information from the following sources:

- "Numerical Simulation of the Effect on Groundwater and Surface Water of the Proposed Zinc and Copper Mine near Crandon, Wisconsin", GeoTrans, Inc., August 1996;
- "Addendum No.1 to Numerical Simulation of the Effect on Groundwater and Surface water of the Proposed Zinc and Copper Mine near Crandon, Wisconsin", HSI Geotrans Inc. 1998;
- "Tailings Management Area Feasibility Report/Plan of Operation for the Crandon Project", Foth and Van Dyke, May 1995;
- "Tailings Management Area Addenda to the Feasibility Report/Plan of Operation for the Crandon Project", Foth and Van Dyke, February 1996;
- Exxon Minerals Internal memorandum from D.E. Moe to J.E. Grimes Re: Tailings grain size analysis and permeability testing, 1982.

- "Bedrock Permeability, Crandon Deposit" (for Exxon Minerals Company), Roger Rowe, May 1984

The initial modeling, reported in March 1997, simulated horizontal flow through a representative elevation, and included sensitivity analyses from which flow patterns at other elevations could be inferred. The revised modeling reported herein includes the effects of anisotropy, as recommended in a letter from WDNR dated May 16, 1997, and more accurately simulates horizontal flow through several elevations.

6.2 Model Description

6.2.1 Conceptual Model

As described by GeoTrans (1996), groundwater flows east to west through the bedrock around the Crandon orebody. A moderately permeable weathered zone surrounds the upper portions of the steeply dipping orebody, and will contain a portion of the upper mine workings. Some downward groundwater flow occurs along the eastern end of the orebody, with upward flow along the western end. As a result of the higher permeabilities associated with the weathered zones and the open mine workings, groundwater in the vicinity of the mine will be channeled through the mine area after reflooding occurs. Within the mine area, the continuity of backfilled stopes and open workings may produce complex flow patterns. These patterns will influence the rate of constituent release to the surrounding groundwater.

In the vicinity of the Crandon orebody, fracture density has been documented at approximately two to three fractures per foot (Agapito and Associates, 1996). Dominant structural orientation is approximately N85W, and subvertical, parallel to the conformable Crandon orebody. Contacts between the Crandon Formation, hanging wall Skunk Lake, Rice Lake and Mole Lake Formations and foot wall Sand Lake Formation all parallel this structural trend, and lie within the local groundwater model domain. In view of the fracture frequency, and the scale of the local model, it is considered that a porous media model is appropriate for establishing flow patterns in and around the mine

workings. Previous groundwater modeling studies have successfully utilized porous media models for similar conditions (Toran and Bradbury, 1988).

6.2.2 Model Structure

The groundwater model was constructed using GMS (Groundwater Modeling Software, Brigham Young University, 1996), a graphical software package for performing groundwater modeling simulations. The current modeling was conducted using the MODFLOW processor package Groundwater Vistas (GV), by Environmental Simulations, Inc. This package was used as it allows for flux estimates through specific sections of the model to be easily carried out.

A horizontal two-dimensional model was chosen for the following reasons:

1. Assessment of local flow variations - construction of a two-dimensional model allowed for a more detailed, highly discretized model that would allow assessment of local flow patterns due to small scale heterogeneities (e.g. open workings, cemented vs. uncemented backfilled tailings);

2. Effect of open workings - because most of the open workings will be horizontal, horizontal flow patterns are expected to be most important;

A 12,000 ft x 8,000 ft variably-spaced orthogonal grid, similar to the larger, regional grid employed by GeoTrans, was constructed around a plan of the 1250 elevation mine workings. The long axis (x-direction) of the grid was oriented at 97 degrees azimuth, parallel to the orebody, the dominant structural trend, and the main direction of horizontal groundwater flow in the vicinity of the Crandon orebody.

The model was run in steady state mode to simulate long term conditions following completion of the mine reflooding. Constant head boundaries were established along the margins of the grid to match head elevations drawn from the GeoTrans Layer 6 (Moderately Weathered Bedrock) head elevations (Geotrans, 1996). Subsequent revisions to the GeoTrans model did not significantly alter the predicted head distribution in this area.

Polygons were constructed to conform to the following hydrogeologic units:

1. Low to weakly weathered hanging wall
2. Moderately weathered hanging wall
3. Strongly weathered hanging wall
4. Low to weakly weathered foot wall
5. Moderately weathered foot wall
6. Unweathered hanging wall
7. Unweathered foot wall
8. Backfilled stopes - uncemented coarse tailings
9. Backfilled stopes - cemented coarse tailings
10. Open mine workings

The geometry of the weathering patterns at each of the simulated elevations was derived from sections presented in Rowe, 1984. The intersections of weathering zone boundaries with each elevation were projected onto the model grid and interpolated. The moderately weathered zones were assumed to terminate near the ends of the orebody.

Areas of the hanging wall and footwall that were not logged on the sections were assumed to be weakly weathered for all mine elevations above 1200 feet. Mine levels below 1200 feet were assumed to be surrounded by unweathered bedrock unless logged as weathered. Furthermore, weathered areas were assumed to pinch out and form a weathered zone parallel to the orebody. Figures 6.1 to 6.4 show the resulting delineation of weathering zones at each of elevations 850, 1050, 1250, and 1350.

In simulations of levels where cut and fill mining would be used, the stopes were assumed to be backfilled with cemented tailings. In simulations of elevations with blasthole stopes, individual stopes were assumed to be 100 ft wide, and an alternating pattern of cemented and uncemented tailings backfill was utilized, as per the mining plan.

In order to provide a conservatively high estimate of groundwater flow through the mine workings, the geometry of the workings at the 1250 foot elevation was used in all simulations. The horizontal cross-sectional width of the backfilled tailings will be greatest in the vicinity of the 1250 elevation; and the hanging wall workings at the 1250 foot elevation are as extensive as at any other elevation.

6.2.3 Hydraulic Conductivity and Transmissivity Estimates

The hydraulic conductivity assigned to each of the model polygons is provided in Table 6.1. Both best engineering judgment (BEJ) and practical worst case (PWC) values were used in the simulations. The hydraulic conductivity values for the weathered bedrock units were obtained from HSI Geotrans, 1998.

Table 6.2 reports the associated transmissivity values. Note that, because the model was representing a 10-foot thick horizontal layer, the transmissivity values (in ft^2/day) are simply ten times the respective hydraulic conductivities (in ft/day)

TABLE 6.1
Assumed Hydraulic Conductivities

Model Material	BEJ Hydraulic Conductivity (ft/ day)	PWC Hydraulic Conductivity (ft^2/ day)
Low to weakly weathered hanging wall rock	Kx = 3.0e-3 Ky = 3.0e-4	Kx = 1.1e-2 Ky = 1.1e-3
Moderately weathered hanging wall rock	Kx = 4.4e-2 Ky = 4.4e-3	Kx = 2.9e-1 Ky = 2.9e-2
Strongly weathered hanging wall rock	4.8e-2	2.4e-1
Low to weakly weathered foot wall rock	Kx = 3.8e-2 Ky = 3.8e-3	Kx = 1.3e-1 Ky = 1.3e-2
Moderately weathered foot wall rock	Kx = 8.8e-2 Ky = 8.8e-3	Kx = 3.0e-1 Ky = 3.0e-2
Strongly weathered foot wall rock	2.3e-1	1.1
Uncemented tailings backfill	2.8e-2	2.8e-1
Cemented tailings backfill	2.8e-3	2.8e-2
Unweathered hanging wall rock	1.8e-3	6.6e-3
Unweathered foot wall rock	2.3e-2	7.8e-2
Hanging wall workings	1.0e+4	1.0e+4

* Note: Kx = Ky = unless indicated otherwise

TABLE 6.2
Assumed Transmissivities

Model Material	BEJ Transmissivity (ft/day)	PWC Transmisivity (ft^2/day)
Low to weakly weathered hanging wall rock	Tx = 3.0e-2 Ty = 3.0e-3	Tx = 1.1e-1 Ty = 1.1e-2
Moderately weathered hanging wall rock	Tx = 4.4e-1 Ty = 4.4e-2	Tx = 2.9 Ty = 2.9e-1
Strongly weathered hanging wall rock	4.8e-1	2.4
Low to weakly weathered foot wall rock	Tx = 3.8e-1 Ty = 3.8e-2	Tx = 1.3 Ty = 1.3e-1
Moderately weathered foot wall rock	Tx = 8.8e-1 Ty = 8.8e-2	Tx = 3.0 Ty = 3.0e-1
Strongly weathered foot wall rock	2.3	11
Uncemented tailings backfill	2.8e-2	2.8e-1
Cemented tailings backfill	2.8e-1	2.8
Unweathered hanging wall rock	1.8e-2	6.6e-2
Unweathered foot wall rock	2.3e-1	7.8e-1
Hanging wall workings	1.0e+5	1.0e+5

* Note: Tx = Ty = unless indicated otherwise

The estimated hydraulic conductivities of the weathered hanging and foot rock units were obtained from Tables 3.2 and 5.2 of the latest model addendum, as supplied by F&VD. The weakly and moderately weathered units were modeled as anisotropic, as documented in HSI Geotrans, 1998.

The estimated hydraulic conductivity of the unweathered hanging and foot wall rock was based on a value equal to 60% of the corresponding weakly weathered material. Unweathered rock was not assumed to be anisotropic.

Hydraulic conductivity values for the uncemented coarse tailings were estimated from conductivity data reported in an Exxon Minerals internal memo (1982). A transmissivity equal to one order of magnitude less than the uncemented tailings was applied to the cemented tailings.

The transmissivity of the open mine workings was initially estimated based on the upper limit of hydraulic conductivity for gravel, published by Freeze and Cherry (1979), modified to account for 100 % porosity. Initial runs demonstrated that the model would be unstable with such a high hydraulic conductivity assigned to the open workings. The value used for the simulations, and reported in Table 6.2, was two orders of magnitude less than the initial estimate. Sensitivity analyses demonstrated that the model was relatively insensitive to changes in the open workings' transmissivity below the assumed value, because the low permeability of the surrounding wall rock constrains the overall flow. Toran and Bradbury (1988) reported a similar groundwater modeling study incorporating flow through underground workings, and applied lower values for open workings transmissivity than was used for this study (Toran and Bradbury, 1988).

6.3 Simulated Cases

Table 6.3 lists the model runs, and summarizes the assumptions used for each run. The runs included simulations of elevations 850, 1050, 1250, and 1350. Each of those elevations was assumed to contain extensive hanging wall workings. Additional runs were completed without the hanging wall workings, to simulate flow at intermediate elevations (approximately elevations 900, 1100, 1300, and 1400). For all cases, both BEJ and PWC runs were completed.

All of the runs were executed using MODFLOW (McDonald and Harbaugh, 1988), the U.S. Geological Survey modular three-dimensional finite-difference groundwater flow code, modified by GV for coupling with the GV software. GeoTrans used MODFLOW for their regional model simulations. Resulting finite-difference equations were solved using the Preconditioned Conjugate Gradient 2 solver.

For each run, both head distribution and particle path solutions were determined, and printed. Predicted fluxes through the mine workings and tailings backfill were then

calculated using the mass balance function for a projected polygon on both the backfilled tailings and the mine workings sections of the model.

TABLE 6.3
Run Descriptions

Run	Weathering Units	Transmissivity	Hanging Wall Workings	Filename
850-BEJ	Figure 6.1	BEJ	Present	850_BEJ_1
850-PWC	Figure 6.1	PWC	Present	850_PWC_1
900-BEJ	Figure 6.1	BEJ	Not present	850_BEJ_NW1
900-PWC	Figure 6.1	PWC	Not present	850_PWC_NW1
1050-BEJ	Figure 6.2	BEJ	Present	1050_BEJ_1
1050-PWC	Figure 6.2	PWC	Present	1050_PWC_1
1100-BEJ	Figure 6.2	BEJ	Not present	1050_BEJ_NW1
1100-PWC	Figure 6.2	PWC	Not present	1050_PWC_NW1
1250-BEJ	Figure 6.3	BEJ	Present	1250_BEJ_2
1250-PWC	Figure 6.3	PWC	Present	1250_PWC_2
1300-BEJ	Figure 6.3	BEJ	Not present	1250_BEJ_NW1
1300-PWC	Figure 6.3	PWC	Not present	1250_PWC_NW1
1350-BEJ	Figure 6.4	BEJ	Present	1350_BEJ_1
1350-PWC	Figure 6.4	PWC	Present	1350_PWC_1
1400-BEJ	Figure 6.4	BEJ	Not present	1350_BEJ_NW1
1400-PWC	Figure 6.4	PWC	Not present	1350_PWC_NW1

6.4 Results

Results of each model run are shown graphically in Appendix D. As a typical example, Figure 6.5 shows the results of run 1250_BEJ. Particle tracking was used to display flowpaths originating within cells on the eastern boundary of the model. The resulting pictures clearly show the strong influence of the mine workings on flow patterns.

Results of the flux calculations are summarized in Table 6.4. The fluxes reported correspond to the 10 foot thick model.

TABLE 6.4
Simulation Results

Run	Total Flow through Workings (ft^3/day)	Flow through Tailings Backfill (ft^3/day)	Flow through Hanging Wall Workings (ft^3/day)
850-BEJ	3.45	2.20	1.25
850-PWC	14.80	9.41	5.39
900-BEJ	0.44	0.44	-
900-PWC	0.44	0.44	-
1050-BEJ	3.75	2.22	1.53
1050-PWC	16.07	9.46	6.61
1100-BEJ	0.50	0.50	-
1100-PWC	1.89	1.89	-
1250-BEJ	4.44	1.33	3.11
1250-PWC	20.41	6.42	13.99
1300-BEJ	0.37	0.37	-
1300-PWC	2.20	2.20	-
1350-BEJ	4.74	1.49	3.25
1350-PWC	21.70	7.05	14.65
1400-BEJ	0.47	0.47	-
1400-PWC	2.98	2.98	-

6.5 Conclusions

There are a number of common features in the simulations of all of elevations that included open workings in the hanging wall. Flow is directed substantially toward the open workings, with the majority of flow passing through the relatively permeable foot wall, through the backfill and into the mine workings. In all cases, significantly more flux flowed from the backfilled tailings into the mine workings than vice versa. Once in the workings, flow is dominantly from east to west.

The total flows through the mine were significantly higher (about 10x higher) in runs with open workings present in the hanging wall than in the respective runs without the hanging wall workings. In the latter runs, there was of course no flow through the hanging wall workings. However, flow through the tailings backfill was also lower (about 3x lower) when hanging wall workings were not present.

The flow estimates provided by the model results represent flow through 10-foot thick layers. Conservative estimates of the total groundwater flow through the mine workings can be obtained by multiplying the flux estimated from each model run by the number of 10-foot thick intervals represented by that run. These calculations are shown in Table 6.5 for the BEJ runs and Table 6.6 for the PWC runs.

The total flow through the mine workings is estimated to be 44 ft^3/day using the BEJ assumptions, and 208 ft^3/day using the PWC assumptions. The implication of these estimates is that the mine workings, with a total pore volume of roughly 120,000,000 ft^3, would take approximately 7500 years to flush in the BEJ case, and 1600 years in the PWC.

The proportion of flow through each of the underground sources is relatively constant from run to run. In both the BEJ and PWC estimates, approximately four-fifth of the total flow is through the tailings backfill, the other one-fifths is through the hanging wall workings. The implication of these estimates is that concentrations in approximately 80% of the groundwater leaving the mine area would be dominated by the concentrations associated with the tailings backfill (i.e. Table 2.7). The remaining 20% of the groundwater leaving the mine area would be expected to exhibit concentrations typical of the hanging wall workings (i.e. Table 3.5).

TABLE 6.5
BEJ Estimates of Total Flows

Run	Number of Levels	Total Flow through Workings (ft^3/day)	Flow through Tailings Backfill (ft^3/day)	Flow through Hanging Wall Workings (ft^3/day)
850-BEJ	1	3.45	2.2	1.25
900-BEJ	24	10.56	10.56	-
1050-BEJ	1	3.75	2.22	1.53
1100-BEJ	19	9.5	9.5	-
1250-BEJ	1	4.44	1.33	3.11
1300-BEJ	9	3.33	3.33	-
1350-BEJ	1	4.74	1.49	3.25
1400-BEJ	9	4.23	4.23	-
BEJ Totals	65	44.00	34.86	9.14

TABLE 6.6
PWC Estimates of Total Flows

Run	Number of Levels	Total Flow through Workings (ft^3/day)	Flow through Tailings Backfill (ft^3/day)	Flow through Hanging Wall Workings (ft^3/day)
850-PWC	1	14.8	9.41	5.39
900-PWC	24	52.56	52.56	-
1050-PWC	1	16.07	9.46	6.61
1100-PWC	19	35.91	35.91	-
1250-PWC	1	20.41	6.42	13.99
1300-PWC	9	19.8	19.8	-
1350-PWC	1	21.7	7.05	14.65
1400-PWC	9	26.82	26.82	-
PWC Totals	65	208.07	167.43	40.64

7.0 CONCLUSIONS REGARDING GROUNDWATER QUALITY

7.1 Concentration Estimates

Table 7.1 summarizes the estimated contribution of each underground source to constituent concentrations in the groundwater that will flood the Crandon Mine.

As discussed in Section 2, the bulk of the backfilled tailings are not expected to contribute significant quantities of sulfate or metals to the reflooding groundwater. Limitations to oxygen transport will restrict oxidation and constituent dissolution to areas near the stope access cross-cuts. These areas will be a very small percentage of the total volume of backfilled tailings. After reflooding, the groundwater model shows that much of the flow will be directed through the access cross-cuts. However, it will pass through the bulk of the backfilled tailings, either on its way to the access workings (on the east end of the mine) or on its way out of the access workings (on the west end of the mine). In both cases, alkalinity from the bulk of the backfilled tailings will be available to neutralize oxidation products that could be accumulated during the mine life. The use of the simple average concentrations shown in row 1 of Table 7.1 to represent the backfilled tailings source term is therefore conservative.

TABLE 7.1
Estimated Concentrations on Reflooding

Source	Estimated Volume (ft^3)	Percentage of total flow	Constituent Concentrations in Groundwater (mg/L)							
			SO_4	As	Ca	Cu	Fe	Mn	Se	Zn
Backfilled Tailings	195,000,000	79%	1006	0.51	404	0.23	11	1.3	0.12	13
Total Wall Rock	12,600,000	1%	17	0.016	10	0.078	2.6	0.12	0.004	0.12
Crown Pillar	950,000	20%	35	0.001	3	1.5	0.8	0.06	0.004	13
Volume weighted average	210,000,000		941	0.48	378	0.22	10	1.2	0.11	12
Flow weighted average		100%	798	0.41	321	0.21	9	1.0	0.10	10

As discussed in Section 3, wall rock in the access developments will be exposed to oxygen throughout the mine life, resulting in oxidation of sulfide minerals and liberation of metals and sulfate. As the groundwater re-floods the access developments, some of these metals and sulfates will be dissolved. The constituent concentrations shown in row 2 in Table 7.1 were estimated under the conservative assumption that all of the liberated metals and sulfate will dissolve into the volume of water required to fill the access developments.

Wall rock from the ore zone is not expected to make a significant contribution of metals or sulfate to the reflooding groundwater. Sulfidic wall rock will remain in the area of the ore body, and may oxidize. However, backfilling of the stopes will result in flushing and/or neutralization of any oxidation products during mining, and they will be captured in the mine water treatment system. As discussed in Section 4, gossan and saprolite zones in the crown pillar are also not expected to make a significant contribution of metals or sulfate to the reflooding groundwater. The gossan and saprolite zones have been oxidized over geologic time and unstable oxidation products have been removed. Deeper in the crown pillar, zones of unmined sulfide mineralization will be left behind after mining. These zones will generally form the backs of the uppermost stopes, and may make a contribution of sulfate and metals to the reflooding groundwater. However, oxidation will be limited to the relatively short period during mining, before the stopes are sealed from contact with the ventilation system. The third row of Table 7.1 summarizes the constituent concentrations that will result if the estimated quantity of accumulated oxidation products conservatively is assumed to dissolve in the groundwater that will fill the void between the stope backs and the tailings backfill.

As discussed in Chapter 5, combustion emissions make an insignificant contribution to the metal mass in the underground workings, and can therefore be considered a de minimus source.

The final two rows of Table 7.1 provide average concentration estimates for each constituent. The first set of averages was obtained by weighting the contribution from each source by the volume of water associated with that source. In effect, the volume-weighted averages represent the concentrations that would be observed in a fully mixed system.

Given the conclusion of the groundwater flow modeling that approximately 20% of the flow through the mine area is through the hanging wall workings, and 80% enters the stopes, the flow-weighted average concentrations may be more representative of concentrations in groundwater flows leaving the underground sources. In any case, the flow-weighted average concentrations are very similar to the volume-weighted average concentrations.

7.2 Uncertainty Analysis

The concentration estimates in Table 7.1 were obtained through relatively simple calculations, supported by generally conservative assumptions. Tables 7.2 to 7.4 list the assumptions that were made and provide a semi-quantitative assessment of the uncertainty that each assumption brings to the resulting concentration estimates. The format of the tables is similar to that recommended by the USEPA for review of exposure pathway models used for human health risk assessments (U.S. EPA, 1989). The intent is to provide an overview of the uncertainty associated with each estimated quantity, and to allow the reader to form an opinion as to how conservative the estimates are likely to be.

Scanning through tables 7.2 to 7.4 shows that the assumptions used in the source term modeling were generally conservative. The resulting estimates of constituent concentrations in the reflooding groundwater are therefore likely to be conservatively high. Table 7.5 provides a similar review of the uncertainties in the groundwater flow modeling. In any further analyses that rely on these estimates, the conservative nature of the calculations should be taken into consideration.

TABLE 7.2
Uncertainty Associated with Estimation of Constituent Contributions from Backfill Tailings

Assumption	Potential for Over-Estimation of Concentrations*	Potential for Under-Estimation of Concentrations*
Gas diffusion coefficients for tailings and waste rock used in oxygen transport modeling are near the upper range of published data	Moderate	–
Assumption that oxygen would be at atmospheric concentrations inside the bulkhead for oxygen diffusion modeling	Moderate	–
Selection of tortuosity values for oxygen transport modeling	Moderate	Low
Use of humidity cell test results on coarse uncemented tailings to estimate constituent concentrations in cemented tailings	Low to Moderate	Low
Use of last 3 cycles of humidity test cell data to estimate constituent concentrations for cemented, unoxidized tailings	Moderate	Moderate
Use of PWC estimates of TMA process water quality to estimate uncemented tailings contribution to groundwater	Moderate	Low
Use of average exposure time of 15 years for tailings	Moderate	Moderate
Use of MINTEQA2 model to estimate concentrations after secondary precipitation	Moderate	Moderate
Use of weighted averages to calculate overall contribution of constituents to reflooding groundwater	Moderate	–

* Uncertainty rated as "Low" may affect estimates of contribution from the individual source by less than a factor of 2; assumptions rated as "Moderate" may affect estimates by less than one order of magnitude; assumptions rated as "High" may affect estimates by greater than one order of magnitude.

TABLE 7.3

Uncertainty Associated with Estimation of Constituent Contributions from Wall Rock

Assumption	Potential for Over-Estimation of Concentrations*	Potential for Under-Estimation of Concentrations *
Estimation of sulfur contents in mine workings wall rock	Low	Low
Contribution from ore zone and foot wall deemed to be negligible due to short exposure period and washing with alkaline water, in addition to collection in mine water system		Low
Use of humidity column tests to estimate release of constituents from wall rock	Moderate	Low
Use of reactive surface area/ mine workings surface area ratios from surface mine workings literature to predict reactive surface area in underground workings	Moderate to High	Low to Moderate
Use of average mine workings oxidation period of 15 years	Low	Low
Assumption that all constituents generated during oxidation period will dissolve in reflooding groundwater	Moderate to High	

* Uncertainty rated as "Low" may affect estimates of contribution from the individual source by less than a factor of 2; assumptions rated as "Moderate" may affect estimates by less than one order of magnitude; assumptions rated as "High" may affect estimates by greater than one order of magnitude.

TABLE 7.4
Uncertainty Associated with Estimation of Constituent Contributions from the Crown Pillar

Assumption	Potential for Over-Estimation of Concentrations*	Potential for Under-Estimation of Concentrations*
Estimation of sulfide content of exposed ore in crown pillar	Low	Low
Assumption that entire mean annual infiltration of 10 inches percolates through overburden to crown pillar, while maintaining theoretical maximum solubility of oxygen	Moderate to High	–
Use of diffusion coefficient which assumes uniformly unsaturated conditions for oxygen transport calculation	Moderate	–
Use of humidity column test results on high-grade Crandon zinc ore to estimate constituent release from exposed copper and zinc ore portions of crown pillar	Moderate	Low
Assumption of average exposure period of 6 weeks	Low	Low to Moderate
Assumption that tight-filling methods will seal off stope access points	–	Low to Moderate
Assumption that all constituents accumulated would be dissolved in the reflooding groundwater	Moderate to High	–
Neglect of cemented tailings immediately below crown pillar as a source of alkalinity	Moderate to High	–

* Uncertainty rated as "Low" may affect estimates of contribution from the individual source by less than a factor of 2; assumptions rated as "Moderate" may affect estimates by less than one order of magnitude; assumptions rated as "High" may affect estimates by greater than one order of magnitude.

8.0 REFERENCES

Agapito and Associates Inc., May 1996. Hydrologic Stability of the Crown Pillar, Crandon Deposit.

Archibald, J.F. and Nantel, J. H., 1984. Prediction of Radiation Levels and Ventilation Requirements in Underground Uranium Mines. CIM Bulletin, Vol. 77, No. 861, January 1984, pp. 60-64.

Blowes, D,W., Reardon, E.J. Jambor, J.L., Cherry, J.A., 1990. The Formation and Potential Importance of Cemented Layers in Inactive Sulfide Mine Tailings. Geochemica et Cosmochimica Acta, Vol. 55, pp. 965-978.

Cussler, E.L., 1984. Mass Transfer in Fluid Systems Cambridge Univ. Press, 525 pp.

Erickson, A.J. Jr., November 1996. Crandon Mining Company. Memo to file Re: Reserves/Permanent Crown Pillar.

Erickson, A.J. Jr. and R. Cote. Geological Summary, Crandon Deposit, January, 1996.

Erickson, A.J. Jr. Memo Re: Hanging Wall Sulfide Content Review, Crandon Deposit Updated, less Appendix 2, to Mr. D.E. Moe, dated July 10, 1996.

Erickson, A.J. Jr. Memo Re: Hanging Wall Sulfide Estimates, to Mr. K. Black, dated December 16, 1996.

Exxon Minerals, 1982. Internal Memo from D.E. Moe to J.E. Grimes Re: Grain Size and Permeability Characteristics of Tailings.

Foth and Van Dyke, May 1995. Environmental Impact Report, Crandon Project.

Foth and Van Dyke, May and September, 1995. Crandon Project Mine Permit Application, pages 35 to 49, 63, 81 to 84, dated September 29, 1995 and May 30, 1995.

Foth and Van Dyke. December 1995. Waste Characterization Update Report, Crandon Project.

Foth and Van Dyke April 1998. Updated Crandon Project Tailings Management Area Groundwater Quality Performance Evaluation.

Freeze, R.A. and Cherry, J. A., 1979. Groundwater. Prentice-Hall, 604 pp.

Gangal, Mahi, Ph.D. Head of Diesel Emissions, CANMET - Mining Research Laboratories, Ontario, Canada. Personal Communication.

Gangal, Mahi, Ph.D. Head of Diesel Emissions, CANMET - Mining Research Laboratories, Ontario, Canada. Personal Communication.

GeoTrans, 1996. Numerical Simulation of the Effect on Groundwater and Surface Water of the Proposed Zinc and Copper Mine near Crandon, Wisconsin.

HSI Geotrans Inc., 1998. Addendum No.1 to Numerical Simulation of the Effect on Groundwater and Surface water of the Proposed Zinc and Copper Mine near Crandon, Wisconsin, HSI Geotrans Inc. 1998;

Johnson, John, Ph.D., Director of Engineering Extension, College of Engineering, Michigan Technological University, Houghton, Michigan, and Mahi Gangal, Ph.D., Head of Diesel Emissions, CANMET - Mining Research Laboratories, Ontario, Canada. Personal Communication.

Morin, K.A., 1990. Acid Drainage from Mine Walls: The Main Zone Pit at Equity Silver Mines. British Columbia Acid Mine Drainage Task Force.

Morin, K.A. and Hutt, N.M., 1995. A Technique for Predicting Water Chemistry in Open Pit and Underground Mines. In: Sudbury '95 Mining and the Environment Conf. Proc.

Nicholson, R.V., 1994. Iron Sulfide Oxidation Mechanisms: Laboratory Studies. In Short Course Handbook on Environmental Geochemistry of Sulfide Mine Wastes, Mineral Association of Canada, 438 pp.

Reardon, E.J. and Moddle, P.M., 1985. Gas Diffusion Coefficient Measurement on Uranium Mill Tailings: Implications to Cover Layer Design. Uranium, Vol. 2 pp 111-131.

Ritchie, A.J.M, 1994. Sulfide Oxidation Mechanism-Controls and Rates of Oxygen Transport. In "The Environmental Geochemistry of Sulfide Mine Wastes", D.A. Blowes J.L. Jambor, Eds. CANMENT, 1994.

Stachulak, J.S., E.D. Dainty, and M.J. McPherson, November 1991. "The Phenomenon of Dust Deposition in Exhaust Ventilation Shafts at Inco Mines". *Journal of the Mine Ventilation Society of South Africa.*

Toran, L. and Bradbury, K.R., 1988. Ground-Water Flow Model of Drawdown and Recovery Near an Underground Mine. *Ground Water*, Vol. 26, No. 6.

U.S. Environmental Protection Agency, April 1989. Estimating Air Toxics Emissions from Coal and Oil Combustion Sources. Radian Corporation. EPA/450/2-89/001.

U.S. Environmental Protection Agency, December 1989. Risk Assessment Guidance for Superfund, Volume 1, Human Health Evaluation Manual (Part A), Interim Final. EPA/540/1-89/002.

U.S. Environmental Protection Agency, September 1993. Locating and Estimating Air Toxic Emissions from Medical Waste Incinerators. Radian Corporation. USEPA Contract No. 68D90054. DCN #96/275/026/42/02.

Watts, W.F., and R.W. Waytulonis, 1990. Why is diesel particulate in mines an issue and how can it be controlled? *Proc. Symp. Environ. Manage for the 1990s*, Denver, CO.

Watts, W.F. and R.W. Wayfulonis, 1991. "Why is Diesel Particulate in Mines an Issue and How Can It Be Controlled?" U.S. Department of the Interior, Bureau of Mines. Proceedings of the Symposium on Environmental Management for the 1990s.

Waytulonis, R.W., 1991. Emission control options for mine diesels. *Mining and Engineering*, Vol. 43, No. 3, pp. 325-328.

Note: As a result of the April 1998 update to the Reflooded Mine Source Term - Crandon Project report, pages 61-65 of the report (pages 4.2-13-66 through 4.2-13-70) have been deleted.

TABLE 7.5
Uncertainty Associated with Estimation of Groundwater Fluxes

Assumption	Potential for Over-Estimation of Fluxes*	Potential for Under-Estimation of Fluxes*
Use of a porous media model	Moderate	Low
Use of an isotropic model	Moderate	–
Assumption that no flow exists below 800 foot elevation	–	Low to Moderate
Use of the 1250 foot elevation as a basis for estimating flows within the middle portions of the mine	Moderate	Low
Use of 1400 elevation to assess flow within the upper portions	Moderate	Low
Use of constant head boundaries along margins of model	Low	Low
Estimation of base case transmissivity values for hydrogeologic units	Low to High	Low to Moderate
Effect of grid discretization on estimation of groundwater fluxes	Low	Low
Use of maximum "Reasonable Model Range" transmissivity values drawn from GeoTrans (1996) to estimate fluxes	Moderate	Low
Use of moderately and highly weathered zones in 1400 elevation model	Moderate	–
Extrapulation of fluxes from 10 foot model to layer thickness of 650 feet in mine	Moderate to High	–

* Uncertainty rated as "Low" may affect estimates of groundwater flux by less than a factor of 2; assumptions rated as "Moderate" may affect estimates by less than one order of magnitude; assumptions rated as "High" may affect estimates by greater than one order of magnitude.

8.0 REFERENCES

Agapito and Associates Inc., May 1996. Hydrologic Stability of the Crown Pillar, Crandon Deposit.

Archibald, J.F. and Nantel, J. H., 1984. Prediction of Radiation Levels and Ventilation Requirements in Underground Uranium Mines. CIM Bulletin, Vol. 77, No. 861, January 1984, pp. 60-64.

Blowes, D,W., Reardon, E.J. Jambor, J.L., Cherry, J.A., 1990. The Formation and Potential Importance of Cemented Layers in Inactive Sulfide Mine Tailings. Geochemica et Cosmochimica Acta, Vol. 55, pp. 965-978.

Cussler, E.L., 1984. Mass Transfer in Fluid Systems Cambridge Univ. Press, 525 pp.

Erickson, A.J. Jr., November 1996. Crandon Mining Company. Memo to file Re: Reserves/Permanent Crown Pillar.

Erickson, A.J. Jr. and R. Cote. Geological Summary, Crandon Deposit, January, 1996.

Erickson, A.J. Jr. Memo Re: Hanging Wall Sulfide Content Review, Crandon Deposit Updated, less Appendix 2, to Mr. D.E. Moe, dated July 10, 1996.

Erickson, A.J. Jr. Memo Re: Hanging Wall Sulfide Estimates, to Mr. K. Black, dated December 16, 1996.

Exxon Minerals, 1982. Internal Memo from D.E. Moe to J.E. Grimes Re: Grain Size and Permeability Characteristics of Tailings.

Foth and Van Dyke, May 1995. Environmental Impact Report, Crandon Project.

Foth and Van Dyke, May and September, 1995. Crandon Project Mine Permit Application, pages 35 to 49, 63, 81 to 84, dated September 29, 1995 and May 30, 1995.

Foth and Van Dyke. December 1995. Waste Characterization Update Report, Crandon Project.

Freeze, R.A. and Cherry, J. A., 1979. Groundwater. Prentice-Hall, 604 pp.

Gangal, Mahi, Ph.D. Head of Diesel Emissions, CANMET - Mining Research Laboratories, Ontario, Canada. Personal Communication.

Gangal, Mahi, Ph.D. Head of Diesel Emissions, CANMET - Mining Research Laboratories, Ontario, Canada. Personal Communication.

GeoTrans, 1996. Numerical Simulation of the Effect on Groundwater and Surface Water of the Proposed Zinc and Copper Mine near Crandon, Wisconsin.

Johnson, John, Ph.D., Director of Engineering Extension, College of Engineering, Michigan Technological University, Houghton, Michigan, and Mahi Gangal, Ph.D., Head of Diesel Emissions, CANMET - Mining Research Laboratories, Ontario, Canada. Personal Communication.

Morin, K.A., 1990. Acid Drainage from Mine Walls: The Main Zone Pit at Equity Silver Mines. British Columbia Acid Mine Drainage Task Force.

Morin, K.A. and Hutt, N.M., 1995. A Technique for Predicting Water Chemistry in Open Pit and Underground Mines. In: Sudbury '95 Mining and the Environment Conf. Proc.

Nicholson, R.V., 1994. Iron Sulfide Oxidation Mechanisms: Laboratory Studies. In Short Course Handbook on Environmental Geochemistry of Sulfide Mine Wastes, Mineral Association of Canada, 438 pp.

Reardon, E.J. and Moddle, P.M., 1985. Gas Diffusion Coefficient Measurement on Uranium Mill Tailings: Implications to Cover Layer Design. Uranium, Vol. 2 pp 111-131.

Ritchie, A.J.M, 1994. Sulfide Oxidation Mechanism-Controls and Rates of Oxygen Transport. In "The Environmental Geochemistry of Sulfide Mine Wastes", D.A. Blowes J.L. Jambor, Eds. CANMENT, 1994.

Stachulak, J.S., E.D. Dainty, and M.J. McPherson, November 1991. "The Phenomenon of Dust Deposition in Exhaust Ventilation Shafts at Inco Mines". *Journal of the Mine Ventilation Society of South Africa.*

Toran, L. and Bradbury, K.R., 1988. Ground-Water Flow Model of Drawdown and Recovery Near an Underground Mine. *Ground Water*, Vol. 26, No. 6.

U.S. Environmental Protection Agency, April 1989. Estimating Air Toxics Emissions from Coal and Oil Combustion Sources. Radian Corporation. EPA/450/2-89/001.

U.S. Environmental Protection Agency, December 1989. Risk Assessment Guidance for Superfund, Volume 1, Human Health Evaluation Manual (Part A), Interim Final. EPA/540/1-89/002.

U.S. Environmental Protection Agency, September 1993. Locating and Estimating Air Toxic Emissions from Medical Waste Incinerators. Radian Corporation. USEPA Contract No. 68D90054. DCN #96/275/026/42/02.

Watts, W.F., and R.W. Waytulonis, 1990. Why is diesel particulate in mines an issue and how can it be controlled? *Proc. Symp. Environ. Manage for the 1990s*, Denver, CO.

Watts, W.F. and R.W. Wayfulonis, 1991. "Why is Diesel Particulate in Mines an Issue and How Can It Be Controlled?" U.S. Department of the Interior, Bureau of Mines. Proceedings of the Symposium on Environmental Management for the 1990s.

Waytulonis, R.W., 1991. Emission control options for mine diesels. *Mining and Engineering*, Vol. 43, No. 3, pp. 325-328.

FIGURES

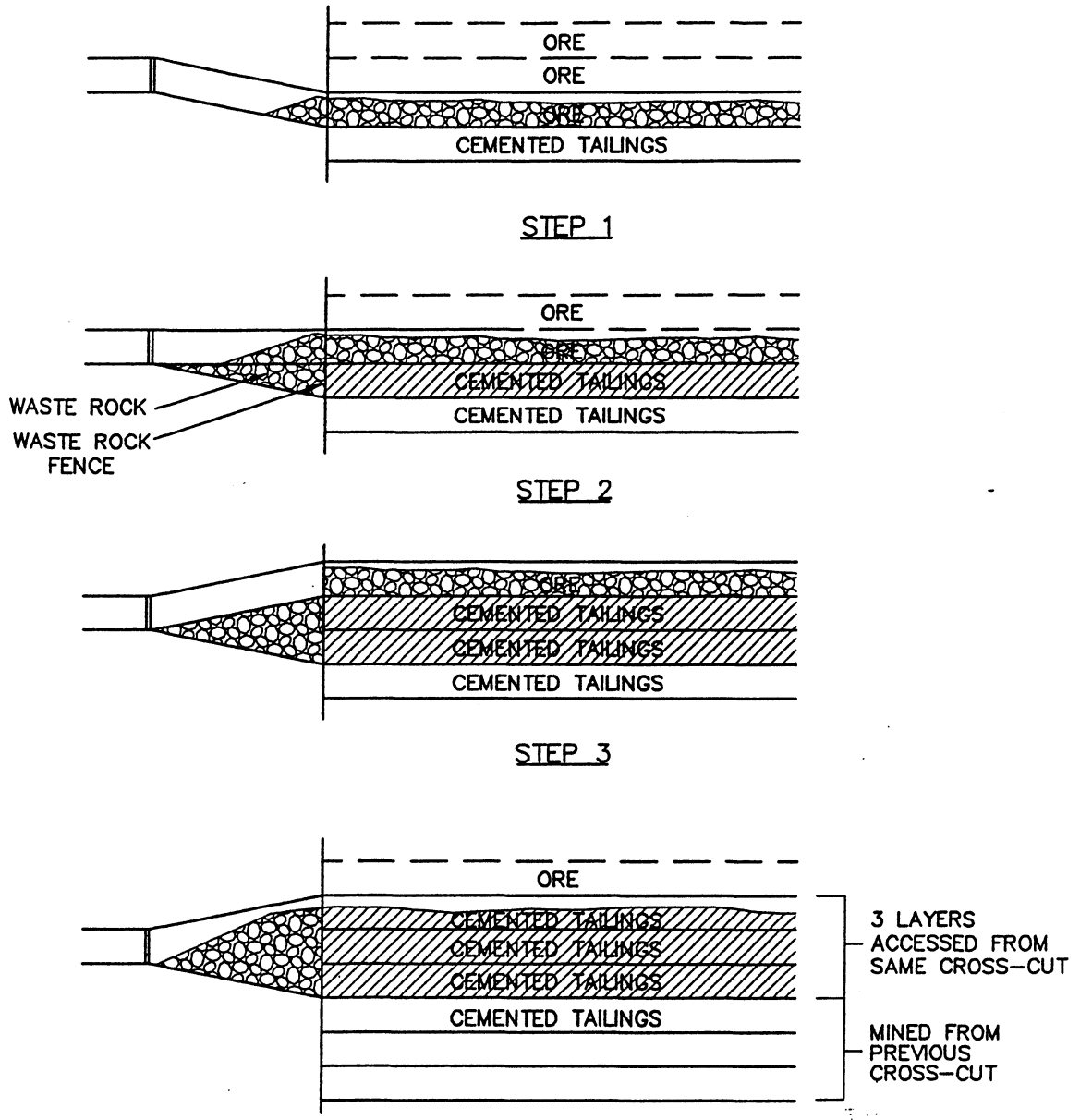

SIDE ELEVATION

STEFFEN ROBERTSON AND KIRSTEN
Consulting Engineers

FOTH & VAN DYKE

REFLOODED MINE SOURCE TERM

CUT AND FILL BACKFILLING CONCEPTUAL MODEL

PROJECT NO.	DATE	APPROVED	FIGURE
F107107	JAN. 1997		2.1

FILE REF: FIG-3-1

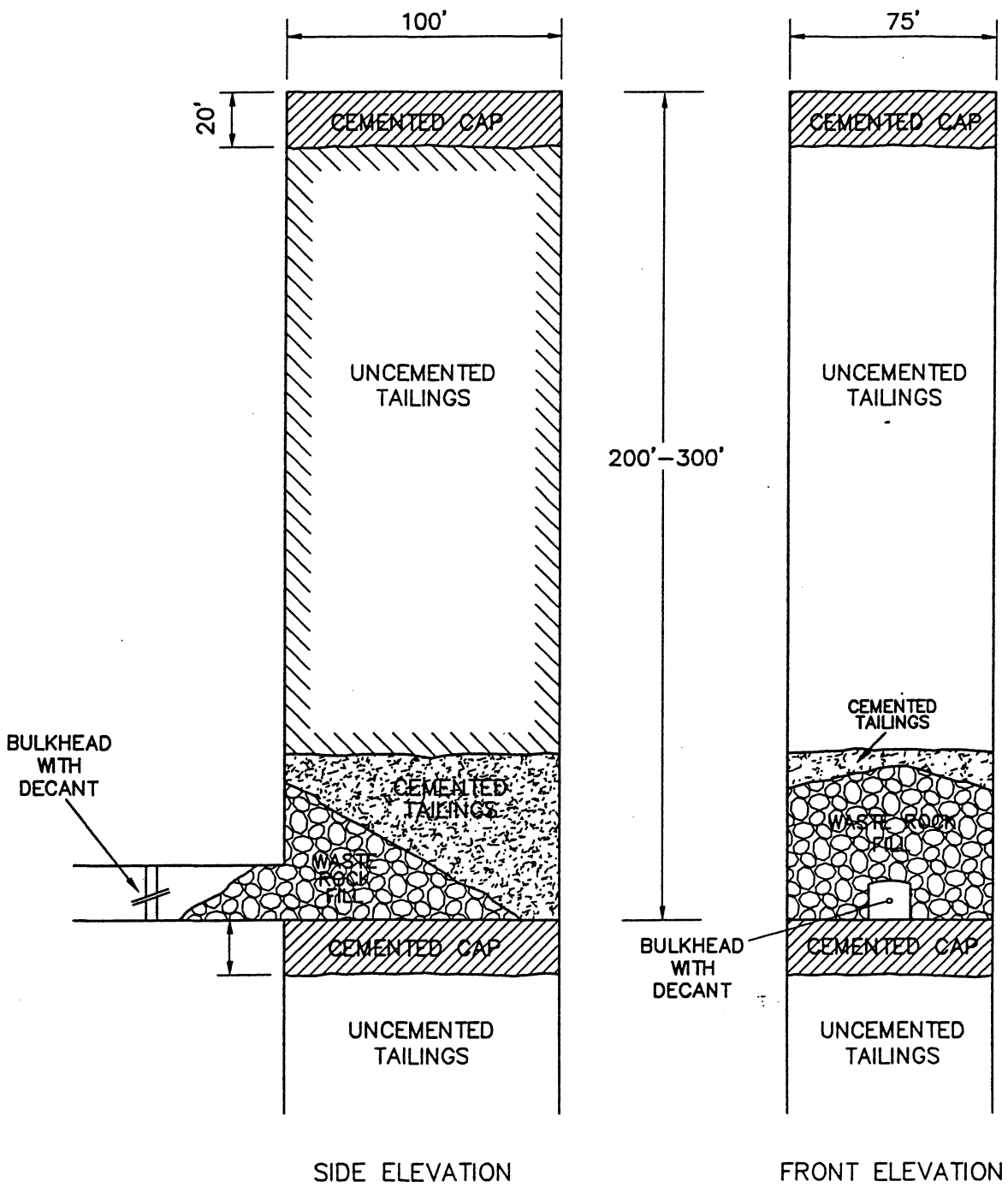

STEFFEN ROBERTSON AND KIRSTEN
Consulting Engineers

FOTH & VAN DYKE

REFLOODED MINE SOURCE TERM

BACKFILLED STOPE (UNCEMENTED TAILINGS)

PROJECT NO.	DATE	APPROVED	FIGURE
F107107	DEC. 1996		2.2

FILE REF: FIG-3-2

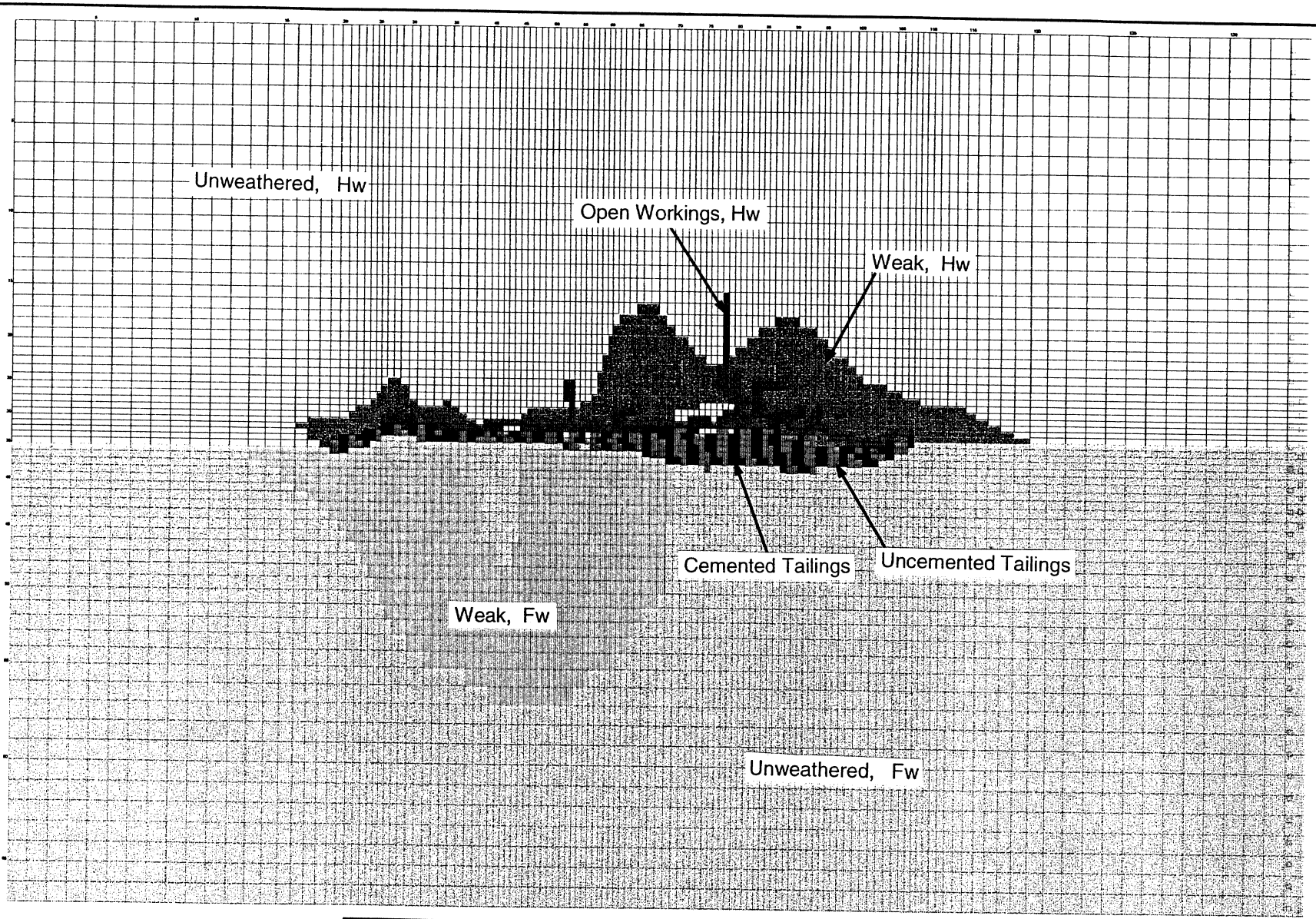

STEFFEN ROBERTSON AND KIRSTEN
Consulting Engineers

FOTH & VAN DYKE

REFLOODED MINE SOURCE TERM

850 FOOT ELEVATION
WEATHERING ZONES

PROJECT NO.	DATE	APPROVED	FIGURE
F107107/2	MARCH 1998		6.1

4.2-13-74

FILE REF: FIG-SIX-ONE

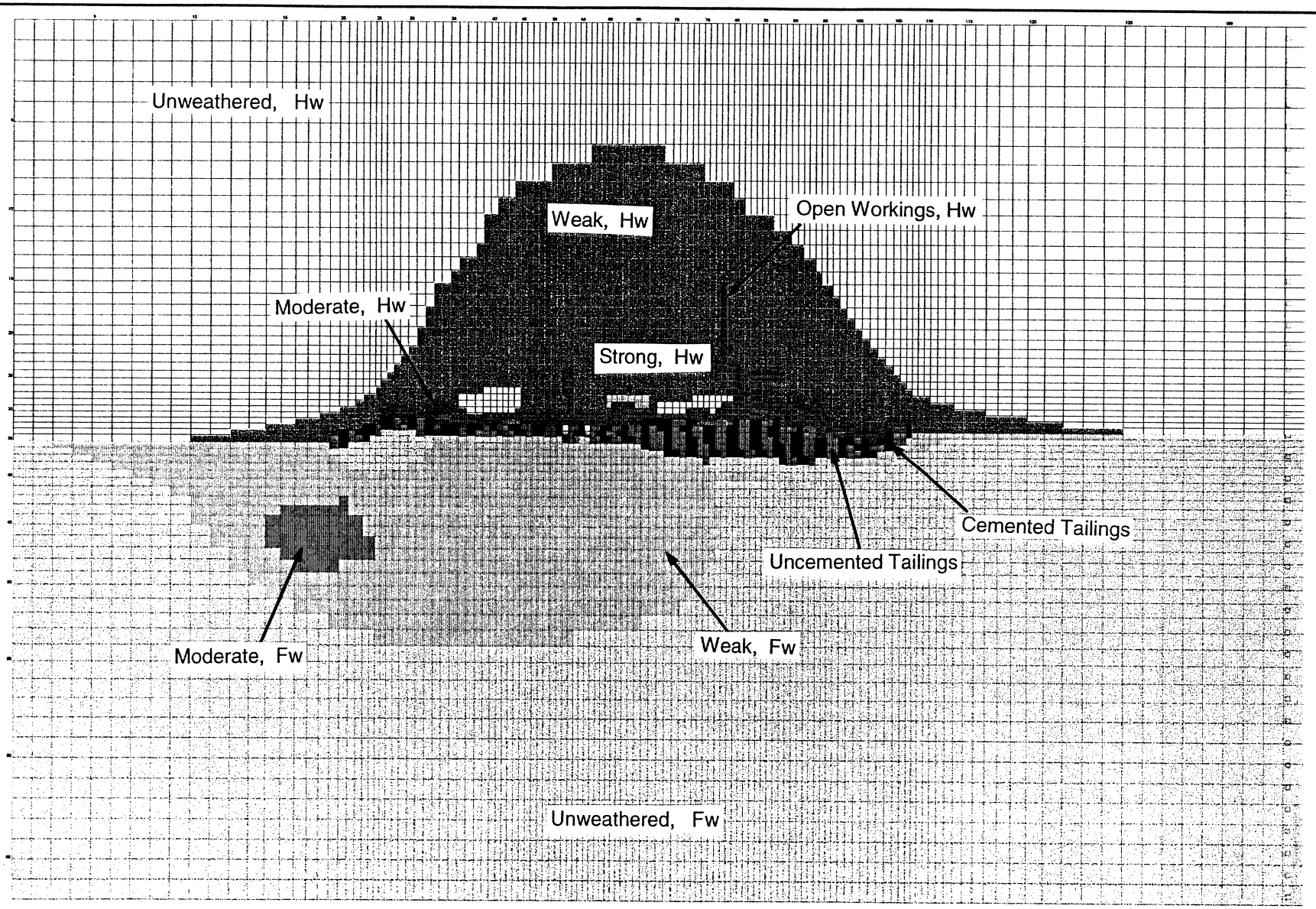

STEFFEN ROBERTSON AND KIRSTEN
Consulting Engineers

FOTH & VAN DYKE

REFLOODED MINE SOURCE TERM

1050 FOOT ELEVATION
WEATHERING ZONES

PROJECT NO.	DATE	APPROVED	FIGURE
F107107/2	MARCH 1998		6.2

4.2-13-75

FILE REF: FIG-SIX-TWO

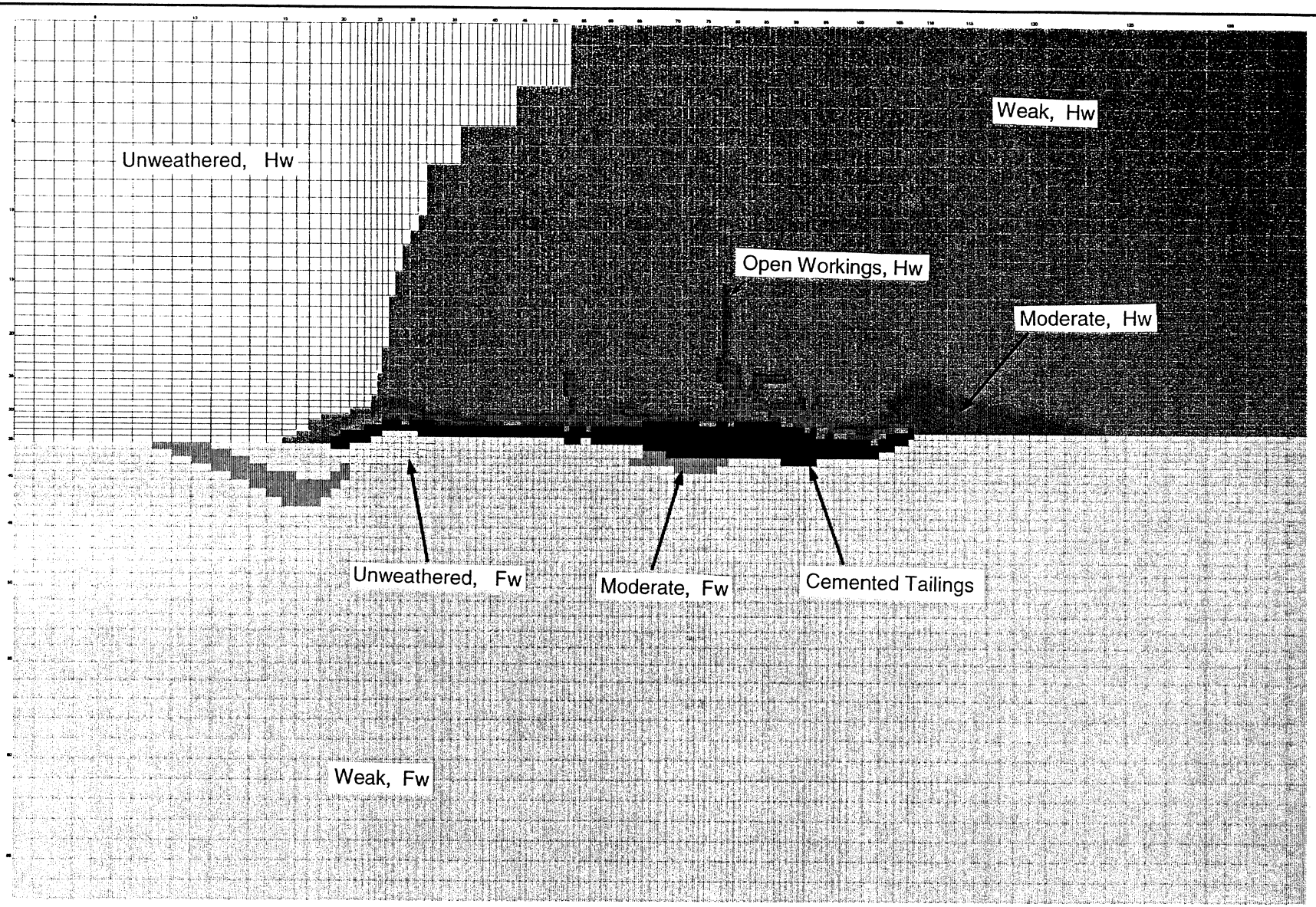

STEFFEN ROBERTSON AND KIRSTEN
Consulting Engineers

FOTH & VAN DYKE

REFLOODED MINE SOURCE TERM

1250 FOOT ELEVATION
WEATHERING ZONES

PROJECT NO.	DATE	APPROVED	FIGURE
F107107/2	MARCH 1998		6.3

FILE REF: FIG-SIX-THREE

4.2-13-75a

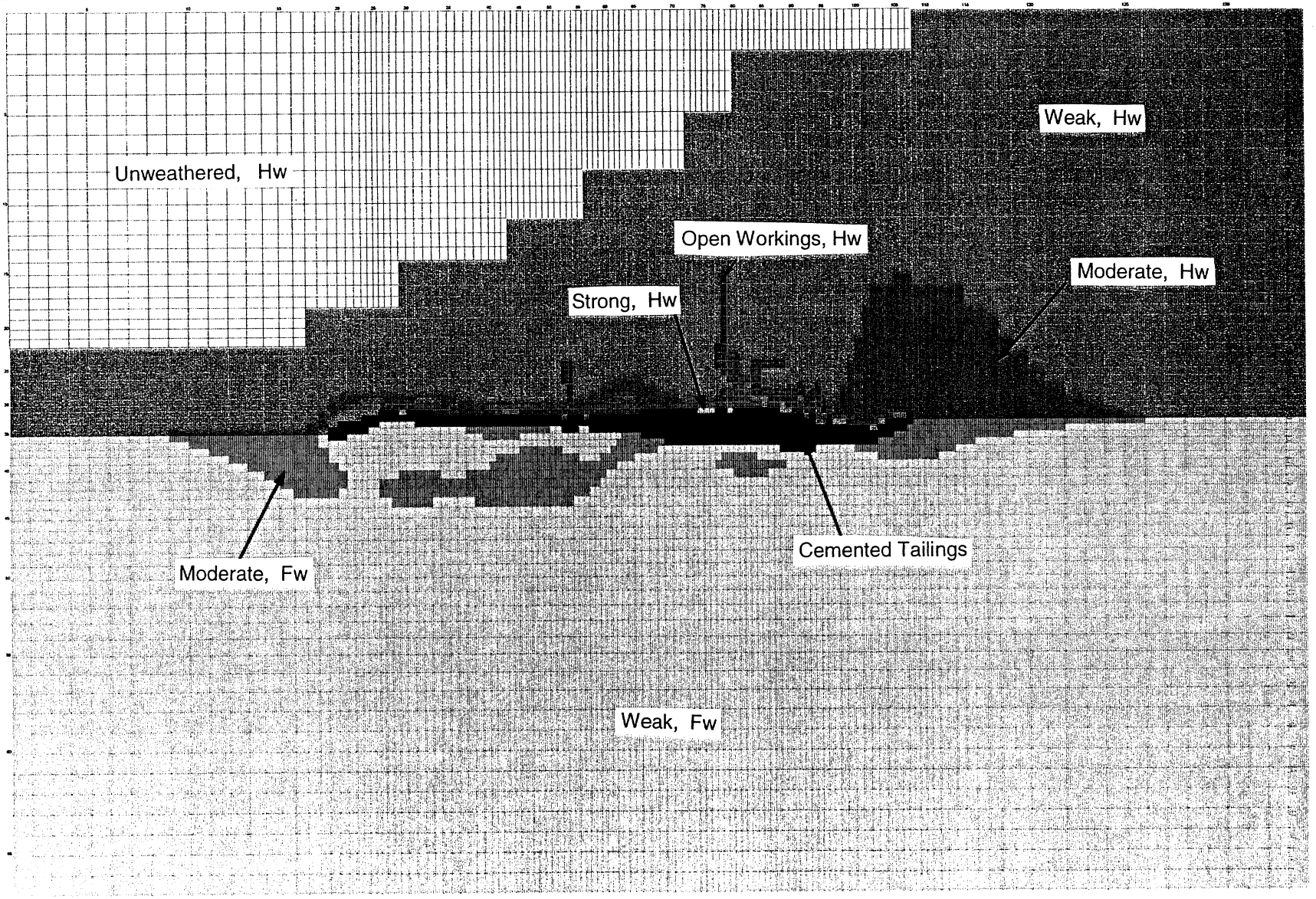

STEFFEN ROBERTSON AND KIRSTEN
Consulting Engineers

FOTH & VAN DYKE

REFLOODED MINE SOURCE TERM

1350 FOOT ELEVATION
WEATHERING ZONES

PROJECT NO.	DATE	APPROVED	FIGURE
F107107/2	MARCH 1998		6.4

FILE REF: FIG-SIX-FOUR

4.2-13-75b

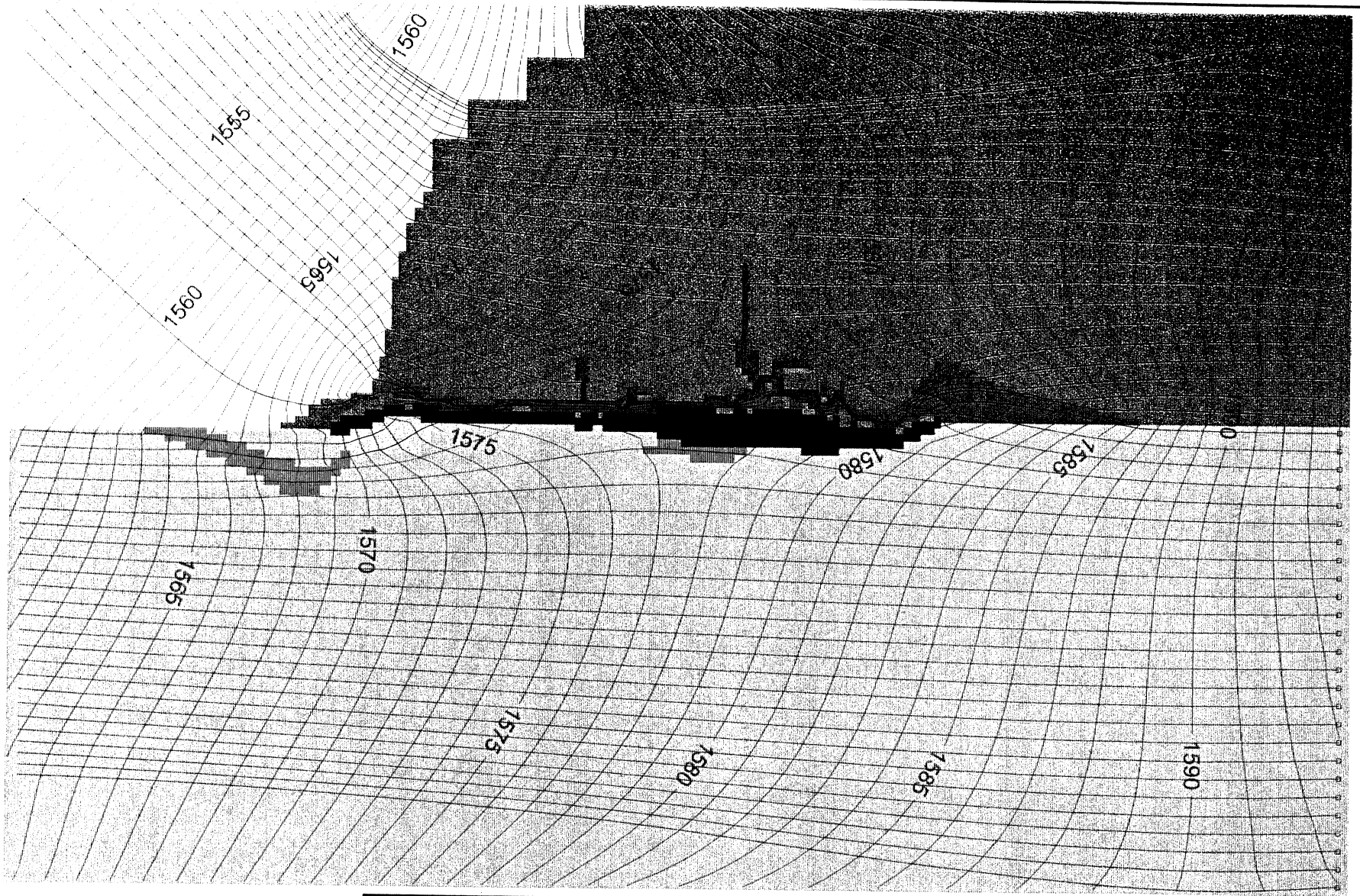

STEFFEN ROBERTSON AND KIRSTEN
Consulting Engineers

FOTH & VAN DYKE

REFLOODED MINE SOURCE TERM

HEAD DISTRIBUTION AND PARTICLE TRACKING : 1250 FOOT ELEVATION (RUN 1250_BEJ)

PROJECT NO.	DATE	APPROVED	FIGURE
F107107/2	MARCH 1998		6.5

FILE REF: FIG-SIX-FIVE

4.2-13-75c

APPENDIX A1
Model Calculations

APPENDIX A1
DESCRIPTION OF CALCULATIONS

Objective:

Determine the amount of oxidation products that will be released to groundwater after flooding.

Assumptions:

Dimensions of drift allowing O_2 into stope: 13 ft. x 16 ft. (3.96 m x 4.88 m)
Distance between bulkhead and stope: 20 ft. (6.096 m)
O_2 at the bulkhead is in equilibrium with the atmosphere. O_2 concentration calculated to be 8.9 mol/m^3.
Cemented tailings density is 2 $tonnes/m^3$.

Step 1: Determining the Amount of O_2 Entering the Stopes

a) Blasthole Stopes

O_2 transport is assumed to be by diffusion through the bulkhead and the waste rock.
Assume that all O_2 passing through the bulkhead will react with the tailings.

Flux of O_2 (rate of O_2 flow per m^2) is given by Fick's Law:

$$\text{Flux } O_2 = \frac{D * C_o}{L}$$

Where:
- D = diffusion coefficient = $6 * 10^{-6}$ m^2/s (from literature)
- C_o = O_2 concentration at bulkhead = 8.9 mol/m^3
- L = distance between bulkhead & stope = 6.096 m

$$\text{Rate of } O_2 \text{ Entry (mol/s)} = O_2 \text{ Flux} * \text{cross-sectional area of entrance drift}$$
$$= 8.76 * 10^{-6} * 3.96 * 4.88$$
$$= 1.69 * 10^{-4} \text{ mol/s}$$

Total O_2 entering stope during mine life (mol) = rate of O_2 entry * exposure time

From the mine plan, the average stope will be exposed to O_2 for 15 years. Therefore,

Total O_2 entering stope during mine life = 80, 132 moles
≈ 80, 000 moles

b) Cut and Fill Stopes

The dimensions of the access drift to the cut and fill stopes and the distance between the bulkhead and the stope will be the same as the access drifts to the blasthole stopes. Therefore, the rate of O_2 entry will be the same. However, the average exposure time will be 3.5 years (from the mine plan):

$$\text{Total } O_2 \text{ entering stope during mine life} = 1.69 * 10^{-4} \text{ mol/s} * 110,451,600 \text{ s}$$
$$= 18,666 \text{ moles}$$
$$\approx 19,000 \text{ moles}$$

Step 2: Determining the Amount of Oxidation

Pyrite oxidizes to iron hydroxide via the following reaction:

$$FeS_2 + 15/4\ O_2 + 7/2\ H_2O \rightarrow Fe(OH)_{3(s)} + 2\ SO_4^{2-} + 4\ H^+$$

Acidity is neutralized by calcite:

$$2\ CaCO_3 + 2\ H_2SO_4 \rightarrow 2\ CaSO_4 + 2\ CO_{2(g)} + 2\ H_2O$$

Therefore, 15/4 mol O_2 converts to 2 mol of $CaCO_3$ equivalent acidity; that is:

$$1 \text{ mol } O_2 = 8/15 \text{ mol } CaCO_3 \text{ equivalent acidity.}$$

a) Blasthole Stopes

From the above stoichiometry:

$$\text{Total Acidity} = \text{total } O_2 \text{ entering stope} * 8/15 * 0.1 \text{ kg CaCO3/mol CaCO3}$$
$$= 4,266 \text{ kg CaCO3 equivalent.}$$

Assuming all acidity will be neutralized:

$$\text{Maximum NP consumption} = \text{total acidity}$$
$$= 4,266 \text{ kg CaCO3 equivalent}$$

The average NP "concentration" in cemented tailings is 128 kg CaCO3 equivalent/tonne tailings (values determined from ABA test work). Therefore:

$$\text{Amount of tailings required to neutralize total acidity} = \frac{\text{maximum NP consumption}}{\text{NP concentration}}$$
$$= 33.3 \text{ tonnes}$$

$$\text{Volume of tailings required to neutralize total acidity} = \frac{\text{amount of tailings}}{\text{Density}}$$
$$= 16.7 \text{ m}^3$$

b) Cut and Fill Stopes

Calculation is the same as for blasthole stopes:

$$\text{Volume of tailings required to neutralize acidity} = \frac{7.8 \text{ tonnes}}{2 \text{ tonnes/m}^3} = 3.9 \text{ m}^3$$

c) Step 3: Estimating Contaminant Concentration in Groundwater

Assume oxidation products are created at the same rate as NP is consumed (128 kg $CaCO_3$ equivalent/tonne):

$$\text{Moles Oxidation Product} = \frac{128 \text{ kg } CaCO_3 \text{ equivalent/tonne}}{0.1 \text{ kg/mol } CaCO_3}$$
$$= 1280 \text{ mol } CaCO_3 \text{ equivalent/tonne}$$
$$= 1.28 \text{ mol } CaCO_3 \text{ equivalent/kg oxidized tailings}$$

From the oxidation and neutralization reactions given in Step 2, the ratio of $CaCO_3$ to sulphide released is 2:1. Therefore:

$$\text{Moles of } S_2 = \text{moles of oxidation product} / 2$$
$$= 0.64 \text{ mol } S_2\text{/kg oxidized tailings}$$

Estimated Constituent Release (g/kg) =
sulphide release * constituent molecular weight * constituent release ratio ,

where the constituent release ratio is given in the TMA Groundwater Quality Performance Evaluation.

The estimated constituent release is compared to the constituent content in unoxidized tailings and the lesser of the two values is used as the maximum constituent release (mg/kg):

$$\text{Max. constituent concentration in groundwater (mg/L)} = \frac{(\text{max. constituent release} * \text{tailings bulk density})}{(\text{porosity} * 1000\text{L/m}^3)}$$

Constituents have solubility controls that limit constituent concentration in water. The maximum constituent concentration in groundwater was compared to the solubility control concentration, as derived from MINTEQA2 geochemical modeling. The lesser value was taken as the estimated constituent concentration.

APPENDIX A2

MINTEQA2 Inputs and Outputs

APPENDIX A2
MINTEQA2 INOUTS AND OUTPUTS

A2.1 MINTEQA2 INPUT FILE

```
Cemented Acidic Tails

15.00 MG/L   0.000  0.00000E-01
0 0 1 0 3 0 0 0 1 1 0 0 0
0   0   0
    330  0.000E-01   -1.70 y                    /H+1
    732  4.000E+04   -1.81 y                    /SO4-2
    231  4.410E+02   -6.00 y                    /Cu+2
    470  3.128E+03   -7.04 y                    /Mn+2
    950  3.609E+04   -5.17 y                    /Zn+2
     60  1.379E+03   -1.96 y                    /H3AsO3
     30  0.000E-01  -20.43 y                    /Al+3
    460  0.000E-01  -20.39 y                    /Mg+2
    280  0.000E-01  -20.75 y                    /Fe+2
    150  0.000E-01  -20.60 y                    /Ca+2
    600  0.000E-01  -21.32 y                    /Pb+2
    100  0.000E-01  -21.14 y                    /Ba+2

  3   7
6003000     3.2300     0.0000                   /ALOHSO4
6046000     2.1400    -2.8200                   /EPSOMITE
6028000     2.4700    -2.8600                   /MELANTERITE
6015001     4.8480    -0.2610                   /GYPSUM
6060003     7.7900    -2.1500                   /ANGLESITE
6010000     9.9760    -6.2800                   /BARITE
    330     1.7000     0.0000                   /H+1
```

A2.2 MINTEQA2 OUTPUT FILE

PART 1 of OUTPUT FILE

PC MINTEQA2 v3.10 DATE OF CALCULATIONS: 11-MAR-97 TIME: 23:53:47

Cemented Acidic Tails

Temperature (Celsius): 15.00
Units of concentration: MG/L
Ionic strength to be computed.
If specified, carbonate concentration represents total inorganic carbon.
Do not automatically terminate if charge imbalance exceeds 30%
Precipitation is allowed only for those solids specified as ALLOWED
in the input file (if any).
The maximum number of iterations is: 200
The method used to compute activity coefficients is: Davies equation
Intermediate output file

330	0.000E-01	-1.70	y
732	4.000E+04	-1.81	y
231	4.410E+02	-6.00	y
470	3.128E+03	-7.04	y
950	3.609E+04	-5.17	y
60	1.379E+03	-1.96	y
30	0.000E-01	-20.43	y
460	0.000E-01	-20.39	y
280	0.000E-01	-20.75	y
150	0.000E-01	-20.60	y
600	0.000E-01	-21.32	y
100	0.000E-01	-21.14	y

H2O has been inserted as a COMPONENT

3 7

6003000	3.2300	0.0000
6046000	2.1400	-2.8200
6028000	2.4700	-2.8600
6015001	4.8480	-0.2610
6060003	7.7900	-2.1500
6010000	9.9760	-6.2800
330	1.7000	0.0000

INPUT DATA BEFORE TYPE MODIFICATIONS

ID	NAME	ACTIVITY GUESS	LOG GUESS	ANAL TOTAL
330	H+1	1.995E-02	-1.700	0.000E-01
732	SO4-2	1.549E-02	-1.810	4.000E+04
231	Cu+2	1.000E-06	-6.000	4.410E+02
470	Mn+2	9.120E-08	-7.040	3.128E+03
950	Zn+2	6.761E-06	-5.170	3.609E+04
60	H3AsO3	1.096E-02	-1.960	1.379E+03
30	Al+3	3.715E-21	-20.430	0.000E-01
460	Mg+2	4.074E-21	-20.390	0.000E-01
280	Fe+2	1.778E-21	-20.750	0.000E-01
150	Ca+2	2.512E-21	-20.600	0.000E-01
600	Pb+2	4.786E-22	-21.320	0.000E-01
100	Ba+2	7.244E-22	-21.140	0.000E-01
2	H2O	1.000E+00	0.000	0.000E-01

Charge Balance: UNSPECIATED

Sum of CATIONS= 1.341E+00 Sum of ANIONS = 9.062E-01

PERCENT DIFFERENCE = 1.933E+01 (ANIONS - CATIONS)/(ANIONS + CATIONS)

IMPROVED ACTIVITY GUESSES PRIOR TO FIRST ITERATION:		
SO4-2	Log activity guess:	-0.74
Cu+2	Log activity guess:	-2.12
Mn+2	Log activity guess:	-1.21
H3AsO3	Log activity guess:	-1.93
H2O	Log activity guess:	0.00

PARAMETERS OF THE COMPONENT MOST OUT OF BALANCE:

ITER	NAME	TOTAL MOL	DIFF FXN	LOG ACTVTY	RESIDUAL
0	Zn+2	6.008E-01	1.340E+29	-5.17000	1.340E+29
1	Zn+2	6.008E-01	6.702E+28	-4.86751	6.701E+28
2	Zn+2	6.008E-01	4.436E+28	-4.56728	4.436E+28
3	Zn+2	6.008E-01	2.218E+28	-4.26596	2.218E+28
4	Zn+2	6.008E-01	1.109E+28	-3.96464	1.109E+28
5	Zn+2	6.008E-01	5.545E+27	-3.66552	5.545E+27
6	Zn+2	6.008E-01	2.772E+27	-3.37075	2.772E+27
7	Zn+2	6.008E-01	1.386E+27	-3.07760	1.386E+27
8	Zn+2	6.008E-01	6.928E+26	-2.79182	6.928E+26
9	Zn+2	6.008E-01	3.461E+26	-2.51704	3.461E+26
10	Zn+2	6.008E-01	1.726E+26	-2.26014	1.726E+26
11	Zn+2	6.008E-01	8.567E+25	-2.03361	8.566E+25
12	Zn+2	6.008E-01	4.204E+25	-1.85183	4.203E+25
13	Zn+2	6.008E-01	2.023E+25	-1.72095	2.023E+25
14	Zn+2	6.008E-01	9.508E+24	-1.63724	9.507E+24
15	Zn+2	6.008E-01	4.382E+24	-1.58593	4.381E+24
16	Zn+2	6.008E-01	1.987E+24	-1.55855	1.987E+24
17	Zn+2	6.008E-01	8.926E+23	-1.54442	8.925E+23
18	Zn+2	6.008E-01	3.989E+23	-1.53718	3.989E+23
19	Zn+2	6.008E-01	1.778E+23	-1.53357	1.778E+23
20	Zn+2	6.008E-01	7.913E+22	-1.53160	7.912E+22
21	Zn+2	6.008E-01	3.519E+22	-1.53068	3.519E+22
22	Zn+2	6.008E-01	1.565E+22	-1.53025	1.565E+22
23	Zn+2	6.008E-01	6.955E+21	-1.53005	6.954E+21
24	Zn+2	6.008E-01	3.091E+21	-1.52993	3.091E+21
25	Zn+2	6.008E-01	1.374E+21	-1.52985	1.374E+21
26	Zn+2	6.008E-01	6.107E+20	-1.52981	6.107E+20
27	Zn+2	6.008E-01	2.714E+20	-1.52978	2.714E+20
28	Zn+2	6.008E-01	1.206E+20	-1.52976	1.206E+20
29	Zn+2	6.008E-01	5.362E+19	-1.52976	5.361E+19
30	Zn+2	6.008E-01	2.383E+19	-1.52976	2.383E+19
31	Zn+2	6.008E-01	1.059E+19	-1.52976	1.059E+19
32	Zn+2	6.008E-01	4.707E+18	-1.52976	4.707E+18
33	Zn+2	6.008E-01	2.092E+18	-1.52976	2.092E+18
34	Zn+2	6.008E-01	9.298E+17	-1.52976	9.297E+17
35	Zn+2	6.008E-01	4.133E+17	-1.52976	4.132E+17
36	Zn+2	6.008E-01	1.837E+17	-1.52975	1.836E+17
37	Zn+2	6.008E-01	8.163E+16	-1.52975	8.162E+16
38	Zn+2	6.008E-01	3.628E+16	-1.52976	3.628E+16
39	Zn+2	6.008E-01	1.612E+16	-1.52976	1.612E+16
40	Zn+2	6.008E-01	7.166E+15	-1.52976	7.166E+15
41	Zn+2	6.008E-01	3.185E+15	-1.52976	3.185E+15
42	Zn+2	6.008E-01	1.416E+15	-1.52976	1.415E+15
43	Zn+2	6.008E-01	6.292E+14	-1.52976	6.291E+14
44	Zn+2	6.008E-01	2.796E+14	-1.52976	2.796E+14
45	Zn+2	6.008E-01	1.243E+14	-1.52976	1.243E+14
46	Zn+2	6.008E-01	5.523E+13	-1.52976	5.523E+13
47	Zn+2	6.008E-01	2.455E+13	-1.52976	2.455E+13
48	Zn+2	6.008E-01	1.091E+13	-1.52975	1.091E+13

49	Zn+2	6.008E-01	4.849E+12	-1.52975	4.849E+12
50	Zn+2	6.008E-01	2.155E+12	-1.52975	2.155E+12
51	Zn+2	6.008E-01	9.578E+11	-1.52975	9.577E+11
52	Zn+2	6.008E-01	4.257E+11	-1.52975	4.257E+11
53	Zn+2	6.008E-01	1.892E+11	-1.52975	1.892E+11
54	Zn+2	6.008E-01	8.409E+10	-1.52975	8.408E+10
55	Zn+2	6.008E-01	3.737E+10	-1.52975	3.737E+10
56	Zn+2	6.008E-01	1.661E+10	-1.52975	1.661E+10
57	Zn+2	6.008E-01	7.382E+09	-1.52975	7.382E+09
58	Zn+2	6.008E-01	3.281E+09	-1.52974	3.281E+09
59	Zn+2	6.008E-01	1.458E+09	-1.52974	1.458E+09
60	Zn+2	6.008E-01	6.481E+08	-1.52973	6.481E+08
61	Zn+2	6.008E-01	2.881E+08	-1.52971	2.880E+08
62	Zn+2	6.008E-01	1.280E+08	-1.52969	1.280E+08
63	Zn+2	6.008E-01	5.690E+07	-1.52966	5.690E+07
64	Zn+2	6.008E-01	2.529E+07	-1.52961	2.529E+07
65	Zn+2	6.008E-01	1.124E+07	-1.52954	1.124E+07
66	Zn+2	6.008E-01	4.997E+06	-1.52943	4.996E+06
67	Zn+2	6.008E-01	2.221E+06	-1.52927	2.221E+06
68	Zn+2	6.008E-01	9.874E+05	-1.52902	9.873E+05
69	Zn+2	6.008E-01	4.390E+05	-1.52866	4.390E+05
70	Zn+2	6.008E-01	1.952E+05	-1.52811	1.952E+05
71	Zn+2	6.008E-01	8.683E+04	-1.52729	8.682E+04
72	Zn+2	6.008E-01	3.864E+04	-1.52605	3.863E+04
73	Zn+2	6.008E-01	1.720E+04	-1.52421	1.720E+04
74	Zn+2	6.008E-01	7.666E+03	-1.52145	7.665E+03
75	Zn+2	6.008E-01	3.421E+03	-1.51733	3.420E+03
76	Zn+2	6.008E-01	1.529E+03	-1.51119	1.529E+03
77	Zn+2	6.008E-01	6.856E+02	-1.50207	6.855E+02
78	Zn+2	6.008E-01	3.086E+02	-1.48858	3.086E+02
79	Zn+2	6.008E-01	1.397E+02	-1.46881	1.397E+02
80	Zn+2	6.008E-01	6.373E+01	-1.44018	6.373E+01
81	Zn+2	6.008E-01	2.937E+01	-1.39957	2.937E+01
82	Zn+2	6.008E-01	1.370E+01	-1.34392	1.369E+01
83	Zn+2	6.008E-01	6.463E+00	-1.27197	6.463E+00
84	Zn+2	6.008E-01	3.069E+00	-1.18830	3.069E+00
85	Zn+2	6.008E-01	1.434E+00	-1.10958	1.434E+00
86	Zn+2	6.008E-01	6.134E-01	-1.06767	6.134E-01
87	Zn+2	6.008E-01	1.944E-01	-1.08680	1.943E-01
88	Zn+2	6.008E-01	2.727E-02	-1.12639	2.721E-02
89	Zn+2	6.008E-01	5.829E-04	-1.13628	5.229E-04
91	Zn+2	6.008E-01	2.464E-01	-1.13651	2.463E-01
92	Zn+2	6.008E-01	-1.923E-01	-1.43453	1.922E-01
93	Zn+2	6.008E-01	1.146E-01	-1.20901	1.145E-01
94	Zn+2	6.008E-01	-1.319E-01	-1.37552	1.318E-01
95	Zn+2	6.008E-01	1.027E-01	-1.21538	1.026E-01
96	Zn+2	6.008E-01	-1.071E-01	-1.35434	1.070E-01
97	Zn+2	6.008E-01	8.507E-02	-1.22500	8.501E-02
98	Zn+2	6.008E-01	-8.637E-02	-1.33762	8.631E-02
99	Zn+2	6.008E-01	7.042E-02	-1.23324	7.036E-02
100	Zn+2	6.008E-01	-6.989E-02	-1.32492	6.983E-02
101	Zn+2	6.008E-01	5.813E-02	-1.24031	5.807E-02
102	Zn+2	6.008E-01	-5.668E-02	-1.31509	5.662E-02
103	Zn+2	6.008E-01	4.791E-02	-1.24631	4.785E-02
104	Zn+2	6.008E-01	-2.771E-03	-1.30739	2.711E-03
106	Zn+2	6.008E-01	-4.435E-02	-1.30568	4.429E-02
107	Zn+2	6.008E-01	4.130E-02	-1.25024	4.124E-02
108	Zn+2	6.008E-01	-3.907E-02	-1.30242	3.901E-02
109	Zn+2	6.008E-01	3.371E-02	-1.25483	3.365E-02
110	Zn+2	6.008E-01	-3.181E-02	-1.29734	3.175E-02
111	Zn+2	6.008E-01	2.769E-02	-1.25851	2.763E-02

112	Zn+2	6.008E-01	-2.593E-02	-1.29329	2.587E-02
113	Zn+2	6.008E-01	2.274E-02	-1.26157	2.268E-02
114	Zn+2	6.008E-01	-2.116E-02	-1.29004	2.110E-02
115	Zn+2	6.008E-01	1.866E-02	-1.26411	1.860E-02
116	Zn+2	6.008E-01	-1.727E-02	-1.28741	1.721E-02
117	Zn+2	6.008E-01	1.530E-02	-1.26622	1.524E-02
118	Zn+2	6.008E-01	-1.411E-02	-1.28529	1.405E-02
119	Zn+2	6.008E-01	-2.210E-04	-1.26796	1.610E-04
121	Zn+2	6.008E-01	1.270E-02	-1.26783	1.264E-02
122	Zn+2	6.008E-01	-1.139E-02	-1.28349	1.133E-02
123	Zn+2	6.008E-01	1.016E-02	-1.26947	1.010E-02
124	Zn+2	6.008E-01	-9.307E-03	-1.28210	9.247E-03
125	Zn+2	6.008E-01	8.325E-03	-1.27064	8.265E-03
126	Zn+2	6.008E-01	-7.608E-03	-1.28098	7.548E-03
127	Zn+2	6.008E-01	6.820E-03	-1.27161	6.760E-03
128	Zn+2	6.008E-01	-6.221E-03	-1.28007	6.161E-03
129	Zn+2	6.008E-01	5.586E-03	-1.27240	5.526E-03
130	Zn+2	6.008E-01	-5.088E-03	-1.27932	5.028E-03
131	Zn+2	6.008E-01	4.574E-03	-1.27305	4.514E-03
132	Zn+2	6.008E-01	-4.161E-03	-1.27872	4.101E-03
133	Zn+2	6.008E-01	3.746E-03	-1.27358	3.686E-03
135	Zn+2	6.008E-01	-3.393E-03	-1.27821	3.333E-03
136	Zn+2	6.008E-01	3.077E-03	-1.27401	3.017E-03
137	Zn+2	6.008E-01	-2.794E-03	-1.27782	2.734E-03
138	Zn+2	6.008E-01	2.519E-03	-1.27437	2.459E-03
139	Zn+2	6.008E-01	-2.286E-03	-1.27749	2.226E-03
140	Zn+2	6.008E-01	2.062E-03	-1.27467	2.002E-03
141	Zn+2	6.008E-01	-1.870E-03	-1.27722	1.810E-03
142	Zn+2	6.008E-01	1.688E-03	-1.27491	1.628E-03
143	Zn+2	6.008E-01	-1.530E-03	-1.27700	1.470E-03
144	Zn+2	6.008E-01	1.382E-03	-1.27511	1.322E-03
145	Zn+2	6.008E-01	-1.252E-03	-1.27682	1.192E-03
146	Zn+2	6.008E-01	1.131E-03	-1.27527	1.071E-03
147	Zn+2	6.008E-01	-1.025E-03	-1.27667	9.645E-04
149	Zn+2	6.008E-01	9.265E-04	-1.27540	8.664E-04
150	Zn+2	6.008E-01	-8.377E-04	-1.27655	7.776E-04
151	Zn+2	6.008E-01	7.570E-04	-1.27551	6.969E-04
152	Zn+2	6.008E-01	-6.855E-04	-1.27645	6.254E-04
153	Zn+2	6.008E-01	6.196E-04	-1.27560	5.595E-04
154	Zn+2	6.008E-01	-5.610E-04	-1.27637	5.009E-04
155	Zn+2	6.008E-01	5.071E-04	-1.27567	4.470E-04
156	Zn+2	6.008E-01	-4.591E-04	-1.27630	3.990E-04
157	Zn+2	6.008E-01	4.151E-04	-1.27573	3.550E-04
158	Zn+2	6.008E-01	-3.757E-04	-1.27625	3.156E-04
159	Zn+2	6.008E-01	3.397E-04	-1.27578	2.796E-04
160	Zn+2	6.008E-01	-3.074E-04	-1.27620	2.474E-04
161	Zn+2	6.008E-01	2.780E-04	-1.27582	2.179E-04
163	Zn+2	6.008E-01	-2.515E-04	-1.27617	1.915E-04
164	Zn+2	6.008E-01	2.276E-04	-1.27586	1.675E-04
165	Zn+2	6.008E-01	-2.060E-04	-1.27614	1.459E-04
166	Zn+2	6.008E-01	1.863E-04	-1.27588	1.262E-04
167	Zn+2	6.008E-01	-1.686E-04	-1.27611	1.085E-04
168	Zn+2	6.008E-01	1.525E-04	-1.27590	9.237E-05
169	Zn+2	6.008E-01	-1.379E-04	-1.27609	7.786E-05
170	Zn+2	6.008E-01	1.248E-04	-1.27592	6.469E-05
171	Zn+2	6.008E-01	-1.129E-04	-1.27608	5.281E-05
172	Zn+2	6.008E-01	1.021E-04	-1.27594	4.204E-05
173	Zn+2	6.008E-01	-9.239E-05	-1.27606	3.231E-05
174	Zn+2	6.008E-01	8.357E-05	-1.27595	2.349E-05
175	Zn+2	6.008E-01	-7.561E-05	-1.27605	1.553E-05
177	Zn+2	6.008E-01	6.840E-05	-1.27596	8.322E-06

178	Zn+2	6.008E-01	-6.188E-05	-1.27604	1.798E-06

ID	NAME	ANAL MOL	CALC MOL	LOG ACTVTY	GAMMA	DIFF FXN
30	Al+3	0.000E-01	1.175E-03	-3.48400	0.279257	-2.069E-05
60	H3AsO3	1.191E-02	1.171E-02	-1.74088	1.551023	4.619E-07
231	Cu+2	7.552E-03	2.134E-03	-2.91708	0.567257	5.039E-07
470	Mn+2	6.196E-02	1.973E-02	-1.95114	0.567257	4.353E-06
950	Zn+2	6.008E-01	9.338E-02	-1.27597	0.567257	5.597E-05
732	SO4-2	4.531E-01	6.439E-02	-1.43738	0.567257	0.000E-01
330	H+1	0.000E-01	2.299E-02	-1.70000	0.867851	0.000E-01
460	Mg+2	0.000E-01	3.405E-01	-0.71405	0.567257	4.752E-19
100	Ba+2	0.000E-01	3.531E-09	-8.69836	0.567257	0.000E-01
280	Fe+2	0.000E-01	1.589E-01	-1.04507	0.567257	0.000E-01
150	Ca+2	0.000E-01	7.018E-04	-3.40003	0.567257	0.000E-01
2	H2O	0.000E-01	1.096E+01	-0.00861	1.000000	1.110E-16
600	Pb+2	0.000E-01	6.901E-07	-6.40731	0.567257	0.000E-01

Type I - COMPONENTS AS SPECIES IN SOLUTION

ID	NAME	CALC MOL	ACTIVITY	LOG ACTVTY	GAMMA	NEW LOGK
330	H+1	2.299E-02	1.995E-02	-1.70000	0.86785	0.062
732	SO4-2	6.439E-02	3.653E-02	-1.43738	0.56726	0.246
231	Cu+2	2.134E-03	1.210E-03	-2.91708	0.56726	0.246
470	Mn+2	1.973E-02	1.119E-02	-1.95114	0.56726	0.246
950	Zn+2	9.338E-02	5.297E-02	-1.27597	0.56726	0.246
60	H3AsO3	1.171E-02	1.816E-02	-1.74088	1.55102	-0.191
30	Al+3	1.175E-03	3.281E-04	-3.48400	0.27926	0.554
460	Mg+2	3.405E-01	1.932E-01	-0.71405	0.56726	0.246
280	Fe+2	1.589E-01	9.014E-02	-1.04507	0.56726	0.246
150	Ca+2	7.018E-04	3.981E-04	-3.40003	0.56726	0.246
600	Pb+2	6.901E-07	3.915E-07	-6.40731	0.56726	0.246
100	Ba+2	3.531E-09	2.003E-09	-8.69836	0.56726	0.246

Type II - OTHER SPECIES IN SOLUTION OR ADSORBED

ID	NAME	CALC MOL	ACTIVITY	LOG ACTVTY	GAMMA	NEW LOGK
3300603	H4AsO3 +	2.069E-04	1.795E-04	-3.74588	0.86785	-0.243
3307320	HSO4 -	6.204E-02	5.384E-02	-1.26887	0.86785	1.930
3300020	OH-	2.603E-13	2.259E-13	-12.64607	0.86785	-14.276
4603300	MgOH +	7.311E-12	6.345E-12	-11.19760	0.86785	-12.113
4607320	MgSO4 AQ	7.454E-01	1.156E+00	0.06298	1.55102	2.024
1503300	CaOH +	2.428E-15	2.107E-15	-14.67637	0.86785	-12.906
1507320	CaSO4 AQ	1.752E-03	2.718E-03	-2.56580	1.55102	2.081
303300	AlOH +2	1.449E-07	8.217E-08	-7.08529	0.56726	-5.046
303301	Al(OH)2 +	7.250E-11	6.292E-11	-10.20123	0.86785	-10.038
303302	Al(OH)4 -	1.669E-21	1.448E-21	-20.83920	0.86785	-24.059
307320	AlSO4 +	1.275E-02	1.106E-02	-1.95607	0.86785	3.027
307321	Al(SO4)2 -	3.553E-02	3.083E-02	-1.51101	0.86785	4.909
303303	Al(OH)3 AQ	2.509E-15	3.892E-15	-14.40985	1.55102	-16.191
2803300	FeOH +	7.450E-10	6.465E-10	-9.18942	0.86785	-9.774
2803301	FeOH3 -1	2.089E-28	1.813E-28	-27.74164	0.86785	-31.709
2807320	FeSO4 AQ	3.124E-01	4.846E-01	-0.31461	1.55102	1.977
2803302	FeOH2 AQ	7.087E-20	1.099E-19	-18.95890	1.55102	-21.487
1003300	BaOH +	2.054E-21	1.783E-21	-20.74894	0.86785	-13.680
4703300	MnOH +	7.007E-12	6.081E-12	-11.21602	0.86785	-10.895
4703301	Mn(OH)3 -1	2.424E-32	2.104E-32	-31.67698	0.86785	-34.738
4707320	MnSO4 AQ	4.223E-02	6.551E-02	-1.18372	1.55102	2.014

2313300	CuOH +	6.853E-10	5.947E-10	-9.22569	0.86785	-7.938
2313301	Cu(OH)2 AQ	3.936E-14	6.105E-14	-13.21431	1.55102	-13.871
2313302	Cu(OH)3 -	2.088E-25	1.812E-25	-24.74192	0.86785	-26.837
2313303	Cu(OH)4 -2	3.124E-36	1.772E-36	-35.75154	0.56726	-39.354
2313304	Cu2(OH)2+2	9.777E-14	5.546E-14	-13.25602	0.56726	-10.558
2317320	CuSO4 AQ	5.419E-03	8.404E-03	-2.07549	1.55102	2.088
9503300	ZnOH +	1.500E-09	1.302E-09	-8.88541	0.86785	-9.239
9503301	Zn(OH)2 AQ	1.040E-15	1.614E-15	-14.79220	1.55102	-17.090
9503302	Zn(OH)3 -	2.889E-25	2.507E-25	-24.60081	0.86785	-28.337
9503303	Zn(OH)4 -2	3.442E-36	1.952E-36	-35.70942	0.56726	-40.953
9507320	ZnSO4 AQ	2.700E-01	4.188E-01	-0.37794	1.55102	2.145
9507321	Zn(SO4)2-2	2.374E-01	1.347E-01	-0.87073	0.56726	3.526
6003300	PbOH +	4.321E-13	3.750E-13	-12.42592	0.86785	-7.648
6003301	Pb(OH)2 AQ	4.622E-21	7.169E-21	-20.14453	1.55102	-17.311
6003302	Pb(OH)3 -	4.660E-30	4.044E-30	-29.39315	0.86785	-27.998
6003303	Pb2OH +3	1.177E-17	3.287E-18	-17.48323	0.27926	-5.806
6007320	PbSO4 AQ	5.184E-06	8.041E-06	-5.09469	1.55102	2.559
6003304	Pb3(OH)4+2	1.721E-37	9.762E-38	-37.01045	0.56726	-24.308
6003305	Pb(OH)4 -2	8.044E-40	4.563E-40	-39.34076	0.56726	-39.453
6007321	Pb(SO4)2-2	2.717E-06	1.541E-06	-5.81207	0.56726	3.716
3300600	H2AsO3 -	4.225E-10	3.667E-10	-9.43575	0.86785	-9.333
3300601	HAsO3 -2	1.637E-20	9.288E-21	-20.03206	0.56726	-21.445
3300602	AsO3 -3	4.508E-32	1.259E-32	-31.89998	0.27926	-34.705

Type III - SPECIES WITH FIXED ACTIVITY

ID	NAME	CALC MOL	LOG MOL	NEW LOGK	DH
2	H2O	1.096E+01	1.040	0.009	0.000
330	H+1	-1.347E-01	-0.871	1.700	0.000
6003000	ALOHSO4	-4.947E-02	-1.306	3.230	0.000
6010000	BARITE	-3.531E-09	-8.452	10.136	-6.280
6046000	EPSOMITE	-1.086E+00	0.036	2.212	-2.820
6015001	GYPSUM	-2.454E-03	-2.610	4.855	-0.261
6028000	MELANTERITE	-4.714E-01	-0.327	2.543	-2.860
6060003	ANGLESITE	-8.592E-06	-5.066	7.845	-2.150

PERCENTAGE DISTRIBUTION OF COMPONENTS AMONG
TYPE I and TYPE II (dissolved and adsorbed) species

Al+3			
	2.4	PERCENT BOUND IN SPECIES # 30	Al+3
	25.8	PERCENT BOUND IN SPECIES # 307320	AlSO4 +
	71.8	PERCENT BOUND IN SPECIES # 307321	Al(SO4)2 -
H3AsO3			
	98.3	PERCENT BOUND IN SPECIES # 60	H3AsO3
	1.7	PERCENT BOUND IN SPECIES #3300603	H4AsO3 +
Cu+2			
	28.3	PERCENT BOUND IN SPECIES # 231	Cu+2
	71.7	PERCENT BOUND IN SPECIES #2317320	CuSO4 AQ
Mn+2			
	31.8	PERCENT BOUND IN SPECIES # 470	Mn+2
	68.2	PERCENT BOUND IN SPECIES #4707320	MnSO4 AQ
Zn+2			
	15.5	PERCENT BOUND IN SPECIES # 950	Zn+2
	44.9	PERCENT BOUND IN SPECIES #9507320	ZnSO4 AQ
	39.5	PERCENT BOUND IN SPECIES #9507321	Zn(SO4)2-2
SO4-2			
	3.1	PERCENT BOUND IN SPECIES # 732	SO4-2
	3.0	PERCENT BOUND IN SPECIES #3307320	HSO4 -
	36.1	PERCENT BOUND IN SPECIES #4607320	MgSO4 AQ
	3.4	PERCENT BOUND IN SPECIES # 307321	Al(SO4)2 -
	15.2	PERCENT BOUND IN SPECIES #2807320	FeSO4 AQ
	2.0	PERCENT BOUND IN SPECIES #4707320	MnSO4 AQ
	13.1	PERCENT BOUND IN SPECIES #9507320	ZnSO4 AQ

	23.0	PERCENT BOUND IN SPECIES #9507321	Zn(SO4)2-2
H+1			
	27.0	PERCENT BOUND IN SPECIES # 330	H+1
	72.8	PERCENT BOUND IN SPECIES #3307320	HSO4 -
Mg+2			
	31.4	PERCENT BOUND IN SPECIES # 460	Mg+2
	68.6	PERCENT BOUND IN SPECIES #4607320	MgSO4 AQ
Ba+2			
	100.0	PERCENT BOUND IN SPECIES # 100	Ba+2
Fe+2			
	33.7	PERCENT BOUND IN SPECIES # 280	Fe+2
	66.3	PERCENT BOUND IN SPECIES #2807320	FeSO4 AQ
Ca+2			
	28.6	PERCENT BOUND IN SPECIES # 150	Ca+2
	71.4	PERCENT BOUND IN SPECIES #1507320	CaSO4 AQ
H2O			
	97.9	PERCENT BOUND IN SPECIES # 303300	AlOH +2
	1.0	PERCENT BOUND IN SPECIES #9503300	ZnOH +
Pb+2			
	8.0	PERCENT BOUND IN SPECIES # 600	Pb+2
	60.3	PERCENT BOUND IN SPECIES #6007320	PbSO4 AQ
	31.6	PERCENT BOUND IN SPECIES #6007321	Pb(SO4)2-2

---------- EQUILIBRATED MASS DISTRIBUTION ----------

IDX	NAME	DISSOLVED		SORBED		PRECIPITATED	
		MOL/KG	PERCENT	MOL/KG	PERCENT	MOL/KG	PERCENT
30	Al+3	4.945E-02	100.0	0.000E-01	0.0	0.000E-01	0.0
60	H3AsO3	1.192E-02	100.0	0.000E-01	0.0	0.000E-01	0.0
231	Cu+2	7.552E-03	100.0	0.000E-01	0.0	0.000E-01	0.0
470	Mn+2	6.196E-02	100.0	0.000E-01	0.0	0.000E-01	0.0
950	Zn+2	6.008E-01	100.0	0.000E-01	0.0	0.000E-01	0.0
732	SO4-2	2.062E+00	100.0	0.000E-01	0.0	0.000E-01	0.0
330	H+1	8.524E-02	100.0	0.000E-01	0.0	0.000E-01	0.0
460	Mg+2	1.086E+00	100.0	0.000E-01	0.0	0.000E-01	0.0
100	Ba+2	3.531E-09	100.0	0.000E-01	0.0	0.000E-01	0.0
280	Fe+2	4.714E-01	100.0	0.000E-01	0.0	0.000E-01	0.0
150	Ca+2	2.454E-03	100.0	0.000E-01	0.0	0.000E-01	0.0
2	H2O	1.479E-07	100.0	0.000E-01	0.0	0.000E-01	0.0
600	Pb+2	8.592E-06	100.0	0.000E-01	0.0	0.000E-01	0.0

Charge Balance: SPECIATED

Sum of CATIONS = 1.270E+00 Sum of ANIONS 7.012E-01

PERCENT DIFFERENCE = 2.887E+01 (ANIONS - CATIONS)/(ANIONS + CATIONS)

EQUILIBRIUM IONIC STRENGTH (m) = 1.906E+00

EQUILIBRIUM pH = 1.700

DATE ID NUMBER: 970311
TIME ID NUMBER: 23535320

Saturation indices and stoichiometry of all minerals

ID #	NAME	Sat. Index	Stoichiometry in [brackets]
2003000	ALOH3(A)	-9.478	[1.000] 30 [3.000] 2 [-3.000] 330
6003000	ALOHSO4	0.000	[-1.000] 330 [1.000] 30 [1.000] 732 [1.000] 2
6003001	AL4(OH)10SO4	-21.160	[-10.000] 330 [4.000] 30 [1.000] 732 [10.000] 2
6015000	ANHYDRITE	-0.296	[1.000] 150 [1.000] 732
6010000	BARITE	0.000	[1.000] 100 [1.000] 732
2003001	BOEHMITE	-7.695	[-3.000] 330 [1.000] 30 [2.000] 2
2046000	BRUCITE	-14.781	[1.000] 460 [2.000] 2 [-2.000] 330
2003002	DIASPORE	-5.901	[-3.000] 330 [1.000] 30 [2.000] 2
6046000	EPSOMITE	0.000	[1.000] 460 [1.000] 732 [7.000] 2
2003003	GIBBSITE (C)	-7.760	[-3.000] 330 [1.000] 30 [3.000] 2
3003000	Al2O3	-19.774	[2.000] 30 [3.000] 2 [-6.000] 330
6015001	GYPSUM	0.000	[1.000] 150 [1.000] 732 [2.000] 2
6028000	MELANTERITE	0.000	[1.000] 280 [1.000] 732 [7.000] 2
2047003	PYROCROITE	-14.231	[-2.000] 330 [1.000] 470 [2.000] 2
6047000	MNSO4	-6.451	[1.000] 470 [1.000] 732
2023100	CU(OH)2	-8.562	[-2.000] 330 [1.000] 231 [2.000] 2
6023100	ANTLERITE	-11.713	[-4.000] 330 [3.000] 231 [4.000] 2 [1.000] 732
6023101	BROCHANTITE	-18.297	[-6.000] 330 [4.000] 231 [6.000] 2 [1.000] 732
6023102	LANGITE	-20.764	[-6.000] 330 [4.000] 231 [7.000] 2 [1.000] 732
2023101	TENORITE	-7.533	[-2.000] 330 [1.000] 231 [1.000] 2
6023103	CUOCUSO4	-16.315	[-2.000] 330 [2.000] 231 [1.000] 2 [1.000] 732
6023104	CUSO4	-7.826	[1.000] 231 [1.000] 732
6023105	CHALCANTHITE	-1.721	[1.000] 231 [1.000] 732 [5.000] 2
2095000	ZN(OH)2 (A)	-10.343	[-2.000] 330 [1.000] 950 [2.000] 2
2095001	ZN(OH)2 (C)	-10.093	[-2.000] 330 [1.000] 950 [2.000] 2
2095002	ZN(OH)2 (B)	-9.643	[-2.000] 330 [1.000] 950 [2.000] 2
2095003	ZN(OH)2 (G)	-9.603	[-2.000] 330 [1.000] 950 [2.000] 2
2095004	ZN(OH)2 (E)	-9.393	[-2.000] 330 [1.000] 950 [2.000] 2
6095000	ZN2(OH)2SO4	-8.107	[-2.000] 330 [2.000] 950 [2.000] 2 [1.000] 732
6095001	ZN4(OH)6SO4	-24.793	[-6.000] 330 [4.000] 950 [6.000] 2 [1.000] 732
2095005	ZNO(ACTIVE)	-9.195	[-2.000] 330 [1.000] 950 [1.000] 2
2095006	ZINCITE	-9.581	[-2.000] 330 [1.000] 950 [1.000] 2
6095002	ZN3O(SO4)2	-23.908	[-2.000] 330 [3.000] 950 [2.000] 732 [1.000] 2
6095003	ZINCOSITE	-6.212	[1.000] 950 [1.000] 732

ID #	NAME	Sat. Index	Stoichiometry in [brackets]							
6095004	ZNSO4, 1H2O	-2.423	[1.000]	950	[1.000]	732	[1.000]	2		
6095005	BIANCHITE	-1.004	[1.000]	950	[1.000]	732	[6.000]	2		
6095006	GOSLARITE	-0.730	[1.000]	950	[1.000]	732	[7.000]	2		
2060000	MASSICOT	-16.353	[-2.000]	330	[1.000]	600	[1.000]	2		
2060001	LITHARGE	-16.153	[-2.000]	330	[1.000]	600	[1.000]	2		
2060002	PBO, .3H2O	-15.999	[-2.000]	330	[1.000]	600	[1.330]	2		
6060000	LARNAKITE	-10.744	[-2.000]	330	[2.000]	600	[1.000]	732		
			[1.000]	2						
6060001	PB3O2SO4	-24.804	[-4.000]	330	[3.000]	600	[1.000]	732		
			[2.000]	2						
6060002	PB4O3SO4	-39.885	[-6.000]	330	[4.000]	600	[1.000]	732		
			[3.000]	2						
6060003	ANGLESITE	0.000	[1.000]	600	[1.000]	732				
2060004	PB(OH)2 (C)	-11.530	[-2.000]	330	[1.000]	600	[2.000]	2		
2060005	PB2O(OH)2	-32.240	[-4.000]	330	[2.000]	600	[3.000]	2		
6060004	PB4(OH)6SO4	-38.018	[-6.000]	330	[4.000]	600	[1.000]	732		
			[6.000]	2						
3006000	ARSENOLITE	-3.746	[4.000]	60	[-6.000]	2				
3006001	CLAUDETITE	-3.509	[4.000]	60	[-6.000]	2				
2015000	LIME	-33.982	[-2.000]	330	[1.000]	150	[1.000]	2		
2015001	PORTLANDITE	-23.473	[-2.000]	330	[1.000]	150	[2.000]	2		
2028000	WUSTITE	-9.917	[-2.000]	330	[0.947]	280	[1.000]	2		
2046001	PERICLASE	-19.752	[-2.000]	330	[1.000]	460	[1.000]	2		
3028001	HERCYNITE	-23.603	[-8.000]	330	[1.000]	280	[2.000]	30		
			[4.000]	2						
3046000	SPINEL	-32.716	[-8.000]	330	[1.000]	460	[2.000]	30		
			[4.000]	2						

Note: As a result of the April 1998 update to the Reflooded Mine Source Term - Crandon Project report, Appendices A1 and A2 replace the existing Appendix A in its entirety. Remove pages 4.2-13-95 through 4.2-13-276.

RESULTS FOR YEAR: 0.0192

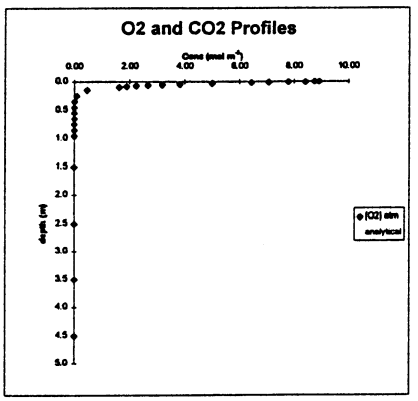

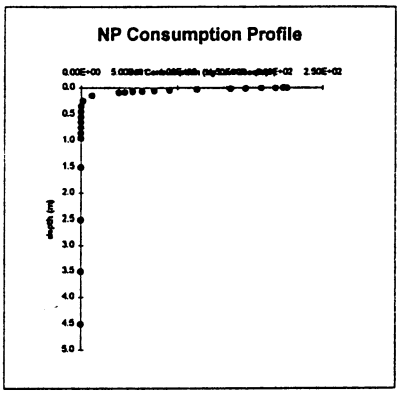

Flux in (mol/m²s)	4.74E-05
O_2 cons. (mol/m²s)	4.92E-05
Dpen (m)	1

t=0.0192												
DEPTH (m)	CONC O2 (mol/m³)	O2 Cons (mol/m³/s)	CO2 Prod (mol/m³/s)	CONC CO2 (mol/m³)	mols O2 cons per m3 rock	NP consmptn kg CaCO3eq/t/yr						Sulf dens mol/m³
0.001	8.900	9.52E-04	-5.08E-04	0.0141	3.81E-04	2.14E+02						10201.94
0.002	8.732	9.34E-04	-4.98E-04	0.0141	3.74E-04	2.10E+02						10239.06
0.004	8.403	8.99E-04	-4.80E-04	0.0141	3.60E-04	2.02E+02						10311.84
0.008	7.783	8.33E-04	-4.44E-04	0.0141	3.33E-04	1.87E+02						10449.06
0.013	7.080	7.58E-04	-4.04E-04	0.0141	3.03E-04	1.70E+02						10604.48
0.018	6.443	6.89E-04	-3.68E-04	0.0141	2.76E-04	1.55E+02						10745.26
0.030	4.999	5.35E-04	-2.85E-04	0.0141	2.14E-04	1.20E+02						11063.91
0.045	3.824	4.09E-04	-2.18E-04	0.0141	1.64E-04	9.19E+01						11322.58
0.055	3.183	3.41E-04	-1.82E-04	0.0141	1.36E-04	7.65E+01						11463.54
0.065	2.659	2.85E-04	-1.52E-04	0.0141	1.14E-04	6.39E+01						11578.34
0.075	2.235	2.39E-04	-1.28E-04	0.0141	9.57E-05	5.37E+01						11671.31
0.085	1.894	2.03E-04	-1.08E-04	0.0141	8.11E-05	4.55E+01						11745.94
0.095	1.623	1.74E-04	-9.26E-05	0.0141	6.95E-05	3.90E+01						11805.07
0.150	0.464	4.97E-05	-2.65E-05	0.0141	1.99E-05	1.12E+01						12057.22
0.250	0.084	8.98E-06	-4.79E-06	0.0141	3.59E-06	2.02E+00						12139.15
0.350	0.015	1.62E-06	-8.65E-07	0.0141	6.49E-07	3.65E-01						12153.78
0.450	0.003	2.93E-07	-1.56E-07	0.0141	1.17E-07	6.59E-02						12156.40
0.550	0.000	5.30E-08	-2.82E-08	0.0141	2.12E-08	1.19E-02						12156.87
0.650	0.000	9.57E-09	-5.10E-09	0.0141	3.83E-09	2.15E-03						12156.96
0.750	0.000	1.73E-09	-9.22E-10	0.0141	6.92E-10	3.89E-04						12156.97
0.850	0.000	3.14E-10	-1.67E-10	0.0141	1.26E-10	7.05E-05						12156.97
0.950	0.000	6.41E-11	-3.42E-11	0.0141	2.56E-11	1.44E-05						12156.97
1.500	0.000	3.11E-13	-1.66E-13	0.0141	1.25E-13	7.00E-08						12156.97
2.500	0.000	1.07E-14	-5.71E-15	0.0141	4.28E-15	2.40E-09						12156.97
3.500	0.000	1.07E-14	-5.71E-15	0.0141	4.28E-15	2.40E-09						12156.97
4.500	0.000	1.07E-14	-5.71E-15	0.0141	4.28E-15	2.40E-09						12156.97
5.500	0.000	1.07E-14	-5.71E-15	0.0141	4.28E-15	2.40E-09						12156.97
6.500	0.000	1.07E-14	-5.71E-15	0.0141	4.28E-15	2.40E-09						12156.97
7.500	0.000	1.07E-14	-5.71E-15	0.0141	4.28E-15	2.40E-09						12156.97
8.500	0.000	1.07E-14	-5.71E-15	0.0141	4.28E-15	2.40E-09						12156.97
9.500	0.000	1.07E-14	-5.71E-15	0.0141	4.28E-15	2.40E-09						12156.97
10.500	0.000	1.07E-14	-5.71E-15	0.0141	4.28E-15	2.40E-09						12156.97
11.500	0.000	1.07E-14	-5.71E-15	0.0141	4.28E-15	2.40E-09						12156.97
12.500	0.000	1.07E-14	-5.71E-15	0.0141	4.28E-15	2.40E-09						12156.97
14.000	0.000	1.07E-14	-5.71E-15	0.0141	4.28E-15	2.40E-09						12156.97
16.000	0.000	1.07E-14	-5.71E-15	0.0141	4.28E-15	2.40E-09						12156.97
18.000	0.000	1.07E-14	-5.71E-15	0.0141	4.28E-15	2.40E-09						12156.97
20.000	0.000	1.07E-14	-5.71E-15	0.0141	4.28E-15	2.40E-09						12156.97
22.000	0.000	1.07E-14	-5.71E-15	0.0141	4.28E-15	2.40E-09						12156.97
25.000	0.000	1.07E-14	-5.71E-15	0.0141	4.28E-15	2.40E-09						12156.97

RESULTS FOR YEAR: 0.0385

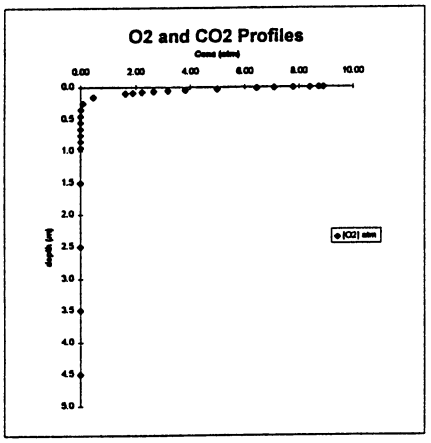

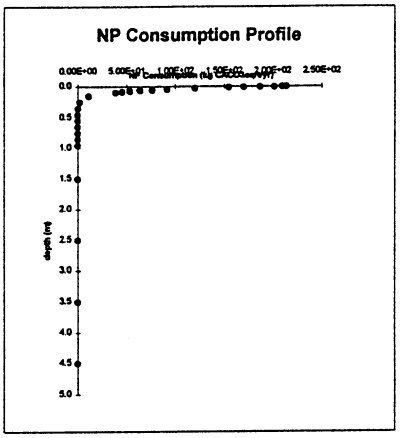

Flux in (mol/m²s)	4.74E-05
O_2 cons. (mol/m²s)	4.92E-05
Dpen (m)	1

t=0.0385												
DEPTH (m)	CONC O2 (mol/m³)	O2 Cons (mol/m³/s)	CO2 Prod (mol/m³/s)	CONC CO2 (mol/m³)	mols O2 cons per m3 rock	NP consmptn kg CaCO3eq/t/yr						Sulf dens mol/m³
0.001	8.900	9.52E-04	-5.06E-04	0.0141	3.81E-04	2.14E+02						8216.89
0.002	8.732	9.34E-04	-4.96E-04	0.0141	3.74E-04	2.10E+02						8291.39
0.004	8.403	8.99E-04	-4.80E-04	0.0141	3.60E-04	2.02E+02						8437.53
0.008	7.783	8.33E-04	-4.44E-04	0.0141	3.33E-04	1.87E+02						8713.11
0.013	7.080	7.58E-04	-4.04E-04	0.0141	3.03E-04	1.70E+02						9025.33
0.018	6.443	6.89E-04	-3.68E-04	0.0141	2.76E-04	1.55E+02						9308.26
0.030	4.999	5.35E-04	-2.85E-04	0.0141	2.14E-04	1.20E+02						9948.89
0.045	3.824	4.09E-04	-2.18E-04	0.0141	1.64E-04	9.19E+01						10469.68
0.055	3.183	3.41E-04	-1.82E-04	0.0141	1.36E-04	7.65E+01						10753.70
0.065	2.659	2.85E-04	-1.52E-04	0.0141	1.14E-04	6.39E+01						10985.18
0.075	2.235	2.39E-04	-1.28E-04	0.0141	9.57E-05	5.37E+01						11172.78
0.085	1.894	2.03E-04	-1.08E-04	0.0141	8.11E-05	4.55E+01						11323.54
0.095	1.623	1.74E-04	-9.26E-05	0.0141	6.95E-05	3.90E+01						11443.09
0.150	0.464	4.97E-05	-2.65E-05	0.0141	1.99E-05	1.12E+01						11953.63
0.250	0.084	8.98E-06	-4.79E-06	0.0141	3.59E-06	2.02E+00						12120.44
0.350	0.015	1.62E-06	-8.65E-07	0.0141	6.49E-07	3.65E-01						12150.41
0.450	0.003	2.93E-07	-1.56E-07	0.0141	1.17E-07	6.59E-02						12155.80
0.550	0.000	5.30E-08	-2.82E-08	0.0141	2.12E-08	1.19E-02						12156.77
0.650	0.000	9.57E-09	-5.10E-09	0.0141	3.83E-09	2.15E-03						12156.94
0.750	0.000	1.73E-09	-9.22E-10	0.0141	6.92E-10	3.89E-04						12156.97
0.850	0.000	3.14E-10	-1.67E-10	0.0141	1.26E-10	7.05E-05						12156.97
0.950	0.000	6.41E-11	-3.42E-11	0.0141	2.56E-11	1.44E-05						12156.97
1.500	0.000	3.11E-13	-1.66E-13	0.0141	1.25E-13	7.00E-08						12156.97
2.500	0.000	1.07E-14	-5.71E-15	0.0141	4.28E-15	2.40E-09						12156.97
3.500	0.000	1.07E-14	-5.71E-15	0.0141	4.28E-15	2.40E-09						12156.97
4.500	0.000	1.07E-14	-5.71E-15	0.0141	4.28E-15	2.40E-09						12156.97
5.500	0.000	1.07E-14	-5.71E-15	0.0141	4.28E-15	2.40E-09						12156.97
6.500	0.000	1.07E-14	-5.71E-15	0.0141	4.28E-15	2.40E-09						12156.97
7.500	0.000	1.07E-14	-5.71E-15	0.0141	4.28E-15	2.40E-09						12156.97
8.500	0.000	1.07E-14	-5.71E-15	0.0141	4.28E-15	2.40E-09						12156.97
9.500	0.000	1.07E-14	-5.71E-15	0.0141	4.28E-15	2.40E-09						12156.97
10.500	0.000	1.07E-14	-5.71E-15	0.0141	4.28E-15	2.40E-09						12156.97
11.500	0.000	1.07E-14	-5.71E-15	0.0141	4.28E-15	2.40E-09						12156.97
12.500	0.000	1.07E-14	-5.71E-15	0.0141	4.28E-15	2.40E-09						12156.97
14.000	0.000	1.07E-14	-5.71E-15	0.0141	4.28E-15	2.40E-09						12156.97
16.000	0.000	1.07E-14	-5.71E-15	0.0141	4.28E-15	2.40E-09						12156.97
18.000	0.000	1.07E-14	-5.71E-15	0.0141	4.28E-15	2.40E-09						12156.97
20.000	0.000	1.07E-14	-5.71E-15	0.0141	4.28E-15	2.40E-09						12156.97
22.000	0.000	1.07E-14	-5.71E-15	0.0141	4.28E-15	2.40E-09						12156.97
25.000	0.000	1.07E-14	-5.71E-15	0.0141	4.28E-15	2.40E-09						12156.97

RESULTS FOR YEAR: 0.0577

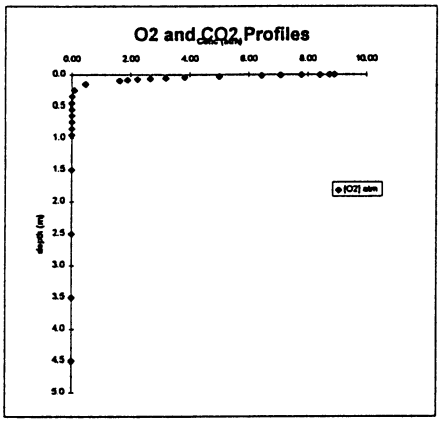

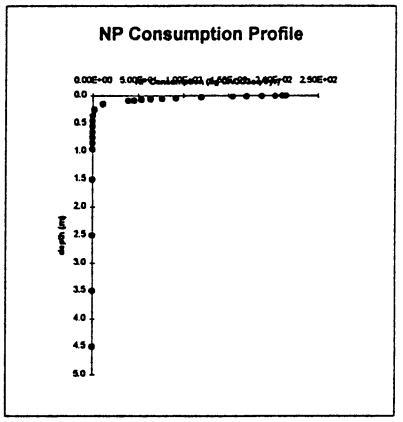

Flux in (mol/m²s)	4.74E-05
O_2 cons. (mol/m²s)	4.92E-05
Dpen (m)	1

t=0.0577												
DEPTH (m)	CONC O2 (mol/m³)	O2 Cons (mol/m³/s)	CO2 Prod (mol/m³/s)	CONC CO2 (mol/m³)	mols O2 cons per m3 rock	NP consmptn kg CaCO3eq/l/yr						Suif dens mol/m³
0.001	8.900	9.52E-04	-5.08E-04	0.0141	3.81E-04	2.14E+02						6231.83
0.002	8.732	9.34E-04	-4.98E-04	0.0141	3.74E-04	2.10E+02						6343.73
0.004	8.403	8.99E-04	-4.80E-04	0.0141	3.60E-04	2.02E+02						6563.22
0.008	7.783	8.33E-04	-4.44E-04	0.0141	3.33E-04	1.87E+02						6977.15
0.013	7.080	7.58E-04	-4.04E-04	0.0141	3.03E-04	1.70E+02						7446.18
0.018	6.443	6.89E-04	-3.68E-04	0.0141	2.76E-04	1.55E+02						7871.26
0.030	4.999	5.35E-04	-2.85E-04	0.0141	2.14E-04	1.20E+02						8833.87
0.045	3.824	4.09E-04	-2.18E-04	0.0141	1.64E-04	9.19E+01						9616.78
0.055	3.183	3.41E-04	-1.82E-04	0.0141	1.36E-04	7.65E+01						10043.65
0.065	2.659	2.85E-04	-1.52E-04	0.0141	1.14E-04	6.39E+01						10392.02
0.075	2.235	2.39E-04	-1.28E-04	0.0141	9.57E-05	5.37E+01						10674.25
0.085	1.894	2.03E-04	-1.08E-04	0.0141	8.11E-05	4.55E+01						10901.14
0.095	1.623	1.74E-04	-9.26E-05	0.0141	6.95E-05	3.90E+01						11081.11
0.150	0.464	4.97E-05	-2.65E-05	0.0141	1.99E-05	1.12E+01						11850.04
0.250	0.084	8.96E-06	-4.79E-06	0.0141	3.59E-06	2.02E+00						12101.73
0.350	0.015	1.62E-06	-8.65E-07	0.0141	6.49E-07	3.65E-01						12147.04
0.450	0.003	2.93E-07	-1.56E-07	0.0141	1.17E-07	6.59E-02						12155.20
0.550	0.000	5.30E-08	-2.82E-08	0.0141	2.12E-08	1.19E-02						12156.66
0.650	0.000	9.57E-09	-5.10E-09	0.0141	3.83E-09	2.15E-03						12156.93
0.750	0.000	1.73E-09	-9.22E-10	0.0141	6.92E-10	3.89E-04						12156.97
0.850	0.000	3.14E-10	-1.67E-10	0.0141	1.26E-10	7.05E-05						12156.97
0.950	0.000	6.41E-11	-3.42E-11	0.0141	2.56E-11	1.44E-05						12156.97
1.500	0.000	3.11E-13	-1.66E-13	0.0141	1.25E-13	7.00E-08						12156.97
2.500	0.000	1.07E-14	-5.71E-15	0.0141	4.28E-15	2.40E-09						12156.97
3.500	0.000	1.07E-14	-5.71E-15	0.0141	4.28E-15	2.40E-09						12156.97
4.500	0.000	1.07E-14	-5.71E-15	0.0141	4.28E-15	2.40E-09						12156.97
5.500	0.000	1.07E-14	-5.71E-15	0.0141	4.28E-15	2.40E-09						12156.97
6.500	0.000	1.07E-14	-5.71E-15	0.0141	4.28E-15	2.40E-09						12156.97
7.500	0.000	1.07E-14	-5.71E-15	0.0141	4.28E-15	2.40E-09						12156.97
8.500	0.000	1.07E-14	-5.71E-15	0.0141	4.28E-15	2.40E-09						12156.97
9.500	0.000	1.07E-14	-5.71E-15	0.0141	4.28E-15	2.40E-09						12156.97
10.500	0.000	1.07E-14	-5.71E-15	0.0141	4.28E-15	2.40E-09						12156.97
11.500	0.000	1.07E-14	-5.71E-15	0.0141	4.28E-15	2.40E-09						12156.97
12.500	0.000	1.07E-14	-5.71E-15	0.0141	4.28E-15	2.40E-09						12156.97
14.000	0.000	1.07E-14	-5.71E-15	0.0141	4.28E-15	2.40E-09						12156.97
16.000	0.000	1.07E-14	-5.71E-15	0.0141	4.28E-15	2.40E-09						12156.97
18.000	0.000	1.07E-14	-5.71E-15	0.0141	4.28E-15	2.40E-09						12156.97
20.000	0.000	1.07E-14	-5.71E-15	0.0141	4.28E-15	2.40E-09						12156.97
22.000	0.000	1.07E-14	-5.71E-15	0.0141	4.28E-15	2.40E-09						12156.97
25.000	0.000	1.07E-14	-5.71E-15	0.0141	4.28E-15	2.40E-09						12156.97

RESULTS FOR YEAR: 0.0769

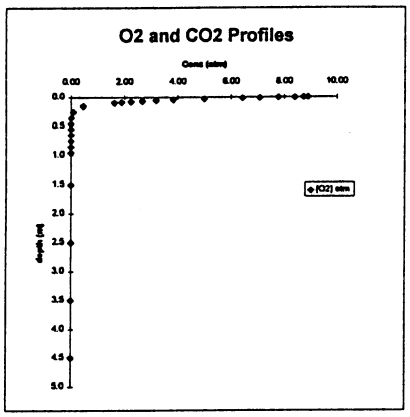

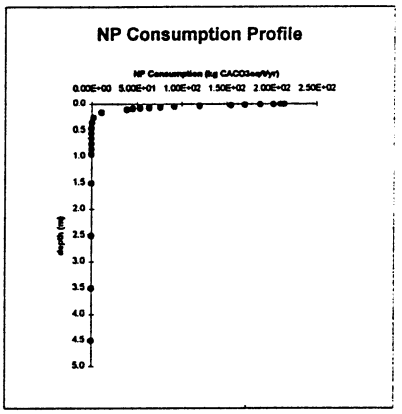

Flux in (mol/m²s)	4.74E-05
O_2 cons. (mol/m²s)	4.92E-05
Dpen (m)	1

t=0.0769												
DEPTH (m)	CONC O2 (mol/m³)	O2 Cons (mol/m³/s)	CO2 Prod (mol/m³/s)	CONC CO2 (mol/m³)	mols O2 cons per m3 rock	NP consmptn kg CaCO3eq/t/yr						Sulf dens mol/m³
0.001	8.900	9.52E-04	-5.08E-04	0.0141	3.81E-04	2.14E+02						4246.76
0.002	8.732	9.34E-04	-4.98E-04	0.0141	3.74E-04	2.10E+02						4396.07
0.004	8.403	8.99E-04	-4.80E-04	0.0141	3.60E-04	2.02E+02						4688.91
0.008	7.783	8.33E-04	-4.44E-04	0.0141	3.33E-04	1.87E+02						5241.19
0.013	7.080	7.58E-04	-4.04E-04	0.0141	3.03E-04	1.70E+02						5867.03
0.018	6.443	6.89E-04	-3.68E-04	0.0141	2.76E-04	1.55E+02						6434.25
0.030	4.999	5.35E-04	-2.85E-04	0.0141	2.14E-04	1.20E+02						7718.85
0.045	3.824	4.09E-04	-2.18E-04	0.0141	1.64E-04	9.19E+01						8763.87
0.055	3.183	3.41E-04	-1.82E-04	0.0141	1.36E-04	7.65E+01						9334.00
0.065	2.659	2.85E-04	-1.52E-04	0.0141	1.14E-04	6.39E+01						9798.86
0.075	2.235	2.39E-04	-1.28E-04	0.0141	9.57E-05	5.37E+01						10175.72
0.085	1.894	2.03E-04	-1.08E-04	0.0141	8.11E-05	4.55E+01						10478.74
0.095	1.623	1.74E-04	-9.26E-05	0.0141	6.95E-05	3.90E+01						10719.14
0.150	0.464	4.97E-05	-2.65E-05	0.0141	1.99E-05	1.12E+01						11746.45
0.250	0.084	8.98E-06	-4.79E-06	0.0141	3.59E-06	2.02E+00						12083.02
0.350	0.015	1.62E-06	-8.65E-07	0.0141	6.49E-07	3.65E-01						12143.67
0.450	0.003	2.93E-07	-1.56E-07	0.0141	1.17E-07	6.59E-02						12154.59
0.550	0.000	5.30E-08	-2.82E-08	0.0141	2.12E-08	1.19E-02						12156.56
0.650	0.000	9.57E-09	-5.10E-09	0.0141	3.83E-09	2.15E-03						12156.92
0.750	0.000	1.73E-09	-9.22E-10	0.0141	6.92E-10	3.89E-04						12156.97
0.850	0.000	3.14E-10	-1.67E-10	0.0141	1.26E-10	7.05E-05						12156.97
0.950	0.000	6.41E-11	-3.42E-11	0.0141	2.56E-11	1.44E-05						12156.97
1.500	0.000	3.11E-13	-1.66E-13	0.0141	1.25E-13	7.00E-08						12156.97
2.500	0.000	1.07E-14	-5.71E-15	0.0141	4.28E-15	2.40E-09						12156.97
3.500	0.000	1.07E-14	-5.71E-15	0.0141	4.28E-15	2.40E-09						12156.97
4.500	0.000	1.07E-14	-5.71E-15	0.0141	4.28E-15	2.40E-09						12156.97
5.500	0.000	1.07E-14	-5.71E-15	0.0141	4.28E-15	2.40E-09						12156.97
6.500	0.000	1.07E-14	-5.71E-15	0.0141	4.28E-15	2.40E-09						12156.97
7.500	0.000	1.07E-14	-5.71E-15	0.0141	4.28E-15	2.40E-09						12156.97
8.500	0.000	1.07E-14	-5.71E-15	0.0141	4.28E-15	2.40E-09						12156.97
9.500	0.000	1.07E-14	-5.71E-15	0.0141	4.28E-15	2.40E-09						12156.97
10.500	0.000	1.07E-14	-5.71E-15	0.0141	4.28E-15	2.40E-09						12156.97
11.500	0.000	1.07E-14	-5.71E-15	0.0141	4.28E-15	2.40E-09						12156.97
12.500	0.000	1.07E-14	-5.71E-15	0.0141	4.28E-15	2.40E-09						12156.97
14.000	0.000	1.07E-14	-5.71E-15	0.0141	4.28E-15	2.40E-09						12156.97
16.000	0.000	1.07E-14	-5.71E-15	0.0141	4.28E-15	2.40E-09						12156.97
18.000	0.000	1.07E-14	-5.71E-15	0.0141	4.28E-15	2.40E-09						12156.97
20.000	0.000	1.07E-14	-5.71E-15	0.0141	4.28E-15	2.40E-09						12156.97
22.000	0.000	1.07E-14	-5.71E-15	0.0141	4.28E-15	2.40E-09						12156.97
25.000	0.000	1.07E-14	-5.71E-15	0.0141	4.28E-15	2.40E-09						12156.97

RESULTS FOR YEAR: 0.096

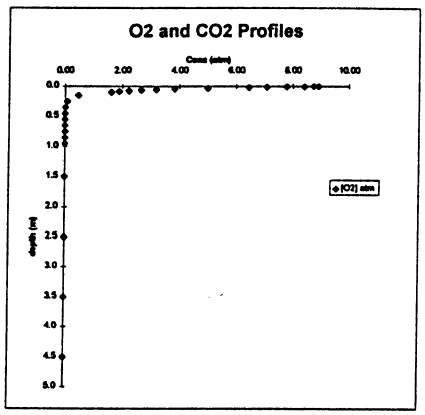

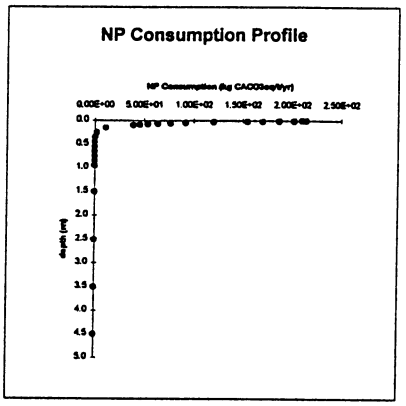

Flux in (mol/m²s)	4.74E-05
O_2 cons. (mol/m²s)	4.92E-05
Dpen (m)	1

t=0.0962												
DEPTH (m)	CONC O2 (mol/m³)	O2 Cons (mol/m³/s)	CO2 Prod (mol/m³/s)	CONC CO2 (mol/m³)	mols O2 cons per m3 rock	NP consmptn kg CaCO3eq/t/yr						Sulf dens mol/m³
0.001	8.900	9.52E-04	-5.08E-04	0.0141	3.81E-04	2.14E+02						2261.70
0.002	8.732	9.34E-04	-4.98E-04	0.0141	3.74E-04	2.10E+02						2448.40
0.004	8.403	8.99E-04	-4.80E-04	0.0141	3.60E-04	2.02E+02						2814.59
0.008	7.783	8.33E-04	-4.44E-04	0.0141	3.33E-04	1.87E+02						3505.23
0.013	7.080	7.58E-04	-4.04E-04	0.0141	3.03E-04	1.70E+02						4287.88
0.018	6.443	6.89E-04	-3.68E-04	0.0141	2.76E-04	1.55E+02						4997.24
0.030	4.999	5.35E-04	-2.85E-04	0.0141	2.14E-04	1.20E+02						6603.83
0.045	3.824	4.09E-04	-2.18E-04	0.0141	1.64E-04	9.19E+01						7910.97
0.055	3.183	3.41E-04	-1.82E-04	0.0141	1.36E-04	7.65E+01						8624.15
0.065	2.659	2.85E-04	-1.52E-04	0.0141	1.14E-04	6.39E+01						9205.70
0.075	2.235	2.39E-04	-1.28E-04	0.0141	9.57E-05	5.37E+01						9677.19
0.085	1.894	2.03E-04	-1.08E-04	0.0141	8.11E-05	4.55E+01						10056.34
0.095	1.623	1.74E-04	-9.28E-05	0.0141	6.95E-05	3.90E+01						10357.16
0.150	0.464	4.97E-05	-2.65E-05	0.0141	1.99E-05	1.12E+01						11642.86
0.250	0.084	8.98E-06	-4.79E-06	0.0141	3.59E-06	2.02E+00						12064.31
0.350	0.015	1.62E-06	-8.65E-07	0.0141	6.49E-07	3.65E-01						12140.31
0.450	0.003	2.93E-07	-1.56E-07	0.0141	1.17E-07	6.59E-02						12153.99
0.550	0.000	5.30E-08	-2.82E-08	0.0141	2.12E-08	1.19E-02						12156.46
0.650	0.000	9.57E-09	-5.10E-09	0.0141	3.83E-09	2.15E-03						12156.90
0.750	0.000	1.73E-09	-9.22E-10	0.0141	6.92E-10	3.89E-04						12156.97
0.850	0.000	3.14E-10	-1.67E-10	0.0141	1.26E-10	7.05E-05						12156.97
0.950	0.000	6.41E-11	-3.42E-11	0.0141	2.56E-11	1.44E-05						12156.97
1.500	0.000	3.11E-13	-1.66E-13	0.0141	1.25E-13	7.00E-08						12156.97
2.500	0.000	1.07E-14	-5.71E-15	0.0141	4.28E-15	2.40E-09						12156.97
3.500	0.000	1.07E-14	-5.71E-15	0.0141	4.28E-15	2.40E-09						12156.97
4.500	0.000	1.07E-14	-5.71E-15	0.0141	4.28E-15	2.40E-09						12156.97
5.500	0.000	1.07E-14	-5.71E-15	0.0141	4.28E-15	2.40E-09						12156.97
6.500	0.000	1.07E-14	-5.71E-15	0.0141	4.28E-15	2.40E-09						12156.97
7.500	0.000	1.07E-14	-5.71E-15	0.0141	4.28E-15	2.40E-09						12156.97
8.500	0.000	1.07E-14	-5.71E-15	0.0141	4.28E-15	2.40E-09						12156.97
9.500	0.000	1.07E-14	-5.71E-15	0.0141	4.28E-15	2.40E-09						12156.97
10.500	0.000	1.07E-14	-5.71E-15	0.0141	4.28E-15	2.40E-09						12156.97
11.500	0.000	1.07E-14	-5.71E-15	0.0141	4.28E-15	2.40E-09						12156.97
12.500	0.000	1.07E-14	-5.71E-15	0.0141	4.28E-15	2.40E-09						12156.97
14.000	0.000	1.07E-14	-5.71E-15	0.0141	4.28E-15	2.40E-09						12156.97
16.000	0.000	1.07E-14	-5.71E-15	0.0141	4.28E-15	2.40E-09						12156.97
18.000	0.000	1.07E-14	-5.71E-15	0.0141	4.28E-15	2.40E-09						12156.97
20.000	0.000	1.07E-14	-5.71E-15	0.0141	4.28E-15	2.40E-09						12156.97
22.000	0.000	1.07E-14	-5.71E-15	0.0141	4.28E-15	2.40E-09						12156.97
25.000	0.000	1.07E-14	-5.71E-15	0.0141	4.28E-15	2.40E-09						12156.97

RESULTS FOR YEAR: 0.1346

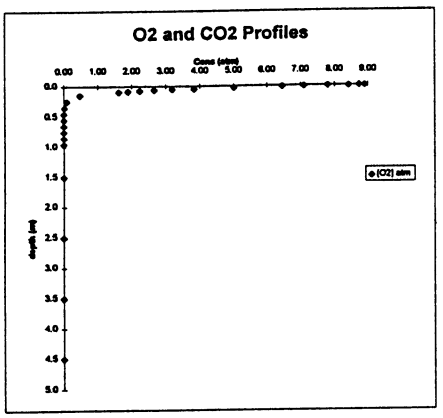

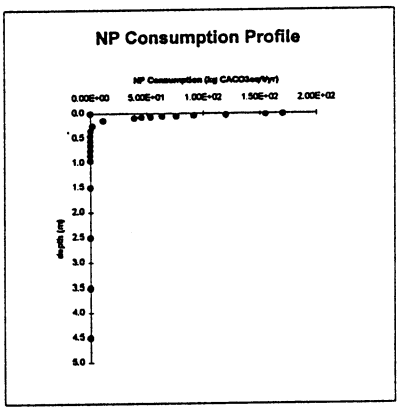

Flux in (mol/m²s)	4.56E-05
O_2 cons. (mol/m²s)	4.06E-05
Dpen (m)	1

t=0.1346												
DEPTH (m)	CONC O2 (mol/m³)	O2 Cons (mol/m³/s)	CO2 Prod (mol/m³/s)	CONC CO2 (mol/m³)	mols O2 cons per m3 rock	NP consmptn kg CaCO3eq/t/yr						Suif dens mol/m³
0.001	8.900	0.00E+00	0.00E+00	0.0141	0.00E+00	0.00E+00						0.00
0.002	8.741	0.00E+00	0.00E+00	0.0141	0.00E+00	0.00E+00						0.00
0.004	8.424	0.00E+00	0.00E+00	0.0141	0.00E+00	0.00E+00						0.00
0.008	7.803	0.00E+00	0.00E+00	0.0141	0.00E+00	0.00E+00						0.00
0.013	7.098	7.59E-04	-4.05E-04	0.0141	3.04E-04	1.71E+02						1001.56
0.018	6.459	6.91E-04	-3.69E-04	0.0141	2.76E-04	1.55E+02						2006.73
0.030	5.012	5.36E-04	-2.86E-04	0.0141	2.15E-04	1.21E+02						4283.43
0.045	3.834	4.10E-04	-2.19E-04	0.0141	1.64E-04	9.22E+01						6136.04
0.055	3.191	3.41E-04	-1.82E-04	0.0141	1.37E-04	7.67E+01						7146.93
0.065	2.667	2.85E-04	-1.52E-04	0.0141	1.14E-04	6.41E+01						7971.30
0.075	2.242	2.40E-04	-1.28E-04	0.0141	9.59E-05	5.39E+01						8639.74
0.085	1.899	2.03E-04	-1.08E-04	0.0141	8.13E-05	4.57E+01						9177.31
0.095	1.628	1.74E-04	-9.29E-05	0.0141	6.97E-05	3.91E+01						9603.88
0.150	0.466	4.99E-05	-2.66E-05	0.0141	1.99E-05	1.12E+01						11427.29
0.250	0.084	9.01E-06	-4.81E-06	0.0141	3.60E-06	2.02E+00						12025.37
0.350	0.015	1.63E-06	-8.68E-07	0.0141	6.51E-07	3.66E-01						12133.28
0.450	0.003	2.94E-07	-1.57E-07	0.0141	1.18E-07	6.61E-02						12152.73
0.550	0.000	5.32E-08	-2.83E-08	0.0141	2.13E-08	1.19E-02						12156.24
0.650	0.000	9.60E-09	-5.12E-09	0.0141	3.84E-09	2.16E-03						12156.87
0.750	0.000	1.74E-09	-9.26E-10	0.0141	6.94E-10	3.90E-04						12156.97
0.850	0.000	3.15E-10	-1.68E-10	0.0141	1.26E-10	7.08E-05						12156.97
0.950	0.000	6.43E-11	-3.43E-11	0.0141	2.57E-11	1.45E-05						12156.97
1.500	0.000	3.12E-13	-1.67E-13	0.0141	1.25E-13	7.02E-08						12156.97
2.500	0.000	1.07E-14	-5.71E-15	0.0141	4.28E-15	2.40E-09						12156.97
3.500	0.000	1.07E-14	-5.71E-15	0.0141	4.28E-15	2.40E-09						12156.97
4.500	0.000	1.07E-14	-5.71E-15	0.0141	4.28E-15	2.40E-09						12156.97
5.500	0.000	1.07E-14	-5.71E-15	0.0141	4.28E-15	2.40E-09						12156.97
6.500	0.000	1.07E-14	-5.71E-15	0.0141	4.28E-15	2.40E-09						12156.97
7.500	0.000	1.07E-14	-5.71E-15	0.0141	4.28E-15	2.40E-09						12156.97
8.500	0.000	1.07E-14	-5.71E-15	0.0141	4.28E-15	2.40E-09						12156.97
9.500	0.000	1.07E-14	-5.71E-15	0.0141	4.28E-15	2.40E-09						12156.97
10.500	0.000	1.07E-14	-5.71E-15	0.0141	4.28E-15	2.40E-09						12156.97
11.500	0.000	1.07E-14	-5.71E-15	0.0141	4.28E-15	2.40E-09						12156.97
12.500	0.000	1.07E-14	-5.71E-15	0.0141	4.28E-15	2.40E-09						12156.97
14.000	0.000	1.07E-14	-5.71E-15	0.0141	4.28E-15	2.40E-09						12156.97
16.000	0.000	1.07E-14	-5.71E-15	0.0141	4.28E-15	2.40E-09						12156.97
18.000	0.000	1.07E-14	-5.71E-15	0.0141	4.28E-15	2.40E-09						12156.97
20.000	0.000	1.07E-14	-5.71E-15	0.0141	4.28E-15	2.40E-09						12156.97
22.000	0.000	1.07E-14	-5.71E-15	0.0141	4.28E-15	2.40E-09						12156.97
25.000	0.000	1.07E-14	-5.71E-15	0.0141	4.28E-15	2.40E-09						12156.97

RESULTS FOR YEAR: 0.1923

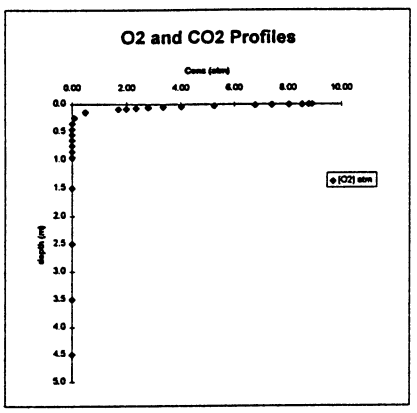

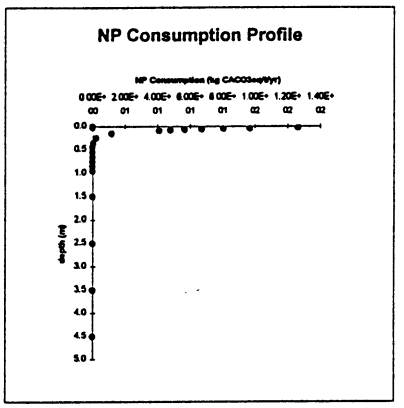

Flux in (mol/m²s)	3.57E-05
O_2 cons. (mol/m²s)	3.50E-05
Dpen (m)	1

t=0.192												
DEPTH (m)	CONC O2 (mol/m³)	O2 Cons (mol/m³/s)	CO2 Prod (mol/m³/s)	CONC CO2 (mol/m³)	mols O2 cons per m3 rock	NP consmptn kg CaCO3eq/t/yr						Sulf dens mol/m³
0.001	8.900	0.00E+00	0.00E+00	0.0141	0.00E+00	0.00E+00						0.00
0.002	8.776	0.00E+00	0.00E+00	0.0141	0.00E+00	0.00E+00						0.00
0.004	8.529	0.00E+00	0.00E+00	0.0141	0.00E+00	0.00E+00						0.00
0.008	8.031	0.00E+00	0.00E+00	0.0141	0.00E+00	0.00E+00						0.00
0.013	7.397	0.00E+00	0.00E+00	0.0141	0.00E+00	0.00E+00						0.00
0.018	6.777	0.00E+00	0.00E+00	0.0141	0.00E+00	0.00E+00						0.00
0.030	5.261	5.63E-04	-3.00E-04	0.0141	2.25E-04	1.26E+02						708.66
0.045	4.026	4.31E-04	-2.30E-04	0.0141	1.72E-04	9.68E+01						3401.71
0.055	3.351	3.59E-04	-1.91E-04	0.0141	1.43E-04	8.06E+01						4871.28
0.065	2.801	3.00E-04	-1.60E-04	0.0141	1.20E-04	6.74E+01						6069.76
0.075	2.355	2.52E-04	-1.34E-04	0.0141	1.01E-04	5.66E+01						7041.64
0.085	1.996	2.14E-04	-1.14E-04	0.0141	8.54E-05	4.80E+01						7823.26
0.095	1.710	1.83E-04	-9.76E-05	0.0141	7.32E-05	4.11E+01						8443.54
0.150	0.490	5.24E-05	-2.80E-05	0.0141	2.10E-05	1.18E+01						11095.26
0.250	0.089	9.48E-06	-5.06E-06	0.0141	3.79E-06	2.13E+00						11965.40
0.350	0.016	1.71E-06	-9.15E-07	0.0141	6.86E-07	3.85E-01						12122.45
0.450	0.003	3.10E-07	-1.65E-07	0.0141	1.24E-07	6.97E-02						12150.78
0.550	0.001	5.60E-08	-2.99E-08	0.0141	2.24E-08	1.26E-02						12155.89
0.650	0.000	1.01E-08	-5.40E-09	0.0141	4.05E-09	2.28E-03						12156.81
0.750	0.000	1.83E-09	-9.76E-10	0.0141	7.32E-10	4.11E-04						12156.97
0.850	0.000	3.32E-10	-1.77E-10	0.0141	1.33E-10	7.46E-05						12156.97
0.950	0.000	6.78E-11	-3.62E-11	0.0141	2.71E-11	1.52E-05						12156.97
1.500	0.000	3.30E-13	-1.76E-13	0.0141	1.32E-13	7.41E-08						12156.97
2.500	0.000	1.07E-14	-5.71E-15	0.0141	4.28E-15	2.40E-09						12156.97
3.500	0.000	1.07E-14	-5.71E-15	0.0141	4.28E-15	2.40E-09						12156.97
4.500	0.000	1.07E-14	-5.71E-15	0.0141	4.28E-15	2.40E-09						12156.97
5.500	0.000	1.07E-14	-5.71E-15	0.0141	4.28E-15	2.40E-09						12156.97
6.500	0.000	1.07E-14	-5.71E-15	0.0141	4.28E-15	2.40E-09						12156.97
7.500	0.000	1.07E-14	-5.71E-15	0.0141	4.28E-15	2.40E-09						12156.97
8.500	0.000	1.07E-14	-5.71E-15	0.0141	4.28E-15	2.40E-09						12156.97
9.500	0.000	1.07E-14	-5.71E-15	0.0141	4.28E-15	2.40E-09						12156.97
10.500	0.000	1.07E-14	-5.71E-15	0.0141	4.28E-15	2.40E-09						12156.97
11.500	0.000	1.07E-14	-5.71E-15	0.0141	4.28E-15	2.40E-09						12156.97
12.500	0.000	1.07E-14	-5.71E-15	0.0141	4.28E-15	2.40E-09						12156.97
14.000	0.000	1.07E-14	-5.71E-15	0.0141	4.28E-15	2.40E-09						12156.97
16.000	0.000	1.07E-14	-5.71E-15	0.0141	4.28E-15	2.40E-09						12156.97
18.000	0.000	1.07E-14	-5.71E-15	0.0141	4.28E-15	2.40E-09						12156.97
20.000	0.000	1.07E-14	-5.71E-15	0.0141	4.28E-15	2.40E-09						12156.97
22.000	0.000	1.07E-14	-5.71E-15	0.0141	4.28E-15	2.40E-09						12156.97
25.000	0.000	1.07E-14	-5.71E-15	0.0141	4.28E-15	2.40E-09						12156.97

APPENDIX A5
Run 2B1, Cut and Fill

COUPLED $O_2/CO_2/Mg/SO_4/Ca$ MODEL

OXYDIFF V2.0

MODEL DETAILS

Filename	BF_CS2b1
Date	27/11/1996
Description:	Steady State Model Of Crandon Cut and Fill Placed Cemented Backfill Tailings
	Part 2 (year 1 to 32)
	First Order Model

INPUT PARAMETERS

Finite Difference Parameters

nodes x	1
nodes y	40
time periods	7
init delt (s)	0.01
[O2] at surface (mol/m³)	8.9
[CO2] at surface (mol/m³))	0.0141

Model Options

CO2 OPTION	0
FES2 OPTION	1
O2 OPTION	1

Geochemical Options

Infiltration (m/s)	1.10E-09
Infiltration Coefficient	1.00
Kgypsum	-
Infiltration (m/s)	1.10E-09
Fraction Flow Paths (G)	1.00

Diffusion Parameters

Dw (m2/s)	2.20E-09
Da (m2/s)	1.80E-05
τ	0.273
α	3.28
H	33.9

OUTPUT TIMES

time (s)	time (y)	Output col
1.6E+07	1	1
6.3E+07	2	6
1.3E+08	4	11
2.5E+08	8	16
5.0E+08	16	21
7.6E+08	24	26
1.0E+09	32	31

FES2 OPTION
0 - No FES2 DEPLETION
1 - ALLOW FES2 DEPLETION

CO2 OPTION:
0 - No CO2 Coupling
1 - CO2 Coupling

O2 OPTION
0 - HALF ORDER REACTION
1 - FIRST ORDER REACTION
2 - MIXED FIRST ORDER / ZERO ORDER
3 - ZERO ORDER SOLUTION

TORTUOSITY

Rock fill	τ	3
Cemented Tailings	τ	100

MODEL INPUTS

Material	DEPTH (m)	Depth (ft)	Cell Sizes (m)	r (s-1)	Porosity	Bulk Dens. (tonnes m^{-3})	Sat. (%)	SulfDens (mol/m^3)	Diff Coeff [1] (m2/s)	Diff Coeff [2] (m2/s)	$[O_2]_{ini}$ (mol/m^3)	$[CO_2]_{ini}$ (mol/m^3)
Waste Rock	0.050	0.164	0.1	0.00E+00	0.40	1.9	15%	0	6.00E-06	6.00E-06	8.89	1.41E-02
Waste Rock	0.225	0.738	0.25	0.00E+00	0.40	1.9	15%	0	6.00E-06	6.00E-06	8.89	1.41E-02
Waste Rock	0.600	1.969	0.5	0.00E+00	0.40	1.9	15%	0	6.00E-06	6.00E-06	8.89	1.41E-02
Waste Rock	1.400	4.593	1.1	0.00E+00	0.40	1.9	15%	0	6.00E-06	6.00E-06	8.89	1.41E-02
Waste Rock	3.200	10.499	2.5	0.00E+00	0.40	1.9	15%	0	6.00E-06	6.00E-06	8.89	1.41E-02
Waste Rock	5.950	19.521	3	0.00E+00	0.40	1.9	15%	0	6.00E-06	6.00E-06	8.89	1.41E-02
Waste Rock	8.950	29.364	3	0.00E+00	0.40	1.9	15%	0	6.00E-06	6.00E-06	8.89	1.41E-02
Waste Rock	11.700	38.386	2.5	0.00E+00	0.40	1.9	15%	0	6.00E-06	6.00E-06	8.89	1.41E-02
Waste Rock	13.450	44.127	1	0.00E+00	0.40	1.9	15%	0	6.00E-06	6.00E-06	8.89	1.41E-02
Waste Rock	14.200	46.588	0.5	0.00E+00	0.40	1.9	15%	0	6.00E-06	6.00E-06	8.89	1.41E-02
Waste Rock	14.508	47.597	0.115	0.00E+00	0.40	1.9	15%	0	6.00E-06	6.00E-06	8.89	1.41E-02
Waste Rock	14.590	47.867	0.05	0.00E+00	0.40	1.9	15%	0	6.00E-06	6.00E-06	8.89	1.41E-02
Waste Rock	14.620	47.966	0.01	0.00E+00	0.40	1.9	15%	0	6.00E-06	6.00E-06	8.89	1.41E-02
Waste Rock	14.628	47.990	0.005	0.00E+00	0.40	1.9	15%	0	6.00E-06	6.00E-06	8.89	1.41E-02
Tailings Backfill	14.631	48.000	0.001	1.07E-04	0.40	3.0	15%	12187	2.88E-08	2.88E-08	8.89	1.41E-02
Tailings Backfill	14.632	48.004	0.001	1.07E-04	0.40	3.0	15%	12187	2.88E-08	2.88E-08	8.89	1.41E-02
Tailings Backfill	14.635	48.013	0.005	1.07E-04	0.40	3.0	15%	12187	2.88E-08	2.88E-08	8.89	1.41E-02
Tailings Backfill	14.640	48.030	0.005	1.07E-04	0.40	3.0	15%	12187	2.88E-08	2.88E-08	8.89	1.41E-02
Tailings Backfill	14.647	48.054	0.01	1.07E-04	0.40	3.0	15%	12187	2.88E-08	2.88E-08	8.89	1.41E-02
Tailings Backfill	14.657	48.087	0.01	1.07E-04	0.40	3.0	15%	12187	2.88E-08	2.88E-08	8.89	1.41E-02
Tailings Backfill	14.687	48.186	0.05	1.07E-04	0.40	3.0	15%	12187	2.88E-08	2.88E-08	8.89	1.41E-02
Tailings Backfill	14.737	48.350	0.05	1.07E-04	0.40	3.0	15%	12187	2.88E-08	2.88E-08	8.89	1.41E-02
Tailings Backfill	14.812	48.596	0.1	1.07E-04	0.40	3.0	15%	12187	2.88E-08	2.88E-08	8.89	1.41E-02
Tailings Backfill	14.912	48.924	0.1	1.07E-04	0.40	3.0	15%	12187	2.88E-08	2.88E-08	8.89	1.41E-02
Tailings Backfill	15.212	49.908	0.5	1.07E-04	0.40	3.0	15%	12187	2.88E-08	2.88E-08	8.89	1.41E-02
Tailings Backfill	15.712	51.549	0.5	1.07E-04	0.40	3.0	15%	12187	2.88E-08	2.88E-08	8.89	1.41E-02
Tailings Backfill	16.212	53.189	0.5	1.07E-04	0.40	3.0	15%	12187	2.88E-08	2.88E-08	8.89	1.41E-02
Tailings Backfill	16.712	54.829	0.5	1.07E-04	0.40	3.0	15%	12187	2.88E-08	2.88E-08	8.89	1.41E-02
Tailings Backfill	17.462	57.290	1	1.07E-04	0.40	3.0	15%	12187	2.88E-08	2.88E-08	8.89	1.41E-02
Tailings Backfill	18.462	60.571	1	1.07E-04	0.40	3.0	15%	12187	2.88E-08	2.88E-08	8.89	1.41E-02
Tailings Backfill	19.462	63.852	1	1.07E-04	0.40	3.0	15%	12187	2.88E-08	2.88E-08	8.89	1.41E-02
Tailings Backfill	20.462	67.133	1	1.07E-04	0.40	3.0	15%	12187	2.88E-08	2.88E-08	8.89	1.41E-02
Tailings Backfill	21.962	72.054	2	1.07E-04	0.40	3.0	15%	12187	2.88E-08	2.88E-08	8.89	1.41E-02
Tailings Backfill	23.962	78.615	2	1.07E-04	0.40	3.0	15%	12187	2.88E-08	2.88E-08	8.89	1.41E-02
Tailings Backfill	26.462	86.818	3	1.07E-04	0.40	3.0	15%	12187	2.88E-08	2.88E-08	8.89	1.41E-02
Tailings Backfill	29.462	96.660	3	1.07E-04	0.40	3.0	15%	12187	2.88E-08	2.88E-08	8.89	1.41E-02
Tailings Backfill	32.962	108.143	4	1.07E-04	0.40	3.0	15%	12187	2.88E-08	2.88E-08	8.89	1.41E-02
Tailings Backfill	36.962	121.266	4	1.07E-04	0.40	3.0	15%	12187	2.88E-08	2.88E-08	8.89	1.41E-02
Tailings Backfill	40.962	134.390	4	1.07E-04	0.40	3.0	15%	12187	2.88E-08	2.88E-08	8.89	1.41E-02
Tailings Backfill	44.962	147.513	4	1.07E-04	0.40	3.0	15%	12187	2.88E-08	2.88E-08	8.89	1.41E-02

1. Diff Coefficient Based on Erbering, B., R.V.Nicholson, E.J.Reardon and P.Tibble, Evaluation of sulphide oxidation rates. Nordic Hydrology, 24(5), 323-338, 1993.
2. Diff Coefficient Based on Reardon, E.J. and P.M. Moddle, Gas Diffusion Coefficient Measurements on Uranium Mill Tailings: Implications to Cover Layer Design. Uranium, 2, 111-131,1985.

RESULTS FOR YEAR: 1

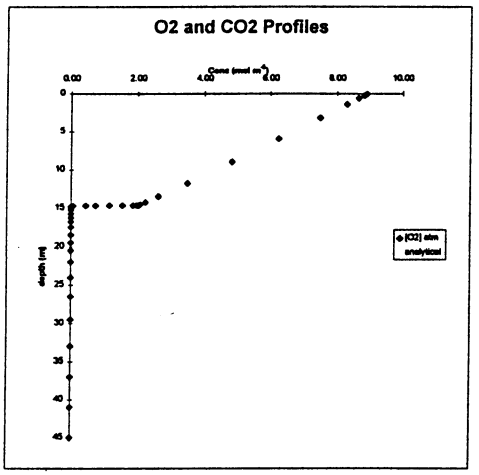

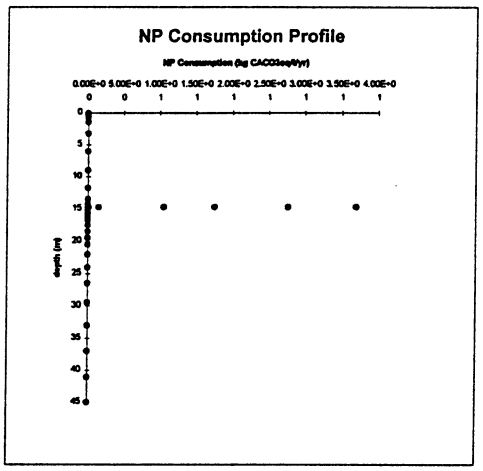

Flux in (mol/m²s)	2.66E-06
O_2 cons. (mol/m²s)	3.06E-06
Dpen (m)	14.962

t=1												
DEPTH (m)	CONC O2 (mol/m³)	O2 Cons (mol/m³/s)	CO2 Prod (mol/m³/s)	CONC CO2 (mol/m³)	mols O2 cons per m³ material	NP consmptn kg CaCO3eq/t/yr						Sulf dens mol/m³
0.050	8.900	0.00E+00	0.00E+00	0.0141	0.00E+00	0.00E+00						0.00
0.225	8.822	0.00E+00	0.00E+00	0.0141	0.00E+00	0.00E+00						0.00
0.600	8.656	0.00E+00	0.00E+00	0.0141	0.00E+00	0.00E+00						0.00
1.400	8.301	0.00E+00	0.00E+00	0.0141	0.00E+00	0.00E+00						0.00
3.200	7.500	0.00E+00	0.00E+00	0.0141	0.00E+00	0.00E+00						0.00
5.950	6.252	0.00E+00	0.00E+00	0.0141	0.00E+00	0.00E+00						0.00
8.950	4.840	0.00E+00	0.00E+00	0.0141	0.00E+00	0.00E+00						0.00
11.700	3.495	0.00E+00	0.00E+00	0.0141	0.00E+00	0.00E+00						0.00
13.450	2.615	0.00E+00	0.00E+00	0.0141	0.00E+00	0.00E+00						0.00
14.200	2.235	0.00E+00	0.00E+00	0.0141	0.00E+00	0.00E+00						0.00
14.508	2.078	0.00E+00	0.00E+00	0.0141	0.00E+00	0.00E+00						0.00
14.590	2.036	0.00E+00	0.00E+00	0.0141	0.00E+00	0.00E+00						0.00
14.620	2.021	0.00E+00	0.00E+00	0.0141	0.00E+00	0.00E+00						0.00
14.628	2.017	0.00E+00	0.00E+00	0.0141	0.00E+00	0.00E+00						0.00
14.631	1.963	0.00E+00	0.00E+00	0.0141	0.00E+00	0.00E+00						0.00
14.632	1.857	0.00E+00	0.00E+00	0.0141	0.00E+00	0.00E+00						0.00
14.635	1.539	1.65E-04	-8.78E-05	0.0141	6.59E-05	3.70E+01						84.58
14.640	1.152	1.23E-04	-6.57E-05	0.0141	4.93E-05	2.77E+01						3123.05
14.647	0.731	7.82E-05	-4.17E-05	0.0141	3.13E-05	1.76E+01						6423.88
14.657	0.441	4.72E-05	-2.52E-05	0.0141	1.89E-05	1.06E+01						8698.00
14.687	0.062	6.64E-06	-3.54E-06	0.0141	2.65E-06	1.49E+00						11670.49
14.737	0.006	6.08E-07	-3.24E-07	0.0141	2.43E-07	1.37E-01						12112.41
14.812	0.000	2.06E-08	-1.10E-08	0.0141	8.22E-09	4.62E-03						12155.45
14.912	0.000	5.35E-10	-2.85E-10	0.0141	2.14E-10	1.20E-04						12156.94
15.212	0.000	9.59E-13	-5.11E-13	0.0141	3.83E-13	2.15E-07						12156.97
15.712	0.000	1.07E-14	-5.71E-15	0.0141	4.28E-15	2.40E-09						12156.97
16.212	0.000	1.07E-14	-5.71E-15	0.0141	4.28E-15	2.40E-09						12156.97
16.712	0.000	1.07E-14	-5.71E-15	0.0141	4.28E-15	2.40E-09						12156.97
17.462	0.000	1.07E-14	-5.71E-15	0.0141	4.28E-15	2.40E-09						12156.97
18.462	0.000	1.07E-14	-5.71E-15	0.0141	4.28E-15	2.40E-09						12156.97
19.462	0.000	1.07E-14	-5.71E-15	0.0141	4.28E-15	2.40E-09						12156.97
20.462	0.000	1.07E-14	-5.71E-15	0.0141	4.28E-15	2.40E-09						12156.97
21.962	0.000	1.07E-14	-5.71E-15	0.0141	4.28E-15	2.40E-09						12156.97
23.962	0.000	1.07E-14	-5.71E-15	0.0141	4.28E-15	2.40E-09						12156.97
26.462	0.000	1.07E-14	-5.71E-15	0.0141	4.28E-15	2.40E-09						12156.97
29.462	0.000	1.07E-14	-5.71E-15	0.0141	4.28E-15	2.40E-09						12156.97
32.962	0.000	1.07E-14	-5.71E-15	0.0141	4.28E-15	2.40E-09						12156.97
36.962	0.000	1.07E-14	-5.71E-15	0.0141	4.28E-15	2.40E-09						12156.97
40.962	0.000	1.07E-14	-5.71E-15	0.0141	4.28E-15	2.40E-09						12156.97
44.962	0.000	1.07E-14	-5.71E-15	0.0141	4.28E-15	2.40E-09						12156.97

RESULTS FOR YEAR: 2

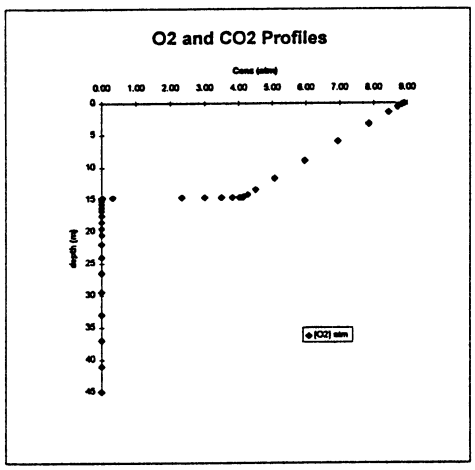

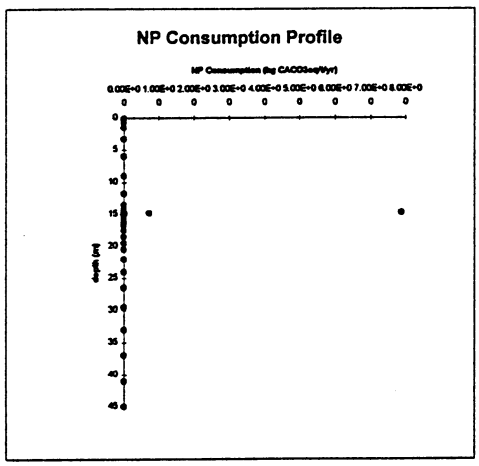

Flux in (mol/m²s)	1.99E-06
O_2 cons. (mol/m²s)	1.93E-06
Dpen (m)	14.962

t=2												
DEPTH (m)	CONC O2 (mol/m³)	O2 Cons (mol/m³/s)	CO2 Prod (mol/m³/s)	CONC CO2 (mol/m³)	mols O2 cons per m3 rock	NP consmptn kg CaCO3eq/t/yr						Sulf dens mol/m³
0.050	8.900	0.00E+00	0.00E+00	0.0141	0.00E+00	0.00E+00						0.00
0.225	8.842	0.00E+00	0.00E+00	0.0141	0.00E+00	0.00E+00						0.00
0.600	8.717	0.00E+00	0.00E+00	0.0141	0.00E+00	0.00E+00						0.00
1.400	8.452	0.00E+00	0.00E+00	0.0141	0.00E+00	0.00E+00						0.00
3.200	7.855	0.00E+00	0.00E+00	0.0141	0.00E+00	0.00E+00						0.00
5.950	6.946	0.00E+00	0.00E+00	0.0141	0.00E+00	0.00E+00						0.00
8.950	5.962	0.00E+00	0.00E+00	0.0141	0.00E+00	0.00E+00						0.00
11.700	5.069	0.00E+00	0.00E+00	0.0141	0.00E+00	0.00E+00						0.00
13.450	4.507	0.00E+00	0.00E+00	0.0141	0.00E+00	0.00E+00						0.00
14.200	4.262	0.00E+00	0.00E+00	0.0141	0.00E+00	0.00E+00						0.00
14.508	4.163	0.00E+00	0.00E+00	0.0141	0.00E+00	0.00E+00						0.00
14.590	4.136	0.00E+00	0.00E+00	0.0141	0.00E+00	0.00E+00						0.00
14.620	4.126	0.00E+00	0.00E+00	0.0141	0.00E+00	0.00E+00						0.00
14.628	4.124	0.00E+00	0.00E+00	0.0141	0.00E+00	0.00E+00						0.00
14.631	4.090	0.00E+00	0.00E+00	0.0141	0.00E+00	0.00E+00						0.00
14.632	4.023	0.00E+00	0.00E+00	0.0141	0.00E+00	0.00E+00						0.00
14.635	3.822	0.00E+00	0.00E+00	0.0141	0.00E+00	0.00E+00						0.00
14.640	3.491	0.00E+00	0.00E+00	0.0141	0.00E+00	0.00E+00						0.00
14.647	2.997	0.00E+00	0.00E+00	0.0141	0.00E+00	0.00E+00						0.00
14.657	2.335	0.00E+00	0.00E+00	0.0141	0.00E+00	0.00E+00						0.00
14.667	0.328	3.51E-05	-1.87E-05	0.0141	1.41E-05	7.89E+00						8028.72
14.737	0.030	3.22E-06	-1.72E-06	0.0141	1.29E-06	7.23E-01						11779.09
14.812	0.001	1.09E-07	-5.80E-08	0.0141	4.35E-08	2.45E-02						12144.18
14.912	0.000	2.83E-09	-1.51E-09	0.0141	1.13E-09	6.36E-04						12156.66
15.212	0.000	5.07E-12	-2.70E-12	0.0141	2.03E-12	1.14E-06						12156.97
15.712	0.000	1.07E-14	-5.71E-15	0.0141	4.28E-15	2.40E-09						12156.97
16.212	0.000	1.07E-14	-5.71E-15	0.0141	4.28E-15	2.40E-09						12156.97
16.712	0.000	1.07E-14	-5.71E-15	0.0141	4.28E-15	2.40E-09						12156.97
17.462	0.000	1.07E-14	-5.71E-15	0.0141	4.28E-15	2.40E-09						12156.97
18.462	0.000	1.07E-14	-5.71E-15	0.0141	4.28E-15	2.40E-09						12156.97
19.462	0.000	1.07E-14	-5.71E-15	0.0141	4.28E-15	2.40E-09						12156.97
20.462	0.000	1.07E-14	-5.71E-15	0.0141	4.28E-15	2.40E-09						12156.97
21.962	0.000	1.07E-14	-5.71E-15	0.0141	4.28E-15	2.40E-09						12156.97
23.962	0.000	1.07E-14	-5.71E-15	0.0141	4.28E-15	2.40E-09						12156.97
26.462	0.000	1.07E-14	-5.71E-15	0.0141	4.28E-15	2.40E-09						12156.97
29.462	0.000	1.07E-14	-5.71E-15	0.0141	4.28E-15	2.40E-09						12156.97
32.962	0.000	1.07E-14	-5.71E-15	0.0141	4.28E-15	2.40E-09						12156.97
36.962	0.000	1.07E-14	-5.71E-15	0.0141	4.28E-15	2.40E-09						12156.97
40.962	0.000	1.07E-14	-5.71E-15	0.0141	4.28E-15	2.40E-09						12156.97
44.962	0.000	1.07E-14	-5.71E-15	0.0141	4.28E-15	2.40E-09						12156.97

RESULTS FOR YEAR: 4

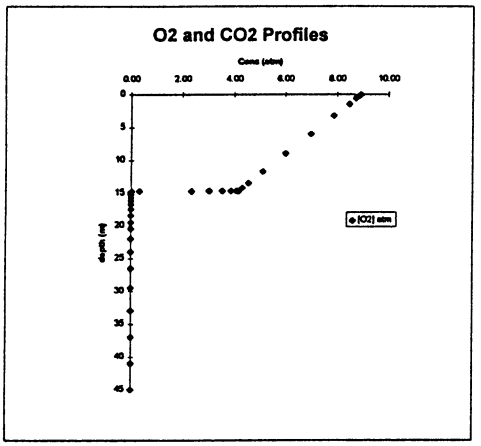

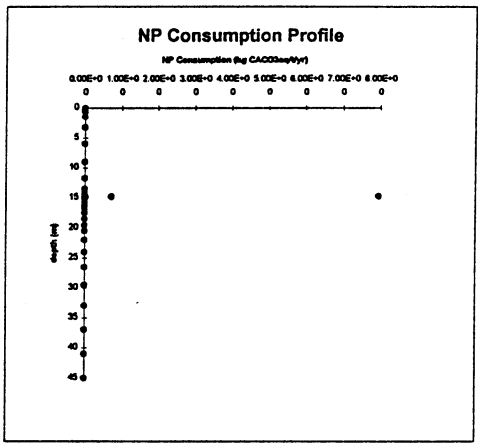

Flux in (mol/m²s)	1.94E-06
O_2 cons. (mol/m²s)	1.94E-06
Dpen (m)	14.962

t=4												
DEPTH (m)	CONC O2 (mol/m³)	O2 Cons (mol/m³/s)	CO2 Prod (mol/m³/s)	CONC CO2 (mol/m³)	mols O2 cons per m3 rock	NP consmptn kg CaCO3eq/t/yr						Sulf dens mol/m³
0.050	8.900	0.00E+00	0.00E+00	0.0141	0.00E+00	0.00E+00						0.00
0.225	8.843	0.00E+00	0.00E+00	0.0141	0.00E+00	0.00E+00						0.00
0.600	8.722	0.00E+00	0.00E+00	0.0141	0.00E+00	0.00E+00						0.00
1.400	8.462	0.00E+00	0.00E+00	0.0141	0.00E+00	0.00E+00						0.00
3.200	7.879	0.00E+00	0.00E+00	0.0141	0.00E+00	0.00E+00						0.00
5.950	6.988	0.00E+00	0.00E+00	0.0141	0.00E+00	0.00E+00						0.00
8.950	6.016	0.00E+00	0.00E+00	0.0141	0.00E+00	0.00E+00						0.00
11.700	5.124	0.00E+00	0.00E+00	0.0141	0.00E+00	0.00E+00						0.00
13.450	4.557	0.00E+00	0.00E+00	0.0141	0.00E+00	0.00E+00						0.00
14.200	4.314	0.00E+00	0.00E+00	0.0141	0.00E+00	0.00E+00						0.00
14.506	4.214	0.00E+00	0.00E+00	0.0141	0.00E+00	0.00E+00						0.00
14.590	4.188	0.00E+00	0.00E+00	0.0141	0.00E+00	0.00E+00						0.00
14.620	4.178	0.00E+00	0.00E+00	0.0141	0.00E+00	0.00E+00						0.00
14.628	4.176	0.00E+00	0.00E+00	0.0141	0.00E+00	0.00E+00						0.00
14.631	4.141	0.00E+00	0.00E+00	0.0141	0.00E+00	0.00E+00						0.00
14.632	4.074	0.00E+00	0.00E+00	0.0141	0.00E+00	0.00E+00						0.00
14.635	3.871	0.00E+00	0.00E+00	0.0141	0.00E+00	0.00E+00						0.00
14.640	3.534	0.00E+00	0.00E+00	0.0141	0.00E+00	0.00E+00						0.00
14.647	3.028	0.00E+00	0.00E+00	0.0141	0.00E+00	0.00E+00						0.00
14.657	2.354	0.00E+00	0.00E+00	0.0141	0.00E+00	0.00E+00						0.00
14.687	0.331	3.54E-05	-1.89E-05	0.0141	1.42E-05	7.96E+00						52.06
14.737	0.030	3.24E-06	-1.73E-06	0.0141	1.30E-06	7.29E-01						11048.69
14.812	0.001	1.10E-07	-5.85E-08	0.0141	4.39E-08	2.47E-02						12119.48
14.912	0.000	2.85E-09	-1.52E-09	0.0141	1.14E-09	6.41E-04						12156.02
15.212	0.000	5.11E-12	-2.73E-12	0.0141	2.05E-12	1.15E-06						12156.97
15.712	0.000	1.07E-14	-5.71E-15	0.0141	4.28E-15	2.40E-09						12156.97
16.212	0.000	1.07E-14	-5.71E-15	0.0141	4.28E-15	2.40E-09						12156.97
16.712	0.000	1.07E-14	-5.71E-15	0.0141	4.28E-15	2.40E-09						12156.97
17.462	0.000	1.07E-14	-5.71E-15	0.0141	4.28E-15	2.40E-09						12156.97
18.462	0.000	1.07E-14	-5.71E-15	0.0141	4.28E-15	2.40E-09						12156.97
19.462	0.000	1.07E-14	-5.71E-15	0.0141	4.28E-15	2.40E-09						12156.97
20.462	0.000	1.07E-14	-5.71E-15	0.0141	4.28E-15	2.40E-09						12156.97
21.962	0.000	1.07E-14	-5.71E-15	0.0141	4.28E-15	2.40E-09						12156.97
23.962	0.000	1.07E-14	-5.71E-15	0.0141	4.28E-15	2.40E-09						12156.97
26.462	0.000	1.07E-14	-5.71E-15	0.0141	4.28E-15	2.40E-09						12156.97
29.462	0.000	1.07E-14	-5.71E-15	0.0141	4.28E-15	2.40E-09						12156.97
32.962	0.000	1.07E-14	-5.71E-15	0.0141	4.28E-15	2.40E-09						12156.97
36.962	0.000	1.07E-14	-5.71E-15	0.0141	4.28E-15	2.40E-09						12156.97
40.962	0.000	1.07E-14	-5.71E-15	0.0141	4.28E-15	2.40E-09						12156.97
44.962	0.000	1.07E-14	-5.71E-15	0.0141	4.28E-15	2.40E-09						12156.97

RESULTS FOR YEAR: 8

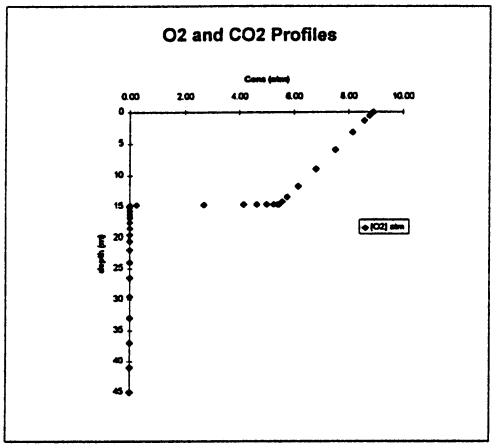

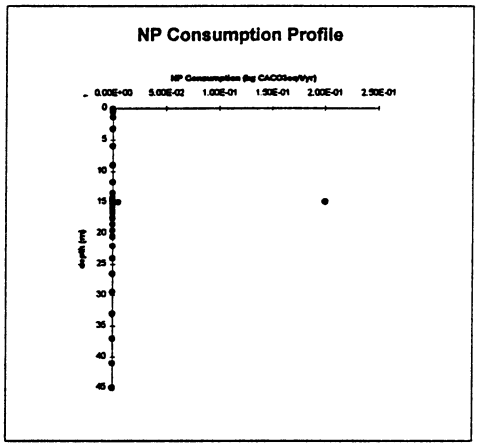

Flux in (mol/m²s)	1.41E-06
O_2 cons. (mol/m²s)	9.15E-08
Dpen (m)	15.462

t=8												
DEPTH (m)	CONC O2 (mol/m³)	O2 Cons (mol/m³/s)	CO2 Prod (mol/m³/s)	CONC CO2 (mol/m³)	mols O2 cons per m3 rock	NP consmptn kg CaCO3eq/t/yr						Sulf dens mol/m²
0.050	8.900	0.00E+00	0.00E+00	0.0141	0.00E+00	0.00E+00						0.00
0.225	8.859	0.00E+00	0.00E+00	0.0141	0.00E+00	0.00E+00						0.00
0.600	8.771	0.00E+00	0.00E+00	0.0141	0.00E+00	0.00E+00						0.00
1.400	8.583	0.00E+00	0.00E+00	0.0141	0.00E+00	0.00E+00						0.00
3.200	8.160	0.00E+00	0.00E+00	0.0141	0.00E+00	0.00E+00						0.00
5.950	7.514	0.00E+00	0.00E+00	0.0141	0.00E+00	0.00E+00						0.00
8.950	6.810	0.00E+00	0.00E+00	0.0141	0.00E+00	0.00E+00						0.00
11.700	6.164	0.00E+00	0.00E+00	0.0141	0.00E+00	0.00E+00						0.00
13.450	5.753	0.00E+00	0.00E+00	0.0141	0.00E+00	0.00E+00						0.00
14.200	5.577	0.00E+00	0.00E+00	0.0141	0.00E+00	0.00E+00						0.00
14.508	5.504	0.00E+00	0.00E+00	0.0141	0.00E+00	0.00E+00						0.00
14.590	5.485	0.00E+00	0.00E+00	0.0141	0.00E+00	0.00E+00						0.00
14.620	5.478	0.00E+00	0.00E+00	0.0141	0.00E+00	0.00E+00						0.00
14.628	5.476	0.00E+00	0.00E+00	0.0141	0.00E+00	0.00E+00						0.00
14.631	5.451	0.00E+00	0.00E+00	0.0141	0.00E+00	0.00E+00						0.00
14.632	5.402	0.00E+00	0.00E+00	0.0141	0.00E+00	0.00E+00						0.00
14.635	5.256	0.00E+00	0.00E+00	0.0141	0.00E+00	0.00E+00						0.00
14.640	5.011	0.00E+00	0.00E+00	0.0141	0.00E+00	0.00E+00						0.00
14.647	4.645	0.00E+00	0.00E+00	0.0141	0.00E+00	0.00E+00						0.00
14.657	4.156	0.00E+00	0.00E+00	0.0141	0.00E+00	0.00E+00						0.00
14.687	2.690	0.00E+00	0.00E+00	0.0141	0.00E+00	0.00E+00						0.00
14.737	0.246	0.00E+00	0.00E+00	0.0141	0.00E+00	0.00E+00						0.00
14.812	0.008	8.92E-07	-4.75E-07	0.0141	3.57E-07	2.00E-01						11727.93
14.912	0.000	2.32E-08	-1.24E-08	0.0141	9.28E-09	5.21E-03						12145.84
15.212	0.000	4.16E-11	-2.22E-11	0.0141	1.66E-11	9.34E-06						12156.96
15.712	0.000	4.47E-14	-2.38E-14	0.0141	1.79E-14	1.00E-08						12156.97
16.212	0.000	1.07E-14	-5.71E-15	0.0141	4.28E-15	2.40E-09						12156.97
16.712	0.000	1.07E-14	-5.71E-15	0.0141	4.28E-15	2.40E-09						12156.97
17.462	0.000	1.07E-14	-5.71E-15	0.0141	4.28E-15	2.40E-09						12156.97
18.462	0.000	1.07E-14	-5.71E-15	0.0141	4.28E-15	2.40E-09						12156.97
19.462	0.000	1.07E-14	-5.71E-15	0.0141	4.28E-15	2.40E-09						12156.97
20.462	0.000	1.07E-14	-5.71E-15	0.0141	4.28E-15	2.40E-09						12156.97
21.962	0.000	1.07E-14	-5.71E-15	0.0141	4.28E-15	2.40E-09						12156.97
23.962	0.000	1.07E-14	-5.71E-15	0.0141	4.28E-15	2.40E-09						12156.97
26.462	0.000	1.07E-14	-5.71E-15	0.0141	4.28E-15	2.40E-09						12156.97
29.462	0.000	1.07E-14	-5.71E-15	0.0141	4.28E-15	2.40E-09						12156.97
32.962	0.000	1.07E-14	-5.71E-15	0.0141	4.28E-15	2.40E-09						12156.97
36.962	0.000	1.07E-14	-5.71E-15	0.0141	4.28E-15	2.40E-09						12156.97
40.962	0.000	1.07E-14	-5.71E-15	0.0141	4.28E-15	2.40E-09						12156.97
44.962	0.000	1.07E-14	-5.71E-15	0.0141	4.28E-15	2.40E-09						12156.97

RESULTS FOR YEAR: 16

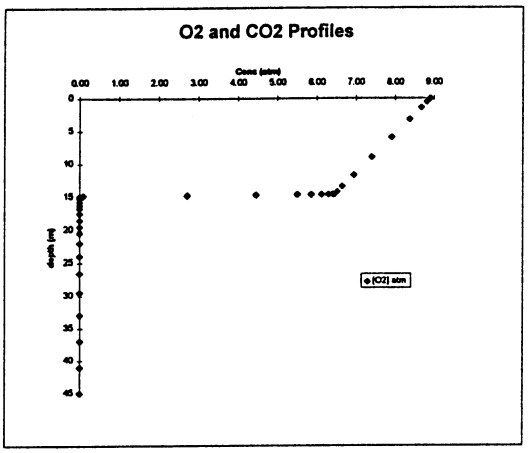

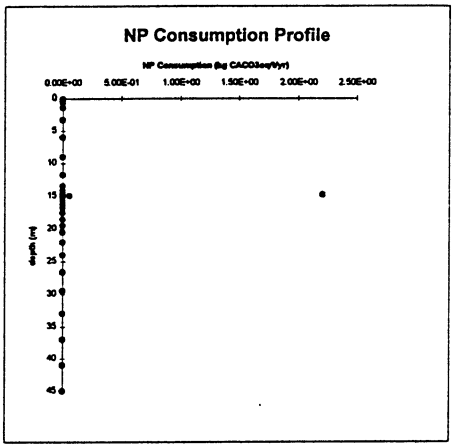

Flux in (mol/m²s)	1.01E-06
O_2 cons. (mol/m²s)	1.01E-06
Dpen (m)	15.462

t=16												
DEPTH (m)	CONC O2 (mol/m³)	O2 Cons (mol/m³/s)	CO2 Prod (mol/m³/s)	CONC CO2 (mol/m³)	mols O2 cons per m3 rock	NP consmptn kg CaCO3eq/t/yr						Sulf dens mol/m³
0.050	8.900	0.00E+00	0.00E+00	0.0141	0.00E+00	0.00E+00						0.00
0.225	8.871	0.00E+00	0.00E+00	0.0141	0.00E+00	0.00E+00						0.00
0.600	8.806	0.00E+00	0.00E+00	0.0141	0.00E+00	0.00E+00						0.00
1.400	8.673	0.00E+00	0.00E+00	0.0141	0.00E+00	0.00E+00						0.00
3.200	8.371	0.00E+00	0.00E+00	0.0141	0.00E+00	0.00E+00						0.00
5.950	7.909	0.00E+00	0.00E+00	0.0141	0.00E+00	0.00E+00						0.00
8.950	7.405	0.00E+00	0.00E+00	0.0141	0.00E+00	0.00E+00						0.00
11.700	6.944	0.00E+00	0.00E+00	0.0141	0.00E+00	0.00E+00						0.00
13.450	6.650	0.00E+00	0.00E+00	0.0141	0.00E+00	0.00E+00						0.00
14.200	6.524	0.00E+00	0.00E+00	0.0141	0.00E+00	0.00E+00						0.00
14.506	6.472	0.00E+00	0.00E+00	0.0141	0.00E+00	0.00E+00						0.00
14.590	6.458	0.00E+00	0.00E+00	0.0141	0.00E+00	0.00E+00						0.00
14.620	6.453	0.00E+00	0.00E+00	0.0141	0.00E+00	0.00E+00						0.00
14.628	6.452	0.00E+00	0.00E+00	0.0141	0.00E+00	0.00E+00						0.00
14.631	6.434	0.00E+00	0.00E+00	0.0141	0.00E+00	0.00E+00						0.00
14.632	6.399	0.00E+00	0.00E+00	0.0141	0.00E+00	0.00E+00						0.00
14.635	6.294	0.00E+00	0.00E+00	0.0141	0.00E+00	0.00E+00						0.00
14.640	6.120	0.00E+00	0.00E+00	0.0141	0.00E+00	0.00E+00						0.00
14.647	5.857	0.00E+00	0.00E+00	0.0141	0.00E+00	0.00E+00						0.00
14.657	5.508	0.00E+00	0.00E+00	0.0141	0.00E+00	0.00E+00						0.00
14.687	4.460	0.00E+00	0.00E+00	0.0141	0.00E+00	0.00E+00						0.00
14.737	2.713	0.00E+00	0.00E+00	0.0141	0.00E+00	0.00E+00						0.00
14.812	0.092	9.62E-06	-5.24E-06	0.0141	3.93E-06	2.21E+00						3095.05
14.912	0.002	2.55E-07	-1.38E-07	0.0141	1.02E-07	5.74E-02						11921.27
15.212	0.000	4.58E-10	-2.44E-10	0.0141	1.83E-10	1.03E-04						12156.56
15.712	0.000	4.92E-13	-2.63E-13	0.0141	1.97E-13	1.11E-07						12156.97
16.212	0.000	1.07E-14	-5.71E-15	0.0141	4.28E-15	2.40E-09						12156.97
16.712	0.000	1.07E-14	-5.71E-15	0.0141	4.28E-15	2.40E-09						12156.97
17.462	0.000	1.07E-14	-5.71E-15	0.0141	4.28E-15	2.40E-09						12156.97
18.462	0.000	1.07E-14	-5.71E-15	0.0141	4.28E-15	2.40E-09						12156.97
19.462	0.000	1.07E-14	-5.71E-15	0.0141	4.28E-15	2.40E-09						12156.97
20.462	0.000	1.07E-14	-5.71E-15	0.0141	4.28E-15	2.40E-09						12156.97
21.962	0.000	1.07E-14	-5.71E-15	0.0141	4.28E-15	2.40E-09						12156.97
23.962	0.000	1.07E-14	-5.71E-15	0.0141	4.28E-15	2.40E-09						12156.97
26.462	0.000	1.07E-14	-5.71E-15	0.0141	4.28E-15	2.40E-09						12156.97
29.462	0.000	1.07E-14	-5.71E-15	0.0141	4.28E-15	2.40E-09						12156.97
32.962	0.000	1.07E-14	-5.71E-15	0.0141	4.28E-15	2.40E-09						12156.97
36.962	0.000	1.07E-14	-5.71E-15	0.0141	4.28E-15	2.40E-09						12156.97
40.962	0.000	1.07E-14	-5.71E-15	0.0141	4.28E-15	2.40E-09						12156.97
44.962	0.000	1.07E-14	-5.71E-15	0.0141	4.28E-15	2.40E-09						12156.97

RESULTS FOR YEAR: 24

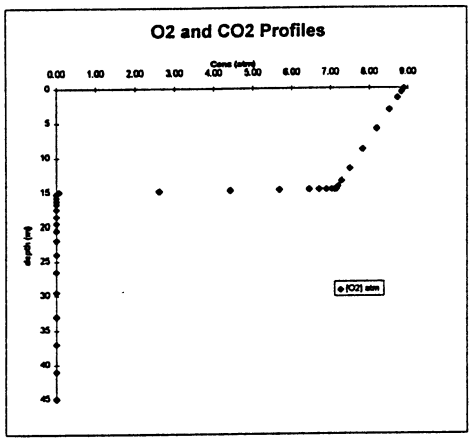

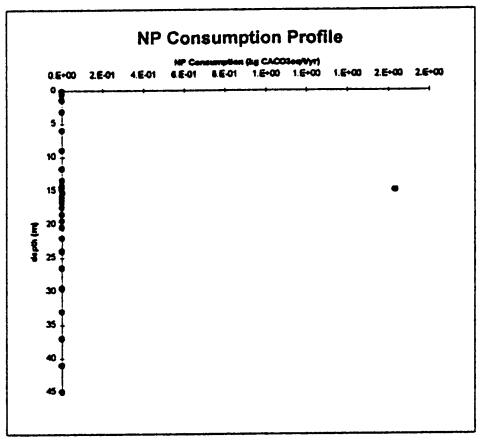

Flux in (mol/m²s)	7.23E-07
O_2 cons. (mol/m²s)	7.33E-07
Open (m)	15.962

t=24												
DEPTH (m)	CONC O2 (mol/m³)	O2 Cons (mol/m³/s)	CO2 Prod (mol/m³/s)	CONC CO2 (mol/m³)	mols O2 cons per m3 rock	NP consmptn kg CaCO3eq/t/yr						Sulf dens mol/m³
0.050	8.900	0.00E+00	0.00E+00	0.0141	0.00E+00	0.00E+00						0.00
0.225	8.879	0.00E+00	0.00E+00	0.0141	0.00E+00	0.00E+00						0.00
0.600	8.834	0.00E+00	0.00E+00	0.0141	0.00E+00	0.00E+00						0.00
1.400	8.737	0.00E+00	0.00E+00	0.0141	0.00E+00	0.00E+00						0.00
3.200	8.520	0.00E+00	0.00E+00	0.0141	0.00E+00	0.00E+00						0.00
5.950	8.189	0.00E+00	0.00E+00	0.0141	0.00E+00	0.00E+00						0.00
8.950	7.827	0.00E+00	0.00E+00	0.0141	0.00E+00	0.00E+00						0.00
11.700	7.496	0.00E+00	0.00E+00	0.0141	0.00E+00	0.00E+00						0.00
13.450	7.286	0.00E+00	0.00E+00	0.0141	0.00E+00	0.00E+00						0.00
14.200	7.195	0.00E+00	0.00E+00	0.0141	0.00E+00	0.00E+00						0.00
14.508	7.157	0.00E+00	0.00E+00	0.0141	0.00E+00	0.00E+00						0.00
14.590	7.147	0.00E+00	0.00E+00	0.0141	0.00E+00	0.00E+00						0.00
14.620	7.143	0.00E+00	0.00E+00	0.0141	0.00E+00	0.00E+00						0.00
14.628	7.142	0.00E+00	0.00E+00	0.0141	0.00E+00	0.00E+00						0.00
14.631	7.129	0.00E+00	0.00E+00	0.0141	0.00E+00	0.00E+00						0.00
14.632	7.103	0.00E+00	0.00E+00	0.0141	0.00E+00	0.00E+00						0.00
14.635	7.027	0.00E+00	0.00E+00	0.0141	0.00E+00	0.00E+00						0.00
14.640	6.898	0.00E+00	0.00E+00	0.0141	0.00E+00	0.00E+00						0.00
14.647	6.706	0.00E+00	0.00E+00	0.0141	0.00E+00	0.00E+00						0.00
14.657	6.450	0.00E+00	0.00E+00	0.0141	0.00E+00	0.00E+00						0.00
14.687	5.682	0.00E+00	0.00E+00	0.0141	0.00E+00	0.00E+00						0.00
14.737	4.416	0.00E+00	0.00E+00	0.0141	0.00E+00	0.00E+00						0.00
14.812	2.611	0.00E+00	0.00E+00	0.0141	0.00E+00	0.00E+00						0.00
14.912	0.068	7.27E-06	-3.88E-06	0.0141	2.91E-06	1.63E+00						7715.24
15.212	0.000	1.30E-08	-6.94E-09	0.0141	5.21E-09	2.93E-03						12149.04
15.712	0.000	1.40E-11	-7.47E-12	0.0141	5.60E-12	3.15E-06						12156.97
16.212	0.000	1.51E-14	-8.03E-15	0.0141	6.02E-15	3.38E-09						12156.97
16.712	0.000	1.07E-14	-5.71E-15	0.0141	4.28E-15	2.40E-09						12156.97
17.462	0.000	1.07E-14	-5.71E-15	0.0141	4.28E-15	2.40E-09						12156.97
18.462	0.000	1.07E-14	-5.71E-15	0.0141	4.28E-15	2.40E-09						12156.97
19.462	0.000	1.07E-14	-5.71E-15	0.0141	4.28E-15	2.40E-09						12156.97
20.462	0.000	1.07E-14	-5.71E-15	0.0141	4.28E-15	2.40E-09						12156.97
21.962	0.000	1.07E-14	-5.71E-15	0.0141	4.28E-15	2.40E-09						12156.97
23.962	0.000	1.07E-14	-5.71E-15	0.0141	4.28E-15	2.40E-09						12156.97
26.462	0.000	1.07E-14	-5.71E-15	0.0141	4.28E-15	2.40E-09						12156.97
29.462	0.000	1.07E-14	-5.71E-15	0.0141	4.28E-15	2.40E-09						12156.97
32.962	0.000	1.07E-14	-5.71E-15	0.0141	4.28E-15	2.40E-09						12156.97
36.962	0.000	1.07E-14	-5.71E-15	0.0141	4.28E-15	2.40E-09						12156.97
40.962	0.000	1.07E-14	-5.71E-15	0.0141	4.28E-15	2.40E-09						12156.97
44.962	0.000	1.07E-14	-5.71E-15	0.0141	4.28E-15	2.40E-09						12156.97

RESULTS FOR YEAR: 32

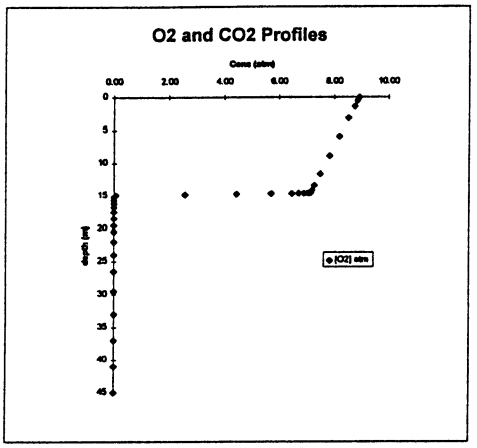

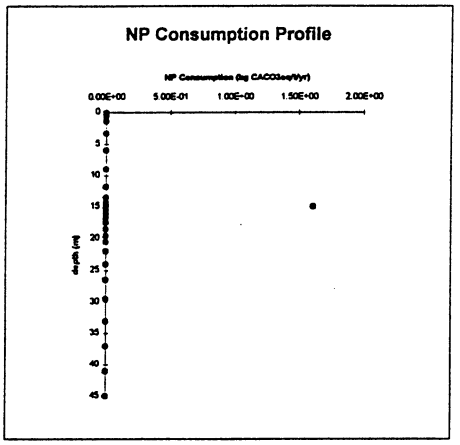

Flux in (mol/m²s)	7.23E-07
O_2 cons. (mol/m²s)	7.23E-07
Dpen (m)	15.962

t=32												
DEPTH (m)	CONC O2 (mol/m³)	O2 Cons (mol/m³/s)	CO2 Prod (mol/m³/s)	CONC CO2 (mol/m³)	mols O2 cons per m3 rock	NP consmptn kg CaCO3eq/t/yr						Sulf dens mol/m³
0.050	8.900	0.00E+00	0.00E+00	0.0141	0.00E+00	0.00E+00						0.00
0.225	8.879	0.00E+00	0.00E+00	0.0141	0.00E+00	0.00E+00						0.00
0.600	8.834	0.00E+00	0.00E+00	0.0141	0.00E+00	0.00E+00						0.00
1.400	8.737	0.00E+00	0.00E+00	0.0141	0.00E+00	0.00E+00						0.00
3.200	8.520	0.00E+00	0.00E+00	0.0141	0.00E+00	0.00E+00						0.00
5.950	8.189	0.00E+00	0.00E+00	0.0141	0.00E+00	0.00E+00						0.00
8.950	7.827	0.00E+00	0.00E+00	0.0141	0.00E+00	0.00E+00						0.00
11.700	7.495	0.00E+00	0.00E+00	0.0141	0.00E+00	0.00E+00						0.00
13.450	7.284	0.00E+00	0.00E+00	0.0141	0.00E+00	0.00E+00						0.00
14.200	7.194	0.00E+00	0.00E+00	0.0141	0.00E+00	0.00E+00						0.00
14.508	7.157	0.00E+00	0.00E+00	0.0141	0.00E+00	0.00E+00						0.00
14.590	7.147	0.00E+00	0.00E+00	0.0141	0.00E+00	0.00E+00						0.00
14.620	7.143	0.00E+00	0.00E+00	0.0141	0.00E+00	0.00E+00						0.00
14.628	7.142	0.00E+00	0.00E+00	0.0141	0.00E+00	0.00E+00						0.00
14.631	7.129	0.00E+00	0.00E+00	0.0141	0.00E+00	0.00E+00						0.00
14.632	7.104	0.00E+00	0.00E+00	0.0141	0.00E+00	0.00E+00						0.00
14.635	7.029	0.00E+00	0.00E+00	0.0141	0.00E+00	0.00E+00						0.00
14.640	6.904	0.00E+00	0.00E+00	0.0141	0.00E+00	0.00E+00						0.00
14.647	6.716	0.00E+00	0.00E+00	0.0141	0.00E+00	0.00E+00						0.00
14.657	6.465	0.00E+00	0.00E+00	0.0141	0.00E+00	0.00E+00						0.00
14.687	5.712	0.00E+00	0.00E+00	0.0141	0.00E+00	0.00E+00						0.00
14.737	4.458	0.00E+00	0.00E+00	0.0141	0.00E+00	0.00E+00						0.00
14.812	2.576	0.00E+00	0.00E+00	0.0141	0.00E+00	0.00E+00						0.00
14.912	0.067	7.17E-06	-3.82E-06	0.0141	2.87E-06	1.61E+00						1376.40
15.212	0.000	1.28E-08	-6.85E-09	0.0141	5.14E-09	2.89E-03						12137.68
15.712	0.000	1.38E-11	-7.37E-12	0.0141	5.53E-12	3.10E-06						12156.96
16.212	0.000	1.49E-14	-7.93E-15	0.0141	5.94E-15	3.34E-09						12156.97
16.712	0.000	1.07E-14	-5.71E-15	0.0141	4.28E-15	2.40E-09						12156.97
17.462	0.000	1.07E-14	-5.71E-15	0.0141	4.28E-15	2.40E-09						12156.97
18.462	0.000	1.07E-14	-5.71E-15	0.0141	4.28E-15	2.40E-09						12156.97
19.462	0.000	1.07E-14	-5.71E-15	0.0141	4.28E-15	2.40E-09						12156.97
20.462	0.000	1.07E-14	-5.71E-15	0.0141	4.28E-15	2.40E-09						12156.97
21.962	0.000	1.07E-14	-5.71E-15	0.0141	4.28E-15	2.40E-09						12156.97
23.962	0.000	1.07E-14	-5.71E-15	0.0141	4.28E-15	2.40E-09						12156.97
26.462	0.000	1.07E-14	-5.71E-15	0.0141	4.28E-15	2.40E-09						12156.97
29.462	0.000	1.07E-14	-5.71E-15	0.0141	4.28E-15	2.40E-09						12156.97
32.962	0.000	1.07E-14	-5.71E-15	0.0141	4.28E-15	2.40E-09						12156.97
36.962	0.000	1.07E-14	-5.71E-15	0.0141	4.28E-15	2.40E-09						12156.97
40.962	0.000	1.07E-14	-5.71E-15	0.0141	4.28E-15	2.40E-09						12156.97
44.962	0.000	1.07E-14	-5.71E-15	0.0141	4.28E-15	2.40E-09						12156.97

APPENDIX A6
Run 2B3, Cut and Fill

COUPLED $O_2/CO_2/Mg/SO_4/Ca$ MODEL

OXYDIFF V2.0

MODEL DETAILS

Filename	BF_CS2b2
Date	27/11/1996
Description:	Steady State Model Of Crandon Cut and Fill Placed Cemented Backfill Tailings
	Part 2 (year 1 to 32)
	First Order Model

INPUT PARAMETERS

Finite Difference Parameters

nodes x	1
nodes y	40
time periods	7
init delt (s)	0.01
[O2] at surface (mol/m³)	8.9
[CO2] at surface (mol/m³))	0.0141

Model Options

CO2 OPTION	0
FES2 OPTION	1
O2 OPTION	1

Geochemical Options

Infiltration (m/s)	1.10E-09
Infiltration Coefficient	1.00
Kgypsum	-
Infiltration (m/s)	1.10E-09
Fraction Flow Paths (G)	1.00

Diffusion Parameters

Dw (m2/s)	2.20E-09
Da (m2/s)	1.80E-05
τ	0.273
α	3.28
H	33.9

OUTPUT TIMES

time (s)	time (y)	Output col
1.6E+07	1	1
6.3E+07	2	6
1.3E+08	4	11
2.5E+08	8	16
5.0E+08	16	21
7.6E+08	24	26
1.0E+09	32	31

FES2 OPTION
0 - No FES2 DEPLETION
1 - ALLOW FES2 DEPLETION

CO2 OPTION:
0 - No CO2 Coupling
1 - CO2 Coupling

O2 OPTION
0 - HALF ORDER REACTION
1 - FIRST ORDER REACTION
2 - MIXED FIRST ORDER / ZERO ORDER
3 - ZERO ORDER SOLUTION

TORTUOSITY

Rockfill	τ	3
Cemented Tailings	τ	10

MODEL INPUTS

Material	DEPTH (m)	Depth (ft)	Cell Sizes (m)	r (s-1)	Porosity	Bulk Dens. (tonnes m^{-3})	Sat. (%)	SulfDens (mol/m^3)	Diff Coeff [1] (m2/s)	Diff Coeff [2] (m2/s)	$[O_2]_{sat}$ (mol/m^3)	$[CO_2]_{sat}$ (mol/m^3)
Waste Rock	0.050	0.164	0.1	0.00E+00	0.40	1.9	15%	0	6.00E-06	6.00E-06	8.89	1.41E-02
Waste Rock	0.225	0.738	0.25	0.00E+00	0.40	1.9	15%	0	6.00E-06	6.00E-06	8.89	1.41E-02
Waste Rock	0.600	1.969	0.5	0.00E+00	0.40	1.9	15%	0	6.00E-06	6.00E-06	8.89	1.41E-02
Waste Rock	1.400	4.593	1.1	0.00E+00	0.40	1.9	15%	0	6.00E-06	6.00E-06	8.89	1.41E-02
Waste Rock	3.200	10.499	2.5	0.00E+00	0.40	1.9	15%	0	6.00E-06	6.00E-06	8.89	1.41E-02
Waste Rock	5.950	19.521	3	0.00E+00	0.40	1.9	15%	0	6.00E-06	6.00E-06	8.89	1.41E-02
Waste Rock	8.950	29.364	3	0.00E+00	0.40	1.9	15%	0	6.00E-06	6.00E-06	8.89	1.41E-02
Waste Rock	11.700	38.386	2.5	0.00E+00	0.40	1.9	15%	0	6.00E-06	6.00E-06	8.89	1.41E-02
Waste Rock	13.450	44.127	1	0.00E+00	0.40	1.9	15%	0	6.00E-06	6.00E-06	8.89	1.41E-02
Waste Rock	14.200	46.588	0.5	0.00E+00	0.40	1.9	15%	0	6.00E-06	6.00E-06	8.89	1.41E-02
Waste Rock	14.508	47.597	0.115	0.00E+00	0.40	1.9	15%	0	6.00E-06	6.00E-06	8.89	1.41E-02
Waste Rock	14.590	47.867	0.05	0.00E+00	0.40	1.9	15%	0	6.00E-06	6.00E-06	8.89	1.41E-02
Waste Rock	14.620	47.966	0.01	0.00E+00	0.40	1.9	15%	0	6.00E-06	6.00E-06	8.89	1.41E-02
Waste Rock	14.628	47.990	0.005	0.00E+00	0.40	1.9	15%	0	6.00E-06	6.00E-06	8.89	1.41E-02
Tailings Backfill	14.631	48.000	0.001	1.07E-04	0.40	3.0	15%	12187	2.88E-07	2.88E-07	8.89	1.41E-02
Tailings Backfill	14.632	48.004	0.001	1.07E-04	0.40	3.0	15%	12187	2.88E-07	2.88E-07	8.89	1.41E-02
Tailings Backfill	14.635	48.013	0.005	1.07E-04	0.40	3.0	15%	12187	2.88E-07	2.88E-07	8.89	1.41E-02
Tailings Backfill	14.640	48.030	0.005	1.07E-04	0.40	3.0	15%	12187	2.88E-07	2.88E-07	8.89	1.41E-02
Tailings Backfill	14.647	48.054	0.01	1.07E-04	0.40	3.0	15%	12187	2.88E-07	2.88E-07	8.89	1.41E-02
Tailings Backfill	14.657	48.087	0.01	1.07E-04	0.40	3.0	15%	12187	2.88E-07	2.88E-07	8.89	1.41E-02
Tailings Backfill	14.667	48.186	0.05	1.07E-04	0.40	3.0	15%	12187	2.88E-07	2.88E-07	8.89	1.41E-02
Tailings Backfill	14.737	48.350	0.05	1.07E-04	0.40	3.0	15%	12187	2.88E-07	2.88E-07	8.89	1.41E-02
Tailings Backfill	14.812	48.596	0.1	1.07E-04	0.40	3.0	15%	12187	2.88E-07	2.88E-07	8.89	1.41E-02
Tailings Backfill	14.912	48.924	0.1	1.07E-04	0.40	3.0	15%	12187	2.88E-07	2.88E-07	8.89	1.41E-02
Tailings Backfill	15.212	49.906	0.5	1.07E-04	0.40	3.0	15%	12187	2.88E-07	2.88E-07	8.89	1.41E-02
Tailings Backfill	15.712	51.549	0.5	1.07E-04	0.40	3.0	15%	12187	2.88E-07	2.88E-07	8.89	1.41E-02
Tailings Backfill	16.212	53.189	0.5	1.07E-04	0.40	3.0	15%	12187	2.88E-07	2.88E-07	8.89	1.41E-02
Tailings Backfill	16.712	54.829	0.5	1.07E-04	0.40	3.0	15%	12187	2.88E-07	2.88E-07	8.89	1.41E-02
Tailings Backfill	17.462	57.290	1	1.07E-04	0.40	3.0	15%	12187	2.88E-07	2.88E-07	8.89	1.41E-02
Tailings Backfill	18.462	60.571	1	1.07E-04	0.40	3.0	15%	12187	2.88E-07	2.88E-07	8.89	1.41E-02
Tailings Backfill	19.462	63.852	1	1.07E-04	0.40	3.0	15%	12187	2.88E-07	2.88E-07	8.89	1.41E-02
Tailings Backfill	20.462	67.133	1	1.07E-04	0.40	3.0	15%	12187	2.88E-07	2.88E-07	8.89	1.41E-02
Tailings Backfill	21.962	72.054	2	1.07E-04	0.40	3.0	15%	12187	2.88E-07	2.88E-07	8.89	1.41E-02
Tailings Backfill	23.962	78.615	2	1.07E-04	0.40	3.0	15%	12187	2.88E-07	2.88E-07	8.89	1.41E-02
Tailings Backfill	26.462	86.818	3	1.07E-04	0.40	3.0	15%	12187	2.88E-07	2.88E-07	8.89	1.41E-02
Tailings Backfill	29.462	96.660	3	1.07E-04	0.40	3.0	15%	12187	2.88E-07	2.88E-07	8.89	1.41E-02
Tailings Backfill	32.962	108.143	4	1.07E-04	0.40	3.0	15%	12187	2.88E-07	2.88E-07	8.89	1.41E-02
Tailings Backfill	36.962	121.266	4	1.07E-04	0.40	3.0	15%	12187	2.88E-07	2.88E-07	8.89	1.41E-02
Tailings Backfill	40.962	134.390	4	1.07E-04	0.40	3.0	15%	12187	2.88E-07	2.88E-07	8.89	1.41E-02
Tailings Backfill	44.962	147.513	4	1.07E-04	0.40	3.0	15%	12187	2.88E-07	2.88E-07	8.89	1.41E-02

1. Diff Coefficient Based on Erberling, B., R.V.Nicholson, E.J.Reardon and P.Tibble, Evaluation of sulphide oxidation rates. Nordic Hydrology, 24(5), 323-338, 1993.
2. Diff Coefficient Based on Reardon, E.J. and P.M. Moddle, Gas Diffusion Coefficient Measurements on Uranium Mill Tailings: Implications to Cover Layer Design. Uranium, 2, 111-131,1985.

RESULTS FOR YEAR: 1

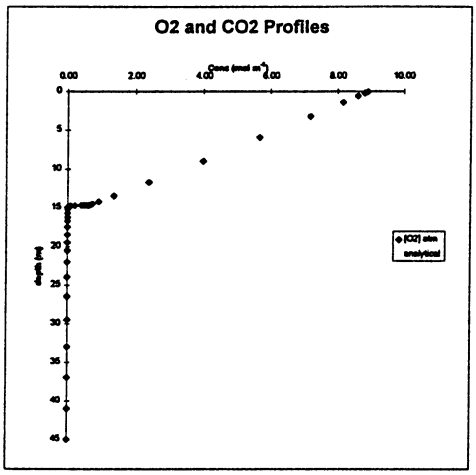

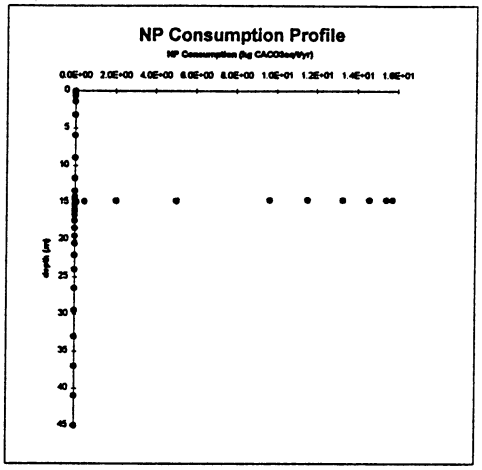

Flux in (mol/m²s)	3.24E-06
O_2 cons. (mol/m²s)	3.56E-06
Dpen (m)	15.962

t=1												
DEPTH (m)	CONC O2 (mol/m³)	O2 Cons (mol/m³/s)	CO2 Prod (mol/m³/s)	CONC CO2 (mol/m³)	mols O2 cons per m³ material	NP consmptn kg CaCO3eq/t/yr						Sulf dens mol/m³
0.050	8.900	0.00E+00	0.00E+00	0.0141	0.00E+00	0.00E+00						0.00
0.225	8.805	0.00E+00	0.00E+00	0.0141	0.00E+00	0.00E+00						0.00
0.600	8.603	0.00E+00	0.00E+00	0.0141	0.00E+00	0.00E+00						0.00
1.400	8.170	0.00E+00	0.00E+00	0.0141	0.00E+00	0.00E+00						0.00
3.200	7.193	0.00E+00	0.00E+00	0.0141	0.00E+00	0.00E+00						0.00
5.950	5.681	0.00E+00	0.00E+00	0.0141	0.00E+00	0.00E+00						0.00
8.950	3.987	0.00E+00	0.00E+00	0.0141	0.00E+00	0.00E+00						0.00
11.700	2.392	0.00E+00	0.00E+00	0.0141	0.00E+00	0.00E+00						0.00
13.450	1.361	0.00E+00	0.00E+00	0.0141	0.00E+00	0.00E+00						0.00
14.200	0.917	0.00E+00	0.00E+00	0.0141	0.00E+00	0.00E+00						0.00
14.508	0.735	0.00E+00	0.00E+00	0.0141	0.00E+00	0.00E+00						0.00
14.590	0.686	0.00E+00	0.00E+00	0.0141	0.00E+00	0.00E+00						0.00
14.620	0.668	0.00E+00	0.00E+00	0.0141	0.00E+00	0.00E+00						0.00
14.628	0.664	0.00E+00	0.00E+00	0.0141	0.00E+00	0.00E+00						0.00
14.631	0.656	7.02E-05	-3.74E-05	0.0141	2.81E-05	1.58E+01						6061.04
14.632	0.644	6.89E-05	-3.67E-05	0.0141	2.76E-05	1.55E+01						6192.94
14.635	0.608	6.51E-05	-3.47E-05	0.0141	2.60E-05	1.46E+01						6522.04
14.640	0.555	5.94E-05	-3.17E-05	0.0141	2.37E-05	1.33E+01						7018.29
14.647	0.482	5.16E-05	-2.75E-05	0.0141	2.06E-05	1.16E+01						7691.22
14.657	0.403	4.31E-05	-2.30E-05	0.0141	1.73E-05	9.69E+00						8422.87
14.667	0.211	2.26E-05	-1.20E-05	0.0141	9.03E-06	5.07E+00						10202.42
14.737	0.086	9.24E-06	-4.93E-06	0.0141	3.70E-06	2.08E+00						11356.43
14.812	0.020	2.11E-06	-1.12E-06	0.0141	8.43E-07	4.74E-01						11974.29
14.912	0.004	4.19E-07	-2.23E-07	0.0141	1.67E-07	9.41E-02						12120.70
15.212	0.000	7.31E-09	-3.90E-09	0.0141	2.93E-09	1.64E-03						12156.33
15.712	0.000	7.72E-11	-4.12E-11	0.0141	3.09E-11	1.73E-05						12156.97
16.212	0.000	8.15E-13	-4.35E-13	0.0141	3.26E-13	1.83E-07						12156.97
16.712	0.000	1.07E-14	-5.71E-15	0.0141	4.28E-15	2.40E-09						12156.97
17.462	0.000	1.07E-14	-5.71E-15	0.0141	4.28E-15	2.40E-09						12156.97
18.462	0.000	1.07E-14	-5.71E-15	0.0141	4.28E-15	2.40E-09						12156.97
19.462	0.000	1.07E-14	-5.71E-15	0.0141	4.28E-15	2.40E-09						12156.97
20.462	0.000	1.07E-14	-5.71E-15	0.0141	4.28E-15	2.40E-09						12156.97
21.962	0.000	1.07E-14	-5.71E-15	0.0141	4.28E-15	2.40E-09						12156.97
23.962	0.000	1.07E-14	-5.71E-15	0.0141	4.28E-15	2.40E-09						12156.97
26.462	0.000	1.07E-14	-5.71E-15	0.0141	4.28E-15	2.40E-09						12156.97
29.462	0.000	1.07E-14	-5.71E-15	0.0141	4.28E-15	2.40E-09						12156.97
32.962	0.000	1.07E-14	-5.71E-15	0.0141	4.28E-15	2.40E-09						12156.97
36.962	0.000	1.07E-14	-5.71E-15	0.0141	4.28E-15	2.40E-09						12156.97
40.962	0.000	1.07E-14	-5.71E-15	0.0141	4.28E-15	2.40E-09						12156.97
44.962	0.000	1.07E-14	-5.71E-15	0.0141	4.28E-15	2.40E-09						12156.97

RESULTS FOR YEAR: 2

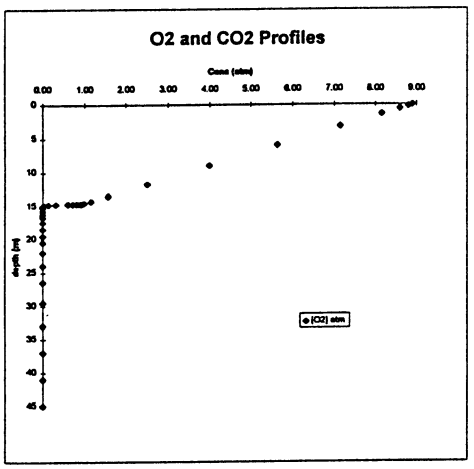

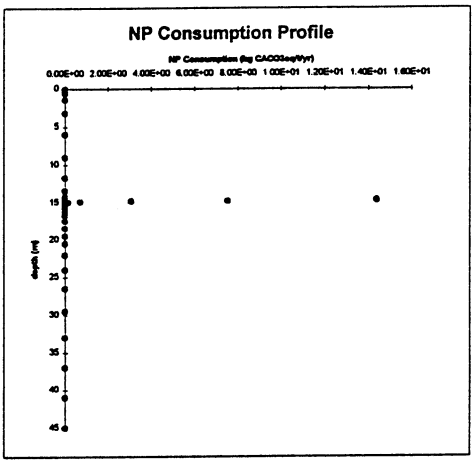

Flux in (mol/m²s)	3.33E-06
O_2 cons. (mol/m²s)	3.38E-06
Dpen (m)	15.962

t=2												
DEPTH (m)	CONC O2 (mol/m³)	O2 Cons (mol/m³/s)	CO2 Prod (mol/m³/s)	CONC CO2 (mol/m³)	mols O2 cons per m3 rock	NP consmptn kg CaCO3eq/t/yr						Sulf dens mol/m³
0.050	8.900	0.00E+00	0.00E+00	0.0141	0.00E+00	0.00E+00						0.00
0.225	8.803	0.00E+00	0.00E+00	0.0141	0.00E+00	0.00E+00						0.00
0.600	8.595	0.00E+00	0.00E+00	0.0141	0.00E+00	0.00E+00						0.00
1.400	8.151	0.00E+00	0.00E+00	0.0141	0.00E+00	0.00E+00						0.00
3.200	7.153	0.00E+00	0.00E+00	0.0141	0.00E+00	0.00E+00						0.00
5.950	5.634	0.00E+00	0.00E+00	0.0141	0.00E+00	0.00E+00						0.00
8.950	3.992	0.00E+00	0.00E+00	0.0141	0.00E+00	0.00E+00						0.00
11.700	2.509	0.00E+00	0.00E+00	0.0141	0.00E+00	0.00E+00						0.00
13.450	1.568	0.00E+00	0.00E+00	0.0141	0.00E+00	0.00E+00						0.00
14.200	1.157	0.00E+00	0.00E+00	0.0141	0.00E+00	0.00E+00						0.00
14.508	0.985	0.00E+00	0.00E+00	0.0141	0.00E+00	0.00E+00						0.00
14.590	0.938	0.00E+00	0.00E+00	0.0141	0.00E+00	0.00E+00						0.00
14.620	0.922	0.00E+00	0.00E+00	0.0141	0.00E+00	0.00E+00						0.00
14.628	0.917	0.00E+00	0.00E+00	0.0141	0.00E+00	0.00E+00						0.00
14.631	0.910	0.00E+00	0.00E+00	0.0141	0.00E+00	0.00E+00						0.00
14.632	0.898	0.00E+00	0.00E+00	0.0141	0.00E+00	0.00E+00						0.00
14.635	0.863	0.00E+00	0.00E+00	0.0141	0.00E+00	0.00E+00						0.00
14.640	0.804	0.00E+00	0.00E+00	0.0141	0.00E+00	0.00E+00						0.00
14.647	0.716	0.00E+00	0.00E+00	0.0141	0.00E+00	0.00E+00						0.00
14.657	0.599	6.41E-05	-3.42E-05	0.0141	2.56E-05	1.44E+01						635.47
14.687	0.313	3.35E-05	-1.79E-05	0.0141	1.34E-05	7.53E+00						6127.48
14.737	0.128	1.37E-05	-7.32E-06	0.0141	5.49E-06	3.09E+00						9688.06
14.812	0.029	3.13E-06	-1.67E-06	0.0141	1.25E-06	7.04E-01						11593.78
14.912	0.006	6.22E-07	-3.32E-07	0.0141	2.49E-07	1.40E-01						12045.19
15.212	0.000	1.09E-08	-5.80E-09	0.0141	4.35E-09	2.44E-03						12155.02
15.712	0.000	1.15E-10	-6.12E-11	0.0141	4.59E-11	2.58E-05						12156.96
16.212	0.000	1.21E-12	-6.46E-13	0.0141	4.85E-13	2.72E-07						12156.97
16.712	0.000	1.28E-14	-6.85E-15	0.0141	5.13E-15	2.88E-09						12156.97
17.462	0.000	1.07E-14	-5.71E-15	0.0141	4.28E-15	2.40E-09						12156.97
18.462	0.000	1.07E-14	-5.71E-15	0.0141	4.28E-15	2.40E-09						12156.97
19.462	0.000	1.07E-14	-5.71E-15	0.0141	4.28E-15	2.40E-09						12156.97
20.462	0.000	1.07E-14	-5.71E-15	0.0141	4.28E-15	2.40E-09						12156.97
21.962	0.000	1.07E-14	-5.71E-15	0.0141	4.28E-15	2.40E-09						12156.97
23.962	0.000	1.07E-14	-5.71E-15	0.0141	4.28E-15	2.40E-09						12156.97
26.462	0.000	1.07E-14	-5.71E-15	0.0141	4.28E-15	2.40E-09						12156.97
29.462	0.000	1.07E-14	-5.71E-15	0.0141	4.28E-15	2.40E-09						12156.97
32.962	0.000	1.07E-14	-5.71E-15	0.0141	4.28E-15	2.40E-09						12156.97
36.962	0.000	1.07E-14	-5.71E-15	0.0141	4.28E-15	2.40E-09						12156.97
40.962	0.000	1.07E-14	-5.71E-15	0.0141	4.28E-15	2.40E-09						12156.97
44.962	0.000	1.07E-14	-5.71E-15	0.0141	4.28E-15	2.40E-09						12156.97

RESULTS FOR YEAR: 4

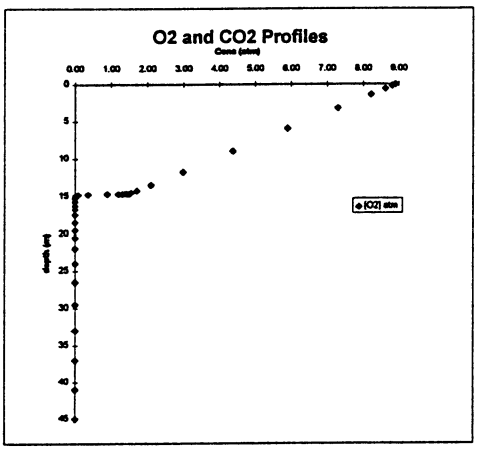

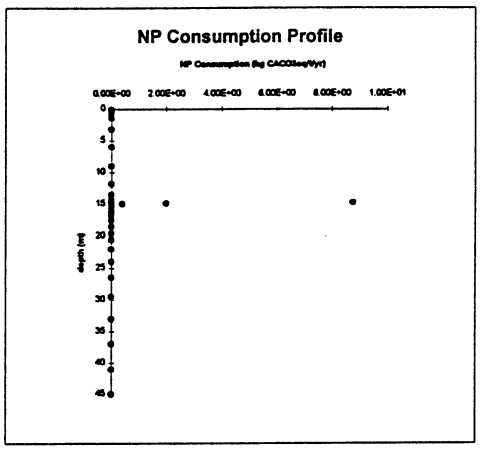

Flux in (mol/m²s)	3.05E-06
O_2 cons. (mol/m²s)	3.03E-06
Dpen (m)	15.962

t=4												
DEPTH (m)	CONC O2 (mol/m³)	O2 Cons (mol/m³/s)	CO2 Prod (mol/m³/s)	CONC CO2 (mol/m³)	mols O2 cons per m3 rock	NP consmptn kg CaCO3eq/t/yr						Sulf dens mol/m³
0.050	8.900	0.00E+00	0.00E+00	0.0141	0.00E+00	0.00E+00						0.00
0.225	8.811	0.00E+00	0.00E+00	0.0141	0.00E+00	0.00E+00						0.00
0.600	8.620	0.00E+00	0.00E+00	0.0141	0.00E+00	0.00E+00						0.00
1.400	8.214	0.00E+00	0.00E+00	0.0141	0.00E+00	0.00E+00						0.00
3.200	7.298	0.00E+00	0.00E+00	0.0141	0.00E+00	0.00E+00						0.00
5.950	5.900	0.00E+00	0.00E+00	0.0141	0.00E+00	0.00E+00						0.00
8.950	4.377	0.00E+00	0.00E+00	0.0141	0.00E+00	0.00E+00						0.00
11.700	2.985	0.00E+00	0.00E+00	0.0141	0.00E+00	0.00E+00						0.00
13.450	2.088	0.00E+00	0.00E+00	0.0141	0.00E+00	0.00E+00						0.00
14.200	1.702	0.00E+00	0.00E+00	0.0141	0.00E+00	0.00E+00						0.00
14.508	1.546	0.00E+00	0.00E+00	0.0141	0.00E+00	0.00E+00						0.00
14.590	1.504	0.00E+00	0.00E+00	0.0141	0.00E+00	0.00E+00						0.00
14.620	1.489	0.00E+00	0.00E+00	0.0141	0.00E+00	0.00E+00						0.00
14.628	1.485	0.00E+00	0.00E+00	0.0141	0.00E+00	0.00E+00						0.00
14.631	1.478	0.00E+00	0.00E+00	0.0141	0.00E+00	0.00E+00						0.00
14.632	1.468	0.00E+00	0.00E+00	0.0141	0.00E+00	0.00E+00						0.00
14.635	1.437	0.00E+00	0.00E+00	0.0141	0.00E+00	0.00E+00						0.00
14.640	1.384	0.00E+00	0.00E+00	0.0141	0.00E+00	0.00E+00						0.00
14.647	1.308	0.00E+00	0.00E+00	0.0141	0.00E+00	0.00E+00						0.00
14.657	1.202	0.00E+00	0.00E+00	0.0141	0.00E+00	0.00E+00						0.00
14.687	0.890	0.00E+00	0.00E+00	0.0141	0.00E+00	0.00E+00						0.00
14.737	0.364	3.90E-05	-2.08E-05	0.0141	1.56E-05	8.76E+00						4470.36
14.812	0.063	8.89E-06	-4.74E-06	0.0141	3.56E-06	2.00E+00						10403.90
14.912	0.016	1.77E-06	-9.42E-07	0.0141	7.06E-07	3.97E-01						11809.08
15.212	0.000	3.06E-08	-1.64E-08	0.0141	1.23E-08	6.93E-03						12150.91
15.712	0.000	3.25E-10	-1.74E-10	0.0141	1.30E-10	7.31E-05						12156.93
16.212	0.000	3.43E-12	-1.83E-12	0.0141	1.37E-12	7.72E-07						12156.97
16.712	0.000	3.64E-14	-1.94E-14	0.0141	1.45E-14	8.17E-09						12156.97
17.462	0.000	1.07E-14	-5.71E-15	0.0141	4.28E-15	2.40E-09						12156.97
18.462	0.000	1.07E-14	-5.71E-15	0.0141	4.28E-15	2.40E-09						12156.97
19.462	0.000	1.07E-14	-5.71E-15	0.0141	4.28E-15	2.40E-09						12156.97
20.462	0.000	1.07E-14	-5.71E-15	0.0141	4.28E-15	2.40E-09						12156.97
21.962	0.000	1.07E-14	-5.71E-15	0.0141	4.28E-15	2.40E-09						12156.97
23.962	0.000	1.07E-14	-5.71E-15	0.0141	4.28E-15	2.40E-09						12156.97
26.462	0.000	1.07E-14	-5.71E-15	0.0141	4.28E-15	2.40E-09						12156.97
29.462	0.000	1.07E-14	-5.71E-15	0.0141	4.28E-15	2.40E-09						12156.97
32.962	0.000	1.07E-14	-5.71E-15	0.0141	4.28E-15	2.40E-09						12156.97
36.962	0.000	1.07E-14	-5.71E-15	0.0141	4.28E-15	2.40E-09						12156.97
40.962	0.000	1.07E-14	-5.71E-15	0.0141	4.28E-15	2.40E-09						12156.97
44.962	0.000	1.07E-14	-5.71E-15	0.0141	4.28E-15	2.40E-09						12156.97

RESULTS FOR YEAR: 8

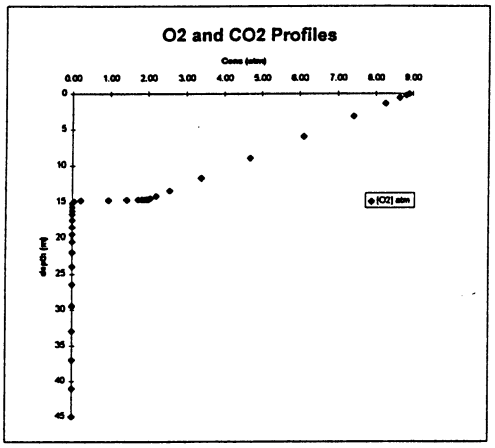

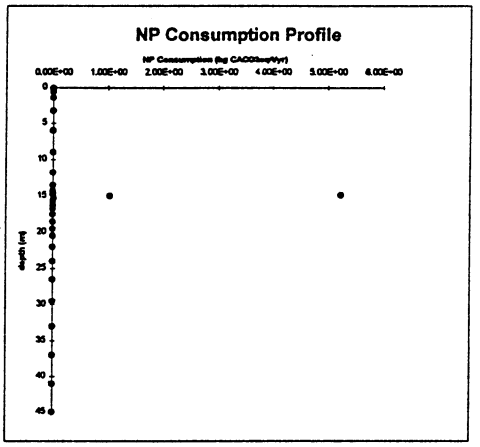

Flux in (mol/m²s)	2.84E-06
O_2 cons. (mol/m²s)	2.83E-06
Dpen (m)	15.962

t=8												
DEPTH (m)	CONC O2 (mol/m³)	O2 Cons (mol/m²/s)	CO2 Prod (mol/m²/s)	CONC CO2 (mol/m³)	mols O2 cons per m3 rock	NP consmptn kg CaCO3eq/t/yr						Sulf dens mol/m³
0.050	8.900	0.00E+00	0.00E+00	0.0141	0.00E+00	0.00E+00						0.00
0.225	8.817	0.00E+00	0.00E+00	0.0141	0.00E+00	0.00E+00						0.00
0.600	8.640	0.00E+00	0.00E+00	0.0141	0.00E+00	0.00E+00						0.00
1.400	8.282	0.00E+00	0.00E+00	0.0141	0.00E+00	0.00E+00						0.00
3.200	7.411	0.00E+00	0.00E+00	0.0141	0.00E+00	0.00E+00						0.00
5.950	6.111	0.00E+00	0.00E+00	0.0141	0.00E+00	0.00E+00						0.00
8.950	4.693	0.00E+00	0.00E+00	0.0141	0.00E+00	0.00E+00						0.00
11.700	3.393	0.00E+00	0.00E+00	0.0141	0.00E+00	0.00E+00						0.00
13.450	2.567	0.00E+00	0.00E+00	0.0141	0.00E+00	0.00E+00						0.00
14.200	2.211	0.00E+00	0.00E+00	0.0141	0.00E+00	0.00E+00						0.00
14.508	2.064	0.00E+00	0.00E+00	0.0141	0.00E+00	0.00E+00						0.00
14.590	2.025	0.00E+00	0.00E+00	0.0141	0.00E+00	0.00E+00						0.00
14.620	2.011	0.00E+00	0.00E+00	0.0141	0.00E+00	0.00E+00						0.00
14.628	2.007	0.00E+00	0.00E+00	0.0141	0.00E+00	0.00E+00						0.00
14.631	2.001	0.00E+00	0.00E+00	0.0141	0.00E+00	0.00E+00						0.00
14.632	1.991	0.00E+00	0.00E+00	0.0141	0.00E+00	0.00E+00						0.00
14.635	1.962	0.00E+00	0.00E+00	0.0141	0.00E+00	0.00E+00						0.00
14.640	1.912	0.00E+00	0.00E+00	0.0141	0.00E+00	0.00E+00						0.00
14.647	1.838	0.00E+00	0.00E+00	0.0141	0.00E+00	0.00E+00						0.00
14.657	1.740	0.00E+00	0.00E+00	0.0141	0.00E+00	0.00E+00						0.00
14.687	1.444	0.00E+00	0.00E+00	0.0141	0.00E+00	0.00E+00						0.00
14.737	0.955	0.00E+00	0.00E+00	0.0141	0.00E+00	0.00E+00						0.00
14.812	0.218	2.33E-05	-1.24E-05	0.0141	9.33E-06	5.24E+00						1680.05
14.912	0.043	4.63E-06	-2.47E-06	0.0141	1.85E-06	1.04E+00						10077.67
15.212	0.001	8.08E-08	-4.31E-08	0.0141	3.23E-08	1.82E-02						12120.67
15.712	0.000	8.53E-10	-4.55E-10	0.0141	3.41E-10	1.92E-04						12156.61
16.212	0.000	9.00E-12	-4.80E-12	0.0141	3.60E-12	2.02E-06						12156.97
16.712	0.000	9.53E-14	-5.08E-14	0.0141	3.81E-14	2.14E-08						12156.97
17.462	0.000	1.07E-14	-5.71E-15	0.0141	4.28E-15	2.40E-09						12156.97
18.462	0.000	1.07E-14	-5.71E-15	0.0141	4.28E-15	2.40E-09						12156.97
19.462	0.000	1.07E-14	-5.71E-15	0.0141	4.28E-15	2.40E-09						12156.97
20.462	0.000	1.07E-14	-5.71E-15	0.0141	4.28E-15	2.40E-09						12156.97
21.962	0.000	1.07E-14	-5.71E-15	0.0141	4.28E-15	2.40E-09						12156.97
23.962	0.000	1.07E-14	-5.71E-15	0.0141	4.28E-15	2.40E-09						12156.97
26.462	0.000	1.07E-14	-5.71E-15	0.0141	4.28E-15	2.40E-09						12156.97
29.462	0.000	1.07E-14	-5.71E-15	0.0141	4.28E-15	2.40E-09						12156.97
32.962	0.000	1.07E-14	-5.71E-15	0.0141	4.28E-15	2.40E-09						12156.97
36.962	0.000	1.07E-14	-5.71E-15	0.0141	4.28E-15	2.40E-09						12156.97
40.962	0.000	1.07E-14	-5.71E-15	0.0141	4.28E-15	2.40E-09						12156.97
44.962	0.000	1.07E-14	-5.71E-15	0.0141	4.28E-15	2.40E-09						12156.97

RESULTS FOR YEAR: 16

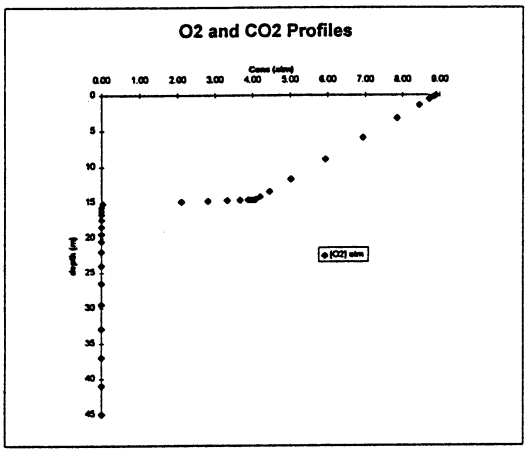

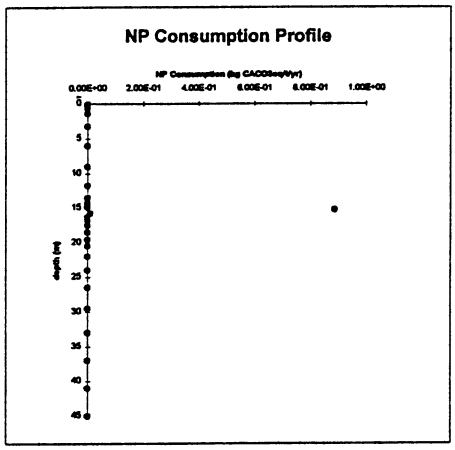

Flux in (mol/m²s)	1.99E-06
O_2 cons. (mol/m²s)	1.99E-06
Dpen (m)	16.462

t=16												
DEPTH (m)	CONC O2 (mol/m³)	O2 Cons (mol/m³/s)	CO2 Prod (mol/m³/s)	CONC CO2 (mol/m³)	mols O2 cons per m3 rock	NP consmptn kg CaCO3eq/t/yr						Sulf dens mol/m³
0.050	8.900	0.00E+00	0.00E+00	0.0141	0.00E+00	0.00E+00						0.00
0.225	8.842	0.00E+00	0.00E+00	0.0141	0.00E+00	0.00E+00						0.00
0.600	8.718	0.00E+00	0.00E+00	0.0141	0.00E+00	0.00E+00						0.00
1.400	8.452	0.00E+00	0.00E+00	0.0141	0.00E+00	0.00E+00						0.00
3.200	7.855	0.00E+00	0.00E+00	0.0141	0.00E+00	0.00E+00						0.00
5.950	6.942	0.00E+00	0.00E+00	0.0141	0.00E+00	0.00E+00						0.00
8.950	5.944	0.00E+00	0.00E+00	0.0141	0.00E+00	0.00E+00						0.00
11.700	5.027	0.00E+00	0.00E+00	0.0141	0.00E+00	0.00E+00						0.00
13.450	4.456	0.00E+00	0.00E+00	0.0141	0.00E+00	0.00E+00						0.00
14.200	4.213	0.00E+00	0.00E+00	0.0141	0.00E+00	0.00E+00						0.00
14.508	4.111	0.00E+00	0.00E+00	0.0141	0.00E+00	0.00E+00						0.00
14.590	4.084	0.00E+00	0.00E+00	0.0141	0.00E+00	0.00E+00						0.00
14.620	4.074	0.00E+00	0.00E+00	0.0141	0.00E+00	0.00E+00						0.00
14.628	4.072	0.00E+00	0.00E+00	0.0141	0.00E+00	0.00E+00						0.00
14.631	4.067	0.00E+00	0.00E+00	0.0141	0.00E+00	0.00E+00						0.00
14.632	4.060	0.00E+00	0.00E+00	0.0141	0.00E+00	0.00E+00						0.00
14.635	4.040	0.00E+00	0.00E+00	0.0141	0.00E+00	0.00E+00						0.00
14.640	4.005	0.00E+00	0.00E+00	0.0141	0.00E+00	0.00E+00						0.00
14.647	3.953	0.00E+00	0.00E+00	0.0141	0.00E+00	0.00E+00						0.00
14.657	3.884	0.00E+00	0.00E+00	0.0141	0.00E+00	0.00E+00						0.00
14.687	3.676	0.00E+00	0.00E+00	0.0141	0.00E+00	0.00E+00						0.00
14.737	3.331	0.00E+00	0.00E+00	0.0141	0.00E+00	0.00E+00						0.00
14.812	2.816	0.00E+00	0.00E+00	0.0141	0.00E+00	0.00E+00						0.00
14.912	2.112	0.00E+00	0.00E+00	0.0141	0.00E+00	0.00E+00						0.00
15.212	0.037	3.95E-06	-2.11E-06	0.0141	1.58E-06	8.87E-01						10339.42
15.712	0.000	4.17E-08	-2.22E-08	0.0141	1.67E-08	9.36E-03						12137.83
16.212	0.000	4.40E-10	-2.34E-10	0.0141	1.76E-10	9.88E-05						12156.78
16.712	0.000	4.66E-12	-2.48E-12	0.0141	1.86E-12	1.05E-06						12156.97
17.462	0.000	1.66E-14	-8.87E-15	0.0141	6.65E-15	3.74E-09						12156.97
18.462	0.000	1.07E-14	-5.71E-15	0.0141	4.28E-15	2.40E-09						12156.97
19.462	0.000	1.07E-14	-5.71E-15	0.0141	4.28E-15	2.40E-09						12156.97
20.462	0.000	1.07E-14	-5.71E-15	0.0141	4.28E-15	2.40E-09						12156.97
21.962	0.000	1.07E-14	-5.71E-15	0.0141	4.28E-15	2.40E-09						12156.97
23.962	0.000	1.07E-14	-5.71E-15	0.0141	4.28E-15	2.40E-09						12156.97
26.462	0.000	1.07E-14	-5.71E-15	0.0141	4.28E-15	2.40E-09						12156.97
29.462	0.000	1.07E-14	-5.71E-15	0.0141	4.28E-15	2.40E-09						12156.97
32.962	0.000	1.07E-14	-5.71E-15	0.0141	4.28E-15	2.40E-09						12156.97
36.962	0.000	1.07E-14	-5.71E-15	0.0141	4.28E-15	2.40E-09						12156.97
40.962	0.000	1.07E-14	-5.71E-15	0.0141	4.28E-15	2.40E-09						12156.97
44.962	0.000	1.07E-14	-5.71E-15	0.0141	4.28E-15	2.40E-09						12156.97

RESULTS FOR YEAR: 24

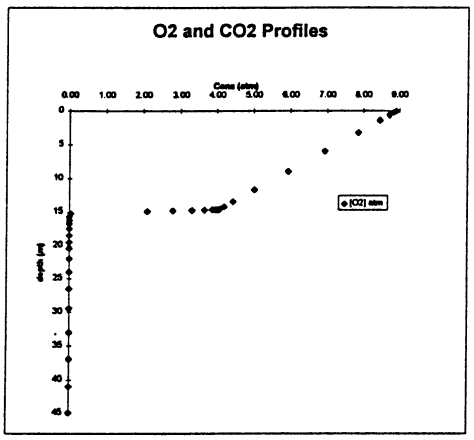

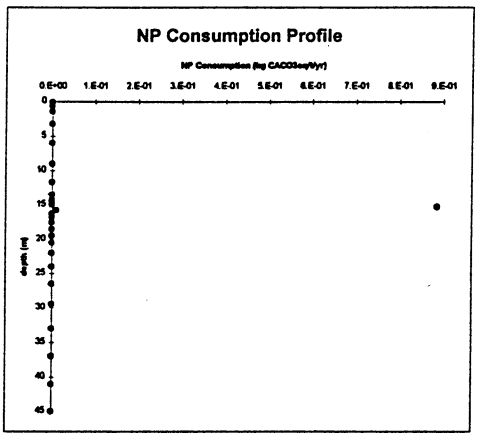

Flux in (mol/m²s)	1.99E-06
O_2 cons. (mol/m²s)	1.99E-06
Dpen (m)	16.462

t=24												
DEPTH (m)	CONC O2 (mol/m³)	O2 Cons (mol/m²/s)	CO2 Prod (mol/m²/s)	CONC CO2 (mol/m³)	mols O2 cons per m3 rock	NP consmptn kg CaCO3eq/t/yr						Sulf dens mol/m³
0.050	8.900	0.00E+00	0.00E+00	0.0141	0.00E+00	0.00E+00						0.00
0.225	8.842	0.00E+00	0.00E+00	0.0141	0.00E+00	0.00E+00						0.00
0.600	8.717	0.00E+00	0.00E+00	0.0141	0.00E+00	0.00E+00						0.00
1.400	8.452	0.00E+00	0.00E+00	0.0141	0.00E+00	0.00E+00						0.00
3.200	7.854	0.00E+00	0.00E+00	0.0141	0.00E+00	0.00E+00						0.00
5.950	6.941	0.00E+00	0.00E+00	0.0141	0.00E+00	0.00E+00						0.00
8.950	5.945	0.00E+00	0.00E+00	0.0141	0.00E+00	0.00E+00						0.00
11.700	5.031	0.00E+00	0.00E+00	0.0141	0.00E+00	0.00E+00						0.00
13.450	4.450	0.00E+00	0.00E+00	0.0141	0.00E+00	0.00E+00						0.00
14.200	4.201	0.00E+00	0.00E+00	0.0141	0.00E+00	0.00E+00						0.00
14.508	4.099	0.00E+00	0.00E+00	0.0141	0.00E+00	0.00E+00						0.00
14.590	4.072	0.00E+00	0.00E+00	0.0141	0.00E+00	0.00E+00						0.00
14.620	4.062	0.00E+00	0.00E+00	0.0141	0.00E+00	0.00E+00						0.00
14.628	4.059	0.00E+00	0.00E+00	0.0141	0.00E+00	0.00E+00						0.00
14.631	4.055	0.00E+00	0.00E+00	0.0141	0.00E+00	0.00E+00						0.00
14.632	4.048	0.00E+00	0.00E+00	0.0141	0.00E+00	0.00E+00						0.00
14.635	4.027	0.00E+00	0.00E+00	0.0141	0.00E+00	0.00E+00						0.00
14.640	3.993	0.00E+00	0.00E+00	0.0141	0.00E+00	0.00E+00						0.00
14.647	3.941	0.00E+00	0.00E+00	0.0141	0.00E+00	0.00E+00						0.00
14.657	3.872	0.00E+00	0.00E+00	0.0141	0.00E+00	0.00E+00						0.00
14.687	3.664	0.00E+00	0.00E+00	0.0141	0.00E+00	0.00E+00						0.00
14.737	3.319	0.00E+00	0.00E+00	0.0141	0.00E+00	0.00E+00						0.00
14.812	2.801	0.00E+00	0.00E+00	0.0141	0.00E+00	0.00E+00						0.00
14.912	2.110	0.00E+00	0.00E+00	0.0141	0.00E+00	0.00E+00						0.00
15.212	0.037	3.94E-06	-2.10E-06	0.0141	1.58E-06	8.86E-01						6853.70
15.712	0.000	4.16E-08	-2.22E-08	0.0141	1.66E-08	9.35E-03						12101.05
16.212	0.000	4.39E-10	-2.34E-10	0.0141	1.76E-10	9.87E-05						12156.40
16.712	0.000	4.65E-12	-2.48E-12	0.0141	1.86E-12	1.04E-06						12156.97
17.462	0.000	1.66E-14	-8.86E-15	0.0141	6.64E-15	3.73E-09						12156.97
18.462	0.000	1.07E-14	-5.71E-15	0.0141	4.28E-15	2.40E-09						12156.97
19.462	0.000	1.07E-14	-5.71E-15	0.0141	4.28E-15	2.40E-09						12156.97
20.462	0.000	1.07E-14	-5.71E-15	0.0141	4.28E-15	2.40E-09						12156.97
21.962	0.000	1.07E-14	-5.71E-15	0.0141	4.28E-15	2.40E-09						12156.97
23.962	0.000	1.07E-14	-5.71E-15	0.0141	4.28E-15	2.40E-09						12156.97
26.462	0.000	1.07E-14	-5.71E-15	0.0141	4.28E-15	2.40E-09						12156.97
29.462	0.000	1.07E-14	-5.71E-15	0.0141	4.28E-15	2.40E-09						12156.97
32.962	0.000	1.07E-14	-5.71E-15	0.0141	4.28E-15	2.40E-09						12156.97
36.962	0.000	1.07E-14	-5.71E-15	0.0141	4.28E-15	2.40E-09						12156.97
40.962	0.000	1.07E-14	-5.71E-15	0.0141	4.28E-15	2.40E-09						12156.97
44.962	0.000	1.07E-14	-5.71E-15	0.0141	4.28E-15	2.40E-09						12156.97

RESULTS FOR YEAR: 32

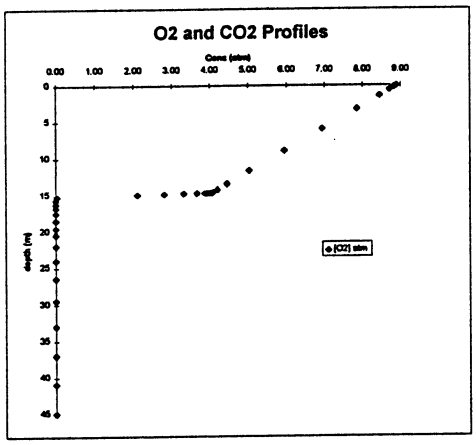

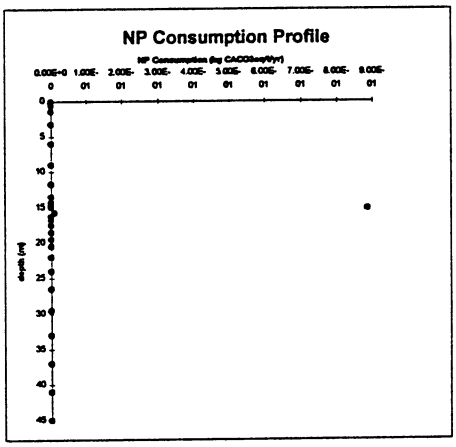

Flux in (mol/m²s)	1.99E-06
O_2 cons. (mol/m²s)	1.99E-06
Dpen (m)	16.462

t=32												
DEPTH (m)	CONC O2 (mol/m³)	O2 Cons (mol/m³/s)	CO2 Prod (mol/m³/s)	CONC CO2 (mol/m³)	mols O2 cons per m3 rock	NP consmptn kg CaCO3eq/t/yr						Sulf dens mol/m³
0.050	8.900	0.00E+00	0.00E+00	0.0141	0.00E+00	0.00E+00						0.00
0.225	8.842	0.00E+00	0.00E+00	0.0141	0.00E+00	0.00E+00						0.00
0.600	8.717	0.00E+00	0.00E+00	0.0141	0.00E+00	0.00E+00						0.00
1.400	8.452	0.00E+00	0.00E+00	0.0141	0.00E+00	0.00E+00						0.00
3.200	7.854	0.00E+00	0.00E+00	0.0141	0.00E+00	0.00E+00						0.00
5.950	6.941	0.00E+00	0.00E+00	0.0141	0.00E+00	0.00E+00						0.00
8.950	5.945	0.00E+00	0.00E+00	0.0141	0.00E+00	0.00E+00						0.00
11.700	5.031	0.00E+00	0.00E+00	0.0141	0.00E+00	0.00E+00						0.00
13.450	4.450	0.00E+00	0.00E+00	0.0141	0.00E+00	0.00E+00						0.00
14.200	4.201	0.00E+00	0.00E+00	0.0141	0.00E+00	0.00E+00						0.00
14.508	4.099	0.00E+00	0.00E+00	0.0141	0.00E+00	0.00E+00						0.00
14.590	4.072	0.00E+00	0.00E+00	0.0141	0.00E+00	0.00E+00						0.00
14.620	4.062	0.00E+00	0.00E+00	0.0141	0.00E+00	0.00E+00						0.00
14.628	4.059	0.00E+00	0.00E+00	0.0141	0.00E+00	0.00E+00						0.00
14.631	4.055	0.00E+00	0.00E+00	0.0141	0.00E+00	0.00E+00						0.00
14.632	4.046	0.00E+00	0.00E+00	0.0141	0.00E+00	0.00E+00						0.00
14.635	4.027	0.00E+00	0.00E+00	0.0141	0.00E+00	0.00E+00						0.00
14.640	3.993	0.00E+00	0.00E+00	0.0141	0.00E+00	0.00E+00						0.00
14.647	3.941	0.00E+00	0.00E+00	0.0141	0.00E+00	0.00E+00						0.00
14.657	3.872	0.00E+00	0.00E+00	0.0141	0.00E+00	0.00E+00						0.00
14.687	3.664	0.00E+00	0.00E+00	0.0141	0.00E+00	0.00E+00						0.00
14.737	3.319	0.00E+00	0.00E+00	0.0141	0.00E+00	0.00E+00						0.00
14.812	2.801	0.00E+00	0.00E+00	0.0141	0.00E+00	0.00E+00						0.00
14.912	2.110	0.00E+00	0.00E+00	0.0141	0.00E+00	0.00E+00						0.00
15.212	0.037	3.94E-06	-2.10E-06	0.0141	1.58E-06	8.86E-01						3368.02
15.712	0.000	4.16E-08	-2.22E-08	0.0141	1.66E-08	9.35E-03						12064.27
16.212	0.000	4.39E-10	-2.34E-10	0.0141	1.76E-10	9.87E-05						12156.01
16.712	0.000	4.65E-12	-2.48E-12	0.0141	1.86E-12	1.04E-06						12156.97
17.462	0.000	1.66E-14	-8.86E-15	0.0141	6.64E-15	3.73E-09						12156.97
18.462	0.000	1.07E-14	-5.71E-15	0.0141	4.28E-15	2.40E-09						12156.97
19.462	0.000	1.07E-14	-5.71E-15	0.0141	4.28E-15	2.40E-09						12156.97
20.462	0.000	1.07E-14	-5.71E-15	0.0141	4.28E-15	2.40E-09						12156.97
21.962	0.000	1.07E-14	-5.71E-15	0.0141	4.28E-15	2.40E-09						12156.97
23.962	0.000	1.07E-14	-5.71E-15	0.0141	4.28E-15	2.40E-09						12156.97
26.462	0.000	1.07E-14	-5.71E-15	0.0141	4.28E-15	2.40E-09						12156.97
29.462	0.000	1.07E-14	-5.71E-15	0.0141	4.28E-15	2.40E-09						12156.97
32.962	0.000	1.07E-14	-5.71E-15	0.0141	4.28E-15	2.40E-09						12156.97
36.962	0.000	1.07E-14	-5.71E-15	0.0141	4.28E-15	2.40E-09						12156.97
40.962	0.000	1.07E-14	-5.71E-15	0.0141	4.28E-15	2.40E-09						12156.97
44.962	0.000	1.07E-14	-5.71E-15	0.0141	4.28E-15	2.40E-09						12156.97

APPENDIX A7
Run 3A1, Open Stope

COUPLED $O_2/CO_2/Mg/SO_4/Ca$ MODEL
OXYDIFF V2.0

MODEL DETAILS

Filename	BF_CS3A1
Date	27/11/1996
Description:	Steady State Model Of Crandon Open Stope Placed Cemented Backfill Tailings
	Part 2 (year 1 to 32)
	First Order Model

INPUT PARAMETERS

Finite Difference Parameters

nodes x	1
nodes y	40
time periods	7
init delt (s)	0.01
[O2] at surface (mol/m³)	8.9
[CO2] at surface (mol/m³))	0.0141

Model Options

CO2 OPTION	0
FES2 OPTION	1
O2 OPTION	1

Geochemical Options

Infiltration (m/s)	1.10E-09
Infiltration Coefficient	1.00
Kgypsum	-
Infiltration (m/s)	1.10E-09
Fraction Flow Paths (G)	1.00

Diffusion Parameters

Dw (m2/s)	2.20E-09
Da (m2/s)	1.80E-05
τ	0.273
α	3.28
H	33.9

OUTPUT TIMES

time (s)	time (y)	Output col
1.6E+07	1	1
6.3E+07	2	6
1.3E+08	4	11
2.5E+08	8	16
5.0E+08	16	21
7.6E+08	24	26
1.0E+09	32	31

FES2 OPTION
0 - No FES2 DEPLETION
1 - ALLOW FES2 DEPLETION

CO2 OPTION:
0 - No CO2 Coupling
1 - CO2 Coupling

O2 OPTION
0 - HALF ORDER REACTION
1 - FIRST ORDER REACTION
2 - MIXED FIRST ORDER / ZERO ORDER
3 - ZERO ORDER SOLUTION

TORTUOSITY

Rockfill	τ	3
Cemented Tailings	τ	10

MODEL INPUTS

Material	DEPTH (m)	Depth (ft)	Cell Sizes (m)	r (s-1)	Porosity	Bulk Dens. (tonnes m⁻³)	Sat. (%)	SolidDens (mol/m³)	Diff Coeff [1] (m2/s)	Diff Coeff [2] (m2/s)	$[O_2]_{BM}$ (mol/m³)	$[CO_2]_{BM}$ (mol/m³)
Waste Rock	0.050	0.164	0.1	0.00E+00	0.40	1.9	15%	0	6.00E-06	6.00E-06	8.89	1.41E-02
Waste Rock	0.225	0.738	0.25	0.00E+00	0.40	1.9	15%	0	6.00E-06	6.00E-06	8.89	1.41E-02
Waste Rock	0.475	1.558	0.25	0.00E+00	0.40	1.9	15%	0	6.00E-06	6.00E-06	8.89	1.41E-02
Waste Rock	0.725	2.379	0.25	0.00E+00	0.40	1.9	15%	0	6.00E-06	6.00E-06	8.89	1.41E-02
Waste Rock	0.993	3.256	0.285	0.00E+00	0.40	1.9	15%	0	6.00E-06	6.00E-06	8.89	1.41E-02
Waste Rock	1.385	4.544	0.5	0.00E+00	0.40	1.9	15%	0	6.00E-06	6.00E-06	8.89	1.41E-02
Waste Rock	1.885	6.184	0.5	0.00E+00	0.40	1.9	15%	0	6.00E-06	6.00E-06	8.89	1.41E-02
Waste Rock	2.385	7.825	0.5	0.00E+00	0.40	1.9	15%	0	6.00E-06	6.00E-06	8.89	1.41E-02
Waste Rock	2.760	9.055	0.25	0.00E+00	0.40	1.9	15%	0	6.00E-06	6.00E-06	8.89	1.41E-02
Waste Rock	2.911	9.551	0.052	0.00E+00	0.40	1.9	15%	0	6.00E-06	6.00E-06	8.89	1.41E-02
Waste Rock	2.962	9.716	0.05	0.00E+00	0.40	1.9	15%	0	6.00E-06	6.00E-06	8.89	1.41E-02
Waste Rock	3.012	9.882	0.05	0.00E+00	0.40	1.9	15%	0	6.00E-06	6.00E-06	8.89	1.41E-02
Waste Rock	3.042	9.980	0.01	0.00E+00	0.40	1.9	15%	0	6.00E-06	6.00E-06	8.89	1.41E-02
Waste Rock	3.050	10.005	0.005	0.00E+00	0.40	1.9	15%	0	6.00E-06	6.00E-06	8.89	1.41E-02
Tailings Backfill	3.053	10.015	0.001	1.07E-04	0.40	3.0	15%	12187	2.88E-07	2.88E-07	8.89	1.41E-02
Tailings Backfill	3.054	10.018	0.001	1.07E-04	0.40	3.0	15%	12187	2.88E-07	2.88E-07	8.89	1.41E-02
Tailings Backfill	3.057	10.028	0.005	1.07E-04	0.40	3.0	15%	12187	2.88E-07	2.88E-07	8.89	1.41E-02
Tailings Backfill	3.062	10.044	0.005	1.07E-04	0.40	3.0	15%	12187	2.88E-07	2.88E-07	8.89	1.41E-02
Tailings Backfill	3.069	10.069	0.01	1.07E-04	0.40	3.0	15%	12187	2.88E-07	2.88E-07	8.89	1.41E-02
Tailings Backfill	3.079	10.102	0.01	1.07E-04	0.40	3.0	15%	12187	2.88E-07	2.88E-07	8.89	1.41E-02
Tailings Backfill	3.109	10.200	0.05	1.07E-04	0.40	3.0	15%	12187	2.88E-07	2.88E-07	8.89	1.41E-02
Tailings Backfill	3.159	10.364	0.05	1.07E-04	0.40	3.0	15%	12187	2.88E-07	2.88E-07	8.89	1.41E-02
Tailings Backfill	3.234	10.610	0.1	1.07E-04	0.40	3.0	15%	12187	2.88E-07	2.88E-07	8.89	1.41E-02
Tailings Backfill	3.334	10.938	0.1	1.07E-04	0.40	3.0	15%	12187	2.88E-07	2.88E-07	8.89	1.41E-02
Tailings Backfill	3.634	11.923	0.5	1.07E-04	0.40	3.0	15%	12187	2.88E-07	2.88E-07	8.89	1.41E-02
Tailings Backfill	4.134	13.563	0.5	1.07E-04	0.40	3.0	15%	12187	2.88E-07	2.88E-07	8.89	1.41E-02
Tailings Backfill	4.634	15.203	0.5	1.07E-04	0.40	3.0	15%	12187	2.88E-07	2.88E-07	8.89	1.41E-02
Tailings Backfill	5.134	16.844	0.5	1.07E-04	0.40	3.0	15%	12187	2.88E-07	2.88E-07	8.89	1.41E-02
Tailings Backfill	5.884	19.304	1	1.07E-04	0.40	3.0	15%	12187	2.88E-07	2.88E-07	8.89	1.41E-02
Tailings Backfill	6.884	22.585	1	1.07E-04	0.40	3.0	15%	12187	2.88E-07	2.88E-07	8.89	1.41E-02
Tailings Backfill	7.884	25.866	1	1.07E-04	0.40	3.0	15%	12187	2.88E-07	2.88E-07	8.89	1.41E-02
Tailings Backfill	8.884	29.147	1	1.07E-04	0.40	3.0	15%	12187	2.88E-07	2.88E-07	8.89	1.41E-02
Tailings Backfill	10.384	34.068	2	1.07E-04	0.40	3.0	15%	12187	2.88E-07	2.88E-07	8.89	1.41E-02
Tailings Backfill	12.384	40.630	2	1.07E-04	0.40	3.0	15%	12187	2.88E-07	2.88E-07	8.89	1.41E-02
Tailings Backfill	14.884	48.832	3	1.07E-04	0.40	3.0	15%	12187	2.88E-07	2.88E-07	8.89	1.41E-02
Tailings Backfill	17.884	58.675	3	1.07E-04	0.40	3.0	15%	12187	2.88E-07	2.88E-07	8.89	1.41E-02
Tailings Backfill	21.384	70.157	4	1.07E-04	0.40	3.0	15%	12187	2.88E-07	2.88E-07	8.89	1.41E-02
Tailings Backfill	25.384	83.281	4	1.07E-04	0.40	3.0	15%	12187	2.88E-07	2.88E-07	8.89	1.41E-02
Tailings Backfill	29.384	96.404	4	1.07E-04	0.40	3.0	15%	12187	2.88E-07	2.88E-07	8.89	1.41E-02
Tailings Backfill	33.384	109.528	4	1.07E-04	0.40	3.0	15%	12187	2.88E-07	2.88E-07	8.89	1.41E-02

1. Diff Coefficient Based on Erbarling, B., R.V.Nicholson, E.J.Reardon and P.Tibble, Evaluation of sulphide oxidation rates. Nordic Hydrology, 24(5), 323-336, 1993.
2. Diff Coefficient Based on Reardon, E.J. and P.M. Moddle, Gas Diffusion Coefficient Measurements on Uranium Mill Tailings: Implicatsions to Cover Layer Design. Uranium, 2, 111-131,1985.

RESULTS FOR YEAR: 1

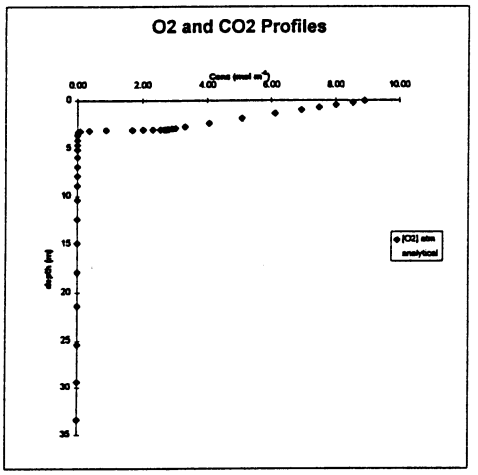

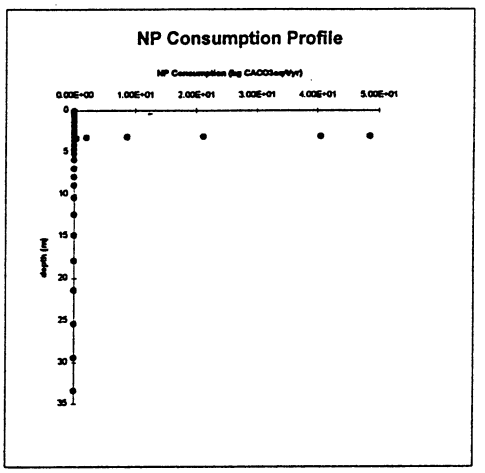

Flux in (mol/m²s)	1.25E-05
O_2 cons. (mol/m²s)	1.17E-05
Dpen (m)	4.384

t=1												
DEPTH (m)	CONC O2 (mol/m³)	O2 Cons (mol/m³/s)	CO2 Prod (mol/m³/s)	CONC CO2 (mol/m³)	mols O2 cons per m³ material	NP consmptn kg CaCO3eq/t/yr						Sulf dens mol/m³
0.050	8.900	0.00E+00	0.00E+00	0.0141	0.00E+00	0.00E+00						0.00
0.225	8.534	0.00E+00	0.00E+00	0.0141	0.00E+00	0.00E+00						0.00
0.475	8.012	0.00E+00	0.00E+00	0.0141	0.00E+00	0.00E+00						0.00
0.725	7.491	0.00E+00	0.00E+00	0.0141	0.00E+00	0.00E+00						0.00
0.993	6.933	0.00E+00	0.00E+00	0.0141	0.00E+00	0.00E+00						0.00
1.385	6.117	0.00E+00	0.00E+00	0.0141	0.00E+00	0.00E+00						0.00
1.885	5.063	0.00E+00	0.00E+00	0.0141	0.00E+00	0.00E+00						0.00
2.385	4.061	0.00E+00	0.00E+00	0.0141	0.00E+00	0.00E+00						0.00
2.760	3.308	0.00E+00	0.00E+00	0.0141	0.00E+00	0.00E+00						0.00
2.911	3.010	0.00E+00	0.00E+00	0.0141	0.00E+00	0.00E+00						0.00
2.962	2.909	0.00E+00	0.00E+00	0.0141	0.00E+00	0.00E+00						0.00
3.012	2.811	0.00E+00	0.00E+00	0.0141	0.00E+00	0.00E+00						0.00
3.042	2.752	0.00E+00	0.00E+00	0.0141	0.00E+00	0.00E+00						0.00
3.050	2.738	0.00E+00	0.00E+00	0.0141	0.00E+00	0.00E+00						0.00
3.053	2.712	0.00E+00	0.00E+00	0.0141	0.00E+00	0.00E+00						0.00
3.054	2.672	0.00E+00	0.00E+00	0.0141	0.00E+00	0.00E+00						0.00
3.057	2.550	0.00E+00	0.00E+00	0.0141	0.00E+00	0.00E+00						0.00
3.062	2.325	0.00E+00	0.00E+00	0.0141	0.00E+00	0.00E+00						0.00
3.069	2.020	2.16E-04	-1.15E-04	0.0141	8.65E-05	4.86E+01						1522.00
3.079	1.689	1.81E-04	-9.64E-05	0.0141	7.23E-05	4.06E+01						3265.29
3.109	0.883	9.45E-05	-5.04E-05	0.0141	3.78E-05	2.12E+01						7504.80
3.159	0.361	3.86E-05	-2.06E-05	0.0141	1.55E-05	8.68E+00						10252.56
3.234	0.062	8.80E-06	-4.69E-06	0.0141	3.52E-06	1.98E+00						11722.74
3.334	0.016	1.74E-06	-9.30E-07	0.0141	6.98E-07	3.92E-01						12070.82
3.634	0.000	3.04E-08	-1.62E-08	0.0141	1.22E-08	6.83E-03						12155.46
4.134	0.000	3.20E-10	-1.71E-10	0.0141	1.28E-10	7.19E-05						12156.96
4.634	0.000	3.37E-12	-1.80E-12	0.0141	1.35E-12	7.58E-07						12156.97
5.134	0.000	3.56E-14	-1.90E-14	0.0141	1.43E-14	8.01E-09						12156.97
5.884	0.000	1.07E-14	-5.71E-15	0.0141	4.28E-15	2.40E-09						12156.97
6.884	0.000	1.07E-14	-5.71E-15	0.0141	4.28E-15	2.40E-09						12156.97
7.884	0.000	1.07E-14	-5.71E-15	0.0141	4.28E-15	2.40E-09						12156.97
8.884	0.000	1.07E-14	-5.71E-15	0.0141	4.28E-15	2.40E-09						12156.97
10.384	0.000	1.07E-14	-5.71E-15	0.0141	4.28E-15	2.40E-09						12156.97
12.384	0.000	1.07E-14	-5.71E-15	0.0141	4.28E-15	2.40E-09						12156.97
14.884	0.000	1.07E-14	-5.71E-15	0.0141	4.28E-15	2.40E-09						12156.97
17.884	0.000	1.07E-14	-5.71E-15	0.0141	4.28E-15	2.40E-09						12156.97
21.384	0.000	1.07E-14	-5.71E-15	0.0141	4.28E-15	2.40E-09						12156.97
25.384	0.000	1.07E-14	-5.71E-15	0.0141	4.28E-15	2.40E-09						12156.97
29.384	0.000	1.07E-14	-5.71E-15	0.0141	4.28E-15	2.40E-09						12156.97
33.384	0.000	1.07E-14	-5.71E-15	0.0141	4.28E-15	2.40E-09						12156.97

RESULTS FOR YEAR: 2

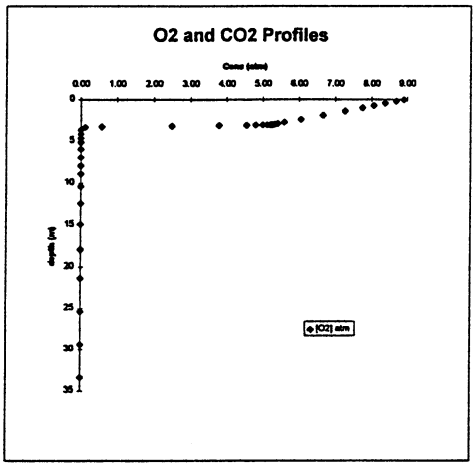

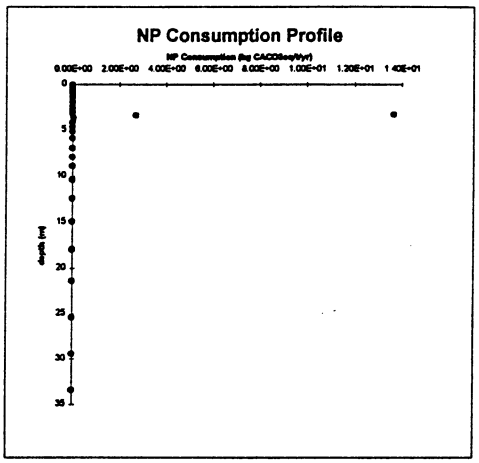

Flux in (mol/m²s)	7.39E-06
O_2 cons. (mol/m²s)	7.38E-06
Dpen (m)	4.884

t=2												
DEPTH (m)	CONC O2 (mol/m³)	O2 Cons (mol/m³/s)	CO2 Prod (mol/m³/s)	CONC CO2 (mol/m³)	mols O2 cons per m3 rock	NP consmptn kg CaCO3eq/t/yr						Sulf dens mol/m²
0.050	8.900	0.00E+00	0.00E+00	0.0141	0.00E+00	0.00E+00						0.00
0.225	8.684	0.00E+00	0.00E+00	0.0141	0.00E+00	0.00E+00						0.00
0.475	8.376	0.00E+00	0.00E+00	0.0141	0.00E+00	0.00E+00						0.00
0.725	8.069	0.00E+00	0.00E+00	0.0141	0.00E+00	0.00E+00						0.00
0.993	7.741	0.00E+00	0.00E+00	0.0141	0.00E+00	0.00E+00						0.00
1.385	7.262	0.00E+00	0.00E+00	0.0141	0.00E+00	0.00E+00						0.00
1.885	6.657	0.00E+00	0.00E+00	0.0141	0.00E+00	0.00E+00						0.00
2.385	6.052	0.00E+00	0.00E+00	0.0141	0.00E+00	0.00E+00						0.00
2.760	5.594	0.00E+00	0.00E+00	0.0141	0.00E+00	0.00E+00						0.00
2.911	5.408	0.00E+00	0.00E+00	0.0141	0.00E+00	0.00E+00						0.00
2.962	5.345	0.00E+00	0.00E+00	0.0141	0.00E+00	0.00E+00						0.00
3.012	5.284	0.00E+00	0.00E+00	0.0141	0.00E+00	0.00E+00						0.00
3.042	5.247	0.00E+00	0.00E+00	0.0141	0.00E+00	0.00E+00						0.00
3.050	5.237	0.00E+00	0.00E+00	0.0141	0.00E+00	0.00E+00						0.00
3.053	5.222	0.00E+00	0.00E+00	0.0141	0.00E+00	0.00E+00						0.00
3.054	5.196	0.00E+00	0.00E+00	0.0141	0.00E+00	0.00E+00						0.00
3.057	5.120	0.00E+00	0.00E+00	0.0141	0.00E+00	0.00E+00						0.00
3.062	4.993	0.00E+00	0.00E+00	0.0141	0.00E+00	0.00E+00						0.00
3.069	4.803	0.00E+00	0.00E+00	0.0141	0.00E+00	0.00E+00						0.00
3.079	4.548	0.00E+00	0.00E+00	0.0141	0.00E+00	0.00E+00						0.00
3.109	3.786	0.00E+00	0.00E+00	0.0141	0.00E+00	0.00E+00						0.00
3.159	2.487	0.00E+00	0.00E+00	0.0141	0.00E+00	0.00E+00						0.00
3.234	0.567	6.07E-05	-3.24E-05	0.0141	2.43E-05	1.36E+01						6471.76
3.334	0.113	1.20E-05	-6.43E-06	0.0141	4.82E-06	2.71E+00						11029.06
3.634	0.002	2.10E-07	-1.12E-07	0.0141	8.42E-08	4.73E-02						12137.29
4.134	0.000	2.22E-09	-1.18E-09	0.0141	8.88E-10	4.99E-04						12156.78
4.634	0.000	2.34E-11	-1.25E-11	0.0141	9.37E-12	5.27E-06						12156.97
5.134	0.000	2.48E-13	-1.32E-13	0.0141	9.93E-14	5.58E-08						12156.97
5.884	0.000	1.07E-14	-5.71E-15	0.0141	4.28E-15	2.40E-09						12156.97
6.884	0.000	1.07E-14	-5.71E-15	0.0141	4.28E-15	2.40E-09						12156.97
7.884	0.000	1.07E-14	-5.71E-15	0.0141	4.28E-15	2.40E-09						12156.97
8.884	0.000	1.07E-14	-5.71E-15	0.0141	4.28E-15	2.40E-09						12156.97
10.384	0.000	1.07E-14	-5.71E-15	0.0141	4.28E-15	2.40E-09						12156.97
12.384	0.000	1.07E-14	-5.71E-15	0.0141	4.28E-15	2.40E-09						12156.97
14.884	0.000	1.07E-14	-5.71E-15	0.0141	4.28E-15	2.40E-09						12156.97
17.884	0.000	1.07E-14	-5.71E-15	0.0141	4.28E-15	2.40E-09						12156.97
21.384	0.000	1.07E-14	-5.71E-15	0.0141	4.28E-15	2.40E-09						12156.97
25.384	0.000	1.07E-14	-5.71E-15	0.0141	4.28E-15	2.40E-09						12156.97
29.384	0.000	1.07E-14	-5.71E-15	0.0141	4.28E-15	2.40E-09						12156.97
33.384	0.000	1.07E-14	-5.71E-15	0.0141	4.28E-15	2.40E-09						12156.97

RESULTS FOR YEAR: 4

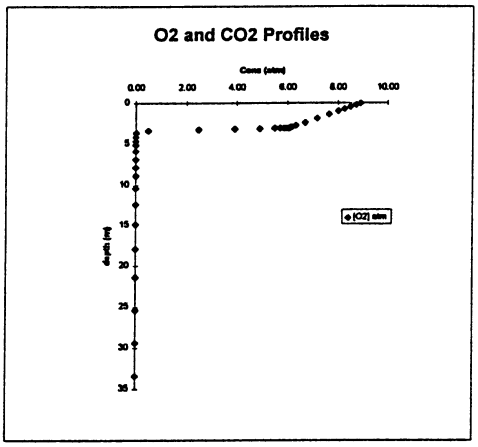

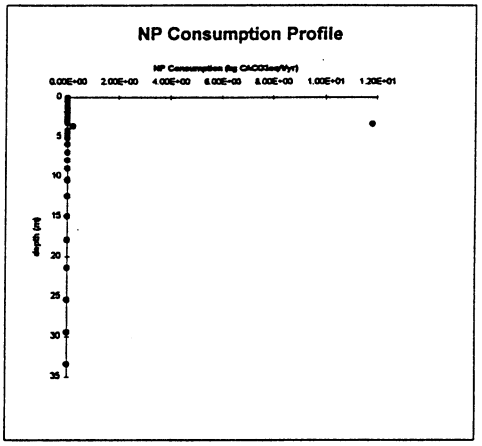

Flux in (mol/m²s)	5.66E-06
O_2 cons. (mol/m²s)	5.72E-06
Dpen (m)	4.884

t=4												
DEPTH (m)	CONC O2 (mol/m³)	O2 Cons (mol/m²/s)	CO2 Prod (mol/m²/s)	CONC CO2 (mol/m³)	mols O2 cons per m3 rock	NP consmptn kg CaCO3eq/t/yr						Sulf dens mol/m³
0.050	8.900	0.00E+00	0.00E+00	0.0141	0.00E+00	0.00E+00						0.00
0.225	8.735	0.00E+00	0.00E+00	0.0141	0.00E+00	0.00E+00						0.00
0.475	8.499	0.00E+00	0.00E+00	0.0141	0.00E+00	0.00E+00						0.00
0.725	8.263	0.00E+00	0.00E+00	0.0141	0.00E+00	0.00E+00						0.00
0.993	8.010	0.00E+00	0.00E+00	0.0141	0.00E+00	0.00E+00						0.00
1.385	7.639	0.00E+00	0.00E+00	0.0141	0.00E+00	0.00E+00						0.00
1.885	7.165	0.00E+00	0.00E+00	0.0141	0.00E+00	0.00E+00						0.00
2.385	6.687	0.00E+00	0.00E+00	0.0141	0.00E+00	0.00E+00						0.00
2.760	6.325	0.00E+00	0.00E+00	0.0141	0.00E+00	0.00E+00						0.00
2.911	6.180	0.00E+00	0.00E+00	0.0141	0.00E+00	0.00E+00						0.00
2.962	6.131	0.00E+00	0.00E+00	0.0141	0.00E+00	0.00E+00						0.00
3.012	6.082	0.00E+00	0.00E+00	0.0141	0.00E+00	0.00E+00						0.00
3.042	6.054	0.00E+00	0.00E+00	0.0141	0.00E+00	0.00E+00						0.00
3.050	6.046	0.00E+00	0.00E+00	0.0141	0.00E+00	0.00E+00						0.00
3.053	6.034	0.00E+00	0.00E+00	0.0141	0.00E+00	0.00E+00						0.00
3.054	6.014	0.00E+00	0.00E+00	0.0141	0.00E+00	0.00E+00						0.00
3.057	5.954	0.00E+00	0.00E+00	0.0141	0.00E+00	0.00E+00						0.00
3.062	5.854	0.00E+00	0.00E+00	0.0141	0.00E+00	0.00E+00						0.00
3.069	5.704	0.00E+00	0.00E+00	0.0141	0.00E+00	0.00E+00						0.00
3.079	5.504	0.00E+00	0.00E+00	0.0141	0.00E+00	0.00E+00						0.00
3.109	4.906	0.00E+00	0.00E+00	0.0141	0.00E+00	0.00E+00						0.00
3.159	3.921	0.00E+00	0.00E+00	0.0141	0.00E+00	0.00E+00						0.00
3.234	2.475	0.00E+00	0.00E+00	0.0141	0.00E+00	0.00E+00						0.00
3.334	0.491	5.26E-05	-2.80E-05	0.0141	2.10E-05	1.18E+01						3415.88
3.634	0.009	9.18E-07	-4.90E-07	0.0141	3.67E-07	2.06E-01						12004.36
4.134	0.000	9.69E-09	-5.17E-09	0.0141	3.88E-09	2.18E-03						12155.38
4.634	0.000	1.02E-10	-5.45E-11	0.0141	4.09E-11	2.30E-05						12156.96
5.134	0.000	1.08E-12	-5.77E-13	0.0141	4.33E-13	2.43E-07						12156.97
5.884	0.000	1.07E-14	-5.71E-15	0.0141	4.28E-15	2.40E-09						12156.97
6.884	0.000	1.07E-14	-5.71E-15	0.0141	4.28E-15	2.40E-09						12156.97
7.884	0.000	1.07E-14	-5.71E-15	0.0141	4.28E-15	2.40E-09						12156.97
8.884	0.000	1.07E-14	-5.71E-15	0.0141	4.28E-15	2.40E-09						12156.97
10.384	0.000	1.07E-14	-5.71E-15	0.0141	4.28E-15	2.40E-09						12156.97
12.384	0.000	1.07E-14	-5.71E-15	0.0141	4.28E-15	2.40E-09						12156.97
14.884	0.000	1.07E-14	-5.71E-15	0.0141	4.28E-15	2.40E-09						12156.97
17.884	0.000	1.07E-14	-5.71E-15	0.0141	4.28E-15	2.40E-09						12156.97
21.384	0.000	1.07E-14	-5.71E-15	0.0141	4.28E-15	2.40E-09						12156.97
25.384	0.000	1.07E-14	-5.71E-15	0.0141	4.28E-15	2.40E-09						12156.97
29.384	0.000	1.07E-14	-5.71E-15	0.0141	4.28E-15	2.40E-09						12156.97
33.384	0.000	1.07E-14	-5.71E-15	0.0141	4.28E-15	2.40E-09						12156.97

RESULTS FOR YEAR: 8

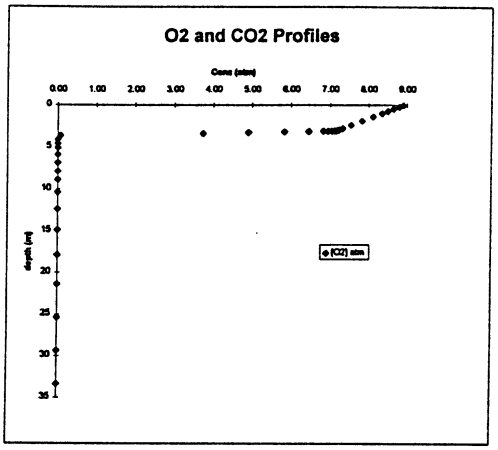

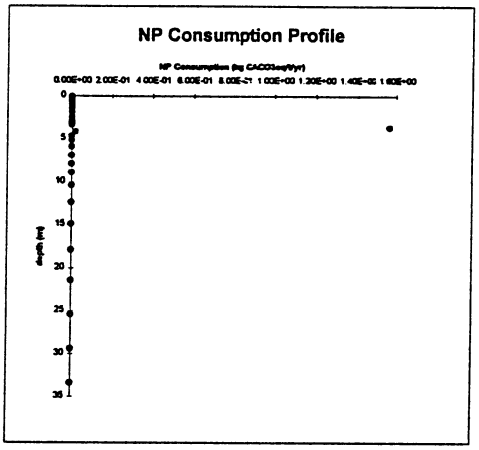

Flux in (mol/m²s)	3.51E-06
O_2 cons. (mol/m²s)	3.52E-06
Dpen (m)	4.884

t=8												
DEPTH (m)	CONC O2 (mol/m³)	O2 Cons (mol/m³/s)	CO2 Prod (mol/m³/s)	CONC CO2 (mol/m³)	mols O2 cons per m3 rock	NP consmptn kg CaCO3eq/t/yr						Sulf dens mol/m³
0.050	8.900	0.00E+00	0.00E+00	0.0141	0.00E+00	0.00E+00						0.00
0.225	8.798	0.00E+00	0.00E+00	0.0141	0.00E+00	0.00E+00						0.00
0.475	8.652	0.00E+00	0.00E+00	0.0141	0.00E+00	0.00E+00						0.00
0.725	8.505	0.00E+00	0.00E+00	0.0141	0.00E+00	0.00E+00						0.00
0.993	8.349	0.00E+00	0.00E+00	0.0141	0.00E+00	0.00E+00						0.00
1.385	8.120	0.00E+00	0.00E+00	0.0141	0.00E+00	0.00E+00						0.00
1.885	7.829	0.00E+00	0.00E+00	0.0141	0.00E+00	0.00E+00						0.00
2.385	7.540	0.00E+00	0.00E+00	0.0141	0.00E+00	0.00E+00						0.00
2.760	7.322	0.00E+00	0.00E+00	0.0141	0.00E+00	0.00E+00						0.00
2.911	7.233	0.00E+00	0.00E+00	0.0141	0.00E+00	0.00E+00						0.00
2.962	7.204	0.00E+00	0.00E+00	0.0141	0.00E+00	0.00E+00						0.00
3.012	7.174	0.00E+00	0.00E+00	0.0141	0.00E+00	0.00E+00						0.00
3.042	7.157	0.00E+00	0.00E+00	0.0141	0.00E+00	0.00E+00						0.00
3.050	7.152	0.00E+00	0.00E+00	0.0141	0.00E+00	0.00E+00						0.00
3.053	7.144	0.00E+00	0.00E+00	0.0141	0.00E+00	0.00E+00						0.00
3.054	7.132	0.00E+00	0.00E+00	0.0141	0.00E+00	0.00E+00						0.00
3.057	7.095	0.00E+00	0.00E+00	0.0141	0.00E+00	0.00E+00						0.00
3.062	7.034	0.00E+00	0.00E+00	0.0141	0.00E+00	0.00E+00						0.00
3.069	6.942	0.00E+00	0.00E+00	0.0141	0.00E+00	0.00E+00						0.00
3.079	6.819	0.00E+00	0.00E+00	0.0141	0.00E+00	0.00E+00						0.00
3.109	6.450	0.00E+00	0.00E+00	0.0141	0.00E+00	0.00E+00						0.00
3.159	5.833	0.00E+00	0.00E+00	0.0141	0.00E+00	0.00E+00						0.00
3.234	4.908	0.00E+00	0.00E+00	0.0141	0.00E+00	0.00E+00						0.00
3.334	3.729	0.00E+00	0.00E+00	0.0141	0.00E+00	0.00E+00						0.00
3.634	0.065	6.97E-06	-3.72E-06	0.0141	2.79E-06	1.57E+00						9292.13
4.134	0.001	7.36E-08	-3.92E-08	0.0141	2.94E-08	1.65E-02						12126.77
4.634	0.000	7.76E-10	-4.14E-10	0.0141	3.10E-10	1.74E-04						12156.66
5.134	0.000	8.22E-12	-4.38E-12	0.0141	3.29E-12	1.85E-06						12156.97
5.884	0.000	2.94E-14	-1.57E-14	0.0141	1.17E-14	6.60E-09						12156.97
6.884	0.000	1.07E-14	-5.71E-15	0.0141	4.28E-15	2.40E-09						12156.97
7.884	0.000	1.07E-14	-5.71E-15	0.0141	4.28E-15	2.40E-09						12156.97
8.884	0.000	1.07E-14	-5.71E-15	0.0141	4.28E-15	2.40E-09						12156.97
10.384	0.000	1.07E-14	-5.71E-15	0.0141	4.28E-15	2.40E-09						12156.97
12.384	0.000	1.07E-14	-5.71E-15	0.0141	4.28E-15	2.40E-09						12156.97
14.884	0.000	1.07E-14	-5.71E-15	0.0141	4.28E-15	2.40E-09						12156.97
17.884	0.000	1.07E-14	-5.71E-15	0.0141	4.28E-15	2.40E-09						12156.97
21.384	0.000	1.07E-14	-5.71E-15	0.0141	4.28E-15	2.40E-09						12156.97
25.384	0.000	1.07E-14	-5.71E-15	0.0141	4.28E-15	2.40E-09						12156.97
29.384	0.000	1.07E-14	-5.71E-15	0.0141	4.28E-15	2.40E-09						12156.97
33.384	0.000	1.07E-14	-5.71E-15	0.0141	4.28E-15	2.40E-09						12156.97

RESULTS FOR YEAR: 16

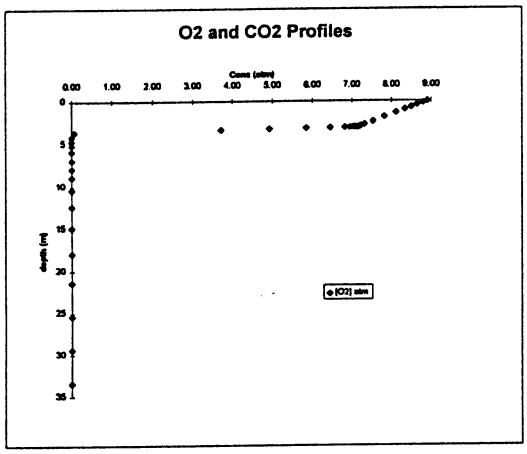

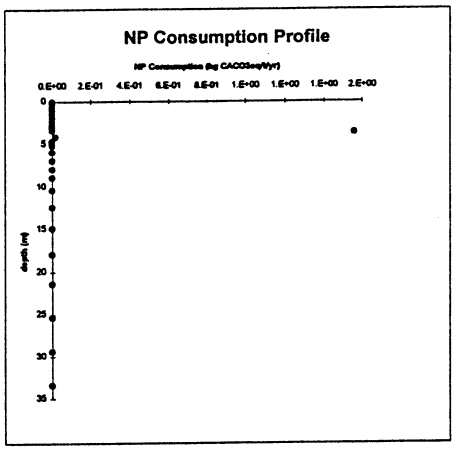

Flux in (mol/m²s)	3.51E-06
O_2 cons. (mol/m²s)	3.51E-06
Dpen (m)	4.884

t=16												
DEPTH (m)	CONC O2 (mol/m³)	O2 Cons (mol/m²/s)	CO2 Prod (mol/m²/s)	CONC CO2 (mol/m³)	mols O2 cons per m3 rock	NP consmptn kg CaCO3eq/t/yr						Sulf dens mol/m³
0.050	8.900	0.00E+00	0.00E+00	0.0141	0.00E+00	0.00E+00						0.00
0.225	8.798	0.00E+00	0.00E+00	0.0141	0.00E+00	0.00E+00						0.00
0.475	8.652	0.00E+00	0.00E+00	0.0141	0.00E+00	0.00E+00						0.00
0.725	8.505	0.00E+00	0.00E+00	0.0141	0.00E+00	0.00E+00						0.00
0.993	8.349	0.00E+00	0.00E+00	0.0141	0.00E+00	0.00E+00						0.00
1.385	8.120	0.00E+00	0.00E+00	0.0141	0.00E+00	0.00E+00						0.00
1.885	7.827	0.00E+00	0.00E+00	0.0141	0.00E+00	0.00E+00						0.00
2.385	7.535	0.00E+00	0.00E+00	0.0141	0.00E+00	0.00E+00						0.00
2.760	7.316	0.00E+00	0.00E+00	0.0141	0.00E+00	0.00E+00						0.00
2.911	7.227	0.00E+00	0.00E+00	0.0141	0.00E+00	0.00E+00						0.00
2.962	7.198	0.00E+00	0.00E+00	0.0141	0.00E+00	0.00E+00						0.00
3.012	7.168	0.00E+00	0.00E+00	0.0141	0.00E+00	0.00E+00						0.00
3.042	7.151	0.00E+00	0.00E+00	0.0141	0.00E+00	0.00E+00						0.00
3.050	7.146	0.00E+00	0.00E+00	0.0141	0.00E+00	0.00E+00						0.00
3.053	7.139	0.00E+00	0.00E+00	0.0141	0.00E+00	0.00E+00						0.00
3.054	7.127	0.00E+00	0.00E+00	0.0141	0.00E+00	0.00E+00						0.00
3.057	7.090	0.00E+00	0.00E+00	0.0141	0.00E+00	0.00E+00						0.00
3.062	7.029	0.00E+00	0.00E+00	0.0141	0.00E+00	0.00E+00						0.00
3.069	6.938	0.00E+00	0.00E+00	0.0141	0.00E+00	0.00E+00						0.00
3.079	6.816	0.00E+00	0.00E+00	0.0141	0.00E+00	0.00E+00						0.00
3.109	6.451	0.00E+00	0.00E+00	0.0141	0.00E+00	0.00E+00						0.00
3.159	5.843	0.00E+00	0.00E+00	0.0141	0.00E+00	0.00E+00						0.00
3.234	4.931	0.00E+00	0.00E+00	0.0141	0.00E+00	0.00E+00						0.00
3.334	3.714	0.00E+00	0.00E+00	0.0141	0.00E+00	0.00E+00						0.00
3.634	0.065	6.94E-06	-3.70E-06	0.0141	2.78E-06	1.56E+00						3155.37
4.134	0.001	7.33E-08	-3.91E-08	0.0141	2.93E-08	1.65E-02						12062.02
4.634	0.000	7.73E-10	-4.12E-10	0.0141	3.09E-10	1.74E-04						12155.98
5.134	0.000	8.19E-12	-4.37E-12	0.0141	3.27E-12	1.84E-06						12156.97
5.884	0.000	2.92E-14	-1.56E-14	0.0141	1.17E-14	6.57E-09						12156.97
6.884	0.000	1.07E-14	-5.71E-15	0.0141	4.28E-15	2.40E-09						12156.97
7.884	0.000	1.07E-14	-5.71E-15	0.0141	4.28E-15	2.40E-09						12156.97
8.884	0.000	1.07E-14	-5.71E-15	0.0141	4.28E-15	2.40E-09						12156.97
10.384	0.000	1.07E-14	-5.71E-15	0.0141	4.28E-15	2.40E-09						12156.97
12.384	0.000	1.07E-14	-5.71E-15	0.0141	4.28E-15	2.40E-09						12156.97
14.884	0.000	1.07E-14	-5.71E-15	0.0141	4.28E-15	2.40E-09						12156.97
17.884	0.000	1.07E-14	-5.71E-15	0.0141	4.28E-15	2.40E-09						12156.97
21.384	0.000	1.07E-14	-5.71E-15	0.0141	4.28E-15	2.40E-09						12156.97
25.384	0.000	1.07E-14	-5.71E-15	0.0141	4.28E-15	2.40E-09						12156.97
29.384	0.000	1.07E-14	-5.71E-15	0.0141	4.28E-15	2.40E-09						12156.97
33.384	0.000	1.07E-14	-5.71E-15	0.0141	4.28E-15	2.40E-09						12156.97

RESULTS FOR YEAR: 24

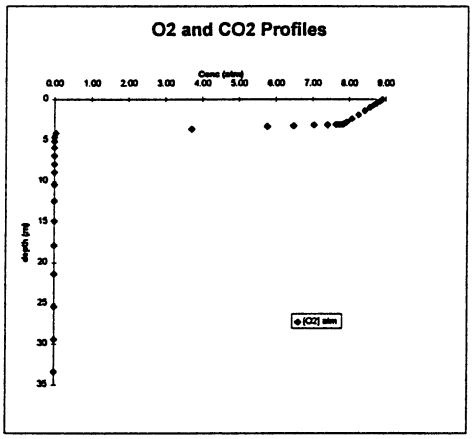

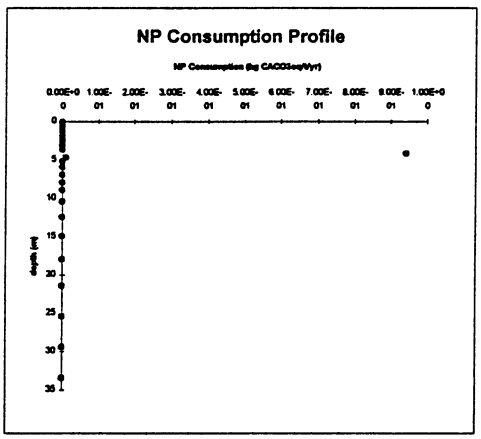

Flux in (mol/m²s)	2.10E-06
O_2 cons. (mol/m²s)	2.12E-06
Dpen (m)	5.384

t=24												
DEPTH (m)	CONC O2 (mol/m³)	O2 Cons (mol/m³/s)	CO2 Prod (mol/m³/s)	CONC CO2 (mol/m³)	mols O2 cons per m3 rock	NP consmptn kg CaCO3eq/t/yr						Sulf dens mol/m³
0.050	8.900	0.00E+00	0.00E+00	0.0141	0.00E+00	0.00E+00						0.00
0.225	8.839	0.00E+00	0.00E+00	0.0141	0.00E+00	0.00E+00						0.00
0.475	8.751	0.00E+00	0.00E+00	0.0141	0.00E+00	0.00E+00						0.00
0.725	8.664	0.00E+00	0.00E+00	0.0141	0.00E+00	0.00E+00						0.00
0.993	8.570	0.00E+00	0.00E+00	0.0141	0.00E+00	0.00E+00						0.00
1.385	8.432	0.00E+00	0.00E+00	0.0141	0.00E+00	0.00E+00						0.00
1.885	8.254	0.00E+00	0.00E+00	0.0141	0.00E+00	0.00E+00						0.00
2.385	8.076	0.00E+00	0.00E+00	0.0141	0.00E+00	0.00E+00						0.00
2.760	7.941	0.00E+00	0.00E+00	0.0141	0.00E+00	0.00E+00						0.00
2.911	7.886	0.00E+00	0.00E+00	0.0141	0.00E+00	0.00E+00						0.00
2.962	7.868	0.00E+00	0.00E+00	0.0141	0.00E+00	0.00E+00						0.00
3.012	7.850	0.00E+00	0.00E+00	0.0141	0.00E+00	0.00E+00						0.00
3.042	7.839	0.00E+00	0.00E+00	0.0141	0.00E+00	0.00E+00						0.00
3.050	7.837	0.00E+00	0.00E+00	0.0141	0.00E+00	0.00E+00						0.00
3.053	7.832	0.00E+00	0.00E+00	0.0141	0.00E+00	0.00E+00						0.00
3.054	7.825	0.00E+00	0.00E+00	0.0141	0.00E+00	0.00E+00						0.00
3.057	7.802	0.00E+00	0.00E+00	0.0141	0.00E+00	0.00E+00						0.00
3.062	7.765	0.00E+00	0.00E+00	0.0141	0.00E+00	0.00E+00						0.00
3.069	7.709	0.00E+00	0.00E+00	0.0141	0.00E+00	0.00E+00						0.00
3.079	7.634	0.00E+00	0.00E+00	0.0141	0.00E+00	0.00E+00						0.00
3.109	7.411	0.00E+00	0.00E+00	0.0141	0.00E+00	0.00E+00						0.00
3.159	7.039	0.00E+00	0.00E+00	0.0141	0.00E+00	0.00E+00						0.00
3.234	6.486	0.00E+00	0.00E+00	0.0141	0.00E+00	0.00E+00						0.00
3.334	5.769	0.00E+00	0.00E+00	0.0141	0.00E+00	0.00E+00						0.00
3.634	3.716	0.00E+00	0.00E+00	0.0141	0.00E+00	0.00E+00						0.00
4.134	0.039	4.20E-06	-2.24E-06	0.0141	1.68E-06	9.43E-01						10252.03
4.634	0.000	4.43E-08	-2.36E-08	0.0141	1.77E-08	9.95E-03						12136.89
5.134	0.000	4.69E-10	-2.50E-10	0.0141	1.88E-10	1.05E-04						12156.77
5.884	0.000	1.67E-12	-8.93E-13	0.0141	6.70E-13	3.76E-07						12156.97
6.884	0.000	1.07E-14	-5.71E-15	0.0141	4.28E-15	2.40E-09						12156.97
7.884	0.000	1.07E-14	-5.71E-15	0.0141	4.28E-15	2.40E-09						12156.97
8.884	0.000	1.07E-14	-5.71E-15	0.0141	4.28E-15	2.40E-09						12156.97
10.384	0.000	1.07E-14	-5.71E-15	0.0141	4.28E-15	2.40E-09						12156.97
12.384	0.000	1.07E-14	-5.71E-15	0.0141	4.28E-15	2.40E-09						12156.97
14.884	0.000	1.07E-14	-5.71E-15	0.0141	4.28E-15	2.40E-09						12156.97
17.884	0.000	1.07E-14	-5.71E-15	0.0141	4.28E-15	2.40E-09						12156.97
21.384	0.000	1.07E-14	-5.71E-15	0.0141	4.28E-15	2.40E-09						12156.97
25.384	0.000	1.07E-14	-5.71E-15	0.0141	4.28E-15	2.40E-09						12156.97
29.384	0.000	1.07E-14	-5.71E-15	0.0141	4.28E-15	2.40E-09						12156.97
33.384	0.000	1.07E-14	-5.71E-15	0.0141	4.28E-15	2.40E-09						12156.97

RESULTS FOR YEAR: 32

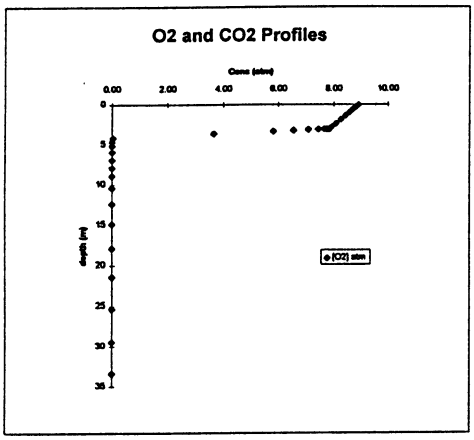

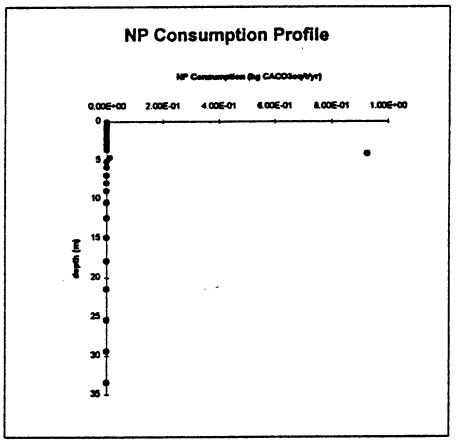

Flux in (mol/m²s)	2.08E-06
O_2 cons. (mol/m²s)	2.08E-06
Dpen (m)	5.384

t=32												
DEPTH (m)	CONC O2 (mol/m³)	O2 Cons (mol/m³/s)	CO2 Prod (mol/m³/s)	CONC CO2 (mol/m³)	mols O2 cons per m3 rock	NP consmptn kg CaCO3eq/t/yr						Sulf dens mol/m³
0.050	8.900	0.00E+00	0.00E+00	0.0141	0.00E+00	0.00E+00						0.00
0.225	8.839	0.00E+00	0.00E+00	0.0141	0.00E+00	0.00E+00						0.00
0.475	8.752	0.00E+00	0.00E+00	0.0141	0.00E+00	0.00E+00						0.00
0.725	8.666	0.00E+00	0.00E+00	0.0141	0.00E+00	0.00E+00						0.00
0.993	8.573	0.00E+00	0.00E+00	0.0141	0.00E+00	0.00E+00						0.00
1.385	8.436	0.00E+00	0.00E+00	0.0141	0.00E+00	0.00E+00						0.00
1.885	8.263	0.00E+00	0.00E+00	0.0141	0.00E+00	0.00E+00						0.00
2.385	8.089	0.00E+00	0.00E+00	0.0141	0.00E+00	0.00E+00						0.00
2.760	7.959	0.00E+00	0.00E+00	0.0141	0.00E+00	0.00E+00						0.00
2.911	7.906	0.00E+00	0.00E+00	0.0141	0.00E+00	0.00E+00						0.00
2.962	7.889	0.00E+00	0.00E+00	0.0141	0.00E+00	0.00E+00						0.00
3.012	7.871	0.00E+00	0.00E+00	0.0141	0.00E+00	0.00E+00						0.00
3.042	7.861	0.00E+00	0.00E+00	0.0141	0.00E+00	0.00E+00						0.00
3.050	7.858	0.00E+00	0.00E+00	0.0141	0.00E+00	0.00E+00						0.00
3.053	7.854	0.00E+00	0.00E+00	0.0141	0.00E+00	0.00E+00						0.00
3.054	7.847	0.00E+00	0.00E+00	0.0141	0.00E+00	0.00E+00						0.00
3.057	7.825	0.00E+00	0.00E+00	0.0141	0.00E+00	0.00E+00						0.00
3.062	7.789	0.00E+00	0.00E+00	0.0141	0.00E+00	0.00E+00						0.00
3.069	7.735	0.00E+00	0.00E+00	0.0141	0.00E+00	0.00E+00						0.00
3.079	7.662	0.00E+00	0.00E+00	0.0141	0.00E+00	0.00E+00						0.00
3.109	7.446	0.00E+00	0.00E+00	0.0141	0.00E+00	0.00E+00						0.00
3.159	7.084	0.00E+00	0.00E+00	0.0141	0.00E+00	0.00E+00						0.00
3.234	6.542	0.00E+00	0.00E+00	0.0141	0.00E+00	0.00E+00						0.00
3.334	5.820	0.00E+00	0.00E+00	0.0141	0.00E+00	0.00E+00						0.00
3.634	3.652	0.00E+00	0.00E+00	0.0141	0.00E+00	0.00E+00						0.00
4.134	0.039	4.12E-06	-2.20E-06	0.0141	1.65E-06	9.27E-01						6606.55
4.634	0.000	4.35E-08	-2.32E-08	0.0141	1.74E-08	9.78E-03						12098.42
5.134	0.000	4.61E-10	-2.46E-10	0.0141	1.84E-10	1.04E-04						12156.37
5.884	0.000	1.65E-12	-8.78E-13	0.0141	6.58E-13	3.70E-07						12156.97
6.884	0.000	1.07E-14	-5.71E-15	0.0141	4.28E-15	2.40E-09						12156.97
7.884	0.000	1.07E-14	-5.71E-15	0.0141	4.28E-15	2.40E-09						12156.97
8.884	0.000	1.07E-14	-5.71E-15	0.0141	4.28E-15	2.40E-09						12156.97
10.384	0.000	1.07E-14	-5.71E-15	0.0141	4.28E-15	2.40E-09						12156.97
12.384	0.000	1.07E-14	-5.71E-15	0.0141	4.28E-15	2.40E-09						12156.97
14.884	0.000	1.07E-14	-5.71E-15	0.0141	4.28E-15	2.40E-09						12156.97
17.884	0.000	1.07E-14	-5.71E-15	0.0141	4.28E-15	2.40E-09						12156.97
21.384	0.000	1.07E-14	-5.71E-15	0.0141	4.28E-15	2.40E-09						12156.97
25.384	0.000	1.07E-14	-5.71E-15	0.0141	4.28E-15	2.40E-09						12156.97
29.384	0.000	1.07E-14	-5.71E-15	0.0141	4.28E-15	2.40E-09						12156.97
33.384	0.000	1.07E-14	-5.71E-15	0.0141	4.28E-15	2.40E-09						12156.97

APPENDIX A8
Run 3B1, Open Stope

COUPLED $O_2/CO_2/Mg/SO_4/Ca$ MODEL

OXYDIFF V2.0

MODEL DETAILS

Filename	BF_CS3b1
Date	27/11/1996
Description:	Steady State Model Of Crandon Open Stope Placed Cemented Backfill Tailings
	Part 2 (year 1 to 32)
	First Order Model

INPUT PARAMETERS

Finite Difference Parameters

nodes x	1
nodes y	40
time periods	7
init delt (s)	0.01
[O2] at surface (mol/m³)	8.9
[CO2] at surface (mol/m³))	0.0141

Model Options

CO2 OPTION	0
FES2 OPTION	1
O2 OPTION	1

Geochemical Options

Infiltration (m/s)	1.10E-09
Infiltration Coefficient	1.00
Kgypsum	-
Infiltration (m/s)	1.10E-09
Fraction Flow Paths (G)	1.00

Diffusion Parameters

Dw (m2/s)	2.20E-09
Da (m2/s)	1.80E-05
τ	0.273
α	3.28
H	33.9

OUTPUT TIMES

time (s)	time (y)	Output col
1.6E+07	1	1
6.3E+07	2	6
1.3E+08	4	11
2.5E+08	8	16
5.0E+08	16	21
7.6E+08	24	26
1.0E+09	32	31

FES2 OPTION
0 - No FES2 DEPLETION
1 - ALLOW FES2 DEPLETION

CO2 OPTION:
0 - No CO2 Coupling
1 - CO2 Coupling

O2 OPTION
0 - HALF ORDER REACTION
1 - FIRST ORDER REACTION
2 - MIXED FIRST ORDER / ZERO ORDER
3 - ZERO ORDER SOLUTION

TORTUOSITY

Rockfill	τ	3
Cemented Tailings	τ	10

MODEL INPUTS

Material	DEPTH (m)	Depth (ft)	Cell Sizes (m)	r (s-1)	Porosity	Bulk Dens. (tonnes m^{-3})	Sat. (%)	SulfDens (mol/m^3)	Diff Coeff [1] (m2/s)	Diff Coeff [2] (m2/s)	$[O_2]_{BM}$ (mol/m^3)	$[CO_2]_{BM}$ (mol/m^3)
Waste Rock	0.050	0.164	0.1	0.00E+00	0.40	1.9	15%	0	6.00E-06	6.00E-06	8.89	1.41E-02
Waste Rock	0.200	0.656	0.2	0.00E+00	0.40	1.9	15%	0	6.00E-06	6.00E-06	8.89	1.41E-02
Waste Rock	0.450	1.476	0.3	0.00E+00	0.40	1.9	15%	0	6.00E-06	6.00E-06	8.89	1.41E-02
Waste Rock	1.100	3.609	1	0.00E+00	0.40	1.9	15%	0	6.00E-06	6.00E-06	8.89	1.41E-02
Waste Rock	2.600	8.530	2	0.00E+00	0.40	1.9	15%	0	6.00E-06	6.00E-06	8.89	1.41E-02
Waste Rock	4.600	15.092	2	0.00E+00	0.40	1.9	15%	0	6.00E-06	6.00E-06	8.89	1.41E-02
Waste Rock	7.600	24.934	4	0.00E+00	0.40	1.9	15%	0	6.00E-06	6.00E-06	8.89	1.41E-02
Waste Rock	11.600	38.058	4	0.00E+00	0.40	1.9	15%	0	6.00E-06	6.00E-06	8.89	1.41E-02
Waste Rock	14.600	47.900	2	0.00E+00	0.40	1.9	15%	0	6.00E-06	6.00E-06	8.89	1.41E-02
Waste Rock	16.100	52.822	1	0.00E+00	0.40	1.9	15%	0	6.00E-06	6.00E-06	8.89	1.41E-02
Waste Rock	16.650	54.626	0.1	0.00E+00	0.40	1.9	15%	0	6.00E-06	6.00E-06	8.89	1.41E-02
Waste Rock	16.725	54.872	0.05	0.00E+00	0.40	1.9	15%	0	6.00E-06	6.00E-06	8.89	1.41E-02
Waste Rock	16.755	54.970	0.01	0.00E+00	0.40	1.9	15%	0	6.00E-06	6.00E-06	8.89	1.41E-02
Waste Rock	16.763	54.995	0.005	0.00E+00	0.40	1.9	15%	0	6.00E-06	6.00E-06	8.89	1.41E-02
Tailings Backfill	16.766	55.005	0.001	1.07E-04	0.40	3.0	15%	12187	2.88E-07	2.88E-07	8.89	1.41E-02
Tailings Backfill	16.767	55.008	0.001	1.07E-04	0.40	3.0	15%	12187	2.88E-07	2.88E-07	8.89	1.41E-02
Tailings Backfill	16.770	55.018	0.005	1.07E-04	0.40	3.0	15%	12187	2.88E-07	2.88E-07	8.89	1.41E-02
Tailings Backfill	16.775	55.034	0.005	1.07E-04	0.40	3.0	15%	12187	2.88E-07	2.88E-07	8.89	1.41E-02
Tailings Backfill	16.782	55.059	0.01	1.07E-04	0.40	3.0	15%	12187	2.88E-07	2.88E-07	8.89	1.41E-02
Tailings Backfill	16.792	55.092	0.01	1.07E-04	0.40	3.0	15%	12187	2.88E-07	2.88E-07	8.89	1.41E-02
Tailings Backfill	16.822	55.190	0.05	1.07E-04	0.40	3.0	15%	12187	2.88E-07	2.88E-07	8.89	1.41E-02
Tailings Backfill	16.872	55.354	0.05	1.07E-04	0.40	3.0	15%	12187	2.88E-07	2.88E-07	8.89	1.41E-02
Tailings Backfill	16.947	55.600	0.1	1.07E-04	0.40	3.0	15%	12187	2.88E-07	2.88E-07	8.89	1.41E-02
Tailings Backfill	17.047	55.928	0.1	1.07E-04	0.40	3.0	15%	12187	2.88E-07	2.88E-07	8.89	1.41E-02
Tailings Backfill	17.347	56.913	0.5	1.07E-04	0.40	3.0	15%	12187	2.88E-07	2.88E-07	8.89	1.41E-02
Tailings Backfill	17.847	58.553	0.5	1.07E-04	0.40	3.0	15%	12187	2.88E-07	2.88E-07	8.89	1.41E-02
Tailings Backfill	18.347	60.194	0.5	1.07E-04	0.40	3.0	15%	12187	2.88E-07	2.88E-07	8.89	1.41E-02
Tailings Backfill	18.847	61.834	0.5	1.07E-04	0.40	3.0	15%	12187	2.88E-07	2.88E-07	8.89	1.41E-02
Tailings Backfill	19.597	64.295	1	1.07E-04	0.40	3.0	15%	12187	2.88E-07	2.88E-07	8.89	1.41E-02
Tailings Backfill	20.597	67.575	1	1.07E-04	0.40	3.0	15%	12187	2.88E-07	2.88E-07	8.89	1.41E-02
Tailings Backfill	21.597	70.856	1	1.07E-04	0.40	3.0	15%	12187	2.88E-07	2.88E-07	8.89	1.41E-02
Tailings Backfill	22.597	74.137	1	1.07E-04	0.40	3.0	15%	12187	2.88E-07	2.88E-07	8.89	1.41E-02
Tailings Backfill	24.097	79.058	2	1.07E-04	0.40	3.0	15%	12187	2.88E-07	2.88E-07	8.89	1.41E-02
Tailings Backfill	26.097	85.620	2	1.07E-04	0.40	3.0	15%	12187	2.88E-07	2.88E-07	8.89	1.41E-02
Tailings Backfill	28.597	93.822	3	1.07E-04	0.40	3.0	15%	12187	2.88E-07	2.88E-07	8.89	1.41E-02
Tailings Backfill	31.597	103.665	3	1.07E-04	0.40	3.0	15%	12187	2.88E-07	2.88E-07	8.89	1.41E-02
Tailings Backfill	35.097	115.148	4	1.07E-04	0.40	3.0	15%	12187	2.88E-07	2.88E-07	8.89	1.41E-02
Tailings Backfill	39.097	128.271	4	1.07E-04	0.40	3.0	15%	12187	2.88E-07	2.88E-07	8.89	1.41E-02
Tailings Backfill	43.097	141.394	4	1.07E-04	0.40	3.0	15%	12187	2.88E-07	2.88E-07	8.89	1.41E-02
Tailings Backfill	47.097	154.518	4	1.07E-04	0.40	3.0	15%	12187	2.88E-07	2.88E-07	8.89	1.41E-02

1. Diff Coefficient Based on Erbering, B., R.V.Nicholson, E.J.Reardon and P.Tibble, Evaluation of sulphide oxidation rates. Nordic Hydrology, 24(5), 323-338, 1993.
2. Diff Coefficient Based on Reardon, E.J. and P.M. Moddle, Gas Diffusion Coefficient Measurements on Uranium Mill Tailings: Implications to Cover Layer Design. Uranium, 2, 111-131,1985.

RESULTS FOR YEAR: 1

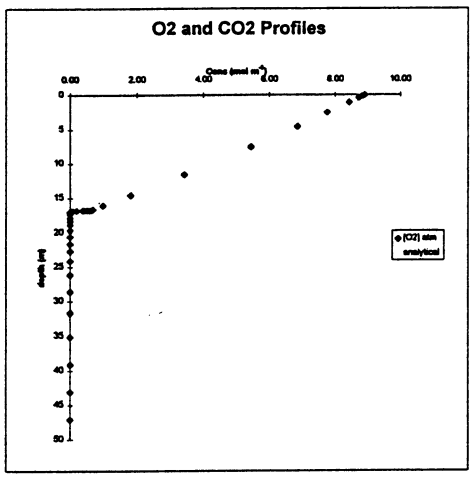

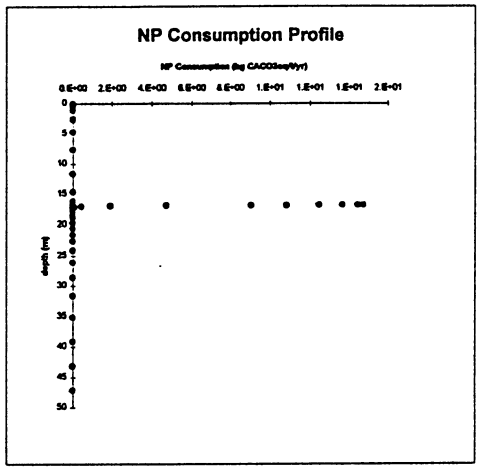

Flux in (mol/m²s)	2.67E-06
O_2 cons. (mol/m²s)	3.32E-06
Dpen (m)	18.097

t=1												
DEPTH (m)	CONC O2 (mol/m³)	O2 Cons (mol/m³/s)	CO2 Prod (mol/m³/s)	CONC CO2 (mol/m³)	mols O2 cons per m³ material	NP consmptn kg CaCO3eq/l/yr						Sulf dens mol/m³
0.050	8.900	0.00E+00	0.00E+00	0.0141	0.00E+00	0.00E+00						0.00
0.200	8.833	0.00E+00	0.00E+00	0.0141	0.00E+00	0.00E+00						0.00
0.450	8.722	0.00E+00	0.00E+00	0.0141	0.00E+00	0.00E+00						0.00
1.100	8.433	0.00E+00	0.00E+00	0.0141	0.00E+00	0.00E+00						0.00
2.600	7.764	0.00E+00	0.00E+00	0.0141	0.00E+00	0.00E+00						0.00
4.600	6.855	0.00E+00	0.00E+00	0.0141	0.00E+00	0.00E+00						0.00
7.600	5.453	0.00E+00	0.00E+00	0.0141	0.00E+00	0.00E+00						0.00
11.600	3.432	0.00E+00	0.00E+00	0.0141	0.00E+00	0.00E+00						0.00
14.600	1.812	0.00E+00	0.00E+00	0.0141	0.00E+00	0.00E+00						0.00
16.100	0.986	0.00E+00	0.00E+00	0.0141	0.00E+00	0.00E+00						0.00
16.650	0.682	0.00E+00	0.00E+00	0.0141	0.00E+00	0.00E+00						0.00
16.725	0.641	0.00E+00	0.00E+00	0.0141	0.00E+00	0.00E+00						0.00
16.755	0.624	0.00E+00	0.00E+00	0.0141	0.00E+00	0.00E+00						0.00
16.763	0.620	0.00E+00	0.00E+00	0.0141	0.00E+00	0.00E+00						0.00
16.766	0.613	6.56E-05	-3.50E-05	0.0141	2.62E-05	1.47E+01						6189.83
16.767	0.601	6.44E-05	-3.43E-05	0.0141	2.57E-05	1.45E+01						6299.74
16.770	0.568	6.08E-05	-3.24E-05	0.0141	2.43E-05	1.37E+01						6622.93
16.775	0.518	5.54E-05	-2.96E-05	0.0141	2.22E-05	1.25E+01						7110.29
16.782	0.450	4.82E-05	-2.57E-05	0.0141	1.93E-05	1.08E+01						7771.16
16.792	0.377	4.03E-05	-2.15E-05	0.0141	1.61E-05	9.05E+00						8489.69
16.822	0.197	2.11E-05	-1.12E-05	0.0141	8.43E-06	4.74E+00						10237.37
16.872	0.081	8.64E-06	-4.61E-06	0.0141	3.45E-06	1.94E+00						11370.73
16.947	0.018	1.97E-06	-1.05E-06	0.0141	7.88E-07	4.43E-01						11977.54
17.047	0.004	3.91E-07	-2.09E-07	0.0141	1.56E-07	8.79E-02						12121.34
17.347	0.000	6.83E-09	-3.64E-09	0.0141	2.73E-09	1.54E-03						12156.34
17.847	0.000	7.21E-11	-3.85E-11	0.0141	2.89E-11	1.62E-05						12156.97
18.347	0.000	7.62E-13	-4.06E-13	0.0141	3.05E-13	1.71E-07						12156.97
18.847	0.000	1.07E-14	-5.71E-15	0.0141	4.28E-15	2.40E-09						12156.97
19.597	0.000	1.07E-14	-5.71E-15	0.0141	4.28E-15	2.40E-09						12156.97
20.597	0.000	1.07E-14	-5.71E-15	0.0141	4.28E-15	2.40E-09						12156.97
21.597	0.000	1.07E-14	-5.71E-15	0.0141	4.28E-15	2.40E-09						12156.97
22.597	0.000	1.07E-14	-5.71E-15	0.0141	4.28E-15	2.40E-09						12156.97
24.097	0.000	1.07E-14	-5.71E-15	0.0141	4.28E-15	2.40E-09						12156.97
26.097	0.000	1.07E-14	-5.71E-15	0.0141	4.28E-15	2.40E-09						12156.97
28.597	0.000	1.07E-14	-5.71E-15	0.0141	4.28E-15	2.40E-09						12156.97
31.597	0.000	1.07E-14	-5.71E-15	0.0141	4.28E-15	2.40E-09						12156.97
35.097	0.000	1.07E-14	-5.71E-15	0.0141	4.28E-15	2.40E-09						12156.97
39.097	0.000	1.07E-14	-5.71E-15	0.0141	4.28E-15	2.40E-09						12156.97
43.097	0.000	1.07E-14	-5.71E-15	0.0141	4.28E-15	2.40E-09						12156.97
47.097	0.000	1.07E-14	-5.71E-15	0.0141	4.28E-15	2.40E-09						12156.97

RESULTS FOR YEAR: 2

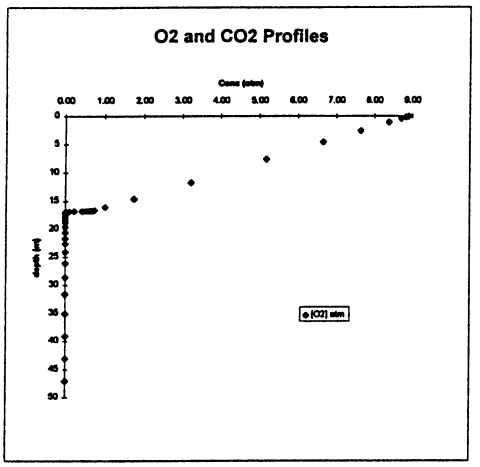

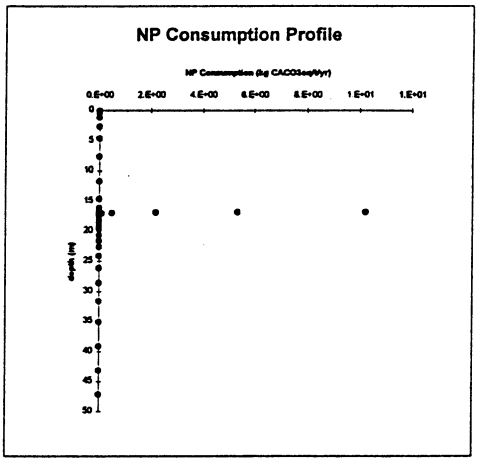

Flux in (mol/m²s)	2.96E-06
O_2 cons. (mol/m²s)	2.40E-06
Dpen (m)	18.097

t=2												
DEPTH (m)	CONC O2 (mol/m³)	O2 Cons (mol/m³/s)	CO2 Prod (mol/m³/s)	CONC CO2 (mol/m³)	mole O2 cons per m3 rock	NP consmptn kg CaCO3eq/t/yr						Sulf dens mol/m³
0.050	8.900	0.00E+00	0.00E+00	0.0141	0.00E+00	0.00E+00						0.00
0.200	8.826	0.00E+00	0.00E+00	0.0141	0.00E+00	0.00E+00						0.00
0.450	8.703	0.00E+00	0.00E+00	0.0141	0.00E+00	0.00E+00						0.00
1.100	8.382	0.00E+00	0.00E+00	0.0141	0.00E+00	0.00E+00						0.00
2.600	7.643	0.00E+00	0.00E+00	0.0141	0.00E+00	0.00E+00						0.00
4.600	6.656	0.00E+00	0.00E+00	0.0141	0.00E+00	0.00E+00						0.00
7.600	5.181	0.00E+00	0.00E+00	0.0141	0.00E+00	0.00E+00						0.00
11.600	3.214	0.00E+00	0.00E+00	0.0141	0.00E+00	0.00E+00						0.00
14.600	1.744	0.00E+00	0.00E+00	0.0141	0.00E+00	0.00E+00						0.00
16.100	1.009	0.00E+00	0.00E+00	0.0141	0.00E+00	0.00E+00						0.00
16.650	0.739	0.00E+00	0.00E+00	0.0141	0.00E+00	0.00E+00						0.00
16.725	0.702	0.00E+00	0.00E+00	0.0141	0.00E+00	0.00E+00						0.00
16.755	0.688	0.00E+00	0.00E+00	0.0141	0.00E+00	0.00E+00						0.00
16.763	0.684	0.00E+00	0.00E+00	0.0141	0.00E+00	0.00E+00						0.00
16.766	0.678	0.00E+00	0.00E+00	0.0141	0.00E+00	0.00E+00						0.00
16.767	0.667	0.00E+00	0.00E+00	0.0141	0.00E+00	0.00E+00						0.00
16.770	0.637	0.00E+00	0.00E+00	0.0141	0.00E+00	0.00E+00						0.00
16.775	0.586	0.00E+00	0.00E+00	0.0141	0.00E+00	0.00E+00						0.00
16.782	0.509	0.00E+00	0.00E+00	0.0141	0.00E+00	0.00E+00						0.00
16.792	0.425	4.55E-05	-2.43E-05	0.0141	1.82E-05	1.02E+01						1883.74
16.822	0.223	2.38E-05	-1.27E-05	0.0141	9.53E-06	5.35E+00						6780.51
16.872	0.091	9.75E-06	-5.20E-06	0.0141	3.90E-06	2.19E+00						9955.34
16.947	0.021	2.22E-06	-1.19E-06	0.0141	8.90E-07	5.00E-01						11654.71
17.047	0.004	4.42E-07	-2.35E-07	0.0141	1.77E-07	9.92E-02						12057.27
17.347	0.000	7.71E-09	-4.11E-09	0.0141	3.08E-09	1.73E-03						12155.23
17.847	0.000	8.14E-11	-4.34E-11	0.0141	3.25E-11	1.83E-05						12156.97
18.347	0.000	8.59E-13	-4.58E-13	0.0141	3.43E-13	1.93E-07						12156.97
18.847	0.000	1.07E-14	-5.71E-15	0.0141	4.28E-15	2.40E-09						12156.97
19.597	0.000	1.07E-14	-5.71E-15	0.0141	4.28E-15	2.40E-09						12156.97
20.597	0.000	1.07E-14	-5.71E-15	0.0141	4.28E-15	2.40E-09						12156.97
21.597	0.000	1.07E-14	-5.71E-15	0.0141	4.28E-15	2.40E-09						12156.97
22.597	0.000	1.07E-14	-5.71E-15	0.0141	4.28E-15	2.40E-09						12156.97
24.097	0.000	1.07E-14	-5.71E-15	0.0141	4.28E-15	2.40E-09						12156.97
26.097	0.000	1.07E-14	-5.71E-15	0.0141	4.28E-15	2.40E-09						12156.97
28.597	0.000	1.07E-14	-5.71E-15	0.0141	4.28E-15	2.40E-09						12156.97
31.597	0.000	1.07E-14	-5.71E-15	0.0141	4.28E-15	2.40E-09						12156.97
35.097	0.000	1.07E-14	-5.71E-15	0.0141	4.28E-15	2.40E-09						12156.97
39.097	0.000	1.07E-14	-5.71E-15	0.0141	4.28E-15	2.40E-09						12156.97
43.097	0.000	1.07E-14	-5.71E-15	0.0141	4.28E-15	2.40E-09						12156.97
47.097	0.000	1.07E-14	-5.71E-15	0.0141	4.28E-15	2.40E-09						12156.97

RESULTS FOR YEAR: 4

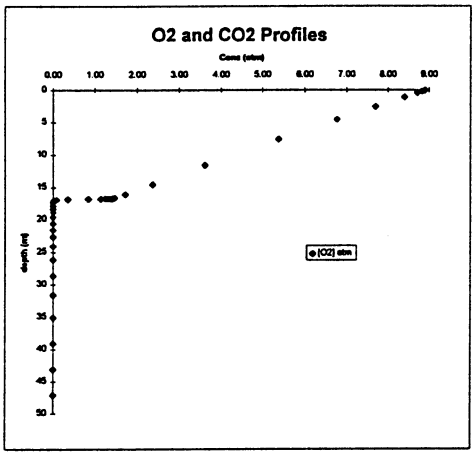

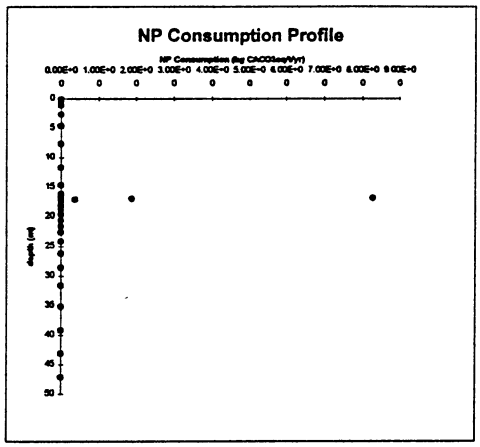

Flux in (mol/m²s)	2.82E-06
O_2 cons. (mol/m²s)	2.86E-06
Dpen (m)	18.097

t=4												
DEPTH (m)	CONC O2 (mol/m³)	O2 Cons (mol/m³/s)	CO2 Prod (mol/m³/s)	CONC CO2 (mol/m³)	mols O2 cons per m3 rock	NP consmptn kg CaCO3eq/t/yr						Sulf dens mol/m³
0.050	8.900	0.00E+00	0.00E+00	0.0141	0.00E+00	0.00E+00						0.00
0.200	8.829	0.00E+00	0.00E+00	0.0141	0.00E+00	0.00E+00						0.00
0.450	8.712	0.00E+00	0.00E+00	0.0141	0.00E+00	0.00E+00						0.00
1.100	8.406	0.00E+00	0.00E+00	0.0141	0.00E+00	0.00E+00						0.00
2.600	7.701	0.00E+00	0.00E+00	0.0141	0.00E+00	0.00E+00						0.00
4.600	6.767	0.00E+00	0.00E+00	0.0141	0.00E+00	0.00E+00						0.00
7.600	5.381	0.00E+00	0.00E+00	0.0141	0.00E+00	0.00E+00						0.00
11.600	3.613	0.00E+00	0.00E+00	0.0141	0.00E+00	0.00E+00						0.00
14.600	2.369	0.00E+00	0.00E+00	0.0141	0.00E+00	0.00E+00						0.00
16.100	1.722	0.00E+00	0.00E+00	0.0141	0.00E+00	0.00E+00						0.00
16.650	1.485	0.00E+00	0.00E+00	0.0141	0.00E+00	0.00E+00						0.00
16.725	1.429	0.00E+00	0.00E+00	0.0141	0.00E+00	0.00E+00						0.00
16.755	1.415	0.00E+00	0.00E+00	0.0141	0.00E+00	0.00E+00						0.00
16.763	1.411	0.00E+00	0.00E+00	0.0141	0.00E+00	0.00E+00						0.00
16.766	1.405	0.00E+00	0.00E+00	0.0141	0.00E+00	0.00E+00						0.00
16.767	1.395	0.00E+00	0.00E+00	0.0141	0.00E+00	0.00E+00						0.00
16.770	1.365	0.00E+00	0.00E+00	0.0141	0.00E+00	0.00E+00						0.00
16.775	1.315	0.00E+00	0.00E+00	0.0141	0.00E+00	0.00E+00						0.00
16.782	1.241	0.00E+00	0.00E+00	0.0141	0.00E+00	0.00E+00						0.00
16.792	1.140	0.00E+00	0.00E+00	0.0141	0.00E+00	0.00E+00						0.00
16.822	0.840	0.00E+00	0.00E+00	0.0141	0.00E+00	0.00E+00						0.00
16.872	0.344	3.68E-05	-1.96E-05	0.0141	1.47E-05	8.28E+00						6251.78
16.947	0.079	8.41E-06	-4.48E-06	0.0141	3.36E-06	1.89E+00						10810.21
17.047	0.016	1.67E-06	-8.91E-07	0.0141	6.68E-07	3.75E-01						11889.71
17.347	0.000	2.92E-08	-1.56E-08	0.0141	1.17E-08	6.57E-03						12152.32
17.847	0.000	3.09E-10	-1.65E-10	0.0141	1.24E-10	6.94E-05						12156.94
18.347	0.000	3.26E-12	-1.74E-12	0.0141	1.31E-12	7.33E-07						12156.97
18.847	0.000	3.46E-14	-1.85E-14	0.0141	1.38E-14	7.78E-09						12156.97
19.597	0.000	1.07E-14	-5.71E-15	0.0141	4.28E-15	2.40E-09						12156.97
20.597	0.000	1.07E-14	-5.71E-15	0.0141	4.28E-15	2.40E-09						12156.97
21.597	0.000	1.07E-14	-5.71E-15	0.0141	4.28E-15	2.40E-09						12156.97
22.597	0.000	1.07E-14	-5.71E-15	0.0141	4.28E-15	2.40E-09						12156.97
24.097	0.000	1.07E-14	-5.71E-15	0.0141	4.28E-15	2.40E-09						12156.97
26.097	0.000	1.07E-14	-5.71E-15	0.0141	4.28E-15	2.40E-09						12156.97
28.597	0.000	1.07E-14	-5.71E-15	0.0141	4.28E-15	2.40E-09						12156.97
31.597	0.000	1.07E-14	-5.71E-15	0.0141	4.28E-15	2.40E-09						12156.97
35.097	0.000	1.07E-14	-5.71E-15	0.0141	4.28E-15	2.40E-09						12156.97
39.097	0.000	1.07E-14	-5.71E-15	0.0141	4.28E-15	2.40E-09						12156.97
43.097	0.000	1.07E-14	-5.71E-15	0.0141	4.28E-15	2.40E-09						12156.97
47.097	0.000	1.07E-14	-5.71E-15	0.0141	4.28E-15	2.40E-09						12156.97

RESULTS FOR YEAR: 8

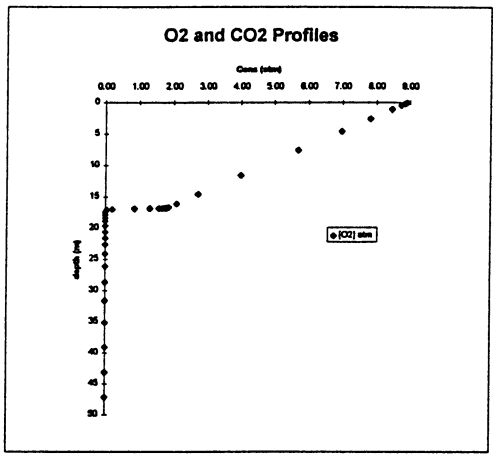

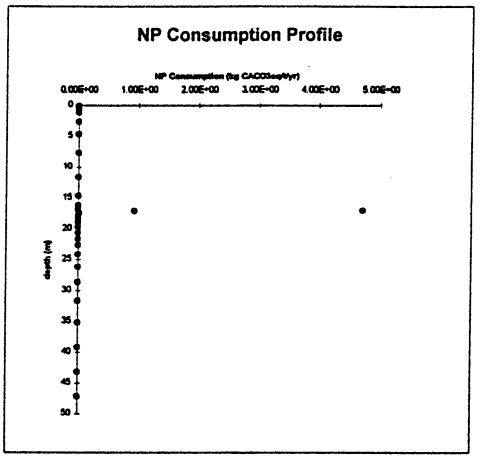

Flux in (mol/m²s)	2.55E-06
O_2 cons. (mol/m²s)	2.55E-06
Dpen (m)	18.097

t=8												
DEPTH (m)	CONC O2 (mol/m³)	O2 Cons (mol/m³/s)	CO2 Prod (mol/m³/s)	CONC CO2 (mol/m³)	mols O2 cons per m3 rock	NP consmptn kg CaCO3eq/t/yr						Sulf dens mol/m³
0.050	8.900	0.00E+00	0.00E+00	0.0141	0.00E+00	0.00E+00						0.00
0.200	8.836	0.00E+00	0.00E+00	0.0141	0.00E+00	0.00E+00						0.00
0.450	8.730	0.00E+00	0.00E+00	0.0141	0.00E+00	0.00E+00						0.00
1.100	8.454	0.00E+00	0.00E+00	0.0141	0.00E+00	0.00E+00						0.00
2.600	7.817	0.00E+00	0.00E+00	0.0141	0.00E+00	0.00E+00						0.00
4.600	6.968	0.00E+00	0.00E+00	0.0141	0.00E+00	0.00E+00						0.00
7.600	5.695	0.00E+00	0.00E+00	0.0141	0.00E+00	0.00E+00						0.00
11.600	3.997	0.00E+00	0.00E+00	0.0141	0.00E+00	0.00E+00						0.00
14.600	2.722	0.00E+00	0.00E+00	0.0141	0.00E+00	0.00E+00						0.00
16.100	2.088	0.00E+00	0.00E+00	0.0141	0.00E+00	0.00E+00						0.00
16.650	1.856	0.00E+00	0.00E+00	0.0141	0.00E+00	0.00E+00						0.00
16.725	1.824	0.00E+00	0.00E+00	0.0141	0.00E+00	0.00E+00						0.00
16.755	1.812	0.00E+00	0.00E+00	0.0141	0.00E+00	0.00E+00						0.00
16.763	1.808	0.00E+00	0.00E+00	0.0141	0.00E+00	0.00E+00						0.00
16.766	1.803	0.00E+00	0.00E+00	0.0141	0.00E+00	0.00E+00						0.00
16.767	1.794	0.00E+00	0.00E+00	0.0141	0.00E+00	0.00E+00						0.00
16.770	1.768	0.00E+00	0.00E+00	0.0141	0.00E+00	0.00E+00						0.00
16.775	1.724	0.00E+00	0.00E+00	0.0141	0.00E+00	0.00E+00						0.00
16.782	1.658	0.00E+00	0.00E+00	0.0141	0.00E+00	0.00E+00						0.00
16.792	1.569	0.00E+00	0.00E+00	0.0141	0.00E+00	0.00E+00						0.00
16.822	1.305	0.00E+00	0.00E+00	0.0141	0.00E+00	0.00E+00						0.00
16.872	0.860	0.00E+00	0.00E+00	0.0141	0.00E+00	0.00E+00						0.00
16.947	0.196	2.10E-05	-1.12E-05	0.0141	8.39E-06	4.72E+00						3806.25
17.047	0.039	4.16E-06	-2.22E-06	0.0141	1.67E-06	9.36E-01						10499.66
17.347	0.001	7.27E-08	-3.88E-08	0.0141	2.91E-08	1.63E-02						12128.04
17.847	0.000	7.68E-10	-4.09E-10	0.0141	3.07E-10	1.72E-04						12156.69
18.347	0.000	8.10E-12	-4.32E-12	0.0141	3.24E-12	1.82E-06						12156.97
18.847	0.000	8.58E-14	-4.58E-14	0.0141	3.43E-14	1.93E-08						12156.97
19.597	0.000	1.07E-14	-5.71E-15	0.0141	4.28E-15	2.40E-09						12156.97
20.597	0.000	1.07E-14	-5.71E-15	0.0141	4.28E-15	2.40E-09						12156.97
21.597	0.000	1.07E-14	-5.71E-15	0.0141	4.28E-15	2.40E-09						12156.97
22.597	0.000	1.07E-14	-5.71E-15	0.0141	4.28E-15	2.40E-09						12156.97
24.097	0.000	1.07E-14	-5.71E-15	0.0141	4.28E-15	2.40E-09						12156.97
26.097	0.000	1.07E-14	-5.71E-15	0.0141	4.28E-15	2.40E-09						12156.97
28.597	0.000	1.07E-14	-5.71E-15	0.0141	4.28E-15	2.40E-09						12156.97
31.597	0.000	1.07E-14	-5.71E-15	0.0141	4.28E-15	2.40E-09						12156.97
35.097	0.000	1.07E-14	-5.71E-15	0.0141	4.28E-15	2.40E-09						12156.97
39.097	0.000	1.07E-14	-5.71E-15	0.0141	4.28E-15	2.40E-09						12156.97
43.097	0.000	1.07E-14	-5.71E-15	0.0141	4.28E-15	2.40E-09						12156.97
47.097	0.000	1.07E-14	-5.71E-15	0.0141	4.28E-15	2.40E-09						12156.97

RESULTS FOR YEAR: 16

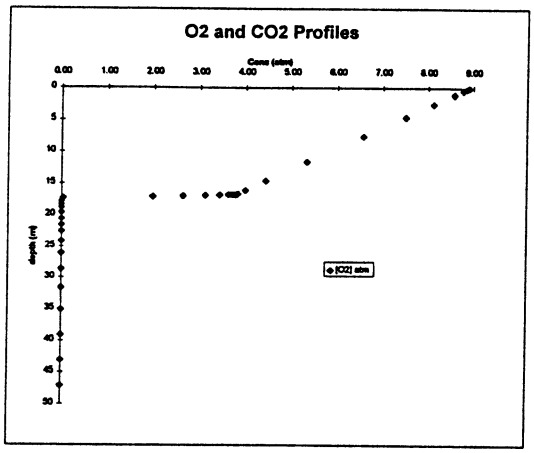

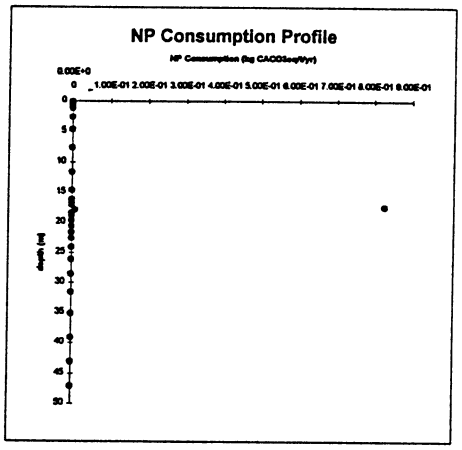

Flux in (mol/m²s)	1.84E-06
O_2 cons. (mol/m²s)	1.86E-06
Dpen (m)	18.597

t=16												
DEPTH (m)	CONC O2 (mol/m³)	O2 Cons (mol/m³/s)	CO2 Prod (mol/m³/s)	CONC CO2 (mol/m³)	mols O2 cons per m3 rock	NP consmptn kg CaCO3eq/t/yr						Sulf dens mol/m³
0.050	8.900	0.00E+00	0.00E+00	0.0141	0.00E+00	0.00E+00						0.00
0.200	8.854	0.00E+00	0.00E+00	0.0141	0.00E+00	0.00E+00						0.00
0.450	8.777	0.00E+00	0.00E+00	0.0141	0.00E+00	0.00E+00						0.00
1.100	8.576	0.00E+00	0.00E+00	0.0141	0.00E+00	0.00E+00						0.00
2.600	8.117	0.00E+00	0.00E+00	0.0141	0.00E+00	0.00E+00						0.00
4.600	7.501	0.00E+00	0.00E+00	0.0141	0.00E+00	0.00E+00						0.00
7.600	6.575	0.00E+00	0.00E+00	0.0141	0.00E+00	0.00E+00						0.00
11.600	5.338	0.00E+00	0.00E+00	0.0141	0.00E+00	0.00E+00						0.00
14.600	4.439	0.00E+00	0.00E+00	0.0141	0.00E+00	0.00E+00						0.00
16.100	3.996	0.00E+00	0.00E+00	0.0141	0.00E+00	0.00E+00						0.00
16.650	3.832	0.00E+00	0.00E+00	0.0141	0.00E+00	0.00E+00						0.00
16.725	3.809	0.00E+00	0.00E+00	0.0141	0.00E+00	0.00E+00						0.00
16.755	3.800	0.00E+00	0.00E+00	0.0141	0.00E+00	0.00E+00						0.00
16.763	3.798	0.00E+00	0.00E+00	0.0141	0.00E+00	0.00E+00						0.00
16.766	3.794	0.00E+00	0.00E+00	0.0141	0.00E+00	0.00E+00						0.00
16.767	3.788	0.00E+00	0.00E+00	0.0141	0.00E+00	0.00E+00						0.00
16.770	3.769	0.00E+00	0.00E+00	0.0141	0.00E+00	0.00E+00						0.00
16.775	3.738	0.00E+00	0.00E+00	0.0141	0.00E+00	0.00E+00						0.00
16.782	3.690	0.00E+00	0.00E+00	0.0141	0.00E+00	0.00E+00						0.00
16.792	3.627	0.00E+00	0.00E+00	0.0141	0.00E+00	0.00E+00						0.00
16.822	3.438	0.00E+00	0.00E+00	0.0141	0.00E+00	0.00E+00						0.00
16.872	3.117	0.00E+00	0.00E+00	0.0141	0.00E+00	0.00E+00						0.00
16.947	2.631	0.00E+00	0.00E+00	0.0141	0.00E+00	0.00E+00						0.00
17.047	1.973	0.00E+00	0.00E+00	0.0141	0.00E+00	0.00E+00						0.00
17.347	0.034	3.89E-06	-1.97E-06	0.0141	1.48E-06	8.29E-01						11041.72
17.847	0.000	3.89E-08	-2.08E-08	0.0141	1.56E-08	8.74E-03						12145.24
18.347	0.000	4.11E-10	-2.19E-10	0.0141	1.64E-10	9.23E-05						12156.85
18.847	0.000	4.35E-12	-2.32E-12	0.0141	1.74E-12	9.77E-07						12156.97
19.597	0.000	1.55E-14	-8.28E-15	0.0141	6.21E-15	3.49E-09						12156.97
20.597	0.000	1.07E-14	-5.71E-15	0.0141	4.28E-15	2.40E-09						12156.97
21.597	0.000	1.07E-14	-5.71E-15	0.0141	4.28E-15	2.40E-09						12156.97
22.597	0.000	1.07E-14	-5.71E-15	0.0141	4.28E-15	2.40E-09						12156.97
24.097	0.000	1.07E-14	-5.71E-15	0.0141	4.28E-15	2.40E-09						12156.97
26.097	0.000	1.07E-14	-5.71E-15	0.0141	4.28E-15	2.40E-09						12156.97
28.597	0.000	1.07E-14	-5.71E-15	0.0141	4.28E-15	2.40E-09						12156.97
31.597	0.000	1.07E-14	-5.71E-15	0.0141	4.28E-15	2.40E-09						12156.97
35.097	0.000	1.07E-14	-5.71E-15	0.0141	4.28E-15	2.40E-09						12156.97
39.097	0.000	1.07E-14	-5.71E-15	0.0141	4.28E-15	2.40E-09						12156.97
43.097	0.000	1.07E-14	-5.71E-15	0.0141	4.28E-15	2.40E-09						12156.97
47.097	0.000	1.07E-14	-5.71E-15	0.0141	4.28E-15	2.40E-09						12156.97

RESULTS FOR YEAR: 24

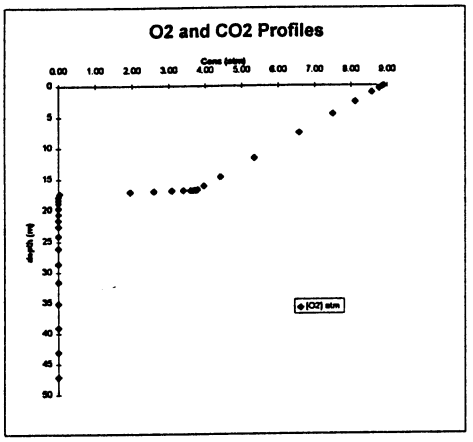

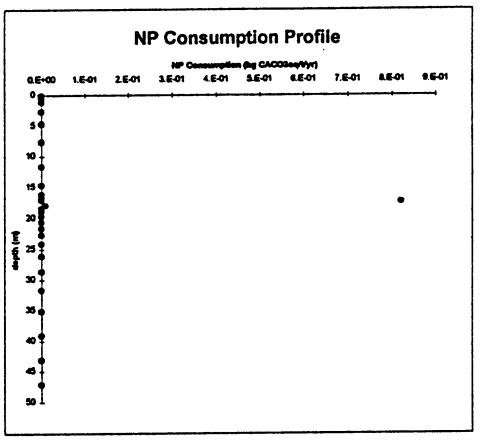

Flux in (mol/m²s)	1.85E-06
O_2 cons. (mol/m²s)	1.85E-06
Dpen (m)	16.597

t=24												
DEPTH (m)	CONC O2 (mol/m³)	O2 Cons (mol/m³/s)	CO2 Prod (mol/m³/s)	CONC CO2 (mol/m³)	mols O2 cons per m3 rock	NP consmptn kg CaCO3eq/t/yr						Sulf dens mol/m³
0.050	8.900	0.00E+00	0.00E+00	0.0141	0.00E+00	0.00E+00						0.00
0.200	8.854	0.00E+00	0.00E+00	0.0141	0.00E+00	0.00E+00						0.00
0.450	8.777	0.00E+00	0.00E+00	0.0141	0.00E+00	0.00E+00						0.00
1.100	8.577	0.00E+00	0.00E+00	0.0141	0.00E+00	0.00E+00						0.00
2.600	8.116	0.00E+00	0.00E+00	0.0141	0.00E+00	0.00E+00						0.00
4.600	7.501	0.00E+00	0.00E+00	0.0141	0.00E+00	0.00E+00						0.00
7.600	6.578	0.00E+00	0.00E+00	0.0141	0.00E+00	0.00E+00						0.00
11.600	5.348	0.00E+00	0.00E+00	0.0141	0.00E+00	0.00E+00						0.00
14.600	4.425	0.00E+00	0.00E+00	0.0141	0.00E+00	0.00E+00						0.00
16.100	3.963	0.00E+00	0.00E+00	0.0141	0.00E+00	0.00E+00						0.00
16.650	3.794	0.00E+00	0.00E+00	0.0141	0.00E+00	0.00E+00						0.00
16.725	3.771	0.00E+00	0.00E+00	0.0141	0.00E+00	0.00E+00						0.00
16.755	3.762	0.00E+00	0.00E+00	0.0141	0.00E+00	0.00E+00						0.00
16.763	3.760	0.00E+00	0.00E+00	0.0141	0.00E+00	0.00E+00						0.00
16.766	3.758	0.00E+00	0.00E+00	0.0141	0.00E+00	0.00E+00						0.00
16.767	3.749	0.00E+00	0.00E+00	0.0141	0.00E+00	0.00E+00						0.00
16.770	3.730	0.00E+00	0.00E+00	0.0141	0.00E+00	0.00E+00						0.00
16.775	3.698	0.00E+00	0.00E+00	0.0141	0.00E+00	0.00E+00						0.00
16.782	3.650	0.00E+00	0.00E+00	0.0141	0.00E+00	0.00E+00						0.00
16.792	3.586	0.00E+00	0.00E+00	0.0141	0.00E+00	0.00E+00						0.00
16.822	3.394	0.00E+00	0.00E+00	0.0141	0.00E+00	0.00E+00						0.00
16.872	3.074	0.00E+00	0.00E+00	0.0141	0.00E+00	0.00E+00						0.00
16.947	2.594	0.00E+00	0.00E+00	0.0141	0.00E+00	0.00E+00						0.00
17.047	1.954	0.00E+00	0.00E+00	0.0141	0.00E+00	0.00E+00						0.00
17.347	0.034	3.65E-06	-1.95E-06	0.0141	1.46E-06	8.21E-01						7813.05
17.847	0.000	3.85E-06	-2.06E-06	0.0141	1.54E-06	8.66E-03						12111.17
18.347	0.000	4.07E-10	-2.17E-10	0.0141	1.63E-10	9.14E-05						12156.50
18.847	0.000	4.31E-12	-2.30E-12	0.0141	1.72E-12	9.68E-07						12156.97
19.597	0.000	1.54E-14	-8.20E-15	0.0141	6.15E-15	3.46E-09						12156.97
20.597	0.000	1.07E-14	-5.71E-15	0.0141	4.28E-15	2.40E-09						12156.97
21.597	0.000	1.07E-14	-5.71E-15	0.0141	4.28E-15	2.40E-09						12156.97
22.597	0.000	1.07E-14	-5.71E-15	0.0141	4.28E-15	2.40E-09						12156.97
24.097	0.000	1.07E-14	-5.71E-15	0.0141	4.28E-15	2.40E-09						12156.97
26.097	0.000	1.07E-14	-5.71E-15	0.0141	4.28E-15	2.40E-09						12156.97
28.597	0.000	1.07E-14	-5.71E-15	0.0141	4.28E-15	2.40E-09						12156.97
31.597	0.000	1.07E-14	-5.71E-15	0.0141	4.28E-15	2.40E-09						12156.97
35.097	0.000	1.07E-14	-5.71E-15	0.0141	4.28E-15	2.40E-09						12156.97
39.097	0.000	1.07E-14	-5.71E-15	0.0141	4.28E-15	2.40E-09						12156.97
43.097	0.000	1.07E-14	-5.71E-15	0.0141	4.28E-15	2.40E-09						12156.97
47.097	0.000	1.07E-14	-5.71E-15	0.0141	4.28E-15	2.40E-09						12156.97

RESULTS FOR YEAR: 32

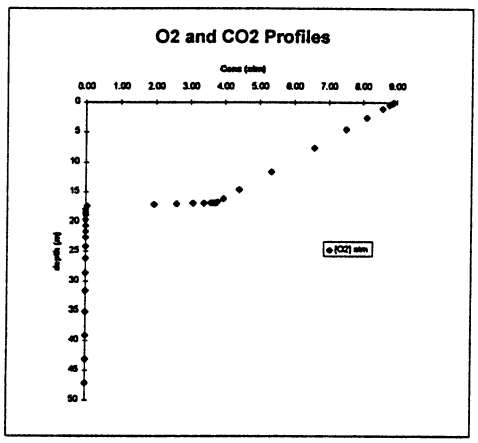

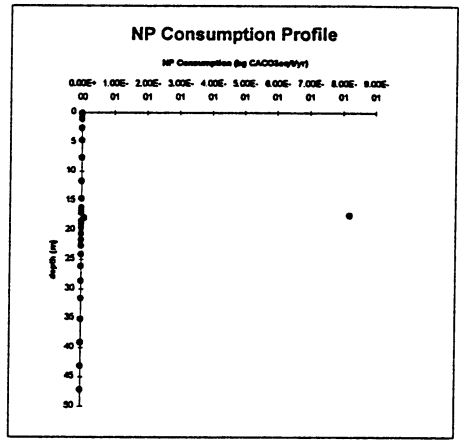

Flux in (mol/m²s)	1.85E-06
O_2 cons. (mol/m²s)	1.85E-06
Dpen (m)	18.597

t=32												
DEPTH (m)	CONC O2 (mol/m³)	O2 Cons (mol/m³/s)	CO2 Prod (mol/m³/s)	CONC CO2 (mol/m³)	mols O2 cons per m3 rock	NP consmptn kg CaCO3eq/t/yr						Suff dens mol/m³
0.050	8.900	0.00E+00	0.00E+00	0.0141	0.00E+00	0.00E+00						0.00
0.200	8.854	0.00E+00	0.00E+00	0.0141	0.00E+00	0.00E+00						0.00
0.450	8.777	0.00E+00	0.00E+00	0.0141	0.00E+00	0.00E+00						0.00
1.100	8.577	0.00E+00	0.00E+00	0.0141	0.00E+00	0.00E+00						0.00
2.600	8.116	0.00E+00	0.00E+00	0.0141	0.00E+00	0.00E+00						0.00
4.600	7.501	0.00E+00	0.00E+00	0.0141	0.00E+00	0.00E+00						0.00
7.600	6.578	0.00E+00	0.00E+00	0.0141	0.00E+00	0.00E+00						0.00
11.600	5.348	0.00E+00	0.00E+00	0.0141	0.00E+00	0.00E+00						0.00
14.600	4.425	0.00E+00	0.00E+00	0.0141	0.00E+00	0.00E+00						0.00
16.100	3.963	0.00E+00	0.00E+00	0.0141	0.00E+00	0.00E+00						0.00
16.650	3.794	0.00E+00	0.00E+00	0.0141	0.00E+00	0.00E+00						0.00
16.725	3.771	0.00E+00	0.00E+00	0.0141	0.00E+00	0.00E+00						0.00
16.755	3.762	0.00E+00	0.00E+00	0.0141	0.00E+00	0.00E+00						0.00
16.763	3.760	0.00E+00	0.00E+00	0.0141	0.00E+00	0.00E+00						0.00
16.766	3.756	0.00E+00	0.00E+00	0.0141	0.00E+00	0.00E+00						0.00
16.767	3.749	0.00E+00	0.00E+00	0.0141	0.00E+00	0.00E+00						0.00
16.770	3.730	0.00E+00	0.00E+00	0.0141	0.00E+00	0.00E+00						0.00
16.775	3.698	0.00E+00	0.00E+00	0.0141	0.00E+00	0.00E+00						0.00
16.782	3.650	0.00E+00	0.00E+00	0.0141	0.00E+00	0.00E+00						0.00
16.792	3.586	0.00E+00	0.00E+00	0.0141	0.00E+00	0.00E+00						0.00
16.822	3.394	0.00E+00	0.00E+00	0.0141	0.00E+00	0.00E+00						0.00
16.872	3.074	0.00E+00	0.00E+00	0.0141	0.00E+00	0.00E+00						0.00
16.947	2.594	0.00E+00	0.00E+00	0.0141	0.00E+00	0.00E+00						0.00
17.047	1.954	0.00E+00	0.00E+00	0.0141	0.00E+00	0.00E+00						0.00
17.347	0.034	3.65E-06	-1.95E-06	0.0141	1.46E-06	8.21E-01						4584.56
17.847	0.000	3.85E-08	-2.06E-08	0.0141	1.54E-08	8.66E-03						12077.11
18.347	0.000	4.07E-10	-2.17E-10	0.0141	1.63E-10	9.14E-05						12156.15
18.847	0.000	4.31E-12	-2.30E-12	0.0141	1.72E-12	9.68E-07						12156.97
19.597	0.000	1.54E-14	-8.20E-15	0.0141	6.15E-15	3.46E-09						12156.97
20.597	0.000	1.07E-14	-5.71E-15	0.0141	4.28E-15	2.40E-09						12156.97
21.597	0.000	1.07E-14	-5.71E-15	0.0141	4.28E-15	2.40E-09						12156.97
22.597	0.000	1.07E-14	-5.71E-15	0.0141	4.28E-15	2.40E-09						12156.97
24.097	0.000	1.07E-14	-5.71E-15	0.0141	4.28E-15	2.40E-09						12156.97
26.097	0.000	1.07E-14	-5.71E-15	0.0141	4.28E-15	2.40E-09						12156.97
28.597	0.000	1.07E-14	-5.71E-15	0.0141	4.28E-15	2.40E-09						12156.97
31.597	0.000	1.07E-14	-5.71E-15	0.0141	4.28E-15	2.40E-09						12156.97
35.097	0.000	1.07E-14	-5.71E-15	0.0141	4.28E-15	2.40E-09						12156.97
39.097	0.000	1.07E-14	-5.71E-15	0.0141	4.28E-15	2.40E-09						12156.97
43.097	0.000	1.07E-14	-5.71E-15	0.0141	4.28E-15	2.40E-09						12156.97
47.097	0.000	1.07E-14	-5.71E-15	0.0141	4.28E-15	2.40E-09						12156.97

APPENDIX A9
Run 3C2, Open Stope

COUPLED $O_2/CO_2/Mg/SO_4/Ca$ MODEL
OXYDIFF V2.0

MODEL DETAILS

Filename	BF_CS3b1
Date	27/11/1996
Description:	Steady State Model Of Crandon Open Stope Placed Cemented Backfill Tailings
	Part 2 (year 1 to 32)
	First Order Model

INPUT PARAMETERS

Finite Difference Parameters

nodes x	1
nodes y	40
time periods	7
init delt (s)	0.01
[O2] at surface (mol/m³)	8.9
[CO2] at surface (mol/m³))	0.0141

Model Options

CO2 OPTION	0
FES2 OPTION	1
O2 OPTION	1

Geochemical Options

Infiltration (m/s)	1.10E-09
Infiltration Coefficient	1.00
Kgypsum	-
Infiltration (m/s)	1.10E-09
Fraction Flow Paths (G)	1.00

Diffusion Parameters

Dw (m2/s)	2.20E-09
Da (m2/s)	1.80E-05
τ	0.273
α	3.28
H	33.9

OUTPUT TIMES

time (s)	time (y)	Output col
1.6E+07	1	1
6.3E+07	2	6
1.3E+08	4	11
2.5E+08	8	16
5.0E+08	16	21
7.6E+08	24	26
1.0E+09	32	31

FES2 OPTION
0 - No FES2 DEPLETION
1 - ALLOW FES2 DEPLETION

CO2 OPTION:
0 - No CO2 Coupling
1 - CO2 Coupling

O2 OPTION
0 - HALF ORDER REACTION
1 - FIRST ORDER REACTION
2 - MIXED FIRST ORDER / ZERO ORDER
3 - ZERO ORDER SOLUTION

TORTUOSITY

Rockfill	τ	3
Cemented Tailings	τ	10

MODEL INPUTS

Material	DEPTH (m)	Depth (ft)	Cell Sizes (m)	r (s-1)	Porosity	Bulk Dens. (tonnes m⁻³)	Sat. (%)	SatDens (mol/m³)	Diff Coeff [1] (m2/s)	Diff Coeff [2] (m2/s)	$[O_2]_{sat}$ (mol/m³)	$[CO_2]_{sat}$ (mol/m³)
Waste Rock	0.050	0.164	0.1	0.00E+00	0.40	1.9	15%	0	6.00E-06	6.00E-06	8.89	1.41E-02
Waste Rock	0.200	0.656	0.2	0.00E+00	0.40	1.9	15%	0	6.00E-06	6.00E-06	8.89	1.41E-02
Waste Rock	0.815	2.674	1.03	0.00E+00	0.40	1.9	15%	0	6.00E-06	6.00E-06	8.89	1.41E-02
Waste Rock	2.830	9.285	3	0.00E+00	0.40	1.9	15%	0	6.00E-06	6.00E-06	8.89	1.41E-02
Waste Rock	7.330	24.049	6	0.00E+00	0.40	1.9	15%	0	6.00E-06	6.00E-06	8.89	1.41E-02
Waste Rock	13.330	43.734	6	0.00E+00	0.40	1.9	15%	0	6.00E-06	6.00E-06	8.89	1.41E-02
Waste Rock	19.330	63.419	6	0.00E+00	0.40	1.9	15%	0	6.00E-06	6.00E-06	8.89	1.41E-02
Waste Rock	25.330	83.104	6	0.00E+00	0.40	1.9	15%	0	6.00E-06	6.00E-06	8.89	1.41E-02
Waste Rock	30.098	98.745	3.535	0.00E+00	0.40	1.9	15%	0	6.00E-06	6.00E-06	8.89	1.41E-02
Waste Rock	32.615	107.005	1.5	0.00E+00	0.40	1.9	15%	0	6.00E-06	6.00E-06	8.89	1.41E-02
Waste Rock	33.415	109.629	0.1	0.00E+00	0.40	1.9	15%	0	6.00E-06	6.00E-06	8.89	1.41E-02
Waste Rock	33.490	109.875	0.05	0.00E+00	0.40	1.9	15%	0	6.00E-06	6.00E-06	8.89	1.41E-02
Waste Rock	33.520	109.974	0.01	0.00E+00	0.40	1.9	15%	0	6.00E-06	6.00E-06	8.89	1.41E-02
Waste Rock	33.528	109.998	0.005	0.00E+00	0.40	1.9	15%	0	6.00E-06	6.00E-06	8.89	1.41E-02
Tailings Backfill	33.531	110.008	0.001	1.07E-04	0.40	3.0	15%	12187	2.88E-07	2.88E-07	8.89	1.41E-02
Tailings Backfill	33.532	110.011	0.001	1.07E-04	0.40	3.0	15%	12187	2.88E-07	2.88E-07	8.89	1.41E-02
Tailings Backfill	33.535	110.021	0.005	1.07E-04	0.40	3.0	15%	12187	2.88E-07	2.88E-07	8.89	1.41E-02
Tailings Backfill	33.540	110.038	0.005	1.07E-04	0.40	3.0	15%	12187	2.88E-07	2.88E-07	8.89	1.41E-02
Tailings Backfill	33.547	110.062	0.01	1.07E-04	0.40	3.0	15%	12187	2.88E-07	2.88E-07	8.89	1.41E-02
Tailings Backfill	33.557	110.095	0.01	1.07E-04	0.40	3.0	15%	12187	2.88E-07	2.88E-07	8.89	1.41E-02
Tailings Backfill	33.567	110.194	0.05	1.07E-04	0.40	3.0	15%	12187	2.88E-07	2.88E-07	8.89	1.41E-02
Tailings Backfill	33.637	110.358	0.05	1.07E-04	0.40	3.0	15%	12187	2.88E-07	2.88E-07	8.89	1.41E-02
Tailings Backfill	33.712	110.604	0.1	1.07E-04	0.40	3.0	15%	12187	2.88E-07	2.88E-07	8.89	1.41E-02
Tailings Backfill	33.812	110.932	0.1	1.07E-04	0.40	3.0	15%	12187	2.88E-07	2.88E-07	8.89	1.41E-02
Tailings Backfill	34.112	111.916	0.5	1.07E-04	0.40	3.0	15%	12187	2.88E-07	2.88E-07	8.89	1.41E-02
Tailings Backfill	34.612	113.556	0.5	1.07E-04	0.40	3.0	15%	12187	2.88E-07	2.88E-07	8.89	1.41E-02
Tailings Backfill	35.112	115.197	0.5	1.07E-04	0.40	3.0	15%	12187	2.88E-07	2.88E-07	8.89	1.41E-02
Tailings Backfill	35.612	116.837	0.5	1.07E-04	0.40	3.0	15%	12187	2.88E-07	2.88E-07	8.89	1.41E-02
Tailings Backfill	36.362	119.298	1	1.07E-04	0.40	3.0	15%	12187	2.88E-07	2.88E-07	8.89	1.41E-02
Tailings Backfill	37.362	122.579	1	1.07E-04	0.40	3.0	15%	12187	2.88E-07	2.88E-07	8.89	1.41E-02
Tailings Backfill	38.362	125.860	1	1.07E-04	0.40	3.0	15%	12187	2.88E-07	2.88E-07	8.89	1.41E-02
Tailings Backfill	39.362	129.140	1	1.07E-04	0.40	3.0	15%	12187	2.88E-07	2.88E-07	8.89	1.41E-02
Tailings Backfill	40.862	134.062	2	1.07E-04	0.40	3.0	15%	12187	2.88E-07	2.88E-07	8.89	1.41E-02
Tailings Backfill	42.862	140.623	2	1.07E-04	0.40	3.0	15%	12187	2.88E-07	2.88E-07	8.89	1.41E-02
Tailings Backfill	45.362	148.825	3	1.07E-04	0.40	3.0	15%	12187	2.88E-07	2.88E-07	8.89	1.41E-02
Tailings Backfill	48.362	158.668	3	1.07E-04	0.40	3.0	15%	12187	2.88E-07	2.88E-07	8.89	1.41E-02
Tailings Backfill	51.862	170.151	4	1.07E-04	0.40	3.0	15%	12187	2.88E-07	2.88E-07	8.89	1.41E-02
Tailings Backfill	55.862	183.274	4	1.07E-04	0.40	3.0	15%	12187	2.88E-07	2.88E-07	8.89	1.41E-02
Tailings Backfill	59.862	196.398	4	1.07E-04	0.40	3.0	15%	12187	2.88E-07	2.88E-07	8.89	1.41E-02
Tailings Backfill	63.862	209.521	4	1.07E-04	0.40	3.0	15%	12187	2.88E-07	2.88E-07	8.89	1.41E-02

1. Diff Coefficient Based on Erberling, B., R.V.Nicholson, E.J.Reardon and P.Tibble, Evaluation of sulphide oxidation rates. Nordic Hydrology, 24(5), 323-336, 1993.
2. Diff Coefficient Based on Reardon, E.J. and P.M. Moddle, Gas Diffusion Coefficient Measurements on Uranium Mill Tailings: Implications to Cover Layer Design. Uranium, 2, 111-131,1985.

RESULTS FOR YEAR: 1

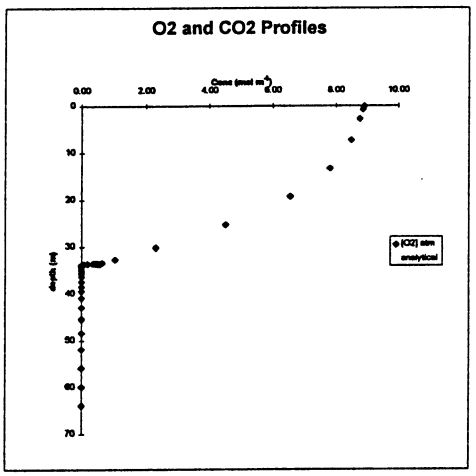

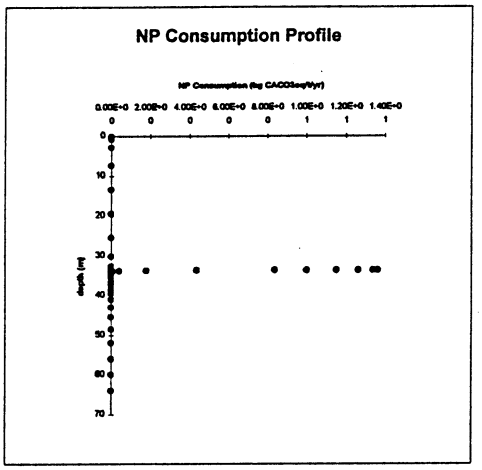

Flux in (mol/m²s)	3.00E-07
O_2 cons. (mol/m²s)	3.08E-06
Dpen (m)	34.862

t=1												
DEPTH (m)	CONC O2 (mol/m³)	O2 Cons (mol/m³/s)	CO2 Prod (mol/m³/s)	CONC CO2 (mol/m³)	mols O2 cons per m³ material	NP consmptn kg CaCO3eq/t/yr						Sulf dens mol/m³
0.050	8.900	0.00E+00	0.00E+00	0.0141	0.00E+00	0.00E+00						0.00
0.200	8.892	0.00E+00	0.00E+00	0.0141	0.00E+00	0.00E+00						0.00
0.815	8.862	0.00E+00	0.00E+00	0.0141	0.00E+00	0.00E+00						0.00
2.830	8.759	0.00E+00	0.00E+00	0.0141	0.00E+00	0.00E+00						0.00
7.330	8.486	0.00E+00	0.00E+00	0.0141	0.00E+00	0.00E+00						0.00
13.330	7.816	0.00E+00	0.00E+00	0.0141	0.00E+00	0.00E+00						0.00
19.330	6.561	0.00E+00	0.00E+00	0.0141	0.00E+00	0.00E+00						0.00
25.330	4.518	0.00E+00	0.00E+00	0.0141	0.00E+00	0.00E+00						0.00
30.098	2.309	0.00E+00	0.00E+00	0.0141	0.00E+00	0.00E+00						0.00
32.615	1.041	0.00E+00	0.00E+00	0.0141	0.00E+00	0.00E+00						0.00
33.415	0.632	0.00E+00	0.00E+00	0.0141	0.00E+00	0.00E+00						0.00
33.490	0.593	0.00E+00	0.00E+00	0.0141	0.00E+00	0.00E+00						0.00
33.520	0.578	0.00E+00	0.00E+00	0.0141	0.00E+00	0.00E+00						0.00
33.528	0.574	0.00E+00	0.00E+00	0.0141	0.00E+00	0.00E+00						0.00
33.531	0.567	6.07E-05	-3.24E-05	0.0141	2.43E-05	1.36E+01						6323.69
33.532	0.557	5.98E-05	-3.18E-05	0.0141	2.38E-05	1.34E+01						6431.13
33.535	0.526	5.63E-05	-3.00E-05	0.0141	2.25E-05	1.26E+01						6747.08
33.540	0.480	5.13E-05	-2.74E-05	0.0141	2.05E-05	1.15E+01						7223.49
33.547	0.417	4.46E-05	-2.38E-05	0.0141	1.78E-05	1.00E+01						7869.52
33.557	0.349	3.73E-05	-1.99E-05	0.0141	1.49E-05	8.38E+00						8571.93
33.587	0.182	1.95E-05	-1.04E-05	0.0141	7.81E-06	4.39E+00						10280.40
33.637	0.075	8.00E-06	-4.26E-06	0.0141	3.20E-06	1.80E+00						11388.35
33.712	0.017	1.82E-06	-9.73E-07	0.0141	7.30E-07	4.10E-01						11981.56
33.812	0.003	3.62E-07	-1.93E-07	0.0141	1.45E-07	8.14E-02						12122.13
34.112	0.000	6.33E-09	-3.38E-09	0.0141	2.53E-09	1.42E-03						12156.36
34.612	0.000	6.69E-11	-3.57E-11	0.0141	2.67E-11	1.50E-05						12156.97
35.112	0.000	7.06E-13	-3.77E-13	0.0141	2.82E-13	1.59E-07						12156.97
35.612	0.000	1.07E-14	-5.71E-15	0.0141	4.28E-15	2.40E-09						12156.97
36.362	0.000	1.07E-14	-5.71E-15	0.0141	4.28E-15	2.40E-09						12156.97
37.362	0.000	1.07E-14	-5.71E-15	0.0141	4.28E-15	2.40E-09						12156.97
38.362	0.000	1.07E-14	-5.71E-15	0.0141	4.28E-15	2.40E-09						12156.97
39.362	0.000	1.07E-14	-5.71E-15	0.0141	4.28E-15	2.40E-09						12156.97
40.862	0.000	1.07E-14	-5.71E-15	0.0141	4.28E-15	2.40E-09						12156.97
42.862	0.000	1.07E-14	-5.71E-15	0.0141	4.28E-15	2.40E-09						12156.97
45.362	0.000	1.07E-14	-5.71E-15	0.0141	4.28E-15	2.40E-09						12156.97
48.362	0.000	1.07E-14	-5.71E-15	0.0141	4.28E-15	2.40E-09						12156.97
51.862	0.000	1.07E-14	-5.71E-15	0.0141	4.28E-15	2.40E-09						12156.97
55.862	0.000	1.07E-14	-5.71E-15	0.0141	4.28E-15	2.40E-09						12156.97
59.862	0.000	1.07E-14	-5.71E-15	0.0141	4.28E-15	2.40E-09						12156.97
63.862	0.000	1.07E-14	-5.71E-15	0.0141	4.28E-15	2.40E-09						12156.97

RESULTS FOR YEAR: 2

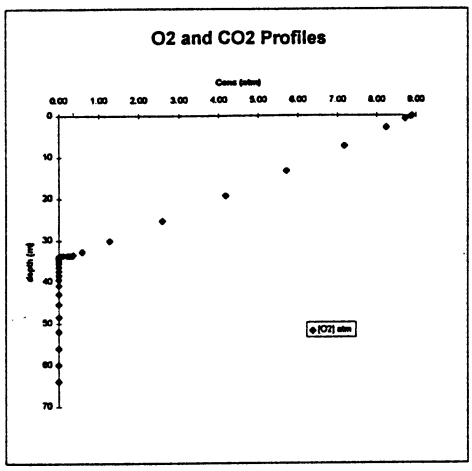

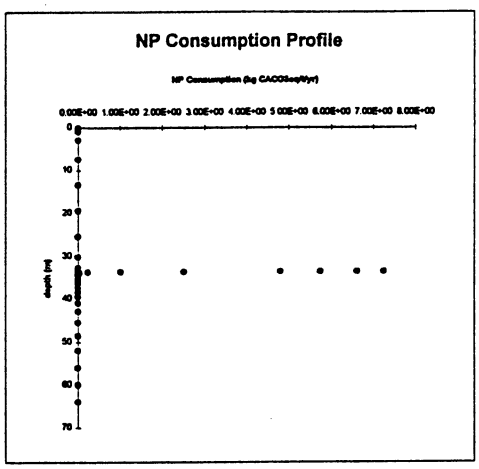

Flux in (mol/m²s)	1.41E-06
O_2 cons. (mol/m²s)	1.69E-06
Dpen (m)	34.862

t=2												
DEPTH (m)	CONC O2 (mol/m³)	O2 Cons (mol/m³/s)	CO2 Prod (mol/m³/s)	CONC CO2 (mol/m³)	mols O2 cons per m3 rock	NP consmptn kg CaCO3eq/t/yr						Satf dens mol/m³
0.050	8.900	0.00E+00	0.00E+00	0.0141	0.00E+00	0.00E+00						0.00
0.200	8.865	0.00E+00	0.00E+00	0.0141	0.00E+00	0.00E+00						0.00
0.815	8.720	0.00E+00	0.00E+00	0.0141	0.00E+00	0.00E+00						0.00
2.830	8.246	0.00E+00	0.00E+00	0.0141	0.00E+00	0.00E+00						0.00
7.330	7.180	0.00E+00	0.00E+00	0.0141	0.00E+00	0.00E+00						0.00
13.330	5.716	0.00E+00	0.00E+00	0.0141	0.00E+00	0.00E+00						0.00
19.330	4.185	0.00E+00	0.00E+00	0.0141	0.00E+00	0.00E+00						0.00
25.330	2.585	0.00E+00	0.00E+00	0.0141	0.00E+00	0.00E+00						0.00
30.098	1.276	0.00E+00	0.00E+00	0.0141	0.00E+00	0.00E+00						0.00
32.615	0.581	0.00E+00	0.00E+00	0.0141	0.00E+00	0.00E+00						0.00
33.415	0.359	0.00E+00	0.00E+00	0.0141	0.00E+00	0.00E+00						0.00
33.490	0.339	0.00E+00	0.00E+00	0.0141	0.00E+00	0.00E+00						0.00
33.520	0.330	0.00E+00	0.00E+00	0.0141	0.00E+00	0.00E+00						0.00
33.528	0.328	0.00E+00	0.00E+00	0.0141	0.00E+00	0.00E+00						0.00
33.531	0.325	0.00E+00	0.00E+00	0.0141	0.00E+00	0.00E+00						0.00
33.532	0.319	0.00E+00	0.00E+00	0.0141	0.00E+00	0.00E+00						0.00
33.535	0.301	3.23E-05	-1.72E-05	0.0141	1.29E-05	7.25E+00						315.18
33.540	0.275	2.94E-05	-1.57E-05	0.0141	1.18E-05	6.61E+00						1358.18
33.547	0.239	2.56E-05	-1.36E-05	0.0141	1.02E-05	5.74E+00						2772.46
33.557	0.200	2.14E-05	-1.14E-05	0.0141	8.55E-06	4.80E+00						4310.12
33.587	0.105	1.12E-05	-5.96E-06	0.0141	4.47E-06	2.51E+00						8050.01
33.637	0.043	4.58E-06	-2.44E-06	0.0141	1.83E-06	1.03E+00						10475.02
33.712	0.010	1.04E-06	-5.57E-07	0.0141	4.18E-07	2.35E-01						11773.22
33.812	0.002	2.07E-07	-1.11E-07	0.0141	8.29E-08	4.66E-02						12060.78
34.112	0.000	3.62E-09	-1.93E-09	0.0141	1.45E-09	8.13E-04						12155.65
34.612	0.000	3.82E-11	-2.04E-11	0.0141	1.53E-11	8.58E-06						12156.97
35.112	0.000	4.03E-13	-2.15E-13	0.0141	1.61E-13	9.06E-08						12156.97
35.612	0.000	1.07E-14	-5.71E-15	0.0141	4.28E-15	2.40E-09						12156.97
36.362	0.000	1.07E-14	-5.71E-15	0.0141	4.28E-15	2.40E-09						12156.97
37.362	0.000	1.07E-14	-5.71E-15	0.0141	4.28E-15	2.40E-09						12156.97
38.362	0.000	1.07E-14	-5.71E-15	0.0141	4.28E-15	2.40E-09						12156.97
39.362	0.000	1.07E-14	-5.71E-15	0.0141	4.28E-15	2.40E-09						12156.97
40.862	0.000	1.07E-14	-5.71E-15	0.0141	4.28E-15	2.40E-09						12156.97
42.862	0.000	1.07E-14	-5.71E-15	0.0141	4.28E-15	2.40E-09						12156.97
45.362	0.000	1.07E-14	-5.71E-15	0.0141	4.28E-15	2.40E-09						12156.97
48.362	0.000	1.07E-14	-5.71E-15	0.0141	4.28E-15	2.40E-09						12156.97
51.862	0.000	1.07E-14	-5.71E-15	0.0141	4.28E-15	2.40E-09						12156.97
55.862	0.000	1.07E-14	-5.71E-15	0.0141	4.28E-15	2.40E-09						12156.97
59.862	0.000	1.07E-14	-5.71E-15	0.0141	4.28E-15	2.40E-09						12156.97
63.862	0.000	1.07E-14	-5.71E-15	0.0141	4.28E-15	2.40E-09						12156.97

RESULTS FOR YEAR: 4

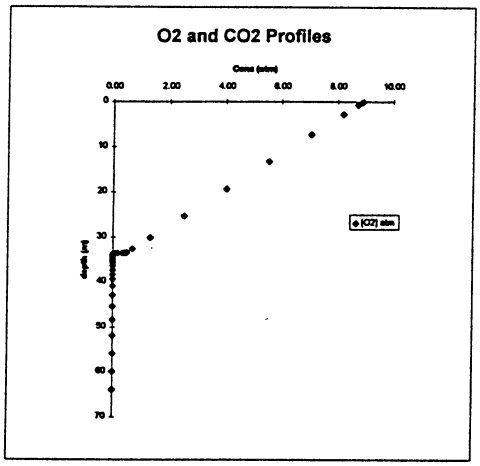

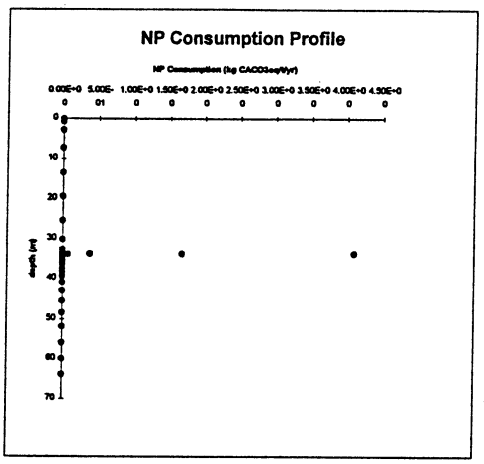

Flux in (mol/m²s)	1.52E-06
O_2 cons. (mol/m²s)	1.49E-06
Open (m)	34.862

t=4

DEPTH (m)	CONC O2 (mol/m³)	O2 Cons (mol/m³/s)	CO2 Prod (mol/m³/s)	CONC CO2 (mol/m³)	mols O2 cons per m3 rock	NP consmptn kg CaCO3eq/t/yr						Sulf dens mol/m³
0.050	8.900	0.00E+00	0.00E+00	0.0141	0.00E+00	0.00E+00						0.00
0.200	8.862	0.00E+00	0.00E+00	0.0141	0.00E+00	0.00E+00						0.00
0.815	8.706	0.00E+00	0.00E+00	0.0141	0.00E+00	0.00E+00						0.00
2.830	8.196	0.00E+00	0.00E+00	0.0141	0.00E+00	0.00E+00						0.00
7.330	7.058	0.00E+00	0.00E+00	0.0141	0.00E+00	0.00E+00						0.00
13.330	5.541	0.00E+00	0.00E+00	0.0141	0.00E+00	0.00E+00						0.00
19.330	4.029	0.00E+00	0.00E+00	0.0141	0.00E+00	0.00E+00						0.00
25.330	2.521	0.00E+00	0.00E+00	0.0141	0.00E+00	0.00E+00						0.00
30.098	1.328	0.00E+00	0.00E+00	0.0141	0.00E+00	0.00E+00						0.00
32.615	0.694	0.00E+00	0.00E+00	0.0141	0.00E+00	0.00E+00						0.00
33.415	0.494	0.00E+00	0.00E+00	0.0141	0.00E+00	0.00E+00						0.00
33.490	0.476	0.00E+00	0.00E+00	0.0141	0.00E+00	0.00E+00						0.00
33.520	0.468	0.00E+00	0.00E+00	0.0141	0.00E+00	0.00E+00						0.00
33.528	0.466	0.00E+00	0.00E+00	0.0141	0.00E+00	0.00E+00						0.00
33.531	0.463	0.00E+00	0.00E+00	0.0141	0.00E+00	0.00E+00						0.00
33.532	0.458	0.00E+00	0.00E+00	0.0141	0.00E+00	0.00E+00						0.00
33.535	0.443	0.00E+00	0.00E+00	0.0141	0.00E+00	0.00E+00						0.00
33.540	0.417	0.00E+00	0.00E+00	0.0141	0.00E+00	0.00E+00						0.00
33.547	0.378	0.00E+00	0.00E+00	0.0141	0.00E+00	0.00E+00						0.00
33.557	0.326	0.00E+00	0.00E+00	0.0141	0.00E+00	0.00E+00						0.00
33.587	0.171	1.83E-05	-9.74E-06	0.0141	7.30E-06	4.10E+00						4764.11
33.637	0.070	7.48E-06	-3.99E-06	0.0141	2.99E-06	1.68E+00						9129.69
33.712	0.016	1.71E-06	-9.09E-07	0.0141	6.82E-07	3.83E-01						11466.38
33.812	0.003	3.38E-07	-1.81E-07	0.0141	1.35E-07	7.61E-02						12019.89
34.112	0.000	5.91E-09	-3.15E-09	0.0141	2.36E-09	1.33E-03						12154.59
34.612	0.000	6.24E-11	-3.33E-11	0.0141	2.50E-11	1.40E-05						12156.97
35.112	0.000	6.59E-13	-3.51E-13	0.0141	2.63E-13	1.48E-07						12156.97
35.612	0.000	1.07E-14	-5.71E-15	0.0141	4.28E-15	2.40E-09						12156.97
36.362	0.000	1.07E-14	-5.71E-15	0.0141	4.28E-15	2.40E-09						12156.97
37.362	0.000	1.07E-14	-5.71E-15	0.0141	4.28E-15	2.40E-09						12156.97
38.362	0.000	1.07E-14	-5.71E-15	0.0141	4.28E-15	2.40E-09						12156.97
39.362	0.000	1.07E-14	-5.71E-15	0.0141	4.28E-15	2.40E-09						12156.97
40.862	0.000	1.07E-14	-5.71E-15	0.0141	4.28E-15	2.40E-09						12156.97
42.862	0.000	1.07E-14	-5.71E-15	0.0141	4.28E-15	2.40E-09						12156.97
45.362	0.000	1.07E-14	-5.71E-15	0.0141	4.28E-15	2.40E-09						12156.97
48.362	0.000	1.07E-14	-5.71E-15	0.0141	4.28E-15	2.40E-09						12156.97
51.862	0.000	1.07E-14	-5.71E-15	0.0141	4.28E-15	2.40E-09						12156.97
55.862	0.000	1.07E-14	-5.71E-15	0.0141	4.28E-15	2.40E-09						12156.97
59.862	0.000	1.07E-14	-5.71E-15	0.0141	4.28E-15	2.40E-09						12156.97
63.862	0.000	1.07E-14	-5.71E-15	0.0141	4.28E-15	2.40E-09						12156.97

RESULTS FOR YEAR: 8

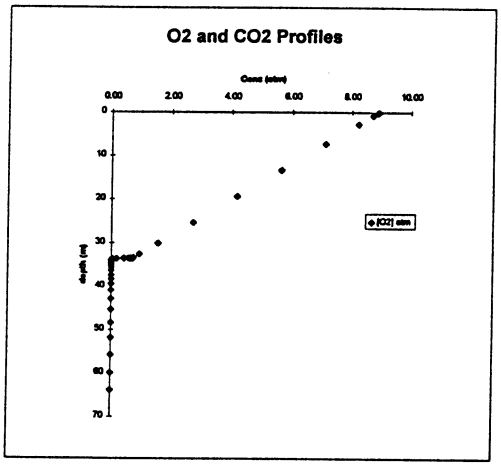

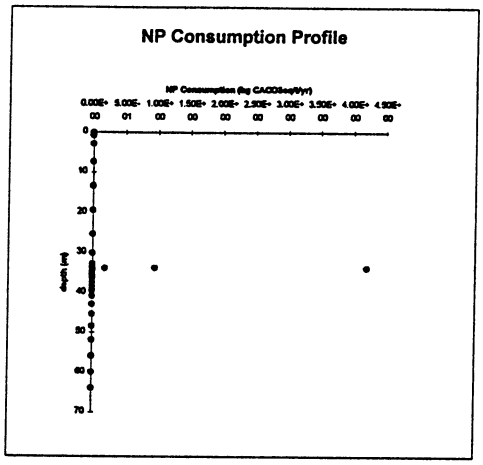

Flux in (mol/m²s)	1.47E-06
O_2 cons. (mol/m²s)	1.46E-06
Dpen (m)	34.862

t=8												
DEPTH (m)	CONC O2 (mol/m³)	O2 Cons (mol/m³/s)	CO2 Prod (mol/m³/s)	CONC CO2 (mol/m³)	mols O2 cons per m3 rock	NP consmptn kg CaCO3eq/t/yr						Sulf dens mol/m³
0.050	8.900	0.00E+00	0.00E+00	0.0141	0.00E+00	0.00E+00						0.00
0.200	8.863	0.00E+00	0.00E+00	0.0141	0.00E+00	0.00E+00						0.00
0.815	8.712	0.00E+00	0.00E+00	0.0141	0.00E+00	0.00E+00						0.00
2.830	8.217	0.00E+00	0.00E+00	0.0141	0.00E+00	0.00E+00						0.00
7.330	7.113	0.00E+00	0.00E+00	0.0141	0.00E+00	0.00E+00						0.00
13.330	5.643	0.00E+00	0.00E+00	0.0141	0.00E+00	0.00E+00						0.00
19.330	4.176	0.00E+00	0.00E+00	0.0141	0.00E+00	0.00E+00						0.00
25.330	2.712	0.00E+00	0.00E+00	0.0141	0.00E+00	0.00E+00						0.00
30.098	1.552	0.00E+00	0.00E+00	0.0141	0.00E+00	0.00E+00						0.00
32.615	0.937	0.00E+00	0.00E+00	0.0141	0.00E+00	0.00E+00						0.00
33.415	0.742	0.00E+00	0.00E+00	0.0141	0.00E+00	0.00E+00						0.00
33.490	0.724	0.00E+00	0.00E+00	0.0141	0.00E+00	0.00E+00						0.00
33.520	0.716	0.00E+00	0.00E+00	0.0141	0.00E+00	0.00E+00						0.00
33.528	0.714	0.00E+00	0.00E+00	0.0141	0.00E+00	0.00E+00						0.00
33.531	0.711	0.00E+00	0.00E+00	0.0141	0.00E+00	0.00E+00						0.00
33.532	0.706	0.00E+00	0.00E+00	0.0141	0.00E+00	0.00E+00						0.00
33.535	0.691	0.00E+00	0.00E+00	0.0141	0.00E+00	0.00E+00						0.00
33.540	0.666	0.00E+00	0.00E+00	0.0141	0.00E+00	0.00E+00						0.00
33.547	0.628	0.00E+00	0.00E+00	0.0141	0.00E+00	0.00E+00						0.00
33.557	0.578	0.00E+00	0.00E+00	0.0141	0.00E+00	0.00E+00						0.00
33.587	0.427	0.00E+00	0.00E+00	0.0141	0.00E+00	0.00E+00						0.00
33.637	0.175	1.87E-05	-9.99E-06	0.0141	7.49E-06	4.21E+00						3621.82
33.712	0.040	4.27E-06	-2.28E-06	0.0141	1.71E-06	9.60E-01						10210.19
33.812	0.008	8.48E-07	-4.52E-07	0.0141	3.39E-07	1.90E-01						11770.59
34.112	0.000	1.48E-08	-7.90E-09	0.0141	5.92E-09	3.33E-03						12150.25
34.612	0.000	1.56E-10	-8.33E-11	0.0141	6.25E-11	3.51E-05						12156.93
35.112	0.000	1.65E-12	-8.79E-13	0.0141	6.60E-13	3.71E-07						12156.97
35.612	0.000	1.75E-14	-9.31E-15	0.0141	6.99E-15	3.92E-09						12156.97
36.362	0.000	1.07E-14	-5.71E-15	0.0141	4.28E-15	2.40E-09						12156.97
37.362	0.000	1.07E-14	-5.71E-15	0.0141	4.28E-15	2.40E-09						12156.97
38.362	0.000	1.07E-14	-5.71E-15	0.0141	4.28E-15	2.40E-09						12156.97
39.362	0.000	1.07E-14	-5.71E-15	0.0141	4.28E-15	2.40E-09						12156.97
40.862	0.000	1.07E-14	-5.71E-15	0.0141	4.28E-15	2.40E-09						12156.97
42.862	0.000	1.07E-14	-5.71E-15	0.0141	4.28E-15	2.40E-09						12156.97
45.362	0.000	1.07E-14	-5.71E-15	0.0141	4.28E-15	2.40E-09						12156.97
48.362	0.000	1.07E-14	-5.71E-15	0.0141	4.28E-15	2.40E-09						12156.97
51.862	0.000	1.07E-14	-5.71E-15	0.0141	4.28E-15	2.40E-09						12156.97
55.862	0.000	1.07E-14	-5.71E-15	0.0141	4.28E-15	2.40E-09						12156.97
59.862	0.000	1.07E-14	-5.71E-15	0.0141	4.28E-15	2.40E-09						12156.97
63.862	0.000	1.07E-14	-5.71E-15	0.0141	4.28E-15	2.40E-09						12156.97

RESULTS FOR YEAR: 16

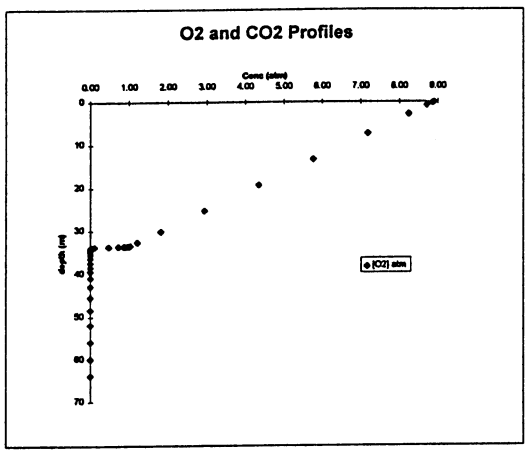

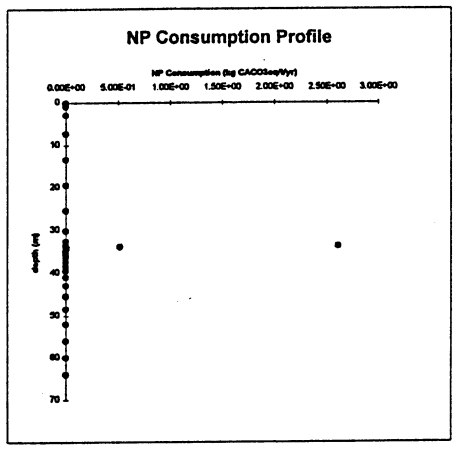

Flux in (mol/m²s)	1.42E-06
O_2 cons. (mol/m²s)	1.41E-06
Dpen (m)	34.862

t=16												
DEPTH (m)	CONC O2 (mol/m³)	O2 Cons (mol/m²/s)	CO2 Prod (mol/m²/s)	CONC CO2 (mol/m³)	mols O2 cons per m3 rock	NP consmptn kg CaCO3eq/t/yr						Sulf dens mol/m³
0.050	8.900	0.00E+00	0.00E+00	0.0141	0.00E+00	0.00E+00						0.00
0.200	8.865	0.00E+00	0.00E+00	0.0141	0.00E+00	0.00E+00						0.00
0.815	8.720	0.00E+00	0.00E+00	0.0141	0.00E+00	0.00E+00						0.00
2.830	8.244	0.00E+00	0.00E+00	0.0141	0.00E+00	0.00E+00						0.00
7.330	7.183	0.00E+00	0.00E+00	0.0141	0.00E+00	0.00E+00						0.00
13.330	5.767	0.00E+00	0.00E+00	0.0141	0.00E+00	0.00E+00						0.00
19.330	4.352	0.00E+00	0.00E+00	0.0141	0.00E+00	0.00E+00						0.00
25.330	2.937	0.00E+00	0.00E+00	0.0141	0.00E+00	0.00E+00						0.00
30.098	1.812	0.00E+00	0.00E+00	0.0141	0.00E+00	0.00E+00						0.00
32.615	1.218	0.00E+00	0.00E+00	0.0141	0.00E+00	0.00E+00						0.00
33.415	1.028	0.00E+00	0.00E+00	0.0141	0.00E+00	0.00E+00						0.00
33.490	1.010	0.00E+00	0.00E+00	0.0141	0.00E+00	0.00E+00						0.00
33.520	1.003	0.00E+00	0.00E+00	0.0141	0.00E+00	0.00E+00						0.00
33.528	1.002	0.00E+00	0.00E+00	0.0141	0.00E+00	0.00E+00						0.00
33.531	0.998	0.00E+00	0.00E+00	0.0141	0.00E+00	0.00E+00						0.00
33.532	0.994	0.00E+00	0.00E+00	0.0141	0.00E+00	0.00E+00						0.00
33.535	0.979	0.00E+00	0.00E+00	0.0141	0.00E+00	0.00E+00						0.00
33.540	0.954	0.00E+00	0.00E+00	0.0141	0.00E+00	0.00E+00						0.00
33.547	0.917	0.00E+00	0.00E+00	0.0141	0.00E+00	0.00E+00						0.00
33.557	0.868	0.00E+00	0.00E+00	0.0141	0.00E+00	0.00E+00						0.00
33.587	0.721	0.00E+00	0.00E+00	0.0141	0.00E+00	0.00E+00						0.00
33.637	0.476	0.00E+00	0.00E+00	0.0141	0.00E+00	0.00E+00						0.00
33.712	0.109	1.16E-05	-6.20E-06	0.0141	4.65E-06	2.61E+00						1357.79
33.812	0.022	2.31E-06	-1.23E-06	0.0141	9.23E-07	5.19E-01						10013.60
34.112	0.000	4.03E-08	-2.15E-08	0.0141	1.61E-08	9.06E-03						12119.56
34.612	0.000	4.25E-10	-2.27E-10	0.0141	1.70E-10	9.56E-05						12156.61
35.112	0.000	4.49E-12	-2.39E-12	0.0141	1.80E-12	1.01E-06						12156.97
35.612	0.000	4.75E-14	-2.54E-14	0.0141	1.90E-14	1.07E-08						12156.97
36.362	0.000	1.07E-14	-5.71E-15	0.0141	4.28E-15	2.40E-09						12156.97
37.362	0.000	1.07E-14	-5.71E-15	0.0141	4.28E-15	2.40E-09						12156.97
38.362	0.000	1.07E-14	-5.71E-15	0.0141	4.28E-15	2.40E-09						12156.97
39.362	0.000	1.07E-14	-5.71E-15	0.0141	4.28E-15	2.40E-09						12156.97
40.862	0.000	1.07E-14	-5.71E-15	0.0141	4.28E-15	2.40E-09						12156.97
42.862	0.000	1.07E-14	-5.71E-15	0.0141	4.28E-15	2.40E-09						12156.97
45.362	0.000	1.07E-14	-5.71E-15	0.0141	4.28E-15	2.40E-09						12156.97
48.362	0.000	1.07E-14	-5.71E-15	0.0141	4.28E-15	2.40E-09						12156.97
51.862	0.000	1.07E-14	-5.71E-15	0.0141	4.28E-15	2.40E-09						12156.97
55.862	0.000	1.07E-14	-5.71E-15	0.0141	4.28E-15	2.40E-09						12156.97
59.862	0.000	1.07E-14	-5.71E-15	0.0141	4.28E-15	2.40E-09						12156.97
63.862	0.000	1.07E-14	-5.71E-15	0.0141	4.28E-15	2.40E-09						12156.97

RESULTS FOR YEAR: 24

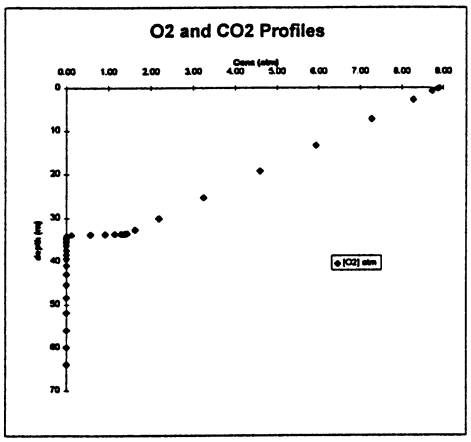

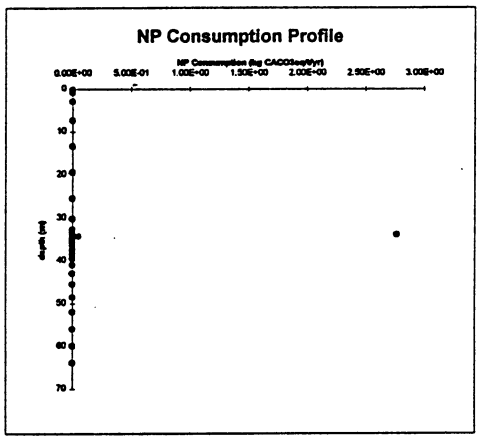

Flux in (mol/m²s)	1.34E-06
O_2 cons. (mol/m²s)	1.34E-06
Dpen (m)	35.362

t=24												
DEPTH (m)	CONC O2 (mol/m³)	O2 Cons (mol/m³/s)	CO2 Prod (mol/m³/s)	CONC CO2 (mol/m³)	mols O2 cons per m3 rock	NP consmptn kg CaCO3eq/t/yr						Sulf dens mol/m³
0.050	8.900	0.00E+00	0.00E+00	0.0141	0.00E+00	0.00E+00						0.00
0.200	8.867	0.00E+00	0.00E+00	0.0141	0.00E+00	0.00E+00						0.00
0.815	8.729	0.00E+00	0.00E+00	0.0141	0.00E+00	0.00E+00						0.00
2.830	8.279	0.00E+00	0.00E+00	0.0141	0.00E+00	0.00E+00						0.00
7.330	7.275	0.00E+00	0.00E+00	0.0141	0.00E+00	0.00E+00						0.00
13.330	5.935	0.00E+00	0.00E+00	0.0141	0.00E+00	0.00E+00						0.00
19.330	4.596	0.00E+00	0.00E+00	0.0141	0.00E+00	0.00E+00						0.00
25.330	3.256	0.00E+00	0.00E+00	0.0141	0.00E+00	0.00E+00						0.00
30.098	2.192	0.00E+00	0.00E+00	0.0141	0.00E+00	0.00E+00						0.00
32.615	1.630	0.00E+00	0.00E+00	0.0141	0.00E+00	0.00E+00						0.00
33.415	1.450	0.00E+00	0.00E+00	0.0141	0.00E+00	0.00E+00						0.00
33.490	1.433	0.00E+00	0.00E+00	0.0141	0.00E+00	0.00E+00						0.00
33.520	1.426	0.00E+00	0.00E+00	0.0141	0.00E+00	0.00E+00						0.00
33.528	1.424	0.00E+00	0.00E+00	0.0141	0.00E+00	0.00E+00						0.00
33.531	1.422	0.00E+00	0.00E+00	0.0141	0.00E+00	0.00E+00						0.00
33.532	1.417	0.00E+00	0.00E+00	0.0141	0.00E+00	0.00E+00						0.00
33.535	1.403	0.00E+00	0.00E+00	0.0141	0.00E+00	0.00E+00						0.00
33.540	1.379	0.00E+00	0.00E+00	0.0141	0.00E+00	0.00E+00						0.00
33.547	1.344	0.00E+00	0.00E+00	0.0141	0.00E+00	0.00E+00						0.00
33.557	1.296	0.00E+00	0.00E+00	0.0141	0.00E+00	0.00E+00						0.00
33.587	1.158	0.00E+00	0.00E+00	0.0141	0.00E+00	0.00E+00						0.00
33.637	0.926	0.00E+00	0.00E+00	0.0141	0.00E+00	0.00E+00						0.00
33.712	0.580	0.00E+00	0.00E+00	0.0141	0.00E+00	0.00E+00						0.00
33.812	0.115	1.23E-05	-6.57E-06	0.0141	4.92E-06	2.77E+00						391.98
34.112	0.002	2.15E-07	-1.15E-07	0.0141	8.60E-08	4.83E-02						11951.53
34.612	0.000	2.27E-09	-1.21E-09	0.0141	9.06E-10	5.10E-04						12154.85
35.112	0.000	2.39E-11	-1.28E-11	0.0141	9.58E-12	5.38E-06						12156.96
35.612	0.000	2.54E-13	-1.35E-13	0.0141	1.01E-13	5.70E-08						12156.97
36.362	0.000	1.07E-14	-5.71E-15	0.0141	4.28E-15	2.40E-09						12156.97
37.362	0.000	1.07E-14	-5.71E-15	0.0141	4.28E-15	2.40E-09						12156.97
38.362	0.000	1.07E-14	-5.71E-15	0.0141	4.28E-15	2.40E-09						12156.97
39.362	0.000	1.07E-14	-5.71E-15	0.0141	4.28E-15	2.40E-09						12156.97
40.862	0.000	1.07E-14	-5.71E-15	0.0141	4.28E-15	2.40E-09						12156.97
42.862	0.000	1.07E-14	-5.71E-15	0.0141	4.28E-15	2.40E-09						12156.97
45.362	0.000	1.07E-14	-5.71E-15	0.0141	4.28E-15	2.40E-09						12156.97
48.362	0.000	1.07E-14	-5.71E-15	0.0141	4.28E-15	2.40E-09						12156.97
51.862	0.000	1.07E-14	-5.71E-15	0.0141	4.28E-15	2.40E-09						12156.97
55.862	0.000	1.07E-14	-5.71E-15	0.0141	4.28E-15	2.40E-09						12156.97
59.862	0.000	1.07E-14	-5.71E-15	0.0141	4.28E-15	2.40E-09						12156.97
63.862	0.000	1.07E-14	-5.71E-15	0.0141	4.28E-15	2.40E-09						12156.97

RESULTS FOR YEAR: 32

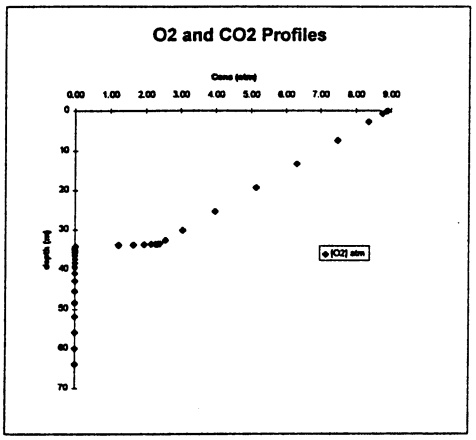

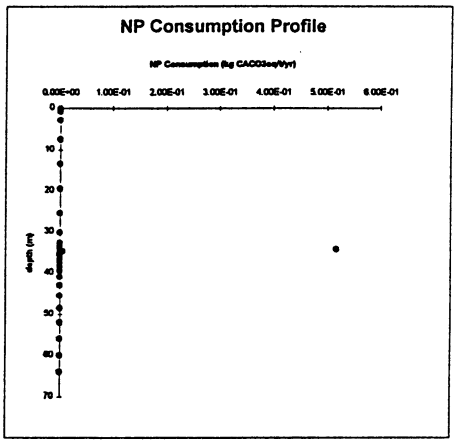

Flux in (mol/m²s)	1.17E-06
O_2 cons. (mol/m²s)	1.16E-06
Dpen (m)	35.362

t=32												
DEPTH (m)	CONC O2 (mol/m³)	O2 Cons (mol/m³/s)	CO2 Prod (mol/m³/s)	CONC CO2 (mol/m³)	mols O2 cons per m3 rock	NP consmptn kg CaCO3eq/t/yr						Sulf dens mol/m³
0.050	8.900	0.00E+00	0.00E+00	0.0141	0.00E+00	0.00E+00						0.00
0.200	8.871	0.00E+00	0.00E+00	0.0141	0.00E+00	0.00E+00						0.00
0.815	8.751	0.00E+00	0.00E+00	0.0141	0.00E+00	0.00E+00						0.00
2.830	8.359	0.00E+00	0.00E+00	0.0141	0.00E+00	0.00E+00						0.00
7.330	7.482	0.00E+00	0.00E+00	0.0141	0.00E+00	0.00E+00						0.00
13.330	6.314	0.00E+00	0.00E+00	0.0141	0.00E+00	0.00E+00						0.00
19.330	5.146	0.00E+00	0.00E+00	0.0141	0.00E+00	0.00E+00						0.00
25.330	3.977	0.00E+00	0.00E+00	0.0141	0.00E+00	0.00E+00						0.00
30.098	3.049	0.00E+00	0.00E+00	0.0141	0.00E+00	0.00E+00						0.00
32.615	2.558	0.00E+00	0.00E+00	0.0141	0.00E+00	0.00E+00						0.00
33.415	2.402	0.00E+00	0.00E+00	0.0141	0.00E+00	0.00E+00						0.00
33.490	2.387	0.00E+00	0.00E+00	0.0141	0.00E+00	0.00E+00						0.00
33.520	2.381	0.00E+00	0.00E+00	0.0141	0.00E+00	0.00E+00						0.00
33.528	2.379	0.00E+00	0.00E+00	0.0141	0.00E+00	0.00E+00						0.00
33.531	2.377	0.00E+00	0.00E+00	0.0141	0.00E+00	0.00E+00						0.00
33.532	2.373	0.00E+00	0.00E+00	0.0141	0.00E+00	0.00E+00						0.00
33.535	2.361	0.00E+00	0.00E+00	0.0141	0.00E+00	0.00E+00						0.00
33.540	2.340	0.00E+00	0.00E+00	0.0141	0.00E+00	0.00E+00						0.00
33.547	2.310	0.00E+00	0.00E+00	0.0141	0.00E+00	0.00E+00						0.00
33.557	2.269	0.00E+00	0.00E+00	0.0141	0.00E+00	0.00E+00						0.00
33.587	2.147	0.00E+00	0.00E+00	0.0141	0.00E+00	0.00E+00						0.00
33.637	1.945	0.00E+00	0.00E+00	0.0141	0.00E+00	0.00E+00						0.00
33.712	1.644	0.00E+00	0.00E+00	0.0141	0.00E+00	0.00E+00						0.00
33.812	1.233	0.00E+00	0.00E+00	0.0141	0.00E+00	0.00E+00						0.00
34.112	0.022	2.30E-06	-1.23E-06	0.0141	9.22E-07	5.16E-01						10025.29
34.612	0.000	2.43E-08	-1.30E-08	0.0141	9.73E-09	5.47E-03						12134.53
35.112	0.000	2.57E-10	-1.37E-10	0.0141	1.03E-10	5.77E-05						12156.74
35.612	0.000	2.72E-12	-1.45E-12	0.0141	1.09E-12	6.11E-07						12156.97
36.362	0.000	1.07E-14	-5.71E-15	0.0141	4.28E-15	2.40E-09						12156.97
37.362	0.000	1.07E-14	-5.71E-15	0.0141	4.28E-15	2.40E-09						12156.97
38.362	0.000	1.07E-14	-5.71E-15	0.0141	4.28E-15	2.40E-09						12156.97
39.362	0.000	1.07E-14	-5.71E-15	0.0141	4.28E-15	2.40E-09						12156.97
40.862	0.000	1.07E-14	-5.71E-15	0.0141	4.28E-15	2.40E-09						12156.97
42.862	0.000	1.07E-14	-5.71E-15	0.0141	4.28E-15	2.40E-09						12156.97
45.362	0.000	1.07E-14	-5.71E-15	0.0141	4.28E-15	2.40E-09						12156.97
48.362	0.000	1.07E-14	-5.71E-15	0.0141	4.28E-15	2.40E-09						12156.97
51.862	0.000	1.07E-14	-5.71E-15	0.0141	4.28E-15	2.40E-09						12156.97
55.862	0.000	1.07E-14	-5.71E-15	0.0141	4.28E-15	2.40E-09						12156.97
59.862	0.000	1.07E-14	-5.71E-15	0.0141	4.28E-15	2.40E-09						12156.97
63.862	0.000	1.07E-14	-5.71E-15	0.0141	4.28E-15	2.40E-09						12156.97

APPENDIX A10
MINTEQA2 Input Files

Uncemented unoxidized tailings

```
15.00 MG/L   0.000  0.00000E-01
0 0 1 0 3 0 0 0 1 1 0 0 0
0   0   0
     330  0.000E-01   -7.00 y                    /H+1
     732  1.500E+03   -1.81 y                    /SO4-2
      30  1.400E+00   -4.28 y                    /Al+3
      61  6.000E-02   -6.45 y                    /H3AsO4
     100  2.000E-02   -6.84 y                    /Ba+2
     160  1.000E-04   -9.05 y                    /Cd+2
     150  2.990E+02   -2.13 y                    /Ca+2
     210  5.600E-02   -5.97 y                    /Cr+2
     231  6.300E-02   -6.00 y                    /Cu+2
     280  4.100E-01   -5.13 y                    /Fe+2
     600  2.700E-01   -5.89 y                    /Pb+2
     460  1.500E-01   -5.21 y                    /Mg+2
     470  5.000E-03   -7.04 y                    /Mn+2
     540  6.000E-03   -6.99 y                    /Ni+2
     762  2.870E-01   -5.70 y                    /SeO4-2
      20  3.000E-03   -7.56 y                    /Ag+1
     950  4.450E-01   -5.17 y                    /Zn+2
     140  0.000E-01  -16.00 y                    /CO3-2
       1  0.000E-01  -16.00 y                    /E-1
     730  0.000E-01  -20.52 y                    /HS-1
     281  1.000E-03  -20.75 y                    /Fe+3

  3   2
1028003    18.4790   -11.3000                    /PYRITE
    330     7.0000     0.0000                    /H+1
  4   1
5015001     8.4750     2.5850   1.000E-03        /CALCITE
  5   8
2003000   -10.3800    27.0450                    /ALOH3(A)
6010000     9.9760    -6.2800                    /BARITE
6015001     4.8480    -0.2610                    /GYPSUM
5028000    10.5500     5.3280                    /SIDERITE
2023101    -7.6200    15.2400                    /TENORITE
5016000    13.7400     0.5800                    /OTAVITE
6060003     7.7900    -2.1500                    /ANGLESITE
7210000     8.9100    -2.6400                    /BA(ASO4)2
  6   1
      1     0.0000     0.0000                    /E-1
```

Cemented Acidic Tails

```
15.00 MG/L   0.000  0.00000E-01
0 0 1 0 3 0 0 0 1 1 0 0 0
0   0   0
     330  0.000E-01   -1.70 y                    /H+1
     732  4.000E+04   -1.81 y                    /SO4-2
     231  4.410E+02   -6.00 y                    /Cu+2
     470  3.128E+03   -7.04 y                    /Mn+2
     950  3.609E+04   -5.17 y                    /Zn+2
      60  1.379E+03   -1.96 y                    /H3AsO3
      30  0.000E-01  -20.43 y                    /Al+3
     460  0.000E-01  -20.39 y                    /Mg+2
     280  0.000E-01  -20.75 y                    /Fe+2
     150  0.000E-01  -20.60 y                    /Ca+2
     600  0.000E-01  -21.32 y                    /Pb+2
     100  0.000E-01  -21.14 y                    /Ba+2

  3   7
6003000     3.2300     0.0000                    /ALOHSO4
```

```
6046000      2.1400     -2.8200                    /EPSOMITE
6028000      2.4700     -2.8600                    /MELANTERITE
6015001      4.8480     -0.2610                    /GYPSUM
6060003      7.7900     -2.1500                    /ANGLESITE
6010000      9.9760     -6.2800                    /BARITE
    330      1.7000      0.0000                    /H+1
```

Cemented oxidized neutral tailings

```
15.00 MG/L    0.000  0.00000E-01
0 0 1 0 3 0 0 0 1 1 0 0 0
0    0    0
    330  0.000E-01   -7.00 y                      /H+1
    732  2.369E+05   -1.81 y                      /SO4-2
     30  4.130E+01   -4.28 y                      /Al+3
     61  3.200E+00   -6.45 y                      /H3AsO4
    100  2.680E+01   -6.84 y                      /Ba+2
    160  1.000E-01   -9.05 y                      /Cd+2
    150  3.368E+04   -2.13 y                      /Ca+2
    210  1.570E+02   -5.97 y                      /Cr+2
    231  4.170E+00   -6.00 y                      /Cu+2
    280  3.600E+01   -5.13 y                      /Fe+2
    600  7.340E+01   -5.89 y                      /Pb+2
    460  1.040E+02   -5.21 y                      /Mg+2
    470  2.609E+00   -7.04 y                      /Mn+2
    762  1.090E+01   -5.70 y                      /SeO4-2
    950  1.040E+01   -5.17 y                      /Zn+2
    140  0.000E-01  -16.00 y                      /CO3-2
      1  0.000E-01  -16.00 y                      /E-1
    730  0.000E-01  -20.52 y                      /HS-1
    281  1.000E-03  -20.75 y                      /Fe+3

  3   2
1028003     18.4790    -11.3000                   /PYRITE
    330      7.0000      0.0000                   /H+1
  4   1
5015001      8.4750      2.5850   1.000E+01       /CALCITE
  5   8
2003000    -10.3800     27.0450                   /ALOH3(A)
6010000      9.9760     -6.2800                   /BARITE
6015001      4.8480     -0.2610                   /GYPSUM
5028000     10.5500      5.3280                   /SIDERITE
2023101     -7.6200     15.2400                   /TENORITE
5016000     13.7400      0.5800                   /OTAVITE
6060003      7.7900     -2.1500                   /ANGLESITE
7210000      8.9100     -2.6400                   /BA(ASO4)2
  6   1
      1      0.0000      0.0000                   /E-1
```

Cemented Unoxidized Tailings

```
15.00 MG/L    0.000  0.00000E-01
0 0 1 0 3 0 0 0 1 1 0 0 0
0    0    0
    330  0.000E-01  -10.00 y                      /H+1
    732  3.296E+02   -1.81 y                      /SO4-2
     30  8.000E-02   -4.28 y                      /Al+3
     61  3.860E-02   -6.45 y                      /H3AsO4
    100  4.300E-02   -6.84 y                      /Ba+2
    160  1.000E-03   -9.05 y                      /Cd+2
    150  3.000E+02   -2.13 y                      /Ca+2
    210  3.000E-03   -5.97 y                      /Cr+2
    231  4.000E-03   -6.00 y                      /Cu+2
```

```
     280  5.000E-02   -5.13 y                    /Fe+2
     600  3.400E-02   -5.89 y                    /Pb+2
     460  2.000E-02   -5.21 y                    /Mg+2
     470  3.000E-03   -7.04 y                    /Mn+2
     540  1.330E-02   -6.99 y                    /Ni+2
     762  1.900E-02   -5.70 y                    /SeO4-2
      20  1.250E-03   -7.56 y                    /Ag+1
     950  2.000E-02   -5.17 y                    /Zn+2
     140  0.000E-01  -16.00 y                    /CO3-2
       1  0.000E-01  -16.00 y                    /E-1
     730  0.000E-01  -20.52 y                    /HS-1
     281  1.000E-03  -20.75 y                    /Fe+3

  3   2
1028003    18.4790   -11.3000                    /PYRITE
    330    10.0000     0.0000                    /H+1
  4   1
5015001     8.4750     2.5850   1.000E-03        /CALCITE
  5   8
2003000   -10.3800    27.0450                    /ALOH3(A)
6010000     9.9760    -6.2800                    /BARITE
6015001     4.8480    -0.2610                    /GYPSUM
5028000    10.5500     5.3280                    /SIDERITE
2023101    -7.6200    15.2400                    /TENORITE
5016000    13.7400     0.5800                    /OTAVITE
6060003     7.7900    -2.1500                    /ANGLESITE
7210000     8.9100    -2.6400                    /BA(ASO4)2
  6   1
      1     0.0000     0.0000                    /E-1
```

APPENDIX A11
MINTEQA2 Output Files

PART 1 of OUTPUT FILE

PC MINTEQA2 v3.10 DATE OF CALCULATIONS: 11-MAR-97 TIME: 23:53:41

Uncemented unoxidized tailings

Temperature (Celsius): 15.00
Units of concentration: MG/L
Ionic strength to be computed.
If specified, carbonate concentration represents total inorganic carbon.
Do not automatically terminate if charge imbalance exceeds 30%
Precipitation is allowed only for those solids specified as ALLOWED in the input file (if any).
The maximum number of iterations is: 200
The method used to compute activity coefficients is: Davies equation
Intermediate output file

330	0.000E-01	-7.00	y
732	1.500E+03	-1.81	y
30	1.400E+00	-4.28	y
61	6.000E-02	-6.45	y
100	2.000E-02	-6.84	y
160	1.000E-04	-9.05	y
150	2.990E+02	-2.13	y
210	5.600E-02	-5.97	y
231	6.300E-02	-6.00	y
280	4.100E-01	-5.13	y
600	2.700E-01	-5.89	y
460	1.500E-01	-5.21	y
470	5.000E-03	-7.04	y
540	6.000E-03	-6.99	y
762	2.870E-01	-5.70	y
20	3.000E-03	-7.56	y
950	4.450E-01	-5.17	y
140	0.000E-01	-16.00	y
1	0.000E-01	-16.00	y
730	0.000E-01	-20.52	y
281	1.000E-03	-20.75	y

H2O has been inserted as a COMPONENT

3	2		
1028003	18.4790	-11.3000	
330	7.0000	0.0000	
4	1		
5015001	8.4750	2.5850	1.000E-03
5	8		
2003000	-10.3800	27.0450	
6010000	9.9760	-6.2800	
6015001	4.8480	-0.2610	
5028000	10.5500	5.3280	
2023101	-7.6200	15.2400	
5016000	13.7400	0.5800	
6060003	7.7900	-2.1500	

```
7210000      8.9100     -2.6400
  6   1
      1      0.0000      0.0000
```

INPUT DATA BEFORE TYPE MODIFICATIONS

ID	NAME	ACTIVITY GUESS	LOG GUESS	ANAL TOTAL
330	H+1	1.000E-07	-7.000	0.000E-01
732	SO4-2	1.549E-02	-1.810	1.500E+03
30	Al+3	5.248E-05	-4.280	1.400E+00
61	H3AsO4	3.548E-07	-6.450	6.000E-02
100	Ba+2	1.445E-07	-6.840	2.000E-02
160	Cd+2	8.913E-10	-9.050	1.000E-04
150	Ca+2	7.413E-03	-2.130	2.990E+02
210	Cr+2	1.072E-06	-5.970	5.600E-02
231	Cu+2	1.000E-06	-6.000	6.300E-02
280	Fe+2	7.413E-06	-5.130	4.100E-01
600	Pb+2	1.288E-06	-5.890	2.700E-01
460	Mg+2	6.166E-06	-5.210	1.500E-01
470	Mn+2	9.120E-08	-7.040	5.000E-03
540	Ni+2	1.023E-07	-6.990	6.000E-03
762	SeO4-2	1.995E-06	-5.700	2.870E-01
20	Ag+1	2.754E-08	-7.560	3.000E-03
950	Zn+2	6.761E-06	-5.170	4.450E-01
140	CO3-2	1.000E-16	-16.000	0.000E-01
1	E-1	1.000E-16	-16.000	0.000E-01
730	HS-1	3.020E-21	-20.520	0.000E-01
281	Fe+3	1.778E-21	-20.750	1.000E-03
2	H2O	1.000E+00	0.000	0.000E-01

Charge Balance: UNSPECIATED

Sum of CATIONS= 1.515E-02 Sum of ANIONS = 3.129E-02

PERCENT DIFFERENCE = 3.475E+01 (ANIONS - CATIONS)/(ANIONS + CATIONS)

IMPROVED ACTIVITY GUESSES PRIOR TO FIRST ITERATION:

SO4-2	Log activity guess:	-1.81
Al+3	Log activity guess:	-9.35
H3AsO4	Log activity guess:	-11.60
Cu+2	Log activity guess:	-6.04
Fe+2	Log activity guess:	-5.13
Mn+2	Log activity guess:	-7.04
SeO4-2	Log activity guess:	-5.70
Fe+3	Log activity guess:	-16.13

PART 3 of OUTPUT FILE

PC MINTEQA2 v3.10 DATE OF CALCULATIONS: 11-MAR-97 TIME: 23:53:42

PARAMETERS OF THE COMPONENT MOST OUT OF BALANCE:

ITER	NAME	TOTAL MOL	DIFF FXN	LOG ACTVTY	RESIDUAL
0	E-1	0.000E-01	-2.195E-03	-16.00000	2.195E-03
1	E-1	0.000E-01	-7.005E-04	-15.95653	7.004E-04
2	E-1	0.000E-01	-3.096E-04	-15.89356	3.096E-04
3	E-1	0.000E-01	-1.233E-04	-15.82441	1.233E-04
4	E-1	0.000E-01	-4.910E-05	-15.74970	4.909E-05
5	E-1	0.000E-01	-1.972E-05	-15.67099	1.971E-05
6	E-1	0.000E-01	-7.923E-06	-15.59186	7.922E-06
7	E-1	0.000E-01	-3.184E-06	-15.51268	3.184E-06
8	E-1	0.000E-01	-1.280E-06	-15.43350	1.279E-06
9	E-1	0.000E-01	-5.142E-07	-15.35432	5.142E-07
10	E-1	0.000E-01	-2.067E-07	-15.27514	2.066E-07
11	E-1	0.000E-01	-8.305E-08	-15.19595	8.304E-08
12	E-1	0.000E-01	-3.338E-08	-15.11677	3.337E-08
13	E-1	0.000E-01	-1.341E-08	-15.03759	1.341E-08
14	E-1	0.000E-01	-5.391E-09	-14.95841	5.390E-09
15	E-1	0.000E-01	-2.166E-09	-14.87923	2.166E-09
16	E-1	0.000E-01	-8.706E-10	-14.80005	8.705E-10
17	E-1	0.000E-01	-3.499E-10	-14.72087	3.498E-10
18	E-1	0.000E-01	-1.406E-10	-14.64168	1.406E-10
19	E-1	0.000E-01	-5.651E-11	-14.56250	5.650E-11
20	E-1	0.000E-01	-2.271E-11	-14.48332	2.271E-11
21	E-1	0.000E-01	-9.126E-12	-14.40414	9.125E-12
22	E-1	0.000E-01	-3.668E-12	-14.32496	3.667E-12
23	E-1	0.000E-01	-1.474E-12	-14.24577	1.474E-12
24	E-1	0.000E-01	-5.924E-13	-14.16659	5.923E-13
25	E-1	0.000E-01	-2.381E-13	-14.08741	2.380E-13
26	E-1	0.000E-01	-9.567E-14	-14.00823	9.566E-14
27	E-1	0.000E-01	-3.845E-14	-13.92904	3.844E-14
28	E-1	0.000E-01	-1.545E-14	-13.84986	1.545E-14
29	E-1	0.000E-01	-6.210E-15	-13.77067	6.209E-15
30	E-1	0.000E-01	-2.496E-15	-13.69149	2.495E-15
31	E-1	0.000E-01	-1.003E-15	-13.61230	1.003E-15
32	E-1	0.000E-01	-4.030E-16	-13.53312	4.030E-16
33	E-1	0.000E-01	-1.620E-16	-13.45393	1.620E-16
34	E-1	0.000E-01	-6.510E-17	-13.37474	6.509E-17
35	E-1	0.000E-01	-2.616E-17	-13.29555	2.616E-17
36	E-1	0.000E-01	-1.051E-17	-13.21637	1.051E-17
37	E-1	0.000E-01	-4.223E-18	-13.13721	4.223E-18
38	E-1	0.000E-01	-1.696E-18	-13.05810	1.695E-18
39	E-1	0.000E-01	-6.793E-19	-12.97917	6.793E-19
40	E-1	0.000E-01	-2.705E-19	-12.90077	2.705E-19
41	E-1	0.000E-01	-1.058E-19	-12.82395	1.058E-19
42	E-1	0.000E-01	-3.918E-20	-12.75159	3.917E-20
43	E-1	0.000E-01	-1.240E-20	-12.69075	1.239E-20
44	E-1	0.000E-01	-2.521E-21	-12.65297	2.519E-21
45	E-1	0.000E-01	-1.634E-22	-12.64146	1.620E-22

ID	NAME	ANAL MOL	CALC MOL	LOG ACTVTY	GAMMA	DIFF FXN
281	Fe+3	1.794E-08	3.264E-16	-16.20010	0.193285	- 4.830E-17

```
  2076200 SeO3          -49.038    [  1.000] 762  [  2.000] 330  [ -
1.000]   2
  6102001 Ag2SeO4       -13.952    [  1.000] 762  [  2.000]  20
  6110001 BaSeO4        -12.546    [  1.000] 762  [  1.000] 100
  6115001 CaSeO4:2H2O    -6.552    [  1.000] 762  [  1.000] 150  [
2.000]   2
  6160000 PbSeO4         -9.995    [  1.000] 762  [  1.000] 600
  2021100 CR(OH)2         1.498    [  1.000] 210  [  2.000]   2  [ -
2.000] 330
    21000 CR METAL      -56.167    [  1.000] 210  [  2.000]   1
```

```
   732  SO4-2          1.564E-02  1.180E-02    -2.24520    0.481676  -
1.395E-10
    30  Al+3           5.198E-05  2.285E-09    -9.35485    0.193285  -
7.651E-15
    61  H3AsO4         4.235E-07  1.425E-12   -11.84204    1.009365  -
4.083E-15
   100  Ba+2           1.459E-07  1.459E-07    -7.15323    0.481676  -
1.743E-15
   160  Cd+2           8.913E-10  4.221E-10    -9.69188    0.481676  -
5.602E-18
   150  Ca+2           7.474E-03  7.556E-03    -2.43896    0.481676  -
7.892E-11
   210  Cr+2           1.079E-06  1.079E-06    -6.28424    0.481676  -
1.289E-14
   231  Cu+2           9.932E-07  1.702E-07    -7.08626    0.481676  -
2.098E-15
   280  Fe+2           7.355E-06  5.253E-06    -5.59686    0.481676  -
6.192E-14
   600  Pb+2           1.306E-06  1.059E-07    -7.29254    0.481676  -
1.351E-15
   460  Mg+2           6.181E-06  4.226E-06    -5.69134    0.481676  -
4.995E-14
   470  Mn+2           9.118E-08  6.250E-08    -7.52138    0.481676  -
7.401E-16
   540  Ni+2           1.024E-07  1.915E-08    -8.03496    0.481676  -
2.103E-16
   762  SeO4-2         2.011E-06  2.011E-06    -6.01385    0.481676  -
2.402E-14
    20  Ag+1           2.786E-08  2.529E-08    -7.67633    0.833084  -
8.320E-17
   950  Zn+2           6.820E-06  3.577E-06    -5.76372    0.481676  -
4.621E-14
     1  E-1            0.000E-01  2.288E-13   -12.64061    0.833084
2.900E-29
     2  H2O            0.000E-01 -1.561E-04    -0.00017    1.000000
0.000E-01
   330  H+1            0.000E-01  1.200E-07    -7.00000    0.833084
0.000E-01
   730  HS-1           0.000E-01  7.144E-27   -26.22540    0.833084
0.000E-01
   140  CO3-2          0.000E-01  2.153E-06    -5.98414    0.481676
0.000E-01

-------------------------------------------------------------------------
-----

 Type I - COMPONENTS AS SPECIES IN SOLUTION

   ID        NAME        CALC MOL    ACTIVITY    LOG ACTVTY     GAMMA
NEW LOGK
    330  H+1             1.200E-07  1.000E-07     -7.00000    0.83308
0.079
    732  SO4-2           1.180E-02  5.686E-03     -2.24520    0.48168
0.317
     30  Al+3            2.285E-09  4.417E-10     -9.35485    0.19329
0.714
     61  H3AsO4          1.425E-12  1.439E-12    -11.84204    1.00937   -
0.004
    100  Ba+2            1.459E-07  7.027E-08     -7.15323    0.48168
0.317
    160  Cd+2            4.221E-10  2.033E-10     -9.69188    0.48168
0.317
    150  Ca+2            7.556E-03  3.639E-03     -2.43896    0.48168
0.317
```

210	Cr+2	1.079E-06	5.197E-07	-6.28424	0.48168	0.317
231	Cu+2	1.702E-07	8.199E-08	-7.08626	0.48168	0.317
280	Fe+2	5.253E-06	2.530E-06	-5.59686	0.48168	0.317
600	Pb+2	1.059E-07	5.099E-08	-7.29254	0.48168	0.317
460	Mg+2	4.226E-06	2.035E-06	-5.69134	0.48168	0.317
470	Mn+2	6.250E-08	3.010E-08	-7.52138	0.48168	0.317
540	Ni+2	1.915E-08	9.226E-09	-8.03496	0.48168	0.317
762	SeO4-2	2.011E-06	9.686E-07	-6.01385	0.48168	0.317
20	Ag+1	2.529E-08	2.107E-08	-7.67633	0.83308	0.079
950	Zn+2	3.577E-06	1.723E-06	-5.76372	0.48168	0.317
140	CO3-2	2.153E-06	1.037E-06	-5.98414	0.48168	0.317
281	Fe+3	3.264E-16	6.308E-17	-16.20010	0.19329	0.714
730	HS-1	7.144E-27	5.951E-27	-26.22540	0.83308	0.079

Type II - OTHER SPECIES IN SOLUTION OR ADSORBED

ID	NAME	CALC MOL	ACTIVITY	LOG ACTVTY	GAMMA	NEW LOGK
1607620	CdSeO4	3.402E-14	3.434E-14	-13.46423	1.00937	2.237
9507620	ZnSeO4	2.632E-10	2.657E-10	-9.57568	1.00937	2.198
9507621	Zn(SeO4)2-2	2.854E-18	1.375E-18	-17.86183	0.48168	0.247
3300020	OH-	5.517E-08	4.596E-08	-7.33762	0.83308	-14.258
4603300	MgOH +	1.633E-11	1.360E-11	-10.86645	0.83308	-12.096
4601400	MgCO3 AQ	1.712E-09	1.728E-09	-8.76245	1.00937	2.909
4601401	MgHCO3 +	7.493E-08	6.243E-08	-7.20463	0.83308	11.550
4607320	MgSO4 AQ	1.879E-06	1.896E-06	-5.72213	1.00937	2.210
1503300	CaOH +	4.704E-09	3.919E-09	-8.40686	0.83308	-12.888
1501400	CaHCO3 +	9.294E-05	7.743E-05	-4.11110	0.83308	11.391
1501401	CaCO3 AQ	4.391E-06	4.432E-06	-5.35336	1.00937	3.066
1507320	CaSO4 AQ	3.832E-03	3.868E-03	-2.41255	1.00937	2.268
303300	AlOH +2	4.673E-08	2.251E-08	-7.64769	0.48168	-4.975
303301	Al(OH)2 +	4.208E-06	3.506E-06	-5.45519	0.83308	-10.021
303302	Al(OH)4 -	4.009E-06	3.340E-06	-5.47628	0.83308	-24.041

307320	AlSO4 +	2.783E-09	2.319E-09	-8.63474	0.83308	3.045
307321	Al(SO4)2 -	1.207E-09	1.006E-09	-8.99748	0.83308	4.927
303303	Al(OH)3 AQ	4.371E-05	4.412E-05	-4.35536	1.00937	-16.004
2803300	FeOH +	4.431E-09	3.692E-09	-8.43278	0.83308	-9.756
2803301	FeOH3 -1	5.143E-17	4.284E-17	-16.36811	0.83308	-31.691
2807320	FeSO4 AQ	2.098E-06	2.117E-06	-5.67422	1.00937	2.164
2803302	FeOH2 AQ	1.265E-13	1.277E-13	-12.89381	1.00937	-21.301
2807300	Fe(HS)2 AQ	7.912E-50	7.986E-50	-49.09766	1.00937	8.946
2807301	Fe(HS)3 -	6.212E-74	5.175E-74	-73.28606	0.83308	11.066
2813300	FeOH +2	4.597E-12	2.214E-12	-11.65479	0.48168	-2.137
2817320	FeSO4 +	2.848E-15	2.373E-15	-14.62475	0.83308	3.900
2813301	FeOH2 +	1.618E-08	1.348E-08	-7.87044	0.83308	-5.591
2813302	FeOH3 AQ	1.568E-09	1.583E-09	-8.80061	1.00937	-13.604
2813303	FeOH4 -	1.899E-10	1.582E-10	-9.80078	0.83308	-21.521
2817321	Fe(SO4)2 -	4.918E-16	4.097E-16	-15.38750	0.83308	5.382
2813304	Fe2(OH)2+4	3.759E-21	2.023E-22	-21.69394	0.05383	-2.024
2813305	Fe3(OH)4+5	5.225E-26	5.436E-28	-27.26473	0.01040	-4.681
1003300	BaOH +	1.527E-14	1.272E-14	-13.89537	0.83308	-13.663
4703300	MnOH +	3.995E-12	3.328E-12	-11.47781	0.83308	-10.877
4703301	Mn(OH)3 -1	5.720E-22	4.765E-22	-21.32189	0.83308	-34.721
4700020	MnO4 -	2.778E-21	2.314E-21	-20.63563	0.83308	-132.237
4700021	MnO4 -2	1.264E-23	6.087E-24	-23.21563	0.48168	-121.939
4707320	MnSO4 AQ	2.718E-08	2.743E-08	-7.56177	1.00937	2.201
4701400	MnHCO3 +	1.492E-09	1.243E-09	-8.90551	0.83308	11.679
2311400	CuCO3 AQ	4.524E-07	4.567E-07	-6.34040	1.00937	6.726
2311401	Cu(CO3)2-2	1.238E-09	5.963E-10	-9.22453	0.48168	10.147
2313300	CuOH +	9.837E-09	8.195E-09	-8.08643	0.83308	-7.921
2313301	Cu(OH)2 AQ	1.696E-07	1.712E-07	-6.76660	1.00937	-13.684
2313302	Cu(OH)3 -	1.240E-13	1.033E-13	-12.98578	0.83308	-26.820
2313303	Cu(OH)4 -2	4.269E-19	2.056E-19	-18.68695	0.48168	-39.283
2313304	Cu2(OH)2+2	2.186E-11	1.053E-11	-10.97750	0.48168	-10.487
2317320	CuSO4 AQ	8.779E-08	8.862E-08	-7.05249	1.00937	2.275

2317300	Cu(HS)3 -	1.644E-60	1.369E-60	-59.86346	0.83308	25.978
2311402	CuHCO3 +	1.021E-07	8.504E-08	-7.07040	0.83308	13.079
9503300	ZnOH +	1.034E-08	8.615E-09	-8.06472	0.83308	-9.222
9503301	Zn(OH)2 AQ	2.152E-09	2.172E-09	-8.66307	1.00937	-16.903
9503302	Zn(OH)3 -	8.243E-14	6.867E-14	-13.16324	0.83308	-28.320
9503303	Zn(OH)4 -2	2.259E-19	1.088E-19	-18.96341	0.48168	-40.882
9507300	Zn(HS)2 AQ	5.265E-44	5.315E-44	-43.27452	1.00937	14.936
9507301	Zn(HS)3 -	5.488E-69	4.572E-69	-68.33992	0.83308	16.179
9507320	ZnSO4 AQ	2.101E-06	2.121E-06	-5.67351	1.00937	2.331
9507321	Zn(SO4)2-2	2.204E-07	1.061E-07	-6.97412	0.48168	3.597
9501400	ZnHCO3 +	5.388E-07	4.489E-07	-6.34786	0.83308	12.479
9501401	ZnCO3 AQ	3.533E-07	3.566E-07	-6.44786	1.00937	5.296
9501402	Zn(CO3)2-2	1.642E-08	7.907E-09	-8.10199	0.48168	9.947
1601400	Cd(CO3)3-4	6.993E-21	3.765E-22	-21.42429	0.05383	7.489
1603300	CdOH +	9.420E-14	7.847E-14	-13.10527	0.83308	-10.334
1603301	Cd(OH)2 AQ	8.989E-17	9.074E-17	-16.04222	1.00937	-20.354
1603302	Cd(OH)3 -	1.222E-22	1.018E-22	-21.99239	0.83308	-33.221
1603303	Cd(OH)4 -2	1.882E-29	9.066E-30	-29.04256	0.48168	-47.033
1603304	Cd2OH +3	4.599E-22	8.889E-23	-22.05116	0.19329	-8.953
1607320	CdSO4 AQ	3.100E-10	3.129E-10	-9.50455	1.00937	2.428
1607300	CdHS +	2.148E-26	1.789E-26	-25.74728	0.83308	10.249
1607301	Cd(HS)2 AQ	2.417E-46	2.440E-46	-45.61268	1.00937	16.526
1607302	Cd(HS)3 -	2.638E-70	2.197E-70	-69.65808	0.83308	18.789
1607303	Cd(HS)4 -2	4.205E-94	2.025E-94	-93.69348	0.48168	21.217
1601400	CdHCO3 +	6.358E-11	5.296E-11	-10.27601	0.83308	12.479
1601401	CdCO3 AQ	5.235E-11	5.284E-11	-10.27701	1.00937	5.395
1607321	Cd(SO4)2-2	4.315E-11	2.078E-11	-10.68227	0.48168	3.817
6001400	Pb(CO3)2-2	4.971E-09	2.394E-09	-8.62081	0.48168	10.957
6003300	PbOH +	1.193E-08	9.938E-09	-8.00271	0.83308	-7.631
6003301	Pb(OH)2 AQ	3.829E-11	3.865E-11	-10.41288	1.00937	-17.124
6003302	Pb(OH)3 -	5.324E-15	4.436E-15	-14.35305	0.83308	-27.981
6003303	Pb2OH +3	5.869E-14	1.134E-14	-13.94525	0.19329	-5.646

6007320	PbSO4 AQ	1.615E-07	1.630E-07	-6.78774	1.00937	
2.746						
6007300	Pb(HS)2 AQ	3.331E-45	3.362E-45	-44.47334	1.00937	
15.266						
6007301	Pb(HS)3 -	4.793E-70	3.993E-70	-69.39874	0.83308	
16.649						
6003304	Pb3(OH)4+2	7.671E-19	3.695E-19	-18.43238	0.48168	-
24.237						
6001401	PbCO3 AQ	9.105E-07	9.190E-07	-6.03668	1.00937	
7.236						
6003305	Pb(OH)4 -2	2.114E-19	1.018E-19	-18.99223	0.48168	-
39.382						
6007321	Pb(SO4)2-2	1.010E-08	4.865E-09	-8.31293	0.48168	
3.787						
6001402	PbHCO3 +	1.006E-07	8.382E-08	-7.07668	0.83308	
13.279						
5403300	NiOH +	7.383E-12	6.151E-12	-11.21106	0.83308	-
10.097						
5403301	Ni(OH)2 AQ	9.134E-14	9.219E-14	-13.03531	1.00937	-
19.004						
5403302	Ni(OH)3 -	1.106E-17	9.216E-18	-17.03548	0.83308	-
29.921						
5407320	NiSO4 AQ	9.271E-09	9.358E-09	-8.02882	1.00937	
2.247						
5401400	NiHCO3 +	3.390E-09	2.824E-09	-8.54910	0.83308	
12.549						
5401401	NiCO3 AQ	7.028E-08	7.094E-08	-7.14910	1.00937	
6.866						
5401402	Ni(CO3)2-2	2.655E-10	1.279E-10	-9.89324	0.48168	
10.427						
5407321	Ni(SO4)2-2	6.485E-12	3.124E-12	-11.50536	0.48168	
1.337						
207300	AgHS AQ	1.394E-20	1.407E-20	-19.85173	1.00937	
14.046						
207301	Ag(HS)2 -	2.525E-42	2.103E-42	-41.67713	0.83308	
18.529						
203300	AgOH AQ	2.087E-13	2.106E-13	-12.67650	1.00937	-
12.004						
203301	Ag(OH)2 -	2.527E-18	2.105E-18	-17.67667	0.83308	-
23.921						
207320	AgSO4 -	2.570E-09	2.141E-09	-8.66942	0.83308	
1.331						
3300611	H2AsO4 -	1.090E-07	9.077E-08	-7.04205	0.83308	-
2.121						
3300612	HAsO4 -2	3.145E-07	1.515E-07	-6.81964	0.48168	-
8.660						
3300613	AsO4 -3	1.540E-11	2.977E-12	-11.52629	0.19329	-
19.970						
3301400	HCO3 -	3.347E-03	2.788E-03	-2.55466	0.83308	
10.509						
3301401	H2CO3 AQ	5.623E-04	5.676E-04	-3.24598	1.00937	
16.734						
3307320	HSO4 -	5.042E-08	4.201E-08	-7.37669	0.83308	
1.948						
3307300	H2S AQ	7.164E-27	7.231E-27	-26.14081	1.00937	
7.081						
3307301	S -2	7.346E-33	3.538E-33	-32.45118	0.48168	-
12.909						
3307620	HSeO4-1	7.319E-12	6.097E-12	-11.21489	0.83308	
1.878						
4707620	MnSeO4	6.187E-12	6.245E-12	-11.20444	1.00937	
2.327						
5407620	NiSeO4	3.139E-12	3.168E-12	-11.49915	1.00937	
2.546						

Type III - SPECIES WITH FIXED ACTIVITY

ID	NAME	CALC MOL	LOG MOL	NEW LOGK	DH
2	H2O	-1.561E-04	-3.807	0.000	0.000
330	H+1	-4.409E-03	-2.356	7.000	0.000
1028003	PYRITE	-6.969E-21	-20.157	18.766	-11.300

Type IV - FINITE SOLIDS (presumed present at equilibrium)

ID	NAME	CALC MOL	LOG MOL	NEW LOGK	DH
5015001	CALCITE	0.000E-01	-2.397	8.423	2.585

Type V - POSSIBLE SOLIDS

ID	NAME	CALC MOL	LOG MOL	NEW LOGK	DH
2003000	ALOH3(A)	3.773E+00	0.577	-11.068	27.045
6015001	GYPSUM	1.480E+00	0.170	4.855	-0.261
6010000	BARITE	5.462E+00	0.737	10.136	-6.280
5028000	SIDERITE	6.815E-02	-1.167	10.414	5.328
2023101	TENORITE	8.052E-02	-1.094	-8.008	15.240
5016000	OTAVITE	1.120E-02	-1.951	13.725	0.580
6060003	ANGLESITE	2.027E-02	-1.693	7.845	-2.150
7210000	BA(ASO4)2	6.814E+05	5.833	8.977	-2.640

Type VI - EXCLUDED SPECIES (not included in mole balance)

ID	NAME	CALC MOL	LOG MOL	NEW LOGK	DH
3301403	CO2 (g)	1.547E-02	-1.810	18.173	-0.530
3300021	O2 (g)	1.091E-08	-7.962	-86.524	133.830
1	E-1	2.288E-13	-12.641	0.000	0.000
2802810	Fe+2/Fe+3	1.103E-10	-9.957	13.286	-10.000
7307320	HS-/SO4-2	0.000E-01	-104.954	35.190	-60.140
3301404	CH4 (g)	0.000E-01	-135.457	41.652	-61.000

PERCENTAGE DISTRIBUTION OF COMPONENTS AMONG
TYPE I and TYPE II (dissolved and adsorbed) species

Fe+3	90.2	PERCENT BOUND IN SPECIES #2813301	
FeOH2 +			
8.7	PERCENT BOUND IN SPECIES #2813302	FeOH3 AQ	
1.1	PERCENT BOUND IN SPECIES #2813303	FeOH4 -	
SO4-2	75.5	PERCENT BOUND IN SPECIES #	732
SO4-2			
24.5	PERCENT BOUND IN SPECIES #1507320	CaSO4 AQ	
Al+3	8.1	PERCENT BOUND IN SPECIES #	303301
Al(OH)2 +			
7.7	PERCENT BOUND IN SPECIES # 303302	Al(OH)4 -	
84.1	PERCENT BOUND IN SPECIES # 303303	Al(OH)3 AQ	
H3AsO4	25.7	PERCENT BOUND IN SPECIES #3300611	
H2AsO4 -			
74.3	PERCENT BOUND IN SPECIES #3300612	HAsO4 -2	
Ba+2	100.0	PERCENT BOUND IN SPECIES #	100
Ba+2			
Cd+2	47.4	PERCENT BOUND IN SPECIES #	160
Cd+2			
34.8	PERCENT BOUND IN SPECIES #1607320	CdSO4 AQ	
7.1	PERCENT BOUND IN SPECIES #1601400	CdHCO3 +	
5.9	PERCENT BOUND IN SPECIES #1601401	CdCO3 AQ	
4.8	PERCENT BOUND IN SPECIES #1607321	Cd(SO4)2-2	
Ca+2	65.8	PERCENT BOUND IN SPECIES #	150
Ca+2			
33.4	PERCENT BOUND IN SPECIES #1507320	CaSO4 AQ	
Cr+2	100.0	PERCENT BOUND IN SPECIES #	210
Cr+2			
Cu+2	17.1	PERCENT BOUND IN SPECIES #	231
Cu+2			
45.6	PERCENT BOUND IN SPECIES #2311400	CuCO3 AQ	
17.1	PERCENT BOUND IN SPECIES #2313301	Cu(OH)2 AQ	
8.8	PERCENT BOUND IN SPECIES #2317320	CuSO4 AQ	
10.3	PERCENT BOUND IN SPECIES #2311402	CuHCO3 +	
Fe+2	71.4	PERCENT BOUND IN SPECIES #	280
Fe+2			
28.5	PERCENT BOUND IN SPECIES #2807320	FeSO4 AQ	
Pb+2	8.1	PERCENT BOUND IN SPECIES #	600
Pb+2			
12.4	PERCENT BOUND IN SPECIES #6007320	PbSO4 AQ	
69.7	PERCENT BOUND IN SPECIES #6001401	PbCO3 AQ	
7.7	PERCENT BOUND IN SPECIES #6001402	PbHCO3 +	

Mg+2	68.4	PERCENT BOUND IN SPECIES # 460
Mg+2		
	1.2	PERCENT BOUND IN SPECIES #4601401 MgHCO3 +
	30.4	PERCENT BOUND IN SPECIES #4607320 MgSO4 AQ
Mn+2	68.5	PERCENT BOUND IN SPECIES # 470
Mn+2		
	29.8	PERCENT BOUND IN SPECIES #4707320 MnSO4 AQ
	1.6	PERCENT BOUND IN SPECIES #4701400 MnHCO3 +
Ni+2	18.7	PERCENT BOUND IN SPECIES # 540
Ni+2		
	9.1	PERCENT BOUND IN SPECIES #5407320 NiSO4 AQ
	3.3	PERCENT BOUND IN SPECIES #5401400 NiHCO3 +
	68.6	PERCENT BOUND IN SPECIES #5401401 NiCO3 AQ
SeO4-2	100.0	PERCENT BOUND IN SPECIES # 762
SeO4-2		
Ag+1	90.8	PERCENT BOUND IN SPECIES # 20
Ag+1		
	9.2	PERCENT BOUND IN SPECIES # 207320 AgSO4 -
Zn+2	52.5	PERCENT BOUND IN SPECIES # 950
Zn+2		
	30.8	PERCENT BOUND IN SPECIES #9507320 ZnSO4 AQ
	3.2	PERCENT BOUND IN SPECIES #9507321 Zn(SO4)2-2
	7.9	PERCENT BOUND IN SPECIES #9501400 ZnHCO3 +
	5.2	PERCENT BOUND IN SPECIES #9501401 ZnCO3 AQ
E-1	99.6	PERCENT BOUND IN SPECIES #4700020
MnO4 -		
H2O	5.4	PERCENT BOUND IN SPECIES # 303301
Al(OH)2 +		
	10.3	PERCENT BOUND IN SPECIES # 303302 Al(OH)4 -
	84.0	PERCENT BOUND IN SPECIES # 303303 Al(OH)3 AQ
H+1	2.1	PERCENT BOUND IN SPECIES #1501400
CaHCO3 +		
	75.9	PERCENT BOUND IN SPECIES #3301400 HCO3 -
	25.5	PERCENT BOUND IN SPECIES #3301401 H2CO3 AQ
HS-1	100.0	PERCENT BOUND IN SPECIES # 207300
AgHS AQ		
CO3-2	2.3	PERCENT BOUND IN SPECIES #1501400
CaHCO3 +		
	83.4	PERCENT BOUND IN SPECIES #3301400 HCO3 -
	14.0	PERCENT BOUND IN SPECIES #3301401 H2CO3 AQ

PART 5 of OUTPUT FILE

PC MINTEQA2 v3.10 DATE OF CALCULATIONS: 11-MAR-97 TIME: 23:53:45

---------- PROVISIONAL MASS DISTRIBUTION ----------

IDX	NAME	DISSOLVED		SORBED		PRECIPITATED
		MOL/KG	PERCENT	MOL/KG	PERCENT	MOL/KG
PERCENT						
281	Fe+3	1.794E-08	100.0	0.000E-01	0.0	0.000E-01
0.0						
732	SO4-2	1.564E-02	100.0	0.000E-01	0.0	0.000E-01
0.0						
30	Al+3	5.198E-05	100.0	0.000E-01	0.0	0.000E-01
0.0						
61	H3AsO4	4.235E-07	100.0	0.000E-01	0.0	0.000E-01
0.0						
100	Ba+2	1.459E-07	100.0	0.000E-01	0.0	0.000E-01
0.0						
160	Cd+2	8.913E-10	100.0	0.000E-01	0.0	0.000E-01
0.0						
150	Ca+2	1.148E-02	100.0	0.000E-01	0.0	0.000E-01
0.0						
210	Cr+2	1.079E-06	100.0	0.000E-01	0.0	0.000E-01
0.0						
231	Cu+2	9.932E-07	100.0	0.000E-01	0.0	0.000E-01
0.0						
280	Fe+2	7.355E-06	100.0	0.000E-01	0.0	0.000E-01
0.0						
600	Pb+2	1.306E-06	100.0	0.000E-01	0.0	0.000E-01
0.0						
460	Mg+2	6.181E-06	100.0	0.000E-01	0.0	0.000E-01
0.0						
470	Mn+2	9.118E-08	100.0	0.000E-01	0.0	0.000E-01
0.0						
540	Ni+2	1.024E-07	100.0	0.000E-01	0.0	0.000E-01
0.0						
762	SeO4-2	2.011E-06	100.0	0.000E-01	0.0	0.000E-01
0.0						
20	Ag+1	2.786E-08	100.0	0.000E-01	0.0	0.000E-01
0.0						
950	Zn+2	6.820E-06	100.0	0.000E-01	0.0	0.000E-01
0.0						
1	E-1	-1.394E-20	100.0	0.000E-01	0.0	0.000E-01
0.0						
2	H2O	1.561E-04	100.0	0.000E-01	0.0	0.000E-01
0.0						
330	H+1	4.409E-03	100.0	0.000E-01	0.0	0.000E-01
0.0						
730	HS-1	1.394E-20	100.0	0.000E-01	0.0	0.000E-01
0.0						
140	CO3-2	4.011E-03	100.0	0.000E-01	0.0	0.000E-01
0.0						

Charge Balance: SPECIATED

Sum of CATIONS = 1.524E-02 Sum of ANIONS 2.697E-02

PERCENT DIFFERENCE = 2.779E+01 (ANIONS - CATIONS)/(ANIONS + CATIONS)

PROVISIONAL IONIC STRENGTH (m) = 4.048E-02

PART 6 of OUTPUT FILE

PC MINTEQA2 v3.10 DATE OF CALCULATIONS: 11-MAR-97 TIME: 23:53:45

Saturation indices and stoichiometry of all undersaturated minerals

ID #	NAME	Sat. Index	Stoichiometry in [brackets]
6003000	ALOHSO4	-1.370	[-1.000] 330 [1.000] 30 [1.000] 732
			[1.000] 2
6015000	ANHYDRITE	-0.143	[1.000] 150 [1.000] 732
5015000	ARAGONITE	-0.173	[1.000] 150 [1.000] 140
5046000	ARTINITE	-13.699	[-2.000] 330 [2.000] 460 [1.000] 140
			[5.000] 2
2046000	BRUCITE	-9.141	[1.000] 460 [2.000] 2 [-2.000] 330
5015001	CALCITE	0.000	[1.000] 150 [1.000] 140
5015002	DOLOMITE	-3.309	[1.000] 150 [1.000] 460 [2.000] 140
6046000	EPSOMITE	-5.726	[1.000] 460 [1.000] 732 [7.000] 2
2028100	FERRIHYDRITE	-0.092	[-3.000] 330 [1.000] 281 [3.000] 2
2028101	FE3(OH)8	-2.220	[-8.000] 330 [2.000] 281 [1.000] 280
			[8.000] 2
1028000	FES PPT	-20.907	[-1.000] 330 [1.000] 280 [1.000] 730
6028100	FE2(SO4)3	-44.220	[2.000] 281 [3.000] 732
1028001	GREIGITE	-69.864	[-4.000] 330 [2.000] 281 [1.000] 280
			[4.000] 730
5015003	HUNTITE	-14.137	[3.000] 460 [1.000] 150 [4.000] 140
5046001	HYDRMAGNESIT	-30.956	[5.000] 460 [4.000] 140 [-2.000] 330
			[6.000] 2
6028101	JAROSITE H	-7.395	[-5.000] 330 [3.000] 281 [2.000] 732
			[7.000] 2
1028002	MACKINAWITE	-20.174	[-1.000] 330 [1.000] 280 [1.000] 730
5046002	MAGNESITE	-3.803	[1.000] 460 [1.000] 140
6028000	MELANTERITE	-5.301	[1.000] 280 [1.000] 732 [7.000] 2
5046003	NESQUEHONITE	-6.202	[1.000] 460 [1.000] 140 [3.000] 2
1028003	PYRITE	0.000	[-2.000] 330 [-2.000] 1 [1.000] 280
			[2.000] 730
5028000	SIDERITE	-1.167	[1.000] 280 [1.000] 140
5010000	WITHERITE	-4.543	[1.000] 100 [1.000] 140
3047000	HAUSMANNITE	-4.862	[-8.000] 330 [-2.000] 1 [3.000] 470
			[4.000] 2
2047003	PYROCROITE	-9.184	[-2.000] 330 [1.000] 470 [2.000] 2
5047000	RHODOCHROSIT	-3.148	[1.000] 470 [1.000] 140

```
  1047000 MNS GREEN      -30.694    [ -1.000] 330  [  1.000] 470  [
1.000] 730
  6047000 MNSO4          -12.829    [  1.000] 470  [  1.000] 732
  1023101 COVELLITE       -2.663    [ -1.000] 330  [  1.000] 231  [
1.000] 730
  5023100 CUCO3           -3.440    [  1.000] 231  [  1.000] 140
  2023100 CU(OH)2         -2.115    [ -2.000] 330  [  1.000] 231  [
2.000]   2
  6023100 ANTLERITE       -3.795    [ -4.000] 330  [  3.000] 231  [
4.000]   2
                                    [  1.000] 732
  6023101 BROCHANTITE     -3.931    [ -6.000] 330  [  4.000] 231  [
6.000]   2
                                    [  1.000] 732
```

ID #	NAME	Sat. Index	Stoichiometry in [brackets]
6023102	LANGITE	-6.389	[-6.000] 330 [4.000] 231 [7.000] 2
			[1.000] 732
2023101	TENORITE	-1.094	[-2.000] 330 [1.000] 231 [1.000] 2
6023103	CUOCUSO4	-14.853	[-2.000] 330 [2.000] 231 [1.000] 2
			[1.000] 732
6023104	CUSO4	-12.803	[1.000] 231 [1.000] 732
6023105	CHALCANTHITE	-6.656	[1.000] 231 [1.000] 732 [5.000] 2
1023102	CHALCOPYRITE	-14.961	[-2.000] 330 [1.000] 231 [1.000] 280
			[2.000] 730
95000	ZN METAL	-57.738	[1.000] 950 [2.000] 1
5095000	SMITHSONITE	-1.859	[1.000] 950 [1.000] 140
5095001	ZNCO3, 1H2O	-1.488	[1.000] 950 [1.000] 140 [1.000] 2
2095000	ZN(OH)2 (A)	-4.214	[-2.000] 330 [1.000] 950 [2.000] 2
2095001	ZN(OH)2 (C)	-3.964	[-2.000] 330 [1.000] 950 [2.000] 2
2095002	ZN(OH)2 (B)	-3.514	[-2.000] 330 [1.000] 950 [2.000] 2
2095003	ZN(OH)2 (G)	-3.474	[-2.000] 330 [1.000] 950 [2.000] 2
2095004	ZN(OH)2 (E)	-3.264	[-2.000] 330 [1.000] 950 [2.000] 2
6095000	ZN2(OH)2SO4	-7.273	[-2.000] 330 [2.000] 950 [2.000] 2
			[1.000] 732
6095001	ZN4(OH)6SO4	-11.701	[-6.000] 330 [4.000] 950 [6.000] 2
			[1.000] 732
2095005	ZNO(ACTIVE)	-3.074	[-2.000] 330 [1.000] 950 [1.000] 2
2095006	ZINCITE	-3.460	[-2.000] 330 [1.000] 950 [1.000] 2
6095002	ZN3O(SO4)2	-28.379	[-2.000] 330 [3.000] 950 [2.000] 732
			[1.000] 2
1095000	ZNS (A)	-15.844	[-1.000] 330 [1.000] 950 [1.000] 730
1095001	SPHALERITE	-13.161	[-1.000] 330 [1.000] 950 [1.000] 730
1095002	WURTZITE	-15.178	[-1.000] 330 [1.000] 950 [1.000] 730
6095003	ZINCOSITE	-11.507	[1.000] 950 [1.000] 732
6095004	ZNSO4, 1H2O	-7.710	[1.000] 950 [1.000] 732 [1.000] 2
6095005	BIANCHITE	-6.249	[1.000] 950 [1.000] 732 [6.000] 2
6095006	GOSLARITE	-5.966	[1.000] 950 [1.000] 732 [7.000] 2
16000	CD METAL	-48.921	[1.000] 160 [2.000] 1
16001	GAMMA CD	-49.025	[1.000] 160 [2.000] 1
5016000	OTAVITE	-1.951	[1.000] 160 [1.000] 140
2016000	CD(OH)2 (A)	-9.951	[-2.000] 330 [1.000] 160 [2.000] 2

```
  2016001 CD(OH)2 (C)     -9.342    [ -2.000] 330  [  1.000] 160  [
2.000]   2
  6016000 CD3(OH)4SO4    -25.882    [ -4.000] 330  [  3.000] 160  [
4.000]   2
                                    [  1.000] 732
  6016001 CD3OH2(SO4)2   -26.276    [ -2.000] 330  [  3.000] 160  [
2.000]   2
                                    [  2.000] 732
  6016002 CD4(OH)6SO4    -27.414    [ -6.000] 330  [  4.000] 160  [
6.000]   2
                                    [  1.000] 732
  2016002 MONTEPONITE    -11.442    [ -2.000] 330  [  1.000] 160  [
1.000]   2
  6016003 CDSO4          -12.212    [  1.000] 160  [  1.000] 732
  6016004 CDSO4, 1H2O    -10.472    [  1.000] 160  [  1.000] 732  [
1.000]   2
  6016005 CDSO4,2.7H2O   -10.174    [  1.000] 160  [  1.000] 732  [
2.670]   2
  1016000 GREENOCKITE    -12.571    [ -1.000] 330  [  1.000] 160  [
1.000] 730
    60000 PB METAL       -36.834    [  1.000] 600  [  2.000]   1
  5060000 CERRUSITE       -0.023    [  1.000] 600  [  1.000] 140
  2060000 MASSICOT        -6.630    [ -2.000] 330  [  1.000] 600  [
1.000]   2
```

ID #	NAME	Sat. Index	Stoichiometry in [brackets]
2060001	LITHARGE	-6.429	[-2.000] 330 [1.000] 600 [1.000] 2
2060002	PBO, .3H2O	-6.273	[-2.000] 330 [1.000] 600 [1.330] 2
5060001	PB2OCO3	-6.361	[-2.000] 330 [2.000] 600 [1.000] 2
			[1.000] 140
6060000	LARNAKITE	-2.714	[-2.000] 330 [2.000] 600 [1.000] 732
			[1.000] 2
6060001	PB3O2SO4	-7.051	[-4.000] 330 [3.000] 600 [1.000] 732
			[2.000] 2
6060002	PB4O3SO4	-12.408	[-6.000] 330 [4.000] 600 [1.000] 732
			[3.000] 2
5060002	PB3O2CO3	-11.554	[-4.000] 330 [3.000] 600 [1.000] 140
			[2.000] 2
6060003	ANGLESITE	-1.693	[1.000] 600 [1.000] 732
1060001	GALENA	-10.892	[-1.000] 330 [1.000] 600 [1.000] 730
2060003	PLATTNERITE	-5.111	[-4.000] 330 [-2.000] 1 [1.000] 600
			[2.000] 2
3060000	PB2O3	-8.344	[-6.000] 330 [-2.000] 1 [2.000] 600
			[3.000] 2
3060001	MINIUM	-16.901	[-8.000] 330 [-2.000] 1 [3.000] 600
			[4.000] 2
2060004	PB(OH)2 (C)	-1.799	[-2.000] 330 [1.000] 600 [2.000] 2
5060003	HYDCERRUSITE	-2.386	[-2.000] 330 [3.000] 600 [2.000] 140
			[2.000] 2
2060005	PB2O(OH)2	-12.786	[-4.000] 330 [2.000] 600 [3.000] 2
6060004	PB4(OH)6SO4	-10.516	[-6.000] 330 [4.000] 600 [1.000] 732
			[6.000] 2
5054000	NICO3	-7.432	[1.000] 540 [1.000] 140
2054000	NI(OH)2	-4.061	[-2.000] 330 [1.000] 540 [2.000] 2
6054000	NI4(OH)6SO4	-24.386	[-6.000] 330 [4.000] 540 [1.000] 732
			[6.000] 2
2054001	BUNSENITE	-7.094	[-2.000] 330 [1.000] 540 [1.000] 2
1054000	MILLERITE	-19.155	[-1.000] 330 [1.000] 540 [1.000] 730
6054001	RETGERSITE	-8.213	[1.000] 540 [1.000] 732 [6.000] 2
6054002	MORENOSITE	-7.847	[1.000] 540 [1.000] 732 [7.000] 2
2000	AG METAL	-6.165	[1.000] 20 [1.000] 1
5002000	AG2CO3	-10.024	[2.000] 20 [1.000] 140
2002000	AG2O	-14.198	[-2.000] 330 [2.000] 20 [1.000] 2
6002000	AG2SO4	-12.570	[2.000] 20 [1.000] 732

```
  5023101 MALACHITE       -1.374    [  2.000] 231  [  2.000]   2  [
1.000] 140
                                    [ -2.000] 330
  5023102 AZURITE         -2.912    [  3.000] 231  [  2.000]   2  [
2.000] 140
                                    [ -2.000] 330
  3006100 AS2O5          -30.520    [  2.000]  61  [ -3.000]   2
  7203000 ALASO4.2W       -4.997    [  1.000]  30  [  1.000]  61  [
2.000]   2
                                    [ -3.000] 330
  7215000 CA3(ASO4)26W   -11.302    [  3.000] 150  [  2.000]  61  [
4.000]   2
                                    [ -6.000] 330
  7223100 CU3(ASO4)26W    -9.043    [  3.000] 231  [  2.000]  61  [
2.000]   2
                                    [ -6.000] 330
  7228100 FEASO4.2W       -7.442    [  1.000] 281  [  1.000]  61  [
2.000]   2
                                    [ -3.000] 330
```

```
    ID #      NAME          Sat. Index        Stoichiometry in [brackets]
  7247000 MN3ASO428W       -16.750    [  3.000] 470  [  2.000]  61  [
8.000]   2
                                       [ -6.000] 330
  7254000 NI3(ASO4)28W     -21.490    [  3.000] 540  [  2.000]  61  [
8.000]   2
                                       [ -6.000] 330
  7260000 PB3(ASO4)2        -9.362    [  3.000] 600  [  2.000]  61  [ -
6.000] 330
  7295000 ZN3ASO422.5W     -12.626    [  3.000] 950  [  2.000]  61  [
2.500]   2
                                       [ -6.000] 330
  2015000 LIME             -22.413    [ -2.000] 330  [  1.000] 150  [
1.000]   2
  2015001 PORTLANDITE      -11.895    [ -2.000] 330  [  1.000] 150  [
2.000]   2
  2028000 WUSTITE           -3.619    [ -2.000] 330  [  0.947] 280  [
1.000]   2
  2046001 PERICLASE        -14.121    [ -2.000] 330  [  1.000] 460  [
1.000]   2
  3046000 SPINEL            -7.001    [ -8.000] 330  [  1.000] 460  [
2.000]  30
                                       [  4.000]   2
  3046001 MAG-FERRITE       -0.552    [ -8.000] 330  [  1.000] 460  [
2.000] 281
                                       [  4.000]   2
  2076200 SeO3             -41.948    [  1.000] 762  [  2.000] 330  [ -
1.000]   2
  6102001 Ag2SeO4          -12.199    [  1.000] 762  [  2.000]  20
  6110001 BaSeO4            -7.927    [  1.000] 762  [  1.000] 100
  6115001 CaSeO4:2H2O       -5.483    [  1.000] 762  [  1.000] 150  [
2.000]   2
  6160000 PbSeO4            -6.371    [  1.000] 762  [  1.000] 600
  2021100 CR(OH)2           -3.320    [  1.000] 210  [  2.000]   2  [ -
2.000] 330
    21000 CR METAL         -64.682    [  1.000] 210  [  2.000]   1

 ITERATIONS=  47:  SOLID CALCITE      DISSOLVES
```

PART 3 of OUTPUT FILE

PC MINTEQA2 v3.10 DATE OF CALCULATIONS: 11-MAR-97 TIME: 23:53:45

PARAMETERS OF THE COMPONENT MOST OUT OF BALANCE:

ITER	NAME	TOTAL MOL	DIFF FXN	LOG ACTVTY	RESIDUAL
47	CO3-2	1.000E-03	2.441E-03	-5.98414	2.441E-03
48	CO3-2	1.000E-03	1.522E-04	-6.51241	1.521E-04
49	CO3-2	1.000E-03	1.698E-05	-6.57411	1.688E-05
50	CO3-2	1.000E-03	1.856E-06	-6.58124	1.756E-06
51	CO3-2	1.000E-03	1.757E-07	-6.58202	7.568E-08

PC MINTEQA2 v3.10 DATE OF CALCULATIONS: 11-MAR-97 TIME: 23:53:45

ITERATIONS= 52: SOLID BA(ASO4)2 PRECIPITATES

PART 3 of OUTPUT FILE

PC MINTEQA2 v3.10 DATE OF CALCULATIONS: 11-MAR-97 TIME: 23:53:45

PARAMETERS OF THE COMPONENT MOST OUT OF BALANCE:

ITER	NAME	TOTAL MOL	DIFF FXN	LOG ACTVTY	RESIDUAL
52	E-1	0.000E-01	2.378E-21	-12.64111	2.377E-21
53	E-1	0.000E-01	-2.537E-21	-12.64368	2.535E-21
54	E-1	0.000E-01	-4.253E-22	-12.63877	4.238E-22
55	E-1	0.000E-01	-1.577E-24	-12.64083	1.803E-25
56	E-1	0.000E-01	-1.726E-24	-12.64111	3.296E-25

PC MINTEQA2 v3.10 DATE OF CALCULATIONS: 11-MAR-97 TIME: 23:53:46

ITERATIONS= 57: SOLID ALOH3(A) PRECIPITATES

PART 3 of OUTPUT FILE

PC MINTEQA2 v3.10 DATE OF CALCULATIONS: 11-MAR-97 TIME: 23:53:46

PARAMETERS OF THE COMPONENT MOST OUT OF BALANCE:

ITER	NAME	TOTAL MOL	DIFF FXN	LOG ACTVTY	RESIDUAL
57	Zn+2	6.820E-06	-2.047E-06	-5.72731	2.046E-06
58	Zn+2	6.820E-06	2.177E-06	-5.70623	2.176E-06
59	Zn+2	6.820E-06	4.124E-07	-5.71314	4.118E-07
60	Zn+2	6.820E-06	2.935E-08	-5.72626	2.867E-08
61	Zn+2	6.820E-06	1.880E-09	-5.72725	1.198E-09

PC MINTEQA2 v3.10 DATE OF CALCULATIONS: 11-MAR-97 TIME: 23:53:46

ITERATIONS= 62: SOLID GYPSUM PRECIPITATES

PART 3 of OUTPUT FILE

PC MINTEQA2 v3.10 DATE OF CALCULATIONS: 11-MAR-97 TIME: 23:53:46

PARAMETERS OF THE COMPONENT MOST OUT OF BALANCE:

ITER	NAME	TOTAL MOL	DIFF FXN	LOG ACTVTY	RESIDUAL
62	Ag+1	2.786E-08	-4.477E-09	-7.67691	4.474E-09
63	Ag+1	2.786E-08	4.350E-09	-7.61476	4.347E-09
64	Ag+1	2.786E-08	7.514E-10	-7.65958	7.486E-10
65	Ag+1	2.786E-08	1.454E-10	-7.67022	1.426E-10
66	Ag+1	2.786E-08	3.026E-11	-7.67209	2.747E-11
67	Ag+1	2.786E-08	6.380E-12	-7.67249	3.594E-12
68	SeO4-2	2.011E-06	3.891E-10	-5.99041	1.879E-10

ID	NAME	ANAL MOL	CALC MOL	LOG ACTVTY	GAMMA	DIFF FXN
281	Fe+3	1.794E-08	2.927E-16	-16.19483	0.218147	1.654E-13
732	SO4-2	1.564E-02	1.178E-02	-2.22293	0.508289	2.933E-07
1	E-1	0.000E-01	2.295E-13	-12.63919	0.844360	- 1.608E-25
61	H3AsO4	4.235E-07	1.153E-12	-11.93496	1.007676	1.068E-11
140	CO3-2	1.000E-03	5.187E-07	-6.57895	0.508289	8.588E-09
160	Cd+2	8.913E-10	4.447E-10	-9.64578	0.508289	1.999E-14
950	Zn+2	6.820E-06	3.805E-06	-5.71351	0.508289	1.649E-10
210	Cr+2	1.079E-06	1.079E-06	-6.26087	0.508289	4.412E-11
231	Cu+2	9.932E-07	2.789E-07	-6.84842	0.508289	1.127E-11
280	Fe+2	7.355E-06	5.089E-06	-5.58724	0.508289	2.055E-10
600	Pb+2	1.306E-06	2.379E-07	-6.91744	0.508289	1.056E-11
460	Mg+2	6.181E-06	4.122E-06	-5.67875	0.508289	1.664E-10
470	Mn+2	9.118E-08	6.118E-08	-7.50727	0.508289	2.471E-12
540	Ni+2	1.024E-07	3.979E-08	-7.69412	0.508289	1.577E-12
762	SeO4-2	2.011E-06	2.011E-06	-5.99049	0.508289	8.223E-11
20	Ag+1	2.786E-08	2.517E-08	-7.67259	0.844360	2.849E-13
150	Ca+2	8.474E-03	4.597E-03	-2.63137	0.508289	0.000E-01
30	Al+3	5.198E-05	5.367E-10	-9.93155	0.218147	1.323E-22
730	HS-1	0.000E-01	6.993E-27	-26.22879	0.844360	0.000E-01
100	Ba+2	1.459E-07	1.812E-09	-9.03574	0.508289	6.617E-24
330	H+1	0.000E-01	1.184E-07	-7.00000	0.844360	- 6.776E-21

2	H2O	0.000E-01	-2.689E-03	-0.00017	1.000000
0.000E-01					

Type I - COMPONENTS AS SPECIES IN SOLUTION

ID	NAME	CALC MOL	ACTIVITY	LOG ACTVTY	GAMMA
NEW LOGK					
330	H+1	1.184E-07	1.000E-07	-7.00000	0.84436
0.073					
732	SO4-2	1.178E-02	5.985E-03	-2.22293	0.50829
0.294					
30	Al+3	5.367E-10	1.171E-10	-9.93155	0.21815
0.661					
61	H3AsO4	1.153E-12	1.162E-12	-11.93496	1.00768
0.003					
100	Ba+2	1.812E-09	9.210E-10	-9.03574	0.50829
0.294					
160	Cd+2	4.447E-10	2.261E-10	-9.64578	0.50829
0.294					
150	Ca+2	4.597E-03	2.337E-03	-2.63137	0.50829
0.294					
210	Cr+2	1.079E-06	5.484E-07	-6.26087	0.50829
0.294					
231	Cu+2	2.789E-07	1.418E-07	-6.84842	0.50829
0.294					
280	Fe+2	5.089E-06	2.587E-06	-5.58724	0.50829
0.294					
600	Pb+2	2.379E-07	1.209E-07	-6.91744	0.50829
0.294					
460	Mg+2	4.122E-06	2.095E-06	-5.67875	0.50829
0.294					
470	Mn+2	6.118E-08	3.110E-08	-7.50727	0.50829
0.294					
540	Ni+2	3.979E-08	2.022E-08	-7.69412	0.50829
0.294					
762	SeO4-2	2.011E-06	1.022E-06	-5.99049	0.50829
0.294					
20	Ag+1	2.517E-08	2.125E-08	-7.67259	0.84436
0.073					
950	Zn+2	3.805E-06	1.934E-06	-5.71351	0.50829
0.294					
140	CO3-2	5.187E-07	2.637E-07	-6.57895	0.50829
0.294					
281	Fe+3	2.927E-16	6.385E-17	-16.19483	0.21815
0.661					
730	HS-1	6.993E-27	5.905E-27	-26.22879	0.84436
0.073					

Type II - OTHER SPECIES IN SOLUTION OR ADSORBED

ID	NAME	CALC MOL	ACTIVITY	LOG ACTVTY	GAMMA
NEW LOGK					
1607620	CdSeO4	3.999E-14	4.029E-14	-13.39478	1.00768
2.238					
9507620	ZnSeO4	3.123E-10	3.147E-10	-9.50210	1.00768
2.199					
9507621	Zn(SeO4)2-2	3.381E-18	1.718E-18	-17.76489	0.50829
0.223					

3300020	OH-	5.443E-08	4.596E-08	-7.33762	0.84436	-
14.264						
4603300	MgOH +	1.658E-11	1.400E-11	-10.85386	0.84436	-
12.101						
4601400	MgCO3 AQ	4.488E-10	4.522E-10	-9.34467	1.00768	
2.910						
4601401	MgHCO3 +	1.935E-08	1.634E-08	-7.78685	0.84436	
11.544						
4607320	MgSO4 AQ	2.039E-06	2.055E-06	-5.68726	1.00768	
2.211						
1503300	CaOH +	2.980E-09	2.516E-09	-8.59926	0.84436	-
12.894						
1501400	CaHCO3 +	1.497E-05	1.264E-05	-4.89832	0.84436	
11.385						
1501401	CaCO3 AQ	7.180E-07	7.235E-07	-6.14058	1.00768	
3.066						
1507320	CaSO4 AQ	2.594E-03	2.614E-03	-2.58269	1.00768	
2.268						
303300	AlOH +2	1.174E-08	5.965E-09	-8.22439	0.50829	-
4.999						
303301	Al(OH)2 +	1.100E-06	9.292E-07	-6.03189	0.84436	-
10.027						
303302	Al(OH)4 -	1.048E-06	8.852E-07	-6.05298	0.84436	-
24.047						
307320	AlSO4 +	7.661E-10	6.469E-10	-9.18916	0.84436	
3.039						
307321	Al(SO4)2 -	3.498E-10	2.954E-10	-9.52964	0.84436	
4.921						
303303	Al(OH)3 AQ	1.160E-05	1.169E-05	-4.93206	1.00768	-
16.003						
2803300	FeOH +	4.470E-09	3.774E-09	-8.42315	0.84436	-
9.762						
2803301	FeOH3 -1	5.188E-17	4.380E-17	-16.35849	0.84436	-
31.697						
2807320	FeSO4 AQ	2.261E-06	2.279E-06	-5.64233	1.00768	
2.165						
2803302	FeOH2 AQ	1.296E-13	1.306E-13	-12.88418	1.00768	-
21.300						
2807300	Fe(HS)2 AQ	7.977E-50	8.039E-50	-49.09481	1.00768	
8.947						
2807301	Fe(HS)3 -	6.122E-74	5.169E-74	-73.28660	0.84436	
11.060						
2813300	FeOH +2	4.409E-12	2.241E-12	-11.64952	0.50829	-
2.161						
2817320	FeSO4 +	2.994E-15	2.528E-15	-14.59721	0.84436	
3.894						
2813301	FeOH2 +	1.615E-08	1.364E-08	-7.86517	0.84436	-
5.597						
2813302	FeOH3 AQ	1.590E-09	1.602E-09	-8.79534	1.00768	-
13.603						
2813303	FeOH4 -	1.897E-10	1.601E-10	-9.79552	0.84436	-
21.527						
2817321	Fe(SO4)2 -	5.442E-16	4.595E-16	-15.33769	0.84436	
5.376						
2813304	Fe2(OH)2+4	3.106E-21	2.073E-22	-21.68340	0.06675	-
2.118						
2813305	Fe3(OH)4+5	3.872E-26	5.637E-28	-27.24892	0.01456	-
4.827						
1003300	BaOH +	1.975E-16	1.668E-16	-15.77788	0.84436	-
13.668						
4703300	MnOH +	4.072E-12	3.438E-12	-11.46370	0.84436	-
10.883						
4703301	Mn(OH)3 -1	5.830E-22	4.923E-22	-21.30778	0.84436	-
34.727						

4700020	MnO4 -	2.785E-21	2.352E-21	-20.62865	0.84436	-132.243
4700021	MnO4 -2	1.221E-23	6.206E-24	-23.20722	0.50829	-121.962
4707320	MnSO4 AQ	2.960E-08	2.983E-08	-7.52539	1.00768	2.201
4701400	MnHCO3 +	3.866E-10	3.264E-10	-9.48622	0.84436	11.673
2311400	CuCO3 AQ	1.992E-07	2.007E-07	-6.69737	1.00768	6.727
2311401	Cu(CO3)2-2	1.311E-10	6.663E-11	-10.17632	0.50829	10.124
2313300	CuOH +	1.678E-08	1.417E-08	-7.84859	0.84436	-7.927
2313301	Cu(OH)2 AQ	2.937E-07	2.960E-07	-6.52876	1.00768	-13.683
2313302	Cu(OH)3 -	2.116E-13	1.787E-13	-12.74793	0.84436	-26.826
2313303	Cu(OH)4 -2	6.995E-19	3.555E-19	-18.44910	0.50829	-39.306
2313304	Cu2(OH)2+2	6.195E-11	3.149E-11	-10.50182	0.50829	-10.511
2317320	CuSO4 AQ	1.601E-07	1.613E-07	-6.79238	1.00768	2.276
2317300	Cu(HS)3 -	2.740E-60	2.313E-60	-59.63578	0.84436	25.972
2311402	CuHCO3 +	4.427E-08	3.738E-08	-7.42737	0.84436	13.073
9503300	ZnOH +	1.145E-08	9.672E-09	-8.01450	0.84436	-9.227
9503301	Zn(OH)2 AQ	2.420E-09	2.439E-09	-8.61285	1.00768	-16.902
9503302	Zn(OH)3 -	9.130E-14	7.709E-14	-13.11302	0.84436	-28.326
9503303	Zn(OH)4 -2	2.403E-19	1.221E-19	-18.91319	0.50829	-40.905
9507300	Zn(HS)2 AQ	5.829E-44	5.874E-44	-43.23108	1.00768	14.937
9507301	Zn(HS)3 -	5.938E-69	5.013E-69	-68.29987	0.84436	16.173
9507320	ZnSO4 AQ	2.487E-06	2.506E-06	-5.60103	1.00768	2.332
9507321	Zn(SO4)2-2	2.597E-07	1.320E-07	-6.87936	0.50829	3.574
9501400	ZnHCO3 +	1.517E-07	1.281E-07	-6.89246	0.84436	12.473
9501401	ZnCO3 AQ	1.010E-07	1.018E-07	-6.99246	1.00768	5.297
9501402	Zn(CO3)2-2	1.128E-09	5.736E-10	-9.24141	0.50829	9.924
1601400	Cd(CO3)3-4	1.030E-22	6.876E-24	-23.16263	0.06675	7.396
1603300	CdOH +	1.033E-13	8.726E-14	-13.05918	0.84436	-10.340
1603301	Cd(OH)2 AQ	1.001E-16	1.009E-16	-15.99613	1.00768	-20.353
1603302	Cd(OH)3 -	1.340E-22	1.132E-22	-21.94630	0.84436	-33.227
1603303	Cd(OH)4 -2	1.983E-29	1.008E-29	-28.99647	0.50829	-47.056
1603304	Cd2OH +3	5.038E-22	1.099E-22	-21.95897	0.21815	-9.006
1607320	CdSO4 AQ	3.635E-10	3.663E-10	-9.43618	1.00768	2.429

1607300	CdHS +	2.338E-26	1.974E-26	-25.70457	0.84436	
10.243						
1607301	Cd(HS)2 AQ	2.650E-46	2.671E-46	-45.57336	1.00768	
16.527						
1607302	Cd(HS)3 -	2.827E-70	2.387E-70	-69.62214	0.84436	
18.783						
1607303	Cd(HS)4 -2	4.295E-94	2.183E-94	-93.66093	0.50829	
21.194						
1601400	CdHCO3 +	1.773E-11	1.497E-11	-10.82473	0.84436	
12.473						
1601401	CdCO3 AQ	1.482E-11	1.494E-11	-10.82573	1.00768	
5.396						
1607321	Cd(SO4)2-2	5.038E-11	2.561E-11	-10.59164	0.50829	
3.794						
6001400	Pb(CO3)2-2	7.220E-10	3.670E-10	-9.43534	0.50829	
10.934						
6003300	PbOH +	2.792E-08	2.357E-08	-7.62761	0.84436	-
7.637						
6003301	Pb(OH)2 AQ	9.097E-11	9.167E-11	-10.03778	1.00768	-
17.123						
6003302	Pb(OH)3 -	1.246E-14	1.052E-14	-13.97795	0.84436	-
27.987						
6003303	Pb2OH +3	2.926E-13	6.382E-14	-13.19505	0.21815	-
5.699						
6007320	PbSO4 AQ	4.039E-07	4.070E-07	-6.39036	1.00768	
2.747						
6007300	Pb(HS)2 AQ	7.792E-45	7.852E-45	-44.10501	1.00768	
15.267						
6007301	Pb(HS)3 -	1.096E-69	9.251E-70	-69.03380	0.84436	
16.643						
6003304	Pb3(OH)4+2	9.701E-18	4.931E-18	-17.30707	0.50829	-
24.260						
6001401	PbCO3 AQ	5.499E-07	5.541E-07	-6.25639	1.00768	
7.237						
6003305	Pb(OH)4 -2	4.751E-19	2.415E-19	-18.61712	0.50829	-
39.405						
6007321	Pb(SO4)2-2	2.515E-08	1.279E-08	-7.89329	0.50829	
3.764						
6001402	PbHCO3 +	5.985E-08	5.054E-08	-7.29639	0.84436	
13.273						
5403300	NiOH +	1.597E-11	1.348E-11	-10.87022	0.84436	-
10.102						
5403301	Ni(OH)2 AQ	2.005E-13	2.021E-13	-12.69446	1.00768	-
19.003						
5403302	Ni(OH)3 -	2.392E-17	2.020E-17	-16.69464	0.84436	-
29.927						
5407320	NiSO4 AQ	2.143E-08	2.159E-08	-7.66571	1.00768	
2.248						
5401400	NiHCO3 +	1.864E-09	1.574E-09	-8.80307	0.84436	
12.543						
5401401	NiCO3 AQ	3.923E-08	3.953E-08	-7.40307	1.00768	
6.867						
5401402	Ni(CO3)2-2	3.563E-11	1.811E-11	-10.74202	0.50829	
10.404						
5407321	Ni(SO4)2-2	1.492E-11	7.586E-12	-11.11998	0.50829	
1.314						
207300	AgHS AQ	1.397E-20	1.408E-20	-19.85137	1.00768	
14.047						
207301	Ag(HS)2 -	2.473E-42	2.089E-42	-41.68016	0.84436	
18.523						
203300	AgOH AQ	2.108E-13	2.124E-13	-12.67276	1.00768	-
12.003						
203301	Ag(OH)2 -	2.515E-18	2.124E-18	-17.67293	0.84436	-
23.927						

207320	AgSO4 -	2.692E-09	2.273E-09	-8.64341	0.84436	1.326
3300611	H2AsO4 -	8.680E-08	7.329E-08	-7.13497	0.84436	-2.127
3300612	HAsO4 -2	2.406E-07	1.223E-07	-6.91256	0.50829	-8.684
3300613	AsO4 -3	1.102E-11	2.403E-12	-11.61921	0.21815	-20.023
3301400	HCO3 -	8.395E-04	7.088E-04	-3.14948	0.84436	10.503
3301401	H2CO3 AQ	1.432E-04	1.443E-04	-3.84079	1.00768	16.735
3307320	HSO4 -	5.237E-08	4.422E-08	-7.35442	0.84436	1.942
3307300	H2S AQ	7.120E-27	7.175E-27	-26.14419	1.00768	7.081
3307301	S -2	6.907E-33	3.511E-33	-32.45457	0.50829	-12.932
3307620	HSeO4-1	7.620E-12	6.434E-12	-11.19153	0.84436	1.872
4707620	MnSeO4	6.756E-12	6.808E-12	-11.16697	1.00768	2.327
5407620	NiSeO4	7.273E-12	7.329E-12	-11.13494	1.00768	2.546

Type III - SPECIES WITH FIXED ACTIVITY

ID	NAME	CALC MOL	LOG MOL	NEW LOGK	DH
2	H2O	-2.689E-03	-2.570	0.000	0.000
330	H+1	-9.838E-04	-3.007	7.000	0.000
1028003	PYRITE	-6.987E-21	-20.156	18.766	-11.300

Type IV - FINITE SOLIDS (present at equilibrium)

ID	NAME	CALC MOL	LOG MOL	NEW LOGK	DH
7210000	BA(ASO4)2	4.802E-08	-7.319	8.977	-2.640
2003000	ALOH3(A)	3.821E-05	-4.418	-11.068	27.045
6015001	GYPSUM	1.266E-03	-2.897	4.855	-0.261

Type V - UNDERSATURATED SOLIDS (not present at equilibrium)

ID	NAME	CALC MOL	LOG MOL	NEW LOGK	DH
6010000	BARITE	7.535E-02	-1.123	10.136	-6.280
5028000	SIDERITE	1.771E-02	-1.752	10.414	5.328
2023101	TENORITE	1.392E-01	-0.856	-8.008	15.240
5016000	OTAVITE	3.166E-03	-2.499	13.725	0.580
6060003	ANGLESITE	5.062E-02	-1.296	7.845	-2.150
5015001	CALCITE	1.632E-01	-0.787	8.423	2.585

Type VI - EXCLUDED SPECIES (not included in mole balance)

ID	NAME	CALC MOL	LOG MOL	NEW LOGK	DH
3301403	CO2 (g)	3.933E-03	-2.405	18.173	-0.530

3300021	O2 (g)	1.077E-08	-7.968	-86.524	133.830
1	E-1	2.295E-13	-12.639	0.000	0.000
2802810	Fe+2/Fe+3	1.095E-10	-9.960	13.286	-10.000
7307320	HS-/SO4-2	0.000E-01	-104.917	35.190	-60.140
3301404	CH4 (g)	0.000E-01	-136.040	41.652	-61.000

PART 4 of OUTPUT FILE

PC MINTEQA2 v3.10 DATE OF CALCULATIONS: 11-MAR-97 TIME: 23:53:47

PERCENTAGE DISTRIBUTION OF COMPONENTS AMONG
TYPE I and TYPE II (dissolved and adsorbed) species

Fe+3	90.1	PERCENT BOUND IN SPECIES #2813301	
FeOH2 +			
	8.9	PERCENT BOUND IN SPECIES #2813302	FeOH3 AQ
	1.1	PERCENT BOUND IN SPECIES #2813303	FeOH4 -
SO4-2	81.9	PERCENT BOUND IN SPECIES #	732
SO4-2			
	18.0	PERCENT BOUND IN SPECIES #1507320	CaSO4 AQ
E-1	99.7	PERCENT BOUND IN SPECIES #4700020	
MnO4 -			
H3AsO4	26.5	PERCENT BOUND IN SPECIES #3300611	
H2AsO4 -			
	73.5	PERCENT BOUND IN SPECIES #3300612	HAsO4 -2
CO3-2	1.5	PERCENT BOUND IN SPECIES #1501400	
CaHCO3 +			
	83.9	PERCENT BOUND IN SPECIES #3301400	HCO3 -
	14.3	PERCENT BOUND IN SPECIES #3301401	H2CO3 AQ
Cd+2	49.9	PERCENT BOUND IN SPECIES #	160
Cd+2			
	40.8	PERCENT BOUND IN SPECIES #1607320	CdSO4 AQ
	2.0	PERCENT BOUND IN SPECIES #1601400	CdHCO3 +
	1.7	PERCENT BOUND IN SPECIES #1601401	CdCO3 AQ
	5.7	PERCENT BOUND IN SPECIES #1607321	Cd(SO4)2-2
Zn+2	55.8	PERCENT BOUND IN SPECIES #	950
Zn+2			
	36.5	PERCENT BOUND IN SPECIES #9507320	ZnSO4 AQ
	3.8	PERCENT BOUND IN SPECIES #9507321	Zn(SO4)2-2
	2.2	PERCENT BOUND IN SPECIES #9501400	ZnHCO3 +
	1.5	PERCENT BOUND IN SPECIES #9501401	ZnCO3 AQ
Cr+2	100.0	PERCENT BOUND IN SPECIES #	210
Cr+2			
Cu+2	28.1	PERCENT BOUND IN SPECIES #	231
Cu+2			
	20.1	PERCENT BOUND IN SPECIES #2311400	CuCO3 AQ
	1.7	PERCENT BOUND IN SPECIES #2313300	CuOH +
	29.6	PERCENT BOUND IN SPECIES #2313301	Cu(OH)2 AQ
	16.1	PERCENT BOUND IN SPECIES #2317320	CuSO4 AQ
	4.5	PERCENT BOUND IN SPECIES #2311402	CuHCO3 +
Fe+2	69.2	PERCENT BOUND IN SPECIES #	280
Fe+2			
	30.7	PERCENT BOUND IN SPECIES #2807320	FeSO4 AQ
Pb+2	18.2	PERCENT BOUND IN SPECIES #	600
Pb+2			

	2.1	PERCENT BOUND IN SPECIES #6003300	PbOH +
	30.9	PERCENT BOUND IN SPECIES #6007320	PbSO4 AQ
	42.1	PERCENT BOUND IN SPECIES #6001401	PbCO3 AQ
	1.9	PERCENT BOUND IN SPECIES #6007321	Pb(SO4)2-2
	4.6	PERCENT BOUND IN SPECIES #6001402	PbHCO3 +
Mg+2	66.7	PERCENT BOUND IN SPECIES #	460
Mg+2			
	33.0	PERCENT BOUND IN SPECIES #4607320	MgSO4 AQ
Mn+2	67.1	PERCENT BOUND IN SPECIES #	470
Mn+2			
	32.5	PERCENT BOUND IN SPECIES #4707320	MnSO4 AQ
Ni+2	38.9	PERCENT BOUND IN SPECIES #	540
Ni+2			
	20.9	PERCENT BOUND IN SPECIES #5407320	NiSO4 AQ
	1.8	PERCENT BOUND IN SPECIES #5401400	NiHCO3 +
	38.3	PERCENT BOUND IN SPECIES #5401401	NiCO3 AQ
SeO4-2	100.0	PERCENT BOUND IN SPECIES #	762
SeO4-2			
Ag+1	90.3	PERCENT BOUND IN SPECIES #	20
Ag+1			
	9.7	PERCENT BOUND IN SPECIES # 207320	AgSO4 -
Ca+2	63.8	PERCENT BOUND IN SPECIES #	150
Ca+2			
	36.0	PERCENT BOUND IN SPECIES #1507320	CaSO4 AQ
Al+3	8.0	PERCENT BOUND IN SPECIES #	303301
Al(OH)2 +			
	7.6	PERCENT BOUND IN SPECIES # 303302	Al(OH)4 -
	84.3	PERCENT BOUND IN SPECIES # 303303	Al(OH)3 AQ
HS-1	100.0	PERCENT BOUND IN SPECIES #	207300
AgHS AQ			
Ba+2	100.0	PERCENT BOUND IN SPECIES #	100
Ba+2			
H+1	1.4	PERCENT BOUND IN SPECIES #1501400	
CaHCO3 +			
	76.4	PERCENT BOUND IN SPECIES #3301400	HCO3 -
	26.1	PERCENT BOUND IN SPECIES #3301401	H2CO3 AQ
H2O	5.2	PERCENT BOUND IN SPECIES #	303301
Al(OH)2 +			
	10.0	PERCENT BOUND IN SPECIES # 303302	Al(OH)4 -
	83.0	PERCENT BOUND IN SPECIES # 303303	Al(OH)3 AQ
	1.4	PERCENT BOUND IN SPECIES #2313301	Cu(OH)2 AQ

PART 5 of OUTPUT FILE

PC MINTEQA2 v3.10 DATE OF CALCULATIONS: 11-MAR-97 TIME: 23:53:47

EQUILIBRATED MASS DISTRIBUTION

IDX	NAME	DISSOLVED		SORBED		PRECIPITATED
		MOL/KG	PERCENT	MOL/KG	PERCENT	MOL/KG
						PERCENT
281	Fe+3	1.794E-08	100.0	0.000E-01	0.0	0.000E-01
0.0						
732	SO4-2	1.438E-02	91.9	0.000E-01	0.0	1.266E-03
8.1						
1	E-1	-1.397E-20	100.0	0.000E-01	0.0	0.000E-01
0.0						
61	H3AsO4	3.274E-07	77.3	0.000E-01	0.0	9.605E-08
22.7						
140	CO3-2	1.000E-03	100.0	0.000E-01	0.0	0.000E-01
0.0						
160	Cd+2	8.913E-10	100.0	0.000E-01	0.0	0.000E-01
0.0						
950	Zn+2	6.820E-06	100.0	0.000E-01	0.0	0.000E-01
0.0						
210	Cr+2	1.079E-06	100.0	0.000E-01	0.0	0.000E-01
0.0						
231	Cu+2	9.932E-07	100.0	0.000E-01	0.0	0.000E-01
0.0						
280	Fe+2	7.355E-06	100.0	0.000E-01	0.0	0.000E-01
0.0						
600	Pb+2	1.306E-06	100.0	0.000E-01	0.0	0.000E-01
0.0						
460	Mg+2	6.181E-06	100.0	0.000E-01	0.0	0.000E-01
0.0						
470	Mn+2	9.118E-08	100.0	0.000E-01	0.0	0.000E-01
0.0						
540	Ni+2	1.024E-07	100.0	0.000E-01	0.0	0.000E-01
0.0						
762	SeO4-2	2.011E-06	100.0	0.000E-01	0.0	0.000E-01
0.0						
20	Ag+1	2.786E-08	100.0	0.000E-01	0.0	0.000E-01
0.0						
150	Ca+2	7.207E-03	85.1	0.000E-01	0.0	1.266E-03
14.9						
30	Al+3	1.377E-05	26.5	0.000E-01	0.0	3.821E-05
73.5						
730	HS-1	1.397E-20	100.0	0.000E-01	0.0	0.000E-01
0.0						
100	Ba+2	1.812E-09	1.2	0.000E-01	0.0	1.441E-07
98.8						
330	H+1	1.099E-03	100.0	0.000E-01	0.0	0.000E-01
0.0						
2	H2O	4.197E-05	100.0	0.000E-01	0.0	0.000E-01
0.0						

Charge Balance: SPECIATED

Sum of CATIONS = 9.241E-03 Sum of ANIONS 2.440E-02

PERCENT DIFFERENCE = 4.506E+01 (ANIONS - CATIONS)/(ANIONS + CATIONS)

EQUILIBRIUM IONIC STRENGTH (m) = 3.321E-02

EQUILIBRIUM pH = 7.000

EQUILIBRIUM pe = 12.639 or Eh = 722.61 mv

DATE ID NUMBER: 970311
TIME ID NUMBER: 23534743

PART 6 of OUTPUT FILE

PC MINTEQA2 v3.10 DATE OF CALCULATIONS: 11-MAR-97 TIME: 23:53:47

Saturation indices and stoichiometry of all minerals

ID #	NAME	Sat. Index	Stoichiometry in [brackets]
2003000	ALOH3(A)	0.000	[1.000] 30 [3.000] 2 [-3.000] 330
6003000	ALOHSO4	-1.925	[-1.000] 330 [1.000] 30 [1.000] 732
			[1.000] 2
6003001	AL4(OH)10SO4	5.349	[-10.000] 330 [4.000] 30 [1.000] 732
			[10.000] 2
6015000	ANHYDRITE	-0.313	[1.000] 150 [1.000] 732
5015000	ARAGONITE	-0.960	[1.000] 150 [1.000] 140
5046000	ARTINITE	-14.268	[-2.000] 330 [2.000] 460 [1.000] 140
			[5.000] 2
6010000	BARITE	-1.123	[1.000] 100 [1.000] 732
2003001	BOEHMITE	1.775	[-3.000] 330 [1.000] 30 [2.000] 2
2046000	BRUCITE	-9.128	[1.000] 460 [2.000] 2 [-2.000] 330
5015001	CALCITE	-0.787	[1.000] 150 [1.000] 140
2003002	DIASPORE	3.569	[-3.000] 330 [1.000] 30 [2.000] 2
5015002	DOLOMITE	-4.679	[1.000] 150 [1.000] 460 [2.000] 140
6046000	EPSOMITE	-5.691	[1.000] 460 [1.000] 732 [7.000] 2
2028100	FERRIHYDRITE	-0.086	[-3.000] 330 [1.000] 281 [3.000] 2
2028101	FE3(OH)8	-2.200	[-8.000] 330 [2.000] 281 [1.000] 280
			[8.000] 2
1028000	FES PPT	-20.901	[-1.000] 330 [1.000] 280 [1.000] 730
6028100	FE2(SO4)3	-44.142	[2.000] 281 [3.000] 732
2003003	GIBBSITE (C)	1.718	[-3.000] 330 [1.000] 30 [3.000] 2
3003000	Al2O3	-0.844	[2.000] 30 [3.000] 2 [-6.000] 330
2028102	GOETHITE	3.937	[-3.000] 330 [1.000] 281 [2.000] 2
1028001	GREIGITE	-69.857	[-4.000] 330 [2.000] 281 [1.000] 280
			[4.000] 730
6015001	GYPSUM	0.000	[1.000] 150 [1.000] 732 [2.000] 2
3028100	HEMATITE	12.833	[-6.000] 330 [2.000] 281 [3.000] 2
5015003	HUNTITE	-16.671	[3.000] 460 [1.000] 150 [4.000] 140
5046001	HYDRMAGNESIT	-33.273	[5.000] 460 [4.000] 140 [-2.000] 330
			[6.000] 2
6028101	JAROSITE H	-7.334	[-5.000] 330 [3.000] 281 [2.000] 732

```
                                        [  7.000]   2
  1028002 MACKINAWITE    -20.168       [ -1.000] 330  [  1.000] 280  [
1.000] 730
  3028101 MAGHEMITE        3.224       [ -6.000] 330  [  2.000] 281  [
3.000]   2
  5046002 MAGNESITE       -4.386       [  1.000] 460  [  1.000] 140
  3028000 MAGNETITE       13.002       [ -8.000] 330  [  2.000] 281  [
1.000] 280
                                        [  4.000]   2
  6028000 MELANTERITE     -5.269       [  1.000] 280  [  1.000] 732  [
7.000]   2
  5046003 NESQUEHONITE    -6.784       [  1.000] 460  [  1.000] 140  [
3.000]   2
  1028003 PYRITE           0.000       [ -2.000] 330  [ -2.000]   1  [
1.000] 280
                                        [  2.000] 730
  5028000 SIDERITE        -1.752       [  1.000] 280  [  1.000] 140
```

ID #	NAME	Sat. Index	Stoichiometry in [brackets]
5010000	WITHERITE	-7.021	[1.000] 100 [1.000] 140
3047000	HAUSMANNITE	-4.823	[-8.000] 330 [-2.000] 1 [3.000] 470
2047003	PYROCROITE	-9.170	[4.000] 2 [-2.000] 330 [1.000] 470 [2.000] 2
5047000	RHODOCHROSIT	-3.729	[1.000] 470 [1.000] 140
1047000	MNS GREEN	-30.683	[-1.000] 330 [1.000] 470 [1.000] 730
6047000	MNSO4	-12.793	[1.000] 470 [1.000] 732
1023101	COVELLITE	-2.428	[-1.000] 330 [1.000] 231 [1.000] 730
5023100	CUCO3	-3.797	[1.000] 231 [1.000] 140
2023100	CU(OH)2	-1.877	[-2.000] 330 [1.000] 231 [2.000] 2
6023100	ANTLERITE	-3.059	[-4.000] 330 [3.000] 231 [4.000] 2
6023101	BROCHANTITE	-2.958	[1.000] 732 [-6.000] 330 [4.000] 231 [6.000] 2
6023102	LANGITE	-5.415	[1.000] 732 [-6.000] 330 [4.000] 231 [7.000] 2
2023101	TENORITE	-0.856	[1.000] 732 [-2.000] 330 [1.000] 231 [1.000] 2
6023103	CUOCUSO4	-14.355	[-2.000] 330 [2.000] 231 [1.000] 2
6023104	CUSO4	-12.543	[1.000] 732 [1.000] 231 [1.000] 732
6023105	CHALCANTHITE	-6.396	[1.000] 231 [1.000] 732 [5.000] 2
3023100	CUPRICFERIT	9.897	[-8.000] 330 [1.000] 231 [2.000] 281
1023102	CHALCOPYRITE	-14.721	[4.000] 2 [-2.000] 330 [1.000] 231 [1.000] 280
95000	ZN METAL	-57.684	[2.000] 730 [1.000] 950 [2.000] 1
5095000	SMITHSONITE	-2.403	[1.000] 950 [1.000] 140
5095001	ZNCO3, 1H2O	-2.033	[1.000] 950 [1.000] 140 [1.000] 2
2095000	ZN(OH)2 (A)	-4.164	[-2.000] 330 [1.000] 950 [2.000] 2
2095001	ZN(OH)2 (C)	-3.914	[-2.000] 330 [1.000] 950 [2.000] 2
2095002	ZN(OH)2 (B)	-3.464	[-2.000] 330 [1.000] 950 [2.000] 2
2095003	ZN(OH)2 (G)	-3.424	[-2.000] 330 [1.000] 950 [2.000] 2
2095004	ZN(OH)2 (E)	-3.214	[-2.000] 330 [1.000] 950 [2.000] 2
6095000	ZN2(OH)2SO4	-7.150	[-2.000] 330 [2.000] 950 [2.000] 2
6095001	ZN4(OH)6SO4	-11.478	[1.000] 732 [-6.000] 330 [4.000] 950 [6.000] 2
2095005	ZNO(ACTIVE)	-3.024	[1.000] 732 [-2.000] 330 [1.000] 950 [1.000] 2

```
  2095006 ZINCITE          -3.410    [ -2.000] 330  [  1.000] 950  [
1.000]   2
  6095002 ZN3O(SO4)2      -28.184    [ -2.000] 330  [  3.000] 950  [
2.000] 732
                                     [  1.000]   2
  1095000 ZNS (A)         -15.797    [ -1.000] 330  [  1.000] 950  [
1.000] 730
  1095001 SPHALERITE      -13.114    [ -1.000] 330  [  1.000] 950  [
1.000] 730
  1095002 WURTZITE        -15.132    [ -1.000] 330  [  1.000] 950  [
1.000] 730
  6095003 ZINCOSITE       -11.435    [  1.000] 950  [  1.000] 732
  6095004 ZNSO4, 1H2O      -7.637    [  1.000] 950  [  1.000] 732  [
1.000]   2
  6095005 BIANCHITE        -6.177    [  1.000] 950  [  1.000] 732  [
6.000]   2
  6095006 GOSLARITE        -5.894    [  1.000] 950  [  1.000] 732  [
7.000]   2
    16000 CD METAL        -48.872    [  1.000] 160  [  2.000]   1
    16001 GAMMA CD        -48.976    [  1.000] 160  [  2.000]   1
  5016000 OTAVITE          -2.499    [  1.000] 160  [  1.000] 140
```

ID #	NAME	Sat. Index	Stoichiometry in [brackets]
2016000	CD(OH)2 (A)	-9.904	[-2.000] 330 [1.000] 160 [2.000] 2
2016001	CD(OH)2 (C)	-9.296	[-2.000] 330 [1.000] 160 [2.000] 2
6016000	CD3(OH)4SO4	-25.721	[-4.000] 330 [3.000] 160 [4.000] 2 [1.000] 732
6016001	CD3OH2(SO4)2	-26.094	[-2.000] 330 [3.000] 160 [2.000] 2 [2.000] 732
6016002	CD4(OH)6SO4	-27.207	[-6.000] 330 [4.000] 160 [6.000] 2 [1.000] 732
2016002	MONTEPONITE	-11.396	[-2.000] 330 [1.000] 160 [1.000] 2
6016003	CDSO4	-12.144	[1.000] 160 [1.000] 732
6016004	CDSO4, 1H2O	-10.403	[1.000] 160 [1.000] 732 [1.000] 2
6016005	CDSO4,2.7H2O	-10.106	[1.000] 160 [1.000] 732 [2.670] 2
1016000	GREENOCKITE	-12.528	[-1.000] 330 [1.000] 160 [1.000] 730
60000	PB METAL	-36.456	[1.000] 600 [2.000] 1
5060000	CERRUSITE	-0.243	[1.000] 600 [1.000] 140
2060000	MASSICOT	-6.254	[-2.000] 330 [1.000] 600 [1.000] 2
2060001	LITHARGE	-6.054	[-2.000] 330 [1.000] 600 [1.000] 2
2060002	PBO, .3H2O	-5.898	[-2.000] 330 [1.000] 600 [1.330] 2
5060001	PB2OCO3	-6.206	[-2.000] 330 [2.000] 600 [1.000] 2 [1.000] 140
6060000	LARNAKITE	-1.942	[-2.000] 330 [2.000] 600 [1.000] 732 [1.000] 2
6060001	PB3O2SO4	-5.903	[-4.000] 330 [3.000] 600 [1.000] 732 [2.000] 2
6060002	PB4O3SO4	-10.885	[-6.000] 330 [4.000] 600 [1.000] 732 [3.000] 2
5060002	PB3O2CO3	-11.024	[-4.000] 330 [3.000] 600 [1.000] 140 [2.000] 2
6060003	ANGLESITE	-1.296	[1.000] 600 [1.000] 732
1060001	GALENA	-10.521	[-1.000] 330 [1.000] 600 [1.000] 730
2060003	PLATTNERITE	-4.739	[-4.000] 330 [-2.000] 1 [1.000] 600 [2.000] 2
3060000	PB2O3	-7.597	[-6.000] 330 [-2.000] 1 [2.000] 600 [3.000] 2
3060001	MINIUM	-15.779	[-8.000] 330 [-2.000] 1 [3.000] 600 [4.000] 2
2060004	PB(OH)2 (C)	-1.424	[-2.000] 330 [1.000] 600 [2.000] 2

```
  5060003 HYDCERRUSITE   -2.451    [ -2.000] 330  [  3.000] 600  [
2.000] 140
                                   [  2.000]   2
  2060005 PB2O(OH)2     -12.035    [ -4.000] 330  [  2.000] 600  [
3.000]   2
  6060004 PB4(OH)6SO4    -8.994    [ -6.000] 330  [  4.000] 600  [
1.000] 732
                                   [  6.000]   2
  5054000 NICO3          -7.686    [  1.000] 540  [  1.000] 140
  2054000 NI(OH)2        -3.720    [ -2.000] 330  [  1.000] 540  [
2.000]   2
  6054000 NI4(OH)6SO4   -23.000    [ -6.000] 330  [  4.000] 540  [
1.000] 732
                                   [  6.000]   2
  2054001 BUNSENITE      -6.753    [ -2.000] 330  [  1.000] 540  [
1.000]   2
  1054000 MILLERITE     -18.817    [ -1.000] 330  [  1.000] 540  [
1.000] 730
  6054001 RETGERSITE     -7.850    [  1.000] 540  [  1.000] 732  [
6.000]   2
  6054002 MORENOSITE     -7.483    [  1.000] 540  [  1.000] 732  [
7.000]   2
     2000 AG METAL       -6.160    [  1.000]  20  [  1.000]   1
```

ID #	NAME	Sat. Index	Stoichiometry in [brackets]
5002000	AG2CO3	-10.612	[2.000] 20 [1.000] 140
2002000	AG2O	-14.191	[-2.000] 330 [2.000] 20 [1.000] 2
1002000	ACANTHITE	2.832	[-1.000] 330 [2.000] 20 [1.000] 730
6002000	AG2SO4	-12.540	[2.000] 20 [1.000] 732
5023101	MALACHITE	-1.493	[2.000] 231 [2.000] 2 [1.000] 140 [-2.000] 330
5023102	AZURITE	-3.388	[3.000] 231 [2.000] 2 [2.000] 140 [-2.000] 330
3006100	AS2O5	-30.706	[2.000] 61 [-3.000] 2
73100	SULFUR	8.053	[1.000] 730 [-1.000] 330 [-2.000] 1
7203000	ALASO4.2W	-5.667	[1.000] 30 [1.000] 61 [2.000] 2
7215000	CA3(ASO4)26W	-12.065	[-3.000] 330 [3.000] 150 [2.000] 61 [4.000] 2
7223100	CU3(ASO4)26W	-8.516	[-6.000] 330 [3.000] 231 [2.000] 61 [2.000] 2
7228100	FEASO4.2W	-7.530	[-6.000] 330 [1.000] 281 [1.000] 61 [2.000] 2
7247000	MN3ASO428W	-16.893	[-3.000] 330 [3.000] 470 [2.000] 61 [8.000] 2
7254000	NI3(ASO4)28W	-20.654	[-6.000] 330 [3.000] 540 [2.000] 61 [8.000] 2
7260000	PB3(ASO4)2	-8.422	[-6.000] 330 [3.000] 600 [2.000] 61 [-6.000] 330
7295000	ZN3ASO422.5W	-12.661	[3.000] 950 [2.000] 61 [2.500] 2 [-6.000] 330
7210000	BA(ASO4)2	0.000	[3.000] 100 [2.000] 61 [-6.000] 330
2015000	LIME	-22.605	[-2.000] 330 [1.000] 150 [1.000] 2
2015001	PORTLANDITE	-12.087	[-2.000] 330 [1.000] 150 [2.000] 2
2028000	WUSTITE	-3.610	[-2.000] 330 [0.947] 280 [1.000] 2
2046001	PERICLASE	-14.108	[-2.000] 330 [1.000] 460 [1.000] 2
3028001	HERCYNITE	1.394	[-8.000] 330 [1.000] 280 [2.000] 30 [4.000] 2
3046000	SPINEL	-8.142	[-8.000] 330 [1.000] 460 [2.000] 30 [4.000] 2
3046001	MAG-FERRITE	-0.529	[-8.000] 330 [1.000] 460 [2.000] 281 [4.000] 2
3028102	LEPIDOCROCIT	3.434	[-3.000] 330 [1.000] 281 [2.000] 2

```
  2076200 SeO3          -41.924    [  1.000] 762  [  2.000] 330  [ -
1.000]   2
  6102001 Ag2SeO4       -12.168    [  1.000] 762  [  2.000]  20
  6110001 BaSeO4         -9.786    [  1.000] 762  [  1.000] 100
  6115001 CaSeO4:2H2O    -5.653    [  1.000] 762  [  1.000] 150  [
2.000]   2
  6160000 PbSeO4         -5.973    [  1.000] 762  [  1.000] 600
  2021100 CR(OH)2        -3.297    [  1.000] 210  [  2.000]   2  [ -
2.000] 330
    21000 CR METAL      -64.656    [  1.000] 210  [  2.000]   1
```

PART 1 of OUTPUT FILE

PC MINTEQA2 v3.10 DATE OF CALCULATIONS: 11-MAR-97 TIME: 23:53:47

Cemented Acidic Tails

```
 Temperature (Celsius):  15.00
 Units of concentration: MG/L
 Ionic strength to be computed.
 If specified, carbonate concentration represents total inorganic
carbon.
 Do not automatically terminate if charge imbalance exceeds 30%
 Precipitation is allowed only for those solids specified as ALLOWED
   in the input file (if any).
 The maximum number of iterations is: 200
 The method used to compute activity coefficients is: Davies equation
 Intermediate output file
```

```
    330  0.000E-01   -1.70 y
    732  4.000E+04   -1.81 y
    231  4.410E+02   -6.00 y
    470  3.128E+03   -7.04 y
    950  3.609E+04   -5.17 y
     60  1.379E+03   -1.96 y
     30  0.000E-01  -20.43 y
    460  0.000E-01  -20.39 y
    280  0.000E-01  -20.75 y
    150  0.000E-01  -20.60 y
    600  0.000E-01  -21.32 y
    100  0.000E-01  -21.14 y

 H2O has been inserted as a COMPONENT
  3   7
6003000     3.2300     0.0000
6046000     2.1400    -2.8200
6028000     2.4700    -2.8600
6015001     4.8480    -0.2610
6060003     7.7900    -2.1500
6010000     9.9760    -6.2800
    330     1.7000     0.0000

INPUT DATA BEFORE TYPE MODIFICATIONS

   ID        NAME        ACTIVITY GUESS     LOG GUESS   ANAL TOTAL
    330  H+1                  1.995E-02         -1.700   0.000E-01
```

732	SO4-2	1.549E-02	-1.810	4.000E+04
231	Cu+2	1.000E-06	-6.000	4.410E+02
470	Mn+2	9.120E-08	-7.040	3.128E+03
950	Zn+2	6.761E-06	-5.170	3.609E+04
60	H3AsO3	1.096E-02	-1.960	1.379E+03
30	Al+3	3.715E-21	-20.430	0.000E-01
460	Mg+2	4.074E-21	-20.390	0.000E-01
280	Fe+2	1.778E-21	-20.750	0.000E-01
150	Ca+2	2.512E-21	-20.600	0.000E-01
600	Pb+2	4.786E-22	-21.320	0.000E-01
100	Ba+2	7.244E-22	-21.140	0.000E-01
2	H2O	1.000E+00	0.000	0.000E-01

Charge Balance: UNSPECIATED

Sum of CATIONS= 1.341E+00 Sum of ANIONS = 9.062E-01

PERCENT DIFFERENCE = 1.933E+01 (ANIONS - CATIONS)/(ANIONS + CATIONS)

IMPROVED ACTIVITY GUESSES PRIOR TO FIRST ITERATION:

SO4-2	Log activity guess:	-0.74
Cu+2	Log activity guess:	-2.12
Mn+2	Log activity guess:	-1.21
H3AsO3	Log activity guess:	-1.93
H2O	Log activity guess:	0.00

PARAMETERS OF THE COMPONENT MOST OUT OF BALANCE:

ITER	NAME	TOTAL MOL	DIFF FXN	LOG ACTVTY	RESIDUAL
0	Zn+2	6.008E-01	1.340E+29	-5.17000	1.340E+29
1	Zn+2	6.008E-01	6.702E+28	-4.86751	6.701E+28
2	Zn+2	6.008E-01	4.436E+28	-4.56728	4.436E+28
3	Zn+2	6.008E-01	2.218E+28	-4.26596	2.218E+28
4	Zn+2	6.008E-01	1.109E+28	-3.96464	1.109E+28
5	Zn+2	6.008E-01	5.545E+27	-3.66552	5.545E+27
6	Zn+2	6.008E-01	2.772E+27	-3.37075	2.772E+27
7	Zn+2	6.008E-01	1.386E+27	-3.07760	1.386E+27
8	Zn+2	6.008E-01	6.928E+26	-2.79182	6.928E+26
9	Zn+2	6.008E-01	3.461E+26	-2.51704	3.461E+26
10	Zn+2	6.008E-01	1.726E+26	-2.26014	1.726E+26
11	Zn+2	6.008E-01	8.567E+25	-2.03361	8.566E+25
12	Zn+2	6.008E-01	4.204E+25	-1.85183	4.203E+25
13	Zn+2	6.008E-01	2.023E+25	-1.72095	2.023E+25
14	Zn+2	6.008E-01	9.508E+24	-1.63724	9.507E+24
15	Zn+2	6.008E-01	4.382E+24	-1.58593	4.381E+24
16	Zn+2	6.008E-01	1.987E+24	-1.55855	1.987E+24
17	Zn+2	6.008E-01	8.926E+23	-1.54442	8.925E+23
18	Zn+2	6.008E-01	3.989E+23	-1.53718	3.989E+23
19	Zn+2	6.008E-01	1.778E+23	-1.53357	1.778E+23
20	Zn+2	6.008E-01	7.913E+22	-1.53160	7.912E+22
21	Zn+2	6.008E-01	3.519E+22	-1.53068	3.519E+22
22	Zn+2	6.008E-01	1.565E+22	-1.53025	1.565E+22
23	Zn+2	6.008E-01	6.955E+21	-1.53005	6.954E+21
24	Zn+2	6.008E-01	3.091E+21	-1.52993	3.091E+21
25	Zn+2	6.008E-01	1.374E+21	-1.52985	1.374E+21
26	Zn+2	6.008E-01	6.107E+20	-1.52981	6.107E+20
27	Zn+2	6.008E-01	2.714E+20	-1.52978	2.714E+20
28	Zn+2	6.008E-01	1.206E+20	-1.52976	1.206E+20
29	Zn+2	6.008E-01	5.362E+19	-1.52976	5.361E+19
30	Zn+2	6.008E-01	2.383E+19	-1.52976	2.383E+19
31	Zn+2	6.008E-01	1.059E+19	-1.52976	1.059E+19
32	Zn+2	6.008E-01	4.707E+18	-1.52976	4.707E+18
33	Zn+2	6.008E-01	2.092E+18	-1.52976	2.092E+18
34	Zn+2	6.008E-01	9.298E+17	-1.52976	9.297E+17
35	Zn+2	6.008E-01	4.133E+17	-1.52976	4.132E+17
36	Zn+2	6.008E-01	1.837E+17	-1.52975	1.836E+17
37	Zn+2	6.008E-01	8.163E+16	-1.52975	8.162E+16
38	Zn+2	6.008E-01	3.628E+16	-1.52976	3.628E+16
39	Zn+2	6.008E-01	1.612E+16	-1.52976	1.612E+16
40	Zn+2	6.008E-01	7.166E+15	-1.52976	7.166E+15
41	Zn+2	6.008E-01	3.185E+15	-1.52976	3.185E+15
42	Zn+2	6.008E-01	1.416E+15	-1.52976	1.415E+15
43	Zn+2	6.008E-01	6.292E+14	-1.52976	6.291E+14
44	Zn+2	6.008E-01	2.796E+14	-1.52976	2.796E+14
45	Zn+2	6.008E-01	1.243E+14	-1.52976	1.243E+14
46	Zn+2	6.008E-01	5.523E+13	-1.52976	5.523E+13
47	Zn+2	6.008E-01	2.455E+13	-1.52976	2.455E+13
48	Zn+2	6.008E-01	1.091E+13	-1.52975	1.091E+13
49	Zn+2	6.008E-01	4.849E+12	-1.52975	4.849E+12
50	Zn+2	6.008E-01	2.155E+12	-1.52975	2.155E+12
51	Zn+2	6.008E-01	9.578E+11	-1.52975	9.577E+11

52	Zn+2	6.008E-01	4.257E+11	-1.52975	4.257E+11
53	Zn+2	6.008E-01	1.892E+11	-1.52975	1.892E+11
54	Zn+2	6.008E-01	8.409E+10	-1.52975	8.408E+10
55	Zn+2	6.008E-01	3.737E+10	-1.52975	3.737E+10
56	Zn+2	6.008E-01	1.661E+10	-1.52975	1.661E+10
57	Zn+2	6.008E-01	7.382E+09	-1.52975	7.382E+09
58	Zn+2	6.008E-01	3.281E+09	-1.52974	3.281E+09
59	Zn+2	6.008E-01	1.458E+09	-1.52974	1.458E+09
60	Zn+2	6.008E-01	6.481E+08	-1.52973	6.481E+08
61	Zn+2	6.008E-01	2.881E+08	-1.52971	2.880E+08
62	Zn+2	6.008E-01	1.280E+08	-1.52969	1.280E+08
63	Zn+2	6.008E-01	5.690E+07	-1.52966	5.690E+07
64	Zn+2	6.008E-01	2.529E+07	-1.52961	2.529E+07
65	Zn+2	6.008E-01	1.124E+07	-1.52954	1.124E+07
66	Zn+2	6.008E-01	4.997E+06	-1.52943	4.996E+06
67	Zn+2	6.008E-01	2.221E+06	-1.52927	2.221E+06
68	Zn+2	6.008E-01	9.874E+05	-1.52902	9.873E+05
69	Zn+2	6.008E-01	4.390E+05	-1.52866	4.390E+05
70	Zn+2	6.008E-01	1.952E+05	-1.52811	1.952E+05
71	Zn+2	6.008E-01	8.683E+04	-1.52729	8.682E+04
72	Zn+2	6.008E-01	3.864E+04	-1.52605	3.863E+04
73	Zn+2	6.008E-01	1.720E+04	-1.52421	1.720E+04
74	Zn+2	6.008E-01	7.666E+03	-1.52145	7.665E+03
75	Zn+2	6.008E-01	3.421E+03	-1.51733	3.420E+03
76	Zn+2	6.008E-01	1.529E+03	-1.51119	1.529E+03
77	Zn+2	6.008E-01	6.856E+02	-1.50207	6.855E+02
78	Zn+2	6.008E-01	3.086E+02	-1.48858	3.086E+02
79	Zn+2	6.008E-01	1.397E+02	-1.46881	1.397E+02
80	Zn+2	6.008E-01	6.373E+01	-1.44018	6.373E+01
81	Zn+2	6.008E-01	2.937E+01	-1.39957	2.937E+01
82	Zn+2	6.008E-01	1.370E+01	-1.34392	1.369E+01
83	Zn+2	6.008E-01	6.463E+00	-1.27197	6.463E+00
84	Zn+2	6.008E-01	3.069E+00	-1.18830	3.069E+00
85	Zn+2	6.008E-01	1.434E+00	-1.10958	1.434E+00
86	Zn+2	6.008E-01	6.134E-01	-1.06767	6.134E-01
87	Zn+2	6.008E-01	1.944E-01	-1.08680	1.943E-01
88	Zn+2	6.008E-01	2.727E-02	-1.12639	2.721E-02
89	Zn+2	6.008E-01	5.829E-04	-1.13628	5.229E-04
91	Zn+2	6.008E-01	2.464E-01	-1.13651	2.463E-01
92	Zn+2	6.008E-01	-1.923E-01	-1.43453	1.922E-01
93	Zn+2	6.008E-01	1.146E-01	-1.20901	1.145E-01
94	Zn+2	6.008E-01	-1.319E-01	-1.37552	1.318E-01
95	Zn+2	6.008E-01	1.027E-01	-1.21538	1.026E-01
96	Zn+2	6.008E-01	-1.071E-01	-1.35434	1.070E-01
97	Zn+2	6.008E-01	8.507E-02	-1.22500	8.501E-02
98	Zn+2	6.008E-01	-8.637E-02	-1.33762	8.631E-02
99	Zn+2	6.008E-01	7.042E-02	-1.23324	7.036E-02
100	Zn+2	6.008E-01	-6.989E-02	-1.32492	6.983E-02
101	Zn+2	6.008E-01	5.813E-02	-1.24031	5.807E-02
102	Zn+2	6.008E-01	-5.668E-02	-1.31509	5.662E-02
103	Zn+2	6.008E-01	4.791E-02	-1.24631	4.785E-02
104	Zn+2	6.008E-01	-2.771E-03	-1.30739	2.711E-03
106	Zn+2	6.008E-01	-4.435E-02	-1.30568	4.429E-02
107	Zn+2	6.008E-01	4.130E-02	-1.25024	4.124E-02
108	Zn+2	6.008E-01	-3.907E-02	-1.30242	3.901E-02
109	Zn+2	6.008E-01	3.371E-02	-1.25483	3.365E-02
110	Zn+2	6.008E-01	-3.181E-02	-1.29734	3.175E-02
111	Zn+2	6.008E-01	2.769E-02	-1.25851	2.763E-02
112	Zn+2	6.008E-01	-2.593E-02	-1.29329	2.587E-02
113	Zn+2	6.008E-01	2.274E-02	-1.26157	2.268E-02
114	Zn+2	6.008E-01	-2.116E-02	-1.29004	2.110E-02
115	Zn+2	6.008E-01	1.866E-02	-1.26411	1.860E-02
116	Zn+2	6.008E-01	-1.727E-02	-1.28741	1.721E-02
117	Zn+2	6.008E-01	1.530E-02	-1.26622	1.524E-02
118	Zn+2	6.008E-01	-1.411E-02	-1.28529	1.405E-02

119	Zn+2	6.008E-01	-2.210E-04	-1.26796	1.610E-04
121	Zn+2	6.008E-01	1.270E-02	-1.26783	1.264E-02
122	Zn+2	6.008E-01	-1.139E-02	-1.28349	1.133E-02
123	Zn+2	6.008E-01	1.016E-02	-1.26947	1.010E-02
124	Zn+2	6.008E-01	-9.307E-03	-1.28210	9.247E-03
125	Zn+2	6.008E-01	8.325E-03	-1.27064	8.265E-03
126	Zn+2	6.008E-01	-7.608E-03	-1.28098	7.548E-03
127	Zn+2	6.008E-01	6.820E-03	-1.27161	6.760E-03
128	Zn+2	6.008E-01	-6.221E-03	-1.28007	6.161E-03
129	Zn+2	6.008E-01	5.586E-03	-1.27240	5.526E-03
130	Zn+2	6.008E-01	-5.088E-03	-1.27932	5.028E-03
131	Zn+2	6.008E-01	4.574E-03	-1.27305	4.514E-03
132	Zn+2	6.008E-01	-4.161E-03	-1.27872	4.101E-03
133	Zn+2	6.008E-01	3.746E-03	-1.27358	3.686E-03
135	Zn+2	6.008E-01	-3.393E-03	-1.27821	3.333E-03
136	Zn+2	6.008E-01	3.077E-03	-1.27401	3.017E-03
137	Zn+2	6.008E-01	-2.794E-03	-1.27782	2.734E-03
138	Zn+2	6.008E-01	2.519E-03	-1.27437	2.459E-03
139	Zn+2	6.008E-01	-2.286E-03	-1.27749	2.226E-03
140	Zn+2	6.008E-01	2.062E-03	-1.27467	2.002E-03
141	Zn+2	6.008E-01	-1.870E-03	-1.27722	1.810E-03
142	Zn+2	6.008E-01	1.688E-03	-1.27491	1.628E-03
143	Zn+2	6.008E-01	-1.530E-03	-1.27700	1.470E-03
144	Zn+2	6.008E-01	1.382E-03	-1.27511	1.322E-03
145	Zn+2	6.008E-01	-1.252E-03	-1.27682	1.192E-03
146	Zn+2	6.008E-01	1.131E-03	-1.27527	1.071E-03
147	Zn+2	6.008E-01	-1.025E-03	-1.27667	9.645E-04
149	Zn+2	6.008E-01	9.265E-04	-1.27540	8.664E-04
150	Zn+2	6.008E-01	-8.377E-04	-1.27655	7.776E-04
151	Zn+2	6.008E-01	7.570E-04	-1.27551	6.969E-04
152	Zn+2	6.008E-01	-6.855E-04	-1.27645	6.254E-04
153	Zn+2	6.008E-01	6.196E-04	-1.27560	5.595E-04
154	Zn+2	6.008E-01	-5.610E-04	-1.27637	5.009E-04
155	Zn+2	6.008E-01	5.071E-04	-1.27567	4.470E-04
156	Zn+2	6.008E-01	-4.591E-04	-1.27630	3.990E-04
157	Zn+2	6.008E-01	4.151E-04	-1.27573	3.550E-04
158	Zn+2	6.008E-01	-3.757E-04	-1.27625	3.156E-04
159	Zn+2	6.008E-01	3.397E-04	-1.27578	2.796E-04
160	Zn+2	6.008E-01	-3.074E-04	-1.27620	2.474E-04
161	Zn+2	6.008E-01	2.780E-04	-1.27582	2.179E-04
163	Zn+2	6.008E-01	-2.515E-04	-1.27617	1.915E-04
164	Zn+2	6.008E-01	2.276E-04	-1.27586	1.675E-04
165	Zn+2	6.008E-01	-2.060E-04	-1.27614	1.459E-04
166	Zn+2	6.008E-01	1.863E-04	-1.27588	1.262E-04
167	Zn+2	6.008E-01	-1.686E-04	-1.27611	1.085E-04
168	Zn+2	6.008E-01	1.525E-04	-1.27590	9.237E-05
169	Zn+2	6.008E-01	-1.379E-04	-1.27609	7.786E-05
170	Zn+2	6.008E-01	1.248E-04	-1.27592	6.469E-05
171	Zn+2	6.008E-01	-1.129E-04	-1.27608	5.281E-05
172	Zn+2	6.008E-01	1.021E-04	-1.27594	4.204E-05
173	Zn+2	6.008E-01	-9.239E-05	-1.27606	3.231E-05
174	Zn+2	6.008E-01	8.357E-05	-1.27595	2.349E-05
175	Zn+2	6.008E-01	-7.561E-05	-1.27605	1.553E-05
177	Zn+2	6.008E-01	6.840E-05	-1.27596	8.322E-06
178	Zn+2	6.008E-01	-6.188E-05	-1.27604	1.798E-06

ID	NAME	ANAL MOL	CALC MOL	LOG ACTVTY	GAMMA	DIFF FXN
30	Al+3	0.000E-01	1.175E-03	-3.48400	0.279257	- 2.069E-05
60	H3AsO3	1.191E-02	1.171E-02	-1.74088	1.551023	4.619E-07
231	Cu+2	7.552E-03	2.134E-03	-2.91708	0.567257	5.039E-07

470	Mn+2	6.196E-02	1.973E-02	-1.95114	0.567257
4.353E-06					
950	Zn+2	6.008E-01	9.338E-02	-1.27597	0.567257
5.597E-05					
732	SO4-2	4.531E-01	6.439E-02	-1.43738	0.567257
0.000E-01					
330	H+1	0.000E-01	2.299E-02	-1.70000	0.867851
0.000E-01					
460	Mg+2	0.000E-01	3.405E-01	-0.71405	0.567257
4.752E-19					
100	Ba+2	0.000E-01	3.531E-09	-8.69836	0.567257
0.000E-01					
280	Fe+2	0.000E-01	1.589E-01	-1.04507	0.567257
0.000E-01					
150	Ca+2	0.000E-01	7.018E-04	-3.40003	0.567257
0.000E-01					
2	H2O	0.000E-01	1.096E+01	-0.00861	1.000000
1.110E-16					
600	Pb+2	0.000E-01	6.901E-07	-6.40731	0.567257
0.000E-01					

Type I - COMPONENTS AS SPECIES IN SOLUTION

ID	NAME	CALC MOL	ACTIVITY	LOG ACTVTY	GAMMA	NEW LOGK
330	H+1	2.299E-02	1.995E-02	-1.70000	0.86785	0.062
732	SO4-2	6.439E-02	3.653E-02	-1.43738	0.56726	0.246
231	Cu+2	2.134E-03	1.210E-03	-2.91708	0.56726	0.246
470	Mn+2	1.973E-02	1.119E-02	-1.95114	0.56726	0.246
950	Zn+2	9.338E-02	5.297E-02	-1.27597	0.56726	0.246
60	H3AsO3	1.171E-02	1.816E-02	-1.74088	1.55102	-0.191
30	Al+3	1.175E-03	3.281E-04	-3.48400	0.27926	0.554
460	Mg+2	3.405E-01	1.932E-01	-0.71405	0.56726	0.246
280	Fe+2	1.589E-01	9.014E-02	-1.04507	0.56726	0.246
150	Ca+2	7.018E-04	3.981E-04	-3.40003	0.56726	0.246
600	Pb+2	6.901E-07	3.915E-07	-6.40731	0.56726	0.246
100	Ba+2	3.531E-09	2.003E-09	-8.69836	0.56726	0.246

Type II - OTHER SPECIES IN SOLUTION OR ADSORBED

ID	NAME	CALC MOL	ACTIVITY	LOG ACTVTY	GAMMA	NEW LOGK
3300603	H4AsO3 +	2.069E-04	1.795E-04	-3.74588	0.86785	-0.243
3307320	HSO4 -	6.204E-02	5.384E-02	-1.26887	0.86785	1.930

3300020	OH-	2.603E-13	2.259E-13	-12.64607	0.86785	-14.276
4603300	MgOH +	7.311E-12	6.345E-12	-11.19760	0.86785	-12.113
4607320	MgSO4 AQ	7.454E-01	1.156E+00	0.06298	1.55102	2.024
1503300	CaOH +	2.428E-15	2.107E-15	-14.67637	0.86785	-12.906
1507320	CaSO4 AQ	1.752E-03	2.718E-03	-2.56580	1.55102	2.081
303300	AlOH +2	1.449E-07	8.217E-08	-7.08529	0.56726	-5.046
303301	Al(OH)2 +	7.250E-11	6.292E-11	-10.20123	0.86785	-10.038
303302	Al(OH)4 -	1.669E-21	1.448E-21	-20.83920	0.86785	-24.059
307320	AlSO4 +	1.275E-02	1.106E-02	-1.95607	0.86785	3.027
307321	Al(SO4)2 -	3.553E-02	3.083E-02	-1.51101	0.86785	4.909
303303	Al(OH)3 AQ	2.509E-15	3.892E-15	-14.40985	1.55102	-16.191
2803300	FeOH +	7.450E-10	6.465E-10	-9.18942	0.86785	-9.774
2803301	FeOH3 -1	2.089E-28	1.813E-28	-27.74164	0.86785	-31.709
2807320	FeSO4 AQ	3.124E-01	4.846E-01	-0.31461	1.55102	1.977
2803302	FeOH2 AQ	7.087E-20	1.099E-19	-18.95890	1.55102	-21.487
1003300	BaOH +	2.054E-21	1.783E-21	-20.74894	0.86785	-13.680
4703300	MnOH +	7.007E-12	6.081E-12	-11.21602	0.86785	-10.895
4703301	Mn(OH)3 -1	2.424E-32	2.104E-32	-31.67698	0.86785	-34.738
4707320	MnSO4 AQ	4.223E-02	6.551E-02	-1.18372	1.55102	2.014
2313300	CuOH +	6.853E-10	5.947E-10	-9.22569	0.86785	-7.938
2313301	Cu(OH)2 AQ	3.936E-14	6.105E-14	-13.21431	1.55102	-13.871
2313302	Cu(OH)3 -	2.088E-25	1.812E-25	-24.74192	0.86785	-26.837
2313303	Cu(OH)4 -2	3.124E-36	1.772E-36	-35.75154	0.56726	-39.354
2313304	Cu2(OH)2+2	9.777E-14	5.546E-14	-13.25602	0.56726	-10.558
2317320	CuSO4 AQ	5.419E-03	8.404E-03	-2.07549	1.55102	2.088
9503300	ZnOH +	1.500E-09	1.302E-09	-8.88541	0.86785	-9.239
9503301	Zn(OH)2 AQ	1.040E-15	1.614E-15	-14.79220	1.55102	-17.090
9503302	Zn(OH)3 -	2.889E-25	2.507E-25	-24.60081	0.86785	-28.337
9503303	Zn(OH)4 -2	3.442E-36	1.952E-36	-35.70942	0.56726	-40.953
9507320	ZnSO4 AQ	2.700E-01	4.188E-01	-0.37794	1.55102	2.145
9507321	Zn(SO4)2-2	2.374E-01	1.347E-01	-0.87073	0.56726	3.526
6003300	PbOH +	4.321E-13	3.750E-13	-12.42592	0.86785	-7.648

6003301	Pb(OH)2 AQ	4.622E-21	7.169E-21	-20.14453	1.55102	-
17.311						
6003302	Pb(OH)3 -	4.660E-30	4.044E-30	-29.39315	0.86785	-
27.998						
6003303	Pb2OH +3	1.177E-17	3.287E-18	-17.48323	0.27926	-
5.806						
6007320	PbSO4 AQ	5.184E-06	8.041E-06	-5.09469	1.55102	
2.559						
6003304	Pb3(OH)4+2	1.721E-37	9.762E-38	-37.01045	0.56726	-
24.308						
6003305	Pb(OH)4 -2	8.044E-40	4.563E-40	-39.34076	0.56726	-
39.453						
6007321	Pb(SO4)2-2	2.717E-06	1.541E-06	-5.81207	0.56726	
3.716						
3300600	H2AsO3 -	4.225E-10	3.667E-10	-9.43575	0.86785	-
9.333						
3300601	HAsO3 -2	1.637E-20	9.288E-21	-20.03206	0.56726	-
21.445						
3300602	AsO3 -3	4.508E-32	1.259E-32	-31.89998	0.27926	-
34.705						

Type III - SPECIES WITH FIXED ACTIVITY

ID	NAME	CALC MOL	LOG MOL	NEW LOGK	DH
2	H2O	1.096E+01	1.040	0.009	0.000
330	H+1	-1.347E-01	-0.871	1.700	0.000
6003000	ALOHSO4	-4.947E-02	-1.306	3.230	0.000
6010000	BARITE	-3.531E-09	-8.452	10.136	-6.280
6046000	EPSOMITE	-1.086E+00	0.036	2.212	-2.820
6015001	GYPSUM	-2.454E-03	-2.610	4.855	-0.261
6028000	MELANTERITE	-4.714E-01	-0.327	2.543	-2.860
6060003	ANGLESITE	-8.592E-06	-5.066	7.845	-2.150

PERCENTAGE DISTRIBUTION OF COMPONENTS AMONG
TYPE I and TYPE II (dissolved and adsorbed) species

Al+3	2.4	PERCENT BOUND IN SPECIES #	30
Al+3			
25.8	PERCENT BOUND IN SPECIES # 307320	AlSO4 +	
71.8	PERCENT BOUND IN SPECIES # 307321	Al(SO4)2 -	
H3AsO3	98.3	PERCENT BOUND IN SPECIES #	60
H3AsO3			
1.7	PERCENT BOUND IN SPECIES #3300603	H4AsO3 +	
Cu+2	28.3	PERCENT BOUND IN SPECIES #	231
Cu+2			
71.7	PERCENT BOUND IN SPECIES #2317320	CuSO4 AQ	
Mn+2	31.8	PERCENT BOUND IN SPECIES #	470
Mn+2			
68.2	PERCENT BOUND IN SPECIES #4707320	MnSO4 AQ	
Zn+2	15.5	PERCENT BOUND IN SPECIES #	950
Zn+2			
44.9	PERCENT BOUND IN SPECIES #9507320	ZnSO4 AQ	
39.5	PERCENT BOUND IN SPECIES #9507321	Zn(SO4)2-2	
SO4-2	3.1	PERCENT BOUND IN SPECIES #	732
SO4-2			
3.0	PERCENT BOUND IN SPECIES #3307320	HSO4 -	
36.1	PERCENT BOUND IN SPECIES #4607320	MgSO4 AQ	
3.4	PERCENT BOUND IN SPECIES # 307321	Al(SO4)2 -	
15.2	PERCENT BOUND IN SPECIES #2807320	FeSO4 AQ	
2.0	PERCENT BOUND IN SPECIES #4707320	MnSO4 AQ	
13.1	PERCENT BOUND IN SPECIES #9507320	ZnSO4 AQ	
23.0	PERCENT BOUND IN SPECIES #9507321	Zn(SO4)2-2	
H+1	27.0	PERCENT BOUND IN SPECIES #	330
H+1			
72.8	PERCENT BOUND IN SPECIES #3307320	HSO4 -	
Mg+2	31.4	PERCENT BOUND IN SPECIES #	460
Mg+2			
68.6	PERCENT BOUND IN SPECIES #4607320	MgSO4 AQ	
Ba+2	100.0	PERCENT BOUND IN SPECIES #	100
Ba+2			
Fe+2	33.7	PERCENT BOUND IN SPECIES #	280
Fe+2			
66.3	PERCENT BOUND IN SPECIES #2807320	FeSO4 AQ	
Ca+2	28.6	PERCENT BOUND IN SPECIES #	150
Ca+2			
71.4	PERCENT BOUND IN SPECIES #1507320	CaSO4 AQ	

H2O	97.9	PERCENT BOUND IN SPECIES # 303300
AlOH +2		
	1.0	PERCENT BOUND IN SPECIES #9503300 ZnOH +
Pb+2	8.0	PERCENT BOUND IN SPECIES # 600
Pb+2		
	60.3	PERCENT BOUND IN SPECIES #6007320 PbSO4 AQ
	31.6	PERCENT BOUND IN SPECIES #6007321 Pb(SO4)2-2

PART 5 of OUTPUT FILE

PC MINTEQA2 v3.10 DATE OF CALCULATIONS: 11-MAR-97 TIME: 23:53:53

EQUILIBRATED MASS DISTRIBUTION

IDX	NAME	DISSOLVED		SORBED		PRECIPITATED
		MOL/KG	PERCENT	MOL/KG	PERCENT	MOL/KG
PERCENT						
30	Al+3	4.945E-02	100.0	0.000E-01	0.0	0.000E-01
0.0						
60	H3AsO3	1.192E-02	100.0	0.000E-01	0.0	0.000E-01
0.0						
231	Cu+2	7.552E-03	100.0	0.000E-01	0.0	0.000E-01
0.0						
470	Mn+2	6.196E-02	100.0	0.000E-01	0.0	0.000E-01
0.0						
950	Zn+2	6.008E-01	100.0	0.000E-01	0.0	0.000E-01
0.0						
732	SO4-2	2.062E+00	100.0	0.000E-01	0.0	0.000E-01
0.0						
330	H+1	8.524E-02	100.0	0.000E-01	0.0	0.000E-01
0.0						
460	Mg+2	1.086E+00	100.0	0.000E-01	0.0	0.000E-01
0.0						
100	Ba+2	3.531E-09	100.0	0.000E-01	0.0	0.000E-01
0.0						
280	Fe+2	4.714E-01	100.0	0.000E-01	0.0	0.000E-01
0.0						
150	Ca+2	2.454E-03	100.0	0.000E-01	0.0	0.000E-01
0.0						
2	H2O	1.479E-07	100.0	0.000E-01	0.0	0.000E-01
0.0						
600	Pb+2	8.592E-06	100.0	0.000E-01	0.0	0.000E-01
0.0						

Charge Balance: SPECIATED

Sum of CATIONS = 1.270E+00 Sum of ANIONS 7.012E-01

PERCENT DIFFERENCE = 2.887E+01 (ANIONS - CATIONS)/(ANIONS + CATIONS)

EQUILIBRIUM IONIC STRENGTH (m) = 1.906E+00

EQUILIBRIUM pH = 1.700

DATE ID NUMBER: 970311
TIME ID NUMBER: 23535320

PC MINTEQA2 v3.10 DATE OF CALCULATIONS: 11-MAR-97 TIME: 23:53:53

Saturation indices and stoichiometry of all minerals

ID #	NAME	Sat. Index	Stoichiometry in [brackets]
2003000	ALOH3(A)	-9.478	[1.000] 30 [3.000] 2 [-3.000] 330
6003000	ALOHSO4	0.000	[-1.000] 330 [1.000] 30 [1.000] 732
			[1.000] 2
6003001	AL4(OH)10SO4	-21.160	[-10.000] 330 [4.000] 30 [1.000] 732
			[10.000] 2
6015000	ANHYDRITE	-0.296	[1.000] 150 [1.000] 732
6010000	BARITE	0.000	[1.000] 100 [1.000] 732
2003001	BOEHMITE	-7.695	[-3.000] 330 [1.000] 30 [2.000] 2
2046000	BRUCITE	-14.781	[1.000] 460 [2.000] 2 [-2.000] 330
2003002	DIASPORE	-5.901	[-3.000] 330 [1.000] 30 [2.000] 2
6046000	EPSOMITE	0.000	[1.000] 460 [1.000] 732 [7.000] 2
2003003	GIBBSITE (C)	-7.760	[-3.000] 330 [1.000] 30 [3.000] 2
3003000	Al2O3	-19.774	[2.000] 30 [3.000] 2 [-6.000] 330
6015001	GYPSUM	0.000	[1.000] 150 [1.000] 732 [2.000] 2
6028000	MELANTERITE	0.000	[1.000] 280 [1.000] 732 [7.000] 2
2047003	PYROCROITE	-14.231	[-2.000] 330 [1.000] 470 [2.000] 2
6047000	MNSO4	-6.451	[1.000] 470 [1.000] 732
2023100	CU(OH)2	-8.562	[-2.000] 330 [1.000] 231 [2.000] 2
6023100	ANTLERITE	-11.713	[-4.000] 330 [3.000] 231 [4.000] 2
			[1.000] 732
6023101	BROCHANTITE	-18.297	[-6.000] 330 [4.000] 231 [6.000] 2
			[1.000] 732
6023102	LANGITE	-20.764	[-6.000] 330 [4.000] 231 [7.000] 2
			[1.000] 732
2023101	TENORITE	-7.533	[-2.000] 330 [1.000] 231 [1.000] 2
6023103	CUOCUSO4	-16.315	[-2.000] 330 [2.000] 231 [1.000] 2
			[1.000] 732
6023104	CUSO4	-7.826	[1.000] 231 [1.000] 732
6023105	CHALCANTHITE	-1.721	[1.000] 231 [1.000] 732 [5.000] 2
2095000	ZN(OH)2 (A)	-10.343	[-2.000] 330 [1.000] 950 [2.000] 2
2095001	ZN(OH)2 (C)	-10.093	[-2.000] 330 [1.000] 950 [2.000] 2

```
  2095002 ZN(OH)2 (B)      -9.643     [ -2.000] 330   [  1.000] 950   [
2.000]    2
  2095003 ZN(OH)2 (G)      -9.603     [ -2.000] 330   [  1.000] 950   [
2.000]    2
  2095004 ZN(OH)2 (E)      -9.393     [ -2.000] 330   [  1.000] 950   [
2.000]    2
  6095000 ZN2(OH)2SO4      -8.107     [ -2.000] 330   [  2.000] 950   [
2.000]    2
                                      [  1.000] 732
  6095001 ZN4(OH)6SO4     -24.793     [ -6.000] 330   [  4.000] 950   [
6.000]    2
                                      [  1.000] 732
  2095005 ZNO(ACTIVE)      -9.195     [ -2.000] 330   [  1.000] 950   [
1.000]    2
  2095006 ZINCITE          -9.581     [ -2.000] 330   [  1.000] 950   [
1.000]    2
  6095002 ZN3O(SO4)2      -23.908     [ -2.000] 330   [  3.000] 950   [
2.000] 732
                                      [  1.000]   2
  6095003 ZINCOSITE        -6.212     [  1.000] 950   [  1.000] 732
```

ID #	NAME	Sat. Index	Stoichiometry in [brackets]
6095004	ZNSO4, 1H2O	-2.423	[1.000] 950 [1.000] 732 [1.000] 2
6095005	BIANCHITE	-1.004	[1.000] 950 [1.000] 732 [6.000] 2
6095006	GOSLARITE	-0.730	[1.000] 950 [1.000] 732 [7.000] 2
2060000	MASSICOT	-16.353	[-2.000] 330 [1.000] 600 [1.000] 2
2060001	LITHARGE	-16.153	[-2.000] 330 [1.000] 600 [1.000] 2
2060002	PBO, .3H2O	-15.999	[-2.000] 330 [1.000] 600 [1.330] 2
6060000	LARNAKITE	-10.744	[-2.000] 330 [2.000] 600 [1.000] 732 [1.000] 2
6060001	PB3O2SO4	-24.804	[-4.000] 330 [3.000] 600 [1.000] 732 [2.000] 2
6060002	PB4O3SO4	-39.885	[-6.000] 330 [4.000] 600 [1.000] 732 [3.000] 2
6060003	ANGLESITE	0.000	[1.000] 600 [1.000] 732
2060004	PB(OH)2 (C)	-11.530	[-2.000] 330 [1.000] 600 [2.000] 2
2060005	PB2O(OH)2	-32.240	[-4.000] 330 [2.000] 600 [3.000] 2
6060004	PB4(OH)6SO4	-38.018	[-6.000] 330 [4.000] 600 [1.000] 732 [6.000] 2
3006000	ARSENOLITE	-3.746	[4.000] 60 [-6.000] 2
3006001	CLAUDETITE	-3.509	[4.000] 60 [-6.000] 2
2015000	LIME	-33.982	[-2.000] 330 [1.000] 150 [1.000] 2
2015001	PORTLANDITE	-23.473	[-2.000] 330 [1.000] 150 [2.000] 2
2028000	WUSTITE	-9.917	[-2.000] 330 [0.947] 280 [1.000] 2
2046001	PERICLASE	-19.752	[-2.000] 330 [1.000] 460 [1.000] 2
3028001	HERCYNITE	-23.603	[-8.000] 330 [1.000] 280 [2.000] 30 [4.000] 2
3046000	SPINEL	-32.716	[-8.000] 330 [1.000] 460 [2.000] 30 [4.000] 2

PART 1 of OUTPUT FILE

PC MINTEQA2 v3.10 DATE OF CALCULATIONS: 11-MAR-97 TIME: 23:53:53

Cemented oxidized neutral tailings

Temperature (Celsius): 15.00

```
 Units of concentration: MG/L
 Ionic strength to be computed.
 If specified, carbonate concentration represents total inorganic
carbon.
 Do not automatically terminate if charge imbalance exceeds 30%
 Precipitation is allowed only for those solids specified as ALLOWED
   in the input file (if any).
 The maximum number of iterations is: 200
 The method used to compute activity coefficients is: Davies equation
 Intermediate output file

-------------------------------------------------------------------------
-------
    330  0.000E-01   -7.00 y
    732  2.369E+05   -1.81 y
     30  4.130E+01   -4.28 y
     61  3.200E+00   -6.45 y
    100  2.680E+01   -6.84 y
    160  1.000E-01   -9.05 y
    150  3.368E+04   -2.13 y
    210  1.570E+02   -5.97 y
    231  4.170E+00   -6.00 y
    280  3.600E+01   -5.13 y
    600  7.340E+01   -5.89 y
    460  1.040E+02   -5.21 y
    470  2.609E+00   -7.04 y
    762  1.090E+01   -5.70 y
    950  1.040E+01   -5.17 y
    140  0.000E-01  -16.00 y
      1  0.000E-01  -16.00 y
    730  0.000E-01  -20.52 y
    281  1.000E-03  -20.75 y

 H2O has been inserted as a COMPONENT
  3   2
1028003    18.4790   -11.3000
    330     7.0000     0.0000
  4   1
5015001     8.4750     2.5850   1.000E+01
  5   8
2003000   -10.3800    27.0450
6010000     9.9760    -6.2800
6015001     4.8480    -0.2610
5028000    10.5500     5.3280
2023101    -7.6200    15.2400
5016000    13.7400     0.5800
6060003     7.7900    -2.1500
7210000     8.9100    -2.6400
  6   1
      1     0.0000     0.0000

INPUT DATA BEFORE TYPE MODIFICATIONS

   ID        NAME       ACTIVITY GUESS     LOG GUESS   ANAL TOTAL
    330  H+1                 1.000E-07         -7.000   0.000E-01
    732  SO4-2               1.549E-02         -1.810   2.369E+05
     30  Al+3                5.248E-05         -4.280   4.130E+01
     61  H3AsO4              3.548E-07         -6.450   3.200E+00
    100  Ba+2                1.445E-07         -6.840   2.680E+01
    160  Cd+2                8.913E-10         -9.050   1.000E-01
    150  Ca+2                7.413E-03         -2.130   3.368E+04
    210  Cr+2                1.072E-06         -5.970   1.570E+02
    231  Cu+2                1.000E-06         -6.000   4.170E+00
    280  Fe+2                7.413E-06         -5.130   3.600E+01
    600  Pb+2                1.288E-06         -5.890   7.340E+01
```

460	Mg+2	6.166E-06	-5.210	1.040E+02
470	Mn+2	9.120E-08	-7.040	2.609E+00
762	SeO4-2	1.995E-06	-5.700	1.090E+01
950	Zn+2	6.761E-06	-5.170	1.040E+01
140	CO3-2	1.000E-16	-16.000	0.000E-01
1	E-1	1.000E-16	-16.000	0.000E-01
730	HS-1	3.020E-21	-20.520	0.000E-01
281	Fe+3	1.778E-21	-20.750	1.000E-03
2	H2O	1.000E+00	0.000	0.000E-01

Charge Balance: UNSPECIATED

Sum of CATIONS= 2.336E+00 Sum of ANIONS = 6.766E+00

PERCENT DIFFERENCE = 4.867E+01 (ANIONS - CATIONS)/(ANIONS + CATIONS)

IMPROVED ACTIVITY GUESSES PRIOR TO FIRST ITERATION:

SO4-2	Log activity guess:	0.53
Al+3	Log activity guess:	-7.74
H3AsO4	Log activity guess:	-9.74
Cu+2	Log activity guess:	-4.13
Fe+2	Log activity guess:	-3.05
Mn+2	Log activity guess:	-4.19
SeO4-2	Log activity guess:	-3.98
Fe+3	Log activity guess:	-15.99

PART 3 of OUTPUT FILE

PC MINTEQA2 v3.10 DATE OF CALCULATIONS: 11-MAR-97 TIME: 23:53:54

PARAMETERS OF THE COMPONENT MOST OUT OF BALANCE:

ITER	NAME	TOTAL MOL	DIFF FXN	LOG ACTVTY	RESIDUAL
0	E-1	0.000E-01	-1.138E+00	-16.00000	1.138E+00
1	E-1	0.000E-01	-2.805E-01	-15.97115	2.805E-01
2	E-1	0.000E-01	-6.036E-04	-15.97016	6.036E-04
3	E-1	0.000E-01	-6.036E+00	-16.97016	6.036E+00
4	E-1	0.000E-01	-7.570E-01	-16.98982	7.570E-01
5	E-1	0.000E-01	-2.873E-01	-16.92608	2.872E-01
6	E-1	0.000E-01	-1.153E-01	-16.84729	1.153E-01
7	E-1	0.000E-01	-4.635E-02	-16.76811	4.635E-02
8	E-1	0.000E-01	-1.863E-02	-16.68893	1.863E-02
9	E-1	0.000E-01	-7.486E-03	-16.60975	7.485E-03
10	E-1	0.000E-01	-3.009E-03	-16.53057	3.008E-03
11	E-1	0.000E-01	-1.209E-03	-16.45139	1.209E-03
12	E-1	0.000E-01	-4.859E-04	-16.37221	4.858E-04
13	E-1	0.000E-01	-1.953E-04	-16.29303	1.952E-04
14	E-1	0.000E-01	-7.847E-05	-16.21384	7.847E-05
15	E-1	0.000E-01	-3.154E-05	-16.13466	3.153E-05
16	E-1	0.000E-01	-1.267E-05	-16.05548	1.267E-05
17	E-1	0.000E-01	-5.093E-06	-15.97630	5.093E-06
18	E-1	0.000E-01	-2.047E-06	-15.89712	2.047E-06
19	E-1	0.000E-01	-8.226E-07	-15.81794	8.225E-07
20	E-1	0.000E-01	-3.306E-07	-15.73876	3.306E-07
21	E-1	0.000E-01	-1.329E-07	-15.65958	1.328E-07
22	E-1	0.000E-01	-5.339E-08	-15.58039	5.339E-08
23	E-1	0.000E-01	-2.146E-08	-15.50121	2.145E-08
24	E-1	0.000E-01	-8.623E-09	-15.42203	8.622E-09
25	E-1	0.000E-01	-3.465E-09	-15.34285	3.465E-09
26	E-1	0.000E-01	-1.393E-09	-15.26367	1.393E-09
27	E-1	0.000E-01	-5.597E-10	-15.18449	5.596E-10
28	E-1	0.000E-01	-2.249E-10	-15.10531	2.249E-10
29	E-1	0.000E-01	-9.039E-11	-15.02613	9.038E-11
30	E-1	0.000E-01	-3.633E-11	-14.94694	3.632E-11
31	E-1	0.000E-01	-1.460E-11	-14.86776	1.460E-11
32	E-1	0.000E-01	-5.867E-12	-14.78858	5.866E-12
33	E-1	0.000E-01	-2.358E-12	-14.70940	2.358E-12
34	E-1	0.000E-01	-9.475E-13	-14.63022	9.475E-13
35	E-1	0.000E-01	-3.808E-13	-14.55104	3.808E-13
36	E-1	0.000E-01	-1.530E-13	-14.47186	1.530E-13
37	E-1	0.000E-01	-6.150E-14	-14.39268	6.149E-14
38	E-1	0.000E-01	-2.472E-14	-14.31349	2.471E-14
39	E-1	0.000E-01	-9.933E-15	-14.23431	9.932E-15
40	E-1	0.000E-01	-3.992E-15	-14.15513	3.991E-15
41	E-1	0.000E-01	-1.604E-15	-14.07595	1.604E-15
42	E-1	0.000E-01	-6.447E-16	-13.99677	6.446E-16
43	E-1	0.000E-01	-2.591E-16	-13.91759	2.591E-16
44	E-1	0.000E-01	-1.041E-16	-13.83841	1.041E-16
45	E-1	0.000E-01	-4.184E-17	-13.75923	4.184E-17
46	E-1	0.000E-01	-1.682E-17	-13.68004	1.681E-17
47	E-1	0.000E-01	-6.758E-18	-13.60086	6.757E-18
48	E-1	0.000E-01	-2.716E-18	-13.52168	2.716E-18
49	E-1	0.000E-01	-1.091E-18	-13.44250	1.091E-18
50	E-1	0.000E-01	-4.386E-19	-13.36332	4.386E-19
51	E-1	0.000E-01	-1.763E-19	-13.28414	1.763E-19

52	E-1	0.000E-01	-7.084E-20	-13.20496	7.083E-20
53	E-1	0.000E-01	-2.847E-20	-13.12578	2.847E-20
54	E-1	0.000E-01	-1.144E-20	-13.04659	1.144E-20
55	E-1	0.000E-01	-4.598E-21	-12.96741	4.598E-21
56	E-1	0.000E-01	-1.848E-21	-12.88823	1.848E-21
57	E-1	0.000E-01	-7.426E-22	-12.80905	7.425E-22
58	E-1	0.000E-01	-2.984E-22	-12.72987	2.984E-22
59	E-1	0.000E-01	-1.199E-22	-12.65069	1.199E-22
60	E-1	0.000E-01	-4.819E-23	-12.57153	4.818E-23
61	E-1	0.000E-01	-1.936E-23	-12.49238	1.936E-23
62	E-1	0.000E-01	-7.769E-24	-12.41332	7.768E-24
63	E-1	0.000E-01	-3.110E-24	-12.33449	3.109E-24
64	E-1	0.000E-01	-1.235E-24	-12.25635	1.235E-24
65	E-1	0.000E-01	-4.790E-25	-12.18022	4.790E-25
66	E-1	0.000E-01	-1.734E-25	-12.10972	1.733E-25
67	E-1	0.000E-01	-5.132E-26	-12.05317	5.131E-26
68	E-1	0.000E-01	-8.715E-27	-12.02198	8.706E-27
69	E-1	0.000E-01	-3.652E-28	-12.01460	3.573E-28

ID	NAME	ANAL MOL	CALC MOL	LOG ACTVTY	GAMMA	DIFF FXN
281	Fe+3	2.456E-08	7.736E-26	-18.62329**********		- 6.617E-24
732	SO4-2	3.383E+00	2.148E+00	3.21567	764.954202	0.000E-01
30	Al+3	2.100E-03	1.887E-20	-13.23601**********		7.806E-18
61	H3AsO4	3.093E-05	3.131E-10	-8.59370	8.138617	- 4.743E-20
100	Ba+2	2.677E-04	2.677E-04	-0.68874	764.954202	- 1.084E-19
160	Cd+2	1.221E-06	1.423E-16	-12.96329	764.954202	1.694E-21
150	Ca+2	1.153E+00	4.228E-08	-4.49026	764.954202	- 8.882E-16
210	Cr+2	4.142E-03	4.142E-03	0.50087	764.954202	- 3.469E-18
231	Cu+2	9.002E-05	3.058E-12	-8.63086	764.954202	1.220E-19
280	Fe+2	8.843E-04	3.891E-11	-7.52635	764.954202	1.193E-18
600	Pb+2	4.860E-04	6.033E-14	-10.33580	764.954202	1.952E-18
460	Mg+2	5.868E-03	2.319E-10	-6.75103	764.954202	- 4.337E-18
470	Mn+2	6.515E-05	2.632E-12	-8.69606	764.954202	2.439E-19
762	SeO4-2	1.046E-04	1.045E-04	-1.09727	764.954202	- 6.776E-20
950	Zn+2	2.183E-04	4.215E-14	-10.49156	764.954202	4.066E-19
1	E-1	0.000E-01	9.677E-13	-12.01426	5.259069	- 2.602E-36
2	H2O	0.000E-01	-1.774E-08	-0.03496	1.000000	0.000E-01
330	H+1	0.000E-01	1.901E-08	-7.00000	5.259069	0.000E-01
730	HS-1	0.000E-01	4.414E-26	-24.63430	5.259069	0.000E-01
140	CO3-2	0.000E-01	1.526E-07	-3.93284	764.954202	0.000E-01

Type I - COMPONENTS AS SPECIES IN SOLUTION

ID	NAME	CALC MOL	ACTIVITY	LOG ACTVTY	GAMMA	NEW LOGK
330	H+1	1.901E-08	1.000E-07	-7.00000	5.25907	- 0.721
732	SO4-2	2.148E+00	1.643E+03	3.21567	********	- 2.884
30	Al+3	1.887E-20	5.808E-14	-13.23601	********	- 6.488
61	H3AsO4	3.131E-10	2.549E-09	-8.59370	8.13862	- 0.911
100	Ba+2	2.677E-04	2.048E-01	-0.68874	********	- 2.884
160	Cd+2	1.423E-16	1.088E-13	-12.96329	********	- 2.884
150	Ca+2	4.228E-08	3.234E-05	-4.49026	********	- 2.884
210	Cr+2	4.142E-03	3.169E+00	0.50087	********	- 2.884
231	Cu+2	3.058E-12	2.340E-09	-8.63086	********	- 2.884
280	Fe+2	3.891E-11	2.976E-08	-7.52635	********	- 2.884
600	Pb+2	6.033E-14	4.615E-11	-10.33580	********	- 2.884
460	Mg+2	2.319E-10	1.774E-07	-6.75103	********	- 2.884
470	Mn+2	2.632E-12	2.013E-09	-8.69606	********	- 2.884
762	SeO4-2	1.045E-04	7.993E-02	-1.09727	********	- 2.884
950	Zn+2	4.215E-14	3.224E-11	-10.49156	********	- 2.884
140	CO3-2	1.526E-07	1.167E-04	-3.93284	********	- 2.884
281	Fe+3	7.736E-26	2.381E-19	-18.62329	********	- 6.488
730	HS-1	4.414E-26	2.321E-25	-24.63430	5.25907	- 0.721

Type II - OTHER SPECIES IN SOLUTION OR ADSORBED

ID	NAME	CALC MOL	ACTIVITY	LOG ACTVTY	GAMMA	NEW LOGK
1607620	CdSeO4	1.864E-13	1.517E-12	-11.81906	8.13862	1.331
9507620	ZnSeO4	5.041E-11	4.103E-10	-9.38693	8.13862	1.291
9507621	Zn(SeO4)2-2	2.290E-16	1.752E-13	-12.75649	********	- 2.954
3300020	OH-	8.066E-09	4.242E-08	-7.37242	5.25907	- 15.058
4603300	MgOH +	2.080E-13	1.094E-12	-11.96093	5.25907	- 12.896
4601400	MgCO3 AQ	2.083E-09	1.695E-08	-7.77084	8.13862	2.002
4601401	MgHCO3 +	1.164E-07	6.123E-07	-6.21302	5.25907	10.750
4607320	MgSO4 AQ	5.868E-03	4.776E-02	-1.32094	8.13862	1.304

1503300	CaOH +	6.111E-12	3.214E-11	-10.49295	5.25907	-
13.689						
1501400	CaHCO3 +	1.472E-05	7.743E-05	-4.11110	5.25907	
10.591						
1501401	CaCO3 AQ	5.446E-07	4.432E-06	-5.35336	8.13862	
2.159						
1507320	CaSO4 AQ	1.220E+00	9.932E+00	0.99702	8.13862	
1.361						
303300	AlOH +2	3.570E-15	2.731E-12	-11.56365	********	-
8.176						
303301	Al(OH)2 +	7.467E-11	3.927E-10	-9.40594	5.25907	-
10.821						
303302	Al(OH)4 -	6.060E-11	3.187E-10	-9.49661	5.25907	-
24.842						
307320	AlSO4 +	1.675E-08	8.810E-08	-7.05503	5.25907	
2.244						
307321	Al(SO4)2 -	2.100E-03	1.104E-02	-1.95691	5.25907	
4.127						
303303	Al(OH)3 AQ	5.605E-10	4.561E-09	-8.34090	8.13862	-
16.911						
2803300	FeOH +	7.621E-12	4.008E-11	-10.39706	5.25907	-
10.557						
2803301	FeOH3 -1	7.535E-20	3.963E-19	-18.40198	5.25907	-
32.492						
2807320	FeSO4 AQ	8.843E-04	7.197E-03	-2.14284	8.13862	
1.257						
2803302	FeOH2 AQ	1.572E-16	1.280E-15	-14.89288	8.13862	-
22.207						
2807300	Fe(HS)2 AQ	1.756E-49	1.429E-48	-47.84496	8.13862	
8.039						
2807301	Fe(HS)3 -	6.868E-72	3.612E-71	-70.44227	5.25907	
10.266						
2813300	FeOH +2	1.008E-17	7.713E-15	-14.11277	********	-
5.338						
2817320	FeSO4 +	4.921E-13	2.588E-12	-11.58707	5.25907	
3.100						
2813301	FeOH2 +	8.239E-12	4.333E-11	-10.36322	5.25907	-
6.391						
2813302	FeOH3 AQ	5.771E-13	4.697E-12	-11.32818	8.13862	-
14.511						
2813303	FeOH4 -	8.240E-14	4.334E-13	-12.36314	5.25907	-
22.321						
2817321	Fe(SO4)2 -	2.455E-08	1.291E-07	-6.88895	5.25907	
4.582						
2813304	Fe2(OH)2+4	7.171E-39	2.455E-27	-26.60990	********	-
14.828						
2813305	Fe3(OH)4+5	2.013E-53	2.121E-35	-34.67346	********	-
24.686						
1003300	BaOH +	6.508E-09	3.422E-08	-7.46567	5.25907	-
14.463						
4703300	MnOH +	3.907E-14	2.055E-13	-12.68729	5.25907	-
11.677						
4703301	Mn(OH)3 -1	4.766E-24	2.506E-23	-22.60095	5.25907	-
35.521						
4700020	MnO4 -	1.577E-26	8.294E-26	-25.08124	5.25907	-
133.038						
4700021	MnO4 -2	1.206E-30	9.228E-28	-27.03488	********	-
125.140						
4707320	MnSO4 AQ	6.514E-05	5.302E-04	-3.27559	8.13862	
1.294						
4701400	MnHCO3 +	1.779E-09	9.356E-09	-8.02889	5.25907	
10.879						
2311400	CuCO3 AQ	1.802E-07	1.467E-06	-5.83370	8.13862	
5.819						

2311401	Cu(CO3)2-2	2.817E-10	2.155E-07	-6.66653	********	
6.946						
2313300	CuOH +	4.105E-11	2.159E-10	-9.66583	5.25907	-
8.721						
2313301	Cu(OH)2 AQ	5.113E-10	4.161E-09	-8.38079	8.13862	-
14.591						
2313302	Cu(OH)3 -	4.409E-16	2.319E-15	-14.63476	5.25907	-
27.620						
2313303	Cu(OH)4 -2	5.567E-24	4.259E-21	-20.37072	********	-
42.484						
2313304	Cu2(OH)2+2	9.552E-18	7.306E-15	-14.13629	********	-
13.688						
2317320	CuSO4 AQ	8.979E-05	7.308E-04	-3.13622	8.13862	
1.368						
2317300	Cu(HS)3 -	4.409E-58	2.319E-57	-56.63478	5.25907	
25.178						
2311402	CuHCO3 +	5.193E-08	2.731E-07	-6.56370	5.25907	
12.279						
9503300	ZnOH +	2.830E-14	1.488E-13	-12.82735	5.25907	-
10.022						
9503301	Zn(OH)2 AQ	4.256E-15	3.463E-14	-13.46049	8.13862	-
17.810						
9503302	Zn(OH)3 -	1.921E-19	1.011E-18	-17.99546	5.25907	-
29.120						
9503303	Zn(OH)4 -2	1.932E-27	1.478E-24	-23.83042	********	-
44.083						
9507300	Zn(HS)2 AQ	1.859E-46	1.513E-45	-44.82017	8.13862	
14.029						
9507301	Zn(HS)3 -	9.652E-70	5.076E-69	-68.29448	5.25907	
15.379						
9507320	ZnSO4 AQ	1.409E-06	1.147E-05	-4.94049	8.13862	
1.425						
9507321	Zn(SO4)2-2	2.168E-04	1.659E-01	-0.78022	********	
0.396						
9501400	ZnHCO3 +	1.798E-10	9.454E-10	-9.02440	5.25907	
11.679						
9501401	ZnCO3 AQ	9.227E-11	7.509E-10	-9.12440	8.13862	
4.389						
9501402	Zn(CO3)2-2	2.450E-12	1.874E-09	-8.72723	********	
6.746						
1601400	Cd(CO3)3-4	8.388E-31	2.872E-19	-18.54180	********	-
5.315						
1603300	CdOH +	7.373E-18	3.877E-17	-16.41148	5.25907	-
11.134						
1603301	Cd(OH)2 AQ	5.084E-21	4.138E-20	-19.38322	8.13862	-
21.261						
1603302	Cd(OH)3 -	8.145E-27	4.284E-26	-25.36818	5.25907	-
34.021						
1603303	Cd(OH)4 -2	4.605E-36	3.523E-33	-32.45315	********	-
50.234						
1603304	Cd2OH +3	7.639E-36	2.351E-29	-28.62878	********	-
16.155						
1607320	CdSO4 AQ	5.948E-09	4.841E-08	-7.31509	8.13862	
1.522						
1607300	CdHS +	7.104E-29	3.736E-28	-27.42759	5.25907	
9.449						
1607301	Cd(HS)2 AQ	2.441E-47	1.987E-46	-45.70190	8.13862	
15.619						
1607302	Cd(HS)3 -	1.327E-69	6.979E-69	-68.15620	5.25907	
17.989						
1607303	Cd(HS)4 -2	3.280E-94	2.509E-91	-90.60051	********	
18.016						
1601400	CdHCO3 +	6.067E-13	3.191E-12	-11.49613	5.25907	
11.679						

1601401	CdCO3 AQ	3.911E-13	3.183E-12	-11.49713	8.13862	4.488
1607321	Cd(SO4)2-2	1.215E-06	9.291E-04	-3.03195	********	0.616
6001400	Pb(CO3)2-2	3.588E-11	2.745E-08	-7.56147	********	7.756
6003300	PbOH +	1.579E-12	8.303E-12	-11.08076	5.25907	-8.431
6003301	Pb(OH)2 AQ	3.662E-15	2.980E-14	-13.52572	8.13862	-18.031
6003302	Pb(OH)3 -	6.003E-19	3.157E-18	-17.50069	5.25907	-28.781
6003303	Pb2OH +3	2.788E-27	8.579E-21	-20.06656	********	-12.848
6007320	PbSO4 AQ	5.240E-06	4.265E-05	-4.37013	8.13862	1.839
6007300	Pb(HS)2 AQ	5.689E-46	4.630E-45	-44.33441	8.13862	14.359
6007301	Pb(HS)3 -	4.077E-69	2.144E-68	-67.66871	5.25907	15.849
6003304	Pb3(OH)4+2	2.600E-31	1.989E-28	-27.70132	********	-27.438
6001401	PbCO3 AQ	1.150E-08	9.362E-08	-7.02863	8.13862	6.329
6003305	Pb(OH)4 -2	8.744E-26	6.689E-23	-22.17465	********	-42.583
6007321	Pb(SO4)2-2	4.807E-04	3.677E-01	-0.43445	********	0.586
6001402	PbHCO3 +	1.624E-09	8.538E-09	-8.06863	5.25907	12.479
3300611	H2AsO4 -	3.058E-05	1.608E-04	-3.79371	5.25907	-2.921
3300612	HAsO4 -2	3.508E-07	2.684E-04	-3.57130	********	-11.861
3300613	AsO4 -3	1.713E-15	5.273E-09	-8.27795	********	-27.172
3301400	HCO3 -	5.967E-02	3.138E-01	-0.50336	5.25907	9.709
3301401	H2CO3 AQ	7.848E-03	6.387E-02	-1.19468	8.13862	15.828
3307320	HSO4 -	2.308E-03	1.214E-02	-1.91582	5.25907	1.148
3307300	H2S AQ	3.465E-26	2.820E-25	-24.54971	8.13862	6.174
3307301	S -2	1.804E-34	1.380E-31	-30.86009	********	-16.109
3307620	HSeO4-1	9.567E-08	5.032E-07	-6.29830	5.25907	1.078
4707620	MnSeO4	4.236E-09	3.447E-08	-7.46254	8.13862	1.420

Type III - SPECIES WITH FIXED ACTIVITY

ID	NAME	CALC MOL	LOG MOL	NEW LOGK	DH
2	H2O	-1.774E-08	-7.751	0.035	0.000
330	H+1	-7.765E-02	-1.110	7.000	0.000
1028003	PYRITE	-3.943E-26	-25.404	18.766	-11.300

Type IV - FINITE SOLIDS (presumed present at equilibrium)

ID	NAME	CALC MOL	LOG MOL	NEW LOGK	DH
5015001	CALCITE	9.932E+00	-1.171	8.423	2.585

Type V - POSSIBLE SOLIDS

ID	NAME	CALC MOL	LOG MOL	NEW LOGK	DH
2003000	ALOH3(A)	3.901E-04	-3.409	-11.068	27.045
6015001	GYPSUM	3.237E+03	3.510	4.855	-0.261
6010000	BARITE	4.599E+12	12.663	10.136	-6.280
5028000	SIDERITE	9.022E-02	-1.045	10.414	5.328
2023101	TENORITE	2.121E-03	-2.673	-8.008	15.240
5016000	OTAVITE	6.747E-04	-3.171	13.725	0.580
6060003	ANGLESITE	5.304E+00	0.725	7.845	-2.150
7210000	BA(ASO4)2	5.291E+31	31.724	8.977	-2.640

Type VI - EXCLUDED SPECIES (not included in mole balance)

ID	NAME	CALC MOL	LOG MOL	NEW LOGK	DH
3301403	CO2 (g)	1.886E+00	0.276	18.173	-0.530
3300021	O2 (g)	2.904E-11	-10.537	-86.524	133.830
1	E-1	9.677E-13	-12.014	0.000	0.000
2802810	Fe+2/Fe+3	1.497E-10	-9.825	13.286	-10.000
7307320	HS-/SO4-2	0.000E-01	-95.935	35.190	-60.140
3301404	CH4 (g)	0.000E-01	-128.290	41.652	-61.000

PART 4 of OUTPUT FILE

PC MINTEQA2 v3.10 DATE OF CALCULATIONS: 11-MAR-97 TIME: 23:53:57

PERCENTAGE DISTRIBUTION OF COMPONENTS AMONG
TYPE I and TYPE II (dissolved and adsorbed) species

Fe+3	100.0	PERCENT BOUND IN SPECIES #2817321
Fe(SO4)2 -		
SO4-2	63.5	PERCENT BOUND IN SPECIES # 732
SO4-2		
	36.1	PERCENT BOUND IN SPECIES #1507320 CaSO4 AQ
Al+3	100.0	PERCENT BOUND IN SPECIES # 307321
Al(SO4)2 -		
H3AsO4	98.9	PERCENT BOUND IN SPECIES #3300611
H2AsO4 -		
	1.1	PERCENT BOUND IN SPECIES #3300612 HAsO4 -2
Ba+2	100.0	PERCENT BOUND IN SPECIES # 100
Ba+2		
Cd+2	99.5	PERCENT BOUND IN SPECIES #1607321
Cd(SO4)2-2		
Ca+2	100.0	PERCENT BOUND IN SPECIES #1507320
CaSO4 AQ		
Cr+2	100.0	PERCENT BOUND IN SPECIES # 210
Cr+2		
Cu+2	99.7	PERCENT BOUND IN SPECIES #2317320
CuSO4 AQ		
Fe+2	100.0	PERCENT BOUND IN SPECIES #2807320
FeSO4 AQ		
Pb+2	1.1	PERCENT BOUND IN SPECIES #6007320
PbSO4 AQ		
	98.9	PERCENT BOUND IN SPECIES #6007321 Pb(SO4)2-2
Mg+2	100.0	PERCENT BOUND IN SPECIES #4607320
MgSO4 AQ		
Mn+2	100.0	PERCENT BOUND IN SPECIES #4707320
MnSO4 AQ		
SeO4-2	99.9	PERCENT BOUND IN SPECIES # 762
SeO4-2		
Zn+2	99.4	PERCENT BOUND IN SPECIES #9507321
Zn(SO4)2-2		
E-1	100.0	PERCENT BOUND IN SPECIES #4700020
MnO4 -		

H2O	45.5	PERCENT BOUND IN SPECIES #3300020	
OH-			
1.4	PERCENT BOUND IN SPECIES # 303302	Al(OH)4 -	
9.5	PERCENT BOUND IN SPECIES # 303303	Al(OH)3 AQ	
36.7	PERCENT BOUND IN SPECIES #1003300	BaOH +	
5.8	PERCENT BOUND IN SPECIES #2313301	Cu(OH)2 AQ	
H+1	76.8	PERCENT BOUND IN SPECIES #3301400	
HCO3 -			
20.2	PERCENT BOUND IN SPECIES #3301401	H2CO3 AQ	
3.0	PERCENT BOUND IN SPECIES #3307320	HSO4 -	
HS-1	56.0	PERCENT BOUND IN SPECIES # 730	
HS-1			
43.9	PERCENT BOUND IN SPECIES #3307300	H2S AQ	
CO3-2	88.4	PERCENT BOUND IN SPECIES #3301400	
HCO3 -			
11.6	PERCENT BOUND IN SPECIES #3301401	H2CO3 AQ	

PART 5 of OUTPUT FILE

PC MINTEQA2 v3.10 DATE OF CALCULATIONS: 11-MAR-97 TIME: 23:53:57

PROVISIONAL MASS DISTRIBUTION

IDX	NAME	DISSOLVED		SORBED		PRECIPITATED
		MOL/KG	PERCENT	MOL/KG	PERCENT	MOL/KG
						PERCENT
281	Fe+3	2.456E-08	100.0	0.000E-01	0.0	0.000E-01
0.0						
732	SO4-2	3.383E+00	100.0	0.000E-01	0.0	0.000E-01
0.0						
30	Al+3	2.100E-03	100.0	0.000E-01	0.0	0.000E-01
0.0						
61	H3AsO4	3.093E-05	100.0	0.000E-01	0.0	0.000E-01
0.0						
100	Ba+2	2.677E-04	100.0	0.000E-01	0.0	0.000E-01
0.0						
160	Cd+2	1.221E-06	100.0	0.000E-01	0.0	0.000E-01
0.0						
150	Ca+2	1.220E+00	10.9	0.000E-01	0.0	9.932E+00
89.1						
210	Cr+2	4.142E-03	100.0	0.000E-01	0.0	0.000E-01
0.0						
231	Cu+2	9.002E-05	100.0	0.000E-01	0.0	0.000E-01
0.0						
280	Fe+2	8.843E-04	100.0	0.000E-01	0.0	0.000E-01
0.0						
600	Pb+2	4.860E-04	100.0	0.000E-01	0.0	0.000E-01
0.0						
460	Mg+2	5.868E-03	100.0	0.000E-01	0.0	0.000E-01
0.0						
470	Mn+2	6.515E-05	100.0	0.000E-01	0.0	0.000E-01
0.0						
762	SeO4-2	1.046E-04	100.0	0.000E-01	0.0	0.000E-01
0.0						
950	Zn+2	2.183E-04	100.0	0.000E-01	0.0	0.000E-01
0.0						
1	E-1	-7.886E-26	100.0	0.000E-01	0.0	0.000E-01
0.0						
2	H2O	1.774E-08	100.0	0.000E-01	0.0	0.000E-01
0.0						
330	H+1	7.765E-02	100.0	0.000E-01	0.0	0.000E-01
0.0						
730	HS-1	7.886E-26	100.0	0.000E-01	0.0	0.000E-01
0.0						
140	CO3-2	6.753E-02	0.7	0.000E-01	0.0	9.932E+00
99.3						

Charge Balance: SPECIATED

Sum of CATIONS = 8.835E-03 Sum of ANIONS 4.362E+00

PERCENT DIFFERENCE = 9.960E+01 (ANIONS - CATIONS)/(ANIONS + CATIONS)

PROVISIONAL IONIC STRENGTH (m) = 9.106E+00

PART 6 of OUTPUT FILE

PC MINTEQA2 v3.10 DATE OF CALCULATIONS: 11-MAR-97 TIME: 23:53:57

Saturation indices and stoichiometry of all supersaturated minerals

ID #	NAME	Sat. Index	Stoichiometry in [brackets]
6003000	ALOHSO4	0.175	[-1.000] 330 [1.000] 30 [1.000] 732
			[1.000] 2
6015000	ANHYDRITE	3.267	[1.000] 150 [1.000] 732
6010000	BARITE	12.663	[1.000] 100 [1.000] 732
5015001	CALCITE	0.000	[1.000] 150 [1.000] 140
2003002	DIASPORE	0.195	[-3.000] 330 [1.000] 30 [2.000] 2
2028102	GOETHITE	1.438	[-3.000] 330 [1.000] 281 [2.000] 2
6015001	GYPSUM	3.510	[1.000] 150 [1.000] 732 [2.000] 2
3028100	HEMATITE	7.872	[-6.000] 330 [2.000] 281 [3.000] 2
3028000	MAGNETITE	6.067	[-8.000] 330 [2.000] 281 [1.000] 280
			[4.000] 2
5010000	WITHERITE	3.973	[1.000] 100 [1.000] 140
3023100	CUPRICFERIT	3.119	[-8.000] 330 [1.000] 231 [2.000] 281
			[4.000] 2
6060003	ANGLESITE	0.725	[1.000] 600 [1.000] 732
73100	SULFUR	8.397	[1.000] 730 [-1.000] 330 [-2.000] 1
7210000	BA(ASO4)2	31.724	[3.000] 100 [2.000] 61 [-6.000] 330
3028102	LEPIDOCROCIT	0.936	[-3.000] 330 [1.000] 281 [2.000] 2
6110001	BaSeO4	3.454	[1.000] 762 [1.000] 100
2021100	CR(OH)2	3.396	[1.000] 210 [2.000] 2 [-2.000] 330

PC MINTEQA2 v3.10 DATE OF CALCULATIONS: 11-MAR-97 TIME: 23:53:57

ITERATIONS= 71: SOLID BARITE PRECIPITATES

PART 3 of OUTPUT FILE

PC MINTEQA2 v3.10 DATE OF CALCULATIONS: 11-MAR-97 TIME: 23:53:57

PARAMETERS OF THE COMPONENT MOST OUT OF BALANCE:

ITER	NAME	TOTAL MOL	DIFF FXN	LOG ACTVTY	RESIDUAL
71	Zn+2	2.183E-04	1.657E-01	-10.49156	1.657E-01
72	Zn+2	2.183E-04	-2.181E-04	-10.19076	2.181E-04
73	Zn+2	2.183E-04	-1.472E-04	-6.98239	1.472E-04
74	Zn+2	2.183E-04	4.126E-02	-7.98239	4.126E-02
75	Zn+2	2.183E-04	1.238E-02	-8.98239	1.238E-02
76	Zn+2	2.183E-04	3.445E-03	-9.26915	3.445E-03
77	Zn+2	2.183E-04	1.896E-05	-10.45551	1.894E-05
78	HS-1	0.000E-01	-4.305E-22	-25.38176	4.305E-22
79	HS-1	0.000E-01	-1.730E-22	-25.30258	1.730E-22
80	HS-1	0.000E-01	-6.953E-23	-25.22341	6.952E-23
81	HS-1	0.000E-01	-2.793E-23	-25.14425	2.793E-23
82	HS-1	0.000E-01	-1.122E-23	-25.06515	1.121E-23
83	HS-1	0.000E-01	-4.496E-24	-24.98619	4.495E-24
84	HS-1	0.000E-01	-1.793E-24	-24.90768	1.793E-24
85	HS-1	0.000E-01	-7.043E-25	-24.83048	7.042E-25
86	HS-1	0.000E-01	-2.645E-25	-24.75704	2.645E-25
87	HS-1	0.000E-01	-8.708E-26	-24.69352	8.707E-26
88	HS-1	0.000E-01	-1.976E-26	-24.65107	1.975E-26
89	HS-1	0.000E-01	-1.683E-27	-24.63585	1.675E-27
90	HS-1	0.000E-01	-1.469E-29	-24.63433	6.807E-30

PC MINTEQA2 v3.10 DATE OF CALCULATIONS: 11-MAR-97 TIME: 23:53:58

ITERATIONS= 92: SOLID GYPSUM PRECIPITATES

PART 3 of OUTPUT FILE

PC MINTEQA2 v3.10 DATE OF CALCULATIONS: 11-MAR-97 TIME: 23:53:58

PARAMETERS OF THE COMPONENT MOST OUT OF BALANCE:

ITER	NAME	TOTAL MOL	DIFF FXN	LOG ACTVTY	RESIDUAL
92	SeO4-2	1.046E-04	7.983E-02	-1.09727	7.982E-02
93	SeO4-2	1.046E-04	-3.127E-05	-3.98051	3.126E-05
94	SeO4-2	1.046E-04	1.346E-05	-3.82626	1.345E-05
95	SeO4-2	1.046E-04	-7.095E-06	-3.87883	7.085E-06
96	SeO4-2	1.046E-04	4.468E-06	-3.84832	4.457E-06
97	SeO4-2	1.046E-04	-2.562E-06	-3.86649	2.552E-06
98	SeO4-2	1.046E-04	1.548E-06	-3.85572	1.538E-06
99	SeO4-2	1.046E-04	-9.068E-07	-3.86210	8.963E-07
100	SeO4-2	1.046E-04	5.410E-07	-3.85832	5.305E-07
101	SeO4-2	1.046E-04	-3.193E-07	-3.86056	3.088E-07
102	SeO4-2	1.046E-04	1.896E-07	-3.85923	1.792E-07
103	SeO4-2	1.046E-04	-1.122E-07	-3.86002	1.017E-07
104	SeO4-2	1.046E-04	6.654E-08	-3.85955	5.608E-08
105	SeO4-2	1.046E-04	-3.941E-08	-3.85983	2.895E-08
107	SeO4-2	1.046E-04	2.336E-08	-3.85966	1.290E-08
108	SeO4-2	1.046E-04	-1.384E-08	-3.85976	3.380E-09

PC MINTEQA2 v3.10 DATE OF CALCULATIONS: 11-MAR-97 TIME: 23:53:59

ITERATIONS= 109: SOLID SIDERITE PRECIPITATES

PART 3 of OUTPUT FILE

PC MINTEQA2 v3.10 DATE OF CALCULATIONS: 11-MAR-97 TIME: 23:53:59

PARAMETERS OF THE COMPONENT MOST OUT OF BALANCE:

ITER	NAME	TOTAL MOL	DIFF FXN	LOG ACTVTY	RESIDUAL
109	Mn+2	6.515E-05	5.557E-05	-6.34912	5.556E-05
110	Mn+2	6.515E-05	-2.731E-05	-6.48192	2.730E-05
111	Mn+2	6.515E-05	6.903E-06	-6.33074	6.896E-06
112	Mn+2	6.515E-05	-1.013E-06	-6.34076	1.006E-06
113	Mn+2	6.515E-05	5.873E-07	-6.35414	5.808E-07
114	Mn+2	6.515E-05	-4.287E-07	-6.34667	4.222E-07
115	Mn+2	6.515E-05	2.277E-07	-6.35074	2.212E-07
116	Mn+2	6.515E-05	-1.438E-07	-6.34821	1.373E-07
117	Mn+2	6.515E-05	8.203E-08	-6.34967	7.551E-08
118	Mn+2	6.515E-05	-4.971E-08	-6.34879	4.320E-08
119	Mn+2	6.515E-05	2.906E-08	-6.34931	2.255E-08
120	Mn+2	6.515E-05	-1.736E-08	-6.34900	1.084E-08
121	Mn+2	6.515E-05	1.024E-08	-6.34918	3.721E-09
122	Pb+2	4.860E-04	-1.387E-07	-7.46836	9.010E-08
124	Pb+2	4.860E-04	8.219E-08	-7.46841	3.359E-08
125	Pb+2	4.860E-04	-4.870E-08	-7.46838	9.610E-11

PC MINTEQA2 v3.10 DATE OF CALCULATIONS: 11-MAR-97 TIME: 23:54: 0

ITERATIONS= 126: SOLID ALOH3(A) PRECIPITATES

PART 3 of OUTPUT FILE

PC MINTEQA2 v3.10 DATE OF CALCULATIONS: 11-MAR-97 TIME: 23:54: 0

PARAMETERS OF THE COMPONENT MOST OUT OF BALANCE:

ITER	NAME	TOTAL MOL	DIFF FXN	LOG ACTVTY	RESIDUAL
126	Mg+2	5.868E-03	5.126E-03	-4.39329	5.125E-03
127	Mg+2	5.868E-03	-2.489E-03	-4.53008	2.489E-03
128	Mg+2	5.868E-03	6.358E-04	-4.37503	6.352E-04
129	Mg+2	5.868E-03	-9.095E-05	-4.38576	9.036E-05
130	Mg+2	5.868E-03	5.310E-05	-4.39928	5.252E-05
131	Mg+2	5.868E-03	-3.884E-05	-4.39176	3.826E-05
132	Mg+2	5.868E-03	2.062E-05	-4.39585	2.003E-05
133	Mg+2	5.868E-03	-1.303E-05	-4.39331	1.244E-05
134	Mg+2	5.868E-03	7.430E-06	-4.39477	6.843E-06
135	Mg+2	5.868E-03	-4.504E-06	-4.39389	3.917E-06
136	Mg+2	5.868E-03	2.633E-06	-4.39441	2.046E-06
137	Mg+2	5.868E-03	-1.573E-06	-4.39410	9.859E-07
138	Mg+2	5.868E-03	9.275E-07	-4.39428	3.407E-07
139	Pb+2	4.860E-04	-1.396E-07	-7.46967	9.100E-08
141	Pb+2	4.860E-04	8.273E-08	-7.46973	3.413E-08
142	Pb+2	4.860E-04	-4.902E-08	-7.46970	4.200E-10

PC MINTEQA2 v3.10 DATE OF CALCULATIONS: 11-MAR-97 TIME: 23:54: 1

ITERATIONS= 143: SOLID ANGLESITE PRECIPITATES

PART 3 of OUTPUT FILE

PC MINTEQA2 v3.10 DATE OF CALCULATIONS: 11-MAR-97 TIME: 23:54: 1

PARAMETERS OF THE COMPONENT MOST OUT OF BALANCE:

ITER	NAME	TOTAL MOL	DIFF FXN	LOG ACTVTY	RESIDUAL
143	Mg+2	5.868E-03	5.131E-03	-4.39422	5.130E-03
144	Mg+2	5.868E-03	-2.488E-03	-4.52995	2.487E-03
145	Mg+2	5.868E-03	6.352E-04	-4.37509	6.346E-04
146	Mg+2	5.868E-03	-9.103E-05	-4.38579	9.044E-05
147	Mg+2	5.868E-03	5.312E-05	-4.39931	5.254E-05
148	Mg+2	5.868E-03	-3.886E-05	-4.39179	3.828E-05
149	Mg+2	5.868E-03	2.063E-05	-4.39588	2.004E-05
150	Mg+2	5.868E-03	-1.304E-05	-4.39334	1.245E-05
151	Mg+2	5.868E-03	7.437E-06	-4.39480	6.850E-06
152	Mg+2	5.868E-03	-4.508E-06	-4.39392	3.922E-06
153	Mg+2	5.868E-03	2.636E-06	-4.39444	2.049E-06
154	Mg+2	5.868E-03	-1.575E-06	-4.39413	9.879E-07
155	Mg+2	5.868E-03	9.288E-07	-4.39431	3.420E-07
156	SeO4-2	1.046E-04	-3.878E-08	-3.85907	2.832E-08
158	SeO4-2	1.046E-04	2.299E-08	-3.85891	1.253E-08
159	SeO4-2	1.046E-04	-1.362E-08	-3.85900	3.161E-09

PC MINTEQA2 v3.10 DATE OF CALCULATIONS: 11-MAR-97 TIME: 23:54: 2

ITERATIONS= 160: SOLID OTAVITE PRECIPITATES

PART 3 of OUTPUT FILE

PC MINTEQA2 v3.10 DATE OF CALCULATIONS: 11-MAR-97 TIME: 23:54: 2

PARAMETERS OF THE COMPONENT MOST OUT OF BALANCE:

ITER	NAME	TOTAL MOL	DIFF FXN	LOG ACTVTY	RESIDUAL
160	SeO4-2	1.046E-04	3.379E-05	-3.85895	3.378E-05
161	SeO4-2	1.046E-04	-3.114E-05	-3.98052	3.113E-05
162	SeO4-2	1.046E-04	1.300E-05	-3.82702	1.299E-05
163	SeO4-2	1.046E-04	-7.012E-06	-3.87790	7.002E-06
164	SeO4-2	1.046E-04	4.391E-06	-3.84776	4.380E-06
165	SeO4-2	1.046E-04	-2.518E-06	-3.86562	2.508E-06
166	SeO4-2	1.046E-04	1.522E-06	-3.85503	1.511E-06
167	SeO4-2	1.046E-04	-8.914E-07	-3.86130	8.810E-07
168	SeO4-2	1.046E-04	5.319E-07	-3.85759	5.214E-07
169	SeO4-2	1.046E-04	-3.139E-07	-3.85979	3.035E-07
170	SeO4-2	1.046E-04	1.865E-07	-3.85848	1.760E-07
171	SeO4-2	1.046E-04	-1.104E-07	-3.85926	9.991E-08
172	SeO4-2	1.046E-04	6.546E-08	-3.85880	5.500E-08
173	SeO4-2	1.046E-04	-3.878E-08	-3.85907	2.832E-08
175	SeO4-2	1.046E-04	2.299E-08	-3.85891	1.253E-08
176	SeO4-2	1.046E-04	-1.362E-08	-3.85900	3.161E-09

PC MINTEQA2 v3.10 DATE OF CALCULATIONS: 11-MAR-97 TIME: 23:54: 3

ITERATIONS= 177: SOLID BA(ASO4)2 PRECIPITATES

PC MINTEQA2 v3.10 DATE OF CALCULATIONS: 11-MAR-97 TIME: 23:54: 3

PARAMETERS OF THE COMPONENT MOST OUT OF BALANCE:

ITER	NAME	TOTAL MOL	DIFF FXN	LOG ACTVTY	RESIDUAL
177	Cu+2	9.002E-05	5.507E-05	-7.38720	5.506E-05
178	Cu+2	9.002E-05	-3.305E-05	-7.44770	3.304E-05
179	Cu+2	9.002E-05	1.156E-05	-7.37143	1.155E-05
180	Cu+2	9.002E-05	-2.624E-06	-7.37839	2.615E-06
181	Cu+2	9.002E-05	1.706E-06	-7.39190	1.697E-06
182	Cu+2	9.002E-05	-1.083E-06	-7.38484	1.074E-06
183	Cu+2	9.002E-05	6.220E-07	-7.38872	6.130E-07
184	Cu+2	9.002E-05	-3.750E-07	-7.38633	3.660E-07
185	Cu+2	9.002E-05	2.199E-07	-7.38772	2.109E-07
186	Cu+2	9.002E-05	-1.311E-07	-7.38689	1.221E-07
187	Cu+2	9.002E-05	7.743E-08	-7.38738	6.843E-08
188	Cu+2	9.002E-05	-4.599E-08	-7.38709	3.699E-08
189	Cu+2	9.002E-05	2.722E-08	-7.38726	1.822E-08
190	Cu+2	9.002E-05	-1.614E-08	-7.38716	7.141E-09
192	Cu+2	9.002E-05	9.565E-09	-7.38722	5.631E-10
193	Cr+2	4.142E-03	-5.395E-07	-2.26125	1.253E-07

ID	NAME	ANAL MOL	CALC MOL	LOG ACTVTY	GAMMA	DIFF FXN
281	Fe+3	2.456E-08	7.187E-17	-15.86998	1.877012	4.742E-13
732	SO4-2	3.383E+00	1.202E+00	0.20148	1.322942	1.127E-04
470	Mn+2	6.515E-05	3.376E-07	-6.35009	1.322942	1.274E-09
762	SeO4-2	1.046E-04	1.046E-04	-3.85895	1.322942	8.074E-09
950	Zn+2	2.183E-04	3.771E-08	-7.30205	1.322942	1.598E-08
460	Mg+2	5.868E-03	3.049E-05	-4.39426	1.322942	1.148E-07
730	HS-1	8.386E-20	2.996E-25	-24.49301	1.072470	- 7.804E-31
210	Cr+2	4.142E-03	4.143E-03	-2.26119	1.322942	3.198E-07
231	Cu+2	9.002E-05	3.099E-08	-7.38720	1.322942	3.359E-09
160	Cd+2	1.221E-06	3.892E-11	-10.28834	1.322942	0.000E-01
61	H3AsO4	3.093E-05	5.371E-11	-9.98274	1.937474	2.168E-18
1	E-1	-8.386E-20	2.520E-12	-11.59857	1.072470	0.000E-01
30	Al+3	2.100E-03	7.932E-11	-9.82717	1.877012	8.132E-19
2	H2O	-1.804E-16	-4.352E+00	-0.03496	1.000000	0.000E-01
150	Ca+2	1.153E+00	7.803E-06	-4.98619	1.322942	0.000E-01
280	Fe+2	8.843E-04	7.960E-08	-6.97756	1.322942	0.000E-01

100	Ba+2	2.677E-04	3.477E-11	-10.33722	1.322942	2.168E-19
600	Pb+2	4.860E-04	6.797E-09	-8.04617	1.322942	0.000E-01
140	CO3-2	0.000E-01	2.764E-04	-3.43691	1.322942	0.000E-01
330	H+1	0.000E-01	9.324E-08	-7.00000	1.072470	- 3.388E-21

Type I - COMPONENTS AS SPECIES IN SOLUTION

ID	NAME	CALC MOL	ACTIVITY	LOG ACTVTY	GAMMA	NEW LOGK
330	H+1	9.324E-08	1.000E-07	-7.00000	1.07247	- 0.030
732	SO4-2	1.202E+00	1.590E+00	0.20148	1.32294	- 0.122
30	Al+3	7.932E-11	1.489E-10	-9.82717	1.87701	- 0.273
61	H3AsO4	5.371E-11	1.041E-10	-9.98274	1.93747	- 0.287
100	Ba+2	3.477E-11	4.600E-11	-10.33722	1.32294	- 0.122
160	Cd+2	3.892E-11	5.148E-11	-10.28834	1.32294	- 0.122
150	Ca+2	7.803E-06	1.032E-05	-4.98619	1.32294	- 0.122
210	Cr+2	4.143E-03	5.480E-03	-2.26119	1.32294	- 0.122
231	Cu+2	3.099E-08	4.100E-08	-7.38720	1.32294	- 0.122
280	Fe+2	7.960E-08	1.053E-07	-6.97756	1.32294	- 0.122
600	Pb+2	6.797E-09	8.991E-09	-8.04617	1.32294	- 0.122
460	Mg+2	3.049E-05	4.034E-05	-4.39426	1.32294	- 0.122
470	Mn+2	3.376E-07	4.466E-07	-6.35009	1.32294	- 0.122
762	SeO4-2	1.046E-04	1.384E-04	-3.85895	1.32294	- 0.122
950	Zn+2	3.771E-08	4.988E-08	-7.30205	1.32294	- 0.122
140	CO3-2	2.764E-04	3.657E-04	-3.43691	1.32294	- 0.122
281	Fe+3	7.187E-17	1.349E-16	-15.86998	1.87701	- 0.273
730	HS-1	2.996E-25	3.214E-25	-24.49301	1.07247	- 0.030

Type II - OTHER SPECIES IN SOLUTION OR ADSORBED

ID	NAME	CALC MOL	ACTIVITY	LOG ACTVTY	GAMMA	NEW LOGK
1607620	CdSeO4	6.412E-13	1.242E-12	-11.90578	1.93747	1.954
9507620	ZnSeO4	5.671E-10	1.099E-09	-8.95909	1.93747	1.915

9507621	Zn(SeO4)2-2	6.139E-16	8.122E-16	-15.09034	1.32294	-
0.192						
3300020	OH-	3.955E-08	4.242E-08	-7.37242	1.07247	-
14.368						
4603300	MgOH +	2.320E-10	2.488E-10	-9.60416	1.07247	-
12.205						
4601400	MgCO3 AQ	6.232E-06	1.207E-05	-4.91814	1.93747	
2.626						
4601401	MgHCO3 +	4.067E-04	4.362E-04	-3.36032	1.07247	
11.440						
4607320	MgSO4 AQ	5.425E-03	1.051E-02	-1.97836	1.93747	
1.927						
1503300	CaOH +	9.566E-12	1.026E-11	-10.98888	1.07247	-
12.998						
1501400	CaHCO3 +	7.220E-05	7.743E-05	-4.11110	1.07247	
11.282						
1501401	CaCO3 AQ	2.288E-06	4.432E-06	-5.35336	1.93747	
2.783						
1507320	CaSO4 AQ	1.584E-03	3.068E-03	-2.51310	1.93747	
1.984						
303300	AlOH +2	5.292E-09	7.002E-09	-8.15481	1.32294	-
5.414						
303301	Al(OH)2 +	9.387E-07	1.007E-06	-5.99710	1.07247	-
10.130						
303302	Al(OH)4 -	7.618E-07	8.170E-07	-6.08777	1.07247	-
24.151						
307320	AlSO4 +	2.038E-07	2.186E-07	-6.66038	1.07247	
2.935						
307321	Al(SO4)2 -	2.473E-05	2.652E-05	-4.57645	1.07247	
4.817						
303303	Al(OH)3 AQ	6.035E-06	1.169E-05	-4.93206	1.93747	-
16.287						
2803300	FeOH +	1.322E-10	1.418E-10	-9.84827	1.07247	-
9.866						
2803301	FeOH3 -1	1.307E-18	1.402E-18	-17.85319	1.07247	-
31.801						
2807320	FeSO4 AQ	1.272E-05	2.465E-05	-4.60825	1.93747	
1.881						
2803302	FeOH2 AQ	2.337E-15	4.528E-15	-14.34409	1.93747	-
21.584						
2807300	Fe(HS)2 AQ	5.002E-48	9.692E-48	-47.01358	1.93747	
8.663						
2807301	Fe(HS)3 -	3.163E-70	3.392E-70	-69.46958	1.07247	
10.957						
2813300	FeOH +2	3.304E-12	4.371E-12	-11.35946	1.32294	-
2.576						
2817320	FeSO4 +	1.323E-12	1.419E-12	-11.84795	1.07247	
3.790						
2813301	FeOH2 +	2.289E-08	2.455E-08	-7.60990	1.07247	-
5.700						
2813302	FeOH3 AQ	1.374E-09	2.662E-09	-8.57487	1.93747	-
13.887						
2813303	FeOH4 -	2.290E-10	2.456E-10	-9.60983	1.07247	-
21.630						
2817321	Fe(SO4)2 -	6.391E-11	6.855E-11	-10.16402	1.07247	
5.273						
2813304	Fe2(OH)2+4	2.574E-22	7.884E-22	-21.10328	3.06312	-
3.780						
2813305	Fe3(OH)4+5	6.712E-28	3.859E-27	-26.41353	5.74951	-
7.423						
1003300	BaOH +	7.169E-18	7.689E-18	-17.11416	1.07247	-
13.772						
4703300	MnOH +	4.249E-11	4.557E-11	-10.34132	1.07247	-
10.987						

4703301	Mn(OH)3 -1	5.184E-21	5.559E-21	-20.25498	1.07247	-
34.830						
4700020	MnO4 -	1.432E-25	1.536E-25	-24.81373	1.07247	-
132.347						
4700021	MnO4 -2	3.363E-27	4.450E-27	-26.35168	1.32294	-
122.378						
4707320	MnSO4 AQ	5.874E-05	1.138E-04	-3.94381	1.93747	
1.918						
4701400	MnHCO3 +	6.062E-06	6.501E-06	-5.18700	1.07247	
11.570						
2311400	CuCO3 AQ	4.156E-05	8.052E-05	-4.09411	1.93747	
6.443						
2311401	Cu(CO3)2-2	2.802E-05	3.707E-05	-4.43102	1.32294	
9.708						
2313300	CuOH +	3.527E-09	3.783E-09	-8.42217	1.07247	-
8.030						
2313301	Cu(OH)2 AQ	3.764E-08	7.292E-08	-7.13713	1.93747	-
13.967						
2313302	Cu(OH)3 -	3.789E-14	4.064E-14	-13.39110	1.07247	-
26.929						
2313303	Cu(OH)4 -2	5.642E-20	7.463E-20	-19.12706	1.32294	-
39.722						
2313304	Cu2(OH)2+2	1.696E-12	2.244E-12	-11.64897	1.32294	-
10.926						
2317320	CuSO4 AQ	6.397E-06	1.239E-05	-4.90676	1.93747	
1.992						
2317300	Cu(HS)3 -	1.006E-55	1.078E-55	-54.96722	1.07247	
25.869						
2311402	CuHCO3 +	1.398E-05	1.499E-05	-4.82411	1.07247	
12.970						
9503300	ZnOH +	2.147E-10	2.302E-10	-9.63784	1.07247	-
9.331						
9503301	Zn(OH)2 AQ	2.766E-11	5.358E-11	-10.27098	1.93747	-
17.186						
9503302	Zn(OH)3 -	1.458E-15	1.563E-15	-14.80594	1.07247	-
28.429						
9503303	Zn(OH)4 -2	1.728E-21	2.286E-21	-20.64090	1.32294	-
41.321						
9507300	Zn(HS)2 AQ	2.316E-42	4.487E-42	-41.34806	1.93747	
14.653						
9507301	Zn(HS)3 -	1.943E-65	2.084E-65	-64.68107	1.07247	
16.070						
9507320	ZnSO4 AQ	8.863E-06	1.717E-05	-4.76516	1.93747	
2.048						
9507321	Zn(SO4)2-2	1.817E-04	2.404E-04	-3.61909	1.32294	
3.158						
9501400	ZnHCO3 +	4.272E-06	4.582E-06	-5.33896	1.07247	
12.370						
9501401	ZnCO3 AQ	1.878E-06	3.640E-06	-5.43896	1.93747	
5.013						
9501402	Zn(CO3)2-2	2.151E-05	2.845E-05	-4.54586	1.32294	
9.508						
1601400	Cd(CO3)3-4	1.364E-15	4.178E-15	-14.37906	3.06312	
5.734						
1603300	CdOH +	1.710E-14	1.834E-14	-13.73652	1.07247	-
10.444						
1603301	Cd(OH)2 AQ	1.010E-17	1.958E-17	-16.70827	1.93747	-
20.637						
1603302	Cd(OH)3 -	1.890E-23	2.027E-23	-22.69323	1.07247	-
33.330						
1603303	Cd(OH)4 -2	1.260E-30	1.666E-30	-29.77820	1.32294	-
47.472						
1603304	Cd2OH +3	2.803E-24	5.262E-24	-23.27888	1.87701	-
9.941						

1607320	CdSO4 AQ	1.144E-08	2.217E-08	-7.65433	1.93747	
2.145						
1607300	CdHS +	2.282E-25	2.447E-25	-24.61134	1.07247	
10.140						
1607301	Cd(HS)2 AQ	9.298E-44	1.802E-43	-42.74435	1.93747	
16.243						
1607302	Cd(HS)3 -	8.171E-66	8.763E-66	-65.05736	1.07247	
18.680						
1607303	Cd(HS)4 -2	3.297E-88	4.361E-88	-87.36036	1.32294	
20.778						
1601400	CdHCO3 +	4.409E-09	4.729E-09	-8.32525	1.07247	
12.370						
1601401	CdCO3 AQ	2.435E-09	4.718E-09	-8.32625	1.93747	
5.112						
1607321	Cd(SO4)2-2	3.112E-07	4.117E-07	-6.38538	1.32294	
3.378						
6001400	Pb(CO3)2-2	3.967E-05	5.248E-05	-4.27999	1.32294	
10.518						
6003300	PbOH +	1.508E-09	1.618E-09	-8.79113	1.07247	-
7.740						
6003301	Pb(OH)2 AQ	2.997E-12	5.806E-12	-11.23610	1.93747	-
17.407						
6003302	Pb(OH)3 -	5.735E-16	6.151E-16	-15.21106	1.07247	-
28.090						
6003303	Pb2OH +3	1.735E-16	3.256E-16	-15.48730	1.87701	-
6.633						
6007320	PbSO4 AQ	4.150E-06	8.041E-06	-5.09469	1.93747	
2.463						
6007300	Pb(HS)2 AQ	8.924E-43	1.729E-42	-41.76218	1.93747	
14.983						
6007301	Pb(HS)3 -	1.034E-65	1.109E-65	-64.95519	1.07247	
16.540						
6003304	Pb3(OH)4+2	1.112E-21	1.471E-21	-20.83244	1.32294	-
24.676						
6001401	PbCO3 AQ	2.949E-05	5.714E-05	-4.24308	1.93747	
6.953						
6003305	Pb(OH)4 -2	9.850E-21	1.303E-20	-19.88503	1.32294	-
39.821						
6007321	Pb(SO4)2-2	5.073E-05	6.711E-05	-4.17321	1.32294	
3.348						
6001402	PbHCO3 +	4.859E-06	5.211E-06	-5.28308	1.07247	
13.170						
3300611	H2AsO4 -	6.122E-06	6.565E-06	-5.18275	1.07247	-
2.230						
3300612	HAsO4 -2	8.282E-06	1.096E-05	-4.96034	1.32294	-
9.099						
3300613	AsO4 -3	1.147E-10	2.153E-10	-9.66699	1.87701	-
20.958						
3301400	HCO3 -	9.166E-01	9.830E-01	-0.00743	1.07247	
10.399						
3301401	H2CO3 AQ	1.033E-01	2.001E-01	-0.69875	1.93747	
16.451						
3307320	HSO4 -	1.095E-05	1.175E-05	-4.93001	1.07247	
1.838						
3307300	H2S AQ	2.015E-25	3.905E-25	-24.40841	1.93747	
6.797						
3307301	S -2	1.444E-31	1.911E-31	-30.71879	1.32294	-
13.347						
3307620	HSeO4-1	8.121E-10	8.710E-10	-9.05998	1.07247	
1.769						
4707620	MnSeO4	6.832E-09	1.324E-08	-7.87825	1.93747	
2.044						

Type III - SPECIES WITH FIXED ACTIVITY

ID	NAME	CALC MOL	LOG MOL	NEW LOGK	DH
2	H2O	-4.352E+00	0.639	0.035	0.000
330	H+1	-1.117E+00	0.048	7.000	0.000
1028003	PYRITE	4.193E-20	-19.377	18.766	-11.300

Type IV - FINITE SOLIDS (present at equilibrium)

ID	NAME	CALC MOL	LOG MOL	NEW LOGK	DH
5015001	CALCITE	8.978E+00	0.009	8.423	2.585
6010000	BARITE	2.429E-04	-3.615	10.136	-6.280
6015001	GYPSUM	2.173E+00	0.337	4.855	-0.261
5028000	SIDERITE	8.715E-04	-3.060	10.414	5.328
2003000	ALOH3(A)	2.067E-03	-2.685	-11.068	27.045
6060003	ANGLESITE	3.571E-04	-3.447	7.845	-2.150
5016000	OTAVITE	8.909E-07	-6.050	13.725	0.580
7210000	BA(ASO4)2	8.262E-06	-5.083	8.977	-2.640

Type V - UNDERSATURATED SOLIDS (not present at equilibrium)

ID	NAME	CALC MOL	LOG MOL	NEW LOGK	DH
2023101	TENORITE	3.717E-02	-1.430	-8.008	15.240

Type VI - EXCLUDED SPECIES (not included in mole balance)

ID	NAME	CALC MOL	LOG MOL	NEW LOGK	DH
3301403	CO2 (g)	5.909E+00	0.772	18.173	-0.530
3300021	O2 (g)	6.312E-13	-12.200	-86.524	133.830
1	E-1	2.520E-12	-11.599	0.000	0.000
2802810	Fe+2/Fe+3	6.243E-08	-7.205	13.286	-10.000
7307320	HS-/SO4-2	0.000E-01	-95.764	35.190	-60.140
3301404	CH4 (g)	0.000E-01	-124.469	41.652	-61.000

PERCENTAGE DISTRIBUTION OF COMPONENTS AMONG
TYPE I and TYPE II (dissolved and adsorbed) species

Fe+3		93.2	PERCENT BOUND IN SPECIES #2813301
FeOH2 +			
	5.6	PERCENT BOUND IN SPECIES #2813302	FeOH3 AQ
SO4-2		99.4	PERCENT BOUND IN SPECIES # 732
SO4-2			
Mn+2		90.2	PERCENT BOUND IN SPECIES #4707320
MnSO4 AQ			
	9.3	PERCENT BOUND IN SPECIES #4701400	MnHCO3 +
SeO4-2		100.0	PERCENT BOUND IN SPECIES # 762
SeO4-2			
Zn+2		4.1	PERCENT BOUND IN SPECIES #9507320
ZnSO4 AQ			
	83.2	PERCENT BOUND IN SPECIES #9507321	Zn(SO4)2-2
	2.0	PERCENT BOUND IN SPECIES #9501400	ZnHCO3 +
	9.9	PERCENT BOUND IN SPECIES #9501402	Zn(CO3)2-2
Mg+2		6.9	PERCENT BOUND IN SPECIES #4601401
MgHCO3 +			
	92.4	PERCENT BOUND IN SPECIES #4607320	MgSO4 AQ
HS-1		41.1	PERCENT BOUND IN SPECIES # 730
HS-1			
	31.3	PERCENT BOUND IN SPECIES #1607300	CdHS +
	27.6	PERCENT BOUND IN SPECIES #3307300	H2S AQ
Cr+2		100.0	PERCENT BOUND IN SPECIES # 210
Cr+2			
Cu+2		46.2	PERCENT BOUND IN SPECIES #2311400
CuCO3 AQ			
	31.1	PERCENT BOUND IN SPECIES #2311401	Cu(CO3)2-2
	7.1	PERCENT BOUND IN SPECIES #2317320	CuSO4 AQ
	15.5	PERCENT BOUND IN SPECIES #2311402	CuHCO3 +
Cd+2		3.5	PERCENT BOUND IN SPECIES #1607320
CdSO4 AQ			
	1.3	PERCENT BOUND IN SPECIES #1601400	CdHCO3 +
	94.4	PERCENT BOUND IN SPECIES #1607321	Cd(SO4)2-2
H3AsO4		42.5	PERCENT BOUND IN SPECIES #3300611
H2AsO4 -			
	57.5	PERCENT BOUND IN SPECIES #3300612	HAsO4 -2
E-1		98.2	PERCENT BOUND IN SPECIES #4700020
MnO4 -			
	1.8	PERCENT BOUND IN SPECIES #4700021	MnO4 -2

Al+3	2.9	PERCENT BOUND IN SPECIES # 303301	
Al(OH)2 +			
2.3	PERCENT BOUND IN SPECIES # 303302	Al(OH)4 -	
75.7	PERCENT BOUND IN SPECIES # 307321	Al(SO4)2 -	
18.5	PERCENT BOUND IN SPECIES # 303303	Al(OH)3 AQ	
H2O	8.1	PERCENT BOUND IN SPECIES # 303301	
Al(OH)2 +			
13.1	PERCENT BOUND IN SPECIES # 303302	Al(OH)4 -	
78.0	PERCENT BOUND IN SPECIES # 303303	Al(OH)3 AQ	
Ca+2	4.3	PERCENT BOUND IN SPECIES #1501400	
CaHCO3 +			
95.1	PERCENT BOUND IN SPECIES #1507320	CaSO4 AQ	
Fe+2	99.4	PERCENT BOUND IN SPECIES #2807320	
FeSO4 AQ			
Ba+2	100.0	PERCENT BOUND IN SPECIES # 100	
Ba+2			
Pb+2	30.8	PERCENT BOUND IN SPECIES #6001400	
Pb(CO3)2-2			
3.2	PERCENT BOUND IN SPECIES #6007320	PbSO4 AQ	
22.9	PERCENT BOUND IN SPECIES #6001401	PbCO3 AQ	
39.4	PERCENT BOUND IN SPECIES #6007321	Pb(SO4)2-2	
3.8	PERCENT BOUND IN SPECIES #6001402	PbHCO3 +	
CO3-2	89.8	PERCENT BOUND IN SPECIES #3301400	
HCO3 -			
10.1	PERCENT BOUND IN SPECIES #3301401	H2CO3 AQ	
H+1	81.6	PERCENT BOUND IN SPECIES #3301400	
HCO3 -			
18.4	PERCENT BOUND IN SPECIES #3301401	H2CO3 AQ	

PART 5 of OUTPUT FILE

PC MINTEQA2 v3.10 DATE OF CALCULATIONS: 11-MAR-97 TIME: 23:54: 4

EQUILIBRATED MASS DISTRIBUTION

IDX	NAME	DISSOLVED		SORBED		PRECIPITATED
		MOL/KG	PERCENT	MOL/KG	PERCENT	MOL/KG
PERCENT						
281	Fe+3	2.456E-08	100.0	0.000E-01	0.0	0.000E-01
0.0						
732	SO4-2	1.210E+00	35.8	0.000E-01	0.0	2.174E+00
64.2						
470	Mn+2	6.515E-05	100.0	0.000E-01	0.0	0.000E-01
0.0						
762	SeO4-2	1.046E-04	100.0	0.000E-01	0.0	0.000E-01
0.0						
950	Zn+2	2.183E-04	100.0	0.000E-01	0.0	0.000E-01
0.0						
460	Mg+2	5.868E-03	100.0	0.000E-01	0.0	0.000E-01
0.0						
730	HS-1	7.294E-25	100.0	0.000E-01	0.0	0.000E-01
0.0						
210	Cr+2	4.143E-03	100.0	0.000E-01	0.0	0.000E-01
0.0						
231	Cu+2	9.003E-05	100.0	0.000E-01	0.0	0.000E-01
0.0						
160	Cd+2	3.296E-07	27.0	0.000E-01	0.0	8.909E-07
73.0						
61	H3AsO4	1.440E-05	46.6	0.000E-01	0.0	1.652E-05
53.4						
1	E-1	-7.294E-25	100.0	0.000E-01	0.0	0.000E-01
0.0						
30	Al+3	3.267E-05	1.6	0.000E-01	0.0	2.067E-03
98.4						
2	H2O	2.321E-05	100.0	0.000E-01	0.0	0.000E-01
0.0						
150	Ca+2	1.666E-03	0.0	0.000E-01	0.0	1.115E+01
100.0						
280	Fe+2	1.280E-05	1.4	0.000E-01	0.0	8.715E-04
98.6						
100	Ba+2	3.477E-11	0.0	0.000E-01	0.0	2.677E-04
100.0						
600	Pb+2	1.289E-04	26.5	0.000E-01	0.0	3.571E-04
73.5						
140	CO3-2	1.021E+00	10.2	0.000E-01	0.0	8.979E+00
89.8						
330	H+1	1.124E+00	100.0	0.000E-01	0.0	0.000E-01
0.0						

Charge Balance: SPECIATED

Sum of CATIONS = 8.872E-03 Sum of ANIONS 3.322E+00

PERCENT DIFFERENCE = 9.947E+01 (ANIONS - CATIONS)/(ANIONS + CATIONS)

EQUILIBRIUM IONIC STRENGTH (m) = 2.872E+00

EQUILIBRIUM pH = 7.000

EQUILIBRIUM pe = 11.599 or Eh = 663.11 mv

DATE ID NUMBER: 970311
TIME ID NUMBER: 23540413

PC MINTEQA2 v3.10 DATE OF CALCULATIONS: 11-MAR-97 TIME: 23:54: 4

Saturation indices and stoichiometry of all minerals

ID #	NAME	Sat. Index	Stoichiometry in [brackets]
2003000	ALOH3(A)	0.000	[1.000] 30 [3.000] 2 [-3.000] 330
6003000	ALOHSO4	0.569	[-1.000] 330 [1.000] 30 [1.000] 732
			[1.000] 2
6003001	AL4(OH)10SO4	7.843	[-10.000] 330 [4.000] 30 [1.000] 732
			[10.000] 2
6015000	ANHYDRITE	-0.244	[1.000] 150 [1.000] 732
5015000	ARAGONITE	-0.173	[1.000] 150 [1.000] 140
5046000	ARTINITE	-8.731	[-2.000] 330 [2.000] 460 [1.000] 140
			[5.000] 2
6010000	BARITE	0.000	[1.000] 100 [1.000] 732
2003001	BOEHMITE	1.809	[-3.000] 330 [1.000] 30 [2.000] 2
2046000	BRUCITE	-7.913	[1.000] 460 [2.000] 2 [-2.000] 330
5015001	CALCITE	0.000	[1.000] 150 [1.000] 140
2003002	DIASPORE	3.603	[-3.000] 330 [1.000] 30 [2.000] 2
5015002	DOLOMITE	0.535	[1.000] 150 [1.000] 460 [2.000] 140
6046000	EPSOMITE	-2.226	[1.000] 460 [1.000] 732 [7.000] 2
2028100	FERRIHYDRITE	0.134	[-3.000] 330 [1.000] 281 [3.000] 2
2028101	FE3(OH)8	-3.219	[-8.000] 330 [2.000] 281 [1.000] 280
			[8.000] 2
1028000	FES PPT	-20.556	[-1.000] 330 [1.000] 280 [1.000] 730
6028100	FE2(SO4)3	-36.219	[2.000] 281 [3.000] 732
2003003	GIBBSITE (C)	1.718	[-3.000] 330 [1.000] 30 [3.000] 2
3003000	Al2O3	-0.739	[2.000] 30 [3.000] 2 [-6.000] 330
2028102	GOETHITE	4.192	[-3.000] 330 [1.000] 281 [2.000] 2
1028001	GREIGITE	-63.655	[-4.000] 330 [2.000] 281 [1.000] 280
			[4.000] 730
6015001	GYPSUM	0.000	[1.000] 150 [1.000] 732 [2.000] 2
3028100	HEMATITE	13.379	[-6.000] 330 [2.000] 281 [3.000] 2
5015003	HUNTITE	-2.604	[3.000] 460 [1.000] 150 [4.000] 140
5046001	HYDRMAGNESIT	-14.491	[5.000] 460 [4.000] 140 [-2.000] 330
			[6.000] 2
6028101	JAROSITE H	-1.755	[-5.000] 330 [3.000] 281 [2.000] 732

```
                                        [  7.000]   2
  1028002 MACKINAWITE      -19.823      [ -1.000] 330  [  1.000] 280  [
1.000] 730
  3028101 MAGHEMITE          3.769      [ -6.000] 330  [  2.000] 281  [
3.000]   2
  5046002 MAGNESITE          0.041      [  1.000] 460  [  1.000] 140
  3028000 MAGNETITE         12.122      [ -8.000] 330  [  2.000] 281  [
1.000] 280
                                        [  4.000]   2
  6028000 MELANTERITE       -4.478      [  1.000] 280  [  1.000] 732  [
7.000]   2
  5046003 NESQUEHONITE      -2.462      [  1.000] 460  [  1.000] 140  [
3.000]   2
  1028003 PYRITE             0.000      [ -2.000] 330  [ -2.000]   1  [
1.000] 280
                                        [  2.000] 730
  5028000 SIDERITE           0.000      [  1.000] 280  [  1.000] 140
```

ID #	NAME	Sat. Index	Stoichiometry in [brackets]
5010000	WITHERITE	-5.180	[1.000] 100 [1.000] 140
3047000	HAUSMANNITE	-3.571	[-8.000] 330 [-2.000] 1 [3.000] 470
			[4.000] 2
2047003	PYROCROITE	-8.083	[-2.000] 330 [1.000] 470 [2.000] 2
5047000	RHODOCHROSIT	0.570	[1.000] 470 [1.000] 140
1047000	MNS GREEN	-27.790	[-1.000] 330 [1.000] 470 [1.000] 730
6047000	MNSO4	-9.211	[1.000] 470 [1.000] 732
1023101	COVELLITE	-1.231	[-1.000] 330 [1.000] 231 [1.000] 730
5023100	CUCO3	-1.194	[1.000] 231 [1.000] 140
2023100	CU(OH)2	-2.485	[-2.000] 330 [1.000] 231 [2.000] 2
6023100	ANTLERITE	-2.390	[-4.000] 330 [3.000] 231 [4.000] 2
			[1.000] 732
6023101	BROCHANTITE	-2.897	[-6.000] 330 [4.000] 231 [6.000] 2
			[1.000] 732
6023102	LANGITE	-5.390	[-6.000] 330 [4.000] 231 [7.000] 2
			[1.000] 732
2023101	TENORITE	-1.430	[-2.000] 330 [1.000] 231 [1.000] 2
6023103	CUOCUSO4	-13.043	[-2.000] 330 [2.000] 231 [1.000] 2
			[1.000] 732
6023104	CUSO4	-10.657	[1.000] 231 [1.000] 732
6023105	CHALCANTHITE	-4.684	[1.000] 231 [1.000] 732 [5.000] 2
3023100	CUPRICFERIT	9.869	[-8.000] 330 [1.000] 231 [2.000] 281
			[4.000] 2
1023102	CHALCOPYRITE	-13.178	[-2.000] 330 [1.000] 231 [1.000] 280
			[2.000] 730
95000	ZN METAL	-57.192	[1.000] 950 [2.000] 1
5095000	SMITHSONITE	-0.850	[1.000] 950 [1.000] 140
5095001	ZNCO3, 1H2O	-0.514	[1.000] 950 [1.000] 140 [1.000] 2
2095000	ZN(OH)2 (A)	-5.822	[-2.000] 330 [1.000] 950 [2.000] 2
2095001	ZN(OH)2 (C)	-5.572	[-2.000] 330 [1.000] 950 [2.000] 2
2095002	ZN(OH)2 (B)	-5.122	[-2.000] 330 [1.000] 950 [2.000] 2
2095003	ZN(OH)2 (G)	-5.082	[-2.000] 330 [1.000] 950 [2.000] 2
2095004	ZN(OH)2 (E)	-4.872	[-2.000] 330 [1.000] 950 [2.000] 2
6095000	ZN2(OH)2SO4	-7.973	[-2.000] 330 [2.000] 950 [2.000] 2
			[1.000] 732
6095001	ZN4(OH)6SO4	-15.616	[-6.000] 330 [4.000] 950 [6.000] 2
			[1.000] 732
2095005	ZNO(ACTIVE)	-4.647	[-2.000] 330 [1.000] 950 [1.000] 2

```
  2095006 ZINCITE          -5.033    [ -2.000] 330  [  1.000] 950  [
1.000]   2
  6095002 ZN3O(SO4)2      -28.135    [ -2.000] 330  [  3.000] 950  [
2.000] 732
                                     [  1.000]   2
  1095000 ZNS (A)         -15.650    [ -1.000] 330  [  1.000] 950  [
1.000] 730
  1095001 SPHALERITE      -12.967    [ -1.000] 330  [  1.000] 950  [
1.000] 730
  1095002 WURTZITE        -14.984    [ -1.000] 330  [  1.000] 950  [
1.000] 730
  6095003 ZINCOSITE       -10.599    [  1.000] 950  [  1.000] 732
  6095004 ZNSO4, 1H2O      -6.836    [  1.000] 950  [  1.000] 732  [
1.000]   2
  6095005 BIANCHITE        -5.549    [  1.000] 950  [  1.000] 732  [
6.000]   2
  6095006 GOSLARITE        -5.301    [  1.000] 950  [  1.000] 732  [
7.000]   2
    16000 CD METAL        -47.433    [  1.000] 160  [  2.000]   1
    16001 GAMMA CD        -47.537    [  1.000] 160  [  2.000]   1
  5016000 OTAVITE           0.000    [  1.000] 160  [  1.000] 140
```

```
    ID #      NAME        Sat. Index        Stoichiometry in [brackets]
  2016000 CD(OH)2 (A)     -10.617     [ -2.000] 330   [  1.000] 160   [
2.000]   2
  2016001 CD(OH)2 (C)     -10.008     [ -2.000] 330   [  1.000] 160   [
2.000]   2
  6016000 CD3(OH)4SO4     -25.363     [ -4.000] 330   [  3.000] 160   [
4.000]   2
                                      [  1.000] 732
  6016001 CD3OH2(SO4)2    -23.242     [ -2.000] 330   [  3.000] 160   [
2.000]   2
                                      [  2.000] 732
  6016002 CD4(OH)6SO4     -27.562     [ -6.000] 330   [  4.000] 160   [
6.000]   2
                                      [  1.000] 732
  2016002 MONTEPONITE     -12.073     [ -2.000] 330   [  1.000] 160   [
1.000]   2
  6016003 CDSO4           -10.362     [  1.000] 160   [  1.000] 732
  6016004 CDSO4, 1H2O      -8.656     [  1.000] 160   [  1.000] 732   [
1.000]   2
  6016005 CDSO4,2.7H2O     -8.417     [  1.000] 160   [  1.000] 732   [
2.670]   2
  1016000 GREENOCKITE     -11.435     [ -1.000] 330   [  1.000] 160   [
1.000] 730
    60000 PB METAL        -35.503     [  1.000] 600   [  2.000]   1
  5060000 CERRUSITE         1.771     [  1.000] 600   [  1.000] 140
  2060000 MASSICOT         -7.418     [ -2.000] 330   [  1.000] 600   [
1.000]   2
  2060001 LITHARGE         -7.218     [ -2.000] 330   [  1.000] 600   [
1.000]   2
  2060002 PBO, .3H2O       -7.073     [ -2.000] 330   [  1.000] 600   [
1.330]   2
  5060001 PB2OCO3          -5.356     [ -2.000] 330   [  2.000] 600   [
1.000]   2
                                      [  1.000] 140
  6060000 LARNAKITE        -1.810     [ -2.000] 330   [  2.000] 600   [
1.000] 732
                                      [  1.000]   2
  6060001 PB3O2SO4         -6.935     [ -4.000] 330   [  3.000] 600   [
1.000] 732
                                      [  2.000]   2
  6060002 PB4O3SO4        -13.080     [ -6.000] 330   [  4.000] 600   [
1.000] 732
                                      [  3.000]   2
  5060002 PB3O2CO3        -11.338     [ -4.000] 330   [  3.000] 600   [
1.000] 140
                                      [  2.000]   2
  6060003 ANGLESITE         0.000     [  1.000] 600   [  1.000] 732
  1060001 GALENA           -9.914     [ -1.000] 330   [  1.000] 600   [
1.000] 730
  2060003 PLATTNERITE      -8.018     [ -4.000] 330   [ -2.000]   1   [
1.000] 600
                                      [  2.000]   2
  3060000 PB2O3           -12.040     [ -6.000] 330   [ -2.000]   1   [
2.000] 600
                                      [  3.000]   2
  3060001 MINIUM          -21.385     [ -8.000] 330   [ -2.000]   1   [
3.000] 600
                                      [  4.000]   2
  2060004 PB(OH)2 (C)      -2.622     [ -2.000] 330   [  1.000] 600   [
2.000]   2
```

```
  5060003 HYDCERRUSITE     0.378    [ -2.000] 330  [  3.000] 600  [
2.000] 140
                                    [  2.000]   2
  2060005 PB2O(OH)2       -14.397   [ -4.000] 330  [  2.000] 600  [
3.000]   2
  6060004 PB4(OH)6SO4     -11.293   [ -6.000] 330  [  4.000] 600  [
1.000] 732
                                    [  6.000]   2
  5023101 MALACHITE         0.502   [  2.000] 231  [  2.000]   2  [
1.000] 140
                                    [ -2.000] 330
  5023102 AZURITE           1.210   [  3.000] 231  [  2.000]   2  [
2.000] 140
                                    [ -2.000] 330
  3006100 AS2O5           -26.697   [  2.000]  61  [ -3.000]   2
    73100 SULFUR            7.707   [  1.000] 730  [ -1.000] 330  [ -
2.000]   1
  7203000 ALASO4.2W        -3.680   [  1.000]  30  [  1.000]  61  [
2.000]   2
                                    [ -3.000] 330
  7215000 CA3(ASO4)26W    -15.364   [  3.000] 150  [  2.000]  61  [
4.000]   2
                                    [ -6.000] 330
```

```
    ID #      NAME        Sat. Index        Stoichiometry in [brackets]
  7223100 CU3(ASO4)26W    -6.297    [  3.000] 231  [  2.000]  61  [
 2.000]   2
                                     [ -6.000] 330
  7228100 FEASO4.2W       -5.323    [  1.000] 281  [  1.000]  61  [
 2.000]   2
                                     [ -3.000] 330
  7247000 MN3ASO428W      -9.795    [  3.000] 470  [  2.000]  61  [
 8.000]   2
                                     [ -6.000] 330
  7260000 PB3(ASO4)2      -7.904    [  3.000] 600  [  2.000]  61  [ -
 6.000] 330
  7295000 ZN3ASO422.5W   -13.609    [  3.000] 950  [  2.000]  61  [
 2.500]   2
                                     [ -6.000] 330
  7210000 BA(ASO4)2        0.000    [  3.000] 100  [  2.000]  61  [ -
 6.000] 330
  2015000 LIME           -24.995    [ -2.000] 330  [  1.000] 150  [
 1.000]   2
  2015001 PORTLANDITE    -14.512    [ -2.000] 330  [  1.000] 150  [
 2.000]   2
  2028000 WUSTITE         -4.962    [ -2.000] 330  [  0.947] 280  [
 1.000]   2
  2046001 PERICLASE      -12.858    [ -2.000] 330  [  1.000] 460  [
 1.000]   2
  3028001 HERCYNITE        0.073    [ -8.000] 330  [  1.000] 280  [
 2.000]  30
                                     [  4.000]   2
  3046000 SPINEL          -6.788    [ -8.000] 330  [  1.000] 460  [
 2.000]  30
                                     [  4.000]   2
  3046001 MAG-FERRITE      1.266    [ -8.000] 330  [  1.000] 460  [
 2.000] 281
                                     [  4.000]   2
  3028102 LEPIDOCROCIT     3.689    [ -3.000] 330  [  1.000] 281  [
 2.000]   2
  2076200 SeO3           -39.758    [  1.000] 762  [  2.000] 330  [ -
 1.000]   2
  6110001 BaSeO4          -8.956    [  1.000] 762  [  1.000] 100
  6115001 CaSeO4:2H2O     -5.945    [  1.000] 762  [  1.000] 150  [
 2.000]   2
  6160000 PbSeO4          -4.970    [  1.000] 762  [  1.000] 600
  2021100 CR(OH)2          0.634    [  1.000] 210  [  2.000]   2  [ -
 2.000] 330
    21000 CR METAL       -58.575    [  1.000] 210  [  2.000]   1
```

PART 1 of OUTPUT FILE

PC MINTEQA2 v3.10 DATE OF CALCULATIONS: 11-MAR-97 TIME: 23:54: 4

Cemented Unoxidized Tailings

Temperature (Celsius): 15.00
Units of concentration: MG/L

```
 Ionic strength to be computed.
 If specified, carbonate concentration represents total inorganic
carbon.
 Do not automatically terminate if charge imbalance exceeds 30%
 Precipitation is allowed only for those solids specified as ALLOWED
   in the input file (if any).
 The maximum number of iterations is: 200
 The method used to compute activity coefficients is: Davies equation
 Intermediate output file

-------------------------------------------------------------------------
-------
    330  0.000E-01  -10.00 y
    732  3.296E+02   -1.81 y
     30  8.000E-02   -4.28 y
     61  3.860E-02   -6.45 y
    100  4.300E-02   -6.84 y
    160  1.000E-03   -9.05 y
    150  3.000E+02   -2.13 y
    210  3.000E-03   -5.97 y
    231  4.000E-03   -6.00 y
    280  5.000E-02   -5.13 y
    600  3.400E-02   -5.89 y
    460  2.000E-02   -5.21 y
    470  3.000E-03   -7.04 y
    540  1.330E-02   -6.99 y
    762  1.900E-02   -5.70 y
     20  1.250E-03   -7.56 y
    950  2.000E-02   -5.17 y
    140  0.000E-01  -16.00 y
      1  0.000E-01  -16.00 y
    730  0.000E-01  -20.52 y
    281  1.000E-03  -20.75 y

 H2O has been inserted as a COMPONENT
  3   2
1028003    18.4790   -11.3000
    330    10.0000     0.0000
  4   1
5015001     8.4750     2.5850   1.000E-03
  5   8
2003000   -10.3800    27.0450
6010000     9.9760    -6.2800
6015001     4.8480    -0.2610
5028000    10.5500     5.3280
2023101    -7.6200    15.2400
5016000    13.7400     0.5800
6060003     7.7900    -2.1500
7210000     8.9100    -2.6400
  6   1
      1     0.0000     0.0000

INPUT DATA BEFORE TYPE MODIFICATIONS

   ID        NAME       ACTIVITY GUESS    LOG GUESS   ANAL TOTAL
    330  H+1                 1.000E-10      -10.000    0.000E-01
    732  SO4-2               1.549E-02       -1.810    3.296E+02
     30  Al+3                5.248E-05       -4.280    8.000E-02
     61  H3AsO4              3.548E-07       -6.450    3.860E-02
    100  Ba+2                1.445E-07       -6.840    4.300E-02
    160  Cd+2                8.913E-10       -9.050    1.000E-03
    150  Ca+2                7.413E-03       -2.130    3.000E+02
    210  Cr+2                1.072E-06       -5.970    3.000E-03
    231  Cu+2                1.000E-06       -6.000    4.000E-03
    280  Fe+2                7.413E-06       -5.130    5.000E-02
```

600	Pb+2	1.288E-06	-5.890	3.400E-02
460	Mg+2	6.166E-06	-5.210	2.000E-02
470	Mn+2	9.120E-08	-7.040	3.000E-03
540	Ni+2	1.023E-07	-6.990	1.330E-02
762	SeO4-2	1.995E-06	-5.700	1.900E-02
20	Ag+1	2.754E-08	-7.560	1.250E-03
950	Zn+2	6.761E-06	-5.170	2.000E-02
140	CO3-2	1.000E-16	-16.000	0.000E-01
1	E-1	1.000E-16	-16.000	0.000E-01
730	HS-1	3.020E-21	-20.520	0.000E-01
281	Fe+3	1.778E-21	-20.750	1.000E-03
2	H2O	1.000E+00	0.000	0.000E-01

Charge Balance: UNSPECIATED

Sum of CATIONS= 1.499E-02 Sum of ANIONS = 6.867E-03

PERCENT DIFFERENCE = 3.718E+01 (ANIONS - CATIONS)/(ANIONS + CATIONS)

IMPROVED ACTIVITY GUESSES PRIOR TO FIRST ITERATION:

SO4-2	Log activity guess:	-2.46
Al+3	Log activity guess:	-21.41
H3AsO4	Log activity guess:	-17.60
Cu+2	Log activity guess:	-10.34
Fe+2	Log activity guess:	-6.45
Mn+2	Log activity guess:	-7.31
SeO4-2	Log activity guess:	-6.88
Fe+3	Log activity guess:	-26.15

PART 3 of OUTPUT FILE

PC MINTEQA2 v3.10 DATE OF CALCULATIONS: 11-MAR-97 TIME: 23:54: 5

PARAMETERS OF THE COMPONENT MOST OUT OF BALANCE:

ITER		NAME	TOTAL MOL	DIFF FXN	LOG ACTVTY	RESIDUAL
0	E-1		0.000E-01	-1.186E+21	-16.00000	1.186E+21
1	E-1		0.000E-01	-1.186E+20	-16.00000	1.186E+20
2	E-1		0.000E-01	-3.236E+11	-16.00000	3.236E+11
3	E-1		0.000E-01	-3.236E+10	-16.00000	3.236E+10
4	E-1		0.000E-01	-4.733E+01	-16.00000	4.733E+01
5	E-1		0.000E-01	-4.323E+00	-15.99296	4.323E+00
6	E-1		0.000E-01	-1.267E+00	-15.95202	1.267E+00
7	E-1		0.000E-01	-4.614E-01	-15.81898	4.613E-01
8	E-1		0.000E-01	-8.216E-02	-15.54671	8.215E-02
9	E-1		0.000E-01	-1.014E-03	-14.92734	1.013E-03
10	E-1		0.000E-01	-2.413E-10	-13.09851	2.413E-10
11	E-1		0.000E-01	3.045E-17	-6.47815	3.044E-17
12	E-1		0.000E-01	-1.865E-04	-11.07143	1.864E-04
13	E-1		0.000E-01	-3.493E-05	-11.05100	3.493E-05
14	E-1		0.000E-01	-1.434E-05	-10.95898	1.433E-05
15	E-1		0.000E-01	-5.675E-06	-10.82690	5.674E-06
16	E-1		0.000E-01	-2.292E-06	-10.70217	2.291E-06
17	E-1		0.000E-01	-9.468E-07	-10.60477	9.467E-07
18	E-1		0.000E-01	-3.869E-07	-10.51747	3.868E-07
19	E-1		0.000E-01	-1.574E-07	-10.43218	1.574E-07
20	E-1		0.000E-01	-6.400E-08	-10.34713	6.400E-08
21	E-1		0.000E-01	-2.602E-08	-10.26173	2.602E-08
22	E-1		0.000E-01	-1.059E-08	-10.17570	1.059E-08
23	E-1		0.000E-01	-4.312E-09	-10.08890	4.312E-09
24	E-1		0.000E-01	-1.758E-09	-10.00126	1.758E-09
25	E-1		0.000E-01	-7.171E-10	-9.91274	7.171E-10
26	E-1		0.000E-01	-2.928E-10	-9.82333	2.928E-10
27	E-1		0.000E-01	-1.196E-10	-9.73305	1.196E-10
28	E-1		0.000E-01	-4.892E-11	-9.64193	4.891E-11
29	E-1		0.000E-01	-2.001E-11	-9.55003	2.001E-11
30	E-1		0.000E-01	-8.187E-12	-9.45741	8.186E-12
31	E-1		0.000E-01	-3.351E-12	-9.36413	3.351E-12
32	E-1		0.000E-01	-1.372E-12	-9.27026	1.372E-12
33	E-1		0.000E-01	-5.617E-13	-9.17589	5.617E-13
34	E-1		0.000E-01	-2.300E-13	-9.08109	2.300E-13
35	E-1		0.000E-01	-9.421E-14	-8.98591	9.420E-14
36	E-1		0.000E-01	-3.858E-14	-8.89042	3.858E-14
37	E-1		0.000E-01	-1.580E-14	-8.79466	1.580E-14
38	E-1		0.000E-01	-6.472E-15	-8.69869	6.472E-15
39	E-1		0.000E-01	-2.651E-15	-8.60255	2.651E-15
40	E-1		0.000E-01	-1.086E-15	-8.50626	1.086E-15
41	E-1		0.000E-01	-4.446E-16	-8.40988	4.445E-16
42	E-1		0.000E-01	-1.819E-16	-8.31345	1.819E-16
43	E-1		0.000E-01	-7.433E-17	-8.21713	7.432E-17
44	E-1		0.000E-01	-3.021E-17	-8.12128	3.021E-17
45	E-1		0.000E-01	-1.208E-17	-8.02700	1.208E-17
46	E-1		0.000E-01	-4.605E-18	-7.93740	4.605E-18
47	E-1		0.000E-01	-1.521E-18	-7.86041	1.521E-18
48	E-1		0.000E-01	-3.347E-19	-7.81021	3.346E-19
49	E-1		0.000E-01	-2.561E-20	-7.79331	2.546E-20
50	E-1		0.000E-01	-1.750E-22	-7.79182	2.719E-23

ID	NAME	ANAL MOL	CALC MOL	LOG ACTVTY	GAMMA	DIFF FXN
281	Fe+3	1.792E-08	2.023E-26	-26.20727	0.306646	- 3.425E-13
732	SO4-2	3.433E-03	2.415E-03	-2.84516	0.591342	- 1.850E-07
30	Al+3	2.967E-06	1.108E-21	-21.46867	0.306646	- 5.654E-11
61	H3AsO4	2.721E-07	1.466E-18	-17.83217	1.004111	- 2.195E-11
100	Ba+2	3.133E-07	3.132E-07	-6.73230	0.591342	- 2.418E-11
160	Cd+2	8.902E-09	4.676E-09	-8.55825	0.591342	- 3.825E-13
150	Ca+2	7.490E-03	6.472E-03	-2.41713	0.591342	- 4.979E-07
210	Cr+2	5.773E-08	5.773E-08	-7.46677	0.591342	- 4.455E-12
231	Cu+2	6.299E-08	5.117E-14	-13.51914	0.591342	8.938E-14
280	Fe+2	8.959E-07	4.168E-07	-6.60820	0.591342	- 4.009E-11
600	Pb+2	1.642E-07	2.525E-10	-9.82593	0.591342	- 8.201E-13
460	Mg+2	8.232E-07	7.202E-07	-6.37069	0.591342	- 5.551E-11
470	Mn+2	5.464E-08	4.518E-08	-7.57324	0.591342	- 3.543E-12
540	Ni+2	2.267E-07	1.816E-08	-7.96895	0.591342	- 1.544E-12
762	SeO4-2	1.330E-07	1.330E-07	-7.10438	0.591342	- 1.026E-11
20	Ag+1	1.160E-08	1.121E-08	-8.00743	0.876919	- 2.217E-13
950	Zn+2	3.061E-07	3.953E-10	-9.63124	0.591342	1.579E-13
1	E-1	0.000E-01	1.615E-08	-7.79181	0.876919	1.158E-22
2	H2O	0.000E-01	-7.080E-05	-0.00008	1.000000	0.000E-01
330	H+1	0.000E-01	1.140E-10	-10.00000	0.876919	0.000E-01
730	HS-1	0.000E-01	1.535E-24	-23.87093	0.876919	0.000E-01
140	CO3-2	0.000E-01	1.668E-06	-6.00596	0.591342	0.000E-01

Type I - COMPONENTS AS SPECIES IN SOLUTION

ID	NAME	CALC MOL	ACTIVITY	LOG ACTVTY	GAMMA	NEW LOGK
330	H+1	1.140E-10	1.000E-10	-10.00000	0.87692	0.057
732	SO4-2	2.415E-03	1.428E-03	-2.84516	0.59134	0.228
30	Al+3	1.108E-21	3.399E-22	-21.46867	0.30665	0.513
61	H3AsO4	1.466E-18	1.472E-18	-17.83217	1.00411	- 0.002
100	Ba+2	3.132E-07	1.852E-07	-6.73230	0.59134	0.228

160	Cd+2	4.676E-09	2.765E-09	-8.55825	0.59134
0.228					
150	Ca+2	6.472E-03	3.827E-03	-2.41713	0.59134
0.228					
210	Cr+2	5.773E-08	3.414E-08	-7.46677	0.59134
0.228					
231	Cu+2	5.117E-14	3.026E-14	-13.51914	0.59134
0.228					
280	Fe+2	4.168E-07	2.465E-07	-6.60820	0.59134
0.228					
600	Pb+2	2.525E-10	1.493E-10	-9.82593	0.59134
0.228					
460	Mg+2	7.202E-07	4.259E-07	-6.37069	0.59134
0.228					
470	Mn+2	4.518E-08	2.672E-08	-7.57324	0.59134
0.228					
540	Ni+2	1.816E-08	1.074E-08	-7.96895	0.59134
0.228					
762	SeO4-2	1.330E-07	7.863E-08	-7.10438	0.59134
0.228					
20	Ag+1	1.121E-08	9.830E-09	-8.00743	0.87692
0.057					
950	Zn+2	3.953E-10	2.338E-10	-9.63124	0.59134
0.228					
140	CO3-2	1.668E-06	9.864E-07	-6.00596	0.59134
0.228					
281	Fe+3	2.023E-26	6.205E-27	-26.20727	0.30665
0.513					
730	HS-1	1.535E-24	1.346E-24	-23.87093	0.87692
0.057					

Type II - OTHER SPECIES IN SOLUTION OR ADSORBED

ID	NAME	CALC MOL	ACTIVITY	LOG ACTVTY	GAMMA	
NEW LOGK						
1607620	CdSeO4	3.776E-14	3.792E-14	-13.42113	1.00411	
2.240						
9507620	ZnSeO4	2.914E-15	2.926E-15	-14.53373	1.00411	
2.200						
9507621	Zn(SeO4)2-2	2.078E-24	1.229E-24	-23.91041	0.59134	
0.158						
3300020	OH-	5.242E-05	4.597E-05	-4.33753	0.87692	-
14.280						
4603300	MgOH +	3.246E-09	2.846E-09	-8.54570	0.87692	-
12.118						
4601400	MgCO3 AQ	3.424E-10	3.439E-10	-9.46362	1.00411	
2.911						
4601401	MgHCO3 +	1.417E-11	1.242E-11	-10.90580	0.87692	
11.528						
4607320	MgSO4 AQ	9.926E-08	9.967E-08	-7.00143	1.00411	
2.213						
1503300	CaOH +	4.700E-06	4.122E-06	-5.38494	0.87692	-
12.911						
1501400	CaHCO3 +	8.830E-08	7.743E-08	-7.11110	0.87692	
11.369						
1501401	CaCO3 AQ	4.414E-06	4.432E-06	-5.35336	1.00411	
3.068						
1507320	CaSO4 AQ	1.017E-03	1.022E-03	-2.99069	1.00411	
2.270						
303300	AlOH +2	2.929E-17	1.732E-17	-16.76142	0.59134	-
5.065						

303301	Al(OH)2 +	3.078E-12	2.699E-12	-11.56883	0.87692	-
10.043						
303302	Al(OH)4 -	2.933E-06	2.572E-06	-5.58973	0.87692	-
24.064						
307320	AlSO4 +	5.111E-22	4.482E-22	-21.34852	0.87692	
3.022						
307321	Al(SO4)2 -	5.569E-23	4.884E-23	-22.31123	0.87692	
4.905						
303303	Al(OH)3 AQ	3.383E-08	3.397E-08	-7.46891	1.00411	-
16.002						
2803300	FeOH +	4.102E-07	3.597E-07	-6.44402	0.87692	-
9.779						
2803301	FeOH3 -1	4.763E-09	4.177E-09	-8.37917	0.87692	-
31.714						
2807320	FeSO4 AQ	5.161E-08	5.182E-08	-7.28552	1.00411	
2.166						
2803302	FeOH2 AQ	1.240E-08	1.245E-08	-7.90496	1.00411	-
21.298						
2807300	Fe(HS)2 AQ	3.964E-46	3.981E-46	-45.40006	1.00411	
8.948						
2807301	Fe(HS)3 -	6.654E-68	5.835E-68	-67.23399	0.87692	
11.044						
2813300	FeOH +2	3.684E-19	2.178E-19	-18.66186	0.59134	-
2.226						
2817320	FeSO4 +	6.686E-26	5.863E-26	-25.23189	0.87692	
3.878						
2813301	FeOH2 +	1.512E-12	1.326E-12	-11.87743	0.87692	-
5.613						
2813302	FeOH3 AQ	1.551E-10	1.558E-10	-9.80751	1.00411	-
13.602						
2813303	FeOH4 -	1.776E-08	1.557E-08	-7.80759	0.87692	-
21.543						
2817321	Fe(SO4)2 -	2.900E-27	2.543E-27	-26.59460	0.87692	
5.360						
2813304	Fe2(OH)2+4	1.602E-35	1.958E-36	-35.70809	0.12228	-
2.381						
2813305	Fe3(OH)4+5	1.381E-44	5.178E-46	-45.28587	0.03750	-
5.238						
1003300	BaOH +	3.826E-11	3.355E-11	-10.47435	0.87692	-
13.685						
4703300	MnOH +	3.369E-09	2.954E-09	-8.52959	0.87692	-
10.899						
4703301	Mn(OH)3 -1	4.826E-13	4.232E-13	-12.37348	0.87692	-
34.743						
4700020	MnO4 -	1.336E-21	1.172E-21	-20.93115	0.87692	-
132.260						
4700021	MnO4 -2	3.680E-19	2.176E-19	-18.66234	0.59134	-
122.028						
4707320	MnSO4 AQ	6.090E-09	6.115E-09	-8.21360	1.00411	
2.203						
4701400	MnHCO3 +	1.196E-12	1.049E-12	-11.97921	0.87692	
11.657						
2311400	CuCO3 AQ	1.596E-13	1.603E-13	-12.79510	1.00411	
6.728						
2311401	Cu(CO3)2-2	3.366E-16	1.990E-16	-15.70107	0.59134	
10.058						
2313300	CuOH +	3.450E-12	3.025E-12	-11.51922	0.87692	-
7.943						
2313301	Cu(OH)2 AQ	6.294E-08	6.320E-08	-7.19930	1.00411	-
13.682						
2313302	Cu(OH)3 -	4.352E-11	3.816E-11	-10.41838	0.87692	-
26.842						
2313303	Cu(OH)4 -2	1.284E-13	7.595E-14	-13.11946	0.59134	-
39.372						

2313304	Cu2(OH)2+2	2.427E-18	1.435E-18	-17.84307	0.59134	-
10.576						
2317320	CuSO4 AQ	8.183E-15	8.216E-15	-14.08533	1.00411	
2.277						
2317300	Cu(HS)3 -	6.670E-60	5.849E-60	-59.23293	0.87692	
25.956						
2311402	CuHCO3 +	3.404E-17	2.985E-17	-16.52510	0.87692	
13.057						
9503300	ZnOH +	1.333E-09	1.169E-09	-8.93215	0.87692	-
9.244						
9503301	Zn(OH)2 AQ	2.936E-07	2.948E-07	-6.53040	1.00411	-
16.901						
9503302	Zn(OH)3 -	1.063E-08	9.322E-09	-8.03049	0.87692	-
28.342						
9503303	Zn(OH)4 -2	2.498E-11	1.477E-11	-10.83057	0.59134	-
40.971						
9507300	Zn(HS)2 AQ	3.674E-43	3.689E-43	-42.43311	1.00411	
14.938						
9507301	Zn(HS)3 -	8.185E-66	7.177E-66	-65.14404	0.87692	
16.157						
9507320	ZnSO4 AQ	7.198E-11	7.228E-11	-10.14100	1.00411	
2.334						
9507321	Zn(SO4)2-2	1.537E-12	9.087E-13	-12.04157	0.59134	
3.508						
9501400	ZnHCO3 +	6.604E-14	5.792E-14	-13.23721	0.87692	
12.457						
9501401	ZnCO3 AQ	4.582E-11	4.600E-11	-10.33721	1.00411	
5.298						
9501402	Zn(CO3)2-2	1.641E-12	9.701E-13	-12.01317	0.59134	
9.858						
1601400	Cd(CO3)3-4	3.602E-20	4.404E-21	-20.35614	0.12228	
7.133						
1603300	CdOH +	1.218E-09	1.068E-09	-8.97155	0.87692	-
10.356						
1603301	Cd(OH)2 AQ	1.230E-09	1.235E-09	-8.90841	1.00411	-
20.352						
1603302	Cd(OH)3 -	1.580E-12	1.385E-12	-11.85849	0.87692	-
33.243						
1603303	Cd(OH)4 -2	2.087E-16	1.234E-16	-15.90857	0.59134	-
47.122						
1603304	Cd2OH +3	5.365E-17	1.645E-17	-16.78381	0.30665	-
9.154						
1607320	CdSO4 AQ	1.065E-09	1.069E-09	-8.97088	1.00411	
2.431						
1607300	CdHS +	6.279E-23	5.506E-23	-22.25918	0.87692	
10.227						
1607301	Cd(HS)2 AQ	1.691E-40	1.698E-40	-39.77011	1.00411	
16.528						
1607302	Cd(HS)3 -	3.945E-62	3.459E-62	-61.46104	0.87692	
18.767						
1607303	Cd(HS)4 -2	1.220E-83	7.212E-84	-83.14197	0.59134	
21.128						
1601400	CdHCO3 +	7.813E-13	6.852E-13	-12.16421	0.87692	
12.457						
1601401	CdCO3 AQ	6.808E-10	6.836E-10	-9.16521	1.00411	
5.397						
1607321	Cd(SO4)2-2	3.017E-11	1.784E-11	-10.74857	0.59134	
3.728						
6001400	Pb(CO3)2-2	1.072E-11	6.341E-12	-11.19786	0.59134	
10.868						
6003300	PbOH +	3.319E-08	2.911E-08	-7.53601	0.87692	-
7.653						
6003301	Pb(OH)2 AQ	1.128E-07	1.132E-07	-6.94609	1.00411	-
17.122						

6003302	Pb(OH)3 -	1.482E-08	1.300E-08	-7.88617	0.87692	-28.003
6003303	Pb2OH +3	3.173E-16	9.729E-17	-16.01194	0.30665	-5.847
6007320	PbSO4 AQ	1.194E-10	1.199E-10	-9.92109	1.00411	2.748
6007300	Pb(HS)2 AQ	5.017E-43	5.037E-43	-42.29779	1.00411	15.268
6007301	Pb(HS)3 -	1.543E-65	1.353E-65	-64.86872	0.87692	16.627
6003304	Pb3(OH)4+2	1.570E-14	9.286E-15	-14.03218	0.59134	-24.326
6001401	PbCO3 AQ	2.549E-09	2.559E-09	-8.59189	1.00411	7.238
6003305	Pb(OH)4 -2	5.046E-10	2.984E-10	-9.52525	0.59134	-39.471
6007321	Pb(SO4)2-2	1.520E-12	8.990E-13	-12.04625	0.59134	3.698
6001402	PbHCO3 +	2.662E-13	2.334E-13	-12.63189	0.87692	13.257
5403300	NiOH +	8.167E-09	7.162E-09	-8.14496	0.87692	-10.119
5403301	Ni(OH)2 AQ	1.069E-07	1.074E-07	-6.96911	1.00411	-19.002
5403302	Ni(OH)3 -	1.224E-08	1.074E-08	-7.96920	0.87692	-29.943
5407320	NiSO4 AQ	2.725E-09	2.737E-09	-8.56278	1.00411	2.250
5401400	NiHCO3 +	3.566E-12	3.127E-12	-11.50492	0.87692	12.527
5401401	NiCO3 AQ	7.822E-08	7.854E-08	-7.10492	1.00411	6.868
5401402	Ni(CO3)2-2	2.277E-10	1.346E-10	-9.87088	0.59134	10.338
5407321	Ni(SO4)2-2	3.880E-13	2.295E-13	-12.63928	0.59134	1.248
207300	AgHS AQ	1.479E-18	1.485E-18	-17.82836	1.00411	14.048
207301	Ag(HS)2 -	5.725E-38	5.020E-38	-37.29929	0.87692	18.507
203300	AgOH AQ	9.788E-11	9.829E-11	-10.00751	1.00411	-12.002
203301	Ag(OH)2 -	1.121E-12	9.827E-13	-12.00759	0.87692	-23.943
207320	AgSO4 -	2.861E-10	2.509E-10	-9.60049	0.87692	1.309
3300611	H2AsO4 -	1.059E-10	9.286E-11	-10.03218	0.87692	-2.143
3300612	HAsO4 -2	2.621E-07	1.550E-07	-6.80977	0.59134	-8.749
3300613	AsO4 -3	9.930E-09	3.045E-09	-8.51642	0.30665	-20.171
3301400	HCO3 -	3.024E-06	2.652E-06	-5.57649	0.87692	10.487
3301401	H2CO3 AQ	5.375E-10	5.397E-10	-9.26781	1.00411	16.736
3307320	HSO4 -	1.203E-11	1.055E-11	-10.97665	0.87692	1.926
3307300	H2S AQ	1.629E-27	1.636E-27	-26.78634	1.00411	7.083
3307301	S -2	1.353E-27	8.004E-28	-27.09672	0.59134	-12.998
3307620	HSeO4-1	5.644E-16	4.950E-16	-15.30542	0.87692	1.856

4707620	MnSeO4	4.481E-13	4.499E-13	-12.34684	1.00411
2.329					
5407620	NiSeO4	2.982E-13	2.995E-13	-12.52367	1.00411
2.548					

Type III - SPECIES WITH FIXED ACTIVITY

ID	NAME	CALC MOL	LOG MOL	NEW LOGK	DH
2	H2O	-7.080E-05	-4.150	0.000	0.000
330	H+1	6.824E-05	-4.166	10.000	0.000
1028003	PYRITE	-7.393E-19	-18.131	18.766	-11.300

Type IV - FINITE SOLIDS (presumed present at equilibrium)

ID	NAME	CALC MOL	LOG MOL	NEW LOGK	DH
5015001	CALCITE	9.907E-04	-5.033	8.423	2.585

Type V - POSSIBLE SOLIDS

ID	NAME	CALC MOL	LOG MOL	NEW LOGK	DH
2003000	ALOH3(A)	2.905E-03	-2.537	-11.068	27.045
6015001	GYPSUM	3.910E-01	-0.408	4.855	-0.261
6010000	BARITE	3.616E+00	0.558	10.136	-6.280
5028000	SIDERITE	6.314E-03	-2.200	10.414	5.328
2023101	TENORITE	2.973E-02	-1.527	-8.008	15.240
5016000	OTAVITE	1.449E-01	-0.839	13.725	0.580
6060003	ANGLESITE	1.491E-05	-4.826	7.845	-2.150
7210000	BA(ASO4)2	1.306E+13	13.116	8.977	-2.640

Type VI - EXCLUDED SPECIES (not included in mole balance)

ID	NAME	CALC MOL	LOG MOL	NEW LOGK	DH
3301403	CO2 (g)	1.471E-08	-7.832	18.173	-0.530
3300021	O2 (g)	4.394E-16	-15.357	-86.524	133.830
1	E-1	1.615E-08	-7.792	0.000	0.000
2802810	Fe+2/Fe+3	7.861E-15	-14.105	13.286	-10.000
7307320	HS-/SO4-2	0.000E-01	-96.119	35.190	-60.140
3301404	CH4 (g)	0.000E-01	-126.689	41.652	-61.000

PERCENTAGE DISTRIBUTION OF COMPONENTS AMONG
TYPE I and TYPE II (dissolved and adsorbed) species

Fe+3	99.1	PERCENT BOUND IN SPECIES #2813303
FeOH4 -		
SO4-2	70.4	PERCENT BOUND IN SPECIES # 732
SO4-2		
	29.6	PERCENT BOUND IN SPECIES #1507320 CaSO4 AQ
Al+3	98.9	PERCENT BOUND IN SPECIES # 303302
Al(OH)4 -		
	1.1	PERCENT BOUND IN SPECIES # 303303 Al(OH)3 AQ
H3AsO4	96.3	PERCENT BOUND IN SPECIES #3300612
HAsO4 -2		
	3.6	PERCENT BOUND IN SPECIES #3300613 AsO4 -3
Ba+2	100.0	PERCENT BOUND IN SPECIES # 100
Ba+2		
Cd+2	52.5	PERCENT BOUND IN SPECIES # 160
Cd+2		
	13.7	PERCENT BOUND IN SPECIES #1603300 CdOH +
	13.8	PERCENT BOUND IN SPECIES #1603301 Cd(OH)2 AQ
	12.0	PERCENT BOUND IN SPECIES #1607320 CdSO4 AQ
	7.6	PERCENT BOUND IN SPECIES #1601401 CdCO3 AQ
Ca+2	86.3	PERCENT BOUND IN SPECIES # 150
Ca+2		
	13.6	PERCENT BOUND IN SPECIES #1507320 CaSO4 AQ
Cr+2	100.0	PERCENT BOUND IN SPECIES # 210
Cr+2		
Cu+2	99.9	PERCENT BOUND IN SPECIES #2313301
Cu(OH)2 AQ		
Fe+2	46.5	PERCENT BOUND IN SPECIES # 280
Fe+2		
	45.8	PERCENT BOUND IN SPECIES #2803300 FeOH +
	5.8	PERCENT BOUND IN SPECIES #2807320 FeSO4 AQ
	1.4	PERCENT BOUND IN SPECIES #2803302 FeOH2 AQ
Pb+2	20.2	PERCENT BOUND IN SPECIES #6003300
PbOH +		
	68.7	PERCENT BOUND IN SPECIES #6003301 Pb(OH)2 AQ
	9.0	PERCENT BOUND IN SPECIES #6003302 Pb(OH)3 -
	1.6	PERCENT BOUND IN SPECIES #6001401 PbCO3 AQ
Mg+2	87.5	PERCENT BOUND IN SPECIES # 460
Mg+2		
	12.1	PERCENT BOUND IN SPECIES #4607320 MgSO4 AQ

Mn+2		82.7	PERCENT BOUND IN SPECIES # 470
Mn+2			
	6.2	PERCENT BOUND IN SPECIES #4703300	MnOH +
	11.1	PERCENT BOUND IN SPECIES #4707320	MnSO4 AQ
Ni+2		8.0	PERCENT BOUND IN SPECIES # 540
Ni+2			
	3.6	PERCENT BOUND IN SPECIES #5403300	NiOH +
	47.2	PERCENT BOUND IN SPECIES #5403301	Ni(OH)2 AQ
	5.4	PERCENT BOUND IN SPECIES #5403302	Ni(OH)3 -
	1.2	PERCENT BOUND IN SPECIES #5407320	NiSO4 AQ
	34.5	PERCENT BOUND IN SPECIES #5401401	NiCO3 AQ
SeO4-2		100.0	PERCENT BOUND IN SPECIES # 762
SeO4-2			
Ag+1		96.7	PERCENT BOUND IN SPECIES # 20
Ag+1			
	2.5	PERCENT BOUND IN SPECIES # 207320	AgSO4 -
Zn+2		95.9	PERCENT BOUND IN SPECIES #9503301
Zn(OH)2 AQ			
	3.5	PERCENT BOUND IN SPECIES #9503302	Zn(OH)3 -
E-1		99.5	PERCENT BOUND IN SPECIES #4700021
MnO4 -2			
H2O		74.0	PERCENT BOUND IN SPECIES #3300020
OH-			
	6.6	PERCENT BOUND IN SPECIES #1503300	CaOH +
	16.6	PERCENT BOUND IN SPECIES # 303302	Al(OH)4 -
H+1		76.8	PERCENT BOUND IN SPECIES #3300020
OH-			
	6.9	PERCENT BOUND IN SPECIES #1503300	CaOH +
	17.2	PERCENT BOUND IN SPECIES # 303302	Al(OH)4 -
HS-1		100.0	PERCENT BOUND IN SPECIES # 207300
AgHS AQ			
CO3-2		18.0	PERCENT BOUND IN SPECIES # 140
CO3-2			
	47.6	PERCENT BOUND IN SPECIES #1501401	CaCO3 AQ
	32.6	PERCENT BOUND IN SPECIES #3301400	HCO3 -

PART 5 of OUTPUT FILE

PC MINTEQA2 v3.10 DATE OF CALCULATIONS: 11-MAR-97 TIME: 23:54: 7

PROVISIONAL MASS DISTRIBUTION

IDX	NAME	DISSOLVED		SORBED		PRECIPITATED
		MOL/KG	PERCENT	MOL/KG	PERCENT	MOL/KG
PERCENT						
281	Fe+3	1.792E-08	100.0	0.000E-01	0.0	0.000E-01
0.0						
732	SO4-2	3.433E-03	100.0	0.000E-01	0.0	0.000E-01
0.0						
30	Al+3	2.967E-06	100.0	0.000E-01	0.0	0.000E-01
0.0						
61	H3AsO4	2.721E-07	100.0	0.000E-01	0.0	0.000E-01
0.0						
100	Ba+2	3.133E-07	100.0	0.000E-01	0.0	0.000E-01
0.0						
160	Cd+2	8.902E-09	100.0	0.000E-01	0.0	0.000E-01
0.0						
150	Ca+2	7.499E-03	88.3	0.000E-01	0.0	9.907E-04
11.7						
210	Cr+2	5.773E-08	100.0	0.000E-01	0.0	0.000E-01
0.0						
231	Cu+2	6.299E-08	100.0	0.000E-01	0.0	0.000E-01
0.0						
280	Fe+2	8.958E-07	100.0	0.000E-01	0.0	0.000E-01
0.0						
600	Pb+2	1.642E-07	100.0	0.000E-01	0.0	0.000E-01
0.0						
460	Mg+2	8.231E-07	100.0	0.000E-01	0.0	0.000E-01
0.0						
470	Mn+2	5.464E-08	100.0	0.000E-01	0.0	0.000E-01
0.0						
540	Ni+2	2.267E-07	100.0	0.000E-01	0.0	0.000E-01
0.0						
762	SeO4-2	1.330E-07	100.0	0.000E-01	0.0	0.000E-01
0.0						
20	Ag+1	1.160E-08	100.0	0.000E-01	0.0	0.000E-01
0.0						
950	Zn+2	3.061E-07	100.0	0.000E-01	0.0	0.000E-01
0.0						
1	E-1	-1.479E-18	100.0	0.000E-01	0.0	0.000E-01
0.0						
2	H2O	7.080E-05	100.0	0.000E-01	0.0	0.000E-01
0.0						
330	H+1	-6.824E-05	100.0	0.000E-01	0.0	0.000E-01
0.0						
730	HS-1	1.479E-18	100.0	0.000E-01	0.0	0.000E-01
0.0						
140	CO3-2	9.277E-06	0.9	0.000E-01	0.0	9.907E-04
99.1						

Charge Balance: SPECIATED

Sum of CATIONS = 1.295E-02 Sum of ANIONS 4.894E-03

PERCENT DIFFERENCE = 4.516E+01 (ANIONS - CATIONS)/(ANIONS + CATIONS)

PROVISIONAL IONIC STRENGTH (m) = 1.782E-02

PART 3 of OUTPUT FILE

PC MINTEQA2 v3.10 DATE OF CALCULATIONS: 11-MAR-97 TIME: 23:54: 7

PARAMETERS OF THE COMPONENT MOST OUT OF BALANCE:

ITER	NAME	TOTAL MOL	DIFF FXN	LOG ACTVTY	RESIDUAL
52	Zn+2	3.061E-07	-4.379E-10	-9.63124	4.073E-10
53	Zn+2	3.061E-07	5.134E-10	-9.63061	4.828E-10
54	Zn+2	3.061E-07	-6.132E-11	-9.63133	3.070E-11
55	SeO4-2	1.330E-07	3.496E-11	-7.10424	2.166E-11

ID	NAME	ANAL MOL	CALC MOL	LOG ACTVTY	GAMMA	DIFF FXN
281	Fe+3	1.792E-08	2.023E-26	-26.20726	0.306658	- 1.143E-13
732	SO4-2	3.433E-03	2.415E-03	-2.84515	0.591352	- 6.155E-08
30	Al+3	2.967E-06	1.108E-21	-21.46866	0.306658	- 1.887E-11
61	H3AsO4	2.721E-07	3.409E-19	-18.46565	1.004110	- 1.703E-12
1	E-1	0.000E-01	1.615E-08	-7.79181	0.876923	3.669E-23
160	Cd+2	8.902E-09	4.677E-09	-8.55823	0.591352	- 1.275E-13
150	Ca+2	7.490E-03	6.472E-03	-2.41711	0.591352	- 1.660E-07
210	Cr+2	5.773E-08	5.773E-08	-7.46674	0.591352	- 1.487E-12
231	Cu+2	6.299E-08	5.117E-14	-13.51914	0.591352	2.982E-14
280	Fe+2	8.959E-07	4.168E-07	-6.60818	0.591352	- 1.337E-11
600	Pb+2	1.642E-07	2.525E-10	-9.82593	0.591352	- 2.734E-13
460	Mg+2	8.232E-07	7.203E-07	-6.37066	0.591352	- 1.851E-11
470	Mn+2	5.464E-08	4.518E-08	-7.57322	0.591352	- 1.181E-12
540	Ni+2	2.267E-07	1.816E-08	-7.96894	0.591352	- 5.102E-13
762	SeO4-2	1.330E-07	1.330E-07	-7.10435	0.591352	- 3.425E-12
20	Ag+1	1.160E-08	1.121E-08	-8.00742	0.876923	- 7.397E-14
950	Zn+2	3.061E-07	3.953E-10	-9.63124	0.591352	5.269E-14
2	H2O	0.000E-01	-7.080E-05	-0.00008	1.000000	0.000E-01
100	Ba+2	3.133E-07	3.517E-11	-10.68195	0.591352	0.000E-01
730	HS-1	0.000E-01	1.535E-24	-23.87094	0.876923	0.000E-01
140	CO3-2	0.000E-01	1.668E-06	-6.00599	0.591352	0.000E-01
330	H+1	0.000E-01	1.140E-10	-10.00000	0.876923	2.647E-23

PART 6 of OUTPUT FILE

PC MINTEQA2 v3.10 DATE OF CALCULATIONS: 11-MAR-97 TIME: 23:54: 7

Saturation indices and stoichiometry of all supersaturated minerals

ID #	NAME	Sat. Index	Stoichiometry in [brackets]
6010000	BARITE	0.558	[1.000] 100 [1.000] 732
5015001	CALCITE	0.000	[1.000] 150 [1.000] 140
2003002	DIASPORE	1.032	[-3.000] 330 [1.000] 30 [2.000] 2
2028101	FE3(OH)8	0.755	[-8.000] 330 [2.000] 281 [1.000] 280 [8.000] 2
2028102	GOETHITE	2.924	[-3.000] 330 [1.000] 281 [2.000] 2
3028100	HEMATITE	10.809	[-6.000] 330 [2.000] 281 [3.000] 2
3028101	MAGHEMITE	1.199	[-6.000] 330 [2.000] 281 [3.000] 2
3028000	MAGNETITE	15.956	[-8.000] 330 [2.000] 281 [1.000] 280 [4.000] 2
1028003	PYRITE	0.000	[-2.000] 330 [-2.000] 1 [1.000] 280 [2.000] 730
3047000	HAUSMANNITE	9.285	[-8.000] 330 [-2.000] 1 [3.000] 470 [4.000] 2
3023100	CUPRICFERIT	7.202	[-8.000] 330 [1.000] 231 [2.000] 281 [4.000] 2
2060004	PB(OH)2 (C)	1.668	[-2.000] 330 [1.000] 600 [2.000] 2
2054000	NI(OH)2	2.005	[-2.000] 330 [1.000] 540 [2.000] 2
1002000	ACANTHITE	7.520	[-1.000] 330 [2.000] 20 [1.000] 730
73100	SULFUR	3.716	[1.000] 730 [-1.000] 330 [-2.000] 1
7210000	BA(ASO4)2	13.116	[3.000] 100 [2.000] 61 [-6.000] 330
2028000	WUSTITE	1.423	[-2.000] 330 [0.947] 280 [1.000] 2
3028001	HERCYNITE	1.299	[-8.000] 330 [1.000] 280 [2.000] 30 [4.000] 2
3046001	MAG-FERRITE	2.754	[-8.000] 330 [1.000] 460 [2.000] 281 [4.000] 2
3028102	LEPIDOCROCIT	2.422	[-3.000] 330 [1.000] 281 [2.000] 2
2021100	CR(OH)2	1.498	[1.000] 210 [2.000] 2 [-2.000] 330

PC MINTEQA2 v3.10 DATE OF CALCULATIONS: 11-MAR-97 TIME: 23:54: 7

ITERATIONS= 52: SOLID BA(ASO4)2 PRECIPITATES

Type I - COMPONENTS AS SPECIES IN SOLUTION

ID	NAME	CALC MOL	ACTIVITY	LOG ACTVTY	GAMMA	NEW LOGK
330	H+1	1.140E-10	1.000E-10	-10.00000	0.87692	0.057
732	SO4-2	2.415E-03	1.428E-03	-2.84515	0.59135	0.228
30	Al+3	1.108E-21	3.399E-22	-21.46866	0.30666	0.513
61	H3AsO4	3.409E-19	3.423E-19	-18.46565	1.00411	- 0.002
100	Ba+2	3.517E-11	2.080E-11	-10.68195	0.59135	0.228
160	Cd+2	4.677E-09	2.765E-09	-8.55823	0.59135	0.228
150	Ca+2	6.472E-03	3.827E-03	-2.41711	0.59135	0.228
210	Cr+2	5.773E-08	3.414E-08	-7.46674	0.59135	0.228
231	Cu+2	5.117E-14	3.026E-14	-13.51914	0.59135	0.228
280	Fe+2	4.168E-07	2.465E-07	-6.60818	0.59135	0.228
600	Pb+2	2.525E-10	1.493E-10	-9.82593	0.59135	0.228
460	Mg+2	7.203E-07	4.259E-07	-6.37066	0.59135	0.228
470	Mn+2	4.518E-08	2.672E-08	-7.57322	0.59135	0.228
540	Ni+2	1.816E-08	1.074E-08	-7.96894	0.59135	0.228
762	SeO4-2	1.330E-07	7.864E-08	-7.10435	0.59135	0.228
20	Ag+1	1.121E-08	9.831E-09	-8.00742	0.87692	0.057
950	Zn+2	3.953E-10	2.338E-10	-9.63124	0.59135	0.228
140	CO3-2	1.668E-06	9.863E-07	-6.00599	0.59135	0.228
281	Fe+3	2.023E-26	6.205E-27	-26.20726	0.30666	0.513
730	HS-1	1.535E-24	1.346E-24	-23.87094	0.87692	0.057

Type II - OTHER SPECIES IN SOLUTION OR ADSORBED

ID	NAME	CALC MOL	ACTIVITY	LOG ACTVTY	GAMMA	NEW LOGK
1607620	CdSeO4	3.777E-14	3.792E-14	-13.42108	1.00411	2.240
9507620	ZnSeO4	2.914E-15	2.926E-15	-14.53370	1.00411	2.200
9507621	Zn(SeO4)2-2	2.079E-24	1.229E-24	-23.91035	0.59135	0.158
3300020	OH-	5.242E-05	4.597E-05	-4.33753	0.87692	- 14.280
4603300	MgOH +	3.246E-09	2.847E-09	-8.54568	0.87692	- 12.118

4601400	MgCO3 AQ	3.424E-10	3.439E-10	-9.46362	1.00411	
2.911						
4601401	MgHCO3 +	1.417E-11	1.242E-11	-10.90580	0.87692	
11.528						
4607320	MgSO4 AQ	9.927E-08	9.968E-08	-7.00140	1.00411	
2.213						
1503300	CaOH +	4.700E-06	4.122E-06	-5.38491	0.87692	-
12.911						
1501400	CaHCO3 +	8.830E-08	7.743E-08	-7.11110	0.87692	
11.369						
1501401	CaCO3 AQ	4.414E-06	4.432E-06	-5.35336	1.00411	
3.068						
1507320	CaSO4 AQ	1.018E-03	1.022E-03	-2.99065	1.00411	
2.270						
303300	AlOH +2	2.929E-17	1.732E-17	-16.76141	0.59135	-
5.065						
303301	Al(OH)2 +	3.078E-12	2.699E-12	-11.56882	0.87692	-
10.043						
303302	Al(OH)4 -	2.933E-06	2.572E-06	-5.58972	0.87692	-
24.064						
307320	AlSO4 +	5.111E-22	4.482E-22	-21.34850	0.87692	
3.022						
307321	Al(SO4)2 -	5.570E-23	4.884E-23	-22.31120	0.87692	
4.905						
303303	Al(OH)3 AQ	3.383E-08	3.397E-08	-7.46890	1.00411	-
16.002						
2803300	FeOH +	4.102E-07	3.597E-07	-6.44400	0.87692	-
9.779						
2803301	FeOH3 -1	4.763E-09	4.177E-09	-8.37916	0.87692	-
31.714						
2807320	FeSO4 AQ	5.161E-08	5.182E-08	-7.28549	1.00411	
2.166						
2803302	FeOH2 AQ	1.240E-08	1.245E-08	-7.90494	1.00411	-
21.298						
2807300	Fe(HS)2 AQ	3.964E-46	3.981E-46	-45.40006	1.00411	
8.948						
2807301	Fe(HS)3 -	6.653E-68	5.834E-68	-67.23400	0.87692	
11.044						
2813300	FeOH +2	3.684E-19	2.178E-19	-18.66186	0.59135	-
2.226						
2817320	FeSO4 +	6.686E-26	5.863E-26	-25.23186	0.87692	
3.878						
2813301	FeOH2 +	1.512E-12	1.326E-12	-11.87742	0.87692	-
5.613						
2813302	FeOH3 AQ	1.551E-10	1.558E-10	-9.80750	1.00411	-
13.602						
2813303	FeOH4 -	1.776E-08	1.557E-08	-7.80758	0.87692	-
21.543						
2817321	Fe(SO4)2 -	2.901E-27	2.544E-27	-26.59456	0.87692	
5.360						
2813304	Fe2(OH)2+4	1.602E-35	1.959E-36	-35.70807	0.12229	-
2.381						
2813305	Fe3(OH)4+5	1.381E-44	5.178E-46	-45.28584	0.03750	-
5.238						
1003300	BaOH +	4.296E-15	3.767E-15	-14.42400	0.87692	-
13.685						
4703300	MnOH +	3.369E-09	2.954E-09	-8.52956	0.87692	-
10.899						
4703301	Mn(OH)3 -1	4.826E-13	4.232E-13	-12.37346	0.87692	-
34.743						
4700020	MnO4 -	1.336E-21	1.172E-21	-20.93112	0.87692	-
132.260						
4700021	MnO4 -2	3.680E-19	2.176E-19	-18.66231	0.59135	-
122.028						

4707320	MnSO4 AQ	6.091E-09	6.116E-09	-8.21356	1.00411	
2.203						
4701400	MnHCO3 +	1.196E-12	1.049E-12	-11.97921	0.87692	
11.657						
2311400	CuCO3 AQ	1.596E-13	1.603E-13	-12.79513	1.00411	
6.728						
2311401	Cu(CO3)2-2	3.365E-16	1.990E-16	-15.70112	0.59135	
10.058						
2313300	CuOH +	3.450E-12	3.025E-12	-11.51922	0.87692	-
7.943						
2313301	Cu(OH)2 AQ	6.294E-08	6.320E-08	-7.19930	1.00411	-
13.682						
2313302	Cu(OH)3 -	4.352E-11	3.816E-11	-10.41838	0.87692	-
26.842						
2313303	Cu(OH)4 -2	1.284E-13	7.595E-14	-13.11946	0.59135	-
39.372						
2313304	Cu2(OH)2+2	2.427E-18	1.435E-18	-17.84308	0.59135	-
10.576						
2317320	CuSO4 AQ	8.183E-15	8.216E-15	-14.08532	1.00411	
2.277						
2317300	Cu(HS)3 -	6.669E-60	5.848E-60	-59.23296	0.87692	
25.956						
2311402	CuHCO3 +	3.403E-17	2.985E-17	-16.52513	0.87692	
13.057						
9503300	ZnOH +	1.333E-09	1.169E-09	-8.93215	0.87692	-
9.244						
9503301	Zn(OH)2 AQ	2.936E-07	2.948E-07	-6.53040	1.00411	-
16.901						
9503302	Zn(OH)3 -	1.063E-08	9.322E-09	-8.03049	0.87692	-
28.342						
9503303	Zn(OH)4 -2	2.498E-11	1.477E-11	-10.83057	0.59135	-
40.971						
9507300	Zn(HS)2 AQ	3.674E-43	3.689E-43	-42.43312	1.00411	
14.938						
9507301	Zn(HS)3 -	8.184E-66	7.177E-66	-65.14407	0.87692	
16.157						
9507320	ZnSO4 AQ	7.198E-11	7.228E-11	-10.14099	1.00411	
2.334						
9507321	Zn(SO4)2-2	1.537E-12	9.088E-13	-12.04154	0.59135	
3.508						
9501400	ZnHCO3 +	6.604E-14	5.791E-14	-13.23723	0.87692	
12.457						
9501401	ZnCO3 AQ	4.581E-11	4.600E-11	-10.33723	1.00411	
5.298						
9501402	Zn(CO3)2-2	1.640E-12	9.700E-13	-12.01322	0.59135	
9.858						
1601400	Cd(CO3)3-4	3.601E-20	4.404E-21	-20.35619	0.12229	
7.133						
1603300	CdOH +	1.218E-09	1.068E-09	-8.97153	0.87692	-
10.356						
1603301	Cd(OH)2 AQ	1.230E-09	1.235E-09	-8.90839	1.00411	-
20.352						
1603302	Cd(OH)3 -	1.580E-12	1.385E-12	-11.85847	0.87692	-
33.243						
1603303	Cd(OH)4 -2	2.087E-16	1.234E-16	-15.90855	0.59135	-
47.122						
1603304	Cd2OH +3	5.365E-17	1.645E-17	-16.78377	0.30666	-
9.154						
1607320	CdSO4 AQ	1.065E-09	1.069E-09	-8.97085	1.00411	
2.431						
1607300	CdHS +	6.279E-23	5.506E-23	-22.25917	0.87692	
10.227						
1607301	Cd(HS)2 AQ	1.691E-40	1.698E-40	-39.77011	1.00411	
16.528						

1607302	Cd(HS)3 -	3.944E-62	3.459E-62	-61.46105	0.87692	
18.767						
1607303	Cd(HS)4 -2	1.219E-83	7.211E-84	-83.14199	0.59135	
21.128						
1601400	CdHCO3 +	7.813E-13	6.851E-13	-12.16422	0.87692	
12.457						
1601401	CdCO3 AQ	6.808E-10	6.836E-10	-9.16522	1.00411	
5.397						
1607321	Cd(SO4)2-2	3.017E-11	1.784E-11	-10.74853	0.59135	
3.728						
6001400	Pb(CO3)2-2	1.072E-11	6.340E-12	-11.19790	0.59135	
10.868						
6003300	PbOH +	3.319E-08	2.911E-08	-7.53601	0.87692	-
7.653						
6003301	Pb(OH)2 AQ	1.128E-07	1.132E-07	-6.94609	1.00411	-
17.122						
6003302	Pb(OH)3 -	1.482E-08	1.300E-08	-7.88617	0.87692	-
28.003						
6003303	Pb2OH +3	3.173E-16	9.729E-17	-16.01193	0.30666	-
5.847						
6007320	PbSO4 AQ	1.194E-10	1.199E-10	-9.92107	1.00411	
2.748						
6007300	Pb(HS)2 AQ	5.017E-43	5.037E-43	-42.29781	1.00411	
15.268						
6007301	Pb(HS)3 -	1.543E-65	1.353E-65	-64.86875	0.87692	
16.627						
6003304	Pb3(OH)4+2	1.570E-14	9.286E-15	-14.03218	0.59135	-
24.326						
6001401	PbCO3 AQ	2.549E-09	2.559E-09	-8.59192	1.00411	
7.238						
6003305	Pb(OH)4 -2	5.046E-10	2.984E-10	-9.52525	0.59135	-
39.471						
6007321	Pb(SO4)2-2	1.520E-12	8.990E-13	-12.04622	0.59135	
3.698						
6001402	PbHCO3 +	2.661E-13	2.334E-13	-12.63192	0.87692	
13.257						
5403300	NiOH +	8.168E-09	7.162E-09	-8.14495	0.87692	-
10.119						
5403301	Ni(OH)2 AQ	1.069E-07	1.074E-07	-6.96910	1.00411	-
19.002						
5403302	Ni(OH)3 -	1.224E-08	1.074E-08	-7.96918	0.87692	-
29.943						
5407320	NiSO4 AQ	2.726E-09	2.737E-09	-8.56275	1.00411	
2.250						
5401400	NiHCO3 +	3.565E-12	3.127E-12	-11.50493	0.87692	
12.527						
5401401	NiCO3 AQ	7.821E-08	7.854E-08	-7.10493	1.00411	
6.868						
5401402	Ni(CO3)2-2	2.276E-10	1.346E-10	-9.87092	0.59135	
10.338						
5407321	Ni(SO4)2-2	3.881E-13	2.295E-13	-12.63924	0.59135	
1.248						
207300	AgHS AQ	1.479E-18	1.485E-18	-17.82836	1.00411	
14.048						
207301	Ag(HS)2 -	5.724E-38	5.020E-38	-37.29930	0.87692	
18.507						
203300	AgOH AQ	9.789E-11	9.829E-11	-10.00750	1.00411	-
12.002						
203301	Ag(OH)2 -	1.121E-12	9.827E-13	-12.00758	0.87692	-
23.943						
207320	AgSO4 -	2.861E-10	2.509E-10	-9.60047	0.87692	
1.309						
3300611	H2AsO4 -	2.462E-11	2.159E-11	-10.66566	0.87692	-
2.143						

3300612	HAsO4 -2	6.094E-08	3.604E-08	-7.44325	0.59135	-8.749
3300613	AsO4 -3	2.309E-09	7.081E-10	-9.14990	0.30666	-20.171
3301400	HCO3 -	3.024E-06	2.651E-06	-5.57651	0.87692	10.487
3301401	H2CO3 AQ	5.375E-10	5.397E-10	-9.26783	1.00411	16.736
3307320	HSO4 -	1.203E-11	1.055E-11	-10.97664	0.87692	1.926
3307300	H2S AQ	1.629E-27	1.636E-27	-26.78635	1.00411	7.083
3307301	S -2	1.353E-27	8.003E-28	-27.09673	0.59135	-12.998
3307620	HSeO4-1	5.645E-16	4.950E-16	-15.30539	0.87692	1.856
4707620	MnSeO4	4.482E-13	4.500E-13	-12.34679	1.00411	2.329
5407620	NiSeO4	2.983E-13	2.995E-13	-12.52363	1.00411	2.548

Type III - SPECIES WITH FIXED ACTIVITY

ID	NAME	CALC MOL	LOG MOL	NEW LOGK	DH
2	H2O	-7.080E-05	-4.150	0.000	0.000
330	H+1	6.844E-05	-4.165	10.000	0.000
1028003	PYRITE	-7.393E-19	-18.131	18.766	-11.300

Type IV - FINITE SOLIDS (present at equilibrium)

ID	NAME	CALC MOL	LOG MOL	NEW LOGK	DH
5015001	CALCITE	9.907E-04	-5.033	8.423	2.585
7210000	BA(ASO4)2	1.044E-07	-6.981	8.977	-2.640

Type V - UNDERSATURATED SOLIDS (not present at equilibrium)

ID	NAME	CALC MOL	LOG MOL	NEW LOGK	DH
6015001	GYPSUM	3.910E-01	-0.408	4.855	-0.261
6010000	BARITE	4.061E-04	-3.391	10.136	-6.280
5028000	SIDERITE	6.314E-03	-2.200	10.414	5.328
2023101	TENORITE	2.973E-02	-1.527	-8.008	15.240
5016000	OTAVITE	1.449E-01	-0.839	13.725	0.580
6060003	ANGLESITE	1.491E-05	-4.826	7.845	-2.150
2003000	ALOH3(A)	2.905E-03	-2.537	-11.068	27.045

Type VI - EXCLUDED SPECIES (not included in mole balance)

ID	NAME	CALC MOL	LOG MOL	NEW LOGK	DH
3301403	CO2 (g)	1.471E-08	-7.832	18.173	-0.530
3300021	O2 (g)	4.394E-16	-15.357	-86.524	133.830
1	E-1	1.615E-08	-7.792	0.000	0.000
2802810	Fe+2/Fe+3	7.861E-15	-14.105	13.286	-10.000
7307320	HS-/SO4-2	0.000E-01	-96.119	35.190	-60.140

3301404	CH4 (g)	0.000E-01	-126.689	41.652	-61.000

PERCENTAGE DISTRIBUTION OF COMPONENTS AMONG
TYPE I and TYPE II (dissolved and adsorbed) species

Fe+3	99.1	PERCENT BOUND IN SPECIES #2813303	
FeOH4 -			
SO4-2	70.4	PERCENT BOUND IN SPECIES #	732
SO4-2			
	29.6	PERCENT BOUND IN SPECIES #1507320	CaSO4 AQ
Al+3	98.9	PERCENT BOUND IN SPECIES # 303302	
Al(OH)4 -			
	1.1	PERCENT BOUND IN SPECIES # 303303	Al(OH)3 AQ
H3AsO4	96.3	PERCENT BOUND IN SPECIES #3300612	
HAsO4 -2			
	3.6	PERCENT BOUND IN SPECIES #3300613	AsO4 -3
E-1	99.5	PERCENT BOUND IN SPECIES #4700021	
MnO4 -2			
Cd+2	52.5	PERCENT BOUND IN SPECIES #	160
Cd+2			
	13.7	PERCENT BOUND IN SPECIES #1603300	CdOH +
	13.8	PERCENT BOUND IN SPECIES #1603301	Cd(OH)2 AQ
	12.0	PERCENT BOUND IN SPECIES #1607320	CdSO4 AQ
	7.6	PERCENT BOUND IN SPECIES #1601401	CdCO3 AQ
Ca+2	86.3	PERCENT BOUND IN SPECIES #	150
Ca+2			
	13.6	PERCENT BOUND IN SPECIES #1507320	CaSO4 AQ
Cr+2	100.0	PERCENT BOUND IN SPECIES #	210
Cr+2			
Cu+2	99.9	PERCENT BOUND IN SPECIES #2313301	
Cu(OH)2 AQ			
Fe+2	46.5	PERCENT BOUND IN SPECIES #	280
Fe+2			
	45.8	PERCENT BOUND IN SPECIES #2803300	FeOH +
	5.8	PERCENT BOUND IN SPECIES #2807320	FeSO4 AQ
	1.4	PERCENT BOUND IN SPECIES #2803302	FeOH2 AQ
Pb+2	20.2	PERCENT BOUND IN SPECIES #6003300	
PbOH +			
	68.7	PERCENT BOUND IN SPECIES #6003301	Pb(OH)2 AQ
	9.0	PERCENT BOUND IN SPECIES #6003302	Pb(OH)3 -
	1.6	PERCENT BOUND IN SPECIES #6001401	PbCO3 AQ
Mg+2	87.5	PERCENT BOUND IN SPECIES #	460
Mg+2			
	12.1	PERCENT BOUND IN SPECIES #4607320	MgSO4 AQ

Mn+2		82.7	PERCENT BOUND IN SPECIES # 470
Mn+2			
	6.2	PERCENT BOUND IN SPECIES #4703300	MnOH +
	11.1	PERCENT BOUND IN SPECIES #4707320	MnSO4 AQ
Ni+2		8.0	PERCENT BOUND IN SPECIES # 540
Ni+2			
	3.6	PERCENT BOUND IN SPECIES #5403300	NiOH +
	47.2	PERCENT BOUND IN SPECIES #5403301	Ni(OH)2 AQ
	5.4	PERCENT BOUND IN SPECIES #5403302	Ni(OH)3 -
	1.2	PERCENT BOUND IN SPECIES #5407320	NiSO4 AQ
	34.5	PERCENT BOUND IN SPECIES #5401401	NiCO3 AQ
SeO4-2		100.0	PERCENT BOUND IN SPECIES # 762
SeO4-2			
Ag+1		96.7	PERCENT BOUND IN SPECIES # 20
Ag+1			
	2.5	PERCENT BOUND IN SPECIES # 207320	AgSO4 -
Zn+2		95.9	PERCENT BOUND IN SPECIES #9503301
Zn(OH)2 AQ			
	3.5	PERCENT BOUND IN SPECIES #9503302	Zn(OH)3 -
H2O		74.0	PERCENT BOUND IN SPECIES #3300020
OH-			
	6.6	PERCENT BOUND IN SPECIES #1503300	CaOH +
	16.6	PERCENT BOUND IN SPECIES # 303302	Al(OH)4 -
Ba+2		100.0	PERCENT BOUND IN SPECIES # 100
Ba+2			
HS-1		100.0	PERCENT BOUND IN SPECIES # 207300
AgHS AQ			
CO3-2		18.0	PERCENT BOUND IN SPECIES # 140
CO3-2			
	47.6	PERCENT BOUND IN SPECIES #1501401	CaCO3 AQ
	32.6	PERCENT BOUND IN SPECIES #3301400	HCO3 -
H+1		77.3	PERCENT BOUND IN SPECIES #3300020
OH-			
	6.9	PERCENT BOUND IN SPECIES #1503300	CaOH +
	17.3	PERCENT BOUND IN SPECIES # 303302	Al(OH)4 -

PART 5 of OUTPUT FILE

PC MINTEQA2 v3.10 DATE OF CALCULATIONS: 11-MAR-97 TIME: 23:54: 8

EQUILIBRATED MASS DISTRIBUTION

IDX	NAME	DISSOLVED		SORBED		PRECIPITATED
		MOL/KG	PERCENT	MOL/KG	PERCENT	MOL/KG
PERCENT						
281	Fe+3	1.792E-08	100.0	0.000E-01	0.0	0.000E-01
0.0						
732	SO4-2	3.433E-03	100.0	0.000E-01	0.0	0.000E-01
0.0						
30	Al+3	2.967E-06	100.0	0.000E-01	0.0	0.000E-01
0.0						
61	H3AsO4	6.327E-08	23.3	0.000E-01	0.0	2.088E-07
76.7						
1	E-1	-1.479E-18	100.0	0.000E-01	0.0	0.000E-01
0.0						
160	Cd+2	8.902E-09	100.0	0.000E-01	0.0	0.000E-01
0.0						
150	Ca+2	7.499E-03	88.3	0.000E-01	0.0	9.907E-04
11.7						
210	Cr+2	5.773E-08	100.0	0.000E-01	0.0	0.000E-01
0.0						
231	Cu+2	6.299E-08	100.0	0.000E-01	0.0	0.000E-01
0.0						
280	Fe+2	8.959E-07	100.0	0.000E-01	0.0	0.000E-01
0.0						
600	Pb+2	1.642E-07	100.0	0.000E-01	0.0	0.000E-01
0.0						
460	Mg+2	8.231E-07	100.0	0.000E-01	0.0	0.000E-01
0.0						
470	Mn+2	5.464E-08	100.0	0.000E-01	0.0	0.000E-01
0.0						
540	Ni+2	2.267E-07	100.0	0.000E-01	0.0	0.000E-01
0.0						
762	SeO4-2	1.330E-07	100.0	0.000E-01	0.0	0.000E-01
0.0						
20	Ag+1	1.160E-08	100.0	0.000E-01	0.0	0.000E-01
0.0						
950	Zn+2	3.061E-07	100.0	0.000E-01	0.0	0.000E-01
0.0						
2	H2O	7.080E-05	100.0	0.000E-01	0.0	0.000E-01
0.0						
100	Ba+2	3.518E-11	0.0	0.000E-01	0.0	3.133E-07
100.0						
730	HS-1	1.479E-18	100.0	0.000E-01	0.0	0.000E-01
0.0						
140	CO3-2	9.277E-06	0.9	0.000E-01	0.0	9.907E-04
99.1						
330	H+1	-6.781E-05	100.0	0.000E-01	0.0	0.000E-01
0.0						

Charge Balance: SPECIATED

Sum of CATIONS = 1.295E-02 Sum of ANIONS 4.893E-03

PERCENT DIFFERENCE = 4.516E+01 (ANIONS - CATIONS)/(ANIONS + CATIONS)

EQUILIBRIUM IONIC STRENGTH (m) = 1.781E-02

EQUILIBRIUM pH = 10.000

EQUILIBRIUM pe = 7.792 or Eh = 445.47 mv

DATE ID NUMBER: 970311
TIME ID NUMBER: 23540836

PC MINTEQA2 v3.10 DATE OF CALCULATIONS: 11-MAR-97 TIME: 23:54: 8

Saturation indices and stoichiometry of all minerals

ID #	NAME	Sat. Index	Stoichiometry in [brackets]
2003000	ALOH3(A)	-2.537	[1.000] 30 [3.000] 2 [-3.000] 330
6003000	ALOHSO4	-11.084	[-1.000] 330 [1.000] 30 [1.000] 732
6003001	AL4(OH)10SO4	-11.421	[1.000] 2 [-10.000] 330 [4.000] 30 [1.000] 732
6015000	ANHYDRITE	-0.721	[10.000] 2 [1.000] 150 [1.000] 732
5015000	ARAGONITE	-0.173	[1.000] 150 [1.000] 140
5046000	ARTINITE	-9.079	[-2.000] 330 [2.000] 460 [1.000] 140
6010000	BARITE	-3.391	[5.000] 2 [1.000] 100 [1.000] 732
2003001	BOEHMITE	-0.762	[-3.000] 330 [1.000] 30 [2.000] 2
2046000	BRUCITE	-3.820	[1.000] 460 [2.000] 2 [-2.000] 330
5015001	CALCITE	0.000	[1.000] 150 [1.000] 140
2003002	DIASPORE	1.032	[-3.000] 330 [1.000] 30 [2.000] 2
5015002	DOLOMITE	-4.011	[1.000] 150 [1.000] 460 [2.000] 140
6046000	EPSOMITE	-7.005	[1.000] 460 [1.000] 732 [7.000] 2
2028100	FERRIHYDRITE	-1.099	[-3.000] 330 [1.000] 281 [3.000] 2
2028101	FE3(OH)8	0.755	[-8.000] 330 [2.000] 281 [1.000] 280
1028000	FES PPT	-16.564	[8.000] 2 [-1.000] 330 [1.000] 280 [1.000] 730
6028100	FE2(SO4)3	-66.034	[2.000] 281 [3.000] 732
2003003	GIBBSITE (C)	-0.819	[-3.000] 330 [1.000] 30 [3.000] 2
3003000	Al2O3	-5.918	[2.000] 30 [3.000] 2 [-6.000] 330
2028102	GOETHITE	2.924	[-3.000] 330 [1.000] 281 [2.000] 2
1028001	GREIGITE	-69.471	[-4.000] 330 [2.000] 281 [1.000] 280
6015001	GYPSUM	-0.408	[4.000] 730 [1.000] 150 [1.000] 732 [2.000] 2
3028100	HEMATITE	10.809	[-6.000] 330 [2.000] 281 [3.000] 2
5015003	HUNTITE	-16.240	[3.000] 460 [1.000] 150 [4.000] 140
5046001	HYDRMAGNESIT	-28.440	[5.000] 460 [4.000] 140 [-2.000] 330
6028101	JAROSITE H	-23.615	[6.000] 2 [-5.000] 330 [3.000] 281 [2.000] 732

```
                                        [  7.000]   2
  1028002 MACKINAWITE    -15.831        [ -1.000] 330   [  1.000] 280   [
1.000] 730
  3028101 MAGHEMITE        1.199        [ -6.000] 330   [  2.000] 281   [
3.000]   2
  5046002 MAGNESITE       -4.505        [  1.000] 460   [  1.000] 140
  3028000 MAGNETITE       15.956        [ -8.000] 330   [  2.000] 281   [
1.000] 280
                                        [  4.000]   2
  6028000 MELANTERITE     -6.911        [  1.000] 280   [  1.000] 732   [
7.000]   2
  5046003 NESQUEHONITE    -6.903        [  1.000] 460   [  1.000] 140   [
3.000]   2
  1028003 PYRITE           0.000        [ -2.000] 330   [ -2.000]   1   [
1.000] 280
                                        [  2.000] 730
  5028000 SIDERITE        -2.200        [  1.000] 280   [  1.000] 140
```

ID #	NAME	Sat. Index	Stoichiometry in [brackets]
5010000	WITHERITE	-8.094	[1.000] 100 [1.000] 140
3047000	HAUSMANNITE	9.285	[-8.000] 330 [-2.000] 1 [3.000] 470
2047003	PYROCROITE	-3.236	[4.000] 2 [-2.000] 330 [1.000] 470 [2.000] 2
5047000	RHODOCHROSIT	-3.222	[1.000] 470 [1.000] 140
1047000	MNS GREEN	-25.391	[-1.000] 330 [1.000] 470 [1.000] 730
6047000	MNSO4	-13.481	[1.000] 470 [1.000] 732
1023101	COVELLITE	-3.741	[-1.000] 330 [1.000] 231 [1.000] 730
5023100	CUCO3	-9.895	[1.000] 231 [1.000] 140
2023100	CU(OH)2	-2.547	[-2.000] 330 [1.000] 231 [2.000] 2
6023100	ANTLERITE	-11.693	[-4.000] 330 [3.000] 231 [4.000] 2
6023101	BROCHANTITE	-12.262	[1.000] 732 [-6.000] 330 [4.000] 231 [6.000] 2
6023102	LANGITE	-14.720	[1.000] 732 [-6.000] 330 [4.000] 231 [7.000] 2
2023101	TENORITE	-1.527	[1.000] 732 [-2.000] 330 [1.000] 231 [1.000] 2
6023103	CUOCUSO4	-22.318	[-2.000] 330 [2.000] 231 [1.000] 2
6023104	CUSO4	-19.836	[1.000] 732 [1.000] 231 [1.000] 732
6023105	CHALCANTHITE	-13.688	[1.000] 231 [1.000] 732 [5.000] 2
3023100	CUPRICFERIT	7.202	[-8.000] 330 [1.000] 231 [2.000] 281
1023102	CHALCOPYRITE	-11.697	[4.000] 2 [-2.000] 330 [1.000] 231 [1.000] 280
95000	ZN METAL	-51.907	[2.000] 730 [1.000] 950 [2.000] 1
5095000	SMITHSONITE	-5.748	[1.000] 950 [1.000] 140
5095001	ZNCO3, 1H2O	-5.377	[1.000] 950 [1.000] 140 [1.000] 2
2095000	ZN(OH)2 (A)	-2.081	[-2.000] 330 [1.000] 950 [2.000] 2
2095001	ZN(OH)2 (C)	-1.831	[-2.000] 330 [1.000] 950 [2.000] 2
2095002	ZN(OH)2 (B)	-1.381	[-2.000] 330 [1.000] 950 [2.000] 2
2095003	ZN(OH)2 (G)	-1.341	[-2.000] 330 [1.000] 950 [2.000] 2
2095004	ZN(OH)2 (E)	-1.131	[-2.000] 330 [1.000] 950 [2.000] 2
6095000	ZN2(OH)2SO4	-9.608	[-2.000] 330 [2.000] 950 [2.000] 2
6095001	ZN4(OH)6SO4	-9.771	[1.000] 732 [-6.000] 330 [4.000] 950 [6.000] 2
2095005	ZNO(ACTIVE)	-0.941	[1.000] 732 [-2.000] 330 [1.000] 950 [1.000] 2

```
  2095006 ZINCITE          -1.327    [ -2.000] 330  [  1.000] 950  [
1.000]   2
  6095002 ZN3O(SO4)2       -35.181   [ -2.000] 330  [  3.000] 950  [
2.000] 732
                                     [  1.000]   2
  1095000 ZNS (A)          -14.357   [ -1.000] 330  [  1.000] 950  [
1.000] 730
  1095001 SPHALERITE       -11.674   [ -1.000] 330  [  1.000] 950  [
1.000] 730
  1095002 WURTZITE         -13.691   [ -1.000] 330  [  1.000] 950  [
1.000] 730
  6095003 ZINCOSITE        -15.975   [  1.000] 950  [  1.000] 732
  6095004 ZNSO4, 1H2O      -12.177   [  1.000] 950  [  1.000] 732  [
1.000]   2
  6095005 BIANCHITE        -10.716   [  1.000] 950  [  1.000] 732  [
6.000]   2
  6095006 GOSLARITE        -10.433   [  1.000] 950  [  1.000] 732  [
7.000]   2
    16000 CD METAL         -38.090   [  1.000] 160  [  2.000]   1
    16001 GAMMA CD         -38.193   [  1.000] 160  [  2.000]   1
  5016000 OTAVITE           -0.839   [  1.000] 160  [  1.000] 140
```

ID #	NAME	Sat. Index	Stoichiometry in [brackets]
5002000	AG2CO3	-10.708	[2.000] 20 [1.000] 140
2002000	AG2O	-8.860	[-2.000] 330 [2.000] 20 [1.000] 2
1002000	ACANTHITE	7.520	[-1.000] 330 [2.000] 20 [1.000] 730
6002000	AG2SO4	-13.832	[2.000] 20 [1.000] 732
5023101	MALACHITE	-8.261	[2.000] 231 [2.000] 2 [1.000] 140 [-2.000] 330
5023102	AZURITE	-16.254	[3.000] 231 [2.000] 2 [2.000] 140 [-2.000] 330
3006100	AS2O5	-43.768	[2.000] 61 [-3.000] 2
73100	SULFUR	3.716	[1.000] 730 [-1.000] 330 [-2.000] 1
7203000	ALASO4.2W	-14.734	[1.000] 30 [1.000] 61 [2.000] 2 [-3.000] 330
7215000	CA3(ASO4)26W	-6.483	[3.000] 150 [2.000] 61 [4.000] 2 [-6.000] 330
7223100	CU3(ASO4)26W	-23.589	[3.000] 231 [2.000] 61 [2.000] 2 [-6.000] 330
7228100	FEASO4.2W	-15.073	[1.000] 281 [1.000] 61 [2.000] 2 [-3.000] 330
7247000	MN3ASO428W	-12.152	[3.000] 470 [2.000] 61 [8.000] 2 [-6.000] 330
7254000	NI3(ASO4)28W	-16.539	[3.000] 540 [2.000] 61 [8.000] 2 [-6.000] 330
7260000	PB3(ASO4)2	-12.209	[3.000] 600 [2.000] 61 [-6.000] 330
7295000	ZN3ASO422.5W	-19.475	[3.000] 950 [2.000] 61 [2.500] 2 [-6.000] 330
7210000	BA(ASO4)2	0.000	[3.000] 100 [2.000] 61 [-6.000] 330
2015000	LIME	-16.391	[-2.000] 330 [1.000] 150 [1.000] 2
2015001	PORTLANDITE	-5.873	[-2.000] 330 [1.000] 150 [2.000] 2
2028000	WUSTITE	1.423	[-2.000] 330 [0.947] 280 [1.000] 2
2046001	PERICLASE	-8.800	[-2.000] 330 [1.000] 460 [1.000] 2
3028001	HERCYNITE	1.299	[-8.000] 330 [1.000] 280 [2.000] 30 [4.000] 2
3046000	SPINEL	-7.907	[-8.000] 330 [1.000] 460 [2.000] 30 [4.000] 2
3046001	MAG-FERRITE	2.754	[-8.000] 330 [1.000] 460 [2.000] 281 [4.000] 2
3028102	LEPIDOCROCIT	2.422	[-3.000] 330 [1.000] 281 [2.000] 2

ID #	NAME	Sat. Index	Stoichiometry in [brackets]
2016000	CD(OH)2 (A)	-2.817	[-2.000] 330 [1.000] 160 [2.000] 2
2016001	CD(OH)2 (C)	-2.208	[-2.000] 330 [1.000] 160 [2.000] 2
6016000	CD3(OH)4SO4	-11.080	[-4.000] 330 [3.000] 160 [4.000] 2 [1.000] 732
6016001	CD3OH2(SO4)2	-18.075	[-2.000] 330 [3.000] 160 [2.000] 2 [2.000] 732
6016002	CD4(OH)6SO4	-5.479	[-6.000] 330 [4.000] 160 [6.000] 2 [1.000] 732
2016002	MONTEPONITE	-4.308	[-2.000] 330 [1.000] 160 [1.000] 2
6016003	CDSO4	-11.678	[1.000] 160 [1.000] 732
6016004	CDSO4, 1H2O	-9.938	[1.000] 160 [1.000] 732 [1.000] 2
6016005	CDSO4,2.7H2O	-9.640	[1.000] 160 [1.000] 732 [2.670] 2
1016000	GREENOCKITE	-6.083	[-1.000] 330 [1.000] 160 [1.000] 730
60000	PB METAL	-29.669	[1.000] 600 [2.000] 1
5060000	CERRUSITE	-2.578	[1.000] 600 [1.000] 140
2060000	MASSICOT	-3.163	[-2.000] 330 [1.000] 600 [1.000] 2
2060001	LITHARGE	-2.963	[-2.000] 330 [1.000] 600 [1.000] 2
2060002	PBO, .3H2O	-2.806	[-2.000] 330 [1.000] 600 [1.330] 2
5060001	PB2OCO3	-5.449	[-2.000] 330 [2.000] 600 [1.000] 2 [1.000] 140
6060000	LARNAKITE	-2.381	[-2.000] 330 [2.000] 600 [1.000] 732
6060001	PB3O2SO4	-3.251	[-4.000] 330 [3.000] 600 [1.000] 2 [1.000] 732
6060002	PB4O3SO4	-5.141	[-6.000] 330 [4.000] 600 [1.000] 2 [1.000] 732
5060002	PB3O2CO3	-7.176	[-4.000] 330 [3.000] 600 [1.000] 2 [1.000] 140
6060003	ANGLESITE	-4.826	[1.000] 600 [1.000] 732
1060001	GALENA	-8.071	[-1.000] 330 [1.000] 600 [1.000] 730
2060003	PLATTNERITE	-5.342	[-4.000] 330 [-2.000] 1 [1.000] 2 [1.000] 600
3060000	PB2O3	-5.108	[-6.000] 330 [-2.000] 1 [2.000] 2 [2.000] 600
3060001	MINIUM	-10.198	[-8.000] 330 [-2.000] 1 [3.000] 2 [3.000] 600
2060004	PB(OH)2 (C)	1.668	[-2.000] 330 [1.000] 600 [2.000] 2

```
  5060003 HYDCERRUSITE    -4.030    [ -2.000] 330  [  3.000] 600  [
2.000] 140
                                  [  2.000]   2
  2060005 PB2O(OH)2       -5.852    [ -4.000] 330  [  2.000] 600  [
3.000]   2
  6060004 PB4(OH)6SO4     -3.249    [ -6.000] 330  [  4.000] 600  [
1.000] 732
                                  [  6.000]   2
  5054000 NICO3           -7.388    [  1.000] 540  [  1.000] 140
  2054000 NI(OH)2          2.005    [ -2.000] 330  [  1.000] 540  [
2.000]   2
  6054000 NI4(OH)6SO4     -6.721    [ -6.000] 330  [  4.000] 540  [
1.000] 732
                                  [  6.000]   2
  2054001 BUNSENITE       -1.027    [ -2.000] 330  [  1.000] 540  [
1.000]   2
  1054000 MILLERITE      -13.734    [ -1.000] 330  [  1.000] 540  [
1.000] 730
  6054001 RETGERSITE      -8.747    [  1.000] 540  [  1.000] 732  [
6.000]   2
  6054002 MORENOSITE      -8.380    [  1.000] 540  [  1.000] 732  [
7.000]   2
     2000 AG METAL        -1.647    [  1.000]  20  [  1.000]   1
```

APPENDIX B
Wall Rock Sulfur Content Estimates

MEMORANDUM

EXXON COAL AND MINERALS COMPANY
Technical Department

February 6, 1997

TO: Ken Black - CMC

FROM: A. J. Erickson Jr

SUBJ: Addendum -- Hanging Wall Sulfide Content Review, Crandon Deposit - Updated

---

The attached are summary and detail calculation sheets for work done in December 1996 on hanging wall sulfide estimates in key development areas of zinc mineralization at the Crandon, Wisconsin property.

A preliminary summary was faxed to K. Black, CMC, 12/16/96 with comments as indicated below. The data represents additional work carried out since 7/10/96, the date of the above titled report.

1. Basis was the same holes as in the 7/10/96 report.

2. Drill holes and sections used are representative of the area.

3. Data from 29 holes, locations as shown on the sections and plans in the 7/10/96 referenced report, were used in this update. These holes provide a representative sample of the ground in which mine development will take place.

4. Estimates on individual logs compiled 7/10/96.

5. Numerical values of estimates in the calculations are shown on the attached sheet SULSUM6.XLS. If the drill log showed trace (tr) sulfide content, the value 0.1% was used in the calculation. If the value of sulfide was estimated at 1.0 to 3.0%, the value of 2.0% was used in the calculations.

6. SULSUM5.XLS is a summary on a hole by hole basis.

7. No holes were included in the West Vent Shaft area as they do not sample the appropriate stratigraphy.

8. As shown on Stope 60 sections (shaft) the sulfides in the Skunk Lake are considerably north of the proposed shaft. Little sulfide is anticipated in the shaft, while the sand fill drift may contain some sulfide.

9. Individual sheets are available for each of the 29 holes.

CRANDON MINING COMPANY
Sulfide Distribution in Hanging Wall - By Formation

Footage Distribution								
	< 5% Sulfide				> 5% Sulfide			
	Ft	%Sulfide	Range(%)	Comment	Ft	%Sulfide	Range(%)	Comment
Sk	6843	0.6	0.0-4.0		226	6.2	4.8-15.0	
Rc	8606	0.4	0.0-3.0		12	6.0	6.0	
Ml	5776	0.5	0.0-2.0		3	26.7	25.0-30.0	
Lml	3395	0.5	0.0-5.0		26	5.0	5.0	

Percentage Distribution								
	< 5% Sulfide				> 5% Sulfide			
	Ft(%)	%Sulfide	Range(%)	Comment	Ft(%)	%Sulfide	Range(%)	Comment
Sk	96.8	0.6	0.0-4.0		3.2	6.2	4.8-15.0	
Rc	99.86	0.4	0.0-3.0		0.14	6.0	6.0	
Ml	99.95	0.5	0.0-2.0		0.05	26.7	25.0-30.0	
Lml	99.24	0.5	0.0-5.0		0.76	5.0	5.0	

% Sulfide	to	%Sulfur
0.1	equals	0.05
0.5	equals	0.27
0.7	equals	0.37
1.0	equals	0.53
1.5	equals	0.80
2.0	equals	1.06
2.5	equals	1.33
3.0	equals	1.59
3.5	equals	1.86
4.0	equals	2.12
4.5	equals	2.39
5.0	equals	2.65
5.5	equals	2.92
5.7	equals	3.00
6.0	equals	3.18

Value estimated Sulfide		
Log Estimate	% Sulfide Range	% Sulfide CalcValue
Nil	0.0	0.0
Nil to Tr	0 to 0.1	0.1
Tr	< 0.1	0.1
Wk	0.5	0.5
Tr to 1.0	0.5	0.5
< 1.0	< 1.0	0.7
< = 1.0	1.0	1.0
1.0 to 3.0	1.0 to 3.0	2.0
5.0 to 7.0	5.0 to 7.0	6.0

CRANDON MINING COMPANY

Sulfide Distribution in Hanging Wall - By Formation

Hole No.	Skunk Lake						Rice Creek						Mole Lake						Lower Mole Lake						Comment
	< 5% sulfide			>5 % sulfide			< 5% sulfide			>5 % sulfide			< 5% sulfide			>5 % sulfide			< 5% sulfide			>5 % sulfide			
	Ft	%	Range	Ft	%	Range	Ft	%	Range	Ft	%	Range	Ft	%	Range	Ft	%	Range	Ft	%	Range	Ft	%	Range	
9	220	1.3	0.5-2.0				370	0.7	0.0-0.7				60	0.6	0.5-0.7				126	0.7	0.5-1.0				
15	380	0.1	0.7-4.0				678	0.8	0.7-1.0				162	0.8	0.0-2.0				114	0.8	0.0-1.5				
20	230	0.1	0.0-0.1				241	0.1	0.0-0.1				78	0.1	0.0-0.1				115	0.5	1.0-1.5				
21	534	0.9	0.0-2.0	117	4.8	3.0-6.5	387	0.7	0.7-1.0				694	0.9	0.7-1.5				152	1.1	1.0-1.5				
				13	6.0	6.0																			
23	671	0.5	0.1-0.7	7	10.0	10.0	429	0.5	1.0-2.0				143	0.5	0.5				67	0.5					
24	854	1.1	0.0-3.0				315	0.5	0.5				174	0.2	0.2-0.7				111	0.1	0.1				
44	523	0.6	0.5-1.5	10	5.0	5	219	0.5	0.5-1.0				198	0.6	0.5-1.0				123	0.0	0.1-0.5				
46	88	0.1	0.1				715	0.3	0.1-2.0				297	0.3	0.1-2.0				123	0.5	0.1-2.0				
73	30	0.1	0.1				348	0.1	0.0-2.0				85	1.6	0.5-2.0				157	0.03	0.0-0.5				
74	254	0.6	0.5-0.7				282	0.1	0.0-0.5				116	0.0	0.0				117	0.5	0.0-0.7				
84	172	1.18	0.0-3.0	10	5.0	5.0	225	0.1	0.1				157	0.5	0.0-1.5	1	30.0	30.0	108	0.0	0.0				
																2	25.0	25.0							
85																			83	1.5	1.0-2.0				NoDetail-936
91	497	0.4	0.1-3.0	10	5.0	5.0	211	0.1	0.0-0.1				73	0.4	0.0-2.0				133	0.5	0.0-1.0				
92	241	0.5	0.5	57	9.0	9.0	182	0.5	0.1-1.0				87	0.6	0.1-0.7				136	0.6	0.1-0.7				
94	201	0.2	0.0-0.5				375	0.0	0.0-0.5				75	0.0	0.0-0.1				123	0.8	0.1-1.0				
98	612	0.6	0.0-2.0	2	15.0	15	273	0.1	0.0-0.7				238	0.03	0.0-0.3				136	0.5	0.0-1.0				
132													190	0.1	0.0-0.5				128	0.4	0.0-1.0				
133													200	0.1	0.01				195	1.0	1.0				
140	587	0.6	0.1-0.7				742	0.7	0.1-0.7				362	0.7	0.0-1.0				120	0.3	0.1-0.5				
143							67	0.0	0				143	0.0					210	0.2	0.0-1.0				
149							112	0.0	0				460	0.3	0.0-2.0				162	0.0	0				
154							106	0.9	0.7-1.5				207	1.0	0.7-1.0				145	0.9	1.0				
155	749	0.0	0.0-2.0				1353	0.2	0.0-6.0	1	6.0	6.00	528	0.3	0.0-6.0										
										11	6.0	6.00													
160							476	0.6	0.1-1.0				409	0.9	0.1-2.0				104	2.0	2.0				
170							250	0.2	0.0-3.0				80	0.0	0				96	0.0	0.0-5.0				
172							230	0.3	0.1-0.7													26	5.0	5.0	
174							20	0.0					150	0.1	0.0-0.1				160	0.0	0.0-1.0				
176													170	0.0	0				151	0.5	0.0-1.5				
214													240	0.2	0.2										
VtAvg	6843	0.6		226	6.2		8606	0.4		12	6.0		5776	0.5		3	26.7		3395	0.5		26	5.0		
%	96.8	0.6		3.2	6.0		99.86	0.6		0.1	6.0		99.95	0.5		0.05	26.7		99.24	0.5		0.76	5.0		

4.2-13-280

CRANDON MINING COMPANY

Sulfide Distribution Preproduction Development

	Logs											
Section	Hole	Fr Ft	To Ft	Tk Ft	Fm	TS Est%	Sulfide Notes	Tk Ft	< 5%WtAvg	> 5%WtAvg	Tk Ft	Fm WtAvg
2278844	9	80	100	20	sk	0.5						
		100	131	31	sk	2.0						
		131	136	5	sk	1.0						
		136	144	8	sk	1.0						
		144	150	6	sk	1.0						
		150	161	11	sk	1.5						
		161	200	39	sk	1.0						
		200	300	100	sk	1.5		220	1.3			
		300	387	87	rc	0.7						
		387	670	283	rc	0.7		370	0.7			
		670	700	30	ml	0.7						
		700	730	30	ml	0.5		60	0.6			
		730	749	19	lml	0.5						
		749	751	2	lml	1.0						
		751	856	105	lml	0.7		126	0.7			
		856										

X

CRANDON MINING COMPANY

Sulfide Distribution Preproduction Development

		Logs											
Section	Hole	Fr Ft	To Ft	Tk Ft	Fm	TS Est%	Sulfide Notes		Tk Ft	< 5%WtAvg	> 5%WtAvg	Tk Ft	Fm WtAvg
2278581	15	1200	1300	100	sk	1.0							
		1300	1358	58	sk	0.7							
		1358	1405	47	sk	0.7							
		1405	1418	13	sk	1.0							
		1418	1425	7	sk	4.0					Close		
		1425	1580	155	sk	0.7			380	0.9			
		1580	1720	140	rc	0.7							
		1720	1772	52	rc	0.7							
		1772	1923	151	rc	0.7							
		1923	2000	77	rc	1.0							
		2000	2209	209	rc	0.7							
		2209	2258	49	rc	1.0			678	0.8			
		2258	2278	20	ml	1.0							
		2278	2345	67	ml	0.7							
		2345	2353	8	ml	2.0							
		2353	2371	18	ml	0.7							
		2371	2375	4	ml	1.5							
		2375	2397	22	ml	0.7							
		2397	2409	12	ml	1.5							
		2409	2420	11	ml	0.0			162	0.8			
		2420	2438	18	lml	0.0							
		2438	2443	5	lml	1.0							
		2443	2460	17	lml	0.7							
		2460	2475	15	lml	1.0							
		2475	2500	25	lml	0.7							
		2500	2516	16	lml	1.0							
		2516	2534	18	lml	1.5			114	0.8			
		2534											
		0											
		0											

x

CRANDON MINING COMPANY

Sulfide Distribution Preproduction Development

		Logs											
Section	Hole	Fr Ft	To Ft	Tk Ft	Fm	TS Est%	Sulfide Notes		Tk Ft	< 5%WtAvg	> 5%WtAvg	Tk Ft	Fm WtAvg
2278581	20	91	142	51	sk	0.1							
		142	176	34	sk	0.0							
		176	200	24	sk	0.0							
		200	321	121	sk	0.0		230					
		321	430	109	rc	0.0							
		430	480	50	rc	0.1							
		480	562	82	rc	0.0		241					
		562	592	30	ml	0.0							
		592	598	6	ml	0.1							
		598	640	42	ml	0.1		78					
		640	680	40	iml	0.1							
		680	720	40	iml	1.5							
		720	755	35	iml	1.5		115	0.5				
		755											
													x

CRANDON MINING COMPANY

Sulfide Distribution Preproduction Development

	Logs											
Section	Hole	Fr Ft	To Ft	Tk Ft	Fm	TS Est%	Sulfide Notes	Tk Ft	< 5%WtAvg	> 5%WtAvg	Tk Ft	Fm WtAvg
2278188	21	149	203	54	sk	0.0	oxide					
		203	246	43	sk	2.0						
		246	271	25	sk	1.0						
		271	300	29	sk	1.5						
		300	313	13	sk	1.0		164	1.0			
		313	323	10	sk	6.5		10		6.5		
		323	389	66	sk	4.5	cp	66		4.5		
		389	400	11	sk	4.0						
		400	421	21	sk	6.0			21.0	6.0		
		421	430	9	sk	3.0	cp	117		4.8		
		430	466	36	sk	0.7						
		466	615	149	sk	1.0						
		615	695	80	sk	0.7						
		695	756	61	sk	0.7						
		756	800	44	sk	0.7		370	0.8			
		800	813	13	sk	6.0	cp5 py1	13		6.0	664	1.7
		813	838	25	rc	1.0						
		838	872	34	rc	1.0						
		872	891	19	rc	0.7						
		891	1200	309	rc	0.7		387	0.7			
		1200	1274	74	ml	1.5						
		1274	1287	13	ml	1.0						
		1287	1300	13	ml	0.7						
		1300	1585	285	ml	1.0		694	0.9			
		1585	1709	124	lml	1.0						
		1709	1737	28	lml	1.5		152	1.1			
		1737										
												x

CRANDON MINING COMPANY

Sulfide Distribution Preproduction Development

	Logs											
Section	Hole	Fr Ft	To Ft	Tk Ft	Fm	TS Est%	Sulfide Notes	Tk Ft	< 5%WtAvg	> 5%WtAvg	Tk Ft	Fm WtAvg
2278581	23	155	203	48	sk	0.1		48	0.1			
		203	210	7	sk	10.0		7		10.0		
		210	330	120	sk	0.1						
		330	360	30	sk	0.5						
		360	444	84	sk	0.7						
		444	464	20	sk	0.7						
		464	474	10	sk	0.7						
		474	754	280	sk	0.5						
		754	764	10	sk	0.5						
		764	833	69	sk	0.5		623	0.5		678	0.5
		833	900	67	rc	0.5						
		900	944	44	rc	0.1						
		944	1043	99	rc	0.5						
		1043	1054	11	rc	0.7						
		1054	1096	42	rc	0.7						
		1096	1110	14	rc	2.0						
		1110	1262	152	rc	0.5		429	0.5			
		1262	1405	143	ml	0.5		143	0.5			
		1405	1472	67	lml	0.5		67	0.5			
		1472										

x

CRANDON MINING COMPANY

Sulfide Distribution Preproduction Development

	Logs											
Section	Hole	Fr Ft	To Ft	Tk Ft	Fm	TS Est%	Sulfide Notes	Tk Ft	< 5%WtAvg	> 5%WtAvg	Tk Ft	Fm WtAvg
2278844	24	107	130	23	sk	0.0						
		130	400	270	sk	2.0						
		400	438	38	sk	2.0						
		438	463	25	sk	3.0						
		463	600	137	sk	1.0						
		600	700	100	sk	0.1						
		700	706	6	sk	0.2						
		706	716	10	sk	0.6						
		716	721	5	sk	0.2						
		721	756	35	sk	0.0						
		756	766	10	sk	0.4						
		766	961	195	sk	0.5		854	1.1			
		961	1276	315	rc	0.5		315	0.5			
		1276	1279	3	ml	0.3						
		1279	1286	7	ml	0.3						
		1286	1311	25	ml	0.7	>1 cp					
		1311	1326	15	ml	0.4						
		1326	1450	124	ml	0.1		174	0.2			
		1450	1561	111	lml	0.1		111	0.1			
		1561										

x

CRANDON MINING COMPANY

Sulfide Distribution Preproduction Development

	Logs											
Section	Hole	Fr Ft	To Ft	Tk Ft	Fm	TS Est%	Sulfide Notes		Tk Ft	< 5%WtAvg	> 5%WtAvg	Tk Ft	Fm WtAvg
2278188	44	105	170	65	sk	0.5							
		170	174	4	sk	1.0							
		174	390	216	sk	0.5							
		390	394	4	sk	0.7							
		394	424	30	sk	1.5							
		424	474	50	sk	1.0							
		474	494	20	sk	1.5			389	0.7			
		494	504	10	sk	5.0			10		5.0		
		504	514	10	sk	1.5							
		514	590	76	sk	0.5							
		590	638	48	sk	0.5			134	0.6		533	0.7
		638	829	191	rc	0.5							
		829	833	4	rc	1.0							
		833	857	24	rc	0.5			219	0.5			
		857	1014	157	ml	0.5							
		1014	1040	26	ml	1.0							
		1040	1055	15	ml	0.5			198	0.6			
		1055	1100	45	lml	0.5							
		1100	1178	78	lml	0.1			123	0.2			
		1178											

x

CRANDON MINING COMPANY

Sulfide Distribution Preproduction Development

	Logs											
Section	Hole	Fr Ft	To Ft	Tk Ft	Fm	TS Est%	Sulfide Notes	Tk Ft	< 5%WtAvg	> 5%WtAvg	Tk Ft	Fm WtAvg
2278844	46	0	1100	1100	sk	0.0		0				
		1100	1188	88	sk	0.1		88		0.1		
		1188	1214	26	rc	0.1						
		1214	1293	79	rc	2.0						
		1293	1903	610	rc	0.1		715		0.3		
		1903	1945	42	ml	0.1						
		1945	1973	28	ml	2.0						
		1973	2200	227	ml	0.1		297		0.3		
		2200	2290	90	lml	0.1						
		2290	2300	10	lml	1.0						
		2300	2323	23	lml	2.0		123		0.5		
		2323										

x

CRANDON MINING COMPANY

Sulfide Distribution Preproduction Development

	Logs											
Section	Hole	Fr Ft	To Ft	Tk Ft	Fm	TS Est%	Sulfide Notes	Tk Ft	< 5%WtAvg	> 5%WtAvg	Tk Ft	Fm WtAvg
2278581	73	960	990	30	sk	0.1		30	0.1			
		990	1050	60	rc	0.1						
		1050	1146	96	rc	0.0						
		1146	1154	8	rc	3.0						
		1154	1329	175	rc	0.0						
		1329	1334	5	rc	2.0						
		1334	1338	4	rc	2.0		348	0.1			
		1338	1400	62	ml	2.0						
		1400	1423	23	ml	0.5		85	1.6			
		1423	1430	7	lml	0.0						
		1430	1465	35	lml	0.0						
		1465	1496	31	lml	0.5						
		1496	1580	84	lml	0.0		157	0.03			
		1580										
		0										
		0										
		0										
		0										
		0										
		0										
												x

CRANDON MINING COMPANY

Sulfide Distribution Preproduction Development

	Logs											
Section	Hole	Fr Ft	To Ft	Tk Ft	Fm	TS Est%	Sulfide Notes	Tk Ft	< 5%WtAvg	> 5%WtAvg	Tk Ft	Fm WtAvg
2278188	74	108	200	92	sk	0.7	oxide					
		200	362	162	sk	0.5		254	0.6			
		362	400	38	rc	0.5						
		400	644	244	rc	0.0		282	0.1			
		644	760	116	ml	0.0		116	0.0			
		760	800	40	lml	0.0						
		800	810	10	lml	0.7						
		810	829	19	lml	0.7						
		829	877	48	lml	0.7		117	0.5			
											67	0.7
												x

CRANDON MINING COMPANY

Sulfide Distribution Preproduction Development

	Logs												
Section	Hole	Fr Ft	To Ft	Tk Ft	Fm	TS Est%	Sulfide Notes		Tk Ft	< 5%WtAvg	> 5%WtAvg	Tk Ft	Fm WtAvg
2279106	84	93	126	33	sk	0.0	Oxidized	s					
		126	184	58	sk	1.5		s					
		184	200	16	sk	3.0		s	107	1.3			
		200	210	10	sk	5.0		s	10		5.0		
		210	225	15	sk	0.0	Oxidized	s					
		225	247	22	sk	3.0		s					
		247	275	28	sk	0.0	Oxidized	s	65	1.0		182	1.4
		275	464	189	rc	0.1		r					
		464	480	16	rc	0.1		r					
		480	500	20	rc	0.0	Oxidized	r	225	0.1		225	0.1
		500	510	10	ml	1.5		m					
		510	526	16	ml	0.0	Oxidized	m	26	0.6			
		526	527	1	ml	30.0		m	1		30.0		
		527	532	5	ml	0.0	Oxidized	m	5				
		532	534	2	ml	25.0		m	2		25.0		
		534	542	8	ml	1.5		m					
		542	635	93	ml	0.5		m					
		635	660	25	ml	0.0		m	126	0.5		160	1.0
		660	768	108	lml	0.0	Oxidized	m	108	0.0		108	0.0
		768			cr								

x

CRANDON MINING COMPANY

Sulfide Distribution Preproduction Development

	Logs											
Section	Hole	Fr Ft	To Ft	Tk Ft	Fm	TS Est%	Sulfide Notes		Tk Ft	< 5%WtAvg	> 5%WtAvg	Tk Ft	Fm WtAvg
2277925	85	130	320	190	sk		no detail						
		320	771	451	rc		no detail						
		771	895	124	ml		no detail						
		895	936	41	lml		no detail						
		936	977	41	lml	2.0							
		977	1019	42	lml	1.0			83	1.5			
		1019											

x

CRANDON MINING COMPANY

Sulfide Distribution Preproduction Development

		Logs											
Section	Hole	Fr Ft	To Ft	Tk Ft	Fm	TS Est%	Sulfide Notes		Tk Ft	< 5%WtAvg	> 5%WtAvg	Tk Ft	Fm WtAvg
2278712	91	73	151	78	sk	0.0	oxidized						
		151	158	7	sk	0.1	ptly oxidized						
		158	175	17	sk	0.5	ptly oxidized		102	0.1			
		175	185	10	sk	5.0			10		5.0		
		185	195	10	sk	0.5							
		195	280	85	sk	0.5							
		280	295	15	sk	1.0							
		295	422	127	sk	0.5							
		422	443	21	sk	0.0							
		443	445	2	sk	3.0							
		445	505	60	sk	0.7							
		505	520	15	sk	1.0							
		520	565	45	sk	0.5							
		565	581	16	sk	0.1			396	0.5		508	0.5
		581	700	119	rc	0.1							
		700	792	92	rc	0.0			211	0.1			
		792	800	8	ml	0.0							
		800	813	13	ml	2.0							
		813	865	52	ml	0.0			73	0.4			
		865	868	3	lml	0.0							
		868	900	32	lml	0.5							
		900	924	24	lml	0.1							
		924	954	30	lml	1.0							
		954	998	44	lml	0.5			133	0.5			
		998											

x

CRANDON MINING COMPANY

Sulfide Distribution Preproduction Development

	Logs												
Section	Hole	Fr Ft	To Ft	Tk Ft	Fm	TS Est%	Sulfide Notes		Tk Ft	< 5%WtAvg	> 5%WtAvg	Tk Ft	Fm WtAvg
2278844	92	81	200	119	sk	0.5		s	119	0.5			
		200	257	57	sk	9.0			57		9.0		
		257	379	122	sk	0.5			122	0.5		298	2.1
		379	527	148	rc	0.5							
		527	532	5	rc	1.0							
		532	538	6	rc	0.5							
		538	546	8	rc	0.1							
		546	561	15	rc	0.7			182	0.5			
		561	571	10	ml	0.1							
		571	577	6	ml	0.7							
		577	593	16	ml	0.5							
		593	602	9	ml	0.1							
		602	630	28	ml	1.0							
		630	648	18	ml	0.7			87	0.6			
		648	663	15	lml	0.1							
		663	670	7	lml	0.1							
		670	750	80	lml	0.7							
		750	782	32	lml	0.7							
		782	784	2	lml	2.0			136	0.6			
		784	800	16	cr	2.0							
		800	809	9	cr	7.0							
		809	813	4	cr	3.0							
		813	821	8	cr	11.0							
		821	835	14	cr	0.5							
		835	851	16	cr	11.0							
		851											

x

CRANDON MINING COMPANY

Sulfide Distribution Preproduction Development

		Logs											
Section	Hole	Fr Ft	To Ft	Tk Ft	Fm	TS Est%	Sulfide Notes		Tk Ft	< 5%WtAvg	> 5%WtAvg	Tk Ft	Fm WtAvg
2278319	94	99	210	111	sk	0.0	oxidezed						
		210	300	90	sk	0.5			201	0.2			
		300	455	155	rc	0.0	oxidized						
		455	627	172	rc	0.0	oxidized						
		627	650	23	rc	0.5	ptly oxidized						
		650	675	25	rc	0.0	ptly oxidized		375	0.0			
		675	700	25	ml	0.0	ptly oxidized						
		700	750	50	ml	0.1	ptly oxidized		75	0.1			
		750	758	8	lml	0.1	ptly oxidized						
		758	825	67	lml	1.0							
		825	873	48	lml	0.7			123	0.8			
		873											
		0											
		0											
		0											
		0											
		0											
		0											
		0											
		0											
		0											
		0											

x

CRANDON MINING COMPANY

Sulfide Distribution Preproduction Development

	Logs												
Section	Hole	Fr Ft	To Ft	Tk Ft	Fm	TS Est%	Sulfide Notes		Tk Ft	< 5%WtAvg	> 5%WtAvg	Tk Ft	Fm WtAvg
2278188	98	138	235	97	sk	0.0							
		235	264	29	sk	1.0							
		264	303	39	sk	0.0							
		303	312	9	sk	1.0							
		312	338	26	sk	1.0							
		338	378	40	sk	2.0							
		378	400	22	sk	0.0							
		400	600	200	sk	0.7							
		600	710	110	sk	0.7			572	0.6			
		710	712	2	sk	15.0	cp		2		15.0		
		712	754	42	sk	0.7			42	0.7		616	0.7
		754	800	46	rc	0.7							
		800	1027	227	rc	0.0			273	0.1			
		1027	1143	116	ml	0.0							
		1143	1145	2	ml	3.0	cp						
		1145	1265	120	ml	0.0			238	0.03			
		1265	1300	35	lml	0.0							
		1300	1332	32	lml	0.7							
		1332	1341	9	lml	1.0							
		1341	1401	60	lml	0.7			136	0.5			
		1401											

x

CRANDON MINING COMPANY

Sulfide Distribution Preproduction Development

	Logs											
Section	Hole	Fr Ft	To Ft	Tk Ft	Fm	TS Est%	Sulfide Notes		Tk Ft	< 5%WtAvg	> 5%WtAvg	Tk Ft	Fm WtAvg
2278319	132	870	1000	130	ml	0.0	oxidized						
		1000	1030	30	ml	0.5	oxidized			0.1			
		1030	1060	30	ml	0.0			190	0.0			
		1060	1094	34	lml	0.0							
		1094	1138	44	lml	1.0							
		1138	1188	50	lml	0.1			128	0.4			
		1188											
		0											
		0											
		0											
		0											
		0											
		0											
		0											
		0											
		0											

x

CRANDON MINING COMPANY

Sulfide Distribution Preproduction Development

	Logs											
Section	Hole	Fr Ft	To Ft	Tk Ft	Fm	TS Est%	Sulfide Notes	Tk Ft	< 5%WtAvg	> 5%WtAvg	Tk Ft	Fm WtAvg
2277925	133	900	1100	200	ml	0.1		200	0.1			
		1100	1160	60	lml	1.0						
		1160	1295	135	lml	1.0		195	1.0			
		1295										

CRANDON MINING COMPANY

Sulfide Distribution Preproduction Development

		Logs											
Section	Hole	Fr Ft	To Ft	Tk Ft	Fm	TS Est%	Sulfide Notes		Tk Ft	< 5%WtAvg	> 5%WtAvg	Tk Ft	Fm WtAvg
2278581	140	1213	1400	187	sk	0.7							
		1400	1449	49	sk	0.7							
		1449	1500	51	sk	0.1							
		1500	1600	100	sk	0.7							
		1600	1638	38	sk	0.7							
		1638	1695	57	sk	0.7							
		1695	1800	105	sk	0.5			587	0.6			
		1800	1815	15	rc	0.7							
		1815	1829	14	rc	0.7							
		1829	1891	62	rc	0.7							
		1891	2535	644	rc	0.7							
		2535	2542	7	rc	0.1			742	0.7			
		2542	2622	80	ml	0.7							
		2622	2800	178	ml	0.7							
		2800	2815	15	ml	0.1							
		2815	2860	45	ml	1.0							
		2860	2900	40	ml	0.7							
		2900	2904	4	ml	0.0			362	0.7			
		2904	2920	16	lml	0.1							
		2920	2929	9	lml	0.1							
		2929	2942	13	lml	0.5							
		2942	2989	47	lml	0.1							
		2989	3024	35	lml	0.1			120	0.3			
		3024											
													x

CRANDON MINING COMPANY

Sulfide Distribution Preproduction Development

	Logs											
Section	Hole	Fr Ft	To Ft	Tk Ft	Fm	TS Est%	Sulfide Notes	Tk Ft	< 5%WtAvg	> 5%WtAvg	Tk Ft	Fm WtAvg
2278844	143	700	767	67	rc	0.0		67	0.0			
		767	910	143	ml	0.0		143	0.0			
		910	965	55	lml	0.0						
		965	1000	35	lml	0.5						
		1000	1100	100	lml	0.0						
		1100	1120	20	lml	1.0		210	0.2			
		1120										
		0										
		0										
		0										

x

CRANDON MINING COMPANY

Sulfide Distribution Preproduction Development

	Logs											
Section	Hole	Fr Ft	To Ft	Tk Ft	Fm	TS Est%	Sulfide Notes	Tk Ft	< 5%WtAvg	> 5%WtAvg	Tk Ft	Fm WtAvg
2278319	149	1100	1212	112	rc	0.0		112	0.0			
		1212	1384	172	ml	0.0						
		1384	1390	6	ml	2.0						
		1390	1560	170	ml	0.0		460	0.03			
		1560	1722	162	lml	0.0		162	0.0			
		1722										

x

CRANDON MINING COMPANY

Sulfide Distribution Preproduction Development

	Logs											
Section	Hole	Fr Ft	To Ft	Tk Ft	Fm	TS Est%	Sulfide Notes	Tk Ft	< 5%WtAvg	> 5%WtAvg	Tk Ft	Fm WtAvg
2278712	154	1202	1226	24	rc	1.5						
		1226	1300	74	rc	0.7						
		1300	1308	8	rc	1.5		106	0.9			
		1308	1354	46	ml	1.0						
		1354	1420	66	ml	1.0						
		1420	1442	22	ml	0.7						
		1442	1452	10	ml	1.0						
		1452	1500	48	ml	1.0						
		1500	1515	15	ml	1.0		207	1.0			
		1515	1588	73	lml	1.0						
		1588	1606	18	lml	1.0						
		1606	1660	54	lml	0.7		145	0.9			
		1660										
		0		0								
		0		0								
		0		0								
		0		0								
		0		0								

x

CRANDON MINING COMPANY

Sulfide Distribution Preproduction Development

		Logs											
Section	Hole	Fr Ft	To Ft	Tk Ft	Fm	TS Est%	Sulfide Notes		Tk Ft	< 5%WtAvg	> 5%WtAvg	Tk Ft	Fm WtAvg
2278188	155	111	200	89	sk	0.0	oxide						
		200	311	111	sk	0.0							
		311	353	42	sk	1.5							
		353	502	149	sk	0.5							
		502	514	12	sk	2.0							
		514	762	248	sk	0.5							
		762	860	98	sk	0.0			749	0.4			
		860	950	90	rc	0.0							
		950	1261	311	rc	0.0							
		1261	1280	19	rc	0.3							
		1280	1553	273	rc	0.0			693	0.0			
		1553	1554	1	rc	6.0			1		6.0		
		1554	1581	27	rc	0.2							
		1581	1583	2	rc	3.0							
		1583	1619	36	rc	0.0			65	0.2			
		1619	1652	33	rc	3.0			3		3.0		
		1652	1663	11	rc	6.0			11		6.0		
		1663	1940	277	rc	0.0							
		1940	1959	19	rc	0.1							
		1959	1965	6	rc	1.0							
		1965	2000	35	rc	0.1							
		2000	2022	22	rc	0.5							
		2022	2124	102	rc	0.1							
		2124	2183	59	rc	0.3							
		2183	2225	42	rc	0.0			562	0.1		1365	0.2
		2225	2470	245	ml	0.0							
		2470	2500	30	ml	0.5							
		2500	2680	180	ml	0.0							
		2680	2760	80	ml	1.0							
		2760	2830	70	ml	0.1							
		2830	2998	168	ml	0.0			528	0.3			
		2998											
													x

CRANDON MINING COMPANY

Sulfide Distribution Preproduction Development

	Logs											
Section	Hole	Fr Ft	To Ft	Tk Ft	Fm	TS Est%	Sulfide Notes	Tk Ft	< 5%WtAvg	> 5%WtAvg	Tk Ft	Fm WtAvg
2278188	160	1580	1600	20	rc	0.1						
		1600	1800	200	rc	0.7						
		1800	1995	195	rc	0.5						
		1995	2019	24	rc	1.0						
		2019	2056	37	rc	0.1		476	0.6			
		2056	2142	86	ml	0.1						
		2142	2254	112	ml	0.7						
		2254	2290	36	ml	0.7						
		2290	2330	40	ml	0.0						
		2330	2465	135	ml	2.0		409	0.9			
		2465	2569	104	lml	2.0		104	2.0			
		2569										
		0										
												x

CRANDON MINING COMPANY

Sulfide Distribution Preproduction Development

	Logs											
Section	Hole	Fr Ft	To Ft	Tk Ft	Fm	TS Est%	Sulfide Notes	Tk Ft	< 5%WtAvg	> 5%WtAvg	Tk Ft	Fm WtAvg
2278319	170	1000	1200	200	rc	0.0			0.0			
		1200	1205	5	rc	1.0						
		1205	1213	8	rc	3.0						
		1213	1250	37	rc	0.7		250	0.2		250	0.2
		1250	1256	6	ml	0.0						
		1256	1330	74	ml	0.0		80	0.0			
		1330	1395	65	lml	0.0						
		1395	1421	26	lml	5.0		26		5.0		
		1421	1452	31	lml	0.1		122	1.1			
		1452										

x

CRANDON MINING COMPANY

Sulfide Distribution Preproduction Development

	Logs											
Section	Hole	Fr Ft	To Ft	Tk Ft	Fm	TS Est%	Sulfide Notes	Tk Ft	< 5%WtAvg	> 5%WtAvg	Tk Ft	Fm WtAvg
2278581	172	1500	1642	142	rc	0.1						
		1642	1730	88	rc	0.7		230	0.3			

x

CRANDON MINING COMPANY

Sulfide Distribution Preproduction Development

		Logs											
Section	Hole	Fr Ft	To Ft	Tk Ft	Fm	TS Est%	Sulfide Notes		Tk Ft	< 5%WtAvg	> 5%WtAvg	Tk Ft	Fm WtAvg
2278844	174	700	720	20	rc	0.0			20	0.0			
		720	729	9	ml	1.0							
		729	870	141	ml	0.0			150	0.1			
		870	913	43	lml	0.0							
		913	928	15	lml	1.0							
		928	1000	72	lml	0.1							
		1000	1030	30	lml	0.0			160	0.1			
		1030											

x

CRANDON MINING COMPANY

Sulfide Distribution Preproduction Development

	Logs											
Section	Hole	Fr Ft	To Ft	Tk Ft	Fm	TS Est%	Sulfide Notes	Tk Ft	< 5%WtAvg	> 5%WtAvg	Tk Ft	Fm WtAvg
2278319	176	700	870	170	ml	0.0		170	0.0			
		870	900	30	lml	0.0						
		900	920	20	lml	1.0						
		920	985	65	lml	0.0						
		985	1021	36	lml	1.5		151	0.5			
		1021										

x

CRANDON MINING COMPANY

Sulfide Distribution Preproduction Development

	Logs											
Section	Hole	Fr Ft	To Ft	Tk Ft	Fm	TS Est%	Sulfide Notes	Tk Ft	< 5%WtAvg	> 5%WtAvg	Tk Ft	Fm WtAvg
2278188	214	0	364	364	sk	0.0	oxide					
		364	425	61	rc	0.0	oxide					
		425	928	503	ml	0.0	tr oxide					
		928	960	32	ml	0.0	tr oxide					
		960	1200	240	ml	0.2		240	0.2			
		1200										
												x

APPENDIX C
Fuel Oil Metal Composition

Fuel Oil Metal Composition

Constituent	Concentration (ppmw)
Arsenic	0.085
Beryllium	0.05
Cadmium	0.21
Chromium (Total)	0.95
Copper	5.6
Lead	0.18
Manganese	0.28
Mercury	0.06
Nickel	3.4

ppmw = parts per million weight

Source: *Estimating Air Toxics from Coal and Oil Combustion*, EPA-450/2-89/001.

APPENDIX D
Groundwater Modelling Plots

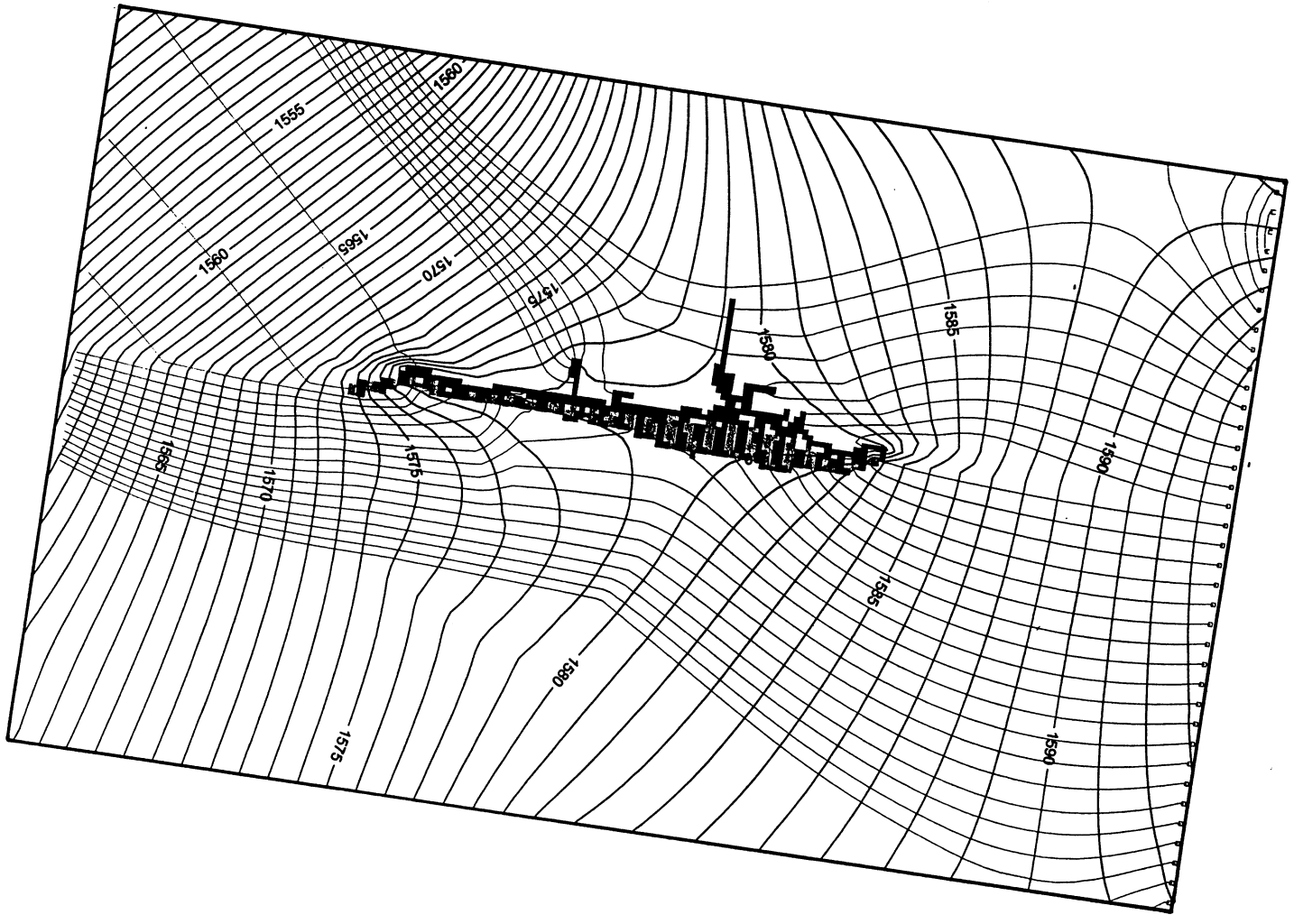

CONTOUR INTERVAL=1'

0 1000 2000 3000 4000 5000 FEET

1"=2000'

STEFFEN ROBERTSON AND KIRSTEN
Consulting Engineers

FOTH & VAN DYKE

REFLOODED MINE SOURCE TERM

GROUNDWATER FLOW MODEL 850 FOOT ELEVATION

PROJECT NO.	DATE	APPROVED	FIGURE
F107107/2	APRIL 1998	MDR	D-1

4.2-13-313

FILE REF: ELEV-850

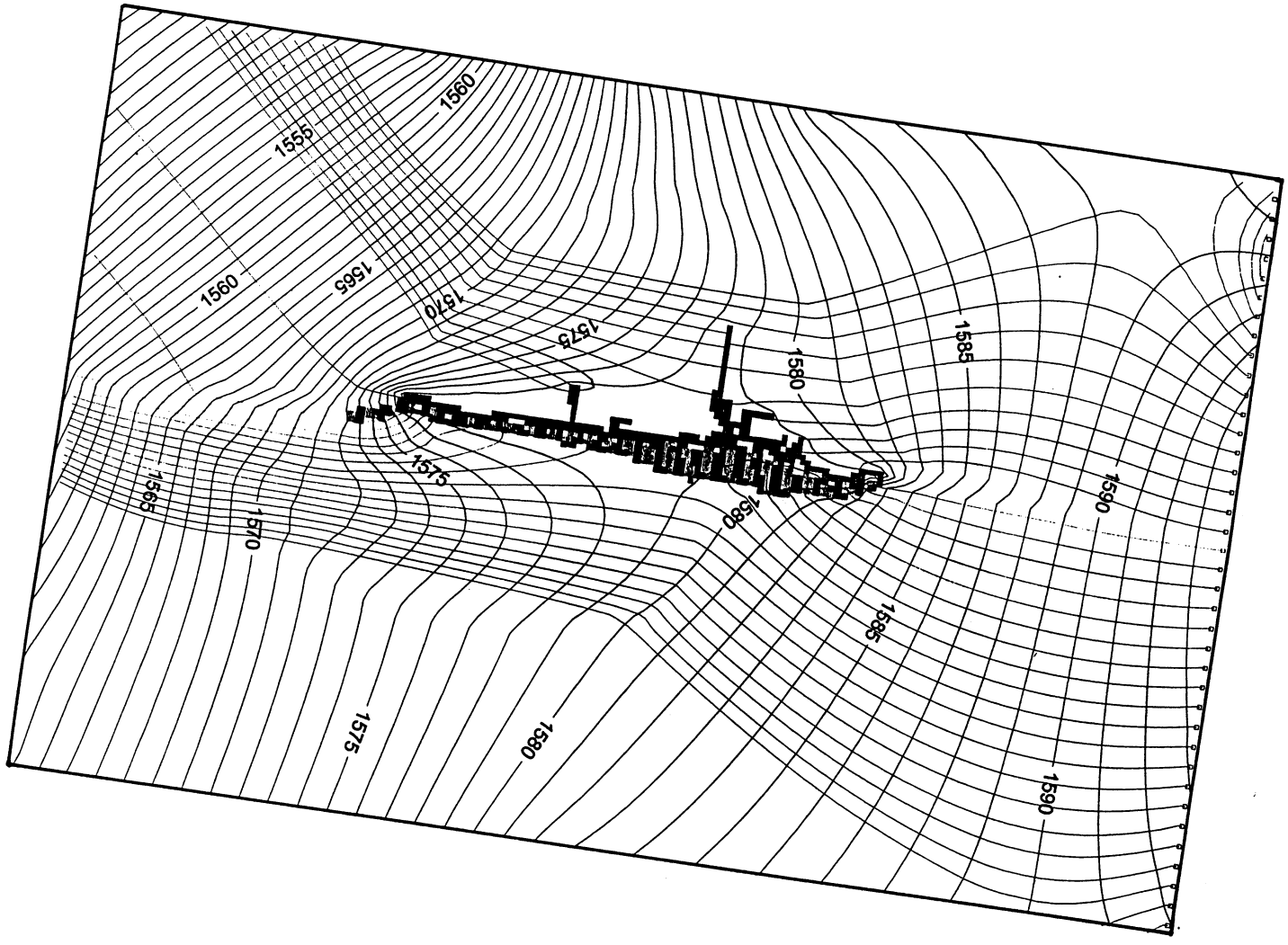

CONTOUR INTERVAL=1'

0 1000 2000 3000 4000 5000 FEET

1"=2000'

STEFFEN ROBERTSON AND KIRSTEN
Consulting Engineers

FOTH & VAN DYKE

REFLOODED MINE SOURCE TERM

GROUNDWATER FLOW MODEL 1050 FOOT ELEVATION

PROJECT NO.	DATE	APPROVED	FIGURE
F107107/2	APRIL 1998	MDR	D-2

4.2-13-314

FILE REF: ELEV-1050

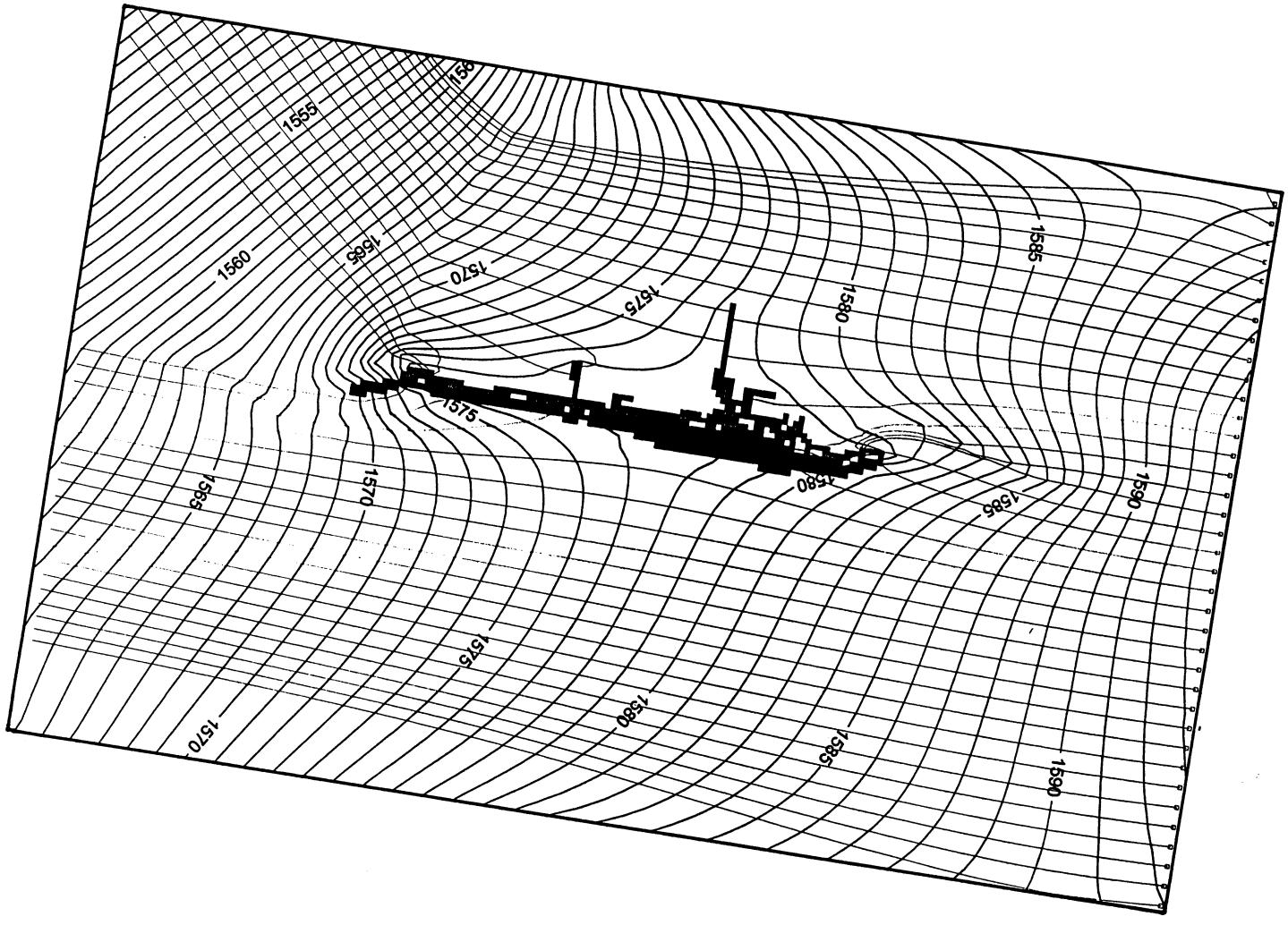

CONTOUR INTERVAL=1'

0 1000 2000 3000 4000 5000 FEET

1"=2000'

4.2-13-315

FILE REF: ELEV-1250

STEFFEN ROBERTSON AND KIRSTEN
Consulting Engineers

FOTH & VAN DYKE

REFLOODED MINE SOURCE TERM

GROUNDWATER FLOW MODEL 1250 FOOT ELEVATION

PROJECT NO.	DATE	APPROVED	FIGURE
F107107/2	APRIL 1998	MDR	D-3

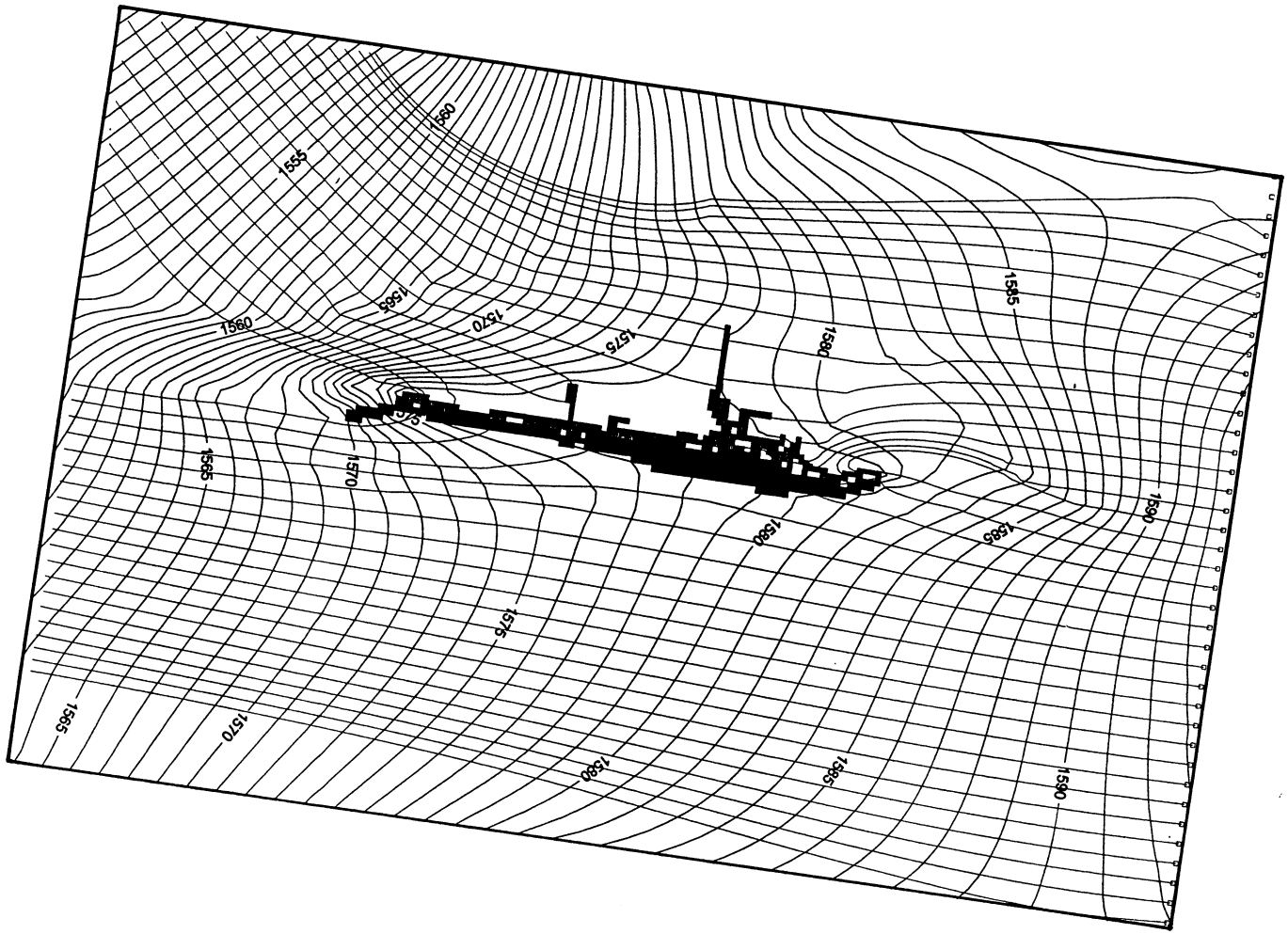

CONTOUR INTERVAL=1'

0 1000 2000 3000 4000 5000 FEET

1"=2000'

4.2-13-316

FILE REF: ELEV-1350

STEFFEN ROBERTSON AND KIRSTEN
Consulting Engineers

FOTH & VAN DYKE

REFLOODED MINE SOURCE TERM

GROUNDWATER FLOW MODEL 1350 FOOT ELEVATION

PROJECT NO.	DATE	APPROVED	FIGURE
F107107/2	APRIL 1998	MDR	D-4

Note: As a result of the April 1998 update to the Reflooded Mine Source Term - Crandon Project report, Figures D-5 through D-11 of Appendix D (pages 4.2-13-318 through 4.2-13-323) have been deleted.

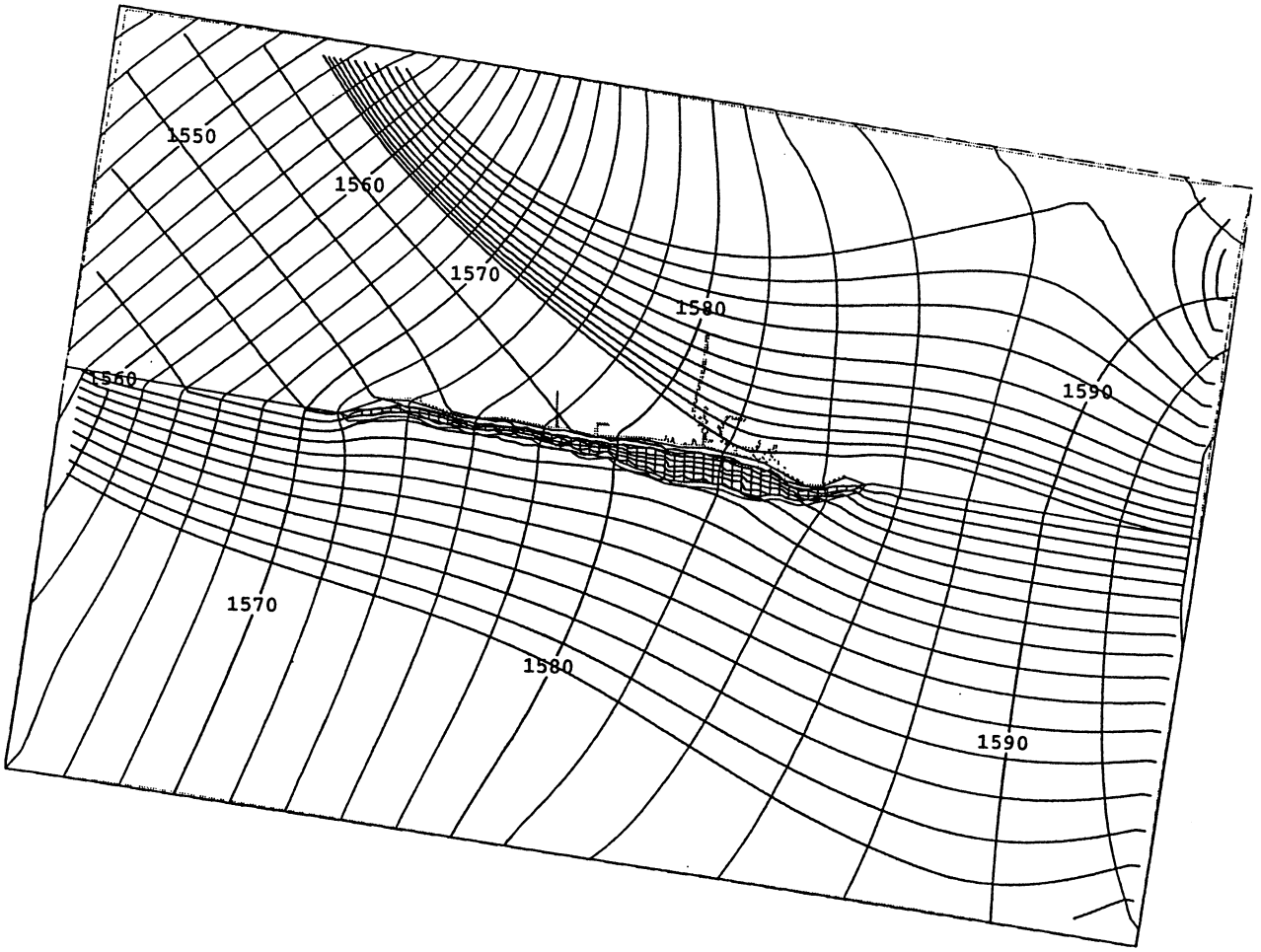

CONTOUR INTERVAL=10'

0 1000 2000 3000 4000 5000 FEET

1"=2000'

STEFFEN ROBERTSON AND KIRSTEN
Consulting Engineers

FOTH & VAN DYKE

REFLOODED MINE SOURCE TERM

GROUNDWATER FLOW MODEL SIMULATION 7–1300 FOOT LEVEL

PROJECT NO.	DATE	APPROVED	FIGURE
F107107	FEB. 1997		D-7

4.2-13-319

FILE REF: FIG-C-7

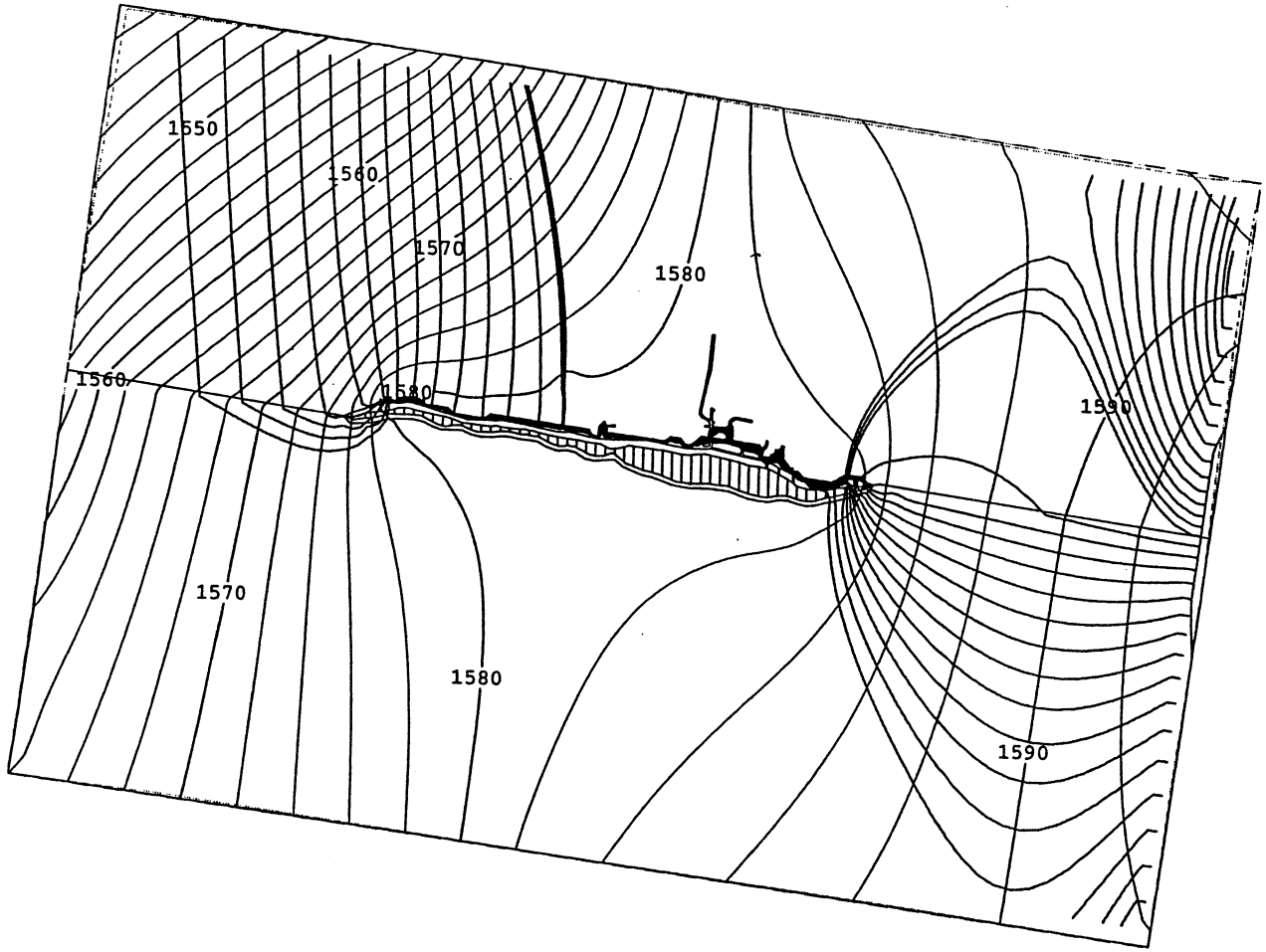

CONTOUR INTERVAL=10'

0 1000 2000 3000 4000 5000 FEET

1"=2000'

STEFFEN ROBERTSON AND KIRSTEN
Consulting Engineers

FOTH & VAN DYKE

REFLOODED MINE SOURCE TERM

GROUNDWATER FLOW MODEL SIMULATION 8–1250 FOOT LEVEL

PROJECT NO.	DATE	APPROVED	FIGURE
F107107	FEB. 1997		D-8

4.2-13-320

FILE REF: FIG-C-8

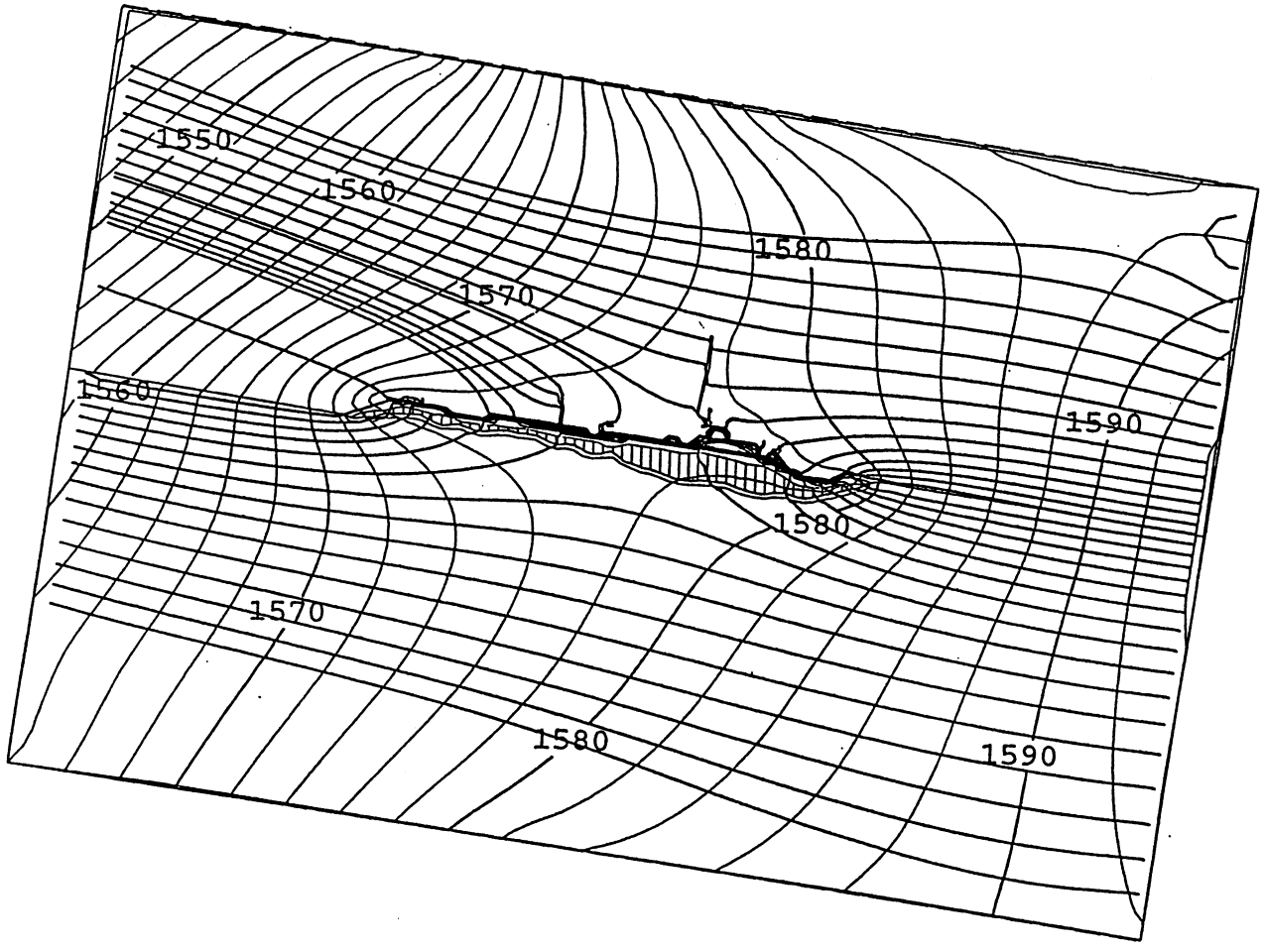

CONTOUR INTERVAL=10'

0 1000 2000 3000 4000 5000 FEET

1"=2000'

STEFFEN ROBERTSON AND KIRSTEN
Consulting Engineers

FOTH & VAN DYKE

REFLOODED MINE SOURCE TERM

GROUNDWATER FLOW MODEL
SIMULATION 9–1250 FOOT LEVEL

PROJECT NO.	DATE	APPROVED	FIGURE
F107107	FEB. 1997		D-9

4.2-13-321

FILE REF: FIG-D-9

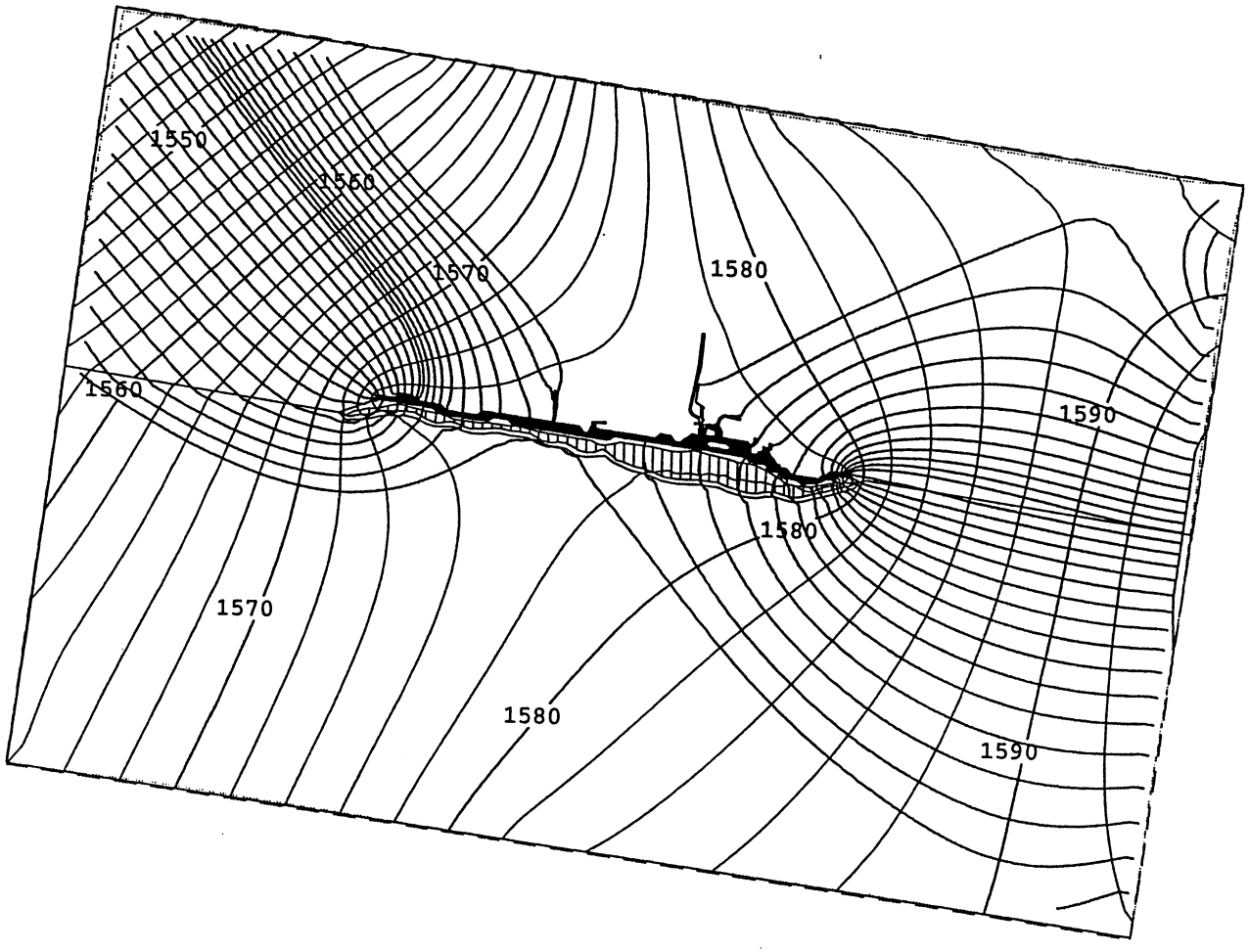

CONTOUR INTERVAL=10'

0 1000 2000 3000 4000 5000 FEET

1"=2000'

STEFFEN ROBERTSON AND KIRSTEN
Consulting Engineers

FOTH & VAN DYKE

REFLOODED MINE SOURCE TERM

GROUNDWATER FLOW MODEL SIMULATION 10–1400 FOOT LEVEL

PROJECT NO.	DATE	APPROVED	FIGURE
F107107	FEB. 1997		D-10

4.2-13-322

FILE REF: FIG-D-10

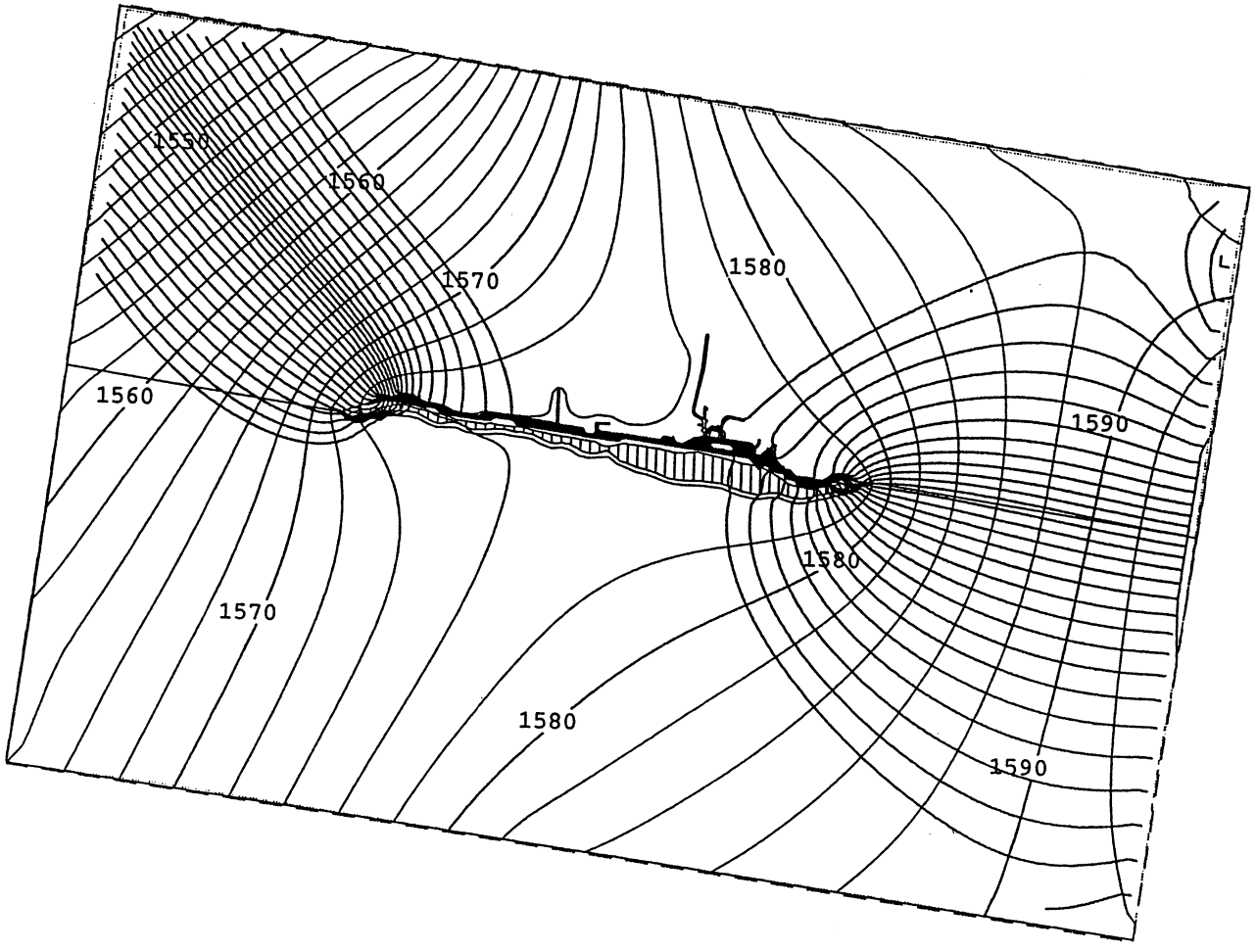

CONTOUR INTERVAL=10'

0 1000 2000 3000 4000 5000 FEET

1"=2000'

STEFFEN ROBERTSON AND KIRSTEN
Consulting Engineers

FOTH & VAN DYKE

REFLOODED MINE SOURCE TERM

GROUNDWATER FLOW MODEL SIMULATION 11–1400 FOOT LEVEL

PROJECT NO.	DATE	APPROVED	FIGURE
F107107	FEB. 1997		D-11

4.2-13-323

FILE REF: FIG-C-11

Appendix 4.2-14

HSI GeoTrans Technical Memorandum Pertaining to the Review of the November 1998 Reflooded Mine Source Term Report

HSI GEOTRANS
A TETRA TECH COMPANY

1080 Holcomb Bridge Road
Building 100, Suite 190
Roswell, Georgia
30076

770-642-1000 FAX 770-642-8808

MEMORANDUM

TO: Jerry Sevick, Foth and Van Dyke

FROM: Peter F. Andersen, HSI GeoTrans PFA

DATE: November 17, 1998

SUBJECT: Reflooded mine source term
HSI GeoTrans Project No. N015-023

INTRODUCTION

Groundwater modeling performed by HSI GeoTrans to assess the potential for solute transport from the orebody into the glacial system following mine reflooding consisted of evaluating:

- potential flow paths from the orebody past a compliance boundary, and;
- travel times from the orebody past a compliance boundary.

These factors were evaluated using the regional groundwater flow model documented in HSI GeoTrans (1998) and will be described in the solute transport model report (HSI GeoTrans, 1999). The analysis used particle tracking techniques to determine flowpaths and travel times. The results of the analysis indicated that particles could migrate within the bedrock or upwards into the glacial system towards a compliance boundary 1,200 feet from the orebody. Upwards migration into the glacial system was primarily restricted to the western side of the orebody following mine reflooding. Particle migration was found to be very slow, with transport times to the compliance boundary being on the order of thousands of years. In addition to the slow migration, the arrival times at the compliance boundary of particles originating at various locations in the orebody were found to be quite variable. The arrival times at the compliance boundary for the first 10 percent of the particles ranged over a 22,000 year period for the Best Engineering Judgement for Transport (BEJT) simulation. The arrival times for the first 50 percent of the particles ranged over a 100,000 year period. For the Practical Worst Case for Transport (PWCT) simulation, the arrival times at the

compliance boundary for the first 10 percent of the particles ranged over a 5,200 year period, while the arrival times for the first 50 percent of the particles ranged over a 24,000 year period.

Discussions with WDNR and USCOE indicated that they would reserve judgement as to whether the particle tracking simulations were a sufficient demonstration of compliance until they had reviewed data regarding the concentrations of source terms associated with the reflooded mine. I have reviewed the original and recently updated reports by SRK (1997, 1998a, and 1998b) and believe that the calculated source term concentrations are sufficiently low to preclude the necessity of additional analysis regarding attenuation between the orebody and the compliance boundary. Two primary reasons have led to this conclusion.

First, the concentrations of constituents *within the mine workings* will be further reduced as they migrate from the vicinity of the orebody and into the glacial system. I have calculated the expected concentration reduction factor under Best Engineering Judgement for Transport (BEJT) to range from 0.000084 to 0.000293 based on an analytical relationship that is shown below. These factors mean that concentrations will be reduced by 3412 (1/0.000293) times to 11905 (1/0.000084) times from the original concentration. These factors result in the concentration of all constituents to be below standards at the compliance boundary. Under Practical Worst Case for Transport (PWCT) conditions, the concentration reduction factor range from 0.000191 to 0.000679, based on the same analytical relationship cited earlier. These factors mean that concentrations will be reduced by 5235 (1/0.000191) times to 1493 (1/0.000670) times from the original concentration. These factors also result in the concentrations of all constituents to be below standards at the compliance boundary.

Second, the analyses that are documented in this memorandum use conservative simplifying assumptions that tend to overstate the concentrations beyond those that would have been determined had a more detailed analysis been performed. Examples of key conservative assumptions include neglecting dispersion, adsorption, and precipitation. These assumptions are discussed further later in this memorandum.

The calculations that were made to determine the concentration reduction factors cited above are based on mixing water that has come in contact with the mine workings with water flowing in the glacial system. The flow rate across the compliance boundary of water originating from the orebody is based on the particle tracking analysis. The number of particles crossing the compliance boundary is weighted to correspond to volume represented by each particle, and

the volumeteric flow rate versus time is computed. The flow in the glacial system is determined with a simple Darcy evaluation of the flow in the glacial system in the vicinity of the orebody.

MIXING CALCULATION

Particles cross the compliance boundary over a 10,000,000 year period in the BEJT case (HSI GeoTrans, 1999). Note that the number of particles crossing the compliance boundary versus time is greatest during the initial 200,000 year period and then gradually decreases with time. For a conservative mixing calculation, the highest flow rate originating from the orebody crossing the compliance boundary is of most interest. This rate was approximated by assigning a volume represented by each particle, based on the volume of the grid cell times porosity, and computing the cumulative volume of flow across the boundary versus time. The greatest flow rate then corresponds to the steepest portion of the cumulative volume plot (Figure 1). For the BEJT case, this flow rate is 460 ft^3/yr, or 1.26 ft^3/d, based on the time period between 20,000 and 40,000 years.

If we assume that this entire quantity exits upward into the overburden prior to crossing the compliance boundary, then it will mix with lateral flow in the glacial system. Lateral flow in the glacial system is governed by Darcy's Law:

$$Q = Kibw$$

where:	Q	=	volumetric flow rate [L^3]
	K	=	horizontal hydraulic conductivity [L/T]
	i	=	horizontal hydraulic gradient [L/L]
	b	=	thickness of flow regime
	w	=	width of flow regime

The lateral flow in the Pre- to Early Wisconsinan Till/massive saprolite may be approximated from Darcy's Law as:

$$Q_{EWT} = Kibw$$

where:

Q_{EWT}	=	lateral flow in Pre- to Early Wisconsinan Till/massive saprolite
K	=	2.0 ft/d, from HSI GeoTrans (1998),
i	=	10 ft / 2000 ft, from potentiometric surface maps,
b	=	100 feet, from geologic cross-sections, and
w	=	4300 feet, from width of flow net in SRK (1998a) (see Figure 2)

therefore:

$$Q_{EWT} = 2.0\ ft/d\ x\ \frac{10\ ft}{2000\ ft}\ x\ 100\ ft\ x\ 4300\ ft$$

$$Q_{EWT} = 4300\ ft^3/d$$

The ratio of upward flow from the bedrock to lateral flow in the Pre- to Early Wisconsinan Till within the compliance boundary is the concentration reduction factor.

$$Concentration\ reduction\ factor = \frac{Q_{Bedrock}}{Q_{EWT}}$$

Substituting the flow crossing the compliance boundary and flows computed above gives:

$$\frac{1.26\ ft^3/d}{4300\ ft^3/d} = 0.000293$$

Some of the flow from the bedrock may continue to flow upwards into the outwash deposits. If we assume that it will mix with flow in the lower 10 feet of the outwash deposits, then

$$Q_{OW} = Kibw$$

where:

Q_{ow}	=	lateral flow in lower 10 ft of the outwash deposits
K	=	50 ft/d, average value of coarse and fine outwash, from HSI GeoTrans (1998),
i	=	10 ft / 2000 ft, from potentiometric surface maps,
b	=	10 feet, conservative assumption for mixing zone,
w	=	4300 feet, from width of flow net in SRK (1998a)

therefore:

$$Q_{OW} = 50\ ft/d\ x\ \frac{10\ ft}{2000\ ft}\ x\ 10\ ft\ x\ 4300\ ft$$

$$Q_{OW} = 10750\ ft^3/d$$

The ratio of upward flow from the bedrock to lateral flow in the glacial deposits (outwash and Pre- to Early Wisconsinan Till) within the compliance boundary is the concentration reduction factor.

$$Concentration\ reduction\ factor = \frac{Q_{Bedrock}}{Q_{EWT} + Q_{OW}}$$

Substituting the flow crossing the compliance boundary and flows computed above gives:

$$\frac{1.26\ ft^3/d}{4300\ ft^3/d + 10750\ ft^3/d} = 0.000084$$

Based on these calculations, the concentration reduction factor under BEJT conditions ranges from 0.000084 to 0.000293.

Under PWCT conditions, the maximum volumetric flow of water originating from the orebody is 1050 ft^3/yr, or 2.88 ft^3/d, based on the particle tracking for the period between 20,000 and 40,000 years (Figure 1).

Using the same methodology as was used for the BEJT calculation, the concentration reduction factor under PWCT conditions is:

$$\frac{2.88\ ft^3/d}{4300\ ft^3/d} = 0.000670$$

for mixing within the Pre- to Early Wisconsinan Till only. For mixing within the till and outwash it is:

$$\frac{2.88\ ft^3/d}{4300\ ft^3/d + 10750\ ft^3/d} = 0.000191$$

Based on these calculations, the concentration reduction factors for the PWCT case ranges from 0.000191 to 0.000670. Note that the flows through the Pre- to Early Wisconsinan Till/massive saprolite and outwash deposits are the same for the PWCT case and the BEJT case. This is because the PWCT case does not alter the outwash hydraulic conductivity or the horizontal Pre- to Early Wisconsinan Till/massive saprolite hydraulic conductivity.

These calculations contain several conservative assumptions that will tend to underestimate the amount of mixing that will occur. First, it is assumed that *all* pore water in the orebody will mix with the glacial deposits. Therefore, the quantity used in the numerator of the concentration reduction factor calculation is conservatively high, resulting in less mixing in the glacial system than will actually occur. The second conservative assumption is that dispersion is neglected, which will tend to provide greater mixing and a reduction in concentration if included in the calculation. Third, adsorption and chemical precipitation are not accounted for, which will tend to further increase the travel time, spread out the time over which the particles cross the compliance boundary, and reduce peak concentrations.

CONCLUSIONS

In summary, we have reviewed the source term concentrations derived by SRK (1998b) and have determined their significance relative to compliance with groundwater standards. We have made mixing calculations for the BEJT and PWCT cases to determine the concentration reduction due to mixing with water

within the compliance boundary. These calculations are relatively simple and contain several assumptions that would tend to underestimate the amount of mixing and overestimate the concentrations.

The calculations show that expected concentration reduction factor for the BEJT case ranges from 0.000084 to 0.000293. This number represents the factor that concentrations in the mine workings should be multiplied by to determine the concentration at the compliance boundary. The calculations show that the concentration reduction factor for the PWCT ranges from 0.000191 to 0.000670.

When these factors are applied to the concentrations within the mine workings (flow weighted average) obtained by SRK (1998b), the concentrations of all constituents at the proposed compliance boundary are below the currently anticipated groundwater standards (see Table 1). In addition, the incremental increases in concentrations are likely to be significantly below background concentrations and therefore the incremental increase at the compliance boundary would not be measurable.

Given the conservatism that has been built into these first order dilution calculations (including neglecting dispersion, adsorption, and precipitation), and the long travel times determined from particle tracking analysis described in the solute transport modeling report (HSI GeoTrans, 1999), we do not believe that there is a reasonable expectation that the groundwater standards would be exceeded at the compliance boundary. Therefore, additional assessment is not necessary to further quantify concentration reductions between the orebody and the compliance boundary for the reflooded mine scenario.

REFERENCES

HSI GeoTrans, 1998. Addendum No. 2 to Numerical Simulation of the Effect on Groundwater and Surface Water of the Proposed Zinc and Copper Mine Near Crandon, Wisconsin. Consulting report prepared for Foth & Van Dyke. August 28, 1998.

HSI GeoTrans, 1999. Update No. 2 to: Numerical Simulation of Potential Solute Transport at the Proposed Zinc and Copper Mine Near Crandon, Wisconsin. Consulting report prepared for Foth & Van Dyke. In preparation.

SRK, 1997. Reflooded Mine Source Term. Consulting report prepared for Foth & Van Dyke. March 1997.

SRK, 1998a. Comments on Reflooded Mine Source Term for the Proposed Crandon Mine. Consulting report prepared for Foth & Van Dyke. April 1998.

SRK, 1998b. Crandon Project - Reflooded Mine Source Term. Assessment for Cemented Pyrite Paste Backfill. Consulting report prepared for Foth & Van Dyke. November, 1998.

Table 1. Estimated Concentration in the Glacial Overburden at the Proposed 1200 Foot Compliance Boundary for the Reflooded Mine

Constituent	concentration (mg/l) in mine workings (SRK, 1998b)	Estimated Concentrations (mg/l)				Anticipated groundwater standard[1] (mg/l)	
		low range BEJT conditions concentration in mine workings x0.000084	high range BEJT conditions concentration in mine workings x0.000293	low range PWCT conditions concentration in mine workings x0.000191	high range PWCT conditions concentration in mine workings x0.00067	Preventative Action Limit	Enforcement Standard
Sulfate	2025	0.17010	0.59333	0.38678	1.35675	125	250
Arsenic	1.22	0.00010	0.00036	0.00023	0.00082	0.005	0.05
Copper	1.01	0.00008	0.00030	0.00019	0.00068	0.13	1.3
Iron	37	0.00311	0.01084	0.00707	0.02479	0.15	0.3
Manganese[2]	2.6	0.00022	0.00076	0.00050	0.00174	0.025	0.05
Selenium	0.35	0.00003	0.00010	0.00007	0.00023	0.01	0.05
Zinc	48	0.00403	0.01406	0.00917	0.03216	2.5	5

[1] NR 140 Enforcement Standards and Preventative Action Limits

[2] Parameter likely to have an alternate concentration level due to background concentrations above the standard.

Prepared by: PFA
Checked by: SVD1
Approved by: JWS

P:\CMC\DOC\REFLD98B.WPD

\Crandon\Flowmod2\Excel\Reflood.xls

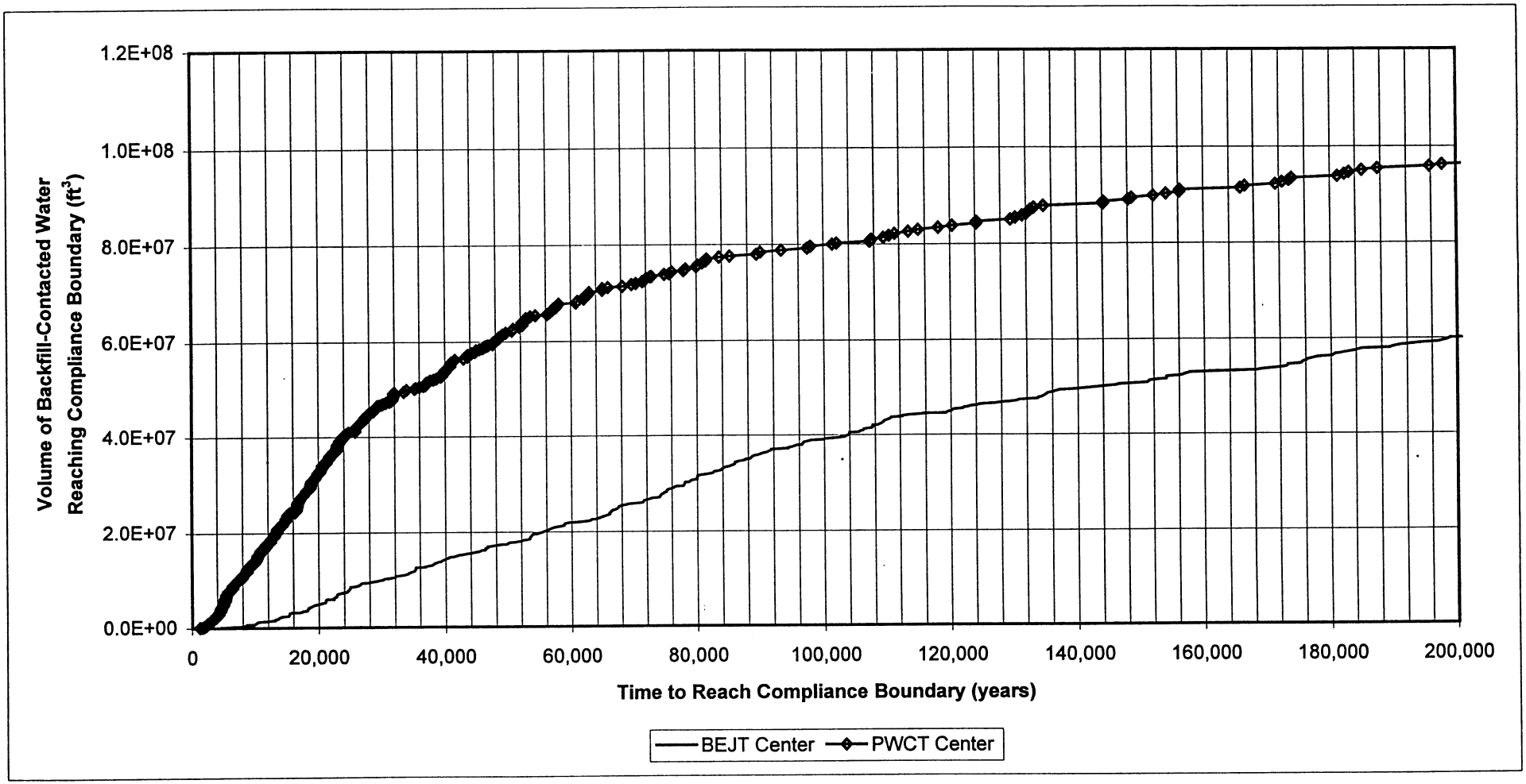

4.2-14-10

HSI GEOTRANS			
REVISED	DATE	BY	DESCRIPTION
CHECKED BY: KMR			DATE: 11/98
APPROVED BY: PFA			DATE: 11/98
APPROVED BY: SVD1			DATE:

Simulation 49T1 & 50T4

Nicolet Minerals COMPANY

Figure 1
Volume-Time Curves for Particle Tracking Simulations

Scale: None	Date: Nov 1998
Prepared By: HSI GEOTRANS	By: GWC

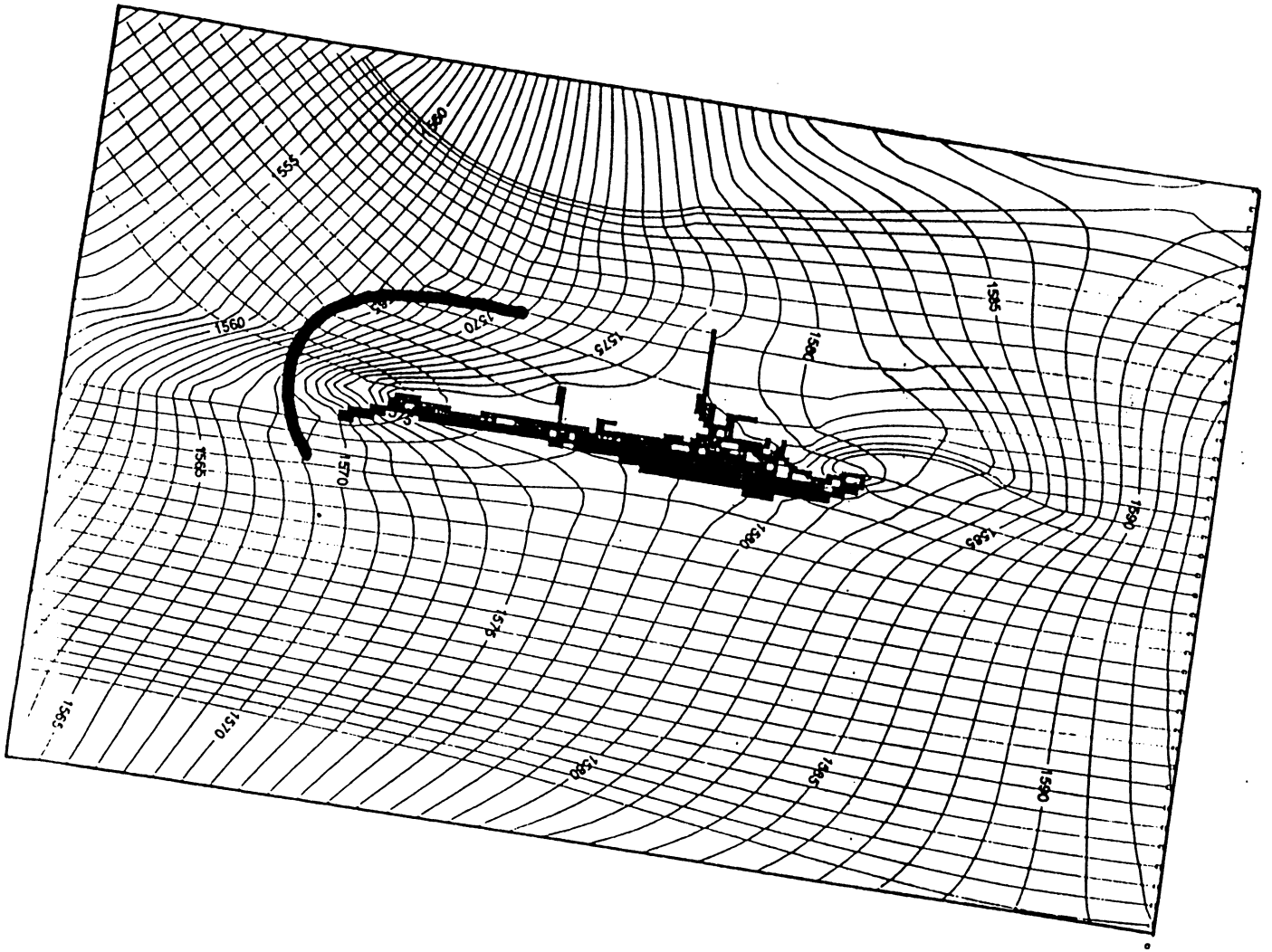

CONTOUR INTERVAL=1'

0 1000 2000 3000 4000 5000 FEET

1"=2000'

STEFFEN ROBERTSON AND KIRSTEN
Consulting Engineers

FOTH & VAN DYKE

REFLOODED MINE SOURCE TERM

GROUNDWATER FLOW MODEL
1350 FOOT ELEVATION

PROJECT NO.	DATE	APPROVED	FIGURE
F107107/2	APRIL 1998	MDR	

FILE REF. FIG-C-1

4.2-14-11

FIGURE 2 FLOW FIELD WIDTH